Bulletin of the Geological Society of Greece
Special Publication No. 10, 2022

OCT **17-19** 2022
PATRAS | GREECE

Our Earth Our Home

16th International Congress Geological Society of Greece

GSG 2022

BOOK OF ABSTRACTS

www.gsg2022.gr

16th International Congress of the Geological Society of Greece

GEOLOGICAL SOCIETY OF GREECE
Board Members

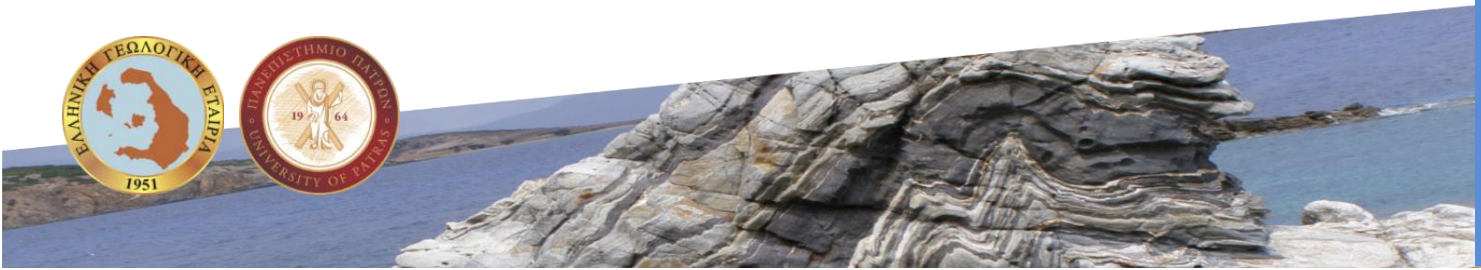

16th INTERNATIONAL CONGRESS of the GEOLOGICAL SOCIETY OF GREECE

Organizing Committee

Chair

Paris XYPOLIAS	University of Patras

Vice-chair

Efthimios SOKOS	University of Patras

Secretariat

Pavlos AVRAMIDIS	University of Patras
Stavros KALAITZIDIS	University of Patras
Sotirios KOKKALAS	University of Patras
Petros KOUTSOVITIS	University of Patras
Zafeiria ROUMELIOTI	University of Patras

Treasurer

Georgios BATHRELLOS	University of Patras

Members

Georgios AGGELOPOULOS	Geotechnical Chamber of Greece – branch of W. Greece & Peloponnese, Association of Greek Geologists
Asimina ANTONARAKOU	National and Kapodistrian University of Athens
Kimon CHRISTANIS	University of Patras
Athanasios GANAS	National Observatory of Athens
Ioannis KOUKOUVELAS	University of Patras
Efthimios LEKKAS	National and Kapodistrian University of Athens, Earthquake Planning and Protection Organization
Constantinos LOUPASAKIS	National Technical University of Athens
Emmanuel MANOUTSOGLOU	Technical University of Crete
Ioannis PAPANIKOLAOU	Agricultural University of Athens
Georgios PAPATHEODOROU	University of Patras
Konstantinos PAPAZACHOS	Aristotle University of Thessaloniki
Efthimios SPYRIDIS	Geotechnical Chamber of Greece
Aristofanis STEFATOS	Hellenic Hydrocarbon Resources Management S.A.
Avraam ZELILIDIS	University of Patras

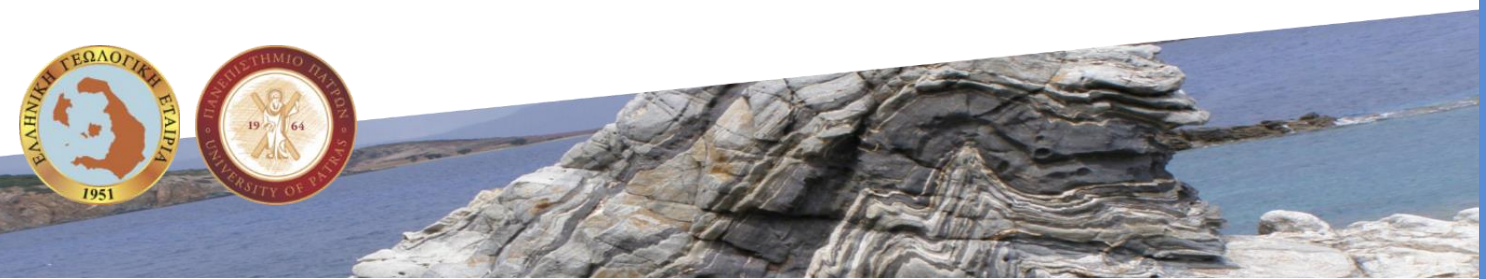

OUR EARTH, OUR HOME

16th INTERNATIONAL CONGRESS of the
GEOLOGICAL SOCIETY OF GREECE

Scientific Committee

Pascal BERNARD	Institut de Physique du Globe de Paris
Pierre BRIOLE	École Normale Supérieure
Pier-Paolo BRUNO	University of Napoli Federico II
Riccardo CAPUTO	University of Ferrara
Konstantinos CHALIKAKIS	University of Avignon
Vasileios CHATZARAS	University of Sydney
Elias CHATZITHEODORIDIS	National Technical University of Athens
Giuseppe ETIOPE	Istituto Nazionale di Geofisica e Vulcanologia
Niki EVELPIDOU	National and Kapodistrian University of Athens
Anne EWING-RASSIOS	Hellenic Survey of Geology and Mineral Exploration
Maria FERENTINOU	Liverpool John Moores University
Anestis FILIPPIDIS	Aristotle University of Thessaloniki
Thomas GENTZIS	Corelabs, USA
Aggeliki GEORGIOPOULOU	University of Brighton
Tassos GRAMMATIKOPOULOS	SGS, Canada
Bernhard GRASEMANN	University of Vienna
Philip HUGHES	University of Manchester
Laurent JOLIVET	Sorbonne University
Anastasia KIRATZI	Aristotle University of Thessaloniki
Kiki MAKRI	National Observatory of Athens
Eleni ZAGGANA	University of Patras
Olga SYKIOTI	National Observatory of Athens
Efthimios KARYMBALIS	Harokopio University
Maria TRIANTAFYLLOU	National and Kapodistrian University of Athens
Nikolaos KOUKOUZAS	Centre for Research and Technology Hellas
Konstantinos KONSTANTINOU	National Central University, Taiwan
Anna KORRE	Imperial College
Andreas MAGGANAS	National and Kapodistrian University of Athens
Hampik MAROUKIAN	National and Kapodistrian University of Athens
Angelos MAVROMATIDIS	Abu Dhabi National Oil Company, UAE
Dimitrios PAPANIKOLAOU	National and Kapodistrian University of Athens
Spyridon PAVLIDES	Aristotle University of Thessaloniki
Maria SACHPAZI	National Observatory of Athens

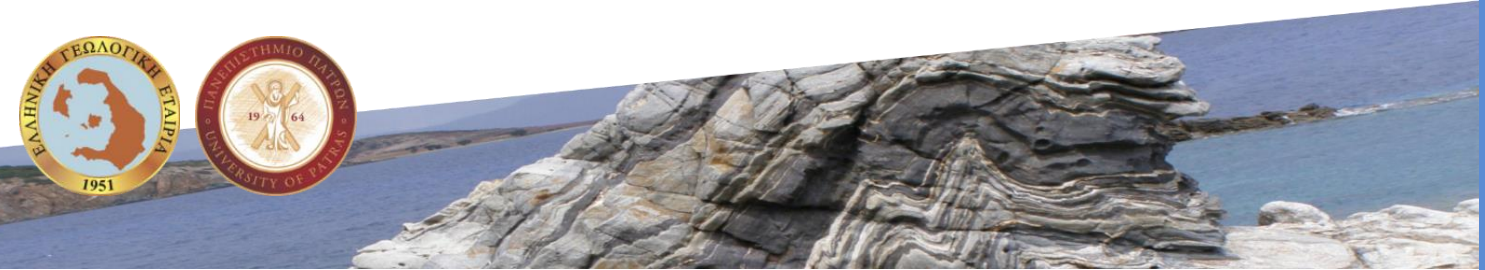

OUR EARTH, OUR HOME

Mike SEARLE	University of Oxford
Margarita SEGOU	British Geological Survey
George SIAVALAS	Shell Global Solutions International
Andreas SKARLATOUDIS	AECOM, USA
Filippos TSIKALAS	University of Oslo
Vasileios TSIKOURAS	University of Brunei Darussalam
Chronis TZEDAKIS	University College London
Eva VALSAMI-JONES	University of Birmingham
Andreas VÖTT	University of Mainz
Christos EVANGELIDIS	National Observatory of Athens
Konstantinos SOUKIS	National and Kapodistrian University of Athens
Charalampos FASSOULAS	Natural History Museum of Crete
Gernold ZULAUF	Goethe University, Germany
Jiří ZAHRADNIK	Charles University, Czech Republic
Theodoros NTAFLOS	University of Vienna, Austria

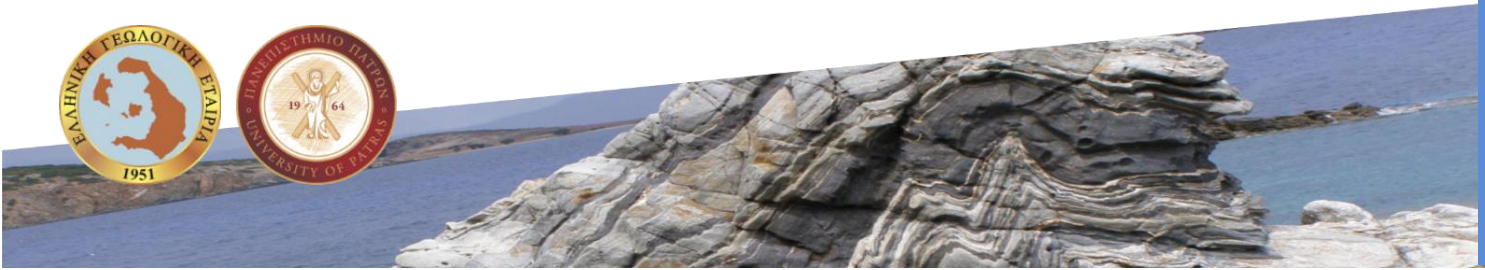

Keynote Speakers

Anna Korre

Co-Director of Energy Futures Lab and Professor of Environmental Engineering at Imperial College London, UK

Professor Korre joined Imperial in 1993 as a Marie Sklodowska Curie Research Fellow, having completed her BSc in Geology at the University of Athens. She became Energy Futures Lab's Co-Director in September 2018. EFL is the College's energy institute, established in 2005 to address global energy challenges by identifying and leading new opportunities to serve industry, government and society at large. Anna also heads the Minerals Energy and Environmental Engineering Research Group, developing engineering solutions to the supply of clean energy, the sustainable production of natural resources, and mitigating environmental impacts and risks. Her research focus is in the areas of modelling risk and uncertainty and the environmental and life cycle assessment of engineering systems. She has led and participated in numerous industry, UKRI, BEIS, The Crown Estate and EU funded projects developing engineering tools to assess the impacts of the minerals and energy industries in terms of operational performance, environmental footprint and cost.

Theodoros Ntaflos

Professor of Petrology and Geochemistry at the University of Vienna, Austria

Member of the Expert Board of the National Science Center, Poland. Guest professor at the Unversity of Bahia Blanca, Argentina (2014, 2016), at the University of Ferrara (2013), Italy and at the University of Wloclaw, Poland (2015, 2017). Guest Editor of the scientific Jounal Lithos. Co-author in 147 peer-reviewed journal papers with over 2000 citations. Expertise in Earth Mantle petrology and geochemistry Patagonia, NE-Siberia, Russia and Pannonian Basin. Expertise in magmatic processes of basaltic rocks Pannonian Basin and in petrology and geochemistry of the explosive lavas of Etna.

Jiří Zahradník

Professor of Geophysics at the Faculty of Mathematics and Physics, Charles University, Prague, Czech Republic

Head of the Department of Geophysics in 1993-2006 and vice-head 2006-2010. Vice-President of the European Seismological Commission in 2004-2006. Associate editor of the Journal of Seismology in 2002-2017. Invited lecture courses in Costa Rica, Colombia, Brasil, Cuba. Co-author of more than 100 journal papers with over 1300 citations. Expertise in seismic source studies, earthquakes of the Eastern Mediterranean. Leader of the Prague group that jointly with the University of Patras has built and co-operated 11 seismic stations and 6 GNSS stations in Greece (since 1997). Award: The Ernst Mach Honorary Medal for Merit in the Physical Sciences (Czech Academy of Sciences, 2018).

Gernold Zulauf

Professor of Geology at Goethe University, Frankfurt a.M., Germany

Founder chair of Geoscience Department of Goethe Universität in 2004-2005. Vice chair (Prodekan) of Geoscience Faculty of Goethe Universität in 2008-2011. Secretary of GV (Geologische Vereinigung) in 2000-2006, Vice Chairman of DGG (Deutsche Gesellschaft für Geowissenschaften) in 2008-2011, Chairman of DGG (Deutsche Gesellschaft für Geowissenschaften) in 2011-2014, Member of DFG Review Board (German Research Foundation) in 2012-2016, Vice Chairman of DGGV (Deutsche Geol. Gesellschaft/Geol. Vereinigung) in 2014-2017. Guest lecturer at Istanbul University (2009, 2010). Co-author of more than 140 peer-reviewed journal papers with over 2500 citations. Expertise in Geodynamic evolution of Hellenides, Variscides and Cadomides; Modelling and assessing geological structures in 3D; Deformation of salt rocks; and Microfabrics and deformation mechanisms of deformed rocks. Award: Hermann-Credner Award 1998 of DGG.

16th INTERNATIONAL CONGRESS of the
GEOLOGICAL SOCIETY OF GREECE

Keynote Abstracts

OUR EARTH, OUR HOME

16th International Congress of the Geological Society of Greece
17-19 October, 2022 - Patras, Greece
Bulletin of the Geological Society of Greece, Sp. Publ. 10
Ext. Abs. GSG2022-A2

The geochemical and petrological evolution of the Etna volcano through the time

Th. Ntaflos
Department of Lithospheric Research, Vienna, Austria, theodoros.ntaflos@univie.ac.at

Mt. Etna with an elevation of 3,340 m is the largest active subaerial volcano in Europe is Mt. Etna. It is located along the eastern coast of Sicily in a complex tectonic setting between the colliding African and European plates (Fig. 1). Upwelling asthenospheric mantle passing through the window that created between the african plate, the subducting and rolled back Ionian lithosphere and the overriding Tyrrenian plate, caused voluminous melting underneath Mt. Etna (Gvitzman & Nur, 1999).

The volcanic activity of Mt. Etna begun around 600 ka ago and it is divided into four phases (Branca *et al.*, 2011): the first phase the Basal Tholeiitic is a long period of volcanic activity (~350-380 ka) characterized by submarine to subaerial eruptions of tholeiitic composition lavas. The second phase, referred as the Timpe phase volcanism, characterizes the period between 220 to 110 ka ago. During this phase, has taken place the transition of the erupted lavas from sub-alkaline to Na-alkaline affinity. The third phase characterizes the time between 110 and 65 ka ago and is associated to the formation of the alkaline central -conduit edifices and to the horse-shoe Valle Del Bove depression in the southern flank of Etna. The fourth phase the Stratovolcano, comprises the time from 65 ka ago to recent and is divided into the periods Ellittico (57-15 ka) and Mongibello (<15 ka). The Ellittico period is characterized by lavas with Na-alkaline composition and pyroclastic products whereas the products of the Mongibello period up to 1971 are basaltic lava flows and explosive eruptions. The post Mongibello period shows a gradual compositional transition from Na- towards to K-alkaline affinity lavas.

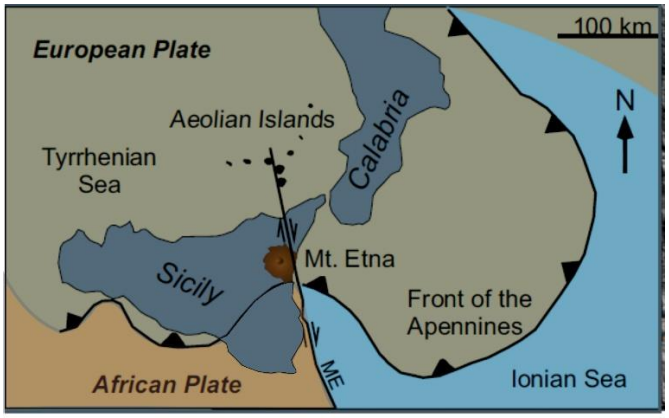

Figure 1. Map showing the plate tectonic constrains and the location of Mt. Etna (modified after Kahl *et al.*, 2015)

Magma mixing and/or mingling are the most frequent process identified in the Mt. Etna lavas. Several studies using the chemical variations of the phenocrysts clinopyroxene (Petrone *et al.*, 2018) and olivine (Kahl *et al.*, 2015) attributed to magma mixing processes are dedicated in deciphering the evolutionary stages of the upwelling magma from the source to the surface.

We studied the 2002-2003 effusive fissure eruption at 2750 m a.s.l. in the NE flank of the volcano. The rocks are trachybasalts, which were collected directly from the fissure and therefore represent the very last effusive lavas of this eruption. The texture is porphyritic and the mineralogical assemblage is dominated by clinopyroxene phenocrysts with olivine and Fe-Ti oxide inclusions and complex zoning followed by olivine and plagioclase, which frequently shows cores with sieve texture. The groundmass consists of clinopyroxene, olivine, plagioclase, Ti-Fe oxides and variable amounts of glass.

High precision EPMA analyses of olivne phenocrysts have shown simultaneous occurrence of normal and complex inverse zoning. According to the detailed elemental profiles of major, minor and trace elements, the olivine is divided into three groups: group A with normal zoning, group B with inverse zoning, and group C overgrowth on existing olivine with normal and inverse zoning. The rim to rim compositional profiles in olivine grains of the group A show a remarkably wide plateau with Mg#=80-83 and Ni=1000-1700 ppm and a narrow up to 50 microns wide rim where the Mg# drops to 75-73 and the Ni content to 420 ppm. The olivine from group B is characterized by inverse zoning. It has, like group A olivine, a wide compositional plateau but rims with variable thickness. The Mg# at the plateau vary systematically from grain to grain between 69 and 74, whereas the up to 100 microns wide rims show a bell-shaped profile with maximum Mg# between 77 and 79 which, at the very rim in contact with matrix, drops to values similar to those in the corresponding

plateau. The Ni-contents at the plateau vary from 100 to 380 ppm and correlate positively with the corresponding Mg#. In the rim, the Ni content increases steeply ranging from 100 to 800 ppm and decreases at the very margin in contact with the matrix to the level of the plateau concentrations. The olivine from group C shows a compositional profile similar to the group A normal zoning and an overgrowth of 50 microns wide rim with a bell shaped Mg# profile, which decreases from 73 in the core to 68 in the rim.

It is evident that an ascending magma, which experienced en-route fractional crystallization mixed with a more mafic magma responsible for the inverse olivine zoning prior to the eruption at relatively shallow depths. The estimated time of the diffusive Fe-Mg exchange between the mafic magma and olivine is very short and ranges from a few days to 100 days. Apparently, the magma mixing is associated with the triggering of the 2002-2003 flank eruption

.

References

Branca, S., Coltelli, M., Groppelli, G., Lentini, F., 2011: Geological map of Etna volcano, 1:50,00 scale 130, 265-291. **[Italian Journal of Geosciences]**

Gvirtzman, Z., Nur, A., 1999: The formation of Mount Etna as the consequence of slab rollback 401, 782-785. **[Nature]**

Kahl, M., Chakraborty, S., Pompilio, M., Costa, F., 2015: Constraints on the Nature and Evolution of the Magma Plumbing System of Mt. Etna Volcano (1991–2008) from a Combined Thermodynamic and Kinetic Modelling of the Compositional Record of Minerals 56, 2025-2068. **[Journal of Petrology]**

Petrone, C.M., Braschi, E., Francalanci, L., Casalini, M., Tommasini, S., 2018: Rapid mixing and short storage timescale in the magma dynamics of a steady-state volcano 492, 206-211. **[Earth and Planetary Science Letters]**

16th International Congress of the Geological Society of Greece

17-19 October, 2022 - Patras, Greece

Bulletin of the Geological Society of Greece, Sp. Publ. 10

Ext. Abs. GSG2022-A3

Mixed-type faulting and non-double-couple earthquakes

J. Zahradník[1]

(1) Faculty of Mathematics and Physics, Charles University, Prague, Czech Republic, jiri.zahradnik@matfyz.cuni.cz

In a seismic sequence, aftershocks may have different focal mechanisms than the mainshock, indicating the activation of several faults. Here I demonstrate mainshocks that themselves involve mixed-type faulting, e.g. strike-slip and thrust-fault episodes. Earthquakes like that improve understanding of active fault zones and are important for seismic and tsunami hazard assessment.

Insight into the earthquake rupture process is provided through seismic moment tensors (MTs). Typical tectonic earthquakes are shear processes, equivalent to double-couple forces (DC events). The mixed-type faulting is signaled by MTs which are deviatoric, i.e. their volume component is vanishing (VOL=0), but their MT still possesses a significant non-double-couple component. The non-DC component of a deviatoric MT is the compensated linear vector dipole (CLVD). Such earthquakes attract our attention because we can interpret them as a superposition of two (or more) DC subevents of different focal mechanisms.

Calculation of full MTs from seismic waveforms is a demanding task, requiring high-quality records and accurate velocity models; otherwise, we can reliably determine just strike/dip/rake angles, and seismic moment, but the non-DC components of MT may be completely false. Even the best-determined DC, CLVD, and VOL components have typical uncertainties of ~10%. Some data centers (e.g. GCMT) calculate MTs under the assumption of the deviatoric process (VOL=0). Such analyses are not sufficient for our purposes. We need methods allowing for VOL≠ 0, and we focus on the events with VOL ~ 0. The latter events are then further analyzed for a possible presence of multiple point-source episodes (subevents), searching the subevents in space and time so that observed waveforms are better fitted than with a single dominant point source. A useful tool for multiple-point inversions is ISOLA software (Zahradník and Sokos, 2018). Its ability to calculate full MT and uncertainty has been tested on regional seismic recordings of the 2017 nuclear test in North Korea, equivalent to Mw 5.7 (Liu *et al.*, 2018). Naturally, in such a man-made event, the non-DC components (small DC, large CLVD, and large VOL) were real, caused by the underground explosion, and subsequent cavity implosion, physically equivalent to the opening and closing cracks. In the following, I present three examples of shallow crustal earthquakes whose CLVD component is not real but apparent, caused by multi-type double-couple faulting. The three earthquakes were studied by many other researchers not focusing on the non-DC part.

The first example is the 2019 Mw 5.7 Silivri earthquake that occurred in a seismic gap of the Marmara Sea, which may host a future M7 event. As shown by our team (Turhan *et al.*, 2022), the earthquake is characterized by small DC ~ 41 (±20) %, large negative CLVD ~ -54 (±20) %, and negligible VOL ~ -5 (±10) %. Formally, the event can be decomposed into two 100% DC parts, the major and minor, represented by a thrust fault (TF), and strike-slip (SS), with a moment ratio TF/SS ~ 2. However, when inverting waveforms for two-point models, the TF subevent is smaller than SS (TF/SS ~ 0.4), and their fault planes slightly differ from the formal decomposition. The first-motion polarities agree with the SS motion. Thus we conclude that the Silivri earthquake started with a dominant strike-slip moment release at or near the Main Marmara Fault, and, within a few kilometers and seconds, the rupture process continued on a reverse fault. Such mixed-type faulting perfectly explains the observed apparent departure from the double-couple mechanism characterized by the large negative CLVD component. As such, when speculating about a future M7 event we should allow for a non-negligible thrust faulting, more important for tsunami hazard than the strike-slip.

In the second example, I discuss the 2018 Mw 6.8 earthquake near Zakynthos. Here, on the western termination of the Hellenic subduction, we may perhaps expect a TF mechanism, but the proximity of the region to the Kefalonia-Lefkada transform fault system makes the SS faulting equally plausible. As indicated by significant CLVD ~ −60%, the event certainly could not be a pure double-couple SS, or TF. It was interpreted as a rupture occurring almost simultaneously (within ~ 15 s) on two nearby faults, a low-dipping TF (10°), and a moderately-dipping (40°) SS. Combining seismic and geodetic (GNSS) data, we resolved the space-time slip distribution on both fault planes, revealing the SS faulting episode on a single compact patch occurring between two TF patches (Sokos *et al.*, 2020). Naturally, specific questions remained unanswered, e.g.: How rupture skipped from one subfault of the mainshock to the other? Did the initial TF faulting trigger the SS faulting, either statically or dynamically? What is the geologic interpretation of the two faults inferred near the subducting slab top? Besides that, we have again seen the importance of careful uncertainty assessment of the non-DC MT components because their values varied widely between agencies (e.g., the CLVD part reported by GCMT and NOA was -44% and -61%, respectively).

The Silivri and Zakynthos earthquakes have two notable similarities. (i) In the regional stress field, only one of the principle stress axes is well defined (the one corresponding to the P-axis of the focal mechanism, i.e. the axis common to the SS and TF subevents). The other two stress axes have similar eigenvalues, causing limited constraint of the T-axis,

thus explaining easy switching between SS and TF nearby faults. (ii) For the same reason, in both studied regions we could observe foreshock/aftershocks of both SS and TF types, indicating transpressional tectonics. In transtensional regions, we may expect analogous mixing of the strike-slip and normal faulting, even within a single event.

The third example of multi-type faulting that we investigated is an event partially triggered by man-made activity. The example concerns the 2019 Mw 5.7 Changning earthquake in Sichuan Basin, China (Liu and Zahradník, 2020). The district is well known for underground salt mining accompanied for many years by intensive water injections. According to the GCMT agency, the double-couple part of the event was as low as 2%. We found small DC ~ 20 (±15) %, large CLVD ~ -70 (± 25) %, and very small VOL ~ -10 (± 15) %. First-motion polarities at more than 100 stations undoubtedly constrained the initial type of rupture to be a thrust. The TF-type mechanism is also prevailing during small earthquakes there. The large CLVD was then explained by a SS faulting following after the TF faulting within a few kilometers and a few seconds. When we analyze the regional stress field (using small earthquakes of previous years), we find that the TF subevent of the mainshock is nearly optimally oriented to the given stress field, thus ready to rupture easily. Contrarily, the SS subfault of the mainshock is quite far from the optimal orientation, explaining why SS faults are stable, and small SS events are rare there. Therefore, to explain the unusual SS faulting component undoubtedly present in the mainshock, we hypothesize elevated pore-pressure effects of the water injections that facilitated rupture of the SS subfault. In this sense, the Changing earthquake might be considered an event whose multi-type faulting was man-made caused.

The three demonstrated cases should not be confused with another almost equally exciting topic – multiple-fault (or multi-segment) earthquakes, where several episodes occur on different faults, but all are of the same type. One such example that we investigated was a complex three-segment strike-slip faulting of the 2020 Mw 6.8 Elazığ earthquake, Turkey (Gallovič *et al.*, 2020). Another one was a two-segment 2021 Mw 5.3 mainshock of the Corinth Gulf sequence that likely involved cascading normal faulting. The rupture started on a small low-dip normal fault in the detachment layer and was shortly followed by a major shallower moment release on a high-angle normal fault, probably the Mornos fault on the western continuation of the Trizonia fault system (Zahradník, *et al.*, 2022).

I conclude that multi-type faulting earthquakes are worth investigating because they illuminate tectonic processes and stress fields existing in active fault zones; moreover, some of them have a direct impact on seismic hazard assessment or may explain man-made earthquake triggering. The primary detection of multiple-type faulting relies on seismology, particularly on non-double-couple components of moment tensors. The current practice of seismic data centers should be considerably improved in terms of uncertainty assessments of the non-DC components. Once earthquakes are identified as multi-type events by seismologists and confirmed as such by geodesists (GNSS, InSAR) these events offer rich data for *subsequent* analyses, e.g., dynamic analyses of the rupture, and tectonic analyses of the segmented faults. My lecture clearly showed that we are still far from satisfactory geologic interpretations of multiple-type faulting. To efficiently proceed forward we should not only enhance joint cooperative seismo-tectonic studies but even improve in the nearest future the corresponding curricula at our universities.

Acknowledgements

I am grateful to the congress organizers who invited me to deliver this lecture. The presentation is based on recent articles that I published with numerous co-authors from Greece, Turkey, France, China, and the Czech Republic, to whom I am thankful for long-term cooperation. My special thanks go to the University of Patras, Seismology Lab of prof. E. Sokos and his staff, my "second home institution". Data used from various seismic and geodetic networks have been acknowledged in the below-referenced papers.

References

Gallovič, F., Zahradník, J., Plicka, V., Sokos, E., Evangelidis, Ch., Fountoulakis, I., & Turhan, F., 2020. Complex rupture dynamics on an immature fault during the 2020 Mw 6.8 Elazığ earthquake, Turkey. Communications Earth & Environment 1, 40, https://doi.org/10.1038/s43247-020-00038-x

Liu, J., Li, L., Zahradník, J., Sokos, E., Liu, C., & Tian, X., 2018. North Korea's 2017 test and its nontectonic aftershock. Geophysical Research Letters 45, https://doi.org/10.1002/2018GL077095

Liu, J., & Zahradník, J., 2020. The 2019 MW 5.7 Changning earthquake, Sichuan Basin, China: A shallow doublet with different faulting styles. Geophysical Research Letters 47, e2019GL085408. https://doi.org/10.1029/2019GL085408

Sokos, E., Gallovič, F., Evangelidis, C. P., Serpetsidaki, A., Plicka, V., Kostelecký, J., & Zahradník, J., 2020. The 2018 Mw 6.8 Zakynthos, Greece, earthquake: Dominant strike-slip faulting near subducting slab. Seismological Research Letters 91, 721–732, https://doi. org/10.1785/0220190169

Turhan, F., Acarel, D., Plicka, V., Bohnhoff, M., Polat, R., & Zahradník, J., 2022. Coseismic faulting complexity of the 2019 Mw5.7 Silivri earthquake in the central Marmara seismic gap, offshore Istanbul. Seismological Research Letters, in press, https://doi.org/10.1785/0220220111

Zahradník, J., & Sokos, E., 2018. ISOLA Code for Multiple-Point Source Modeling—Review. In: D'Amico, S. (ed) Moment Tensor Solutions. Springer Natural Hazards. Springer, Cham, Switzerland; pp. 1-28, https://doi.org/10.1007/978-3-319-77359-9_1

Zahradník, J., Aissaoui, M., Bernard, P., Briole, P., Bufféral, S., De Barros, L., Deschamps, A., Elias, P., Evangelidis, C.P., Fountoulakis, I., Gallovič, F., Kapetanidis, V., Kaviris, G., Ktenidou, O.-J., Lambotte, S., Lengliné, O., Lyon-Caen, H., Noble, M., Plicka, V., Rigo, A., Roumelioti, Z., Serpetsidaki, A., Sokos, E. & Voulgaris, N., 2022. An atypical shallow Mw 5.3, 2021 earthquake in the western Corinth Rift (Greece). Journal of Geophysical Research: Solid Earth, in press, https://doi.org/10.1029/2022JB024221

16th International Congress of the Geological Society of Greece
17-19 October, 2022 - Patras, Greece
Bulletin of the Geological Society of Greece, Sp. Publ. 10
Ext. Abs. GSG2022-A4

The nappe pile of Crete: Records of orogenic activity since Precambrian times

G. Zulauf[1]
(1) Institut für Geowissenschaften, Universität Frankfurt a.M., Germany (g.zulauf@em.uni-frankfurt.de)

The nappe pile of Crete consists of two different parts, which are separated by the Pindos suture. The lower part is attributed to the External Hellenides and consists of the Plattenkalk, Trypali, Phyllite-Quartzite s.str., Pre-Cimmerian Basement, Tyros, Tripolitza and Pindos Unit. The upper part (Uppermost Unit) is attributed to the Internal Hellenides and consists of the Arvi, Preveli, Vatos, Miamou, Ophiolite, Mourne and Asteroussia Unit. The stacking of these nappes results from Cadomian, Variscan, Eocimmerian, Eohellenic and Alpine events, which are briefly described below.

Cadomian events

The oldest orogenic events are documented in the Cadomian basement of eastern Crete that was intruded by Cambrian granites. Still older granites are present as boulders in Cadomian wildflysch, the youngest detrital zircon of which is 541 Ma, meaning that the flysch was probably deposited in Cambrian times. The zircons of the granitic boulder yielded a concordant U-Pb intrusion age at 600 ±7 Ma. This is the oldest magmatic rock of Crete probably derived from the Arabian Nubian shield. Together with the Minoan age spectrum of detrital zircons (with a typical Tonian/Stenian peak), these granitoids suggest that the basement of Crete did not travel for long distances since Neoproterozoic times.

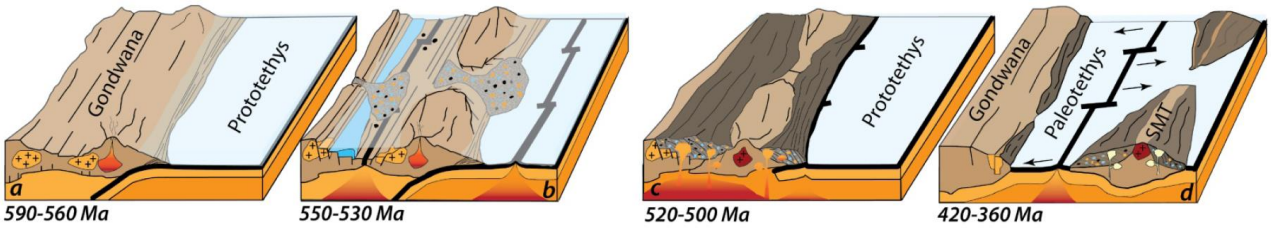

Fig. 1. Cadomian orogenic activity in the eastern Mediterranean (a-c) and Devonian separation of the Minoan Terranes (d) (after S. Fisher-Spurlock, in prep.); SMT = South Minoan Terrane.

Variscan events

During the Devonian opening of the Paleotethys, the South (SMT) and the North Minoan Terrane (NMT) were detached from Gondwana drifting towards the north. These terranes were accreted to Laurussia in Viséan and early Permian times while Paleotethys lithosphere was subducted towards the north. Almost half of the detrital zircons separated from the Variscan basement of Crete are Pennsylvanian in age. The basement is unconformably overlain by early Permian (285 ±2 Ma, U-Pb on zircon) arc-related volcanics of the Tyros back-arc basin, meaning that the (meta)trench sediments of the basement were deposited, metamorphosed and exhumed in latest Carboniferous to early Permian times (302 - 283 Ma). Magmatic activity during this late Variscan phase is also indicated by igneous boulders within Olenekian (meta)conglomerates of the Tyros Unit, which yielded concordant U-Pb zircon ages at 291 ±2 and 310 ±2 Ma. These late Carboniferous/early Permian ages are widespread in entire Europe.

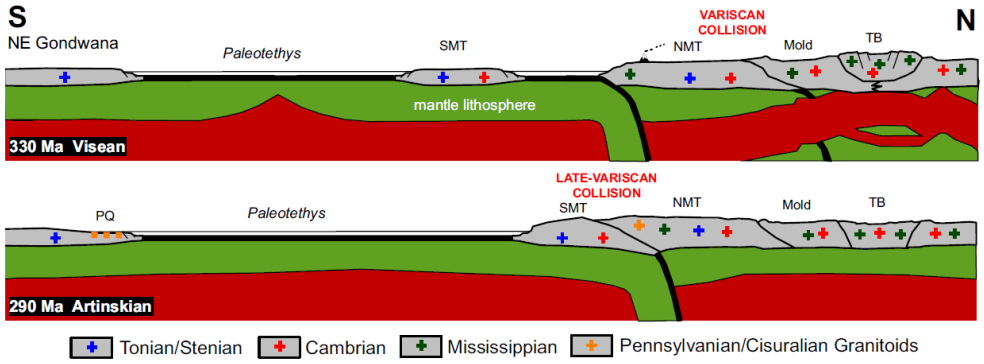

Fig. 2. Variscan orogenic activity in the eastern Mediterranean. NMT = North Minoan Terrane, SMT = South Minoan Terrane, PQ = Phyllite-Quartzite Unit s.str., Mold = Moldanubian Unit, TB = Tepla-Barrandian Unit (Bohemian Massif)

Eocimmerian events

The plate tectonic situation changed with the Permian opening of the Neotethys and the coeval separation of the Cimmerian ribbon continent from Gondwana. The Plattenkalk and the Typali basins were situated along the southern and northern passive margins of the Neotethys, respectively. The sediments of the Phyllite-Quartzite Unit s.str. (PQU s.str.) were deposited along the southern passive margin of the Paleotethys. The volcano-sedimentary records and the age spectra of detrital zircons of the PQU s.str. and the Tyros Unit suggest that their different settings persisted until the Anisian, as long as the Paleotethys was open, but approximated in Ladinian times, when both units collided during the Eocimmerian closure of the Paleotethys. Subsequent thermal relaxation in the northern domain led to the opening of the Tripolitza and Pindos basins.

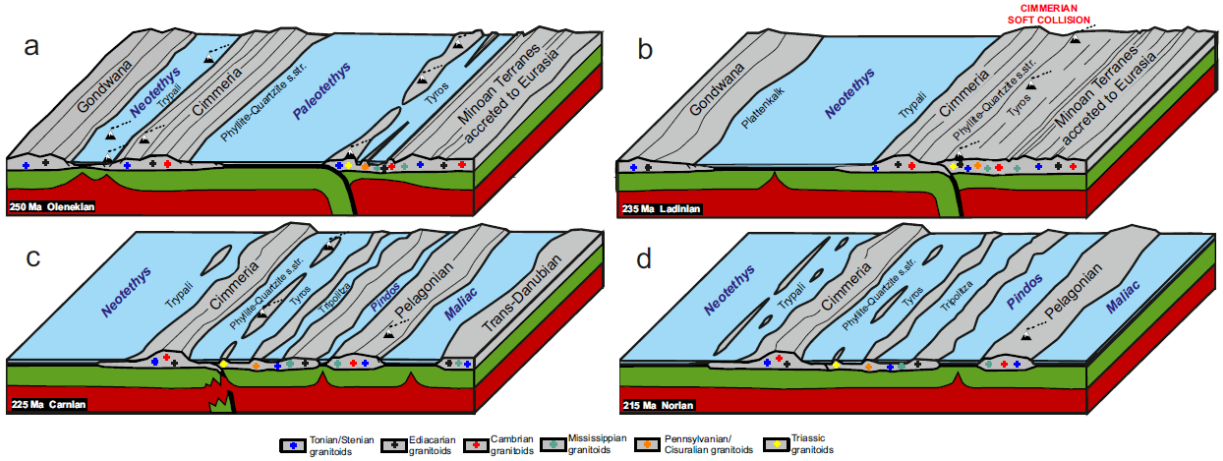

Fig. 3. (a) Opening of the Neotethys and separation of the Cimmerian ribbon continent from Gondwana, (b) Closure of the Paleotethys during Eocimmerian soft collision. (c) and (d) Opening of the Tripolitza and Pindos basins.

Eohellenic events

Records of the Eohellenic phase are lacking in the nappes of the External Hellenides mentioned above, but are well preserved in the basal part of the Uppermost Unit, particularly in the area of Preveli-Kerames-Spili of central Crete and Gavdos. The following sequence of nappes (from bottom to top) has been thrust on top of the Pindos Unit: (1) Preveli nappe, rocks of which underwent Jurassic to lower Cretaceous blueschist facies metamorphism; (2) Vatos nappe, consisting of fore-arc basin and trench (meta)sediments of late Jurassic/Creaceous age, (3) Jurassic ophiolite, and (4) mafic volcanics and marbles of the Mourne nappe, which underwent late Jurassic blueschist facies metamorphism. In contrast to the top-to-the S kinematics of the External Hellenides, this sequence of nappes was stacked during top-to-the SW and top-to-the W sense of shear. The age of the final emplacement on top of the Pindos Unit is constrained by the Eocene age of the youngest Pindos flysch.

Alpine events

Alpine imprints in the Aegean region result from Cretaceous to recent subduction/collision, which led to the closure of the Neotethys. First U-Pb ages obtained from aragonite marble of the PQU s.str. of western Crete suggest that HP-LT metamorphism should have started during the late Eocene (ca. 38 Ma). The situation is different in eastern Crete, where a metaaplite yielded a U-Pb concordia age at 25.1 ±0.2 Ma (the youngest magmatic rock of the External Hellenides). As the metaaplite underwent ductile deformation during subduction, the age of the HP-LT metamorphism must be <24 Ma, which is compatible with the first U-Pb calcite ages obtained from subduction-related cleavage (ca. 23 Ma). Thus, the peak of HP-LT metamorphism in the PQU s.str. was attained >10 m.yr. earlier in western Crete than in eastern Crete.
The middle Miocene emplacement of the Tripolitza Unit (with the Pindos and Uppermost Unit on top) post-dates the deposition of the oldest Neogene sediments and is also indicated by new U-Pb ages of calcite (7 - 10 Ma), which developed in late veins of Eocene Tripolitza (meta)limestone.

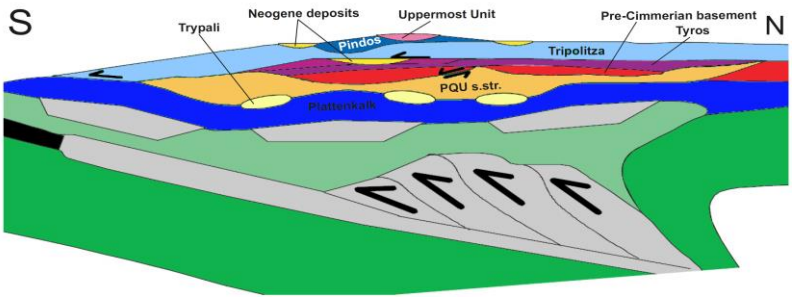

Fig. 4. Recent nappe stack of Crete without young normal faulting (modified after Klein et al., 2012, IJES, 102, 139–182)

16th INTERNATIONAL CONGRESS of the
GEOLOGICAL SOCIETY OF GREECE

GENERAL SESSIONS

OUR EARTH, OUR HOME

T1. Stratigraphy, Palaeontology and Sedimentology

Conveners:

***Pavlos Avramidis**, University of Patras;*
***Maria Triantaphyllou**, National and Kapodistrian University of Athens;*
***Dimitris Kostopoulos**, Aristotle University of Thessaloniki*

T2. Structural Geology and Tectonics

Conveners:

***Sotirios Kokkalas**, University of Patras;*
***Ioannis Papanikolaou**, Agricultural University of Athens;*
***Markos Tranos**, Aristotle University of Thessaloniki*

T3. Geophysics, Seismology and Geodynamics

Conveners:

***Zafeiria Roumelioti**, University of Patras;*
***George Vargemezis**, Aristotle University of Thessaloniki;*
***Christos Evangelidis**, National Observatory of Athens*

T4. Geomorphology and Quaternary Geology

Conveners:

***George Bathrellos**, University of Patras;*
***Efthimios Karymbalis**, Harokopio University;*
***Niki Evelpidou**, National and Kapodistrian University of Athens*

T5. Marine Geology and Oceanography

Conveners:

***George Papatheodorou**, University of Patras;*
***Serafeim Poulos**, National and Kapodistrian University of Athens;*
***Dimitris Sakellariou**, Hellenic Centre for Marine Research*

T6. Geochemistry, Mineralogy, Petrology and Volcanology

Conveners:

***Petros Koutsovitis**, University of Patras;*
***Ariadne Argyraki**, National and Kapodistrian University of Athens;*
***Vasileios Melfos**, Aristotle University of Thessaloniki*

T7. Economic Geology, Raw Materials, Energy Resources, Circular Economy

Conveners:

***Stavros Kalaitzidis**, University of Patras;*
***Andreas Georgakopoulos**, Aristotle University of Thessaloniki;*
***Konstantinos Laskaridis**, Hellenic Survey of Geology and Mineral Exploration*

T8a. Information Technologies in Geosciences

Conveners:
***Konstantinos Nikolakopoulos**, University of Patras;*
***Isaak Parharidis**, Harokopio University;*
***Olga Sykioti**, National Observatory of Athens*

T8b. Natural Hazards and Information Technologies

Conveners:
***Ioannis Koukouvelas**, University of Patras;*
***Efthymios Lekkas**, National and Kapodistrian University of Athens;*
***Alexandros Chatzipetros**, Aristotle University of Thessaloniki*

T9. Engineering Geology and Hydrogeology

Conveners:
***Nikolaos Depountis**, University of Patras;*
***Eleni Zaggana**, University of Patras;*
***Vasileios Marinos**, National Technical University of Athens*

T10. Environmental Geosciences and Climate Change

Conveners:
***Maria Geraga**, University of Patras;*
***Konstantinos Vouvalidis**, Aristotle University of Thessaloniki;*
***Katerina Kouli**, National and Kapodistrian University of Athens*

T11. Geosciences for Society, Education and Geoheritage

Conveners:
***Ioannis Iliopoulos**, University of Patras;*
***Nikolaos Zouros**, University of the Aegean;*
***Charalampos Fassoulas**, Natural History Museum of Crete, University of Crete*

16th INTERNATIONAL CONGRESS of the
GEOLOGICAL SOCIETY OF GREECE

SPECIAL SESSIONS

OUR EARTH, OUR HOME

S1. Evolving techniques in the study of sediments

Conveners:
***George Kontakiotis**, National and Kapodistrian University of Athens;*
***Angelos G. Maravelis**, Aristotle University of Thessaloniki;*
***Avraam Zelilidis**, University of Patras*

S2. Quaternary processes and geoenvironments in the active Corinth Rift

Conveners:
***Maria Geraga**, University of Patras;*
***Katerina Kouli**, National and Kapodistrian University of Athens;*
***Lisa McNeill**, University of Southampton UK;*
***Georgios Michas**, National and Kapodistrian University of Athens*

S3. The Hellenides: Tectonostratigraphic terranes, tectonic units and orogenic evolution

Conveners:
***Dimitris Papanikolaou**, National and Kapodistrian University of Athens;*
***Bernhard Grasemann**, University of Vienna AT;*
***Paris Xypolias**, University of Patras*

S4. Recent Advances in InSAR and GNSS Applications for Crustal Deformation mapping and monitoring

Conveners:
***Athanassios Ganas**, National Observatory of Athens;*
***Panagiotis Elias**, National Observatory of Athens;*
***Vassilis Sakkas**, National and Kapodistrian University of Athens*

S5. Insights into the Nature of the Earth's Upper Mantle approached from the study of Ophiolites and Volcanic Rocks

Conveners:
***Petros Koutsovitis**, University of Patras;*
***Andreas Magganas**, National and Kapodistrian University of Athens;*
***Panagiotis Pomonis**, National and Kapodistrian University of Athens*

S6. The Hydrocarbon prospectivity of SE Mediterranean: targets and opportunities

Conveners:
***Avraam Zelilidis**, Hydrocarbon Research Institute, P.E.K. University of Patras;*
***Nikolaos Pasadakis**, Institute of Petroleum Research, Foundation for Research and Technology – Hellas;*
***Aristofanis Stefatos**, Hellenic Hydrocarbon Resources Management SA.*

S7. Remote Sensing Techniques in Geohazards

Conveners:
***Sotiris Valkaniotis**, Democritus University of Thrace;*
***Emmanuel Vassilakis**, National and Kapodistrian University of Athens;*
***George Papathanassiou**, Aristotle University of Thessaloniki*

S8. New perspectives for the monitoring and early detection of Geohazards

Conveners:
***Constantinos Loupasakis**, National Technical University of Athens;*
***Harry Saroglou**, National Technical University of Athens;*
***George Papathanassiou**, Aristotle University of Thessaloniki*

S9. Geological heritage for education and sustainable development

Sub-session 1**: **Geoheritage, geoconservation, geoeducation, geoethics
Conveners:
***Hara Drinia**, National and Kapodistrian University of Athens;*
***Nikolaos Zouros**, University of the Aegean;*
***Asimina Antonarakou**, National and Kapodistrian University of Athens*

S9. Geological heritage for education and sustainable development

Sub-session 2**: **Achieving sustainable development through geoheritage
Conveners:
***Charalampos Fassoulas**, University of Crete;*
***Georgios Iliopoulos**, University of Patras;*
***Nikolaos Zouros**, University of the Aegean*

16th INTERNATIONAL CONGRESS of the
GEOLOGICAL SOCIETY OF GREECE

T1. Stratigraphy, Palaeontology and Sedimentology

OUR EARTH, OUR HOME

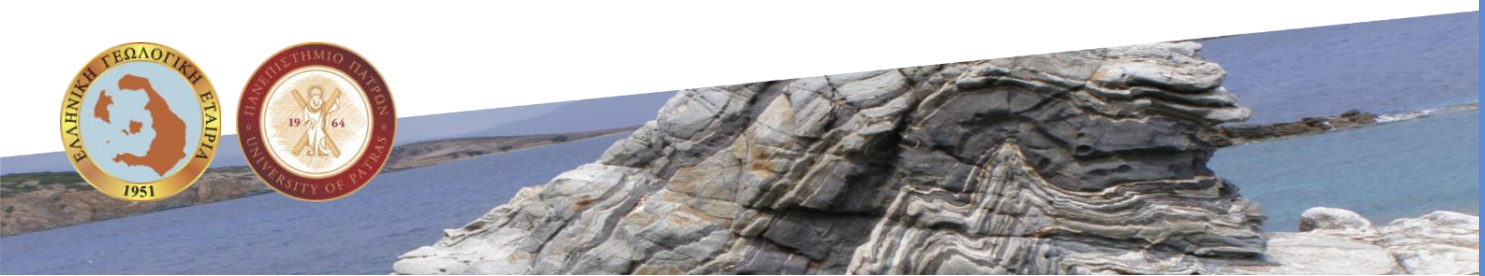

16th International Congress of the Geological Society of Greece
17-19 October, 2022 - Patras, Greece
Bulletin of the Geological Society of Greece, Sp. Publ. 10
Ext. Abs. GSG2022-016

On the oncoid-rich facies in the Dachstein-type platform carbonates of the Sofiko area, Peloponnesus, Greece

V. Kostopoulou[1], F. Pomoni-Papaioannou[1]

(1) National and Kapodistrian University of Athens, Department of Geology & Geoenvironment, Panepistimiopolis, 15784 Athens, Greece, vakofil@gmail.com

Introduction

Dachstein-type cyclic carbonates (Pantokrator facies) have been developed during the Upper Triassic-Lower Jurassic times at the extended carbonate platform that geotectonically belongs to the zone of the internal Hellenides known as Eastern Greece (i.e., referred to in this work as Pelagonian carbonate palaeoplatform). In the Argolis peninsula (e.g., Didymi area, Karnezeika) as well as, in the eastern-southern Corinthia (e.g., Korfos, Sofiko), the Dachstein-type cyclic successions are dominant, thick and well exposed, representing the inner platform domain (e.g., Schäfer & Senowbari-Daryan, 1982; Gaitanakis et al., 1985, 2007). They are made up of discontinuity-bounded, meter-scale lagoonal- peritidal cycles showing deepening- and/or shallowing-upward trend and consisting of three units that correspond, respectively, to the members A, B and C of the Fischer's (1964) typical Lofer cyclothem (Pomoni-Papaioannou, 2008; Haas et al., 2009; Kostopoulou, 2018): supratidal/terrestrial unit (represented by calcrete/dolocrete crusts containing pisoids, black pebbles, root and alveolar-like structures, karstified surfaces with solution vugs and fossil molds, unfossiliferous mudstones, intraformational conglomerates), intertidal unit (represented by often dolomitized, horizontal or slightly crinkled stromatolites and algal mat loferites), and subtidal unit (represented by megalodontid wackestones-floatstones and foraminiferal-algal-peloidal packstones-wackestones). Shallow subtidal units consisting of oncoid-rich facies have also been detected. Oncoids are microbially formed nodular coated grains exhibiting concentric laminae around a nucleus and are generally regarded as a type of microbialites (Riding, 2000; Flügel, 2004). Oncoids have been noted as components of the platform subtidal part (e.g., Fisher 1964).

Aim and Methods

Aim of this work was the study of the oncoid-bearing beds, constituting the shallow subtidal facies of the Late Triassic (Rhaetian)-?Liassic (Dercourt 1964) Dachstein-type carbonates (limestones/dolomitized limestones) that crop out few km from Sofiko village (Corinthia). For the microfacies analysis thin sections were prepared, stained and studied in transmitted light. Microfacies types were defined according to Flügel (2004), and classified following Dunham (1962).

Results and Discussion-Conclusions

From the macroscopic observations and the microfacies analysis performed at the material collected at Sofiko locality, three different microfacies have been recognized and are interpreted in terms of paleoenvironment.

MF_{S1} - Oncoidal floatstone/boundstone: composed by oncoids usually spherical to sub-elliptical with smooth contours (irregular forms with wavy contours occasionally occur). They consist of a nucleous (commonly of microbial nature) and a cortex (coatings). Large forms display a thick, concentrically laminated cortex with alternating micritic and clotted-fine peloidal laminae (Fig. 1/i). Smaller forms are composed by thin micritic or crudely laminated cortices. The oncoids are coalesced with a micritic (locally fenestral) matrix that is probably of microbial origin and includes fine and coarser peloids and relics of calcimicrobes (oncoidal boundstones). Other allochems are aggregate grains consisting of peloids, a few foraminifers and fragments of bivalves (Megalodontids).

MF_{S2} – Bioclastic oncoidal wackestone/boundstone: composed by bioclasts, intraclasts, peloids (?fecal pellets) and small-sized oncoids in a clotted-very fine peloidal micritic to homogeneous matrix, likely generated by microbial activity (Fig. 1/ii). Bioclastic components include occasional green algae (dasyclads?) and small thin-shelled gastropods, calcimicrobes, fragments of thaumatoporellids and tiny benthic foraminifera.

MF_{S3} - Calcimicrobe boundstone/floatstone: predominantly composed of calcified cyanobacteria. Abundant tufts of porostromate calcimicrobes (?Rivulariaceae) can be observed (Fig. 1/iii), forming a well-preserved framework. Small or larger fenestral pores occluded by sparry cement are common. Oncoids with a cyanobacteria fragment as nucleus and a dark-coloured micritic cortex, occur as well locally.

In some cases, vadose meteoric diagenetic features (e.g., pisoids, pendant cements, dissolution features) have been observed, overprinting the oncoidal facies/microfacies.

The microfacies described are interpreted as corresponding to a shallow subtidal depositional setting within the platform interior where cyanobacterial calcimicrobes occurred in abundance. The characteristics of microfacies suggest a transitional zone from protected (lower-energy) to more open lagoonal to back-reef (higher-energy) environments, near

to the platform margin. Oncoids are commonly considered as indicators of shallow (inter- to subtidal) and agitated depositional settings (e.g., Wright & Tucker, 1990). Porostromate calcimicrobes are common in Mesozoic shallow- water carbonates and their occurrence in association with aggregate grains and fenestral structures implies an open marine lagoonal/back-reef area (Kiessling & Flügel, 2000; Flügel, 2004; Peybernes et al., 2016). Furthermore, based on the probably underlying and/or coeval coral boundstones, found in close vicinity to the sampled outcrop, the microfacies defined were likely associated with small reefs (patch-reefs). Colonial and solitary corals of Rhaetian age were reported by Dercourt (1964) from the area of Sofiko. Regarding the meteoric early diagenesis traces that affected the oncolite facies, they are proof of subaerial exposure events (episodes of sea-level fall).

Microbial carbonates or microbialites are significant component within the Dachstein-type Pantokrator facies, including attached laminated (stromatolites) and unattached nodular (oncolites) types. The former are thick and highly represented in the Argolis peninsula (e.g., Didymi area), corresponding to a low-energy peritidal setting whereas the oncoidal facies have only been observed in the Sofiko locality, corresponding to more open and agitated lagoonal/back- reef environments near the marginal zone of the carbonate palaeoplatform. The recognized oncoid-rich facies are comparable with the oncoidal facies of the Dachstein Limestone (oncoidal Dachstein Limestone) in the Transdanubian Range and the Dachstein Plateau (Haas et al., 2010).

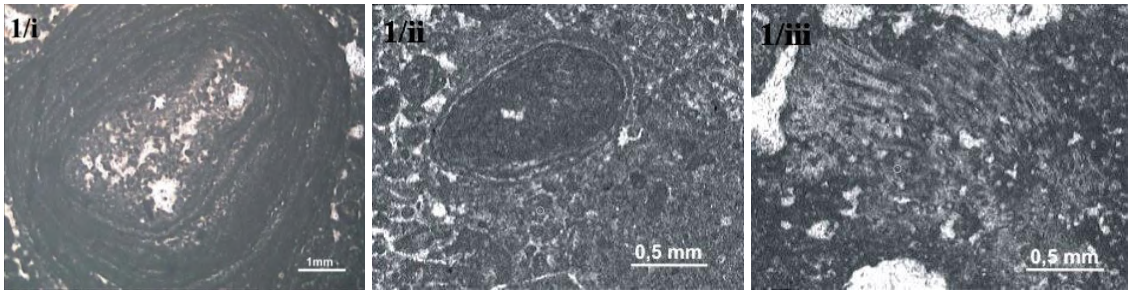

Figure 1: (i) Large, spherical oncoid with well-laminated and concentric cortex. (ii) Distinct small oncoid with a thin laminated cortex, embedded in a fine peloidal micrite matrix. (iii) Porostromate calcimicrobes inter-grown with microbial micrite.

References

Dercourt, J. 1964. Contribution à l' étude géologique d' un secteur du Péloponnèse septentrional. Annalles géologiques des pays Helléniques 15, 1-417 (Thèse Univ Paris).

Dunham, R.J. 1962. Classification of carbonate rocks according to depositional texture. American Association Petroleum Geologists, Memoir 1, 108-121.

Fischer, A.G. 1964. The Lofer cyclothems of the Alpine Triassic, in: Merriam, D.F. (Ed.) Symposium on cyclic sedimentation. Kansas Geological Survey Bulletin 169, 107-149.

Flügel, E. 2004. Microfacies of carbonate rocks: Analysis, interpretation and application. Springer.

Gaitanakis, P., Mettos, A., Fytikas, M., Tsaila-Monopolis, St., Tsapralis, V., Ioakim, Chr. 1985. Geological map of Greece, Sofiko Sheet 1:50.000, Institute of Geology and Mineral Exploration, Athens, Greece.

Gaitanakis, P., Photiades, A., Tsaila-Monopolis, St., Tsapralis, V. 2007. Geological map of Greece, Spetses-Spetsopoula Sheet 1:50.000. Institute of Geology and Mineral Exploration, Athens, Greece.

Haas, J., Pomoni-Papaioannou, F., Kostopoulou, V. 2009. Comparison of the Late Triassic carbonate platform evolution and Lofer cyclicity in the Transdanubian Range, Hungary and Pelagonian Zone, Greece. Central European Geology 52, 153–184.

Haas, J., Piros, O., Budai, T., Görög, A., Mandl, G.W., Lobitzer, H. 2010. Transition between the massive reef-backreef and cyclic lagoon facies of the Dachstein Limestone in the southern part of the Dachstein Plateau, Northern Calcareous Alps, Upper Austria and Styria. Abhandlungen der Geologischen Bundesanstalt 65, 35–56.

Kiessling, W., Flügel, E. 2000. Late Paleozoic and Late Triassic limestones from North Palawan block (Philippines): microfacies and paleogeographical implications. Facies 43, 39–77.

Kostopoulou, V. 2018. Lofer cycles in the Upper Triassic-Lower Jurassic carbonate platform of the Eastern Greece zone. Ph.D. Thesis, National & Kapodistrian University of Athens, Athens, 362 p.

Peybernes, C., Chablais, J., Onoue, T., Martini, R. 2016. Mid-oceanic shallow-water carbonates of the Panthalassa domain: new microfacies data from the Sambosan Accretionary Complex, Shikoku Island, Japan. Facies 62/4, 1-27.

Pomoni-Papaioannou, F. 2008. Facies analysis of Lofer cycles (Upper Triassic), in the Argolis Peninsula (Greece). Sedimentary Geology 208, 79-87.

Riding, R., 2000. Microbial carbonates: the geological record of calcified bacterial–algal mats and biofilms. Sedimentology 47, 179–214.

Schäfer, P., Senowbari-Daryan, B. 1982. The Upper Triassic Pantokrator limestone of Hydra, Greece: An example of a prograding reef complex. Facies 6, 147-164.

Tucker, M.E., Wright, V.P. 1990. Carbonate Sedimentology. Blackwells, Oxford.

16th International Congress of the Geological Society of Greece

17-19 October, 2022 - Patras, Greece

Bulletin of the Geological Society of Greece, Sp. Publ. 10

Ext. Abs. GSG2022-039

Syn-orogenic deposits on Ionian islands: the case of Katelios section, SE Kefalonia

M. V. Triantaphyllou[1], Th. Tsourou[1], M.D. Dimiza[1], L. Beza Zerihun[1], H. Drinia[1]

(1) Faculty of Geology & Geoenvironment, National and Kapodistrian University of Athens, Panepistimioupolis 15784, Zographou, Greece, mtriant@geol.uoa.gr

The widespread of Pliocene deposits in the Mediterranean area, is usually interpreted as a result of the abrupt marine transgression at the earliest Zanclean, which terminated the Messinian salinity crisis. Since the end of the Messinian the Mediterranean has been continuously connected to the Atlantic Ocean through the shallow Strait of Gibraltar and consequently changing the water budget for the Mediterranean (e.g. Kouwenhoven et al., 2006). Microfossils have proven to be reliable indicators of past environments and numerous high-resolution microfossil studies have revealed paleoenvironmental changes related to the Miocene-Pliocene transition and the re-establishing of normal marine conditions (among others, Castradori, 1998; Iaccarino et al., 1999).

Kefalonia is part of the Ionian group of islands that lie at the west segment of Hellenic arc-trench system. The geological structure of Kefalonia Island includes the relative autochthon Mesozoic–Cenozoic unit of Paxos, occurring on Paliki peninsula in the west and on the major part of the central Kefalonia, and the allochthon tectonic nappe of the Ionian unit, occurring along the eastern part. The thick Early Cretaceous to Early Miocene shallow water carbonate platform of Paxos unit is followed by Middle Miocene-Late Pliocene clastic sequences of flysch type. Upper Jurassic to Lower Cretaceous limestones of the Ionian geotectonic zone that overthrusted the Paxos sediments, are present in the eastern part of the island (Nikolaou, 1986; Underhill, 1989). Overthrusting of the Ionian nappe took place at Middle-Late Miocene but affected the top of the Paxos sequence till the Late Miocene – Early Pliocene (Mercier, 1972; van Hinsbergen et al, 2006) or even till the Quaternary (Underhill, 1989; Papanikolaou and Triantaphyllou, 2013). Plio-Quaternary sediments are abundant in the area, laying uncomformably mainly at the southeastern coast of the island and the largest part of the Paliki peninsula (Triantaphyllou, 2001; Triantaphyllou et al., 1999), also featured by tectonic deformation (Underhill, 1989; Papanikolaou and Triantaphyllou, 2013).

In this work, we have performed a synthesis of the biostratigraphical and palaeoenvironmental study carried out by analysis of the distribution of the calcareous nannofossil, foraminifer and ostracod assemblages from the Early Pliocene section Katelios in Kefalonia, in order to evaluate the impact of the Ionian overthrusting on the Paxos syn-orogenic deposits as also to detect the paleoenvironmental conditions during the late Zanclean in the study area. Katelios section (approx. 90 m thick) located at the southeastern coast of the island below the Ionian thrust, consists of marls alternating with sandy layers and marly limestones (Fig. 1).

Calcareous nannofossils are abundant throughout the Katelios section and generally well-preserved in all samples. The sequence is featured by the dominance of *Reticulofenestra pseudoumbilicus* (abundance >20%) and the presence of *Pseudoemiliania lacunosa* and *Discoaster asymmetricus, D. pentaradiatus, D. surculus* that enable the biostratigraphic assignment within the NN14-15 nannofossil biozone (4.04-3.82 Ma) during the late Zanclean. The nannofossil assemblages indicate warm-temperate and high-productivity conditions due to the abundance of *R. pseudoumbilicus*. Additionally the dominating discoasterid species *D. pentaradiatus, D. asymmetricus* (abundance >5%), favor warm and more productive intervals, in contrast to rare *D. variabilis* and *D. surculus* which are mostly associated with colder conditions. The benthic foraminiferal fauna corresponds to inner-middle neritic zone (~70m, van Hinsbergen et al., 2006), with few planktonic foraminifera [P/(P+B) max 30%]. The studied foraminiferal assemblages show high diversity throughout Katelios section. The lowermost samples are characterized by high frequencies of shallow-water epiphytic taxa such as *Asterigerinata planorbis, Elphidium* spp., *Cibicides lobatulus/refulgens*. An increase in frequency of open marine mesotrophic species *Bolivina punctata, Bulimina aculeata, Melonis* spp., *Hanzawaia boueana, Valvulineria bradyana, Cibicides dutemplei* marks the middle part of the section (in between 20-40 m height), related to a respective paleodepth increase combined with a simultaneous increase of organic matter content in the depositional paleoenvironment. Ostracod assemblages from the lower part of the Katelios sequence are dominated by *Aurila*, accompanied mainly by *Cytherella* spp., *Callistocythere* spp. and *Loxoconcha* spp., all typical of the inner infralittoral zone. In the samples from the middle part of the Katelios sequence, *Aurila* is found together with *Xestoleberis* spp., *Semicytherura* spp., *Callistocythere* spp. and *Loxoconcha* spp., marking a shallow depositional environment with rich algal vegetation, however species representing the outer shelf-upper bathyal environments adapted to clayey-silty substrates, such as *Henryhouwella asperrima*, *Cytherella* spp., *Buntonia sublatissima, B. textilis, Pterygocythereis jonesi, Acanthocythereis* sp. and *Rectobuntonia subulate*, are increasing in abundance also indicating higher trophic content. Finally, *Aurila* is again the dominant ostracod in the upper part of the Katelios sequence accompanied mainly by *Callistocythere* spp., *Loxoconcha* spp., *Cytherella* spp.

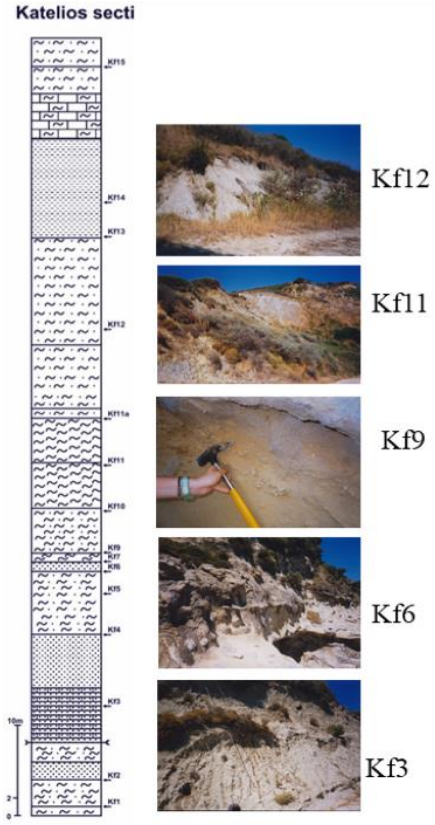

Figure 1: Lithostratigraphic column of Katelios section. Photos of different parts of the section and the samples which were collected from these levels.

The Katelios syn-orogenic shallow deposits reflect the uplift and subsequent emergence and erosion as also the increase of Paxos foreland space, caused by the Ionian overthrusting during the warm late Zanclean time interval.

References

Castradori, D., 1998. Calcareous nannofossil in the basal Zanclean of the eastern Mediterranean Sea: remarks on paleoceanography and sapropel formation. *Proceedings of the Ocean Drilling Program. Scientific Results* 160, 113-123.

Iaccarino, S.M., Castradori, D., Cita, M.B., Di Stefano, E., Gaboardi, S., McKenzie, J.A., Spezzaferri, S., Sprovieri, R., 1999. The Miocene-Pliocene boundary and the significance of the earliest Pliocene flooding in the Mediterranean. *Memorie della Societa Geologica Italiana* 54, 109-131.

Kouwenhoven, T.J., Morigi, C., Negri, A., Giunta, S., Krijgsman, W., Rouchy, J.-M., 2006. Paleoenvironmental evolution of the eastern Mediterranean during the Messinian: constraints from integrated microfossil data of the Pissouri Basin (Cyprus). *Marine Micropaleontology* 60, 17-44.

Mercier JL, Bousquet B, Delibassis N, et al. (1972). Deformations en compression dans le Quaternaire de rivages ioniens (Cephalonie, Grece). Donnes neotectoniques et sismiques. *Comptes Rend. Acad. Sci.*, 175, 2307–2310.

Nikolaou, C., 1986. Contribution to the study of Neogene and Geological concepts of the Ionian and Preapulian zone and their boundaries in relation to hydrocarbon exploration mainly on Strophades, Zakynthos and Cephallonia. *PhD thesis*, National and Kapodistrian University of Athens, 350, Athens.

Papanikolaou, M., Papanikolaou, D., Triantaphyllou, M.V., 2010. Post-alpine Late Pliocene-Middle Pleistocene uplifted marine sequences in Zakynthos Island. *Proceedings of the 12th International Congress, Patras, May, 2010, Bulletin of the Geological Society of Greece* XLIII(2): 475-485.

Papanikolaou, D., Triantaphyllou, M., 2013. Growth folding and uplift of Lower and Middle Pleistocene marine terraces in Kephalonia: Implications to active tectonics, in: *Proceedings of the 4th International INQUA Meeting on Paleoseismology*, Active Tectonics and Archeoseismology (PATA), Aachen, Germany. pp. 9–15.

Triantaphyllou, M.V., (2001). Quantitative calcareous nannofossil biostratigraphy of Bay Akrotiri section (Cefallinia island, W.Greece*). Bull. Geol. Soc. Greece*, XXXIV/2, 645-652.

Triantaphyllou, M.V., Dimiza, M.D., Papanikolaou, M.D., (2010). Early Pliocene deposits in Kephallonia (Ionian Islands): Biostratigraphy and paleoenvironmental-paleoclimatic implications. *XIX CBGA Congress*. Thessaloniki, 2010, *Geologica Balcanica*, 39, 1-2:398-399.

Triantaphyllou, M.V., Drinia, H. & M.D. Dermitzakis, 1999. Biostratigraphical and paleoenvironmental determination of a marine Plio/Pleistocene outcrop in Cefallinia island. *Geologie Mediterraneenne* XXVI, 1 / 2, pp.3-18.

Underhill, J.R., 1989. Late Cenozoic deformation of the Hellenide foreland, western Greece. Geological Society of America Bulletin, 101, 613-634.

Van Hinsbergen, D.J.J., D.G. van der Meer, W.J. Zachariasse, and J.E. Meulenkamp (2006). Deformation of western Greece during Neogene clockwise rotation and collision with Apulia, Int. J. Earth Sci., 95, 463–490.

16th International Congress of the Geological Society of Greece
17-19 October, 2022 - Patras, Greece
Bulletin of the Geological Society of Greece, Sp. Publ. 10
Ext. Abs. GSG2022-041

Intense Marine Reworking of Tephra on the flanks of Yali Island, at the Southeastern End of the South Aegean Volcanic Arc

A. Koutroulli[1], G. Anastasakis[1], S. C. Kuehn[2], D.J.W. Piper[3], G. Pe-Piper[4], G.Kontakiotis[1]

(1) Section of Historical Geology-Paleontology, Department of Geology and Geoenvironment, National & Kapodistrian University of Athens, Panepistimiopolis, Athens 15784, Greece, annkout@geol.uoa.gr; akoutroulli@gmail.com (2) Department of Physical Sciences, Concord University, Athens, WV, 24712, USA (3) Geological Survey of Canada, Atlantic, Bedford Institute of Oceanography, P.O Box 1006, Dartmouth, Nova Scotia, B2Y 4A2, Canada (4) Department of Geology, Saint Mary's University, Halifax, Nova Scotia, B3H 3C3, Canada.

Research Highlights

New chronological and tephrostratigraphic data covering the last 30,000 years of volcanic activity at the southeastern end of the South Aegean Volcanic Arc. Evidence for the most recent Yali eruptions.

Background

The Kos-Yali-Nisyros volcanic center displays intense Late Quaternary volcanic activity marking the easternmost end of the South Aegean Volcanic Arc. The major phreatoplinian eruption of the Kos Plateau Tuff (161 ka BP, Smith et al. (1996) constitutes the largest event which took place in this area during the Quaternary (Di Paola, 1974; Keller et al., 1990; Allen and Cas, 1998; Allen et al., 1999) and is well represented in the distal marine tephrostratigraphic record (Keller et al., 1978; Federman and Carey, 1980). The volcanic islands of Nisyros and Yali, which formed after the Kos Plateau Tuff eruption, comprise significant pyroclastic units, however, the chronology and stratigraphy of these rocks has long been a subject of debate (Pe-Piper and Piper, 2002; Volentik et al., 2002; Tomlinson et al., 2012;). Dates obtained by different methods add to the uncertainty of the timing of the volcanic eruptions. Specifically on Yali, the most recent years of volcanic activity are represented by poorly dated thin tephra layers associated with Neolithic artifacts (Galloway and Liritzis, 1992; Liritzis et al., 1996).

Objectives

This study is focused on new chronostratigraphy, sedimentological and geochemical data in order to elucidate the most recent, ca 30 ka to present, volcanic activity of the southeastern end of the South Aegean Volcanic Arc.

Methods

Two deep-sea sediment cores, PAG-12-10 and -13 retrieved respectively about 10 km to the south and north of Yali Island, were investigated at high resolution (Fig. 1). Cores were scanned for magnetic susceptibility, split, logged and sampled at 1 cm. Carbonate content was measured for all samples, whereas selected intervals were analyzed for their textural parameters, sediment grain density, organic carbon and bulk X-ray mineralogy. Samples with elevated feldspar contents were selected for Electron Microprobe-WDS major element analyses of glass and pumice grains. Seven samples from both cores were AMS ^{14}C dated.

Results and Conclusions

In all the examined lithostratigraphic levels, totaling 30 WDS analyses, we identify mostly volcaniclastic shards correlating to the various Yali eruptions. Samples within the uppermost Holocene sapropel are dominated by shards and pumice clasts of the Yali topmost eruption. At stratigraphic levels older than 18 ka, at the base of the cores, we identify shard populations belonging to a previously unreported Yali eruption, presumably of only local significance. Distribution of the various shards suggests intense marine reworking, caused, most probably, by turbidites which flowed downhill the island slopes.

Figures and Figure Captions

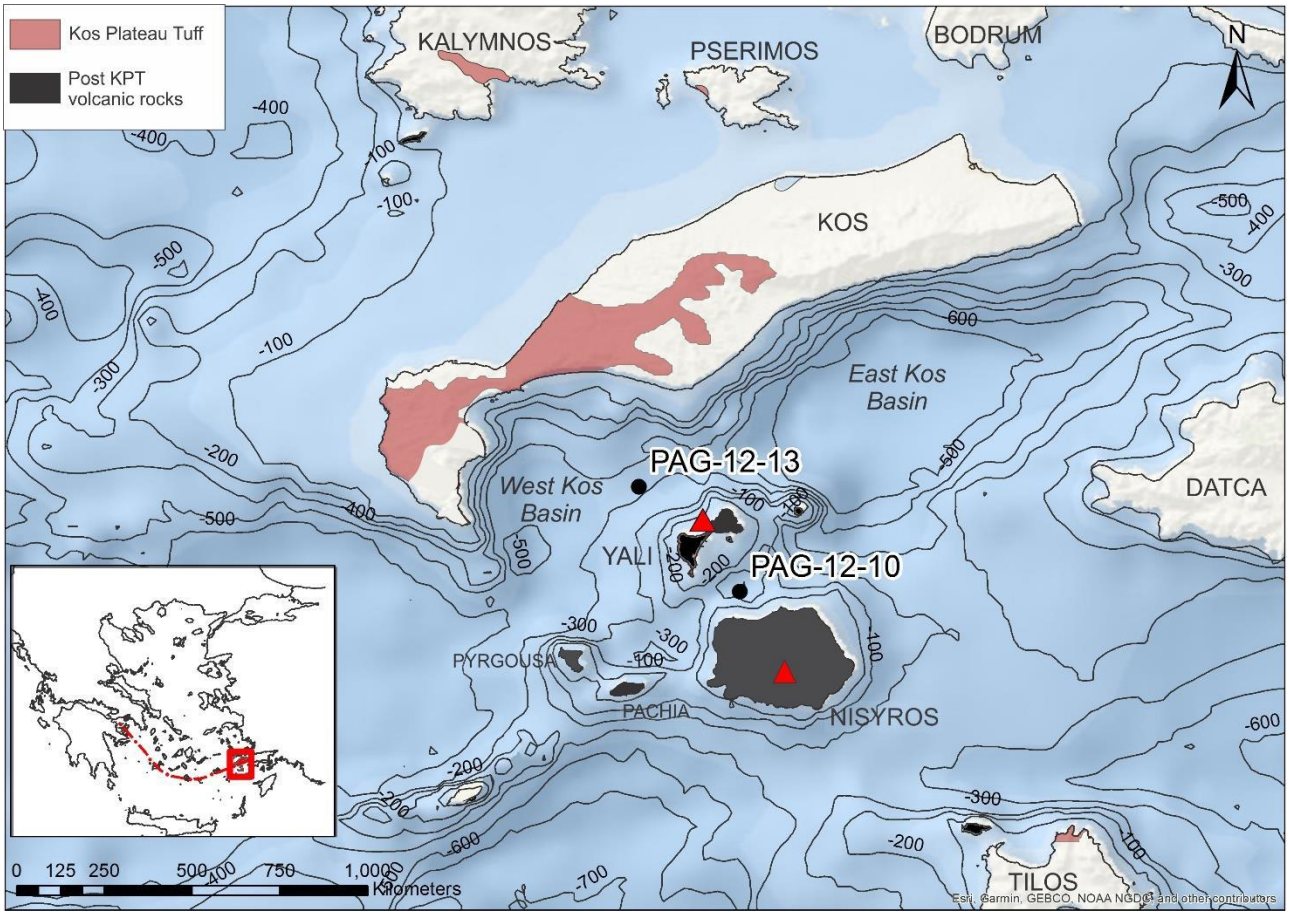

Figure 1: Bathymetric map showing the location of the cores of this study.

Acknowledgements

Anna Koutroulli wishes to acknowledge her supervising Professors.

References

Allen, S.R., Cas, R.A.F., 1998. Lateral variations within coarse coignimbrite lithic breccias of the Kos Plateau Tuff, Greece. Bull. Volcanol. 59, 356–377.

Allen, S.R., Stadlbauer, E., Keller, J., 1999. Stratigraphy of the Kos Plateau Tuff: product of a major Quaternary explosive rhyolitic eruption in the eastern Aegean, Greece. Int. J. Earth Sci. 88, 132–156.

Di Paola, G.M., 1974. Volcanology and Petrology of Nisyros island (Dodecanese, Greece). Bull. Volcanol. 381, 944–987. Galloway, R.B., Liritzis, Y., 1992. Provenance of Aegean volcanic tephras by high resolution gamma spectrometry. Int. J. Radiat. Appl. Instrum. Part E 6 (3), 405–411.

Keller, J., Ryan, W.B.F., Ninkovich, D., Altherr, R., 1978. Explosive volcanic activity in the Mediterranean over the past 200,000 yr as recorded in deep-sea sediments. Geol. Soc. Am. Bull. 89, 591–604.

Keller, J., Rehren, T.H., Stadlbauer, E., 1990. Explosive volcanism in the Hellenic arc. In: Doumas, C. (Ed.), Thera and the Aegean World, Athens, pp. 13–26.

Liritzis, I., Michael, C., Galloway, R.B.A., 1996. A significant Aegean volcanic eruption during the second millennium B.C. revealed by thermoluminescence dating. Geoarch. Internat. 11 (4), 361–371.

Pe-Piper, G., Piper, D.J.W., 2002. The Igneous Rocks of Greece. Gebruder Borntraeger, Berlin, p. 573.

Smith P.E., York D., Chen Y., Evensen N.M. (1996). Single crystal $^{40}Ar/^{39}Ar$ dating of a Late Quaternary paroxysm on Kos, Greece: concordance of terrestrial and marine ages. Geophys. Res. Lett. 23: 3047–3050.

Tomlinson, E.L., Kinvig, H.S., Smith, V.C., Blundy, J.D., Gottsmann, J., Müller, W., Menzies, M.A., 2012. The Upper and Lower Nisyros Pumices: revisions to the Mediterranean tephrostratigraphic record based on micron-beam glass geochemistry. J. Volcanol. Geotherm. Res. 243–244, 69–80.

Volentik, A., Vanderkluysen, L., Principe, C., Hunziker, J.C., (2002). Stratigraphy of Nisyros volcano (Greece). In: Hunziker JC, Marini L (eds) The geology, geochemistry and evolution of Nisyros Volcano (Greece). Implications for the volcanic hazards, vol. 44. Memoires de Geologie (Lausanne), pp 26–66.

16th International Congress of the Geological Society of Greece
17-19 October, 2022 - Patras, Greece
Bulletin of the Geological Society of Greece, Sp. Publ. 10
Ext. Abs. GSG2022-042

High Resolution Tephrostratigraphic Record of a deep-water SE Aegean Sea Core spanning the last 110 ka

A. Koutroulli[1], G. Anastasakis[1], S.C. Kuehn[2], D.J.W. Piper[3], G. Pe-Piper[4], G.Kontakiotis[1]

(1) Section of Historical Geology-Paleontology, Department of Geology and Geoenvironment, National & Kapodistrian University of Athens, Panepistimiopolis, Athens 15784, Greece, annkout@geol.uoa.gr; akoutroulli@gmail.com (2) Department of Physical Sciences, Concord University, Athens, WV, 24712, USA (3) Geological Survey of Canada, Atlantic, Bedford Institute of Oceanography, P.O Box 1006, Dartmouth, Nova Scotia, B2Y 4A2, Canada (4) Department of Geology, Saint Mary's University, Halifax, Nova Scotia, B3H 3C3, Canada.

Research Highlights

The first core reported from the SE Aegean Sea to contain a full record back to Campanian X-5 of major eruptions originating from Santorini, Nisyros-Yali and Italian volcanic centers. The pre-Minoan M12 scoria deposits are recognized.

Background

In the Aegean Sea the late Quaternary marine sedimentary record contains several distinct tephra layers originating from major explosive eruptions in the Hellenic and Italian volcanic arcs (Ninkovich and Heezen, 1965; Keller et al., 1978; Federman and Carey, 1980; McCoy, 1981). Less well defined tephra and/ or cryptotephra layers, attributed to local smaller eruptions, are also identified.

In the SE Aegean Sea, in particular, chronological data (e.g. Grant et al., 2012) were provided mostly in order to compliment previous paleo-oceanographic studies (incl. Hayes et al., 1999; de Rijk et al., 1999; Rohling et al., 2002 Casford et al., 2002; Marino et al., 2007; Osborne et al., 2010), whereas, recently, synthetic chronology and tephrostratigraphic records were published (Satow et al., 2015; Wulf et al., 2020), aiming to refine the tephrostratigraphic and chronostratigraphic framework of the southeastern Aegean and the eastern Mediterranean Sea.

Objectives

This study is based on numerous new chronological, sedimentological and geochemical data, obtained on core M-15-221, in an attempt to decipher the tephrostratigraphy of the last 110 ka in the SE Aegean Sea.

Methods

An over 5 m long, deep-sea core recovered from the NW margin of Karpathos Basin (SE Aegean Sea, Greece) was scanned for magnetic susceptibility, split, logged and sampled at 0.5 cm or 1 cm resolution (Fig.1). Carbonate content was measured for all samples, whereas selected intervals were analyzed for their grain size, density and organic carbon content. Layers with elevated magnetic susceptibility and relatively low carbonate content were selected for Electron Microprobe-WDS major element analyses of glass and pumice grains. Five (5) radiocarbon dates were obtained providing a robust chronostratigraphic framework for the upper half of the core, further facilitating an extrapolation of chronology to the base of the core.

Results and Conclusions

Tephra layers which comprise only one chemical population of volcanic grains correlating to the well-established Santorini Cape Riva Y-2, Yali-C, Campanian Y-5, Nisyros Upper and Lower Pumice deposits, are identified within the upper 65 ka of the examined core. Between the Minoan Z-2 and Cape Riva Y-2 deposits we identify, for the first time, the marine expression of two members of the M12 scoria fall deposit, as detected in Phira Quarry by Vespa et al., (2006). Below the Nisyros Lower Pumice tephra the sedimentary column is characterized by several turbiditic intercalations resulting in higher sedimentation rates. Within this interval, spanning from 67 to 110 ka, we identify several geochemically consistent tephra layers attributed to the Santorini Upper Scoriae 1, Nisyros Kyra and Campanian X-5 events.

Figures and Figure Captions

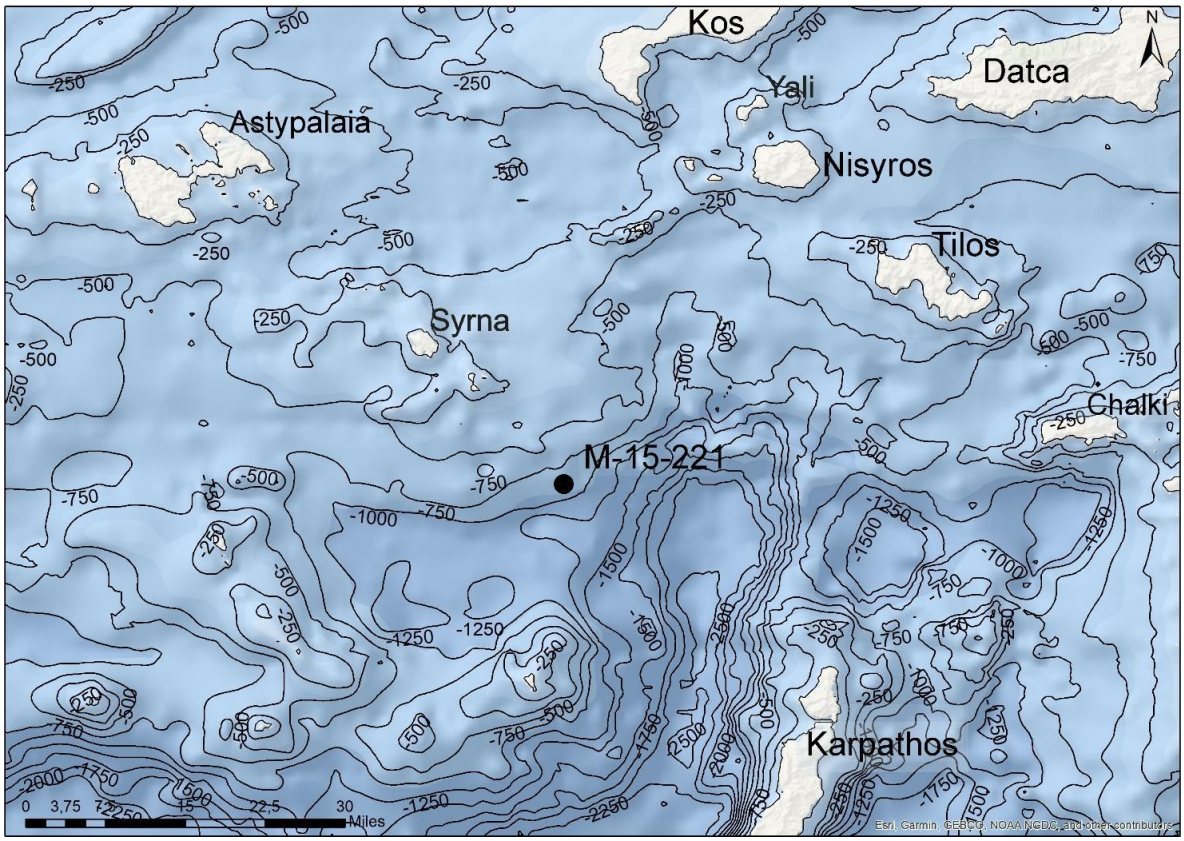

Figure 1: Bathymetric map showing the location of the examined core.

Acknowledgements

Anna Koutroulli wishes to acknowledge her supervising Professors.

References

De Rijk, S., Hayes, A., Rohling., E.J., 1999. Eastern Mediterranean sapropel S1 interruption: and expression of the climatic deterioration around 7 ka BP. Mar. Geol. 153, 337–343.

Casford, J.S.L., Rohling, E.J., Abu-Zied, R., Cooke, S., Fontanier, C., Leng, M., Lykousis, V., 2002. Circulation changes and nutrient concentrations in the late Quaternary Aegean Sea: a non-steady state concept for sapropel formation. Paleoceanography 17, 14.1–14.11.

Federman, A.N., Carey, S.N., 1980. Electron microprobe correlation of tephra layers from Eastern Mediterranean. Quat. Res. 13, 160–171.

Grant, K.M., Rohling, E.J., Bar-Matthews, M., Ayalon, A., Medina-Elizalde, M., Bronk Ramsey, C., Satow, C., Roberts, A.P., 2012. Rapid response of ice volume to polar temperature variations. Nature 491, 744–747.

Hayes, A., Rohling, E.J., De Rijk, S., Kroon, D., Zachariesse, W.J., 1999. Mediterranean planktonic foraminiferal faunas during the Last Glacial cycle. Mar. Geol. 153, 239–252.

Keller, J., Ryan, W.B.F., Ninkovich, D., Altherr, R., 1978. Explosive volcanic activity in the Mediterranean over the past 200,000 yrs. as recorded in deep-sea sediments. Geol. Soc. Am. Bull. 89, 591–604.

Marino, G., Rohling, E.J., Rijpstra, W.I.C., Sangiorgi, F., Schouten, S., Sininghe Damste, J.S., 2007. Aegean Sea as driver of hydrographic and ecological changes in the eastern Mediterranean. Geology 35, 675–678.

McCoy, F.W., 1981. Areal distribution, redeposition and mixing of tephra within deep sea sediments of the eastern Mediterranean sea. In: Self, S., Sparks, R.S.J. (Eds.), Tephra Studies. D. Reidel Publishing Company, pp. 255–280.

Ninkovich, D., Heezen, B.C., 1965. Santorini tephra. Proceedings of the Seventeenth Symposium of the Colston Res.Society. Colston Research Papers. Vol. 17. Butterworths Scientific Publications, London, pp. 413–452.

Osbourne, A.H., Marino, G., Vance, D., Rohling, E.J., 2010. Eastern Mediterranean surface water Nd during Eemian sapropel S5: monitoring northerly (mid-latitude) versus southerly (sub-tropical) freshwater contributions. Quat. Sci. Rev. 29, 2473–2483.

Rohling, E.J., Cane, T.R., Cooke, S., Sprovieri, M., Bouloubassi, I., Emeis, K.C., Schiebel, R., Kroon, D., Jorissen, F.J., Lorre, A., Kemp, A.E.S., 2002a. African monsoon variability during the previous interglacial maximum. Earth Planet.Sci. Lett. 202, 61–75.

Satow, C., Tomlinson, E.L., Grant, K.M., Albert, P.G., Smith, V.C., Manning, C.J., Ottolini, L., Wulf, S., Rohling, E.J., Lowe, J.J., Blockley, S.P.E., Menzies, M.A., 2015. A new contribution to the Late Quaternary tephrostratigraphy of the Mediterranean: Aegean Sea core LC21. Quat. Sci. Rev. 117, 96–112.

Vespa, M., Keller, J., Gertisser, R., 2006. Interplinian explosive activity of Santorini volcano (Greece) during the past 150,000 years. J. Volcanol. Geotherm. Res. 153, 262–286.

Wulf, S., Keller, J., Satow, C., Gertisser, R., Kraml, M., Grant, K. M., et al. (2020). Advancing Santorini's tephrostratigraphy: New glass geochemical data and improved marine-terrestrial tephra correlations for the past ~360 kyrs. Earth-Science Reviews, 200.

16th International Congress of the Geological Society of Greece
17-19 October, 2022 - Patras, Greece
Bulletin of the Geological Society of Greece, Sp. Publ. 10
Ext. Abs. GSG2022-055

Paleoclimate Study Of Skeletal Material Of The Pygmy Hippo *Phanourios Minor* From Ayia Napa (Cyprus) Based On Oxygen and Carbon Isotope Analysis.

M. A. Nakasi[1], E. Stathopoulou[1], M. Tassi [2], P. Karalis[2], E. Dotsika[2], G. Theodorou[1], E. Tsiolakis[3]

(1) Department of Historical Geology & Palaeontology, Faculty of Geology & Geoenvironment, National and Kapodistrian University of Athens, Panepistimiopolis, 15784 Zographou, Greece, mariannakv@yahoo.com (2) Stable Isotope Unit, Institute of Nanoscience and Nanotechnology, National Center of Scientific Research "Demokritos", GR15310 Ag. Paraskevi Attikis, Greece (3) Cyprus Geological Survey Department, 2064 Strovolos, Cyprus

Dwarf elephants, pygmy hippos and various species of micromammals are some of the animals that lived in Cyprus, 11.000 to 13.000 years ago (Theodorou et al., 2007). Fossil skeletal material of the pygmy hippopotamus *Phanourios minor* has been excavated from the fossiliferous site in Ayia Napa (Theodorou et al., 2004) and is considered as the smallest of all known insular hippopotamuses (Hadjisterkotis et al., 2008). In this study, material from Ayia Napa was used in order to attempt to reconstruct the climate in which this species lived. The method used to determine the living conditions of this extinct species is the isotopic analysis of oxygen and carbonate bioapatite of bones and tooth samples. The ^{13}C / ^{12}C ($\delta^{13}C$) and ^{18}O / ^{16}O ($\delta^{18}O$) ratios used function as a paleoclimatic index.

Studying area

The site of Ayia Napa is located less than 1km east of the town center, at an altitude of 25 m and was discovered in 2000. The numerous fossils are embedded in red clays, deposited in a littoral rock – shelter comprised from limestones. The site is dominated by skeletal material of the pygmy Hippopotamus species *Phanourios minor*, an endemic species that lived exclusively on Cyprus. The material has been dated back to the Upper Pleistocene (11-13,500 years B.P.) (Theodorou et al, 2007). When the elephants and hippos were isolated on the island, they gradually evolved into dwarfs. In contrast, small mammals evolved to gigantic sizes (Theodorou et al., 2007). The fossiliferous assemblage is spread in a total area of about 72 m^2 and a thickness of between 1 and 1.5 meters and the estimated fossil density of 817 remains/m^3, verifies an extremely high-density assemblage of skeletal material (Fillipidi et al., 2013).

Figure 1. Paleontological excavation in Ayia Napa (Cyprus), 2014

Materials and Methods

In the case of skeletal material, the study of stable isotopes can be based on the extracted collagen or the material's bioapatite. In our case, all attempts to extract collagen failed as the material was totally dissolved during purification. Thus, the analysis continued based on the study of the phosphates and carbonates of the bone and tooth bioapatite. In the case of teeth, tooth enamel was preferred. Furthermore, several possible parameters that may have affected the isotopic composition of apatite were investigated, including age, sex, tooth type and diagenesis (Clemenz, 2012; Dotsika et al, 2011).

Essentially, ten long bones and ten teeth (canines and molars) were used to determine the living conditions of this species. From each sample, 100-200 mg was ground in the mortar. The samples were analyzed with a ThermoScientific Delta V Plus mass spectrometer, after reaction for 1 hour with orthophosphoric acid (99%) at 72°C, for CO_2 production (GasBench II instrument) and $\delta^{18}O$ and $\delta^{13}C$ were measured. The analysis was done at the Institute of Nanosciences and Nanotechnology (INN) of NCSR Demokritos, in the isotope laboratory.

Results

To interpret the results we converted the oxygen values of the apatite to drinking water values and calculated an average value -4,56‰. The values were compared with the isotope values of September-April 2000/2001 precipitation in Kouri region of Cyprus, which is located at an altitude of 242m. For this region the isotopic value is -4.93‰ (Boronina et al, 2005). Our study area is located at an altitude of 25m. For every 100m the oxygen value changes by -0.27‰. Therefore,

the isotopic value becomes -4.39‰. The average value from our results is more negative, so the climate of Cyprus was colder. It also appears that this species lived during *Younger dryas* wich was a cold period. It would also be worth mentioning their disappearance, which could be due to the lack of adaptation to the cold period.

Table 1. Carbon and Oxygen isotope results for the hippopotamus Phanourios minor samples from the Aghia Napa area of Cyprus. Measurements by the isotope laboratory NCSR Demokritos.

Bone Code	Bone or Tooth	d13CV-PDB	d18OapV-PDB	d18Oap-VSMOW	d18Ow-VSMOW
AN01A225	bone	-6.99	-2.15	28.69	-3.68
AN01A2336	tooth	-10.56	-2.58	28.25	-4.13
AN02475	canine	-7.52	-3.17	27.64	-4.75
AN03 2513	canine	-8.10	-3.40	27.41	-4.99
AN01 2328	tooth	-10.60	-2.00	28.85	-3.52
AN02 1099	canine	-9.24	-3.04	27.78	-4.61
AN07 2451	canine	-6.93	-3.53	27.27	-5.13
AN01 2805	tooth	-9.21	-1.14	29.73	-2.61
AN8 1915	bone	-9.14	-3.39	27.42	-4.98
AN8 572	bone	-9.30	-2.20	28.64	-3.73
AN8 1141	bone	-8.86	-2.95	27.86	-4.52
AN07 753	bone	-9.40	-3.68	27.11	-5.29
AN02 A51x	bone	-8.87	-3.56	27.24	-5.16
AN02 1095	bone	-9.67	-2.86	27.96	-4.42
AN07 3556	bone	-10.00	-3.00	27.82	-4.57
AN02 1578	bone	-8.95	-3.14	27.68	-4.71
AN07 3451	bone	-9.96	-3.12	27.69	-4.69
AN01 2661	bone	-9.32	-3.22	27.59	-4.80
AN01 3037	bone	-8.90	-3.90	26.89	-5.51
AN01 4012	tooth	-8.96	-3.89	26.90	-5.51

Acknowledgements

The authors would like to thank the people who helped me and supported me either cognitively or psychologically. I would also like to thank the team of the isotope laboratory at the NCSR Demokritos research center for accepting me at their place for the processing of the material and the Cyprus Geological Survey, which allowed us access to the material and excavations in the area.

References

Boronina A., Balderera W., Renardb P., Stichlerc W., 2005. Study of stable isotopes in the Kouris catchment (Cyprus) for the description of the regional groundwater flow, Journal of Hydrology 308 (2005) 214–226.

Clemenz, M. T., 2012. New insight from old bones: stable isotope analysis of fossil mammals, Journal of Mammalogy, 93(2), 368-380.

Dotsika, E., Zisi, N., Tsoukala, E., Poutoukis, D., Lykoudis, S. and Giannakopoulos, A., 2011. Palaeoclimatic information from isotopic signatures of Late Pleistocene Ursus ingressus bone and teeth apatite (Loutra Arideas Cave, Macedonia, Greece), Quaternary International, 245 (2), 291-301.

Filippidi, A., Stathopoulou, E. T., & Theodorou, G. E., 2013. Taphonomical observations on the pygmy hippopotamus site in Aghia Napa, Cyprus. Bulletin of the Geological Society of Greece, 47, 122–135.

Hadjisterkotis E. and Reese S.D. 2008. Considerations on the potential use of cliffs and caves by the extinct endemic late Pleistocene hippopotami and elephants of Cyprus, European Journal of Wildlife Research, 54: 122-133

Stathopoulou, E. 2005. First results on the fossilization of Dwarf Hippo skeletal remains from Aghia Napa, Cyprus. Monografies de la Societat d'Història Natural de les Balears, 12: 319-324.

Theodorou G., Panayides I., Stathopoulou E., Papaspyropoulos C., Agiadi K. and Tsolakis E., 2004. Remarks on the endemic fossil Hippopotamus from Aghia Napa (Cyprus), Proceedings of the 5th International Symposium on Eastern Mediterranean Geology, 1, 355-358.

Theodorou, G., Roussiakis, S., Athanassiou, A., Giaourtsakis, I., and Panayides, I., 2007. A late Pleistocene endemic Genet (Carnivora, Viverridae) from Aghia Napa, Cyprus, Bulletin of the Geological Society of Greece, 40(1), 201-208.

Sondaar, P.Y., 1977. Insularity and its effect on mammal evolution. In: Hecht, M.N., P.L. Goody, & B.M. Hecht (eds). Major Patterns in Vertebrate Evolution: 671-707. New York: Plenum Publ. Co.

16th International Congress of the Geological Society of Greece

17-19 October, 2022 - Patras, Greece

Bulletin of the Geological Society of Greece, Sp. Publ. 10

Ext. Abs. GSG2022-071

New Paleoceanographic Constraints for the Tortonian-Messinian Transition: Carbon Cycle and Hydroclimate Insights from the Potamida Section (Crete Island, Eastern Mediterranean).

E. Besiou[1], G. Kontakiotis[1], A. Antonarakou[1], A. Mulch[2,3], I. Vasiliev[2]

(1) National and Kapodistrian University of Athens, Department of Historical Geology and Paleontology, Faculty of Geology and Geoenvironment, 15784, Athens, Greece, evabesiou@geol.gr (2) Senckenberg Biodiversity and Climate Research Centre (BiK-F), Senckenberganlage 25, D-60325 Frankfurt am Main, Germany (3) Goethe University, 60438 Frankfurt am Main, Germany

Background

The Latest Miocene (8.0–5.33 Ma) has been considered as one of the most climatically stable periods of the Cenozoic, characterized by minor long-term cooling and ice growth compared to the entire Neogene (Zachos *et al*., 2001). Especially, the Tortonian-Messinian Transition (TMT) is recognized as a priority for paleoenvironmental reconstruction and climate modelling due to the significant paleoenvironmental changes preceding the Messinian Salinity Crisis (MSC) and the resemblance with the modern Mediterranean-type climate respectively (Kontakiotis *et al*., 2019, 2022).

Objectives

The Mediterranean region was affected by astonishing changes in its hydrological cycle, making it ideal to explore the sea level fluctuations and climate perturbations in the circum-Mediterranean region, during the TMT. On this regard, an integrated study was carried out in Potamida section (western Crete, eastern Mediterranean) that covers the TMT (Fig. 1).

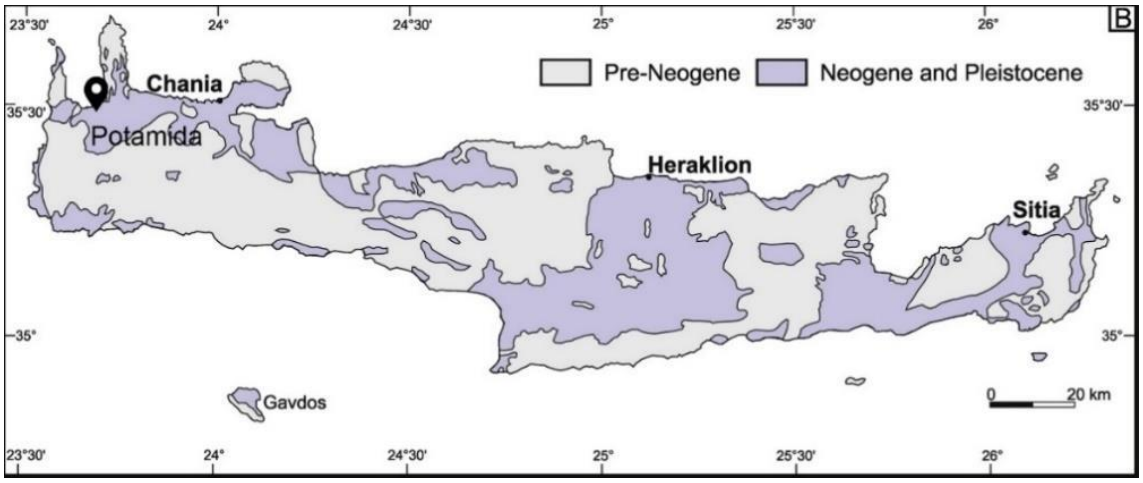

Figure 1: Geological sketch map of Crete Island including the location of the study section.

Methods

Methodology consists of integrated geochemical analyses in terms of biomarkers and stable isotopes. Biomarkers based on isoprenoid glycerol dialkyl tetraethers-based TEX_{86} proxies (Schouten *et al*., 2002) used estimating Sea Surface Temperature (SST). Stable carbon ($\delta^{13}C$) and oxygen ($\delta^{18}O$) isotopes measured on both benthic (*Cibicides kullenbergi*) and planktonic foraminifera (*Globigerinoides obliquus*). Foraminiferal $\delta^{18}O$ combining biomarker-derived SST values resulted in the Sea Surface Salinity (SSS).

Results

The resulting foraminiferal oxygen isotopes indicative a decoupling between the bottom and the surface water column starting before the Tortonian-Messinian boundary. The difference between planktonic and benthic oxygen isotope signals ($\Delta\delta^{18}O$) further shows an estimate of the degree of water masses stratification during that time. The $\delta^{13}C$ data display a trend to lighter values in accordance with the global Late Miocene Carbon Isotope Shift (LMCIS; 7.6-6.6 Ma), due to progressive restriction of the Mediterranean basin. However, an exception is observed the time interval from 7.38-7.26 Ma, where the estimated $\delta^{13}C$ demonstrate heavier values in both records. These changes in carbon cycle through a 6-cycle development are more pronounced to planktonic $\delta^{13}C$ representing the surface waters. The calculated SSTs indicate warm sea surface waters with average temperatures of 270C, during latest Tortonian, following by a strong cooling event

when the values drop as low as 200C. The SSSs results show an increasing trend on surface waters already before the Messinian, while at the TMT, the conditions in the surface waters changed towards cooler (~240C) and normal salinity conditions (Fig. 2).

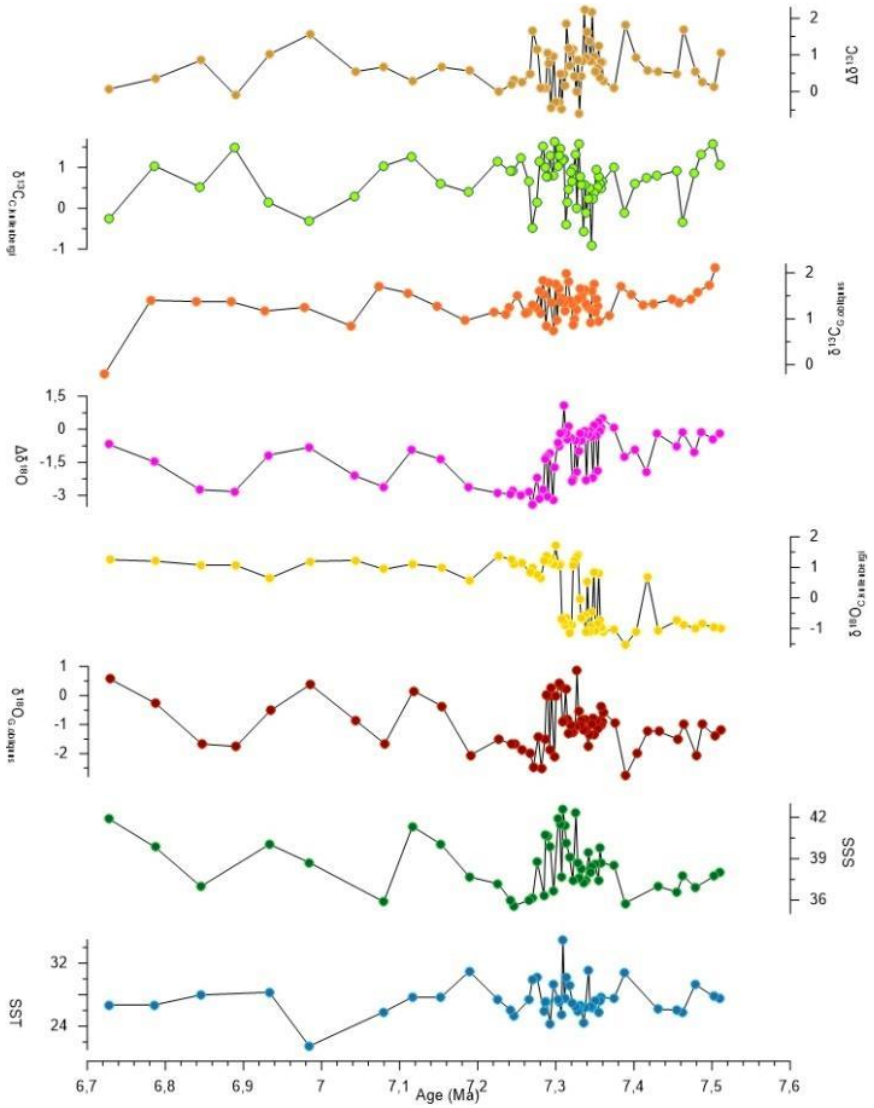

Figure 2: Potamida A) Sea surface temperature calculated based on TEXH86 (SST-TEXH86); B) sea surface salinities (SSS) based on SST TEXH86 and δ18OG. Obliquus; C) δ13C measured on Globigerinoides obliquus (δ13CG. Obliquus) and on Cibicides kullenbergi (δ13CC. Kullenbergi)), Δδ13C; D) δ18O measured on Globigerinoides obliquus (δ18OG. obliquus) and on Cibicides kullenbergi (δ18OC. Kullenbergi)), Δδ18O.

Conclusions

Results of this study indicate a warm water column until 7.3 Ma, afterwards is observed a strong cooling event. Contrary, a progressive surface salinity increase is documented. At the same time, the benthic oxygen isotopes display a salinity increase in the bottom waters. Additionally, the difference between benthic and planktonic $\delta^{18}O$ reflects stratification of water masses. Finally, the $\delta^{13}C$ records point to a productivity driven cyclicity, which is more pronounced to the surface waters.

References

Kontakiotis G., Besiou E., Antonarakou A., Zarkogiannis S., Kostis A., Mortyn P. G., Moissette p., Cornée J. J., Schulbert C., Drinia H., Anastasakis G. & Karakitsios V., 2019. Decoding sea surface and paleoclimate conditions in the eastern Mediterranean over the Tortonian-Messinian Transition. Palaeogeography, Palaeoclimatology, Palaeoecology, 534, 109312.

Kontakiotis et al., 2022 Kontakiotis, G., Butiseacă, G.A., Antonarakou, A., Agiadi, K., Zarkogiannis, S.D., Krsnik, E., Besiou, E., Zachariasse, W.J., Lourens, L., Thivaiou, D., Koskeridou, E., Moissette, P., Mulch, A., Karakitsios, V., Vasiliev, I., 2022. Hypersalinity accompanies tectonic restriction in the eastern Mediterranean prior to the Messinian Salinity Crisis. Palaeogeography, Palaeoclimatology, Palaeoecology, 592.

Schouten, S., Hopmans, E. C., Schefuss, E. & Sinninghe Damsté, J. S. Distributional variations in marine crenarchaeotal membrane lipids: a new tool for reconstructing ancient sea water temperatures? Earth Planet. Sci. Lett. 204, 265–274 (2002).

Zachos, J., Pagani, M., Sloan, L., Thomas, E., Billups, K., 2001. Trends, rhythms, and aberrations in global climate 65 Ma to present. Science, 292, 686–693.

16th International Congress of the Geological Society of Greece
17-19 October, 2022 - Patras, Greece
Bulletin of the Geological Society of Greece, Sp. Publ. 10
Ext. Abs. GSG2022-075

Caenozoic Gastropods from France; part of the P.G. Moazzo Collection of the Goulandris Natural History Museum

C. Giamali
(1) The Goulandris Natural History Museum, Kifissia, Greece, ch.giamali@gnhm.gr

Invertebrate palaeontological collection constitute a large part of the Goulandris Natural History Museum (GNHM). In order to shed light to some of the hidden palaeontological treasures of the GNHM collections, the Caenozoic Gastropod Moazzo Collection is here studied. Polychronis G. Moazzo (1893-1975) born in Egypt, to Greek parents. Initially he studied agronomic engineering, though soon he followed zoological studies at the Natural History Museum of Paris, and worked alongside molluscan experts of his time (Goulandris, 1977). Moazzo was devoted to marine biology and travels, and became an exceptional collector of recent and fossils marine invertebrates (mainly molluscs), though he also collected entomological material (Dimaki and Tylianakis, 2006). After Moazzo's death, his family donated his collections to the GNHM.

The palaeontological P.G. Moazzo collection consists of about 1021 lots of molluscs (Bivalvia, Gastropoda, Cephalopoda, and Scaphopoda), brachiopods, corrals, and echinoids, from Mesozoic and Caenozoic deposits of Europe (France, Spain, Italy, and Portugal), Africa (Egypt, Somalia, and Algeria), Central and South America (Mexico and Peru). Most of the specimens were collected by Moazzo between the World War I and World War II, however, some specimens are part of the Berlier Collection.

In this study, Caenozoic gastropods from France are revealed. This part of the collection comprises 247 lots (473 specimens) placed in cartons and boxes, made appropriate by P. G. Moazzo, with details concerning the nomenclature, origin, age and/or formation. In case of gifted specimens this is stated at the back of the cartons. The collection represents 224 species (plus 13 indeterminate), belonging to 50 families, from 43 fossiliferous sites of Eocene, Oligocene and Miocene Epoch. Particularly, the majority of the samples derives from the Paris Basin (Grignon, Damery, Montmirail, Cuise-la-Motte, Chaussy, Chamery, Chambors, Parnes, Le Fayel, Mouchy, St. Ouen, Vaudacourt, Mary, Saulxmarchais, Beynes, Liancourt, Le Guépelle, Auvers, Chaumont, Houdan, Châtillon, Requiécourt, Montjavoult, Ver, Brasles prés Chateau Thierry, Porte de Gentilly, Le Ruel, Chécy, Chéry-Chartreuve, Mortefontaine), whereas representatives of Aquitaine Basin (Gaas, Dax, Bordeaux, Saucats, Mérignac), Côte d'Or (Dijon, Magny-Saint-Médard, Varois, Vesyrottes), Loire-Atlantique, Cotentin, and Loire-et-Cher are also included. Families with the most numerous representatives are Cerithiidae (26 species), Volutidae (24 species), Turritellidae (18 species) and Fasciolariidae (16 species). The majority of the species are of marine environment, though terrestrial and fresh water species are also included (11 species).

In the frame of this work, is underlined that the collection is of historical importance and constitute a comparative tool for molluscan studies. The disclosure of Moazzo's collection highlights the need of curation, scientific revision and integration into the data base of the GNHM. These actions will enhance the accessibility and the recognition of a collection, which was up to know well hidden in the drawers of the GNHM.

Acknowledgements

I would like to thank the volunteers Niovi Roussou and Konstantina Tsoulou for their assistance in cataloguing. Furthermore Dr. Evi Vardala – Theodorou is kindly appreciated for her constructive comments.

References

Goulandris, N., 1977. Georgi P. Moazzo (1893 – 1975), Greek conchologist. Annales Musei Goulandris 3, 105-122.
Dimaki, M., Tylianakis, J., 2006. A catalogue of the G.P. Moazzo collection in the Goulandris Natural History Museum. Part I. Annales Musei Goulandris 11, 281-287.

16th International Congress of the Geological Society of Greece

17-19 October, 2022 - Patras, Greece

Bulletin of the Geological Society of Greece, Sp. Publ. 10

Ext. Abs. GSG2022-103

Comparison of the Eocene Larger Benthic Foraminifera Assemblages of Two Paleogene Molassic Basins of the Greek Territory

V.-G. Dimou1, O. Koukousioura1, G. Less2, M. V. Triantaphyllou3, M. D. Dimiza3, G. Syrides1

(1) Aristotle University of Thessaloniki, School of Geology, Thessaloniki, Greece, dimouvaso@geo.auth.gr (2) University of Miskolc, Department of Geology and Mineral Resources, Miskolc, Hungary (3) National and Kapodistrian University of Athens, Faculty of Geology and Geoenvironment, Athens, Greece.

During the Paleogene, two molassic basins (Mesohellenic Trough and Thrace Basin) operated in the Greek peninsula. Sedimentation of both basins seems to begin almost simultaneously (middle Eocene) however their stratigraphic evolution is differentiated. The Mesohellenic Trough is located in NW Greece and Albania, and comprises a succession (Rizoma, Krania, Eptachori, Pentalophos, Tsotyli and Ondria Fms) of molasse-type formations (Brunn, 1956; Wielandt-Schuster *et al*., 2004; Ferrière *et al*., 2013; Kilias *et al*., 2015). The sampling area is located in Vasiliki Trikala (NW of Trikala) and belongs to the late Eocene Rizoma FM (Ferrière *et al*., 2013). Sampling was carried out at two sites (Vsl 1, Vsl 2), considering the composition alternation in the nummulitic-bearing Vasiliki limestones. The greek part of the Thrace basin is expanded in the Northern Greece and according to Papanikolaou and Triantaphyllou (2010, 2019) a variation in the stratigraphy occurs (Kirki, Chorafaki, Avas, Pylaea Fms). Three sites were studied Kirki, Fanari and Avandas. Kirki's samples derived from an argillaceous horizon (Kirki Fm), Avandas' from the Avas limestone and Fanari samples came from sandstone and siltstone. The sampled sites were selected as they should be representative of larger benthic foraminifera (LBF) assemblages of middle-upper Eocene corresponding to almost the same paleoenvironmental conditions.

The objectives of this study are: (1) to determine the LBF assemblages of the Eocene, in accordance with biometric analysis when possible and morphological features (internal/external), (2) to provide a biostratigraphic framework and finally (3) to compare all the above between the two basins.

Samples originated from hard consolidated sediments (Vasiliki limestone, Avas limestone) were studied mainly in thin sections. In case of Vasiliki, a few isolated specimens were also collected. These along with the isolated specimens, which were extracted from the loose sediments of Kirki and Fanari, were submitted to dichotomy. Morphometrical measurements were performed on the bisected specimens to support and amplify the taxonomic identification of LBF. On the other hand, measurements were not possible to take upon thin section due to the lack of equatorial sections and the existence of plethora randomly oriented sections of LBF.

The association of Vasiliki Trikala includes *Nummulites* ex. gr. *perforatus* together with several other giant and rare small *Nummulites*, *Operculina* ex. gr. *gomezi* Colom and Bauzá, *Amphistegina* sp., *Discocyclina* sp., *Silvestriella tetraedra* (Gümbel), other orthophragmines and small rotaliids Additionally, gastropods (Trochinae), regular echinoids and red algae were observed. This association corresponds to the Bartonian (SBZ 17-18A; Dimou *et al.*, 2021).

The association of Kirki comprises *N. perforatus* de Montfort, *N. maximus* d'Archiac, and *Assilina exponens* (Sowerby), accompanied by gastropods (Turritellidae) and corals. The faunal composition indicates Shallow Benthic zones SBZ 16/17 (Dimou *et al.*, 2021).

The assemblage of Fanari is characterized by *N. fabianii* (Prever), *N. incrassatus* de la Harpe, *N. garnieri* de la Harpe, *N. chavannesi* de la Harpe, *N. budensis* Hantken, *N. stellatus* Roveda, *Heterostegina gracilis* Herb, *H. reticulata* Herb, *Spiroclypeus carpaticus* (Uhlig), *Operculina* ex. gr. *gomezi* Colom & Bauzá, *Assilina alpina* Douvillé, *Discocyclina dispansa* (Sowerby) *umbilicata* (Deprat), *D. radians labatlanensis* (Less), *D. euaensis* Whipple, *D. augustae* van der Weijden, *Orbitoclypeus varians* (Kaufmann) cf. *scalaris* (Schlumberger), *O. furcatus* (Rütimeyer), *Asterocyclina stellata* (d'Archiac) *stellaris* (Brünner, in Rütimeyer), *A. stella stella* (Gümbel), *A. alticostata danubica* (Nuttall), *Pellatispira madaraszi* (Hantken), *Sivlestriella tetraedra* (Gümbel), *Sphaerogypsina* sp., and *Fabiania* sp. The foraminiferal assemblage corresponds to the uppermost Eocene, SBZ 20 (Dimou *et al.* submitted).

The association of Avandas constitute of *N. fabianii* (Prever), *Nummulites* sp., *Operculina* ex. gr. *gomezi* Colom & Bauzá, *Spiroclypeus* sp., *Heterostegina* sp., *Discocyclina* sp., *D. radians* (d'Archiac), *Asterocyclina* sp., *Orbitoclypeus* sp., *Silvestriella tetraedra* (Gümbel), *Fabiania* sp., *Sphaerogypsina* sp., *Amphistegina* sp., small rotalids, miliolids, fragments of coralline algae, bryozoan, gastropods and bivalves. The age of this assemblage can be defined as middle-upper Priabonian, SBZ 19-20.

Based on the biostratigraphic assignment of Vasiliki (SBZ 17-18A) and Kirki (SBZ 16/17) assemblages, the concept of the almost simultaneously beginning of the sedimentation is supported. However, the oldest Kirki's assemblage is clearly redeposited; hence it allows us only to assume the existence of a late Lutetian to early Bartonian platform that is demolished. *N. perforatus* is a characteristic and common species for the two basins. Fanari and Avandas assemblages imply the operation of a younger platform of middle-late Priabonian, that is not traced in the Mesohellenic Trough.

According to Soliman and Zygojiannis (1979) the upper Eocene deposits of the Mesohellenic Trough are featured mainly by planktonic foraminifera responding to an open marine environment; indeed Zygogiannis and Muller (1982) had documented the late Eocene calcareous nannofossil biozones NP19-20, in Nea Zoi, between Kalambaka and Trikala. Concluding, the evolutionary/ paleoenvironmental history of the Eocene of Mesohellenic Trough is marked by a transgressive episode overlapping the shallow marine deposits of middle Eocene. Unlike, throughout Eocene the paleoenvironmental conditions in Thrace basin are more or less stable and such shift to open marine settings took place in later stages of the Paleogene. The micropaleontological data from Thrace basin leads to several question about the period of the operation and demise of the Lutetian- Bartonian (SBZ 16/17) platform, that needs further investigation.

Acknowledgements

This research (V.-G. Dimou) is co-financed by Greece and the European Union (European Social Fund-ESF) through the Operational Programme "Human Resources Development, Education and Lifelong Learning" in the context of the Act "Enhancing Human Resources Research Potential by undertaking a Doctoral Research" Sub-action 2, implemented by the Scholarship Programme (IKY) for PhD candidates in the Greek Universities. The work of G. Less was carried out at the University of Miskolc, within the framework of the Thematic Excellence Program funded by the Ministry of Innovation and Technology of Hungary (Grant Contract reg. nr.: NKFIH-846-8/2019).

References

Brunn, J.H., 1956. Etude géologique du Pinde septentrional et de la Macédoine occidentale Thèse, Paris, 1955. Annales Géologiques des Pays Helléniques 7, 358 pp.

Dimou, V.G., Koukousioura, O., Dimiza, D.M., Triantaphyllou, V.M., Less, G., Pomoni-Papaioannou, F., Syrides, G., 2021. A preliminary investigation of Eocene larger benthic foraminifera assemblages from Alpine and molasse-type deposits of the Hellenic peninsula (Greece). Revue de Micropaléontologie 70, 100468.

Dimou, V.G., Koukousioura, O., Less, G., Triantaphyllou D.M., Dimiza, V.M., Syrides, G., submitted. Systematic paleontology and biostratigraphy of the upper Eocene Large Benthic Foraminifera of Fanari (Thrace Basin, Greece).

Ferrière, J., Chanier, F., Reynaud, J., Pavlopoulos, A., Ditbanjong, P., Coutand, I., 2013. Evolution of the Mesohellenic Basin (Greece): a synthesis, in: Skourtsos, E. (Eds), The Geology of Greece - Part II. Journal of the Virtual Explorer Electronic Edition, ISSN 1441-8142 volume 45, paper 1.

Kilias, A., Vamvaka, A., Falalakis, G., Sfeikos, A., Papadimitriou, E., Gkarlaouni, C., Karakostas, B., 2015. The Mesohellenic Trough and the Paleogene Thrace Basin on the Rhodope Massif, their structural evolution and geotectonic significance in the Hellenides. Journal of Geology and Geophysics 4, 2.

Papanikolaou, D., Triantaphyllou, M., 2010. Tectonostratigraphic observations in the western Thrace Basin in Greece and correlations with the eastern part in Turkey. Geologica Balcanica 39 (1-2), 293-294.

Papanikolaou, D., Triantaphyllou, M., 2019. New stratigraphic data of the Limnos volcanosedimentary sequence and correlations with the Thrace Basin. Proceedings of the 15th International Congress of the Geological Society of Greece, 22-24 May, Athens, Greece, Bulletin of the Geological Society of Greece Sp. Pub. 7, Ext. Abs. GSG2019-240, 71-72.

Soliman, H.A., Zygojannis, N., 1977. Foraminiferal assemblages from the Eocene of the Mesohellenic Basin, Northern Greece. VI Colloquium on the Geology of the Aegean Region 3, 1095-1104.

Wielandt-Schuster, U., Schuster, F., Harzhauser, M., Mandic, O., Kroh, A., Rogl, F., Reisinger, J., Liebetrau, V., Steininger, F.F., Piller, W.E., 2004. Stratigraphy and palaeoecology of Oligocene and Early Miocene sedimentary sequences of the Mesohellenic Basin (NW Greece). CFS Courier Forschungsinstitut Senckenberg 248, 1-55.

Zygojannis, N., Müller, C., 1982. Nannoplankton Biostratigraphie der tertiären Mesohellenischen Molasse (Nordwest-Griechenland). Zeitschrift der Deutschen Geologischen Gesellschaft 133, 445-455.

16th International Congress of the Geological Society of Greece
17-19 October, 2022 - Patras, Greece
Bulletin of the Geological Society of Greece, Sp. Publ. 10
Ext. Abs. GSG2022-114

Depositional Trends In The Extreme Discovery Deep Environment (Red Sea)

S. Matsagou[1], I.P. Panagiotopoulos[1], H. Drinia[1], P. Avramidis[2]

(1) Faculty of Geology and Geoenvironment, National and Kapodistrian University of Athens, Zografou, Greece, sofia_matsagou_sofiamatsagou93@gmail.com (2) Department of Geology, University of Patras, Patras, Greece.

Research Highlights

Differentiating between pelagic and hydrothermal deposition in a sedimentary archive from the Discovery Deep hot (~45 ºC) brine pool, and identifying the impact of hydrothermal venting on the autochthonous benthic foraminifera.

Background

The peculiar geotectonic regime of the Red Sea has attracted the attention of various oceanographic missions during the last 60-65 years, with hydrothermal geochemistry/mineralogy being the most important field of interest primarily due to the potential economic benefits. The central and southern sections of Red Sea are characterized by an axial trough with a continuous rift valley, where the largest Red Sea hydrothermal venting sites, i.e., Atlantis II and Discovery deeps, are located. In contrast, the northern part has not any axial rift valley but only a few isolated deeps (Botz *et al.*, 2007). Most of the discovered deeps reflect the early initial phase of seafloor spreading with punctiform emplacement of oceanic crust, while they are brine-filled due to the leaching of the sub-bottom Miocene evaporites resulting in salinities up to 27%. Also, except the amount of leaching salt, the thickness of the brine is affected by the diffusion processes at the seawater-brine interface.

Even though significant emphasis has been given to the geochemistry/mineralogy of the metalliferous sediments of Atlantis II Deep (chemically precipitated from the hot, up to 66 ºC, brine), which is undoubtedly the most mineralized deep of Red Sea and one of the largest present-day ore-forming environments, the studies concerning the Discovery Deep are quite limited and rather old. Firstly, Swallow and Crease (1965) reported the presence of iron-bearing sediments in the deep, while afterwards Miller *et al*. (1966), Degens and Ross (1969), and Ross *et al*. (1973) provided in detail the results of their investigations on recent iron deposits in the area. In addition, Bischoff (1969) identified a variety of authigenic minerals, including goethite, iron-montmorillonite, manganosiderite, lepidocrocite and pyrite, as well as detrital material consisting of pteropods, coccoliths and foraminiferal shells, along with minor amounts of quartz, feldspar and clays.

Objectives

- Detection of the more recent depositional trends in the Discovery Deep in order to unravel the temporal evolution of the physico-chemical conditions in the local hypersaline environment, which has resulted from changes in the composition, temperature and flow rate of ascending hydrothermal solutions, and/or mixing events of the brine with seawater.
- Identification of the hydrothermal fluid influence on the autochthonous benthic foraminiferal assemblages, examining their transformation patterns (e.g., due to dissolution) and vertical distribution, in order to indicate influxes (from below) of diffuse acid solutions to the occurring sediments. These data could be useful as a criterion for defining potential active hydrothermal sources in deep-water environments elsewhere.

Methods

A ~1.7-m-long gravity core was retrieved (at a water depth of ~2 km; 38º02.90' E, 21º17.09' N) from the hot brine pool of Discovery Deep in the central Red Sea during an oceanographic expedition (in 2010) with the R/V Aegaeo and was investigated to accomplish the objectives of the present study. Specific stratigraphic intervals, based on the sediment color and texture variability examined via the unaided eye and a low-power (x10) hand lens, were selected for grain size, XRF and XRD analysis, TC and TOC determinations, AMS radiocarbon dating and, finally, identification of the benthic foraminiferal composition, abundance and diversity.

First Results and Conclusions

In terms of sedimentation processes, based on the performed XRF and grain size analysis (see Fig 1, 2), three stratigraphic intervals may be distinguished: (i) an upper interval (0-80 cm) analogous to the background biogenic sediments of Red Sea, suggesting that the hydrothermal system in the Discovery Deep is presently rather found in a state of inactivity; (ii) an intermediate interval (80-115 cm), displaying light- and dark-colored layers, most probably influenced by hydrothermal venting (Backer and Fellerer, 1986) without, however, affecting the metal contents in the sediment (only some slight enhancement of the Zn content can be observed); and, eventually, (iii) a bottom interval (115-170 cm) strikingly marked by a dramatic increase in the Mn content (up to 21,000 ppm, on a carbonate-free basis)

and by the occurrence of a black sticky layer (bitumen?) with strong petroliferous odor, indicating a robust hydrothermal impact. A sudden increase in the sand fraction (up to 45% dw) of the bottom stratigraphic interval has probably resulted from sub-bottom erosion processes during the vigorous hydrothermal venting, even though a turbiditic origin of the sand could be feasible too due to the numerous earthquake swarms in Red Sea; however, the visual sediment inspection did not reveal any structures (e.g., ripple or convolute laminations, sole marks, flame structures) diagnostic of the Bouma/Lowe sequence. Finally, it must be noticed that diagenesis should partly contribute to the general Mn enrichment throughout the studied sediment core via diffusion, while a hydrogenous precipitation/scavenging of Mn from the normal seawater is rather questionable because an analogous concomitant enrichment of metals such as Fe, Ni, Co and Cu is not observed (Ergin, 1994).

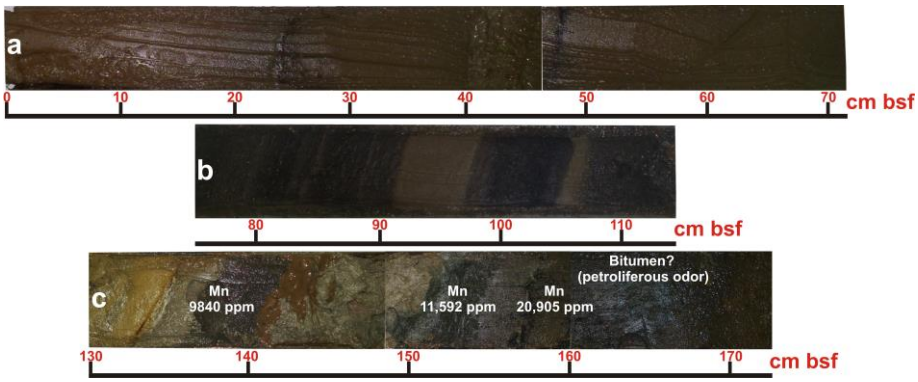

Figure 1. Image of the gravity core sections immediately after its recovery (in 2010) from the Discovery Deep brine pool. (a) Typical pelagic sedimentation; (b), (c) Hydrothermal impact on sedimentation.

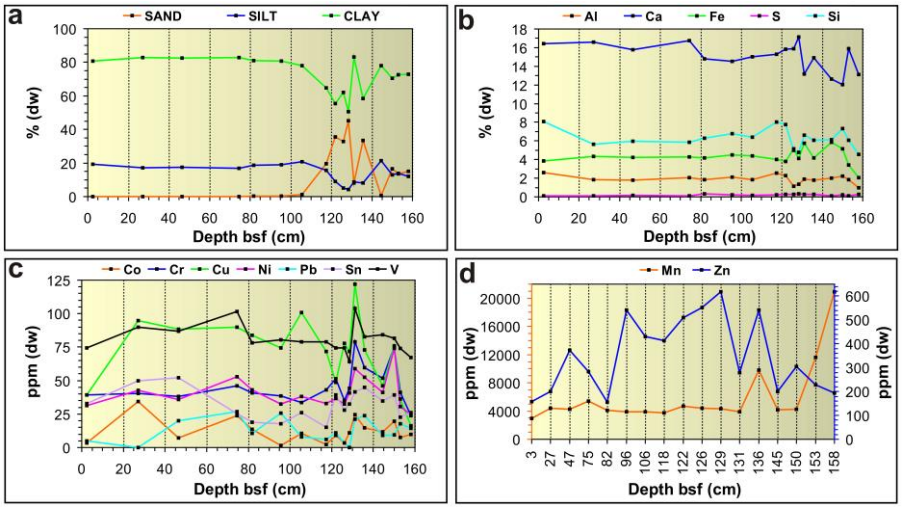

Figure 2. (a) Vertical distribution of grain size in the studied sedimentary archive; (b), (c), (d) Vertical distribution of representative metal contents in the studied sedimentary archive.

Acknowledgements

The authors are grateful to the Hellenic Centre for Marine Research for the provision of the investigated sediment core.

References

Backer, H., Fellerer, R., 1986. Chapter 7: Marine mineral exploration examples, in: Kunzendorf, H. (Ed.), Marine mineral exploration, 191-244.

Bischoff, J.L, 1969. Red Sea geothermal brine deposits: their mineralogy, chemistry, and genesis, in: Degens, E.T., Ross, D.A. (Eds.), Hot brines and recent heavy metal deposits in the Red Sea, 368-401.

Bontz, R., Schmidt, M., Wehner, H., Hufnagel, H., Stoffers, P., 2007. Organic-rich sediments in brine-filled Shaban and Kebrit deeps, northern Red Sea. Chemical Geology 244, 520-553.

Degens, E.T., Ross, D.A., 1969. Hot brines and recent heavy metal deposits in the Red Sea. Springer Verlag.

Ergin, M., 1994. Possible sources and mechanisms of manganese enrichment in the deep-sea sediments of the Marmara Trough depressions (NE-Mediterranean, Turkey). Oceanologica Acta 17, 535-546.

Miller, A.R., Densmore, C.D., Degens, E.T., Hathaway, J.C., Manheim, F.T., McFarlin, P.F., Pocklington, R., Jokela, A., 1966. Hot brines and recent iron deposits in deeps of the Red Sea. Geochimica Cosmochimica Acta 30, 341-359.

Ross, D.A., Whitmarsh, R.B., Ali, S.A., Boudreaux, J.E., Coleman, R., Fleisher, R.L., Girdler, R., Manheim, F., Matter, A., Nigrini, C., Stoffers, P., Supko, P.R., 1973. Red Sea drilling. Science 179, 377-380.

Swallow, J.C., Crease, J., 1965. Hot salty water at the bottom of the Red Sea. Nature 205, 165-166.

16th International Congress of the Geological Society of Greece

17-19 October, 2022 - Patras, Greece

Bulletin of the Geological Society of Greece, Sp. Publ. 10

Ext. Abs. GSG2022-136

The Geological Structure of the wider Samaria Gorge Area, White Mountains, Crete (Greece) – A Comprehensive Review of the Geological Models

E. Manoutsoglou[1], I. Lazos[1], E. Steiakakis[1], A. Vafidis[1]

(1) School of Mineral Resources Engineering, Technical University of Crete, University campus, 73100 Chania, Greece, emanoutsoglou@tuc.gr

Samaria gorge is situated in White Mountains region in the southwestern part of Crete Island. It is extended for 13 km in N-S direction and it consist the major geological-geomorphological structure of the Samaria National Park. Moreover, it represents the geological profile of the region, highlighting the Plattenkalk Group geological formations, which is the tectonically lower parautochthonous group of all the sequences, structing the White Mountains core, as well as the major mountain masses of Crete (Mt Talea, Mt Psiloritis, Mt Lasithiotika etc).

The geology of the study area consists of the Upper and Lower Quaternary and the Alpine formations, which includes the metamorphic parautochthonous part of the External Hellenides. In particular, two bedrock units have been identified in the wider area, showing distinct lithological features: 1) the Trypali Unit, characterized by intensively cracked, metamorphic, mostly carbonate rocks, showing cellular texture, which resemble cargneules and 2) the Plattenkalk Group, characterized by thin-bedded marbles, including chert intercalations and/or nodules.

Based on all above, various approaches have been revised contributing decisively to the theoretical background improvement, and clarifying the geology of the wider region. More specifically, three different geological models have been proposed for the Samaria gorge wider area by: 1) Tataris and Christodoulou (1969 – 1st model), 2) Pavlaki and Perleros (2015 – 2nd model), 3) Manutsoglu et al. (1999, 2001 – 3rd model).

Regarding the 1st model (Tataris and Christodoulou, 1965), the underlying system of the Plattenkalk (after Chalikiopoulos, 1903) is characterized by the following lithologies (from the upper to the lower): a) Phyllites, b) Gray – white grayish, massive carbonates with sparse chert nodules, c) Gray limestones with cellular texture (in some locations), d) Thin-bedded limestones with marl intercalations, e) Dark, massive limestones with chert nodules and phyllite intercalations, f) Calcitic phyllites and dark, crystalline limestones alternations, g) crystalline limestones, h) Similarly, calcitic phyllites and dark, crystalline limestones alternations and i) Calcitic phyllites. The Plattenkalk of this model consists of thin-bedded, crystalline limestones, including nodules and/or thin chert intercalations and thin phyllite intercalations, while these limestones are locally documented in a thick-bedded form, without chert occurrences, maintaining the crystallization. Moreover, the transition of these formations to calcitic phyllites is observed. The overlying Plattenkalk formation of this model includes a lower sequence, consisting of limestones and dolomites, and an upper sequence, consisting of phyllites, cargneules, gypsum, limestones, quartzites, eruptive formations and iron ores.

According to the 2nd model (Pavlaki and Perleros, 2015), the underlying of the Plattenkalk includes: a) Thin-bedded alternations of clay phyllites and (meta)sandstones (with low grade metamorphism), marls, as well as sparse thin-bedded limestones and chert occurrences. These sequence is also known as “Gigilos beds”, and b) A carbonate system, subjected to different tectonic facies folding and uplift, while it is characterized by significant thickness in the greatest part of White Mountains region and it is divided into: i) White grayish – whitish marbles, locally cracked, showing karstic phenomena, b) Stromatolitic dolomites, c) Black dolomites, showing cellular texture, strongly cracked with karstic phenomena. Regarding the Plattenkalk, the upper members (White Mountains metaflysch) consist of thick-bedded carbonate formations, alternating with green, calcitic phyllites, which dominate at the upper parts, while brown-black slates are locally documented. On the other hand, the lower members consist of thin-bedded and strongly recrystallized, gray-black limestones and dolomites, forming beds with thin chert intercalations and nodules. Finally, the overlying Trypali Unit, strongly karstic and tectonically affected, includes (meta)carbonate formations, which locally show a conglomerate-breccia form. In particular, the upper horizons consist of coarse, carbonate conglomerate-breccia formations and recrystallized limestones-dolomitic limestones, white the corresponding lower ones include strongly recrystallized, white grayish, squamiform to thick-bedded and cracked limestones, as well as dark dolomites.

According to the 3rd model (Manutsoglu et al., 1999; 2001), which considers the study of Soujon et al. (1998), the Plattenkalk Group of the White Mountains consists of the Mavri formation and the “Aloides formation” (after Soujon et al., 1998), includes the following lithologies (from the upper to the lower): a) Carbonate breccia, b) Dolomitic marbles with chert nodules, c) Chert-clay-carbonate sequence, d) Thin-bedded, calcitic marbles with chert intercalations and nodules, e) Medium-bedded to thin-bedded, calcitic marbles with chert nodules and layers and f) Thin-bedded marbles with red/green calc-silt horizons and cherts. In addition, the upper part includes marls and calc-schists

(Kalavros formation), which are considered as the White Mountains metaflysch. Finally, the overlying of the Plattenkalk Group sequence is the Trypali Unit (also known as Madara-Kalke). Considering the aforementioned viewpoints, we correlated the geological-lithological formations of the models highlighting the similarities and the differences between them. The results are summarized in Table 1.

Table 1. Correlation of the proposed geological models for the wider Samaria gorge area.

1st model (Tataris and Christodoulou, 1965)	**2nd model (Pavlaki and Perleros, 2015)**	**3rd model (Manutsoglu et al., 1999; 2001)**
Lower sequence - Madara-Kalke (limestones and dolomites)	Trypali Unit	Trypali Formation
Plattenkalk: crystalline, light gray - dark gray limestones with phyllite intercalations. Thin-bedded with chert intercalations and nodules. The uppermost horizons are thick-bedded without cherts, changing locally into calcitic phyllites.	White Mountains metaflysch: Thick-bedded carbonate formations with intercalations of green, calcitic phyllites	Aloides Formation
	Plattenkalk: (detailed lithological description in the text)	
System underlying the Plattenkalk: phyllites, dolomites, limestones, quartz sandstones and slates. These formations are documented in the Klados and Trypiti gorges, as well as within the Gigilos and Poria areas.	System underlying the Plattenkalk: division into metacarbonate and metaclastic formations (detailed lithological description in the text)	Gigilos formation

Acknowledgements

This research is financially supported by the Applied Research Project “3D geological structure modelling of Samaria Gorge, aiming at the investigation of hydrogeological conditions and water reservoir levels in the core of Samaria National Park (Lefka Ori), Western Crete”, funded by the Green Fund “Forest Protection and Upgrading 2019” under “Other Nationals. Green Fund”.

References

Chalikiopoulos L. (1903). Sitia, die Osthalbinsel Kreta's. Veroff. Inst. Meereskunde Berlin, 4, 1-138.

Fytrolakis, N., 1980. The geological structure of Crete (in Greek). Ph.D. thesis. National Technical University of Athens.

Manutsoglu, E., Jacobshagen, V., Spyridonos, E. Skala, W., 1999. Geologische 3D-Modellierung der Plattenkalk-Gruppe West-Kretas. Mathem. Geol., 4, 73-79.

Manutsoglu, E., Spyridonos, E., Soujon, A., Jacobshagen, V., 2001. Revision of the Geological Map and 3D Modelling of the Geological Structure of the Samaria Gorge Region, W. Crete (in greek). Bull. Geol. Soc. Greece, 34 (1), 29-36.

Pavlaki, A., Perleros, V., 2015. Updated Geological Map of the Lefka Ori National Park with Determination and Mapping og Geotope Locations (in greek). Development Organization of Crete S.A.

Soujon, A., Jacobshagen, V., Manutsoglu, E., 1998. A Lithostratigraphic Correlation of the Plattenkalk Occurrences of Crete (Greece). Bull. Geol. Soc. Greece, 32 (1), 41-48.

Tataris, A.A., Christodoulou, G., 1965. The Geological Structure of White Mountains (Western Crete) (in Greek). Bull. Geol. Soc. Greece, 6 (2), 319-347.

16th International Congress of the Geological Society of Greece
17-19 October, 2022 - Patras, Greece
Bulletin of the Geological Society of Greece, Sp. Publ. 10
Ext. Abs. GSG2022-138

Krimni-3: A New Lower Pleistocene Vertebrate Site in Mygdonia Basin

G.E. Konidaris[1], M. Amanatidou[2], K. Chitoglou[2], E. Fragkioudakis[2], N. Gerakakis[2], V. Giannakou[2], A. Gkeme[2], C. Kalaitzi[2], A. Ladas[2], C. Tsakalidis[2], V. Tsatsalis[2], D.S. Kostopoulos[2]

(1) Eberhard Karls University of Tübingen and Senckenberg Centre for Human Evolution and Palaeoenvironment, Tübingen, Germany, geo.konidaris@gmail.com (2) School of Geology Aristotle University of Thessaloniki, Thessaloniki, Greece, dkostop@geo.auth.gr

Introduction – Fossiliferous site

In this paper, we present the new Lower Pleistocene vertebrate site Krimni-3 (KMN; Figure 1) in the Mygdonia Basin (Central Macedonia, Greece), one of the most important and richest fossiliferous basins in southeastern Europe. The ongoing since 2019 research at KMN revealed a rather rich and diversified fauna, and the first results on its stratigraphy, faunal composition, taphonomic context and chronology are provided herein.

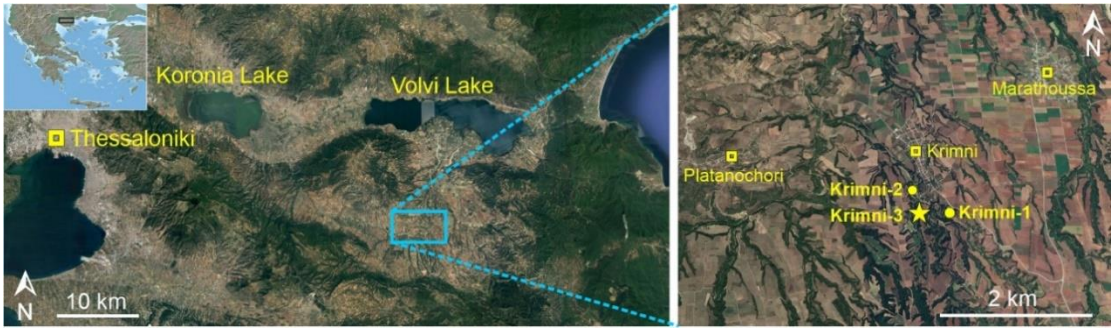

Figure 1. Geographic position of the Krimni fossiliferous sites (map from Copernicus Land Monitoring Service; satellite images from Google Earth).

KMN is placed in the upper levels of the Gerakarou Formation, which consists of red-brown sands, gravels, sandy silts and clays of fluvial/fluvio-torrential origin (Koufos *et al*., 1995; Konidaris *et al*., 2015). The fossiliferous section at KMN is divided into four 0.5-1 m-thick layers. The lowermost layer consists of parallel laminated alternating gravelly and coarse-grained reddish sands; the next layer shows the highest abundance of fossils (Figure 2) and consists of dark yellowish to reddish unconsolidated sands; the overlying layer is composed of reddish-pale brown silty sands. The section ends to the top by a cross bedded layer of thin gravels to coarse grained sands. Most of the fossil assemblage belongs to large-sized ungulates and many of the postcranial remains appear articulated (Figure 2). Bone surfaces are mainly fresh or slightly weathered. Considering the minor to moderate rounding and polishing, and the presence of calcareous concretions on some bones, as well as the several green breakages and tooth marks that they possess, a combination of water and carnivore activity is suggested.

The Krimni-3 Fauna

The KMN fossil mammal fauna consists of the following taxa: *Erinaceus* sp., Elephantidae indet. (a cheek tooth fragment with lamellae, discovered in the 2022 excavation season), *Canis* sp., Hyaenidae indet., *Ursus* sp., *Equus altidens*, *Equus* sp. (large-sized), *Stephanorhinus* cf. *hundsheimensis*, *Sus* sp., *Palaeotragus inexpectatus*, Cervidae indet. (medium-sized), *Praemegaceros* sp., *Bison* cf. *degiulii*, *Soergelia brigittae*, and *Hemitragus* sp. In addition to mammals, a complete, large-sized avian femur was discovered. The comparison of the physical attributes of the avian specimen, such as its stoutness index and morphology, with other ostrich specimens from the late Miocene to Early Pleistocene of Eurasia permits its attribution to the giant ostrich *Pachystruthio dmanisensis*. This is the first occurrence of a giant ostrich in Greece and southeastern Europe in general, and by recording its southernmost occurrence it expands greatly its known geographical distribution.

Figure 2. Krimni-3 excavation photos. a, panoramic view of the site at its discovery and close-up view of the first fossil remains in 2019; b-d, isolated and articulated specimens of several taxa in situ in the following years 2020-2022, respectively.

Biochronology – Conclusions

Based on the available faunal data, a late Villafranchian age, within the 1.8–1.5 Ma time frame is proposed for KMN, intermediate between Tsiotra Vryssi (between 1.78 and ~1.5 Ma; Konidaris *et al.*, 2021) and Apollonia-1 (~1.2–1.0 Ma; Koufos and Kostopoulos, 2016). At a regional scale KMN is placed biochronologically perhaps close to Kalamoto-2 (Tsoukala and Chatzopoulou, 2005), while at a wider scale it shows affinities with faunas dated between ca. 1.8 and 1.5 Ma from eastern territories (e.g., Dmanisi, Trlica 11–10, Taurida Cave). Importantly for the Pleistocene biostratigraphy of Greece and the southern Balkans, KMN may document the last occurrence of *Palaeotragus* and *Sus strozzi*, and the first occurrence of *Soergelia*. Albeit research is at its beginning, KMN provides new and promising insights into the Early Pleistocene terrestrial ecosystems of western Eurasia during a crucial period for mammal turnovers and dispersal events. Thus overall, along with additional taxonomical and biostratigraphical data, further research at KMN and the wider region is deemed essential in order to provide valuable palaeogeographical, palaeoenvironmental and taphonomic insights. Detailed data on KNM fauna, taphonomy, and chronology are provided by Kostopoulos *et al.* (2022)

Acknowledgements

We thank all field team members for their contribution during the fieldwork and the subsequent preparation of fossils.

References

Konidaris, G.E., Kostopoulos, D.S., Maron, M., Schaller, M., Ehlers, T.A., Aidona, E., Marini, M., Tourloukis, V., Muttoni, G., Koufos, G.D., Harvati, K., 2021. Dating of the Lower Pleistocene vertebrate site of Tsiotra Vryssi (Mygdonia Basin, Greece): Biochronology, magnetostratigraphy, and cosmogenic radionuclides. Quaternary 4, 1-18.

Konidaris, G.E., Tourloukis, V., Kostopoulos, D.S., Thompson, N., Giusti, D., Michailidis, D., Koufos, G.D., Harvati, K., 2015. Two new vertebrate localities from the Early Pleistocene of Mygdonia Basin (Macedonia, Greece): Preliminary results. Comptes Rendus Palevol 14, 353-362.

Kostopoulos, D.S., Konidaris, G.E., Amanatidou, M., Chitoglou, K., Fragkioudakis, E., Gerakakis, N., Giannakou, V.,· Gkeme, A., Kalaitzi, Ch., Tsakalidis, Ch, Tsatsalis, V., 2022. The new fossil site Krimni-3 in Mygdonia Basin and the first evidence of a giant ostrich in the Early Pleistocene of Greece. Palaeontologische Zeitschrift. https://doi.org/10.1007/s12542-022-00632-8

Koufos, G.D., Kostopoulos, D.S., 2016. The Plio-Pleistocene large mammal record of Greece: Implications for early human dispersals into Europe, in: Harvati, K., Roksandic, M. (Eds.), Paleoanthropology of the Balkans and Anatolia: Human evolution and its context, 269-280.

Koufos, G.D., Syrides, G., Kostopoulos, D.S., Koliadimou, K., 1995. Preliminary results about the stratigraphy and the palaeoenvironment of Mygdonia basin, Macedonia, Greece. Geobios M.S. 18, 243-249.

Tsoukala, E., Chatzopoulou, K., 2005. A new Early Pleistocene (latest Villafranchian) site with mammals in Kalamotó (Mygdonia Basin, Macedonia, Greece) – Preliminary report. Mitteilungen der Kommission für Quartärforschung der Österreichischen Akademie der Wissenschaften 14, 213-233.

16th International Congress of the Geological Society of Greece
23-25 May, 2022 - Patras, Greece
Bulletin of the Geological Society of Greece, Sp. Publ. 10
Ext. Abs. GSG2022-139

An Early Pliocene Monitor Lizard (genus *Varanus*) from the Locality of Megalo Emvolon (Northern Greece)

C. Drakopoulou[1], G. L. Georgalis[2], G. Lazaridis[1], D. S. Kostopoulos[1]

(1) Aristotle University of Thessaloniki, Thessaloniki, Greece, drakopcc@geo.auth.gr (2) Institute of Systematics and Evolution of Animals, Polish Academy of Sciences, Krakow, Poland

New finds of *Varanus marathonensis* (Squamata, Varanidae) from the Lower Pliocene locality of Megalo Emvolon, N. Greece increase its local and European record.

Despite the fact that important reptile fossil finds were described already in the 19th century, Greek herpetofauna has been systematically ignored by palaeontologists in Greece until the last decade (Georgalis & Delfino, 2022). Of all the extant reptiles few are as studied as the monitor lizard (Varanidae). In Europe, varanids are represented in the fossil record by two genera: *Saniwa*, confined to the Eocene of Belgium and France, and the extant genus *Varanus*, distributed across multiple localities of the continent and spanning from the Early Miocene up to the Middle Pleistocene (Georgalis *et al.* 2017, 2021). Their distribution in Greece is sparse, spanning from the Late Miocene to the Middle Pleistocene. The earliest Greek occurrence of *Varanus* is recorded in the locality of Ravin de la Pluie of Axios Valley bearing a late Vallesian (MN 10) mammal fauna (Georgalis *et al.*, 2018). The youngest Greek occurrence of the genus, which pertains also to the ultimate European record of varanids, is documented from the Middle Pleistocene of Tourkobounia 5 near Athens (Georgalis *et al.*, 2017). Other Varanidae fossils have also been recovered from the Upper Miocene of Pikermi, certain sites in Samos, Kryopigi in Chalkidiki end the Miocene/earliest Pliocene of Maramena (Georgalis & Delfino, 2022).

Megalo Emvolon (Fig. 1a) is a relatively rich and one of the few Lower Pliocene fossiliferous sites in Greece. Located on the eastern coast of Thermaikos Gulf, near Thessaloniki, it is situated at the center of the Axios-Thermaikos Basin filled by Neogene-Quaternary deposits grouped into six formations. Clays, marls, marly limestones, and sandstones exposed around Megalo Emvolon area are indicative of a fluvio-lacustrine depositional environment and are included into the Lower Pliocene Gonia Formation (Fm) (Syrides, 1990). The Gonia Fm lies in between the Upper Miocene Trilophos Fm and the Upper Pliocene/Lower Pleistocene Moudania Fm respectively. The vertebrate fauna of Megalo Emvolon is rich and diverse, including mammals and micromammals, birds, and reptiles (Koufos *et al.*, 1991). Known reptilian fossils from the site so far include a giant viperid snake (*Laophis crotaloides*), as well as small and giant tortoises (Georgalis *et al.*, 2016; Fig. 1b). According to the mammals, the fauna corresponds to the European Land Mammal Zone 15 (MN 15; late Ruscinian), estimated at 4.2 - 3.2 Ma (Koufos *et al.*, 1991). The dispersed fossil concentrations of Megalo Emvolon have been grouped into three levels, namely Megalo Emvolon 1 (MEV) which is the base level and consists of grey argillaceous sands, Megalo Emvolon 2 (MEM) which is situated 20 meters above MEV with gravel-beds intercalated with red sands, and Megalo Emvolon 3 (MEL) deposited roughly 10 meters higher than MEM. The material of this study was recovered some years ago from a new site named Megalo Emvolon 4 (MVL) which correlates to the two lower fossiliferous levels (MEV, MEM) previously known.

Overall, the varanid material of this study is well-preserved, with only a few incomplete specimens or fragments in poor condition. It comprises of 40 specimens, out of which 10 are cranial, 25 are postcranial and 5 are indeterminate. The cranial material contains a parietal, a frontal, a postorbitofrontal, a quadrate, an exoccipital, a dentary, two maxillae fragments and two isolated teeth. The teeth are trenchant and transversely narrow, with the presence of plicidentine being distinctive. The postcranial material consists of trunk, sacral and caudal vertebrae (Fig. 1c), chevron bones, rib fragments, carpals, and phalanges. The trunk vertebrae are relatively large, their condyles and cotyles are dorsoventrally compressed with triangular centra. They exhibit a noticeable precondylar constriction. The caudal vertebrae are distinguished by a single pair of transverse processes and are accompanied by chevron bones. Both the vertebrae and the cranial material allow a definitive referral to *Varanus* (Villa *et al.*, 2018) and, due to the nature of their recovery (found within the same MVL spot of 3m x 0.5m), could possibly pertain to a single individual.

In Europe only two taxonomically valid *Varanus* species are currently accepted: *Varanus marathonensis* from various Neogene localities and *Varanus mokrensis* from the Early Miocene of Czech Republic (Ivanov *et al.*, 2018; Villa *et al.*, 2018). One anatomical character in the Megalo Emvolon material observed on the postorbitofrontal, the angle formed between the squamosal and parietal processes which is rather wide almost shaping a right angle (Villa *et al.*, 2018) compared to a very acute angle in *V. mokrensis* (Ivanov *et al.*, 2018), points to a possible attribution of the material to *V. marathonensis*. This is also supported by the well preserved parietal which is characterized by narrower anterolateral processes and a rounder pineal foramen situated closer to the anterior margin of the bone. Lastly, the two phalanges (distal and non-terminal) that were recovered do not seem to have completed the ossification process, although they each appear to have their epiphyses with their diaphysis attached. That, combined with the fact that the rest of the bones are large and

have been fully ossified could indicate that the adult lizard had simply not reached its potential maximum size before its death (de Buffrénil *et al.*, 2004). However, additional research is needed before we can conclude with these results.

Figure 1: (a): Megalo Emvolon 4 site in northern Greece, (b): a small tortoise excavated at the site, (c): block of two vertebrae of the Varanus marathonensis cemented by matrix from the MVL site.

Acknowledgements

C. D. would like to thank Andrea Villa for providing her with guidance in her Erasmus+ traineeship which majorly helped this study, as well as all of the Institut Català de Palaeontologia Miquel Crusafont members who proved to be great friends and mentors in palaeontology for the four months that her Erasmus+ traineeship lasted.

References

De Buffrénil, V., Ineich, I., Böhme, W., 2004. Comparative data on epiphyseal development in the family Varanidae. Journal of Herpetology 37(3), 328-335.

Georgalis, G.L., Čerňanský, A., Klembara, J., 2021. Osteological atlas of new lizards from the Phosphorites du Quercy (France), based on historical, forgotten, fossil material. Geodiversitas 43(9), 219-293.

Georgalis, G.L., Delfino, M., 2022. The fossil record of lizards and snakes (Reptilia: Squamata) in Greece, in: Vlachos, E. (Ed.), Fossil Vertebrates of Greece Vol. 1. Basal vertebrates, amphibians, reptiles, afrotherians, glires and primates, 205-235.

Georgalis, G.L., Szyndlar, Z., Kear, B.P., Delfino, M., 2016. New material of *Laophis crotaloides*, an enigmatic giant snake from Greece, with an overview of the largest fossil European vipers. Swiss Journal of Geosciences 109, 103-116.

Georgalis, G.L., Rage, J.C., de Bonis, L., Koufos, G.D., 2018. Lizards and snakes from the Late Miocene hominoid locality of Ravin de la Pluie (Axios Valley, Greece). Swiss Journal of Geosciences 111, 169-181.

Georgalis, G.L., Villa, A., Delfino, M., 2017. The last European varanid: demise and extinction of monitor lizards (Squamata, Varanidae) from Europe. Journal of Vertebrate Paleontology e1301946, 1-7.

Ivanov, M., Ruta, M., Klembara, J., Böhme, M., 2018. A new species of *Varanus* (Anguimorpha: Varanidae) from the early Miocene of Czech Republic, and its relationships and palaeoecology. Journal of Systematic Palaeontology 16(9), 767-797.

Koufos, G.D., Syrides, G.E., Koliadimou, K.K., 1991. A Pliocene primate from Macedonia (Greece). Journal of Human Evolution 21, 283-294.

Syrides, G., 1990. Lithostratigraphic, biostratigraphic and palaeogeographic study of the Neogene – Quaternary sedimentary deposits of Chalkidiki Peninsula, Macedonia, Greece. Ph.D. Thesis, Aristotle University of Thessaloniki, Thessaloniki, 243 p.

Villa, A., Abella, J., Alba, D.M., Almécija, S., Bolet, A., Koufos, G.D., Knoll, F., Luján, À.H., Morales, J., Robles, J.M., Sánchez, I.M., Delfino, M., 2018. Revision of *Varanus marathonensis* (Squamata, Varanidae) based on historical and new material: morphology, systematics, paleobiogeography of the European monitor lizards. PLoS ONE 13(12):e0207719, 1-46.

16th International Congress of the Geological Society of Greece

17-19 October, 2022 - Patras, Greece

Bulletin of the Geological Society of Greece, Sp. Publ. 10

Ext. Abs. GSG2022-175

A holistic approach for reconstructing environmental dynamics during Holocene in Agia Bay (Lemnos Island, Greece)

O. Koukousioura[1], K. Kouli[2], G. Syrides[1], N. Theocharidis[1], M. Gkouma[3], P. Avramidis[4], M. Ntinou[5], P. Tsourlos[1], A. Chalkioti[5], E. Aidona[1], V.-G. Dimou[1], K. Vouvalidis[1], N. Efstratiou[4]

(1) Aristotle University of Thessaloniki, School of Geology, Thessaloniki, Greece, okoukous@geo.auth.gr (2) National and Kapodistrian University of Athens, Faculty of Geology and Geoenvironment, Athens, Greece (3) 3M. H. Wiener Laboratory for Archaeological Science, The American School of Classical Studies at Athens, Athens, Greece (4) University of Patras, Department of Geology, Patras, Greece (5) Aristotle University of Thessaloniki, School of History and Archaeology, Thessaloniki, Greece.

Lemnos island is located at the center of the NE Aegean Sea, a key point for interpreting temporal environmental, vegetational and climatic changes since Last Glacial Maximum for the entire northern Aegean. The island bears a long record of human presence, initiated, as suggested by archaeological evidence, with the Late Paleolithic hunting campsite of Ouriakos (~12.000 BP; Efstratiou *et al.*, 2014; Efstratiou, 2015), located at the SE part of the island. In the vicinity of Ouriakos site lays the Agia Bay, a small river valley resulting in an embayment formed into the Paleogene molassic basement (Innocenti *et al.*, 1994; Papanikolaou and Triantaphyllou, 2019) and which is overlain by Holocene deposits. The surrounding area is characterized by a low smooth topography, inclining towards the NE, aeolian deposits and a small river which is discharging into the bay.

During the last decades multi-approach analyses became a valuable tool for geoarchaeological studies providing insights on the paleoenvironmental evolution of coastal plains (e.g., Triantaphyllou *et al.*, 2010, 2021; Koukousioura *et al.*, 2019, 2020, Emmanouilidis et al., 2022a, b), although only a few have been conducted in the NE Aegean coastal plains (Syrides *et al.*, 2009; Pavlopoulos *et al.*, 2013). The systematic investigation of a 15.5-m long sediment core from the coastal plain of Agia Bay aims (1) to set light to the environmental dynamics of the area (2) to reconstruct the paleoenvironmental and plant landscape evolution of the NE Aegean during Holocene and (3) to reconstruct the paleoenvironmental background on which the early Holocene human presence occurred.

The sedimentary core AGIA was obtained by a rotating rig, 120 m from the coastline and is characterized by alternations of silty and sandy, as well as peat deposits. Prior a geophysical survey (ERT, Electrical Resistivity Tomography) has been conducted, in order to standardize the coring location through obtaining indirect information concerning the subsurface sedimentary strata geometry and lithology of the study area. The exhaustive study of the faunal and floral remains of the deposits, including benthic foraminifera, ostracods, molluscs, seeds, charophytes, pollen and NPPs was further supported by sedimentological, micromorphological, elemental and anthracological analyses as well as magnetic susceptibility measurements integrated with radiocarbon dating. In total 163 sediment samples were carefully selected for the needs of the micro- (foraminifera and ostracoda), macropaleontological (molluscs) and anthracological analyses, wet sieved and dried. A total of 59 samples from the same core were selected for pollen and NPPs study and were chemically treated following the standard palynological protocol including sieving through a 10 μm mesh (Faegri and Iversen, 1989). Additional samples were collected as well for the micromorphological analysis, magnetic susceptibility measurements and radiocarbon dating, while the determination of the sand and mud fractions was achieved by sieving all samples in a 63 μm mesh size sieve. Elemental analysis measurements were performed directly on the core with a portable XRF device.

This plethoric dataset enabled us to distinguish four main evolutionary stages:

(a) at the base of the sequence the fluvial activity is dominating the sedimentation in the area, forming a wetland with shallow stagnant waters, while progressively seawater intrusions are observed as suggested by reworked marine foraminifera and mollusc specimens. Before c.a. 11000 yr BP periodic desiccations of the wetland are recorded

(b) At c.a. 7500 to 6000 yr BP a restricted fresh-water wetland with sedge vegetation is evidenced by the occurrence of Cyperacea pollen, aquatic plant seeds, as well as land snails, while detritus material inputs suggest erosional processes occurring in the basin

(c) during c.a. 6000-4000 yr BP, the occurrence of euryhaline foraminifera (*Ammonia tepida*, *Haynesina germanica*), ostracoda (*Cyprideis torosa*, *Cyprinotus salinus*) and mollusc (*Cerastoderma glaucum*, *Abra* sp., *Hydrobia* sp.) assemblages accompanied by marine dinoflagellate cysts indicate the existence of a connection of the wetland to the sea. An inner lagoon is established, with fresh-water inputs as suggested by the intense presence of charophytes and seeds

(d) since c.a. 4000 yr BP a nearshore environment is developed due the sea-level rise. It is characterized by a marine assemblage including *Peneroplis pertusus*, rotaliids and miliolids as well as *Loxoconcha* sp., *Cerithium* sp. and reworked foraminifera and mollusc specimens. Pollen assemblages record the occurrence of mixed deciduous oak forest with *Ulmus* and *Carpinus*/*Ostrya* in the island interior, while agricultural activities are inferred by pollen indicator species.

Acknowledgements

The research work was supported by the Hellenic Foundation of Research and Innovation (H.F.R.I) under the "First Call for H.F.R.I. Research Projects to support Faculty members and Researchers and the procurement of high-cost research equipment grant" (Project Number: 1609, Aegean islands: Palaeoenvironment and early human settlement: EGEOLAND).

References

Efstratiou, N., 2015. The Final Palaeolithic hunting camp of Ouriakos on the island of Lemnos, Eurasian Prehistory 11, 75-96.

Efstratiou, N., Biagi, P., Starnini, E., 2014. The Epipalaeolithic site of Fyssini-Ouriakos in the island of Lemnos (Northeastern Aegean Sea, Greece) and its Place in the Late Pleistocene Peopling of the East Mediterranean Region. Adalya XVII, 1-25.

Emmanouilidis, A., Katrantsiotis, C., Dotsika, E., Kokkalas, S., Unkel, I., Avramidis, P., 2022a. Holocene paleoclimate variability in the eastern Mediterranean, inferred from the multi-proxy record of Lake Vouliagmeni, Greece. Palaeogeography, Palaeoclimatology, Palaeoecology 595, 110964.

Emmanouilidis, A., Panagiotopoulos, K., Kouli, K., Avramidis, P., 2022b. Late-Holocene paleoenvironmental and land-use changes in Western Greece based on a sediment record from Klisova lagoon. The Holocene 32 (6), 485-500.

Faegri, K., Iversen, J., 1989. Textbook of pollen analysis. J. Willey and Sons, 328 p.

Innocenti, F., Manetti, P., Mazzuoli, R., Pertusati, P., Fytikas, M., Kolios, N.,1994. The geology and geodynamic significance of the island of Limnos, North Aegean Sea, Greece. Neues Jahrbuch für Geologie und Paläontologie, Monatschefte H11, 661-691.

Koukousioura, O., Dimiza, M.D., Kyriazidou, E., Triantaphyllou, M.V., Syrides, G., Aidona, E., Vouvalidis, K., Panagiotopoulos, I.P., Papadopoulou, L., 2019. Environmental evolution of the Paliouras coastal lagoon in the eastern Thermaikos gulf (Greece) during Holocene. Environmental Earth Sciences 78, 313. https://doi.org/10.1007/s12665-019-8316-y

Koukousioura, O., Kouli, K., Vouvalidis, K., Aidona, E., Karadimou, G., Syrides, G., 2020. A multi-proxy approach for reconstructing environmental dynamics since the mid Holocene in Lake Ismarida (Thrace, N. Greece). Revue de Micropaléontologie 68, 100443.

Papanikolaou, D., Triantaphyllou, M., 2019. New stratigraphic data of the Limnos volcanosedimentary sequence and correlations with the Thrace Basin. Proceedings of the 15th International Congress of the Geological Society of Greece, 22-24 May, Athens, Greece, Bulletin of the Geological Society of Greece Sp. Pub. 7, Ext. Abs. GSG2019-240, 71-72.

Pavlopoulos, K., Fouache, E., Sidiropoulou, M., Triantaphyllou, M., Vouvalidis, K., Syrides, G., Gonnete, A., Greco, E., 2013. Palaeoenvironmental evolution and sea-level changes in the coastal area of NE Lemnos Island (Greece) during the Holocene. Quaternary International 308-309, 80-88.

Syrides, G, Vouvalidis, K., Albanakis, K., Tsourlos, P., Matsas, D., 2009. Paleogeographical evolution and sea level changes during Holocene in the Prehistoric settlement of Mikro Vouni (Samotrhace Island, Greece). Zeitschrift für Geomorphologie Supplementary Issues 53(1), 39-54.

Triantaphyllou, M.V., Kouli, K., Tsourou, T., Koukousioura, O., Pavlopoulos, K., Dermitzakis, M.D., 2010. Paleoenvironmental changes since 3000 BC in the coastal marsh of Vravron (Attica, SE Greece). Quaternary International 216, 14-22.

Triantaphyllou, M.V., Tsourou, T., Kouli, K., Koukousioura, O., Dimiza, M.D., Aidona, E.V., Syrides, G., Antoniou, V., Panagiotopoulos, I.P., Vandarakis, D., Pallikarakis, A., Cheilaris, S., Skampa, E., Goiran, J.-P., Fouache, E., Pavlopoulos, K.P., 2021. Paleoenvironmental Evolution and Sea Level Change in Saronikos Gulf (Aegean Sea, Greece): Evidence from the Piraeus Coastal Plain and Elefsis Bay Sedimentary Records. Water 13, 1621. https://doi.org/10.3390/w13121621.

16th International Congress of the Geological Society of Greece
17-19 October, 2022 - Patras, Greece
Bulletin of the Geological Society of Greece, Sp. Publ. 10
Ext. Abs. GSG2022-185

Assessment of the Upper Holocene paleoenvironment and vegetation shifts in the Natura 2000 coastal lagoon Prokopos (W. Greece)

M. Haut-Labourdette[1], K. Kouli[1], I. Prevedouros[2], A. Emmanoulidis[3], P. Avramidis[2]

(1) National and Kapodistrian University of Athens, Department of Geology and Geoenvironment, Athens, Greece, (2) University of Patras, Department of Geology, Patras, Greece p.avramidis@upatras.gr, (3) Institute for Ecosystem Research, Kiel University, Germany

Transitional sedimentary environments in the coastal zone comprise a wide range of dynamic and vulnerable ecosystems. Nevertheless, past environmental changes imprinted in the coastal areas' sedimentary deposits, provide valuable information concerning geomorphological processes, vegetation dynamics, climate variability and human activity. During the last decades, a rising number of Holocene paleoenvironmental and paleovegetation studies have emerged from lagoonal deposits in Greece (e.g. Pavlopoulos *et al.*, 2010; Triantaphyllou *et al.*, 2010; Lazarova *et al.*, 2012; Avramidis et al. 2017ab, Emmanouilidis *et al.*, 2020; 2022).

Prokopos lagoon is situated on the coastline of north-western Peloponnesus (38°08'47" N 21°23'52" E) within the Kotychi-Strofylia National Park. Due to the great ecological significance of the ecosystems present in the park, the area is protected by the Ramsar Convention and the European community network Natura2000. The overall area includes Kotychi, Pappas, Lamia, Prokopos and Kaiafas Lagoons as well as one of the most important stone pine (*Pinus pinea*) forests in Europe and Mediterranean shrublands. At the same time, it hosts a great diversity of bird and fish species. Prokopos is a chocked coastal lagoon receiving freshwater from two small rivers and seawater from the Ionian Sea through an artificial and narrow channel (Apostolopoulos et al., 2022). It is characterized by seasonal variations in salinity and water depth depending on the precipitation/evaporation regime (Fyttis, 2011).

The aim of this study is to investigate the vegetation history, as well as the local paleoenvironment evolution of Prokopos lagoon and evaluate the diachronic impact of human activities in the surrounding area through sedimentological and palynological analysis. To achieve this, a 120 cm long sediment core was retrieved from the deepocenter of the lagoon in 2021 using an Uwitec gravity corer with hammer action. The recovered deposits consist of mud, rich in polychaetes and bivalve fragments. The chronological framework sets at 4000 cal BP, based on nine AMS ^{14}C datings. Reservoir correction was determined through a modern *Cerastoderma glaucum* shell at 102 ± 2 years. The age-depth model was constructed using the R package rbacon (v.2.5.0; Blaauw and Christeney, 2011) and IntCal20 calibration curve (Reimer et al., 2020). A total of 23 sediment samples were analyzed for their grain size, TOC and TN. Additionally, 24 sediment samples were palynologically studied through an intricate laboratory protocol followed by microscope analysis. A minimum of 200 terrestrial pollen were counted per sample, while all Non-Pollen Palynomorphs (NPPs) present in each slide were identified and counted. Microscopic analysis results were processed through Tilia (Grimm 1991), intending the construction of palynological diagrams highlighting the pollen and NPPs variations through time. Percentages and concentration diagrams were obtained. Zonation of the diagrams was generated by the cluster analysis CONISS (Grimm, 1987), based on the terrestrial pollen.

A total of 74 pollen taxa have been identified: 31 trees and shrubs, 35 herb taxa, 8 taxa of aquatic vascular plants, as well as 32 taxa of Non-Pollen Palynomorphs (NPPs). Four pollen assemblage zones (A-D) were identified. The vegetation record revealed a plant landscape and its evolution through time. From Mediterranean shrubland dominated by Ericaceae in low altitudes and a deciduous forest in intermediate altitudes mainly represented by deciduous *Quercus*, *Ostrya/Carpinus* and *Corylus*, followed by a shift within the Mediterranean vegetation with the decrease of the shrubs and increase of the maquis vegetation in low altitudes depicted by *Phillyrea*, evergreen *Quercus* and *Pistacia* and the expansion of the deciduous forest in intermediate altitudes. Finally, the former Mediterranean vegetation was replaced by a Pine dominated forest covering the low and intermediate altitudes as the deciduous forest retreated.

Within the wetland, aquatic vascular plants such as *Isoëtes*, *Typha*, *Sparganium*, *Myriophyllum*, *Callitriche* and Nymphaeaceae were detected and the green algae *Botryococcus* was recognized as the most abundant element of the lagoon. Their fluctuations through time were associated with the variations of the conditions within the lagoons. The latter are controlled by the influxes received within the system. Nowadays, both riverine and marine inflows are conveyed into the lagoon and Prokopos record revealed that these influxes have been fluctuating over time. Freshwater indicators such a *Pseudoschizea*, Rhabdocoela, *Gloetrichia*, *Pediastrum* and Zygnemataceae were identified within the record. Marine water indicators (foraminifera test linnings and dinoflagellate cysts) with significative abundancies were detected as well, meaning that sea incursions were diachronic in the system. Moreover, *Gloetrichia*, *Pediastrum* and *Botryococcus* displayed simultaneous abundancy in some part of the profile inducing periodic eutrophication of the lagoon.

The present study eventually revealed how human impact on its environment was featured in the past vegetation record and how it can be traced through time. Clear evidence of human influence was identified within the pollen record. Pollen

of cultivable plants (*Juglans*, *Vitis*, Poaceae Cerealia-type), forest clearance signs and biofertilizer traces were distinguished in zone D of the palynological diagrams, suggesting an intensification of the human activities in the vicinity of Prokopos lagoon. However, the indexes API (Anthropogenic Pollen indicator; Mercuri et al., 2013b) and PDI (Pollen Disturbance Index; Kouli, 2015) show relatively lower values over time, implying that there is no direct land use in Prokopos or its closest surroundings.

Acknowledgements

This study was financially supported by the Green Fund of the Hellenic Ministry of the Environment and Energy (181.6.5/2020). We thank the National Park personnel for their support during sampling.

References

Apostolopoulos, D.N.; Avramidis, P.; Nikolakopoulos, K.G., 2022. Estimating Quantitative Morphometric Parameters and Spatiotemporal Evolution of the Prokopos Lagoon Using Remote Sensing Techniques. Journal of Marine Science and Engineering 10, 931.

Avramidis, P., Iliopoulos, G., Nikolaou, K., Kontopoulos, N., Koutsodendris, A., van Wijngaarden, G.J. 2017a. Holocene sedimentology and coastal geomorphology of Zakynthos Island, Ionian Sea: A history of a divided Mediterranean island. Palaeogeography, Palaeoclimatology, Palaeoecology, 487, pp. 340-354.

Avramidis, P., Nikolaou, K., Poulos, K., Bekiari, V., Vantarakis, A. 2017b. Environmental characterization of a Mediterranean protected shallow brackish coastal aquatic system, Klisova Lagoon, Western Greece: a case study. Journal of Coastal Conservation, 21 (1), pp. 115-125.

Blaauw, M., Christeny, J.A., 2011. Flexible paleoclimate age-depth models using an autogressive gamma process. Bayesian Analysis 6, 457-474.

Emmanouilidis, A., Panagiotopoulos, K., Kouli, K., Avramidis, P. 2022. Late-Holocene paleoenvironmental and land-use changes in Western Greece based on a sediment record from Klisova lagoon. Holocene 32, 485-500.

Emmanouilidis, A., Unkel, I., Triantaphyllou, M., Avramidis, P. 2020. Late-Holocene coastal depositional environments and climate changes in the Gulf of Corinth, Greece. Holocene, 30 (1), pp. 77-89.

Fyttis G., 2011. Monitoring the ecological quality of the western Greek lagoons Kotychi and Prokopos: Analysis of the biocoenosis of the aquatic macrophytes and macromolluscs in the frame of the directive 2000/60/EE for the water. MSc thesis, University of Patras, Patras, 255 p.

Grimm, E.C., 1991. Tilia and tiliagraph. Illinois State Museum, Springfield, p.101.

Grimm, E.C., 1987. CONISS: A Fortran 77 program for stratigraphycally constrained cluster analysis by the method of incremental sum of squares. Computers & Geosciences 13, 13-35.

Kouli, K., 2015. Plant landscape and land use at the Neolithic lake settlement of Dispilio (Macedonia, northern Greece). Plant Biosystems 149, 195-204

Lazarova, M, Koutsios, A., Kontopoulos, N., 2012. Holocene vegetation history of the Kotihi Lagoon (north-western Peloponnesus, Greece). Quat Int. 261, 138-145.

Mercuri, A.M., Bandini Mazzanti, M., Florenzano A., Montecchi, M., Rattighieri, E., Torri, P., 2013b. Anthropogenic pollen indicators (API) from archeological sites as local evidence of human-induced environments in the Italian peninsula, Annali di Botanica 3, 143-53

Pavlopoulos, K., Triantaphyllou, M.V., Karkanas, P., Kouli, K., Syrides, G., Vouvalidis, K., Palyvos, N., Tsourou, T., 2010. Paleoenvironmental evolution and prehistoric human environment, in the embayment of Palamari (Skyros Island, Greece) during Middle-Late Holocene. Quat. Int. 216, 41–53.

Reimer, P.J.,et al, 2020. The IntCal20 Northern Hemisphere Radiocarbon Age Calibration Curve (0–55 cal kBP). Radiocarbon 62, 725–757.

Triantaphyllou, M.V., Kouli, K., Tsourou, T., Koukousioura, O., Pavlopoulos, K., Dermitzakis, M.D., 2010. Paleoenvironmental changes since 3000 BC in the coastal marsh of Vravron (Attica, SE Greece). Quat. Int. 216, 14-22

16th International Congress of the Geological Society of Greece
17-19 October 2022 - Patras, Greece
Bulletin of the Geological Society of Greece, Sp. Publ. 10
Ext. Abs. GSG2022-187

Preliminary results on living ostracods in the lacustrine environments of Lake Vegoritis, Greece

V. Navrozidou[1,2], O. Koukousioura[1], P. Frenzel[3], M. V. Triantaphyllou[4], P. Avramidis[5], I. Prevedouros[5], E. Aidona[1], G. Syrides[1]

(1) School of Geology, Aristotle University of Thessaloniki, Thessaloniki, Greece, (2) Greek Biotope/Wetland Centre, The Goulandris Natural History Museum, Thessaloniki, Greece, vnavrozidou@gmail.com, (3) Institute of Earth Sciences, Friedrich-Schiller-Universität Jena, Jena, Germany, (4) Faculty of Geology and Geoenvironment, National and Kapodistrian University of Athens, Athens, Greece, (5) Department of Geology, University of Patras, Rio-Patras, Greece.

Background and Objectives

Ostracods are a diverse microfossil group mostly encountered in aquatic (palaeo)environments, marine and non-marine (Gouramanis, 2020). Studies on their biogeography, biology, ecology, and shell geochemistry provide useful insights during both paleoenvironmental investigations and evaluations regarding the impact of human activities on aquatic ecosystems (Ruiz *et al.*, 2013). Ostracods are sensitive to changes in water quality but also show different response and tolerance to distinctive environmental variables, thus considered valuable environmental tracers in freshwater ecosystems (Külköylüoğlu, 2003). Lake Vegoritis (40°45′N, 21°47′E) (Northwestern Greece) is one of the largest lakes in Greece located at 540 m a.s.l with an area of 55 km^2 and a maximum depth of ~52 m.

Vegoritis as a karstic lake had a naturally fluctuating water level until 1950's (Vavliakis *et al*., 1994). Over the past few decades, due to intense human interventions the lake has experienced a severe water level decrease (new agricultural land on the exposed former bottom) and has started exhibiting eutrophication symptoms (e.g., algal blooms) due to various anthropogenic land use activities (agriculture, mining) in its catchment (Stephanidis and Papastergiadou, 2013). However, during the last decade seems that the lake is "reclaiming" its former bottom, as a constant rise of the lake water level resulted in flooding of agricultural areas and the general expansion of its surface.

Lake Vegoritis, despite being one of the biggest lakes in Greece, has been very limited studied concerning ostracod fauna. The only documentation of the lake so far was performed by Petkovski and Keyser (1992), but their study focused on only one species. Our preliminary results provide a detailed documentation of the lake's ostracod fauna accompanied by a complete dataset of sedimentological and geochemical measurements.

The composition and distribution of recent ostracod assemblages were analyzed in Lake Vegoritis, in relation to various environmental parameters (temperature, conductivity, pH, TDS, DO), geochemical, sedimentological analyses and magnetic susceptibility measurements, in order to test their ability to serve as environmental proxies in lacustrine environments.

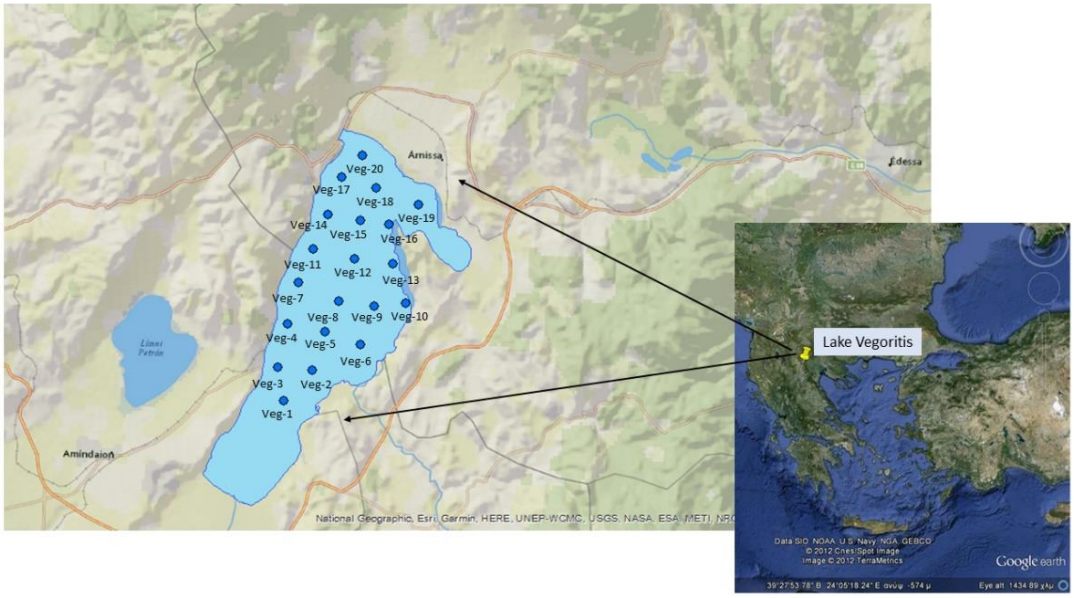

Figure 1. Lake Vegoritis and corresponding sampling stations

Materials and Methods

Sampling was conducted by boat in twenty stations all over the lake during 2015 (Fig. 1). Samples were collected from the upper 1 cm of the lake surface sediment down to a sediment depth of 5 cm, by using an Ekman grab and then fixed in 70% ethyl alcohol. Physicochemical measurements were performed in situ using a Thermo Scientific Orion Star A329 Portable multi-probe. Water transparency was estimated using a Secchi disk. For ostracod analysis, 50 ml sediment of each sample was wet sieved with tap water through a 250 μm mesh size standard sieve. All specimens (both living + dead) were collected, identified, and counted using a binocular stereomicroscope. Absolute abundances and relative frequencies were calculated along with diversity indices.

Furthermore, Magnetic Susceptibility, Total Organic Carbon, Nitrogen and Phosphorus were measured for the present study. Magnetic Susceptibility measurements were performed using the Bartington MS2D loop (Bartington Ltd., UK). Sediment's grain size distribution was calculated using a Malvern Mastersizer 2000 and fractions of clay silt and sand as well as textural names were calculated. Total organic carbon (TOC%) and Total Nitrogen (TN) were measured with a ShimadzuTOC-VCSH TOC/TN analyzer (Avramidis and Bekiari, 2021), while Total Phosphorus (TP) was measured with the ascorbic acid method according to APHA 4500P (2005).

Results and concluding remarks

In total about 1650 ostracod valves have been collected (both dead and living), and assigned to eight taxa (*Candona* spp., *Candona neglecta*, *C. angulata*, *Cyclocypris ovum*, cf. *Cypris* sp., *Darwinula stevensoni*, *Limnocythere* spp.) with the most dominant being *Candona* spp., mostly juveniles. The highest total abundances were recorded at the southern stations (Veg-4, Veg-5), while in eight stations no ostracod fauna was documented. Two to six taxa were recorded in each station, with the southern stations being most diversified. In general, the ostracod abundance and diversity display a gradual decrease with increasing depths, resulting in total absence in stations with depths exceeding 40 m (northern part of the lake).

The magnetic susceptibility showed fluctuations among the stations with a mean value of 27.510^{-5}SI. Based on grain size, the bottom lake sediments reflect a uniform geographical distribution as the sediments consist mainly of silt and clayey silt. Sediment TOC concentration ranged between 0.78% and 2.59%, with a mean of 1.73%, while TN showed relatively significant variation among the stations ranging from 0.7 to 3 mg/g. TP is the limited nutrient with concentrations ranging from 0.09 to 0.46 mg/g and a mean of 0.28 mg/g.

Further investigation will enable us to evaluate ostracod assemblage's response to the various environmental variables.

Acknowledgements

Sampling and physicochemical parameter measurements were supported by the Greek Biotope Wetland Centre, through the National Water Monitoring Network for lakes of Greece, according to the Joint Ministerial Decision 140384/2011. Specials thanks to Dr Petros Kakouros for his help during field work.

References

APHA, 2005. 4500-P Standard methods for the examination of water and waste water, 21st edn. American Public Health Association, Washington.

Avramidis, P., Bekiari, V., 2021. Application of a catalytic oxidation method for the simultaneous determination of total organic carbon and total nitrogen in marine sediments and soils. PloS ONE 16 (6), e0252308.

Gouramanis, C., 2020. Ostracoda in extreme-wave deposits, in: Engel, M., Pilarczyk, J., May, S.M., Brill, D., Garrett, E., (Eds.), Geological Records of Tsunamis and Other Extreme Waves, 261-290.

Külköylüoğlu, O., 2003. Ecology of Freshwater Ostracoda (Crustacea) from Lakes and Reservoirs in Bolu, Turkey. Journal of Freshwater Ecology 18 (3), 343-347.

Petkovski, T., Keyser, D., 1992. Leptocythere ostrovskensis sp. n., Crustacea, Ostracoda, Cytheracea aus dem See Vegoritis (Ostrovsko Ezero) in NW Griechenland. Mit kurzer Übersicht der Süsswasserarten des Genus Leptocythere G.O. Sars, 1925 vom Westbalkan. Mitteilungen aus dem Hamburgischen Zoologischen Museum und Institut 89, 227-237.

Ruiz, F., Abad, M., Bodergat, A.M., Carbonel, P., Rodríguez-Lázaro, J., González-Regalado, M.L., Toscano, A., García, E.X., Prenda, J., 2013. Freshwater ostracods as environmental tracers. International Journal of Environmental Science and Technology 10 (5), 1115-1128.

Stefanidis, K., Papastergiadou, E., 2013. Effects of a long term water level reduction on the ecology and water quality in an eastern Mediterranean lake. Knowledge and Management of Aquatic Ecosystems 411, 05.

Vavliakis, E., Albanakis, K., Antonopoulou, E., Geramian, A., 1994. Anthropogenic influences on the evolution of the Lake Vegoritida. Proceedings of the 3rd Panhellenic Geographical Congress B, 275-289, (in Greek).

16th International Congress of the Geological Society of Greece
17-19 October, 2022 - Patras, Greece
Bulletin of the Geological Society of Greece, Sp. Publ. 10
Ext. Abs. GSG2022-190

First recording of the ostracod assemblage of Lake Kournas (Crete, Greece)

V. Navrozidou[1,2], O. Koukousioura[1], P. Frenzel[3], M. V. Triantaphyllou[4], P. Avramidis[5], E. Aidona[1], G. Syrides[1]

(1) School of Geology, Aristotle University of Thessaloniki, Thessaloniki, Greece, (2) Greek Biotope/Wetland Centre, The Goulandris Natural History Museum, Thessaloniki, Greece, vnavrozidou@gmail.com, (3) Institute of Earth Sciences, Friedrich-Schiller-Universität Jena, Jena, Germany, (4) Faculty of Geology and Geoenvironment, National and Kapodistrian University of Athens, Athens, Greece, (5) Department of Geology, University of Patras, Rio-Patras, Greece

Ostracods are excellent bioindicators of physicochemical conditions, with a remarkable response to variable salinities, water depth, temperature ranges, or pH (Ruiz, 2013). Both with foraminifers have been described as the most important microfossils for brackish waters systems (Frenzel and Boomer, 2005). For the present study, recent ostracod fauna was analyzed in order to investigate their composition and distribution in Lake Kournas and to interpret their relationships between various physicochemical parameters.

Lake Kournas (35°21′, 0″N, 24°16′26″E, ~16 m a.s.l., max depth: 23 m) is the only natural lake in Crete Island and the southernmost lake of Europe. It is monitored for its environmental quality status and is characterized by a continuous degradation due to the extensive human activities in the surrounding area, considered as the main factor of the ecosystem change already since ~8000 years ago (Jouffroy-Bapicot et al., 2021). The degradation of the lake during the last few years is moreover confirmed by the monitoring of Greek Lakes program of the Greek Biotope Wetland Centre and specifically the macrophyte assemblages, as it is observed a decrease of the abundance through time (Dr Zervas – personal communication). The lake is slightly brackish (Moustaka-Gouni *et al.*, 2019; present study) and receives water from underground springs. Sampling of the top 1 cm of the surface sediment was conducted in three stations in 2017 and in twelve stations in 2020, with depth ranging from 11.5 to 22.5 m.

In total almost 2000 ostracod valves have been collected and assigned to seven taxa, with the most dominant species being *Cyprideis torosa* followed by *Candona* spp. In 2017, the highest abundance reached almost 600 valves while in 2020, 450 (Fig.1). One to six taxa were recorded in each station. In general, the lowest abundances were observed at the eastern part of the lake which is the most anthropogenically impacted area. In two stations (one in 2017 and one in 2020) no ostracod fauna was recorded. The brackish character of Lake Kournas is supported both by salinity measurements and the majority of the ostracod species recorded, which are known for their brackish preference or tolerance (Meisch, 2000).

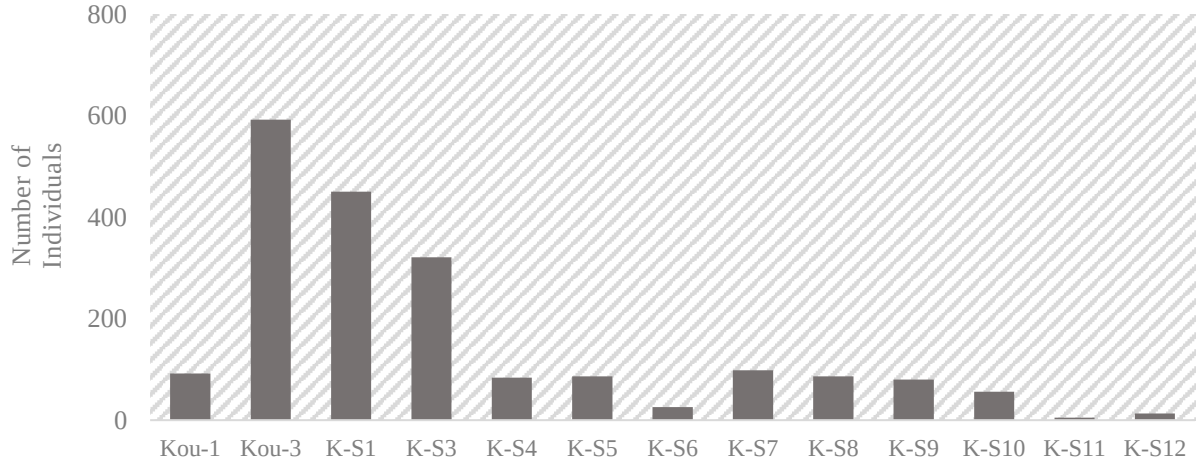

Figure 1. Total abundance of ostracods in each station of Lake Kournas

Based on grain size analysis the lake bottom sediments were silty to sandy silt and are characterized by relatively uniform distribution. Total organic carbon (TOC%) concentrations presented high values at the eastern, anthropogenically most impacted part of the lake; total Nitrogen (TN) showed relatively high values while Total Phosphorus (TP) displayed low concentrations. Nevertheless, the lateral distribution of the nutrients in the sediments showed a significant variation between the northern and southern part, with the highest values to be observed at the eastern side, which is in general the most affected by human activities.

The performed Canonical Correspondence analysis distinguished two groups of stations. The northwestern part of the lake that is mostly defined by the high abundances of *Cyprideis torosa* and the southeastern stations which are affected by high nutrient concentrations, high TOC (%) and fine sediments. Since the ostracod fauna of Lake Kournas was never

investigated before, the documentation of the ostracod assemblage provides reference information for the Cretan inland waters and can contribute to the evaluation of the environmental conditions in this vulnerable environment. Ostracod abundances and nutrient concentrations clearly reflect anthropogenic impact at the eastern part. Further investigation in the area will provide more precise information about the environment of the lake.

Acknowledgements

Sampling and physicochemical parameter measurements were supported by the Greek Biotope Wetland Centre, through the National Water Monitoring Network for lakes of Greece, according to the Joint Ministerial Decision 140384/2011. Specials thanks to Dr. Dimitrios Zervas for his help during field work.

References

Frenzel, P., Boomer, I., 2005. The use of ostracods from marginal marine, brackish waters as bioindicators of modern and Quaternary environmental change. Palaeogeography, Palaeoclimatology, Palaeoecology 225 (1-4), 68-92.

Jouffroy-Bapicot, I., Pedrotta, T., Debret, M., Field, S., Sulpizio, R., Zanchetta, G., Sabatier, P., Roberts, N., Tinner, W., Walsh, K., Vannière, B., 2021. Olive groves around the lake. A ten-thousand-year history of a Cretan landscape (Greece) reveals the dominant role of humans in making this Mediterranean ecosystem. Quaternary Science Reviews 267, 107072.

Meisch, C., 2000. Bd. 8/3: Crustacea: Ostracoda. Heidelberg [etc.]: Spektrum Akademischer Verlag.

Moustaka-Gouni, M., Sommer, U., Economou-Amilli, A., Arhonditsis, G.B., Katsiapi, M., Papastergiadou, E., Kormas, K.A., Vardaka, E., Karayanni, H., Papadimitriou, T., 2019. Implementation of the Water Framework Directive: Lessons learned and future perspectives for an ecologically meaningful classification based on phytoplankton of the status of Greek lakes, Mediterranean region. Environmental Management 64 (6), 675-688.

Ruiz, F., Abad, M., Bodergat, A.M., Carbonel, P., Rodríguez-Lázaro, J., González-Regalado, M.L., Toscano, A., García, E.X., Prenda, J., 2013. Freshwater ostracods as environmental tracers. International Journal of Environmental Science and Technology 10 (5), 1115-1128.

16th International Congress of the Geological Society of Greece
17-19 October, 2022 - Patras, Greece
Bulletin of the Geological Society of Greece, Sp. Publ. 10
Ext. Abs. GSG2022-193

Rhizoliths within aeolianites at the ancient quarry of Stavros, Akrotiri, Chania, Greece

E. Manoutsoglou[1]

(1) School of Mineral Resources Engineering, Technical University of Crete, University Campus, GR-73100 Chania, Greece, emanoutsoglou@tuc.gr

Observations on uplift beach phenomena at the coasts of western Crete were first performed by Spratt in the early 1850'S and used to postulate tectonic uplift of the western end of the island during historical times. Then, the uplift of the western coast of Crete during Pleistocene - Holocene has been the subject of observation and study of many researchers for more than 100 years. Isostatic model predictions for this area suggest the occurrence of a gradual relative sea-level rise of over 1.5m since 2000 years BP and of over 6m since 6000 years BP (i.e. about 1 mm/yr) by Lambeck and Johnston (1995). Beyond the uplift, due to the eustatic phenomena, various researchers studied the effect of tectonic activity on local uplifts and subsidences. Along the coasts of western Crete widespread evidence of uplifted and submerged tidal notches, beachrocks and coastal ancient remains were revealed. The coast on the peninsula of Akrotiri in Chania have abundant geomorphological and archaeological relative sea level change indicators.

In their paper on the morphotectonic evolution of the Akrotiri peninsula in the prefecture of Chania, Zamani & Maroukian (1981) described remnants of calcareous, well-cemented, red-brown or yellow sands bearing numerous shell fragments are observed. It is aeolianite, known in Greece as “poros”, composed of coarse to medium calcareous sand, cross-bedded with almost horizontal to steeply dipping thin layers including numerous mollusc shell fragments. Based on the a l,5 to 2 m notch in the aeolianites of this area, they concluded that the current morphology of peninsula of Akrotiri generally was formed due to the tectonic instability of the area and only locally to eustatism (Zamani & Marakian, 1981).

The aeolianites developed on beachrocks, a rapidly forming rock composed of beach sand and gravel cemented by a calcareous cement of aragonite or magnesium-calcite precipitated from seawater. After Fytrolakis (1986) the beachrocks were formed during the gradual subsidence of the sea level. Aeolianites formed next, when sea retreat reached the maximum level. This results from the fact that the aeolianites (2-4 m thick) have been deposited on the beachrocks and that a large part of the aeolianites are below sea level or wetted by the wave and are relatively fine-grained. Pleistocene aeolianite sandstones, which were easily excavated, were mostly used during the Venetian period (Κοκκορού-Αλευρά et al., 2014) at Stavros in Akrotiri, as well as during the Bronze Age (Moody et al., 1985).

At the western area, in the aeolianite quarry of Stavros rhizoliths were documented, which are defined as organosedimentary structures resulting in the preservation of roots of higher plants, or mineral matter remains. They are abundant and characteristic features of Quaternary paleosoils developed mainly within aeolianites from coastal regions. Rhizoliths, like animal burrows, are commonly circular in cross-section and cylindrical in shape. Lengths of rhizoliths vary from a few centimeters to several meters. The diameters of rhizoliths range from 0.1 mm to (approximately) 20 cm. Downward bifurcations with decreasing diameters of second, third and fourth order branches distinguish rhizoliths from animal burrows. Burrowing systems usually have uniform diameters. Rhizoliths show many orientations although the commonest forms occur as vertical, isolated or branching structures and as ramifying horizontal networks. Although roots prefer to grow in unconsolidated sediments, they can also bore through indurated rock. Rhizoliths and associated features of the rhizosphere (zone of soil around root which is affected by root activity) such as soil fungi indicate terrestrial conditions and subaerial exposure of marine or lacustrine sediments. Filling of a root mould, either by sediment or cement, or both, produces a root cast. Rhizoliths can be used to help identify pedogenetically modified substrates. Rhizoliths are exclusively documented within the vadose zone. They are formed in climatic regimes ranging from subtropical humid to semiarid; however, they decrease as long as the aridity increases (Klappa, 1980).

Rhizoliths are abundant within the ancient quarry. The calcitic rhizoliths reported here can be easily distinguished from burrows and non-biogenic concretions. Rhizoliths (Figs. 1) occur on the planar erosional surfaces of aeolianites. The features interpreted here as rhizoliths are rods of micritic limestone varying in diameter and length. Although the rhizome parts differ in length and diameter, they do not probably belong to different tree species.

The plants represented by the rhizoliths described here were clearly capable of penetrating several meters of eolian sand. The rhizoliths have not been studied by paleobotanists, remaining unknown. Based on the rhizoliths comparisons with the external morphology of recent plant root, documented in the wider area, they resemble the rhizome genus *Tamarix* L.. Tamarix is usually deep rooted. Tap roots may reach 30 m in depth; subsuperficial side roots may reach a length of 50 m and are capable of producing adventitious buds. Adventitious roots are abundantly produced when the plant is buried by shifting dunes, and some species of Tamarix are therefore excellent dune binders (Baum 1978). Aeolian dunes, like modern ones, mainly restricted to arid and semi-arid settings.

Figure 1. Various sizes rhizoliths within the aeolianites at the western part of the ancient quarry of Stavros, Akrotiri, Chania, scale 0,5 m.

Rhizoliths are excellent soil carbonates for studying not only the terrestrial ecosystem but sub millennial cycles of long-term seasonal anomalies (Wang et al., 2004). Calcitic rhizoliths are abundant and easily recognized structures within aeolianite on the Venetian quarry of Stavros in Akrotiri Peninsula. Rhizoliths are remarkable, as their distribution may provide indices of paleoecological aspects (Loope, 1988). Reconstruction of Pleistocene-Holocene environments and processes in the sensitive geographical location like western Crete, facing the sea, is crucial for understanding impacts on early human communities.

References

Klappa K., 1980. Rhizoliths in terrestrial carbonates: classification, recognition, genesis and significance. Sedimentology, 27, 613-629.

Lambeck, K., Johnston, P., 1995. Land subsidence and sea-level change: contributions from the melting of the last great ice sheets and the isostatic adjustment of the Earth. In: Barends, F.B.J., et al. (Eds.), Land Subsidence. Balkema, Rotterdam, pp. 3–18.

Loope D.B., 1988. Rhizoliths in ancient eolianites. Sedimentary Geology, 56, 301-314.

Moody, J.A., Rackham, O., Rapp Jr., G. 1985. The Development of a Bronze Age Coarse Ware Chronology for the Khania Region of West Crete,10th Temple University Aegean Symposium, Philadelphia: Temple University Department of Art History, 51-65.

Wang H., Ambrose S. H., Fouke B.W., 2004. Evidence of long-term seasonal climate forcing in rhizolith isotopes during the last glaciations. Geophysical Research Letters, vol. 31, L13203, https://doi.org/10.1029/2004GL020207

Κοκκορού-Αλευρά, Γ., Πουπάκη, Ε., Ευσταθόπουλος Α., Χατζηκωνσταντίνου., Α., 2014. 2014. Corpus αρχαίων λατομείων: Λατομεία του ελλαδικού χώρου από τους προϊστορικούς έως τους μεσαιωνικούς χρόνους, Αθήνα.

Φυτρολάκης, Ν., 1986. Γεωλογική έρευνα ορισμένων αιολικών ιζημάτων στην Κρήτη. Δελτίο Ελληνικής Γεωλογικής Εταιρίας, Τόμος XVIII, 243 – 267.

16th International Congress of the Geological Society of Greece

17-19 October, 2022 - Patras, Greece

Bulletin of the Geological Society of Greece, Sp. Publ. 10

Ext. Abs. GSG2022-211

Observations On The Enamel Microstructure Of *Phanourios minor,* The Dwarf Hippo From Aghia Napa, Cyprus

V. Noulis[1], E. Stathopoulou[1], G. Theodorou[1], E. Tsiolakis[2]

(1) Department of Historical Geology & Palaeontology, Faculty of Geology & Geoenvironment, National and Kapodistrian University of Athens, Panepistimiopolis, 15784 Zographou, Greece, vasilisgnoulis@gmail.com (2) Cyprus Geological Survery Department, 2064 Strovolos, Cyprus.

Research Highlights

Description and interpretation of enamel microstructure of the pygmy hippo Phanourios minor in means of species identification.

Background

The microstructure of tooth enamel exhibits unique diversity that often allows for the identification and classification of mammals, shedding light also on their phylogenetic relations. Tooth enamel microstructure is known to be an indicator of dietary adaptations and biomechanical stress due to its unalterable nature (Koenigswald *et al.,* 1991; Koenigswald *et al.,* 1994).

Objective

Up to now there was but little information concerning the dental microstructure of the species *Phanourios minor,* an endemic pygmy hippo of the Upper Quaternary, located in Cyprus (Pfretzschner, 1994; Stathopoulou, 2005). The objective of this study was to describe and interpret the particular traits of its enamel in comparison to *Hippopotamus amphibius*. Any unique characteristics could offer crucial phylogenetic information and even be used for the identification of the species.

Material

The dental material used for this study consists of ten molar teeth of the species *Phanourios minor* from the fossiliferous site of Aghia Napa in Cyprus as well as two tooth fragments of the species *Hippopotamus amphibius* (courtesy of the University of Bonn) to be used in means of comparison. The site of Aghia Napa is located less than 1km east of the town center, at an altitude of 25 m and was discovered in 2000. The site consists of a littoral rockshelter and is dominated by skeletal material of the pygmy Hippopotamus species *Phanourios minor,* an endemic species that lived exclusively on Cyprus. The material at the site has been dated back to the Upper Pleistocene (11-13,500 years B.P.) (Fillipidi *et al*., 2013).

Methodology

In order to study the enamel microstructure of the selected teeth, 28 embedded samples and 10 thin sections were prepared. The embedded samples were prepared according to a specific procedure which includes etching with HCl, to enhance the enamel's characteristic features (Koeningswald *et al*., 1992). Thin sections were studied with a Polarizing Optical Microscope while the embedded samples with a Jeol JSM 6390 Scanning Electron Microscope. Scanning electron microscopy was used in our study, because when it comes both to archeological and paleontological findings, SEM is considered essential for the observation of specimen histology.

Results

The enamel microstructure of *Phanourios minor* exhibits two enamel types. Starting from the enamel – dentine junction (EDJ), the dominant enamel type is horizontal Hunter – Schreger bands, which is then followed by primitive radial enamel. The latter covers about 5-10% of the enamel. The enamel microstructure of *Hippopotamus amphibius* on the other hand, exhibits 3 different types of enamel. Near the enamel – dentine junction (EDJ), modified radial enamel is present, followed then by horizontal Hunter – Schreger bands, which covers the largest part of the enamel. The outer 5 – 8% consists of primitive radial enamel. The differences between the two species were indicated, thus allowing for their discrimination (Alloing-Séguier *et al.*, 2014; Lihoreau *et al*., 2015; Pfretzschner, 1994).

During the study of the adjacent dentine areas, further findings concerning dentine preservation and bioerosion have provided us with evidence beyond our objective. Intriguing features, such as fossilized odontoblastic processes were observed and described. The odontoblastic processes are extensions of cells called odontoblasts, which forms dentin in a tooth and are located within the dentinal tubules, which are easy to be seen in the dentine area. In our samples, the odntoblast processes are found either intact or cropped, in groups or isolated, and mainly inside the dentinal tubules.

At the same time, bioerosional phenomena were observed throughout the dentinal tissue, such as bacteria colonies and

filaments. The bacteria colonies are exhibited as pores and tunnels within characteristic dissolution rims and are the result of dissolution of dentine caused by bacteria feeding on collagen. Filaments are fossilized bacteria, forming 3D structures, resembling tubes and tunnels.

Conclusions

The *Phanourios minor* enamel microstructure exhibits a distinct pattern, which can be discriminated from that of *Hippopotamus amphibius*. In both species enamel is constructed in such a way, that maximum resistance can be achieved in order to avoid the propagation of cracks during mastication. It is obvious that mechanical stability and functionality of mammal dentition is linked inseparably to enamel microstructure (Koenigswald *et al.*, 1994).

The bacteria colonies are attributed to exogenous microbes indicating relatively humid aerobic terrestrial environments with high temperature and a pH: 4–9 (Hedges *et al.*, 1995). The filaments (fossilized bacteria) detected, could possibly be attributed to the endogenous symbiotic bacteria Actinomycetales (Kalthoff *et al.*, 2011).

Hopefully in the future, the systematic documentation of enamel microstructure of the *Phanourios minor* species could prove to be more informative about its past and habits.

References

Alloing-Séguier, L., Lihoreau, F., Boisserie, J. R., Charruault, A. L., Orliac, M., Tabuce, R., 2014. Enamel microstructure evolution in anthracotheres (Mammalia, Cetartiodactyla) and new insights on hippopotamoid phylogeny. Zoological Journal of the Linnean Society, 171(3).

Fillipidi, A., Stathopoulou, E. T., Theodorou, G., 2013. Taphonomical observations on the pygmy Hippopotamus site in Aghia Napa, Cyprus, Bulletin of the Geological Society of Greece, vol. XLVII.

Hedges, R.E.M., Millard, A.R., 1995. Bones and groundwater: towards the modelling of diagenetic processes. Journal of Archaeological Science. 22, 155–164.

Kalthoff, D., Rose, K., Koenigswald, W., 2011. Dental microstructure in Palaeanodon and Tubulodon (Palaeanodonta) and bioerosional tunneling as a widespread phenomenon in fossil mammal teeth, Journal of Vertebrate Paleontology 31:6, 1303-1313.

Koeningswald, W., Clemens, 1992. Levels of complexity in the microstructure of mammalian enamel and their application in studies of systematics, Scanning Microscopy, 6(1): 195-218.

Koenigswald, W., Pfretzschner, H. U., 1991. Biomechanics in the Enamel of Mammalian Teeth, Constructional Morphology and Evolution, 113–125.

Koenigswald, W., Sander, P. M. 1994. Tooth Enamel Microstructure Proceedings of the enamel microstructure workshop. University of Bonn, Andernach, Rhine.

.Lihoreau, F., Boisserie, J. R., Manthi, F. K., Ducrocq, S., 2015. Hippos stem from the longest sequence of terrestrial cetartiodactyl evolution in Africa. Nature Communications, 6.

Pfretzschner, H. U., 1994. Biomechanik der Schmelzmikrostruktur in den Backenzähnen von Großsäugern. Palaeontographica Abteilung, A Band A234 Lieferung 1-3, p1 - 88. Schweizerbart Science Publishers. Stuttgart, Germany.

Stathopoulou, E. T., 2005. First results on the fossilization of dwarf hippo skeletal remains from Aghia Napa, Cyprus, Proceedings of the International Symposium “Insular Vertebrate Evolution: The Palaeontological Approach,” Monografies de la Societat d’ História Natural de les Balears, 12, 319–324.

16th International Congress of the Geological Society of Greece
23-25 May, 2022 - Patras, Greece
Bulletin of the Geological Society of Greece, Sp. Publ. 10
Ext. Abs. GSG2022-238

Dental hypoplasias in the late Miocene hornless rhinocerotid *Chilotherium* (Mammalia, Rhinocerotidae) from Eurasia

P. Kampouridis[1], G. Svorligkou[2], C. Kyriakouli[3], N. Kargopoulos[1,2], S. Roussiakis[2], M. Böhme[1,3]

(1) Eberhard Karls University of Tübingen, Tübingen, Germany, panagiotis.kampouridis.@uni-tuebingen.de (2) National and Kapodistrian University of Athens, Athens, Greece (3) Senckenberg Centre for Human Evolution and Palaeoenvironment, Tübingen, Germany.

Research Highlights

Linear enamel hypoplasias are consistently present in the d4/D4 of *Chilotherium* spp. and associated with elevated stress levels during or shortly after birth of the individual. This is in marked contrast to the very rare hypoplasias seen in any other tooth position in *Chilotherium* spp.

Background

The hornless rhino genus *Chilotherium* was an autochthonous taxon to Eurasia, which lived only during the late Miocene (Deng, 2006). Its geographical distribution ranged from eastern China to the Balkan Peninsula (Deng, 2006; Kampouridis *et al.*, 2022). The genus was initially described by Ringström (1924), who revised several hornless rhinos, most of which had been attributed to the genus *Aceratherium* till then. The most notable features that connected these species were the depression in their frontal bones, the separated parietal crests, the wide mandibular symphysis with huge tusk-like lower second incisors, and the short limb bones (Ringström, 1924).

Objectives

The aim of this study is to investigate the deciduous dentition of *Chilotherium* spp. across Eurasia and their enamel hypoplasias in order to identify patterns in their occurrence and correlate these to physiological or environmental factors that may have affected the amelogenesis.

Chilotherium species studied

- *Chilotherium persiae* (Pohlig, 1886) from the late Miocene of Maragheh (Iran)
- *Chilotherium habereri* (Schlosser, 1903) from the late Miocene of China
- *Chilotherium schlosseri* (Weber, 1905) from the late Miocene of Samos (Greece)
- *Chilotherium anderssoni* Ringström, 1924, the type species of the genus, from the late Miocene of China

Taxonomy

The milk teeth in Aceratheriini are often extremely uniform and do not differ significantly in their morphology. The lower deciduous dentition lacks any specialised characters and therefore cannot be used to distinguish any of the *Chilotherium* species from each other. Ringström (1924) already pointed out that the species *C. habereri* and *C. anderssoni* cannot be distinguished based on their deciduous dentition, which is confirmed in the current study. Similarly, the deciduous teeth of *C. persiae* do not exhibit any consistent features that may be used for their separation from the two Chinese species. All three of these species exhibit strong intraspecific variation in the deciduous teeth leading to a great overlap in their morphologies, thus, preventing their use for the identification of the species. However, the deciduous teeth of the European *C. schlosseri* demonstrate a somewhat more complex morphology, with more prominent enamel folds, a consistently closed medifossette, an enlarged lingual cingulum, and some enamel plications in the median valley in the D2; the presence of a small crista and a (discontinuous) lingual cingulum in the D3; and the presence of a (discontinuous) lingual cingulum and enamel plications in the D4.

Enamel Hypoplasia

In total, 51 specimens of juvenile *Chilotherium* spp. were studied (29 *C. persiae*, 11 *C. habereri*, 9 *C. schlosseri*, and 2 *C. anderssoni*), including (partial) maxillae, mandibles, and isolated teeth, which in total exhibited 131 teeth. The material included 40 d4/D4s that were erupted but not completely worn down. Every d4/D4s exhibited at least one linear hypoplasia (in 2 cases a second hypoplasia was also visible). Only very few other deciduous teeth exhibited hypoplasias (4 specimens in total). In *C. persiae*, *C. habereri* and *C. anderssoni* the d4/D4 hypoplasias were positioned more or less at the same height of the tooth crown at its centrum and ω-shaped (Fig. 1A). On the other hand, in *C. schlosseri* the hypoplasia was a straight line, situated at the base of the tooth crown (Fig. 1B, C).

The position of the enamel defect of the buccal side of the d4/D4 is comparable to the hypoplasia reported in *Prosantorhinus germanicus* from the Miocene of Sandelzhausen (Germany) (Böhmer and Rössner, 2018) and *Teleoceras* from the Miocene of North America (Mead, 1999). Other cases of hypoplasia in fossil rhinoceroses had been reported by

Bratlund (1999), who studied a large collection of *Stephanorhinus kirchbergensis* specimens, including 368 teeth from which only nine featured some kind of enamel hypoplasia. Recently, the study of enamel hypoplasias in rhinoceroses has significantly increased (Hullot *et al.*, 2021, 2022; Hullot and Antoine, 2022).

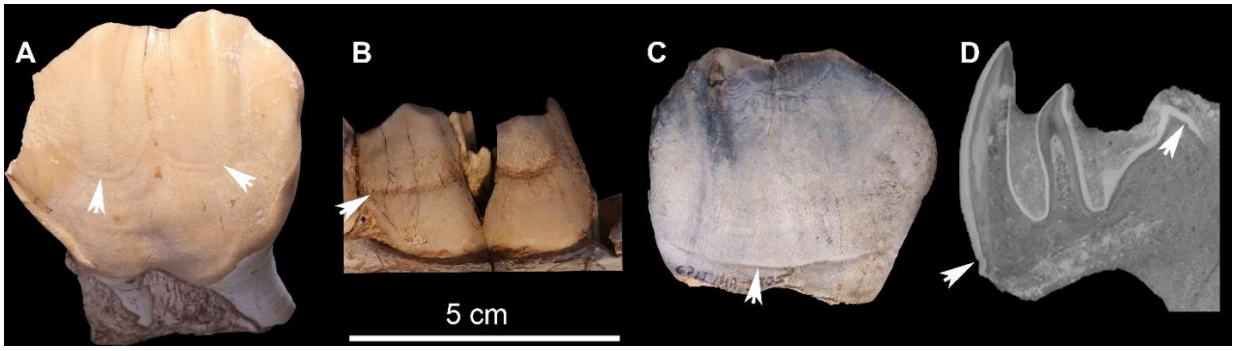

Figure 1. Chilotherium spp. fourth deciduous premolars, A, D4 of C. habereri B, d4 of C. habereri; C, D4 of C. schlosseri in buccal view; and D, CT-scan buccal-lingual cross section of a D4 of C. schlosseri. White arrows indicate the hypoplasias.

In the extant white rhinoceros (*Ceratotherium simum*), the d4 can start erupting as early as the second postnatal month (Hillman-Smith *et al.*, 1986). Based on a radiographical images provided by Goddard (1970), in the extant black rhinoceros (*Diceros bicornis*) the d4, which starts erupting few months after birth, is already fully formed in a 5.5-month-old calf. Thus, Mead (1999) correlated the hypoplasias in the d4/D4 of *Teleoceras* with the timing of birth of the individuals. Enamel hypoplasias in different mammalian groups have been linked to stress situation like birth and a study concerning hypoplasias in extant white-tailed deers correlated linear enamel hypoplasias in the d4 to the timing of birth or the first week following the birth (Davis and Mead, 2013).

These hypoplasias reported herein in *Chilotherium* are consistent throughout several individuals of four distinct species, being situated at a similar portion of the tooth crown (except *C. schlosseri*), while other enamel defects were very rare. Therefore, a random event that caused a hypoplasia at almost the same position in the d4/D4s in 39 individuals can be excluded. On the contrary, an event that could cause such a defect in the amelogenesis and is regular in the life of all individuals and at a common ontogenetic stage (during the formation of the d4/D4) must be looked for as a cause. The only such event that could cause a stressful situation during the formation of the d4/D4 is the birth of the animal. Therefore, we follow Mead (1999) and support that the enamel hypoplasia was caused during birth or during the week(s) following the birth.

Acknowledgements

We would like to thank Eli Amson (Stuttgart), Ursula Göhlich (Vienna), Ingmar Werneburg (Tübingen), Rainer Brocke (Frankfurt), Maximilian Albrecht (Halle), Spyridoula Pappa (London), and Georgios Theodorou (Athens) for access to comparative collections. We would like to thank Gabriel de Souza Ferreira (Tübingen) and the imaging lab of the Senckenberg Centre for Human Evolution and Palaeoenvironment in Tübingen and the Eberhard Karls University of Tübingen for CT-scanning several of the specimens. This research received support from the SYNTHESYS+ project http://www.synthesys.info/ which is financed by European Community Research Infrastructure Action under the H2020 Integrating Activities Programme, Project number 823827 (AT-TAF-TA3-9 to PK and AT-TAF-3924 to GS).

References

Böhmer, C., Rössner, G.E., 2018. Dental paleopathology in fossil rhinoceroses: etiology and implications. Journal of Zoology 304, 3-12.

Bratlund, B., 1999. Taubach revisited. Jahrbuch Des Römisch-Germanischen Zentralmuseums Mainz 46, 61–174.

Davis, H., Mead, A.J., 2013. Enamel Hypoplasia as an Indicator of Nutritional Stress in Juvenile White-Tailed Deer. Georgia Journal of Science 71, 95-101.

Deng, T., 2006. Neogene Rhinoceroses of the Linxia Basin (Gansu, China). Courier Des Forschungsinstituts Senckenberg 256,43-56.

Goddard, J., 1970. Age criteria and vital statistics of a black rhinoceros population. East African Wildlife Journal 8, 105-121.

Hullot, M., Antoine, P.-O., 2022. Enamel hypoplasia on rhinocerotoid teeth: Does CT-scan imaging detect the defects better than the naked eye? Palaeovertebrata 45, e2.

Hullot, M., Laurent, Y., Merceron, G., Antoine, P.-O., 2021. Paleoecology of the Rhinocerotidae (Mammalia, Perissodactyla) from Béon 1, Montréal-du-Gers (late early Miocene, SW France): Insights from dental microwear texture analysis, mesowear, and enamel hypoplasia. Palaeontologia Electronica 24, a27.

Hullot, M., Antoine, P.-O., Spassov, N., Koufos, G.D., Merceron, G., 2022. Late Miocene rhinocerotids from the Balkan-Iranian province: ecological insights from dental microwear textures and enamel hypoplasia. Historical Biology 1-18.

Kampouridis, P., Svorligkou, G., Kargopoulos, N., F. J. Augustin, F.J., 2022. Reassessment of '*Chilotherium wegneri*' (Mammalia, Rhinocerotidae) from the late Miocene of Samos (Greece) and the European record of *Chilotherium*. Historical Biology 34, 412-420.

Mead, A.J., 1999. Enamel hypoplasia in Miocene rhinoceroses (*Teleoceras*) from Nebraska: evidence of severe physiological stress. Journal of Vertebrate Paleontology 19, 391-397.

Ringström, T., 1924. Nashörner der Hipparion-Fauna Nord-Chinas. Palaeontologia Sinica 1, 1-156.

16th International Congress of the Geological Society of Greece
17-19 October, 2022 - Patras, Greece
Bulletin of the Geological Society of Greece, Sp. Publ. 10
Ext. Abs. GSG2022-244

Environmental monitoring of a coastal lagoon dominated by the reef-building polychaete *Ficopomatus enigmaticus*

S. Faulwetter[1], A. Ramfos[2], O. Katsani[1], I. Prevedouros[1], A. Emmanouilidis[1,3], D. Panagiotaras[4], M. Alexandridis[1], K. Nikolakopoulos[1], G. Droukas[1], A.-V. Ntzoumani[1,5], V. Bekiari[6], P. Avramidis[1]

(1) Department of Geology, University of Patras, 26504 Rio, Patras, Greece sarahfaulwetter@gmail.com (2) Department of Fisheries and Aquaculture, University of Patras, 30200 Messolonghi, Greece. (3) Institute for Ecosystem Research, Kiel University, Olshausenstr. 75, 24118 Kiel, Germany. (4) Department of Environment, Ionian University, 29100 Zakynthos, Greece. (5) Department of Biology, University of Patras, 26504 Rio, Patras, Greece. (6) Department of Agriculture, University of Patras, 30200 Messolonghi, Greece

Research Highlights

The spatiotemporal hydro-/ geochemical characteristics and benthic community distributions of a Greek coastal lagoon were studied with regard to the presence of massive biological reefs. These reefs cover a large area of the lagoon and possibly contribute to its reduced water exchange and spatial zonation.

Background and Objectives

Prokopos lagoon is located in northwestern Peloponnese, Greece. Its size is approximately 1.5 km^2, and its depth fluctuates from 0.5 m (summer) to 1.5 m (winter). The lagoon is divided into two main basins: the shallower northern basin, which is connected to the sea by a 10–20 m wide and 2.3 km long inlet, and the deeper southern basin, which receives freshwater from the river Larissos and the surrounding wetlands (Katsaros *et al*., 2017). Environmental monitoring as part of the Water Framework Directive has classified the ecological status of the lagoon as Moderate. The lagoon is characterised by the colonization of the invasive polychaete *Ficopomatus enigmaticus* (Fauvel, 1923), which constructs calcium carbonate tubes aggregated as large reef structures several meters in size. This species has invaded brackish waters worldwide, often causing changes to habitats, hydrology, biodiversity and human uses (Dittmann *et al.*, 2009). Since the characteristics and potential impacts of the reef structures on the ecosystem of Prokopos are unknown, the aims of this study are: a) estimation of the reef coverage, b) one-year monitoring of water and sediment characteristics, c) seasonal monitoring of ecological quality through macrobenthic analyses, d) comparison of present and past environmental conditions through micropaleontological analysis of surficial and sediment core samples.

Methods

Reef coverage was mapped through photogrammetric flights using a drone. In total, >3500 high-resolution images were acquired to build the georeferenced mosaic of the lagoon that was later converted to a precise digital surface model with <10 cm offset. Calculating of the reef coverage area was conducted on 50 x 50m subareas.

Sampling was performed from April 2021 to June 2022 at eleven stations and included: a) water samples for nutrient analyses (monthly sampling except for August 2021 and December 2021), b) seasonal sediment samples for geochemical and macrofaunal analyses, c) surficial sediments for micropaleontological analyses (January 2022). A geological core (120 cm length) was retrieved in April 2021 from the central part of the southern basin using an Uwitec gravity corer with hammer action. Physicochemical parameters (temperature, salinity, pH, dissolved oxygen) were measured in situ with a multi-meter. Water samples for laboratory analyses were collected from the upper part of the water column. Sediment samples were taken with a Van-Veen grab with a surface of 0.025m². Two replicates were taken for macrofaunal analyses, sieved over 0.5 mm mesh, fixed in 4% formaldehyde, and stained with Rose Bengal.

Total organic carbon (TOC) and total nitrogen (TN) in water and sediment were measured using a Shimadzu TOC-VCSH TOC/TN analyzer. Total phosphorus (TP) in sediments was measured with a Hach photometer according to the APHA 2005-4500-P method. Nitrate, nitrite and ammonium concentrations in the water column were measured with a HACH-LANGE DR3800 absorption spectrophotometer, using cuvette tests (LCK). Chlororophyll-α concentrations were determined according to the APHA 10200-H method. Sediment grain size was determined through dry sieving for coarser materials and with a Malvern Mastersizer 2000 Hydro for the fine fractions. For the macrobenthic samples, organisms were removed from the sediment manually and identified to species level using stereo- and light microscopes. Biodiversity (no. of species and individuals, Shannon-Wiener, Pielou's) and ecological indices (M-AMBI) were calculated on the averaged replicates. For multivariate analyses, abiotic data were standardised and biotic data log(x+1) transformed. A PERMANOVA analysis was performed on the multivariate datasets to test for differences between seasons and basins (significance level α=0.05). Statistical analyses were performed in R 4.1.2.

Results and Conclusions

Analysis of the georeferenced mosaic showed that in a sub-area of 2500 m² size approximately 607.64 m² were covered by polychaete reefs, i.e., 24.3%.

Physiochemical conditions of Prokopos drastically fluctuated seasonally and seem to be mainly driven by the annual precipitation regime and evaporation magnitude. In September 2021, close-to-marine conditions (36.1 psu) prevailed in the northern basin and brackish (26.6 psu) in the southern basin, whereas close-to-freshwater conditions (<1.5 psu) prevailed in the entire lagoon from January to February 2022. Water temperatures ranged from 9.4°C to 32.4°C in the northern basin and 8.2°C to 30.7°C in the southern basin (January 2022 / July 2021, respectively). Dissolved oxygen content was generally high (93% of oxygen measurements >6.5mg/l), especially in early summer due to high abundance of macrophytes and angiosperms which led to increased photosynthesis. This was also reflected in pH measurements (mean: 8.71± standard deviation: 0.48). Nutrient load levels in the water column were overall moderately elevated (TOC: 10.2±6.24 mg/l, max. 34.4 mg/l; TN: 0.97±0.45 mg/l, max. 2.77 mg/l; phosphates: 0.16±0.19 mg/l, max. 0.95 mg/l; NH_4^+: 0.05±0.06 mg/l, max. 0.32 mg/l; NO_3-: 0.35±0.16 mg/l, max. 0.93 mg/l; NO_2-: 0.05±0.13 mg/l, max. 0.88 mg/l). Peaks in nutrient loads occurred primarily after precipitation extremes, as recorded by the nearest meteorological station. Chlorophyll-α content was high throughout the year (28.3±24.0 mg/m³ max. 99.6 mg/m³).

Prokopos lagoon is dominated by fine sediments (silts, sandy silts), often intermixed with fragments of polychaete tubes. Nutrient concentrations in the sediment were 1.33±0.68 mg/g for TN (max. 3.02 mg/g), 2.29±1.3% for TOC (max. 5.20%) and 0.48±0.12 mg/g for TP (max. 0.7mg/g). Concentrations for TN and TOC were similar in both basins, but TP values were constantly higher in the southern basin.

The macrofauna in the lagoon was impoverished, with a maximum of 12 species found in October 2021 at one station in the Northern basin. Overall, the northern basin showed a higher species richness and diversity. The ecological quality of the lagoon was estimated as poor to moderate (highest M-AMBI value: 0.54, in October 2021 in the northern basin).

The multivariate analyses showed that water parameters followed a seasonal pattern, with the pairwise PERMANOVA analysis showing significant differences between all seasons ($p < 0.001$, adjusted significant level $\alpha = 0.006$), whereas geochemical parameters showed significant differences between seasons and basins ($p < 0.05$). The macrofaunal community composition showed significant differences between basins and seasons ($p < 0.05$), however, Bonferroni-Holm corrected pairwise comparisons between seasons were only significant within the northern basin ($p < 0.006$).

Micropaleontological analyses also distinguished the environmental variations between the two basins, with samples from the southern basin being dominated by the brackish and freshwater ostracods *Cyprideis torosa* and *Candona* spp., whereas the northern basin samples were totally dominated by the presence of *Cyprideis torosa* (>97% of total abundance). The upper 40 cm of the sediment core were dominated by *F. enigmaticus* fragments, but no traces of them were found after that point. From 40 cm until 120 cm the core was dominated by *Cyprideis torosa*, accompanied by sporadic presence of the ostracods *Loxoconcha elliptica* and *Candona* spp.

Our results show that Prokopos lagoon is subjected to both natural stress through strong annual fluctuations in salinity and temperature but also receives significant nutrient input from the surrounding agricultural areas, as seen in pulses of elevated nutrient concentrations in the water column. The fine sediments in the lagoon retain the nutrients (especially phosphorus in the southern basin, which is the first to receive agricultural runoffs and seems to act as a sink). The high coverage of the lagoon with *Ficopomatus* reefs possibly contributes to changes in water circulation and sediment transport and thus may also affect nutrient input to the sediments. The two basins show different physicochemical characteristics, but also sediment textural characteristics, macrofaunal, and microfossil community composition. The southern basin is strongly influenced by freshwater and does not show a seasonal pattern in macrofaunal composition, indicating limited water renewal rates from the sea towards the southern part. The macro- and microfossil communities are impoverished in Prokopos lagoon. However, analyses of the sediment core also revealed similar natural stressors in the past (distinct seasonal salinity fluctuations), thus communities are not only influenced by anthropogenic impacts but also by osmotic stress through salinity and temperature changes, corroborating previous findings (Iliopoulos *et al.*, 2015). As the lagoon is also being destabilised by water surface loss (Apostolopoulos *et al.*, 2022), continuous monitoring of all environmental aspects is crucial for the management of this important ecosystem.

Acknowledgements

This study was supported by the Green Fund of the Hellenic Ministry of the Environment and Energy (181.6.5/2020). We thank the National Park personnel for their support during sampling.

References

Apostolopoulos, D.N.; Avramidis, P.; Nikolakopoulos, K.G., 2022. Estimating Quantitative Morphometric Parameters and Spatiotemporal Evolution of the Prokopos Lagoon Using Remote Sensing Techniques. Journal of Marine Science and Engineering 10, 931.

Dittmann, S., Rolston, A., Benger, S.N., Kupriyanova, E.K., 2009. Habitat requirements, distribution and colonisation of the tubeworm *Ficopomatus enigmaticus* in the Lower Lakes and Coorong. Report for the South Australian Murray-Darling Basin Natural Resources Management Board, 104 p.

Iliopoulos G., Emmanouilidis A., Katsaros D., Papadopoulou P., Avramidis P., 2015, Palaeoecological evidence for a declining shallow coastal lagoon, Prokopos Lagoon, Western Greece. 15th International Multidisciplinar Scientific Conferences, p. 369 – 375.

Katsaros, D. Panagiotaras, D. Kontopoulos, N., Avramidis, P., 2017. Sediments characteristics and heavy metals distribution of a very shallow protected coastal lagoon, Prokopos Lagoon, Mediterranean Sea western Greece. Fresenius Environmental Bulletin 26, 6093-6103.

16th International Congress of the Geological Society of Greece

17-19 October, 2022 - Patras, Greece

Bulletin of the Geological Society of Greece, Sp. Publ. 10

Ext. Abs. GSG2022-276

Variation in Pneumatisation and Brain Expansion in Bovids from the Late Miocene of Greece

D. Liakopoulou[1], M. Georgitsis[1], S. Roussiakis[1]

(1) National and Kapodistrian University of Athens, Faculty of Geology and Geoenvironment, Panepistimioupoli Zografou, 15784 Athens, Greece. dliakopoulou@geol.uoa.gr.

Pneumatisation is the process known as the resorption and deposition of bone responding to biomechanical stress that results to cranial sinuses (Rae and Koppe, 2003; Farke, 2010; Sharp, 2016; Buck *et al.*, 2019; Liakopoulou *et al.*, 2021). Frontal sinuses are air-filled spaces within the cranial bones that are surrounding the nasal chambers (Edinger 1950; Rae 2008; Farke 2010). Mammal skulls possess the maxillary, ethmoidal, sphenoidal, and frontal sinuses all of them forming the paranasal sinuses (Rae, 2008; Alsafy, 2013; Buck *et al.*, 2019). There are several hypotheses suggested explaining the extensive volume of these structures in literature, e.g. decrease of the cranial mass, thermoregulation of the brain, shock absorption during feeding and combat, and yet their functional role and their phylogenetic weight remain elusive (Rae and Koppe, 2003; Farke, 2007, 2008a, 2008b, 2010; Badlangana *et al*., 2011; Snively and Theodor, 2011; Curtis, 2014; Curtis *et al.*, 2015).

Three-dimensional models of taxa of two tribes of Bovidae (Antilopini, Boselaphini) with variable frontal bone size and frontal sinus size and morphology are examined herein. The bovids present an exceptional diversity in cranial characters in terms of size and shape, something that provides an excellent opportunity for identifying important morphological aspects. This study reveals a previously unknown diversity in the morphology of frontal sinuses in these taxa. Cranial anatomy is largely studied and described in the literature, however these structures are scarcely studied in literature and mainly focused on extant or primate species (Rae and Koppe, 2003; Rae, 2008; Farke, 2008b, 2010; Miguel and Higgins, 2018; Buck *et al.*, 2019; Liakopoulou *et al.*, 2021).

The advances in digital visualization allow to investigate hypotheses regarding the structure and the evolution of these cranial structures. Therefore, X-ray computed tomography is extensively used in this study, because it is the only high-resolution and non-invasive/non-destructive method available that provides information to inaccessible areas and structures of the skull. Additionally, it gives the opportunity to work on available Museum/University specimens, thus providing more information to the final results. In this context, a Philips CT 64-slice tomographer from the Konstantopouleio General Hospital 'Agia Olga', the 'Attikon' University Hospital and an Optima LG CT 64-slice tomographer from the University General Hospital of Thessaloniki 'AHEPA' were used to scan the available specimens.

The CT data obtained are imported to advance imaging software to generate internal and external digital reconstructions of the skulls, in order to provide a volumetric assessment of the endocast and the cranial sinuses. Sinus volume strongly correlates to the frontal bone size and the brain size. Brain size scales negatively with the skull size, hence a thicker frontal bone will result in more space for frontal sinus volume (Farke, 2010; Sharp, 2016). In large sized bovids the brain fills approximately 10% of the total endocranial volume. On the contrary, in medium to small sized taxa this percentage increases and the frontal sinus volume decreases or it is even absent.

Acknowledgements

For access to material from Aristotle University of Thessaloniki and permission to CT scan them we thank Prof. Emeritus G. Koufos and Prof. D. S. Kostopoulos. For access to CT medical equipment special thanks deserve to Dr. N. Koliakos and I. Saradeas at the Attikon University Hospital, to Dr. P. Maniatis and his team (especially to Dr. P. Moschouris and Dr. E. Tsipra) at the Konstantopouleio General Hospital 'Agia Olga' and Dr. A. Kalogera and her team at the University General Hospital of Thessaloniki 'AHEPA'. Finally, for his constant help and support we would like to thank Prof. Emeritus G. Theodorou (AMPG).

Some data concerning extant taxa studied herein were accessed on MorphoSource.org.

Part of this research is co-financed by Greece and the European Union (European Social Fund-ESF) through the Operational Programme «Human Resources Development, Education and Lifelong Learning» in the context of the Act "Enhancing Human Resources Research Potential by undertaking a Doctoral Research" Sub-action 2: IKY Scholarship Programme for PhD candidates in the Greek Universities.

References

Alsafy, M.A.M., El-Gendy, S.A.A., El Sharaby, A.A., 2013. Anatomic reference for computed tomography of paranasal sinuses and their communication in the Egyptian buffalo (*Bubalus bubalis*). Journal of Veterinary Medicine Series C: Anatomia Histologia Embryologia,Anat. Histologia Embryol., 42(3), 220-231.

Badlangana, N. L., Adams, J.W., Manger, J.R., 2011. A Comparative Assessment of the Size of the Frontal Air Sinus in the Giraffe (*Giraffa Camelopardalis*). The Anatomical Record 294, 931–940.

Buck, L.T., Stringer, C.B., Mac Larnon, A.M., Rae, T.C., 2019. Variation in paranasal pneumatisation between mid-late Pleistocene hominins. Bull Mem Soc Anthropol Paris. 31(1–2):14–33.

Curtis, A.A., Lai, G., Wei, F., Van Valkenburgh, B., 2015. Repeated loss of frontal sinuses in arctoid carnivorans. Journal of

Morphology 276, 22-32
Curtis, A.A., 2014. A three-dimensional quantitative investigation of frontal sinus morphology and function in mammalian carnivores. Ph.D. Thesis in Biology, University of California, 128 p.
Edinger, T., 1950. Frontal sinus evolution particularly in the Equidae. Bulletin of the Museum of Comparative Zoology at Harvard 103, 409-496.
Farke, A.A., 2007. Morphology, constraints, and scaling of frontal sinuses in the hartebeest, *Alcelaphus buselaphus* (Mammalia: Artiodactlya, Bovidae). Journal of Morphology 268, 243–253
Farke, A.A., 2008a. Frontal sinuses and head-butting in goats: a finite element analysis. Journal of Experimental Biology 211, 3085–3094.
Farke, A.A., 2008b. Function and evolution of the cranial sinuses in bovid mammals and ceratopsian Dinosaurs. Ph.D. Thesis in Anatomical Sciences, Stony Brook University.
Farke, A.A., 2010. Evolution and functional morphology of the frontal sinuses in Bovidae (Mammalia: Artiodactyla), and implications for the evolution of cranial pneumaticity. Zoological Journal of the Linnean Society, 159, 988-1014.
Liakopoulou, D., Georgitsis, M., Roussiakis, S., 2021. Frontal bone pneumatisation in *Tragoportax* and *Miotragocerus* (Mammalia, Bovidae) from the Late Miocene of Greece, Historical Biology, 34:6, 1019-1028.
Miguel, R., Higgins, P. O., 2018. The biomechanical significance of the frontal sinus in Kabwe 1 (*Homo heidelbergensis*). Journal of Human Evolution, 114, 141–153. doi: 10.1016/j.jhevol.2017.10.007.
Rae, T.C., Koppe, T., 2003. The term ‘lateral recess’ and craniofacial pneumatization in Old World monkeys (Mammalia, Primates, Cercopithecoidea). Journal of Morphology 258, 193–199.
Rae, T.C., 2008. Paranasal pneumatization in extant and fossil Cercopithecoidea. Journal of Human Evolution, 54(3): 279–286.
Sharp, A.C., 2016. A quantitative comparative analysis of the size of the frontoparietal sinuses and brain in vombatiform marsupials. Memoires of Museum Victoria. 74:331–342.
Snively, E., Theodor, J.M., 2011. Common Functional Correlates of Head-Strike Behavior in the *Pachycephalosaur Stegoceras validum* (Ornithischia, Dinosauria) and Combative Artiodactyls. PloS ONE 6: e21422

16th International Congress of the Geological Society of Greece
17-19 October, 2022 - Patras, Greece
Bulletin of the Geological Society of Greece, Sp. Publ. 10
Ext. Abs. GSG2022-291

Upper Miocene (MN9) *Chelydropsis* Remains from Höwenegg (Germany): Preliminary Results

I. Pappa[1], E. Frey[2], E. Vlachos[3], G. Iliopoulos[1]

(1) Department of Geology, University of Patras. University Campus, 26504, Rio, Greece. irpappa89@gmail.com. (2) Department of Biology, Karlsruhe Institute of Technology, University of Karlsruhe. Kaiserstraße 1276131, Karlsrouhe, Germany (3) CONICET and Museo Paleontológico Egidio Feruglio. U9100GYO, Trelew, Chubut, Argentina.

Our study area is the well-known Upper Miocene (Vallesian stage, MN9) Lagerstätte site of Höwenegg, part of the volcanic district in Hegau, South Germany, where very important findings of vertebrates, invertebrates and plant fossils have been found

Periodical excavations during the last decades revealed a large number of chelonian fossils, which makes Höwenegg one of the most diverse chelono-fossil localities of Western Paleoarctic during the Neogene. At least four cryptodiran clades (Trionychidae, Chelydridae, Geoemydidae, Testudinidae) of tortoises and freshwater turtles have been discovered. Among freshwater turtles, *Chelydropsis* remains stand out for their completeness and preservation.

The revision of the clade Pan- Chelydridae (Joyce, 2016) attributes almost all the Middle Miocene samples of chelydrids from East and Central Europe in the species *Chelydropsis murchisoni* Bell, 1836, including as well its subjective junior synonyms: *Chelydra allingensis* Fuchs, 1939, *Chelydropsis carinata* Peters, 1868, *Chelydropsis murchisoni staeschei* Mlynarski, 1980b, *Macrocephalochelys pontica* Pidoplichko and Tarashchuk, 1960, and *Trionyx sansaniensis* Bergounioux, 1935.

The studied material consists an almost complete *Chelydropsis* skeleton, as well as other isolated skeletal remains. It belongs to the palaeontological collections of the Natural History Museums of Karlsruhe, Mainz, Freiburg and Darmstadt. Notably, the *Chelydropsis* skeleton stands out, being one of the most complete *Chelydropsis* skeletons found to-date. The skeleton shares the main characters with other described species of chelydrids from the middle and upper Miocene of Eastern and Central Europe. Nevertheless, the skeleton presents also some unique characters which have not been observed in any other *C. murchisoni* specimen found until now, and thus further investigation is required.

The skeleton is lacking the carapace, which is quite inportant for the identification of the species. Nevertheless, the study of this skeleton will be combined with 3D modelling of the preserved skull, as well as with the study of the isolated remains (some of them from the carapace) and which could provide additional information concerning the identification of the species.

The presence of important material in the study area, including the almost entire skeleton enables us to investigate more systematically the taxonomic status of available *Chelydropsis* spp. from the Miocene of Europe and analyze whether the material of this study area could most likely belong to a new species, providing new data on the phylogeny and palaeogeography of Western Paleoarctic chelonians.

Acknowledgements

We would like to thank Natural History Museums of Karlsruhe, Mainz, Darmstadt, and Geological Institute of Freiburg for giving permission to study Höwenegg's chelonian skeletal material. Furthermore, we would like to thank the stuff of Natural History Museum of Karlsruhe for all their help. Also, we would like to thank Walter Joyce for his help in providing comparative material.
IP thanks Erasmus + Placement Trainsheep 2017 and DAAD Short-Term Grant, 2021 (57552336), Programs under which she was able to visit the collections in the Natural History Museum of Karlsruhe and study part of material stored there.
The implementation of the doctoral thesis was co-financed by Greece and the European Union (European Social Fund) through the Operational Program "Human Resource Development, Education and Lifelong Learning", 2014-2020, within the framework of the Action "Strengthening human resources through the implementation of doctoral research - Sub-Action 2: IKY grant program for doctoral candidates of Greek universities".

References

Bell, T., 1836. Zoological observations on a new fossil species of *Chelydra*, from Öhningen. Transactions of the Geological Society of London 4, 379–381.

Bergounioux, F., 1935. Contribution à l'étude paléontologique des Chéloniens: Chéloniens fossiles du Bassin d'Aquitaine. Mémoires de la Société Géologique de France 25, 1–216.

Fuchs, E., 1939. Die Schildkrotenreste aus dem oberpfalzer Braunkohlentertiar. Paleontographica 89A, 57- 104.

Joyce, W.G., 2016. A review of the fossil record of turtles of the clade Pan- *Chelydridae*. Bulletin of the Peabody Museum of Natural History 57(1), 21- 55.

Mlynarski, M., 1980. Die schildkrote des steinheimer beckens: b. Chelydridae mit einem nachtrag zu den Testudinoidea. Paleontographica Suppl. Vlll, Ttil II, 8, 1-35.

Peters, K.F., 1868. Zur Kenntnis der Wirbelthiere aus den Miocenschichten von Eibiswald in Steiermark. Die

Schildkrötenreste. Sitzungsberichte der Kaiserlichen Akademie der Wissenschaften, mathematisch-naturwissenschaftliche Classe 57, 72–74.
Pidoplichko, I.G. and Tarashchuk, V.I., 1960. New genus of large-headed turtle from the Pontian beds surrounding Odessa. Zbirnik Prac Zoologichnogo Muzeyu 29, 105–110.

16th International Congress of the Geological Society of Greece
17-19 October, 2022 - Patras, Greece
Bulletin of the Geological Society of Greece, Sp. Publ. 10
Ext. Abs. GSG2022-311

The Late Miocene Rhinocerotids (Perissodactyla, Rhinocerotidae) from Samos Island - New Insights from the Historical T. Skoufos Collection

G. Svorligkou[1], P. Kampouridis[2], E. Alifieri,[3] S. Roussiakis[1]

National and Kapodistrian University of Athens, Athens, Greece, geosvorligk@geol.uoa.gr (2) Eberhard Karls Universität Tübingen, Tübingen, Germany (3) Aristotle University of Thessaloniki, Thessaloniki, Greece

Research Highlights

Report of craniodental material of the rhinocerotids *Chilotherium schlosseri*, *Miodiceros neumayri* and *Dihoplus pikermiensis* from the late Miocene of Samos Island, Greece, from the T. Skoufos collection. Based on the study of the mesowear, *C. schlosseri* is interpreted as a mixed feeder engaged in browsing.

Samos island is famous for its late Miocene fossil mammals, most of which come from localities in the Mytilinii Formation. Koufos et al. (2011) distinguished four successive mammal assemblages, covering a timespan between 8.0—6.7 Ma. The Samos rhinocerotids (Perissodactyla, Rhinocerotidae) are represented by four species: the tandem-horned *Dihoplus pikermiensis* (Toula, 1906) and *Miodiceros neumayri* (Osborn, 1900) along with the hornless *Chilotherium schlosseri* (Weber, 1905) and *Chilotherium samium* (Weber, 1905).

In the present work, we examined the systematic classification of unpublished rhinocerotid craniodental material from Samos, excavated in 1903 by Professor Theodoros Skoufos of the National and Kapodistrian University of Athens, and currently stored in the Athens Museum of Palaeontology and Geology (AMPG). The species identified in the collection are *M. neumayri*, *D. pikermiensis* and *C. schlosseri*. Amidst the most significant specimens were an almost complete juvenile *M. neumayri* maxilla, an adult *D. pikermiensis* mandible partly preserving both clades, a *C. schlosseri* mandible bearing part of the lower incisors, two partly preserved adult *C. schlosseri* skulls, and the skull of a juvenile *C. schlosseri*. For the present work we applied a preliminary mesowear scoring on the dentitions of the two *C. schlosseri* skulls (Fig. 1) following Mihlbachler et al. (2011).

The specimens were enclosed in two different types of fossil matrix. Type-A Matrix is a tuffaceous conglomerate of variant cocometry levels, whereas Type-B Matrix is a yellowish calcitic sandstone. Therefore, it can be deduced that the material originates from at least two different fossiliferous horizons, one characterized by the coexistence of *C. schlosseri* (n = 8) and *M. neumayri* (n = 1) and another, bearing both *C. schlosseri* (n = 1) and *D. pikermiensis* (n = 1). However, due to the lack of stratigraphic data, it was impossible to correlate the material to any known fossiliferous horizon and further geochemical studies are needed in order to check the validity of this observation.

The sympatry of *D. pikermiensis* and *M. neumayri*, along with an aceratheriine genus such as the derived *Chilotherium* or the more primitive *Acerorhinus* Kretzoi, 1942 is common in the Turolian localities of the Balkano-Iranian Province (Athanassiou et al., 2014; Giaourtsakis, 2022; Kampouridis et al., 2022). Concerning their autecology, different herbivory types have been proposed for the Samos rhinocerotids. Brachydont *D. pikermiensis* is interpreted as a browser and *C. schlosseri* as a mixed feeder, whereas *M. neumayri* as a grazer, based on the limited available material (Hullot et al., 2022). Consequently, a clear niche partitioning between the 3 species is proposed. The results of our mesowear analysis indicate that *C. schlosseri* was indeed a mixed feeder, probably more engaged in browsing. However, a more thorough study of the dental wear signal of the Samos rhinos is recommended for an accurate interpretation.

The majority of the craniodental material of the Samos rhinocerotids stored at the AMPG collection was assigned to *C. schlosseri. Chilotherium* is a genus very common in the relatively more open and arid late Miocene habitats of Anatolia and China, lacking from the more humid, forest-type habitats of Central Europe (Kampouridis et al., 2022). Therefore, a more arid, open habitat could be proposed for Samos during the Turolian, rather than those of the classical localities of Pikermi, Attica (Roussiakis et al., 2019) and Kerassia, Euboea Island (Kampouridis et al., 2019). This conclusion comes in agreement with previous research discussing the homogeneity of the Pikermian Biome (Kostopoulos 2009; Hullot et al., 2022).

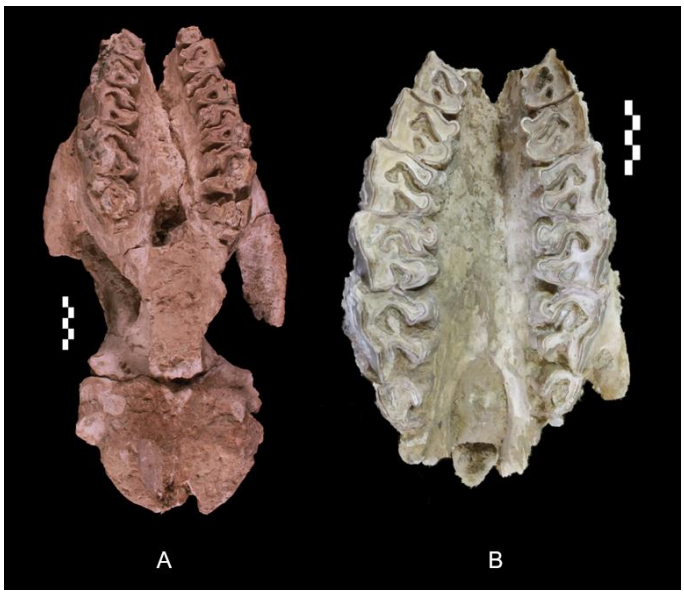

Figure 1. AMPG-SAM513 (A) and AMPG-SAM506 (B), *C. schlosseri* skulls, occlusal view. Scale: 5 cm.

Acknowledgements

We would like to thank Georgios Theodorou and Efterpi Koskeridou (University of Athens), former and current Director of the Athens Museum of Palaeontology and Geology respectively, for providing us access to the Samos material. We are obliged to Ursula Göhlich and Karin Wiltske (Naturhistorisches Museum Wien, Vienna) for providing us access to the Paleontology Collections during 2 SYNTHESYS+ research visits (AT-TAF-3924 to GS and AT-TAF-TA3-9 to PK) for the study of comparative material. We are grateful to Christine Argot (Muséum National d'Histoire Naturelle, Paris), Eli Amson (Staatliches Museum für Naturkunde Stuttgart), Maximilian Albrecht (Zentralmagazin Naturwissenschaftlicher Sammlungen der Martin-Luther-Universität Halle-Wittenberg), Rainer Brocke (Senckenberg Museum Frankfurt), Markus Bertling (Geologisch-Paläontologisches Museum der Westfälischen Wilhelms-Universität Münster), Madelaine Böhme and Ingmar Werneburg (Geologisches und Paläontologisches Institut der Universität Tübingen).

References

Athanassiou, A., Roussiakis, S. J., Giaourtsakis, I. X., Theodorou, G. E., Iliopoulos, G. 2014. A new hornless rhinoceros of the genus Acerorhinus (Perissodactyla: Rhinocerotidae) from the Upper Miocene of Kerassiá (Euboea, Greece), with a revision of related forms. Palaeontographica Abteilung A, 303 (1–3), 23-59.

Giaourtsakis, I. X. 2022. The fossil record of rhinocerotids (Mammalia: Perissodactyla: Rhinocerotidae) in Greece, in: Vlachos, E. (Ed.), Fossil Vertebrates of Greece Vol. 2, 409-500.

Hullot, M., Antoine, P. O., Spassov, N., Koufos, G. D., Merceron, G. 2022. Late Miocene rhinocerotids from the Balkan-Iranian province: ecological insights from dental microwear textures and enamel hypoplasia. Historical Biology, 1-18, https://doi.org/10.1080/08912963.2022.2095910.

Kampouridis, P., Svorligkou, G., Kargopoulos, N., Augustin, F. J. 2022. Reassessment of 'Chilotherium wegneri'(Mammalia, Rhinocerotidae) from the late Miocene of Samos (Greece) and the European record of Chilotherium. Historical Biology 34 (3), 412-420, https://doi.org/10.1080/08912963.2021.1920939.

Kampouridis, P., Roussiakis, S., Kargopoulos, N., Giaourtsakis, I., Dimakopoulos, G., Iliopoulos, G., Svorligkou, G., Theodorou, G. 2019. Faunal diversity at the Turolian locality of Kerassia (northern Euboea, Greece). Bulletin of the Geological Society of Greece, Sp. Pub. 7 (122), 52-53.

Kostopoulos, D. S. (2009). The Pikermian Event: temporal and spatial resolution of the Turolian large mammal fauna in SE Europe. Palaeogeography, Palaeoclimatology, Palaeoecology 274(1-2), 82-95.

Koufos, G. D., Kostopoulos, D. S., Vlachou, T. D., Konidaris, G. E., 2011. A synopsis of the late Miocene mammal fauna of Samos Island, Aegean Sea, Greece. Geobios 44 (2-3), 237-251.

Kretzoi, M. 1942. Praokkupierte und durch altere zu ersetzende Saugetiernamen. Foltani Kozlony 72, 345-349.

Mihlbachler, M. C., Rivals, F., Solounias, N., Semprebon, G. M. 2011. Dietary change and evolution of horses in North America. Science 331(6021), 1178-1181.

Roussiakis, S., Filis, P., Sklavounou, S., Giaourtsakis, I., Kargopoulos, N., Theodorou, G. 2019. Pikermi: a classical European fossil mammal geotope in the spotlight. European Geologist 48, 28-32.

Osborn H. F. 1900. Phylogeny of Rhinoceroses of Europe. Memoirs of the American Museum of Natural History, New York 13, 229-267.

Toula F. 1906. Das Gebiss und Reste der Nasenbeine von Rhinoceros (Ceratorhinus Osborn) hundsheimensis. Abhandlungen der Kaiser-Königlichen Geologische Reichs-Ausz., 1-38.

Weber M. 1905. Über tertiäre Rhinocerotiden von der Insel Samos II. Bulletin de la Société impériale des Naturalistes in Moscou 18: 345–363.

16th International Congress of the Geological Society of Greece
17-19 October, 2022 - Patras, Greece
Bulletin of the Geological Society of Greece, Sp. Publ. 10
Ext. Abs. GSG2022-314

Conodont Colouration Alteration Index pattern in Greece: a First Attempt to Study its Distribution

C. Georgopoulos[1], E. Stathopoulou[1], A. Zambetaki-Lekkas[1], H. Kranis[1]

(1) National and Kapodistrian University of Athens, Department of Geology & Geoenvironment, Panepistimiopolis, 15784 Zographou, Greece, Christosgeorgopoulosgeol@gmail.com

Research Highlights

Conodonts from numerous outcrops in Greece are described and graded, according to the Conodont Colour Alteration Index (CAI), to study its distribution and correlation to lithology, geotectonic conditions and diagenesis.

Background

Conodonts are an extinct group of Palaeozoic to Triassic elongated soft bodied marine chordates, whose feeding apparatus consists of small phosphatic tooth-like elements (Sweet *et al.*, 2001). These elements were the first evidence of these organisms but their attribution to a specific taxonomic group remained elusive for decades. The first unequivocal soft bodied conodont was only described in 1983 (Briggs *et al*., 1983). Conodonts are generally found scattered in marine sedimentary rocks of Cambrian to Triassic age and are of immense biostratigraphical significance (Metcalfe *et al*., 2010). The conodont elements consist of carbonated hydroxylapatite but also contain amounts of organic material (Eipstein *et al.*, 1977; Golding *et al.*, 2021). When these elements are heated or subject to metamorphism in the subsurface, they progressively and irreversibly change colour (Metcalfe *et al*., 2010). Colour alteration in conodonts is directly related to the depth and duration of burial and the geothermal gradient. In addition, their microstructure is altered texturally, leading to recrystallization, pitting, distortion or even destruction. Studies of conodont colour and textural alteration have led to the establishment of a scale of Conodont Colour Alteration Indices (CAI) and textural alteration types (Epstein *et al.*, 1977; Rejebian *et al.*, 1987). These changes in conodont colour and texture has been used extensively in the petroleum industry as an index of thermal maturation, as an indication of mineralization temperature (Rejebian *et al.*, 1987; Jones, 1992) and in regional basin history and tectonic studies (Metcalfe, 2003). It is a useful method that covers a large temperature range, from 50 to 600 °C, used mainly in carbonate rocks and in zones where temperature distribution in rocks is mainly the result of burial. A reasonable approximation to palaeo-temperatures and geothermal palaeo-gradients is possible from CAI data if the thickness of the stratigraphic succession, and the boundaries of the chronostratigraphic units are known (Garcia-Lopez *et al.*, 2003). The CAI is widely used to determine the maximum temperature in carbonate rocks, even though conodont colour may also be affected by other factors, such as diagenesis (Golding *et al.*, 2021).

Objectives

Conodonts have been reported from several formations/outcrops throughout the Hellenic peninsula, ever since the beginning of the 60's by a great number of researchers. These conodont assemblages date from the Silurian to the Triassic. Most of these outcrops can be found in localities across different regions of the central, south, as well as on islands of the Hellenic territory. These usually belong to deposits of the Sub-Pelagonian, Pindos Trypali (Crete), or even the Ionian geotectonic unit (Koukousioura *et al.*, 2022). The objective of this study is to grade conodont assemblages from numerous outcrops of the Greek territory according to the CAI established by Eipstein et al. (1977), for the first time. The CAIs will then be correlated to specific formations/rock types and geotectonic units found throughout Greece as a preliminary attempt to attribute them to specific geotectonic conditions due to burial. The possibility of the effect of diagenetic procedures (enrichment in Mn, Fe oxides), will also be examined. In time this data base will be enriched with yet more material from other outcrops.

Material

The material used in this study consists of conodont assemblages from nine locations, coming from A.Z.L.'s personal collection. These locations, belong to the Sub-Pelagonian, Pindos and Ionian geotectonic units. From each location and outcrop, numerous samples were studied, while more than 1000 conodont elements were described and graded.

Methods

The CAI of conodonts is a valuable tool for assessing organic metamorphism because it is a rapid and inexpensive method requiring only standard laboratory techniques and a binocular microscope. The conodont elements were studied and graded according to Eipstein *et al.*, 1977. The Conodont Colouration Alteration Index was used, which ranges from 1 to 8. At CAl 1, conodont colour is assumed to be unaltered, and conodonts are generally pale yellow. Very pale brown conodonts mark the beginning of colour alteration (CAl=1.5). CAl 2 is brown to dark brown, and so on to CAl 5 which is black. Each CAl is distinctive enough that half indexes frequently may be determined. With continued heating, black

conodonts become gray, then opaque white, and in the last stage before decomposition, crystal clear. The fixed carbon of the black conodont is driven out of the conodont element (volatilized) at these high temperatures, thus clearing the conodont element. The change from opaque white to crystal clear conodonts may result from the release of water of crystallization as well as from recrystallization (Eipstein *et al.*, 1977). Naturally occurring conodont collections that have a CAl of 4.5 or higher, show changes in surface texture as well as colour. At these high indexes, conodont surfaces change from smooth and vitreous to pitted and grainy (Rejebian *et al.*, 1987).

Results

According to the study of our material, conodonts were found in limestones, dolomitic limestones and limestones with chert of Triassic age. These usually belong to the Sub-Pelagonian and Pindos geotectonic units, with the exception of Corfu outcrops, which belong to the Ionian unit. Conodont Colour Alteration Indices (CAI) values in the Greek peninsula, based on the studied material, show a large range of 3-8, the majority being a value of about 7-8. A map exhibiting the exact distribution of the CAI's was constructed in order to better understand its correlation to the geology and tectonics of every outcrop. In zones where temperature distribution in rocks is mainly the result of burial, colour alteration in conodonts is directly related to the depth and duration of burial and the geothermal gradient. In our case, this could mean that the conodont assemblages have been subjected to temperatures between 110o and 600o C. Speculations are made, on the basis of the duration of burial (geological age of formations, etc.), depth of burial (minimum thickness of overlying formations) etc.

Conclusions

The CAI values are a result of the sedimentary and tectonic history of each region. Lower values of CAI can be interpreted to be due to the thinner sedimentary cover in that area while relatively high values of CAI probably reflect a thicker cover, always taking under consideration the diagenetic history of the formations, as well the presence of igneous events, reheating and mineralization. This study is only a first attempt to grade and describe this characteristic feature of conodonts and create a distribution map, which will be enriched in time with new material from other locations.

References

Briggs, D. E. G., Clarkson, E. N. K., Aldridge, R. J., 1983. The conodont animal. Lethaia, 16, 1–14.

Epstein, A G, Epstein, J.B., Harris, L. D., 1977. Conodont colour alteration-an index to organic metamorphism, Geological Survey professional paper; 995, 1-25.

Garcia-Lopez, S., Bastida, F., Aller, J., Sanz-Lopez, J., 2003. Geothermal palaeogradients and metamorphic zonation from the conodont colour alteration index (CAI), Terra Nova, 13, 79-83.

Golding, M. L., McMillan, R., 2021. The impacts of diagenesis on the geochemical characteristics and Colour Alteration Index of conodonts, Palaeobiodiversity and Palaeoenvironments, 101:803–821.

Jones, G. L. 1992. Irish Carboniferous conodonts record maturation levels and the influence of tectonism, igneous activity and mineralization. Terra Nova, 4, 238–244.

Koukousioura, O., Dimou, V. G., 2022. The Fossil Record of Conodonts in Greece, in: Vlachos, E. (ed.), Fossil Vertebrates of Greece, Vol. 1, 33-89.

Metcalfe, I. 2003. Colour and textural alteration of Palaeozoic and Triassic conodonts from Peninsular Malaysia: implications for tectonic evolution and hydrocarbon generation. Courier Forschungsinstitut Senckenberg, 245, 261–280.

Metcalfe, I., Riley, N. J., 2010. Conodont Colour Alteration pattern in the Carboniferous of the Craven Basin and adjacent areas, northern England. Proceedings of the Yorkshire Geological Society, 58 (1), 1–8.

Rejebian, V.A., Harris, A.G., Huebner, J.S., 1987. Conodont colour and textural alteration: An index to regional metamorphism and hydrothermal alteration. Bulletin of the Geological Society of America, 99, 471-479.

Sweet, W. C., Donogue, P. C. J., 2001. Conodonts: Past, Present, Future. Journal of Paleontology, 75, 1174–1184.

16th International Congress of the Geological Society of Greece
17-19 October, 2022 - Patras, Greece
Bulletin of the Geological Society of Greece, Sp. Publ. 10
Ext. Abs. GSG2022-353

A Stratigraphic Contribution To The Geological History of Lesvos Petrified Forest: Preliminary Results From the West Akrocheiras Section

Penelope Papadopoulou[1,2], G. Iliopoulos[1], K. Perleros[1], K. Christanis[1], S. Kalaitzidis[1], N. Zouros [2,3]

(1) University of Patras, Patras, Greece, penelpapadop@upatras.gr (2) Natural History Museum of the Lesvos Petrified Forest, Sigri, Greece (3) Department of Geography, University of the Aegean, Mytilene, Greece.

Background

The Petrified Forest of Lesvos Island is a Natural Monument of International value and the main geological heritage site of the Lesvos Island UNESCO Global Geopark. It is well known that spectacular silicified tree trunks, branches and leaves pop up from different stratigraphic levels of the Sigri Pyroclastic Formation (Fig.1) (Pe-Piper et al., 2019a,b). Sigri pyroclastics cover the northwestern part of Lesbos Island and derive from a volcanic province that existed in the northeastern Aegean Sea and Anatolia during the Lower Miocene (Pe-Piper et al., 2018). Several hundred meters of stratified tuffs and volcaniclastic sediments intercalate with palaeosoils The Sigri Formation presents a complex stratigraphy due to multiple eruption events and their different generation mechanisms. The intense tectonism, however, complicates the stratigraphic interpretation of the volcaniclastic sequence and the reconstruction of the respective eruption history. The construction of the new Kalloni-Sigri road with several new road cuts has exposed a significant part of the Sigri Pyroclastic Formation, which otherwise remains mostly covered by colluvium and/or is extensively eroded.

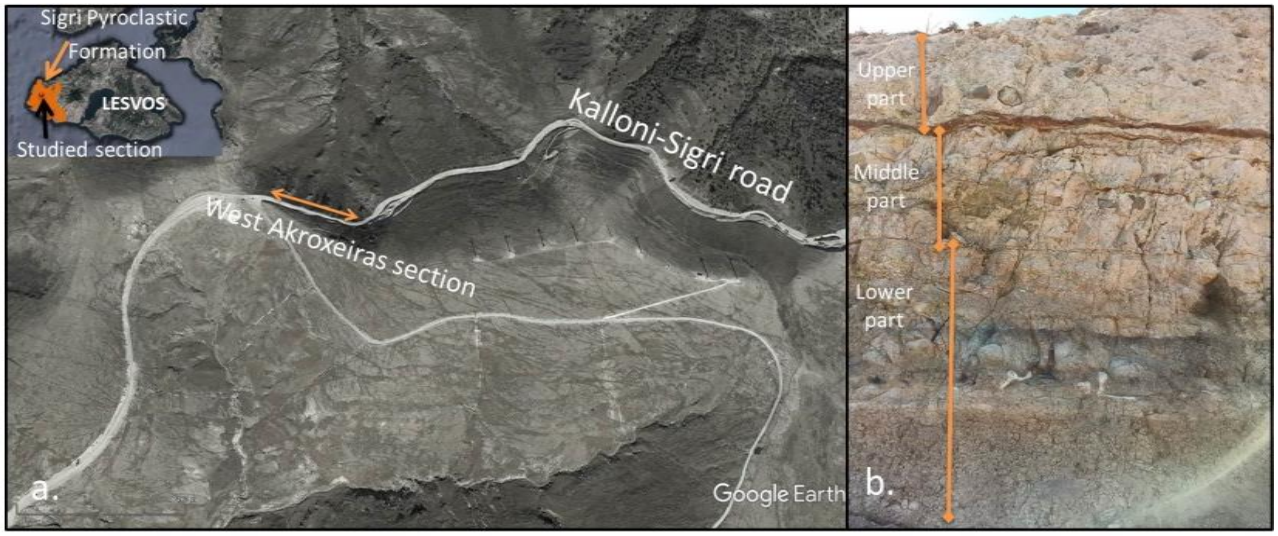

Figure 1: a. Satellite image (Google Earth) with the location of the study area b. Photo of the lower stratigraphic layers of West Acrocheiras section were the three parts of the section have been noted.

Objectives

The West Akrocheiras section is about 330m long and comprises more than 25-m-thick volcaniclastic sediments and tuffs exposed at three different elevational stages. The objectives of this study are to provide new stratigraphic data, and to establish temporal and spatial correlations for the Sigri Formation in the West Akrocheiras area, by determining the facies changes, recording the stratigraphic position of fossil plant horizons as well as their taphonomy. The aim is to reconstruct the depositional palaeoenvironments in the basin and, to elucidate their evolution in time and space.

Methods

Detailed lithostratigraphic logging and sampling of the section, as well as mapping and measurements of the faults were conducted. The various pyroclastic layers were characterized according to Fisher (1984) using terms for mixed pyroclastic-epiclastic rocks. Additionally, color attribution was often used as an indication of different volcanic source amongst others. Because of the significant lateral changes of the nature of the pyroclastic rocks, twelve separate stratigraphic loggings were recorded. Detailed stratigraphic columns were constructed using STRATER software. Stratigraphic correlation was performed using characteristic layers. Palaeosoils represent significant stratigraphic

hiatuses in a volcanic sequence and are often used as index horizons in order to separate the different eruption events. Samples from characteristic palaeosoils were submitted to tephra and maceral analysis in order to acquire information regarding their origin and composition. XRD analysis was also carried out in three samples. The origin and nature of the volcaniclastic sediments (e.g. riverine, lacustrine etc.) and the adjacent sedimentary basins was sought and the volcaniclastic evolution of the studied section has been determined.

Results and Conclusion

The detailed stratigraphic logging resulted in the recording of several different pyroclastic layers with substantially different thicknesses from 1cm to more than 6m in some cases. Coarse tuffs, lapilli tuffs and tuff breccias many times containing fallen tree trunks and branches, are dominating. Tuffaceous siltstones, sandstones and conglomerates have been recorded in several cases, especially at the lower part of the sequence. Palaeosoils with red, green or/and black coloring and thicknesses no more than a few centimeters thick, interrupt the sequence. In one case petrified tree trunks standing on the palaeosoil were recorded. In many cases lenses of riverine origin were also noticed. The layers are severely affected by tectonic movements and thus, their lateral continuity has been interrupted many times.

The lower part of the sequence, with a thickness of 3.80m, consists mostly of fine grained rocks. At the western part tuffaceous sediments exist, implying the presence of a water body at the lowest stratigraphic levels. The Huminite/Vitrinite reflectance from one sample from this unit varies from 0.42-0.5%, with a mean value of 0.47%, indicating a sub-bituminous rank, which has been reached not due to a normal geothermal gradient but due to thermal affection. Moreover, maceral analysis of a soil-resembling sample from this unit points to a surface pyrolysis of fresh and/or slightly peatified organic matter, probably resembling root systems (as corpohuminite macerals are prevailing) or of arboreal origin. These data imply evolution of the water body to a mire, in which plant material had been burnt. In the upper part of this unit conglomerate lenses occur implying the presence of a riverine system on the top. The middle part of the sequence (3.80-6.80m) consists of lapilli tuffs with intercalations of two palaeosoils. The base of this unit consists of a palaeosoil with standing tree trunks. According to maceral analysis, this is characterized as a carbonaceous or sapropelic coaly horizon with limited thermal affection, which has been deposited in a water-logged limnic/limnotelmatic environment. In this unit several horizons with leaf fossils exist either deposited as leaf litter or scattered in the different layers. XRD analysis in the palaeosoil samples from both the lower and the middle unit revealed that the samples consisted mostly of crystalline intermediate feldspars and clay or/and zeolites. Amorphous or/and organic material also exists. The upper part of the sequence (6.80-25m) consists mostly of thick lapilli tuffs and tuff breccias with intercalations of thin palaeosoils and conglomerate lenses. Fallen tree trunks have been recorded in these layers.

The stratigraphic record of West Akroxeiras section has revealed the presence of a water body at the base of the sequence, which possibly developed in the mires, where a big tropical forest grew during the lower Miocene. At this stage the volcanic activity was low, allowing the formation of palaeosoils. At the upper part of the sequence the volume of provided volcanic material has increased dramatically.

Acknowledgements

We would like to sincerely thank Ass. Prof. Lambropoulou Paraskevi for the XRD analysis.

References

Fisher, R., Schminke, H.U., 1984. Pyroclastic rocks. Springer Berlin, Heidelberg

Pe-Piper, G., Imperial, A., Piper, D.W.J., Zouros, N., Anastasakis, G., 2019. Nature of the hydrothermal alteration of the Miocene Sogri Petrified Forest and host pyroclastic rocks, western Lesbos, Greece. Journal of Volcanology and Geothermal Research. 369: 172-187.

Pe-Piper, G., Piper, D.W.J, Zouros, N., Anastasakis, G., 2019. Age, stratigraphy, sedimentology and tectonic setting of the Sigri Pyroclastic Formation and its fossil forests, Early Miocene, Lesbos, Greece. Basin Research 31: 1178-1197

16th International Congress of the Geological Society of Greece
17-19 October, 2022 - Patras, Greece
Bulletin of the Geological Society of Greece, Sp. Publ. 10
Ext. Abs. GSG2022-354

Mountainous vegetation succession during the last 2000 years: A case study from an upland site in the Peloponnese

K. Kouli[1,4], G. Vasileiadi[1,2], A. Emmamouilidis[3], I. Prevedouros[4], P. Avramidis[4], G. Liakopoulos[5], C. Vignola[6], A. Masi[5,6], A. Izdebski[4]

(1) National and Kapodistrian University of Athens, Department of Geology and Geoenvironment, Athens, Greece, akouli@geol.uoa.gr (2) Aristotle University of Thessaloniki, School of Geology, Thessaloniki, Greece (3) Institute for Ecosystem Research, Kiel University, Germany (4) University of Patras, Department of Geology, Patras, Greece (5) Max Planck Institute for Geoanthropology, Jena, Germany (6) Department of Environmental Biology, Sapienza University of Rome, Rome, Italy

Introduction

The intricate plant landscape evolution in southern Greece during the Upper Holocene has been the scope of numerous paleovegetation studies (e.g. Jahns, 1993; Kouli, 2012; Lazarova *et al.*, 2012; Vignola *et al.*, 2022; Emmanouilidis *et al.*, 2022) in the last decades. The significant regional topographic and climatic variability and human activities are the main shaping factors of the vegetation development in southern Greece and especially the Peloponnese (Weiberg *et al.*, 2016; Kouli *et al.*, 2018) that has been the scenery for the rise and the fall of numerous human communities. So far, the existing paleovegetation records from the Peloponnese derive from coastal and lowland sites and eventually, the vegetation succession of the mountainous areas is far from being clearly understood.

Rakita wetland is located at an altitude of c. 1100 meters above sea level on a plateau of Panachaiko Mountain (northwestern Peloponnese). Its most remarkable ancient monument in the area is the Geometric temple of Artemis dated in the late 8th c. BCE (Petropoulos, 2001). Even though the area has been inhabited from the Mycenaean times, authoritative demographic figures can be monitored only after the mid-15th century CE. On the basis of the data obtained from Ottoman taxation registers and Venetian cadastral and population surveys (15th–18th c. CE), the area appears to hold a number of small and medium-sized settlements, of which Ano Mazaraki was the largest (Liakopoulos, 2019). An alpine vegetation zone and fir forests occur in the nearby high altitude areas, while pine or mixed pine with deciduous oak forests are also recorded in the lower parts. Nowadays, a significant part of the plant landscape around the site is shaped by human activity, mainly animal husbandry and arboriculture.

The present study aims to investigate the late Holocene vegetation development and feature human land-use practices in a mountainous area of the Peloponnese. To evidence the vegetation response and decipher the human impact, a detailed palynological analysis was conducted.

Material and Methods

From Rakita wetland a 3 m long sediment core (RKT-2) was retrieved. The upper 150 cm of the core consists of peat and gyttja intercalations, while silty sand with rare pebbles is predominant in the lower part. The age of the recovered deposits is based on 9 AMS radiocarbon dates. In the present study, the core interval between 26 and 164 cm, covering the last 2000 BP is being discussed. In total, 54 sediment samples of approximately 2 gr at a mean 1.5 cm interval were used for pollen analysis. Subsamples were spiked and chemically treated with acids (HCl and HF), boiled repeatedly in KOH, sieved through a 10μm mesh to concentrate the pollen content and eventually mounted in glycerine. Microscopic palynological analysis revealed a rich and well-preserved pollen assemblage accompanied by numerous green algae, fungal remains and other Non-Pollen Palynomorphs (NPPs). A mean of 250 terrestrial pollen grains per sample and all (NPPs) within the same spectra were counted. Pollen percentages were calculated on the basis of all terrestrial pollen. Palynological percentage and concentration diagrams were constructed. Pollen assemblage zones were defined based on Stratigraphically constrained cluster analysis.

Results and Discussion

Microscopic analysis revealed a rich and well preserved pollen flora accompanied by numerous green algae, fungal remains and other NPPs. The distinct local pollen assemblage zones recognized in the Rakita record highlight significant shifts in the vegetation during the last 2000 years, providing the first insights of the plant landscape evolution from an upland site in Peloponnese. The base of the sequence is characterized by the dominance of open herbaceous vegetation, while the deciduous *Quercus* woodland and the upland coniferous forest components, such as *Abies*, *Pinus* and *Juniperus* appear restricted. The concurrent high abundance of Cerealia-type and the presence of several pollen connected with human activities, feature an interval of significant anthropogenic activity in the area, roughly corresponding to the Roman Period. Following, the increase of deciduous *Quercus* and the drop in all human pollen indicators mark the expansion of the mixed deciduous oak forest, as a result of the retreat of human pressure on the mountainous environment. The sharp

retreat of deciduous oaks and the expansion of Cichorieae recorded up-core is most likely associated with forest clearance and landscape opening as a result of pastoralism. Evidence of arboriculture -mainly *Vitis* and *Juglans*- complement the land-use practices of the upland communities, during the last c.a.600 years in the area.

Acknowledgments

This work was funded by the Palaeo-Science and History Independent Research Group of the Max Planck Institute for the Science of Human History and the NKUA grand 16302.

References

Emmanouilidis, A., Panagiotopoulos, K., Kouli, K., Avramidis, P. 2022. Late-Holocene paleoenvironmental and land-use changes in Western Greece based on a sediment record from Klisova lagoon. Holocene 32, 485-500.

Jahns, S.,1993. On the Holocene vegetation history of the Argive Plain (Peloponnese, southern Greece). Veg Hist Archaeobot. 2, 187-203.

Kouli, K., 2012. Vegetation development and human activities in Attiki (SE Greece) during the last 5,000 years. Veg Hist Archaeobot. 21, 267-278

Kouli, K., Masi, A., Mercuri, A.M., Florenzano, A., Sadori, L., 2018. Regional vegetation histories: an overview of the pollen evidence from the Central Mediterranean. Late Antiq. Archaeol. 11, 69-82

Liakopoulos G.C., 2019. The early Ottoman Peloponnese. A study in the light of an annotated *editio princeps* of the TT10–1/14662 Ottoman taxation cadastre (ca. 1460–1463). Royal Asiatic Society, The Ibrahim Pasha of Egypt Fund Series, The Gingko Library, London

Lazarova, M, Koutsios, A., Kontopoulos, N., 2012. Holocene vegetation history of the Kotihi Lagoon (north-western Peloponnesus, Greece). Quat Int. 261, 138-145.

Petropoulos M., 2001. Γεωμετρικός ναός Ρακίτας-Λατρευόμενη θεότητα. In: Forschungen in der Peloponnes, Akten des Symposions anlasslich der Feier "100 Jahre Österreichisches Archäologisches Institut Athen", V. Mitsopoulos-Leon (ed.), Athen 5.3.-7.3.1998, Osterreichisches Archaologisches Institut, Sonderschriften Band 38, p. 39-45.

Vignola, C., Hättestrand, M., Bonnier, A., Finné, M., Izdebski, A., Katrantsiotis, C., *et al.*, 2022. Mid-late Holocene vegetation history of the Argive Plain (Peloponnese, Greece) as inferred from a pollen record from ancient Lake Lerna. PLoS ONE 17(7), e0271548

Weiberg, E., Unkel, I., Kouli, K., Holmgren, K., Avramidis, P., Bonnier, A., *et al.*, 2016. The socio-environmental history of the Peloponnese during the Holocene: Towards an integrated understanding of the past. Quat. Sci Rev. 136, 40-65

16th International Congress of the Geological Society of Greece
17-19 October, 2022 - Patras, Greece
Bulletin of the Geological Society of Greece, Sp. Publ. 10
Ext. Abs. GSG2022-355

Collagen extraction and evaluation of organic preservation in Greek & Cypriot fossilized bones

J. Iliopoulos[1], E. Stathopoulou[1, 2]

(1) Department of Historical Geology and Palaeontology, Faculty of Geology and Geoenvironment, National and Kapodistrian University of Athens, Panepistimiopolis, 15784 Zografou, Greece, James1997@windowslive.com
(2) Wiener Laboratory, American School of Classical Studies at Athens ASCSA, 54 Souidias st., 10676 Athens, Greece

Application of collagen extraction protocols and infrared spectroscopy on fossilized material from Greece and Cyprus and correlation of organic preservation to the diagenetic profile of samples.

The degree of preservation and the extractability of organic molecules in both archeological and paleontological skeletal material has been the objective of many studies during the last decades and have shown extremely promising and interesting results (Poulakakis *et al.*, 2002; Dotsika *et al*., 2011; Schweitzer *et al.*, 2014). Studies on such molecules via various protocols of extraction as well as isotopic and spectroscopic analyses (Stathopoulou *et al.*, 2008; Dotsika *et al*., 2011; Kontopoulos *et al*., 2019) have led to important information concerning evolutionary, environmental and diagenetic issues. Collagen is one of the most abundant proteins in skeletal material and its presence in fossils may indicate the preservation of other extremely important biomolecules such as DNA (Turner-Walker *et al*., 2008).

This paper aims to present results concerning the evaluation of organic preservation as well as the extraction and quantification of collagen in samples from the locations of Pikermi, Samos, Kerassia (7,3 Ma), Sesklo (1,3-1,1 Ma), Megalopoli (500-400 ka), Tilos (45-3,5 ka), Dispilio (7,5-7 ka) (Greece) and Aghia Napa (11,5-9,5 ka) (Cyprus). In total 41 samples were used; 40 were selected from the aforementioned locations and 1 served as reference sample (bovine bone). According to previous studies (Stathopoulou *et al*., 2008) the Dispilio material specifically has been grouped based on bone coloration variance, attributed to the presence of Mn and Fe oxides. For the purpose of this study we have chosen material from 2 colour types described as light colored and dark colored (rich in oxides).

Infrared Spectroscopy (ATR and NIR) was applied to all samples, prior to extraction in means of collagen prescreening and following extraction (where successful), to study the exact composition of the extracts and examine the correlation between collagen preservation and the samples' diagenetic profile (Stathopoulou *et al.*, 2008; Kuczumow *et al.*, 2010; Stathopoulou *et al*., 2019). The extraction of collagen was attempted via modifications of the Longin (1971) method and specifically those of Maspero *et al*. (2011), Semal and Orban (1995) and Ambrose (1990).

The IR analysis prior to extraction indicated the presence of organic material in all samples however the older samples (Pikermi – Aghia) exhibited only trace amounts of organic remains.

Of the extraction methods applied, only the Ambrose method led to successful collagen extraction and specifically only in the Dispilio samples (Figure 1). The collagen yield values for this material varied significantly (0,3 – 6,1 % w/w) and seemed to strongly correlate to the different contexts found within the archaeological site.

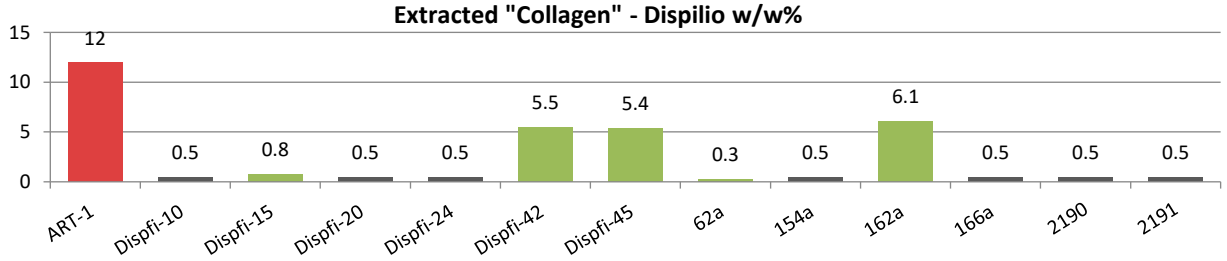

Figure 1: Results of collagen extraction from the Dispilio material (green: light coloured samples, grey: dark coloured samples) in comparison to the fresh bovine bone (red).

The light coloured material appears to contain more collagen than the dark coloured bones on average. The IR analysis after the extraction indicated that the reference sample contained solely collagen and various other organics while the extracted Dispilio collagen also contained impurities such as carbonates and subsequently raised questions relating to the efficacy of the extraction method (Figure 2).

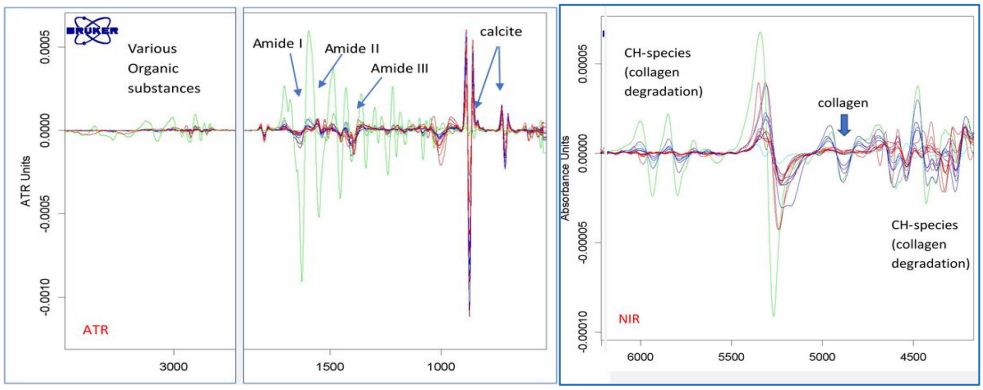

Figure 2: ATR (left) and NIR (right) spectra of the Dispilio material (red: dark coloured samples, blue: light coloured samples)and the fresh bone (green) extraction residue.

Concerning the coloration variances in the Dispilio samples, most dark colored samples are indicative of a waterlogged environment while the light colored samples reflect a more terrestrial environment (Stathopoulou *et al*., 2019). According to Stathopoulou *et al*. (2019), microbial activity is not a major phenomenon, so the collagen values most likely correlate with the presence of Mn and Fe oxides. This has also been noted by Kuczumow *et al*. (2010).

As mentioned above, the older samples contained only trace amounts of collagen therefore the type of extraction method applied was not successful. In the case of older material a more detailed approach is necessary (Schweitzer *et al*., 2014). However the Tilos and Aghia Napa (Stathopoulou *et al*., 2008) material is promising in terms of organic preservation and specifically from the former location DNA extraction has been successful (Poulakakis *et al.*, 2002). A more careful selection of material including petrous bone might provide better results (Kontopoulos *et al*., 2019).

In regard to the impurities that remained in the final stage of extraction, we need to examine if using bone powder accomplishes better results in terms of purity without significant reduction in overall yield. Taking all of the above under consideration we will hopefully be able to pinpoint more accurately the effects of diagenesis on collagen preservation and refine the extraction methodology for optimal results.

Acknowledgments

Thanks are owed to Dr. Dotsika and her team from the Stable Isotope laboratory at NCSR Demokritos, for their help and guidance during our experiments.

References

Ambrose, S.H., 1990. Preparation and characterization of bone and tooth collagen for isotopic analysis. *Journal of archaeological science*, *17*(4), pp.431-451.

Dotsika, E., Zisi, N., Tsoukala, E., Poutoukis, D., Lykoudis, S. and Giannakopoulos, A., 2011. Palaeoclimatic information from isotopic signatures of Late Pleistocene Ursus ingressus bone and teeth apatite (Loutra Arideas Cave, Macedonia, Greece). *Quaternary International*, *245*(2), pp.291-301.

Kontopoulos, I., Penkman, K., McAllister, G.D., Lynnerup, N., Damgaard, P.B., Hansen, H.B., Allentoft, M.E. and Collins, M.J., 2019. Petrous bone diagenesis: a multi-analytical approach. *Palaeogeography, Palaeoclimatology, Palaeoecology*, *518*, pp.143-154.

Kuczumow, A., Cukrowska, E., Stachniuk, A., Gawęda, R., Mroczka, R., Paszkowicz, W., Skrzypiec, K., Falkenberg, R. and Backwell, L., 2010. Investigation of chemical changes in bone material from South African fossil hominid deposits. *Journal of Archaeological Science*, *37*(1), pp.107-115.

Maspero, F., Sala, S., Fedi, M.E., Martini, M. and Papagni, A., 2011. A new procedure for extraction of collagen from modern and archaeological bones for 14C dating. *Analytical and bioanalytical chemistry*, *401*(6), pp.2019-2023.

Poulakakis, N., Theodorou, G.E., Zouros, E. and Mylonas, M., 2002. Molecular phylogeny of the extinct Pleistocene dwarf elephant Palaeoloxodon antiquus falconeri from Tilos Island, Dodekanisa, Greece. *Journal of Molecular Evolution*, *55*(3), pp.364-374.

Schweitzer, M.H., Schroeter, E.R. and Goshe, M.B., 2014. Protein molecular data from ancient (> 1 million years old) fossil material: pitfalls, possibilities and grand challenges. *Analytical chemistry*, *86*(14), pp.6731-6740.

Semal, P. and Orban, R., 1995. Collagen extraction from recent and fossil bones: quantitative and qualitative aspects. *Journal of Archaeological Science*, *22*(4), pp.463-467.

Stathopoulou, E., Cosmetatou, N.P., Theodoropoulou, T., Mallouchou, M., Margariti, E. and Psycharis, V., 2019. Origin of archaeological black bones within a waterlogged context: A multidisciplinary approach. *Palaeogeography, Palaeoclimatology, Palaeoecology*, *534*, p.109334.

Stathopoulou, E.T., Psycharis, V., Chryssikos, G.D., Gionis, V. and Theodorou, G., 2008. Bone diagenesis: New data from infrared spectroscopy and X-ray diffraction. *Palaeogeography, Palaeoclimatology, Palaeoecology*, *266*(3-4), pp.168-174.

Turner-Walker, G., Peacock, E.E., Gilbert, T. and Koon, H.E., 2008. An experimental study of morphological and chemical degradation of bone in wetlands: Potential for DNA extraction and amplification. *PARIS3 preserving archaeological remains in situ. Geoarchaeological and Bioarchaeological Studies*, *10*, pp.75-84.

16th International Congress of the Geological Society of Greece
17-19 October, 2022 - Patras, Greece
Bulletin of the Geological Society of Greece, Sp. Publ. 10
Ext. Abs. GSG2022-359

Undergraduate students ready for micropalaeontology: unraveling the lower Pleistocene palaeoecology of Rio-Antirio Basin

P. Papadopoulou[1], M. Tsoni[1], A. Arvanitis[1], T. Dougios[1], K. Goukos[1], A.M. Kiritsi[1], C. Nikolaou[1], A. Rekouti[1], D. Theodorakopoulou[1], G. Iliopoulos[1]

(1) University of Patras, Rion, Greece, penelpapadop@upatras.gr

Background

The Corinth-Patras rift system is a worldwide known laboratory for studying early rifting processes. Its high seismicity and fast deformation rates are attracting the scientific interest (Koukouvelas et al. 2001, Rohais and Moretti 2016). Rio-Antirio Graben is part of this rift system, nevertheless, it still remains relatively less studied. However, it presents major stratigraphic and palaeontological interest as it records in great detail the environmental changes that result from the combined effect of tectonism and eustatic changes (Tsoni et al., 2021).

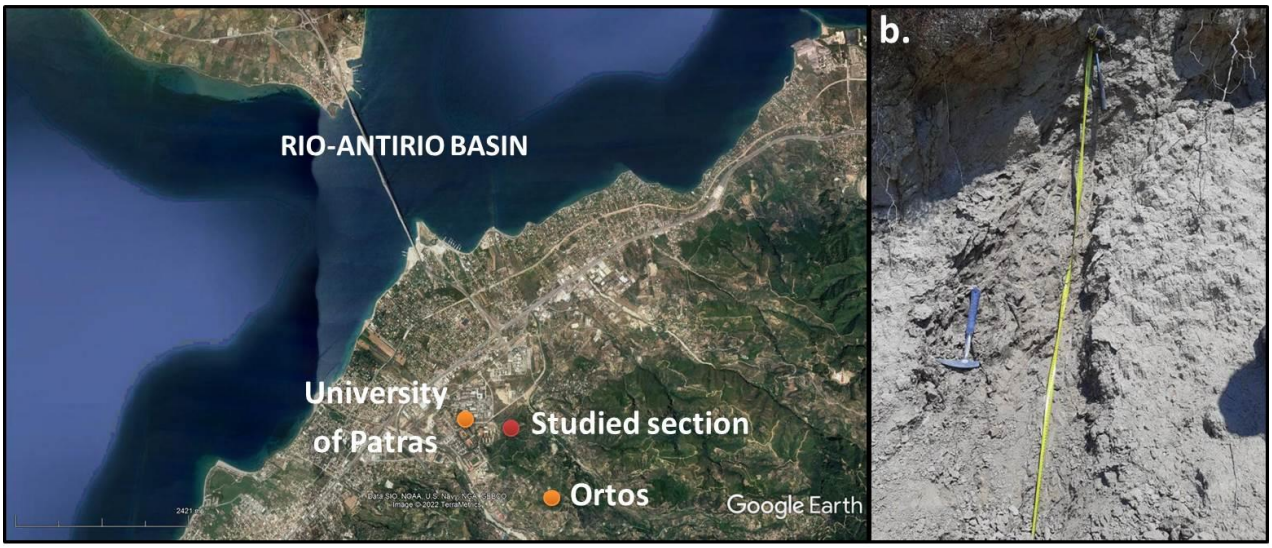

Figure 1: a. Satellite image (Google Earth) showing the study area b. Photo of the studied section

Objectives

The purpose of this work is to contribute to the study of the micropalaeontological record of the area through an educational process. In the frame of the undergraduate module "Micropalaeontology", students have used standard methods of micropalaeontology in order to familiarize with this specific scientific field and also provide new data for the study of the area. The studied section lies at the southern border of Rio-Antirio Basin, (38.28664N, 21.79624S, altitude 110m). The area is covered by early- middle Pleistocene sediments (Tsoni et al., 2021).

Methods

Stratigraphic logging and sampling of the studied section took place. The stratigraphic column was constructed using SedLog Free software. Microfaunal analysis was carried out in 8 samples collected every 20cm from a 2.90m thick natural section. 50-100 gr of sediment were washed through 500 and 63μm mesh sieves. A maximum of 300 fossil tests were collected whenever possible. Identification of the microfossils (especially foraminifera and ostracods) followed using standard bibliography (e.g. Cimerman & Langer 1991, Relative volumes of the Stereo-atlas of ostracod shells). Also, the ecological characteristics of the determined species were examined.

Results and Conclusions

The studied section consists of gray silty clay, rich in organic material. In the studied samples a total of 37 taxa (28 foraminifera and 9 ostracod taxa) were identified, either to the genus or species level. The species number varies between 10 and 20. A uniform assemblage has been revealed throughout the section. *Elphidium crispum* and

Quinqueloculina seminula dominate in all samples. They are accompanied by typical shallow marine foraminifera taxa (*Ammonia becarii, Bulimina, Hyanesina, Valvulineria*, several Miliolidae taxa and other less common foraminifera). As far as ostracods are concerned *Aurilla* spp and *Bosquetina* are found quite often, while other shallow marine ostracods also exist (*Cytherella, Costa edwardsii, Cimbaurila cimbaeformis, Pterygocythereis, Acanthocythereis* etc). Small sized Globigirinidae exist in some samples. Typical brackish species have been noticed in small numbers (*Ammonia tepida, Cyprideis torosa*). Mollusk shells were found especially between 20-80cm and 120-140cm.

The taphocoenosis revealed the prevalence of an overall uniform marine inner circalittoral environment with elevated nutrient content throughout the studied section. The presence of *Aurila* spp. may imply a vegetated bottom. The small numbers of brackish species are considered transported from a nearby lagoonal area. Moreover, the presence of the ostracod species *C. cimbaeformis* sets the age of the studied section at the early Pleistocene. The studied assemblage is in good agreement with the data retrieved at the Ortos section by Tsoni (2021). More detailed stratigraphic and micropalaeontological studies are needed in order to provide a more complete picture for the Lower Pleistocene record of the Rio-Antirio Basin.

References

Cimerman, F. & Langer, M.R., 1991. Mediterranean Foraminifera: Slovenska Akademija Znanosti, Ljubljana, 118

Koukouvelas, I., Stamatopoulos, L., Katsonopoulou, D., Pavlides, S. 2001. A paleoseismological and geoarchaeological investigation of Eliki fault, Gulf of Corinth, Greece. Journal of Structural Geology, 23: 531 – 543.

Rohais, S., Moretti, I. 2016. Structural and Stratigraphic Architecture of the Corinth Rift (Greece): An Integrated Onshore to Offshore Basin-Scale Synthesis. Lithosphere Dynamics and Sedimentary Basins of the Arabian Plate and Surrounding Areas. Frontiers in Earth Sciences, Springer, Cham.

Tsoni, M., Iliopoulos, G., Valavani, D., Liapi, E., Papadopoulou, P., Stamoulis, K., Koukouvelas, I. , Kontopoulos, N. 2021. Palaeoenvionmental inferences on the Pleistocene deposits of the Charadros River (Rio graben, Western Corinth Gulf, Greece). Quaternary International 589: 39-54

Tsoni, M, 2021. Stratigraphic, palaeontological and palaeoecological study of Quaternary deposits in Rio- Antirio basin (Unpublished doctoral dissertation). University of Patras

16th International Congress of the Geological Society of Greece
17-19 October, 2022 - Patras, Greece
Bulletin of the Geological Society of Greece, Sp. Publ. 10
Ext. Abs. GSG2022-395

New floristic data of the Early Miocene Lesvos Petrified Forest − Part A: Non-vascular plants, ferns and monocots from the West Akrocheiras outcrop

E. Liapi[1], G. Zidianakis[2,3], E. Tsitsou[1], G. Iliopoulos[3], N. Zouros[1,4]

(1) Natural History Museum of the Lesvos Petrified Forest, Sigri 81103, Lesvos, Greece, geo11066@upnet.gr (2) Department of Agriculture, Hellenic Mediterranean University, 71410 Heraklion, Crete, Greece (3) Department of Geology, University of Patras, 26504 Rio, Patras, Greece (4) Department of Geography, University of the Aegean, 81100 Mytilene, Lesvos, Greece.

Research Highlights

Documentation, description and taxonomic identification of newly reported plant taxa (Cryptogams and monocots) from West Akrocheiras outcrop: enriching the flora list of Lesvos Petrified Forest.

Background

Lesvos UNESCO Global Geopark (NE Aegean Sea, Greece) is widely known for its unique and extensive Petrified Forest at the western part of Lesvos Island. The early Miocene Petrified Forest represents an important source of taxonomic data, as it includes a great variety of plant macro-remains (mostly tree trunks, roots, branches and leaf imprints). Previous palaeobotanical studies have focused on both fossilized wood (e.g., Süss and Velitzelos, 1994, 2010; Velitzelos *et al*., 2019, Iamandei *et al*., 2022) and leaf material (e.g., Velitzelos *et al*., 1981; Velitzelos and Zouros, 1998; Zouros *et al*., 2007; Velitzelos *et al*., 2014; Kafetzidou *et al*., 2022) of the broader area of the Petrified Forest. In the last few years, during the reconstruction of the Sigri–Antissa road that crosses the protected area of the Petrified Forest, systematic and rescue excavations have revealed impressive fossilized tree trunks and mass-occurrences of leaf remains in several outcrops along the Akrocheiras hill range.

Objectives and Methods

In this study, new floristic data are documented, described and identified from the West Akrocheiras outcrop of the Lesvos Petrified Forest. The plant macro-assemblage comprises 4,700 fossiliferous blocks containing more than 40,000 plant remains, collected by the Natural History Museum of the Lesvos Petrified Forest. The fossil material occurs within the volcanic tuff beds of the well-exposed 'Sigri Pyroclastic deposits' (Pe-Piper and Piper, 1993). At least five different fossiliferous horizons of fine to coarse tuffs intercalated with paleosols have been recognized. The taxonomic identification is based on macro-morphological features of the leaf architecture. Comparative bibliographic data from other Neogene palaeofloras are included for the ecological interpretation of the identified fossils.

Results

Based on leaf and thalloid material, this ongoing systematic research reveals the occurrence of several Cryptogamae (bryophytes and ferns) and Monocotyledons (excluding palms) in the West Akrocheiras assemblage. Some of them are reported for the first time in the Lesvos Petrified Forest, including two non-vascular plants (Bryophyta) with insufficient diagnostic details for an accurate classification, two new ferns presenting affinities with the families of Dryopteridaceae and Polypodiaceae as well as two monocots *Smilax weberi* P. WESSEL (Kafetzidou *et al*., 2022) and Zingiberales fam. et gen. indet. (Fig. 1). Bryophytes are scarce in the assemblage, while ferns and herbaceous monocots are common.

Conclusions

Our results provide additional facts regarding the palaeoenvironmental conditions of the study area back to the early Miocene. The ecological preferences of the identified morphotaxa come to enhance the vegetation analysis of West Akrocheiras outcrop, described by Kafetzidou *et al*. (2022). During the early Miocene, West Akrocheiras area comprised a rich flora with several dicots, monocots and ferns dominating on the fertile volcanogenic soils of a lowland/riparian forest and the well-drained mesophytic forests. Each of the herein reported taxa could belong to one or more different vegetation units of West Akrocheiras area. In shady places under the forest canopy of riparian or well-drained lowland plant associations, stands of ferns and herbaceous monocots probably thrived. The bryophytes might have lived in humid environments of the area, while the lianas of *Smilax* could have been an accessory element. Further research is needed for the conclusive assignment of the fossil material and vegetation reconstruction, as well as the establishment of the palaeoclimatic and palaeobiogeographic patterns.

Figure 1. Monocots and Cryptogams from the West Akrocheiras outcrop of the Lesvos Petrified Forest: 1. Zingiberales fam. et gen. indet., leaf, Nr. AKY3252A, scale bar 2 cm; 2. *Smilax weberi* P. WESSEL, leaf, Nr. AKY3203, scale bar 1 cm; 3–4. Bryophyta, thalli, scale bar 1 cm, 3. Nr. AKY453, 4. Nr. AKY2445; 5–6. aff. Dryopteridaceae, frond, 5. Nr. AKY2249, scale bar 1 cm, 6. Close-up of AKY2249, fertile pinnule with dentate margin, scale bar 2 mm; 7–8. aff. Polypodiaceae, frond, 7. Nr. AKY2071, scale bar 1 cm, 8. Close-up of AKY2071, capitate endings of the veinlets (hydathodes), scale bar 1 mm.

References

Iamandei, S., Iamandei, E., Velitzelos, D., Velitzelos, E., 2022. Palaeoxylotomical studies in the Cenozoic petrified forests of Greece. Part two – conifers. Acta Palaeontologica Romaniae 18 (1), 65–111.

Kafetzidou, A., Kouli, K., Zidianakis, G., Kostopoulos, D., Zouros, N., 2022. The early Miocene angiosperm flora of Akrocheiras in Lesvos Petrified Forest (North Aegean, Greece) – Preliminary results. Review of Palaeobotany and Palynology 296, 104559, doi.org/10.1016/j.revpalbo.2021.104559.

Pe-Piper, G., Piper, D.J.W., 1993. Revised stratigraphy of the Miocene volcanic rocks of Lesvos, Greece. Neues Jahrbuch für Geologie und Paläontologie 2, 97–110.

Süss, H., Velitzelos, E., 1994. Zwei neue tertiäre Hölzer der Gattung *Pinoxylon* Knowlton emend. Read aus dem Versteinerten Wald von Lesvos, Griechenland. Feddes Repertorium 105, 403–423.

Süss, H., Velitzelos, E., 2010. *Lesboxylon* gen. nov., eine neue Morphogattung mit dem Typus *Lesvosoxylon ventricosuradiatum* sp. nova aus dem Tertiar der Insel Lesvos, Griechenland. Feddes Repertorium 121, 18–26.

Velitzelos, E., Petrescu, I., Symeonidis, N., 1981. Tertiäre Pflanzenreste aus der Ägäis. Die Makroflora der Insel Lesvos (Griechenland). Annales Géologiques des Pays Helléniques 30, 500–514.

Velitzelos, E., Zouros, N., 1998. New results on the petrified forest of Lesvos. Bulletin of the Geological Society of Greece 32, 133–142.

Velitzelos, D., Bouchal, J.M., Denk, T., 2014. Review of the Cenozoic floras and vegetation of Greece. Review of Palaeobotany and Palynology 204, 56–117.

Velitzelos, D., Iamandei, S., Iamandei, E., Velitzelos, E., 2019. Palaeoxylotomical studies in the Cenozoic petrified forests of Greece. Part one – palms. Acta Palaeobotanica 59 (2), 289–350.

Zouros, N., Velitzelos, E., Valiakos, I., Labaki, O., 2007. The Plaka Petrified Forest Park in Western Lesvos – Greece. Bulletin of the Geological Society of Greece 40, 1880–1891.

16th International Congress of the Geological Society of Greece
17-19 October, 2022 - Patras, Greece
Bulletin of the Geological Society of Greece, Sp. Publ. 10
Ext. Abs. GSG2022-398

New floristic data of the Early Miocene Lesvos Petrified Forest − Part B: Dicotyledon taxa from the West Akrocheiras outcrop

E. Tsitsou[1], G. Zidianakis[2,3], E. Liapi[1], G. Iliopoulos[3], N. Zouros[1,4]

(1) Natural History Museum of the Lesvos Petrified Forest, Sigri, 81103 Lesvos, Greece, ef.tsits@gmail.com (2) Agriculture Department, Hellenic Mediterranean University, Estauromenos Heraklion, Crete, Greece (3) Department of Geology, University of Patras, University Camp, 26504 Rio, Greece (4) Geography Department, University of the Aegean, 81100 Mytilene, Greece.

Documentation, description and taxonomic identification of newly reported plant taxa (dicots) from West Akrocheiras outcrop: enriching the flora list of Lesvos Petrified Forest.

The Lesvos Petrified Forest, located in western Lesvos at the NE Aegean Sea, is a unique natural monument representing a rare, fossilized forest ecosystem with several assemblages of tree trunks and foliage imprints. Most fossils are embedded in volcanic rocks, belonging to the Sigri Pyroclastic Formation. These rocks consist of pyroclastic flow tuffs, interbedded with fluvial conglomerate, volcaniclastic sandstone, mudstone and paleosol, dated in Early Miocene, at approximately 22–18 Ma (Pe-Piper *et al.*, 2019).

During the last decades, researchers investigating the palaeoflora of the Petrified Forest, have focused on the study of both wood and leaf remains (e.g. Velitzelos *et. al*, 1981; Zouros *et al*., 2007; Süss & Velitzelos, 2010; Iamandei *et al*., 2022; Kafetzidou *et al.*, 2022). Since 2014, a large number of fossiliferous sites have been discovered due to the reconstruction of the Kalloni–Sigri road, which intersects the protected area of the Lesvos Petrified Forest. Hence, the road cuts in the Akrocheiras site exposed part of the Sigri pyroclastic formation (Pe-Piper *et al.*, 2019). This provided the opportunity to the Natural History Museum of the Lesvos Petrified Forest to conduct targeted excavations, revealing numerous fossilized tree trunks and abundant leaf imprints.

Herein, we deal with a new collection of leaf and fruit imprints found recently in the West Akrocheiras outcrop. Our study focuses on the recording, identification and description of some newly reported taxa, in order to enrich our knowledge about the palaeoflora of Lesvos Island. The unearthed material from West Akrocheiras consists of 4,700 blocks with around 40,000 plant remains, curated in the Natural History Museum of the Lesvos Petrified Forest. It was collected from a 10-meter-long sequence comprising lapilli and fine tuff beds from at least five different fossiliferous horizons, either as thin layers of paleosol, where the leaf litter is usually found, or as leaf imprints scattered in the matrix of fine or lapilli tuffs representing leaf lamellae transported by mud flows. The study of the leaf imprints was mainly done during the period 2020-2022. The observation and the descriptions of the leaf architecture were accomplished using standard macromorphological methods based mainly on Ellis *et al.* (2009). The specimens were examined under an Optika SLX-5 stereomicroscope and were photographed with a Nikon Coolpix B500 compact digital camera. The images were edited with Adobe Photoshop Software 2020 version 21.0.

Five newly reported dicot taxa from the West Akrocheiras outcrop are determined and descripted herein. The dicotyledon morphotypes, belonging to Lauraceae (*Laurophyllum* sp.), Rosaceae (*Rosa* sp.), Juglandaceae (*Carya* cf. *serrifolia*), Sapindaceae (cf. *Acer* sp.) and incertae sedis (*Myrtophyllum* sp.), have been identified and were added in the Early Miocene Lesvos palaeoflora record list. The studied specimens have been classified based on observations of their foliage, except from cf. *Acer* sp. which is represented by fruit remains (Fig. 1). The taxa present different abundances, *Myrtophyllum* sp. is dominant, *Laurophyllum* sp. and *Rosa* sp. are common, while *Carya* cf. *serrifolia* and cf. *Acer* sp. are rare (Table 1).

Table 1. The abundance and the ecological preferences of the reported dicot taxa.

Taxon	Family	Plant Part/Organ	Abundance	Ecology − Vegetation units (sensu Denk, 2016; Denk *et al.*, 2017; 2022)
Laurophyllum sp.	Lauraceae	Leaves	Common	Riparian, well-drained lowland and upland forests (VU4, VU5, VU6)
Rosa sp.	Rosaceae	Leaflets	Common	Riparian, well-drained lowland and upland forest, including hummocks (VU4, VU5, VU6, VU7)
Carya cf. *serrifolia*	Juglandaceae	Leaflets	Rare	Riparian, well-drained lowland forest (VU4, VU5)
Myrtophyllum sp.	Indet.	Leaves/leaflets	Dominant	Indifferent
cf. *Acer* sp.	Sapindaceae	Fruits	Rare	Indifferent

These preliminary results provide new floristic data on the Lesvos Petrified Forest, since *Laurophyllum* sp., *Rosa* sp., *Carya* cf. *serrifolia*, *Myrtophyllum* sp. and cf. *Acer* sp. are recorded for the first time in Lesvos Early Miocene. Remarkably, within the rich studied material, no conifer remains have been detected. The above-mentioned dicots represent mainly the riparian and well drained zone of the existed forests (Table 1). In West Akrocheiras, *Laurophyllum* sp. frequently coexists and is probably associated with *Myrtophyllum* sp., and *Rosa* sp. is accompanied by *Daphnogene polymorpha*, one of the most dominant taxa.

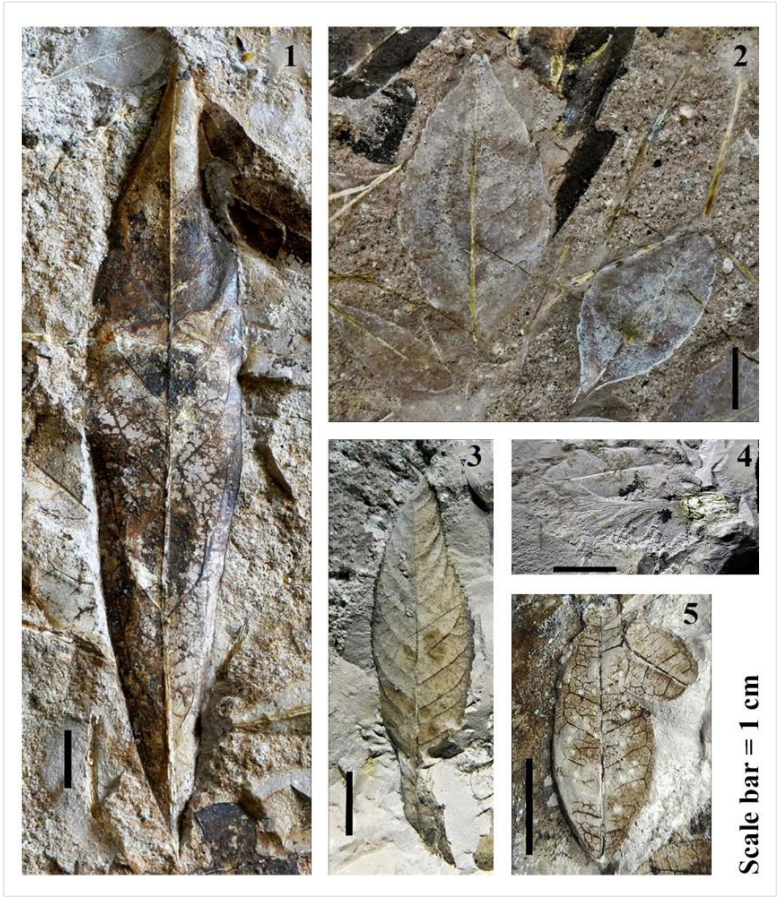

Figure 1. New dicotyledon taxa from West Akrocheiras: 1. Laurophyllum sp. 1, leaf, Nr. AKY2775; 2. Rosa sp., leaflets, Nr. AKY812; 3. Carya cf. serrifolia, leaflet, Nr. AKY3711A; 4. cf. Acer sp., winged fruit, Nr. AKY2504; 5. Myrtophyllum sp., leaves/leaflets, Nr. AKY2559A.

References

Denk, T., 2016. Palaeoecological interpretation of the late Miocene landscapes and vegetation of northern Greece: a comment to Merceron et al., 2016 (Geobios 49, 135–146). Geobios 49, 423–431.

Denk, T., Güner, H.T., Bouchal, J.M., 2022. Catalogue of revised and new plant macrofossils from the Aquitanian-Burdigalian of Soma (W Turkey) – Biogeographic and palaeoclimatic implications. Rev. Palaeobot. Palynol. 296, 104550, doi.org/10.1016/j.revpalbo.2021.104550.

Denk, T., Güner, H.T., Kvaček, Z., Bouchal, J.M., 2017. The early Miocene flora of Güvem (Central Anatolia, Turkey): a window into early Neogene vegetation and environments in the Eastern Mediterranean. Acta Palaeobot. 57, 237–338.

Ellis, B., Daly, D., Hickey, L., Johnson, K., Mitchell, J., Wilf, P., Wing, S., 2009. Manual of Leaf Architecture, The New York Botanical Garden Press.

Iamandei, S., Iamandei, E., Velitzelos, D., Velitzelos, E., 2022. Palaeoxylotomical studies in the Cenozoic petrified forests of Greece. Part two – Conifers. Acta Palaeontologica Romaniae 18 (1), 65–111.

Kafetzidou, A., Kouli, K., Zidianakis, G., Kostopoulos, D., Zouros, N., 2022. The early Miocene angiosperm flora of Akrocheiras in Lesvos Petrified Forest (North Aegean, Greece) – Preliminary results. Rev. Palaeobot. Palynol. 296, 104559, doi.org/10.1016/j.revpalbo.2021.104559.

Pe-Piper, G., Piper, D.W.J., Zouros, N., Anastasakis, G., 2019. Age, stratigraphy, sedimentology and tectonic setting of the Sigri Pyroclastic Formation and its fossil forests, Early Miocene, Lesbos, Greece. Basin Research 31, 1178–1197.

Süss, H., Velitzelos, E., 2010. Lesboxylon gen. nov., eine neue Morphogattung mit dem Typus Lesvosoxylon ventricosuradiatum sp. nova aus dem Tertiar der Insel Lesvos, Griechenland. Fed. Repert. 121, 18–26.

Velitzelos, E., Petrescu, I., Symeonidis, N., 1981. Tertiäre Pflanzenreste aus der Ägäis. Die Makroflora der Insel Lesvos (Griechenland). Ann. Géol. Pays Hellén. 30, 500–514.

Zouros, N., Velitzelos, E., Valiakos, I., Labaki, O., 2007. The Plaka Petrified Forest Park in Western Lesvos – Greece. Bull. Geol. Soc. Greece 40, 1880–1891.

16th INTERNATIONAL CONGRESS of the
GEOLOGICAL SOCIETY OF GREECE

T2. Structural Geology and Tectonics

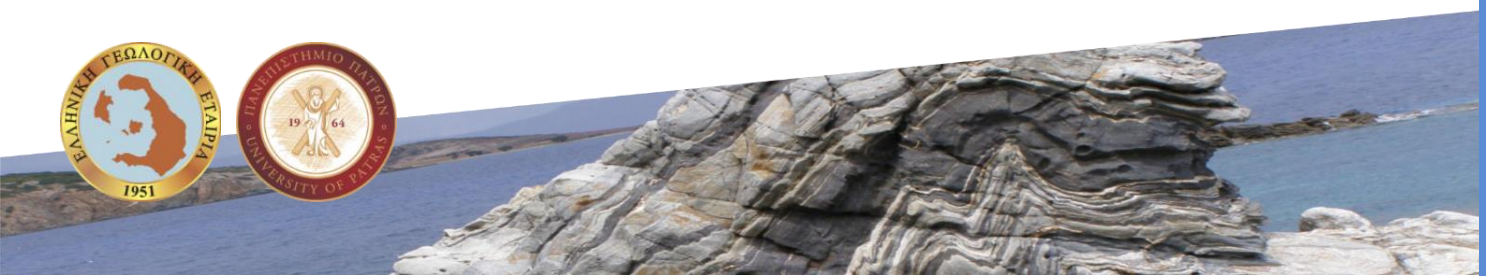

OUR EARTH, OUR HOME

16th International Congress of the Geological Society of Greece
17-19 October, 2022 - Patras, Greece
Bulletin of the Geological Society of Greece, Sp. Publ. 10
Ext. Abs. GSG2022-024

Kinematic Analysis and Structural Restoration of Dunga Gali-Kuza Gali Area, Southern Hazara Basin, Lesser Himalayas, Pakistan

M. A. F. Miraj[1], M. Ishfaq[1], N. Ahsan[1]
(1) Institute of Geology, University of the Punjab, Lahore-54590, Pakistan, armghan.geo@pu.edu.pk

The study area is located near the western limb of Hazara-Kashmir Syntaxis, northwest Himalayas, Pakistan. It is comprised of NE-SW trending fold and thrust belt bearing Jurassic to Eocene sediments partially overlying low-grade metamorphosed rock unit of Pre-Cambrian age. The study area is bounded by two major faults, Nathia Gali Thrust (NGT) and Main Boundary Thrust (MBT) in the north and south, respectively (Ahsan and Chaudhary, 2008). These two major faults and their subordinating parallel to sub-parallel high angle reverse faults severely deformed the stratigraphy of the area. Intraformational folding is also present in thick sequence of Hazara Formation (Pre-Cambrian), Samana Suk Formation (Jurassic) and Kawagarh Formation (Cretaceous). The prime objectives of the research are (1) modification of structural and stratigraphic cross-section of Dunga Gali-Kuza Gali area, (2) restoration of the cross-section and (3) calculation of the total crustal shortening in this area. A very complicated structure is restored using MOVE™ and rock units are aligned to its pre-deformed state, which shows the shortening. It is interpreted from the results that overall area lies in purely compressive tectonic regime along with some of the segments related to strike-slip (transpression).

To understand and interpret the structural geology and stratigraphy of the area, a traverse from SE Dunga Gali to NW Kuza Gali is drawn, along which a balanced cross-section A-A' (Figure 1 and 2) is constructed for the mapped area. It covers the central to southern part of the mapped area. The thicknesses of the formations in the cross-section are acquired from literature (Shah, 1977). The northeast trending Nathia Gali Thrust (NGT) passes about 2km north of the cross-section and in the south of the cross-section a regional fault, Main Boundary Thrust (MBT) passes. These two major faults play an important role in deformation of the structure and geometry of the area. The rotation of faults and intense folding in the area was also addressed by Chaudhry and Ghazanfar (1990).

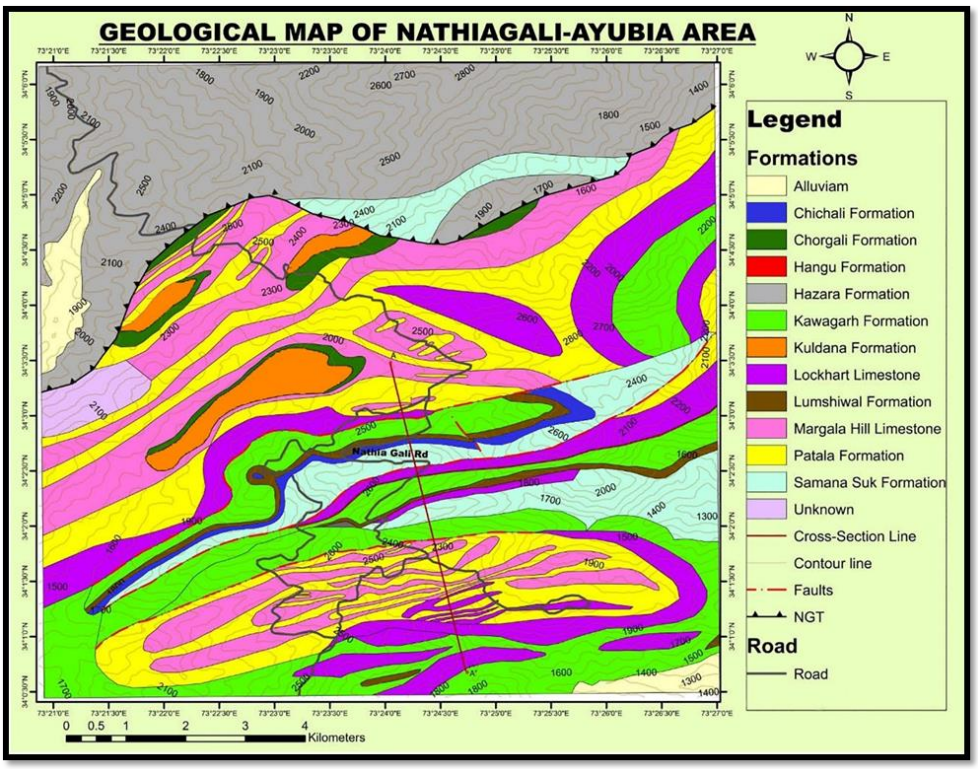

Figure 1. Geological map of a part of southern Hazara Basin, Pakistan. Nathia Gali Thrust (NGT) in the north and Main Boundary Thrust (MBT) in the south. The rock units present in the mapped area are the oldest Hazara Formation (Precambrian age), Samana Suk Formation (Jurassic age), Chichali, Lumshiwal and Kawagarh Formations (Cretaceous age), thin band of Hangu Formation, Lockhart Limestone and Patala Formation (Paleocene age), Margala Hill Limestone, Chorgali Formation, and the youngest Kuldana Formation (Eocene age).

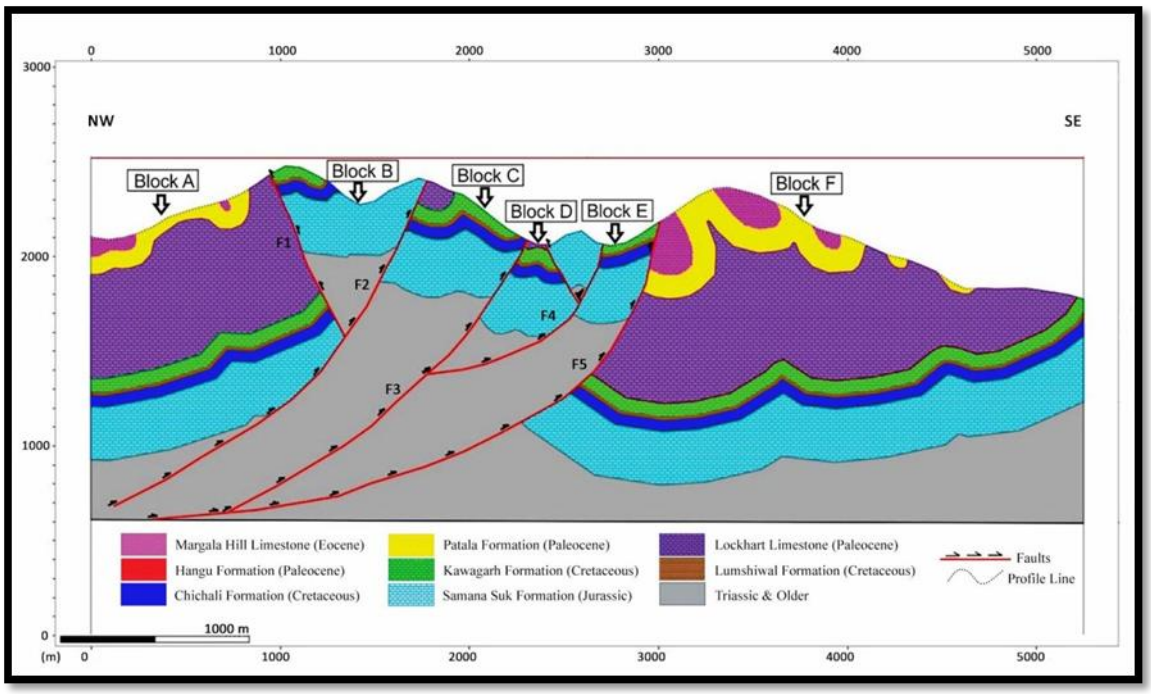

Figure 2: A geological Cross-Section A-A' from Dunga Gali to Kuza Gali area, southern Hazara Basin. Blocks from A to F and Faults are highlighted in the cross-section. As the faults in the cross-section are high angle having small heave value, so the resultant extension after performing "2D Move on Fault" Module on all blocks is less than 85m.

The average shortening in the area calculated is about 29.98% (1570 km). The main reason of deformation, complexity and shortening in this area is due to the tectonic forces, which are applied from north toward south direction.

References

Ahsan, N., & Chaudhry, M. N., 2008. Geology of Hettangian to middle Eocene rocks of Hazara and Kashmir basins, Northwest lesser Himalayas, Pakistan. Geological Bulletin of Panjab University, 43, 131-152.

Chaudhry, M.N., Ghazanfar, M., 1990. Position of the Main Central Thrust in the tectonic framework of Western Himalaya. Tectonophysics 174, 321-329.

Shah, S.M.I., 1977. "Stratigraphy of Pakistan", Geol. Surv. Pakistan. Mem., Vol. 12, 138 p.

16th International Congress of the Geological Society of Greece
17-19 October, 2022 - Patras, Greece
Bulletin of the Geological Society of Greece, Sp. Publ. 10
Ext. Abs. GSG2022-028

A tool to explore slip/separation relationships in faults that offset inclined or folded surfaces. Examples from the Asturian Basin (NW Iberian Peninsula)

M. Magán[1], M. Bulnes[1], J. Poblet[1]
(1) Departamento de Geología, Universidad de Oviedo, Oviedo, Spain, maganmarta@uniovi.es

Research highlights

Graphs to predict dip and strike separation in faults offsetting dipping beds and apparently reverse/normal segments in post-folding faults. Examples of strike-slip faults offsetting inclined and folded layers.

Introduction

The most common classification of faults (normal, reverse, left-lateral, right-lateral or oblique) is based on their kinematics; when we know how two fault blocks have moved, we can state what type of fault it is. The fault trace is an element easy to recognise as it corresponds to a discontinuity. However, the fault slip is usually more difficult to establish, as kinematics indicators are needed (e.g., fault striations, slickensides) and even more complex is to estimate the net slip as two homologous points on both fault blocks need to be identified. Even so, in the absence of clear kinematic criteria, it is relatively common to classify faults according to the observed separation of planar markers, usually bedding. These interpretations are correct when the displaced marker is a horizontal surface or its strike and that of the fault are parallel. However, when the planar marker had a previous dip and its strike is different from that of the fault, these deductions may be wrong, and thus, a classification based on separation may cause misleading structural interpretations (fig. 1). The concepts of slip and separation are well known from classical works of the past century (e.g., Reid et al., 1913; Straley III, 1934; Crowell, 1959; Billings, 1972) and they have been extensively discussed in many Structural Geology books (e.g., Ragan, 2009). In the coastal outcrops of Lower Jurassic rocks in the Asturian Basin, NW Iberian Peninsula, some faults, including kinematic criteria, cut and offset inclined layers and their separation disagrees with slip. This led us to explore this relationship further and develop a tool to facilitate the classification of faults that cut and offset previously tilted or folded surfaces. This tool consists of graphs that predict how the separation will be in cross sections and maps. The validity of the graphs is tested through its application to two Asturian Basin field examples of strike-slip faults offsetting inclined layers and a fold train.

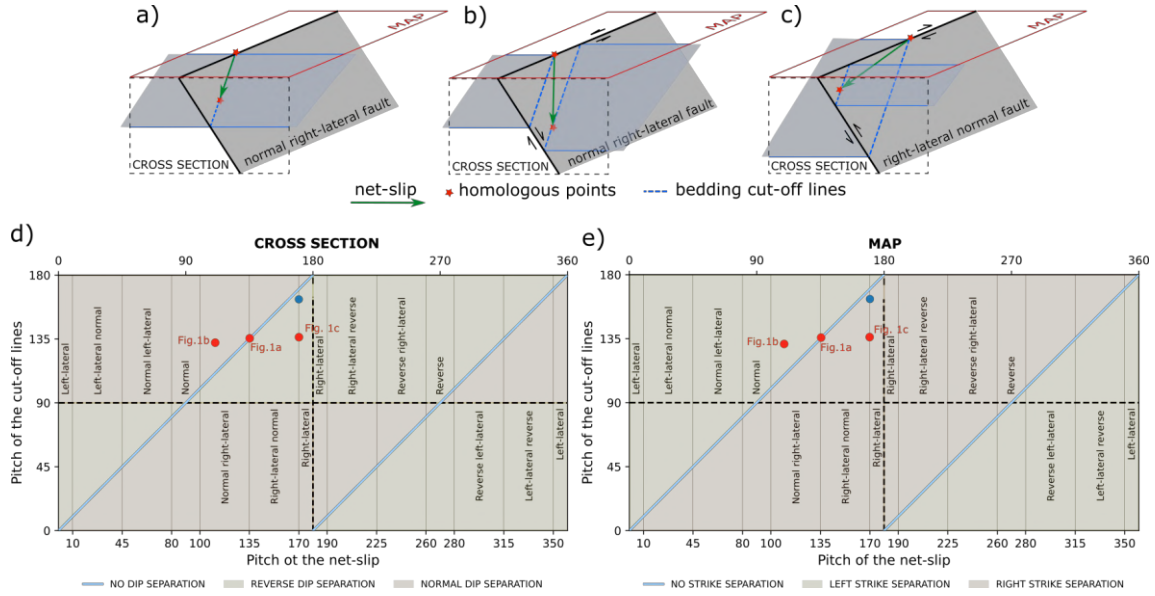

Figure 1. a-c) Block diagrams showing misleading slip / separation relationships. d-e) graphs to predict separation.

Faults displacing previously inclined layers

To show how the fault dip and strike separation would look like in cross sections and maps, we have constructed two graphs (Figs. 1 d-e) where we have represented the different types of faults according to their kinematics based on the pitch of the slip vector as a function of the pitch of the bedding cut-off lines on the fault plane. The analysis of these graphs has allowed us to draw the confusing situations set out below.

1) If the slip vector and the bedding cut-off lines are parallel, regardless of the fault type, any fault will show neither strike

nor dip separation. Figure 1a shows a normal right-lateral fault whose dip and strike separation are null because the net-slip vector and the bedding cut-off lines are parallel, and therefore, the fault causes apparently no bed offset in cross-sectional and map views.

2) When the slip vector pitches in the same direction than the bedding cut-off lines but at greater angle, then the dip separation will agree with the fault slip, whereas the strike separation will disagree with the fault slip. Figure 1b shows a normal right-lateral fault that appears as a normal fault in cross-sectional view and as a left-lateral fault in map view.

3) When the slip vector pitches in the same direction than the bedding cut-off lines but at smaller angle, then the dip separation will disagree with the fault slip, whereas the strike separation will agree with the fault slip. Figure 1c shows a right-lateral normal fault that appears as a reverse fault in cross-sectional view and as a right-lateral fault in map.

Faults displacing previously folded layers

In a region where cylindrical folds, with axes parallel to the strike of the axial planes, are cut and offset by a fault whose strike is parallel to the axial plane strike and the dip of both the axial planes and the fault are constant along strike, then the fault maintains the same character along its entire trace, i.e., the geological map shows a fault in which the oldest rocks are always in one fault block and the youngest rocks in the other. However, in other cases there may be segments of the same fault where the youngest rocks are in one fault block and segments where the youngest rocks are in the other fault block (fig. 2). To illustrate these situations in map view, we have constructed a graph where we have represented the different types of faults according to their kinematics based on the pitch of the slip vector as a function of the pitch of the axial planes cut-off lines on the fault plane. The following conclusions can be drawn from the analysis of this graph.

1) When the slip vector and the axial plane cut-off lines are parallel, the fault maintains the same character along strike on a geological map, i.e., the fault acts as an apparent normal or as an apparent reverse fault.

2) In all other cases, regardless of the fault type, the faults may have segments where the fault acts as an apparent normal fault and segments of the fault where it appears to be reverse.

The segments where the fault acts as an apparent reverse fault and those where it acts as an apparent normal fault are separated by null points (term adapted from Williams et al., 1989, originally applied to inversion tectonics) in which the outcropping layers in both fault blocks have the same age, and therefore, no strike separation occurs at these points.

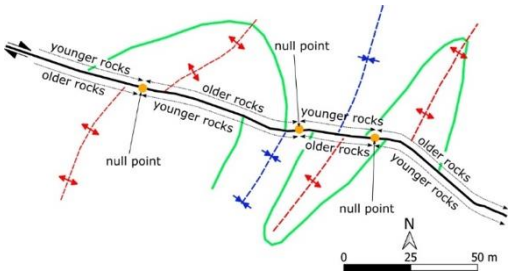

Figure 2. Structural sketch of a field example showing the apparently reverse and apparently normal segments of the fault and the null points.

Conclusions

Basing fault classification on separation may lead to incorrect structural interpretations. Amongst other parameters, the observed separation depends on the angular relationship between the cut-off line of the planar marker on the fault plane and the slip vector. The graphs presented here explore this relationship and can improve geological interpretations, irrespective whether kinematic criteria are or are not available. The graphs can be used in three different ways: 1) As a tool to improve our structural interpretations in cases where observations are apparently contradictory. 2) From the predictive point of view in regions where we know the existence of faults that cut and offset previously tilted and/or folded layers. 3) To check whether in a region the layers were tilted and/or folded before fault development.

Acknowledgements

Spanish Ministry of Economy and Competitivity and the European Fund for Regional Development (FEDER) (CGL2015-66997-R), Spanish Ministry for Science and Innovation (PID2021-126357NB-100), Asturias Government (FC-GRUPIN-IDI/2018/000216), Repsol Exploración S.A (CN-16-014, CN-16-015 and CN-16-016) and The Andrew Whitham CASP Fieldwork Award 2019. Marta Magán thanks the support by the Asturias Government via Severo Ochoa grant.

References

Billings, M. P., 1972. Structural geology. Prentice-Hall, Englewood Cliffs.

Crowell, J. C., 1959. Problems of fault nomenclature. AAPG Bulletin, 43(11), 2653-2674.

Ragan, D. M., 2009. Structural Geology: An Introduction to Geometrical Techniques. Cambridge University Press, Cambridge.

Straley III, H. W., 1934. Some notes on the nomenclature of faults. The Journal of Geology, 42(7), 756-763.

Reid, H. F., Davis, W. M., Lawson, A. C. & Ransome, F. L. 1913. Report of the committee on the nomenclature of faults. Bulletin of the Geological Society of America 24(1), 163-186.

Williams, G. D., Powell, C. M. & Cooper, M. A., 1989. Geometry and kinematics of inversion tectonics. In: Cooper, M.A. & Williams, G.D. (eds.), Inversion tectonics. Geological Society, London, Special Publications, 44: 3-15

16th International Congress of the Geological Society of Greece
17-19 October, 2022 - Patras, Greece
Bulletin of the Geological Society of Greece, Sp. Publ. 10
Ext. Abs. GSG2022-093

Is the Mesochori Fault a key structure for understanding the earthquake activity during the 2021 Damasi earthquake in the NW Thessaly, Greece?

I. Koukouvelas[1], R. Caputo[2], K. Nikolakopoulos[1], S. Verroios[1], V. Zygouri[1]

(1) Department of Geology, University of Patras, Rion, Greece, iannis@upatras.gr (2) Department of Physics and Earth Sciences, University of Ferrara, Ferrara, Italy, rcaputo@unife.it

Research Highlights

In this paper, we investigate the role of south and north dipping faults during the 2021 Damasi earthquake. In this seismotectonic framework, we provide palaeoseismological results across the Mesochori Fault that show repeated ground ruptures before the 2021 event.

Introduction

It is a common topic among geoscientists that earthquakes form two categories of geomorphic features, those directly related to tectonic structures affecting a large part of the earth's surface and seismo-gravitational landforms that are concentrated close with an active structure as its surface expression (McCalpin, 2009). Repeated morphogenic earthquakes (Caputo, 2005) on a fault especially the "linear" ones, have the potential to generate colluvial wedges that record various earthquake cycles highlighting tectonic forcing on the landscapes. Also, it is worth noting that worldwide examples of previously unknown or poorly mapped active faults were related to unexpected earthquakes. These poor exposed or unknown short faults are capable to accommodate active deformation and are widely underestimated, see the examples of the Kozani-Grevena 1995, the Athens 1999 and the Movri Mnt. 2008 earthquakes. All these earthquakes were hosted on poor expressed or unmapped active faults (see Zygouri et al. 2015). A powerful tool for recognizing active faults and their role during earthquakes is the paleoseismological trenching method. In Greece, palaeoseismological trenching is a powerful tool for recognizing strong past earthquakes (i.e. Tsodoulos et al. 2016). In this paper, we investigate the short active Mesochori Fault which, was clearly associated with the surface ruptures observed during the 2021 Damasi earthquake. It is noteworthy that the Mesochori Fault was mapped for the first time after the earthquake in an area with unknown historical seismicity.

Geological Setting

The area affected by the Damasi earthquake corresponds with a large sector of Northern Thessaly, which belongs to the Pelagonian superterrane. It consists of gneiss and schists Palaeozoic in age, Triassic recrystallized carbonates, and post-Alpine sediments. The Titarisios River valley, which dissects the epicentral area, and drains a large portion of the Antichasia Mountains and the western Olympus Mount, is a fault-controlled axial river (Koukouvelas et al. 2021). On a large scale, the present-day Thessaly geomorphology is controlled by Pliocene-Early Pleistocene NW- trending and the Middle Pleistocene E-W-to-ESE-WNW oriented normal faults (Caputo et al. 2021). These faults and their evolution control the regional drainage pattern and the fluvial geomorphology in Thessaly. In particular, these active faults appear to exert complete control on the flow of the Titarisios River in the study area. The river in the past was flowing towards Pineiada, but likely during Late Pleistocene its course was governed by the activity of some major faults, among which the Vlachogianni Fault, and since then the river was captured and diverted eastwards flowing into the northern Larissa Plain where the Tyrnavos Basin had just started forming.

Materials and Methods

The paleoseismological investigation has been conducted in the area where the Mesochori Fault shows the maximum surface displacement across its trace. In this area we excavated three trenches across the rupture. All performed trenches are single-slot "California style", following the standard trenching methods outlined by McCalpin (2009). One of them exposing the best stratigraphy is presented in this work. The trench was 15 m long and 2 m wide, while its maximum depth was almost 2.5 m. The trench walls were cleaned and mapped manually using a 1 × 1 m reference grid of non-stretch string. Photomosaic of the trench is composed using the image processing software Agisoft (Figure 1). The ages of stratigraphic units or the deposits derived after seismic events in the trench based on the collection of the available radiocarbon samples. Among these samples, we selected seven as the most promising for dating the stratigraphic horizons exposed in the trench. AMS radiometric analyses performed at the Laboratory of Ion Beam Physics, ETH Zurich, Switzerland.

Results and Conclusions

Seismological and primarily on InSAR data used for investigating the 2021 seismic sequence, indicate that the central-eastern sector of the seismogenic volume was affected by a major blind N-dipping fault, although several morphotectonic

and co-seismic field evidence suggest that the Vlachogianni Fault (Koukouvelas et al., 2021) has also acted as a high-angle splay structure, likely bearing only a small amount of displacement. In this seismotectonic framework, it would be crucial to understand the role played by the Mesochori Fault as far as our palaeoseismological results clearly show that the trench site was repeatedly affected by ground ruptures also prior the 2021 event. On the other hand, field evidence suggests cumulative displacement along the morphological scarp. It is thus clear that the Mesochori Fault is somehow directly related with seismogenic processes at depth and it possibly represents an antithetic structure of the Vlachogianni Fault accommodating some downdip geometrical irregularity. The same irregularity could have also favored a different dynamic up dip path of the slip surface along the low-angle blind segment. We do not know whether in concomitance of M>6 past earthquakes the upper portion of the rupture reactivated the same 2021 blind segment or instead the higher angle Vlachogianni Fault, there generating co-seismic surface ruptures. Notwithstanding the secondary role of the Mesochori Fault in the overall kinematics and strain release of this seismogenic crustal volume corresponding to the western sector of the Tyrnavos Graben, the investigated tectonic structure has provided crucial information on the seismotectonics of the region. Although there it is not uncommon for some faults combined with surface expression (i.e. escarpments) to remain under debate whether or not they are active, even after paleoseismological analysis, or surface ruptures during earthquakes, as is the case of the Edgecumbe Faults (New Zealand), and Jericho (Dead Sea Fault Zone) respectively, we will provide here the results for three earthquakes on the Mesochori Faults. Based on the palaeoseismological and dating results we conclude that the Mesochori Fault is directly related with three Late Quaternary earthquake events. These are recognized to juxtapose the post last glacial maximum (LGM) period i.e. 17 ka BP strata. The three events are the March 2021, the ca. 2.5 ka BP event and a ca. 5.0 ka BP event. If this interpretation is correct each event is related with an offset of 15-17 cm indicating a rather stable recurrence interval and co-seismic surface displacement.

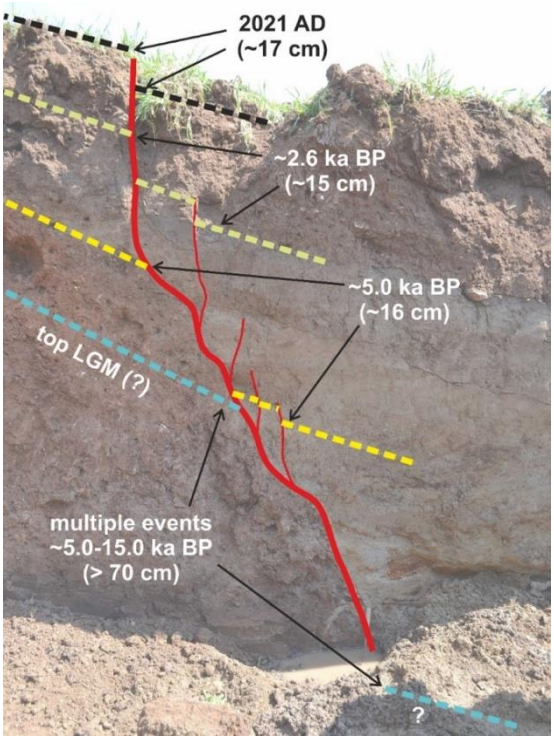

Figure 1: Eastern wall of one of the investigated trenches where are emphasized the recognized horizon events documenting showing (at least) 3 co-seismic ruptures during (late) Holocene and likely 3-5 additional ones in the time window 5-15 ka BP (post-LGM).

References

Caputo, R., 2005. Ground effects of large morphogenic earthquakesl: preface, J. Geodyn., 40(2–3), 113– 118.

Caputo, R., Helly, B., Rapti, D., Valkaniotis, S., 2021. Late Quaternary hydrographic evolution in Thessaly (Central Greece): The crucial role of the Piniada Valley. Quat. Int. 2021, in press.

Koukouvelas, I.K., Nikolakopoulos, K.G., Kyriou, A., Caputo, R., Belesis, A., Zygouri, V., Verroios, S., Apostolopoulos, D., Tsentzos, I. 2021. The March 2021 Damasi Earthquake Sequence, Central Greece: Reactivation Evidence across the Westward Propagating Tyrnavos Graben. Geosciences, 11, 328. https://doi.org/10.3390/ geosciences11080328

McCalpin, J.P., 2009. Paleoseismology. Academic Press, San Diego, CA 613.

Tsodoulos, I.M., Stamoulis, K., Caputo, R., Koukouvelas, I., Chatzipetros, A., Pavlides, S., Gallousi, C., Papachristodoulou, C., Ioannides, K., 2016. Middle-Late Holocene earthquake history of the Gyrtoni Fault, Central Greece: Insight from optically stimulated luminescence (OSL) dating and paleoseismology. Tectonophysics 687, 14–27

Zygouri, V., Koukouvelas, I.K., Kokkalas, S., Xypolias, P., Papadopoulos, G.A., 2015. The Nisi Fault as a Key structure for understanding the active deformation of the NW Peloponnese, Greece. Geomorphology 237, 142-156

16th International Congress of the Geological Society of Greece
17-19 October, 2022 - Patras, Greece
Bulletin of the Geological Society of Greece, Sp. Publ. 10
Ext. Abs. GSG2022-105

Quantitative Seismic Interpretation of Lower Goru Formation in Kadanwari-Latif Area, Central Indus Basin, Pakistan

A. Ali[1], K. B. Zafar[2], M. Ehsan[2]

(1) Institute of Geology, University of the Punjab, Lahore, 54590 Pakistan, abidali306@gmail.com (2) Department of Earth and Environmental Sciences, Bahria University, Islamabad, Pakistan

Central Indus Basin (CIB) in Pakistan is a hydrocarbon bearing area comprises of many producing fields. Kadanwari field in Kadanwari-Latif area is in the CIB mainly consists of combination traps. Faults present in the study area are providing seal at the level of Lower Goru Formation (LGF). On the western portions of the area, Lower Goru 'G' sand (member of LGF) has been producing while 'E' and 'D' members of the formation are contributing in the eastern part. The primary aim of this study was to analyze the architecture and hydrocarbon potential of LGF in north-eastern part of Kadanwari area (Figure 1). The quantitative seismic interpretation using 3D seismic volume of 12 km² and two wells Kadanwari-10 and Kadanwari-11 were conducted. Structural seismic interpretations were made, and depth maps were generated. Multi-attribute analysis was performed in which structures at the reservoir level are further confirmed by utilizing variance, chaos, curvature, instantaneous and cosine of phase attributes whereas the reservoir quality was estimated using other attributes such as relative acoustic impedance and Root Mean Square. Petrophysical analysis was carried out on the wells for the estimation of reservoir properties including effective porosity, volume of shale and water saturation etc. Model based seismic inversion technique had been applied for the reservoir characterization. Structural interpretation revealed the presence of two steep to high-angle normal faults which provided the lateral seal to the formation prospective zones. Seismic structural attributes did not provide much in the demarcation of small fractures and discontinuities while relative acoustic impedance and RMS attributes provided the reservoir quality throughout the volume. Petrophysical studies marked the prospective zones in Lower Goru probable E Sand member in both of the wells where the porosities are ranging from 12% to 22 %, low to moderate volume of shale about 5%-26% and water saturation is in range of 12% to 38%. Model-based seismic inversion applied on 3D seismic cube and wireline log data was quite helpful in predicting reservoir properties in the Lower Goru probable E Sand member. The integrated approach applied in this has provided great deal of information to determine the reservoir properties spatially and between the interfaces.

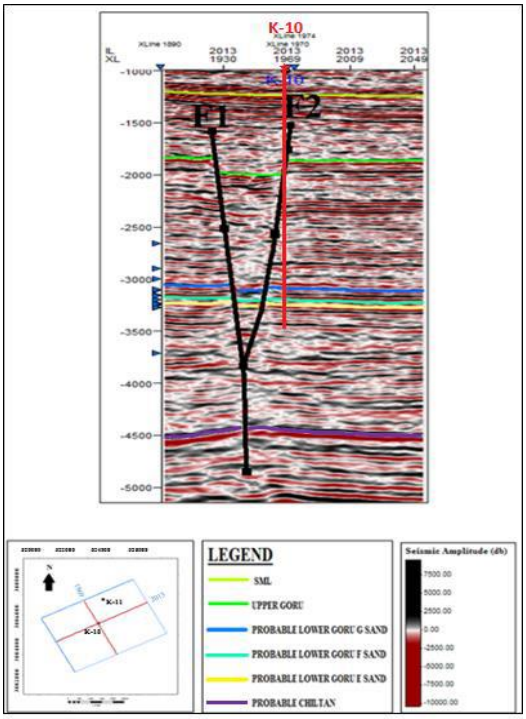

Figure 1. An interpreted seismic section and well data (K-10) used to get a control on the seismic interpretation.

Acknowledgements

The authors would like to acknowledge the Director General of Petroleum Concessions (DGPC), Pakistan and Landmark Resources for providing the seismic and well data to conduct the present study.

16th International Congress of the Geological Society of Greece
17-19 October, 2022 - Patras, Greece
Bulletin of the Geological Society of Greece, Sp. Publ. 10
Ext. Abs. GSG2022-144

Fracture attributes variability and distribution of fracture network from digital outcrops in the Upper Cretaceous Kruja carbonate platform (Dinarides, Montenegro).

S. Kokkalas[1], R.R., Jones[2], S. Gilment[2], G. Panagopoulos[3], T. Konstantopoulos[3], L. Gouliotis[3], D. Anestoudis[3]

(1) Department of Geology, University of Patras, Patras, Greece, skokalas@upatras.gr (2) Geospatial Research Ltd., Durham, UK (3) Energean Oil & Gas, Athens, Greece.

Background-Objectives

Targeting of permeable fracture horizons in hydrocarbon or geothermal fields can be aided significantly by outcrop analogue studies, which can improve the understanding of fracture characteristics and their impact on fluid flow. Most carbonate platforms show high variation in lithology, diagenetic evolution and fracture abundance, both laterally and vertically, and this can have a great impact in reservoir quality. For this reason, examining the variability and distribution of fracture populations in a carbonate sequence can provide good feedback for predictive fracture models in the subsurface.

The study area belongs to Kruja Unit, which forms part of the fold-and-thrust belt of western Dinarides and includes a Mesozoic thrust-imbricate carbonate sequence overlain by Oligocene synorogenic turbiditic siliciclastics. The stratigraphic succession commences with evaporites and limestone breccias of late Early Cretaceous, followed by Late Cretaceous neritic carbonates and Eocene nummulitic limestones. The laser-scanned outcrop analogues are stratigraphically located in the Upper Cretaceous to Paleocene-Eocene shallow water carbonate sequence exposed along the coastal area of Montenegro (Fig.1; Radovici, Bar and Kruce).

Methods

Following data acquisition conducted by field work and lidar, the virtual outcrops were further processed to derive fracture geometries. Once the fracture network is picked, further processing is carried out to define dominant fracture sets and then to derive spatial parameters that characterize the fracture system for that outcrop (Fig. 1). Fracture orientation data from each studied location are sub-divided into color-coded sets (i.e., G: green, R: red, T: turquoise) based upon their orientation and abundance, together with other key manual field observations. Prior to this sub-division, each dataset is bedding-restored in a pre-tilted horizontal reference plane allowing comparisons of fracture sets in all studied locations. Additionally, fracture intensities and spacings of fractures per set were estimated from each outcrop, taking into account the sampling problems and uncertainties that encounter with such estimations in the subsurface (Ortega et al., 2006).

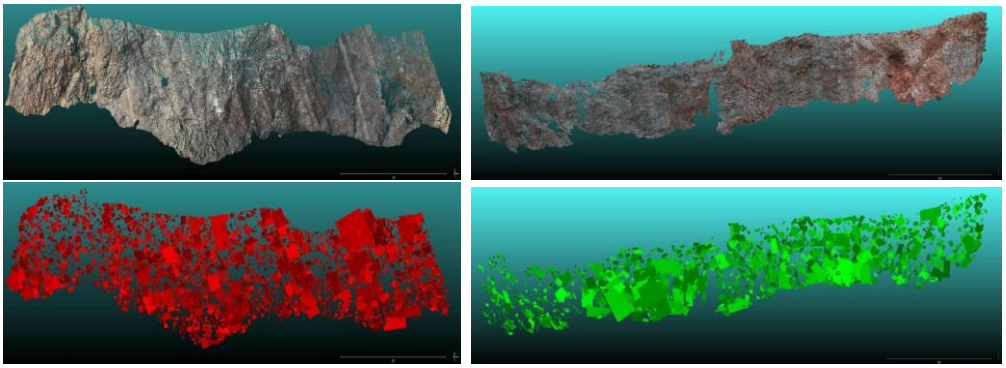

Figure 1. Left column: Screenshots of lidar outcrop data from Radovići Quarry (NW Montenegro), looking horizontally towards WNW. Length of section is 63m. (top): point cloud data; (bottom): best-fit fracture planes derived from the picked patches. N=4,367 fracture planes. Right column: Screenshots of lidar outcrop data from Bar Quarry (SE Montenegro), looking horizontally towards NW. Length of section is 53m. (Top): laser point cloud data; (Bottom): best-fit fracture planes derived from the picked patches. N=1654 fracture planes.

Results

Most of the studied outcrops in the region are cut by a pervasive network of natural fractures. P_{10} fracture intensities recorded from outcrop TLS data are generally high to extremely high. Upscaled estimates of P_{32} fracture intensity (m^2 of fracture per m^3 of rock) are between $12m^{-1}$ for the low case example of fracture network development (i.e., Kruce which is considered as background values) and reach 50-60 m^{-1} in the high case examples of Bar-Radovici sites, possibly representing the fracture development in locally faulted anticline structures.

The spatial arrangement of fracture systems can be quantified using statistical laws (e.g., power law, log normal, and exponential law; Marrett et al., 2018) or other statistical parameters, such as the coefficient of variability (C_v) along 1D

sections, with main goal to enhance the fracture distribution understanding (clustered, random, or uniform distribution) and its effects on connectivity. Broad interpretations on the fracture size-intensity in Radovici outcrop suggest that on the outcrop scale exponential and log-normal distributions appear to be the most appropriate for sets R and T, respectively (Fig. 2). However, the data span less than two orders of magnitude of fracture sizes, and further analysis is needed over a wider scale range to better understand scaling of fracture sizes. Fracture spacing is best modeled by a log-normal distribution at this locality (Fig. 2). Size- dependent coefficient of variation (C_v) data shows that the spatial distribution of Set R fractures is strongly clustered across the measured scale range, while Set T fractures lie on the upper threshold and there is not sufficient evidence to conclude that are strongly clustered.

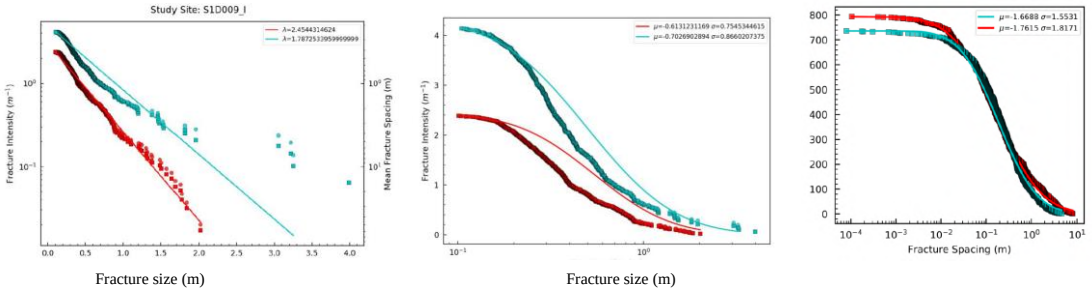

Figure 2. Cumulative linked size-intensity plots from fracture transects from Radovići SW Quarry. Fractures are plotted according to set (Sets R and T). The same data are plotted in each graph: note the different linear vs. log axes. (left): exponential, (center): log-normal, (right): cumulative number plots for fracture spacing in same outcrop.

In comparison, the linked fracture size-intensity data for the Bar area towards the SE Montenegro suggest that on the outcrop scale a log-normal distribution is more appropriate than a typical power-law model for Sets T and R (Fig. 3). Additionally, interpretation of fracture spacing suggests that either exponential or log-normal distributions are the most appropriate distribution to model fracture spacing for Set R, while log-normal is best for Set T at this locality. Set G is considered over-sampled and not reliable for more interpretations. Regarding the fracture distribution, coefficient of variation (C_v) suggests that at this outcrop the spatial distribution of fractures in Set G, as well as in Set R over the limited size range available, cannot be statistically distinguished from random; i.e., there is no evidence that fractures are clustered (into fracture zones or corridors) or are very regular spaced (anticlustered).

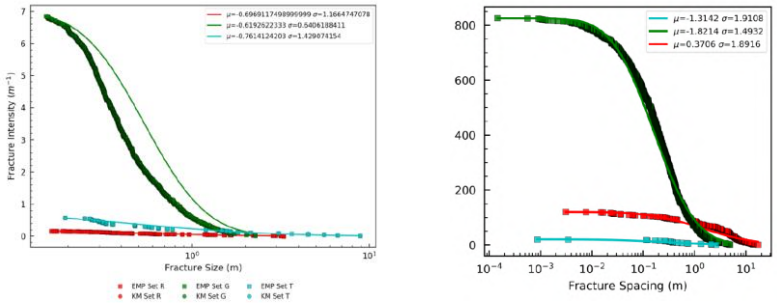

Figure 3. Cumulative linked size-intensity plot (left) and fracture spacing plot (right) from fracture transects at Bar area. Fractures are plotted according to set (Sets R, G, and T) and best fit a log-normal distribution. In each case the best-fit curve is shown for comparison alongside the data (with curve parameters stated in the inset box).

Conclusions

Fracture models are mostly based on the knowledge of the statistical distribution of fracture geometric properties across a range of scales. Power-law distributions are devoid of characteristic scale and often indicate clustering, while on the other hand fracture spacing (as a proxy of fracture intensity) are better modeled by distributions with characteristic scale e.g., as the log-normal, indicative of layered formations with strata-bound fractures. The spatial arrangement of fracture networks in Kruja unit in Montenegro gives indications that are controlled by the layered nature of the carbonate sequence (with two characteristic bed thicknesses of 0.3 m and 1.5 m in the stratigraphic sequence), as well as the later effect of major fault zones that developed during folding that possibly developed fracture 'ladders' and promote fracture clustering, where applicable. Best practices in quantifying and compare fracture intensity in similar units can be reasonable only if considering a common minimum fracture size.

Acknowledgements

This work is part of a project funded and supported by Energean Oil & Gas.

References

Marrett, R., Gale, J.F.W., Gómez, L.A., Laubach, S.E., 2018. Correlation Analysis of Fracture Arrangement in Space. J. Struct. Geol., 108, 16–33.

Ortega, O., Marrett, R., Laubach, S.E., 2006. A scale-independent approach to fracture intensity and average spacing measurement. AAPG Bulletin, 90, 2, 193-208.

16th International Congress of the Geological Society of Greece
17-19 October, 2022 - Patras, Greece
Bulletin of the Geological Society of Greece, Sp. Publ. 10
Ext. Abs. GSG2022-145

Reservoir-Scale Fracture network variation computed from 3D cross-section restoration in Jebel Hafit anticline, UAE.

S. Kokkalas[1], M. Zampos[1]
(1) Department of Geology, University of Patras, Patras, Greece, skokalas@upatras.gr

Introduction-Geological setting

Anticlinal fold structures comprise common traps for hydrocarbons. Such structures are often influenced by faults and fractures that operate as either conduits to channel fluids into a reservoir or as pathways to disperse accumulated fluids out of a reservoir (Coward et al., 1998; Aydin, 2000). In order to generate reservoir scale fracture models representative fracture properties across a wider range of scales are needed. Prediction of fracture network variation from curved fold shapes and kinematics still remains poorly understood in terms of spatial and temporal distribution of fracture sets. We use the Jebel Hafit pericline (UAE-Oman border) as an outcrop analogue to a folded carbonate reservoir in the UAE foreland fold-and-thrust belt. The Jebel Hafeet structure is a 24 km long and 5 km wide asymmetric, ENE-facing, 'whale-back' anticline, which rises to around 1200 m above the surrounding plains. It has a fold core of Early-Middle Eocene limestones, which is enveloped at its opposing limb ends by incomplete elliptical-shaped ridges made up of limestones with marl intercalations, belonging to the Late Eocene to Middle Oligocene Dammam and Asmari formations (Warrak, 1996). The Jebel Hafit anticline comprises a world-class analogue since it is an extremely well exposed fractured anticline that can be a pilot study for other similar buried anticlines in the broader area. The anticlinal, four-way closure structure is affected by a conjugate set of reactivated strike-slip faults cross-cutting the whole structure, as well as an emergent, partially blind back-thrust in the core anticline and different lithofacies on the fold limbs make the fracture network more complicated and the fracture analysis a more challenging task.

Methods

In order to compare the theoretical, field-based and predicted geomechanical fracture models we applied 3D restoration of large scale geological cross sections, together with available published ones across the fold structure (Warrak, 1996). Additionally, available seismic profiles and borehole data were taken into account, providing additional constraints on the sub-surface fold geometry and existence of large-scale thrusting, in the core of the anticline (Ali et al., 2009). The 3D retro-deformation model (Fig. 1) was created using 2D/3D Move suite of IPM (Petex) software. The 3D faults and triangulated surfaces were created by extrapolating horizons, derived from the published seismic profiles, and geological cross sections, which were modified and constrained by our field structural measurements (Kokkalas et al., 2015). The modules '3D Move on Fault' and '3D Unfolding' of Move suite were used for the structural restoration of the 3D model, in order to reach to a pre-deformational state applying the 'fault parallel flow' and 'flexural slip' algorithms, respectively. The successive stages of restoration procedure involve (Fig. 1): a) decompaction of the Upper Tertiary units, b) restoration of the upper thrust (Tarabat thrust) displacement for the Dammam formation, c) restoration of Tarabat thrust fault displacement for the Rus and Umm er Radhuma, Simsima and Fiqa formations, d) restoration of the deformation associated with the basement listric-geometry reverse fault, which offset the Mesozoic shelf carbonates and e) unfolding of Dammam and Rus formations. Next steps in the analysis include the calculation of strain and joint intensity (Fig. 2) by computing the strain attributes between the different geometric states at every restoration sub-stage. The module '3D Unfolding' and the 'flexural slip' algorithm was used for capturing the strain of structural restoration.

Results

The generated fracture sets from fracture modeling with input based on strain calculated from retro-deformation analysis and calibrated by fracture parameters from our digital outcrop analogues (Kokkalas et al., 2015) display high intensity, mainly on the west limb and fold nose, and show consistent fracture orientation in the fold hinge area. Less prominent are the transverse fractures mostly in the eastern limb close to the curved nose and in the central fold hinge zone. Conceptual models commonly assume a more systematic and simple relationship between fractures, stress and strain in fold structures, inferring relatively homogeneous fracture patterns, either controlled by curvature of folded beds or the structural position on a fold. The fracture network variation across the folded structure, based on our analyses is more complex than that predicted from conceptual models and display deviation from the generated geomechanical fracture modelling. Mechanical stratigraphy, pre-existing structures and

sedimentation during fold growth seem to exert a critical influence in the development of fracture systems within Jebel Hafeet anticline and directly affect fracture orientations, spacing/intensity, segmentation and connectivity. This complexity of the relationship between fold geometry and fracture orientation and intensity can have a great impact in naturally fractured reservoir by either increasing the storage capacity and productivity or compartmentalize reservoir horizons.

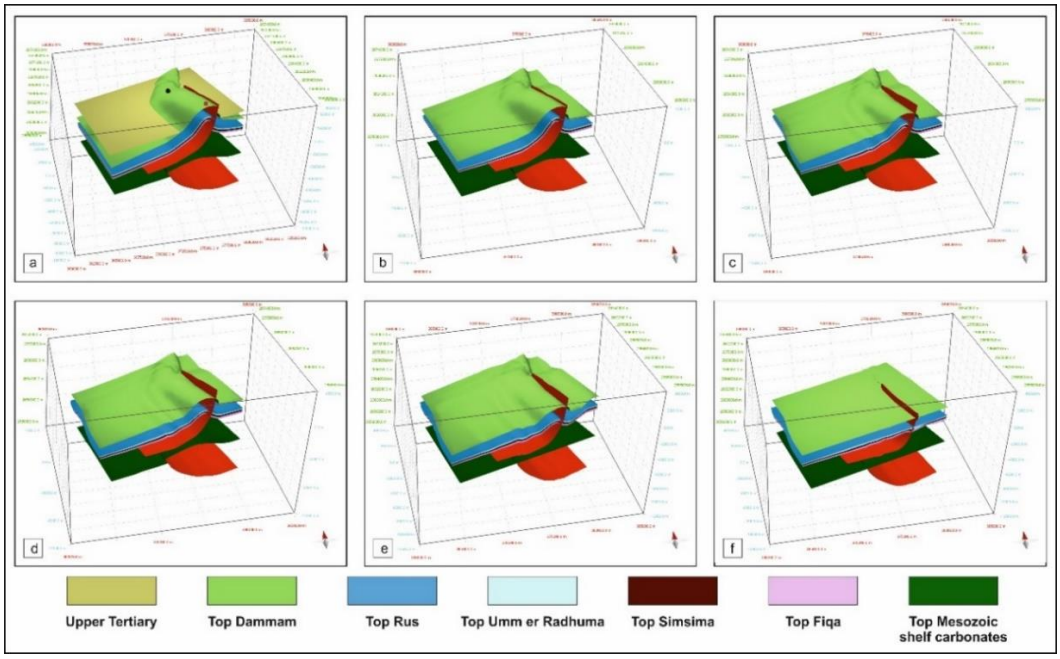

Figure 1. Successive stages of the 3D restoration in Jebel Hafit anticline (a to f stages from the final to the initial configuration); black dot: Mosque in Mubazarah park, red dot: parking, end-top of J. Hafit)

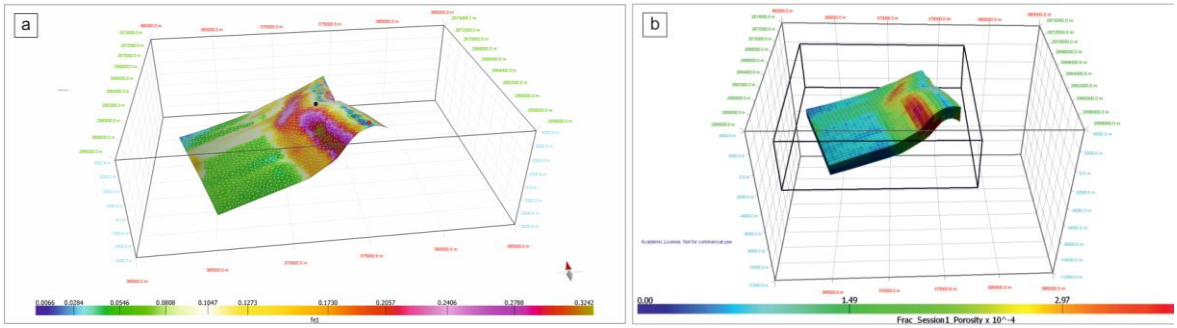

Figure 2. Calculation of the strain e_1 of the Dammam formation along the anticline structure showing the high strain in the western-limb area and towards the propagating fold nose. b) Calculation of the fracture porosity P_{32} based on the strain calculations and application of fracture analysis on Move suite.

Acknowledgments

We would like to thank Petroleum Experts (Petex) for the academic licenses kindly donated to the Department of Geology, University of Patras. S.K. would like to thank Geospatial Research Ltd. for collaboration on a previous research project (RIFP 15312-funded by PI R&D) conducted in J. Hafit that provided the rich dataset on fracture network variation.

References

Ali, M., Sirat, M., Small, J., 2009. Integrated gravity and seismic investigation over the Jabal Hafit structure: implications for basement configuration of the frontal fold and thrust belt of the Northern Oman Mountains. J. Petr. Geol., 32, 1-18.

Aydin, A., 2000, Fractures, faults, and hydrocarbon entrapment, migration and flow. Marine Petroleum Geology, v. 17, p. 797–814

Coward, M.P., Daltaban, T.S., Johnson, H., 1998. Structural Geology in Reservoir Characterization. In: Fleet, A.J. (Ed.), Geological Society Special Publication. The Geological Society of London, London, vol. 127, p. 266.

Kokkalas, S., Jones, R.R., Long, J., Woods, C., Gilment, S. 2015. Structural evolution of the Jebel Hafeet anticline (Al Ain, UAE): a multi-scale approach to model fracture patterns and kinematic fold evolution. GSA Annual Meeting, USA.

Warrak, M., 1996. Origin of the Hafit structure: implications for timing the Tertiary deformation in Northern Oman Mountains. Journal of Structural Geology, 18, No6, 813-818.

16th International Congress of the Geological Society of Greece
17-19 October, 2022 - Patras, Greece
Bulletin of the Geological Society of Greece, Sp. Publ. 10
Ext. Abs. GSG2022-154

Structural evolution and fabric-forming amphiboles in the Cycladic Blueschists

P. Xypolias[1], N. Gerogiannis[1], E. Aravadinou[1], V. Chatzaras[2]

(1) Department of Geology, University of Patras, 26500 Patras, Greece; p.xypolias@upatras.gr (2) School of Geosciences, The University of Sydney, NSW, 2006, Sydney, Australia

Research Highlights

Early ductile deformation in the Cycladic Blueschists caused internal duplication at deep subduction levels.

Subsequent ductile exhumation of the Cycladic Blueschists was accomplished during a single deformation phase from blueschist to greenschist facies conditions.

Objectives

The Cycladic Blueschists of the Internal Hellenides are characterized by a controversial deformation and metamorphic history during the subduction-exhumation cycle (e.g., Ring *et al*., 2007; Jolivet and Brun, 2010; Xypolias *et al*., 2010). Much of the controversy is due to the fact that polyphase deformation in combination with mineralogical transformations impede the distinction between subduction- and exhumation-related structures, as well as the identification of the internal structure of the Cycladic Blueschists. In this work, we combine detailed structural mapping of the Cycladic Blueschists exposed on Evia, Andros, and Sifnos islands with compositional and textural data of fabric-forming amphiboles in order to correlate the main ductile deformation phases with metamorphic conditions.

Geological setting

Within the nappe pile of the Cycladic Massif, the Blueschist unit occupies an intermediate position (e.g., Dürr, 1986). It represents a metamorphosed late Palaeozoic – Mesozoic unit, which mainly consists of an upper metaigneous-rich sequence (e.g., Ochi and Makrotantalo nappes) and a lower marble-schist sequence (e.g., North Cyclades nappe). These rocks were subjected to an Eocene blueschist to eclogite facies metamorphism, followed by retrograde metamorphism of greenschist facies conditions at early Miocene (e.g., Okrusch and Bröcker, 1990). On most islands, the greenschist retrogression becomes increasingly dominant in successively lower structural levels of the unit and was broadly synchronous with the formation of mylonitic rocks related with the ductile thrust zone defining the contact between the Cycladic Blueschist unit and the underlying Basal unit of the Cycladic Massif (e.g., Xypolias *et al*., 2010).

Results

Structural mapping showed that the early deformation phase in the Cycladic Blueschists is mainly expressed by a homogeneously developed mylonitic folia-ion, which is relatively well-preserved in competent lithologies and commonly parallel to the meta-morphic/compositional layering. This phase is related with ESE-directed thrusting resulting to the stacking of individual unit that constitute the Cycladic Blueschists. The second main ductile deformation occurred coeval with ENE-directed thrusting of the Cycladic Blueschists over the Basal unit. This phase is represented by a gently dipping, planar fabric, which varies in intensity from a widely spaced crenulation cleavage to a penetrative mylonitic foliation. Associated with the high-strain foliation is an ENE-trending stretching lineation. The second foliation is commonly axial planar to open to isoclinal, recumbent or gently inclined folds. The variation in intensity and style of foliation is mainly the result of localization of deformation into ductile shear zones that range in thickness from several meters to several hundreds of meters.

Amphiboles defining the first foliation are compositionally characterized as glaucophane. Locally, these glaucophane grains display a compositional zoning from core to rim expressed by an increase in Al^{VI}, Fe^{+2}, and Na_B content. The second foliation is defined by the shape-preferred orientation of acicular sodic, sodic-calcic and calcic amphiboles. Sodic amphiboles are (ferro-)glaucophane and show a systematic decrease in $Fe^{+3}/(Fe^{+3}+Al^{VI})$ ratio towards the grain rims. Sodic-calcic and calcic amphiboles are typically represented by (ferro-) winchite and actinolite, respectively. (Ferro-)winchite and actinolite occur either as isolated grains oriented parallel to the fabrics of the second phase or grow at the edges and necks of fractured (ferro-)glaucophane grains or on the outermost rims of (ferro-)glaucophane grains. Moreover, barroisite grows locally at the rims of sodic amphiboles (e.g., Sifnos).

Conclusions

Compositional data from amphiboles defining the first foliation indicate increase in metamorphic pressure during the syn-kinematic growth of glaucophane. Therefore, the emplacement of the metaigneous-rich sequence over the marble-schist sequence occurred at deep subduction levels before or contemporaneously with peak metamorphism. The zoning pattern of amphiboles defining the second-phase fabrics show that these rocks passed from the stability field of glaucophane to that of actinolite during progressive deformation. Therefore, the second deformation phase is associated with the main exhumation of the Cycladic Blueschists. Several studies suggest that exhumation was achieved by a mechanism of ductile

extrusion. Our observations indicate that the ductile extrusion of the Cycladic Blueschists commenced under blueschist facies conditions and continued up to greenschist facies conditions. Therefore, the Cycladic Blueschists represent a natural example, which shows that ductile extrusion/exhumation can be accomplished during a single deformation phase.

Acknowledgements

This work was supported by Grants C924 and E045 from the Research Committee of the University of Patras (Programme K. Karatheodori).

References

Dürr, S., 1986. Das Attisch–Kykladische Kristallin, in: Jacobshagen, V. (Ed.), Geologie von Griechenland. Bornträger, Berlin, 116-148.

Jolivet, L., Brun, Z.J.P., 2010. Cenozoic geodynamic evolution of the Aegean. International Journal of Earth Sciences, 99, 109-138.

Okrusch, M., Bröcker, M., 1990. Eclogites associated with high grade blueschists in the Cyclades archipelago, Greece: A review, European Journal of Mineralogy, 2, 451-478.

Ring, U., Glodny, J., Will, T., Thomson, S.N., 2007. An Oligocene extrusion wedge of blueschist-facies nappes on Evia, Aegean Sea, Greece: implications for the early exhumation of high-pressure rocks. Journal of the Geological Society London, 164, 637-652.

Xypolias, P., Spanos, D., Chatzaras, V., Kokkalas, S., Koukouvelas, I., 2010. Vorticity of flow in ductile thrust zones: Examples from the Attico-Cycladic Massif (Internal Hellenides, Greece). Geological Society, London, Special Publication, 335, 687-714.

16th International Congress of the Geological Society of Greece
17-19 October, 2022 - Patras, Greece
Bulletin of the Geological Society of Greece, Sp. Publ. 10
Ext. Abs. GSG2022-164

Structural Analysis of the Granodiorite of Paliokamariza in Lavrio (Attiki, Greece) and the Associated Secondary Uranium Mineralization.

P. Karoutsos[1], S. Kokkalas[1]
(1) Department of Geology, University of Patras, Patras, Greece, panoskaroutsos@hotmail.com

Introduction

This study presents results from the structural analysis of the Paliokamariza granodiorite in Lavrio (Attiki), as well as field mapping and the 3D illustration of the mine gallery 18, where the accompanying uranium mineralization can be found. Fieldwork was carried out in this area in order to collect structural data (foliation-lineations) and correlate the tectonostratigraphy of the wider area of the Attic-Cycladic massif, both on the surface and subsurface inside the mine gallery 18, and especially the granodiorite intrusion's subsurface extend and the upper marble unit of the BU unit.

Throughout this work, a composite imaging method was applied inside the mine gallery, which enabled us to map its interior. This composite method can illustrate the interior of the mine gallery by collecting a 3D point cloud, which later can be used for the generation of 2D images or 3D models from a different kind of software, with the GeoSLAM ZEB-REVO (Fig.1a), a light hand-held rotating laser-scanner that can achieve an accuracy of 2-3cm with a scanning speed of 43200 points/second. This output is complemented by the Matterport Pro2 3D Camera (Fig.1b) that provides a high-quality 3D scan, producing stunning 3D virtual tours. The choice of the method was related to the clarity of the walls in the gallery's interior and the effort to capture better details. The application of these methods was done comparatively to examine the level of data extraction from each method. Furthermore, besides applying the techniques, the main purpose of this work was to explore and map all types of contacts between the rock units and gather structural measurements to define the structural features and kinematics.

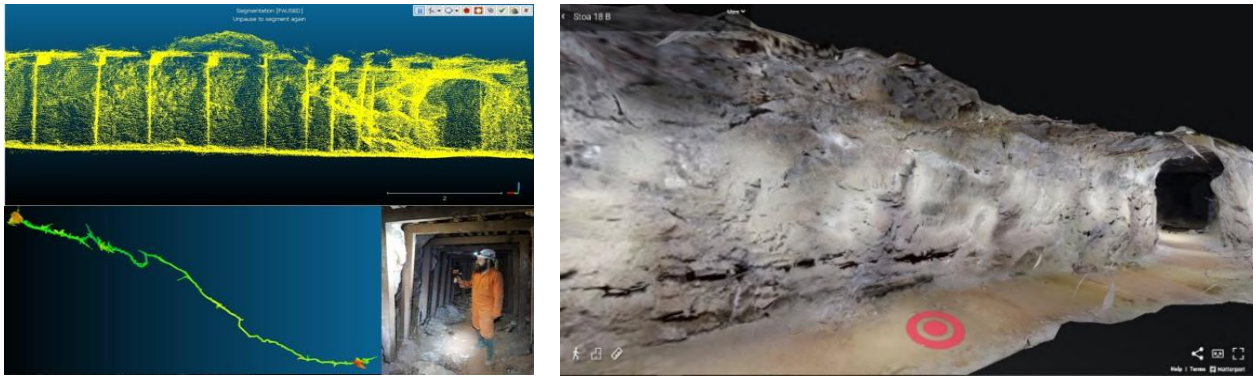

Figure 1. a) Segment of the 3D mapping of the mine gallery using the GeoSLAM ZEB-REVO b) 3D mapping of the mine gallery using the Matterport Pro2 3D Camera.

Results and implications

The study area is located in the wider area of Lavrion peninsula, which corresponds to the western boundary of the Attic-Cycladic massif (Tarantola et al., 2021). This area comprises a stack of polyphased deformed nappes, which below an upper non metamorphic unit, is composed of a middle unit dominated by the Lavrion schists (Cycladic Blueschist unit, CBU) and the basal unit (Kamariza unit-BU) dominated by marbles alternating with Kamariza schists (considered as para-autochthonous; Scheffer et al., 2016). In the study area, the upper marble of the Kamariza unit displays two main foliation orientations, one with NE-SW strike and dipping to the NW and another with NW-SE direction and dipping to either NE or SW, displaying in general low dip values. Above the marbles, we find the Lavrion schists of the CBU, which have a NE-SW foliation orientation, dipping to the NW. In the broader area, we identified occurrences of plutonic bodies of granodioritic composition (Liati et al., 2009). Such plutonic bodies were also found inside the mine gallery18 (Fig.2), as sills and stocks in the upper marbles of the Kamariza unit. A characteristic feature on the roof of this subsurface intrusion is an asymmetric NW-trending sigmoidal structure identified along a brittle-ductile shear zone, as part of a secondary detachment zone within the BU marbles (Fig.2a and 3a). This kinematic indicator with a vergence to the ESE implies the progressive deformation and slip along the detachment zone in a ductile to brittle regime and postdates the granodiorite intrusion, and thus, in a sense, it gives a younger than 9-8 Ma age for the late stage kinematics of this detachment zone. Throughout the length of the mine gallery, we also found small cavities filled with gypsum and baryte deposits. We have also identified cupola structures forming domes on the roof of the mine, suggesting that the system is

hypogene. The creation of these cavities-domes is a result of the rising hydrothermal solutions (Scheffer et al., 2016). In several places, we have also observed breccia zones (Figs 2 and 3b), especially in the last meters of the gallery at its western end, with numerous wall-rock marble fragments, iron oxides, and baryte deposits (Scheffer et al., 2019).

In an access gallery, 6m above this location, there is a cavity filled with gypsum where secondary uranium minerals were identified. The macroscopic localization of the secondary uranium minerals in the gypsum-bearing karst cavities was done with ultraviolet (UV) light. Rock samples from this formation were also collected to confirm the presence of uranium minerals within the gypsum. In order to study the mineralogical composition of these samples, XRD analysis was performed (Fig. 3b). At this point, their identification and existence require further research and more analytical data on their mineral chemistry.

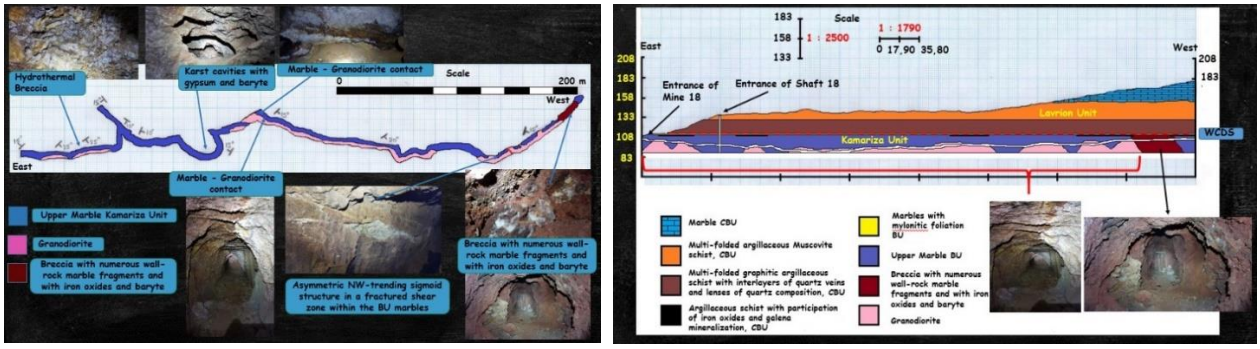

Figure 2. Mine gallery 18 mapping (view from above), cross section with the location of secondary detachment zone and WCDZ and characteristic features with the localities of breccia zones, karst cavities, domes and intrusion of the granodiorite in the upper marbles.

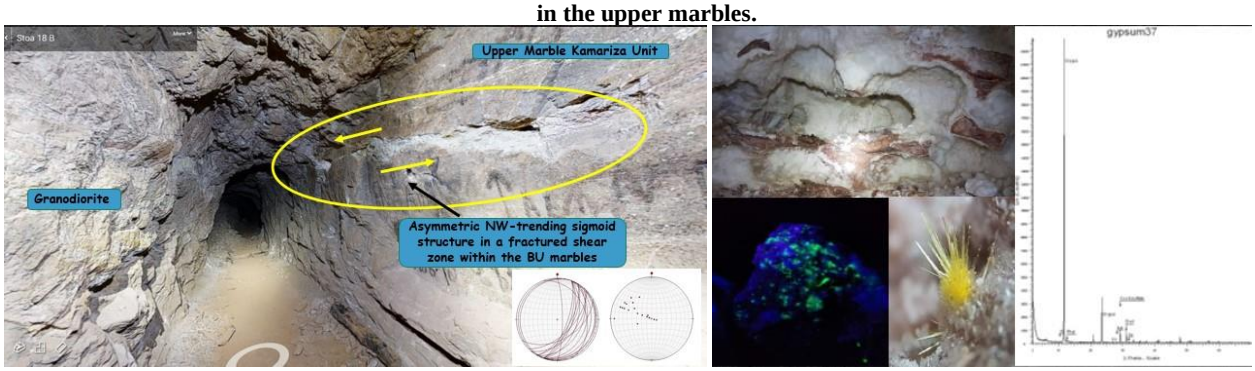

Figure 3. a) Oblique view of the asymmetric NW-trending sigmoid structure in the brittle-ductile shear zone within the BU marbles b) View of the cavity filled with gypsum and the secondary uranium minerals. XRD composition diagram and image of the secondary uranium minerals shown in magnification and under ultraviolet (UV) light.

Acknowledgments

Special thanks go to Landmark–G. Loutridis Company and Yiannis Psaltakis for kindly providing the mapping equipment. Markos Vaxevanopoulos (Ph.D. Post Doc at Ecole Normale Supérieure de Lyon) is also thanked for his essential help in carrying out the mapping of the mine gallery and the processing of the data, and also Dimitris Syrigos. The latter indicated to us the importance of researching gallery 18 in the area of Paliokamariza in Lavrio District. P. Lampropoulou (University of Patras) is also thanked for helping us with the XRD analysis.

References

Liati, A., Skarpelis, N, Pe-Piper, G., 2009. Late Miocene magmatic activity in the Attic-Cycladic Belt of the Aegean (Lavrion, SE Attica, Greece): implications for the geodynamic evolution and timing of ore deposition. Geological Magazine, 146, 732-742.

Scheffer C, Tarantola A, Vanderhaeghe O, Voudouris P, Rigaudier T, Photiadis A, Morin D, Alloucherie A., 2017. The Lavrion Pb-Zn-Fe-Cu-Ag detachment-related district (Attica, Greece): Structural control on hydrothermal flow and element transfer-deposition. Tectonophysics, 717:607-627.

Scheffer C., Vanderhaeghe, Lanari, P., Tarantola, A., Ponthus, L., Photiades, A., France, L., 2016. Syn- to post-orogenic exhumation of metamorphic nappes: Structure and thermobarometry of the western Attic-Cycladic metamorphic complex (Lavrion, Greece). Journal of Geodynamics, v. 96, 174–193.

Scheffer C, Tarantola A, Vanderhaeghe O, Voudouris P, Paul G. Spry, Rigaudier T, and Photiades A., 2019. The Lavrion Pb-Zn-Ag–Rich Vein and Breccia Detachment-Related Deposits (Greece): Involvement of Evaporated Seawater and Meteoric Fluids During Postorogenic Exhumation. Economic Geology, v. 114, (7), 1415–1442.

Tarantola, A.; Scheffer, C.; Vanderhaeghe, O.; Voudouris, P.; Photiades, A.; Morin, D. 2021. Geologic and metallogenic overview of the Lavrion mining district: A guide for archaeological exploration. *Der Anschnitt, in press.*

16th International Congress of the Geological Society of Greece
17-19 October, 2022 - Patras, Greece
Bulletin of the Geological Society of Greece, Sp. Publ. 10
Ext. Abs. GSG2022-166

What is the proper Misfit Angle for the stress inversion of heterogeneous fault-slip data?

M. D. Tranos[1]

(1) Aristotle University of Thessaloniki, Thessaloniki, Greece, tranos@geo.auth.gr.

Research Highlights

Choosing Misfit angle between fault slickenlines and Slip Preferences of faults.

The importance of the Tensor Ratio diagrams in finding the Misfit angle for the paleostress analysis.

Introduction

All the stress inversion methods, dealing with the 'inverse problem', i.e., to resolve the driving reduced stress tensor of no less than four fault-slip data, use algorithms based on the Wallace-Bott hypothesis (Angelier, 1994). This hypothesis takes into account that the slip preference (SP) on a fault (Tranos, 2012) occurs in the direction of the maximum resolved shear stress (Wallace, 1951; Bott, 1959). A fault's SP depends on the orientation of the four variables of the resolved stress tensor, which are the principal stresses (σ_1, σ_2, σ_3) and the stress ratio $R = \sigma_1-\sigma_3/\sigma_2-\sigma_3$ with $0 \leq R \leq 1$ (Carey and Brunier, 1974; Angelier, 1994). The optimal stress tensor should best minimize a misfit function related to the Misfit Angle (MA), i.e., the angle between the real slip (defined by the kinematic indicators-microstructures) and the SP on each fault plane. The MA varies in intervals [0°, 180°] or ([0°, 90°] regarding a common sense-of-slip (SOS)). However, a critical question in applying the stress inversion methods to heterogeneous fault-slip data is: What misfit angle (MA) should one use when applying the stress inversion methods and aiming at obtaining the optimal stress tensors? Lisle (2013) recommends that the MA should have a tolerance of ± 26° for making decisions regarding attributing fault-slip data to particular stress tensors calculated by the stress inversion methods. Indeed, most stress inversion applications consider MA≤ 20° to 30° for each fault-slip datum, but several published stress tensors explain fault-slip data with the mean MA (MMA) instead of the MA for each fault-slip datum. Although the resolved MMA should be less than 20° for having homogeneous fault-slip data (Tranos, 2017, 2018), there are cases where the stress tensors are calculated with MMA > 20°, and therefore there are fault-slip data with MA >> 20°. Herein, by using the Tensor Ratio diagrams used in the Tensor Ratio Method (TRM) (Tranos, 2015), I will indicate what should be the proper MA for applying the stress inversion methods and the reasons for it.

The Tensor Ratio diagrams (TR diagrams)

TRM is a simple graphical and semi-automatic method devised to separate heterogeneous or polyphase fault-slip data into homogeneous groups and define for each group the driving 'enhanced' Andersonian stress tensors, i.e., Andersonian stress tensors with the addition of the stress ratio (Tranos, 2015). The homogeneity of each group is based not only on the MA minimization criteria as used in other stress inversion methods but additional compatibility criteria related to the stress ratio of the stress tensor as shown in the Tensor Ratio (TR) diagrams (Tranos 2012, 2013, 2015). The TR diagrams are XY plots constructed for enhanced Andersonian stress tensors, i.e., stress tensors which have one of the principal stress axes in a vertical position, and they vary depending on the stress ratio if the orientations of the principal stress axes remain stable. In the TR diagram, each fault-slip datum is shown with a point whose X value is the slip deviation (SD) of the fault's real slip from the dip-slip fault activation (either normal or reverse), i.e., the absolute difference that the pitch α° of the real fault slickenline (or striation) has from the value of 90°, and the Y value is the absolute value of the acute angle between the trend of the horizontal principal stress axis, σ_1 or σ_3, and the dip direction of the fault in compressional or extensional stress regimes, respectively.

TR diagrams and the misfit angle

Figure 1 shows TR diagrams of enhanced Andersonian stress regimes with similar stress axes orientations (σ_3 or σ_1 axis at the same trend) but stress ratios at 0, 0.25, 0.5, 0.75, and 1. The TR diagrams show the SP areas of the optimally driven fault-slip data by taking into account the slip tendency (Ts), i.e., the ratio of shear stress to normal stress on a fault plane (Morris et al., 1996) equal to or above 0.6 (dry conditions). In the extensional stress regimes (Fig. 1a), the optimal faults dipping at trends ± 30° away from the horizontal σ_3 axis, i.e., Y= 30°, show the largest X value differences varying from 9° to 34° depending on their dip angles for a common stress ratio. Also, the X values of such faults show the highest differences among the different stress ratios (Fig. 1a).

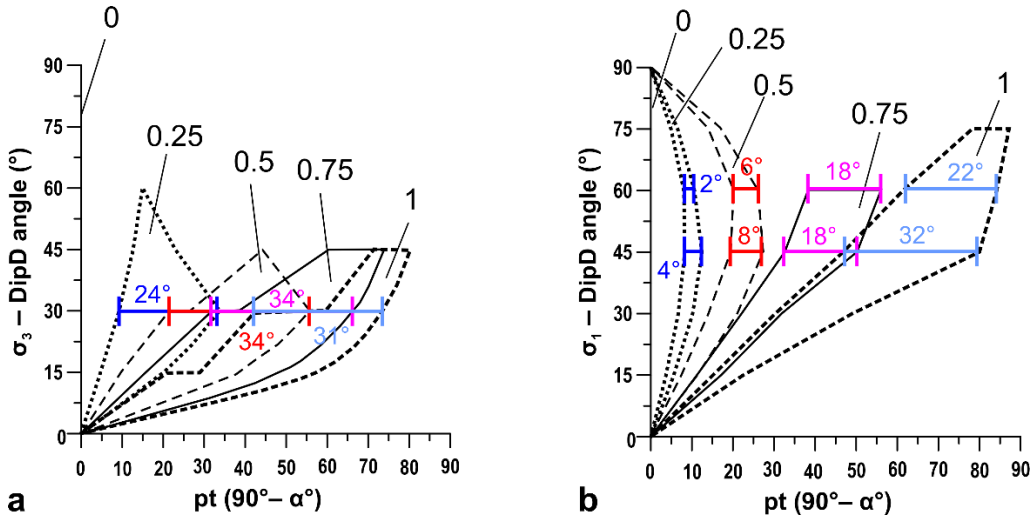

Figure 1. Slip Preference (SP) areas in the TR diagrams of the optimal faults activated by (a) extensional and (b) compressional enhanced Andersonian stress regimes with R equal to 0, 0.25, 0.5, 0,75 and 1 (modified from Tranos, 2015). Colored bars and numbers show the X values of the faults, which dip at a specific trend away from the trend of the horizontal σ3 or σ1 axis but have various dip angles.

Analogous TR diagrams for compressional stress regimes (Fig. 1b) show that the optimal contractional faults dipping at trends ± 60° and ± 45° away from the horizontal σ_1 axis, respectively, and having different dip angles show the largest X value differences varying from 8° to 22° and 4° to 32°, for a common stress ratio. The faults of such dip direction reveal the largest X values among the stress regimes (Fig. 1b).

On the other hand, the TR diagrams show that the SP areas of the different stress ratios converge towards the (0,0) value showing that when the dip directions of the input fault planes are less than 30° with the σ_3 or σ_1 trend, respectively, then the distinction between the varied stress regimes is much more difficult when the orientation of the stresses are quite close. In such cases, the inverse problem is hard to solve.

Conclusions

The TR diagrams show that the MA chosen for the paleostress analysis depends on the orientations of the input fault-slip data, but it should be no more than 22° making the angle of 20° the proper and default MA for inverting fault-slip data. Moreover, the MA = 20° for each fault-slip datum seems to function well for separating stress regimes even when the driving stress regimes vary only in the stress ratio values. In the last case, the faults with oblique and oblique to strike-slip displacements are needed to exist among the input fault-slip data. On the other hand, when the majority of the fault-slip data have pitches > 60°, and the number of the fault-slip data is not enough, then the distinction between the varied stress regimes regarding the stress ratio is much more difficult, and in such cases, a smaller MA, e.g., MA = 10°, might be considered as a default angle. The usage of the TRM and the TR diagrams allows the user to directly inspect what should be the final misfit angle for defining the optimal fault-slip data for each of the driven enhanced Andersonian stress regimes. The misfit angle might differ among the homogeneous fault-slip data groups, but the MMA should not be greater than 20°.

References

Angelier, J., 1994. Fault-slip analysis and palaeostress construction, in: Hancock, P.L. (Ed.), Continental Deformation, 53-100.

Bott, M.H.P., 1959. The mechanics of oblique slip faulting. Geological Magazine 96, 109–117.

Carey, E., Brunier. B., 1974. Analyse théorique et numérique d'un modèle mécanique élémentaire appliquè à I' étude d'une population de failles. Comptes Rendus de l' Académie des Sciences, D., 279, 891–894.

Lisle, R., 2013. A critical look at the Wallace-Bott hypothesis in fault-slip analysis. Bull. Soc. géol. France, 2013, 184, 4-5, 299-306.

Morris, A.P., Ferrill, D.A., Henderson, D.B., 1996. Slip tendency and fault reactivation. Geology, 24, 275–278.

Tranos, M.D., 2012. Slip preference on pre-existing faults: a guide tool for the separation of heterogeneous fault-slip data in extensional stress regimes. Tectonophysics, 544–545, 60–74, doi: 10.1016/j.tecto.2012.03.032.

Tranos, MD, 2013. The TR method: the use of slip preference to separate heterogeneous fault-slip data in compressional stress regimes. The surface rupture of the 1999 Chi-Chi Taiwan earthquake as a case study. Tectonophysics, 608, 622–641, doi:10.1016/j.tecto.2013.08.017.

Tranos, MD, 2015. TR method (TRM): A separation and stress inversion method for heterogeneous fault-slip data driven by Andersonian extensional and compressional stress regimes. J. Struct. Geol., 79, 57–74, doi: 10.1016/j.jsg.2015.07.006.

Tranos, MD, 2017. The use of Stress Tensor Discriminator Faults in separating heterogeneous fault-slip data with best-fit stress inversion methods. J. Struct. Geol., 102, 168-178, doi:10.1016/j.jsg.2017.08.002.

Tranos, MD, 2018. The use of Stress Tensor Discriminator Faults in separating heterogeneous fault-slip data with best-fit stress inversion methods. II. Compressional stress regimes. J. Struct. Geol., 107, 153-162, doi: 10.1016/j.jsg.2017.12.015.

Wallace, R.E., 1951. Geometry of shearing stress and relation to faulting. Journal of Geology, 59, 118–130.

16th International Congress of the Geological Society of Greece
17-19 October, 2022 - Patras, Greece
Bulletin of the Geological Society of Greece, Sp. Publ. 10
Ext. Abs. GSG2022-167

Late orogenic basement faults and their control on active fault segmentation and seismic hazard of the Serbomacedonian massif, Central Macedonia (Northern Greece)

M.D. Tranos[1], G.A., Georgiadis[1], P.G., Neofotistos[1], A.P., Plougarlis[1]
(1) Aristotle University of Thessaloniki, Thessaloniki, Greece, tranos@geo.auth.gr.

Research Highlights

The critical aspect of the late orogenic basement faults on the present fault pattern of the Serbomacedonian massif.

The kinematics of the late orogenic basement faults and the related morphotectonics.

Introduction

The Serbomacedonian massif in Central Macedonia (Northern Greece) is characterized by intense seismicity with strong and destructive earthquakes up to 6.5 in magnitude (Tranos et al., 2003, Mountrakis et al., 2006). This seismic activity occurs mainly along rupture zones consisting of E-W trending normal faults and subsidiary NW-SE trending left-lateral oblique extensional fault zones, the latter bounding a series of Late Neogene-Quaternary basins (e.g., Kerkini, Sochos, Mygdonia, Anthemountas, Zagkliveri-Rizia, Stratoni-Ierissos). These basins, interrupting the mountainous terrain of the Serbomacedonian massif, have been developed due to a NE-SW extension dated in Late Miocene-Pliocene and a N-S extension from the Quaternary to the present.

The seismically active faults are characterized by strike changes and various lengths up to a few tens of kilometers showing that their growth results from the coalescence of various inherited fault segments (Pavlides and Kilias, 1987; Tranos et al., 2003, Mountrakis et al., 2006) striking mainly ± 30° from the E-W. However, the present fault segmentation is critical in the localization of the rupture and propagation of these zones, especially throughgoing the mountainous terrain (Tranos et al., 2003) and the size of the resulting earthquakes and seismic hazard assessment of the Serbomacedonian massif. We present in this study that among the several factors controlling the fault growth and segmentation of these rupture zones, a significant factor is the existence of the inherited late orogenic basement faults that strike mainly NNE-SSW to NE-SW and, less frequently, NNW-SSE to N-S.

Late orogenic basement faults

The late orogenic basement faults (LOBF) strike mainly NNE-SSW to NE-SW and, less frequently, NNW-SSE to N-S. Several of them have already been mapped in published geological maps and papers, e.g., Kockel et al. (1977) and Tranos et al. (2003), and their length is commonly up to 10 km. Based on the satellite image interpretation, those with the former strike are better recognized because they crosscut the NW-SE orogenic fabric at high angles or orthogonal. Regardless of the strike, they constitute the mountainous terrain's main drifts or streams, usually forming a sinusoidal alignment. Also, along them, changes in the orogenic fabric trend can be observed. Generally, they occur as discontinuous, rectilinear lineaments presenting two main morphotectonic features related to their kinematics. These features are (1) prolonged valleys run by a sinusoidal stream, juxtaposing blocks without remarkable relief differences due to strike-slip displacements, and (2) small but well-defined depocenters filled with Neogene and Quaternary sediments which are related to oblique-normal to normal displacements along these faults. In the last case, most faults forming the depocenters dip at steep angles towards WNW.

The strike-slip and the oblique-normal to normal displacements have been driven by a strike-slip to transpression stress regime with contraction N-S to NNE-SSW and a NW–SE extensional stress regime, respectively (Tranos, 1998; Georgiadis et al., 2007; Tranos, 2011; Tranos and Lacombe, 2014). These stress regimes relate to the late-orogenic processes between the Apulia and Eurasia plates in Early-Middle Miocene (Tranos, 1998; Tranos and Lacombe, 2014).

Types of fault segmentation

The existence of the LOBFs controls the growth and coalescence of the seismically active rupture zones because of the following recognized fault patterns. These fault patterns are formed between active or more fault segments and a LOBF or LOBF zone. They can be described as follows (Fig. 1):

a) An active fault segment terminates against a late orogenic basement fault (T shape pattern). In this case, the angle between the LOBF and the fault segment is high to orthogonal (cases 1, 2).
b) Two active fault segments of the same or slightly different strikes are joined through a LOBF (X or Y shape pattern). The LOBF and the angle between it and the fault segments vary in this case and control the coalescence of the two active fault segments (cases 3-6).
c) Two active in-line fault segments with similar or slightly different strikes bypass the LOBF in-between by using part of the latter. In most cases, the LOBF does not stand at high angles to these fault segments (case 7).

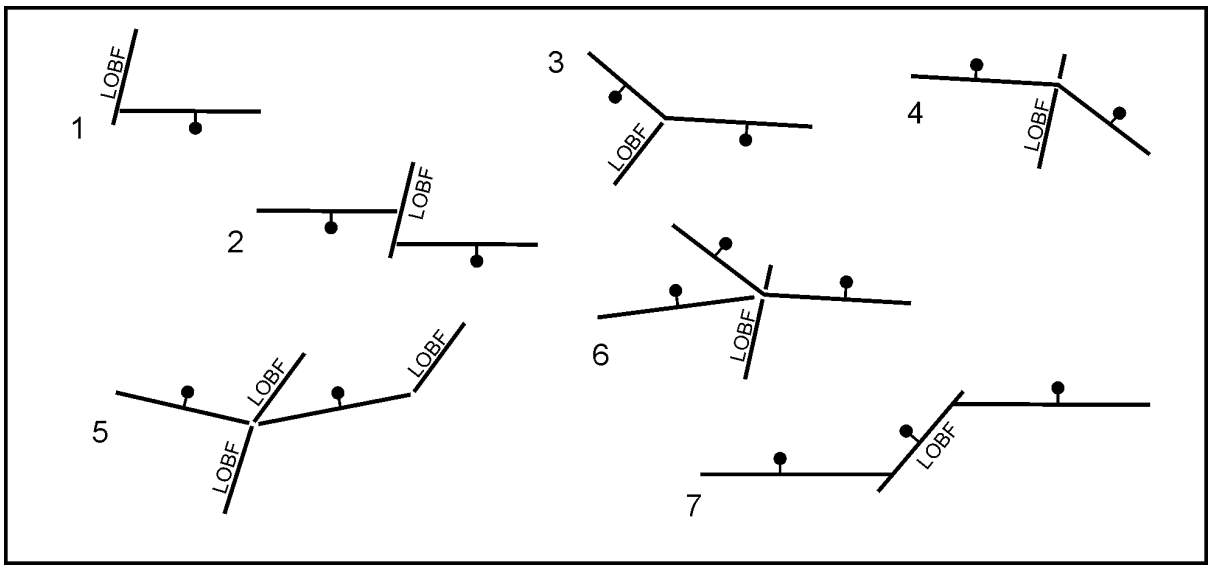

Figure 1. Examples 1 through 7 of the Late orogenic basement faults (LOBF) and their control on active fault segmentation in the Serbomacedonian massif. Balls indicate the hangingwall of the active fault or active fault segment.

The coalescence and unique activity of these active fault segments depend on the features of the LOBF, e.g., if it is a single fault or a wide fault zone and the angles formed by the strikes of the engaged faults. The types mentioned above are valid even if the LOBF is not in direct contact with the fault segments because of sediments covering it or it being a blind fault not exposed to the Earth's surface.

Conclusion

The LOBFs strike mainly NNE-SSW to NE-SW and less frequently NNW-SSE to N-S with lengths up to about 10km. They are faults activated as strike-slip and normal by the late orogenic stresses dated in Early-Middle Miocene. These faults control, to a large degree, the segmentation of the E-W seismically active rupture zones in the Serbomacedonian massif, and in several cases, they become parts of the active rupture zones. Therefore, considering the presence and the geometric and morphotectonic features of the late orogenic basement faults, the latter constitutes a vital element in studying the active faults of the Serbomacedonian massif and the seismic risk assessment in the area.

References

Georgiadis, G.A., Tranos, M.D., Mountrakis, D.M., 2007. Late- and post-Alpine tectonic evolution of the southern part of the Athos peninsula, northern Greece. Bulletin of the Geological Society of Greece 40, 309–320.

Kockel, F., Mollat, H., Walther, H.W., 1977. Erlauterungen zur Geologischen Karte der Chalkidiki und angrenzender Gebiete 1:100000 (Nord-Griechenland). Bundesanstalt fur Geowisseschaften und Rohstoffe, Hannover, 119 pp.

Mountrakis, D., Tranos, M., Papazachos, C., Thomaidou, E., Karagianni, E., Vamvakaris, D., 2006. New neotectonic and seismological data about the main active faults and stress regime of Northern Greece. Journal of Geological Society, London, Special Publications 260, 649–670.

Pavlides, S.B., Kilias, A.A., 1987. Neotectonic and active faults along the Serbomacedonian zone (Chalkidiki, N. Greece). Annales Tectonicae 1, 97–104.

Tranos, M.D., 1998. Contribution to the study of the neotectonic deformation in the region of Central Macedonia and North Aegean. Ph.D. Thesis, Aristotle University of Thessaloniki (in Greek with extended English abstract).

Tranos, M.D., 2011. Strymon and Strymonikos Gulf basins (Northern Greece): implications on their formation and evolution from faulting. Journal of Geodynamics51, 285–305, http://dx.doi.org/10.1016/j.jog.2010.10.002.

Tranos, M.D., Lacombe, O., 2014. Late Cenozoic faulting in SW Bulgaria: Fault geometry, kinematics and driving stress regimes. Implications for late orogenic processes in the Hellenic hinterland. Journal of Geodynamics, 74, 32-55, doi: 10.1016/j.jog.2013.12.001.

Tranos, M. D., Papadimitriou, E. E., Kilias, A. A. 2003. Thessaloniki–Gerakarou Fault Zone (TGFZ): the western extension of the 1978 Thessaloniki earthquake fault (Northern Greece) and seismic hazard assessment. Journal of Structural Geology, 25, 2109–2123.

16th International Congress of the Geological Society of Greece
17-19 October, 2022 - Patras, Greece
Bulletin of the Geological Society of Greece, Sp. Publ. 10
Ext. Abs. GSG2022-212

Can 'old' geological maps from IGME be structurally rejuvenated with Geographic Information System software?

P. G. Neofotistos[1], A. P. Plougarlis[1], M. Savvidou[1], M.D. Tranos[1]
(1) Aristotle University of Thessaloniki, Thessaloniki, Greece, petrosgn@geo.auth.gr.

Research Highlights

Using structural data from published IGME geological maps to structurally analyze a study area and answer crucial questions regarding its deformation.

Extracting fundamental structural information from published geological maps with GIS software.

Introduction

For decades now, the Institute of Geology and Mineral Exploration (IGME) (a successor of the Institute of Geology and Underground Exploration (IGEY), the initial foundation and activity of which was in 1952), has undertaken the geological mapping of Greece in the form of 352 published analogical map sheets. These map sheets, as a whole, were the infrastructural work for the planning and implementation of developmental projects, mainly functioning as an important tool for the sustainable management and resolution of environmental-economic-social problems related to the surrounding geological environment (Zervakou et al., 2008).

However, because they have been outdated over the years, their role and significance have been gradually constrained in recent research, making them considered 'fossilized'. Nevertheless, these map sheets potentially contain important structural information in the form of primary structural data, e.g., foliation, lineation, and fold axis measurements, which, if extracted, processed and analyzed with the proper tools, can give insight into the deformation of the region under research.

Two IGME map sheets, the Sithonia and Lachanas, have been selected as case studies from two areas located in Central Macedonia (Northern Greece). The Sithonia area is largely occupied by an Eocene granitoid, which intrudes the multiply deformed, and Alpine reworked Serbomacedonian Massif and the rocks of the Circum Rhodope Belt (Kockel et al., 1977; Tranos et al., 1993 and references therein). In particular, the two-mica gneisses and amphibolite rocks of the Serbo-Macedonian massif constitute the envelope mainly in the northern and eastern part of the granitoid, whereas Lower-Middle Jurassic phyllites and quartzites of the Circum Rhodope Belt metamorphosed in the greenschist facies and greenschists and greenstones complete the granitoid's envelope in the west and south, respectively (Kockel et al., 1977; Tranos et al., 1993). The Lachanas area constitutes a gneissic terrain with two-mica gneisses and amphibolites rocks of the Serbo-Macedonian massif (Kockel et al., 1977) and intruded by Mesozoic, well-foliated granite bodies, incorporated to the Arnea Granite (Plougarlis et al., 2021 and references therein).

Our purpose is to show that, with the aid of Geographic Information System (GIS) software, outdated map sheets can potentially be structurally rejuvenated and provide crucial information to answer complex questions in a simple manner regarding the deformation of the mapped areas. We achieve this by extracting primary data depicted in the map sheets, such as the main foliation.

Concept, methodology and results

Sithonia and Lachanas map sheets have an adequate number and spatial distribution of structural data, which constituted them as adequate candidate maps and sources for fundamental structural analysis, thus, setting a quantitative and qualitative criterion for the future application of the same methodology to other map sheets published by IGME.

So, the two chosen map sheets were initially introduced to the QGIS software as georeferenced images. Then, a plug-in was used, based on a simple algorithm, to extract the primary data of foliation in both map sheets regarding dip direction and dip angle. Once collected, the foliation data were input to a stereonet plot software for plotting and visualizing them (Fig. 1). The results were the following:

a) Sithonia map sheet: The Sithonia granitoid was divided into two subareas, i.e., northern and southern, based on the spatial distribution of the foliation data along its margins. In the northern subarea, the granitoid's foliation generally strikes NW-SE, dipping to SW with medium to high angles (Fig. 1a). In the southern subarea, it strikes ENE-WSW dipping towards NNW with high angles (Figs. 1b). These foliation orientations are in concordance with the foliations depicted in the envelope rocks in the northern (Fig. 1c) and southern area (Fig. 1d), respectively. The granitoid's foliation constitutes a planar fabric, increasing in intensity towards its margins as shown in the map sheet and has been distinguished (Figs. 1a, b) to a magmatic in the interior, and a solid-state foliation to the margins of the granitoid (Tranos et al., 1993). The concordance between the foliation from the envelope and the granitoid (Figs. 1a-d) suggests

that the Sithonia granitoid is a syn-tectonically emplaced intrusive body during Eocene times, as already suggested by Tranos et al. (1993).

b) Lachanas map sheet: The foliation in the two-mica gneisses and amphibolites of the Serbo-Macedonian Massif shows two concentrations that strike WNW-ESE and dip towards the two opposite directions, NNE and SSW, with moderate to low angles (Fig. 1e). These two concentrations constitute the limbs of a mega-scale, open fold, with a WNW-ESE trending fold axis, which is related to a NNE-SSW shortening. The latter deformational event can only be concluded through the insight provided by analyzing the foliation data on the map scale. The reason is that, in such monotonous and intensely vegetated gneissic terrain, such open folds can hardly be observed at mesoscale in the field. This NNE-SSW shortening fits well with a N-S, late Alpine shortening reported for other parts of the Serbo-Macedonian Massif (Tranos et al., 1993, 1999; Georgiadis et al., 2007; Tranos, 2011; Neofotistos, 2020) but also with the kinematics implied for the Nestos Shear zone in SW Bulgaria (Tranos et al. 2008) and Eastern Macedonia (Tranos et al., 2009).

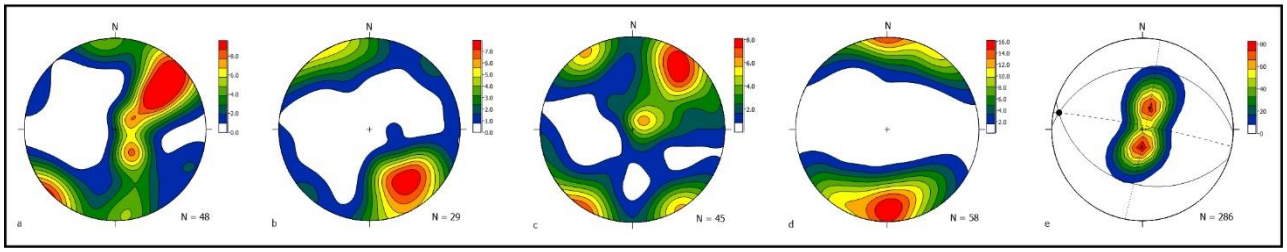

Figure 1. Equal area, lower hemisphere density diagrams of the foliation planes extracted from the Sithonia and Lachanas map sheets. Foliation of the Sithonia granitoid in the (a) and (b), and the envelope rocks in the (c) and (d), from the northern and southern subareas, respectively, of the Sithonia map sheet. (e) Foliation of the metamorphic rocks of the Lachanas map sheet. In (e), the two maximum concentrations are shown with the great circles and poles representing the flanks of WNW-ESE open folds.

Conclusions

Two map sheets of the IGME, the Sithonia and Lachanas map sheets, are used, and the foliation of the basement and intrusive rocks is extracted with the aid of QGIS software. Through processing and analyzing these data, we concluded that: a) the Sithonia granitoid body exhibits a planar fabric which is geometrically similar to the foliation of its envelope, thus constituting the former a syn-tectonically emplaced intrusive body in the Sithonia peninsula, and b) the foliation in the crystalline rocks of Lachanas map sheet depicts WNW-ESE trending, map-scale open folds related with a NNE-SSW shortening, similar in trend with the shortening of other parts of the Serbo-Macedonian massif and the activity of the Nestos Shear Zone.

We, therefore, introduce a new aspect, where the existing IGME map sheets surpass their paper 'fossilized' view and contribute to the recent research related to the deformation of the mapped areas, highlighting, at the same time, the role of GIS software as a useful tool in their digital transformation.

References

Georgiadis, G.A., Tranos, M.D., Mountrakis, D.M., 2007. Late- and post-Alpine tectonic evolution of the southern part of the Athos peninsula, northern Greece. Bulletin of the Geological Society of Greece 40, 309–320.

IGME, 1978. Peninsula of Sithonia geological map sheet, scale 1:50.000.

IGME, 1979. Lachanas geological map sheet, scale 1:50.000.

Kockel, F., Mollat, H., Walther, H.W., 1977. Erlauterungenzur Geologischen Karte der Chalkidiki und angrenzender Gebiete 1:100000 (Nord-Griechenland). Bundesanstalt fur Geowisseschaften und Rohstoffe, Hannover, 119 pp.

Neofotistos, P., 2020. Geology and deformation of the Northern part of the Athos Peninsula, Northern Greece. Ph.D. thesis, 253 pp.

Plougarlis, A., Tranos, M., & Papadopoulou, L. (2021). The tectonostratigraphic architecture of the Serbo-Macedonian massif in the Vertiskos and Kerdilion mountains (Northern Greece). Bulletin of the Geological Society of Greece 57(1), 1–22. https://doi.org/10.12681/bgsg.25054.

Tranos, M., Kilias, A., Mountrakis, D., 1993. Emplacement and deformation of the Sithonia granitoid pluton (Macedonia, Hellas). Bulletin of the Geological Society of Greece 28, 195-210.

Tranos, M. D., Kilias, A. A., Mountrakis, D. M., 1999. Geometry and kinematics of the Tertiary post-metamorphic Circum Rhodope Belt Thrust System (CRBTS), Northern Greece. Bulletin of Geological Society of Greece 33, 5–16.

Tranos, M.D., Eleftheriadis, G.E., Kilias, A.A., 2009. Philippi granitoid as a proxy for the Oligocene and Miocene crustal deformation in the Rhodope Massif (Eastern Macedonia, Greece). Geotectonic Research 96 (1), 69–85, doi:10.1127/1864-5658/09/96-0069.

Tranos, M.D., 2011. Strymon and Strymonikos Gulf basins (Northern Greece): implications on their formation and evolution from faulting. Journal of Geodynamics 51, 285–305, http://dx.doi.org/10.1016/j.jog.2010.10.002.

Zervakou, A., Tsombos, P., Photiades, A., Hademenos, V., 2008. Σύγχρονοι γεωλογικοί χάρτες Ι.Γ.Μ.Ε.: Ψηφιοποίηση, ενιαία γεωλογική ψηφιακή βάση, χαρτοσύνθεση. 10° Εθνικό Συνέδριο Χαρτογραφίας ΧΕΕΕ: Η χαρτογραφία της ηπειρωτικής περιφέρειας.

QGIS Development Team (2021). QGIS Geographic Information System. Open Source Geospatial Foundation Project. http://qgis.osgeo.org.

16th International Congress of the Geological Society of Greece
23-25 May, 2022 - Patras, Greece
Bulletin of the Geological Society of Greece, Sp. Publ. 10
Ext. Abs. GSG2022-257

Remote Sensing of Lineaments as Assisting Elements in Neotectonic Research: a Case Study in Mygdonia Basin, Northern Greece.

E. Papadopoulou[1], A. Dretaki[1]
(1) Department of Geography, University of the Aegean, Mytilene, Greece, evdokiapap97@gmail.com

The purpose of this research is the correlation of fault segments, in large scale, using Remote Sensing data, with the neotectonic map of Lagyna area, at the southern margin of Mygdonia basin (Chatzipetros *et al*., 2019, Papadopoulou, 2020, Papadopoulou *et al*., 2020). Remote Sensing contributes in detecting and monitoring the physical characteristics of an area and collecting useful data without the need of visiting the region itself. The three different fault segments, which were mapped at the study area, will be compared with the extracted results of analyzed satellite images. For the analysis, Sentinel-2 satellite images (acquired on 25 September 2021) and SRTM (1 Arc-Second) DEM were used (Earth Explorer), as well as ArcGIS Pro for processing the analysis methods and construction of the final maps.

The study area is a tectonic basin, located near Thessaloniki city, northern Greece. Mygdonia basin is bounded by two major fault zones, the southern of which is the active one. Figure 1 shows the study area, with the three parallel fault segments of the southern fault zone (Papadopoulou, 2020), where fault migration towards the center of the basin (Chatzipetros *et al*., 2019). Segment A represents a shear zone within the metamorphic bedrock. Segment B forms a clear fault scarp, which gave the destructive M6.5 earthquake event in 1978, and defines the contact between the bedrock and the Pleistocene sedimentary cover. Segment C is entirely within the Quaternary sequence, and the deformation created is only traceable on man-made structures, such as pavements, streets, houses and buildings (Chatzipetros *et al*., 2019).

For this research, two different methodologies where applied, using ArcGIS Pro. The first methodology is visualization of slope direction, which was achieved with DEM data and Hillshade Raster Function, to detect linear features on the produced map. Four hillshade maps were created with different azimuth, however the one that highlights the linear features is Figure 2, with azimuth and altitude 45º and 50º respectively. The second methodology is combining bands from Sentinel-2 level 2 satellite images and further processing with raster functions toolbox (Figure 3) (ten Veen, 1998). The map created with the combination RGB = 12, 11, 2 (User guide for https://platform.pulchra-schools.eu/supporting-tools/remote-sensing-tool/), that brings out the geology (Figure 3a), confirms the presence of the mapped fault segments, but the one that gives the most accurate results is the combination RGB = 2/8, 3/11, 4/12, which reveals the geology and lineaments (Figure 3b). Multiple maps were produced by Figure 3b, using Raster Functions, such as Line detection, Gradient and Laplacian, all with good correlation. A good example of the maps mentioned above is gradient with northeast direction and line detection with left direction (Figures 3c and 3d) that emphasize segments A and B.

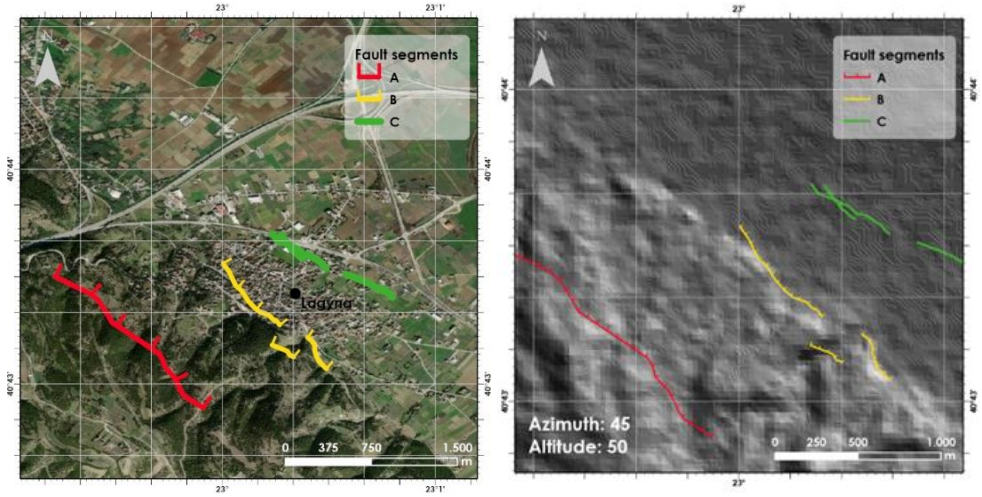

Figure 1: Study area with the three mapped fault segments (Papadopoulou, 2020).

Figure 2: Hillshade map (azimuth 45o and altitude 50o) derived from SRTM (1 Arc-Second) DEM data.

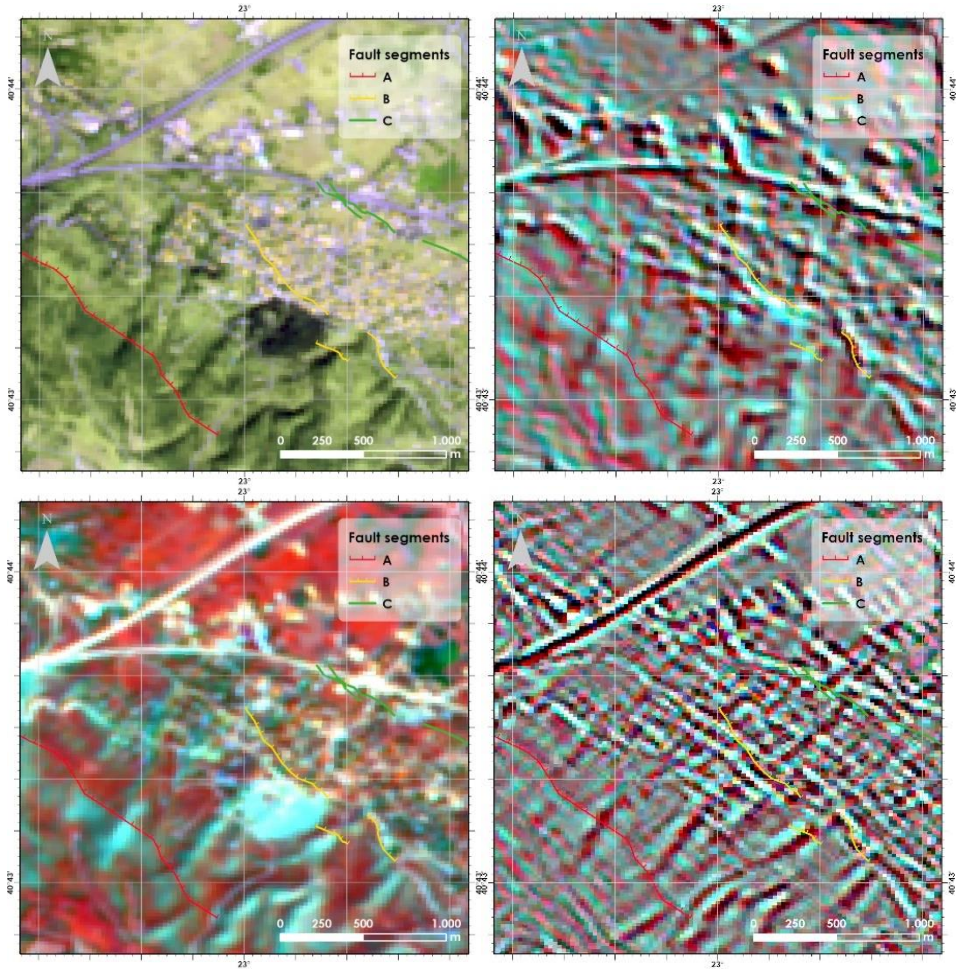

Figure 3. a. Geology band combination RGB = 12, 11, 2 map, b. Band combination RGB = 2/8, 3/11, 4/12 (ten Veen, 1998), c. Gradient northeast direction map, d. Line detection left direction map.

The produced maps show, in general, good correlation with the mapped fault segments of the Mygdonia basin. More specifically, segment A is more detectable with the band combination method, as it represents an old tectonic structure, and it is untraceable with Hillshade method. Segment B is visible with both methods because it represents a prominent tectonic structure of the area and a contact between the bedrock and the Quaternary sequence. However, the Hillshade method is more consistent as it represents a relief related structure. Segment C is not visible, as predicted, considering that is located entirely within the Quaternary sequence, as mentioned above.

This research shows that, even though these methodologies are commonly used in small scale line detection, they can be applied to larger scale as well. The proposed methodology works as a verification tool to the preliminary remote neotectonic study of an area since the results are in fairly good agreement with the existing mapped structures, and can supplement the field data.

Acknowledgements

We would like to thank our colleagues Efstathios Lymperis and Pavlos Fachouridis for their useful advice, and our professor Alexandros Chatzipetros for his valuable support.

References

Chatzipetros, A., Papadopoulou, E., 2019. A case of active fault migration in Mygdonia basin, northern Greece. IESCA – International Earth Science Colloquium on the Aegean Region, Izmir, Turkey, 7-11 October 2019.

Papadopoulou E., 2020. Neotectonic mapping in the southern margin of Mygdonia basin. Bachelor thesis, Aristotle University of Thessaloniki, Dept. Of Geology, Thessaloniki, 79 p.

Papadopoulou, E., Chatzipetros A. and Dretaki A., 2020. Neotectonic mapping and morphotectonic analysis of the southern margin of Mygdonia basin using G.I.S., Geography Conference – Geography in a Changing World, Mytilene 2-4 June 2020.

Earth Explorer; 2000; FS; 083-00; Geological Survey (U.S.) PULCHRA City Challenges Platform. Retrieved from Remote Sensing Tool: https://platform.pulchra-schools.eu/supportingtools/remote-sensing-tool/

Ten Veen, J. H., 1998. Neogene outer-arc evolution in the Cretan segment of the Hellenic arc: Tectonic, sedimentary and geodynamic reconstructions (Vol. 160, pp. 1-192). Utrecht University.

16th International Congress of the Geological Society of Greece

17-19 October, 2022 - Patras, Greece

Bulletin of the Geological Society of Greece, Sp. Publ. 10

Ext. Abs. GSG2022-260

The Flyschoidal Mélange Unit of the Adheres Massif (SE Argolis), in Relation to the Geological Mapping of Trizina Sheet at a Scale of 1:50.000.

A. Photiades[1], G. Deligiannakis[1]

(1) Hellenic Survey of Geology and Mineral Exploration (HSGME), Athens, Greece, fotiadis@igme.gr

The Hellenic Survey of Geology and Mineral Exploration (HSGME), in the frame of the GEOINFRA project (2019-2023) is updating, amongst others, the geological map sheet of Trizina – scale 1:50,000. In this context, we focused on the Adheres massif, which extends in parts of the existing Methana, Kranidi, and Hydra sheets, which are also to be updated. Previously, the Adheres massif was interpreted as a continuous stratigraphic Mesozoic carbonate sequence of the Pelagonian flysch succession of the Argolis peninsula. This area was named after "Ermioni Complex" by Robertson *et al.* (1987) and Clift (1996), while Bortolotti *et al.* (2003) described the stack of tectonic slices and olistoliths of heterogeneous lithologies as "Adheres Mélange Unit".

The Adheres massif is a flyschoidal tectonic unit of Campanian-Maastrichtian age, rich in pelagic limestone and turbidites (Bachman and Risch 1979; Bortolotti *et al.*, 2003). It is emplaced tectonically over the Paleocene flysch of the underlying bearing-ophiolite limestone Mesozoic sequences of the Argolis Basal Unit in the peninsula (Baumgartner 1985; Bortolotti *et al.*, 2003). Upwards the massif is overlain tectonically by the upper tectonic unit of Akros, consisting of late Cretaceous limestones with a serpentinite tectonic sole (Photiades, 1986; Mermighis, 1989).

The map-view of the Adheres massif reveals an imbricate complex thrusting system. Fold-and-thrust belts associated with NE and SE folding shears are present, while deeper faults refolding overlying thrust sheets indicate large-scale folding of the area. The thrust segment areas are duplicated by mostly northeast- and southeast-dipping thrust faults, forming an imbricate stack which preserves fine-grained to coarse-grained siliciclastic slices. The flyschoidal unit of the Adheres originates from various paleogeographical environments of the Internal Hellenides ranges and, among others, especially those deriving from the Pelagonian domain. It was probably assembled during two tectonic phases; first, it was emplaced onto the margin of the Argolis Basal Unit during the post-flysch thrusting (post-Paleocene). Then, it was deformed by a subsequent post-Eocene thrusting when the Akros Unit (Kastro, Skapeti, Poros outcrops) of the upper Cretaceous limestone sequence with the schistose serpentinite sole comprised the highest structural level of the nappe.

The flyschoidal block-in-matrix mélange consists of a wide range of siliciclastic deposits, which are affected by intense pervasive deformations that compose the matrix of a tectonic mélange (Figure 1a). Sandstones up to 1.5 m thick are often lensoidal with lateral axes of the order of several meters. Fine-grained sandstone, rich in mudstones or shales, alternate with thick-bedded lenticular coarse-grained sandstones, interbedded with debris flows (up to 3 m thick), containing mixtures of well-rounded pebbles of metamorphosed psammitic, carbonate and pelitic rocks up to 10 cm in diameter. Locally, graded bedding and various divisions of the Bouma sequence turbidites of siltstones and sandstones are present. The siliciclastics consist mainly of deep marine channelized coarse-grained turbidites, derived from quartzo-feldspathic metamorphic and limestone terranes. The quartzose sandstones are mostly lithic sandstones, containing polycrystalline quartz, muscovite, plagioclase, orthoclase, biotite, and opaque minerals. Lithoclasts comprise recrystallized carbonate, indurated shale, and psammitic schist. A variable abundance of siliciclastic sediment is also observed, including monocrystalline and polycrystalline quartz, schist, and shale. Multiple tectonic segments are placed within this mélange, including a) Upper Jurassic limestone olistholite (near Baroutospilia and Thermissi), associated with scattered quartz grains and shale lithoclasts with conglomeratic horizons, including phyllite and quartzite clasts; b) Mesozoic oceanic crust sediments interbedded with the basalts succession comprise up to several meter-thick packets of ribbon radiolarian chert (near Baroutospilia) of the Middle-Late Jurassic age and serpentinite slivers (see also Bortolotti et al. 2003); c) Basalts (MORB and IAT, according to Clift and Robertson, 1989); d) Andesitic rocks originating from a convergent setting on a continental margin (Sideris *et al.*, 1987); e) Jurassic granodiorites (170-144 Ma, Photiades and Keay, 2000); f) Upper Jurassic neritic carbonate, Upper Cretaceous pelagic carbonate, finely red mudstones, and shaly carbonate of Turonian-Maastrichtian (Bachman and Risch 1979); g) Upper Cretaceous metalliferous deposits interstratified with terrigenous turbidites (65-66 Ma, Triantafyllidis *et al.*, 2021); and h) Numerous km-sized detached marble sequence slivers, which are affected by folding deformation, diffuse fragmentation by fluid overpressure, and are cross-cut by calcite and quartz veining processes (Figure 1b). They are tectonically imbricated within NE-dipping at the top of the massif and the eastern part of the Tselevinia area. The coarse- to fine-grained and thick- to thin-platy bearing-chert marble sequence resembled a stratigraphic bottom with alternations of highly sheared metatuff layers, metabasalts, metamudstones, shales, and schists, where they metamorphosed in greenschist facies conditions.

These formations represent the final block-in-matrix in a shale-dominated shear zone (Ogata *et al.*, 2012) of that protracted deformational episodes, via already deformed/disrupted units from broken formations to olistostromes and evolving to tectono-sedimentary mélanges. Therefore, they imply different deformational processes from ductile deformation to

progressively more brittle and deeper mechanisms (Figure 1c) and suggest that part of the Adheres mélange occurs in exhumed metamorphic and poly-deformed subduction complexes (Festa *et al.*, 2022).

The flyschoidal mélange of Adheres massif tectonically overlies the Triassic-Jurassic limestone series, the Malm ophiolitic mélanges, and the Cretaceous limestone series of the Argolis (Figure 1d). The whole tectonic structure is the result of two compressional regimes creating sheared inclined folds: a) A NE to SW compression, which took place during the post-flysch compressional episode, and b) a SE to NW compression, during the post- Eocene continental collision of the Hellenides, which is thrusting the Akros Unit. It is analogous to the non-metamorphic upper Cycladic Unit, and refolds the implicated mélange of the massif transversally.

Figure 1: a) flyschoidal block-in-matrix mélange, b) folded thin-banded marble with meta-chert, c) crystalline limestone breccia of brittle origin, bearing red and olive-green schistose clasts, d) multi-folded alternations of thin-banded limestone and red mudstone, which is overlain by the Paleocene psammitic flysch of the Argolis Basal Unit.

Acknowledgements

The current work was carried out in the frame of the project "GEOINFRA: Geological Mapping of Greece for the support of innovation and entrepreneurship" (2019-2023), funded by the National Strategic Reference Framework (2014-2020).

References

Bachmann, G.H., Risch, H., 1979. Die geologische Entwicklung der Argolis-Halbinsel (Peloponnes, Griechenland). Geol. Jb.,B32: 3-177.

Baumgartner, P.O., 1985. Jurassic sedimentary evolution and nappe emplacement in the Argolis Peninsula (Peloponnesus, Greece). Mém. Soc. Helv. Sci. Nat. 99: 1-111.

Bortolotti, V., Carras, N, Chiari, M., Fazzuoli, M., Marcucci, M., Photiades, A., Principi, G., 2003. The Argolis Peninsula in the palaeogeographic and geodynamic frame of the Hellenides. Ofioliti, 28/2, 79-94.

Clift, P.D., Robertson, A.H.F., 1989. Evidence of a late Mesozoic ocean basin and subduction/accretion in southern Greek Neo-Tethys. Geology, 17: 559-563.

Clift, P.D., 1996. Accretion tectonics of the Neotethyan Ermioni Complex, Peloponnesos, Greece. J. Geol. Soc. London, 153: 745-757.

Festa, A., Barbero, E., Remitti, F., Ogata, K., Pini, G.A., 2022. Mélanges and chaotic rock units: implications for exhumed subduction complexes and orogenic belts. Geosystems and Geoenvironment (2022), doi.org/10.1016/j.geogeo.2022.100030.

Mermighis, A., 1989. Plates-formes carbonatées et récifs à rudistes du Crétacé supérieur de l'Argolide septentrionale (Péloponnèse NE, Grèce). Thèse Sciences, Univ. Provence, 171pp.

Ogata, K., Pini, G. A., Carè, D., Zélic, M., Dellisanti, F., 2012. Progressive development of block-in-matrix fabric ina shale-dominated shear zone: Insights from the Bobbio Tectonic Window (Northern Apennines, Italy), Tectonics,31, TC1003,doi:10.1029/2011TC002924.

Photiades, A., 1986. Contribution à l'étude géologique et métallogénique des unités ophiolitiques de l'Argolide septentrionale (Grèce). Thèse 3e cycle, Univ. Besançon, 261 pp.

Photiades, A., Keay, S, 2000. Mid-late Jurassic granodioritic basement in southern Argolis Peninsula (Greece): Tectonostratigrapic implications. In: I. Panayides, C. Xenophontos and J. Malpas (eds.), Proceed. 3rd Intern. Conf. Geology of the Eastern Mediterranean. Geol. Surv. Dpt. Cyprus, Nicosia, p. 233-239.

Robertson, A.H.F., Varnavas, S.P., Panagos, A.G., 1987. Ocean ridge origin and tectonic setting of Mesozoic sulphide and oxide deposits of the Argolis Peninsula of the Peloponnesus, Greece. *Sedimentary Geology*, 53/1, 1-32.

Sideris, C, Skounakis, S., and Simantov, J., 1987. Trace and REE geochemistry of a basic lava series from the Ermioni area (Argolis peninsula) Greece, Ofioliti, 12/1, 107-112.

Triantafyllidis, S., Tombros, S.T., Zhai, D., Kokkalas, S., 2021. The upper Cretaceous Ermioni VMS deposit, Argolis Peninsula, Peloponnese, Greece: Type, genesis, and geotectonic setting. Ore Geology Reviews 138, doi.org/10.1016/j.oregeorev.2021.104403

16th International Congress of the Geological Society of Greece
17-19 October, 2022 - Patras, Greece
Bulletin of the Geological Society of Greece, Sp. Publ. 10
Ext. Abs. GSG2022-261

The Stacked Tectonic Units Implicated in SW Othrys Massif: Regarding the Geological Mapping Update of the Northern Parts of Lamia and Sperchias Sheets at a 1:50.000 Scale

A. Photiades[1], N. Kalogiannis[1]
(1) Hellenic Survey of Geology & Mineral Exploration (HSGME), Athens, Greece, fotiadis@igme.gr

The Hellenic Survey of Geology and Mineral Exploration (HSGME), in the frame of the GEOINFRA project (2019-2023) is updating, amongst others, the geological map sheets of Lamia and Sperchias – scale 1:50,000. The fieldwork covered the SW Othrys massif including the northern parts of the geological sheets of Lamia (Marinos *et al.,* 1967) and Sperchias (Kallergis *et al.,* 1970) which extend north of the Sperchios river valley. The area as a part of the Pelagonian *s.l.* domain (Internal Hellenides) consists of extensive thrust units of Triassic pillow-lavas – radiolarites, Triassic-Jurassic hemipelagic siliceous carbonate series and ophiolites, which successively stacked during pre-Upper Cretaceous tectonic compressive phases that affected the area and involved towards the SW in successive Tertiary thrusts over both the calcarenite series (Asvesti village) of the Beotian unit and then on the sandstone-pelitic formation of the Pindos flysch unit.

The pre-Neogene tectono-stratigraphic stack is composed of successive overlapping thrust units facing southwestwards, where the following tectonic units, from bottom to top, are distinguished:

- **Kastri series** (**T.sh,k**), in the South of Grammeni village, is a clastic moderately metamorphic unit with shale, limestone-bearing filaments and conodonts of the middle-upper Triassic age, equivalent to the Maliac hemipelagic series (Ferriere, 1982), intercalated by radiolarian red-yellow mudstone, metasandstone series and pyroclastic deposits. It is affected by isoclinal folds with ENE trends that mainly verging to the SE but few of them to the NW;
- **Flyschoidal unit** (**T.fl**), in Karia railway station, is composed of flyschoidal siliciclastic coherent deposits in trailing imbricate fan inclined to the NE and bearing metasandstone up to coarse-grained arenitic (rich in poly-crystalline quartz, siltstone, silty sandstone, and volcanic grains) detrital input of various siliciclastic sedimentary rocks derived probably from erosional denudation of a Paleozoic crystalline basement, and bearing intercalation of shales and pyroclastic deposits. This sequence is affected by slaty cleavage and fracture schistosity. Also, the association of brittle structures (Riedel shears) under left-lateral and right-lateral oblique-slip normal faults reveals that both formed under the same compression direction (ENE–WSW);
- **Agrilia tectonic unit** (**$T_{i\text{-}s}$.vol,hn**) consists of the lower part of Loggitsi nappe. However, it is particularly challenging to be determined through mapping from the dominant hemipelagic tectonic unit of the region that is accepted as the Loggitsi nappe (Ferriere, 1982). However, the formations composing this unit are the following from base to top: purple vesicular pillow alkaline basalts and tuffs followed by siliceous beds and dark picrite lavas, upwards by radiolarian red chert and then overlain by folded platy siliceous limestones of Norian age alternating with filament-bearing gray limestone and red jasper beds intercalated by red mudstone and carbonate breccias, where the recumbent folds trend WNW and verge mainly to the NE. The upper part of the Agrilia unit is composed of rhythmically bedded, redeposited radiolarites and is also related to the extended Maliac hemipelagic unit (Ferriere, 1982);
- **Archani–Grammeni series** (**$T_{m\text{-}s}$.br**) is affected by brittle shear bands of SW-NE direction and consists of a volcaniclastic tectonic complex rich in limestone-matrix material, entraining blocks of red nodular carbonates of middle Triassic and lower Carnian age (in Kallergis *et al.*,1970), tectonic collapse breccias of upper Triassic neritic carbonate always tectonically associated with volcanic rocks (south of Trilofon) and rich in fragments of red radiolarites and sandstones. In addition, a mapped-size tectonosome of vesicular-porphyritic lavas that could be analogous to the short-lived and may be abortive volcanism is observed. This tectonosome is dated from Permo-Triassic up to middle Triassic and is associated with Anisian carbonate hemipelagic series;
- **Hemipelagic tectonic unit** (**T-J_i.k,hn**), consisting of siliceous limestones with red radiolarian cherts intercalated with red siliceous mudstone of Triassic-Jurassic age. In addition, it shows up to 300 m thick syn-rift volcanics (purple pillow lavas predominantly MORB and OIB) and deep pelagic sediments, often similar to those of the Fourka pillow lava unit (see below). This unit is composed of the upper part of Loggitsi nappe and thus, as a transitional hemipelagic unit of distal origin of the Maliac series, overthrusts during late Jurassic-early Cretaceous time on the Pelagonian carbonate platform outcropping northward and northeastward within the Efxinoupolis (former Anavra), and Almyros map sheets. This unit outcrops recumbent folds, trend NE and verges mainly towards the NW, but few folds trend WNW and ENE;
- **Mélange unit (**J_s**.mg)** of Malm age (Ferriere *et al.,* 1988), consists of a tectono-sedimentary mélange like Agoriani melange and is the base of the ophiolite unit (Photiades *et al.,* 2003; Bortolotti *et al.,* 2008). It is rich in clastic-supported collapse breccias and matrix-supported with red clay shale-red mudstone bearing various reworking and

some localities outcropping blocks-in-matrix and olisthostromes rich in radiolarites, lavas, and thin slivers of schistose serpentinites, includes alkaline within-plate basaltic and normal-type mid-ocean ridge sequences in the pillow facies, locally exhibit island arc tholeiite and boninitic composition (Photiades *et al.*, 2003; Bortolotti *et al.*, 2008);

- **Pillow lava unit with radiolarites** (**T.vol**), also referred to as Fourka unit, and its dating from Middle and Upper Triassic after radiolarian assemblages (Ferriere, 1982; Bortolotti *et al.*, 2008) and is made of pillow-lavas showing mainly MOR, within plate (WPB) and ocean island (OIB) basalts (Ferriere, 1982; Bortolotti *et al.*, 2008). It is a significant unit more than 300 m thick, being the most remarkable remnant of the Triassic oceanic crust corresponding to the initial activity of the divergence period within the MOR, and which constitutes the principal unit of the period before the oceanic crust convergence. Apart from pillow-lavas, pillow-lava collapse breccia and massive lava flows are also found and related with bedded radiolarian red cherts up to radiolarian red mudstone, locally bearing manganiferous nodules in red clay-shale matrix. Furthermore, in the Lamia sheet, the pillow-lavas are locally implicated by tectonic slices of nodular red siliceous limestones or neritic white limestones of Ladinian-Upper Triassic age. In general, the associated ribbon red cherts are characterized by isoclinal to recumbent up to chevron folds (trending NW and verging mainly to the NE, but few folds trend ENE and verging to NW), or warped folded red cherts tectonic slices imbricated in pillow lavas. In general, the mesoscopic scale fold architecture confirms the top-to-the-SW translation of this thrust unit;
- **Ophiolite unit (π,σ),** of Jurassic age is tectonically thrust on the previous Triassic-Jurassic series and consists of diverse suite of mantle rocks, ranging from fertile lherzolites (at the southern slope of Mega Isoma, Tourla areas in Sperchias sheet) to depleted harzburgites (in Lamia sheet) indicative of both anhydrous MOR-type and hydrous SSZ-type melting regimes (Saccani and Photiades, 2004; Barth *et al.*, 2008). Locally, some imbricated thin thrust cumulate and amphibolite slices drifted and incorporated at their basal thrust zone displaying ductile to brittle laminated and C-S shear bands. They are analyzed to have been derived from a supra-subduction zone (SSZ) environment with dated metamorphic soles in the range of 171–165 Ma (Spray and Roddick, 1980).
- Finally, the stacked tectonic units are sealed upwards through the transgressive carbonate formations of the Lower Cretaceous (at Stavros village and eastern Lamia areas with Hauterivian-Berriasian age) on the roof, passing then into the shallow-water carbonate succession up to deepening upwards with the deposition of platy limestone pelagic series of the Middle-Upper Cretaceous (Ks.k). At the top parts the clastic flysch formation (fg) of the Paleocene is deposited.

The northern parts of Lamia and Sperchias are stacked syn-thrust units of Triassic-Jurassic continental margin and oceanic crust, which were successively accreted during the early tectonic compression phase in late Jurassic-early Cretaceous and then, during the compressive post-flysch phase, in Eocene period, where the wider Pelagonian domain suffered showing within SW Othrys units' inter-thrusts and whole overthrust towards the W-SW on the Boeotian unit formations and the Pindos flysch unit.

The Sperchios tectonic structure plays a significant role since the Middle Triassic-Middle Jurassic could be a transform fault zone (Ferriere, 1982), contributing to the palaeogeographic differentiation on both sides of this transverse fault zones (E-W to ENE-WSW), providing to significant geological changes in the areas both north and south of the valley like the ophiolite unit bounded by the ENE-WSW faults. Still, the fold trending ENE to NE during the post-flysch period could be related to back folding activity, connected with the Cycladic blueschist formation, during the Eocene continental collision of the Hellenides (Mercier &Vergely, 1977 in Ferriere, 1982; Gerogiannis & Xypolias, 2017).

Acknowledgements

The current work was carried out in the frame of the project "GEOINFRA: Geological Mapping of Greece for the support of innovation and entrepreneurship" (2019-2023), funded by the National Strategic Reference Framework (2014-2020).

References

Barth, M. G., Mason, P. R. D., Davies, G. R., Drury, M. R., 2008. The Othris Ophiolite, Greece: A snapshot of subduction initiation at a mid-ocean ridge. Lithos, 100(1-4), 234–254.

Bortolotti, V., Chiari, M., Marcucci, M., Photiades, A., Principi, G., Saccani, E., 2008. New geochemical and age data on the ophiolites from the Othrys area (Greece): Implication for the Triassic evolution of the Vardar Ocean. Ofioliti, 33/2, 135–151.

Ferriere, J., 1982. Paleogeographies et tectoniques superposees dans les hellenides internes au niveau de l'Othrys et du Pelion (Grece). Soc Geol Nord Publ 8, 970 pp.

Gerogiannis, N., Xypolias, P., 2017. Retroward extrusion of high-pressure rocks: an example from the Hellenides (Pelion Blueschist Nappe, NW Aegean). Terra Nova, 29/1,372-381.

Kallergis, G.A., Koch, K.E., Nicolaus H.J., 1970. Geological map in scale 1:50.000: Sperchias sheet. Inst. Geol, Subs. Res., Athens.

Marinos, G., Anastopoulos, J., Maratos, G., Melidonis, N., Andronopoulos, V., 1967. Geological map in scale 1:50.000: northern part of Lamia sheet. Inst. Geol, Subs. Res., Athens.

Photiades, A., Saccani, E., Tassinari, R., 2003. Petrogenesis and tectonic setting of volcanic rocks from the subpelagonian ophiolitic mélange in the Agoriani area (Othrys, Greece). Ofioliti, 28(2), 121–135.

Spray, J.G., Roddick, J.C., 1980. Petrology and Ar geochemistry of some Hellenic subophiolite metamorphic rocks. Contrib. Mineral Petrol. 72:43–55.

16th International Congress of the Geological Society of Greece
17-19 October, 2022 - Patras, Greece
Bulletin of the Geological Society of Greece, Sp. Publ. 10
Ext. Abs. GSG2022-263

The Kourkoula Massif of Molai Area: a Tectonic Window Analogous to the Plattenkalk Series in South Peloponnese

A. Photiades[1], A. Zervakou[1]
(1) Hellenic Survey of Geology & Mineral Exploration (HSGME), Athens, Greece, fotiadis@igme.gr

Geological mapping/study

The Hellenic Survey of Geology and Mineral Exploration (HSGME), in the frame of the GEOINFRA project (2019-2023) is updating, amongst others, the geological map sheet of Molai – scale 1:50,000. Previous studies on the lithostratigraphic structure of the Kourkoula massif (Molai area, south Peloponnese) attribute it to the Tyros beds subbasement and, therefore, the whole massif to the Tripolis unit (Exindavelonis & Taktikos, 1979). Furthermore, throughout the Peloponnese region, covered by HSGME 1:50.000 scale geological map sheets (revised in the current period), no such metamorphic carbonate and metaclastic sequences of that thickness, like Kourkoula massif, are mapped and interconnected or even identified as composing the stratigraphic basis of the Tyros beds and, by extension, to be interconnected with the Tripolis unit.

Preliminary geological mapping of the Kourkoula massif at 1:25.000 scale (Figure 1) showed that:

1. The massif forms an NW/SE-trending morphological "anticline", more than 10 km long and 5 km wide, is structurally separated by an SW-dipping thrust zone in two folded compartments: the northern one of Ano Glykovryssi-Kourkoula, which is affected by isoclinal folds trend NNW and verge mainly to the NE, and the Astropeleki-Strongyla southern compartment, that is structured by NW trending isoclinal folds but verge to the SW.
2. From NE to SW, this massif entirely consists of a metaclastic sequence, as a metaflysch formation, of considerable thickness, composed of meta-siltstone lithologies, alternating with thin metasandstone horizons. The locally variegated (reddish, greenish) to foliated basal metaflysch section in the underlying marbles is characterized by transitional layers of calc-schists, bearing thin-platy dolomitic marbles, while the upper members are violet to multi-coloured thin-banded marbles with gray nodular chert. The whole sequence is isoclinal folded with a clearly developed axial planar cleavage. Colorful marbles (Figure 2) are also found at the northwestern end of Kourkoula massif, always at the base of the metaflysch sequence. In the western-central slope of the massif (Glykovryssi), several matrix-supported metaconglomerates outcropping in metaclastic sequence and include pebbles up to 10 cm in size, consisting of marble, quartz, quartzite, metasandstone, and rarely phyllite. In the area of Profitis Ilias chapel, the section of the transitional beds of the basis to the downwards banded marbles consists of thick-platy medium- to coarse-grained polygenic metabreccia marbles with heteroblastic fabrics, bearing metasandstone elements surrounded by a low matrix.

To the NE of Pakia village, the following formations outcrop successively, such as:

- dark grey thin-medium banded to nodular dolomitic marbles;
- South of Paliokastro (west of Pakia) banded dolomites occur. At their base, grey clastic horizons developed with rhythmic alternations from coarse-grained sandstones to arkoses, alternating with chlorite schists. Both dolomites and sandstones are cross-cut by Fe-rich veins;
- the Tyros beds, from Permian to lower Triassic age, are subdivided to a lower clastic member and an upper volcano-sedimentary sequence (Skarpelis, 1982), where the thickness of the last one, based on IGME (now HSGME) drilling data, is more than 500 m. The lower clastic member exclusively consists of turbiditic series, bearing alternations of pelites-sandstone and shale-sandstone. At the Sotiros Chapel, the clastic formation is conformably overlaid by Carnian limestone bed (Brauer *et al*., 1980), over which an upper volcano-sedimentary sequence is developed, consisting of basalt, andesite, rare dacite, rhyolite, and flows, together with voluminous pyroclastic and volcaniclastic bedded deposits, with shale-sandstone intercalations locally occurred, suffered by very-low grade metamorphism. The volcano-sedimentary sequence is overlaid by Norian and younger limestone beds derived from Tripolis unit (Thiebault and Kozur, 1979). Furthermore, Doutsos *et al.* (2000) demonstrated that an extensive arcuate backthrust, *the Molai Thrust*, carries the marbles and schists of the Kourkoula series eastwards, above the Tyros beds, while the Tripolis unit is affected by westward directed regional shearing.
- More northeastward, in the Gagania area, above the volcano-sedimentary sequence, the transitional layers to dolomites and fossil-bearing dolomitic limestones of Tripolis-derived unit of middle-upper Triassic age, are grey to dark grey, passing upwards to light-coloured, white to pink medium-bedded fossiliferous limestones of lower Jurassic age.

Conclusion/Discussion

Whereas the known Phyllites-Quartzites unit is absent at Molai area, the Kourkoula massif could be similar to Taygetos

and Parnon Plattenkalk series (PLK), that consist of the deepest structural unit in the Peloponnese. The PLK series comprise of chert-bearing pelagic carbonate rocks (multi-coloured carbonates exposed on the top of the multi-coloured marble sequence) of Jurassic to Upper Eocene age (Thiebault, 1982). A metaflysch sequence of probably lower Oligocene age (Bizon and Thiebault, 1974) rests conformably on these Mesozoic carbonate rocks. The PLK series in Taygetos and Parnon massifs corresponds to the southern prolongation of the Ionian zone, whereas other researchers place the PLK series in a more external position, between the Ionian and Pre-Apulian zones.

The preliminary geological mapping at 1:25.000 scale and ongoing structural and petrographic determinations showed that the Kourkoula massif outcrop in the southern prolongation of the Parnon and parallel to the Taygetos could be part of these tectonic windows in the south Peloponnese. It is structured equivalently to the platy carbonate series of the Plattenkalk on which both, the volcanic-sedimentary series of the Tyros beds and the Mesozoic limestones of Tripolis, are developed as nappe, without any presence of Phyllites-Quartzites unit, structurally implicated between them.

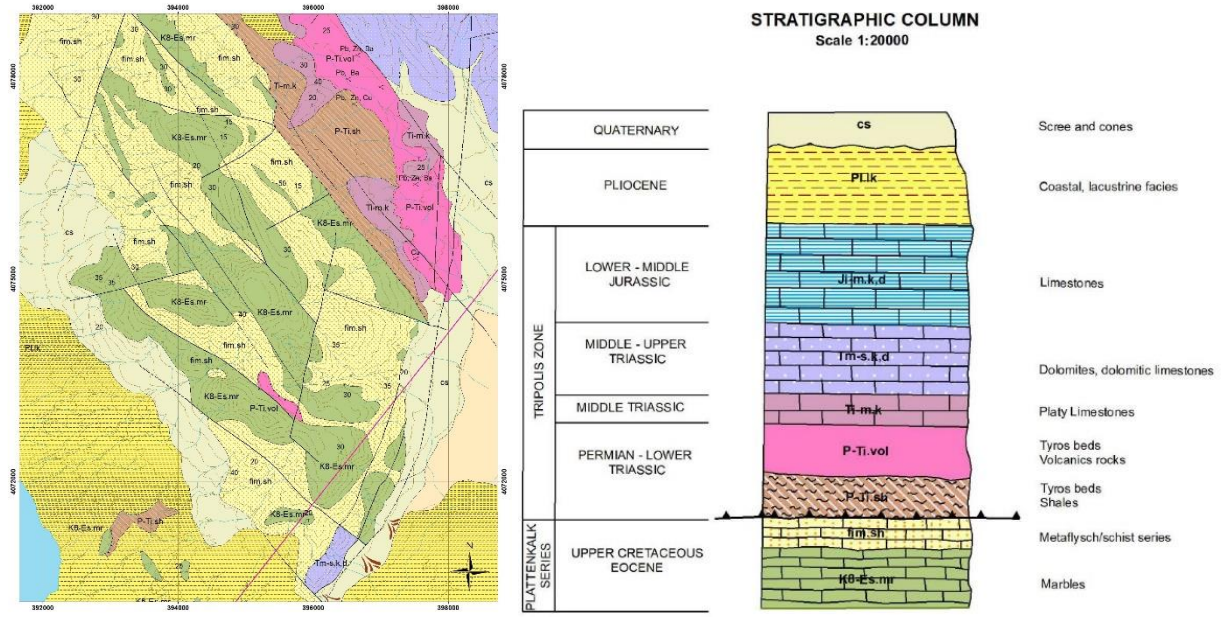

Figure 1. (a) Part of the 1:25.000 scale geological map of the Molai broader area and the relevant stratigraphic column.

Figure 2. Marble outcrop in the Kourkoula massif (Pakia village).

Acknowledgements

The current work was carried out in the frame of the project "GEOINFRA: Geological Mapping of Greece for the support of innovation and entrepreneurship" (2019-2023), funded by the National Strategic Reference Framework (2014-2020).

References

Bizon, G., Thiebault, F., 1974. Donnees nouvelles sur l' age des marbres et quartzites du Taygete (Peloponnese meridional, Grece). C. R. Acad. Sci., Paris, Ser. D, 278, 9–12.

Brauer, R., Ittner, R., Kowalczyk, G., 1980. Ergebnisse aus der "Phyllit-Serie" SE-Lakoniens (Peloponnes, Griechenland). N. Jb. Geol. Paläont. Mh. , 1980 (3), 129-144.

Doutsos, T., Koukouvelas, I., Poulimenos, G., Kokkalas, S., Xypolias, P., Skourlis, K., 2000. An exhumation model of the south Peloponnesus, Greece. Int J Earth Sci 89, 350–365.

Thiebault, F., 1982.Evolution géodynamique des Hellenides externes en Péloponnèse méridional (Grèce). Soc. Geol. Nord 6, 1—574.

Skarpelis, N., 1982. Metallogeny of massive sulfides and petrology of the External Metamorphic Belt of the Hellenides (SE-Peloponnesus). PhD Thesis, University of Athens, Athens, 1-149 (in Greek).

Thiebault, F., Kozur, H., 1979. Precisions sur l' age de la formation de Tyros (Paleozoique Superieur-Carnien) et la base de la serie de Garvrovo-Tripolitza (Carnien) (Peloponnese meridonal, Grece). C. R. Acad. Sci., Paris , Ser. D, 288, p. 23-26.

Exindavelonis, P, Taktikos, S., 1979. 1:50.000 scale Geological Map, Molai Sheet. IGME, Greece.

16th International Congress of the Geological Society of Greece

17-19 October, 2022 - Patras, Greece

Bulletin of the Geological Society of Greece, Sp. Publ. 10

Ext. Abs. GSG2022-305

Preliminary tectonostratigraphy results from the Small Trocharis mountain, north-east Lefka Ori, western Crete

D. Moraetis[1], C. Fassoulas[2], F. Alzhra[1], H. Khan[1], A. Leontaritis[3] K. Pavlopoulos[4] A. Scharf[5], M Vaxevanopoulos[6], K Adamopoulos[7], M. Digenis[8] C. Pennos[9], N. Nikolaidis[10].

(1) University of Sharjah, Department of Applied Physics and Astronomy Sharjah, UAE, dmoraitis@sharjah.ac.ae (2) University of Crete, Natural History Museum, Iraklion, Greece (3) National Technical University of Athens, Greece (4) Paris Sorbonne University Abu Dhabi, UAE (5) Sultan Qaboos University, Department of Earth Sciences, Muscat, Oman (6) Natural History Museum, Volos, Greece (7) Platonos Str, 132, Moschato, Athens, Greece (8) Ionian University, Department of Environment, , Zakynthos, Greece (9) University of Bergen, Department of Geography, Bergen, Norway (10) Technical University of Crete, School of Chemical and Environmental Engineering, Chania, Greece

Highlight

Here we describe our mapping results, for the updated stratigraphy of the Plattenkalk unit, and the tectonic contacts in Small Trocharis Mountain at north-east Lefka Ori of the island of Crete. The most prominent finding is that in the north-east, close to the peak of Ag Pneuma Melidoniou the thin bedded marble with silex (upper Jurassic-Eocene) is overlain by the upper Triassic to lower Jurassic white marble (Plattenkalk unit, both) and the contact between them appears as a primary conformable depositional contact. The previous shows a possible overturned structure.

Background and Objective

Nikolaidis *et al.* (2013) estimated the capacity of the karstic aquifer at $500x10^6$ m^3 for the Koiliaris watershed and the associated extended karstified area outside the watershed. The extended karst area is delineated in the region of the two deepest caves (sinkholes) in Greece, the Liontari (1100 m deep) and the Gourgouthakas caves (1208 m deep). Our study covers the extended karstic watershed. The objective of this work, under the IGCP-715 project, is to update our existing understanding of the geological model in the area and as well as to provide detailed lithological and structural insights for the extended karst area.

Geological Setting

The lithostratigrapy of Crete has been describe by Fytrolakis (1980), Soujon *et al*. (1998), Manutsoglu *et al*. (2003), Fassoulas & Nikolakakis (2005) and Papanikolaou *et al*. (2010). The western part of Lefka Ori area is characterized by a non-overturned continued sequence of Plattenkalk unit (Manutsoglu *et al*., 2003, IGME 1972, Vrisses sheet, 1:50,000). The general stratigraphy from old to young is: (1) Lias stromatolitic, dolomitic marble (Mavri formation), (2) The upper Jurassic Gigilos beds (marble with schist and chert), (3) the upper Jurassic to Eocene thin bedded marble with silex (also called *Typical* Plattenkalk), and (4) the Oligocene metaflysch (Kalavros layers-limeschists; Manutsoglu *et al.*, 2003). The Triassic to Jurassic Trypali unit is mainly recrystallized marble and appears to overlay with a thrust at different age formations of the Plattenkalk unit. In the Vrisses sheet (1:50,000), the Lias stromatolitic is missing and a white-grey limestone is alternating with very karstified black dolomite of the same age.

Results-Area 1 and Area 2

We have mapped 4 different formations of the Plattenkalk unit in the Small Trocharis mountain (area 1) and Ag Pneuma Melidoniou (area 2) as it is shown in Figure 1a. From top to bottom in the stratigraphy column we have identified (1) white marbles of the Plattenkalk unit (Wl) alternating with grey brecciated dolomite (BrD2) sometimes not only vertical but also within cavities, thus we consider it as one formation WI+BrD2, (2) black and white alternating stromatolitic dolomitic layers which are dipping SE (Str), which are not described in the Vrisses sheet (1:50,000) (3) black massive dolomite alternating with brecciated dolomite (BrD1). In the area around Gourgouthakas cave, Wl+BrD2 is reappearing and the nature of the contact between the BrD1 and WI+BrD2 has not yet clarified (Figure 1b). At Ag Pneuma Pemoniano chapel (close to area 1), there is the tectonic contact of the Trypali unit (Tr) in the hangingwall and the Ca-phyllites of the thin bedded marble (Plk) in the footwall, however, we were not able to identify the tectonostratigraphic relationship of the youngest Plk with the older formations of the Plattenkalk unit in the area 1 (WI-BrD2, Str, BrD1). The Plk are dipping towards NE with very shallow dipping angle (12-17°). On the contrary, in the area 2, the Plk is overlain by the Wl+BrD2 (Figure 1c). The measured faults in the area are striking E-W and NW-SE and they are characterized as thrust and normal faults, respectively.

Interestingly, in the area 2, the younger formation of the Plattenkalk unit, the thin bedded marble with silex (Plk) is overlain by the white marble (Wl+BrD2) (Figure 2a, 2b and 1c). We were able to measure the dipping of the Plk which dips NE with 30°. The contact appeared sedimentary conformable (Figure 2a, 2b). This is the first time we observe in western Crete the Plk to be overlain by the Wl+BrD2 and that denotes a possible overturned structure. The same observation has been reported also from the 2022 expedition in Gourgouthakas cave (Unpublished data).

Area 3 and Area 4

Area 3 is in the road to Ag. Pneuma Melidoniou and area 4 in Gournes valley (Figure 1a). A thrust contact between the Trypali Unit (Tr) (hanging wall) above the Plattenkalk (footwall) has been described. The thrust dips to the NE with an angle of 30°. The Trypali unit is strongly tectonized. The Plattenkalk unit dips shallowly to the NE. In the area 3, the thrust shows evidence of reactivation as normal fault, probably related with later than the thrust, extensional phase.

Conclusions

We have identified four formations at Small Trocharis mountain, and we described the stromatolitic layers and their stratigraphic position relative to the other formations in north Lefka Ori. East of the deep caves the younger formation Plk of the Plattenkalk unit appears stratigraphically bellow the older formation WI+BrD2 of the Plattenkalk unit. The previous denotes an overturned structure which has been observed also at Gourgouthakas cave at equivalent elevation of 1260 m. Further petrographic analysis will be used to correlate with the tectonostratigraphy of the central Crete.

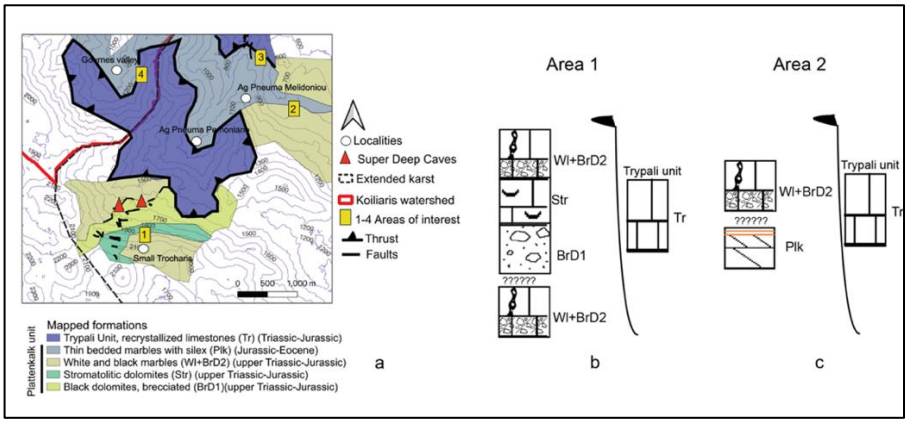

Figure 1. a) Mapping results and the identified lithologies. IGME 1972, Vrisses sheet 1:50,000 has been also utilized to identify the extend of the mapped lithologies. Contour elevation in meters and contour interval 100 m. b) stratigraphy column in area 1. c) stratigraphy column in area 2, below the contact the thin marble change to Ca-phyllite.

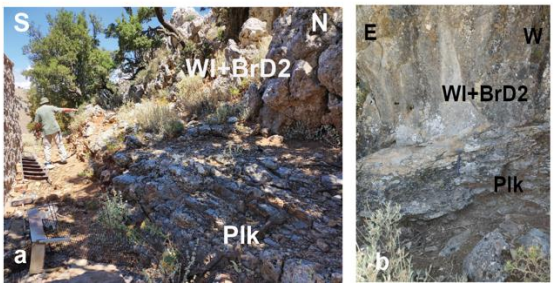

Figure 2. a) White limestone with pockets of dolomitic breccia (Wl+BrD2) overlay the thin bedded limestones with silex (Plk) in the area 2. b) Close view of the white limestone (Wl+BrD2) which overlies Plk in the area 2.

Acknowledgements

We are grateful for the UNESCO-IGCP-715 project and their financial support to organize the workshop in Crete-Greece in June 2022. We also acknowledge the Paris Sorbonne University Abu Dhabi for supporting the same workshop. Finally, we deliver our praise to all members of the Speleological expedition, Gourgouthakas 2022, for the sampling and the support of this work.

References

Fassoulas C. &. Nikolakakis E. 2005. Landscape response to the tectonic uplift of Crete, Greece. Bulletin Geological Society Greece, XXXVII 201-217.

Fytrolakis, N., 1980. The geological structure of Crete. Problems, observations and conclusions. Habil. thesis, National Technical University Athens, 143p.

Institute of Geology and Mineral Exploration, 1972. Geological map of Greece at scale 1:50.000, sheet Vrisses.

Manutsoglu E., Soujon A. and Jacobshagen V. 2003. 'Tectonic structure and fabric development of the Plattenkalk unit around the Samaria gorge, Western Crete, Greece'. Zeitschrift der Deutschen Geologischen Gesellschaft 154, 85-100.

Nikolaidis, N.P., Bouraoui, F, Bidoglio G, 2013. Hydrologic and geochemical modeling of a karstic Mediterranean watershed. Journal of Hydrology 477, 129-138.

Papanikolaou D, Vassilakis E, 2010. Thrust faults and extensional detachment faults in Cretan tectono-stratigraphy: Implications for Middle Miocene extension. Tectonophysics, 488, 233–24.

Soujon A., Jacobshagen V. & Manutsoglu, E. 1998. A lithostratigraphic correlation of the Plattenkalk occurrences of Crete (Greece), Bulletin Geological Society Greece, XXXII/1 41-48.

16th International Congress of the Geological Society of Greece
17-19 October, 2022 - Patras, Greece
Bulletin of the Geological Society of Greece, Sp. Publ. 10
Ext. Abs. GSG2022-320

Revisiting active faulting in Northern Greece: E-W and NW-SE trending structures

I. Papanikolaou[1], P. Dafnis[2], G. Deligiannakis[1], J. Hengesh[2], A. Panagopoulos[2], E. Lymperis[4]

(1) Mineralogy-Geology Laboratory, Agricultural University of Athens, Athens, Greece, i.pap@aua.gr (2) Geoskopio SA - Edafomichaniki group Athens, N. Iraklio Athens, Greece (3) Interface Geohazard Consulting LLC, Lahaina, USA (4) Edafos Engineering Consultants SA, Athens, Greece

Introduction

The Central Macedonia landscape and geological structure is dominated by large NW–SE trending fault-bounded basins, such as the Axios, Mygdonia, Strymon and Drama basins. These basins formed during Late Miocene to Pliocene NE–SW directed extension that primarily activated NW–SE striking normal faults (Dinter and Royden, 1993; Tranos, 2011). Since the Quaternary, the stress field has changed and is now dominated by N–S extension and formation of E-W trending normal faults that have reshaped the pre-existing basins (e.g. Pavlides and Kilias, 1987; Chatzipetros and Pavlides, 1998; Pavlides *et al.*, 2010; Tranos, 2011). The current N–S extension direction is also confirmed by geodetic (McClusky *et al.*, 2000; Müller *et al.*, 2013) and seismicity data (Vamvakaris *et al.*, 2006). Therefore, the existence of E-W trending active normal faults in a N-S extensional stress field is straightforward and confirmed by neotectonic and paleoseismological data (e.g. Chatzipetros *et al.*, 2005) as well as by strong surface rupturing earthquakes (e.g. in 1978 the M=6.5 event occurred along a fault towards the southern part of the Mygdonia basin (Figure 1b), generating primary and secondary surface ruptures (Papazachos *et al.*, 1979; Mercier *et al.*, 1983)).

Key Question

Following the above, a key question concerns the NW-SE trending faults. Are they still active today? We have some strong indications of their potential activity since: a) they bound Quaternary sediments and control Holocene sedimentation processes, b) they still influence the topography preserving steep gradients that are not expected for structures considered inactive since the Pliocene, c) surface ruptures from the 1978 M=6.5 earthquake that were trending not only E-W, but continue to pre-existing fault plains with NW-SE directions and d) we have elongated isoseismals trending NW-SE in some recent strong historical events (e.g. 1902 M=6.6 Assiros and 1932 M=7.0 Ierrisos earthquakes, Voidomatis *et al.*, 1990, Papazachos and Papazachou 2003). Although a limited number of prior paleoseismological investigations have been completed along some of the E-W oriented fault zones in northern Greece (Chatzipetros *et al.*, 2005), none previously have been carried out on the NW-SE oriented fault zones in the region to confirm or reject this hypothesis.

Methodology and Results

Paleoseismological trenching investigations supported by radiometric dating have been conducted in the Mygdonia, Strymon and Drama basins (Papanikolaou *et al.*, 2018, Papanikolaou *et al.*, in press). These studies: i) confirmed that three NW-SE trending faults are indeed active and ii) identified a new E-W trending active fault in North Mygdonia basin approximately 20km northwards the town of Thessaloniki. In particular:

1) The Symvoli - Fotolivos fault zone (SFFZ) dips to the NE and forms the western boundary of the Drama basin (Figure 1a). Two Holocene surface rupturing events are inferred for this fault with vertical displacements of 75 and 66cm, yielding a Holocene slip rate of 0.15±0.1mm/yr and an average recurrence interval of 5700yrs.
2) The Tholos - Nea Zichni fault zone (TNFZ) dips to the SW and forms the eastern boundary of the Strymon basin (Figure 1a). Paleoseismic trenching revealed that this is a complex fault zone with deformation distributed across several synthetic and antithetic planes involving also Holocene events. It is interpreted as a low slip-rate fault (0.20 ± 0.1 mm/yr), with recurrence intervals on the order of 2500±1000yrs.
3) The Drimos fault zone (DFZ) dips to the NE (Figure 1b), is characterized by distributed deformation with eight major and secondary fault planes observed at four different sites, has hosted Holocene events and has a slip-rate on the order of 0.1–0.3 mm/yr.
4) The Assiros - Krithia fault AKF is an E-W trending, north facing structure that has deflected the local drainage system and forms the northern boundary of the Mygdonia basin (Figure 1b). Radiocarbon dates suggest that at least two events have occurred since the mid-Holocene. The total displacement over the last 18620 years is 185 cm, implying a ~0.10 mm/yr slip-rate.

Discussion and Conclusions

Paleoseismological trenching provided geological evidence for Holocene deformation along the NW-SE trending Drimos, Symvoli - Fotolivos and Tholos - Nea Zichni basin bounding fault zones, demonstrating that the NW-SE trending structures can also be active in the current N–S extensional stress regime. As a result, we should treat all these NW-SE trending faults that bound such basins, as potentially active and proceed with intensive paleoseismological studies. We

also observe that in several fault zones, E-W trending faults are interfingering with and interconnected along the older NW-SE structures (e.g. AKF, Serres fault), smoothly reshaping the older basins. All the studied faults have long recurrence intervals justifying why they were not activated during the period covered by the historical record and emphasise, once again, the necessity of paleoseismological studies and the implementation of fault specific approaches in seismic hazard assessment.

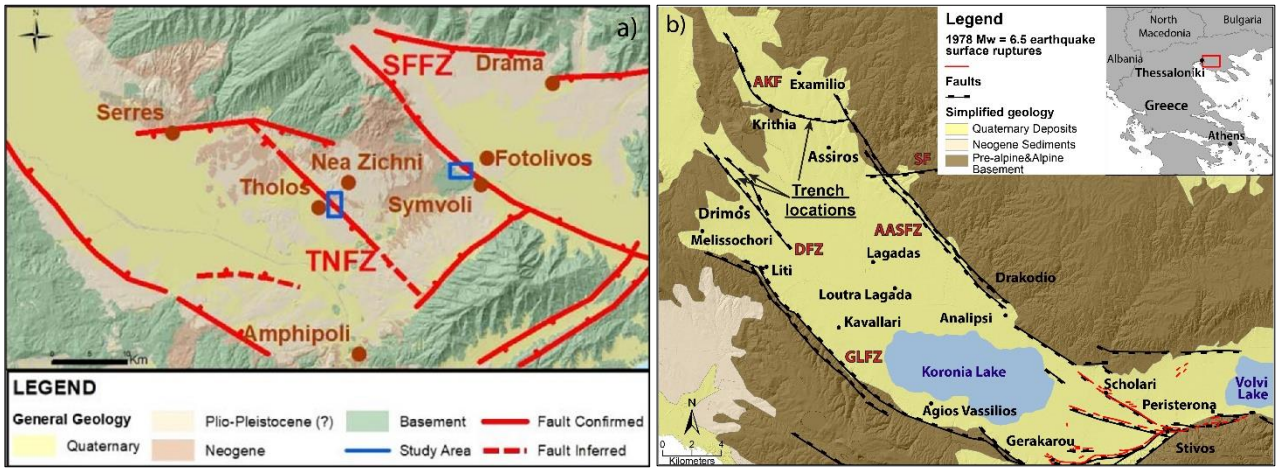

Figure 1 a) Simplified geological map showing the main faults of the Drama and Strymon Basins. b) Simplified Geological Map of the Mygdonia Basin (modified from Mountrakis *et al.*, 1996a, 1996b; Neotectonic Maps) , showing the active faults (with thick traces the Assiros-Krithia fault and the Drimos fault zone), the trench locations and the surface ruptures of the 1978 M = 6.5 event (highlighted in red).

References

Chatzipetros, A.A., Pavlides, S.B., 1998. A quantitative morphotectonic approach to the study of active faults; Mygdonia basin, northern Greece. Bull. Geol. Soc. Greece 32, 155–164.

Chatzipetros, A., Kokkalas, S., Pavlides, S., Koukouvelas, I., 2005. Palaeoseismic data and their implication for active deformation in Greece. J. Geodyn. 40, 170–188.

Dinter, D.A., Royden, L., 1993. Late Cenozoic extension in north-eastern Greece: Strymon Valley detachment system and Rhodope metamorphic core complex. Geology 21, 45–48.

McClusky, S., et al., 2000. Global positioning system constraints on plate kinematics and dynamics in the eastern Mediterranean and Caucasus. J. Geophys. Res. 105, 5695–5719.

Mercier, J., Carey-Gailhardis, E., Mouyaris, N., Simeakis, K., Rondoyiannis, T., Anghelidhis, C., 1983. Structural analysis of recent and active faults and regional state of stress in the epicentral area of the 1978 Thessaloniki earthquakes (northern Greece). Tectonics 2, 577–600.

Mountrakis, D., Tranos, M., Papazachos, C., Thomaidou, E., Karagianni, E., Vamvakaris, D., 2006. New Neotectonic and Seismological Data about the Main Active Faults and Stress Regime of Northern Greece, 260. Geological Society of London, Special Publications, pp. 649–670.

Müller, M.D., Geiger, A., Kahle, H.-G., Veis, G., Billiris, H., Paradissis, D., Felekis, S., 2013. Velocity and deformation fields in the North Aegean domain, Greece, and implications for fault kinematics, derived from GPS data 1993–2009. Tectonophysics 598, 34–49.

Papanikolaou, I.; Deligiannakis, G.; Hengesh, J.; Dafnis, P.; Panagopoulos, A.; Lymperis, E. (2018). Paleoseismic Trenching and Evaluation of the Symvoli-Fotolivos and Tholos-Nea Zichni Fault Zones in Northern Greece. In Proceedings of the 9th International INQUA Meeting on Paleoseismology, Active Tectonics and Archeoseismology (PATA); Possidi, Greece,pp. 205–208.

Papanikolaou, I.; Dafnis, P.; Deligiannakis, G.; Hengesh, J.; Panagopoulos, A. (in press). Active Faults, Paleoseismological Trenching and Seismic Hazard Assessment in the Northern Mygdonia Basin, Northern Greece: The Assiros-Krithia Fault and the Drimos Fault Zone. Quaternary International 2022, doi:10.1016/J.QUAINT.2022.02.001.

Papazachos, B., Mountrakis, D., Psilovikos, A., Leventakis, G., 1979. surface fault ruptures and fault plane solutions of the may-June 1978 June major shocks in the Thessaloniki area, Greece. Tectonophysics 53, 171–183.

Papazachos, B.C., Papazachou, C.B., 2003. The Earthquakes of Greece. Ziti editions.

Pavlides, S.B., Kilias, A.A., 1987. Neotectonic and active faults along the Servomacedonian zone (SE Chalkidiki, northern Greece). Ann. Tect. I (2), 9–104.

Pavlides, S., Caputo, R., Sboras, S., Chatzipetros, A., Papathanasiou, G., Valkaniotis, S., 2010. The Greek catalogue OF active faults and database OF seismogenic sources. Bull. Geol. Soc. Greece 43 (1), 486–494.

Tranos, M., Papadimitriou, E., Kilias, A., 2003. Thessaloniki-Gerakarou Fault Zone (TGFZ): the western extension of the 1978 Thessaloniki earthquake fault (Northern Greece) and seismic hazard assessment. J. Struct. Geol. 25, 2109–2123.

Tranos, M.D., 2011. Strymon and Strymonikos Gulf basins (Northern Greece): implications on their formation and evolution from faulting. J. Geodyn. 51, 285–305.

Vamvakaris, D.A., Papazachos, C.B., Karagianni, E.E., Scordilis, E.M., Hatzidimitriou, P. M., 2006. Small-scale spatial variation of the stress field in the back-arc Aegean area: results from the seismotectonic study of the broader area of Mygdonia basin (N. Greece). Tectonophysics 417, 249–267.

Voidomatis, Ph S., Pavlides, S.B., Papadopoulos, G.A., 1990. Active deformation and seismic potential in the Serbomacedonian zone, northern Greece. Tectonophysics 179, 1–9.

16th International Congress of the Geological Society of Greece
17-19 October, 2022 - Patras, Greece
Bulletin of the Geological Society of Greece, Sp. Publ. 10
Ext. Abs. GSG2022-334

The East Tower of the Phyle Fortress: A Deformation Pattern Suggesting an additional contributing factor to the ground motion of Athens 1999 earthquake

I. Kampolis[1,2], E. Kamperis[3], I. Vakalas[1], St. Triantafyllidis[1], Th. Georgousopoulou[4]

(1) National Technical University of Athens, Athens, Greece, (2) National Center for Scientific Research 'Demokritos', Agia Paraskevi, Greece, kampolisigeo@gmail.com (3) Epidomos Ltd, Lykovryssi, Greece, (4) Ephorate of Antiquities of West Attica, Athens, Greece

Research Highlights

The observed damages on the east tower of the Phyle Fortress reveal additional scientific data regarding an unknown earthquake event and its associated damages.

Abstract

The fortress of Phyle is mentioned in several ancient sources. Xenophon holds that it was captured by Thracyboulos in 404 B.C. when he set off against the 30 tyrants (Xenophon Hellenica II, 4, 2-7). Archaeological evidence, however, points towards a later dating of the fortress in the first quarter of the 4th century B.C. It was constructed as part of the defensive system of Athens in the 4th century B.C., a product of Athenian concerns for territorial defense (Leriou *et al.*, 2010). The Phyle Fortress is located at 666 m altitude (its central gate) in the mountainous area of Western Parnes and about 10.5 km NW from the modern town of Fyli. It has been constructed on a horst consisting of Upper Cretaceous Limestone of the Pelagonian Unit (IGME, 1986 – Geological Sheet 'Athinai-Elefsis'). On top of this horst, a paleo-peneplain can be found which attracted the attention of the ancient people and thus, they took advantage of this landform and fortified the area. The fortified area (that is the peneplain) has a 112 m-long major axis trending N098º. The walls were reinforced by four towers, three of which are rectangular and one cylindrical, which is partly collapsed. Two gates rendered the fortress accessible, the main one, which is partly collapsed, on the east, and a smaller one on the south.

The area of the archaeological monument was shaken by a Mw=6 earthquake in September 7th 1999 provoking extended damages in the NW suburbs of Athens (Seismological Lab, University of Athens). This event left 700 people injured and 7000 homeless (Papadopoulos *et al*., 2000), whereas the fatalities reached the 143. Of course, the earthquake, having an epicenter about 9 km SW of the Fortress, did not leave the archaeological site unaffected. This case where an archaeological monument is impacted by an earthquake constitutes an important opportunity for an archaeoseismological approach to be applied in order to explain the observed damages. Nevertheless, several studies of this type, based on quantitative methods have shown the ambiguity arising for the causative factor between earthquake ground motion and alternative causes (Hinzen and Weiner, 2009; Hinzen *et al*., 2010).

The days following the main shock, an autopsy was performed by personnel of the Ministry of Culture in order to assess the site damages. Partial collapses of the surrounding fortification wall occurred and the east tower of the fortress revealed patterns of deformation (Fig. 1). The emerged collapses and deformation, directly after the 1999 temblor, was linked to the released seismic energy. By analyzing the overall geomorphology as well as the tectonic elements on the east area of the fortification wall in combination with the deformation patterns of the east tower, we attempted to link /relate the tectonic elements with the triggered deformation. Our work was also assisted by laser scanning of the archaeological site as well as a 3D model generated by employing structure from motion (SfM) photogrammetry at the east tower, methods increasingly used in archaeoseismology (Hinzen *et al*, 2011).

During fieldwork we measured a NW trending fault (dip direction 065º/69º) close to the northern leg of the east tower bearing a light band on its surface (Fig.1). Its fresh surface without any signs of weathering, implies a relatively young movement and may be attributed to an older earthquake episode (before 1999). Although, the wider area of Athens as well as of the fortress was considered aseismic or of very low seismic activity (Pavlides *et al*., 2002), the most recent known earthquake event of similar size and before 1999, took place in 1705 (Ambraseys, 1994). With a close-up observation on the fault, we were able to assess and measure the sense of movement which presented a low-angle NNW-bearing direction (354º /25º). Thus, the measured fault is marginally in the category of normal faults but with a significant oblique motion. Also, another fresh surface on a NNW-trending fault (dip direction 083º /56º) was detected in a distance of about 3 m eastwards of the previous fault. The sense of movement on the latter could not be defined. Similar small fault scarps were reported by Pavlides *et al*. (2002).

The deformation of the East Tower was produced mainly, due to the strong ground motion provoked by the 1999 Athens earthquake. The latter have triggered up to 0.32 g of peak ground acceleration (Pavlides *et al*., 2002). However, there is a possibility that the observed NW-SE oblique-slip fault had already impacted the structural stability of the tower, which showed a strong deformation only after the 1999 Athens earthquake and its intense shaking. The aforementioned fault delineates the façade of the east tower and may have contributed to the triggered deformation pattern of the tower. The NE corner of the tower has undergone an eastward torsion due to the slip on the NW-SE fault (Fig. 1), which was able to

emerge only after the released earthquake energy of 1999. Noteworthy, is the fact that the building block of the tower's NE corner presents a slight tilt (5°) towards the NE, whereas the respective blocks in the unaffected part of the tower have a horizontal inclination.

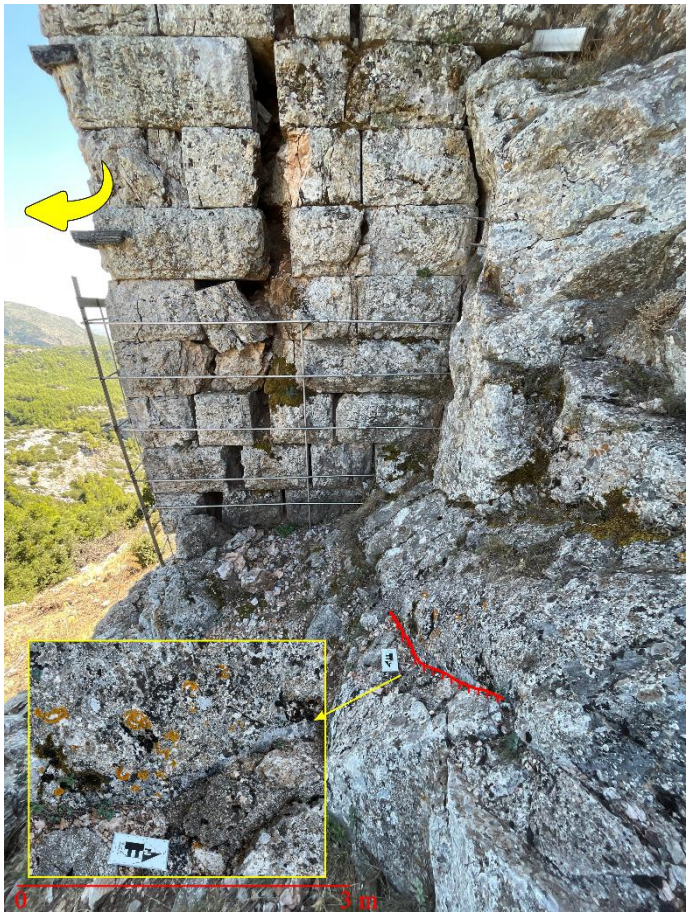

Figure 1. The east tower of the Phyle Fortress and the NW-SE fault (red line). The embedded image depicts the fresh surface of the scarp. The large yellow arrow represents the direction of the tower's torsion.

The present study highlights the potential of the archaeological monument of Phyle on revealing additional scientific data regarding an unknown earthquake event and its associated damages.

Acknowledgements

We would like to express our sincere thanks to Mr. Christos Pappous, Mayor of the Fyli Municipality for the embracement and the funding of the current project. Special thanks are also, addressed to the Ephorate of Antiquities of West Attica for granting permit in order to digitally record the site.

References

Ambraseys, N., 1994. Material for the investigation of the seismicity of central Greece, in: Albini P., Moroni A. (Eds), Historical Investigation of the Seismicity of European Earthquakes, Vol. 2, 1–10.

Dodwell, E., 1834. Views and Descriptions of Cyclopian, or Pelasgic Remains, in Greece and Italy; with Constructions of a Later Period. Adolphus Richter and Co.

Hinzen, K.-G., Weiner, J., 2009. Testing a Seismic Scenario for the Damage of the Neolithic Wooden Well of Erkelenz-Kueckhoven, Germany. Geological Society, London. Special Publications 316, 189-205.

Hinzen, K.-G., Schreiber, S., Yerli, B., 2010. The Lycian sarcophagus of Arttumpara, Pınara (Turkey): Testing seismogenic and anthropogenic damage scenarios. Bulletin of the Seismological Society of America, 100(6): 3148–3164.

Hinzen, K.-G., Fleischer, C., Reamer, K. S., Schreiber, S., Schütte, S., Yerli, B., 2011. Quantitative methods in archaeoseismology. Quaternary International 242, 31-41.

IGME, 1986. Geological Sheet 'Athinai-Elefsis'. scale 1:50000.

Leriou, A., Athanassakou V., Mourouglou, A., Ghini, M., 2010. WESTERN ATTICA: HISTORY-CULTURE. E.E.-Ellinikes Ekdoseis S.A.

Papadopoulos, G. A., Drakatos, G., Papanastassiou, D., Kalogeras, I., Stavrakakis, G., 2000. Preliminary results about the catastrophic earthquake of 7 September 1999 in Athens, Greece. Seismological Research Letters 71, 318–329.

Pavlides, B. S., Papadoloulos, G., Ganas, A., 2002. The Fault that Caused the Athens September 1999 Ms=5.9 Earthquake: Field Observations. Natural Hazards 27: 61–84.

Xenophon. Hellenica. Book II, Chapter 4, 2-7. (in Greek)

16th International Congress of the Geological Society of Greece
17-19 October, 2022 - Patras, Greece
Bulletin of the Geological Society of Greece, Sp. Publ. 10
Ext. Abs. GSG2022-335

Preliminary results on the geological and structural setting of the Mamonia Complex in SW Cyprus

A. Varnava[1], A. Chatzipetros[1], E. Katrivanos[1], L. Papadopoulou[1], A. Kilias[1]
(1) Department of Geology, Aristotle University of Thessaloniki, Thessaloniki, Greece, avarnava@geo.auth.gr

Research Highlights

Preliminary results on the geological and structural setting of the Mamonia Complex and the imbricated amphibolite slices in between it.

In this paper, we present the preliminary results on the structural setting of the Mamonia Complex tectonostratigraphic units and of imbricated between them amphibolite slices. The complicated Mamonia allochthon complex in SW Cyprus (Fig.1a) is an important tectono-sedimentary unit for the understanding of the geodynamic evolution and paleogeography of the Tethyan ocean (Dercourt *et al.*, 1993; Robertson & Woodcock, 1979; Lapierre, *et al.*, 2007; Torley & Robertson, 2018). Mamonia Complex can be subdivided into two essential tectono-stratigraphic units, the Dhiarizos Group, and the Ayios Photios Group (Swarbrick & Robertson, 1980).

Dhiarizos Group is the lower tectonic unit of Mamonia Complex and comprises mostly of volcanic rocks of mafic to felsic composition which are a pillow lava assemblage (Phasoula Formation) that accompanied with reefal and brecciated carbonates (Petra tou Romiou Formation) (Malpas *et al.*, 1992; Lapierre, *et al.*, 2007). Also, Dhiarizos Group comprises of lava breccias (Loutra tis Aphroditis Formation) and a thin unit that consists of turbidity current redeposited as periplatformal mud across the volcanic basement, while radiolarian horizons were deposited in deeper environment below the calcium carbonate compensation depth (Kholetria member) (Malpas *et al.*, 1992). Ayios Photios Group is the upper tectonic unit of Mamonia Complex and consists predominantly of sedimentary rocks, and according to Robertson & Woodcock (1979) and Swarbrick & Robertson (1980) is further subdivided into three lithostratigraphic units: Vlampouros, Marona and Episkopi Formations. Vlampouros Fm is an essentially terrigenous sedimentary sequence containing grey sandstones, micritic limestones and calcarenites shallow-water clasts; it is ca. 30 m-thick and Late Triassic (Carnian-Norian) in age, as established by radiolarians (Ealey & Knox, 1975; Bragin & Krylov, 1996). Marona Fm is consisted of a ca.25-thick pelagic carbonate sequence that is mostly calcilutites and includes abundant pelagic bivalve Halobia, Upper Triassic ages (Robertson & Woodcock, 1979). At many sites Vlampouros Fm passes through directly to Episkopi Fm and this the reason why Marona Fm considered by Bragin & Krylov (1996) as a member of the Vlampouros Fm. Episkopi Fm is a ca. 100m-thick sequence of radiolarites that are couplets of cm-thick radiolarian cherts an mm-thick shales, which contain few intercalations of redeposited limestones and terrigenous sediments. By the few paleontological data available, Episkopi Fm is assumed as a unit of late Middle Jurassic-Early Cretaceous age. More specifically, Bragin & Krylov (1999) have observed radiolarian assemblages suggestive of three separate time intervals: Callovian-Oxfordian, Oxfordian and Kimmerigian-Valanginian. However, Varnava *et al.*, (2021) present a new radiolarian age evidence that established for the first time an explicit and short-range Middle Jurassic (Middle Bathonian) age for a small part of radiolarites of this unit, which is established that radiolarian ooze accumulation begun at least since the Middle Bathonian. Therefore, according to the results of Varnava *et al.*, (2021) that reduce the age range of the previously known hiatus between the Upper Triassic and Jurassic sequences of the Ayios Photios Group such as presented. Kathikas Fm and Lefkara Fm are overlying the Mamonia Complex and the Troodos ophiolitic Complex. Kathikas Fm is an olistostromal unit containing blocks of both Troodos and Mamonia which seals (c. 70 Ma, Maastrichtian; Swarbrick & Robertson, 1980) the structural contacts within Mamonia Complex and the fundamental tectonic contacts between the Mamonia and Troodos Complexes. Kathikas Fm passes upwards into the deep-water limestones of the Lefkara Fm, but in some places the two Complexes are overlaid directly by the latest (Fig.1b).

According to Malpas *et al.*, (1992) serpentinite and amphibolite appear as a discontinuous acuate belt. Usually, amphibolite slices are less than 50-100 m in length, however, there is a large slice of amphibolite, approximately 2 km in length, in the vicinity of Ayia Varvara village (Ayia Varvara Formation). Isotopic data analysis date the metamorphic event of the amphibolite as Upper Cretaceous ages (c. 92-90 Ma; Mukasa & Ludden, 1987). We regard the amphibolite as a metamorphic amphibolite sole created in a North-wards directed Neo-Tethyan intra-oceanic subduction during the Upper Cretaceous.

The study of relevant thin sections shows that the amphibolite contains abundant scattered quartz and, more often, quartz in veins, plagioclase, amphiboles (hornblende and actinolite), biotite, epidote, titanite and rutile. A few thin sections have olivine, chlorite, rutile, and very small crystals of garnet and zircon. Additionally, calcite in veins is present in several thin sections which could be associated with a subsequent brittle phase of deformation.

As we present in the geological column (Fig.1b) and the schematic geological cross-section (Fig.1d) the Mamonia

Complex together with the amphibolites and the Troodos ophiolites are strongly imbricated. According to the discordant transgression of Maastrichtian shallow water sediments on the imbricated slices and thrusts, we support that the imbrication took place during the period of 90 to 70 Ma. Ductile, as well as brittle shear sense indicators show a mainly kinematic sense to-wards W-SW (Fig.1c, d). Occasionally simultaneous with the dominant W-SWwards kinematics, in some places appears opposite sense of shear of the trusts to the NE (Fig. 1d).

In conclusion, we suggest that the Mamonia Complex and the described associated units constitute an imbricated wedge in between the Troodos ophiolitic Complex, which was occurred during 90 to 70 Ma. The mainly kinematic sense of shear is regarded to-wards W-SW.

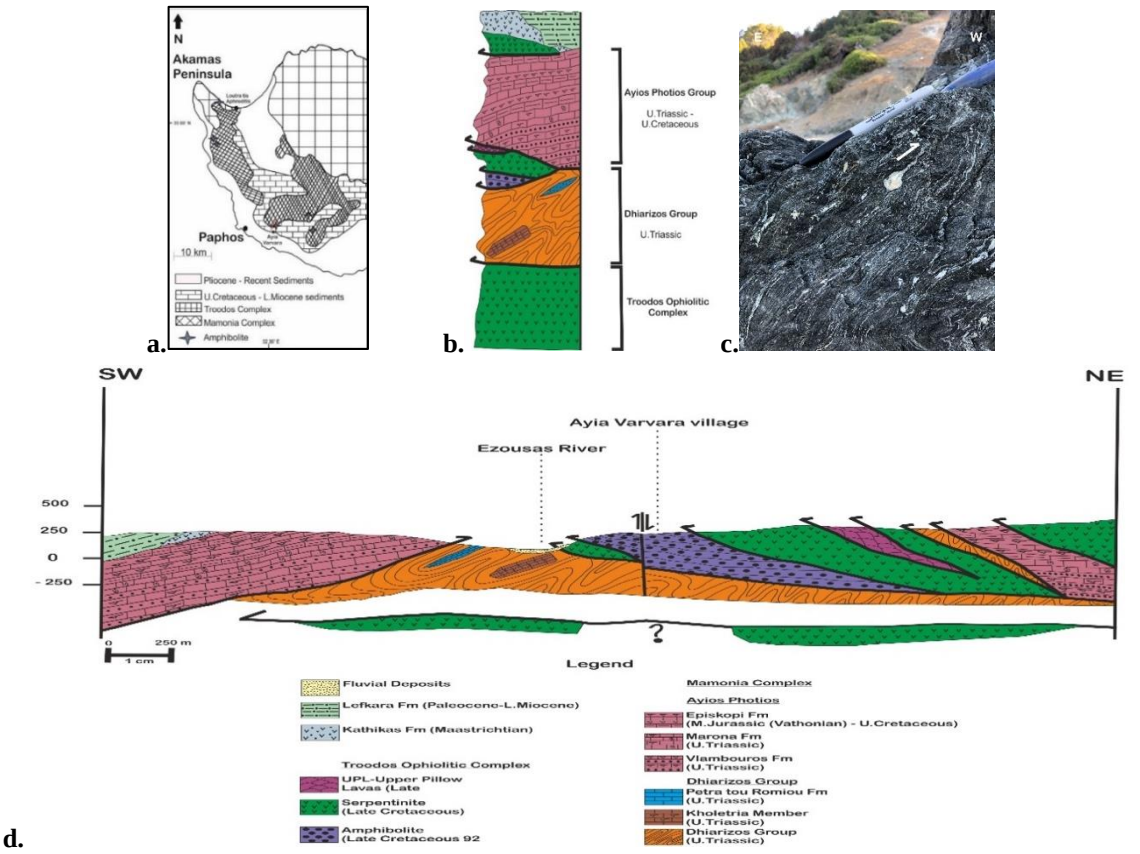

Figure 1. a) Geological map of Mamonia Complex, b) Tectono-stratigraphy of Mamonia Complex, c) Mainly kinematic sense of amphibolite is regarded to W-SW, d) Schematic geological cross-section in SW Cyprus.

References

Bragin, N., Krylov, K. (1996). Stratigraphy and lithology of the Upper Triassic deposits of southwestern Cyprus (Vlambouros Formation). Stratigraphy and Geological Correlation, 4(2), pp. 132-140.

Bragin, N., Krylov, K. (1999). Early Norian Radiolaria from Cyprus. Geodiversitas, 21(4), pp. 539-569.

Dercourt, J., Vrielynck, B., Ricou, L. (1993). Atlas Tethys Palaeoenvironmental Maps Gauthier-Villars. Paris 307pp, 14. Paris.

Ealey, P., Knox, G. (1975). The pre-Tertiary rocks of S.W. Cyprus. Geologie Mijnb. 54, pp. 85-100.

Lapierre, H., Bosch, D., Narros, A., Mascle , G., Tardy, M., Demant, A. (2007). The Mamonia Complex (SW Cyprus) revisited: remnant of Late Triassic intra-oceanic volcanism along the Tethyan southwestern passive margin. Geological Magazine, 144(1).

Malpas, J., Xenophontos, C., Williams, D. (1992). The Ayia Varvara Formation of SW Cyprus: a product of complex collisional tectonics. Tectonophysics, 212(3-4), pp. 193-211.

Mukasa, S., Ludden, J. (1987). Uranium-lead isotopic ages of plagiogranites from the Troodos ophiolite, Cyprus, and their tectonic significance. Geology, 15(9), pp. 825-828.

Robertson, A., Woodcock, N. (1979). Mamonia Complex, southwest Cyprus: Evolution and emplacement of a Mesozoic continental margin. Geological Society of America Bulletin 90.7, pp. 651-665.

Swarbrick, R., Robertson, A. (1980). Revised stratigraphy of the Mesozoic rocks of southern Cyprus. Geological Magazine, 117(6), pp. 547-563.

Torley, J., Robertson, A. (2018). New evidence and interpretation of facies, provenance and geochemistry of late Triassic-early Cretaceous Tethyan deep-water passive margin-related sedimentary rocks (Ayios Photios Group), SW Cyprus in the context of eastern Mediterranean geodynamics. Sedimentary Geology (377), pp. 82-110.

Varnava, A., Danelian, T., Regnier, S., Devaere, L. (2021). Radiolarian evidence for Middle Bathonian radiolarites in the Episkopi Formation (Ayios Photios Group, Mamonia Complex, SW Cyprus). Revue de Micropaléontologie, 73, p. 100549.

16th International Congress of the Geological Society of Greece
17-19 October, 2022 - Patras, Greece
Bulletin of the Geological Society of Greece, Sp. Publ. 10
Ext. Abs. GSG2022-382

Fine slope geomorphology and fracture mapping using imagery acquired by a UAV: an example of Avlakia area, Samos Island.

I. Vakalas[1,2], I. Zananiri[1]

(1) Hellenic Survey of Geology and Mineral Exploration (HSGME), Acharnae, Greece, izanan@igme.gr (2) National Technical University of Athens (NTUA), Athens, Greece

Introduction

During the past years remote sensing technology has experienced significant advances in geosciences, yielding it a useful and handy tool for the field geologist. Though traditional techniques (geological mapping, sampling, compass readings) are still necessary, aerial images can greatly support the field geologist. The Hellenic Survey of Geology & Mineral Exploration (HSGME), in the frame of the GEOINFRA project (2019-2023), has been incorporating new techniques in standard fieldwork, to achieve rapid, reliable, and detailed data acquisition. Towards this scope, a characteristic slope at the Area of Avlakia (Samos Island), exhibiting instability issues (Galanakis & Kontodimos, 2020) after a recent strong earthquake (30th October 2020, Mw: 7.0) and the adjacent area was mapped using an Unmanned Aircraft Vehicle (UAV).

Methodology

The detailed data collection using an UAV aimed at: a) the optimum visualization of rockfalls and instabilities from different angles, and b) the creation of a slope visualization model. During fieldwork, area mapping was conducted using a DJI Phantom Pro V2 quadrorotor UAV, equipped with a an 1-inch 20 MP CMOS sensor with mechanical shutter (Aspect Ratio: 5472 × 3648 pixels). A total of 475 high resolution photos were collected, with an overlap of more than 80% both horizontally and vertically.

Figure 1. Examples of high-resolution images acquired from vertical and horizontal flights.

During the fieldwork two distinct approaches were implemented: a) to capture the almost vertical slope, the flights were done manually by an operator who was at its base, and b) an automated predefined flight pattern, designed and controlled using the Drone Deploy application, was used to map the hill top morphology (Fig. 1). Moreover, to complement the UAV dataset, during fieldwork tectonic measurements were collected by traditional means (Fig. 2).

Figure 2. Characteristic structures at the study area.

Data processing and results

Standard photogrammetry techniques were applied in data processing, using the Agisoft Metashape 1.7.2 Professional Edition software. Data elaboration followed several steps (Fig. 3) and the corresponding models were produced: Align photos (181.007 points, 474/474 cameras aligned), Dense point cloud (high quality, 57.207.480 points), 3D Model (high quality, 11.393.981 faces), Tiled model (8 levels, 1.42 cm/pix), DEM (1.42 cm/pix), Orthomosaic (1.42 cm/pix) (Fig. 4).

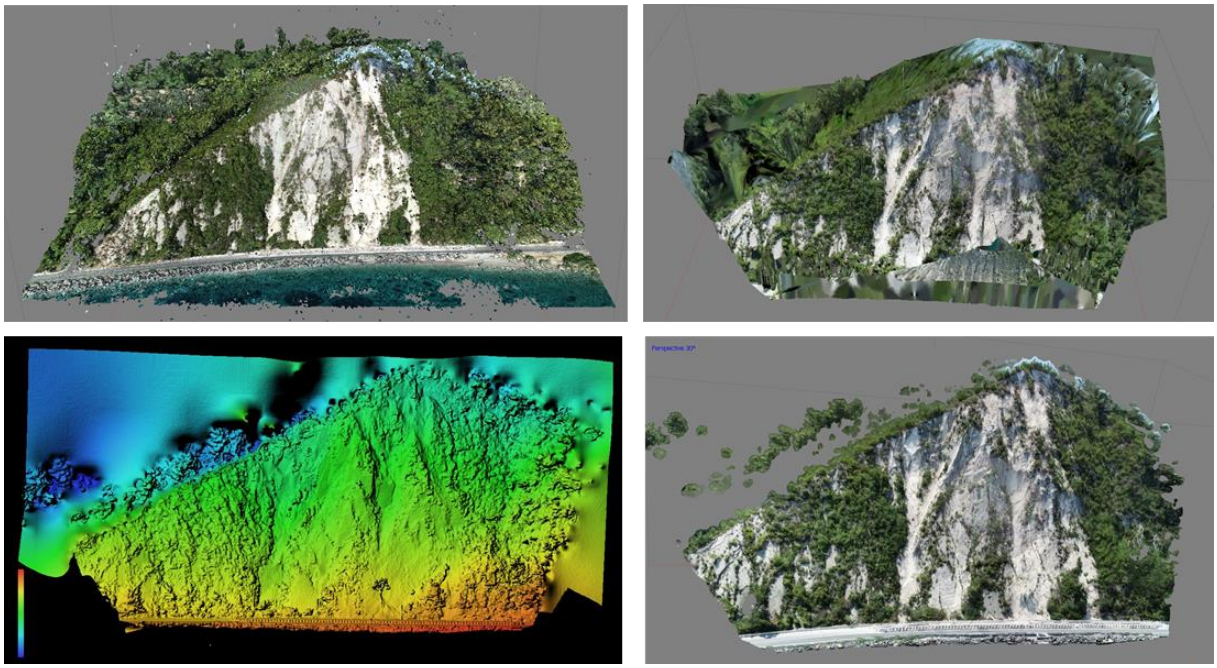

Figure 3. Basic steps of UAV images processing: Dense point cloud, 3D model, DEM, tiled model.

The high-resolution data allowed the detailed observation of the slope, its fractures, inclinations and instabilities, as well as the extraction of data (sections) for further use by the local authorities and towards the design of slope stability measures.

Figure 4. High resolution orthomosaic created from UAV image processing.

Acknowledgements

The current work was carried out in the frame of the project "GEOINFRA: Geological Mapping of Greece for the support of innovation and entrepreneurship" (2019-2023), funded by the National Strategic Reference Framework (2014-2020).

References

Galanakis, D. and Kontodimos, K., 2020. Technical geological identification of landslide phenomena on the island of Samos after the catastrophic earthquake of 30-10-2020. HSGME Internal Report, Athens, pp. 1-18.

16th International Congress of the Geological Society of Greece
17-19 October, 2022 - Patras, Greece
Bulletin of the Geological Society of Greece, Sp. Publ. 10
Ext. Abs. GSG2022-416

Fracture Analysis in the Eastern Limb of the North Paramythia Anticline and micro-structural characteristics for carbonate reservoir quality (Elataria, NW-Greece).

I. Panetas-Felouris[1], S. Kokkalas[1], G. Iliopoulos[1], S. Tombros[2], K. Kappis[2]

(1) Department of Geology, University of Patras, Patras, Greece, up1052529@upnet.gr (2) Department of Material Sciences, University of Patras, Greece.

Background

Paramythia anticline is a well-exposed structure in Epirus, NW Greece, a region intensively affected by the westward compressional deformation, acting in a continental collision setting (Kokkalas et al., 2006). The study area belongs to the Ionian zone, which is considered to comprise three distinct stratigraphic sequences: a) a pre-rift sequence (Triassic–Early Jurassic) represented by a thick evaporitic succession overlain by shallow marine carbonates, b) a syn-rift sequence (Early to Late Jurassic) where the basin was compartmentalized, and a half-graben geometry was favored reflected in variations in sediment thickness and type (pelagic carbonates and deep water clastics), c) A post-rift sequence (Early Cretaceous to Eocene) marked by the deposition of pelagic carbonates Mobilization of evaporites at the base of the carbonate platform significantly affected the deformation style in the area, with several cases of diapiric intrusions along the thrusts. (Karakitsios, 1995).

Methods and objectives

Representative outcrop sites along the eastern limb of the north Paramythia anticline (Elataria) were analyzed in detail regarding their key characteristics of the fracture network, as well as their depositional environment, using a combination of structural field observations and site sampling. Structural analysis along various types of scanlines allowed us to decipher the fracture set orientations, fracture intensity, fracture spacing, and connectivity. Structural data include measurements of bedding, fractures, and mesoscale fold axes. Regarding the fracture analysis methodology, three distinct techniques were employed in order to measure fracture intensity: the Linear Scanline Method (LSM), the Areal Sampling Method (ASM), and the Circular Scanline Method (CSM) (Fig. 1; Conny et al., 2013). A total of 19 outcrop sections were studied, spawning the eastern limb of the anticline (5 LSM, 5 ASM, 9 CSM) and including most lithological formations (Pantokrator, Vigla, Senonian, and Paleocene-Eocene unit). Additionally, from the images acquired in the field, an analysis of the topology of the 2D fracture networks was conducted so that the relationship between the fractures is described using the techniques presented by Sanderson (2016). For a better understanding of fracture abundance in the fold limb, the depositional environment of the carbonate platform, as well as the porosity type and size of the pores, were evaluated in a total of eight representative samples collected in the field through N_2 absorption/desorption method and optical microscopy. In order to measure the specific surface area (SSA), size, and distribution of pores within samples, a N_2 absorption-desorption device (Micromeritics TriStar 3000, Laboratory of the Department of Material Science, University of Patras) was used. The interpretation of the obtained diagrams was done using the classification of Lowell (2004).

Results

The lithological units show bedding with a general NW to NNW orientation, dipping to the ENE with intermediate to low dip values, while the strata dip progressively higher towards the center of the anticline. In contrast, the western flank of the anticline displays steeper dips, indicative of the west-verging asymmetry of the anticline. Fold axes show a main NNW-SSE orientation and a secondary NE-SW orientation, mainly observable in the southern part of the anticline, closer to the major strike-slip transfer fault of Ag. Kiriaki. Regarding the fracture analysis results, the Eocene 1 lithologies showed values of bulk fracture intensity P_{10}: 25.4m^{-1}, with fracture spacing of 0.04m and a mean fracture length of 43cm, whereas Eocene 2 shows a higher intensity of 41.8 m^{-1}, fracture spacing of 0.023m, and average fracture length of 10cm. For a comparison with the western limb, the Polydrosso outcrop showed rather similar results to those of Eocene 2 (P_{10}: 36.06m^{-1}, S: 0.027m, $I_{m;SLS}$: 0,31m^{-1}), further deviating significantly from that of Vigla unit (P_{10}: 8.1 m^{-1}, S:0.12m, $I_{m;SLS}$: 0.38), implying that it probably should be considered more as Senonian or at least a transitional phase to Vigla unit. Lastly, the Pantokrator limestones show an increase in mean fracture length with an average of 1.9 m and values of P_{10}: 21.4m^{-1}, and fracture spacing of 0.048m.

Figure 1. Representative outcrop images with application of circular and area sampling methods for fracture analysis.

Finally, the lithological and microfacies contrast in the carbonate platform units is further examined by thin section petrographic and microfacies analysis in order to give information about the depositional environment. The Eocene and Vigla limestones were deposited in a pelagic environment, while the Senonian calcarenites with characteristic microbreccia and fragments of Orbitoinid, rudists etc., indicate a slope. The Posidonia shale unit indicates a deep shelf environment while the Pantokrator packstone to floatstones deposited in a shallow water depositional environment (i.e., back reef). Regarding the reservoir quality, all studied carbonate units are mesoporous with a porous diameter of 4-6 nm and, based on the N_2 absorption-desorption diagrams, suggest split to sphere-like pores in the deeper carbonate facies and well-sorted needle-like pores in the shallower facies. The SSA shows higher values in Eocene, Senonian and Vigla samples (3.1 to 5.5 m^2/g) in contrast to the Pantokrator and Posidonia shales (0.1 to 0.6 m^2/g), possibly representing the differences in particle size, as well as the structure and porosity of the carbonate material. Microscopic observations show low to absent optical porosity, while microfractures are mainly filled with secondary calcite and initiate from clasts and fossil fragments, developing in cases overlapping zones between them.

Acknowledgments

We would like to thank Assoc. Prof. George Avgouropoulos for providing us the access in the laboratories of the Department of Materials Science (Univ. of Patras) for the measurements in physical absorption of N2.

References

Conny Z., Gomez-Rivas E., Bons P., Blum P., 2013. Evaluation of sampling methods for fracture network characterization using outcrops. AAPG Bulletin, vol.97, 9, 1545–1566.

Karakitsios, V., 1995. The influence of preexisting structure and halokinesis on organic matter preservation and thrust system evolution in the Ionian Basin, Northwest Greece. The American Association of Petroleum Geologists Bulletin, 7, 960–980.

Kokkalas S., Xypolias, P., Koukouvelas, I., Doutsos, T., 2006. Post-collisional contractional and extensional deformation in the Aegean region, in Dilek, Y., and Pavlides, S., eds., Post-collisional tectonics and magmatism in the Mediterranean region and Asia: Geological Society of America Special Paper 409, p. 97–123, doi: 10.1130/2006.2409(06).

Lowell S., 2004. Characterization of Porous Solids and Powders: Surface Area, Pore Size and Density. Springer Netherlands.

Sanderson, D.J., 2016. Field-based structural studies as analogues to sub-surface reservoirs. In: Bowman, M., Smyth, H.R., Good, T.R., Passey, S.R., Hirst, J.P.P. and C.J. Jordan. 'The Value of Outcrop Studies in Reducing Subsurface Uncertainty and Risk in Hydrocarbon Exploration and Production', GSL Special Publications, 436, doi.org/10.1144/SP436.

16th INTERNATIONAL CONGRESS of the
GEOLOGICAL SOCIETY OF GREECE

T3. Geophysics, Seismology and Geodynamics

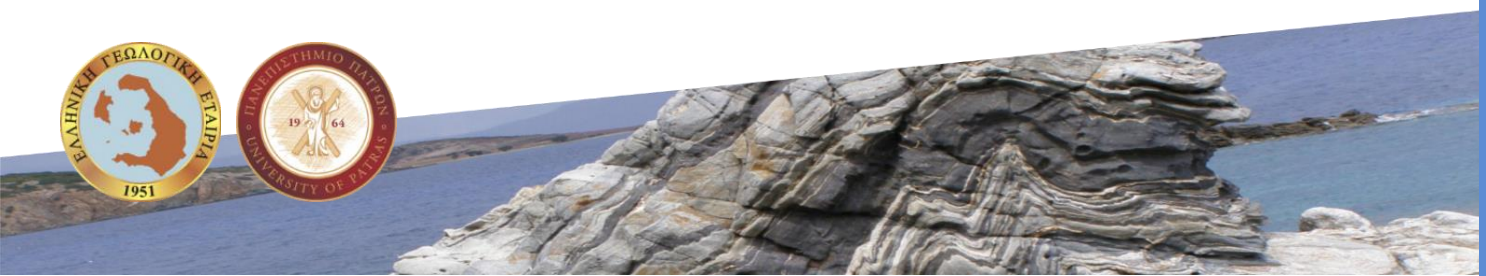

OUR EARTH, OUR HOME

16th International Congress of the Geological Society of Greece
17-19 October, 2022 - Patras, Greece
Bulletin of the Geological Society of Greece, Sp. Publ. 10
Ext. Abs. GSG2022-026

The geophysical identification of lateritic bauxite formation at Mandra area, Attiki (Greece)

I.K. Giannopoulos[1], J.D. Alexopoulos[1], S. Dilalos[1], V. Gkosios[1], G.S. Mitsika[1], M. Stamatakis[2], N. Voulgaris[1]

(1) National and Kapodistrian University of Athens, Faculty of Geology and Geoenvironment, Section of Geophysics and Geothermy, jkgianno@geol.uoa.gr (2) National and Kapodistrian University of Athens, Faculty of Geology and Geoenvironment, Section of Economic Geology and Geochemistry

Determination of the physical parameters of lateritic bauxite formation with the contribution of geophysical methods. In this paper we present the results of a near-surface geophysical survey carried out for the investigation of geotechnical engineering characteristics in selected locations of the seismological stations of the National Network, Section of Geophysics and Geothermy of National and Kapodistrian University of Athens. The studied area is located at Mandra (Attiki), close to the MDRA seismological station (Figure 1) and the main task of the study was the geophysical identification of buried bauxite deposits in the area.

Geological setting

The study area is mainly covered with carbonate formations of the *Sub-Pelagonian Unit*. These formations comprise of limestones of the Upper Cretaceous (*Ks*) which overly the dolostones, dolomitic limestones and limestones of the Upper Triassic (*TRm*). In places, between the Triassic dolostones/limestones and the Cretaceous limestones, lateritic bauxite ores can be observed. Due to the mining processes that had been carried out until the early '80s, most of these bauxitic ores have been extracted and replaced by their mining wastes.

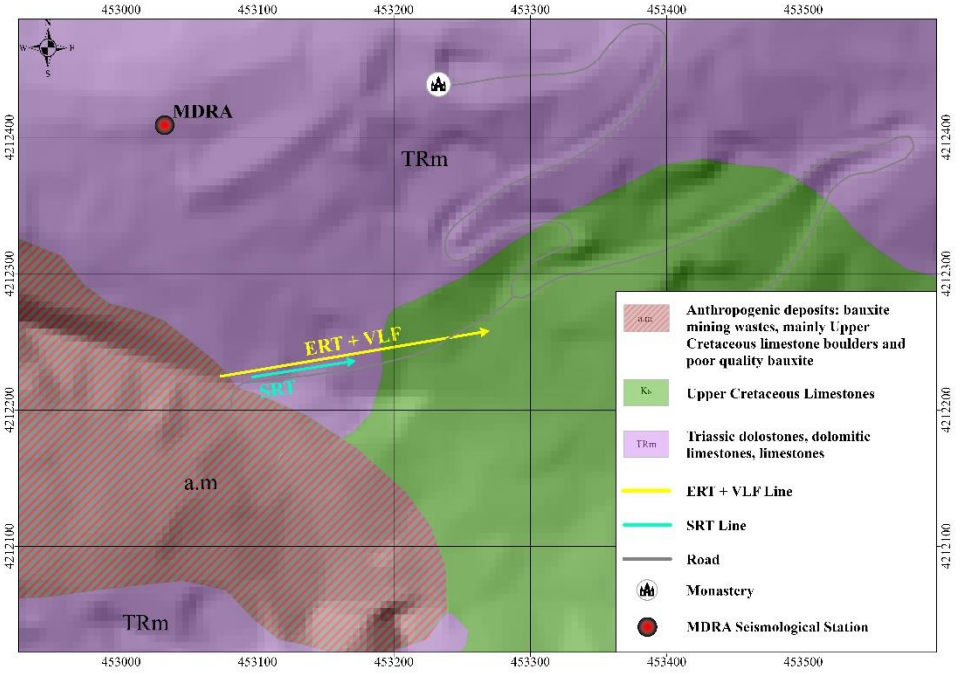

Figure 1. Modified geological map (Dounas, 1971) of the study area along with the location of the geophysical measurements

Methodology

In the context of the geophysical-geotechnical investigation of the geological formations close to the MDRA seismological station, four (4) different methodologies have been applied in order to achieve a multi-disciplinary approach. More specifically, we carried out i) an Electrical Resistivity Tomography of 200 meters total length and 2.5 meters electrode spacing, ii) a seismic refraction tomography section of 47 meters and geophone spacing 1 meter, with 48 geophones of 10Hz iii) a MASW section of 23 meters with 24 geophones of 4.5Hz (1 meter geophone spacing) and finally iv) an electromagnetic VLF section of 200 meters with a 5-meter spacing. Finally, we determined the density of the geological formations from laboratory measurements of 30 samples from each one. The determined density of the Triassic dolostones and limestones is equal to 2.71 gr/cm^3, the one of the bauxites is 3.36 gr/cm^3, while the one of the Cretaceous limestones is 2.71 gr/cm^3.

In Figure 2, the results of the Electrical Resistivity Tomography illustrate a zone of relatively vertical high electrical resistivity values (>2.500 Ohm.m) between 80 and 130 meters, up to depths of 40 meters. The first part of the

geoelectrical section, up to 100 meters, we observe relatively lower resistivity values (< 500 Ohm.m), while form the 120 meters to the end of the section even lower resistivity values have been determined (<200 Ohm.m).

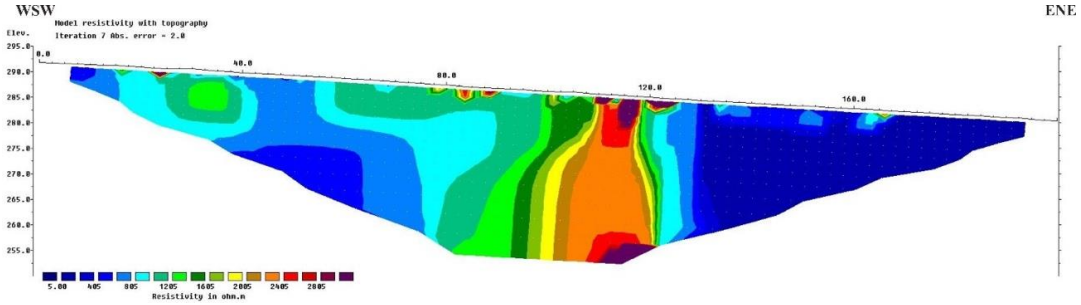

Figure 2. Electrical Resistivity Tomography

As it concerns the electromagnetic VLF section, the processing results, after the 3-point smoothing and the Karous-Hjelt filter the pseudo-section of the current density distribution has been produced (Figure 3). The results are similar to the resistivity model of Figure 2, since a zone of low current density is located between 70 and 135 meters. At this part of the Resistivity Tomography we investigated a resistant formation.

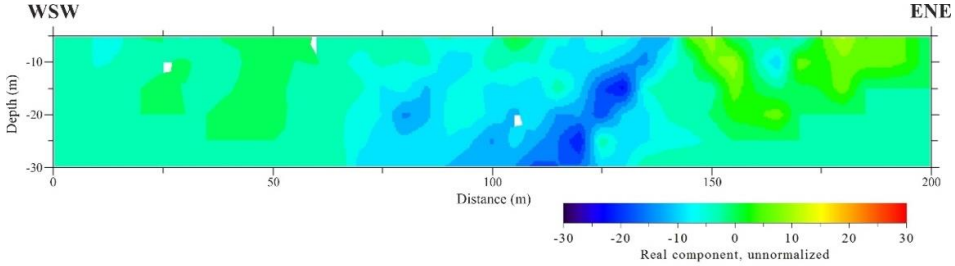

Figure 3. The Karous-Hjelt pseudo-section for current density distribution

Finally, for the estimation of P-waves velocity the geophysical method of Seismic Refraction Tomography was applied. In total, thirteen (13) shots were carried out, with a spacing of four (4) meters, using a 6kg seismic source (sledgehammer). In Figure 4, we can observe the upper formation with reddish colors, thickness 1-3 meters and V_1=1.940–2.200 m/s but also the underlying one with V_2=2.400-3.650 m/s and thickness ranging from 1,0 to 2,5 meters. Finally, the deeper formation has been investigated with V_3=3.800-4.135 m/s at depths from 3,0 meters (middle of the section) up to 6,0 meters (end of section).

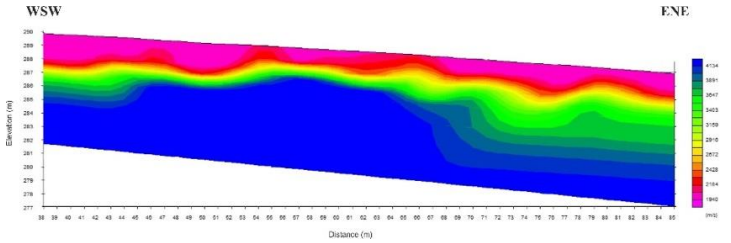

Figure 4. Seismic Refraction Tomography (the distance axis is referred to ERT meters)

Conclusions

The results of the geophysical measurements reveal an intense lateral inhomogenous zone between 90 and 120 meters of the ERT profile. Taking into consideration that the existence of the contact between the Triassic dolostones/ limestones and the Cretaceous limestones has been verified from field observations of the authors, the prementioned area could be interpreted as a possible fracture zone, where bauxite ore remains are expected to be found. Therefore, the Triassic dolostones and limestones have been investigated with values of 500-1200 Ohm.m, the Cretaceous limestones with values <800 Ohm.m, while the bauxites seem to have values >1700 Ohm.m, similar with published literature from other researchers (Amosun *et al.*, 2020; Eluwole *et al.*, 2019).

Acknowledgements

The project was founded by "HELPOS-Hellenic System for Lithosphere Monitoring" (MIS 5002697), which is implemented under the action "Reinforcement of the Research and Innovation Infrastructure", funded by the Operational Programme "Competitiveness, Entrepreneurship and Innovation" (NSRF 2014-2020) and co-financed by Greece and the European Union.

References

Amosun J.O., Alagbe O.A., Fagbemigun T.S., Sanuade O.A., Olaseeni O.G., 2020. Imaging lateritic bauxite bearing zones in Ekiti, Southwestern Nigeria, using magnetic and electrical resistivity tomography techniques. SN Applied Sciences, 2(12), 1-14.

Dounas A., 1971. Geological map of Greece, sheet "Erythrai", Scale 1:50.000. Institute of Geological and Mineralogical of Greece

Eluwole A.B., Ademilua O.L., Oyinloye A., Adebayo O.F., Obasi R.A., Talabi, A.O., Olaolorun O.A., 2019. Geoelectric assessments of the bauxite ore deposit at orin-ekiti, southwestern Nigeria. Int J Appl Environ Sci, 14(2), 197-210.

16th International Congress of the Geological Society of Greece
17-19 October, 2022 - Patras, Greece
Bulletin of the Geological Society of Greece, Sp. Publ. 10
Ext. Abs. GSG2022-031

Determination of the subsurface geological regime and geotechnical characteristics at the area of Goudi (Athens, Greece) derived from geophysical measurements

V. Gkosios[1], J.D. Alexopoulos[1], I.K. Giannopoulos[1], G.S. Mitsika[1], S. Dilalos[1], I. Barbaresos[2], N. Voulgaris[1]

(1) National and Kapodistrian University of Athens, Faculty of Geology and Geoenvironment, Section of Geophysics and Geothermy, (2) National and Kapodistrian University of Athens, Directorate of Technical Services, Project Execution Department vgkosios@geol.uoa.gr

Research Highlights

- Seismic velocity and density calculations for the estimation of the elastic moduli of the *Athens schist* formation.

In this paper we present the results of the near-surface geophysical survey for the investigation of the geological and geotechnical characteristics at the construction area of the new building of the Dental School of National and Kapodistrian University of Athens (Fig. 1). Three sampling boreholes, carried out during January of 2022, have also been taken into consideration for the interpretation of the geophysical measurements.

The area is covered with post-alpine sediments and more specifically with diluvial deposits (Fig. 1), formed from the weathering products of the surrounding rocks. Underlying, the *Schists of Athens* are expected to be found. The boreholes have verified their existence at depths 11-13 meters. It is a complex mélange without internal geometry, comprised of unmetamorphic clastic sediments, such as sandstones, pelites, clays, sandstone marls, greywackes, tuffs and argillic schists (Papanikolaou *et al.*, 2002). Based on the results of the sampling boreholes the study area is structured by 8,5 meters of anthropogenic coarse-grained materials, probably due to the fact that the area had been excavated on 2010 up to 7,25 meters and then was refilled. The water table level during the period of the measurements was defined at almost 10 meters depth. The shallow aquifer presents alterations, which may affect the building and for that reason we monitor its level from two boreholes.

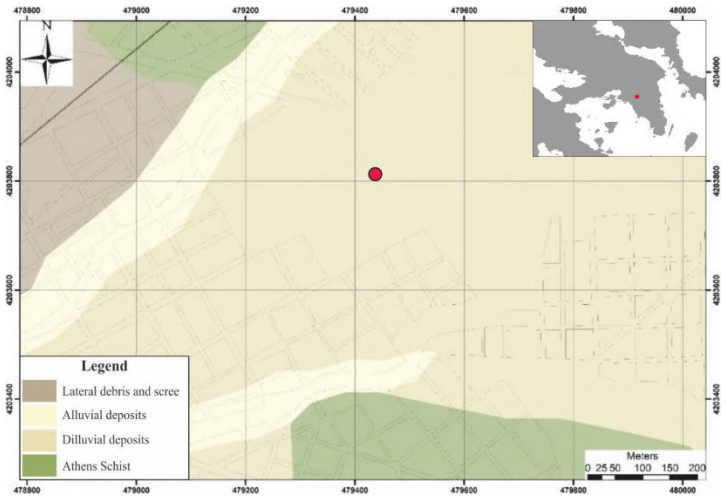

Figure 1. Geological map of the study area indicated with the red circle (Papanikolaou et al., 2002)

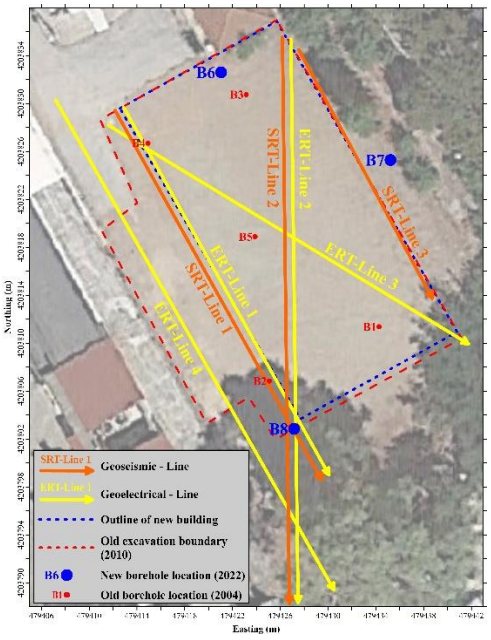

Figure 2. Location of ERT-SRT measurements, boreholes and the outline of the new building

Methodology

In the context of the geophysical investigation of the subsurface at the building site, three (3) different geophysical techniques have been applied in order to have a multi-disciplinary approach (Al-Heety *et al.*, 2021). More specifically (Fig. 2), we carried out i) four (4) electrical resistivity tomography (ert) sections, of totally 165 meters length, using the *IRIS Syscal Pro* unit, ii) three (3) seismic refraction and MASW sections, of totally 105 meters length, using the *Geometrics Strata View* unit. For the generation of seismic waves, a 6kg sledgehammer was used and the seismic energy was detected by 48 geophones of 4,5 Hz arranged in a linear deployment. iii) 52 GPR sections on a 1x1 meter grid, with dimensions 20x30 meters. The geophysical measurements were positioned based on the RTK-NTRIP technique,

providing horizontal and vertical accuracy of 8 mm and 15 mm, respectively. Additionally, we carried out density laboratory measurements for the geological formations of borehole samples.

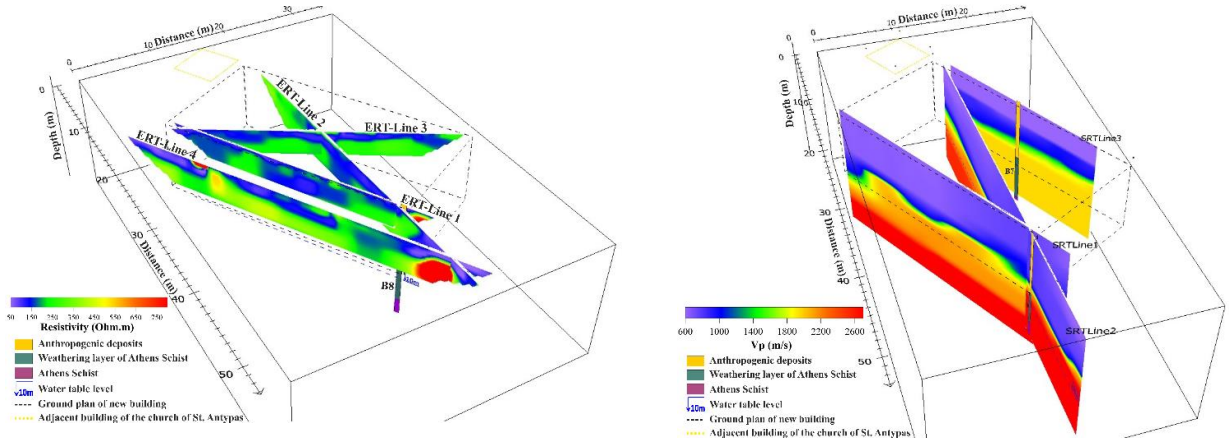

Figure 3. 3-D view of the Electrical Resistivity Tomography Sections (left) and the Seismic Refraction Tomography Sections (right). The dashed line represents the volume of the excavation

In Figure 3 (left), a 3-D presentation of the ert technique results is illustrated (processed with *Res2Dinv*), where we can observe a conductive zone (<100 Ohm.m) located up to the first 2 meters depth. On the other hand, a relatively resistant formation (>600 Ohm.m) has been adumbrated at the southeast part, at depths between 2-4 meters. The investigation depth from the ert measurements is practically the same with the lower level of the building (~8,6 meters). Due to the restricted available area for the geophysical measurements the investigation depth was limited.

Regarding the seismic refraction sections, the processing results, carried out with *SeisImager/2D*, are illustrated in a 3-D presentation in Figure 3 (right). We can observe an upper seismic layer with V_P = 600-1.000 m/s and thickness 8 meters and an underlying one with V_P = 1.200-2.000 m/s and thickness 5 meters. As basement, there is a third seismic layer with V_P > 2.200 m/s, located at depth >13 meters. According to the borehole cores, the first layer seems to be the anthropogenic deposits, the second one the weathering layer of *Athens schists* while the third one the compact formation of *Athens schists*. The corresponding V_S values were calculated from the MASW processing technique, with *SeisImager/SW*. Unfortunately, the GPR measurements hadn't penetrate deep enough to provide information due to the high percentage of clay in the anthropogenic materials of the area that caused the high attenuation of the electromagnetic waves.

Conclusions

Due to the restricted available area for resistivity measurements, we weren't able to investigate the *Athens schists* compact formation. Instead, a resistant formation (>600 Ohm.m) has been delineated at the southeast area, just 4,5 meters out of the excavation boundaries. Its geometry could be interpreted as an old subsurface small tunnel, possible connecting the older buildings. On the other hand, the seismic measurements reached greater depths of investigation, up to almost 15 meters, allowing us to identify the uppermost part of the compact *Athens schists* formation. In Table 1 we present the elastic moduli of the geological formations, calculated after the laboratory determination of their densities. At this point we have to mention that the V_S values of *Athens schists* are affected due to the acquirer's existence.

Table 1. Seismic velocity, density and elastic moduli determination

Geological formations	***Vp (m/s)***	***Vs (m/s)***	***Density (g/cm^3)***	***Poisson's Ratio (σ)***	***Shear modulus G (GPa)***	***Young's modulus E (GPa)***	***Bulk modulus k (GPa)***
Anthropogenic materials	800	400	2,51	0,33	0,40	1,07	1,31
Weathering layer of *Athens schists*	1.600	680	2,66	0,39	1,23	3,42	5,88
Athens schists	2.600	1.300	2,67	0,33	4,52	12,05	14,68

Acknowledgements

The authors would like to thank all the graduate and post-graduate students for their contribution during the field measurements.

References

Papanikolaou D., Lozios S., Sideris Ch., Kranis Ch., Danamos G., Soukis K., Skourtsos E., Basi E., 2002. Geological – Geotechnical study of Athens basin. OASP Applied research program, 152p., Athens.

Al-Heety, A. J., Hassouneh, M., & Abdullah, F. M., 2021. Application of MASW and ERT methods for geotechnical site characterization: A case study for roads construction and infrastructure assessment in Abu Dhabi, UAE. *Journal of Applied Geophysics*, 193, 104408.

16th International Congress of the Geological Society of Greece
17-19 October, 2022 - Patras, Greece
Bulletin of the Geological Society of Greece, Sp. Publ. 10
Ext. Abs. GSG2022-036

Probabilistic Seismic Hazard Assessment for the islands of the Administrative Region of Attica (Greece)

G. Kaviris[1], A. Zymvragakis[1], I. Spingos[1], V. Kapetanidis[1], I. Kassaras[1†], S. Mavroulis[2], E. Kotsi[2], E. Lekkas[2], N. Voulgaris[1]

(1) Section of Geophysics–Geothermics, Department of Geology and Geoenvironment, National and Kapodistrian University of Athens, Athens, Greece, gkaviris@geol.uoa.gr (2) Section of Dynamic Tectonic Applied Geology, Department of Geology and Geoenvironment, National and Kapodistrian University of Athens, Athens, Greece.

Research Highlights

- We present a probabilistic seismic hazard assessment for the islands of the Administrative Region of Attica (Greece).
- The Peak Ground Acceleration (PGA) values reveal that only Spetses and Ydra comply with the current National Building Code. Salamina, Agina, Methana, Poros, Kithira and Antikithira surpass the EAK reference value.

The islands of the administrative region of Attica (central and southern Greece) are divided into four (4) groups from north to south: 1) Salamina and Aegina, 2) Methana and Poros, 3) Spetses and Ydra, and 4) Kythira and Antikythira (areas with black shoreline in Figure 1). The ground motions of the first group are mainly influenced by the high seismicity of the Eastern Gulf of Corinth, whereas those of the last group are strongly affected by its proximity to the Hellenic arc (Figure 1). The seismicity in the remaining islands of the Saronic and Argolikos gulfs (groups 2 and 3) is intermediate. In this study, seismic hazard is assessed for each group via the probabilistic method proposed by Cornell (1968) and McGuire (1976). The Area-Source zones of the Euro-Mediterranean Seismic Hazard Model (ESHM13; Giardini et al., 2014) were selected as the seismotectonic model (Figure 1). For each zone, Ground Motion Prediction Equations (GMPEs) proposed for Greece were taken into account. The results of Peak Ground Acceleration (PGA) for a return period of 475 years were computed by constructing a logic tree, where each branch is a hybrid GMPE model to account qualitatively for epistemic uncertainties.

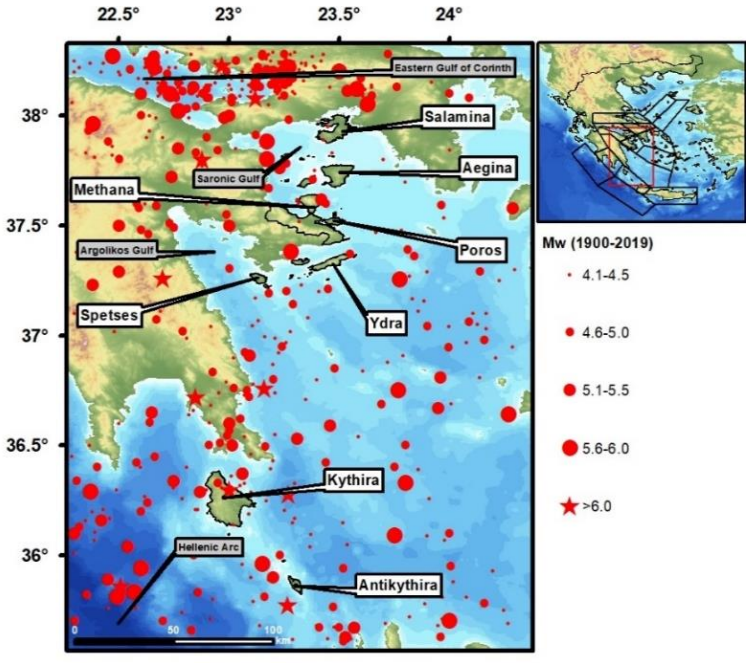

Figure 1. Left: Seismicity of the study area. The Makropoulos et al. (2012) earthquake catalogue is used and extended up to 2019. Right: The red rectangle represents the study area. Black polygons denote the ESHM13 zones used in the study.

The instrumental seismicity catalogue of Makropoulos et al. (2012) was used. To perform the probabilistic method of seismic hazard assessment, the calculation of the following seismic parameters for each zone is necessary: a) the b-value of the Gutenberg-Richter relation, b) the magnitude of completeness, M_c, c) the annual rate of M_c exceedance, $\lambda(M_c)$ and d) the maximum expected magnitude, M_u. The b-value and M_c were calculated using the Maximum

Curvature method, $\lambda(M_c)$ was calculated manually and M_u was adopted from ESHM13. The GMPEs of Margaris et al. (2002), Skarlatoudis et al. (2003), Danciu and Tselentis (2007), Sakkas (2016) and Chousianitis et al. (2018) were used. Each GMPE was converted to a hybrid one, to account for the types of focal mechanisms for each zone in percentages. The results were computed via an equal-weight logic-tree approach, where every branch is a hybrid GMPE.

The spatial distribution of the calculated PGA values follows the seismicity level of the groups (Figure 2). Specifically, group 4 (Kythira-Antikythira) has the highest PGA values, [300-330] cm/sec^2, while groups 2 and 3 have the lowest values, [225-250] cm/sec^2. The first group has intermediate PGA values, [230-290] cm/sec^2.

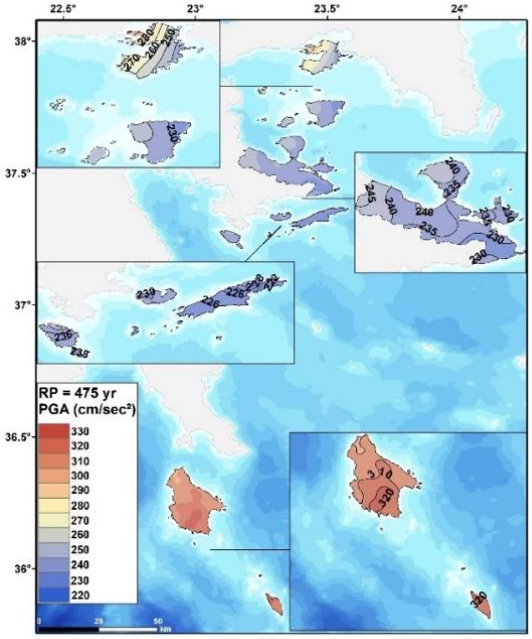

Figure 2. Spatial distribution of PGA values for a return period of 475 years.

According to the current Greek National Building Code (EAK, 2003), only group 3 (Spetses and Ydra) belongs to zone I (PGA ~160 cm/sec^2, approximately), while the remaining groups belong to zone II (~240 cm/sec^2). In group 1, regarding Salamina, only the obtained values at its easternmost part follow EAK (2003), while the entire Aegina Island is in agreement with EAK (2003). The PGA values for group 2 comply with the EAK (2003), with only the western part of the land slightly exceeding it by ~5 cm/sec^2. The other two groups exceed EAK (2003) throughout their entire land. The highest calculated PGA values for both groups exceed EAK (2003) by ~80 cm/sec^2.

Acknowledgements

The research is partially funded by the "Assessment of Seismic, Fire and Flood hazard in Attica Region" project, signed by Attica Region, the National Observatory of Athens (NOA) and the National and Kapodistrian University of Athens (NKUA; Athens, Greece) (Special Account for Research Grants of NKUA, project code: 17531). The present work is dedicated to Ioannis Kassaras who actively participated to this work, even until his last days.

References

Chousianitis, K., Del Gaudio, V., Pierri, P., Tselentis, G.A., 2018. Regional ground-motion prediction equations for amplitude, frequency response, and duration-based parameters for Greece. Earthquake Engineering and Structural Dynamics 47, 2252–2274.

Cornell, C., A., 1968. Engineering seismic risk analysis. Bulletin Seismological Society of America 58, 1583–1606.

Danciu, L., Tselentis, G.A., 2007. Engineering ground-motion parameters attenuation relationships for Greece. Bulletin of the Seismological Society of America, 97, 162–183.

E.A.K., 2003. Greek seismic code edited by: Earthquake planning and protection organization. Athens—Greece, 72 pp., 7 appendixes, 2003 (in Greek).

Giardini, D., Wossner, J., Danciu, L., 2014. Mapping Europe's Seismic Hazard. Eos, Transactions, American Geophysical Union, 95, 261–262. https://doi.org/10.1002/2014EO290001

Makropoulos, K., Kaviris, G., Kouskouna, V., 2012. An updated and extended earthquake catalogue for Greece and adjacent areas since 1900. Natural Hazards and Earth System Sciences, 12, 1425–1430. https://doi.org/10.5194/nhess-12-1425-2012

Margaris, B., Papazachos, C., Papaioannou, C., Theodoulidis, N., Kalogeras, I., Skarlatoudis, A., 2002. Ground motion attenuation relations for shallow earthquakes in Greece. In: Proceedings of the 12th European conference on earthquake engineering, 385.

McGuire, R., K., 1976. FORTRAN computer program for seismic risk analysis. Us geological Survey 20, 76–67.

Sakkas, G., 2016. Calculation and analysis of the seismic motion rotational components in Greece. Ph.D. Thesis, National and Kapodistrian University of Athens, Athens, p. 278.

Skarlatoudis, A. A., Papazachos, C. B., Margaris, B. N., Theodulidis, N., Papaioannou, Ch., Kalogeras, I., Scordilis, E. M., Karakostas, V., 2003. Empirical peak ground-motion predictive relations for shallow earthquakes in Greece. Bulletin of the Seismological Society of America 93, 2591–2603.

16th International Congress of the Geological Society of Greece
17-19 October, 2022 - Patras, Greece
Bulletin of the Geological Society of Greece, Sp. Publ. 10
Ext. Abs. GSG2022-062

Preliminary results of near-surface geophysical survey in Lefkada town (Greece).

G.S. Mitsika[1], J.D. Alexopoulos[1], I.K. Giannopoulos[1], V. Gkosios[1], S. Dilalos[1], C. Filis, Emm. Vassilakis[1], G. Kaviris[1], V. Sakkas[1], N. Voulgaris[1]

(1) Faculty of Geology and Geoenvironment, National and Kapodistrian University of Athens, g.mitsika@geol.uoa.gr

Investigation of the subsurface structure of Lefkada town using a multi-disciplinary geophysical approach.

In this paper we present the preliminary results of a near-surface geophysical research carried out on Lefkada island, for the investigation of the geological setting of Lefkada town. The geophysical survey has also been extended in selected locations of Peratia region (Fig. 1), for a more accurate perspective of the subsurface geological structure.

The post-alpine formations that outcrop throughout the broader study area, mainly consist of alluvial deposits (Fig. 1). Coastal sandy deposits and beach rocks are observed along the shoreline, whilst lagoon deposits are cropping out at several locations surrounding Lefkada town. Miocene deposits of sandstones and marls are observed at the south-eastern and south-western areas, on both sides of the canal. The alpine basement consists of the *Pantocrator Limestones* and with *Dolomites of Upper Triassic* formations that are cropping out at the southern-western part of the study area and at the eastern area, respectively. The active fault system that bounds the northern margin of *Pantocrator Limestones* (Lekkas *et al.*, 2001) is trending along NW-SE direction and dipping towards NNE, beneath the alluvial deposits and the downtown area that is located at the south coast of the lagoon.

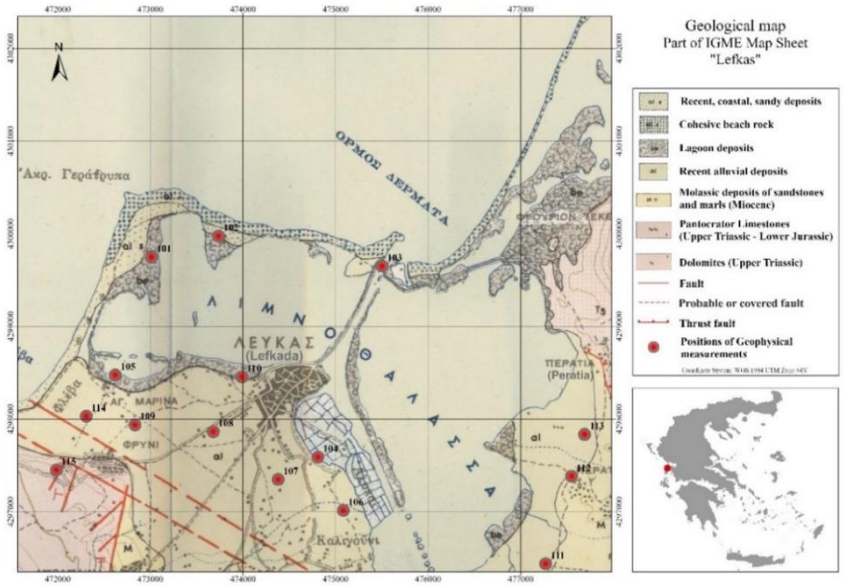

Figure 1. Geological map of the study area (Bornovas, 1964) along with the sites of the geophysical measurements.

Methodology

In the context of the near-surface geophysical investigation of the subsurface structure of Lefkada town we acquired geophysical measurements at fourteen (14) selected sites (Fig. 1). At each site we executed three (3) different techniques, in order to have a multi-disciplinary approach. More specifically, we carried out i) an electrical resistivity tomography (ERT) of 47 meters length (Fig. 2), ii) a seismic refraction tomography (SRT) of 23 meters length (Fig. 2) and iii) a multichannel analysis of surface waves (MASW) measurement at the midpoint of the previously mentioned seismic line. The ERT and SRT lines were designed in a frame to share the same midpoint, since successful combination of geoelectrical and seismic methods has been reported in suburban and coastal environments (Calamita *et al*, 2019; Hammock *et al.*, 2021).

In Figure 3, the results of the ERT at measurement site 114 illustrate a relatively homogeneous conductive zone (<25 Ohm.m) as a first geoelectrical layer, down to an absolute elevation of -1,5 meters. A more resistant formation, more than 35 Ohm.m, was investigated across the bottom part of the section.

At the same site, regarding the seismic measurements processing, two seismic layers were investigated (Fig. 4); the upper one with thickness almost 3,0 meters and V_1=660 m/s and the underlying one with V_2=1.600 m/s.

Figure 2. Geophysical field measurements at site 101 (left) and site 111 (right).

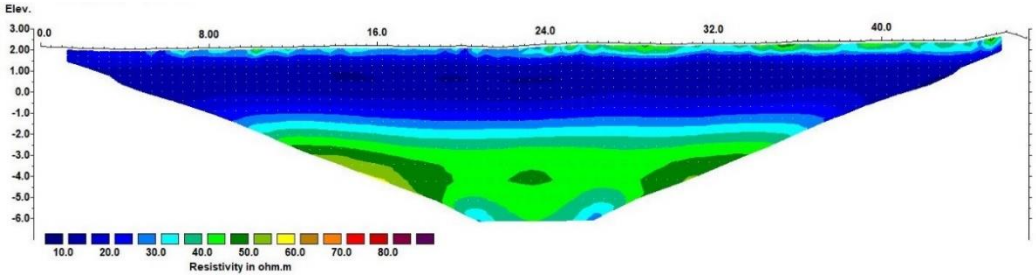

Figure 3. Electrical resistivity tomography at measurement site 114.

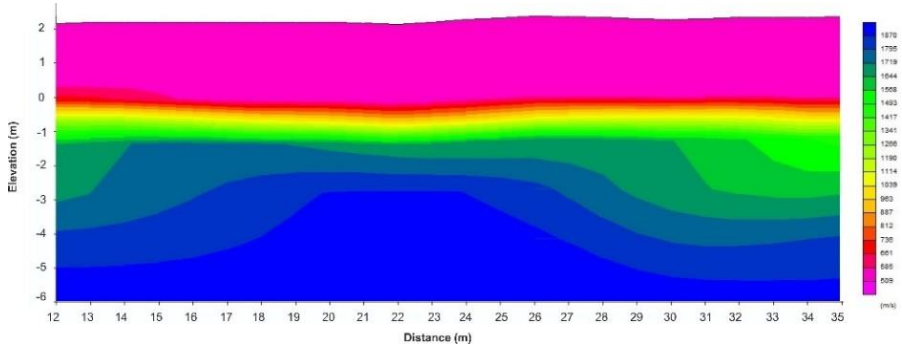

Figure 4. Seismic refraction tomography line at site 114. Distance axis is referred to ERT meters.

Conclusions

Interpreting the geoelectrical measurements at site 114, it seems that we managed to determine the marl formation with a mean resistivity value of more than 35 Ohm.m and seismic velocity of 1.600 m/s. Its upper boundary at the illustrated tomograms of Figures 3 and 4 is estimated to be at -1,5 meters absolute elevation. The preliminary interpretation of all the acquired geophysical measurements, reveal that the marl formation has been investigated at similar absolute elevations, across all the non-coastal sites of Lefkada town, as long as at the sites at Peratia region. On the other hand, at the coastal sites of Lefkada town, the marl formation has not been found down to the investigation depth of the present study. This could be explained by the existence of a possible fault zone parallel to the one illustrated in Figure 1.

Acknowledgements

This research was funded by the project “Telemachus Innovative Seismic Risk Management Operational System of the Ionian Islands” (MIS 5007986) which is part of the Regional Operational Programme «Ionian Islands 2014 2020» and is co-financed by the European Regional Development Fund (ERDF) (National Strategic Reference Framework NSRF 2014 20).

References

Bornovas J., 1964. Geologie de l’ île de Lefkade. Geol Geophys Res (I.G.S.R.) 10(1), 14

Calamita G., Serlenga V., Stabile T.A., Gallipoli M.R., Bellanova J., Bonano M., Casu F., Vignola L., Piscitelli S., Perrone A. 2019. An integrated geophysical approach for urban underground characterization: the Avigliano town (southern Italy) case study, Geomatics, Natural Hazards and Risk, 10:1, 412-432

Hammock C. P., Kulessa B., Hiemstra, J. F., Hodson A. J., & Hubbard A., 2021. Seismic and electrical geophysical characterization of an incipient coastal open-system pingo: Lagoon Pingo, Svalbard. Earth and Space Science, 9, e2021EA002093.

Lekkas E., Danamos G., Lozios S., 2001. Neotectonic structure and evolution of Lefkas Island, Bulletin of the Geological Society of Greece, 34(1), 157-163

16th International Congress of the Geological Society of Greece
17-19 October, 2022 - Patras, Greece
Bulletin of the Geological Society of Greece, Sp. Publ. 10
Ext. Abs. GSG2022-118

Micro-seismicity Monitoring (2015-2018) In Aetolia-Akarnanian Region: Earthquake Clustering And Active Faulting Implications

V. Lefils, A. Rigo[1], E. Sokos[2], C. Duverger[3]

(1) Laboratoire de Géologie, Ecole Normale Supérieure, PSL Research University, CNRS, Paris, France, valentine.lefils@gmail.com . (2) Department of Geology, Seismological Laboratory of Patras, Patras, Greece. (3) CEA, DAM, DIF F-91297 Arpajon, France.

The micro-seismic analysis constrains the active faulting on the Aetolia-Akarnanian region and the geodynamic of the Ionian Island-Akarnanian Block microplate.

The Aetolia-Akarnanian region, in Western Greece, is considered to be part of a microplate in formation, named the Ionian Island-Akarnanian Block (IAB), in the larger-scale tectonic context of Central Mediterranean area. Characterized for the first time in 2013 (Pérouse, 2013 and Pérouse *et al.*, 2017), this microplate accommodates the deformation between the surrounding tectonic structures of the Corinth Gulf (South-East), the Hellenic subduction (South), the Kefalonia Transform Fault (West) and the Apulian collision (North-West).

The Aetolia-Akarnanian seismicity was until now mainly recorded by two permanent seismic networks. The Corinth Rift Laboratory Network (CRLnet) is a local network installed around the Western Corinth Gulf (e.g. Duverger, 2017). The Hellenic Unified Seismological Network (HUSN) collects data from the whole territory of Greece thanks to different Greek networks (Evangelidis *et al.*, 2021). To increase the accuracy and the seismic detection in the Aetolia-Akarnanian region, we started a micro-seismic survey (MADAM) in late 2015 with a dense seismological network over the area (from the Amvrakikos Gulf to the Patras Gulf). Our network has been designed to avoid gaps in terms of magnitudes and to allow the recording of a major part of the Aetolia-Akarnania seismicity. With a semi-automatic event detection and picking program, and a new local velocity model, we precisely locate 12 723 events from October 2015 to December 2018 (Figure 1). That actually represents the most important catalog for the Aetolia-Akarnania with a magnitude range between $0 < M_L < 4,6$ and a magnitude of completeness Mc = 1,0.

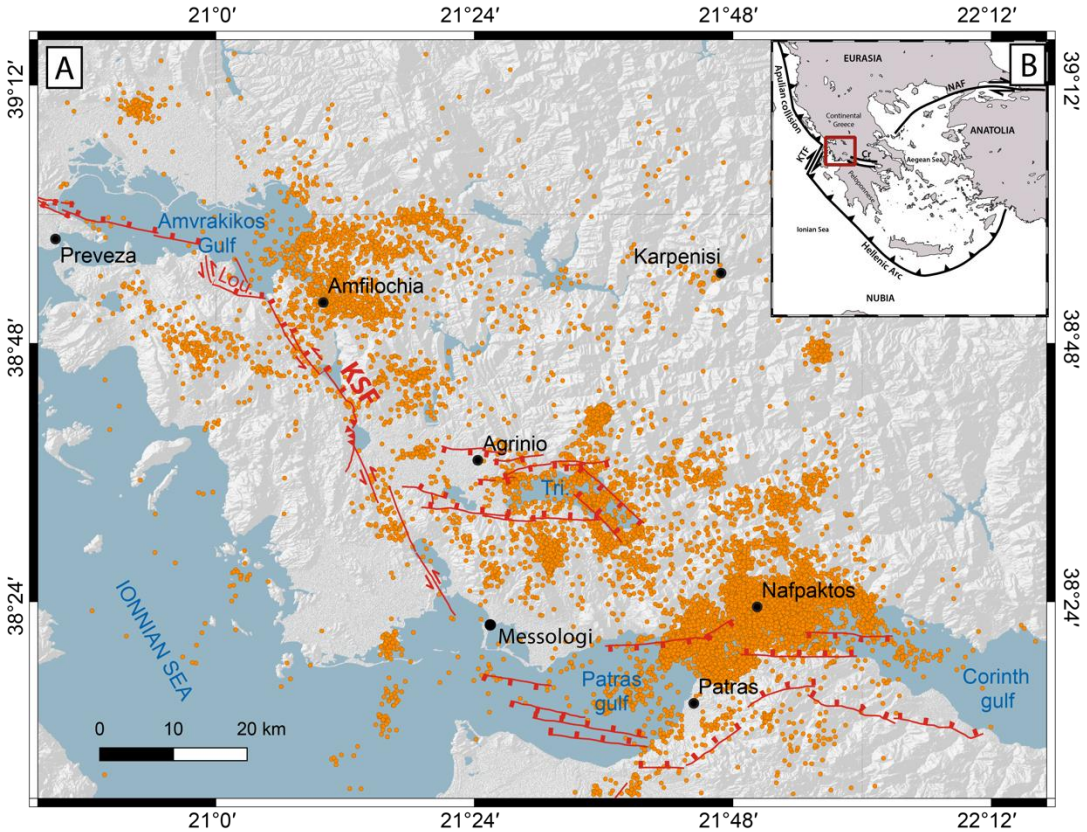

Figure 1. A) Located seismic events map from the MADAM catalog. The locations are from hypo71 software with the new local velocity model. Red traces correspond to fault traces from Pérouse, 2013 and Pérouse *et al.*, 2017. Tri; for Trichonis Lake, KSF for Katouna-Stamna Fault System. B) General tectonic map, red retangle locating the study area.

The observed seismicity highlights specific seismic structures as clusters and a seismic layer below the West of Corinth Gulf. Clusters are spatio-temporal combinations of seismic events. In the whole region, 77 clusters are individually identified. This clustered seismicity is governed by geometry and associated physical processes. Some of these clusters have a geometry similar to a plane and others are elongated vertically with a cone shape. Two distinct physical processes have been identified and studied : a Mainshock-Aftershock (MS-AS) process whose temporal decay corresponds to an Omori law, and a fluid migration process associated with slow slip events (De-Barros *et al.*, 2020) exclusively identified around the Trichonis lake. A link between geometry and process is possibly highlighted with MS-AS clusters mainly located on fault plane type geometries and fluid migration clusters associated with slow earthquakes located on the cone geometry. The seismic layer detected in the western part of the Corinth Gulf have been already observed by previous studies (Rigo *et al.*, 1996 ; Godano *et al.*, 2014 ; Lambotte *et al.*, 2014 ; Duverger, *et al.*, 2018 ; Kaviris *et al.*, 2021) and presents a permanent seismicity in time. This north dipping layer is made of normal faulting seismic events with a shallow dip angle below the Corinth Gulf, then a steeper dip angle toward the north, to end a steeply dipping angle at the latitude of the Trichonis Lake. For the first time, this seismic layer is observed below 15 km depth and above 38°30' latitude. Our different observations are in agreement with the hypothesis of an immature detachment reaching the brittle-ductile boundary. After specific structures analysis the remaining seismicity is named the background seismicity. That correspond to the seismicity after clusters and seismic layer extraction. The detailed studies (by zone) of this seismicity associated with focal mechanisms studies (Weng, 2021) allow us to determine the active faults planes of the region but also the type and direction of the associated deformation. Moreover, some structural observations made from background seismicity allow the identification of previously unknown surface faults.

With all those seismic observations and interpretations associated with the preexisting geodynamic framework, we are able to propose geodynamic and structural model for the Aetolia-Akarnanian region, and finally have a better understanding of the deformation mode of the IAB microplate.

Acknowledgements

This work benefited from the support of CNRS/INSU Tellus/Aleas 2016 and 2017. E.S. acknowledges financial support by the HELPOS project, "Hellenic Plate Observing System" (MIS 5002697). We thanks George Andriopoulos, Nicos Germenis, Dimitri Giannopoulos and Paris Paraskevopoulos for their help in the field, Christos Evangelidis for the loan of instruments during the campaign and Hélène Lyon-Caen for her help in the magnitude determinations.

References

De-Barros, L., Cappa, F., Deschamps, A., and Dublanchet, P. (2020). Imbricated aseismic slip and fluid diffusion drive a seismic swarm in the corinth. Geophysical Research Letter, 47 :1–9.

Duverger, C. (2017). Sismicité, couplages sismique-asismiques et processus transitoires de déformation dans un système de failles actives : le rift de corinthe, grèce, PhD thesis.

Duverger, C., Lambotte, S., Bernard, P., Lyon-Caen, H., Deschamps, A., and Nercessian, A. (2018). Dynamics of microseismicity and its relationship with the active structures in the western corinth rift (greece). Geophysical Journal International, 215 :196–221.

Evangelidis, C. P., Triantafyllis, N., Samios, M., Boukouras, K., Kontakos, K., Ktenidou, O.-J., Fountoulakis, I., Kalogeras, I., Melis, N. S., Galanis, O., et al. (2021). Seismic waveform data from greece and cyprus : Integration, archival, and open access. Seismological Society of America, 92(3) :1672–1684.

Kaviris, G., Elias, P., Kapetanidis, V., Serpetsidaki, A., Karakonstantis, A., Plicka, V., Barros, L. D., Sokos, E., Kassaras, I., Sakkas, V., Spingos, I., Lambotte, S., Duverger, C., Lengliné, O., Evangelidis, C. P., Fountoulakis, I., Ktenidou, O.-J., Gallovi , F., Bufféral, S., Klein, E., Aissaoui, E. M., Scotti, O., Lyon-Caen, H., Rigo, A., Papadimitriou, P., Voulgaris, N., Zahradnik, J., Deschamps, A., Briole, P., and Bernard, P. (2021). The western gulf of corinth (greece) 2020–2021 seismic crisis and cascading events : First results from the corinth rift laboratory network. The Seismic Record, 1 :85–95.

Lambotte, S., Lyon-Caen, H., Bernard, P., Deschamps, A., Patau, G., Nercessian, A., Pacchiani, F., Bourouis, S., Drilleau, M., and Adamova, P. (2014). Reassessment of the rifting process in the western corinth rift from relocated seismicity. Geophysical Journal International, 197 :1822–1844.

Pérouse, E. (2013). Cinématique et tectonique active de l'ouest de la grèce dans le cadre géodynamique de la méditerranée centrale et orientale.

Pérouse, E., Sébrier, M., Braucher, R., Chamot-Rooke, N., Bourlès, D., Briole, P., Sorel, D., Dimitrov, D., and Arsenikos, S. (2017). Transition from collision to subduction in western greece : the katouna–stamna active fault system and regional kinematics. International Journal of Earth Sciences, 106 :967–989.

Rigo, A., Lyon-Caen, H., Armijo, R., Deschamps, A., Hatzfeld, D., Makropoulos, K., Papadimitriou, P., and Kassaras, I. (1996). A microseismic study in the western part of the gulf of corinth (greece) : Implications for large-scale normal faulting mechanisms. Geophysical Journal International, 126 :663–688.

Weng, M. (2021). Détermination de mécanismes au foyer d'un essaim de séismes du Golfe Ambracique (Grèce), master thesis, Ecole Normale Supérieure de Paris.

16th International Congress of the Geological Society of Greece
17-19 October, 2022 - Patras, Greece
Bulletin of the Geological Society of Greece, Sp. Publ. 10
Ext. Abs. GSG2022-127

Normal faulting for five of the ten strong (Mw ≥ 6.0) earthquakes that occurred during the last 5 years in the Aegean

S. Sboras[1,2], D. Galanakis[2], I. Lazos[3], E. Mouzakiotis[1], V. Karastathis[1], S. Pavlides[4]

(1) National Observatory of Athens, Athens, Greece, sboras@noa.gr (2) Hellenic Survey of Geology & Mineral Exploration, Acharnae, Greece (3) School of Mineral Resources Engineering, Technical University, Crete, Greece (4) Geology Department, Aristotle University, Thessaloniki, Greece.

Research Highlights

- Normal faulting prevailed in the Aegean plate during the last quinquennium by producing strong intraplate earthquakes in geodynamically complex areas.

In the last five years (2017-Today), ten earthquakes of Mw ≥ 6.0 have occurred in the broader Aegean region. Eight of them had epicentral locations offshore; two of the offshore ones had hypocentral depths much greater than 40 km and were located along the forearc basin of the Hellenic Arc. Half of the ten earthquakes, all shallow events, demonstrated normal dip-slip kinematics. Three were located along the Anatolian coast (Lesvos, June 12, 2017, M_w6.3; Kos-Bodrum, July 20, 2017, M_w6.6; Samos, October 30, 2020, M_w7.0), one in northern Thessaly, central Greece (Elassona-Tyrnavos, March 3, 2021, M_w6.3), and one in Crete, southern Aegean (Arkalochori, September 27, 2021, M_w6.0). Remote sensing technologies, improved seismographic networks and advanced analytical techniques, combined with conventional, but crucial, methods such as field work mapping, allow the deeper understanding of fault rupturing behaviour.

The 2017 Lesvos earthquake was produced by an offshore, ESE-WNW-striking (SSW-dipping), normal dip-slip fault (*e.g.* Kiratzi, 2018; Chousianitis & Konca, 2018). The causative fault is related with the Plomari-Polichnitos fault (Chatzipetros *et al*., 2013) which controls the local coastline.

The 2017 Kos-Bodrum earthquake occurred in the Gökova (Kerameikos) Gulf just east of Kos Island. Following the local tectonic setting, the earthquake was generated by an emerging ENE-WSW-striking (SSE-dipping), normal dip-slip fault, although the rupture never reached the surface (*e.g.* Sboras *et al*., 2020). The fault is not entirely located offshore; its western tip runs along the northern front of Mt Dikaeos, a tectonically controlled, ENE-WSW-trending horst. Moreover, the mainshock triggered smaller neighbouring faults as seen from the relocated aftershock spatiotemporal distribution and the Coulomb stress changes. The causative fault belongs to a horst-graben fault system that dominates the gulf (*e.g.* Yilmaz *et al*., 2000; Kurt *et al*., 1999).

The 2020 Samos earthquake is the third offshore event in a row occurring in the eastern Aegean – western Anatolia. An E-W-striking (N-dipping), normal dip-slip fault was ruptured, running along and controlling the northern coastline of the island. The aftershock spatiotemporal distribution and the Coulomb stress changes suggest partial reactivation of nearby faults (Sboras *et al*., 2021).

The 2021 Elassona-Tyrnavos seismic sequence is located in the Domeniko-Amouri sub-basin of the larger Elassona – Domeniko-Amouri basin. The latter is the smallest and less well-formed basin of the three ones that prevail in Thessaly. Our pre-earthquake knowledge dictated us that the extension in northern Thessaly is roughly N-S, and hence, the normal active faults direction is *ca.* WNW-ESE. The mainshock, however, revealed a different fault orientation, striking NW-SE (NE-dipping), but maintaining normal dip-slip kinematics. Consequently, the extensional axis strikes NE-SW. The mainshock was followed by a strong (M_w5.9) aftershock (March 4), probably generated by an adjacent fault segment as the spatiotemporal aftershock evolution and Coulomb stress transfer suggest. The coseismic ruptures that were observed in both the Titarissios valley and the intermontane alpine area, the focal mechanisms, and the hypocentral location, imply the occurrence of a NE-dipping, low-angle (detachment-type) fault, bifurcating upwards in several branches.

The 2021 Arkalochori mainshock came after a quite long period of seismic activity in this area. Just a few scattered microearthquakes were recorded in the very beginning of 2021 until the M_L4.2 of June 4 and the swarm that followed. The September 27, M_w6.0 mainshock marked a new outburst. Until very recently, on July 20, 2022, a small shock (M_L4.5) was recorded in the same epicentral area. Tangled among various candidate fault directions that have been proposed as active for central Crete, the mainshock clarified that, at least, the NNE-SSW-striking, normal dip-slip faulting is definitely active. Dipping to the WNW, the seismic fault distinctively bounds the eastern margin of the Heraklion basin. However, the spatiotemporal hypocentral distribution strongly suggests the triggering of more than one nearby faults.

All the above five normal-slip earthquakes occurred within the Aegean (micro-)plate (intraplate events). The rest five strong, other than normal dip-slip earthquakes of the last 5 years, occurred along the Aegean plate boundary, and more specifically along the Aegean-Nubian convergent boundary (interplate events), *i.e.* the Hellenic Arc. During this period no significant activity was recorded along the northern boundary of the Aegean (micro-)plate, *i.e.* the North Aegean

Trough and North Aegean Basin (the westward continuation of the North Anatolian Fault). Thus, extensional deformation in the inner Aegean (micro-)plate during this period was quite intense if we also consider smaller sequences and swarms.

Normal faulting also prevailed in the central part of the Aegean – western Anatolia coast (Lesvos and Samos earthquakes), an area demonstrating a complex seismotectonic setting with both normal dip-slip and strike-slip faulting being active (Chatzipetros *et al*., 2013; Caputo *et al*., 2012). The 2021 Arkalochori earthquake revealed that NNE-SSW normal faulting, one of the many fault directions that are supposed to be active in Crete, is indeed active. However, nature never ceases to surprise us: the 2021 northern Thessaly sequence changed our insight about the roughly N-S extension in this part of the Aegean.

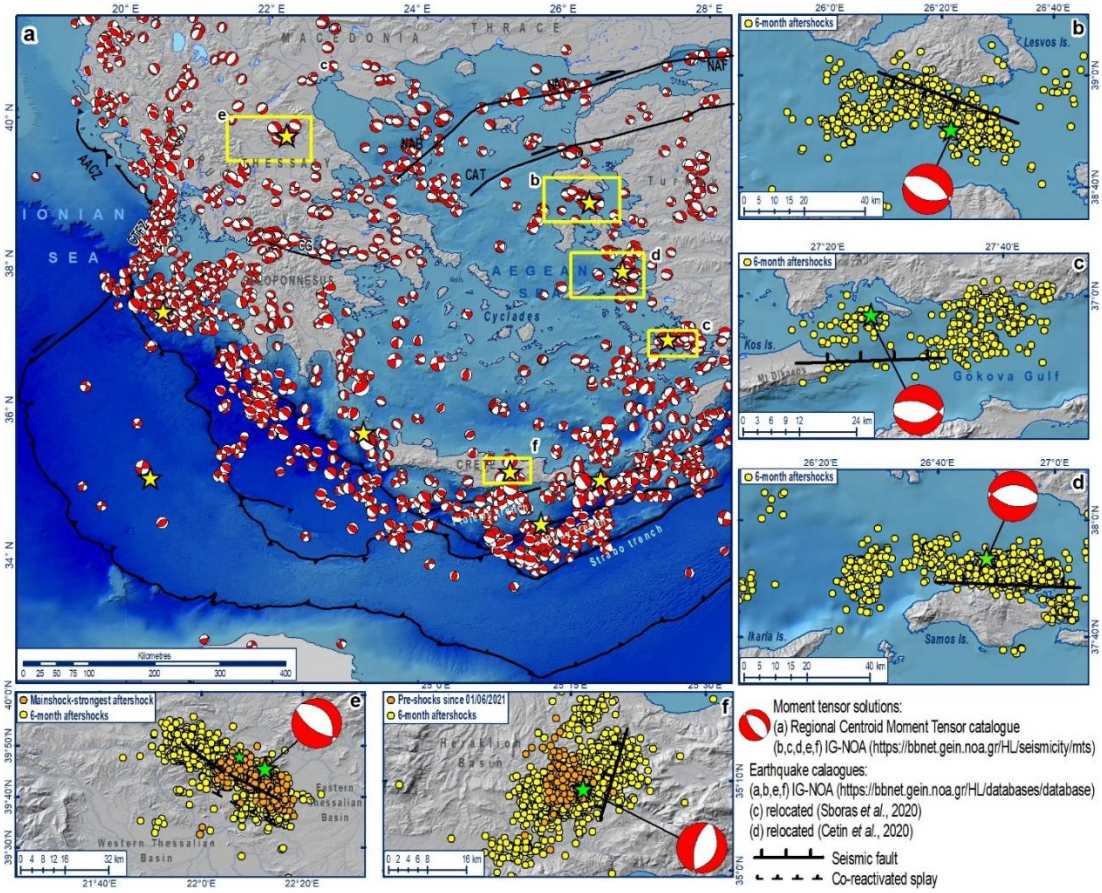

Figure 1. (a) The major tectonic structures with moment tensor solutions since 1997 and the 10 strong earthquake epicentres (stars) of the last 5 years in the broader Aegean region. Inset maps focus on the five study cases described in the main text. NAT: North Aegean Trough, NAB: North Aegean Basin, NAF: North Anatolian Fault, CAT: Central Aegean Trough, AACZ: Apulian-Aegean Collision Zone, CTFZ: Cephalonia Transform Fault Zone.

References

Caputo, R., Chatzipetros, A., Pavlides, S., Sboras, S. 2012. The Greek Database of Seismogenic Sources (GreDaSS): state-of-the-art for northern Greece. Annals of Geophysics 55(5), 859-894. https://doi.10.4401/ag-5168

Cetin, K.O., Mylonakis, G., Sextos, A., Stewart, J.P., 2021. Seismological and Engineering Effects of the M 7.0 Samos Island (Aegean Sea) Earthquake. Geotechnical Extreme Events Reconnaissance Association: Report Geer-069. https://doi.10.18118/G6H088

Chatzipetros, A., Kiratzi, A., Sboras, S., Zouros, N., Pavlides, S., 2013. Active faulting in the north-eastern Aegean Sea Islands. Tectonophysics 597, 106-122.

Chousianitis, K., Konca, A.O., 2018. Coseismic slip distribution of the 12 June 2017 M_w= 6.3 Lesvos earthquake and imparted static stress changes to the neighboring crust. Journal of Geophysical Research: Solid Earth 123(10), 8926-8936.

Kiratzi, A., 2018. The 12 June 2017 Mw 6.3 Lesvos Island (Aegean Sea) earthquake: Slip model and directivity estimated with finite-fault inversion. Tectonophysics 724, 1-10.

Kurt, H., Demirbağ, E., Kuşçu, İ. 1999. Investigation of the submarine active tectonism in the Gulf of Gökova, southwest Anatolia–southeast Aegean Sea, by multi-channel seismic reflection data. Tectonophysics 305(4), 477-496.

Sboras, S., Lazos, I., Mouzakiotis, E., Karastathis, V., Pavlides, S., Chatzipetros, A., 2020. Fault modelling, seismic sequence evolution and stress transfer scenarios for the July 20, 2017 (MW 6.6) Kos–Gökova Gulf earthquake, SE Aegean. Acta Geophysica, 68(5), 1245-1261.

Sboras, S., Lazos, I., Bitharis, S., Pikridas, C., Galanakis, D., Fotiou, A., Chatzipetros, A., Pavlides, S., 2021. Source modelling and stress transfer scenarios of the October 30, 2020 Samos earthquake: seismotectonic implications. Turkish Journal of Earth Sciences 30(8), 699-717.

Yilmaz, Y., Genç, Ş.C., Gürer, F., Bozcu, M., Yilmaz, K., Karacik, Z., Altunkaynak, Ş., Elmas, A., 2000. When did the western Anatolian grabens begin to develop? Geological Society, London, Special Publications 173(1), 353-384.

16th International Congress of the Geological Society of Greece
17-19 October, 2022 - Patras, Greece
Bulletin of the Geological Society of Greece, Sp. Publ. 10
Ext. Abs. GSG2022-149

Spatial analysis of seismic noise estimation on Italy by statistical methods: a comparison with the magnitude completeness map

M. Catania[1], G. Vitale[2], A. Figlioli[1], A. D'Alessandro[2]

(1) Università degli studi di Palermo, Dipartimento di Scienze della Terra e del Mare, Palermo, Italy, maria.catania03@unipa.it (2) Istituto Nazionale di Geofisica e vulcanologia, Osservatorio Nazionale Terremoti, Rome, Italy.

Seismic noise has been the subject of study for many eras, as in many fields at the beginning the scientific effort was related to military applications to identify the enemy from a distance. So right from the start it was necessary to understand if the vibrations detected are produced by natural and / or anthropogenic sources. Historical (Gutenberg1911) (Frantti1962) (Asten1978) (Asten1984) and recent (Bonnefoy-Claudet1984) (Grecu2012) scientific works divide seismic noise into two classes: natural sources (microsisms) at lower frequencies; anthropogenic sources (microtremors) at high frequencies. However, it is possible to identify in the bibliography just cited an interval of intermediate frequencies (from 1 to 5 Hz) in which it is possible to observe both types of sources. Site characteristics such as: geology, meteorological phenomena, site effects, distance from the coastline, etc., can influence natural seismic noise. Human activities such as: traffic, power plants, factories, industrial machinery etc. influence anthropogenic noise. It should also be noted that the works based on foreign national seismic networks stop at spectral analysis (Dimitrova2016) (Grecu2012) (Abd el-aal2013) (Custodio2014) (Anthony2014) (Guo2015) (Demuth2016) (Jana2017).

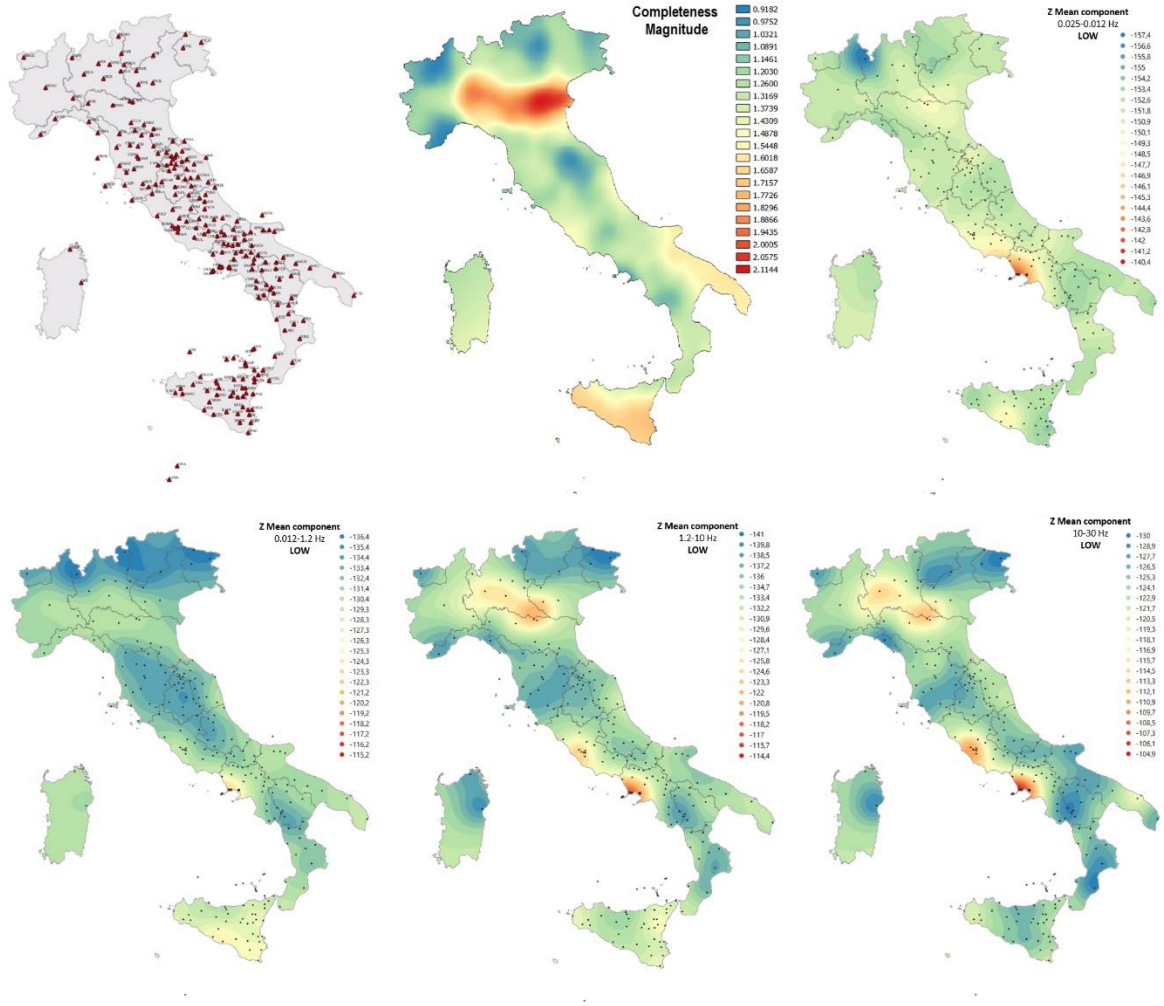

Figure 1. Starting from the top left: map of the ISN station (red triangles), magnitude completeness map and spatial low-pass filtered maps of the average noise power spectrum for the four frequency ranges analyzed.

The literature does not report much information on the Italian territory and reference is made to local studies (Marzorati2006) (Vassallo2012). (D'Alessandro2010) presented for the first time a noise power map relating to the entire Italian territory for the Italian Seismic Network (ISN) managed by the Istituto Nazionale di Geofisica e Vulcanologia in an estimated range 1-12 Hz, and subsequently in (D'Alessandro2021) the entire Italian Seismic Network through a spectral / statistical approach to develop a seismic noise model for Italy. In this work we want to show a comparison between two types of independent spatial data: seismic noise power distribution and the catalog of seismic events as magnitude of completeness. We want to observe whether the data that are independent of each other lead to the same results throughout the Italian territory and justify any anomalies.

Much attention is paid to the spatial and statistical analysis of the power of background noise recorded by the ISN in the three-year period 2015-2017. We studied the variation of seismic noise by calculating the power spectral densities (PSD) and the probability density function (PDF), following the method of Peterson (Peterson1993) and second (McNamara2004) to make a comparison. There are currently no other works in the literature in which an Italian noise model has been verified with a statistical approach or in which an attempt is made to correlate the local completeness magnitude to the local seismic noise level. This involves a new statistical approach with an imported and applied feedback, the local completeness magnitude map. The local completeness magnitude map was obtained by downloading the entire INGV catalog and then processing the data using the ZMAP application. This methodology could also be applicable to other seismic networks around the world. Therefore, this work aims to lay the foundations for further future research on the study of seismic noise, not leaving it to the interpretation of the researcher, but to develop a method in which different types of information allow to have feedback on the results and obtain more robust national seismic models. Furthermore, it is possible to observe anomalies between the two types of data that lead to important considerations and conclusions, difficult to identify if you do not have a detailed knowledge of the whole territory. These works could be of great operational importance, as they allow the performance of the ISN to be assessed, in particular in terms of detection magnitude and quality of the hypo-central location, and for future upgrades of the monitoring infrastructure.

References

Gutenberg, B., 1911. Die seismische bodenunruhe, Ph.D. thesisUniversity of Gottigen, Germany. (In German).

Frantti, G., Willis, D.E. & Wilson, J.T., 1962. The spectrum of seismic noise, Bulletin of the Seismological Society of America, 52(1), 113–121.

Asten, M.W. (1978). Geological control of the three-component spectra of rayleigh-wave microseisms, Bull. Seism. Soc. Am., 68, 1623-1636.

Asten, M.W. & Henstridge, J.D., 1984. Array estimators and use of microseisms for reconnaissance of sedimentary basins, Geophysics, 49, 1828-1837.

Bonnefoy-Claudet, S., Cotton, F., & Bard, P.Y., 2006. The nature of noise wavefield and its applications for site effects studies: A literature review, Earth-Science Reviews, 79(3–4), 205–227

Grecu, B., Neagoe, C., & Tataru, D., 2012. Seismic noise characteristics at the Romanian broadband seismic network, Journal of Earthquake Engineering, 16(5), 644-661.

Dimitrova, L., & Nikolova, S., 2010. Analysis of the ambient seismic noise at Bulgarian seismic stations, In EGU General Assembly Conference Abstracts, 6736.

Abd el-aal, A. E. A. K., 2013. Very broadband seismic background noise analysis of permanent good vaulted seismic stations, Journal of Seismology, 17, 223-237.

Custodio, S., Dias, N.A., Caldeira, B., Carrilho, F., Carvalho, S., Corela, ´ C., D´ıaz, J., Narciso, J., Madureira, G., Matias, L. & Haberland, C., 2014. Ambient noise recorded by a dense broadband seismic deployment in western Iberia, Bulletin of the Seismological Society of America, 104(6), 2985-3007

Anthony, R. E., Aster, R. C., Wiens, D., Nyblade, A., Anandakrishnan, S., Huerta, A. & Rowe, C., 2014. The seismic noise environment of Antarctica, Seismological Research Letters, 86, LA-UR-14-28568.

Guo, Z., & Aydin, A., 2015. Double-Frequency Microseisms in Ambient Noise Recorded in Mississippi, Bulletin of the Seismological Society of America, 105(3), 1691-1710.

Demuth, A., Ottemoller, L., & Keers, H., 2016. Ambient noise levels and ¨ detection threshold in Norway., Journal of seismology, 20(3), 889-904.

Jana, N., Singh, C., Biswas, R., Grewal, N. & Singh, A., 2017. Seismic noise analysis of broadband stations in the Eastern Ghat mobile belt of India using power spectral density, Geomatics, Natural Hazards and Risk, 8(2), 1622–1630.

Marzorati, S. & Bindi, D., 2006. Ambient noise levels in north central Italy, Geochemistry, Geophysics, Geosystems, 7(9).

Vassallo, M., Festa, G., & Bobbio, A., 2012. Seismic ambient noise analysis in southern Italy, Bulletin of the Seismological Society of America, 102(2), 574-586.

D'Alessandro, A., Luzio, D., D'Anna, G., & Mangano, G., 2010. Valutazione della performance di localizzazione della RSN-INGV tramite simulazione numerica, Quaderni di Geofisica, 2010-06-2483, 1-33.

D'Alessandro, A., Greco, L., Scudero, S., & Lauciani, V., 2021. Spectral characterization and spatiotemporal variability of the background seismic noise in Italy, Earth and Space Science, 8(10), e2020EA001579.

Peterson, J. R., 1993. Observations and modeling of seismic background noise, US Geological Survey.

McNamara, D. E. & Buland, R. P., 2004. Ambient noise levels in the continental United States, Bulletin of the Seismological Society of America, 94(4), 1517–1527.

16th International Congress of the Geological Society of Greece
17-19 October, 2022 - Patras, Greece
Bulletin of the Geological Society of Greece, Sp. Publ. 10
Ext. Abs. GSG2022-150

The earthquake monitoring network in Taiwan: general considerations about its coverage and performance

S. Scudero[1], A. D'Alessandro[1], A. Figlioli[2]

(1) Istituto Nazionale di Geofisica e Vulcanologia, Osservatorio Nazionale dei Terremoti, Rome, Italy, salvatore.scudero@ingv.it (2) Università degli studi di Palermo, Dipartimento di Scienze della Terra e del Mare, Palermo, Italy.

Abstract

In this contribution, we perform the evaluation of the national seismic network operating in Taiwan. We analyze the Magnitude-frequency distribution of earthquakes; moreover, the distributions of seismic network and earthquakes have been jointly analyzed with spatial statistics techniques and used to retrieve information about their consistency. We highlight the overall high quality of the network established in Taiwan for seismic surveillance purposes. The proposed approach can be generalized to retrieve quantitative information on the coverage of other earthquake monitoring networks, identifying possible critical areas and addressing future developments.

Introduction

Taiwan island is characterized by a considerable seismicity. The beginning of instrumental earthquake monitoring in Taiwan dates back to 1897 when the very first seismograph was installed (Shin et al., 2013). Since then, a network has been established and expanded over the whole country, mainly boosted later by the technological advancements in the 1970s and 1990s and it is still expanding and improving at present (Wang, 1989; Shin et al., 2013). For this study, we considered only the part of the network which includes the broad-band velocimeters (*Real-time Seismic Monitoring Network*), namely the network mainly used to locate the earthquakes, excluding the nodes equipped with accelerometers whose purpose is sometimes different. The distribution of the network's nodes is then analysed in comparison with the catalogue of instrumental earthquakes according to the method proposed by Siino et al (2020). Moreover, we also compare the intensity map of the *Real-time Seismic Monitoring Network* with the map of the magnitude of completeness.

Data and methods

The datasets used for data analysis were downloaded from the website of the Seismological Centre of the Central Weather Bureau (https://scweb.cwb.gov.tw/en-us/earthquake/data). For the earthquakes, the time period selected for the analysis runs from 1995/01/01 to 2020/12/31; the catalogue counts 11,857 events, with magnitude in the interval 2.0 - 7.3. For the calculation of the completeness magnitude, the range goes from 2000/01/01 to 2022/08/02. The locations of the monitoring stations are limited to those sites equipped with broad-band sensors (274 sites).

Data are analysed by means of descriptive spatial statistics and point process methods. A spatial point pattern is a set of unordered points within a given region of space. For a spatial point process, the first-order intensity is the expected number of points in a unit region around a generic location divided by its area. For spatial point patterns, the intensity is estimated non-parametrically to understand the spatial trend. The estimated intensities of the point patterns (i.e. earthquakes and seismic stations) are considered as raster data sets; pairs of rasters can be compared to determine if the spatial information within the raster data is locally correlated. The local correlation coefficient for a pair of raster maps is computed considering a grid resolution of 3 km and a neighborhood of 5x5 cells (15*15 km2) around each cell. To calculate the magnitude of completeness, the Maximum technique has been employed (Wiemer and Wyss, 2000). It consists of evaluating the maximum curvature of the frequency-magnitude curve by computing the maximum value of the first derivative. This method is fast and straightforward, it performs very well to small catalogues and gives a stable completeness magnitude. For this catalogue, the frequency-magnitude distribution completeness magnitude is 4.1.

Discussion and conclusions

The intensities have been calculated with a kernel estimator, given the spatial point patterns (Figure 1). Having fixed the grid resolution to 3 km, the values reported in the intensity plots indicate the number of stations over a 9 km^2 area. The intensity of stations appears to be almost constant over the study area: relatively higher intensity values mark the northern and western portions of the country. The intensity of the earthquakes shows very high values of intensity extending along a portion of the eastern coast. Their relationship (i.e. local correlation) is evaluated by mapping the correlation coefficient of the 25 pairs of values within the focal area (5x5 cells). Both zones with positive and negative correlation emerge (Figure 1). The positive correlation indicates coherence between the two considered variables, conversely the negative correlation indicates discordance between the distributions of the stations and the instrumental seismicity. Considering the almost

uniform station intensity, most of these negative areas are likely the result of a significant network coverage in zones with moderate or low recorded seismicity. Figure 2 shows the map of the magnitude of completeness. The areas characterized by the highest values of intensity (Figure 1) match with the areas characterized by low values of completeness magnitude (2.5-3.5). On the other hand, low intensity values appear to be correlated with high values of completeness magnitude, that is, greater than 3.5. Therefore, there is a relationship between the number of stations installed in the field and the minimum magnitude of a catalogue.

In conclusion, it appears that at large scales there are no major inconsistencies between the geometry of the seismic network and the distribution of the earthquakes. As expected, the magnitude of completion is controlled by the distribution of the network, and their values are relatively high. This can be ascribable to the characteristics of the seismicity and deserves further investigation.

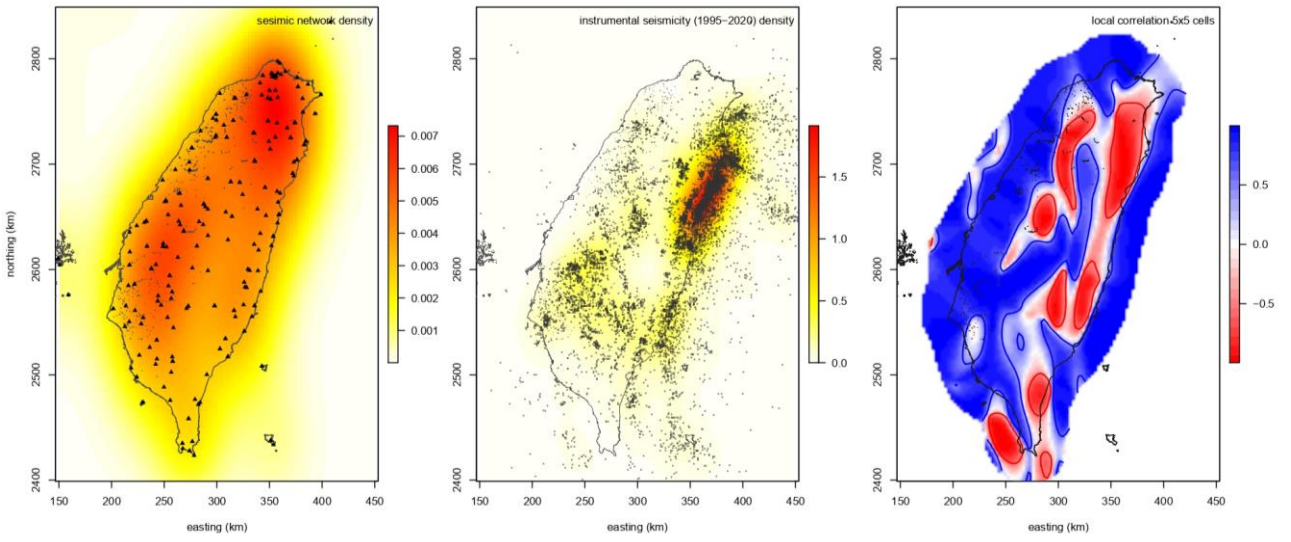

Figure 1. Kernel intensity estimation for the earthquake monitoring network (left), kernel intensity estimations (centre), and local correlation coefficients (right), calculated for the Taiwan Real-time Seismic Network

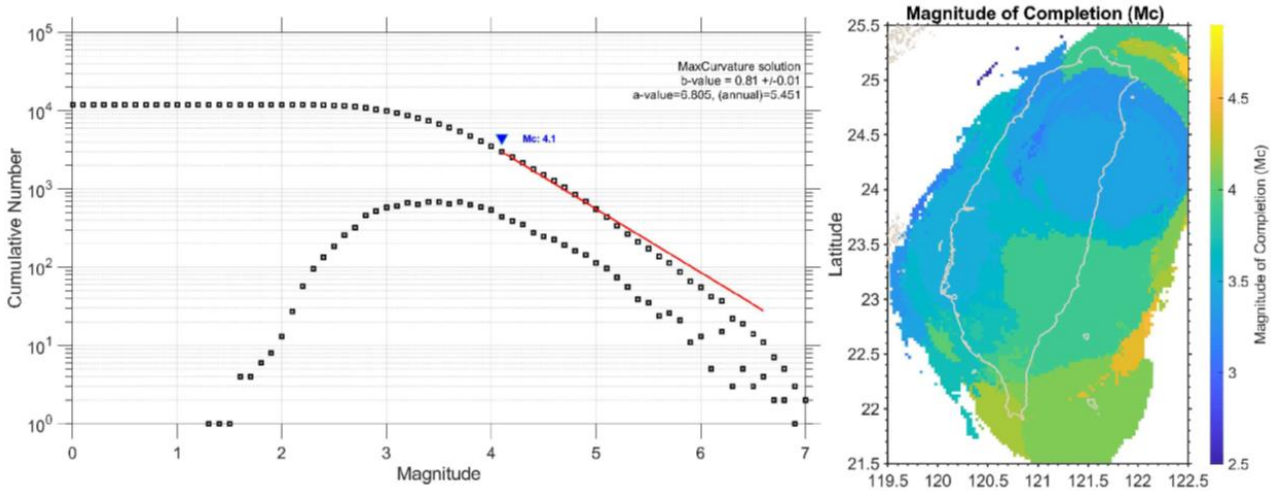

Figure 2. Magnitude-frequency relationship for Taiwan earthquake catalogue (left) and spatial distribution of the magnitude of completion (right).

References

Shin, T.-C., C.-H. Chang, H.-C. Pu, L. Hsiao-Wei, and P.-L. Leu, 2013. The geophysical database management system in Taiwan. TAO: Terrestrial, Atmospheric and Oceanic Sciences, 24 (1), 11

Siino, M., S. Scudero, L. Greco, and A. D'Alessandro, 2020: Spatial analysis for an evaluation of monitoring networks: examples from the italian seismic and accelerometric network. Journal of Seismology, 24 (6), 1045–1061, doi:https://doi.org/10.1007/s10950-020-09937-0

Wang, J. H., 1989: The Taiwan telemetered seismographic network. Physics of the Earth and Planetary Interiors, 58 (1), 9–18.

Wiemer, S., & Wyss, M. (2000). Minimum magnitude of completeness in earthquake catalogs: Examples from Alaska, the western United States, and Japan. Bulletin of the Seismological Society of America, 90(4), 859-869

16th International Congress of the Geological Society of Greece

17-19 October, 2022 - Patras, Greece

Bulletin of the Geological Society of Greece, Sp. Publ. 10

Ext. Abs. GSG2022-159

Complex Anisotropy in the Habanero Geothermal Field, Cooper Basin, Australia

I. Spingos[1], G. Michas[1], V. Kapetanidis[1], G. Kaviris[1], F. Vallianatos[1,2]

(1) National and Kapodistrian University of Athens, Department of Geology & Geoenvironment, Section of Geophysics-Geothermics, Athens, Greece, ispingos@geol.uoa.gr (2) Institute of Physics of Earth's Interior and Geohazards, UNESCO Chair on Solid Earth Physics and Geohazards Risk Reduction, Hellenic Mediterranean University Research Center, Chania, Greece

Research Highlights

- First time analysis of shear-wave splitting in the Habanero geothermal field.
- Fast polarizations suggest complex anisotropy associated with fracture geometry and regional stress

Introduction

Shear-wave Splitting (SwS) is a phenomenon caused by anisotropic media. As a shear-wave enters such a medium, it splits in two orthogonally-polarized waves, travelling with different velocities. The fast wave (S_{fast}) is polarized according to the anisotropic feature of the medium, while the polarization of the slow one (S_{slow}) is perpendicular. SwS has long been connected to stress variations in rocks permeated by fluid-filled microcracks or dominated by large tectonic structures. Studying the properties of SwS can offer valuable information for the geometry (through φ, the polarization direction of $\underline{S_{fast}}$) and intensity (via t_d, the time-delay between the arrivals of S_{fast} and S_{slow}) of these features.

Herein, we study seismic anisotropy via SwS in the Habanero geothermal field in the Cooper Basin, Australia. A series of wells have been drilled in this area since 2002, to explore its geothermal potential. In 2012, a hydraulic stimulation experiment was conducted in the Habanero-4 well, leading to the seismic activation of a sub-horizontal fault plane of only few-meters thickness at ~4 km depth, within the granite basement (Baisch *et al.*, 2015). The maximum regional stress (S_{Hmax}) in Cooper Basin is oriented at N101ºE (Reynolds *et al.*, 2005). Focal mechanisms determined from past injection experiments (2003 and 2005) in the Habanero field showcased two types of faulting; (a) a dominant reverse Type I (157º/09º/065º) and, (b) a minority of Type II fractures (074º/020º/150º). Type I agrees with the WNW-ESE maximum stress component, while Type II is assumed to be related to conjugate fracturing (Baisch *et al.*, 2009).

Data and Methods

Our initial seismic catalogue consisted of 29,283 detected earthquakes, out of which 7,499 could not be located. The catalogue spans a period from 9th September 2012 to 23rd January 2013. The bulk of seismicity started with the first injection and lasted for a brief time after the end of the main phase (from 14th November 2012 to 15th December 2012). Magnitudes in the catalogue varied between -1.7 and 3.0, with a magnitude of completeness equal to -1.2. Depths were constrained in the 3.92 to 4.46 km range. As this is a first step towards exploring SwS in the area, we selected a subset of the initial catalogue for analysis, i.e. all events with a M≥1.0 (379 earthquakes).

During 2012, a network of 24 sensors was monitoring the area around Habanero, consisting of 10 short-period (1 Hz) seismometers installed at the surface and 14 downhole geophones. Our analysis was conducted using recordings from the surface instruments, as their orientation is known.

We used an automated processing scheme for SwS, through the Pytheas software (Spingos *et al.*, 2020). Splitting parameters were determined with the eigenvalue method (Silver and Chan, 1991). This process was repeated for multiple signal windows at each event-station pair. The optimal signal window and measurement was selected with cluster analysis (Teanby *et al.*, 2004).

Results

Our analysis led to the procurement of 708 good quality measurements out of the 10 stations. We can identify two main groups of sites, based on φ (Fig. 1); (a) NE-SW: SS02, SS05, SS08 and (b) WNW-ESE to NW-SE: MS06, SS01, SS03, SS06, SS07, WA03. Stations SS03 and SS07, however, exhibit a strong secondary direction, perpendicular to the primary one. It is noted that the number of observations at WA03 is low (8 measurements) and, therefore, can be considered unreliable. There are at least 20 results at each of the other sites. Station SS04 showcases highly scattered φ values, rendering the assignment of a dominant direction arguable.

Concerning time-delays, assuming t_d accumulates linearly along the ray path, the normalized (per the hypocentral distance) time-delay (t_n) can be obtained. Three groups of t_n are identifiable: (a) low (SS02, SS07, SS08), (b) medium (SS01, SS05, SS06), and (c) high (SS03, MS06, WA03).

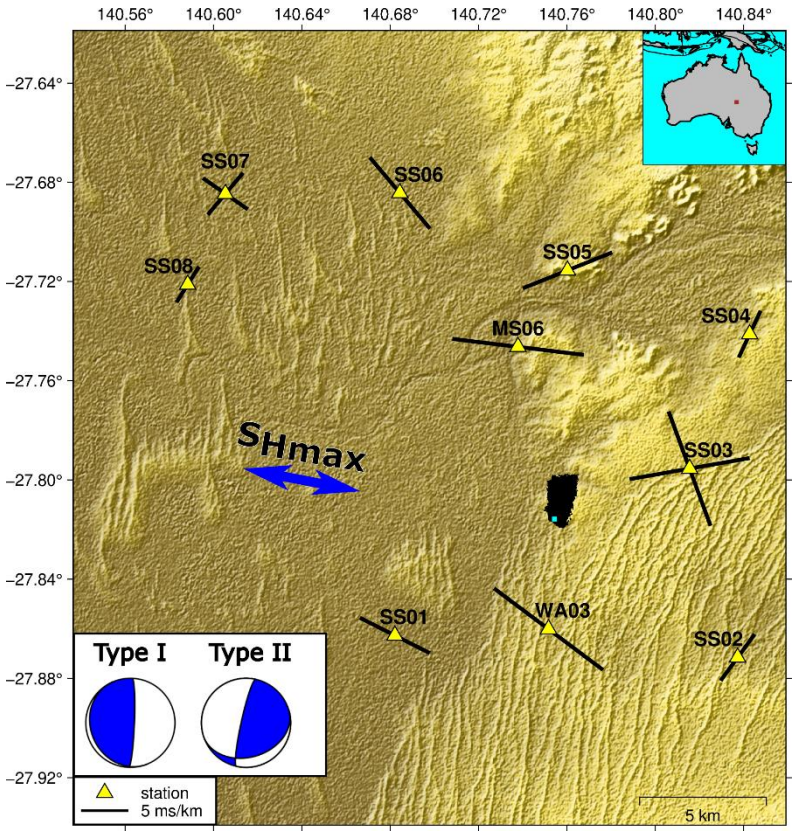

Figure 1. Map of the study area, showcasing dominant polarization directions at each site (black lines, length proportionate to the average tn). The earthquake epicenters (black area) are constrained near the eastern edge of the network, close to the Habanero-4 well (cyan square). The direction SHmax (blue arrow) and the focal mechanisms of Type I and II (Baisch et al., 2009) fractures are also shown. Inset: study area (brown square) in the context of Australia.

Conclusions

Preliminary analysis of 379 M≥1.0 earthquakes from the 2012 injection stimulation at Habanero field (Cooper Basin, Australia) showcases an underlying intricate anisotropic medium. The general direction of S_{Hmax} is followed by four sites, while both Type I and Type II fracture directions are represented, by three sites each. Neither φ nor t_n follow specific temporal patterns. The existence of two φ directions at a single site is usually an indication of 90º-flips due to increased pore pressure; however, in this case, observations of different φ co-exist in time.

Further work is required to process the whole dataset and obtain a much more populous sample. Moreover, identifying the orientation of downhole sensors would greatly enrich available data. Even so, the presented preliminary sample of results revealed the existence of a complex anisotropic uppermost crust beneath Habanero, permitting extensive analysis to identify patterns between splitting and well injections.

Acknowledgements

The authors are grateful to the Department of State Development of South Australia for providing event catalogues, station information and waveform data from the Habanero-4 experiment. This study was supported by the Hellenic Foundation for Research and Innovation (H.F.R.I.) under the "2nd Call for H.F.R.I. Research Projects to support Post-Doctoral Researchers" (Project Number: 00256).

References

Baisch, S., Rothert, E., Stang, H., Vörös, R., Koch, C., McMahon, A., 2015. Continued Geothermal Reservoir Stimulation Experiments in the Cooper Basin (Australia). Bulletin of the Seismological Society of America, 105(1), 198–209. doi: 10.1785/0120140208

Baisch, S., Vörös, R., Weidler, R., Wyborn, D., 2009. Investigation of fault mechanisms during geothermal reservoir stimulation experiments in the Cooper Basin, Australia. Bulletin of the Seismological Society of America, 99(1), 148–158. doi: 10.1785/0120080055

Reynolds, S. D., Mildren, S. D., Hillis, R. R., Meyer, J. J., Flottmann, T., 2005. Maximum horizontal stress orientations in the Cooper Basin, Australia: Implications for plate-scale tectonics and local stress sources. Geophysical Journal International, 160(1), 332–344. doi: 10.1111/j.1365-246X.2004.02461.x

Silver, P. G., Chan, W. W., 1991. Shear Wave Splitting and Sub continental Mantle Deformation. Journal of Geophysical Research, 96, 429–454. doi: 10.1029/91JB00899

Spingos, I., Kaviris, G., Millas, C., Papadimitriou, P., Voulgaris, N., 2020. Pytheas: An open-source software solution for local shear-wave splitting studies. Computers & Geosciences, 134, 104346. doi: 10.1016/j.cageo.2019.104346

Teanby, N., Kendall, J.-M., van der Baan, M., 2004. Automation of shear-wave splitting measurements using cluster analysis. Bulletin of the Seismological Society of America, 94(2), 453–463. doi: 10.1785/0120030123

16th International Congress of the Geological Society of Greece
17-19 October, 2022 - Patras, Greece
Bulletin of the Geological Society of Greece, Sp. Publ. 10
Ext. Abs. GSG2022-161

Spatiotemporal Evolution of the 2020 Perachora Earthquake Swarm and Inferences for the Triggering Mechanism

G. Michas[1], V. Kapetanidis[1], I. Spingos[1], G. Kaviris[1], F. Vallianatos[1,2]

(1) Section of Geophysics – Geothermics, Department of Geology and Geoenvironment, National and Kapodistrian University of Athens, Athens, Greece, gemichas@geol.uoa.gr (2) Institute of Physics of Earth's Interior and Geohazards, UNESCO Chair on Solid Earth Physics and Geohazards Risk Reduction, Hellenic Mediterranean University Research Center, Crete, Greece.

Research Highlights

- We present a relocated catalogue for the pronounced earthquake swarm that occurred in 2020 at the Perachora peninsula, East Corinth Rift.
- The spatiotemporal evolution of the swarm indicates pore-fluid pressure diffusion as the primary triggering mechanism.

Background and Objectives

The Corinth Rift, a high-strain zone of extensional deformation in the back-arc region of the Hellenic subduction zone, represents one of the most seismically active areas in the Eastern Mediterranean. Several large and damaging earthquakes have been reported in this area in both historic and modern times (e.g., Makropoulos *et al*., 2012). While abundant microseismicity and frequent earthquake swarms have routinely been recorded in the western part (e.g., Michas *et al*., 2021; Kapetanidis *et al*., 2021), in the eastern part seismic activity is more sparse. However, occasional seismic outbursts do occur in this area. Recently, during April – August 2020, a pronounced earthquake sequence was recorded at the broader area of the Perachora peninsula. The sequence evolved as a swarm and was widely felt by the local population, raising public concern regarding its evolution and a possibly impending stronger and damaging event.

In this work, we study the spatiotemporal properties of the 2020 Perachora swarm and investigate the possible triggering mechanisms. Initially, earthquake hypocenters in the area were relocated with the double-difference method to enhance the spatial resolution of the catalogue. Then, we investigated the migration patterns of seismicity in terms of migration velocities and diffusion rates that can provide significant insights regarding the triggering mechanism.

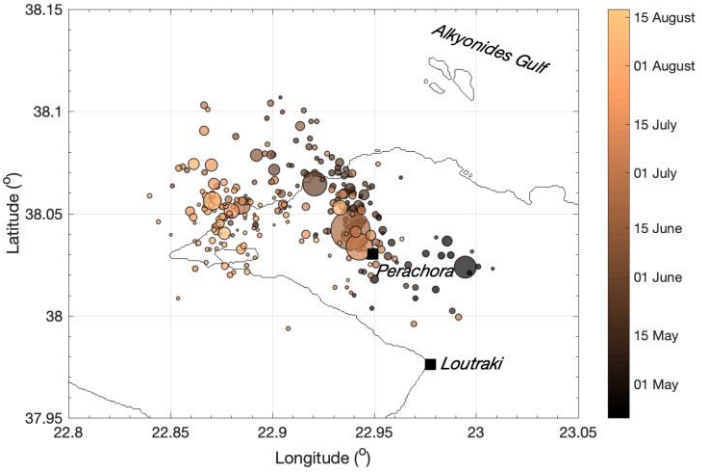

Figure 1. Spatial distribution of the relocated 2020 Perachora swarm. Earthquakes, shown as circles, are sized and colored according to magnitude and origin time, respectively.

Methods

Initially, catalogue and arrival-time data were collected from the databases of the Seismological Laboratory of the National and Kapodistrian University of Athens (SL-NKUA) and the Geodynamic Institute of the National Observatory of Athens (GI-NOA) for 828 events that occurred at the Eastern Gulf of Corinth between January 2020 and June 2021. Preliminary event absolute locations were obtained with HypoInverse and the 1D velocity model of Karakonstantis (2017). An error minimization procedure was then performed to acquire an optimum velocity model for the sequence. As a final step, the earthquake hypocenters were relocated with the double-difference method (Waldhauser, 2001), using both catalogue and cross-correlation differential travel-time data. The final relocated catalogue consists of 788 events, with median horizontal and vertical errors of the relocated hypocenters of the order of 0.175 km and 0.340 km, respectively.

Results

The catalogue presents a *b*-value of 1.20±0.06 and a magnitude of completeness of 1.6 (Michas *et al*., 2022). The largest event during the studied period was an M_w 3.9 earthquake that occurred at the Alkyonides Gulf on 7 March 2020, while the second largest of M_w 3.7 occurred on 23 June 2020 close to Perachora.

An increased seismicity rate was observed in the broader area of the Perachora peninsula between April and August 2020 (Figure 1), marking the period of the swarm activity. The activated zone covers an area of ~161 km^2, with a 1st principal semi-axis length of ~9.9 km pointing toward N103ºE, as indicated by the Principal Component Analysis (PCA) applied to the sequence (Michas *et al*., 2022). The seismic activity presented distinct characteristics of earthquake migration from the eastern part of the peninsula towards northwest and then west of the activated area (Figure 1), with successive deepening of the events. This migration pattern of seismicity along the direction of the maximum spatial variance indicated by PCA is consistent with a pore-fluid pressure triggering front of hydraulic diffusivity of D=2.8 m^2/s (Shapiro *et al*., 1997) and an average speed of 0.22 km/day (Figure 2). Furthermore, the sequence presents a diffusion exponent of a=0.89±0.06, which is consistent with anomalous fluid transport phenomena in heterogeneous and fractured media (Michas *et al*., 2022). Such results indicate pore-fluid pressure diffusion as the primary triggering mechanism of the Perachora swarm.

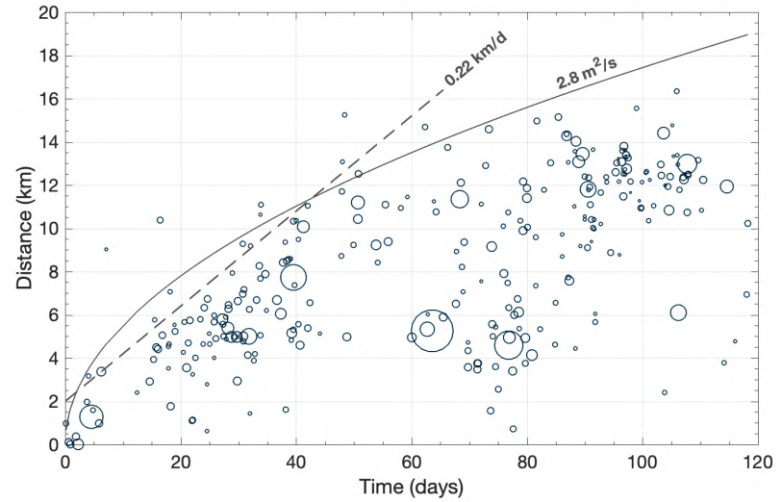

Figure 2. Distance-Time plot of the relocated 2020 Perachora swarm. The events, shown as circles, are sized according to magnitude. The solid and dashed lines represent the parabolic and linear triggering fronts, respectively.

Conclusions

The analysis and results indicate, overall, that the 2020 Perachora swarm was initially triggered at shallow depths by fluid overpressures, possibly generated by the increased precipitation in the area during November 2019 – April 2020, and was then driven by pore-fluid pressure diffusion along a local, possibly blind, northwest-dipping structure.

Acknowledgements

The research project was supported by the Hellenic Foundation for Research and Innovation (H.F.R.I.) under the "2nd Call for H.F.R.I. Research Projects to support Post-Doctoral Researchers" (Project Number: 00256).

References

Kapetanidis, V., Michas G, Kaviris, G., Vallianatos, F., 2021. Spatiotemporal properties of seismicity and variations of shear-wave splitting parameters in the Western Gulf of Corinth (Greece). Applied Sciences 11, 6573. https://doi.org/10.3390/app11146573

Karakonstantis, A. 2017. 3-D simulation of crust and upper mantle structure in the broader Hellenic area through Seismic Tomography. Ph.D. Thesis, National and Kapodistrian University of Athens, Greece.

Makropoulos, K., Kaviris, G., Kouskouna, V., 2012. An updated and extended earthquake catalogue for Greece and adjacent areas since 1900. Natural Hazards Earth System Science 12(5), 1425–1430. https://doi. org/10.5194/nhess-12-1425-2012

Michas, G., Kapetanidis, V., Kaviris, G., Vallianatos, F., 2021. Earthquake diffusion variations in the Western Gulf of Corinth (Greece). Pure and Applied Geophysics 178, 2855–2870. https://doi.org/10.1007/ s00024-021-02769-0

Michas, G., Kapetanidis, V., Spingos, I., Kaviris, G., Vallianatos, F., 2022. The 2020 Perachora peninsula earthquake sequence (East Corinth Rift, Greece): spatiotemporal evolution and implications for the triggering mechanism. Acta Geophysica. https://doi.org/10.1007/s11600-022-00864-x

Shapiro, S.A., Huenges, E., Borm, G., 1997. Estimating the crust permeability from fluid-injection-induced seismic emission at the KTB site. Geophysical Journal International 131, F15–F18. https://doi.org/10.1111/j.1365- 246X.1997.tb01215.x

Waldhauser, F., 2001. hypoDD-A program to compute double-difference hypocenter locations. US Geological Survey Open File Report 01,113-125.

16th International Congress of the Geological Society of Greece
17-19 October, 2022 - Patras, Greece
Bulletin of the Geological Society of Greece, Sp. Publ. 10
Ext. Abs. GSG2022-174

Estimating the ground motion frequency response with the use of mean normalized spectral acceleration.

G. Chatzopoulos[1]

(1) Institute of Physics of the Earth's Interior and Geohazards, UNESCO Chair on Solid Earth Physics and Geohazards Risk Reduction, Hellenic Mediterranean University Research Center, 73133 Crete, Greece, ggh1983@hotmail.com

Research Highlights

This research study presents results on the estimation of the ground motion response in areas characterized by complex geological settings with formations that vary in stiffness and thickness such as a tectonic basin. The study uses a large dataset with seismic events to calculate the mean normalized response spectra for a site.

Introduction

The city of Chania, located on the west part of Crete Island (Greece), has been built on a sedimentary basin filled with Neogene and Quaternary deposits. The following description of the geological formation of the Chania basin area are from (Mountrakis *et al*., 2012). The Neogene formations (brown and beige color in Figure 1), which consist mainly of marls and carbonates and present average values in seismic wave velocities, are on the top of a stiff layer (bedrock, gray and magenta color in Figure 1) with high seismic wave velocities. The loose Quaternary deposits (white color in Figure 1) which are mainly sands, clays and gravels present very low seismic wave velocities. Their thickness based on borehole logs is about 150m. The Neogene and Quaternary deposits combined thickness is estimated to 400–500m (Papadopoulos *et al*., 2017). The local site effects attributed to the velocity contrasts due to formations change are not uniform as there are considerable differences in the stiffness and thickness of the basin materials. In addition, the city presents elevated seismic hazard due to the seismic energy being released from the subduction of the African plate beneath the Aegean microplate.

Since the fall of 2015, the Hellenic Seismological Network of Crete (HSNC) is operating a Strong Ground Motion Network (SGMN) focused on monitoring the urban part of Chania and its Southern basin. After a 'felt' seismic event, the HSNC personnel carries out a manual Strong Ground Motion (SGM) analysis of the earthquake and provide typical measurements such as the Peak Ground Acceleration (PGA), the Peak Ground Velocity (PGV), the Peak Ground Displacement (PGD) and Arias Intensity (Chatzopoulos *et al*., 2021). In addition, the PGA is interpolated with Co-Kriging method and illustrated in 'shakemaps' with the aid of ArcGIS environment (www.arcgis.com/index.html, accessed on 01/08/2022). Lastly, the Spectral Acceleration (SA) for each site is calculated with Boore's method (Boore *et al*., 2006).

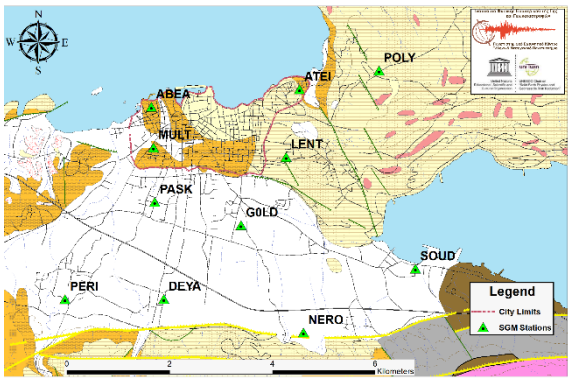

Figure 1. The Strong Ground Motion sensors topology in the geological map modified from (Mountrakis et al., 2012).

Data and Method

The recordings from the permanent SGMN located in Chania, have been used to calculate the mean response spectra. The dataset contains seismic events since 2016 up to the middle of 2022. The dataset was built with 'felt' seismic events with local magnitudes from 3.2 up to 6.1. The selected seismic events in this research had adequate signal to noise ratio. The SGMN is equipped with 24bit integrated tri-axial accelerometers constructed by REF TEK (https://reftek.com/, accessed on 01/08/2022). The SGMN was built gradually, thus the seismic events from the first couple of years of operations, have recordings from fewer SGM sensors. The waveforms since June 2021, are available for distribution through the National European Integrated Data Archive (EIDA) node (http://eida.gein.noa.gr/, accessed on 01/08/2022) while the waveforms from the previous years are available with personal communication.

The response spectra have been calculated with Boore's method (Boore *et al*., 2006) which negates the orientation of the horizontal components. To calculate the ground motion intensity with this method, one non-overlap rotation of the horizontal axis has been caried out to find the geometric mean of the period dependent response spectra. The period independent response spectra are obtained through the minimization (based on the rotation angle) of a penalty function (Boore *et al*., 2006). The available waveforms were cut few seconds (8–15 seconds) before P waves arrival up to the coda and then the REF TEK format files were transformed into SAC format in order to remove the instrument response with SAC and EVALRESP code (ds.iris.edu/files/sac-manual/commands/transfer.html, accessed on 01/08/2022).

Results and Discussion

The examination of the dataset shows that the SA main peak appears to vary in each case (withing some limits), which is based on the magnitude, the depth and the epicentral distance of the earthquake. In order to evaluate all the available peaks, the data were normalized (Figure 2a), and the mean value of the SA was calculated for each site. The seismic events with distance larger than 250km were omitted from this study as the main peak in SA was considerably deviant from the rest results. The possible variations of the normalized peaks (different period values) affect the normalized mean value. The sharpness and the height of the peak in the mean normalized SA results are higher when most of the normalized peaks are in the same period as in the case of the MULT site (Figure 2b). The opposite occurs for site NERO (Figure 2c) where the mean normalized SA presents no clear peak. The final results along with a dataset containing peak ground parameters, can be used to examine the predominant frequencies and assess the strength of the local site effects and the vulnerability of the site.

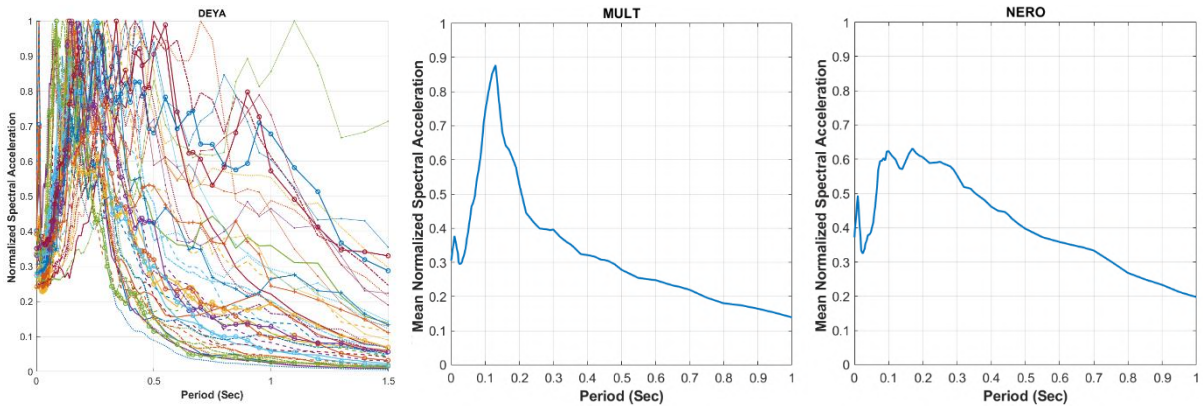

Figure 2. Examples from three case studies: a) The summary of the normalized SA peaks for the station DEYA. b) The mean normalized SA that presents a clear and high peak in the station MULT. c) The mean normalized SA with no clear peak from station NERO.

Acknowledgements

We acknowledge support of Region of Crete by the project "Operation of the Hellenic Seismological Network of Crete".

References

Boore, D.M., Watson-Lamprey, J., Abrahamson, N.A., 2006. Orientation-Independent Measures of Ground Motion. Bulletin of the Seismological Society of America, Volume 96, No. 4A, 1502–1511.

Chatzopoulos, G., Papadopoulos, I., Vallianatos, F., Makris, J.P., Kouli, M., 2021. Strong Ground Motion Sensor Network for Civil Protection Rapid Decision Support Systems. Sensors, 21, 2833, https://doi.org/10.3390/s21082833.

Mountrakis, D., Killias, A., Pavlaki, A., Fassoulas, C., Thomaidou, E., Papazachos, C., Papaioannou, C., Roumelioti, Z., Benetatos, C., Vamvakaris, D., 2012. Neotectonic study of Western Crete and implications for seismic hazard assessment. Journal of the Virtual Explorer, 42, 19–20.

Papadopoulos, I., Papazachos, C., Savvaidis, A., Theodoulidis, N., Vallianatos, F., 2017. Seismic microzonation of the broader Chania basin area (Southern Greece) from the joint evaluation of ambient noise and earthquake recordings. Bulletin of Earthquake Engineering, 15, 861–888.

16th International Congress of the Geological Society of Greece
17-19 October, 2022 - Patras, Greece
Bulletin of the Geological Society of Greece, Sp. Publ. 10
Ext. Abs. GSG2022-184

Probabilistic and Stochastic Seismic Hazard Assessment for the Western Gulf of Corinth (Greece)

A. Zymvragakis[1], G. Kaviris[1], V. Kapetanidis[1], P. Bonatis[2], N. Voulgaris[1]

(1) Section of Geophysics–Geothermics, Department of Geology and Geoenvironment, National and Kapodistrian University of Athens, Athens, Greece, gkaviris@geol.uoa.gr (2) Geophysics Department, Aristotle University of Thessaloniki, Thessaloniki, Greece.

Research Highlights

- We present a Probabilistic and Stochastic Seismic Hazard Assessment for the Western Gulf of Corinth (Greece).
- The results of both the Probabilistic and the Scenario – Based Seismic Hazard Assessment indicated that PGA throughout the Western Gulf of Corinth exceed the PGA reference value of the current National Building Code.

The Western Gulf of Corinth (WGoC), located in central Greece, constitutes one of the most tectonically active continental rifts worldwide. An important number of earthquakes with $M_w > 4.0$, reflecting the predominant extensional stress field, affect the seismic hazard of the area (Figure 1). In this study, seismic hazard is evaluated by combining two approaches: a) probabilistic (PSHA) and b) stochastic assessment through earthquake scenarios. Regarding the PSHA, three seismotectonic models were used: the 2013 and 2020 Euro-Mediterranean Seismic Hazard Model (ESHM13; Giardini et al., 2014 and ESHM20; Danciu et al., 2021) and the one of Vamvakaris et al. (2016) for Greece. Ground Motion Prediction Equations (GMPEs), proposed for the Greek territory, were chosen and reconstructed as hybrid models to account for all types of focal mechanisms. Peak Ground Acceleration (PGA) values for a return period of 475 years were computed via a logic tree approach.

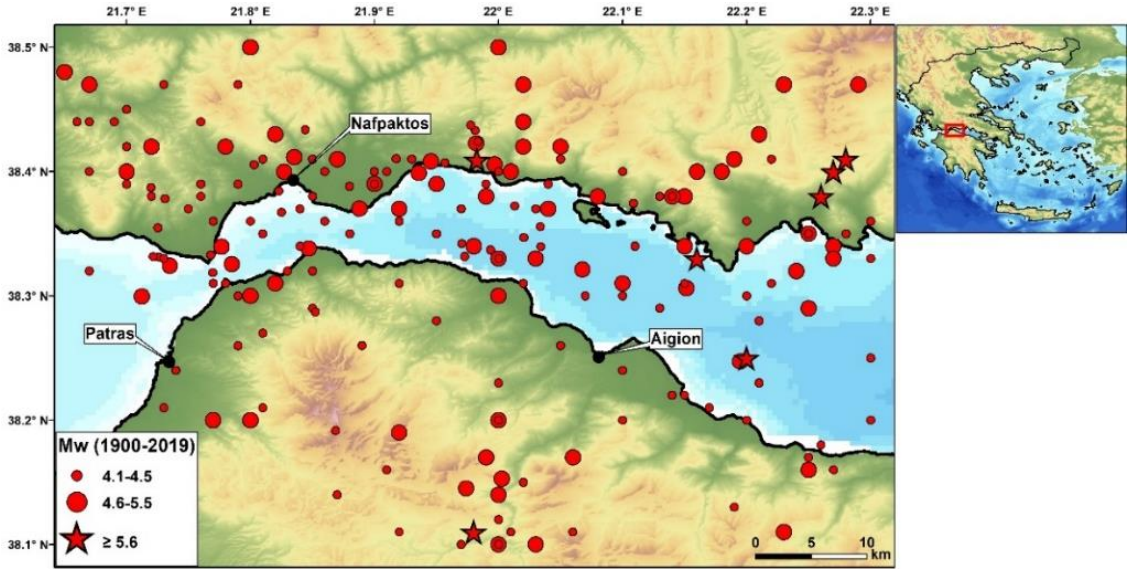

Figure 1. Instrumental seismicity of the WGoC. Epicenters are adopted from the Makropoulos et al. (2012) earthquake catalogue, extended up to 2019.

The earthquake catalogue of Makropoulos et al. (2012), extended up to 2019 for the broader study area, was used to calculate the seismic parameters for each seismic zone: a) *b*-value of the Gutenberg-Richter relation, b) magnitude of completeness, M_c, c) annual rate of M_c exceedance, $\lambda(M_c)$ and d) maximum expected magnitude, M_u. The *b*-value and M_c were calculated using the Maximum Curvature method, $\lambda(M_c)$ was calculated manually and M_u was estimated using the Robson - Whitlock - Cooke (R-W-C) procedure (Robson & Whitlock, 1964; Cooke, 1979). The GMPEs of Margaris et al. (2002), Skarlatoudis et al. (2003), Danciu and Tselentis (2007), Sakkas (2016) and Chousianitis et al. (2018) were employed. Each GMPE was converted into a hybrid one. The results were computed via an equal-weight logic tree approach, where every major branch is a different seismotectonic model and every minor branch is a hybrid GMPE.

Aiming to predict ground motion parameters due to the occurrence of future strong earthquakes, stochastic ground motion simulations were performed through the finite-fault model approach, implemented in the EXSIM code (Assatourians and Atkinson, 2012; Boore, 2009; Motazedian and Atkinson, 2005). The M_w 6.5 Aigion 1995 earthquake was used as a case study to calibrate the path and site components of strong ground motion. The recorded strong motion data, as well as widely adopted GMPEs (e.g., Boore et al., 2020) were used to effectively compare the simulated ground motions. Afterwards, stochastic simulations were performed through a worst-case scenario approach on known faults in

the study area. Multiple iterations of possible slip distribution models for various positions of rupture nucleation points onto the fault surface were considered. Maps of the resulting spatial distribution of PGA were produced, as well as maximum PGA values and Fourier Amplitude Spectra (FAS) for the largest cities of the study area.

Results of PSHA, in terms of PGA values, increase near the coastline, which is reasonable as most earthquakes occur offshore (Figure 1). Specifically, the highest PGA value is 325 cm/sec^2 in the vicinity of Aigion. On the northern side, the contour of 320 cm/sec^2 is found 15 km NNE of Patras and 5 km west of Nafpaktos.

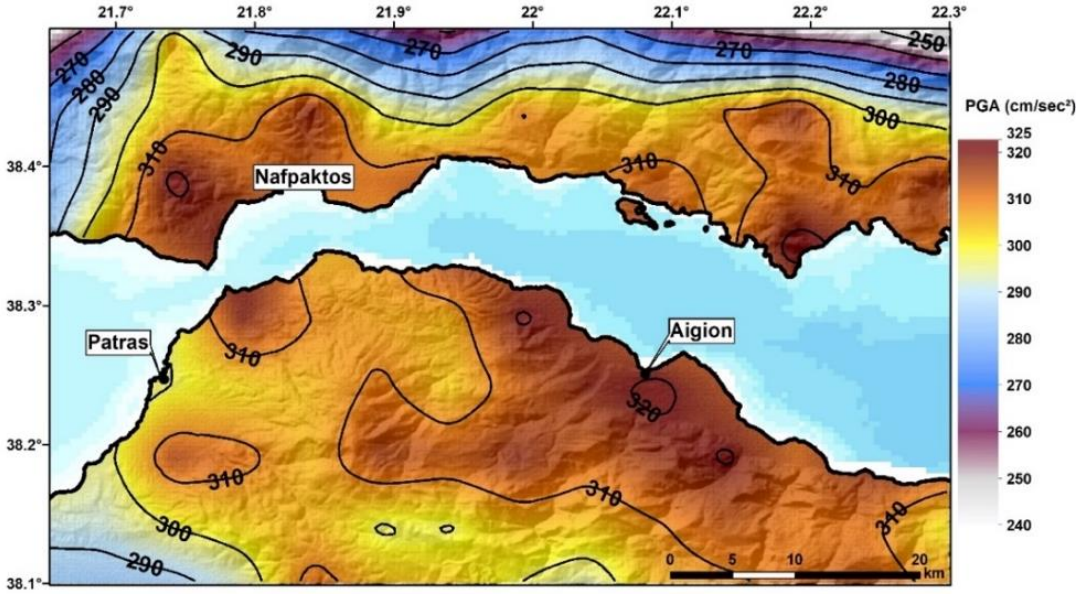

Figure 2. Spatial distribution of PGA values for a return period of 475 years.

The value of 235 cm/sec^2 is only encountered in the northeastern part of the map (Figure 2) and is the smallest PGA value. Therefore, the whole study area exceeds the reference value set by EAK (2003), equal to 0.24g (235 cm/sec^2) for the area. The largest difference between EAK and the model of this study is about 80 cm/sec^2. The fact that the final PGA values were obtained from the equal contribution of three distinct seismotectonic models, where each zone incorporates hybrid GMPEs, indicates that the scientific uncertainties have been qualitatively reduced.

References

Assatourians, K., Atkinson, G., 2012. EXSIM12: a Stochastic Finite- Fault Computer Program in FORTRAN.

Boore, D. M., 2009. Comparing stochastic point-source and finitesource ground-motion simulations: SMSIM and EXSIM. Bulletin of the Seismological Society of America, 99(6), 3202–3216.

Boore, D. M., Stewart, J. P., Skarlatoudis, A. A., Seyhan, E., Margaris, B., Theodoulidis, N., Scordilis, E., Kalogeras, I., Klimis, N., & Melis, N. S., 2020. A Ground-motion prediction model for shallow crustal earthquakes in Greece. Bulletin of the Seismological Society of America, 111(2), 857–874.

Cooke, P., 1979. Statistical inference for bounds of random variables, Biometrika 66, 367-374.

Chousianitis, K., Del Gaudio, V., Pierri, P., Tselentis, G.A., 2018. Regional ground-motion prediction equations for amplitude, frequency response, and duration-based parameters for Greece. Earthquake Engineering and Structural Dynamics 47, 2252–2274.

Danciu L., Nandan S., Reyes C., Basili R., Weatherill G., Beauval C., Rovida A., Vilanova S., Sesetyan K., Bard P-Y., Cotton F., Wiemer S., Giardini D., 2021. The 2020 update of the European Seismic Hazard Model: Model Overview. EFEHR Technical Report 001, v1.0.0

Danciu, L., Tselentis, G.A., 2007. Engineering ground-motion parameters attenuation relationships for Greece. Bulletin of the Seismological Society of America, 97, 162–183.

E.A.K., 2003. Greek seismic code edited by: Earthquake planning and protection organization. Athens—Greece, 72 pp., 7 appendixes, 2003 (in Greek).

Giardini, D., Wossner, J., Danciu, L., 2014. Mapping Europe's Seismic Hazard. Eos, Transactions, American Geophysical Union, 95, 261–262. https://doi.org/10.1002/2014EO290001

Makropoulos, K., Kaviris, G., Kouskouna, V., 2012. An updated and extended earthquake catalogue for Greece and adjacent areas since 1900. Natural Hazards and Earth System Sciences, 12, 1425–1430. https://doi.org/10.5194/nhess-12-1425-2012

Margaris, B., Papazachos, C., Papaioannou, C., Theodoulidis, N., Kalogeras, I., Skarlatoudis, A., 2002. Ground motion attenuation relations for shallow earthquakes in Greece. In: Proceedings of the 12th European conference on earthquake engineering, 385.

Motazedian, D., & Atkinson, G. M., 2005. Stochastic finite-fault modeling based on a dynamic corner frequency. Bulletin of the Seismological Society of America, 95, 995–1010.

Robson, D.S., Whitlock, J.H., 1964. Estimation of a truncation point, Biometrika 51, 33-39.

Sakkas, G., 2016. Calculation and analysis of the seismic motion rotational components in Greece. Ph.D. Thesis, National and Kapodistrian University of Athens, Athens, p. 278.

Skarlatoudis, A. A., Papazachos, C. B., Margaris, B. N., Theodulidis, N., Papaioannou, Ch., Kalogeras, I., Scordilis, E. M., Karakostas, V., 2003. Empirical peak ground-motion predictive relations for shallow earthquakes in Greece. Bulletin of the Seismological Society of America 93, 2591–2603.

Vamvakaris, D.A., Papazachos, C.B., Papaioannou, Ch.A., Scordilis, E.M., Karakaisis, G.F., 2016. A detailed seismic zonation model for shallow earthquakes in the broader Aegean area. Natural Hazards and Earth System Sciences 16, 55–84.

16th International Congress of the Geological Society of Greece
17-19 October, 2022 - Patras, Greece
Bulletin of the Geological Society of Greece, Sp. Publ. 10
Ext. Abs. GSG2022-202

Locating Local And Regional Earthquakes Using Distributed Acoustic Sensing (DAS) On A Fibre-Optic Cable As A Seismic Array

K. Lentas[1], D. Bowden[2], N. S. Melis[1], A. Fichtner[2], M. Koroni[2], K. Smolinski[2], A. Bogris[3], T. Nikas[4], C. Simos[5], I. Simos[6]

(1) National Observatory of Athens, Institute of Geodynamics, Lofos Nimfon, Athens, 11810, Greece, k.lentas@noa.gr (2) Department of Earth Sciences, ETH Zurich, Zurich, Switzerland (3) Department of Informatics and Computer Engineering, University of West Attica, Aghiou Spiridonos, 12243, Egaleo, Greece (4) Department of Informatics and Telecommunications, National and Kapodistrian University of Athens, 15784, Athens, Greece (5) Electronics & Photonics Laboratory, Department of Physics, University of Thessaly, 35100, Lamia, Greece (6) Department of Electrical and Electronics Engineering, University of West Attica, Aghiou Spiridonos, 12243, Egaleo, Greece.

- A local earthquake was successfully located by the use of DAS signals in an L-shaped seismic array.

From late September to mid-October 2021, a Distributed Acoustic Sensing (DAS) system was installed at the premises of OTE Academy (Hellenic Telecommunications Organisation S.A.) in Marousi (Attica, Greece). The system was connected to a 25 km-long link (50 km in closed-loop configuration) and an experimental integrated fibre-optic sensing system, also known as the Microwave Frequency Fibre Interferometer (MFFI) was tested against it (*Bogris et al.*, 2022; *Bowden et al.*, 2022). Theory on phase transmission fibre-optic deformation sensing was developed and the fibre geometry, specifically the effect of the local curvature was studied (*Fichtner et al.*, 2022a, 2022b).

In situ tapping tests were carried out in order to associate DAS channels (distances) with geographic coordinates along the path of the fibre-optic cable as accurately as possible, whilst an interpolating algorithm was used to extract the coordinates of all other intermediate DAS channels.

During the operational time period both systems recorded a number of local and regional earthquakes, i.e. with magnitude spanning from ML=2.8, located in Marousi to a Mw=6.3, located off the coast of Crete, whereas the DAS system showing lower noise levels was capable to record even lower magnitude local earthquakes (ML~1.0).

In this study we focus on the southern part of the fibre-optic cable which is located in the vicinity of the OTE Academy building in Marousi and we first examine the coherency of the recorded DAS signals in different distances along the cable by means of waveform cross-correlation. We observed a few cases where the signal was almost lost and others with substantial amplitude fluctuations within just few tens of meters, which is most likely due to the way that the fibre-optic cable is deployed. In some cases, these observations are supported by the presence of telecommunication vaults and distributing boxes where fibre-optic cables are strongly bent and connected together. Assuming a velocity model and the elastic parameters for the cable, one could simulate the wrapping angle of the cable by the seismic waves incidence angles based on a known earthquake location (*Wuestefeld &Wilks*, 2019).

Overall, we found high coherency between channels within straight segments, whereas phase changes were associated with cable bends. We then chose to use parts of the fibre-optic cable with the highest coherency as an L-shaped seismic array with nodes at 10 m intervals which is the DAS cable gauge length, and we calculated the array transfer function suggesting an ellipsoid shape. We attempted to locate the 2021/09/23, ML=3.4, Thiva earthquake, based on frequency-wavenumber analysis (f-k analysis) for estimating the slowness. Since the P-wave signal-to-noise ratio in our recordings is too low, we used a three-second S-wave time window filtered within two frequency bands (0.5 Hz – 2.5 Hz, and 1.0 Hz - 5.0 Hz). Both bands showed similar results, notably, a back-azimuth of 300° - 305° and a slowness of 0.32 s/km – 0.35 s/km, suggesting that the obtained location is roughly 10 km away from the location reported by the Institute of Geodynamics, National Observatory of Athens (GEIN-NOA). On the contrary, the location that we obtained for the near-regional earthquake (2021/10/12, Mw=6.3, off the coast of Crete), suggested larger errors in distance, projected in our slowness estimation, possibly due to the longer epicentral distance and the complex structure of the Hellenic subduction zone, whereas the estimated back-azimuth from the f-k analysis (145° - 150°) is in good agreement with the GEIN-NOA location.

Acknowledgements

We wish to thank Christina Lessi, Dimitris Polydorou, Diomidis Skalistis and Petros Voudas from OTE S.A. for their efforts in setting up the links that were used in this experiment. We also acknowledge Athena Chalari for helping us with the iDAS setup.

References

Bogris, A., Nikas, T., Simos, C. Simos, I., Lentas, K., Melis, N.S., Fichtner, A., Bowden, D., Smolinski, K., Mesaritakis, C., Chochliouros, I., 2022. Sensitive seismic sensors based on microwave frequency fiber interferometry in commercially deployed cables. Sci Rep 12, 14000. https://doi.org/10.1038/s41598-022-18130-x

Bowden, D. C., Fichtner, A., Nikas, T., Bogris, A., Simos, C., Smolinski, K., Koroni, M., Lentas, K., Simos, I., Melis, N.S., 2022.

Linking distributed and integrated fiber-optic sensing. Geophysical Research Letters, 49, e2022GL098727. https://doi.org/10.1029/2022GL098727

Fichtner, A., Bogris, A., Bowden, D., Lentas, K., Melis, N.S., Nikas, T., Simos, C., Simos, I., Smolinski, K., 2022a. Sensitivity kernels for transmission fibre optics, Geophysical Journal International, Volume 231, Issue 2, Pages 1040–1044, https://doi.org/10.1093/gji/ggac238

Fichtner, A., Bogris, A., Nikas, T., Bowden, D., Lentas, K., Melis, N.S., Simos, C., Simos, I., Smolinski, K., 2022b. Theory of phase transmission fibre-optic deformation sensing, Geophysical Journal International, Volume 231, Issue 2, Pages 1031–1039, https://doi.org/10.1093/gji/ggac237

Wuestefeld, A., Wilks, M., 2019. How to twist and turn a fiber: Performance modeling for optimal DAS acquisitions. The Leading Edge, 38 (3), 226–231. doi: https://doi.org/10.1190/tle38030226.1

16th International Congress of the Geological Society of Greece
17-19 October, 2022 - Patras, Greece
Bulletin of the Geological Society of Greece, Sp. Publ. 10
Ext. Abs. GSG2022-207

The 12 October 2021, Mw=6.3, offshore Zakros (Crete) earthquake

C.G. Gkarlaouni[1], K. Lentas[1], N. Kalligeris[1], N. S. Melis[1]

(1) National Observatory of Athens, Institute of Geodynamics, Lofos Nimfon, Athens, 11810, Greece, ch.gkarlaouni@noa.gr.

- The focal coordinates of the 2021 M6.3 off-shore Zakros earthquake were improved following the IASPEI standards and the slip model was determined.
- A potential generated tsunami was simulated based on gauge record analysis.

The properties of the Mw=6.3, 12 October 2021, offshore Zakros, Crete earthquake, and its seismotectonic implications are studied in the present work. The epicentral area lies within a complex seismotectonic regime where the southern prolongation of the deep Karpathos basin meets the Hellenic Arc. The area has been repeatedly struck by strong tsunamigenic earthquakes. No casualties have been reported in the 2021 earthquake but shaking was widely felt in Dodecanese islands and Crete with maximum macroseismic intensity equal to VII. Advisory messages for possible small-amplitude tsunami waves at a local scale were issued by the regional Tsunami Service Providers, which were later cancelled. The post-earthquake tide gauge recording at the harbour of Kasos island (operated by the National Observatory of Athens, Institute of Geodynamics) is examined here.

Since this part of the Aegean Sea in our study lies outside the local Hellenic Seismological Network, questions are rising regarding the accuracy of the mainshock location reported by NOA. In this study we attempted to improve the offshore Zakros earthquake location by exploiting local seismic phases reported by NOA along with regional and teleseismic phases obtained from the International Seismological Centre (ISC). The ISC locator algorithm (Bondar and Storchak, 2011) was used, since it takes into account the structure-correlated errors and allows conversions of phase characterizations according to travel times following the IASPEI Standard Seismic Phase List. Several tests were carried out in order to determine a free depth solution with balanced residuals across zero seconds. The resulted solution yielded an epicentre which is shifted to the northeast compared to other agencies and the depth was constrained at 19.9 km with an associated azimuthal gap equal to 17°.

In the absence of rich aftershock activity, probably due to low network detectability (possibly, small number of stations recording the small magnitude aftershocks), the initial dimensions of the mainshock rupture model for the kinematic slip inversion analysis and tsunami modelling were empirically approximated. The kinematic slip inversion based on the methodology developed by Gallovic et al. (2015), using three-component strong motion data (i.e. recorded by strong motion stations of the agencies: National Observatory of Athens, Institute of Geodynamics, Athens, 1997; ITSAK, Institute of Engineering Seismology Earthquake Engineering, 1981) highlighted a simple, single slip episode on a NE-SW oriented, NW dipping, fault plane, instead of the Zakros, NE-SW oriented, seismic fault. An anti-correlation of the maximum slip (~ 30 cm) with the aftershocks further supported this possibility, although the accuracy of the aftershock hypocentral locations could be somewhat questionable.

Coulomb stress changes are also calculated for the rupture which best describes the kinematic model. The causative seismogenic fault is approximated with a planar normal fault obtained from our kinematic inversion. Aftershock seismicity within three months after the main shock is distributed in the shadow zone of negative stress changes induced by the main shock and the southern termination of the fault where two lobes of enhanced stress changes are developed. The Kasos island tide gauge record analysis reveals the signature of some disturbance being recorded after the earthquake, but it can hardly demonstrate the existence of tsunami waves due to the low signal-to-noise ratio. Tsunami simulations computed for the two nodal planes using the Method Of Splitting Tsunamis code (MOST; Titov and Synolakis, 1998) are compared to the high-pass filtered Kasos island tide gauge record. Results do not yield conclusive evidence to highlight whether the causative fault plane is NW, or SE dipping, however, the power spectrum analysis of the NW dipping nodal plane matches the spectral peak at 8 s period and is overall closer to the spectrum of the tide gauge record.

The focal coordinates of the offshore 2021 Zakros earthquake were improved by exhaustively exploiting all available seismic phases. Distinct methodology results reached in this study, slightly imply a rather westward low dipping offshore fault zone, being antithetic to the Zakros high-angle normal fault which shapes the coast of eastern Crete and is perpendicular to the direction of Ptolemy Trench in this area. This result agrees with seismotectonic and bathymetric evidence which support the existence of approximately N-S trending grabens, east and northeast of Crete.

Acknowledgements

This research was supported by the ARISTOTLE-eENHSP (All Risk Integrated System TOwards Trans-boundary hoListic Early-warning—enhanced European Natural Hazards Scientifc Partnership) Project (Contract ECHO/SER/2020/830887+830888).

References

Bondar, I. and Storchak, D., 2011. Improved location procedures at the International Seismological Centre, Geophysical Journal International, 186(3), 1220–1244.

Gallovic, F., Imperatori, W., and Mai, P. M., 2015. Effects of three-dimensional crustal structure and smoothing constraint on earthquake slip inversions: Case study of the mw 6.3 2009 L' Aquila earthquake, Journal of Geophysical Research: Solid Earth, 120(1), 428–449.

ITSAK Institute of Engineering Seismology Earthquake Engineering, 1981. ITSAK strong motion network. DOI 10.7914/SN/HI.

National Observatory of Athens IOG, 1997. National Observatory of Athens seismic network. DOI 10.7914/SN/HL.

Titov, V. V. and Synolakis, C. E., 1998. Numerical modeling of tidal wave runup, Journal of Waterway, Port, Coastal, and Ocean Engineering, 124(4), 157–171.

16th International Congress of the Geological Society of Greece
17-19 October, 2022 - Patras, Greece
Bulletin of the Geological Society of Greece, Sp. Publ. 10
Ext. Abs. GSG2022-215

The evolution of recent seismicity in the Ionian Islands (W. Greece) with implications on seismic hazard assessment

V. Kapetanidis[1], G. Kaviris[1], I. Spingos[1], I. Kassaras[1†], V. Sakkas[1], D. Kazantzidou-Firtinidou[1], S. Mavroulis[2], M. Diakakis[2], J. D. Alexopoulos[1], S. Dilalos[1], E. Vassilakis[3], E. Kotsi[2], G.-A. Tselentis[1,4], E. Lekkas[2], N. Voulgaris[1]

(1) Section of Geophysics–Geothermics, Department of Geology and Geoenvironment, National and Kapodistrian University of Athens, Athens, Greece, vkapetan@geol.uoa.gr (2) Section of Dynamic Tectonic Applied Geology, Department of Geology and Geoenvironment, National and Kapodistrian University of Athens, Athens, Greece (3) Section of Geography & Climatology, Department of Geology and Geoenvironment, National and Kapodistrian University of Athens, Athens, Greece (4) Institute of Geodynamics, National Observatory of Athens, Athens, Greece

Research Highlights

- An overview of the recent seismicity in the Ionian Islands is presented, focusing on the period of 2014-2018.
- Probabilistic Seismic Hazard Assessment indicates PGA values that surpass the provisions of EAK2003.

The Ionian Sea, in western Greece, is undoubtedly one of the most seismically active areas in Greece. From north to south, the dominant structures include the Apulian collision zone, near Corfu Island, the dextral Cephalonia-Lefkada Transform Fault Zone (CLTFZ) and the north-western end of the Hellenic subduction zone, near Zakynthos Island. Herein, we present the past seismicity in the Ionian Sea area, with emphasis on the last decade; particularly during the period between 2014 and 2018, which was marked by strong earthquakes striking the islands of Cephalonia, Lefkada and Zakynthos. To this purpose, we employed a catalogue of ~62,000 earthquakes for the period between February 2011 and November 2021 (Sakkas *et al.*, 2022), with data collected from the databases of the Geodynamics Institute of the National Observatory of Athens (GI-NOA) and the Seismological Laboratory of the National and Kapodistrian University of Athens (SL-NKUA), as well as relocated seismicity catalogues for the major aftershock sequences (Papadimitriou *et al.*, 2021; Kapetanidis, 2017). The spatiotemporal evolution of seismicity projected along a south-north axis (A-B) is presented in **Fig. 1**. Low seismicity is observed in the north, where the collision between the Apulian platform and the Hellenic foreland is taking place. At the Central Ionian Sea, where CTLFZ is the prevailing structure generating intense seismic activity, the 2014 Mw6.1 and Mw5.9 Cephalonia earthquakes occurred on an adjacent local faulting zone, with the aftershock sequence expanding in the vicinity of the activated area along the Paliki peninsula, and offshore northwards (group #1/red in **Fig. 1**). Few months later, on 17 November 2015, another strong earthquake (Mw6.4) occurred on or parallel to the Lefkada segment of the CLTFZ (group #2/green in **Fig. 1**). The post-seismic activity expanded along the CLTFZ and southwards, in the same area as the 2014 sequence. Its temporal evolution shows a long relaxation period, reaching its background levels (0.1–0.2 events/day) between late 2016 and mid-2017. The two seismic sequences are linked in space and time, with the 2014 activity likely accelerating the 2015 event. The October 2018 Mw6.7 Zakynthos earthquake occurred close to the northwestern tip of the Hellenic Arc, with aftershocks expanding in the vicinity of the epicentral area, but mainly offshore south and west of Zakynthos Island (group #3/blue in **Fig. 1**). The seismicity rate has remained at higher values than the background (0.2 events/day) for more than three years.

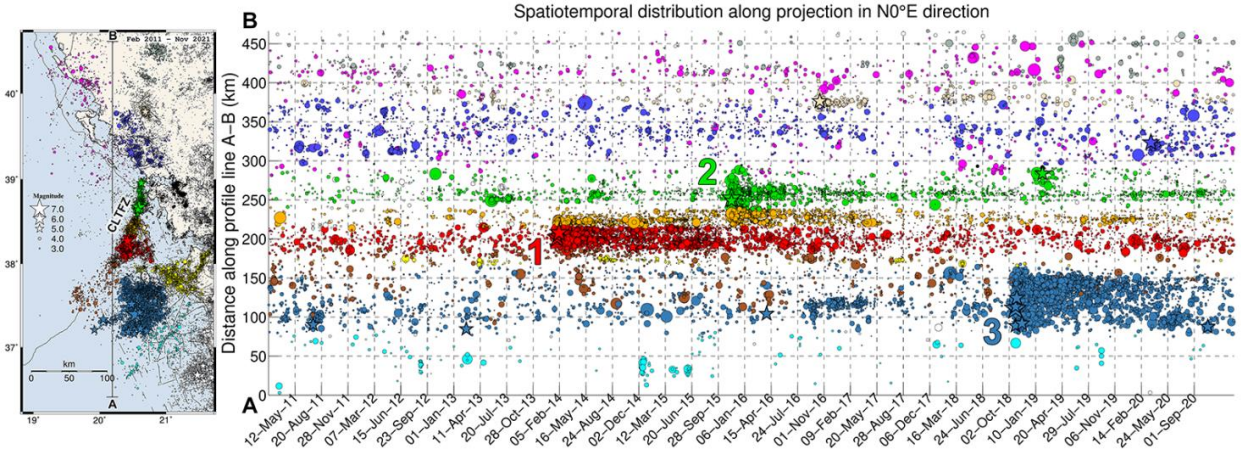

Figure 1. Left: Map of seismicity in the Ionian Sea, from the compiled catalogue of this study. Right: spatiotemporal projection along the south-north oriented profile A-B (see map). Colours correspond to different spatial groups.

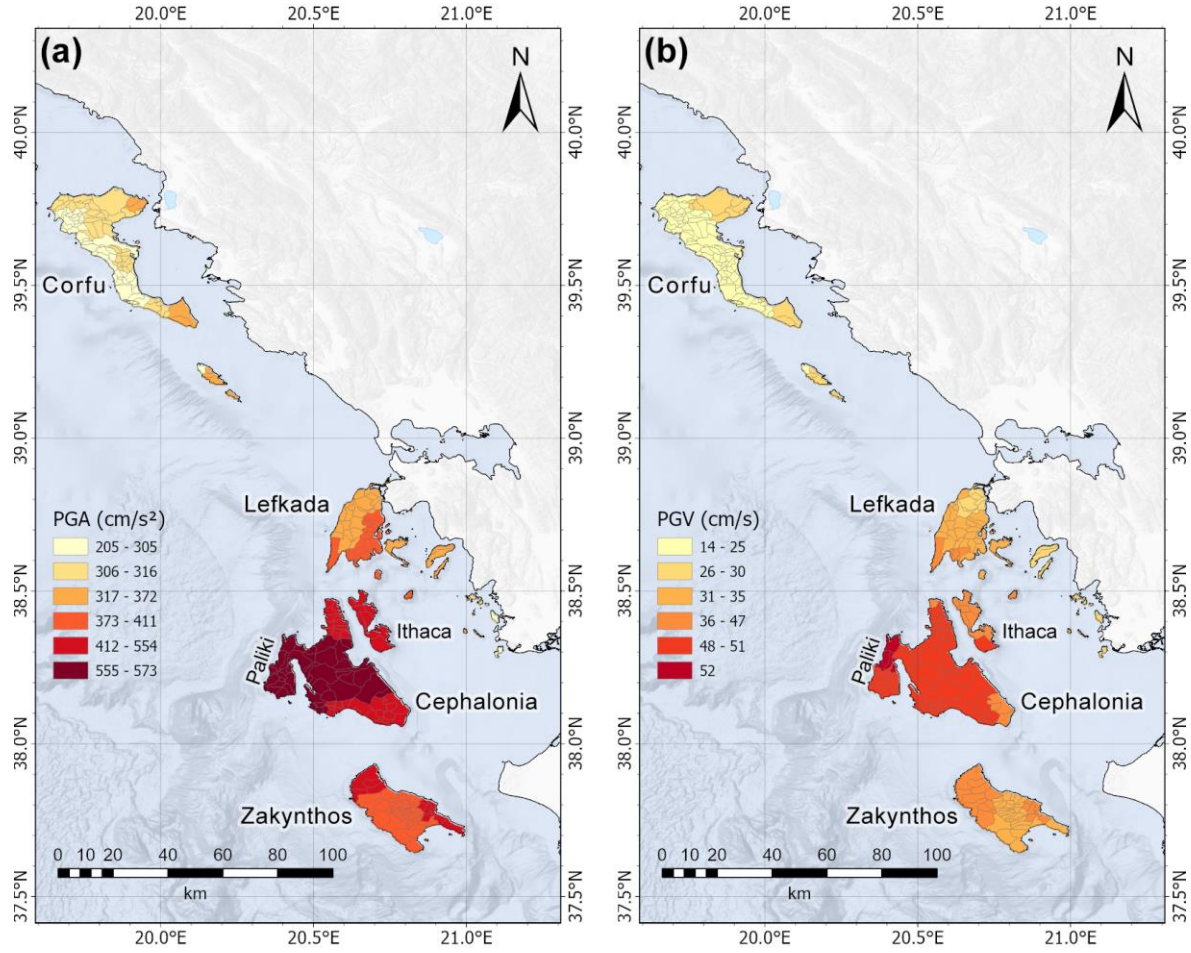

Figure 2. Spatial distribution of (a) PGA and (b) PGV values, for a return period of 475 years.

In the framework of this study, the seismic hazard of the Ionian Islands was evaluated using a probabilistic seismic hazard assessment (PSHA) method, including earthquake data since 1900 (Makropoulos *et al.*, 2012), whereas the Area-Source zones of the Euro-Mediterranean Seismic Hazard Model (ESHM13; Giardini *et al.*, 2014) were selected as the seismotectonic model. The PSHA revealed high PGA and PGV expected values in the central Ionian and lower values on Corfu Island (**Fig. 2**). The largest values are observed in Cephalonia and Ithaca islands, with PGA surpassing 412 cm/s^2 for a return period of 475 years. These values are higher than those proposed by the current Greek Building Code (EAK, 2003), which makes provision for an estimate PGA of 353 cm/s^2 (0.36 g) for the same return period.

Acknowledgements

The research was funded by the project "Telemachus Innovative Seismic Risk Management Operational System of the Ionian Islands" (MIS 5007986) which is part of the Regional Operational Programme «Ionian Islands 2014 - 2020» and is co-financed by the European Regional Development Fund (ERDF) (National Strategic Reference Framework NSRF 2014-20). The present work is dedicated to Ioannis Kassaras who actively participated to this study, even until his last days.

References

EAK, 2003. Greek Seismic Code edited by: Earthquake Planning & Protection Organization. Athens Greece, 72, 7. (In Greek)

Giardini, D., Wossner, J., Danciu, L., 2014. Mapping Europe's Seismic Hazard. Eos, Transactions, AGU, 95, 261–262.

Makropoulos, K., Kaviris, G., Kouskouna, V., 2012. An updated and extended earthquake catalogue for Greece and adjacent areas since 1900. Nat. Hazards Earth Syst. Sci. 12, 1425–1430. https://doi.org/10.5194/nhess-12-1425-2012

Papadimitriou, P., Kapetanidis, V., Karakonstantis, A., Spingos, I., Pavlou, K., Kaviris, G., Kassaras, I., Sakkas, V., Voulgaris, N., 2021. The 25 October, 2018 Zakynthos (Greece) earthquake: seismic activity at the transition between a transform fault and a subduction zone. Geophys. J. Int., 225, 15–36. doi:10.1093/gji/ggaa575

Kapetanidis, V. Spatiotemporal Patterns of Microseismicity for the Identification of Active Fault Structures Using Seismic Waveform Cross-Correlation and Double-Difference Relocation. Ph.D. Thesis, Department of Geophysics-Geothermics, Faculty of Geology and Geoenvironment, University of Athens, Athens, Greece, 2017.

Sakkas, V., Kapetanidis, V., Kaviris, G., Spingos, I., Mavroulis, S., Diakakis, M., Alexopoulos, J.D., Kazantzidou-firtinidou, D., Kassaras, I., Dilalos, S., Vassilakis, E., Kotsi, E., Tselentis, G., Lekkas, E., Voulgaris, N., 2022. Seismological and Ground Deformation Study of the Ionian Islands (W. Greece) during 2014–2018, a Period of Intense Seismic Activity. Applied Sciences, 12 (5), art. no. 2331.

16th International Congress of the Geological Society of Greece
17-19 October, 2022 - Patras, Greece
Bulletin of the Geological Society of Greece, Sp. Publ. 10
Ext. Abs. GSG2022-230

Frequency Magnitude Distribution of Aftershock Sequences Related to Major Subduction Zone Worldwide Earthquakes in Terms of Tsallis Entropy

E.A. Anyfadi[1], S.A. Avgerinou[1], G. Michas[1], F. Vallianatos[1,2]

(1) Section of Geophysics-Geothermics, Department of Geology and Geoenvironment, National and Kapodistrian University of Athens, 15784 Panepistimiopolis, Athens, Greece, eleniapanif@geol.uoa.gr. (2) Institute of Physics of Earth's Interior and Geohazards, UNESCO Chair on Solid Earth Physics and Geohazards Risk Reduction, Hellenic Mediterranean University Research Center, Crete, Greece.

Research Highlights

- The cumulative distribution with respect to earthquake magnitude was examined for 44 aftershock sequences of M≥7.0 earthquakes in subduction zones worldwide.
- Based on the fragment-asperity model, the entropic index q_M was estimated, with a range of 0.82 – 1.80.

Applied Methodology

Sotolongo-Costa and Posadas (2004), based on the fragment-asperity model, presented a physical model based on the first principles of statistical physics for the earthquake frequency-size distribution. According to this model, as long-range interactions arise among all parts of the fragmented piece as a result of the severe fractioning of the material, deriving the size distribution function of the fragments would necessitate the use of non-extensive statistical physics as Tsallis (2009) suggested as a potential generalization of BG statistical physics.

Telesca (2012) proposed a modified function based on the non-extensive statistical physics theory, which relates the cumulative number of earthquakes with the magnitude, normalized by the total number of earthquakes (Papadakis *et al*., 2014)

$$\log\left(\frac{N>M}{N}\right) = \frac{2-q_M}{1-q_M}\log\left(\frac{1-\left(\frac{1-q_M}{2-q_M}\right)\left(\frac{10^M}{A^{2/3}}\right)}{1-\left(\frac{1-q_M}{2-q_M}\right)\left(\frac{10^{M_C}}{A^{2/3}}\right)}\right) \qquad (1)$$

where M is the earthquake magnitude, Mc is the magnitude threshold, A is proportional to the volumetric energy density and q_M is the entropic index (Michas *et al*., 2013). In comparison to the Gutenberg–Richter scaling relation, the fragment-asperity model gives a reasonable explanation of recorded earthquake magnitudes over a larger range of scales. In addition, the b-value may be obtained as a special case for values over a certain threshold magnitude (Vallianatos *et al*., 2016)

$$b = \frac{2-q_M}{q_M-1} \qquad (2)$$

Results

The cumulative distribution in terms of the earthquake magnitude is examined via non-extensive statistical physics with equation (1) (Telesca, 2012) taking into account the threshold magnitude Mc in a seismic region. We estimated the entropic index q_M with a value close to 1.5 which informs us on the degree of long-range interactions. In the table below (Table 1), among the 44 sequences, the results for 10 characteristic aftershock sequences are presented. Figure 1 shows the frequency magnitude distribution for the 2003 M_w 8.3 Japan earthquake, while Figure 2 refers to the 2010 M_w 8.8 Chile earthquake. The bold red line indicates the model of equation (1) for the current q_M, while the other two lines illustrate the corresponding 95% confidence intervals.

Table 1. Summary of results for 10 subduction aftershock sequences.

Date	Epicenter	Depth	Mainshock Magnitude (M_w)	Number of aftershocks	Mc	q_M	b value
16/08/95	-5.51, 153.64	45.60	7.7	100	5.2	1.50	0.99
03/12/95	44.82, 150.17	25.90	7.9	138	5.2	1.50	0.99
16/11/00	-4.56, 152.79	24.00	8.0	165	5.5	1.50	0.99
25/09/03	42.21, 143.84	28.20	8.3	110	5.2	1.52	0.92
28/03/05	1.67, 97.07	25.80	8.6	210	5.1	1.50	0.99
27/02/10	-35.98, -73.15	23.20	7.8	154	5.1	1.47	1.12
11/03/11	37.52, 143.05	20.20	9.1	435	5.0	1.51	0.96

16/09/15	-31.57, -71.67	22.40	8.3	213	4.6	1.50	0.99
08/12/16	-10.68, 161.33	40.00	7.8	100	5.0	1.51	0.96
05/12/18	-21.95, 169.43	10.00	7.5	166	4.8	1.52	0.92

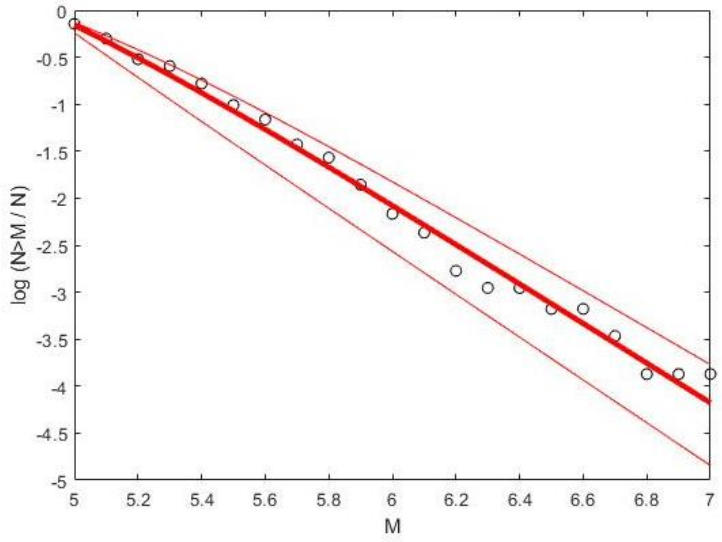

Figure 1. The frequency-magnitude distribution of the 2003 Japan earthquake Mw 8.3.

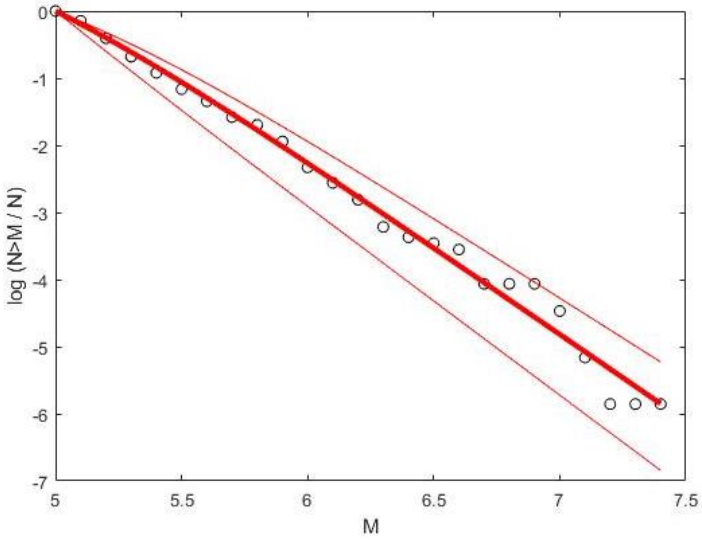

Figure 2. The frequency-magnitude distribution of the 2010 Chile earthquake Mw 8.8.

Acknowledgements

This presentation was supported by the Post Graduate Program (No 15305) of the Department of Geology and Geoenvironment, University of Athens (NKUA).

References

Sotolongo-Costa, O., Posadas, A., 2004. Fragment-Asperity Interaction Model for Earthquakes, Physical Review Letters, 92, 048501.

Tsallis, C., 2009. Learning with Boltzzmann-Gibbs Statistical Mechanics, in: Introduction to Nonextensive Statistical Mechanics, Springer, 19-37.

Telesca L., 2012. Maximum Likelihood Estimation of the Nonextensive Parameters of the Earthquake Cumulative Magnitude Distribution. Bulletin of the Seismological Society of America 102, 886–891.

Papadakis G., Vallianatos F., Sammonds P., 2015. A Nonextensive Statistical Physics Analysis of the 1995 Kobe, Japan Earthquake, Pure and Applied Geophysics 172, 1923–1931.

Michas, G., Papadakis, G., Vallianatos, F., 2013. A Non-Extensive approach in investigating Greek seismicity. Bulletin of the Geological Society of Greece 47, 1177–1187.

Vallianatos, F., Papadakis, G., Michas G., 2016. Generalized statistical mechanics approaches to earthquakes and tectonics. Proceedings of the Royal Society A 472, 1364-5021.

16th International Congress of the Geological Society of Greece
17-19 October, 2022 - Patras, Greece
Bulletin of the Geological Society of Greece, Sp. Publ. 10
Ext. Abs. GSG2022-231

Study of the Frequency Magnitude Distribution of recent Aftershock Sequences of Earthquakes in Greece, in Terms of Tsallis Entropy.

S.E. Avgerinou[1], E.A. Anyfadi[1], G. Michas[1], F. Vallianatos [1,2]

(1) Section of Geophysics – Geothermics, Department of Geology and Geoenvironment, National and Kapodistrian University of Athens, 15784 Panepistimiopolis, Athens, Greece, sophiavg@geol.uoa.gr (2) Institute of Physics of Earth's Interior and Geohazards, UNESCO Chair on Solid Earth Physics and Geohazards Risk Reduction, Hellenic Mediterranean University Research Center, Grete, Greece

Introduction

This work presents an analysis of the earthquake frequency-magnitudes distribution for the aftershock sequences of recent strong earthquakes in Greece, with magnitudes that reach up to M_w=7.0. Our analysis is focused on the recent events, as that of the Elassona M_w6.0 (03/03/2021), Parnitha M_w5.1 (19/07/2019), Zakynthos M_w6.6 (25/10/2018), Kos M_w6.6 (20/07/2017) and M_w6.1 Mytilene (12/06/2017) earthquakes. The frequency–magnitude distribution analysis is performed in a non-extensive statistical physics context. The non-extensive parameter q_M, which is related to the frequency-magnitude distribution, reflects the existence of long-range correlations and is used as an index of the physical state of the studied area.

Applied Methodology

Telesca (2012) took into account the threshold magnitude Mc while examining the frequency distribution of earthquake magnitude (M) presenting a modified expression that connects the cumulative number of earthquakes to magnitude (Papadakis *et al*., 2014), as follows:

$$\log\left(\frac{N(>M)}{N}\right) = \frac{2-q_M}{1-q_M}\log\left(\frac{1-\left(\frac{1-q_M}{2-q_M}\right)\left(\frac{10^M}{A^{2/3}}\right)}{1-\left(\frac{1-q_M}{2-q_M}\right)\left(\frac{10^{M_c}}{A^{2/3}}\right)}\right) \quad (1)$$

where M is the earthquake magnitude, Mc is the threshold magnitude and A is proportional to the volumetric energy density. Equation (1) presents a generalization of Gutenberg–Richter law in terms of Tsallis Entropy.

Results and Conclusions

In this study our interest focus on the estimation of the parameter q_M in some recent aftershock sequences in Greece. For the calculation of the non-extensive parameter q_M equation 1 was used.

Table 1. Mainshock location parameters and detailed statistics for the estimation of aftershocks decay parameters.

Event No.	Date	Time (G.M.T.)	Lat. (°N)	Long. (°E)	Magnitude	Number of Aftershocks	q_M
1. Mytilene	12/06/2017	12:28:37	38.85	26.31	6.3	1610	1.54
2. Kos	20/07/2017	22:31:10	36.97	27.41	6.6	6492	1.53
3. Zakynthos	25/10/2018	22:54:50	37.35	20.49	6.6	1668	1.54
4. Parnitha	19/07/2019	11:13:15	38.13	23.53	5.1	436	1.56
5. Elassona	03/03/2021	10:16:08	39.73	22.22	6.0	676	1.54

Here we present an analysis of the October 25th, 2018 aftershock sequence of 1668 events recorded after a shallow Mw = 6.6 earthquake located offshore Zakynthos island (Ionian Sea, Greece) following the catalogue of the Hellenic Unified Seismological Network (see Geodynamics Institute of the National Observatory of Athens, GI-NOA). The second example presented here, refers to the Elassona earthquake in the Thessaly Region on March 3rd, 2021. The mainshock had a magnitude M_w6.0 (see the catalogue of the Geophysical Laboratory of the Aristotle University of Thessaloniki, GL-AUTH) and occurred at 10:16:08 GMT (see details in Michas *et al*., 2022).

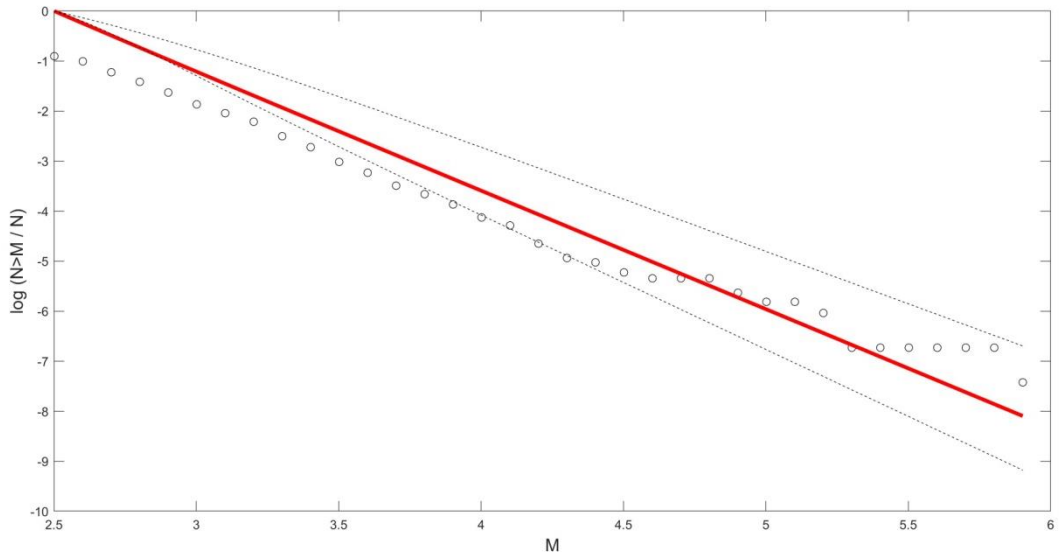

Figure 1. Normalized cumulative magnitude distribution and the fitting curve (red continuous line) according to Eq.1 for the 2021 Elassona earthquake. The non-extensive parameter is estimated equal to qM=1.54.

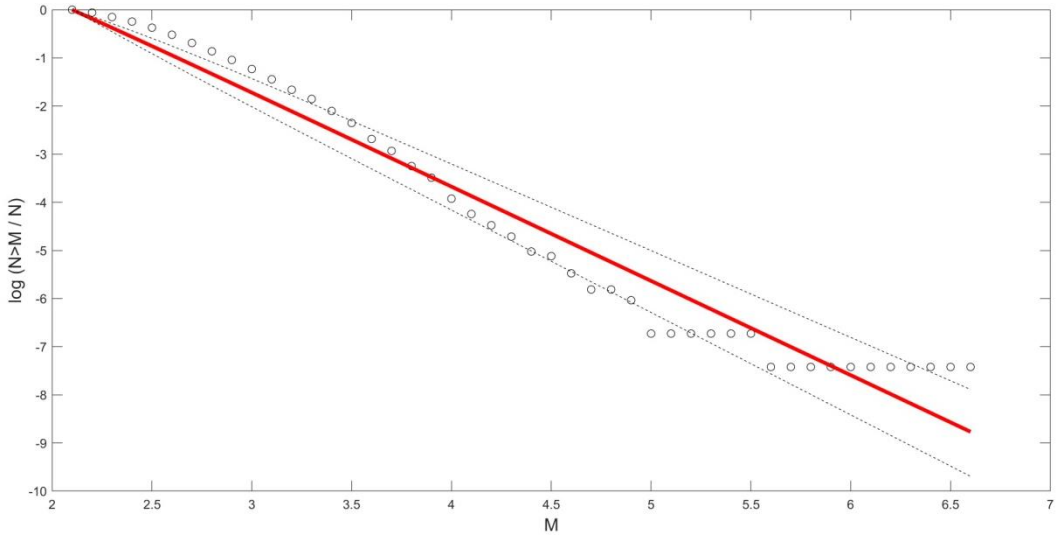

Figure 2. Normalized cumulative magnitude distribution and the fitting curve (red continuous line) according to Eq.1 for the 2018 Zakynthos earthquake. The non-extensive parameter is estimated equal to qM=1.54.

Figure 1 and 2 shows the distribution of the relative cumulative number of earthquakes as a function of magnitude and the associated fitting curve according to equation for the two earthquakes. The non-extensive parameters are estimated equal to q_M=1.54 for both aftershock sequences.

Acknowledgements

This presentation was supported by the Post Graduate program (No 15305) of the Department of Geology and Geoenvironment, University of Athens.

References

Papadakis, G., Vallianatos, F., Sammonds, P., 2014. A Non-extensive Statistical Physics Analysis of the 1995 Kobe, Japan Earthquake. Pure and Applied Geophysics 172, 1923-1931.

Telesca, L., 2012. Maximum Likelihood Estimation of the Non-Extensive Parameters of the Earthquake Cumulative Magnitude Distribution. Bulletin of the Seismological Society of America 102, 886–891.

Michas, G., Pavlou, K., Avgerinou, S.E., Anyfadi, E.A., Vallianatos, F., 2022. Aftershock Patterns of the 2021 Mw6.3 Northern Thessaly (Greece) Earthquake. Journal of Seismology 26, 201-225.

16th International Congress of the Geological Society of Greece
17-19 October, 2022 - Patras, Greece
Bulletin of the Geological Society of Greece, Sp. Publ. 10
Ext. Abs. GSG2022-237

On the VES over a Complex Fractal Layered Medium. Preliminary Results.

I. Zanesis[1], F. Vallianatos[1,2]

(1) National and Kapodistrian University of Athens, Faculty of Geology and Geoenvironment, Department of Geophysics–Geothermics, University Campus, Panepistmiopolis – Athens 157 84, Greece, giannis.zanesis@gmail.com
(2) Institute of Physics of Earth's Interior and Geohazards, UNESCO Chair on Solid Earth Physics & Geohazards Risk Reduction, Hellenic Mediterranean University Research Center, Crete, Greece

Research Highlights

In this study, the simulated results of simulations of VES in a layered medium with a) fat fractal geometry and b) structures whose resistivities follow a distribution around an average resistivity are presented. The results suggest a power law could be observed that could be used as an indicator of the complexity of the structure.

Introduction

This work was inspired by the variations of resistivity observed in log data. Here we study the VES response over a layered medium with a) fat fractal geometry and b) structures whose resistivities follow a distribution around an average resistivity. It is well known that subsurface (Xu et al., 2002) or highly fractured rocks (Sui et al., 2019) follow fat fractal structures. The fat fractals have finite measures and integral dimensions as the underlying space. For this reason, their dimension is insensitive to their structure (Eykholt et al., 1988). Fat fractals are characterized by an exponent β, which shows how the fractal fattens. On the other hand, we model the resistivities fluctuations following Pareto and Gaussian distributions, and we search for the possibility to distinguish using VES the patterns and if there is, a measure to characterize the degree of their structural complexity.

Methodology

Here, six different models were analyzed. The structure of the models consists of a 100m "complex" layer placed over a 100ohm.m half-space. In the first layer, we construct a fat fractal structure with two resistivity patterns of 10ohm.m and 50ohm.m. The thicknesses of one pattern remain constant while the thicknesses of the other will vary following a power law and vice versa. We will consider the same structure for different power law exponents α, which practically determines how fat the thickness of the constant thicknesses will be. The larger α is, the fatter the thickness of the constant thicknesses. We will consider three different α=2,3,5 for both cases. The mathematical approach is as follows. For $\rho_o(z)=\rho_1$, there are 2^n length intervals with thickness $Ln=2^{-n}f_\alpha(n)L$. While, there are $N_n(k)=2^{k-1}$ (k=1,2,3…n) intrusive layers with thickness $l_k=L_{l-1}/\alpha^k$ and resistivity $\rho^*_n(z)=\rho_2$. The total layers are $N_l=2^{n+1}-1$. Next, we randomly mix all intervals keeping the thickness alternation between ρ_1 and ρ_2. We obtain a fat fractal as a mathematical object by restricting $n\rightarrow\infty$. Depending on the type of smearing, an exponent β can be obtained for the fat fractal, and this exponent allows us to write: $L_n-L_\alpha \propto l^\beta_{n+1}$ where $L_\alpha=f_a\infty L$ and $\beta=\log\alpha/\log_2\alpha$. The physical idea behind the model is the distribution of intrusive layers concerning their size governed by power law: $N_n(k)=l_k^{\beta-1}$ (n>>1) (Vallianatos, 1997). In our work, we will stop in the 7th step (n=7), and the total layers of the structures will be 127.

In the second part, we will consider three more models where in the structure, the thicknesses will be constant at 0.5m up to a depth of 500m, while the resistivities will be around an average value $\rho=\rho_o+\xi(z)$ where ξ(z) a stochastic random variable that follows a given distribution. To avoid negative or close to zero resistivities ρ, when such a case appears, the resistivity value is replaced by $\rho=\rho_o-2\sigma$. In the first case presented, the variance ξ(z) follows a Gaussian distribution with mean zero and standard deviation σ=1 ohm.m with mean resistivity ρ_o=5ohm.m. For the second case, σ=5ohm.m with mean ρ_o=12ohm.m. In the latter model, the variance values ξ(z) will follow a Pareto power law distribution.

Results and Conclusions

The apparent resistivity of the particular structure is estimated by taking into account the distance between current electrodes (AB/2), the potential electrodes (MN/2), and the given geometry of the study structure. We repeat these procedures 1000 times for each model to extract reliable statistics. Then, we estimate the mean and standard deviation of resistivity in every AB/2 for every response and extract the apparent resistivity plot. As the last step, the cumulative probability distribution of the apparent resistivity as the response given for each of the tested models, i.e., we plot in a log-log scale the $N(>\rho_a)/No$ versus the apparent resistivity ρ_a. As given in Figures 1 and 2, a power law is presented.

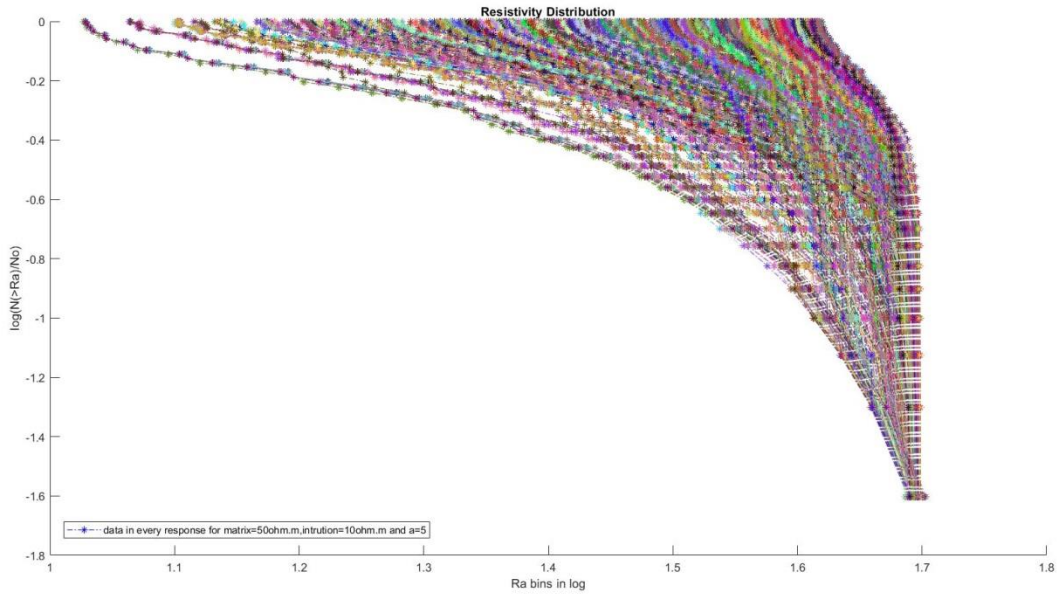

Figure 1. Resistivity distribution for a fat fractal layered structure with matrix resistivity 50 Ohm.m, intrusions resistivity 10 Ohm.m, and fat fractal parameter α =5

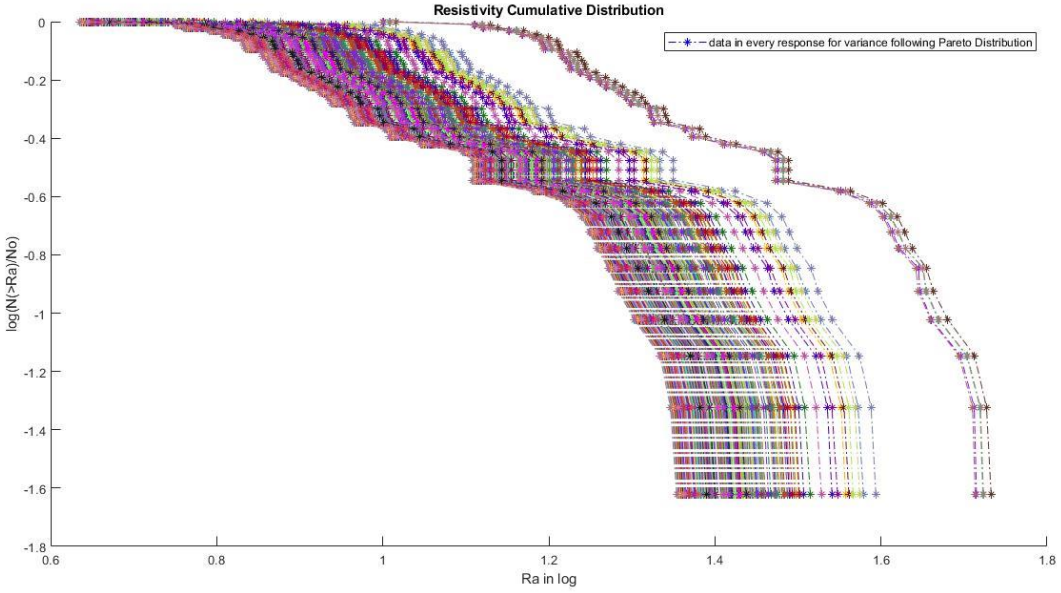

Figure 2. Resistivity distribution which the a patterns following Pareto Distribution

References

Bulgakov, S.A., Konotop, V.V., Vasquez L., 1995. Wave interaction with a random fat fractal dimension of the reflection coefficient. Waves in random media 5, 9-18.

Eykholt, R., Umberger, D.K., 1988. Relating the various scaling exponents used to characterize fat fractals in nonlinear dynamical system. Physica D 30, 43-60.

Sui, L., Yu, J., Cang, D., Miao, W., Wang, H., Zhang, J., Yin, S., Chang, K., 2019. The fractal description model of rock fracture networks characterization. Chaos Solitons and Fractals 129, 71-79.

Vallianatos, F., 1997. Electromagnetic wave propagation in a random fat fractal medium. Marelec97 International conference in Marine Electromagnetics, London, UK.

Xu, Y.F., Sun, D, A., 2002. A fractal model for soils pores and its application to determination water permeability. Physica A 316, 56-64.

16th International Congress of the Geological Society of Greece
17-19 October, 2022 - Patras, Greece
Bulletin of the Geological Society of Greece, Sp. Publ. 10
Ext. Abs. GSG2022-242

Statistical Seismology in view of Tsallis entropy and Beck-Cohen Superstatistics. A Tutorial.

F. Vallianatos[1,2]

(1) National and Kapodistrian University of Athens, Faculty of Geology and Geoenvironment, Department of Geophysics–Geothermics, University Campus, Panepistmiopolis – Athens 157 84, Greece, fvallian@geol.uoa.gr.
(2) Institute of Physics of Earth's Interior and Geohazards, UNESCO Chair on Solid Earth Physics & Geohazards Risk Reduction, Hellenic Mediterranean University Research Center, Crete, Greece, fvallian@hmu.gr

Research Highlights

The fundamental laws of Statistical seismology as that of Gutenberg-Richter (GR) and Omori law are analysed using the ideas of Tsallis entropy and the dynamical superstatistical interpretation offered by Beck-Cohen.

Quo Vademus ?

Earthquake physics is one of the most intriguing fields in science. It is not only the abruptness of the phenomenon that attracts our interest and wonder, but also the devastating consequences that earthquakes can have for the anthropogenic environment that require our better understanding of the fundamental physics of this phenomenon in order to mitigate the risks. The earthquake generation process is a complex phenomenon, manifested in the nonlinear dynamics and in the wide range of spatial and temporal scales that are incorporated in the process (Sornette, 2004). Despite the significant progress that has been achieved since the beginning of instrumental seismology in the late 19th century in understanding the mechanisms that lead to the nucleation of individual earthquakes, understanding the exact physics that govern the earthquake generation process and the subsequent prediction of future earthquakes still represent an outstanding challenge for scientists (e.g., Turcotte et. al., 2000). Despite the complexity of the earthquake generation process and our limited knowledge on the physical processes that lead to the initiation and propagation of a seismic rupture giving rise to earthquakes, the collective properties of many earthquakes present patterns that seem universally valid. The most prominent is scale-invariance, which is manifested in the size of faults, the frequency of earthquake sizes and the spatial and temporal scales of seismicity.

Since the beginning of the 20th century and the early years of modern seismology, it became apparent that small earthquakes are considerably more frequent than larger ones. The number of small to larger size earthquakes, in terms of the earthquake magnitude M, is commonly expressed with the cumulative distribution $N(>M)$ of earthquake magnitudes, which indicates the number of earthquakes with magnitude equal or greater than M. The cumulative distribution $N(>M)$ exhibits a decay that is commonly expressed with the well-known Gutenberg-Richter (G-R) law :

$$\log N(M) = a - bM \ , \qquad (1)$$

where a and b are positive fitting parameters. The parameter a describes the regional level of seismicity and b, known as the seismic b-value, is the slope of the cumulative distribution that estimates the proportion of small to large events.

The aftershock production rate following a main event generally decays as a power-law with time according to the modified Omori formula (Utsu et al., 1995):

$$n(t) = K(t+c)^{-p} \ , \qquad (2)$$

where $n(t)$ is the production rate, t is the time after the main shock and K, c and p are empirical constants. The power-law exponent p usually takes values close to 1. The constant K depicts the total number of aftershocks, while the constant c the onset of the power-law decay.

Scale-invariance and (multi)fractality are also manifested in the temporal evolution of seismicity and the distribution of earthquake epicentres (Sornette and Werner,2009). The organization patterns that earthquakes and faults exhibit have motivated the statistical physics approach to earthquake occurrence (Sornette and Werner,2009; Vallianatos et al., 2016). Statistical physics bridges the gap between the underlying physics that characterize seismic rupture at the microscopic scale and the laws that govern friction, chemical reactions, fluid-rock interactions and so on, to the macroscopic scale of large earthquakes and faults (Sornette and Werner, 2009).

Based on statistical physics and the entropy principle, a unified framework that produces the collective properties of earthquakes and faults from the specification of their microscopic elements and their interactions, has recently been introduced. This framework, called nonextensive statistical mechanics (NESM) was introduced by Tsallis (1988), as a generalization of classic statistical mechanics due to Boltzmann and Gibbs (BG), to describe the macroscopic behaviour of complex systems that present strong correlations among their elements, violating some of the essential properties of BG statistical mechanics (Tsallis, 2009). Such complex systems typically present power-law distributions, enhanced by

(multi)fractal geometries, long-range interactions and/or large fluctuations between the various possible states, properties that correspond well to the collective behaviour of earthquakes and faults. Many applications during the last decade have highlighted that NESM is a powerful framework for describing the macroscopic behaviour of earthquakes and faults in a wide range of scales (Vallianatos et al., 2016 and references therein), introducing the field of nonextensive statistical seismology (NESS). The dynamical characteristics that lead to a NESP behaviour were demonstrated by Beck and Cohen (2003). Here, we provide an overview on the fundamental properties and applications of NESS. Initially, we provide an overview of the collective properties of earthquake populations and the main empirical statistical models that have been introduced to describe them. We describe the main statistical physics models that have been introduced to describe earthquake occurrence and we summarize the classic (BG) statistical mechanics approach to the phenomenology of earthquakes. We provide an analytic description of the fundamental theory and the models that have been derived within the NESM framework to describe the collective properties of earthquakes.

The fundamental laws of Statistical seismology as that of Gutenberg-Richter (GR) and Omori law a analysed using the ideas of Tsallis entropy and its dynamical superstatistical interpretation offered by Beck and Cohen. The open question are presented for discussion.

Acknowledgements

We acknowledge support of Region of Crete by the project "Operation of the Hellenic Seismological Network of Crete". This is a contribution of the UNESCO Chair on Solid Earth Physics & Geohazards Risk Reduction, Hellenic Mediterranean University Research Center, Crete, Greece

Selected References:

Beck C., 2004. Superstatistics: Theory and applications**,** Contin. Mech. Thermodyn., 16, 293-304.

Beck C., 2005. From time series to superstatistics, E. G. D. Cohen, H. L. Swinney, **P**hys. Rev. E, 72, 1-8.

Beck C., 2006. Superstatistical Brownian Motion, Progr. Theoret. Phys. Suppl., 162, 29-36.

Beck, C., Cohen , E.G.D., 2003. Superstatistics, Physica A, 322, 267-275.

Michas, G.; Vallianatos, F.; Sammonds, P., 2015. Statistical Mechanics and scaling of fault population with increasing strain in the Corinth Rift. Earth and Planetary Science letters, 431, 150-163.

Silva, R.; Franca, G.S.; Vilar, C.S.; Alcaniz, J.S., 2006. Nonextensive models for earthquakes. Phys. Rev. E., 73, 026102.

Sornette, D., 2004. Critical Phenomena in Natural Sciences: Chaos, Fractals, Self organization and Disorder (2nd Edition), Springer, New York.

Sornette, D.; Werner, M. J., Statistical physics approaches to seismicity. In: Meyers, R. A. (Ed.), Encyclopedia of Complexity and Systems Science, Springer, New York **2009**, 7872–7891.

Telesca, L., 2010. Analysis of Italian seismicity by using a nonextensive approach**,** Tectonophysics, 494, 155-162.

Tsallis C., 1988. Possible generalization of Boltzmann-Gibbs statistics. J. Stat. Phys. 52, 479–487.

Tsallis C., 2009. Introduction to nonextensive statistical mechanics-Approaching a Complex World. Springer, New York.

Turcotte D.L.; Newman W. I.; Gabrielov A., 2000.A statistical physics approach to earthquakes, Geocomplexity and the Physics of Earthquakes, American Geophysical Union, Washington D.C. 2000.

Vallianatos, F. 2011. A non-extensive statistical physics approach to the polarity reversals of the geomagnetic field. Physica A: Statistical Mechanics and its Applications, 390(10), 1773-1778.

Vallianatos, F., 2009. A non-extensive approach to risk assessment. *Nat. Hazards Earth Syst. Sci.*, 9, 211-216.

Vallianatos, F.; Michas, G.; Papadakis, G., 2015. A description of seismicity based on non-extensive statistical physics: A review. In Earthquakes and Their Impact on Society, Series Title: Springer Natural Hazard, Springer.

Vallianatos, F.; Michas, G.; Papadakis, G., 2018. Non Extensive statistical Seismology: An overview , in Complexity of Seismic Time Series .Measurement and Application, 1st edition, T. Chelidze F. Vallianatos L. Telesca (eds.,) Elsevier. [Book chapter]

Vallianatos, F.; Papadakis, G.; Michas, G., 2016. Generalized statistical mechanics approaches to earthquakes and tectonics. Proc. R. Soc. A Math. Phys. Eng. Sci.**,** 472:20160497.

Vallianatos, F.; Sammonds, P. 2013. Evidence of non-extensive statistical physics of the lithospheric instability approaching the 2004 Sumatran-Andaman and 2011 Honshu mega-earthquakes. Tectonophysics, 590 , 52-58.

Vallianatos, F.; Sammonds, P., 2010. Is plate tectonics a case of non-extensive thermodynamics? Physica A: Statistical Mechanics and its Applications, 389(21), 4989-4993 .

16th International Congress of the Geological Society of Greece
17-19 October, 2022 - Patras, Greece
Bulletin of the Geological Society of Greece, Sp. Publ. 10
Ext. Abs. GSG2022-245

The North Euboea (Greece) Volcanic Field as Outlined by its Magnetic Anomalies

Andreas Tzanis[1], Stylianos Chailas[1] and M. Sagredou[1]
(1) Section of Geophysics – Geothermy, National and Kapodistrian University of Athens; atzanis@geol.uoa.gr.

Introduction

N. Euboea is situated in the westward extension of the North Aegean Fault (NAF) into mainland Greece through the Trikeri and Oreoi straits. The area is known to host a volcanic field; as evident in Fig. 1 numerous hot springs discharge hydrothermal fluids (Geothermica Italiana, 1984), but only four small volcanic outcrops have been identified, at the Lichades Islets and Hagios Ioannis location (0.5 Ma of age), near Achileion (3.4 – 2.7 Ma) and at Chronia (eastern coast of N. Euboea); they comprise trachyandesites with high-K calc-alkaline affinities (Innocenti et al., 2010). Beyond this, little is known about the number, location and configuration of individual volcanic centres. Because trachyandesites are magnetisable, herein we take a first step in addressing this question with aeromagnetic data extracted from the unified aeromagnetic map of Greece (Chailas et al., 2010; Chailas and Tzanis, 2019), shown in Fig. 1 in reduced-to-pole form.

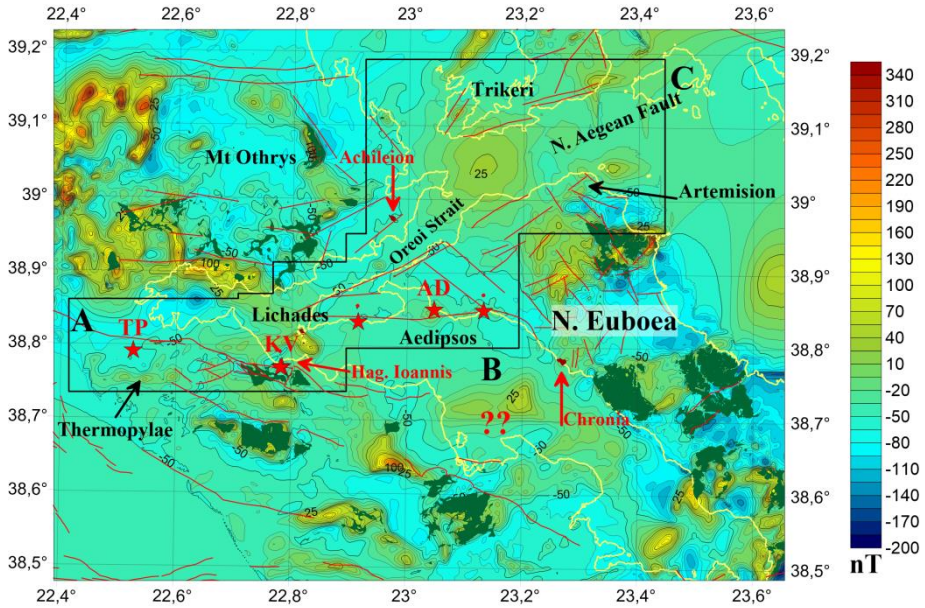

Figure 1: Reduced-to-Pole aeromagnetic anomaly map observed at constant ground clearance of 300m. Superimposed are the ophiolite outcrops observed in the area (dark green patches). Red stars mark the locations of hot springs. Faults (red lines) have been extracted from the New Seismotectonic Atlas of Greece v1.0 (Kassaras et al., 2020).

Volcanigenic Magnetic Anomalies.

Thermopylae – Lichades – Aedipsos group of anomalies (boxes A and B in Fig. 1): These align in a ~N70° orientation but i*ndividually* exhibit W-E elongation with lengths of ~16, ~12.5 and ~5.6 km and W-E/N-S aspect ratios of 3.2, 3.2 and 1.4 respectively. They are invariably parallel to local W-E faults. Thermal springs exist near each anomaly. The *Lichades anomaly* is collocated with outcrops of Quaternary volcanic rocks at the Lichades islets: this is the Lichades volcano, presumably associated with the Kammena Vourla hot springs (KV in Fig 1) and seismically imaged by Makris et al. (2001). The low amplitude *Thermopylae anomaly* cannot be attributed to outcropping magnetic rock formations in its vicinity. By its similitude to the Lichades anomaly and the presence of the hot springs (TP in Fig 1), it is presumed to be magmatic of origin. The *Aedipsos anomaly* lies directly beneath the Aedipsos hot springs (AD in Fig. 1); in the absence of other magnetic rock formations it is reasonable to assume a magmatic origin.

The Trikeri Strait – Cape Artemision group (box C in Fig. 1): The most prominent feature is an offshore round anomaly between N. Euboea and Cape Trikeri. Its shape is suggestive of a massive intrusive magmatic body (pluton) of approximately right cylindrical shape with a diameter of ~10 km; the main anomaly is decorated with smaller-scale features, presumably formed by apophyses of the main pluton. In this area, the seismic reflection Profile 1 of Makris et al. (2001) indicates significant updoming of the deeper crust, suggestive of intrusive/diapiric processes. The group

includes a lesser W-E oriented offshore anomaly, located a few km NE of Cape Artemision; the configuration is similar to that of the Lichades anomaly and also suggestive of a pluton with apophyses branching to shallower depths. In other words, the Trikeri Strait – Cape Artemision anomalies have attributes of a *failed volcano*.

Depth analysis

To study the scale and distribution of geological magnetic field sources with depth and separate their contributions to the total observed anomalies, it is customary to implement the analysis of the radially averaged power spectrum (RAS) pioneered by Spector and Grant (1970). Fig. 2a illustrates the RAS of the Trikeri–Artemision anomaly group. The basal (deepest) ensemble of magnetized structures appears to be depth-limited: the causative bodies, either are confined to depths of a few km below the surface or are demagnetized at depth due to elevated temperatures. Given Karastathis et al. (2011), the latter is plausible. The RAS is modelled with three depth-limited ensembles and the parametric function

$$\hat{P}_r(k) = \sum_{j=1}^{3} A_j k^2 e^{-2kZ_j} + A_n$$

where Aj are the ensemble strengths, Zj are the depths to the ensemble ceilings and An is the noise level. The problem was solved with non-linear least squares that produced a best-fitting model with R2 > 0.99 (Fig. 2a).

The basal depth-limited sources are located at depths greater than approx. 4 km below flight level (BFL), provide the most significant contribution to the observed anomalies and represents the "massive intrusive bodies". In geological terms, these should be calc-alkaline batholiths. The second ensemble is distributed at depths between 1.3 and 4 km BFL and may comprise large-scale apophyses of the plutons. Finally, sources at depths 0.5–1 km BFL may represent upper-stage, small-scale apophyses of the intrusive bodies and parts of the ophiolitic formations of N. Euboea and Mt. Othrys.

A corresponding analysis of the Lichades-Thermopylae-Aedipsos group required two ensembles (Fig. 2b). The basal depth-limited sources are located at depths of the order of 2 km BFL and are interpreted to comprise warm batholiths of presumably calc-alkaline composition. The second ensemble is distributed between 0.3 and 2 km BFL and represents apophyses of the main batholiths, one of which outcrops at the Lichades islets.

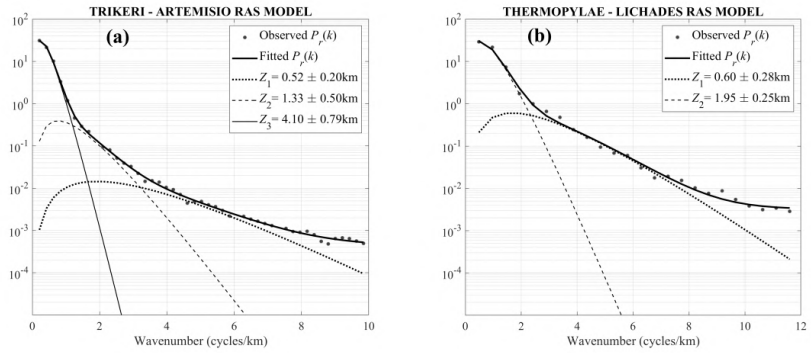

Figure 2: a) Modelling the RAS of the Trikeri – Cape Artemision anomaly. Solid grey circles: observed RAS. Solid black line: best fitting model. Other lines: responses of ensembles buried at depths Z1-Z3. b) Same for the Thermopylae–Lichades anomaly but only two ensembles required here.

Conclusions

The North Euboea Volcanic Field develops along a WSW-ENE zone from Thermopylae (west) to beyond Cape Artemision (east). It appears to consist of at least 5 centres, three of which (western group, Thermopylae, Lichades and Aedipsos) were known/suspected and two (eastern group, Trikeri–Artemision) were not. The western group's centres exhibit W-E elongation; they are located at depths >2 km and date to ~0.5 Ma. The eastern group comprises large intrusions at depths >4 km decorated with apophyses of various scales and attributes of "failed volcanoes"; their age is undeterminable from magnetic data but their proximity to Achileion may date them to 3.4 – 2.7 Ma. Given the location of both groups in the westward extension of the very active NAF and their conformity with local faulting features, we opine that albeit at different times, they have been syn-tectonically emplaced.

References

Chailas, S. et al., 2010, *Bull. Geol. Soc. Greece*, **43** (4), 1919-1929, available through http://www.geosociety.gr/images/arxeio-teuxwn/GSG_XLIII_4.pdf (last accessed August 2022).

Chailas, S. and Tzanis, A., 2019, *Bull. Geol. Soc. Greece, Sp. Pub.* 7: Extended Abstract GSG2019-328, 289-290, available through https://ejournals.epublishing.ekt.gr/index.php/geosociety/issue/view/1265 (last accessed August 2022).

Geotermica Italiana, 1984. Final reports on Methana –Poros, Loutraki- Sousaki, Platystomon, Aedipsos Geothermal projects, IGME, Athens, Greece.

Innocenti, F. et al., 2010, *J. Geol. Soc. London*, **167** (3), 475-489, https://doi.org/10.1144/0016-76492009-14.

Karastathis V. K. et al., 2011, *J. Volcanol. Geotherm. Res.*, **206**, 106–120, https://doi.org/10.1016/j.jvolgeores.2011.06.00.

Kassaras, I., et al., 2020, *Geosciences*, **10** (11), 447, https://doi.org/10.3390/geosciences10110447

Makris, J. et al., 2001, *Tectonophysics*, **341** (1–4), 225-236, https://doi.org/10.1016/S0040-1951(01)00186-X .

Spector, A. and Grant, F.S., 1970, Statistical models for interpreting aeromagnetic data, *Geophysics*, **35** (2), 294-302.

16th International Congress of the Geological Society of Greece

17-19 October, 2022 - Patras, Greece

Bulletin of the Geological Society of Greece, Sp. Publ. 10

Ext. Abs. GSG2022-246

Methana volcanic observatory: A seismic network to monitor seismicity and volcanic activity

C.P. Evangelidis[1], E. Sokos[2], I. Fountoulakis[1,2], F. Gkika[1], S. Kanakaki[2], A. Thermos[2], K. Kontakos[1], S. Liakopoulos[1]

(1) Institute of Geodynamics, National Observatory of Athens, Athens, Greece, cevan@noa.gr (2) Department of Geology, University of Patras, Rio, Greece.

Monitoring seismicity and deformation across the Methana volcanic complex continues since the beginning of 2019. Our target is to monitor continuously any potential volcanic activity and deformation across the volcano using pilot applications of innovative seismic methods. Thus, we can assess the volcanic risk in the broader area that may affect maritime and air transport, in order to determine preventive measures. During this volcanic quiescence period, seismological and geodetic data, derived from a permanent and temporary infrastructure, can define the level of volcanic status, hence the continuous (background) seismic-volcanic activity. We have deployed a network of permanent broadband and temporary short period seismic stations at the volcano and the neighboring areas. We established two independent workflows to detect the microseismicity in the area. The first automatic one, without human intervention, makes use of machine learning algorithms, a state of the art associator and waveform crosscorrelation techniques to build clusters and relocate the events. An additional manual workflow that uses a semi-automatic picker and associator triggers the analysis of the dataset following the established procedures for National Observatory of Athens (NOA) catalogue. Ambient noise interferometry (ANI) methods are used to detect temporal seismic velocity changes in the volcano. Any relative velocity changes within the crust in the area are likely to be caused by the change of stress and/or volume within the edifice and are accounted as precursors to volcanic events.

Methana volcano

Methana peninsula, located in the Saronicos Gulf at the westernmost part of the South Aegean active volcanic arc and 50km south of Athens, shows a long recorded volcanic history from Upper Pliocene to recent times. It is composed by andesitic and dacitic volcanic rocks with the more recent dated at 0.2 ± 0.3 Ma (Pe-Piper and Piper, 2013). The latest eruption giving andesitic lava is described by the ancient geographer Strabo at about 230 BCE. Moreover, Pausanias volcanic field is the offshore continuation of northern Methana. The long lived volcanic field is characterized by relatively low rates of magma supply and absence of Plinian phreatomagmatic eruptions. Recent tomographic results of the Hellenic arc show a thinned lithosphere associated with an horizontal slab tear that coincides with the volcanic centers in this area (Hansen et. al., 2018).

Volcanic observatory network

Past permanent seismic networks were not covering adequately the Saronikos Gulf area. Thus, the completeness of the recorded seismicity in the area was considered inaccurate. Our aim is to operate a local network surrounding the Methana peninsula able to detect microseismicity (Fig. 1). Four temporary short -period stations were installed at Ano Fanari (MET3), Agious Theodorous (MET4), Makriloggos (MET5) and Megalochori (MET6) at Methana peninsula starting on February 2019 (Fig. 1). The vaults of two permanent broadband seismic stations were constructed at Methana town (MET1) and Kameni Chora (MET2) and the stations were installed on May and July 2019, respectively. A permanent co-located GNSS station is operating in MET2 since 2019 and a co-located strong motion sensor is operating in MET1.

Building a seismic catalogue

We analyse continuous waveforms from 6 stations on the volcano (MET1-6) in combination with permanent seismic stations located at distances less than 100 km from the volcano from the HL, HA and HT networks (HL network, doi: 10.7914/SN/HL, HA network, doi: 10.7914/SN/HA and HT network, doi: 10.7914/SN/HT). We use the EQTransformer signal detector (Mousavi et al., 2020) to identify seismic signals and to detect P and S wave seismic arrivals. Our workflow continues with the association of the independently identified arrivals and the initial location of the seismic events using the REAL method (Zhang et al., 2019). Then, we locate the sequence with HYPOINVERSE (Klein, 2002). and further improve the earthquake locations using algorithms that incorporates techniques for hierachical clustering and relocation based on cross-correlation (CC) values. Finally, after successful relocation we calculate the local magnitude. Additionally, an independent manual analysis workflow is estabilished. Based on PhasePApy picker and associator (Chen and Holland, 2017) the detected events are manually corrected and refined using the SeisComp3 analysis platform. All manually detected events are incorporated in NOAIG catalogue (eida.gein.noa.gr/fdsnws/event).
Our aim is to compare the results between the independent automatic and manual workflows. Further analysis following template matching techniques will be followed.

Monitoring temporal changes within the volcanic edifice

Apart from monitoring the ongoing microseismicity in the area, we are interested in monitoring volcanic edifices for temporal changes of the velocity of the seismic waves. When magma pressure increases inside a volcano, the added pressure results into the inflation of the volcano, and small cracks around the magma chamber will decrease the velocity of seismic waves. That small decrease in velocity can be detected successfully using ambient noise interferometry (ANI) techniques. Based on previous ANI studies in Milos and Santorini (Daskalakis et. Al, 2016) we can resolve any potential velocity change of ±0.1%.

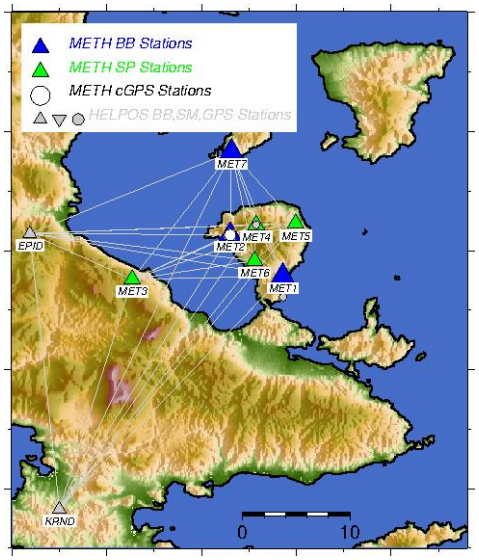

Figure 1. Network of permanent (blue) and temporary (green) seismic stations in Methana and their inter-station paths. MET7 station in Agkistri Island has not been installed yet.

Acknowledgements

The local municipality of Troizinia-Methana supported the network deployment in terms of granting land permissions, seismic vault construction, power supply and telecommunication links. We acknowledge support of this abstract by the project "GEORISK – Developing Infrastructure and Provision of Services through Actions of Excellence to Reduce the Impact of Geodynamic Hazards" (MIS 5002541) which is implemented under the "Action for the Strategic Development of Research and Technology Organizations", funded by the Operational Programme "Competitiveness, Entrepreneurship and Innovation" (NSRF 2014-2020) and co-financed by Greece and the European Union (European Regional Development Fund).

References

Aristotle University of Thessaloniki. (1981). Aristotle University of Thessaloniki Seismological Network [Data set]. International Federation of Digital Seismograph Networks. https://doi.org/10.7914/SN/HT

Chen Chen, Austin A. Holland; PhasePApy: A Robust Pure Python Package for Automatic Identification of Seismic Phases. *Seismological Research Letters* 2017; 87 (6): 1384–1396. doi: https://doi.org/10.1785/0220160019

Daskalakis E., C.P. Evangelidis, J. Garnier, N.S. Melis, G. Papanicolaou and C. Tsogka, Robust seismic velocity change estimation using ambient noise recordings, Geophys.J.Int, doi: 10.1093/gji/ggw142, 2016

Pe-Piper Γ., DJW Piper, The effect of changing regional tectonics on an arc volcano: Methana, Greece, Journal of Volcanology and Geothermal Research 260, 146-163, 2013

Hansen, S. E., Evangelidis, C. P., & Papadopoulos, G. A. (2019). Imaging slab detachment within the Western Hellenic Subduction Zone. Geochemistry, Geophysics, Geosystems, 20, 895– 912. https://doi.org/10.1029/2018GC007810

Klein, F. W. (2002). User's guide to HYPOINVERSE-2000: A Fortran program to solve for earthquake locations and magnitudes. U.S. Geol. Surv. Open-File Report.

Mousavi, M. S., Ellsworth, W. L., Zhu, W., Chuang, L. Y., & Beroza, G. C. (2020). Earthquake transformer—an attentive deep-learning model for simultaneous earthquake detection and phase picking. Nature Communications, 11 , 3952. doi: 10.1038/s41467-020-17591-w

National Observatory of Athens, Institute of Geodynamics, Athens. (1975). National Observatory of Athens Seismic Network [Data set]. International Federation of Digital Seismograph Networks. https://doi.org/10.7914/SN/HL

University of Athens. (2008). Hellenic Seismological Network, University of Athens, Seismological Laboratory [Data set]. International Federation of Digital Seismograph Networks. https://doi.org/10.7914/SN/HA

Zhang, M., Ellsworth, W. L., & Beroza, G. C. (2019). Rapid Earthquake Association and Location. Seismological Research Letters, 90 (6), 2276-2284. doi: 10.1785/0220190052

16th International Congress of the Geological Society of Greece
17-19 October, 2022 - Patras, Greece
Bulletin of the Geological Society of Greece, Sp. Publ. 10
Ext. Abs. GSG2022-267

Damage distribution of a recent (2016, M5.3) and a historical mainshock (1898, M6.3) in the area of Ioannina using a finite fault stochastic simulation approach

M. Ravnalis[1], C. Kkallas[1], C. Papazachos[1]
(1) Geophysical Laboratory, Aristotle University of Thessaloniki, Thessaloniki, Greece, mravnalis@gmail.com

Epirus is located on the northwestern edge of Greece, in which the transition of the extensional Aegean regime to the compressional outer Aegean occurs (Mercier et al., 1972; Hatzfeld et al., 1995). The main tectonic structures are thrust belts that trend north-northwest because of the east–west shortening, changing to normal (and sometimes strike-slip) faults as we move to the east. In 1898, just before the start of the instrumental period of Seismology in Greece, a strong **M**~6.3 earthquake occurred in Archimandrion (Ioannina), with a highest macroseismic intensity of I_{MM} = VIII (Papazachos et al., 1997) (**Figure 1**), causing significant damage in Ioannina. Almost one century later, on 15/10/2016 (20:14 UTC) a moderate earthquake measuring **M**5.3 was recorded in northwestern Greece, with its epicenter located 12 km northwest of the city of Ioannina (depth of ~10km) near the Pogoni village, northwest of Ioannina. There have been no reports of damage or injuries, though several landslides in the mountainous road network have been reported. In this work, we relocate the epicenters of the seismic sequence using a locally derived velocity model and appropriate station corrections. Macroseismic data were collected from the published databank of macroseismic information for the Aegean area (Papazachos et al., 1997) for the historical earthquake (1898, **M**6.3), whereas for the modern earthquake (2016, **M**5.3) we used macroseismic data from online databases of USGS – DYFI (Did You Feel It) and EMSC (European Mediterranean Seismological Centre) (Bossu et al., 2018). Furthermore, we used the finite fault stochastic simulation approach with the EXSIM code (Motazedian & Atkinson, 2005), as adapted by Boore (2009) to assess the strong ground motion due to the events, as well the expected damage distribution.

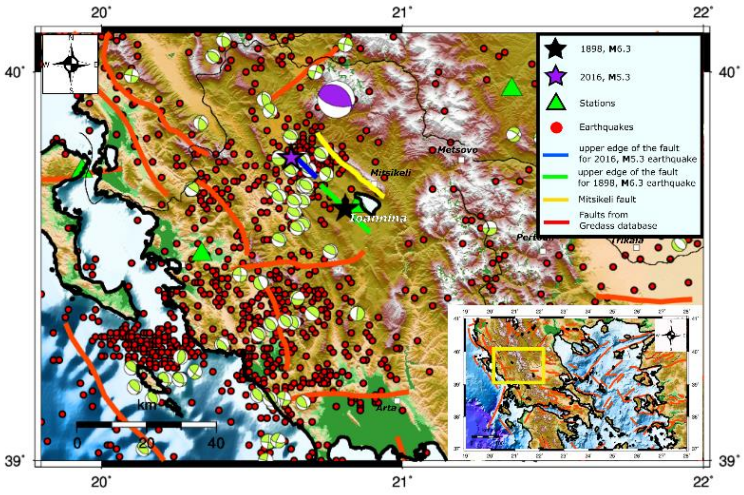

Figure 1 Map of the broader study area showing the major faults, and the events which occurred between 01/01/1960 – 14/07/2022; yellow rectangular denotes the zoomed area in the area of Ioannina. Fault model (upper fault edge) used to simulate the 2016, M5.3 and the earthquake damage pattern (blue solid line). The focal mechanism (with purple color), the stations for which strong motion records were used (green triangles), as well as main surface faulting traces observed after the earthquake in the study area by GredaSS database (Caputo et al., 2013) are depicted. Fault model (upper fault edge) used to simulate the 1898, M6.3 earthquake (green solid line), as well as the focal mechanisms between 01/01/1960 – 14/07/2022 (with yellow color) are also shown.

Considering the importance of the site-effect assessment for the simulation approach, the SRTM3 morphological model was adopted to determine Vs30 values from slope proxies, following Wald and Allen (2007). Generic transfer site amplification functions for NEHRP (1994) site conditions A/B, C and D, were adopted from the work of Margaris and Boore (1998) and Klimis et al. (1999) and used for each IDP site in the simulation with the EXSIM code. Furthermore, we have adopted a simple approach, where the PGA & PGV values from the synthetic waveforms were converted into macroseismic intensities. For this conversion we used the relations proposed by Kkallas et al., 2018 (modified from Wald et al., 1999) (**Figure 2a and 2b**). The simulated macroseismic results show a good agreement of the spatial distribution of the observed and modeled (simulated) macroseismic intensities, verifying that we can reliably reconstruct the main features of the damage distribution approach for these two earthquakes (**Figure 2c**).

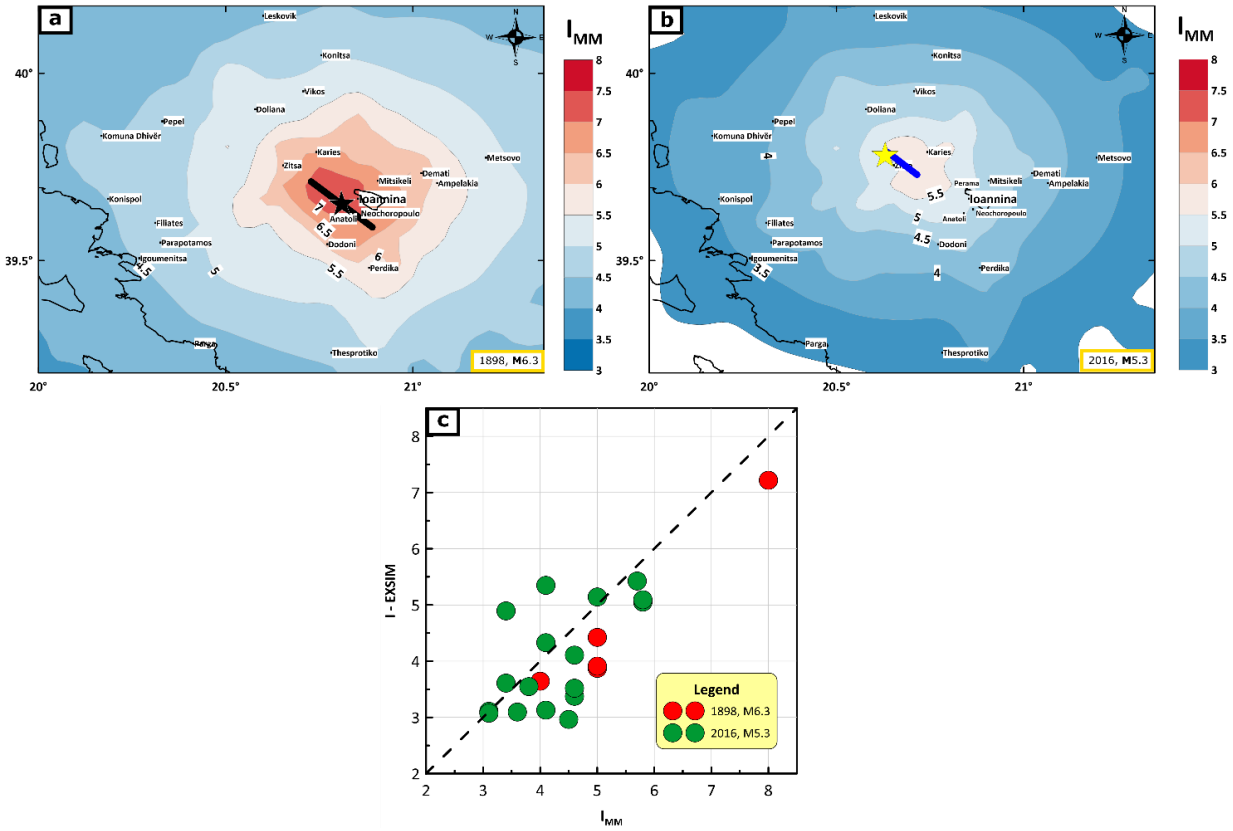

Figure 2 (a) Spatial distribution of synthetic I_{MM} values of 1898, M6.3 earthquake (the epicenter is depicted with a black star). Fault model (upper fault edge) used for the simulation is also depicted (black solid line). (b) Same as (a) for the 2016, M5.3 earthquake (The upper fault edge is depicted with a blue solid line, and the epicenter with a yellow star). (c) Comparison of the modelled (synthetic), I – EXSIM, and observed, I_{MM}, macroseismic intensities for the historical (1898, M6.3) and the recent earthquakes (2016, M5.3) using the EXSIM code (red and green solid circles respectively).

References

Boore, D. M. (2009). Comparing Stochastic Point-Source and Finite-Source Ground-Motion Simulations: SMSIM and EXSIM, Bull. Seism. Soc. Am., 99(6), 3202-3216, doi:10.1785/0120090056.

Bossu, R., Roussel, F., Fallou, L., Landès, M., Steed, R., Mazet-Roux, G., Dupont, A., Frobert, L., & Petersen, L. (2018). LastQuake: From rapid information to global seismic risk reduction. Int. J. Disaster Risk Reduct., 28, 32–42. https://doi.org/10.1016/j.ijdrr.2018.02.024.

Caputo, R., Chatzipetros, A., Pavlides, S., & Sboras, S. (2013). The Greek Database of Seismogenic Sources (GreDaSS): State-of-the-art for northern Greece. Ann. Geophys., 55(5). https://doi.org/10.4401/ag-5168.

Hatzfeld, D., Kassaras, L., Panagiotopoulos, D., Amorese, D., Makropoulos, K., Karakaisis, G., & Coutand, O., (1995). Microseismicity and strain pattern in northwestern Greece, Tectonics 14, 773–785.

Kkallas, Ch., Papazachos, C. B., Boore, D., Ventouzi, Ch., & Margaris, B. N. (2018). Historical intermediate-depth earthquakes in the southern Aegean Sea Benioff zone: Modeling their anomalous macroseismic patterns with stochastic ground-motion simulations. Bull. Earthq. Eng, 16(11), 5121–5150. https://doi.org/10.1007/s10518-018-0342-8.

Klimis, N. S., Margaris, B. N., & Koliopoulos, P. K. (1999). Site-dependent amplification functions and response spectra in Greece. J. Earthq. Eng., 3(2), 237–270. https://doi.org/10.1080/13632469909350346.

Margaris, B. N., & Boore, D. M. (1998). Determination of Δσ and Ko from Response Spectra of Large Earthquakes in Greece. Bull Seism Soc Am 88: 170-182.

Mercier, J., Bousquet, B., Delibasis, N., Drakopoulos, I., Kerarden, B., Lemell, F., & Sorel, D. (1972). Deformations en compression dans le quartinaire des ravages Ioniens. Donnes neotectoniques et seismiques. C. R. Acad. Sci. Paris, 275, 2307–2310.

Motazedian, D., & Atkinson, G.M. (2005), Stochastic Finite-Fault Modeling Based on a Dynamic Corner Frequency, Bull. Seismol. Soc. Am., 95(3), 995-1010, doi:10.1785/0120030207.

Papazachos, B.C., Papaioannou, Ch., Papazachos, C.B., & Savvaidis, A.S. (1997). Atlas of Isoseismal Maps for Strong Shallow Earthquakes in Greece and Surrounding Area (426BC-1995), Ziti publications, Thessaloniki, 176.

Wald, D. J., & Allen, T. I. (2007). Topographic Slope as a Proxy for Seismic Site Conditions and Amplification. Bull Seism Soc Am, 97:1379–1395 97(5), 1379–1395. https://doi.org/10.1785/0120060267.

Wald, D. J., Quitoriano, V., Heaton, T. H., & Kanamori, H. (1999). Relationships between Peak Ground Acceleration, Peak Ground Velocity, and Modified Mercalli Intensity in California. Earthq. Spectra, 15(3), 557–564. https://doi.org/10.1193/1.1586058.

16th International Congress of the Geological Society of Greece
17-19 October, 2022 - Patras, Greece
Bulletin of the Geological Society of Greece, Sp. Publ. 10
Ext. Abs. GSG2022-275

Seismicity Relocation Reveals Unstudied Seismotectonic Features in the Broader Patras Gulf Area

I. Nikolopoulou[1], Z. Roumelioti[1], E. Sokos[1], V. Mouslopoulou [2]

(1) Geology Department University of Patras, Rio, Greece, up1052555@upnet.gr (2) National Observatory of Athens, Athens, Greece

Introduction

Patras Gulf lies at the western end of the Corinth Gulf continental rift, an area of intense N-S extension. Further west, in the Ionian Islands area, continental collision and oceanic subduction takes place. Despite its significance in accommodating crustal strain between the Corinth rift in the east and the Ionian Islands in the west, the Gulf of Patras has not been studied adequately to date, using the available high quality earthquake data. Previous studies are limited in number, i.e., the work of Melis et al. (1989), who installed a microseismic network in the area, and two studies focused on the 1993 Patras earthquake (M_s=5.4), aftershock sequence (Karakostas et al., 1994, Tselentis et al., 1994).

In this paper we use eleven years (2011-2022) of seismic data - collected after the establishment of the Hellenic Unified Seismological Network (HUSN) in 2008 - to accurately relocate the seismicity within the geographical area of 38-38.45N^o and 21-21.8E^o. The relocated events reveal active structures in the area over a broad range of depths and provide an improved understanding of the seismotectonics along the western termination of the Corinth Rift.

Data

The initial catalog includes P- and S- phase data of 6601 events provided by the Institute of Geodynamics of the National Observatory of Athens (NOA, www.gein.noa.gr). Since the crustal velocity model is crucial for earthquake location, four local and/or regional models were tested to pick the most suitable for the area. The selected models were published by Rigo et al. (1996), Haslinger et al. (1998), Kassaras et al. (2016), and Lefils (2022).

Location procedure

Event location was performed with the Hypoinverse code (Klein, 2002). Phase data were filtered based on their quality i.e., minimum number of phases for location was set to 12, maximum event station distance was 180km for minimizing the crustal model effect, and the starting depth was set at 10km, a value suitable for the area. These restrictions resulted in location of 5389 out of 6601 events in the initial catalog. Among all tested velocity models, the model of Lefils (2022) presented the best data fitting. Nevertheless, all models were characterized by similar error values.

Relocation procedure

After the initial location, events were relocated using the double difference relocation algorithm HypoDD (Waldhauser and Ellsworth, 2000). We used catalog differential times calculated based on the P- and S-wave arrival picks. Relocation of the epicenters was performed several times to test different combinations of P- and S- phases weighting schemes. After many tests at the selected run, 4959 events (92% of the initial catalog) passed the HypoDD criteria and were accurately relocated. The final HypoDD run was executed using a P- and S- waves data weighting scheme of 1.0 and 0.5, respectively.

Results and Discussion

In Figure 1, we present the spatial distribution of the earthquake epicenters before relocation (Figure 1a), after the location with the Hypoinverse code (Figure 1b) and after relocation with HypoDD (Figure 1c). It is obvious that after each step, despite that the number of events gradually decreases, earthquake clusters get tighter to form clear linear features. The relocated seismicity for the last eleven years in the Patras Gulf (Figure 1c) reveals some interesting features.

- A striking feature is the abrupt termination of the western Corinth Gulf intense seismicity, a few kilometers west of the Rio-Antirio Strait, along a line of NW-SE orientation.
- Another important observation from Figure 1c is a concentration of relatively deep events (~40km depth), most probably related to the subduction. This deep cluster appears to be the only one observed within the study area.
- The Achaia-Elia fault zone is clearly delineated by seismicity, but its northern extend, proximal to the Patras coastline, is less clear as the seismicity becomes distributed, stepping northeastward through a series of NE-SW trending clusters.
- Finally, maybe the most significant features are the three NW-SE lineaments in the eastern part of the Patras Gulf, clearly observed at the relocated seismicity. These lineaments present an orientation similar to the strike of the March 1993, M_w 5.8 Patras earthquake, which caused considerable damage in the city of Patras (largest beachball in Figure 1d). Their significant spatial extent and their proximity to Patras city suggest that they may be important in terms of seismic hazard and, thus call for a more careful study.

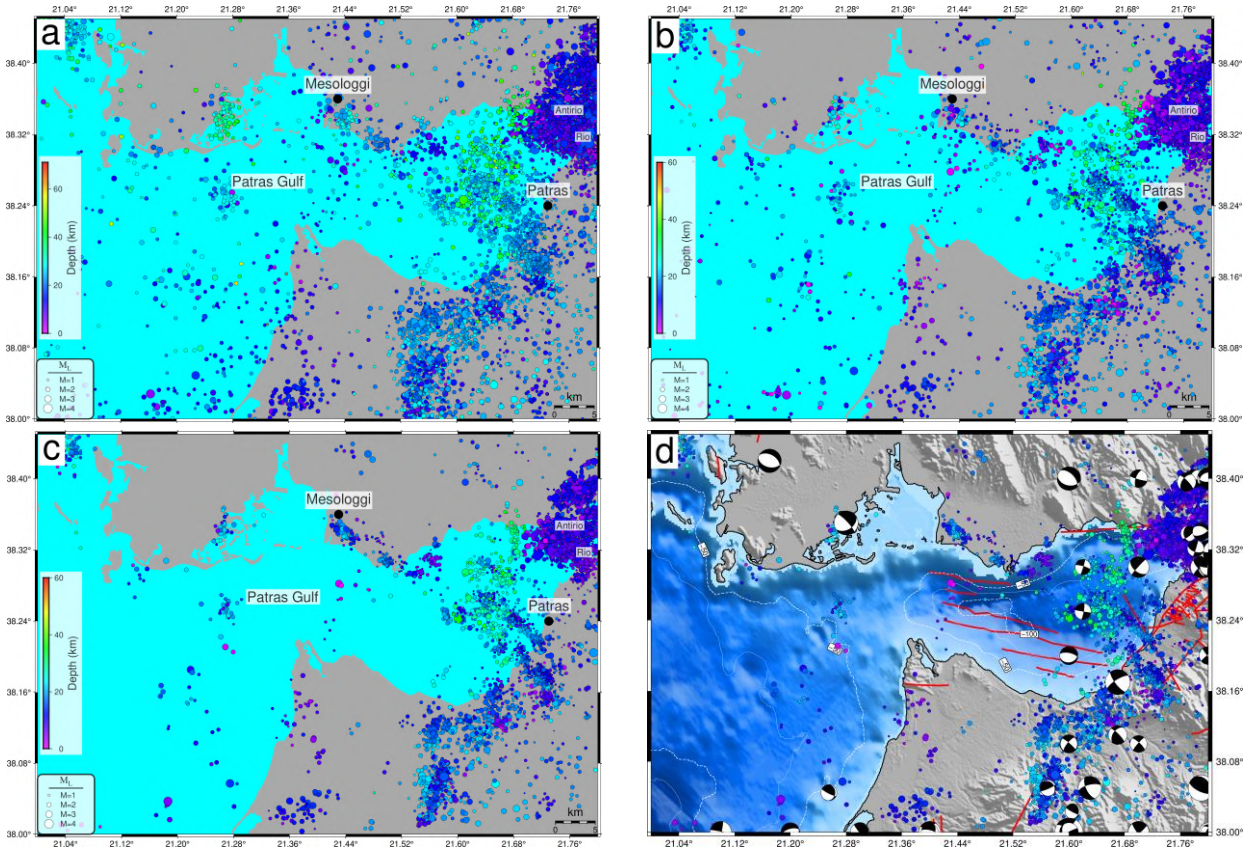

Figure 1. Distribution of earthquake epicenters in and around the Patras Gulf that occurred in the period 2011-2022. a) Locations provided by NOA. b) Locations using the Hypoinverse code and the velocity model of Lefils (2022). c) Relocated seismicity using the double-differences method. The color scale shows variation in earthquake depth. d) Relocated seismicity, including topography, mapped faults (Ganas, 2022) and focal mechanisms (https://www.globalcmt.org/; https://www.emsc-csem.org/).

References

Ganas, A. (2022). NOAFAULTS KMZ layer version 4.0 (v4.0) [Data set]. Zenodo, https://doi.org/10.5281/zenodo.6326260.

Haslinger, F., Kissling, E., Ansorge, J., Hatzfeld, D., Papadimitriou E., Karakostas, V., Makropoulos, K., Kahle, H.-G., Peter, Y., (1999). 3D crustal structure from local earthquake tomography around the Gulf of Arta (Ionian region, NW Greece). Tectonophysics 304, 201-218.

Karakostas, B., Papadimitriou, E., Hatzfeld, D., Makaris, D., Makropoulos, K., Diagourtas, D., Papaioannou, D., Stavrakakis, G., Drakopoulos, J., Papazachos, B., 1994. The aftershock sequence and focal properties of the July 14, 1993 (M_S= 5.4) Patras earthquake. 7th Congress of the Geological Society of Greece, Thessaloniki, Greece, p. 167-174.

Kassaras, I., Kapetanidis, V., Karakonstantis, A., (2016). On the spatial distribution of seismicity and the 3D tectonic stress field in western Greece. Physics and Chemistry of the Earth 95, 50-72.

Klein, F. W., 2002. User's Guide to HYPOINVERSE-2000, a Fortran program to solve for earthquake locations and magnitudes, Open File Report 02-171, U.S. Geological Survey, 123 p.

Lefils, V., 2022. Experience MADAM: Caractérisation sismotectonique d'une microplaque en formation (Grèce). Ph.D. Thesis, PSL University, Paris, 222p.

Melis, N.S., Brooks, M., Pearce, R.G., 1989. A microearthquake study in the Gulf of Patras region, western Greece, and its seismotectonic interpretation. Geophysical Journal 98, 515-524.

Rigo, A., Lyon-Caen, H., Armijo, R., Deschamps, A., Hatzfeld, D., Makropoulos, K., Papadimitriou, P., Kassaras, I. (1996). A microseismic study in the western part of the Gulf of Corinth (Greece): implications for large-scale normal faulting mechanisms. Geophysical Journal International 126, 663-668.

Tselentis, G., Melis, N., Sokos, E., 1994. The Patras (July 14, 1993; M_S= 5.4) earthquake sequence. 7th Congress of the Geological Society of Greece, Thessaloniki, Greece, p. 159-165.

Waldhauser, F., Ellsworth, W. L., 2000. A Double-Difference Earthquake Location Algorithm: Method and Application to the Northern Hayward Fault, California. Bulletin of the Seismological Society of America 90, 6, pp. 1353-1368.

Waldhauser, F., 2001. hypoDD – A Program to Compute Double-Difference Hypocenter Locations, Open File Report 01-113, U.S. Geological Survey, 25 p.

16th International Congress of the Geological Society of Greece
17-19 October, 2022 - Patras, Greece
Bulletin of the Geological Society of Greece, Sp. Publ. 10
Ext. Abs. GSG2022-277

Microseismicity in Mesara Basin, Crete: Observations from a local seismic monitoring network

E. Dafnioti[1], G. Chatzopoulos[2], S. Pytharouli[1], F. Vallianatos[2], G. Hloupis[3] and R. Lunn[1]

(1) University of Strathclyde, Glasgow, United Kingdom, eleni.dafnioti@strath.ac.uk (2) National and Kapodistrian University of Athens, Athens, Greece/ Institute of Physics of the Earth's Interior and Geohazards, UNESCO Chair on Solid Earth Physics and Geohazards Risk Reduction, Hellenic Mediterranean University Research Center, Chania, Greece, (3) University of West Attica, Athens, Greece

The occurrence of microseismicity is often overlooked as non significant, yet it can reveal important aspects of the evolution of seismicity at a region and the geological structures that accommodate this seismicity (Ross et al., 2019; Helmstetter et al., 2005; Marsan D., 2005; Helmstetter, 2003). Permanent seismic monitoring networks do not allow for the recording of all small in magnitude (< M1) earthquakes at longer distances. These events have higher frequencies that attenuate fast, making detection challenging, if not impossible, at stations located 10s of kilometres away.

This work focuses on the study of the characteristics of natural microseismicity (frequency of occurrence, magnitude distribution, depth of hypocentres etc.) in an effort to understand whether microseismicity follows the same characteristics as larger earthquakes and whether it can be used as a precursor for the occurrence of larger earthquakes.

In July 2022, along with the Hellenic Seismological Network of Crete (https://doi.org/10.7914/SN/HC) we deployed a local, temporary microseismic monitoring network in the south of Heraklion prefecture (Crete, Greece) aiming to record very small in magnitude earthquakes (within the range of $-0.5 < M < 3$, i.e. two orders of magnitude below the current completeness magnitude of M_c2.0). The network consisted of seven short period Guralp CMG-40T-1 seismometers with a flat response between 1Hz and 100Hz paired with REF TEK 130 24bit digitizers. The utilized sensors were set to record in continuous mode with a sample rate 200Hz. The seismometers were deployed in an almost circular geometry, with one seismometer deployed at the centre and the remaining six in a circle of radius approximately 6.1km. This geometry provided a good azimuthal coverage and constraints for determining the hypocentres. In this work, we present the first results from the evaluation of the monitoring network and analysis of microseismic data collected during the first week of monitoring.

H/V analysis of ambient noise recordings acquired using a GEObit GEOtiny 10sec seismometer, showed that two out of seven stations are located on top of bedrock, while four are located on top of sedimentary layers of with a considerable thickness.

We modelled the sensitivity (detection capability) of the local monitoring network that can be achieved with the adopted deployment geometry using the InSite software (InSite-Lab™(v.3.15.1)). Results are consistent with the magnitude detection threshold as estimated using catalogued events (Figure 1).

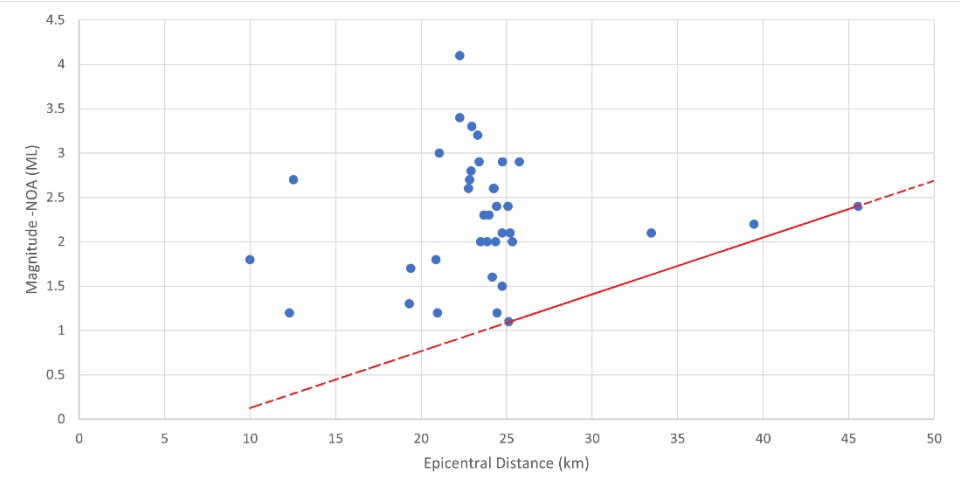

Figure 1. Detection Magnitude threshold of the local monitoring network deployed in this study. Red solid line indicates the magnitude threshold above which an event can be detected by the network.

We manually picked the P and S phase arrivals of 23 catalogued, by the Hellenic Unified Seismological Network (see Institute of Geodynamics, National Observatory of Athens, https://doi.org/10.7914/SN/HL), events occurring within an

area of 50km radius from the central station of our monitoring network during the week under investigation. We used the picks and Wadati diagrams (Havskov et al., 2009) to estimate the Vp/Vs value for the area. We find an average value of Vp/Vs = 1.78 ± 0.05. This is consistent with the values specified in Nicolintaga et al (2007) for the same region.

Further analysis of our recordings revealed the occurrence of a large number of microseismic events, at least 10 times more than the number of officially reported events in the published seismic catalogue for the same time period. The seismicity we report here refers to events that can be visually observed in the recordings. We anticipate that further, more advanced signal processing analysis will reveal a much larger number of masked by noise, smaller in magnitude events. This indicates the significance of local monitoring networks in providing more detailed information over fault activity.

We examine the characteristics of the newly detected microseismic events, the magnitude distribution and the depth of the hypocentres. The analysis was performed using SEISAN (2021. SEISAN (v.12.0)). The velocity model used for the analysis was the one suggested by Meier *et al.* (2004).

Further analysis is required and is currently ongoing in order to achieve a better understanding on the evolution of seismicity in the Heraklion prefecture, Central Crete. Future steps include the analysis of recordings covering a longer time period and the determination of the moment tensors to help in understanding of the nature of the events and the geological structures that accommodate this seismicity.

Acknowledgements

This work was funded by GeoNetZero CDT and the University of Strathclyde. We acknowledge support by the Region of Crete and the project "Operation of the Hellenic Seismological Network of Crete". The authors would like to thank the Municipality of Archanes-Asterousia and the Municipatity of Kofina and particularly Mr E. Kokosalis, Mr T. Chatzakis and Mr G. Kalogiannakis for their support on the deployment of the local seismic network. The authors are grateful to the Leaders of the local councils within the aforementioned Municipalities for their continuous help and patience and for providing access to the buildings where the seismometers have been deployed.

References

Havskov, J., Bormann, P. and Schweitzer, J., 2009. Earthquake location. In New Manual of Seismological Observatory Practice (NMSOP) (pp. 1-28). Deutsches GeoForschungsZentrum GFZ.

Helmstetter, A., 2003. Is earthquake triggering driven by small earthquakes?. Physical review letters, 91(5), p.058501.

Helmstetter, A., Kagan, Y.Y. and Jackson, D.D., 2005. Importance of small earthquakes for stress transfers and earthquake triggering. Journal of Geophysical Research: Solid Earth, 110(B5).

Marsan, D., 2005. The role of small earthquakes in redistributing crustal elastic stress. Geophysical Journal International, 163(1), pp.141-151.

Nikolintaga, I., Karakostas, V., Papadimitriou, E., Vallianatos, F. and Panopoulou, G., 2007. Velocity models inferred from p-waves travel time curves in South Aegean. Bulletin of the Geological Society of Greece, 40(3), pp.1187-1198.

Ottemöller, L., Voss, P.H. and Havskov J. (2021). SEISAN Earthquake Analysis Software for Windows, Solaris, Linux and Macosx, Version 12.0. 607 pp. University of Bergen. ISBN 978-82-8088-501-2, URL http://seisan.info.

Ross, Z.E., Trugman, D.T., Hauksson, E. and Shearer, P.M., 2019. Searching for hidden earthquakes in Southern California. Science, 364(6442), pp.767-771.

16th International Congress of the Geological Society of Greece

17-19 October, 2022 - Patras, Greece

Bulletin of the Geological Society of Greece, Sp. Publ. 10

Ext. Abs. GSG2022-278

Moderate to Strong recoded earthquakes during 2020-2022 in the Hellenic peninsula and neighbouring regions.

Andreas Karakonstantis[1,2], Panayotis Papadimitriou[1], Vasilis Kapetanidis[1], George Kaviris[1], Nicholaos Voulgaris[1] and Ioannis Kassaras[1, †]

(1) Department of Geology and Geoenvironment, National and Kapodistrian University of Athens, Athens, Greece
(2) Institute of Physics of the Earth's Interior and Geohazards, Hellenic Mediterranean University Research Center, Chania, Crete, Greece

From 2020 to the first half of 2022, more than 30,000 events, recorded by stations of the Hellenic Unified Seismological Network (HUSN; Evangelidis et al. 2021), were analyzed by the Seismological Laboratory of the National and Kapodistrian University of Athens (SL_NKUA). Recently, data from the Hellenic Strong Motion Network (HSMN; Theodulidis et al. 2004; Kassaras et al. 2016) that were also included. The scolv tool of the SeisComP3 software package was used to manually revise the automatic located events, also enriching the catalogue with events that weren't in the database, extracting waveform data according to an initial origin time after visual inspection of the 24-hour recording of reference stations.

In the present study, we focus on significant seismic activity during the early months of 2020 until the end of the first semester of 2022. Specifically, the results of the earthquake sequences of moderate and strong earthquakes are presented, along with some moderate, intermediate-depth (H≥40 km) earthquakes, such as:

- The 30 October 2020, Samos M_w=6.9 earthquake,
- The March 2021, Damasi (Northern Thessaly), M_w~6.0 seismic sequence,
- The 2021-2022 Arkalochorion earthquakes,
- A series of moderate events during April-August 2021 in the broader area of Nisyros Volcanic complex,
- The intermediate-depth earthquakes on Rhodes Island, on 28 June, 2020 (M_L=5.3), and at Kythera, December 18th, 2021 (M_L=5.3).

As a first case, the shallow activity associated with the earthquakes that occurred during the last quarter of 2020, in the broader area of Samos Island, are presented. On 30 October 2020 11:51 UTC, a M_w=6.9 earthquake occurred in the offshore area north of Samos Island, in the Gulf of Ephesos / Kuşadasi, causing two fatalities and 19 minor injuries at Samos Island. Manual analysis of more than 1,000 events since 30 October, 2020, was used to obtain an optimized local velocity model. The newly developed seismic catalogue revealed distinct spatial ~E-W oriented seismic clusters, compatible with the strike of Quaternary faults in the area. The spatial distribution of hypocenters appeared similar with that of the 2017 Kos earthquake (Ganas *et al.*, 2019), in the sense that the eastern part of the aftershocks sequence was more densely populated with events than the western part, while a significant lack of aftershocks is observed between the two halves. This gap could coincide with the region of the fault surface where most of the co-seismic slip occurred, i.e. a large asperity that ruptured during the mainshock, thus only few aftershocks are observed therein (Papadimitriou et al. 2020).

Following, from 3 March, 2021, a seismic sequence affected north Thessaly, with major epicenters located 20–30 km WNW of Larissa, the fifth most populated city in Greece. Specifically, on 3 March 2021, an earthquake of magnitude M_w = 6.3 occurred at 10:16 UTC in the mountainous area of Damasi-Tyrnavos (Ganas et al., 2021, Karakostas et al., 2021, Kassaras et al. 2022). Near the epicentral region, where the M_w = 6.3 mainshock occurred, foreshock activity was observed in the catalogue, between 28 February and 3 March 2021. On 4 March an M_w = 6.0 earthquake took place about 12 km to the northwest of the first one, inside the basin formed by the Titarisios river. Lastly, on 12 March, another major event of M_w = 5.6 occurred 7 km further NNW, near the NW edge of the basin. An optimum 1-D velocity model was estimated for each temporal group of the seismic sequence. The search of the best solution concerns multiple iterations per layer (velocity, thickness), using the generic 1-D velocity profile as starting model. The new region-specific velocity models provided hypocentral solutions with smaller uncertainties than those derived with the generic one, used during the analysis procedure with scolv (Kassaras et al. 2022).

On 27 September 2021, an M_w=6.0 event, linked to an approximately N-S trending normal fault at the central part of the island of Crete, Greece, occurred ~20 km to the south of the prefecture's capital. The occurrence of the mainshock took place after a long time of foreshocks since the first half of June 2021 with the strongest event occurring on 28 September with local magnitude M_L=5.3. Its focal mechanism is characterized by an SSW-NNE to SW-NE-trending, nearly dip-slip normal faulting. Its strike generally ranges from N200° E–N230° E and its dip angle varies between 40° and 60°. The active fault associated with the main event is the Kastelli Fault, which has a progressive change in the strike from 225° to 265° northeastwards and dips between 60°–80° northwestwards (Triantaphyllou et al. 2022;

Vassilakis et al. 2022; Ganas et al. 2022; Vallianatos et al. 2022).

The earthquake activity in the broader area of the Eastern Hellenic Volcanic Arc (HVA) is strongly connected with the tectonic regime, as well as with the volcanic processes (Papadimitriou et al., 2015, Papadimitriou et al. 2018, Karakonstantis et al. 2019). After the occurrence of the M_L=4.9 event on 1 October, 2020 the activity increased in the Southern Nisyros Basin and on 13 April, 2021 a moderate earthquake of M_L=5.2 occurred in the basin. After this event, more than 350 earthquakes followed. The activity remained in high levels and on 21 June, 2021 another moderate earthquake of M=5.6 took place further to the south in the basin. All the determined focal mechanism solutions of the Seismological Laboratory of NKUA indicate NNE-SSW-trending normal faulting. This is supported by both the hypocenters and the mapped faults in the area, suggesting the activation of an ESE-dipping normal fault, bounding the Southern Nisyros Basin. Both waveform analysis (HF) and focal mechanism solutions (absence of Non-Double Couple component) have shown that these events are mainly characterized as tectonic.

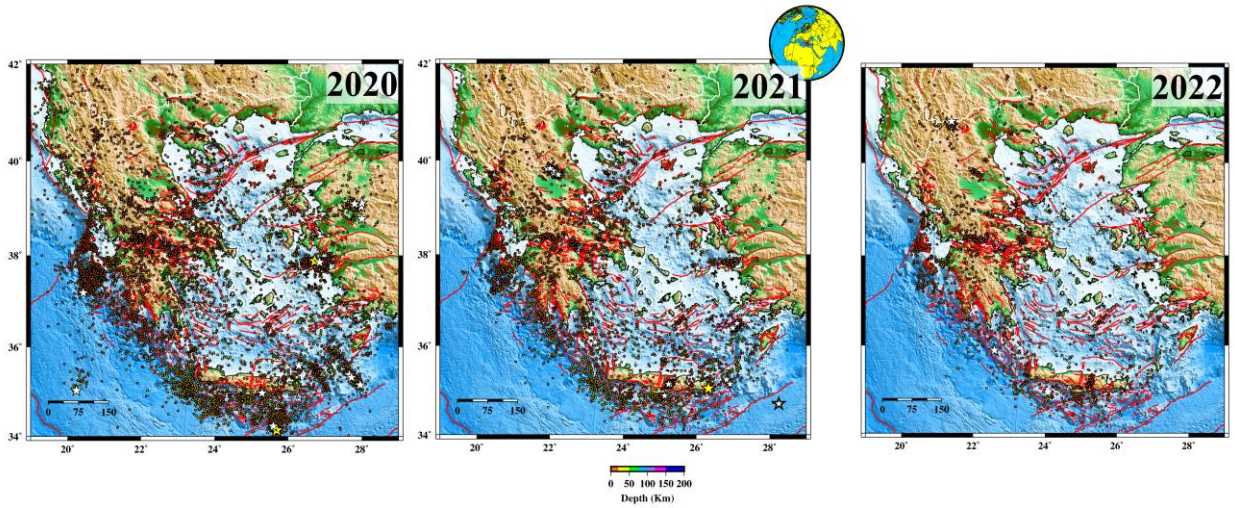

Figure 1. Location of the earthquakes with M≥2.0 in 2020 (left), 2021 (middle) and 2022 (right) derived by the analysis of the Seismological Laboratory of NKUA. Seismic events of M≥6.0 are marked with yellow stars while the events with 5.0≤M<6.0 with white ones. Fault traces are modified by Ganas (2022) and marked in red colour.

References

Evangelidis, Ch. et al., 2021. Seismic waveform data from Greece and Cyprus: Integration, archival, and open access. Seismological Soci ety of America, 92(3), 1672-1684.

Ganas A. et al., 2019. The 20 July 2017 M6.6 Kos Earthquake: Seismic and Geodetic Evidence for an Active North-Dipping Normal Fault at the Western End of the Gulf of Gökova (SE Aegean Sea). Pure Appl. Geophys. 176, 4177–4211.

Ganas, A. 2022. NOAFAULTS KMZ layer Version 4.0. https://doi.org/10.5281/ZENODO.6326260

Ganas A. et al., 2022. The Arkalochori Mw = 5.9 Earthquake of 27 September 2021 Inside the Heraklion Basin: A Shallow, Blind Rupture Event Highlighting the Orthogonal Extension of Central Crete. Geosciences. 2022; 12(6):220.

Karakonstantis, A. et al., 2019. Tomographic imaging of the NW edge of the Hellenic volcanic arc. J Seismol 23, 995–1016.

Karakostas, V. et al., 2021. The March 2021 Tyrnavos, central Greece, doublet (Mw6.3 and Mw6.0): aftershock relocation, faulting details, coseismic slip and deformation. Bull. Geol. Soc. Greece 58 (131).

Kassaras, I. et al., 2016. ACCELEROMETRIC DATA AND WEB PORTAL FOR THE VERTICAL CORINTH GULF SOFT SOIL ARRAY (CORSSA). Bulletin of the Geological Society of Greece, 50(2), 1081–1090. https://doi.org/10.12681/bgsg.11813

Kassaras et al., 2022. Seismotectonic analysis of the 2021 Damasi-Tyrnavos (Thessaly, Central Greece) earthquake sequence and implications on the stress field rotations, Journal of Geodynamics, 150 (2022).

Papadimitriou, P. et al., 2015. The Santorini Volcanic Complex: A detailed multi-parameter seismological approach with emphasis on the 2011–2012 unrest period. J. Geodyn., 85, 32–57, doi: 10.1016/j.jog.2014.12.004.

Papadimitriou, P. et al., 2018. Seismicity and Tomographic Imaging of the Broader Nisyros Region (Greece), "Nisyros volcano. The Kos - Yali - Nisyros volcanic field" e-book. Springer, 245–271.

Papadimitriou, P. et al., 2020. First Results on the Mw=6.9 Samos Earthquake of 30 October 2020. *Bulletin of the Geological Society of Greece*, *56*(1), 251–279. https://doi.org/10.12681/bgsg.25359

Theodulidis N. et al., 2004. HEAD1.0 : A unified accelerogram database", Seism. Research. Lett, 75, 41-50.

Triantafyllou I. et al. (2022). The Crete Isl. (Greece) Mw6.0 Earthquake of 27 September 2021: Expecting the Unexpected. GeoHazards. 2022; 3(1):106-124.

Vallianatos F. et al. 2022. On the Patterns and Scaling Properties of the 2021–2022 Arkalochori Earthquake Sequence (Central Crete, Greece) Based on Seismological, Geophysical and Satellite Observations. Applied Sciences. 2022; 12(15):7716.

Vassilakis E. et al., 2022. The 27 September 2021 Earthquake in Central Crete (Greece)—Detailed Analysis of the Earthquake Sequence and Indications for Contemporary Arc-Parallel Extension to the Hellenic Arc. Applied Sciences [Internet]. 2022;12(6):2815.

16th International Congress of the Geological Society of Greece
17-19 October, 2022 - Patras, Greece
Bulletin of the Geological Society of Greece, Sp. Publ. 10
Ext. Abs. GSG2022-281

Site-Effect Studies Through the Joint Inversion and Interpretation of Earthquake and Noise Data in South-Central Santorini Island

N. Chatzis[1], A. Castano[2], C. Papazachos[1], M. Ohrnberger[2], P. Chatzidimitriou[1], N. Theodoulidis[3], M. Anthymidis[1], Ch. Ventouzi[1]

(1) Department of Geophysics, Aristotle University of Thessaloniki, Thessaloniki, Greece, chatniko@geo.auth.gr (2) Institute of Geosciences, University of Potsdam, Potsdam, Germany (3) Institute of Engineering Seismology & Earthquake Engineering, Thessaloniki, Greece.

Site effects studies are widely used for the determination of the amplification of strong motion, thus contributing to the reliable seismic hazard assessment. Significant damage has been observed in the Santorini island by the large **M**7.5 1956 Amorgos earthquake, which occurred along the Santorini-Amorgos fault zone. The heaviest damage was observed at Oia, Fira, Imerovigli and Pirgos, with high marcoseismic intensities (VIII and VIII+) (Papazachos and Papazachou, 2003). The spatial distribution suggests that the damage pattern can be probably explained by the impact of topographic effects (Kkallas et al., 2018) due to the Santorini caldera, as well as the site-effects due to the contrast of the volcanic formations with the metamorphic basement. Site-effects can be directly estimated by seismological methods with the use of earthquake records, as well as with geophysical techniques e.g. with the use of surface-waves from passive (noise) and active sources or boreholes data. In this study we explore the applicability of the joint inversion and interpretation of noise and earthquake data for the site-effect determination along the central-southern part of the Santorini island.

Santorini is the most active volcano of the Aegean volcanic arc and part of the south Cycladic islands. The present shape of the island is a result of multiple volcanic eruptions and tectonic events. The main tectonic episodes took place during the Oligocene-Miocene, with and extensional phase along a WNW-ESE direction which continued and evolved to the present NW-SE extension (Mercier et al., 1989; Bohnhoff et al., 2006; Jolivet et al., 2013). These tectonic events shaped the metamorphic basement of the island, by forming deep basins, where volcanic formations were deposited. Volcanic activity started before ~650ka, mostly with lava flows in the south-west part of the island. Then, the volcanic activity continued during the first and the second explosive cycles (360-3.6ka) and pyroclastic deposits were produced by large explosive eruptions, many of which are considered to be of Plinian intensity (Druitt et al., 1999). The latest large eruption of the second cycle took place during the Bronze Age (~1560BCE, Ehrlich et al., 2021) and produced pyroclastic deposits above the upper-most layers. This eruption is also known as the Minoan eruption. During these explosive cycles, parts of the central island collapsed and formed the present shape of the caldera (Druitt, 2014).

The present work focuses on site-effects studies, employing the joint-inversion of earthquake and noise data for the 1D shear-waves velocity model estimation at selected sites in the south-central part of Santorini island. A large number (>300) of single-station noise data were collected and the Horizontal to Spectral Noise Ratio (HVSR, Nakamura, 1989) curves were computed for each site. Noise array (Foti et al., 2017) and Multichannel Analysis of Surface Waves, MASW (Park et al., 1999), measurements were performed at four sites for the dispersion curve computation with the use of the High-Resolution Frequency-Wavenumber (HRFK) and Frequency-Wavenumber (FK) methods (Capon, 1969), respectively, as implemented by the Geopsy software (www.geopsy.org). Also, a temporal seismological network was installed at these 4 sites, with Guralp-40T (30sec) 3-component sensors and RefTek130 digitizers for the collection of earthquake records. The Standard Spectral Ratio, SSR (Borcherdt, 1970), method was applied at these records to determine the empirical transfer function (SSR) curves. Finally, a joint Monde Carlo (Wathelet, 2008) inversion of the dispersion and the SSR curves was performed for the 1D shear-waves velocity model estimation with the implementation of the external module of the Dinver module included in the Geopsy software package. The reliability of the inversion results was validated by the use of the simulated Annealing (Kirkpatrick et al., 1983) inversion approach.

Prominent maximum amplitude peaks (HVSR amplitude >5, e.g., Fig. 1 right) are observed in the HVSR curves, with fundamental frequencies in the range of 0.7-2 Hz (locally >2Hz, close to basement outcrops) in the south-central Santorini island. We assume that this pattern is due to the high impedance contrast between the pyroclastic deposits and the metamorphic basement. This is also evidenced by the geological stratigraphy of the caldera walls in the area of Athinios, as well as two deep boreholes (>200m), in which the contact of the pyroclastic deposits with the metamorphic basement is well observed. To the north (Fira and Monolithos) and to the south-west (Akrotiri) more complex HVSR curves are observed, and a decrease of the maximum amplitude is evidenced. For that reason, the HVSR data in these areas cannot be explained by the simple pyroclastics-basement structural model. The SSR curves also show this high velocity contrast between the pyroclastic deposits above the basement (Fig. 1 left), that it is also observed in the HVSR curve (Fig. 1 right). Moreover, they also show amplifications at higher frequencies (~10Hz), due to a second impedance contrast inside the pyroclastic formations, such as the contact between the Minoan and the lower pyroclastic deposits. Joint inversion results of the dispersion and SSR curves show 1D models with moderate shear-waves velocities (~600m/sec) and very low

densities (~1350 Kg/m^3) for the pyroclastic deposits above the metamorphic basement, which exhibits very high shear-wave velocities (>2500m/sec) and densities (~2500Kg/m^3). These results show that the high impedance contrast is due to the moderate-velocities and low-densities of the pyroclastic deposits above the high-velocity/high-density metamorphic basement in the central-south Santorini island. These findings are in very good agreement with the results of Tzanis et al. (2019), who proposed low densities for the upper pyroclastic layers from both gravity and rock sample data.

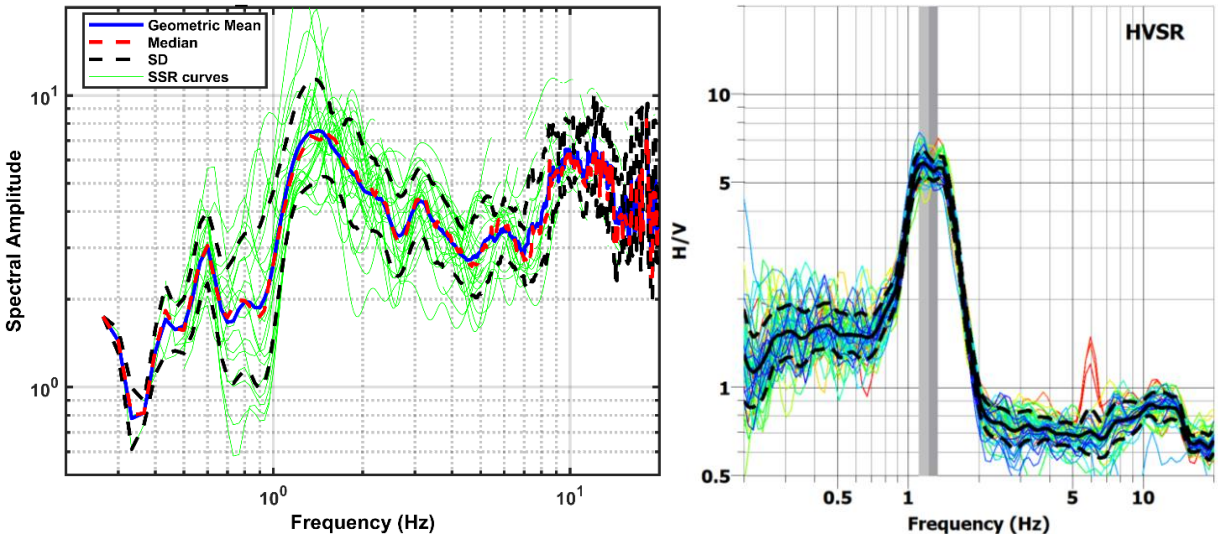

Figure 1. SSR (left) and HVSR (right) curves in Megalochori site.

Acknowledgements

This research was co-financed by Greece and the European Union (European Social Fund- ESF) through the Operational Programme «Human Resources Development, Education and Lifelong Learning» in the context of the project "Strengthening Human Resources Research Potential via Doctorate Research" (MIS-5000432), implemented by the State Scholarships Foundation (IKY), and the Hellenic Foundation for Research and Innovation (HFRI) under the "First Call for HFRI Research Projects to support Faculty members and Researchers and the procurement of high-cost research equipment grant" (Project Number: 2924, Acronym PROTECTANT). We would like to thank K. Polydoropoulos and I. Grendas for their assistance in HVSR data collection.

References

Bohnhoff, M., Rische, M., Meier, T., Becker, D., Stavrakakis, G., Harjes, H. P., 2006. Microseismic activity in the Hellenic Volcanic Arc, Greece, with emphasis on the seismotectonic setting of the Santorini–Amorgos zone. Tectonophysics, 423(1-4), 17-33.

Borcherdt, R. D., 1970. Effects of local geology on ground motion near San Francisco Bay. Bulletin of the Seismological Society of America, 60(1), 29-61.

Capon, J., 1969. High-resolution frequency-wavenumber spectrum analysis. Proceedings of the IEEE, 57(8), 1408-1418.

Druitt, T. H. (2014). New insights into the initiation and venting of the Bronze-Age eruption of Santorini (Greece), from component analysis. Bulletin of Volcanology, 76(2), 1-21.

Druitt, T. H., Edwards, L., Mellors, R. M., Pyle, D. M., Sparks, R. S. J., Lanphere, M., Davies, M., Barreirio, B., 1999. Santorini volcano. Geological Society Memoir, 19.

Ehrlich, Y., Regev, L., Boaretto, E., 2021. Discovery of annual growth in a modern olive branch based on carbon isotopes and implications for the Bronze Age volcanic eruption of Santorini. Scientific reports, 11(1), 1-11.

Foti, S., Hollender, F., Garofalo, F., Albarello, D., Asten, M., Bard, P. Y., ..., Socco, V., 2018. Guidelines for the good practice of surface wave analysis: a product of the InterPACIFIC project. Bulletin of Earthquake Engineering, 16(6), 2367-2420.

Jolivet, L., Faccenna, C., Huet, B., Labrousse, L., Le Pourhiet, L., Lacombe, O., ..., Driussi, O., 2013. Aegean tectonics: Strain localisation, slab tearing and trench retreat. Tectonophysics, 597, 1-33.

Kirkpatrick, S., Gelatt Jr, C.D., Vecchi, M. P. (1983). Optimization by simulated annealing. science, 220(4598), 671-680.

Kkallas, C., Papazachos, C., Skarlatoudis, A., Anthymidis, M., Ventouzi, C., 2018. Topographic amplification effects on seismic motions: the case of the large (M=7.4) 1956 Amorgos earthquake and its impact in the area of Santorini, 16th Eur. Conf. Earth. Eng., paper 10430, Thessaloniki, 18-21 June.

Mercier, J.L., Sorel, D., Vergely, P., Simeakis, K., 1989. Extensional tectonic regimes in the Aegean basins during the Cenozoic. Basin research, 2(1), 49-71.

Nakamura, Y., 1989. A method for dynamic characteristics estimation of subsurface using microtremor on the ground surface. Railway Technical Research Institute, Quarterly Reports, 30(1).

Papazachos, B.C., Papazachou, C., 2003. The earthquakes of Greece. Ziti publications, Thessaloniki, Greece, 286 pp. (in Greek).

Park, C.B., Miller, R.D., Xia, J., 1999. Multichannel analysis of surface waves. Geophysics, 64(3), 800-808.

Tzanis, A., Chailas, S., Sakkas, V., Lagios, E., 2020. Tectonic deformation in the Santorini volcanic complex (Greece) as inferred by joint analysis of gravity, magnetotelluric and DGPS observations. Geophysical Journal International, 220(1), 461-489.

Wathelet, M, 2008. An improved neighborhood algorithm: Parameter conditions and dynamic scaling. Geophysical Research Letters 35.9.

16th International Congress of the Geological Society of Greece

17-19 October, 2022 - Patras, Greece

Bulletin of the Geological Society of Greece, Sp. Publ. 10

Ext. Abs. GSG2022-284

1981-2022: 40 years of seismological investigations in the Gulf of Corinth and surrounding areas (Central Greece).

Panayotis Papadimitriou[1], Andreas Karakonstantis[1], Vasilis Kapetanidis[1], George Kaviris[1] and Ioannis Kassaras[1, †]

(1) Department of Geology and Geoenvironment, National and Kapodistrian University of Athens, Athens, Greece

The Gulf of Corinth has been identified as one of the faster expanding (1.0 to 1.5 cm/year of ~north-south extension) and most seismically active continental rifts around the world, characterized by normal faulting in an approximate E-W direction (Makropoulos and Burton, 1981; Rigo et al., 1996; Papadimitriou et al., 2020). The most active normal faults of the Gulf are dipping north, resulting in a long-term subsidence of the northern coast and an upward displacement of the main footwalls, forming an asymmetrical rift structure (Armijo et al., 1996). The area of study is dominated by Alpine Carbonate formations of the H1 (External Hellenides Platform) and H2 (Cyclades-Pindus Ocean crust) terrains, and Plio-quaternary sediments in the northern shores of Peloponnese. The subsiding Hellenides limestone nappes to the north of the gulf are outcropping in the majority of sites, whereas to the south, these formations are mostly covered by a conglomerate layer of several hundreds of meters thickness that outcrops only on the footwall of the southern active faults (Armijo et al., 1996; Cornet et al., 2004).

In the eastern part of the Gulf, the Cornet telemetric seismological network, the first digital permanent network in Greece, was operational for 10 years, since 1995, by the Seismological Laboratory of the Section of Geophysics – Geothermics of the National and Kapodistrian University of Athens (SL-NKUA) (Kaviris, 2003; Kaviris et al., 2007; Papadimitriou et al., 2010). The area was chosen due to its vicinity to destructive earthquakes, the most recent being the 1981 Alkyonides earthquake sequence (Jackson et al., 1982), as well as high seismicity rates. The relatively small distance between the Alkyonides Gulf and Athens makes the Gulf a source of seismic risk for the capital of Greece.

In the western part of the Gulf, in the early 2000s, the Corinth Rift Laboratory network (CRLnet) was established, covering a 30 km × 30 km area (Cornet et al., 2004). CRL is one of the Near-Fault Observatories (NFO) of the European Plate Observing System (EPOS), and the only one with an international status. It is administered and maintained by the Centre National de la Recherche Scientifique (France), the National and Kapodistrian University of Athens (Greece), the University of Patras (Greece) and the National Observatory of Athens (Greece), with the participation of Charles University Prague (Czech Republic). The western Gulf of Corinth is characterized by high level of seismicity during the instrumental era (Makropoulos et al., 2012).

In the present study, the seismic activity during the last 40 years (1981-2021) is reviewed. Specifically, the results of the earthquake sequences of moderate and strong earthquakes are presented, along with certain moderate intermediate-depth (H≥40 km) earthquakes, such as:

- The 1981 Alkyonides earthquake sequence, with three major events i.e., the 24 February (M=6.7), the 25 February (M=6.4) and the 4 March, 1981 (M=6.3) major events (Jackson et al., 1982; Papazachos et al., 1983),
- The Ms=5.9 Galaxidi earthquake, which occurred on 18 November 1992 (Hatzfeld et al., 1996),
- The Ms=6.2 Aigion earthquake of 15 June 1995 (Bernard et al. 1997),
- The January 2010, Mw 5.2–5.3 Efpalio doublet (Kapetanidis and Papadimitriou 2011; Sokos et al. 2012),
- The 2020 Perachora peninsula earthquake sequence (East Corinth Rift, Greece) (Michas et al., 2022),
- The 2020-2021 Psathopyrgos-Trizonia seismic crisis (Kaviris et al., 2021).

It is demonstrated that the Corinth Gulf exhibits high rates of seismic activity in certain locations, while remaining unbroken in others. The areas of low activity are likely to host sources of upcoming moderate to strong events. Both parts of the Gulf are active, with the more intense microseismicity occurring at the western part, which is frequented by the occurrence of seismic swarms, such as the 2003–2004 offshore WGoC (Duverger et al., 2015), the 2013 Helike (Kapetanidis et al., 2015; Mesimeri et al., 2016) and the 2015 Malamata (De Barros et al., 2020) swarms. However, the largest events of the last 40 years have occurred at the eastern part, during the 1981 Alkyonides earthquake sequence.

The dense local network at the western part of the Gulf of Corinth permitted the conduction of detailed upper-crust shear-wave splitting studies (Kaviris et al., 2017, 2018). The results revealed a dominant WNW – ESE mean anisotropy direction, in agreement with the orientation of the maximum horizontal stress component (σ_{Hmax}). In sites with deviating NE-SW mean fast shear-wave polarization directions, mainly at the northern coast of the Gulf, seismic anisotropy could reveal the existence of faults or structures with similar orientation, that overpower the regional stress field.

References

Armijo, R., Meyer, B., King, G.C.P., Rigo, A., Papanastassiou, D., 1996. Quaternary evolution of the Corinth Rift and its

implications for the Late Cenozoic evolution of the Aegean. Geophys. J. Int. 126, 11–53. https://doi.org/10.1111/j.1365-246X.1996.tb05264.x
Bernard, P., Briole, P., Meyer, B., Gomez, J., Tiberi, C., Berge, C., Cattin, R., Hatzfeld, D., Lachet, C., Lebrun, B., Deschamps, a., Courboulex, F., Larroque, C., Rigo, a., Massonnet, D., Papadimitriou, P., Kassaras, J., Diagourtas, D., Makropoulos, K., Veis, G., Papazisi, E., Mitsakaki, C., Karakostas, V., Papadimitriou, E., 1997. The Ms=6.2, June 15, 1995 Aigion earthquake (Greece): evidence for low-angle normal faulting in the Corinth rift. J. Seismol. 1, 131–150.
Cornet, F.H., Doan, M.L., Moretti, I., Borm, G., 2004. Drilling through the active Aigion Fault: the AIG10 well observatory. Comptes Rendus Geosci. 336, 395–406. https://doi.org/10.1016/j.crte.2004.02.002
De Barros, L., Cappa, F., Deschamps, A., Dublanchet, P., 2020. Imbricated Aseismic Slip and Fluid Diffusion Drive a Seismic Swarm in the Corinth Gulf, Greece. Geophys. Res. Lett. 47, e2020GL087142. https://doi.org/10.1029/2020GL087142
Duverger, C., Godano, M., Bernard, P., Lyon-Caen, H., Lambotte, S., 2015. The 2003-2004 seismic swarm in the western Corinth rift: Evidence for a multiscale pore pressure diffusion process along a permeable fault system. Geophys. Res. Lett. 42, 7374–7382. https://doi.org/10.1002/2015GL065298
Hatzfeld, D., Kementzetzidou, D., Karakostas, V., Ziazia, M., Nothard, S., Diagourtas, D., Deschamps, A., Karakaisis, G., Papadimitriou, P., Scordilis, M., Smith, R., Voulgaris, N., Kiratzi, S., Makropoulos, K., Bouin, M.P., Bernard, P., 1996. The Galaxidi earthquake of 18 November 1992: A possible asperity within the normal fault system of the Gulf of Corinth (Greece). Bull. Seismol. Soc. Am. 86, 1987–1991.
Jackson, J.A., Gagnepain, J., Houseman, G., King, G.C.P., Papadimitriou, P., Soufleris, C., Virieux, J., 1982. Seismicity, normal faulting, and the geomorphological development of the Gulf of Corinth (Greece): the Corinth earthquakes of February and March 1981. Earth Planet. Sci. Lett. 57 (2), 377-397. https://doi.org/10.1016/0012-821X(82)90158-3
Kapetanidis, V., Deschamps, A., Papadimitriou, P., Matrullo, E., Karakonstantis, A., Bozionelos, G., Kaviris, G., Serpetsidaki, A., Lyon-Caen, H., Voulgaris, N., Bernard, P., Sokos, E., Makropoulos, K., 2015. The 2013 earthquake swarm in Helike, Greece: seismic activity at the root of old normal faults. Geophys. J. Int. 202, 2044–2073. https://doi.org/10.1093/gji/ggv249
Kapetanidis, V., Papadimitriou, P., 2011. Estimation of arrival-times in intense seismic sequences using a Master-Events methodology based on waveform similarity. Geophys. J. Int. 187, 889–917. https://doi.org/10.1111/j.1365-246X.2011.05178.x
Karakostas, V., Mirek, K., Mesimeri, M., Papadimitriou, E., Mirek, J., 2017. The Aftershock Sequence of the 2008 Achaia, Greece, Earthquake: Joint Analysis of Seismicity Relocation and Persistent Scatterers Interferometry. Pure Appl. Geophys. 174, 151–176. https://doi.org/10.1007/s00024-016-1368-y
Kaviris, G., 2003. Study of Seismic Source Properties of the Eastern Gulf of Corinth. Ph D. Thesis, Geophysics-Geothermics Department, Faculty of Geology, University of Athens, Greece, 2003 (in Greek).
Kaviris, G., Elias, P., Kapetanidis, V., Serpetsidaki, A., Karakonstantis, A., Plicka, V., De Barros, L., Sokos, E., Kassaras, I., Sakkas, V., Spingos, I., Lambotte, S., Duverger, C., Lengliné, O., Evangelidis, C.P., Fountoulakis, I., Ktenidou, O.-J., Gallovič, F., Bufféral, S., Klein, E., Aissaoui, E.M., Scotti, O., Lyon-Caen, H., Rigo, A., Papadimitriou, P., Voulgaris, N., Zahradnik, J., Deschamps, A., Briole, P., Bernard, P., 2021. The Western Gulf of Corinth (Greece) 2020–2021 Seismic Crisis and Cascading Events: First Results from the Corinth Rift Laboratory Network. Seism. Rec. 1, 85–95. https://doi.org/10.1785/0320210021
Kaviris, G., Millas, C., Spingos, I., Kapetanidis, V., Fountoulakis, I., Papadimitriou, P., Voulgaris, N., Makropoulos, K., 2018. Observations of shear-wave splitting parameters in the Western Gulf of Corinth focusing on the 2014 M w = 5.0 earthquake. Phys. Earth Planet. Inter. 282, 60–76. https://doi.org/10.1016/j.pepi.2018.07.005
Kaviris, G., Papadimitriou, P., Makropoulos, K., 2007. Magnitude Scales in Central Greece. Bull. Geol. Soc. Greece 40, 1114–1124. https://doi.org/10.12681/bgsg.16838
Kaviris, G., Spingos, I., Kapetanidis, V., Papadimitriou, P., Voulgaris, N., Makropoulos, K., 2017. Upper crust seismic anisotropy study and temporal variations of shear-wave splitting parameters in the western Gulf of Corinth (Greece) during 2013. Phys. Earth Planet. Inter. 269, 148–164. https://doi.org/10.1016/j.pepi.2017.06.006
Makropoulos, K., Kaviris, G., Kouskouna, V., 2012. An updated and extended earthquake catalogue for Greece and adjacent areas since 1900. Nat. Hazards Earth Syst. Sci. 12, 1425–1430. https://doi.org/10.5194/nhess-12-1425-2012
Makropoulos, K.C., Burton, P.W., 1981. A catalogue of seismicity in Greece and adjacent areas. Geophys. J. Int. 65, 741–762. https://doi.org/10.1111/j.1365-246X.1981.tb04881.x
Mesimeri, M., Karakostas, V., Papadimitriou, E., Schaff, D., Tsaklidis, G., 2016. Spatio-temporal properties and evolution of the 2013 Aigion earthquake swarm (Corinth Gulf, Greece). J. Seismol. 20, 595–614. https://doi.org/10.1007/s10950-015-9546-4
Michas, G., Kapetanidis, V., Spingos, I., Kaviris, G., Vallianatos, F., 2022. The 2020 Perachora peninsula earthquake sequence (East Corinth Rift, Greece): spatiotemporal evolution and implications for the triggering mechanism. Acta Geophys. https://doi.org/10.1007/s11600-022-00864-x
Papadimitriou, P. et al., 2020. The 25 October 2018 Zakynthos (Greece) earthquake: seismic activity at the transition between a transform fault and a subduction zone. Geophys J Int., 225(1), 15-36. https://doi.org/10.1093/gji/ggaa575
Papadimitriou, P., Kaviris, G., Karakonstantis, A., Makropoulos, K, 2010. The Cornet seismological network: 10 years of operation, recorded seismicity and significant applications. Ann. Geol Des Pays Hell., 45, 193–208.
Papazachos, B. C., Panagiotopoulos, D. G., Tsapanos, T. M., Mountrakis, D. M. and Dimopoulos, G. Ch., 1983. A study of the 1980 summer seismic sequence in the Magnesia region of central Greece. Geophysical J. R. Astron. Society, 75, 155-168, 1983.
Rigo, A., Lyon-Caen, H., Armijo, R., Deschamps, A., Hatzfeld, D., Makropoulos, K., Papadimitriou, P., Kassaras, I., 1996. A microseismic study in the western part of the Gulf of Corinth (Greece): Implications for large-scale normal faulting mechanisms. Geophys. J. Int. 126, 663–688. https://doi.org/10.1111/j.1365-246X.1996.tb04697.x
Serpetsidaki, A., Elias, P., Ilieva, M., Bernard, P., Briole, P., Deschamps, A., Lambotte, S., Lyon-Caen, H., Sokos, E., Tselentis, G.A., 2014. New constraints from seismology and geodesy on the Mw = 6.4 2008 Movri (Greece) earthquake: Evidence for a growing strike-slip fault system. Geophys. J. Int. 198, 1373–1386. https://doi.org/10.1093/gji/ggu212
Serpetsidaki, A., Sokos, E., Tselentis, G.-A., 2010. Study of the 2Nd December 2002 Vartholomio Earthquake (Western Peloponnese) M5.5 Aftershock Sequence. Bull. Geol. Soc. Greece 43, 2174. https://doi.org/10.12681/bgsg.11408
Sokos, E., Zahradník, J., Kiratzi, A., Janský, J., Gallovič, F., Novotny, O., Kostelecký, J., Serpetsidaki, A., Tselentis, G.A., 2012. The January 2010 Efpalio earthquake sequence in the western Corinth Gulf (Greece). Tectonophysics 530–531, 299–309. https://doi.org/10.1016/j.tecto.2012.01.005

16th International Congress of the Geological Society of Greece
17-19 October, 2022 - Patras, Greece
Bulletin of the Geological Society of Greece, Sp. Publ. 10
Ext. Abs. GSG2022-298

Preliminary Results For The Near-Surface Geophysical Structure In Urban Environment By Ambient Noise Tomography: Integrating Two Ambient Noise Arrays For The Metropolitan Area Of Thessaloniki (Northern Greece)

M. Anthymidis[1], C. Papazachos[1], N. Chatzis[1], C. Ventouzi[1]

(1) Aristotle University of Thessaloniki, School of Geology, Department of Geophysics, Thessaloniki, Greece, manthymi@geo.auth.gr.

Implementation of ambient noise array tomography is feasible in the challenging conditions of urban environments, providing useful insights for the geophysical structure of the near-surface subsurface (top 100-200m).

Introduction

Near-surface geophysical structure is usually one of the most important information for earthquake engineering and engineering seismology applications. Typical geotechnical surveys and active geophysical measurements (e.g., boreholes, seismic refraction, etc.) provide reliable estimates for various properties of the subsurface structure, although their application confronts several problems in urban areas. Some of them are the high application cost, the necessity of considerable human resources, the inability to use high energy active sources and the bureaucracy needed to get the appropriate permissions, especially in densely populated cities.

An alternative approach to evaluate the 2D/3D geophysical subsurface structure of the uppermost layers in an urban environment is based on the acquisition and processing of ambient noise measurements with the installation of suitable arrays of recording stations. In particular, part of the Green's function can emerge from the cross-correlation of ambient noise data obtained from two spatially separated recording stations (Gouedard et al., 2008). Considering that ambient noise wavefield is dominated by surface waves (Bonnefoy-Claudet et al., 2006), the cross-correlation traces can be exploited to derive information about their travel-times at different frequencies. Thus, the application of a tomographic approach on the travel-time datasets provides the spatial distribution of the surface waves phase or group velocity for the same frequencies. The abovementioned procedure is usually referred as ambient noise array tomography and it has been implemented during the last decades for the evaluation of the geophysical subsurface structure in a variety of spatial scales and environments, ranging from deep crustal studies to near-surface (geotechnical) surveys in volcanic, rural and urban environments.

In the present study, we employed the ambient noise array tomography to determine the shallow geophysical structure, integrating two array configurations temporarily installed at the challenging and demanding conditions of the city of Thessaloniki city (Northern Greece, Fig. 1). The geological setting exhibits a rather 2D pattern, where the bedrock outcrop is detected in the NE part of the study area (Fig. 1a) and is rapidly dipping to the SW, possibly exceeding the depth of 200m near the city's coastline (Anastasiadis et al. 2001; Panou et al 2005; Skarlatoudis et al. 2010).

Data Acquisition

Two ambient noise arrays operated during different time periods, with a different total number of deployed stations and spatial extent. More specifically, for the array geometry in the SE part of the study area (red circles in Fig. 1) 34 stations were installed, providing continuous ambient noise recordings for almost one month. The minimum and maximum distance of the installed stations was 50 and 900m, respectively. The second array in the NW part of the study area (green circles in Fig. 1) incorporated the deployment of 30 stations and operated for a larger time span, recording continuously ambient noise for almost three months. The spatial extend of this array covered a wider area, with the minimum and maximum inter-station distance ranging between 100 and 1300m, respectively.

The recording stations were installed inside buildings for both arrays, to prevent the possible contamination of the seismic signals from weather conditions and anthropogenic intervention. The acquisition of ground motion data was performed with 3-component, broadband, seismometers, all equipped with 24-bit digitizers, whereas the sample rate was set to 100Hz.

Processing of Ambient Noise Data

The processing of the ambient noise data was divided in two different phases. In the first phase, we calculated the HVSR (Horizontal to Vertical Spectral Ratio) curves (Nakamura 1989) at every recording station position for both arrays to recover the fundamental resonance frequency (f_0) for the upper sedimentary layers of the subsurface (Hagshenas et al. 2008). The f_0 distribution provided a preliminary and qualitative estimation of the sediment thickness (above bedrock), thus allowing to roughly access the subsurface structure in the study area. The second phase concerned the implementation of ambient noise tomography and consisted of three main steps, namely: a) the cross-correlation of the corresponding vertical and transverse components of the ground motion for all the available station pairs of the arrays, b) the computation

of the surface waves travel-times for specific frequencies and, c) the derivation of group velocity maps, applying an adjusted tomographic approach on the travel-time datasets. This approach incorporated approximate Fresnel volumes for the ray paths (Cerveny and Soares 1999), smoothing and damping constraints to stabilize the inversion, and an iterative procedure to discard outliers from the inversion.

An example of the Rayleigh group slowness distribution for the frequency of 4Hz in the study area is shown in Fig. 1b. Low group slowness values (high group velocities) are observed in the NE part, following the surficial contact of the bedrock and sedimentary formations. The group slowness values gradually increase to the SW (decrease of group velocities), where a sediment thickening is expected. The determined group slowness maps are in very good agreement with the available geological and geotechnical information for the study area, as well as with the f_0 spatial variability.

Conclusions

In the present study we implement the ambient noise tomography in an urban environment and on geotechnical scale (spatial extend of few hundred meters) to evaluate the surficial geophysical structure of the subsurface. In addition, we used the HVSR method to the ambient noise recordings to estimate the response of the sedimentary cover in the study area, and roughly assess the bedrock depth and geometry. The results are in good agreement with the available information for local geology, suggesting that the application of ambient noise tomography is feasible in the demanding and challenging conditions of an urban area, such as Thessaloniki.

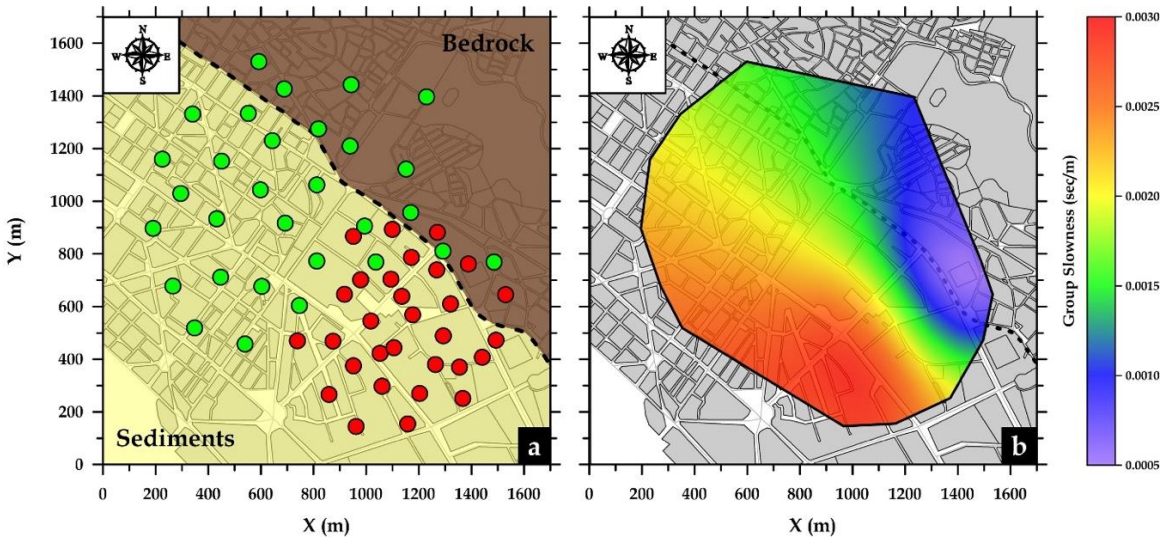

Figure 1. (a) Ambient noise recording stations from two ambient noise arrays (green and red circles, respectively) in the study area, superimposed on the geological map, which indicates the contact of bedrock formations and sedimentary deposits at the surface (dashed line). (b) Rayleigh wave group slowness distribution for the frequency of 4Hz in the study area.

Acknowledgements

The present work has been supported by the Hellenic Foundation for Research and Innovation (H.F.R.I.) under the "1st Call for H.F.R.I. research projects to support faculty members & researchers & the procurement of high-cost research equipment grant" (Project PROTECTANT, Number 2924).

References

Anastasiadis, A., Raptakis, D., Pitilakis K., 2001. Thessaloniki's detailed microzoning: Subsurface structure as basis for site response analysis. Pure Appl. Geophys., 158, 2597–2633.

Bonnefoy-Claudet, S., Cotton, F., Bard P.-Y., 2006. The nature of noise wavefield and its applications for site effects studies. A literature review. Earth Sci. Rev., 79, 205–227.

Cerveny, V., Soares J. E. P., 1992. Fresnel volume ray tracing. Geophys. 57, 902–915.

Gouédard, P., L., Stehly, F., Brenguier, M., Campillo, Y., Colin De Verdière, E., Larose, L., Margerin, P., Roux, F. J., Sánchez-Sesma, N. M., Shapiro, Weaver R. L., 2008. Cross-correlation of random fields: Mathematical approach and applications. Geophys. Prospect., 56, 375–393.

Haghshenas, E., Bard, P.-Y., Theodulidis N., 2008. Empirical evaluation of microtremor H/V spectral ratio. Bull. Earthquake Eng., 6, 75-108.

Nakamura Y., 1989. A method for dynamic characteristics estimation of subsurface using microtremor on the ground surface. Q. Rep. Railw. Tech. Res. Inst., 30, 25–33.

Panou, A., Theodulidis, N., Hatzidimitriou, P., Stylianidis, K., Papazachos C., 2005. Ambient noise horizontal-to-vertical spectral ratio in site effects estimation and correlation with seismic damage distribution in urban environment: The case of the city of Thessaloniki (Northern Greece). Soil Dyn. Earthquake Eng., 25, 261–274.

Skarlatoudis, A., Papazachos, C., Theodoulidis, N., Kristek, J., Moczo P., 2010. Local site-effects for the city of Thessaloniki (N. Greece) using a 3-D finite-difference method: A case of complex dependence on source and model parameters. Geophys. J. Int., 182, 279–298.

16th International Congress of the Geological Society of Greece
17-19 October, 2022 - Patras, Greece
Bulletin of the Geological Society of Greece, Sp. Publ. 10
Ext. Abs. GSG2022-301

The non-Gaussian characteristics of Seismic S-Coda Waves on Mars in terms of Tsallis Statistics.

M. Bantouvaki[1], F. Vallianatos[1,2], F. Karakostas[3]

(1) National and Kapodistrian University of Athens, Faculty of Geology and Geoenvironment, Department of Geophysics–Geothermics, University Campus, Panepistimiopolis – Athens 157 84, Greece, melibanto@gmail.com (2) Institute of Physics of Earth's Interior and Geohazards, UNESCO Chair on Solid Earth Physics & Geohazards Risk Reduction, Hellenic Mediterranean University Research Center, Crete, Greece (3) Istituto Nazionale di Geofisica e Vulcanologia, Via Donato Creti 12, Bologna (BO) 40100, Italy.

Research Highlights

The last decades a lot of progress has been made in studying planetary Physics based on the science of complexity and the application of generalized formalisms of statistical physics and entropy. The results of the present work suggests that the seismic S-coda waves recorded on Mars by NASA's InSight Mission stations, present increments that deviate from the Gaussian shape and their respective probability density function could be adequately described by a q-Gaussian. This observation implies that seismic S-coda wave complexity originating by multiscattering effects, can be described by Tsallis entropy terms (Tsallis, 2019, Tsallis and Brigatti, 2004).

Introduction

Investigation of the dynamical features of seismic waves is of fundamental importance since they could provide information on the statistical properties of the scatterers in the wave propagation path. The non-extensive statistical mechanics (NESM) seems to be a promising framework for studying complex earthquake systems that exhibit long-range interactions and memory effects. In this work, S-coda waves recorded on Mars are studied from the point of view of non-extensive statistical mechanics. Our aim is to demonstrate the applicability of non-extensive statistical mechanics to the fluctuations of S-coda amplitudes and to define the entropic q parameters obtained in the S-coda waves recorded by seismological stations on Mars (Clinton *et al*., 2021).

Methodology

We defined the increment function X(t)=V(t+1) −Vt, where V(t) is the measured ground velocity. We proceed by analyzing the normalized increments X(t) constructing the probability density function PDF p(x), where x =(X−<X>)/σ_X, σ_X being the standard deviation of X(t) and <X> the observed mean value on the same data set. The observed probability density function deviates from the standard Gaussian shape due to the existence of heavy tails and can be rather described by the q-Gaussian function of the form

$$p(x) = A[1 + B(q-1)x^2]^{-\frac{1}{q-1}} \qquad (1)$$

Results and Conclusions

The results of the present work suggest that the seismic S-coda waves increments deviate from the Gaussian shape and their respective probability density function p(x), could be adequately described by a q-Gaussian and thus presenting power-law tails with slope −2/ (q − 1). This observation implies that seismic S-coda wave complexity originating by multiscattering effects on Mars, can be described by Tsallis entropy, with the same way as it was discovered for Earth (Koutalonis *et al.,* 2019). An example is given in Fig.1a, b, c.

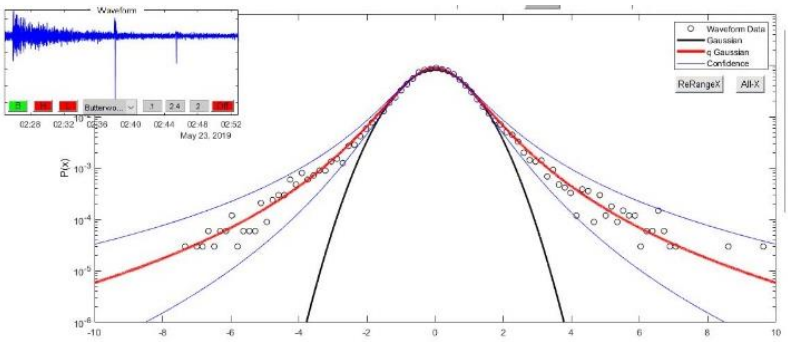

Event S0173a, Type Low Frequency, Quality A, BHE with q=1.48

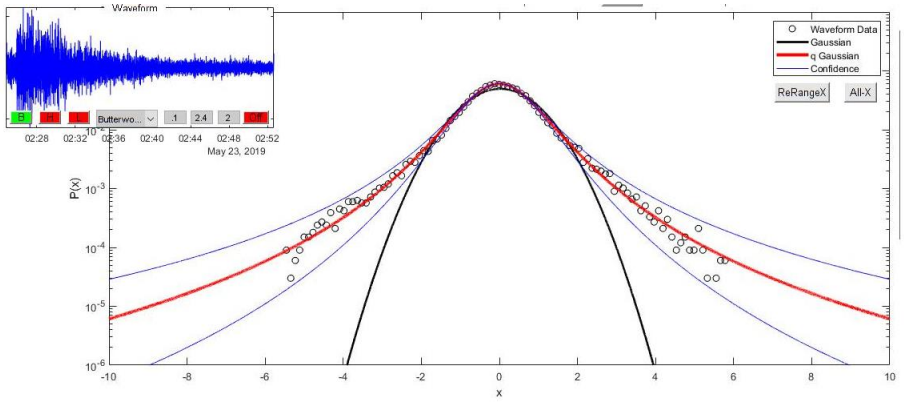

Event S0173a, Type Low Frequency, Quality A, BHN with q=1.40

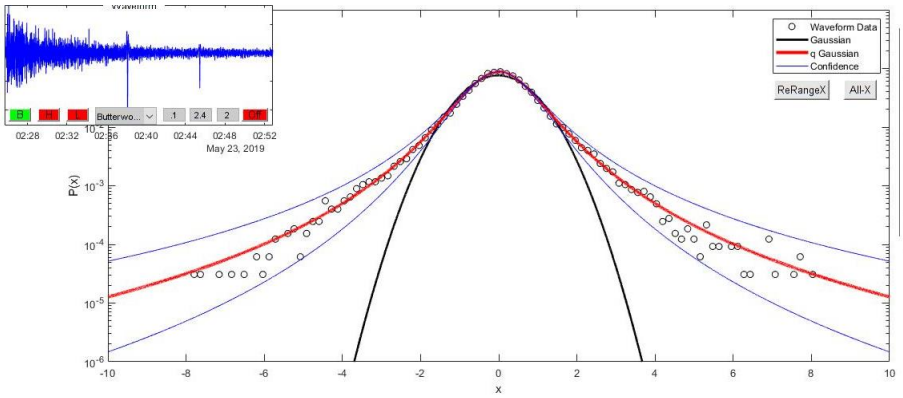

Event S0173a, Type Low Frequency, Quality A, BHZ with q=1.44

Figure 1. The incremental PDFs of all the components (a: BHE, b: BHN, c: BHZ) of the seismic S-coda waves generated by the event S0173a, Type Low Frequency, Quality A, as recorded from NASA's InSight Mission stations. The PDFs are fitted to Eq. (1) (Red line). The q-values are presented in the panels along with the 95% Confidence bounds (Blue lines) yielding an error of $\delta q \approx \pm 0.05$.

Acknowledgements

We acknowledge NASA, CNES, their partner agencies and Institutions (UKSA, SSO, DLR, JPL, IPGP-CNRS, ETHZ, IC, MPS-MPG) and the flight operations team at JPL, SISMOC, MSDS, IRIS-DMC and PDS for providing SEED SEIS data (Inshight Mars SEIS Data Service 2019, Inshight Marsquake Service 2021). We would also like to thank Ted Aspiotis for his MATLAB program, that we used for the analysis and Ioannis Spingos for his help with the data elaboration.

References

Clinton, J. F., Ceylan, S., van Driel, M., Giardini, D., Stähler, S. C., Böse, M., Stott, A. E., 2021. The Marsquake catalogue from InSight, sols 0–478. Physics of the Earth and Planetary Interiors, 310, 106595. https://doi:10.1016/j.pepi.2020.106595

InSight Mars SEIS Data Service. (2019). SEIS raw data, Insight Mission. IPGP, JPL, CNES, ETHZ, ICL, MPS, ISAE-Supaero, LPG, MFSC. https://doi.org/10.18715/SEIS.INSIGHT.XB_2016

InSight Marsquake Service (2021). Mars Seismic Catalogue, InSight Mission; V6 2021-04-01. ETHZ, IPGP, JPL, ICL, MPS, Univ. Bristol. doi:10.12686/a11

Karakostas, F., N. Schmerr, R. Maguire, Q. Huang, D. Kim, V. Lekic, L. Margerin, C. Nunn, S. Menina, T. Kawamura, et al., 2021. Scattering Attenuation of the Martian Interior through Coda-Wave Analysis, Bull. Seismol. Soc. Am. 111, 3035–3054, doi: 10.1785/0120210253

Koutalonis I., Vallianatos F., Observational evidence of non-extensive behavior of seismic coda waves, 2020. Physica A: Statistical Mechanics and Its Applications, 550 , https://doi.org/10.1016/j.physa.2020.124523

Tsallis, C. Introduction to Nonextensive Statistical Mechanics: Approaching a Complex World, Springer,New York, 2009

Tsallis, C., Brigatti, E., Nonextensive statistical mechanics: a brief introduction, 2004. Continuum Mechanics and Thermodynamics 16 , 223–235

16th International Congress of the Geological Society of Greece
17-19 October, 2022 - Patras, Greece
Bulletin of the Geological Society of Greece, Sp. Publ. 10
Ext. Abs. GSG2022-312

Local site effects investigation in Durres city (Albania) using ambient noise, after the Nov. 26, 2019 (Mw6.4) destructive earthquake

N. Theodoulidis[1], E. Dushi[2], L. Duni[2], I. Grendas[1], A. Panou[3], Hajrrulai A.[4], N. Kuka[2], R. Koci[2]

(1) Institute of Engineering Seismology and Earthquake Engineering, Thessaloniki (ITSAK), Greece, ntheo@itsak.gr (2) Department of Seismology, Institute of Geosciences, Polytechnic University Tirana, Albania (3) Geophysical Department, Aristotle University Thessaloniki, Greece (4) GeoSeis-IT Consulting

Research Highlights

- In this work fundamental frequencies and corresponding amplitudes are estimated for the Durres city (Albania) as well as site categorization classification (four zones) is proposed based on ambient noise measurements.

Site characterization of metropolitan areas, especially after an earthquake disaster, is of paramount importance for interpreting spatial damage distribution and take all those measures assuring realistic design actions to strengthen existing and construct new buildings. Such a case is the Durres city (Albania) that was hit by a disastrous earthquake in Nov. 26, 2019. (Mw6.4). A variety of damage in the city was observed though its similar source-to-city distance; this fact could be due either to different vulnerability of affected constructions or/and to spatial variation of strong ground motion in the city due to local site effects, with the latter factor to be deemed under investigation.

To this purpose, a first campaign for single station ambient noise measurements within the city was decided and planned a few months after the mainshock (Fig. 1). The reason for such a choice was based on the easiness and effectiveness to acquire ambient noise data - as a noninvasive approach - within built environment. Processing of the measurements were made using the widely applied Horizontal-to-Vertical Spectral Ratio (HVSR) method following the SESAME project (2004) guidelines. Their fundamental and dominant frequencies, f_o and f_d, respectively, as well as their corresponding amplitudes, A_o, and A_d, were calculated and related to the iso-depth contours of the investigated area. Based on the entire HVSR curve of all examined sites, a clustering of four categories exhibiting similar shapes and amplitudes were proposed for the Durres city (see Figs. 2, 3). This map could be utilized as a first level zonation of local site effect of the city. In addition, available dynamic properties of soil profiles in selected sites were validated based on 1D synthetic ambient noise data using the Hisada (1994, 1995) 1D simulation method and observed HVSRs close to the selected sites. The proposed in this study categorization of the expected similar local site effects can be used as a first level seismic microzonation of the Durres city. Certainly, corrections for 2D/3D effects on ground shaking must be applied for sites lying in the edges of the Durres basin.

Finally, HVSRs of 1D ambient noise synthetics in combination with actual HVSRs at the same sites, can effectively validate 1D geophysical profiles to be used as seismic response input to any earthquake excitation scenario. In the case of Durres city it seems that the 1D approximation is in general satisfactory. However, seismic site response corrections due to 2D/3D effects especially in the edge of the basin must be the goal for a more realistic assessment of future ground shaking in Durres.

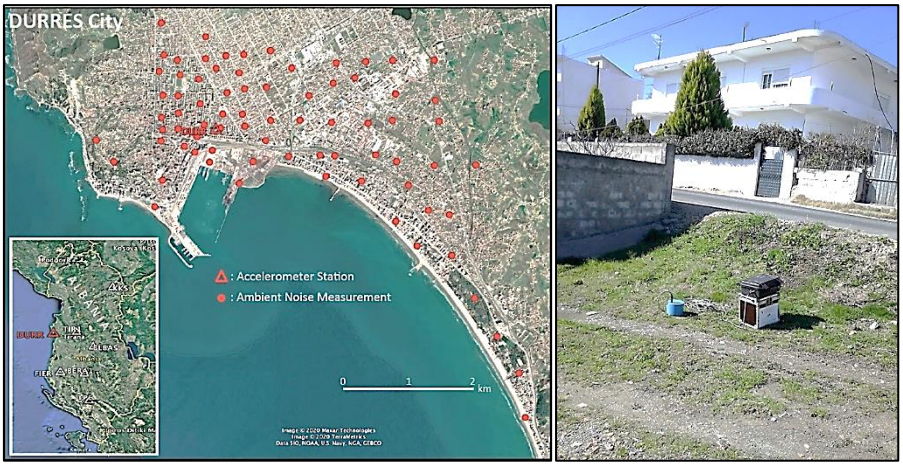

Figure 1: (left)Measurement points within the Durres city; (right) An example of a measurement site

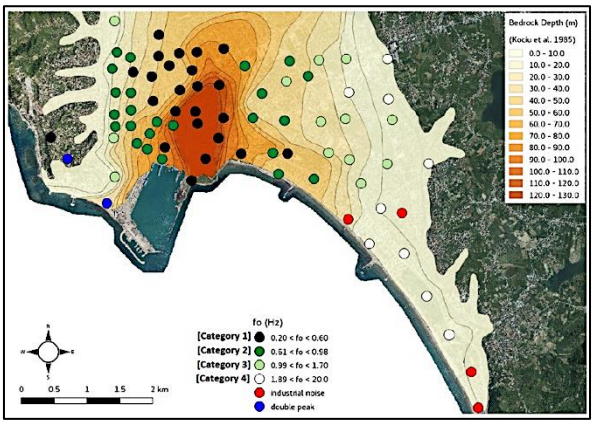

Figure 2: Spatial distribution of the four HVSR site categories in the Durres city together with iso-depth contours.

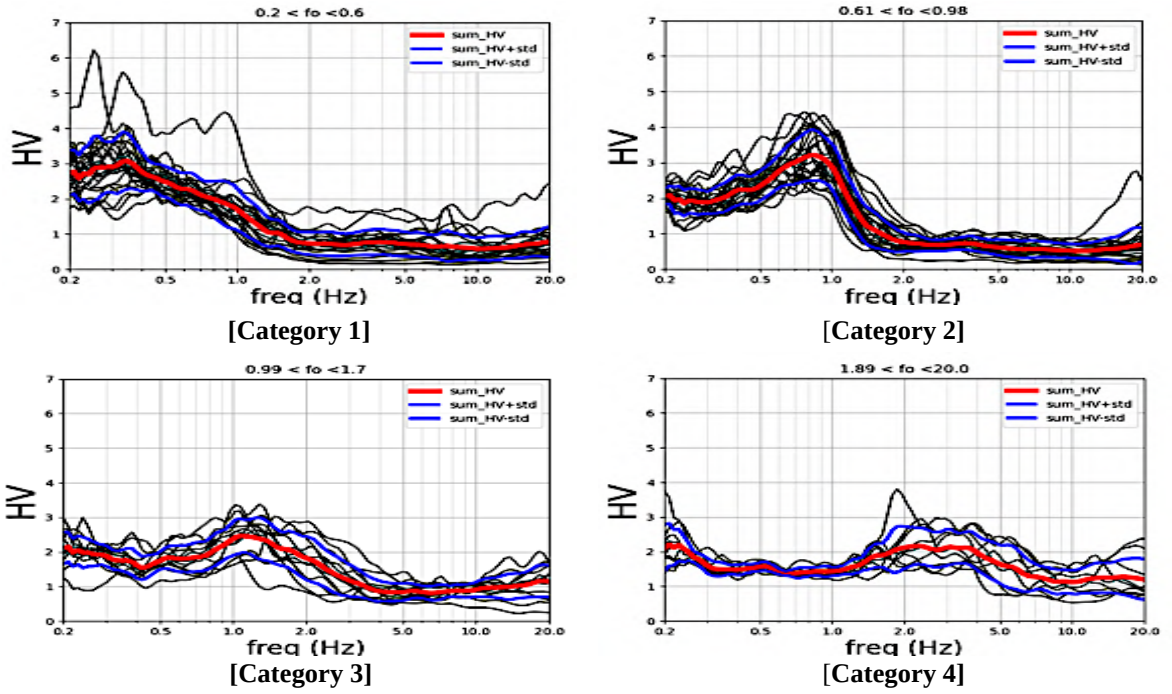

Figure 3: Four categories of HVSRs for the Durres city (average red line ± one standard deviation blue lines).

References

Arai H. and Tokimatsu K.(2005). S-wave velocity profiling by joint inversion of microtremor dispersion curve and horizontal-to-vertical (H/V) spectrum. Bull Seism. Soc Am 95: 1766-1778

Bard P-Y. and the SESAME Participants (2004). The SESAME project: an overview and main results, Proc. 13th WCEE, Paper No 2207.

Bard, P.-Y. (1999). "Microtremor Measurements: A tool for site effect estimation?", in the Effects of Surface Geology on Seismic Motion, (ed. Irikura, Kudo, Okada and Sasatani) Balkema, Rotterdam, 1251-1279.

Duni Ll., Theodoulidis N. (2019). Short note on the November 26, 2019, Durrës (Albania) M6.4 earthquake: Strong ground motion with emphasis in Durrës City. https://www.emsc-csem.org/Files/news/Earthquakes_reports/Short-Note_EMSC_31122019.pdf

Geopsy software [http://www.geopsy.org] , last accessed date: 30/8/2022

Hisada Y. (1994). An efficient method for computing Green's functions for a layered half-space with sources and receivers at close depths," Bull. Seism. Soc. Am., 84, 5, 1456-1472.

Hisada Y. (1995)."An efficient method for computing Green's functions for a layered half-space with sources and receivers at close depths (part 2), Bull. Seism. Soc. Am., 85, Issue 4, 1080-93, 1995.

Koçiu S, Sulstarova E, Aliaj Sh, Duni Ll, Peçi V, Konomi N, Dakoli H, Fuga I, Goga K, Zeqo A, Kapllani L, Kozmaj S, Lika M. (1985). Seismic microzonation of Durresi town, internal report, (in Albanian), IGEWE, Tirana, Albania.

SESAME Guidelines (2004) [http://sesame.geopsy.org/SES_Reports.htm]

16th International Congress of the Geological Society of Greece
17-19 October, 2022 - Patras, Greece
Bulletin of the Geological Society of Greece, Sp. Publ. 10
Ext. Abs. GSG2022-323

Seismic Hazard maps of Aitolo-Akarnania Prefecture based on Deterministic Seismic Hazard Methodology

E. Lyros[1], Z. Roumelioti[1], K. Nikolakopoulos[1], E. Sokos[1]
(1) Department of Geology, University of Patras, 26504 Rio, Patras, Greece, lyrosepam@upatras.gr.

Introduction

Aitolo-Akarnania prefecture, western Greece, is an area with strong earthquakes and large active fault systems. Seismic hazard assessment attracts the interest of the scientific community especially in earthquake pone areas where there are complex fault systems The most prominent fault systems in the area, are the Katouna sinistral strike slip fault and the Trichonis Lake normal fault system. Their proximity to large cities, and the lack of detailed information about their seismogenic potential, calls for a multiparametric research. Ideally this research will start with the quantification of fault movements, through a detailed GNSS study, and will continue with the assessment of their possible future ground motions. The traditional seismic hazard assessment methods suffer from large uncertainty and incompleteness problems. This paper summarizes the seismic hazard assessment methodology follow fault specific approaches where seismic sources are geologically constrained active faults. The main goal is the extraction of reliable results and to obtain a higher spatial resolution of hazard assessment in the examined area of Aitolo – Akarnania.

Data and Methods

Since 2013, the crustal deformation in Aitolo-Akarnania has been monitored by a dense GNSS Network (PPGNet), consisting of five stations, equipped with Leica and Septentrio receivers. The objective of this network is to define the rate of deformation across these two main fault systems. Data is recorded using two sampling frequencies, 1 Hz and 10Hz, producing hourly and daily files. Daily data is processed using Bernese GNSS Processing Software using final orbits of International GNSS Service. Double-difference solution is computed using phase measurements from the PPGNet network complemented by four stations from Athens' National Observatory GNSS network and six stations from METRICA network. The results show a NNE movement at PVOG station of 12 mm/y and a similar movement at RETS station of about 9 mm/y. This means that the Trichonis Lake normal fault system, located between these two stations, depicts a slip rate of 3 mm/y. KTCH and RGNI stations move eastwards at a velocity of about 5 mm/y due to the Katouna - Stamna fault system. Data from PPGNet has provided important results on crustal deformation in the area, i.e. slip rates have been attributed to specific fault systems (Lyros et al. 2021).

Different case studies were calculated for the faults of the research area by the use of the OpenQuake software (https://platform.openquake.org/). The hazard methodology goes as follows:

1. A place of interest was selected by adding a site location.
2. A hazard model was selected. Only models with data available at the point of interest are displayed.
3. An intensity measurement type was selected. Choices are PGA (peak ground acceleration) and SA 1s (spectral acceleration, with spectral period in corner brackets.)
4. A site class was selected (note that the options available may be different from the true soil conditions at your site of interest). The probability of exceedance that was studied is 5% and 10%.
5. An aggregation type was selected. Aggregation types describe how the selected values were derived from the set of single-branch results of a logic tree model. Typical choices are mean, median, and fractiles. For our study mean values have been used.

Results

Detailed hazard maps have been planned for every important mapped fault of this specific area using the Deterministic Seismic Hazard Assessment. The analysis of the hazard maps took place with the OpenQuake and QGIS (https://www.qgis.org/en/site/). The comparison and links of these data with broader geodynamic models is now possible and we expect, in a later phase that will provide a more detailed image of the associated seismic hazard for Aitolo-Akarnania.

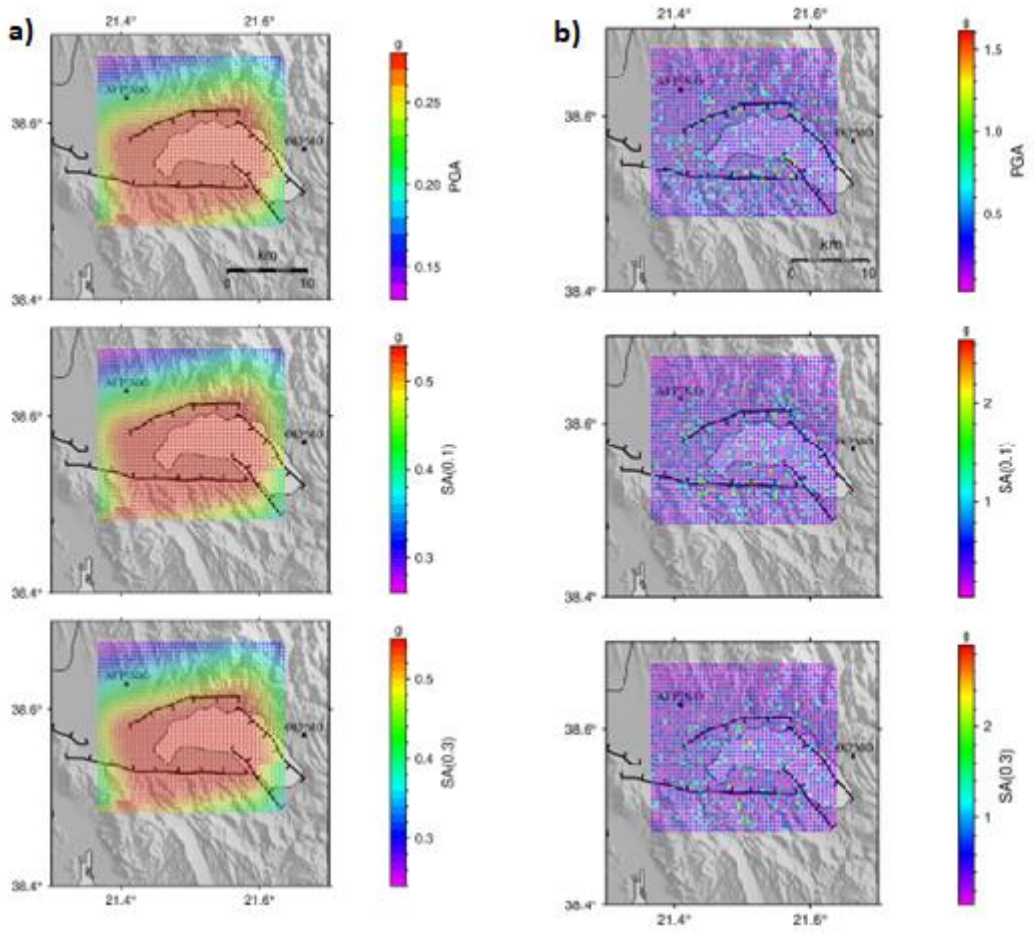

Fig. 1: a) Hazard maps of maximum values of the ground motion. From top to bottom: PGA, SA (0.1s) & SA (0.3s) for a seismic scenario of M = 6.0 on A10Z fault. The mean values are mapped according to the different empirical models. b) Hazard maps of maximum values of the ground motion. From top to bottom: PGA, SA (0.1s) & SA (0.3s) for a seismic scenario of M = 6.0 on A10Z fault. In the calculations was taken into account the uncertainty of the empirical ground motion prediction equation (± 3 standard deviation of the mean value).

Acknowledgements

E. Lyros, Z. Roumelioti, K. Nikolakopoulos & E. Sokos acknowledge that the hazard analysis was done by the use of the OpenQuake software (www.openquake.org/) & the QGIS software (https://www.qgis.org/en/site/), and the map design with the GMT software (https://www.generic-mapping-tools.org/)

References

Baker, C., Hatzfeld, D., Lyon–Caen, H., Papadimitriou, E. and Rigo, A., (1997). Earthquake mechanisms of the Adriatic Sea and western Greece: implications for the oceanic subduction – continental collision transition. Geophysical Journal International, 131, 559– 594.

Henrion, E., Masson, F., Doubre, C., Ulrich, P., Meghraoui, M., 2020. Present-day deformation in the Upper Rhine Graben from GNSS data. Geophys. J. Int. 223, 599-611. doi:10.1093/gji/ggaa320.

Lyros, E., (2022). "Crustal deformation in Aitolo-Akarnania prefecture using permanent GNSS stations". Ph.D. Thesis, University of Patras, Greece, 181 – 238.

Lyros, E., Kostelecky J., Plicka V., Vratislav F., Sokos E., Nikolakopoulos K., (2021). Detection of Tectonic and Crustal Deformation using GNSS Data Processing: The Case of PPGnet. Vol. 7, No 01, p. 14-23, Doi: 10.28991/cej-2021-03091633

Perouse, E., et al. (2016). Transition from collision to subduction in Western Greece: The Katouna– Stamna active fault system and regional kinematics. International Journal of Earth Sciences volume 106, pages 967–989 (2017).

Pérouse, E., Sébrier, M., Braucher, R., Chamot-Rooke, N., Bourlès, D., Briole, P., Sorel, D., Dimitrov, D., Arsenikos, S., (2017). Transition from collision to subduction in Western Greece: The Katouna– Stamna active fault system and regional kinematics. Int. J. Earth Sci. 106, 967–989. https://doi.org/10.1007/s00531-016-1345-9.

16th International Congress of the Geological Society of Greece
17-19October, 2022 -Patras, Greece
Bulletin of the Geological Society of Greece, Sp. Publ. 10
Ext. Abs. GSG2022-356

Seismic Hazard Deaggregation With The Use Of Random Catalogues: An Application For The Broader Aegean Area

A. Kerkenou[1], C. Papazachos[1], B. Margaris[2], C. Papaioannou[2]

(1) Aristotle University of Thessaloniki, Thessaloniki, Greece, akerkeno@geo.auth.gr (2) Institute of Engineering Seismology and Earthquake Engineering (ITSAK), Thessaloniki, Greece.

Research Highlights

A new seismic hazard deaggregation analysis is conducted for the area of Greece, with the use of updated seismicity models and recent data.The results show that in most cases the seismic hazard level of the examined cities is affected by earthquakes of medium to large magnitude (4.5-6.5) that occur at close distances (0-50 km), while several sites - especially along the Hellenic Arc- are mostly affected by medium to large magnitude events, at large distances (up to ~200 km). This pattern is justified by the seismotectonic features of their adjacent regions (e.g., large thrust events along the Hellenic arc) and should be critically considered for the appropriate selection of design earthquakes.

Background

Probabilistic Seismic Hazard Analysis (PSHA) results typically correspond to the determination of a ground motion parameter, that is characterized by a specific annual probability of exceedance. For the computation of this value, usually all possible combinations of seismic sources, earthquake magnitudes and source-to-site distances are considered (Cornell, 1968). As a result, the seismic hazard level of a site is not directly connected to a specific event. Seismic hazard deaggregation is an approach that allows to partly overcome this issue and determine the dominant earthquakes that contribute most to the seismic hazard level. This is performed by calculating the most likely M-R-ε combination, where ε is the number of standard deviations applied to the Ground Motion Prediction Equation (GMPE) of an earthquake of magnitude M at a distance R, corresponding to the bias between the calculated and the predicted ground motion value (3-D deaggregation), as initially proposed by McGuire (1995). Since the distance R is not indicative of the direction from which seismic hazard originates, Bazzuro and Cornell (1999) proposed the 4-D deaggregation, that is the definition of the most likely Lon-Lat-M-ε combination, which is able to identify the most effective seismic sources/locations.

Earlier deaggregation studies for the broader Aegean area [e.g., Tselentis and Danciu (2010)] have shown that the seismic hazard is mainly affected by moderate events, located at rather short distances (R<40 km). Results obtained during the last decade suggest that an updated seismic deaggregation computation, with the use of more recent seismic source models and GMPEs, could possibly lead to different results.

Method

The standard PGA value with 10.0% probability of exceedance, for a typical mean return period of 50 years is considered. A Monte Carlo simulation technique was followed, using synthetic catalogues of seismicity.PGA value is computed for each catalogue event, using a GMPE-logic tree. Then, the synthetic catalogue is divided to 50-year duration sub-catalogues, and the maximum PGA value of each sub-catalogue is computed. The corresponding PGA maxima form a histogram, which can be approximately described by a Gumbel-III distribution. The value with the desirable probability of exceedance corresponds to the desired seismic hazard level. The PGA values above the determined seismic hazard level correspond to those destructive events that would result in larger PGA values. The characteristics of these events (e.g., Lon, Lat, M, ε but also fault type, etc.) are already available in the synthetic seismic catalogue for further analysis.

Results

Figures 1 and 2 present two indicative deaggregation results for two different sites of interest in the Aegean area, namely Kefalonia Island and Chania, respectively. Kefalonia Island (Figure 1) is characterized by the highest values of seismic hazard in Greece. The deaggregation results for Kefalonia Island are quite representative for most of the sites examined, since the events that are responsible for PGA values $\geq$0.72 g (Figure 1, left) are located at relatively short distances, while their magnitude varies mainly in the range 5.5 to 7.0. This is clearly shown in the M-R diagram (Figure 1, right), where the possibility of each M-R combination is shown, where the higher possibilities cluster in the area limited by magnitudes 5.5-7.0 and distances 0-20 km. The corresponding mean and median values (depicted on the Figure) are in good agreement with the epicenter distribution, as well as the M-R diagram.

The city of Chania (Figure 2) is located at the NW part of Crete Island, which corresponds to the outer Hellenic Arc, controlled by the subduction of the eastern Mediterranean lithosphere under the Eurasian plate. As a result, it is affected

both by events of small-medium magnitude (4.5-6.5) located at seismic sources at short distances, as well as by events of relatively large magnitude (7.0-8.0) located at a large distance, along the outer Hellenic Arc (dark-coloured events in Figure 2, left). These two clusters of earthquakes are also visible in the M-R diagram (Figure 2, right). While higher possibilities of exceedance are observed for the magnitudes range 4.5-6.0 and distances 0-40 km, several events exceeding the expected seismic hazard level span magnitudes in the rage 6.5-8.0 and distances between 50 and 150 km. This is an example where the mean and median values of M and R do not fully describe the seismic hazard origin, as they neglect the bimodal character of the distribution and the fact that distant events of significant importance for this site. In this case, the definition of two (or generally more than one) design earthquakes is clearly recommended.

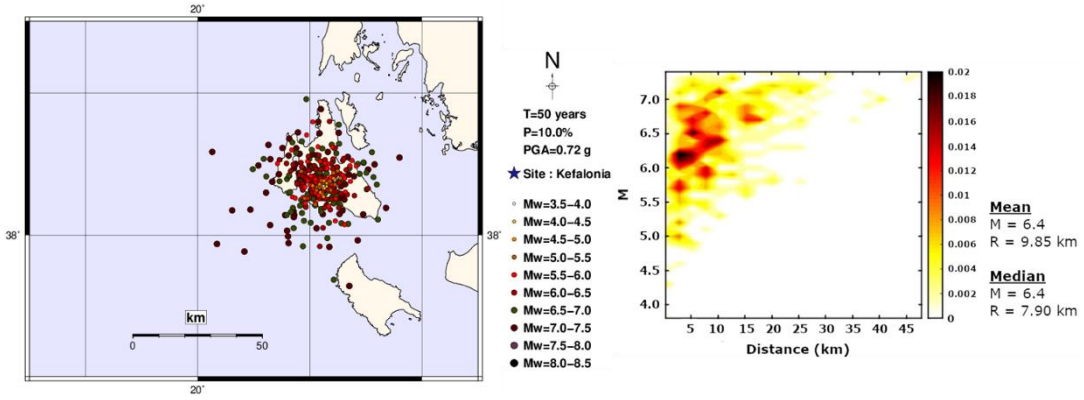

Figure 1. Map of the epicenters causing a PGA value of 0.72 g (or higher) for Kefalonia Island (left). Probability distribution of each MR combination to cause the above-mentioned PGA value (right).

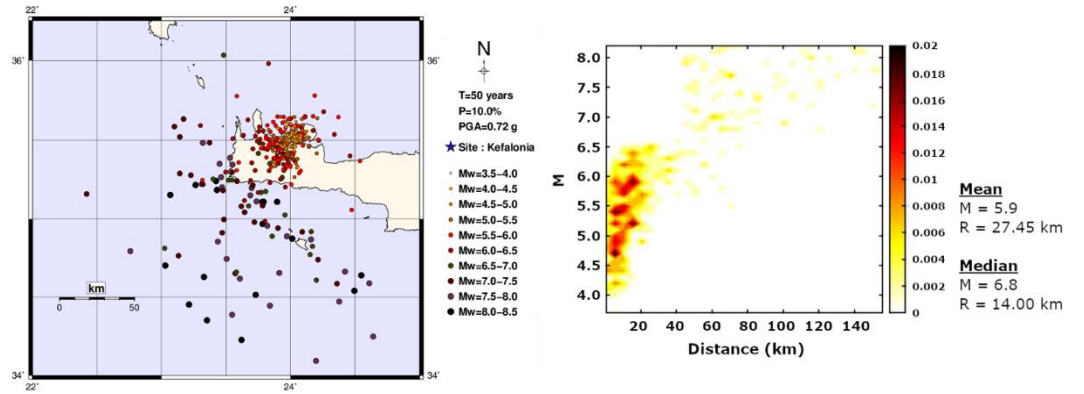

Figure 2. Map of the epicenters causing a PGA value of 0.19 g (or higher) for the site of Chania (left). Probability distribution of each MR combination to cause the above-mentioned PGA value (right).

Conclusions

The use of random catalogue (Monte Carlo-type) seismic hazard modelling provides an easy approach to deaggregate seismic hazard. Seismic hazard in Greece is dominated by events of small to medium magnitudes at close distances, a result that is in good agreement with the results of Tselentis and Danciu (2010). However, several sites are also affected by larger-magnitude events, originating at larger distances, due to the seismotectonic setting of the broader Aegean area. A typical case concerns the regions affected by events occurring due to the subduction of the eastern Mediterranean lithosphere beneath the Aegean microplate, or events originated at the North Aegean Trough.

Acknowledgements

This work was partly co-financed by Greece and the European Union (European Social Fund) through the OP“Human Resource Development, Education and Lifelong Learning 2014-2020” of the Action “Strengthening human resources through doctoral research-Sub-Action2:IKY Scholarships Program for Ph.D. Candidates of Greek Universities”.

References

Bazzuro, P., Cornell, C.A., 1999. Disaggregation of Seismic Hazard. Bull. Seismol. Soc. Am. 89, 501-520.

Cornell, C.A., 1968. Engineering seismic risk analysis. Bull. Seismol. Soc. Am. 58, 1583-1606.

McGuire, R.K., 1995. Probabilistic seismic hazard analysis and design earthquakes: closing the loop. Bull. Seismol. Soc. Am. 85, 1275-1284.

Tselentis, G.A., Danciu, L, 2010. Probabilistic seismic hazard assessment in Greece – Part 3: Deaggregation. Nat. Hazards Earth Syst. Sci. 10, 51-59.

16th International Congress of the Geological Society of Greece

17-19 October, 2022 - Patras, Greece

Bulletin of the Geological Society of Greece, Sp. Publ. 10

Ext. Abs. GSG2022-360

Rheological Modelling of the 26 November 2019 Durres Epicentral Area

D. Russo[1,2], M. Maggini[1,2], R. Caputo[1,2]

(1) Department of Physics and Earth Sciences, University of Ferrara, Ferrara, Italy, davide.russo@unife.it (2) CRUST – UR Ferrara, Ferrara, Italy.

The definition of the brittle-ductile transition (BDT) depth could be used to improve seismic hazard assessment studies in seismically active regions (Maggini and Caputo, 2021). The BDT represents a proxy of the seismic/aseismic transition and fundamentally corresponds to a mechanical boundary for coseismic rupture propagation processes. Close to this transition, deformation within the viscous crustal body generally induces elastic deformation also within the contiguous elasto-brittle body and when sufficient energy has been accumulated it is commonly released seismically. A rheological modelling was previously performed by Maggini and Caputo (2020, 2021) in the broader Aegean Region including the southern Balkans. Moreover, the seismicity cutoff depth of several seismogenic volumes was compared with the modelled BDT depth thus confirming that the rheological and seismological transitions are tightly correlated. Accordingly, the brittle-ductile transition depth is a very reliable marker for constraining the width of seismogenic sources.

Based on these premises, we investigated the epicentral area of the November 2019 seismic sequence which mainly affected the city of Durres. It corresponds to the north-western sector of Albania characterized by an on-going compressional regime due to the persistent continental-continental collision between the Adria microplate and European block that has is maximum expression in the Dinarides-Hellenides fold-and-thrust belt. In this sector of the accretionary wedge, the thrust front is segmented and the kinematics partitioned by the ENE-WSW Shkodra and Lushnje transfer faults (Caputo and Pavlides, 2013). The mainshock occurred on the 26th November 2019 in the Durres area with a Mw = 6.4. Following the inversion of InSAR and GNSS data (i.e. Caporali et al., 2020; Ganas et al., 2020; Govorcin et al., 2020; Papadopoulos et al., 2020; Pezzo et al., 2021; Vittori et al., 2021), it is well constrained that the event was associated with a blind thrust fault. However, authors interpretations differ in terms of dip-angle and dip-direction of the causative source. In particular, some authors suggest a low-angle NE-dipping blind thrust (i.e. Caporali et al., 2020; Ganas et al., 2020; Papadopoulos et al., 2020; Vittori et al., 2021), while some others prefer a high-angle SW-dipping back-thrust plane (Govorcin et al., 2020; Pezzo et al., 2021).

Solving this ambiguity is not among the principal aims of this research, instead it is to provide an additional constraint, independent from seismological data, on the seismotectonics of this sector of the Albanides fold-and-thrust belt and particularly on the maximum depth of the seismogenic sources and hence on their maximum width.

Following a similar methodology from Maggini and Caputo (2020b) we obtained, with dedicated MatLab scripts, a pseudo 3D rheological model of the 26th November 2019 epicentral area from which an ENE-WSW oriented profile is then extracted. The transect, which runs from Adria to western Balkans (A-B; Fig. 1) across the epicentral volume and perpendicular to the major tectonic structures, clearly shows the presence of different brittle and ductile layers characterizing the broader seismogenic volume. By plotting the hypocentral locations proposed by the different authors on the same profile, it is possible to observe the presence of a lense-shaped ductile body at ca. 18-25 km-depth within the upper plate delimited to the west by the major shear zone of the basal detachment. As above mentioned, such conditions are ideal for accumulating stresses within the contiguous elasto-brittle rock volume and this indeed is where the hypocentre of the mainshock has been located (Papadopoulos et al., 2020; http://terremoti.ingv.it; www.emsc-csem.org)

Furthermore, and considering that the plate boundary represents a major weakness zone, it is likely that rupture propagation has then followed the basal detachment up-dip towards the west. Based on this reconstruction, the focal depth of ca. 22 km and the estimated seismic moment, the rupture surface remained entirely blind.

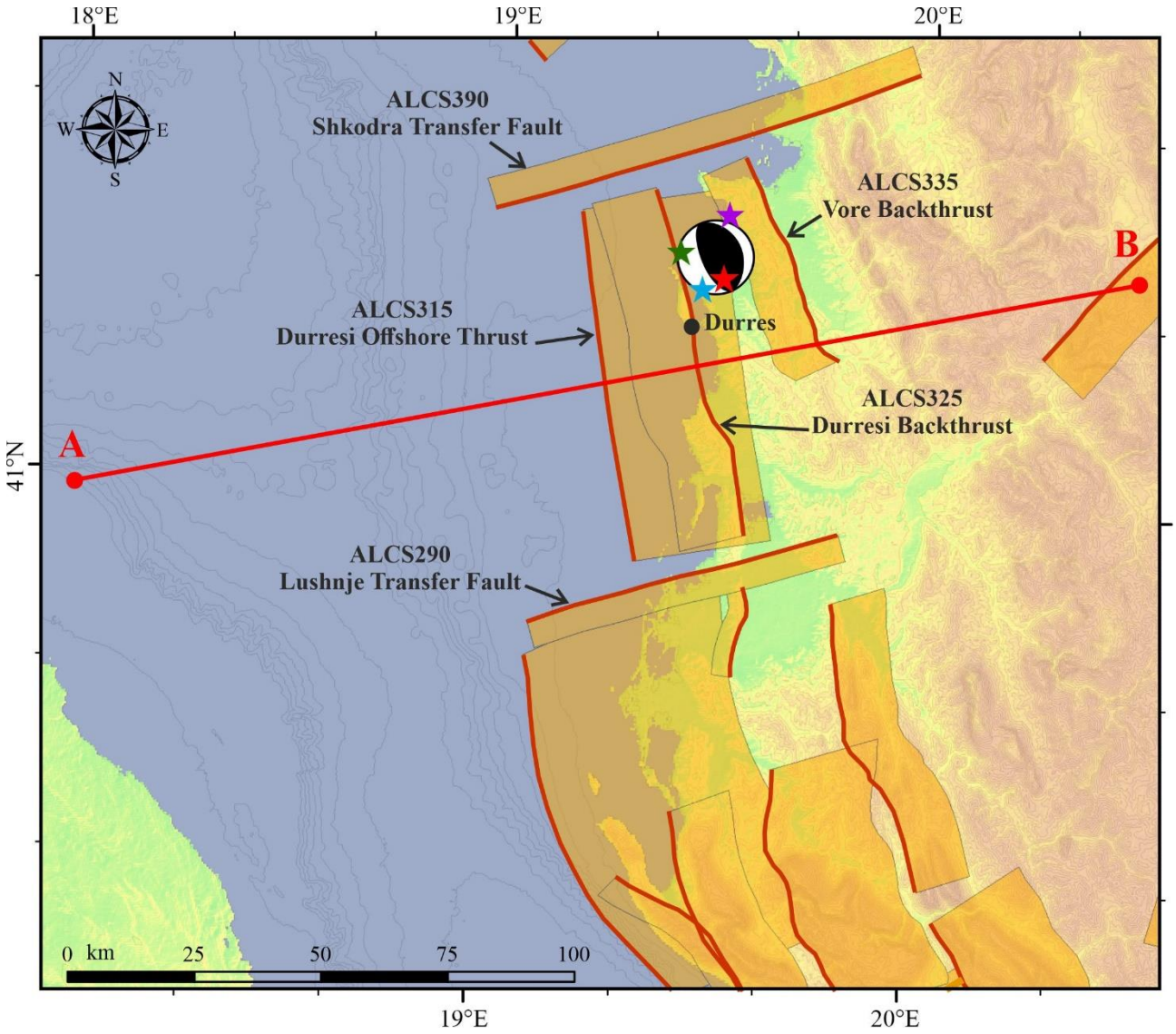

Figure 1. Investigated area showing section A-B trace; contour interval at 100 m; CSSs from GreDaSS database (Caputo and Pavlides, 2013); possible epicenters of the 26 November 2019 mainshock as determined by various authors and catalogues (USGS catalogue, purple star; Papadopoulos et al. [2020], green star; CSEM-EMSC catalogue, blue star; ISIDe network, red star); focal mechanism solution from USGS catalogue.

References

Caporali, A., Floris, M., Chen, X., Nurce, B., Bertocco, M., 2020. The November 2019 seismic sequence in Albania: Geodetic constraints and fault interaction. Remote Sens. 12(5), 846.

Caputo, R., Pavlides, S., 2013. The Greek Database of Seismogenic Sources (GreDaSS), version 2.0.0: A compilation of potential seismogenic sources (Mw > 5.5) in the Aegean Region.

Ganas, A., Elias, P., Briole, P., Cannavo, F., Valkaniotis, S., Tsironi, V., Partheniou, E.I., 2020. Ground deformation and seismic fault model of the M6.4 Durres (Albania) Nov. 26, 2019 earthquake, based on GNSS/INSAR observations. Geosciences 10(6), 210.

Govorcin, M., Wdowinski, S., Matos, B., Funning, G.J., 2020. Geodetic source modelling of the 2019 Mw 6.3 Durres, Albania, earthquake: Partial rupture of a blind reverse fault. Geophysical Research Letters 47, 22.

Maggini, M., Caputo, R., 2020. Rheological behaviour in continental and oceanic subduction: Inferences for the seismotectonic of the Aegean Region. Turkish J. Earth Sci. 29, 381-405.

Maggini, M., Caputo, R., 2020. Sensitivity analysis for crustal rheological profiles: Examples from the Aegean Region. Annals of Geophysics 63,3, GT334.

Maggini, M., Caputo, R., 2021. Seismological data versus rheological modelling: Comparison across the Aegean Region for improving the seismic hazard assessment. Journal of Structural Geology 145, 104312.

Papadopoulos, G.A., Agalos, A., Carydis, P., Lekkas, E., Mavroulis, S., Triantafyllou, I., 2020. The 26 November 2019 Mw6.4 Albania destructive earthquake. Seismol. Res. Lett. 91(6), 3129-3138.

Pezzo, G., Palano, M., Chiarabba, C., 2022. Rotation at subduction margins: How complexity at fault-scale (the 2019 Albanian Mw 6.4 earthquake) mirrors the regional deformation. Terra Nova 34(3), 244-252.

Vittori, E., Blumetti, A.M., Comerci, V., Di Manna, P., Piccardi, L., Gega, D., Hoxha, I., 2021. Geological effects and tectonic environment of the 26 November 2019, Mw 6.4 Durres earthquake (Albania). Geophys. J. Int. 225, 1174-1191.

16th International Congress of the Geological Society of Greece
17-19 October, 2022 - Patras, Greece
Bulletin of the Geological Society of Greece, Sp. Publ. 10
Ext. Abs. GSG2022-378

Geophysics: A valuable tool for management of bioreactor landfills

I. Fikos[1], F. Chitea[2], L. Pavel[3], G. Vargemezis[1]
(1) Laboratory of Applied Geophysics Aristotle University of Thessaloniki, Greece, ifikos@geo.auth.gr
(2) Faculty of Geology and Geophysics, University of Bucharest, Romania.
(3) Klarwin, Romania

Introduction

Operation of Municipal Waste Deposit areas is a very complex procedure with one of the most important aspects being the treatment of leachate produced and accumulated in the body of the wastes. To achieve faster degradation and increase the capacity operation of a MWD the idea of recirculation of leachate had been proposed since the 1970s (Pohland, 1975). By the proposed process the leachate flow can be managed taking care of peak flow buffering and the absorption capacity. The recirculation also helps in stimulating gas generation, accelerates the stabilization of organic waste, controls the leachate feed to the treatment plants, accelerates settlement by increasing the airspace. The MWD are of course dynamic systems changing constantly both in the phase of full operation but also during the post-closure care phase when only the degradation process is taking place. Therefore, snapshot of leachate distribution provides an excellent decision-making tool for optimizing the treatment and recirculation process.

To this goal the method of Electrical Resistivity Tomography was applied in bioreactor landfill in west Romania in such a way so that it would provide a detailed 3D estimation of the total volume and current distribution of leachate in the body of the wastes and at the same time identify possible gas accumulation and leakage below the liner.

Methodology

The characteristically high conductivity of the leachate makes them an ideal target for electrical resistivity method. The target area is a cell approximately 280X160 meters that became operational in 2011 and was full by the end of 2017. The method used was the 2D ERT measured in such a pattern so that at the end it would provide a set of parallel ERT lines suitable for a full 3D inversion (Kim 2009, Kim et al 2010). To achieve that we implemented 22 ERT lines that covered almost the compete area of the cell. For the 20 parallel lines (figure 1), to increase the length and the DOI, we modified the original 3 meters spacing between the spacing between electrodes 1 – 2 and 47 – 48 to 9 meters while for the electrodes 2 – 47 the spacing remained 3 meters providing very good resolution. The remaining 2 ERT lines were measured with a 50% overlap on the north slope of the cell to provide information on the part of the cell that was not fully covered by the previous measurements. The datasets for the 2 lines were joined and treated like one long ERT line of 72 electrodes.

Table 1. Parameters for measured ERTs in Cell#1.

Name	# electrodes	Spacing (m)	Length (m)
ERT-01 – ERT-20	48	3 and 9	153
ERT-29	72	3	213

Figure 1. Map of the location of the ERTs measured in cell#1.

Results

The 2d and 3d images results suggest a rather complicated distribution of the leachate forming preferential flow paths mainly towards the west half of the cell. The areas where leachate appears (low resistivity – blue color) to accumulate are at different depths and sometimes close to the slopes, coinciding with small ponds that are observed on the surface near the edges of the cell. Higher resistivity areas (red color) are most likely to correspond to areas where gas accumulates.

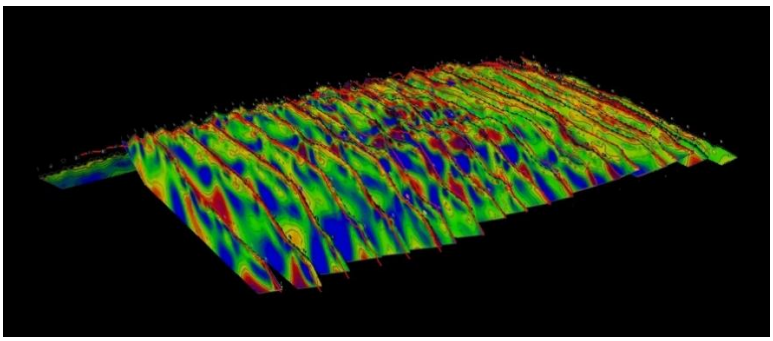

Figure 2. Image of the 2D ERT results measured in cell#1.

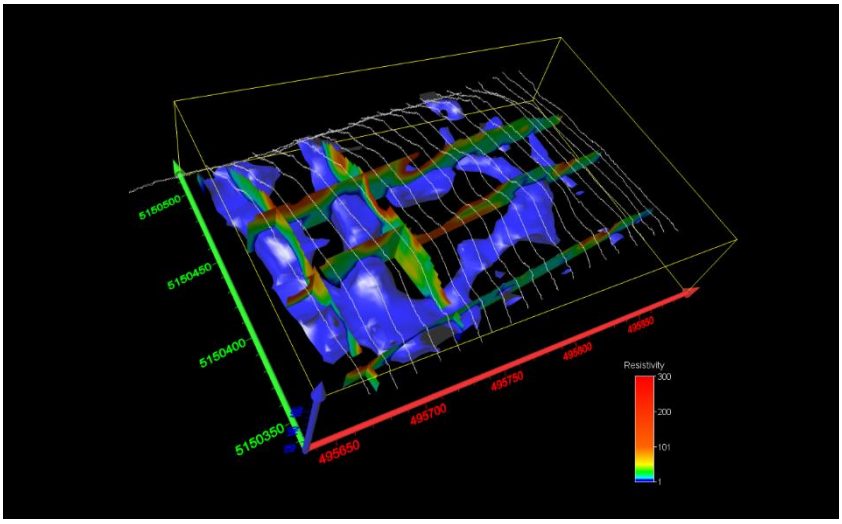

Figure 3. Distribution of the leachate from the 3D inversion of the ERTs measured in cell#1.

Conclusions

The survey provided very useful insights identifying the areas where the leachate accumulates. In the 2-dimensional and 3-dimensional images the cells proves to be extremely heterogeneous in terms of resistivity, corresponding to different type of wastes, different degree of decomposition, different phase (accumulated gas) or different degree of saturation with leachate.

Acknowledgements

The work in this paper resulted trough a cooperation between Romanian Society of Applied Geophysics, Klarwin and the Laboratory of applied geophysics of AUTH.

References

Pohland, F., 1975. Sanitary Landfill Stabilization with Leachate Recycle and Residual Treatment, Report for EPA Grant No. R-801397, USEPA National Environmental Research Center, Cincinnati, OH.

Kim, J. H. 2009. DC2DPro-2D Interpretation System of DC Resistivity Tomography. User's Manual and Theory, Publisher: KIGAM, S. Korea.

Kim, J. H., Yi, M. J. 2010. DC3DPRO - 3D Geoelectrical Modelling and Inversion, User's Manual.KIGAM, S. Korea.

16th International Congress of the Geological Society of Greece
17-19 October, 2022 - Patras, Greece
Bulletin of the Geological Society of Greece, Sp. Publ. 10
Ext. Abs. GSG2022-379

Evaluation of the Damasi earthquake environmental effects by using the ESI-2007 intensity scale

E. Papadopoulou[1], A. Chatzipetros[2], S. Pavlides[2]

(1) Department of Geography, University of the Aegean, Mytilene, Lesvos, Greece, evdokiapap97@gmail.com
(2) Department of Geology, Aristotle University, Thessaloniki, Greece

In order to quantify the effects of an earthquake, various intensity scales have been proposed, e.g. modified Mercalli (MM), EMS-98, JMA, MSK-64, etc. However, they are all based on effects on man-made structures, therefore lacking in detail in sparsely populated areas. This is partly covered by the introduction of the Environmental Seismic Intensity (ESI) scale, that was released in 2007 (Michetti et al. 2007). It takes into account primary and secondary environmental effects (e.g. ruptures, landslides, liquefaction, etc.) and assigns their magnitude to a prespecified intensity level.

In the present paper, the ESI-2007 scale was applied to the surface effects of the 2021 Damasi earthquake sequence. Environmental effects were observed in a rather large area of northern Thessaly. Coseismic effects were detected in predominantly two different regions in and around Pinios and Titarisios river valleys. Since the earthquake was produced by a blind fault as shown by field evidence and seismological data (e.g. Chatzipetros *et al.*, 2021a,b; Galanakis *et al.*, 2021; Karakostas *et al.*, 2021), the effects are mainly secondary ones and disperse. These effects manifest themselves as surface ruptures, landslides, ground cracks, liquefaction and hydrological anomalies. Most of the surface ruptures and quite limited liquefaction were observed in Titarisios river valley, in the vicinity of Damasi, Mesochori, Vlachogianni, Amouri, Domenico and Pretori villages. Widespread liquefaction was observed in Pinios valley, especially in the vicinity of Piniada and Koutsouchero villages.

In order to produce ESI-2007 isoseismal maps, all environmental effects have to be collected, processed and evaluated. This was performed using a GIS platform and the relevant methodology is described below:

The first step was the collection and digitization of all the effects. To this effect, all available information (gathered in the field or published) was collected, analyzed and evaluated (e.g. Chatzipetros *et al.*, 2021a and the papers within, Papathanasiou *et al*. 2021, Ganas *et al*. 2021; Koukouvelas *et al*. 2021). The evaluated effects were then digitized to scale and inserted into the GIS platform as separate layers. Wherever applicable (e.g. the effects included in the database of Papathanasiou *et al.* 2022 were compared and cross-checked against the drone data of Pavlides *et al*. 2021 and Chatzipetros *et al.* 2021b.

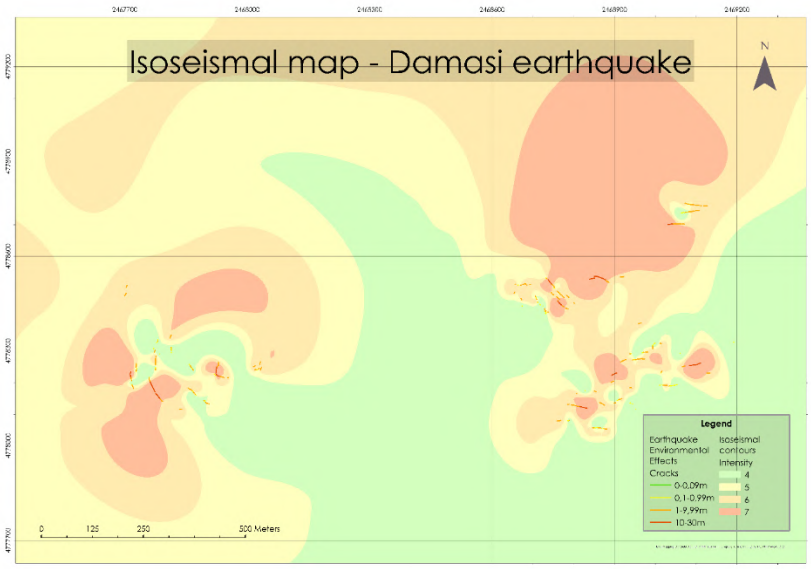

Figure 1. Isoseismal map of Damasi earthquake environmental effects using the automatic contour lines in ArcGIS (Spatial Analyst).

The next step was to correlate the observed surface effects with the relevant intensities in the ESI-2007 scale. Since rockfalls and landslides were rather limited in extend and volume, the main factors used were the surface area of liquefaction and the length of ground cracks. The calculated intensities were mostly ESI=4 and ESI=5, however intensities of ESI=6 and ESI=7 were observed locally within the liquefied area of Pinios valley.

The first map (Fig. 1) was produced using the Spatial Analyst tool for drawing the automated contour lines in ArcGIS. However, the second map (Fig. 2) was created by drawing the isoseismal contours associated with the intensities that were extrapolated from the length of cracks and the surface area of the liquefaction. By comparing the two methods, it can be deduced that the maps have a quite good correlation, especially in the areas where there are lots of measured data. Both of those methods are in agreement with the actual observed data, showing that the highest intensities were controlled primarily by the liquefaction and secondary by the surface cracks and rockfalls. It is important to note that the two ESI-2007 calculated macroseismic epicentres cannot be associated with the epicentral locations of the main shocks and the earthquake sequence at large.

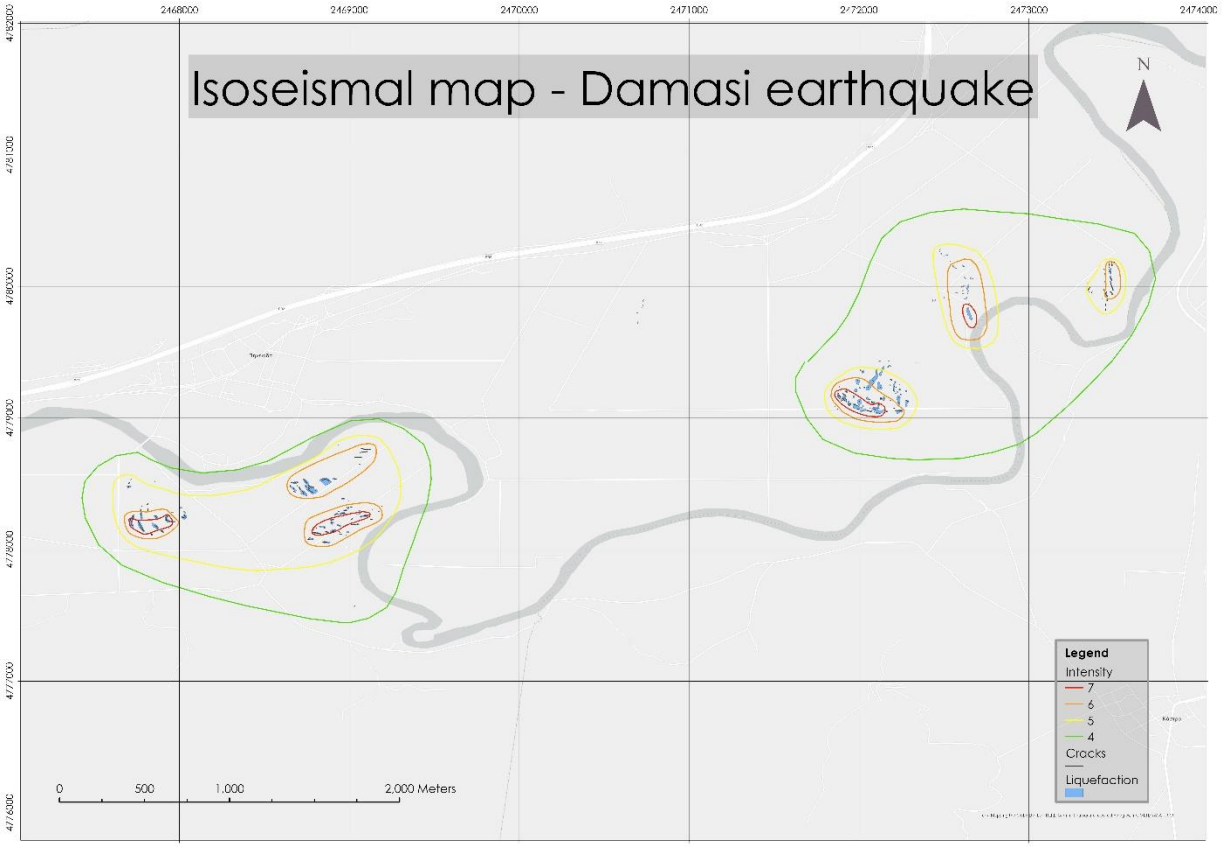

Figure 2. Isoseismal map of Damasi earthquake by drawing the contour lines of intensity in GIS.

References

Chatzipetros, A., Grützner, C., Kranis, H., (Eds.) 2021a. Preface: The March 2021 Thessaly Earthquake Sequence. Bulletin of the Geological Society of Greece 58, i-vii.

Chatzipetros, A., Pavlides, S., Foumelis, M., Sboras, S., Galanakis, D., Pikridas, C., Bitharis, S., Kremastas, E., Chatziioannou, A., Papaioannou, I., 2021b. The northern Thessaly strong earthquakes of March 3 and 4, 2021, and their neotectonic setting. Bulletin of the Geological Society of Greece 58, 222-255.

Galanakis, D., Sboras, S., Konstantopoulou, G., Xenakis, M., 2021. Neogene-Quaternary tectonic regime and macroseismic observations in the Tyrnavos-Elassona broader epicentral area of the March 2021, intense earthquake sequence. Bulletin of the Geological Society of Greece 58, 200-221.

Ganas, A, Valkaniotis, S, Briole, P et al. (13 more authors) 2021. Domino-style earthquakes along blind normal faults in Northern Thessaly (Greece): kinematic evidence from field observations, seismology, SAR interferometry and GNSS. Bulletin of the Geological Society of Greece, 58. pp. 37-86. ISSN 0438-9557

Karakostas, V., Papazachos, C., Papadimitriou, E., Foumelis, M., Kiratzi, A., Pikridas, C., Kostoglou, A., Kkallas, C., Chatzis, N., Bitharis, S., Chatzipetros, A., Fotiou, A., Ventouzi, C., Karagianni, E., Bonatis, P., Kourouklas, C., Paradisopoulou, P., Scordilis, E., Vamvakaris, D., Grendas, I., Kementzetzidou, D., Panou, A., Karakaisis, G., Karagianni, I., Hatzidimitriou, P., Galanis, O., 2021. The March 2021 Tyrnavos, central Greece, doublet (Mw6.3 and Mw6.0): Aftershock relocation, faulting details, coseismic slip and deformation. Bulletin of the Geological Society of Greece 58, 131-178.

Koukouvelas, I.K, Nikolakopoulos, K.G, Kyriou, A., Caputo, R., Belesis, A., Zygouri, V., Verroios, S., Apostolopoulos, D., Tsentzos, I. The March 2021 Damasi Earthquake Sequence, Central Greece: Reactivation Evidence across the Westward Propagating Tyrnavos Graben. Geosciences. 2021; 11(8):328. https://doi.org/10.3390/geosciences11080328

Michetti, A. M., Esposito, E., Guerrieri, L., Porfido, S., Serva, L., Tatevossian, R. & Roghozin, E. 2007. Environmental seismic intensity scale-ESI 2007. Mem. Descr. Carta Geol. D'Ital, 74, 7-23.

Papathanasiou, G., Valkaniotis, S., Ganas A., Stampolidis A., Rapti D., Caputo R., 2022 Floodplain evolution and its influence on liquefaction clustering: The case study of March 2021 Thessaly, Greece, seismic sequence, Engineering Geology, Volume 298, 106542, ISSN 0013-7952.

16th International Congress of the Geological Society of Greece
17-19 October, 2022 - Patras, Greece
Bulletin of the Geological Society of Greece, Sp. Publ. 10
Ext. Abs. GSG2022-391

Tectonic Settings and Neo-Tectonics of the Aegean Sea Deduced from Satellite Altimeter and Gravity Data

Khalid H. Zahran[1]
(1) National Research Institute of Astronomy and Geophysics, Cairo, Egypt, zahran@nriag.sci.eg

Introduction

The Aegean Sea is one of the key regions for the understanding of fundamental tectonic processes, including continental rifting, passive margins, ophiolites, subduction, accretion, collision and post-collisional exhumation. It is also ideal for understanding the interaction of tectonic, sedimentary, igneous and metamorphic processes through time that eventually lead to the development of an orogenic belt. Below, we will outline some milestones in the development of tectonic-related research in the Aegean Sea region. In addition, the continuous seismicity attributed to its tectonic settings, which affect almost all countries surrounding this region indicates the activities of these tectonics, fig.1. Thus, tectonics and geodynamics of this region have been always the attention of many interested in earth sciences.

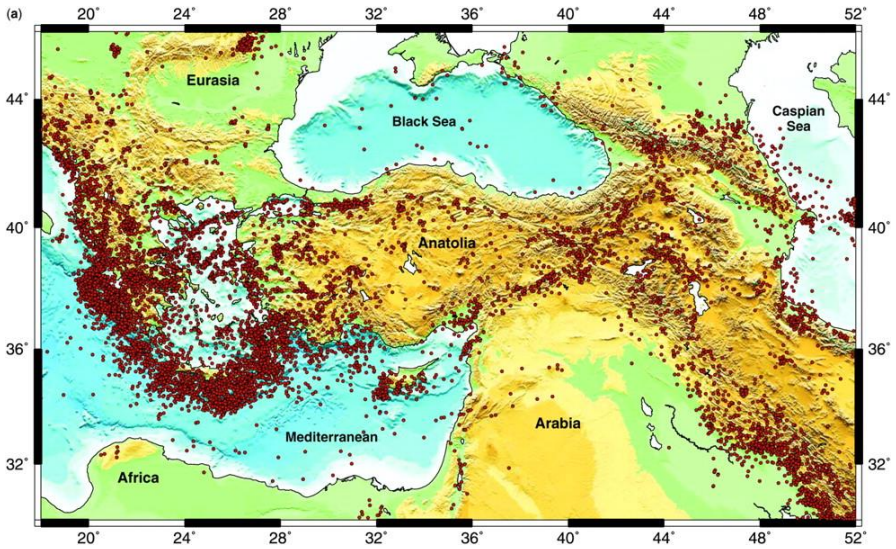

Figure 1 Seismicity of the Aegean Sea region, geologic society, London.

Background

Modern interpretations of this region in terms of plate tectonics effectively began with the pioneering work of Smith (1971). During the 1970s a scientific project (French-led Tethys) proposed the existence of a Mesozoic-Early Tertiary Tethyan ocean dating from Triassic time, bordered by the African and Eurasian continents. They interpreted the Mesozoic ophiolites as forming at mid-ocean ridges. The Tethyan ocean was sub-ducted northwards beneath Eurasia (Dercourt et al. 1986). A major advance in recent years has been the testing and confirmation of the early plate tectonics using a combination of field evidence and geophysical modeling (Jackson & McKenzie 1984). In addition to the palaeo-tectonics, which refers to stress regimes that are no longer active, there has also been an increasing focus on the neo-tectonic development, which refers to the strain resulting from a stress regime that essentially remains active at the present time of the region (Taymaz et al. 2004). Neo-tectonics is broadly from Miocene to Recent in the Eastern Mediterranean region. Other advances include the results of ocean drilling in the Eastern Mediterranean Sea that allowed a closer integration of tectonic processes operating on land and under the sea (Robertson et al. 1998).

Methodology

The main objective of this study is to figure out the tectonic settings and the geodynamics behavior of the Arabian Peninsula using integrated recent satellite data. Radar altimetry data has been used to derive gravity and its variations over the world's oceans and an excellent tool for mapping sea floor structures, including tectonics, sea mounts and rifts. Satellite altimeter data has been used to determine spatial gravity map of the marine region of the studied area and to delineate the attributed to the stress-strain accumulation and its relation to the earthquake occurrence. The Gravity Recovery and Climates Experiment (GRACE) have been monitoring time-varying changes of the earth's gravitational

field on a near global scale since 2002. Thus, data from GRACE has been used to determine the regional trends of the gravity variation along Cairo region. Moreover, data from GOCE gravity mission will be used to determine the tectonic boundaries of the selected region. Finally, integrated satellite data will be utilized to figure out the geodynamics behavior of the studied region and its neo-tectonic activities.

1. Results

According to the study the following results can be outline:

- Geoid map deduced from satellite altimeter reflects deep seated mass discontinuity zones.
- After removing the long-wavelength range, the residual geoid indicates that forces affect the rifting system is of local and regional tectonic sources.
- The satellite free air gravity map shows important zones of mass discontinuities and was able to delineate sub and minor rifting and transformation zones.
- Bathymetry map deduced from satellite altimeter data were capable to figure out possible transform faults.
- Temporal gravity variation from GRACE shows significant mass redistribution correlated well with the tectonic settings and the seismicity of the Aegean Sea region.
- Temporal gravity variations from GRACE show significant complimentary information about the kinematics and dynamics of the rifting system and the transformation fault.
- GOCE gravity anomaly map indicates less local features, suggests the importance of linking theses data with ground-based data for detecting small scale features.
- Integrated recent satellite data sets is a potential data source of monitoring neo-tectonic and seismo-active zones.

Conclusion

Evaluation the tectonic setting of this region regarding to the mass discontinuities has been made using gravity-based satellite altimeter data. The gravity map show important zones of mass discontinuities along plates and sub-plates margins. Gravity data enable the revealing the complicated fault pattern of this region on term of gravity anomalies. The temporal gravity variation from GRACE has been used to detect a possible mass distribution along plates boundaries attributed to the neo-tectonics. Temporal gravity variation indicates that the seismic activities on this region are attributed to a significant mass redistribution around the seismo-active zones. In addition, it gives important information about mass sources responsible for neo-tectonics. Due to spatial limitations of GRACE, it is not possible to reveal The study indicates the importance of considering spatial and temporal gravity to the deformation and tectonic studies for completeness of the geodynamic studies. Generally, it can be stated that the satellite data offer additional and complementary data sets to help the geoscientists to determine the Earth's internal structure and tectonics. Determination of spatial and temporal earth's gravity field from satellite opened new perspectives on earth sciences and provides valuable information of the geodynamic studies. .

References

Dercourt, J., Zonenshain, L. P., Rjcou, L. E. et al. 1986. Geological evolution of the Tethys belt from the Atlantic to the Pamirs since the Lias. Tectonophysics, 123, 241-315.

Jackson, J. & Mckenzie, D. P. 1984. Active tectonics of the Alpine-Himalayan belt between western Turkey and Pakistan. Geophysical Journal of the Royal Astronomical Society, 77, 185-264.

Robertson, A. H. F., & Mountrakis, D. 2006, Tectonic development of the Eastern Mediterranean region: an introduction. In ROBERTSON, A. H. F. & MOUNTRAKIS, D. (eds) 2006. Tectonic Development of the Eastern Mediterranean Region. Geological Society, London, Special Publications, 260, 1-9.

Smith, A. G. 1971. Alpine deformation and the alpine areas of Tethys, Mediterranean and Atlantic. Geo- logical Society of America Bulletin, 82, 2039-2070.

Taymaz, T., Westaway, R. & Reilinger, R. (eds) 2004. Active Faulting and Crustal Deformation in the Eastern Mediterranean Region. Tectonophysics, Special Issue, 391.

16th International Congress of the Geological Society of Greece
17-19 October, 2022 - Patras, Greece
Bulletin of the Geological Society of Greece, Sp. Publ. 10
Ext. Abs. GSG2022-391

Seismic Source Spectrum estimation, for the January 26, 2014, Cephalonia earthquake (Mw~6.1), based on Coda wave analysis.

I. Grendas[1], N. Theodoulidis[1], F. Hollender[2] and P. Hatzidimitriou[3]

(1) Institute of Engineering Seismology and Earthquake Engineering, Thessaloniki, Greece, igrendas@geo.auth.gr (2) Atomic Energy and Alternative Energies Commission (CEA), Cadarache, France (3) Aristotle University of Thessaloniki, Greece

Introduction

The Seismic Source Spectrum (SSS) estimation for high magnitude earthquakes, aiming to retrieve the maximum possible broad-band frequency range, is essential in engineering seismology attempting to retrieve the source characteristics. The quick estimation of these characteristics and of the SSS after a high magnitude earthquake is significant in attempting to simulate ground motion spectra in sites where no seismic records are available. In general, the common applied methodologies in retrieving the Source Time Function (STF) of an earthquake (e.g. the one based on Green's functions, Courboulex et al., 1997, Benetatos et al., 2005) and consequently its Fourier Spectrum, require a satisfying number of earthquake records, relevant close to the seismic source and usually provide information in covering the lower frequency band (< ~1 Hz). In this study, the Seismic Source Spectrum of Cephalonia earthquake in 26/01/2014 (Mw~6.1) is estimated as a characteristic example of a coda wave analysis introduced by Sèbe et al., (2018). In this analysis the available, good quality, coda wave part of a single station earthquake record can be used to retrieve the SSS of an earthquake, after computing and removing from the coda waveform the frequency dependent attenuation factor.

Data & Methodology

Five earthquake records from five permanent installed accelerographs (KAC1, MSL1, PAT4, PRE2 and ZAK2) which belong to the Institute of Engineering Seismology and Earthquake Engineering (ITSAK, http://www.itsak.gr) (Figure 1), were analyzed by the Spectral Factorization Method of coda waves (SFC) algorithm developed by Grendas et al., (2022), based on the study of Sèbe et al., (2018), in order to retrieve the Seismic Source Spectrum of the January, 26, 2014 Cephalonia earthquake (Figure 1).

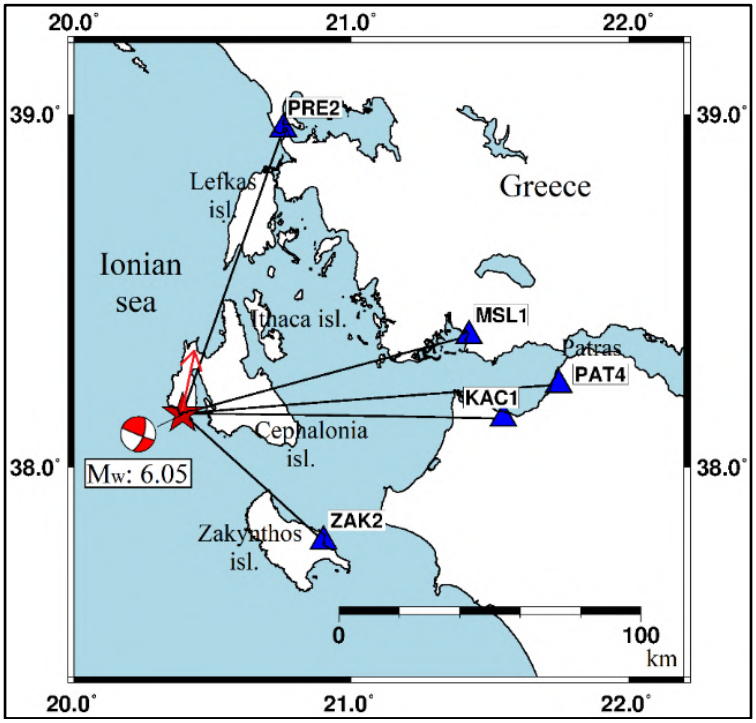

Figure 1. The western Greece area. In red asterisk the epicenter of the examined Cephalonia earthquake and its focal mechanism (Karakostas et al., 2015) are depicted (20140126). In blue triangles the five examined stations are also presented.

The SFC algorithm is based on the following fundamental equation (Aki, 1969; Aki and Chouet, 1975):

$$R_{ij}(f,t') = W_i(f)\cdot E_c\cdot|A_C(f,t')|^2\cdot N_j(f)$$

where for an earthquake, i and a station, j, the Power Spectral Density, $R_{ij}(f,t')$ of a coda wave window, centered in time, t', is analyzed, in terms of energy, as the product of Seismic Source, $W_i(f)$, of attenuation factor $A_C(f,t')$, of site effects, $N_j(f)$, and of the known by previous studies, coda excitation factor, E_c (Aki, 1980; Sato, 1977), which controls the fractional loss of energy per unit travel distance of the shear waves from the source to the receiver, due to the wave scattering by the lithosphere heterogeneities.

Results & Conclusions

The Seismic Source Spectra of the Mw~6.1, Cephalonia earthquake (26/01/2014) computed in this study by the Spectral Factorization of coda waves (SFC) (Figure 2), seems to be in a relevant good agreement to the Fourier Amplitude Spectra of the STF, determined by Sokos et al., (2015), up to ~2 Hz. Moreover, the calculated moment Magnitudes are also in agreement to the one determined by Sokos et al., (2015) and by the Seismological Station of Aristotle university of Thessaloniki (http://geophysics.geo.auth.gr/ss/, Mw = 6.1±0.2). The results encourage the further use and development of the SFC method, in application to high magnitude earthquakes.

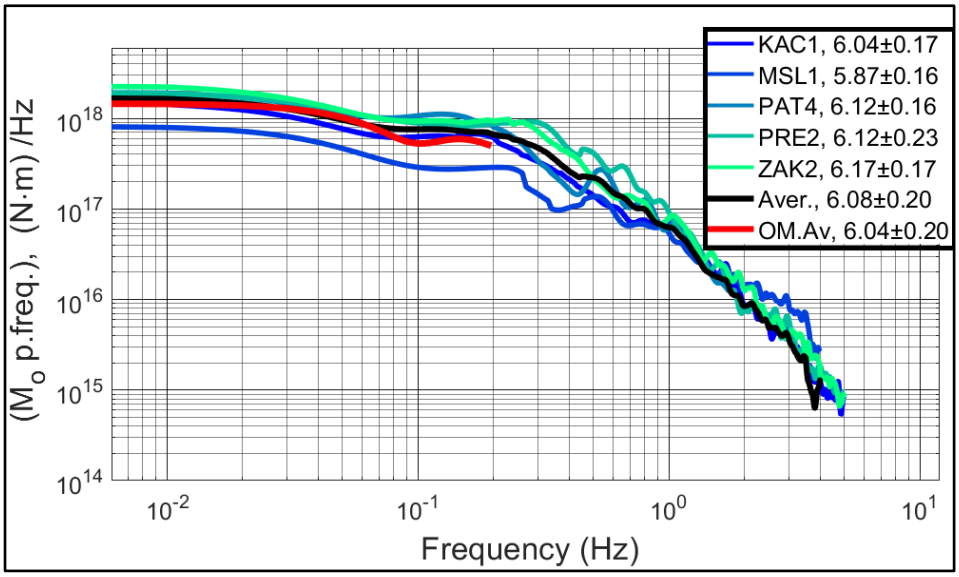

Figure 2. The Seismic Source Spectra and the corresponding moment Magnitudes, as computed in this study for the five stations (multi color lines) (Figure 1), their average (black line) and the one (red line) computed by Other Method by Sokos et al., (2015).

Acknowledgements

This work was funded by the SIREAT (KE 2.027) project. Pierre-Yves Bard has greatly contributed understanding the theoretical background of the applied methodology.

References

Aki, K., 1969. Analysis of the Seismic Coda of Local Earthquakes as Scattered Waves. J. Geophys. Res. 74, 615–631.

Aki, K., 1980. Scattering and attenuation of shear waves in the lithosphere. J. Geophys. Res. 85, 6496–6504.

Aki, K., Chouet, B., 1975. Origin of coda waves: Source, attenuation, and scattering effects. J. Geophys. Res. 80, 3322–3342.

Benetatos, C., Kiratzi, A., Roumelioti, Z., Stavrakakis, G., Drakatos, G., Latoussakis, I., 2005. The 14 August 2003 Lefkada Island (Greece) earthquake: Focal mechanisms of the mainshock and of the aftershock sequence. J. Seismol. 9, 171–190.

Courboulex, F., Santoyo, M.A., Pacheco, J.F., Singh, S.K., 1997. The 14 September 1995 (M = 7.3) Copala, Mexico, earthquake: a source study using teleseismic, regional, and local data. Bull. Seism. Soc. Am. 87–4, 999–1010.

Grendas, I., Theodoulidis, N., Bard, P.Y., Perron, V., Hatzidimitriou, P., Hollender, F., 2022. Can site effects be estimated with respect to a distant reference station? Performance of the spectral factorization of coda waves. Geophys. J. Int. 230, 1–28.

Karakostas, V., Papadimitriou, E., Mesimeri, M., Gkarlaouni, C., Paradisopoulou, P., 2015. The 2014 Kefalonia Doublet (Mw6.1 and Mw6.0), central Ionian Islands, Greece: Seismotectonic implications along the Kefalonia transform fault zone. Acta Geophys. 63, 1–16.

Sato, H., 1977. Energy propagation including scattering effects single isotropic scattering approximation. J. Phys. Earth 25, 27–41.

Sèbe, O., Guilbert, J., Bard, P.-Y., 2018. Spectral factorization of the source time function of an earthquake from coda waves, application to the 2003 rambervillers, France, earthquake. Bull. Seismol. Soc. Am. 108, 2521–2542.

Sokos, E., Kiratzi, A., Gallovič, F., Zahradník, J., Serpetsidaki, A., Plicka, V., Janský, J., Kostelecký, J., Tselentis, G.A., 2015. Rupture process of the 2014 Cephalonia, Greece, earthquake doublet (Mw6) as inferred from regional and local seismic data. Tectonophysics 656, 131–141.

16th International Congress of the Geological Society of Greece

17-19 October 2022 - Patras, Greece

Bulletin of the Geological Society of Greece, Sp. Publ. 10

Ext. Abs. GSG2022-404

A Comprehensive Moho Surface from Arabia to Italy Based on Gravity Data: Significance on the Geodynamic Regime

S. Chailas[1], A. Tzanis[1], Ch. Kranis[1]

(1) Section of Geophysics – Geothermy, National and Kapodistrian University of Athens, Athens, Greece; schailas@geol.uoa.gr. (2) Section of Dynamic and Applied Geology, National and Kapodistrian University of Athens, Athens, Greece

Abstract

A model of the Moho surface for the Westernmost part of the Alpine-Himalayan system is presented herein, based on gravity data. We introduce the finite element method as a means of examining complicated structural models by considering the deformation of the oceanic plate at the Eastern Mediterranean, along with the adoption of spectral techniques in the calculation and inversion of the isostatic correction for the rest of the area. The examination of the Arabia-Turkey-Aegean system indicated the existence of mantle flow which is of significance to the compensation mechanism. The relation of crustal thickness fluctuations with the active tectonics is also examined.

Introduction

Our study area is hosting three (or four, depending on the author) subduction systems two of which are active orogenetic fronts, two small closing oceans and one of the fastest spreading plates on earth (Aegean) that also comprises the second most seismically active domain on earth.

The study of the isostatic regime of convergent plate margins is always challenging. Classical isostatic models involving local compensation are not sufficient to describe the relationship between the observed topography/ bathymetry and gravity anomalies, hence the topography of the base of the lithosphere. On the other hand, elastic plate models require forward modeling in combination with realistic geodynamic scenaria, so as to achieve a sufficiently accurate gravitational solution. The typical approach is to examine flexural profile models, assuming the loading of a thin beam lying on a weak foundation (Hetenyi, 1947). During the last few decades finite differences have been implemented in modelling the flexure of elastic plates with considerable success. This method, however, cannot efficiently incorporate large discontinuities, such as regional scale faults cutting through the crust. Herein, we introduce an implementation of the finite element method in calculating flexure, while incorporating representative models of the geodynamic and tectonic regimes. The approach is computationally expensive but very efficient.

Data Analysis

The gravity data for the entire study area were extracted from TOPEX Global Gravity Model. In its current version (v29) this combines the global marine gravity model (Sandwell, *et al.*, 2014) for offshore areas, and the EGM 2008 gravity model (Pavlis *et al.*, 2012) for onshore/land areas. The TOPEX data are provided in the form of free air anomalies. We applied the Bouguer correction using the SRTM30_PLUS topography extracted from the same source, and a Bouguer correction density of 2.67 gr/cm^3. We also calculated the isostatic anomaly of the entire study area based on the Airy model and using the 3DINVER software (Gómez-Ortiz & Agarwal, 2005) to model the isostatic correction. This can be taken to represent the Moho surface in the areas in which the topographic load is isostatically compensated. Because significant and extensive negative isostatic anomalies were observed in the fore-arc areas of all three convergent margins (which are not justified by the lithology), we implemented flexural modeling in an attempt to explain their presence, amplitude and configuration. To this effect, we developed a finite element code for calculating the deflection in response to a topographic load, of an irregular thin elastic plate with varying flexural rigidity floating on, or partly dipping in a fluid. This facilitated the incorporation of regional scale faults and allowed us to highlight the catalytic significance of some of those (e.g. Medina Fault, Cyrenaica Fault) in the modulation or relaxation of the Mediterranean crust in "seismically quiet" areas. We note that this is ongoing research and the results presented in Fig. 1 are only preliminary.

Results and Interpretation

In Fig. 1, the dotted line separates the areas in which the classical Airy model was sufficient to explain the observed isostatic anomalies, from the areas in which it was inadequate and flexural modeling was necessary.

Although details cannot be shown here, the implementation of the Airy model showed that an ever increasing 'hidden load' is needed in order to completely predict the gravity anomaly as one moves from Arabia towards Turkey and Europe. Such hidden loads are commonly used to model, for example, the *underthrusting pressure* in convergent margins or the *underplating pressure* due to hot spots (which produces a gravitational similitude of undercompensated

topography). Letting *R* be the ratio of root load to surface load, in our case one transits from the completely compensated topography of the Arabian plate in the Middle East (*R* =1), to a block with *R* =1.1 in the mountainous areas of Eastern Anatolia and Caucasus (deep blue areas in Fig. 1), and then to *R* =1.25 in western Anatolia and the Aegean. We suggest that this observation could be attributed to the existence of mantle flow that contributes to the motion of the Anatolian microplate.

As far as Greece and its closer vicinity is concerned, the computed Moho is in *absolute* accordance with the configuration of active faulting and the distribution of seismicity. In the inner part of the Hellenic Arc the shallow Moho outlines the area undergoing extension and crustal thinning, while along the Arc the deeper Moho outlines the area of convergence and crustal thickening.

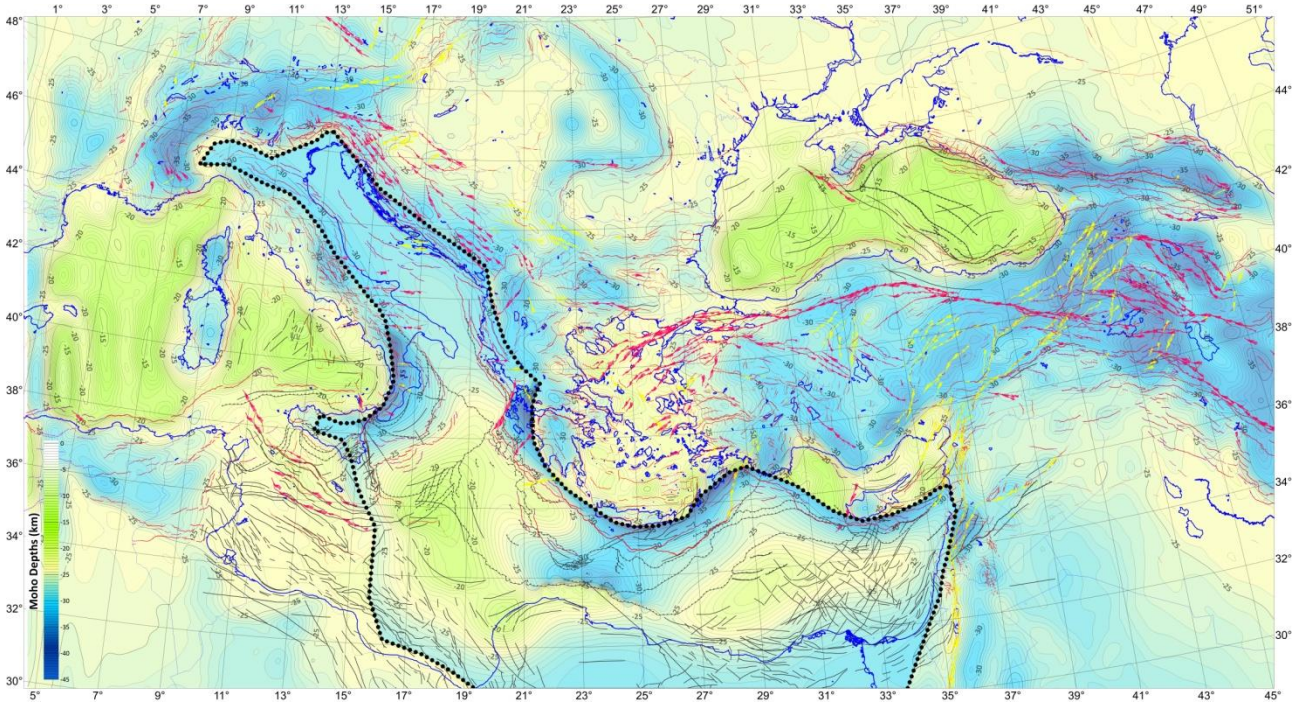

Figure 1. The Moho Depth model resulting from a combination of two different methods: the Airy isostatic model (surrounding area) and a flexural model for the central part. Black lines illustrate fault and thrust lines taken from Chamot-Rooke *et al.* (2001), Frizon de Lammote *et al.*, (2011) and Tugend *et al.* (2019). Red lines illustrate active faults taken from Bachmanov *et al.* (2017).

References

Bachmanov, D.M., Kozhurin, A.I., Trifonov, V.G., 2017. The Active Faults of Eurasia Database. *Geodynamics & Tectonophysics* 8(4), 711–736. (In Russian); http://neotec.ginras.ru/index/english/database_eng.html

Bondár, I., E.R. Engdahl, A. Villaseñor, J. Harris and D.A. Storchak, 2015. Phys. Earth Planet. Int., 239, 2-13, https://doi.org/10.1016/j.pepi.2014.06.002.

Chailas, S. and Tzanis, A., 2019, *Bull. Geol. Soc. Greece*, *Sp. Pub.* 7: Extended Abstract GSG2019-328, 289-290, available through https://ejournals.epublishing.ekt.gr/index.php/geosociety/issue/view/1265 (last accessed August 2022).

Chailas, S. et al., 2010, *Bull. Geol. Soc. Greece*, **43** (4), 1919-1929, available through http://www.geosociety.gr/images/arxeio-teuxwn/GSG_XLIII_4.pdf (last accessed August 2022).

Chamot-Rooke et al. 2001. DOTS Consortium Final Scientific Report.

Frizon de Lamotte, D., Raulin, C., Mouchot, N., Wrobel-Daveau, J. C., Blanpied, C., Ringenbach, J. C., 2011. The southernmost margin of the Tethys realm during the Mesozoic and Cenozoic: initial geometry and timing of the inversion processes. *Tectonics*, 30, TC3002. https://doi.org/10.1029/2010TC002691

Gómez-Ortiz, D., Agarwal, B.N.P., 2005, 3DINVER.M: a MATLAB program to invert the gravity anomaly over a 3D horizontal density interface by Parker–Oldenburg's algorithm. *Computers & Geosciences*, 31, 513–520

Hetenyi, 1947. Beams on elastic foundation. (*2nd printing*) The University of Michigan Press

International Seismological Centre (ISC) 2022, On-line Bulletin, https://doi.org/10.31905/D808B830

Pavlis, N. K., S. A. Holmes, S. C. Kenyon, and J. K. Factor (2012), The development and evaluation of the Earth Gravitational Model 2008 (EGM2008),J. Geophys. Res.,117, B04406, doi:10.1029/2011JB008916.

Pavlis, N. K., S. A. Holmes, S. C. Kenyon, Factor, J. K., 2012, The development and evaluation of the Earth Gravitational Model 2008 (EGM2008). JGR, 117, B04406, https://doi.org/10.1029/2011JB008916

Sandwell , D.T., Müllerwalter, R. D., Smith, H. F., Garcia, E., Francis, R. 2014. New global marine gravity model from CryoSat-2 and Jason-1 reveals buried tectonic structure. Science, 346/6205, pp. 65-67, https://doi.org/10.1126/science.1258213

Tugend, J., Chamot-Rooke, N., Arsenikos, S., Blanpied, C., Frizon de Lamotte, D. 2019. The southernmost margin of the Tethys realm during the Mesozoic and Cenozoic: initial geometry and timing of the inversion processes. *Tectonics* (AGU), 38(8), 2668-2702. https://doi.org/10.1029/2018TC005472.

16th International Congress of the Geological Society of Greece
17-19 October 2022 - Patras, Greece
Bulletin of the Geological Society of Greece, Sp. Publ. 10
Ext. Abs. GSG2022-405

An Evaluation of the Magnetic Anomalies of SE Europe in the Context of Active Tectonics.

S. Chailas[1], A. Tzanis[1], Ch. Kranis[1]

(1) Section of Geophysics – Geothermy, National and Kapodistrian University of Athens, Athens, Greece; schailas@geol.uoa.gr. (2) Section of Dynamic and Applied Geology, National and Kapodistrian University of Athens, Athens, Greece

The recompiled magnetic anomaly map of Greece (Chailas and Tzanis, 2019; Kassaras *et al.* 2020) was merged with the regional magnetic anomaly map available through the EMAG2 V3 model (Meyer *et al.* 2017), by Chailas *et al.* (2021). The resulting regional data set, henceforth Digital Magnetic Anomaly Model (D-MAM) can readily be used for the large-scale analysis of magnetized rock formations.

The fore-arc region of the Hellenic subduction system (HSS) extends up to the African coast towards the south, and as far as the Ionian Basin to the west, whose deformation is simultaneously affected by the Calabrian arc. To the north, the Adriatic plate is thicker and more rigid and interacts with the thinner Ionian and Aegean plates thus contributing to the geodynamic complexity of the HSS. To the east, the subduction doesn't stop at the southeast sector of the Aegean Sea (Dodecanese) but continues eastwards and changes direction. The back-arc extension of the Aegean plate is not confined within the expanse of the Aegean Sea but extends further to the east.

It has been established that the shape of the magnetic anomalies of magnetized alpine rock formations (e.g. ophiolites) as well as post-alpine magnetized igneous rock formations, is extensively influenced by later stage active tectonics (e.g. Tzanis *et al.* 2010). Analogous observations can be made on the regional D-MAM: The configuration (zonation) of ophiolites and their associated magnetic anomalies is collocated with the traces of later-stage active faults. The same holds for the shapes amplitudes and alignments of intrusive and extrusive igneous rock formations.

In Fig. 1, the RTP anomaly map is shown together with the major active faults and geotectonic units of the study area. For the area east of 18°E, the outcrops of igneous rock formations (including ophiolites) are also shown.

It is apparent that the different geotectonic units of the study area exhibit different and occasionally distinctive textures of magnetic anomalies. A quasi-linear configuration of magnetic anomalies is prominent in the Anatolian plate, in accordance with the alignment of active faults. The outcropping ophiolite and calc-alkaline igneous formations not only align with, but also appear to be delimited by active faulting.

In the fore-arc region of the HSS, the anomalies are confined to the accretionary wedge area. A difference in the character of the magnetic anomalies can be seen between the northern and the southern Aegean Sea. In the northern half of the Aegean, elongated anomalies collocated with seismic activity along the branches of the North Aegean Fault dominate while in the southern half the anomalies are distributed and of local character, albeit always associated with local active faults.

References

Bachmanov, D.M., Kozhurin, A.I., Trifonov, V.G., 2017. The Active Faults of Eurasia Database. *Geodynamics & Tectonophysics* 8(4), 711–736. (In Russian); http://neotec.ginras.ru/index/english/database_eng.html

Chailas, S., Tzanis, A. 2019; A new improved version of the Aeromagnetic Map of Greece. 5th International Congress of the Geological Society of GreeceAt: Athens, 22-24 May, 2019, Sp. Pub. 7, Ext. Abs. GSG2019-305, 289-290; https://ejournals.epublishing.ekt.gr/index.php/geosociety/issue/view/1265

Chailas, S., Tzanis, A., Kranis, H., 2021. Integration of the Gravity and Magnetic Anomaly fields of Greece into the respective anomaly maps of Southeastern Europe and comments on their relation to contemporary tectonics and seismicity. 37th General Assembly of the European Seismological Commission (ESC2021) Virtual Conference. http://dx.doi.org/10.13140/RG.2.2.31024.69128

Frizon de Lamotte, D., Raulin, C., Mouchot, N., Wrobel-Daveau, J. C., Blanpied, C., Ringenbach, J. C., 2011. The southernmost margin of the Tethys realm during the Mesozoic and Cenozoic: initial geometry and timing of the inversion processes. *Tectonics*, 30, TC3002. https://doi.org/10.1029/2010TC002691

Kassaras, I.; Kapetanidis, V.; Ganas, A.; Tzanis, A.; Kosma, C.; Karakonstantis, A.; Valkaniotis, S.; Chailas, S.; Kouskouna, V.; Papadimitriou, P. The New Seismotectonic Atlas of Greece (v1.0) and Its Implementation. *Geosciences*, 10, 447, https://doi.org/10.3390/geosciences10110447 .

Meyer, B., Saltus, R., Chulliat, A.. 2017: EMAG2v3: Earth Magnetic Anomaly Grid (2-arc-minute resolution). Version 3. NOAA National Centers for Environmental Information. https://doi.org/10.7289/V5H70CVX. Accessed [2017/05/30].

Tzanis, A., Kranis, H., Chailas, S., 2010. An Investigation of the Active Tectonics in Central-Eastern Mainland Greece with Imaging and Decomposition of Topographic and Aeromagnetic Data *Journal of Geodynamics* 49(2):55-67. https://doi.org/10.1016/j.jog.2009.09.042

Tzanis, A., Chailas, S., Sagredou, M., 2022. The North Euboea (Greece) Volcanic Field as Outlined by its Magnetic Anomalies. GSG2022 (245).

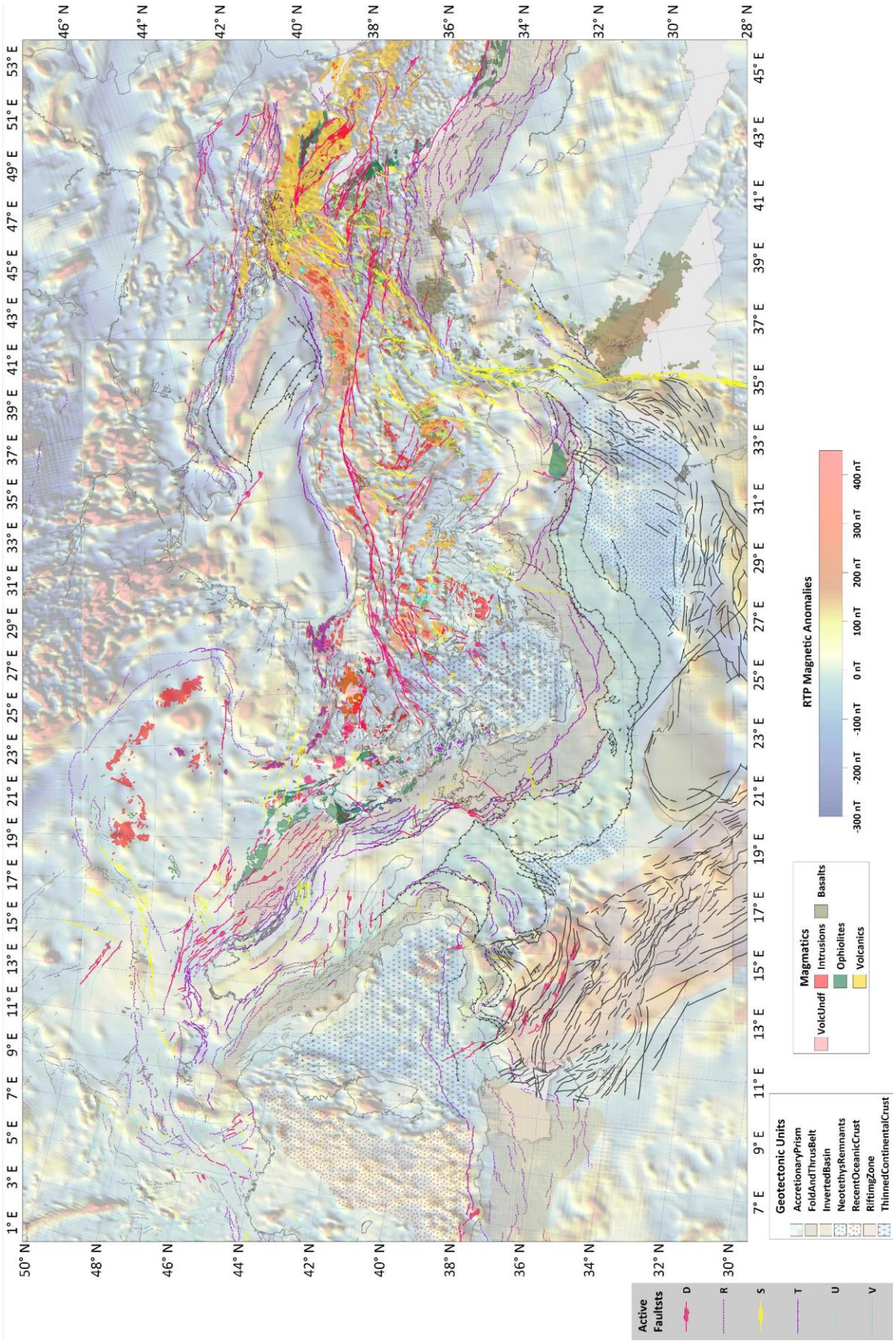

Figure 1. RTP Magnetic Anomaly coloured relief Map of the SE Europe and Northern Africa.(Data from EMAG-2 [Meyer *et al.* 2013]) for Greece, our map of Aeromagnetic Anomalies was incorporated. The main tectonic structural figure (Frizon de Lammote *et al.*, 2011) and, the active faults of the area (Bachmanov *et al.* 2017) are also depicted, as well as the the formations of magmatic origin and the ophiolitic exposures (taken from various sources)

16th International Congress of the Geological Society of Greece

17-19 October, 2022 - Patras, Greece

Bulletin of the Geological Society of Greece, Sp. Publ. 10

Ext. Abs. GSG2022-410

Evaluation of the Hellenic Arc seismic monitoring network

S. Scudero[1], A. D'Alessandro[1], A. Figlioli[2], G. Vitale[1]

(1) Istituto Nazionale di Geofisica e Vulcanologia-Osservatorio Nazionale dei Terremoti, Rome, Italy, salvatore.scudero@ingv.it (2) Università degli studi di Palermo-Dipartimento di Scienze della Terra e del Mare, Palermo, Italy.

Abstract

In this contribution, we analyse the instrumental seismicity recorded in the Greek region in the period from 1995 to 2022 and the Hellenic seismic network geometry. By analysing the Magnitude-frequency distribution of the seismic events, and by comparing their spatial distribution with the distribution of the seismic stations, we are able to get insights about the coverage and the performance of the earthquake monitoring network. The results indicate a non-uniformity of the coverage of the network over the investigated area.

Introduction

Greece and its surrounding regions are characterized by the highest seismic release in the whole Mediterranean region. In order to perform the seismic monitoring of the territory, several regional networks developed over time; their union into a national, homogeneous network started in 2005, and it has been operational since 2007. This network is today referred as the Hellenic Unified Seismological Network (HUSN). The analysis of the location performance of the HUSN was performed by D'Alessandro et al (2011) using the SNES (Seismic Network Evaluation through Simulation) method which provides, for given magnitude, hypocentral depth and confidence level, the spatial distribution of the: number of active stations in the location procedure and their relative azimuthal gaps and confidence intervals in hypocentral parameters regarding both the geometry of the seismic network and the use of an inadequate velocity model. D'Alessandro et al. (2011) proved the non-uniform monitoring coverage of the network, which does not adequately cover the southern part of Greece. In this paper we aim to further investigate the coverage and the performance of the HUSN, exploiting a methodology proposed by Siino et al., (2020), which includes the application of spatial statistics and point process method and evaluation of the Magnitude of Completeness (M_c).

Data and methods

The dataset used for data analysis was downloaded from the available website Seismological Centre of the Central Weather Bureau. The time period selected for the analysis runs from January 1, 1995 to July 4, 2022 and counts 116,894 events, with magnitude in the interval 0.10 - 7.1. For the calculation of the M_c, the range goes from 1 January 2000 to 2 August 2022.

The Maximum Curvature technique (MAXC) (Wiemer and Wyss, 2000) was used to calculate the M_c. This technique consists of evaluating the maximum curvature by computing the maximum value of the first derivative of the frequency-magnitude curve. This method is fast and uncomplicated, it is very performing to a small catalogue and gives a stable M_c. For this catalogue, the frequency-magnitude distribution (FMD) completeness magnitude is 3.0 (Figure 1). With the same method, it is possible to calculate the spatial distribution of M_c (and also of the *b* value) over the region. In particular, these values have been computed considering a minimum number of 100 events within a radius of 90 km around each map unit.

In this paper, seismicity and seismic stations are also analysed by means of point process methods. For a spatial point process, the first-order intensity is the expected number of points in a unit region around a generic location divided by its area. For spatial point patterns, the intensity is estimated non-parametrically to understand the spatial trend. The estimated intensities of the point patterns (i.e. earthquakes and seismic stations) are considered as raster data sets; pairs of rasters can be compared to determine if the spatial information within the raster data is locally correlated. The local correlation coefficient for a pair of raster maps is computed considering a grid resolution of 5 km and a neighborhood of 5x5 cells (25*25 km^2) around each cell. In this phase, the seismic catalogue has been filtered to include only the crustal events (depth >= 30km) and above the M_c threshold (M>=3.0).

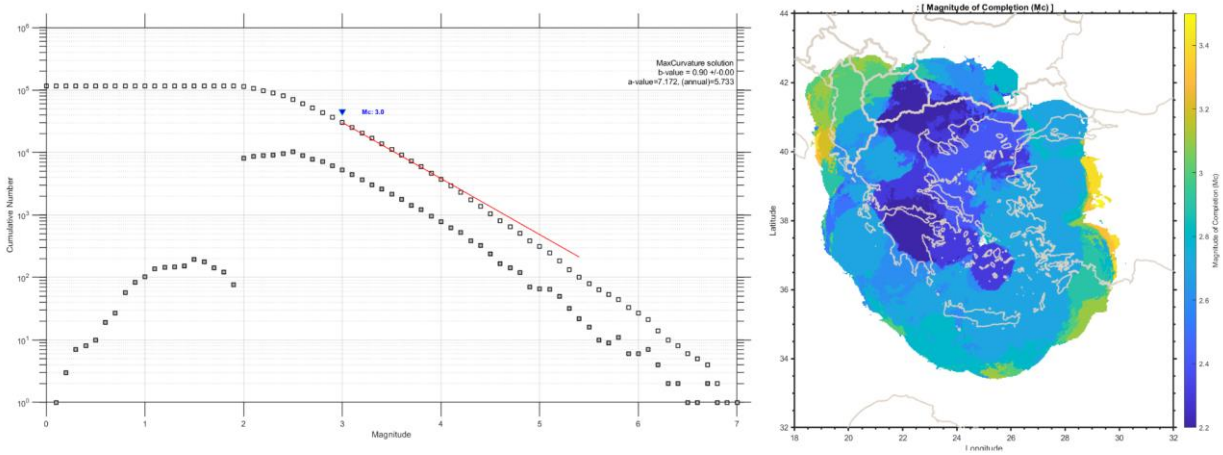

Figure 1. Magnitude-frequency relationship of the instrumental seismicity recorded in the Greece region during 1995-2022 and spatial distributions of Magnitude of completion (Mc) .

Discussion and conclusions

The earthquake and network intensities have been calculated with the grid resolution to 5 km, the values reported in the intensity plots indicate the number of stations over a 25 km^2 area The intensity of stations is characterized by two areas where more stations are clustered; the earthquake intensity shows higher values forming ring pattern, with the maximum intensity values in the western part (Figure 2).

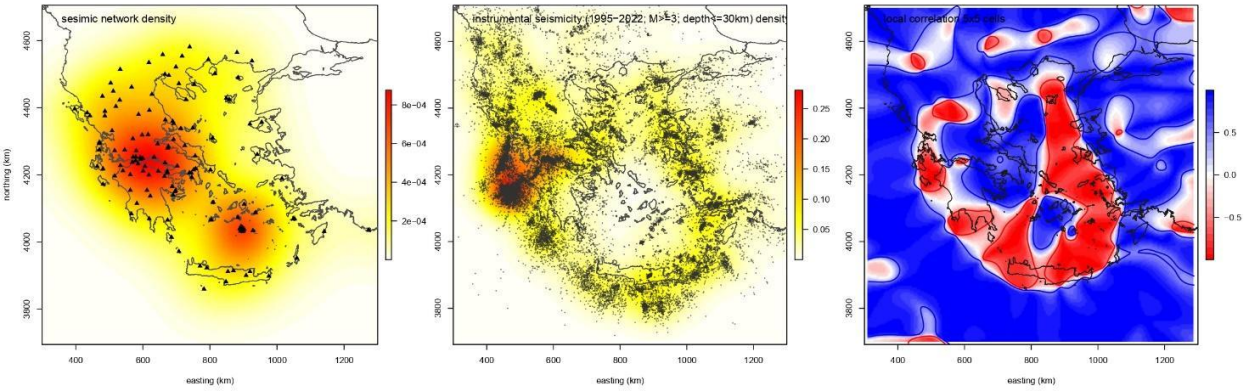

Figure 2. Kernel intensity estimation for the earthquake monitoring networks (left), kernel intensity estimations for the instrumental seismicity (centre), and their local correlation (right).

Their relationship (i.e. local correlation) is evaluated by mapping the correlation coefficient of the 25 pairs of values within the focal area (5x5 cells). Both zones with positive and negative correlation emerge (Fig. 2). The positive correlation indicates coherence between the two considered variables, conversely the negative correlation indicates discordance between the distributions of the stations and the instrumental seismicity. Two possible cases may arise: poor seismicity in a well-covered area, or lack of stations in a seismic area. Of course, the latter case is the one to avoid.

It's interesting to note that the local correlation and the M_c distribution show the same pattern. The inner part of the region, characterised by two adjacent zones of positive values (Fig. 2), correspond to the areas with lowest values of M_c (Figure 1); conversely, the areas with negative correlation (Fig. 2) correspond to the highest value of M_c (Fig. 1).

In conclusion, the zones with the negative correlations represent those areas which probably are not adequately covered by the seismic network. The geographical framework of these regions (i.e. distribution of islands across the Greek archipelago) certainly involves a control on the distribution of the seismic network. However, especially for the southern region, this work suggest to enhance the seismic network, as just suggested by D'Alessandro et al., (2011).

References

D'Alessandro, A., Papanastassiou, D., & Baskoutas, I. (2011). Hellenic Unified Seismological Network: an evaluation of its performance through SNES method. Geophysical Journal International, 185(3), 1417-1430.

Siino, M., S. Scudero, L. Greco, and A. D'Alessandro, 2020: Spatial analysis for an evaluation of monitoring networks: examples from the italian seismic and accelerometric network. Journal of Seismology, 24 (6), 1045–1061, doi:https://doi.org/10.1007/s10950-020-09937-0.

Wiemer, S., & Wyss, M. (2000). Minimum magnitude of completeness in earthquake catalogs: Examples from Alaska, the western United States, and Japan. Bulletin of the Seismological Society of America, 90(4), 859-869.

16th International Congress of the Geological Society of Greece
17-19 October, 2022 - Patras, Greece
Bulletin of the Geological Society of Greece, Sp. Publ. 10
Ext. Abs. GSG2022-422

Exploring the use of magnetic properties of playground sands as a pollution proxy from the broader area of Thessaloniki, Greece

A. Bourliva[1], E. Aidona[1], L. Papadopoulou[1], Ch. Sarafidis[2], N. Kantiranis[1]

(1) Aristotle University of Thessaloniki, School of Geology, Thessaloniki, Greece, aidona@geo.auth.gr (2) Aristotle University of Thessaloniki, School of Physics, Thessaloniki, Greece.

Recreation and green areas play a vital role in the socio-economic development and sustainability of large urban centers. Many researchers have highlighted the need to control soil/dust quality in recreation sites of urban agglomerations, especially in those where children are exposed. Particularly, in children's play sites it is imperative to quantify the levels of Potential Harmful Elements (PHEs) in soils and dusts, with a large number of researchers focusing on the determination of their chemical composition. On the other hand, extensive reports in the international literature on the observed relationship between anthropogenic pollution and magnetic signature of soils/dusts, reinforce the effectiveness of magnetic mapping of urban areas in determining their degree of pollution. Specifically, the use of magnetic methods is proposed as a quick and inexpensive first step in assessing soil/dust pollution by providing qualitative data on its degree and extent. However, the studies focused on magnetic measurements in children's recreation and exposure areas are to our knowledge rather limited. The aim of the present study was to perform thorough magnetic analyses in order to provide information regarding the type, concentration, and relative grain-size distribution of iron-bearing magnetic phases in playground sand. For this reason, sand samples were collected within the top layer at 37 public playgrounds in the broader area of the city of Thessaloniki. Composite samples from 2-5 different points from the playground were collected. The sampling criteria used were the following: the sampling spots were not covered by the treetops, they were not at the edge of the playground or near to vegetation or urban furniture and they were visibly dry. Unexposed samples were not dispensable, however freshly replaced sand samples were gathered. Sampling was conducted in a dry period (August-September 2019) when no rain event had occurred for several weeks. Information regarding maintenance activities (i.e. disinfection, sand renewal) were not available. Magnetic measurements including mass specific magnetic susceptibility (χ) at low and high frequencies, frequency-dependent susceptibility (χFD%), temperature-dependence magnetic susceptibility represented by thermomagnetic curves, anhysteretic remanent magnetization (ARM) and isothermal remanent magnetization (IRM) were carried out.

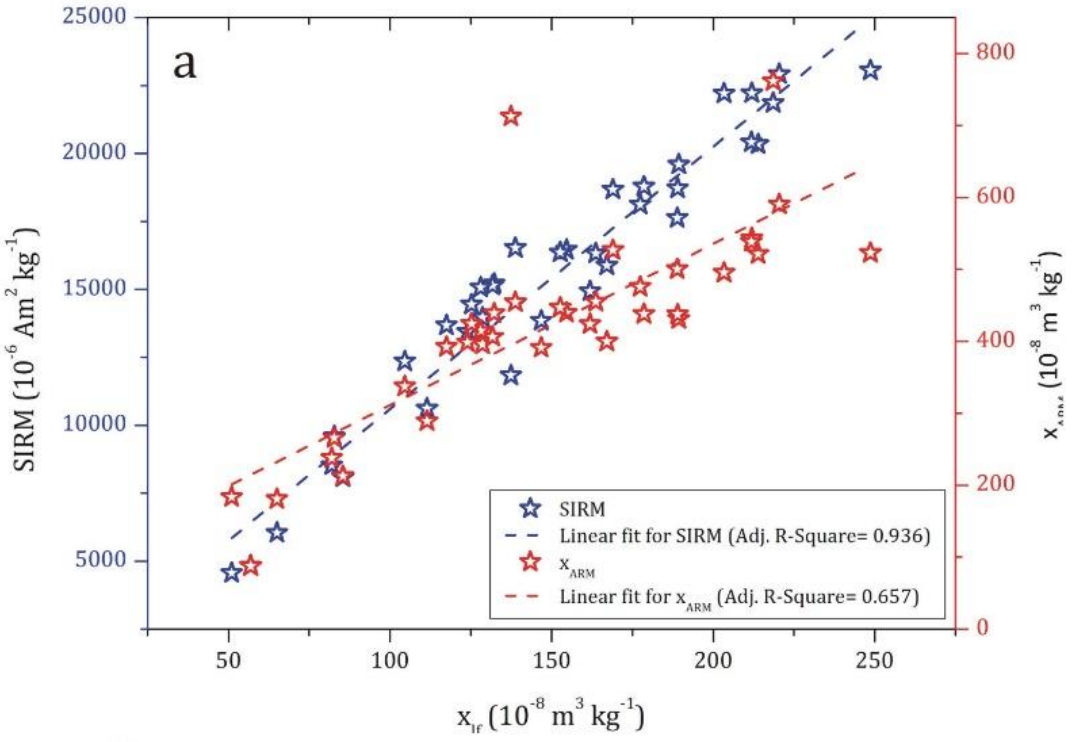

Figure 1. Scatter plots of SIRM and χARM versus χlf, showing strong correlation

Magnetic susceptibility ranged between 51 to 248.7×10^{-8} m^3 kg^{-1} (with a median of 149.8×10^{-8} m^3 kg^{-1}) indicating an enhanced level of anthropogenic sand bound magnetic components in the PG sands. Despite the limited data, the obtained χlf values were lower than the ones reported by other researchers for playground dusts (Ng et al., 2003; Yang et al., 2017), while they are notably higher than the χlf values referred for urban park soils (Lu and Bai, 2006; Wang et al., 2017) and street dusts (Dytłow et al., 2019). In addition, SIRM and χARM, which are characteristic concentration related magnetic parameters, were evaluated. SIRM ranged between 456.5 ×10^{-5} Am^2 kg^{-1} to 2306 ×10^{-5} Am^2 kg^{-1} with a median value of 1554.6×10^{-5} Am^2 kg^{-1}. A strong positive linear correlation among χlf and SIRM was evident (Fig. 1) underscoring the dominance of ferrimagnetic minerals to the magnetic signal of the PG sands. On the other hand, χARM, exhibited a range of 87.6–761.7 ×10^{-8} m^3 $kg^{-1}$with a median value of 434.4×10^{-8} m^3 kg^{-1}, while the significant correlation with the χlf values (Fig. 1) revealed the dominant control of SSD grains on the magnetic load of PG sands.

Additionally, geochemical analyses in magnetic extracts separated from PG sands were performed, indicating that metal(loid) contents were notably enriched in the magnetic fraction validating their strong affinity with sand-bound magnetic particles. Finally, bioaccessibility tests revealed lower UBM-extracted fractions for the magnetic extracts of PG sands compared to bulk samples. However, arsenic (As) was more bioaccessible in the sand-bound magnetic particles raising serious concerns for the children exposed to playground sands.

References

Dytłow, S., Winkel, A., Górka-Kostrubiec, B., Sagnotti, L., 2019. Magnetic, geochemical and granulometric properties of street dust from Warsaw (Poland). J. Appl. Geophys. 169, 58–73.

Lu, S.G., Bai, S.Q., 2006. Study on the correlation of magnetic properties and heavy metals content in urban soils of Hangzhou City, China. J. Appl. Geophys. 60, 1–12.

Ng, S.L., Chan, L.S., Lam, K.C., Chan,W.K., 2003. Heavy metal contents and magnetic properties of playground dust in Hong-Kong. Environ. Monit. Assess. 89, 221–232.

Wang, G., Ren, F., Chen, J., Liu, Y., Ye, F., Oldfield, F., Zhang, W., Zhang, X., 2017. Magnetic evidence of anthropogenic dust deposition in urban soils of Shanghai, China. Chem. Erde 77, 421–428.

Yang, M., Li, H.-M., Li, F.-Y., Wang, J.-H., Diao, Y.-W., Qian, X., Yang, Z.-P., Wang, C., 2017. Magnetic response of heavy metal pollution in playground dust of an industrial area. Huanjing Kexue 38, 5282–5291.

16th International Congress of the Geological Society of Greece
17-19 October, 2022 - Patras, Greece
Bulletin of the Geological Society of Greece, Sp. Publ. 10
Ext. Abs. GSG2022-423

The January 2022 Florina (Northwestern Greece) Earthquake: Source Process and Interactivity of Active Tectonics and CO2 Gas Emissions

N. Vavlas[1], A. Kiratzi[1], Z. Roumelioti[2]

(1) Aristotle University of Thessaloniki, Thessaloniki, Greece, navavlas@geo.auth.gr (2) University of Patras, Patras, Greece.

Research Highlights

The slip model of the January 9, 2022, M5.5 earthquake in Florina (Northwestern Greece), derived by inverting regional broad band and strong ground motion waveforms, revealed west-dipping normal faulting with slip on a single patch at relatively large depth (12-19 km).

Introduction

On January 9 of 2022 (21:43:47 UTC) a M5.5 earthquake occurred just underneath the highly populated town of Florina. The earthquake ruptured a previously unmapped fault, panicked the citizens but the damage in Florina town was limited to mainly old and disused houses. The area that the aftershock sequence spatially extended belongs to the homonymous Florina Basin, located in northwestern Greece and being characterized by NE-SW striking normal faults. The region has been shaken only by small to moderate magnitude earthquakes during the instrumental era of seismicity. The most recent events include the swarm that took place in 2013-2014 (Mesimeri et al., 2017) and its occurrence was linked to fluid migration and CO2 gas emissions. In terms of seismic hazard, it belongs to the zone of lowest design peak acceleration (0.16g) according to the Greek seismic code. Against this background, the moderate magnitude event of January 9, 2022, being the strongest instrumentally recorded event that occurred within the Florina natural CO2 field motivates further study. In this work, we aim to study the slip distribution on the fault by retrieving the source model using kinematic slip inversion.

Methodology

To study the source, we used the methodology and code of Gallovič et al. (2015) that provides a kinematic finite-fault description of the rupture. In essence, the rupture process is discretized in space and time along a given fault plane, and the model parameters are the spatial-temporal samples of the slip rates, spanning the whole rupture duration. An advantage of the methodology is that rupture is not forced to nucleate at hypocenter and so its location is not required as an input. For our case, the fault was modelled as a rectangle, 12km × 9km along strike and along dip, respectively. Its orientation, e.g., strike, dip, and rake, was grid searched in the vicinity of the centroid solution reported by NOA (National Observatory of Athens).

The data used are displacement waveforms acquired either by single integration of broadband stations or double integration of strong motion stations. Green's functions were calculated for the assumed fault orientation, position and faulting mechanism and were filtered exactly the same way as the real data. The inversion was done in the frequency range 0.05-0.13 Hz in terms of a 4th order causal (single-pass) Butterworth filter.

Results

The inversion results are presented on Fig.1a where the slip model on map view is shown alongside the moment rate function on the top right part of the figure. The optimal strike/dip/rake angles for the inversion were 277°/59°/-66°, in the sense that they provided the best waveform fit and the least amount of ghost features (unphysical occurrences of slip). Both nodal planes were tested, and a NW dipping fault provided a better fit. More tests are needed together with geological evidence and seismic cross sections for the verification of the dip direction. It is worth noting that the published moment tensors from NOA(shown on Fig.1a) and GMT report a depth of 16km and 18km respectively while the hypocenter from NOA is also at located at 14km depth. This range of depth values is also evident on the geometry of the preferred fault model that extends at 12km-19km depth.

As depicted on the map, slip is concentrated above the hypocenter (red star) according to the modeled NW dipping fault plane. The town of Florina is located at the fault's upper edge just ~2km away from the hypocenter and very close to the locus of peak slip. This signifies that despite the moderate amount of moment released during the earthquake, the highly populated town may be susceptible to damage from future events. This slip distribution on fault from the inferred slip model comprises one single asperity. There are no signs of rupture complexity which can be ruled out given the magnitude of the event. Fig.1b shows the waveform fit between real (black) and synthetic (red) waveforms obtained by forward simulation from the obtained slip model. Overall, a good variance reduction (0.58) was obtained given the moderate magnitude of the event.

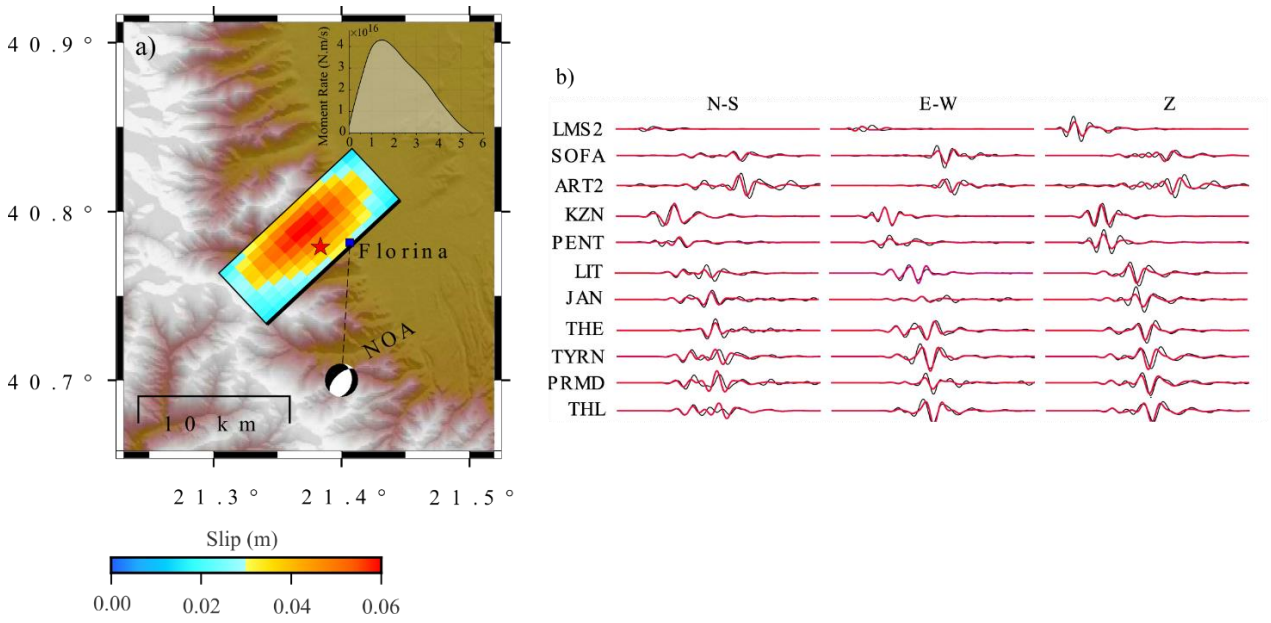

Figure 1. a) Slip distribution of the (NW) fault on map view resulting from the kinematic inversion. Moment rate function of the model is show on the top right part of the figure that depicts the ~5s source duration. Red asterisk marks the epicenter. a) Waveform fit between real(black) and synthetic(red) data for the 3 components of both strong motion and broadband stations.

Conclusions

The 9 January 2022 earthquake sequence in Florina basin provided the first instrumentally recorded evidence for the continuity of active extension along NE-SW striking normal faults in western Greece. The mainshock is the strongest earthquake to be instrumentally recorded in this otherwise moderate seismicity region. The focal mechanism indicates activation of a blind normal fault striking NE-SW and dipping to the west. The strike of the causative fault is parallel to the western margin of the Florina Basin and parallel to the fault zone that created the basin itself. In the broader area of the Florina sedimentary basin, CO2 leakage creates widespread mineral springs and wells connected to a slow upward migration of CO2 along rock fractures. Previous swarm activity in the same seismogenic region, occurred in 2013-2014 was related to gas migration (Mesimeri et al., 2017; Kaviris et al., 2020).

The inferred slip model, obtained from finite-fault inversion using regional broad band and strong ground motion waveforms, shows breakage of a single asperity. The locus of peak slip and the majority of slip concentration is located above the hypocenter. The upper edge of the fault is buried at a depth of ~12 km, and this partly explains the limited damage to the town of Florina, considering that the hypocenter was literally beneath it.

Even though the 2022 mainshock is in accordance with the tectonic regime and contemporary stress field, its activation might have been enhanced by the widespread fluid circulation.

Acknowledgements

This research was supported by the Hellenic Foundation for Research and Innovation (H.F.R.I.) under the “2nd Call for H.F.R.I. Research Projects to support Faculty Members & Researchers” (Project Number: 2724). AK and NV acknowledge support by the project “Safe-Schools” which is implemented under the Action “Reinforcement of the Research and Innovation Infrastructure”, funded by the Operational Programme "Competitiveness, Entrepreneurship and Innovation" (NSRF 2014-2020) and co-financed by Greece and the EU (European Regional Development Fund).

References

Gallovič, F., Imperatori, W., Mai, P. M., 2015. Effects of three-dimensional crustal structure and smoothing constraint on earthquake slip inversions: Case study of the Mw6. 3 2009 L’Aquila earthquake. *Journal of Geophysical Research: Solid Earth*, *120*(1), 428–449.

Kaviris, G., Spingos, I., Karakostas, V., Papadimitriou, E., & Tsapanos, T., 2020. Shear-wave splitting properties of the upper crust, during the 2013–2014 seismic crisis, in the CO2-rich field of Florina Basin, Greece. Physics of the Earth and Planetary Interiors, 303, 106503. https://doi.org/10.1016/j.pepi.2020.106503

Mesimeri M., Karakostas V., Papadimitriou E., Tsaklidis G., Tsapanos T., 2017. Detailed microseismicity study in the area of Florina (Greece) Evidence for fluid driven seismicity. Tectonophysics, 694:424–435. /10.1016/j.tecto.2016.11.027.

16th International Congress of the Geological Society of Greece
17-19 October, 2022 - Patras, Greece
Bulletin of the Geological Society of Greece, Sp. Publ. 10
Ext. Abs. GSG2022-424

The good, the bad and the ugly: Computing high-frequency attenuation from otherwise unusable seismic recordings thanks to noise modelling

E.V. Pikoulis [1], O.J. Ktenidou [2]
(1) University of Patras, Patras, Greece, pikoulis@ceid.upatras.gr (2) National Observatory of Athens, Athens, Greece.

Research Highlights

By modeling rather than avoiding the noisy part of the Fourier spectrum, we demonstrate a technique to render high-noise seismic recordings usable. We achieve a more robust estimate of high-frequency spectral parameters, , succeeding at using very low-quality data down to around SNR=1.

Scope and method

The high-frequency attenuation parameter, kappa (κ; Anderson and Hough, 1984), is measured on the Fourier amplitude spectrum of recorded ground motions. There are several methods to do this, including band-limited ones focusing on the spectral slope and broadband ones inverting several seismic parameters. What they all have in common, however, is that the user must select the frequency band in which to apply them based on a judgment of the signal quality. This is typically done (if at all) by applying the traditional signal-to-noise ratio (SNR) and excluding frequencies where the noise is strong. This typically penalizes higher frequencies.

In this work, we use the recent technique proposed by Pikoulis et al. (2020), which stochastically models the noise spectrum with the aim of improving the signal spectrum and rendering it usable at higher frequencies. We demonstrate the discrepancy between the traditional (noise-avoiding) and new (noise-modeling) technique on recorded as well as simulated data. By modeling rather than avoiding the noise, we achieve a more robust estimate of kappa by using data down to around SNR=1. We do not need to rely on any particular theoretical model or assumption, and it is also possible to go beyond conventional noise models to more unfavorable conditions such as spectral peaks, etc.

Results and conclusions

In the context of the INL project described by Silva *et al.* (2021), the maximum likelihood (ML) method of Pikoulis *et al.* (2020) was successfully used on a limited ground-motion dataset from a low-seismicity, stable continental region, increasing the number of usable recordings by about 25%. This was achieved despite the unusual spectral shape of the background noise at the sites under study, which included spectral peaks such as those shown in grey in Figure 1 at 30 Hz.

The entire dataset included only one high-quality recording with ample frequency band to estimate high-frequency attenuation κ (Figure 1 – top). This was used to demonstrate the ability of the ML method to go well within the noise and through the spectral peak, doubling the usable bandwidth and retrieving a spectral slope (κ) similar to the one computed when using the traditional criterion of SNR>3 (72 ms out to 45 Hz, as opposed to 67 ms with the classic method out to 25 Hz indicated by the thick arrow).

The dataset included numerous recordings of poor quality that afforded a limited bandwidth to compute κ in (Figure 1 – middle). Such estimates are not considered robust, as they may be frequency-dependent. The ML method confirmed and improved the classic estimates, multiplying the usable bandwidth (e.g. 145 ms out to 30 Hz, as opposed to 142 ms out to 12 Hz) and decreasing the uncertainty of the estimate.

Finally, the dataset included several very poor recordings where the signal hardly exceeded the noise level at any frequency, rendering it impossible to use them to any purpose, much less to compute κ, due to a usable bandwidth of only a couple of Hz, as indicated by the thick arrow (Figure 1 – bottom). The ML method rendered these recordings usable and yielded a robust estimate of κ that was stable for different frequency ranges (e.g. 140 ms out to 25 Hz, as opposed to no estimate).

Impact

This demonstration opens the way towards a more robust estimate of any high-frequency spectral parameter from low-quality or even unusable seismic recordings. We believe it should be a valuable tool not only for κ, but also for the study of stress drop, especially in the context of small events and microseismicity.

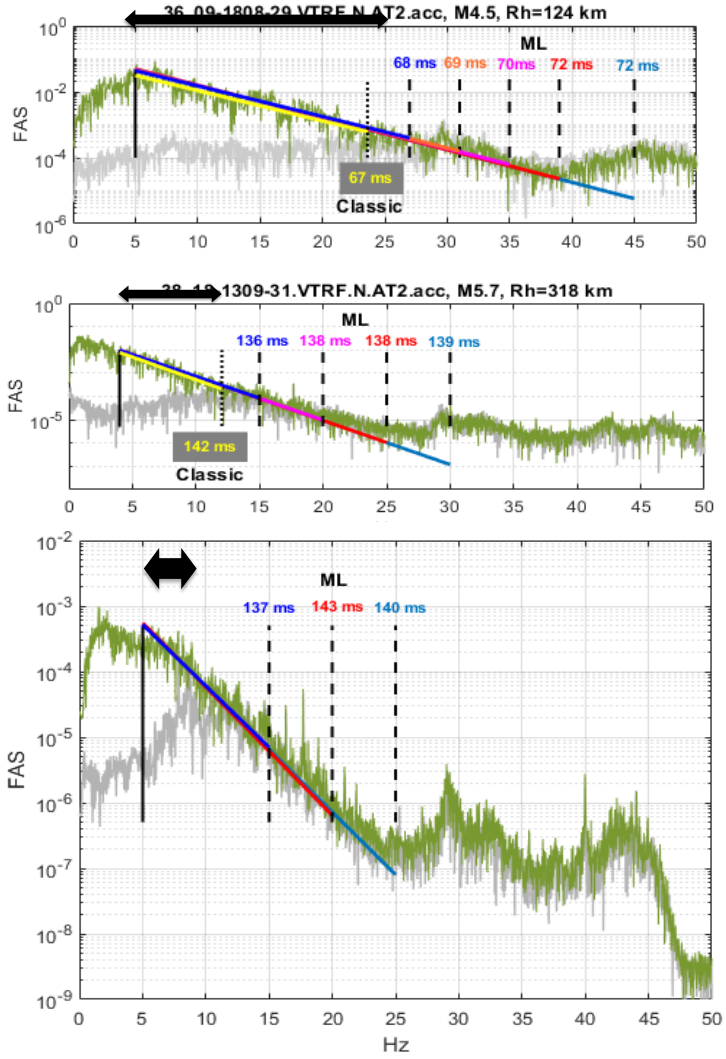

Figure 1. Top to bottom: examples of the estimation of κ on signals of deteriorating quality (from top to bottom). Usable bandwidth according to the classic noise-avoiding method is indicated by the thick arrows, while estimates in colour indicate ML estimates out to various frequencies well within the noise.

Acknowledgements

This work stems from work done together with profs Norm Abrahamson (UC Berkeley, US) and Emmanuel Psarakis (University of Patras) and their early contributions are gratefully acknowledged.

References

Anderson, J.G., Hough, S.E., 1984. A model for the shape of the Fourier amplitude spectrum of acceleration at high frequencies, Bull. Seismol. Soc. Am. 74, 1969–1993.

Pikoulis, E-V., Ktenidou, O-J., Psarakis, E.Z., Abrahamson, N.A., 2020. Stochastic modeling as a method of arriving at higher frequencies: An application to κ estimation, J. Geophys. Res. 125.

Silva, W.J., Darragh, R.B., Kishida, T., Ktenidou, O.-J., Pikoulis, E.-V., 2021. INL SSHAC Level 3 study: Estimation of source, path, and site parameters and their uncertainty. INL Report INL/EXT-21-65281, Idaho National Laboratory, Idaho Falls, p. 259.

16th International Congress of the Geological Society of Greece

17-19 October, 2022 - Patras, Greece

Bulletin of the Geological Society of Greece, Sp. Publ. 10

Ext. Abs. GSG2022-425

Turning A Linear Geometry Force Balance Accelerometer To A Broad-Band Seismometer: Design, Modelling, And Evaluation

N. Germenis[1,2,4], G. Dimitrakakis[1], E. Sokos[2], P. Nikolakopoulos[3]

(1) GEObit-Instruments, Patra – Greece, ngermenis@geobit-instruments.com (2) Laboratory of Seismology, Dept. of Geology, University of Patras, Rio – Greece (3) Machine Design Laboratory, Dept. of Mechanical Engineering & Aeronautics, University of Patras, Rio – Greece

Research Highlights

- A newly designed force-balance seismometer is presented.

Introduction

The problem of ground motion recording, over a wide band of frequencies and amplitudes, has been a key point for seismology and has been studied extensively by various researchers (see Bormann, 2002; Wielandt 2002; Wielandt and Streckeisen, 1982 and references therein). A number of seismometer designs have been proposed e.g., Usher *et al*, 1977; Habbak *et al*, 2015; Koutsoukos and Melis, 2005, and most of them are based on rotational pendulum seismic mass systems and electronic controllers with a Proportional-Derivative-Integral (PID) controller architecture. In this paper we investigate the performance of a new broadband seismometer design, which is based on a combination of a high-performance seismic accelerometer, followed by a continuous time analogue integrator. This combination produces analogue velocity seismic signals, with a flat response range extending from 120s to 85Hz. Instrument's sensitivity is adjustable due to a gain differential output amplifier that follows the analogue integrator. Its mechanical system is an evolution of a previously linear based geometry setup, used for the implementation of a high-performance seismic accelerometer (Germenis *et al*, 2022). To achieve a better performance, the accelerometer's mechanical system had to be significantly modified compared to that in Germenis *et al*, 2022, with adding a much larger seismic mass, lowering the spring stiffness, and using a wider area for the capacitive displacement transducer; the rest of the architecture principles, e.g., the linear motion geometry, remain basically unaltered. The electronic continuous time analogue integrator, developed for the purposes of the present work, was carefully designed to provide a self-noise level below NLNM down to at least 100s, a feature that, accordingly, results to the high performance of the instrument in terms of total noise. Based on initial tests, in a seismic vault, the instrument's self-noise is lower than the low-noise model, described by Peterson, 1993, between 80s and 16Hz.

Sensor design - General description

The seismic sensor's design is based on two main parts: a) a mechanical accelerometer spring-mass system, along with a double electromagnetic force actuator and b) the electronics board. The block diagram of the sensor is presented in Fig.1 (horizontal component). The same design is used for the vertical component if rotated by 90°. The mechanical system is firmly positioned in a hollow aluminum frame. The acceleration is applied to the frame along the axial direction of the sensing element and causes a displacement of the mass relative to the frame. The mass displacement is sensed by a capacitance transducer with a sensitivity At [V/m]. The transducer's output voltage is fed to a low noise preamplifier with gain A_1. Then, the signal is fed to a demodulator that derives the seismic signal from the amplitude modulated carrier signal. The carrier signal is generated by the signal generator "sin" (Fig.1). The output goes to amplifier A_2 at the open loop path which is the only trimmable amplifier stage in the loop. Its output is converted to a current signal by an R-C network, that implements a Proportional-Derivative (PD) control logic, and its current is fed to the double electromagnetic force actuator, which applies a restoring force to the seismic mass, with a proportionality constant Gc [N/A]. The output of A_2 amplifier represents the acceleration signal and it is driven to the analogue integrator $\int A(t)dt$ to obtain the velocity equivalent seismic signal. Unit A_0 is the final output amplifier.

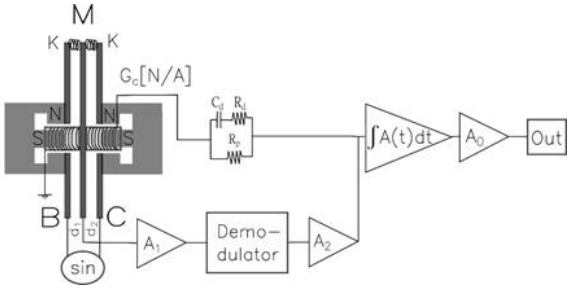

Figure 1. Simplified block diagram of the seismic sensor component.

Sensor's noise – noise power spectral density evaluation

The prototype sensor was tested at the seismic vault of the Seismological Laboratory of the University of Patras, to derive its ability to properly resolve seismic signals. The sensor was attached to a six channel GEObit 32bit ADC seismic digitizer. For sensor's self-noise calculation, one Nanometrics Trillium 120s sensor was used as the reference. Both seismometers were connected to the six-channel digitizer, which was left to record for several days at 100sps, 40Vpp for both sensors. The total noise power spectral density (PSD) of each sensor, has been derived using long term recordings. The method described in McNamara and Boaz, 2006, was used for the calculation of the power spectra density (PSD) of a six-day data segment for both seismometers. The PSD analysis was made for all the components (Z, N, E). Results are presented in Fig.2, plots on the top panels belong to the reference instrument, while the prototype instrument's plots are presented on the bottom panels of Fig.2. It is evident that the two sensors depict the same behavior in all recording components.

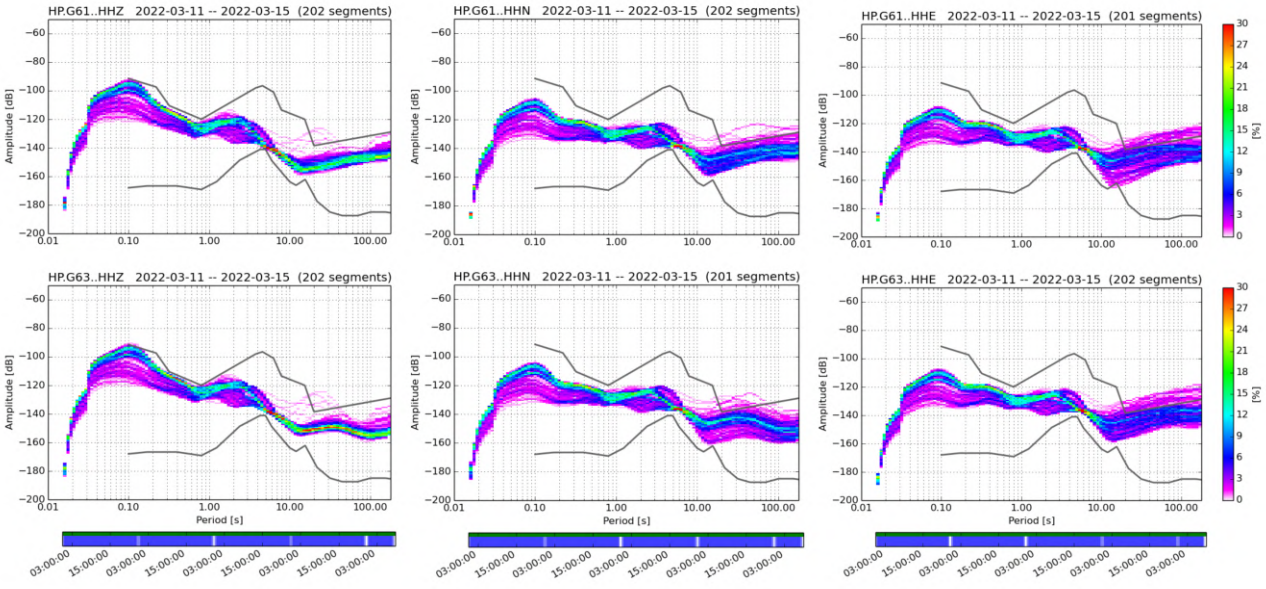

Figure 2. Power spectral density plots for the reference instrument (top) and the prototype (bottom). From left to right the Z, N and E component is presented.

Conclusions

We present here a newly designed force-balance seismometer. Its core is a spring-mass mechanism with two leaf springs and a double coil forcer, attached on a movable conductive plate in between two stationary plates, which form a capacitive displacement transducer. The double-spring and the double-coil ensure a linear motion of the seismic mass and a symmetrical operation on both sides of the sensor's rest position. The instrument's performance, in terms of signal fidelity and noise level, is evaluated in comparison to a well-established commercial product. The new seismometer was found to satisfy the expectations of its suggested specifications (120sec-85Hz bandwidth, 1200V/m/s). Its low-cost characteristics (raw materials, easy design process, available electronic components) guarantee easy manufacturing and high repeatability in a production line.

References

Bormann, P (2002) Seismic signals and noise, chapter 4. In: Bormann P (ed) New manual of seismological observatory practice, vol 1. GeoForschungsZentrum, Potsdam

Germenis, N., Dimitrakakis, G., Sokos, E., Nikolakopoulos, P., 2022. Design, Modeling, and Evaluation of a Class-A Triaxial Force-Balance Accelerometer of Linear Based Geometry. Seismological Research Letters 2022; 93 (4): 2138–2146. doi: https://doi.org/10.1785/0220210102

Habbak, E., Nofal, H., Lotfy, E., El-Sabban, S., Nossair, Z., 2015. Design and simulation of a vertical broadband seismometer, Arab J Geosci 9, 408 (2016). https://doi.org/10.1007/s12517-016-2422-x

Koutsoukos, E.T., Melis, N.S., 2005. A Horizontal Component Broadband Seismic Sensor Based on an Inverted Pendulum, Bulletin of the Seismological Society of America 2005; 95 (6): 2462–2471. doi: https://doi.org/10.1785/0120050040

McNamara, D.E., Boaz, R.I., 2006. Seismic Noise Analysis System Using Power Spectral Density Probability Density Functions—A Stand-Alone Software Package. Open-file report 2005-1483, US Geological Survey.

Peterson, J., 1993. Observations and modeling of seismic background noise. Open-file report 93–322. US Geological Survey, Albuquerque

Usher, M.J., Buckner, I.W., Burch, R.F., 1977. A miniature wideband horizontal-component feedback seismometer. J. Phys. E Sci. Instrum. 10, 1253–1260.

Wielandt, E., 2002. Seismic sensors and their calibration, chapter 5. In: Bormann P. (ed), New manual of seismological observatory practice, vol 1. GeoForschungsZentrum, Potsdam

Wielandt, E., Streckeisen, G., 1982. The leaf-spring seismometer – design and performance. Bull Seis Soc Am 72(6):2349–2367.

16th International Congress of the Geological Society of Greece
17-19 October, 2022 - Patras, Greece
Bulletin of the Geological Society of Greece, Sp. Publ. 10
Ext. Abs. GSG2022-426

A New Force Balance Accelerograph for Earthquake and Structural Monitoring Based On A Linear Geometry Accelerometer

N. Germenis[1,2,4], G. Dimitrakakis[1], E. Sokos[2], P. Nikolakopoulos[3]

(1) GEObit-Instruments, Patra – Greece, ngermenis@geobit-instruments.com (2) Laboratory of Seismology, Dept. of Geology, University of Patras, Rio – Greece (3) Machine Design Laboratory, Dept. of Mechanical Engineering & Aeronautics, University of Patras, Rio – Greece

Research Highlights

- A newly designed force-balance accelerograph for earthquake and structural monitoring, is presented.

Introduction

Seismic accelerometers are classified according to their incorporated technology or principle of operation. Some main types are the piezo-electric, the micro-electromechanical (MEM) and the force-balance accelerometers (FBA) (Piersal and Paez, 2010; Santos *et al.*, 2019; Ringler, 2015, 2020). The self-noise of an accelerometer is a key parameter in earthquake and structural monitoring where ambient noise measurements are required. The highest dynamic range is provided by the FBA accelerometers that exceeds 150dB and therefore these sensors are ideal for seismic or ambient noise measurements. For example, most of the sensors used in structural monitoring of bridges, are FBAs. In such applications the bridge's modal analysis is performed (Talha *et al.*, 2003). Several pendulum spring-mass mechanism FBAs have been described in the past, e.g., Hitachi Ltd. (1985) and Kinemetrics Inc. (1997, 2005). In this work we describe a linear motion mechanical system, abutted on two leaf springs, and carefully shaped to minimize unwanted torsional motion. With the use of carefully selected electronic components, like ultra-low noise operational amplifiers and with careful design of the feedback loop, a high-performance FBA with a wide bandwidth from DC to 200Hz and dynamic range over 150dB is built. The digitizer of the accelerograph is implemented over a single high density, multilayer PCB board. It is mainly designed according to a two-processor architecture, channel sampling and data timestamping are in dedicated real-time CPU board section. The Seedlink encoding, streaming and local storage through locally running open-source components, is ported on the ARM Linux board section. On-demand streaming, based on local Seedlink server chains, local signal processing and trigger detection, based on multiple schemes (amplitude, STA/LTA etc.) through open-source components, is ported from the Earthworm toolchain. MQTT-based signaling for trigger event distribution is supporting multiple centralized or distributed schemes (https://mqtt.org/). The overall performance of the instrument is described in terms of its transfer function; its excellent noise behavior is illustrated in a comprehensive manner with spectral density noise plots (Fig.3). Finally, the power spectral density plots of some common earthquake recordings of the presented FBA and of a reference instrument are presented. (Fig. 4) It results that the proposed FBA design has a performance like that of other well-established strong motion sensors, while being more robust and cost effective.

Sensor design - General description

The accelerometer sensor design is based on two main parts: a) a mechanical accelerometer spring-mass system, along with a double electromagnetic force actuator and b) an electronics board. The mechanical system has been extensively simulated to calculate the spring shape and material. The simulation showed that an ellipsoid shape spring must be used. The main free oscillation mode was found at 58.16Hz (Fig. 2) and all other oscillation modes have a frequency far outside the recording band (DC-200Hz) The block diagram of a horizontal FBA component is presented in Fig.1.

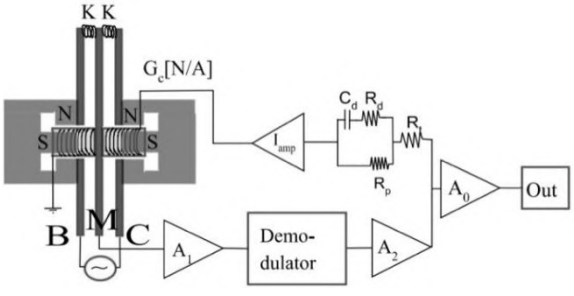

Figure 1. Simplified block diagram of the FBA accelerometer

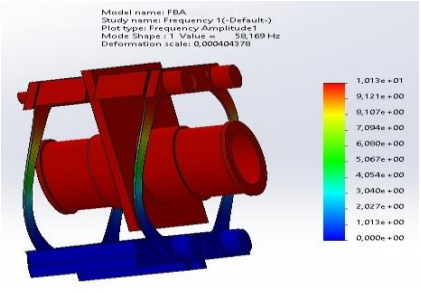

Figure 2. 3D view of the spring-mass system, at the first normal oscillation mode.

The same design can be used as a vertical component if rotated by 90°, after the proper mechanical adjustment of seismic mass position. The mechanical system is firmly positioned in a hollow aluminum frame, which in turn is tightly anchored, on a steel base. The acceleration is applied to the frame along the axial direction of the sensing element and causes a displacement of the mass relative to the frame. The mass displacement is sensed by a capacitance transducer with a sensitivity A_t [V/m]. The transducer's output voltage is fed to a low noise preamplifier with gain A_1. In the next step, the signal is fed to a demodulator that derives the seismic signal from the amplitude modulated carrier signal. The carrier signal is generated by the signal generator "~" (Fig.1), which is a sinusoidal signal, with amplitude 15Vpp, frequency 30kHz and 180° phase difference between the two capacitor plates. The output goes to amplifier A_2 at the open loop path. Its output is converted to a current signal by an R-C network, and through a dual stage current amplifier goes to the double coil force transducer (forcer). The forcer applies a restoring force to the seismic mass, with a proportionality constant G_c [N/A]. The term "double" denotes that there are two coils on the seismic mass, electrically connected in series, interacting with two permanent magnets placed on both inner sides of the metal frame, as illustrated in Fig.1. The output of A_0 amplifier represents the acceleration signal and it is driven to the digitizer which is connected to the output of each acceleration sensor (three channels digitizer).

Sensor's noise – noise power spectral density evaluation

The prototype accelerograph was tested at the seismic vault of the Seismological Laboratory of the University of Patras, to derive its ability to properly resolve seismic signals. For the sensor's self-noise calculation, one Guralp 5T sensor connected to a GEObit digitizer was used as the reference instrument. Both recording systems were left to record for several days at 100sps. The total noise power spectral density (PSD) of each sensor, which is the sum of the instrument's self-noise plus the site's ground noise, has been derived using a quiet signal part. The Welch averaging method (Welch, 1967) was used for the calculation of the power spectra density (PSD) for both recording systems. Results are presented in Fig.3, where the red line represents the noise PSD of the proposed accelerograph, and the blue line represents the noise PSD of the reference sensor. It is evident that the two recording systems depict similar behavior over all the recording band. This is a direct proof of prototype's ability to accurately record ground motion in a broad band range.

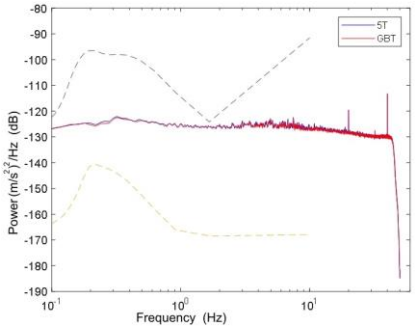

Figure 3. Total noise PSD diagrams for the proposed accelerometer (GBT) and the reference instrument (5T).

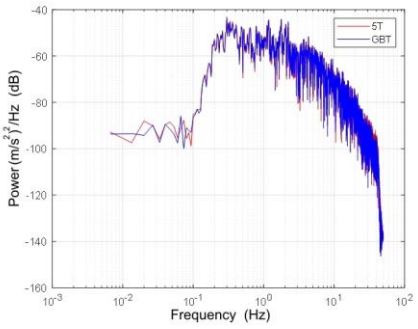

Figure 4. PSD diagram of an earthquake signal, for the reference instrument and the prototype

Conclusions

We present here a newly designed accelerograph based on force-balance accelerometers. The accelerometer's spring-mass mechanism has two leaf springs and a double coil forcer, attached on a movable conductive plate in between two stationary plates, which form a capacitive displacement transducer. The double-spring and the double-coil ensure a linear motion of the seismic mass and a symmetrical operation on both sides of the sensor's rest position. The output signal is connected to high resolution 32 bits ADC digitizer, with a Linux board running open-source components ported on the ARM processor. The instrument's performance, in terms of noise level and signal response, is evaluated in comparison to a well-established commercial product. The new accelerograph was found to satisfy the expectations of its suggested specifications (200Hz bandwidth, +/- 4G). Its low-cost characteristics (raw materials, easy design process, available electronic components) guarantee easy manufacturing and high repeatability in a production line.

References

Hitachi Ltd. (1985). European Patent Application 0338688A1

Kinemetrics Inc. (1997). The FBA-23 Force Balance Accelerometer – User's Guide

Kinemetrics Inc. (2005). EpiSensor Force Balance Accelerometer Model FBA ES-T– User's Guide

Piersal A. and Paez T (2010). Harris' Shock and Vibration Handbook 6th Ed., McGraw Hill, Ch. 10.

Ringler A, Evans J, and Hutt C, (2015). Self-noise models of five commercial strong-motion accelerometers, Seismological Research Letters, 86 (4), 1143-1147.

Ringler A. and Bastien P, (2020). A brief introduction to seismic instrumentation: Where does my data come from?, Seismological Research Letters, 91 (2A), 1074-1083.

Santos J, Catapang , and Reyta E, (2019). Understanding the fundamentals of earthquake signal sensing networks, Analogue Dialogue, 53 (3).

Talha M A, Elattar A G, and Khalil A H, (2003) Dynamic monitoring of a long span bridge. – Jourlal of engineering and applied science Vol. 50, No. 2, Apr. 2003, PP. 351-370 Faculty of Engineering, Cairo University.

Welch P, (1967). The use of fast Fourier transform for the estimation of power spectra: A method based on time averaging over short, modified periodograms, IEEE Trans. Audio, AU-15, pp. 70–73.

16th International Congress of the Geological Society of Greece
17-19 October, 2022 - Patras, Greece
Bulletin of the Geological Society of Greece, Sp. Publ. 10
Ext. Abs. GSG2022-428

Detecting and Mapping the Buried Past: GPR surveys at two Archaeological Sites in Achaea, Greece

Z. Roumelioti[1], P. Paraskevopoulos[1], H. Moustakas[1], M. Koilanitis[1], E. Sokos[1], P. Avramidis[1], K. Aktypi[2], M. Gazis[2]

(1) Department of Geology, University of Patras, Patras, Greece, zroumelioti@upatras.gr (2) Ephorate of Antiquities of Achaea, Greek Ministry of Culture and Sports, Patras, Greece.

Research Highlights

The Ground Penetrating Radar (GPR) method successfully identified unexcavated Mycenaean tombs and classical/hellenistic building remains at the archaeological sites of Voudeni and ancient Kleitor (Achaea, Greece), respectively.

Background and Method

Geophysical prospecting has been aiding archaeological research for several decades, especially in the surveying phase of broad areas of interest (e.g., Gaffney, 2008; Conyers, 2012, 2013; Deiana et al., 2018). Among the various broadly applied, non-catastrophic, shallow prospecting geophysical methods appropriate for archaeological applications, GPR stands out not only because it is relatively easy and fast to apply, but also because it provides information for both the horizontal and vertical distribution of targets. In this work, we investigate the efficiency of the GPR method in identifying two different types of buried archaeological targets: tombs and building remains. GPR surveys have been conducted at the archaeological sites of the Mycenaean cemetery of Voudeni in Patras and of ancient Kleitor, close to the village of Kleitoria in the Municipality of Kalavryta. Both sites fall under the jurisdiction of the Greek Ministry of Culture and Sports, through the Ephorate of Antiquities of Achaea.

In the applications presented here, GPR measurements were collected using a GSSI SIR-3000 system with a 400MHz center-frequency antenna. A time window of 70 ns was adopted for the recorded signal, which was a-priori filtered between 100 and 800 MHz. Data were processed using the software packages GPR Viewer, GPR Process (http://www.gpr-archaeology.com/software/) and Radan (https://www.geophysical.com/software). Basic processing included the zero-time correction of the traces, removal of background noise when necessary, adjusting gain values and computing, through hyperbola fitting, the relative dielectric permittivity of the surveyed formations.

GPR Application in the Mycenaean Cemetery of Voudeni

The Mycenaean cemetery of Voudeni (Kolonas, 2021), one of the largest in the Peloponnese, includes 78 already excavated burial monuments which had been dug into the marl formations of the area 30-35 centuries ago. The dimensions of the burial chambers vary from less than 1m^2 to several tens of m^2, whereas their ceilings, especially those of smaller tombs, are often found at very shallow depths (even at <1m) from today's ground surface. Archaeological evidence suggests that the cemetery hosts a much larger number of tombs than that excavated so far.

Our GPR survey at the cemetery of Voudeni initiated with single-profile reconnaissance measurements above a small-sized excavated tomb (Figure 1; tomb 28; Kolonas, 2021) with the purpose of a) testing the method in terms of its capability to actually detect the archaeological targets and more specifically the entrance and the main chamber of the tomb and b) calibrating the value of the Relative Dielectric Permittivity (RDP) or dielectric constant in the area of interest, which is needed to translate the double travel times measured by the GPR system to actual depth values of the identified targets. Results showed that the method is capable to identify voids (Figure 1), at least down to the depth of ~2m and even provide information on the dimensions of the chamber. Individual parts of the tomb, i.e., its entrance (Figure 1c) and its chamber (Figure 1d) were identified as strong reflections.

Grid measurements in unexcavated parts of the cemetery and subsequent analysis and interpretation of individual profiles and spatial variation of reflections amplitudes at various depths pointed out to several areas of possible archaeological interest. The interpretation of GPR data suggests features such as excavations corresponding to the entrance passages (dromoi) to the tombs, as well as to voids or piled reflections corresponding to the main chambers and their "walls", respectively. GPR clearly distinguished areas of intact rock from those that have experienced human intervention. Strong reflections were found to systematically initiate close to the depth of 0.8m, which implies some consistency in the building practices followed by the tomb constructors of the time.

GPR Application in the Area of Ancient Kleitor

Kleitor was an ancient Arcadian city-state, presently found ~3 km west of the village of Kleitoria in the Municipality of Kalavryta. Remains of the ancient city are buried at shallow depth and only limited and targeted excavations have taken place in the past (Petritaki, 2005 and references therein). However, remains of the fortification walls and other elements

of the city are evident throughout an area of more than 2 km^2.

Our GPR investigation covered an area of 20×27m, a few tens of meters away from the partly excavated SW gate of the ancient city. Profiles were collected unidirectionally, in an almost S-N direction and spaced every 50 cm. All collected profiles were processed individually, but were also combined in a single grid file to provide a three-dimensional view of varying reflections amplitudes in space. The co-interpretation of individual profiles and amplitude maps at various depths clearly revealed an underground structure of considerable dimensions and possible remains of a street.

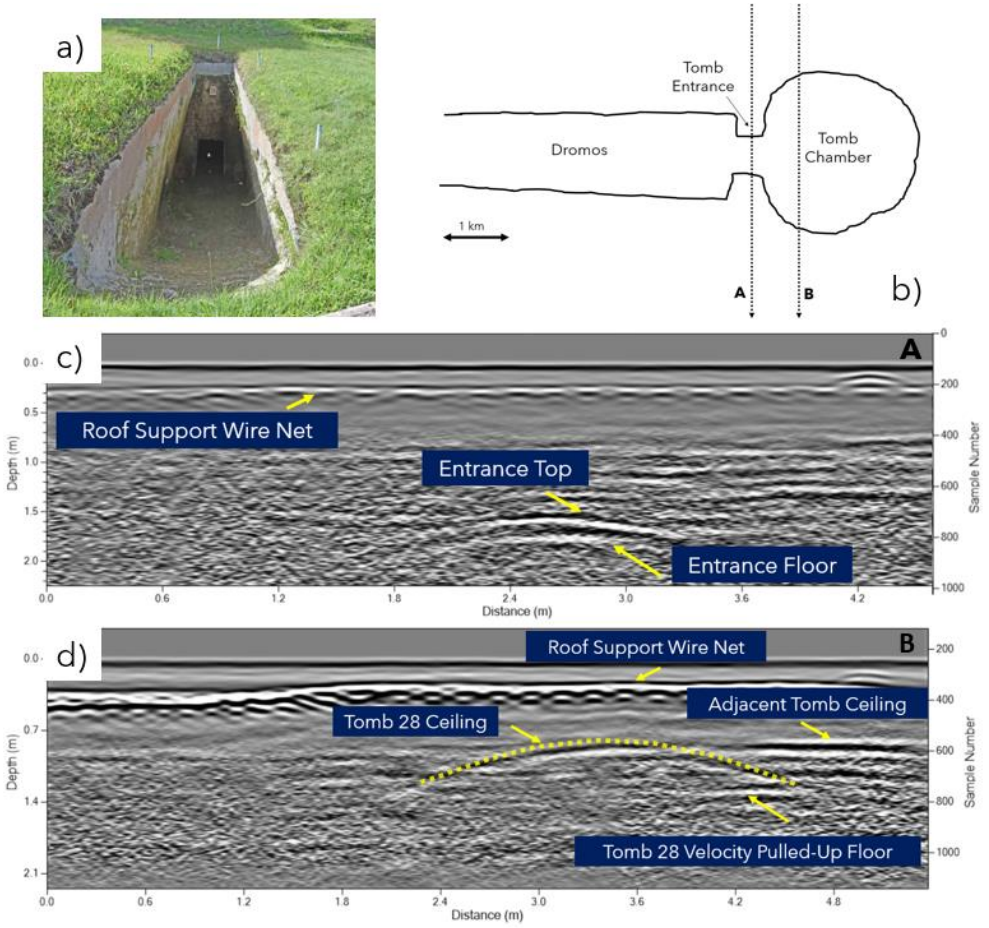

Figure 1. a) Photo from the outside and b) ground plan of Voudeni's Tomb 28 (modified from Kolonas, 2021). The two reconnaissance lines (A, B), along which GPR profiles were collected, are marked using dashed lines, c) GPR profile A and d) profile B. Stronger reflections are marked and interpreted.

Conclusions

We successfully applied the GPR method to detect and map reflections from underground tomb chambers in the Mycenaean cemetery of Voudeni in Patras and to investigate a very small part of the unexcavated city of Ancient Kleitor, close to present village of Kleitoria in Achaea, Greece. Individual-profile and grid measurements at unexcavated parts of both archaeological sites have revealed numerous areas of possible archaeological interest. Overall, the results are particularly encouraging in terms of the contribution of the method to archaeological research, at least under conditions resembling those of present measurements.

Acknowledgements

We are grateful to the students of the Geology Department of the University of Patras (in alphabetical order) Ch. Dedopoulou, S. Kanakaki, M. Mavridis and P. Karoutsos for their help and enthusiasm in the field. We are also thankful to the director of the Ephorate of Antiquities of Achaea, Dr. A. Koumousi for facilitating this cooperation and to the Municipality of Kalavryta for the warm hospitality during our measurements at ancient Kleitor.

References

Conyers, L.B., 2012. Interpreting Ground-penetrating Radar for Archaeology. Routledge, Taylor and Francis Group, New York.

Conyers, L.B., 2013. Ground-penetrating Radar for Archaeology. 3rd edn. Rowman and Littlefield, Lantham, MD, USA.

Deiana, R., Leucci, G., Martorana, R., 2018. New perspectives on geophysics for archaeology: a special issue. Surv. Geophys. 39, 1035–1038. https://doi.org/10.1007/s10712- 018-9500-4.

Gaffney, C., 2008. Detecting trends in the prediction of the buried past: a review of geophysical techniques in archaeology. Archaeometry 50 (2), 313–336. https://doi.org/ 10.1111/j.1475-4754.2008.00388.x.

Kolonas, L., 2021. Voudeni. An important Mycenaean center of Achaea, (in Greek).

Petritaki, M., 2005. Kleitor: the city in the light of the excavations. General consideration of excavation data, in Østby, E. (ed.), Ancient Arcadia (Athens and Sävedalen, Sweden: Norwegian Institute at Athens and Åström), 351–62 (in Greek).

16th International Congress of the Geological Society of Greece
17-19 October, 2022 - Patras, Greece
Bulletin of the Geological Society of Greece, Sp. Publ. 10
Ext. Abs. GSG2022-430

Non-linear site Response During Earthquakes Sequence on Early March 2021 in Thessaly (central Greece): Analysis of Strong Motion Data and Synthetics

T. Novikova[1], E. Mouzakiotis,[1], V. Karastathis[1], and G.-A. Tselentis[1]
(1) Institute of Geodynamics, NOA, Athens, Greece, Novikova Tatyana tatyana@noa.gr

Research highlights

The analysis of strong motion data and synthetics can be helpful in assessment of liquefaction potential of the sites close to the fault. Significant criteria derived in present study, can be employed for a quick, preliminary assessment of liquefaction susceptibility before detailed investigation of the region is carried-out.

Background

A sequence of strong earthquakes with Mw5.6 and M6.3 which occurred on the 3rd and 4th of March 2021 on previously unknown (according to deformation model), normal faults in Thessaly, caused extensive liquefaction in several sites in the broader region, as well as extensive damage in several local villages. The most notable liquefaction cases such as sand blows, craters fissures, surface cracks and ruptures were reported (Caputo et al 2021) for the Piniada valley (Figure 1a) and along Titarisios river floodplain- between the villages Varko and Damasi (Figure 1a), which are all situated at the epicentral area of both earthquakes at distances up to 20 km.

Objectives

The main objective of the present work is to simulate seismic response of the sites within the investigated area (Figure 1a). Among them are following locations: liquefaction spots; sites of geophysical tests and locations in proximity of the fault, where seismic data were available. Then to conduct the frequency analysis of the available records and obtained synthetics at those locations to clarify which frequency is related to liquefaction in our case study. Further to obtain and analyze time and depth distribution of excess pore water pressure for all events of seismic sequence and at all localities of studied area to clarify which event was responsible for liquefaction phenomenon. Eventually, based on the obtained results to derive specific criteria that can be used for a preliminary estimation of the liquefaction susceptibility of the site, before detailed investigation of the region is carried-out (Figure 1b).

Methodology

At the first stage of the research we obtained the Vs velocity profiles (Figure 2) which were derived from MASW seismic surveys at the investigated sites. The data were of a very high quality and provided quite reliable results.

At the second step for the calculation of the strong ground motion caused by the events on the tested sites, we used the EXSIM algorithm, which utilizes the stochastic simulation of ground motion methodology for finite sources with a dynamic corner frequency (Motazedian & Atkinson, 2005). At final stage the seismic response of all investigated sites was computed, employing a fully nonlinear analysis, based on the effective stress (Matasović, 1993 Matasović & Vucetic, 1993, 1995a, b) that is able to calculate directly the soil liquefaction potential, accommodating for pore-water pressure-induced soil softening (reduction in shear modulus and strength). This analysis allowed us to model cases of large earthquakes and soft soils, when shear strains in excess of 1.0% can be induced.

Results and Conclusions

Performed non-linear analysis allows us to understand better the development of the liquefaction phenomenon during the seismic sequence, to define frequency contents related to this phenomenon and to explain quite low values of recorded acceleration at stations Lar1, Lar 2 approximately 20 km far from the epicenter of the main shock. The results of the simulation confirm the initiation of liquefaction during the main shock with Mw=6.3.

Carrying out the analysis for a large number of sites within the investigated region, we are able to obtain some specific criteria which can assist in the preliminary estimation of liquefaction susceptibility, before any cost and time consuming methodology is applied. This is: the presence of alluvial deposits, shallow position of water table (< 5m) in combination with generally low Vs values (<300 m/sec.) as well as unexpectedly low values of PGA (from recorded or synthetic data) close to the potentially liquefiable sites. It should be noted, however, that these criteria were obtained by applying our methodology only for three specific seismic events (of the sequence) and therefore for specific strong ground motion time-series. In order to obtain an actual accurate relation between the Vs values of a site, the ground motion and the liquefaction susceptibility, it is important to perform the above analysis for a large number of events. In spite of the above fact, the criteria can still be considered as first indicators for the initiation of the phenomenon after a strong seismic event.

This research will be helpful to reach broad consistency between the present and accumulated previous results and further can be employed to other areas, providing basic constraints for modeling pore-pressure development during seismic

events of different magnitudes and in areas where the records of strong motion are not available.

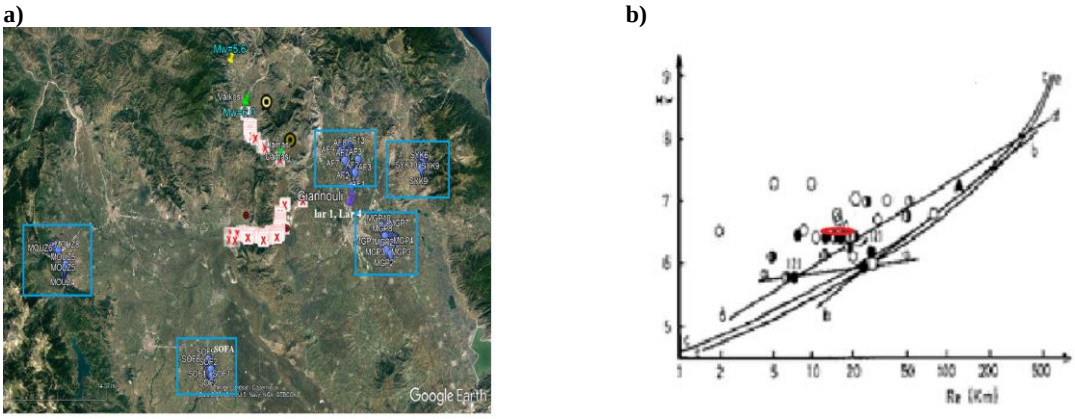

Figure 1. (a) location of sites, where geophysical experiment was carried out (blue squares); liquefaction reported sites (red dots, Papathanassiou et. al., 2022); stations, where the events of seismic sequence were recorded (Lar 1, Lar 4, Giannouli, Sofa); (b) maximum epicentral distance R of liquefied sites versus moment magnitude Mw of shallow earthquakes (based on data of Greek, New Zealand, Loma Prieta and Japanese earthquakes (Papadopoulos & Lefkopoulos, 1993). Red circle corresponds to the liquefaction cases discussed in present article.

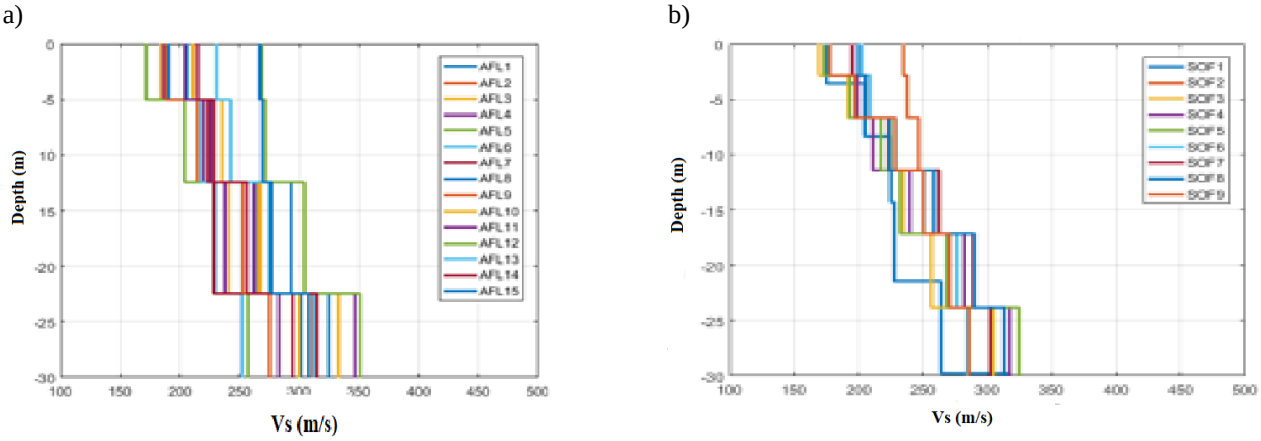

Figure 2. Example of resulting Vs profiles from the local geophysical surveys are given for Ampelonas (a) and Sofades (b) sites.

Acknowledgements

We acknowledge support of this study by the project ‘‘HELPOS -Hellenic Plate Observing System’’ (MIS 5002697) which is implemented under the Action ‘‘Reinforcement of the Research and Innovation Infrastructure’’, funded by the Operational Program ‘‘Competitiveness, Entrepreneurship and Innovation’’ (NSRF 2014–2020) and co-financed by Greece and the European Union (European Regional Development Fund).

References

Caputo R., Helly B., Rapti D., Valkaniotis S. 2021. Late Quaternary hydrographic evolution in Thessaly (Central Greece): The crucial role of the Piniada Valley. Quaternary International, https://doi.org/10.1016/j.quaint.2021.02.013.

Matasovic N, M., Vucetic 1995b. Seismic response of soil deposits composed of fully saturated clay and sand layers. In: Kenji Ishihara AA (ed) Proceedings of the IS-Tokyo’95, the 1st international conf. on earthquake geotechnical engineering, Balkema, Rotterdam.

Matasovic N., 1993. Seismic response of composite horizontally layered soil deposits. PhD dissertation, Civil and Environmental Engineering Department, University of California, Los Angeles, 452 p

Matasovic N., M. Vucetic, 1995a. Generalized cyclic degradation-pore pressure generation model for clays. ASCE J Geotech Eng 121(1):33–42.

Matasović, N., M. Vucetic, 1993. Cyclic characterization of liquefiable sands, *Journal of Geotechnical Eng.*, **119**(11), 1805-1822.

Motazedian, D. G. Atkinson, 2005. Stochastic Finite-Fault Modeling Based on a Dynamic Corner Frequency. Bulletin of the Seismological Society of America, 95, 995-1010. http://dx.doi.org/10.1785/0120030207.

Papadopoulos, G., G. Lefkopoulos, 1993. Magnitude-distance relations for liquefaction in soil from earthquakes. Bulletin of the Seismological Society of America, Vol. 83, No. 3, pp. 925 938.

Papathanassiou, G., Valkaniotis, S., Ganas, A., Stampolidis, A., Rapti, D., R. Caputo, 2022. Floodplain evolution and its influence on liquefaction clustering: The case study of March 2021 Thessaly, Greece, seismic sequence, Engineering Geology, 298, 106542.

Sarhosis, V., Giarlelis, C., Karakostas, C., Smyrou, E., Bal, I., Valkaniotis, V., A. Ganas. 2022. Observations from the March 2021 Thessaly Earthquakes: an earthquake engineering perspective for masonry structures, Bulletin of Earthquake Engineering https://doi.org/10.1007/s10518-022-01416-w.

16th INTERNATIONAL CONGRESS of the
GEOLOGICAL SOCIETY OF GREECE

T4. Geomorphology and Quaternary Geology

OUR EARTH, OUR HOME

16th International Congress of the Geological Society of Greece
23-25 May, 2022 - Patras, Greece
Bulletin of the Geological Society of Greece, Sp. Publ. 10
Ext. Abs. GSG2022-006

The Geomorphological Map of Northeastern Messinia (Andania), Greece, for the delimitation of potential archaeological sites of great importance.

D. Vandarakis [1], N. Liosis [2], V. Chondraki [3], C. Petrakou [4], V. Kapsimalis [1], I. Panagiotopoulos [5] and Eleni Zimi [6]

(1) Institute of Oceanography, Hellenic Centre for Marine Research (HCMR), 19013 Anavyssos P.C., Greece; divandarakis@hcmr.gr. (2) MELETI AEME Geospatial Engineering Company, 143 Kymis ave., 15122 Marousi, Greece. (3) Aristotle University of Thessaloniki, Thessaloniki 54124, Greece. (4) Hellenic Survey of Geology & Mineral Exploration –HSGME, Spirou Loui 1, 13677, Acharnai, Greece. (5) National and Kapodistrian University of Athens, Department of Historical Geology and Paleontology, Faculty of Geology and Geoenvironment, School of Science, University Campus - Zografou, P.C. 15784, Greece (6) University of Peloponesse. Faculty of Humanities and Cultural Studies. Department of History, Archaeology and Cultural Resources Management, Palaio Stratopedo, Kalamata 24100, Greece.

Abstract

Messinia is a prefecture of Greece located in the southwest part of Peloponnese. Has a diverse landscape with extensive beaches and mountainous areas combined with large plains, ideal for rural activities. Its strategic location makes Messinia one of the most inhabitated regions in Greece, consequently, there are indications of habitation since Neolithic Period (Syriopoulos, 1994). Consequently, for all the above mentioned arguments, archaeological findings are observed throughout Messinia.

Our study area is located in the Northeastern end of Messinia Prefecture, called Steniklariko basin-Andania (Fig. 1). Its limit in the north is near the village “Kato Melpeia”, in the east “Filia” in the South “Meligalas” and in the West “Konstantinoi”. It is named by the ancient city located in the area, which along with ancient Messini were the most significant political, military and cultural centers of the ancient times. The selection of the area is based also on the significancy that is self-evident, plus few research is done in the area.

The geographical setting of the study area includes, geological-geographical-geomorphological information, along with tectonism, erosion, and depositional processes, which all of these combined have resulted in the development of the current relief. This complex landscape played a significant role for the development of the cultural status of the area.

The main process resulting the current landscape is tectonism. Since it is only 60 Km from the Hellenic Trench, where the collision between the African and Eurasian plate occurs. Messinia is one of the most tectonically active areas in the Hellenic Arc. This can be justified also by the presence of numerous faults such as Pidima fault in south east of the study area, near Pidima village (Karamitros et al., 2018).

The first stage of the research was the collection of analogue maps (in digital form) and remote sensing data of the area. The spatial information used was by different sources and various scales. To represent as accurate as possible the different layers of the study area a common scale was decided and implemented.

Firstly, analogue maps were collected including the large scale (1/5.000) topographic sheets by the Hellenic Military Geographical Service. As well as the medium scale (1/50.000) geological maps from the Institute of Geology and Mineral Exploration sheets of (Meligalas, Kalamai, Kato Figalia and Megalopolis).

Remote sensing data include large scale Digital Elevation Model (Dem) cell size 5m, by the National Cadastre of Greece. DEM was the most important layer extracted from the topographic information of the area, compiled by the elevation, peak points, contours. Slope, Aspect and Hillshade models were also derived from the interpretation of the DEM. In addition, aerial photos and the high-resolution images were used by the open-source Google earth Pro for the first evaluation of the DEM.

The second stage in order to complete the geomorphological mapping, was the fieldwork. Made for the Andania Survey Project in 6th August 2021. During the fieldwork crucial data was gathered in order to represent the current relief as accurate as possible and to retrieve important information to understand the processes that carved the landscape and affected the human activities throughout the ages.

Furthermore, in this study the Semi automated methods were used for geomorphological mapping. This method is the most widespread-state of the art, in the scientific community (Vandarakis et al. 2014 a,b; Gustavsson et al., 2009; Gustavsson et al., 2006; Gustavsson et al., 2005; Van Asselen S. & Seijmonsbergen., 2006).

This method allowed the automatic retrieval of the spatial data by the use of the current spatial technologies as Geographic Information System and remote sensing data (Gustavsson et al., 2006).

The use of those technologies with the combination of the scientific knowledge, has offered significant advantages in the geomorphological research. Specifically has important effect in the reduction of the time.

The classification of the features was made according to their characteristics following the rules of cartographic

generalization, abstraction and simplification (Gustavsson, 2005).

In this study the mapping scale for the whole study area, is been set to a scale of 1:50.000. This scale class is generally applied for same studies, and it represents the relief with great accuracy, allowing the geomorphologists to include as many information as possible. The software used for the data collection, processing and the map composition was Arc GIS 10,4 by ESRI and the open source QGIS v 3,6.

In the study area the most significant landforms encountered are the "V" shaped valleys (down cutting erosion), which are formed by the action of the accumulation of the water through the hydrographic network. Also, cliffs are observed in high altitude areas (mainly near the peaks) formed also by the activity of the erosion and the tectonism (Fig. 1).

The geological formations, mostly limestones, favor the preservation of such landforms. The sediments derived from erosion were deposited in lowlands at the borders of the plain of Andania forming alluvial-colluvial fans (transported by the accumulation of the water) and debris cones (formed by gravitational processes). These formations are observed on all sides of the plain of Andania, but the most significant alluvial-colluvial fans and debris cones can be found in the eastern side of the study area (Fig. 1).

The main feature is the plain of Andania which is a deposition area of the sediments accumulated from the surrounding high-altitude areas (hills and mountains). Inside the plain the hydrographic network present "Π" shaped valleys since the inclinations are so low and the relief so smooth that allow the main torrent bed to augment its width (Fig. 1).

During this step the basic geomorphological characteristics-processes have been documented and mapped. More studies will be carried out in order to acquire as many information as possible by applying new technologies in combination with the available data.

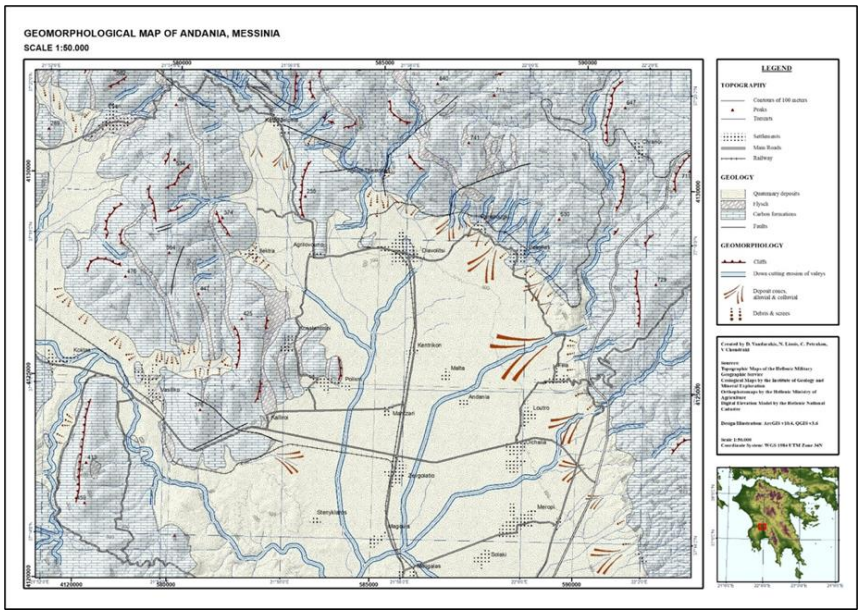

Figure 1. Geomorphological map of the study area.

References

Gustavsson M., Seijmonsbergen A. C., Kolstrup E., 2009. Combining digital elevation data (SRTM/ASTER), high resolution satellite imagery (Quickbird) and GIS for geomorphological mapping: A multi-component case study on Mediterranean karst in Central Crete, *Geomorphology 112*, 106 – 121.

Gustavsson M., Kolstrup E., Seijmonsbergen A. C., 2006. A new symbol-and-GIS based detailed geomorphological mapping system: Renewal of a scientific discipline for understanding landscape development, *Geomorphology 77*, 90 – 111.

Gustavsson M. 2005. Development of a Detailed Geomorphological Mapping System and GIS Geodatabase in Sweden, Licentiate Thesis, 20.

Gustavsson M., Kolstrup E. and Seijmonsbergen A.C. 2006. A new symbol-and-GIS based detailed geomorphological mapping system: Renewal of a scientific discipline for understanding landscape development, Geomorphology 77, 90 – 111. XLVII, No 1 - 342 http://epublishing.ekt.gr | e-Publisher: EKT | Downloaded at 05/02/2018 06:25:13.

Gustavsson M., Seijmonsbergen A. C. and Kolstrup E. 2009. Combining digital elevation data (SRTM/ASTER), high resolution satellite imagery (Quickbird) and GIS for geomorphological mapping: A multi-component case study on Mediterranean karst in Central Crete, Geomorphology 112, 106 – 121.

Karamitros, I., Ganas, A., & Chatzipetros, A., 2018. Terrestrial Lidar surveying of active normal faults: Preliminary results from The Pidima fault scarp, Messinia, Greece.

Van Asselen S. and Seijmonsbergen A.C. (2006). Expert-driven semi-automated geomorphological mapping for a mountainous area using a laser DTM, Geomorphology 78. 309 – 320.

Vandarakis Dimitrios, Nikolaos Liosis, Kosmas Pavlopoulos, 2014a. "The Geomorphological mapping of Keros island (Cyclades, Greece)". Bulletin of 10th Geographical Conference, Thessaloniki 22-24 October 2014.

Vandarakis Dimitrios, Liosis Nikolaos, Pavlopoulos Kosmas, Fachard Sylvian, Knodell Alex, 2014b. "Geomorphological mapping of the Mazi-Oinoe area, Northwest Attica, Greece". Bulletin of 10th Geographical Conference, Thessaloniki 22-24 October 2014.

16th International Congress of the Geological Society of Greece
17-19 October, 2022 - Patras, Greece
Bulletin of the Geological Society of Greece, Sp. Publ. 10
Ext. Abs. GSG2022-146

Nationwide geomorphological mapping: Introducing the geomorphological map of Greece

E. Karymbalis[1], K. Tsanakas[1], K. Valkanou[1], D. Griva[1], D.-V. Batzakis[1]

(1) Department of Geography, Harokopio University, Athens, Greece, karymbalis@hua.gr

Introduction

The systematic study of the origin and development of different types of landforms on the earth's surface is essential for understanding the geomorphological processes that create and modify them (Costa *et al.,* 1984). Understanding the processes provides significant insight into the dynamics of planet earth, which can then be used as a background for landscape, environmental and resource evaluation and management (Gustavsson *et al.,* 2006). From this perspective, geomorphological maps i.e. the accurate depiction of landforms on a map and their interrelated processes, are increasingly becoming essential tools for stakeholders and decision makers, so that the necessary policies are taken in the direction of a sustainable future (Smith *et al.,* 2002).

Although recent years have seen a great resurgence in the production of large-scale geomorphological maps, the scientific interest for small-scale geomorphological mapping remains relatively limited (Serrano, 2005; Smith *et al.,* 2011). In the last decades a great amount of geomorphological information has been provided for Greece through geomorphological studies (among others Karymbalis *et al.,* 2013; Karymbalis *et al.,* 2016; Tsanakas *et al.,* 2019). However, when mapping on a small scale, the high degree of generalization required to represent landforms originally mapped at larger scales, did not yet allow to bring together all this geomorphological knowledge into a national-scale geomorphological map.

The present study is a geomorphological overview of Greece mapped on a 1:1,000,000 scale cartographic synthesis. This is the first attempt that aims to collect and interpret the geological and geomorphological factors that contributed to the landscape formation and evolution of Greece on a national scale. The map provides a tool for the evaluation of landscape evolution and dynamics and can be used as a base for geomorphic analysis and other purposes of landscape evaluation and valorization.

Study area

Geomorphological mapping was performed at the mainland, as well as on the islands of Greece. Greece is located at the south-eastern part of Europe between 19º 22΄E - 29º 38΄E and 34º 48΄N - 41º 44΄N. More than 80% of the Greek territory exhibits a mountainous or hilly terrain. Extensive plains are also present and are primarily located in the regions of Thessaly, Central Macedonia and Thrace. The geology of Greece is structurally highly complex due to its position at the junction between the European and African tectonic plates (Papanikolaou, 2021). Its high seismic activity shows that the area is tectonically very active (Makropoulos et al., 1984). In terms of geological structure, Greece can be divided from South to North into the following main features:

- The Mediterranean ridge which extends from the Ionian Sea to Cyprus.
- The Hellenic trench which consists of a series of depressions to a depth of 5000 m and parallels the Hellenic arc.
- The Hellenic arc which is formed by the outer sedimentary arc (consisting of Palaeozoic to Tertiary rocks, folded and faulted in several phases of the Apline orogeny) and the inner volcanic arc.
- The northern Aegean Sea which lies immediately north of the volcanic arc and is a rather stable block of folded palaeozoic and granitoid masses.

The climate in Greece is predominantly Mediterranean with mild and wet winters and hot, dry summers. Past climatic conditions and especially late Quaternary climatic variations have played an important role in the configuration of the present-day relief.

Data and methods

The production of the geomorphological map was based on the literature review of previous geomorphological studies of Greek inland and coastal areas on different scales as well as on the application of semi-automated, GIS techniques. The methodological procedure can be divided into three phases:

- 1st phase: Collection and preparation of literature and data, determination of the appropriate methodology and mapping protocols and organization of available data into a GIS spatial geodatabase. High resolution topography obtained from the Hellenic Cadastre as well as the geological maps of Greece on a scale of 1:50,000 obtained from the Institute of Geology and Mineral Exploration of Greece were used during this phase as initial inputs in the geodatabase for the production of a series of derivatives, which included a hillshade map, a slope-aspect map, and a red relief image map
- 2nd phase: Delineation of morphological features based on the GIS analysis performed in the previous phase. At this point, large- and small-scale landforms such as alluvial fans and cones, mass wasting forms, planation surfaces, brakes of slope, etc., were identified. The preliminary morphological sketch was then evaluated using Google Earth imagery for the interpretation of the morphological features and the determination of the landforms.

- 3rd phase: Evaluation of the morphological sketch, graphic design – symbolization and production of the final geomorphological map.

A series of accompanying maps and tables were also produced, providing topographic parameters as well as information about the geotectonic setting and the climatic regime of Greece. A graphic outline of the methodological procedures is provided in Figure 1.

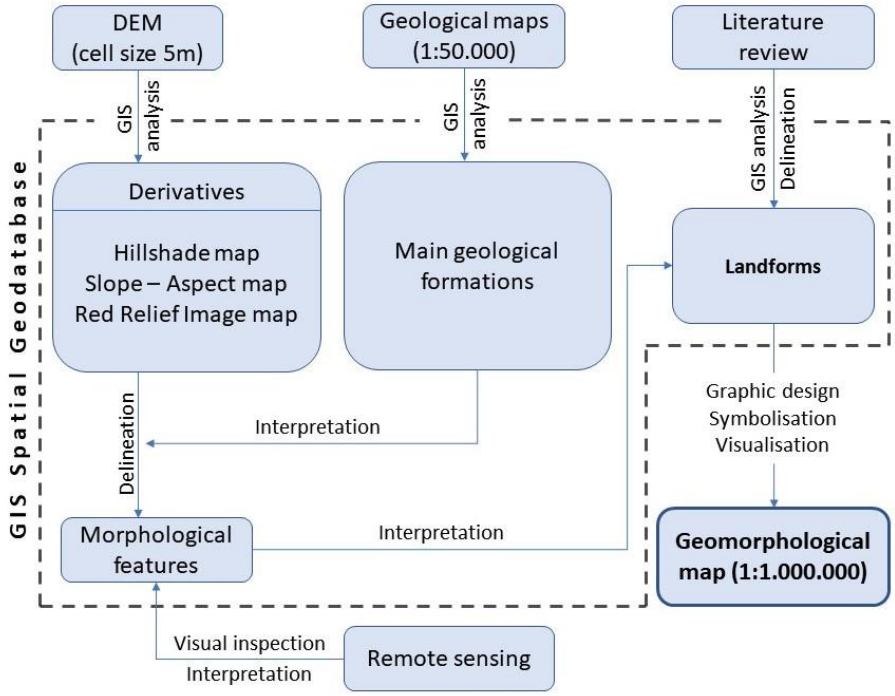

Figure 1. Flow diagram outlying the main methodological steps of the map production.

Results and conclusions

The final map incorporates landforms of both endogenic and exogenic origin. The legend was organized genetically including structural landforms, landforms due to fluvial erosional and depositional processes, gravity induced landforms as well as coastal, karst, volcanic, glacial and periglacial landforms and anthropogenic facilities.

The results show that the Greek territory comprises a landscape with heterogeneous geomorphological environments, the formation and evolution of which, is the result of primarily active tectonics, and exogenic processes.

The map reflects the extent of recent developments of geomorphology of Greece and can be used as reference for further interdisciplinary research as well as a management tool for stakeholders. It also provides information on the long-term geomorphological history of Greece and comprises a 'first approach' land classification on a national scale for Greece.

References

Costa, J.E., Graf, W.I., 1984. The geography of geomorphologists in the United States. Prof. Geogr. 36, 82-89.

Gustavsson, M., Kolstrup, E., Seijmonsbergen, A.C., 2006. A new symbol-and-GIS based detailed geomorphological mapping system:renewal of a scientific discipline for understanding landscape development. Geomorphology 77, 90-111.

I.G.M.E. Geological Map of Greece (Scale 1:50,000) Institute of Geology and Mineral Exploration of Greece: Athens, Greece.

Karymbalis, E., Papanastassiou, D., Gaki-Papanastassiou, K., Tsanakas, K., Maroukian, H., 2013. Geomorphological study of Cephalonia Island, Ionian Sea, Western Greece. Journal of Maps, 9(1), 121-134.

Karymbalis, E., Gaki-Papanastassiou, K., Tsanakas, K., Ferentinou, M., 2016. Geomorphology of the Pinios River delta, Central Greece. Journal of Maps, 12,12-21 DOI: 10.1080/17445647.2016.1153356.

Makropoulos, K.C., Burton, P.W., 1984. Greek tectonics and seismicity. Tectonophysics, 106, 275-304.

Papanikolaou, D., 2021. The Geology of Greece. Regional geology reviews. 1st ed. Springer

Serrano, A.M., 2005. Mapa geomorfologico de Espana y del margen continental a escala 1:1.000.000. Instituto Geologico y Minero de Espana.

Smith, B.J., Warke, P.A., Whalley, W.B., 2002. Landscape development, collective amnesia and the need for integration in geomorphological research. Area 33 (4), 409-418.

Smith, M.J., Paron, P., Griffiths, J.S., 2011. Geomorphological mapping, methods and applications. Elsevier

Tsanakas, K., Karymbalis, E., Gaki – Papanastassiou, K., Maroukian, H., 2019. Geomorphology of the Pieria Mtns, Northern Greece. Journal of Maps, 15(2), 499-508, DOI: 10.1080/17445647.2019.1619630.

16th International Congress of the Geological Society of Greece
17-19 October, 2022 - Patras, Greece
Bulletin of the Geological Society of Greece, Sp. Publ. 10
Ext. Abs. GSG2022-151

Cave evolution in Strymonas Valley, Greece

G. Lazaridis[1], A. Karampelas[1], D. Dora[1], P. Koulelis[2]
(1) School of Geology, Aristotle University of Thessaloniki, GR-54124, Thessaloniki, Greece, geolaz@geo.auth.gr
(2) Proteas Speleological Club, Thessaloniki

Lakis Cave is a karstic cave studied in detail in terms of geomorphology and processes involved in its evolution and the formation of various dissolutional features.

Methods

The cave was surveyed according to standard cave techniques (i.e. Dasher, 1994) and scanned with a LIDAR sensor built in iPhone13 pro and application Polycam. Rock discontinuities were measured with FieldMove Clino application. Terminology of dissolutional forms follows Lauritzen and Lundberg (2000), Gunn (2004), White and Culver (2005) and Ford and Williams (2007). Morphometrical parameters are estimated according to Klimchouk (2003) and Frumkin & Fischhendler (2005).

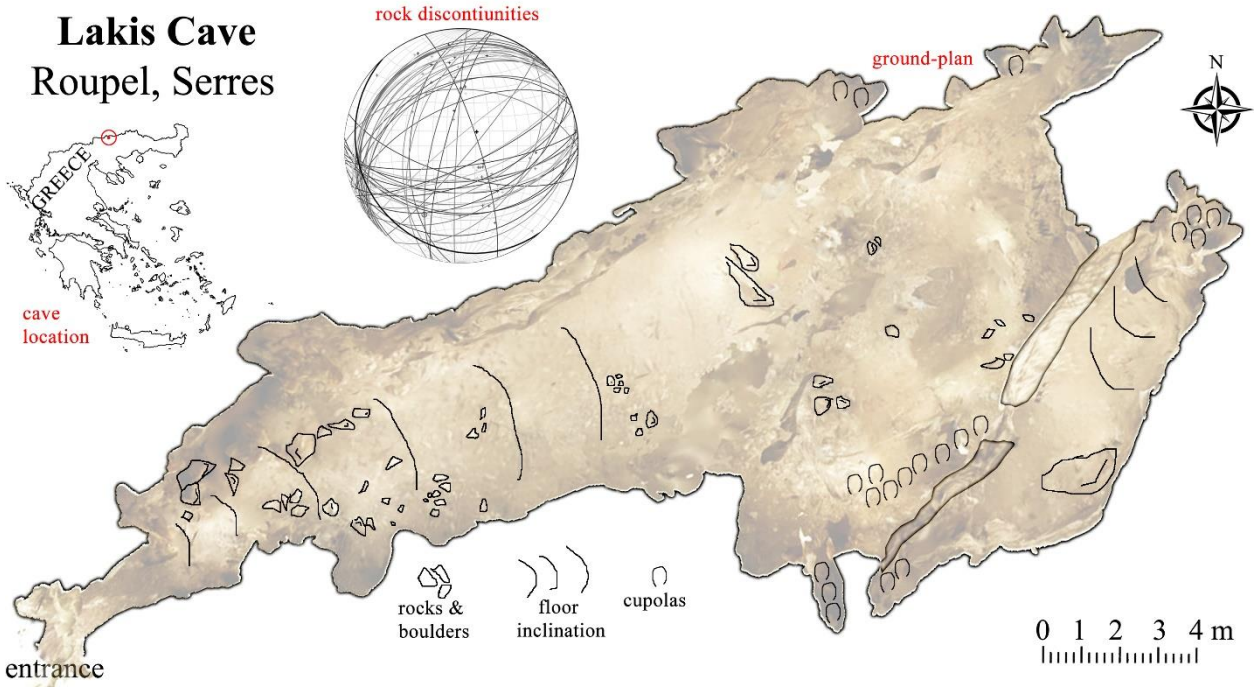

Figure 1. Lakis Cave in Strymonas Valley. Geographic location, ground-plan and Schmidt diagram of rock discontinuities.

Cave Description

Lakis Cave is a horizontal cave that consists mainly of two elongated chambers with WSW-ENE and SW-NE orientation, respectively (Fig.1), formed in marbles of the crystalline rocks of the Rilla-Rhodope Massif (Pangeo Unit) that are intercalated with schists. Entry is via a small triangular hole with SW orientation, about 310 m above sea level that lies on a stream feeding Strymonas river drainage, close to Roupel bunker. The cave covers an area of approximately 240 m^2 and total passage length reaches 60 m. Cave perimeter is 135 m; and fits in a quadrangular of 33.5 to 14 m. Cave field is 343 m^2 and 469 m^2 as a convex hull and as a rectangular, respectively. The floor is inclined inwards with about 15° inclination and it is covered with clastic sediments. Basic measures and morphometric indices were calculated using the rectangular cave field. In the central part of the main chamber there is a partial ceiling collapse as indicated by a sub-horizontal partition. Below the collapsed boulders, mud and sand layers have been deposited. At the SE part of the first chamber a small passage leads to the second one. The second chamber leads to a well-developed rising passage, at its NE corner, where the consolidated sedimentation has been followed by erosion. The sediments are both fine and coarse-grained and cover part of the side-walls till the upper part of the passage. The northern wall of the chamber displays an inclined line that marks an old level of the sediments inside the chamber, which is located about half a meter higher than the current level. Micro-scale dissolutional forms include various assemblages of ceiling cupolas, especially in the SE part of the main chamber, but also in the smaller passages. Many of them display stepped, rough surfaces depending on

the rock foliation (Fig. 2). The NE and SW ends of the second chamber display also cupola-related morphology. Indicators of forced lateral flow along a pressure head, such as scallops, are found only in the northern side-wall of the main chamber. However, they seem to be corroded by condensation corrosion that also characterizes in general the cave walls. The cave is currently dry, and dripwater speleothems are almost absent, with exception of a few places where small stalactites occur.

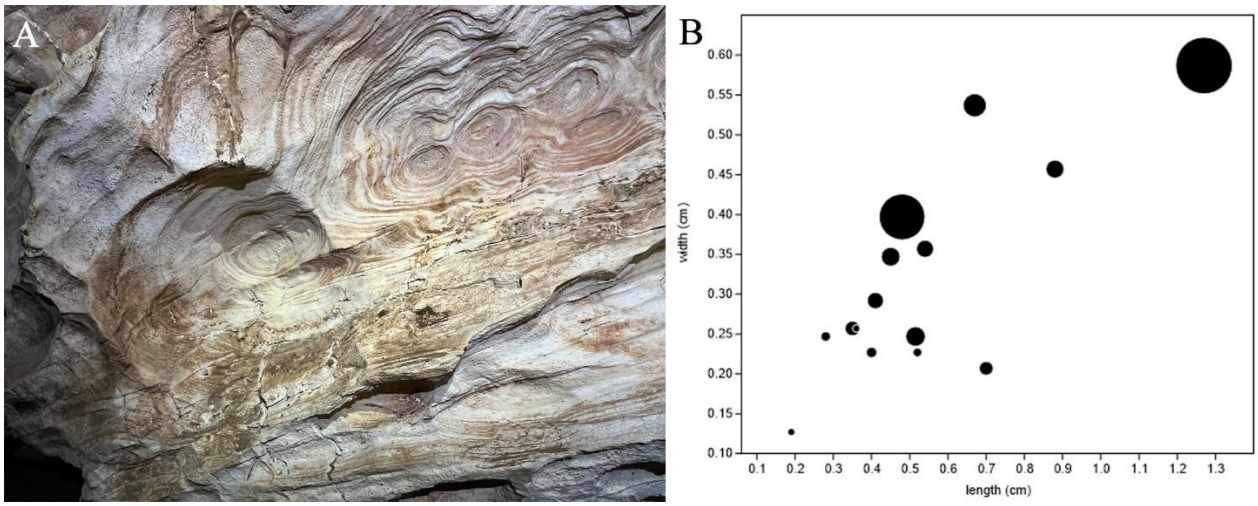

Figure 2. Cupolas in Lakis Cave of Strymonas Valley. A. Shallow cupolas with rough surface in the main chamber. B. Diagram of width versus length; circle diameter increases with cupola's height (3rd axis).

Discussion and conclusions

Field work in Lakis Cave, has resulted in its detailed mapping and 3d representation available to watch in the link https://streamable.com/u06egx. Basic measurements allow the calculation of morphometric indices that have been used in the discrimination of caves formed in confined and unconfined aquifers (Klimchouk, 2003) as well as between chamber and maze cave morphologies (Frumkin, & Fischhendler, 2005). Lakis cave is morphologically an isolated chamber cave according to the length to width ratio (L/W). Furthermore, areal coverage is 68% and passage density is 9.9%; indicating morphological difference from both maze cave and brancwork networks.

The micro-scale morphological features of the cave are mainly the cupolas found in the large rooms and in ascending passages. The shallowest cupolas are found in the main chamber and display rough surfaces (Fig. 2A), which is interpreted as the result of condensation corrosion that acts on already formed cupolas. In the ascending passages the cupolas are deeper and with relatively smoother surface. Although cupolas are polygenetic forms, these small passages can be considered indicative of phreatic conditions. The presence of a small patch with scallops at the main chamber is indicative of lateral flow that could reflect speleogenesis close to water table or later invasion of the nearby stream water. The pattern of the cave in ground-plan resembles phreatic caves. Its development has been affected by the rock discontinuities and in particular along the junction of the foliation that dips to the SSE and a joint group that dips to the NNW (Fig. 1). Other joints with high dip-angles guide the small ascending blind passages at the SE part of the cave.

The sediments found are in general indicative of low energy depositional environment. The presence of eroded sediments reflects water table drop. Main events supported by evidence found in this study are of the following order: phreatic speleogenesis, sedimentation, water level drop, condensation corrosion, ceiling breakdown, new sediment filling.

References

Dasher, G.R., 1994, On Station: A complete handbook for surveying and mapping caves, Huntsville, Ala, National Speleological Society, 242 p.

Ford, D., Williams, P.D., 2007. Karst hydrogeology and geomorphology. John Wiley and Sons Inc.

Frumkin, A., & Fischhendler, I. (2005). Morphometry and distribution of isolated caves as a guide for phreatic and confined paleohydrological conditions. Geomorphology, 67(3-4), 457-471.

Gunn, J. (Ed.), 2004. Encyclopedia of caves and karst science. Taylor & Francis.

Klimchouk, A., 2003. Unconfined versus confined speleogenetic settings: variations of solution porosity. Speleogenesis and Evolution of Karst Aquifers, 1-7.

Lauritzen, S., Lundberg, J., 2000. Solutional and erosional morphology of caves. Klimchouk, A., Ford, D.C., Palmer, A.N., Dreybrodt, W. (eds.) Speleogenesis. Evolution of Karst Aquifers. Huntsville: National Speleological Society.

Palmer, A., 2000. Hydrogeologic control of cave patterns. Speleogenesis: Evolution of Karst Aquifers. Huntsville: National. Speleological Society, 77-90.

White, W.B., Culver, D.C., 2005. Encyclopedia of caves, Elsevier Amsterdam (The Netherlands).

16th International Congress of the Geological Society of Greece
17-19 October, 2022 - Patras, Greece
Bulletin of the Geological Society of Greece, Sp. Publ. 10
Ext. Abs. GSG2022-198

Palaeogeographic Reconstruction of the Ancient Course of Eridanos River (Athens, Greece): A Review

Th. Karympali[1], K. Tsanakas[2]

(1) Department of History & Archaeology, National & Kapodistrian University of Athens, Athens, Greece, theodorak2000@gmail.com (2) Department of Geography, Harokopio University, Athens, Greece.

Introduction

Attica has always faced a significant problem of lack of water resources. However, in antiquity, Athens' basin had a constant source of water from two rivers namely the Kifissos and the Ilissos, whereas a third in size stream (in terms of water flow) of ancient Athens was Eridanos which was a tributary of the Ilissos River. The discharge of these rivers was variable, thus during intense rainfall events, they turned into fast-flowing streams, which flooded their overbank areas, while in periods of no rain they were small perennial streams. A significant length of the channels of these rivers is no longer visible since they have either been artificially filled or gradually converted into rainwater runoff conduits covered under concrete, as a result of the urban expansion of Athens. The main reason for the "disappearance" of the streams was flooding since overflow events were frequent and had devastating consequences for the residential areas adjacent to the channels. Thus, Athens is the only European capital that has no river flowing through it.

The aim of this short review paper is the palaeogeographic representation of the ancient course of the Eridanos River beneath the modern city of Athens. Furthermore, the diachronic human impact on the river is also discussed. Eridanos was a small stream that originated from the southern slopes of the Lycabettus hill and flowed into the Ilissos River. It drained an area of approximately 2 km^2 (Karymbalis and Pavlopoulos, 2002), and it received the water from the surface runoff of the area of Acropolis and Philopappos. Since ancient times, the channel of this river, which was an integral part of the city's landscape, has been gradually almost totally covered.

Methodology

To represent the ancient course of the Eridanos River we took into consideration the topography of the city, the Athenian landscape descriptions of ancient historical writers, and locations of the modern city where the buried river channel or traces of fluvial flow (such as sedimentary-stratigraphic records) have been verified (Figure 1). The record of the diachronic human impact on the river channel was based on both ancient literature and the results of the archeological excavations.

Results – Conclusions

Today, the Eridanos River is almost totally buried under the modern city of Athens except for a channel segment that is still visible at the archaeological site of Kerameikos (next to the Sacred Gate), crossing the excavation site from east to west for about 250 m (Figure 2a). The course of the river can be traced in various locations in the city center where the presence of the ancient channel has been verified by several approaches (Figure 1).

According to Strabo, the Eridanos River originated from the southern foothills of Lycabettus, opposite the Gates of Diocharous, where the Panopos fountain was located (today it is placed NW of the Syntagma square). The buried channel of the river was identified on Filellinon Street and Amalias Ave. (southeast of Syntagma Square) with the use of Georadar and electrical sounding methods respectively (Papamarinopoulos *et al*., 1997, Papaioannou *et al*., 2008). The buried channel had a width of about 17 m, and its deepest part was found about 6 m below the surface. Stratigraphic data collected from boreholes drilled for the construction of the Athens metro (Dounas *et al*., 1976, Dounas and Gakis, 1977) along the probable ancient valley of the river (Figure 1), showed the presence of buried coarse-grained sedimentary layers which possibly correspond to the channel deposits of Eridanos. Such layers were found in Amalias Ave., the intersection of Mitropoleos Str. and Nikis Str., Mitropoleos square, the intersection of Ermou Str. and Miaouli Str., and Asomaton Square (Figure 1). A borehole at the intersection of Thermopilon Str. and Kerameikou Str. showed the presence of a thick fine grained (clay) sediment layer indicative of the presence of a marsh adjacent to the channel of the river. Recent archaeological excavations, held during the construction of the metro, revealed the artificially arranged ancient channel of the river under Monastiraki Square (Figure 2b), as well as under the intersection of Iera Odos Str. and Pireos Str. (at the depth of 3.5-4 m) (Ministry of Culture, 2000a). According to the Greek traveler and geographer Pausanias (2nd century AD), the river drained into the main channel of Ilissos (Papachatzis, 1992) and the confluence of these two rivers is believed to be at the intersection of Iera Odos Str. and Pireos Str.

From the Classical Period (480-330 BC) the Eridanos River flowed through the city center of Athens, and gradually became part of the city's sewage system due to urban growth. As the river often flooded, its channel was unstable,

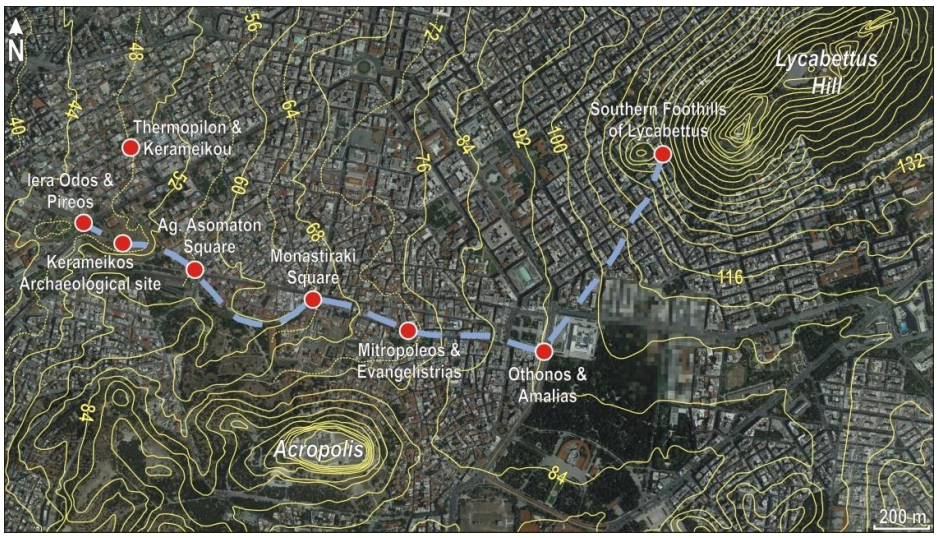

Figure 1. Map of the center of Athens depicting the course of Eridanos River (blue dashed line). Red colored dots correspond to spots where the channel of the river has been identified.

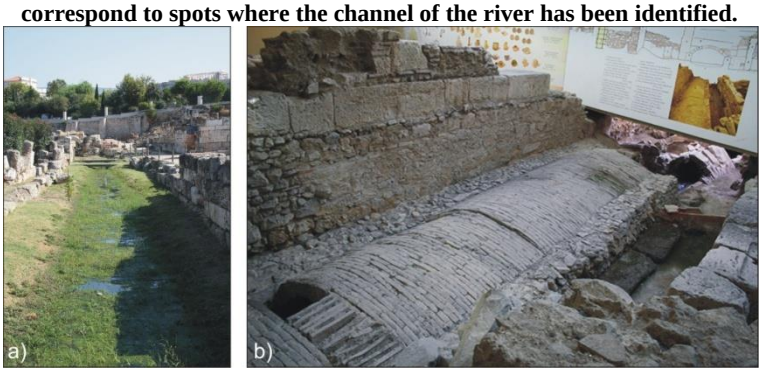

Figure 2. Photos of the Erianos River channel a) Archaeological site of Kerameikos, b) Monastiraki Athens metro station.

changing its position from time to time. In an attempt to control the riverbed and to limit flood damage in the surrounding areas, the Athenians channelized the river. Until the contraction of the Themistoclean wall, the river was flowing freely. In 478 BC, the channel was built, arranged, and enclosed within the city walls. A segment of its course along the Sacred Road was artificially aligned and the bed was enclosed with the construction of artificial levees made of stone. An indication of human intervention in the river is the discovery of several thousands of small ceramic pieces that have writing scratched into them, which were used to artificially fill parts of the channel. The artificial arrangement of the channel is believed that started in the late Classical and Hellenistic Period (330-30 BC). Indicative of the quality of the water of Eridanos during the Hellenistic Period (330-30 BC), is the reference of the poet and scholar Callimachus of Cyrene, according to which "….*the waters of the Eridanos were clear along the segment of the river channel between the Diocharous Gates and the Lyceum*…." (this area today is located somewhere at the upper part of Vassilissis Sofias Str. close to the source of the river), while downstream "….*along the part of the river's course inside the city its water was not even suitable for the animals*…." (Ministry of Culture, 2000b). In 124-125 AD, Hadrian (the Roman emperor) converted the river into a sewer by constructing a masonry vault over it and then covering the vault with soil (Ministry of Culture, 2000a). A major project that dramatically altered the landscape at the end of the 19th century, was the installation of the electric railroad, which cut the Ancient Agora in two.

References

Dounas, A., Gakis, A., 1977. Fluctuation in ground water level of piezometric wells of the Athens metro area, Hydrological and Hydrogeological Research, 22, Institute of Geology and Mineral Exploration.

Dounas, A., Kallergis, G., Morfis, A., 1976. Hydrogeological research within the frame of the study of Athens metro, Hydrological and Hydrogeological Research, 19, Institute of Geology and Mineral Exploration.

Karymbalis, E., Pavlopoulos, K., 2002. Paleogeographic representation of the flow of Iridanos River and human interference. Geographies 3, 9-23.

Ministry of Culture, 2000a. The city under the city, KAPON.

Ministry of Culture, 2000b. Eridanos, the river of the ancient city, Archaeological Receipts Fund.

Papachatzis, N., 1992. Pausaniou Ellados periigisis, "Attica", Athens, Ekdotiki Athinon.

Papaioannou, M.G., Papamarinopoulos, S.P., Stefanopoulos, P., 2008. Geophysical Research at Syntagma square, Athens – Relationship to Geology and Ancient Texts. Proceedings of the 4th Symposium of the Hellenic Society for Archaeometry, National Hellenic Research Foundation, Athens, Greece, p. 85-88.

Papamarinopoulos, S.P., Papaioannou, M.G., Stefanopoulos, P., 1997. New geological evidence in the center of Athens using the georadar. Proceedings of the International Symposium on Engineering Geology and the Environment, Athens, Greece, p. 121-126.

16th International Congress of the Geological Society of Greece
17-19October, 2022 -Patras, Greece
Bulletin of the Geological Society of Greece, Sp. Publ. 10
Ext. Abs. GSG2022-216

Detecting Recent Surface Deformation in the Evinos River Delta, Western Greece, Using SBAS Interferometry

I. Papadopoulos[1], A. Karavias[1,2], E. Karymbalis[1], I. Parcharidis[1], K. Tsanakas[1]

(1) Department of Geography, Harokopio University, Athens, Greece, papasmlnros13@gmail.com (2) Centre for Research & Technology Hellas (CERTH), 15125 Athens, Greece

Introduction

River deltas are extremely dynamic and complex depositional landforms shaped by the competition between fluvial sediment discharge and marine processes (Wright and Coleman, 1973). They are important ecological systems, as well as hot spots for economic, urban and agricultural development since approximately 25% of the world's population lives on deltaic coastlines and wetlands (Syvitski and Saito, 2007). River deltas are subject to a range of fluvial, climatic, tectonic, and sea-level controls and their physical characteristics (low-lying topography, subsidence due to compaction of deltaic sediments, etc.) make them vulnerable to the effects of climate change-related coastal hazards (such as storm surges and sea-level rise) (Milliman *et al*., 1989).

Land subsidence is a common phenomenon in modern delta plains because of sediments compaction by consolidation of the dewatered material, compression of the load of the subsequent overlain deposits, and groundwater or oil pumping (Meckel, *et al.*, 2007). Coastal subsidence of low-lying delta plains results in sea-level rise, shoreline erosion, and wetland loss, which causes a threat to coastal populations (Parcharidis *et al*., 2013). Thus, quantitative understanding of subsidence is important for predicting relative sea-level rise, storm-surge flooding, as well as for successful wetland restoration.

This study deals with the estimation of subtle ground deformation at millimetric accuracy over the deltaic plain of the Evinos River and its spatio-temporal distribution for the period between 2015 and 2020 through the method of Small Baseline Subset (SBAS) Interferometry. The Evinos River delta is located on the northern shore of the Gulf of Patras, Western Greece. It covers an area of approximately 92 km^2 and belongs to the Messologi wetland, one of the most significant ecosystems in Western Greece protected by the Ramsar Convention (Maroukian and Karymbalis, 2004, Karymbalis *et al*., 2022). According to Galloway's (1975) proposed delta classification it should be classified among those deltas affected by fluvial sediment supply and wave activity.

Methodology

To analyze the mobility of the Evinos River delta the interferometric method of Small Baseline Subset (SBAS) has been performed (Figure 1) using the SARscape software 5.3, which runs on the ENVI platform 5.3, whereas the visualization of the results has been made with ArcGIS 10.4. 222 Single Look Complex (SLC) scenes, 100 in ascending orbit and 122 in descending orbit, VV polarization and operating C-band from Sentinel 1A and 1B satellites were used, covering the time period between August 2015 and October 2020. The digital terrain model Shuttle Radar Topography Mission (SRTM) 3 version 4, provided by NASA, with a resolution of 90 m was also used.

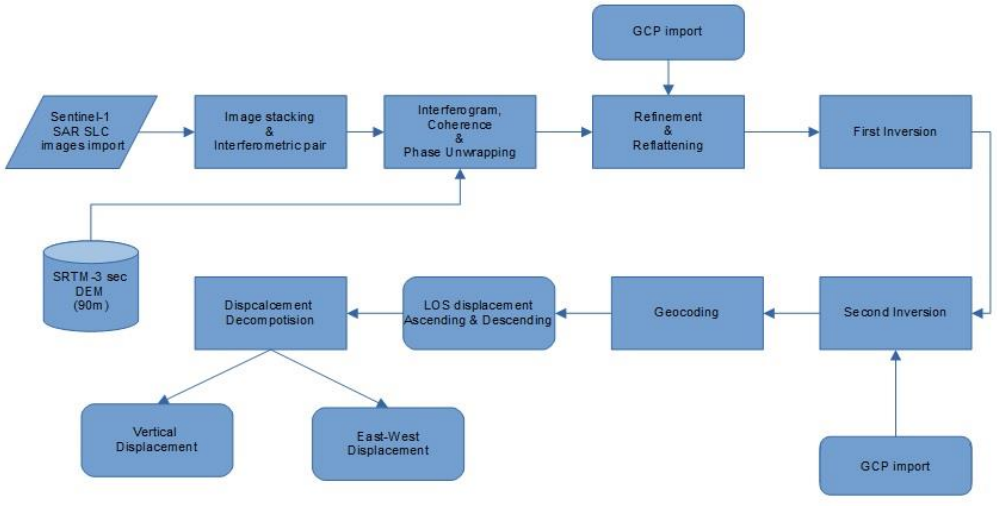

Figure 1. Flow chart of the processing.

To investigate the influence of sediment compaction on the differential subsidence in the deltaic plain, boring log sediment descriptions of 13 boreholes were considered. Borehole data were obtained from a study conducted by the

Ministry of Agriculture during the late 1970s at the deltaic plain. For each borehole the percentages of coarse- and fine-grained sediments in the drilling log was estimated. Buffer zone of 200 m around the location of each borehole were created, and mean annual subsidence rates were calculated for the time period under study. Then a plot of the percentage of fine sediments in the boring logs vs. mean annual subsidence rate was created.

Results - Conclusions

The results indicate that the maximum subsidence observed for the period 2015-2020 is approximately -40 mm/yr, while the maximum uplift is about +5 mm/yr (Figure 2a). The urbanized area of Messologi at the northwestern part of the delta can be characterized as a stable zone, since the values of velocity are close to 0. Negative velocity values, indicative of subsidence, were recorded along Louros, west of Akra Evinou. Louros is an elongated low-lying barrier feature, made up of a series of beach ridges, with maximum elevation of approximately 50 cm, which separates Klissova lagoon from the Gulf of Patras. It is obvious that due to the combined action of land subsidence and the anticipated sea-level rise the lagoon will be totally connected to the Gulf of Patras in the near future. Another subsiding part of the deltaic plain is its southern part, on both sides of the lower reaches of the Evinos River main channel (Figure 2a). These areas correspond to paleo-distributaries of delta paleo-lobes, as well as to an abandoned mouth of the river (east of the currently active one). A probable reason for this subsidence is the lack of river sediment supply.

Positive velocity values are displayed along the main distributary channel of the River as well as along the eastern shore of the Klisova Lagoon (Figure 2a). The positive values along the main channel are the result of the bedload transport since the Evinos River has a braided channel with "moving" coarse grained bars. As for the Klisova shore positive velocity values are the result of artificial constructions along the road that connects Akra Evinou with Messologi.

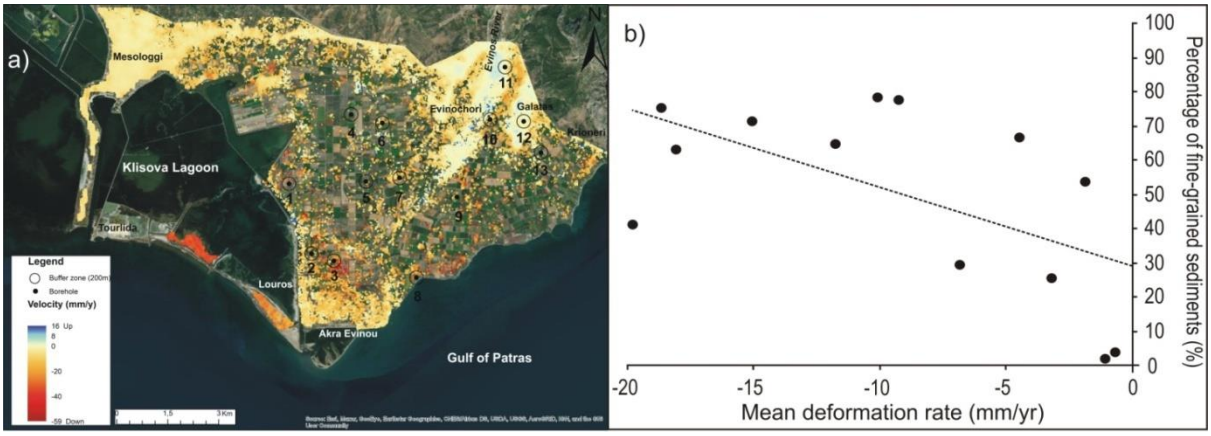

Figure 2. a) Linear component of ground deformation over the broader Evinos River delta area for the period 2015-2020. b) Diagram of percentage of fine sediments of the boring log vs. subsidence rates. The locations of the boreholes are displayed on the map.

The "percentage of fine sediments of the boring log vs. subsidence rates" plot shows a positive correlation between subsidence rate and the thickness of the fine-grained sediment participation in the subsurface deltaic sedimentary sequence (Figure 2b). Hence, differential natural compaction of Holocene deposits, attributable to subjacent grain-size variability, seems to be the main reason for the observed ground subsidence of the delta plain. Natural compaction happens as new sediment (weight) is added to the deltaic sedimentary sequence, and the underlying sediment is reduced of its water content because of reduction of the void spaces between sediment grains (Meckel *et al*., 2007).

References

Galloway, W.E., 1975. Process framework for describing the morphological and stratigraphic evolution of deltaic depositional systems, in: Broussard, M.L. (Ed.), Deltas, models for exploration, 87-98.

Karymbalis, E., Gallousi, C., Cundy, A., Tsnakas, K., Gaki-Papanastassiou, K., Tsodoulos, I., Batzakis, D.V., Papnstassiou, D., Liapis, I., Maroukian, H., 2022. Long-term spatial and temporal shoreline changes of the Evinos River delta, Gulf of Patras, Western Greece. Zeitschrift für Geomorphologie 63/2, 141-155.

Maroukian, H., Karymbalis, E., 2004. Geomorphic evolution of the fan-delta of the Evinos River in western Greece and human impacts in the last 150 years. Zeitschrift für Geomorphologie 48/2, 201-217.

Meckel, T.A., ten Brink, U.S., Williams, S., 2007. Sediment compaction rates and subsidence in deltaic plains: numerical constraints and stratigraphic influences. Basin Research 19/1, 19-31.

Milliman, J.D., Qin, Y.S., Park, Y.A., 1989. Sediment and sedimentary processes in the Yellow and East China Seas, in: Taira, A., Masuda, F. (Eds.), Sedimentary facies in the active plate margin, 233-249.

Parcharidis, I., Kourkouli, P., Karymbalis, E., Foumelis, M., Karathanassi, V., 2013. Time series Synthetic Aperture Interferometry for ground deformation monitoring over a small scale tectonically active environment (Mornos, Central Greece). Journal of Coastal Research 29/2, 325-338.

Syvitski, J.P., Saito, Y., 2007. Morphodynamics of deltas under the influence of humans. Global and Planetary Change 57/3-4, 261-282.

Wright, L.D., Coleman, J.M., 1973. Variations in morphology of major river deltas as functions on ocean wave and river discharge regimes. The American Association of Petroleum Geologists Bulletin, 57, 370–398.

16th International Congress of the Geological Society of Greece
17-19 October, 2022 - Patras, Greece
Bulletin of the Geological Society of Greece, Sp. Publ. 10
Ext. Abs. GSG2022-224

The caves of Greece: archive analysis and modern field-work data

G. Lazaridis[1], D. Dora[1], I. Nikolaidou[1], P. Karakoulakis[1], A. Almpanopoulou[1], S. Pantali[1], K. Kamadanis[1], M. Karagkiozi[1], M. Kokovaki[1], F. Sdraka[1], A. Karampelas[1], A. Panora[1], S. Ntasioti[1], M. Georgiadou[1], F. Konstantinakis[1], M.-D. Gkari[1], K. Vouvalidis[1]

(1) School of Geology, Aristotle University of Thessaloniki, GR-54124, Thessaloniki, Greece, geolaz@geo.auth.gr

Cave density along Greek territory, the dominant morphological types and, the main speleogenetic processes that formed Greek caves are investigated in a solid statistical analysis combined with field work data.

Introduction

This work is based on a new cadastral of caves that is developed by the undergraduate students of School of Geology in Aristotle University of Thessaloniki who are focused on the topic of speleology. A database was built which aims to the management of scientific information on the geology and speleology of Greek caves. The first step was to fill in the various fields of the database with published information about caves in Greece that can be found in explorational and scientific papers. In a further step, the database was reinforced with information retrieved from various exploration reports and as well as from unpublished data derived from field work performed by or in collaboration with our speleological team, which significantly increased the total number of records. Few main questions included in this statistical analysis, such as which is the cave density along Greek territory, which are the main morphological types and under which processes have formed the recorded caves, are being answered.

Methods

Data: The statistical sample used in this analysis includes the records retrieved by the students from the bulletin of the Hellenic Speleological Society. The benefit of using this sample is that the data used are accessible to everyone and the results repetitive. However, additional sources are discussed below in order to clarify certain perspectives of this study. Quantitative analysis: Exact information on the geographic location of cave entrances is quite rare in that sample because of the lack in georeferencing tools in those early years that explorations took place, restricting a detailed spatial analysis of cave distribution. Caves are being represented as point features to the geographical area that belong and then illustrated in a Kernel density map (Silverman, 1986). The geographical unit used is the prefecture. Cave morphology is used to identify main types of karst caves. It is worth to note that the database includes all cave types that can be found in Greece; not only karst ones. Qualitative analysis: Caves are classified on the following categories that describe their morphology according to their pattern, as derived from the available cave maps, limiting the statistical sample in 340 caves: 1. vertical shaft and complex vertical structure; 2. horizontal single passage; 3. chamber; 4. horizontal with multiple passages/chambers; 5. combination of single vertical and horizontal passage; 6. complex caves of multiple horizontal and vertical passages; 7. sinkhole; 8. complex branchwork. Furthermore, speleological information based on field work is used for the interpretation of speleogenesis.

Results

The sample size is n=1491 caves and corresponds to about 20% of the registered Greek caves. Their geographical density is illustrated in the map of figure 1A. The southern center of highest density appears in Crete Island and the northern one in region of Attica. Northern Greece appears to be in the zone of less than twenty caves in most of its regions. According to the morphological classification (Fig. 1B) most caves included in the dataset are falling into the single chamber category and the category with caves of vertical development is coming next. Complex caves of horizontal development with (17.3%) or without (17.3%) vertically developed sectors are about one third of the dataset. Maze caves, such as some hypogene ones, are included in these categories. Other large systems that form branchwork networks are representing only the 5% of the sample.

The cadastral of Greek caves include both constructional and destructional caves after Mylroie, 2019. Constructional caves found in Greece include caves in travertine such as progradational in waterfalls, travertine bridges and aggradational caves. Destructional caves include karst caves that formed by corrosion and those formed by weathering/erosion of rocks. Karstic caves that have been recorded are both hypergene and hypogene caves. Hypergene caves are phreatic, epiphreatic, vadose primary and drawdown caves. Hypogene caves fall in the categories of endogenous and caves in aquifers side-open to the sea that are related to Sulfuric Acid Speleogenesis (SAS). Caves from mechanical erosion include several types such as wave-cut caves, riverbank caves (i.e. Lazaridis, 2014), eolian caves (i.e. for Meteora area; Rassios et al., 2013), suffosional/piping caves and salt weathering caves.

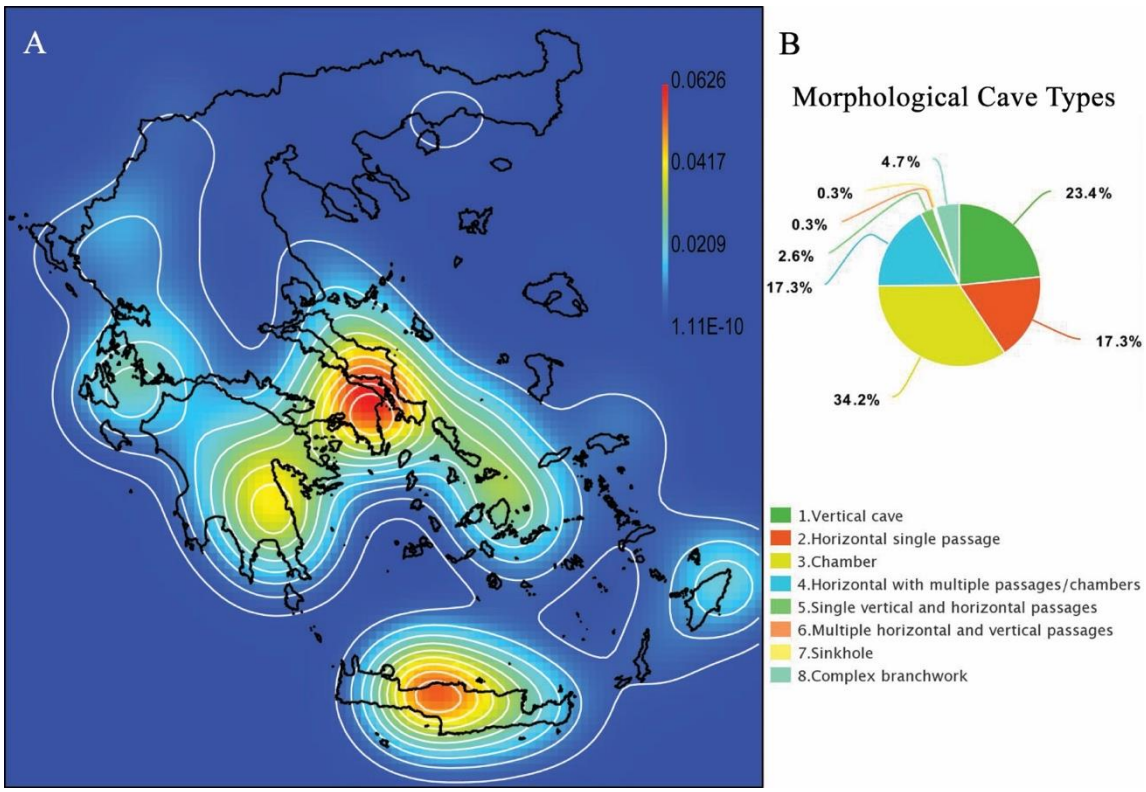

Figure 1. A. Kernel density map of Greece of the cave population included in the dataset. B. Morphological categories of caves as derived from the cave maps.

Discussion and conclusions

Figure 1A is describing the spatial relationship between the geographical area and the cave explorations in Greece. The great difference in the number of explored caves per geographical area is not only due to the distribution of the caves, but mainly due to uneven explorational efforts. This leads to over-interpretation of the cave density in the area of Attica, where the most speleological clubs are located. The density of caves in northern Greece is low because only few cavers and speleologists have worked in the area between 1950 and 2000, which is the time window covered by the dataset. The density map radically changes with the addition of new data for hundreds of caves, located in Northern Greece, in the dataset. These new data are the result of the systematic investigation of caves in northern Greece from the School of Geology in Aristotle University of Thessaloniki since 2001. The cave expeditions and the following conduction of the scientific research has enriched the cadastral of caves in Greece.

Cave pattern in ground-plan is informative of speleogenesis (Palmer, 2000; White and Culver, 2005). Chamber cave is the predominant morphological type, which can have different speleogenetic origin. Registered chamber caves can be categorized either as phreatic karst caves, or weathering caves or as littoral caves, which are all very common speleogenetic categories in Greece. Vertical caves appear all over the country and present a particularly high frequency of development in Crete Island and in general to the geotectonical zones of external Hellenides, that correspond to the west and southwest territory of Greece. These caves are mainly primary vadose caves that mark rapid tectonic uplift (Ford and Williams, 2007). The presence of multiple speleogenetic types along Greece, is depended on the variations in lithology, hydrogeology, climate, tectonics etc.

This work provided useful information in terms of both quantitative and qualitative perspectives. In the future it will be expanded by further analyzing the data and examining various morphological and speleogenetical types in separate maps.

Regarding the educational perspective of this project, it is concluded that this work was comprehensive and well understood by the students who acquired new skills in respect to speleology and data mining.

References

Ford, D., Williams, P.D., 2007. Karst hydrogeology and geomorphology. John Wiley and Sons Inc.

Lazaridis, G., 2014. Processes of rock-shelter and shelter cave development. Examples from Greece. Спелеология и спелестология, (5), 85-92.

Mylroie, J., 2019. Caves in space. Journal of Cave & Karst Studies, 81(1).

Palmer, A., 2000. Hydrogeologic control of cave patterns. Speleogenesis: Evolution of Karst Aquifers. Huntsville: National. Speleological Society, 77-90.

Rassios, A. E., Ghikas, D., Dilek, Y., Vamvaka, A., Batsi, A., & Koutsovitis, P., 2020. Meteora: A billion years of geological history in Greece to create a World Heritage Site. Geoheritage, 12(4), 1-16.

Silverman, B. W., 1986. Density Estimation for Statistics and Data Analysis. New York: Chapman and Hall.

White, W.B., Culver, D.C., 2005. Encyclopedia of caves, Elsevier Amsterdam (The Netherlands).

16th International Congress of the Geological Society of Greece
17-19 October, 2022 - Patras, Greece
Bulletin of the Geological Society of Greece, Sp. Publ. 10
Ext. Abs. GSG2022-225

Identification and Mapping of Beach Ridges in the Acheron River delta (Western Greece)

D. Griva[1], E. Karymbalis[1], M. Poscolieri[2], I. Parcharidis[1], V. Kapsimalis[3], K. Tsanakas[1], D.-V. Batzakis[1]

(1) Department of Geography, Harokopio University, Athens, Greece, dgriva@hua.gr, (2) Section of Acoustics and Sensors O.M. Corbino, CNR-INM, Rome, Italy (3) Institute of Oceanography, Hellenic Centre for Marine Research, Anavyssos, Greece

Introduction

A beach ridge is a coastal depositional landform defined as a relict shore ridge that is more or less parallel with the coastline and with other landward-adjacent ridges. It is built by wave swash that may be surmounted by wind-deposited sediments (Otvos, 2000). Once such a ridge becomes isolated from daily active beach processes by coastal progradation, it becomes a beach ridge (Otvos, 2000). These landforms can serve as indicators of the positions of past shorelines and as former sea-level markers (Mason, 1990). The older beach ridges are located further inland, and new ones are built progressively seaward. They generally prograde when an abundance of sediment exists and the offshore gradient is low.

The main aim of this study is to identify and map in detail a series of beach ridges developed and preserved at the delta of the Acheron River, in Western Greece (Figure 1). The part of the deltaic plain north of the main river channel is characterized by a "ridge and swale topography" consisting of several beach ridges alternating with marshy depressions almost parallel to the present-day Phanari Bay shoreline. These beach ridges have accreted rapidly and gradually filled Phanari Bay over the last 900 years (Besonen et al., 2003).

Figure 1. Location of the study area.

Methodology

Three different methodologies have been applied to recognize and map the beach ridges. The first method is based on the application of indicators on PlanetScope and Sentinel-2 satellite images (Tables 1 and 2) for inverting the swales since sometimes it is difficult to discriminate the ridges themselves.

Table 1. Characteristics of the Sentinel-2 satellite images used.

Orbit Pass Direction	Spectral bands	Period	Relative Orbit Number
Descending	13(VIS, NIR, SWIR)	25/5/2021	93
Descending	13(VIS, NIR, SWIR)	13/1/2022	93

VIS: visual, NIR: near-infrared, SWIR: short-wave infrared

Table 2. Characteristics of the PlanetScope Dove microsatellites' images used.

Number of images	Period	Bands
1	29/05/2021	R,G,B,NIR
1	30/01/2022	R,G,B,NIR

VIS: visual, NIR: near-infrared, SWIR: short-wave infrared

The Normalized Difference Vegetation Index (NDVI), an index that describes the difference between visible and near-infrared reflectance of vegetation cover, was used to discriminate swales based on their vegetation. NDVI is calculated by the following formula (Tucker, 1979) and its values range from -1 to +1:

$$\mathrm{NDVI} = \frac{\mathrm{RED} - \mathrm{NIR}}{\mathrm{RED} + \mathrm{NIR}}$$

In addition, the Normalized Difference Water Index (NDWI), the most suitable index for mapping water bodies, was used to separate the swales from the ridges. NDWI allowed us to detect swales using satellite images taken in the winter months since topographic depressions are covered by water during this period of the year. NDWI is calculated through the following equation (McFeeters, 1996):

$$\mathrm{NDWI} = \frac{\mathrm{Green} - \mathrm{NIR}}{\mathrm{Green} + \mathrm{NIR}}$$

NDWI values vary from -1 to +1 with values greater than 0.3 usually corresponding to water bodies.

The second methodological approach for the identification of the beach ridges was the application of a Red Relief Image Map (RRIM), using a 2 m cell size Digital Elevation Model (DEM) of the study area, obtained from the Hellenic Cadastre. RRIM is a ground surface visualization method based on the combination of three landform element layers i.e. topographic slope, positive openness, and negative openness, and is considered ideal for the delineation of linear morphological features.

The third method was a landform classification procedure of the geomorphological characteristics of the deltaic plain (ridges and swales) based on the application of multivariate statistics to an eight-layer stack, which describes the topographic gradients, measured along the eight azimuth orientations of the neighborhood of every DEM pixel (Parcharidis et al., 2001).

This approach allowed a rapid assessment of the spatial distribution of different types of slope gradients and the discrimination of landforms with similar geomorphic characteristics (in particular ridges and swales).

Results - Conclusions

The results of the application of the above-mentioned techniques are presented in Figure 2. The combination of the three crossing methods results led to the construction of a preliminary map of the beach ridge system, which was verified in the field to produce the final map.

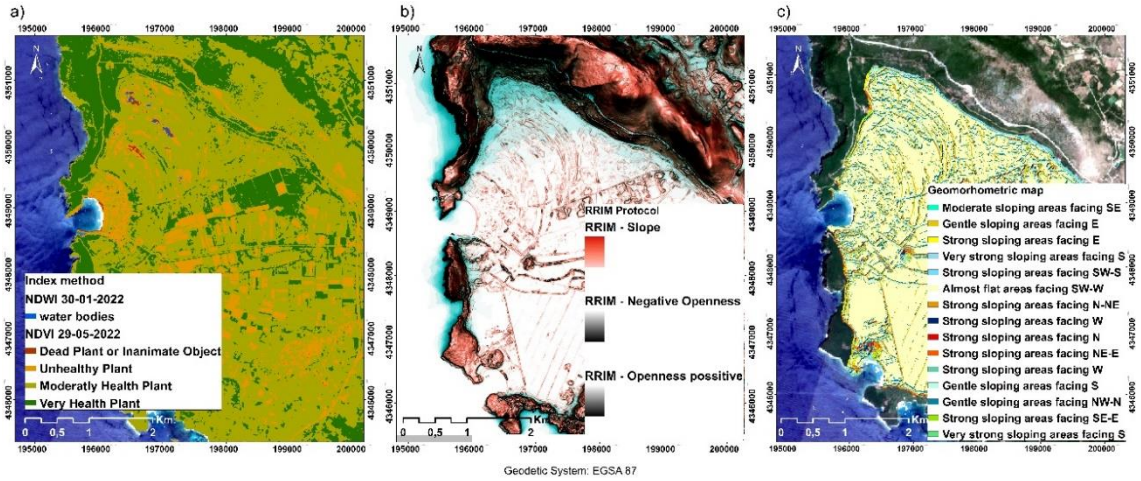

Figure 2. The results of the three different methodological approaches for the recognition of the Acheron River delta beach ridges: a) NDVI and NDWI calculation from PlanetScope and Sentinel-2 satellite images, b) Red Relief Image Map (RRIM), and c) aspect and slope calculation from DEM.

Approximately 10 beach ridges, the present-day shoreline of Phanari Bay, have been recognized. The maximum elevation of the ridges is ~8.3 m above mean sea level (m.s.l.), whereas the minimum elevation of the swales is 0.1 m below m.s.l. Identifying and mapping of the beach ridges were the first necessary steps to trace the palaeogeographic evolution as well as to reconstruct the accretion history of this part of the Acheron River delta over the last 900 years.

References

Besonen, M.R., Rapp, G., Jing, Z., 2003. The lower Acheron River valley: Ancient accounts and the changing landscape. Hesperia Supplements 32, 199-263.

Mason, O.K., 1990. Beach Ridge Geomorphology of Kotzebue Sound: Implications or Paleoclimatology and Archeology. Ph.D. Thesis, University of Alaska, Fairbanks, 291 p.

McFeeters, S.K., 1996. The use of the Normalized Difference Water Index (NDWI) in the delineation of open water features. International Journal of Remote Sensing 17, 1425-1432.

Otvos, E.G., 2000. Beach ridges – definitions and significance. Geomorphology 32/1, 83-108.

Parcharidis, I., Pavlopoulos, A., Poscolieri, M., 2001. Geomorphometric analysis of the Vulcano and Nysiros island: clues of the definitions of their volcanic landforms. Proceedings of the International Workshop “The Bridge between Big Bang and Biology”, Stromboli, Messina, Italy, 310-320.

Tucker, C.J., 1979. Red and photographic infrared linear combinations for monitoring vegetation. Remote Sensing of Environment 8, 127-150.

16th International Congress of the Geological Society of Greece
17-19 October, 2022 - Patras, Greece
Bulletin of the Geological Society of Greece, Sp. Publ. 10
Ext. Abs. GSG2022-318

Relative Tectonic Activity Assessment of the Trichonis Lake Graben (Western Greece) Using Geomorphometry and Artificial Intelligence

E. Karymbalis[1], K. Valkanou[1], G. Fubelli[2], M. Ferentinou[3], P.T. Giles[4], K. Tsanakas[1], D.-V. Batzakis[1], D. Papanastassiou[5], K. Gaki-Papanastassiou[6]

(1) Department of Geography, Harokopio University, Athens, Greece, karymbalis@hua.gr (2) Department of Earth Sciences, University of Turin, Turin, Italy (3) School of Civil Engineering and the Built Environment, Liverpool John Moores University, Liverpool, United Kingdom (4) Department of Geography and Environmental Studies, Saint Mary's University, Halifax, Nova Scotia, Canada (5) Institute of Geodynamics, National Observatory of Athens, Athens, Greece (6) Faculty of Geology and Geoenvironment, University of Athens, Athens, Greece.

Introduction

Landscape morphology can provide insights into the interactions of surface processes and tectonic activity. In tectonically active areas fluvial systems and mountain fronts are controlled by the type, geometry, and recent activity of faults. Therefore, the geomorphological analysis of mountain fronts, drainage networks, and catchments can provide valuable information about the recorded tectonic history (Burbank and Anderson, 2008).

The quantitative measurements of the landscape are mainly based on the calculation of geomorphic indices. Individual geomorphic indices of active tectonics, based on estimations of the characteristics of the drainage networks, catchments and mountain fronts, provide a quantitative approach for evaluating the influence of active tectonics on the morphology of the landscape in a given area. For the assessment of the relative tectonic activity of an area, a single analysis can be made but the results are more meaningful if more indices are applied. Some attempts used a combination of two indices (e.g. the mountain front sinuosity index Smf and the valley width/height ratio Vf) to provide semi-quantitative information of the relative degree of tectonic activity of fault-generated mountain fronts. Similar approaches, which take into account not only geomorphic indices of mountain fronts but also variables of drainage networks and catchments, have been found to be useful for the evaluation of relative active tectonics in various tectonically active areas around the world. Several recent studies proposed a single index produced from the combination of multiple quantitative geomorphological parameters to make a more accurate and objective evaluation of relative active tectonics (e.g. El Hamdouni *et al.*, 2008, Valkanou *et al.* 2020).

A widely used method for the assessment of the clustering tendency of datasets (such as morphometric indices of mountain fronts, drainage networks, and catchments) is Self-Organizing Map (SOM), which is a clustering and projection algorithm of high-dimensional data to a lower dimensional space (Karymbalis *et al.*, 2022). SOM is a special type of Artificial Neural Network (ANN) that is trained using unsupervised learning to produce a low-dimensional projection of the input space, called the map.

This study aims to assess the relative tectonic activity around the Trichonis Lake graben coupling quantitative morphometric analysis and SOM. 35 catchments around the Lake were analyzed using nine geomorphic indices.

Study Area

The Trichonis Lake graben is located in western continental Greece. It is a late Plio-Quaternary extensional basin created by back-arc extensional faulting. It strikes WNW-ESE for a distance of 32 km, has a width of 10 km, and cuts across the early Tertiary NW-SE fold and thrust structures of the Pindos Mountains (Doutsos *et al.*, 1987). The seismicity, the focal mechanisms of microearthquakes, and the GPS measurements (Kiratzi *et al*., 2008, Kassaras *et al.*, 2014) indicate that Trichonis graben, like the other active structures in the broader area (Amvrakikos Gulf, Gulf of Corinth and Gulf of Patras), is controlled by N-S extension. The north and south flanks of the Trichonis tectonic depression are bounded by E-W and NW-SE trending faults. Two segmented E-W trending antithetic normal faults, buried locally by Pleistocene deposits and thick alluvial fans, have been mapped along the margins of the lake (Doutsos *et al.*, 1987): An E-W trending and south-dipping low-angle normal fault, related to the major Agrinio Fault Zone (AFZ), parallel to the northern bank of the lake and an E-W striking and north-dipping normal fault (the Trichonis Fault Zone: TFZ), located south of the lake. A 1975 shallow earthquake sequence along with a 2007 earthquake swarm revealed a NW-SE striking normal fault that dips to the NE which bounds the southeastern bank of the lake (Kato Makrinou Fault: KMF) (Kiratzi *et al*., 2008). The focal mechanism analysis of the same earthquakes showed the existence of a conjugate NW-SE striking and SW-dipping marginal fault along the northeastern flanks of the lake (Petrochorion Fault: PF) (Kassaras *et al.*, 2014). The Neotectonic map of the area by Lekkas and Papanikolaou (1997) shows the existence of a less prominent NE-SW trending probable normal fault running parallel to the southeastern shore of the Lake (Sitaralona Probable Fault: SPF).

Methodology

To evaluate the relative tectonic activity in the study area, various morphometric indices including stream length - gradient index (SL), drainage basin asymmetry (Af), hypsometric integral (Hi), valley floor width-valley height ratio (Vf), drainage basin shape (Bs), mountain front sinuosity (Smf), Basin slope (Bs), Relief ratio (Rh) and Melton's ruggedness number (M) were calculated for 35 catchments. In addition, mountain-front sinuosity index has been estimated for 20 mountain fronts around the lake. For the measurement of the geomorphic indices a digital elevation model (with 5 m cell size), obtained from the Hellenic Cadastre, was used. The catchments of the study area were classified into four classes based on the morphometric variables and a series of maps showing their spatial distribution were produced by applying GIS techniques. The combination of these morphometric variables yielded two indices of relative tectonic activity (named IRTA: Index of Relative Tectonic Activity proposed by Valkanou *et al*. (2020), and IAT (Index of Active Tectonics), initially proposed by El Hamdouni *et al*. (2008). Based on the values of IRTA and IAT, the area was classified into three classes of relative tectonic activity (low, medium, and high). Additionally, to evaluate the landscape of the study area in terms of relative tectonic activity the SOM method was used. The application of SOM classified the catchments into four groups based on the values of the nine geomorphic indices.

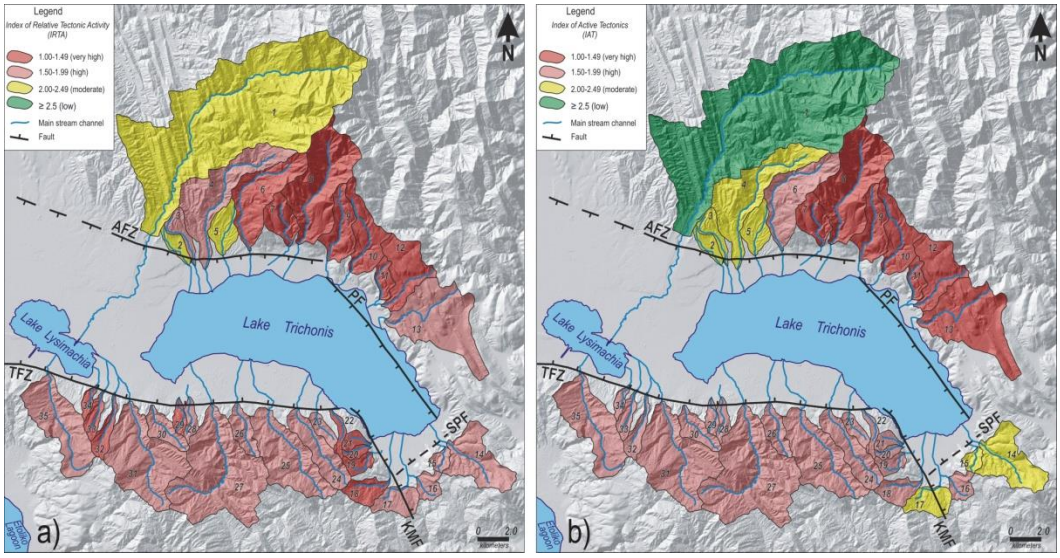

Figure 1. Spatial distribution maps of the integrated indices a) IRTA, and b) IAT. AFZ: Agrinio Fault Zone, TFZ: Trichonis Fault Zone, PF: Petrochorion Fault, KMF: Kato Makrinou Fault, SPF: Sitaralona Probable Fault.

Results and Conclusions

The results of the classification of the catchments into four classes of relative tectonic activity, according to the values of IRTA and IAT, are depicted in Figure 1. In general, the spatial distribution maps of IRTA and IAT suggest that the catchments of the footwalls of the western segment of the AFZ, as well as of the PF are affected by very high relative tectonic activity. It is worth mentioning that although the graben shows asymmetry with the topography along the north shore of the lake being less pronounced pointing to the existence of a less active margin in comparison to the south, the results of the analysis indicate that the development of the landscape of the central and western parts of the northern flanks of the graben has been highly influenced by the tectonic uplift due to the activity of both the AFZ and the PF. the catchments' classification results of the application of the SOM technique are in general agreement with the IAT and IRTA grouping.

References

Burbank, D.W., Anderson, R.S., 2008. Tectonic Geomorphology. Blackwell Science.

Doutsos, T., Kontopoulos, N., Frydas, D., 1987. Neotectonic evolution of northwestern continental Greece. Geologische Rundschau, 76(2), 433-450.

El Hamdouni, R., Irigaray, C., Fernandez, T., Chacon, J., Keller, E.A., 2008. Assessment of relative active tectonics, southwest border of the Sierra Nevada (southern Spain). Geomorphology 96, 150-173.

Karymbalis, E., Ferentinou, M., Fubelli, G., Giles, P., Tsanakas, K., Valkanou, K., Batzakis, D.V., Karalis, S., 2022. Classification of Trichonis Lake graben (Western Greece) alluvial fans and catchments using geomorphometry and artificial intelligence. Zeitschrift fur Geomorphologie, 63/2-3, 295-312.

Kassaras, I., Kapetanidis, V., Karakonstantis, A., Kaviris, G., Papadimitriou, P., Voulgaris, Makropoulos, K., Popandopoulos, G., Moshou, A., 2014. The April-June 2007 Trichonis Lake earthquake swarm (W. Greece): New implications toward the causative fault zone. Journal of Geodynamics 73, 60-80.

Kiratzi, A., Sokos, E., Ganas, A., Tselentis, A., Benetatos, C., Roumelioti, Z., Serpetsidaki, A., Andriopoulos, G., Galanis, O., Petrou, P., 2008. The April 2007 earthquake swarm near Lake Trichonis and implications for active tectonics in western Greece. Tectonophysics, 452(1-4), 51–65.

Lekkas, E., Papanikolaou, D., 1997. Neotectonic Map of Greece, Aitolia-Akarnania sheet (scale 1:100.000), Applied scientific program, Unicersity of Athens, Dept of Dynamic, Tectonic and Appplied Geology, Technical report.

Valkanou, K., Karymbalis, E., Papanastassiou, D., Soldati, M., Chalkias, C., Gki-Papanastassiou, K., 2020. Morphometric analysis for the assessment of relative tectonic activity in Evia Island, Greece. Geosciences 10, 264.

16th International Congress of the Geological Society of Greece
17-19 October, 2022 - Patras, Greece
Bulletin of the Geological Society of Greece, Sp. Publ. 10
Ext. Abs. GSG2022-321

Coastal Vulnerability Assessment of Mirabelo Gulf-NE Crete

M. Kazantzaki[1], E. Tsakalos[1], E. Filippaki[1], Y. Bassiakos[1]
(1) National Centre for Scientific Research, NCSR "Demokritos", Athens, Greece, .kazantzaki@inn.demokritos.gr

The impact assessment for the Mirabello Gulf (NE Crete), based on three different sea level rise scenarios (0.5, 1 and 2 m), revealed that ~7 km of its coastal zone is characterized as of high vulnerability while ~13 km of the coastal zone is classified as of "moderate" vulnerability. In addition, a total land of ~95, ~102 and ~137 km^2 respectively, will be flooded in the case of 0.5, 1 and 2 m rise of sea level, something that will exacerbate the already existing environmental and socio-economic impact of rising sea level.

The main purpose of this research was to investigate the coastal vulnerability of Mirabello Gulf due to sea level rise. In this regard, the Coastal Vulnerability Index (CVI) was calculated, using data from geological maps, past relative sea level fluctuations, mean tide range, aerial photographs, the Digital Elevation Model (DEM) as well as the wind and wave Atlas for the Hellenic seas-Poseidon System..

Mediterranean areas are characterized by intense seismic and volcanic activity as well as eustatic changes, the result of which is the creation of particularly vulnerable coastal zones. The most vulnerable are low-lying coastal areas, the geomorphological evolution of which are highly affected by both natural processes and anthropogenic interventions (EUROSION, 2004). Therefore, assessing changes that take place along coastal zones is of great importance in order to enable the development of integrated coastal management plans (e.g., IPCC, 2013). A characteristic case is the Gulf of Mirabello in N.E Crete, where intense coastal erosion, in combination with the tectonic subsidence of the area threatens a large part the coastal zone, resulting in direct socio-economic impacts. The present study assesses the temporal geomorphological changes that have taken place in the coastal zone of Mirabello Gulf, to provide a clear frame of the coastal zone evolution over time and performs a vulnerability assessment, based on the coastal vulnerability index (CVI) methodology by Thieler and Hammar-Klose (1999), considering geological features, coastal slope, shoreline erosion/accretion rates, relative sea-level change and mean significant wave height, as well as mean tide range in the area (Karymbalis, et al., 2012). In light of this, an impact assessment, based on three different sea level rise scenarios, is also performed and presented. The ArcGIS 10.5 software was used to calculate the CVI index. A database consequently was created containing a risk value for each data variable. The vulnerability index along the coastline was presented using the ArcMap software.

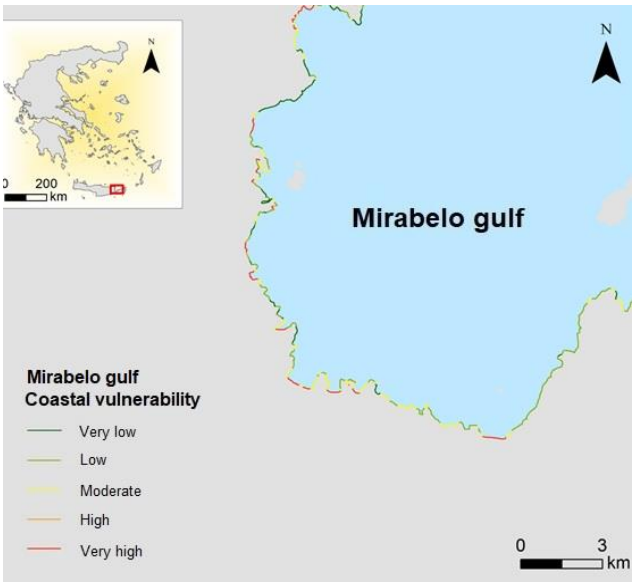

Figure 1: Coastal Vulnerability Index (CVI) of Mirabello Gulf

CVI revealed that Mirabello Gulf coast line experiences very high to very low vulnerability (Fig. 1). In several parts along the coast, the low degree of vulnerability could be attributed to the ports which reduce the rate of sediment removal. However, there are many sections that show very high vulnerability, especially in places where sandy beaches are found.

Based on a quantitative calculation of the CVI, it appears that the part that shows the lowest vulnerability along the coastline stretches over ~10 km which corresponds to 18.7%. The coastline with a low vulnerability has a length of ~23

km (42.1%), moderate vulnerability ~13.3 km (24.8%), high vulnerability ~0.5 km (0.9%), while very high vulnerability ~7.3 km (13.5%). Furthermore, taking into account three different sea level rise scenarios of 0.5, 1 and 2 m rise, a total land of ~95, ~102 and ~137 km^2 respectively, will be flooded (Fig. 2).

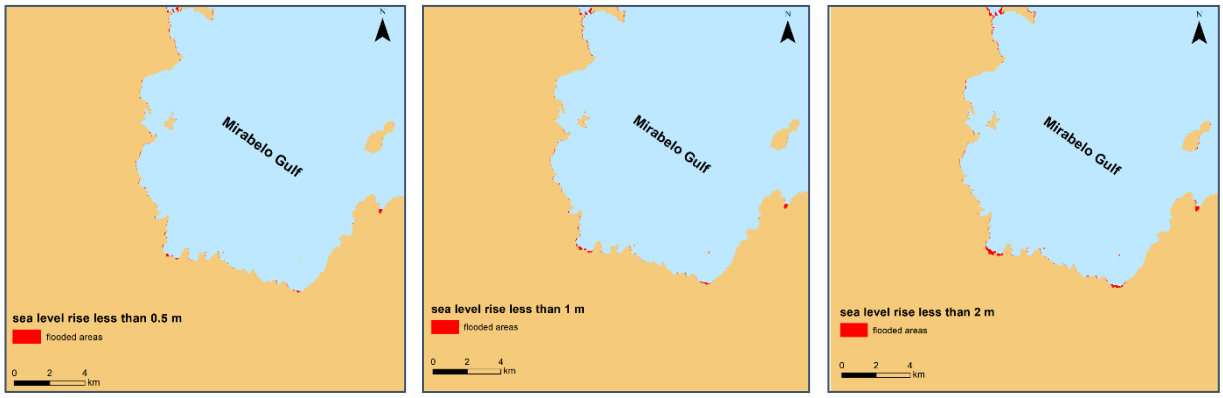

Figure 2: Flooded areas after a sea level rise of a) 0.5 m, b) 1 m and c) 2 m

Conclusions

The present study assessed the temporal geomorphological changes that have taken place in the coastal zone of Mirabello Gulf and provided the frame of the coastal zone evolution and vulnerability of the coast. CVI revealed that coastal vulnerability at Mirabello Gulf coastline ranges from very high to very low. Furthermore, future sea level rise of 0.5, 1 and 2 m, will lead to a total land loss of ~95, ~102 and ~137 km^2 respectively.

Acknowledgements

This study was a part of a master dissertation supported by both Harokopio University-Department of Geography and National Centre for Scientific Research "Demokrios"- Laboratory of Palaeoenvironment and Ancient Metal Studies.

MSc Thesis: Shoreline vulnerability assessment of Mirabelo Gulf-NE Crete.National Technical University of Athens, faculty of Geological Sciences, School of Mining and Metallurgical Engineering.

References

EUROSION, 2004. Living with coastal erosion in Europe. Final report of the project 'Coastal erosion – Evaluation of the need for action'. Directorate General Environment, European Commission.

IPCC (Intergovernmental Panel on Climate Change), 2013. Climate Change-2013: The Physical Science Basis. Contribution of Working Group I to the Fifth Assessment Report of the Intergovernmental Panel on Climate Change [Stocker T.F., Qin D., Plattner G.K., Tignor M., Allen S.K., Boschung J., Nauels A., Xia Y., Bex V. and Midgley P.M. (Eds.)]. Cambridge University Press, Cambridge, United Kingdom and New York, NY, USA, 1535.

Karymbalis, E., Chalkias, C., Chalkias, G., Grigoropoulou, E., Manthos, G. et al., 2012. Assessment of the Sensitivity of the Southern Coast of the Gulf of Corinth (Peloponnese, Greece) to Sea-level Rise. Central European Journal of Geosciences, 4 (4), 561-577.

Thieler E.R., Hammar-Klose E.S., 1999. «National Assessment of Coastal Vulnerability to Future Sea-Level Rise: Preliminary Results for the U.S. Atlantic Coast, U.S». Geological Survey, Open-File Report, 99-593.

16th International Congress of the Geological Society of Greece
17-19 October, 2022 - Patras, Greece
Bulletin of the Geological Society of Greece, Sp. Publ. 10
Ext. Abs. GSG2022-336

Geomorphological Map of Greece at 1:1,000,000 Scale – Pilot 1:50,000 scale geomorphological mapping of Naxos Sheet

A. Petropoulos[1,2], N. Evelpidou[2], A. Zervakou[1] I. Zananiri[1]

(1) Hellenic Survey of Geology and Mineral Exploration, Acharnae, Greece, apetropoulos@igme.gr. (2) Faculty of Geology and Geoenvironment, National and Kapodistrian University of Athens, Panepistimiopolis, Athens, Greece.

Introduction

In the frame of recording, management and highlighting of the geological and geomorphological heritage of Greece, the Hellenic Survey of Geology & Mineral Exploration (HSGME) in collaboration with the National and Kapodistrian University of Athens (NKUA) has implemented a research project focusing on the systematic recording of the geomorphological landforms of the Greek area. Through the project entitled "GEOMORPHOLOGICAL MAP OF GREECE ON A SCALE OF 1:1,000,000 AND PILOT GEOMORPHOLOGICAL MAPPING ON A LARGE SCALE", HSGME and NKUA will compile the first geomorphological map of Greece at a scale of 1:1,000,000 and a pilot geomorphological 1:50,000 scale map of Naxos Island. Additionally, the methodology and specifications of the geomorphological mapping of the country will be determined and defined in order to display the relevant spatial information at standard medium and small-scale geomorphological maps (e.g., 1:50,000, 1:1,000,000). The need of a complete national geomorphological map is imminent, as it is a preliminary tool for land management, but also for geomorphological-geological risk management, providing basic data for other scientific fields of environmental research, such as ecology, forestry, or soil science. Finally, the derived spatial database can be a reference point for the national and local authorities, as well as other public bodies, regarding the protection of the natural environment, the implementation of technical projects, the management of natural resources and the study of natural disasters.

Database and Geomorphological map of Greece 1:1,000,000

Through this project, a more systematic and organized study of the geomorphological landforms of Greece is foreseen, while the comprehensive mapping of the available information and the definition of the standards for systematic geomorphological mapping on a large scale is deemed necessary (scale 1:1M).

Basic research aims are:

- The design of an Integrated Database of geomorphological features according to international standards
- The recording of relevant information from available databases into the Integrated Database
- The bibliographic review of the most important landforms in Greece and their recording in the Integrated Database
- The definition of a standard methodology and specifications for geomorphological mapping (according to the distribution of Geological Maps of HSGME)

Each landform is categorized by a classification scheme combining geomorphological characteristics with emphasis on morphography, morpho-genesis & morpho-structure, adopting all the geomorphic and landform units required for such projects. The hierarchical classification system is a modification of the purely genetic classification system of the INSPIRE code list register on geology and geomorphology. A total of 9 genetic classifications categories of natural and man-made processes are captured in the database and spatially distributed as points, lines and polygons depending on the source of origin.

The National Cadastre and the HSGME geological maps have been used as basic geospatial reference and information maps of landforms, as they constitute a unified and continuously updated information system of high spatial resolution (pixel resolution: 5m x 5m). Landforms and their geomorphological characteristics have been recorded in a specially designed database, incorporated into a GIS environment. Following data analysis and processing, multiple maps displaying the categorization of the chosen landforms have been produced using ArcGIS Pro.

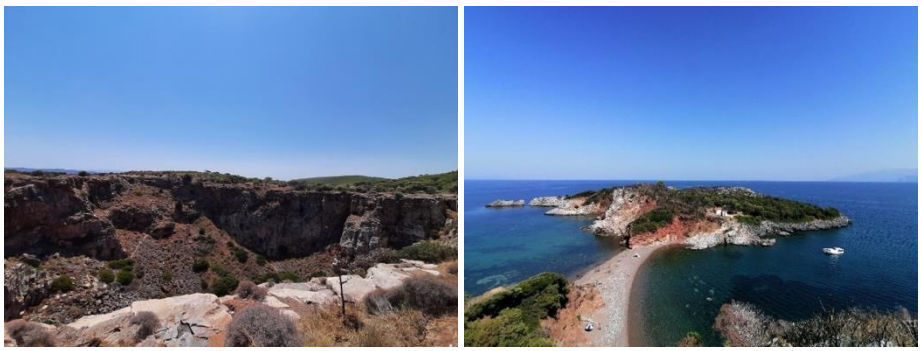

Figure 1. Examples of characteristic landforms from Greece. A karst landform (doline) from Lavrio (Chaos) (left) - A tombolo landform from North Evia (right)

Pilot Geomorphological Map of Naxos (1:50,000)

Naxos, the largest of the Cyclades islands in Central Aegean, exhibits a complex relief and a wide variety of landforms of natural beauty and rarity, due to the lithology, intense tectonics and natural processes that shaped its morphology. Different high ecological value landforms are formed as a result of varying sea level fluctuations, erosion, weathering, tectonics, drainage networks and depositional processes. On 2001, NKUA prepared the first geomorphological map of the island of Naxos at 1:50,000 scale (Evelpidou, 2001), using a combination of modern methods, techniques, and tools such as photo interpretation methods (photogrammetry, photointerpretation), aerial photographs, orthophoto maps, UAV aerial mapping, satellite images, field work data (with the use of GPS and if needed d-GPS), and GIS. Today, with the use of upgraded GIS tools and techniques, a new pilot geomorphological map of the Island map is to be produced, based on international standards of symbology and cartography, in order to serve as a foundation for the promotion, conservation, and management of Naxos Isl. geomorphological legacy.

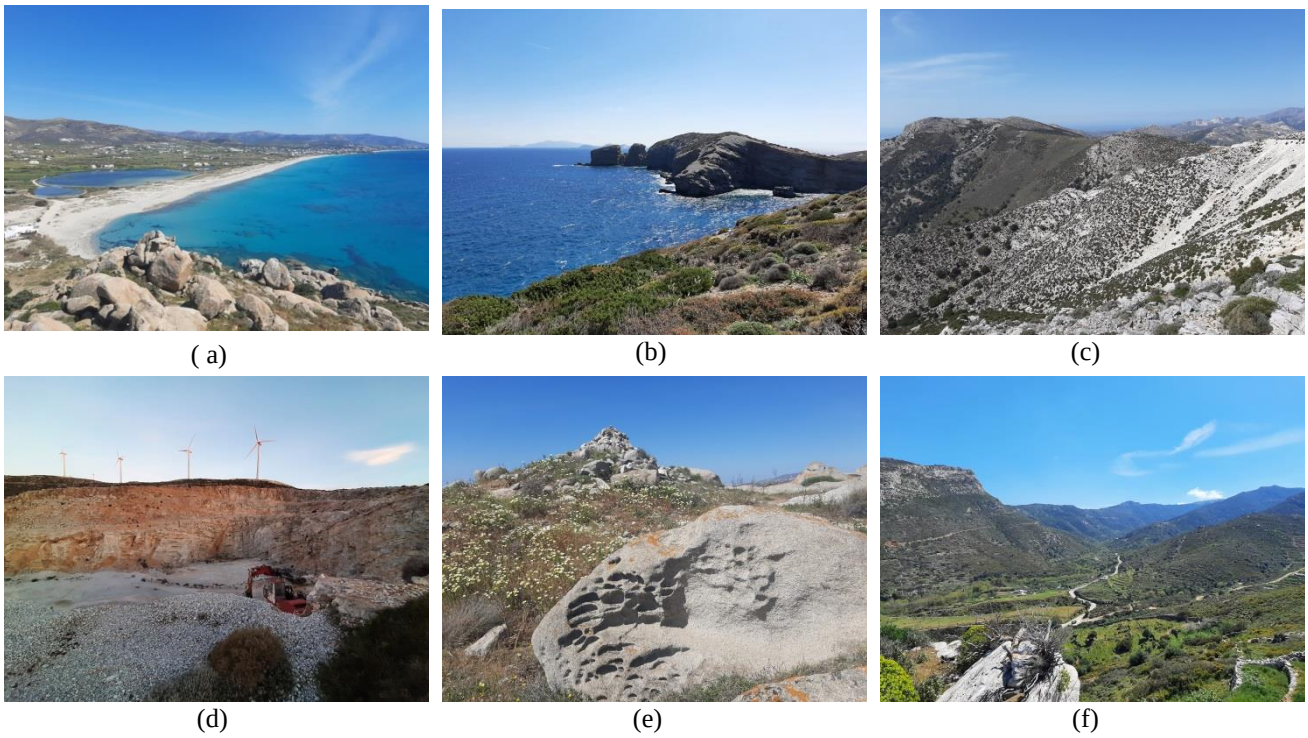

Figure 2. Examples of characteristic landforms and geomorphic features from Naxos Isl. (Cyclades). a) Coastal landforms from Vigla (e.g. lagoon, coastal sand dunes, beachrocks, tor). b) Stack at Moutsouna area. c) Debris flow at Za Mountain. d) Man-made landform (quarry) at Koronos. e) Tafoni at Vigla. f) V-Valley and alluvial fan from Appolona.

Acknowledgements

The current work was carried out in the frame of the project "GEOMORPHOLOGICAL MAP OF GREECE ON A SCALE OF 1:1,000,000 AND PILOT GEOMORPHOLOGICAL MAPPING ON A LARGE SCALE" (2020-2023), supported by the National Funds Programme and coordinated by the Hellenic Survey of Geology & Mineral Exploration.

References

Evelpidou Niki. 2001. Γεωμορφολογικές και περιβαλλοντικές παρατηρήσεις στη νήσο Νάξο με τη χρησιμοποίηση μεθόδων Τηλεανίχνευσης και GIS. Thesis. ISBN 960-8313-30-9 ISSN 1107-311X.

16th International Congress of the Geological Society of Greece
17-19 October, 2022 - Patras, Greece
Bulletin of the Geological Society of Greece, Sp. Publ. 10
Ext. Abs. GSG2022-351

Spatial distribution of caves in Crete

I. Antoniou[1], F. Livanos[1], H. Skilodimou[2], G. Bathrellos[2]

(1) Department of Geography & Climatology, Faculty of Geology & Geoenvironment, National and Kapodistrian University of Athens, University Campus, 15784, Zografou, Athens, Greece, eiriniantoniu@gmail.com (2) Department of Geology, University of Patras, Rio Patras 26504, Greece

Background

Crete is the largest island in Greece and the fifth largest island in the Mediterranean Sea. It is located in the southern part of the Aegean Sea separating the Aegean from the Libyan Sea and covers an area of 8,939 km^2. The length of the island reaches up to 260 km, while its width varies from 60 to 12 km. The total length of the coastline of the island is more than 1,000 km. The island of Crete is divided into four Regional units. From west to east these are: Chania, Rethymno, Heraklion, and Lasithi.

Crete is situated as a horst in the forearc of the subduction system of the African and the Aegean plates. The topography of Crete, due to its position in the Aegean geotectonic regime, is mainly characterized by a mountainous relief, which suggests young and rapid uplift (Kokinou et al. 2015). The mountainous relief includes high mountains, crossing from west to east, such as: the White Mountains in the western part of the island, with a maximum altitude of 2,453 m, in the central Crete Ida (Psiloritis) Mt., which reaches up to 2,456 m, and in the eastern part of the island Dikti Mt., with an altitude of 2,148 m.

Crete is one of the regions in Greece where there are karstification phenomena. The prevailing geological and climatic conditions favor the development of karst formations. The intense morphology of the island is directly linked to the appearance of surface and underground karst forms. Surface karst formations develop on the island such as gorges, polges, and dolines. Regarding endokarst formations, many caves and caverns have been mapped throughout Crete. It is worth noting that the three deepest caves that have been explored are located in the island (Bornovas, 1999; Fasoulas, 2001).

The speleological and ecological importance of many caves in Crete is enormous. Areas that host a large number of caves, ideal for speleologists, are the area of Mount Stroumboula in Heraklion, Geoparks of Sitia and Psiloritis Mt., and Melidoni in the White Mountains (Petrocheilou 1984; Adamopoulos, 1993).

Objectives

The purpose of this work is to record caves in the island of Crete. The recorded caves were entered into a database and then a statistical processing of the data was carried out. The spatial distribution of the caves and their density in each Regional unit of the island was studied while the caves and their altitude were correlated.

Methods

In the context of the present study, the selection of caves of Crete was carried out. The selection of data was based on relevant records of speleological companies and scientific papers (Petrocheilou 1984; Adamopoulos, 1993; Bornovas, 1999). A database was created incorporating information such as the geographical location of each cave, the Regional unit it belongs to and its altitude. The database was entered into a Geographical Information System. The spatial distribution of caves in Crete along with their density per 100 km^2 in each Regional unit were analyzed. The distribution of the caves was also studied in relation to the altitude at which they are located.

Results

The total number of caves recorded and entered the database was 170. The highest spatial concentrations of caves are observed in the western and central part of the island.

The results of the statistical processing of the data are presented in Figure 1. Specifically, the figure shows the number of caves expressed as a percentage in each Regional unit of Crete. The Regional unit with most of the recorded caves is the Chania Regional unit. It contains 32% of the total number of caves. The Regional units of Heraklion and Lasithi follow, while the smallest number of recorded caves was found in the regional unit of Rethymno.

Table 1 presents the regional units of Crete, their area, the number of caves in each one of them and the density of caves per 100 km^2. The Regional unit of Chania contains the largest number of caves. The density of caves in this regional unit is the highest and equal to 2.3 cave per 100 km^2. The remaining regional units present approximately the same density, equal to 2 cave per 100 km^2.

Figure 2 shows the distribution of caves in relation to their altitude. Most caves appear at an altitude of less than 100 meters. The number of caves decreases as the altitude increases. More generally, most caves develop at an altitude of less than 700 meters. The smallest number of caves is observed at altitudes greater than 900 meters.

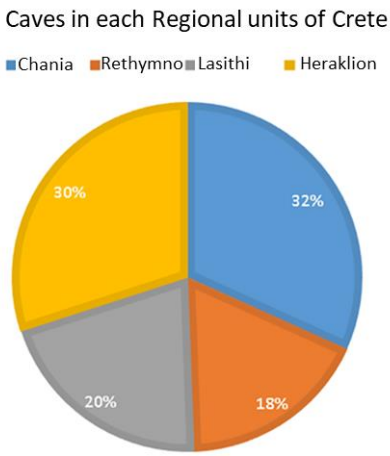

Figure 1. The distribution of caves (in percentages) in each Regional unit of Crete.

Table 1. The area of the regional units of Crete, the number of caves in each one of them and the density of caves per 100 km^2.

Regional unit	Area (km^2)	Number of caves	Density
Chania	2376	54	2.3
Rethymno	1494	30	2
Lasithi	1827	35	1.9
Heraklion	2641	51	1.9

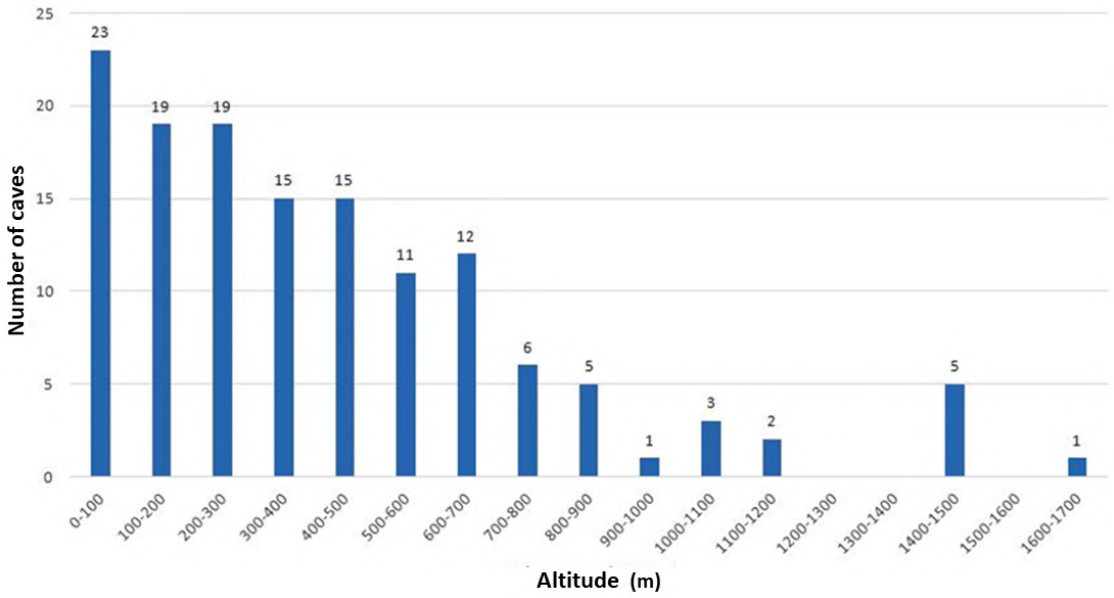

Figure 2. The distribution of caves in relation to their altitude.

Conclusions

The processing of the data showed that the Regional unit containing most of the recorded caves is that of Chania. The density of caves in Chania is equal to 2.3 cave /100 km^2. Most caves are found at an altitude of less than 700 meters. The number of caves decreases as the altitude increases.

References

Adamopoulos, C.1993. The largest potholes and caves of Crete. Bulletin of Hellenic Speleological Society, 21, 393-399.

Kokinou, E., Skilodimou, H.D., Bathrellos, G.D., Antonarakou, A., Kamberis, E. 2015. Morphotectonic analysis, structural evolution/pattern of a contractional ridge: Giouchtas Mt., Central Crete, Greece. J Earth Syst Sci, 124 (3): 587 – 602.

Bornovas J. 1999. Natural monuments of Greece. Ed. Kaktos.

Petrochilou A., 1984. The caves of Greece. Ed. Athinon.

16th International Congress of the Geological Society of Greece
17-19 October, 2022 - Patras, Greece
Bulletin of the Geological Society of Greece, Sp. Publ. 10
Ext. Abs. GSG2022-357

Disaster Risk Reduction Strategies in Secondary Education: A Teaching Intervention at Schools In The River Basin of Xerias River, Corinth (Greece)

Maria Karpouza[1], George Bathrellos[2], Hariklia Skilodimou[2], George Kaviris[1], Assimina Antonarakou[1], Eleni Tsami[3]

(1) Faculty of Geology and Geoenvironment, National and Kapodistrian University of Athens, University Campus, Zografou, 15784 Athens, Greece, mkarpouza@geol.uoa.gr, aantonar@geol.uoa.gr, gkaviris@geol.uoa.gr (2) Department of Geology, University of Patras, 26500 Patras, Greece, gbathrellos@upatras.gr, hskilodimou@upatras.gr, (3) School of Finance and Statistics, University of Piraeus, etsami@unipi.gr

Background

The Sendai Framework for Disaster Risk Reduction 2015-2030 was adopted at the Third UN World Conference in Sendai, Japan, on March 18, 2015. It suggests measures to be taken at all levels of administration by the member countries, such as Greece, to reduce the impact of natural disasters, which burden all mankind. Extreme natural phenomena are best dealt with-appropriate civil protection measures in advance and not at the time of the incident or after their occurrence, by simply remedying their consequences (Piangamore et al., 2015). The same logic should be followed at all levels of education as students of today will become the active society members of tomorrow.

Objectives

The present study presents an approved educational intervention, related to natural disasters, that was designed, implemented and evaluated to contribute towards the achievement of the following purpose: The mitigation of the impacts due to various geo hazards at high schools in the prefecture of Corinthia, Greece, and specifically in the basin of Xerias stream. The goals that were set for the achievement of the aforementioned purpose can be separated into educational- and scientific-related ones. Regarding the former, the goals related to the students involved are:

- Raise awareness on natural phenomena and disasters.
- Inform about the types of natural disasters that can potentially threaten their residence area.
- Communicate the message that natural disasters that had occurred in the past will occur again in the future.
- Inform about the factors that influence the occurrence of natural disasters.
- Facilitate the development of critical and scientific thinking about natural disasters.
- Record the students' knowledge concerning the natural phenomena and disasters and inspect their progress after the implementation of the educational intervention.
- Familiarize students with Geographic Information Systems that were used in calculating and creating Hazard Susceptibility maps, enhance cartographic skills and develop their spatial thinking, through case studies concerning the local community (Bednarz, 2004).
- Become aware about the critical actions that should be taken before and during a natural disaster.

Methods

The study of the natural and geological conditions in the basin of Xerias stream began in 2018 to calculate the susceptibility of the study area to six geo hazards (i.e. seismic landslides, liquefaction, floods, landslides, tsunamis and forest fires) using spatial multi-criteria analysis and GIS (Karpouza et al., 2021). It was critical to present the results of the aforementioned research to the students of the area, via a 2 hours' lesson about geohazards, their triggering factors and their mitigation. The educational intervention was approved by the Institute of Educational Policy in April 2022 and took place in May 2022 at the 1st High School of Corinth (119 students participated) and at the High School of Athikia (53 students participated) to students of all three grades. It consisted of a questionnaire of closed-ended responses and a slideshow presentation. Research questionnaires have been repeatedly used in schools (Strange et al., 2003) and in hazards' mitigation (Bird, 2009), while videos and presentations comprise essential tools for the understanding of the concept of natural disasters in high schools (Dewi et al., 2022). The selection of the two schools was made in order to get and process answers from students living in different environments (the city of Corinth and the smaller rural settlement of Athikia). Also, the responses were evaluated according to their age (12-13 years, 13-14 years and 14-15 years) which is associated both to their experiences and their level of knowledge, as well as to their emotional maturity.

After the Schools' directors informed students and their parents about the educational intervention, the questionnaire was given to the students (in Google forms) in digital and hard-copy format and were prompted to answer to 46 closed – ended questions (Yes, No, Maybe, I don't know / I don't answer). The questionnaire was divided into sections and aimed at the

respondents' knowledge on natural disasters, namely definition, occurrence, triggering factors, impact and actions to be taken. There were also questions about the usage of susceptibility maps of various geohazards.

Afterwards, a slideshow presentation was given to the students, consisting of information on each question of the questionnaire. After the presentation, the participants asked questions and a classroom discussion was held. Upon completion of the presentation and the discussion, the students responded again to the same questionnaire, but this time after having being educated about natural hazards through the presentation and the discussion.

Results

The inspection of the students' responses to the questionnaire after the completion of the teaching intervention revealed an undeniable increase (more than 50% in many cases) of the correct answers. Accordingly, the answers "I don't know/ I don't answer", "No", and "Maybe" strongly decreased. During the filling of the questionnaires for the first time, the students of the first grade gave more positive answers, even on specialized topics that there was little chance of knowing them, while the students of the third grade were more restrained in their answers. However, the third grades' percentages in "Yes" increased the most after attending the presentation and the discussion. Concerning the landslides phenomenon, some of them weren't aware of it at all upon answering the questionnaire for the first time. Regarding the students of the second grade, they in general moved in between the other two grades, without severe deviations.

The students in Corinth achieved better results in the flood section, because a severe flood event with human loses occurred there in 1997. On the other hand, the students of Athikia had more correct answers overall in questions that needed experience of living near nature. During the presentation and discussion, the students in Athikia seemed to maintain a more pleasant and participatory mood. It is worth noting that no student expressed dissatisfaction with the topic of natural hazards or any negative emotional state even when presenting details for past natural disasters in the broader area of their residence. However, there were incidents where students expressed tiredness in Corinth, because in only two hours they had to deal with two questionnaires, attend the presentation and participate in the discussion.

Conclusions

The prime conclusion that was drawn after the inspection of the questionnaires was the positive effect of the educational intervention about natural disasters both on a scientific and emotional level for the students who participated. This is justified by the increase of the percentage of correct answers after the presentation as well as by the decrease in false and negative answers. The answers "No" and "I don't know/ I don't respond", except from lack of relevant knowledge and experience, often suggest insecurity or indifference of the respondents. Therefore, the awareness of students in all age groups was increased (with small variations from topic to topic in general) since they realized that their area had been damaged in the past from geohazards, phenomena that may occur again in the future. They also perceived that even children like them, can act and effectively help themselves and others during a natural disaster. In addition, their self-confidence rose as they managed to respond to difficult questions that required complicated and critical thinking. Also, an interesting conclusion that was drawn from the answers coming from the two schools -among which one is located within a large city whereas the other is located in rural area- was that the proximity of children to the natural environment is important towards a better understanding of the natural phenomena and the danger they pose. The educational intervention also proved that children worry for events that have or may occur mainly in the broader area of their residence. That was the case also in this research, where the students in Corinth paid more attention in the floods' section of the educational intervention, while the students in Athikia were motivated the most by the forest fires' section, as this phenomenon occurred near their town in 2021. All the above warrant the necessity of adding lesson activities on natural disasters in the regular curriculum of the course Geology – Geography in A' and B' grades and as a project in the C' grade of Junior High School. Such additions could include games (Taillandier, 2018), indoor and outdoor activities, projects and lectures given by specialized and experienced in the field scientists, in collaboration with the teacher of each class, to ensure the dissemination of scientific knowledge in the right way.

References

Bednarz, S.W., 2004. Geographic Information Systems: A Tool to Support Geography and Environmental Education. GeoJournal 60, 191–199.

Bird, D.K., 2009. The use of questionnaires for acquiring information on public perception of natural hazards and risk mitigation – a review of current knowledge and practice, Nat. Hazards Earth Syst. Sci. 9, 1307–1325.

Karpouza, M., Chousianitis, K., Bathrellos, G.D., Skilodimou, H.D., Kaviris, G., Antonarakou, A., 2021. Hazard zonation mapping of earthquake-induced secondary effects using spatial multi-criteria analysis. Nat. Hazards 109, 637–669.

Piangiamore, G.L., Musacchio, G., Pino, N.A., 2015. Natural hazards revealed to children: the other side of prevention. Geological Society, London, Special Publications 419(1), 171–181.

Dewi, R.P., Fatonah, A., Wahyuningsih, Y., 2022. Improving natural disater understanding of junior high school students. IOP Conference Series: Earth and Environmental Science 986 (1), 012010.

Strange, V., Forrest, S., Oakley, A., the Ripple Study Team, 2003. Using research questionnaires with young people in schools: the influence of the social context. International Journal of Social Research Methodology 6(4), 337-346.

Taillandier, F., Adam, C., 2018. Games Ready to Use: A Serious Game for Teaching Natural Risk Management. Simulation & Gaming 49(4), 441-470.

16th International Congress of the Geological Society of Greece
17-19 October, 2022 - Patras, Greece
Bulletin of the Geological Society of Greece, Sp. Publ. 10
Ext. Abs. GSG2022-358

Differentiated Learning – Digital Game Based Learning in Geology and Mathematics in Primary School Students.

Eleni Tsami[1], George Bathrellos[2], Hariklia Skilodimou[2], George Lyras[3], Assimina Antonarakou[3]

(1) School of Finance and Statistics, University of Piraeus, 80 Karaoli & Dimitriou st., 18534 Piraeus, Greece, etsami@unipi.gr (2) Department of Geology, University of Patras, 26504 Patras, Greece, (3) Faculty of Geology and Geoenvironment, National and Kapodistrian University of Athens, University Campus, Zografou, 15784 Athens, Greece,

Background

Geology and Mathematics curricula within the scope of secondary education are often rich in content and have traditionally been seen as a means of favoring above average students, perhaps to the detriment of the lower performing tail in the class. It is therefore no surprise that students from countries like Greece, Cyprus, Italy, Hungary, Bulgaria or even Luxembourg are consistently scoring below the OECD average scores, and substantially below the top performing nationalities in the math and science PISA tests. This systemic failure indicates that secondary education is highly segmented in many countries and it further hints that primary education, perhaps, has not been particularly successful in establishing a uniform standard with regards to mathematical aptitude.

Objectives

In this context, the University of Piraeus has launched the project KIDEDU (Play Create Learn) in order to provide an engaging and creative learning framework, addressing pupils in their early stages of education. The specific project entails a series of 3D animation interactive games which seek to cultivate the "The Planet Earth" and "Everyday Arithmetic" skills of children between 6 and 12 years of age. This is an innovative and student-friendly mode that utilizes sophisticated digital technology—much favored by the younger generations—instead of traditional means such as books, notebooks, pencils and blackboards, in order to create an appealing environment for guided exploratory learning.

The project

We seek to present subjects in a simple and student-friendly manner in order to have children developing their skills through guided exploratory learning. During the games, basic knowledge will be narrated and transferred, where this is deemed necessary by the children. Note that we use children voices in order to make the game more appealing to younger individuals.

Every theory of learning is based on certain conditions and principles for the way a person learns. Learning processes involve experiences and stimuli from the environment, as well as certain mental processes. So, the main question for learning is what happens in relation to the stimuli of the environment and what processes occur in the mind in order to achieve learning.

The exploratory approach, as a basic principle, is supported by most educators, because it activates children and makes them participants in the learning process. The effectiveness of the discovery approach in specific circumstances has been extensively discussed.

Below we can see two photos from the game's environment, specifically from the Geopark (Figure 1) and from the Forest (Figure 2) in which the hero will wander, solve puzzles and move from level to level.

Results

Teaching, assisted by games and computers, is almost as cost-effective but probably costs more than conventional pedagogy. Computer-based study systems seem to be more effective than games and simulations, especially for low-achieving students. Curricula are cost-effective because they bring students to a certain level of proficiency in less time, and are generally liked by students. Students enjoy being taught at their personal pace which seems to increase their performance. Contemporary research shows mixed and controversial results regarding the use of computers in the teaching. Particular attention should be paid to the fact that computers in the classroom should be used for a specific purpose in the lesson and should in no way be a new game for students because there will be no benefit in the long run.

An important advantage that students can gain by following the new teaching method is that unlike the traditional method the process becomes less passive. This way the children can and do understand the presentations more clearly and with more interest, as a result of which learning is enhanced. A computer-based lesson format offers a teaching method in which student participation is particularly intensive even in large classrooms. A basic condition is that the design of teaching tools should be done in light of the various learning objectives and in combination with pedagogical principles. Multimedia can also be used as they combine the attributes of databases with modern tools for visualization and processing of the relevant data. Interactive multimedia allow the user to control the learning process and to access/read the material, choosing each time, among many alternatives, which one to follow in order to obtain the information he deems necessary for his endeavor.

Figure 1. Geopark

Figure 2. Forest

Conclusions

Both aspects of new technologies utilized, provide a real boost in the quality of mathematical and natural science education. The results of this study suggest beneficial effects of implementing new technologies and its enhancements.

Clarity in presentation, along with enthusiasm and attention to the student views resulted in very positive influence on the lesson evaluation by the students. On the way, teachers tend to underestimate significantly these two factors and overestimate the importance of being well prepared for the lesson and knowing their subject-matter.

Students' effort plays a key role in achieving high grades. Students claiming to have tried harder at a module, acquired higher grades. Thus, we could support that the studying focus and the total amount of time spent on studying affects the learning outcomes in Mathematics and Natural Sciences.

Teaching assisted by games and computers is almost as effective as conventional teaching but probably costs more. Computer based study systems appear to be more effective than game and simulations especially for students of weaker performance.

Educational programmes are effective because students can reach a standard level of qualification sufficiency in less time but students are not very fond of them. Students enjoy being taught according to their personal preferences and this increases performance in some cases. In general, research results show that the advantages of applying computers in teaching mathematic and natural science modules are controversial.

References

Çankayaa, S., Karameteb, A., 2009. The effects of educational computer games on students' attitudes towards mathematics course and educational computer games, Procedia Social and Behavioral Sciences 1, 145–149.

Tom Lowrie, T., Jorgensen R., (2011). Gender differences in students' mathematics game playing, Computers & Education, 57 (4), 2244-2248.

16th International Congress of the Geological Society of Greece
17-19 October, 2022 - Patras, Greece
Bulletin of the Geological Society of Greece, Sp. Publ. 10
Ext. Abs. GSG2022-376

From fuzzy sets to normal cloud model. An application to an environmental problem.

T. Gournelos[1], V. Kotinas[1], N.-A. Gournelos[2]

(1) National and Kapodistrian University of Athens, Athens, Greece, gournelos@geol.uoa.gr (2) National Technical University of Athens, Athens, Greece.

Background

In many problems of earth sciences, the available data are characterized by non crisp sets of values and in such cases we can use fuzzy sets which operate based on linguistic variables. These variables contain discrete fuzzy values (for example the gradient of topographic slope can be described as low, moderate, high (L, M, H). Fuzzy sets and especially normal cloud models are useful tools to study a wide variety of environmental problems including the erosional processes. It has to be noted that in general normal cloud models give more precise results, in comparison to simple fuzzy sets and as such normal cloud models are becoming more popular in environmental research works.

Normal cloud models are based on fuzzy sets and probability theory are characterized by 3 parameters: the expectation, the entropy and hyper-entropy. Cloud models map the conversion from qualitative to quantitative variables. The expectation is the numerical value that represents better the concept of the linguistic variable, while the entropy expresses the range of the values of the membership function of the expectation. Finally, the hyper-entropy is a measure of the uncertainty of the entropy of the qualitative variable.

We use the proposed model to estimate erosion in a small coastal drainage basin in the island of Samos, Greece. This basin (Fourniotiko river basin) is characterized by the presence of schists and marls, forest vegetation and relatively steep slopes in its upper part, while the lower part (flood plain) demonstrates gentler slopes, quaternary lithological formations and areas of agricultural activity (mainly vineyards).

Objectives

The purpose of this work is to apply a normal cloud model to an important environmental problem, i.e. erosion, using as input variables easily obtainable data that have an important impact on the erosional processes. Through G.I.S. and cloud models we aim to identify the spatial distribution of soil erosion intensity more precisely than by using simple fuzzy models.

Methodology

In this research we use a normal cloud model (Li et al., 1995; Li & Du, 2008) to estimate soil erosion by using various data inputs (slope, lithology, land use). Based on the above variables a cloud model was developed which transforms the input variables to the output variable (erosion degree) using an inference mechanism of logical rules. This cloud model accepts also the same linguistic variables (L, M, H) as simple fuzzy models but the membership function of these variables is normally distributed, as demonstrated in Fig. 1.

The cloud model was developed using MATLAB and Python. We apply this model to a small drainage basin of Samos Island for which the geological map (scale 1:50.000), land use (CLC2018, Büttner et al.,2017) and DEM of 5m spatial resolution are obtained (Kotinas, 2020). These data are organized in a geodatabase and are analyzed through G.I.S. to create suitable inputs for our model (e.g. through classification of variables and normalization of their values). The GIS environment is interconnected to the cloud model and after passing through the model the data for our study area, we estimate the intensity of erosion for various parts of the watershed.

Results - Conclusions

The final results show that areas in this coastal drainage basin with soft lithology (allouvial formations, marls) and medium to high topographic slopes present high erosion rates, while areas dominated by resistant lithology (carbonates) and covered by forests area present low erosion rates. To sum up, the application of the cloud model to develop spatial erosion maps is a useful tool. It maps the areas with high vulnerability degree with relatively high precision and helps researchers and stakeholders suggest the application of the right conservation strategy to manage and control soil erosion.

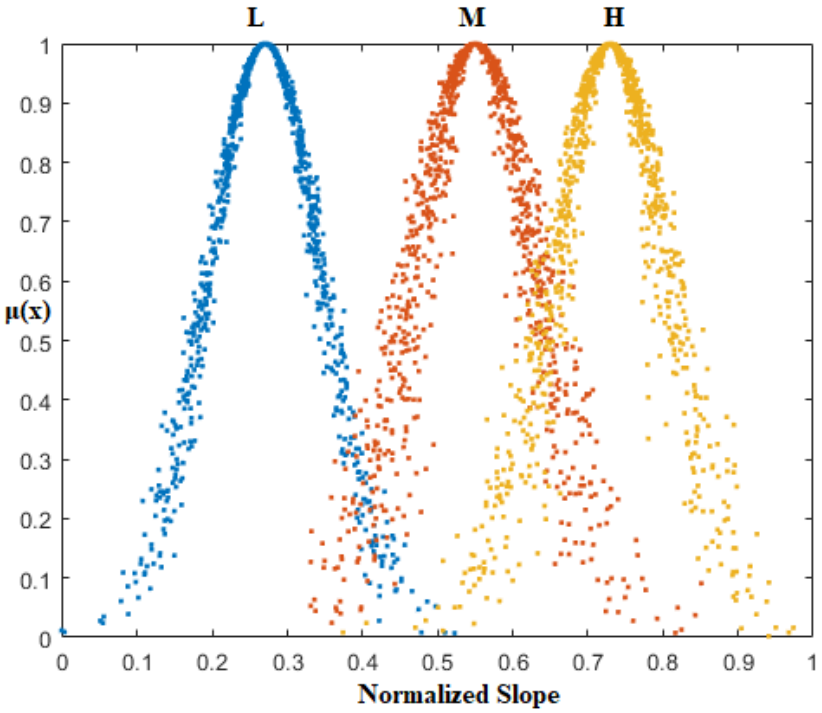

Figure 1. The distribution of the slope, one of the input variables in the cloud model.

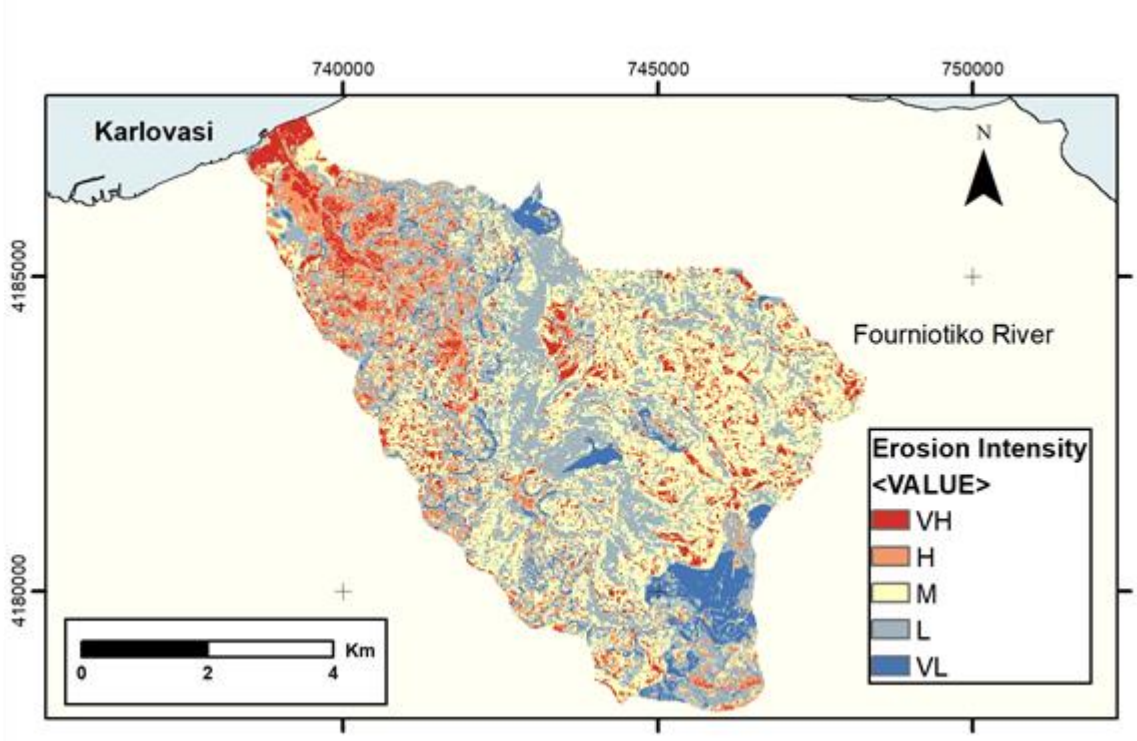

Figure 2. Erosion intensity in the study area (Fourniotiko river) as calculated by the cloud model.

Selected References

Büttner, G.; Kosztra, B., 2017. CLC2018 Technical Guidelines; European Environmental Agency: Wien, Austria. Available online: https://land.copernicus.eu/user-corner/technical-library/clc2018technicalguidelines_final.pdf .

Kotinas, V. ,2020. Study of Soil Erosion and Flash Floods with the use of Artificial Intelligence (Fuzzy Logic, Artificial Neural Networks) and Geographic Information Systems. A study case in the island of Samos, Greece. Faculty of Geology and Geoenvironment. Ph.D Thesis, National Kapodistrian University of Athens.

Li, D. Y., Meng, H. J., & Shi, X. M., 1995. Affiliated cloud and affiliated cloud generator. Computer Research and Development, 32(6), 15-20.

Li, D., & Du, Y.,2008. Artificial intelligence with uncertainty. CRC press.

16th International Congress of the Geological Society of Greece
17-19 October, 2022 - Patras, Greece
Bulletin of the Geological Society of Greece, Sp. Publ. 10
Ext. Abs. GSG2022-387

Evaluation of soil erosion risk using Neural Networks (SOM) in a GIS platform: Study case in the island of Samos.

V. Kotinas[1], G.D. Bathrellos[2], H.D. Skilodimou[2]

(1) National and Kapodistrian University of Athens, Athens, Greece, vkotinas@geol.uoa.gr (2) University of Patras, Patras, Greece.

Background

Soil is one of the most valuable natural resources supporting life on our planet. Soil erosion is a slow process caused mainly by water. Rainfall characteristics and land use change affect the erosion rate, and for areas around the Mediterranean, because of climate change, erosion is expected to increase until 2100 significantly. Modelling of soil erosion risk is a challenging task because of the vast number of variables that are interconnected with fuzzy relations and determine the spatial distribution of soil erosion. With the implementation of new technologies like neural networks, the capacity of disaster risk governance and mitigation can be greatly improved.

A Self Organizing Map (SOM; Kohonen, 1982) is a neural network consisting of a simple input layer and an output layer that typically consists of a 2D lattice (of m x n neurons). The SOM is a fully connected neural network i.e. all output neurons are connected to all input neurons. The network is trained through competitive learning, and is able to identify similarities and connections inside the data of the training data set. In more detail the training algorithm of SOM searches for the most similar neuron (in relation to the input pattern using the Euclidean distance) and selects this neuron as the winner-takes-all neuron (also called Best Matching Unit). Also neurons that are in close proximity with the BMU adjust their weights and participate in the learning process making the model more robust. The learning rate is an important hyper-parameter on any neural network and can affect the quality of the model and it is common to use an exponential decay function for its calculation (learning rate decreases after each epoch).

We apply our methodology to the island of Samos, Greece which demonstrates a variety of lithological, morphological and vegetation formations. In general the island is characterized by steep slopes in the mountainous areas (Kerketeas and Ambelos mountains) which consist mainly of marbles and schists, while neogene and quaternary sediments are located to the two neotectonic basins of the island (Karlovasi and Mytilinii basins). There are large forest areas mainly in the central part of the island and low vegetation in the eastern and western parts of the island.

Objectives

This study aims to use Geographic Information Systems (G.I.S.) to model the processes of soil erosion, when data is limited, through the use of neural networks (Self Organising Maps), which has proved its usefulness in various spatial analysis problems (e.g. Gorricha & Lobo, 2012, Li &Juhola, 2014), to estimate the most vulnerable areas to erosion.

Methodology

The methodology presented in this study was tested in the island of Samos. A geodatabase consisting of the digitized geological map (scale 1:50.000), land use (CLC2018, Büttner et al.,2017) and DEM of 30 m spatial resolution was created for the study area. The spatial data were analyzed further through G.I.S. to export the lithological map of Samos (and its relative vulnerability), the slope map and the relative vulnerability of the vegetation. These variables were normalized to a range between 0 and 1 and passed through the SOM network that was designed in MATLAB using a decaying learning rate and an exponential decaying neighborhood size. The proposed model (consisting of a 10x10 mesh of output neurons) transforms the input variables (land use, lithology, morphology), to the output variable, which represents erosion risk. For the training dataset we used a dataset with size n=50.000. After the training phase we continue to the prediction phase where we estimate the output for all the dataset (all the island of Samos). The spatial data are processed through GIS and MATLAB and the output is visualized to produce a soil erosion risk map representing the spatial distribution of erosion susceptibility. To identify the optimal number of clusters we apply the "Silhouette" index (Rousseeuw, 1987).

Results - Conclusions

The optimal number of clusters as identified by the "Silhouette" index is three (Low, Medium, high). After examining the weight distances of neighbor neurons we can clearly distinguish the neurons that are fired when a specific class is detected. As demonstrated in Figure 2 the central part of the island demonstrates moderate susceptibility with higher values along the cliffs of Ambelos mountain, while the eastern and western part demonstrate high erosion potential. The Neogene basins of the island have a low susceptibility to erosion, which is in accordance with field observations (deposition zones). Through the proposed model we can obtain a susceptibility map of erosion, when data is limited, which can prove fundamental to improve management of areas sensitive to soil loss, which is a huge problem in the Mediterranean area and is highly related to climatic change.

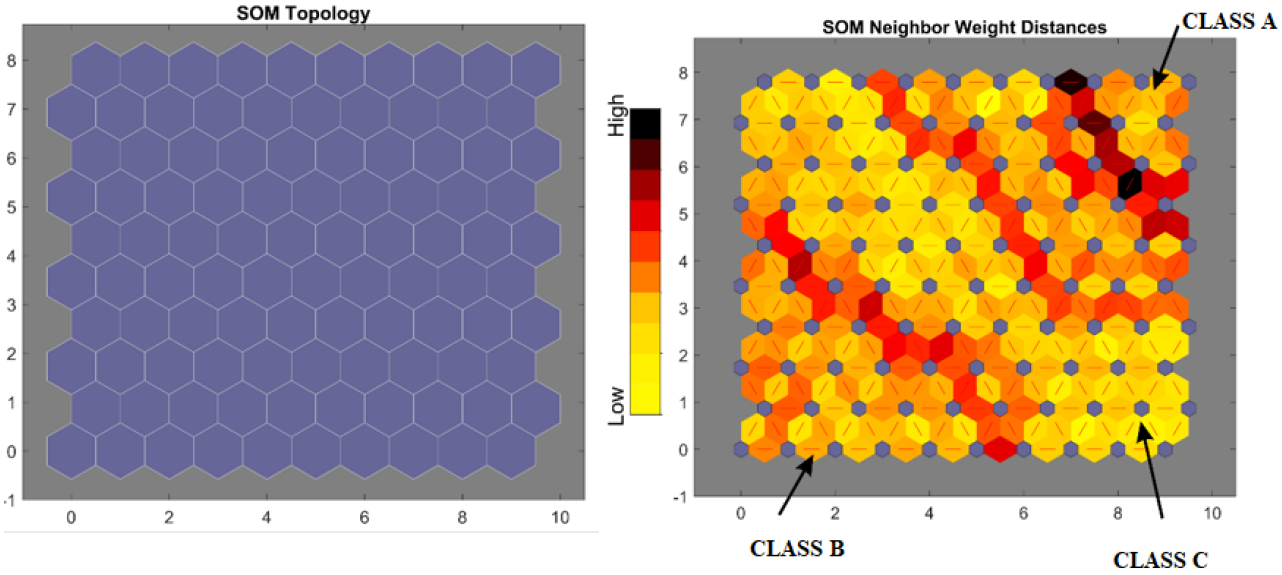

Figure 1. The topology of the Self Organised Map that we used, and the weights between nearby neurons.

Figure 2. Soil Erosion Risk for the study area (estimated using a 3 parameter SOM neural network)

References

Gorricha, J., & Lobo, V., 2012. Improvements on the visualization of clusters in geo-referenced data using Self-Organizing Maps. Computers and Geosciences, 43, 177-186. https://doi.org/10.1016/j.cageo.2011.10.008

Kohonen, T., 1982. Self-organized formation of topologically correct feature maps. Biological Cybernetics, 43, 59–69.

Kotinas, V. ,2020. Study of Soil Erosion and Flash Floods with the use of Artificial Intelligence (Fuzzy Logic, Artificial Neural Networks) and Geographic Information Systems. A study case in the island of Samos, Greece. Faculty of Geology and Geoenvironment. Ph.D Thesis, National Kapodistrian University of Athens.

Li, X., & Juhola, M., 2014. Country crime analysis using the self-organizing map, with special regard to demographic factors. AI and Society, 29 (1). https://doi.org/10.1007/s00146-013-0441-7

Rousseeuw, P. J., 1987. Silhouettes: A graphical aid to the interpretation and validation of cluster analysis. Journal of Computational and Applied Mathematics. https://doi.org/10.1016/0377-0427(87)90125-7

16th INTERNATIONAL CONGRESS of the
GEOLOGICAL SOCIETY OF GREECE

T5. Marine Geology and Oceanography

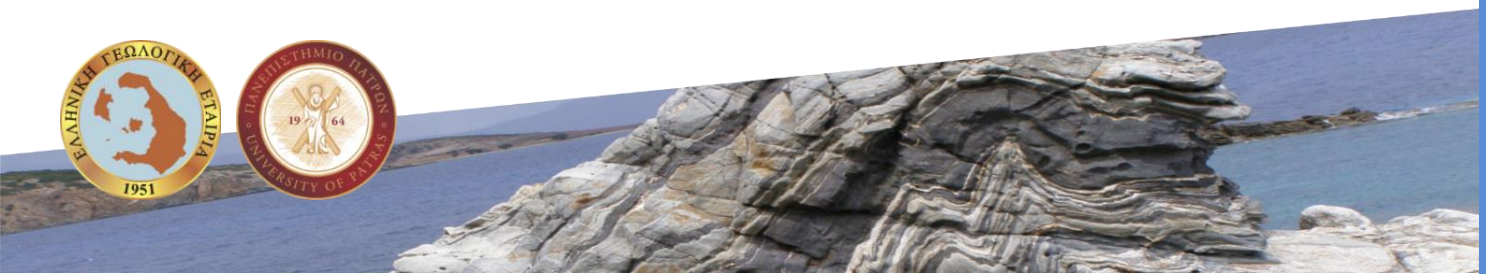

OUR EARTH, OUR HOME

16th International Congress of the Geological Society of Greece

23-25 May, 2022 - Patras, Greece

Bulletin of the Geological Society of Greece, Sp. Publ. 10

Ext. Abs. GSG2022-014

Assessment of the effect of Posidonia Banquettes on shoreline changes: Preliminary results from the case of Schinias-Marathon National Park, Attica, Greece.

I. Kourliaftis, D. Vandarakis, V. Gerakaris, Y. Issaris, V. Kapsimalis, I. Panagiotopoulos, M. Salomidi

Institute of Oceanography, Hellenic Centre for Marine Research (HCMR), 46.7 km Athens-Sounion, 19013, Anavyssos, Greece. g.kourliaftis@hcmr.gr.

Introduction

The purpose of this study is the determination of shoreline changes along a coastal front surrounded by *Posidonia oceanica* meadows, at the easternmost part of the beach of Schinias - Marathon National Park (SMNP). The broader area of Schinias and Marathon is an area of special ecological and socio-economic importance due to the presence of several historical monuments, sports and military facilities, while also of intense agricultural and touristic activities in Attica. Additionally, SMNP is part of the Natura 2000 European Network of protected areas, comprising both a Special Protection Area for its rich avifauna (GR3000016 - Schinias Wetland), and a Site of Conservation Importance for its rich diversity in numerous terrestrial, coastal, and marine species and habitats of conservation interest (GR 3000003 – Schinias-Marathon National Park). The marine counterpart of the area has been mainly designated for the presence of extensive *Posidonia oceanica* meadows, which is of conservation priority for the EU (Habitat's Directive, 92/43/EC). Depending on local coastal hydrodynamics, part of *P. oceanica* withered leaves and other organic debris (necromass), is regularly washed ashore, forming wedge structure deposits also known as banquettes (Boudouresque and Jeudy de Grissac, 1983). These formations are unique coastal habitats for several species, including several endemic ones, and are known to contribute to beach erosion prevention, coastal dune formation, and nutrient and calcium carbonate supply to adjacent littoral and sublittoral habitats (Otero et al, 2018). At least for the past 4 decades, *Posidonia* banquettes of variable extend form along the eastern part of the beach all year round. Due to a general misperception of banquettes as a downgrade of beach appeal, local business demanded their seasonal removal up until 2018. Later on, regulations set forth by the SMNP Management Board of eventually forbade this practice, allowing for the opportunity to examine its effects on the coastal front.

Methods

The survey of long-term shoreline displacements was carried out by comparing historical and contemporary aerial photographs (1945, 1960, 1969, 1988, 1996, 2001, 2010) along with high resolution satellite imagery (2012, 2014, 2018) and orthophotomosaic from photographs obtained using Unmanned Aerial Vehicle (2021) covering a period of 76 years (1945 - 2021).The quantification of long-term shoreline displacements was made with the use of the add-on application of Digital Shoreline Analysis System (DSAS) within the GIS platform ArcMap 10.6 (Himmelstoss et al., 2018). This was accomplished by assessing 68 transects (every 10 meters), placed perpendicular relatively to the historical shorelines from a stable baseline (Tsokos et al., 2018). At each transect the Net Shoreline Movement (NSM), the Shoreline Change Envelope (SCE), the End Point Rate (EPR) and Linear Regression Rate (LRR) (Thieler et al. 2009) was calculated and analyzed. All distances were calculated in meters, while the rate of change in meters per year (m / y). The shoreline uncertainty variable for each coastline was defined as the spatial resolution (cell size) of the corresponding orthophotomosaic or image whose coastline was digitized. Additionally, 4 UAV flight missions were conducted over the study area on 10/7/2020, 28/9/2020, 24/2/2021 and 8/6/2021, in order to map the spatial distribution of *P. oceanica* banquettes on the coast and study seasonal changes. Results

Based on the UAV surveying, the surface covered by *P. oceanica* banquettes on the coast for the study period, range from 2292.5 m^2 (on 10/7/2020) to 11468.49 m^2 (on 24/2/2021), seasonal change of 9176 m^2. (Figure 1a). The results of NSM shown that the coastline has undergone retreat in the last 76 years. The largest changes (25 - 30 m) are observed at the eastern part, with the maximum value (-30 m) at transect 3 at the eastern end of the beach. From east to west, values gradually decrease (from transect 30 to 68 values range from -10 to -12.5 meters). The average change of the coastline across the study site is –15.3 m. The SCE values range from 20 m (transect 61) to 40 m (transect 6). Based on the EPR, the average displacement rate in the study area shows only negative values (regression) for the period 1945 – 2021 (Figure 1a). The maximum setback value is found in transect 3 (-0.39 m / yr.) and the minimum in transect 43 (-0.14 m / yr.). The overall average coastline retreat rate for the study site is 0.2 m / yr. The study of the Linear Regression Rate (LRR) shown that the regression rate has been estimated not to have been constant (Figure 1b,c,d and e): changes from the period 1945 – 1969, where the coastline is constantly eroding with the higher rates, to the period 1969 – 1996, where erosion rates decreased significantly. Within 1996 advance of the coastline is first observed, then alternating with periods of setback until 2010. Within 2010 - 2018, shoreline advance becomes more frequent (while again alternating with periods of regression). Also 2014 – 2018, milder setback (and even advance) values are generally observed along the study area,

particularly pronounced at the easternmost part of beach where the greatest setbacks had been previously detected. Finally, a rather remarkable shoreline accretion is observed for the latest period (2018 - 2021).

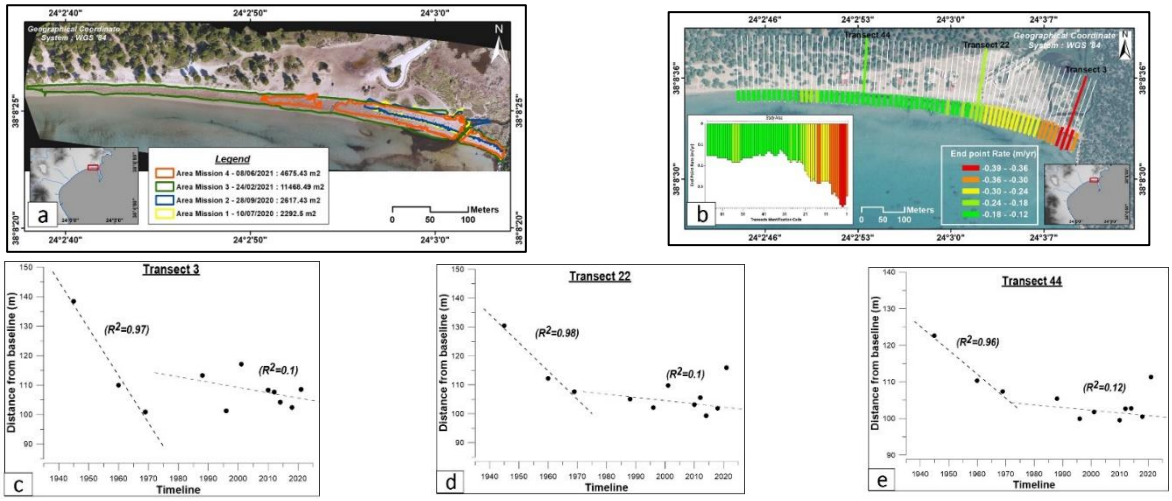

Figure 1. Representation of the surface covered by *P. oceanica banquettes* at each one of the 4 UAV missions (a) and the **shoreline displacement rate (EPR) at each transect (in meters per year) across the study area, for the period 1945 – 2021(b) and the positions where the representative transect 3 (c), 22 (d), 44 (e) intersects the coastlines as well as the linear correlation of the points at each transect.**

Conclusions

The study area seems to be subjected to coastal erosion since 1945, resulting to a loss of land surface of the order of 10,189 m^2. The operation of the Marathon Dam in 1929 severely disturbed the sedimentological balance of the wider coast resulting high rates of coastline regression for the period 1945 – 1969. Part of the coastal sedimentological balance was rather restored from the 80's onwards, when regression rates decrease and periods of shoreline advance appear. Although the study area appears more sheltered due to Kynosoura cape, it presents higher changes and regression rates as compared to the western part of Schinias beach. At the study area, more intense beach erosion and deposition of sediments at shallow sublittoral depths (mainly until 1996) is due to coastal hydrodynamic regime in combination with the finer sediments and the lower beach foreshore slopes (Kourliaftis, 2019). Regarding the correlation of the coastline with the *Posidonia* banquettes, noteworthy is the position of the coastline on 2018, when a non-removal strategy for Posidonia banquettes was set forth by the Management Body of SMNP, presenting lower setback values and even mild advance at the study area, where indeed the greatest setbacks had been previously detected. Moreover, this finding stands out against the general situation characterizing the wider beach of Schinias (beyond the study area), where setback values remain constant for the same period (Kourliaftis, 2019). Also, a rather remarkable shoreline accretion is observed for the latest period (2018 - 2021) across the study area, which is in sheer contrast to the generally high erosion rates previously characterizing this area, and are likely directly related with the extensive *Posidonia* banquettes that have undisturbed accumulated here this last couple of years. More extensive monitoring, considering both long-term and seasonal changes is required for better discernment of the effect of *Posidonia* banquettes on the coastal front of the beach.

Acknowledgements

This research was funded by the Hellenic Society for the Protection of Nature (HSPN) and carried out in the scope of the international InterregMED project "POSBEMED2: Governance and Management of Posidonia Beach-Dune Systems Across the Mediterranean".

References

Boudouresque, C.F. and Jeudy de Grissac, A., 1983. L'herbier à Posidonia oceanica en Méditerranée: les interactions entre la plante et le sédiment. Journal de recherche océanographique, 8(2-3), pp.99-122.

Himmelstoss, E.A., Henderson, R.E., Kratzmann, M.G. and Farris, A.S., 2018. Digital shoreline analysis system (DSAS) version 5.0 user guide (No. 2018-1179). US Geological Survey.

Kourliaftis, I., 2019. Morphodynamic processes and evolution of the coastline of Marathonas Gulf – Shinias beach area. Msc Thesis, National and Kapodistrian University of Athens, 207 p.

Otero, M.M., Simeone, S., Aljinovic, B., Salomidi, M., Mossone, P., Giunta Fornasin M.E., Gerakaris, V., Guala, I., Milano, P., Heurtefeux H., Issaris, Y., Guido, M., Adamopoulou, M., 2018. Governance and management of Posidonia beach-dune system. POSBEMED Interreg Med Project. 66pp+ Annexes.

Thieler, E.R., Himmelstoss, E.A., Zichichi, J.L. and Ergul, A., 2009. The Digital Shoreline Analysis System (DSAS) version 4.0-an ArcGIS extension for calculating shoreline change (No. 2008-1278). US Geological Survey.

Tsokos, A., Kotsi, E., Petrakis, S. and Vassilakis, E., 2018. Combining series of multi-source high spatial resolution remote sensing datasets for the detection of shoreline displacement rates and the effectiveness of coastal zone protection measures. Journal of Coastal Conservation, 22(2), pp.431-441.

16th International Congress of the Geological Society of Greece

17-19 October, 2022 - Patras, Greece

Bulletin of the Geological Society of Greece, Sp. Publ. 10

Ext. Abs. GSG2022-038

Inventory of submarine landslides in the Aegean Sea: A database in progress

D. Sakellariou[1], M. Iatrou[1], K. Tsampouraki-Kraounaki[1], K. Manta[1,2], I. Morfis[1,2], I. Livanos[1], P. Drakopoulou[1], Ch. Kyriakidou[1], V. Loukaidi[1], G. Rousakis[1]

(1) Inst. Oceanography, Hellenic Centre for Marine Research, Anavyssos, Greece, sakell@hcmr.gr (2) Department of Geology, Patras University, Rio, Greece.

This work presents the current state of the first effort for the compilation of a data base of submarine landslides in the Aegean Sea. The aim is to improve knowledge on occurrence, distribution of submarine landslides and hence to provide better understanding of their triggering mechanisms and their tsunamigenic potential.

Introduction

Submarine landslides are very common in the marine domain and constitute a major marine geohazard (Gamboa *et al*., 2021). They occur in literally all kinds of marine environments spanning from the shallow coastal zone to the deep seafloor, including (but not limited to) passive and active margins, river deltas, submarine canyons, open slopes, volcanoes, etc. (Lee, 2009). Earthquake activity, tectonic steepening of slopes, sea-level changes, rapidly increasing sediment load, pore pressure changes and wave activity are some of the most common trigger mechanisms for slope failure (e.g. Canals *et al*., 2004). Slope failures and subsequent submarine mass movements have the potential to cause destructive impact on installations and infrastructures on the seafloor (cables, pipelines, etc.) as well as on the coastal zone. In addition, submarine landslides are a major triggering mechanism for the generation of tsunamis that can have severe impact on the coastline.

The Aegean Sea is an actively deforming back- arc area developed above the NNE-wards subducting East Mediterranean slab. SSW-ward extension is mainly accommodated by NE-SW, NW-SE and E-W striking, oblique to strike slip and normal faults (Sakellariou & Tsampouraki-Kraounaki, 2018 and references therein). They create a variety of landforms on the seafloor including shallow flat shelves, narrow variably steeping slopes, deep, elongate to spindle-shaped basins and troughs, seamounts and ridges of tectonic or volcanic origin. The morphological configuration of the seafloor along with the active tectonic movements and the high seismicity are the major triggering mechanisms for slope failures and submarine landslides that can generate or have generated tsunamis in the Aegean (Okal *et al.,* 2009; Papadopoulos *et al.*, 2014 and references therein).

It is thus crucial to understand the spatial occurrence of submarine landslides in respect to the local/regional morphology and tectonic activity, to describe their morphometric characteristics and gain insights into their potential as triggering mechanisms for tsunamis. Herewith, we present the concept, the structure and the current state of a new (first) data base of submarine landslides in the Aegean Sea, with the aim to improve our understanding on slope failure processes and contribute to the assessment of tsunami hazard.

Methods

Data bases of submarine landslides are already available in the literature for various marine settings (e.g. Moscardelli & Wood, 2015) and regional seas, e.g. the North Atlantic (Chaytor *et al*., 2009), the Mediterranean Sea (Urgeles & Camerlenghi, 2013), the Caribbean (ten Brink *et al*., 2006) and others. The compilation of the Aegean data base and the morphometric measurements therein are based on a combination of Urgeles & Camerlenghi (2013) and Clare *et al*. (2018) approaches. Digital Elevation Models (DEMs) compiled from swath bathymetry data obtained during various cruises at variable resolution between <10 and 50 m grid cell size have been used as the primary data set for the identification and accurate measurements in GIS platform. Landslide scars are identified on the base of the evaluation of slope maps and examination of multiple perspective views of the DEMs using different illumination azimuths. The area of a failure scar is calculated as the planar area within a manually digitized bounding polygon that encompasses the region of negative elevation within the landslide's headwall and sidewalls (Chaytor *et al*., 2009). Failure volumes are calculated using three different methods depending on each location's characteristics: 1) estimation of the missing volume from a scar following ten Brink's *et al.* (2006) and Gamboa's *et al*. (2021) methods which aim to reconstruct failure topography, 2) modeling of the landslide volume as a wedge geometry (McAdoo *et al.,* 2000) and, 3) measurement of the dimensions of the landslide deposits, especially when scar is not preserved or surveyed.

Results: Landslide morphology and morphometric measurements

Morphological analysis of swath bathymetry data reveals the following: roughly 30% of the total surface of the Aegean's seafloor is steeper than 5% and may reach slope values up to 40% or higher; 90% of the seafloor is shallower than 1000 m; the steep slopes are oriented preferentially along NE-SW and NW-SE directions and are controlled by active faults; the majority of the observed slope failures occur at the shelf edge or the upper slopes; shallower slope failures occur mostly off river mouths. However, less than 30% - 35% of the Aegean seafloor has been surveyed by means of multi

beam bathymetry.

Currently, more than eighty (80) submarine landslides have been identified in areas covered by swath bathymetry and have been entered into the data base. They are of various types, including (i) slides when sliding occurs on a roughly planner surface such as the Arkitsa slide in North Evia Gulf (Sakellariou *et al.,* 2005), (ii) glides when a translational slide moves laterally with no rotation such as Thasos landslide (Lykousis *et al.*, 2002), (iii) slumps when the failed mass rotates along a curved slip surface and the failed material does not exceed the downslope limit of the scar such as Malia landslide (Strozyk, *et al*., 2009), (iv) debris avalanches with characteristic chaotic distribution of blocks, a flow morphology and angularity of fragments which are mainly associated with volcanic slopes (Bell *et al.,* 2012) and other.

In general, the observed submarine landslides vary in size from $<1^2$ km^2 to 10^2 km^2 and are characterized as small to medium. Water depths also vary from shallow shelf to the margins of deep basins (~1800 m). The height of scars ranges between less than 10 m and roughly 30 m, while their width ranges between tens of meters and a few kilometers. The slope gradient mode in the scars ranges between 6°and16° but may locally exceed 30°. Run-out distances vary from few km to 20 km and can reach or exceed 40 km in cases of debris avalanches.

The volume ranges between 0.1 km^3 and 4.4 km^3, however the majority of the observed landslides is characterized by volume <1 km^3. Debris avalanches and flows are in general larger than 1 km^3 and may reach volume of 8 km^3 or more. Some discrepancies have been observed when using different methods for the volume estimation. They can be attributed either to additional sources of sediment that add to the volume released from the headwall scar, or loss of sediment from the main deposition area due to more or less dilute flows (Canals *et al.,* 2004).

Both, simple and composite landslide features have been identified and mapped. The first ones comprise a single slope failure event with arc-like scar shape and well concentrated deposit. The latter result from multiple failures, they display complicated structure and may show a hierarchical pattern of failures.

Conclusions

This work presents the current state of the first effort for the compilation of a data base of submarine landslides in the Aegean Sea. The aim of the data base is to improve knowledge on occurrence, distribution of submarine landslides and hence to provide better understanding of their triggering mechanisms and their tsunamigenic potential. The assessment of landslide risk zones in the Aegean region, which consists of dozens of inhabited islands, is necessary as submarine landslides are one of the most important potential marine geo-hazards in the region. Mapping, spatial distribution and structural analysis of submarine landslides, can be furtherly correlated with active offshore faults and geomorphological characteristics of the seafloor with the aim to identify submarine slopes prone to failure and assess tsunami probability.

References

Bell, K.L.C., Carey, S.N., Nomikou, P., *et al*., 2012. Submarine evidence of a debris avalanche deposit on the eastern slope of Santorini volcano, Greece, Tectonophysics.

Canals, M., Lastras, G., Urgeles, R., *et al*., 2004. Slope failure dynamics and impacts from seafloor and shallow sub-seafloor geophysical data: case studies from the Costa Project. Marine Geology, 213, 9–72.

Chaytor, J. D., ten Brink, U. S., Solow, A.R., Andrews, B.D., 2009. Size distribution of submarine landslides along the US Atlantic margin. Marine Geology, 264, 16–27.

Clare, M. Chaytor, J., Dabson, O., *et al*., 2018. A consistent global approach for the morphometric characterization of subaqueous landslides, in: Lintern, D.G., Mosher, D.C., Moscardelli, L.G., *et al* (Eds.), Subaqueous Mass Movements and Their Consequences. Geological Society, London, Special Publications, 477, 455–477.

Gamboa, D., Omira, R., Terrinha, P., 2021. A database of submarine landslides offshore West and Southwest Iberia. Nature Scientific Data, 8:185.

Lee, H.J., 2009. Timing of occurrence of large submarine landslides on the Atlantic Ocean margin. Marine Geology, 264, 53–64.

Lykousis, V., Roussakis, G., Alexandri, M., *et al.,* 2002. Sliding and regional slope stability in active margins: North Aegean Trough (Mediterranean). Marine Geology, 186, 281-298.

McAdoo, B.G., Pratson, L.F., Orange, D.L., 2000. Submarine landslide geomorphology, US continental slope. Marine Geology, 169, 103–136.

Moscardelli, L., Wood, L., 2016. Morphometry of mass-transport deposits as a predictive tool. Geological Society of America Bulletin, 128, 47–80.

Okal, E.A., Synolakis, C.E., Uslu, B., *et al.,* 2009. The 1956 earthquake and tsunami in Amorgos, Greece. Geophysical Journal International 178, 1533–1554.

Papadopoulos, G., Gràcia, E., Urgeles R., *et al.,* 2014. Historical and pre-historical tsunamis in the Mediterranean and its connected seas: Geological signatures, generation mechanisms and coastal impacts. Marine Geology, 354, 81–109.

Sakellariou D., Karambas, Th., Lykousis, V., *et al.,* 2005. Tsunami hazard in the North Evia Gulf: Source areas, triggering mechanism and propagation of past and future tsunamis. 22nd IUGG International Tsunami Symposium, Chania.

Sakellariou, D., Tsampouraki-Kraounaki, K., 2019. Plio-Quaternary extension and strike-slip tectonics in the Aegean, in: J. Duarte (Ed.): Transform Plate Boundaries and Fracture Zones, 339-374.

Strozyk, F., Huhn, K., Strasser, M., *et al*., 2009. New evidence for massive gravitational mass-transport deposits in the southern Cretan Sea, eastern Mediterranean. Marine Geology, 263, 97-107.

Ten Brink, U.S., Geist, E.L., Andrews, B.D., 2006. Size distribution of submarine landslides and its implication to tsunami hazard in Puerto Rico. Geophysical Research Letters, 33, L11307.

Urgeles, R., Camerlenghi, A., 2013. Submarine landslides of the Mediterranean Sea: Trigger mechanisms, dynamics, and frequency-magnitude distribution. Journal of Geophysical Research: Earth Surface, 118, 2600–2618

16th International Congress of the Geological Society of Greece
17-19 October, 2022 - Patras, Greece
Bulletin of the Geological Society of Greece, Sp. Publ. 10
Ext. Abs. GSG2022-206

Late Quaternary Sedimentary Processes Around Lesvos Island (NE Aegean Sea, Greece): Preliminary Results

D. Evangelinos[1], E. Benetou[2], T. Hasiotis[2], I. Zananiri[3]

(1), Department of Earth and Ocean Dynamics, Spain, devangelinos@ub.edu (2) Department of Marine Sciences, Mytilene, Greece (3) Hellenic Survey of Geology and Mineral Exploration, Acharnae, Greece.

Introduction

Lesvos is the third largest island of Greece, located in the northeastern Aegean Sea. Its complex neo-tectonic activity, which is responsible for the geomorphology of the island, attracted numerous onshore studies mainly focusing on the geological characteristics and tectonic structures (i.e., Katsikatsos *et al*., 1982; Pavlides *et al.,* 2009). In general, volcanic rocks occupy the northern part of the island and metamorphic and plutonic rocks the southern part. Quaternary deposits are mainly distributed in the lower-lying areas. Coastal and marine surveys discussed on the beach morphodynamics (i.e., Velegrakis *et al.,* 2008) and the geomorphology of the two semi-closed gulfs (Kalloni and Gera) of the island (Chronis *et al.,* 2014; Manoutsouglou *et al*., 2018). On the contrary, regarding the offshore part, only recently Hasiotis *et al*., (2020) provided sedimentary characteristics at certain locations of the shelf around Lesvos, for the detection of marine aggregates, whilst Nomikou *et al.,* (2021a, 2021b) discuss the morphotectonic structures along the southwestern margin of Lesvos, next to the epicenter of the 6.3 R earthquake of 2017. Thus, the main depositional environments and sedimentary patterns around Lesvos Island remain unknown. This contribution aims to determine the recent sedimentary processes and main geomorphological features, as well as their spatial variability around the island.

Methods

The study is based on a dataset of high-resolution analogue 3.5 kHz (O.R.E.) sub-bottom profiles collected onboard a vessel of opportunity (Irini) by the Hellenic Survey of Geology and Mineral Exploration (EAGME, former IGME), under the EUROSEISMIC project. Data collection took place during two surveys (June 1987 and May 1988). A total of 744.5 km of sub-bottom profiles collected, covering an area of about 1265 km^2 within the territorial waters (Fig. 1a). Bathymetry was extracted from Emodnet. The main echo-types were identified based on a determination of the geometry and internal configuration of surface and subsurface reflections following Damuth, (1975). Unfortunately, no sediment cores were available for ground-truthing the results. Moreover, major geomorphological (erosional, depositional, and mass movement) features, their geometries and positions were distinguished. ArcGIS was used for mapping purposes (echo-types and geomorphology).

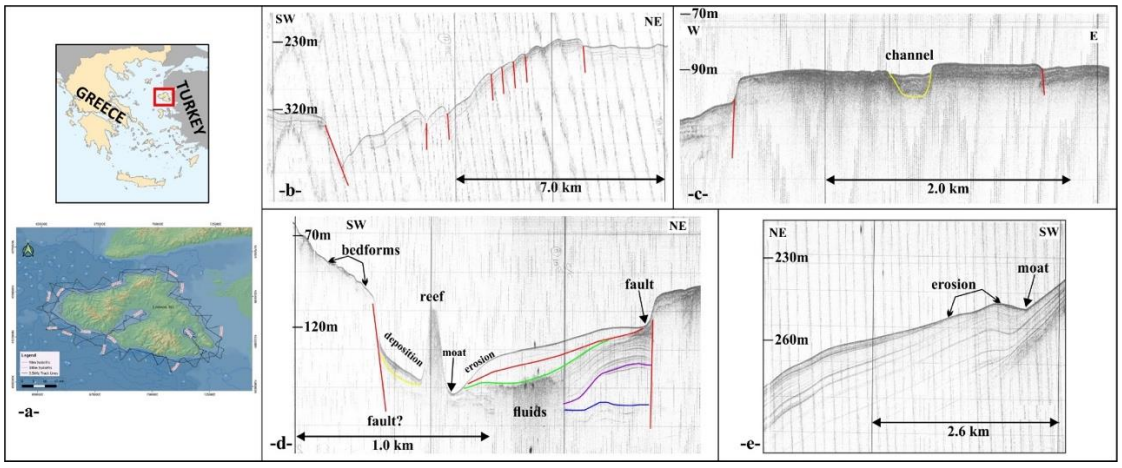

Figure 1. (a) Location of the study area and grid of 3.5 kHz survey lines around Lesvos Island, (b-d) 3.5 kHz profiles displaying various tectonic and morphological features, major unconformities and acoustic anomalies and patterns around Lesvos (see text for details).

Results and Discussion

The shelf around Lesvos extends down to ~150 m water depth and has a general flat surface with mean gradients up to 0.2º, except from areas where bedrock or harder substrate outcrops. The eastern part of Lesvos is the shallowest (less than 100 m water depth). The shelf width varies between ~1 km and 8 km. Shelf-edge morphology has been intermittently detected to the north, west and south. The slope extends to ~350 m and is < 1 km (southern part) to 8 km wide in western

part, with gradients ranging from 3.5° to 13.5 °. A deep basin (700 m water depth) to the southeast (off Vatera), is bounded by a steep slope (to the north), while a shallower basin at the northwestern part reaches 300 m depth.

Seven echo-types (ET) were recognized in the 3.5 kHz subbottom profiles. ET I corresponds to coarse-grained sediments, attains penetration up to ~10 m and develops at the shallow waters to the east. ET II is attributed to a surficial (up to 4 m) homogeneous mixed (sand to mud) sedimentary cover, lying over coarser or more compacted sediments or the acoustic basement and it is distributed shallower than 40 m around the island. ET III is related to fine-grained stratified sediments alternating with turbidites and it is sub-divided into two sub-types. ET IIIa attains higher penetration (~60 m), and it is found to the south and southwest (along Vatera basin and towards the base of the bounding lower slope), whereas ET IIIb has a lower penetration (~30 m), probably corresponding to slightly coarser deposits and it is found deeper from the shelf-edge to the north and west. ET IV shows no penetration under the relatively smooth surficial echo indicating a very coarse sedimentary cover preventing penetration and it is distributed to the northwest at the shallower waters. Locally, a thin layer of finer material is observed. ET V corresponds to areas of hard substrate outcropping with various relief, locally with a limited thickness of coarse sediments. It is randomly distributed around the island but more often is found to the northwest and north. ET VI is associated to recent mass movements forming a micro-relief and occupies restricted areas at the base of the slope to the south. ET VII has an irregular morphology distributed along the slope bounding Vatera basin and it is related to channels and small canyons of varying relief.

The results show that the dominant types of sedimentation is hemipelagic and shelf sedimentation driven by coastal erosion and transport by currents. Moreover, mass movements, mainly in the form of mass flow deposits were detected either lying on the seafloor producing an anomalous relief or buried under the seabed as lens-shaped deposits. At the base of the slopes and/or along the basins the higher intensity of the subbottom reflections could be also attributed to turbiditic deposits. These instability processes are most probably related to the relatively intense seismic activity, which has been known from ancient times and continues until today (Nomikou *et al*., 2021b). Numerous faults (Fig. 1b,c,d) have been also detected in the seismic records distributed to the south, west and to the north, some of them possibly related to onshore fault zones. The faults are either displaying the seafloor or they are buried, or they form fault zones confirming the active seismic character of the region. Several gullies/channels of various sizes were also recognized, many of which seem to remain still active, in particular along the slope. Additionally, buried paleo channels (Fig. 1c) were identified usually in the vicinity to the modern onshore hydrographic network and locally paleo-deltaic deposits were recognized. The undulating relief of the shelf deposits at north and east Lesvos that is detected in the seismic profiles probably suggest bedforms due to bottom current activity (Fig. 1d). Yet, erosional surfaces and moat-like features in deeper areas covered by finer sediments may be also related to contourite drifts (Fig. 1e). Anomalous seismic characters close to areas of well-known onshore hydrothermal activity could possibly indicate the presence of fluids in the sediments (Fig. 1d).

This study provides the first insights into the main sedimentary processes and geomorphological features of the offshore part around Lesvos Island. The sedimentary processes are governed by a complex interplay between hemipelagic sedimentation, mass wasting processes and bottom current activity. It becomes obvious that since different hydrographic provinces are encountered around the island, the depositional environments and the sedimentation processes vary, and they are also controlled by the active tectonism of the region and the Quaternary sea-level fluctuations. A detailed seafloor mapping in association with the acquisition of lower resolution seismic data, sediment coring and hydrodynamic measurements/modelling is expected to advance our understanding on the relationship and links between geological and oceanographic processes on local-to regional scales around Lesvos Island.

Acknowledgements

We would like to thank the Hellenic Survey of Geology and Mineral Exploration (EAGME) Greece for providing the seismic dataset.

References

Chronis, A., Hasiotis, T., Lowag, J., 2014. Relationship between gas-bearing sediments and biogenic mounds. Hydro International 18 (8), 22-25.

Damuth, J.E., 1975. Echo character of the western equatorial Atlantic floor and its relationship to the dispersal and distribution of terrigenous sediments. Marine Geology 18, 17-45.

Hasiotis T., Gazis I-Z., Anastasatou M., Manoutsoglou E., Velegrakis et al., 2020. Searching for potential marine sand resources to mitigate beach erosion in island settings. Marine Georesources and Geotechnology 39 (5), 527-542.

Katsikatsos, G., Mataragas, D., Migiros, G., Triandafillou, E., 1982. Geological study of Lesbos Island. Special Report, IGME.

Manoutsoglou, E., Hasiotis, T., Kyriakoudi, D., Velegrakis, A., Lowag, J., 2018. Puzzling micro-relief (mounds) of a soft-bottomed, semi-enclosed shallow marine environment. Geo-Marine Letters 38, 359–370.

Nomikou, P., Papanikolaou, D., Lampridou, D., Blum, M., Hubscher, C., 2021a. The active tectonic structures along the southern margins of Lesvos Island, related to the seismic activity of July 2017, Aegean Sea, Greece. Geo-Marine Letters 41: 49.

Nomikou, P., Evangelidis, D., Papanikolaou, D., Lampridou, D., Litsas, D., Tsaparas, Y., Koliopanos, I., Petroulia, M., 2021b. Morphotectonic structures along the southwestern margin of Lesvos Island, and their interrelation with the southern strand of the North Anatolian Fault, Aegean Sea, Greece. GeoHazards 2, 415–429.

Pavlides, S., Tsapanos, T., Zouros, N., Sboras, S., Koravos, G., Chatzipetros, A., 2009. Using active fault data for assessing seismic hazard: a case study from NE Aegean Sea, Greece. XVIIth International Conference on Soil Mechanics & Geotechnical Engineering, Alexandria, Egypt, paper 3.5.20.

Velegrakis, A., Vousdoukas, M., Andreadis, O., Adamakis, G., Pasakalidou, E., Meligonitis, R., Kokolatos. G.,2008. Influence of dams on downstream beaches: Eressos, Lesbos, Eastern Mediterranean. Marine Georesources & Geotechnology 26 (4), 350–371.

16th International Congress of the Geological Society of Greece
17-19 October, 2022 - Patras, Greece
Bulletin of the Geological Society of Greece, Sp. Publ. 10
Ext. Abs. GSG2022-209

Evidence of mass transport deposits in the south Serifos slope in western Cyclades, Greece

A. Poulos[1], T. Hasiotis[1], S. Missias[2], A. Paleokrassas[2]

(1) Department of Marine Sciences, University of the Aegean, Mytilene, Greece, marm21024@marine.aegean.gr (2) Akti Engineering, Piraeus, Greece.

Introduction

Gravitative mass movements have been documented in various marine settings in Greece, from shallow to deep water environments (i.e., Ferentinos *et al*., 1992; Hasiotis *et al*., 2002; Strozyk *et al*., 2010). The main mechanism being responsible for the initiation of mass wasting seems to be earthquakes, although other factors exerting a key role in slope-failure development include topographic steepening (due to faulting or to uplifting of underlying diapiric structures) and excess pore pressures due to the presence of fluids and high rates of sedimentation (Ferentinos, 1992). Bottom flows have not been considered until now as a potential factor contributing to mass failures in Greece. This paper examines mass transport deposits in the southern margin of Serifos Island, an area being part of the corridor that has been recently investigated for the power interconnection between Lavrio (in Attica) and Milos Island.

Serifos Island belongs to the western Cyclades, bounded to the west by Myrtoon Basin and towards the south by Sifnos Island and the southwestern part of the Aegean Volcanic Arc. The wider marine area has been investigated by Piper and Perissoratis (2003), Anastasakis *et al*., (2006) in respect to the sedimentary and tectonic evolution. Lykousis (2001) observed morphological and sedimentological evidence in the Cyclades plateau implying strong near-bed unidirectional currents flowing in a NE-SW direction. Moreover, Tripsanas *et al*., (2016) report erosional gullies, abraded surfaces and channel-related sediment drifts, neighboring Serifos slope (north Milos basin), all associated with the presence of strong bottom currents, usually being episodic, even during the Holocene at higher sea-level stands. Apart from this general information little is known about the recent depositional processes in the study area. Within this context, this study aims to provide evidence regarding the potential hazards of the south Serifos slope, which may also support design, laying and safe burial operations of the submarine power cables in this area.

Methods

Bathymetric and geomorphological information was collected in 2020, with the multipurpose support vessel "HYDNA". The study comprised data from a Kongsberg EM710-MK2 multibeam echo-sounder (MBES), a Geopulse 3.5 kHz subbottom profiler (SBP) and an EdgeTech 4200-MP side scan sonar (SSS). Sound velocity casts were provided from a MIDAS SVP 650 MARK II (Valeport). A 3-m gravity corer was employed for the collection of 11 sediment cores along Serifos slope for sedimentological and geotechnical analysis. For vessel positioning a Kongsberg Seapath 320 system comprising of 2 GNSS receivers was used, whilst a Kongsberg μPAP USBL acoustic tracking system was used for the SSS tracking. Navigation was supported by Hypack-Max software. For processing and mapping purposes the SonarWiz, AutoCAD and QGIS softwares were utilized. Geophysical interpretation was based on changes of the backscatter intensity in the SSS images and variations in the acoustic character of the SBP profiles.

Results and Discussion

The study area along Serifos slope develops from 130-140 m water depth down to the ~480 m, has an aerial extent of ~14 km^2 (Fig. 1a) and it can be crudely separated into 3 sections: (i) the upper slope section (down to 310 m), (ii) the middle slope section (310 m to 410 m) and (iii) the lower slope section (410 m to ~470-480 m). Although the mean slope gradient is less than 8° in the upper section, inclinations may reach ~18°, and locally (along slide scars) they attain values of ~30°. The middle section is, also, marked by a steep sloping step (~10-16°) that extends almost throughout the surveyed area. Within this section the mean gradient is ~5.5°, and progressively (from the 380 m isobath down to 410 m) attains lower values. The lower section (base of slope) is characterized by very low gradients (< 2°) that only locally may reach 12°.

Along the Serifos slope various acoustic patterns appear on both the SBP and the SSS records, suggesting a puzzling subbottom and surficial relief. More specifically, the SBP profiles show that the seabed is composed, in general, of a layered muddy surficial sequence, which thins and wedges out, or it is erosional truncated along with sudden slope changes (Fig. 1b). The SSS images exhibit various backscatter tones accompanied with scattered positive targets and locally arcuate areas of high reflectivity (Fig. 1c), indicating that the seafloor has an irregular relief composed of blocks or material of different composition and micro-relief resting over the seafloor. It becomes obvious that Serifos slope suffers from instability processes, which have an extensive and complex pattern, in the form of blocky mass flows and sheet-like deposits. Amphitheatric-shaped or almost elongated scarps in the upper and middle sections of the slope suggest evacuation zones and they are associated with sediment blocks found downslope implying a gradual disintegration of the slided material. Numerous shallow and narrow bottom scars observed behind sediment slabs (Fig.

1c) are interpreted as glide tracks of outrunner blocks that had been separated from the main body of the mass transport deposit and moved independently for a few hundred meters. However, some of these scars could be also caused by the sediment slabs that were dragged together with the main body of the slided material. At the northeastern limit of the surveyed area the MBES derived morphology suggests that instabilities may have taken place even along or very close to the shelf-edge. The aforementioned geomorphological instability features might have resulted in the local exposure of deeper-seated more compacted sedimentary strata on the seafloor. The SBP profiles along the lower slope section have revealed detached blocks and mass flow deposits (Fig. 1b) from the adjacent steeper slope, usually resembling rafted blocks.

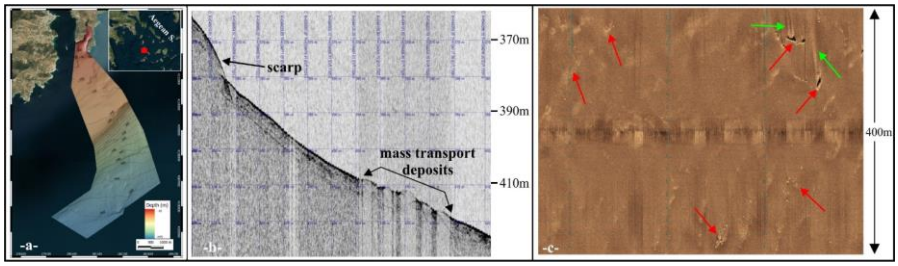

Figure 1. (a) Location and bathymetry of south Serifos slope, (b) 3.5 kHz profile showing a scarp and mass transport deposits and (c) SSS image demonstrating rafted sediment blocks (red arrows) and glide tracks of outrunner blocks (green arrows).

The retrieved sediment cores were 18-264 cm long and their analysis revealed four (4) sediment types (ST1 to ST4). ST1 corresponds to very soft to soft mud to sandy mud with small biogenic fragments locally found in a relatively remolded state. ST2, found only in 3 cores, is Sapropel S1. In one case it resembles a water-rich episapropelic layer. ST3 corresponds to very soft to soft water-rich sandy mud to muddy sand with biogenic and coral fragments, locally with a disturbed texture and usually indistinct basal contacts implying deposits of a gravitational origin. ST4 is water-rich (very loose) muddy sand to sand with terrigenous grains occasionally hosting biogenic fragments of species thriving in shallow water, and with distinct or indistinct basal contacts. ST4 has a thickness of up to 25 cm, it is found down to 175 cm under the seabed and is interpreted as turbidites.

Data analysis revealed that recent mass transport deposits are widespread and represent the main sedimentation process on south Serifos slope. Deposition in the upper ~2.5 m seabed is not constant, but it is interrupted by muddy sand to sandy turbidites. The absence of ST2 (sapropel) in most of the sediment cores verifies that recent sediment failures took place the last ~9000 years. Yet, in the case that ST2 is buried under the sediment recovered by coring, or it was disturbed, and transported downslope deposited as episapropelic layers, then the gravitative processes could be younger than ~6500 years. The area under consideration is characterized by low to medium seismic activity, thus other factors must have contributed to the destabilization of the sediment structure. Serifos slope is not directly connected to any fluvial drainage system, nor fluids in the sediments, or relevant morphological features were detected in the geophysical data. Tripsanas *et al*., (2016) reported buried mass transport deposits south of Serifos margin suggesting mass wasting history over a long period of time. The same authors described mounded, levee-like drifts and channel like features (moats) suggesting the presence of strong bottom currents. Sakellariou and Tsampouraki-Kraounaki (2019) indicate an inferred fault line bounding the south Serifos slope, possibly related to the Myrtoon-Ikaria fault zone. The high topographic gradient of south Serifos slope cannot directly be linked with this fault unless high energy seismic sources are to be used. However, based on the abovementioned findings, it is inferred that bottom current activity might be responsible for continuous sediment erosion and maintenance of steep slopes, whereas sediment undercutting due to flowing water at various bathymetric levels along the slope may have contributed to shear strength reduction and gradual sediment collapse. Therefore, recurrence of mass-wasting events is thereby likely controlled by the progressive steepening of the slope. Thus, bottom currents may precondition the slope and even small earthquakes could trigger mass movements along the slope.

References

Anastasakis, G., Piper, D.J.W., 2005. Late Neogene evolution of the western South Aegean volcanic arc: sedimentary imprint of volcanicity around Milos. Marine Geology 215, 135–158.

Ferentinos, G., 1992. Recent gravitative mass movements in a highly tectonically active arc system: The Hellenic Arc. Marine Geology 104, 93-107.

Hasiotis, T., Papatheodorou, G., Bouckovalas, G., Corbau, C., Ferentinos, G., 2002. Earthquake-induced coastal sediment instabilities in the western Gulf of Corinth, Greece. Marine Geology 186, 319-335.

Lykousis, V., 2001. Subaqueous bedforms on the Cyclades plateau (NE Mediterranean) - evidence of Cretan deep-water formation. Continental Shelf Research 21, 495–507.

Piper, D.J.W., Perissoratis, C., 2003. Quaternary neotectonics of the south Aegean arc. Marine Geology 198, 259–288.

Sakellariou, D., Tsampouraki-Kraounaki, K., 2019. Plio-Quaternary extension and strike slip tectonics in the Aegean, in: Duarte, J., (Ed.), Transform Plate Boundaries and Fracture Zones, 339-374.

Strozyk, F., Strasser, M., Krastel, S., Meyer, M., Huhn, K., 2010. Reconstruction of retreating mass wasting in response to progressive slope steepening of the northeastern Cretan margin, eastern Mediterranean. Marine Geology 271, 44-54.

Tripsanas, E., Panagiotopoulos, I., Lykousis, V., Morfis, I., Karageorgis, A., Anastasakis, G., Kontogonis, G., 2016. Late quaternary bottom-current activity in the south Aegean Sea reflecting climate-driven dense-water production. Marine Geology 375, 99-119.

16th International Congress of the Geological Society of Greece

17-19 October, 2022 - Patras, Greece

Bulletin of the Geological Society of Greece, Sp. Publ. 10

Ext. Abs. GSG2022-319

Beneath the lapilli and the post-volcanic torrential depositions: locating the prehistoric port at Akrotiri, Thera – Preliminary results

Y. Bassiakos, E. Tsakalos, M. Kazantzaki, E. Filippaki

Laboratory of Archaeometry, Institute of Nanoscience and Nanotechnology, NCSR "Demokritos" Athens, Greece

It happened around 1620 BC, the cataclysmic prehistoric eruption of the Thera volcano, covering the entire island with a thick tephra mantle which exterminated almost every kind of life on the island. The width of the associated extant caldera (*ca*. 11 km in diameter, the largest in the world), implies the plausible presumption that one of the most important and violent Holocene volcanic eruptions has taken place at Thera.

Ongoing archaeological excavations near the southern bays of the island, have revealed a prehistoric coastal city (known as "Akrotiri") buried beneath the siliceous pyroclastic successions. Besides, numerous luxurious findings, such as ivory masterpieces, precious imported stones, and depictions of exotic themes (e.g., "the Antelopes", "the Blue Monkeys", "the Nilotic landscapes") clearly indicate well-established maritime contacts between "Akrotiri" and the eastern Mediterranean lands. Obviously, such maritime operations required adequate harbor facilities (Doumas, 1991) and the needed anchorage. However, in spite of the repeated relevant attempts, undertaken by a number of scholars during the last decades (Friedrich and Sørensen, 2010), the location of the buried harbor (although reasonably hypothesized) remained an unrealized aim.

In recent years, the Archaeometry Laboratory of NCSR "Demokritos" initiated an ambitious geoarchaeological project with the major objective the localisation of the "lost" prehistoric harbor. As such, a wide range of geological approaches was employed including, field reconnaissance studies, satellite image assisted GIS processing, land vertical movements assessment caused by volcanism and local tectonics, eustatic and relative sea-rise changes, palaeovalleys drainage pattern assessment, diachronic torrents outfall including terrestrial sedimentation, as well as surface geological sampling for chemical/petrographic analysis. Geophysical studies, by employing Seismic Refraction (SR) and Electrical Resistivity Tomography (ERT), in all three seaside valleys near Akrotiri, had been conducted by Heidelberg University-Geography Department, during the first stages of the project (Theodorakopoulou *et al.*, 2018).

Based on pedometric data as well as geomorphological observations of the area around "Akrotiri", the project was oriented towards drilling/coring activities at one of the three near-Akrotiri valleys (two of them once constituted bays, see Fig. 1) known as Mavrorachidi (located between Kokkino Vouno and Mesovouna hills) *ca*. 700 meters west of excavated "Akrotiri" settlement. Although all three valleys around Akrotiri settlement may be seen as potential candidate areas for hosting the prehistoric anchorage, for two of them such a possibility may be severely restricted since:

- A little bay (now comprising a small creek/valley) known as "Potamos", situated *ca.* 170 meters east of "Akrotiri" excavation, receives the outfalls of a rather extended drainage basin and exhibits a consolidated fluvial formation at the coast, indicating longitudinal stream deposits. Moreover, emerged pre-Minoan ignimbrites, at both sides of the torrent, are less than 50 meters apart, so obstructing vessels maneuvers for mooring.
- A bay once existed between "Akrotiri" excavations and "Mesovouna hill" seems not suitable strand area for hosting harbor facilities. Today, the distance between the western fringes of the settlement and the "Mesovouna hill" is less than 150 meters; and the actual length of the ancient bay might be even smaller at lower levels. On the contrary, the physical distance between "Mesovouna" and "Kokkino Vouno" (at "Mavrorachidi") valley, where the two boreholes were accomplished, is longer than 200 meters.

One first-pilot borehole was drilled at Mavrorachidi valley, ~240 meters north from the modern coastline, where the bedrock (pre-Minoan ignimbrite) was reached at 23 meters in depth, although no sea-bottom (marine) indicators were detected. The next two geotechnical' drillings were conducted in March 2019, 165 and 105 meters north from today's strand, yielding undisturbed and solid "dark" cores, the latter required for luminescence (OSL) dating studies.

The drilling cores retrieved were quite enlightening for the purposes of the study: while the top 80 cm discard, as it was mainly disturbed soils, the lower levels exhibited features of a quasi-crossed sedimentation, an indication of fluvial sedimentation. Fine to coarse gravel was the main core content and the grains were consisted of a mixture of volcanic material (ash, pre-Minoan ignimbrites, scoriae and andesites) along with sub-angular carbonaceous chips and limited fine clay. These fluvial-type components were predominant from 0.80 to 11.00 meters below the modern surface, while compact andesitic boulders up to 70 cm (hindering the drilling), were met rather frequently.

Below the mixed-gravel layer that exceeds 10 meters in thickness, the borehole met soft and fine volcanic ash of white-yellowish color, often containing minute rounded grains of blackish andesitic crumbs. This bed was met at depths from

11.05 to 17.10 meters below the modern surface. Beneath this *ca.* seven (7) meters layer, the borehole met fine-grained black to reddish sand of approximately three (3) meters in thickness, consisting of volcanic rounded constituents, similar to the well-known Theran black-sands which are commonly found at the modern coastlines of southern Thera (e.g., Perissa and elsewhere). Following the black-reddish sand, a dense ignimbrite formation at 20.50 meters in depth was met, and the drilling operations were concluded as the pre-Minoan volcanic background of the area was reached.

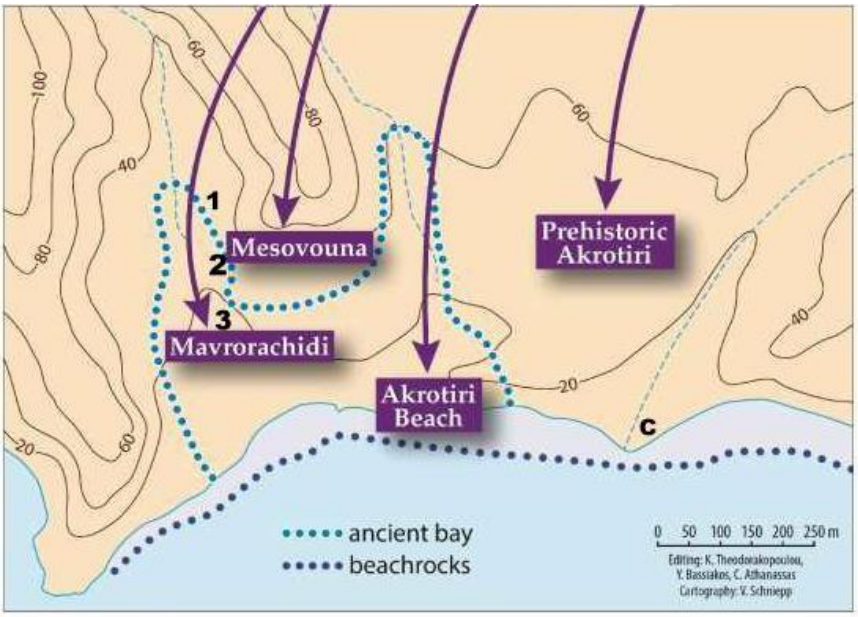

Figure 1. The investigated area near Akrotiri /Thera coastline; 1: point of the pilot borehole, 2 and 3: points of the drilling/coring boreholes, C: little consolidated fluvial formation

Summing up, it is believed that an ancient strand has been discovered at a distance more than 100 meters north of the modern beach, at "Mavrorachidi" valley, where it was probably used as a prehistoric anchorage, and that the flooding phenomenon happened directly after the Minoan four stages eruption, is fairly verified by the findings of the coring undertakings. Nevertheless, further research is recommended to affirm these findings.

The next stages of the project include detailed absolute dating (luminescence and radiocarbon) of the extracted core material, micro-morphological analyses as well as other palaeoenvironmental/analytical techniques, to further confirm the location of the prehistoric harbor of Thera but also to get an insight into the post-Minoan evolution of the important Theran/Akrotiri landscape.

Acknowledgments:

The authors are grateful to Professor C. Doumas, Director of Akrotiri Excavation and his collaborators for inducement and multiple endorsements of the project, to the Ephorate of Antiquities of Cyclades for substantial support in the field, and to the Institute of Aegean Prehistory (INSTAP) for funding the costly drilling and coring works.

References

Doumas C., 1991. Thera's prehistoric harbor. *The Illustrated London*, *News Historical Archive*, Royal Issue, 76-78.

Friedrich W., Sørensen A.H., 2010. New light on the Ship Fresco from Late Bronze Age Thera. *Prähistorische Zeitschrift*, 85.2, 243-257.

Theodorakopoulou, K., Bassiakos, Y., Athanassas, C., Schukraft, G., Holzhauer, I., Hecht, S., Mächtle. B., Wagner, G.A., (2018). A geoarchaeological approach for the localization of the prehistoric harbor of Akrotiri, Thera. In: C. Siart, M. Forbriger and O. Bubenzer (eds) *Digital Geoarchaeology – New techniques for interdisciplinary human-environmental research*, Springer, Heidelberg, 237–251.

16th International Congress of the Geological Society of Greece
17-19 October, 2022 - Patras, Greece
Bulletin of the Geological Society of Greece, Sp. Publ. 10
Ext. Abs. GSG2022-324

Sediment transport patterns of coastal areas. The examples of Igoumenitsa Gulf and Volos coast, Greece.

I. Zananiri[1], I. Vakalas[1]

(1) Hellenic Survey of Geology and Mineral Exploration (HSGME), Acharnae, Greece, izanan@igme.gr (2) National Technical University of Athens (NTUA), Athens, Greece

Research Highlights

Grain size parameters (mean size, sorting, skewness) can reveal sediment transport patterns providing useful information for various aspects of marine sediments exploration.

Abstract

The textural tendencies of grain size parameters (McLaren and Bowles, 1985; Gao and Collins, 1991, 1994) can provide useful information about the transport direction of the sedimentary material in coastal or open marine settings. The knowledge of sediment transport patterns in modern or ancient marine areas (Huang, X. and W. Jokat, 2016) is an important tool for various applications such as mineral exploration, coastal management, HC exploration, etc. In this context, the methodological approach proposed by Gao (1996) was applied in two coastal areas: Igoumenitsa Gulf and Volos coastal area, where a total of 52 and 58 surficial samples for grain size analysis was acquired respectively. Data acquisition was carried out in the frame of the GEOCHART project (NSRF 2007-2013), while analysis of the collected samples was performed on the basis of the HSGME Marine Geology Laboratory procedures according to international protocols (Folk 1954). For the interpretation of the results MATLAB R2022a version was used.

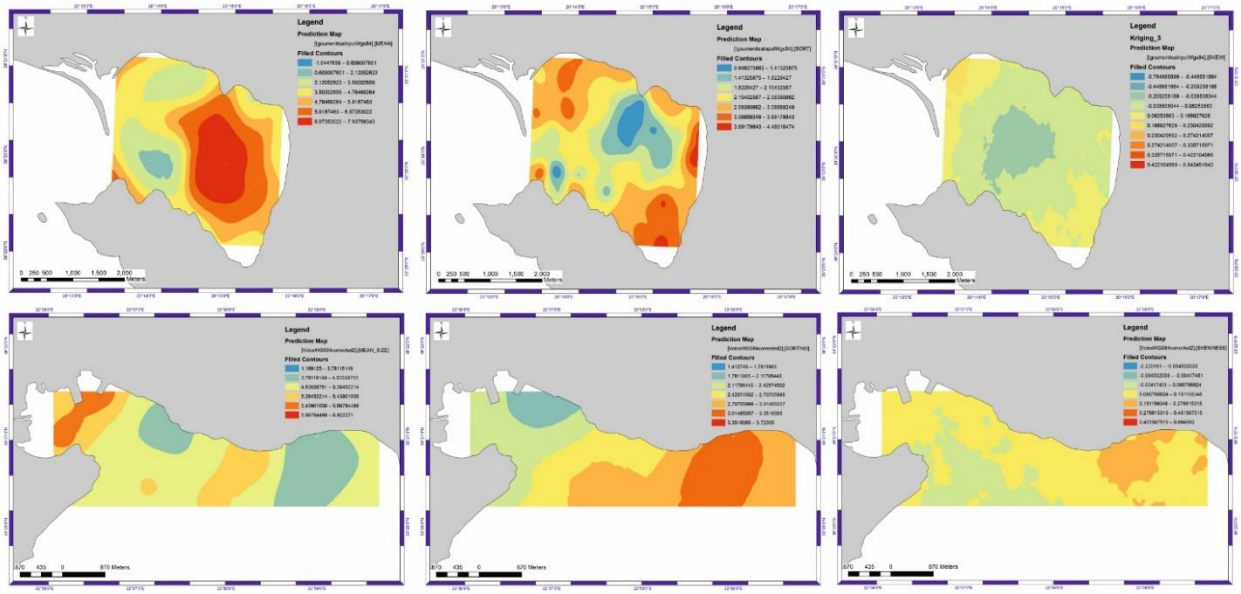

Figure 1. Spatial distributions of the mean diameter of the surface sediment (left), the sorting coefficient (center) and the skewness (right) (Igoumenitsa gulf at the top, Volos coastal area at the bottom).

The surficial sediment transport seems relatively complicated due to the comprehensive influence of the topographical conditions, hydrodynamic characteristics, anthropogenic influence and sediment sources in the study area. The spatial distribution of the mean diameter of the surface sediments (Fig. 1) shows a clear coarse-fine trend from the shallow water to the deep water in the nearshore area of Igoumenitsa Gulf. Volos coastal areas presents a more complex pattern with coarser sediments in the central and eastern areas while relatively finer sediments are deposited near the port. These variations are in accordance with the major sediment inlets. Sorting values have a clear trend in Volos area. Eastwards poor sorting characterizes the coastal area while towards the west sorting values reduce, presenting the lower values in the port. In Igoumenitsa gulf sorting values are greater near the coast while at the slopes that delineate the deeper part of the gulf sorting values reduce. Skewness values in Igoumenitsa suggest a coarse skewed to near symmetrical trend (Folk and Ward, 1957) indicating a depletion of finer material and deposition in the deeper parts of the basin. In Volos coastal area skewness values present a more symmetrical trend. Slightly fine skewed values are observed at the easternmost areas.

The correlativity between the sorting coefficient, skewness and mean diameter is presented in Fig. 2. These plots reveal that for Volos area as grain size decreases, sediments are better sorted (Fig.2a). In Igoumenitsa Gulf (Fig.2c) a trend cannot be implied. Skewness versus mean size indicates that independently of the grain size, sediments are generally symmetrical for Volos area while for Igoumenitsa slightly fine skewed. The absence of clear trends is the result of the multi feeding sources while anthropogenic interference plays also a significant role.

The net sediment transport patterns, obtained by the grainsize trend analysis, reveal several distinct characteristics in both areas (Fig. 3). The white arrows indicate the direction of sediment transport while their lengths depict the significance of transport trends (Gao and Collins, 1994). As expected, the surficial sediment transport pattern is complicated. This fact is common in areas where the physical parameters and processes (sediment sources, topographic relief, hydrodynamic processes and climate) are interacting with anthropogenic activities. In Volos coastal area sediment transport pathways are significant in the eastern part indicating that the sediment enteering Pagasitikos gulf is transported probably by longshore drift towards the west. In the central part sediment transport patterns are weak, while near the port a clear SW

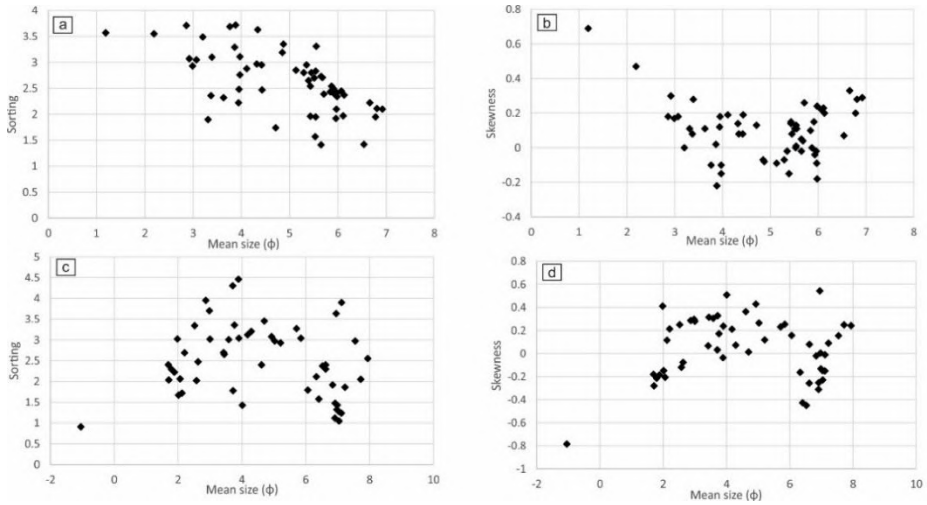

Figure 2. Cross plots of mean size versus sorting and skewness (a&b Volos coast, c&d Igoumenitsa Gulf).

trend is identified. This trend combined with the good sorting and fine-grained character of the sediments suggests the influx of fine material by the prevailing winds towards the port. In Igoumenitsa gulf a clear transport trend is observed in the southeastern area where a stream feeds the gulf with sediment that moves towards the NW in the deeper parts of the gulf. Minor feeding points are located also in the N – NE areas showing also a trend towards the central parts of the basin. At the western margins of the gulf, a northwards sediment transport direction is identified which is not well understood in the context of physical processes. In this area, an artificial channel has been excavated in order to secure marine traffic. Probably, this adjustment has interfered the physical processes resulting in the aforementioned elusive transport pattern.

Figure 3. Sediment transport patterns (white arrows) in Igoumenitsa Gulf (left) and Volos coastal zone (right). Dashed lines represent bathymetric contours while white dots sampling locations.

References

Folk, R.L. and Ward, W.C., 1957. A Study in the Significance of Grain-Size Parameters. Journal of Sedimentary Petrology, 27, 3-26.

Gao, S., 1996. A FORTRAN program for grain-size trend analysis to define net sediment transport pathways. Comput. Geosci. 22 (4), 449-452

Gao, S., Collins, M., 1994. Net sediment transport patterns inferred from grain-size trends, based upon definition of "transport vectors" - reply. Sediment. Geol. 90 (1-2), 157-159

Gao, S., Collins, M., 1991. A critique of the "McLaren Method" for defining sediment transport paths. J. Sed. Petrol. 61 (1), 143-146

Huang, X. and W. Jokat (2016). "Middle Miocene to present sediment transport and deposits in the Southeastern Weddell Sea, Antarctica." Global and Planetary Change 139: 211-225.

McLaren, P., Bowles, D., 1985. The effects of sediment transport on grain-size distributions. J. Sediment. Res. 55 (4), 0457-0470.

16th International Congress of the Geological Society of Greece
17-19 October, 2022 - Patras, Greece
Bulletin of the Geological Society of Greece, Sp. Publ. 10
Ext. Abs. GSG2022-364

Geophysical Study Of Patras Gulf Pockmark Field and Long-Term Monitoring Using Distributed Temperature Sensors (DTS): Preliminary Results.

G. Papatheodorou[1], D. Christodoulou[1], M. Geraga[1], E. Fakiris[1], X. Dimas[1], N. Georgiou[1], E. Sokos[2], Z. Roumelioti[2], G. Etiope[3], S. Kokkalas[4], G. Giannaraki[5], M. Papakonstantinou[1]

(1) Laboratory of Marine Geology & Physical Oceanography, Department of Geology, University of Patras, 26504 Patras, Greece, g.papathe@upatras.gr (2) Laboratory of Seismology, Department of Geology, University of Patras, 26504 Patras,, Greece. (3) Istituto Nazionale Geofisica e Vulcanologia (I.N.G.V.), Rome, Italy. (4) Laboratory of Structural Geology & Tectonics, Department of Geology, University of Patras, 26504 Patras, Greece. (5) National Observation of Athens, 11810 Athens, Greece.

Research Highlights

A systematic geophysical survey was carried out in the Patras Gulf active pockmark field. Moreover, a long-term monitoring survey using DTS system is in progress in order to investigate the relationship between the pockmark activity and the seismicity in western Greece.

Background

Seabed fluid flows and related seabed morphological features (e.g. pockmarks, mud volcanoes) describe a wide range of fluids (gases and liquids) passing from sediments to seawater. Although the fluid release from the seabed has been linked to tectonics, the exact relationship between seabed gas release and the seismic activity is very poorly known and is based on very sparse measurements (Hasiotis *et al*., 1996).

A well-developed field of pockmarks, associated with fluid flows is situated in the gulf of Patras, Greece. There, in one occasion, in earlies '90s, temperature anomalies that had been recorded in a hydrographic station, within the pockmark field, prior to a major earthquake (5.4 R, 14/7/1993), had been attributed to changes in the fluid flow behavior due to earthquake (Hasiotis *et al*., 1996, Papatheodorou *et al*., 2007), providing documentation for the links between fluid seepages and earthquakes. Moreover, on June 8th 2008 (12:25 GMT) a major earthquake, MW=6.4R, occurred on the Northwestern Peloponnese. Side scan sonar data and methane measurements that collected in the pockmarks immediately after the earthquake showed evidence of activation of the field (gas plumes in the water column) (Christodoulou *et al*, 2009).

DTS system is an effective tool for gas seepage monitoring since the seabed fluids are characterized by slightly lower temperature compared to the bottom waters. So far, DTS system has been successfully used for the short-term monitoring of gas bubbles emitting for the seafloor of Katakolo bay (W. Greece) (Wood, 2013).

Objectives

The aim of the present work is to study in great detail the Patras gulf pockmark field using state-of-the-art geophysical means. The major objective of this work is to monitor, in long-term, the fluid flow from the pockmark field using DTS system and to investigate its relationship to earthquake activity in western Greece. Moreover, the impact of the Patras new harbor to the pockmark field and vice versa will be also assessed.

Methods

A systematic geophysical survey was conducted in the pockmark field using multibeam echosounders, subbottom profiling systems, side scan sonars and ground truthing techniques (R.O.V.). The selection of the specific site, within the pockmark field, for seepage monitoring was made on the results of: (a) the geophysical survey and (b) the geochemical investigation using CH_4 - H_2S in-situ sensors and analytical procedures. A Distributed Temperature Sensors (DTS) system has been deployed on the seabed of the specific site and a microseismic monitoring network and a meteorological station have been also established in the wider area.

Results

The interpretation of multibeam bathymetric data and side scan sonar sonograms revealed a very accurate map of the pockmarks of the field. The pockmark field consists of 129 pockmarks and extends over an area of about 2.5 km^2 (Fig. 1a). The pockmarks, based on their shape characteristics, are divided into two morphological classes: (i) normal pockmarks which are mostly circular or oval in plan view, ranging from 50 to 150m in diameter and up to 15m in depth and (ii) complex or composite pockmarks having irregular shape in plan view and occurring as amalgamation of normal pockmarks. Pockmark distribution shows a clear spatial pattern that distinguishes the pockmark field in two sectors. The northern sector contains 84 pockmarks within an area of about 1 km^2 while the southern sector consists of 45 pockmarks (Fig. 1a). In the northern sector, 35 pockmarks are located inside the Patras harbor basin and 49 out of the harbor (Fig. 1a). The northern sector of the field is dominated by composite pockmarks. One complex pockmark has

been detected at the southern end of the field. It has a diameter of about 250 m, a maximum depth of 40 m and is about 25 m deeper than the surrounding area (Fig. 1a). The field comprises at least two groups of pockmarks (pockmark strings) which appear to follow linear trends of W-E to W.SW-E.NE orientations (Fig. 1a).

The comparison of the detail bathymetric map of the present study with previous datasets showed that the construction of the new Patras harbor has heavily affected the spatial distribution of the pockmarks.

The interpretation of high resolution CHIRP and 3.5 kHz seismic profiles acquired at the northern end of the field displays the trace of a W.SW-E.NE trending normal fault which dips to the south (Fig. 1b). This fault coincides well with a pockmark string suggesting that the fault acts as permeable pathways for gas. This fault can be considered as the offshore continuation of the active fault of Ag. Triada (A.T.F) that was activated during the major earthquake 5.4 R of 14/7/1993. Faults of almost the same orientation have been also detected suggesting that the field is tectonically controlled (Fig. 1a).

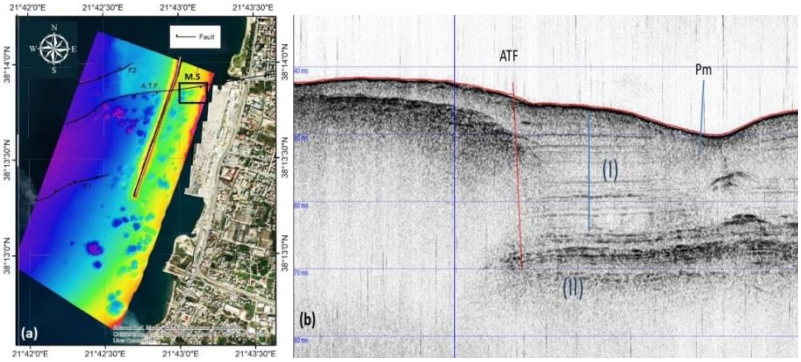

Figure 1. (a) Bathymetric map of the Patras Gulf pockmark field showing the main active faults (ATF, F1, F2) and the DTS monitoring site (M.S.), (b) CHIRP seismic profile showing the Ag. Triada fault (ATF) (Pm: pockmark, I: stratified sediments, II: acoustic turbid zone).

Based on the acquired geophysical and geochemical data, a specific site located at the shallowest part of the AT Fault/pockmark string was selected for the deployment of the Distributed Temperature Sensor (DTS) (Fig. 1a). During the first months of monitoring, the DTS system successfully performed a continuous, long-term temperature recording. An example of sequence of the temperature data recorded by the DTS is presented in Figure 2. The seismological and meteorological data for the DTS monitoring period were retrieved. So far no effect of seismic activity on the dataset was detected. This is probably because the seismic events were weak (<3.5 M) and/or not in sufficient proximity to the DTS deployment site to significantly affect methane flux variation.

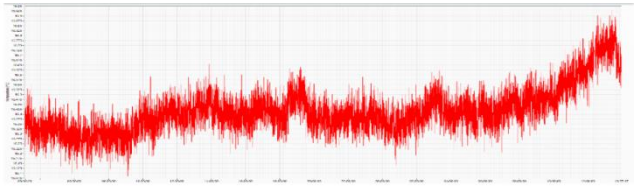

Figure 2. Example of sequence of the temperature data recorded by the DTS in the monitoring site.

Acknowledgements

This study was conducted as part of the BLUEL project (https://bluel.upatras.gr/) financed by Hellenic Foundation for Research and Innovation (H.F.R.I).

References

Christodoulou, D., Papatheodorou, G., Fakiris, E., Etiope, G., Ferentinos, G. 2009. The activation of the Patras Gulf pockmark field triggered by the June 8, 2008 eartquake. 9th Symposium on Oceanography & Fisheries, Patras, Greece, p. 3-8.

Hasiotis, T., Papatheodorou, G., Kastanos, N., Ferentinos, G. 1996. A pock-mark field in the Patras Gulf (Greece) and its activation during the 14/7/1993 seismic event. Marine Geology 130, 333-344.

Papatheodorou, G., Christodoulou, D., Geraga, M., Etiope, G., Ferentinos, G. 2007. The pockmark field of the Gulf of Patras: An ideal natural laboratory for studying seabed fluid flow. 25th IAS Meeting of Sedimentology, Patras, Greece, Field Trip Guidebook, 43-62.

Wood, P. 2013. Hearing with light. GEO ExPro 10, 3, 54-56.

16th International Congress of the Geological Society of Greece
17-19 October, 2022 - Patras, Greece
Bulletin of the Geological Society of Greece, Sp. Publ. 10
Ext. Abs. GSG2022-417

Geophysical and Sedimentological Investigation of Marathon Lake dam reservoir

N. Georgiou[1], D. Christodoulou[1], E. Fakiris[1], X. Dimas[1], S. Sergiou[1], M. Geraga[1], G. Papatheodorou[1], S. Nalpantidou[2], G. Antonakopoulos[2] (1) Laboratory of Marine Geology & Physical Oceanography, Department of Geology, University of Patras, Patra, Greece, (2) Water Intake Division, EYDAP, Athens Water Supply and Sewerage Company, Athens, Greece

Research Highlights. This work uses an interdisciplinary approach including marine remote sensing techniques and sediment core analysis for the study of the Marathon Lake Reservoir floor and for the assessment of the sedimentation processes that occur in after the construction of the concrete dam. The study indicated two sedimentation infill phases of different energy conditions, which affected the storage capacity of the Marathon Reservoir.

Background. Marathon Lake/Reservoir was developed by the construction of a concrete dam, in 1931, at the intersection of the Charadros and Varnavas torrents, at NE Attica, and was for many years the main water supplier for the capital city of Athens and its Metropolitan. The need to preserve the existing reservoir storage capacity demands the continuous monitoring and evaluation of the freshwater resources. In 2017, for the very first time after the Marathon dam construction, a very detailed geophysical and sedimentological survey was carried out at the artificial lake area.

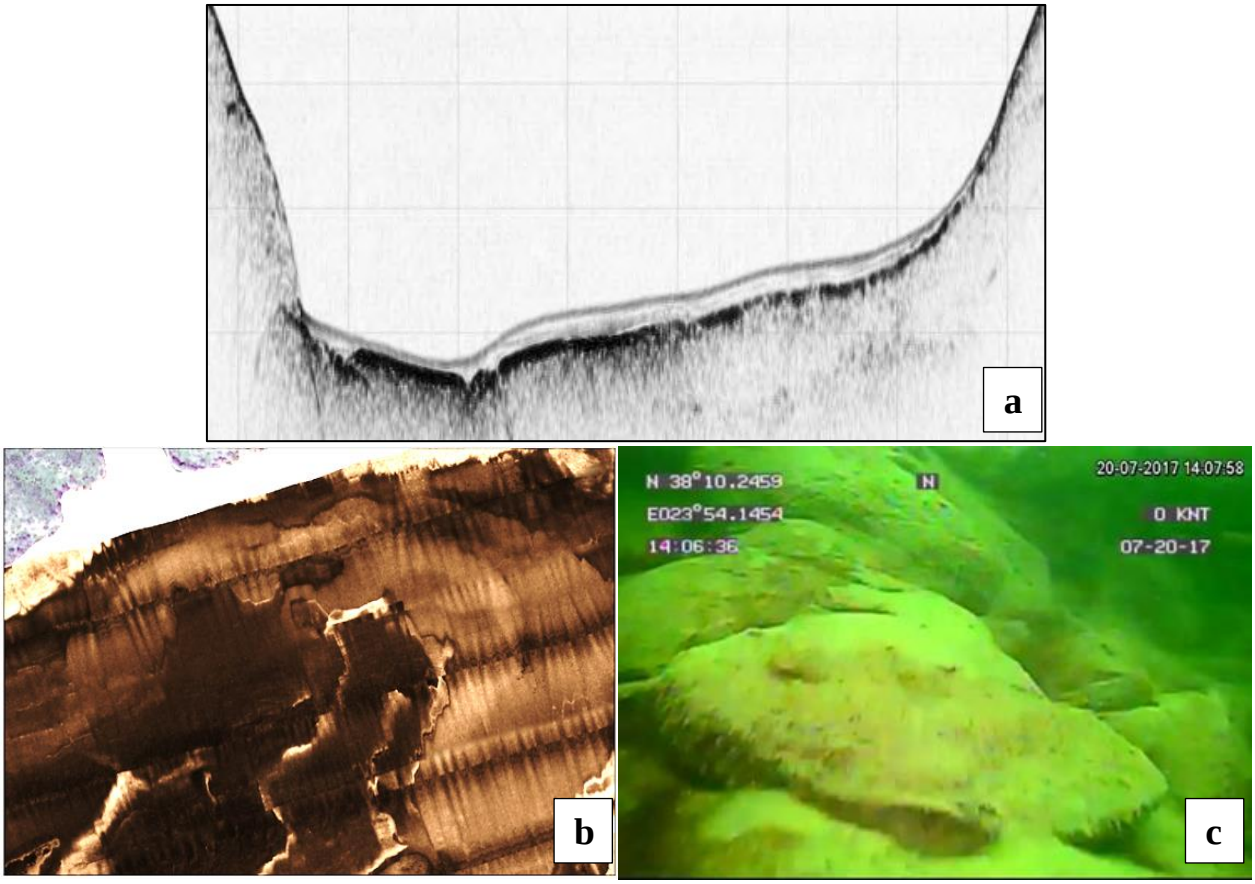

Figure 1. (a) High resolution seismic profile showing the seismic stratigraphy of the sediments of the reservoir, (b) Side scan sonar mosaic of the central part of the reservoir (backscatter: high, moderate, low), (c) underwater photo of submerged ruins.

Objectives. The main objectives were: i) to study the morphodynamical evolution of the reservoir, with an emphasis on mapping and defining the bottom morphology and the thickness of sediment alluvial deposits, ii) to calculate its storage capacity and surface as a function of water level and iii) to examine the condition of the underwater structures or other anthropogenic artifacts (Fakiris et al. 2016).

Methods. Swathe Bathymetry, side scan sonar, and high-resolution seismic profiling datasets, all integrated with real-time kinematic (RTK) positioning (Phase A), were acquired and analyzed to fulfill the above objectives (Fig. 1a,b).

Ground truthing techniques (Phase B) were also used consisting of ROV visual inspection in selected sites and sediment coring in selected location on the basis of subbottom profiling data (Fig.1c). The combined interpretation of the datasets acquired during the two methodological phases led to the estimation of the spatial and temporal sedimentation variability. Sedimentation rates were calculated in the collected sediments using the radioactive isotope ^{210}Pb (Appleby & Oldfield, 1978).

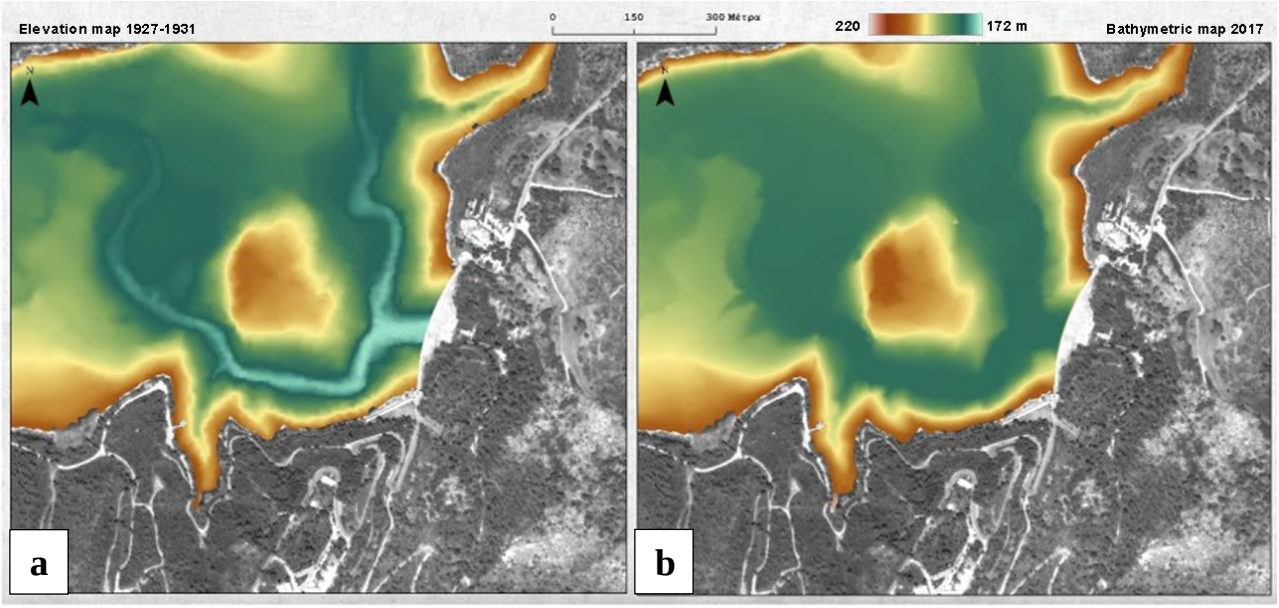

Figure 2. Part of the Marathon Dam area showing the a) elevation map before the dam construction (1972-1931), b) bathymetric map of the reservoir in 2017 (common color scale).

Results & Conclusions.

The bathymetric survey showed that the maximum lake depth is 36.5m while the elevation of the lake ranges from 184m to 220.5m (Fig. 2) (Papatheodorou *et al.*, 2018). The spatial distribution pattern of backscatter as emerged from the interpretation side sonar data coincides well with the steep slopes of the reservoir (high), the submerged river bed (moderate), and the accumulation of soft sediment (low). Through the early stage of the dam (first sedimentation infill), which was recognized only through the geophysical data interpretation, the streams and torrents were rapidly filled by coarse-grained sediment of 2-13m thickness range, while the highest thickness was detected close to the dam foot. During the second phase of the sediment infill, when the system reached a hydrodynamic balance and fine-grained sediment (lake sediment) was settling, the mean sedimentation rate was estimated at 1.84 cm/yr, while adding a sediment layer of 1.6m maximum. Increased sedimentation rate up to 2cm/yr after 2009 is probably attributed to increased erosion rates due to a major fire that occurred then in the surrounding area. The lake sedimentary unit presents a complex spatial distribution pattern due to the hydrodynamic regime and the various freshwater sources. Delivery of freshwater services highly depends on sustaining adequate storage capacity, hence monitoring and management of the reservoirs are essential for the indefinite operation of this critical infrastructure.

References

Appleby, P. G., & Oldfield, F. (1978). The Calculation of Lead-210 Dates Assuming a Constant Rate of Supply of Unsupported 210Pb to the Sediment. Catena, 5, 1-8. https://doi.org/10.1016/S0341-8162(78)80002-2.

Fakiris, E., Papatheodorou, G., Geraga, M., Ferentinos, G., 2016. An automatic target detection algorithm for swath Sonar backscatter imagery, using image texture and independent component analysis. Remote Sensing 8(5), 373.

Papatheodorou G., Christodoulou D., Fakiris E., Georgiou N., Dimas X., Sergiou S., Geraga M., 2018, Geological, Geomorphological And Sedimentary Exploration of the Bottom And Lake Deposits Of The Artificial Lake Of Marathon. Technical Report submitted to EYDAP, pp.164.

16th INTERNATIONAL CONGRESS of the
GEOLOGICAL SOCIETY OF GREECE

T6. Geochemistry, Mineralogy, Petrology and Volcanology

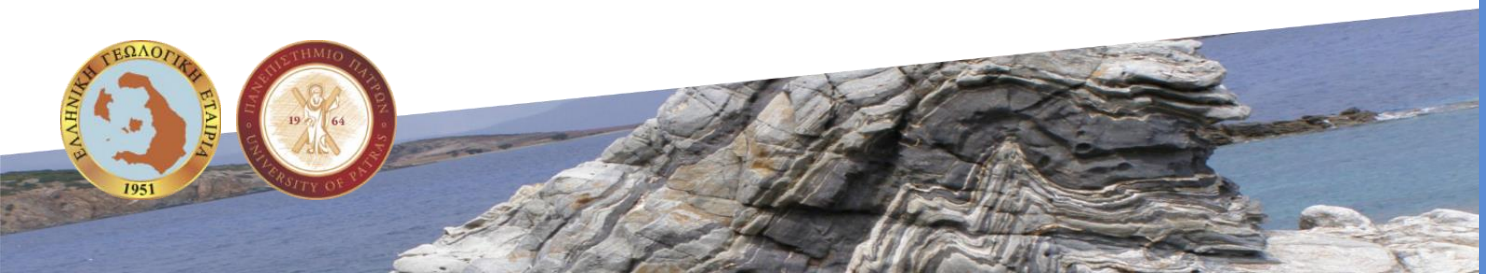

OUR EARTH, OUR HOME

16th International Congress of the Geological Society of Greece

17-19 October, 2022 - Patras, Greece

Bulletin of the Geological Society of Greece, Sp. Publ. 10

Ext. Abs. GSG2022-017

The Polychnitos Ignimbrite and Other MegaCaldera Stories of the Aegean Sea.

M. Kouli[1,2], S. Lamera[3], K.St.Seymour[3] , D. Zouzias[3]

(1) Hellenic Mediterranean University, Institute of Physics of the Earth's Interior & Geohazards, Chania, Greece, mkouli@hmu.gr (2) Mediterranean University, Faculty of Electronic Engineering, Chania, Greece, (3) Patras University, Department of Geology, Patras, Greece.

In a geologist's perception Lesvos represents a superb volcanic field. The volcanic stratigraphy of the island has been pioneered by Pe Piper & Piper (1993), whilst its numerous caldera structures were first identified and reported by Kouli & St.Seymour (2006) (Fig.1). Possible caldera structure in the Gurf of Kalloni agrees with Lamera's (2006) findings about the source of the autochthonous PU member (Fig.2) of the Polychnitos Ignimbrite. More recent work by Ferier *et al.*, (2019), has proposed as caldera-originated structures two features proximal to the Agra caldera (Fig.1). The largest caldera on Lesvos exists in its western half, the 25km Sigri Caldera (Fig.1). This extensive structure is responsible for the cataclysmic deposition of the Sigri Pyroclastics that cover most of the renown Lithified Forest with petrified tree trunks even up to 30m long. Remnant Sigri Caldera features in the field constitute the flat caldera floor, the western caldera wall, with the town of Antissa amphitheatrically exposed on it and the huge megabreccia of the breached western caldera wall, clearly visible from the autoroute. The more salient features establishing the Sigri and other Lesvos calderas were accomplished by Kouli (2004) using satellite imagery. Lamera (2006) has established two main autochthonous ignimbrite sheets (PU and MGF I,II, III) and three allochthon units (Fig.2) using volcanological field methods of detailed mapping and measuring the dimensions of pumices and lithic fragments. The most extensive autochthonous (source-wise) ignimbrite sheets of Lesvos are: (1) the Purple Ignimbrite (PU) and (2) the MegaFiamma Ignimnrite (MGF I, II, III) (Fig.2). Allochthon units include: (3) the Pink Ignimbrite (PI), (4) the Gray Ignimbrite (GI) and (5) the White Ignimbrite (WI). As for the Basal Breccia to the autochthonous ignimbrite sheets most probably represent a Lahar Unit (6). The Quarry Ignimbrite (ZV) (7) overlies all other ignimbrite sheets (Fig.2) and has an allochthon origin. The **Purple Ignimbrite (PU)** is characterized by black, intensely welded, long fiammae of isotropic glass with flame-like endings. The fiammae have length of several cm (near its source of Kalloni Bay) down to a few mm. The lithics of PU are rounded fragments of lavas and peridotite i.e. the basement of which the PU has flown. The color of PU is purple to gray. It displays columnar jointing and a base that looks like black obsidian glass, features that advocate emplacement at high temperatures. The base of the PU is enriched in lithics. The **Megafiamma (MGF) I, II & III Ignimbrite** is a unit of high density and hardness, of pink-mauve color which consists of 3 cooling units which represent the emptying of a layered magma chamber, successively emplaced and cooled together. Their source is the Stipsi caldera (Fig.1). The unit is characterized by fiammae of large size which have not been intensely welded. The larger fiammae belong to the upper member i.e. MGF III. The unit displays cooling diaclases and remnant chimneys of loss of gasses. The size of lithics increases in the lower units. The base of the MGF Ignimbrite consists of black glass and red fiammae and is thought to represent the base of the unit which has been subjected to intense welding.

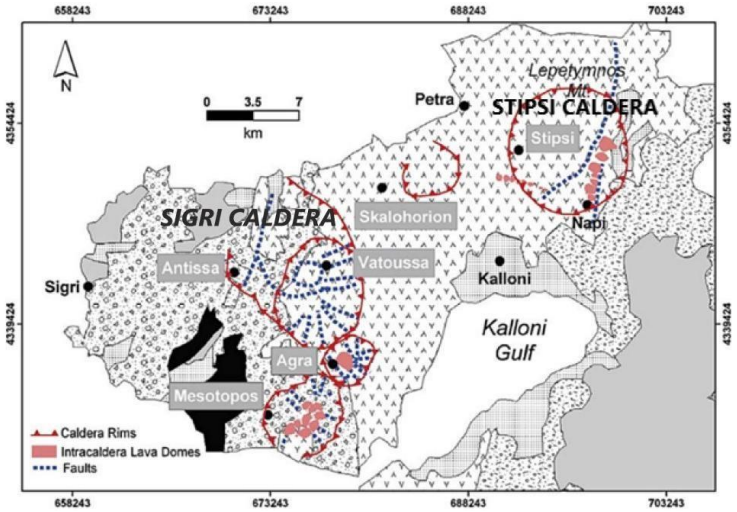

Figure 1. Integration of the calderas located on the Lesvos volcanic field into the geological context of the island (adopted

from Kouli & St.Seymour, 2006).

ZV	QUARRY IGNIMBRITE
MGF III	MEGAFIAMMA IGNIMBRITE III
MGF II	MEGAFIAMMA IGNIMBRITE II
MGF I	MEGAFIAMMA IGNIMBRITE I
PU	PURPLE IGNIMBRITE
PI	PINK IGNIMBRITE
GR	GRAY IGNIMBRITE
WH	WHITE IGNIMBRITE
BR	BASAL BRECCIA

Figure 2. Stratigraphic column of Polychnitos ignimbrite.

Other **Megacalderas in the Aegean** are the Kos Megacaldera between Kos and Nisyros (Fig.3a) and the Apollonia (Saraceneco) Megacaldera in the Northern shore of Milos (Fig.3b).

The **Kos Megacaldera** (Zouzias *et al.*, 2011) has a 20 km maximum axis and is the source of the Kos Plateau Tuff dated 160,000 years.

In **Milos**, 3 caldera structures successively open from the open sea towards and including the Gulf of Adamas (Fig.3b). However, the northern shore of Milos is occupied by the Apollonia or Saraceneco Megacaldera structure visible clearly by satellite imagery. This caldera includes also the western shore of Kimolos (Fig.3b). "Mushroom" structures with a stem of felsic tuff with an umbrella of meter-long unwelded felsic pumice fragment on top decorate the shores of this Megacaldera on Milos and also on Kimolos testifying events of cataclysmic explosive activity. Further research should investigate if the mega pumice accumulating Fyriplaka originates from Saraceneco caldera. A thermal contact zone of a few centimeters testifies the effect of hot pumice emplaced on the tuff. In the western part of this caldera a package of tuff-derived sedimentary rocks display microfaults rather attributed to microseismic activity in the caldera area (Zelelidis, personal communication).

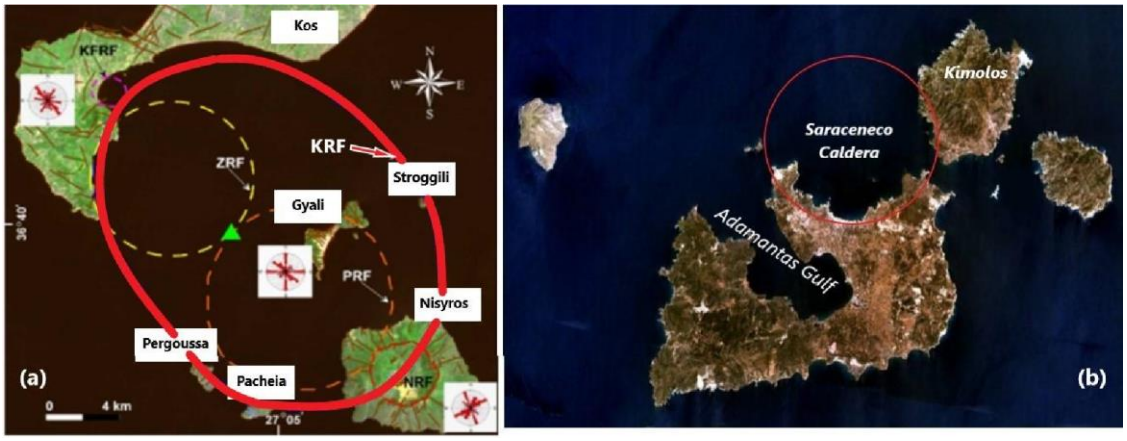

Figure 3. Other Megacalderas in the Aegean: **(a) the Kos Megacaldera between Kos and Nisyros (KRF: The radial fault of the Kos Megacaldera. The dashed circles indicate other radial faults), (b) the Apollonia or Saraceneco Megacaldera in Milos.**

References

Ferrier, G., Ganas, A., Pope, R., 2019. Prospectivity mapping for high sulfidation epithermal porphyry deposits using an integrated compositional and topographic remote sensing dataset. Ore Geology Reviews, 107, pp 353-363.

Kouli, M., 2004. Application of Modern Technology to the Solution of Volcanological Problems: I. Use of NDIC to Compare Magma Mixing Plg Textures from the Volcanoes of Teide and Lesvos, II. Identification of Volcanic Structures with the Use of Remote Sensing Technique. Ph.D. Thesis, University of Patras, Patras, pp 453.

Kouli, M., St. Seymour, K., 2006. Contribution of remote sensing techniques to the identification and characterization of Miocene calderas, Lesvos Island, Aegean Sea, Hellas. Geomorphology 77, 1-16.

Lamera, S., 2006. The Polychnitos Ignimbrite of Lesvos Island, Ph.D. Thesis, University of Patras, Patras, pp 272.

Pe-Piper, G., Piper, D.J.W., 1993. Revised stratigraphy of the Miocene volcanic rocks of Lesvos, Greece. N. Jb. Geol. Paläont. Mh, H2, pp. 97-110.

Plimer, I., 2000. Milos Geological History, KOAN Publishing House, Athens, pp.262.

Zouzias, D., Miliaresis, G., St. Seymour, K., 2011. Interpretation of Nisyros volcanic terrain using land surface parameters generated from the ASTER Global Digital Elevation Model. Journal of Volcanology and Geothermal Research, 200, pp 159-170.

16th International Congress of the Geological Society of Greece
17-19 October, 2022 - Patras, Greece
Bulletin of the Geological Society of Greece, Sp. Publ. 10
Ext. Abs. GSG2022-023

Magmatic and late-magmatic geochemical modifications within an evolving geodynamic environment: The case of the Jerissos granites, Macedonia, Greece

C. Vasilatos[1], A. Papoutsa[1], C. Stouraiti[1]

(1) Department of Geology and Geoenvironment, National and Kapodistrian University of Athens, Athens, Greece, vasilatos@geol.uoa.gr.

Introduction and Objectives

Granitoid rocks comprise the dominant igneous lithology of the continental crust and therefore their geochemistry has been extensively utilized to decipher the geodynamic evolution in their respective geological province. Several classification schemes categorize these rocks based on their major and trace element compositions (Pearce et *al*. 1989; Maniar and Picolli, 1989). While these classification systems should be used with caution in cases where post-magmatic processes have affected the whole-rock composition, it is less clear how magmatic processes may affect the geodynamic classification of these rocks.

The Jerissos pluton in Northern Greece is a Tertiary (45-55 Ma) subduction-related, granitic pluton, that intrudes paragneisses of the Vertiskos Formation and metabasites of the Therma-Volvi-Gomati (TVG) Complex, (Plougarlis et *al*., 2021; Frei, 1996; Vasilatos, 2013). The pluton presents a geochemical inhomogeneity, interpreted to reflect different evolutional stages during a shift from syn-orogenic to post-orogenic settings (Vasilatos, 2013). The purpose of this study is to investigate geochemical characteristics that are widely used in the geodynamic classification of granitoids and determine whether they may also result from specific magmatic processes.

Mineralogy and Geochemistry of Jerissos granites

Mineralogically, the Jerissos granites are divided into three main groups: a) a two-mica granite with residual amphibole (Group 1), b) a two-mica granite with no amphibole (Group 2), and c) a muscovite granite (Group 3). All granites are coarse to medium-grained rocks with equigranular texture. In groups 1 and 3 plagioclase dominates over alkali feldspar, whereas in Group 2 plagioclase is lesser. K-feldspar is found, locally, as large crystals with inclusions of partially dissolved plagioclase, however, all feldspars appear homogeneous and lack zoning. Biotite and muscovite occur as homogeneous, idiomorphic crystals, and in Group 1, biotite replaces residual amphibole. Alteration in these rocks is limited and is expressed by chloritization in biotite and saussuritization of feldspars.

All granites are weakly peraluminous, with groups 2 and 3 being alkali-calcic, and ferroan, whereas Group 1 presents calc-alkalic, magnesian affinities. There are distinct differences in the trace element spider diagrams, between these three groups (Fig. 1A). Groups 1 and 2 present a distinct pattern that differs from Group 3. Group 3 has pronounced negative anomalies in Ba, Sr, P, and Ti. Groups 1 and 2, on the other hand, have weak negative Ba anomaly, and have positive Sr anomalies. For P and Ti, Group 2 deviates from the joint Group 1-2 pattern and shows negative anomalies as in Group 3. In the source classification of Laurent et al. (2014) the magmatic source of Group 1 appears to be enriched in a high-K mafic component, whereas the other two groups appear to be derived mainly from a tonalitic source (Fig. 1B).

Discussion and Conclusions

Geochemical variations in Ti and Nb are extensively used in tectonic classification diagrams of granitoids. However, the variations in Ti in Jerissos granites also correlate with the replacement of amphibole by biotite. Such replacement has been reported during the formation of anatectic melts from an amphibolitic source and (Carvalho et *al.* 2017). These melts would appear enriched in Ti, CaO and MgO as the granites of Group 1 do. In Jerissos, such an origin for Group 1 granites would be consistent with a) derivation of mid-lower, crustal felsic melt, sourcing possibly from gneisses of Kerdyllion Unit and b) an input from amphibolite-derived partial melts (either those intercalated in Kerdyllion Unit or from the overlying TVG complex upon ascent). However, further interaction of these melts with the upper meta-sedimentary rocks of the Vertiskos formation could result in their enrichment in Al and K, forming Group 2 granites (Fig. 2B). A latemagmatic contamination by a K-rich crustal component affected the crystallization of magmatic biotite and K-feldspar as suggested by the Pb isotopic composition of these minerals (Frei, 1996). The biotite chemistry from groups 1 and 2 is indicative of recalibrated magmatic biotites (Fig. 1A), confirming their late-magmatic origin. Compared to the other two groups, the Group 3 granites are enriched in Nb (Fig. 2B) and have higher Rb/Sr and lower Ba/Rb ratios (Fig. 1C) indicating greater degrees of magmatic differentiation. As such, the relative enrichment in Nb could be consistent with its behavior as an incompatible element.

Thus, the Jerissos pluton is constructed by magmatically modified melts. The distribution of affected trace elements that are used in tectonic classification, such as Ti and Nb does not necessarily reflect a change in regional regime upon granite formation. The case of Jerissos granites demonstrates that besides hydrothermal alteration, in cases where there is

evidence of mixed magmatic sources, trace element tectonic classification should be used with caution.

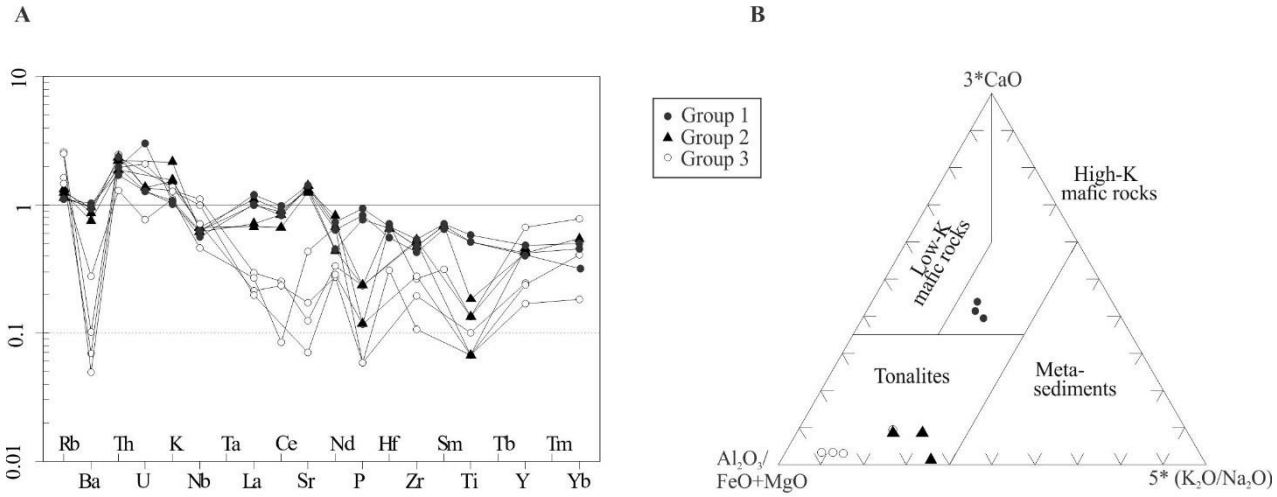

Figure 1. Spider diagram normalized for upper crust (A) and source classification diagram (B) for the Jerissos granites. Fields after Laurent et *al.* (2014).

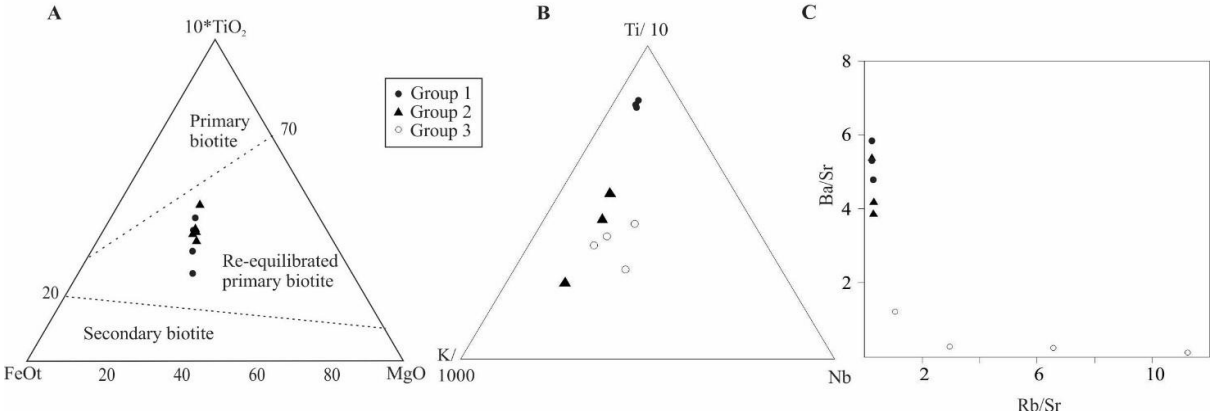

Figure 2. Biotite compositions from Jerissos granites (A), covariation between whole-rock Ti-K-Nb (B), Ba/Rb vs. Rb/Sr ratios. Numerical modifiers are for scaling purposes. Fields in (A) as in Kamali et *al.* 2020.

Acknowledgements

Whole-rock analyses of major and trace elements as well as mineral analyses were conducted in the Department of Geology at the University of Leicester and at NCSR Demokritos Institute of Nuclear Technology and Radiation Protection. National and Kapodistrian University of Athens (Special Account for Research Grands) is kindly thanked for funding the presentation of this work.

References

Carvalho, B.B., Sawyer, E.W., and Janasi, V.A., 2017. Enhancing Maficity of Granitic Magma during Anatexis: Entrainment of Infertile Mafic Lithologies. Journal of Petrology 58, 1333-1362.

Frei, R., 1996. The extent of inter-mineral isotope equilibrium: a systematic bulk U-Pb and step-leach Pb isotope study of individual phases from the Tertiary granite of Jerisssos (Northern Greece). European Journal of Mineralogy 8, 1175-1189.

Kamali, A.A., Moayyed, M., Amel, N., Mohammad, F., Brenna, M.,Saumur, B.M., and Santos, J.F., 2020. Mineralogy, mineral chemistry and thermobarometry of post-mineralization dykes of the Sungun Cu–Mo porphyry deposit (Northwest Iran). Open Geosciences 12, 764-790.

Laurent, O., Martin, H., Moyen, J.F., and Ducelance, R., 2014. The diversity and evolution of late-Archean granitoids: Evidence for the onset of "modern-style" plate tectonics between 3.0 and 2.5 Ga. Lithos 205, 208-235.

Maniar, P.D. and Piccoli, P.M., 1989. Tectonic Discrimination of Granitoids. Geological Society of America Bulletin 101, 635-643.

Plougarlis, A., Tranos, M., and Papadopoulou, L., 2021. The tectonostratigraphic architecture of the Serbo-Macedonian massif in the Vertiskos and Kerdilion mountains (Northern Greece). Bulletin of the Geological Society of Greece 57, 1–22.

Pearce, J.A., Harris, N.B.W, and Tindle, A.G., 1984. Trace element discrimination diagrams for the tectonic interpretation of granitic rocks. Journal of Petrology 25m 956-983.

Vasilatos, C., 2013. A Comparative study in the geochemistry of the trace and the Rare Earth Elements in Tertiary granites in central Macedonia, related or not, with known mineralizations- Definition of the geotectonic environment for the granites' genesis. Department of Geology and Geoenvironment, Ph.D. Thesis 474 p., National and Kapodistrian University of Athens.

16th International Congress of the Geological Society of Greece
17-19 October, 2022 - Patras, Greece
Bulletin of the Geological Society of Greece, Sp. Publ. 10
Ext. Abs. GSG2022-049

A Comparative Study of Oral Bioaccessibility of potentially toxic elements in soil and house dust from the urban environments of Athens and Volos

Evangelia Sigala[1], Efstratios Kelepertzis[1]

(1) National and Kapodistrian University of Athens, Department of Geology and Geoenvironment, Panepistimiopolis, Zografou 15784, Athens, Greece, euaggelia.sigala@gmail.com, kelepert@geol.uoa.gr

Research Highlights

- The source (industrial/traffic emissions) may determine the oral bioaccessibility of anthropogenic Pb and Zn in urban soil and house dust material.
- House dust exhibit high PTEs bioaccessibilities (%) irrespective of the source of PTEs in the two areas (Athens and Volos).

Soil contamination in urban and industrial areas is a significant environmental problem worldwide. In such environments, potentially toxic elements (PTEs) have been used as tracers of anthropogenic contamination. (Luo et al., 2012) Particularly, urban soil is a complex component of the urban landscape that is influenced by both natural and anthropogenic factors. A variety of anthropogenic sources including traffic and industrial emissions contribute to the accumulation of PTEs in various environmental materials with different responses to contamination. Moreover, house dust contains PTEs, which are hazardous for human health. Household dust may be defined as fine (≤100 μm), settled or airborne particulate material encountered in the indoor domestic setting. Of all the heterogeneous environmental geosolids, household dust is the most significant in terms of exposure and effects on the general population (Turner, 2011).

Prolonged presence of PTEs in the urban environment can significantly amplify the exposure of the urban population via inhalation, ingestion, and dermal contact. Specifically, PTEs can have long-term and far-reaching health implications via oral bioaccessibility (Wong et al., 2006). Bioaccessibility of an element is defined as the fraction of the element that is soluble in the gastrointestinal or pulmonary environment, representing the maximum amount of contaminant that is available for absorption (USEPA, 2007). A simplified extraction method (SBET) has been applied to several studies, providing useful information on the solubility of PTEs in a medium of composition similar to acidic gastric fluids (Kelepertzis and Argyraki, 2015).

Previous studies regarding the oral bioaccessibility of PTEs in Athens and Volos in soil and house dust samples have been conducted (Kelepertzis et al., 2015; Kelepertzis et al., 2021), but no comparison between the two has been made. This comparison is of great interest, as the concentration of some PTEs (especially Pb, Zn) in each area is principally influenced by different sources, such as vehicle emissions for Athens and industrial emissions for Volos (Kelepertzis and Argyraki, 2015; Kelepertzis et al., 2020), and correlations can be drawn among these sources and the bioaccessibility of PTEs found in these urban environments. In this study, we performed a comparative evaluation of bioaccesibility of PTEs, (Cr, Cu, Mn, Ni, Pb, Zn) in soils and house dust samples from the urban environments of Volos and Athens and the main objective was a discussion concerning the influence of the sources of PTEs on their oral bioaccessibility.

A total number of 10 soils (0-10 cm depth) and 15 house dust samples were selected from the sample data set of an earlier survey in the wider area of Volos. On the other hand, a total number of 33 soils (0-10 cm depth) and 43 samples of house dusts were processed from the area of Athens. The criteria for sample selection were the total content of anthropogenic Pb and Zn as determined by a strong acid dissolution for Volos samples and the highly urbanized samples for Athens. The selected soil samples from both areas were located around the city centers. Laboratory sample preparation included sieving through 2 mm and subsequently 100 μm nylon sieves to focus on bioaccessible particles. Details on sample collection, preparation and analytical methods for the determination of total concentrations of PTEs are described in previous studies (Kelepertzis and Argyraki, 2015; Kelepertzis et al., 2020). The oral bioaccessibility of PTEs was determined by using a 0.4 M glycine extraction solution (adjusted to pH 1.5 with concentrated HCl), simulating the low pH conditions of the human gastric fluids (USEPA, 2013: Method 1340). Procedural blanks, Certified Reference Materials (CRMs) and analytical duplicates were added for quality control purposes. Details for the analytical procedure of bioaccessibility assessment following the Simplified Bioaccessibility Extraction Test (SBET) can be found in the studies of Kelepertzis and Argyraki (2015) and Kelepertzis et al. (2021).

The bioaccessible fraction percentage was calculated as follows:

$$\%\ bioaccessibility = \frac{Cbio}{Ctot} \times 100$$

where C_{bio} is the bioaccessible concentration of PTE (in mg/kg), and C_{total} is the total content of PTE (in mg/kg), determined by a strong acid (HNO_3-$HClO_4$-HF) dissolution.

The median bioaccessibility of Pb and of Zn in urban soil in Athens was 63% (range from 32% to 85%) and 34% (range from 4% to 69%), respectively (Fig. 1). The median bioaccessibility of Pb and of Zn in house dust in Athens was 77% for Pb (range from 52% to 100%) and 72% for Zn (range from 44% to 100%). On the other hand, the median bioaccessibility of Pb in urban soils in Volos was 51% (range from 34% to 58%), of Zn was 48% (range from 29% to 64%) and in house dust was 50% for Pb (range from 36% to 72%) and 80% for Zn (range from 56% to 85%). Bioaccessible Pb in soil and house dust in Athens is higher than Volos (Mann Whitney test, $p < 0.05$), so traffic emissions may result to higher Pb bioaccessible amounts compared to the corresponding from industrial emissions in soil and house dust. On the other hand, Zn bioaccessibility in soil and house dust is higher in Volos (Mann Whitney test, $p < 0.05$). Industrial emissions may be more significant for determining Zn bioaccessibility in the two environmental materials. No statistical differences were found for Cu bioaccessibility between the two materials in both areas (Fig. 1), whereas Cr, Ni and Mn bioaccessible amounts were statistically higher (Mann Whitney test, $p < 0.05$) in Athens compared to the corresponding in Volos.

Comparisons among the sampling media showed that the oral bioaccessible fractions of Pb, Mn, Zn, Ni, and Cr were higher in the house dust compared to urban soil (Mann Whitney test, $p < 0.05$), in both Volos and Athens, suggesting the presence of PTEs forms highly soluble in the SBET solution in this sampling medium. This happened because, in addition to outdoor sources, PTEs in house dusts may derive from various indoor activities, such as smoking, cooking, domestic heating, wall paints, and decorative materials.

Conclusively, the sources of Pb and Zn may have a dominant influence on their bioaccessiblity in both soil and hou se dust materials. Industrial emissions from the steel plant in Volos could result to higher Zn bioaccessible amounts; on the other hand, vehicular emissions in the more urbanized area of Athens could be responsible for the higher Pb bioaccessibility compared to industrially-derived Pb. Such variability should be the result of the different response of Pb and Zn-related sources to the simulated gastric solution. Moreover, house dust material from both Athens and Volos exhibited higher PTEs bioaccessibilities (%) in relation to those measured in soils, regardless of the source of PTEs, confirming the importance of this sampling medium in terms of human exposure to PTEs.

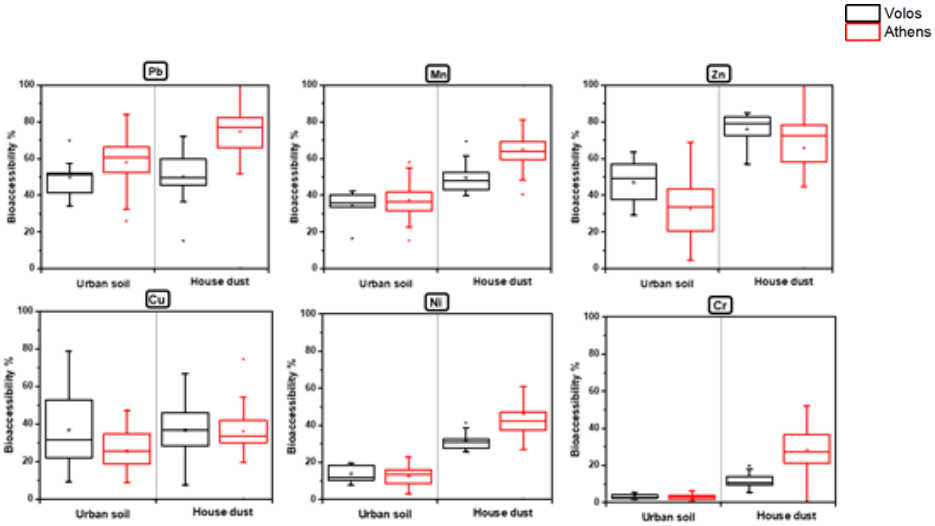

Figure 1: Bioaccessibility results of PTEs for the soil and house dust samples from the urban areas of Volos and Athens.

References

Huang, M., Wang, W., Chan, C.Y., Cheung, K.C., Man, Y.B., Wang, X., Wong, M.H., 2014. Contamination and risk assessment (based on bioaccessibility via ingestion and inhalation) of metal(loid)s in outdoor and indoor particles from urban centers of Guangzhou, China. Science of the Total Environment 479-480, 117-124.

Kelepertzis, E., Argyraki, A., 2015. Geochemical associations for evaluating the availability of potentially harmful elements in urban soils: lessons learnt from Athens. Appl. Geochem. 59, 63–73.

Kelepertzis, E., Argyraki A., Botsou F., Aidona, E., Szab, A., Szab, C., 2019. Tracking the occurrence of anthropogenic magnetic particles and potentially toxic elements (PTEs) in house dust using magnetic and geochemical analyses. Environmental Pollution 245, 909–920.

Kelepertzis, E., Argyraki, A., Chrastný, V., Botsou, F., Skordas, K., Komárek, M., Fouskas, A., 2020. Metal(loid) and isotopic tracing of Pb in soils, road and house dusts from the industrial area of Volos (central Greece). Sci. Total Environ. 725, 138300.

Kelepertzis, E., Chrastný, V., Botsou, F., Sigala, E., Kypritidou, Z., Komárek, M., Skordas, K., Argyraki, A., 2021. Tracing the sources of bioaccessiblemetal(loid)s in urban environments: A multidisciplinary approach. Science of the Total Environment 771, 144827.

Luo, X-s., Yu, S., Zhu, Y-g., Li, X-d., 2012. Trace metal contamination in urban soils of China. Science of the Total Environment, 421-422, 17-30.

Turner, A., 2011. Oral bioaccessibility of trace metals in household dust: a review. Environ Geochem Health (2011) 33:331–341.

USEPA, 2007. Framework for Metals Risk Assessment (EPA 120/R-07/001).

USEPA, 2013: Method 1340. In vitro bioaccessibility assay for lead in soil. SW-846 hazardous waste test methods.

Wong, C., Li, X., Thornton, I., 2006. Urban environmental geochemistry of trace metals. Environmental Pollution 142, 1–16.

16th International Congress of the Geological Society of Greece
17-19 October, 2022 - Patras, Greece
Bulletin of the Geological Society of Greece, Sp. Publ. 10
Ext. Abs. GSG2022-052

Granite magma genesis and emplacement conditions within evolving metamorphic core complexes: a case study from the Tinos core complex of Cyclades, Central Aegean, Greece

C. Stouraiti[1], A. Papoutsa[1], C. Soukis[1], P. Alvanos[1]

(1) Faculty of Geology and Geoenvironment, National and Kapodistrian University of Athens, Greece, chstouraiti@geol.uoa.gr.

In Miocene, the Aegean region experienced rapid N-S crustal extension, accommodated by a series of large-scale detachments, namely the North Cycladic Detachment System (NCDS), and the West Cycladic Detachment System (WCDS) (Brun and Sokoutis, 2010; Bargnesi et al. 2013). This extensional event has been associated with subduction zone retreat and led to the exhumation of the Cycladic metamorphic core complexes (MCCs), decompression and partial melting of the middle and lower crust (Stouraiti et al. 2010; Rabillard *et al*. 2018). As a result, several MCCs in Cyclades are intruded by syn-kinematic intrusions. It is noteworthy, that although P-T conditions have been studied in the metamorphic rocks (Lamont *et al*., 2020), thermobarometric estimations are currently lacking for the Miocene plutons. Thus, the purpose of this study is to employ empirical thermobarometers and investigate the intensive parameters of magma genesis, emplacement conditions and potential sources of the Tinos granites and correlate them to the MCC evolution.

The tectonostratigraphy of Tinos comprises an upper unit (UU) and a lower unit that are separated by Tinos Detachment (Jolivet *et al*., 2010) overlying a lowermost, Pre-Alpine basement consisting of para- and orthogneisses (Bargnesi *et al*., 2013). The LU corresponds to the Cycladic Blueschist Unit (CBU) and consists of meta-sedimentary and meta-volcanic rocks metamorphosed up to the eclogite facies, and later retrogressed to blueschist and finally to the greenschist facies. The UU comprises (meta-)ophiolitic rocks, rare gabbros, and widespread intermediate-basic volcanics and mica-rich phyllites, weakly metamorphosed, at greenschist facies with no evidence of high-pressure metamorphism. The NE part of the metamorphic dome is intruded by a weakly metaluminous I-type, Bio-Hbl granite, surrounded by smaller bodies of peraluminous (Fig. 1A) Kfs- Grn-bearing S-type granites. Zircon U-Pb dating indicates that the two different types of granitoids were synchronous, i.e., 14.73 ± 0.22 Ma and 14.4 ± 0.2 Ma for I-type and S-type, respectively (Bolhar *et al*. 2010). The applied geothermometers, geobarometers and hygrometers (Anderson et al. 2008, and references therein) indicate that the I-type granites crystallized under higher temperatures, whereas crystallization pressures are within the same range for both types (Table 1). Although the S-type melt appears more hydrous than the I-type melt, both compositions indicate H_2O-undersaturated conditions, compatible with dehydration melting. These empirical observations are consistent with the geochemistry of these granites, suggesting a derivation through dehydration melting of Bio-Ms schist for the S-type and Bio-gneiss/amphibolite for the I-type granites (Fig. 1C). I-type granites appear enriched in Zr possibly associated with higher magmatic temperatures and with their metaluminous affinity that enhances the solubility of Zr, in contrast to peraluminous melts.

Upper-crust normalized compositions of the I-type granites point to a metasedimentary source (Fig. 1B), with mild negative Ba anomalies, and mildly positive- to no-anomaly in Sr suggesting presence of plagioclase in the source rock. The S-type granites, on the other hand, have pronounced negative Ba and Sr anomalies and high Rb/Sr. The Rb-Sr concentrations in Tinos granites appear to have been controlled by the dehydration melting of predominately muscovite and biotite for the I-type and S-type melts, respectively (Fig. 1D). For the S-type granites this is consistent with the dehydration melting reaction: Bt+Plg+Als+Qz= Grn+Kfs+Melt at ~ 5.5 kbar (Weinberg and Hasalová, 2015, and references therein), as also indicated by the Grn-Bio-Plg barometer (Table 1). Peritectic garnet has been found in the Tinos S-type granites showing resorption features and containing inclusions of quartz, K-feldspar and melt. The melt inclusion is enriched in K_2O (4 wt.%) suggesting a reaction with a K-enriched melt, presumably formed due to the consumption of biotite in the host rock. Biotite-dehydration melting triggers a strong increase in the Rb/Sr ratio with little effect on either Ba or Sr, since these are hosted mainly in plagioclase (Fig. 1D) (Weinberg and Hasalova 2015).

The assemblage of biotite gneisses and amphibolites, potential source rocks of the I-type melt, correlates with the ortho, para-gneisses and amphibolites of the Pre-Alpine basement. The similarity in crystallization pressures of the S- and Itype granites could imply that crystallization occurred at the structural level of emplacement along with the S-type magma, and therefore its ascent was probably rather rapid and at high temperatures. This could be due to a lower viscosity resulting from its drier and high-T nature, and from rapid crustal extension and uplift during MCC exhumation. Thus, it is postulated that elevated temperatures at the lower crust during crustal extension and probably asthenospheric upwelling, resulted in the dehydration melting of the Pre-Alpine basement, producing the I-type melt. The ongoing crustal thinning and the lower melt viscosity enhanced magma ascent and resulted in a rapid emplacement at the middle crust, within the CBU unit. The thermal anomaly produced by the trapped I-type melt, initiated partial melting of the surrounding rocks, producing bodies of S-type granites that crystallized at the same crustal level, peripheral to the I-type granite.

Table 1: Summary of P-T and water estimates for the Tinos granites

Granitic Type	Magmatic Temperatures (C°)				P estimates (kbar)		Magmatic water (wt.%)
I-type	**Plg-melt**	**Zr-sat.**	**Plg-Hbl**	**Ti-in-Bio**	**Al-in-Hbl**	**Plg-Hbl**	**Plg-melt**
	1030-1060	700-750	520-732	590-670	3.2-6.8	3.1-5.9	1.8-3.3
S-type	**Plg-melt**	**Zr-sat.**	**Ti-in-Bio**		**Grn-Bio-Plg**		**Plg-melt**
	943-955	560-680	537-730		5.6		3.3-3.7

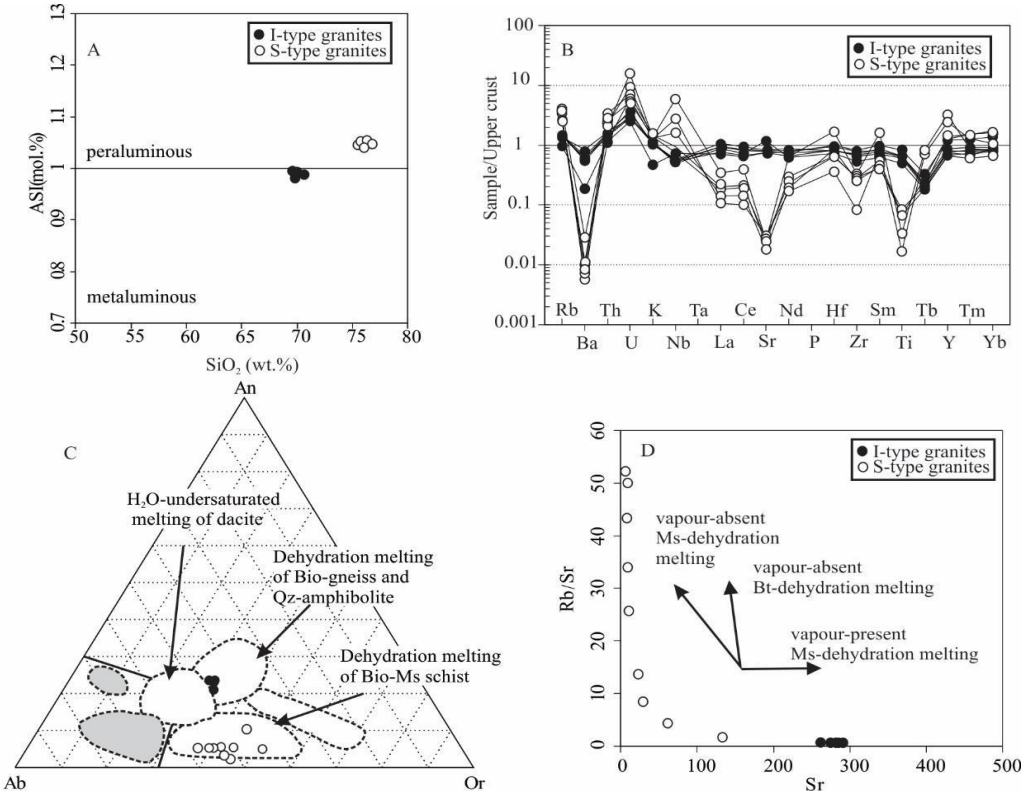

Figure 1: A: Aluminum Saturation Index classification of Tinos granites, B: upper crust-normalized spider diagram, C: normative Ab-An-Or diagram, D: Rb/Sr vs. Sr diagram (Weinberg and Hasalová, 2015 and references therein).

Acknowledgements

The Authors are grateful to the American School of Classical Studies in Athens for their assistance during SEM-EDS analyses.

References

Anderson, J.L., Barth, A.P., Wooden, J.L, Mazdab, F., 2008. Thermometers and Thermobarometers in Granitic Systems. Reviews in Mineralogy and Geochemistry 69, 121-142.

Bargnesi, E.A., Stockli, D.F., Mancktelow, N., Soukis, K., 2013. Miocene core complex development and coeval supradetachment basin evolution of Paros, Greece, insights from (U–Th)/He thermochronometry. Tectonophysics 595-596, 165–182.

Bolhar, R., Ring, U.,Allen, C.M., 2010. An integrated zircon geochronological and geochemical investigation into the Miocene plutonic evolution of the Cyclades, Aegean Sea, Greece: Part 1: Geochronology: Contributions to Mineralogy and Petrology, 160, 719–742.

Brun, J.P., Sokoutis, D., 2010. 45 m.y. of Aegean crust and mantle flow driven by trench retreat. Geology 38, 815–818.

Jolivet, L., Lecomte, E., Huet, B., Denèle, Y., Lacombe, O., Labrousse, L., Le Pourhiet, L., and Mehl, C., 2010. The North Cycladic Detachment System: Earth and Planetary Science Letters, 289, p. 87–104.

Lamont, T.N., Searle, M.P., Gopon, P., Roberts, N.M.W., Wade, J., Palin, R M., Waters, D. J., 2020. The Cycladic Blueschist Unit on Tinos, Greece: Cold NE subduction and SW directed extrusion of the Cycladic continental margin under the Tsiknias Ophiolite. Tectonics, 39, e2019TC005890. doi.org/10.1029/2019TC005890

Stouraiti, C., Mitropoulos, P., Tarney, J., Barreiro, B., McGrath, A.M., Baltatzis, E., 2010. Geochemistry and petrogenesis of late Miocene granitoids, Cyclades, southern Aegean: Nature of source components. Lithos 114, 337-352. doi.org/10.1016/j.lithos.2009.09.010

Rabillard, A., Jolivet, L., Arbaret, L., Bessière, E., Laurent, V., Menant, A., Augier, R., Beaudoin, A., 2018. Synextensional Granitoids and Detachment Systems Within Cycladic Metamorphic Core Complexes (Aegean Sea, Greece): Toward a Regional Tectonomagmatic Model. Tectonics 37, 2328–2362.

Weinberg, R.F., Hasalová, P., 2015. Water-fluxed melting of the continental crust: A review. Lithos 212-215, 158-188.

16th International Congress of the Geological Society of Greece
17-19 October, 2022 - Patras, Greece
Bulletin of the Geological Society of Greece, Sp. Publ. 10
Ext. Abs. GSG2022-066

Mineralogical characterization of Brochantite from Kimmeria, Xanthi, N. Greece.

M. Nikopoulou[1], T. Zorba[2], L. Papadopoulou[1], V. Melfos[1], N. Kantiranis[1]

(1) Department of Mineralogy, Petrology, Economic Geology, School of Geology, Aristotle University of Thessaloniki, 54124, Thessaloniki, Greece, e-mail: marthonik@geo.auth.gr (2) Department of Solid State Physics, Faculty of Physics, Aristotle University of Thessaloniki, 52124 Thessaloniki, Greece.

Introduction

The present study has been carried out to determine the mineralogical and chemical characteristics of brochantite from the contact metamorphic aureole of the Xanthi pluton, in Kimmeria, N. Greece. Brochantite is a secondary copper hydrous sulphate mineral with the following chemical formula: $Cu_4(SO_4)(OH)_6$ (Helliwel & Smith, 1997), and it is characterized by an intensely deep emerald-green color. It is found in metamorphic deposits and may be observed as pseudomorphs of malachite (Schmidt & Lutz, 1992) while it can be altered to chrysocolla. Brochantite crystallizes in the monoclinic crystal system (Merlino et al., 2003) and has a hardness between 3.5 and 4 on Mohs scale. Though it is an uncommon mineral, brochantite occurs in numerous places around the world such as USA, Chile and Greece. In Greece it is mostly found in Lavrion-Attiki and Serifos-Cyclades. Brochantite is used as a pigment in various artifacts such as paintings; thus, there is an interest for this material among archeologists and art conservators. Sometimes, it can be used as a decorative gemstone but due to its low hardness it is not suitable for jewelry.

Analytical techniques

In order to determine the mineralogical composition of brochantite from Kimmeria, a polished-thin section was prepared and studied under a light polarizing microscope. Also, a scanning electron microscope (SEM) was used, connected to an energy dispersive spectrometer (EDS). Fourier-transform infrared (FTIR) spectroscopy was also applied to a powdered part of the mineral for a better understanding of its chemical composition and hydrous phase. The chemical composition of the neighboring minerals was identified by SEM-EDS analysis.

Results

Macroscopically, the samples of brochantite are very similar to chrysocolla and other copper bearing minerals (such as malachite, antlerite, chalcocyanite etc.). Brochantite crystals have a bluish-green color with pearly-vitreous luster and forms botryoids (Fig. 1). When cut and polished, brochantite appears as needle-like crystals forming veins. Under plane polarized light (Fig. 2) brochantite shows a pale green color with distinct pleochroism. Under cross-polarized light, radial aggregates of brochantite are observed with second order interference colors. Other minerals that were identified in the thin section are quartz, pyroxene orthoclase and garnet. Mean chemical composition of brochantite was determined at 71.57 wt% CuO and 16.37 wt% SO_3. Pyroxene has a chemical composition of diopside while garnets belong to the grandite group (grossular-andradite series). They exhibit chemical zoning with a composition of grossular 54.84-57.53 mol% in the core, reaching 98.2 mol % of andradite in the rim.

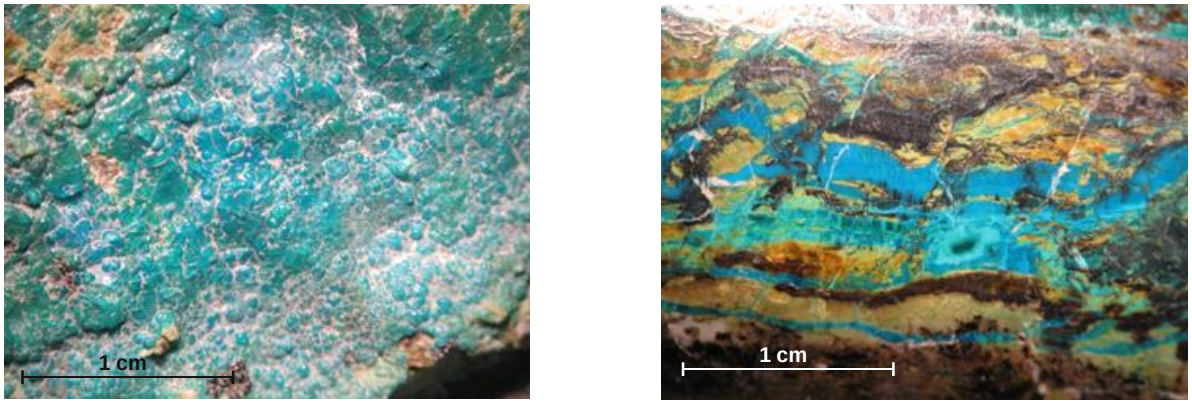

(a) **(b)**

Figure 1. Photos of brochantite samples. (a) Rough sample with botryoid formation and (b) polished section under stereoscope.

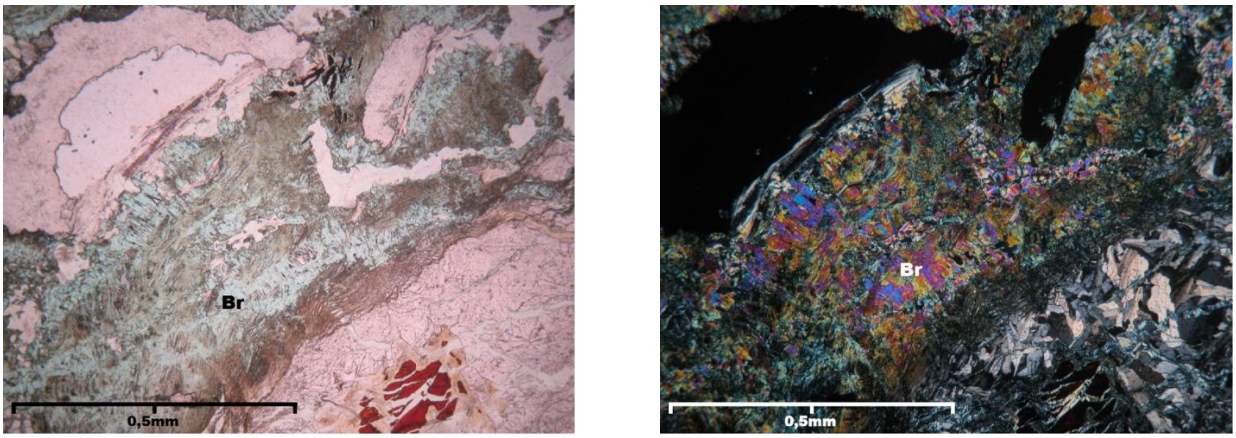

(a) **(b)**

Figure 2. Photomicrographs of brochantite (a) under plane polarized light exhibiting distinct pleochroism and (b) under cross-polarized light displaying radial aggregates and second order interference colors.

FTIR spectrum (Fig. 3) helped to determine the type of the copper sulphate mineral. Absorption double bands at 3587 and 3565 cm^{-1} are due to stretching vibrations of O-H (free hydroxyls). The characteristic band at 1633cm^{-1} confirms the presence of H_2O within the structure. The wide peak between 3410-3360cm^{-1} has secondary absorptions at 3403, 3383, 3369 cm^{-1} which are due to OH groups which form weak hydrogen bonds in the crystal structure. But, rough peak at 3262cm^{-1} is correlated with OH groups which form very strong hydrogen bonds. Further peaks whose presence is due to Cu-O-H vibrations show up at 990 and 943cm^{-1} (strong H-bonded OH), 872 and 849 cm^{-1} (medium H-bonded OH), 780 and 732 cm^{-1} (free OH). Moreover, absorption bands at 1121, 1088, 1040 cm^{-1} are associated with SO_4 vibrations and they are characteristic for brochantite crystals (Secco, 1988; Valdas et al., 2015). According to these results, brochantite is formed as a secondary mineral in the Fe-Cu-Bi-W-Au skarn deposit of the Xanthi pluton.

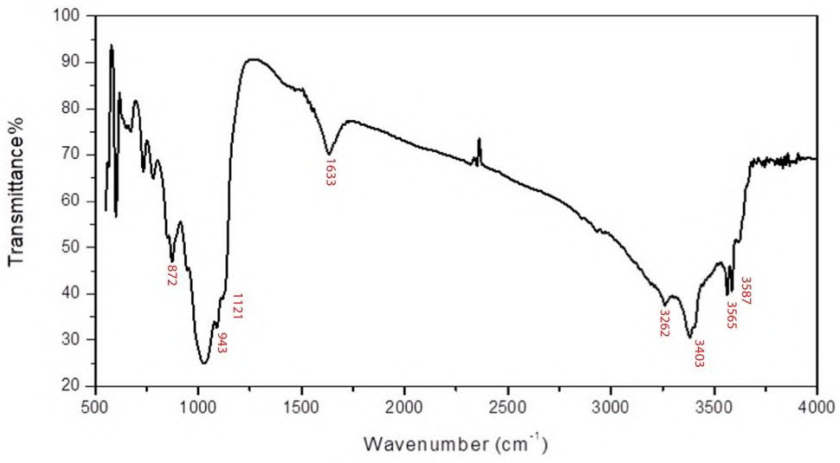

Figure 3. FTIR spectra of brochantite from Kimmeria.

Acknowledgements

The authors wish to thank Geologist N. Kipouros for the preparation of the polished-thin sections. We are also grateful to the mineral collectors Mr. A. Tsinidis and Mr. N. Bacharidis for providing the samples.

References

Helliwell, M., & Smith, J. V., 1997. Brochantite. Acta Crystallographica Section C Crystal Structure Communications, 53(10), 1369–1371.

Merlino, S., Perchiazzi, N., Franco, D., 2003. Brochantite, Cu4SO4(OH)6: OD character, polytypism and crystal structures European, Journal of Mineralogy 15, 267-275.

Schmidt, M. & Lutz, H.D., 1993. Hydrogen bonding in basic copper salts; a spectroscopic study of malachite, Cu2(OH)2CO3, and brochantite, Cu4(OH)6SO4. Phys. Chem. Mineral., 20, 27-32.

Secco, E.A., 1988. Spectroscopic properties of SO4 (and OH) in different molecular and crystalline environments. I. Infrared spectra of Cu4(OH)6SO4, Cu4(OH)4OSO4 and Cu3(OH)4SO4, Can. J. Chem. 66, 329

Valadas, S., Freire, R.V., Cardoso, A., Mirão, J., Dias, C.B., Vandenabeele, P. and Candeias, A., 2015. On the Use of the Unusual Green Pigment Brochantite (Cu4(SO4)(OH)6) in the 16th-Century Portuguese-Flemish Paintings Attributed to The Master Frei Carlos Workshop, Microscopy Society of America, Microsc. Microanal. 21, 518–525.

16th International Congress of the Geological Society of Greece
17-19 October, 2022 - Patras, Greece
Bulletin of the Geological Society of Greece, Sp. Publ. 10
Ext. Abs. GSG2022-067

Mineralogical Study of Blue-Lace Agate from Aetochori-Evros, NE Greece

M. Nikopoulou[1], L. Papadopoulou, V. Melfos, N. Kantiranis

(1) Department of Mineralogy, Petrology, Economic Geology, School of Geology, Aristotle University of Thessaloniki, 54124, Thessaloniki, Greece, e-mail: marthoniki@geo.auth.gr

Introduction

The present study is focused on the mineralogical and chemical characterization of blue-lace agate from Aetochori-Evros in Greece. Agate is a variety of chalcedony with concentrically colored bands (Heaney, 2021). Chalcedony is a microcrystalline type of quartz and according to its color, pattern and optical phenomena it can be categorized in different varieties (jasper, carnelian, agate etc.). Agate responds in a wide range of geological environments thus it is one of the most affordable type of gemstones. It is one of the oldest minerals that have been used by humans since prehistoric times (Lüle, 2021). Blue-lace agate is quite common in Greece and especially in Evros area (Voudouris et al., 2019). One of the most important tasks of this study is the determination of the chromophore element that is responsible for the blue-violet color of blue-lace agates at Aetochori, Evros district. Blue agate occurs in veins cross-cutting dacitic lavas or as loose fragments around the area (Voudouris et al., 2019). According to previous studies, the exact mechanism that gives agates their color has not yet been determined but the most common chromophore elements in agates are Mn and Fe (Michalski & Foord, 2005) in the form of oxides, which are responsible for the sky blue color in combination with Rayleigh scattering phenomenon. Chromophore elements can insert in crystal lattice after the crystallization of agate by the influence of later hydrothermal fluids or water solutions (Wicht & Miller, 2020) rich in Mn and Fe. Colored bands due to high levels of porosity, absorb water and fluids rich in Mn and Fe hydroxides. Milky and colorless bands in agates can be observed due to structural defects and low porosity.

Analytical techniques

Samples of blue-lace agate were observed under stereoscope (ZEISS model Stemi 2000-C). A polished-thin section was prepared, cut perpendicular to the color bands and was studied under the polarizing microscope. Chemical composition of the agate was determined by Scanning Electron Microscopy connected to Energy Dispersive Spectrometer (SEM-EDS, JEOL, JSM-6390LV).

Results

Macroscopically, the samples show alternating bands of different color (blue, violet and white) with conchoidal fracture (Fig. 1). Some zones of the agate are coarse-grained and at the center of the concentric zones large transparent quartz crystals can be observed.

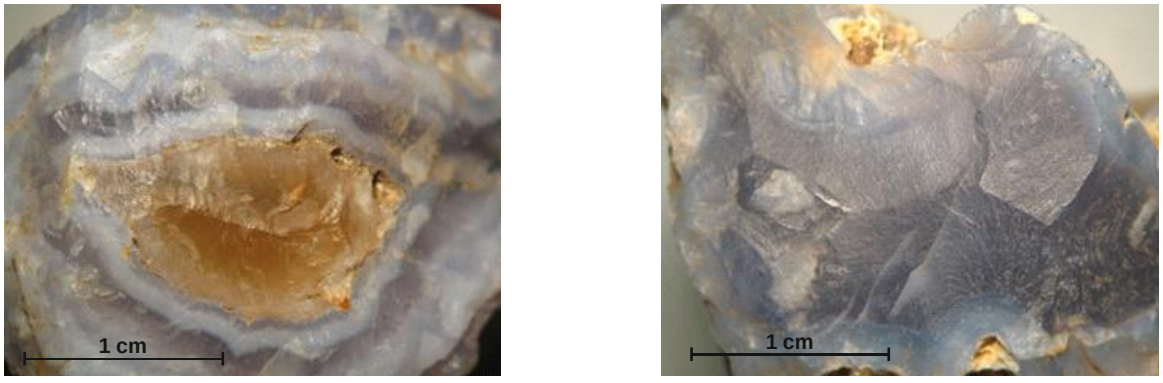

(a) **(b)**

Figure 1. Macroscopic images of blue-lace agate from Aetochori-Evros. (a) Concentric zones of agate around a large transparent quartz crystal, (b) conchoidal fracture of blue-lace agate.

Under cross polarized light, colored bands and quartz crystal layers with low polarizing colors can be distinguished (Fig. 2). Some parts of the thin section with milky-white bands show irregular arrangement of microcrystalline quartz crystals that probably lead to low porosity and eventually, lack of color in these areas. Chemical analyses along a line perpendicular to the agate zones show that there is no significant variation in the chemical composition of the agate zones with the exception of FeO (0.14 - 0.49 wt%), which appears in small but significant amounts in the colored zones of the agate.

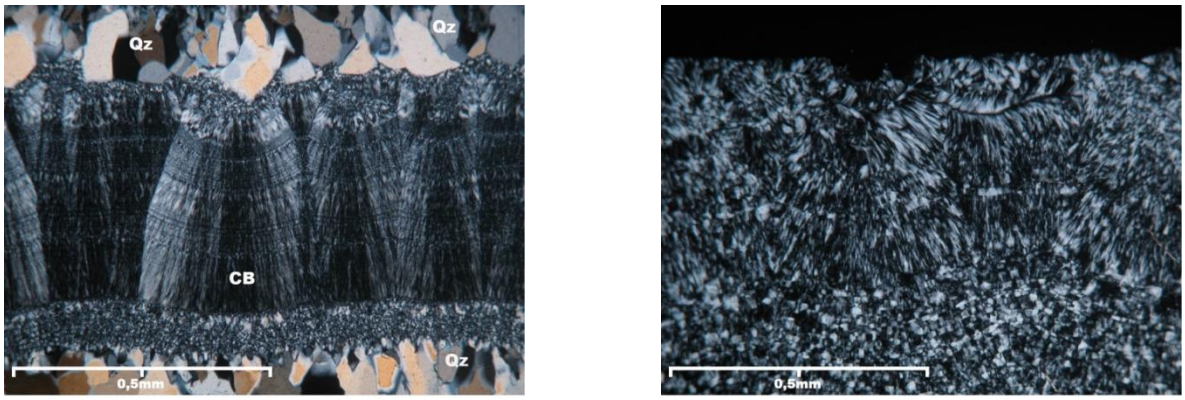

(a) **(b)**

Figure 2. Photomicrographs of blue-lace agate from Aetochori under cross polarized light. (a) Blue-lace agate (CB) between coarse-grained quartz crystals (Qz), (b) irregular arrangement of microcrystalline quartz crystals with low porosity.

The content of MnO is below the detection limit showing that FeO is the main oxide responsible for the sky blue color in combination with Rayleigh scattering phenomenon. Significant presence of other elements is also worth to mention: MgO (0.05-0.12 wt%), Al_2O_3 (0.04-0.32 wt%) and TiO_2 (0.03-0.05 wt%). These elements have no or very little impact on the color of agate (Michalski & Foord, 2005) and they were possibly absorbed by water solutions during weathering processes after the crystallization of the agate.

Acknowledgements

The authors wish to thank Geologist N. Kipouros for the preparation of the thin-polished sections and Mr. N. Baharidis for providing the samples.

References

Heaney P.J., 2021. Iris Agates and Color Dusts: The Textural Complexity of Agates. Seventeenth Annual Sinkankas Symposium – Agate and Chalcedony. Pala International, Inc. Fallbrook, California, United States, 29-39.

Lüle Ç., 2021. From Neolithic to Modern Day. Seventeenth Annual Sinkankas Symposium – Agate and Chalcedony. Pala International, Inc.Fallbrook, California, United States, 51-55.

Michalski T.C., Foord E.E., 2005. Seven Causes of Color in Banded Agates. Symposium on Agate and Cryptocrystalline Quartz, Sponsored by Friends of Mineralogy, Colorado Chapter, Colorado School of Mines Geology Museum, and U.S. Geological Survey, 60-66.

Voudouris P., Mavrogonatos C., Graham I., Giuliani G., Tarantola A., Melfos V., Karampelas S., Katerinopoulos A., Magganas A., 2019. Gemstones of Greece: Geology and Crystallizing Environments. Minerals 2019, 9, 461, 29.

Wicht J., Miller D., 2020. Blue Lace Agate from Ysterputs, Southern Namibia. The Official Newsletter of the Cape Town Gem and Mineral Club. Mineral Chapter, 3-12.

16th International Congress of the Geological Society of Greece

17-19 October, 2022 - Patras, Greece

Bulletin of the Geological Society of Greece, Sp. Publ. 10

Ext. Abs. GSG2022-101

Colour and chemical variations in adamite-olivenite solid solution minerals from the Lavrion mines, Attica, Greece.

C. Mavrogonatos[1], C. Kanellopoulos[1,2], I. Megremi[1], S. Klemme[3], J. Berndt[3], P. Voudouris[1], C. Stouraiti[1], M. Anastasatou[1], I. Iliopoulos[2], V. Xanthopoulou[2].

(1) National and Kapodistrian University of Athens, Athens, Greece, kmavrogon@geol.uoa.gr (2) University of Patras, Patras, Greece (3) Westfälische-Wilhelms Univerität Münster, Munster, Germany

The Lavrion mining district is as world-class site of geological and historical value. In terms of geology, an impressive succession of geodynamic processes i.e., metamorphism, tectonic and magmatic activity, ore-formation, and supergene oxidation, created over time a unique diversity of primary and secondary minerals. Until today, more than 600 minerals have been remarked at the broad Lavreotiki area, corresponding to nearly 12% of all known species (Voudouris *et al.*, 2021, and references therein). Historically, Lavrion comprises one of the most important mining districts on Earth, exhibiting mining works that date back to at least the 3rd millennium B.C. However, it is mostly known for its silver mines that flourished during the classical period (6th-4th centuries B.C.). Among other mineral species, adamite-olivenite solid solution mineral specimens (hereafter "adamite") from Lavrion, are of exceptional quality since they exhibit significant morphological and colour variations. Collectors use several names (e.g., cuproadamite, aluminium-adamite, zincian olivenite, etc.) to describe "adamite" specimens based on colouration and/or crystal habit. However, the terminology used often does not reflect either the chemistry of the specimen, or the official nomenclature. Thus, a proper characterization of "adamite" specimens from Lavrion remains partly inaccurate. Here we present preliminary mineral-chemical data for the Lavrion "adamites" collected by SEM-EDS (HSGME, Athens, Greece) and EPMA (WWU-Institute of Mineralogy, Munster, Germany).

Figure 1. Colourful varieties of adamite group minerals from the Lavrion mines.

Among other arsenates, minerals of the adamite group and especially adamite [$Zn_2(AsO_4)(OH)$] and olivenite [$Cu_2(AsO_4)(OH)$] are scarcely present in oxidation zones of polymetallic deposits (Southwood *et al.*, 2020). Zinc can be completely substituted by Cu, thus forming a solid solution series between the two end-member species. Other impurities commonly comprise Fe, Co and Mn substituting for the cation sites and P replacing As. Recently, zincolivenite was identified as new mineral species with intermediate composition and an ideal Zn:Cu ratio of 1:1, corresponding to a compositional range of [$Cu_{0.5}Zn_{1.5}(AsO_4)(OH)$] to $Cu_{1.5}Zn_{0.5}(AsO_4)(OH)$], (Chukanov *et al.* 2007).

At Lavrion, "adamite" exhibits a significant variety of both crystal habits and colours. It is found in many localities throughout the mining district (e.g., Kamariza, Plaka, Sounion) forming fine, radiating crusts or fan-shaped rosettes, pseudo-octahedral, bow-tie shaped or prismatic crystals, commonly set on a limonitic matrix (Fig. 1). It is commonly associated with other minerals like calcite, aragonite, smithsonite, hemimorphite, zincaluminite, etc., forming very aesthetic specimens. Colours range from various shades of green to blue, colourless, or rarely, black or with a yellowish tint. Traditionally, green-coloured varieties are described as 'cuproadamite" or "cuprian adamite", a term partly applicable to blue-colored varieties as well. Vivid blue crystals are often referred to as "aluminian adamite". Pinkish/purple varieties are extremely rare at Lavrion and are described as "cobaltoan or manganoan adamite". The latter two varieties are not considered in the present study.

Blue crystals correspond to adamite composition (Fig. 2 and 3a-c) with a limited substitution of Zn by Cu (up to 2.73 wt %). No other impurities were found (e.g., Fe, Co, Al, Mn, P are mostly below the detection limit). An increasing Cu

content results in greenish hues: green "adamite" specimens yielded a compositional range covering both fields of zincolivenite and olivenite (Cu content from 26 wt % to 58.16 wt %). None of the green-coloured crystals yielded Cu content lower that 0.5 apfu (Fig 2), at least in the studied specimens. Many analyses cluster around the Zn:Cu ratio of 1:1, corresponding to typical, green-coloured zincolivenite.

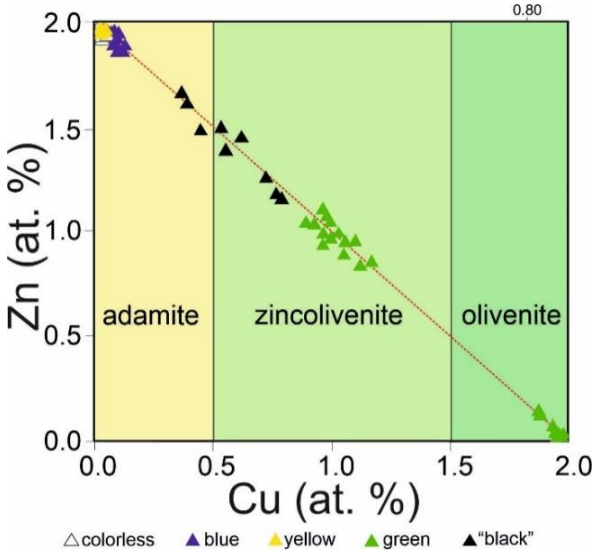

Figure 2. Cu *vesrus* Zn (apfu) classification diagram of analysed "adamite" compositions from the Lavrion mines.

The rare "black adamite" is built of a μm-sized film of colourless to light bluish adamite that grows on top of green zincolivenite (Figs. 2 and 3d-f), thus giving the overall impression of a black tint to the crystals. This adamite carries significantly more Cu (aver. 8.34 wt %) compared to the pure, blue-colored crystals, and evolves into zincolivenite as the Cu content exceeds 0.5 apfu towards the inner part of the crystals. Both yellowish and transparent crystals carry no significant impurities: the analyses plot in the adamite s.s. field and exhibit very minor Cu content (up to 0.30 wt% Cu). Based on EPM analyses, we conclude that adamite s.s. from Lavrion exhibits significant colour variations, from transparent, to yellow, to blue. No green-coloured adamite s.s. was identified in the studied samples. Crystals with green hues cover a significant compositional range from zincolivenite to olivenite. Further study will include other colourful varieties of "adamite" and will also investigate a larger number of trace elements using LA-ICP-MS, to fully define the chromophore elements responsible for the large variation in the colour of the desirable "adamite" specimens from Lavrion and RAMAN spectroscopy for identifying their spectral signature.

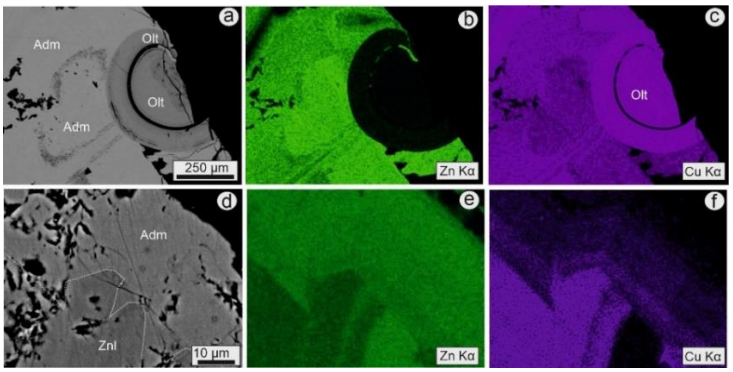

Figure 3. SEM-BSE images and SEM-EDS elemental maps showing the distribution of Zn and Cu in blue- (a-c) and black-colored (d-f) "adamite" specimens. Abbreviations: Adm = adamite; Olt = olivenite; Znl = zincolivenite.

Acknowledgements

Special thanks are due to K. Kapellas and S. Rust for providing material for analyses, Paulos Tsigas for providing photographs 1b and 1d, and B. Schmitte and M. Sakkalis for assisting us with the EPM analyses and SEM-EDS mapping, respectively.

References

Chukanov, N.V., Pushcharovsky, D. Yu., Zubkova, N.V., *et al.*, 2007. Zincolivenite CuZn(AsO4)(OH): A new adamite-group mineral with ordered distribution of Cu and Zn. Dokl. Earth Sc., Vol. 415A, No. 6, 841-845. **[Journal Article]**

Southwood, M., Števko, M., Carr, P., 2020. Tsumeb: Zincolivenite and the Adamite-Olivenite Series. Rocks & Minerals, 95:3, 210-233, doi:10.1080/00357529.2020.1716168. **[Journal Article]**

Voudouris, P., Melfos, M., Mavrogonatos, C., *et al.*, 2021. The Lavrion mines: A unique site of geological and mineralogical heritage. Minerals 11, 76., https://doi.org/10.3390/min11010076. **[Journal Article]**

16th International Congress of the Geological Society of Greece
17-19 October, 2022 - Patras, Greece
Bulletin of the Geological Society of Greece, Sp. Publ. 10
Ext. Abs. GSG2022-102

Morphological Growth Model for Modern Polymetallic and Au-rich CO_2 Diffuser Chimneys from Kolumbo Submarine Volcano, Hellenic Arc: implications for SMS formation

N. Zegkinoglou[1], V. Pletsas[1], S. P. Kilias[1], E. Zygouri[1], M. Keith[2] P. Nomikou[1], P. Polymenakou[3]

(1) National and Kapodistrian University of Athens, Athens, Greece, nikolaoszegkinoglou@yahoo.com (2) Friedrich-Alexander-Universitat (FAU), Erlangen-Nurnberg, Germany (3) Hellenic Centre for Marine Research, Heraklion, Greece

Research Highlights

A new morphological type of polymetallic and Au-rich CO_2 diffuser chimneys is very efficient for the precipitation of Au and the epithermal suite of elements, in shallow-marine arc-related settings.

Background

Studies of seafloor massive sulphide (SMS) hydrothermal precipitates at mid-ocean ridge vent sites, have suggested that chimney morphology and venting style may influence hot vent fluid-seawater mixing, and base, precious and strategic metal precipitation (e.g., Knight et al., 2018; Fouquet et al., 1993). For example, diffuser-type chimneys with "beehive" structures, and a range of venting temperatures from shimmering water to ~350°C black smoker fluid, are closely related to diffuse, low velocity venting, and Au-rich polymetallic SMS deposition (Fouquet et al., 1993; Weber et al., 2017). On the other hand, organ-style chimneys that focus high-temperature (~350–400°C) fluids are less propitious for Au precipitation, because > 90% of their contained metals are lost to the black smoker discharge (Fouquet et al. 1993; Knight et al., 2018). Moreover, submarine arc volcanoes have been found to be venting a free gas phase, composed mainly of CO_2, over a range of depths (Mariana Arc and Tonga-Kermadec Arc), suggesting the importance of magma degassing and metal contribution on hydrothermal systems on volcanic arcs (Lupton et al., 2008). Understanding of any linkage between the internal complex structure and growth morphology, and, the effusive velocity of venting of CO_2 degassing SMS chimneys, and their metal(loid) precipitation, in arc-related hydrothermal vent sites, is still in its infancy. To address this, actively forming, polymetallic and Au-rich SMS samples from diffuser chimneys, emitting shimmering water to ~265°C pure gaseous CO_2 fluid, at the Kolumbo arc-volcano hydrothermal vent field, Greece (Kilias et al. 2022), were mineralogically, geochemically, and texturally examined.

Objective –Research Hypothesis

The main objective of this study is to test the following research hypothesis: low-velocity CO_2 degassing from pumice-hosted, shallow-marine, arc-related hydrothermal vent sites, is likely linked to the formation of "polymetallic and Au-rich CO_2 diffuser chimney, hereafter "Kolumbo diffusers" (KDs), Kolumbo submarine volcano, Hellenic Arc, which do not develop "beehive" structures.

Methods

Reflected and transmitted light microscopy was used to study the sulphide-sulphate mineralogy. The samples were further geochemically and texturally examined using combined FEG-SEM-EDS imaging, EMPA-EDS and LA-ICP-MS spot analyses.

Results

The Kolumbo SMS is enriched in the epithermal suite of volatile elements (Au, Ag, Tl, Sb, Hg, As, Te) (ESVE), base metals (Cu, Pb and Zn), and barite. The sulphide-sulphosalt mineralization consist of pyrite, marcasite, galena, sphalerite, chalcopyrite, (Tl-As-Ag-Mo) Pb-Sb sulphosalts, stibnite, jamesonite, and X-ray amorphous, orpiment- and realgar like As-sulphides, and Fe-(oxy)hydroxides. All sulphide phases are variably enriched in Au and ESVE (Kilias et al., 2022). This study shows that KDs follow a four-stage chimney growth model (see Berkenbosch et al., 2012). The KDs begin with the formation of an initial massive anhydrite mound once hot CO_2-rich hydrothermal fluids mix with seawater. Anhydrite, however, is dissolved during the enduring hydrothermal fluid flow, and replaced by a massive barite wall, that lacks internal conduits and segregates inner hotter vent fluids from seawater. As a result, early colloform pyrite precipitates into the interior barite wall pores. The insulated hot vent fluids form porous channels, via dissolution of the early barite-dominated wall, resulting in an internal complex structure of anastomosing, multiple sulphide-lined conduits, creating a labyrinthine structure with a high proportion of porous channels (Stage 1, Fig. 1). Stage 2 (Fig. 1) is dominated by two highly porous assemblages, consisting of pyrite, sphalerite, Pb-Sb sulphosalts ± galena, and, recrystallized pyrite, marcasite, galena±chalcopyrite, respectively, which precipitate inside the main porous channels. Barite intergrown with pyrite+sphalerite, indicates lower-temperature sulphide precipitation due to fluid-seawater mixing. The lack of barite from the latter assemblage, indicates that some interior conduits gradually lose contact with seawater allowing for the

prevalence of hotter hydrothermal fluids. This labyrinthine chimney structure allows stages 3 and 4 (Fig. 1) to develop. Stage 3 is characterized by the inflow of new hotter vent fluids, which is indicated by the precipitation of chalcopyrite lining some main flow conduits within the porous interior, intergrown with galena, marcasite and lesser sphalerite, which develops at the expense of the early sulphide/sulphate insulating wall that consists of barite, colloform and recrystallized pyrite, Pb-Sb sulfosalts and sphalerite. Stage 4 is characterized by slow diffusion of hot vent fluids through the highly porous axial zone to the top, and laterally to the sides of the chimney, while allowing ingress of seawater to cool the fluid and, synchronous upward advancement of the barite "hot fluid-seawater mixing front", with some lateral growth through the chimney walls, allowing for both upward and outward chimney growth. Thus, the hot hydrothermal fluids can mix with ambient seawater and be cooled to much lower temperatures on the margins of the chimney structure, resulting in a chimney outermost skin consisting of X-ray amorphous orpiment-like As-sulphides, intergrown with stibnite, jamesonite, colloform pyrite and Pb-Sb sulphosalts.

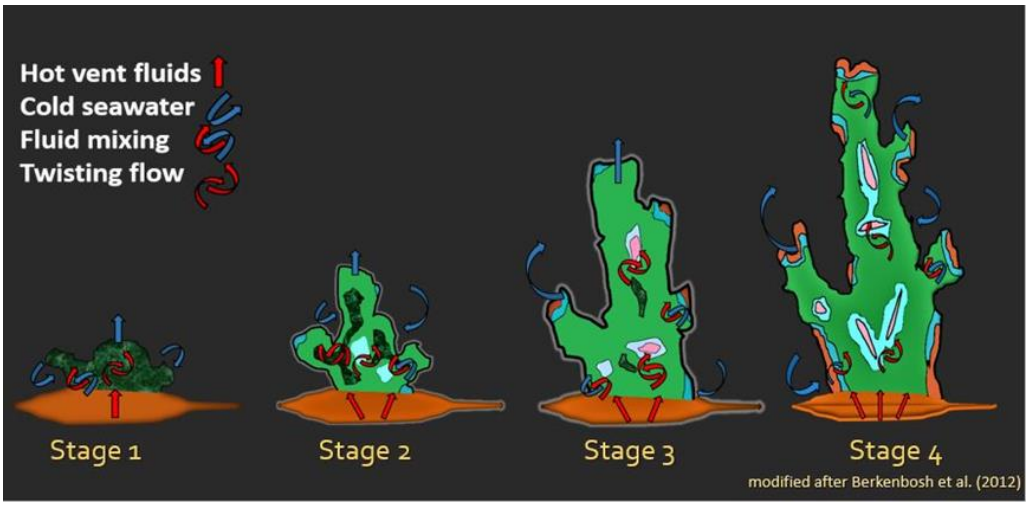

Figure 1. **Four stages model for growth of the modern polymetallic and Au-rich CO_2 diffuser chimneys (KDs), at the Kolumbo hydrothermal vent field. Figure not to scale. Time increases toward the right of the figure (see text for details). Dark green: anhydrite and barite; green: barite, colloform and recrystallized pyrite, sphalerite, Pb-Sb sulphosalts ± galena; light blue: recrystallized pyrite, marcasite, galena ± barite, sphalerite, chalcopyrite; pink: recrystallized pyrite, galena, marcasite, chalcopyrite ± sphalerite; blue: barite, colloform pyrite, Pb-Sb sulphosalts, stibnite, jamesonite ± sphalerite, galena, recrystallized pyrite; brownish orange: barite, colloform pyrite, Pb-Sb sulphosalts, As-sulphides ± stibnite, recrystallized pyrite, sphalerite, galena.**

Conclusions

This complex KD chimney structure is very efficient for the precipitation of Au and the epithermal suite of elements, in shallow-marine arc-related settings. All the aforementioned sulphide/sulphosalt phases, which built the KDs, are variably enriched in invisible Au, and ESVE, therefore, this wide dispersion of Au incorporation in sulphides/sulphosalts could likely be due to the influence of chimney morphology and the venting style.

Acknowledgements

This is part of ongoing international joined research: SANTORY (https://santory.gr/) and IODP PROGRAM EXPEDITION 398.

References

Berkenbosch, H.A., de Ronde, C.E.J., Gemmell, J.B., McNeill, A.W., Goemann, K., 2012. Mineralogy and Formation of Black Smoker Chimneys from Brothers Submarine Volcano, Kermadec Arc. Economic Geology, 107(8): 1613–1633.

Fouquet, Y., Wafik, A., Cambon, P., Mevel, C., Meyer, G., Gente, P., 1993. Tectonic setting and mineralogical and geochemical zonation in the Snake Pit sulfide deposit (Mid-Atlantic Ridge at 23o N). Economic Geology 88, 2018-2036.

Kilias, S.P., Zygouri, E., Zegkinoglou, N., Nomikou, P., Keith, M., Zack, T., Smith, D.J., Polymenakou, P., 2022. Fluid-Mediated Coupled Dissolution-Reprecipitation (CDR) Reaction Drives Gold Remobilization in Shallow-Water Massive Sulfides at the Kolumbo Arc-Volcano, Greece. Proceedings of the 16th SGA Biennial Meeting, Rotorua, New Zealand, 1, 168-171.

Knight, R.D., Roberts, S., Webber, A.P., 2018. The influence of spreading rate, basement composition, fluid chemistry and chimney morphology on the formation of gold-rich SMS deposits at slow and ultraslow mid-ocean ridges. Mineralium Deposita 53, 143-152.

Lupton, J., Lilley, M., Butterfield, D., Evans, L., Embley, R., Massoth, G., Christenson, B., Nakamura, K., Schmidt, M., 2008. Venting of a separate CO_2-rich gas phase from submarine arc volcanoes: Examples from the Mariana and Tonga-Kermadec arcs: Journal of Geophysical Research 113(B8), 8-12.

16th International Congress of the Geological Society of Greece
17-19 October, 2022 - Patras, Greece
Bulletin of the Geological Society of Greece, Sp. Publ. 10
Ext. Abs. GSG2022-106

Assessment of Marl Samples from Kefalonia Island (Western Greece) for their Potential Use in Pelotherapy

E. Sofianska[1], K. Athanassoulis[1], D. Tarenides[1], M. Gkagka[1]

(1) Hellenic Survey of Geology and Mineral Exploration, 1 S. Louis st., 13677, Acharnes, Athens, Greece
eths_n@yahoo.gr

Mud therapy or pelotherapy is the topical application of peloids for medical or cosmetic purposes, and it is known since ancient times (Veniale et al., 2007). These applications are carried out either at natural sites or in thermal centers (SPAs) for the treatment of chronic illnesses, like rheumatism, arthritis, bone-muscle traumatic damages and skin diseases, as local or generalized cataplasms, or in beauty therapy as cosmetic cleaning masks and aesthetic baths (Rebelo et al., 2010).

Peloids are matured muds composed of a complex mixture of fine-grained geological materials, mineral water or sea/lake water and very often organic compounds from biological metabolic activity (Gomes et al., 2013, Maraver et al., 2021). Naturally occurring peloids are rare, but they can be made artificially from their constituents. The growing interest in human health and welfare has increased the scientific investigation on the selection of potentially suitable materials for the formulation of thermal muds to be used in pelotherapy.

The curative efficiency of peloids depends mainly on the grain size, mineralogy, and chemical composition, as well as on some physicochemical properties of the initial geological material (Carretero et al., 2014). Clay mineral constituents in the solid phase of peloids are of great importance, determining properties like absorption of water, cation exchange capacity (CEC), plasticity, and thermal characteristics. With regard to chemical composition, in pelotherapy it is important to know the concentration of elements either beneficial (Ca, Mg, Na, K, Fe among others), or potentially toxic (PTEs, Hg, As, Cu, Cr, Pb, Zn, Co, Ni, Sb, Ba, V, U), since both can pass through the skin of the patient during treatment (Veniale et al., 2007, Carretero et al., 2014).

In the present investigation the texture, mineralogy, chemistry and some physicochemical characteristics of representative marl samples from Kefalonia Island (western Greece) were studied at an effort to evaluate their potential use as row material for peloids in pelotherapy. At the Xi site, a coastal area of Kefalonia Island, marl muds are currently used in pelotherapy, but no detailed data exist on their characteristics.

Six row material samples in this investigation were collected at four beach sites of the south part of the island and specifically, Xi (3 samples, SPXK1, SPXK2, SPXK3), Ai Helis (SPAHK), Paliolinos (SPPK), and Koroni (SPKK).

The analyzed samples belong geologically to Plio-Quaternary sedimentary deposits.

Portions of the samples were used to determine their characteristics following relative ASTM or ISO methodologies. Optical microscopy and X-ray powder diffraction (XRD) analysis ware used for the study of the mineralogical composition of marl samples from Kefalonia. Bulk samples in random aggregates and the separated clay fraction (<2μm) in oriented, glycolized and heated to 550°C samples were used.

Semiquantitative estimates of mineral constituents were obtained from diagnostic basal reflections of the minerals in the difractograms. Final mineral percentages were calculated combining XRD semiquantitative estimates and samples chemistry, following López-Galindo et al. (1996) method.

The major and minor element oxides were determined by X-ray fluorence analysis (XRF), whereas the concentration of trace elements and exchangeable elements during CEC evaluation were determined by inductively couple plasma mass spectrometry (ICP-MS). All the analytical work was conducted at the Laboratories of the Hellenic Survey of Geology and Mineral Exploration (HSGME). Table 1 presents the main characteristics of the studied marl samples from Kefalonia Island.

Results showed that in terms of granulometry Kefalonia marls were characterized as clayey silts with 8.38% sand, 15.97% clay and 75.65% silt on average (Curtis 2005). Best peloids should contain higher percentages of the clay fraction (<2μm). Nevertheless, Spanish peloids (Carretero et al., 2014) and Turkish thermal muds (Karakaya et al., 2010) have similar clay fraction contents and are in use in pelotherapy.

XRD analyses revealed that the principal clay minerals include illite (8-19%), kaolinite (7-10%), chlorite (0-8%) and muscovite (4-9%), while interstratified illite-smectite and smectite are present in some samples. Non clay minerals include quartz (21-37%), carbonates (21-32%), albite (5-9%), and in a few samples traces of gypsum and pyrite.

The chemical composition of Kefalonia marls showed high SiO_2 (39.17-42.43%) and CaO (14.56-25.24%) contents, reflecting the presence of quartz and carbonates, respectively. Microfossil shells contribute part of the carbonate content of the samples. Lower Al_2O_3 (7.14-9.55), followed by Fe_2O_3 (2.73-4.84%), MgO (1.78-4.38%), K_2O (1.24-1.93%) and Na_2O (0.80-1.81%) were found. The most abundant trace elements measured in Kefalonia marls Island were Mn, Sr and

Ba (Table 1). Among the analyzed potentially toxic elements (values in mg/kg) As (5-10), Cd (1-2), Cu (16-26), (Zn 64-175), Ni (105-150) and Cr (90-150) were found to exceed significantly the composition of the Earth's upper crust (Li, 2000). However, many examples of peloids applied in pelotherapy are referred to contain similar or even higher levels of these elements (Quintela et al., 2012, Carretero et all., 2014).

The CEC of the samples investigated are relatively low and were found ranging from 11.09 to 25.72 meq/100g (average 19.65 meq/100g) and reflecting the clay minerals contents. Similar CEC values are, however, referred for Spanish peloids (Pozo et al., 2013). CEC of clay mineral particles affects ion exchange between peloid and the skin of the patient and thus contributes to a cleansing process (Tateo et al., 2009).

The liquid limit values, and the plasticity indices found are low, varying between 28 and 37% (average 31.7%) and 7 to 17% (average 11.5%), respectively, classifying the samples into low plasticity clays in the Casagrande chart. This is probably due to the large number (>58%) of non-clay components and the low clay fraction (9.83-22.94%).

It is worth noting that marl samples from the Xi site have the higher clay size fraction, clay mineral content, plasticity, and CEC, compared to the other sites.

In conclusion, particle size, clay mineral content and chemistry render the investigated marls potentially suitable for use in pelotherapy. However, a sieving process is recommended to enhance the clay-size fraction particles of them and consequently improve their CEC and plasticity. A further investigation is needed to study the technical properties of a derivative peloid formed from the mixture of Kefalonia marls with a medicinal mineralise water or sea water, after a maturation process. Besides, the study of elements bioavailability and their potential enter into the patient's body is more important than their concentration in the peloid constituents.

Table 1. Maine physical and chemical characteristics of the Kefalonia islands marls.

Sample	Particle size (%)			CEC meq/100g	Clay mineral content (%)					Non clay min. (%)	LL (%)	PI (%)
	Sand	Silt	Clay		Ill	Kln	Chl	Smc	Ill/Smc			
SPXK1	2.76	79.90	17.34	23.00	13	8	8	3	-	68	32	12
SPXK2	4.55	72.51	22.94	25.72	19	8	6	-	-	67	37	17
SPXK3	8.38	74.31	17.31	22.49	13	9	6	-	8	64	33	13
SPKK	11.05	73.31	15.64	18.59	8	10	5	-	5	72	28	11
SPPK	10.83	79.84	9.33	17.00	9	7	3	3	2	76	30	7
SPAHK	12.72	74.05	13.23	11.09	8	7	4	5	-	76	30	9
Average	8.38	75.65	15.97	19.65	11.67	8.17	5.33	1.83	2.50	64.17	31.70	11.5

CEC: Cation exchange capacity, Ill: Illite, Kln: Kaolinite, Chl: Chlorite, Ms: Muscovite, Smc: Smectite, Ill/Smc: Illite/Smectite, LL: Liquid Limit, PI: Plastic Index. Xi - SPXK1, SPXK2, SPXK3, Koroni – SPKK, Paliolinos - SPPK, Ai Helis -SPAHK.

References

Carretero, M. I., Pozo, M., Legido, J. L., Fernández-González, M. V., Delgado, R., Gómez, I., Armijo, F., Maraver, F., 2014. Assessment of three Spanish clays for their use in pelotherapy. Applied Clay Science, 99, 131–143.

Curtis, J.O. 2005. Electromagnetic Poser Attenuation in Soils. ERDC/EL TR-05-5. Vicksburg, MS: U.S. Army Engineer Research and Development Center.

Gomes, C., Carretero, M. I., Pozo, M., Maraver, F., Cantista, P., Armijo, F., Legido, J., Texeira, F., Rautureau, M., Delgado, R., 2013. Peloids and pelotherapy: Historical evolution, classification and glossary. Applied Clay Science, 75-76, 28–38.

Karakaya, M.C., Karakaya, N., Sarıoğlan, S., Koral, M., 2010. Some properties of thermal muds of some spas in Turkey. Applied Clay Science, 48, 531–537.

Li, YH.A., 2009. A compendium of geochemistry. Princeton: Princeton University Press.

Lopez-Galindo, A., Torres-Ruiz, J., Gonzalez-Lopez, J.M., 1996. Mineral quantification in sepiolite–palygorskite deposits using X-ray diffraction and chemical data. Clay Miner. 31, 217–224.

Maraver, F., Armijo F., Fernández-Toran, M.A., Armijo, O., Ejeda J.M., Vazquez, I., Corvillo I., Torres-Piles, S. 2021. Peloids as thermotherapeutic agents. International Journal of Environmental Research and Public Health, 18 (4), 1-17.

Pozo, M, Carretero, M.I, Maraver, F, Pozo, E, Gómez, I, Armijo, F, Martín-Rubí, JA 2013. Composition and physico-chemical properties of peloids used in Spanish spas: a comparative study. Applied Clay Science, 83–84, 270–279.

Quintela, A., Terroso, D., Da Silva, E. F., Rocha, F., 2012. Certification and quality criteria of peloids used for therapeutic purposes. Clay Minerals, 47, 441–451.

Rebelo, M., Viseras C., Lopez Galindo, A., Rocha F., Fereira da Silva, E., 2011. Characterization of Portugese geological materials to be used in medical hydrology. Applied Clay Science 51, 258-66.

Rizo, O.D., Rudnikas, A.G., Rodrigues, K.D., Padila, D.B., 2000. Assessment of historical heavy metal content in healing muds from San Diego (Cuba) using nuclear analytical techniques. Nucleaus 53, 19-23.

Tateo, F., Ravaglioli, A., Andreoli, C., Bonina, F., Coiro, V., Degetto, S., Giaretta, A., Menconi Orsini, A., Puglia, C., Summa, V., 2009. The in-vitro percutaneous migration of chemical elements from a thermal mud for healing use. Applied Clay Science, 44, 83–94.

Veniale, F Battero, A., Jobstraibizer, P.G., Setti M., 2007. Thermal muds: Perspectives of innovations. Applied clay science, 36, 141-147.

16th International Congress of the Geological Society of Greece
17-19 October, 2022 - Patras, Greece
Bulletin of the Geological Society of Greece, Sp. Publ. 10
Ext. Abs. GSG2022-107

Geochemical characterization of the waste dump and mine waters of Kardia lignite mine, Western Macedonia, Greece

K. Pyrgaki[1], C. Karkalis[1], G. Louloudis[2], C. Roumpos[2], P. Krassakis[1], N. Koukouzas[1], E. Mertiri[2] and G. Kasfikis[2]
(1) Centre for Research and Technology, Hellas (CERTH), 15125 Athens, Greece; pyrgaki@certh.gr (2) Public Power Corporation of Greece, Mining Engineering and Closure Planning Department, 10432 Athens, Greece

Background and Objectives,

According to the energy transition plan and the gradual phase-out of the lignite mines in Greece, the Kardia lignite field stopped operating in 2021. In this framework, the main objectives of the present study are 1) the hydrogeochemical assessment of mine waters of Kardia lignite field and 2) the chemical & mineralogical characterization of Kardia waste dump site. Our findings are of great significance for land rehabilitation and land and water repurposing of the Kardia lignite field in order to identify future open pit lakes' water quality (Louloudis et al., 2022).

Sampling procedure and analytical methods

Eight mine water samples (six groundwater samples, Soulou stream and water sump) and 11 samples from the inside waste dump were collected during the wet season of March 2022 from the Kardia lignite field (**Fig.1**). During water sampling, the following parameters were measured in situ: pH, electrical conductivity (EC), total dissolved solids (TDS), dissolved oxygen (DO) and temperature (θ). All major ions and trace elements were analyzed shortly after sampling in the Centre for Research and Technology Hellas laboratories. The waste dump material has been collected by sampling a composite sample (triangle method) of about 2 kg. The chemical composition of the lignite dump samples was analyzed by X-ray Fluorescence (XRF) and the mineralogical composition by X-ray Diffraction (XRD). XRD analyses were conducted in 10 lignite dump samples using a Siemens D500 X-ray diffractometer, operating with Cu radiation at 40 kV, whereas interpretation of the XRD patterns was accomplished with the use of the DIFFRACplus EVA software v.11 (Bruker-AXS, USA) and the ICDD Powder Diffraction File (2006).

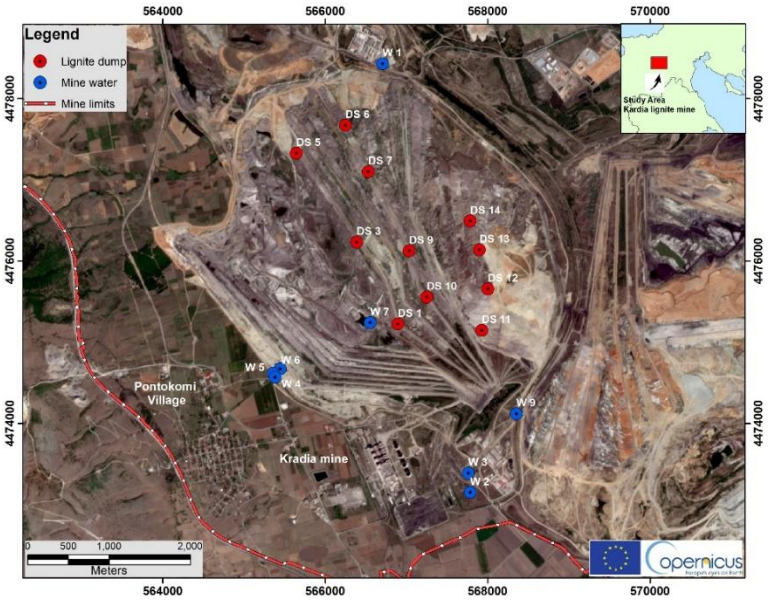

Figure 1. Sampling stations in the Kardia lignite field.

Results and Conclusions

Mine waters are alkaline with a pH ranging from 7.5 to 8.3 and hydraulic conductivities from 404 to 875 μS/cm. The minimum measured dissolved oxygen value is 2.1 mg/L, and the maximum is 9.1 mg/L. The main hydrochemical types are bicarbonate or mixed type waters (**Fig.2**). Nitrate concentrations range from below 0.8 mg/L to 125 mg/L, sulfates from 10 mg/L to 149 mg/L and chlorides from 5 mg/L to 108 mg/L.

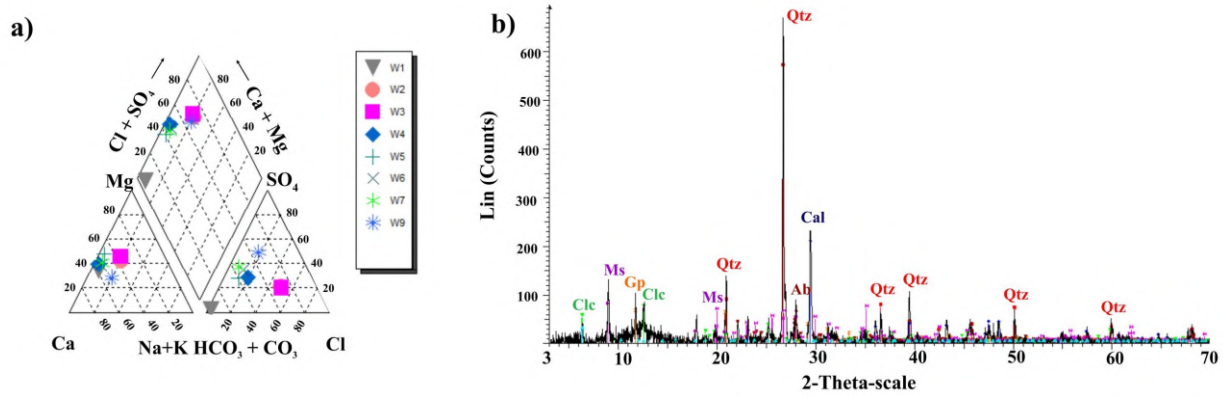

Figure 2. a. Piper diagram of mine waters, b. XRD pattern of a representative lignite dump sample from the Kardia mine, Qtz: quartz, Cal: calcite, Ms: muscovite, Ab: albite, Clc: clinochlore, Gp: gypsum.

The mineralogical composition of the lignite dump samples is characterized by the occurrence of calcite + quartz ± microcline ± muscovite ± albite ± sanidine (**Table 1**). Accessory minerals include gehlenite ± gypsum ± hematite ± faujasite ± clinochlore ± ettringite ± brucite ± osbornite ± zinnwaldite ± ilmenite± kaolinite ± dolomite ± anorthite. In some cases, albite, calcite and quartz appear as accessory minerals. The samples also contain remarkable quantities of amorphous glass material.

Table 1. Quantitative estimations of the mineralogical composition of the lignite dumps from Kardia mine.

Sample	Qtz	Gel	Cal	Gp	San	Hem	Fau	Clc	Ab	Ms	Ett	Mic	Brc	Ilm	Kao	Dol	An	Zin
DS1P	xx	x	xxx	x														
DS3P			xxx															
DS5P			xxx		xx	x												
DS6P	xx		x	x			TR	x	xx	xxx								
DS7P			xxx			x												
DS9P	x		xxx			x												
DS10P	x		xxx															
DS12P	xxx		xxx						xxx									
DS13P	xx		xxx						x		xx			x	x	x		x
DS14P	x		xxx														x	x

Abbreviations: qtz: quartz, cal: calcite, gp: gypsum, fau: faujasite, clc: clinochlore, ab: albite, ms: muscovite, brc: brucite, zinn: zinnwaldite, ilm: ilmenite, kao: kaolinite, dol: dolomite, an: anorthite

The observed minerals are distinguished into naturally formed types derived from geological processes and secondary types resulting from lignite processing during combustion. In particular, feldspars, including albite, are assigned to the presence of volcanic ash beds within the Ptolemais basin, alternate with sedimentary sequences and lignite beds (Steenbrink et al., 1999). The sedimentary formations of the Ptolemais basin include clastic rocks such as siltstones and sandstones, justifying the occurrence of quartz and clay minerals in the studied lignite dumps, whereas calcite and dolomite are assigned to the presence of marls. Gypsum is a common mineralogical component of the Kardia lignites (Nikolaidou et al., 2016). Faujasite is a zeolite-group mineral that appears in scarce traces, probably due to alteration of the volcanic ash. Oxide and hydroxide mineral phases such as hematite, ilmenite and brucite were probably derived from the produced fly ash during coal combustion. Similar processes may explain the formation of gehlenite, which has been linked with dehydration and melting Ca-clays during coal combustion (Valentim et al., 2018). Ettringite is also assigned to secondary processes.

Acknowledgements

We would like to thank Mr Ioakim Kalogiros for his valuable help during the sampling and Ms Marina Christopoulou (Geologist) for her support in the interpretation of the XRD patterns.

References

Louloudis, G., Roumpos, C., Louloudis, E., Mertiri, E., Kasfikis, G. 2022. Spatiotemporal Analysis of a Mined-out Pit Lake Considering Land Repurposing, 12th International Hydrogeological Conference. Nicosia (Lefkosia), Cyprus [Conference Proceedings]

Steenbrink, J., Van Vugt, N., Hilgen, F.J., Wijbrans, J.R., Meulenkamp, J.E., 1999. Sedimentary cycles and volcanic ash beds in the Lower Pliocene lacustrine succession of Ptolemais (NW Greece): Discrepancy between 40Ar/39Ar and astronomical ages. Palaeogeogr. Palaeoclimatol. Palaeoecol. 152, 283–303. doi:10.1016/S0031- 0182(99)00044-9. **[Journal Article]**

Nikolaidou, P., Triantafyllou, A., Kantiranis, N., & Filippidis, A. 2016. Mineralogical composition of suspended particles PM10 in the Ptolemais-Kozani area, Macedonia, Greece. Bulletin of the Geological Society of Greece, 50(2), 1046–1051. https://doi.org/10.12681/bgsg.11809. **[Journal Article]**

Valentim , B., Białecka , B., Gonçalves , P.A., Guedes, A., Guimarães, R., Cruceru, M., Całus-Moszko, J., Popescu, LG., Predeanu, G., Santos, A.C. 2018. Undifferentiated Inorganics in Coal Fly Ash and Bottom Ash: Calcispheres, Magnesiacalcispheres, and Magnesiaspheres. Minerals, *8*, 140; doi:10.3390/min8040140. **[Journal Article]**

16th International Congress of the Geological Society of Greece
17-19 October, 2022 - Patras, Greece
Bulletin of the Geological Society of Greece, Sp. Publ. 10
Ext. Abs. GSG2022-110

Triassic Basic and Intermediate Rift-related Volcanic Rocks from Akritas-Metallikon area, Circum-Rhodope Belt, northern Greece

A. Asvesta[1], S. Dimitriadis[2]

(1) Department of Mineral Resources Engineering, School of Engineering, University of Western Macedonia, Kozani, Greece, aasvesta@uowm.gr (2) Department of Geology, Aristotle University of Thessaloniki, Thessaloniki, Greece.

Introduction and Geological setting

The main formation of the Circum-Rhodope Belt (CRB) in northern Greece is the Silicic Volcano-Sedimentary (SVS) succession, the result of A-type silicic volcanism and neritic sedimentation evolved during Permo-Triassic in a post-collision extensional environment (Asvesta and Dimitriadis, 2019). It probably represents the early stages of the opening of a post-Variscan, neo-Tethyan oceanic strand (Vardar-Axios-oceanic basin; Asvesta, 1992; Dimitriadis and Asvesta, 1993; Asvesta and Dimitriadis, 2010, 2013, 2019). Minor basic volcanic rocks, probably of Late Ladinian to Late Triassic age (Ferrière and Stais, 1995) are locally intercalated with the A-type silicic volcanic rocks and the Upper Triassic pelagic limestones of Metallikon and Megali Sterna Unit. They are mainly exposed in the area between the villages Akritas and Cherso and near Metallikon village, north of the town of Kilkis (Asvesta, 1992; Dimitriadis and Asvesta, 1993; Ferrière and Stais, 1995; Asvesta and Dimitriadis, 2010, 2013). Subordinate intermediate volcanic rocks are also exposed only near Akritas. All these rocks have been subjected to lower greenschist-facies metamorphism and related deformation. This study examines the petrographic and geochemical features of these basic and intermediate volcanic rocks focusing on their origin and geotectonic setting.

Results and Discussion

The intermediate volcanic rocks are geochemically classified as trachydacites (SiO_2: 61.90-63.47 wt.%) and andesites (SiO_2: 53.57-55.16 wt.%). Textures are hyalo-ophitic. Plagioclase crystals occur in a mass of stilpnomelane, probably formed by crystallization of ferrous glassy groundmass (Figure 1A). Tiny magnetite crystals are widespread. The rocks classified as andesites contain in addition Fe-rich biotite (electron microprobe data; Asvesta, 1992) (Figure 1B). The TiO_2 contents range from 0.84 to 0.96 wt.% in trachydacites and 2.5 wt.% (invariable) in andesites, Al_2O_3 from 13.67 to 14.21 wt.% in trachydacites and 13.18 to 13.20 wt.% in andesites, Na_2O from 5.77 to 6.96 wt.% in trachydacites and 3.81 to 4.01 wt.% in andesites, K_2O from 0.39 to 1.37 wt.% in trachydacites and 1.93 to 3.28 wt.% in andesites and CaO from 1.69 to 2.15 wt.% in trachydacites and 2.13 to 3.32 wt.% in andesites. They all have relatively high Fe_2O_3 contents (8.94-9.73 wt.% in trachydacites and 13.30-13.50 wt.% in andesites) and low MgO contents (0.87-1.65 wt.% in trachydacites and 3.92-4.20 wt.% in andesites), with low $Mg^{\#}$ values (18-31 for trachydacites and 42-44 for andesites).

The basic volcanic rocks are geochemically classified as sub-alkaline basalts (SiO_2: 46.00-48.38 wt.%; Nb/Y<0.7). They are altered doleritic dykes and basaltic lavas, green-grey in color, locally exhibiting spheroidal weathering. Some preserve relict ophitic texture and have disequilibrium mineral assemblages, characterized by relict subhedral plagioclase enclosed in relict clinopyroxene crystals (Figure 1C). The clinopyroxene is diopside, largely converted to actinolite (electron microprobe data; Asvesta and Dimitriadis, 2013) and chlorite due to greenschist metamorphism. Albite, zoisite, clinozoisite and calcite have been also formed after the primary plagioclase. Sphene and leucoxene have replaced ilmenite. Tiny magnetite crystals are also present. The basic volcanic rocks have TiO_2 contents range from 1.20 to 2.22 wt.%, Al_2O_3 from 14.91 to 17.27 wt.%, Na_2O from 1.44 to 4.78 wt.% and K_2O from 0.06 to 3.09 wt.%. The CaO contents span a range of 6.08 to 10.74 wt.%. They have Fe_2O_3 contents from 8.82 to 12.24 wt.% and high MgO contents from 6.89 to 10.75 wt.%, with $Mg^{\#}$ values of 62 to 75 close to that of mantle-derived magmas.

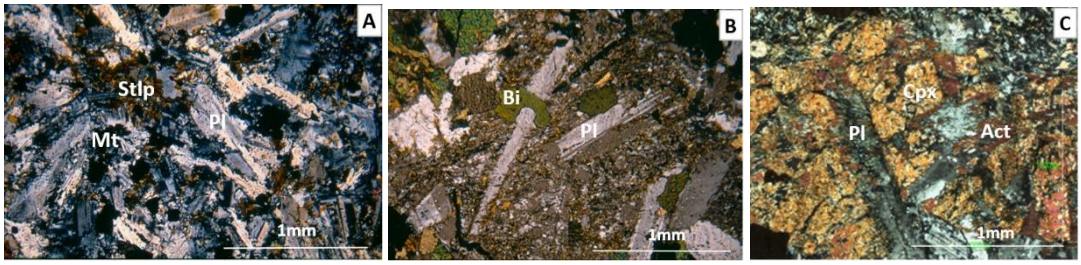

Figure 1. Photomicrographs of the studied volcanic rocks (crossed nicols). A) Intermediate volcanic rock (trachydacite). B) Intermediate volcanic rock (andesite). C) Basic volcanic rock (basalt-dolerite). Plagioclase (Pl), Stilpnomelane (Stlp), Biotite (Bi), Magnetite (Mt), Clinopyroxene (Cpx), Actinolite (Act).

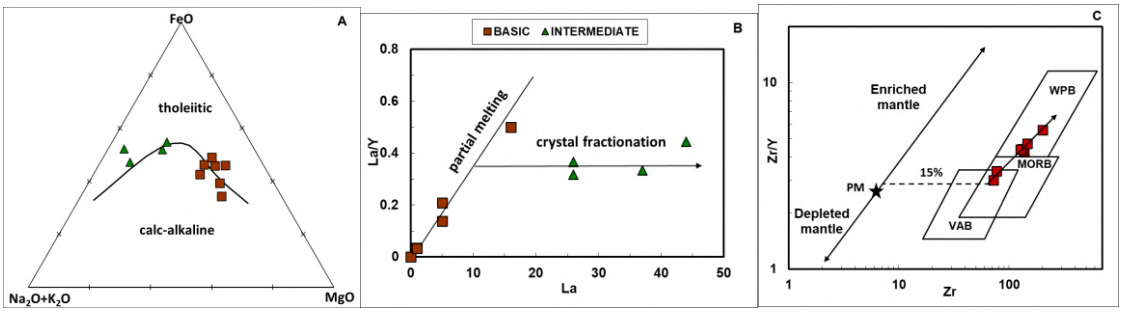

Figure 2. Major and trace element diagrams from the Akritas-Metallikon basic and intermediate volcanic rocks. A) AFM diagram (Irvine and Baragar, 1971). B) La *vs.* La/Y diagram. C) Zr *vs.* Zr/Y diagram (Pearce and Norry, 1979). WPB = Within Plate Basalts, MORB = Mid Ocean Ridge Basalts, VAB = Volcanic Arc Basalts, PM =Primary Mantle.

The tholeiitic character of the basic-intermediate volcanic rocks of Akritas-Metallikon is obvious in the AFM ternary diagram (Irvine and Baragar, 1971) (Figure 2A). The ratios of incompatible elements do not change much with crystal fractionation. The nearly constant La/Y ratios over a wide range of La contents for the intermediate volcanic rocks highlight the role of crystal fractionation in their generation (Figure 2B). In contrast, La/Y ratios of the basic volcanic rocks increase with increasing La contents, a trend that is best interpreted as variable degrees of partial melting (Allègre and Minister, 1978). It is therefore highly likely that the parent magma of the basic volcanic rocks was directly derived from a primary mantle source. This is consistent with their high $Mg^{\#}$ (62-75), Ni (54-152 ppm) and Cr (145-430 ppm) contents.

Mantle source, degree of melting and tectonic setting for the basic volcanic rocks are well defined by the Zr *vs.* Zr/Y diagram (Pearce and Norry, 1979). In this diagram, the basic volcanic rock samples fall into the MORB and WPB field and the most likely petrogenetic pathway indicates about 15 % partial melting of a normal MORB (not enriched) source (Figure 2C). It is also estimated that the main fractionally crystallized phase was clinopyroxene, consistent with the observed diopside crystals. Using the thermobarometer of Albaréde (1992), the calculated P–T conditions of magma generation (Temperature: 1219-1342 °C, Pressure: 1.01-1.61 GPa) imply a depth < ~50 km corresponding to a spinel-peridotite source. Additionally, the very high values of Y/Nb ratios (5-12) suggest the absence of garnet in the source. This implies that spinel-lherzolite was the parent source of magma of these basic volcanic rocks.

Conclusions

The Triassic Akritas-Metallikon tholeiitic volcanic rocks in the CRB are derived from 15% partial melting of a spinel-peridotite source, apparently as a result of adiabatic upwelling and decompression melting of a MORB-type asthenosphere that was accompanied by extension and consequent thinning of the overlying Vertiskos Variscan crust. The produced basic melts underplated, intruded and partly extruded, perhaps near the axis of the continental rift which eventually evolved to the Vardar-Axios oceanic basin. The basic magmatic underplating of the thinned Vertiskos basement provided heat for crustal fusion and generation of the A-type silicic volcanic rocks in a post-collision extensional stage.

Acknowledgements

The University of Western Macedonia is kindly acknowledged for the financial support for the presentation of this research work at the congress.

References

Albaréde, F., 1992. How deep do common basalts form and differentiate? J. Geophys. Res. 97, 10997-11009.

Allègre, C.J., Minister, J.F.,1978. Quantitative models of trace element behavior in magmatic processes. Earth and Planetary Science Letters 38, 1-25.

Asvesta, A., 1992. Magmatism and associated sedimentation during the first stage of the opening of the Vardar oceanic basin in Triassic times. Ph.D. Thesis, University of Thessaloniki, Greece, 439 p. (in Greek with English summary).

Asvesta, A., Dimitriadis, S., 2010. Facies architecture of a Triassic rift-related Silicic Volcano-Sedimentary succession in the Tethyan realm, Peonias subzone, Vardar (Axios) Zone, northern Greece. J. Volcanol. Geotherm. Res. 193, 245-269.

Asvesta, A., Dimitriadis, S., 2013. Magma-sediment interaction during the emplacement of syn-sedimentary silicic and mafic intrusions and lavas into and onto Triassic strata (Circum-Rhodope Belt, northern Greece). Geologica Carpathica 64(3), 181-194.

Asvesta, A., Dimitriadis, S., 2019. Geochemical characteristics and Tectonic significance of Permo-Triassic Silicic Volcanic rocks from Circum-Rhodope Belt, Vardar (Axios) Zone, northern Greece. 15th International Congress of the Geological Society of Greece, Athens, 22-24 May, 2019, Harokopio University of Athens, Greece, Bulletin of the Geological Society of Greece, Sp. Pub. 7 Ext. Abs. GSG2019-005, 307-308.

Dimitriadis, S., Asvesta, A., 1993. Sedimentation and magmatism related to the Triassic rifting and later events in the Vardar-Axios zone. Bull. Geol. Soc. Greece XXVIII(2), 149-168.

Ferrière, J., Stais, A., 1995. Nouvelle interprétation de la suture téthysienne vardarienne d'apres l'analyse des séries de Péonias (Vardar oriental, Hellénides internes). Bull. Soc. Géol. France 166, 4, 327-339.

Irvine, T.N., Baragar, W.P.A., 1971. A guide to the chemical classification of common volcanic rocks. Can. J. Earth Sci. 8, 523-548.

Pearce, J.A., Norry, M.J., 1979. Petrogenetic implications of Ti, Zr, Y, and Nb variations in volcanic rocks. Contrib. Miner. Petrol. 69, 33-47.

16th International Congress of the Geological Society of Greece
17-19 October, 2022 - Patras, Greece
Bulletin of the Geological Society of Greece, Sp. Publ. 10
Ext. Abs. GSG2022-116

Carbon isotope signature as tracer of deep degassing from big karst aquifers of Greece

Li Vigni L.[1], Cardellini C.[2-3], D'Alessandro W.[4], Calabrese S.[1,4], Daskalopoulou K.[5], Chiodini G.[3], Caliro S.[6], Parello F.[1]

(1) University of Palermo, Palermo, Italy, livignilorenza@gmail.com; (2) University of Perugia, Perugia, Italy; (3) Istituto Nazionale di Geofisica e Vulcanologia, sez. Bologna, Italy; (4) Istituto Nazionale di Geofisica e Vulcanologia, sez. Palermo, Italy; (5) University of Potsdam, Potsdam Golm, Germany; (6) Istituto Nazionale di Geofisica e Vulcanologia, Osservatorio Vesuviano, Napoli, Italy.

Research Highlights

Regional karst aquifers can transport elevated amount of geogenic carbon to the atmosphere. The regional diffuse degassing plays an important role within the global carbon budget.

Introduction

The global carbon cycle is very complex network of sources, where endogenic and exogenic sources are interconnected, operating in a multiple spatial and temporal scale (Lee *et al.*, 2019). The estimation of regional diffuse carbon degassing from tectonic structures plays an important role within the global carbon cycle (Frondini *et al.*, 2019). Due to the elevated solubility of CO_2 in water, regional aquifers can trap, transport and release huge amounts of CO_2-rich fluids into the atmosphere (Tamburello *et al.*, 2018). The carbon mass-balance is a useful approach to discriminate and quantify the amount of deeply derived carbon (Chiodini *et al.*, 2000).
Greece is considered one of the geodynamically most active region and is characterized by intense degassing, with different sources of geogenic carbon degassing, such as volcanic and hydrothermal sources. Daskalopoulou *et al.*, 2019, estimates a CO_2 degassing of 10^5 t a^{-1} from the main gas manifestation of its territory.
The main aim of this work is the estimation of geogenic CO_2 dissolved in big karst aquifers. Indeed, the carbonate formations cover about 35% of the country, whilst the karst aquifers are developed in limestones and dolomites (Triassic – Cretaceous), and in marbles (Paleozoic – Mesozoic). About 45% of karst aquifers is located inland, while the rest is in coastal areas. Their hydrogeological behaviour is controlled by tectonic deformation (Voudouris & Kazakis, 2018).

Methods

From 2016 to 2022, more of 180 karst springs were sampled (Fig.1), selected on the base of their flow rate (> 60 L s^{-1}). Physicochemical parameters (temperature, pH, electric conductivity, and redox potential) were measured in situ with portable instruments, whilst total alkalinity was determined by titration with 0.1 M HCl on unfiltered samples, expressed as mgHCO_3^- L^{-1}. Analyses of chemical and isotopic composition of water and gases were performed at the laboratories of INGV of Palermo, Italy. In order to discriminate the carbon sources, the carbon mass-balance was applied for each sample.

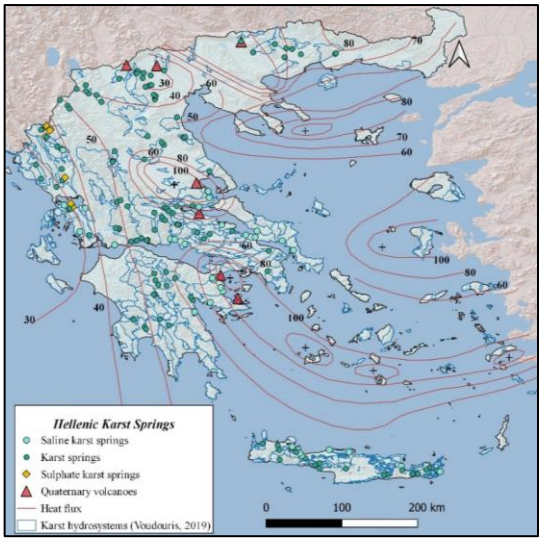

Figure 1. Geographic distribution of the sampling site

Results

Temperature values range between 5.6 and 33.5 °C, pH values vary from 6.5 to 8.5, whereas Electrical conductivity ranges from 174 to 44,000 µS cm^{-1} and Eh from -38 to 399 mV. On the basis of the chemical composition of waters, the karst springs can be subdivided into three groups with different geochemical compositions: a) characterized by Ca-HCO_3 composition and low saline content (< 1,200 mg L^{-1} of TDS); b) characterized by Na-Cl composition and high saline content (up to 25,717 mg L^{-1} of TDS); c) characterized by Ca-SO_4 composition and intermediate saline content (up to 2,424 mg L^{-1} of TDS).

Based on the chemical composition of dissolved gas, the sampled karst springs are dominated by N_2 (up to 985,252 µmol mol^{-1}); carbon dioxide ranges between 941 and 63,715 µmol mol^{-1}, whilst helium varies from <3 to 273 µmol mol^{-1}.

Total dissolved inorganic carbon (TDIC) and carbon isotopic composition ($\delta^{13}C_{TDIC}$) present a wide range, the former varies from 1.82 mmol L^{-1} to 21.8 mmol L^{-1}, whilst $\delta^{13}C_{TDIC}$ ranges between -16.6 to 3.95 ‰ vs. VPDB (Fig.1a). These ranges are evidence of the occurrence of multiple sources of CO_2. In order to discriminate the carbon origin, the contribution of carbonate dissolution (C_{carb}) was removed and a cumulative probability graphs of external carbon (C_{ext}), deriving from the infiltration and from the geogenic sources, was created. Two populations have been recognized (Fig.2b). The biogenic source has mean value $\delta^{13}C_{ext}$ of -20.7 ‰ and mean value C_{ext} of 2.6 mmol L^{-1}, representing the composition of infiltration waters. The second group indicates an input of deeply derived carbon to the infiltrating waters. A preliminary estimation of geogenic carbon output from karst springs has been made, showing a discharge of ~ $1.1*10^9$ mol a^{-1}. Karst springs with evidence of geogenic carbon input are mostly located close to the Quaternary volcanic areas.

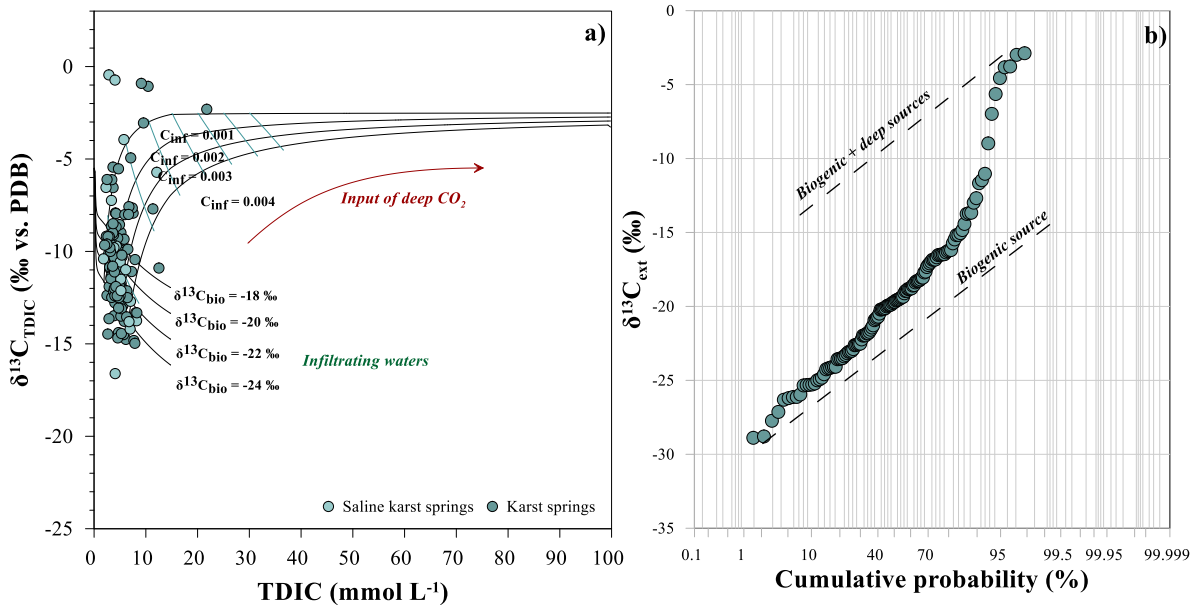

Figure 2. a) TDIC versus $\delta^{13}C_{TDIC}$ diagram of sampled karst springs; b) Probability plot of $\delta^{13}C_{ext}$

References

Lee C.A., Jiang H., Dasgupta R., Torres M., 2019. A framework for understanding whole-Earth Carbon cycling. In: Orcutt B. et al. (eds) Deep Carbon: Past to Present. Cambridge University Press, pp. 313-357.

Frondini F., Cardellini C., Caliro S., Beddini G., Rosiello A., Chiodini G., 2019. Measuring and interpreting CO_2 fluxes at regional scale: the case of the Apennines, Italy. J. Geol. Soc. 176, 408-416.

Tamburello G., Pondrelli S., Chiodini G., Rouwet D., 2018. Global-scale control of extensional tectonics on CO_2 earth degassing. Nature communications, 9:4608.

Chiodini G., Frondini F., Cardellini C., Parello F., Peruzzi L., 2000. Rate of diffuse carbon dioxide Earth degassing estimated from carbon balance of regional aquifers: The case of central Apennine, Italy. Journal of Geophysical Research, 105(B4), 8423-8434.

Daskalopoulou K., Calabrese S., Gagliano A.L. & D'Alessandro W., 2019. Estimation of the geogenic carbon degassing of Greece, Applied Geochemistry, 106, 60-74.

Voudouris K. & Kazakis N., 2018. General characteristics and classification of karst aquifers in Greece. Review Bulg. Geol. Soc., 79(3), 159-160.

16th International Congress of the Geological Society of Greece
17-19 October, 2022 - Patras, Greece
Bulletin of the Geological Society of Greece, Sp. Publ. 10
Ext. Abs. GSG2022-126

The First Soil Geochemical Atlas of Greece: Outline of a Promising New Project.

A. Kontomichalou[1,2], A. Liakopoulos[1], A. Argyraki[2]
(1) HSGME, Department of Geochemistry and Environment, Acharnai, Greece, akontomichalou@igme.gr (2) National and Kapodistrian University of Athens, Department of Geology and Geoenvironment, Athens, Greece

Background and research objectives

Geochemical mapping of soil composition has been a central topic of applied geochemistry, initially aimed at mineral prospecting. Following the development of state-of-the-art technology, geochemical mapping has evolved to be a very useful tool for defining the geochemical baseline of elements for multi-purpose use (Négrel et *al.*, 2021). The resulting geochemical databases have a wide range of applications, including mineral exploration, policy implementation regarding environmental regulatory standards, agriculture, land use planning, forensic science, crisis management, etc. (European Commission, 2021).

Many countries have already published their national geochemical atlases namely the United Kingdom (Johnson et *al.*, 2005), Croatia (Halamić et *al.*, 2009), Cyprus (Cohen et *al.*, 2011) and Sweden (Andersson et *al.*, 2014) by employing a variety of sampling and analytical protocols, however, a unified approach has been lacking. The recent publication of the Manual of Standard Methods for Establishing the Global Geochemical Reference Network (MSM) (Demetriades et *al.*, 2022) by the International Union of Geochemical Sciences- Commission of Global Geochemical Baselines provides for the first time a comprehensive overview of the standardised methods that should be employed across the land surface of the Earth to map the distribution of chemical elements in rock, soil, sediment and water. This guide safeguards that the generated geochemical data are of high quality, integrity and consistency. In Greece, research has been performed extensively in the field of soil geochemistry however only at a local scale: Athens (Argyraki and Kelepertzis, 2014), Euboea (Kanellopoulos and Argyraki., 2013), Lavrion (Demetriades, 2011) etc.

The present project is of high national priority and implemented by the Department of Geochemistry and Environment of HSGME (Hellenic Survey for Geology and Mineral Exploration) through National Funds, in collaboration with the Laboratory of Economic Geology and Geochemistry of NKUA. The project aspires to serve as a preliminary study with the ultimate aim of publishing the first Soil Geochemical Atlas of Greece. Specifically, the present project aims at establishing the sampling protocols for Greek soil geochemical mapping and create a rich database of soil geochemical properties at a selected pilot area. The Attiki- Voiotia region has been selected for the pilot scale survey because it provides sufficient variety of land uses containing urban, suburban, industrial and natural areas, rich geology and geomorphology and a range of soil types, as well as ease of access.

Methods

The parameters to be studied in the pilot survey have been determined upon a thorough literature review of related projects conducted by other European countries. Furthermore, the sampling, sampling preparation procedures and analytical protocols utilised, follow the general guidance provided by the MSM and are adjusted to the Greek natural and anthropogenic environment. In the first stage of the project a detailed sampling and analytical methods manual has been drafted. In the second stage, the methods are being tested in the field by collecting top-soil and bottom-soil samples from approximately 150 locations on a 5 km x 5 km grid within the pilot area of about 2500 km^2. Sample preparation includes drying, gently disaggregating the soil and sieving to produce the < 2 mm fraction to be subjected to further analysis. The analytical methods include chemical analysis by ICP-MS following aqua regia dissolution for trace element determination, measurement of physicochemical soil properties (Eh, pH, particle size distribution, magnetic susceptibility), and mineralogical analysis by X-Ray Diffraction to specify the mineral composition of selected samples. A set of leaching tests will also be performed on a sub-set of the soil samples. The deliverables of the project include but are not limited to: a comprehensive database of geochemical data and trace element maps of the pilot area, statistical interpretation of the dataset, as well as an updated guide for sampling of the Greek soils.

Results and Conclusions

Although still at its primary stages, this ambitious project of HSGME is expected to fill a significant gap in the national geochemical databases of Greece. During the sampling stages of this research, valuable experience has been gained by testing on real terrane the outlined protocols (Fig. 1). Logistics play a very significant role in this type of studies and empirical knowledge gained in the field is extremely valuable. The pilot study will form the basis of research at a larger scale to define the background/baseline level of major and trace elements at regional/national scale. Further, research on mapping will also contribute to continental/global elemental mapping of soil. In subsequent stages of research development of sophisticated applications and new features, integrating modern computing and geoinformation,

computer-based modelling of compositional data is one of the main innovation elements of the research. Furthermore, the outcome of this research will allow, for the first time, the application of geochemical background in developing guideline/intervention values and form an objective basis for the evaluation of potential environmental risks. Expected output of the research comprises a comprehensive sampling manual, including guidance on sample preparation for analysis and a feasibility study for the implementation of the full-scale project of the Soil Geochemical Atlas of Greece.

The scientific, as well as the social impact of this research is highly ranked as the applications of baseline geochemical data that will be produced have a wide range of applications as follows:

- support and supply of information to local and regulatory authorities, land use planners, developers and the general public on the state of environmental soil quality;
- identify anomalous environmental conditions resulting from, for example, mineralisation and industrial sources;
- assess the condition and health of soil for agricultural and ecosystem functions;
- identify and quantify human impact on the environment, if it exists, with well documented data;
- identify new opportunities for mineral exploration, and
- improve understanding of earth system processes over the Greek territory.

Figure 1. Example of field sample collection from a sampling location at Lavreotiki, Attica.

Acknowledgements

This work is conducted by HSGME, and financed by the National Funds Programme, project no. 2020ΣΕ06100004 (HSGME no 22204). We would like to sincerely thank *EurGeol* Alexandros Demetriades for the fruitful discussions, his valuable advice and general support throughout the preparation and implementation of the project.

References

Andersson, M., Carlsson, M., Ladenberger, A., Morris, G., Sadeghi, M., & Uhlback, J., 2014. Geochemical atlas of Sweden.

Argyraki, A. & Kelepertzis, E., 2014. Urban soil geochemistry in Athens, Greece: The importance of local geology in controlling the distribution of potentially harmful trace elements, Science of The Total Environment 482–483, 366-377, ISSN 0048-9697

Cohen, D., & Rutherford, N., 2011. Technical Report on the Development of a Geochemical Atlas of Cyprus. Volume 1 – Text. 1(June), 1–104.

Demetriades, A., 2011. The Lavrion urban geochemistry study, Hellas. Chapter 25 In C.C. Johnson, A. Demetriades, J. Locutura & R.T. Ottesen (Editors), Mapping the Chemical Environment of Urban Areas. Wiley-Blackwell, John Wiley & Sons Ltd., Chichester, U.K., 424–456.

Demetriades, A., Johnson, C.C., Smith, D.B., Ladenberger, A., Adánez Sanjuan, P.A., Argyraki, A., Stouraiti, C., Caritat, P. de, Knights, K.V., Prieto Rincón, G. & Simubali, G.N. (Editors), 2022. International Union of GeologicalSciencesManual of Standard Methods for Establishing the Global Geochemical Reference Network. IUGS Commission on Global Geochemical Baselines, Athens, Hellenic Republic, Special Publication, 2, 515 pages, 375 figures, 35 Tables, 5 Annexes and 1 Appendix, ISBN: 978-618-85049-1-2

European Commission., 2021. EU Soil Strategy for 2030: Reaping the benefits of healthy soils for people, food, nature and climate

Halamić, J., Miko, S., Peh, Z., Galović, L., & Šorša, A., 2009. Geochemical Atlas of the Republic of Croatia.

Johnson, C. C., 2005. 2005 G-BASE Field Procedures Manual. British Geological Survey Internal Report, IR/05/097. 130.

Kanellopoulos, Ch. And Argyraki, A., 2013. Soil baseline geochemistry and plant response in areas of complex geology. Application to NW Euboea, Greece. Chemie der Erde- Geochemistry, 73 (4), 519-532.

Négrel, P., Ladenberger, A., Reimann, C., Birke, M., Demetriades, A., Sadeghi, M., Albanese, S., Andersson, M., Baritz, R., Batista, M. J., Flem, B., Bel-lan, A., Cicchella, D., de Vivo, B., de Vos, W., Dinelli, E., Ďuriš, M., Dusza-Dobek, A., Eggen, O. A., … Zomeni, Z., 2019. GEMAS: Geochemical background and mineral potential of emerging tech-critical elements in Europe revealed from low-sampling density geochemical mapping. Applied Geochemistry, 111(April).

16th International Congress of the Geological Society of Greece
17-19 October, 2022 - Patras, Greece
Bulletin of the Geological Society of Greece, Sp. Publ. 10
Ext. Abs. GSG2022-182

Major Arsenic contamination hot spots. Two case studies: Thermopyles Spring and Pineios River (Greece)

D'Alessandro W.[1], Li Vigni L.[2], Brusca L.[1]

(1) Istituto Nazionale di Geofisica e Vulcanologia, sez. Palermo, Italy, walter.dalessandro@ingv.it; (2) University of Palermo, Palermo, Italy.

Research Highlights

Arsenic is considered the "king of poison", its evaluation in terms of environmental impact and human health is a global concern.

Introduction

Arsenic (As) is a common trace element in groundwaters. Arsenic is known as toxic metalloid and its distribution is a global environmental health concern. In groundwaters, As exists in two main oxidation states; under oxidizing conditions, it is mostly present as arsenate, As(V), whilst in reducing waters, it is present as arsenite, As(III) (IPCS, 2001). Due to its harmful potential to human health, WHO and US-EPA have established the value of 10 µg L^{-1} as the maximum contaminant level (MCL), value yet adopted by the European Council since 1998 (98/83/EC).

Geogenic contamination of arsenic can derive from dissolution of sulfide ore deposits or from geothermal fluids, but As can also derive from anthropogenic sources, such as industrial waste, mining activities or from use of fertilizers in agriculture (Varnavas *et al.*, 2001).

In Greece, many regions are affected by higher concentrations of Arsenic in groundwaters. According Gamaletsos *et al.*, 2013, the main geogenic sources are leaching of sulfide ore deposits and the fluids arising from hydrothermal and volcanic areas.

The main aim of this study is estimating the Arsenic output from springs and evaluating its impact on riverine and marine ecosystems.

Methods

Water samples were collected in Thermopyles spring, in Sperchios basin (Central Greece) and in Agia Paraskevi spring, along the Pineios river (Thessaly) (Fig.1). For the latter, samples at different distance from springs were collected also in order to evaluate the possible impact on the river.

Physico-chemical parameters (temperature, pH, redox potential and electric conductivity) were measured *in situ*, and the total alkalinity was determined *in situ* by titration with 0.1 M HCl on unfiltered samples. Major anions (F^-, Cl^-, NO_3^- and SO_4^{2-}) and major cations (Na^+, K^+, Mg^{2+} and Ca^{2+}) were determined by ionic chromatography (IC; Dionex ICS 1100). Trace elements were analysed by Agilent 7800 - Inductively Coupled Plasma Mass Spectrometry (ICP-MS). Analyses were carried out at the laboratory of Istituto Nazionale di Geofisica e Vulcanologia of Palermo, Italy.

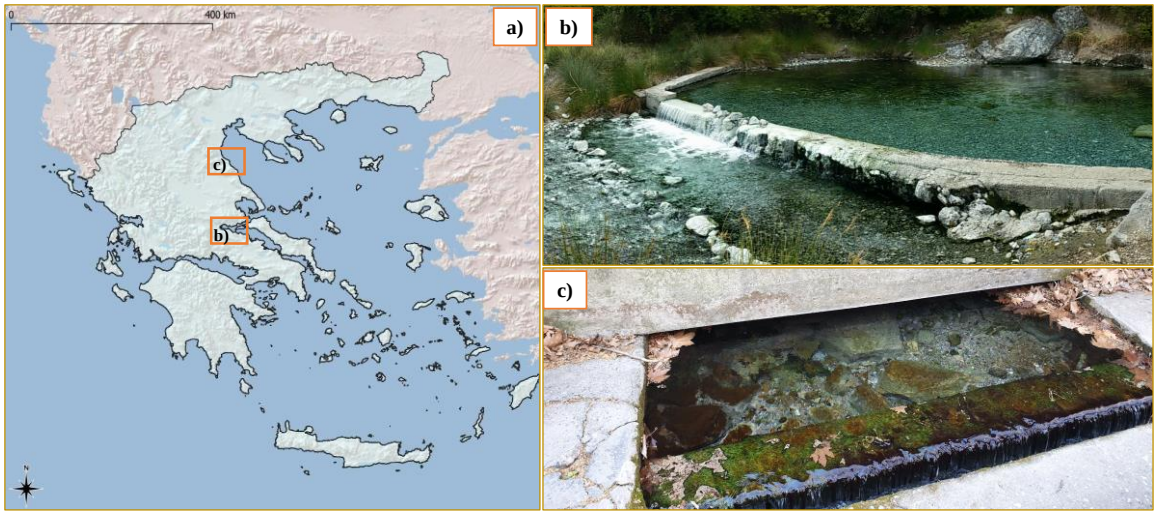

Figure 1. Geographic distribution of the sampling sites (a); Thermopyles spring, in Sperchios Basin (b); Agia Paraskevi spring, Tempi valley, Thessaly (c)

Results

From 2005, several water samples were collected at Thermopyles spring, a thermal spring with abundant gas bubbling that discharge in a channel. The spring has a bicarbonate alkaline composition. Due to its closeness to the sea, the hydrothermal system is by sea water contamination (D'Alessandro *et al.*, 2014). Furthermore, Thermopyles spring shows a wide range of Arsenic content, comprised between 52.3 and 386 µg L^{-1}, likely of hydrothermal origin. Elevated arsenic concentrations were found also along the channel

Table 1. Arsenic output from Thermopyles and Agia Paraskevi springs

Site	Flow rate (L s^{-1})	Arsenic (µg L^{-1})	As output (t a^{-1})
Thermopyles	260	52.3 - 386	0.429 – 3.16
Tempi (Agia Paraskevi)	772	11.1 - 17	0.270 – 0.413

Agia Paraskevi is a cold karst spring, sited in Tempi Valley, close to the delta of the Pineios river. This system presents several springs, some inside the river. The Agia Paraskevi spring is one of the biggest, which shows arsenic content comprised 11.1 and 17 µg L^{-1}. In July 2021, water samples were collected from spring and from upstream and downstream sites along the river. The spring sites are enriched in Ca^{2+} and HCO_3^- and in some trace elements (Li, B, Cr, As, Se, Sr, Mo, Sb, Cs, U) respect to the river. The chemical composition of the upstream site represents the background composition of the river, whilst the downstream site is influenced by the spring. For instance, Arsenic composition varies from 2.09 µg L^{-1} of the upstream site to 10.5 µg L^{-1} of downstream site (Fig.2), suggesting the strong influence of the springs system in the river.

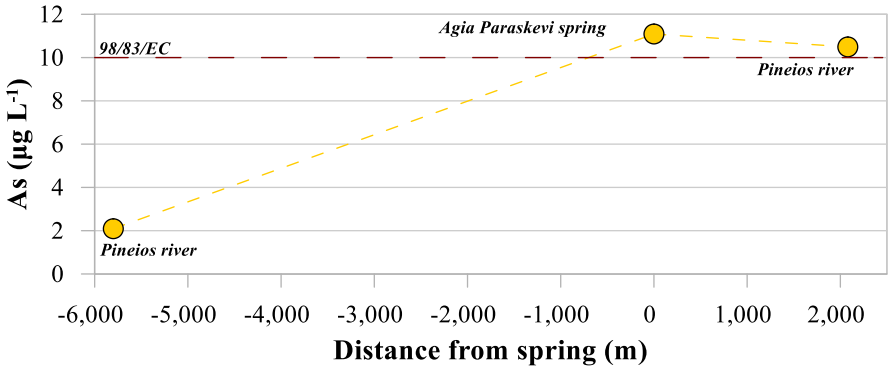

Figure 2. Variations of the arsenic concentration along the Pineios rivers. The distance "0" corresponds to spring site

Generally, the two study springs show high arsenic output (> 10 µg L^{-1}). Arsenic flux was calculated for each spring, multiplying the flow rate (L s^{-1}) of the spring and the arsenic concentration (µg L^{-1}). Thermopyles spring shows an elevated arsenic output, with values that arrives up to 3.16 ton a^{-1}.

The arsenic and other harmful metal elements, occurrence on these systems may have implications not only for river ecosystems, but also for marine ecosystems being the inflow into the sea only few km away from these strong As-sources.

References

D'Alessandro W., Brusca L., Kyriakopoulos K., Bellomo S., Calabrese S., 2014. A geochemical traverse along the "Sperchios Basin – Evoikos Gulf" graben (Central Greece): Origin and evolution of the emitted fluids. Marine and Petroleum Geology 55, 295-308.

E.U. Council Directive 98/83/EC about water quality intended for human consumption. Official Paper Eur Communities L330:32-54, 1998.

Gamaletsos, P., Godelitsas, A., Dotsika, E., Tzamos, E., Göttlicher, J., Filippidis, A., 2013. Geological sources of As in the environment of Greece: A review. In: Threats to the Quality of Groundwater Resources: Prevention and Control; Scozzari, A., Dotsika, E., Eds.; Hdb. Env. Chem. 40, 77–113.

IPCS, International Programe on Chemical Safety, 2001. Arsenic and arsenic compounds. Environmental Health Criteria, 224, World Health Organization, Geneva.

Varnavas, S.P., Forstner, U., Calmano, W., 2001. Environmental assessment and human health in a highly metal polluted coastal zone associated with toxic solid waste. The need of immediate action. In Proceedings of the 7th International Conference on Environmental Science and Technology, Ermoupolis, Greece, 3–6 September 2001; pp. 903–908.

16th International Congress of the Geological Society of Greece
17-19 October, 2022 - Patras, Greece
Bulletin of the Geological Society of Greece, Sp. Publ. 10
Ext. Abs. GSG2022-186

Permo-Triassic granitic magmatism in Serbomacedonian massif and Pelagonian zone: comparative geochemical and petrogenetic study of Kerkini, Arnea and Ardassa granites

K. Panora[1], A. Koroneos[1]

(1) Department of Mineralogy-Petrology-Economic Geology, Aristotle University of Thessaloniki, Thessaloniki, Greece aikatpanor@geo.auth.gr

The Kerkini, Arnea and Ardassa granitic complexes, situated eastern and western of Axios zone respectively, are studied and compared from petrographic and geochemical point of view.

The study area is located in northern Greece. The Kerkini and Arnea granitic complexes intrude the Serbomacedonian massif (Vertiskos Unit) while Ardassa granite intrudes the Pelagonian Zone. Axios Zone (representing the Vardar Ocean) exists between the two continental zones. The Serbomacedonian massif is part of the greek hinterland and consists of a crystalline basement (metamorphic rocks) and magmatic intrusions. The zone is divided into Vertiskos (younger) and Kerdyllia (older) units. The Pelagonian zone covers the most part of central Greece with a NNW-SSE direction and it comprises of Mesozoic sediments that cover a sequence of crystalline rocks. Plutonic rocks, deformed from the alpine metamorphism, intrude the Pelagonian zone (Mountrakis, 2010). The three granites under study have similar Permian-Triassic age.

The granitic complexes of Kerkini and Arnea intrude crystalline rocks, such as gneisses (Paleozoic), of the Serbomacedonian massif (Christofides et al., 1999). On the other hand, Ardassa granite intrudes two-mica schists of Pelagonian zone's pro-alpine geological basement (Petarouda, 2015).

All three magmatic intrusions have similar petrography, as they differ only in some minerals. They are classified as alkali-granites, are leucocratic, medium-grained, and intensively deformed. They have typical granitic texture. Their primary minerals are quartz, K-feldspars, albite, and mica (muscovite and biotite). Biotite appears to be Fe-enriched in all intrusions. Accessory minerals such as allanite, apatite, zircon, and titanite are present. The secondary minerals present are epidote, chlorite, sericite and, in some cases, actinolite, spinel and garnet. All the granites have been subjected to metamorphism.

The major elements variations, for all granites, show similar trends; most of them decrease with the increase of SiO_2. The same applies to trace elements of the three granites. They all have similar trace element contents, with few exceptions. They majority of the trace elements decrease with the increase of SiO_2 percentage, Nb increases, and few elements show no trend.

All rock samples are enriched in LREE compared to HREE and most of them show negative Eu anomaly. In multi-element diagram (Fig.1a) the patterns are similar in the samples of all studied granites. The samples show positive Pb, Nd, Rb and K anomalies, as well as negative Nb, Ti anomaly, which usually indicate magmas related to subduction zones. Negative Ba and Sr anomalies indicate increased crustal involvement in the magma source composition.

According to previous studies, the Kerkini and Arnea magma originated by partial melting of crustal rocks with tonalitic composition, under anhydrous conditions and high temperatures (T >900°C). The Ardassa parental magma could have been derived from gneisses, mica schists or other high-metamorphic rocks (T = 800-900°C) (Christofides, 1999; Poli et al., 2007).

Discrimination diagrams (Batchelor & Bowden, 1985; Streckeisen & LeMaitre, 1979; Pearce et al., 1984; Peccerillo & Taylor, 1976) show that the three plutonites are considered anorogenic, are alkali-granites of intraplate magmatism and they belong to the shoshonitic and high-K calc-alkaline series. Furthermore, based on Whalen et al. (1987), their geochemistry and criteria depicted in Fig.1b, the rocks under study are considered as A-type granites.

The granites of Kerkini, Arnea and Ardassa yielded zircon crystallization ages of 247 Ma (Christofides et al., 1999), 243 Ma (Poli et al., 2008) and 257 Ma (Alagna, 2006), respectively.

It is to note that further to the South, in Thessaly, a small pluton, the Deskati granite, intrudes two-mica schists of Pelagonian zone's pro-alpine geological basement (Katerinopoulos et al., 1994). It is an alkali-granite, with porphyritic texture having quartz, microcline, albite, Fe - biotite and muscovite as primary minerals, allanite, actinolite, zircon, apatite, titanite and chlorite as accessories and epidote, muscovite, and garnet as secondary. Deskati granite is geochemically very similar to the other three granites that were previously mentioned – it has similar trace element trends, it is anorogenic, alkali-granite of inter-plate magmatism and it belongs to the shoshonitic and high-K calc-alkaline series (Paleologou, 2014). According to previous studies, the Deskati magma originated by partial melting of crustal rocks, such as gneisses, charnockite or granulite, under pressure (3kbar) and high temperatures (T~800°C). Also, as shown in Fig.1b, Deskati's granite is considered as A-type granite, like the other three magmatic intrusions. Deskati granite was dated at 233±3 Ma (Katerinopoulos et al., 1999) by Rb-Sr in micas. However, later geochronological

studies have placed this granite at ~700 Ma (Alagna, 2006; Zlatkin et al., 2014), characterizing it as an upper Proterozoic intrusion.

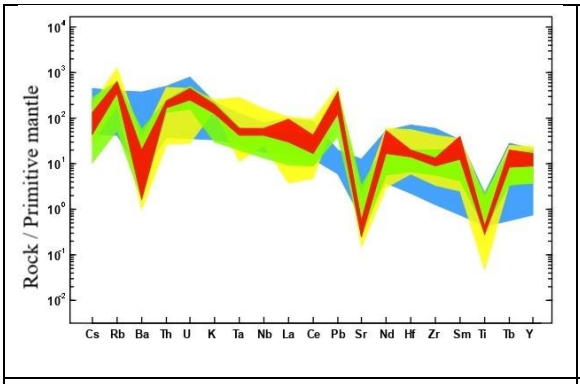

Figure 1a. Multi-element patterns of the four granites, (normalization after McDonough & Sun, 1992). Blue: Kerkini, green: Arnea, red: Ardassa and yellow: Deskati.

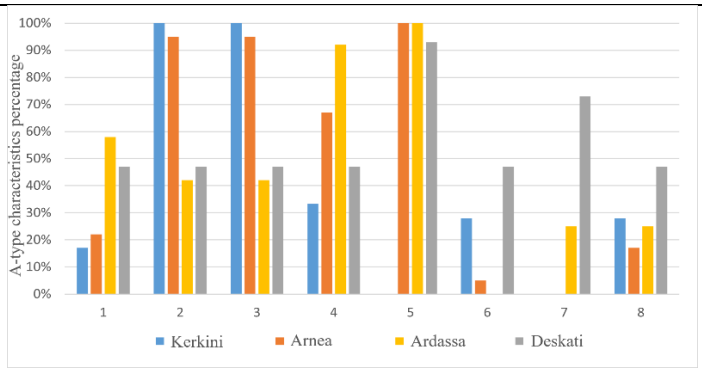

Figure 1b. Histogram depicting the percentage (0% – zero and 100% – completely) of samples of the 4 granites that show A-type characteristics (Bonin et al., 2007 and references therein). 1: FeOt/MgO, 2: NK/A, 3: NK/A, 4: Y+Nb & Y+Ta, 5: Ga/Al, 6: ZNCY, 7: Y/Nb and 8: Tetrad Effect.

Conclusions

In conclusion, the three plutons have characteristics of A-type granites and intrude continental zones on either side of Axios zone (representing the ocean). They are of Permo-Triassic age, while Deskati granite, having similar geochemical features, is placed controversially at upper Proterozoic. Their geochemistry along with their age (apart Deskati), imply that these rocks originate in a geotectonic environment of continental rifting. Specifically, they may represent parts of the acid magmatism – related to the Permo - Triassic continental rifting that led to the opening of Axios ocean.

References

Alagna, K., E., 2006. Geocronologia U-Pb su zirconi tramite spettrometria di massa accoppiata ad ablazione laser: sviluppo della metodologia e applicazione ai plutoni di Ardassa e Deskati (Grecia Nord-Occidentale), unpublished Ph.D thesis, University of Perugia, 161 p.

Batchelor, R. A., Bowden, P., 1985. Petrogenetic interpretation of granitoid rock series using multicationic parameters. Chemical Geology, **48**, 43-55.

Bonin, B., 2007. A-type granites and related rocks: evolution of a concept, problems and prospects. Lithos, **97** (1-2), 1-29.

Christofides, G., Koroneos, A., Pe-Piper, G., Katirtzoglou, K., Chatzikirkou, A., 1999. Pre-Tertiary A-Type magmatism in the Serbomacedonian massif (N. Greece): Kerkini granitic complex. Bulletin of the Hellenic Geological Society, **XXXIII**, 131-148.

Katerinopoulos, A., Kokkinakis, A., Kyriakopoulos, K., 1994. Petrology and chemical characteristics of Deskati granitic rocks, Thessaly, Greece. Bulletin of the Hellenic Geological Society, Proceedings of the 7th Scientific Conference, May 1994, Thessaloniki, **XXX/3**, 79-88.

McDonough, W.F., Sun S.-S., Ringwood, A.E., Jagoutz, E. and Hofmann, A.W., 1992. Potassium, Rubidium and Cesium in the Earth and Moon and the evolution of the mantle of the Earth. Geochim. Cosmochim. Acta, **56**, 1001-1012.

Mountrakis, D., 2010. Geology and Geotectonic Evolution of Greece. University Studio Press, Thessaloniki, 321 p.

Paleologou, M., 2014. Geochemistry and genesis of Deskati granite (Thessaly). Bachelor Thesis, Department of Geology, Aristotle University of Thessaloniki, 68 p.

Pearce, J. A., Harris, N. W., Tindle, A. G., 1984. Trace element discrimination diagrams for the tectonic interpretation of granitic rocks. J. Petrol., **25**, 956–983.

Peccerillo, A., Taylor, S. R., 1976. Geochemistry of Eocene calc-alkaline volcanic rocks from the Kastamonu area, Northern Turkey. Mineralogy and Petrology, **58**, 63–81.

Petarouda, D., 2015. Geochemistry, petrogenesis and geochronology of the leucogranite of Ardassa (Western Macedonia). Bachelor Thesis, Department of Geology, Aristotle University of Thessaloniki, 47 p.

Poli, G., Ghristofides, G., Perugi, S., Triantafyllos, K., 2008 - 2009. Early Triassic Granitic Magmatism (Arnea and Kerkini Granitic Complexes) in the Vertiskos Unit (Serbo-Macedonian Massif, North-Eastern Greece) and its significance in the Geodynamic Evolution of the area. Acta Vulcanologica, **20 - 21**, 28 p.

Streckeisen, A., LeMaitre, R. W., 1979. A chemical approximation to the modal QAPF classification of the igneous rocks. Neues Jahrbuch fur Mineralogie, **136**, 169-206.

Whalen, J. B., Currie, K. L., Chappell, B. W., 1987. A-type granites: geochemical characteristics, discrimination and petrogenesis. Contrib. Mineral Petrol., **95**, 407-419.

Zlatkin, O., Avigad, D., Gerdes, A., 2014. Peri-Amazonian provenance of the Proto-Pelagonian basement (Greece), from zircon U–Pb geochronology and Lu–Hf isotopic geochemistry. Lithos, **184-187**, 379-392.

16th International Congress of the Geological Society of Greece
17-19 October, 2022 - Patras, Greece
Bulletin of the Geological Society of Greece, Sp. Publ. 10
Ext. Abs. GSG2022-205

The Post-Variscan to Pre-Jurassic, Mafic Northern Pelagonian Magmatism: A Comparative Study.

I. Gerontidou[1], A. Koroneos[1], G. Vogdopoulos[1]

(1) Department of Mineralogy-Petrology-Economic Geology, Faculty of Geology, Aristotle University of Thessaloniki, Thessaloniki, Greece, ioangero@geo.auth.gr.

Mafic rocks intruding the Northern Pelagonian zone are studied and distinguished in calc-alkaline rocks of Carboniferous age and tholeiitic rocks of Permian-Triassic age.

The crystalline basement of the Pelagonian zone consists of Paleozoic highly deformed and metamorphosed rocks (Mountrakis, 1983). Papanikolaou (1984) divided the Pelagonian basement into two units. The Northern, Kastoria unit and the Southern, Flambouron unit. Upper Paleozoic plutons intrude both units. These plutons are deformed and metamorphosed in the greenschist, low grade phase due to the Alpine deformation of Late Jurassic-Early Cretaceous. The majority of the plutonic rocks contain acid to intermediate and basic members. Moreover, mafic dykes intrude these plutons. Some of these dykes are referred as "amphibolites" due to the metamorphism they have been subjected to, although they are not typical amphibolites. The aim of this study is to present new analytical data for dykes intruding the East Varnountas pluton and compare the former with the rest mafic igneous rocks (both plutonic and dykes).

The study areas are the pluton of Varnountas (VAR) (Koroneos, 1991), Namata-Ardassa (ARD) (Spyropoulos, 1992), Olympiada (OLY) (Pe-Piper et al., 1993a), Verdikoussa (VER) (Pe-Piper et al., 1993b), the plutonic complex of Pieria and specifically Pieria-Katafygion (KAT) (Kotopouli et al., 2000) and Pieria-Kastania (KAST) (Schenker et al., 2014), and lastly Livadi (LIV) (Nance, 1977).

The data/characteristics for these igneous rocks and their mafic intrusions are gathered and summarized in Table 1.

Table 1. Data for North Pelagonian plutons with mafic intrusions

Areas		**Rock types**	**SiO_2**	**K_2O vs SiO_2**	**Age**	**Group**
	Varnountas (VAR)	Granitoids intermediate-acid	51-76%	Calc-alkaline	297±5 Ma & 290-280 Ma	I
		Mafic member (MME+Mz-diorite)	48-57%			
		Dolerites	44-49%	Tholeiitic	292± 4.1 Ma ?	III
	Namata-Ardassa (ARD)	Dolerites	45-49%	Tholeiitic	< Permian-Triassic	III
	Olympiada (OLY)	Granitoids intermediate-acid	62-69%	Calc-alkaline	290 Ma	I
		Mafic member (MME+diorite)	47-54%			
		Diabase	56-60%	Calc-alkaline	< 290 Ma	II
	Verdikousa (VER)	Granitoids intermediate-acid	63-74%	Calc-alkaline	288±7 Ma	I
		Mafic member (early diorite)	48-52%			
		Diorite Intrusion (late diorite)	46-49%	Tholeiitic	< 288±7 Ma	III
Pieria		Granitoids intermediate-acid	60-79%	Calc-alkaline	302±5 Ma	I
	Katafygion (KAT)	Meta-diorite sheets	47-50%	Tholeiitic	< Permian-Triassic	III
		Amphibolitic dykes	46-47%	Tholeiitic	< Permian-Triassic	III
	Kastania (KAST)	Andesitic dyke	60%	Calc-alkaline	279 Ma	II
		Amphibolitic dykes	49-52%	Tholeiitic	245±1.3 Ma	III
	Livadi (LIV)	Granitoids		Calc-alkaline	307±4 Ma	I
		Phengitic Amphibolitic dykes			< 307±4 Ma	(II)
		Feldspar Amphibolitic dykes			< Permian-Triassic	(III)

On the basis of the geochemical features and age, the mafic igneous rocks of Table 1 can be divided into three groups:

The first (I) group (Late Carboniferous ~300 Ma) consists of the high-K calc-alkaline to shoshonitic mafic rocks with SiO_2 content ranging from 47 to 57%. They are result of the main calc-alkaline magmatism, during the Variscan orogen

in Europe. The intrusion age for (LIV) granite was studied by Zlatkin et al. (2017) who dated the (LIV) granite with U/Pb method resulting to the age of 307±4 Ma. The intrusion age for the (VAR) pluton (Table 1) was measured by Koroneos (1991) with Rb/Sr method. Additionally, Anders et al. (2007) dated the (VAR) pluton with single zircon Pb/Pb evaporation method, measuring mafic to felsic rocks, thus indicating the magma evolution. They proposed that the magma chamber was active for a few Ma (ca. 14), beginning at ca. 290 Ma up to ca. 280 Ma. The most mafic sample resulted to an age of 296±6 Ma. The geochemical characteristics of group I rocks are related with subduction.

The second (II) group consists of the calc-alkaline intrusions (SiO_2 ranges from 56 to 60%) with trachyandesitic-andesitic composition, i.e. (OLY) diabase, intruding the 290 Ma granitoids and (KAST) andesitic dyke. The latter has been studied geochronologically by Schenker et al. (2014) with U-Pb method on zircons resulting to an intrusion age at 279±8.1 Ma. The phengitic amphibolitic greenish dykes intrude the Livadi (LIV) granite (Nance, 1977), with sharp contacts. Since their composition is unknown, it's not clear whether they are part of group II. The calc-alkaline dykes of group II are attributed to the extension during the last stages of the subduction (Schenker et al., 2014).

The third (III) group consists of the tholeiitic intrusions (SiO_2 ranges from 44 to 50%) with basaltic and andesitic composition, i.e. (VAR) dolerites, (ARD) dolerites, (VER) diorite intrusion, (KAT) meta-diorite sheets and amphibolitic dykes and (KAST) amphibolitic dykes. The age of the (ARD), (KAT) and (LIV) (Feldspar Amphibolitic dykes) intrusions is estimated, using relative dating. These rocks intrude the upper Permian-Triassic volcano-sedimentary sequence, so they are younger than at least ca. 260 Ma. Schenker et al. (2014) consider the age of the (KAST) amphibolitic dykes to be similar to that of the augengneiss (245±1.3 Ma) in which they are within, since the dykes represent the mafic magma of bimodal magmatism. The tholeiitic dykes of this group are attributed to the Triassic rifting of Tethys Ocean that developed the Vardar/Axios basin (Schenker et al., 2014). It is to note that the tholeiitic (VAR) dolerites, intruding the calc-alkaline (VAR) pluton, have been dated with U/Pb method (SHRIMP) in zircons (Katerinopoulos, 2008) yielding an intrusion age of 292±4.1 Ma similar to the age of the (VAR) pluton (297±5 Ma). Whereas, according to Anders et al. (2007) at ca. 292 Ma the (VAR) pluton was still crystalizing. However, despite the age of the (VAR) dolerites, which is similar to the group I and II rocks, their composition and geochemical characteristics resemble those of the group III rocks (tholeiitic affinity, REE patterns, multi-element spider diagrams etc.) and are significantly different from those of the group I and II rocks. In detail, a comparison of the (VAR) dolerites with the (VAR) mafic rocks (with similar SiO_2 content) indicates significant differences in ΣREE content, LREE/HREE enrichment and multi-element spider diagrams. They differ also in the $^{87}Sr/^{86}Sr_{T=300}$ ratio which is 0.7040 and 0.7052 in (VAR) dolerites (2 samples) whereas it is 0.7058 in one (VAR) mafic rock (Mz-diorite).

The common tholeiitic composition along with many other geochemical similarities among the (VAR) dolerites and the rest of the tholeiitic intrusions imply their common genesis, which would be Permian-Triassic and/or younger, related to the Triassic rifting of Tethys Ocean. On the contrary, the significant geochemical differences between the (VAR) dolerites and the (VAR) mafic rocks indicate that they are different magmatic products, originated by different mantle melts, related to different geotectonic environment. The above differences, imply that an age difference between the (VAR) dolerites and the (VAR) mafic rocks exists.

References

Anders, B., Reischmann, T., and Kostopoulos, D., 2007. Zircon geochronology of basement rocks from the Pelagonian Zone, Greece: constraints on the pre-Alpine evolution of the westernmost Internal Hellenides. Int. J. Earth Sci., 96, 639-661.

Katerinopoulos, A., 2008. Variscan basic dykes in the Pelagonian (Northern Greece and south FYROM): Geodynamic significance based on petrological, geochemical and geochronological studies. Chemie der Erde, 68, 93-103.

Koroneos, A., 1991. Mineralogy, petrology and geochemistry of Eastern Varnountas plutonite. Ph.D. Thesis, Aristotle University of Thessaloniki, Thessaloniki, 451p (in Greek with English abstr.).

Kotopouli, N.C., Pe-Piper, G., Piper, J. W. D., 2000. Petrology and evolution of the Hercynian Pieria Granitoid Complex Thessaly, Greece): paleogeographic and geodynamic Implications. Lithos, 50, 137-152.

Mountrakis, D. M., 1983. Structural geology of the North Pelagonian zone s.l. and geotectonic evolution of the Internal Hellenides (Macedonia, Greece). Doz. Thesis, Aristotle University of Thessaloniki, Thessaloniki, 289p (in Greek with English abstr.).

Nance, R. D., 1977. The Livadi Mafic-Ultramafic Complex and its metamorphic basement, NE Greece. Ph.D. Thesis. University of Cambridge, Cambridge, 184p.

Papanikolaou, D. J., 1984. The three metamorphic belts of the Hellenides: a review and a kinematic interpretation, in Dixon, J.E. & Robertson, A.H.F. (Eds), The Geological Evolution of the Eastern Mediterranean. Geol. Soc. London, 17, 649-659.

Pe-Piper, G., Doutsos, T., Mijara, A., 1993a. Petrology and regional significance of the Hercynian granitoid rocks of the Olympiada area, northern Thessaly, Greece. Chemie der Erde, 53, 21–36.

Pe-Piper, G., Doutsos, T., Mporonkay, C., 1993b. Structure, geochemistry and mineralogy of Hercynian granitoid rocks of the Verdikoussa area, northern Thessaly, Greece and their regional significance. Neues. Jahrb. Mineral., Abh., 165, 267–296.

Schenker, F. L., Burg, J. P., Kostopoulos, D., Moulas, E., Larionov, A., von Quadt, A., 2014. From Mesoproterozoic magmatism to collisional Cretaceous anatexis: Tectonomagmatic history of the Pelagonian Zone, Greece. Tectonics, 33, 1552–1576.

Spyropoulos, N., 1992. Contribution to the study of the geological structure of the Pelagonian zone on Mountain Askio (Western Macedonia). Ph.D. Thesis, Aristotle University of Thessaloniki, Thessaloniki, 251p (in Greek with English abstr.).

Zlatkin, O., Avigad, D., & Gerdes, A., 2017. The Pelagonian terrane of Greece in the peri-Gondwanan mosaic of the eastern Mediterranean: Implications for the geological evolution of Avalonia. Precambrian Research, 290, 163– 183.

16th International Congress of the Geological Society of Greece
17-19 October, 2022 - Patras, Greece
Bulletin of the Geological Society of Greece, Sp. Publ. 10
Ext. Abs. GSG2022-208

Petrology and geochemistry of the Variscan Kastoria pluton

I. Gerontidou[1], A. Koroneos[1], A. Dretaki[2]

(1) Department of Mineralogy-Petrology-Economic Geology, Faculty of Geology, Aristotle University of Thessaloniki, Thessaloniki, Greece, ioangero@geo.auth.gr. (2) Department of Geography, University of Aegean, Mytilene, Greece.

The petrography and geochemistry of the Carboniferous Kastoria pluton, consisting of granites, aplites and MME is studied. Enriched mantle is the magma source and its genesis is related to an active continental margin.

Introduction

The Kastoria pluton is located in Mt. Vernon, NE of Kastoria city, Macedonia, Greece, intruding the Pelagonian zone basement (Mountrakis, 1983). The aim of this study is to present new analytical data for the granitoids and mafic microgranular enclaves (MME) consisting the Kastoria pluton and examine their petrography and geochemistry. The Kastoria pluton was dated by Zlatkin et al. (2017) using U/Pb method on zircons yielding a Late Carboniferous intrusion age (302±2 Ma) identical to the age given by Mountrakis (1983) and similar with other Variscan plutons intruding the Pelagonian zone (Koroneos et al., 2000).

Petrography and mineralogy

The Kastoria granitoids are coarse-grained porphyritic rocks, showing a greenish-grey colour due to the alteration of the plagioclase. They are weakly to intensively deformed and epizonal metamorphosed. MME of variable shape, reaching up to 50 cm in length are abundant. They are fine to medium grained and more melanocratic than their host rocks with crenulated margins. Aplitic veins are rare. The granitoids are classified as Bi-Hb-granites and the MME as quartz-monzonite to monzonite. The granitoids consist of quartz, plagioclase, K-feldspar, biotite and amphibole (Grigoriadou et al., 2003). The accessory minerals are apatite, titanite, zircon and allanite. Secondary minerals such as sericite, epidote after plagioclase, chlorite after hornblende and iron-oxides are also present. Biotite is mainly altered to chlorite and to colourless mica mainly in MME. The MME have similar mineralogy to their host granites but with a higher proportion of ferromagnesian minerals. K-feldspar, in the granites, is slightly caolinized and perthitic microcline. The megacrysts, of up to 5 cm in length contain quartz and albite after plagioclase. Microcline in MME is more abundant than plagioclase, perthitic and slightly caolinized.

K-feldspar varies from $Or_{94}Ab_6$ to $Or_{97}Ab_3$ in the granite and from $Or_{92}Ab_8$ to $Or_{95}Ab_5$ in the MME. Plagioclase is entirely altered to albite with a composition ranging from $Ab_{97.3}$ to $Ab_{99.7}$ in the granite and $Ab_{95.6}$ to $Ab_{98.5}$ in the MME. Amphiboles are of magnesiohornblende to edenite (hornblende) in composition. In many cases crystals have been marginally altered to actinolite; sometimes it is entirely altered to actinolite and not rarely to chlorite. Biotite is present in both rock types. The MgO content of the biotites in granite ranges from 10.9 to 13.5%, whereas it is lower than 4% in the colourless biotites of MME. TiO_2 ranges from 0.5 to 1.2% in the granites and 0.2 to 0.4% in the MME. Epidote is present in both rock types as idiomorphic to hypidiomorphic secondary mineral. The Ps in epidote ranges from 29 to 36%, implying their secondary origin (Naney, 1983). Dark brown allanite enriched in LREE (LREE=16-17%) is also present.

The plagioclase replacement by epidote plus albite, the formation of chlorite at the expense of biotite, the existence of actinolite in replacing of magmatic amphibole and the large idiomorphic crystals of titanite along with the fine-grained white mica parallel to the schistosity and the granoblastic quartz grain fabric are all indications of greenschist-facies metamorphism.

Geochemistry

The SiO_2 content of the host granitoid rocks ranges from 66 to 72%, whereas in the MME ranges from 49 to 61%. Their composition varies from high-K calc-alkaline to shoshonitic (Peccerillo & Taylor, 1976). The granites range from peraluminous to metaluminous and the MME are metaluminous (Maniar & Piccoli, 1989). Al_2O_3, Fe_2O_3, MgO, CaO, TiO_2 and P_2O_5 decrease with increasing SiO_2, and total alkalies increase. MME are more enriched in TiO_2 (0.6-1.5%) than the granites (0.2-0.5%). The trace elements Sr, Ba, V, Y, Zn and Zr decrease with differentiation while Rb increases. The transitional elements Ni and Cr remain almost constant. The major and trace elements of the MME show similar behaviour except the Al_2O_3, and Na_2O increase, the Ni and Cr decrease and K_2O, Ba and Zn that remain constant. Two groups of enclaves can be recognized on the basis of Zr content; one with Zr content higher than 280 ppm and another with lower than 240 ppm.

The LREE of granites and MME are enriched relative to the HREE as indicated by the $(La/Yb)_{CN}$ values ranging from 9.3 to 13.2 in granites and 5.4 to 13.6 in MME. $(La)_{CN}$ is 26 to 64 in granites and 32 to 88 in MME. MME are more enriched in REE than granites. ΣREE ranges from 94 to 148 in granites and 143 to 313 in MME. ΣREE decreases with

differentiation in both rock types, from the MME to the granites implying that the accessory minerals control the REE behavior. The REE pattern (Fig.1b) show negative Eu anomaly (Eu/Eu* ranges from 0.87 to 0.99 in granites and 0.74 to 0.81 in MME). The samples analyzed show negative Nb, Ba and Ti anomalies and positive U, Rb and Pb anomalies in the multi-element spider diagram (Fig.1a).

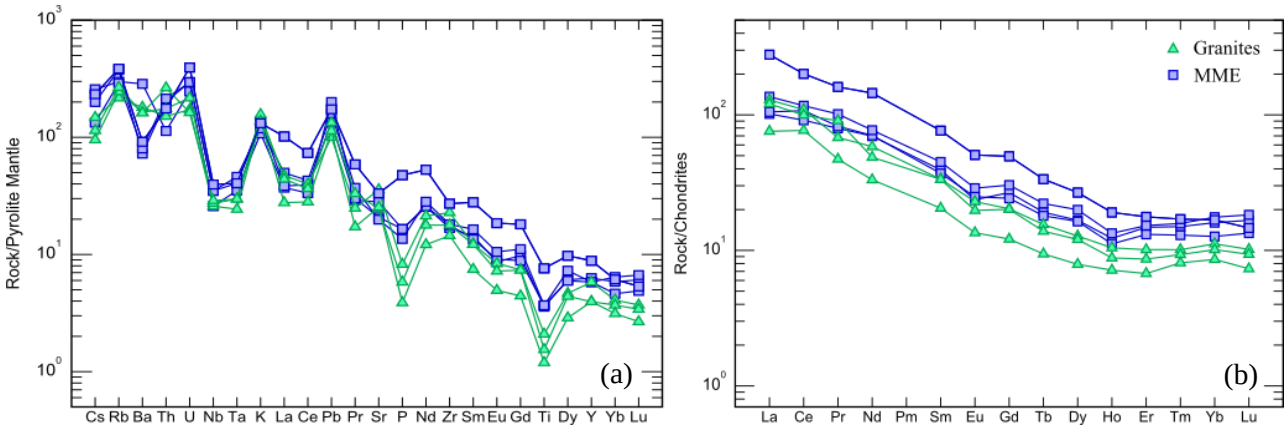

Figure 1. Multi-element spider diagram (a) and REE spider diagram (b) (McDonough & Sun 1995) for Kastoria rocks.

Isotopic data

Whole rock $(^{87}Sr/^{86}Sr)_{T=300}$ ratio ranges from 0.70576 to 0.70587 for the granites and from 0.70577 to 0.70674 for the MME. $(^{143}Nd/^{144}Nd)_{T=300}$ ratio ranges from 0.5121 to 0.51211 for the granites and from 0.51212 to 0.51218 for the MME. On a $(^{87}Sr/^{86}Sr)_{T=300}$ vs $(^{143}Nd/^{144}Nd)_{T=300}$ plot, two different trends are formed for granites and MME respectively, thus implying two different magma sources. Using the isotope correlation diagram of Zindler & Hart (1986) both the granites and the MME plot between the Enriched Mantle I and Enriched Mantle II field.

Petrogenesis

According to the Al-in-hornblende barometer of Schmidt (1992) the crystallization pressure varies from 3.8 to 4.1 kb for the MME and from 2.3 to 4.4 kb for the host rocks. This is in accordance with the absence of magmatic epidote.

The rocks plot in the field of active continental margin granites in the tectonic discrimination diagrams of Pearce et al. (1984) and Gorton & Schandl (2002). Using the petrogenetic discrimination diagrams the granites plot in the field of I-type granites, mantle derived with crustal contamination.

The characteristic anomalies in the multi-element spider diagrams are typical for subduction related magmas. The similarities of the REE and the multi-element spider patterns imply that the granites and MME are co-magmatic, however this is not supported by the two different trends, for granites and MME, on the $(^{87}Sr/^{86}Sr)_{T=300}$ vs $(^{143}Nd/^{144}Nd)_{T=300}$ plot.

A process of mixing plus fractional crystallization is considered responsible for the evolution of the Kastoria pluton. The least evolved MME represent the mafic end member.

References

Gorton, M. P. & Schandl, E. S., 2002. From Continents to Island Arc: A Geochemical Index of Tectonic Setting for Arc-Related and within Plate Felsic to Intermediate Volcanic Rocks. Canadian Mineralogist, 38, 1065-1073.

Grigoriadou, A., Koroneos A., Eleftheriadis, G., 2003. Mineralogy of The Kastoria pluton (W. Macedonia). Bull. Geol. Soc. Greece, 35, 46-60 (in Greek with English abstr.).

Koroneos, A., Soldatos, T., Christofides, G., Gerouki, F., 2000. Comparative geochemical study of north pelagonian zone plutons. Proc. Irst Symp. Com. Econ Geol. Min. Petrol. Geol. Soc. Greece, 243-260 (in Greek with English abstr.).

Maniar, P. D., & Piccoli, P. M., 1989. Tectonic discrimination of granitoids. GSA Bulletin, 101, 635-643.

McDonough, W. & Sun, S., 1995. The composition of the earth. Chemical Geology, 120, 223-253.

Mountrakis, D. M., 1983. Structural geology of the North Pelagonian zone s.l. and geotectonic evolution of the Internal Hellenides (Macedonia, Greece). Doz. Thesis, Aristotle University of Thessaloniki, Thessaloniki, 289p. (in Greek with English abstr.).

Naney, M. T., 1983. Phase equilibria of rock-forming ferromagnesian silicates in granitic systems. Am. J. Sci, 283, 993-1033.

Pearce, J. A., Harris, N. B., Tindle, A. G., 1984. Trace Element Discrimination Diagrams for the Tectonic Interpretation of Granitic Rocks. Journal of Petrology, 25, 956–983.

Peccerillo, A., & Taylor, S. R., 1976. Geochemistry of Eocene calc-alkaline volcanic rocks from the Kastamonu area, Northern Turkey. Contrib. Mineral Petrol., 58, 63-81.

Schmidt, M. W., 1992. Amphibole composition in tonalite as a function of pressure: an experimental calibration of the AI-in-hornblende barometer. Contrib. Mineral Petrol., 110, 304-310.

Zindler, A. & Hart, S. R., 1986. Nd, Sr and Pb isotopic systematics in a three-component mantle: a new perspective. Nature, 298, 519-523.

Zlatkin, O., Avigad, D., Gerdes, A., 2017. The Pelagonian terrane of Greece in the peri-Gondwanan mosaic of the eastern Mediterranean: Implications for the geological evolution of Avalonia. Precambrian Research, 290, 163– 183.

16th International Congress of the Geological Society of Greece

17-19 October, 2022 - Patras, Greece

Bulletin of the Geological Society of Greece, Sp. Publ. 10

Ext. Abs. GSG2022-221

High-pressure minerals and hydrated phases in the Kakowa (L6) ordinary chondrite meteorite

I. P. Baziotis[1], C. Ma[2], Y. Guan[2], L. Ferrière[3], S. Xydous[1], J. Hu[2], M. A. Kipp[2], F. L. H. Tissot[2], P. D. Asimow[2]

(1) Agricultural University of Athens, Athens, Greece, ibaziotis@aua.gr (2) California Institute of Technology, Pasadena, USA (3) Natural History Museum Vienna, Vienna, Austria

Herein, we report on the finding and characterization of high-pressure (HP) minerals as well as an assemblage of detrital fracture-fill minerals, including hydrous phases like margarite, in the Kakowa L6 ordinary chondrite meteorite (fall in Romania on May 19th 1858; shock stage S4-S5) (Baziotis *et al*., 2022).

The effects of collisions on the evolution of asteroids, from local brecciation to catastrophic disruption, depend primarily on the encounter velocity and their relative sizes. The most direct evidence for the strong collisions is the preservation of HP phases in meteorites. Moreover, the meteorites preserve evidence of the modifications that primitive solar system material experienced due to processes such as thermal metamorphism and fluid alteration on their parent bodies. As such, evidence for the action of liquid water is the preservation of secondary hydrous minerals, which have so far mostly been documented in carbonaceous chondrites (e.g., Brearley and Krot, 2013).

The discovered HP minerals and detrital minerals were studied using optical and electron microscopy, electron probe microanalysis (EPMA), micro-Raman spectroscopy, and electron back-scatter diffraction (EBSD). In addition, we also obtained in situ oxygen isotope ratios of some mineral phases by secondary ion mass spectrometry (nanoSIMS) and Pb isotope ratios by multi-collector inductively-coupled plasma mass spectrometry (MC-ICP-MS).

A high-velocity collision led to the formation of melt veins (MV; 300-360 μm wide) that preserve the HP minerals (Figs. 1A-F,2) majorite (two groups: $Na_{0.05–0.09}Ca_{0.12–0.19}Mg_{3.22–3.35}Fe_{0.45–0.67}Al_{0.21–0.38}Si_{3.69–3.75}O_{12}$ and $Ca_{0.04–0.05}Mg_{3.20–3.29}Fe_{0.75–0.89}Mn_{0.02–0.03}Al_{0.01–0.02}Si_{3.87–3.92}O_{12}$), magnesiowüstite, ringwoodite, wadsleyite, and albitic jadeite [$Na_{0.65}Ca_{0.08}K_{0.05}\square_{0.22})(Al_{0.81}Si_{0.17}Fe_{0.02})Si_2O_6$]. The maximum P-T conditions recorded by the HP polymorphs are 23 GPa and 2100 °C.

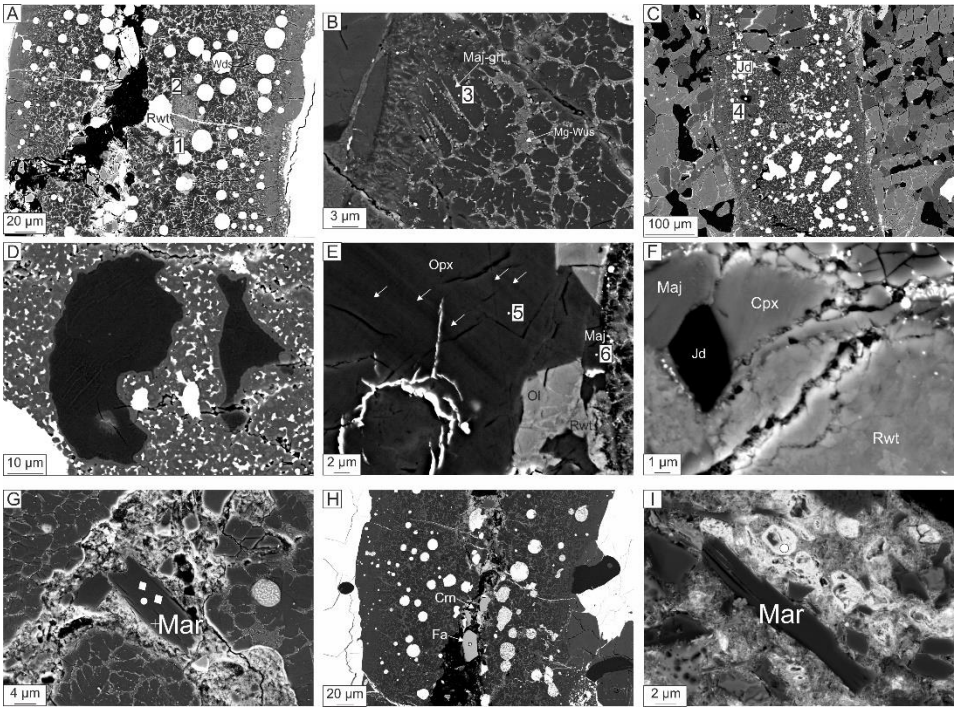

Figure 1. (A-F) BSE images of MVs in Kakowa. (A) MV1a, showing ringwoodite (Rwt) (#1; Raman spectrum MV1a-1 in Fig. 2) in close association with wadsleyite (#2; Raman spectrum MV1a-2 in Fig. 2). (B) MV1b, with fine intergrowth of majorite-pyrope solid solution (Maj-grt) (#3, Raman spectrum MV1b-3 in Fig. 2) and magnesiowüstite (Mg-Wus). (C) MV2, hosting albitic jadeite (Jd) (#4; Raman spectrum MV2-4 in Fig. 2). (D) Glass of feldspathic composition in MV2 showing albitic jadeite lamellae. (E) Groundmass orthopyroxene (Opx) (#5; Raman spectrum MV1b-5 in Fig. 2) in contact with MV1b. The bands across the Opx are likely mechanical twin planes (indicated by white arrows) due to shock. Further, at the

contact with MV, Opx is transformed to majorite (#6; Raman spectrum MV1b-6 in Fig. 2) and olivine (Ol) is partly transformed to ringwoodite. (F) MV2, Albitic jadeite in contact with majorite and ringwoodite. (G-I) BSE images of the occurrence of exogenous material in Kakowa. (G) Margarite crystal; the white squares indicate the location of nano-SIMS O-isotope analysis points. The white circle indicates the location of margarite Raman spectrum given in Fig. 2. The white cross indicates the location of margarite EBSD analysis. (H) Corundum (Crn) and Fayalite (Fa) crystals in the exogenous material show an angular shape. (I) BSE image of elongated margarite in fine-grained material from exogenous fracture fill.

A subsequent low-velocity impact event created through-going fractures that cross-cut the melt veins and are filled with a unique assemblage of detrital grains from a brecciated and aqueously-altered object, including corundum, albite, silica, fayalite ($Fa_{99–100}$), forsterite ($Fa_{25–26}$), and the hydrous phase margarite [$Ca_{0.97}Na_{0.03}Fe_{0.06}Al_{3.94}Si_{2.02}O_{10}(OH)_2$] in a Pb-/Fe-rich matrix (Fig. 1G-I).

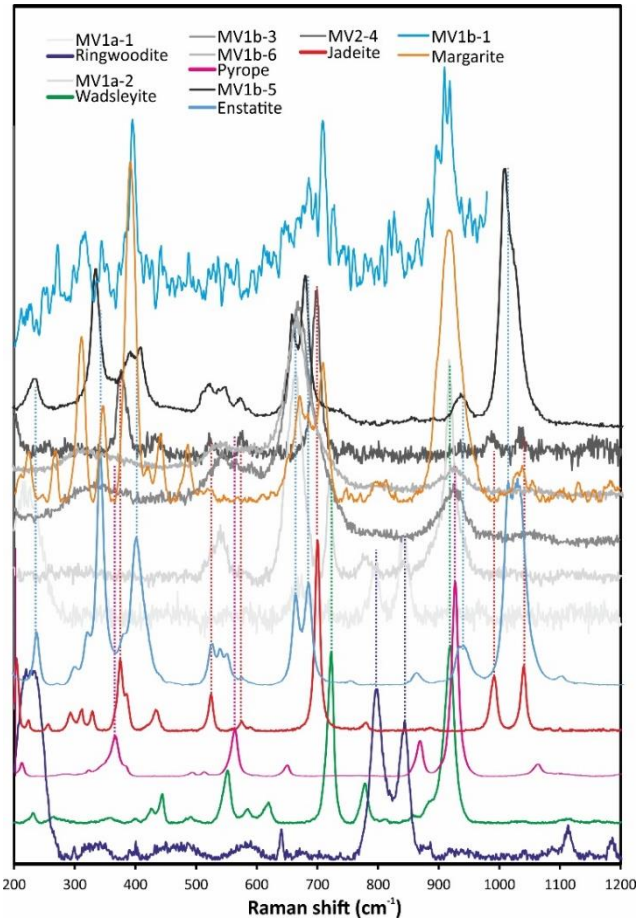

Figure 2. Selected Raman spectra of HP and hydrated minerals in the Kakowa meteorite compared to reference spectra for ringwoodite (RRUFF R070079), wadsleyite (RRUFF R090004), jadeite (RRUFF R050220.2), pyrope (RRUFF R080060), enstatite (RRUFF R040094-3), and margarite (RRUFF R060839).

Isotope ratios of oxygen in the detrital phases and of lead ($^{206}Pb/^{204}Pb = 18.385$, $^{207}Pb/^{204}Pb = 15.615$, $^{208}Pb/^{204}Pb = 38.692$) in the fracture matrix together exclude a carbonaceous chondrite origin and suggest a likely ordinary chondrite source.

Kakowa is unique among ordinary chondrites, as it preserves both indications of a strong collision that disrupted the L-chondrite parent body, and of a weak collision that injected a novel hydrous assemblage into the meteorite mass.

Acknowledgements

I.B. thanks the EU-funded SYNTHESYS [AT-TAF-30] project, which provided funds for travel, accommodation funds, and instrument costs while using SEM and EPMA at the NHMW. Stamatios Xydous greatly thanks “The Barringer Family Fund for Meteorite Impact Research” for support. The authors are grateful to Dan Topa for assistance with the EPMA analyses.

References

Baziotis, I. P., Ma, C., Guan, Y., Ferrière, L., Xydous, S., Hu, J., ... Asimow, P. D. (2022). Unique evidence of fluid alteration in the Kakowa (L6) ordinary chondrite. Scientific reports, 12(1), 1-15.

Brearley, A. J., Krot, A. N. (2013). Metasomatism in the early solar system: The record from chondritic meteorites. In Metasomatism and the chemical transformation of rock (pp. 659-789). Springer, Berlin, Heidelberg.

16th International Congress of the Geological Society of Greece
17-19 October, 2022 - Patras, Greece
Bulletin of the Geological Society of Greece, Sp. Publ. 10
Ext. Abs. GSG2022-234

Potentially Toxic Elements in House Dust of Cyprus Homes: Contribution to the Global DustSafe Database

A. Argyraki[1], A. Pitsillis[1], J.A. Entwistle[2], L. Bramwell[2], A. Zissimos[3], I. Christoforou[3]

(1) National and Kapodistrian University of Athens, Department of Geology and Geoenvironment, 15784 Athens, Greece, argyraki@geol.uoa.gr, (2) Northumbria University, Department of Geography and Environmental Sciences, Engineering and Environment, Newcastle, NE1 8ST, UK, (3) Ministry of Agriculture Natural Resources and Environment, Geological Survey Department, 2064 Lefkosia, Cyprus

Research Highlights

Concentrations of Potentially Toxic Elements (PTEs) in house dust of Cyprus homes are presented for the first time. House dust is enriched in Cr, Cu, Pb and Zn against respective contents in Cyprus soil and slightly enriched in Cr, Mn and Ni compared to the global DustSafe residential dust database as well as house dust of urban areas in Greece.

Background and Research Objectives

House dust is a heterogeneous mixture of organic and inorganic particles that serves as a reservoir for a variety of pollutants and can provide insight into both geogenic and technogenic sources of Potentially Toxic Elements (PTEs) in residential environments. The pollutants encountered in a living space might include PTEs and a variety of organic pollutants (Turner, 2011; Kurt-Karakus, 2012). Soil and street dust particles are common sources of interior house dust, while indoor sources of harmful elements in household dusts include cigarette smoking, cosmetics, paint chips, etc. Research interest concerning the composition of house dust has been on a rise during recent years, especially because of the noted health risks from exposure to PTEs laden finely grained material globally (Isley et al., 2021).

The objectives of the present study is to provide for the first time estimates of PTEs contents in house dust of Cyprus homes and compare them to those reported in Greece and worldwide as part of the global DustSafe database (www.mapmyenvironment.org), as well as to concentrations in Cyprus soil reported in the literature. Specifically, the study is focused on seven PTEs (As, Cr, Cu, Mn, Ni, Pb, Zn) in house dust collected from homes located within the urban areas of Nicosia (Lefkosia) and Limassol (Lemesos), and from Mitsero village which lies in close proximity to an abandoned open pit Cu-mine.

Materials and Methods

Thirty-eight vacuum dust samples were collected from homes of Nicosia (10), Limassol (19), and Mitsero (9), following the protocol of the Home Biome –DustSafe citizen-science study (Isley et al., 2021) from May to September 2021. Participants filled out an online questionnaire which records household information and handed in their vacuum cleaner bags. In the laboratory, samples were sieved to 250 μm using a single-use polypropylene mesh and analyzed for the seven trace elements using energy-dispersive X-ray fluorescence spectrometry (EDXRF). Summary statistic calculations and ANOVA comparisons were performed in Minitab 17 using the Tukey-Kramer multiple comparison tests to assess differences in concentrations between the 3 sampling locations.

Results and Conclusions

The ranges of PTE concentrations are presented as boxplots in Figure 1. The summary statistics of all samples and the comparison with literature data are presented in Table 1.

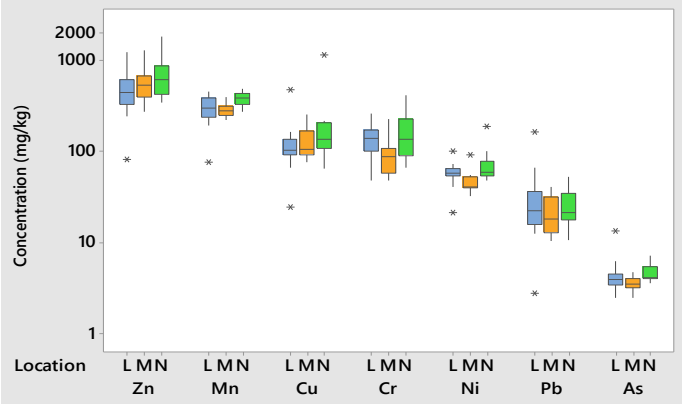

Figure 1. Ranges of PTE concentrations in house dust from Limassol (L), Mitsero (M) and Nicosia (N) in Cyprus.

In general, samples from the urban area of Nicosia presented higher median values than Limassol and Mitsero for all studied elements. However, statistically significant differences (ANOVA on log-transformed data, $p<0.05$) were calculated only for Cr and Ni between Nicosia and Mitsero, and Mn between Nicosia and Limassol. The mining legacy of Mitsero was not evident based on the data of present research.

The order of decreasing medians of all studied elements and all samples is: Zn > Mn > Cr > Cu > Ni >Pb >As. Enrichment factors (EF) were calculated using eq. 1 to provide indication of the impact of anthropogenic activities on dust concentrations. Manganese was selected as the reference element (RE) as being mainly a geogenic element and to achieve comparable results with the global DustSafe study (Isley et al., 2021).

$$EF = \frac{\left(\frac{TE}{RE}\right)dust}{\left(\frac{TE}{RE}\right)crust} \quad \text{(eq. 1)}$$

EFs greater than 2, suggesting anthropogenic influence, were calculated for Zn (EF=9.9), Cu (EF=4.6), Cr (EF=2.3) and Pb (EF=2.0), while the cumulative EF, calculated using the sum of EFs, was found equal to 21.2. It is noted that a lower cumulative EF has been reported only for Nigeria (cEF=10.5) in the DustSafe study.

Table 1. Summary statistics of elemental concentrations (mg/kg) in house dust of Cyprus (n=38) and comparison with literature data for dust and soil.

Element	As	Cr	Cu	Mn	Ni	Pb	Zn
Mean	4.30	139	157	316	60.0	28.8	579
Standard Deviation	1.79	75.0	181	86.1	26.7	26.4	324
Median	3.97	120	114	302	56.9	21.0	516
Minimum	2.45	47.3	24.5	75.4	21.3	2.73	81.2
Maximum	13.3	415	1150	488	187	162	1820
DustSafe database median[1] (n=1703)	13.3	86.0	176	257	39.0	94.0	1110
Greek house dust median[1] (n=35)	6.90	97.9	158	230	52.3	57.0	664
Volos (Greece) house dust median[2] (n=24)	31.7	163	167	274	81.0	63.2	785
Cyprus soil mean[3] (n=5377)	4.90	73.7	87.9	981	111	11.0	67.0
Nicosia soil median[4] (n=441)	5.50	36.0	44.5	617	33.3	7.70	60.5
Limassol soil median[5] (n=411)	4.50	55.4	42.5	531	52.2	8.69	49.0

1: Isley et al. 2021, 2: Kelepertzis et al., 2020, 3: Cohen et al., 2012, 4: Zissimos et al. 2018, 5: Zissimos et al. 2021

Further comparisons based on the median values reported in the DustSafe study reveal slight enrichment of Cyprus dust in Mn, Cr, and Ni possibly reflecting the influence of geogenic factors on the dust contents of these elements. The same pattern is observed after comparison with Greek dusts, while Mn content in Cyprus dust exceeds Mn in house dust of the industrial city of Volos in Greece (Kelepertzis et al., 2020). House dust is also enriched in Cr, Cu, Pb and Zn against respective contents in Cyprus soil (Cohen et al. 2012; Zissimos et al. 2018; Zissimos et al. 2021).

Overall, the present study is a further contribution to the open global DustSafe database and expands our knowledge on the country-specific characteristics of residential dust composition. Ongoing research will focus on the bioaccessibility of PTEs in order to shed more light on potential health risks related to PTEs in Cyprus house dust.

Acknowledgements

The authors are grateful for the support provided by the citizen scientists of Cyprus that shared their dust. This work was partially supported by the Natural Environment Research Council (Research Grant NE/T004401/1, U.K.) to J.E.

References

Cohen, D.R., Rutherford, N.F., Morisseau, E., Zissimos, A.M., 2012. Geochemical patterns in the soils of Cyprus. Sci. Tot. Environ., 420, 250–262.

Isley, C.F., Fry, K.L., Liu, X., Filippelli, G.M., Entwistle, J.A. et al., 2021. International Analysis of Sources and Human Health Risk Associated with Trace Metal Contaminants in Residential Indoor Dust. Environmental Science & Technology, 56, 2, 1053–1068.

Kelepertzis, E., Argyraki, A., Chrastny, V., Botsou, F., Skordas, K., Komárek, M., Fouskas, A., 2020. Metal(loid) and isotopic tracing of Pb in soils, road and house dusts from the industrial area of Volos (central Greece). Sci. Total Environ., 725, 138300.

Kurt-Karakus, P.B., 2012. Determination of heavy metals in indoor dust from Istanbul, Turkey: Estimation of the health risk. Environment International, 50, 47-55.

Turner, A., 2011. Oral bioaccessibility of trace metals in household dust: A review. Environmental Geochemistry and Health, 33, 331–341.

Zissimos, A.M., Cohen, D.R., Christoforou, I.C., 2018. Land use influences on soil geochemistry in Lefkosia (Nicosia) Cyprus. Journal of Geochemical Exploration, 187, 6–20.

Zissimos, A.M., Cohen, D.R., Christoforou, I.C., Sadeghi, B., Rutherford, N.F., 2021. Controls on soil geochemistry fractal characteristics in Lemesos (Limassol), Cyprus. Journal of Geochemical Exploration, 220, 106682.

16th International Congress of the Geological Society of Greece
17-19 October, 2022 - Patras, Greece
Bulletin of the Geological Society of Greece, Sp. Publ. 10
Ext. Abs. GSG2022-236

International Union of Geological Sciences Manual of Standard Methods for Establishing the Global Geochemical Reference Network

A. Demetriades[1], C.C. Johnson[2], D.B. Smith[3], A. Ladenberger[4], P. Adánez Sanjuan[5], A. Argyraki[6], C. Stouraiti[6], P. de Caritat[7], K.V. Knights[8], G. Prieto Rincón[9], G.N. Simubali[10]

(1) Institute of Geology and Mineral Exploration, Athens, Hellenic Republic, alecos.demetriades@gmail.com, (2) GeoElementary, Derby, United Kingdom, (3) IUGS Commission on Global Geochemical Baselines, Denver, USA, (4) Geological Survey of Sweden, Uppsala, Sweden, (5) Instituto Geológico y Minero de España, Madrid, Spain, (6) Department of Geology and Geoenvironment, National and Kapodistrian University of Athens, Athens, Hellenic Republic, (7) IUGS Commission on Global Geochemical Baselines, Canberra, Australia, (8) Dublin, Ireland, (9) Servicio Geológico Colombiano, Bogotá, Columbia, (10) Geological Survey of Namibia, Windhoek, Namibia.

Abstract

The mandate of Commissions of the International Union of Geological Sciences (IUGS) is to set standards in their own discipline. Therefore, the obligation of the Commission on Global Geochemical Baselines (CGGB) is to provide the standards for establishing the Global Geochemical Reference Network. The CGGB has recently published a Manual of Standard Methods for Establishing the Global Geochemical Reference Network (Demetriades *et al.*, 2022a). It presents, for the first time, a comprehensive overview of the standardised geochemical methods that should be employed across the land surface of the Earth to map the distribution of chemical elements in various media. Applying these methods will produce internally consistent quality-controlled data sets for each sampling medium for multipurpose use. The Manual provides extensive information on sampling protocols for rocks, residual soil, humus, stream water, stream sediments, overbank and floodplain sediments. There are also chapters discussing sample site selection; sample preparation; quality control procedures, including the development of project reference materials; analytical methods; data management; map preparation; project management; and information on how to level existing geochemical data sets. Any applied geochemist carrying out a geochemical mapping project at any scale should find a wealth of useful information within the pages of this Manual.

Introduction

The aims of the IUGS-CGGB are:

- To provide high quality geochemical baseline data for the terrestrial part of our home planet Earth,
- To establish a Geochemical Reference Network for levelling data sets of existing regional geochemical projects, and
- To provide reference samples and sites for future monitoring of the chemical state of the world's terrestrial surface.

Hence, the generated geochemical data must be of high quality, integrity and consistency.

Darnley *et al*. (1995) introduced the concept of producing a global-scale, multi-media geochemical atlas based on sampling according to the Global Geochemical Reference Network (GRN). The GRN is a grid-based sampling scheme comprised of 19,833 cells covering the whole globe (Fig. 1). Of these, 7356 cells, approximately 160x160 km in size, cover the land surface of the Earth, and are known as the Global Terrestrial Network (GTN). Figure 2 shows the catchment basin sampling scheme for a grid cell.

Methods

The Manual describes in detail all the necessary methods from planning the sampling campaign, through sample preparation, development of project reference materials, analytical methods, quality control and assurance procedures for the production of harmonised data sets, data levelling of existing regional geochemical data sets with respect to the established Global Terrestrial Network datum, data conditioning for the production of seamless geochemical maps, data management and map plotting and, finally, to project management (Demetriades *et al*., 2022a). As the sampling will cover the whole globe the sampling procedure must be consistent for all sample types and, therefore, is standardised to be applicable in all morphoclimatic environments. Taking into consideration the mode of formation of residual soil, stream, overbank and floodplain sediments, the medium that needs special attention is residual soil. The residual soil chapter has two annexes. The first describes the characteristics of the 28 major soil mapping units, namely Regosols, Leptosols, Gleysols, Cambisols, Podzols, Arenosols, Calcisols, Histosols, Luvisols, Fluvisols, Podzoluvisols, Acrisols, Ferralsols, Kastanozems, Chernozems, Phaeozems, Solonetz, Vertisols, Lixisols, Solonchaks, Gypsisols, Greyzems, Andosols, Planosols, Nitisols, Plinthosols, Anthrosols and Alisols. The second annexe provides annotated soil profiles and instructions on how to overcome sampling difficulties. The supplementary material provided in different chapters is useful not only for the global project, but also for geochemical mapping surveys at any scale.

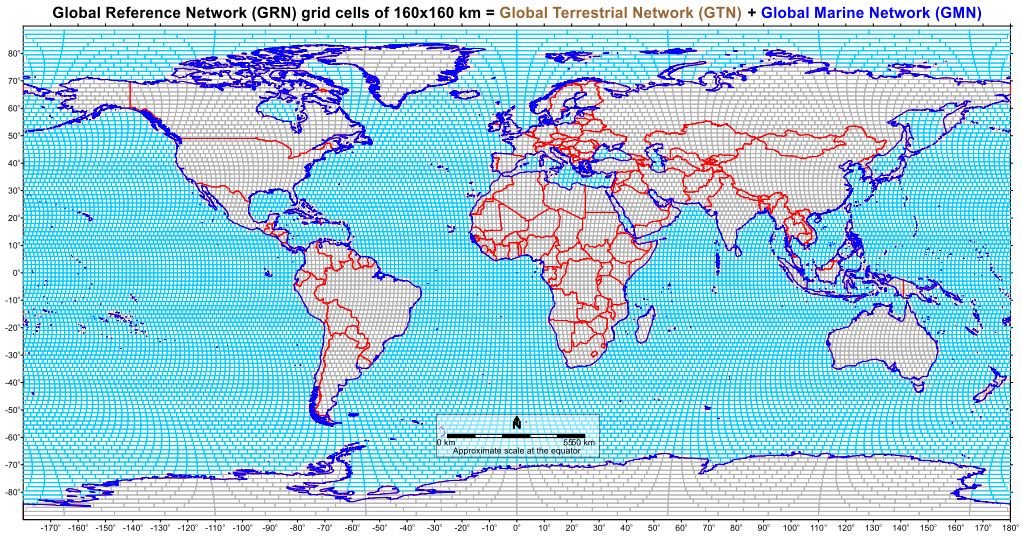

Figure 1. Map of the Global Reference Network (from Demetriades *et al.*, 2022b, Fig. 2.1, p.16).

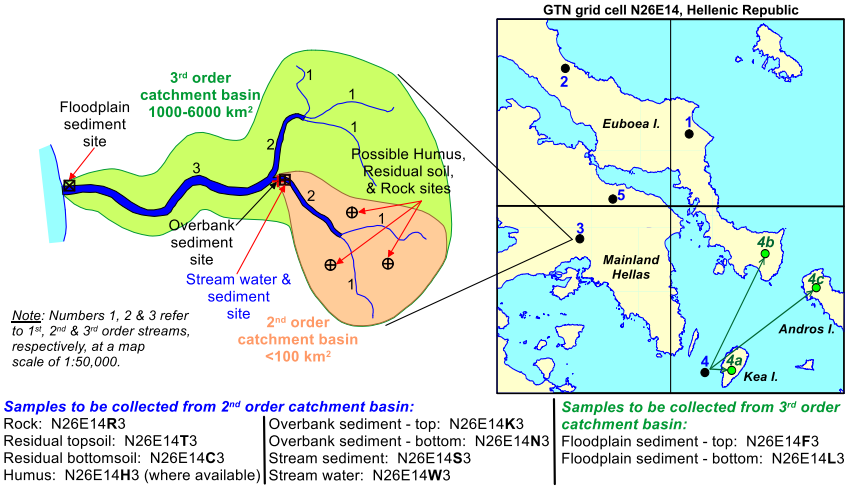

Figure 2. Example of GTN grid cell N26E14 with 5 random points, and a schematic diagram showing the catchment basin approach for collecting samples of rock, residual soil, humus, stream water and sediment, overbank and floodplain sediment (from Demetriades *et al.*, 2022b, Fig. 2.8, p.23).

Conclusions

The main aim of the Global Geochemical Reference Network project is the establishment of the geochemical baseline of chemical elements and compounds in natural surficial materials against which future changes can be quantified, whether natural or human-induced. Further, the generated analytical data, apart from their use as reference data for levelling the more detailed national geochemical data sets, will be used by many disciplines and for different purposes, including compliance with international or national regulatory limits.

References

Darnley, A.G., Björklund, A., Bølviken, B., Gustavsson, N., Koval, P.V., Plant, J.A., Steenfelt, A., Tauchid, M., Xuejing, X., Garrett, R.G., Hall, G.E.M., 1995. A global geochemical database for environmental and resource management. Final report of IGCP Project 259. Earth Sciences, 19, UNESCO Publishing, Paris, 122 pp., http://globalgeochemicalbaselines.eu.176-31-41-129.hs-servers.gr/datafiles/file/Blue_Book_GGD_IGCP259.pdf.

Demetriades, A., Johnson, C.C., Smith, D.B., Ladenberger, A., Adánez Sanjuan, P., Argyraki, A., Stouraiti, C., Caritat, P. de, Knights, K.V., Prieto Rincón, G., Simubali, G.N. (Eds.), 2022a. International Union of Geological Sciences Manual of Standard Methods for Establishing the Global Geochemical Reference Network. IUGS Commission on Global Geochemical Baselines, Athens, Hellenic Republic, Special Publication, 2, 515 pp., https://www.globalgeochemicalbaselines.eu/content/174/iugs-manual-of-standard-methods-for-establishing-the-global-geochemical-reference-network-/.

Demetriades, A., Johnson, C.C., Smith, D.B., Batista, M.J., 2022b. Global Terrestrial Network Grid Cells, Selection of Sample Sites and Sample Types to be Collected, in: Demetriades, A., Johnson, C.C., Smith, D.B., Ladenberger, A., Adánez Sanjuan, P., Argyraki, A., Stouraiti, C., Caritat, P. de, Knights, K.V., Prieto Rincón, G., Simubali, G.N. (Eds.), International Union of Geological Sciences Manual of Standard Methods for Establishing the Global Geochemical Reference Network. IUGS Commission on Global Geochemical Baselines, Athens, Hellenic Republic, Special Publication, 2, 11−26.

16th International Congress of the Geological Society of Greece
17-19 October, 2022 - Patras, Greece
Bulletin of the Geological Society of Greece, Sp. Publ. 10
Ext. Abs. GSG2022-243

Differentiation and storage conditions of mafic magmas in Milos Volcanic Field: Insights from crystal cargo in basaltic andesites and gabbroic nodules

S. Xydous[1], I. Baziotis[1], A. Periferakis[2], J. Berndt[3], S. Klemme[3]

(1) Department of Natural Resources Management & Agricultural Engineering, Agricultural Univ. of Athens, Iera Odos 75, 11855 Athens, Greece, stxydous@aua.gr, (2), Deoartment of Physiology, The Carol Davila Univ. of Medicine and Pharmacy, 050474 Bucharest, Romania (3) Institute for Mineralogy, Westfälische Wilhelms-Universität Münster, Corrensstrasse 24, 48149, Münster, Germany

Detailed chemical characterization of gabbroic xenoliths and phenocrysts from the SW Milos basaltic andesites, indicate that the most mafic units in Milos, rather represent extracts from mid-upper crustal mushes, instead of primitive arc magmas. Plutonic xenoliths in volcanic deposits can provide valuable insights into deep magmatic processes in systems (e.g., arc magmas) that have experienced polybaric fractionation. The ~2.6 Ma basaltic andesite (BA) dykes and subordinate scorias of Katsibardos in SW Milos, intruded the submarine pumice breccias of the Basal Pyroclastic Unit (Fytikas *et al*., 1986; Zhou *et al*., 2021). This small center comprises the most mafic composition erupted in Milos, second only to mafic enclaves in intermediate domes. Recharge filtering within upper crustal mushes (Kent *et al*., 2010) is the most likely scenario for explaining the paucity of mafic magmas erupted on the surface (Xydous *et al*., 2021), with the scarce mafic centers representing eccentric activity from the main edifice. Therefore, the presence of gabbroic nodules (GN) and their relation to the host basaltic andesites (BA), offers rare insights into the petrogenetic evolution of primitive arc magmas, which were not severely modified while ascending through the arc crust.

Mineral major and trace element compositions in two polished thin section of GN and one of the host lavas were determined using a JEOL JXA8530F EPMA and a Thermo Fisher Scientific Element 2 sector field ICP-MS coupled to a Photon Machines Analyte G2 Excimer laser system, at the Institute für Mineralogie, University of Münster (Germany). The BA dykes display a moderately porphyritic texture, comprising plagioclase (An_{60-83}), clinopyroxene ($Wo_{35-49}En_{28-56}Fs_{5-23}$), low-Ca pyroxene ($Wo_{0-8}$; #Mg 57-73) and magnetite phenocrysts. Olivine (Fo_{73-77}) has been reported (Fytikas et al., 1986), although it was not found in the studied sections. The gabbroic nodules display a cumulate texture with plagioclase (An_{85-93}), clinopyroxene ($Wo_{40-49}En_{38-52}Fs_{5-15}$; 2.31-6.39 wt. %$Al_2O_3$; #Mg 74-91), and interstitial tholeiitic basaltic andesite glass (54.1-57.4 wt. % SiO2; #Mg 37-44), locally associated with cellular rims in cpx. Clinopyroxene in GN is characterized by variable Cr (2-715 μg/g), and low Sr (13-52 μg/g), Y (8-24 μg/g) and Zr (6-45 μg/g) contents. Chondrite normalized REE patterns are concave-downwards, with depleted LREE (La/Sm_N~0.22-0.56), absent to negative Eu anomaly (Eu/Eu*~0.64-1.05) and slightly fractionated MREE relative to HREE (Dy/Yb_N~1.04-1.55).

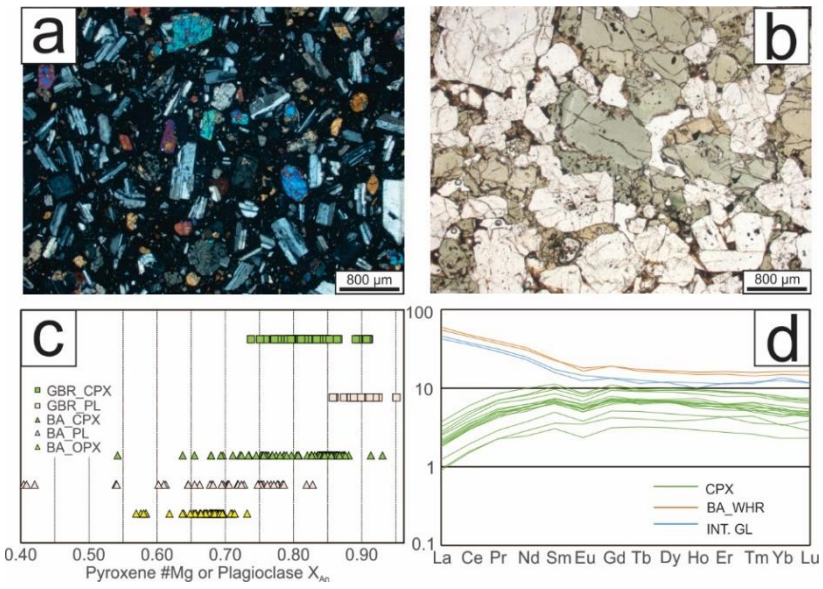

Figure 1. Representative photomicrographs of (a) basaltic andesite and (b) gabbroic nodule. Comparative mineral chemistry (c) between host lava and nodule minerals expressed as range of #Mg and X_{An}, (d) CI-chondrite normalized REE concentration of nodule cpx, interstitial glass and host lava whole rocks.

Gabbroic nodules from the SW Milos are characterized by the co-occurrence of primitive pl (An>85) and relatively evolved cpx (#Mg:74-91; Cr<1000 μg/g). Such an association has been reported from Nysiros (Klaver *et al*., 2017) and

other arc settings rich in plutonic xenoliths (e.g., Lesser Antilles; Cooper *et al*., 2016), and has been interpreted to result from shallow crystallization of already fractionated hydrous melts. Experimental studies (e.g., Sisson and Grove, 1993; Andujar *et al*., 2015) report this mineral assemblage at middle/upper crustal pressures (0.2-0.4 GPa) and in H_2O-saturated conditions. Geothermobarometry, using the cpx-only model (Higgins *et al*., 2022), yields pressure estimates in a similar range (0.2-0.5 GPa), and T ranging from 950-1090°C. Low Sr/Y ratio (0.69-2.5) in variable Y contents in GN cpx, holds additional evidence for shallow crystallization, where pl was a dominant fractionating phase. Significant involvement of amphibole is unlikely, as it would have resulted in near vertical trends in the Sr/Y vs Y space, and a would also have driven derivative melts to more silicic compositions. Simple FC modelling of REE of nodule interstitial glass yields similar patterns with BA after ~30% fractionation of $pl_{0.55}opx_{0.25}cpx_{0.1}ol_{0.1}$, rendering a plausible scenario that GN may represent mush fragments, where BA were extracted from. Whereas compositional gaps between BA and GN plagioclase may reflect different stages of magma evolution and a possible cumulate origin for the latter, clinopyroxenes seem to record a common fractionation history. Aluminum content in calculated cpx-equilibrium-melts from lavas and nodules, displays a negative trend until ~5.5 wt. % MgO, where a positive overturn, marks the appearance of pl. Thermodynamic modeling (using MELTS) reproduces the liquid line of decent outlined by cpx-eq. melts, in runs between 0.3-0.55 GPa under relatively dry conditions 1.5-2.5 wt % H2O, using an average continental arc basalt composition and fO_2 set at NNO. Our preliminary results, suggest that the mafic magmas erupted in Milos may represent extracts from gabbroic mushes in the middle crust, which subsequently evolved via degassing induced crystallization during their ascent to the surface.

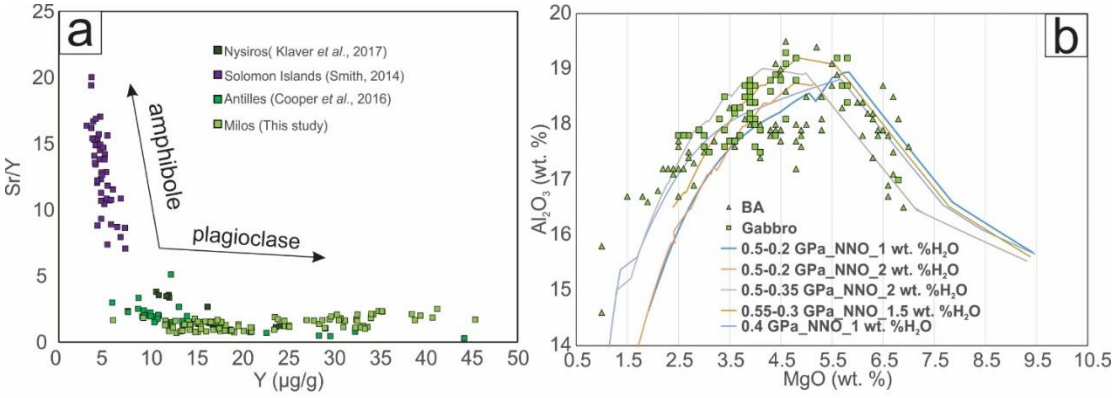

Figure 2. (a) Trace element content of cpx from SW Milos gabbroic nodules, plotted against cpx from various arc cumulate suites, (b) MELTS FC modelling of the LLD outlined from cpx-equilibrium melts.

Acknowledgements

The research work was supported by the Hellenic Foundation for Research and Innovation (HFRI) under the HFRI PhD Fellowship grant (Fellowship Number:364).

References

Andújar, J., Scaillet, B., Pichavant, M., & Druitt, T. H. (2015). Differentiation conditions of a basaltic magma from Santorini, and its bearing on the production of andesite in arc settings. Journal of Petrology, 56(4), 765-794.

Cooper, G. F., Davidson, J. P., & Blundy, J. D. (2016). Plutonic xenoliths from Martinique, Lesser Antilles: evidence for open system processes and reactive melt flow in island arc crust. Contributions to Mineralogy and Petrology, 171(10), 1-21.

Fytikas, M., Innocenti, F., Kolios, N., Manetti, P., Mazzuoli, R., Poli, G., ... & Villari, L. (1986). Volcanology and petrology of volcanic products from the island of Milos and neighbouring islets. Journal of Volcanology and Geothermal Research, 28(3-4), 297-317.

Higgins, O., Sheldrake, T., & Caricchi, L. (2022). Machine learning thermobarometry and chemometry using amphibole and clinopyroxene: a window into the roots of an arc volcano (Mount Liamuiga, Saint Kitts). Contributions to Mineralogy and Petrology, 177(1), 1-22.

Kent, A. J., Darr, C., Koleszar, A. M., Salisbury, M. J., & Cooper, K. M. (2010). Preferential eruption of andesitic magmas through recharge filtering. Nature geoscience, 3(9), 631-636.

Klaver, M., Matveev, S., Berndt, J., Lissenberg, C. J., & Vroon, P. Z. (2017). A mineral and cumulate perspective to magma differentiation at Nisyros volcano, Aegean arc. Contributions to Mineralogy and Petrology, 172(11), 1-23.

Sisson, T. W., & Grove, T. L. (1993). Experimental investigations of the role of H2O in calc-alkaline differentiation and subduction zone magmatism. Contributions to mineralogy and petrology, 113(2), 143-166.

Xydous, S., Baziotis, I., Bizimis, M., Klemme, S., Berndt, J., & Asimow, P. D. (2021, April). Identifying the components of Milos Island subvolcanic plumbing system (South Aegean Volcanic Arc, Greece): An amphibole perspective. In EGU General Assembly Conference Abstracts (pp. EGU21-4922).

Zhou, X., Kuiper, K., Wijbrans, J., Boehm, K., & Vroon, P. (2021). Eruptive history and 40 Ar⁄ 39 Ar geochronology of the Milos volcanic field, Greece. Geochronology, 3(1), 273-297.

16th International Congress of the Geological Society of Greece

17-19 October, 2022 - Patras, Greece

Bulletin of the Geological Society of Greece, Sp. Publ. 10

Ext. Abs. GSG2022-247

P-T constraints on upper and lower metamorphic unit rocks from Skyros Island

D. Boundi[1], I. Baziotis[2], J. Berndt[3], S. Klemme[3].

(1) National and Kapodistrian University of Athens, Athens, Greece, boundi.dimitra@hotmail.com (2) Agricultural University of Athens, Athens, Greece (3) Westfälische Wilhelms-Univ. Münster, Münster, Germany

We estimated the thermobarometric conditions for two tectonic units located in Skyros island; the Upper Metamorphic Unit-UMU of Olympus and the Lower Metamorphic Unit-LMU of Skyros. The methods we used were the multi-equilibrium method (MEM), the graphite thermometry and the pseudosections. Despite the fine-grained nature of the samples, we attempted to evaluate the peak conditions by using core compositions, while for the retrograde stage we analysed the rims. The pressure (*P*)–temperature (*T*) conditions calculated using the MEM based on the assumption of local equilibrium between the minerals chosen (Vidal & Parra, 2000; Parra et al., 2002a,b). The average results of the equilibria between the different chlorite-phengite pairs, were calculated with winTERSX (ver. 2.34). The thermodynamic dataset, and solid-solution models (SSM) are the same with those used in Baziotis et al. (2009).

We acquired Raman Spectra (RS), and then applied a Gaussian-Lorentzian fitting to remove their background; after that, we estimated the full width at half maximum (FWHM). We applied the equations by Kouketsu et al. (2014) for the RS carbonaceous material (CM): $T(^oC)=-2.15 \times D_1^{FWHM} + 478$ (1), and $T(^oC)=-6.78 \times D_2^{FWHM} + 535$ (2), where $D1^{FWHM}$ represents the FWHM of the D1 peak, and $D2^{FWHM}$ the FWHM of the D2 peak. The equation (1) is more accurate in the *T* range of 200-400 ºC, while the equation (2) works better for the *T* range 150-200 ºC.

For the pseudosections (Figs. 1,2), we used the bulk-rock compositions as proxies for the UMU (sample SK-110b) and the LMU (sample SK-51). P-T pseudosections were calculated in the system STAFMCNK, employing Perple_X (ver. 6.9.1; Connolly 2009). The used SSM were: Bio(HP), Carp(M), Chl(HP), Ctd(HP), Gt(HP), Pheng(HP), Mica(M), Sud(M), Pu(M), Act(M), Stlp(M), Omph(GHP), Ep(HP), MtUl(A), IlGkPy, and feldspar (Andersen & Lindsley 1988; Fuhrman & Lindsley 1988; Green et al. 2007; Massonne & Willner 2008; Powell & Holland 1999). The bulk-rock compositions was based on whole-rock analysis, thus, the derived phase assemblage, is assumed to be in equilibrium over the scale of a hand specimen. However, since the analysed rocks are fine-grained, the analysed composition can be regarded as the "effective" one. Thus, the calculated pseudosections, combined with the observed textural relations, mineral mode/chemistry data provide a unique frame of *P-T* conditions for a specific bulk-rock composition, and also serves as a good proxy to derive the peak and post-peak stages along the metamorphic evolution.

LMU *P-T* (Sample SK51b): The MEM has been applied successfully only for the *Chl-Ph* pairs. Then, the calculated invariant points define the maximum *P* at 11±1.5 kbar and *T* 280±15ºC; the maximum *T* is calculated at 384±13 ºC (*P* 9.2±0.4 kbar). Subsequently, one more pair of *Chl-Ph* calculated to be stable at 380±20 ºC and P 7.5±0.6 kbar, indicating decompression at constant *T*. The RSCM [equation (1)] revealed *T* 375±25 ºC. As such, the maximum *T* (~400 ºC) estimated from RSCM, was in accordance with the maximum *T* estimated from the local-equilibria method.

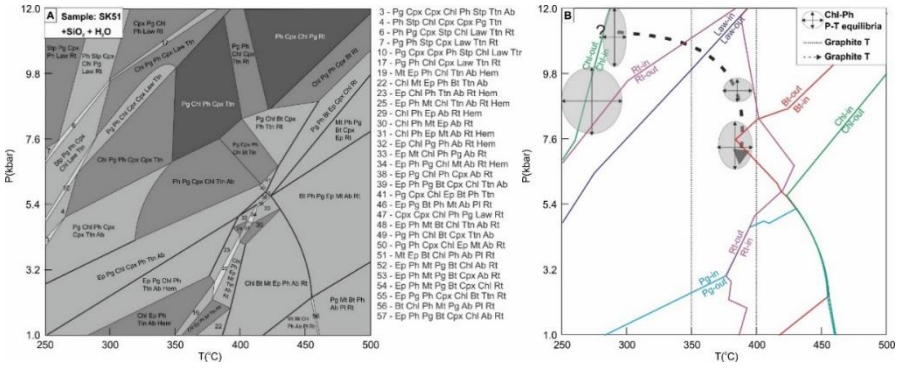

Figure 1. (A) P-T pseudosection (SiO_2 undefined but saturated) calculated for the sample SK51 (bulk composition in wt%: TiO_2: 0.69; Al_2O_3: 14.3; FeO: 4.86; MgO: 2.28; CaO: 1.00; Na_2O: 1.76; K_2O: 2.77; O_2: 0.1). (B) P-T diagram showing the mineral stabilities as calculated in (A). Further, the estimated chl-ph equilibrium conditions and the low/max-*T* estimates from the RSCM method, are also given. Mineral abbreviations as in Whitney and Evans (2010).

The *P-T* pseudosection (Fig. 1) for LMU (sample SK51) displays the following features: (1) *Pmp* is not stable at any *P*/*T*, (2) *Law* stability field displays a positive correlation with increasing *P*/*T* being stable up to ~385 ºC at 12 kbar, (3) the *Rt* stability is restricted at high-*P* and relatively low-*T*; (4) chlorite is stable from low-*T* ~250 ºC (at *P* <7.5 kbar) up to *T*

~500 ºC (at P >10 kbar), (5) *Ms* is stable throughout the *P-T* pseudosection, (6) *Bt* stability is confined at *T* >380 ºC. Based on the absence of *Law*, *Rt*, and *Bt* from the observed assemblage the peak *T* represented by the assemblage Pg+Chl+Ph+Cpx+Ttn. The predicted *Cpx* is not observed (Fig. 1), which may associated with the following: 1) the calculations are correct (appearance of *Cpx* at relatively low P-T conditions) but due to energetic barriers *Cpx* cannot form at such *P-T* conditions, (2) The thermodynamic data are not adequate. Hence, along with the calculated *T* from the RSCM, the peak *T* is in accordance with the results estimated by the MEM at *P* ~9.2 kbar, and *T* ~385 ºC. These conditions should be regarded as tentative until we have additional *in-situ* analyses, and thermodynamic data.

UMU *P-T* (sample SK110b): Several Chl-Ph pairs analysed was not possible to define local equilibria conditions. Similarly, the same sample was C-free, and therefore was not possible to apply the RSCM method. Using the calculated pseudosection, the peak *T* has been estimated based on the *Grt* and *Ph* chemistry. In particular, the isopleths for *Grt* end-members, and the Si-in *Ph* were plotted on the pseudosection (Fig. 2).

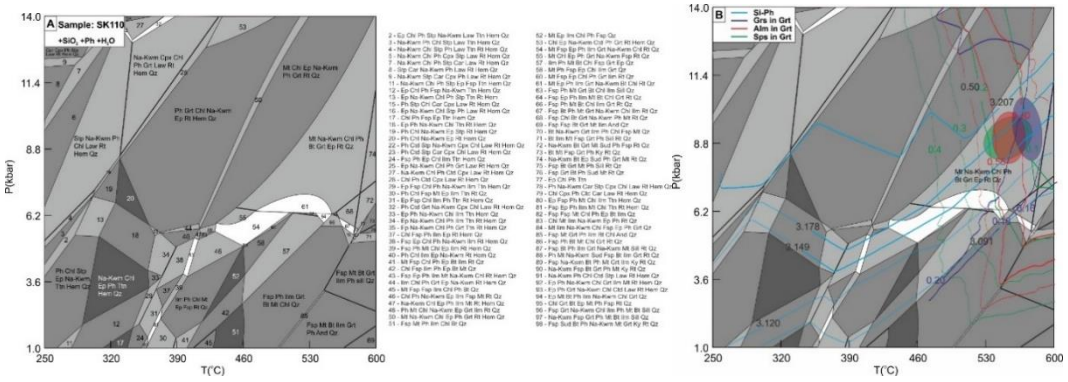

Figure 2. (A) P-T pseudosection calculated for the sample SK110b (bulk composition in wt%: SiO_2: 73.5; TiO_2: 0.53; Al_2O_3: 11.3; FeO: 4.58; MnO: 0.24; MgO: 1.83; CaO: 0.95; Na_2O: 0.28; K_2O: 2.55; O_2: 0.1). (B) P-T pseudosection superimposed with the garnet (spessartine, almandine, grossular), and Si-in phengite isopleths. Mineral abbreviations as in figure 1.

The petrographic inspection of the sample suggest equilibrium between *Grt* and phengitic muscovite. The *Grt* isopleths converged for the three end-members, and when compared with the observed compositions indicate *T* ~550 ±30 ºC at *P* 9.2 ±1 kbar. The Si-in *Ph* isopleths lying between the *P* estimated from the *Grt* isopleths, suggesting compositional equilibrium with the latter. The estimated *T* should be regarded as the peak one (peak assemblage: Kwm+Chl+Ph+Bt+Grt+Ep+Rt+Qz+Mt). The *Bt* was not observed, because it has been retrogressed to chloritized *Bt*. Furthermore, the *Ep*, it is predicted at very low modal content (~1 vol.%), which is possible –due to kinetic reasons or local-equilibrium composition– to not formed in our sample. In the studied sample, another *Ph* (Si up to ~3.45 a.p.f.u.) probably represents relic of an earlier high-*P* event.

Acknowledgements

I.B. greatfully acknowledges the National Hellenic Research Foundation for access to Raman facilities.

References

Andersen, D.J., Lindsley, D.H., 1988. Internally consistent solution models for Fe-Mg-Mn-Ti oxides; Fe-Ti oxides. Am Min, 73(7-8), 714-726.

Baziotis, I., Proyer, A., Mposkos, E., 2009. High-pressure/low-temperature metamorphism of basalts in Lavrion (Greece): implications for the preservation of peak metamorphic assemblages in blueschists and greenschists. EJM, 21(1), 133-148.

Connolly, J. A. D. 2009. The geodynamic equation of state: what and how. G^3, 10(10).

Fuhrman, M.L., Lindsley, D.H., 1988. Ternary-feldspar modeling and thermometry. Am Min, 73(3-4), 201-215.

Green, E., Holland, T., Powell, R., 2007. An order-disorder model for omphacitic pyroxenes in the system jadeite-diopside-hedenbergite-acmite, with applications to eclogitic rocks. Am Min, 92(7), 1181-1189.

Kouketsu, Y., Mizukami, T., Mori, H., Endo, S., Aoya, M., Hara, H., … Wallis, S., 2014. A new approach to develop the R aman carbonaceous material geothermometer for low-grade metamorphism using peak width. Island Arc, 23(1), 33-50.

Massonne, H.J., Willner, A.P., 2008. Phase relations and dehydration behaviour of psammopelite and mid-ocean ridge basalt at very-low-grade to low-grade metamorphic conditions. EJM, 20(5), 867-879.

Parra, T., Vidal, O., Agard, P., 2002a. A thermodynamic model for Fe–Mg dioctahedral K white micas using data from phase-equilibrium experiments and natural pelitic assemblages. CTMP, 143(6), 706-732.

Parra, T., Vidal, O., Jolivet, L., 2002b. Relation between the intensity of deformation and retrogression in blueschist metapelites of Tinos Island (Greece) evidenced by chlorite–mica local equilibria. Lithos, 63(1-2), 41-66.

Powell, R., Holland, T., 1999. Relating formulations of the thermodynamics of mineral solid solutions; activity modeling of pyroxenes, amphiboles, and micas. Am Min, 84(1-2), 1-14.

Vidal, O., Parra, T., 2000. Exhumation paths of high-pressure metapelites obtained from local equilibria for chlorite–phengite assemblages. Geological Journal, 35(3-4), 139-161.

Whitney, D.L., Evans, B.W., 2010. Abbreviations for names of rock-forming minerals. Am Min, 95(1), 185-187.

16th International Congress of the Geological Society of Greece

17-19 October 2022 - Patras, Greece

Bulletin of the Geological Society of Greece, Sp. Publ. 10

Ext. Abs. GSG2022-270

Mineralogical characterization of Greek zeolitic tuffs and their insect repellent effect on the olive fruit fly *Bactrocera (Dacus) oleae*

Kovaiou Soultana Kyriaki[1], Kokkari Anastasia[2], Kouloussis Nikolaos[2], Kantiranis Nikolaos[1]

(1) Department of Mineralogy-Petrology-Economic Geology, School of Geology, Aristotle University of Thessaloniki, Thessaloniki, Greece, skovaiou@geo.auth.gr (2) Laboratory of Applied Zoology and Parasitology, School of Agriculture, Aristotle University of Thessaloniki, Thessaloniki, Greece.

Research Highlights

Zeolitic tuff samples rich in HEU-type zeolite, from Petrota of the Evros Region in Greece, have a significant effect against the olive fruit fly *Bactrocera oleae* (Diptera: Tephritidae).

Background

Zeolites are a class of nanoporous materials with outstanding properties because of their large pore volume, high surface area and thermal stability (Meier, 1986, Rehakova et al., 2004). A siliceous zeolite contains tetrahedral structures of SiO_4 that are linked to each other to give an infinite framework structure with uniform micropores. Because of their various structural arrangements, they have been widely used in many industrial applications, such as ion exchangers, adsorbents, and catalysts (Mumpton, 1999). Zeolitic tuffs, volcanic rocks that are rich in HEU-type zeolites (clinoptilolite - heulandite), have important properties, resulting in high efficiency worldwide in numerous applications. The most widely used zeolitic tuff is the one that contains HEU-type zeolite (clinoptilolite – heulandite). As non-toxic, ecologically advantageous and affordable materials, natural zeolites are appropriate for agricultural uses, such as soil and pest management (Eroglu et al., 2017). Earlier work by our group has proved that high quality natural zeolite formulation, when applied as dust on bean seeds, have a high insecticidal activity against the bean weevil *Acanthoscelides obtectus* (Coleoptera: Bruchidae) (Floros et al., 2018).

Objectives and Methods

Four representative samples of zeolitic tuffs (samples t1-t4) were collected from specific layers of the volcanic deposits of Petrota of the Evros Region in Greece. The samples were studied in their bulk form, ground (<125 μm), homogenized, and grounded further for mineralogical and chemical analysis. From the representative samples, polished thin sections were prepared to determine the petrographic characteristics. The sections were studied under a polarizing and scanning electron microscope. The analysis of the mineralogical composition was derived from the X-ray diffraction method. Also, we studied the analysis of morphological and chemical characteristics by SEM-EDS. To determine the sorption ability, each sample was treated according to the AMAS method.

Regarding the effectiveness of zeolitic tuffs against the olive fruit fly *B. oleae*, we used our studied samples with a grain-size distribution <63μm, after procession. The laboratory colony of *B. oleae* was established with adults emerged from infested olives collected in Kassandra, Chalkidiki, northern Greece. Each zeolitic tuff sample was dissolved in water at a rate of 5% by weight (5 g powder / 100 ml water), mixed with sticker adjuvant, forming aqueous solutions. Olive fruits were immersed in these aqueous solutions, later dried, and then transferred to cages with adult mated females. The number of eggs laid in the olives was used as a criterion for the insect repellent effect. Measurements were taken in total of five days after application. All experiments were performed at 25 °C and a photoperiod of 16:8. Data were analyzed using statistical analysis of variance (ANOVA).

Results

Samples t1-t4 contain clinoptilolite (zeolite), feldspars (potassium+plagioclase), cristobalite+quartz, micas (muscovite, biotite), celadonite, ± chlorite, fragments, and amorphous/vitreous mass (Table 1). They are free of fibrous minerals. They consist of 53-69 wt % clinoptilolite (type-HEU zeolite) and are characterized as clinoptilolitic zeolitic tuffs. The consistence of quartz varies from 0-2 wt%. Regarding the chemical composition (Table 2), samples t1-t4 contain SiO_2 between 64.29 (t4) and 68.03 wt. % (t3). The Al_2O_3 content varied from 12.01 (t3) to 13.11 wt. % (t1), and low amounts of Fe_2O_{3T} and MnO were measured.

When applied on the surface of olives, the zeolitic tuff samples used in our experiments caused a significant reduction in the number of the eggs laid on the olive fruits (Table 3). The reduction, and therefore the inhibitory effect on oviposition of the olive fruit fly, was significant in comparison to the control. The maximum reduction in the number of eggs was found after the application of sample t1 (64 wt% clinoptilolite) and t3 (69 wt% clinoptilolite). Specifically, after 8 days of exposure of the olive fruits to adult females, without the application of zeolitic tuff (Control), a mean number of 162.3 eggs were laid on the olives, whereas after the application of t1, t3 samples, the number of eggs was significantly reduced

(96.7 and 92.1 eggs respectively).

Table 1. Semi-quantitative mineralogical composition (wt. %) and uptake ability (meq/100g) of the studied zeolitic tuff samples.

Samples	t1	t2	t3	t4
Type HEU zeolite (clinoptilolite-heulandite)	64	53	69	66
Mica + clay minerals	3	2	-	4
Quartz + Cristobalite	5	4	3	4
Feldspars + Plagioclase	8	14	6	7
Amorphous	20	27	22	19
Total	100	100	100	100
Uptake ability (meq/100g)	160	134	195	179

Table 2. Chemical composition (wt. %) of the studied zeolitic tuff samples.

	Constituent oxides (wt%)											
Samples	**SiO_2**	**Al_2O_3**	**Fe_2O_{3tot}**	**MnO**	**MgO**	**CaO**	**SrO**	**BaO**	**Na_2O**	**K_2O**	**H_2O**	**Total**
t1	65.09	13.11	0.00	0.00	0.18	0.96	0.00	0.00	2.20	4.48	13.98	100.00
t2	66.68	12.85	0.00	0.00	0.92	3.62	0.00	0.00	0.64	2.22	13.07	100.00
t3	68,03	12.01	0.00	0.00	0.16	3.50	0.00	0.00	0.38	2.54	13.38	100.00
t4	64.29	12.22	0.00	0.00	0.09	1.69	0.00	0.00	1.48	5.12	15.11	100.00

Table 3. Effect of the studied zeolitic tuff samples against the olive fruit fly *B. oleae*.

Treatment	**Mean number of eggs (± SE)**			
Days after application	**2**	**4**	**6**	**8**
Control	47,3 ± 6,9a*	104,5 ± 19,6a	139,4 ± 24,1a	162,3 ± 22,1a
t1	31,1 ± 18,9a	52,1 ± 30,9b	90,5 ± 36,5b	96,7 ± 35,9b
t2	30,7 ± 17,1a	72,7 ± 33,2b	92,3 ± 29,8b	104,5 ± 27,6a
t3	21,1 ± 9,9a	58,2 ± 23,4b	84,9 ± 16,5b	92,1 ± 11,8b
t4	22,5 ± 11,8a	65,1 ± 15,3b	114,4 ± 6,2a	146,2 ± 7,5a

*: Means in a column followed by the same letter are not significantly different (Student-Newman-Keuels test, P>0,05).

Conclusions

Greek zeolitic tuffs, with high concentration of HEU-type zeolite, when applied on the olives' surface, were found to have a substantial repellent effect against adult females of the olive fruit fly *Bactrocera (Dacus) oleae*. This deterrent effect seems to be attributed to the creation of a thin layer (hymen) of zeolitic tuff on the surface of the fruits. Future laboratory and field research is required in order to verify the present results and improve the effectiveness of zeolites for the control of the olive fly and other pests.

Acknowledgements

The present research was in collaboration with the Laboratory of Applied Zoology and Parasitology, of the Faculty of Agriculture of the Aristotle University of Thessaloniki.

References

Eroglu, N., Emekci, M., Athanassiou, C. G., 2017. Applications of natural zeolites on agriculture and food production. Journal of the Science of Food and Agriculture 97, 3487-3499.

Floros, G. D., Kokkari, A. I., Kouloussis, N. A., Kantiranis, N. A., Damos, P., Filippidis, A. A., Koveos, D. S., 2018. Evaluation of the natural zeolite lethal effects on adults of the bean weevil under different temperatures and relative humidity regimes. Journal of economic entomology 111, 482-490.

Meier, W.M., 1986. Zeolites and Zeolite-Like Materials. Seventh International Zeolite Conference, Tokyo, Japan, p. 13–22.

Rehakova, M., Čuvanová, S., Dzivak, M., Rimár, J., & Gaval'Ová, Z., 2004. Agricultural and agrochemical uses of natural zeolite of the clinoptilolite type. Current Opinion in Solid State and Materials Science 8, 397-404.

Mumpton, F. A., 1999. La roca magica: Uses of natural zeolites in agriculture and industry. Proceedings of the National Academy of Sciences 96, 3463-3470.

16th International Congress of the Geological Society of Greece

17-19 October, 2022 - Patras, Greece

Bulletin of the Geological Society of Greece, Sp. Publ. 10

Ext. Abs. GSG2022-293

The Kolumbo Submarine Volcanic-Hydrothermal Vent Ecosystem: The Epitome of Study Sites in the Hellenic Volcanic Arc with Relevance to Ocean Policy and Governance

V. Pletsas[1], S. P. Kilias[1], N. Zegkinoglou[1], P. Nomikou[1], T. J. Mertzimekis[1] P. Polymenakou[2], A. Gondikas[1]

(1) National and Kapodistrian University of Athens, Athens, Greece, vapletsa@gmail.com (2) Hellenic Center for Marine Research, Heraklion, Greece

Research Highlights

The hydrothermal vent ecosystem of the multi-stressor crater of the Kolumbo submarine arc-volcano, will be monitored with multidisciplinary and high-resolution sampling and measurements instrumentation, as part of a new *in situ* submarine observatory (SANTORini's sea floor volcanic observatorY, SANTORY). SANTORY is in line with actions endorsed by the United Nations Decade of Ocean Science for Sustainable Development and the European Green Deal.

Background

The world's seas and oceans (S&Os) are essential for life on Earth, human well-being, and economic growth, as climate buffers, carbon removers, suppliers of natural green metals and biotechnology resources, and by playing a crucial role in addressing pressing global challenges such as food and energy(biofuel) supply, and the interlinked ocean and climate change. The S&Os are under intense stress from human activities, guiding the European Union (EU) to promote for the first time in 2016, a stronger ocean governance around the globe, by introducing an International Ocean Governance (IOG) Agenda, in order to sustainably manage and use the world's ocean. The IOG Agenda is in line with the UN 2030 Agenda and its Sustainable Development Goal 14, the European Green Deal (EGD) (Christodoulou et. al., 2021), and the United Nations decade of Ocean Science for Sustainable Development 2021-2030 (OSSD 2021-2030) (UNESCO-IOC, 2021). Relevant environmental knowledge is not enough to support science-informed EU priority actions on the IOG Agenda, e.g., fight marine pollution, and protect the seabed, commanding S&Os science, observation, environmental monitoring, and prediction, and innovation capacity. The increasing variability and complexity of anthropogenic stressors have recently drawn attention to the necessity for studying the synergistic or additive impacts of natural geologic stressors, on S&Os, which are overlooked (Carrier-Belleau et al., 2021). The Aegean, active Hellenic Volcanic Arc (HVA), is one of the two most volcanically and hydrothermally active areas within Exclusive Economic Zones of EU countries, and perhaps the only place on Earth where the intensity of both anthropogenic and natural stressors is so pronounced. Aegean is therefore an ideal site to study the S&Os ecosystem responses to natural geological stressors, such as submarine volcanic eruption and hydrothermal vent activity, seismicity etc. Here we investigate the active *Kolumbo **Su**bmarine **V**olcanic-**H**ydrothermal **Ec**osystem (SUVHEC)*, as a role model for a volcanic-hosted deep-sea ecosystem (>200 m below sea level) that is influenced by multiple stressors of geological origin. Our aim is to increase knowledge to enable a science-based sustainable management strategy for effective protection and restoration, and monitoring, for Aegean deep-sea ecosystems. Such research on shallow submarine arc volcanoes is still in its infancy, worldwide (Wisz et al, 2020).

Main natural threats for the Kolumbo submarine volcanic ecosystem

Kolumbo is the most dynamic submarine Mediterranean volcano, which hosts an active hydrothermal vent ecosystem on its crater floor (~504 m.b.s.l.). The hydrothermal vents discharge pure gaseous CO_2 fluids (~265 °C), leading to the buildup of stratified, acidic (pH 5.0) seawater at ~15 m above the vents (Carey et al., 2013). Moreover, actively forming hydrothermal polymetallic seafloor massive sulfide (SMS) chimney/mound deposits, are uniquely enriched in Sb, Tl, Au, Ag, Pb, Zn, As, and Hg (Kilias et al, 2013). The chimney/mound walls and crater harbor highly complex prokaryotic communities and microbes with an enhanced co-tolerance to acidity and antibiotics (Bravakos et al., 2021). The HVA has been described as the largest submarine volcanic ecosystem and a considerable resource of novel genes and pathways with potential biotechnological applications (Chrousos et al., 2020); the SMS deposits include critical metal(loid)s that are essential to the EGD (e.g., Sb, Sr, barite), and may be potentially exploitable (Sb, Tl, Au, Ag, Pb, Zn). Accordingly, major natural geological stressors for Kolumbo's deep-sea species/habitats/ecosystems include: **(1) *Potential toxicity and biomagnification of active SMS deposits***: SMS deposits host metal(loid)s (As, Sb, Hg, Tl, Ag, Cd), which are potentially hazardous, if not managed, especially for the Santorini coastal environments and areas exploited by fishing and tourism (Kilias et al., 2013). Understanding the SMS mineralogy and geochemistry, chemical speciation and bioavailability of SMS-hosted metallic or organic pollutants in dissolved species or particles, and the potential toxicity impact associated with SMS preservation, and/or active discharge, is incomplete and needs greater scientific focus (Fallon et al., 2019). Moreover and there is enduring international debate about sustainable exploitation of SMS resources, and whether their development is worth the environmental and ecological risk (Wisz et al., 2020); **(2) *Geological and environmental diversity:*** Nearly exposed volcanic flanks and sheltered crater within relatively shallow waters (~500 m.b.s.l.), combined with changing sediment inputs from islands and continental landmasses, and submarine metal(loid) discharge related to episodic plumes of SMS-laden vent−detritus, or failure of hydrothermally weakened volcanic edifices, vigorous volcanic

hazard activity, with unknown ecosystem impact, which affect rates and levels of mass wasting, may affect seafloor toxic-metal budget and liberation potential (Nomikou et al., 2022); **(3) D*egassing of climate relevant CO_2 from hydrothermal vents:*** The potential impacts of the accumulation of acidic, stably stratified CO_2-rich water on the deep-crater ecological variables such as biodiversity, ecosystem functions and conservation, and the risk assessment for catastrophic release of climate relevant gases at the surface (i.e seismic activity, submarine landslides) are unknown (Carey et al., 2013). Consequently, a geochemical monitoring program of hydrothermal fluids, and CO_2 levels in the seawater column, are strongly recommended; **(4)** ***Radioactivity***: emerging as an environmental issue; large-scale releases due to natural disasters (e.g., seismic, or volcanic activity), with unknown ecosystem impact.

Conclusions and future perspectives

Cutting-edge and innovative deep-sea instrumentation and multidisciplinary research is needed to inform environmental management of the multi-stressor SUVHEC. A new sea floor observatory (SANTORini's sea floor volcanic observatorY, SANTORY), will be developed and installed within the Kolumbo crater to monitor its SUVHEC and mitigate potential hazards (Nomikou et al., 2022). SANTORY includes cutting-edge and innovative marine-technology that integrates hyperspectral imaging, temperature sensors, a radiation spectrometer, fluid/gas samplers, and pressure gauges, which will be integrated into a monitoring platform aimed at geochemical and biological monitoring and sampling. SANTORY will establishe exchange of information with relevant projects, such as: IODP Drilling Expedition 398 (Druitt, et al., 2022), RAMONES (Mertzimekis et al., 2022), and NEXUS-MONARC, a recently funded HORIZON project (Proposal number: 101079156). These results will be communicated to governmental officials, and to actions endorsed by the EU IOG Agenda, and the United Nations Decade of Ocean Science for Sustainable Development.

Acknowledgements

This work represents ideas of ongoing international joined research projects: SANTORY, RAMONES and IODP PROGRAM EXPEDITION 398.

References

Bravakos, P., Mandalakis, M., Nomikou, P., Anastasiou, T.I., Kristoffersen, J.B., Stavroulaki, M., Kilias, S., Kotoulas, G., Magoulas, A. and Polymenakou, P.N., 2021. Genomic adaptation of Pseudomonas strains to acidity and antibiotics in hydrothermal vents at Kolumbo submarine volcano, Greece. Sci Rep 11, 1336.

Carey, S., Nomikou, P., Bell, K.C., Lilley, M., Lupton, J., Roman, C., Stathopoulou, E., Bejelou, K. and Ballard, R., 2013. CO2 degassing from hydrothermal vents at Kolumbo submarine volcano, Greece, and the accumulation of acidic crater water. Geology 41(9), 1035-1038.

Carrier-Belleau, C., Drolet, D. C. W. McKindsey, and P. Archambault, 2021. "Environmental stressors, complex interactions and marine benthic communities' responses," Sci Rep 11, 4194.

Chrousos, G.P., Mentis, AF.A. & Dardiotis, E., 2020. Biomedical research: lessons from the last decade's crisis and austerity-stricken small countries for the current COVID-19-related crisis. Nat Med 26, 644–646.

Druitt, T., Kutterolf, S., and Höfig, T.W., 2022. Expedition 398 Scientific Prospectus: Hellenic Arc Volcanic Field. International Ocean Discovery Program.

Christodoulou, A., Echebarria Fernández, J. (2021). Maritime Governance and International Maritime Organization Instruments Focused on Sustainability in the Light of United Nations' Sustainable Development Goals. In: Carpenter, A., Johansson, T.M., Skinner, J.A. (Eds)., Sustainability in the Maritime Domain. Strategies for Sustainability. Springer, Cham, 415-461.

Fallon, E.K., Frische, M., Petersen, S., Brooker, R.A. and Scott, T.B., 2019. Geological, mineralogical and textural impacts on the distribution of environmentally toxic trace elements in seafloor massive sulfide occurrences. Minerals 9(3), 162.

Kilias, S. P., Nomikou, P., Papanikolaou, D., Polymenakou, P. N., Godelitsas, A., Argyraki, A., Carey, S., Gamaletsos, P., Mertzimekis, T. J., Stathopoulou, E., Goettlicher, J., Steininger, R., Betzelou, K., Livanos, I., Christakis, C., Bell, C. K., and Skoulos, M., (2013)., New insights into hydrothermal vent processes in the unique shallow submarine arc-volcano, Kolumbo (Santorini), Greece, Sci Rep 3, 2421.

Mertzimekis T. J., Nomikou P., Petra E., Batista P., Cabecinhas D., Pascoal A., et al. (2021). "Radioactivity Monitoring in Ocean Ecosystems (RAMONES)," in *Proceedings of the Conference on Information Technology for Social Good (Goodit '21)* (New York, NY, USA: Association for Computing Machinery), 216–220.

Nomikou P, Polymenakou PN, Rizzo AL, Petersen S, Hannington M, Kilias SP, Papanikolaou D, Escartin J, Karantzalos K, Mertzimekis TJ, Antoniou V, Krokos M, Grammatikopoulos L, Italiano F, Caruso CG, Lazzaro G, Longo M, Scire´ Scappuzzo S, D'Alessandro W, Grassa F, Bejelou K, Lampridou D, Katsigera A and Dura A (2022) SANTORY: SANTORini's Seafloor Volcanic ObservatorY. Front. Mar. Sci. 9:796376.

UNESCO-IOC 2021. The United Nations Decade of Ocean Science for Sustainable Development (2021-2030) Implementation Plan. UNESCO, Paris (IOC Ocean Decade Series, 20.)

Wisz MS, Satterthwaite EV, Fudge M, Fischer M, Polejack A, St. John M, Fletcher S and Rudd MA (2020) 100 Opportunities for More Inclusive Ocean Research: Cross-Disciplinary Research Questions for Sustainable Ocean Governance and Management. Front. Mar. Sci. 7:576.

16th International Congress of the Geological Society of Greece
17-19 October, 2022 - Patras, Greece
Bulletin of the Geological Society of Greece, Sp. Publ. 10
Ext. Abs. GSG2022-349

Chromium-Bearing Mineral Phases and Water-Rock/Soil Interaction Process: Insights and Lessons Learned from a Geochemical Modeling Approach

P. Papazotos[1], D. Psarraki[1], E. Vasileiou[1], M. Perraki[1]

(1) School of Mining and Metallurgical Engineering, Division of Geo-sciences, National Technical University of Athens, 9 Heroon Polytechniou St., 15773 Zografou, Greece, papazotos@metal.ntua.gr

It is widely accepted that the occurrence, mobilization, transport, and fate of Potentially Toxic Elements (PTEs) in natural waters depend mainly on the prevailing geological, environmental, and geochemical conditions (Guo et al., 2014; Papazotos et al., 2020; Tziritis et al., 2012). Generally, the source of PTEs in the environment, including water resources, can be both geogenic and anthropogenic; one of the most harmful PTE in groundwater is chromium (Cr) due to its mobilization in the usual groundwater pH range (i.e., 6.5-8.5). This study aims to enrich the thermodynamic data of Cr-bearing mineral phases by adding Cr to their chemical formula and calculating the new saturation indices (SIs). The geochemical modeling was performed through the frequently used geochemical PHREEQC software package (Parkhurst & Appelo, 1999). This approach could help geoscientists and engineers understand the Cr release mechanism in the dynamic water-rock/soil interaction system.

The mineralogical study of the studied rocks included optical microscopy, X-ray diffraction analysis (XRD; Bruker D-8 Focus), and scanning electron microscopy (SEM; JEOL6380LV). The analytical determinations included a large set of physical and chemical parameters, containing the necessary input parameters for the geochemical modeling software PHREEQC (i.e., pH, Eh, Ca^{2+}, Mg^{2+}, Cr, Si, etc.). The chemical reactions in groundwater were evaluated by calculating the SI with respect to mineral phases using the geochemical software PHREEQC with the MINTEQv.4 as the main thermodynamic database (Allison et al., 1991). The SI of the water samples was defined with the following equation:

$$SI = log\ (\frac{IAP}{K_{sp}})$$

where IAP is the Ion Activity Product and K_{sp} is the equilibrium constant.

When the SI value is equal to 0, the solution is in equilibrium with the mineral phase; when the SI value is > 0, the solution is oversaturated, resulting in mineral precipitation, and when the SI value is < 0, the solution is undersaturated indicating that dissolution is required to reach equilibrium.

Mineralogical and groundwater data from different ultramafic-dominated areas (e.g.., Psachna Basin in Central Euboea, Loutraki, Schinos, Gerania Mountains) were used to calculate the new saturation indices of the modified Cr-bearing serpentine (lizardite and chrysotile) and pyroxene (diopside and enstatite); two of the common Cr-bearing silicate minerals of ultramafic rocks. The common feature of the study areas is that they are composed of ultramafic rocks; serpentinites and serpentinized peridotites were the main lithotypes studied. Chromium-bearing mineral phases such as spinels (chromite and Cr-magnetite), serpentine, pyroxene, amphibole, chlorite, etc. were identified (Papazotos, 2020). Chemical analyses of soils and rocks showed a geological environment enriched in Cr, as in all cases their Cr content far exceeded the average content of the Earth's crust. Generally, ultramafic rocks are rich in MgO and FeO and enriched in As, Co, Cr, Ni (Kelepertzis et al., 2013; Oze et al., 2004; Ryan et al., 2011; Vithanage et al., 2014). Although SiO_2 content in ultramafic rocks is the lowest (<45 %) among other igneous rocks, however it is much higher than in other widely occurring rocks in Greece such as carbonates (e.g., limestones, dolostones). Thus, ultramafic rocks could be considered the source of Si in groundwater. Selected Cr-bearing minerals that were identified in the studied areas and their dissolution reaction equations are given in Table 1; the Cr-content in the dissolution reaction equations is indicative.

Table 1. Modified Cr-bearing mineral phases (serpentine and pyroxene minerals) and their dissolution reaction equations to aqueous species.

Mineral phase	Reaction equation
Lizardite	$Mg_3Si_2O_5(OH)_4 + 6H^+ = H_2O + 2H_4SiO_4 + 3Mg^{+2}$
Cr-bearing Lizardite	$Mg_{2.25}Cr_{0.5}Si_2O_5(OH)_4 + 6H^+ = H_2O + 2H_4SiO_4 + 2.25Mg^{+2} + 0.5Cr^{+3}$
Chrysotile	$Mg_3Si_2O_5(OH)_4 + 6H^+ = H_2O + 2H_4SiO_4 + 3Mg^{+2}$
Cr-bearing Chrysotile	$Cr_{0.5}Mg_{2.25}Si_2O_5(OH)_4 + 6H^+ = H_2O + 2H_4SiO_4 + 2.25Mg^{+2} + 0.5Cr^{+3}$
Enstatite	$MgSiO_3 + 2H^+ + H_2O = Mg^{+2} + H_4SiO_4$
Cr-bearing Enstatite	$Cr_{0.3}Mg_{0.55}SiO_3 + 2H^+ + H_2O = 0.3Cr^{+3} + 0.55Mg^{+2} + H_4SiO_4$
Diopside	$CaMg(SiO_3)_2 + 4H^+ + 2H_2O = Ca^{+2} + 2H_4SiO_4 + Mg^{+2}$
Cr-bearing Diopside	$Cr_{0.4}Ca_{0.7}Mg_{0.7}(SiO_3)_2 + 4H^+ + 2H_2O = 0.4Cr^{+3} + 0.7Ca^{+2} + 0.7Mg^{+2} + 2H_4SiO_4$
Ferrosilite	$FeSiO_3 + 2H^+ + H_2O = Fe^{+2} + H_4SiO_4$
Cr-bearing Ferrosilite	$Cr_{0.3}Fe_{0.55}SiO_3 + 2H^+ + H_2O = 0.3Cr^{+3} + 0.55Fe^{+2} + H_4SiO_4$

The results revealed that modified Cr-bearing mineral phases have lower SI values than the Mg and Fe-end members

(Figure 1), suggesting that they are more soluble in the aqueous solution (i.e., groundwater) and strengthening the view that water-rock/soil interaction is a dominate process for Cr-release in groundwater resources. The approach of this study is based on the assumption of using the thermodynamic data such as K_{sp} of Mg and Fe-silicates for the Cr-bearing silicates as well, because of the lack of the respective data for the latter.

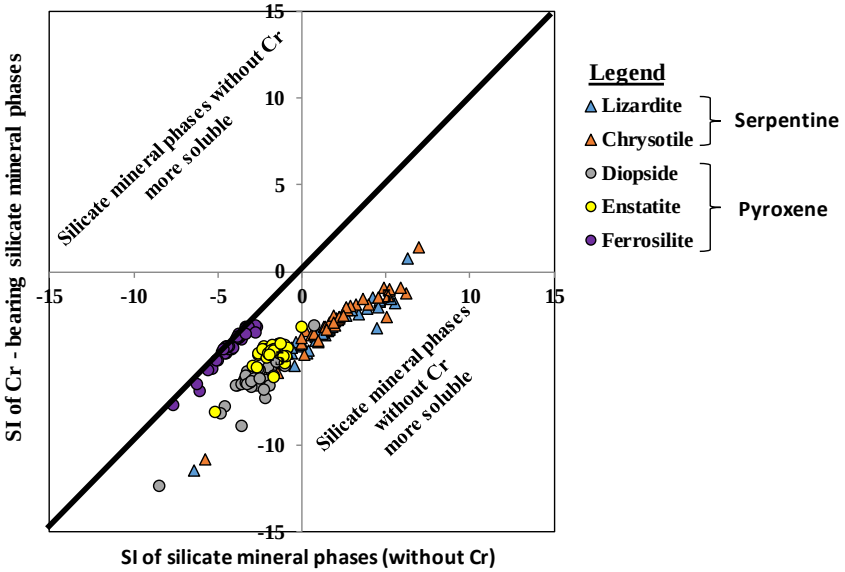

Figure 1. SI of Cr-bearing serpentine and pyroxene mineral phases vs. SI of pure Mg-end and Fe-end members mineral phases of various ultramafic-dominated areas (e.g., Psachna Basin in Central Euboea, Loutraki, Schinos, Gerania Mountains).

Several limitations need to be considered in a comprehensive geochemical modeling approach:

- Many studies misuse geochemical modeling without considering silicate mineral phases because of the lack of data for dissolved Si concentrations in aqueous solutions. In this way, the geoscientists ignore the largest and most important part of the geological and geochemical environment that is associated with aquatic chemistry providing misleading results and losing valuable data of the water-rock/soil interaction process.
- Most scientific papers using the PHREEQC software do not consider the mineralogy of the study area. Therefore, the results provided cannot be geologically interpreted. In this work, we linked mineralogical and hydrogeochemical data with geochemical modeling scenarios that are likely to correspond to real geological conditions.
- The most widely used thermodynamic mineral databases (e.g., MINTEQ, MINTEQ.v4, PHREEQC, llnl.dat, etc.) do not include the majority of the PTE-bearing mineral phases. However, as shown in this work, chemical modifications in the silicates' formula by adding a low content of PTEs result in different SIs and consequently in a different geochemical behavior during dissolution/precipitation processes.

References

Allison, J. D., Brown, D. S., & Novo-Gradac, K. J., 1991. Minteqa2/Prodefa2, a Geochemical Assessment Model for Environmental Systems: Version 3.0 User'S Manual. U. S. Environmental Protection Agency EPA/600/3-91/021. **[Book]**

Guo, H., Wen, D., Liu, Z., Jia, Y., & Guo, Q., 2014. A review of high arsenic groundwater in Mainland and Taiwan, China: Distribution, characteristics and geochemical processes. Applied Geochemistry 41, 196-217. **[Journal Article]**

Kelepertzis, E., Galanos, E., & Mitsis, I., 2013. Origin, mineral speciation and geochemical baseline mapping of Ni and Cr in agricultural topsoils of Thiva Valley (central Greece). Journal of Geochemical Exploration, 125, 56-68. **[Journal Article]**

Oze, C., Fendorf, S., Bird, D. K., & Coleman, R. G., 2004. Chromium geochemistry in serpentinized ultramafic rocks and serpentine soils from the Franciscan complex of California. American Journal of Science, 304, 67-101. **[Journal Article]**

Papazotos, P., 2020. Geochemical fingerprint of ultramafic environments in groundwater quality with emphasis on chromium and arsenic. Ph.D. Thesis, National Technical University of Athens, 830p. **[Dissertation]**

Papazotos, P., Vasileiou, E., & Perraki, M., 2020. Elevated groundwater concentrations of arsenic and chromium in ultramafic environments controlled by seawater intrusion, the nitrogen cycle, and anthropogenic activities: The case of the Gerania Mountains, NE Peloponnese, Greece. Applied Geochemistry, 121, 104697. **[Journal Article]**

Parkhurst, D. L., & Appelo, C. A. J., 1999. User's Guide to PHREEQC (Version 2): A Computer Program for Speciation, Batch-Reaction, One-Dimensional Transport, and Inverse Geochemical Calculations. Water-Resources Investigations Report, 99-4259. **[Book]**

Ryan, P. C., Kim, J., Wall, A. J., Moen, J. C., Corenthal, L. G., Chow, D. R., Sullivan C. M., & Bright K. S., 2011. Ultramafic-derived arsenic in a fractured bedrock aquifer. Applied Geochemistry, 26, 444-457. **[Journal Article]**

Tziritis, E., Kelepertzis, E., Korres, G., Perivolaris, D., & Repani, S., 2012. Hexavalent chromium contamination in groundwaters of Thiva Basin, Central Greece. Bulletin of Environmental Contamination and Toxicology, 89, 1073-1077. **[Journal Article]**

Vithanage, M., Rajapaksha, A. U., Oze, C., Rajakaruna, N., & Dissanayake, C. B., 2014. Metal release from serpentine soils in Sri Lanka. Environmental Monitoring and Assessment, 186, 3415-3429. **[Journal Article]**

16th International Congress of the Geological Society of Greece
17-19 October, 2022 - Patras, Greece
Bulletin of the Geological Society of Greece, Sp. Publ. 10
Ext. Abs. GSG2022-366

Compositional Variability of Epidote-Group Minerals from Black Sands of the Kavala District, Northern Greece.

E. Peristeridou[1], V. Melfos[1], L. Papadopoulou[1], N. Kantiranis[1], P. Voudouris[2]

(1) Department of Mineralogy, Petrology, Economic Geology, Faculty of Geology, Aristotle University of Thessaloniki, 54124, Thessaloniki, Greece, peristee@geo.auth.gr (2) Department of Mineralogy and Petrology, Faculty of Geology & Geoenvironment, National and Kapodistrian University of Athens, 15784, Athens, Greece.

Introduction

The black sands from the coastal area of the Kavala district contain one of the most favorable occurrences of rare earth elements (REE) in Greece (Eliopoulos et al., 2014; Peristeridou et al., 2022). They contain dark horizons on the surface and in small depths, with heavy minerals, derived mainly from the Kavala (Symvolon) pluton. This Miocene pluton has intruded the metamorphic basement and is situated along the coast of North Aegean. The REE enrichment is ascribed to the presence of REE-bearing silicate and phosphate minerals, including allanite, epidote, thorite, titanite, zircon and monazite. The present publication focuses on the spot analyses of grain minerals of the epidote-group, examining the complex patchy patterns associated with REE differentiations and compositional chemical exchange schemes.

The epidote-group minerals are described by the general chemical formula $A_2M_3[T_2O_7][TO_4](O,F)(OH,O)$, where T is composed of Si, the A is separated into two different sites, and M into three structurally different octahedral sites, M1, M2 and M3. A1 is dominated by Ca, in the A2 site are incorporated the excess Ca, the cations Sr, Pb^{2+}, Mn^{2+}, REE^{3+}, Th and U. The cations Al, Fe^{3+}, Fe^{2+}, Mn^{3+}, Mn^{2+}, Mg, Cr^{3+} and V^{3+} are distributed in the M sites (Gieré and Sorensen, 2004**).** On the chemical formula of allanite, REE dominate on the A2 site with ΣREE_2O_3 concentration exceeding 3 wt%, and ΣREE^{3+} is >0.5 atoms per formula unit (apfu)**.** Epidotes with ΣREE^{3+} content between 0.1 and 0.5 apfu are referred to as REE-rich epidotes. In the M3 site, the Fe^{3+} of epidote or the Al^{3+} of clinozoisite are replaced by Fe^{2+} of allanite (Armbruster et al., 2006).

Materials and Methods

Black sand samples were collected from beaches, close to the Kavala pluton outcrops. The preconcentration of heavy minerals was performed with magnetic separation, using Frantz L-1 Isodynamic Magnetic Separator (15° forward, 25° sideways slope). The epidote-group minerals were selected using a binocular stereoscope (Leica Wild M10), and polished epoxy mounts of these minerals were prepared for the identification and detailed mineralogical observations. The chemical composition of the epidote-group minerals was determined by a JEOL JSM- 6390LV scanning electron microscope (SEM) (JEOL Ltd., Tokyo, Japan) equipped with an OXFORD INCA 300 energy dispersive system (EDS) in the School of Sciences at Aristotle University of Thessaloniki.

Results and Discussion

The major REE carrier of the black sands from Kavala is allanite-(Ce), which occurs as tabular or prismatic grains with sizes up to 0.8 mm and is suggested to have a magmatic-hydrothermal origin. The SEM–BSE images demonstrate variations in brightness within a single crystal, indicating variances in the REE content (Fig 1a). The typical crystals of magmatic origin display a REE leaching from core to the rim, possibly reflecting the fractionation of allanite and the approaching LREE depletion of the melt; allanite-(Ce) occurs as core that progressively lapses into REE-rich epidote and finally to epidote in the rims. A common illustration of allanite-(Ce) in the SEM–BSE images reveals patchy internal textures, displaying darker and lighter gray domains with irregular limits that are ascribed to REE leaching of allanite-(Ce) because of the penetration of hydrothermal fluids along the grain fractures **(**Gieré and Sorensen, 2004**).**

Several point analyses within mineral crystals of the epidote group were performed. Their structural formula was calculated on the basis of 12.5 oxygens and 8 cations per formula unit (Σ_{A+M+T} = 8), according to the structure refinement described by Armbruster et al. (2006). The value Fe^{2+}/Fe^{3+} was calculated until the total cation charges were equal to 25, as well as the ratio Fe_{ox} that ensues from Fe^{3+}/Fe_{tot}. The content of the rare earths in allanite-(Ce) from Kavala varies between 14.78 and 23.24 wt % in total.

The epidote-group minerals from the Kavala district are characterized by compositional variations of major and minor elements, as well as Fe_{ox} and variable solid solution phases in a single crystal, shown in Fig. 1b. The graphic illustration of the cationic proportions of REE+Y/A site (apfu) vs. M^{2+}/M site (apfu) (Fig. 2a) demonstrates a very good correlation (r^2= 0.95) and indicates the presence of extensive solid solutions between allanite and epidote end-members, since the compositional data are attributed along the epidote- allanite range. The shifting data from the ideal allanite end-member is ascribed to the strong presence of Fe^{3+} in the M sites. The proposed by Gieré and Sorensen (2004) plot of Al_{tot} against REE + Y (apfu) exhibits the compositional variations between the ferriallanite, allanite, epidote and clinozoisite end-

members (Fig. 2b). This diagram can be used to estimate the Fe_{ox} values from the lines radiating from the clinozoisite end member; however, these values are slightly different from the Fe_{ox} that was calculated from the microanalyses, because the plot factors out the trace elements that contribute to the chemical balance of allanite. The REE-enriched allanites plot within the area between allanite and ferriallanite, indicating a sufficient ferriallanite component with significant Fe^{3+} incorporation in the composition of the allanite. The distribution of the data in the diagram suggests that the modifications follow the exchange scheme $[REE^{3+}Fe^{2+}]_{+1}[Ca^{2+}Fe^{3+}]_{-1}$ for the REE-poor analytical points which are gradually adjusted by the scheme $[REE^{3+}Fe^{2+}]_{+1}[Ca^{2+}Al^{3+}]_{-1}$; the remaining chemical elements and their site occupancy are the determinative factors that make the substitution more complicated.

Conclusions

According to the chemical characteristics and the compositional variations of the epidote-group minerals, the chemical balance of the crystal structure is attained by composite substitution mechanisms that follow the scheme $[Ca+(Fe^{3+},Al)]_{-1}[(REE,Y,Th,U)+(Fe^{2+},Mg,Mn)]_{-1}$.

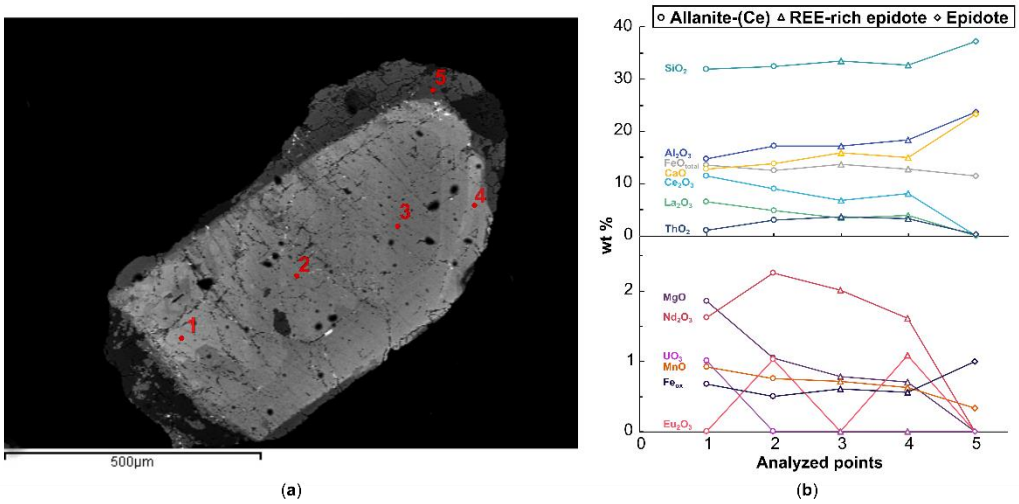

Figure 1. (a) BSE image of allanite grain and the analyzed points, (b) Oxide variations of the analyzed points.

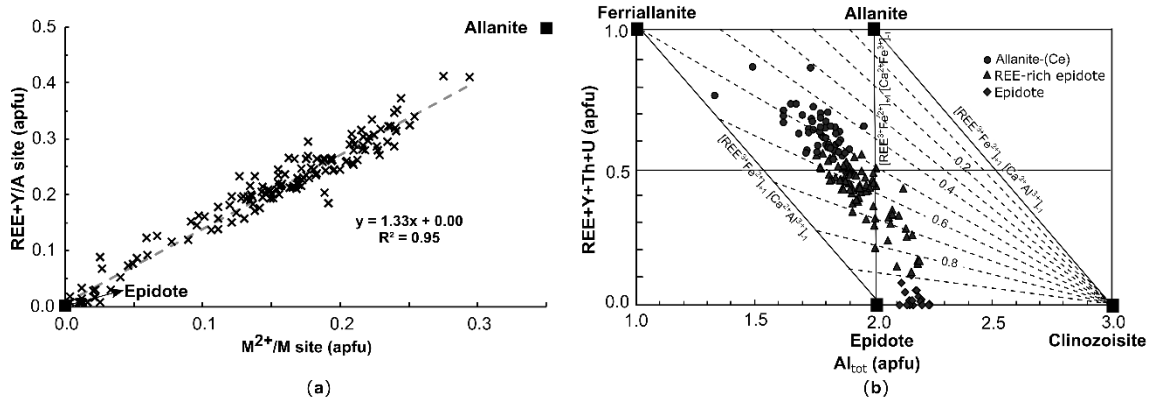

Figure 2. (a) REE+Y/A site vs M^{2+}/M site occupancies (after Gieré and Sorensen, 2004). Full squares indicate ideal compositions of epidote and allanite end-members (b) Al_{tot} vs. REE+Y+Th+U (apfu) diagram, showing the position of the studied epidote-group minerals in the ferriallanite–allanite–epidote–clinozoisite system. Comments in the text.

Acknowledgments

E. Peristeridou received a scholarship funded by HELPE S.A. through the Special Account for Research Grants (S.A.R.G.) A.U.Th.

References

Eliopoulos, D., Economou, G., Tzifas, I., & Papatrechas, C., 2014. The potential of rare earth elements in Greece. In Proceedings of the ERES2014: First European Rare Earth Resources Conference, Milos, Greece, pp. 4-7.

Peristeridou, E., Melfos, V., Papadopoulou, L., Kantiranis, N., Voudouris, P., 2022. Mineralogy and Mineral Chemistry of the REE-Rich Black Sands in Beaches of the Kavala District, Northern Greece. Geosciences, 12, 277.

Giere, R., Sorenson, S. S., 2004. Allanite and other REE-rich epidote-group minerals: Reviews in Mineralogy and Geochemistry, v. 56.

Armbruster, T., Bonazzi, P., Akasaka, M., Bermanec, V., Chopin, C., Gieré, R., Heuss-Assbichler, S., Liebscher, A., Menchetti, S., Pan, Y., Pasero, M., 2006. Recommended nomenclature of epidote-group minerals. European Journal of Mineralogy, 18, 551-567.

16th International Congress of the Geological Society of Greece
17-19 October, 2022 - Patras, Greece
Bulletin of the Geological Society of Greece, Sp. Publ. 10
Ext. Abs. GSG2022-367

X-Ray diffraction quantitative analysis of clay minerals using external standards mixtures: A case study of clays from Ventzia basin, Grevena, West Macedonia, Greece.

C. Mytiglaki[1], D. Papadimitriou[1], N. Kantiranis[1]

(1) Department of Mineralogy-Petrology-Economic Geology, School of Geology, Faculty of Sciences, Aristotle University of Thessaloniki, Thessaloniki, Greece, michristi@geo.auth.gr,

Introduction and Objectives

For the quantitative and qualitative evaluation of natural and synthetic materials, the X-Ray diffraction analysis (XRD) is widely used. There are a lot of research works on the quantitative or qualitative analysis of geological samples based on this method (Clark et al., 1936; Bish et al., 1988). According to the purpose of the analysis, the composition of the investigated material, and the and the available equipment and software, different methods can be used, such as: a) Method of internal standard addition, b) Method of external standards, c) Method of intensity ratio, and d) Method of Rietveld refinement. For instance, clay minerals, due to their various chemical composition, different physical properties, complex structure and arrangement, need specifically conditions and methods in order their minerals percentages to be measured. Still, their quantitative investigation remains a challenge (Moore et al., 1997). The purpose of this work is to evaluate the percentage of mineral content in samples, rich in clay minerals, with the use of external standards. Samples have been taken from the clay deposits of the Ventzia basin (Grevena, West Macedonia, Greece).

Materials and Methods

Palygorskite, smectite, quartz and serpentine were the main mineralogical phases of the Ventzia basin clay deposits. Pure samples of palygorskite (STD1) and smectite (STD2) from specific horizons of the Ventzia basin clay deposits and quartz, serpentine from the collection of the Dept. of Mineralogy-Petrology-Economic Geology, School of Geology, Aristotle University, were used as reference materials. These minerals were used for the preparation of the three standards (STD3, STD4, STD5) mixtures, each one weighted 1g in proportions presented in Table 1. Finally, four representative samples (d1-d4), referred as test samples, from the examined basin, were used to implement the method. The mineralogical composition of the mixtures, the reference minerals and the test samples were determined using X-ray diffractometry under the same conditions. The XRD analysis was performed using a Philips PW1710 diffractometer with Ni-filtered CuKα radiation on randomly oriented bulk samples. The counting statistics were: start angle 3º, end angle 63º (2θ), step size 0.02º (2θ), time per step 1 sec and scan speed 0.02º/sec.

Table 1. Percentage proportion (% wt) of the standard mixtures

Mineral	STD3	STD4	STD5
Palygorskite	40	55	20
Smectite	40	20	50
Serpentine	10	20	15
Quartz	10	5	15

Experimental results and conclusions

An initial qualitative X-ray diffraction analysis proved that the standard reference sample (STD1) consists only of palygorskite while the second (STD2) consists only of smectite. The XRD data of the standard mixtures STD3-STD5 are presented in Table 2. In this table, the amount (wt%) of each mineral phase in the standard mixtures and the intensity (cps) of minerals main reflection measured from the X-ray pattern, are presented. Diagrams between these two variables were created and the trendline and correlation coefficient were calculated (Graph 1), highlighting an important linear correlation.

Table 2 XRD data of the studied standard mixtures.

Mineral	Reflection	STD3		STD4		STD5	
		% wt	cps	% wt	cps	% wt	cps
Palygorskite	≈10,5Å	40	380	55	506	20	193
Smectite	≈15Å	40	388	20	188	50	511
Serpentine	≈7,3Å	10	243	20	392	15	310
Quartz	3,34Å	10	1325	5	692	15	2153

Graph 1. External standard mixtures mineral correlations.

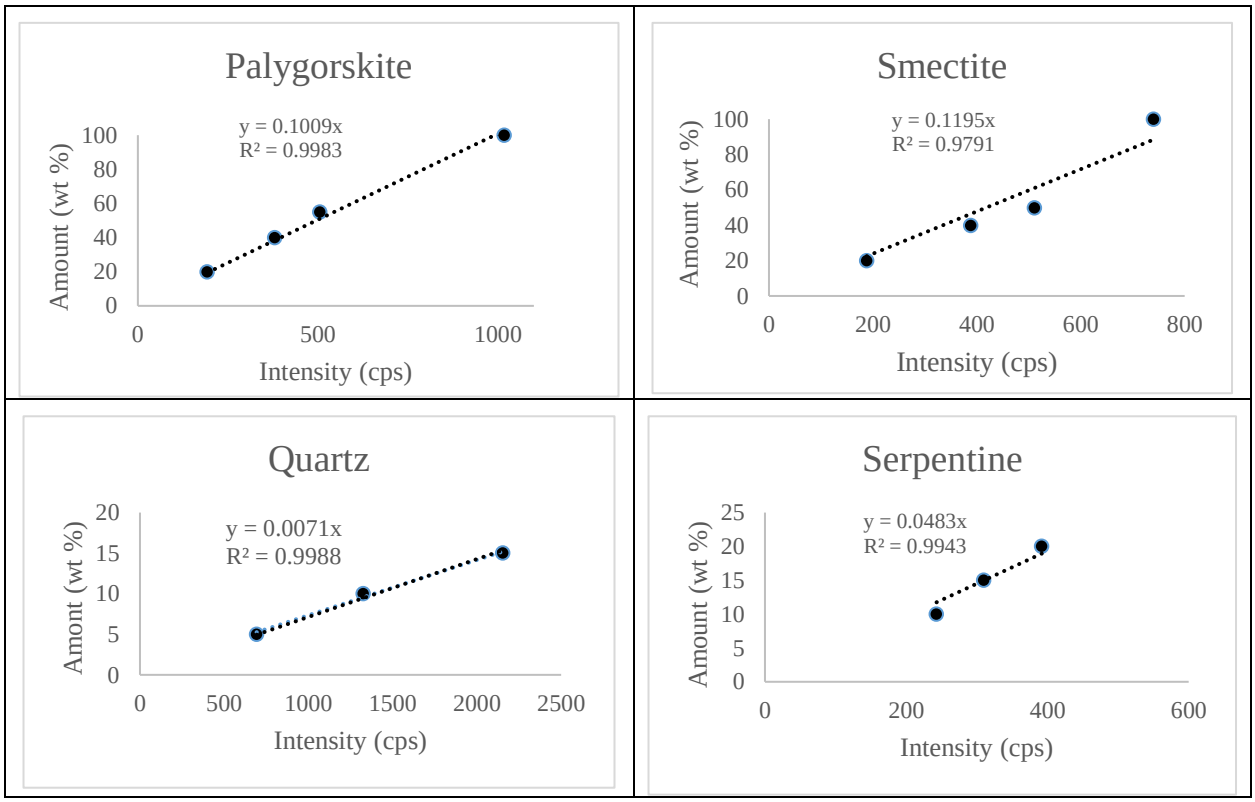

Using the data of Graph 1, the quantitative mineralogical composition of four (d1-d4) clay-rich samples from the Ventzia basin was measured. It was found that the sample d1 is rich in palygorskite, the sample d2 is rich in smectite, while samples d3 and d4 contain equal amounts of palygorksite+smectite (Table 3). From the results of Tab. 3, it is concluded that the method of the external standards can give the quantitative mineralogical composition of an unknown sample with very high precision at amounts well below 1 wt.%. In conclusion, the method of external standard mixtures, is an efficient mineralogical quantitative method for the evaluation of the contained amount of clay minerals in a clay-rich sample.

Table 3. Quantitative mineral composition (wt.%) of the test samples applying the method of the external standards

	Smectite	**Palygorskite**	**Lizardite**	**Quartz**
d1	6.0	93.0	0.6	0.4
d2	67.0	28.0	5.0	0.2
d3	39.9	59.1	0.8	0.1
d4	54.0	45.0	0.8	0.1

Acknowledgements

This research is co-financed by Greece and the European Union (European Social Fund -ESF) through the operational programme «Human Resources Development, Education and Lifelong Learning», 2014-2020, in the context of the project "Strengthening human resources through of the implementation of doctoral research - Sub-Action 2: Program for awarding IKY scholarships to PhDs candidates from Greek universities". Also, the authors would like to thank Geohellas S.A company for the sample supply.

References

G.L. Clark, D.H. Reynolds, 1936. Quantitative analysis of mine Dust Ind. Eng. Chem. Anal. Ed, 8, pp. 36-40

D.L. Bish, S.A. Howard 1988. Quantitative phase analysis using the Rietveld method J. Appl. Crystallogr., 21 (1988), pp. 86-91

D.M. Moore, R.C. Reynolds 1997. X-ray Diffraction and the Identification and Analysis of Clay Minerals (second ed.), Oxford University Press, Oxford

16th International Congress of the Geological Society of Greece
17-19 October, 2022 - Patras, Greece
Bulletin of the Geological Society of Greece, Sp. Publ. 10
Ext. Abs. GSG2022-369

Removal of Cr(VI) from industrial wastewater using coagulants and clinoptilolite zeolitic tuff

C. Mytiglaki[1], N. Kantiranis[1], S. Symeonidou[2] and A. Filippidis[1]

(1) Department of Mineralogy-Petrology-Economic Geology, School of Geology, Faculty of Sciences, Aristotle University of Thessaloniki, Thessaloniki, Greece, michristi@geo.auth.gr (2) Department of Hydraulics and Environmental Engineering, School of Civil Engineering, Faculty of Engineering, Aristotle University of Thessaloniki, Thessaloniki, Greece.

Introduction and Objectives

The world's industrial needs are continuously increasing. The increase rate is in proportion to the growth of the earth's population. A result of this fact is the high production of wastewaters alongside with the high consumption of freshwater. Wastewaters contain a variety of suspended, dissolved as long as colloidal organic and inorganic harmful compounds. Hexavalent chromium constitutes one of them. Anthropogenic Cr derives from different industrial activities (e.g., leather tanning, fertilizers, paints, wood preserving, steel production, ore refining, coal and oil combustion, etc.). One of the most negative consequences of the anthropogenic Cr is that contributes significantly to the existing Cr content of soils, surface and ground waters (Megalovasilis et al., 2016; Kazakis et al., 2018). The Cr, as an element, exists in soils, minerals, surface and ground waters in different oxidation states such as the trivalent (Cr-III) and hexavalent (Cr-VI) chromium. The Cr(III) in comparison with Cr(VI) is characterized by less toxicity and modest immobility. Specifically, hexavalent chromium Cr(VI) occurs as a dissolved anion in aqueous phases. It can be present in waters and in different types of industrial wastewaters, as highly mobile anion with an acute and chronic aquatic toxicant character. The Cr(VI) is also carcinogenic for humans. Common side effects are: skin irritations, dermatitis, stomach ulceration, liver damage, kidney circulation, damage at nerve tissues etc. In large quantities it can be fatal to living organisms (Costa et al.,2006). Concerning the zeolitic tuff, it corresponds to a volcaniclastic rock which contains one or more from the different (>65) phases of zeolites. Clinoptilolite constitutes a type of natural zeolite with wide variety of environmental, industrial and agricultural applications. These abilities derives from the mineral's crystal framework and the containning nano/micro-pores. The channels of the crystal framework form 10- and 8-member rings, in dimensions of 7.5x3.1 Å, 4.6x3.6 Å and 4.7x2.8 Å. Also, the macro pores of the zeolitic tuff contributes to the previously mentioned abilities (Filippidis et al., 2015; Filippidis et al., 2008). The present study investigates, the removal of Cr(VI) from industrial wastewater using 0.0, 0.1, 0.2, 0.3, 0.4 gr of clinoptilolite zeolitic tuff in comparison with the use of 2.1 mL of coagulants.

Materials and Methods

The mineralogical composition of the sample was determined by X-Ray Powder Diffraction (XRPD) method. The XRPD-sample was powdered in agate mortar and passed all through sieve <0.063 mm. The XRPD analysis was performed using a Philips PW1710 diffractometer with Ni-filtered CuKα radiation on randomly oriented samples. The counting statistics were: start angle 3º, end angle 63º (2θ), step size 0.02º (2θ), time per step 1 sec and scan speed 0.02º/sec. Semi-quantitative estimates of the abundance of the mineral phases were derived from the XRPD data, using the intensity (counts) of certain reflections, the density and the mass absorption coefficient of the identified minerals for CuKα radiation, the software MAUD-Material Analysis Using Diffraction with the RIETVELD method. Clay mineralogy was identified from air-dried, glycolated and heat-treated oriented samples scanned from 3º to 23º 2θ at a scanning speed of 1.2º/min. The chemical composition of the zeolitic tuff sample was determined by the Fusion-Inductively Coupled Plasma (FUS-ICP) method. The ammonia ion exchange capacity (sorption ability) of the zeolitic tuff was measured by the Ammonium Acetate Saturation (AMAS) method. The AMAS-sample was powdered in agate mortar and passed all through sieve <0.125 mm. The chemical composition of the clinoptilolite (average of 7 microanalyses) contained in the zeolitic tuff was performed on polished thin section by Scanning Electron Microscopy-Energy Dispersive Spectroscopy (SEM-EDS) with LINK-AN 10000 EDS system. To minimize volatilization of alkalis in the clinoptilolite, the electron beam spot size was enlarged and the counting time decreased. The zeolitic tuff was powdered in agate mortar and passed all through sieve <0.250 mm. The industrial wastewater was treated at room temperature with <0.250 mm grain-size of the zeolitic tuff in batch-type experiments. In 300 mL of wastewater and in five (5) different experiments, 0.0, 0.1, 0.2, 0.3 and 0.4 gr of zeolitic tuff was added under continuous stirring for 2 minutes and at the final stage of each experiment, coagulants were added (0.1 mL of polyaluminium chloride and 2 mL of cationic polyelectrolyte). The overflow clear water and the precipitated zeosludge were separated by filtering. The initial wastewater and the produced overflowed clear water were analyzed for pH electrometric (detection limit 0.1) and Cr(VI) content by the Molecular Absorption Spectrophotometry (MAS) method (detection limit 0.01 mg/L).

Experimental results and conclusions

The grain-size distribution of the <0.250 mm zeolitic tuff is, 29 wt.% (<0.250-0.125 mm), 31 wt.% (<0.125-0.063 mm)

and 40 wt.% (<0.063 mm).

The zeolitic tuff consists of 84 wt.% clinoptilolite, 4 wt.% mica + clay minerals (smectite, illite), 5 wt.% quartz, 2 wt.% cristobalite and 5 wt.% feldspars (al-kali-feldspar + plagioclase). The total microporous minerals (clinoptilolite + mica + clays) is 88 wt.%. Chemically, the zeolitic tuff consists mainly (in descending order) of SiO_2, Al_2O_3, CaO, K_2O, Fe_2O_3, MgO and Na_2O. The chemical formula of the Ca-rich clinoptilolite, contained in the zeolitic tuff is $Ca_{1.8}K_{0.9}Mg_{0.7}Na_{0.5}Al_{6.4}Si_{29.6}O_{72}{\cdot}20.8H_2O$.

The main exchangeable cations of the clinoptilolite, in descending order, are Ca, K, Mg and Na. and its ammonia ion exchange capacity (sorption ability) was measured to 182 meq/100g.

From the treatment of industrial wastewater (500 mL) of pH 8.2 and Cr(VI) 0.12 mg/L with 2.1 mL coagulants (0.1 mL polyaluminium chloride + 2 mL Cationic poly-electrolyte), resulted the production of overflowing clear water with pH values 7.8 and Cr(VI) 0.06 mg/L. Also, a 5% improvement observed in quality parameters to the pH values and 50% to Cr(VI) content. The treatment of wastewater, combined coagulants and 0.1-0.4 gr of the Clinoptilolite Zeolitic Tuff (CZT) resulted the production of overflowing clear water, free of odours and improved to the quality parameters. Especially the pH values improved by 10-11%, from 7.8 to 7.4-7.3. Regarding the Cr(VI) content, the increase of the added amount of Clinoptilolite Zeolitic Tuff (CZT) from 0.1 gr to 0.4 gr, resulted in improvement by 75% to more than 92%, from 0.03 mg/L to <0.01 mg/L. Compared to the treatment with only coagulants, the addition of 0.4 gr of the Clinoptilolite Zeolitic Tuff (CZT) improves the removal of Cr(VI) by more than 42%, from 50% to more than 92%.

The properties of the zeolitic tuff are duo to the contained nano/micro-pores in a framework of channels with 10- and 8-member rings with three dimensions (7.5x3.1 Å, 4.6x3.6 Å, 4.7x2.8 Å) [4, -7]. Generally, the clinoptilolite zeolitic tuff could sorb bacteria, gases, inorganic, organic and organometallic compounds from soils and waters. The sorption of the different components by the nano/micro-pores of clinoptilolite, as well as the meso- and macro-pores of the zeolitic tuff, is attributed to absorption (ion exchange), adsorption and surface precipitation processes. The clinoptilolite, because of the existence of the surface Broensted acidic active sites and the Lewis basic active sites, reacts with the negatively or/and positively charged chemical components. These chemical processes are related to sorption physicochemical phenomena of ions and molecules, and concerns both the structural void spaces (nano/micro-pores) and the surface of the clinoptilolite crystals, consequently the meso- and macro-pores of the zeolitic tuff (Filippidis et al., 2015; Filippidis et al., 2007).

The clinoptilolite zeolitic tuff shows an ability to neutralize the pH of the basic wastewater, acting as a proton donor. The decrease of pH from 7.8 to 7.3, can be at-tributed to the removal of protons (OH-) from the surface Broensted acidic sites and/or the removal of protons from water molecules coordinated to exchangeable cations through interactions between the OH- ions present in the solutions and the clinoptilolite crystals (Filippidis et al., 1996)

The sorption of the Cr(VI) from the wastewater by the clinoptilolite zeolitic tuff and the decrease from 0.06 mg/L to <0.01 mg/L, can be attributed mainly, exclusively to absorption (ion exchange) by the nano/micro-pores of the clinoptilolite and probably to a very low extent to adsorption and surface precipitation processes on the meso- and macro-pores of the zeolitic tuff (Mytiglaki et al., 2020; Godelitsas et al., 2001).

References

Megalovasilis, P., Papastergios, G., Filippidis, A. 2016. Mineralogy, geochemistry and leachability of ashes produced after lignite combustion in Amyntaio Power Station, northern Greece. Energy Sources, 38(10), 1385-1392.

Kazakis, N., Kantiranis, N., Kalaitzidou, K., Kaprara, E., Mitrakas, M., Frei, R., Vargemezis, G., Vogiatzis, D., Zouboulis, A., Filippidis, A. 2018. Environmentally available hexavalent chromium in soils and sediments impacted by dispersed fly ash in Sarigkiol basin (Northern Greece). Environmental Pollution, 235, 632-641.

Costa, M., Klein, C.B. 2006. Toxicity and carcinogenicity of chromium compounds in humans. Critical Reviews in Toxicology, 36(2), 155–163.

Filippidis, A., Kantiranis, N., Papastergios, G., Filippidis, S. 2015 Safe management of municipal wastewater and sludge by fixation of pollutants in very high quality HEU-type zeolitic tuff. Journal of Basic and Applied Research International, 7(1), 1-8.

Mytiglaki, C., Kantiranis, N., Misaelides, P., Noli, F., & Filippidis, A. 2020. Comparative study of the cesium uptake ability between HEU-type (clinoptilolite-heulandite) zeolitic tuff and pure heulandite. Bulletin of the Geological Society of Greece, 56(1), 56-69.

Filippidis, A., Kantiranis, N. 2007. Experimental neutralization of lake and stream waters from N. Greece using domestic HEU-type rich natural zeolitic material. Desalination, 213, 47-55.

Filippidis, A., Apostolidis, N., Paragios, I., Filippidis, S. 2008. Zeolites clean up. Industrial Minerals, 487, 68-71.

Filippidis, A., Godelitsas, A., Charistos, D., Misaelides, P., Kassoli-Fournaraki, A. 1996. The chemical behavior of natural zeolites in aqueous environments: Interactions between low-silica zeolites and 1M NaCl solutions of different initial pH-values. Applied Clay Science, 11, 199-209.

Godelitsas, A., Charistos, D., Tsipis, A., Tsipis, C., Filippidis, A., Triantafyllidis, C., Manos, G., Siapkas, D. 2001. Characterization of zeolitic materials with a HEU-type structure modified by transition metal elements: Definition of acid sites in Nickel-loaded crystals in the light of experimental and quantum-chemical results. Chemistry - A European Journal, 7, 3705-3721.

16th International Congress of the Geological Society of Greece

17-19 October, 2022 - Patras, Greece

Bulletin of the Geological Society of Greece, Sp. Publ. 10

Ext. Abs. GSG2022-375

Absence of anorogenic magmatic signatures in the Late Cretaceous subduction-related granitoids from Anafi island

P. Koutsovitis[1], K. Soukis[2], P. Voudouris[2], S. Lozios[2], T. Ntaflos[3], C. Stouraiti[2], N. Koukouzas[4]

(1) Section of Earth Materials, Department of Geology, University of Patras, Patras 26504, Greece; (pkoutsovitis@upatras.gr) (2) Department of Geology and Geoenvironment, National & Kapodistrian University of Athens, Panepistimioupoli Zografou, Athens, GR- 15784 (3) University of Vienna, Department of Lithospheric Research, Althanstr. 14, Vienna, Austria (4) Centre for Research and Technology-Hellas (CERTH), Marousi, Attica, Greece

In Anafi Island, the Late Cretaceous granitoids compositionally vary between intermediate to felsic and are exposed as intrusions within variably metamorphosed exhumed formations that comprise mostly of amphibolites, serpentinized ultramafics but also of metasedimentary rocks. Recent research findings (Koutsovitis et al. 2022) attribute the formation of the granitoids at arc settings, corresponding to I-type rocks, with a clear calc-alkaline geochemical imprint. Despite the relatively wide variety of lithotypes identified, this is most likely attributed to fractional removal of plagioclase and/or of K-feldspar but also of mafic mineral fractionation (magnesiohornblende and biotite); similar fractionation mechanisms have also been identified in other localities with compositionally comparableLate Cretaceous granitoids in the Aegean (e.g. East Crete, Donousa island), suggesting that this type of magmatic activity was not a local event.

Selected major element ratios point to melting temperatures of ~930 °C and ~800 °C for the intermediate and felsic granitoids respectively, whereas amphibole and zircon saturation thermometry yields crystallization temperatures of ~150 °C lower than of the aforementioned melting ones. Amphibole-based geobarometry but also empirical equations based on the normative (Qz), (Ab) and (Or) suggest shallow intrusion conditions (~4.5 avg. kbar); these temperature/pressure conditions as well as the presence of hydrous mineral phases points to melt/fluid percolation above a subducting slab and not to the effects from interaction with anorogenic alkaline enriched magmas associated with deeper source melting. Apart from fractional crystallization, trace element indicators reveal that assimilation of crustal rocks occurred to some extent affecting the ascending magmas. The most probable scenario for the formation of the Anafi granitoids is their incorporation within the hydrated mantle wedge aiming towards the metamorphic units of the Pindos - CBU domain, a mechanism that was likely facilitated via corner flow. Prolonged underplating of subducted material assisted the exhumation of the granitoids along with their host units above the parautochtonous flysch during the Late Eocene-Oligocene (Koutsovitis et al. 2022).

References

Koutsovitis, P., Soukis, K., Voudouris, P., et al., 2021. The Late Cretaceous magmatic arc of the south Aegean: geodynamic implications from petrological and geochemical studies of granitoids from Anafi Island (Cyclades – Greece). International Geology Review 63, 1-24. https://doi.org/10.1080/00206814.2021.1884906

16th International Congress of the Geological Society of Greece
17-19 October, 2022 - Patras, Greece
Bulletin of the Geological Society of Greece, Sp. Publ. 10
Ext. Abs. GSG2022-381

Mineralogy and fluid inclusion study of the Loutros epithermal mineralization, Rhodope, Greece

M. Melfou[1], P. Voudouris[2], V. Melfos[1], R. Klemd[3], N. Kantiranis[1]

(1) Faculty of Geology, Aristotle University of Thessaloniki, Thessaloniki, Greece, melfoumv@geo.auth.gr (2) Faculty of Geology and Geoenvironment, National and Kapodistrian University of Athens, Athens, Greece (3) Department of Geography and Geosciences, University of Erlangen-Nuremberg, Erlangen, Germany

Research Highlights

Pyrite-marcasite and Ag-enriched galena veins and disseminations are present in the Loutros epithermal system. Fluid inclusion data suggest that the ore-forming fluids had a meteoric/seawater origin, with minor magmatic contribution at the 1st pyrite-marcasite stage and increased meteoric and/or seawater contribution at the 2nd galena stage.

Abstract

A highly prosperous district for epithermal mineralization hosted in Oligocene-Miocene volcanic rocks is the Rhodope metallogenic province in Greece, located in the broader Western Tethyan metallogenic belt (Melfos and Voudouris 2017; Voudouris *et al*., 2019). The Evros (Pefka-Loutros) ore district located within the Rhodopes comprises numerous high-sulfidation (HS) and intermediate-sulfidation (IS) epithermal systems in hydrothermally altered volcanic rocks. Among others, the Loutros IS epithermal mineralization is an important prospect that is hosted in a silicified, sericite and zeolite-altered rhyolitic dome (Melfos and Voudouris, 2017). This felsic intrusion of high-K calc-alkaline affinity has been dated at 19.53 ± 0.75 Ma (K-Ar at whole-rock; Christofides *et al*., 2004). The objective of this study is to present preliminary data on the mineralogy, the ore styles, and the temperatures of formation of the mineralization of the Loutros IS system.

Seven samples were studied under polarized and/or reflected light and three samples were imaged and analyzed with scanning electron microscopy/energy dispersive X-ray spectrometry (SEM/EDS) at the School of Sciences, of the Aristotle University of Thessaloniki (AUTh). Three samples have been analyzed for whole rock trace element analyses at Bureau Veritas Commodities Canada, Vancouver, Canada. Six doubly-polished wafers of barite and quartz veins, were used for fluid inclusion microthermometry at the Department of Mineralogy-Petrology-Economic Geology, AUTh.

The host rock of the Loutros IS mineralization is an altered rhyolite (Fig. 1a) that displays porphyritic texture. The ore minerals form veins, breccias and disseminations, and consist of pyrite, marcasite, galena, and minor sphalerite and chalcopyrite. Two types of veins have been identified: (i) early northwest-trending massive pyrite-marcasite veins with straight borders (Fig. 1a,b), and (ii) late-stage barite-galena veins that either crosscut the rhyolite (Fig. 1c) or occur as late-stage ore deposition in pyrite-marcasite veins (Fig. 1b). Minor sphalerite (Fig. 1d) and chalcopyrite may be present in intergrowths with galena and barite (Melfos and Voudouris, 2017). Framboidal pyrite (Fig. 1e,f) is found in disseminated aggregates. Combined with the widespread barite, this indicates a possible shallow submarine condition during deposition of at least part of the mineralization (e.g. epithermal mineralizations at Milos; Alfieris *et al.*, 2013). Other structures include non-mineralized chalcedony veins that are found in proximity to the pyrite-marcasite vein, and hydrothermal breccias that crosscut the rhyolite.

Bulk ore trace element analyses showed that the pyrite-marcasite mineralization contains traces of As (579 ppm), Mo (9 ppm), and Co (2 ppm). The galena mineralization contains trace amounts of Sb (≤305 ppm), Ag (≤32 ppm), and Cu (≤62 ppm) (Voudouris *et al*., 2019). The pyrite-marcasite vein is depleted in Sb (0.4 ppm), Ag (2 ppm) and Cu (11 ppm), compared with the galena mineralization, while the latter is depleted in As (≤137 ppm), and Mo (4 ppm) related to the pyrite-marcasite vein.

Barite- and quartz-hosted fluid inclusions are concentrated in clusters and are considered to be primary, based on the criteria proposed by Roedder (1984) and Goldstein and Reynolds (1994). Only two-phase aqueous liquid-vapor inclusions, containing a vapor bubble occupying 10-20 vol.%, were observed. These inclusions homogenized into the liquid phase upon heating. Post-entrapment modifications, such as necking down or leakage, have affected many of these fluid inclusions. In order to eliminate the effects of the post-entrapment modifications, only inclusions with constant liquid-to-vapor ratios were selected for the microthermometry. The microthermometric measurements of fluid inclusions in quartz, which is synchronous with the pyrite-marcasite mineralization, showed a homogenization temperature range of 259° to 329°C (Fig. 2a), and a salinity between 2.8 and 3.9 wt.% NaCl equiv. (Fig. 2b), indicating that the fluids had a meteoric and/or seawater origin, with a minor magmatic contribution. The microthermometric measurements on barite- and quartz-hosted fluid inclusions showed that the stage of the galena mineralization may have taken place between 201° and 255°C (Fig. 2a) from a less saline fluid (1.0 - 1.8 wt.% NaCl equiv.; Fig. 2b), indicating an increased contribution of meteoric and/or seawater fluids in the system.

In summary, the Loutros IS epithermal mineralization is hosted in altered rhyolites and is characterized by quartz-pyrite-marcasite veins and disseminations, and barite-galena veins. Textural relationships show that galena postdates the pyrite-marcasite mineralization. This is confirmed by the microthermometric data that show that the pyrite-marcasite event was formed at a temperature range of 259° to 329°C, while the galena stage was formed at lower temperatures (201°-255°C) from a low-saline hydrothermal fluid. Trace element analyses of whole rock samples imply that the galena-associated ore is enriched in Ag (≤32 ppm). Further analysis (whole-rock, fluid inclusions microthermometry, LA-ICP-MS and Raman) and sulfur isotopes are in progress to discriminate the two ore stages and to examine the physicochemical conditions of the ore-forming events.

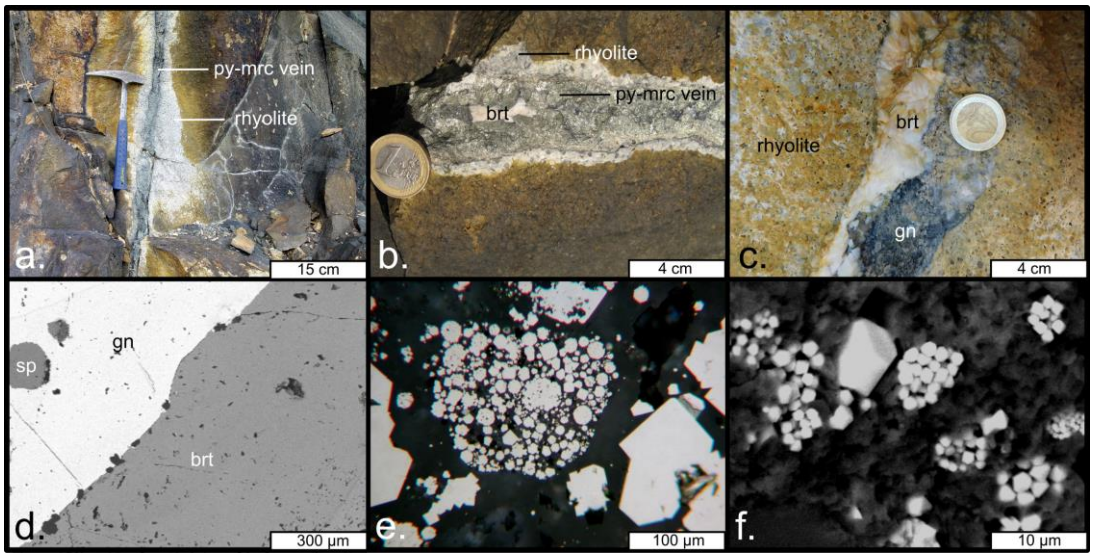

Figure 1. Outcrop, macroscopic and microscopic images from the Loutros epithermal mineralization. (a) Outcrop image of a massive pyrite-marcasite vein that crosscut the altered rhyolite. (b) A barite vein in a pyrite-marcasite vein. (c) A late-stage barite-galena vein that crosscuts the rhyolite. (d) Galena and sphalerite intergrow with barite (SEM). (e) Framboidal pyrite with euhedral pyrite grains (reflected light). (f) Framboidal pyrite (SEM). Mineral abbreviations from Whitney and Evans (2010); py: pyrite; mrc: marcasite; gn: galena; brt: barite; sp: sphalerite.

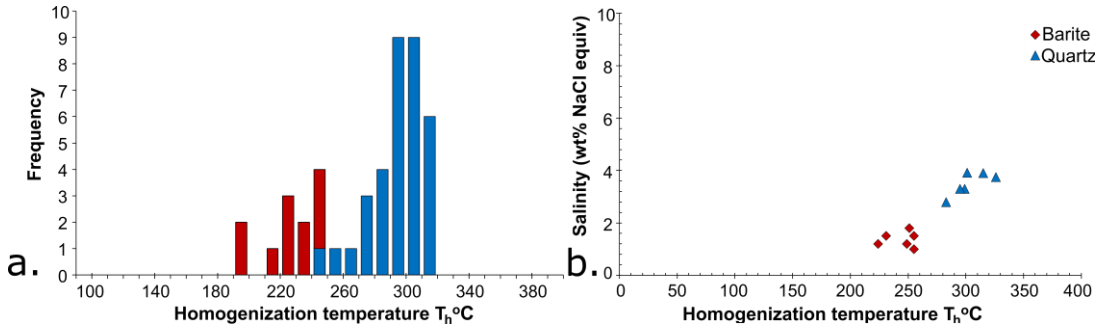

Figure 2. Microthermometric data from the quartz and the barite- and quartz-hosted fluid inclusions of the Loutros IS epithermal mineralization. (a) Homogenization temperatures. (b) Salinity versus homogenization temperatures.

References

Alfieris, D., Voudouris, P., & Spry, P. G. (2013). Shallow submarine epithermal Pb–Zn–Cu–Au–Ag–Te mineralization on western Milos Island, Aegean Volcanic Arc, Greece: Mineralogical, geological and geochemical constraints. *Ore Geology Reviews, 53*, 159–180.

Christofides, G., Pecskay, Z., Eleftheriadis, G., Soldatos, T., & Koroneos, A. (2004). Tertiary Evros volcanic rocks, Thrace, Northeastern Greece: Petrology, K/Ar geochronology and volcanism evolution. Geologica Carpathica, 55, 397-409.

Goldstein, R. H., & Reynolds, T. J. (1994). Fluid inclusion microthermometry.

Melfos, V., & Voudouris, P. (2017). Cenozoic metallogeny of Greece and potential for precious, critical and rare metals exploration. Ore Geology Reviews, 89, 1030–1057.

Roedder, E. (1984). Volume 12: Fluid inclusions. Reviews in Mineralogy, 12, 644.

Voudouris, P., Mavrogonatos, C., Spry, P. G., Baker, T., Melfos, V., Klemd, R., Haase, K., Repstock, A., Djiba, A., Bismayer, U., Tarantola, A., Scheffer, C., Moritz, R., Kouzmanov, K., Alfieris, D., Papavassiliou, K., Schaarschmidt, A., Galanopoulos, E., Galanos, E., … Melfou, M. (2019). Porphyry and epithermal deposits in Greece: An overview, new discoveries, and mineralogical constraints on their genesis. Ore Geology Reviews, 107, 654–691.

Whitney, D., & Evans, B. (2010). Abbreviations for Names of Rock-Forming Minerals. American Mineralogist, 95, 185–187.

16th INTERNATIONAL CONGRESS of the
GEOLOGICAL SOCIETY OF GREECE

T7. Economic Geology, Raw Materials, Energy Resources, Circular Economy

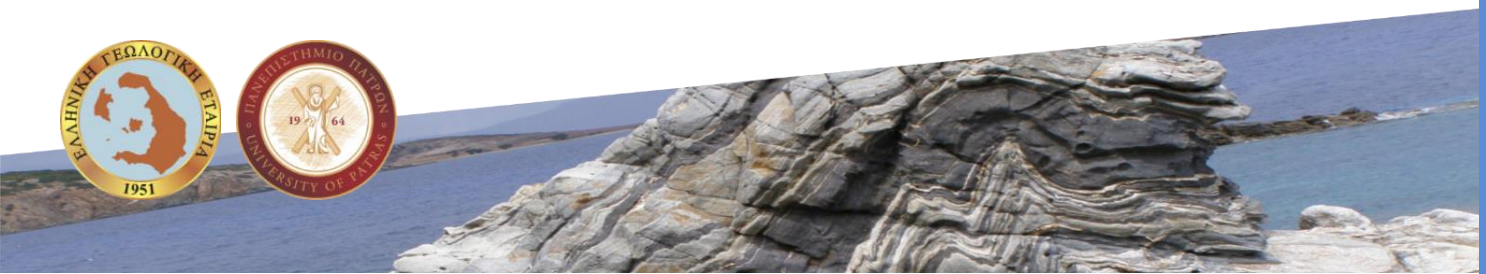

OUR EARTH, OUR HOME

16th International Congress of the Geological Society of Greece
17-19 October, 2022 - Patras, Greece
Bulletin of the Geological Society of Greece, Sp. Publ. 10
Ext. Abs. GSG2022-010

On the Occurrence of Polymetallic Micronodules in Plio-Pleistocene Continental Clay Deposits of Ventzia Basin, Western Macedonia, Greece

K. Vythoulkas[1], M. Stamatakis[2], M. Pozo[3], A. Argyraki[2]

(1) GEOHELLAS S.A., 8A Pentelis Street, 17564, Paleo Faliro, Greece, kvythoulkas@geohellas.com (2) National and Kapodistrian University of Athens, Panepistimiopolis Zografou, 15784 Athens, Greece (3) Universidad Autónoma de Madrid, 28049 Madrid, Spain.

Ferromanganese, or polymetallic nodules have been described from lacustrine, soil, shallow marine, but mainly from deep-sea environments (Lee and Xu, 2016; Gasparatos *et al.*, 2019; Hein *et al.*, 2020; Maciag *et al.*, 2020). In marine environments, and especially in the Pacific Ocean (Clarion Clipperton Zone), Ni-Co-rich polymetallic nodules have been located on the seabed, forming substantial ore deposits, which are planned to be extracted within a short period of time, as the demand of Ni and Co increases rapidly due to their use in batteries of EV cars, to name only a few. In continental deposits, the trace element enrichments of manganese nodules, sizing of some mm up to a few cm, are poorer in trace elements and more variable in their nature (Belzile *et al.* 2001; Segvic *et al.*, 2018; Maciag *et al.*, 2020).

In Ventzia basin, western Macedonia, Greece, a thick Plio-Pleistocene succession composed of clayey and sandy/conglomeratic fluvial sediments overlies altered ultrabasic rocks of the Vourinos ophiolite complex and the Tsotyli formation of the Mesohellenic Trough. These sedimentary rocks have a brownish-greenish color that host significant palygorskite and palygorskite/smectite ore deposits. Besides palygorskite and smectite, other minerals identified in these rocks include sepiolite, and a series of inherited minerals such as serpentine, quartz, as well as feldspar and enstatite in minor amounts. Carbonates are also present, such as magnesite, dolomite and rarely calcite, the latter two occurring mainly as fissure fillings. During fieldwork, scattered medium-hard micro nodules were detected on the weathered surface of the clay deposits, exposed on the surface of old quarry faces, or on natural surfaces on the ground. They occur as small sub-rounded dark brown to massive black structures that range in diameter between 1 to 4mm. Micronodules investigated through the stereoscope reveal black metallic grains scattered in an off-white amorphous groundmass (Figure 1).

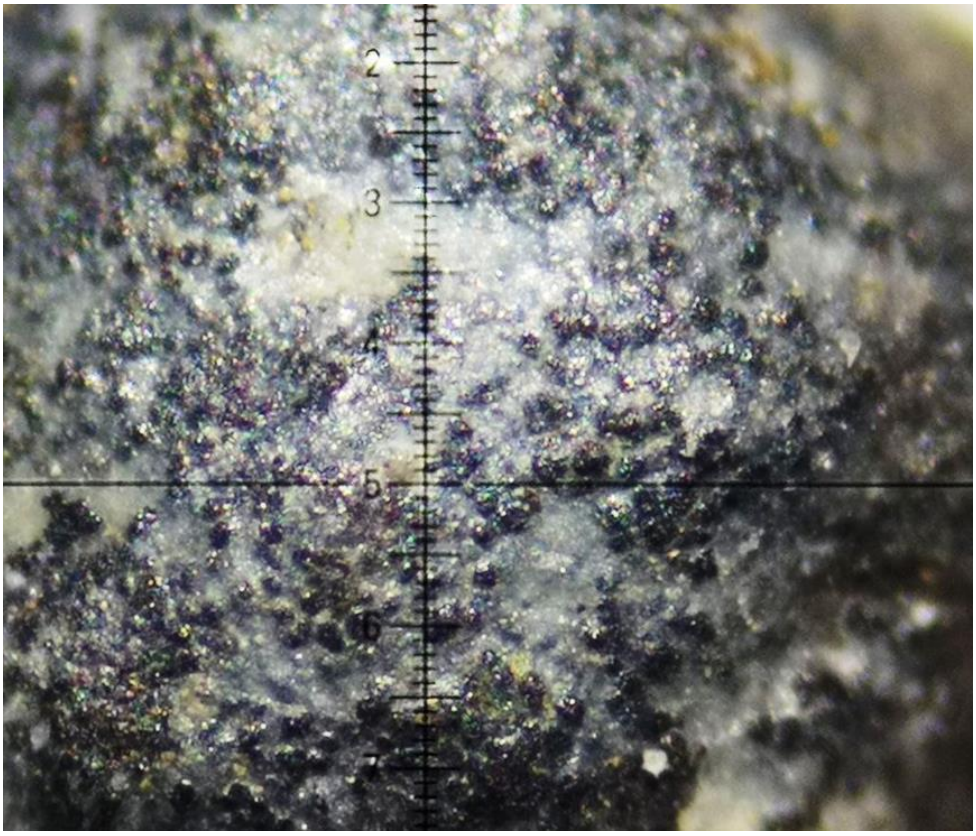

Figure 1: Photo image view from a stereoscope of a micronodule full of metallic grains from the Knidi deposit (scale in mm).

The SEM-EDS micro analyses of a series of these nodules revealed that they are mostly composed of concretional Fe/Mn oxides which are accompanied by high amounts of nickel and cobalt. These metal-rich micro grains are randomly distributed in a magnesium/iron silicate groundmass (Figure 2). The present paper is a preliminary study on the nature and origin of these nodules, which are detected for the first time in a continental basin in Greece.

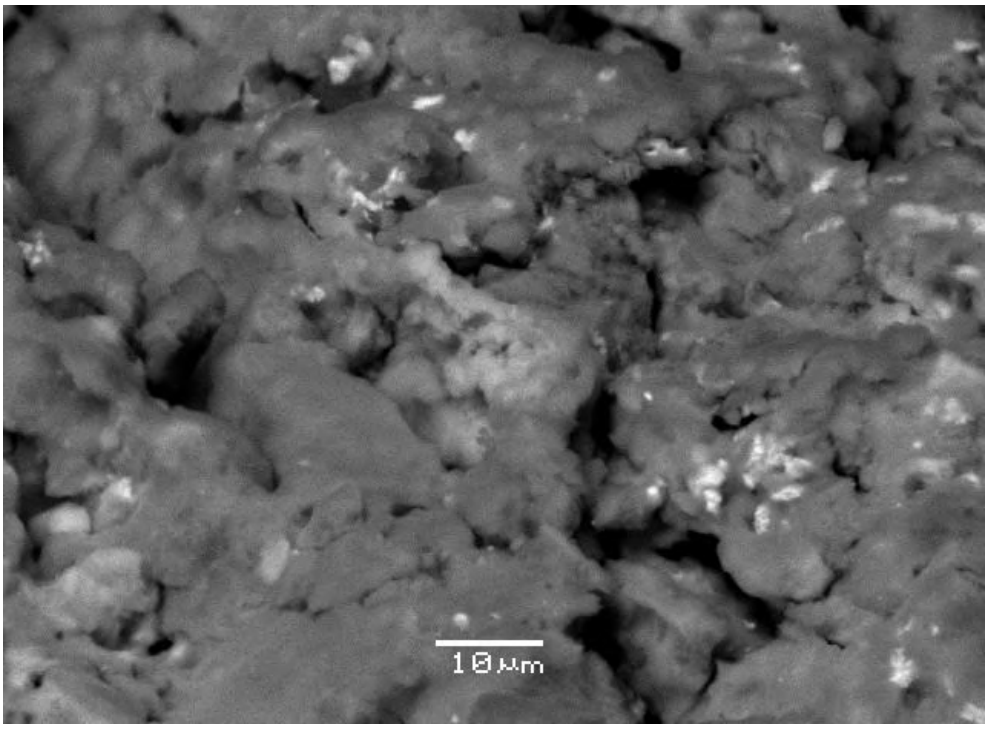

Figure 2: SEM image of Mn-Fe-Ni-Co-rich micro-grains (white spots) hosted in a nodular siliceous Mg-Fe-rich groundmass.

Methods used in the current study were X-ray diffraction (XRD) and scanning electron microscopy (SEM) coupled by energy dispersion spectrometry (EDS). The XRD analysis of the micronodules shows that they contain palygorskite, talc, amphiboles, serpentine, and feldspars, along with a substantial amount of amorphous phases and traces of smectite, chlorite and quartz. Trace amounts of opal was also detected by SEM, having botryoidal texture. SEM-EDS analysis revealed the presence of two chemical types of micronodules, Type-1 Mn-Ni-Co-rich (i.e., Harami palygorskite deposit) and secondarily in Fe, and Type-2 Fe-Mn-Ni-rich and secondarily in Co (i.e., Knidi palygorskite deposit). The spot analyses demonstrated enrichments ranging between 2.70-7.50% for Ni, 1.20-6.30% for Co (Type 1), and 3.30-8.85% for Ni, 0.73-2.84% for Co (Type 2). Based on geochemical and mineralogical data, as well as diagenetic reactions within the basin, it is concluded that during dry periods, Ni-Co-rich residual fluids deposited these metals, along with iron and manganese under fluctuating redox conditions in pore spaces and voids of the clayey sediments. The only possible source of these metals in the Plio-Pleistocene basins is the ultrabasic rocks of the Vourinos Mountain, as all the other formations of the geological substrate are poor in Ni, Co, Mn, and Fe.

Acknowledgements

We would like to thank GEOHELLAS S.A. for the financial support of this study, Mr. V. Skounakis of the NKUA for assistance in the SEM study and Dr. K. Aspiotis of Thrakon S.A. for providing stereoscope images.

References

Belzile, N., Chen, Y.W., Grenier M., 2001. Freshwater metallic concretions from an acidic lake characterized by X-ray energy dispersive spectrometry. Canadian Journal of Analytical Sciences and Spectroscopy 46, 146-151.

Gasparatos, D., Massas, I., Godelitsas, A., 2019. Fe-Mn concretions and nodules formation in redoximorphic soils and their role on soil phosphorus dynamics: Current knowledge and gaps. Catena 182, 104106.

Hein, J.R., Koschinsky, A., Kuhn, T., 2020. Deep-ocean polymetallic nodules as a resource for critical materials. Nature Reviews Earth & Environment 1, 158–169. doi.org/10.1038/s43017-020-0027-0.

Lee S., Xu H., 2016. XRD and TEM studies on nanophase manganese oxides in freshwater ferromanganese nodules from Green Bay, Lake Michigan. Clays and Clay Minerals 64, 488-501.

Maciag L., Rydzewska U., Skowronek A., Salwa S., 2020. Mineralogy and Geochemistry of Fluvial-Lacustrine Pisolith Micronodules from the Roztoka Odrzanska, Odra River, NW Poland. Geosciences 3, 1-27.

Segvic B., Girardclos S., Zanoni G., Gonzalez C.A., Steimer-Herbet T., Besse M., 2018. Origin and paleoenvironmental significance of Fe-Mn nodules in the Holocene perialpine sediments of the Geneva Basin, western Switzerland. Applied Clay Science 160, 22-39.

16th International Congress of the Geological Society of Greece
17-19 October, 2022 - Patras, Greece
Bulletin of the Geological Society of Greece, Sp. Publ. 10
Ext. Abs. GSG2022-011

Online Harmonized Database of Greek Ornamental Stones Developed in the Context of EuroLithos Project

K. Laskaridis[1], A. Arapakou[1]

(1) Hellenic Survey of Geology and Mineral Exploration (HSGME), Lithos Laboratory, Acharnae, Athens, Greece, laskaridis@igme.gr

A harmonized database of the broad range of information regarding Greek Ornamental Stones has been created in the context of EuroLithos project and has been made accessible to the public. The scope of the database is to make widely available key information that could support the promotion and use of European stone, and to contribute to the increased awareness, maintenance, and preservation of Greek cultural heritage. This online database provides important information for each ornamental stone concerning composition, petrography, geological setting, properties characterizing the stone (physical – mechanical, chemical), position of the corresponding quarry, as well applications in buildings, monuments, and other uses. Sixty-six Greek ornamental stones (marbles, limestones, slates, sandstones and miscellaneous ornamental stones) have been included into the platform until now with the ability to add more information. Fourteen countries have participated until today in the Eurolithos project.

Background

Ornamental stone is a raw material produced all over Europe, requiring special skills for its quarrying and transformation to final product. Despite the vast diversity of European natural stone resources, the actual use of local and regional stone resources is decreasing, and so is the knowledge about the available resources, traditions, and skills. EuroLithos has been founded on the idea that increased knowledge of the geology, quality and history of use of natural stone in Europe will stimulate more sustainable use of stone resources in Europe, for the benefit of SME's and our cultural heritage, as well as a sound land use management for the safeguarding of ornamental stone deposits (https://www.eurolithos.org). Thus, a directory of European ornamental stone properties has been developed, including guidelines for valorizing ornamental stone heritage. Greece is one of the participants in this project, providing the corresponding information for its most well-known and widely used ornamental stones.

Objectives

This online database has been created due to the need for a harmonised directory, or "identity card" for Ornamental stone. It has been focused on the collection of data and the evaluation from active ornamental stone quarries for establishing a relevant evaluation database. Although there are many stone "libraries" and databases in the world which are being digitalized, either they are still under development or they display promotional materials (data from private companies) or they contain a trade name of the materials and not a name according to the EN 12440 (2017): Natural Stone – – Denomination Criteria. The definition content of the "identity card" of each ornamental stone refers to the name of the stone according to the European standard EN 12440 (2017) Natural Stone – Denomination Criteria, its commodity type for distinguishing the main kinds of ornamental stones (i.e. marble, granite, limestone, etc) and its lithology (i.e. calcitic marble, gneiss, travertine, etc), its typical colour based on the corresponding code list of Stone colours, as well as its place of origin, petrographic information, geological context, physical – mechanical properties, geochemical properties, performance criteria (Laskaridis and Heldal, 2021). The intention for this project has been to establish structure for data delivery and storage, and connection to Atlas and other databases.

Results

The information provided in the online database of EuroLithos project for each ornamental stone is the following:

- Name of natural stone, based on the European Standard EN 12440: Natural stone – Denomination Criteria
- Representative photograph and macroscopic characterization of the ornamental stone. The macroscopic description includes colour, rock structure, grain size, macroscopic cracks, pores, cavities, weathering and alteration, macrofossils, xenolithic or autolithic inclusions, etc.
- Commodity of the stone, referring to rocks of igneous, sedimentary, or metamorphic origin, and providing the lithology, i.e. basalt, granite, limestone, marble, sandstone, slate, miscellaneous ornamental stones.
- Lithology, for example, calcitic marble, dolomitic marble, dolomite, travertine, dolomitic limestone, andesite, monzonite, greywacke, schist, serpentinite.
- Geological Setting, providing the relevant geological map and information about the geology of the area where the ornamental stone is quarried.
- Petrography, including photographic record of a thin section of each stone and microscopic description which includes fabric, constituents, discontinuities, alterations. The petrographic classification is assigned to each stone according to the European Standard EN 12670 (2019): Natural stone – Terminology.

- Mineral composition which identifies the main, subordinate, or accessory minerals, according to EN 12407 (2019).
- Physical-Mechanical properties assessed through testing in compliance of European Standards, and chemical properties. Freeze-thaw resistance, flexural and compressive strength, abrasion resistance, water absorption, open porosity, apparent density, rupture energy and breaking load at dowel hole are the determined properties of each ornamental stone.
- Brief description of uses and applications of each stone in remarkable constructions, either historical or new structures including relevant photographic record of examples

The 66 Greek ornamental stones which have been uploaded to the EuroLithos platform are given in Table 1, categorized according to their commodity and lithology.

Table 1. Greek ornamental stones uploaded to EuroLithos project

Total No. of stones uploaded	**Commodity**	**Lithology**	**No. of Stones**
35	Marble	Calcitic marble	17
		Dolomitic marble	10
		Cipollino marble	4
		Other marbles (calcitic-dolomitic, onyx marble)	4
22	Limestones	Dolomite	4
		Travertine	3
		Bioclastic, biomicrite, pelmicrite, sparitic	9
		Dolomitic limestone	2
		Other limestones	4
2	Sandstones	Calcitic graywacke	1
		Lithic feldspar arenite	1
4	Slates	Gneiss-schist	1
		Mylonite	2
		Schist	1
3	Miscellaneous ornamental stones	Ignimbrite	1
		Calcitic pelite	1
		Ophicalcite	1

Conclusions

The Eurolithos online database has been founded upon the evidence that increased knowledge of the geological quality and historical use of natural stone in Europe can stimulate more sustainable use of this resource, which will in turn benefit enterprises, promote cultural heritage, and contribute to developing effective land-use practices. The Greek participation in the EuroLithos project is very important providing corresponding information for 66 ornamental stones quarried in different places all over Greece. The project has successfully achieved its goals, to create a harmonized directory database for stones and their properties, to make a natural stone Atlas on a European and country level linked to databases and directories, to identify heritage values and establish guidelines for assessing the heritage value of natural stone.

Acknowledgements

2017/H2020-LCE-2016-ERA, Grant Agreement number 731166.The authors gratefully acknowledge the financial support received by the EC in the frame of the GeoERA project, H2020-LCE-2016-

References

Laskaridis, K. and Heldal, T., 2021. Deliverables D4.1 – D4.2: Working version of the directory containing information from selected countries and Guideline for using the Directory. EuroLithos – European Ornamental Stone Resources, GeoEra – Raw Material, https://www.eurolithos.org/_files/ugd/2b8de6_0eb1a71825d34acb8d2f1cc0013e5387.pdf

EUROLITHOS. Post-Project Community. European Ornamental Sone Resources. (2021). https://www.eurolithos.org

EN 12407: 2019. *Natural Stone Test Methods – Petrographic examination;* EN Standards; CEN/TC 246.

EN 12440: 2017. *Natural Stone—Denomination criteria*; EN Standards; CEN/TC 246.

EN 12670: 2019. *Natural stone – Terminology;* EN Standards; CEN/TC 246.

16th International Congress of the Geological Society of Greece
17-19 October, 2022 - Patras, Greece
Bulletin of the Geological Society of Greece, Sp. Publ. 10
Ext. Abs. GSG2022-015

Issues and constraints for the energy transition and achieving zero Carbon Emissions in 2050 -The role of Critical Metals

K. Papavasileiou[1]
(1) National and Kapodistrian University of Athens, Faculty of Geology and Geoenvironment, Athens, Greece

The European Commission by presenting in 2019 the "European Green Deal", which was then established as European Climate Law, Set a very ambitious final goal: Zero greenhouse gas emissions and energy transition to clean

forms of energy by 2050. They considered that mainly with a significant financing package and with the active internal policies of the Member States in the framework of the Internal Energy Policy, it will be able to achieve these goals by 2050 (E.U Publication 2021).

However, the European authorities omitted a key factor in this equation: They did not consider the huge amount of critical mineral raw materials necessary for the energy transition in achieving the ambitious final goal, especially their uninterrupted availability in this course until 2050!

Achieving this goal means that a fivefold increase in global renewable energy production by 2030 will be needed to meet the global zero-carbon target by the middle of the century. A recent report by the International Energy Agency (IEA) on the global energy outlook for greenhouse gas emissions by 2050 states the demand for critical minerals. Furthermore, the same report continues, "The prospect of a rapid increase in demand for critical minerals - far above anything we have seen past decades and, in most cases - raises severe questions about the availability and reliability of the offer ". The significant increase in demand used by the IEA implies, for example, an increase in lithium production "100 times compared to current levels" according to the IEA's calculations! (IEA Publication 2021), Special Report-IEA. 2020).

Unfortunately, many technocrats and politicians, especially in the European Union, are unaware of a critical fact: that the expansion of renewable energy sources also implies an operation of high-intensity mining and the essential use of mineral raw materials, which of course, cannot be done without an environmental and energy footprint with a parallel non- interrupted flow of these mineral raw materials by 2050!

From the point of view of geology, there is no shortage in the ores that need to be mined. The problem is whether supply can keep up with ever-increasing demand. Mining activity should increase by 20 to 50% for some critical metals by 2050. All major industrial countries struggle for these metals, increasing geopolitical tension. As mentioned above, we will also see a shift in geopolitical power as metal ores are not located in the same countries where coal, oil and gas are.

It is now clear from well-documented studies by international organizations on these issues that: **The energy transition begins and ends with critical minerals and metals. Practically the energy transition requires a transition from fossil fuels to metals.** Achieving zero global carbon emissions is inextricably linked to the supply of critical minerals and metals. It is estimated that any capital investment in exploration, development, and metallurgy processing of all these critical minerals and metals will have to quadruple to about $ 2 trillion to achieve an accelerated energy transition. There is much evidence that the carbon offset targets by 2050, without plans to find and develop new deposits, and mining investments, especially in critical minerals and metals, are meaningless! (Kettle and Wlazly 2021). Therefore achieving zero carbon emissions is inextricably linked to the supply of critical metals.

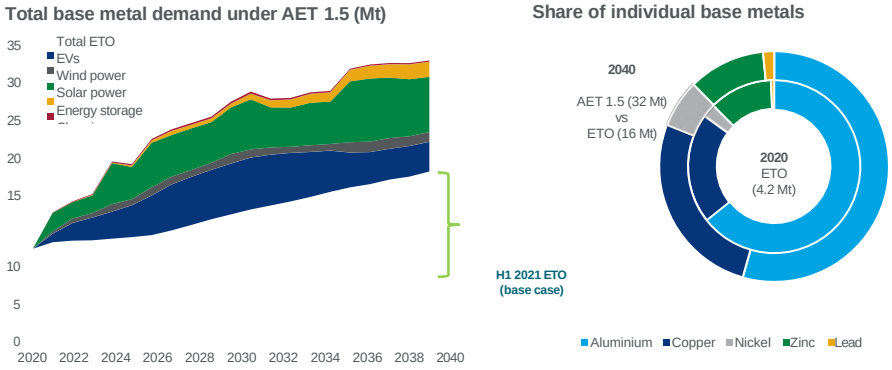

Figure 1 To meet the demand required by the 1.5º C global temperature reduction scenario, a fivefold increase in the supply of critical metals is required by 2040 compared to 2020 (ETO: Energy Transition Outlook; AET :Accelerated Energy Transition, after Wood Mackenzie, 2021).

1. Any energy transition begins and ends with critical metals.

The energy transition depends primarily on the rate at which sufficient reserves of exploitable critical minerals can be identified, developed, mined and processed into finished products. In parallel, if the metal recovery technologies and scrap processing are not improved and maximized, then the problem will be even more significant. On the other hand, if the metal recovery technologies and scrap processing are not improved and maximized, then the problem will be even more significant. Given all these limitations, the critical metal industry will need to invest about half a trillion Euros over the next 20-25 years to supply the critical metals needed for the energy transition to significantly reduce greenhouse gases, which will result in reducing global warming by 2.5 ° C.

2. The challenge of scaling up the primary supply of critical metals

Our prospects for the energy transition concerning critical metals are linked to the rigid limits set by nature and technology themselves, which refer to increasing supply in the long run, including several key factors such as long durations of mineral deposits exploration, mining research, development of a mine and after metallurgical treatment. Finally, until the first delivery of the ultimate product, a process that often takes more than ten years, and at the same time, significant capital investments are required. In order to achieve the zero-carbon emission target by 2050, the critical mineral and metal requirements required for clean energy technologies will increase up to six times by 2050, with exceptionally high growth for critical metals related to electric vehicles. wind turbines and photovoltaics. It is estimated that achieving this goal requires a considerable investment: capital expenditures for the entire chain of discovery-evaluation and extraction of critical minerals and metals, approximately $ 2 trillion over the next 15 years are required. (Hund *et al*., 2020.)

No accelerated energy transition can be achieved if this investment is not found and materialized in time. With the current and medium-term data, we believe that the goal of reducing global warming by 1.5 or 2º C based on critical minerals and metals by 2050 exceeds the limit of technology and industrial capacity available in humanity today. On the other hand, the required ores are mined in only a few specific countries, and the processing of these ores is concentrated in even fewer countries. The geopolitical dimension changes as it steps from countries dictated by hydrocarbons to countries dictated by the mining and metallurgical processing of critical minerals and raw materials.

For example, China is a major producer of many of these materials, including cobalt. Its deposits are found and mined mainly in the Congo, while the ore is then directly transported to China for final metallurgical processing.

Under these new circumstances, it is now unbelievable that Europe has invested so little in its refinery capacities. We have mainly become entirely dependent on other countries – for oil, coal and gas and the critical metals we need to fulfil the energy transition. As it turns out, the production of many critical minerals and metals that we need for the energy transition is geographically much more concentrated than hydrocarbons.

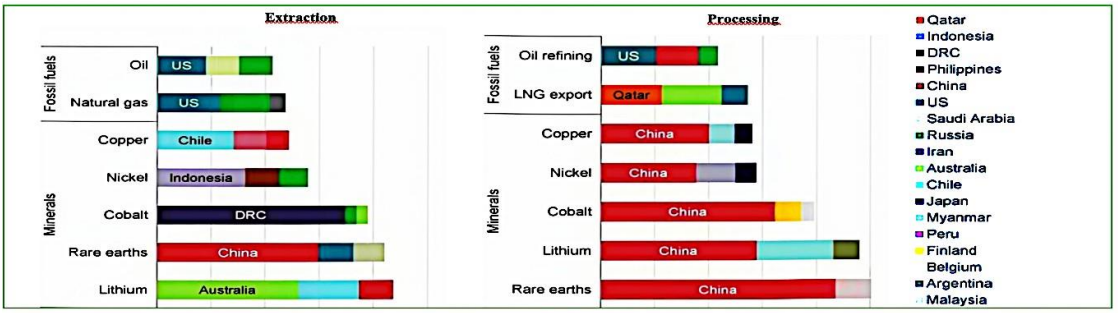

Figure 2. Notes: LNG = liquefied natural gas; US - United States. The values for copper processing are for refining operations. Sources: IEA (2020); USGS (2021), World Bureau of Metal Statistics (2020); Adamas Intelligence (2020).

References

Adamas Intelligence, 2020. Rare earth magnet market outlook to 2030**,** Adamas Intelligence, www.adamasintel.com/.

European Union, 2021. From ambition to action-Acting together for the planet, E.U, https://ec.europa.eu/commission/presscorner/detail/en/fs_21_5485.

Hund, K., La Porta, D., Fabregas, T.P., Laing, T., Drexhage J., 2020. Minerals for Climate Action: The Mineral Intensity of the Clean Energy Transition-Climate-smart Mining Facility, World Bank.

IEA, 2020. The Role of Critical Minerals in Clean Energy Transitions, IEA.

IEA, 2021. World Energy Outlook, IEA.

Kettle, J., Wlazly, K., 2021. Mission impossible: supplying the base metals for accelerated decarbonization-COP26 briefing. Wood Mackenzie.

USGS, 2020. Mineral Commodity Summaries 2020, USGS**, https://pubs.usgs.gov/periodicals/mcs2020/mcs2020.pdf.**

World Bureau of Metal Statistics, 2020. World Metal Statistics Yearbook 2020, https://world-bureau.co.uk/.

16th International Congress of the Geological Society of Greece

17-19 October, 2022 - Patras, Greece

Bulletin of the Geological Society of Greece, Sp. Publ. 10

Ext. Abs. GSG2022-032

A Guide on Mineral Raw Materials of Greece

K. Hatzilazaridou[1], F. Chalkiopoulou[1], K. Laskaridis[1]

(1) Hellenic Survey of Geology and Mineral Exploration, Athens, Greece, kikihatz@igme.gr (2) Hellenic Survey of Geology and Mineral Exploration, Athens, Greece.

The Guide on Mineral Raw Materials of Greece is structured to serve as a general guidance document to those who are interested in evaluating the mining landscape of Greece.

It is the first of its kind and consists of summarized information on the legal framework regulating the exploration and exploitation of Mineral Raw Materials (MRM), the procedures one needs to follow to obtain the ownership right to explore and exploit MRM in Greece and, through a web GIS application, information on areas of potential interest to those who contemplate the possibility of developing new mines in the country. The web GIS application was developed to demonstrate the Guide's content with a geographic reference. It also includes an overview of the extractive sector, a list of the competent permitting/licensing authorities and a comprehensive list of definitions on key terms of the mining and quarrying legislation.

First published in 2022, the Guide has been designed to be easily consulted, distributed, and updated. Its digital version is presented through a tailor-made webpage which is hosted on the HSGME portal. Through the Guide's webpage one may have access to the user-friendly web GIS application and vice versa.

Acknowledgements

This Guide was delivered within the framework of the project titled "A Guide for Mineral Raw Materials of Greece" and was commissioned to the Hellenic Survey of Geology and Mineral Exploration (HSGME) by the Ministry of Environment and Energy. It was funded by the Public Investment Programme. We wish to express our appreciation to the Directorate General of HSGME for its support. Our special thanks are owed to colleagues from the e-Government Unit of HSGME for their contribution to the versatile aspects of this Guide.

16th International Congress of the Geological Society of Greece
17-19 October, 2022 - Patras, Greece
Bulletin of the Geological Society of Greece, Sp. Publ. 10
Ext. Abs. GSG2022-040

On the Role of Cobalt in the Production of Batteries for Electric Vehicles

E. Varotsos[1] and M. Stamatakis[1]
(1) NKUA, Department of Geology & Geoenvironment, Panepistimiopolis, Ano Ilissia, 15784, Athens, Greece, stamatakis@geol.uoa.gr

The main objective of the present study is to report current trends and developments in the cobalt use cycle in electric batteries to produce electric vehicles. This issue addresses a huge contemporary problem with geological, energy, environmental, economic, and social implications.
The plethora of recent research publications and the organization of international conferences and workshops (Varotsos 2021 and References therein) on the crucial role of cobalt in the supply chain of electric vehicles demonstrates the global interest in this issue (Table 1). An example is the recent Cobalt Institute 2021 Conference held on 18-19 May 2021 on this topic, with an emphasis on the role of cobalt in a sustainable future. This Conference also hosted the Benchmark's Cobalt Special (held on Wednesday, May 19, 2021) which discussed in detail the latest developments in lithium-ion batteries and cobalt cells as well as related topics for raw material extraction, chemical processing, cell production and recycling.

Table 1. Major electric vehicle models as of 2017 (from Horowitz and Coffin, 2018)

Manufacturer	Model	Range (miles)	Assembly location	Battery size (kWh)	Battery manufacturer	Battery pack assembly location	Battery cell production location
Tesla	Model S	259–335	United States	75 or 100	Panasonic/ Tesla[a]	United States	Japan
Tesla	Model X	295	United States	75 or 100	Panasonic/ Tesla[a]	United States	Japan
Tesla	Model 3	220–310	United States	50–74	Panasonic/ Tesla[a]	United States	United States
Chevrolet	Bolt EV	238	United States	60	LG Chem	United states	South Korea
Nissan	Leaf	151	United States	30	Automotive Energy Supply Corp.	United States	United States
Fiat	500e	84	Mexico	24	SB LiMotive	United States	United States
VW	e-Golf	126	Germany	35.8	Samsung SDI	Hungary	South Korea
Ford	Focus Electric	118	United States	33.5	LG Chem	United States	United States
BMW	i3	114	Germany	22–33	Samsung SDI	Hungary	South Korea
Kia	Soul EV	111	South Korea	27	SK innovation	South Korea	South Korea

In this context the present paper discusses extensively the role of cobalt as a critical raw material - as well as other battery materials - its unique characteristics as a metal, the compounds it forms, and its concentrations on land and the seabed that are or will be future economic mineral deposits worldwide, and especially in Europe (Fig. 1). Special reference is made to the methods of processing, recovery of cobalt, as well as the production levels of the metal to be exploited (Fig. 2). A detailed analysis is then made on current and future promising applications of cobalt, in addition to electrical propulsion, modern recycling trends, the supply chain of electric vehicle batteries and the development of the battery industry internationally.
Finally, the conclusions of the current situation on this research issue are summarized and the relevant perspectives are discussed as follows:

- It is possible to develop another type of battery that will store more energy in the future, but until then, lithium-ion batteries will be the most important part of an EV. As EVs have a growing share of car sales, the battery supply chain will become increasingly important.
- Understanding the supply chain can help businesses and governments understand how trade flows and resources will be affected by increased EV demand. China and the US appear to be the largest suppliers of lithium-ion batteries in the future, with competition from Japan and South Korea. In addition, as cells are more easily imported / exported over longer distances, they are likely to continue to be traded internationally.
- Vehicle manufacturers' decisions about where to produce EVs (and in what quantities) are likely to be the primary determinants of lithium-ion batteries and their locations. Due to the lack of more detailed international trade data for lithium-ion batteries, it is difficult to separate information from the components of the battery supply chain.
- However, based on recent estimates, the US and Japan seem to provide the most added value to lithium-ion batteries used in EVs and sold in the US. Much of the estimated value in the US comes from assembling arrays.

- According to a recent survey, due to China's high level of sales of domestically produced EVs with batteries and cells produced in the domestic market, China probably represents most of the added value of lithium-ion batteries in Chinese EVs worldwide and to the added value for EV batteries.

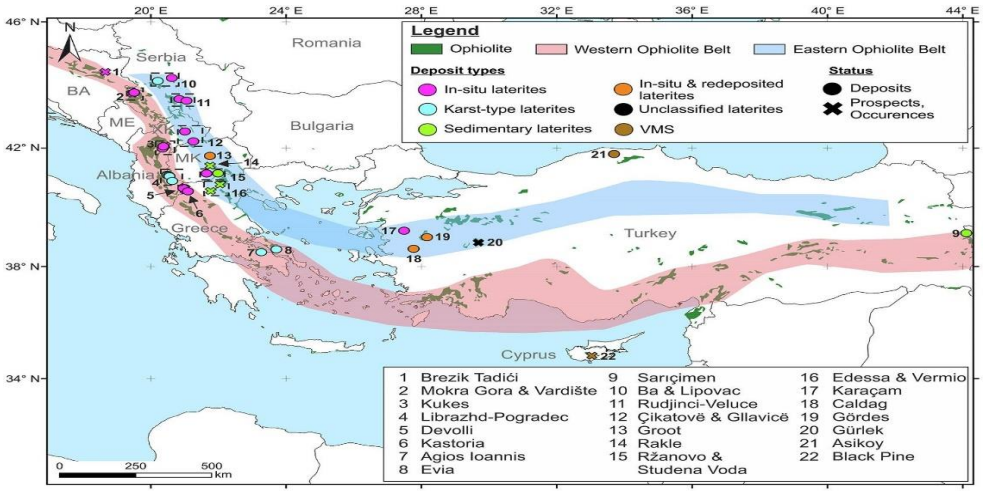

Figure 1. Mesozoic to Palaeozoic nickel–cobalt laterite deposits in the Balkans and Turkey (from Horn *et al*., 2020).

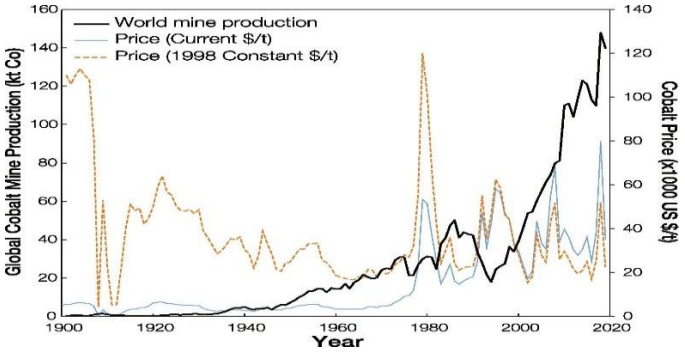

Figure 2. World annual Co mine production and price (during 1900–2019) in current and 1998 (constant $) (by Consumer Price Index for All Urban Consumers). Constant $ remove the effect of inflation on the unit value (Dehaine *et al*., 2021).

According to a recent announcement by Metals Company (MC) [https://metals.co/deepgreen-acquires-third-seabed-contract-area-to-explore-for-polymetallic-nodules/] that it has acquired Tonga Offshore Mining Limited (TOML) from Deep Sea Mining Finance Ltd, thus acquiring the exploration rights to a 74,713 km2 block of Clarion Clipperton Zone seabed containing an inferred resource of $756x10^3$ wet tons of polymetallic nodules. As part of the acquisition The MC benefits from existing environmental studies, a Canadian NI 43-101 compliant technical resource report and an intellectual property portfolio. TOML will allow bringing more critical mineral resources to market to move away from fossil fuels. Research shows that polymetallic nodules can provide minerals preserving the environment.

References

Dehaine, Q., Tijsseling, L. T., Glass, H. J., Törmänen, T., Butcher, A. R., 2021. Geometallurgy of cobalt ores: A review. Minerals Engineering, 160, 106656.

Horn, S., Gunn, A. G., Petavratzi, E., Shaw, R., Eilu, P., Törmänen, T., Wall, F., 2020. Cobalt resources in Europe and the potential for new discoveries. Ore Geology Reviews, 103915.

Horowitz, J., Coffin, D., 2018. The Supply Chain for Electric Vehicle Batteries. Journal of International Commerce and Economics, 1. Available at SSRN: https://ssrn.com/abstract=

Varotsos, E., 2021. Cobalt in the production of Electric vehicles batteries. BSc Thesis National and Kapodistrian University of Athens, Department of Geology & Geoenvironment, 125p.

16th International Congress of the Geological Society of Greece
17-19October, 2022 -Patras, Greece
Bulletin of the Geological Society of Greece, Sp. Publ. 10
Ext. Abs. GSG2022-045

Mineralogical and Geochemical Features of the Fe-Oxide Mineralization, Loutraki, north-central Crete, Greece

S. Triantafyllidis[1], N. Katsiavrias[1]
(1) National Technical University of Athens, School of Mining and Metallurgical Engineering, Athens, Greece, striantafyllidis@metal.ntua.gr

Research highlights: The Loutraki (Crete) Fe-oxide mineralization is developed along a cataclastic and fractured zone (detachment fault) at the lower part of the Gavrovo-Tripoli Unit in north-central Crete. Hematite and goethite predominate, and the ore geochemistry shows very low content in base and critical metals.

Background

The geology of the Loutraki area involves highly deformed Permian-Triassic clastic rocks of the Gavrovo-Tripoli basement (**Fig. 1**). In the Loutraki area, the intermediate Kateriana Beds and Marathos Dolomites formations as well as the lower members of the Damasta Limestones and the upper part of the Faratsi Formation clastic rocks, are either destroyed or dismembered due to tectonism. The mineralization is lenticular and approximately 80 m in length with 2 m maximum thickness. The ore texture changes from the flanks towards the central part. At the edges of the ore body, the mineralization is disseminated and cohesive, forming mainly veins and veinlets, whereas at the central part the mineralization is massive and brittle.

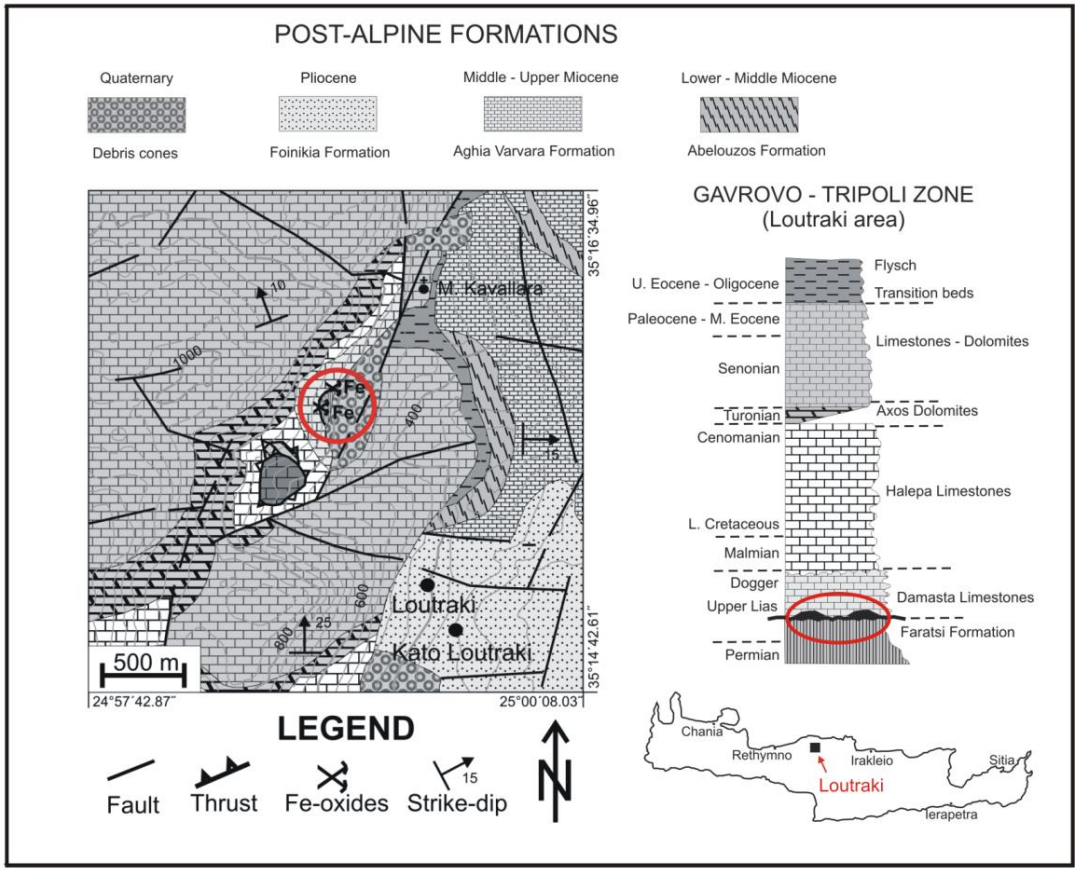

Figure 1: Simplified geological map of the Loutraki area, including the under-investigation Fe-oxide/hydroxide mineralization (modified after Katsiavrias, 2008).

Results and discussion

The mineralogy of the Loutraki Fe- ore is predominated by hematite and goethite with minor pyrolusite and manganite, and traces of sulfides. The Loutraki gangue assemblage includes calcite, Mg-calcite and minor quartz and phyllosilicates (chlorite group phases), whereas no clasts of other rock types are identified that could provide information on the origin

of the protoliths.
The simple ore mineralogy is also depicted in the geochemistry of the massive and semi-massive ore (Table 1). Iron is the major constituent of the mineralization (Table 1), whereas the relatively constant Mn content is related to Mn enrichment in both hematite and goethite, as well as the presence of disseminations and veinlets of pyrolusite and manganite. The Loutraki Fe-oxide mineralization shows very low Al content (0.14 wt% maximum) and very low base and critical metal content (Table 1).
Three different ore textures are identified including:

- Massive ore with fine-grained hematite and goethite
- Massive ore with botryoidal hematite and fine-grained goethite
- Semi-massive/Stockwork ore and disseminated ore

The first two textures are observed at the central part of the ore body, whereas the latter is observed at the flanks. Two stages of ore formation are distinguished. The first (Stage I) is related to the formation of primary hematite after circulation of Fe-rich hydrothermal fluids, dissolution of primary carbonates and precipitation of fine-grained hematite.
Ongoing and limited-scale tectonism during this stage resulted in cracking and brecciation of the ore and deposition of secondary carbonates, mainly calcite, in veins and veinlets cementing the massive ore. The second stage (Stage II) is related to retrograde phenomena that affected the primary mineralization, resulting in hematite alteration to goethite, as well as circulation of secondary Fe-rich fluids that led to the formation of goethite within cracks and fissures of the formerly brecciated ore. In the disseminated/stockwork ore, carbonates predominate over Fe-oxides, and the latter are developed along edges and crystallographic plains of coarse-grained and euhedral calcite. Ongoing tectonism resulted in brecciation of the disseminated ore, which was cemented by later fine-grained and anhedral calcite forming veins and veinlets that cut the primary ore. The later stage calcite veins are distinguished from the primary disseminated ore by the complete absence of Fe-bearing phases. At the same time, primary hematite was partially replaced by goethite (Stage II).

Table 1: Representative major and trace elements analyses (in wt%) from the Fe-oxide mineralization, Loutraki, Central Crete.

Ore type	**SiO_2**	**Al_2O_3**	**Fe_2O_3**	**CaO**	**MgO**	**Na_2O**	**K_2O**	**MnO**	**P_2O_5**	**SrO**	**LOI**	**Total**
Massive ore	5.27	0.14	73.23	4.05	1.14	0.012	0.026	4.03	0.073	0.013	11.67	99.65
Massive ore	1.20	0.08	74.33	9.57	0.40	b.d.l.	0.017	3.42	0.007	0.009	11.04	100.08
Massive ore	0.98	0.03	85.19	2.85	0.17	b.d.l.	0.005	4.11	0.009	0.024	6.42	99.79
Semi-massive ore	2.65	0.08	65.68	11.25	0.70	b.d.l.	0.018	3.39	0.025	0.007	14.99	98.80
Ore type	**As**	**Ba**	**Co**	**Cu**	**Ni**	**Pb**	**Sn**	**S**	**V**	**Zn**	**Zr**	
Massive ore	0.002	0.09	b.d.l.	0.025	0.001	0.002	b.d.l.	0.032	b.d.l.	0.013	0.003	
Massive ore	0.005	0.099	b.d.l.	0.099	0.001	0.006	0.001	0.012	b.d.l.	0.017	0.003	
Massive ore	b.d.l.	0.022	0.001	0.039	0.001	0.005	b.d.l.	0.005	b.d.l.	0.006	0.004	
Semi-massive ore	0.003	0.16	b.d.l.	0.009	b.d.l.	0.002	b.d.l.	0.03	b.d.l.	0.011	b.d.l.	
LOI: Loss on Ignition; b.d.l.: below detection limit; Cr_2O_3 and TiO_2 below detection limit												

Concluding, the Loutraki Fe-oxide mineralization is formed due to ongoing tectonism (detachment fault-cataclasis-fracturing) at the lower part of a single tectonic Unit (Gavrovo-Tripoli). This characteristic differentiates the Loutraki Fe-oxide ore from other similar mineralizations in Crete and other parts of Greece, including the Rabdoucha – Kakopetros mineralization in western Crete (Seidel *et al*., 2005), the Ano Valsamonero mineralization in central Crete (Alevizos *et al*., 2010), the Aghios Elissaios mineralization in SE Peloponnese (Sofis, 2017), and the Sesi mineralization in Attika (Stouraiti *et al*., 2016), that are related to detachment faults developed between different tectonic units.

References

Alevizos, G., Stratakis, A., Petrakis, E., 2010. Mineralogical examination and mineral processing of the iron ore form Ano Valsamonero area (Rethymno). Mineral Wealth, 155, 33-46.

Katsiavrias, N., 2008. Geological map of Anoyia Crete of Greece (scale 1:50.000), Athens, Greece.

Seidel, M., Pack, A., Sharp, Z.D., Seidel. E., 2005. The Kakopetros and Rbdoucha Fe-oxide deposits, Western Crete: fluid transport and mineralization within a detachment zone. Econ. Geol., 100, 165-174.

Sofis, N., 2017. The Aghios Elissaios Fe-oxide mineralzation, Lakonia, Peloponnese, Greece. Unpubl. MSc Thesis (in Greek with English abstract), Department of Geology, University of Patras, 75p.

Stouraiti, C., Lekkas, S., Lozios, S., Kanellopoulos, C., 2016. Iron-oxide mineralization of Sesi, Koropi (S. Hymittos, Greece): mineralization within a detachment zone. Bull. Geol. Soc. Greece, 50, 4, 2025-2036.

16th International Congress of the Geological Society of Greece
17-19 October, 2022 - Patras, Greece
Bulletin of the Geological Society of Greece, Sp. Publ. 10
Ext. Abs. GSG2022-053

New insights into the mineralogical characterization and application of manganese oxide minerals with porous structure from the Drama Mn deposits of Greece.

G. Soulamidis[1], C. Stouraiti[1], H. Tsikos[2], P. Voudouris[1], C. Mavrogonatos[1]

(1) Department of Geology and Geoenvironment, National and Kapodistrian University of Athens, Panepistimiopolis 15784, Athens, Greece. gsoulamidis@geol.uoa.gr; chstouraiti@geol.uoa.gr; voudouris@geol.uoa.gr; kmavrogon@geol.uoa.gr (2) Department of Geology, University of Patras, Rio, Greece. htsikos@upatras.gr

Introduction and Objectives

The western Rhodope massif contains a significant number of battery-grade Mn oxide deposits which are best developed in the area near Kato Nevrokopi, Drama District, N. Greece. Economic Mn oxide concentrations are confined to fault zones and related karsts in marbles. The Mn mineralization is thought to originate from supergene weathering of earlier hydrothermal veins that are genetically linked to acid magmatism of Oligocene age (Nimfopoulos 1988). At Kato Nevrokopi, the veins contain rhodochrosite along with sulphides, quartz and mixed calcite-todorokite (previously termed "black calcite"; Nimfopoulos *et al*. 1991). Protracted weathering of the vein material has resulted in the supergene assemblage: amorphous Mn oxide-todorokite-azurite-goethite-cerussite, while associated karstic cavities host amorphous Mn/Fe oxides-nsutite-birnessite-chalcophanite-cryptomelane-pyrolusite-malachite (Nimfopoulos *et al*. 1991). The main objective of this study is the geochemical and mineralogical characterization of the natural porous Mn oxides from the supergene manganese oxide deposits of Drama. Emphasis will be placed on elucidating the structure and chemistry of tunnel-structured Mn oxides (1×1, 2×2, 3×3), using a combination of advanced techniques suitable for nanomaterials. Thorough understanding of the structure of tunnel-structured Mn oxides through adsorption experiments and electrochemical measurements, will hopefully open new perspectives for the future industrial uses and applications of such materials as catalysts and supercapacitors.

Background on Manganese Ore Mineralogy of Kato Nevrokopi

Based on their setting and mineralogy, the Mn ore zones at Kato Nevrokopi have been previously divided into three categories (Nimfopoulos & Patrick 1991): (a) Deeper (hypogene) mineralized sulphide-carbonate-rich zones, which at the time of primary formation are interpreted to have been located at significant depth. They are currently exposed only in deeply eroded areas such as in the Pyrgi mines and contain amorphous Mn oxide and todorokite in "black calcite" veins; (b) Shallow, Mn oxide-rich veins (25th km Drama-K. Nevrokopi, Mavro Xylo; 28th km Drama-K. Nevrokopi, Karposluk and Tartana mines) exposed in the higher altitude regions of the Falakron Mountain. Similarly to the hypogene veins (a), they contain mainly amorphous Mn oxides and todorokite; (c) Secondary karstic cavities filled with Mn oxide-rich assemblages (nsutite, chalcophanite, birnessite, cryptomelane, pyrolusite), which are derived from weathering of primary mineralization and re-concentration in karsts. Karst-hosted orebodies appear to have originated mainly from shallow vein-type mineralization of the abovementioned type (b), and therefore the ore types (b) and (c) are typically found in close spatial association.

Discussion and Conclusions

The first phase of this study is the identification of the chemical composition of the ore minerals from the first sampling session that was performed at the sites of interest (25th km Drama-K. Nevrokopi/Mavro Xylo). The ore was analyzed for its mineralogy and bulk geochemistry by X-Ray diffraction (XRD) and X-ray fluorescence (XRF), combined with petrographic observations under a dual transmitted-reflected LEICA DM/LP microscope. The study of Mn mineral assemblages at Kato Nevrokopi was particularly challenging due to their poor crystallinity which caused very broad and low intensity peaks and occasionally peakless XRD traces, especially since some of the manganese oxides have similar optical properties which hinders confident identification. Despite these problems, we were able to identify two out of the three ore zones. XRD results showed that the samples from the site at the 25th km Drama-K. Nevrokopi contain mostly the peaks of nsutite and pyrolusite (type "c" assemblage) whereas the samples from the Mavro Xylo (MX) site contain calcite and todorokite (type "b" assemblage). The results from XRF analyses confirmed the enrichment in bulk Mn oxide at both localities (Table 1). The Mavro Xylo ore additionally shows high concentrations of CaO, K_2O and Sr which supports the occurrence of todorokite. By contrast, the low alkali content in the results from the site at the 25th km Drama-K. Nevrokopi combined with the very high bulk Mn oxide content, point to a highly concentrated and essentially pure Mn oxide assemblage dominated by tetravalent Mn oxides such as pyrolusite and nsutite along with possibly some manganite. Petrographic study of the Mavro Xylo samples confirmed the occurrence of apparently weathered todorokite in combination with calcite (Figure 1b) while the samples from the 25th km Drama-K. Nevrokopi confirmed the appearance of nsutite in association with veinlets of chalcophanite (Figure 1a). In a ternary diagram traditionally used for the genetic classification of Mn oxides (Conly *et al*., 2011 and references therein) Mn oxide ores from two of the most

important Mn deposits of Greece, namely Drama (this study) and Milos (Aspro Gialoudi deposit-AG and Vani-V) have been plotted (Figure 1c). According to this diagram, the ore from the site at 25th km Drama-K. Nevrokopi can be classified as supergene ore, whereas Mn ore from Mavro Xylo points to a hydrothermal-terrestrial origin.

Table 1 X-Ray fluorescence analyses of manganese oxide ore from the sites Mavro Xylo and 25th km Drama-K. Nevrokopi.

	Oxides (%)							Minor and Trace Elements (ppm)						LOI	
Sample	MnO	SiO_2	CaO	Fe_2O_3	Al_2O_3	K_2O	MgO	Zn	Sr	Pb	As	Cu	Ag	(%)	TOTAL
MX	47.27	6.51	15.19	0.27	1.03	0.24	0.15	630	659	184	530	17	63	28.86	97.73
25thkm	71.61	2.57	1.28	0.44	1.15	0.14	n.d.	12600	1100	2600	510	138	67	20.53	99.42

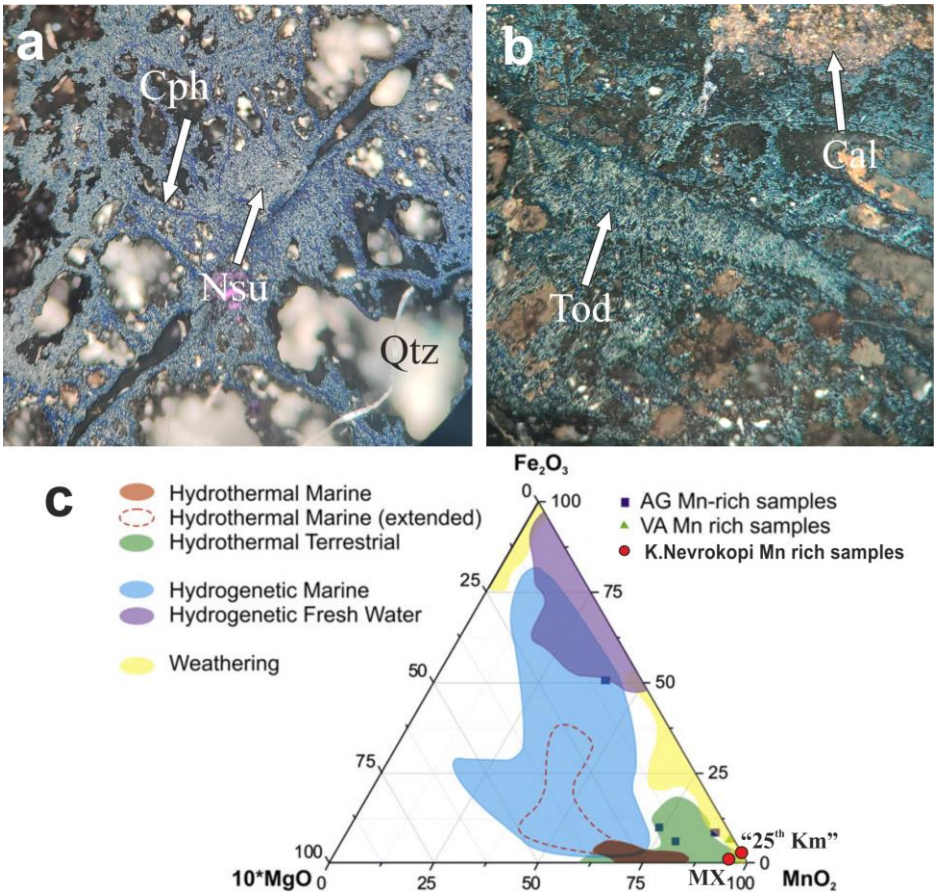

Figure 1. a) Photomicrograph of a Mn ore sample from the site 25th km Drama-K. Nevrokopi (partially crossed polars x20) showing microcrystalline nsutite (Nsu) with its distinctive bluish-grey to creamy-white pleochroic tint, along with chalcophanite veinlets (Cph) which appear with a stronger bluish tint. b) Photomicrograph of a Mn ore sample from locality Mavro Xylo (partially crossed polars x20) showing weathered todorokite (Tod) in contact with crystals of calcite (Cal). c) MnO_2-Fe_2O_3-MgO (×10) ternary diagram for discrimination of Mn oxides (after Conly *et al*., 2011 and Papavassiliou *et al*., 2016)

Acknowledgements

X-ray fluorescence analyses for major/trace elements were conducted in the School of Mining and Metallurgical Engineering, NTUA.

References

Conly A., Scott S., Bellon H., 2011. Metalliferous Manganese Oxide Mineralization Associated with the Boléo Cu-Co-Zn District, Mexico, Economic Geology, 106, 1173-1196

Nimfopoulos M. 1988. Manganese Mineralization near Kato Nevrokopi, Drama, Greece. Ph.D. Thesis, Victoria University of Manchester.

Nimfopoulos M. and Pattrick R., 1991. Mineralogical and textural evolution of the economic manganese mineralisation in western Rhodope massif, N. Greece, Mineralogical Magazine, 55, 423-434

Papavassiliou K., Voudouris P., Kanellopoulos C., Glasby G., Alfieris D., Mitsis I., 2016. New geochemical and mineralogical constraints on the genesis of the Vani hydrothermal manganese deposit at NW Milos island, Greece: Comparison with the Aspro Gialoudi deposit and implications for the formation of the Milos manganese mineralization, Ore Geology Reviews, 80, 594-611

16th International Congress of the Geological Society of Greece
17-19 October, 2022 - Patras, Greece
Bulletin of the Geological Society of Greece, Sp. Publ. 10
Ext. Abs. GSG2022-089

In-situ isotopic and chemical study of pyrite from Zoovch-Ovoo roll-front type uranium deposit in Mongolia

D. Rallakis[1,2], R. Michels[2], M. Cathelineau[2]

(1) Department of Geology, University of Patras, Greece, rallakis@upatras.gr (2) CNRS, CREGU, Université de Lorraine, GeoRessources, 54504, Vandoeuvre-lès-Nancy, France

Research Highlights: *The concentration of trace elements in pyrite in roll-front systems can be hundreds of times higher in the case that it is associated to uranium mineralization.*

Background and Objectives

The Zoovch-Ovoo roll-front type uranium deposit is located in East Gobi Basin, Mongolia. It is hosted within the fluvio-lacustrine deposits of the Late Cretaceous Sainshand Formation, composed of clay to sand layers and sporadic dolomite-cemented sandstone layers. Pyrite is present in the reduced sediments but is also found in the reduced part of the roll-front in association to uranium mineralisation, and thus genetically linked. The recognized petrographic habits of pyrite are: i) isolated framboids within the detrital mineral network, ii) framboids within organic matter particles, iii) concentric overgrowth of framboids, iv) framboids embedded within euhedral pyrite, v) successions of euhedral pyrite, vi) isolated euhedral pyrite, vii) marcasite on isolated euhedral pyrite and viii) framboidal and euhedral pyrite inside post-uranium dolomite. These various pyrite forms were positioned within the overall paragenetic succession of the ore deposit.

The objective of the present study is to present the petrographic habits, trace element concentration and isotopic composition of pyrite and explain the differences as a function of the roll-front system evolution.

Methods

Samples that cover all petrographic types were selected and studied by means of SEM-EDS, EPMA and LA/ICP-MS techniques. The $\delta^{34}S$ was also determined on the various pyrite types and generations at the microscale using a CAMECA IMS 1270 ion probe (Jean Lamour Institute of the School of Mines, Nancy).

Results and Conclusions

The results from the SEM-EDS and EPMA indicated at first place that certain pyrite phases i.e. the polymorph marcasite and certain euhedral pyrite phases are As enriched. Hence, by studying pyrite by means of LA/ICP-MS (high precision), it was possible to identify several geochemical trends for the following trace elements As, Co, Cd, Ni, V, Zn, Pb, Ag, Mo and Cu. It was observed that the morphology of pyrite i.e. framboidal or euhedral plays minor role on trace element concentration, while in every investigated geochemical plot there are always at least two trends visible, the first with pyrite being depleted and the second being enriched in specific trace elements (Co, Ni, Zn, Cd, Mo, Cu), always irrespective of morphology. This specificity is linked to roll-front activity and association to uranium.

The $\delta^{34}S$ of the different pyrite occurrences shows a very large range of isotopic fractionation (between -50 to +50‰). Isolated framboidal pyrite has a preference for positive $\delta^{34}S$ concentrations at the range of 10±5 ‰, while euhedral pyrite tends to be negative at the range of -18±5 ‰.

The interpretation of the petrographical and geochemical data allowed to decipher the genetic origin of these various pyrite forms. According to literature, initial isotopic composition of evaporites may reach +20 to +35‰ (Makhnach *et al*., 2000). Isotopic fractionation of sulfur may be controlled by at least two major mechanisms, bacterial activity (Bacterial Sulfate Reduction) and sulfate disproportionation. In addition, the composition of the sulfate isotopic pool may depend on the intensity of roll-front activity which depends on the transient hydrological activity (from open to closed isotopic system). The overall range of fractionation may therefore be the result of the fluctuating combination of all three phenomena. Most negative sulfur fractionation values (to -52‰ in our case) are attributed to BSR. Intermediate isotopic values can be reported along the Rayleigh fractionation curve proposed by Hough *et al*. (2019). Most positive $\delta^{34}S$ (+50‰) could be explained by isotopic closed systems in which Rayleigh fractionation was most intense.

The availability of sulfur in these overall detrital sediments is linked to the presence of sulfate leached by circulating fluids. It originates either from evaporites (primary sulfates) present in the basin and from the oxidation of pyrite (secondary sulfates) in the oxidized part of the roll front system. On the reduced part of the roll-front, sulfate may be reduced into sulfur to form pyrite. Pyrite sulfur isotopic compositions therefore reflect the various conditions of roll-front activity at Zoovch-Ovoo. Especially bacterial activity occurs during the whole diagenetic history of the deposit and exerts major controls on redox conditions concerning sulfur but most importantly uranium. Therefore, the Zoovch-Ovoo deposit

may be considered as a uranium deposit under biogeochemical control.

To conclude, striking differences regarding the trace element content between the pyrite types associated to uranium phases and the non-associated, were confirmed. An attempt was made to characterize ore stage pyrite based on trace element concentration. The results were very promising, especially when using Co, Ni, Zn and Mo as indicators. Ore stage pyrite tends to be enriched in these trace elements compared to non-associated pyrite which is very lean. The pyrite study was concluded with an isotopic study. In particular the $\delta^{34}S$ of the different pyrite occurrences was analyzed in order to understand more about their origin. The results though very diverse, fluctuating in extreme cases between -50 to +50 per mille for $\delta^{34}S$, show that there are more than four pyrite generations, as was previously concluded by petrography.

Acknowledgements

This work was financed by ORANO Mines through CREGU (Centre de Recherches sur la Géologie des Matières Premières Minérales et Energétiques). The analytical experiments were carried out mainly in the Laboratory of GeoRessources (Université de Lorraine, Nancy, France) and partly in CRPG (Centre de Recherches Pétrographiques et Géochimiques, Vandoeuvre-lès-Nancy) and in the Laboratory IJL (Institut Jean Lamour, Nancy). The field mission in Mongolia was conducted between July-August 2017 with the vital contribution of COGEGOBI, the subsidiary company of ORANO in Mongolia.

References

Hough, G., Swapp, S., Frost, C., Fayek, M., 2019. Sulfur Isotopes in Biogenically and Abiogenically Derived Uranium Roll-Front Deposits. Economic Geology, v. 114, no. 2, pp. 353-373.

Makhnach, A., Mikhajlov, N., Kolosov, I., Gulis, L., Shimanovich, V., Demeneva, O., 2000. Comparative analysis of sulfur isotope behavior in the basins with evaporites of chloride and sulfate types. Sed. Geol. 134, 343–360.

16th International Congress of the Geological Society of Greece
17-19 October, 2022 - Patras, Greece
Bulletin of the Geological Society of Greece, Sp. Publ. 10
Ext. Abs. GSG2022-099

Database Design, Implementation and Management of the Greek Lignite Potential

A. Chatziapostolou[1], M. Xenakis[1]
(1) Hellenic Survey of Geology and Mineral Exploration, Acharnae, Greece, achatzia@igme.gr.

The global energy crisis resulting from the Ukrainian war is leading all the countries depended on Russian natural gas to make new decisions about their energy policy. In Greece the only short-term solution of this crisis is to use the domestic energy raw materials, such as lignite. Nowadays the need to record the lignite potential of Greece is becoming more necessary than ever. Many attempts have been made for the development of a lignite database to date, but none has been completed. The first of these, go back to the first half of the 20th century, during plans for the economic reconstruction of the country (Solomos, 1918; Nicosias, 1948; Ministry of Commerce 1963). During that period the recorded data for each lignite deposit were limited in number because the focus was purely financial (reserves and exploitation). The need for a more systematic recording, completion, correction and renewal of the data arose in the late '70s, after the extensive research that yielded a wealth of new information and data (Koukouzas, 1977). With the entry of technology and computers in the workplace, the electronic recording of the available data and the database development became necessary in all the scientific fields. In late 90s several efforts were made to create and develop an information and data bank for Greek lignite (Koukouzas, 1996a; 1996b; Koukouzas et al., 2000). The latest one was designed by Hatzigiannis et al. (2001), and the main aspect was the digital mapping of energy raw material deposits using geographical information systems. Undoubtedly these databases contributed to the deep knowledge of the Greek lignite potential, but what still remains as a target is to have an updatable database, with an easy open access to the stakeholders.

The philosophy of this project is the implementation of a database that will provide to users (entrepreneur, researcher, investor, scientist), all the information and data for the Greek lignite and should be comprehensive, useful, updatable, and easy to manage. The design of the database is adapted to the specificities of the recorded objects, namely the lignite deposits and the lignite-bearing basins that host them. The ultimate goal is the preparation of an interactive website with digital maps of the lignite basins, deposits, drillings, etc. and all the available quantitative and qualitative data, in which access to the general public will be open. This goal will be achieved by performing the tasks below:

- Design and creation of the lignite database.
- Processing of the data with a special software.
- Digital production of a large series of maps at various scales.

The first task of this study includes the update, completion, maintenance, and expansion of the oldest database on a permanent basis. This database has the particularity that almost all its elements are being revised and completed based on the latest research information, as well as the changes in the economic-technical parameters of the lignite deposits during the mining processes or changes in the global energy and economic policies. The analytical structure of the lignite database is based on international standards for the best design and creation of databases, and includes mainly two log sheets, the lignite-bearing basin log sheet and the lignite deposit or lignite field log sheet. The lignite-bearing basin log sheet contains general information (name and location), as well as information about the main depositional characteristics, such as the age, the number of seams, fields and operating mines in the basin and the extent of the basin. The lignite deposit or lignite field log sheet contains geographical, administrative, and mining information, the extent and the age of the deposit or field, the number of drilling cores, the type of coal and lithological data, the lignite thickness, the tectonic condition, and the main mining parameters of the deposit (roof depth and roof condition of the upper lignite seam, floor condition, upper and middle lignite seam composition, thickness of the lignite seams, extractable reserves etc.). All the available qualitative characteristics of the deposit are also included in this sheet, such as data resulting from proximate (ash, moisture, organic matter and fixed carbon content, volatile matter, and gross calorific value) and ultimate analyses (C, H, N, S, O composition), organic petrographical analyses (maceral composition, huminite reflectance, coal-facies diagrams) and mineralogical composition. Information about the mining history regarding the operation of lignite mines in the deposit, the exploitation method, the annual and total production, the lignite waste disposals and their possible uses and the environmental restoration of the closed mines are also parts of the lignite deposit or lignite field log sheet. It is worth noting that at the end of each log sheet all the references from which the data were taken are mentioned.

The database has been created and updated in Microsoft Access software, which runs under Windows operating system. The reason for this selection was the friendliness and easy use of the interface during computer application development, the ability to develop parts of the application using the Visual Basic software on which Access is based and the easy exchange of data between Access and other applications, apart from Microsoft. Overall, Microsoft Access is the user interface to view, import and edit data but then the actual data are being stored in an SQLite database. All the spatial data are being stored in a free and open-source database system PostgreSQL (Object-Relational Database Management System – ORDBMS), that fully supports SQL queries and works seamlessly with QuantumGIS (QGIS), which is an open-source

GIS system, necessary for the visual representation of all related spatial data.

Overall, the need for the database design, implementation and management of the Greek lignite potential is continuous and urgent, especially nowadays that the weaning off non-domestic energy raw materials is necessary and essential. The Hellenic Survey of Geology and Mineral Exploration is working actively in implementing this complicated technically project following the above-mentioned methodological approach.

Acknowledgements

The authors would like to thank all those who worked at the former Department of Energy Raw Materials of the Greek Institute of Geological and Mineral Exploration, in producing raw data and creating the first original handwritten database, with special thanks to the former Director C. Koukouzas. Additionally, we would like to thank Dr. N. Koukouzas, the former Director of Research at the Centre for Research and Technology Hellas/Chemical Process and Energy Resources Institute (CERTH/CPERI), for providing us the first digital database and technical data. All the data concerning the mining operation, the exploitation methods, some of the drillings and lithostratigraphy data etc., were obtained due to the cooperation with Mr. Roubos (Director) and Mr. Kostaridis from the Department of Central Mine Support of PPC S.A. Special thanks to G. Hatziyannis, the former Director of the Department of Geothermal and Thermometallic Waters at IGME, for the first implementation of digital mapping of energy raw material deposits using geographical information systems, in which this project is based.

References

Hatziyiannis, G., Androulakakis, N., Xenakis, M., 2001. Digital mapping of energy raw materials deposits using geographic information systems, IGME, Athens. [in Greek]

Ministry of Commerce, 1963. Study for the Greek lignite, Edition of the Special Experimental Laboratory of the Ministry of Commerce 36, Athens, 76 p. [in Greek]

Nikosias, N., 1948. Greek lignites and sub-bituminous coals, Ministry of Supply and Distribution, Athens, 47 p. [in Greek]

Koukouzas, C., 1977. Coals of Greece. Potential – research - prospects. Technical Chamber of Greece Conference, Athens, Greece, Technical Chronicles 78, 158-166. [in Greek]

Koukouzas, N., 1996a. Inventory of the Greek lignite deposits – A first approach, Center for Technology and Applications of Solid Fuels, Athens. [in Greek]

Koukouzas, N., 1996b. Creation of data cards with the main characteristics of the lignite deposits of Greece, Center for Technology and Applications of Solid Fuels, Athens. [in Greek]

Koukouzas, N., Hatziyiannis, G., Papatheodorou, C., Kakaras, E., 2000. Systematic record of Greek lignite deposits (qualitative and quantitative characteristics) and database development, Center for Technology and Applications of Solid Fuels, IGME, National Centre for Scientific Research “Demokritos”, Athens. [in Greek]

Solomos, I., 1918. Greek lignites, Ministry of National Economy, Athens, 187 p. [in Greek]

16th International Congress of the Geological Society of Greece
17-19 October, 2022 - Patras, Greece
Bulletin of the Geological Society of Greece, Sp. Publ. 10
Ext. Abs. GSG2022-100

Trace Elements Distribution In Sphalerite From Epithermal-Style Veins At The Pagoni Rachi And Konos Hill Porphyry/Epithermal Prospects, NE Greece

C. Mavrogonatos[1], P. Voudouris[1], V. Melfos[2], P.G. Spry[3], S. Klemme[4], J. Berndt[4], F. Zaccarini[5], C. Stouraiti[1], K. Soukis[1], M. Anastasatou[1]

(1) National and Kapodistrian University of Athens, Greece, kmavrogon@geol.uoa.gr (2) Aristotle University of Thessaloniki, Greece (3) Iowa State University, Ames-Iowa, USA (4) Westfälische-Wilhelms Universität Münster, Germany (5) Faculty of Science, Physical and Geological Sciences, Universiti Brunei Darussalam, Brunei Darussalam

The Sapes and Kirki prospects in NE Greece belong to the Rhodope metallogenic district and host significant porphyry and epithermal type mineralization, which are enriched in several precious and critical metals. Host rocks are mostly magmatic and/or sedimentary rocks of Middle-Upper Eocene to Oligocene age, which intrude or unconformably overlie the metamorphic basement of the Rhodope and Circum-Rhodope units. Porphyry-style Mo-Re-Cu-Au mineralization, which occurs at Konos Hill (broad Sapes area) and Pagoni Rachi (Kirki area) is overprinted by quartz-calcite veins with epithermal affinities ("E-type" veins, Fig. 1a-d). These veins are associated with lateral sericitic and/or argillic alteration of the granodiorite host rock and contain various amounts of base metal sulfides (pyrite, galena, sphalerite, chalcopyrite) along with minor sulfosalts (e.g., tetrahedrite/tennantite group minerals) and Ag-Au alloy.

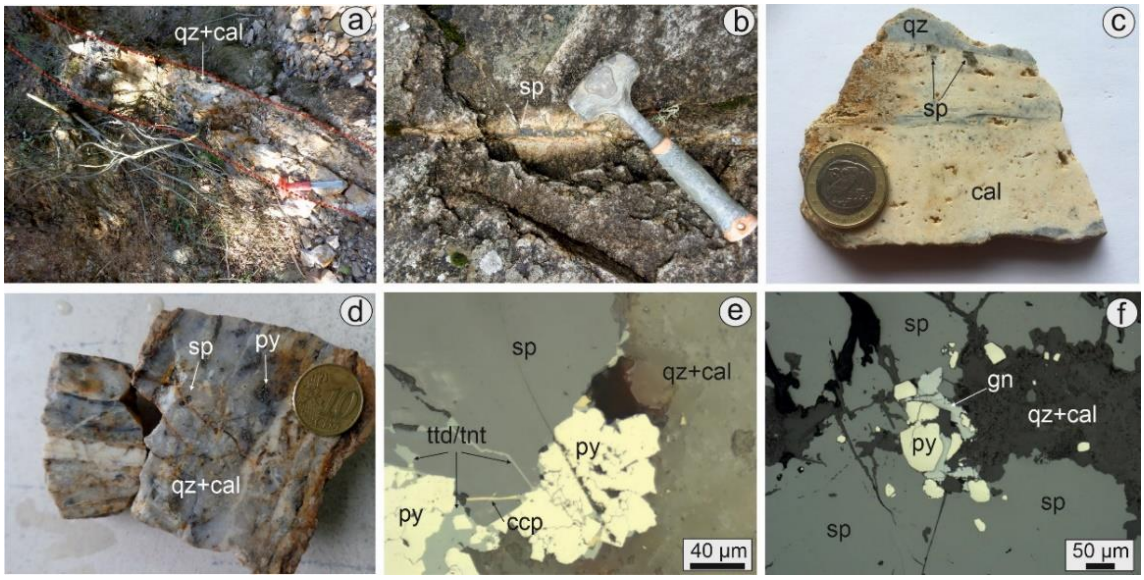

Figure 1. Field (a, b) and hand-specimens photographs (c, d), and reflected light photomicrographs (e, f) of sphalerite-bearing, quartz-calcite E-type veins at Konos Hill (a, c, e) and Pagoni Rachi (b, d, f) areas. Abbreviations: cal: calcite; ccp: chalcopyrite; gn: galena; py: pyrite; quartz; sp: sphalerite; ttd/tnt: tetrahedrite/tennantite group minerals.

Sphalerite is abundant in E-type veins at both prospects, forming coarse-grained (up to 0.5 cm), euhedral to subhedral crystals associated with pyrite, galena, chalcopyrite, and tetrahedrite/tennantite group minerals (Fig. 1e, f). EPMA and preliminary LA-ICP-MS analyses (Table 1, Figure 2) reveal differences in the chemistry of sphalerite between the two prospects: At Konos Hill, sphalerite contains high Cd values (up to 39434 ppm) exhibiting a positive trend with Fe. In contrast, at Pagoni Rachi the Cd content of sphalerite is much lower (up to 4577 ppm) and correlates negatively with Fe. The Fe content is slightly variable in the two prospects (up to 2.75 wt% corresponding to 4.81 mol % FeS at Konos Hill, and up to 3.39 wt% corresponding to 5.93 mol % FeS at Pagoni Rachi, respectively) and is (along with Cd) responsible for the zoned nature of sphalerite. The Mn content is much higher in sphalerite from Pagoni Rachi than in Konos Hill (up to 2620 ppm and 222 ppm, respectively), while a positive relationship occurs between Mn-Fe and Mn-Cd at Konos Hill. Copper has a higher concentration in sphalerite from Pagoni Rachi (up to 817 ppm) than Konos Hill/ Sapes (up to 78 ppm) and exhibits a positive trend with Sn at both prospects. Indium and Cu correlate negatively in sphalerite from Konos Hill/Sapes but show a slightly positive correlation in sphalerite from Pagoni Rachi. Gallium is enriched in sphalerite Konos Hill and Pagoni Rachi, reaching up to 1852 ppm and 2043 ppm, respectively. Indium is present in sphalerite from Konos Hill (average 540 ppm). A single spot analysis yielded 2049 ppm, implying the presence of a submicroscopic In-bearing inclusion. Germanium is characterized by low concentrations at both prospects, reaching up to 51 ppm in sphalerite from Pagoni Rachi. Other trace elements (e.g., Ag, Au, W, Ni, etc.) are present in very small concentrations

(e.g., <10 ppm) or are below the detection limit.

Table 1: LA-ICP-MS analyses of sphalerite (selected elements). All values are reported in ppm.

Prospect	Konos Hill – Sapes (n = 10)				Pagoni Rachi (n = 10)			
Element	**Min**	**Max**	**Std**	**Aver.**	**Min**	**Max**	**Std**	**Aver.**
Mn	113	222	30	176	1014	2620	553	1460
Fe	2541	4363	531	3681	3010	4468	458	3798
Co	0.23	7.13	2.49	3.02	0.21	0.27	0.03	0.24
Cu	13	78	20	31	6.83	817	236	184
Ga	2.12	1852	719	356	2.00	2043	643	214
Ge	0.46	7.25	2.35	2.48	0.41	51	35.77	25.71
As	1.42	1.42	bdl	1.42	0.59	0.71	0.08	0.65
Se	bdl	bdl	bdl	bdl	1.87	2.90	0.35	2.34
Mo	0.04	0.26	0.08	0.11	0.03	0.12	0.03	0.08
Ag	0.44	1.28	0.29	0.88	0.83	4.05	1.10	2.07
Cd	12385	39434	8382	23635	3548	4577	335	4135
In	0.81	2049	876	540	0.02	9.14	3.16	1.33
Sn	2.43	21	5.17	8.01	0.22	49.07	16.14	17.04
Sb	0.07	3.00	1.32	1.22	0.06	0.46	0.20	0.31
Au	bdl	0.01	bdl	bdl	0.01	0.04	0.01	0.02
Pb	0.04	2.21	0.69	0.49	0.04	6.53	2.39	1.94
Bi	bdl	0.01	bdl	bdl	0.01	0.09	0.04	0.03

n = number of analyses; bdl = below detection limit; Min = minimum; Max = maximum; Std = standard deviation (1σ); Aver.= average

The trace element budget of the sphalerite reflects a series of substitution mechanisms and reveals the existence of submicroscopic inclusions that carry significant amounts of critical metals like Mn, Cd, In, and Sn. The presence of bivalent elements like Fe, Mn, and Cd, suggests a simple cation exchange mechanism ($Zn^{2+} \leftrightarrow M^{2+}$) that is also supported by the smooth ablation profiles, thus implying a homogeneous distribution. The positive trend between Sn and Cu observed in both prospect is attributed to submicroscopic inclusions of Sn-bearing minerals, rather than a $3Zn^{2+} \leftrightarrow 2Cu^{+}+Sn^{4+}$ substitution mechanism, since Cu/Sn ratios are ≫2 (Cook *et al*., 2009). At Pagoni Rachi, In is incorporated within sphalerite via the coupled substitution $Cu^{+}+In^{3+} \leftrightarrow Zn^{2+}+Fe^{2+}$. However, such a substitution mechanism cannot be supported for sphalerite from Konos Hill/Sapes, where submicroscopic In-bearing inclusions occur.

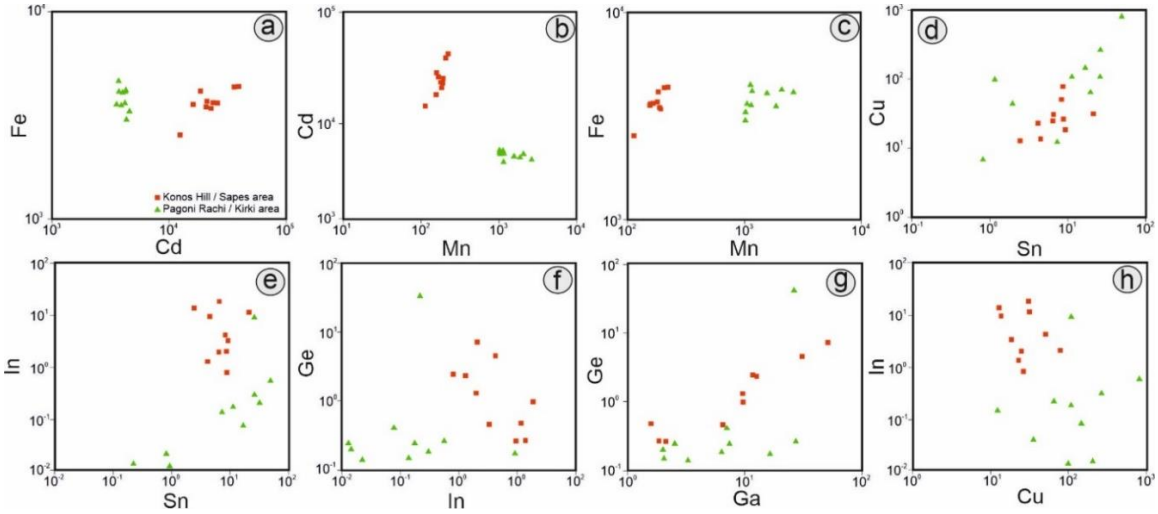

Figure 2. Binary plots for selected elements based on LA-ICP-MS analyses in sphalerite.

Application of the GGIMFis geothermometer (Frenzel *et al*., 2016) to constrain the temperature of sphalerite deposition, yielded T of 222-250ºC (aver. 236 ºC) at Konos Hill/Sapes and 242-275 ºC (aver. 259 ºC) at Pagoni Rachi respectively, which are consistent with previously acquired microthermometric data for both prospects.

References

Cook, N.J., N.J., Ciobanu, C.L., Pring, A., Skinner, W., Danyushevsky, L., Shimizu, M., Saini-Eidukat, B., Melcher, F., 2009. Trace and minor elements in sphalerite: an LA-ICP-MS study. Geochimica et. Cosmochimica Acta 73, 4761-4791.

Frenzel M., Hirsch, T., Gutzmer, J., 2016. Gallium, germanium, indium, and other trace and minor elements in sphalerite as a function of deposit type-A meta-analysis. Ore Geology Reviews 76, 52-78.

16th International Congress of the Geological Society of Greece
17-19 October, 2022 - Patras, Greece
Bulletin of the Geological Society of Greece, Sp. Publ. 10
Ext. Abs. GSG2022-111

Prinos Complex Developments: Past, Present and the Next 30 Years

S. Zervopoulou[1], I. Ismail[1], E. Tartaras[1], A. Stefatos[1]
(1) Hellenic Hydrocarbon Resources Management S.A., Athens, Greece, s.zervopoulou@greekhydrocarbons.gr

1. Overview of Prinos Complex

The Prinos-Kavala offshore basin is located in the North Aegean Sea, 6km northwest of the Island of Thasos (Fig. 1) in water depths ranging between 30-50m. The Prinos-Kavala basin was formed by a system of NW-SE striking faults, hosting clastic and evaporitic sediments with a maximum thickness of 5800m, deposited during Miocene to Pleistocene. The Prinos-Kavala basin was developed in the Miocene, whereas during the Upper Miocene the South Kavala ridge emerged and separated the Prinos-Kavala basin from the open sea. This event has led to the deposition of seven evaporitic cycles, the three deepest of which are thick salt layers (up to 350m), whereas during the Pliocene the subsidence accelerated again to leave the Prinos-Kavala basin in its present configuration. Exploration in this area began with extensive seismic campaigns east and west of the Island of Thasos in the early 70s. The first well, East Thasos-1, was drilled 20km east of Thasos on a large anticline in 1971 and encountered a light oil accumulation. The next two wells were drilled west of the island in 1972-73 on a fault bounded anticline combined with a stratigraphic pinch-out that has resulted in the discovery of South Kavala (SK) gas field, which is located 12km southwestern of the Prinos oil field. It is the first gas discovery in Greece with initial gas reserves estimated at 1bcm and cumulative production of 0.89bcm as of today. Furthermore, the existence of hydrocarbons in the area encouraged further drilling that resulted in the discovery of Prinos oil field with two wells Prinos 1&2 (Proedrou and Papaconstantinou, 2004). Prinos came on stream by early 1981 with initial production rates of 8 and 10 Mbopd reaching the peak at more than 27 Mbopd, in 1985. The second oil field discovery in the area was Prinos North (Prinos N.), which was initially identified as potential exploration opportunity in 1976, when Prinos-4 well encountered small quantities of oil to the north of Prinos field. Later on, it was appraised and developed as a satellite field in 1996, showing an initial rate from the first well of 3 Mbopd. Epsilon field on the other hand was later identified on 2D seismic data, whereas in early 2000s, the E-1 well was drilled and confirmed sour crude oil reserves at a depth of about 2800mTVDSS. In more recent exploration activities, Energean Oil and Gas S.A, the operator of Prinos concessions fields in the Prinos area, conducted in 2015 a 340km^2 broadband 3D seismic survey over the Prinos area leading to an increase in fields 2P reserves and 2C, also in the identification of several potential plays and prospects in the vicinity that need to be confirmed.

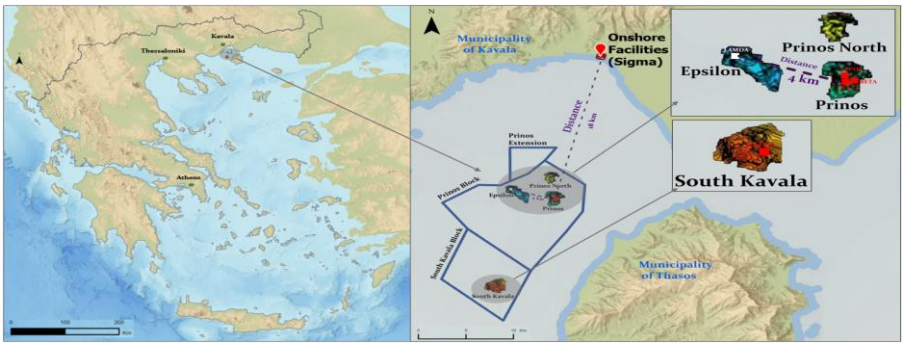

Figure 1. Kavala Basin and Prinos Complex.

2. Prinos Area Development Planning: 2022-2050

In response to the collapse of the market in 2020, a consequence of the COVID19 pandemic outbreak, the Greek state responded to the request of the operator for emergency support measures by approving a state support package. In the beginning of 2022, a €100M state baked up loan was made available to the operator in order to ensure the life extension of Greece's sole hydrocarbon producing asset for several years. The loan comprises €90.5M provided by private bank and €9.5M provided directly by the state itself. This state measure is considered a critical and major support scheme that will primarily extend the lifespan of Prinos development, through the production of the Epsilon field but also set the foundation for later subsequent transformation of the Prinos fields into a carbon-neutral industrial complex that will be a landmark in the Mediterranean, and will lead it into the new energy era. The development projects planned in the area for the coming years are the following:

2.1. Green-Field Epsilon: On Stream

An immediate plan is set for the development of Epsilon field involving the installation of the new satellite Lamda platform equipped with 15 well slots. The Lamda platform will be installed approximately 4km west of the existing Prinos

platforms (Fig.1) and will be connected to processing Delta platform via three sub-marine pipelines. The Epsilon reservoirs exhibit poor porosity and permeability properties compared to those of Prinos due to the fact that Epsilon lies deeper (weight overlay, clay content and dolomitization). Thus, the Epsilon field carries risks of lower production than that achieved in Prinos, and thus higher uncertainty with regard to forecasted production. Therefore, after the platform installation is complete, the three pre-drilled wells will be hocked up and placed on stream for a couple years allowing enough time to investigate further the geology and test reservoir behavior, confirming and/or adjusting production projections. If the field and production data exhibit lower values than those expected, this will result in the need for additional investments in terms of additional drilling, sidetracking, longer horizontal wells etc. to boost the field's production. Consequently, at this stage the determination of a concrete number of wells required to produce recoverable oil from the Epsilon field, is considered premature. Meanwhile, in the most likely scenario as of today, we expect that the production from Epsilon field will contribute 2 Mbopd in addition to production from Prinos and Prinos N. oil fields, when the three predrilled wells will be placed on stream (Energean, 2022).

2.2. Brown-Field Prinos: Production Enhancement, Carbon Capture and Storage (CCS) and Eco Hydrogen

To enhance further the production from Prinos fields, major workover activities and enhancement of production will be needed at Prinos field after the commissioning of the Epsilon field. However, the operator has already submitted conceptual plans for a CCS project proposal at the Prinos Complex. In response the Greek state has included provisions to include such a CCS project in the country's recovery and resilience fund, hoping to utilize the existing infrastructure and extend the local economic activity into the future, beyond hydrocarbon production. The submitted grant proposal, has been approved by the European Commission due to the importance of the project to the energy transition and to the decarbonization targets set at national and EU level. Following this approval, the current field Operator started conducting several studies (e.g., pre-FEED for the Prinos CCS project, Storage Complex Assessment). At a national level the Prinos CCS project will be able to provide a solution for long-term capture and storage of CO_2 emissions from both local industry (e.g., aluminum and steel plants, cement factories, and refineries) as well as remote emitters. The project's stated objective in the first phase aims on capturing and storing 1 Mtpa of CO_2 from carbon emissions sources within 150km of Prinos onshore Sigma Plant. According to preliminary estimates, the theoretical geological storage capacity in Prinos amounts to 100Mt of CO_2. Along with the CCS activity, other plans have been announced by the operator, like the development of a small-scale eco hydrogen plan within the existing Sigma Plant, which could potentially achieve negative CO_2 emissions by using bio-gas, biomass and other waste materials as a source of energy (Energean, 2021; 2022).

2.3. UGS South Kavala: Underground Gas Storage Enhancing National Energy Security

Currently the field is at late-stage production and is considered almost depleted, whereas the future plan relies on the conversion of the South Kavala reservoir to underground gas storage (UGS) facility, boosting the energy security within the country. The Hellenic Republic Asset Development Fund launched in June 2020 a formal international tender process to select the Concessionaire for the UGS Project. Meanwhile, the project has been included in the list of Projects of Common Interest (PCI) adopted in 2017 by the European Commission and included in the 4th PCI list of European Commission in October 2019. The Project covers development and operation of the storage facility for a duration up to 50 years following the licensing (HRADF). To our understanding there are several possible scenarios/plans for the operation of the UGS facility at the South Kavala field. The different operational strategies are related to the working gas volume for which relatively small or large cycle can be operated. The chosen operator will be the one to ultimately establish the operational strategy for the field. However, we foresee two feasible strategies: i. operation of 1 cycle (injection and withdrawal with a duration of approximately 11 months) ii. operation of 2 small cycles each with a duration of 6 months. Both operational strategies involve cycles with 55% working gas (≈ 530MCM) and 45% cushion gas (≈ 430MCM). The operation of either of these cycles is dependent on the investments that will be made on infrastructure. The South Kavala UGS will be the first such facility in Greece, a strategic asset and an energy infrastructure that will enhance the security of supply in the Greek market, as well as in Southeastern Europe, ensuring gas supply to end users.

Conclusions

In summary, the Prinos complex/area presents new opportunities both in hydrocarbon production, as well as in energy transition and decarbonization activities. The production of hydrocarbons in combination with CCS technology and possibly blue hydrogen production constitute a sustainable and appropriate development allowing the country to transit appropriately to Net Zero Economy by 2050.

References

Proedrou, P., Papaconstantinou, M. C., 2004. Primus Basin - A Model for Oil Exploration. Bulletin of the Geological Society of Greece, 36(1), p.p. 327–333.

Energean Plc, Annual Report – Strategic Report, 2021, Energean AR21

Energean Corporate Presentation, 2022, Energean Corporate Presentation HRADF S.A. Underground Gas Storage South Kavala, South Kavala Underground Natural Gas Storage – HRADF

16th International Congress of the Geological Society of Greece

17-19 October, 2022 - Patras, Greece

Bulletin of the Geological Society of Greece, Sp. Publ. 10

Ext. Abs. GSG2022-112

Framework for the Development of a Mineral Resource Digital Twin

A. Patra[1], I. Kapageridis[1], A. Asvesta[1], I. Sinatkas[2]

(1) Department of Mineral Resources Engineering, University of Western Macedonia, Kozani, Greece, a.patra@dei.gr
(2) Department of Informatics, University of Western Macedonia, Kastoria, Greece.

Research Highlights

A framework for the development of a digital twin that represents a mineral resource, enabling effortless and dynamic integration of new information and updating of the mineral resource model.

Background and Objectives

A mineral resource is a concentration of solid material of economic interest in or on the Earth's crust with reasonable prospects for eventual economic extraction. Mineral resource models are commonly generated using specialised software applications, based mostly on information from exploration programmes and mine production. Updating of mineral resource models with new information involves repeating most, if not all, of the modelling stages, even if the new information only affects part of the model. Mineral resources represent static entities (deposits) that change only due to human intervention (mining). Digital twins are virtual representations of entities that span their lifecycle, are updated from real-time data, and use various simulation, machine learning and reasoning algorithms to help decision-making. So, one could question the need for the development of a digital twin to represent a mineral resource. However, our perception of a mineral resource is dynamic and changes through time during various stages of mineral exploration and later during mining with the inflow of new information from various sources. A few researchers have worked recently on finding ways to automate the process of generating a mineral resource / reserve model. Benndorf *et al.* (2016) introduced the concept of an integrated framework for real-time reserve management incorporating sensor-based material characterisation, geostatistical modelling under uncertainty, modern data assimilation methods for a sequential model updating and mining system simulation and optimisation. Wambeke *et al.* (2018) performed a pilot study to demonstrate a new process for updating block estimates using actual mill performance data. Hodjkinson *et al.* (2020 provided an overview of digital twin concepts and how these can be considered in the case of geological models. Servin *et al.* (2021) provide an example of a system for tracking material from mine to mill using digital twin technology. Kumar and Dimitrakopoulos (2022) describe a system for updating geostatistically simulated models of mineral deposits in real-time with new information using reinforcement learning.

Our study aims at developing a digital twin of a mineral resource by breaking down the mineral resource modelling process to all applicable steps, identifying, formalising, and organising information from the available sources, identifying and configuring all the required model entities (grids, triangulations, block models, etc), and, selecting and configuring the necessary data processing and modelling algorithms.

Methodology

The Workflow Editor (WE) from Maptek was chosen as the software platform to develop and test prototype digital twins of mineral resources. WE allows users to design, save and run automated software procedures called *workflows.* They consist of a series of *components* connected by arrows indicating the sequence of execution and the flow of data. Workflows may be fully automated or may consist of a combination of manual and automated steps, alternate paths of execution based on user input (decision-making ability), and customised behaviour. Workflow components generate data called *attributes* that are transported to other components via *connections*. WE provides a number of components, ideal for the development of mineral resource digital twins:

- **Data Editor:** provides a snapshot of the current state of the workflow's data. It allows inspection, adding or removing attributes, items, and files and changing of their value.
- **Data Filter**: used to remove attributes or items from input data.
- **Data Trigger**: used to detect an event within the Workbench or on the file system to trigger actions in a workflow.
- **Decision**: used to alter the flow of execution depending on user input.
- **End of Loop**: used to mark the end of looping over several components. When there are loops defined that span multiple components, it returns control to the top of the loop for the next iteration item.
- **Timer**: delays the execution of the previous component. The timer starts when the component is activated, and the component is completed when the time has expired.
- **Waypoints**: used to make diagrams clearer to navigate for the user and provide control over the flow of data.

Figure 1 shows a simplified workflow used to generate a mineral resource model using three basic sources of information (drilling, topography, and geology) that reacts to any changes to the source data and repeats associated process(es).

Processes unaffected by the changes stay inactive and any downstream processes run using the results of unaffected higher processes derived earlier.

Conclusions

Representing the process of modelling a mineral resource as a workflow in WE allowed the utilisation of certain components that can make modelling dynamic, responding to changes in the input data provided at any stage. The flow of data as attributes of the workflow, allows modelling processes to be reconfigured according to changes to the input data. Overall, with the system discussed in this paper, it is possible to develop digital twins of mineral resources that dynamically react to data changes, not only by simply repeating some or all the modelling processes, but also by adjusting the processes themselves to suit the new data.

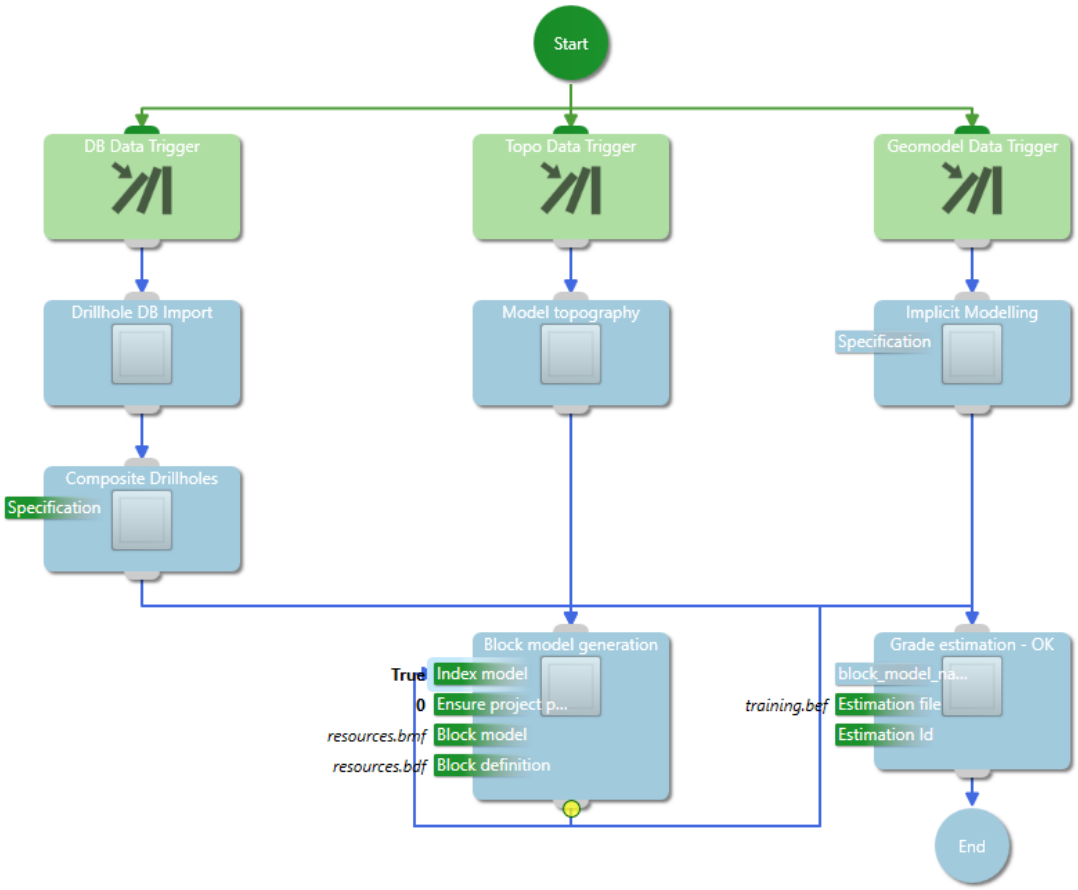

Figure 1. Simple workflow used to generate and estimate a resource block model from drillhole, geological and topographical data, after an update triggered by a change in drillhole data.

Acknowledgements

The authors gratefully acknowledge the financial support of the University of Western Macedonia and funding of this PhD research.

References

Benndorf, J., W. N. Buxton, M.W.N., 2016. Sensor-based real-time resource model reconciliation for improved mine production control – a conceptual framework, Mining Technology, 125:1, 54-64, DOI: 10.1080/14749009.2015.1107342.

Hodjkinson, J.H., Elmouttie, M., 2020. Cousins, Siblings and Twins: A Review of the Geological Model's Place in the Digital Mine. Resources 2020, 9, 24; DOI:10.3390/resources9030024.

Kumar, A., Dimitrakopoulos, R., 2022. Updating geostatistically simulated models of mineral deposits in real-time with incoming new information using actor-critic reinforcement learning. Computers & Geosciences 158 (2022) 104962, DOI: 10.1016/j.cageo.2021.104962.

Servin, M., Vesterlund, F., Wallin, E., 2021. Digital Twins with Distributed Particle Simulation for Mine-to-Mill Material Tracking. Minerals 2021, 11, 524. DOI: 10.3390/min11050524.

Wambeke, T., Elder, D., Miller, A., Benndorf, J., Peattie, R., 2018. Realtime reconciliation of a geometallurgical model based on ball mill performance measurements – a pilot study at the Tropicana gold mine. Mining Technology, 127:3, 115-130, DOI: 10.1080/25726668.2018.1436957.

16th International Congress of the Geological Society of Greece
17-19October, 2022 -Patras, Greece
Bulletin of the Geological Society of Greece, Sp. Publ. 10
Ext. Abs. GSG2022-128

Potential CO_2 sequestration in alkaline rhyolites: the case studies of Milos active and Antiparos fossilized volcanoes

S. Tombros[1], J. Papavasiliou[1].

(1) Department of Material Sciences, University of Patras, Rio, Greece, stel@upatras.gr, ipapavas@upatras.gr.

Research highlights: Sequestration in alkaline rhyolites can be accommodated via precipitation of dawsonite [$(NaAlCO_3(OH)_2$]. The CO_2 storage capacity for Milos alkaline rhyolites corresponds to ~48 Kt of sequestered CO_2, whereas for Antiparos to ~29 Kt.

Background and objectives

The Islands of Antiparos and Milos are placed in the South Aegean volcanic arc, where calc-alkaline volcanism began ~4.7 Ma and is still active, and geotectonically belong to the southern segment of the Attico-Cycladic Massif (Fytikas *et al*., 1984, Fig. 1a, b). Milos Island occupies the outer end of the South Aegean volcanic arc and consists of a volcanosedimentary sequence with ages of 3.5 to 0.1 Ma covering the Cyclades Blueschist Unit, as a result of explosive volcanism of submarine volcanic edifices. An initial volcanic activity comprising calc-alkaline, pumice flows, ignimbrites and tuffs (Phase I, dated from 3.5 to 3.0 Ma), was followed by effusive volcanism that formed numerous domes and lava flows of dacites-to-rhyolites (Stewart and McPhie, 2006) erupted in shallow seawater environment (Phase II, ~2.7 to 1.4 Ma, Fig. 1a). The rhyolites develop porphyritic texture with quartz, plagioclase, sanidine and hornblende ± biotite phenocrysts set in a groundmass of fine-grained quartz and albite (Stewart and McPhie, 2006). Antiparos Island lies on the inner end of the South Aegean volcanic arc and consists of Pliocene rhyolites, dated at ~5.4 Ma, forming two lava domes. The rhyolites occur as massive and aphanitic lava flows, accompanied by pyroclastics (Fig. 1b, Acquafredda *et al*., 2019). They consist of sanidine and quartz phenocrysts (± traces of hornblende, and oligoclase) set in a groundmass of cryptocrystalline sanidine and quartz.

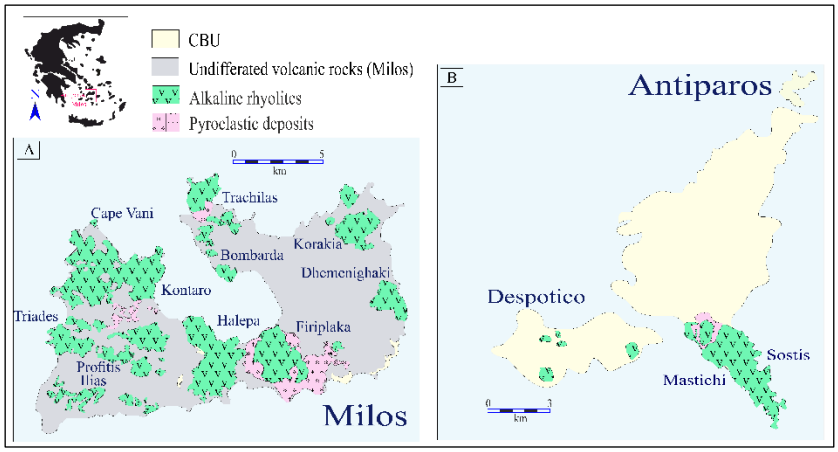

Figure 1. (a): Simplified volcanic maps of Milos and (b): Antiparos with emphasis on the exposure of alkaline rhyolites (modified after Stewart and McPhie, 2006; Acquafredda *et al*., 2019).

Carbon mineralization is indorsed as a policy for CO_2 sequestration. Currently, the most suitable candidates for CO_2 sequestration are considered to be the mafic and ultramafic intrusive and extrusive rocks (e.g., gabbros, peridotites, basalts and tephrites, Dasgupta, 2013); using *in-situ* carbon capture technologies based on CO_2 circulation and storage in mafic volcanic sequences. The case of acidic volcanic rocks, such as the Milos and Antiparos volcanics has not yet been investigated. Towards this end, major and trace element analyses were obtained from Milos and Antiparos rhyolites and SEM microanalyses of their sanidine phenocrysts. We have analyzed the sanidines from Firiplaka in Milos and Mastichi in Antiparos. The petrochemical whole-rock analyses and sanidine microanalyses were performed at the ActLabs Ancaster, Ontario and the Department of Materials Science, University of Patras, respectively.

Results and discussion

Our petrochemical results (combined with the published data from Fytikas *et al*., 1984; Stewart and McPhie, 2006; Acquafredda *et al*., 2019) from Milos and Antiparos volcanic rocks are given in the SiO_2 vs K_2O and vs K_2O+Na_2O plots (in wt. %, Fig. 2 a, b). Our results suggest that CO_2 sequestration in acid volcanic rocks can be accomplished, and so must be further explored, only for the case of alkaline rhyolites (i.e., rhyolites that comprise ≤ 70 wt. % SiO_2, ≤ 10 wt. % (K_2O + Na_2O) and ≤ 3 wt. % K_2O). Furthermore, based on our results, we propose that CO_2 sequestration using as storage reservoirs the alkaline rhyolites can be accommodated via precipitation of dawsonite. Precipitation of dawsonite is proposed to be accomplished though the hydrothermal breakdown of the sodic sanidine [$K(AlSi_3O_8)$] phenocrysts and

most probably of albite [$Na(AlSi_3O_8)$] and their groundmass, which are major constituents of the alkaline rhyolites in Milos and Antiparos. The composition of sanidine is Or_{79-100} for Milos (Firiplaka) and Or_{7-61} for Antiparos (Mastichi) alkaline rhyolites (Fig. 3).

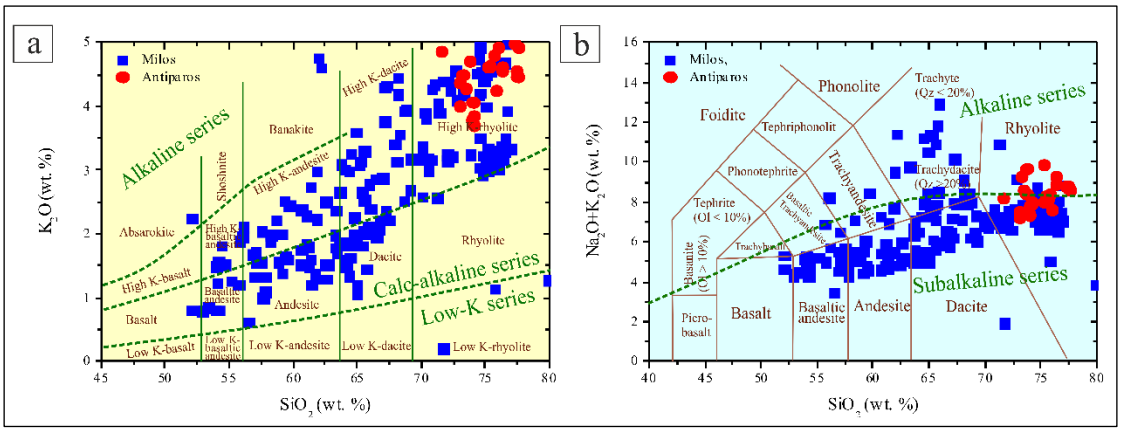

Figure 2. (a): SiO_2 vs K_2O (wt. %) and (b): SiO_2 vs (Na_2O+K_2O) (wt. %) plots of alkaline rhyolites from Milos and Antiparos.

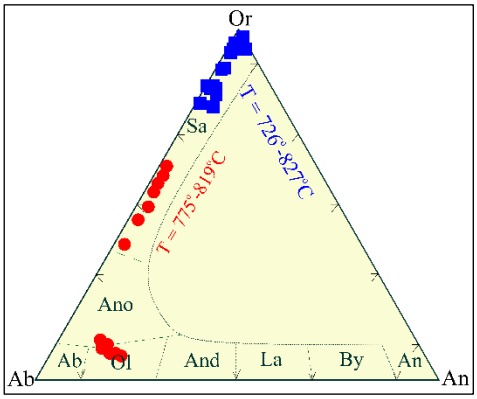

Figure 3. Composition and temperature of formation of the Antiparos and Milos sanidines on the Ab-An-Or plot.

The dawsonite formation reaction associated to CO_2 sequestration proposed herein is: $KAlSi_3O_{8(s)} + NaAlSi_3O_{8(s)} + Na^+_{(aq)} + 2CO_{2(aq)} + 2H_2O_{(l)} \leftrightarrow 2NaAlCO_3(OH)_{2(s)} + 6SiO_{2(s)} + K^+_{(aq)}$ (reaction 1). Experimental data (Li *et al*., 2019; Hellevang *et al*., 2010) combined with the logK values of this reaction, i.e., $logK = log(K^+/Na^+) + 6 \cdot log(SiO_2) - 2 \cdot logfCO_2$, suggest that dawsonite precipitation and sanidine and albite dissolution rates (for albite, sanidine and dawsonite are -9.6, -10.1 and -8.7 to -5.5 in $log(mol \cdot m^{-2} \cdot s^{-1})$, respectively) are enhanced by higher $Na^+_{(aq)}$ and $K^+_{(aq)}$ concentrations (for SiO_2 of 70-75 wt. %), CO_2 fugacities, temperatures (Fig. 3) and porosity, and pH decrease. So the phenocrysts are the first phases expected to be dissolved and then, replaced by dawsonite. In the alkaline rhyolites the phenocrysts occupy ~5% of their total mass and the average (Na_2O + K_2O) content is ~6.7 ± 1.7% (Milos) and ~8.4 ± 0.7 % (Antiparos). The alkaline rhyolites have intermediate diffusivity (e.g., log diffusion coefficient of -6.3) with 6.7 (Milos) and 8.3 wt. % (Antiparos) averages of (Na_2O+K_2O) that correspond to 0.073 to 0.091 CO_2 g/g of rhyolite converted to dawsonite. They also display an estimated average porosity of ~16% and a CO_2 storage ratio ~2.5% (Dasgupta, 2013) and a rock volume of ~20 Mm^3 (Milos) and ~7 Mm^3 (Antiparos) (e.g., exposure surface of ~20 Km^2 for Milos and ~7 km^2 for Antiparos and a reservoir depth of 1 km). Considering that the specific gravity of the CO_2 is ~ 120 kg/m^3 (P = 100 bars and T = 200 °C) their CO_2 storage capacity via dawsonite mineralization for Milos corresponds to ~ 48Kt of sequestered CO_2, whereas for Antiparos to ~ 29 Kt.

References

Acquafredda, P., Micheletti, F., Muntoni, I.M., Pallara, M., Tykot, R.H. 2019. Petroarchaeometric data on Antiparos Obsidian (Greece) for Provenance Study by SEM-EDS and XRF. Open Archaeology, doi.org/10.1515/opar-2019-0003.

Dasgupta, R. 2013. Ingassing, storage, and outgassing of terrestrial carbon through geologic time. Reviews in Mineralogy and Geochemistry, doi.org/10.2138/rmg.2013.75.7.

Fytikas, M., Innocenti, F., Manetti, P., Peccerillo, A., Mazzuoli, R., Villari, L. 1984. Tertiary to Quaternary evolution of volcanism in the Aegean region. Geological Society, London, Special Publications, 17, 687-699.

Hellevang, H., Declercq, J., Kvamme, B., Aagaard, P. 2010. The dissolution rates of dawsonite at pH 0.9 to 5 and temperatures of 22, 60 and 77°C. Applied Geochemistry, doi.org/10.1016/j.apgeochem.2010.08.007.

Li, M., Li, C., Xing, J. et al. An experimental study on dynamic coupling process of alkaline feldspar dissolution and secondary mineral precipitation. Acta Geochimica, 38, 872-882.

Stewart, A.L., McPhie, J. 2006. Facies architecture and Late Pliocene-Pleistocene evolution of a felsic volcanic island, Milos, Greece. Bulletin of Volcanology, doi.org/10.1007/s00445-005-0045-

16th International Congress of the Geological Society of Greece
17-19October, 2022 -Patras, Greece
Bulletin of the Geological Society of Greece, Sp. Publ. 10
Ext. Abs. GSG2022-129

The isotopic signature of wollastonites in Rhodope Massif (Greece) for CO_2 sequestration

A. Spiliopoulou[1], S. Tombros[2], S. Triantafyllidis[1], S. Kokkalas[3], D. Zhai[4], J. Papavasiliou[2].

(1) National Technical University of Athens, School of Mining and Metallurgical Engineering, Athens, Greece kspiliopoulou@mail.ntua.gr, (2) Department of Material Sciences, University of Patras, Rio, Greece, (3) Department of Geology, University of Patras, Rio, Greece, (4) State Key Laboratory of Geological Processes and Mineral Resources, China University of Geosciences, Beijing, 100083, Beijing, China.

Research highlights: Oxygen and calcium isotopes are useful tracers for quantifying wollastonite carbonation and sequestration of CO_2. Wollastonite from Xanthi can sequestrate CO_2 with an overall storage capacity of ~ 97.2 ± 0.5%.

Background and objectives

Rising demands for automotive plastics, healthcare, ceramics and metallurgical processing and constant growth forecast of ~ 9.0% makes the global wollastonite market look promising until the end of 2050 (Wollastonite Market Report, 2021). Wollastonite ($CaSiO_3$), a versatile industrial single chain silicate, is also considered as an excellent model candidate for CO_2 sequestration via mineral carbonation. In Greece the most promising wollastonite skarn deposits are exposed at Kalapoti, Panorama in Drama and Kimmeria and Kalamou in Xanthi, which belong to the Rhodope Massif (Fig. 1). Their estimated reserves are more than 1.2 Mt at ~ 50% recoverable wollastonite suitable to be used for CO_2-mineral sequestration via carbonation, with an estimated value of 20M € (Belardi *et al*., 2008).

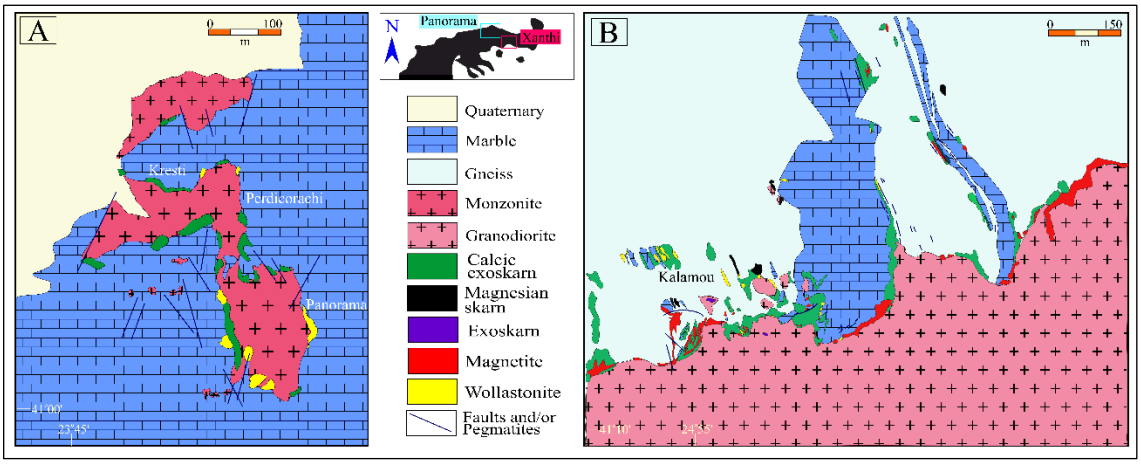

Figure 1. Simplified geological maps of: (a) Panorama, Drama and (b): Xanthi wollastonites (modified after Belardi et al., 2008 and Skarpelis and Liati, 1991).

The wollastonite ore bodies (with dimensions on cm-to-m scale) are genetically related to the Panorama monzonite and Xanthi granodiorite. They are enclosed in calcic exoskarns in both areas, and occur as coarse-grained contact-controlled bodies at the expense of impure marbles (Fig. 1a, b). The calcic skarns comprise three successive zones, i.e., a wollastonite-garnet (Wo-Grt) zone near the marble front, followed by a pyroxene-garnet (Pyx-Grt) zone, and then by a later epidote-garnet (Ep-Grt) zone distal from, and towards the aforesaid granitoids. The Wo-Grt zone consists of fibrous monomineralic wollastonite or by the assemblage wollastonite (≈ 80 and ≈ 78 vol. % for Panorama and Xanthi, respectively), andradite, diopside, subordinate plagioclase, magnetite and veinlets filled with calcite, quartz and calcite-quartz intergrowths (5-10 vol. %) (Georgiadis *et al*., 2012; Voudouris *et al*., 2013).

Sample material of 500-mg splits were obtained for oxygen and hydrogen (vs V-SMOW), silicon (vs NBS-28) and calcium (vs BSE) isotope studies from Panorama and Xanthi wollastonite intergrowth with andradite (Fig. 2a, b; Wo-Grt zone), in order to quantify their CO_2 sequestration potential for carbonation. The isotope analyses were performed at the Beijing Research Institute of Uranium Geology, Nanjing University, China and Chinese Academy of Geological Sciences (CAGS), Beijing. The AlphaDelta software was used to compute the isotopic fractionation factors and temperatures for the isotope wollastonite-andradite pairs.

Results and Discussion

Oxygen and hydrogen isotopic compositions that obtained from wollastonite from Xanthi and Panorama are $\delta^{18}O$ = 8.49 ± 0.03 (n = 9) and +5.85 ± 0.05 (n = 10), and δD = -67.7 ± 6.0 and -64.8 ± 12.5 per mil, respectively. For andradite the isotopic compositions gave $\delta^{18}O$ = 8.78 ± 0.03 (n = 3) and +6.09 ± 0.04 (n = 3), and δD = -63.0 ± 3.0 and -72.8 ± 6.5, respectively. The wollastonite-andradite isotope pair geothermometer of Zheng (1993) suggests temperatures of 555° ± 5° (for Panorama), and 533° ± 6°C (for Xanthi), much lower than the ones reported in the literature (Georgiadis *et al*., 2012). The calculated $\delta^{18}O_{H2O}$ values for wollastonite and andradite are 3.15 ± 0.13 and 5.85 ± 0.19, from Panorama and

5.81 ± 0.12, 3.21 ± 0.15 per mil from Xanthi. Furthermore, the silicon isotopic values for wollastonite and andradite are $\delta^{30}Si_{NBS28}$ = -0.41 ± -0.1 and -0.4 (Panorama), and -0.39 ± -0.1 and -0.38 (Xanthi). The calcium isotopic compositions for the same minerals are $\delta^{44}Ca_{BSE}$ = 0.83 ± 0.05 and 0.43± 0.04 (Panorama), and 0.58 ± 0.04 and 0.60 ± 0.02 (Xanthi).

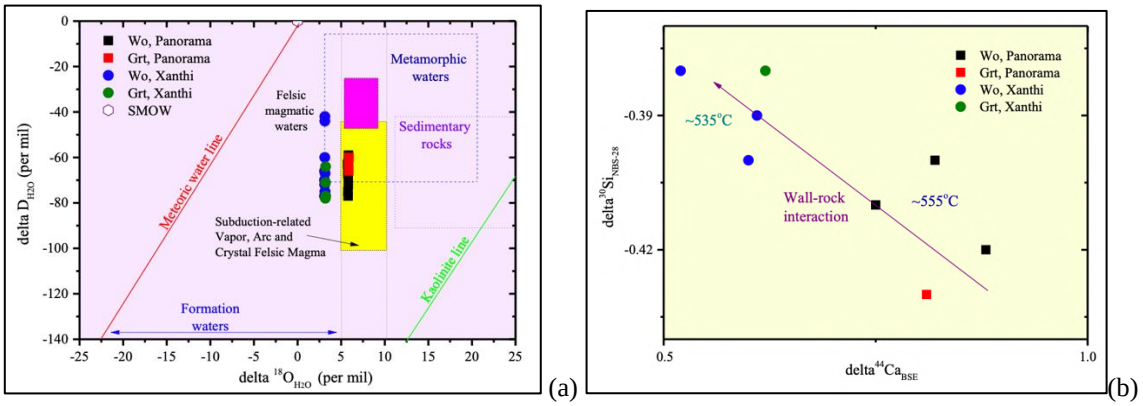

Figure 2. $\delta^{18}O_{H2O}$ vs δD_{H2O} and $\delta^{44}Ca_{BSE}$ vs $\delta^{30}Si_{NBS-28}$ isotope plots for wollastonite and andradite from Xanthi and Panorama.

From the $\delta^{18}O_{H2O}$ vs $\delta^{18}D_{H2O}$ plot (Fig. 2a) it is suggested that wollastonite from both Panorama and Xanthi is genetically related to the Panorama monzonite and Xanthi granodiorite, although for Xanthi it is evident that wall-rock interaction with the marbles modified the original magmatic signature of the skarn-forming fluids. Based on the $\delta^{44}Ca_{BSE}$ vs $\delta^{30}Si_{NBS-28}$ plot (Fig. 2b) the silicon isotopes of wollastonite (and andradite) also suggest that silicon originates from the Panorama and Xanthi granitoids. For calcium incorporated in wollastonite two different sources for the metasomatic fluids are implied (Fig. 1b), i.e., the host marbles as the main source of calcium, with minor contribution from the granitoids.

For Xanthi the fraction of calcium that remains in metasomatic fluid relative to that incorporated into wollastonite can be calculated based on $\delta^{18}O_{wollastonite}$ values using the Rayleigh fractionation equation (Eq. 1): $\delta^{18}O_{wollastonite} - \delta^{18}O_{H2O} = 1000 \cdot (\alpha\text{-}1) \cdot \ln f$, where $\delta^{18}O_{wollastonite}$ = 8.49 ± 0.03, $\delta^{18}O_{H2O}$ = 5.81 ± 0.012, where α = the isotopic fractionation factor with a value of 0.9973534 (T = 533°C) and f is the fraction of calcium remaining in solution (Zheng, 1993). For Xanthi the calculated f values are f = 0.360531 ± 0.01 (against 0.395359 ± 0.15 determined for Panorama for $\delta^{18}O_{wollastonite}$ = 5.85 ± 0.05, $\delta^{18}O_{H2O}$ = 3.15 ± 0.013, α = 0.9973383, T = 555°C). The f values are converted to product calcite, using the equilibrium: $CO_2+H_2O+CaSiO_3 = CaCO_3+H_2O+SiO_2$, and thus the CO_2 sequestration rates are calculated by the equation (Eq. 2): $[x]_{Calcite} = [\frac{(x)_{Wollastonite}}{f} - (x)_{Wollastonite}] \cdot D$, where $[x]_{Calcite}$ and $(x)_{Wollastonite}$ are the $\delta^{44}Ca_{BSE}$ values in product calcite and reactant wollastonite, and D is the partition coefficient (D ≈ 1, Pogge von Strandmann *et al.*, 2019). The obtained $\delta^{44}Ca_{BSE}$ value for calcite from Xanthi is 0.5921 (against 0.3667 for Panorama) and the predicted ratio of CO_2 sequestration for the equilibrium wollastonite to calcite is ~ 97.2% (against ~ 69.4 for Panorama).

At the exoskarn Wo-Grt zone, the Panorama wollastonite comprises higher $\delta^{18}O_{H2O}$ (~ 2.7) and $\delta^{44}Ca_{BSE}$ (~ 0.2) and lower $\delta^{18}D_{H2O}$ (~ 10) and $\delta^{30}Si_{NBS-28}$ (~ 0.02) isotopic compositions in respect to the Xanthi wollastonite (Fig 2a, b). This explicit isotopic signature of wollastonite from Panorama makes it more suitable for applications in ceramics. However, the Xanthi wollastonite bears a predicted ratio of CO_2 sequestration of ~ 97.2 ± 0.5% (against ~ 69.4 ± 0.2% for Panorama) that corresponds to a captured mass of CO_2 of 225 ± 0.9 (2σ, in tons, via calcite precipitation).

References

Belardi, G., Spaziani, E., Passeri, L., 2008. Beneficiation of wollastonite ores from Swedish, Greek and Spanish deposits. Minerals to Materials Conference - M2M 08, Bridging the Gap between Minerals and Materials, 2008, Cairo, Egypt, pp. 1-32.

Georgiadis, I., Tzamos, E., Kantiranis, N., Papadopoulou, L., Tsirambides, A., Filippidis, A., 2012. On the mineralogy of the wollastonite from Xanthi-Kimmeria (Thrace, Greece). Scientific Annals, Aristotle University of Thessaloniki, XIX CBGA Congress, Thessaloniki, Greece, Special volume 101, 17-21 (in Greek with English abstract).

Pogge von Strandmann, P., Burton, K.W., Snæbjörnsdóttir, S.O., Sigfússon, B., Árnadóttir, E.S., Gunnarsson, I., Alfredsson, H.A., Mesfin, K.G., Oelkers, E.H., Gislason, S.R. 2019. Rapid CO_2 mineralisation into calcite at the Carfax storage site quantified using calcium isotopes. Nature communications, 10, 1983, https://doi.org/10.1038/s41467-019-10003-8.

Skarpelis, N., Liati, A., 1991. Wollastonite and associated copper mineralization in the contact metamorphic aureole of Kimmeria, Xanthi, N. Greece. Bulletin of the Geological Society of Greece, 25, 369-377.

Voudouris, P., Xinou, A., Kanellopoulos, C., Kati, M., Mavrogonatos, C., Lyberopoulos, P, 2013. A new occurrence of pyrophanite from the amphibolite-hosted skarn in western Kimmeria, Xanthi, Northern Greece. Bulletin of the Geological Society of Greece 47, 487-496.

Wollastonite Market 2021. Global Industry Analysis, Size, Share, Growth, Trends, and Forecast, 2021-2031. Report, Transparency Market Research, p. 149.

Zheng, Y.F., 1993. Calculation of oxygen isotope fractionation in anhydrous silicate minerals. Geochimica et Cosmochimica Acta, 57, 1079-1091.

16th International Congress of the Geological Society of Greece
17-19October, 2022 -Patras, Greece
Bulletin of the Geological Society of Greece, Sp. Publ. 10
Ext. Abs. GSG2022-147

Mineralogical, petrographic and geochemical study of different steel slag samples used as aggregates

P. Lampropoulou[1], P. Petrounias[1], A. Rogkala[1], S. Liogris[2], P.P. Giannakopoulou[1], N. Koukouzas[3]

(1) University of Patras, Department of Geology, GR-26504, Rio Patras, Greece, p.lampropoulou@upatras.gr (2) Wasco Coatings Europe B.V, Thisvi Industrial Area, Domvrena 32010, Viotia, Greece (3) Chemical Process & Energy Resources Institute, Centre for Research &Technology Hellas, 15125 Maroussi, Greece

In this work, a qualitative/semi-quantitative determination of phases and a petrographic-geochemical study of slag samples of different origins (Greece and Qatar) were carried out. They were supplied by the Wasco Coatings Europe B.V Company and arise as by-product during the steel production process. The aim of this work is the complete textural and chemical characterization of these materials, in order to assess their properties for use as aggregates in the production of underwater concrete. The petrographic analyses combined with the geochemical one constitute a first basic study for the selection or not of these samples for further laboratory tests of their physical and mechanical properties. At the same time, in case of testing as aggregate in concrete, these results can help to explain or even forecast their behavior, preventing possible failures during their use, and also contributing to the successful design of the initial concrete mixes. For this reason, X-ray diffractometry (XRD) analyses (Table 1) and petrographic observation of thin-sections under a polarizing microscope were carried out in the laboratories of the Department of Geology, University of Patras. Phase and microstructure analyses were also carried out with scanning electron microscope (SEM), as well as geochemical analyses (XRF) at the LEMM Lab of the University of Patras.

Table 1:Results of crystalline phases (semi-quantitative evaluation) of studied samples determined by X-ray diffractometry.

Name	Chemical Formula	Sample (% phase)		
		Qf	Qc	Gr
Spinel group	(Mg, Fe, Mn,)(Cr, Al, Fe, V)O_4	21	21	35
Wustite	FeO	30	29	45
Merwinite 1	C_3MS_2	16	14	7
Beta dicalcium silicate	C_2S	5	9	11
Gehlenite 1	C_2AS	10	12	<3
Mayenite	$C_{12}A_{14}$	3	5	-
Anorthite	$CaAl_2Si_2O_8$	4	4	-
Tricalcium silicate	C_3S	<3	3	-
Quartz	SiO_2	4	<3	-
periclase	MgO	3	-	-

[1]: C: CaO, M: MgO, S: SiO_2, A:Al_2O_3

Steel slag is a by-product of steel manufacturing, and ~160 kg of slag is generated per ton of steel production (Furlani *et al.*, 2011). Although previous investigations have indicated that steel slag can be used in several applications e.g. ceramic material, cement and other construction materials (Liu *et al.*, 2015, Tzevelekou *et al*., 2020, Petrounias *et al*., 2022) a large amount of global steel slag is still stockpiled and could be utilized (Mombelli *et al*, 2019). It has been referred that coarse or fine steel slag can be used as aggregate for concrete, substituting limestone and providing satisfied mechanical properties, as well as higher density, due to the higher density of steel slag than limestone aggregate. However, the content of hazardous metals and their release to the environment consist a significant limitation to their use, especially in cases where unbounded slag-bearing materials are in contact with water. For this reason the role of chemical and phase composition in accordance with microstructure characteristics are crucial parameters for investigation before slag utilization (Mombelli *et al*, 2019).

From the results of the chemical analyses of the samples, it is shown that they consist mainly of iron, calcium, silicon oxides and less of others such as magnesium, aluminum, while the alkalis potassium and sodium vary in percentages lower than 1% by weight. The LOI in the samples ranges below ~1.2%. More specifically, the samples of Qatar origin (Qf, and Qc: fine<5mm and coarse: 5-10mm respectively) show the highest percentages in silicon oxides, as well as high in iron and calcium. Regarding the trace elements, samples derived from Qatar indicate the lowest concentrations in the chromium and the highest in the vanadium compared to the Greek sample (Gr). The Greek slag is characterized by lower concentrations of silicon and calcium than the rest but higher of iron and nickel. Similar mineral phases were detected in the studied samples, whilst differences in their amounts are presented. In general, wustite, spinels and also

alumino-calcium-silicate phases constitute their parageneses (Table 1). The highest percentages of wustite-spinel phases are shown in sample Gr reflecting the geochemical results, since it contains the lowest percentages of calcium, silica and highest iron oxides. Moreover, mineralogical analyses indicate participation of amorphous phase in their mass (up to ~20-30%).

They generally present a heterogranular texture consisted of minerals or usually polymineralic fragments. Also, their examination under the microscope proves that they are rich in opaque minerals, mainly in wustite and spinels, while microcrystalline to cryptocrystalline mainly anisotropic alumino-calcium-silicate phases, as well as silicon dioxide minerals complete the overall mineralogical composition. Frequently spinel or wustite crystals are joined by a strong direct bond forming aggregates that are expected to react positively against to the corrosion and in general to resistance due to the stable crystal structures of these phases.

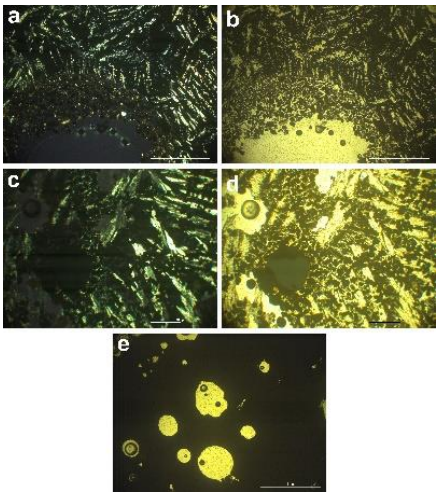

Figure 1: Representative polarizing microscope image of Qatar slag coarse sample (a,c,e cross Nicols and b,d parallel Nicols). It has a medium-grained to coarse-grained texture. Opaque minerals mainly wustite (black in color in cross and parallel Nicols), mainly iron-spinels (brown-black in color in parallel, isotropic in cross Nicols) and other anisotropic minerals with birefringence in cross Nicols of the 1st and 2nd order polarization colors are observed.

Conclusions

- Wustite, spinels as well as alumino-calcium-silicate phases participate mainly in the structure of the materials while amorphous material is contained up to 20-30%. Greek slag contains lower percentages of silicon compared to the rest of the samples.
- In the examined samples, free silicon dioxide appears in low percentages in the quartz structure and in the amorphous phase, while it is mainly associated with other elements in the structures of alumina- calcium-silicate phases, which does not favour the alkalosilicite reactions.
- The alkalis K, Na participate in very low percentages in the composition of the materials (with the lowest contents in the Greek sample).Harmful trace elements such as Cr, V, etc. participate in the spinel or wustite phases with strong bonds, so they are not expected to be easily leached.
- Further laboratory tests (such as strength, corrosion, petrography, porosity) with the participation of the tested slags in different fractions and percentages in concrete mixes are recommended to fully control their behaviour and suitability in real conditions.

Acknowledgements

The authors wish to thank the staff of the Laboratory of Electron Microscopy and Microanalysis, University of Patras for their assistance with the microanalyses and SEM observations. The Program “MEDICUS” of the University of Patras is acknowledged for financial support.

References

Furlani, E., Tonello, G., Maschio, S., 2010. Recycling of steel slag and glass cullet from energy saving lamps by fast ring production of ceramics. Waste Management 30, 1714–1719.

Liu, J., Guo, R., 2018. Applications of Steel Slag Powder and Steel Slag Aggregate in Ultra-High Performance Concrete. Hindawi, Advances in Civil Engineering Article ID 1426037, 1-8.

Tzevelekou, T., Lampropoulou, P., Giannakopoulou, P.P., Rogkala, A., Koutsovitis, P., Koukouzas, N., Petrounias, P., 2020. Valorization of Slags Produced by Smelting of Metallurgical Dusts and Lateritic Ore Fines in Manufacturing of Slag Cements. Applied. Sciences 10, 4670.

Petrounias, P., Rogkala, A., Giannakopoulou, P.P., Christogerou, A., Lampropoulou, P., Liogris, S., Koutsovitis, P., Koukouzas, N., 2022.Utilization of industrial Ferronickel slags as recycled concrete aggregates. Applied Sciences 12, 1-22.

Mombelli, D., Gruttadauria, A., Barella, S.,Mapelli, C., 2019. The Influence of Slag Tapping Method on the Efficiency of Stabilization Treatment of Electric Arc Furnace Carbon Steel Slag (EAF-C). Minerals 9, 706.

16th International Congress of the Geological Society of Greece
17-19October, 2022 -Patras, Greece
Bulletin of the Geological Society of Greece, Sp. Publ. 10
Ext. Abs. GSG2022-148

Characterization of spent refractory materials and other by-products of Greek steelmaking for use as raw materials in new refractory or other ceramic syntheses

P. Lampropoulou[1], P. Petrounias[1], K. Lolos[2], A. Chasiotis[2], Th. Tzevelekou[3], A. Rogkala[1], P.P. Giannakopoulou[1], M. Christopoulou[1]

(1) University of Patras, Department of Geology, GR-26504,Rio Patras, Greece, p.lampropoulou@upatras.gr (2) Aeiforos Metal Processing SA, Almyros, Thessaly, 37100, Greece (3) ELKEME, Hellenic Research Centre for Metals S.A., 61stkm Athens-Lamia National Road, 32011 Oinofyta, Greece

This study deals with the characterization of spent basic dolomitic refractory bricks after use in Greek steelmaking plants in view of their potential utilization in refractory and ceramic sector, employing circular economy principles. Synergy with the other typical by-products and/or wastes of steelmaking production is also examined based on their chemical and mineralogical composition, to enhance new final products properties, while realizing sustainable manufacturing practices. Dolomitic refractories are produced from natural dolomite after sintering at high temperatures (>1500ºC). The aim of this work is the investigation of the recycling of these end-of-live inorganic materials in the production of new high added value refractories or other ceramic materials in order to be utilized mainly at the steel industry, offering additional financial and environmental benefits. In the present work, geochemical (XRF), and mineralogical results (XRD) of spent refractories and chemical analysis (ICP) of carbon steelmaking by-products supplied by AEIFOROS S.A are presented, accompanied by a preliminary assessment on their potential recycling manufacturing routes.

Even though up to 28 million tons of spent refractories are generated every year, low attention has been given in the past for their recycling. Nevertheless, there is an increase of interest for their utilization the last years driven by the global environmental, energy and economic megatrends. In case of dolomitic spent refractories, they have been used unsuccessfully as road bed aggregates due to their rapid hydration, while they are used as slag former or conditioner in metallurgical processes, or soil utilizers (Horckmans *et al.*, 2019). Application of spent magnesia and dolomite refractories as slag former and conditioner to increase MgO saturation of slag and reduce the wear of refractory lining in the EAF(Electric Arc Furnace), as well as BOF (Basic Oxygen Furnace) steelmaking has been reported (Viklund-White *et al.*, 2000). Additionally, even though previous investigations have indicated that steel slag can be used in several applications e.g. ceramics, cement and other construction materials a large amount worldwide of such by-products remains unutilized (Mombelli*et al.*, 2019). Regarding the development of ceramic materials, steel dust and slag have been used in clay-based structural products especially as construction ceramic materials e.g. bricks and tiles (Shakir *et al.*, 2013, Spiliotis *et al.*, 2014). Generally, nowadays there is a mandate to maximize the recycling of products with high environmental footprint, such as spent refractories in the production of new ones or other ceramics. For this reason, there is astrong demand for refractory producers, users and recyclers to work close together on the valorization of their wastes, as well as their mixtures (Horckmans *et al.*, 2019). In this work random samples were collected from the deposits without a previous treatment in order to obtain more representative results. The typical characteristics of dolomite raw material are presented in Table 1. This analysis represents the composition of the produced dolomitic refractory too. The spent refractory is possible enriched in SiO_2, Fe_2O_3 and Al_2O_3. XRD results of four samples of spent refractories indicate similar qualitative composition but they vary in the amounts of phases. They are consisted mainly of brucite (25-48 wt%) and portlandite (22-42wt%) and less of quartz (< 21wt), calcite (<15wt%) and periclase (<13wt%). Additionally, leaching tests classified these refractories in the inert wastes (Kantiranis, 2017). According to these preliminary results the idea of reproduction new refractory from the spent ones is introduced: It is recommended that the alternative raw material of the spent refractory to be tested at lower temperatures of those applied during the commercial refractory production in industrial scale, since it is an already sintered material. Moreover, the initial mixture will contain higher amounts of fine fraction compared with the proposed in the industrial "recipe", in order to increase the binder material and the kinetic of reactions during the processing. However, the excess of iron oxides in spent refractory can contribute as flux enhancing the sintering too. Alternatively, steel dust (Table 2) without pretreatment is suggested to be added in the previous mixture of spent refractory substituting the fine fraction, and testing for new refractory or other ceramics. This waste material will be utilized as flux material due to its high iron and zinc oxides content. The results of typical chemical composition of EAF and ladle furnace steelmaking slags (Table 2) are also encouraging to commence laboratory experiments in order to be utilized in low cost geopolymer ceramic syntheses. The role of calcium in geopolymerization and the final strength of products will be investigated. In case of mill scale even though it has been used in clay ceramics tile as flux agent (Spiliotis *et al.*, 2014) it will be investigated further for improved ceramic or refractory applications.

Table 1: Typical chemical composition of dolomite refractory material.

Oxides	wt %

MgO	43.00
CaO	56.00
SiO_2	0.6
Fe_2O_3	0.5

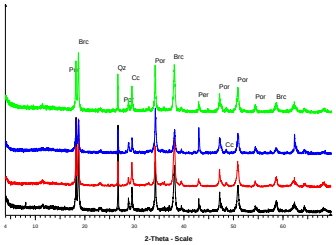

Figure 1. XRD analyses of spent refractory samples, Brc: brucite, Cc: calcite, Per: Periclase, Por: portlandite, Qz: quartz.

Table 2. Representative chemical data of steelmaking by-products

wt %	**EAF Slag**	**Ladle furnace Slag**	**EAF Dust**	**Mill scale**
Fetotal	19.46	3.21	14.91	75.30
MnO	4.57	0.61	2.13	1.54
Cr_2O_3	1.43	-	0.31	0.13
CaO	32.03	65.70	4.76	0.35
Al_2O_3	10.50	3.31	0.96	0.17
SiO_2	16.13	22.14	4.19	1.52
Na	0.09	0.03	3.54	0.03
K	-	-	2.46	-
TiO_2	0.63	0.25	0.10	-
V_2O_5	0.07	0.00	0.00	-
NiO	-	-	-	0.05
Cu_2O	-	-	0,34	0.14
ZnO	-	-	44.02	0.04
SnO	-	-	0.09	-
Sb_2O_3	-	-	0.06	-
BaO	0.23	0.04	0.07	-
MgO	7.89	4.54	2.32	-
Cl^-	-	-	5.58	-
SO_4^{2-}	-	0.02	2.75	-

Conclusions

This work introduces the idea of the utilization of spent refractories after use in steelmaking, as alternative raw materials for the production of new refractories. Moreover, it is recommended the synergy of spent refractories with other by-products of steelmaking used as raw materials for the production of new low cost ceramic-refractories for different uses, in or out of steel industry, realizing circular economy concepts in accordance with EC norms. Further investigation and experimental testing, especially on the texture characterization and physic-mechanical properties of raw materials and products, is in progress.

Acknowledgements

The authors wish to thank the staff of the labs of Section of Earth Materials, Department of Geology, University of Patras and those of AEIFOROS S.A. and ELKEME for their assistance with the petrogeochemical analyses. Furthermore, the Program “MEDICUS” of the University of Patras is acknowledged for financial support.

References

Viklund-White, C., Håkan Johansson, Risto Ponkala, 2000. Utilization of spent refractories as slag formers in steelmaking. Molten Slags 2000, https://pyrometallurgy.co.za/MoltenSlags2000/pdfs/212.pdf.

Horckmans, L., Nielsena, P., Dierckxa, Ph., Ducastelc, A., 2019. Recycling of refractory bricks used in basic steelmaking: A review. Resources, Conservation & Recycling 140, 297-304.

Mombelli, D., Gruttadauria, A., Barella, S., Mapelli, C., 2019. The Influence of Slag Tapping Method on the Efficiency of Stabilization Treatment of Electric Arc Furnace Carbon Steel Slag (EAF-C). Minerals 9, 706.

Shakir, A.A., Naganathan, S., Nasharuddin K., Mustapha, B., 2013. Development of Bricks from waste material: A Review Paper. Australian Journal of Basic and Applied Sciences 7(8), 812-818.

Spiliotis, X., Ntampegliotis, K., Kasiteropoulou, D., Lamprakopoulos, S., Lolos, K., Karayannis V., Papapolymerou, G., 2014. Valorization of Mill Scale Waste by its Incorporation in Fired Clay Bricks. Key Engineering Materials 608, 8-13.

Kantiranis, N., 2017. Report and certificate of analysis. Aristotle University of Thessaloniki, Faculty of sciences, 1-7 (unpublished).

16th International Congress of the Geological Society of Greece
17-19 October, 2022 - Patras, Greece
Bulletin of the Geological Society of Greece, Sp. Publ. 10
Ext. Abs. GSG2022-171

MINERALOGICAL STUDY AND SPATIAL DISTRIBUTION OF MAGNETIC PARTICLES IN SOILS OF SARIGIOL BASIN, KOZANI (GREECE)

C. Chrysakopoulou[1], D. Vogiatzis[1], A. Drakoulis[1], N. Kantiranis[1]
(1) Department of Geology, Aristotle University of Thessaloniki, 54124 Thessaloniki, Greece, chrysakop@geo.auth.gr

Research highlights

Accumulation of magnetic particles at different locations in Sarigiol basin with potential significant contribution of ophiolite complexes.

Background

The source of soil formation is mainly the inorganic material of the bedrock with silicate minerals dominating at 45-80%, while iron, magnesium and aluminum oxides account for 1% (Kabata-Pendias, 2011). Over the last decades the growth of industrialization has caused an adverse redistribution of metals in the environment and therefore in the soils. In Greece and especially to Kozani region the main potential environmental pollutants are produced from the steam generated electric power stations. Magnetic soil particles could be potential tracers of environmental pollution. Magnetic particles in fly ash from fossil fuel combustion at high temperatures are probably the most common source of anthropogenic particles in the upper soil horizons (Kapicka *et al*., 2001). In soils that have not undergone any kind of anthropogenic activity, the presence of natural magnetite is due to the presence of ultramafic rocks such us ophiolite complexes. The aim of this study is the separation and the mineralogical study of magnetic particles from soils and sediments of Sarigiol basin in the region of Kozani (northwestern Greece) and the mapping of their spatial distribution.

Objectives and Methods

The sampling was carried out in Sarigiol basin from 59 different locations. In total, 47 samples of surface sediment (0-10 cm) and 12 samples of soil from the weathering mantle above the bedrock, were collected. For the separation of the magnetic fraction, 20 g of representative material (<2 mm) disaggregated slightly in an agate mortar by hand. Then, this material was mixed with 250 mL of deionized water, 10mL of dispersing agent [$(NaPO_3)_6$, 50g/L] and they were placed with a magnet in a beaker in order to extract the strongly magnetic particles, using a magnetic stirrer at low speed and without heat in order to achieve particle dispersion. The separation repeated three times, after a period of 5, 2, and 1 min (Grimley *et al*., 2021). Magnetic particles extracted from each sample were dried at 110 ºC to constant weight and then weighed and placed in plastic vials for mineralogical study. The mineralogical composition of the magnetic fraction was determined using the X-ray diffractometry (XRD) method in a randomly oriented powder sample, which was pulverized by hand in an agate mortar. The ICDD (International Center of Diffraction Data) diffraction files were used as a database for the identification of the mineralogical phases. For the mapping of the distribution of the magnetic fraction, Surfer was used to create a grid with the spatial interpolation kriging method (for sediment samples) and later, in order to create the map, it was imported into QGIS 3.16.15. The extracted maps were presented through a scaled color gradation of filled contours (for sediment samples) and through colored circles with increased diameters (for soil samples) based on the ranges of the magnetic fraction of each sample.

Results and discussion

Based on the results of the magnetic fraction mineralogical analysis, the major mineral phase of the studied samples is magnetite (42-59 wt.%), while serpentine (probably lizardite), is found in significant amounts. Clay minerals, calcite, quartz, olivine and pyroxene are also present at minor amounts. Magnetite has dual origin as its possible sources are the ophiolite complexes at the NE and SW part of the area but also the fly ash of the two power stations located in the area, Agios Dimitrios plant at the E part and Kardia plant at the NW part of the research area. Serpentine and olivine have lithogenic origin, as they are components of the surrounding ultrabasic rocks. Quartz, pyroxene, calcite and clay minerals are possibly components of the lithological formations of the research area, particularly enriched with these specific minerals, however they also contained in the fly ash of Agios Dimitrios and Kardia plants as components of the burning lignite transferred to fly ash due to incomplete combustion of lignite in some parts of the burning unit (Filippidis *et al*., 1996).

From the separation of the magnetic particles in the studied samples, it is emerged that the magnetic fraction for soil samples shows an average value of 3.36 wt.%, while for sediment samples is 0.67 wt.%. The high amount of magnetic fraction of soil samples attributed to the presence of magnetic minerals in the parent rocks from which the overlying soils are derived (Fig.1). On the other hand, the distribution of the magnetic fraction of the sediment samples showed highest values at the NE and SW part of the research area (Fig. 2). Ophiolite rocks in the NE and SW part of the research area seems to be the main source for the highest values of the magnetic fraction, however the contribution of the two power

plants, through the dispersion of the fly ash, cannot be excluded. According to Kassoli-Fournaraki *et al*. (1992) opaque minerals like hematite, spinels and pyrite contained in the lignite of the Ptolemais basin and transferred to the produced fly ash after burning at the Power Plants of the area.

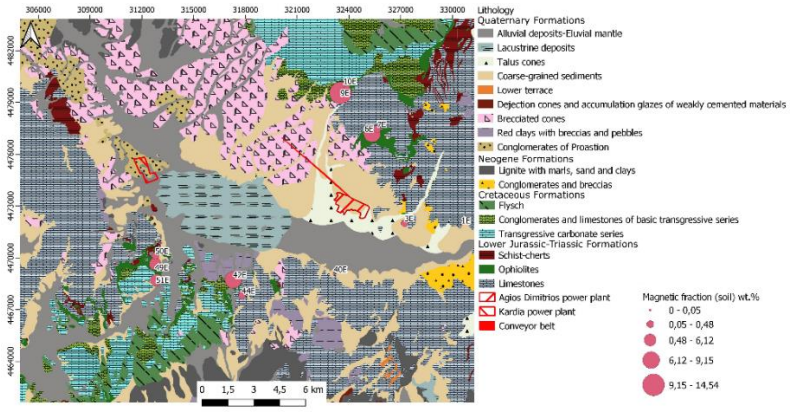

Figure 1. Distribution of magnetic fraction of surface soil samples in the study area.

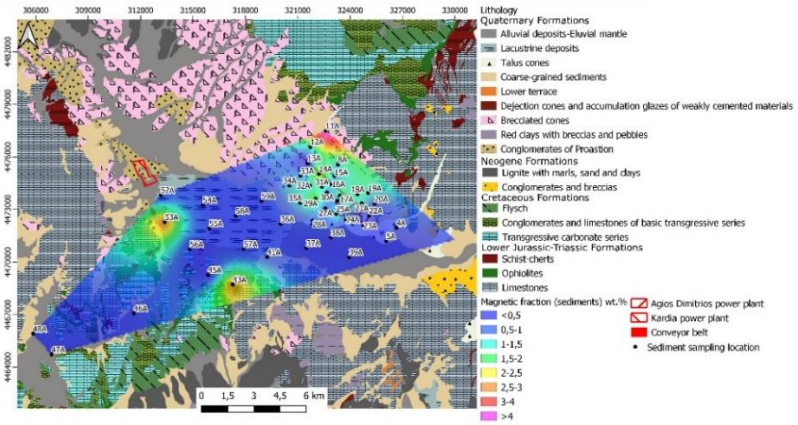

Figure 2. Distribution of magnetic fraction of sediment samples of the study area.

Conclusions

Soil (12 samples) and sediment (47) samples from the Sarigiol basin from 59 different locations were collected in order to study their magnetic particles and spatial distribution. The magnetic fraction for soil samples shows an average value of 3.36 wt.%, while for sediment samples is 0.67 wt.%. The high amount of magnetic fraction of soil samples attributed to the presence of magnetic minerals in the parent rocks from which the overlying soils are derived. The distribution of the magnetic fraction of the sediment samples showed highest values at the NE and SW part of the Sarigiol basin. Ophiolite rocks in the NE and SW part of the research area seems to be the main source for the highest values of the magnetic fraction, however the contribution of the Kardia and Agios Dimitrios power plants, through the dispersion of the fly ash, cannot be excluded. Further research, concerning the mineralogical, morphological and chemical characteristics of the studied magnetic particles, will clarify the sources of these materials and the extent of anthropogenic pollution.

Acknowledgements

Mrs Chrysakopoulou would like to express her gratitude and sincere acknowledgements to Hellenic Petroleum S.A as with the fellowship they provided her they supported significantly and contributed decisively to the completion of her MSc Thesis.

References

Filippidis, A., Georgakopoulos, A., Kassoli-Fournaraki, A., 1996. Mineralogical components of some thermally decomposed lignite and lignite ash from the Ptolemais basin, Greece. International Journal of Coal Geology, 30, 303-314.

Grimley, D.A, Lynn, A.S, Brown, C.W., Blair, N.E., 2021. Magnetic Fly Ash as a Chronological Marker in Post-Settlement Alluvial and Lacustrine Sediment: Examples from North Carolina and Illinois. Minerals 11, 2-20.

Kabata-Pendias, A, 2011. Trace Elements in Soils and Plants, 4th ed. Taylor and Francis Group, LLC, U.S.A.

Kapicka, A., Jordanova, N., Petrovsky, E., Ustjak, S., 2001. Effect of different soil conditions on magnetic parameters of power-plant fly ashes. Journal of Applied Geophysics 48, 291-297.

Kassoli-Fournaraki, A., Georgakopoulos A., Filippidis A., 1992. Heating experiments of the Ptolemais lignite in the temperature range from 100 °C to 500 °C. Neues Jahrbuch fur Mineralogie Monatshefte, 11, 487-493.

16th International Congress of the Geological Society of Greece
17-19 October, 2022 - Patras, Greece
Bulletin of the Geological Society of Greece, Sp. Publ. 10
Ext. Abs. GSG2022-192

Improving performance of Mg-Fe-smectite-rich clay water suspensions by inorganic additives

D. Papadimitriou[1,2], C. Mytiglaki[1], D. Vogiatzis[1], E. Typa[2], N. Kantiranis[1]
(1) Aristotle University, Thessaloniki, Greece, psdimitrio@geo.auth.gr. (2) GEOHELLAS S.A., Knidi Grevena, Greece

Introduction

Clay minerals of the smectite group have a wide range of industrial applications due to their unique properties (Odom, 1984). The high viscosity, swelling capacity, and low filtration loss account for the commercial use of smectite clays as additives in drilling fluids according to international specifications (API SPEC 13A, 2019). The performance improvement of the bentonite water suspensions is achieved by chemical and physical activation.

The aim of this research is to investigate the performance improvement of Mg-Fe-smectite water suspensions using inorganic additives such as sodium carbonate (SC) and a dispersant such as sodium acid pyrophosphate (SAPP). Traditionally, the activation of a bentonite is carried out by applying sodium carbonate at a ratio of 2-4% w/w on mined bentonite (Karaguzel et al., 2010). The use of thinners, such as SAPP, is required to reduce the viscosity of the fluids to modify rheology, helping drilling fluids circulation (Sikorski, 1983).

Materials and methods

A sample rich in smectite (PI35) from the Ventzia basin, Grevena, Greece, was used in the present study. Mineralogical analysis was carried out by X-ray diffraction (XRD, Philips PW1710 with CuKa Ni-filtered radiation, 3-63° 2theta at step size 0.02°/sec, and scan speed 1.2°/min) on a random oriented sample using the method of external standard mixtures for the quantitative analysis. Clay mineralogy was performed on oriented, glycolated and heated at 550℃ samples. In addition, an activated Mg-Fe-smectite sample with 5% w/w SC was also studied by X-ray diffraction. Chemical analysis was done by ICP-ES analysis on $LiBO_2/LiB_4O_7$ fused disks of the studied samples in Bureau Veritas laboratories, Canada.

Laboratory experiments was initiated by the activation process. SC was applied to the studied sample with its natural moisture content (41% w/w) for its activation at ratios sample:SC of 1%, 2%, 3%, 4%, 5%, 6%, 7%, 8%, 10%, 12%, 14%, 16% w/w. The samples were left for aging for a period of 30 days (Karaguzel et al., 2010) and afterwards were subjected to extrusion, drying at 60℃ and grinding <120μm. However, a sample of raw material without activation and extrusion, as well as a sample with extrusion only was also prepared for comparison.

Suspensions of the smectite-rich clay were prepared according to API 13A (2019) specifications. More specific, 22.5 g of bentonite are added to 350 ml deionized water and stirred (Fann multimixer model 9B) for twenty minutes. After aging at least 16 hours the suspensions were stirred for five minutes and their viscosity was measured (Fann 35SA rotary coaxial viscometer). After stirring for 1 minute, the filtration test was performed with a Fann filter press in a period of 30 minutes. The parameters of the test were: PV=Θ600-Θ300, YP= Θ300-PV, where Θ600 and Θ300 are the dial reading at 600 and 300rpm, respectively. The filtrate volume is V= 2*Vc, where Vc is the filtrate loss volume between 7.5 and 30 minutes of the experiment duration. Accordingly, water suspensions of the smectite-rich clay were prepared with activated samples of 3%, 4%, 5%, 6%, 7%, 8%, 10% SC, as above with the addition of 0.17g of SAPP.

Results and discussion

Mineralogical analysis showed a smectite-rich clay (76 wt% smectite), and minor amounts of palygorskite 7 wt%, serpentine 8 wt%, and quartz 9 wt%. Traces (<1 wt%) of plagioclase, pyroxene, and amphibole were also identified. The main reflection of natural smectite sample was determined at 2theta 5.81° and d=15.29Å, while for palygorskite at 2theta 8.38° and d=10.62Å. Activated smectite show a main reflection at 2theta 6.61° and d=13.37Å, while palygorskite at 2theta 8.45° and d=10.46Å. For glycolated samples, the main reflection shifts at about d=17.46Å for untreated smectite, and at d=17.20Å for treated with SC smectite, while palygorskite show reflections at d=10.78Å and at d=10.50Å, respectively. Furthermore, after heating, smectite collapse to about 10Å, while palygorskite structure destroyed.

According to the chemical analysis, the main clay mineral of the studied sample corresponds to an magnesium-iron-rich smectite, which is characteristic phase for the clays of the Ventzia continental basin. The studied sample mainly contains SiO_2 56.99, TiO 0.58, Al_2O_3 11.56, Fe_2O_{3t} 12.40, MnO 0.10, MgO 6.51, CaO 0.73, K_2O 0.66, Na_2O 0.24, P_2O_5 and LOI 9.30 wt%.

The results of the Mg-Fe-smectite-rich clay suspensions are presented in Table 1. The activated samples increased their performance as showed by direct viscometer measurements reaching a maximum when sodium carbonate participated at a ratio 5% w/w. Dial reading at 600rpm decreased by further increase in sodium carbonate amount. The requirement of international specifications for a dial reading of the instrument >30 at 600rpm is achieved after Mg-Fe-smectite-rich clay activation using 2% sodium carbonate. The YP/PV ratio does not meet specifications when the instrument dial reading at 600rpm is >30. The optimum value of the YP/PV ratio is obtained with the participation of 3% sodium carbonate.

Filtration loss showed a noticeable improvement when sodium carbonate participates in a percentage of 3-10%.

Table 1. Performance of Mg-Fe-smectite-rich clay suspensions in distilled water before and after the addition of Na_2CO_3.

Sample	Na_2CO_3 %	600rpm	300rpm	PV (cP)	YP ($lb/100ft^2$)	YP/PV	pH	V7.5 (ml)	Vc (ml)	V (ml)
PI35A0	0%	4	3	1	2	2.0	8.19	30.6	40.0	80.0
PI35A0extr	0%	5	3	2	1	0.5	8.15	29.0	31.0	62.0
PI35A1	1%	25	21	4	17	4.3	9.64	13.3	15.8	31.6
PI35A2	2%	41	39	2	37	18.5	9.64	9.9	10.6	21.2
PI35A3	3%	76	68	8	60	7.5	10.02	8.2	8.9	17.8
PI35A4	4%	111	110	1	109	109.0	10.01	7.8	8.0	16.0
PI35A5	5%	127	121	6	115	19.2	10.10	7.8	8.2	16.4
PI35A6	6%	113	112	1	111	111.0	10.12	8.0	8.4	16.8
PI35A7	7%	107	100	7	93	13.3	10.15	8.2	8.4	16.8
PI35A8	8%	112	111	1	110	110.0	10.28	7.7	8.0	16.0
PI35A10	10%	100	97	3	94	31.3	10.32	8.0	8.2	16.4
PI35A12	12%	87	86	1	85	85.0	10.26	8.5	8.8	17.6
PI35A14	14%	67	66	1	65	65.0	10.36	8.5	9.0	18.0
PI35A16	16%	46	43	3	40	13.3	10.43	10.8	11.2	22.4

The rheological behavior of Mg-Fe-smectite-rich clay suspensions was modified by the addition of sodium acid pyrophosphate (Du et al., 2020). Dial reading at 600rpm was significantly reduced. The plastic viscosity altered, and the yield point decreased significantly. As a result, the plastic viscosity to yield point ratio was reduced to <6 according to OCMA grade bentonite. Filtration loss was excessively reduced (<15ml) with a minimum value of 12.8 ml and a maximum value of 14.0 ml (Table 2). Activated Mg-Fe-smectite-rich clay suspensions with a sodium carbonate content of 5-8% meet the requirements of international standards according to OCMA grade bentonite (API 13A, 2019).

Table 2. Performance of Mg-Fe-smectite-rich clay-**Na_2CO_3 suspensions in distilled water after the addition of 0.17g SAPP.**

Sample	Na_2CO_3 %	600rpm	300rpm	PV (cP)	YP ($lb/100ft^2$)	YP/PV	pH	V7.5 (ml)	Vc (ml)	V (ml)
PI35A3	3%	23	19	4	15	3.8	9.86	6.2	7.0	14.0
PI35A4	4%	25	21	4	17	4.3	10.17	6.6	6.7	13.4
PI35A5	5%	36	30	6	24	4.0	10.13	6.4	6.4	12.8
PI35A6	6%	32	27	5	22	4.4	10.20	6.4	7.0	14.0
PI35A7	7%	31	26	5	21	4.2	10.21	6.2	6.7	13.4
PI35A8	8%	30	25	5	20	4.0	10.32	6.6	6.8	13.6
PI35A10	10%	23	20	3	17	5.7	10.19	7.1	7.0	14.0

Conclusions

The performance of Mg-Fe-smectite-rich clay water suspensions was significantly improved after the activation and extrusion process. The produced fluids exhibited unusually high viscosity. YP/PV ratio was recorded to be >6 and filtration loss were measured >15ml in all suspensions. However, in some suspensions the filtration loss was reduced to near the 16ml limit, according to OCMA grade bentonite specifications. The use of sodium acidic pyrophosphate affects the performance of the suspensions, which comply with the requirements of the standard specifications. In particular, the effect of sodium acid pyrophosphate decreased the viscosity, altered the plastic viscosity, decreased the yield point as a characteristic rheology modifier as reported in the international literature. Additionally, filtrate loss of the produced fluids was drastically reduced. The significant reduction in filtrate loss using sodium acid pyrophosphate, paves the way for extensive study of the Ventzia Basin clays for use in drilling fluids. It is noteworthy that sodium acid pyrophosphate is not mentioned as a fluid loss reducer in the international literature.

Acknowledgements

Mr Papadimitriou would like to thank Geohellas S.A. for the continuous supporting of his investigation on the field of drilling fluids and Ms E. Typa for her help in the Geohellas S.A. laboratory.

References

API SPEC 13A, 2019. Specifications for drilling fluids materials. American Petroleum Institute.

Du, M., Liu, P., Clode, P. L., Liu, J., Haq, B., Leong YK., 2020. Impact of additives with opposing effects on the rheological properties of bentonite drilling mud: Flow, ageing, microstructure and preparation method. Journal of Petroleum Science and Engineering, 192, 107282.

Karaguzel, C., Cetinel, T., Boylu., Cinku, K., Celik, M. S., 2010. Activation of (Na, Ca)-bentonites with soda and MgO and their utilization as drilling mud. Applied Clay Science, 48, 398-404.

Odom, I. E., 1984. Smectite clay minerals: Properties and uses. Philosophical Transactions of the Royal Society A, Mathematical, Physical and Engineering Sciences, 311(1517), 391-409.

Sikorski, C. F. and Weintritt, D.J. 1983. Polyphosphate drilling – mud thinners deserve second look. Oil & Gas Journal 81(27),71-78.

16th International Congress of the Geological Society of Greece
17-19 October, 2022 - Patras, Greece
Bulletin of the Geological Society of Greece, Sp. Publ. 10
Ext. Abs. GSG2022-195

Effect of sodium polyphosphates on rheological behavior and filtration properties of Mg-Fe-smectite-rich clay slurries

D. Papadimitriou[1,2], C. Mytiglaki[1], D. Vogiatzis[1], E. Typa[2], N. Kantiranis[1]
(1) Aristotle University, Thessaloniki, Greece, psdimitrio@geo.auth.gr (2) GEOHELLAS S.A., Knidi Grevena, Greece

Introduction

Sodium polyphosphates like sodium acid pyrophosphate (SAPP), sodium tripolyphosphate (STPP), sodium hexametaphosphate (SHMP) and tetrasodium pyrophosphate (TSPP) are used traditionally as rheology modifiers to improve rotary drilling fluids performance (Sikorski and Weintritt, 1983). They represent a group of drilling mud thinners that are cost effective and suitable for use in various types of freshwater muds at temperatures up to 82 °C. Polyphosphate salts reduce viscosity and prevent flocculation and cement contamination of drilling muds. The temperature limitation is the main disadvantage of these additives.

In the present study, the effect of polyphosphate salts on the rheological behavior of water-smectite suspensions was investigated. The main purpose of this research was to produce activate bentonite powder suitable for use in drilling fluids, by applying inorganic thinners and sodium carbonate on raw smectite samples. The international literature suggests the use of sodium carbonate as an activator of clays but there are no extensive reports on the use of sodium polyphosphate salts on raw bentonite samples.

Materials and methods

Two clay samples rich in smectite minerals were collected from the Ventzia sedimentary continental basin. The mineral composition was identified by X-ray diffraction (XRD, Philips PW1710 with CuKa Ni-filtered radiation, 3-63° 2theta at step size 0.02°/sec, and scan speed 1.2°/min) on random oriented samples using the method of external standard mixtures, while clay mineralogy was performed on oriented, glycolated and heated at 550 ℃ samples. Chemical analysis was done by ICP-ES analysis on $LiBO_2/LiB_4O_7$ fused disks of the studied samples in Bureau Veritas laboratories, Canada.

Samples SL38 and P15 were treated with a percentage of 4 and 5% w/w sodium carbonate to activate. After that smectite-rich samples left for aging for one month (Papadimitriou, 2020; Karaguzel *et al*., 2010). Sodium salts were applied in various percentages on activated smectite, and the half amounts of these mixtures was extruded. Extruded and non-extruded activated and treated by sodium carbonate and sodium polyphosphates smectite-rich materials were dried at 60°C and grinding at <120 μm.

The rheological and filtration behavior of the produced smectite suspensions were determined according to American Petroleum Institute specifications (API 13A, 2019). The slurries were prepared by the Fann multimixer model 9B and the measurements were obtained by a rotary viscometer (Fann 35SA), while filtration tests were caried out by a Fann filter press applying pressure of 100 psi.

Results and discussion

The mineralogical composition of the Ventzia basin smectites indicated smectite-rich clays (79 wt% smectite) with minor amounts of palygorskite (8 wt%), serpentine (6 wt%) and quartz (7 wt%), and traces (<1 wt%) of amphibole and plagioclase. Untreated smectite and palygorskite was identified at d-values 15.77Å and 10.50 Å, respectively. Characteristic d value reflection was obtained from activated materials in a range of d=12.88Å and 13.37Å from smectite and 10.67Å and 10.70Å for palygorskite. Representative chemical analysis of the untreated smectite-rich clays showed that they are rich in iron and magnesium (Table 1).

Table 1. Chemical analysis (wt.%) of the studied smectite-rich clays.

Sample	SiO_2	TiO_2	Al_2O_3	Fe_2O_{3t}	MnO	MgO	CaO	K_2O	Na_2O	P_2O_5	L.O.I. (1050 °C/2h)	Total
P15	55.84	0.58	11.55	12.34	0.08	6.49	0.67	0.63	0.23	0.01	9.30	97.72
SL38	56.23	0.55	10.82	11.66	0.13	6.81	1.46	0.75	2.21	0.02	8.40	99.04

The rheological and filtration characteristics of P15 sample are shown in Table 2. The presence of sodium polyphosphates on smectite suspensions decrease dial reading at 600rpm, reduce yield point to plastic viscosity ratio and reduce filtrate volume. The extruded SL38 sample presents excellent rheological and filtration behavior, that is conforming to OCMA grade bentonite specifications (API 13A, 2019), which are: Dial reading at 600rpm >30, YP/PV <6, filtration volume <16 ml. The results are listed in the Table 3.

Table 2. P15 activated smectite-rich clay (5% sodium carbonate) + 0.75% thinners.

Sample	Non extruded smectite-rich clay				Extruded smectite-rich clay			
	600rpm	YP/PV	V (ml)	pH	600rpm	YP/PV	V (ml)	pH
P15A5	102	23.5	17.6	9.9	124	39.3	17.0	10.2
P15A5 (TSPP)	46	13.3	15.6	10.1	36	10.0	16.4	10.1
P15A5 (SAPP)	39	11.0	14.6	10.0	49	6.2	15.0	10.1
P15A5 (SHMP)	41	18.5	15.2	10.1	40	11.3	16.8	10.2
P15A5 (STPP)	37	16.5	16.0	10.1	33	9.0	16.4	10.1

Table 3. SL38 activated smectite-rich clay (4% sodium carbonate) + 0.5% thinners.

Sample	Non extruded smectite-rich clay				Extruded smectite-rich clay			
	600rpm	YP/PV	V (ml)	pH	600rpm	YP/PV	V (ml)	pH
SL38	41	18.5	17.6	10.2	72	16.0	17.2	10.2
SL38 (TSPP)	23	5.7	15.8	10.3	33	3.5	15.8	10.3
SL38 (SAPP)	21	3.3	15.4	10.0	39	4.5	15.6	10.3
SL38 (SHMP)	22	5.3	15.2	10.2	32	4.4	15.0	10.2
SL38 (STPP)	25	6.3	16.8	10.3	37	5.4	15.6	10.3

Various amounts of sodium acid pyrophosphate and sodium hexametaphosphate were used for producing slurries of non-extruded SL38 material (Table 3). Fluid loss, dial reading at 600 rpm and YP to PV ratio were changed significantly. Rheological behavior was improved, and filtration loss was reduced in a range from 16.4 ml to 17.4 ml. In addition, the treatment of smectite-rich clay by partially hydrolyzed polyacrylamide (PHPA) and sodium acid pyrophosphate gave a product suitable for drilling muds, according to API 13A (2019) specifications.

Table 3. SL38 non extruded activated smectite-rich clays (4% sodium carbonate) + thinners

		SAPP				SHMP			
Sample	Thinner %	600rpm	YP/PV	V (ml)	pH	600rpm	YP/PV	V (ml)	pH
SL38	0.00%	41	18.5	17.6	10.2	42	8.5	19.6	9.7
SL38	0.25%	24	2.8	17.4	10.2	33	9.0	16.8	10.1
SL38	0.50%	21	3.3	16.0	10.3	28	3.6	16.4	10.1
SL38	0.75%	16	1.2	16.0	10.2	25	3.0	14.4	10.0
SL38	1.00%	15	1.0	15.4	10.3	24	2.8	15.0	10.0

The better results were obtained from an activated P15 sample prepared by addition of 3% w/w sodium carbonate and 0.65% w/w sodium hexametaphosphate, which are listed below: 600rpm: 40, 300rpm: 32, PV: 8 cP, YP: 24 lb/100ft^2, and V: 12.4 ml.

Conclusions

Numerous experiments with Mg-Fe-smectite-rich clays were conducted in the presence study. The results showed that rheological behavior was improved, whereas filtration loss significantly decreased by the addition of sodium polyphosphate salts. Suspensions of the studied Mg-Fe-smectite-rich clay produced with the addition of sodium salts conformed to the international standards. Also, treated Mg-Fe-smectite-rich clay with PHPA and SAPP salts can produce slurries with properties that are in accordance with American Petroleum Institute specifications.

References

API SPEC 13A, 2019. Specifications for drilling fluids materials. American Petroleum institute.

Du, M., Liu, P., Clode, P. L., Liu, J., Haq, B., Leong YK., 2020. Impact of additives with opposing effects on the rheological properties of bentonite drilling mud: Flow, ageing, microstructure and preparation method. Journal of Petroleum Science and Engineering, 192, 107282.

Karaguzel, C., Cetinel, T., Boylu., Cinku, K., Celik, M. S., 2010. Activation of (Na, Ca)-bentonites with soda and MgO and their utilization as drilling mud. Applied Clay Science, 48, 398-404.

Papadimitriou, D. S., 2020. Rheological properties of suspensions of activated palygorskite and Mg-Fe-smectite from Grevena using polymers. MSc Thesis, Aristotle University, Thessaloniki, 149 p.

Sikorski, C. F. and Weintritt, D.J. 1983. Polyphosphate drilling – mud thinners deserve second look. Oil & Gas Journal 81(27),71-78.

16th International Congress of the Geological Society of Greece

17-19 October, 2022 - Patras, Greece

Bulletin of the Geological Society of Greece, Sp. Publ. 10

Ext. Abs. GSG2022-233

Strength Development of Lime Pastes with the Addition of Natural Pozzolanas from the Islands of Milos, Yali and Kimolos

G. Triantafyllou, G. Kourtaki, G. Christidis, M. Galetakis

Technical University of Crete, School Of Mineral Resources Engineering, Chania, Greece, gtriant@mred.tuc.gr

This study investigates key parameters which determine the development of strength in lime-pozzolana pastes. The percentage and the reactivity of amorphous matter, the bulk mineralogy and texture of the samples and the grain size distribution of the materials, are the most significant parameters that affect the mechanical behaviour of the pastes. Pozzolanas are materials, used in numerous applications in the construction industry (Qiang *et al.*, 2017). The pozzolanic activity of a material, expressed by its ability to combine with calcium hydroxide $Ca(OH)_2$ and form compounds with hydraulic properties, is strongly related with factors associated with its chemical and mineralogical composition and its physical characteristics (Walker *et al.*, 2011). Main objective of this study was to monitor the mechanical behaviour of lime mixtures with the addition of Pozzolanas, without addition of inert materials or other additives. The three Natural Pozzolanas used in this paper are commercially available volcanic cementitious materials, namely an unwedded ignimbrite from Kimolos Island, a pumice stone from Yali Island and a pyroclastic breccia from Milos Island, locations which belong to the Volcanic Arc of the South Aegean. X-ray powder diffraction (XRD), X-ray fluorescence (XRF), laser scattering particle size distribution analyses and uniaxial compressive strength tests of the pastes, were used to characterize samples. Furthermore, the pozzolanic activity of the samples was monitored with a set of physicochemical experiments including, the Chapelle test that measures the reduction of $Ca(OH)_2$ by combination of the reactive siliceous and aluminosilicate content present in Pozzolanas and the change in conductivity of pozzolan/calcium hydroxide saturated solution mixtures, which is a method that imprints the rate of the pozzolanic reaction. The received samples, were homogenized by the cone and quarter method and a representative quantity was crushed using a jaw crusher for primary and a cone crusher for secondary crushing. Then, they were ground for two hours in a laboratory rod mill and sieved through a No. 170 sieve (90 μm opening). The Kimolos Pozzolana with a median particle size (d_{50}) of approximately 1.36 μm was observed to have the finest particle size distribution among the materials tested (Fig. 1a). Furthermore, in order to achieve optimal homogenization of the Lime-Pozzolana mixtures before adding the appropriate water quantity for the preparation of each set of pastes, the pozzolanic materials were co-ground with a commercial calcium quicklime binder (CL90-EN 459-1:2010) in a 1:1 ratio, with the aid of a micro-Deval apparatus (Fig. 1b). Three hollow drums accompanied with steel balls, were filed with both ingredients and left to rotate at a speed of 100 rpm, for three hours. The produced pastes were casted in cubic molds of 5x5x5 cm, stored in standard conditions (RH = 90%, T = 25 °C) and evaluated for their strength development and their mineralogy, via compressive strength tests and XRD analyses, up to 120 days of curing. The chemical composition of the raw samples determined by XRF showed, that the sum of the three main oxides which comprise the reactive chemical composition of Pozzolanas (SiO_2, Al_2O_3 and Fe_2O_3), were 71.48%, 82.31% and 83.46% wt. for the Milos, Yali and Kimolos samples, respectively. The pozzolanic materials used are calc-alkaline and range in composition form rhyolitic/dacitic (Kimolos & Yali) to andesitic (Milos). The percentages of amorphous material (ranging from 68.74 for the Milos sample to 93.36% by weight in the Kimolos pozzolana), are strongly related to the activity presented by these samples (Christidis *et al.*, 2021), in the results of the physicochemical methods of analyses (Table 1 & Fig. 2).

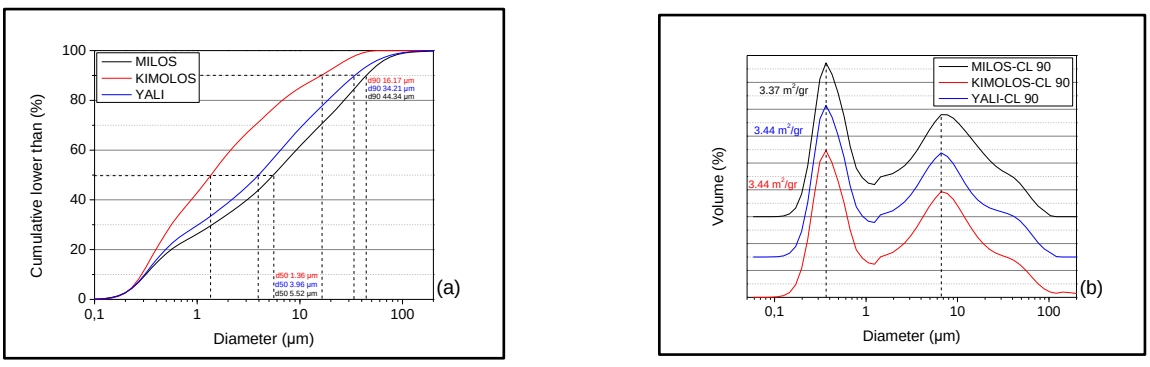

Figure 1 (a & b). Particle size distribution of Pozzolanas after the procedure of individual grinding (a) and the resulted granulometry of the Lime-Pozzolana mixtures (b), after co-grinding them with the aid of a micro-Deval apparatus.

Table 1. Chapelle test results.

Sample	d50 (μm)	mg $Ca(OH)_2$ /g pozz.
MILOS	5.52	528
KIMOLOS	1.36	1531
YALI	3.96	1519

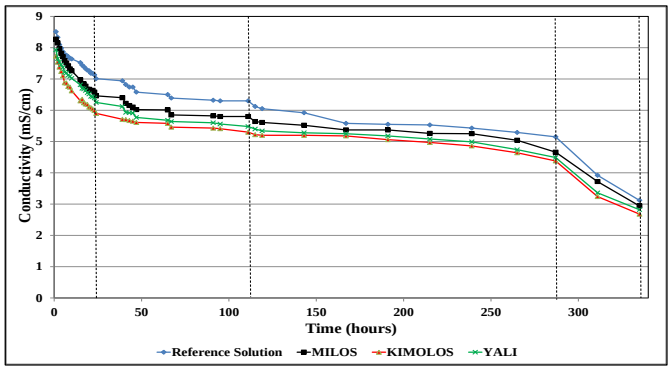

Figure 2. Pozzolanic activity index of the studied samples, expressed as changes in the values of conductivity of saturated lime-pozzolan solutions.

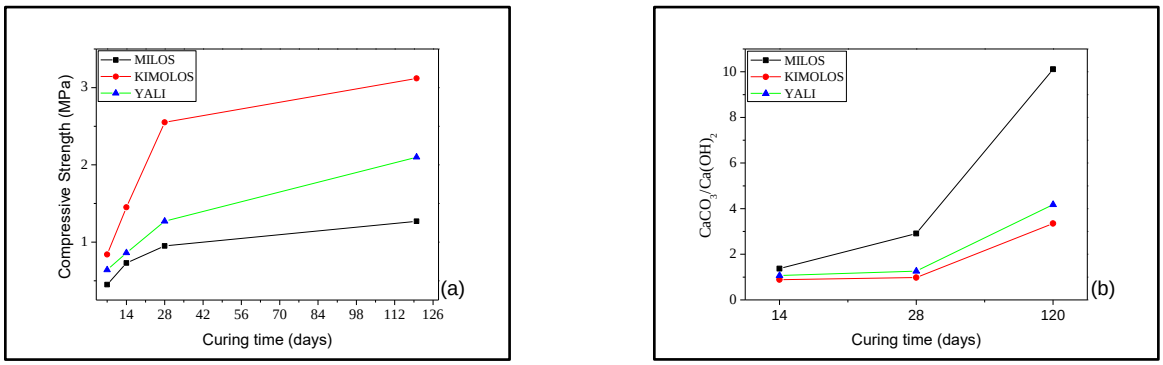

Figure 3 (a & b). Strength development of the lime-pozzolana pastes (a) and evolution of the carbonation process in different curing times (b), respectively.

The evolution of the mechanical characteristics of the mixtures at different curing times differs among the three Pozzolanas. After 28 days of curing of the pastes, the addition of pozzolanic material from Yali and to a greater extent that of Kimolos, significantly enhance the mechanical behaviour of the mixtures, with uniaxial compression strength values reaching 2.10 and 3.12 MPa respectively, after 120 days of curing (Fig. 3a). The evolution of the carbonation reaction which is related to the conversion of the contained percentage of calcium hydroxide in the Lime-Pozzolana mixtures into calcite ($CaCO_3$) (Fig. 3b), was found to be inversely proportional to that of the development of the mechanical strengths recorded in the different curing times. Pozzolanic reaction products such as calcium aluminate hydrate (ICDD-PDF-011-0203) and larnite (ICDD-PDF-033-0302) were identified in the XRD patterns of Kimolos pastes even in the early ages of curing, revealing a highly reactive nature of the certain material. The inferior properties observed in the Milos sample is related to the composition of the specific raw material and more specifically the existence of certain impurities such as carbonates and alteration mineral components like smectite, but also to the comparatively less content of amorphous material, which renders this Pozzolana less active. Taking into consideration that pozzolanic material with both similar mineralogical and chemical characteristics (Yali & Kimolos) and performance in tests which monitor their pozzolanic activity, yield different performance in the development of strength in Lime-Pozzolana pastes, it is concluded that the "nature" of the Pozzolanas as well as the finer particle size of each material each self (Seraj *et al.*, 2017), strongly affects the pozzolanic reactivity of the active phases present in such supplementary cementitious materials.

Acknowledgements

The authors wish to thank the BENTOMINE S.A. and LAVA Mining & Quarrying S.A. companies, for the provision of materials used it the terms of this study.

References

Christidis, G.E., Dimitriadi, M., Triantafyllou, G. and Tsoumeleas, C., 2021. Quantitative Analysis of Portland Cement Clinker with Rietveld Refinement: Implications of the Amorphous Matter. Materials Proceedings 5(1), 75.

Qiang, Y., Zanqun, L., Keren, Z., Cong, M., 2021. Portland cement Concrete: Natural Pozzolans, in: Qiang, Y., Zanqun, L., Keren, Z., Cong, M. (Eds.), Civil Engineering Materials: From Theory to Practice, 59-204.

Seraj, S., Cano, R., Ferron, R.D., Juenger, C.G., 2017. The role of particle size on the performance of pumice as a supplementary cementitious material. Cement and Concrete Composites, 80, 135-142.

Walker, R., Pavia, S., 2011. Physical properties and reactivity of Pozzolans, and their influence on the properties of Lime-Pozzolan pastes. Materials and Structures 44, 1139-1150.

16th International Congress of the Geological Society of Greece

17-19 October, 2022 - Patras, Greece

Bulletin of the Geological Society of Greece, Sp. Publ. 10

Ext. Abs. GSG2022-258

Quality Control of Charcoal Briquettes from Greek Market

M. Georgaki[1], M. Wojtaszek-Kalaitzidi[2], S. Kalaitzidis[1], K. Christanis[1]

(1) Department of Geology, University of Patras, Patras, Greece, christan@upatras.gr (2) Institute of Energy and Fuel Processing Technology, 1 Zamkowa Street, Zabrze, Poland

Research Highlights: *Charcoal Briquettes in the Greek Market do not meet the European quality standards.*

Background and Objectives

Charcoal is one of the first materials human has used since ancient times. Rock paintings in caves and primitive hearths in the form of a handful of stones in a circle are proof of charcoal use. Charcoal has been an important source of energy for centuries and remains till today. Nowadays charcoal is used to generate energy, mostly for cooking and heating purposes, but it also plays important role in metallurgy and other sectors of heavy industry. Up to 17% of the wood used worldwide, is converted to charcoal. Global charcoal production keeps increasing and is expected to grow more in the coming decades since charcoal is considered to be a cleaner fuel than the fossil ones (FAO, 2017). Charcoal produced by using sustainably managed resources and improved technologies, can be a low net emitter of greenhouse gases, with the potential to reduce emissions by more than 80% along the charcoal value chain, ensuring access to affordable, reliable, sustainable, and modern form of energy. The weak point of charcoal production is that it is largely informal, lacking regulations, thus resulting in inefficient and maleficent raw material management, inefficient production yield, emissions control, charcoal quality, and purity control. Charcoal is used in the form of lumps, or as processed briquettes.

Charcoal briquettes are made of charcoal fractions. Fine charcoal particles and dust are mixed with water and starch binder, which are subsequently dried to form the briquettes.

The European standard EN 1860-2 (2005) defines the values of barbecue charcoal briquettes characteristics. According to this standard the moisture shall not be above 8 wt.%, the ash yield shall be maximum 1 wt.% and the total of all detected inadmissible additions should not exceed 1% by volume.

The main purpose of this study is to investigate the quality of charcoal briquettes from the Greek market, by mainly applying standardized organic petrographical techniques.

Methods

The analyzed samples were collected from various vendors in the city of Patras. In total, nine packages imported to the Greek market, were studied, including five from Europe, three from Africa and one from Asia. For each sample proximate, mineralogical and petrographical analyses were conducted according to the EN 1860-2 (2005) standard.

Mineralogical determinations were conducted by applying X-ray diffraction on dry powder samples (∅ < 50 μm) by using a Bruker D8 X-ray Diffractometer equipped with a LynxEye® detector. EVA® and Topas® softwares were used to determine the qualitative and the semi-quantitative features of the mineral phases, respectively.

Polished blocks were prepared from crushed (∅ < 1 mm) samples according to ISO 7404-2 (2014). The blocks were examined by using the Leica DMRX coal-petrography microscope (under both white incident light and fluorescence modes); oil-immersion X50 objective; total magnification X500.

Results and Conclusions

According to the EN 1860-2 (2005) standard, the moisture of the samples is within the permissible limit, but the ash values slightly exceed the maximum threshold in two of the tested samples. The evaluation of the X-ray diffraction data indicates similar mineralogical features for all samples. The dominant minerals are quartz, illite, muscovite, calcite, and feldspars. The quality control based on reflected light microscopy, allows the identification of, and the range of biomass-derived charcoals, and impurities; the latter include raw (fresh) biomass, mineral matter, plastics, rust, metal, coal-particles, and pyrolytic carbon (Fig. 1; see also Jelonek *et al*., 2020; Drobniak *et al*., 2022). The petrographic analysis reveals that the impurity content exceeds 1 vol.% in all samples, and actually four out of nine samples consist almost exclusively of coal particles.

In light of the above and considering the public health hazard that is posed by using grill fuel of questionable quality, the petrographic analysis of charcoal briquettes should be prerequisite for getting allowance to enter the market.

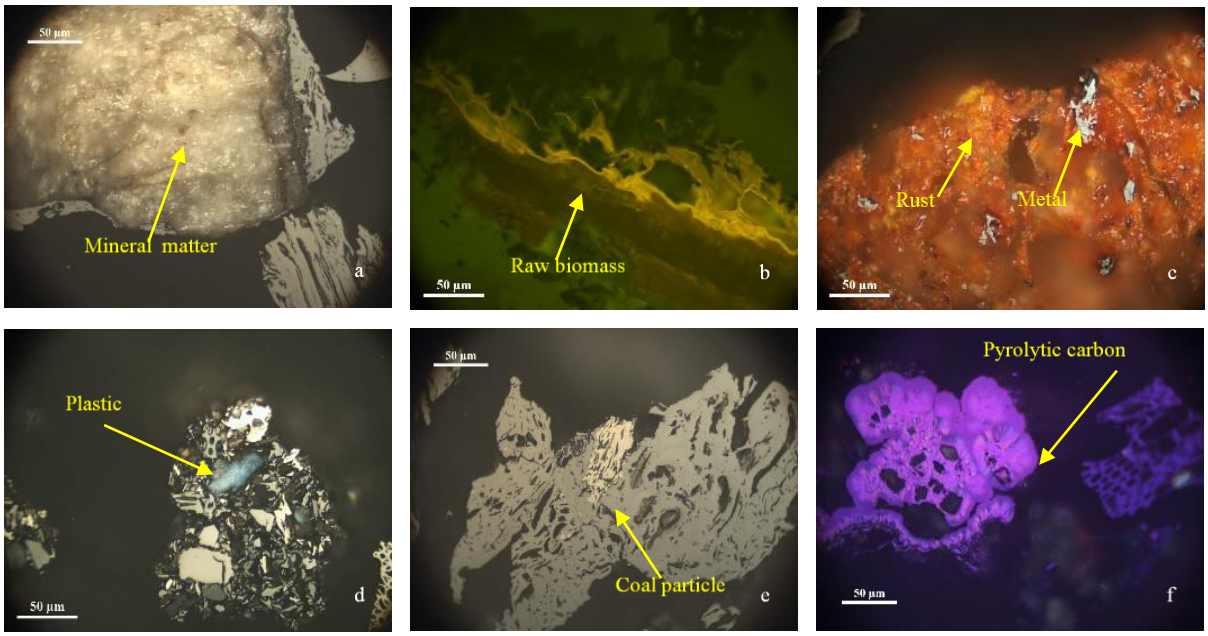

Figure 1. Photomicrographs (a-f) of various inadmissible additions in barbecue charcoal briquettes from Greek market.

Acknowledgements

The authors would like to thank Dr. Paraskevi Lampropoulou, Section of Earth Materials, Department of Geology, University of Patras, for running the XRD analyses.

References

Drobniak, A., Jelonek, I., Jelonek, Z., Mastalerz, M., 2022. Developing methodology for petrographic analysis of solid biomass in reflected light. Int. J. Coal Geol., 253, 103959.

EN 1860-2, 2005. Appliances, solid fuels and firelighters for barbecueing - Part 2: Barbecue charcoal and barbecue charcoal briquettes. Requirements and test methods. European Committee for Standardization.

FAO, 2017. The charcoal transition: greening the charcoal value chain to mitigate climate change and improve local livelihoods, Rome, Food and Agriculture Organization of the United Nations ISBN 978-92-5-109680-2, 179 p.

ISO 7404-2, 2009. Methods for the Petrographic Analysis of Coals — Part 2: Methods of Preparing Coal Samples. International Organization for Standardization, Geneva, Switzerland

Jelonek, Z., Drobniak, A., Mastalerz, M., Jelonek, I., 2020. Environmental implications of the quality of charcoal briquettes and lump charcoal used for grilling. Sci. Total Environ., 747, 141267.

16th International Congress of the Geological Society of Greece

17-19 October, 2022 - Patras, Greece

Bulletin of the Geological Society of Greece, Sp. Publ. 10

Ext. Abs. GSG2022-274

Recycled materials, construction and industrial wastes as aggregates for different types of concrete

P. Petrounias[1,2], P.P. Giannakopoulou[1], A. Rogkala[1], P. Lampropoulou[1], E. Antoniou[1], C. Fourkalidi[1], A. Chronaki[1], M. Kalpogiannaki[3], N. Koukouzas[2]

(1) Section of Earth Materials, Department of Geology, University of Patras, 265 04 Patras, Greece, Geo.plan@outlook.com, (2) Chemical Process & Energy Resources Institute, Centre for Research & Technology Hellas (CERTH), Maroussi, Athens, 15125, Greece, (3) Department of Geology and Geoenvironment, National and Kapodistrian University of Athens, Panepistimioupolis Zografou, 15784 Athens, Greece

This work examines variable recycled materials, construction and industrial wastes as aggregates for normal and pervious concrete specimens, respectively, and is divided into two parts. More specifically, this study presents the results of the examination of variable recycled materials such as beer green glass, waste tile, and asphalt used in variable mixtures in order to prepare concrete specimens (Fig. 1). In addition, the study demonstrates their effect on the strength of the produced normal concrete and how their petrographic characteristics of the various recycled materials influence, in general, the durability of C25/30 strength class concrete. Particular emphasis is given to the influence of the artificial microroughness of glassy and smooth surfaces of recycled materials on their final concrete strength. Concrete specimens made by a mixture of beer green glass with quartz primer, as well as of tile with quartz primer showed the optimum compressive strength's results even the concrete strength values do not show great variance (Petrounias *et al.*, 2019). These limited differences introduce a new promising petrographic methodology, including the study of the surface texture of the used aggregate materials.

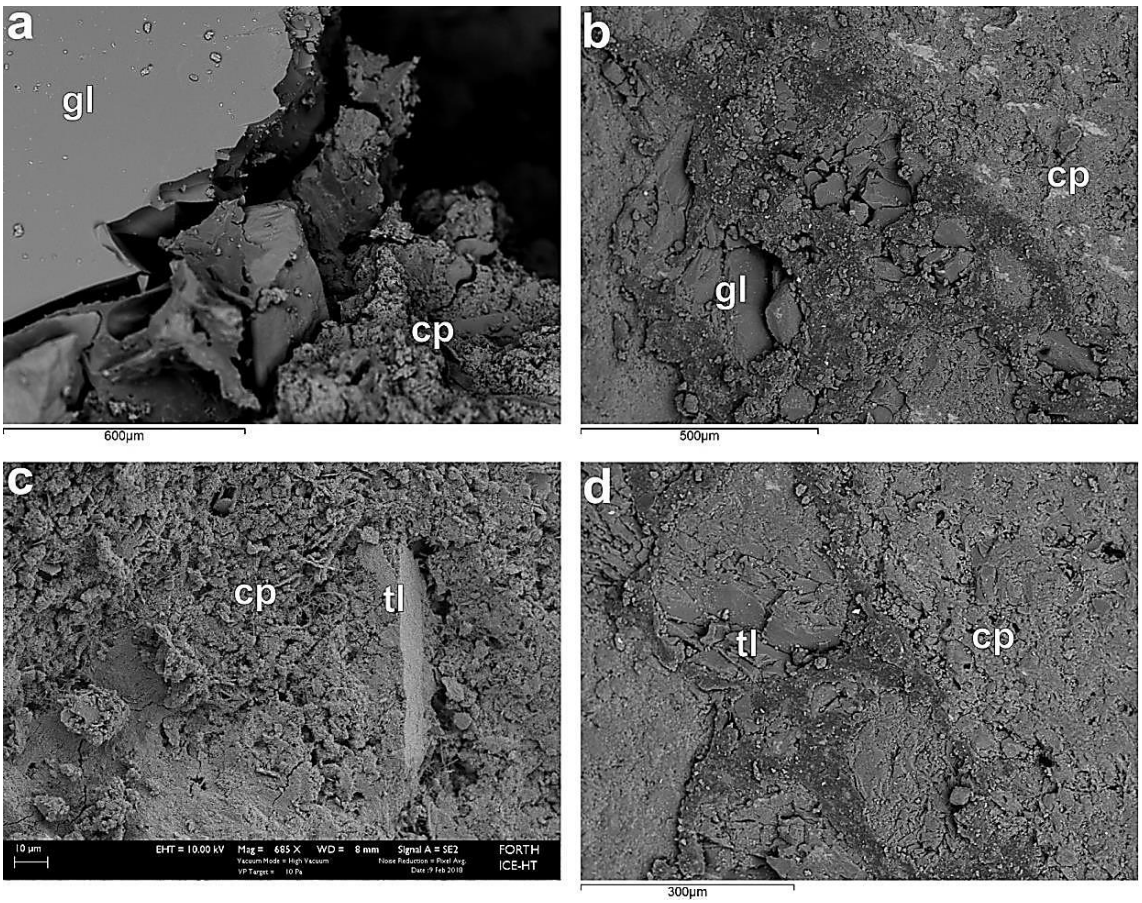

Figure 1. Secondary electron images showing microstructures at the interface between cement paste and: (a) beer green glass; (b) beer green glass with quartz primer; (c) waste tile; and, (d) waste tile with quartz primer. gl: glass, cp: cement paste, tl: tile.

The second part of this study deals with sterile natural rocks (limestones, basalts), industrial by-products (slags), construction wastes (bathroom wastes) and electronic wastes (e-wastes) tested for their suitability as pervious concrete

aggregates (Fig. 2). The physical properties of the tested raw materials are closely related to their petrographic characteristics and they have also played a determinant role to the permeability of the produced concrete specimens (Petrounias *et al.,* 2022). These properties have also influenced the mechanical behaviour of the produced pervious concrete and on their freeze-thaw test results. Quite encouraging results were obtained from this study as concrete made by variable wastes and by-products can be compatible for concrete production, as they show similar performance both in mechanical strength test and in freeze thaw test with those made by natural aggregates.

Figure 2. Representative photos of aggregate components showing: (a) Limestone; (b) Basalt; (c) construction wastes; (d) E-wastes.

Acknowledgements

We kindly thank Dr. V. Xanthopoulou of the Laboratory of Electron Microscopy and Microanalysis, University of Patras for her assistance for the XRF analyses. We would also like to thank Mr. S. Liogris from Wasco Coating Europe BV for providing the slags. We also wish to thank Dr. Drakopoulos from the Foundation for Research and Technology-Hellas (FORTH) Institute of Chemical Engineering and High Temperature Chemical Processes (ICE/HT) Rio-Patras, Greece and A.K Seferlis of the Laboratory of Electron Microscopy and Microanalysis, University of Patras for his assistance with the microanalyses and SEM imaging.

References

Petrounias, P., Giannakopoulou, P.P., Rogkala, A., Lampropoulou, P., Tsikouras, B., Rigopoulos, I., Hatzipanagiotou, K. 2019. Petrographic and mechanical characteristics of concrete produced by different type of recycled materials. Geosciences, 9, 264.

Petrounias, P., Giannakopoulou, P.P., Rogkala, A., Kalpogiannaki, M., Laskaris, N., Lampropoulou, P., Mouzakis, P., Panagiotaras, D., Koukouzas, N. 2022. Sustainable use of by-products and wastes from Greece to produce innovative eco-friendly pervious concrete. Appl. Sci. 12, 5861. https://doi.org/10.3390/app12125861.

16th International Congress of the Geological Society of Greece
17-19 October, 2022 - Patras, Greece
Bulletin of the Geological Society of Greece, Sp. Publ. 10
Ext. Abs. GSG2022-288

Study of mechanical properties and adsorption capacity of heat-treated smectite clays

P. Velli[1], A. Argyraki[1], V. Zotiadis[2]
(1) Department of Geology and Geoenvironment, National and Kapodistrian University of Athens, Panepistimiopolis, Zographou, Athens, Greece, Vivian_Vel@outlook.com (2) Edafomichaniki S.A., Athens, Greece

Research Highlights

The studied Ca-bentonite and Mg-smectite in raw and sodium-activated form, showed resistance to elevated temperatures and maintained their low hydraulic conductivity and high adsorption capacity.

Background and research objectives

The concepts of zero-pollution, circular economy and sustainability for the benefit of the society require novel approaches, where emphasis is given to processes and agents potentially beneficial for both environmental pollution protection and engineering property improvement. For example, geological disposal programs for radioactive waste take advantage of the safety-relevant properties of clays used as engineered barriers (Sellin and Leupin, 2013). Bentonite clay and bentonite clay mixtures are used as buffers, seals, or backfills in almost every program for radioactive-waste disposal worldwide. However, research questions remain on the impact of heating in conjunction with water uptake of the buffer clay under disposal conditions, where temperature gradients of up to 2 ºC per centimeter can develop (Kasbohm *et al*., 2013). Within this frame, the objective of the present research focuses on the study of different smectite clays, i.e. Ca-bentonite and Mg-smectite rich bentonite with respect to their mechanical properties and adsorption capacity before and after heat treatment.

Materials and methods

The following 3 different clay materials were tested: a) a commercial Ca-bentonite (BEN), b) a Mg-smectite rich clay of green color in raw form (PS1R) and c) a Mg-smectite rich clay of green color, Na-converted (PS1A). The raw material of bentonite originated from Milos Island, Greece, while the Mg-smectites originated from Grevena, Greece. The samples underwent heat treatment at temperatures of 150ºC, 180ºC and 210ºC in a muffle furnace for 2h before the experiments. Mineralogical analysis was performed by powder X-ray diffraction (Figure 1). Atterberg limits, hydraulic conductivity (Figure 2), swell index, and methylene blue adsorption (MBA) were measured in all samples. Furthermore, adsorption experiments using ionic standard solutions of Cr(VI) (25 mg/L), Ni (50 mg/L), and Pb (50 mg/L), were performed.

Results and Conclusions

A summary of the mechanical properties and MBA determined in the samples is presented in Table 1.

Table 1. Measured properties of the samples treated at various temperatures.

Sample	Swell Index (%)	Liquid limit (%)	Plasticity limit (%)	Plasticity index (%)	Permeability Factor ($cm \cdot s^{-1}$)	Fluid loss (mL)	MBA (mL)
BEN_25	24.3±2.08	424	41.6±2.98	383	$2.0 \cdot 10^{-7}$	16.0	29.0
BEN_150	25.8±0.76	486	38.7±1.43	447	$7.5 \cdot 10^{-8}$	18.0	26.5
BEN_180	23.2±1.04	413	41.6±3.63	371	$4.1 \cdot 10^{-8}$	18.8	26.2
BEN_210	23.0±0.50	394	43.0±4.67	351	$4.0 \cdot 10^{-7}$	19.0	25.0
PS1R_25	7.80±0.76	145	44.5±6.35	100	$5.5 \cdot 10^{-7}$	122	29.1
PS1R_150	7.30±0.29	141	47.5±9.89	93.5	$8.4 \cdot 10^{-7}$	110	28.9
PS1R_180	7.30±0.58	129	46.0±0.40	82.7	$3.5 \cdot 10^{-7}$	112	29.1
PS1R_210	7.70±1.20	144	52.1±3.18	91.5	$5.1 \cdot 10^{-6}$	112	28.5
PS1A_25	23.5±0.50	353	54.7±0.37	298	$8.9 \cdot 10^{-7}$	26.0	23.6
PS1A_150	18.0±0.50	317	51.9±1.73	265	$1.3 \cdot 10^{-6}$	34.0	23.4
PS1A_180	16.2±0.76	284	50.1±1.04	234	$1.1 \cdot 10^{-7}$	36.0	23.1
PS1A_210	14.3±1.04	261	54.1±0.06	206	$5.4 \cdot 10^{-7}$	38.0	22.9

All materials tested tend to maintain their properties after thermal treatment. Specifically, no significant differences appear between the samples in the plasticity limit and MBA values. On the contrary, a small decrease of liquid limit and plasticity index is observed with increasing temperature. Bentonite samples with or without thermal modification maintain a high swell index (23-26%). According to Holtz and Dibbs (1956) the samples of bentonite are characterized by high swelling capacity, while the green smectite samples and sodium activated green smectite samples with medium and low swelling capacity, respectively. The highest liquid limit was observed in the bentonite samples (394 - 486%), while the highest

plasticity limit was demonstrated by the activated green smectite samples (50-55%). The samples can be characterized as highly plastic materials with plasticity index > 80%, liquid limit between 129 and 486% and plasticity limit range between 39-55% (Sayed and Shehab, 2020).

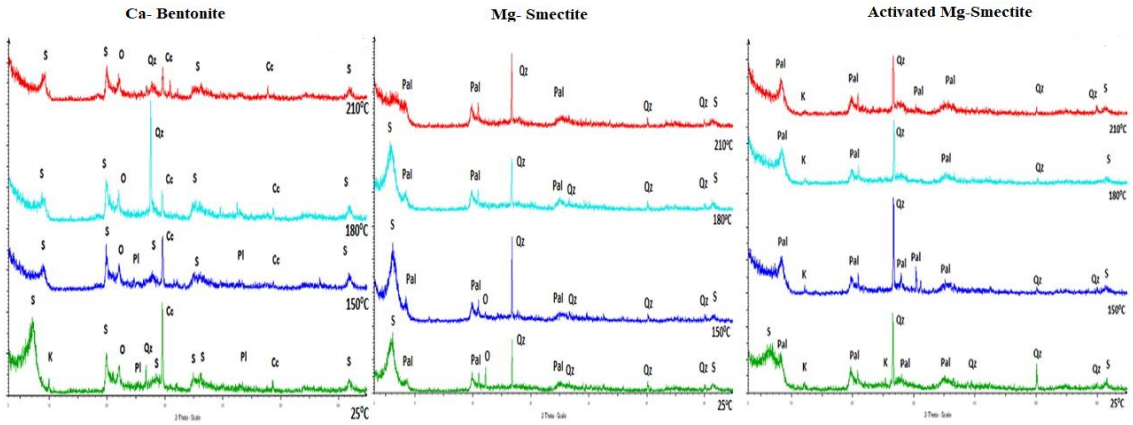

Figure 1: XRD patterns of the tested samples at different temperatures. (Cc = calcite, K = kaolinite, O = opal-CT, Pal = palygorskite, Pl = plagioclase, Qz = quartz, S = smectite).

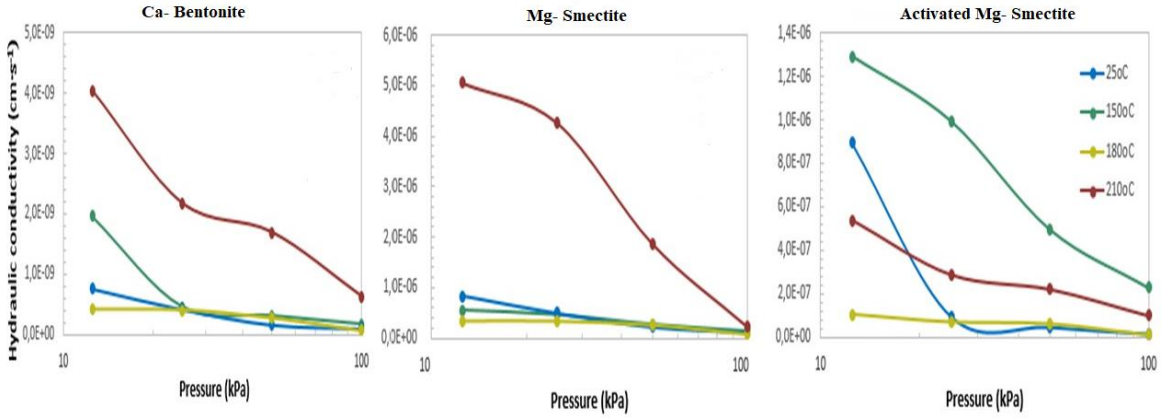

Figure 2: Change of hydraulic conductivity of the samples according to applied pressure.

The samples can be characterized as almost impermeable, due to low value of K factor ($K<10^{-7}$) (Surendra and Sanjeev, 2015). It is noticed that the samples that were heat treated at 180ºC show lower permeability values compared to the others. All samples showed high absorption capacity for Pb (removal ranged from 86% to 100% in tested solutions). High removal rates (44-61%) were also observed for Ni, while levels of Cr(VI) removal were relatively lower (7-20%). The samples showed the same absorption capacity for Pb regardless of temperature, while the removal of Ni increases with increasing thermal treatment of the clay. A slight increase of Cr(VI) removal by the Ca-bentonite was observed with increasing temperature, while a decrease was observed in the activated samples.

In conclusion, it is observed that the hydraulic conductivity of the samples decreases in general with increasing temperature, the best performance is observed for Ca-bentonite. Furthermore, the samples maintain their high absorption capacity for heavy metals at elevated temperatures.

Acknowledgements

The authors thank Edafomichaniki S.A. for assistance with geotechnical measurements and Geohellas S.A. for the MBA testing. Also, we thank Dr. Z. Kypritidou of NKUA for her help during laboratory work.

References

Holtz, W.G., Gibbs, H.J., 1956. Engineering properties of expansive clays. Transactions of the American Society of Civil Engineers 121, 641–663.

Kasbohm, J., Pusch, R., Nguyen-Thanh, L., Hoang-Minh, T., 2013. Lab-scale performance of selected expandable clays under HLW repository conditions. Environ Earth Sci, 69, 2569-2579.

Sayed, M.A., Shehab, S.A., 2020. Strength and stiffness characterization of clays using Atterberg limits, Transportation Geotechnics 25, 100420.

Sellin, P., Leupin, O.X., 2013. The use of clay as an engineered barrier in radioactive-waste management- a review. Clays and Clay Minerals, 61, 477-498.

Surendra, R., Sanjeev, B., 2017. Role of Geotechnical Properties of Soil on Civil Engineering Structures. Resources and Environment, 7, 103-109.

16th International Congress of the Geological Society of Greece
17-19 October, 2022 - Patras, Greece
Bulletin of the Geological Society of Greece, Sp. Publ. 10
Ext. Abs. GSG2022-310

Offshore Synergy: The Transfer of Oil and Gas Experience to the Offshore Wind Sector

I. Ismail[1], E. Kaikas[1], E. Tartaras[1], A. Stefatos[1]
(1) Hellenic Hydrocarbons Resources Management S.A., Athens, Greece, i.ismail@greekhydrocarbons.gr

1. Background:

Offshore wind energy is a rapidly developing renewable energy technology that will play a major role in the future energy mix. Based on current and proposed policies, the analysis of International Energy Agency (IEA, 2019) shows that global offshore wind power capacity is set to increase 15-fold over the next two decades turning it into a $1 trillion business. Moreover, offshore wind will not only help put the global power sector on track for full decarbonization, but it will also provide the means for clean electricity and hydrogen production in the upcoming decades, thus enabling reducing emissions from hard to decarbonize sectors such as the cement, steel and transportation industries.

Meanwhile, cost reduction is considered a crucial element for maintaining offshore wind energy growth. While the EU is providing financial support to the offshore wind industry in Europe in the form of feed-in tariffs and feed-in premiums reducing investments risks, other supporting measures are needed to build an industry of scale and ultimately bring down the cost of offshore wind energy. To do so, the incorporation of best practices and experiences from other sectors such as Oil and Gas (O&G) is critical for both cost reduction and HSE, therefore maintaining a robust growth of offshore wind industry. In this work, we study the areas that exhibit high level of synergy between offshore wind industry and the O&G sector, so that the first can benefit from O&G industry experience and supply chain capabilities to potentially reduce costs and enhance HSE standards in its operations.

2. High level of Synergy: Oil & Gas Experience Serving Offshore Wind Technology for Sustainable Energy

Typically, an offshore wind farm lifecycle exceeds 30-35 years from initial concept planning till decommissioning. To address properly the synergies between the two industries, we consider screening the six main supply chain elements in the lifetime of a typical offshore wind farm project against the O&G industry, described briefly as follows:

1) Development and project management: represents the development and management of the offshore wind farm from signing a lease agreement to the construction works completion date.
2) Turbine: constitutes the manufacturing, assembly and system level functional test of all electrical and mechanical components that make up a turbine
3) Balance of plant: comprises all aspects of the supply of cables, turbine foundations and offshore and onshore substations
4) Installation and commissioning: reflect the commission work on all balance of plant and sub elements
5) Operation, maintenance and service: incorporate all operational, inspection and service costs (e.g., day to day control-repair or replacement)
6) Decommissioning: includes all relevant activities to the removal of end-of-life wind turbines.

The **development and project management** phase includes four main sub-elements: i) Environmental surveys, ii) Consenting and development services, iii) Site investigations, and iv) Project management.

Regarding the site investigations sub-element, typically it comprises two stages. The first stage regards the choice of areas and sites for the development of Offshore Wind Farms (OWF) by the relevant national authority, such as HEREMA in Greece, where a number of various exclusion zones have to be defined and managed. Later on, once the development areas have been identified and exploration permits have been awarded to successful applicants, detailed site investigations are conducted by the exploration permit holders, in order to characterize the specific sites for OWF development and to understand the technical requirements and cost implications for OWF development in each site of interest.

In both of these stages, the suitability of the site for OWF development is investigated. During this investigation, several geotechnical and geophysical surveys/studies are carried out to identify suitable locations for deployment (Velenturf *et al*., 2021), including cable routes. Examples of the geophysical surveys that need to be conducted are multi-beam to determine water depth and seabed bathymetry, marine magnetometer/gradiometer surveys to identify anomalies (deviations from the background field), side-scan sonar determining seabed features/obstructions, and sub-bottom profiler for shallow subsurface geology and geohazards, as well as other geotechnical surveys such as Cone Penetration Tests, boreholes, and core samples to define seabed conditions and sublayers characteristics. Many of these surveys are considered pre-requisites and they have been undertaken for decades in the O&G industry for identifying geological targets, conducting drilling activities and confirming O&G discoveries. Consequently, it is clear that a quite high degree of synergy exists between offshore wind and O&G industries on the site investigation sub-element of development and project management main element of offshore wind projects.

Furthermore, the development and project management element of offshore wind farm makes up 3% of lifetime expenditure. Although this represents a comparatively small cost element over the 30+ year life cycle of a wind farm, expenditure on project management alone, is still in the order of 125 million euro for a representative 500MW project (Scottish Enterprise, 2016). Meanwhile, OWF developers are aware that O&G companies have world class project management capabilities, but also the experience of managing O&G projects in harsh marine environments ensuing implications for HSE, for example, similar to the expertise required in the development of offshore wind farms. On top of that, strong project management will reduce project risk and will be a factor in cost of capital calculations.

On the other hand, **turbine** supply involves the design, manufacture and assembly of all electrical and mechanical components and systems that make up a wind turbine. The wind turbine main components are the nacelle, the rotor and the tower for which no part of the turbine supply seems to show synergy with oil and gas industry. However, when it comes to **balance of plant** element, high synergy with the O&G sector is present. More specifically, the sub elements of the balance of plant are noted as follows: i) array cables, ii) export cables, iii) electrical transmission, iv) substation structures, v) turbine foundation and vi) secondary steelwork. Taking into account the array cables which connect the individual turbines to one another and to the substation, if present, the requirements of offshore wind array cable, although slightly different, are still quite similar to those in the O&G sector, and most O&G suppliers are capable of supplying offshore wind projects without significant investment. Evidence of that is the successful entry of JDR Cables company into the offshore wind sector from the O&G sector, thus becoming the number one array cable supplier in Europe. Similar to the array cables, the same is true for all other sub-elements of balance of plant except of the export cables and transmission electrical ones. The reason for this is that export cable is served by large cable manufacturing companies operating across multiple industries (e.g., Prysmian and Nexans), whereas for Transmission electrical supply is already supported by global engineering companies such as Siemens (Scottish Enterprise, 2016).

On the **Installation and commissioning** part, cable installation, installation equipment and installation support services sub-elements exhibit good synergies with the O&G industry. When cable installations are considered, O&G suppliers have a solid track-record in this aspect, while cable installation equipment and services, such as diving support, cable protection, marine engineering, carousel supply and handling equipment, are already supplied by O&G companies. However, one of the key areas where O&G industry lacks experience is the pull-in of cables on much larger geographical installation areas such as offshore wind projects, as cable pull-in at the turbine is a complex task and may be performed over 100 times at a wind farm. The same applies to installation equipment and installation support services as strong synergies exist for most pieces of O&G equipment whereas O&G skills can be readily applied to offshore wind.

Maintenance and inspection services, as a sub-element of **operation, maintenance and service** main project element, present high synergies with the O&G sector. This element covers a wide range of activities, notably blade inspection and repair, cable fault detection and repair, foundation health monitoring and repair as well as wildlife survey and environmental services (Scottish Enterprise, 2016). Meanwhile O&G suppliers have a vast amount of experience in maintaining assets in the North Sea and synergies in terms of defect detection, planned maintenance and asset repair are extremely high. Furthermore, O&G offshore safety standards and maintenance practices are highly transferrable to offshore wind. Also, a strong O&G service supply chain has been developed over a number of years, and a number of specialist disciplines are highly transferrable.

Meanwhile, **decommissioning** is the process of removing all wind turbines and returning the area to its original condition whereas only one small offshore wind farm has been decommissioned and the strategies for large-scale projects are highly uncertain. Although there is no regulation specific to the decommissioning lifecycle stage of offshore wind installations, it is anticipated that offshore regulations will be applied in a similar manner as O&G licensing and environmental protection regimes. O&G suppliers are likely to be well placed to provide decommissioning services when relevant activities start taking place.

3. Conclusions

Synergies between the O&G industry and the offshore wind sector are clearly presented in this work. Transfer of O&G knowledge and experience to the offshore wind industry is of paramount importance to accelerate wind energy growth, reduce costs, but also to maintain the highest health, safety and environmental standards, considering the lessons learned and best practices of the O&G industry in harsh marine environments.

References

IEA, 2019. Offshore Wind Outlook 2019.

Scottish Enterprise, 2016. Oil and Gas "Seize the Opportunity' Guides, Offshore Wind.

Velenturf, A. P. M., Emery, A. R., Hodgson, D. M., Barlow, N. L. M., Mohtaj Khorasani, A. M., Van Alstine, J. Peterson, E.L., Piazolo S. & Thorp, M., 2021. Geoscience Solutions for Sustainable Offshore Wind Development. Earth Science, Systems and Society, 4.

16th International Congress of the Geological Society of Greece
17-19 October, 2022 - Patras, Greece
Bulletin of the Geological Society of Greece, Sp. Publ. 10
Ext. Abs. GSG2022-333

Monitoring of Key Parameters of the Neo Erasmio-Magana Geothermal Field

Apostolos Arvanitis[1], Markos Xenakis[1], Polyanthi Trimi[1], Marios Amvrazis[1], Christos Mylonas[1]
(1) Hellenic Survey of Geology and Mineral Exploration (H.S.G.M.E.), Athens, Greece, arvanitis@igme.gr

Research Highlights

Temperature and pressure variation caused by production at the Neo Erasmio-Magana geothermal field.

Background

Geothermal energy is a valuable resource of expanding usage; its exploitation, however, possess questions about its sustainability and long-term impacts. In order to prevent the exhaustion of the resource, monitoring of key parameters such as hydraulic head and temperature, on a systematic basis is necessary, taking remedy measures when required. These parameters can be monitored either with the placement of permanent monitoring stations providing data for the reservoir or by conducting periodic field measurements. This practice has been applied to the Neo Erasmio-Magana low enthalpy geothermal field located 24 km SW from Xanthi covering an area of 24 km^2. Wellbore temperature ranges from 22 to 73^{o}C. N70° and N160° faults are responsible for the geothermal fluid circulation with the latter being the main inflowing fault (Kolios *et al*., 2005). The reservoir is a confined one at depths between 200 and 400 m; it consists mainly of sandstone (eastern part) and conglomerate (western part) overlying the faulted gneiss basement (Kolios *et al*., 2000). This field is under exploitation (Dalabakis *et al*., 2015) and the produced fluid is used for greenhouse heating. As a result, the production scheme alters from high exploitation intensity periods to almost zero production periods.

The main objective of these measurements is to ensure the sustainability of the geothermal resource and prevent its possible exhaustion. By this practice any variation can be spotted early enough and remedy measures can be applied. Moreover, the collected data is valuable as it allows a better understanding of the reservoir behavior at different production periods, the way pressure and temperature vary over the years and to observe the reversibility of the processes are taking place. On top of that, this dataset is also used to improve its simulation model which in turn can provide us with more reliable predictions.

Methodology

The Neo Erasmio-Magana geothermal field is constantly monitored by 4 new telemetry stations (Table 1), installed inside pre-existing exploration wells and located nearby production wells. Two field measurements per year are conducted, one during the production period (winter) and another during the relaxation period (summer). The main parts of a telemetry monitoring station are: (a) the pressure and temperature sensors that are plunged into the well; (b) the data logger; (c) the energy supply system; and (d) the data transmission system. The pressure sensor is installed below the lowest known water level, whereas the thermometer sensor is installed at reservoir depth. The data is collected every 5 minutes, the hourly mean value is then calculated and stored. The mean values are daily transmitted to the central HSGME's server. Station data was used to create hydraulic head (m) referenced to mean sea level (msl) and reservoir temperature (°C) diagrams. Moreover, stations hydraulic head (m) msl and reservoir temperature (°C) values were correlated for each station separately. On top of that, field's measurement data along with the stations data are used to create hydraulic head (m) msl and reservoir temperature (°C) distribution maps. The latter are used for the magnitude calculation of changes of the overall median value of the aforementioned reservoir parameters from initial conditions and the rate of hydraulic head build up during the relaxation period (summer).

Table 1. Telemetry monitoring stations.

Well	X (GGRS87)	Y (GGRS87)	Depth of pressure sensor (m)	Depth of temperature sensor (m)	Installation Date	Nearest Production Well	Station-Producer distance (m)
THTH2	570421.00	4530265.00	45.70	246.00	25/6/2021-Present	THTH2a	10
M6	570671.85	4530723.60	51.60	185.00	3/10/2020-Present	GP6	10
GP9	571056.11	4530289.47	32.49	175.00	2/4/2021-Present	THTH6	19

M15	569548.98	4530176.23	44.40	369.30	6/10/2020-Present	GP15	19

Results

From the dataset it is obvious the immediate decline of hydraulic head with production start. Moreover, it was found that GP9 (Figure 1) and THTH2 hydraulic head (m) msl and reservoir temperature (°C) strongly correlate with positive covariance, which means that by a hydraulic head decline temperature also declines. On the other hand, M6 data reveals too weak correlation. One possible reason behind this difference is that M6 (Figure 2) is closer to an inflowing fault, a fact that contributes to preserve a more stable and not sensitive to hydraulic head changes, temperature profile. On the contrary, production of wells THTH6 and THTH2a (GP9 and THTH2 stations) located in greater distance from the inflowing area, results in cooler fluid inflow the well. Moreover, to all stations a sinusoidal behavior over the time is apparent visualizing the reversibility of the processes taking place into the reservoir. From the distribution maps is apparent that the hydraulic head median value has decreased about 55% from initial conditions, while its build up between March and September 2021 was equal to 51% which are not alarming yet as the water table overcomes by far the reservoir cap rock. Regarding temperature, field and station measurements revealed that from initial conditions in September 2021 temperature median value declined by 1.69% (from 40.3°C to 39.6°C), although from September 2021 to May 2022 this was raised by 1.67% almost reaching the initial conditions value. In a nutshell, from all the above can be concluded that production has a minor effect on reservoir sustainability.

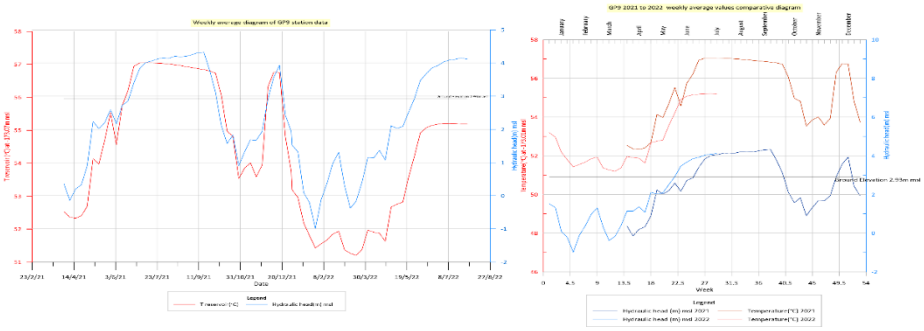

Figure 1. GP9 monitoring station diagrams for the period April 2021 - August 2022.

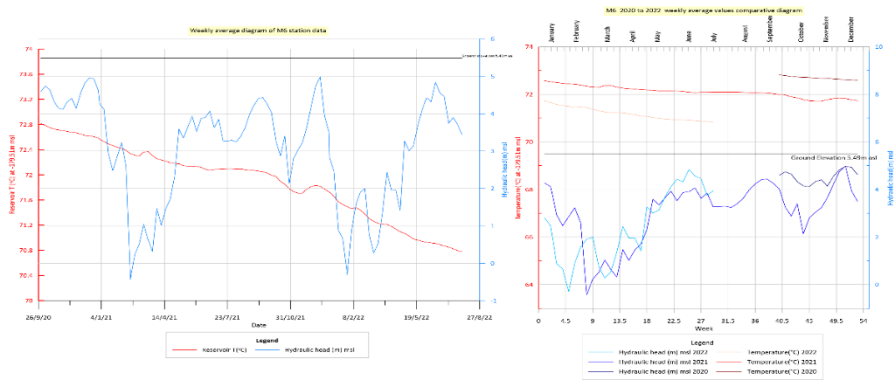

Figure 2. M6 monitoring station diagrams for the period October 2020 - August 2022.

Acknowledgements

This paper was created in the framework of two projects “Actions for the Rational and Sustainable Utilization of Geothermal Energy - GEOTHERM” and “Management Plans of Low Temperature Geothermal Fields in Greece” funded in the frame of NSRF 2014-2020. Moreover, credits should be given to Thrace Greenhouses S.A. and the Decentralized Administration of Macedonia and Thrace for providing data and support.

References

Dalabakis, P., Papachristou, M., Kolios, P., Arvanitis, A., and Kolios N., 2015. Geothermal exploitation in Neo Erasmio (Xanthi). Proceedings, 9th Panhellenic Congress of the Hellenic Society of Agricultural Engineers (Thessaloniki 8-9 October 2015), 711-718

Kolios, N. and Karydakis, G., 2000. Geothermal exploration in the Neo Erasmio-Magana area (Xanthi Prefecture). Technical Report, IGME.

Kolios, N., Koutsinos, S., Arvanitis, A., and Karydakis G., 2005. Geothermal Situation in Northeastern Greece. Proceedings, World Geothermal Congress, Antalya, Turkey, 14p.

16th International Congress of the Geological Society of Greece

17-19 October, 2022 - Patras, Greece

Bulletin of the Geological Society of Greece, Sp. Publ. 10

Ext. Abs. GSG2022-390

An Innovative Experimental Study of Concrete made with shredded recycled tire rubber: the effect of Posidonia balls addition

C. Giannakis[1], G. Liapis[1], V. Mastrokostas[1], E.M. Takoumaki[1], P. Petrounias[1,2], P. P. Giannakopoulou[1], A. Rogkala[1], P. Koutsovitis[1], P. Lampropoulou[1], N. Koukouzas[2]

(1) Section of Earth Materials, Department of Geology, University of Patras, 265 04 Patras, Greece, xaralamposgiannakis49@gmail.com (2) Chemical Process & Energy Resources Institute, Centre for Research & Technology Hellas (CERTH), Maroussi, Athens, 15125, Greece

Increasing waste volumes and escalating disposal costs have forced a reassessment of public attitudes regarding the way society handles its wastes. This expanding awareness has given rise to a definite trend toward recycling or use of a wide variety of solid waste materials. Nowadays, independently of political, economic and ecological reasons, recycling has been encouraged throughout the world. In this study, the criteria of sustainability is emphasized and applied to concrete (and structural concrete). Concrete is the most widely used building material due to its versatility, the easily obtainment of raw materials and fabrication, its low cost, high mechanical strength, impermeability to water and great durability (Petrounias *et al.*, 2019, 2022). Thus, rubberized concrete can support construction sustainability, as well as can contribute to the development of the civil engineering area by using industrial waste, in minimizing the consumption of natural resources and producing a more efficient material (Rad, 1967, Fang *et al.*, 1992, Lougheed and Papagiannakis, 1996, Dogan, 2005, Sukontasukkul and Chaikaew, 2006, Petrounias *et al.*, 2022). Recycled materials such as plastics can be used as aggregates (through suitable formulations and for specific applications) for concrete production, cementitious sheets for sealing systems and other concrete products, such as concrete floors, walls and roof tiles. *Posidonia oceanica*, a marine biomass, which is lignocellulosic, renewable, light, and inexpensive fiber can be exploited to reinforce cement matrix and is considered as a new industrial application. In fact, the availability of large quantities of such fibers and the well-known mechanical properties are a general prerequisite for the successful use of these materials. Recycling or reusing of any kind of discarded material is always a better option than dumping it as a waste, taking into account the environmental impacts as well as the country's economy. To accomplish this objective, the use of plastics, derived from waste tyres, as coarse aggregate in concrete mixes is an option that is being tested nowadays. This work examines a new innovative method for a new eco friendly concrete produced by plastic wastes and posidonia balls as variable recycled materials, for normal concrete specimens. More specifically, this study presents on the one hand the results of the examination of plastics for their suitability as concrete aggregates (Fig. 1a), while on the other hand presents the results of the investigation of the use of *Posidonia oceanica* fibres on the concrete behavior (Fig. 1b). Particular emphasis was given on the influence of the artificial microroughness of glassy and smooth surfaces of recycled plastic materials on their final concrete strength. Concrete specimens made by a mixture of *Posidonia oceanica* and plastics with high microroughness provided better results regarding all the other mixes, which are characterized by low microtopography and of absence of posidonia fibres; the latter seem to act as mesh structures increasing the strength of the mortar by exactly the same mechanism as is the case with silica fibers, which are widely used in mortars today. These limited differences introduce a new promising petrographic methodology, including the study of the surface texture of the used aggregate materials.

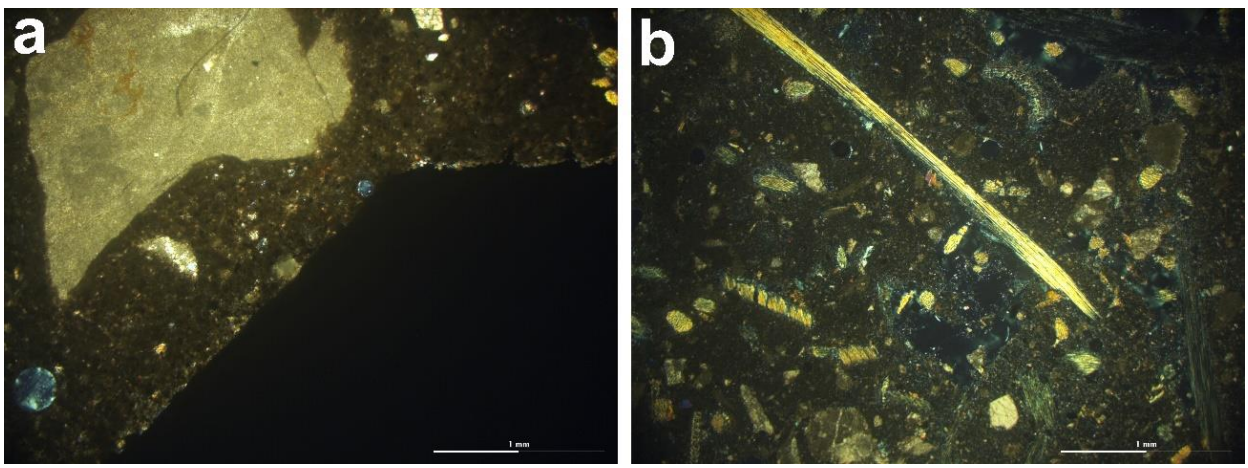

Figure 1. a) Recycled plastics as concrete aggregate, b) Posidonia oceanica fibres in concrete.

References

Petrounias, P., Giannakopoulou, P.P., Rogkala, A., Lampropoulou, P., Tsikouras, B., Rigopoulos, I., Hatzipanagiotou, K., 2019. Petrographic and Mechanical Characteristics of Concrete Produced by Different Type of Recycled Materials. Geosciences 9, 264.

Petrounias, P., Giannakopoulou, P.P., Rogkala, A., Kalpogiannaki, M., Laskaris, N., Lampropoulou, P., Mouzakis, P., Panagiotaras, D., Koukouzas, N., 2022. Sustainable Use of By-Products and Wastes from Greece to Produce Innovative Eco-Friendly Pervious Concrete. Applied Sciences 12.

Dogan O., 2005. Investigation of rubberized concrete characteristics with experiments, Unpublished M.Sc. Thesis, Gazi University, Institute of Science and Technology, Ankara.

Fang, H.Y., Topçu, I.B., Hitchens, D., Hontz, D. 1992. Use of scrap rubber tires for construction materials, Proc. 24th Mid-Atlantic Industrial Waste Conf., West Virginia University, Morgantown, USA. 563-72.

Lougheed, T.J., Papagiannakis, A., 1996. Viscosity characteristics of rubber-modified asphalts. Journal of Materials in Civil Engineering, ASCE 8 (3), 153-156.

Rad, R. 1967, Rubberized concrete, New Horizons in Construction Materials l, 287-292.

Sukontasukkul P, Chaikaew C., 2006. Properties of concrete pedestrian block mixed with crumb rubber. Construction and Building Materials 20 (7), 450-457.

16th International Congress of the Geological Society of Greece
17-19 October, 2022 - Patras, Greece
Bulletin of the Geological Society of Greece, Sp. Publ. 10
Ext. Abs. GSG2022-406

Adsorption capacity of bentonites determined with the plate test and methylene blue test

G.E. Christidis[1], G. Grypaiou-Iskenderidou[1], P. Makri[1]
(1) Technical University of Crete, School of Mineral Resources Engineering, Chania, Greece, gchristidis@tuc.gr

The purpose of this contribution is to determine the adsorption capacity of 15 bentonites from Greece, the USA, South Africa and India for water and methylene blue dye and the influence of smectite content of the bentonites on adsorption. The Greek bentonites originate from Milos and were supplied by the S&B Industrial Minerals (Angeria and Aspro Horio deposits, sample codes S0) and the Hellenic Mining Co. Ltd (Agia Irini deposit, sample codes FB). The Angeria bentonites were received as Na-activated materials, whereas the Agia Irini bentonites were Ca-Mg-rich and were activated with 3.5% Na_2CO_3 in the laboratory of Petrology and Economic Geology of Technical University of Crete. The USA bentonites were procured by the CMS source clay project and Haliburton (Wyoming bentonites, sample codes SWy-2, Blue and Yellow) and from the G.E. Christidis collection (Kinney bentonite, Nevada, USA, sample code Kinney). Finally, the South Africa bentonite (Na-activated) was supplied from G.W. Gates (Deakin University, Australia, sample code Africa) and the Indian bentonite was obtained from Ashapura Co (India, sample code A2). The Wyoming bentonites are natural Na-bentonites, whereas Kinney and India bentonites are natural Ca-rich bentonites. Prior to analyses, the bentonites were ground to pass through a 63 μm sieve. Quantitative mineralogical analysis was determined with the Rietveld approach using the BMGN code (Autoquan 2.80 software). Water adsorption was evaluated with the plate test (ASTM E946-83, 1983) and methylene blue adsorption was determined according to Nevins and Weintritt (1965). The Na-activated bentonites were examined in two preparations, namely a) as received, and b) soaked in water overnight to facilitate Na-exchange and ground again to pass through the 63μm sieve. Finally, the Ag. Irini bentonites were heated at 550°C for 2 h and the plate test and methylene blue test were repeated. Determination of water and methylene blue adsorption after heating at 550°C is indicative of the thermal stability of the bentonites and dictates use in the foundry industry.

All bentonites consist mainly of smectite (58-95%) with variable amounts of K-feldspar, plagioclase, anatase and opal-CT ± carbonates. Finally, the Wyoming bentonites contain minor/trace biotite. The smectite content of the Na-activated bentonites was almost identical to that of the soaked-in-water bentonites (± 1% absolute error), strongly suggesting that the Rietveld approach is a very reliable method for determination of quantitative mineralogical composition of bentonites. The water adsorption with the plate test showed a clear positive trend between smectite content and water adsorption (Fig. 1). However, there are several outlier samples, that do not follow that trend. These samples are the FB heat treated bentonites (with one exception) and the Ca-bentonites (original FB, Kinney and Indian). Na-activation and soaking of Na-activated bentonites increased water adsorption.

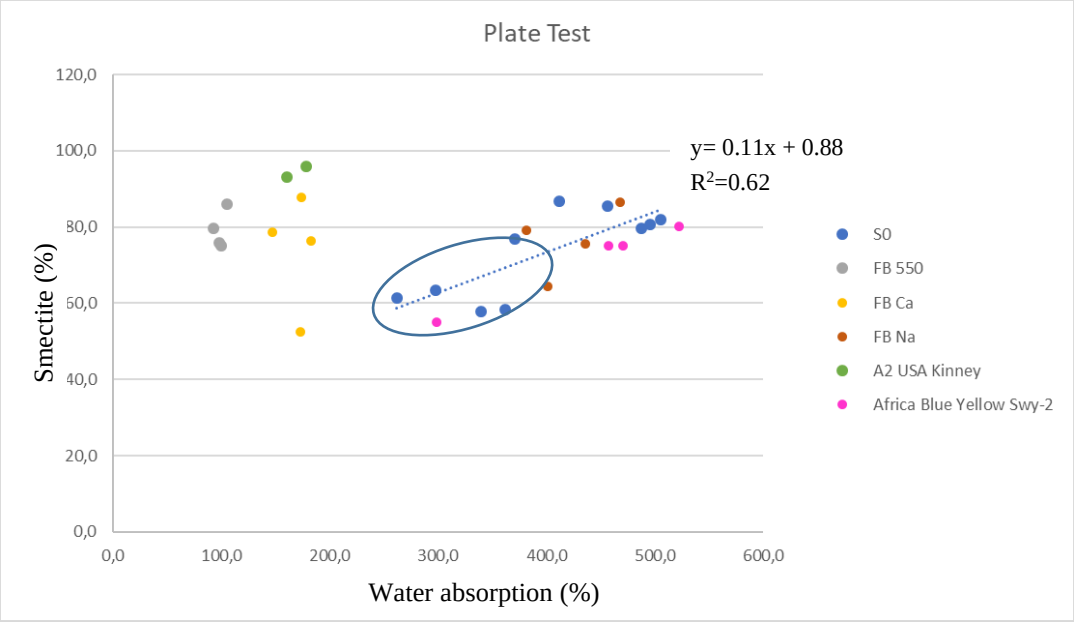

Figure 1. Water adsorption (wt. % with the plate test) *vs.* smectite content. The encircled points are the original (unsoaked) S0 Angeria bentonite samples from Milos.

A similar, although less well expressed linear trend was observed between the smectite content and the volume (ml) of methylene blue adsorbed by the bentonites (data not shown). Again, this linear trend holds for the natural Na-bentonites and the Na-activated bentonites. In contrast, the heated FB bentonites and the Ca-bentonites do not follow this trend and display lower methylene blue adsorption than their Na-rich counterparts. In addition, activation with Na increased methylene blue adsorption.

In conclusion, this study showed that water adsorption and methylene blue adsorption depends on the smectite content, and the type of exchangeable cation (Na *vs.* Ca and/or Mg). While the influence of exchangeable cation is expected in water adsorption, it seems that it holds also in methylene blue adsorption. This is attributed to the difficulty of dye molecules to replace bivalent cations, due to the presence of thick quasicrystals, i.e. due to steric effects. This is enhanced in smectites with high layer charge such as the Kinney smectite (Christidis *et al*. 2006). Finally, the Agia Irini bentonites do not have adequate thermal stability to be used in foundry applications.

Acknowledgements

The authors wish to thank the S&B Industrial Minerals (now Imerys), Bentomine S.A. Ashapura, Halliburton and Will Gates for supplying the bentonite samples for this study.

References

ASTM E946-83 (1983) Standard test method for water absorption of bentonite porous plate method. Annual book of ASTM standards, 681-683.

Christidis, G.E., Blum, A.E and Eberl, D.D (2006). Influence of layer charge and charge distribution of smectites on the flow behaviour and swelling of bentonites. Applied Clay Science, 34, 125-138.

Nevins, M.J and Weintritt, D.J (1967). Determination of cation exchange capacity by methylene blue adsorption. Ceramic Buletin, 46, 587- 592.

16th International Congress of the Geological Society of Greece
17-19 October, 2022 - Patras, Greece
Bulletin of the Geological Society of Greece, Sp. Publ. 10
Ext. Abs. GSG2022-421

Petrographical and geochemical features of the Lower (B1) Karstic Bauxite Horizon at Timios Prodromos Outcrop, Parnassos – Ghiona Unit

N. Sofis[1], G. Papapavlou[1], S. Kalaitzidis[1]
(1) Department of Geology, University of Patras, Rion, Greece, skalait@upatras.gr

Background

The Mesozoic carbonate sequence of the Parnassos-Ghiona Unit (PGU) hosts three bauxite horizons referred to as B1, B2, B3. The latter has been the focus of research interest because it is the main exploitable horizon (e.g. Mondillo et al., 2022). The general geological framework of the bauxite mining district in PGU, and the mineralogical and geochemical features of the bauxite have been well documented (e.g., Valeton et al., 1987; Gamaletsos et al., 2017). However, the focus is currently on the potential exploration of the REE from the metallurgical wastes.

The lower B1 bauxite horizon is characterized by limited vertical and lateral extensions, and is lower in Al grade and quality than the B1 and B2 horizons. Thus, it is not well studied, and its geochemical features and petrogenesis is not well understood.

Objectives

The objective of this study is to characterize the petrographic, mineralogical and geochemical features of the B1 horizon to better understand the depositional conditions, and provenance of the lateritic mud.

Methods

Samples of the B1 bauxite and the hosting limestone were obtained from the known Timios Prodromos (PR) outcrop in the PGU. Petrographic examination was conducted on both thin and polished sections with a polarized optical microscope. The bulk mineralogy was determined with a Bruker D8 X-ray Diffractometer equipped with a LynxEye® detector. EVA® and Topas® software. The geochemical features were determined with a RIGAKU NEXCG Energy Dispersive X-Ray Fluorescence Spectrometer (EDXRF) with a 4 kW Rh X-ray tube to quantify the major elements, and ICP-MS the trace elements.

Results and Conclusions

The B1 bauxite samples consist of varied amounts of hematite, goethite, diaspore, gibbsite, boehmite, anatase, kaolinite, and ±calcite.

A lithology discrimination diagram (Fig. 1), using Fe_2O_3, Al_2O_3 and SiO_2, illustrates that the PR samples fall mainly in the bauxite lithotype, and, less commonly, in the range of kaolinitic to ferritic bauxite.

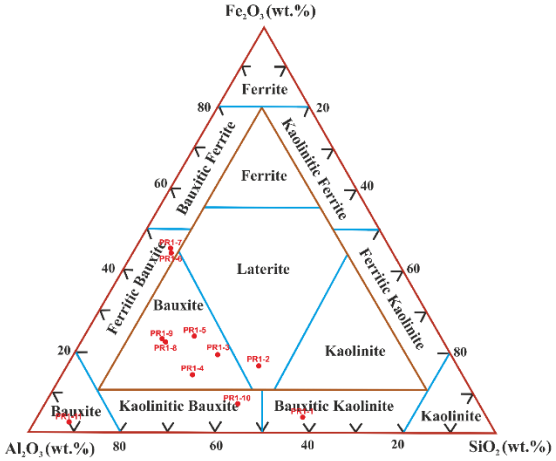

Fig. 1: Ternary diagram illustrating the lithotypes in PR1 outcrop (after Aleva, 1994).

In general, the geochemical results reveal that the PR samples represent a low-grade bauxite, but rich in Fe. Ni grades are up to 907 mg/kg, Co up to 512 mg/kg, Cr up to 342 mg/kg and Cu up to 130 mg/kg. The elevated Ni values probably reflect the mafic/ultramafic origin of the lateritic mud. The ΣREE grades (from 4 bauxite samples) range from 241 to 647 mg/kg, most of which is accounted by Ce, and thus lack a significant REE enrichment.

Acknowledgements

The present work was financially supported by the «Andreas Mentzelopoulos Foundation». The authors would like to thank Dr. Paraskevi Lampropoulou, Section of Earth Materials, Department of Geology, University of Patras, for the XRD analyses, and Dr. Vayia Xantopoulou, Laboratory of Electron Microscopy and Microanalysis of the Faculty of Natural Science, University of Patras, for conducting the XRF analyses. Finally, SGS Canada is acknowledged for the ICP-MS analyses.

References

Aleva, G.J.J., 1994. Laterites: Concepts, Geology, Morphology and Chemistry. Wageningen, the Netherlands: ISIRC, ISBN: 90.6672.053.0., 169 p.

Gamaletsos, P. N., Godelitsas, A., Kasama, T., Church, N. S., Douvalis, A. P., Göttlicher, J., Steininger, R., Boubnov, A., Pontikes, Y., Tzamos, E., Bakas, T., Fillippidis, A., 2017. Nano-mineralogy and -geochemistry of high-grade diasporic karst-type bauxite from Parnassos-Ghiona mines, Greece. Ore Geol. Rev., 84, 228-244.

Mondillo, N., Di Nuzzo, M., Kalaitzidis, S., Boni, M., Santoro, L., Balassone, G., 2022. Petrographic and geochemical features of the B3 bauxite horizon (Cenomanian-Turonian) in the Parnassos-Ghiona area: a contribution towards the genesis of the Greek karst bauxites. Ore Geol. Rev., 143, 104759.

Valeton, I., Biermann, M., Reche, R., Rosenberg, F., 1987. Genesis of nickel laterites and bauxites in Greece during the Jurassic and the Cretaceous and their relation to ultrabasic rocks. Ore Geol. Rev., 2, 359–404.

16th INTERNATIONAL CONGRESS of the
GEOLOGICAL SOCIETY OF GREECE

T8. Natural Hazards and Information Technologies in Geosciences

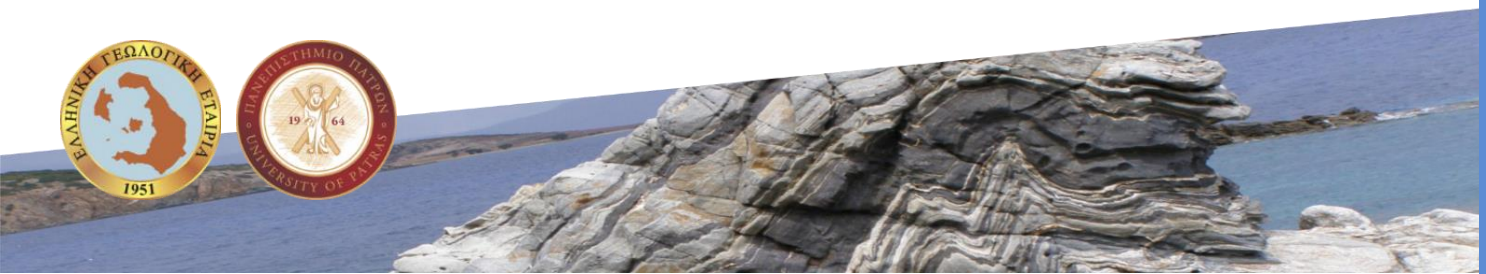

OUR EARTH, OUR HOME

16th International Congress of the Geological Society of Greece
17-19 October, 2022 - Patras, Greece
Bulletin of the Geological Society of Greece, Sp. Publ. 10
Ext. Abs. GSG2022-001

New data of remote sensing: the case of the Khachovi ore occurrence, Georgia.

G. Mindiashvili[1]
(1) Ivane Javakhishvili Tbilisi State University, Tbilisi, Georgia. Giorgi.mindiashvili030@ens.tsu.edu.ge

As it known, the last few years, developed countries successfully use remote sensing to determine structures and search for minerals. In general, remote sensing data collection and interpretation of high-tech production-gene method does not require physical contact with the object. At present all of Earth remote sensing methods are used by science, mainly for the identification of structures of Geology and Earth Resources testing.
Khachkovi area is covered by forests and is characterized by cloudiness. Therefore, the best of satellite ASTER image data were selected, including the minimum cloudiness. Satellite data from the date of 15.06.2007 were investigated. The study area is shown in Figure 1. These data were obtained using remote sensing analysis and techniques through which the geological structures and the possible hydrothermally altered zones are identified.

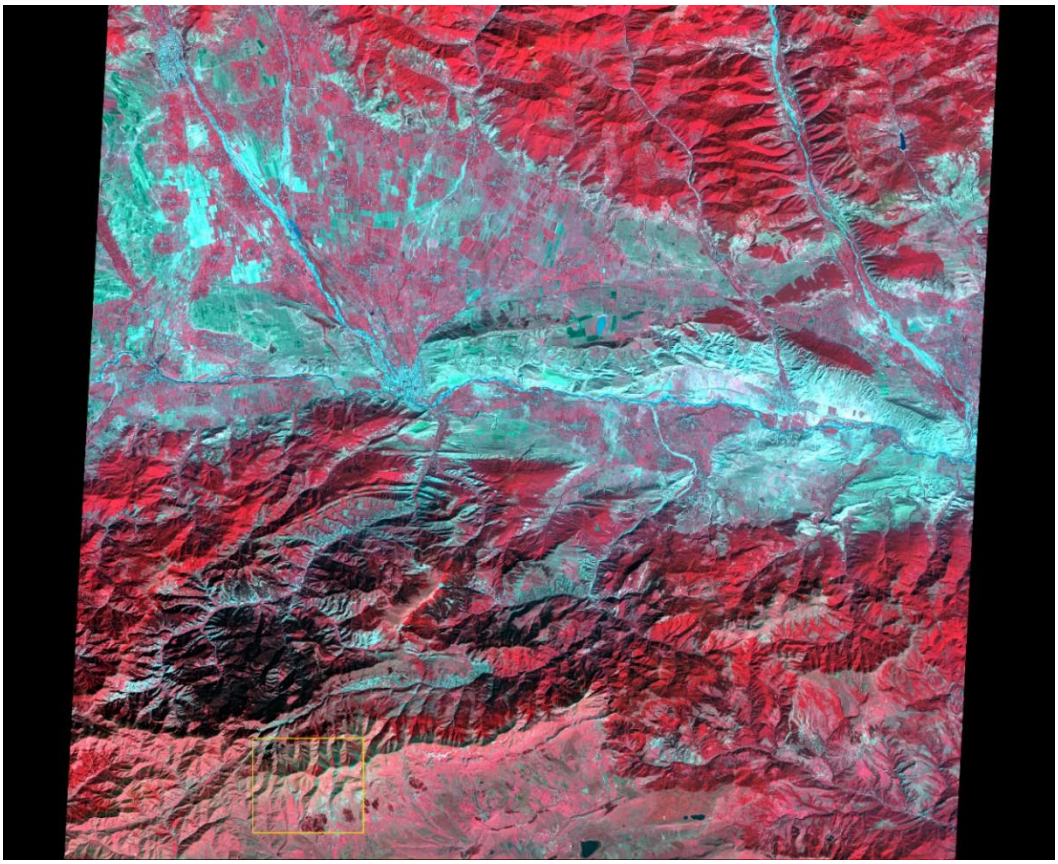

Figure 1. ASTER satellite image of the study area (RGB: 321)

Our research was confined to UTM, WGS84, Zone 38-created coordinates to 1. X-411197.420 Y-4622491.279 2. X-412570.241 Y-4624637.288 3. X-413236.992 Y- 4622827.534 4. X- 415253.122 Y- 4622748.159 5. X- 416491.374 Y-4622525.909 6. X- 417729.626 Y- 4622494.159 7. X- 416920.000 Y- 4621335.281 8. X- 416554.874 Y- 4620620.905 9. X- 415507.122 Y- 4620097.029 10. X- 414999.121 Y- 4619954.154 11. X- 414411.745 Y-4619985.904 12. X-414443.495 Y-4620255.779 13. X-414554.620 Y- 4620271.654 14. X-413792.619 Y-4620144.654 15. X-413459.243 Y-4620255.779 16. X-412150.952 Y- 4619301.316 17. X-412435.941 Y-4620156.282 18. X-412486.233 Y-4620424.507 19. X- 411933.020 Y- 4622084.146.

The coordinates were investigated and conducted a series of tests ASTER-s picture. Structural features and altered zones (Figure 2) were analyzed using a variety of algorithms.

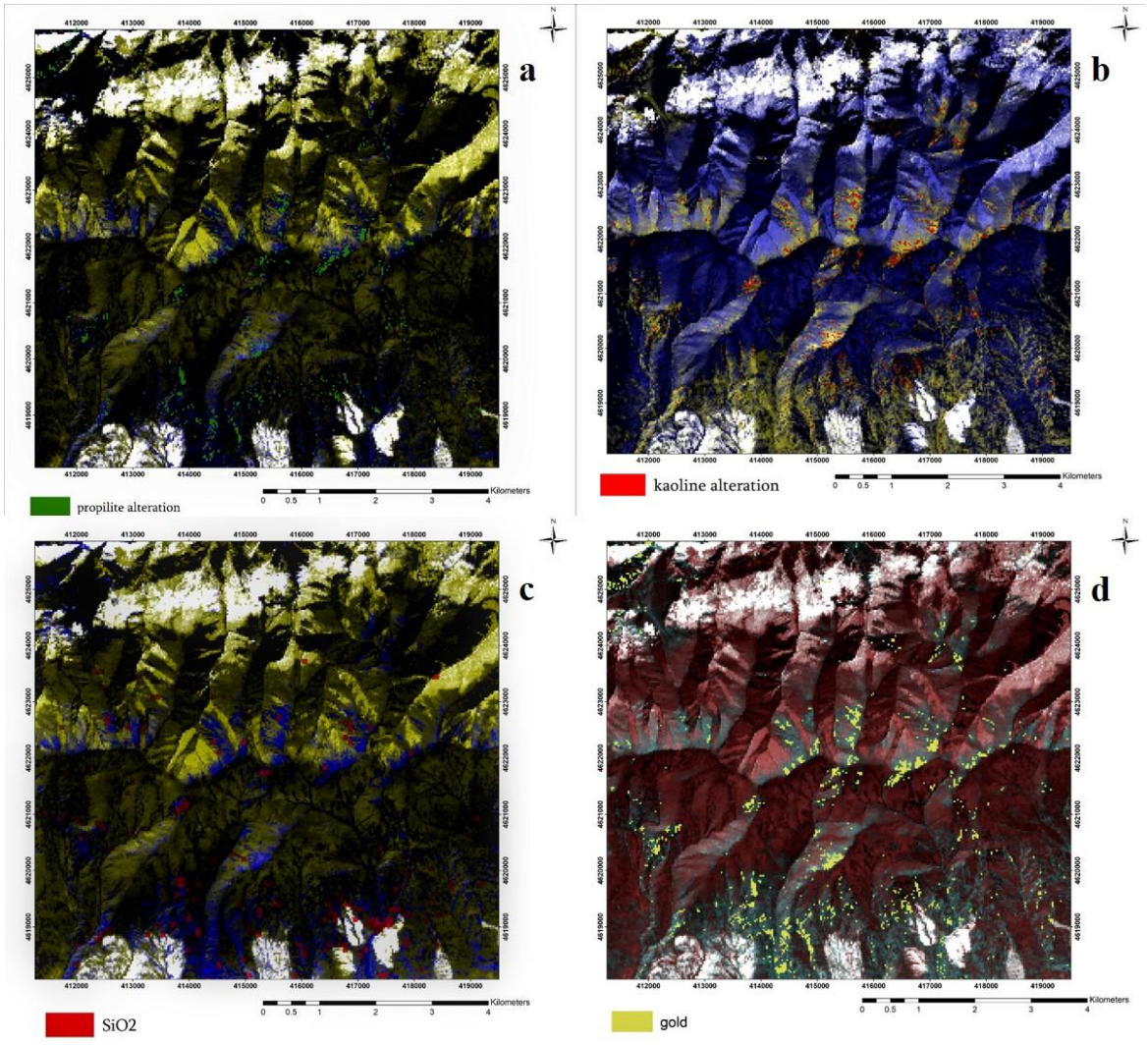

Figure 2. a: Alteration SWIR Band4/SWIR Band5; b: Kaolin alteration SWIR Band4+SWIR Band6+SWIR Band8; c: Sio2 rich rocks TIR Band14/TIR Band12; d: Anomaly of gold-bearing potential zones SWIR Band7/SWIR Band8

As a result of the conducted research work using Remote Sensing methods, unknown mineralized zones on the Khachkovi ore-occurrence were detected. New gold-bearing areas were identified by spectrometric, principal component analyses and international standards of mathematical models. The results of the survey were checked in the field and were found to coincide to previous researchers data.

Acknowledgements

This research [PHDF-21-179] has been supported by Shota Rustaveli National Science Foundation of Georgia (SRNSFG).

References

Bluashvili D. Benashvili K. Mindiashvili G. Makadze D. Bulletion of the Georgian National academy of sciences. Vol. 14, no.3, 2020. New data on the Dzama-Gujareti ore Knot (Georgia). Tbilisi

Bluashvili D. Mindiashvili G. Mining Journal. Structural-Geological position of Gudjareti-Khachkovi orefield.Tbilisi, Georgia.2020.

Yujun, Z., Jianmin, Y., Fojun, Y., 2007. The potentials of multi-spectral remote sensing techniques for mineral prognostication taking Mongolian Oyu Tolgoi Cu–Au deposit as an example. Earth Sci. Front. 14 (5), 63–70.

Ninomiya, Y., Fu, B., Cudahy, T.J., 2005. Detecting lithology with Advanced Spaceborne Thermal Emission and Reflection Radiometer (ASTER) multispectral thermal infrared "radiance-at-sensor" data. Remote Sens. Environ. 99 (1–2), 127–139.

M. Tskhelishvili and Others. Results of general exploration activities in the region of Rekha-Gujareti and Khachkov gold and polimetallic occurrence. Tbilisi, Georgia, 1985

Zhu Liangpu, Geologic remote sensing, 1994.

Gamkrelidze I.P Mechanism of formation of tectonic structure and some problems of tectogenesis. Ed. I need it. Tbilisi, 1976.

16th International Congress of the Geological Society of Greece
17-19 October, 2022 - Patras, Greece
Bulletin of the Geological Society of Greece, Sp. Publ. 10
Ext. Abs. GSG2022-012

Mapping of the non-seismic surface ruptures in Stratoniki village, NE Chalkidiki

A. Chatziioannou[1], A. Chatzipetros[2]

(1) University of the Aegean, Mytilene, Greece, geoha20025@geo.aegean.gr (2) Aristotle University of Thessaloniki, Thessaloniki, Greece.

The development of a surface rupture system not induced by a seismic source has become the main problem of Stratoniki village in NE Chalkidiki since at least 2001. These ruptures not only appear on the asphalted streets, but also on fences and houses compelling the owners to repair them or live at a risk. Moreover, the situation seems to grow bigger with time and cracks appear even on repaired parts of the village. This research focuses only on the ruptures that appear on the public streets of the village. It provides updated maps of their expansion as well as a statistical analysis of their growth and their geometric characteristics.

Stratoniki is built on a small horst bounded by two normal faults as found by I.G.M.E.'s geophysical survey (Arvanitidis et al., 2008). The small formation is located on the top surface of a large normal fault's hanging wall. The Stratoni-Barbara active fault is a large fault (~25km) with an E-W general direction and a seismic potential of M6.8. This fault zone has contributed to the development of hydrothermal mineralizations that have been exploited since the ancient times. Today, the mining activity has been expanded in the area below the village.

From a geological point of view, the area belongs to the Serbo-Macedonian massif with a relatively simple structure. The geohazard is occurring entirely in Pleistocene age sediments that overly the Paleozoic age basement. The sedimentary layer consists of silt and clay and is thinner in the northern part of the village, on the foot of Mount Stratonikon. It also is saturated, since the aquifer is closer to the ground than it seemed to be. Moreover, geophysical surveys have shown a few internal voids below the village. All these factors compose a heterogenous ground with areas of instability lead to ruptures and subsidence phenomena that have been recorded in the past.

During our survey in the summer of 2019, 279 street ruptures were mapped and recorded (208 linear and 71 irregular) within the boundaries of the village. Compared to the 49 recorded in a previous mapping that took place in 2008 by the Institute of Geological and Mineral Exploration of Greece, the growth of the ruptures is significant. The statistical analysis of their geometric characteristics has shown two main trends of direction, NNE-SSW and ESE-WNW, that correspond with the main fault zone of the area. Analyzing the displacement vector, it seems to encompass in two trends too: ENEWSW and NNW-SSE. Furthermore, a geospatial analysis was necessary to understand the phenomenon's growth direction. Comparing the new ruptures' central tendency characteristics to the 2008 mapping, they seem to be expanding southwards.

These findings contribute in several ways to our understanding of the spatiotemporal evolution of this surface rupture system and provide a basis for scientific discussion on the problem. The relationship of the surface ruptures with the area's faults indicates the existence of active horizontal tectonic stresses. This is a common cause of ground fissures but does not suffice for the situation here considering its complexity. Every factor that seems to affect the geohazard should be investigated and quantified. Thus, detailed hydrological research with borehole drillings is necessary to examine for a possible compaction of the aquifer-system. Furthermore, a gravimetric survey would be useful providing data about the potential contribution of the mining activity and the existing voids to the multifaceted geohazard. This method is an asset because it can relate density changes with ground instability areas (Kortas, 2021), but it needs a sufficient time period of monitoring to provide considerable results.

References

Arvanitidis, N., Atzemoglou, A., Maltzaris F., Pogiatzi, E., 2008. Geophysical and Geotechnical Survey of Stratoniki-Stagira region. Institute of Geological and Mineral Exploration (IGME), Thessaloniki. **[Technical report]**

Kortas, Ł., 2021. Gravity field changes during deep exploitation of the coal longwall and their relation to stress distribution and seismic activity, Journal of Sustainable Mining, 20(4), 228–239. **[Journal Article]**

16th International Congress of the Geological Society of Greece
17-19 October, 2022 - Patras, Greece
Bulletin of the Geological Society of Greece, Sp. Publ. 10
Ext. Abs. GSG2022-068

Exploratory Data Analysis of Climate Change and its Relation to the Occurrence and Economic Impact of Natural Hazards.

A.A. Chrysafi[1], P. Tsangaratos[1]

(1) National Technical University of Athens, Athens, Greece, alexchrysafi@mail.ntua.gr

Introduction

According to Fifth Assessment Report of IPCC (IPCC, 2013b), human influence on climate has been the dominant cause of observed warming since the mid-20th century, while global average surface temperature warmed by 0.85°C between 1880 and 2012. Many regions of the world have already greater regional-scale warming, with 20–40% of the global population having experienced over 1.5°C of warming in at least one season. Temperature rise to date has already resulted in profound alterations to human and natural systems, including increases natural hazards such us droughts, floods, extreme temperatures etc.– changes which are causing unprecedented risks to vulnerable persons and populations (IPCC, 2012a; IPCC, 2014a; Mysiak et al., 2016). Based to United Nations Office for Disaster Risk Reduction (UNDRR, 2009) as a natural hazard is considered a "Natural process or phenomenon that may cause loss of life, injury or other health impacts, property damage, loss of livelihoods and services, social and economic disruption or environmental damage". Natural hazards may have severe consequences for society, including threats to human life, economic losses, and damage to ecosystems (Rutgersson et al., 2021). According to the Centre for Research on the Epidemiology of Disasters (CRED), these can be droughts, earthquakes, extreme temperatures, floods, landslides, mass movements, storms, volcanic activities or wildfires. Since 1990, natural hazards have led to over 1.6 million fatalities globally, and economic losses are estimated at an average of around $260–310 billion per year (Ward et al., 2019). In this context, the objective of this study is to explore and analyze climate change and its relation to natural hazards (occurrence and economic impact). For this analysis, global temperature rise is used as an indicator of climate change.

Material & Methods

The data used in this study concern global temperatures for the period 1850-2015 which were extracted from the Berkeley Earth database (http://berkeleyearth.org/data). Moreover, natural hazards data was taken for the period 19002018 from Emergency Events Database (EM-DAT (2019)) which are available via https://ourworldindata.org/naturaldisasters. The processing of the data was carried out through the programming language R (via open software Rstudio) which is considered as the primary tool in data analysis (Lai et al., 2019).

Results and Conclusions

From the data used for the period 1850-2015, observed that the warmest year was 2015. Since the 1970s, the anomalies are positive, which shows that the warming has been strong and ongoing, and even accelerating faster in recent years. Figure 1 depicts the total number of natural hazards such as floods, droughts, wildfires, landslides, extreme temperatures, volcanic activity, mass movements and extreme weather, globally, in relation to the temperature anomaly from 1900 to 2015. There is a positive correlation between the rising occurrence of natural hazards and increasing temperature, however, this relationship is at least partially driven by better detection and recording of hazards. Natural disasters not only have devastating impacts in terms of the loss of human life, but can also cause severe destruction with economic costs. Figure 2 shows that for the period 1900-2018, the year with the greatest economic loss due to natural disasters worldwide was observed in 2011 which amounted to about 364 billion U.S. dollars.

In times of increasing losses from disasters, an in-depth understanding of their impacts is required in order to reduce natural hazards through the development of forms of sustainable risk management as well as risk mitigation and adaptation strategies.

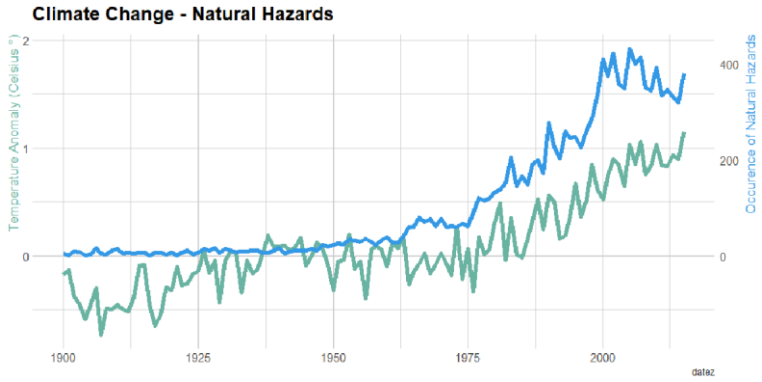

Figure 1. Number of natural hazards in relate to the temperature anomaly globally for the period 1900-2015.

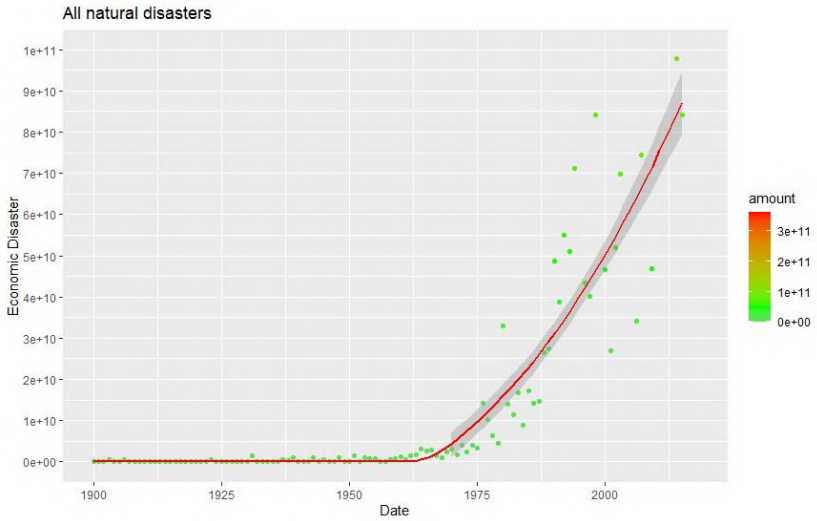

Figure 2. Economic loss of natural hazards for the period 1900-2018.

References

IPCC, 2012a. Summary for Policymakers. In: Managing the Risks of Extreme Events and Disasters to Advance Climate Change Adaptation [Field, C.B., V.R. Barros, T.F. Stocker, D. Qin, D.J. Dokken, K.L. Ebi, M.D. Mastrandrea, K.J. Mach, G.-K. Plattner, S.K. Allen, M. Tignor, and P.M. Midgley (eds.)]. Cambridge University Press, Cambridge, United Kingdom and New York, NY, USA, pp. 3–21.

IPCC, 2013b. Summary for Policymakers. In: Climate Change 2013: The Physical Science Basis. Contribution of Working Group I to the Fifth Assessment Report of the Intergovernmental Panel on Climate Change [Stocker, T.F., D. Qin, G.K. Plattner, M. Tignor, S.K. Allen, J. Boschung, A. Nauels, Y. Xia, V. Bex, and P.M. Midgley (eds.)]. Cambridge University Press, Cambridge, United Kingdom and New York, NY, USA, pp. 3–29.

IPCC, 2014a. Summary for Policymakers. In: Climate Change 2014: Impacts, Adaptation, and Vulnerability. Part A: Global and Sectoral Aspects. Contribution of Working Group II to the Fifth Assessment Report of the Intergovernmental Panel on Climate Change [Field, C.B., V.R. Barros, D.J. Dokken, K.J. Mach, M.D. Mastrandrea, T.E. Bilir, M. Chatterjee, K.L. Ebi, Y.O. Estrada, R.C. Genova, B. Girma, E.S. Kissel, A.N. Levy, S. MacCracken, P.R. Mastrandrea, and L.L. White (eds.)]. Cambridge University Press, Cambridge, United Kingdom and New York, NY, USA, pp. 1–32.

Lai, J., Lortie, C. J., Muenchen, R. A., Yang, J., and Ma, K., 2019. Evaluating the popularity of R in ecology. Ecosphere 10 (1):e02567, https://doi.org/10.1002/ecs2.2567

Mysiak, J., Surminski, S., Thieken, A., Mechler, R., and Aerts, J., 2016. Brief communication: Sendai framework for disaster risk reduction – success or warning sign for Paris?, Nat. Hazards Earth Syst. Sci., 16, 2189–2193, https://doi.org/10.5194/nhess-162189-2016.

Rutgersson, A., Kjellström, E., Haapala, J., Stendel, M., Danilovich, I., Drews, M., Jylhä, K., Kujala, P., Larsén, X. G., Halsnæs, K., Lehtonen, I., Luomaranta, A., Nilsson, E., Olsson, T., Särkkä, J., Tuomi, L., and Wasmund, N., 2022. Natural hazards and extreme events in the Baltic Sea region, Earth Syst. Dynam., 13, 251–301, https://doi.org/10.5194/esd-13-251-2022

UNDRR, 2009. Global Assessment Report 2009. Risk and Poverty in a Changing Climate. Global Assessment Report on Disaster Risk Reduction. UN Office for Disaster Risk Reduction, Geneva

Ward, P. J., Blauhut, V., Bloemendaal, N., Daniell, J. E., de Ruiter, M. C., Duncan, M. J., Emberson, R., Jenkins, S. F., Kirschbaum, D., Kunz, M., Mohr, S., Muis, S., Riddell, G. A., Schäfer, A., Stanley, T., Veldkamp, T. I. E., and Winsemius, H. C., 2020: Review article: Natural hazard risk assessments at the global scale, Nat. Hazards Earth Syst. Sci., 20, 1069–1096, https://doi.org/10.5194/nhess-20-1069-2020

16th International Congress of the Geological Society of Greece
17-19 October, 2022 - Patras, Greece
Bulletin of the Geological Society of Greece, Sp. Publ. 10
Ext. Abs. GSG2022-073

Launching a geophysical campaign on Santorini using muography: simulation of geological targets and geometries

S. Zormpas[1], G. Nyitrai[2], C.D. Athanassas[1], D. Varga[2], E. Hristoforou[1], Th. Alexopoulos[1], G. Hamar[2], G. Surányi[2]
(1) National Technical University of Athens (NTUA), Zografos, 15780, Athens, Greece (2) Wigner Research Center for Physics, Konkoly-Thege Miklós, 1121, Budapest, Hungar

Muography constitutes a novel remote sensing geophysical technique which exploits the penetration of the cosmic rays in the upper solid earth to produce images of the geological structure at high spatial resolution. Muography has been used as a remote sensing method to explore the density variations of volcanoes (e.g. Oláh et al., 2022; Tanaka, 2000), monitor the magma kinetics therein (e.g. Tanaka et al. 2009, 2014; Oláh et al. 2019), and nowcast volcanic hazards in Japan (Tanaka et al. 2009, 2014) by employing cutting-edge particle detector technologies (e.g. Varga et al. 2016; Bouteille et al. 2016). Muography has also revolutionized non-invasive imaging of archaeological monuments (e.g. the great void in Khufu's Pyramid, Morishima et al. 2017).

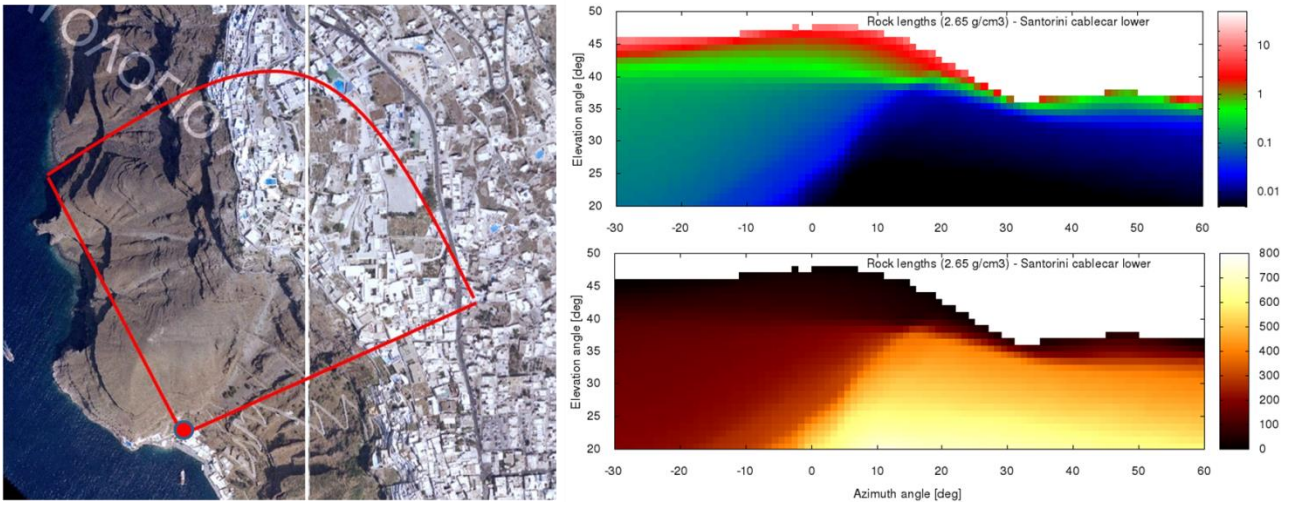

Fig.1. Left: Proposed position of the muographic telescope. Right top: simulated muon flux through the Fira fault, Santorini, for various azimuth angles. Right bottom: calculated rock length around the Fira fault for various azimuth angles (G. Nyitrai).

Gaseous tracking detectors (Oláh et al. 2018) enable the observation of density fluctuations in real time (Varga et al. 2016). Developments have made it possible to image blind deep-seated shear zones, such as the fault zone of Itoigawa-Shizuoaka, Japan (Tanaka et al. 2011) and the Cernon fault, Aveyron, France (Lesparre et al. 2016). Greece is particularly rich in muography targets, including archeological sites, as well as regions with high seismic and volcanic activity with many of these in densely populated areas. Muography , therefore, opens up the possibility of imaging of blind, deep-seated structural failures on Santorini. Santorini is the southernmost active volcanic center in the Aegean and emerges from a NE–SW trending rift zone bounded by normal faults with a right-lateral component of movement (Nomikou et al. 2018). Among them the Fira fault draws particular attention due to its adjacency with the namesake town which is the largest urban center on Santorini. A proposed Hungarian-Greek muography campaign at the Fira fault will have substantial economic and social impact besides the scientific aspect. Muography of the Fira fault is not only a valid scientific case, by contributing to the success of the emerging international "Muographers" community (http://muographers.org/), but has high impact for the society, and can boost Greece to the forefront of the muon imaging research (Athanassas, 2020).

Here, the performance of muography in mapping Fira fault on Santorini, is evaluated on the basis of simulation experiments. Simulations based on DEM data from Fira fault led to estimations of rock lengths and the prediction of the muon flux through Fira fault (Fig. 1). The simulation suggests that for optimal acquisition the detector should be installed near the lower cable car station (right above the port), facing to the north-east. For azimuth angles between 0° and -30° (west), data acquisition would require a few weeks. Still, the fault-related region lies between azimuth angles 10° - 30° (300-500 m rock). Here the cosmic muon fluxes range between 0.1 - 0.01 [$m^{-2} \cdot sr^{-1} s^{-1}$]. In this cease a large setup (80 cm × 80 cm detector chambers) is recommended. The expected counting frequency within a 1 × 1 deg angle

bin is one muon per every 1-2 days. Therefore, in order to image at high resolution the subsurface below the town of Fira within at a depth of ~50 m the measurement time is estimated to a few months. However, if the fault zone falls in the 0 - 100 meter rock-length region in north direction, and 50 cm × 50 cm detector would be sufficient.

References

Athanassas, C.D. 2020. Muography for geological hazard assessment in the South Aegean active volcanic (SAAVA). Mediterranean Geoscience Reviews, 2, 233–246

Bouteille, S., Attié, D., Baron, P., Calvet, D., Magnier, P., Mandjavidze, I., Procureur, S., Riallot, M., Winker, M. 2016. A Micromegas-based telescope for muon tomography: the watTo experiment. Nucl Instrum Methods Phys Res Sect A, 834,223–228

Lesparre, N., Boyle, A., Grychtol, B., Cabrera, J., Marteau, J., Adler, A. 2016. Electrical resistivity imaging in transmission between surface and underground tunnel for fault characterization. J. Appl. Geophys., 128, 163–178

Morishima, K., Kuno, M., Nishio, A. et al. 2017. Discovery of a big void in Khufu's Pyramid by observation of cosmic-ray muons. Nature, 552, 386–390.

Nomikou P., Hübscher, C., Papanikolaou, D., Farangitakis, G.P., Ruhnau, M., Lambridou, D. 2018. Expanding extension, subsidence and lateral segmentation within the Santorin-Amorgos basins during Quaternary: implications for the 1956 Amorgos events, central-south Aegean Sea, Greece. Tectonophysics 722:138–153

Oláh, L., Tanaka, H., Ohminato, T., Nyitrai, G., Hamar, G., and Varga, D. 2022. Muography of the Active Sakurajima Volcano: Recent Results and Future Perspectives of Hazard Assessment. Journal of Advanced Instrumentation in Science, vol. 2022.

Oláh, L., Tanaka, H.K.M., Ohminato, T., Varga. D. 2018. High-deifinition and low-noise muography of the Sakarajima volcano with gaseous tracking detectors. Sci. Rep., 8, 3207

Tanaka, H. 2022. Principles of Muography and Pioneering Works. In: L. Oláh, H.K.M. Tanaka, D. Varga: Muography: Exploring Earth's Subsurface with Elementary Particles, American Geophysical Union (AGU).

Tanaka, H.K.M., Kusagaya, T., Shinohara, H. 2014. Radiographic visualization of magma dynamics in an erupting volcano. Nat. Commun., 5:3381.

Tanaka, H.K.M., Uchida, T., Tanaka, M., Takeo, M., Oikawa, J., Ohminato, T., Aoki, Y., Koyama, E., Tsuji, H. 2009. Detecting a mass change inside a volcano by cosmic-ray muon radiography (muography): first results from measurements at Asama volcano, Japan. Geophys Res Lett 36:L17302.

Tanaka, H.M.K., Miyajima, H., Kuasagaya, T., Taketa, A., Uchida, T., Tanaka, M. 2011. Cosmic muon imaging of hidden sesimc fault zones: rainwater permeation into the mechanical fractured zones in Itoigawa-Shizuoka Tectonic Line, Japan. Earth Planet Sci Lett. 306, 156–162

Varga, D., Nyitrai, G., Hamar, G., Oláh, L. 2016. High efficiency gaseous tracking detector for cosmic muon radiography. Adv High Energy Phys. 1962317

16th International Congress of the Geological Society of Greece
17-19 October, 2022 - Patras, Greece
Bulletin of the Geological Society of Greece, Sp. Publ. 10
Ext. Abs. GSG2022-092

Wildfire mapping in the Region of Western Greece using Sentinel-2 and Landsat imagery.

E. Dimitriou[1], A. Kyriou [1], K. Nikolakopoulos [1]
(1) University of Patras, Department of Geology, 26504 Patras, Greece, eirini.dimitriou99@gmail.com

Research Highlights

Ten-year wildfire mapping in the prefecture of Western Greece using multispectral Sentinel-2 and Landsat data.

Background-Objectives

Wildfires are among the most common natural disasters, which occur mainly in extremely dry conditions (summer period) due to natural causes or human activities. They can potentially lead to permanent vegetation loss, soil erosion and consequently flooding and desertification, while they can also be particularly harmful to humans themselves. In recent years, a rapid increase in the number of fires has been observed, especially in areas such as Siberia, California, Australia as well as in regions with Mediterranean climate. In the current study, we mapped the burned areas in the northwestern Peloponnese for a ten-year period (2011-2021) using spaceborne remote sensing data. The use of remote sensing in burned land mapping has a 30-year long history as tool in mapping and monitoring of forest fire. Despite this long period, burned land mapping using satellite data is still an active research topic in satellite remote sensing. Many characteristic examples of satellite remote sensing studies of burned land mapping and monitoring can be found in the literature (Sali et. al., 2021; Syifa et. al., 2020), however studies dealing with a multisource data set for the same fire event are limited.

Methodology

In more detail, we obtained Sentinel-2 and Landsat data -provided free of charge to all users- covering the study area before and after wildfires (Tables 1,2). Firstly, classical image processing algorithms were applied to correct geometrically, and radiometrically the images used. The processing of satellite products, derived from Landsat and Sentinel-2 satellites, were carried out into ERDAS Imagine and SNAP software. The identification and the subsequent mapping of the burnt areas was based on the calculation of the Normalized Difference Vegetation Index (NDVI) as well as on the estimation of the Normalized Burn Ratio (NBR) index. Burnt areas arising from both missions were integrated into an ArcGIS environment in order to be measured and compared. The assessment of the results was carried out using burnt areas, acquired by the European Forest Fire Information System (EFFIS).

Table 1. Sentinel-2 data

NO	Date	No	Date
1	19 May 18	5	08 May 20
2	21 September 18	6	15 September 20
3	29 April 19	7	08 May 21
4	16 September 19	8	15 September 21

Table 2. Landsat-8 data

NO	Date	NO	Date
1	10 May 14	9	19 April 18
2	01 October 14	10	10 September 18
3	27 April 15	11	26 March 19
4	18 September 15	12	17 October 19
5	13 April 16	13	24 April 20
6	04 September 16	14	05 September 20
7	02 May 17	15	11 April 21
8	07 September 17	16	18 September 21

Results

Sentinel-2 as well as Landsat data were successfully used for the mapping of the wildfires, occurred in the Region of Western Greece between 2011-2021. The total percentage of burnt areas for each year was calculated. Figure 1 displays a region in western Peloponnese before and after a wildfire, as captured by Sentinel-2 mission (band combination 12-11-8A). In particular, the burnt area was marked with orange color, while the boundaries of the burnt part have been digitized.

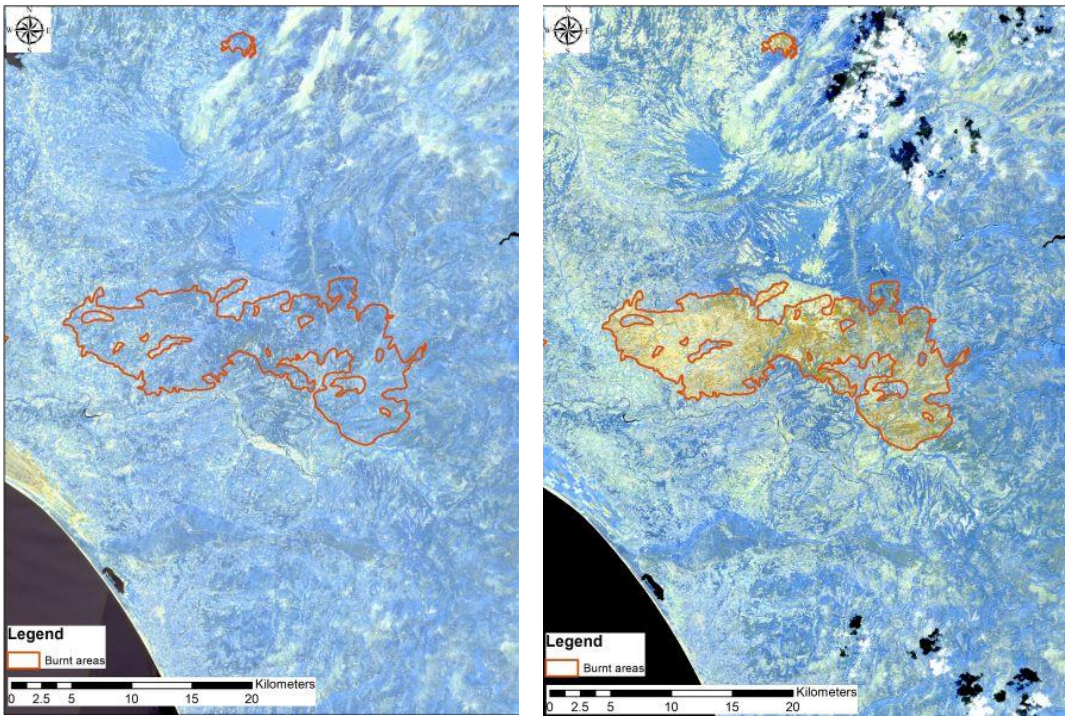

(a) **(b)**

Figure 1. (a) Sentinel-1 pre-fire image (12-11-8A), (b) Sentinel-1 post-fire image (12-11-8A).

Acknowledgements

The authors would like to thank the European Space Agency (ESA) and National Aeronautics and Space Administration (NASA) for the provision of Sentinel-2 and Landsat data.

References

Sali, M., Piaser, E., Boschetti, M., Brivio, P.A., Sona, G., Bordogna, G., Stroppiana, D., 2021. A Burned Area Mapping Algorithm for Sentinel-2 Data Based on Approximate Reasoning and Region Growing. Remote Sens., 13, 2214.

Syifa, M., Panahi, M., Lee, C.-W., 2020. Mapping of Post-Wildfire Burned Area Using a Hybrid Algorithm and Satellite Data: The Case of the Camp Fire Wildfire in California, USA. Remote Sens, 12, 623.

16th International Congress of the Geological Society of Greece
17-19 October, 2022 - Patras, Greece
Bulletin of the Geological Society of Greece, Sp. Publ. 10
Ext. Abs. GSG2022-094

A Multi-Temporal Landslide Inventory in Landslide Hazard Assessment: Statistics and Geometry of Landslides triggered by the 2008 Movri Mnt Earthquake (West Achaia, Greece)

A. Litoseliti[1], I. Koukouvelas[1], K. Nikolakopoulos[1]
(1) University of Patras, Department of Geology, 26504 Rion-Patras, Greece, aspal@upatras.gr

Abstract

Assessment of landslide hazard across mountains is imperative for public safety. Pre- and post-earthquake landslide mapping envisage that landslides show significant size changes during and after the earthquake activity. One of the purposes of earthquake-induced landslide investigation is to determine the landslide state and geometry and draw conclusions on their mobility. This study was based on remote sensing data that covered 72 years, and focused on the west slopes of the Skolis Mountain, in the west Achaia (northwest Peloponnese). On 8 June 2008, during the strong Movri Mountain earthquake (Mw = 6.4), we mapped the extremely abundant landslide occurrence. Historical seismicity and remote sensing data indicate that the Skolis Mountain west slope is prone to landslides. We recognized that 89 landslides developed over the last 72 years. These landslides increased their width (W), called herein as inflation or their length (L), termed as enlargement. Length and width changes were used to describe their aspect ratio (L/W). Based on the aspect ratio, the 89 landslides were classified into three types: I, J, and Δ. Taluses, developed at the base of the slope and belonging to the J- and Δ-landslide types, are supplied by narrow or irregular channels commonly testifying I-type landslides. During the earthquakes, the landslide channels migrated upward and downward, outlining the mobility of the earthquake-induced landslides. Landslide mobility was defined by the reach angle. The reach angle is the arctangent of the landslide's height to length ratio. Furthermore, we analyzed the present slope stability across the Skolis Mountain by using the landslide density (LD), landslide area percentage (LAP), and landslide frequency (LF). All these parameters were used to evaluate the spatial and temporal landslide distribution and evolution with the earthquake activity. Moreover, the investigation of correlations between spatial distribution and statistical parameters has been done using regression analysis. High positive correlations observed between the latter indicating that Skolis slopes are controlled by reactivated landslides, which occur within pre-existing landslide masses, triggered by critical seismic events that determine the beginning and end of seismic periods. These results can be considered as a powerful tool for earthquake-induced landslide disaster mitigation.

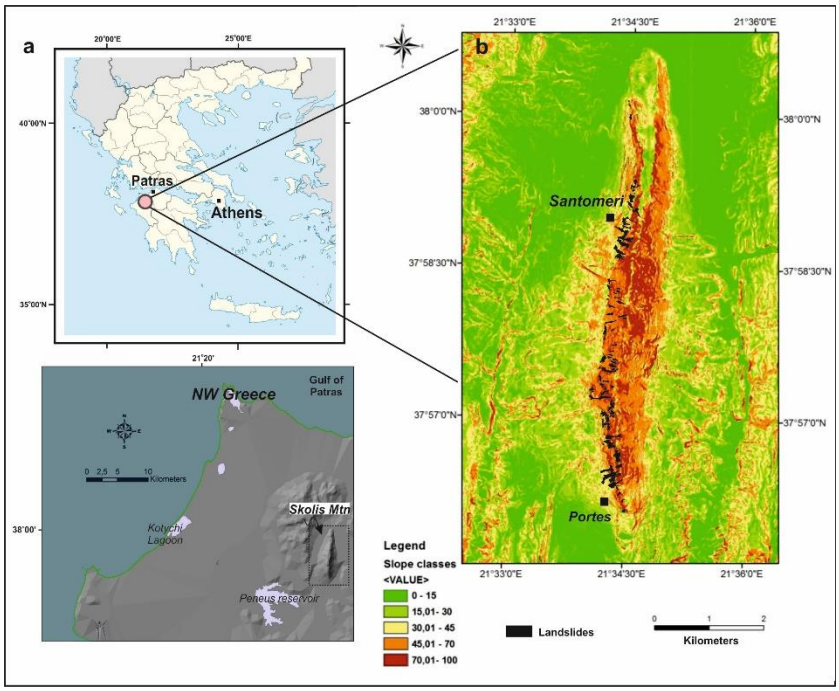

Figure 1. (a) Location map and (b) shaded relief map of the study area; (c) Slope map of Skolis Mtn (west Achaia).

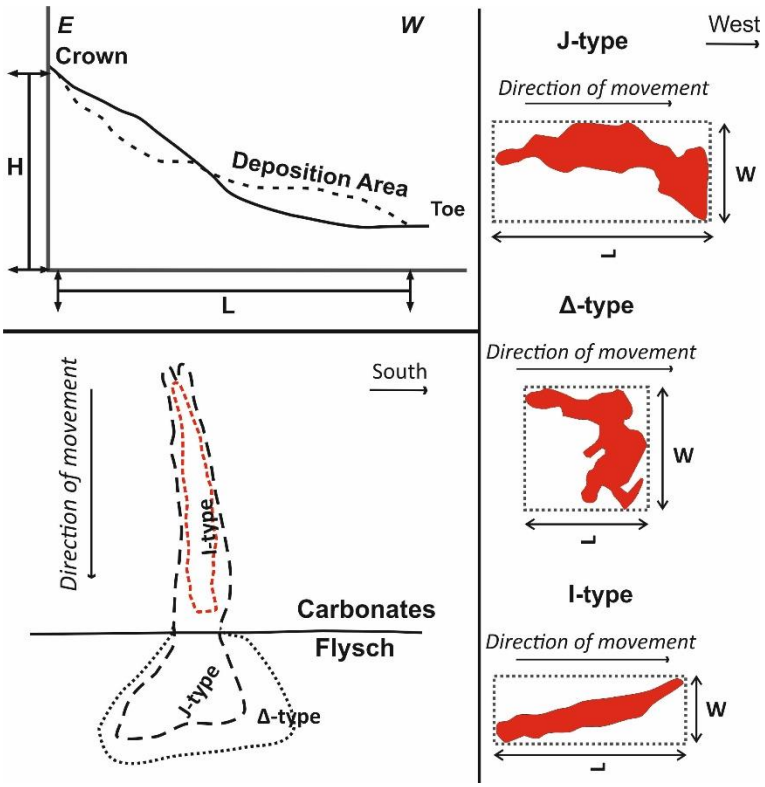

Figure 2. Definitions of geometric parameters of Skolis Mtn landslides and the minimum bounding rectangle method.

References

Koukouvelas, I., Kokkalas, S., Xypolias, P., 2010. Surface deformation during the Mw 6.4 (8 June 2008) Movri Mountain earthquake in the Peloponnese, and its implications for the seismotectonics of western Greece. Int. Geol. Rev. 52, 249–268.

Koukouvelas, I., Litoseliti, A., Nikolakopoulos, K. and Zygouri, V., 2015. Earthquake triggered rock falls and their role in the development of a rock slope: The case of Skolis Mountain, Greece. Eng. Geol. 191, 71-85.

Litoseliti, A., Koukouvelas, I.K., Nikolakopoulos, K.G., Zygouri, V., 2020. An Event-Based Inventory Approach in Landslide Hazard Assessment: The Case of the Skolis Mountain, Northwest Peloponnese, Greece. ISPRS Int. J. Geo-Inf., 9, 457.

16th International Congress of the Geological Society of Greece

17-19 October, 2022 - Patras, Greece

Bulletin of the Geological Society of Greece, Sp. Publ. 10

Ext. Abs. GSG2022-096

Detection of mineralized zones at an igneous intrusion in the Koutala islet, Lavreotiki, Greece using Sentinel-2 satellite data and mineralogical analysis

O. Sykioti[1], A. Ganas[2], C. Vasilatos[3], Z. Kypritidou[3]

(1) Institute of Astronomy, Astrophysics, Space Applications and Remote Sensing, National Observatory of Athens, Athens, Greece, sykioti@noa.gr (2) Institute of Geodynamics, National Observatory of Athens, Athens, Greece (3) Department of Geology and Geoenvironment, National and Kapodistrian University of Athens, Athens, Greece

Introduction and Objectives

The Lavreotiki area (Attica, Greece) has been famous for mining since the 5th century BC producing silver and lead contributing to the economic development of ancient Athens during the classic era (Voudouris *et al.*, 2021). The geology and metallogeny of the Lavreotiki area (Attica, Greece) were studied by Marinos and Petrascheck (1956), Skarpelis *et al.* (2008), Voudouris *et al.* (2021) among others, including the petrology and emplacement of magmatic intrusions (granitoids). These igneous rocks in SE Attica are the most westerly occurrence of a series of Middle to Late Miocene plutons in the Attic–Cycladic belt that were emplaced following the widespread extension of the Cyclades area (located in the back-arc area of the Hellenic Subduction) and the exhumation of high-pressure rocks (blueschists). A west-dipping major detachment fault has been mapped by Skarpelis *et al.* (2008) and Scheffer *et al.* (2016) a few km west of the city of Lavrion with a N-S orientation. In this paper, we present the findings of a joint remote-sensing and laboratory examination of the mineralization zones induced by the intrusion of an igneous body onshore the islet of "Koutala" (Fig.1a) about 5 km NNE of the city of Lavrion. The islet has a form of a rocky promontory, forming a characteristic tombolo feature with the mainland (in geomorphologic terms). Its size is about 240 m in E-W by 40-60 N-S direction. Our objective was to investigate the potential of Sentinel-2 to detect and map minerals which were detected from the laboratory analysis of samples collected in-situ and that they could be linked to Fe-Mn mineralization.

Data and analysis

During a field campaign conducted in 18/7/2022, 18 GPS measurements were collected at the eastern part of the islet in order to delineate the contact between the granitoid and the schists. Furthermore, four samples were collected and analyzed in the laboratory using the XRD method, one of schist, two of granitoid and one of Fe- Mn- mineralization identified at the granitoid/schist contact. The XRD analysis detected, among other minerals, the presence of hydrothermal alteration minerals in all samples. In particular, micas and chlorite were found in the granitoid and schist samples while goethite Mn-oxide/hydroxides and micas, were identified in the ore sample. Mn-oxide/hydroxides were also identified in the schist sample (Fig. 1b).

Following the mineralogical study, four minerals, that could be related to this type of alteration, were selected, namely muscovite, chlorite, goethite and Mn-oxides/hydroxides for the spectral study of the Sentinel-2 image. Their spectral signatures were retrieved from the USGS Spectral Library (average grain size 30-70μm) convolved to the Sentinel-2 spectral bands (named hereafter as reference minerals and/or spectral signatures). A Sentinel-2 satellite image was retrieved, acquired in 19/7/2022. The image was georeferenced, atmospherically corrected and subset to the study area. The output reflectance image (pixel values [0,1]) consists of 12 spectral bands, resampled to 10m spatial resolution. Two distinct methods were then applied: (i) band ratios and (ii) absorption feature analysis. Concerning the former, two spectral indices (SIs) were calculated that detect the presence of iron-bearing minerals, namely the ferric iron SI (b4/b3) and the ferrous iron SI [(b12/b8)+(b3/b4)] (van der Meer *et al.*, 2014). In Fig. 2(a,b), the corresponding maps SI maps are shown. Concerning the second method, the center wavelength(s) of diagnostic absorption feature(s) of each reference mineral was identified in its continuum removed spectrum (Clark, 1999). The analysis showed that each one of the reference minerals presented a diagnostic absorption feature that does not exist in the corresponding signatures of all detected minerals in the study area. This feature is centered at 490nm (band 2) for goethite, at 560nm (band 3) for Mn-oxides//hydroxides, at 783nm (band 7) for muscovite and at 865nm (band 8A) for chlorite. We then produced the corresponding absorption maps. In each map, pixels presenting an absorption greater than 0.01 (0 indicates no absorption and 1 indicates full absorption) were retained while the others were masked (Fig. 2c,d,e and f) indicating thus the spatial distribution of the specific mineral on the islet.

Discussion and Conclusions

XRD analyses and both methods of reflectance spectroscopy applied on the Sentinel-2 satellite image were consistent. They both showed significant mineralization due to the igneous intrusion. Hydrothermal alteration to a different degree is observed on both schists and the granitoid on the entire surface of the island. However, it seems that alteration is stronger at the center of eastern part of the islet where the granitoid/schist contact is located.

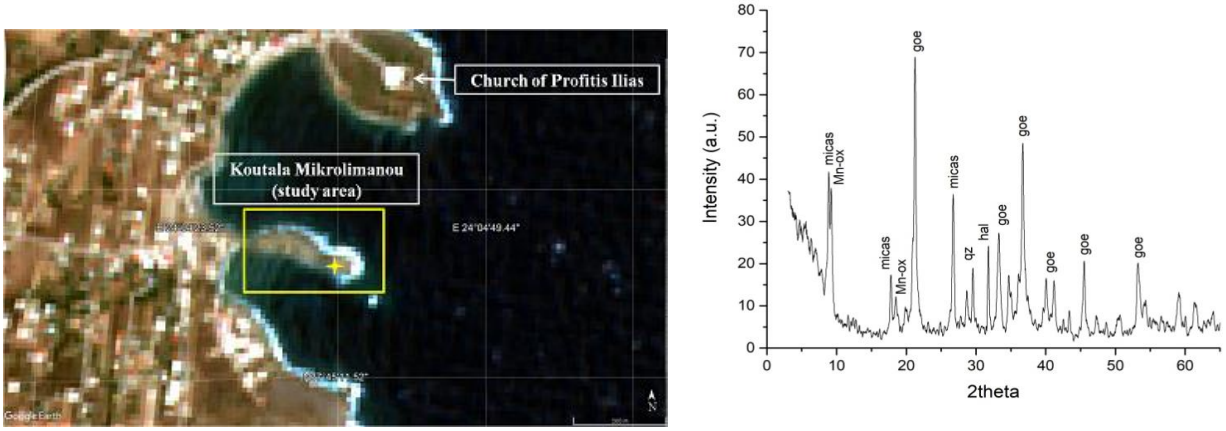

(a) (b)

Figure 1. (a) Location of the study area on the true color composition of the Sentinel-2 image (19/7/2022) (yellow frame). The yellow cross shows the location of the oxides sample collection; (b) XRD plot of the oxides sample.

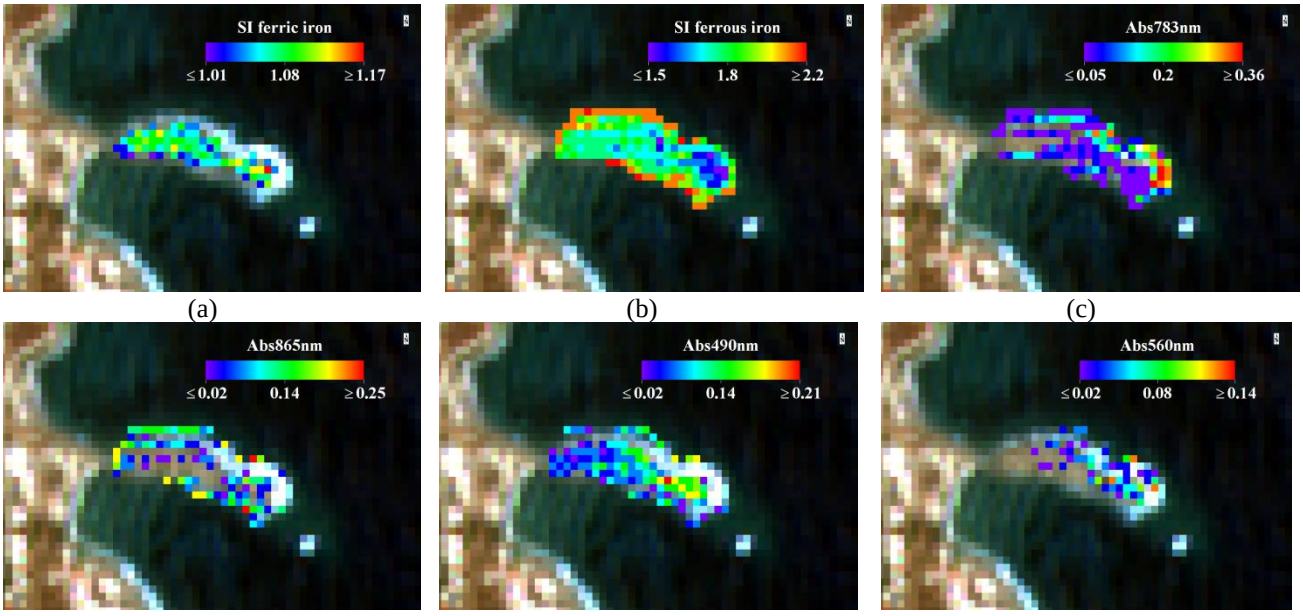

(a) (b) (c)

(d) (e) (f)

Figure 2. Mineral thematic maps issued from Sentinel-2 satellite image. (a) Normalized SI ferric iron (goethite); (b) normalized SI ferrous iron (micas, chlorite); (c) absorption map centered at 783nm (muscovite); (d) absorption map centered at 865nm (chlorite); (e) absorption map centered at 490nm (goethite); (f) absorption map centered at 560nm (Mn-oxides/hydroxides). The background image is the true color composite of the Sentinel 2A image used in this study.

Acknowledgements

The authors would like to thank colleagues geologists Mrs. Evgenia Moraiti (HSGME, Scientific Responsible of the Geopark of Lavreotiki) and Mr. Hercules Katsaros (Geopark of Lavreotiki) for their contribution to the geology of the area.

References

Clark, R., 1999. Spectroscopy of Rocks and Minerals, and Principles of Spectroscopy, in: A. N., Rencz (Eds), Remote Sensing for the Earth Sciences: Manual of Remote Sensing Volume 3, 3-58.

Marinos, G. P. and Petrascheck, W. E. 1956. *Laurium.* Geological & Geophysical Research 4/1, Institute for Geology and Subsurface Research, 1–247.

Scheffer, C., Vanderhaeghe, O., Lanari, P., Tarantola, A., Ponthus, L., Photiades, A., France, L. 2016. Syn- to post-orogenic exhumation of metamorphic nappes: Structure and thermobarometry of the western Attic-Cycladic metamorphic complex (Lavrion, Greece). Journal of Geodynamics 96, 174– 193

Skarpelis, N., Tsikouras, B., Pe-Piper, G. 2008, The Miocene igneous rocks in the Basal unit of Lavrion (SE Attica, Greece): Petrology and geodynamic implications. Geol. Mag. 145, 1–15.

Van der Meer, F.D., Van der Werff, H.M.A., van Ruitenbeck, F.J.A., 2014. Potential of ESA's Sentinel-2 for geological applications. Remote Sensing of Environment 148, 124-133.

Voudouris, P., Melfos, V., Mavrogonatos, C., Photiades, A., Moraiti, E., et al. 2021. The Lavrion Mines: A Unique Site of Geological and Mineralogical Heritage. Minerals 11, 76.

16th International Congress of the Geological Society of Greece
17-19 October, 2022 - Patras, Greece
Bulletin of the Geological Society of Greece, Sp. Publ. 10
Ext. Abs. GSG2022-142

Assessing and Mapping Multi-Hazard Susceptibility in Evia Island Greece Using Integrated Weighting Methods and Geospatial Techniques

K. Valkanou [1], E. Karymbalis [1], K. Tsanakas [1], G. Bathrellos [2], H. Skilodimou [2], D. Papanastassiou [3] and K. Gaki-Papanastassiou [4]

(1) Department of Geography, Harokopio University, Athens, Greece, elnel@otenet.gr, karymbalis@hua.gr, ktsanakas@hua.gr (2) Department of Geology, University of Patras, Rio Patras, Greece, gbathrellos@upatras.gr, hskilodimou@upatras.gr (3)Institute of Geodynamics, National Observatory of Athens, Athens, Greece, d.papan@noa.gr (4) Department of Geography and Climatology, Faulty of Geology and Geoenvironment, University of Athens, Athens, Greece, gaki@geol.uoa.gr

Introduction

Many locations around the world are exposed to- or may be threatened by more than one hazard of different types. In such prone to multiple hazards areas an ideal risk assessment plan and/or a mitigation strategy with the use of realistic and integrated composite spatial approaches is necessary. Based on the glossary of the United Nations Office for Disaster Risk Reduction (UNDRR, 2020-2022), the multi-hazard concept refers to the selection of multiple major hazards that a region faces. There are two kinds of multi-hazard research approaches. Approaches where hazards are treated as independent phenomena and are then overlaid, and approaches that focus on the potential interactions between multiple hazards.

This study attempts to assess and map the susceptibility of the northern part of Evia Island, in central Greece, to landslides and floods via a single multi-hazard approach, using statistical methods along with GIS and geospatial techniques.

Study area

The study area is the north part of Evia Island in central Greece and covers 1,842.3 km^2. It is a particularly prone to natural hazards area since over the years it has been affected by landslides (Rozos et al., 2013), flash floods (Karkani et al., 2021), earthquakes (Valkanou et al., 2020), and devastating wildfires (Giannaros et al., 2022). Human life and property, infrastructure, ecosystems and the natural environment have suffered from these natural hazards. Hence, the identification of the spatial distribution of hazard-causative factors along with susceptibility zoning is of crucial importance.

Methodology

The assessment of the landslide and flood susceptibility of the study area was attempted by the use of selected causative factors. For the calculation of the landslide susceptibility index, the predictive factors included slope, elevation, hydrology, aspect, curvature, lithology, structure, land use and rainfall. The same factors except aspect and curvature were considered for the estimation of the flood susceptibility index. The causal factors were classified and weighted based on the existing available landslide and flood inventories. The subclasses' frequency ratios were calculated in order to indicate the relative importance of the factors' subclasses that were used as criteria in the Analytical Hierarchy Process pair-wise comparison (Frequency ratio- Analytical Hierarchy Process (FR-AHP) assembling method) (Zhou et al., 2016; Rehman et al., 2022). The factors were then combined with the use of the weighted sum (the weights of the factors were obtained through AHP) and the produced landslide and flood susceptibility maps were synthesized to create the final multi-hazard susceptibility map. The results of the predictive method were validated through three different methods, namely the Area Under the Curve (AUC) of the Receiver Operating Characteristic (ROC) curve, the Seed Cell Area Index (SCAI), and the Frequency Ratio (FR).

Results - conclusions

The results of this multi-hazard analysis delineate the most susceptible to landslides and floods areas based on selected causal factors and previous events and can be used as an initial baseline for both future disaster and urban development planning. The spatial distribution of the multi-hazard susceptibility is depicted on the map of Figure 1, while Table 1 includes the percentage area, as well as the density of the recorded landslide and flood events for each susceptibility zone. The results indicate that more than 30% of the study area belongs to the high and very high susceptibility zones regarding both hazards. The results of the validation methods of the model are also demonstrated in Table 1. All three validation methods showed that the model is a reliable approach for the classification of the study area into multi-hazard susceptibility zones that can provide accurate results. The SCAI found to be high for very low susceptibility classes, the FR model showed an inverse increase from the very low to the very high susceptibility class, while the AUC found to have fairly high modeling accuracy that quantitatively corresponds to good to very good accuracy (76% to 86%).

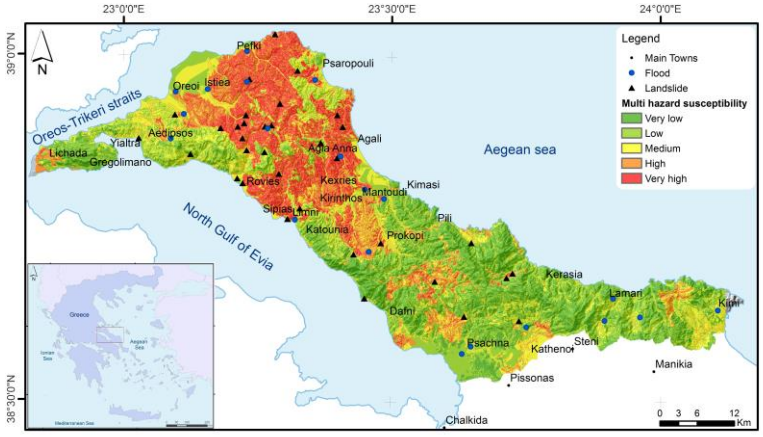

Figure 1. Multi-hazard susceptibility map.

Table 1. Area, and landslide (LSA), flood (FSA) and multi-hazard (MSA) density for each susceptibility class. The results of the validation methods (SCAI, frequency values and AUC) are also included.

Geohazard	Class	Very low	Low	Medium	High	Very high
LSA	% area	31.2	25.6	16.2	14.1	12.9
	% landslide	8.8	17.6	17.6	14.7	41.2
	SCAI	3.54	1.45	0.92	0.96	0.31
	frequency	0.28	0.69	1.09	1.04	3.18
	% AUC	79.6				
FSA	% area	27.3	34.1	23.2	13.5	1.9
	% flood	0.0	20.0	35.0	30.0	15.0
	SCAI		1.71	0.66	0.45	0.13
	frequency	0.00	0.59	1.51	2.22	7.81
	% AUC	86.3				
MSA	% area	20.3	29.3	19.7	16.4	14.3
	% landslide	5.9	8.8	20.6	23.5	41.2
	SCAI	3.46	3.32	0.96	0.70	0.35
	frequency	0.29	0.30	1.05	1.43	2.88
	% AUC	81.20				
	% flood	0.0	30.0	20.0	20.0	30.0
	SCAI		0.98	0.98	0.82	0.48
	frequency	0.00	1.02	1.02	1.22	2.10
	% AUC	75.9				

Acknowledgements

We would like to thank the Organizing Committee of the Congress and the Geological Society of Greece.

References

UNDRR, 2020-2022. Terminology, Online glossary, Hazard. https://www.undrr.org/terminology/hazard, accessed on 8/8/2022

Rozos, D.; Skilodimou, H.D.; Loupasakis, C.; Bathrellos, G.D., 2013. Application of the revised universal soil loss equation model on landslide prevention. An example from N. Euboea (Evia) Island, Greece. Environ Earth Sci., 70, 3255–3266. https://doi.org/10.1007/s12665-013-2390-3

Karkani, A.; Evelpidou, N.; Tzouxanioti, M.; Petropoulos, A.; Santangelo, N.; Maroukian, H.; Spyrou, E.; Lakidi, L., 2021. Flash Flood Susceptibility Evaluation in Human-Affected Areas Using Geomorphological Methods—The Case of 9 August 2020, Euboea, Greece. A GIS-Based Approach. GeoHazards, 2, 366-382. https://doi.org/10.3390/geohazards2040020

Valkanou, K.; Karymbalis, E.; Papanastassiou, D.; Soldati, M.; Chalkias, C.; Gaki-Papanastassiou, K., 2020. Morphometric Analysis for the Assessment of Relative Tectonic Activity in Evia Island, Greece. Geosciences, 10, 264. https://doi.org/10.3390/geosciences10070264

Giannaros, T.M.; Papavasileiou, G.; Lagouvardos, K.; Kotroni, V.; Dafis, S.; Karagiannidis, A.; Dragozi, E., 2022. Meteorological Analysis of the 2021 Extreme Wildfires in Greece: Lessons Learned and Implications for Early Warning of the Potential for Pyroconvection. Atmosphere, 13, 475. https://doi.org/10.3390/atmos13030475

Rehman, A.; Song, J.; Haq, F.; Mahmood, S.; Ahamad, M.I.; Basharat, M.; Sajid, M.; Mehmood, M.S, 2022. Multi-Hazard Susceptibility Assessment Using the Analytical Hierarchy Process and Frequency Ratio Techniques in the Northwest Himalayas, Pakistan. Remote Sens., 14, 554. https://doi.org/10.3390/rs14030554

Zhou, S.; Chen, G.; Fang, L.; Nie, Y., 2016. GIS-Based Integration of Subjective and Objective Weighting Methods for Regional Landslides Susceptibility Mapping. Sustainability, 8, 334. https://doi.org/10.3390/su8040334

16th International Congress of the Geological Society of Greece

17-19 October, 2022 – Patras, Greece

Bulletin of the Geological Society of Greece, Sp. Publ. 10

Ext. Abs. GSG2022-178

An exploratory analysis of EM-DAT database for Greece

F. Botsolis[1], G. Makrygiannis[2], M. V. Mavraki[3], A. F. Mavrakis[4]

(1) Directorate of Secondary Education in Dodecanese, Greek Ministry of Education, 2 G. Mavrou str, GR–85100, Rhodes, Greece, fbotsolis@yahoo.gr, (2) Analysis and Management of Man-made and Natural Disasters, International Hellenic University, Attica, Greece, gmakrigian@gmail.com, (3) Department of Public and One Health, University of Thessaly, Karditsa, Greece, marmavraki23@gmail.com, (4) West Attica Secondary Education Directorate, Greek Ministry of Education, 24 I. Dragoumi str., GR–19200, Elefsis – Attica, Greece, mavrakisan@yahoo.gr.

Abstract

During last decades there is an increase number of natural disasters in Greece, triggering consequences and public awareness. This research highlights the evolution of the number of natural disasters in Greece, using data adopted from the international database EM-DAT (https://www.emdat.be/) and explore their consequences in human resources and financial costs, for those cases with data availability.

The results obtained regarding natural disasters, confirm the increase number of hydrological and meteorological ones, with earthquakes still being the main category of disasters in Greece. From the recorded data, it seems that the parameters of losses (human and material), follow the categories of disasters that are recorded.

Data Used

All data use were adopted from The Emergency Database (the so called EM-DAT) which is an effort undertaken by the Centre for Research on the Epidemiology of Disasters, Louvain (Belgium), providing a unified platform for events' registration. Registered disasters on EM-DAT platform offers a relevant information base for vulnerability assessment and rational decision-making in disaster situations. In Greece, the Hellenic General Secretariat for Civil Protection (GSCP) has been responsible for the registration of natural or technological disasters to EM-DAT database, following the norms, classifications, and thresholds adopted by the same organization. This time series of registered disasters, covering 117 years between 1904 and 2021, was retrieved from EM-DAT (2021).

Results

According to EM-DAT, 146 disasters were recorded in Greece from 1904 to 2020; 100 and 46 events were classified respectively as natural and technological disasters. The period 1980–2021 records a total of 83 out of 100 natural disasters. The results obtained from the analysis of the database show a significant increase in disasters per year, after 1980. The categories of the natural disasters included in the database do not vary, but there is a striking increase in the number of meteorological, hydrological and climatic ones during the period 1980–2021 (Fig 1a & 1b).

Geophysical disasters, and especially earthquakes as sole subcategory, have been the most significant category of all natural disasters in Greece. In the EM-DAT database, there are no geophysical hazard subcategories other than earthquakes (total 44 out of which 26 registered after 1980).

However, the case is not the same concerning the other main disaster classifications (Fig 1c). Specifically, meteorological disasters (total 17 out of which 15 registered after 1980), hydrological (23, all of them registered after 1980) and climatic ones (16, all of them registered after 1980). Meteorological disasters contain the subcategories "Storms" (9 cases) and "Extreme Temperatures" (8 cases), with the latter containing the sub-subcategories "Heat" (5), "Cold Waves" (2) and "Extreme Winter" (1 case). Hydrological disasters contain the sub-categories "River Floods" (20 cases) and "Flash Floods" (3 cases). Finally, Climatic disasters contain the subcategories "Extreme Fires" (15 cases) and "Drought" (1 case).

The percentages of each category for human and property loses, are the following: fatalities: both geophysical and meteorological disasters account a 29%, hydrological 3% and 5% climatological disasters; injuries: 85,7%, 3,4%, 0,3%, 7,7% respectively; number of homeless registered: 96,2%, 0,0%, 0,0%, 2,1%; the number of total affected population: 96,2%, 0,1%, 1,8%, 1,6% by natural disaster category; with the total cost of disasters in US$000's adjusted value: 63,9%, 5,3%, 8,7%, 21,9% respectively.

Conclusions

In Greece the main category of natural disasters are geophysical ones and especially earthquakes (Fig 1a and 1b), with a significant contribution to the registered numbers of deaths and injuries (Botsolis, 2022). Up to now, the efforts of precaution measures and actions to reduce the effects of natural hazards have been focused on this category. The disasters during the last decades show the need for actions and protection measures for the other categories as well (Palmos et al., 2021). According the data of the EM-DAT database, however, one fact emerged: The non-registered

disasters, which according to the existing framework, only the General Secretariat of Civil Protection has the right to do so. It is absolutely clear and understandable that every geological or other phenomenon is not a natural disaster (eg an earthquake that occurs at sea, far from populated areas). An example for Greece, is the absence of registrations regarding Biological disasters, despite the fact that at least in the last decades we had epidemics of influenza (H1N1), West Nile Virus (Mavrakis et al., 2021), the ongoing Covid-19 pandemic, etc. But the more complete the database, the better the results from its investigation. Natural disasters usually cause a series of long-term damaging problems (human casualties, health, infrastructure, environmental, planning, etc.) that need long-term monitoring. It is important to record and register in international databases all available data on natural disasters in Greece. Lack of data due to unrecorded disasters, as well as incomplete international databases, affect policy decision-making issues.

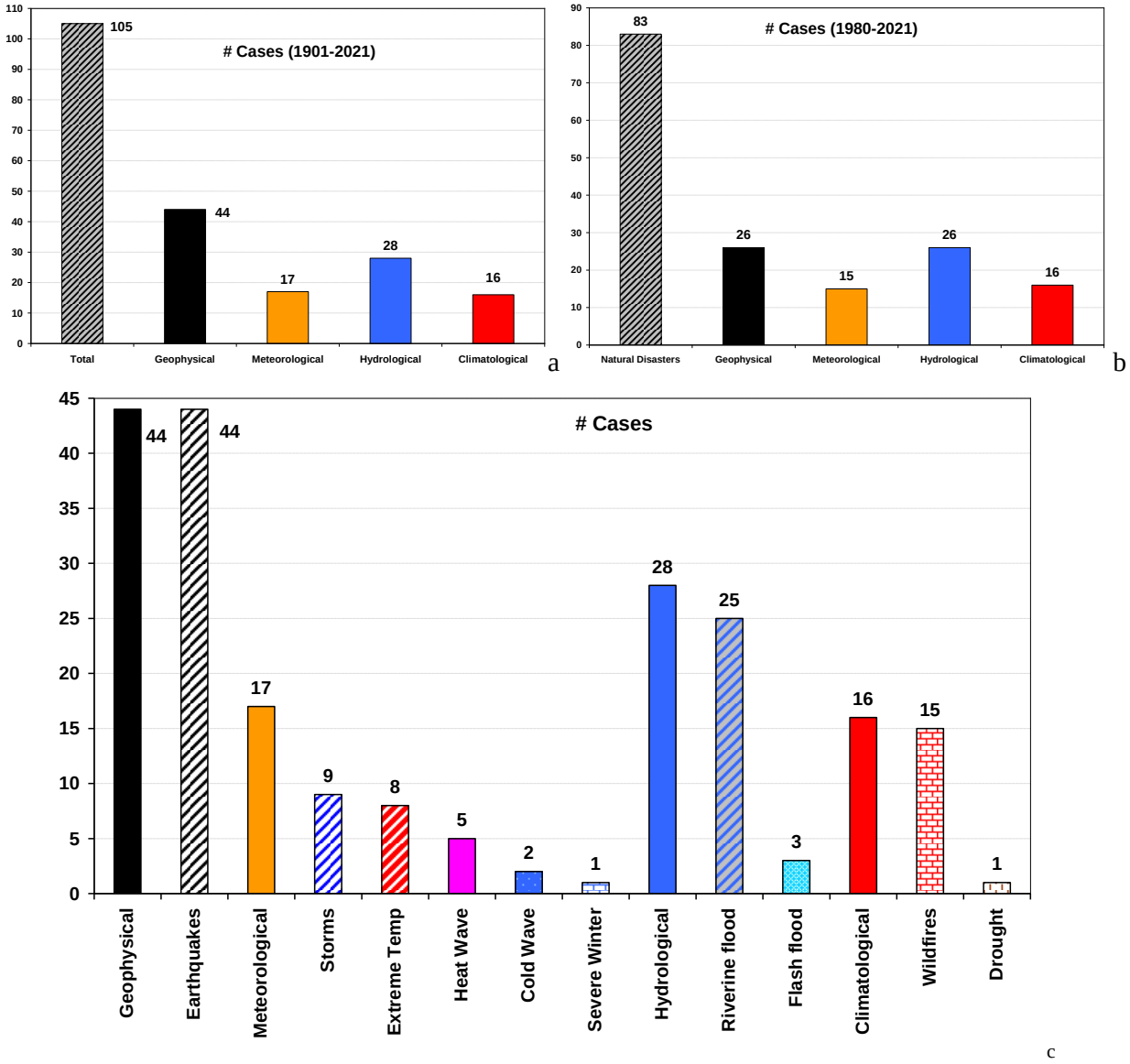

Figure 1. Total number and categories of natural disasters in Greece: a) during the period 1901 – 2021, b) during the period 1980 – 2021 and c) number of disasters by category and sub type.

References

Botsolis F., 2022. Natural disasters and environmental education. Master Thesis, Department of Sciences of Preschool Education and Educational Planning, University of Aegean. http://hdl.handle.net/11610/24151

EM-DAT (2021). The Emergency Events Database – Université catholique de Louvain (U C Louvain) – CRED, D. Guha-Sapir – www.emdat.be, Brussels, Belgium.

Mavrakis A., Papavasileiou C., Alexakis D., Papakitsos C. E., Salvati L., 2021. Meteorological patterns and the evolution of West Nile virus in an environmentally stressed Mediterranean area. Environmental Monitoring and Assessment, 193, 4, 227. https://doi.org/10.1007/s10661-021-09011-3

Palmos D., Papavasileiou C., Papakitsos C. E., Vamvakeros X., Mavrakis A., 2021. Enhancing the environmental programmes of secondary education by using web-tools concerning precaution measures in civil protection: The case of Western Attica (Greece). Safety Science, 135, 105117. https://doi.org/10.1016/j.ssci.2020.105117

16th International Congress of the Geological Society of Greece

17-19 October, 2022 – Patras, Greece

Bulletin of the Geological Society of Greece, Sp. Publ. 10

Ext. Abs. GSG2022-179

Some comments on results obtained from two questionnaires regarding evacuation drills in Greek schools.

G. Makrygiannis[1], F. Botsolis[2], C. Papavasileiou[3], M. V. Mavraki[4], A. F. Mavrakis[5]

(1) Analysis and Management of Man-made and Natural Disasters, International Hellenic University, Attica, Greece, gmakrigian@gmail.com, (2) Directorate of Secondary Education in Dodecanese, Greek Ministry of Education, 2 G. Mavrou str, GR–85100, Rhodes, Greece, fbotsolis@yahoo.gr, (3) Second Athens Secondary Education Directorate, Greek Ministry of Education, Pappa E & Filellinon str, GR–14234, Nea Ionia – Attica, Greece; e-mail: xripapav@gmail.com, (4) Department of Public and One Health, University of Thessaly, Karditsa, Greece, marmavraki23@gmail.com, (5) West Attica Secondary Education Directorate, Greek Ministry of Education, 24 I. Dragoumi str., GR–19200, Elefsis – Attica, Greece, mavrakisan@yahoo.gr.

Abstract

Geophysical disasters and especially earthquakes have been the most important cause of deaths and injuries due to natural disasters in Greece. Until now, the efforts of precaution measures and actions to reduce the effects of natural disasters focus on this hazard. In this short paper and based on answers from two different questionnaires focusing on teacher's perception for hazards and disasters, we make some comments regarding the implementation of evacuation drills in Greek schools. Answers show that 50% of schools make only once per year such drills, while there is a significant number of teachers (about 50% of responders) who do not participate in those drills, possibly because they are note organized at all.

Data Used

For the purpose of this study responses from two questionnaires were used. The first one was completed during 2019 "Investigating the education community's perception of natural and technological hazards: Case study the Thriassio Plain Area" (Papavasileiou, 2021). Respondents were primary and secondary school teachers working in West Attica Secondary (WASED) and Primary (WAPED) Education Directorates. Also answers were received from Second Athens Secondary (SASED) and Primary (SAPED) Education Directorates. A total of 210 responses were collected. The second questionnaire was completed at the end of 2021 and was entitled "Natural disasters and environmental education" (Botsolis, 2022). A total of 110 responses from teachers working in Directorate of Secondary Education in Dodecanese (DSED) were received. The two questionnaires were quite similar with common questions.

Results

The aforementioned question in both questionnaires was: "How often are preparedness (evacuation) drills organized at your school?" Results are shown in Fig 1. A summary for the Attica region follows: Among all respondents there was a large number who did not answer, (about 50% of responders) possibly because they do not participate in those drills, or because those drills not organized at all, or for unspecified reasons, perhaps due to a lack of information if many times the exercises take place on a day when they may be absent either on leave or because they work at another school. In addition, teachers may also be indifferent and consider the time of the exercises "time lost from the lesson". "I don't answer" could also mean "I don't participate". According to the rest answers, it is clear that drills are held in the schools of the secondary education, at least once per year and in fewer cases 2 or even 3 times per year, whereas at the Primary Schools, the frequency is more than 3 times per year at the schools of Western Attica compared to those located in North Athens where the frequency ranges from 2 to 3 times per year, which is consistent with the Earthquake Planning and Protection Organization guidelines (Papavasileiou et al., 2022).

From the answers of the second questionnaire it is evident that preparedness (evacuation) drills take place in the schools of the DESD at least once per year (53%) and in fewer cases 2 or even 3 times, while 11% answer that no readiness exercises are organized which is a very worrying fact indeed. Also, the answer "Never" varies between 2% and 11%, which are significant numbers regarding the vulnerability of the country Fig 2a and Fig 2b (EM-DAT, 2021).

Conclusions

The contribution of education and preparedness drills, as part of the precaution measures in civil protection, is considered crucial. In situ drills and Formal Education (Primary, Secondary and Adult Education) is one of the means that are used by modern states for informing and raising the awareness of pupils (i.e., future adults) about Natural Disaster. Therefore, updating the natural disasters curriculum, enriching the pupil's books and training, and/or updating teachers' knowledge through their training agencies, on a regular basis, may ensures the validity of training (Mavrakis et al., 2021; Palmos et al., 2021; Papavasileiou et al., 2021; Mavrakis et al., 2022).

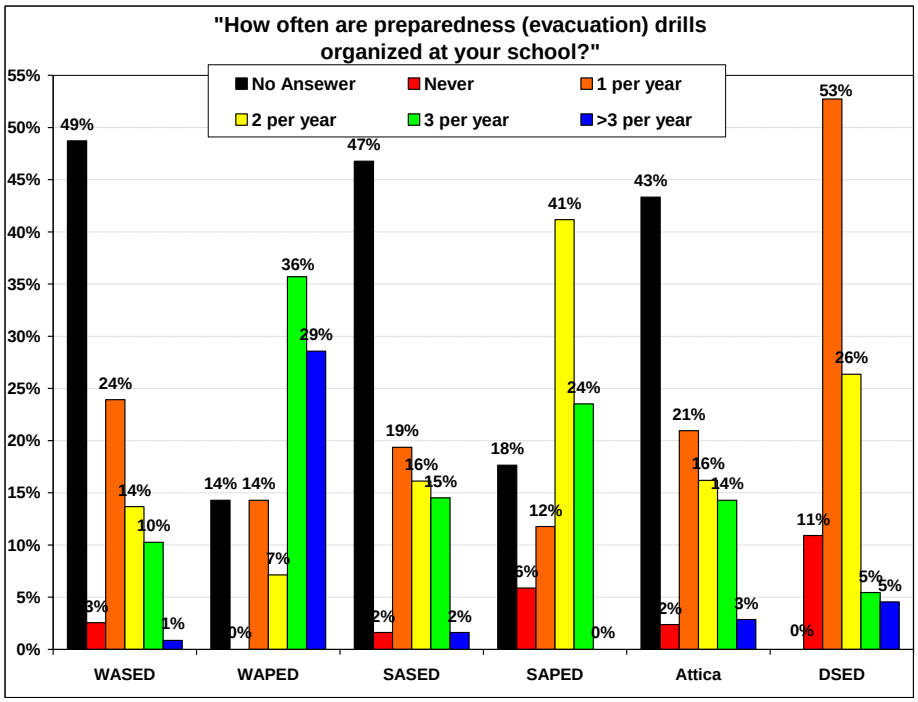

Figure 1. Responses collected from two different questionnaires which include the same question.

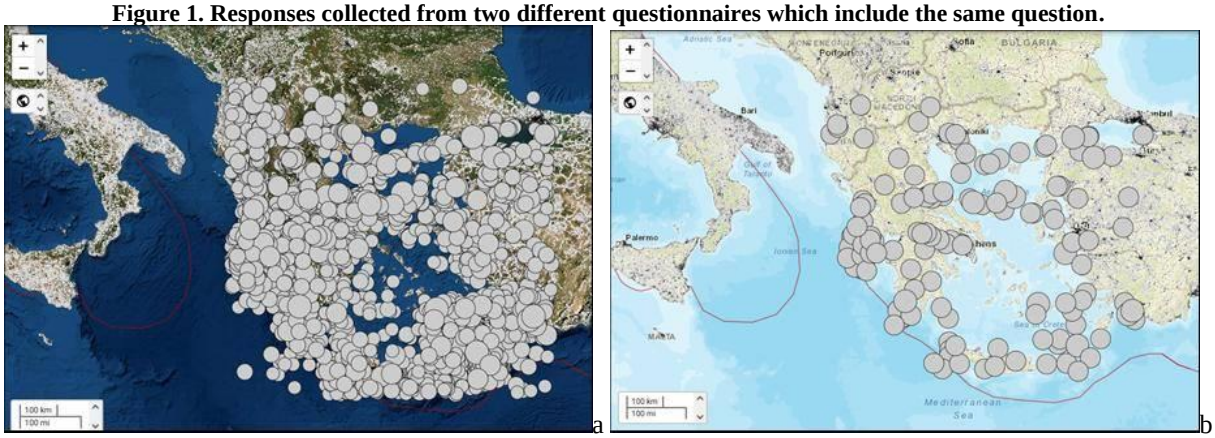

Figure 2. a) 2735 earthquakes with a magnitude greater than 4.5 R, (2000–2021) and b) 133 earthquakes with a magnitude greater than 6 R (2000–2021). Source https://earthquake.usgs.gov/earthquakes/map/

References

Botsolis F., 2022. Natural disasters and environmental education. Master Thesis, Department of Sciences of Preschool Education and Educational Planning, University of Aegean. http://hdl.handle.net/11610/24151

EM-DAT (2021). The Emergency Events Database – Université catholique de Louvain (U C Louvain) – CRED, D. Guha-Sapir – www.emdat.be, Brussels, Belgium.

Mavrakis A., Papavasileiou C., Alexakis D., Papakitsos C. E., Salvati L., 2021. Meteorological patterns and the evolution of West Nile virus in an environmentally stressed Mediterranean area. Environmental Monitoring and Assessment, 193, 4, 227. https://doi.org/10.1007/s10661-021-09011-3.

Mavrakis A., Tsigkou A., Papavasileiou C., Sigalos G., Dasaclis S., Vamvakeros X., Papakitsos C. E., 2022. An application of Systems Science in the context of Greek environmental education for planning interventions against volcanic hazards. International Journal of research in Educational Sciences, 5, 3 (July 2022), 41–76, http://dx.doi.org/10.29009/ijres.5.3.1

Palmos D., Papavasileiou C., Papakitsos C. E., Vamvakeros X., Mavrakis A., 2021. Enhancing the environmental programmes of secondary education by using web-tools concerning precaution measures in civil protection: The case of Western Attica (Greece). Safety Science, 135, 105117. https://doi.org/10.1016/j.ssci.2020.105117

Papavasileiou C., 2021. Investigating the education community's perception of natural and technological hazards: Case study the Thriassio Plain Area. Master Thesis, National and Kapodestrian University of Athens, Athens, Greece. https://pergamos.lib.uoa.gr/uoa/dl/object/2940808

Papavasileiou C., Kourou A., Mavrakis A., Salvati L., 2022. Assessing school teachers' perception of disasters: Insights from a socio-environmentally stressed Mediterranean area (Attica, Greece). International Journal of Disaster Risk Reduction, 2022, 103134. https://doi.org/10.1016/j.ijdrr.2022.103134

Papavasileiou C., Mavrakis A., Kourou A., Salvati L., 2021: Perception of biohazards: a focus on schools in Western Attica, Greece. Euro-Mediterranean Journal for Environmental Integration, 6, 27 2–6. https://doi.org/10.1007/s41207-020-00231-6

16th International Congress of the Geological Society of Greece
17-19 October, 2022 - Patras, Greece
Bulletin of the Geological Society of Greece, Sp. Publ. 10
Ext. Abs. GSG2022-181

Investigating the capability of Sentinel-2 and Worldview-3 SWIR to map the main mineralogical composition of bauxite through spectral unmixing. Case Study: Itea, Greece.

A. Anifadi[1,2], O. Sykioti[3], K. Koutroumbas[3], E. Vassilakis[2], E. Georgiou[4], C. Vasilatos[2]

(1) Faculty of Geology & Geoenvironment, National and Kapodistrian University of Athens, Athens, Greece (2) LARCO GMM S.A., Greece (3) Institute of Astronomy, Astrophysics, Space Applications and Remote Sensing, National Observatory of Athens, Athens, Greece, sykioti@noa.gr (4) Titan Cement Co. S.A., Athens, Greece

Introduction and Objectives

During the last decades, geological remote sensing, including hyperspectral/multispectral data, has grown rapidly in applications such as mineral/ore exploration and mineral resource mapping (Anifadi *et al.*, 2022; Anifadi *et al.*, 2019; van der Meer *et al.*, 2014). Sentinel-2 (S-2) (12 spectral bands within the VNIR-SWIR region of the H/M spectrum), has added new significant capabilities in terms of spatial resolution and spectral information, especially in the VNIR region (Burns, 1993; Clark and Roush, 1984). In parallel, DigitalGlobe's Worldview-3 (WV3) satellite provides very high spatial resolution (1.24m/pixel in the VNIR and 3.7m/pixel in the SWIR) and eight SWIR bands with valuable information on mineralogy, especially on alteration.

Spectral unmixing (SU) is a well-known image processing method at sub-pixel level. The aim of SU is the decomposition of the spectral signatures of mixed pixels into a selection of spectral signatures (represented as vectors) corresponding to the reflectance of pure physical materials (endmembers) (Keshava, 2003). SU results in a set of fractions (abundances) images, which indicate the degree of presence of each endmember within each pixel. Although several SU approaches have been proposed in literature, when working with multispectral data, the most widely used are those adopting the linear mixing model, where the spectral signature (vector) of each pixel is assumed to be expressed as a linear combination of a set of endmember signatures (vectors). The coefficients (abundances) of this combination can be estimated through various unmixing procedures, such as the constrained/unconstrained least squares methods. The objective of this study is to investigate the potential of the capability of S-2 and WV3-SWIR through linear SU to detect minerals which are typical to a bauxite composition. The study is conducted on two selected stock piles of bauxite in the transport zone in Itea Greece.

Data and analysis

For the purpose of this study, two satellite images were utilized, a S-2 image acquired in 3/7/2018 and a WV3-SWIR image acquired in 26/06/2015. Both datasets were georeferenced and atmospherically corrected. All spectral bands of the S-2 output reflectance image were resampled to 10m spatial resolution. The WV-3 SWIR image was co-registered to the S-2 image. Two subset images were then extracted using two Regions of Interest (ROIs) delineating two bauxite stock piles (Fig. 1a,b), named hereafter as A1 and A2. The number of pixels that are included within A1 is 10 for S-2 and 51 for the WV-3 SWIR image and the corresponding number of pixels included within A2 is 8 for S-2 and 36 for the WV-3 SWIR image. Next, five minerals were selected as typical of greek bauxites composition (Mondillo *et al.*, 2022), namely diaspore, goethite, hematite, anatase and kaolinite (there is no available spectral signature of boehmite and quartz is almost featureless in the two datasets spectral bands). The spectral signatures of the five minerals were retrieved from the USGS Spectral Library, convolved to the S-2 and WV3-SWIR spectral bands. The five spectral signatures of each dataset (Fig. 2a, b) were used as endmembers in SU. We performed (i) unconstrained (UC) linear SU and (ii) linear SU with non-negativity constraint (NNG) (the sum-to-one constraint SU and the non-negativity and sum-to-one constraint SU both failed to provide realistic results). The abundance values of the (i) and (ii) SU procedures were calculated for each endmember and each pixel of each one of the two datasets. The larger (positive) the abundance values are, the more indicative of the mineral's presence within the pixel are. For each pixel of each area, its abundance values were normalized in order to sum to one. We then calculated the mean abundance value for each mineral for each study area and the corresponding standard deviation.

Discussion and Conclusions

In general, the results obtained by SU UC and SU NNG methods are consistent to each other, in the sense that the numerical ordering between the abundance values of two minerals is the same for the two datasets and for both areas. For each area, the processing of both datasets resulted in high presence of diaspore (main bauxite mineral), especially for S-2 (>0.80). In all cases, the relatively low standard deviation values of diaspore (<0.11) indicate its uniform presence within each area, in contrast to the corresponding distribution of the other minerals, especially the iron-bearing ones. Furthermore, in the case of S-2, diaspore seems to prevail to the iron phases (goethite <0.19, hematite <0.28) while in the case of WV3 SWIR, the difference between diaspore and iron minerals abundances is not so sharp

(diaspore >0.30 reaching 0.46 in the case NNG, goethite >0.30, hematite <0.31). However, in contrast to S-2, WV3-SWIR is capable to detect the presence of all five minerals, even if it is weak (e.g. kaolinite <0.0003), with the exception of anatase in A2 which is not detected.

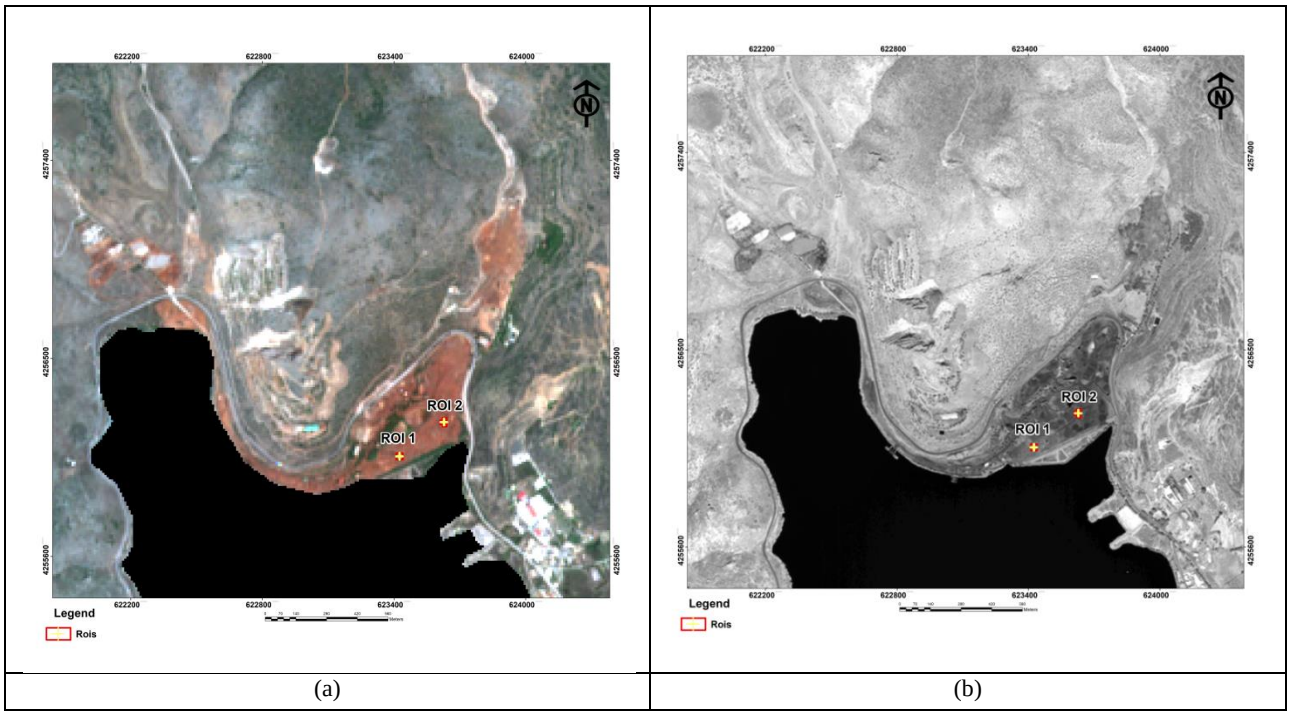

Figure 1. Location of the two bauxite stock piles under study (ROI1, ROI2 in yellow crosses) on (a) the true color composition of the S-2 image; (b) on a pseudo-color composition of the WV3-SWIR image.

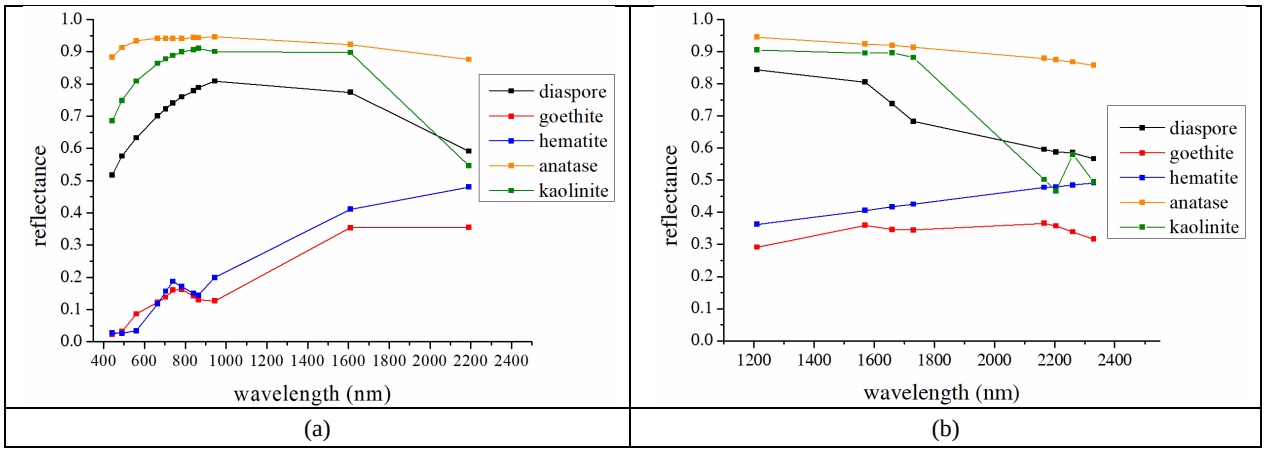

Figure 2. Plot of the five endmembers used in the SU procedure on the a) S-2 and b) WV3-SWIR spectral bands.

References

Anifadi, A., Sykioti, O., Koutroumbas, K., Vassilakis, E., 2022. A Novel Spectral Index for Identifying Ferronickel (Fe–Ni) Laterites from Sentinel 2 Satellite Data. Natural Resources Research 31, 1203-1244.

Anifadi, A., Sykioti, O., Vassilakis, E., 2019. Detection of chromite minerals using Spectral Linear Unmixing on Sentinel-2 imagery. Case study: Ingessana Hills, Blue Nile Province, Soudan. 15th International Congress of the Geological Society of Greece, Athens, Greece, 199.

Burns, R.G., 1993. Mineralogical Applications of Crystal Field Theory. 2nd Ed. Cambridge University Press.

Clark, R.N., Roush, T.L. 1984. Reflectance spectroscopy—quantitative analysis techniques for remote sensing applications. Journal of Geophysical Research 89, 6329–6340.

Keshava, N. 2003. A survey of spectral unmixing algorithms. Lincoln Laboratory Journal 14 (1), 55–78.

Mondillo, N., Di Nuzzo, M. , Kalaitzidis, S., Boni, M, Santoro, L., Balassone G., 2022. Petrographic and geochemical features of the B3 bauxite horizon (Cenomanian-Turonian) in the Parnassos-Ghiona area: A contribution towards the genesis of the Greek karst bauxites. Ore Geology Reviews 143, 104759.

Van der Meer, F.D., Van der Werff, H.M.A., van Ruitenbeek, F.J.A. 2014. Potential of ESA's Sentinel-2 for geological applications. Remote Sensing of Environment 148, 124-133.

16th International Congress of the Geological Society of Greece
17-19 October, 2022 - Patras, Greece
Bulletin of the Geological Society of Greece, Sp. Publ. 10
Ext. Abs. GSG2022-197

Landslide inventory and preliminary susceptibility mapping of Corfu Island, Greece

G. Konstantopoulou [1], K. Kavoura [1], A. Exintaridi [1], P. Paschos [1]
(1) Hellenic Survey of Geology and Mineral Exploration (HSGME) (Greece), kongar@igme.gr.

Up to now, little research has been done to assess landslide susceptibility in the island of Corfu, Greece. However, updated information reveals a long history of landslides, affecting both residential areas and infrastructures. In the present study, a preliminary landslide susceptibility assessment is made using Frequency Ratio (FR) statistical model. To highlight the landslide-hazard the Hellenic Survey of Geology and Mineral Exploration (HSGME) digitized existing landslides data from past reports conducted by the survey over the last 60 years in Corfu (Konstantopoulou *et al*.,2019). The historical archives include landslide locations, timing of landslide events, landslide type, triggering factors, volume and area data, as well as the impact of each landslide, when such information is available. However, this data deals with a level of uncertainty about the geospatial accuracy, that depends on the age of the report. For that reason, information is evaluated by field reconnaissance survey, to increase the accuracy and the reliability of the inventory as well as the landslide susceptibility maps of the island. Moreover, an abundance of new landslide locations was identified during a couple of new field surveys. The landslide inventory consists of 76 landslides based on historical archives and 127 landslides derived from new field observation. As a result, a total of 203 occurrences in a 592 km^2 area were mapped and a multi-temporal landslide inventory map was created (Fig.1).

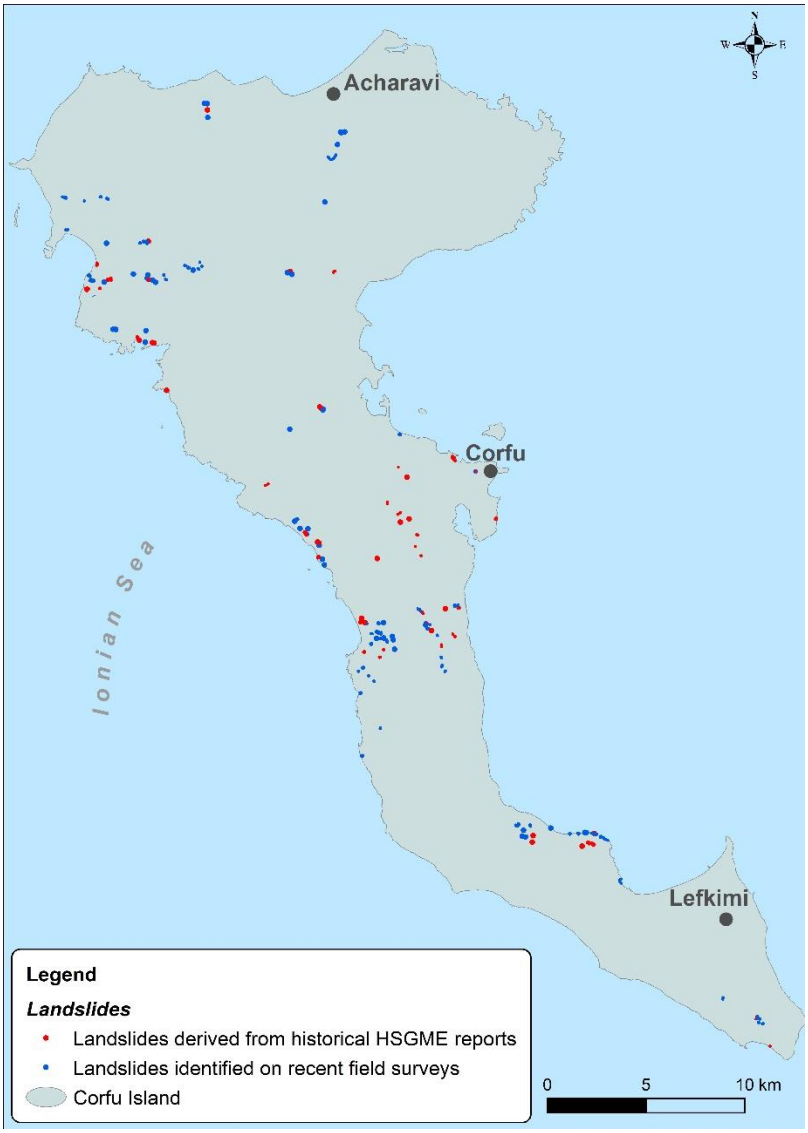

Figure 1: Updated landslide inventory map of Corfu Island.

Due to the variety of information and the abundance of data provided, some interesting outcomes were reached, concerning the characteristics of the landslides, after applying simple statistical analysis. Geological formation, landslide type, land use or impacts of landslides are some of the parameters that were examined. This analysis has shown that 77% of the landslides are hosted in Neogene sediments following by Quaternary formations and artificial fills. Several rockfalls occur in limestones. Serious instability phenomena are often observed as rotational or translational slides (80%), while in some cases complex landslides occur. Moreover, soil creep often be an important process on extensive areas of the island. Almost 85% of the recorded landslides are located within residential areas and road network, while the rest within forests and cultivated lands.

As regards the landslide susceptibility assessment, four (4) commonly used predisposing factors (lithology, land use, slope, distance from road network) were selected to join the procedure. In particular, the procedure applied the Frequency Ratio (FR) statistical model to define weights for each factor (Kavoura and Sabatakakis, 2020). These weights are referred to as evidence of the impact of landslide susceptibility in a given area. The Landslide Susceptibility Index (LSI) was used for landslide susceptibility mapping in ArcGIS environment. This index was expressed as an algebraic summary of weights according to bivariate statistical analysis. Checking the reliability of the proposed susceptibility model Success Rate Curves were also derived (Chung and Fabbri, 1999). Thus, the landslide susceptibility map of Corfu classifies the study area into five landslide susceptibility zones.

The findings reported here contribute to the existing knowledge that HSGME has on the topic of landslides. This work presents the first landslide susceptibility map in Corfu Island while highlighting the impact of landslides in residential and touristic areas. While HSGME serves the Nation by providing reliable scientific information and thus minimizing loss of life and property from natural disasters, this research could be a basic tool for managing a sustainable hazard and risk mitigation program in landslide prone areas.

Acknowledgements

This study was conducted in the framework of the Operational Program entitled "Competitiveness, Entrepreneurship and Innovation (2015-2020), Project «Studies and researches support to the energy sector, industry and entrepreneurship», Sub-Project «Susceptibility assessment of landslides in the Greek territory - Volcanic study and risk assessment», financed by the European Regional Development Fund.

References

Chung C.-J.F., Fabbri A.G., 1999. Probabilistic prediction models for landslide hazard mapping. Photogramm Eng Remote Sens 65(12),1389–1399 **[Journal Article]**

Kavoura, K., Sabatakakis, N., 2020. Investigating landslide susceptibility procedures in Greece. Landslides 17, 127–145 **[Journal Article]**

Konstantopoulou, G., Exintaridi, A., Paschos, P., Nikolaou, N., 2019. Landslide hazard in Corfu Island, Greece. SafeCorfu 2019 - 6th International Conference on Civil Protection & New Technology. **[Conference Proceedings]**

16th International Congress of the Geological Society of Greece

23-25 May, 2022 - Patras, Greece

Bulletin of the Geological Society of Greece, Sp. Publ. 10

Ext. Abs. GSG2022-229

Site effects and surface deformation associated with the M 6.3 Sitia (eastern Crete) earthquake of October 12, 2021

A. Dretaki[1], A. Chatzipetros[2], S. Psomadakis[3]

(1) Department of Geography, University of Aegean, Mytilene, Greece, antoniadret@hotmail.com (2) School of Geology, Aristotle University, Thessaloniki, Greece (3) Rural and Surveying Engineer, G. Gennimata 1, 72300, Sitia, Greece

On October 12, 2021, at 9:24 UTC, a strong (Mw 6.3) shallow earthquake occurred, near the area of Sitia, Crete. According to the National Observatory of Athens (NOA), its epicenter was located approximately 23 km East of Xerocampos, Crete (N35.0748°, E26.4651°) and at a depth of 8.2 km. Its intensity (MM) was determined at VII (according to National Observatory of Athens), with moderate damages across the area, except of the old church of Aghios Nikolaos at Xerocambos, which collapsed. Extensive cracks were observed at several houses and pavements of nearby villages, as well as in Sitia town. Water turbidity was observed for a few hours at Zakros and Zou springs. The earthquake occurred on an oblique normal fault with dextral lateral movement, as shown in most of the published moment tensor solutions, which agrees with the tectonic setting of the area. The aftershock sequence, that lasted from 12/10/2021 to 19/01/2022, is plotted in Figure 1, categorized by depth and magnitude. According to the National Observatory of Athens (NOA), the value of maximum PGA (%g) is 35.1683, at Sitia Sensor (SIT2).

The objective of this paper is to review the Xerocambos earthquake, and the spatial distribution of the earthquake surface effects and their characteristics, as well as the assessment of its macroseismic intensity based on its environmental effects. To this end, a field survey to collect primary data was conducted from 13 to 15 October 2021. Furthermore, a specifically designed topographic campaign was performed at the eastern part of Sitia region, to compare the results with previous measurements and identify any displacements in the area. The high accuracy dual frequency GNSS receivers used were SP60 and SP85 (GPS, GLONASS, BeiDou, Galileo etc) and ProMark 120 (GPS, GLONASS) from Spectra Precision. The measurements were carried out with fast static and high-precision static methods, on 11 pedestals, embedded into solid basement at Aghios Nikolaos Church, Xerocambos, 3 trigonometric points of HMGS (334016-Ambelos, 334024-Plativolo, 334066-Entihtis) and one static control point (T35, Xerocambos). The previous measurements where taken on 2008, for the trigonometric point of HMGS 334016 (Ambelos) and the 11 pedestals, and on 2014 the static control point, all trigonometric points and 7 of the pedestals, which leads to an accurate long-term detection of micromovevents on the area. To quantify the earthquake effects, in situ measurements of their physical characteristics (e.g. volume of rockfalls) took place during the fieldwork and they were further processed using ArcGIS Pro. Using the quantitative measurements of the environmental effects, the requisites of the Environmental Seismic Intensity scale ESI-07 (Michetti *et al.*, 2007), as well as appropriate kriging methods, the map of the spatial distribution of the macroseismic intensity of the earthquake was created.

The environmental effects of the earthquake can be associated with the local geology (Papastamatiou *et al.*, 1959a,b,c). Highly fractured hard rock masses and low cohesion of the sedimentary rock units, together with high angle slopes were the main reasons of the induced phenomena. The rockfall with the highest volume and most significance is located at Argilos beach, Xerocambos (No 9 in figure 1), one of the most visited of the area. Figure 1 indicates that the areas with the highest intensity relate to epicentral distance of the earthquake and geology, as the highest values are observed at the sedimentary rock units, whereas areas with harder rock units demonstrate lower intensity values. There is however a significant anomaly SW of Sitia town, which is attributed to the geological structure of this particular area (post-orogenic sedimentary units). The south-east area of Crete showed no signs of uplift, where at Aghios Nikolaos a 3-5.5cm displacement to the south-east was measured, due to the tensile cracks on the crown of the No 9, 10 and 11 landslides and rockfalls.

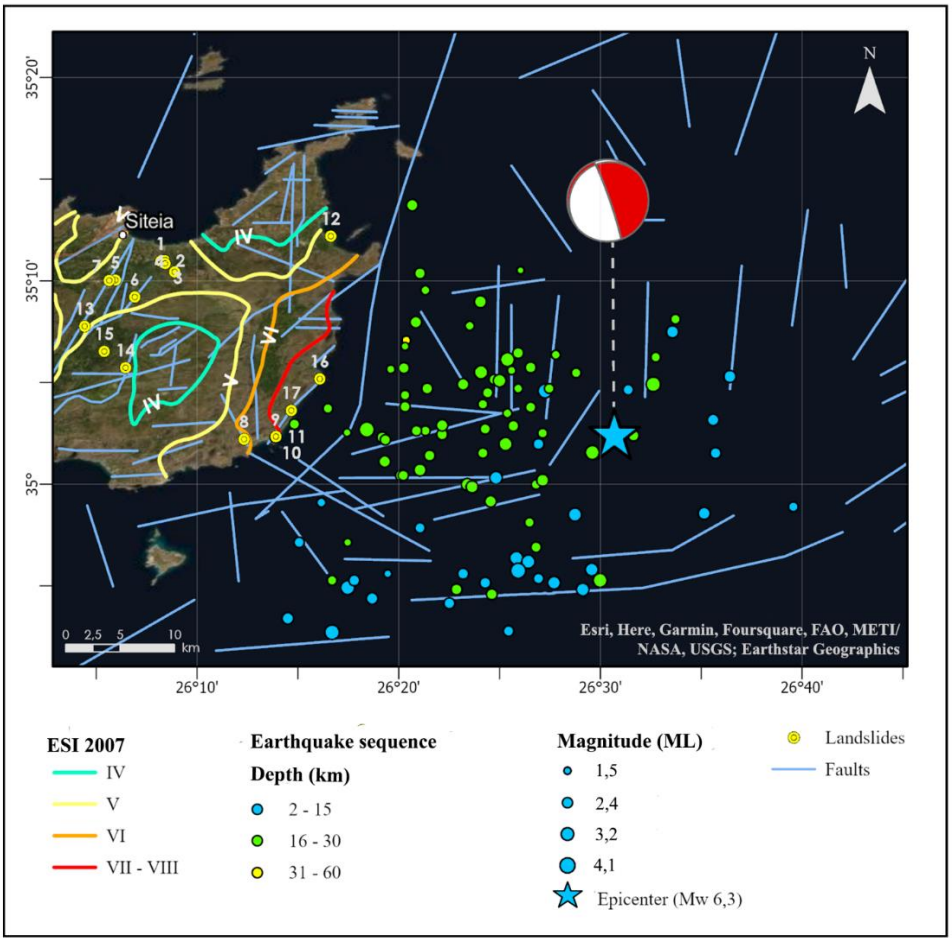

Figure 1. Map of the affected area and the observed environmental effects (landslides and rock falls), the mapped faults (Fytrolakis and Dermitzakis, 1996; Caputo and Pavlides, 2010; Kokinou *et al.*, 2012; Nicol *et al.*, 2020), the earthquake sequence with the epicenter (data from the Institute of Geodynamics, National Observatory of Athens) and its moment tensor solution and the ESI 2007 intensity contour lines (after Michetti *et al.*, 2007)

Acknowledgements

Special thanks to the people of Sitia region for all the helpful information and provided data from their areas.

References

Caputo, R., and S. Pavlides. 2013. *The Greek Database of Seismogenic Sources (GreDaSS), version 2.0.0: A compilation of potential seismogenic sources (Mw > 5.5) in the Aegean Region.* doi:10.15160/unife/gredass/0200.

Dziewonski, A. M., T.-A. Chou, and J. H. Woodhouse. 1981. "Determination of earthquake source parameters from waveform data for studies of global and regional seismicity." *J. Geophys. Res.* 86: 86. doi:10.1029/JB086iB04p02825.

Ekström, G., M. Nettles, and A. M. Dziewonski. 2012. "The global CMT project 2004-2010: Centroid-moment tensors for 13,017 earthquakes." *Phys. Earth Planet. Inter.* 1-9: 200-201. doi:10.1016/j.pepi.2012.04.002.

EMSC-CSEM. 2021. *M 6.4 - CRETE, GREECE - 2021-10-12 09:24:04 UTC.* 10 12. https://www.emsc-csem.org/Earthquake/earthquake.php?id=1047368#pics),%20which.

Fitrolakis, N., and M. Dermitzakis. 1996. "Map of active faults in the area of Crete." Research program of the Organization of Seismic Design and Protection , Athens.

Institute of Geodynamics, National Observatory of Athens. 2022. http://bbnet.gein.noa.gr/.

Kokinou, E., T. Alves, and E. Kamperis. 2012. "Structural decoupling in a convergent forearc setting (southern Crete, Eastern Mediterranean)." (Geological Society of America Bulletin) 124: 1352–1364. doi:10.1130/B30492.1.

Michetti, A. M., E. Esposito, L. Guerrieri, S. Porfido, L. Serva, R. Tatevossian, E. Vittori, et al. 2007. "Environmental Seismic Intensity Scale 2007, ESI 2007." In *Memorie descrittive della Carta Geologica d' Italia*, by L. Guerrieri and E. Vittori, 7-54.

Nicol, A., V. Mouslopoulou, J. Begg, and O. Oncken. 2020. "Displacement accumulation and sampling of paleoearthquakes on active normal faults of Crete in the eastern Mediterranean." *Geochemistry, Geophysics, Geosystems.* doi:10.1029/2020gc009265.

Papastamatiou, J., D. Vetoulis, A. Tataris, J. Bornovas, G. Christodoulou, and G. Katsikatsos. 1959a. *Geological map of Greece - sheet of Ierapetra.* I.G.M.E.

Papastamatiou, J., D. Vetoulis, J. Bornovas, G. Christodoulou, and A. Tataris. 1959b. *Geological map of Greece - sheet of SITIA.* I.G.M.E.

Papastamatiou, J., D. Vetoulis, J. Bornovas, G. Christodoulou, and G. Katsikatsos. 1959c. *Geological map of Greece - sheet of Ziros.* I.G.M.E.

16th International Congress of the Geological Society of Greece
17-19 October, 2022 - Patras, Greece
Bulletin of the Geological Society of Greece, Sp. Publ. 10
Ext. Abs. GSG2022-266

Effects on the Natural and Man-Made Environment from the Occurrence of Floods in Areas of the Western Sector of Athens.

M. Teskou[1], I. Ilia[2]

(1) Hellenic Open University, Patra, Greece, kithnos_maria@yahoo.com (2) National Technical University of Athens, School of Mining and Metallurgical Engineering, Athens, Greece, gilia@metal.ntua.gr

Extended Abstract

One of the most important global problems is climate change and the related consequences on the natural and man-made environment. Several studies report that climate change comes along with increase in extreme natural events, such as flood phenomena, extreme weather, typhoons, wildfires etc, whereas an important portion of the scientific community focus its research in identifying areas which are susceptible to natural disasters and also developing strategies to reduce as far as possible their adverse effect (Khan, 2011; Roy et al., 2020).

In this context, the main objective of the present study was to produce a flood susceptible map concerning Municipalities of the Western Sector of Athens, Attica, Greece taking into account several geomorphologic and hydrogeologic parameters and the related elements at risk. Specifically, the wetness topographic index, the slope length and steepness, and the hydrological characterization of the geological formation of the study area, were used as the primary related parameters. Each parameter was weighted according to their influence to flood susceptibility, whereas the final index of flood susceptibility was estimated by the method of Weighted Linear Combination - WLC (Malczewski, 1999). The map was reclassified into three zones, low, moderate and high susceptibility based on the Natural Break classification scheme (ESRI, 2015).

From the conducted analysis, it was estimated that around 39,40% of the research area has been characterized as high susceptible, 36,93% as moderate susceptible and the 23,68% as low susceptible. The municipality of the highest coverage concerning the flood susceptibility is the Municipality of Aigaleo (84,55%) followed by the Municipality of Peristeri with coverage (63,09%), the Municipality of Iliou (61,27%), the Municipality of Agion Anargiron (39,16%), the Municipality of Agias Varvaras (30,83%), the Municipality of Kamaterou (27,31%), the Municipality of Chaidariou (18,36%) and the Municipality of Petroupoli (16,51%). In order to verify the correctness of the susceptibility model, a superposition was made of the damages on man-made structures that have been recorded after a relevant call received by the Fire Department during extensive rains that occurred in October 2013. It was found that 78.77% (115) of the events are located within the category of high susceptibility and the remaining 21.23% (31) are located within the category of moderate susceptibility (Figure 1). Taking into account the population density of each Municipality, which partially captures the residential development, it was found that, both the Municipality of Peristeri and the Municipality of Aigaleou, municipalities with a high population density show a correspondingly large percentage of areas characterized by high flood susceptibility. In both municipalities, quite adverse effects are expected in the event of a flood event. Regarding land uses, it was found that the category of high flood susceptibility occupies 67.38% of the continuous urban complex, 10.56% of the discontinuous urban complex, 12.68% of industrial and commercial zones and 4.83% of urban green areas. With regard to the road network that may be used for the immediate evacuation and access of the intervention teams to the various parts of the city to provide assistance, (Figure 2), the greater percentage of the road network is characterized by high susceptibility. Specifically, 58.38% are characterized by high susceptibility, 39.94% by moderate susceptibility and only 1.69% by low susceptibility.

Therefore, in terms of impacts and considering that the estimated flood susceptibility is the worst-case scenario, the functionality of the road network is greatly reduced, while several and significant problems are expected to occur.

Based on the results of this analysis, a fairly high percentage of the road network requires the immediate intervention of the local authorities. Their focus should be to implement appropriate measures so as to prevent and mitigate potential negative effects from flooding phenomena, measures that may include the construction and maintenance of the rainwater network, cleaning of existing natural streams, review and redesign of the regulated and unregulated stream network, etc.

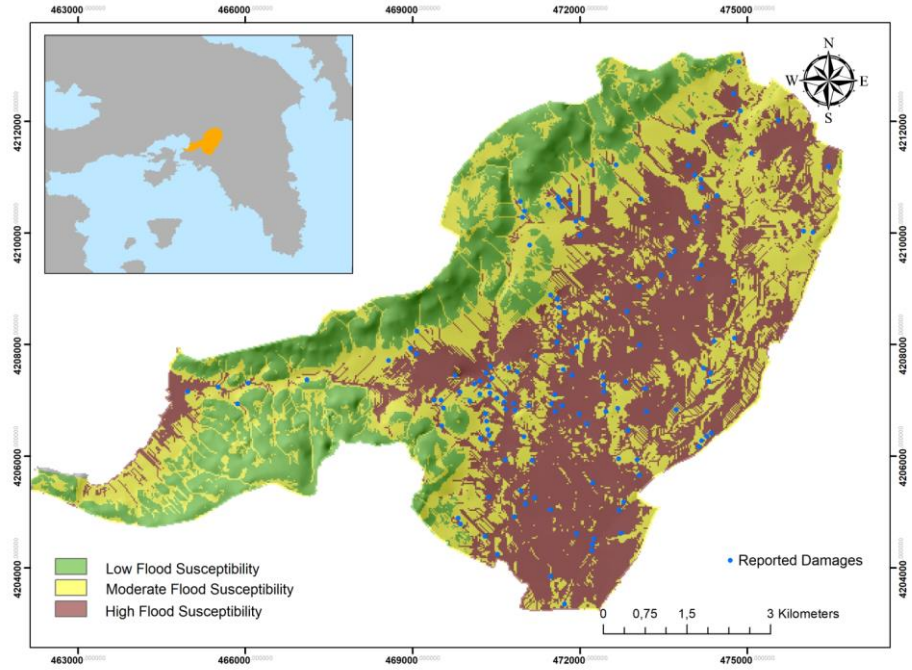

Figure 1 Flood Susceptibility Map

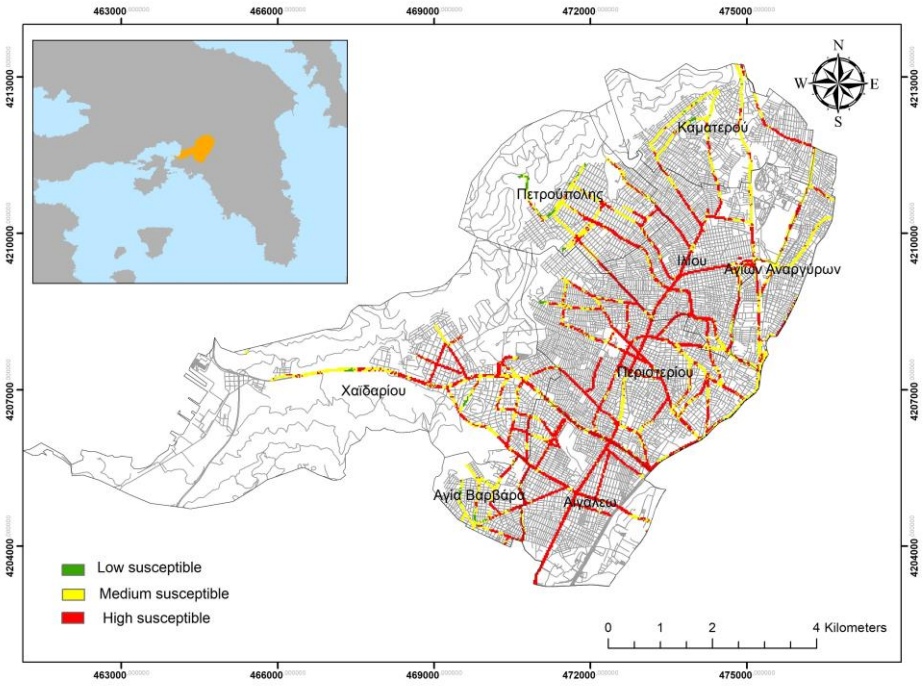

Figure 2. Road Network characterized based on susceptibility to flood

References

ESRI (2015). ArcGIS Desktop: Release 10.3 Redlands, CA: Environmental Systems Research Institute.

Khan, A.N. Analysis of flood causes and associated socio-economic damages in the Hindukush region. Nat. Hazards 2011, 59, 1239

Malczewski, J. (1999) GIS and Multi-Criteria Decision Analysis. John Wiley & Sons, Inc., New York.

Roy, P.; Pal, S.C.; Chakrabortty, R.; Chowdhuri, I.; Malik, S.; Das, B. Threats of climate and land use change on future flood susceptibility. J. Clean. Prod. 2020, 272, 122757

16th International Congress of the Geological Society of Greece
17-19 October, 2022 - Patras, Greece
Bulletin of the Geological Society of Greece, Sp. Publ. 10
Ext. Abs. GSG2022-280

Preliminary results of Antimilos geology and volcanic hazard assessment.

G. Vougioukalakis[1], C. Kanellopoulos[1,3,4], L. Francalanci[2], I. Koufogiannis[1,5]

(1) Hellenic Survey of Geology and Mineral Exploration – HSGME, Greece, e-mail: gvoug@igme.gr , ckanellopoulos@gmail.com (2) Dipartimento di Scienze della Terra, Università di Firenze, Italy, e-mail: lorella.francalanci@unifi.it (3) Faculty of Geology and Geoenvironment, National and Kapodistrian University of Athens, Panepistimiopolis, Zografou, 15784, Athens, Greece (4) Department of Geology, University of Patras, 26504, Patras, Greece (5) Institute of Applied Mineralogy and Economic Geology, RWTH Aachen University, Aachen, Germany e-mail: ilias.koufogiannis@emr.rwth-aachen.de

Antimilos belongs to the Milos volcanic field, along with Kimolos, Polyegos and Ananes islets. All these islands are mainly or entirely constituted by volcanic products and are part of the South Aegean Active Volcanic Arc (SAAVA).

The Antimilos islet (Fig. 1), also called Erimomilos, with a maximum altitude of 686 m, is located at a distance of about 19 km from the port of Adamas at NW of the Milos island. It covers about 8 km^2, and it is uninhabited. The last human residents left the island in about 1960. The island is particularly steep and without roads and paths.

The geological information about Antimilos is limited (Fielder, 1841; Ehrenburg, 1889; Sonder, 1925, Marinos, 1960; Fytikas et al., 1986). The first and only detailed geological study of the island was published by Marinos (1960), and the only radiometric age available is 320 ± 50 ka (K-Ar method, rhyolitic lava) reported by Fytikas et al. (1986).

Due to these conditions and the limited geological knowledge concerning the area, the Hellenic Survey of Geology and Mineral Exploration (HSGME) organised a field expedition with an overnight stay at the island. The aim of that expedition and several others that will follow is to achieve a complete understanding of the geology of Antimilos, with the publication of a geological map, and an assessment of the possible volcanic hazard.

Nine different geological formations were identified and sampled on Antimilos. Additionally, several volcano-tectonic information and structures were recorded. The island consists of volcanic rock formations; no Alpine basement formations were found. The only post-Alpine sedimentary formation on the island is thin eluvial mantles in areas dominated by fragmented volcanic rocks. They consist of fine-grained materials resulting from aeolian and thermal erosion.

The main structures and formations are small volcanic domes and lava flows, mainly of andesitic and rhyolitic composition (Francalanci et al., 2005). The thin and long lava flows are usually andesites, while the thicker and shorter ones are more acidic, i.e. dacites or rhyolites. Domes and lavas are usually highly porphyritic, often characterized by large (up to ca. 0.5 cm) feldspars, and contain mafic enclaves.

Debris and ash flow fed by the collapse of lava fronts or steep dome slopes are also present. In a few cases, small units - horizons of mud flows were identified. The composition of their clasts is the same of the composition of the collapsed lavas from which they originate. Only in one case, on the steep slopes of the NE coast, an andesitic pyroclastic tephra layer outcrops, deposited by dense pyroclastic flows.

Based on the until now available information, pyroclastic deposits, which could be related to large destructive explosions, were not identified. The two main craters, located at the centre of the northern part (Fig. 1B) and at the southern part (Agriokastro; Fig. 1C), are not explosive. They ought to be created in the late phase of the volcanic activity, after the retreat and shrinkage of the magma due to cooling processes. Accordingly, the island was mainly formed by a mild effusive-extrusive activity.

Tectonic features are rare. Two major faults were identified, both on the NE steep slopes of the island. However, the arrangement of the volcanic centers strongly suggests tectonic discontinuities that functioned as magma supply routes and controlled the positions of the craters in a NNE-SSW direction. Some dykes are present, also having a NNE-SSW direction. Similarly, in Milos island, the main tectonic structures, which have been active from the Pleistocene until now, have a NNW-SSE direction.

Among the geological formations and structures identified on the island, no depositional or erosional horizons were observed that could suggest significant intervals of cessation of volcanic activity. So, it could be assumed that the volcanic activity was continuous.

Additionally, based on the until now available information, no hydrothermal manifestations, i.e. hot springs and fumaroles or hydrothermal alterations, are present. Also, no base or precious metal ore or industrial mineral occurrences were identified, in contrast to the Milos island.

Based on the fact that until now, they are not any new dating available, no solid suggestions concerning Antimilos' time interval of creation could be made. The only available dating (320 ± 50 ka; Fytikas et al., 1986) concerns the oldest rhyolitic lavas of the island outcropping along the northern coast (Fig. 1A). Comparing the volume and sequence of the

volcanic products with corresponding volcanic edifices of the southern Aegean, we could consider that the island was built during the last phase of volcanic activity of Milos, when the volcanic centres of Trachila and Phyriplaka were created, i.e. around 360 ka and 110 ka, respectively (Fytikas et al., 1986; Zhou et al., 2020). Of course, this hypothesis remains to be verified after the dating of a sufficient number of selected volcanic samples, which have already been sampled.

Figure 1. Antimilos island. (A) The northern side of Antimilos island. (B) Main crater. (C) Volcanic domes in the southern part of the island and the center of Agriokasto lava dome.

References

Ehrenburg, K., 1889. Die Inselgruppe von Milos. Leipzig.

Fielder, L., 1841. Reise durch alle Theile des Konigreiches Griechenland. Leipzig.

Francalanci L., Vougioukalakis G.E., Perini G., Manetti P., 2005. A West-East traverse along the magmatism of the South Aegean volcanic arc in the light of volcanological, chemical and isotope data. Developments in Volcanology (Amsterdam, Olanda), "*The South Aegean Active Volcanic Arc, Present Knowledge and Future Perspectives*", M. Fitykas and G.E. Vougioukalakis Eds., vol.7, 65-111. [ISBN-13: 978-0-444-52046-3, ISBN-10: 0-444-52046-5].

Fytikas, M., Innocenti, F., Kolios, N., Manetti, P., Mazzuoli, R., Poli, G., Rita, F., Villari, L., 1986. Volcanology and petrology of volcanic products from the island of Milos and neighbouring islets. Journal of Volcanology and Geothermal Research, 28 (3–4), 297-317, https://doi.org/10.1016/0377-0273(86)90028-4.

Marinos, G. 1960. Antimilos volcano. EGE, ΕΓΕ, 4(1), 38-50.

Sonder, A., 1925. Zur Geo1ogie und Petrograpbie der Inselgruppe von Milos Zeitschir. für Vulkanol., 8, Heft 4, S. 957, Berlin.

Vougioukalakis, G., 2001. Study of Cenozoic Volcanism of Greece for the assessment of geothermal energy sources. IGME technical report.

Zhou, X., Kuiper, K., Wijbrans, J., Boehm, K., Vroon, P., 2020. Eruptive history and 719 40Ar/39Ar geochronology of the Milos volcanic field, Greece. Geochronology Discussions, 720, 1–40. https://doi.org/10.5194/gchron-2020-30.

16th International Congress of the Geological Society of Greece

17-19 October, 2022 - Patras, Greece

Bulletin of the Geological Society of Greece, Sp. Publ. 10

Ext. Abs. GSG2022-282

Review of Methana volcano geology aiming at the volcanic hazard assessment in the area.

G. Vougioukalakis[1], C. Kanellopoulos[1,2,3], L. Francalanci[4]

(1) Hellenic Survey of Geology and Mineral Exploration – HSGME, Greece, e-mail: gvoug@igme.gr, ckanellopoulos@gmail.com (2) Faculty of Geology and Geoenvironment, National and Kapodistrian University of Athens, Panepistimiopolis, Zografou, 15784, Athens, Greece (3) Department of Geology, University of Patras, 26504, Patras, Greece (4) Dipartimento di Scienze della Terra, Università di Firenze, Italy, e-mail: lorella.francalanci@unifi.it

The Methana peninsula is mainly composed of volcanic products and hosts Kameni Hora, the westernmost of the active volcanic centers of the South Aegean Volcanic Arc (SAVA). It belongs to the Aegina-Poros-Methana volcanic field, one of the four volcanic fields of the SAVA.

The Methana peninsula hosts the youngest products of the volcanic field, with the main volume of the products deposited from 3.6 to 0.2 Ma (Pe-Piper & Piper, 2013). The products are mostly lava domes and block- and- ash flows, with a prevalent andesitic to dacitic composition (Francalanci et al., 2005; Elburg et al., 2018). An accurate reconstruction of Methana's volcanic history is difficult because there are no distinctive marker beds, but available data favour a low, continuous rate of activity throughout the Quaternary. The most recent volcanic event in the area, i.e. Kameni Hora, took place during the historic times at ca. 230 BC, as reported by Strabo and Pausanias that described it. According to the description of these authors, the activity was relatively calm, effusive and extrusive, building up the lava domes and flows of Kameni Hora, at the NW edge of the peninsula (Fytikas et al., 1986, Pe-Piper & Piper, 2013) (Fig. 1). Lavas are porphyritic, with silica around 60-63 wt%, and are characterized by variable-sized mafic enclaves (Elburg et al., 2018). Other young volcanic centers occur a few kilometres NW offshore of Kameno Vuno; the absence of sedimentary cover suggests a possible historical age for these edifices as well (Foutrakis & Anastasakis, 2018).

We review here the volcano geology, as it has been mapped in the existing geological maps of Fytikas et al. (1986) and Detrich and Gaitanakis (1995) and published in different relative papers, aiming at the volcanic hazard and risk assessment of the area.

Based on the new field observations, no significant explosive eruptions occurred in the area of Methana. No pyroclastic formation could be linked to a large-caldera forming event. Moreover, there are not any volcano-tectonic and structural data suggesting significant collapses or eruptions. The only deposits attributed to sub-plinian events outcrop at the SW Methana area, consisting of four fallout layers of grey andesitic pumice in very proximal facies, suggesting local centres in the nearby area (Fig. 2).

Furthermore, the hydrothermal alteration is limited in very small areas, and no hydrothermal explosion craters and relative products exist.

These preliminary data indicate that in case of volcanic unrest in the Methana area, the most probable scenario to consider is an initial extrusive - effusive activity, building up a lava dome and related flows field, with probable late block and ash flow events when the edifice achieve a height and instability due to the creation of steep slopes in dome flanks or lava flow fronts. These phenomena could induce relatively low risk only in the most proximal area to the vents.

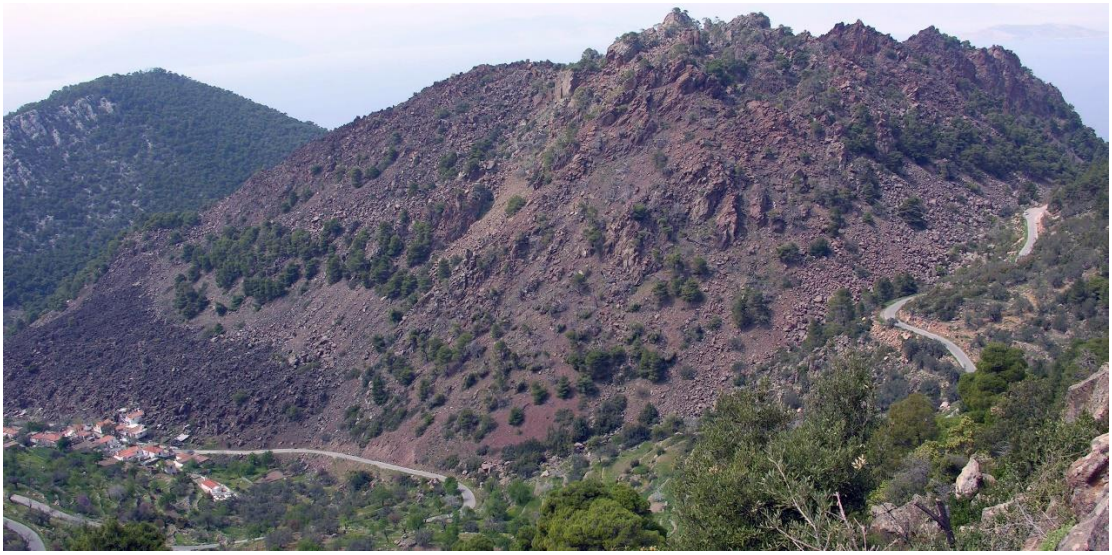

Figure 1. Kameni Hora historical lava dome

Figure 2. Cave Punta pyroclastic deposits, at SW Methana coast.

References

Dietrich, V., Gaitanakis, P., 1995. Geological Map of Methana Peninsula (Greece). ETH Zürich, Switzerland.

Elburg, M.A. Smet, I., Van den haute, P., Vanhaecke, F., Klaver, M., Andersen, T., 2018. Extreme isotopic variation documents extensional tectonics in arc magmas from Methana, Greece. Lithos, 318–319, 386–398.

Foutrakis, P.M., Anastasakis, G., 2018. The active submarine NW termination of the South Aegean Active Volcanic Arc: The Submarine Pausanias Volcanic Field. Journal of Volcanology and Geothermal Research 357 399-417.

Francalanci, L., Vougioukalakis, G.E., Perini, G., Manetti, P., 2005. A West-East traverse along the magmatism of the South Aegean volcanic arc in the light of volcanological, chemical and isotope data. Developments in Volcanology (Amsterdam, Olanda), "The South Aegean Active Volcanic Arc, Present Knowledge and Future Perspectives", M. Fitykas and G.E. Vougioukalakis Eds., vol.7, 65-111. [ISBN-13: 978-0-444-52046-3, ISBN-10: 0-444-52046-5].

Fytikas, M., Giuliani, O., Innocenti, F., Kolios, N., Manetti, P., Mazzuoli, R., 1986. The Plio-Quaternary volcanism of Saronikos area (western part of the active Aegean volcanic Arc). Ann. Geol. Pays Hell., 33: 23-45.

Pe-Piper, G., Piper D.J.W., 2013. The effect of changing regional tectonics on an arc volcano: Methana, Greece. Journal of Volcanology and Geothermal Research 260: 146-163.

Vougioukalakis, G.E., Fytikas, M., 2005. Volcanic hazards in the Aegean area, relative risk evaluation, monitoring and present state of the active volcanic centers. Developments in Volcanology 7, 161-183.

16th International Congress of the Geological Society of Greece

17-19 October, 2022 - Patras, Greece

Bulletin of the Geological Society of Greece, Sp. Publ. 10

Ext. Abs. GSG2022-286

Historical hydrothermal explosive events and present volcanic hazard at Milos island, Greece

G. Vougioukalakis[1], C. Kanellopoulos[1,2,3], S. Massaro[4,5], R. Sulpizio[4,5], F. Lucchi[6], C. Tranne[6], G. Chiodini[5], F. Tassi[7], O. Vaselli[7], G. Bini[5], P. Pantou[8]

(1) Hellenic Survey of Geology and Mineral Exploration – HSGME, Greece, e-mail: gvoug@igme.gr, ckanellopoulos@gmail.com (2) Faculty of Geology and Geoenvironment, National and Kapodistrian University of Athens, Panepistimiopolis, Zografou, 15784, Athens, Greece (3) Department of Geology, University of Patras, 26504, Patras, Greece (4) Dipartimento di Scienze della Terra e Geoambientali, Università di Bari, Italy (5) Istituto Nazionale di Geofisica e Vulcanologia, Bologna, Italy (6) Dipartimento di Scienze Biologiche, Geologiche e Geoambientali, Università di Bologna, Italy (7) Dipartimento di Scienze della Terra, Università di Firenze, Italy (8) School of Archaeology, Hellenic Ministry of Culture, Greece

The Island of Milos belongs to the South Aegean Active Volcanic Arc (SAAVA). The island is mainly composed by volcanic products covering remnants of crystalline basement. Several hot springs and fumarolic fields (inland and offshore) occur. Based on geothermal surveys and deep drilling projects, the presence of a high enthalpy geothermal field was evidenced. Excessive hydrothermal alterations creating industrial mineral deposits and base and precious metal ore deposits also occur due to the intense and continuous hydrothermal-volcanic activity. The active tectonic setting and the high seismicity of the area also play a significant role.

Volcanic activity on subaerial Milos island started at about 3.5 Ma ago, nevertheless, tephrostratigraphic studies on marine sediments of South Milos suggested that volcanic activity likely started earlier, i.e. 4.5-3.7 Ma (Fytikas et al., 1986; Zhou et al., 2020, VanHinsbergen et al., 2004).

Milos, together with the nearby volcanic islands, i.e., Kimolos and Polyegos, is a volcanic complex consisting of different volcanic edifices, lava domes and thick volcaniclastic deposits (Fytikas et al., 1986; Fytikas and Vougioukalakis, 1993; Francalanci et al., 1994, 2003; Stewart and McPhie, 2003; Francalanci et al., 2005). From 3.5 to 1.6 Ma, explosive and effusive activity built up Kimolos island and most of the present Milos island (Francalanci et al., 2005). During the Quaternary, volcanic activity mainly took place at the center of Milos Island, during which acidic magmas were produced. Three main eruptive periods can be distinguished, as follows: (i) 1.1-0.9 Ma: rhyolitic activity in a N-S trending area in the central part of the island where a lava field and domes were emplaced, (ii) 0.38 Ma: rhyolitic activity forming lava flows and the Trachylas (perlitic) tuff ring, in the northernmost sector of the aforementioned N-S trending lineament and (iii): 90 - 70 ka rhyolitic activity forming lava flows and the Fyriplaka (perlitic) tuff ring in the southern edge of the aforementioned N-S trending lineament.

Recurrent hydrothermal (phreatic) explosions of various magnitude occurred, favoured by intense hydrothermal fluid circulation and likely triggered by earthquakes, either before and after the last volcanic eruption of Fyriplaka. Some of these explosions emplaced wide debris and mudflow deposits, rich in crystalline basement fragments, i.e. the so-called "Green Lahar" formation in the central-eastern Milos (Fytikas et al., 1986). Hydrothermal explosions continued during historical times (80-200 AD, Traineau and Dalabakis, 1989) in the Agia Kyriaki area, where a geothermal anomaly currently occurs, as testified by the presence of fumarolic discharges (up to 100 °C, Figure 1).

New findings of a series of hydrothermal craters and volcaniclastic layers of hydrothermal explosion breccias, related to hydrothermal explosions, in the south eastern part of Milos, reveal extensive destruction during the Roman period, as testified by a large number of pottery fragments found at the base of these deposits (Figure 2). A preliminary study of the pottery fragments dates them to the 2nd/3rd century AD. The presence of anthropogenic activity in that period was intense and especially focused on mining and trade activities. At the same time, archaeological studies proved a decline in human presence and activity in the 4th century AD, likely related to hydrothermal eruptions which induced the local population to abandon the island.

These evidences of hystorical hydrothermal explosive activity make imperative the assessment of the volcanic hazard of the island, and strongly suggest that further investigations and monitoring activities are required to understand the physical dynamics that produced the hydrothermal activity to minimize possible future events.

Figure 1. Active fumaroles at Agia Kyriaki area.

Figure 2. Destruction layer with several fragments of pottery.

References

Francalanci, L., Fytikas, M. and Vougioukalakis, G.E., 1994. Volcanological and geochemical evolution of Kimolos and Polyegos centers, Milos Island Group, Greece. IAVCEI Congress, Sember 1994, Ankara, Turkey, Book of Abstracts.

Francalanci, L., Fytikas, M. and Vougioukalakis, G.E., 2003. Kimolos and Polyegos volcanoes, South Aegean Arc, Greece: volcanological and magmatological evolution based on stratigraphic and geochemical data. Meeting on "The South Aegean Volcanic Arc: Present knowledge and future perspectives", in the frame of the “Milos Conferences – Magmatism in convergent plate margins”, Milos island, Greece. Book of abstracts, pp. 25-26.

Francalanci, L., Vougioukalakis, G.E., Perini, G., Manetti, P., 2005. A West-East Traverse along the magmatism of the south Aegean volcanic arc in the light of volcanological, chemical and isotope data. Developments in Volcanology 7, 65-111.

Fytikas, M. and Vougioukalakis, G., 1993. Volcanic Structure and Evolution of Kimolos and Polyegos (Milos island group). Greek Geol. Soc. Bull., XXVIII/2: 221-237.

Fytikas, M., Innocenti, F., Kolios, N., Manetti, P., Mazzuoli, R., Poli, G., Rita, F., Villari, L., 1986. Volcanology and petrology of volcanic products from the island of Milos and neighbouring islets. J. Volcanol. Geotherm. Res., 28: 297-317.

Principe, C., Arias, A. and Zoppi, U., 2003. Hydrothermal explosions on Milos: from debris avalanches to debris flows deposits. In “The South Aegean Active Volcanic Arc: Present Knowledge and Future Perspectives” international conference, Milos 2003. Book of abstracts 95.

Stewart A.L. and McPhie J., 2003. Facies architecture of the submarine-to-subaerial volcanic succession on Milos, Greece. In "The South Aegean Active Volcanic Arc: Present Knowledge and Future Perspectives” international conference, Milos 2003. Book of abstracts 24

Traineau, H. and Dalabakis, P., 1989. Mise en evidence d´une éruption phreatique historique sur l´ile de Milos (Grece). C.R. Acad. Sci. Paris, t. 308, Serie II: 247-252.

Van Hinsbergen, D.J.J., Snel, E., Garstman, S.A., Marunteanu, M., Langereis, C.G., Wortel, M.J.R., Meulenkamp, J.E., 2004. Vertical motions in the Aegean volcanic arc: Evidence for rapid subsidence preceding volcanic activity on Milos and Aegina, Marine Geology, Vol 209, 1-4 329-345.

Zhou, X., Kuiper, K., Wijbrans, J., Boehm, K., Vroon, P., 2020. Eruptive history and 719 40Ar/39Ar geochronology of the Milos volcanic field, Greece. Geochronology Discussions, 720, 1–40. https://doi.org/10.5194/gchron-2020-30.

16th International Congress of the Geological Society of Greece
17-19 October, 2022 - Patras, Greece
Bulletin of the Geological Society of Greece, Sp. Publ. 10
Ext. Abs. GSG2022-290

UAV and LiDAR Technologies for Validating Soil Erosion Models in The Field

S. Alexiou[1], I. Papanikolaou[1], G. Deligiannakis[1], A. Pallikarakis[1], K. Reicherter[2], M. Karamesouti[3], E. Psomiadis[1], N. Efthimiou[1,4], N. Charizopoulos[1]

(1) Department of Natural Resources Development & Agricultural Engineering, Laboratory of Mineralogy and Geology, Agricultural University of Athens, Athens, Greece, sim.alexiou@aua.gr (2) Institute of Neotectonics and Natural Hazards, RWTH Aachen University, Aachen, Germany (3) Geoinformation Science Lab, Geography Department, Humboldt-Universität zu Berlin, Berlin, Germany; IRI THESys, Humboldt-Universität zu Berlin, Berlin, Germany (4) Faculty of Environmental Sciences, Czech University of Life Sciences Prague, Praha, Czech Republic

This research focuses on the application of an emerging technique such as the UAV (Unmanned Aerial Vehicle) photogrammetry and the widely used terrestrial LiDAR (Light Detection And Ranging) in geomorphological change detection (Gulyaev and Buckeridge, 2004, Niethammer et al., 2012, Rosca et al., 2018) and soil erosion modeling validation. The UAV and LiDAR methods are well established in our research, aiming for high-accuracy results, through the multi-source (UAV and LiDAR) comparison of point clouds. The detailed LiDAR and UAV-derived surface reconstruction leads to direct comparison and change detection of the soil surface in various temporal scales. Multi-temporal point cloud analysis is considered a suitable 3D process for accurate soil erosion and sediment yield estimation (Neugirg, 2016). The first study area is a semi-mountainous slope in Evia Island, Greece, that was selected based on a severe fire event in 2019, where significant and rapid topsoil change occurred due to the vegetation cover absence. The calculation of vertical distances through the M3C2 algorithm (Lague et al., 2013) resulted in topsoil difference assessment in the order of a few centimeters within the first 4-months following the wildfire event (Alexiou et al 2021). UAV-derived products were found to quantify localized channel erosion more accurately compared to the LiDAR method, estimating an annual erosion rate of 48 cm. Yet, the slope wash often depicted on slopes following intense rainfall events was delineated more precisely by the LiDAR sensor due to low-height vegetation. To this content, an additional study through UAV SfM (Structure-from-Motion) photogrammetry was developed in a sediment retention dam in the Platana region, Central Greece. This site was selected due to the absence of any fire event in the dam's watershed since its construction (2005). The concrete dam acts as a sufficient sediment trap so that annual sediment deposition processes can be quantified with high accuracy through the UAV point cloud comparison. The UAV- SfM technique yielded an annual volume of 1,620 m^3 that has been deposited in the upland dam area.

Several soil erosion models are widely used over the last decades (Pandey et al., 2021). Yet, the application of different soil erosion models demonstrates that their results differ significantly, highlighting the need for validation (Van Rompaey et al., 2003, Karamesouti et al., 2016, Waltner et al., 2020). For this case study we selected the application of the RUSLE model (Renard et al., 1997). The RUSLE was found to perform well in the studied watershed, where 5.8 t/ha/yr yields mean sediment of 1,552 m^3 when the SDR (Sediment Delivery Ratio) of 40% was applied. This is in agreement with the field measurements.

In conclusion, our study aims to quantify soil erosion and deposition with high accuracy through advanced technological tools and to provide valuable information for soil erosion modeling validation that is currently missing.

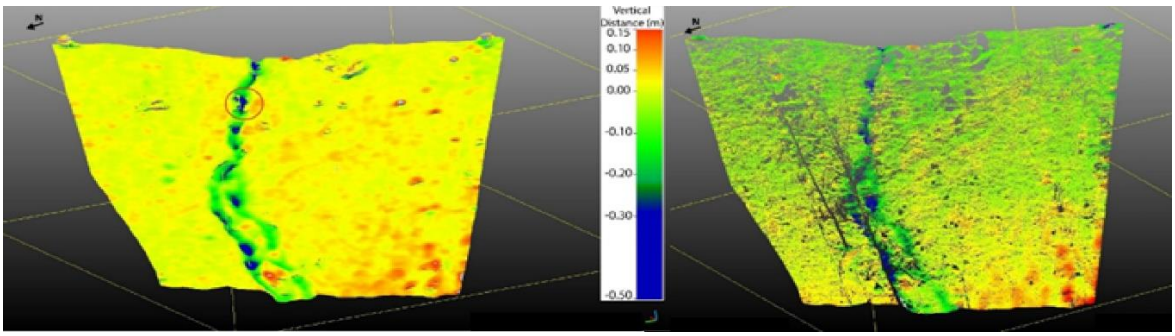

Figure 1. Annual erosion (m) using UAV (on the left) and TLS (on the right) techniques in Evia Island, Greece

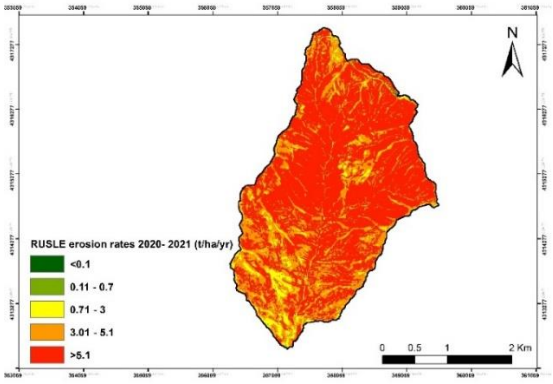

Figure 2. RUSLE annual erosion rate (9/2020 to 8/2021) in Platana dam watershed, Central Greece.

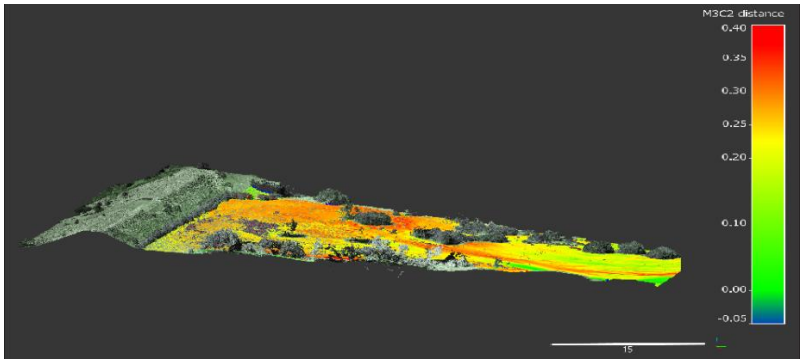

Figure 3. Annual deposition (m) in Platana dam through M3C2 algorithm (vertical difference) implementation

Acknowledgements

This research is co-financed by Greece and the European Union (European Social Fund- ESF) through the Operational Programme «Human Resources Development, Education and Lifelong Learning» in the context of the project "Strengthening Human Resources Research Potential via Doctorate Research – 2nd Cycle" (MIS-5000432), implemented by the State Scholarships Foundation (IKY).

References

Alexiou, S., Deligiannakis, G., Pallikarakis, A., Papanikolaou, I., Psomiadis, E., Reicherter, K., 2021. Comparing High Accuracy t-LiDAR and UAV-SfM Derived Point Clouds for Geomorphological Change Detection. ISPRS Int. J. Geo-Inf., 10, 367.

Gulyaev, S.A., Buckeridge, J.S., 2004. Terrestrial methods for monitoring cliff erosion in an urban environment. Journal of Coastal Research, v. 20(3), 871-878.

Karamesouti, M., Petropoulos, G. P., Papanikolaou, I. D., Kairis, O., & Kosmas, K. (2016). Erosion rate predictions from PESERA and RUSLE at a Mediterranean site before and after a wildfire: Comparison & implications. Geoderma, 261, 44–58.

Lague, D.; Brodu, N.; Leroux, J. Accurate 3D comparison of complex topography with terrestrial laser scanner: Application to the Rangitikei canyon (N-Z). ISPRS J. Photogramm. Remote Sens. 2013, 82, 10–26

Neugirg, F., Stark, M., Kaiser, A., Vlacilova, M., Della Seta, M., Vergari, F., Schmidt, J., Becht, M., Haas, F., 2016. Erosion processes in calanchi in the Upper Orcia Valley, Southern Tuscany, Italy based on multitemporal high-resolution terrestrial LiDAR and UAV surveys. Geomorphology, 269, 8–22.

Niethammer, U., James, M.R., Rothmund, S., Travelletti, J., Joswig, M., 2012. UAV-based remote sensing of the Super-Sauze landslide: Evaluation and results, Engineering Geology, v. 128, 2–11.

Pandey, S., Kumar, P., Zlatic, M., Nautiyal, R., & Panwar, V. P. (2021). Recent advances in assessment of soil erosion vulnerability in a watershed. International Soil and Water Conservation Research, 9(3), 305–318.

Renard, K., Foster, G., Weessies, G., McCool, D. (1997). Predicting soil erosion by water: a guide to conservation planning with the revised universal soil loss equation (RUSLE). In Agriculture Handbook 703, Ed. Yoder DC. U.S.D.A, DC.

Roşca, S., Suomalainen, J., Bartholomeus, H., Herold, M., 2018. Comparing terrestrial laser scanning and unmanned aerial vehicle structure from motion to assess top of canopy structure in tropical forests. Interface Focus, 8.

Van Rompaey, A. J., Vieillefont, V., Jones, R. J. A., Montanarella, L., Verstraeten, G., Bazzoffi, P., Dostal, T., Krasa, J. , de Vente, J., & Poesen, J. (2003). Validation of soil erosion estimates at European scale. European Soil Bureau Research Report No.13, p. 26

Waltner, I., Saeidi, S., Grósz, J., Centeri, C., Laborczi, A., & Pásztor, L. (2020). Spatial assessment of the effects of land cover change on soil erosion in hungary from 1990 to 2018. ISPRS International Journal of Geo-Information, 9(11).

16th International Congress of the Geological Society of Greece
17-19 October, 2022 - Patras, Greece
Bulletin of the Geological Society of Greece, Sp. Publ. 10
Ext. Abs. GSG2022-292

How Land Use/Cover and Landscape Characteristics Along with Fire Severity and Frequency can Affect the Potential Vegetation Recovery: The case of Varibobi Wildfire

E. Psomiadis[1], , S. Alexiou[1], E. Zevgoli[1], M. Avramidou[1], D. Veropoulou[1], P. Mecaj[1], K.X. Soulis[1], I. Papanikolaou[1]
(1) Agricultural University of Athens, Iera Odos 75, 11855, Athens, Greece, mpsomiadis@aua.gr.

Introduction

In recent years, forest fires have increased in terms of frequency, extent and intensity, especially in Mediterranean countries Wildfires affect the ecological functioning of ecosystems as they partially or completely burn the vegetation layers and affect post-fire vegetation and soil processes such as soil erosion and vegetation recovery. Moreover, wildfires involve a great threat to property and human life, especially in Wildland-Urban Interface (WUI) areas, id est "the transition zones between cities and wildland, where structures and other human development meet undeveloped wildland or vegetative fuels". The vegetation recovery is directly correlated with post-fire effect drivers such as fire characteristics (intensity, duration, and severity), local topography, the type of existing flora, bedrock, etc (Efthimiou *et al*., 2020).

The present study, carried out by a targeted project of the Agricultural University of Athens with the assistance of concerned promoters and explores the consequences of the 2021 wildfire that occurred in the broader area of Varibobi district of Acharnes municipality, by examining the fire severity and fire frequency throughout the last decades, along with land use/cover and landscape characteristics. Moreover, it aims to enlighten the impact of these factors on vegetation recovery and landscape restoration.

Materials and Methods

The methodological part of this study comprises the following steps and materials:

- The comprehensive delineation of the burned area using high-resolution Sentinel-2 (S2; Copernicus program) and Landsat-8 (USGS-NASA data; Figure 1)
- The detailed pre- and post-fire land use/cover mapping using very high resolution (0.5m) WorldView-2 data (MAXAR; Figure 2i), before, after and will also be examined the vegetation regrowth two years after the fire.
- the analysis of the geomorphological, geological, hydrological and meteorological characteristics of the affected area (Figure 2ii)

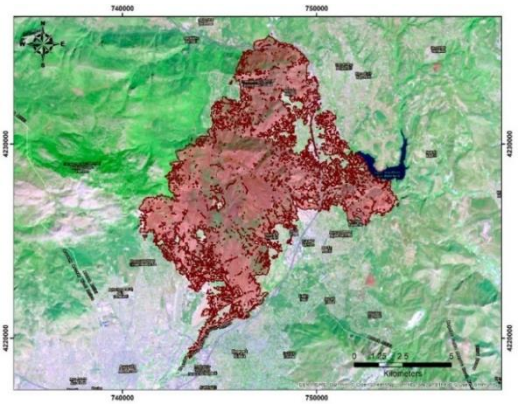

Figure 1. The detailed extraction of the wildfire-affected area (coordinate system: WGS 1984 UTM Zone 34N) using False Color Composites and Ratios (Normalized Difference Vegetation Index) of the spectral bands

- The collection of long-term Landsat data (form the years 1983, 1986, 1987, 1992, 1998, 2001, 2004, 2008, 2011, 2012 & 2021) using the USGS portal (earthexplorer.usgs.com) to create a fire frequency map of the area for the last 40 years (Figure 3i).
- Burn Severity calculation, through SNAP software of ESA and Google Earth Engine, by computing the Normalized Burn Ratio (NBR) before and after the fire event using S2 the equation NBR= (B8-B12)/(B8+B12), where B8 is the near-infrared (NIR) and B12 the short wave infrared (SWIR) bands, using also cloud and water masks. Then the subtraction of these indices provides the burn severity through the equation: $dNBR=NBR_{prefire}-NBR_{postfire}$. The dNBR was classified according to EFFIS classification (Figure 3ii). However, the dNBR is an absolute difference which can present problems in areas with low pre-fire vegetation cover, where the absolute change between pre-fire and post-fire NBR will be small. In such cases the relativized version of burn severity is advantageous. Therefore, the Relativized Burn Ratio (RBR) was calculated utilizing the equation: $RBR = [dNBR / (NBR_{prefire}+1.001)]$.

- field surveys to estimate using Composite Burn Index (CBI) proposed by Key & Benson (2006) method to examine the soil condition and how affected by the fire event, and the correlation of its results with the outcomes from the high and very high-resolution satellite data. The CBI was created to quantify fire burn severity data, describe the heterogeneity of severity that can be observed in the field after a fire, present a comprehensive view of fire effects, and directly assess the magnitude of environmental change in large and hard-to-reach fires.
- The vegetation regrowth control process and its relation to the fire severity and fire frequency, and additionally to geomorphological, geological and hydrological characteristics of the area, and the LULC and vegetation types.

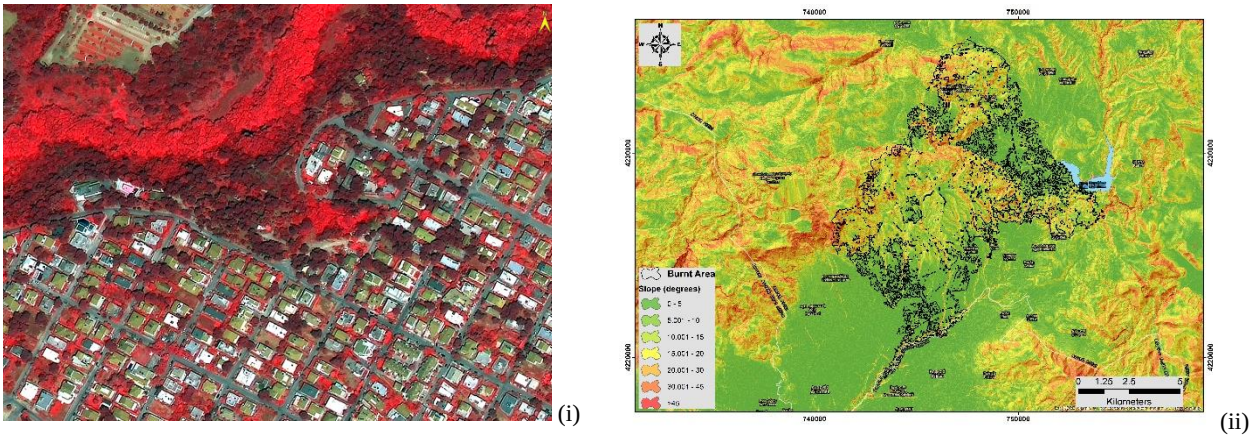

(i) (ii)

Figure 2. (i) Land use/cover classification (LULC) classification image of the Bramianos dam broader area, (ii) Map of flood arrival time, utilizing DSM in the piping scenario.

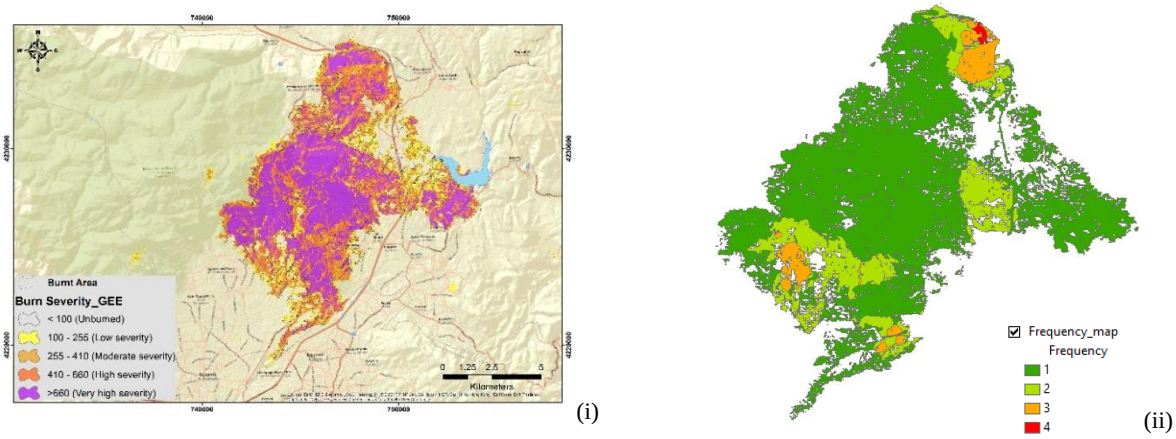

(i) (ii)

Figure 3. (i) The burn severity map, (ii) Frequency map showing how many times each part of the Varibobi-burnt area has been affected by other fire events in the past

Results and Conclusions

The primary results of this study show so far that an area of 73,38 km^2 was affected by the wildfire, from which 12,6 km^2 (17,12%) were burned for the second time and 3,61 (4,93%) and 0.28 km^2 (0,28%) for the third and fourth time, respectively. Taking into account that a big part of the affected area is comprised of man-made concrete constructions (buildings, roads etc.) leads us to the conclusion that these percentages are much higher.

As far as concerns the burn severity, 35,9% (26,36 km^2) and 49% (35,92 km^2) of the total affected area belongs to high and very high burn severity classes. The research is ongoing and further and more detailed results and concusions will be obtained soon.

Acknowledgements

This research is financed by GlaxoSmithKline SA in the framework of the initiative VARIBOPI RESET

References

Efthimiou, N., Psomiadis, E., Panagos, P., 2020. Fire severity and soil erosion susceptibility mapping using multi-temporal Earth Observation data: The case of Mati fatal wildfire in Eastern Attica, Greece. Catena, 187, 1-16 (104320). https://doi.org/10.1016/j.catena.2019.104320

Key, C. & Benson, N. 2006. Landscape Assessment: Ground measure of severity, the Composite Burn Index; and Remote sensing of severity, the Normalized Burn Ratio.In book: FIREMON: Fire Effects Monitoring and Inventory System.Edition: RMRS-GTR-164

Psomiadis, E., Soulis, K.X., Efthimiou, N., 2020. Using SCS-CN and Earth Observation for the comparative assessment of the hydrological effect of gradual and abrupt Spatio-temporal land cover changes. Water, 12 (5), 1386. https://doi.org/10.3390/w12051386

16th International Congress of the Geological Society of Greece

17-19 October, 2022 - Patras, Greece

Bulletin of the Geological Society of Greece, Sp. Publ. 10

Ext. Abs. GSG2022-302

Field Data Collection Using Drone Technology and Ground Sensors for the Estimation of Crop Water Requirements

E. Psomiadis[1], S. Alexandris[1], N. Proutsos[2], I. Charalampopoulos[1]

(1) Agricultural University of Athens, Iera Odos 75, 11855, Athens, Greece, mpsomiadis@aua.gr (2) Institution, Town, Country.

Introduction

Precision agriculture has been at the cutting edge of research during the recent decade, aiming to reduce water consumption and ensure sustainability in agriculture (Darra *et al.*, 2021).

The present study aims to use extensive and innovative field data and implement an integrated analysis of multispectral and thermal drone data along with micrometeorological measurements to estimate the actual water requirements of potato and watermelon fields. The proposed methodology was based on the Crop Water Stress Index (CWSI) and was applied to experimental vegetable crops within the ongoing research project GreenWaterDrone (Alexandris *et al.*, 2021). The innovative approach combines real spatial data, such as infrared canopy temperature, air temperature, air relative humidity, near-infrared and thermal infrared image data, taken above the crop field using an aerial micrometeorological station (AMMS), a multispectral and a thermal camera installed on an unmanned aerial vehicle (UAV). Aerial and ground measurements were transferred in real-time to sophisticated databases and applications over existing mobile networks for further processing and estimation of the actual water requirements of a specific crop at the field level and then an upscale at the regional level was applied.

The increasing demand for freshwater, especially for irrigation purposes could lead to groundwater overexploitation and potential deterioration of coastal aquifers (Giannoulopoulos *et al.*, 2002).

Materials and Methods

The study area was situated in the prefecture of Messinia (western Peloponnese), close to the city of Kyparissia in the Municipality of Trifilia. The experimentation was conducted in two fields with two different crops that are representative of the area, i.e., potato and watermelon, which were utilized for the validation procedure of the project methodology.

Automatic micrometeorological stations were installed in the middle of each field for observations of the upper atmospheric layer of the crops and measurements within the soil profile (at the root zone). This was an indispensable condition for the accurate estimations of CWSI and the determination of all the biophysical attributes of the cultivations during all stages of the growing season.

In the present study, the quadcopter DJI Matrice 200 was used for the measurements of the multispectral, thermal and IR-TH data, and was selected due to the compatibility of incorporating both multispectral (Sentera AGX710, five bands cover blue, green, red, red edge, and near-infrared parts of the electromagnetic spectrum) and thermal (DJI Zenmuse XT2, incorporates a high-resolution forward-looking infrared FLIR Tau 2 thermal sensor) cameras. The high-resolution multispectral and thermal imagery acquired using the UAV platform ideally enables the extraction and identification of crop conditions (vegetation vigour, spatial distribution, canopy cover, and bare ground gaps) and the temperature of the canopy.

For the IR-TH measurements four sensors: data logger, IR radiometer (SI-111-SS Apogee), miniature Thermo-Hygrometer EE08, and an accurate GPS were installed (Figure 1i). The radiation shield plates (which protected the temperature and RH sensors), the watertight box (which protected the data logger), and all the sensors' mounts were designed in a 3D CAD program and printed using a 3D printer in the lab. Particular attention was paid to the placement of the thermo-hygrometer so that it was not affected by the flow of the drone propellers. The vertical positioning of the radiation shield on top of the UAV ensured mild air vortexing and mixing, avoiding the violent airflow from the downside of the drone due to the propellers. Moreover, one of the most important parts of the IR instrument sampling workflow was the calculation and design of the most suitable flight planning to have the best point samples coverage and complementarity to ideally cover the whole cultivated area. The flight height depends on the sensor type and the characteristics of the crop. For a specific IRT sensor, the visible surface area is a function of height. For the sensor SI-111 that was placed on the UAV in such a way to be vertical to the foliage for a flight height of 4 m (h), the surface area was estimated to be 8.2 m^2 (E), and the diameter of the circular surface was about 3.2 m (Figure 1ii).

Results and Conclusions

The pilot flights were conducted around midday having a clear sky with maximum global solar and net radiation flux densities. The Normalized Difference Red Edge index was calculated from the multispectral data. The index demonstrates

the plant health status and the existing gaps in the canopy cover and along the cultivation lines, which are important to distinguish and exclude by applying a binary mask since the reflection from the soil significantly affects the calculation results of the CWSI (Figure 2i). The thermal image was classified, keeping only the pixels of the crop canopy area to separate and present reliable foliage temperature values.

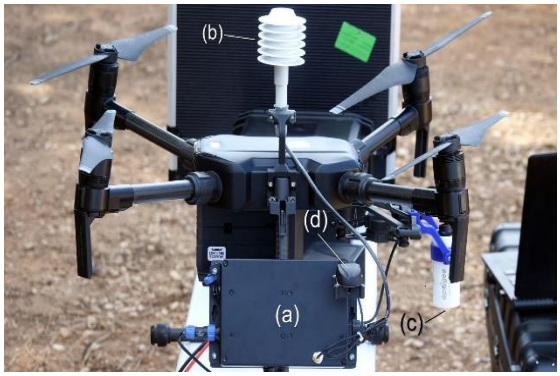

(i)

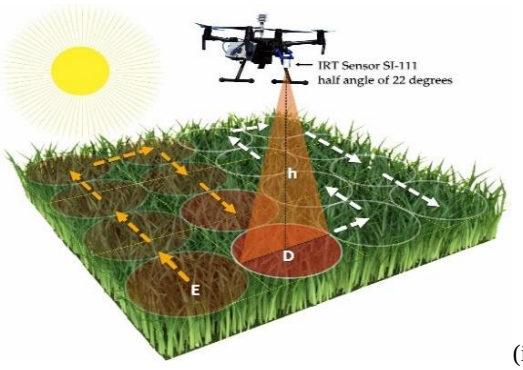

(ii)

Figure 1. (i) (a) Data logger Stylitis-12; (b) thermo-hygrometer sensor; (c) IR-TH infrared sensor; (d) GPS sensor, (ii) Graphic illustration of the measurement process with an infrared radiometer adapted to a UAV over dense cultivation foliage under a clear sky. The flight height depends on the sensor type and the characteristics of the crop.

The evaluation of the CWSI index was calculated through the IR-TH measurements and assisted by the measurements derived from the ground meteorological station, the portable IRT radiometers and the thermal image. These data produced a suitable thermal image (created from point samples) from the surface of the crop and consequently, the CWSI was estimated (Figure 2ii).

The analysis of these results showed that the excess amount of irrigation water supplied by crop irrigation (in mm) in the rhizosphere far exceeds the maximum crop needs [expressed in crop evapotranspiration (ETc)]. A typical example is the spring potato crop where while the average maximum daily irrigation requirement was 5.1 m^3/ha, the average volume of excess irrigation water in the rhizosphere was 20.1 m^3/ha. This difference corresponds to 394% of the maximum required amount of irrigation water. In general, this was confirmed for all the crops examined to a lesser or greater extent.

This intensive use of both water-consuming crops and improper agricultural practices (over-irrigation) led the entire coastal area to salinization (EC>2000 μE/cm). The nowadays practice of utilizing water from boreholes sited several kilometres away from the coastal region could be causing the further deterioration of groundwater aquifers in the area. Therefore, it is indisputable that proper irrigation water management is the only solution for groundwater sustainability.

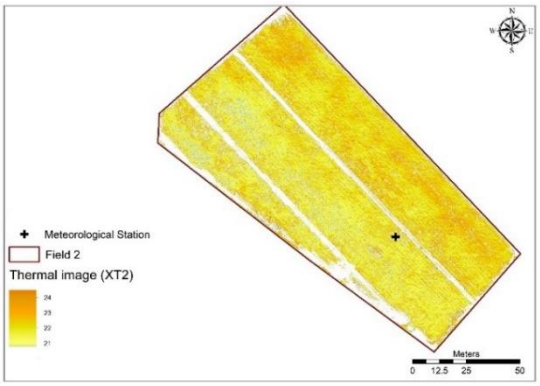

(i)

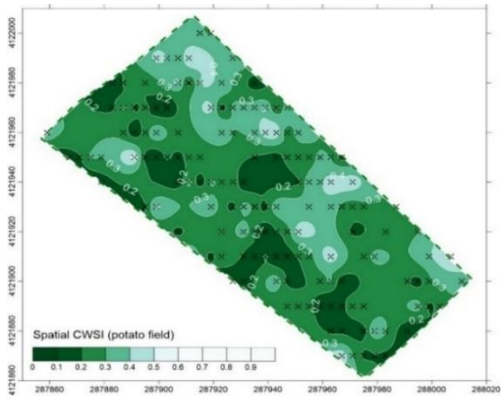

(ii)

Figure 2. (i) Thermal image acquired by the Zenmuse XT2 camera showing only the crop vegetation's temperature values by masking all the non-vegetation pixels, (ii) Spatial estimated isolines of CWSI derived from the AMMS point data

Acknowledgements

This research has been co-financed by the European Regional Development Fund of the European Union and Greek national funds through the Operational Program Competitiveness, Entrepreneurship and Innovation, under the call RESEARCH—CREATE—INNOVATE (project code: T1EΔK-04021).

References

Alexandris, S., Psomiadis, E., Proutsos, N., Philippopoulos, P., Charalampopoulos, I., Kakaletris, G., Vassilakis, S., Papoutsi, E-M., Paraskevopoulos, A., 2021. Integrating drone technology into an innovative agrometeorological methodology for the precise and real-time estimation of crop water requirements. Hydrology, 8(3), 131; https://doi.org/10.3390/hydrology8030131.

Darra, N., Psomiadis, E., Kasimati, A., Anastasiou, A., Anastasiou, V., Fountas, S., 2021 Remote and Proximal Sensing Derived Spectral Indices and Biophysical Variables for Spatial Variation Determination in Vineyards. Agronomy, 11(4), 741. https://doi.org/10.3390/agronomy11040741.

Giannoulopoulos, P., Alexandris, S., Psychogiou, M., Poulovasilis, A., 2002. Proceedings of the 6th Hydrogeological Congress of the Hellenic Hydrogeological Committee, Xanthi, p. 1-12.

16th International Congress of the Geological Society of Greece
17-19 October, 2022 - Patras, Greece
Bulletin of the Geological Society of Greece, Sp. Publ. 10
Ext. Abs. GSG2022-306

Oil and Gas Data Management – Workflow and Future Industry Trends

K. Oikonomopoulos[1], E. Kaikas[1], K. Farmakis[1], A. Stefatos[1]
(1) Hellenic Hydrocarbon Resources Management S.A., Athens, Greece, k.oikonomopoulos@greekhydrocarbons.gr

Research Highlights

How to approach and manage outdated data specifically within the oil and gas industry and what are the industry future trends.

Introduction

Hellenic Hydrocarbon Resources Management S.A. (HHRM), being the oil and gas authority of Greece, is responsible for regulating the oil and gas exploration industry as well as for assisting with the country's energy transition through its new roles as the Carbon Capture and Storage (CCS) and Offshore Wind Farms (OWF) licensing authority. Additionally, HHRM aims to be a value creator for Greece, through several projects such as digitisation and innovation.

The company manages a broad scope of data volumes that aid in decision-making in each phase of the upstream business. Much of the data is of various vintages – primarily from the 1980s – and for the most part in paper format. This indeed has an impact in its everyday activities and may prevent productivity growth. However, this sort of unconditioned data, is discouraging and not particularly attractive to the industry and therefore, in its current form, limits the growth of the oil and gas industry and its potential economic benefits for Greece.

Against this background, it is of utmost importance that all this data must be digitised and treated in such a way that it is brought into a condition through which it can be effectively used for exploration purposes. In addition, such outdated data that is conditioned and well-maintained can be made available to academic and research institutions aiming to produce new ideas and added value.

Data types

The data managed and handled by HHRM originates from disciplines such as geology, geophysics, and engineering and comprises the following:

- geophysical data (2D/3D seismic data, gravity, magnetics, magnetotellurics, etc.).
- well log data (e.g., composite logs, also films, scans)
- reports (e.g., geologic/structural maps, test and production data, etc.)
- images (e.g., composite logs, etc.)
- maps
- cores, cuttings and samples
- reservoir, facilities and well engineering data

Methodology – Workflow

As mentioned above, the majority of the legacy data is in paper format. Therefore, the first step is to have them scanned and reviewed regarding their image quality, resolution, size and save them within the appropriate folder, according to HHRM's filing system (Fig. 1).

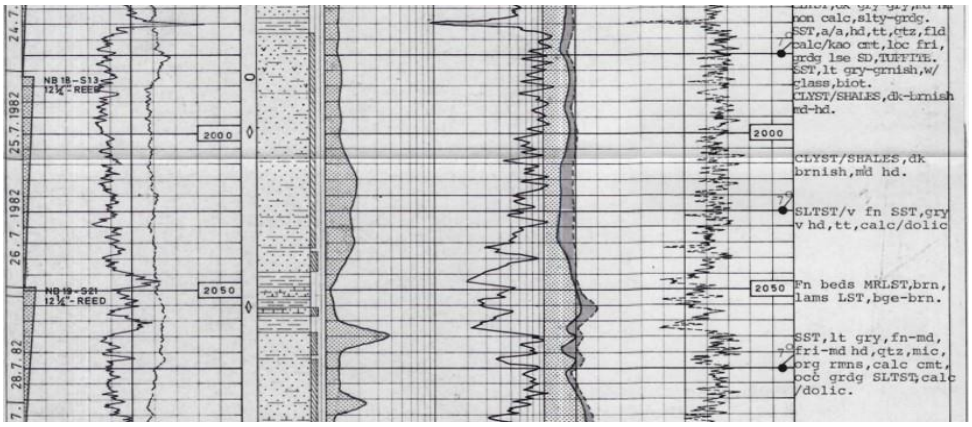

Figure 1. Several well logs, scanned from paper. The next step would be to start digitising the log curves into a LAS file, which can be then used by geoscientists during their studies.

As long as the data corresponds to a well log, before filing them as per HHRM's filing guidelines, the next step is to digitise the log and export it into a proper workstation file format – a LAS file. This procedure is relatively straightforward, but time consuming and nonetheless can be carried out within HHRM's premises, using licensed specialised software (Fig. 2).

On the other hand, in case the data is seismic – either 2D or 3D – it follows that digitisation can only be performed by a company specialising in such services and the exported file is a SEG-Y. The resulting file is then organised into the appropriate folder to be used later by the geoscience team.

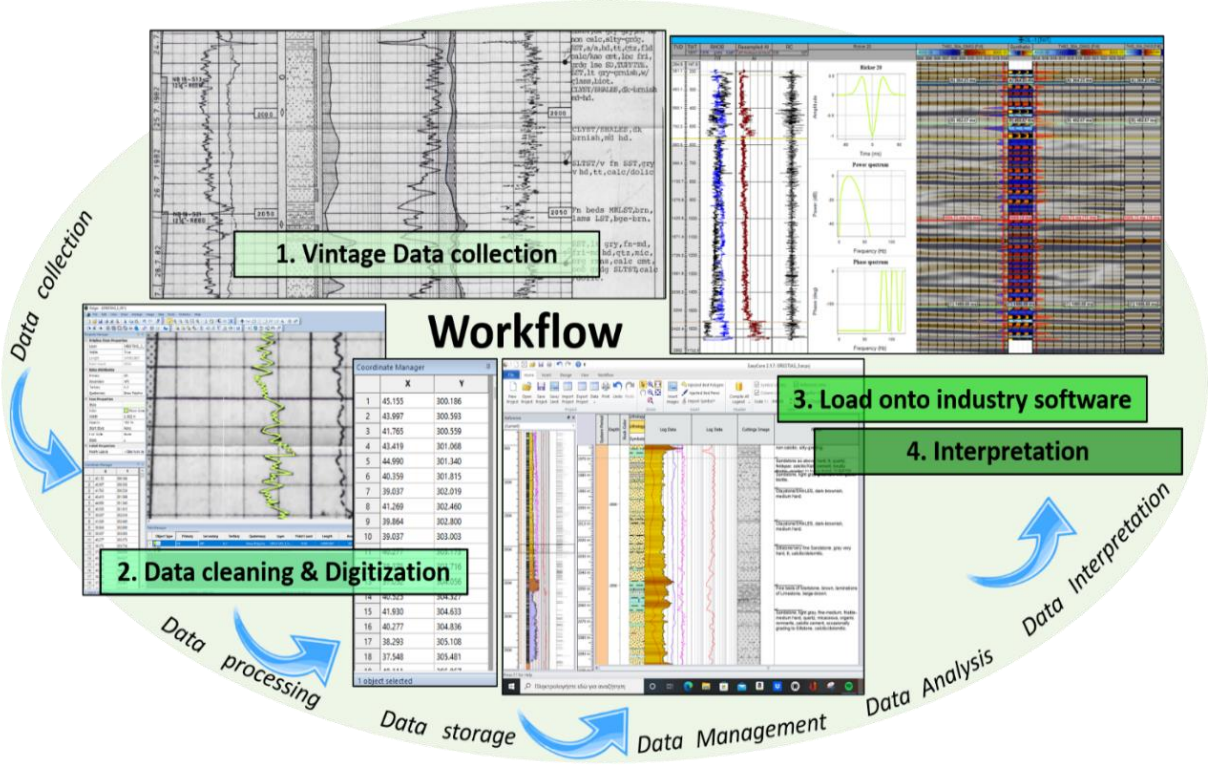

Figure 2. A typical example of a well data management and digitisation workflow.

Data management industry trends

Much like everything else nowadays, data management tends to follow the technological advances and the available solutions. The oil and gas industry needs holistic data management solutions in order to address the complexity and challenges of the upstream data and activities. Therefore, the demand in organised, well-conditioned data and above all data that is accessible at any given time and from any location is growing significantly.

Automated and optimised workflows based on Cloud and Artificial Intelligence (AI) technology is the future in data management. Acquisition, processing, storage, analysis and transfer are part of the management systems companies try to implement and integrate with advanced search functionalities.

Objectives

Ultimately, through improved data management approaches, the oil and gas companies as well as regulators – like HHRM – aim to reduce data retrieval time, improve productivity and minimise the effort of IT and support teams for data loading and quality control.

For regulators specifically, optimised data management can help unlock the hydrocarbon potential of the country and it is a key factor for attracting investments and promoting the upstream activities within a challenging and demanding world market. Digital well data (LAS files) for instance, will open up new potential in data processing, Computer Petrophysical Interpretations (CPIs) and ultimately AI applications in petrophysical analysis, in an attempt to address and fill any data gaps and reconsider data strategies.

Regulators also need these optimised and well-maintained data collections with the intent to preserve the country's natural resources, with an eye toward creating value where it does not currently exist.

Acknowledgements

HHRM SA would like to thank Angelos Tagalidis, Zafiria Chatzi, Niki Marina Rokana students from the University of Thessaloniki as well as Panagiotis Antonakopoulos, Pavlos Tsikouras and Loukas Tolias, students from the University of Patras for their help in the digitisation work of the available well data, during their internship and individual projects. Their outstanding work is greatly appreciated and assisted HHRM's efforts towards an up-to-date and functional database.

16th International Congress of the Geological Society of Greece
17-19 October, 2022 - Patras, Greece
Bulletin of the Geological Society of Greece, Sp. Publ. 10
Ext. Abs. GSG2022-322

Natural Hazard Risk Assessment and Inventory of the Hellenic Geosites

I. Kampolis[1], I. Zananiri[1], E. Moraiti[1], V. Barsaki[1]
(1) Hellenic Survey of Geology and Mineral Exploration (HSGME), Acharnae, Greece, ikampolis@igme.gr

Research Highlights

The Hellenic geosites are mainly threatened by geophysical hazards and less by hydrological or climatological ones.

Abstract

Greece hosts "114" geosites which are considered of high importance as they bear exceptional scientific, educational and touristic value, while representing unique natural monuments of the country. In general, geosites are perceived as geological or geomorphological sites which have been distinguished through an audit, assessment and selection process (Prosser *et al*., 2018). Moreover, geosites represent a key locality or area with geological features providing the appropriate information for the reconstruction of certain stages during Earth's evolution (PROGEO, 2011). Thus, their contribution in informing the public for the natural system as well as shaping the public's awareness regarding its fragility is vital. Unfortunately, their significance comes together with a great vulnerability (PROGEO, 2011). Geosites are part of the geo-environment, therefore they are exposed and vulnerable to natural hazards (Grecu, 2017). Under this threat which is capable of negatively impacting and degrading the natural environment of these monuments, we implemented an assessment for the natural hazard risk on the Hellenic geosites. Each hazard and its impact probability were evaluated by taking into account the geotectonic regime of every single geosite and the geomorphic processes shaping it. Unfortunately, no other effort has taken place to date with the scope of recording and classifying the different potential hazards. Furthermore, considering the fact that geodiversity - which is represented by the Hellenic geosites – is absent in the Greek Law (Zafeiropoulos *et al*., 2021) from a protection issue perspective, the assessment will act supportively to the effort for raising awareness about the fragility of the national geosites and will benefit geoeducational activities. It will also stand as a preliminary approach for the natural hazard assessment of geosites, something which is missing on a global scale.

The current hazard risk assessment was implemented through a scientific project coordinated by the Hellenic Survey of Geology and Mineral Exploration (HSGME). The scope was the evaluation of the different hazard types affecting each site and the establishment of a hazard-related inventory. We classified the different hazards in three main categories: a) geophysical (earthquakes, landslides and volcano-related), b) hydrological (fluvial and coastal floods and erosion) and c) climatological (sea-level rise). These categories include six hazard types named after 1-6: a) seismic (1), b) landslide (2), c) flood (3), d) erosional (4), d) sea-level rise (5) and volcanic hazard (6). Among these, the seismic hazard was further distinguished into three categories in respect to the three zones of seismic risk in Greece. If a geosite is located in zone I, we assign number 1a, whereas for zones II and III, we assign numbers 1b and 1c, respectively. The numbers facilitate the inventorying of the hazards, thus allowing for the establishment of a data base in order to proceed in a qualitative analysis. All the geosites and the different hazards were organized in an excel sheet file (Table 1). By applying filtering on each hazard category, we measured the number/percentage of the affected geosites. Also, the filtering allows the combination of two or more hazard types, thus revealing a combined hazard threat. For the evaluation of geophysical hazards, we used the online database of the Seismotectonic Atlas of Greece (Kassaras *et al*., 2020), whereas for the hydrological one, we extracted data from the published flood hazard maps by the Ministry of Environment & Energy. The landslide hazard was assessed by the HSGME database consisting of 1238 landslide locations (Vassiliadis, 2010) (Fig. 1). The climatological hazard was assessed according to the sea level rise scenarios of the Special Report on Ocean and Cryosphere in a Changing Climate (Oppenheimer *et al*., 2019) and by applying a maximum ~ +1m sea level rise till the end of this century. Additionally, data regarding the geotectonic regime and geomorphological processes governing each geosite was found in the published literature.

Table 1. Sample of the database with the Hellenic geosites and their hazard risk assessment.

Hellenic Geosites	Natural Hazards					
Mani, Alepotrypa Cave	1b	2	-	-	-	-
Kalavryta, Vouraikos Gorge	1b	2	3	-	-	-
Thassos – Ancient Marble Quarries	1c	-	-	4	5	-
Kalymnos – Horst of Telendos	1c	2	-	-	-	-
Kythnos – Kolona Tombolo	1c	-	-	4	5	-
Nisyros – Volcanic complex	1b	2	-	-	-	6

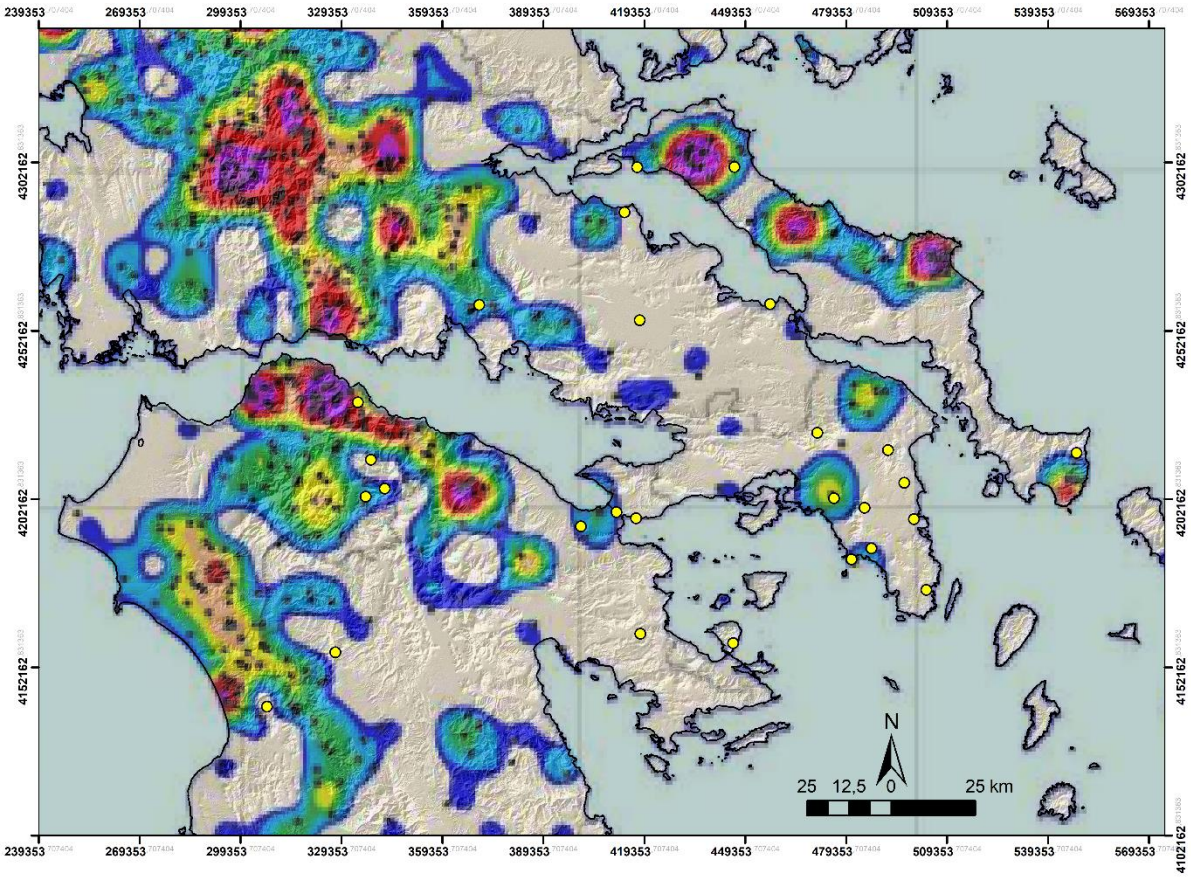

Figure 1. Map of the Hellenic geosites (yellow circles) in Central Greece with landslide frequency zones (modified after Vassiliadis, 2010). The number of landslide events increases from blue to violet. The black dots represent landslide locations.

All the Hellenic geosites are exposed to the earthquake hazard with 5.3% experiencing a high seismic risk (1a), 51.8% a medium seismic risk (1b) and 42.1% a low seismic risk (1c). Regarding the other types of geophysical hazards that is landslides and volcanic-related, 59.6% are affected by landslides and only 4.4% are threatened by volcanic hazards. The risk from the hydrological and climatological hazards on the overall number of the geosites is lower than the geophysical ones. The erosional hazard deriving from fluvial and coastal processes affects 28.1% of the geosites, whereas the flood hazard only 12.3%. The impact of the future sea level rise threatens only 12.3% of the Hellenic geosites which are mainly located close to/on the coastline.

Acknowledgements

The current work was carried out in the frame of the project "Recording the effects of natural disasters on the geotopes of the Greek area – proposing protection measures" (2019-2022), supported by the National Funds Programme.

References

Grecu, F., 2017. Interconditionality geomorphosites and natural hazards. RISCURI ŞI CATASTROFE, NR. XVI, 20: 41-51.

Kassaras, I., Kapetanidis, V., Ganas, A., Tzanis, A., Kosma, Ch., Karakonstantis, A., Valkaniotis, S., Chailas, St., Kouskouna, V., Papadimitriou, P., 2020. The New Seismotectonic Atlas of Greece (v1.0) and Its Implementation. Geosciences 10, 11: 447.

Oppenheimer, M., Glavovic, B.C., Hinkel, J., van de Wal, R., Magnan, A.K., Abd-Elgawad, A., Cai, R., Cifuentes-Jara, M., DeConto, R.M., Ghosh, T., Hay, J., Isla, F., Marzeion, B., Meyssignac, B., Sebesvari, Z., 2019. Sea Level Rise and Implications for Low-Lying Islands, Coasts and Communities, in: Pörtner, H.-O., Roberts, D.C., Masson-Delmotte, V., Zhai, P., Tignor, M., Poloczanska, E., Mintenbeck, K., Alegría, A., Nicolai, M., Okem, A., Petzold, J., Rama, B., Weyer, N.M. (Eds.), IPCC Special Report on the Ocean and Cryosphere in a Changing Climate, 321–445.

PROGEO, 2011. Conserving our shared Geoheritage – A protocol on geoconservation principles, sustainable site use, management, fieldwork, fossil and mineral collecting. 10 p.

Prosser, D.C., Díaz-Martínez, E., Larwood G.J., 2018. The Conservation of Geosites: Principles and Practice, in: Reynard, E., Brilla J. (Eds.), Geoheritage: Assessment, Protection and Management, 193-212.

Vassiliadis, E., 2010. Risk zonation of landslide events in the Hellenic Region. Development and application of GIS-based models. Ph.D. Thesis, University of Patras, 220 p.

Zafeiropoulos, G., Drinia, H., Antonarakou, A., Zouros, N., 2021. From Geoheritage to Geoeducation, Geoethics and Geotourism: A Critical Evaluation of the Greek Region. Geosciences 2021, 11: 381.

16th International Congress of the Geological Society of Greece
17-19 October, 2022 - Patras, Greece
Bulletin of the Geological Society of Greece, Sp. Publ. 10
Ext. Abs. GSG2022-326

Detecting flooded areas using Deep Learning Methods

P. Tsangaratos[1]
(1) National Technical University of Athens, Athens, Greece, ptsag@metal.ntua.gr

Extended Abstract

In recent decades, it has been well documented in numerous research studies that there is a significant increase in the number and intensity of natural disasters around the world that threatens human health, infrastructure, and natural systems. What is of interest in any case is the development of information systems capable of providing accurate, timely and comprehensible information, a capability that is to revolutionize natural disaster management. In the event of a flash flood, rapid response and recovery can be achieved by leveraging technologies based on access to aerial images which are extremely critical sources of information for the response team. The design of small unmanned aerial vehicles (UAV) as well as the corresponding development of sensors for the analysis of environmental elements, gives the opportunity to collect thousands of high-resolution images, even in inaccessible areas and under dangerous conditions for humans. However, despite the amazing potential of collecting such large data sets, extracting from them meaningful information remains a major challenge. In this context, the main objective of the present study was to develop a machine learning model based on Convolutional Neural Network (CNN) to identify flooded areas from images captured by UAV and provide a preliminary status of the number of elements at risk that are within the flooded area taking advantage of methods and techniques from the domain of Computer Vision.

Concerning the followed methodology, it could be separated into two phases of analysis. The first one involves identifying the areas that are flooded and the second one identifying elements at risk. During the first phase, a CNN model, a web-based tool (https://teachablemachine.withgoogle.com/) was utilized, whereas the second phase used an customized CNN model capable of detecting object of interest which in our case was automobiles. The web-based tool was trained using the pre-trained MobileNet model, which uses depth wise separable convolutions to construct lightweight deep convolutional neural networks (Howard et al., 2017), with only tuning three parameters, epochs, batch size and learning rate. On the second phase, the customized CNN was developed using a Keras Sequential API, with a stack of Conv2D and MaxPooling2D layers that define the convolutional base and three Dense layers to perform the final classification task (Dong and Lin, 2019). The data used during this study was derived from the FloodNet database (Rahnemoonfaret et al., 2020). The database contained images collected with a small UAS platform, DJI Mavic Pro quadcopters, after Hurricane Harvey, which consisted of 400 labeled images of flooded and non-flooded areas. Eighty five percent were used as training samples, whereas the rest were used to check how well the model is performing on new, unknown samples. Figure 1 illustrates two images of flooded and non-flooded areas that were used as training samples.

Figure 1 a. flooded area, b. non-flooded area

The accuracy per class (flooded and non-flooded areas), have achieved a high performance on the testing dataset, with the non - flood areas having the highest value, 0.94 followed by the predictive ability of the model concerning the flooded areas (0.88). Figure 2 illustrates the results of the second phase, (green bounding boxes) the detection of the automobiles within the flooded areas. The second model achieved a satisfactory performance (0.71). Although the

implementation of the models achieved a satisfactory outcome, further improvement is necessary by including more training samples or using different approaches from the domain of deep learning methods. Another issue is that from the UAV images which only include top view of the elements of risk, it is very difficult to estimate how much damages is done. Also, the followed methodology also suffers from the uncertainty of the object direction angle, in our cases the angle that the automobiles are captured by the UAV, which causes big trouble to the learning of the algorithm. Apply more sophisticated algorithms that address the above issue would enhance the developed methodology.

Figure 2. Automobile detection in flooded area

Despite, the drawbacks of the developed methodology, it is an innovative approach that in the coming years will be the usual practice in the assessment of natural disasters.

References

Dong, Z., Lin, B., 2019. Learning a robust CNN-based rotation insensitive model for ship detection in VHR remote sensing images. International Journal of Remote Sensing, 41(9), 3614-3626

Howard, A. G., Zhu, M., Chen B., Kalenichenko, D., Wang, W., Weyand, T., Andreetto, M., Adam, H., 2017. Mobilenets: efficient convolutional neural networks for mobile vision applications, https://arxiv.org/abs/1704.04861.

Rahnemoonfar, M., Chowdhury, T., Sarkar, A., Varshney, D., Yari, M., Murphy R., 2020. FloodNet: A High Resolution Aerial Imagery Dataset for Post Flood Scene Understanding. https://doi.org/10.48550/arxiv.2012.02951

16th International Congress of the Geological Society of Greece
17-19 October, 2022 - Patras, Greece
Bulletin of the Geological Society of Greece, Sp. Publ. 10
Ext. Abs. GSG2022-361

The large underground karst system of Maaras Cave through 3D laser Scanning

I. Kampolis[1,2,3], V. Trizonis[3], Y. Psaltakis[3]

(1) National Technical University of Athens, Athens, Greece, (2) National Center for Scientific Research 'Demokritos', Agia Paraskevi, Greece, kampolisigeo@gmail.com (3) SPELEO Caving Club, Athens, Greece

Research Highlights

The 3D laser mapping of Maaras Cave produced the first accurate and in-high-detail digital twin of the cave.

Abstract

Maaras Cave or the cave of the Aggitis River is located in the NW part of Drama basin in the homonymous prefecture of Northern Greece. The entrance of the cave lies close to the small village Aggitis, where the Aggitis River springs can be found. The groundwater feeding the springs derives from the area of Kato Nevrokopi, an enclosed basin, and through sinkholes enters the underground karst system of Maaras. The latter forms the Aggitis springs at its exit as well as the Aggitis River which drains the Drama basin and the former marshes of Philippi (Astaras, 2010). Maaras Cave was explored by the Hellenic Speleological Society in 1952, but due to equipment restrictions the progress was limited. The first large-scale exploration took place in 1978 by a joint French-Greek expedition. To this day, the known development of the cave is about 12-km long (SPELEO, 2015). In the past, the cave was exploited for its voluminous water discharge by the local residents. Thus, they constructed a hydraulic wheel for the pumping of groundwater and its usage for irrigation as well as drinking purposes. The wheel can be found in the big hall of the cave, close to the entrance (Fig. 1).

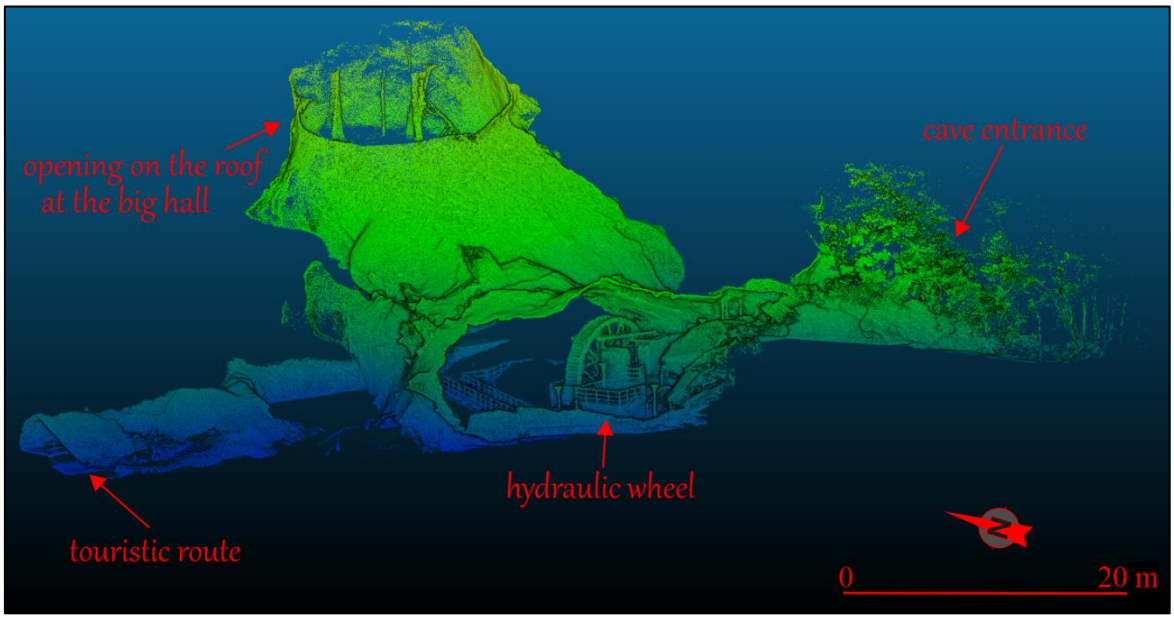

Figure 1. Section of the point cloud from the first chamber of the cave (3D point cloud).

Maaras Cave develops in the grey to whitish, massive to bedded marbles, belonging to the metamorphic formations of the Rhodope Massif (IGME, 1988). It represents the largest underground river in Greece and today, a small part of the cave is open to the public as a show cave. Maaras is one of the most prominent solutional Greek caves and the longest in terms of horizontal development. Due to its uniqueness, we attempted a laser scanning expedition in spring of 2018 with the use of a ZEB-REVO portable laser scanner of GeoSLAM. This device employs the SLAM technology that stands for Simultaneous Localization and Mapping and provides the ability to the scanner of mapping the preferred environment and in the same time locating its position in it. The same method has been used in other Greek caves with exceptional results which benefit both the public as well as the scientific community (Kampolis *et al.*, 2022a; 2022b). The aim of the project was to document the cave environment in high accuracy and produce the first accurate digital twin of the cave. The whole endeavor took place in two consecutive days at the challenging environment of Maaras with the constant presence of water. The total recording comprises of 59 scanning sessions and was implemented in 17 hours. This is the first time that a large system as Maaras Cave is documented with laser scanning technology and in this scale in Greece.

The main passage of Maaras Cave was recorded in great detail, resulting in a point cloud of almost 560 million points. The overall morphology of the cave resembles the surficial geometry of Aggiti's main collector and has a length of 7.736 km (Fig. 2). It presents a general NW-SE trend (N300º) which is probably controlled by the same tectonic directions

defining the Drama basin. Along the route of the cave system, a wealth of structural data can be revealed throughout the point cloud regarding the geometry of the bedding plane as well as the faults controlling its development. Moreover, the laser mapping documented in great detail the clastic sediments and terraces along the route of the underground river.

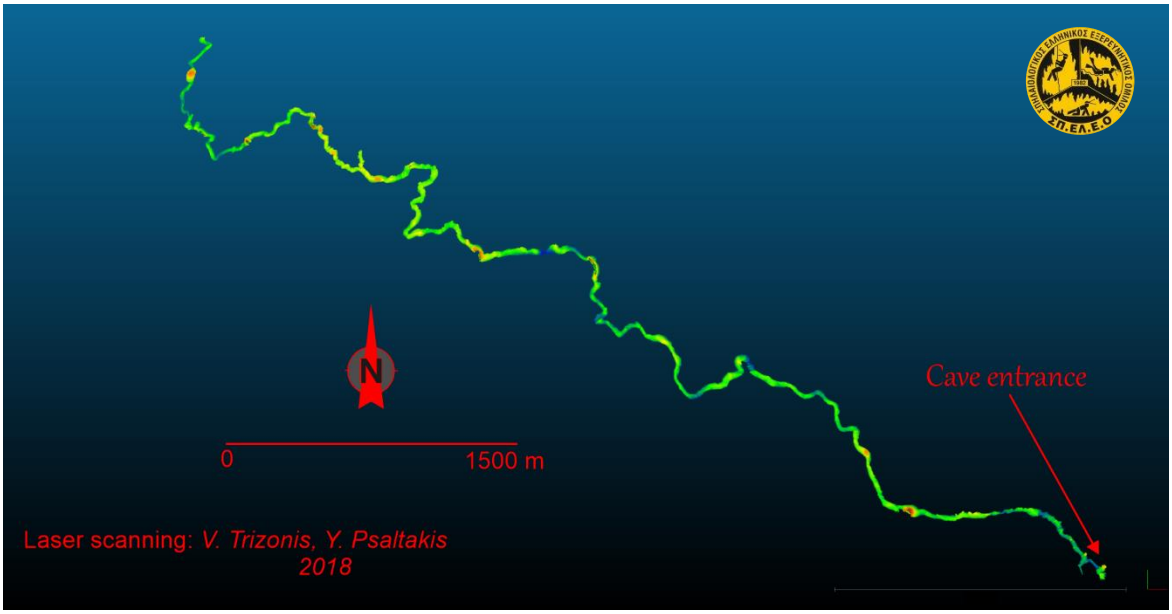

Figure 2. Top view of the main passage of Maaras Cave (3D point cloud).

Despite, the digital visualization of the cave and its scientific or educational value, the 3D point cloud of Maaras Cave can be regarded as a reference state of the cave for future work regarding the influence of climatic stresses or natural hazards in the speleomorphology of Maaras.

Acknowledgements

We would like to express our sincere thanks to the Municipal Company for the Touristic Development of the Aggitis River Cave "DESPATA" for the unique support.

References

Aastaras, Th., 2010. The Gorge of the Angitis River at "Stena Petras" Near the Alistrati Cave. A Magnificent Piece of Natural Architecture in Eastern Macedonia, Greece. in: Evelpidou, N., Figueiredo, T., de Mauro, F., Tecim, V., Vassilopoulos, A. (Eds.), Natural Heritage from East to West, 59-70.

IGME, 1988. Geological Sheet 'Prosotsani'. 1:50000 scale.

Kampolis, I., Triantafyllidis, St., Skliros, V., Kamperis, E., 2022a. Quaternary evolutionary stages of Selinitsa Cave (SW Peloponnese, Greece) revealing sea level changes based on 3D scanning, geomorphological, biological and sedimentological indicators. Quaternary, 5 (2), 24.

Kampolis, I., Triantafyllidis, S., Kokkalas, S., 2022b. Revisiting the speleomorphology of the Cave of Lakes in northern Peloponnese (S. Greece) from a 3D laser scanning perspective. Proceedings of the 18th International Congress of Speleology, Vol. VI – Karstologia Mémoires no 26.

SPELEO, 2015. SPELEO Caving Club Archives.

16th International Congress of the Geological Society of Greece
17-19 October, 2022 - Patras, Greece
Bulletin of the Geological Society of Greece, Sp. Publ. 10
Ext. Abs. GSG2022-368

The forgotten earthquakes of the Peloponnese

A. Barberopoulou[1], V. Kouskouna[2], A. Ganas[3], G. Malaperdas[4], M. Nielsen[1]

(1) Tufts University, Medford, Massachusetts, United States Aggeliki.Barberopoulou@tufts.edu (2) National and Kapodistrian University of Athens, Athens, Greece (3) National Observatory of Athens, Athens, Greece (4) University of the Peloponnese, Kalamata, Greece (5) Tufts, University, Medford, Massachusetts, United States

Abstract
Preliminary work is presented for 2 earthquakes that happened in the first half of the 20th century in the Peloponnese region. This work is part of a new project on *historical earthquakes* recorded prior to the adoption of digital seismographs. The availability of many European earthquake databases allows us to revisit or analyze for the first-time old events utilizing new tools.

Background
Thanks to the Greek and other civilizations which evolved around the Mediterranean Sea, the Greek region has records of significant earthquakes going back to few thousands of years. As part of national, regional, European or global efforts, historical data have been collected, and organized in various databases (e.g., Kouskouna and Sakkas 2013, Ferrari, G. 2022, Locati *et al.* 2014). One of the purposes of the historical earthquake databases is to promote understanding of earthquake hazard through making data observations available to the scientific community for further analysis.
Several earthquake databases exist for the European Mediterranean region that contain data of relevance to Greece. These databases have been compiled with different goals in mind and therefore provide different data. Some contain data for events prior to the 20th century (AHEAD), others contain data only for recent events post-digital instrumental period (ITSAK). Access between these databases also varies. AHEAD is "fed" by various regional European databases but only covers up to 1899AD. ISC in the UK also contains information about historical earthquakes, but information is obtained from processed analog seismograms operating in the 19th and 20th century that are not provided. Analog seismograms provide precious data for analysis of relevant earthquakes but cover a narrow time window (100-150 yrs). Of particular interest to the authors are those events whose observations have not been analyzed or are largely "forgotten". Two such events occurred in the Peloponnese on the 30th of August 1926 and 1st of July 1927. Both events are of similar magnitude (~7-7.2) appear to be intermediate depth earthquakes and have had intensities of at least VIII.

Objectives
This work has few major goals:

1. To identify earthquakes in databases that have not been studied before or their presence in the literature is minimal.
2. To determine whether new 12-point modern – Intensity scales offer significant improvement in describing damage impact from old (>>40 yrs) earthquakes.
3. Revisit old events utilizing new tools such as GIS for an improved analysis
4. Look for primary sources of data to increase density in existing data for earthquakes
5. With respect to the 1926 and 1927 events to a) conclude on the focal depth of both events and b) propose a mechanism based on a different radiation pattern of seismic waves in the case of a i) strike-slip event like Leonidio 2008 (Zahradník et al.,2008)or a b) thrust type event like Methoni 2008.

Data
The data we are using comes from local, regional, or European databases with primary sources given a special "weight". For example, newspapers, magazines, bulletins, and other printed materials such as books or diaries are collected and where necessary digitized (Figure 1). Five criteria were used to identify earthquakes for further analysis, including but not limited to magnitude, intensity, and publications of the event. For the 1926 event the most comprehensive reference is the NOA bulletin.

Discussion
Both 1926 & 1927 events are mentioned in Papazachos and Papazachou (2003) with a summary of their impact. However, the naming of the two events is inconsistent in the literature and in the European databases. For example, Papazachos and Papazachou (2003) refer to the earthquakes as Sparti and Oitylo while ISC refers to them as Southern Greece (Table 1). This may be a result of the four different epicentral locations provided from ISC which are very far from each other. Disagreement seems to also exist among the literature as to the depth of the two earthquakes (Galanopoulos, 1967; Ambraseys & Jackson, 1990) although likely both are intermediate depth earthquakes. The 1926 event is also not included in the isoseismal atlas by Papazachos et al. (1997).

By focusing on these earthquakes, particularly those with minimal previous analysis, we hope to publicize information regarding these events in order to facilitate further research and discussion.

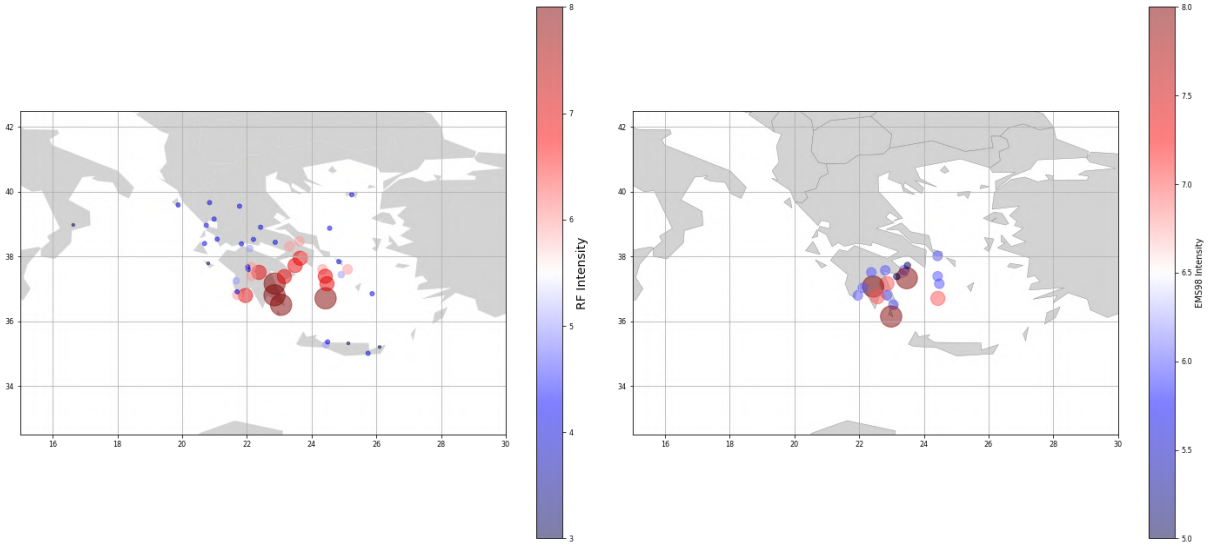

Figure 1. Intensities for the 30/08/1926 earthquake as reported in the NOA Bulletin (Left) Intensities in Rossi-Forel Scale (Right) Intensities reassigned to locations in EMS 98.

Table 1. Summary of the 30/08/1926 earthquake from sampled publications

Publication/Source	**Papazachos and Papazachos (2003)**	**International Seismological Centre**	**Galanopoulos (1967)**	**NOA Bulletin**	**Ambraseys and Jackson (1990)**
Epicentral Location	Sparti	Southern Greece (4 epicentral locations are provided)	-	Laconia	S. Peloponnesus
Depth	100 km	50 km	100 km	N/A	75 km
Magnitude	7.2	Four magnitudes are listed ranging from 6.2-7.1	7	N/A	6.63 (Ms), 7.4(mb)
Intensity	VIII	N/A	-	VIII-IX	N/A

Acknowledgements

We would like to thank Panayiotis Andrianopoulos with the State Archives in Kalamata, the Popular Library of Kalamata, newspaper Neologos Patron and Public Library of Sparti for their help and support of our work. Global Tufts funded Maja Nielsen.

References

Ambraseys N.N., Jackson J., 1990. Seismicity and associated strain of central Greece between 1890 and 1988. Geophysical Journal International, 101, 3, 663-708. https://doi.org/10.1111/j.1365-246X.1990.tb05577.x

Galanopoulos, A.G., 1967. The seismotectonic regime in Greece, Ann. Geofis., 20, 109-119

International Seismological Centre (2022). Seismological Dataset Repository, https://doi.org/10.31905/6TJZECEY

Kouskouna V., G. Sakkas, 2013. The University of Athens Hellenic Macroseismic Database (HMDB.UoA): historical earthquakes. Journal of Seismology, October 2013, Volume 17, Issue 4, pp 1253-1280, DOI 10.1007/s10950-013-9390-3

Ferrari, G. “Euroseismos.” EUROSEISMOS, INGV, 2005, http://storing.ingv.it/es_web/. Accessed 3 August 2022.

Locati M., Rovida A., Albini P., and Stucchi M., 2014. The AHEAD Portal: A Gateway to European Historical Earthquake Data. Seismological Research Letters, 85, 3, pp.727-734.https://doi.org/10.1785/0220130113

Papazachos, BC, C. Papazachou, 2003. The earthquakes of Greece, Ziti Editions, Thessaloniki.

Papazachos, BC, 1997. Atlas of Isoseismal Maps for Strong (M >=5.5) Shallow (h < 60 Km) Earthquakes in Greece and Surrounding Area, 426 BC – 1995, 1997. University of Thessaloniki, Geophysical Laboratory, p.189

Zahradnik, Z., Sokos, E., Serpetsidaki, A. and G. Tselentis, 2008. The Mw 6.2 Leonidio, southern Greece earthquake of January 6, 2008: Preliminary identification of the fault plane, EMSC on-line report.

Howell, A., Palamartchouk, K,Papanikolaou, X., Paradissis, D., Raptakis, C., Copley, A., England, P., Jackson, J., 2017. The 2008 Methoni earthquake sequence: the relationship between the earthquake cycle on the subduction interface and coastal uplift in SW Greece, *Geophysical Journal International*, Volume 208, Issue 3,1592–1610, https://doi.org/10.1093/gji/ggw462

16th International Congress of the Geological Society of Greece
17-19 October, 2022 - Patras, Greece
Bulletin of the Geological Society of Greece, Sp. Publ. 10
Ext. Abs. GSG2022-374

How the aggregate shape influences the compressive strength of concrete? The use of a new micro geo-informatics methodology

P. P. Giannakopoulou[1], A. Litoseliti[1], A. Rogkala[1], M. Kalpogiannaki[2], P. Lampropoulou[1], V. Giamas[1], P. Koutsovitis[1], P. Petrounias[1,3]

(1) Section of Earth Materials, Department of Geology, University of Patras, 265 04 Patras, Greece, peny_giannakopoulou88@outlook.com, (2) Department of Geology and Geoenvironment, National and Kapodistrian University of Athens, Panepistimioupolis Zografou, 15784 Athens, Greece, (3) Chemical Process & Energy Resources Institute, Centre for Research & Technology Hellas (CERTH), Maroussi, Athens, 15125, Greece

Scientists have used quite many techniques mainly such as point counting, image analysis, while lesser have been used more innovative methods like Geographic Information System (GIS) and MatLab software as an efficient and low-cost method, in order to quantify/semi-quantify the mineralogical composition and the textural characteristics of various type of rocks (Petrounias *et al.*, 2020) (fig.1,2). The latter plays a significant role in influencing the engineering performance of the aggregate rocks (Petrounias *et al.*, 2018b). This paper investigates an alternative low-cost, low-energy way to predict the behavior of an aggregate within a concrete and more specifically the shape parameters of aggregates that are found to strongly influence the final concrete strength. This was achieved by using a combination of petrographic methods with GIS and MatLab software in a variety of lithologies when at the same time using the micropetrographic index (*Mshape*) (Petrounias *et al.*, 2022). So, various rocks such as sandstones, ultramafic, mafic and volcanic ones have been selected from Greece and they were used and tested as aggregates. Their petrographic features and their geometrical properties were also studied and hence their influence on concrete production. The new micro-petrographic index which was used is based on the aforementioned methodology and it may act as a predictor of the aggregates shape and as a result of their general behavior and suitability. *Mshape* index is strongly correlated with the geometrical indices of shape I_E and I_F as well as with the concrete strength. Strong relationship was observed between the geometrical parameters of the aggregates such as flakiness and elongation index and the shape parameters expressed through the min/max ratio and the eccentricity. It should be mentioned that determinant factors for the microshape parameters of the aggregate rocks are their micro petrographic features. The *Mshape* index, which is strongly correlated with the geometrical indices such as I_E and I_F as well as with the concrete strength constitutes a useful tool for the prediction of the behavior of a construction project without previous energy-consuming tests, while at the same time technical failures could have been predicted and avoided.

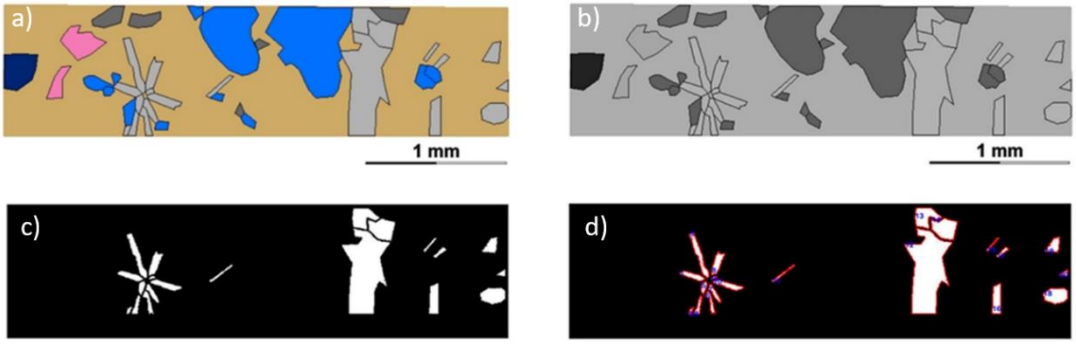

Figure 1. a) ArcMap Digitized image of thin section, b) grayscale equivalent, c) binary version for plg mineral phases and d) plg phases numbered and with their boundaries.

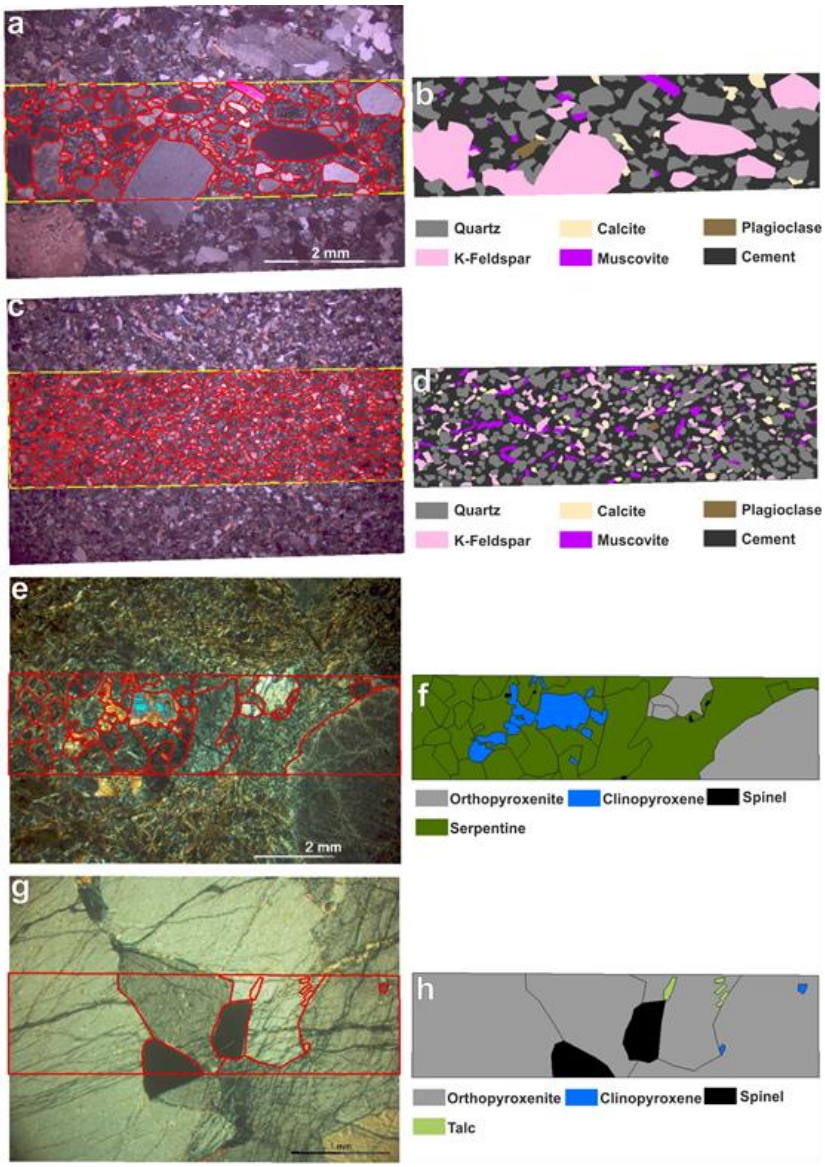

Figure 2. Representative images from the studied Groups I and II derived from the ArcMap 10.1 software showing: a) the part of the thin section of a coarse grained sandstone which has been analysed, b) the output after the digitalization of the investigated part of each thin section where each mineral phase has been attributed by different colours, c) the part of the thin section of a fine grained sandstone which has been analysed, d) the output after the digitalization of the investigated part of each thin section where each mineral phase has been attributed by different colours, e) the part of the thin section of a serpentinized harzburgite which has been analysed, f) the output after the digitalization of the investigated part of each thin section where each mineral phase has been attributed by different colours, g) the part of the thin section of a pyroxenite which has been analysed, h) the output after the digitalization of the investigated part of each thin section where each mineral phase has been attributed by different colours.

Acknowledgements

The authors wish to thank the Konstantin Hatzipanagiotou for his contribution during the whole research.

References

Petrounias, P., Rogkala, A., Giannakopoulou, P.P., Kalpogiannaki, M., Laskaris, N., Lampropoulou, P. 2022. The Role of the Aggregate Shape on the Compressive Strength of Concrete Using a New Micro Geo-Informatics Methodology. Micron, 161, 103333.

Petrounias, P., Giannakopoulou, P.P., Rogkala, A., Lampropoulou, P., Koutsopoulou, E., Papoulis, D., Tsikouras, B., Hatzipanagiotou, K., 2018b. The impact of secondary phyllosilicate minerals on the engineering properties of various igneous aggregates from Greece. Minerals 8, 329.

Petrounias, P., Giannakopoulou, P.P., Rogkala, A., Kalpogiannaki, M., Koutsovitis, P., Damoulianou, M.-E., Koukouzas, N., 2020. Petrographic characteristics of sandstones as a basis to evaluate their suitability in construction and energy storage applications. A case study from Klepa Nafpaktias (Central Western Greece). Energies 13 (5), 1119.

16th International Congress of the Geological Society of Greece
17-19 October, 2022 - Patras, Greece
Bulletin of the Geological Society of Greece, Sp. Publ. 10
Ext. Abs. GSG2022-377

Landslide Susceptibility Assessment Using Multi-Criteria Analysis in Agrafa Municipality, Concerning Hydrological and Hydrogeological Factors.

G. Ntelis[1], I. Koumantakis[2], E. Vasileiou[2]

(1) National Technical University of Athens, School of Civil Engineering, Department of Water Resources and Environmental Engineering, Heroon Polytechneiou 9, Athens, Greece, ntelisgeo@gmail.com (2) National Technical University of Athens, School of Mining and Metallurgy Engineering, Department of Geological Sciences, Heroon Polytechneiou 9, Athens, Greece, koumantakisioannis@gmail.com, elvas@metal.ntua.gr

Abstract

Landslide phenomena are strongly affected by physical factors such as the precipitation (mainly rainfall) combined with the geological structure that exists in a region. In addition, the influence of the anthropogenic activities on the natural environment is proven to be a crucial factor in the appearance of geological failures. This study examines the phenomenon of landslides and in particular the distinguishment of those factors which act as an activating cause. In order to achieve this goal three factors were examined as very important. The case study that was investigated was Agrafa Municipality. Rainfall data of fifty year-period, the historical data of landslides in the area and the integrated system of data management system of Geographic Information Systems were used for the evaluation of all these. The models which were developed to achieve the final result are as follows: i) multi-criteria analysis with weighting factors, ii) analytical hierarchy process method and iii) use of same methods without the participation of hydrogeological factors. The results clearly demonstrate the initial belief, as the final hazard maps verify the importance of rainfall in landslides.

Background

In order to create reliable hazard maps for the research area, thematic information levels (known as layers) were created through the GIS software. In particular, the layers that were created are the following: 1) digital elevation model, 2) slope, 3) aspect, 4) average annual rainfall, 5) climate zone, 6) geology, 7) lithology, 8) soil erosion, 9) hydrographic network, 10) drainage basins, 11) tectonic elements, 12) land use, 13) anthropogenic influence on vegetation, 14) soil depth and 15) a fifty-year landslide area history layer. Moreover, it is noted that for the purpose of create the average annual rainfall map, data for the aforementioned period i.e., from 1967 to 2017, were used. Finally, it should be underlined that landslide history data signify elements, that can be distinguished through the repeatability of the phenomenon, as a tendency in the occurrence of failures. These data were categorized into percentage tables for every known and applicable landslide factor.

Objectives

The aim of this study is to assess landslide susceptibility and to determine the importance of both hydrological and lithological factors in these phenomena, emphasizing in the contribution of rain intense.

Methods

Before the usage of the methodology and after the necessary layer creation, some admissions were made which aimed to categorize in zones the scale of danger for each landslide factor. These admissions are mentioning below in text in bullets.

- The geology of the area giving special emphasis to the unity of the flysch.
- The lithological composition of the formations and especially the rocks of high-water permeability.
- The distance from the hydrographic network highlighting the locations near major streams.
- The morphology of the area and mostly the altitudinal zones that seem more susceptible.
- The distance from the tectonic elements after it is established that the formations are affected.
- The gradients of slopes and gravity strata where there are abrupt changes.
- The uses of land as well as all kinds of human activities that affect them.
- The aspect of the slopes concentrating and focusing on the North-West slopes.
- Atmospheric precipitation with an emphasis on heavy or prolonged rains.

The first method that used in order to estimate landslide hazard for the municipality of Agrafa was a multi-criteria analysis with weighting factors using in total nine (9) factors which have been categorized and calibrated according to landslide history and based on previous authoritative studies of the area. The model has been developed through GIS application. The second method that applied was analytical hierarchy process (AHP) model which is basically correlates pairwise and

simultaneously compares the failure factors so that can approximate landslide hazard assessment. GIS software was used and the same nine (9) factors for this method also as well as for the previous. Briefly, the nine (9) mentioned factors are: a) altitude, b) slope, c) geology, d) hydrolithology, e) aspect, f) land use, g) precipitation, h) distance from hydrographic network and i) distance from tectonic elements. Eventually, two (2) more models were developed using the same methods but this time without involving both hydrolithology and precipitation factor, so that can be proven the importance of them.

Results

The results from each one model are captured below in Figure 1. The landslide hazard maps from left to right are referring to the corresponding models that mentioned previously in the same order. Additionally, Table 1 reflecting the percentages for each hazard class in square kilometer (km^2) of study area, giving in such way a more comprehensive quantity picture.

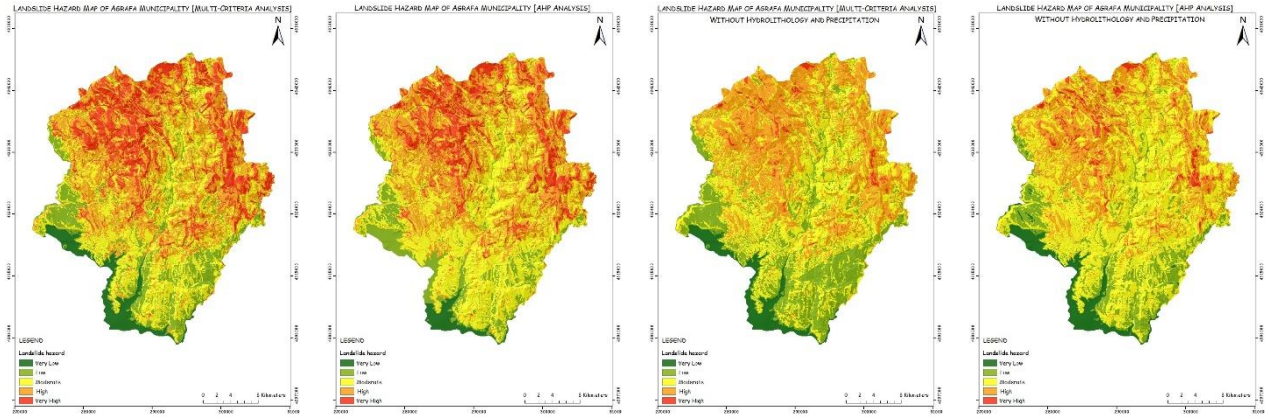

Figure 1. Landslide hazard maps using GIS software and by developing the four (4) different model approaches.

	multi-criteria analysis model	**analytical hierarchy process model**	**multi-criteria analysis 2nd model**	**analytical hierarchy process 2nd model**
Very Low	43.80 km^2	19.80 km^2	43.80 km^2	49.13 km^2
Low	126.15 km^2	94.24 km^2	198.30 km^2	129.50 km^2
Moderate	270.60 km^2	343.75 km^2	333.17 km^2	437.52 km^2
High	301.34 km^2	322.26 km^2	324.40 km^2	265.34 km^2
Very High	175.93 km^2	137.77 km^2	18.15 km^2	36.63 km^2

Table 1. Hazard zones quantification of the study area divided in five (5) classes for each model.

From the hazard zones shown in Table 1, it is demonstrating that there is an important deviation between model that includes precipitation and hydrolithology parameters from those that not incorporate them. Especially in "Very High" class, multi-criteria analysis and analytical hierarchy process models an area of 19% and 15% are allocated, while second models yield a percentage of just 2% and 4% respectively. "Very Low" and "Low" classes remained almost unaffected in all models.

Conclusions

Landslide hazards have been studied by applying several methodologies and new approaches have been applied in order to confront the high risk of this phenomenon. Landslide hazard could be alterated in disasters considering the caused impacts (Valency, 2007). Necessary measures and efforts must be taken for preventing the high risks. The susceptibility map could be linked and inform urban and land use planning, as an important source for different users and particularly for the risk managers (Nahayo et al., 2017). It turns out that hydrological factors are crucial for causing geological failures and potentially could trigger a landslide phenomenon.

References

Nahayo, L.; Mupenzi, C.; Kayiranga, A.; Karamage, F.; Ndayisaba, F.; Nyesheja, E.M.; Li, L. Early alert and community involvement: Approach for disaster risk reduction in Rwanda. Nat. Hazards 2017, 86, 505-517. **[Journal Article]**

Valency, R. Building Disaster Resilient Communities: Good Practices and Lessons Learned; UNISDR (United NationsInternational Strategy for Disaster Reduction): Geneva, Switzerland, 2007. **[Publication]**

16th International Congress of the Geological Society of Greece
17-19 October, 2022 - Patras, Greece
Bulletin of the Geological Society of Greece, Sp. Publ. 10
Ext. Abs. GSG2022-393

Disaster Interrelations In A Multi-Hazard Risk Framework

M.-C. Tsoutsos[1], V. Vescoukis[1]

(1) School of Rural and Surveying Engineering, National Technical University of Athens (NTUA), Athens 15780, Greece, michalis.tsoutsos@gmail.com

Research Highlights

Natural hazards trigger secondary events due to the stable and trigger factors of their geophysical environment. Considering that one or more hazards can be occurred by the same event and/or by human activities, interrelations matter.

Background

Multi-hazard risk refers to the risk arising from multiple hazards (Kappes, *et al.*, 2012) and multi-hazards reflect the occurrence and the interactions of all possible hazards in a given spatial region and/or temporal period (Gill and Malamud, 2014). Murray *et al.* (2021) classified natural hazards into 8 hazard types, which are divided into 47 cluster types, where each cluster type contains specific hazards which in total are 302: the Meteorological and Hydrological hazards with 9 hazards clusters and 60 specific hazards; the Extraterrestrial hazards with 1 hazard cluster and 9 specific hazards; the Geohazards with 3 hazard clusters and 35 specific hazards; the Environmental hazards with 2 hazard clusters and 24 specific hazards; the Chemical hazards with 9 hazard clusters and 25 specific hazards; the Biological hazards with 10 hazard clusters and 88 specific hazards; the Technological hazards with 9 hazard clusters and 53 specific hazards; the Societal hazards with 4 hazard clusters and 8 specific hazards. Considering that 302 natural hazards exist, there will inevitably be interactions between them, namely effect(s) of one hazard on another (Gill and Malamud, 2014), which incorporate both interaction relationships initiated, triggered, catalyzed and impeded by natural hazards, anthropogenic processes and technological hazards/disasters (Gill and Malamud, 2016).

Objectives

The aim of this research is to highlight the importance of multi-hazard approaches and particularly the interaction relationships between natural hazards, anthropogenic processes and technological hazards/disasters, as well as, the types of their interactions, which must be incorporated into disaster risk reduction plans instead of single hazard approaches.

Methods

Cascading natural hazards of great importance have been observed in the volcanic eruption of the volcano Mount Unzen in Japan in 1792, the earthquake in Alaska in 1964, the volcanic eruption in Philippines in 1991 and the tropical storm in Guatemala in 2010 (Gill and Malamud, 2014). Considering the severity of cascade effects of the aforementioned case studies, Gill and Malamud (2014) identified the interactions of 21 major natural hazards which result in 90 natural hazard interactions, including both triggered relationships and relationships where one hazard increases the probability of another. Thus, Gill and Malamud (2014) determined the number and the type of secondary hazards that each primary hazard can trigger, for example, 9 secondary hazards can be triggered by a volcanic eruption (earthquake, tsunami, landslide, avalanche, flood, lightning, hot extreme temperature, cold extreme temperature, wildfires), as well as, the number and the type of primary hazards which can trigger a specific secondary hazard, for example, landslides can be triggered by 13 primary hazards (earthquake, tsunami, volcano, landslide, avalanche, flood, ground collapse, soil (local) subsidence, ground heave, storm, hailstorm, snowstorm, hot extreme temperature). Human activities influence the occurrence and the interaction of natural hazards and therefore Gill and Malamud (2017) identified 18 anthropogenic process types which are associated with interactions (ground water abstraction, oil/gas extraction, subsurface infrastructure construction, subsurface mining, material (fluid injection), vegetation removal, argicultural practice change, urbanisation, infrastructure construction (unloading), quarrying/surface mining (unloading), infrastructure (loading), infilled (made ground), reservoir and dam construction, drainage and dewatering, water addition, chemical explosion, nuclear explosion, fire). Gill and Malamud (2016) define the technological hazards/disasters as unintentional, non-malicious or negligent failures of technology or industry, citing as their examples the structural collapse, the nuclear reactor failure, the urban fire, the chemical pollution, the dam collapse, the industrial explosion and the transport accident.

The interactions between natural hazards can be characterized by independence, triggering (cascading) relations, change of environmental conditions between them, a common primary event for their co-occurrence resulting in compound hazard and mutual exclusion (Tilloy *et al.*, 2019). More specifically, independence between two or more natural hazards means that two natural hazards can be occurred spatial and temporarily, at the same area in different times, without any dependence or triggering relationship, such as the coincidence of the eruption of the volcano Pacaya and the tropical storm Agatha at Pacific coastline of Guatemala in 2010 (Tilloy *et al.*, 2019). Triggering (cascading) relations implies that the occurrence of a primary event, such as an earthquake, can trigger the occurrence of a secondary event, such as submarine landslides and in turn the submarine landslides to trigger a tertiary event, such as tsunami waves, as occurred

in the case of the earthquake in Alaska in 1964 (Gill and Malamud, 2014). Change of environmental conditions between two hazards means that a primary event, such as a wildfire, can change the hazard-forming environment and increase the probability of another hazard, in particular to denude an area of vegetation and harden the soil and thereby a secondary event can be occurred in a shorter period of time than expected, such as an increased flood just one month later, as happened in the case of wildfires in Las Conchas in New Mexico in 2011 (Tilloy *et al.*, 2019). A primary event or large scale processes, such a tropical cyclone, can be the cause, namely the common primary event, for two different natural hazards to be generated simultaneously, such as a river flooding and a sea surge (Tilloy *et al.*, 2019). Thus, the two hazards are considered as dependent and they form a multi-hazard event named compound hazard. Mutual exclusion on the occurrence of two hazards means either that two natural hazards cannot occur together because the changes in their trigger factors, namely the factors that determine the frequency and magnitude of each hazard, are mutually exclusive since one trigger factor cannot move in two directions simultaneously (Liu *et al.*, 2016), or that one hazard alters the frequency or magnitude of another such as to decrease its probability of occurrence (Gill and Malamud, 2014). For example, a tropical storm and a wildfire have a negative dependence (Tilloy *et al.*, 2019) as their trigger factors are mutually exclusive, as well as that a heavy rainfall increases the surface moisture and thus the probability of occurrence of wildfires in the immediate aftermath is decreased (Gill and Malamud, 2014). Furthermore, when two or more natural hazards, anthropogenic processes and technological disasters are characterized by cascading relations, it is possible this triggering relationship to be catalysed or impeded. For example, according to Gill and Malamud (2016), anthropogenic processes, such as urbanisation, can catalyze a triggering relationship between two natural hazards, such as storm-triggered flooding, or technological hazards/disasters, such as a dam collapse, can catalyze a triggering relationship between two natural hazards, such as flood triggered landslides, or natural hazards, such as storms, can impede a triggering relationship between two technological hazards/disasters, such as structural-collapse-triggered urban fires.

Results

The occurrence of a natural hazard does not imply only the consequences of this event, as every natural hazard can trigger a secondary event which in turn can generate a tertiary one. It is worth noting that another natural hazard can be occurred simultaneously with the primary event resulting in adverse effects when taking into account its secondary hazards. Human activities can influence natural hazards by triggering them or catalyse/impede their interactions and therefore technological disasters can be occurred.

Conclusions

Considering the disaster interrelations, the mitigation plans of the hazards' consequences must reflect the multi-hazard landscape of a region, by incorporating the identification of all identified individual hazards and their possible interactions, the probability of their spatial and temporal coincidence and the community's vulnerability, taking into consideration the influence of human activities for which it is imperative to be integrated into multi-hazard approaches.

Acknowledgements

I am especially grateful to the Research Committee of the National Technical University of Athens (N.T.U.A.) who awarded me with a Doctoral Scholarship and, thus, enabled me to carry out the research required for this kind of study.

References

Gill, J.C., Malamud, B.D., 2017. Anthropogenic processes, natural hazards, and interactions in a multi-hazard framework, Earth-Sci. Rev., 166, 246–269.

Gill, J.C., Malamud, B.D., 2016. Hazard interactions and interaction networks (cascades) within multi-hazard methodologies. Earth Syst. Dyn. 7:659–679.

Gill, J.C., Malamud, B.D., 2014. Reviewing and visualizing the interactions of natural hazards, Rev. Geophys., 52, 680–722.

Kappes, M.S., Keiler, M., Von Elverfeldt, K., Glade, T. 2012. Challenges of analyzing multi-hazard risk: a review. Nat Hazards 64, 1925–1958.

Liu, B., Siu, Y.L., Mitchell, G., 2016. Hazard interaction analysis formulti-hazard risk assessment: a systematic classification based on hazard-forming environment. Nat. Hazards Earth Syst. Sci. 16 (2):629–642.

Murray, V., Abrahams, J., Abdallah, C., Ahmed, K., Angeles, L., Benouar, D., Brenes Torres, A., Chang Hun, C., Cox, S., Douris, J., Fagan, L., Fra Paleo, U., Han, Q., Handmer, J., Hodson, S., Khim, W., Mayner, L., Moody, N., Moraes, O.L.L., Nagy, M., Norris, J., Peduzzi, P., Perwaiz, A., Peters, K., Radisch, J., Reichstein, M., Schneider, J., Smith, A., Souch, C., Stevance, A-S., Triyanti, A., Weir, M., Wright, N., 2021. Hazard Information Profiles: Supplement to UNDRR-ISC Hazard Definition & Classification Review: Technical Report: Geneva, Switzerland, United Nations Office for Disaster Risk Reduction; Paris, France, International Science Council.

Tilloy, A., Malamuda, B.D., Winter, H., Joly-Laugel, A., 2019. A review of quantification methodologies for multi-hazard interrelationships. Earth-Science Reviews 196, 102881.

16th International Congress of the Geological Society of Greece
17-19 October, 2022 - Patras, Greece
Bulletin of the Geological Society of Greece, Sp. Publ. 10
Ext. Abs. GSG2022-407

Landslide Phenomena in Greece in the Frame of the GEOKA Research Project

N. Spanou[1], E. Apostolidis[1], G. Konstantopoulou[1], A. Exintaridi[1], K. Kavoura[1], A. Kepas[1], V. Ieronymakis[1], P. Paschos[1]

(1) Hellenic Survey of Geology & Mineral Exploration, Acharnes, Greece, spanou@igme.gr

The GEOKA research project launched in 2018, involves studies in the field of Natural Hazards, focusing on the landslide phenomena as well as the volcanic activity and risk assessment in Greece. The Action 1 of the project is pointing to landslides that constitute one of the most important natural disaster in Greece, showing widespread manifestation and causing considerable damage and fatalities every year.

The Hellenic Survey of Geology & Mineral Exploration (HSGME) representing the national geological survey of Greece, officiates as the geoscientific adviser of the government and keeps an up-to-date file of about 3000 engineering geology reports on the study of landslide phenomena. It refers to the Greek Territory from the half of the last century till today and integrates constantly the recent events. The Engineering Geology Division of HSGME has formed a Landslide Research Team which directly revise the suffered site after a landslide occurrence and composes a report including the event's characteristics (place, time, dimensions etc), the causes and the triggering factor, as well as the implications.

A large number of the information recorded in these technical reports are digitally stored into a Geographical Information System (GIS) as geo-database that was designed during the development of the Geo-Information system of Institute of Geology and Mineral Exploration (IGME). This relational database management system summarized over 4000 landslide records. A unique identification number to each studied landslide event attached to more information concerning the evolution of the phenomenon, date of manifestation, type of movement, geometry, state and type of activity, triggering factor, causes, consequences, proposed remedial measures and the degree of their compliance. Moreover, information concerning the manifestation's location is filled in the database, such as geographic and administrative specification, dip slope, land use, erosion, geotectonic zone, geological setting, lithological composition, inclination of strata, thickness of weathered zone, seismic risk zone and more (WP/WLI, 1990; Koukis, Ziourkas, 1991; WP/WLI, 1991; WP/WLI, 1993; WP/WLI, 1994; WP/WLI, 1995; Pyrgiotis, 1997).

Objective of the GEOKA research project is to update the existing landslide database by entering records of more than 5000 landslide events approximately, matching the landslides data with European and International standards and increasing data accuracy and integration by field survey in reactivated landslides. Result of the above will be a revised inventory map of the occurred landslides in national scale (Figure 1). Taking into account the spatial distribution of landslides, the relevant landslide density map will be also provided. Furthermore, landslide susceptibility map in regional and national scale will be produced (Corominas *et al.*, 2014), as a result of the analysis between the spatial distribution of the landslides and a group of causative factors (geological, topographical, hydrological characteristics of the area and more) based on the fact that landslides in the future will occur under the same circumstances that they occurred in the past (Fell *et al.*, 2008).

The GEOKA research project aims to:

- Better geo-hazard management, providing a valuable tool to the Civil Protection Authority.
- Safer design of energy networks and industrial infrastructures, as well as road network, a necessary mean for the unhindered movement of citizens and goods.
- Determine the accurate conditions for highlighting the most endangered regions and the appropriate models for landslide hazard and risk zonation.
- Exploitation and harmonization of the data and the maps according the directives and the general policy of the European Union and the United Nations on the need to draw up risk maps of natural disasters (multi-hazard maps).
- Preventive preparation in areas of high landslide susceptibility, avoiding the damages by the implementation of the required technical works.

Some constrains and challenges spotted in the research process are the different levels of detail, scale, and accuracy of the data, the fact that most of recorded events appear only in urban areas or along the road and the rail network.

Concluding, the GEOKA research project, updating landslide database and producing inventory, density and susceptibility maps, will be the basic step for better understanding the landslide-hazard in Greece. This knowledge will contribute to increase the safety of vital technical works, reduce the constructions' cost, manage land use planning and decrease the vulnerability of people and goods.

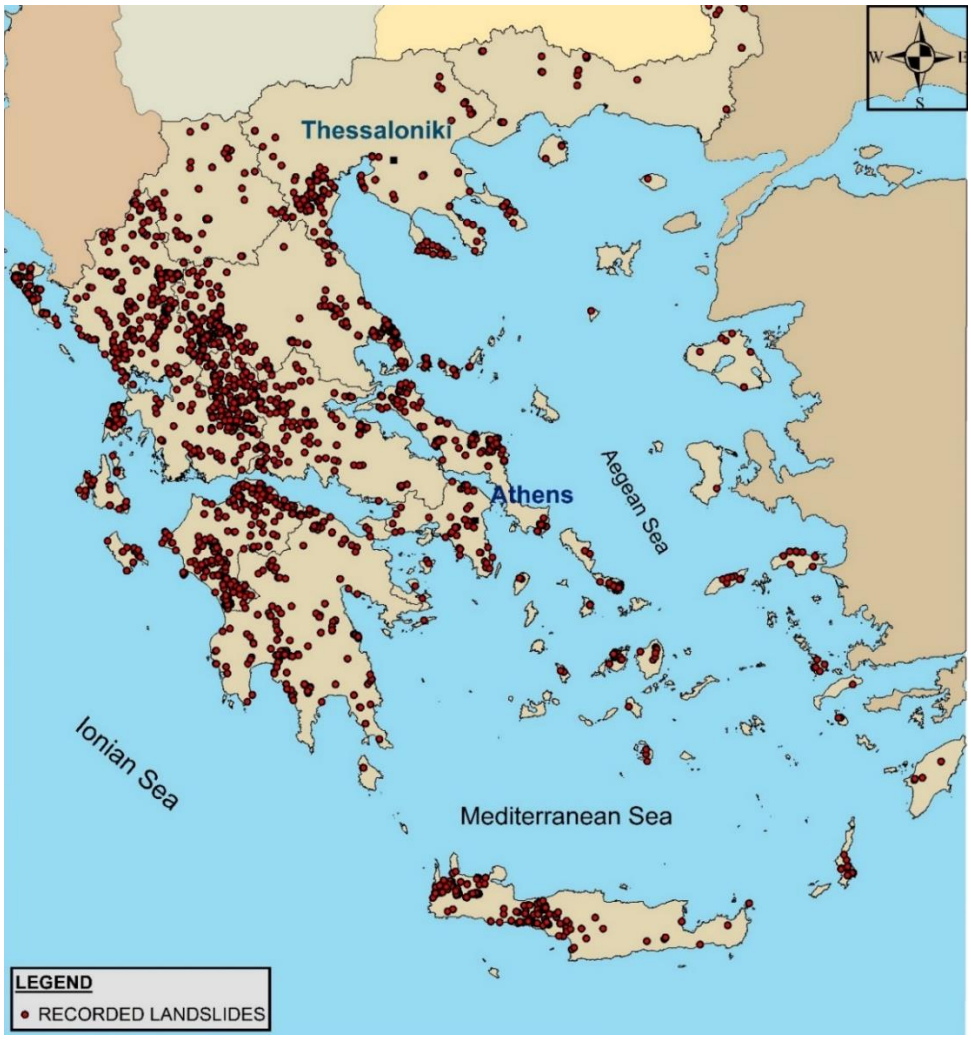

Figure 1. Current inventory map of recorded landslides from engineering geology reports.

Acknowledgements

This study was conducted in the framework of the Operational Program entitled "Competitiveness, Entrepreneurship and Innovation (2015-2020), Project “Studies and researches support to the energy sector, industry and entrepreneurship”, Sub-Project “Susceptibility assessment of landslides in the Greek territory - Volcanic study and risk assessment”, financed by the European Regional Development Fund.

References

Corominas, J., van Westen, C., Frattini, P., Cascini, L., Malet, J., Fotopoulou, S., Catani, F., Mavrouli, O., Pitilakis, K., Winter, M. Recommendations for the quantitative analysis of landslide risk. "Bulletin of engineering geology and the environment", Maig 2014, vol. 73, núm. 2, p. 209-263.

Fell R., Corominas J., Bonnard C., Cascini L., Leroi E., Savage W.Z., on behalf of the JTC-1 Joint Technical Committee on Landslides and Engineered Slopes, 2008. Guidelines for landslide susceptibility, hazard and risk zoning for land-use planning. Eng Geol 102 (3–4): 99–111.

Koukis, G., Ziourkas, C., 1991. Slope instability phenomena in Greece: A statistical analysis. Bulletin of the International Association of Engineering Geology 43, 47–60.

Pyrgiotis, L., 1997. Engineering geological conditions in Karditsa country: landslides phenomena in flysch formations. Ph.D. Thesis, University of Patras, Patras, 612 p.

WP/WLI, 1990. A suggested method for reporting a landslide. International Geotechnical Societies’ UNESCO Working Party on World Landslide Inventory (Chairman D Cruden) Bull Eng Geol Env 41(1):5–12.

WP/WLI, 1991. A suggested method for a landslide summary. International Geotechnical Societies’ UNESCO Working Party on World Landslide Inventory (Chairman D Cruden) Bull Eng Geol Env 43:101–110.

WP/WLI, 1993. Multilingual landslide glossary. International Geotechnical Societies’ UNESCO Working Party on World Landslide Inventory (Chairman D Cruden). BiTech, Richmond, p 59.

WP/WLI, 1994. A suggested method for reporting landslide causes. International Geotechnical Societies’UNESCO Working Party for World Landslide Inventory (Chairman ME Popescu) Bull Eng Geol Env 50(1):71–74.

WP/WLI, 1995. A suggested method for describing the rate of movement of a landslide. International Geotechnical Societies’ UNESCO Working Party for World Landslide Inventory (Chairman ME Popescu). Bull Eng Geol Env 52(1):75–78.

16th INTERNATIONAL CONGRESS of the
GEOLOGICAL SOCIETY OF GREECE

T9. Engineering Geology and Hydrogeology

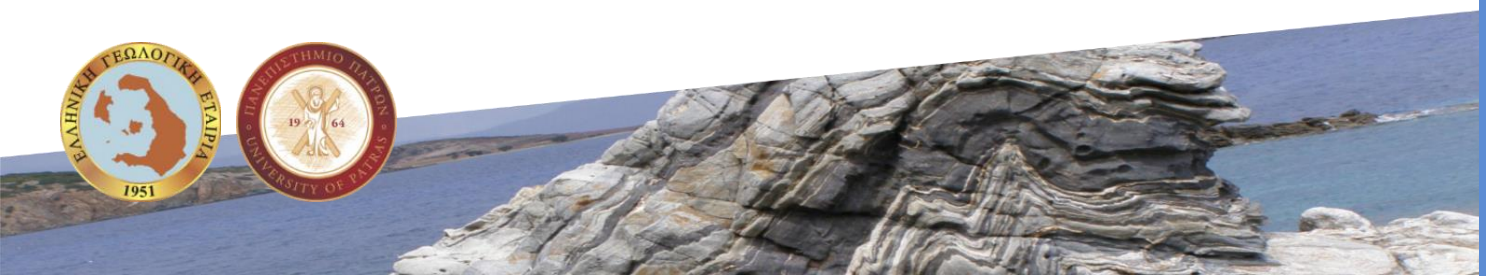

OUR EARTH, OUR HOME

16th International Congress of the Geological Society of Greece
17-19 October, 2022 - Patras, Greece
Bulletin of the Geological Society of Greece, Sp. Publ. 10
Ext. Abs. GSG2022-007

Determination of Groundwater Potential Zones using Geographical Information Systems (GIS) and Analytical Hierarchy Process (AHP) in Tanauan, Batangas, Philippines

Mon Carlo L. Ronquillo[1], Maritza Roneen G. Lopez[1], Federico B. Dela Peña[1]
(1) Mapúa University Intramuros, Manila, Philippines, ronquillomon1125@gmail.com

The efforts necessary to observe the subsurface where groundwater is present can be costly. Existing groundwater studies in Tanauan, Batangas, used geologic, hydrologic, and meteorological data from well inventory, water sampling, and geophysical surveys. This study offers a straightforward and cost-effective alternative by conducting spatial analyses exclusively using computer applications: remote sensing (RS) and geographic information systems (GIS). The Analytical Hierarchy Process (AHP), a multi-criteria decision-making process, will be integrated to ensure the outcomes are reliable. This method will help areas that desire to examine their water resources but lack funds. This goal was achieved by ranking seven geoenvironmental parameters based on their influence on groundwater potentiality. The parameters' established rankings are as follows: Geomorphology, Geology, Lineament Density, Slope Degree, Drainage Density, Soil, and Land Use/Land Cover. A weighted overlay analysis in ArcGIS generated a map outlining the area's groundwater potential. Poor potential zones covered 25.39% of the city's land area; Moderate potential zones covered 50.56%; Good potential zones covered 23.63%, and Very Good potential zones covered 0.40%. To verify their findings, the researchers plotted 15 well locations on the final map, and their water table depth was matched with the category of the area to which they belonged. Fourteen of the fifteen wells were within their zone's depth to groundwater ranges. Areas with good groundwater potential are characterized by quaternary alluvium units in the low-slope alluvial plains found in barangays Ambulong and Banadero.

Background

The groundwater resources in the Philippines serve about 14% of the population, and 50% use them as potable drinking water. Since groundwater is a major source of water in the country, frequent water pumping is carried out; however, this event causes groundwater depletion and pollution. As recent as 2020, the Water Organization pointed out that 5 million people in the Philippines lack access to safe water, and over 9 million people do not suffice for improved sanitation of water (Water Organization, 2020). Given that the country has an extensive groundwater reservoir and that these resources are recharged by rain and seepage constantly at a 20,000 MCM/year rate, this ongoing issue can be ameliorated by identifying the country's groundwater potential zones (GWPZ's) (Environmental Management Bureau, 2006).

Although there are existing studies about groundwater assessment in Tanauan, these were done through a combination of geologic, hydrologic, and meteorological information obtained from well inventory, water sampling, and geophysical surveys. Since these methods are usually money and time costly, the study will make use of a fully remote method which can benefit the field of groundwater studies by providing an alternative and easier way to conduct these studies, which generally would take a lot of labor.

Objectives

This research aims to apply new technology to identify potential groundwater areas in Tanauan, Batangas Province. To achieve this main goal, the following sub-goals were proposed:

- Rank the following geoenvironmental parameters based on their influence on groundwater potential through AHP
- Develop a map that will delineate the groundwater profile of the city in ArcGIS based on the ranking generated
- Provide recommendations on areas for future groundwater development

Methods

Various geo-environmental parameters were examined in the study to have an apparent understanding of the factors that will affect the groundwater potentiality of the area. These parameters are geomorphology, slope, lineament density, land use/land cover, drainage density, geology, and soil. These were chosen based on several factors, such as its percolation characteristics and groundwater holding capacities. The correlation of these parameters to the elements that affect the groundwater recharge of an area was the basis in identifying poor to excellent groundwater potential zones in the study area.

Results and Conclusions

The authors of this study chose to conduct groundwater studies in a different and easier way, relying entirely on remote sensing and GIS-based technology. Such an approach can be used by communities that do not have the funds to conduct groundwater studies, which can be costly. Their main goal is to delineate groundwater potential zones in Tan auan City, Batangas, using previously created thematic layers and validating the results with field data.

An Analytical Hierarchal Process based on Topographic Slope, Soil Class, Land Use/Land Class, Geomorphology,

Geology, Lineament Density, Drainage Density was used to determine the Groundwater Potential Indices (GWPI))Rao, & Briz-Kishore, 1991) in Tanauan Batangas which resulted in a Final Groundwater Potential Map with zones classified into “Poor”, “Moderate”, “Good”, and “Very Good” groundwater potential as seen on Figure 2. The poor potential zones encompassed 25.39% of the city’s area; moderate potential zones encompassed 50.56% of the city’s area; good potential zones encompassed 23.63% of the city’s area, and very good potential zones only encompassed 0.40% of the city’s vicinity.

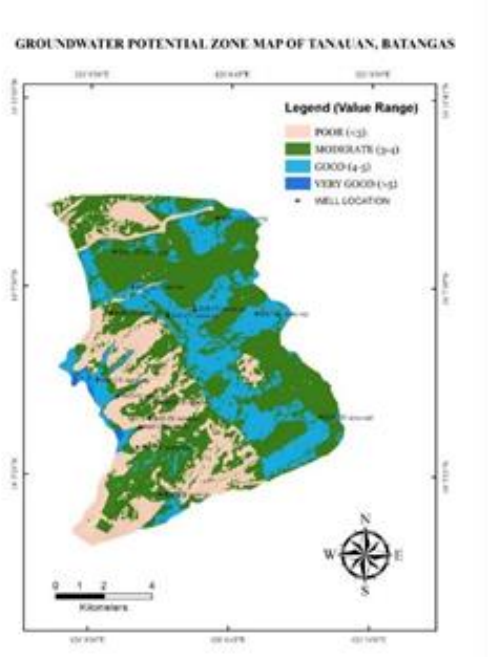

Figure 2. Final generated groundwater potential map of Tanauan, Batangas.

The barangays located near or within very good to good groundwater potential zones were Ambulong and Banadero, which were areas characterized by alluvial plain features and quaternary alluvium units with very low lineament density and slope degrees. Depth to groundwater table was used to validate the groundwater potential in the zone classes since groundwater extraction involves lowering the water table and causes drawdown; hence a shallower water table is generally preferred and associated with higher groundwater. Only one outlier well data point was classified by the GWPI zone as “Moderate” but had a groundwater table depth closer to that of the “Poor” class.

These suggest that the AHP method in delineating GWPI for determining groundwater potential is generally accurate and can provide a systematic method for preliminary exploration for groundwater as it employs an objective way to calculate the weights or relative importance of geologic and topographic features in determining groundwater potential while still incorporating the judgments of experts in the groundwater field.This author kit is designed to assist authors in preparing their submission. It is an exact representation of the format expected by the editor for the final version of the Extended Abstracts (EA).

Acknowledgments

The authors would like to extend their gratitude to their families and friends for their unending support and encouragement. They would also like to acknowledge the paper’s readers Marianne V. Fernandez and Arturo S. Daag, PhD for contributing to the betterment of the study’s content from start to beginning. Lastly, they would like to give praise and gratitude to God for imparting to them knowledge and strength to write this paper.

References

Water Organization., 2020. Philippines Water Crisis - Water In The Philippines 020. Retrieved rom Water.org: https://water.org/our-impact/where-we-work/philippines/.

Environmental Management Bureau., 2006. National Water Quality Status Report 2001 to 2005. Quezon City: Environmental Management Bureau.

Rao, B., Briz-Kishore, B., 1991. A methodology for locating potential aquifers in a typical semi-arid region in India using resistivity and hydrogeologic parameters. Geoexploration, 55-64. doi:10.1016/0016-7142(91)90014-4.

16th International Congress of the Geological Society of Greece
17-19 October, 2022 - Patras, Greece
Bulletin of the Geological Society of Greece, Sp. Publ. 10
Ext. Abs. GSG2022-022

Engineering Geological evaluation of the fault revealed during the foundation excavations of the water supply tank D1 and geotechnical risks mitigation measures.

N. Kazilis[1], N. Linardos[2],
(1) Free Lancer Consulting Engineering Geologist, Thermi, Thessaloniki, Greece, nkazilis@gmail.com (2) Consulting Engineering Geologist, Kalamaria, Thessaloniki, Greece.

During the foundation excavations of the two rooms water supply Tank D1 of Thermi Municipality, in Thessaloniki (and while these had reached the level of the intermediate bench of the total depth) there was revealed the presence of a non-expected normal fault system on the north-west side of the foundation pit. The revealed fault system is part of a wider normal fault system zone of width of a few decades of meters. During our site reconnaissance it was made clear that, a) there existed one main plane being the limit of a normal fault with general maximum dip towards the South, accompanied by few other smaller antithetic and synthetic faults and b) a wider zone of sheared and shattered geological material was formed south of the main fault plane which could develop serious conditions of differential settlements of the two structures of the water tank. Therefore, the accurate location of the main fault plane and the wider shattered zone in the very foundation of the water tank level was of utmost importance together with the assessment of its total risks and of course their mitigation measures determination. It has to be mentioned that during the carrying out of the geotechnical and structural design of the water tank system (prior to construction), there had been provided the possibility of differential settlements in the two structures of the water tank but without the knowledge of the existence of the revealed fault. Thus, it was immediately assessed the potential of a serious problem if the main fault plane (potentially active which practically separated the non-tectonically disturbed zone from the sheared and shattered block) was passing under the one room of the water tank. The accurate location of the main fault plane (north limit of the fault zone) in the foundation of the water tank as it is understood, it was of extreme importance for the safe construction and the trouble free, long term operation of the water tank.

After an extensive engineering geological reconnaissance of the water tank site carried out on the partial excavations, it was evaluated that there were unfavourable geological and geotechnical conditions for the foundation of the two room water tank. In particular, the potentially active fault could split the foundation (formation) level of the one room of the tank into two sub-areas with different physical and engineering properties with great potential for differential settlements (at either side of the main fault plane) in addition to the main potential shearing rupture risk of the tank, in the case of the seismic activation of the fault. Due to the fact that the wider hilly area around the tank foundation excavations was covered with vegetation and man-made deposits carried out by the contractor in order to ease the access to the site, it was made clear that there were not favorable conditions for the carrying out of the accurate scale classical geological mapping alone. Thus, the needed high accuracy mapping and in general the adequate scale engineering geological mapping of the fault system should have been focused on specific areas of the excavations crest, on the excavated cut slopes and primarily on the existing temporary excavation floor of the intermediate bench (mid depth of the total excavations). For that reason, the site investigations were carried out by means of exploratory pits and trenches following the trace indications of the main fault plane. In addition, the trenches and pits were engineering geologically mapped and many measurements of the strike and dip of the main fault plane were taken for further evaluation. Concurrently, there were proposals by academicians and University professors for the carrying out of studies for the evaluation of the seismic activity of the revealed fault system and the carrying out of geophysical investigations for the accurate mapping of the fault system and the evaluation of its location on the expected foundation level of the water tank. However, within an environment of tight budget and lack of needed time on behalf of the Municipality (Client), it had been evaluated by us that the physical and mechanical (engineering) properties of the geological materials cropping out at either side of the fault would not have expected to be critical giving vague results not necessarily satisfactory for the accurate location of the main fault plane at the water tank foundation level and consequently they were ruled out at that moment. Of course, the results of the appropriate geophysical investigations could have supplementary add up on the results of the geotechnical site investigations, but at that case, both the time needed for the carrying out of the proposed investigations and the relevant expenses were such that were not selected in order to achieve results in the shortest possible time and with the least possible expenses. For the above obvious reasons there was proposed by us the carrying out of studies and site investigations including: a) the carrying out of significant trial trenches and pits with the appropriate very accurate engineering geological mapping of the trench faces and the taking of many measurements of strike and dip of the main fault plane cropping out into the trench faces, b) great scale accurate engineering geological mapping of the wider area based on the findings and measurements of the previously mentioned site investigations, c) statistical analyses of the strike and dip measurements of the main fault plane, d) drafting engineering geological sections in order to locate the trace of the main fault plane on the expected to be encountered water tank foundation level and e) the preparation of all the design documentation (reports and drawings) provided by the Greek state procedures together with preparation of

proposals for the confrontation of the geological hazards and the relevant risks mitigation measures.

Taking into consideration the available geological data and primarily the evaluated geological hazards (presence of the extended normal fault zone with sheared and shattered geological materials expected to be encountered on the foundation level of the water tank separating two foundation zones with geotechnically different characteristics and the great potential for seismic activity of the fault), the evaluated geotechnical risks were as following: (i) potential extensive settlements of the part of the water tank that would be founded on extensively sheared and shattered rockmass (south of the main fault plane) to greater levels that the ones calculated in the geotechnical design of the tank, leading to serious differential settlements, (ii) the potential development of seismic acceleration (in the case of seismic activity) much greater than the one provided by the Greek Seismic Design norms (EAK 2000) that has been applied in the structural calculations of the water tank and (iii) potential seismic rupture along the main fault plane in the case of the case of an earthquake.

According to the revised Greek Seismic Design Norm (EAK 2000), the construction of structures with severity of Σ2, Σ3 and Σ4 is not allowed in the narrow vicinity of seismo-tectonic faults which are considered active. However, according to the valid Greek Seismic Design Norm, the characterization of faults as active, should be done on the basis of earthquake historical and tectonic data taking into account the potential scale of the seismic rupture. In addition, according to the Greek EAK 2000, the characterization of the seismo-tectonic active faults, is part of special studies which refer to wider building areas and not the isolated structures. Such studies in the main refer to necessary data for the planning of development of one area that is subject to approval and control by the state. Studies for the presence of general active faults are not needed in wider town developed areas, unless if there exist indications of the opposite, based on official (state published) geological – tectonic maps. In the cases that there exist specific reasons for building structures in the direct vicinity of seismo-tectonic faults which are considered active, according to EAK 2000, this is allowed only after the carrying out of special seismic-geological-geotechnical-structural design. In that case, there must be investigated the impact of the nearby fault and there must be designed and taken measures for the effective confrontation. The design seismic action in the vicinity of such faults, according to EAK 2000, should be taken increased at least by 25% in relation to the one provided by the Norm for that area.

Taking into consideration and evaluating all the data that were revealed from the carried out site investigations works and without having determined the seismic activity of the revealed fault, for the confrontation and the water tank geotechnical risks mitigation there were proposed the following: (i) transfer and rotation of the water tank layout in such a way that the whole of the water tank structure (two rooms and a valve structure) to be founded on the non-sheared and not shattered block of the fault, within the limits of the plot owned by the Municipality, with the appropriate revision of the structural design of the tank with the use of seismic acceleration coefficient increased by 25% that is, A=1.16%X1.25=0.20g. Alternatively and towards a more conservative approach, it could be applied the provision of the Greek Seismic Design Norm for the Zone II which is fairly close to the area of the water tank, that is A=0.24g as well as, (iii) an additional artificial and not costly foundation soil reinforcement (with application of systematic pattern of grouted dowels, or micropiles structure) of a limited zone towards the trace of the main fault plane in order to increase the compactness of the non-sheared fault block and the avoidance of any potential deformation of the foundation level in the case of earthquake activity.

Figure 1. General image of the normal fault system revealed in the Water Tank D1 partial foundations excavations.

16th International Congress of the Geological Society of Greece

17-19 October, 2022 - Patras, Greece

Bulletin of the Geological Society of Greece, Sp. Publ. 10

Ext. Abs. GSG2022-043

Tracing Nitrogen Sources and Transformations by using the Nitrate dual Isotopic Composition of Groundwaters from Atalanti, Fthiotida, Greece

C. Antonopoulou[1], E. Kelepertzis[1], I. Matiatos[2], F. Botsou[3], S. Karavoltsos[3], P. Boeckx[4]

(1) Department of Geology and Geoenvironment, National and Kapodistrian University of Athens, Panepistimiopolis, Zographou, 15784, Athens, Greece, christinaant@geol.uoa.gr (2) Hellenic Centre for Marine Research, 46.7 km of Athens-Sounio Ave., 19013, Anavissos Attikis, Greece (3) Department of Chemistry, National and Kapodistrian University of Athens, Panepistimiopolis, Zographou, 157 84 Athens, Greece (4) Isotope Bioscience Laboratory- ISOFYS, Department of Green Chemistry and Technology, Ghent University, Belgium.

Research Highlights

Two major nitrate sources were identified in the Atalanti basin: fertilizers and untreated wastes from septic systems with the processes of nitrification and denitrification occurring in the central and northern parts of the basin, respectively.

Nitrate pollution in water resources is a global issue of major concern, given its impact on health, as it is responsible for infant diseases and carcinogenesis, and the ecosystems (Kendall & Aravena, 2000). For this reason, the World Health Organization (WHO) and the European Union (Directive 98/83/EC), have set threshold value of 50 ppm for nitrate ion (NO_3^-) concentration in drinking water (WHO, 2004). Increased nitrate concentrations in the groundwater have been associate to land-uses and particularly agricultural and rural areas. The use of nitrate and ammonium fertilizers and manure, as well as the absence of centralized systems for the collection and treatment of domestic wastewater, are mainly responsible for nitrate pollution. In the Greek territory, many areas undergo groundwater deterioration due to strong nitrate pollution, such as in Schinos, Thiva and Central Euboea (Kelepertzis *et al*, 2019). Nitrogen (^{14}N, ^{15}N) and oxygen (^{16}O, ^{18}O) isotopes of the nitrate molecule (NO_3^-), have been widely used to identify and evaluate the origin of nitrate pollution, as well as the biogeochemical transformation of nitrogen species (Matiatos *et al*., 2021). In Greece, the application of nitrate isotopes in water studies, is still limited and sporadic, such as the case studies of the Asopos river basin (Matiatos, 2016) and the Central's Greece basins (Pyrgaki *et al*., 2022) focusing on the water quality deterioration in alluvial aquifers.

The Atalanti basin is located in Eastern Central Greece and is an intensively cultivated area with a relatively small urban fabric, which nevertheless does not have a centralized system for the collection and treatment of domestic sewage. As a result, it is an area that faces groundwater quality deterioration threats, especially from nitrate contamination. The purpose of this work is to assess the nitrate pollution in groundwater in the wider area of Atalanti basin and to determine the sources of nitrate pollution, using nitrate isotope techniques ($\delta^{15}N$ and $\delta^{18}O$ of NO_3^-).

A single sampling campaign was carried out in June 2021, i.e., during the dry season. In total, 41 groundwater samples were collected from productive irrigation boreholes, several of which were also used for drinking water supply purposes. The depths of the boreholes ranged from 20 to 200 m, with an average depth of 60 m. During sampling, *in-situ* parameters were determined such as pH, dissolved oxygen (DO), redox potential (Eh), electrical conductivity (EC) and total dissolved solids (TDS), using a pre-calibrated portable multiparameter meter. All samples were analyzed for major cations (Ca^{2+}, K^+, Mg^{2+}, Na^+) and trace elements, nutrient ions (NO_3^-, NO_2^-, NH_4^+, PO_4^{3-}) and main anions (Cl^-, HCO^-, SO_4^{-2-}). In addition, 32 of the 41 samples, were analyzed for nitrate isotopes ($\delta^{15}N$ and $\delta^{18}O$ of NO_3^-). The 32 samples were selected with the intention to cover the whole range of nitrate concentration values from the lowest to the highest ones. The determination of nitrate ions concentrations was done in the laboratory of Environmental Chemistry, of the Department of Chemistry of NKUA, using an ion chromatography system, whereas the samples were analyzed for nitrate isotopes at the Isotope Bioscience Laboratory – ISOFYS, Ghent University, Gent, Belgium using a bacteria denitrification method (Casciotti et al., 2002). The analytical uncertainties were ± 0.2 ‰ and ± 0.4 ‰ for $\delta^{15}N$ and $\delta^{18}O$ of NO_3^-, respectively.

The pH ranged from 7.00 to 7.69 indicating neutral to slightly alkaline conditions. The Dissolved O_2 (DO) and Eh values ranged from 1.47 to 8.06 mg L^{-1} (median 6.13 mg L^{-1}) and from -333 to 291 mV (median 89.3 mV), respectively. These indicated that most of the samples are under oxic conditions. All chemical ion concentrations were below the threshold values for drinking water (WHO, 2004), except for nitrate ions. Overall, the nitrate values ranged from below detection limit (DL = 0.5 mg L^{-1}) to 337 mg L^{-1} (median 68.8 mg L^{-1}) but exceeded the threshold value of 50 mg NO_3^- L^{-1} (WHO, 2004) in ~66 % of the samples. The $\delta^{15}N$-NO_3^- values in the groundwater samples ranged between +2.0 ‰ and +14.5 ‰, with an average of 6.5±3.3 ‰, whereas the $\delta^{18}O$-NO_3- values were between ±0.3 ‰ and +11.0 ‰, with an average of ±4.7±2.4 ‰. Most of the samples (~72 %) fell within the overlapping ranges for organic N in soil, NH_4^+ fertilizers, manure, and sewage effluents, indicating that multiple nitrate sources are responsible for the nitrate contamination of the aquifer (Fig. 1). The $\delta^{15}N$-NO_3^- and $\delta^{18}O$-NO_3^- values exhibited spatial variability reflecting diverse N sources in the aquifer. For example, the groundwater samples located closer to the urban area showed the highest $\delta^{15}N$ - NO_3^- values,

whereas those from the central part of the basin, which is mostly agricultural, had much lower (Fig. 2). Some samplesexhibited negative correlation between of $\delta^{15}N$- NO_3^- values and NO_3^- concentrations, DO and Eh values reflecting the possible occurrence of denitrification processes under reducing conditions in some parts of the aquifer (Nikolenko et al.,2017). On the other hand, the samples, mainly from the central part of the basin, showed lower $\delta^{18}O$ - NO_3^-, and high DOvalues, which could be indicative of nitrification processes (Nikolenko et al., 2017).

In this study, two major nitrate sources were identified in the Atalanti basin during dry season using chemical and isotope tracers: fertilizers are mostrly responsible for nitrate pollution in the central part of the basin, whereas leaching of untreated wastes from septic systems deteriorated the groundwater near the settlement of Livanates. The relationship between the physicochemical parameters, such as redox (Eh) and dissolved oxygen (DO) and nitrate isotopes lead to the conclusion that the denitrification most likely occurs in the northern part of the basin, near the Livanates settlement, whereas nitrification was more evidently detected in the central part.

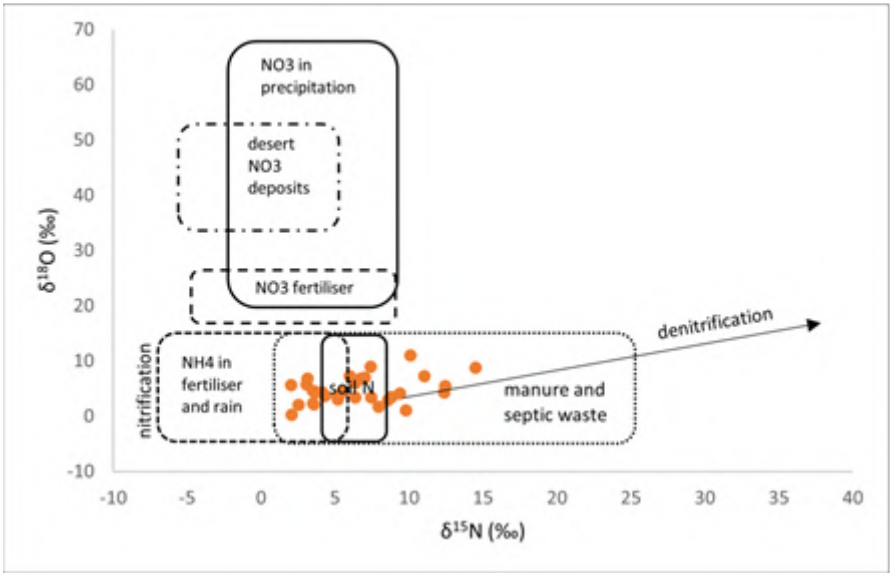

Figure 2. $\delta^{15}N$ vs $\delta^{18}O$ of NO_3^- in the groundwater samples of Atalanti basin (the $\delta^{15}N$ and $\delta^{18}O$ ranges of nitrate sources were taken from Kendall & Aravena, 2000).

Acknowledgements

The authors would like to thank Anastasia Malliou and Katerina Margelou for their assistance during chemical analyses and the local farmers for all their assistance and hospitality.

References

Casciotti, K.L., Sigman, D.M., Hastings, M.G., Böhlke, J.K. and Hilkert, A., (2002). Measurement of the oxygen isotopic composition of nitrate in seawater and freshwater using the denitrifier method. Analytical chemistry, 74(19), pp.4905-4912.

Kelepertzis,E., Pyrgaki, K., Argyraki, A., Botsou, F., Boeckx, P., Megremi, I., Karavolotsos, S., Dassenakis, M., 2019. Application of dual isotopes (δ15N, δ18O) to determine nitrate contamination sources in Cr(VI)-impacted groundwater of central Greece aquifers. 15th International Congress of the Geological Society of Greece.

Kendall, C., Aravena, R., 2000. Nitrate Isotopes in Groundwater Systems: Nitrate Isotopes in Groundwater Systems, 261-291. Matiatos, I., 2016. Nitrate source identification in groundwater of multiple land-use areas by combining isotopes and multivariate statistical analysis: A case study of Asopos basin (Central Greece). Science of the Total Environment, 541, 803-814.

Matiatos, I., Wassenaar, L.I., Monteiro, L.R., Venkiteswaran, J.J., Gooddy, D.C., Boeckx, P., Sacchi, E., Yue, F.J., Michalski, G., Alonso-Hernández, C. and Biasi, C., 2021. Global patterns of nitrate isotope composition in rivers and adjacent aquifers reveal reactive nitrogen cascading. Communications Earth & Environment, 2(1), pp.1-10.

Nikolenko, O., Jurabo, A., Borges, A., Knöller, K., Brouyère, S., 2017. Isotopic composition of nitrogen species in groundwater under agricultural areas: A review. Science of the Total Environment, 621, 1415-1432.

Pyrgaki, K., Kelepertzis, E., Argyraki, A., Boeckx, P., Botsou, F., Dassenakis, E., 2022. Identifcation of sources and transformations of nitrate in Cr(VI)-impacted alluvial aquifers by a hydrogeochemical and δ15N-NO3− and δ18O-NO3− isotopes approach. Environmental Science and Pollution Research. DOI: https://doi.org/10.1007/s11356-022-19837-0.WHO (2004) The World Health Report 2004: Changing History. 96 p.

16th International Congress of the Geological Society of Greece

17-19 October, 2022 - Patras, Greece

Bulletin of the Geological Society of Greece, Sp. Publ. 10

Ext. Abs. GSG2022-046

Toxic chromium and human health risk: A systematic review of epidemiological studies

M. N. Georgaki[1] and M. Charalambous[1]

(1) Department of Health Sciences, School of Sciences, European University Cyprus, Nicosia, Cyprus, nefgeor@gmail.com

Research Highlights

There is a significant association between exposure to hexavalent chromium through the oral route and human health impact. A study indicates a positive correlation of the two factors with an improved health outcome for the study population (decrease in mortality), while the majority of studies highlight the negative impact that hexavalent chromium has on the human body, both short-term health problems (with an emphasis on the gastrointestinal and urinary system) and long term (cancer).

Background

Water contamination with harmful substances is a serious issue for public health (WHO, 2000). Any animal or human exposure to the potentially dangerous chemicals which are widespread in groundwater poses a significant risk to their health, both immediately and over time (Ullah et al., 2009). It is claimed that chromium exposure can induce major diseases in the exposed population. Human life is always significantly impacted by the type of chromium (Cr3+, Cr6+), the mode of absorption, and the duration of exposure (Health Protection Agency, 2007). Any organism can absorb chromium through its skin, lungs, or both. According to epidemiological research, being exposed to hexavalent chromium can cause DNA damage, skin diseases, significant problems with the immune and respiratory systems, as well as impaired liver and kidney function (McCarroll et al. 2010). Hexavalent chromium exposure is associated with many cancers, including stomach, lung, liver, and Hodgkin's disease (Khosravi et al., 2014). The US Environmental Protection Agency categorizes substances into four classes based on their carcinogenic activities (EPA). Hexavalent chromium is classified as a Category A carcinogen. A significant number of studies, both experimental and non-experimental, methodically design, evaluate, and demonstrate the health risk caused by hexavalent chromium exposure in the environment (ATSDR, 2012). The information and epidemiologic research on the effects of hexavalent chromium through drinking water is limited, despite the huge number of epidemiologic studies on respiratory exposure to hexavalent chromium and the risk of lung cancer or other disorders. Provided that previous research's results, explanations, and conclusions have been called into doubt, it is especially crucial to analyze the association in a timely and systematic way.

Methods

Research question

The research question is "What is the relationship between toxic chromium through water, especially drinking water, and the risk of human health? ». The concept of PICOS gives the variables of the research question P=General population, E=Hexavalent chromium via aquifer and drinking water, C=No exposure to hexavalent chromium via aquifer and drinking water, O=Body diseases, development of various types of cancer and death, S=Patient control studies, cohort studies, cross-sectional and ecological studies.

Search strategy

Conducting the systematic review is based on specific inclusion and exclusion criteria. Specifically:

- Language and time: Studies published in English, in the years from 2005 to 2022.
- Type and content of study: Observational and experimental studies. Randomized and non-randomized controlled studies, which analyze the association of toxic chromium in drinking water and the effect on human health, emphasizing the development of cancer, disease, or death. Although the potential health impacts of several chemical substances in the environment are investigated and evaluated using the index of Health Risk Assessment (HRA) and water quality degradation, the studies were not included in the final study set of the systematic review, as they are not epidemiological studies.
- Study sample: General population, regardless of gender, age, and occupation.
- Exposure: Exposure to toxic chromium through drinking water. Air and food exposure studies are not included.
- Outcome: Effects of exposure (various types of cancer, physical illnesses, or death) are analysed.

Final number of articles

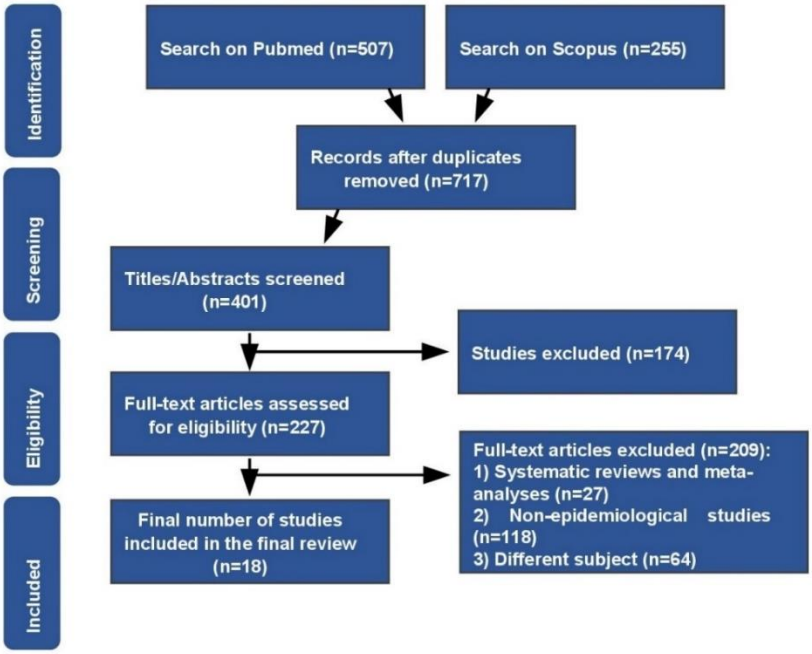

Figure 1. Flow chart illustrating the results of the systematic review search.

Results

Most research concludes that hexavalent chromium is a risk factor for humans, as opposed to trivalent chromium is a protective factor for human health. Ten (10) of the 18 studies indicated a positive association between chromium exposure in humans through the use or consumption of water and its impact on health, while the other 8 found a negative correlation. One study indicated a positive association with an improved health outcome of the population study, but nine (9) out of the ten studies had a positive association with a negative health outcome. Finally, chromium was reported as a non-detectable element in water in 1 of 8 studies.

Conclusions

According to this review, the connection between toxic chromium and its impact on the human body is related to the following health issues: gastrointestinal, immune, genitourinary, and genitourinary system disorders, stomach, lung, kidney, and general urinary cancers, dermatological and hematological disorders, the diseases of the gall bladder, renal impairment, chronic obstructive pulmonary disease, arterial hypertension, and motor neuron disease. As a result, knowing about the existence of these diseases improves the systematic control of their possible association with chromium toxicity. The appropriate implementation of programs for systematic monitoring and management of the quality of drinking and domestic water will ensure safe water for all citizens. Environmental and public health experts should constantly monitor the presence of hexavalent chromium in surface and groundwater as well as in drinking water supplies.

References

World Health Organization (WHO) and Unisef, 2000. Global water supply and sanitation assessment 2000 report. USA: World Health Organization and United Nations Children's Fund. (online) Available at:https://www.who.int/water_sanitation_health/monitoring/jmp2000.pdf Accessed 16 July 2022).

Ullah, R., Malik, R. N. and Qadir, A., 2009. Assessment of groundwater contamination in an industrial city, Sialkot, Pakistan. African Journal of Environmental Science and Technology, 3 (12).

Health protection agency. (2007). Chromium: health effects, incident management and toxicology. Available at: https://www.gov.uk/government/publications/chromium-general-information-incident-management-and-toxicology (Accessed 13/11/21)

McCarroll, N., Keshava, N., Chen, J., Akerman, G., Kligerman, A., & Rinde, E. (2010). An evaluation of the mode of action framework for mutagenic carcinogens case study II: chromium (VI). Environmental and molecular mutagenesis, 51(2), 89-111.

Khosravi, R., Fazlzadehdavil, M., Barikbin, B., & Taghizadeh, A. A. (2014). Removal of hexavalent chromium from aqueous solution by granular and powdered Peganum Harmala. Applied Surface Science, 292, 670-677.

United Nations Educational, Scientific and Cultural Organization (UNESCO), 2003. Water for people water for life. The United Nations World Water Development Report. (UNESCO) and Berghahn Books. Available at: https://unesdoc.unesco.org/ark:/48223/pf0000129726 (Accessed 10 July 2022).

Agency for Toxic Substances and Disease Registry (ATSDR), 2012. Toxicological Profile for Chromium, U.S. Department of Health, and Human Services, Public health Service. (online) Available at: https://www.atsdr.cdc.gov/toxprofiles/tp7.pdf (Accessed 10 July 2022).

16th International Congress of the Geological Society of Greece
17-19 October, 2022 - Patras, Greece
Bulletin of the Geological Society of Greece, Sp. Publ. 10
Ext. Abs. GSG2022-058

Introducing an innovative methodology for mapping rock-discontinuities, based on the interpretation of 3D photogrammetry products. The case of Akronafplia castle

Emm. Vassilakis[1], M. Stavropoulou[1], A. Konsolaki[1], I.K. Giannopoulos[1], S. Petrakis[1,2], E. Kotsi[1], E. Lekkas[1], A. Kokkoromytis[1]

(1) Dpt of Geology & Geoenvironment, National and Kapodistrian University of Athens, Zographou, Greece, evasilak@geol.uoa.gr (2) Institute of Oceanography, Hellenic Centre for Marine Research (HCMR), Anavissos, Greece.

Recent advances in the use of Unmanned Aerial Systems (UAS) and photogrammetry processing have opened new opportunities for collecting data of discontinuity properties and have made it possible to overcome safety issues using conventional methods (Ismail et al., 2022). The orientation of discontinuities (dip/strike), number of joint sets, and other relevant geological data are collected during geological survey field mapping. However, this method has several drawbacks, including site accessibility difficulties, limitations for the use of traditional tools to evaluate the rock characteristics, restrictions on the identification and localisation of site structural features, not to mention that is time-consuming. Additionally, the data acquisition ends up being impossible to the unreachable sections of the area of interest and this makes the data to be deficient. So, the accessibility to state-of-the-art close-range remote sensing technologies grants comprehensive and up-to-date data over the study area (Migliazza et al., 2021).

The described methodology is applied at the steep slopes of the "Path of Arvanitia", at the outer walls of Akronafplia castle, located in the southern border of the old city of Nafplio and aims to map and analyze the rock-discontinuities of the alpine basement of the castle. A historical promenade has been formed along the rocky coastline that surrounds the peninsula of Akronafplia, and it is frequently used by the city inhabitants during the last few centuries. It is a rather risky trail characterized by strong relief with steep, almost vertical, rocky slopes, mainly at its southern and western parts.

We used a DJI Phantom 4 pro RTK drone, equipped with an FC6310R camera and a focal length of 8.8mm for the 3D representation of the Akronafplia peninsula. The field work was accomplished in three different phases, either vertical to the slope, by mapping the north, east and south parts of the obverse face and in a single horizontal plane (Fig. 1a). In addition, the establishment of several topographic bases was carried out, along the entire route trail, with surveying equipment (total station). Also, eleven (11) targets were placed on the slopes, and measured with the same high-precision equipment, to maximize the accuracy of the photogrammetry processing that followed. The dataset was completed with the acquisition of 1678 images that were processed based on Structure-from-Motion photogrammetry techniques, to produce (a) DSMs (0.03m resolution) and (b) ortho-mosaics (0.015m resolution), of different aspects of the cliff face (Fig. 1b), based on a dense point cloud that consisted of ~248 million points.

The data acquisition and the photogrammetric process were followed by structural analysis, focused on the examination of all possible modes of slope failure in a jointed rock mass (Yoon et al., 2002). First, the rock joints were traced across the entire 3D model and digitized (Fig. 1c) for the construction of a failure density map for each of the three obverse faces. This resulted in the identification of the largest joint intersections and failure concentrations, yielding the high-risk locations of the peninsula steep slopes (Fig. 1d). Following, the slopes were divided into 18 different segments and the analysis was performed in each segment separately, due to the continuous change of their orientation and slope angle. The point clouds of each segment were used for extracting the facets of the planes that form the rock failures, followed by rock failure analysis. The latter provides way more accurate and larger number of structural measurements than the classic field work with the use of a geological compass.

The derived datasets were in turn used for the inspection of rock block stability at each one of the segments, including the statistical analysis of discontinuities for assigning them into clusters (Wang et al., 2019). In particular, the geotechnical analysis for the determination of potentially unsafe rock masses included, initially, the statistical processing of discontinuities and the creation of structural analysis stereo-diagrams. Furthermore, specialized software was used for the examination of possible wedge and plane sliding and eventually the possibility of rock falls (Martino and Mazzanti, 2014). The statistical analysis and the examination of all possible rock mass failures was carried out using a safety factor for static (SF=1.4) and for seismic (SF=1.0) conditions. For the estimation of the safety factor of all possible wedge and plane failures, the height and orientation of the slope along with discontinuity orientations and their strength parameters were imported, taking into consideration the Mohr-Coulomb shear strength criterion. Rock falls analyses were also carried out at selected cross-sections that were identified on the photogrammetric products and verified during the in-situ inspections to have increased risk.

From the analysis it was found that the highest risk of the above three modes of slope instabilities and especially of wedge failure is in the Northern part of the study area. Therefore, immediate actions are required, which should focus on measures to reduce the risk of these structural instabilities. These measures pertain to the nailing of individual rock blocks, the removal of unsafe rock blocks and the installation of either restraining nets or dynamic rockfall barriers at several places.

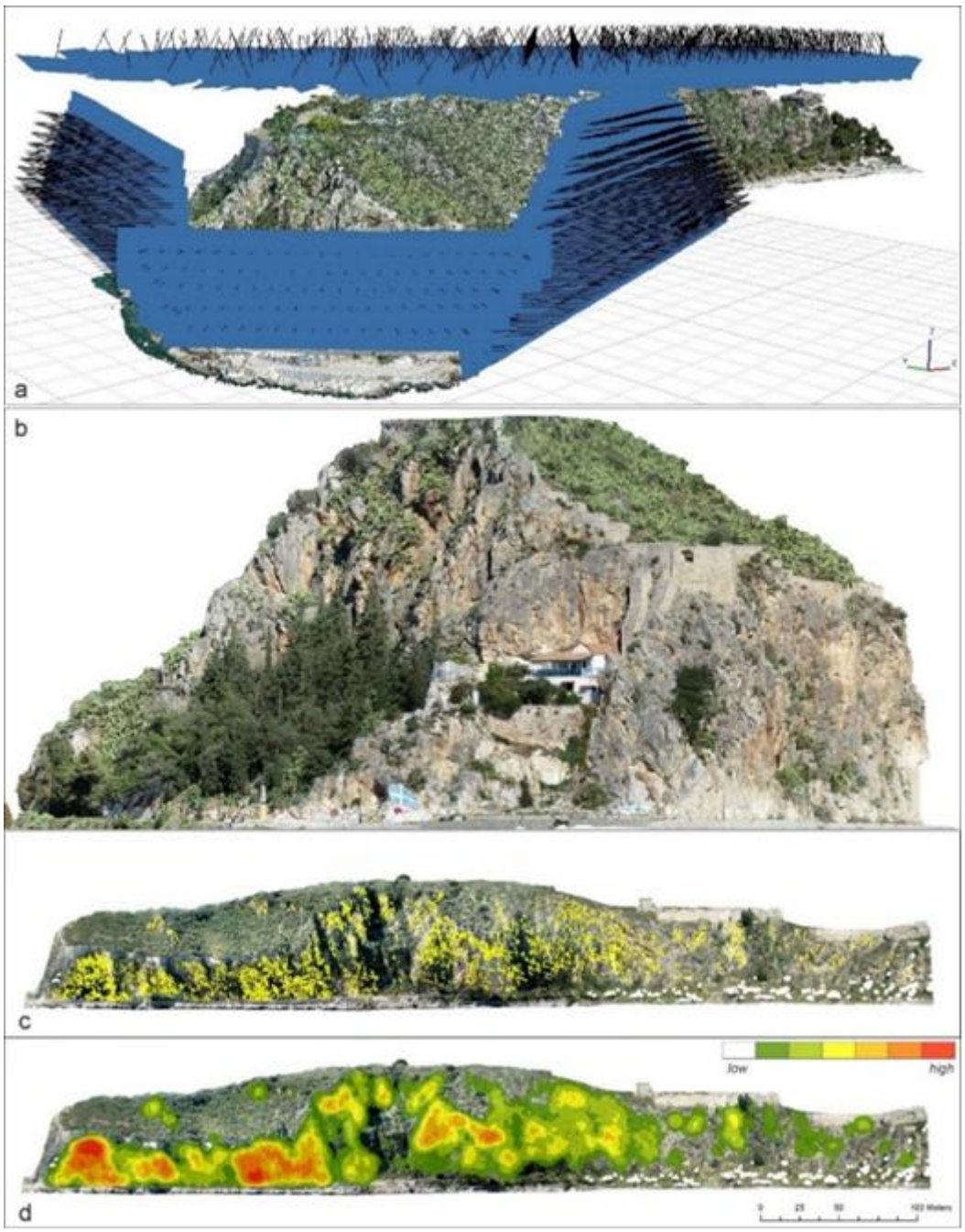

Figure 1. Distribution of the drone flights (a) for the 3D representation of the area of Akronafplia with very high resolution (b). After the data acquisition, the main discontinuities where mapped (c) and the density was measured (d).

Acknowledgements

The authors appreciate the contribution of rope access technician P. Sarelas during the fieldwork. This research was funded by the municipality of Nafplio, the Port Funds of Nafplio and the Ministry of Culture through the research grant "Research of the rockfall risk at the Arvanitia route trail of the Municipality of Nafplio, with innovative techniques".

References

Ismail, A., Ahmad Safuan, A.R., Sa'ari, R., Wahid Rasib, A., Mustaffar, M., Asnida Abdullah, R., Kassim, A., Mohd Yusof, N., Abd Rahaman, N., Kalatehjari, R., 2022. Application of combined terrestrial laser scanning and unmanned aerial vehicle digital photogrammetry method in high rock slope stability analysis: A case study. Measurement, 195, 111161.

Martino, S., Mazzanti, P., 2014. Integrating geomechanical surveys and remote sensing for sea cliff slope stability analysis: the Mt. Pucci case study (Italy). Nat. Hazards Earth Syst. Sci., 14(4), 831-848.

Migliazza, M., Carriero, M.T., Lingua, A., Pontoglio, E., Scavia, C., 2021. Rock Mass Characterization by UAV and Close-Range Photogrammetry: A Multiscale Approach Applied along the Vallone dell'Elva Road (Italy). Geosciences, 11(11), 436.

Wang, S., Zhang, Z., Wang, C., Zhu, C., Ren, Y., 2019. Multistep rocky slope stability analysis based on unmanned aerial vehicle photogrammetry. Environmental Earth Sciences, 78(8), 260.

Yoon, W.S., Jeong, U.J., Kim, J.H., 2002. Kinematic analysis for sliding failure of multi-faced rock slopes. Engineering Geology, 67(1), 51-61.

16th International Congress of the Geological Society of Greece
17-19 October, 2022 - Patras, Greece
Bulletin of the Geological Society of Greece, Sp. Publ. 10
Ext. Abs. GSG2022-081

The SCIENCE project at the Acropolis Hill of Athens, Greece - Developing an Instability Index Model of the rock slopes using advanced spatial analysis

C. Loupasakis [1], P. Tsangaratos[1], Is. Parcharidis [2], V. Eleftheriou [3], D. Michalopoulou [3], R. Christodoulopoulou [3], D. Mavromati [3]

(1) National Technical University of Athens, Athens, Greece, cloupasakis@metal.ntua.gr & ptsag@metal.ntua.gr (2) Harokopio University of Athens, Athens, Greece (3) Acropolis Restoration Service, Ministry of Culture and Sports, Athens, Greece.

Introduction

According to the World Heritage Convention, the Acropolis of Athens is considered as the most striking and complete ancient Greek monumental complex still existing in our times (UNESCO World Heritage Centre - World Heritage List). It is situated on a hill of average height (156m) and dimensions approximately 170 by 350m that rises in the basin of Athens, Greece. The Acropolis Hill is geologically composed mainly by limestone overlying the Athens Schist series, that includes a schist-sand-marly phase, with a horizon of breccia-conglomerate in it (Koukis et al., 2015). Also, one can observe recent loose deposits covering the underlying rock formations on the slopes and artificial earthfill on the upper surface of the Acropolis Hill. All geological formations appear folded into a syncline structure with a folding axis floating around the East - West direction, whereas major faults and joints follow two main directions, East - West and North - South. Significant karstic caves and voids, which in most cases are filled with calcitic material, can also been identified through the entire Acropolis Hill (Andronopoulos and Koukis, 1976).

Over the long history of Acropolis Hill and its monuments, there have been numeral efforts to monitor and evaluate the response of the structures and monuments along with the surrounding rock formations to natural and man-made hazards (Egglezos et al., 2013; Sakellariou et al., 2016; Kapogianni et al., 2020). In this context, the main objective of the current study conducted within the framework of the SIENCE project was to develop an Instability Index Model (IIM) to identify potentially unstable areas of the slopes` rock formations due to geomorphological, weathering and erosion agents. The developed IIM estimated an Instability Index that could be defined as the indicator that captures the probability of instability problems occurring within an area by assessing only the local conditions, ignoring the time parameter and any activation factor. As a result, the IIM determined the spatial distribution of the variables responsible for the occurrence of instability phenomenon and created zones within the research area that were susceptible to instability.

Methods and Data

The methodology followed during the present study could be separated into three phases: (a) collecting and processing data, (b) developing the Instability Index Model and (c) validating the performance of the Instability Index Model. Concerning the first phase, aiming to develop the Instability Index Model and construct the Instability Index Map, the following parameters were analyzed: slope angle, density of discontinuities, density of faults, density of surface runoff elements and the orientation of geological formations in relation to the orientation of the slope. All the parameters were normalized having the same range of values (0.1 – 0.9) with the maximum values indicating most susceptible classes to slide. The data were analyzed using Geographical Information System and by using a weighted sum algorithm the final Instability Index Map was constructed (ESRI, 2015). The algorithm multiplied each parameter by their given weight and summed them together. All parameters were considered to have the same influence on the Instability Index, thus had the same weight. Applying the Natural Break classification algorithm (Jenks, 1967) the produced map was reclassified in a five level of instability format, namely: very low, low, moderate, high, and very high instability. The last phase involved validating the accuracy of the model. The validation process involved overlying the vulnerable areas that have been identified by field surveys and past reports on the Instability Index Map and estimate their similarity.

Results and discussion

Figure 1 illustrates the final Instability Index Map (only moderate, high, and very high instability can be seen), for the entire research area. The North side of the Acropolis Hill, based on the IIM present the most susceptible to instability issues section. At least four sites were identified and as can be seen are in accordance with the findings of field surveys and past research studies (lined polygons). The South side seems to have less instability issues that may be attribute to the fact of favorable orientation of geological formations in relation to the orientation of the slope. To the South-East section, the IIM identified a small in extent instability area which is occupied by fractured unbedded grey limestone. The area is characterized by a dense network of joints and significant degree of weathering. Overall, the most susceptible areas are characterized by steep slope angles, dense arrangement of open cracks, fissures, and discontinuities of significant range, which are mainly zones of loose and fractured limestone masses. These areas are

identified as possible detachment areas and areas with high possibility of instability issues. Although weathering and erosion agents influence the degree of instability, it seems that have a less effect on the overall stability of the rock formations.

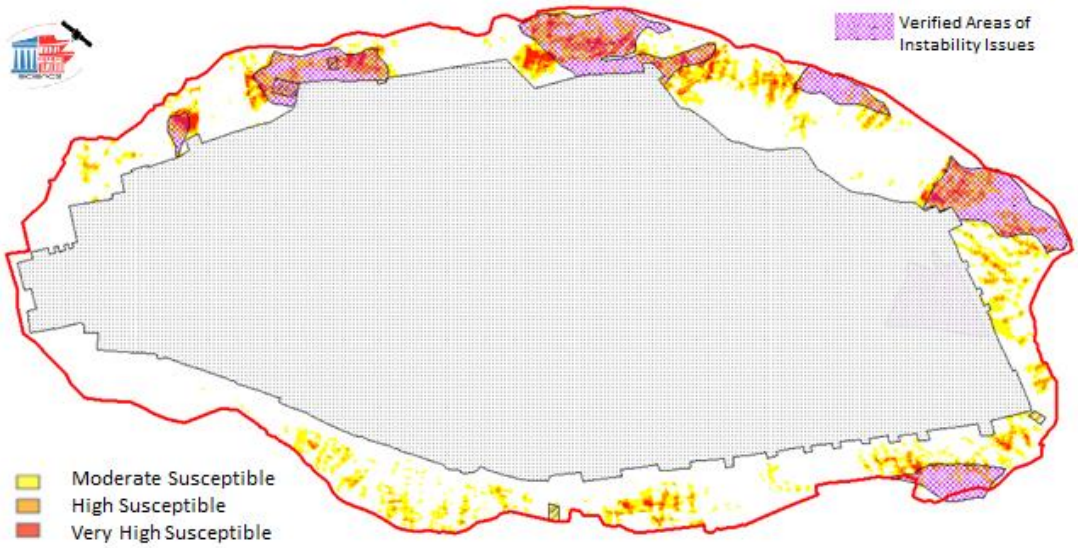

Figure 1. Instability Index

Even if the outcomes of the IIM could be characterized as sufficient accurate, still improvements could be made concerning mainly the weighting of the variables. Future works could involve applying weighting methods based either on expert knowledge or data-driven to differentiate the influence of each variable that have been used in the model and produce a more accurate outcome.

Conclusion

The main objective of the present study was to develop an IIM to locate critical zones that are characterized by significant instability issues across the Acropolis Hill of Athens, Greece. The developed IIM revealed several highly susceptible areas, with the most susceptible identified at the N – NW faces of the hill and some less in number sites at the N-E of the hill. Three main factors that contribute to the occurrence of instability issues were identified: the existence of steep slope angles, the presence of intense ruptures, fissures, joints and discontinuities and the effects of weathering and erosion agents. The outcomes of the study could be used in the decision-making process for the protection, conservation, restoration, and enhancement of the monuments of the Athenian Acropolis, whereas the IIM could serve as alterative investigation tool for other historical cultural monuments of the country.

Acknowledgements

SCIENCE project has received funding from European structural and investment funds, Partnership Agreement 2014–2020, and is supervised by General Secretariat for Research &Technology in the context of National action for bilateral cooperation between Greece-China.

References

Andronopoulos, V., Koukis, G., 1976. Engineering Geology study in the Acropolis area - Athens, IGME, p.66.

Egglezos D., Ioannidou M., Moullou D. , Kalogeras I., ´´Geotechnical issues of the Athenian Acropolis´´, Geotechnics and Heritage, Bilotta E., Flora A., Lirer S. & Viggiani C., University of Naples Federico II, Italy, 2013.

Environmental Systems Research Institute (ESRI), (2015). ArcGIS Desktop 10.3

Jenks, George F. 1967. "The Data Model Concept in Statistical Mapping", International Yearbook of Cartography 7: 186–190.

Kapogianni, E., Psarropoulos, P.N., Kokoris, D., Kalogeras I., Michalopoulou, D., Eleftheriou, V., Sakellariou M.G., 2020. Impact of Local Site Conditions on the Seismic Response of the Athenian Acropolis Hill. Geotechnical and Geological Engineering, Springer International Publishing. https://doi.org/10.1007/s10706-020-01589-8

Koukis, G., Pyrgiotis, L.& Kouki, A., 2015. "The Acropolis Hill of Athens: Engineering Geological Investigations and Protective Measures for the Preservation of the Site and the Monuments", Engineering Geology for Society and Territory - Volume 8, pp. 89-93

Sakellariou, M., Kalogeras, I., Kapogianni, E. & Psarropoulos, P., 2016. Investigation of the Structural Response of the Acropolis Wall due to seismic loading, via optical fibre sensors and accelerographs, Report to the Acropolis Restoration Service-YSMA, 85 pages (in Greek).

UNESCO World Heritage Centre - World Heritage List. https://whc.unesco.org/en/list/404 (last accessed 25/07/2022)

16th International Congress of the Geological Society of Greece
17-19 October, 2022 - Patras, Greece
Bulletin of the Geological Society of Greece, Sp. Publ. 10
Ext. Abs. GSG2022-085

Hydrochemical conditions of the granular aquifer system in the region of North - West Achaia

E. Chrysanthopoulos[1], A. Kallioras[1]
(1) National Technical University of Athens, Athens, Greece, echrysanthopoulos@metal.ntua.gr

Introduction

Considering the division of the sources of groundwater contamination into point and diffuse (Bowen, 1986), this research aims to identify the potential impact of anthropogenic activities on the aquifer system of the research area. The research area comes up to approximately 413 km^2 and it is located within the north and the west boundaries of the regional unit Achaia. The wide variety of landscape shapes is a distinctive characteristic of the area and as a result the diverse land uses account for the development of various activities throughout the area. Geomorphology varies from the lowland coastal zone of Patraikos gulf and the central lowland zone, where agricultural land is considered to be highly productive, to semi-mountainous area in the south of the regional unit.

The geological setting of the lowland zone, which constitutes the largest part of the research area, is characterized by sediments and alluvial deposits of Neogene and Quaternary. In this specific morphological zone, a low, almost horizontal, relief landscape is observed, which is conducive to the development of agriculture, considering the increased fertility, due to the rich ingredients of the alluvial deposits. Apart from the agricultural activities, industrial activities and livestock are taken place within the research area. In the north – west part of the lowland area is located the national park of Strofylia wetlands, which are protected by the Ramsar Convention (1971). The boundaries of the Ramsar region also include Strofylia forest, the most extensive Pinus pinea in Greece and one the of the largest in Europe.

In the semi – mountainous zone the predominant geological formations are flysch and limestone and the relief landscape is considered to be high, to the greatest extent of the area. Human interventions to the natural landscape have formed a lower relief in the area and as a result agricultural activities have been developed intensively throughout the area.

The hydrographic network of the research area is described by rivers and streams which flow through the lowland area and spring from the mountains at the south and south - east of the area. The main rivers that exhibit flow almost during the entire year are Peiros, Parapeiros and Larissos. The catchment of Peiros incorporates the catchments of Parapeiros and other streams of the research area (Stavropoulos, 1992). Several other ephemeral streams flow through the research area and the major of them is called Serdini, which is a tributary of Peiros. The springs of Serdini are located in the vicinity of the village Flokas. A sanitary landfill has been constructed next to the village Flokas, for the disposal of urban waste of West Achaia municipality and neighboring municipalities according to the emerging requirements for waste disposal.

The climate is typical Mediterranean with warm - dry summers and mild – wet winters.

Groundwater flow in the research area occurs in three different types of aquifer systems. According to the classification proposed by Struckmeier et al. (1995) the alluvial granular aquifer of the research area, which is highly productive, consists from alluvial deposits, side scree and scree cones. The rest of the two aquifer systems are considered to be insignificant with local and limited groundwater resources (Nikas et al.,2010) and they consist from flysch (Tripolis zone) and sandstones, sands, marls (Pliocene). In this study, the hydrochemical conditions of the alluvial granular aquifer of the area are investigated, which are developed within the area of the alluvial deposits of Peiros' and Larissos' catchments. These formations are consisted from fine and coarse materials and their permeability is strongly related to primary porosity.

Methods

To investigate the hydrochemical conditions of alluvial granular aquifer and the main surface water bodies of the research area, a sampling campaign was organized after the wet period during the hydrologic year of 2016. During the sampling campaign 28 samples were collected from boreholes pumping water from several layers of the alluvial granular aquifer and 7 samples were collected from Peiros, Parapeiros, Serdinh and Strofylia wetland. As can be concluded from the borehole sections from previous studies (Nikas et al., 2010) water is beared in multiple layers of the formations. However, the intermediate layers cannot be characterized as water-bearing formations. Consequently, it can be assumed that the multiple layers form a uniform aquifer with vertically fluctuating hydraulic characteristics.

Several water quality parameters such as electrical conductivity, pH and temperature were measured in-situ during the sampling campaign both for ground- and surface-water samples. The above samples were analyzed as to their major ions (Cl^-, NO_3^-, SO_4^{2-}, HCO_3^-, Ca^{2+}, Mg^{2+}, Na^+, K^+, PO_4^{3-}).

Results

The outcomes of the hydrochemical analysis were initially interpreted in maps in order to examine the spatial distribution of the water quality parameters. The major ions values of the groundwater samples were interpolated using kriging method. Concerning the major ions values of the surface water samples, they depicted with a point scaling method according to the range of the value.

Then, the water type of both groundwater samples and surface water samples was estimated by calculating the percent contribution of each cation and anion to the total concentration of ions in solution on a equivalents per liter basis. The water type of a sample can be influenced by the interaction of the water with the minerals that it has been in contact with. These types of interactions include precipitation, dissolution, ion exchange, geological structure, and the mineralogy of watershed/aquifer. The dominant cations among groundwater samples were magnesium (Mg^{2+}) and calcium (Ca^{2+}), apart from a specific groundwater sample collected from a distance of 5 km away from a sanitary landfill in Flokas, in which the dominant cation was sodium (Na^{+}). The dominant anions among groundwater samples were bicarbonate (HCO_3^{-}), certifying literature citations that bicarbonate are the prevailing anions in the fresh water (Voudouris, 2009). In terms of the surface water samples the prevailing cations between them were were magnesium (Mg^{2+}) and calcium (Ca^{2+}), besides the sample collected from Strofylia wetland in which sodium (Na^{+}) is the second more dominant cation in the water type of the sample. This can be easily explained by the hydraulic connection of Strofylia wetland with the sea, which occurs both through a physical canal as well as via the limestones at the NW of the wetland.

Finally, the cations and anions values of groundwater samples and surface water samples were plotted and classified according to Piper, Durov and Wilcox diagrams. Durov and Piper diagrams confirm the results of the water type, indicating that the groundwater sample collected in the vicinity of Flokas sanitary landfill is characterized by the cations of sodium (Na^{+}) and potassium (K^{+}), contrary to the remaining samples in which the predominant cations are magnesium (Mg^{2+}) and calcium (Ca^{2+}) and bicarbonate anions (HCO_3^{-}). Wilcox diagram is used to assess the viability of the water in terms of its use for irrigation purposes. It is a scatter plot of points displayed based on the values of the Sodium Adsorption Coefficient, SAR, on the vertical axis, and based on the values of the Specific Electrical Conductivity (salinity), SEC (in μS/cm), on the horizontal axis, the values of which are listed on a logarithmic scale. According to the outcomes of the Wilcox diagram the groundwater samples of the research area were classified in C3S1 class indicating that their condition is considered moderate for irrigation purposes. Nevertheless, several of these wells are used for domestic water supply.

Discussion

The general quality condition of the alluvial granular aquifer of the research area is deemed satisfactory, at least for irrigation purposes, considering that seawater intrusion is only observed at the NW part of the area. The majority of the groundwater samples can be characterized as of good quality for irrigation purposes, apart from the sample collected from the vicinity of the sanitary landfill. In terms of surface water samples, those collected from Serdini exhibit higher values at specific anions, such as nitrates (NO_3^{-}), sulfates (SO_4^{2-}) and clorides (Cl^{-}), than the values of the samples which collected from Peiros and Parapeiros flowing in the same area.

References

Bowen, R., 1986. Groundwater, 2nd ed. Elsevier Applied Science Publishers

Nikas, K., Antonakos, A., 2010. Survey of water reserves of the northern Peloponnese, with an emphasis on quality characteristics and seawater intrusion phenomenon, Institute of Geological and Mining Surveys

Stavropoulos, X., 1992. Hydrogeological conditions in the Kato Achaia - Nea Manolas area (NW Peloponnesus), Ph.D. Thesis, School of Mining and Metallurgical Engineering, National and Technical University of Athens, Athens

Struckmeier, F., W., Margat, J., 1995. Hydrogeological Maps A Guide and a Standard Legend, Volume 17, International Association of Hydrogeologists, HEISE

Voudouris, K., 2009. Enviromental Hydrogeology, Groundwater and Enviroment, Tziola

16th International Congress of the Geological Society of Greece
17-19 October, 2022 - Patras, Greece
Bulletin of the Geological Society of Greece, Sp. Publ. 10
Ext. Abs. GSG2022-086

Research for the Conceptual Model Development of River Lissos Coastal Aquifer System, NE Greece

I. Gkiougkis[1], I. Empliouk[1], A. Adamidis[1], C. Pliaka[1], D. Karasogiannidis[1], F.-K. Pliakas[1], T. Tzevelekis[1]

(1) Democritus University of Thrace, Department of Civil Engineering, Laboratory of Engineering Geology and Groundwater Research, 67100 Xanthi, Greece, jgiougis@civil.duth.gr

Introduction

Conceptual models are defined as simplified versions of real-world systems (Anderson *et al.*, 1992, Zhou and Herath, 2017). The conjugation of hydrogeological research and survey involves the application of a number of methodologies in compiling a conceptual model containing basic exploratory data, hydro-chemical typology, etc (Bentacur *et al.*, 2012). Gkiougkis *et al.* (2021) note that accurate conceptual model is directly related to a thorough investigation of the natural system involving subsurface investigations (groundwater well logging, geophysical investigations, pumping tests), hydrological (groundwater level monitoring, surface and unsaturated zone studies) and hydrochemical measurements (groundwater sampling and analyses). According to Bear *et al.* (1992), selecting the appropriate conceptual model for a given problem is one of the most important steps in the modelling process. Zeng *et al.* (2013) state that the power of the groundwater model is determined by the conceptual model.

The present work deals with the groundwater system conceptual model development of River Lissos, NE Greece, using updated data in addition to information and data from previous relevant research in the wider study area (Pliakas *et al.*, 2007, Kallioras *et al.*, 2011, Eminoglou *et al.*, 2017).

Study area

The plain area of River Lissos coastal area has mild morphologic characteristics with low elevation, extended between Lissos River and the western foot of Ismaros Mount, whereas Thracian Sea covers the southern boundaries of the area (Figure 1). The geological environment of the study area includes recent sediments originated from Lissos River -and some other branches of the same river overlying Neogene deposits or Paleogene deposits of Rhodope massif. The main cultivation type of the area is cotton, while the southern part of the area of investigation is not arable due to groundwater salinization (Pliakas et al., 2007, Eminoglou, 2017). According to Kallioras et al. (2011), the aquifer system of the study area contains clay materials and appears in the form of successive layers composed of clay-sands and sands with a width ranging from 1 to 10 m, with many interferences of clay layers.

Meteorological data

After processing the available hydrological data, which have been recorded at the meteorological stations of Imeros located in the SE part of the study area, the average annual rainfall value is estimated at 495.2 mm for the period 2011 – 2021 (maximum annual rainfall: 709.6 mm (2017), minimum annual rainfall: 204.8 mm (2011)), while the maximum temperature value for the same period is 27.9 ºC (July 2012) and the minimum is 1.6 ºC (January 2017), the average annual temperature values showing an increasing trend approximately of the order of 1.0 °C.

Methodology

Groundwater level measurements, in situ measurements of groundwater temperature, pH and Electrical Conductivity, and groundwater sampling from twenty-five (25) wells at the study area were carried out in two (2) time periods (July and October 2021). Then, relevant analyses were performed at the Laboratory of Engineering Geology and Groundwater Research of the Civil Engineering Department, DUTH, Greece. Piezometric and hydrochemical maps were compiled presenting the spatial distribution of several parameters such as temperature, pH, electrical conductivity (EC), NH_4^+, NO_3^-, NO_2^-, Cl^-, Na^+, Ca^{2+}, Mg^{2+}, Mn^{2+}, Fe^{2+}, SAR, SO_4^{2-}, some of which are presented in Figure 1.

Results

The groundwater level gradually increases from October to March, due to natural recharge from direct infiltration from precipitation (at parts of the aquifer where it appears semi-confined or unconfined), percolation from Lissos River and main lateral inflows from the western and NE parts of the study area where there is a hydraulic connection with the mountainous zones (Figure 1). The spatial distribution of nitrate ion (NO_3^-) concentration values (Figure 1) in the study area indicates E and NE parts of the aquifer system (50 – 90 mg/L), at the wider area of Xylagani, potentially affected by anthropogenic factors (urban wastewater, use of phosphate fertilizers in agriculture). It is worth mentioning that high values of Electrical Conductivity are detected in the coastal part of the study area, exceeding the value of 7500 μS/cm, while at the same area, the chloride (Cl^-) concentration values range from 200 to more than 1800 mg/L, which imposes the argument of seawater intrusion conditions.

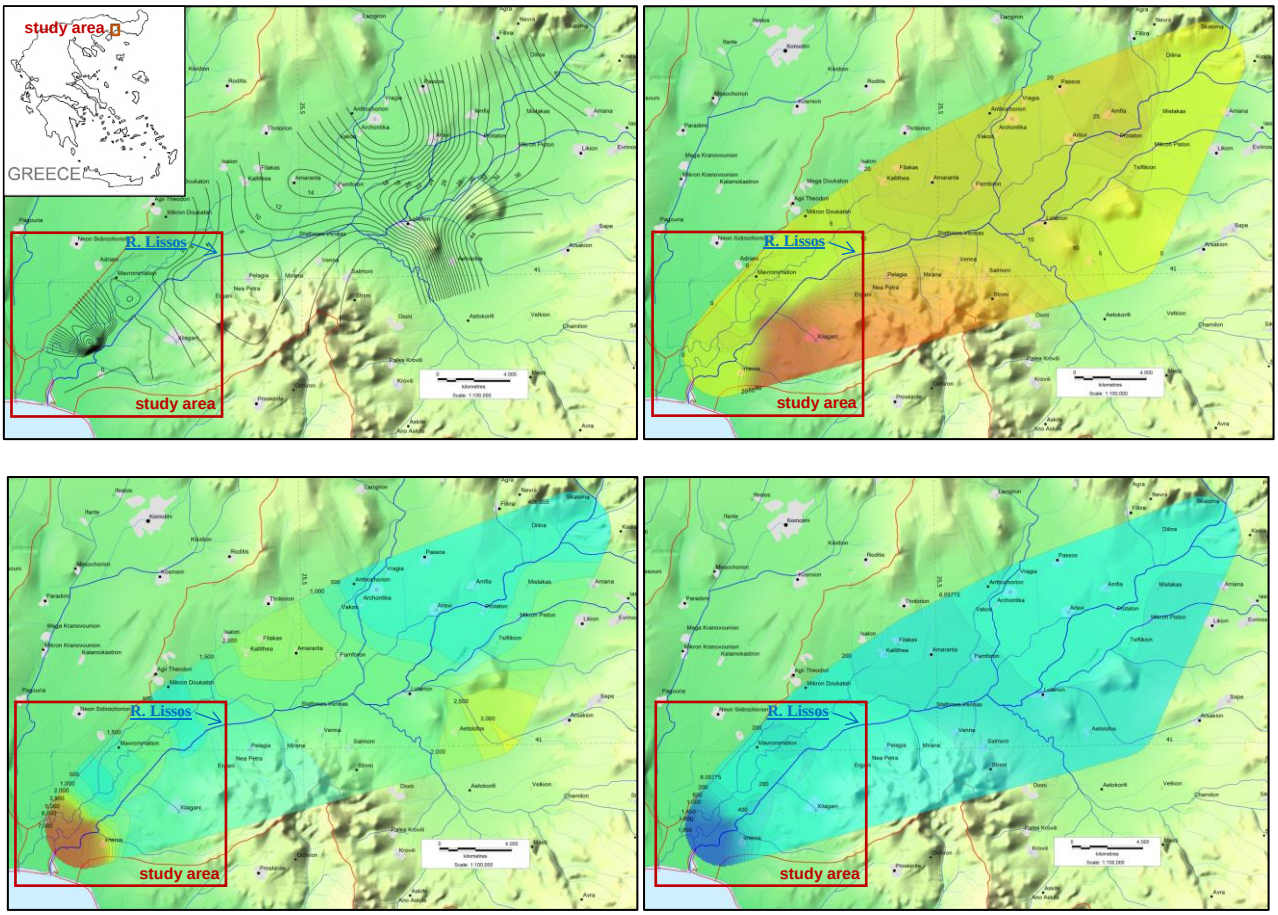

Figure 1. Upper left: Study area, monitoring wells network, piezometric map of the studied aquifer system (October 2021). Upper right: Nitrates (NO_3^-) distribution map (mg/L), July 2021. Lower left: Electrical Conductivity distribution (EC) map (μS/cm), July 2021. Lower right: Chloride ions (Cl^-) distribution map (mg/L), July 2021.

Conclusions

The research work in the study area included data, information, findings and valuations, which can contribute to the further investigation of the hydrogeological status of the aquifer system in the area in the context of the development and management of groundwater and surface waters in the wider area.

Acknowledgements

The research was funded by Eye4Water project (eye4water.com), MIS 5047246, implemented under the action: "Support for Research Infrastructure and Innovation" by the Operational Program "Competitiveness, Entrepreneurship and Innovation" in the framework of the Co-financed by Greece and the European Union-European Regional Development Fund.

References

Anderson, M.P., Woessner, W.W., 1992. Applied Groundwater Modeling— Simulation of Flow and Advective Transport. Academic Press. Inc. San Diego. CA., 381p.

Bear, J., Beljin, M.S., Ross, R.R., 1992. Fundamentals of Ground-Water Modeling. Ground Water Issue. United States Environmental Protection Agency. Office of Solid Waste and Emergency. Response Office of Research and Development. EPA/540/S-92/005.

Betancur, T., Palacio, C.A., Escobar, J.F., 2012.Conceptual Models in Hydrogeology. Methodology and Results. Hydrogeology - A Global Per-spective. Edited by Gholam A. Kazemi. ISBN 978-953-51-0048-5, 232 pages. Publisher: InTech.

Eminoglou, G., Gkiougkis, I., Kallioras, A., Pliakas, F.-K., 2017. Updated groundwater vulnerability evaluation at a coastal aquifer system in NE Greece. European Water, E.W. Publications, 57, 423-428.

Gkiougkis, I., Pouliaris, C., Pliakas, F.-K., Diamantis, I., Kallioras, A., 2021. Conceptual and Mathematical Modeling of a Coastal Aquifer in Eastern Delta of R. Nestos (N. Greece). Hydrology Journal, MDPI, 8(1) 23, https://doi.org/10.3390/hydrology8010023.

Kallioras, A., F. Pliakas, S. Skias, I. Gkiougkis, 2011. Groundwater vulnerability assessment at SW Rhodope aquifer system in NE Greece. Advances in the Research of Aquatic Environment, Environmental Earth Sciences, Springer, Vol. 2, ISBN: 978-3-642-24075-1, 351-358.

Pliakas, F., A. Mouzaliotis, A. Kallioras, I. Diamantis, 2007. Hydrogeological assessment of the salinization problem of Xilagani – Imeros aquifer system in SW plain area of Rhodope Prefecture, Greece. Proceedings of the 11th International Conference of the Geological Society of Greece, Athens, Greece, 24-26/5/2007, 2, 536-547.

Zeng, X., Wang, D., Wu, J., Chen, X., 2013. Reliability Analysis of the Groundwater Conceptual Model. Human and Ecological Risk Assessment: An International Journal, 19(2), 515-525.

Zhou, Y., Herath, H., 2017. Evaluation of alternative conceptual models for groundwater modelling. Geoscience Frontiers, 8, 437-443.

16th International Congress of the Geological Society of Greece

17-19 October, 2022 - Patras, Greece

Bulletin of the Geological Society of Greece, Sp. Publ. 10

Ext. Abs. GSG2022-087

Research for the Conceptual Model Development of River Laspias Coastal Aquifer System, NE Greece

I. Gkiougkis, D. Karasogiannidis, C. Pliaka, A. Adamidis, I. Empliouk, F.-K. Pliakas, T. Tzevelekis

Democritus University of Thrace, Department of Civil Engineering, Laboratory of Engineering Geology and Groundwater Research, 67100 Xanthi, Greece, jgiougis@civil.duth.gr

Introduction

Conceptual models are defined as simplified versions of real-world systems (Anderson *et al*., 1992, Zhou and Herath, 2017). The conjugation of hydrogeological research and survey involves the application of a number of methodologies in compiling a conceptual model containing basic exploratory data, hydro-chemical typology, etc (Bentacur *et al.*, 2012). Gkiougkis *et al.* (2021) note that accurate conceptual model is directly related to a thorough investigation of the natural system involving subsurface investigations (groundwater well logging, geophysical investigations, pumping tests), hydrological (groundwater level monitoring, surface and unsaturated zone studies) and hydrochemical measurements (groundwater sampling and analyses). According to Bear *et al.* (1992), selecting the appropriate conceptual model for a given problem is one of the most important steps in the modelling process. Zeng *et al.* (2013) state that the power of the groundwater model is determined by the conceptual model.

The present work deals with the groundwater system conceptual model development of River Laspias, NE Greece, using updated data in addition to information and data from previous relevant research in the wider study area (Pedreira *et al*., 2015, Gkiougkis *et al.*, 2011, 2015, 2021).

Study area

The plain area of River Laspias coastal area has mild morphologic characteristics with low elevation is mainly coved by clay, sandy clay, sand and in some cases pebbles (Figure 1). River Laspias is situated along the eastern boundaries of the eastern River Nestos Delta and is the area where the degraded industrial and sewage treatment effluents are discharged. The wider study area faces serious environmental problems due to (Gkiougkis *et al.*, 2021): (i) seawater intrusion, (ii) quality degradation of fresh water from different sources such as applied fertilizers and pesticides, irrigation return flows and disposal of municipal and industrial waste, (iii) use of wetlands for grazing and fishing, (iv) rural development of the coastal zone.

According to Gkiougkis *et al.*, (2021), the aquifer system of the wider study area consists of two hydrogeological systems, situated within the quaternary coastal and alluvial deposits of the broader region: (a) the shallow hydrogeological consisted of phreatic to semi-confined aquifers with a thickness of approximately 30 m, is recharged mainly from precipitation and partly from nearby small streams and canals, and (b) the deeper hydrogeological system incorporates alternate confined aquifers with a thickness of approximately 200 m recharged from River Nestos infiltration through old buried river beds, and partly from lateral groundwater inflows originated from the neighboring hydrogeological basin of Vistonida lagoon.

Meteorological data

After processing the available hydrological data, which have been recorded at the meteorological stations of Xanthi located in the NE part of the study area, the average annual rainfall value is estimated at 639.1 mm for the period 2009 – 2021 (maximum annual rainfall: 1028.4 mm (2019), minimum annual rainfall: 277.8 mm (2011)), while the maximum temperature value for the same period is 28.2 ºC (August 2010) and the minimum is 2.8 ºC (January 2017), the average annual temperature values showing an increasing trend approximately of the order of 1.0 °C.

Methodology

Groundwater level measurements, in situ measurements of groundwater temperature, pH and Electrical Conductivity, and groundwater sampling from twenty-three (23) wells at the study area were carried out in two (2) time periods (July and October 2021). Then, relevant analyses were performed at the Laboratory of Engineering Geology and Groundwater Research of the Civil Engineering Department, DUTH, Greece. Piezometric and hydrochemical maps were compiled presenting the spatial distribution of several parameters such as temperature, pH, electrical conductivity (EC), NH_4^+, NO_3^-, NO_2^-, Cl^-, Na^+, Ca^{2+}, Mg^{2+}, Mn^{2+}, Fe^{2+}, SAR, SO_4^{2-}, some of which are presented in Figure 1.

Results

The groundwater level gradually increases from October to March, due to natural recharge from direct infiltration from precipitation (at parts of the upper aquifer where it appears semi-confined or unconfined), percolation from River Laspias and main lateral inflows from the western and NE parts of the study area where there is a hydraulic connection with the mountainous zones (Figure 1). The spatial distribution of nitrate ion (NO_3^-) concentration values (Figure 1) in the study

area indicates E and NE parts of the aquifer system (50 – 150 mg/L), potentially affected by anthropogenic factors (urban wastewater, use of phosphate fertilizers in agriculture). It is worth mentioning that high values of Electrical Conductivity are detected in the coastal part of the study area, exceeding the value of 3000 μS/cm, while at the same area, the chloride (Cl^-) concentration values range from 250 to more than 600 mg/L, which imposes the argument of seawater intrusion conditions.

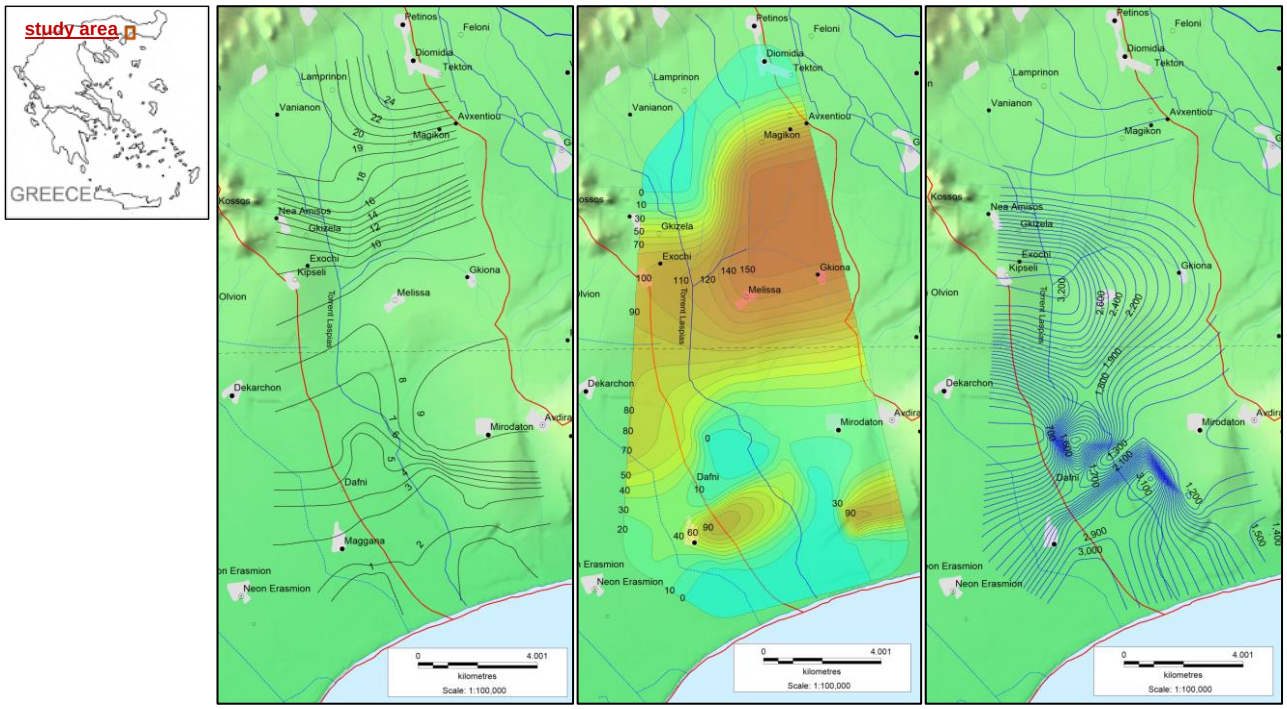

Figure 1. Left: Study area, piezometric map of the studied aquifer system (October 2021), Center: Nitrates (NO_3^-) distribution map (mg/L), July 2021, Right: Electrical Conductivity distribution map (μS/cm), July 2021.

Conclusions

The research work in the study area included data, information, findings and valuations, which can contribute to the further investigation of the hydrogeological status of the aquifer system in the area in the context of the development and management of groundwater and surface waters in the wider area.

Acknowledgements

The research was funded by Eye4Water project (eye4water.com), MIS 5047246, implemented under the action: "Support for Research Infrastructure and Innovation" by the Operational Program "Competitiveness, Entrepreneurship and Innovation" in the framework of the Co-financed by Greece and the European Union-European Regional Development Fund.

References

Anderson, M.P., Woessner, W.W., 1992. Applied Groundwater Modeling— Simulation of Flow and Advective Transport. Academic Press. Inc. San Diego. CA., 381p.

Bear, J., Beljin, M.S., Ross, R.R., 1992. Fundamentals of Ground-Water Modeling. Ground Water Issue. United States Environmental Protection Agency. Office of Solid Waste and Emergency. Response Office of Research and Development. EPA/540/S-92/005.

Betancur, T., Palacio, C.A., Escobar, J.F., 2012.Conceptual Models in Hydrogeology. Methodology and Results. Hydrogeology - A Global Per-spective. Edited by Gholam A. Kazemi. ISBN 978-953-51-0048-5, 232 pages. Publisher: InTech.

Gkiougkis I., Kallioras, A., Pliakas, F., Pechtelidis, A., Diamantis, V., Diamantis, I., Ziogas, A., Dafnis, I., 2015. Assessment of soil salinization at the eastern Nestos River Delta, N.E. Greece. Catena, Elsevier, 128, 238-251.

Gkiougkis I., Pouliaris, C., Pliakas, F.-K., Diamantis, I., Kallioras, A., 2021. Conceptual and Mathematical Modeling of a Coastal Aquifer in Eastern Delta of R. Nestos (N. Greece). Hydrology Journal, MDPI, 8(1), 23, https://doi.org/10.3390/hydrology8010023.

Gkiougkis I., Tzevelekis, T., Pliakas, F., Diamantis, I., Pechtelidis, A., 2011. Geophysical research of groundwater degradation at the eastern Nestos River Delta, NE Greece. Advances in the Research of Aquatic Environment, Environmental Earth Sciences, Springer, Vol. 1, ISBN: 978-3-642-19901-1, 259-266.

Pedreira, R., Kallioras, A., Pliakas, F., Gkiougkis, I., Schuth, C., 2015. Groundwater vulnerability assessment of a coastal aquifer system at River Nestos eastern Delta, NE Greece, Environmental Earth Sciences, Springer, 73, 6387–6415, DOI 10.1007/s12665-014-3864-7.

Zeng, X., Wang, D., Wu, J., Chen, X., 2013. Reliability Analysis of the Groundwater Conceptual Model. Human and Ecological Risk Assessment: An International Journal, 19(2), 515-525.

Zhou, Y., Herath, H., 2017. Evaluation of alternative conceptual models for groundwater modelling. Geoscience Frontiers, 8, 437-443.

16th International Congress of the Geological Society of Greece
17-19 October, 2022 - Patras, Greece
Bulletin of the Geological Society of Greece, Sp. Publ. 10
Ext. Abs. GSG2022-117

Well Inspectors: Giving Greek Geologists a Chance

P. Ntontos
Freelance Geologist, Naflpio, Greece, ntontosp@gmail.com

Introduction

The science of Geology has worldwide applications in numerous social and financial areas. However, although the title of Geologist has been an autonomous educational qualification in Greece since the 70s, its application has been limited. Moreover, the science of Geology is essentially state-devouring as it is heavily subsidized by the state. Geologists will either be exclusively employed by the state or work as freelancers in studies or contracting companies whose main focus studies public works.

Offering services and receiving fees directly to and from individuals is extremely rare. The employment of geologists by individuals to solve problems has not been institutionalized by the Greek State and there are almost no specifications for geological works. Moreover, Geology as a vocation is gradually being divided into the realms of engineers (mineralogist engineers, civil engineers, etc.) with insufficient or no geological knowledge. The PD 99/2018 (FEK 187/A') is the most characteristic example as it entitles civil engineer graduates of all Greek Polytechnic Schools to draw up and sign hydrogeological studies. By looking into the study programmes of these schools, one will find out there are schools where the only contact of students with Geology is an induction lesson with the general title of "Geology for Engineers" and also an additional elective course regarding underground aquifers, underground hydraulics and water resources management.

At this time, when state insufficiencies (understaffing, malfunctions) in conjunction with intense environmental pressures (droughts, salinisation, etc.) and the need for the development of the primary sector production in an international environment facing numerous problems (food, energy and financial crises etc.) there is a chance for upgrading and developing Geology. This field can provide indispensable services to numerous aspects of both society and finance. The institution of "Well Inspector" will constitute an important step for the realm.

The Institution of Well Inspector

Although there are more than 250,000 functioning wells in Greece (Ntontos, 2017), the involvement of geologists in their licensing and function was only institutionalized in 2005 according to JMD 43504/2005 (FEK 1784/B'). However, according to current legislation, the involvement of geologists only takes place in the phase of licensing, while it is the state and its inspecting mechanisms which are responsible for their monitoring. For instance, the inspection of the water quantities pumped or the monitoring of the chemical condition of underground waters through time is in the jurisdiction of the respective directorates of water resources management.

The institution of Well Inspector aims at the training and certification of the appropriate scientific specialisation of Geologists who will play a double role. They will provide services to individual users on an individual well level and provide services as well as important data for the management of water resources to the state on a river basin level.

The responsibilities of Well Inspectors for each well will include a minimum of:

- Monitoring aquifer levels twice yearly. In problematic areas, conductivity measurements will also be conducted
- Registering of the quantities pumped twice yearly.
- The energy consumed twice yearly
- Water sampling for chemical analysis will be conducted as frequently as the water use permit dictates

The data acquired via monitoring (measurements, chemical analyses etc.) will be entered into an electronic database which will be kept in the respective responsible body.

In addition to the monitoring of the wells, the certified inspector will have to conduct an appropriate pumping test so that the hydraulic characteristics of the aquifer such as transmissivity (T), Storativity (S), critical discharge rates, etc. as well as those of the well itself such as specific capacity. These characteristics will constitute part of the well identity.

Furthermore, the responsibilities of the Well Inspector may include a great proportion of the well-licensing process which constitutes the greatest volume of the decisions issued by the Directorates of Water Management of the country. Just to name one, the water use permits of the existing water use rights constituted 81% of the total number of water directorate decisions (Ntontos, 2017). Through an electronic licensing system, similar to the one used by the system of arbitrary building arrangements used by the TCG, Well Inspectors will issue decisions such as:

- Water use permits of existing water rights
- Revisions of water use permits

- Project permit and water use permit in Underground Water Systems which are in good quantitative and chemical condition according to the River Basin Management Plan
- Other more simple decisions required for the function and/or the construction of wells

Well instruction Institution Benefits

The simple or more complicated data collected by well instructors will constitute services to individuals (natural or legal entities) through which they can:

- Save money through the optimisation of the pumping programme to lower the reduction of the water level in the well being pumped and, consequently, the quantity of energy consumed
- Save money through timely problem detection such as screen clogging which causes unnecessary and expensive action to be taken (well deepening, well replacement, etc.) or income loss due to reduced well performance
- Protect water resources from exhausting or salinisation phenomena. As in many cases (e.g. irrigation wells) their good quantitative and qualitative condition constitutes the requirements for farm production.

Moreover, the ability of certified inspectors to issue simple decisions will minimize the time required for individuals to deal with the problems that arise. Currently, these individuals are distressed and possibly lose income due to the significant bureaucracy involved.

There will be multiple benefits for the state on different levels. The understaffing in services such as the Directorates of Water Management (Ntontos, 2017), in conjunction with the lack of coordination between the relevant bodies responsible, as well as the inadequacies and the errors of the administrative tools such as the River Basin Management Plan (Ntontos, 2017) have reduced the management of water resources plans from an essential tool of environmental management and financial development to merely a meaningless bureaucratic procedure. Through the institution of the Well Inspectors the state will:

- Save financial and human resources and the employees will be able to deal with issues more important than well licencing
- Acquire a reliable database according to which the inspectors will be able to design Riven Basin Management Plans more appropriately and control the course of action to be followed
- Acquire the monitoring mechanism which is impossible to take place due to the current financial conditions, as more employees are needed
- Will be able to implement energy-saving plans in times of energy crisis such as the one we are facing now

Finally, the most important benefit for the field of Geology will be that, if this institution is implemented, there will be hundreds or even thousands of work positions available, which will absorb a large proportion of the unemployed reaching 41% according to GCG data for the year 2019 (Ntontos et al, 2022).

Conclusions

The implementation of Well Inspectors will directly benefit the state, the society and the geological realm itself on multiple levels. The adoption of the proposed plan and its implementation must be claimed by the field of Geology itself aiming to promote its usefulness and development.

References

Ntontos, P., 2017. Hydrowells permit issuing: Existing legislation, current situation and future prospects. Hellenic Chapter of IAH International Hydrogeological Conference, Athens, Greece, p. 309.

Ntontos, P., 2022. River Water Management Plans: Weaknesses and Errors. Hellenic Chapter of IAH & CAGME International Hydrogeological Conference, Nicosia, Cyprus, p. 362.

Ntontos, P., Pasialis, V., 2022. Brackish aquifers in Greece: A different approach. Hellenic Chapter of IAH & CAGME International Hydrogeological Conference, Nicosia, Cyprus, p. 366.

16th International Congress of the Geological Society of Greece
17-19 October, 2022 - Patras, Greece
Bulletin of the Geological Society of Greece, Sp. Publ. 10
Ext. Abs. GSG2022-120

Correlation of the macroscopic shear failure of intact rocks with the sliding friction on pre-existing rock surfaces

A. Tsikrikis[1,3], V. Marinos[2], T. Papaliangas[3]

(1) Aristotle University, Department of Geology, Thessaloniki, Greece, tsikrika@geo.auth.gr (2) National Technical University, School of Civil Engineering, Athens, Greece. (3) International Hellenic University, Department of Environmental Engineering, Thessaloniki, Greece.

Research Highlights

The friction angle of a flat rock surface decreases linearly with the constant m_i of the Hoek-Brown criterion and increases linearly with the Brinell penetration hardness.

Background

The macroscopic failure of an intact rock in triaxial compression is generally controlled by shear in the entire brittle field. Accordingly, the shear strength parameters of the failure surface along which the shear displacement occurs might be related to the friction angle of a pre-fractured naturally textured flat surface of the same rock. In the case of a rough rock surface, this angle (non-dilational friction angle) is best determined from the peak friction angle after elimination of the effect of dilation (Hencher and Richards 2015, Papaliangas *et al.*, 1995,1996). Therefore, independent measurements from direct shear tests on pre-existing joints may be useful in the prediction of triaxial failure envelopes of intact rocks.

Objectives

This study aims to present the results of a research concerning the link between the parameters controlling the macroscopic failure of intact rock and the sliding friction of rock joints (Tsikrikis, 2021). The parameters m_i and σ_{ci} of the Hoek-Brown criterion for intact rocks, the brittle-ductile transition pressure and the Brinell indentation hardness, as well as the sliding friction angle of rock surfaces, are experimentally studied, and the established interrelations are presented.

Methods

Two independent laboratory test programs were carried out consisting of a series of triaxial compression tests on dry cylindrical specimens from intact rock samples and a second series of direct shear tests on artificial rock joints generated by tensile splitting or bending fracturing of prisms from natural rocks of the same rocks. Blocks from twelve rock types (seven silicates and five carbonates) with porosities ranged from 0.3% to 24.0%, including three igneous (diorite, granodiorite and metadolerite), four metamorphic (amphibolite and 3 types of marble) and five sedimentary (2 types of sandstone, 2 types of limestone and graywacke), were collected from natural outcrops, stone and marble quarries and tested in the laboratory. The triaxial compression tests were conducted on dry cylindrical specimens with confining pressures in the range of 0-70 MPa, using a standard Hoek cell. The triaxial compression failure envelope and especially the parameters m_i and σ_{ci} of the Hoek-Brown criterion were determined. Special emphasis was given to the brittle-ductile transition since this state generally occurs under non-dilational shearing. The direct shear tests were performed under constant normal load (CNL) conditions using the multi-stage shear procedure with repositioning of the joint in its initial natural position before each shearing stage (ISRM, 2014). Five normal stresses were used in the range 0-2 MPa and a total relative shear displacement of at least 5%. Special attention was paid to the detailed recording of the dilation of the specimen, which was used to separate the total shear strength into a frictional component (non-dilational) and a geometrical component (dilation). In addition, an independent part of the research was devoted to the determination of the Brinell penetration hardness (BHN), which is a fundamental property of friction (Bowden and Tabor, 1950). A standard spherical indenter with a 10 mm diameter, that is better suited for larger grain as well as for polymineralic rock materials, with a vertical indentation force of 500 kgf was used.

Results

(a) The values of the non-dilational friction angle resulting from the direct shear tests on joints were found to be practically equal to the values of the friction angle determined from the analysis of the stress state of the intact rock at the brittle-ductile transition.
(b) The critical ratio of the major principal stress (σ_{1T}) to the confining pressure (σ_{3T}) corresponding to the brittle-ductile transition depends on the mineralogy. The mean value found for the tested silicate rocks was 4.07 and for carbonate rocks 5.57. These values are in line with those found by Mogi (1966), i.e. 4.4 for silicates and higher for carbonates.
(c) The average ratio of the transition pressure (σ_{3T}) to the unconfined compressive strength (σ_{ci}) is highly dependent on the mineralogy, being more than three times higher for silicates (2.37) than for that of carbonates (0.73).
(d) The constant m_i of the Hoek and Brown criterion, the non-dilational friction angle of joints and the Brinell hardness number are interconnected with linear relationships shown in Figure 1, with their correlation coefficients. The constant m_i depends on the porosity, decreases linearly with the value of the non-dilational friction angle (Fig. 1a) and increases linearly with the value of the Brinell penetration hardness (Fig. 1b). In addition, the non-dilational friction angle decreases

linearly with the Brinell hardness number (Fig. 1c).

(e) A simple relationship of the form m_i σ_ci=kσ_3T among the constant mi, the unconfined compressive strength σci and the brittle-ductile transition pressure σ3T was fitted separately for the silicate and the carbonate rocks. The values of the constant k and the correlation coefficient (in parenthesis) were found to be 9.24 (0.96) and 19.58 (0.99) respectively.

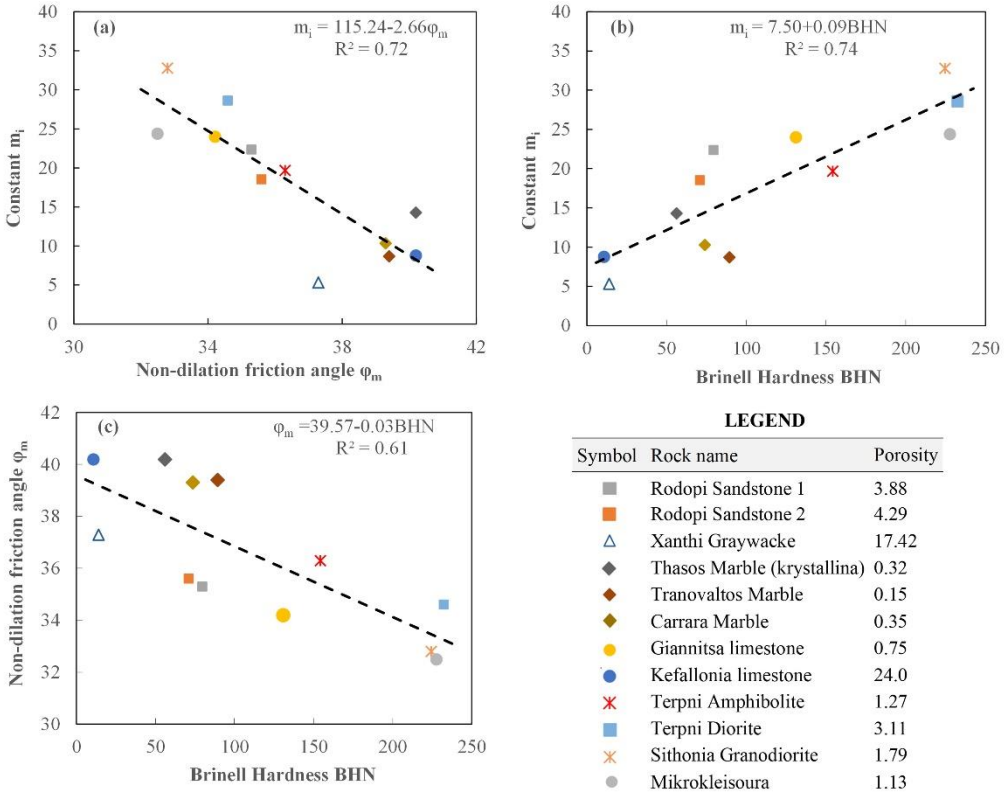

Figure 1. Graphical representation of the interrelations among non-dilational friction angle of joints φ_m, constant m_i of Hoek-Brown criterion and Brinell Hardness Number BHN. (a) constant m_i vs. non-dilational friction angle φ_m. (b) constant m_i vs. Brinell Hardness Number BHN. (c).Non-dilational friction angle φ_m vs. Brinell Hardness Number BHN.

Conclusions

A connection between the strength parameters of triaxial compression failure of intact rocks and the sliding friction of pre-existing rock surfaces is experimentally established. In addition, hardness is shown to have a considerable effect on the triaxial compression and the shear strength envelopes. Acceptable linear relationships among the non-dilational friction angle, the constant m_i of Hoek-Brown criterion and the Brinell hardness number are proposed. Therefore, independent experimental data from sliding friction tests may be used for the prediction of triaxial fracture envelope of an intact rock.

Acknowledgements

This research is co-financed by Greece and the European Union (European Social Fund- ESF) through the Operational Programme «Human Resources Development, Education and Lifelong Learning» in the context of the project "Strengthening Human Resources Research Potential via Doctorate Research" (MIS-5000432), implemented by the State Scholarships Foundation (IKY).

References

Bowden F. P., Tabor D., 1950. The Friction and Lubrication of Solids. Oxford Univ. Press.

Mogi K., 1966. Pressure Dependence of Rock Strength and Transition from brittle fracture to ductile flow. Bull. Earthquake Res Inst. Tokyo Univ., 44, 215-232.

Hencher, S., Richards, L., 2015. Assessing the Shear Strength of Rock Discontinuities at Laboratory and Field Scales. Rock Mechanics and Rock Engineering, 48(3), 883-905.

ISRM, 2014. ISRM Suggested Method for Laboratory Determination of the Shear Strength of Rock Joints: Revised Version Rock Mechanics and Rock Engineering 47, 291–302.

Papaliangas, T. T., Hencher, S.R., Lumsden, A.C., 1995. A comprehensive peak shear strength criterion for rock joints. 8th International Congress ISRM, Tokyo, Japan, Vol. 1, p. 359.

Papaliangas, T.T., Lumsden, A.C., Hencher, S.R., 1996. Prediction of in situ peak shear strength of rock joints. EUROCK' 96. Prediction and Performance in Rock Mechanics and Rock Engineering., Torino, Italy, p. 143.

Tsikrikis, A., 2021. Correlation between the shear strength parameters of discontinuities and intact rock. Ph.D. Thesis, School of Geology, Aristotle University of Thessaloniki, 616 p.

16th International Congress of the Geological Society of Greece

17-19 October, 2022 - Patras, Greece

Bulletin of the Geological Society of Greece, Sp. Publ. 10

Ext. Abs. GSG2022-121

Engineering Geological And Geotechnical Big Data Management For Planning And Protecting Smart Cities: The Pilot Case Of The City Of Thessaloniki.

A. Kokkala[1], V. Marinos[2]

(1) School of Geology, Faculty of Sciences, Aristotle University of Thessaloniki, Thessaloniki, Greece, Aliki_Kokkala_kokkalaa@geo.auth.gr (2) Geotechnical Department, School of Civil Engineering, Nation and Technical University of Athens, Athens, Greece.

The key aim of this paper is to highlight how geological, engineering geological and geotechnical knowledge can be managed in a well-organized database, which is able to develop various correlations and to present useful information for both the design and construction stages of important projects of civil protection, municipality and technical companies.

The present research demonstrates the implementation of such work in the city of Thessaloniki, northern Greece, where a large amount of geological and geotechnical data for more than 600 boreholes, mainly based on borehole geological information, laboratory testing, geotechnical characterization and in situ field tests collected from fill, Quaternary and Neogene deposits, is stored in a georeferenced database. The presented database, is targeted to the management and processing of geo-engineering datasets for various geotechnical projects but also for the protection against natural hazards.

The research emerged from the experience of Tunnel Information and Analysis System (TIAS), a geotechnical tunnel database developed for the design and construction of Egnatia highway in northern Greece (AGS, 1999; Marinos et al., 2013). The motivation for conducting this research was the absence of an engineering geological database presenting a vast amount of information regarding detailed geological and engineering geological data, discrete in depth and grouped properly, in the urban area of Thessaloniki. Thessaloniki, is located mainly on post-Alpine sediments and partly on bedrock which consists of a medium to coarse-grained green schist-gneiss complex. The basement complex is overlain by a Neogene sedimentary sequence. Sediments of Neogene age are divided into two units, the red clay series and sandstone-marl series. The formation that follows is sediments of Quaternary age which are present throughout the largest part of the city and encompass nearly the entire historical center. Both sediments of Neogene and Quaternary age are covered in places by fill material during different phases of the historical development of the city.

In the present work, big data from different sources are efficiently compiled, processed, and exploited in a large urban area to develop knowledge and enhance smart city geotechnical services. An extensive number of datasets from over 600 boreholes with geological information and mainly in situ and laboratory test data, such as the standard penetration test, unconfined compression strength, Atterberg limits, consistency index and natural moisture content, are stored in an engineering geological database. Datasets are analyzed and correlated to thoroughly determine the complex nature of the ground surface of Thessaloniki city, while at the same time, representative value ranges for geological and geotechnical parameters, as well as statistical distributions and classification charts with depth, can be assessed to estimate the geological conditions and geotechnical behavior of the examined geomaterials.

The purpose of this approach, besides integrating multisource datasets, is to provide a tool to effortlessly and directly analyze, correlate and display data on maps, tables and diagrams for stakeholders. For this analysis, the present study offers a geographic information system method, coupling the use of geostatistical techniques along with the cross validation. The final outcome is to establish geotechnical zonation maps in order to define units with specific geotechnical characteristics, highlight hazardous areas prone to liquefaction and settlement and to indicate an area's adaptability for different infrastructure projects, at surface or underground. In that context, the performance of three different interpolation techniques, is analyzed by applying different statistical methods, such as root mean square error (RMSE) and Pearson's correlation coefficient (r).

The existing engineering geological map of the Thessaloniki area has been revised with modifications in range values of properties and with transformations of formation boundaries. Thematic maps showing the distribution of several physical and mechanical parameters, accompanied by value ranges, were created for different depths. The construction and combination of these maps provide a superior understanding, in range and depth, of the geological formations examined and their geotechnical properties. Therefore, understanding construction conditions is further enhanced, providing a tool for safe urban planning and risk management.

Additionally, specific value ranges for several physical and mechanical properties are proposed from the assessment and correlation of the information originating from the database and spatial variability, providing geological and geotechnical knowledge in safe urban extensions suitable for construction in the research area environment. Furthermore, a set of reliable structural and high-precision informative engineering geological models to comprehensively understand the superficial and subsurface conditions of the research area was established. Several cross-sections, representing the stratigraphy of a selected section, were constructed and exported in a 3D environment by using the software Leapfrog

Works (Seequent Limited), as shown in Fig. 1. Such tools are capable of assisting in the design of an underground project, be it a road or a railway tunnel, or in the analysis of the liquefaction potential of a specific area.

Another major application of this database is to depict areas where deep foundations could be required for major structures. Fig. 2 illustrates two different zones of SPT values for the first 15 m of the examined formations. Areas of low SPT values (0–15) are demonstrated in the central coastal area, as well as in regions of eastern and western part of the basin. These values are observed within the first 7 to 12 m depth and indicate zones of poor geotechnical behavior with very low shear strength values. In such cases, the construction of high buildings and highway embankments are usually established deeper on pile foundations. As for the other investigated areas, where for the same depths SPT values are beyond 15, and higher strength properties are met, shallower foundations can be applicable (Kokkala, A., Marinos, V., 2022).

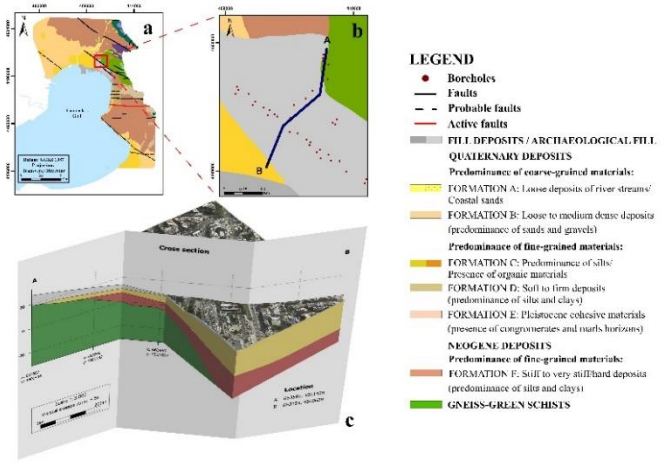

Figure 1. (a) Engineering geological map of the city of Thessaloniki, illustrating the spatial distribution of formations in the research area (modified by the authors from Rozos et al., 1998), (b) Generated cross-section for the central region and (c) 3-D model created by Leapfrog Works Software (Copyright © Seequent Limited).

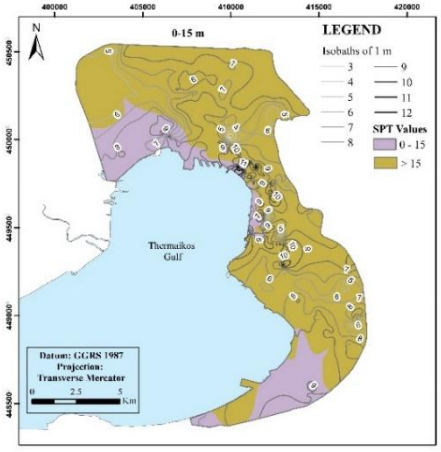

Figure 2. Thematic map of the city of Thessaloniki, showing the distribution of SPT values of fill deposits and of Quaternary and Neogene age sediments, up to a range of depth of 0–15 m.

Acknowledgements

The research work was supported by the Hellenic Foundation for Research and Innovation (HFRI) under the HFRI PhD Fellowship grant (Fellowship Number: 99319). The authors would like to thank the Central Laboratory of Public Works, Geognosi S.A., Attiko Metro S.A., Egnatia Odos S.A., National Cadastre and Mapping Agency S.A. and the Engineering Geologist Th. Stimaratzis for their kindness in encouraging and providing relevant data for carrying out our academic research activities. Finally, the authors would also like to recognize the support team of Seequent Leapfrog Works software for academic licensing.

References

Association of Geotechnical and Geoenvironmental Specialists (AGS), 1999. Electronic Transfer of Geotechnical and Geoenvironmental Data, 3rd ed.

Kokkala, A., Marinos, V., 2022. An engineering geological database for managing, planning and protecting intelligent cities: The case of Thessaloniki city in Northern Greece. Engineering Geology 301.

Marinos, V., Prountzopoulos, G., Fortsakis, P., Koumoutsakos, D., Korkaris, K., Papouli, D., 2013. Tunnel information and analysis system: a geotechnical database for tunnels. Geotechnical and Geological Engineering 31, 891–910.

Rozos, D., Apostolidis, E., Hadzinakos, I., 1998. Engineering-Geological Map of the Wider Thessaloniki Area, 1:25,000 Scale. I.G.M.E, Athens.

16th International Congress of the Geological Society of Greece
23-25 May, 2022 - Patras, Greece
Bulletin of the Geological Society of Greece, Sp. Publ. 10
Ext. Abs. GSG2022-124

Geotechnical properties of the geological formations in Southwestern Cyprus

P. Tzampoglou[1,2], D. Loukidis[2], A. Anastasiades[1]

(1) GeoImaging Ltd, 2021 Nicosia, Cyprus, ptzampoglou@geoimaging.com.cy (2) Department of Civil & Environmental Engineering, University of Cyprus, 1678 Nicosia, Cyprus

The activation as well as the consequences of natural geohazards, such as landslides, are difficult to predict, as they depend on factors characterized by large uncertainties, such as the geological and geotechnical conditions, and the influence of human activities. Due its particular geology and relatively high seismicity, the island of Cyprus has historically suffered from landslide phenomena. Numerous occurrences of new landslides and reactivation of old ones in the recent decades pose serious threat to the human infrastructure and the sustainable development of the build environment. The most affected regions of Cyprus are the Paphos District and the western part of Limassol District (Myronidis, 2016). According to the study of Hart and Hearn (2013), 1842 landslides of various types have been recorded in an area covering 40% (546km^2) of the Paphos District (3.4 landslides per km^2).

The present study constitutes the first stage of a research effort aiming at producing landslide susceptibility and hazard maps for the entire southwestern Cyprus using novel computational methodologies. In the context of this stage, maps and geotechnical data and reports from the Geological Survey Department of Cyprus (GSD) were evaluated. Over 700 geotechnical boreholes contained in the files of GSD were processed. The geological formation members with same lithological characteristics were merged into geotechnical units using geospatial functions within ArcGIS (Figure 1).

The geology of this region is characterized by extensive outcrops of fine grained clastic sedimentary rocks (e.g. shales, mudstones, marls) of low strength. The rock masses are often folded and sheared. This is particularly true for the rocks of the Mamonia Complex, which is a group of allochthonous Mesozoic geological formations that were thrusted on Cyprus and were originally part of the accretionary prism formed during the early stages of the subduction of the African tectonic plate under the Eurasian plate (Constantinou et al. 2002). Another particularity of the geology of the area is the existence of extensive outcrops of bentonitic clays and mélange (i.e. fragments of the Mamonia complex and igneous rocks inside a bentonitic matrix). A thorough experimental study of these geomaterials of Cyprus conducted in the '80s jointly by the British Geological Survey (BGS) and the Cyprus Geological Survey (CGS) revealed that their effective peak friction angle is often lower than 20^o, while the residual friction angle occasionally falls below 10^o.

Tables 1 to 3 presents a summary of the processed geotechnical data. It can be seen that bentonitic materials (Kannaviou formation and Mélange) exhibit low specific gravity and densities (Table 1). These values can be attributed to the high smectite content. Regarding the grain size distribution, it seems that all the formations which are located in the study area contain argillaceous materials that have relatively high percentage of clay, with average values in the 30%-45% range.

Table 1. Physical properties of the geological formations located at the study area.

	Dry unit weight (kN/m^3)				Bulk unit weight (kN/m^3)				Specific Gravity				Silt content (%)				Clay content (%)			
	Average	Min	Max	Count	Average	Min	Max	Count	Average	Min	Max	Count	Average	Min	Max	Count	Average	Min	Max	Count
Quaternary	16.06	11.99	20.08	20	20.38	16.78	24.76	18	2.52	2.21	2.67	29	45	11	73	20	29	2	61	23
Nicosia Fm.	15.19	11.54	22.23	87	19.47	14.48	27.12	96	2.58	2.38	2.76	38	53	20	93	115	36	2	71	124
Kalavasos Fm.	-	-	-	-	17.78	17.78	17.78	1	2.43	2.43	2.43	1	52	43	61	2	41	37	44	2
Pacnha Fm.	15.62	12.74	17.5	14	21.10	17.56	22.96	14	2.56	2.44	2.67	13	49	30	68	21	44	22	65	21
Lefkara Fm.	17.73	12.86	22.37	28	21.65	17.95	26.19	21	2.66	2.52	2.75	13	42	16	66	46	40	7	81	46
Kannaviou Fm.	13.81	11.38	19.25	10	18.45	15.51	23.98	18	2.37	2.17	2.64	20	46	10	96	230	43	1	90	235
Pera Pedi Fm.	-	-	-	-	-	-	-	-	-	-	-	-	55	34	74	10	34	19	49	10
Bentonitic Mélange	13.51	9.56	17.7	5	19.26	14.68	24.81	6	2.13	2.08	2.18	2	36	9	93	189	35	2	83	191

With respect to argillaceous materials (Table 2), the formations appear to have substantial values of montmorillonite content, with the Kannaviou formation having the highest values. It should be stressed that most of the montmorillonite content data originates from tests using the methylene blue method. The high values of PI and LL in Kannaviou formation and Mélange are due to the presence of bentonitic clays. In addition, the high values of the samples belonging to the Kalavasos formation (which, in general, is mostly gypsum) can be attributed to the fact that the samples were taken from the transition zone with the Nicosia formation, indicating that the first marl beds on top of the gypsum can be highly plastic. The marls of the highly calcareous Pachna and Lefkara formations have the largest undrained shear strength (obtained from UU triaxial tests), while bentonitic materials (Kannaviou clays and Mélange) the smallest. For the Nicosia formation, UU tests on samples with water content less than 30% were excluded in order to limit the effects of high matric suction due to desiccation. Table 3 shows data on unconfined compressive strength (UCS) of rocky materials. It can be seen that limestones (reef and recrystallized) are the strongest rocks. The chalks of the Lefkara and Pachna formations have substantial UCS due to the fact that they are silicified.

Table 2. Montmorillonite content, Atterberg limits and undrained strength of argillaceous materials.

Argillaceous material	Montmorillonite (%)				LL (%)				PI (%)				Undrained shear strength		
	Average	Min	Max	Count	Average	Min	Max	Count	Average	Min	Max	Count	$c_{u,aver}$ (kPa)	$\varphi_{u,aver}$ (^{o})	Count
Quaternary	15.9	3.1	39.0	16	60.2	34	99	17	31.2	12	60	17	87	20	11
Nicosia Fm. Marls	13.9	3.7	38.1	99	57.7	23	112	130	27.3	9	47	130	229	16	58
Kalavasos Fm. Marls	16.3	16.3	16.3	1	97.5	67	128	2	60.5	37	84	2	-	-	-
Pachna Fm. Marls	15.1	9.0	21.0	9	63.9	52	135	21	33.5	25	88	21	283	14	6
Lefkara Fm. Marls	15.3	8.8	48.0	28	61.2	38	199	41	35.0	17	167	41	322	18	3
Kannaviou Fm.	27.9	2.5	53.0	68	109.1	52	298	238	66.2	4	257	238	68	16	18
Pera Pedi Fm.	23.5	11.3	36.3	8	82.4	69	109	8	37.9	26	54	8	-	-	-
Bentonitic Mélange	16.1	5.0	38.8	68	62.8	32	200	206	40.2	10	156	203	48	21	3

Table 3. Unconfined compressive strength of rocky materials

Rocks	Uniaxial Compressive Strength (MPa)			
	Average	Min	Max	Count
Quaternary Sandstones-Calcarenites	16.0	4.8	39.5	6
Nicosia Fm. Sandstones	18.0	14.6	22.8	7
Kalavasos Fm. Gypsum	8.5	2.2	14.8	2
Pachna Fm. Chalks-Calcarenites	27.5	6.2	56.0	56
Lefkara Fm. Chalks	39.1	10.4	85.8	43
Kannaviou Fm. Sandstones	4.6	3.8	5.4	2
Limestones	51.4	33.1	75.6	4

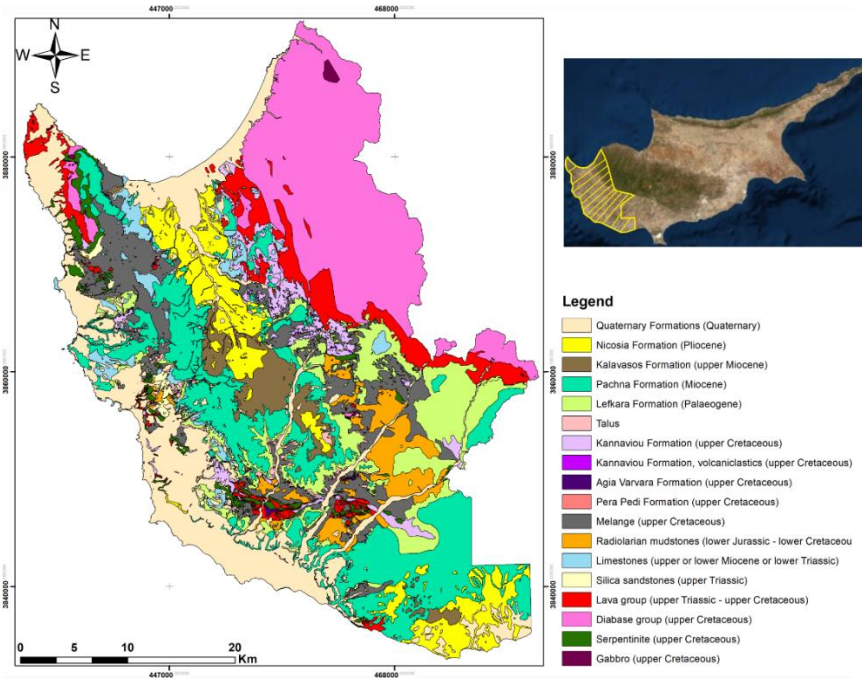

Figure 1. Map of geotechnical units of the study area.

Acknowledgements

The authors would like to express their gratitude to Dr Zomenia Zomeni and Ms Niki Koulermou of the Geological Survey Department for providing the data used in this research.

Funding

This research was funded by the European Commission (Marie Sklodowska-Curie Actions, Hybland-Society and Enterprise panel, Project No.: 101027880).

References

Constantinou, G., Panagides I., Xenophontos, K., Afrodisis, S., Michaelides, P. & Kramvis, S. (2002). The Geology of Cyprus, Bulletin No. 10, Cyprus Geological Survey, Nicosia, Cyprus.

Hart, A.B., Hearn, G.J., (2013). Landslide assessment for land use planning and infrastructure management in the Paphos District of Cyprus. Bull Eng Geol Environ, 72:173–188.

Myronidis D., Papageorgiou Ch., Theophanous S., (2016). Landslide susceptibility mapping based on landslide history and analytic hierarchy process (AHP). Nat Hazards, 81:245–263.

16th International Congress of the Geological Society of Greece

23-25 May, 2022 - Patras, Greece

Bulletin of the Geological Society of Greece, Sp. Publ. 10

Ext. Abs. GSG2022-132

Laboratory investigation of the swelling behavior of high plasticity Nicosia Marl

P. Tzampoglou[1], T. Stylianou[1], G. Lazarou[1], D. Loukidis[1]

(1) Department of Civil & Environmental Engineering, University of Cyprus, 1678 Nicosia, Cyprus, tzampoglou.ploutarchos@ucy.ac.cy

Extensive damages are observed worldwide in structures built over swelling clays formations. The mechanism of this phenomenon is complex and the factors that play an active role include the geotechnical, climate and weather conditions. The soil expansiveness can be expressed by the free swelling strain and the swelling pressure, which are functions of a number of variables such as the initial dry density and the initial degree of saturation. Soil expansiveness increases with initial dry density. On the other hand, the tendency for swelling decreases with increasing initial degree of saturation and vanishes completely in the case of the soil being fully saturated. Moreover, the swelling tendency is a decreasing function of the applied vertical stress and vanishes when the vertical stress is equal to the swelling pressure.

This study aims at investigating the swelling response of the clayey soil called Nicosia marl. This formation mainly consists of silty clay with some sandier intercalations. It can be divided into two distinct horizons, the upper light brown (khaki) marl and the lower grey marl (Constantinou et al. 2002), and its total thickness in the region of the city of Nicosia exceeds one hundred meters. In the context of this research, a comprehensive experimental program for the determination of the physical and mechanical properties of the expansive Nicosia marl was conducted. The samples were collected using U100 samplers from five locations in order to reflect the natural heterogeneity of this geomaterial.

The soil expansiveness was investigated by a series of swelling/collapse tests in the oedometer. At the beginning of this procedure, samples were trimmed and placed in controlled humidity chambers (glass desiccators) for at least 30 days aiming to achieve the equilibrium of the moisture conditions at three different levels of water content and, consequently, levels of suction. More specifically, the first batch of samples was tested at their natural moisture content, the second one was dried by placing the samples in a desiccator filled with saturated NaCl solution, and the third one was wetted and placed in a desiccator filled with distilled water. After that, each batch of samples was formed into oedometer specimens (5 cm in diameter and 2 cm thick) inside steel rings to perform series of swelling/collapse tests at various values of constant vertical stress. The oedometer cells were sealed carefully using cling film to prevent moisture loss and the samples were allowed to settle under a target vertical pressure at partial saturation conditions for two days. Then, the samples were inundated with distilled water, keeping the vertical stress constant and recording the development of vertical (swelling or collapse) deformation (Bardanis & Grifiza 2016).

Grain size distribution and Atterberg limits were determined for all samples. The clay content (<2μm) ranges from 30% to 49% and the plasticity index is in the 37-50 range, with the exception of one low plasticity sample. Furthermore, consolidation tests were conducted by adding extra loads on a limited number of specimens after the completion of a "free" swelling stage in order to determine the compression and swelling indexes. The load was doubled every 24 hours until the vertical pressure of 3200 kPa was reached. The specimens were unloaded at similar stages.

Figures 1 shows the swelling/collapse test results (which are grouped in ranges of initial degree of saturation S_r and initial dry density ρ_d) in terms of vertical (swelling or collapse) strain (%) versus applied vertical stress (kPa). The strains at vertical stress of 4 kPa (considered as the free swelling strain) for the various batches of initial S_r are shown (averaged) in Table 1 along with the physical characteristics of the samples. It can be observed that the free swelling strain decreases intensely with increasing initial degree of saturation and decreasing initial dry density. The maximum strain value was recorded for marl from borehole BH3 (17%) on a specimen that was left to lose moisture in a desiccator filled with NaCl, reducing the S_r below 50%. Yet, the marl of BH3 remains highly expansive even for S_r as high as 80%-85%, with the free swelling strain being close to 10%. Even more interesting is the fact that the decreased initial degree of saturation does not enhance only the potential for swelling at low vertical stresses, but also the potential for collapse at stresses larger than the swelling pressure. Collapse strains of the order of 8%-10% can be seen in Figure 1 at vertical stress 6400kPa for the initially desiccated specimens. This can be explained by the fact that, unlike the wet specimens, the vertical strain that develops in the desiccated specimens during the application of the vertical load before the inundation phase is very small due to the high suction (which increases the soil strength and stiffness), in conjunction with the fact that the marl has inherent calcite cementation. With inundation, the suction vanishes and the cemented matrix of the marl cannot withstand the high vertical stress, leading to the abrupt collapse of the matrix.

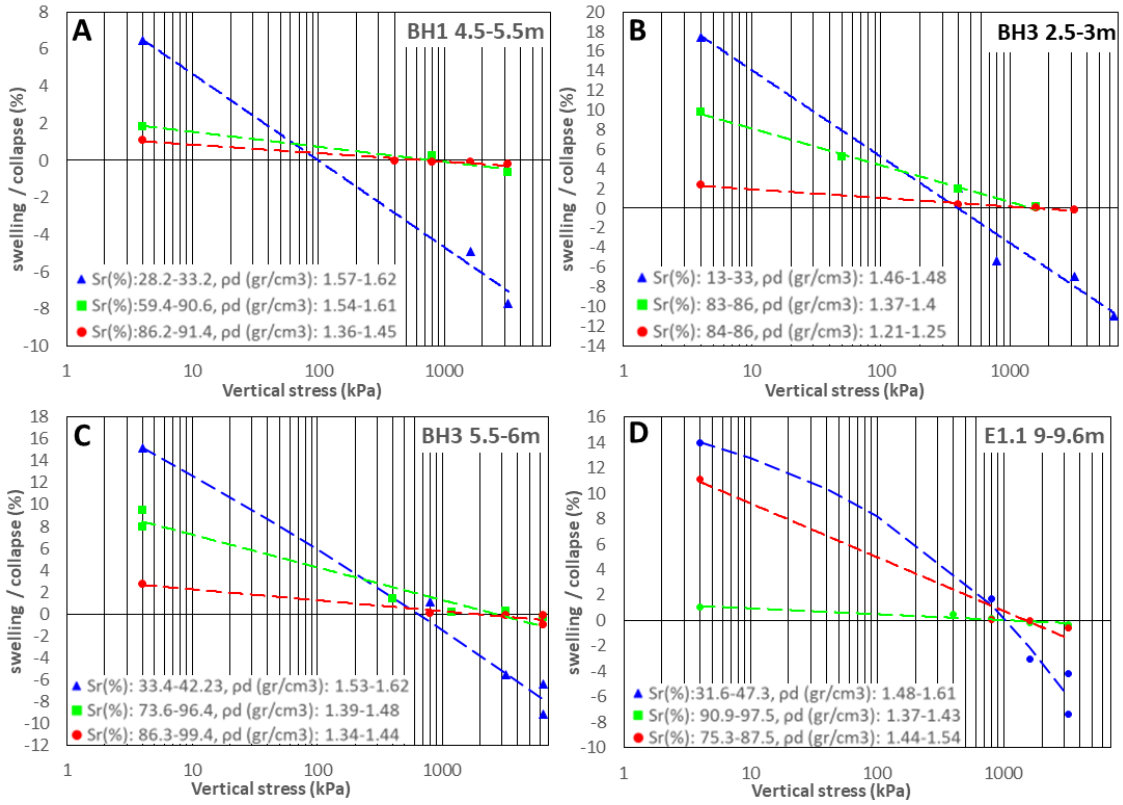

Figure 1. Volumetric strain due to inundation versus applied vertical stress at three different levels of initial S_r.

Table 1. Free swelling strain in relation to classification test data.

Borehole	Depth (m)	PI (%)	LL (%)	Clay content (%)	$CaCO_3$	Compression Index (C_c)	Swelling Index (C_s)	Degree of Saturation S_r (%)	ρ_d (gr/cm^3)	Free swelling (%)
BH1	4.5-5.5	37-48	67-78	34-40	37.1-40.0	0.187	0.048	30.3	1.605	6.4
								89.3	1.584	1.8
								90.5	1.414	1.1
BH2	4.5-5.5	44.6	74.0	30.3	43.0-46.6	0.443	0.058	29.7	1.458	3.8
								75.3	1.364	0.9
								70.3	1.283	0.9
BH3	2.5-3	40.3	90.6	49.0	29.8	-	-	86.3	1.402	9.8
								33.6	1.469	17.4
								84.4	1.257	2.3
BH3	5.5-6	44.0	83.4	43.0	28.9	0.281	0.023	33.7	1.563	15.2
								87.9	1.479	9.4
								93.4	1.355	2.7
E1.1	9-9.6	50.1	77.9	45.2	24.2	0.267	0.078	47.3	1.607	14.0
								87.5	1.542	11.1
								93.1	1.396	1.0
A2 (GREY)	12-12.6							20.9	1.568	4.9
								32.6	1.487	3.8

Funding

This research was funded by the Research and Innovation Foundation of Cyprus (Project INTEGRATED/0916/0049).

References

Constantinou, G., Petrides, G., Kyrou, K., Chrysostomou, C. 2002. Swelling Clays: A Continuous Threat to the Built Environment of Cyprus. UNOPS Project Final Report, Technical Chamber of Cyprus, Nicosia, Cyprus.

Bardanis, M. and Grifiza, S., 2016. Swelling and collapse of compacted soils to be used as earth dam cores. In 3rd European Conference on Unsaturated Soils – E-UNSAT 2016, Volume 9, E3S Web of Conferences.

16th International Congress of the Geological Society of Greece
23-25 May, 2022 - Patras, Greece
Bulletin of the Geological Society of Greece, Sp. Publ. 10
Ext. Abs. GSG2022-133

Measurements of seasonal vertical ground movement in high plasticity Nicosia marl

P. Tzampoglou[1], T. Stylianou[1], G. Lazarou[1], D. Loukidis[1]

(1) Department of Civil & Environmental Engineering, University of Cyprus, 1678 Nicosia, Cyprus, tzampoglou.ploutarchos@ucy.ac.cy

Expansive soils are the geomaterials that exhibit significant tendency for volume change due to variation of their degree of saturation. Such tendencies for volume change cause significant damages to civil engineering structures (Jahangir et al. 2012), especially in regions with arid climate. In fact, the annual cost of damages due to expansive soils surpasses that of other natural hazards, namely landslides and earthquakes (Chen 2012). To improve our understanding of this complex phenomenon, this research aims to investigate the amplitude of seasonal vertical ground movement via field topographic measurements.

The study area is in the city of Nicosia, the capital of the Republic of Cyprus, which is largely outcropped by the Nicosia geological formation that contains a swelling clayey geomaterial called Nicosia marl. Nicosia marl contains substantial amounts of the clay mineral montmorillonite (Hobbs et al. 1986). The soil stratigraphy down to a depth of 15m (which encompasses the active zone) was established via a borehole that was drilled using auger. Four undisturbed U100 samples were collected at depths 1.0m, 2.5m, 4.0m, 5.5m. A series of classification tests were conducted at the Geomechanics Laboratory of UCY. Figure 1 presents the stratigraphic column in combination with the variation of the marl's geotechnical parameters. The first 0.5m consists of brownish silty-clay marl which overlies the brownish silty clay marl of high plasticity (at a depth of 0.5 to 6m). Underneath this layer, the clay content and Plasticity Index (PI) increase significantly. The grey marl, which exhibits similar physical parameters with the brown Nicosia Marl, was found below 13.6m. Generally, in the study area the Nicosia marl has substantially higher clay content than in other parts of Nicosia, ranging from 43% to 63% and increasing with depth, while the amount of sand never exceeds 3%.

Two bored piles 15m deep and with 0.8m diameter were constructed in the study area during the period 9-11 December 2019. The pile drilling and construction was undertaken by Themeliotechniki Ltd. In order to monitor the heave and settlement of the ground at depth in the free field, two vertical rod extensometers (ExtFF1 and ExtFF2), with depth 2.50m and 1.20m, respectively, were constructed in 21-24 May 2020. The diameter of each extensometer borehole was 10cm and the distance (center-to-center) between them is 1.50m. After the drilling, a steel rod was inserted in each hole and fixed at the bottom by a 30cm plug of cement grout. The cement left for about an hour to harden and subsequently a short plastic casing was inserted near the surface in order to fill the borehole with uniform sand. Each extensometer was capped by a plastic box grouted to the ground surface to protect the extensometer from direct rainwater percolation through the sand.

In order to monitor the motion of the ground surface, eight monitoring points, consisting of 8cm long wood screws surrounded by a cement apron on the upper part, were installed in a scattered pattern across the study area. The two bored piles were used as fixed reference points given that their length exceeds by far the active zone and that they were installed during the winter, and thus any negative friction during wet periods will result in negligible pile movement. Measurements of the elevations of monitoring points, rod extensometers and reference points were done using a Leica laser level.

Figure 2 shows the evolution of the vertical surface movement over time. As it can be observed, all the ground surface points (1 to 8) settle about 1.5cm to 2.5cm during the period 15th June 2020 - 30th September 2020 (end of hydrological year) due to ground drying and the complete absence of rainfall. After this period, it can be seen that the ground continued to shrink until mid-November 2020 despite the rain that fell during early November. Subsequently, the ground surface monitoring points start to heave and reach their peak values at the end of January to mid-February 2021. In the period that follows until September 2021, the ground shrinks and the vertical deformations follow the trends of the previous year. It is interesting to note that the ground surface settles during the period February to April despite that it is still in the rainy season. This indicates that apart from the rainfall there are other climatic factors, such as temperature and total hours of sunshine, that play a role in the amount of water that enters the ground to increase its moisture. Based on the measurements made during the period 6/2020-9/2021, the amplitude of seasonal vertical motion of the ground surface is of the order of 2.5cm-3cm.

Finally, the amplitude of vertical displacement at the ground surface is much higher than that at a depth of 2.5m, since the motion of the extensometer (ExtFF1) is one order of magnitude smaller (0.1cm to 0.3cm). It must be pointed out that extensometer ExtFF2 (1.5m deep) exhibits a progressive monotonic heave since June 2020. This is because of the execution of two ground wetting experiments (performed in the summers of 2020 and 2021 and achieving full saturation of the ground down to a depth of at least 1.5m) that were done in close proximity to ExtFF2 (roughly 2m away) and inducing significant ground heave even at a depth of 1.5m.

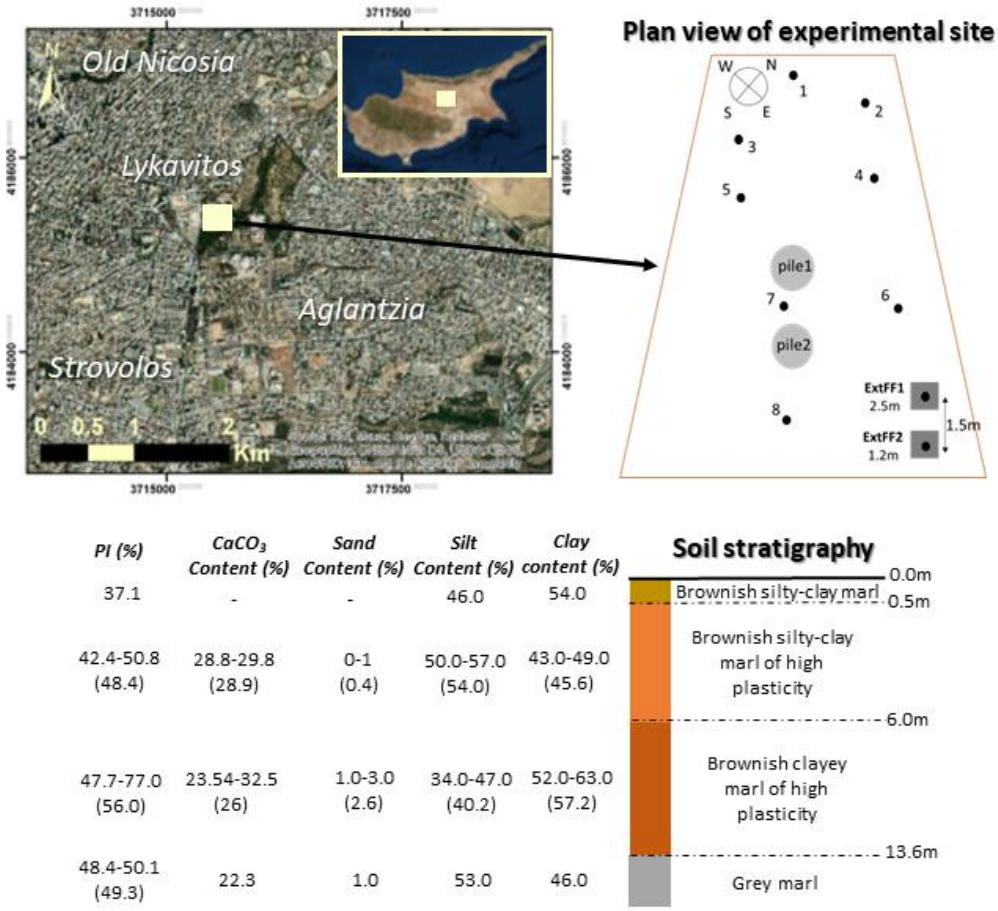

Figure 1. Plan view of the field works carried out in the study area along with thestratigraphic column (values in parenthesis pertain to average properties).

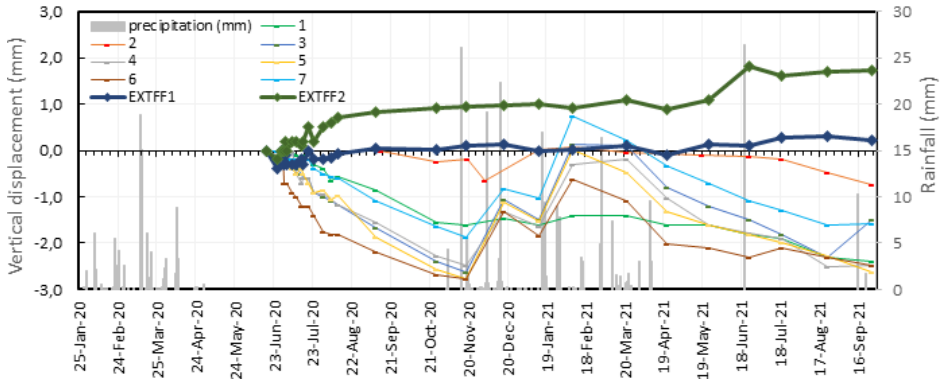

Figure 2. Variation of the vertical displacement with time in correlation with the rainfall data.

Funding

This research was funded by the Research and Innovation Foundation of Cyprus (Project INTEGRATED/0916/0049).

References

Chen, F. H., 2012. Foundations on expansive soils, Elsevier.

Hobbs, P.R.N., Loucaides, G. and Petrides, G., 1986. Geotechnical properties and behaviour of Pliocene marl in Nicosia, Cyprus. British Geological Survey / Cyprus Geological Survey Department, Nicosia, Cyprus.

Jahangir, E., Deck, O., Masrouri, F., 2012. Estimation of ground settlement beneath foundations due to shrinkage of clayey soils. Canadian Geotechnical Journal 49(7), 835-852.

16th International Congress of the Geological Society of Greece
17-19 October, 2022 - Patras, Greece
Bulletin of the Geological Society of Greece, Sp. Publ. 10
Ext. Abs. GSG2022-137

Groundwater flow simulation in the Tymbaki aquifer by using different subsurface geological models

P. Diakoparaskevas[1], E.A. Varouchakis[2], G. Panagopoulos[2], P. Soupios[3], A. Vafidis[2], G.P Karatzas[1], E. Manoutsoglou[2]

(1) School of Environmental and Chemical Engineering, Technical University of Crete, University campus, 73100 Chania, Greece, diako_par@hotmail.com , (2) School of Mineral Resources Engineering, Technical University of Crete, University campus, 73100 Chania, Greece, (3) Department of Geosciences, College of Petroleum Engineering & Geosciences, King Fahd University of Petroleum and Minerals – KFUPM, PO Box 5070, Dhahran 31261, Kingdom of Saudi Arabia.

Groundwater resources in Mediterranean coastal aquifers are under threat due to overexploitation of the water resources. Efficient management and monitoring of groundwater systems require interpreting all available data sources. Geostatistics and geophysics can be successfully combined to interpretating the hydrogeological characteristics of an aquifer system. This work is based on geological and geophysical surveys held in the coastal alluvial aquifer of the Tympaki basin in the south and central part of the island of Crete, Greece. This research work aims to develop a set of plausible 3D geological models combining data of geological maps and mapping, 1D and 2D geophysical profiles, spatial well data analytics, and geostatistical simulation techniques. The resulting set of models represents possible scenarios of the structure of the coastal aquifer system under investigation and identify regions associated with higher uncertainty.

Management and monitoring of groundwater systems require a sufficient understanding of hydrogeology and the subsurface configuration. This work employs the development of a 3D geological model by using two different approaches to assess the impact that each one has on the groundwater flow simulation. The first approach is based on geophysical data using geostatistical and simulation techniques such as 3D Kriging and Sequential Gaussian Simulation (SGS) to provide the structure of the coastal aquifer system. A geophysical survey (Pipatpan and Blindow 2005) provided data in the study area that were inverted to hydraulic conductivity. Therefore, the inverted geophysical data were used to estimate the spatial distribution of the hydraulic conductivity in the study area.

The modified Box–Cox technique was applied to transform the data close to normal distribution to allow the application of the SGS method. SGS is a stochastic approach for producing equiprobable realizations (maps) of spatial distribution of a variable on a grid by means of kriging methodology. Variogram analysis was employed to investigate the spatial dependence of the monitoring data, while the simulation analysis provided the spatial distribution of hydraulic conductivity considering the bounds of estimations uncertainty.

The second approach uses the lithostratigraphic interpretation of the available geophysical and water-well data to define the subsurface structure of the alluvial aquifer and the associated fault patterns (Panagopoulos et al., 2021). Then, the geological model is further populated with resistivity and lithological values by applying stochastic algorithms of gaussian random function simulation and the sequential indicator simulation, respectively (Schlumberger, 2016). Finally, the two approaches were combined to run a new groundwater flow simulation and assess the benefits of using a more detailed subsurface geological model as the basis for the simulation.

The proposed methodologies exploit the spatial information from geophysical surveys to provide the spatial distribution of the hydrogeological structure of the coastal aquifer system in three dimensions inside the convex hull of the measurements. The resulting models will be imported under the same parameterization (e.g., boundary conditions) to a numerical groundwater flow model (Feflow), considering time series of groundwater level in 20 monitoring wells and 6 observation wells for validation, to determine the groundwater level field in the study area.

The 3D property distribution of hydraulic conductivity, resistivity and lithologies have been constructed to understand the aquifer's behavior better. The property model helps to identify the areas where the coarser material is expected as well as areas of low resistivity that could be related to seawater intrusion.

Comparing the two approaches will help identify similarities and differences in groundwater flow modeling using different data interpretation tools. In addition, it will provide valuable information on the hydrogeological structure detail which is required to acquire optimal groundwater flow modelling results. Such approaches can help develop typical hydrogeological models, which will aid the management and monitoring of the area's groundwater resources. This work will support the development of a reliable groundwater flow model to investigate future groundwater level fluctuations in the study area under climate change scenarios.

References

Panagopoulos, G.; Soupios, P.; Vafidis, A.; Manoutsoglou, E.: Integrated use of well and geophysical data for constructing 3D geological models in shallow aquifers: a case study at the Tymbakion basin, Crete. Greece. Environm. Earth Sci. 80, 142 (2021).

https://doi.org/10.1007/s12665-021-09461-5
Pipatpan, S., Blindow, N., 2005. Geophysical Saltwater-Intrusion Mapping in Timbaki / Crete (Report within MEDIS (EVK1-CT-2001-00092): Towards sustainable water use on Mediterranean islands: addressing conflicting demands and varying hydrological, social and economical conditions). Institute for Geophysics, Westfälische Wilhelms-Universität, Münster.
Schlumberger (2016) Accessed August 2020, <https ://www.software.slb.com/software-news/support-news/petrel/petrel-2014-8>

16th International Congress of the Geological Society of Greece
17-19 October, 2022 - Patras, Greece
Bulletin of the Geological Society of Greece, Sp. Publ. 10
Ext. Abs. GSG2022-143

Correlation of mineralogical/petrographic characteristics and physical and mechanical properties of carbonate rocks from the Ionian unit of Lefkada Island, western Greece

V. Kallimogianis[1], M. Kati[2], Ch. Saroglou[1]

(1) National Technical University of Athens, Greece, vkallim@hotmail.com (2) National and Kapodistrian University of Athens, Greece.

The mechanical properties of carbonate rocks (limestones and dolomites) present a wide range of values and are related to their lithology, depositional features, and diagenetic processes. Besides the sedimentary characteristics, the dominant tectonic regime throughout their evolution further influences their physical and mechanical properties. The studied carbonate rocks belong to the Ionian tectonic unit that outcrops on the island of Lefkada in western Greece. The unit consists of Triassic evaporates, Late Triassic to Late Eocene carbonate rocks interbedded with minor cherts and shales, and flysch sediments of the Late Eocene-Oligocene age (Bornovas, 1964). Paleogeographically, it constitutes part of the External Hellenides Carbonate Platform (Papanikolaou, 1997) which, after the Early-Middle Jurassic rifting phase, functioned as a deep intraplatform basin, as opposed to the shallow-water carbonate platforms that continued to operate in the east and west (the Gavrovo and Paxos or Pre-Apulian units, respectively). The latter is also present in the southwestern part of the island, bounded by the Ionian thrust. The geodynamic evolution of the island is largely associated with the dominant post-Eocene compressive stresses expressed in the formation of numerous folds and thrusts (Rondoyanni et al., 2012) and NE-SW to NNE-SSW trending neotectonic faults (Papathanassiou et al., 2013). The intense tectonic activity has resulted in the formation of various carbonate fault rocks with poor mechanical properties. Quantifying their strength and deformability is of great importance to protect the local infrastructure and prevent the loss of human life. In 2015, nearly 700 co-seismic landslides occurred along the western coastline of the island during the M_w 6.5 earthquake (2015).

The study was performed on several samples of different carbonate formations of the Ionian unit, taken from three quarry areas located in the central-northern part of the island (i.e., Chortata, Pefkoulia, and Apolpaina - Figure 1a). Polished slabs and thin sections were prepared from all the samples, which were also stained with alizarin red S and potassium ferricyanide. Petrographic analysis was performed by using transmitted light microscopy, while the mineralogical composition was determined by X-ray diffraction (XRD) analysis. In addition, the same samples were prepared to derive their physical and mechanical properties, which were then correlated with their sedimentary features.

Based on the mineralogical and petrographic analyses, three main rock types were identified that are characterized as follows:

Chortata (Type X): White, massive allochemical limestone with abundant peloids and intraclasts but also a few scattered bioclasts in a packstone-grainstone fabric. Primary cavities are mainly occluded by early marine fibrous cement locally forming multiphase crusts of finely crystalline calcite (Figure 1b). Major cracks are not observed. Mineralogical analysis showed only non-ferroan low-magnesian calcite. This rock type comprises typical shallow-water marine limestone formed in a broad carbonate subtidal depositional setting.

Pefkoulia (Type P): Monomictic carbonate breccia consisting entirely of dolomitic fragments of dark brownish-grey coloured, mostly angular and elongated, platy or even isometric shapes. Their size varies from very coarse pebble to granule (2-30mm). Mineralogical analysis showed pure dolomite, but some low magnesium calcite (probably dedolomite) was revealed through staining of the samples. Dolomite fragments are characterized by two main mosaic textures, a coarsely (>0.25mm) crystalline subhedral/planar-s to unhedral/nonplanar dolomite and, to a lesser extent, a medium (up to 0.2mm) crystalline euhedral/planar-e dolomite, often exhibiting cloudy cores and light-coloured rims. The minor matrix is also a finely to medium-crystalline (0.1-0.25mm) subhedral dolomite. Major characteristics of the rock are also the numerous dissolution seams (due to chemical compaction), which often surround the larger dolomite fragments (Figure 1b), as well as the presence of several microfractures that crosscut or dislocate the above seams. Overall, the multistage dolomitization along with the several brecciation events (pre- and post-compaction) that affected the studied dolomite rocks show their complex tectono-diagenetic origin.

Apolpaina (Type A): Soft, whitish to light yellow-coloured micritic limestone. Mineralogical study revealed dominant low magnesium calcite with minor amounts of smectite (montmorillonite) and muscovite. Although macroscopically it appears as a homogeneous and massive lime mudstone, microscopically, however, some scattered non-identified bioclasts and areas with burrows were observed. Additionally, abundant, multi-generation microcracks are usually filled with microcrystalline calcite (Figure 1b). This rock type represents a pelagic limestone with some transported skeletal fragments and minor clay minerals of detrital origin.

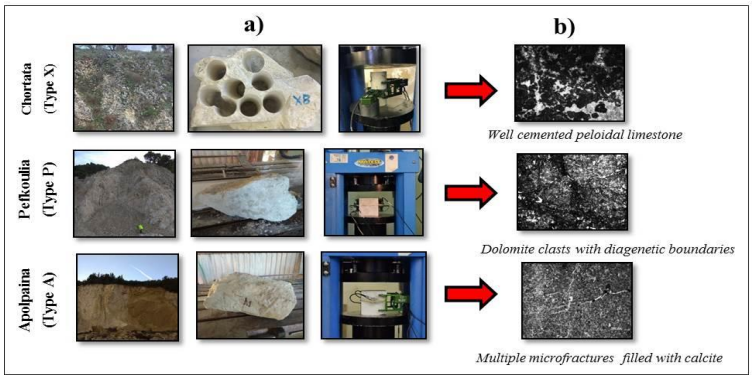

Figure 1. a) Photographs from the locations of block sampling, typical blocks from each rock type and specimens tested in uniaxial compression; b) Thin sections photomicrographs (PPL) from the three rock types.

The physical and mechanical properties of the studied rocks were derived in accordance with ISRM standards (ISRM, 1979). In particular, the uniaxial compressive strength (UCS), the modulus of elasticity (E), and the porosity (n) were measured. Figure 2 presents the results from these properties per rock type, including the individual values from each test and the average values. The UCS and E of the intact limestone specimens (Type X) are significantly higher compared to Types P and A (more than 2.5 times, on average). On the other hand, the higher porosity values were measured for Type A followed by Type P. UCS and E tends to present a positive correlation, whilst UCS and porosity a negative correlation, therefore, the findings are reasonable.

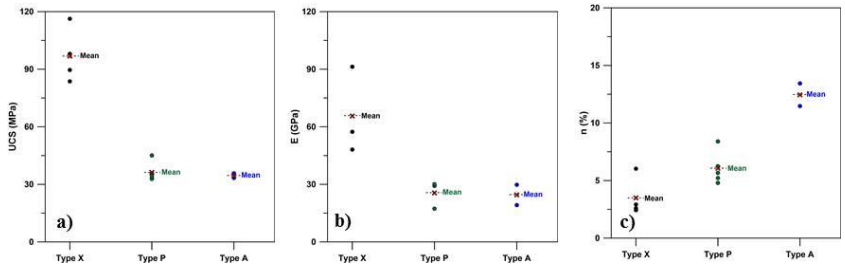

Figure 2. Physical & mechanical properties measured for the three (3) rock types (X, P, A): a) Uniaxial Compressive Strength (UCS); b) Modulus of elasticity (E); c) Porosity (n).

Type X is characterized as a strong rock (UCS~50-100MPa), while Types P and A are characterized as medium-strong rocks (UCS~25-50MPa), as per ISRM (1981). Type X is homogenous (in terms of mineralogy), massive, and well-lithified; therefore, the high mechanical properties measured are justified. However, the presence of cement (crystalline calcite) may create zones of reduced tensile/shear strength affecting the overall behavior of the material. These explain the observed variability in the measured UCS (Figure 2a). The lower mechanical properties of Type P specimens (compared to Type X) can be attributed to their tectono-diagenetic origin. Apart from the different mineralogy (almost pure dolomite) and the variety of mosaic textures, the presence of abundant dissolution seams (that act as shear zones) and the intense brecciation processes are the main factors that control their mechanical properties. The mechanical response of Type A samples is mostly determined by the mineralogy (slightly marly limestone) and the kinds of components. Despite the prevalence of micrite (microcrystalline calcite), the presence of coarser crystalline calcite (as fracture-filling material) and bioclasts causes a certain degree of heterogeneity and reduces the mechanical rock properties. Furthermore, several microcracks (of tectonic origin) mainly control the strength and deformability of the Type A samples. In the uniaxial compression test, the latter act as tensile stress concentrators from which new microcracks initiate and propagate towards failure. The assessment of the mineralogical composition and the depositional and diagenetic characteristics of the studied rocks enable interpretation of their properties.

References

Bornovas, I., 1964. Geology of Lefkada Island. Ph.D. Thesis.

ISRM, 1979. Suggested Methods for Determining the Uniaxial Compressive Strength and Deformability of Rock Materials. International Journal of Rock Mechanics and Mining Sciences & Geomechanics Abstracts. 16, 2.

ISRM, 1981. Rock Characterization Testing and Monitoring. ISRM Suggested Methods. *International Society for Rock Mechanics*. Pergamon Press, Oxford, pp: 32.

Papanikolaou, D., 1997. The tectonostratigraphic terranes of the Hellenides.. Ann. Géol. des Pays Helléniques, 37: 495–514.

Papathanassiou, G., Valkaniotis, S., Pavlides, S., 2013. Evaluation of the Temporal Probability of Earthquake-Induced Landslides in the Island of Lefkada, Greece. In: Margottini C., Canuti P., Sassa K. (eds) Landslide Science and Practice. Springer, Berlin, Heidelberg. https://doi.org/10.1007/978-3-642-31427-8_27

Rondoyanni, Th., Sakellariou, M., Baskoutas, J., Christodoulou, N., 2012. Evaluation of active faulting and earthquake secondary effects in Lefkas Island, Ionian Sea, Greece: an overview. Nat Hazards 61:843–860. https://doi.org/10.1007/s11069-011-0080-6.

16th International Congress of the Geological Society of Greece
17-19 October, 2022 - Patras, Greece
Bulletin of the Geological Society of Greece, Sp. Publ. 10
Ext. Abs. GSG2022-152

Hydrochemical regime of the fractured rock aquifer of Simonos Petra Monastery, Holy Mountain

N. Kazakis[1], M.M. Ntona[1,2], I. Krajcar Bronić[3], J. Barešić[3], J. Parlov[4], Z. Kovač[4], D. Lampropoulou[1], V. Koulos[5], P. Neofotistos[1], A. Plougarlis[1], K. Voudouris[1]

(1) Aristotle University of Thessaloniki, Thessaloniki, Greece, kazakis@geo.auth.gr (2) Università degli Studi della Campania "Luigi Vanvitelli", Caserta, Italy (3) Ruđer Bošković Institute, Zagreb, Croatia (4) University of Zagreb, Zagreb, Croatia (5) Koulos: BD Inventions.

Research highlights

- The fractured rock aquifer of Simonos Petra Monastery in Holy Mountain discharges from a fracture zone artesian spring.
- The spring water is characterized by low electrical conductivity (127 μS/cm), and the absence of anthropogenic pollution such as nitrogen species and potentially toxic elements.

The Athos peninsula is located in Northern Greece and constitute one of the last unexplored areas of Greece regarding hydrogeological conditions (Figure 1). This study is focused on the Hydrosystem of the Holy Monastery of Simonos Petra with the aim of determining the hydrochemical regime of the fracture zone aquifer. The Territory of the Holy Monastery of Simonos Petra covers an area of 13 km^2, has a coastline of 5.9 km, the mean elevation is 473 m, and the maximum is 892 m in Tsamantara peak. The study area is located at the boundary of the Hellenic Hinterland and the Internal Hellenides and consists of granitoid rocks, of the Eocene age (Christofides *et al.*, 1990). It constitutes facies of extensive magmatism, which geotectonically belongs to the late-Alpine stage of the Hellenic Hinterland and the Innermost Hellenides deformation and is characterized by such granitic bodies. The Gregoriou type granite is, according to Kockel *et al.*, (1977), a mainly biotitic granite, rich in quartz, perthitic orthoclase, microcline, plagioclase with a 30% anorthite, biotite, and hornblende. Frequently enough veins of leucocratic aplitic muscovite granite occur rich in quartz, perthite and orthoclase, microcline, and plagioclase with a 15-20% anorthite, muscovite and secondary minerals. The main aquifer of the Simonos Petra spring stretches in an area of 0.87 km^2 and is developed within the fractured formation of the Granodiorite, Gabbro, and Diorite (Figure 1). The aquifer discharge from a fracture zone artesian spring (Busico *et al.*, 2022). The gush points of the spring are more than 15, however**,** five gushes are the main discharge points that we focused this hydrochemical research. The water demands of the study area are exclusively covered by the spring water.

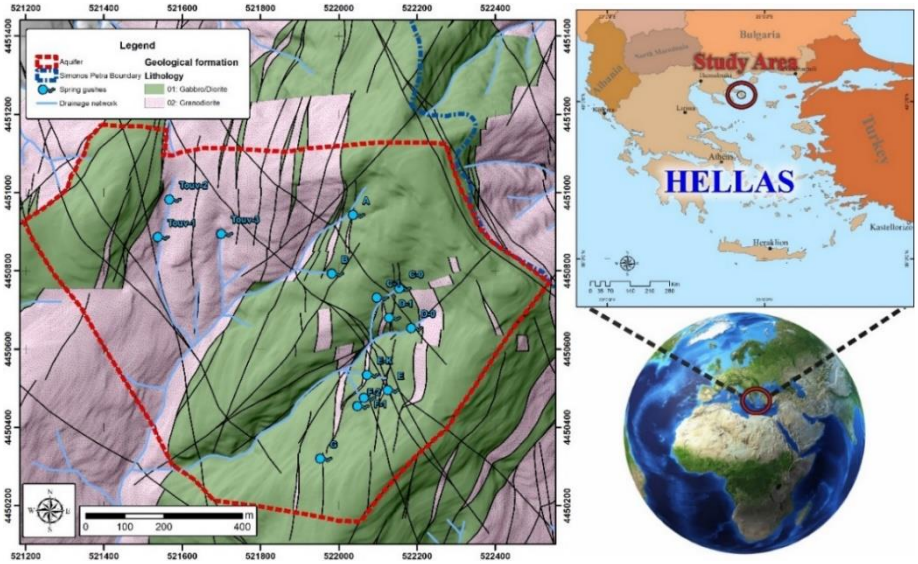

Figure 1. Geological map of the study area.

Water samples were collected from 5 gushes from the Simonos Petra aquifer in November 2020 for hydrochemical, isotope and tritium analysis. The physicochemical parameters of temperature (T), pH, and electrical conductivity (EC) were measured in situ using a multi-parametric probe, HANNA (HI98194). All water samples were filtered using a 0.45

μm millipore filter and stored in two 50 mL PE bottles (one acidified with ultrapure HNO_3) for laboratory analysis (ICP-MS) according to standard methods (Lenore *et al.* 1998). According to the hydrochemical data all gushes have similar water quality verifying the spring mechanism. The spring pH is 7.1, the electrical conductivity 126.8 μS/cm and the temperature 9.6 ºC, with the absence of potentially toxic elements, nitrate, nitrite, and ammonium ions (Table 1). Based on the sample classification in the Piper (Piper, 1944) and Durov (Durov, 1948) diagrams in Figure 2, the water type of the spring is Mg-HCO_3.

Table 1. Results from the underground water isotope analyses from the spring systems of Mount Athos Simonopetra spring for the sampling period of November 2020.

Spring gushes	δ18O	δ2H	A(3H)	Mg^{2+}	Ca^{2+}	NO_3^-	NO_2^-	NH_4^+	Cr	As	U
	‰ VSMOW	‰ VSMOW	TU	mg/L	mg/L	mg/L	mg/L	mg/L	μg/L	μg/L	μg/L
E	-8.76	-50.53	3.1	3.2	5.3	ND	ND	ND	ND	ND	ND
C0	-8.55	-49.75	3.2	3.3	5.7	ND	ND	ND	ND	ND	ND
C1	-8.78	-50.34	3.6	3.3	6.5	ND	ND	ND	ND	ND	ND
D0	-8.89	-51.2	3.4	2.8	5.6	ND	ND	ND	ND	ND	ND
D1	-8.73	-51.27	3.5	3.1	6.5	ND	ND	ND	ND	ND	ND

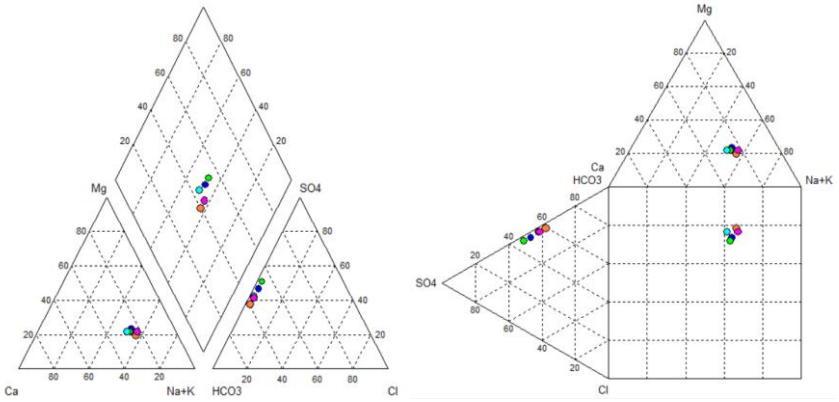

Figure 2. Classification of the water samples from the main spring system in Piper (left) and Durov (right) diagrams for the sampling period of November 2020.

The meteoric water line for Greece was used to characterize the samples, developed by Argiriou and Lykoudis (2006). The relationship of the Greek meteoric water line (HellasMWL) is given by the formula: $\delta^2H = 7.2 \times \delta^{18}O + 8.2‰$. According to the stable isotope analysis, groundwater of the Simonopetra aquifer has meteoric origin and has not been subject to secondary evaporation (Table 1). Additionally, this aquifer recharged from a maximum altitude of 890 m. Regarding the tritium analyses of groundwater of the Simonopetra aquifer, it is characterized as contemporary water, according to classification by Clark and Fritz (1997). The relatively young age of the aquifer's groundwater fortifies the theory of the high flow speed of the aquifer, as well as its direct supply from atmospheric precipitation (meteoric origin).

Conclusions

In the study area, there is an absence of human activity, therefore, the physicochemical characteristics of groundwater solely depend on the interaction and hydrodynamics of water with the geological formations. Groundwater of Simonos Petra aquifer is characterized as potable with the absence of potentially toxic elements, nitrate, nitrite, and ammonium ions. The aquifer recharge occurs from a maximum altitude of 890 meters and is characterized as contemporary water. The next step of this work is the time-series analysis of the hydrochemical data from the Simonos Petra aquifer and its correlation with the hydrodynamic analysis of the Simonos Petra spring.

References

Argiriou, A.A., Lykoudis, S., 2006. Isotopic composition of precipitation in Greece. Journal of Hydrology, 327, 486-495.

Busico G., Ntona M.M., Kazakis N., Mastroccico M., 2022. Simulating historical, actual and future water balance in mountainous watershed. 12th International Hydrogeological Conference, Cyprus, 20-22 March 2022, pp. 172-175.

Clark, I.D., Fritz, P., 1997. Environmental Isotopes in Hydrogeology. Lewis Publishers, New York, p. 328.

Christofides, G., D'Amico, C., Del Moro, A., Eleftheriadis, G., Kyriakopoulos, C., 1990. Rb-Sr-geochronology and geochemical characters of the Sithonia plutonic complex (Greece). European Journal of Mineralogy, 2, 79–87.

Durov, S.A., 1948. Natural water and graphical representation of their composition. Dokl. Akad. Nauk. U.S.S.R., 59, 87-90.

Kockel, F., Mollat, H., Walther, H.W., 1977. Erlauterungenzur Geologischen Karte der Chalkidiki und angrenzender Gebiete 1:100000 (Nord-Griechenland). Bundesanstalt fur Geowisseschaften und Rohstoffe, Hannover, 119.

Lenore, S.C., Arnold, E.G., Andrew, D.E. 1998. Standard Methods for Examination of Water and Wastewater, 20th ed. American Public Health Association, American Water Works Association, World Environment Federation: Washington, DC, USA.

Piper, A.M., 1944. A graphic procedure in the geochemical interpretation of water analyses. American Geophysical Union, Transactions, 25, 914 – 923.

16th International Congress of the Geological Society of Greece

17-19 October, 2022 - Patras, Greece

Bulletin of the Geological Society of Greece, Sp. Publ. 10

Ext. Abs. GSG2022-157

Preliminary Investigation of Geotechnical Properties of Quaternary Deposits of Kopais Plain, Viotia County, Central Greece

El. Chatzicharalampous[1], G. Tsapralis[1], C. Loupasakis[1]

(1) School of Mining and Metallurgical Engineering, National Technical University of Athens, Athens, Greece, chatzieliza@central.ntua.gr.

Research Highlights

In the framework of an ongoing investigation concerning the extensive deformations occurring in the Kopais plain the geotechnical properties of Quaternary deposits covering the plain were investigated in detail. The deformations appear to cause damage to buildings and infrastructure in Aliartos and several other villages, mainly in the western area of Kopais plain.

Area of Study

Kopais plain is located in the Viotia regional unit, central Greece, approximately 100km NW of Athens and has a general W-E direction (figure 1). It is the last part of the Fokiko-Beotian depression which extends from Gravia with a WNW-ESE direction, continuous through Tithorea and Xaironia and passing between the mountain chains of Chlomos-Ptoos to the north and Parnassos-Elikonas to the south and it ends up to Kopais plain (Papadopoulou-Vrynioti, 1990). It came from the drainage of the homonymous lake and expands into an area of about 250000 acres. The lake was extending at the eastern part of the basin with 23km in length and 13km in width. Its' maximum depth was 4m and its creation was the result of tectonic and erosional processes. Drainage works were carried out in various historical periods. It is worth mentioning the effort of "French Kopaida Company" that was completed in 1886 with drainage of the lake that was followed by a fire caused by self-ignite of peat, which resulted getting all peat burned and the lake being reformed (Lappas, 1983). It was in 1931 that the English company "Lake Copais" completed successfully the draining project and since then cultivation, stock raising and industry were developed. In parallel, preexisting settlements expanded and new ones were created.

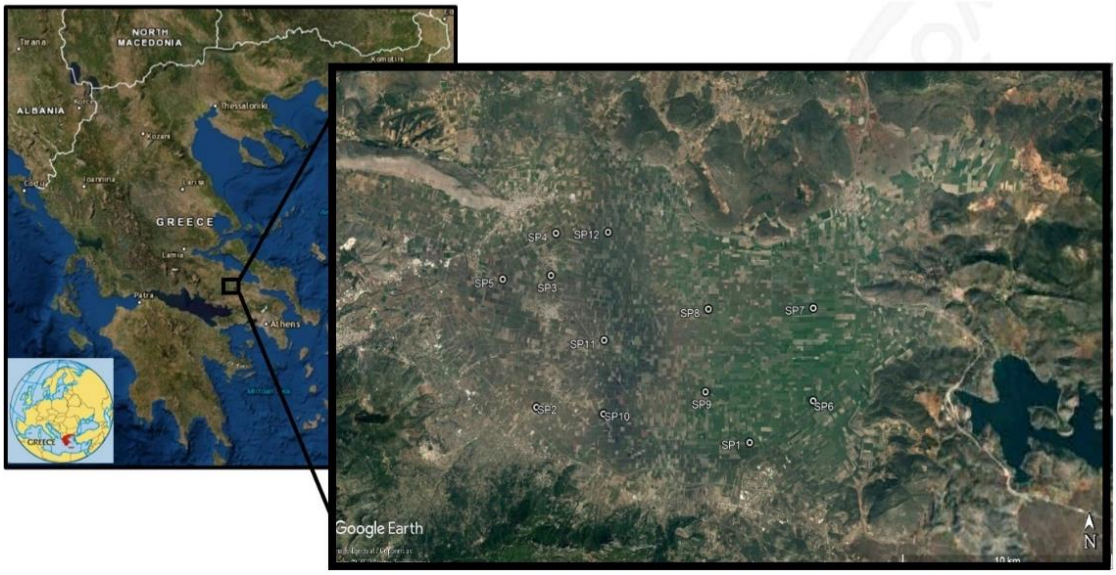

Figure 1. Location of Kopais plain (Google Earth) and map with sampling positions (map from Google Earth)

Methodology

For the determination of physical and mechanical characteristics of soils covering Kopais plain, several samples were collected covering the whole range of the plain (figure 1) and tests were done as follows:

- Particle size analysis with sieves and hydrometer analysis, particle size distribution curves were plotted
- The density of solid grains was valued and the results were expressed with a 0.01 accuracy for 20ºC. Three tests were performed for each sample and in cases where the results differed more than 0.03 between them, the tests were

repeated. From the accepted results, the average values were calculated for each sample.

- Atterberg limits (liquid and plastic) and Plasticity Index were specified. Atterberg limits were performed to soil fraction passing through sieve no 40. The liquid limit was calculated by the use of the Casagrande device and for some of the samples, the cone penetrometer method was also applied.
- Voids ratio of soils was calculated by cylindrical specimens that were formed for this reason. Also, for that purpose, the density of solid grains as was calculated for our samples was used.
- Direct determination of organic matter content.
- One-dimensional consolidation test was applied, consolidation factor was calculated by applying Casagrande method and also compression factor and elasticity modulus and relative diagrams were plotted.
- Direct shear strength-rapid solidified test (CU) was also applied for the determination of cohesion and internal friction angle of the samples.

Results-Discussion

During the field campaigns Kopais plain damages to buildings and infrastructure in the town of Aliartos and several villages in the area were discovered (figure 2). It is considered that these damages are caused by land subsidence phenomena. Analysis of the soil samples collected from the plain showed that the area mainly consists of loose silt and soft to very soft clay soils of low plasticity or close to the limit between low and high plasticity. Soils are compressible, but according to consolidation factors determined, subsidence occurring in the plain progress at a slow rate. The density of soil grains varies from 2.53-2.67gr/cm^3 and it is considered that low-density values are ascribed to the presence of organic material in the soils.

Figure 2. Indicative photos showing damages caused by land subsidence phenomena in Mavrogia (left photo), Aliartos (photo center-up), Agios Dimitrios (photo center-down), Alalkomenes (right photo)

References

Lappas, T., 1983. The Kopaida, N. Mavrommatis Co Ltd (in Greek)

Papadpoulou-Vrynioti, K., 1990. Geomorphological study of Kopaida area (Viotia). Ph.D. Thesis, National and Kapodistrian University of Athens, Geological Department, Athens, 160p.

16th International Congress of the Geological Society of Greece

17-19 October, 2022 - Patras, Greece

Bulletin of the Geological Society of Greece, Sp. Publ. 10

Ext. Abs. GSG2022-165

Assessment of Groundwater Quality in Ooeides Aquifer System, NE Greece

A. Adamidis[1], A. Kallioras[2], P. Angelidis[3], I. Gkiougkis[1], F.-K. Pliakas[1]

(1) Democritus University of Thrace, Department of Civil Engineering, Laboratory of Engineering Geology and Groundwater Research, 67100 Xanthi, Greece, adamidi@otenet.gr (2) National Technical University of Athens, School of Mining and Metallurgical Engineering, Iroon Polytechniou 9 str., 15773 Zografou Campus, Athens, Greece (3) Democritus University of Thrace, Department of Civil Engineering, Division of Hydraulics, 67100 Xanthi, Greece.

Introduction

Zhang (2015) mentions that the use of groundwater as a free source of water has been an effective means to meet the ever-increasing water demands and addressing the problems of surface water scarcity. Gkiougkis et al. (2021) argue that accurate conceptual model is directly related to a thorough investigation of the natural system involving subsurface investigations (groundwater well logging, geophysical investigations, pumping tests), hydrological (groundwater level monitoring, surface and unsaturated zone studies) and hydrochemical measurements (groundwater sampling and analyses). Groundwater resources play the most important role in the supply of irrigation water to rural communities in Orestiada Region in Evros Prefecture, NE Greece, while surface water sources are related to rivers Evros and Ardas. This research work deals with the assessment of groundwater quality and main controls on groundwater chemistry in the aquifer system of Ooeides, Orestiada Region. Statistical analysis and conventional hydrochemical plots were employed in the analysis of 85 groundwater samples from the study area during sampling campaigns for the years 2018, 2019 and 2020.

Study area

The study area is located in River Evros Trough, Orestiada Region in Evros Prefecture, NE Greece (Figure 1) covering a narrow land strip of 160 km^2, called "Ooeides", which means oval because of its shape. The eastern border is River Evros. The lithological composition of the study area is made up of Holocene alluvials, consisting of alternations of cobbles, sands, gravels and clays in interlocking horizons in vertical and horizontal sense creating a heterogeneity in the material. According to Adamidis *et al.* (2022), the sedimentation of Plio – Plistocene represents the main formation of the study area. Located to the edges of River Ardas basin and the Neochori stream basin, continues submerged under the alluvial depositions. Irrigation needs for rural activities are met by pumping of groundwater from over a hundred wells, then supplied through a pipe network.

Methodology and results

In the context of the development of the conceptual model of the study area, hydrochemical research was carried out in a network of thirty (30) monitoring wells. Three groundwater sampling campaigns were performed in August and September of 2018, 2019 and 2020. The relevant groundwater chemical analyses were executed in the Laboratory of Engineering Geology and Groundwater Research, Department of Civil Engineering, DUTH. The chemical parameters examined were the following: Ca^{2+}, Mg^{2+}, SO_4^{2-}, HCO_3^-, PO_4^{3-}, NO_3^-, NO_2^-, NH_4^+, Cl^-, Electrical Conductivity (EC), TDS, pH, K^+, Na^+, Fe^{2+}, Mn^{2+}. The analyses were carried out using mainly the HACH DR4000 spectrophotometer within an error margin of less than 5%, resulting in the production of relevant hydrochemical diagrams (Figure 1): Piper plot (Piper, 1944) presenting cation pass from calcium to sodium and potassium type, Chadha diagram (Chadha, 1999) defining main water type as Ca–Mg–HCO_3, Chlor-alkaline index (CAI) plot demonstrating the inversion of ionic exchange. Additionally, Gibbs diagram was constructed to identify hydrogeochemical evolution, which involves precipitation, rock weathering, and evaporation - crystallization processes, as well as scatter plot Ca+Mg vs HCO_3+SO_4 (meq/L) was designed showing that the main procedure affecting groundwater hydrochemistry evolution is due to ionic exchange.

Conclusions

The research work in the study area included data, information and valuations regarding mainly the hydrochemical type of groundwater and the impact on groundwater quality from anthropogenic activities (cultivation activities, municipal waste). The whole procedure is evaluated as very important for the further investigation of the hydrogeological and hydrochemical status of the aquifer system in the area in the context of the development and management of groundwater and surface waters in the wider area.

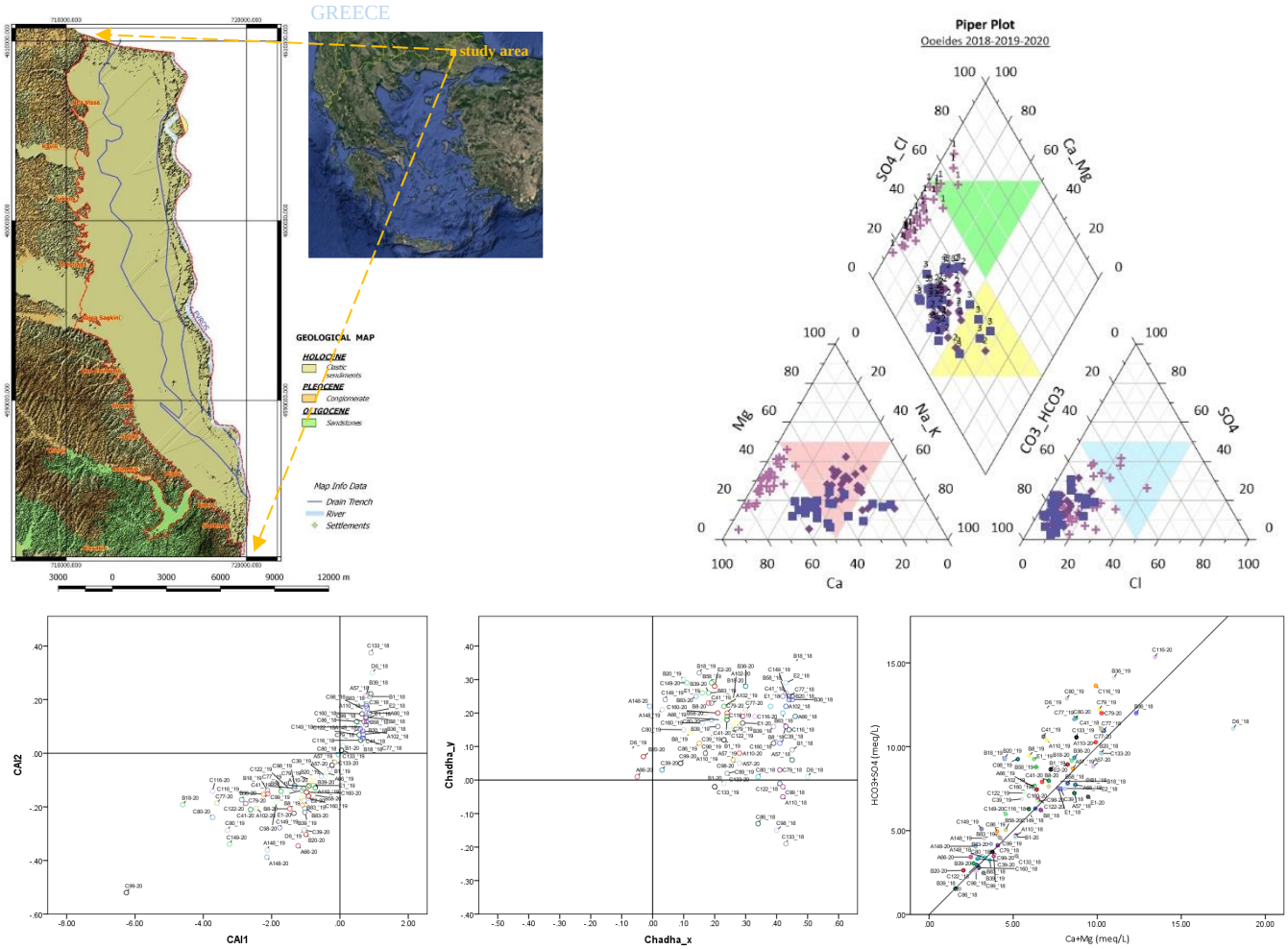

Figure 1. Upper left: Study area and geological map (Adamidis *et al.*, 2022). Upper right: Piper plot. Lower left: Cholo-alkaline index plot. Lower center: Chadha diagram. Lower right: Scatter plot Ca+Mg vs HCO_3+SO_4 (meq/L).

References

Adamidis, A., Despotakis, I., Kallioras, A., Angelidis, P., Pliakas, F.-K., 2022. Conceptual model of an aquifer system in the region of Orestiada, North Greece. Proceedings of the 12th International Hydrogeological Congress of Greece and Cyprus / Nicosia, 2022, Book of Extended Abstracts, 52-55.

Chadha, D.K., 1999. A Proposed New Diagram for Geochemical Classification of Natural Waters and Interpretation of Chemical Data. Hydrogeology Journal, 7, 431-439.

Gkiougkis, I., Pouliaris, C., Pliakas, F.-K., Diamantis, I., Kallioras, A., 2021. Conceptual and Mathematical Modeling of a Coastal Aquifer in Eastern Delta of R. Nestos (N. Greece). Hydrology Journal, MDPI, 8(1) 23, https://doi.org/10.3390/hydrology8010023.

Piper, A.M., 1944. A graphic procedure in the geochemical interpretation of water analyses. American Geophysical Union, Transactions, 25, 914-923.

Zhang, X., 2015. Conjunctive surface water and groundwater management under climate change. Frontiers in Environmental Science, 3:59, doi.org/10.3389/fenvs.2015.00059.

16th International Congress of the Geological Society of Greece
17-19 October, 2022 - Patras, Greece
Bulletin of the Geological Society of Greece, Sp. Publ. 10
Ext. Abs. GSG2022-177

A MATLAB code for simulating rockfalls

N. Vagenas[1], E. Papadopoulos[1], N. Depountis[1], N. Sabatakakis[1]
(1)University of Patras, Patras, Greece, nikolaosvagenas@upatras.gr.

Research Highlights

A code developed in MATLAB for calculating more precisely the coefficients of restitution in rockfall simulations.

Introduction

This research aims to investigate the rockfall kinetics and particularly the individual parameters affecting rockfall's kinetic energy with a more meticulous analysis of the restitution coefficients (vertical R_N and tangential R_T). For this purpose, a mathematical model was developed using Matlab software based on the kinematic analysis of rock blocks and focusing on their impact on the slope. The model aims to calculate the values of R_N and R_T, using as input data the initial impact speed of a rock block, the inclination of the slope and the distance of the start and end impact points of rock blocks. The presented code aims to determine the restitution coefficients with a more detailed and accurate procedure and investigate possible correlations with the characteristics of the falling rocks such as the shape, volume, and velocity.

Methodology

For the development and calibration of the mathematical model, real cases of rockfalls that have occurred in Western Greece (Figure 1) were used and restitution coefficient data from other similar studies in Western Greece (Depountis *et al.*, 2020; Sabatakakis *et al.*, 2015) were collected and analyzed.

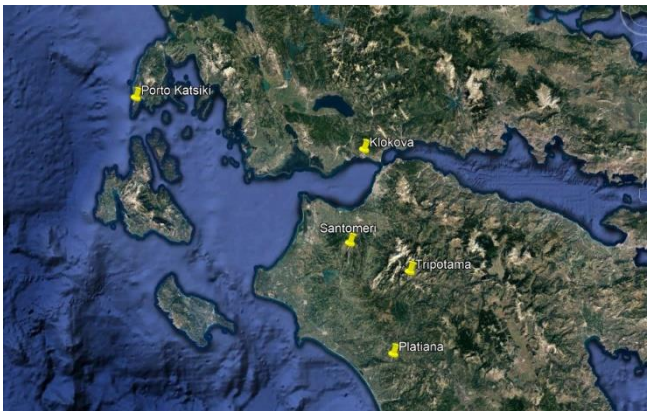

Figure 1. Google Earth map with the positions of rockfalls used for the development and calibration of the model.

Accurate topographic surveying and detailed geotechnical investigation in these areas led to the identification of the most representative trajectories of the fallen rock blocks to survey. Then a back analysis was followed to determine the restitution coefficients using the Rocscience Rocfall software with the actual bounce locations being identified in the field. The resulting data served as a benchmark of the presented mathematical model, named Ana-rock.

Code description

The Ana-rock code was initially developed in Wolfram Mathematica (Vagenas, 2020) and translated later into Matlab language. It is a mathematical solution of the motion of falling rock blocks, which focuses on the bounce of the blocks. The initial speed of the block before the impact, the gradient of the slope and the distance of the start and end points, are required as input data. Equations of motion are applied for two or more cases and the resulting system of equations calculates the R_N, and R_T values that verify the given conditions. The total reduction of the kinetic energy of the block during its bounce is thus calculated. The effectiveness of the back analysis depends on the accuracy of the topographic mapping, the estimation of the initial velocity of the rock block and the bounce points distance detection. The method's calculations become more accurate if additional impact points are added for back-analysis pairs. A flowchart of the applied methodology (Vagenas, 2020) and a snapshot of the code are presented in Figures 2 and 3 respectively.

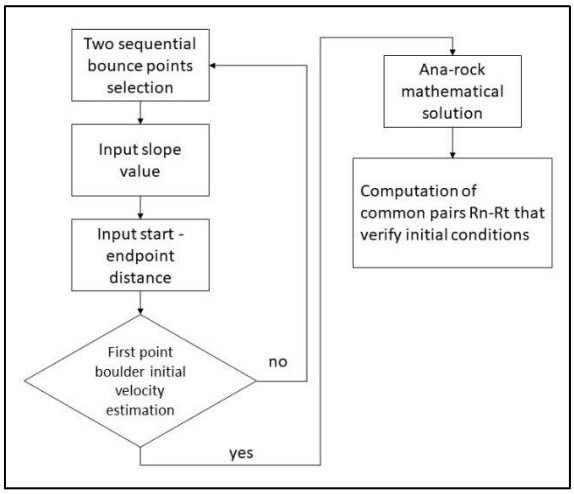

Figure 2. Flowchart of the applied methodology.

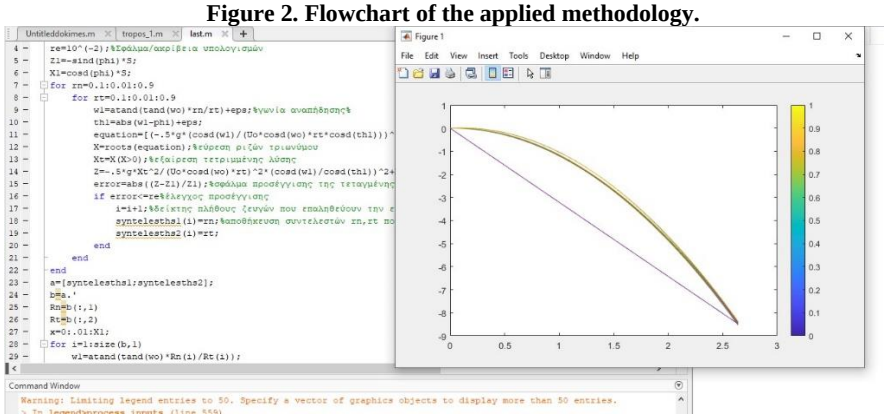

Figure 3. Snapshot of the code.

Discussion and Results

The proposed mathematical model, Ana-rock, works supplementary to the classical back analysis of rockfall simulation and determines the restitution coefficients as both the rotational motion developed by the rock block as well as the intermediate parts of the total fall trajectory, can be included in the calculations. Through this model, the energy factors estimated by back analysis are adjusted in all test sites, thus validating its applicability in field conditions. As a result, more realistic trajectories are obtained during the simulation and therefore the resulting restitution coefficients are better adapted to local conditions.

One limitation of the code is that it requires knowledge of the speed of the rock block before its impact on the slope, which is not easy to be estimated in the field. To overcome this obstacle, points with extreme changes in the relief were chosen, and it was assumed that the initial velocity of the falling blocks is similar to the velocity of a free fall.

The differences in the estimation of the coefficients of restitution between the Ana-rock code and the Rocscience Rocfall software seem to be related not only to the geological material but more to the shape and size of the rock blocks. The new simulation with the coefficients derived from the mathematical model generally is lowering the bounce heights of rocks, compared to the procedure with the traditional Rockfall back analysis. Another correlation that emerges is between the change of the coefficients and the relative angle of incidence velocity - slope gradient. The rate of change of the R_N and R_T depends on the value of this angle. R_T has a stronger effect on bounce height and impact distance, as the velocity-slope angle decreases. On the contrary, the normal coefficient of restitution is more effective as this angle increases. In any case, the effect of R_N is stronger than that of R_T. For this reason, the value of the normal coefficient is more sensitive to changes.

References

Depountis, N., Nikolakopoulos, K., Kavoura, K., & Sabatakakis, N. (2020). Description of a GIS-based rockfall hazard assessment methodology and its application in mountainous sites. *Bulletin of Engineering Geology and the Environment*, *79*(2), 645–658. https://doi.org/10.1007/s10064-019-01590-3

Sabatakakis, N., Depountis, N., & Vagenas, N. (2015). Evaluation of Rockfall Restitution Coefficients. In G. Lollino, D. Giordan, G. B. Crosta, J. Corominas, R. Azzam, J. Wasowski, & N. Sciarra (Eds.), *Engineering Geology for Society and Territory—Volume 2* (pp. 2023–2026). Springer International Publishing. https://doi.org/10.1007/978-3-319-09057-3_359

Vagenas, N. 2020. *Rockfall simulation by analytical methods. Correlation of rockfall energy dissipation parameters and rock mass characteristics*, https://nemertes.library.upatras.gr/jspui/handle/10889/14727?mode=full

MATLAB, 2010. version 7.10.0 (R2010a), Natick, Massachusetts: The MathWorks Inc.

Rocscience RocFall, 2002 software—for risk analysis of falling rocks on steep slopes. Rocscience user's guide

16th International Congress of the Geological Society of Greece
17-19 October, 2022 - Patras, Greece
Bulletin of the Geological Society of Greece, Sp. Publ. 10
Ext. Abs. GSG2022-183

Natural and anthropogenic impacts on Greek karst water quality

Li Vigni L.[1], D'Alessandro W.[2] Calabrese S.[1,2], Cardellini C.[3,4], Daskalopoulou K.[5,6], Brugnone F.[1], Parello F.[1]

(1) University of Palermo, Palermo, Italy, livignilorenza@gmail.com; (2) Istituto Nazionale di Geofisica e Vulcanologia, sez. Palermo, Italy; (3) University of Perugia, Perugia, Italy; (4) Istituto Nazionale di Geofisica e Vulcanologia, sez. Bologna, Italy; (4) (5) University of Potsdam, Potsdam-Golm, Germany; (6) Deutsches GeoForschungsZentrum, Potsdam, Germany.

Research Highlights

Water is life. Although karst aquifers represent the main drinking freshwater source, thus a precious resource to protect, they are extremely vulnerable to anthropogenic pollution and overexploitation.

Introduction

Karst hydrosystems represent a worldwide drinking water resource thanks to their storing capacity of large amounts of good quality freshwater (Ford & Williams, 2007). At the same time, they are extremely vulnerable to chemical and microbial contamination and overexploitation (Bakalowicz, 2005). Karst aquifers are the result of intense water-gas-rock interactions. The karstification process is a chemical dissolution of carbonate or evaporite formations by water rich in dissolved carbon dioxide (Bakalowicz, 2005).

In Greece, karst aquifers represent an important resource for the population. The main sources of the deterioration of karst resources are the salinization of aquifers near coastal areas and the use of fertilizers in agriculture (Daskalaki & Voudouris, 2008).

The main aim of this study is to evaluate the chemical status of the big karst hydrosystems of Greece and to discriminate the possible geogenic and anthropogenic sources of contamination.

Methods

From 2016 to 2022, more than 180 karst springs were sampled (Fig.1). These were selected on the basis of their flow rate (> 60 L s^{-1}). Physico-chemical parameters (temperature, pH, electric conductivity, and redox potential) were measured *in situ* with portable instruments, and total alkalinity was determined by titration with 0.1 M HCl on unfiltered samples, expressed as mgHCO_3^- L^{-1}. Analyses of the chemical composition of major ions and trace elements were performed at the laboratories of INGV of Palermo, Italy.

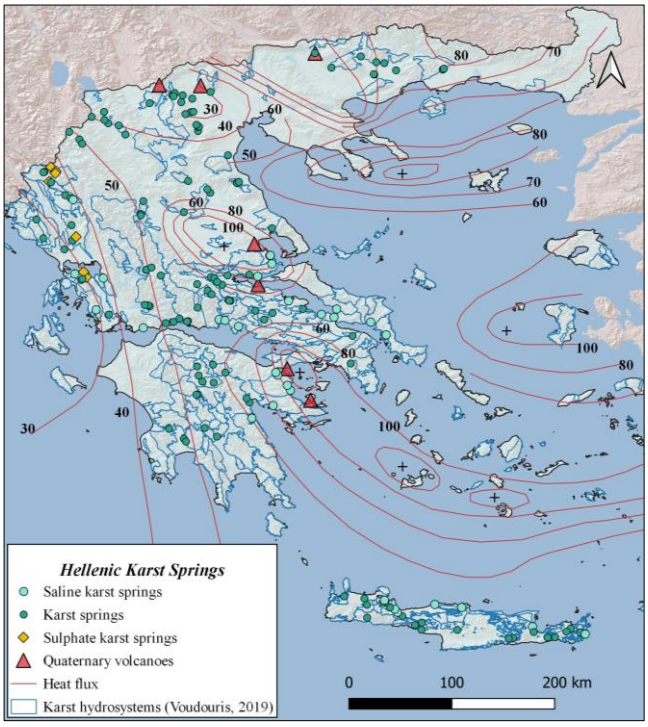

Figure 1. Geographic distribution of the sampling site.

Results

Temperature values range between 5.6 °C and 33.5 °C, pH values vary from 6.5 to 8.5, whereas both electrical conductivity and Eh show a wide spectrum of values; from 174 μS cm^{-1} to 44,000 μS cm^{-1} and from -38 mV to 399 mV, respectively. Based on the chemical composition of waters, the karst springs are subdivided into three groups with different geochemical compositions. Group (a) is characterized by Ca-HCO_3 composition and low saline content (TDS < 1,200 mg L^{-1}), showing the typical composition of groundwater circulating in carbonate aquifers. Group (b) is characterized by Na-Cl composition and high saline content (TDS up to 25,717 mg L^{-1}). According to Voudouris (2019), the saline springs show important seawater contamination of their aquifers due to their coastal location and the overexploitation of their aquifers. The high concentrations of chloride and boron, sometimes exceeding the limit set by European Council for drinking waters, make them not suitable for human consumption. Lastly, group (c) is characterized by Ca-SO_4 composition and intermediate saline content (TDS up to 2,424 mg L^{-1}). This composition derives from gypsum dissolution processes. Indeed, these springs are located in the Epirus region, where the aquifers comprise the Triassic evaporite formations of the Ionian zone (Katsanou *et al.*, 2017).

Nitrate is an important nutrient, but also a widespread pollutant mainly deriving from agricultural fertilizers; the content of nitrates in the collected samples never exceeds the European limit for drinking water (98/83/EC), suggesting good quality of sampled karst groundwater. Nevertheless, high NO_3^- contents (up to 31 mg L^{-1}) were identified in some springs, mainly located close to urban centers or intensively cultivated areas.

According to USEPA, high concentrations of Sr (< 4,000 μg L^{-1}) may have negative effects on human health, although no limit has been set for its content in drinking waters. In our research, significant strontium concentrations (up to 7,081 μg L^{-1}) were measured in some springs. These elevated contents derive from mixing between fresh and sea water for saline springs and from the dissolution of celestine and strontianite minerals for calcium-sulfate springs.

Another extremely toxic trace element is arsenic. Some of the studied karst springs show arsenic concentrations (up to 17 μg L^{-1}) exceeding the EU limit for drinking waters (10 μg L^{-1}). These high concentrations were found in Thessaly and Central Greece, likely originate from the development of aquifers within carbonate formation at contact with metamorphic and metavolcanic formations.

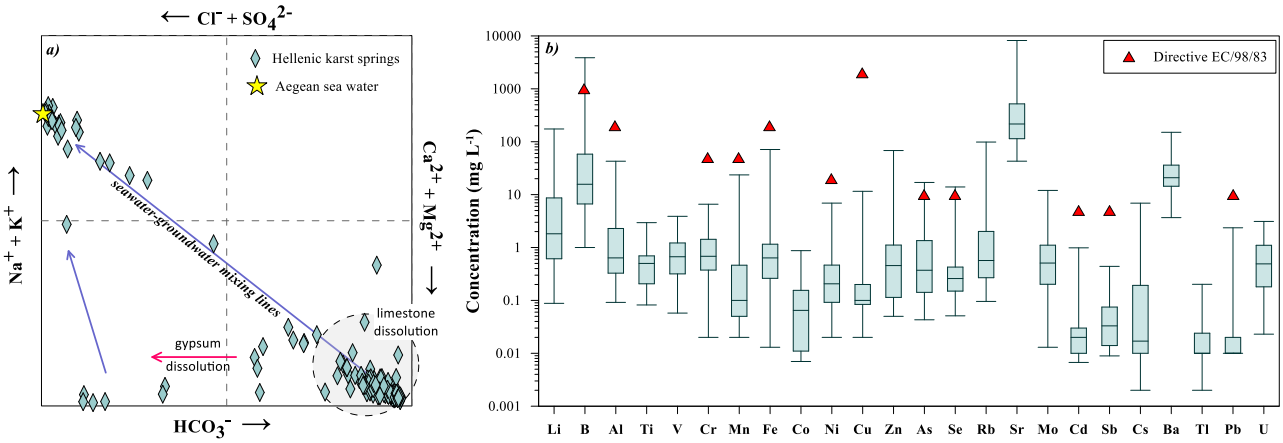

Figure 2. (a) Langelier-Ludwig diagram; (b) box plot of trace elements of karst springs, comparing with the limit set by European Council for drinking waters.

Generally the Hellenic karst aquifers show a good quality of their waters. The main causes of water deterioration are the intrusion of seawater within the karst aquifers andmetal enrichment due to the local geogenic environment, such as the dissolution of minerals bearing toxic trace elements.

References

Bakalowicz M. 2005. Karst groundwater: a challenge for new resources. Hydrogeology Journal 13:148-160.

Daskalaki P., Voudouris K., 2008. Groundwater quality of porous aquifers in Greece: a synoptic review. Environ Geol, 54:505-513.

E.U. Council Directive 98/83/EC about water quality intended for human consumption. Official Paper Eur Communities L330:32-54, 1998.

Ford D.C., Williams P.W., 2007. Karst Hydrogeology and Geomorphology. Wiley, Chichester.

Katsanou K., Lambrakis N., D'Alessandro W., Siavalas G., 2017. Chemical parameters as natural tracers in hydrogeology: A case study of Louros Karst System, Greece. Hydrogeology Journal 25, 487-499.

Voudouris K., 2019. Status and codification of karst aquifer systems in Greece. Bulletin Geological Society of Greece, 57, 23-51.

16th International Congress of the Geological Society of Greece
17-19 October, 2022 - Patras, Greece
Bulletin of the Geological Society of Greece, Sp. Publ. 10
Ext. Abs. GSG2022-199

Ultimate and Residual Shear Strength of the Weathered Flysch in Wet and Dry conditions

S. Anagnostopoulou[1], N. Depountis[1], N. Sabatakakis[1]
(1) Laboratory of Engineering Geology, University of Patras, 26504, Greece, anagnostopoyloy_sofia@upnet.gr,

Research Highlights

Calculation of the residual and ultimate shear strength of weathered flysch materials in a large and a ring shear apparatus for modeling their behavior in landslide problems.

Background

The weathered zone of flysch is described as the most critical, prone to landslides, geological formation in Greece and constitutes a major predisposing factor in the induced landslide movements. In this research, a laboratory approach is attempted to investigate the behavior of the tectonically highly sheared, decomposed, and weathered flysch material, with the performance of large shear and ring shear testing in reconstituted specimens. The testing program was conducted on five flysch specimens derived from three landslides: a) Panagopoula (PAN sample), b) Karya (KAR1 and KAR2 samples) and c) Platanitis (PLAT1 and PLAT2 samples), located in Western Greece. The tests included direct large shearing (300×300×120 mm), conducted in moisture and density-controlled conditions and ring shear tests in the finer material.

Methods

From each material type of the three sites, a series of large shear tests were carried out according to ASTM D3080 using a VJT/2780A direct shear machine, on reconstituted 120 mm thick specimens prepared inside the shear box carriage (Figure 1)

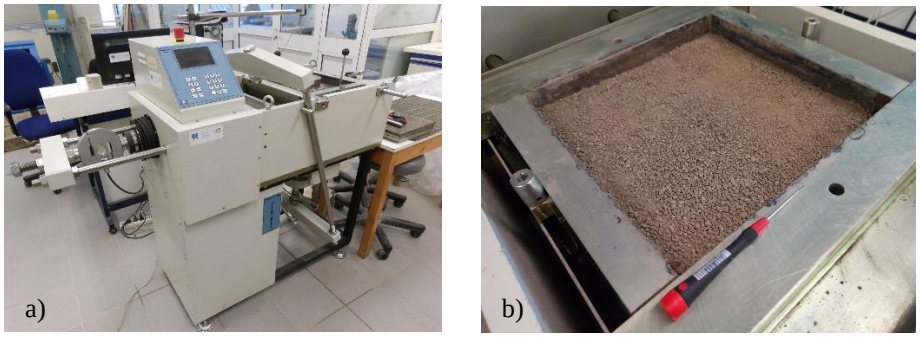

Figure 1. Large shear box apparatus. a) Prior starting the testing procedure, and b) with a compacted specimen.

Low-density (loose) specimens were obtained by pouring the flysch material into the shear box carriage from a funnel with a very low drop height (up to 20 cm). The funnel was moved from the center to the periphery of the box and vice versa. This method produced an initial bulk unit weight (γb) range of 13.1 to 19.4 kN/m^3. Dense specimens were prepared inside the apparatus carriage by manual dynamic compaction (tapping) in several layers so that the shear plane coincides with the middle of the central layer. A material, with an initial bulk unit weight (γb) of 14.3 to 20.5 kN/m^3 was produced. Both loose and dense specimens were tested in dry and wet conditions. The wet conditions included partially saturated, as well as saturated states to simulate all potential situations. Wet specimens were prepared by mixing the soil material with a predetermined quantity of water and were tested in optimum dense conditions according to ASTM D1557, partially saturated, as well as fully saturated. An additional water content check was always performed in the shear zone material just after shearing. Saturated specimens were prepared by pouring (loose state) or tapping the material (dense state) and then pouring water into the carriage so that it had been percolated very slowly upwards through the specimen. This procedure was used to avoid material segregation phenomena due to the fine-grained contents.

Ring shear tests were also conducted according to ASTM D6467-21 to determine the residual angle of friction of the finer material. For this purpose, the ring shear apparatus developed by Bromhead (1979, 1986) was used by applying four different normal stresses σ_n' (50, 100, 200 and 400 kPa). The apparatus allowed testing of ring-shaped test specimens having an outer and inner diameter of 100 mm and 70 mm, respectively and a thickness of 5mm (Figure 2).

Those tests were performed under consolidated drained conditions on remolded materials passing the No 200 ASTM sieve (<0.075mm), first mixed at a water content lying between the plastic limit PL and the liquid limit LL. All specimens were sheared at a displacement rate of 0.048 deg/min (or 0.036 mm/min), to allow induced pore pressures to dissipate.

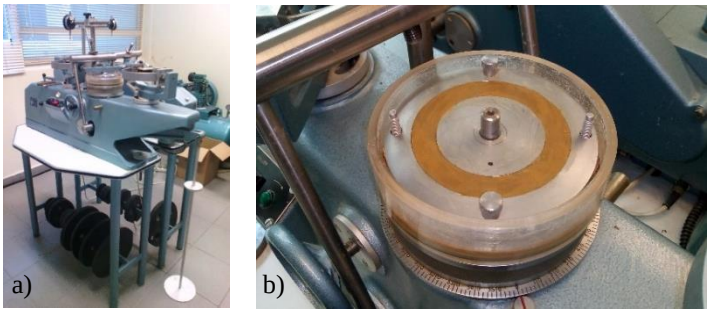

Figure 2. Ring shear apparatus. a) Loading plate adjusted, and b) compacted specimen.

Results

Analyzing the obtained results is evident that ultimate shear strength decreases as water content increases. A definite decrease in the effective angle of friction is observed with an increase in water content up to the saturation state ($\varphi' > 40°$ in the dry state which is reduced to values $\varphi' < 30°$ in the saturation state). Moreover, the density significantly affects the soil strength in the case of dry and wet specimens, while unexpectedly, the strength of dense and loose saturated specimens is generally identical and are dependent on the angle of friction ranging from 25° to 30°. Finally, under fully saturation conditions, the soil matrix dominates the strength behavior, and the strength of dense and loose dry specimens is quite high with large effective friction angles because of the granular material structure that mainly influences its behavior. Figure 3 presents the failure envelops of the ultimate and residual state of the flysch material used in the laboratory tests.

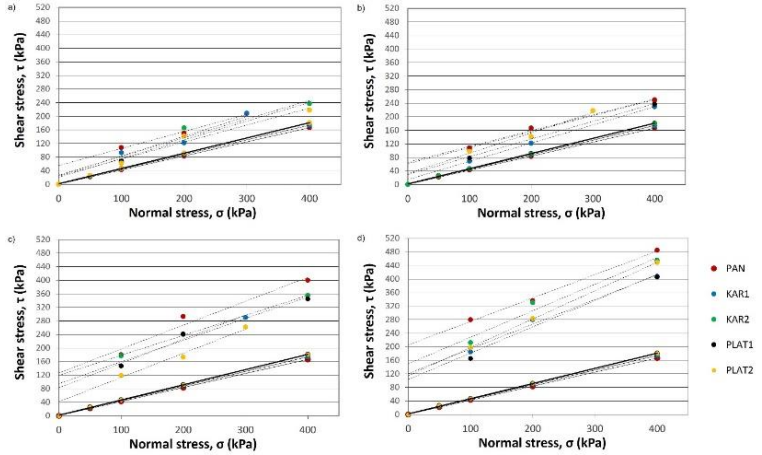

Figure 3. Large shear (dashed lines) and ring shear (solid lines) failure envelops of the flysch specimens in (a) loose saturated, (b) dense saturated, (c) dense partially saturated, and (d) dense optimum conditions (Anagnostopoulou *et al.*, 2022).

Conclusions

Large shear test results revealed that the values of effective angle of friction in the weathered flysch material decrease with the increasing water content. Moreover, in the fully saturated state the ultimate angle of friction was found to be 1–6° higher than the residual one. This is an expected difference that exists in granular materials such as flysch, on which the ultimate shear strength is slightly higher than the residual. In the wet, normally consolidated specimens, the peak shear stress was found to be equal to the ultimate. This suggests that the normally consolidated flysch specimens provide a lower shear strength compared to their similar over-consolidated specimens and may be more representative for landslide analysis when using reconstituted specimens. It is concluded that the large shear apparatus may overcome the problem of modeling representative samples of "difficult" soil materials, such as the strongly sheared and decomposed flysch, and seems to be a better approach to describe the strength behavior of weathered soils in landslide problems.

References

American Society for Testing and Materials (ASTM) D3080-11, 2011. Standard Test Method for Direct Shear Test of Soils Under Consolidated Drained Conditions.

American Society for Testing and Materials (ASTM) D1557-12, 2021. Standard Test Methods for Laboratory Compaction Characteristics of Soil Using Modified Effort (56,000 Ft-Lbf/Ft3 (2,700 KN-m/M3)).

American Society for Testing and Materials (ASTM) D6467-21e1, 2021. Standard Test Method for Torsional Ring Shear Test to Determine Drained Residual Shear Strength of Fine-Grained Soils.

Bromhead, E.N., 1979. A Simple Ring Shear Apparatus. EMAP CONSTRUCT LIMITED, Vol. 12, pp. 40–44.

Bromhead, E.N., 1986. The Stability of Slopes. Surrey University Press. London, p. 373.2.

Anagnostopoulou, S., Depountis, N., Sabatakakis, N., Pelekis, P., 2022. Large Shear Strength Parameters for Landslide Analyses on Highly Weathered Flysch. Land, 11(8), 1353.

16th International Congress of the Geological Society of Greece
17-19 October, 2022 - Patras, Greece
Bulletin of the Geological Society of Greece, Sp. Publ. 10
Ext. Abs. GSG2022-200

The impacts of drought on groundwater resources in the Upper Volturno basin, Southern Italy

M.M. Ntona[1,2], G. Busico[1], M. Mastroccico[1], N. Kazakis[2]
(1)Università degli Studi della Campania "Luigi Vanvitelli", Caserta, Italy, mariamargaritantona@unicampania.it
(2)Aristotle University of Thessaloniki, Thessaloniki, Greece.

Highlights

- The study area is prone to low-duration drought events.
- Groundwater resources have been slightly impacted by drought events.

In this research, the Standardized Precipitation Index (SPI) (McKee, 1993) and the Standardized Precipitation Evapotranspiration Index (SPEI) (Vicente-Serrano *et al.*, 2010) were applied to identify the drought severity in the Upper Volturno basin. The study area is located in the northern part of the Campania province, Southern Italy, and covers 1532 km^2. The mean precipitation is 1039 mm and the mean annual temperature is 15.7 ºC, with an increasing trend of atmospheric minimum temperatures observed in the last years (Mastroccico *et al.*, 2019). According to the climate classification by Köppen (1936), the study area is characterized as Csa (Hot summer Mediterranean).

The Upper Volturno basin is located in the Central-Southern Apennines. The average elevation of the study area ranges from 20 m to 1,618 m where steep slopes and a valley of a long extent which is covered by agricultural fields are observed. From the geological point of view, the area consists of (i) late orogenic molasses and terrigenous units (Upper Miocene-Pliocene), (ii) pre-orogenic and syn-orogenic terrigenous units of inner and thrust-top basins series (Cretaceous-Upper Miocene), (iii) siliceous-marly units of outer basin series (Trias-Paleogene), (vi) limestone and dolomitic limestone units of carbonate platform series (Jurassic-Paleogene), and (v) dolomitic units of carbonate platform series (Trias-Jurassic) (De Vita *et al*., 2012). In the study area, the mountainous part is covered by karst and fractured aquifers while the valley is constituted by alluvial aquifers. Most of the area is covered by mixed systems that are generally low-permeable, with few discontinuous aquifers (Ducci *et al*., 2017).

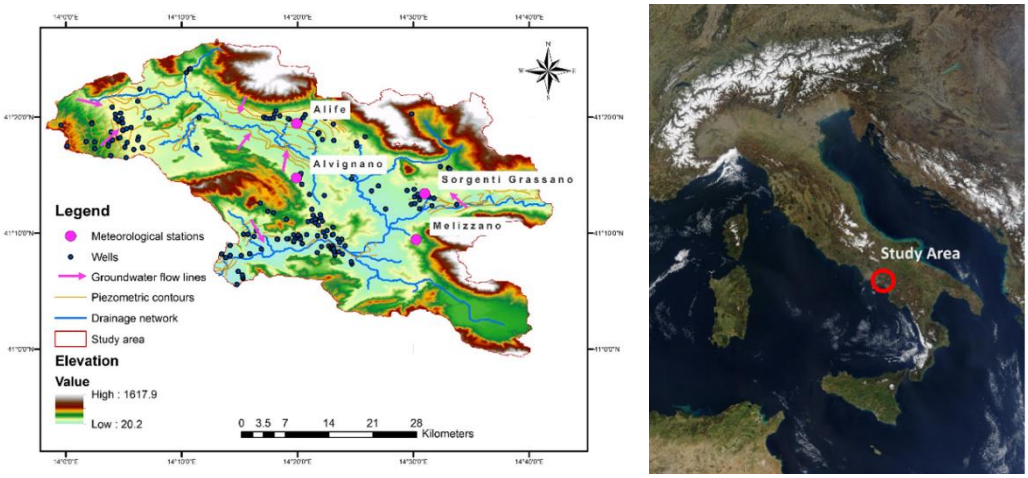

Figure 1. Morphological map of the study area.

Methodology

Monthly data of minimum, maximum temperature, and rainfall values were collected from four meteorological stations (Alife, Alvignano, Melizzano, and Sorgenti Grassano) for a period of nineteen years. Moreover, groundwater level data have been collected and analyzed to investigate the groundwater flow directions in the area (Figure 1). Statistical assessment of the two drought indices is performed using Pearson correlation coefficient and root mean square error (RMSE). Both drought indices were calculated for different aggregation periods (1, 3, and 6 months) in R programming. SPEI was calculated with Hargreaves method, which requires minimum and maximum temperature values and latitude of the point data. The selection of these two drought indices was applied due to their limited data needs.

Results

According to the statistical analysis, all correlations are significant at a 99% coefficient level. The results of Pearson's correlation between SPI and SPEI showed the higher correlation on the 6-month time scale. SPEI has the same RMSE value in all aggregation periods and less error than SPI (Table 1). Although both indices are highly correlated with each other, SPEI performed better than SPI because evaporative demand has a positive impact on defining drought conditions.

Table 1. Correlation coefficient (r) and root mean square error (RMSE) between SPI and SPEI.

Drought indices	R	RMSE
1-month SPI	0.93	1.06
1-month SPEI	0.93	0.97
3-month SPI	0.94	1.03
3-month SPEI	0.94	0.97
6-month SPI	0.96	0.98
6-month SPEI	0.96	0.97

Figure 2 presents the monthly temporal time series of drought index (SPEI6) based on the data from meteorological stations Alife and Sorgenti Grassano. The spatial distribution is not possible due to the absence of meteorological stations with the same recording period in all the extent of the area. However, according to the categories of drought by McKee *et al.* (1993), extreme drought events were highlighted during 2006-2008 and 2017-2018. In addition, many periods of moderate and severe droughts are observed during the years. Thus, the area is prone to low-duration drought events. The deeper groundwater values appear in the NW part of the basin while in the SE and SW parts are mentioned the higher levels of the aquifer with approximate values of 210-170 m and 80-20 m, respectively. The small extent of the aquifers in combination with the low drought events in the valley of the basin represents a favorable condition for groundwater recharge.

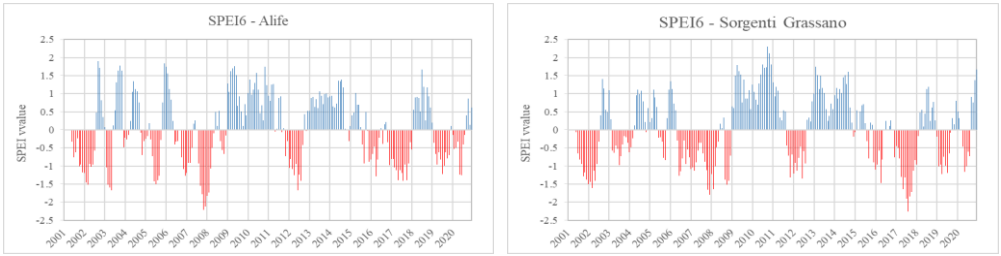

Figure 2. SPEI in the period 2001-2020 for (a) Alife and (b) Sorgenti Grassano meteorological stations. The year marks are centered on 1 January of each year.

Discussion and Conclusion

The complex hydrogeological system with the absence of long-period data sets in the area presents a significant challenge. For this reason, the current study provides a brief drought analysis using SPI and SPEI and demonstrates their potential use for drought analysis with minimal data requirements in connection with the hydrological regime of the area. The results showed that the area is affected by short-duration droughts. The small extent of the aquifers in combination with the low drought events in the valley of the basin represents a favorable condition for groundwater recharge. The current approach provides the results of the first drought analysis in the Upper Volturno basin and therefore, it has to be mentioned that multi-indices of drought assessment are required in order to reach a robust conclusion.

Acknowledgments

This research project was supported by the Hellenic Foundation for Research and Innovation (H.F.R.I.) under the "Second Call for H.F.R.I. Research Projects to support Post-Doctoral Researchers" (Project Number: 00138, Title: Groundwater Depletion. Are Eco-Friendly Energy Recharge Dams a Solution?), and by the VALERE 2020 Program (VAnviteLli pEr la RicErca) of the University of Campania "Luigi Vanvitelli".

References

De Vita, P., Allocca, V., Manna, F., and Fabbrocino, S., 2012. Coupled decadal variability of the North Atlantic Oscillation, regional rainfall and karst spring discharges in the Campania region (southern Italy), Hydrol. Earth Syst. Sci., 16, 1389–1399.

Ducci, D., Della Morte, R., Mottola, A., Onorati, G., Pugliano, G., 2017. Nitrate trends in groundwater of the Campania region (southern Italy). Environmental Science and Pollution Research, 26, 1–12.

Köppen, W., 1936. Das geographische System der Klimat. Handbuch der Klimatologie, 46.

Mastrocicco, M., Busico, G., Colombani, N., 2019. Deciphering Interannual Temperature Variations in Springs of the Campania Region (Italy). Water, 11(2), 288.

McKee, T.B., N.J. Doesken, J. Kleist, 1993. The relationship of drought frequency and duration of time scales. Eighth Conference on Applied Climatology, American Meteorological Society, Jan17-23, 1993, Anaheim CA, pp.179-186.

McKee, T.B., Doesken, N.J., Kleist, J., 1993. The relationship of drought frequency and duration to time scales. In Proceedings of the Eight Conference on Applied Climatoligy, Anaheim, CA, USA, 17–22.

Vicente-Serrano, S.M., Beguería, S., López-Moreno, J.I., 2010. A Multi-scalar drought index sensitive to global warming: The Standardized Precipitation Evapotranspiration Index – SPEI. Journal of Climate, 23, 1696-1718.

16th International Congress of the Geological Society of Greece
17-19 October, 2022 - Patras, Greece
Bulletin of the Geological Society of Greece, Sp. Publ. 10
Ext. Abs. RGR2022-204

Rock Mass Characteristics and Block Volumes Detached After Earthquake Events in Lefkada Island, Greece and their Significance in Rock Fall Analyses

A. Servou[1], N. Depountis[1], N. Sabatakakis[1]

(1) Laboratory of Engineering Geology, Department of Geology, University of Patras, 26504 Patras, Greece, servoy_aikaterini@upnet.gr

Research Highlights

The rock block volumes measured in the field after a rock fall event do not necessarily follow the rock mass discontinuity statistical rules. The coefficient of restitution is directly dependent on the rock block volume and rock mass characteristics.

Background

Greece is a country particularly covered by limestone formations that offer natural beauty due to the karstic phenomena. However, depending on the slopes' geological and geometrical characteristics they could pose in danger to infrastructures and human activities. In the framework of this study, the three prevailing limestone rock masses (Pantokratoras, Vigla, and Paxos) of Lefkada island, Greece, are investigated regarding their discontinuities' characteristics, block volume, and their potential for rockfalls. The study is focused on the western part of the island because is characterized by steep slopes (mean angle >50°) and most importantly the slopes intersect the road network and are close to beaches. This fact makes the rockfall analysis of high necessity as it affects human safety and other socio-economic factors. A crucial step in rockfall analyses and hazard assessment is the investigation of the local engineering geological conditions that characterize the rock masses (Depountis et al., 2020). For instance, the identification of the rock block volume which could be detached from the limestone slopes of the Lefkada island, after an earthquake event, is a very important parameter for calculating the kinetic energy, the bounce height, and the total rockfall trajectory.

Methods

The first step for the identification of the rock mass characteristics was the detailed mapping of all rockfalls in the broader area of the island two days after the earthquake of 17th November 2015. Furthermore, the western part of the island was divided into three sections according to the prevailing limestone formations, namely site A covered by the Pantokratoras limestone, site B, by the Vigla limestone, and site C by the Paxos limestone (Figure 1).

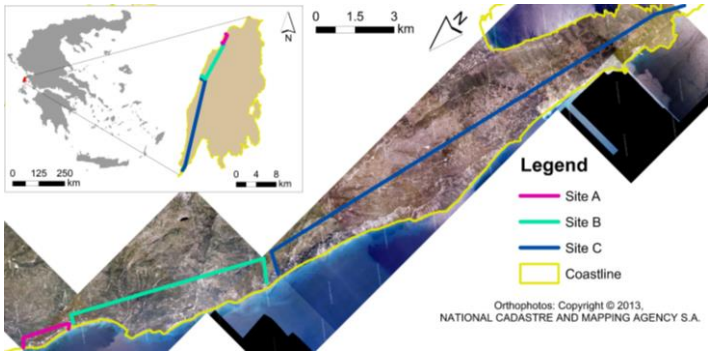

Figure 1: Location of the study area with the limestone sections

Consequently, an analytical rockfall database was compiled including the detached rock block volumes identified in the field, the measured discontinuities' parameters, such as dip and dip direction, spacing, aperture, infilling material, roughness, etc., and the rock mass classification using the Geological Strength Index (GSI) (Marinos & Hoek, 2000), and the Slope Mass Rating (SMR) (Romana, 1985). Subsequently, statistical analysis of the in-situ measurements was employed to determine the most representative rock block volume for rock fall analyses. In specific, frequency distribution tests were employed for each limestone set, and the volume with the higher frequency was selected as the most representative for each one of the three limestones. In addition, the rock block volumes were calculated using analytical methods based on the equations proposed by Morelli (2016) and Palmstrom (1982). By using data from other studies (Sabatakakis et al., 2015) and performing back analysis the mean coefficients of restitution R_N and R_T of the three limestones were determined and they were re-adjusted by using the ana-rock algorithm developed by Vagenas (2020).

Results

Table 1 shows the discontinuity characteristics and the classification of the rock masses, which were derived from in situ measurements, as well as the calculated and measured rock block volumes. All three limestone rock masses are moderate

to strongly weathered and they are intersected by three or four discontinuity sets.

Table 1. Discontinuity, rock mass classification, and block volumes of the studied limestones

Limestone type	S_{mean} (m)	J_v (J/m^3)	JRC	JCS (MPa)	GSI	SMR	V_{calc1} (m^3)	V_{calc2} (m^3)	V_{insitu} (m^3)
Pantokratoras-1	0.15	30	10-12	170 ± 50	35-40	48	0.0011	0.0009	1.57
Pantokratoras-2	0.14	28	10-12	170 ± 50	35-40	<20	0.0030	0.0003	1.32
Vigla-1	0.16	31	8-10	125 ± 40	50-55	36	0.0012	0.0006	0.35
Vigla-2	0.15	31	10-12	95 ± 40	40-45	42	0.0011	0.0008	0.39
Vigla-3	0.13	32	8-10	95 ± 40	30-35	36	0.0007	0.0004	0.22
Paxos	0.09	34	6-8	63 ± 30	20-30	32	0.0008	0.0015	0.025

S_{mean}: mean spacing of discontinuities, J_v: volumetric joint count, JRC: joint roughness condition, JCS: joint compression strength, GSI: Geological Strength Index, SMR: Slope Mass Rating, V_{calc1}: calculated mean rock block volume without considering the shape factor, V_{calc2}: calculated mean rock block volume considering the shape factor, V_{insitu}: in situ measured rock block volume

The rock block volumes (V_{insitu}) of Table 1 refer to the mean values recorded in each site, however, frequency analyses for all detached rocks were employed. Out of the 49 recordings of Pantokratoras limestone, 65% are smaller than 1.65 m^3, while for 42 recordings of Vigla limestone 55% are smaller than 0.35 m^3 and for 46 recordings of Paxos limestone, 75% are smaller than 0.045 m^3 (Figure 2). However, the high disintegration of the rock mass in some sites, made the discontinuity measurements impossible, so the calculated volumes refer to smaller samples. It was observed that considering the rock block shape factor in analytical calculations derives smaller volumes (see V_{calc2} of Table 1). The in-situ volume measurements are quite bigger than the calculated ones and are considered to be more representative for rockfall analyses, since they were recorded after the earthquake event of 17th November 2015.

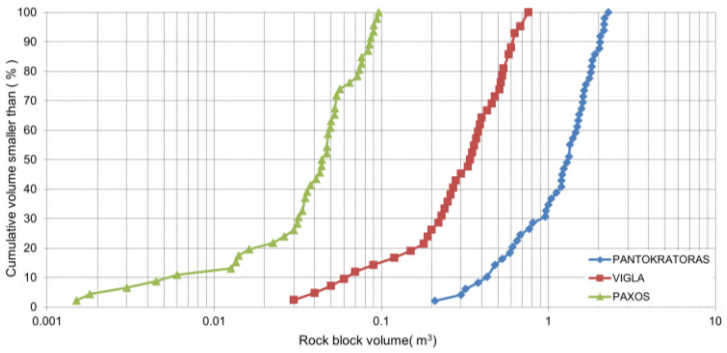

Figure 2: Cumulative distribution of in situ measured rock block volumes of each limestone type.

Conclusions

Although the discontinuity structure throughout the rock mass plays a crucial role in the calculated volume that could be detached from the slope, in reality, bigger volumes were detached in the western part of Lefkada, strongly connected to the earthquake ground motion parameters. The bigger rock block volumes and the higher JCS values of Pantokratoras limestone justify the selection of the specific values and proportionally for the other limestones too. Based on the in-situ rock block recordings, and the rock mass characteristics, the coefficients of restitution were finally determined as follows: Pantokratoras limestone R_N= 0.32 and R_T=0.85, Vigla R_N= 0.30 and R_T=0.75, and Paxos R_N= 0.26 and R_T=0.65.

References

Depountis, N., Nikolakopoulos, K., Kavoura, K., Sabatakakis, N., 2020. Description of a GIS-based rockfall hazard assessment methodology and its application in mountainous sites. Bulletin of Engineering Geology and the Environment, 79(2), 645–658.

Marinos P., Hoek E., 2000. GSI-a geologically friendly tool for rock mass strength estimation. GeoEng2000 Conference, Melbourne, Australia, 1422-1442.

Morelli, G. L., 2016. Empirical Assessment of the Mean Block Volume of Rock Masses Intersected by Four Joint Sets. Rock Mechanics and Rock Engineering, 49(5), 1759–1771.

Palmstrom, A., 1982. The volumetric joint count - A useful and simple measure of the degree of rock mass jointing. 4th International Congress IAEG, New Delhi, India, 221-228.

Romana M., 1985. New adjustment ratings for application of Bieniawski classification to slopes. International Symposium on the Role of Rock Mechanics in Excavations for Mining and Civil Works, 49–53.

Sabatakakis, N., Depountis, N., Vagenas, N., 2015. Evaluation of Rockfall Restitution Coefficients. In Lollino, G., et. al. (Eds.), Engineering Geology for Society and Territory-Volume 2, Springer International Publishing, 2023–2026.

Vagenas, N., 2020. Rockfall simulation by analytical methods. Correlation of rockfall energy dissipation parameters and rock mass characteristics, Ph.D. Thesis, University of Patras, Patras, Greece, 266 p.

16th International Congress of the Geological Society of Greece

17-19 October, 2022 - Patras, Greece

Bulletin of the Geological Society of Greece, Sp. Publ. 10

Ext. Abs. GSG2022-213

Need for a holistic approach to groundwater exploration

D. Rapti[1,2]

(1) Ferrara University, Department of Chemical, Pharmaceutical and Agricultural Sciences, via L. Borsari, 46 – I-44121 Ferrara - Italy, cpr@unife.it (2) New Energies And environment, Spin-off Company of Ferrara University, Dept. of Physics and Earth Sciences, via Saragat, 1 – I-44122 Ferrara, Italy.

During the last decades, climate change, the growing need for drinking, industrial and agricultural water, as well as local demographic pressure, have strongly contributed to a progressive qualitative and quantitative degradation of groundwater resources in large sectors of the Mediterranean area. For these regions, developing and implementing sustainable groundwater management, plans and protection of the underground resources are necessary especially in high and medium priority basins, for avoiding undesirable results and thus mitigating the effects. Sustainable development of water resources consists in the exploitation of groundwater resources to meet current and future beneficial uses without causing unacceptable environmental or socioeconomic consequences. In order to formulate effective sustainable management and strategies, a sufficient knowledge on the behavior of different groundwater systems and their interaction with the environment is crucial.

In line with this premise and in order to understand the hydrodynamic behaviour of the underground water resources within the deltaic region of the Po River, Northern Italy, numerous stratigraphic, hydrogeological, hydrological and hydrochemical data were collected and interpreted. The main purpose of this research is i) the determination of the geometric and hydraulic characteristics of the underground resources; ii) the recognition of mixing phenomena between unconfined and confined aquifer systems; iii) the identification of the recharge area; iv) the assessment of the evolution of the qualitative and quantitative state; v) the inference on the equilibrium between the amount of pumping and the quality of the water; and vi) the evaluation of the average residence time of groundwater within the Ferrara water basins.

In the deltaic Po Plain, up to a depth of 300 m, the geometrical parameter of the aquifers (thickness and lateral distribution), hydrodynamic geochemical and characteristics strongly depend on the lateral and vertical facies variations of the sedimentary successions, which in turn are a consequence of the tectonic structures and the continuous geomorphological and especially hydrographic evolution that led to the generation of variable depositional environments (marine, continental, lacustrine, ...) especially in the more recent times.

As a consequence, the Pliocene-Quaternary deposits are characterised by silty-muddy layers alternating with sandy and sometimes gravel lenses (REGIONE EMILIA-ROMAGNA-ENI-AGIP, 1998; Rapti-Caputo, 2000). The last sedimentary cycle (Middle Pleistocene-Holocene) characterized by cyclic alternations of fine-grained material (silts and clays) and coarser deposits with sands and gravels texture, where the aquifer system of the group A is developed.

Within this group, the aquifer systems called A1, A2, A3 and A4 (Fig. 1) develop in correspondence with the permeable layers. In figure 1, it should be noted that a) the influence of the deep tectonic structures in correspondence of the Casaglia anticline (named Dorsale ferrarese), on the thickness and depth of the diverse aquifer systems; b) the variable spatial distribution of salinity within the aquifers (values greater than 2.000 microS/cm at 20°C). Consequently, their natural chemical compositions are mainly due to the different original depositional environments developed within the low delta Po plain.

The present paper focused on the upper zone of the aquifer system A (aquifers A1 and A2) while, due to the lack of an adequate monitoring network, the deeper aquifers A3 and A4 will not be analyzed.

Also, the integrated analysis of stratigraphical, hydrogeological, hydrochemical and isotopic data and adopting a holistic approach, allowed for the definition that (Rapti-Caputo, 2000; Rapti-Caputo and Martinelli, 2009):

a) the unconfined aquifer, mainly developed in sandy or locally sandy-silty lenses, shows high vulnerability and degree of pollution due to its shallow depth to water and the intensive farming activities (high NO3 and SO4 concentrations). The alimentation comes mainly from the precipitations and secondarily via lateral infiltration from the hydrographic network as it is also demonstrated by the isotopic composition (δD and δ18O); indicating the strongly affected by meteorological events while the mean residence time of the water in the underground reservoir is about few years.

b) in the confined aquifer system A1, which is mainly developed in Würmian sandy layers, bodies representing the infilling of deltaic channels of the Po River covered by the fine-grained sediments associated with the Flandrian transgression. From a hydrochemical point of view, the calcium bicarbonate (Ca–HCO3) facies prevails. The low oxygen-18 (δ18O<–9.2 VSMOW) and deuterium values suggest the occurrence of a slow Po River recharge regime mixed with local precipitation, while the mean residence time of the water in the reservoir is about 40.000-50.000 years (Carbon-13 and Carbon-14 data). The aquifer recharges are mainly from the Alps; while along the main rivers, also via lateral infiltration as shown by i) the occurrence of the alimentation limit after about 1 hour from the start of pumping tests; ii)

the proportional relationship between the hydrometric level of the river and the piezometric level of the aquifer; iii) the increase in electrical conductivity values with the distance from the axis of the river and iv) from the high tritium content value of the water near the Po River (>7 TU) due to mixing phenomena between the 'old' water of the confined aquifer and the 'recent additions' from the hydrological channel network.

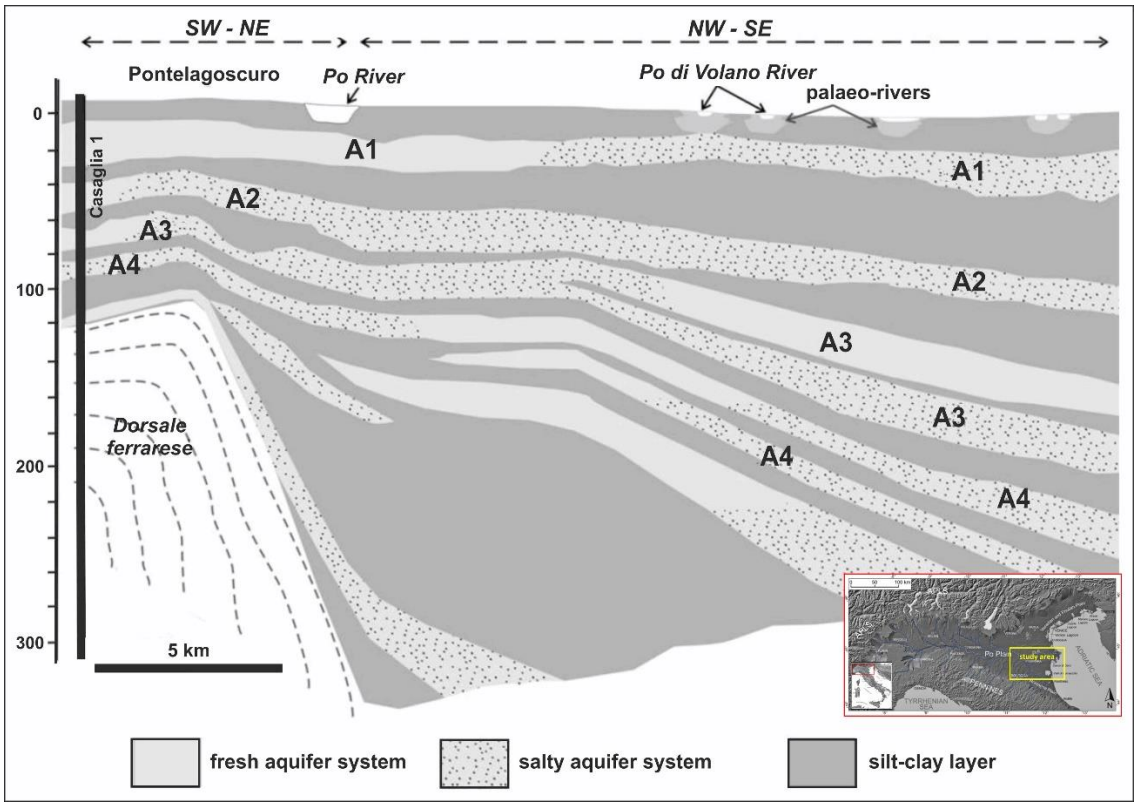

Figure 1. Study area and hydrostratigraphic section.

Consequently, along the major water courses, the vulnerability to pollution of this aquifer body is particularly high. Also, in the eastern sector of the plain, along the coastal area, salinization phenomena have been manifest since 1973 (the year in which data collection began). These phenomena are attributed to the over-exploitation of the aquifer.

c) the confined aquifer system A2 is also composed of continental sandy deposits and the calcium bicarbonate (Ca-HCO3) facies prevails; while the lower part of the aquifer is deposited in the marine environment and the sodium bicarbonate (Na-HCO3) geochemical facies is dominant. In the eastern sector there are evident phenomena of mixing between fresh water and high salinity water.

References

Rapti-Caputo D., 2000. Underground water resources east of Ferrara: investigations on the hydrogeological and hydrochemical behaviour: proposal for the best management. PhD Thesis, University of Ferrara, Italy, 215 p.

Rapti-Caputo D., Martinelli G., 2009. The geochemical and isotopic composition of aquifer systems in the deltaic region of the Po River plain (northern Italy). Hydrogeology Journal, 17 (2), 467-480.

Regione Emilia-Romagna, ENI-AGIP, 1998.Underground water reservoirs in the Emilia-Romagna region. S.EL.CA., Florence, 120 p.

16th International Congress of the Geological Society of Greece

17-19 October, 2022 - Patras, Greece

Bulletin of the Geological Society of Greece, Sp. Publ. 10

Ext. Abs. GSG2022-218

Hydrogeological approach as a key for the exploration of shallow geothermal resources

D. Rapti[1,2] R. Caputo[2,3]

(1) Department of Chemical, Pharmaceutical and Agricultural Sciences, Ferrara University, via L. Borsari, 46 – I-44121 Ferrara - Italy, cpr@unife.it (2) New Energies And environment, Spin-off Company of Ferrara University, Dept. of Physics and Earth Sciences, via G. Saragat, 1 – I-44122 Ferrara, Italy (3) Department of Physics and Earth Sciences, Ferrara University, via G. Saragat, 1 – I-44122 Ferrara – Italy.

The undergoing climate change and the spread of micro-polluting particles in the atmosphere, both effects strongly associated with the large use of fossil sources, urged energy and environmental policies, at all levels from international down to municipal ones, towards a rapid transition.

As a consequence, theoretical research and real examples of successful applications of renewable and eco-sustainable resources represent an important support to the energy transition towards 2030. In line with this, a Public Company has recently decided to expand its district heating which is at present supported by a co-generator fuelled with gas.

In order to fill the added energetical needs they oriented towards the exploitation of the shallow geothermal capacity of their subsoil. For better defining the workflow of this problem-solving process, we used the above mentioned environmental and energy needs as starting points and integrated the process with design-thinking methodologies. The test site is located within the northern alluvial plain of the Modena province; notwithstanding the apparently uniform morphological setting, the stratigraphy and the hydrogeological conditions have been strongly influenced by the recent tectonics causing important heterogeneities in the subsoil.

On the other hand, the most energy-intensive customer of the district heating is represented by the head-quarter offices of the Company itself, where the building's thermal needs consist of approximately 750 MWh/year for heating and the production of domestic hot water. It should be mentioned that at present the buildings also need more than 500 MWh/year for summer cooling, which is provided by another fossil fuelled machine.

Due to the complex geological system and the articulated energy sources and in order to optimize the whole project, a holistic approach was applied taking into account both the energy needs on the side of the buildings and the hydrogeological, chemical and thermophysical characteristics of the subsoil, as well as the presence of other possible constraints.

At the investigated site, we collected i) litho-stratigraphic, ii) hydrogeological, iii) hydrochemical and iv) thermophysical data acquired by means of in situ tests and analysed on the basis of integrated methods. All these tests allowed us to properly define the hydrodynamic and thermophysical behaviour of the underlying aquifers and the response of the subsoil to the thermal stresses applied.

Considering the long season of heat extraction for the district heating and the consequent energetic overexploitation of the subsoil, we planned to energetically balance the system by inverting during the summer the role of the geo-exchangers to provide cooling to the buildings by means of a dedicated heat-pump characterized by a high EER value.

The complex geological conditions and the energy needs, lead us to design a hybrid shallow geothermal supply system, where static and dynamic closed-loop geo-exchangers have been integrated, and innovative monitoring methods have been installed. The investigated site also represented an occasion to test and properly evaluate the energy and environmental sustainability of the innovative dynamic closed loop exchangers.

16th International Congress of the Geological Society of Greece
17-19 October, 2022 - Patras, Greece
Bulletin of the Geological Society of Greece, Sp. Publ. 10
Ext. Abs. GSG2022-219

Revisiting the engineering geological appraisal and interpretation towards the geotechnical design of tunnels based on experiences from over than 70 tunnels in Greece.

V. Marinos[1]
(1) School of Civil Engineering, National Technical University of Athens, Athens, Greece, marinosv@civil.ntua.gr

Generally, knowledge and understanding of the role of the geological material and its implication in design is reinforced with advances in site investigation methods, the development of the geotechnical classification systems and the consequent quantification of the rock masses. Initially, RMR (Bieniawski, 1976) and Q (Barton et al., 1974) systems were developed in order to provide tunnel support estimates through a rating of rock masses. The development of powerful microcomputers and of user-friendly software though, prompted a demand for data related to rock mass properties required as input for numerical analysis or close form solutions for designing tunnels. This necessity preceded the development of the Geological Strength Index (GSI) (Hoek, 1994, Marinos & Hoek, 2000). The Hoek and Brown failure criterion (Hoek & Brown, 2018) is closely connected to the GSI, covering a wide range of geological conditions.

The role of the ground characteristics and its effect in tunnel design, strengthened with progresses in site investigation techniques, cannot be exclusively based and represented in the design only by one rating - classification value. Temporary support measures for rock masses with equivalent classification values can be diverse (Marinos, 2012). The design methodology discussed here incorporates the assessment of the tunnel behaviour type in the selection of design parameters and the definition of the type of the temporary support measures. After the appraisal of the tunnel failure mode, the appropriate numerical modelling can be performed, the conditions can be more soundly analysed, and the principles of tunnel support can be more precisely considered (Figure 1).

The work presented in this study is based on experience gained by the design and construction of over than 70 tunnels along the Greek region, through a wide variety of geological conditions. The engineering geological appraisal towards the geotechnical design starts with the definition of the Geological Model (Step I) of the site-specific area. This is followed by in situ conditions (stresses, hydrogeological conditions and other boundaries) and Tunnel Geometry (Step II). The next step identifies the rock characteristic – "keys" which dictates the stability or instability of the tunnel (Step III). At this point, the practitioner must choose if the behaviour is controlled by the overall rock mass or by the discontinuities or both. The rock mass behaviour during excavation of the tunnel is then assessed (Step IV). The assessment of the rock mass behaviour in tunnelling can be done through the Tunnel Behaviour Chart (TBC) (Marinos, 2012), based on three (3) basic parameters: the rock mass structure, the overburden (H) and the intact rock strength (σ_{ci}). Afterward, the suitable Design Parameters are entered, according to the principles of the failure mechanism (Step V). Parameters of a geotechnical classification systems GSI, RMR, Q can be reported here (Step V). Since most tunnel designs now involve numerical analyses, the question is whether to use rock mass parameters, when the rock mass behaves isotropically or to include the discontinuity parameters, when the behaviour is controlled by the joints or influenced by the resulting anisotropy. Next, the Tunnel Support Philosophy (support type) is discussed (Step VI) and finally, the Remaining Risk after the installation of the temporary support is reported (Step VII). A detailed example of how the ground type characterization is linked with the tunnel behaviour mode towards geotechnical design is illustrated in Figure 2.

Acknowledgements

All the experience and constructive comments, provided, all these years, by Dr. Evert Hoek and the late Emeritus Professor Paul Marinos, my dear father, are gratefully acknowledged. The author would like to thank Egnatia Odos S.A. for its support and the data provided during the years. I am also thankful for the helpful discussions and deep collaboration with Mr. Nikos Kazilis, Mr. Nikos Rachaniotis and Mr. Giorgos Aggistalis, throughout tunnelling construction. Ms. D. Papouli, Geologist, M.Sc. gave valuable assistance in editing the figures.

References

Barton N.R, Lien R and Lunde J. 1974. Engineering classification of rock masses for the design of tunnel support. In: Rock Mech. 6 (4), pp 189-239.

Bieniawski Z.T. 1976. Rock mass classification in rock engineering. In Exploration for Rock Engineering, Proc. of the Symp., (ed. Z.T. Bieniawski) 1, 97-106. Cape Town, Balkema.

Hoek E. Strength of rock and rock masses. ISRM News Journal 1994; 2(2): 4–16.

Hoek E, Brown E. T. 2018. The Hoek-Brown failure criterion and GSI – 2018 edition. In: Journal of Rock Mechanics and Geotechnical Engineering 11(3), Pages 445-463. https://doi.org/10.1016/j.jrmge.2018.08.001.

Marinos P, Hoek E. GSI: a geologically friendly tool for rock mass strength estimation. In: Proceedings of the International Conference on Geotechnical and Geological Engineering (GeoEng2000). Lancaster: Technomic Publishers, 2000. pp. 1422–46.

Marinos V. Assessing rock mass behaviour for tunneling. Environmental and Engineering Geoscience 2012; 18(4): 327–41.

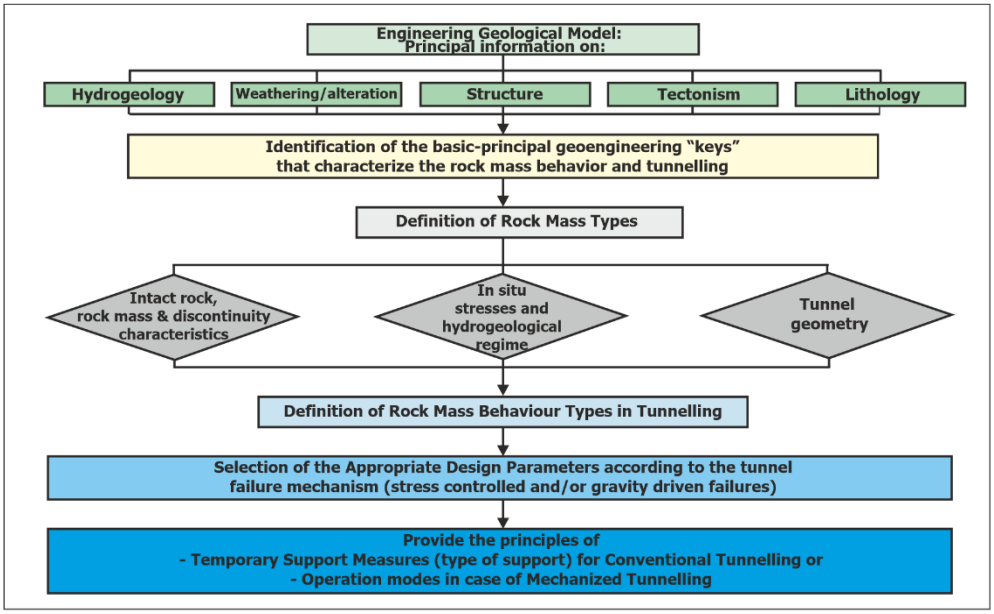

Figure 1. Engineering geological appraisal and interpretation towards the geotechnical design of tunnels.

Ground type	Ground type 1 (GT1)	Ground type 2: (GT2)	Ground type 3 (GT3)	Ground type 4 (GT4)
Schematic representation	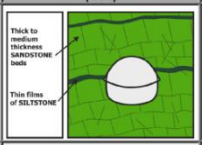	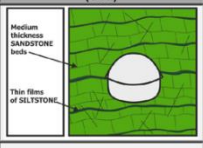	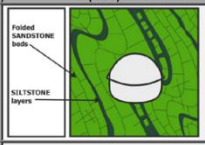	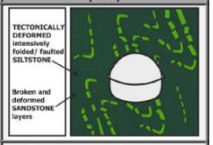
Description	**Undisturbed to moderately disturbed** rock mass with thick to medium thickness sandstone beds with sporadic thin films of siltstone	**Moderately disturbed** rock mass with medium thickness sandstone beds (90%) with thin films of siltstone	**Strongly disturbed,** folded rock mass that retains its structure, with sandstone beds (80%) dominating the siltstone ones (20%)	**Tectonically deformed** rock mass, intensely folded / faulted siltstone with broken and deformed sandstone layers forming an almost chaotic structure
Key parameters				
Lithology	Flysch - Sandstone	Flysch - Sandstone	Flysch – Sandstone/ Siltstone	Flysch – Siltstone/ Sandstone
UCS intact [MPa]	32 – 38 (35)	28 – 32 (30)	12 – 28 (20)	8 - 14
GSI [-]	50 - 60	40 - 50	30 - 40	18 - 23
Distance of discont. [cm]	0.4 - 0.6	0.4 - 0.6	0.4 - 0.6	n.a.
Friction of discont. [°]	35	30 - 35	30	20 - 24
JRC [-]	6 - 12	6 - 10	6 - 8	2 – 6
Persistence [m]	2 - 4	2 - 4	1 - 3	n.a.
Determined parameters (*)				
UCS rock mass [MPa]	7.7 – 9.4	5.4 – 6.7	2.4 – 3.1	0.8 – 0.95
c [MPa]	2.0 – 2.3	1.5 – 1.75	0.75 – 0.90	0.29 – 0.31
Friction angle [°]	35 – 38	32 – 35	26 – 29	19 – 21
E [MN/m²]	3100 - 5200	1800 – 3100	1000 - 1200	400 - 600

Behaviour type	Behaviour type 1 Discontinuity controlled overbreaks	Behaviour type 2 Crown failure	Behaviour type 3 Shallow shear failure
Schematic representation	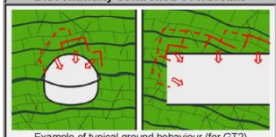 Example of typical ground behaviour (for GT2)	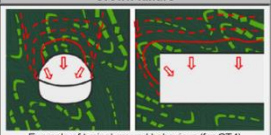 Example of typical ground behaviour (for GT4)	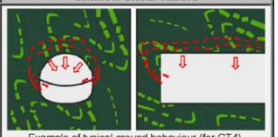 Example of typical ground behaviour (for GT4)
Ground type	GT1, GT2, GT3	GT4	GT3, GT4
Orientation of main joint set	Bedding planes dipping medium steep towards eastern portal	Mechanism is independent to orientation	Mechanism is independent to orientation
Primary stress condition	The secondary stresses are below the rock mass strength	Shallow overburden in combination with low stresses and low confinement stresses	The stresses at the tunnel perimeter exceed the rock mass strength
Groundwater	The water conditions vary from dry to minor water inflow. The water pressure is low	The water conditions vary from dry to minor water inflow. The water pressure is low	The water conditions vary from dry to minor water inflow. The water pressure is low
Rock mass behaviour (failure mechanism and behaviour during failure)	Voluminous discontinuity controlled, gravity induced falling and sliding of blocks from crown and side walls. Sliding preferred along weaker siltstone-layers. The volume of potential overbreak depends on the degree of fracturing and varies for the three ground types	Progressive roof failure (day lighting failure) due to low shear strength of the ground in combination with low confinement stresses. In sections with varying ground, layers with low cohesion and local water inflow, potential for extensive roof failure	Shallow stress induced shear failures at the side walls in combination with voluminous gravity controlled failure of the ground. In sections with varying ground, layers with low cohesion and local water inflow, potential for extensive roof failure
Radial displacements	In the range of some millimetres to a few centimetres	In the range of some decimetres leading to collapse	In the range of a several centimetres to decimetres
Face stability	Potential of wedge sliding along bedding planes in case of excavation from east to west	Unstable conditions due to low shear strength of the ground and low confinement stresses. Potential for voluminous overbreaks and progressive shear failure	Potential of local shear failure and instabilities in case of low cohesion and local water inflows

* To estimate the geotechnical properties of the ground types (I to IV), the code RSdata of Rocscience was used and the Mohr-Coulomb failure envelope derived for the «General application» (max overburden 35 m).

Figure 2. Example of ground type characterization linked with the tunnel behaviour mode towards geotechnical design

16th International Congress of the Geological Society of Greece
17-19 October, 2022 - Patras, Greece
Bulletin of the Geological Society of Greece, Sp. Publ. 10
Ext. Abs. GSG2022-223

Parametric simulations on the stability conditions of the masonry wall of Chandakas, Heraklion City, Crete, Greece

C. Loupasakis[1], N. Antoniadis[1], I. Parcharidis[2], V. Sythiakaki[3], E. Kanaki[3], P. Tsangaratos[1], P. Soupios[4], E. Grigorakou[1], G. Kalousi[5]

(1) Department of Geological Sciences, School of Mining & Metallurgical Engineering, National Technical University of Athens, Greece, cloupasakis@metal.ntua.gr (2) Department of Geography, School of Environment, Geography and Applied Economics, Harokopio University of Athens, Greece (3) Ephorate of Antiquities of Heraklion, Ministry of Culture and Sports, Heraklion, Greece (4) Geosciences Department, College of Petroleum Engineering and Geosciences, King Fahd University of Petroleum and Minerals, Saudi Arabia (5) Terra Spatium S.A., Athens, Greece

Research Highlights

The stability conditions of the Bembo-Saint Francis line-segment have been examined by means of parametric simulations. Through this study various methods of restoration and support are recommended, significantly increasing the safety factor of the monument.

Background

The history of the walls for the Heraklion city begins in the 7th-8th century A.D. where the first zone of fortifications was constructed. These fortifications were later repeatedly repaired in Byzantine times and in early Venetian times (15th century). (Sythiakaki et al. 2013) Later in the 15th century the mechanics designed a new fortification system, called Bastion fortification system or "Fronte Bastiano". This system has a polygon shape at the edges of which seven (7) bastions (baluardi or belovardi) were constructed (Fig. 1a). These bastions relate to line-segments (cortine). (Tzompanaki 2012).

Figure 1. (a) A satellite image of the Heraklion City bastion fortification system (Google Earth) (b) The three (3) construction phases of the line-segment Bembo-Saint Francis can be easily distinguished. A vertical crack is also visible

This study focuses on the line-segment Bembo-Saint Francis of the masonry walls of Chandakas. The line-segment is composed of stone masonry and from a geotechnical point of view, acts as a gravity retaining wall, due to the existence of backfilling material. During the centuries it suffered severe damages and reconstruction works. For instance, it was severely damaged during the long siege by the Ottomans (1648-1669). Also, during 1982 an extensive earth fill was added behind the wall, for the reconstruction of the Duke Beaufort Street. For several years, before the earth fill addition, part of the line-segment of the street served as bus parking spot. The loads applied by the earth fill and the heavy vehicles were proved an unfavorable factor for the stability conditions of the wall (Fig. 1b). Due to the deformations recorded, the authorities forbid parking and currently a wide sidewalk has been constructed along the line-segment. In the line-segment 3 construction phases can be distinguished.

- A lower phase, made by the Venetians with Neogene calcareous sandstones and fossiliferous Mesozoic limestone.
- A middle phase, which is an addition by the Ottomans, with different building materials (dolomized Mesozoic limestone).
- An upper phase, a modern construction (20th century) added during the reconstruction of Duke Beaufort Street, made with Neogene marly limestone.

Objectives - Methods

Through this study the stability conditions of the Bembo-Saint Francis line-segment have been examined by means of parametric simulations. Various equations and formulas from literature and international codes were used for the estimation of the Elastic modulus of the wall, such as Eurocode 6 (1996), Tomazevic (1999), D.M. Farshchi et al. (2008) and others. The mechanical characteristics of the building stones and the mortar were taken from the geotechnical report performed by Xatzistergiou & Skopelitis (2010) and were used to calculated the mechanical characteristics of the wall.

The results were implemented in a numerical investigation performed using the Finite Element code Plaxis2D. The overall stability of the wall-ground system was evaluated through 2 groups of parametric simulations. In the 1st Group, the cohesion and friction angle of the soil layers were altered between the MIN and the MAX values, while maintaining a constant value for the modulus of elasticity of the soil layers and the wall. In the 2nd Group, all possible combinations of values for the modulus of elasticity of the wall were applied, while the mechanical parameters of the soil layers were kept constant (considering them to be the most unfavorable). Regarding the masonry wall, at the Ottoman phase the mechanical parameters of the dolomitized limestone were assigned, while at the Venetian either those of the fossiliferous limestone or those of the calcareous sandstone. Both simulation groups were aiming to evaluate the sensitivity of the models on the values of the masonry wall`s modulus of elasticity.

Results and Conclusions

The results from parametric analyses that were performed indicate that the geometry of the masonry wall must be the key parameter affecting the operation of the wall as a retaining structure. The distribution of the total displacements (Fig. 2) indicates that the Ottoman phase is affected the most by the deformations. The main factor that caused these deformations is believed to be the inability of the Ottoman construction phase to receive earth pressures due to its reduced thickness. Also, the fact that this phase was built with thick layers of mortar presenting inferior quality also affect its bearing capacity.

Finally, various methods of restoration and support are recommended, significantly increasing the safety factor, and decreasing the deformations. As shown in Table 1, the support systems with long piles and anchors (tensioned or not) offers by far the best safety factor values.

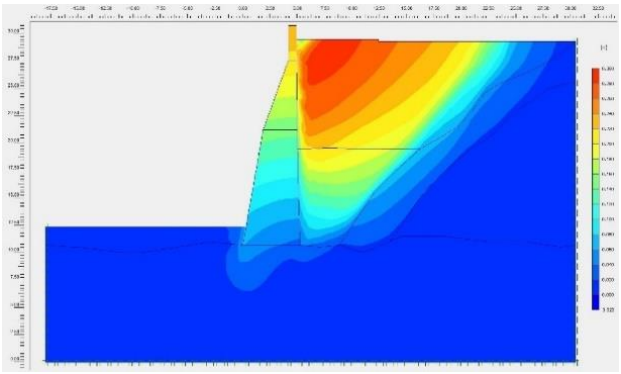

Figure 2. Total displacements contour

Table 1. Safety factors provided by for each support system.

Analysis	SF
Reference analysis with no support measures	1.079
Vertical Piles (21m)	1.185
Vertical Piles (23m)	1.283
Vertical Piles (21m) with a series of anchors	1.513
Vertical Piles (23m) with a series of anchors	1.550
Vertical Piles (23m) with a series of tensioned anchors	1.512

Acknowledgements

SCIENCE project has received funding from European structural and investment funds, Partnership Agreement 2014-2020, and is supervised by General Secretariat for Research & Technology in the context of National action for bilateral cooperation between Greece-China.

References

EN 1996-1-1. 2005. (English): Eurocode 6: Design of masonry structures - Part 1-1: General rules for reinforced and unreinforced masonry structures [Authority: The European Union Per Regulation 305/2011, Directive 98/34/EC, Directive 2004/18/EC]

Farshchi, D. M., Masoud, M., Schumacher, A. & Marefat, M. S. 2009. Numerical modelling of in-plane behaviour of URM walls and an investigation into the aspect ratio, vertical and horizontal post-tensioning and head joint as a parametric study. Archives of Civil and Mechanical Engineering. 9(1): 5-27. doi: 10.1016/s1644-9665(12)60037-5.

Tzompanaki, C. 2012. CHANDAKAS. THE CITY AND THE WALLS. (2). Heraklion. Greece: VIKELAIA PUBLIC LIBRARY.

Xatzistergiou, G., & Skopelitis, I. 2010. Restoration study for the line-segment Bembo-Saint Francis and for the orrechione of Sabbionara bastion of the Venetian walls (Duke Beaufort Street). Heraklion. Greece: Xatzistergiou & Associates

Sithiakaki, V., Kanaki, E. & Bilmezi, X. 2013. Older fortifications of Heraklion: A different approach based on recent excavation data. In Archaeological work in Crete. Proceedings of the 3rd Meeting Rethymnon: 395-410, 5-8 December 2013. Rethymno: Department of Philosophy and Social studies. University of Crete – Ephorate of Antiquities of Rethymno

16th International Congress of the Geological Society of Greece
17-19 October, 2022 - Patras, Greece
Bulletin of the Geological Society of Greece, Sp. Publ. 10
Ext. Abs. GSG2022-241

Study on the engineering geological characteristics and the mechanism of a mudflow in the Perivoli, Grevena area.

P. Sotiriou[1], V. Marinos[2], G. Papathanasiou[1]

(1) Laboratory of Engineering Geology & Hydrogeology, School of Geology, Aristotle University of Thessaloniki, Greece, penelopesot315@gmail.com (2) Geotechnical Division, School of Civil Engineering, National Technical University of Athens, Athens, Greece.

Research Highlights

After the continuous rainfall, the water content of the involved soil exceeded its Liquid Limit (LL), causing a mudflow phenomenon. The possible retreat of this instability can reach the hotel foundation area and cut the forest road in the area of Perivoli, Grevena.

Background

In recent years there have been many cases of mudflow events in various areas of Greece. These flow events occurred in soil materials consisting of 50% sand, mud and clay, and with high water content. (Coussot, et al., 1998). These phenomena are generally triggered by heavy rainfalls, although they appear to be favoured by steep geometric characteristics of the slope, especially when there is negligible vegetation. The monitoring, as well as the method of reaction in such cases, are some of the most difficult and elaborate assessments in geoengineering, due to the rapid movement of the phenomenon and a large amount of debris.

The phenomenon studied in this case study is the mudflow that occurred in Perivoli, Grevena, on the 13th of January 2019, closing the road network below. The area of interest is located in Pindos geotectonic zone (Mountrakis et al 1983). Specifically, the affected area is composed of ophiolite under the compound form of mélange of Abdela. The involved formations of a typical mélange are ophiolite, sedimentary and metamorphic rocks. The area has suffered from multiple and severe tectonic movements. These movements led also to the disarrangement and disintegration of the bedrock of the area. Therefore, the formations now appear as laminated and tectonically sheared weak rock masses. Completely soiled materials have been deposited on the surface, which reduces the mechanical properties causing serious stability problems.

The source area of the mudflow appears to be in the hotel's courtyard, where it caused the cut of the forest road on 13/12/2019, after the mudflow event. After the continuous rainfall on the 10th, 11th and 12th of December and the heavy rainfall on the 13th of December, the water content of the involved soil exceeded its Liquid Limit (LL), causing mudflow. The mudflow is segmented into three (3) main axes of transportation (the second axis is the main caterer). All three are characterized as very narrow and fast-paced passages, leading to the North boundary of the affected area where the transported material was deposited. The transported material blocked the north access road to the hotel in three different deposition locations. The possible retreat of this instability can reach the hotel foundation area and cut the forest road in the area.

Methodology

The aim of this study was initiated to determine the nature of the mudflow and subsequently to identify and quantify the factors and the parameters that related to its occurrence with the implementation of high-end remote sensing technologies, such as the LiDAR scanner. For these goals to be achieved, this study was segmented into four (4) main sections.

- The main triggering factors and manifestations of the Perivoli's mudflow are evaluated. The three (3) main axes of data collection in the current study were a) the climatic conditions in the area of interest which led to the event, b) the testimonies of the residents who witnessed the event, and c) the field surveys that were performed after the flow event.
- The followed methodology and the results of the laboratory tests of the soil samples that were collected from the area are evaluated. These analyses led to the classification of the soil material in terms of, particle size distribution, characteristics, and strength. (O'Brien, et al., 1988). Also, they led to the identification of the material's origin, type, and parameterization. They carried out the following laboratory analysis: water content, Granular analysis, Atterberg limits, and instant shearing.
- The fourth section includes a detailed presentation of the methodology that was followed regarding the mudflow monitoring with the usage of the LiDAR scanner. The dense vegetation in the area prevented the LiDAR from penetrating the thick tree trunks, providing unreliable data (unreliable DEM). In order to create the susceptibility map, a digital terrain model (DTM) with a resolution of 5m was used.
- The result of this aforementioned analysis was the creation of a susceptibility map of the area via the Flow -R software (Horton, et al., 2011). As a result of using a terrain model, the final susceptibility map had numerous errors. A noteworthy aspect is that Flow-R is a tool for susceptibility assessment, but it is not suitable for individual event

modelling because the calculated propagation provides a range of possible events. Therefore, a smaller-scale area analysis to identify bigger susceptible areas in Perivoli would make more sense.

Results

Based on the results of the analysis via Flow-R the wider investigation area was found susceptible to mudflow occurrence without distinctive, unified flows. This result is due to incomplete data because of the dense vegetation of the area. The obtained results from the laboratory tests are summarized in Table 1.

Table 1. Laboratory test results.

Laboratory analysis			**Deposit location 1**	**Deposit location 2**	**Deposit location 2**
Water content (%)			14,37	8,46	16,49
Granular analysis	Granular		Thin to medium sand	Thin to medium sand	Thin to medium sand
	Uniformity coefficient		U>15. Very uneven	U>15. Very uneven	U>15. Very uneven
	Rating scale		Good rating	Good rating	Good rating
Attenberg Limits	LL	medium plasticity silt to medium plasticity clay	35,20	38.10	40,30
	PL		23,50	25,14	26,87
Instant shearing	Cohesion c (kPa)		14		
	Friction angle φ (°)		17		

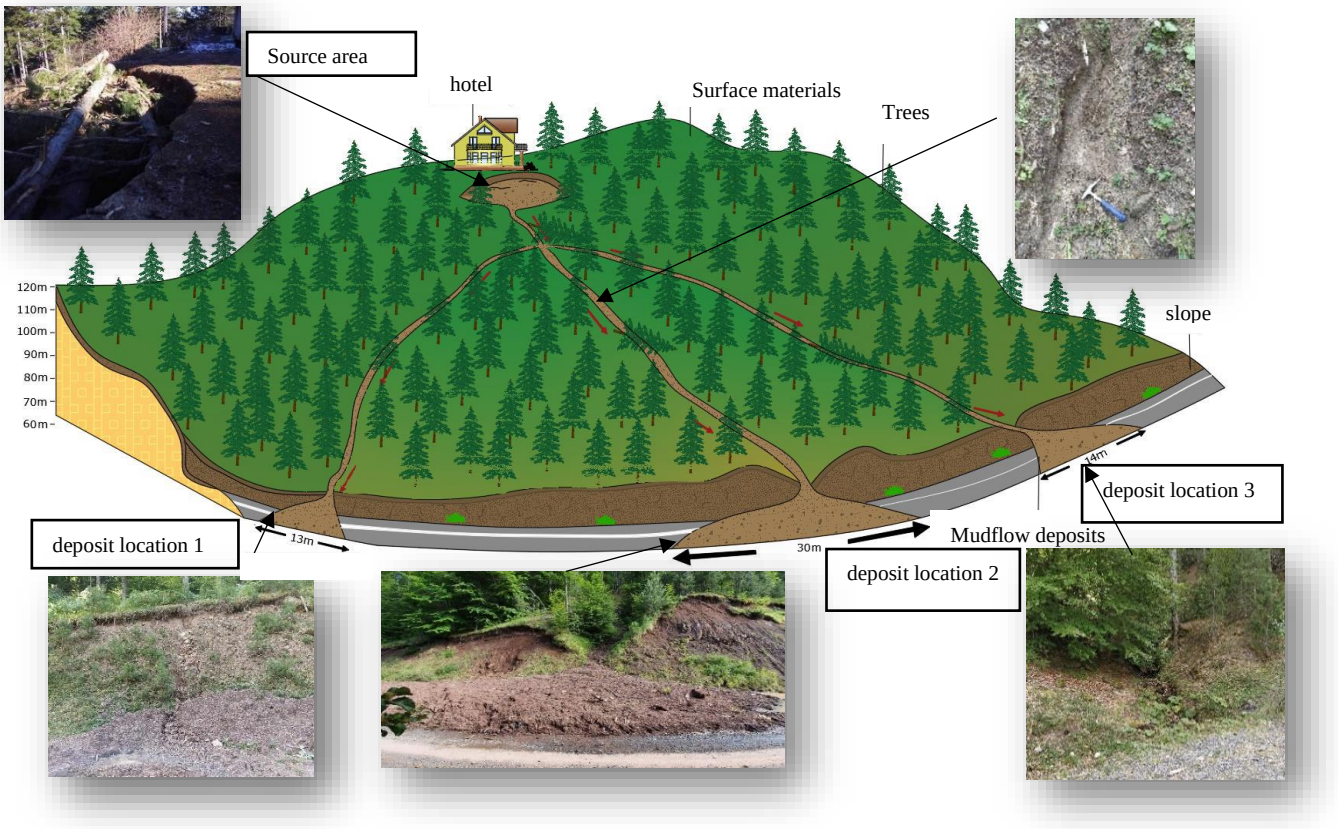

Figure 1: 3D Model of the area

References

Coussot, Ph., Laigle, D., Arattano, M., Deganutti, A.M., Marchi, L., 1998. Direct determination of rheological characteristics of debris flow. Journal of Hydraulic Engineering ASCE 124 (8), 865 – 868.

Horton, P., Jaboyedoff, M., Zimmermann, M., Mozotti, B., Longchamp, C., 2011. Flow-R, a model for debris flow susceptibility mapping at a regional scale - some case studies. Italian Journal of Engineering Geology 2, 875–884.

Mountrakis, D. (2010). Geology and Geo-tectonic Evolution of Greece, pp 132-143.

O'Brien, J.S., and Julien, P.Y. 1988. Laboratory analysis of mudflow properties. Journal of Hydraulics Engineering, ASCE, 114: 877–887.

16th International Congress of the Geological Society of Greece
17-19 October, 2022 - Patras, Greece
Bulletin of the Geological Society of Greece, Sp. Publ. 10
Ext. Abs. GSG2022-248

SAMY II Project. Borehole Inventory for Drawing Water and Groundwater Resources in Greek Territory. Koronia's Ground Water Body Case Study.

C. Christidis[1], P. Sabatakakis, M. Lazaridou, S. Chatzidima, K. Gardiakos, A. Kouskouras, C. Papadopoulos, M. Theodoropoulou, E. Tsolaki, M. Tzima.

[1]Hellenic Survey of Geology and Mineral Exploration (H.S.G.M.E) 1 Spirou Loui St., 13677 Acharne, Greece, christidis@igme.gr

Introduction

SAMY II project is carried out by Hellenic Survey of Geology and Mineral Exploration (H.S.G.M.E.) Project main activities in Greek Territory are: a) borehole inventory by recording drilling technical data and on line measurements, b) database production based to all recorded data and c) groundwater abstraction related to groundwater resources in ground water bodies. During inventory field work, recording data concerns geographical coordinates, drilling operational status and borehole technical characteristics (depth, diameter drill hole and pipeline, pump type). Also, borehole usage such as irrigation, drinking water, stock farming are basic features of recording data with details of pumping.

Based on inventory data final reports are drawn up for all Ground Water Bodies in the field area including also geomorphological, geological, hydrogeological conditions, land use area, statistics with processing of all recording raw data, drawing water estimation and aquifer water balance.

Case Study of Koronia Groundwater Body (EL1000071 - GWB)

Koronia GWB (275,75 Km^2) is located at western part of Mygdonia basin including Koronia's lake acreage 22 – 25 km^2. Its basement belongs to Serbomacedonian massif and consists mainly of flysch, quartzite, quartzite sandstones, two - mica gneiss, amphibolites and marbles. The sediments that fill GWB area can be classified into two main units. Neogene lower unit, composed of sediments, limestones, sandstones, marls, and red clays and upper Quaternary unit, consist of alluvial deposits, lacustrine sediments, clays, sands, and terrestrial phase conglomerates. Groundwater flow (hydrogeological conditions) is characterized by unconfined (upper unit) and semi-confined aquifers (lower unit).

In SAMY II project, more than 1.787 boreholes have been recorded in Koronia's GWB. The rate of 77% (1.337 boreholes) are active, 5% are unexploited (83 boreholes) and 18% are inactive (327 boreholes). Borehole main uses are 90% (1.243 boreholes) for irrigation, 5% (71 boreholes) for domestic water, 3% (37 boreholes) for livestock uses, 2% (21 boreholes) for industrial use and for less than 1% for other uses.

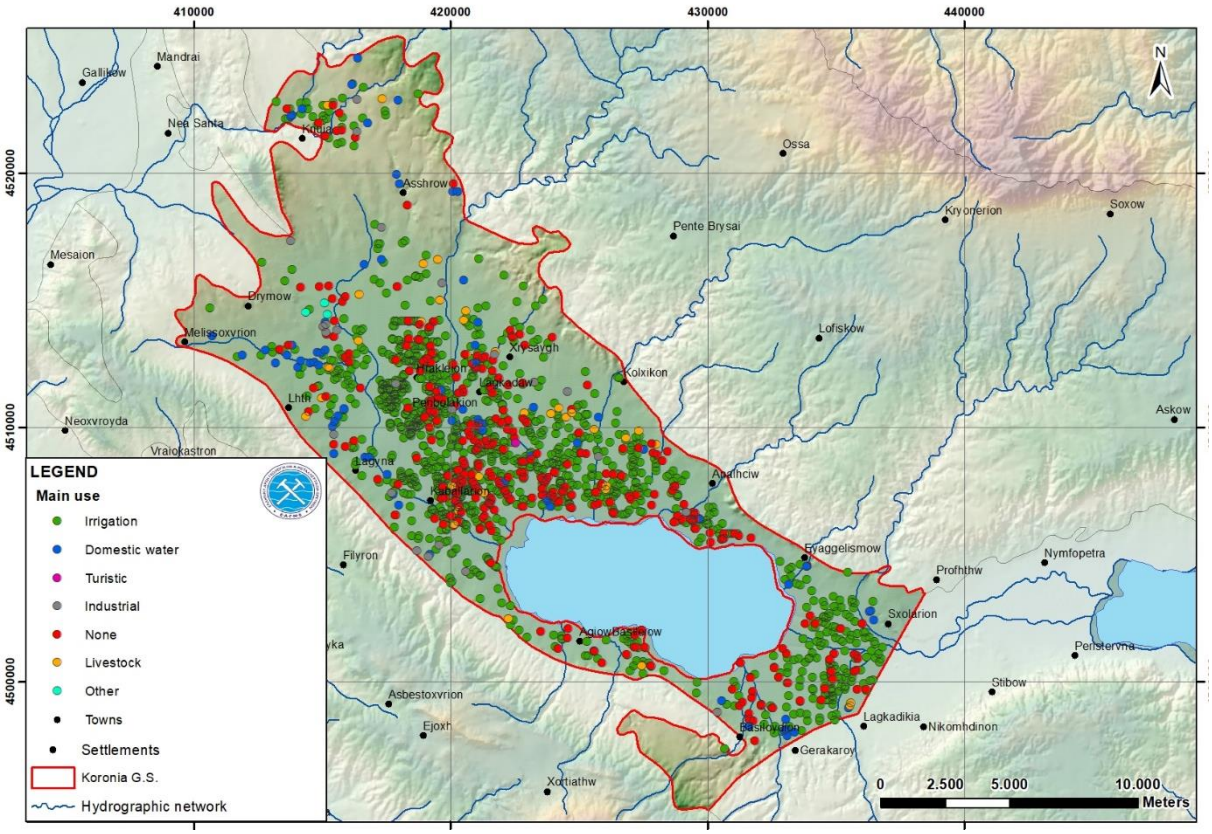

Figure 1. Boreholes mainly use in Koronia's GWB.

Borehole's main depth ranges from 50 – 300 m. Most of them have depth 50-100m. (397 boreholes), 100-150m. (176

boreholes) and 10-50m. (163 boreholes). Boreholes yield, according to raw field data, range from 20 to 40 m^3/h in higher topographic areas, at the margins of the system and 40 to 180 m^3/h in the plain area at Quaternary sediments.

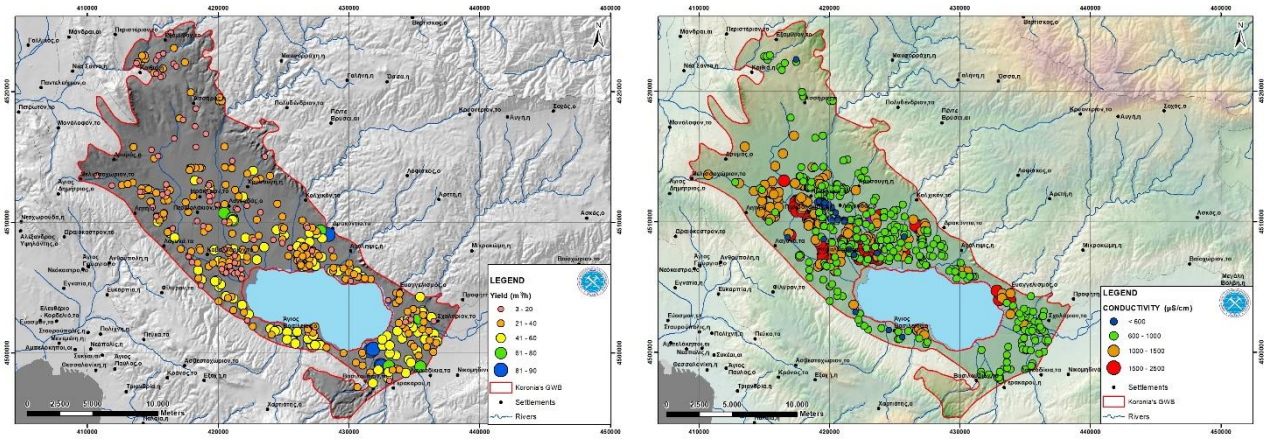

Figure 2. Boreholes yield and conductivity map for Koronia's GWB.

Water electrical conductivity E.C. (μS/cm) measurements were carried out in the field (395 - 9.690 μS/cm). Highest values were determined mainly in Cavalari plain, where intense industrial activity was taking place. Aquifer water level also ranges from +1,25m to +60 mentioned that in plain areas such as Cavarlari artesian water flows in land surface. Total irrigated area is 54.369 km^2.

Groundwater abstraction in Koronia's GWB:

- Irrigation 25.757.608 m^3
- Domestic water 5.548.768 m^3
- Industrial use 276.453 m^3
- Livestock 347.250 m^3
- Other uses 2.650 m^3
- **Total** **31.932.729 m^3**

The groundwater balance assessment made using the water balance equation P = ET + I + R + GA

Precipitation: The average annual precipitation is P= 275.75×10^6 m^2 × 0.49 m = 135.12×10^6 m^3/year.

Evapotranspiration: The average annual evapotranspiration is ET= 275.75×10^6 m 0.383m=105.61×10^6 m^3/year / 78.16 % of precipitation.

Infiltration: Infiltration rate in Koronia's GWB is 14%. Thus, the average annual infiltration is 23.12×10^6 m^3 of water / 17.11% of precipitation.

Surface Runoff: The average annual surface runoff is 6.39×10^6 m^3/ 4.73% of precipitation.

Groundwater abstraction: Drawing water estimated at 31.9×10^6 m^3 (HSGME, 2021). All the calculations for the groundwater equilibrium were made using raster files for each parameter.

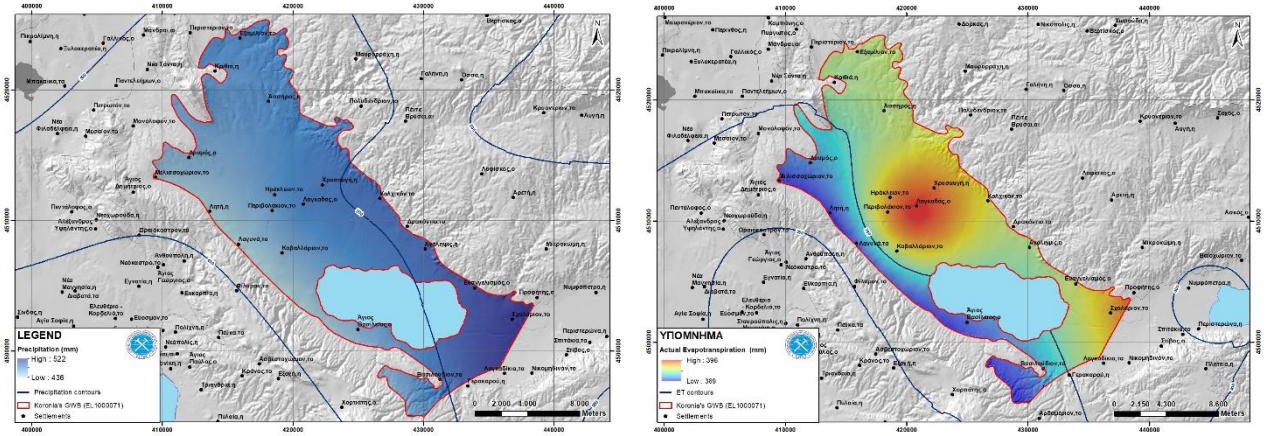

Figure 3. Multiannual precipitation and evapotranspiration maps for Koronia's GWB.

GWB Balance: Koronia's GWB is defined (characterized) as **DEFICIENT**.

References

HSGME, 2021. Results from the hydro-census work and water balance calculation of Koronia groundwater system. Technical Report. (in Greek).

16th International Congress of the Geological Society of Greece
17-19 October, 2022 - Patras, Greece
Bulletin of the Geological Society of Greece, Sp. Publ. 10
Ext. Abs. GSG2022-249

Hydrogeological evaluation using VLF method in the fractured aquifer system of Sithonia peninsula, Chalkidiki, N. Greece

C. Christidis[1], G. Vargemezis[1], K. Voudouris[1]
(1) Aristotle University of Thessaloniki, Greece, christidisc@hotmail.com.

Introduction

Hard rock aquifers are the less studied and exploitable aquifers in Greece. Water demands in Sithonia Peninsula, located in Northern Greece, have risen during the last decades because of the increase of tourist interest of the area. These demands are mainly covered by groundwater abstracted from the coastal alluvial aquifers via numerous boreholes and partly by springwater in semi mountainous area. During the summertime, the population of the area is increasing significantly due to the influx of tourists. The region has the further advantage of being very near to Thessaloniki and is one of the most attractive tourist destinations.

The present – preliminary – results are part of PhD thesis and are based on the data that came up by the geophysical survey in the area, using Very Low Frequency (VLF) method.

The results from the drilling show that due to the intense tectonic stress of the area, the fracture zones in hard rocks, mainly of schists, phyllites, quartzites and sandstones, are located at depths that can reach up to 320 m below ground level, thus forming aquifers of hydrogeological interest.

The main scope of VLF surveys is to detect extended fault zones which are filled up with fresh water. Those zones act as conductive bodies. The major question for this type of survey is to understand when the high conductivity of the fault is caused by the water's existence or by clay minerals.

In this part of the study, VLF surveys were made only in productive and successful boreholes, in order to determine the hydrogeological conditions of the area. In the future, more VLF surveys will be done in target areas which have been delineated using Landsat images.

Materials and methods

Sithonia Peninsula mainly belongs to the Circum Rhodope Belt which composed by Mesozoic sedimentary and metavolcanic rocks. The rest and smallest part of the area belongs to the Serbomacedonian Massif and composed by amphibolites and gneisses (Vergely, 1984). The Sithonia Plutonic Complex is a NW-SE trending plutonic complex which occupies an area of 350 Km^2 mostly composed of granitoids. The metamorphic rocks of Sithonia peninsula have been affected on multiple deformation facies during the Alpine orogeny resulting to the extend growth of cleavages, macro and micro folds. Despite that, during the middle – upper Miocene until nowadays, the neo-tectonic and seismic activity of the area contribute to the extend fracturing of the rocks that generates secondary porosity. Sithonia is described as a tectonic horst with NNW-SSE direction as part of a bigger transportation zone (Mercier, 1981). The hydrogeological behaviour of metamorphic and igneous rocks is related to the discontinuities created by tectonic stress (Domenico and Schwartz, 1998).

Lineaments are linear features which act as evidence for a possible tectonic structure. The extend tectonic stress in hard rocks creates a secondary porosity forming a fractured aquifer. The fractures can be filled up or with water or with argillic minerals, as a result of the tectonic stress in the area.

The VLF method is a widely used geophysical electromagnetic method for the detection of underground water in fractured aquifers. The advantages of this method are that it is a quick, easy and cheap method where the collected data can be easily interpreted and exact useful conclusions about the underground water occurence.

VLF-EM method takes the advantage of electromagnetic radiation which is generated in the low frequency band of 15-30 kHz by military radio transmitters (42 worldwide) for communication and navigation purposes (Parasnis, 1995). VLF magnetic field measurement makes use of E-polarization in which a transmitter is selected in the direction of strike and measuring profiles are taken perpendicular to the strike direction. Generally, the horizontal and vertical components of magnetic fields are measured, and real and imaginary anomalies are computed. The method measures the secondary magnetic field produced by eddy currents that are induced in the ground due to the presence of VLF waves and is suitable for detecting conductive structures up to approximately 200 m deep in terrain with high electrical resistivity.

The data were collected using an ABEM-WADI instrument. Traverses of different directions and stations were made in each area with 10 m interval step.

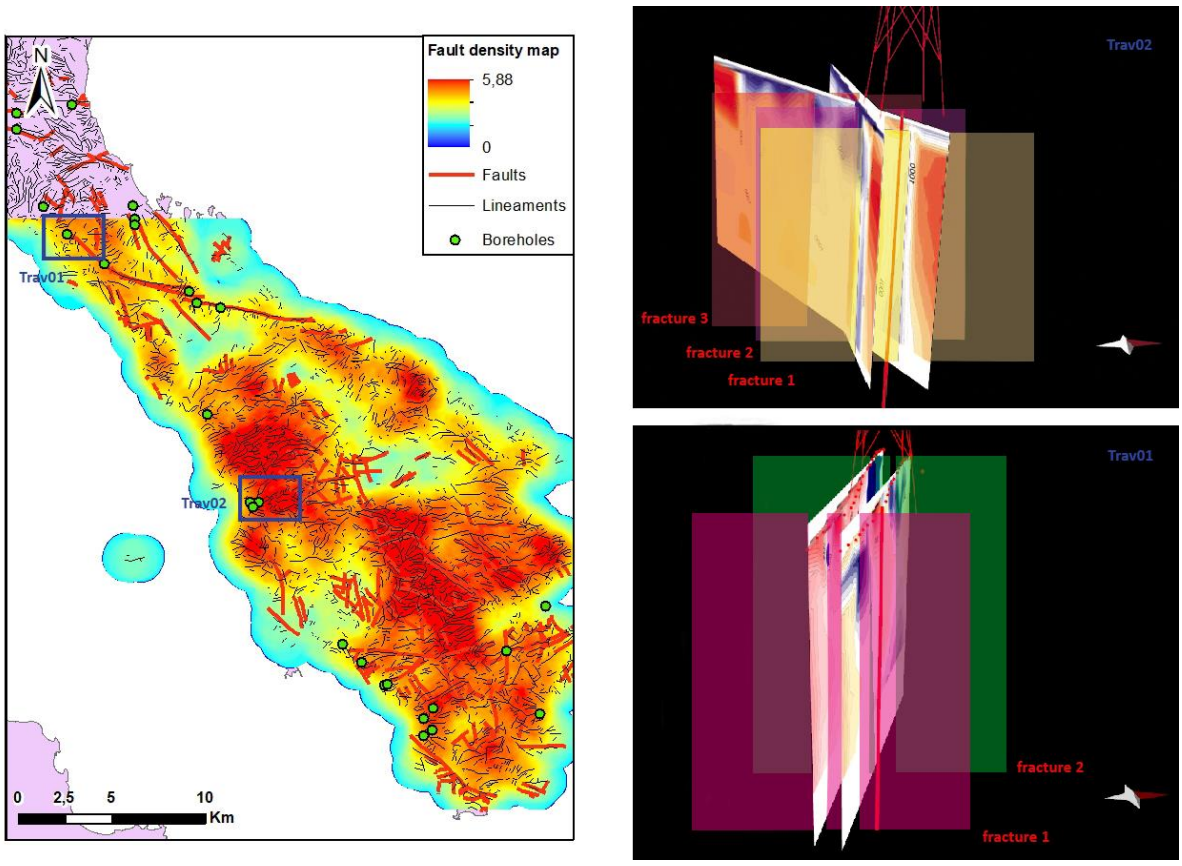

Figure 1. Fault density map with the two project areas (left) and the traverses in those areas (right).

Results

On both of the project areas the geophysical study that carried out, confirmed the reason why the boreholes that exist in those areas where successful.

In the project area 01, two traverses were made with the same direction (NW-SE) and a between them distance of about 50 m. The two traverses were encounter two main fracture zones that probably are filled with fresh water. The borehole is located near fracture 1. The depth of the borehole is 190 m and the yield is 20 m^3/h.

In project area 02, also two traverses were made but with different direction (E-W direction the first one and NE-SW direction the second). The two traverses were encounter three main fracture zones that are probably filled with fresh water. The borehole is located near fracture 1 and has about 250 m depth. The yield of the borehole is not known.

Next step of our research will be a further geophysical study in areas which are extended fractured, according the fault density map that was created for the area (Christidis C., 2022; Gegas et. al., 2022), and productive boreholes exist already. Also, geophysical study in new target areas which have delineated using the lineaments that extracted using satellite images (Landsat) and Digital Terrain Models of the area in order to verify the existence of fracture zones that are filled with fresh water.

Acknowledgements

A part of this research was carried out in the framework of the PhD Thesis of C. Christidis, Laboratory of Engineering Geology and Hydrogeology, Dept. of Geology, Aristotle University of Thessaloniki, Greece (Supervisor K. Voudouris).

References

Christidis C., 2022. Delineation of groundwater potential zones in hard rock aquifers using satellite images, in Sithonia Peninsula, N. Greece. E-proceedings of the Online Youth Water Congress "Emerging water challenges since COVID-19". 6-8 April 2022

Domenico P.A. and Schwartz F.W., 1998. Physical and Chemical Hydrogeology. 2nd Edition, John Wiley & Sons Inc., New York.

Gegas N., Manakos A., Christidis C., Dounou A., Breska E., 2022. New facts about the underground water conditions of fractured hard rocks in the Sithonia peninsula of Halkidiki. 12th International Hydrogeological Conference of Greece. 20-22 March, 2022 Nicosia, Cyprus

Mercier J.L., 1981. Extensional-Compressional Tectonics Associated with the Aegean Arc: Comparison with the Andean Cordillera of South Peru - North Bolivia. Phil. Trans. R. Soc. A., 300, 337-355

Parasnis D.S., 1995. Principles of Applied Geophysics, Chapman et Hall Ed., Fifth Edition, 429pp.

Vergely P., 1984. Tectonique des ophiolites dans le Hellenides internes. Consequences sur l'evolution des regions Tethysiennes occidentales. These Doctorat d'Etat, Paris/Sud (in French).

16th International Congress of the Geological Society of Greece
17-19 October, 2022 - Patras, Greece
Bulletin of the Geological Society of Greece, Sp. Publ. 10
Ext. Abs. GSG2022-250

Slope Stability Analysis of the Earthquake-induced Landslide on October 30th, 2020 in the Avlakia Area, Samos Island, Greece

N. Spanou[1], V. Kontogianni[1], D. Galanakis[1], I. Vakalas[1], I. Zananiri[1], N. Nikolaou[1]
(1) Hellenic Survey of Geology & Mineral Exploration, Acharnes, Greece. spanou@igme.gr

On October 30th, 2020, a strong earthquake (Mw 7.0) occurred offshore, just north of Samos Island, causing life losses, injuries and damages, especially in Turkey. An E-W striking (N-dipping), normal dip-slip fault was ruptured, running along and controlling the northern coastline of the island (Sboras *et al*., 2021). The broader area is characterized by a complex geodynamic setting with both rich seismic history and numerous active faults of different directions and kinematics (Chatzipetros *et al*., 2013; Caputo *et al*., 2012). The slope failure near Avlakia area (Figure 1a) occurred on a steep slope of a NW-SE orientated low ridge consisting of steeply NW-dipping Miocene marly limestone (Figure 1b). Although there was no access to the southwestern side of the ridge, there is a strong suspicion that the valley that follows is tectonically controlled. This fault can be related to the Kokkari-Avlakia fault shown in (Figure 1a, b).

The wider studied area is structured by lacustrine thin-stratigraphic marly limestone, which consists the upper series of the Neogene sediments of Mytilinion basin. It is whitish to gray, containing loose marls, and clays intercalations, as well it usually appears covered by weathering mantle about 1.5 m thick. The series belong to Miocene sediments, in some areas fractured and folded. The total thickness reaches 650 m approximately.

The limestone forming the considered landslide in Avlakia (Figure 1b), shows varying thickness, usually thin-bedded (<6 cm) and marly, while in places it develops a wider bedding (6-20 cm) with more compact limestone horizons. From the northern edge of the landsliding hill and a length 140 m to the south, the slope is covered by former sliding materials until the altitude 40 m. Furthermore, in places, there are debris from the recent landslides and rockfalls which occurred as secondary effects of the earthquake on October 30th, 2020 (Figure 1c, d & 2b).

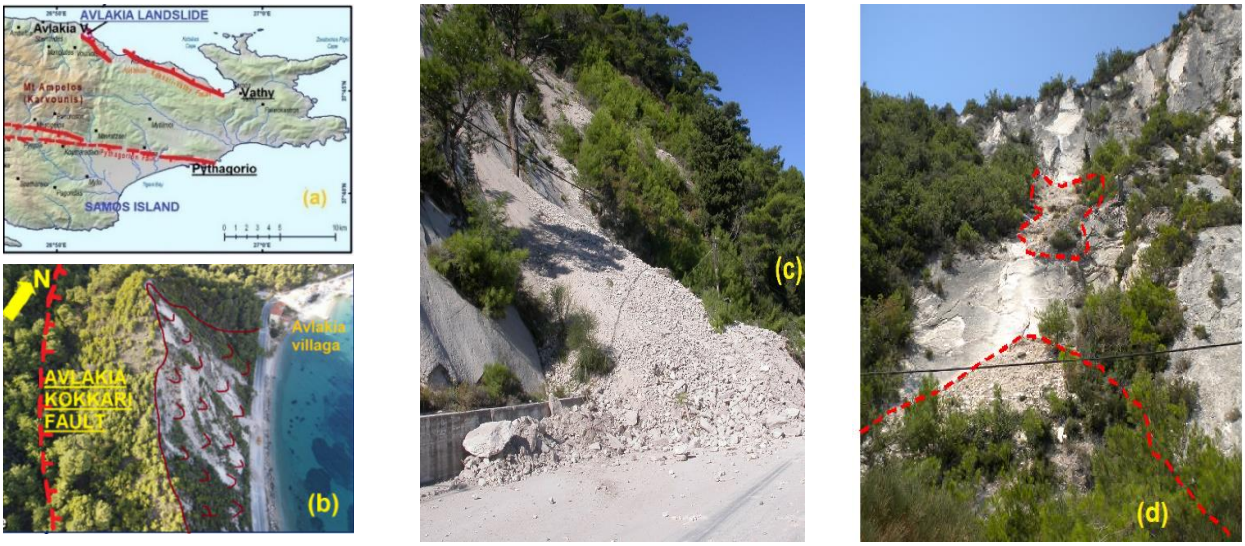

Figures 1: The location of Avlakia landslide on Samos island (a), Avlakia landslide occurred on a steep slope of a NE-SW direction orientated low ridge consisting of steeply NE-dipping Miocene marly limestones (b), the limestones of the landslide show various thicknesses and NE dip exceeding 55° (c), landsliding materials due to the October 30th, 2020 earthquake (c, d).

Laboratory tests were performed on samples for the determination of the strength of rock material which indicated a medium to high strength. Furthermore, microtectonic analysis of joints has been conducted and the characteristics of the fractured rock leaded to the geotechnical classification of the rock mass via the Geological Strength Index (GSI) scoring 45 and the Rock mass rating (RMR_{bas}) scoring 41. However, taking into consideration the high density of joints formed by the limestone's thin bedding and its marly texture, the final rates are much lower classifying the rock mass to poor quality.

Additionally, kinematic analysis was completed for 2 critical slope dips (55° and almost vertical) using the computer program Dips (Rocscience) (Konstantopoulou *et al*., 2015). Two of the results are shown in Figure 2c, referring to the almost vertical dip of the study slope. The left one corresponds to planar sliding, then the right corresponds to wedge

sliding. Relatively to toppling, the statistical analysis of the recorded joints did not reveal much of potential sliding, however rockfall hazard was estimated as highly dangerous because of numerous overhanging rock fragments.

Analyses of the motion and resulting paths of potentially unstable rocks along the pathway were conducted (see also Kontogianni et al., 2019). The rockfall simulations were carried out on the 5 most critical profiles selected during field work, corresponding to the highest profile of the slope or locations where the October 30th rockfalls were observed. Cross section geometry was developed using the digital elevation model produced by a UAV (Figure 2a). Rockfall modeling was completed for all 5 critical slope sections using the computer simulation program RocFall Built 8.015 (2021). Field observations on detached rocks were used as input to the modelling. Other input parameters including source zones, block size, shape, surface roughness and friction coefficients were based on field observations, laboratory testing and rock mass description. Rockfall simulations produced reasonable predictions of the rockfall paths for rock masses of 300 kg breaking up after first crash for both cases of no seismic and seismic loading (Figure 2a). For each one of the examined slope sections, the most effective protection system was determined based on an iterative process of various measures. The support system proposed after the rockfall pathway analyses was a 5m high rockfall barrier built on the top of a 3m high concrete wall. A gravel embankment at the back side of the wall will further contribute to the entrapment of the rocks.

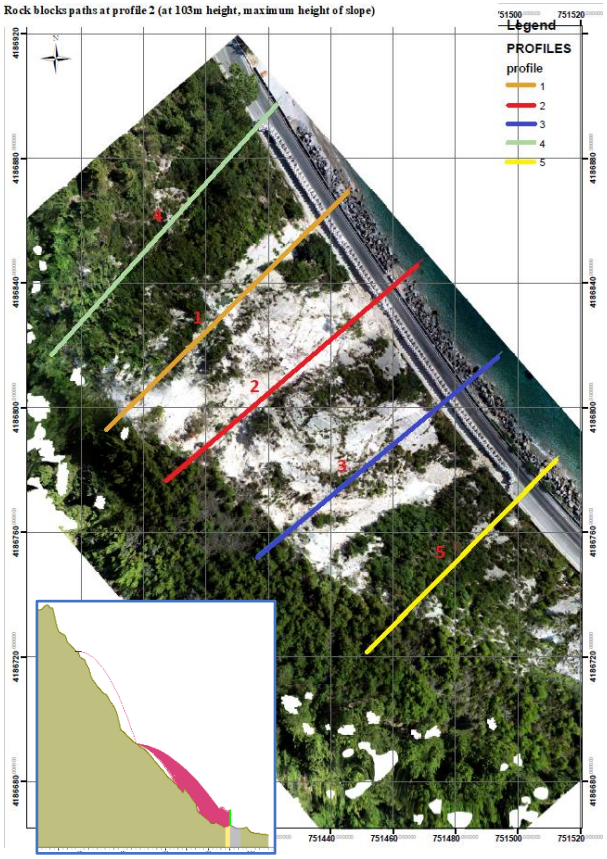

(a)

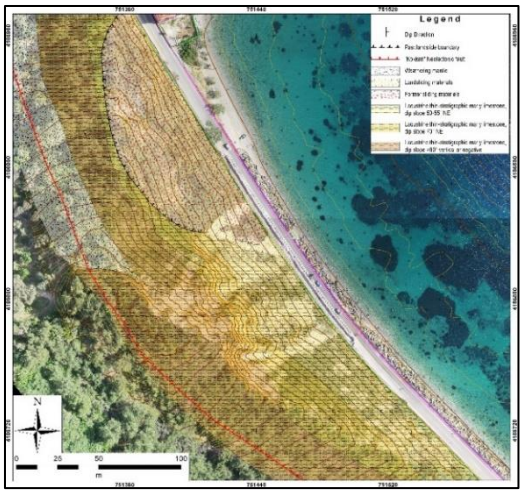

(b)

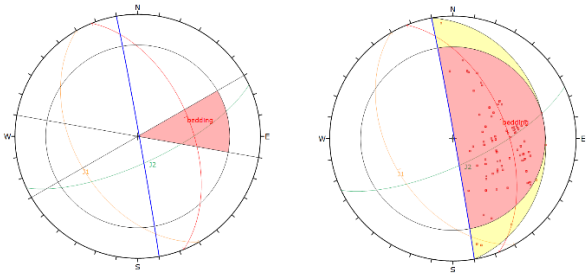

(c)

Figures 2: Orthophoto of the Avlakia slope from drone (map and DEM produced by HSGME 2021). Inset: Rockfall paths at profile 2 (at 103 m height, maximum height of slope) with seismic loading, assuming 0.3g seismic acceleration (a), Engineering Geology map of the study area (b) and kinematic analysis results for planar (left) and wedge (right) sliding on stereographic projection (c).

References

Caputo, R., Chatzipetros, A., Pavlides, S., Sboras, S., 2012. The Greek Database of Seismogenic Sources (GreDaSS): state-of-the-art for northern Greece. Annals of Geophysics 55(5), 859-894. https://doi.10.4401/ag-5168

Chatzipetros, A., Kiratzi, A., Sboras, S., Zouros, N., Pavlides, S., 2013. Active faulting in the north-eastern Aegean Sea Islands. Tectonophysics 597, 106-122.

Konstantopoulou, G., Spanou, N. and Kontogianni V., 2015. Rockfall at the Arvanitia Pathway, Nafplio, Greece: Protection of the Site with Respect to Its Unique Natural Beauty and Archaeological Interest. Engineering Geology for Society and Territory, Springer, 8, pp 431–436.

Kontogianni V., Spanou N. and Nikolaou N., 2019. Vulnerability of critical infrastructures to rock fall hazard: the case of the Wastewater Treatment Facility of Tolo, Greece. 15th International Congress of the Geological Society of Greece, Athens, 22-24 May, 2019 Bulletin of the Geological Society of Greece.

Sboras, S., Lazos, I., Bitharis, S., Pikridas, C., Galanakis, D., Fotiou, A., Chatzipetros, A., Pavlides, S., 2021. Source modelling and stress transfer scenarios of the October 30, 2020 Samos earthquake: seismotectonic implications. Turkish Journal of Earth Sciences 30(8), 699-717.

16th International Congress of the Geological Society of Greece
17-19 October, 2022 - Patras, Greece
Bulletin of the Geological Society of Greece, Sp. Publ. 10
Ext. Abs. GSG2022-251

New insights in the correlation of liquefaction phenomena with the evolution of a floodplain

G. Papathanassiou[1], S. Valkaniotits[2], M. Taftsoglou[2], R. Caputo[3]

(1) Aristotle University of Thessaloniki, Thessaloniki, Greece, gpapatha@geo.auth.gr (2) Democritus University of Thrace, Xanthi, Greece (3) Department of Physics and Earth Sciences, University of Ferrara, Italy.

Liquefaction phenomena are considered as lesser hazardous earthquake-induced secondary effects than those of coseismic landslides and tsunamis. However, the triggering of liquefaction is related not only to free-field effects, inducing low severity damages to farmlands, but also to structural failures that can heavily affect the community resilience, like the ones induced by the 2010-2011 Canterbury sequence, the 2012 Emilia sequence etc. (Cubrinovski et al., 2011; Emergeo WG, 2013; Dolce and Di Bucci, 2014; Papathanassiou et al., 2022).

Studying the occurrence of liquefaction phenomena is a multiparameter task, where geologists, seismologists and engineers must cooperate (Papathanassiou et al., 2022). Initially, the susceptibility to liquefaction should be assessed either on local or regional scale by taking into account quantitative and qualitative information, respectively. At a regional scale, this assessment is mainly based on the statement that the depositional environment and the age of shallow sediments, which are among the most crucial parameters for the classification of a geological unit regarding the liquefaction susceptibility.

This general statement is strengthened by the outcomes arose from studies conducted the last decade in New Zealand, Italy and Greece, highlighting that most of the liquefaction phenomena were concentrated in areas where river channels had been reclaimed or in old/abandoned channels (Wotherspoon et al., 2012; Di Manna et al., 2012; Bastin et al., 2015; Papathanassiou et al., 2012; 2015; Civico et al., 2015). In particular, it is shown that even active floodplains behave heterogeneously in terms of liquefaction and that the spatial distribution of clustered liquefaction phenomena is strongly related to current and former river channels, point-bars, abandoned meanders and oxbow lakes. Recently, Papathanassiou et al. (2022) have shown the influence of the evolution of the geomorphology in the alluvial plain of Piniada Valley, Thessaly, central Greece, by plotting the spatial distribution of liquefaction manifestations on the historical aerial photograph of 1945 (Figure 1).

Figure 1. Correlation of liquefaction manifestations triggered by the March 2021 Thessaly earthquakes with the geomorphological features as they are shown on the aerial photograph of 1945 (Papathanassiou et al. 2022).

Nowadays, the paleoenvironmental features of a meandering river system can be reconstructed by analyzing remote sensing data such as satellite imageries, historical aerial photographs in conjunction with topographic maps and archives

describing the impact of anthropogenic factor i.e., diversion of a river channel, to the evolution of a meander river. Having traced these features e.g., abandoned river channels, oxbow lakes, swamps and crevasse splays, the most prone to liquefaction areas can be targeted in advance. This could result in a reduction of the area where detailed engineering geology investigations (e.g., boreholes with in-situ tests) are required for the evaluation of the liquefaction hazard and consequently reducing the relevant cost of the project (Papathanassiou et al, 2022).

References

Bastin, S., Quigley, M., Bassett, K., 2015. Paleoliquefaction in easter Christchurch. New Zealand Geological Society America Bulletin, 12, 1348-1365.

Civico, R., Brunori, C.A., De Martini, P.M., Pucci, S., Cinti, F.R, Pantosti, D., 2015. Liquefaction susceptibility assessment in fluvial plains using airborne lidar: The case of the 2012 Emilia earthquake sequence area (Italy). Natural Hazard Earth System Science, 15, 2473-2483.

Cubrinovski, M., Bradley, B., Wotherspoon, L., Green, R., Bray, J., Wood, C., Pender, M., Allen, J., Bradshaw, A., Rix, Gl., Taylor, M., Robinson, K., Henderson, D., Giorgini, S., Ma, K., Winkley, A., Zupan, J., O' Rourke, T., De Pascale, G., Wells, D., 2011. Geotechnical aspects of the 22 February 2011 Christchurch earthquake. Bulletin New Zealand Society Earthquake Engineering, 44, 205-226.

Di Manna, P., Guerrieri, L., Piccardi, L., Vittori, E., Castaldini, D., Berlusconi, A., Bonadeo, L., Comerci, V., Ferrario, F., Gambillara, R., Livio, F., Lucarini, M., Michetti, A.M., 2012. Ground effects induced by the 2012 seismic sequence in Emilia: implications for seismic hazard assessment in the Po Plain. Annales Geophysicae, 55(4), 697–703.

Dolce, M., Di Bucci, D. (2014): National Civil Protection Organization and technical activities in the 2012 Emilia earthquakes (Italy). Bulletin Earthquake Engineering, 12, 2231-2253, https://doi.org/10.1007/s10518-014-9597-x.

Emergeo Working Group (2013): Liquefaction phenomena associated with the Emilia earthquake sequence of May–June 2012 (Northern Italy). Natural Hazards Earth System Science, 13, 1-13, https://doi.org/10.5194/nhess-12-1-2013.

Papathanassiou G, Valkaniotis S, Ganas Ath, Stampolidis Al, Rapti D, Caputo R. 2022. Floodplain evolution and its influence on liquefaction clustering: The case study of March 2021 Thessaly, Greece, seismic sequence, Engineering Geology, Volume 298, 106542, https://doi.org/10.1016/j.enggeo.2022.106542.

Wotherspoon, L., Pender, M., Orense, R.P., 2012. Relationship between observed liquefaction at Kaiapoi following the 2010 Darfield earthquake and former channels of the Waimakariri River. Engineering Geology, 125, 45-55. https://doi.org/10.1016/j.enggeo.2011.11.001, 2012.

16th International Congress of the Geological Society of Greece
17-19 October, 2022 - Patras, Greece
Bulletin of the Geological Society of Greece, Sp. Publ. 10
Ext. Abs. GSG2022-256

Comparison Between Different Multi-Criteria Decision Analysis (MCDA) Approaches in Coastal Vulnerability Index Calculations

V. Boumpoulis[1], N. Depountis[1]
(1) University of Patras, Patra, Greece, vasileios_boumpoulis@upnet.gr

Research Highlights

Calculation of CVI incorporating different weight factors and using MCDA methods.

Introduction

As one of the vastest natural hazards, coastal erosion, and sea level rise, threats to the coastline with increasing frequency and intensity, while their impacts in coastal zones are considered to be huge (IPCC, 2022). Moreover, the population in the coastal zone is increasing and half of the EU population lives in regions within 50 km of the coast (ESTAT, 2009), whereas 50% of the world's population lives within 200 km of a coastline (Kummu *et al.*, 2016). Therefore, the assessment of coastal vulnerability has become an important aspect for the protection of the environment, infrastructure, and human population.

Numerous studies have been proposed for the evaluation of the vulnerability in coastal zones with the most common method being the Coastal Vulnerability Index (CVI). The calculation of CVI requires the integration of different data and parameters focused on hydrodynamic, physical, geological, and socio-economic variables. However, in the majority of the CVI studies the parameters used are considered to have equal contribution to the vulnerability assessment. To overcome this consideration, Multi-Criteria Decision Analysis (MCDA) methods have been used to give weights and prioritize the parameters used, with the application of the Analytical Hierarchy Process (AHP) (Saaty *et al.*, 1977). The main aim of this study is to compare the results of using different MCDA methods for the calculation of CVI, by applying them in the coastal area of the Gulf of Patras.

Methodology

The selected key parameters of CVI and the modified CVI_{WF} used in this study, as they have been presented by Boumpoulis et al. (2021) are: i) the use of geological-geomorphological (CVI) and geotechnical (CVI_{WF}) data, ii) the significant mean wave height with a return period of 10 years, iii) the coastal slope which has been calculated by using a Digital Elevation Model (DEM) (5X5 m), iv) the shoreline evolution (2006-2018), v) the average tidal range and vi) the Sea Level Rise (SLR). For the weighting of each one of these parameters, the AHP and Fuzzy AHP (FAHP) techniques were implemented and the calculation of CVI was performed using the following equations: a) the classic formula of CVI (1), b) the modified formula CVI_{WF} (2) with a weight factor in the geotechnical parameter and c) the CVI_{AHP} and CVI_{FAHP} formulas (3):

$$CVI = \sqrt{\frac{a * b * c * d * e * f}{6}} \quad (1)$$

$$CVI_{WF} = \sqrt{\frac{a^3 * b * c * d * e * f}{6}} \quad (2)$$

where a: Geotechnical properties and units b: Significant wave height c: Coastal Slope d: Shoreline evolution e: Tidal range f: Sea level rise (SLR)

$$CVI_{AHP} \text{ and } CVI_{FAHP} = W1 * V1 + W2 * V2 + \cdots + Wi * Vi \quad (3)$$

where: Wi is the weight value and Vi is the vulnerability score of the i-th parameter. The ranking of CVI values into vulnerability classes was performed by applying the equal interval classification method.

Results

In Table 1 are presented the results from the weighting of the CVI parameters using the AHP and FAHP methods. The results indicate that both methods provide similar weights in the parameters with negligible differences.

Table 1: Weight factor of CVI parameters by applying AHP and FAHP methods

Variables	Geotechnical properties	Significant mean height wave	Coastal slope	Shoreline evolution	Average tidal range	Sea Level Rise
AHP_Weight	0.35	0.12	0.20	0.22	0.04	0.07
FAHP_Weight	0.38	0.10	0.21	0.24	0.04	0.03

Application of the coastal vulnerability index using the CVI and CVI_{WF} equations shows that the high and very high vulnerability classes have a smaller proportion in comparison with the CVI_{AHP} and CVI_{FAHP} equations. Specifically, the regime of the coastline of the Gulf of Patras can be characterized with low to high vulnerability using the CVI and CVI_{WF}, while the application of CVI_{AHP} and CVI_{FAHP} indicates that the regime of the coastline is under high and very vulnerability (Figure 1). Furthermore, the increase in the very high vulnerability class using the CVI_{AHP} and CVI_{FAHP}, is almost 25%, which is much higher than the respective values of CVI and CVI_{WF} (3% - 5%). In addition, the very low vulnerability class has a significant percentage using the CVI and CVI_{WF} methods (15-20%), which becomes much smaller using the CVI_{AHP} and CVI_{FAHP} equations (4%).

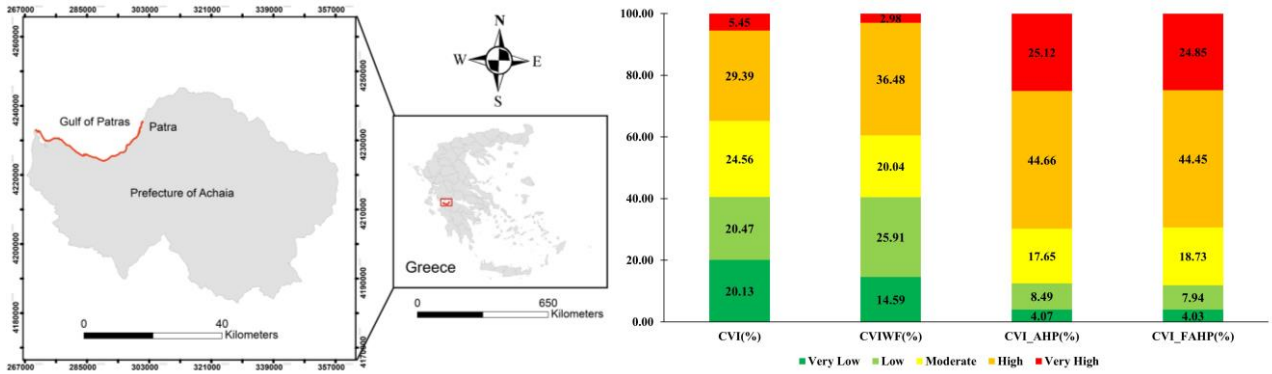

Figure 1: Study area and outputs of MCDA Approaches in CVI calculations.

Conclusions

Many researchers tried to apply the CVI using MCDA methods and especially AHP (Sekovski *et al.*, 2019, Diaz-Cuevas *et al.*, 2020) to insert weight factors in the CVI parameters. The classical formulation of CVI may underestimate the vulnerability and this fact is mentioned also in other papers (De Serio *et al.*, 2018). Hence, the introduction of weight factors in CVI calculation should increase the reliability and accuracy of the vulnerability model, as each parameter has a different contribution to vulnerability assessment. The comparison between AHP and FAHP weights in each one of the CVI parameters of the Gulf of Patras did not reveal important differences, but compared with the application of these weights in the CVI formulation, the increase in the coastal vulnerability proved to be very high. In any case, this result needs further investigation before deciding if MCDA methods are more reliable in CVI calculations or they may overestimate the final results.

Acknowledgements

The authors acknowledge that the raw data used in the CVI calculations came primarily from the "TRITON/Greece-Italy/Interreg V/A 2014-2020 cooperation project" and secondarily from the "EROSION-SENSE/Human Resources Development, Education and Lifelong Learning 2014-2020 operational project".

References

Boumboulis V, Apostolopoulos D, Depountis N, Nikolakopoulos K., 2021. The Importance of Geotechnical Evaluation and Shoreline Evolution in Coastal Vulnerability Index Calculations. Journal of Marine Science and Engineering 9, 423. https://doi.org/10.3390/jmse9040423

De Serio F, Armenio E, Mossa M, Petrillo A.F., 2018. How to define priorities in coastal vulnerability assessment, Geosciences 8, 415. https://doi.org/10.3390/geosciences8110415

Díaz-Cuevas P, Prieto-Campos A, Ojeda-Zújar J., 2020. Developing a beach erosion sensitivity indicator using relational spatial databases and Analytic Hierarchy Process. Ocean Coastal Management 189, 105146. https://doi.org/10.1016/j.ocecoaman.2020.105146

ESTAT. Nearly Half of the Population of EU Countries With a sea Border is Located in Coastal Regions; EUROSTAT: Luxembourg, 2009.

Kummu M., de Moel H., Salvucci G., Viviroli D., Ward P.J., Varis O., 2016. Over the hills and further away from coast: Global geospatial patterns of human and environment over the 20th–21st centuries. Environmental Research Letters, Volume 11, Number 3.

IPCC, 2022: Climate Change 2022: Impacts, Adaptation, and Vulnerability. Contribution of Working Group II to the Sixth Assessment Report of the Intergovernmental Panel on Climate Change [H.-O. Pörtner, D.C. Roberts, M. Tignor, E.S. Poloczanska, K. Mintenbeck, A. Alegría, M. Craig, S. Langsdorf, S. Löschke, V. Möller, A. Okem, B. Rama (eds.)]. Cambridge University Press. In Press.

Sekovski I., Del Rio L., Armaroli C., 2019. Development of a coastal vulnerability index using analytical hierarchy process and application to Ravenna province (Italy). Ocean and Coastal Management 183, 104982. https://doi.org/10.1016/j.ocecoaman.2019.104982

Saaty T.L., 1977. A scaling method for priorities in hierarchical structures. Journal of Mathematical Psychology, *15*, 234–281.

16th International Congress of the Geological Society of Greece
17-19 October, 2022 - Patras, Greece
Bulletin of the Geological Society of Greece, Sp. Publ. 10
Ext. Abs. GSG2022-287

Displacement rates in the coastal zone of Panagopoula landslide, Greece, after an earthquake event

Christos Theodoropoulos[1], Zoe Misiri[2], Katerina Kavoura[2], Kurosch Thuro[1], Nikolaos Depountis[2]
(1) Technical University of Munich, Munich, Germany, christos.theodoropoulos@tum.de (2) Laboratory of Engineering Geology, University of Patras, 26504, Greece

Research Highlights

The seismic event of 17.02.2021 caused a clear acceleration to the landslide of Panagopoula, while the calculated average annual rates of movements provided a characterization of an extremely slow landslide with N to NE direction.

Introduction

The southern part of the Gulf of Corinth in Northern Peloponnese, Greece, is highly connected with numerous landslide events triggered by heavy rainfall, earthquakes, and anthropogenic activity, combined with an already tectonically highly active area. The area of interest, Panagopoula, is highly susceptible to landslides, diachronically affecting the existing motorway and railway connecting Athens with the city of Patras. On 25-27 April and 3 May 1971, large-scale failures were recorded, and as a result, the traffic connections were interrupted (Sabatakakis et al., 2015).

Even though this landslide occurred 50 years ago, it is still active and has been a subject of many studies. Although many protective measures have been constructed, the inclinometers show continuous, slow movement during the last twenty years (Kavoura et al., 2016). Besides that, during the first months of 2021, the Gulf of Corinth presented considerable seismic activity and on 17 February 2021, a sequence of seismic events took place, with the largest on the scale of 5 Richter (National Observatory of Athens/Institute of Geodynamics). As a result, extensive surface cracks appeared in a 1.5-2 km longitudinal direction parallel to the Panagopoula-Psathopyrgos fault (Figure 1).

This study aims to calculate the different rates of movement of the landslide's failure surface before and after the seismic event of 17.02.2021 and examine if the landslide has been accelerated, decelerated or remained at the same levels. Furthermore, the direction of movement has been calculated and in a second phase, several models of the landslide area were produced and analysed with the SLIDE 6.0 software. The latter is out of the frames of this work.

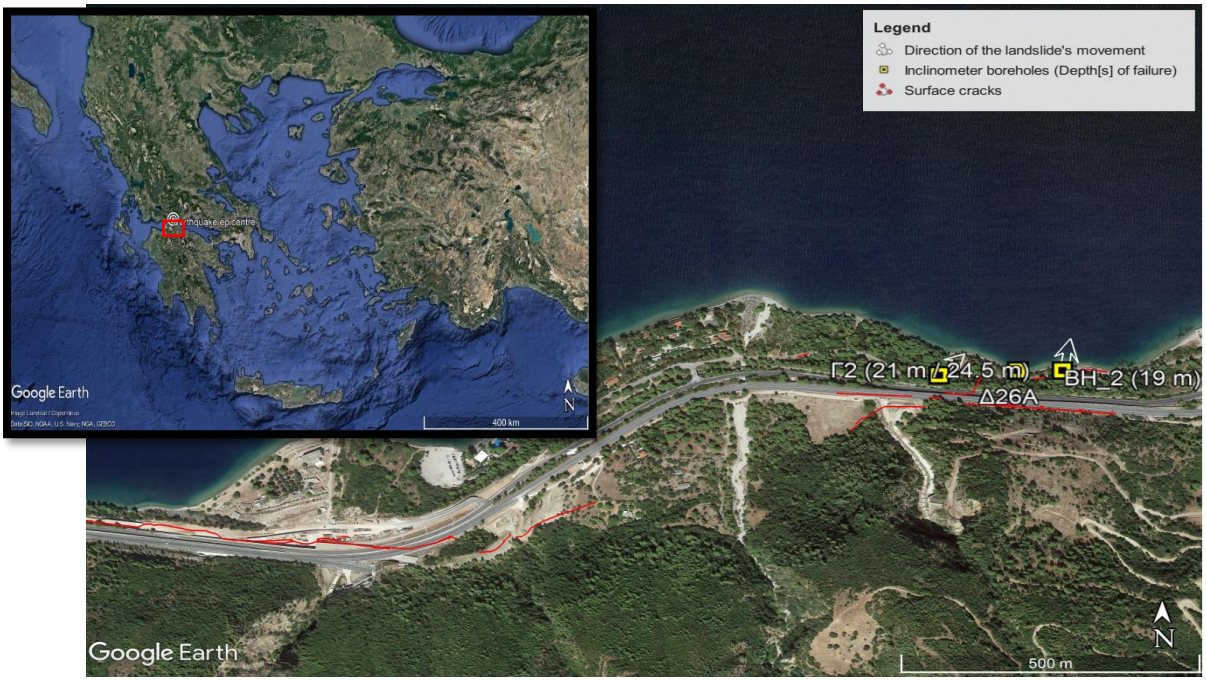

Figure 1: The wider area of the Panagopoula landslide with its movement characteristics and crack development after the seismic event of 17.02.2021.

Methodology

In the last decade, three inclinometer boreholes (Γ2, Δ26A and BH_2) are continually recorded by the laboratory of Engineering Geology, University of Patras. These boreholes are located on the coastal road, below an old national road.

During the on-site visits together with the inclinometer measurements (taken with the ITMSOIL DIGITAL INCLINOMETER) a detailed topographic survey of the surface cracks, caused by the seismic event, took place. These cracks are still observed parallel to the Panagopoula-Psathopyrgos fault (Figure 1).

Newly acquired inclinometric data, (after the seismic event of 17.02.2021) were combined for the first time with older data (before the seismic event of 17.02.2021) and the rates and directions of movement (according to the method suggested by Stark & Choi, 2008) were calculated, together with the average annual rates of movements. Furthermore "**Displacement [mm] – Dates of Measurements**" curves have been produced for the landslide failure depths, which were determined according to the incremental and cumulative data of each borehole.

Results

The results present a clear acceleration rate of movement after the seismic event for the Γ2 and BH_2 boreholes, while the Δ26A borehole did not present any displacement at all. The Γ2 borehole presents two failure surfaces, one at 21 m depth and the other at 24.5 m depth, which gives larger displacements. The BH_2 borehole presents one failure surface at 19 m depth with an even large displacement. These two boreholes have been accelerated by the factors of approx. 4 (BH_2 and Γ2 at the depth of 24.5 m) and 2 (Γ2 borehole at the depth of 21 m) regarding their average annual rate of movement (Figure 2) and the direction of movement has a N to NE direction (Figure 1).

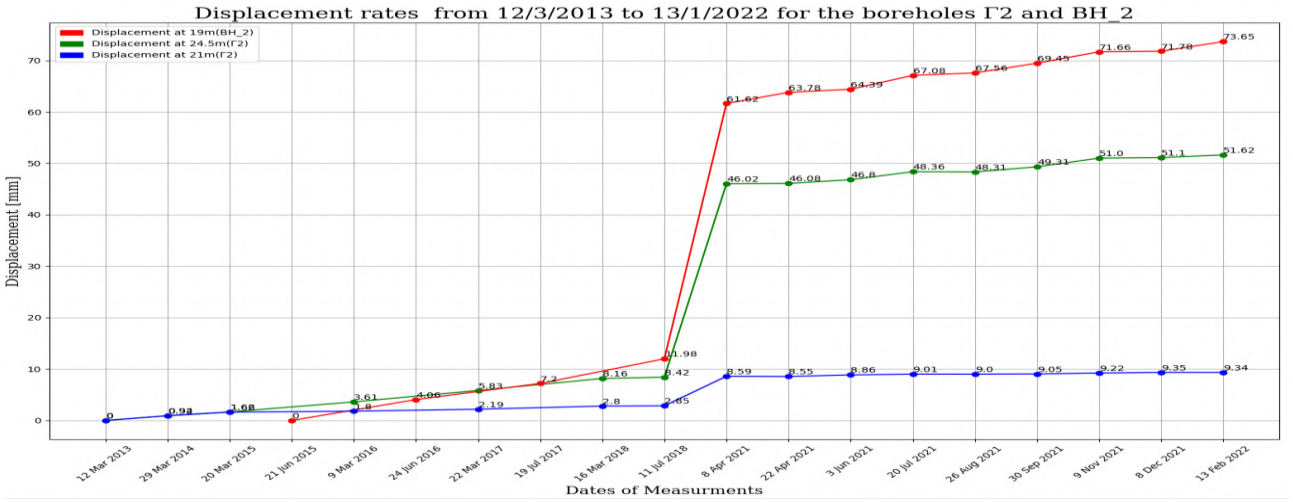

Figure 2: Displacement rates from 12.03.2013 to 13.01.2022 for boreholes Γ2 and BH_2.

Conclusions

The seismic event of 17.02.2021 has accelerated the coastal zone of the Pangopoula by a factor of approx. 4 in the BH_2 borehole (at 19 m depth) and in the Γ2 borehole (at 24.5 m depth), while the same factor is approx. 2 in the Γ2 borehole (at 21 m depth). Moreover, the Γ2 borehole presents a rate of movement of 0.53 mm/year before the seismic event of 17.02.2021, while this turned into 0.98 mm/year after the seismic event, at the depth of 21 m. The same borehole presented a rate of movement of 1.58 mm/year before the seismic event, while this turned into 7.27 mm/year, after the seismic event, for the failure surface at the depth of 24.5 m. In the BH_2 borehole at the depth of 19 m, the rate of movement was calculated at 3.92 mm/year before the seismic event, while this turned into 15.62 mm/year after the seismic event of 17.02.2021. According to Cruden & Varnes, 1996 and the Australian Geomechanics Society, 2002, the landslide of Panagopoula could be characterized as extremely slow, with N to NE direction of movement.

References

Australian Geomechanics Society, 2002: Landslide risk management concepts and guidelines, in: Australian Geomechanics Society Sub-committee on Landslide Risk Management (ed.): Australian Geomechanics, 51-70.

Cruden, D., Varnes, D., 1996: Landslide types and processes, in: Turner, A.K., Schuster, R.L. (eds.): Landslides: investigation and mitigation, 36-75.

Kavoura, K., Anagnostopoulou, S., Servou, K., Depoundis, N., Nikolakopoulos, K., Sabatakakis, N., 2016. Kinematic analysis evolution of extended landslides: two case studies from western Greece. Bulletin of the Geological Society of Greece, 50(2): 730-739.

Sabatakakis, N., Tsiambaos, G., Rondoyanni, T., Papanakli, S., Kavoura, K., 2015. Deep-seated structurally controlled landslides of Corinth Gulf rift zone, Greece: the case of Panagopoula Landslide. 13th ISRM International Congress of Rock Mechanics, Montreal, Canada, p. 7.

National Observatory of Athens/Institute of Geodynamics, 2022. https://www.gein.noa.gr/en/services-products/database-search/. accessed on 03.03.2022.

Stark, T.D., Choi, H., 2008. Slope inclinometers for landslides. Landslides, 5(3): 339-350.

16th International Congress of the Geological Society of Greece
17-19 October, 2022 - Patras, Greece
Bulletin of the Geological Society of Greece, Sp. Publ. 10
Ext. Abs. GSG2022-295

Groundwater Modelling and Data Dependence: Getting Insight on the Simulated Processes Through Fit-Independent Statistics

C. Pouliaris[1], E. Chrysanthopoulos[1], M. Perdikaki[1], E. Koltsida[1], C. Myriounis[1], K. Markantonis[1], A. Kallioras[1]
(1) National Technical University of Athens, Athens, Greece, pouliaris@metal.ntua.gr

Research Highlights

The present study demonstrates that the use of fit-independent statistics for the evaluation of groundwater modelling results can become a useful tool for assisting regional water resources management planners, providing a deep understanding on the hydrological processes through the statistical analysis of relevant data.

Background

Water resources management in agricultural areas are usually heavily exploited, leading to the degradation of quality and quantity. In areas like Greece, where precipitation is in most areas low, this effect can be magnified (Pouliaris et al., 2018). However, even in areas with high precipitation, such as the plain area of Arta, Epirus, the poor management can lead to inaccessibility of water resources.

The study area is an alluvial plain where the local aquifers develop in confined conditions that close to Amvrakikos also become artesian. The thickness of the sediments is at least 200 m and the main aquifers develop between 4-7 m and 60-70 m with the groundwater used entirely in agriculture. Karstic aquifers are formed in limestone formations that are adjacent to the granular aquifer, with the presence of springs showing that there is hydraulic connection between the two aquifer types. In addition, there are two main surface watercourses in the area; Louros and Arachthos travel through the alluvial plain, with both of them expected to highly affect the groundwater regime locally.

Groundwater models can be a valuable tool in water resources management when they are built using a representative conceptual model and reliable data. For the granular aquifer in Arta, a MODFLOW-2005 (Harbaugh, 2005) model is built using data from previous studies. This model is used for assessing the groundwater dynamics in an area with a hydrological regime that shows a high level of complexity. The long-term goal of the model is to become a tool for the management of groundwater resources in this area with intensive agriculture.

Methods

The groundwater flow model consists of three layers; two confined aquifers and an interfering unit with poor hydraulic properties. The cell used has a size of 250 m X 250 m and the simulation period is December 1993 - May 1995 (transient conditions). The boundary conditions used in the model (and the represented processes) are the following:

- Time variant specified head (CHD): As an output to Amvrakikos (hydraulic head of 0 m.a.s.l.) and an input from the adjacent karstic aquifers. The hydraulic head for the karstic aquifers is included in the sensitivity analysis.
- Drain (DRN): For the simulation of the drainage network. The boundary conductance is included in the sensitivity analysis.
- Recharge (RCH): Distributed uniformly in the model. The starting value is 5 % of precipitation that is included in the sensitivity analysis.
- River (RIV): For the simulation of the rivers in the area (Louros and Arachthos). The conductance of the boundary for both rivers is included in the sensitivity analysis.
- Head observation (HOB): For the introduction of hydraulic head observations. This data is also used in the sensitivity analysis and parameter estimation processes and is taken from a previous study (Ministry of Agriculture, 1997).

The sensitivity analysis that follows is done using fit-independent statistics, more specifically the dimensionless scaled sensitivity (DSS). Using the DSS results for each parameter the composite scaled sensitivity (CSS) is calculated. The parameters with the highest CSS are used in the parameter estimation process, where a non-linear Gauss – Newton regression objective function is used. After the parameter estimation, two indexes (Cook's D and DFBetas) were also used to evaluate the impact of specific parameters in the final results of the parameter estimation process. Further information about the methods can be found in Hill and Tiedman (2007) and Poeter et al. (2014), along with other publications that used some of these methods (Koltsida and Kallioras, 2019; Pouliaris, 2019; Perdikaki et al., 2022; Pouliaris et al., 2022).

Results

The results of the sensitivity analysis (Figure 1, left) show that the most important parameters in the model are the constant head boundaries that are related to discharge from the adjacent karstic aquifers. The recharge also had a high impact, along with the conductance assigned to the drainage network. The rest of the parameters showed lower CSSs, so they were excluded from the parameter estimation process. CHD NE and the DRN conductance final estimates were very close

to the initial values, while for CHD E and the recharge there was a dramatic decrease in their values during the parameter estimation.

The final results of the hydraulic heads (Figure 1, right) show that there is a good fit between observed and simulated values, with the sum of squared residuals (SSR) decreasing from about $45*e^6$ m^2 to 4,477 m^2 for 528 observations in the end. Furthermore, the discharge from the karstic aquifers towards the granular ones is represented in the overall water budget, while there is also significant surface water – groundwater interaction, especially in the area where Arachthos is.

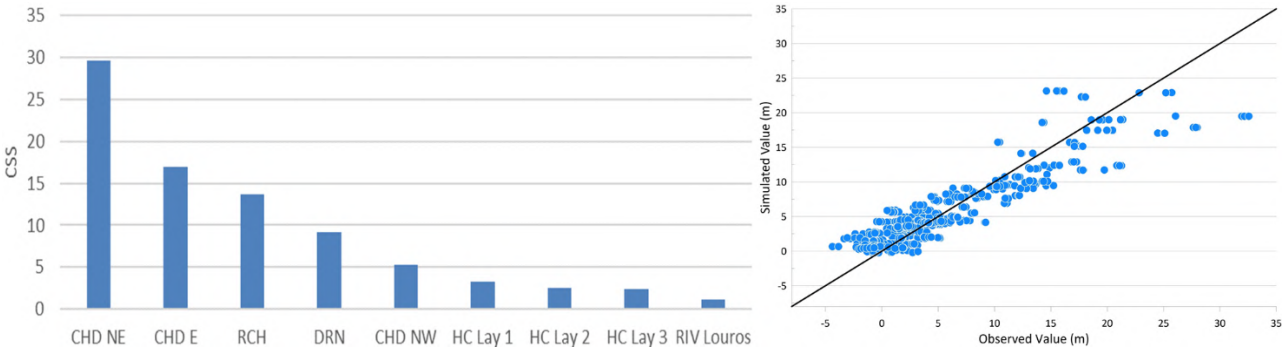

Figure 1: CSS results of the sensitivity analysis (left) and results of the calibrated model (right).

The analysis with the use of Cook's D showed that there are parts of the model, mostly in the northern part of the study area, where specific observations are affecting the modelling results more than others. In addition, DFBetas showed that some parameters are affected more by individual observations. This gives an insight on the local dynamics, highlighting the areas where further investigations could provide more information to the model about the local hydrological processes.

Conclusions

The combination of groundwater models and fit-independent statistics can provide a whole new approach to the modelling process. The main advantage is that, by using this approach, the sensitivity analysis and parameter estimation are done at a mathematical basis. This can actually be very beneficial compared to "trial and error" method in the case a parameter is expected to either have a high or low impact and eventually the results are different. Furthermore, the user can direct the data collection strategy towards the areas that can benefit the model results. Whether more investigation is required for a specific area or hydrological process, fit-independent statistics can recognize the specific data needs, improving the model performance or even leadign to the re-evaluation of the conceptual model of the study area.

Acknowledgements

This research has been co-financed by the European Union and Greek national funds through the Operational Program Competitiveness, Entrepreneurship and Innovation, under the call SUPPORT OF REGIONAL EXCELLENCE (project code MIS: 5047059).

References

Harbaugh, A.W., 2005. MODFLOW-2005, The U.S. Geological Survey modular ground-water model—The ground-water flow process: U.S. Geological Survey Techniques and Methods 6- A16, variously p.

Hill, M.C., Tiedman, C.R., 2007. Effective groundwater model calibration, 978 John Wiley & Sons Inc., Hoboken, New Jersey

Koltsida, E., Kallioras, A., 2019. Groundwater flow simulation through the application of the FREEWAT modeling platform. Journal of Hydroinformatics, 21 (5): 812–833.

Ministry of Agriculture, 1997. Final hydrogeological water balance reform study of the Arta plain (in Greek). Athens, September 1997.

Perdikaki, M., Pouliaris, C., Makropoulos, C., Kallioras, A., 2022. Simulation of horizontal injection wells in Managed Aquifer Recharge facilities using the conduit flow process (CFP) code for MODFLOW-2005. Environmental Modelling and Software, 148, 105289.

Poeter, E. P., Hill, M.C., Lu, D., Tiedeman, C.R., Mehl, S., 2014. UCODE_2014, with new capabilities to define parameters unique to predictions, calculate weights using simulated values, estimate parameters with SVD, evaluate uncertainty with MCMC, and more: Integrated Groundwater Modeling Center Report Number GWMI 2014–02.

Pouliaris, C., 2019. Groundwater modelling of a coastal semiarid hydrogeological system, Institute of Applied Geosciences. Ph.D. Thesis, Technical University of Darmstadt, Darmstadt, 112 p.

Pouliaris, C., Foglia, L., Schüth, C., Kallioras, A., 2021. Groundwater flow model calibration of a coastal multilayer aquifers system based on statistical sensitivity analysis. Environmental Modeling & Assessment.

Pouliaris, C., Perdikaki, M., Foglia, L., Schüth, C., Kallioras, A., 2018. Hydrodynamic analysis of a Mediterranean aquifer system with the use of hydrochemical and isotopical analysis as supporting tools. Environmental Earth Sciences.

16th International Congress of the Geological Society of Greece
17-19 October, 2022 - Patras, Greece
Bulletin of the Geological Society of Greece, Sp. Publ. 10
Ext. Abs. GSG2022-299

Estimation of Soil Loss and Sediment Export with the InVEST SDR Model

M. Michalopoulou[1], N. Depountis[1]
(1) University of Patras, Rio, Greece, maria_michalopoulou@upnet.gr

Research Highlights

Calculation of the amount of soil loss and sediment export using the Sediment Delivery Ratio model of the InVEST suite.

Introduction

Sedimentation is one of the most significant outcomes of soil erosion and a major threat, especially for dam water reservoirs. The deposition of sediment may lead to an increased aggradation rate and reduced water storage capacity of the dam. This study aims to use the Integrated Valuation of Ecosystem Services and Tradeoffs (InVEST) Sediment Delivery Ratio (SDR) model for the estimation of soil loss and sediment export in the pilot area of the Pinios Dam drainage basin, Greece. This model is using the Revised Universal Soil Loss Equation (RUSLE) for the calculation of soil loss, which requires the rainfall-runoff erosivity data, soil erodibility, the Digital Elevation Model (DEM) of the pilot area, land cover and vegetation data. The SDR model also estimates the amount of sediment that is exported from each pixel and reaches the streams. The results for the research area indicate that the soil loss values range from 0 to 162,157 ton/ha/year with an average value of 287 ton/ha/year. The calculated SDR values range from 0 to 0.41 with an average value equal to 0.09 and the sediment export values range from 0 to 40,880 tons/ha/year with an average value of about 40 tons/ha/year.

Research area

The research area is the drainage basin of the Pinios earth-filled dam, which is located in the Ilia regional unit, Western Greece. The Pinios river hydrological basin occupies an area of 1026 km^2, whereas the dam's drainage basin occupies an area of approximately 700 km^2 (Figure 1). Surface water run-off from the dam's drainage basin is collected in a large water reservoir that occupies an area of approximately 20 km^2 (Depountis *et al.*, 2020). The research area is characterized by varied topography. Steep slopes characterize most of the eastern and northern parts of the catchment area, where Mount Scollis and Erymanthos are located, whereas more gentle slopes occur in the western part of the study area. The coordinate system that was used in this study is the Hellenic Geodetic Reference System 1987 (HGRS/EGSA87).

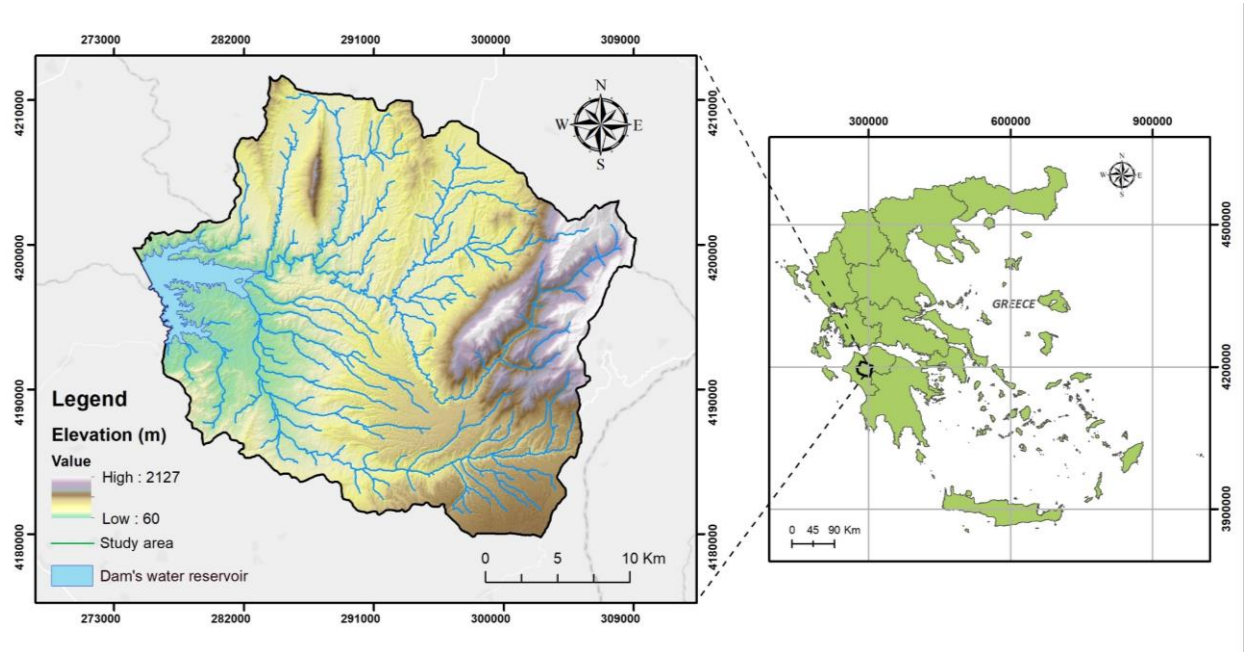

Figure 1. The research area of Pinios Dam drainage basin.

Methodology

The InVEST Sediment Delivery Ratio (SDR) model's goal is to map the production and delivery of overland sediment to the streams. This type of information and data may be used to explore the effect of sediment retention in a watershed,

especially in the context of global change (Sharp *et al.*, 2018). Furthermore, the usefulness of this process is apparent in the instream water quality management as well as in the reservoir management, both of which could have economic worth. The SDR is a spatial model which is working at the spatial resolution of the input digital elevation model (DEM) and calculates the amount of soil loss and sediment exported from each pixel and reaches the stream. This approach was proposed by Borselli *et al.*, 2008 and considers that the sediment that reaches the stream will end up eventually at the catchment outlet (dam reservoir).

The InVEST SDR model acquires the Revised Universal Soil Loss Equation (Renard *et al.*, 1997) which includes the parameters of rainfall-runoff erosivity, soil erodibility, slope length and slope steepness, land cover management, and support practices. The input data of the SDR model were preprocessed in ArcGIS 10.8 according to the InVEST requirements. For this research, rainfall, geological, topographical and land cover data were used. The SDR model also requires a table with the biophysical characteristics which include the land cover categories and the corresponding C factor and P factor values of the watershed (Figure 2).

Results

The soil erosion in the research area was quantified with the use of the SDR model of the InVEST model suite. Based on the results of the SDR model analysis, the calculated soil loss values range from 0 to 162,157 ton/ha/year and an average value of 287 ton/ha/year. The SDR values range from 0 to 0.41 with an average value equal to 0.09 (Figure 2). The catchment area of the Pinios dam drainage basin has sediment export values ranging from 0 to 40,880 tons/ha/year with an average value of about 40 tons/ha/year (pixel size 5 m x 5 m) and the total sediment export is estimated to be equal to 2,948,381 ton/watershed.

DESCRIPTION	LUCODE	C FACTOR	P FACTOR
Discontinuous urban fabric	112	0	1
Industrial or commercial units	121	0	1
Non irrigated arable land	211	0.3	1
Vineyards	221	0.3	1
Olive groves	223	0.3	1
Pastures	231	0.1	1
Complex cultivation patterns	242	0.2	1
Land principally occupied by agriculture	243	0.3	1
Broad-leaved forest	311	0.003	1
Coniferous forest	312	0.001	1
Mixed forest	313	0.001	1
Natural grasslands	321	0.05	1
Sclerophyllous vegetation	323	0.05	1
Transitional woodland shrub	324	0.04	1
Beaches dunes sands	331	1	1
Bare rocks	332	0.001	1
Sparsely vegetated areas	333	0.3	1

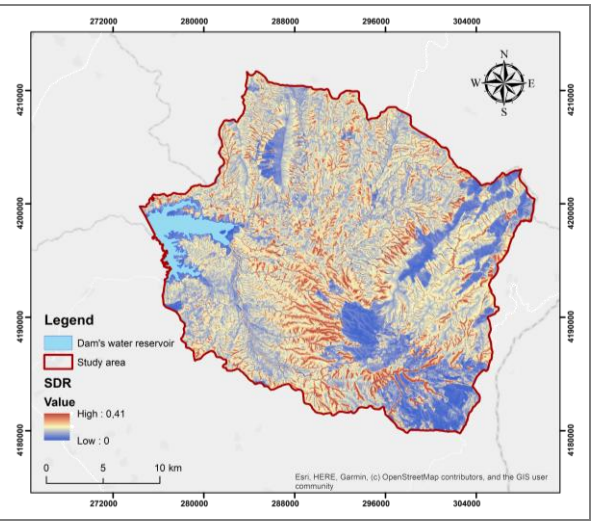

Figure 2. Biophysical table with land cover categories and values for C and P factor of RUSLE model and the SDR map for the research area.

Acknowledgements

The present work was financially supported by the «Andreas Mentzelopoulos Foundation».

References

Depountis, N., Michalopoulou M., Kavoura K., Nikolakopoulos K., Sabatakakis N., 2020. "Estimating Soil Erosion Rate Changes in Areas Affected by Wildfires" ISPRS International Journal of Geo-Information 9, no. 10: 562. https://doi.org/10.3390/ijgi9100562

Sharp, R., Tallis, H.T., Ricketts, T., Guerry, A.D., Wood, S.A., Chaplin-Kramer, R., Nelson, E., Ennaanay, D., Wolny, S., Olwero, N., Vigerstol, K., Pennington, D., Mendoza, G., Aukema, J., Foster, J., Forrest, J., Cameron, D., Arkema, K., Lonsdorf, E., Kennedy, C., Verutes, G., Kim, C.K., Guannel, G., Papenfus, M., Toft, J., Marsik, M., Bernhardt, J., Griffin, R., Glowinski, K., Chaumont, N., Perelman, A., Lacayo, M. Mandle, L., Hamel, P., Vogl, A.L., Rogers, L., Bierbower, W., Denu, D., and Douglass, J. 2018. InVEST +VERSION+ User's Guide. The Natural Capital Project, Stanford University, University of Minnesota, The Nature Conservancy, and World Wildlife Fund.

Borselli L, Cassi P and Torri D 2008 Prolegomena to sediment and flow connectivity in the landscape: A GIS and field numerical assessment Catena 75 268-77

Renard, K.G., Foster, G.R., Weesies, G.A., McCool, D.K., Yoder, D.C., 1997, Predicting soil erosion by water: a guide to conservation planning with the Revised Universal Soil Loss Equation (RUSLE), Agriculture Handbook, No.703, USDA-ARS. United States Department of Agriculture, Washington, D.C., USA. pp.384

16th International Congress of the Geological Society of Greece
17-19 October, 2022 - Patras, Greece
Bulletin of the Geological Society of Greece, Sp. Publ. 10
Ext. Abs. GSG2022-315

Geological, Tectonic and Hydrogeological conditions at Ethia, Asteroussia Mnts, Crete, Greece

G. Tzorbatzakis[1], I. Tzorbatzakis[1], H. Kranis[1], E. Skourtsos[1], L. Moforis[1], A. Alexopoulos[1], G. Kontakiotis[1]

(1) Department of Geology and Geoenvironment, National and Kapodistrian University of Athens, 15784 Zographou, Athens Greece Institution, Town, Country, giorgos.tzorbatzakis@gmail.com.

Introduction

The accumulation and flow of subsurface water is heavily dependent on the geological and structural conditions. In this sense, the knowledge about the geological structure is a crucial factor in groundwater exploration, as well as in the formation subterranean flow models. Asteroussia Mountains, on the southern part of the island of Crete, is a range built of geological formations that belong to geotectonic units of the Internal and External Hellenides. A series of deformation episodes that affected these units have led to a complicated geological structure, thus affecting the prevailing hydrogeological conditions. This study presents the preliminary research results on the geological and hydrogeological conditions in the broader area of Ethia, at the eastern part of Asteroussia Mnts, based on detailed geological mapping (at 1:5,000 scale), structural and sedimentological observations, and palaeontological sampling and analysis.

Geology and Tectonics

Asteroussia Mountains, central-southern Crete, (max. elev 1231 m) is an elongate, E-W mountain range between the Messara plain in the north and the Libyan Sea in the south. The range is built of alpine formations that belong to three geotectonic Units, while post-orogenic deposits crop out mainly along the foot of the mountain. Tripolis Unit, a carbonate platform topped by flysch clastics, is the lowermost one in the area, forming the backbone of the range. The Tripolis formations in the study area include carbonate sediments that crop out in limited, elongated outcrops bounded by high-angle normal faults. These carbonates are thick or unbedded dark or grey limestones and dolostones, that overall dip towards the North. Their upper members are fossiliferous, containing Nummulites, Alveolinae and Rudists. The thick flysch of yellow siltstones, clays and sandstones comes in faulted contact or lies unconformably over the carbonates.

The Ethia (Pindos) Unit that overlies tectonically the Tripolis Unit, is a pelagic sequence, comprising variety of lithological types, including (i) a clastic series, with some platy limestone intervals and clastic limestone intercalations towards the top (ii) A bipartite series, containing a lower member of rosy, platy limestones, intercalated with red pelites, marls and thin chert bands. Radiolaria and filaments were found within the carbonate horizons. The upper member is characterized by thin- to medium bedded carbonates with rare pelite intervals. The carbonate lithologies include unbedded micrit, oolitic to pseudo-oolitic limestones, bearing corals, algae, echinoid fragments, of Upper Jurassic age (ii) a siliclastic series follows, comprising a lower member of black, red, and green radiolarites, interbedded with red marls (Radiolarites fm.) and an upper member of sandstones and marly limestones (First Flysch fm.). (iv) Upper Cretaceous to Eocene carbonates. Multimictic conglomeratic breccia are at the base, evolving into thin-bedded limestones with frequent chert intercalations. Carbonate sedimentation continued towards the Eocene, characterized by micritic platy and micro-brecciated limestones with rare pelite intervals, while the uppermost horizons show a shallower, more neritic environment. Various planktonic foraminifera were identified (i.e. Globigerina, Globorotalia, etc.) while some samples contained benthic forms, such as Thaumatoporella sp. (v) During the Eocene, the carbonate sedimentation was succeeded by flysch clastics, while the upper part contains outcrops of olistoliths of varying composition and size.

The low-angle tectonic contacts between the aforementioned geotectonic units display a sense of displacement towards the South. In particular, the Pindos Unit is intensely folded, comprising sets of imbricated stacks. Large, E-W normal faults bound Asteroussia Mnts, both, along their northern (Messara) and southern (Libyan Sea) boundaries. Post- Mid-Miocene extensional faulting (with E-W and N-S normal faults) have affected the alpine formations and control the deposition of quaternary sediments along the boundaries of the mountain range.

Hydrogeological conditions

The aforementioned geological formations can be distinguished in the following hydrolithological types, according to the International Association of Hydrogeologists (Struckmeier & Margat, 1995; Nikas et al., 2010). (a) Local and thin, porous, unconsolidated aquifers of high yield, or extended aquifers of medium yield. This sub-category corresponds to the coarse members of the alluvial deposits, scree and talus. (b) Extended, high yield aquifers, that correspond to the Tripolis carbonates, some of which discharge at the southern coastal part of the area. (c) Local, thin and high yield carbonate aquifers with secondary permeability, or extended aquifers of medium yield. Pindos intensely fractured and karstified carbonates fall in this category. Medium potential karstic aquifers develop within these formations, owing to their limited thickness and the presence of siliceous and clay intercalations. (d) Porous, unconsolidated formations with limited or absent subsurface water accumulation. These are the fine members of the post-orogenic deposits, including marls and

clays, interbedded with silt and thin bands of coarser material. (e) Consolidated formations with limited water potential, as the ones that belong to the Ethia Unit, which exhibit broad variety of lithological types and intense deformation, resulting in secondary porosity and a thick regolith cover, that leads to the formation of local and low potential aquifers. (f) Aquifers of no practical importance, or aquicludes, such as the flysch of Tripolis and Ethia Units. Intense deformation of these of formations has led to the accumulation of secondary material (clay) within their fractures.

The mountainous part of the study area contains superposed aquifers within the Ethia Unit members, but their limited extent, their relatively small thickness, intense fracturing and folding have led to the development of small hydrogeological basins the quickly discharge through low potential springs, most of which are active during and shortly after the rainfall periods. The Pervola and Ampas gorge springs are an exception, however. Along the southern border of the Messara plain, the carbonates are in faulted contact or underlie unconformably the quaternary fill, leading to hydraulic communication between them. The aquifers in the plain area are (i) a shallow alluvial aquifer, (ii) a confined or leaking aquifer of medium to great depth, developed within the Pleistocene sediments, (iii) intermediate confined thin aquifers between the former two, and (iv) deep aquifers within the bedrock, close to the mountain range. In addition, the water quality in the aforementioned aquifers is good for irrigation.

Discussion and conclusions

The detailed geological and structural mapping, coupled with stratigraphic and hydrogeological observations and re-evaluation of hydrogeological data has led to the revision of the prevailing hydrogeological conditions in the broader area of Ethia, eastern Asteroussia Mnts. The granular and karstic aquifers that prevail in the area are controlled both the lithological and stratigraphic variations and the complexity of the geological structure. The most important water occurrence is located at the northern part of the study area, where a complex aquiferous system within the karstified formations of the Ethia Unit and the granular formations at the border of the Messara plain. However, this complex system is subjected to over-exploitation, through a large number of boreholes.

References

Nikas, K, Antonakos, A, Kallergis, G, Kounis, G., 2010. International Hydrogeological Map of Europe: Sheet D6 “Athina”. Proceedings of the 12th International Congress, Patras, 2010 Bulletin of the Geological Society of Greece, Volume XLIII No 4, p. 1821-1830

Struckmeier, W.F., & Margat, J., 1995. Hydrogeological maps: a guide and a standard legend (Vol. 17). Hannover: Heise

16th International Congress of the Geological Society of Greece
17-19 October, 2022 - Patras, Greece
Bulletin of the Geological Society of Greece, Sp. Publ. 10
Ext. Abs. GSG2022-344

The evidence of potential correlation hydrocarbons and thermal-mineral water: Kyllini's Baths, NW Peloponnese, Greece

V. Stavropoulou[1], E. Zagana[1], N. Lambrakis[1] G. Iliopoulos[2]
(1) Laboratory of Hydrology, Department of Geology, University of Patras, Greece, vstavropoulou@upnet.gr (2) Laboratory of Palaeontology and Stratigraphy, Department of Geology, University of Patras, Greece.

Introduction

Numerous studies have been accomplished on potential presence of hydrocarbons in NW Peloponnese. The geological background and tectonical evolution of the area are very important for the hydrocarbons' research. The presence of source rocks in the research area has been confirmed (Rigakis and Karakitsios, 1998). Petroleum fields occur in deep carbonates and clastic sequences from the Jurassic to Eocene, belonging to the external Ionian tectonic Zone of the Hellenides (Kamberis et al, 2000a, Rigakis 1999). The diapiric movements of evaporites and their evolution in time control the deposition of the Holocene sedimentary sequences (Nikolaou, 1988). Water chemistry is a useful indicator of hydrocarbon migration, occurrence and accumulation processes (Kurchikov, 2009). In NW Peloponnese, thermal water spring of Kyllini is of research interest in terms of their hydrochemical composition and possible association with hydrocarbons. Deep fault systems or fissured zones act as preferential pathways for the rise on the surface of groundwaters, producing water occurrences with specific characteristics, such as rotten egg smell, relatively high temperature and total dissolved solids. All these manifestations tend to occur in groups, each group being related to the same geological features. Thus the character and distribution of thermal occurrences in W. Peloponnese were suspected to be closely related to geological features and neo-tectonic activity, which control the circulation of groundwater, and hence, influence the chemistry of spring waters.

Geological and Tectonical setting of the area

The study area is located in Ilia Prefecture, in the northwestern part of Peloponnese. The Ionian Sea laved Ilia westwards and eastwards the mountainous mass of the region is extended. The study area is characterized mainly as lowland apart from mountains Lampeia, with 1797 m elevation. The alpine formations constitute the geological background of the area and display a small surface spread, while the postalpine formations (Neogene - Quaternary sediments) have covered the geological background and appear in the greater area of the region. The sediments of Plio-Pleistocene and Holocene age are deposited unconformably on the Alpine formations, cover the greater area of Ilia and develop subterranean, almost throughout the Neogene basin of the Western Peloponnese. Peloponnese has been affected by a NNW directed tectonic uplift as a result of tensile stresses and be accomplished during the Middle Miocene. Two fault systems are presented as a consequence of the tensile stresses and the subsequent tectonic uplift. A NW to NWW oriented fault system that formed both the tectonic windows that appear in the central Peloponnese and a NW to SWW oriented system that created several trenches. Specifically, in the NW Peloponnese the Pyrgos graben extends from Mount Lapithas to the edge of Mount Skolis and Kyllini. The current form of the basin is a result of the fault tectonics that appeared from the Upper Vourdigalio onwards and which could be a reflection of pre-existing axes (antiques, tectonic dips) of the alpine tectonics. Diapiric movements benefited from the Alpine and later tectonics to load the tectonic structure of the basin with typical deformations, such as salinization. During Neogene deposition, differential movements of evaporites submerge or uplift the Neogene relief irregularly. These movements are particularly important for the vertical and horizontal evolution of the phases and the thickness of the Neogene deposits. Figure 1 presents a geological section showing the stratigraphic and tectonic setting of the basins in the NW Peloponnese where the diapiric movements of evaporites are established.

Results and Discussion

During oil exploration in western Peloponnese, deep onshore and offshore boreholes were carried out in order to study the geological formations. The Upper Cenozoic successions of the research area present a highly complex pattern of mainly terrigenous-clastic deposits. These sediments prove repeated changes in marine influences and provision of sediment in a palaeogeographic arrangement dominated by lagoonal and fluvio-lacustrine systems (Fig. 2). According to the lithostratigraphy of the area in the complex stratigraphic column, the aquifer is the Peristeri formation which consists of horizons of mixed conglomerates and the series of limestones of the Ionian Zone (Fig. 2).

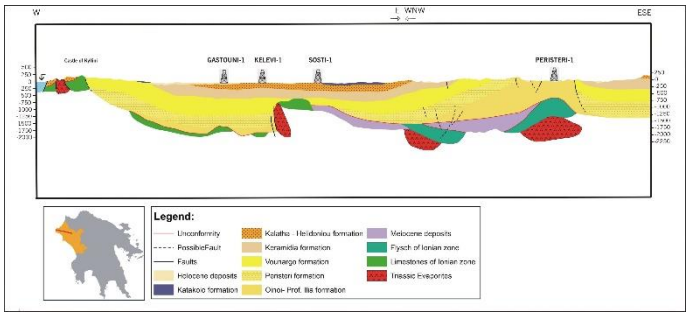

Figure 1: Geological Section of the area (Modified by Kamberis 1987)

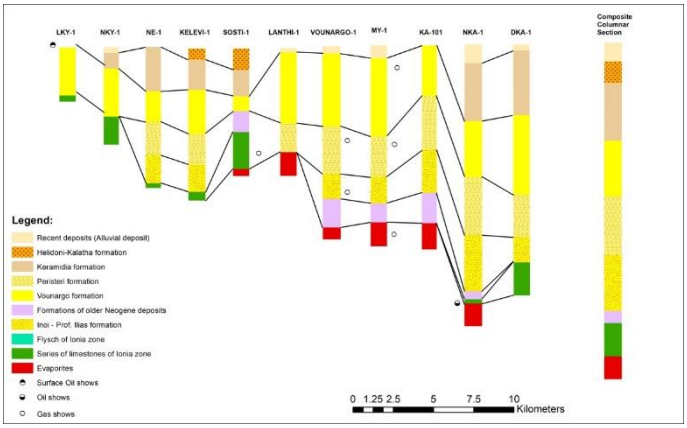

Figure 2: Stratigraphic correlation of boreholes and Composite Column Section (modified by Kamberis 1987)

The thermal water of the Kyllini's spring is hosted in limestone rocks through which it arrives at large depths and then it rises through faults E-W direction. As the water rises under increased pressure some of it is dispersed into the successive confined aquifers of the Plio-Pleistocene through faults.

Conclusions

The thermo-mineral water of the Kyllini's baths is characterized by the water type Na-Cl-HCO_3 and by very strong reducing conditions which expressed by high amounts of ammonia, low concentration of nitrate and high concentration of sulfide. Moreover, the water samples show an excess in sulfate which could be explained by the dissolution of the evaporites (gypsum) that appear in the base of the complex stratigraphic column. The water of Kyllini's Baths with the total dissolved solids over 2250 mg/l is characterized as brackish water. The analyses of minor elements were displayed high concentration of boron, lithium and strodium. The presence of CH4 in the Kyllini spring shows the close relationship of hot water and hydrocarbons expected at the contact between the old alpine rock and the Neogene formations while H_2S is dispersed over longer distances.

Keywords: Hydrocarbons, Thermal-mineral water, Diapiric structure, Composite columnar section

Acknowledgements

The present work was financially supported by the «Andreas Mentzelopoulos Scholarships for the University of Patras».

References

Kamberis, E. (1987) Geological and oil study of NW Peloponnese.Ph.D. thesis, National Technical University of Athens, 141 pp

Kamberis, E. (1992) Geodynamic and Paleogeographic evolution of western Peloponnesus (Greece) during the Neogene. Paleontologia I Evolucio, v. 24-25, 363-376.

Koukouvelas, I., Mpresiakas, A., Sokos, E. and Doutsos. T. (1996) The tectonic setting and earthquake ground hazards of the 1993 Pyrgos earthquake, Peloponnese, Greece. Journal Geol. Soc. Lond. 152, 39-49.

Kurchikov, A.R. and Plavnik, A.G., 2009. Clustering of groundwater chemistry data with implications for reservoir appraisal in West Siberia. Russian Geology and Geophysics 50, 943-949.

Nikolaou, K.A. (1986) Contribution to the knowledge of the Neogene, the geology and the Ionian and pre-Apulian limits in relation to the petroleum geology observations in Strofades, Zakynthos and Kephalinia islands. PhD thesis, University of Athens, 1–228

Nikolaou, K.A. (1988) Neodiapiric movements of Triassic evaporites in Zakynthos and Strofades. Bulletin Geological Society Greece Athens, 1, 213-219.

Rigakis, N., and Karakitsios, V., 1998. The source rock horizons of the Ionian Basin (NW Greece). Marine and Petroleum Geology, 15, 593-617.

16th International Congress of the Geological Society of Greece
17-19 October, 2022 - Patras, Greece
Bulletin of the Geological Society of Greece, Sp. Publ. 10
Ext. Abs. GSG2022-350

Large scale shear tests on soil-geosynthetic interfaces

N. Depountis[1], M. Ferentinou[2], V. Boumpoulis[1], S. Perdikis[1], P. Alexopoulos[1], A. Athanasiou[1]

(1) Laboratory of Engineering Geology, University of Patras, 26504, Greece, ndepountis@upatras.gr (2) Liverpool John Moores University.

Research Highlights

The test results show that the shear strength on soil-geosynthetic interface varies based on the type of geosynthetic used. Geotextiles provide a minimum shear strength compared to a soil compacted material or reinforced with a geogrid.

Background

The understanding of shear strength behaviour of soil-geotextile interface is very important in the analysis, design, and modelling of embankments. The interaction between soils and geosynthetics mainly depends on the type and characteristics of the soil and geosynthetic used. Many researchers have investigated the shear strength behaviour of reinforced soil by conducting direct shear tests (Makkar et al., 2019; Stark et al., 2015; Vieira et al., 2013). In most of these studies, the effectiveness of reinforcement depends on the form in which is the geosynthetic material intersects into the soil. The present study investigates the interaction between soil and a planar geotextile as well a geogrid by performing large scale shear tests. The purpose of the study is to understand the strength interaction between soil and geosynthetics which is vital in the design of earth road embankments.

Materials and Methods

A series of large shear tests were carried out according to ASTM D3080 and ASTM D5321 standards using the VJT/2780A large shear apparatus (Figure 1a), at the Laboratory of Engineering Geology, University of Patras . We conducted test on compacted 120 mm thick soil specimens unreinforced or reinforced with a geotextile (Figure 1b) or a geogrid (Figure 1c).

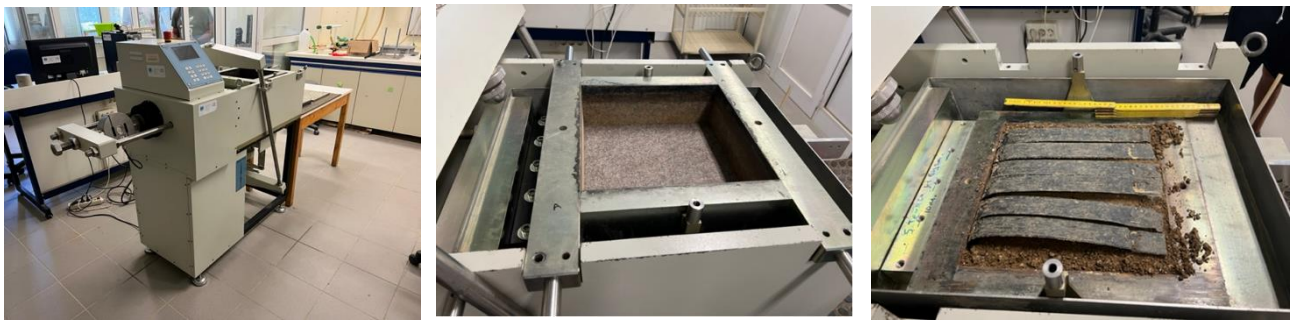

Figure 1. a) Large shear apparatus, b) installation of a geotextile inside the shear box, c) reinforced specimen with a geogrid.

The direct shear tests were performed on samples of well graded sand with silt and gravel (SW-SM) properly compacted inside the shear box. According to the Hellenic Technical Specifications, on construction of embankments with suitable excavation or borrow materials (ELOT TP 1501-02-07-01-00:2009) the material used belongs to the category E3-E4, which is suitable for the construction of road embankments. More specifically, the soil material was non-plastic, had 5% of fines content (<0.075 mm), and a maximum grain size of 9.52 mm.

Dense specimens were prepared inside the shear box by manual dynamic compaction in several layers to reproduce the maximum dry density γ_d = 2,17 gr/cm^3 and the optimum moisture content w_{opt} = 5,30% of a similar compacted embankment, as had been previously calculated with the ASTM D1557 compaction test.

Three series of tests were performed: a) soil compacted material, b) soil - geotextile placed on the top of a spacer block representing the soil's shear surface and c) soil - geogrid positioned on top of the lower shear box and wrapped around the soil at the edge of the box. The tests were performed under normal loads which correspond to nominal normal stresses of 50, 100, 200, and 400 kPa, respectively with a shear displacement rate of 0,5 mm/min.

The geotextile specimen used was a separation and filtration nonwoven continuous filament geosynthetic of 3.6mm thickness (Figure 1b) and the geogrid was a strip bonded polyester material with a nominal tensile strength of 150 kN. The geogrid was modified to account for scale factor effect by increasing its surface interface so that the stripes were aligned together with a spacing of 0.4cm (Figure 1c).

Results

The peak and ultimate shear strength obtained from the results are slightly lower on the soil-geogrid interface compared to the respective values on the soil's without geotextile shear surface for the normal loads 100-400 kPa (Figure 2). A large decrease is observed on the soil-geotextile interface for the same loads (Figure 2). Concerning the angle of friction, a small increase is observed on the soil-geogrid interface and a large decrease on the geotextile-soil interface compared to the respective values of the soil's shear surface. On the contrary, a large decrease is observed on the soil-geogrid interface and on the soil without geotextile interface compared with the respective values soil's shear surface (Table 1).

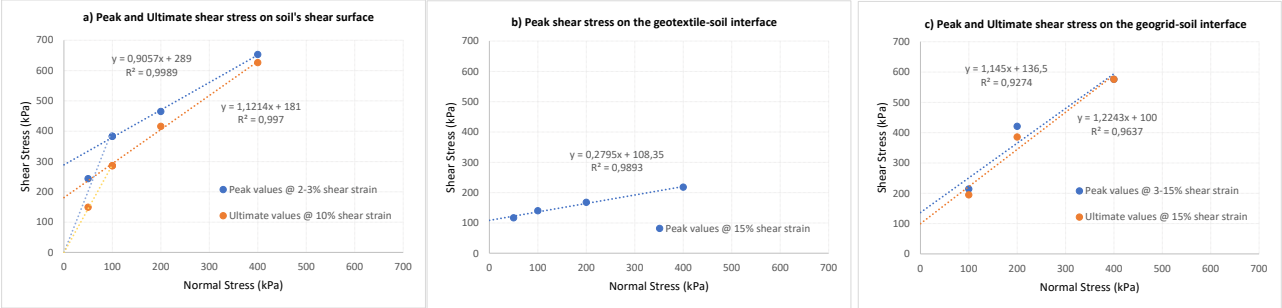

Figure 3. a) Failure envelope of soil at peak and ultimate state, b) Failure envelope on the soil-geotextile interface at peak state, c) Failure envelope on the soil-geotextile interface at peak and ultimate state

Table 1. Shear strength parameters of the preformed large shear tests

State of large shear test	Apparent cohesion (kPa)	Angle of friction (^{0})
Peak values at 2-3% shear strain on soil's shear surface	289	42
Ultimate values at 10% shear strain on soil's shear surface	181	48
Peak values at 3-15% shear strain on the geogrid-soil interface	136,5	49
Ultimate values at 10% shear strain on soil's shear surface	100	51
Peak values at 15% shear strain on the geotextile-soil interface	108,35	16

Conclusions

Large-scale direct shear tests were conducted to study the interaction between selective embankment materials with geotextiles and geogrids under direct shear mode. According to the Hellenic Technical Specifications the material used belongs to the category E3-E4 and was compacted in its optimum dry density and moisture content. Planar geotextile and geogrid were also used to compare the effect of reinforcement on the shear strength of the compacted material. From the results obtained, it is observed that the interface shear strength of geosynthetic-reinforced sand greatly depends on the form in which it is used. Compared to soil without geotextile, no significant increase in interface shear strength or angle of friction was provided by the soil reinforced with a planar geogrid, whereas a definite decrease was provided by the soil reinforced with a planar geotextile.

Acknowledgments

The fellow Dr. Maria Ferentinou and the host Dr. Nikolaos Depountis acknowledge the financial support of the Greek Diaspora Fellowship Program (GDFP) in the project activities that made this publication possible.

References

American Society for Testing and Materials (ASTM) D3080/D3080-M-11, 2011. Standard Test Method for Direct Shear Test of Soils Under Consolidated Drained Conditions.

American Society for Testing and Materials (ASTM) D5321/D5321M-21, 2021. Standard Test Method for Determining the Shear Strength of Soil-Geosynthetic and Geosynthetic-Geosynthetic Interfaces by Direct Shear.

American Society for Testing and Materials (ASTM) D1557-12, 2021. Standard Test Methods for Laboratory Compaction Characteristics of Soil Using Modified Effort.

Hellenic Technical Specifications (ELOT TP 1501-02-07-01-00:2009). Construction of embankments with suitable excavation or borrow materials.

Makkar, F.M., Chandrakaran, S., Sankar N., 2019. Performance of 3-D geogrid-reinforced sand under direct shear mode. International Journal of Geotechnical Engineering, 13:3, 227-235, doi: 10.1080/19386362.2017.1336297.

Stark, T.D., Niazi, F.S., Keuscher, T.C., 2015. Strength Envelopes from S8ingle and Multi Geosynthetic Interface. Geotech Geol Eng, 33:1351-1367, doi: 10.1007/s10706-015-9906-4.

Vieira, C.S., Lopes, M.L., Caldeira, L., 2013. Soil-Geosynthtic Interface Shear Strength by Simple and Direct Shear Tests. Proceedings of the 18th International Conference on Soil Mechanics and Geotechnical Engineering, Paris, 3497-3500.

16th International Congress of the Geological Society of Greece
17-19 October, 2022 - Patras, Greece
Bulletin of the Geological Society of Greece, Sp. Publ. 10
Ext. Abs. GSG2022-385

Experiences from the application of the GSI system for rock engineering design in the last two decades in Greece. Respecting the geological particularities.

V. Marinos[1]
(1) School of Civil Engineering, National Technical University of Athens, Athens, Greece, marinosv@civil.ntua.gr

With the rapid growth of improved numerical design tools, which now allow progressive failure processes and also sequentially installed support to be analyzed, and synthetic rockmasses to be built, the need for acquisition of more reliable rock mass parameters has also grown (Marinos and Carter, 2018). While the Hoek-Brown criterion (Hoek and Brown, 2018) has aided the revolution in rock engineering, it has over the years also suffered a lack of precision in definition of input constants. The need for geological definition of rock mass properties required as inputs into numerical analysis, constitutes one of the greatest reasons for application of the GSI chart (initially introduced by Hoek, 1994, but then improved in subsequent papers published by Marinos & Hoek, 2000), allowing characterization of even difficult-to-describe rock masses, including tackling even the most problematic of weak and complex geological processes of tectonism, weathering and/or alteration. An extension of the original GSI application charts for heterogeneous and structurally complex rockmasses, such as flysch, in most cases forming weak rock masses, for molassic formations, ophiolites, including particularly weak rock masses, gneiss (in its disturbed or weathered form) have been developed (in Marinos, 2007). Back-analyses of tunnels, slopes and foundation behaviour using GSI and its reliable application in rock engineering designs confirm to its reliability. The GSI classification is set up to avoid including other factors, such as intact strength, in situ stresses and/or groundwater pressures, because these factors normally would be allowed for in any analyses. With continuing use worldwide, the GSI system has continued to evolve, but greater understanding is needed in the definition of input constants, for establishing both GSI and intact rock properties.

GSI system and the Hoek and Brown failure criteria was mainly used in the rock engineering design of works in the Greek territory the last two decades. The experiences from the use of the GSI system, without overlooking the geological particularities, by a practitioner are presented here. Geological processes of tectonism, weathering and alteration all affect GSI (Figure 1). When tectonism is low, GSI values are generally high to very high (Intact to Blocky structure). In this case lower GSI values can however be acquired when rockmasses are crossed by discontinuities formed by genesis such as frequent thin bedding or well-expressed schistosity planes, often with conditions of these discontinuities to be Fair to Very Good. In tectonic areas, particularly if compressional, GSI values may be considerably reduced since the structure is more fractured (more joints) or even sheared; such rock behaves in a more ductile manner (e.g. mudstones, shales, siltstones). In the last case, the conditions of joints are most probably Poor to Very Poor (in cases with slickensided or soft clay coatings due to shearing) (Figure 1A).

The influence of weathering that either process exerts on the credited value of GSI is that both degrade not just the parent intact rock material but also, they change the character and competence of the rockmass structure (Figure 1B). According to the weathering degree the discontinuity surface condition becomes poorer and the interlocking of rock blocks becomes loosened. The structure on the other hand may not be in principle affected, at least if weathering is not very advanced.

Alteration in principle also affects both the intact rock properties of the material and the joint surface condition. Slightly to moderately altered rockmasses often exhibit smoother or slickensided joint surfaces (e.g. though serpentinization). The structure, σ_{ci} and m_i in this case are not or only slightly affected. With severe alteration, rock mass structure and surface conditions can be reduced considerably (Figure 1C). The structure becomes disturbed (e.g. from Blocky to Very Blocky or perhaps to Sheared) according to the alteration degree (e.g. formation of schistose or laminated planes). Joint condition in this case is Poor to Very poor. The intact properties σ_{ci} and m_i are considerably reduced. However, there are cases, eg., contact metamorphism, where alteration may result in stronger rocks (such as keratites).

The most common GSI ranges in conjunction with the Hoek and Brown intact rock parameters σ_{ci} and m_i for various example rock units are presented in Figure 2 (Marinos & Carter, 2018).

References

Hoek E. Strength of rock and rock masses. ISRM News Journal 1994; 2(2): 4–16.
Hoek E, Brown E. T. 2018. The Hoek-Brown failure criterion and GSI – 2018 edition. In: Journal of Rock Mechanics and Geotechnical Engineering 11(3), Pages 445-463. https://doi.org/10.1016/j.jrmge.2018.08.001.
Marinos P, Hoek E. 2000. GSI: a geologically friendly tool for rock mass strength estimation. In: Proceedings of the International Conference on Geotechnical and Geological Engineering (GeoEng2000). Lancaster: Technomic Publishers. pp. 1422–46.
Marinos V. 2007. Geotechnical classification and engineering geological behaviour of weak and complex rock masses in tunneling, Doctoral thesis, School of Civil Engineering, Geotechnical Division, National Technical University of Athens (in Greek)
Marinos, V.,&Carter T.G. 2018. Maintaining Geological Reality inApplication of GSI for Design of Engineering Structures in Rock. (2018) J. Eng. Geo.Vol 239 pp282-297

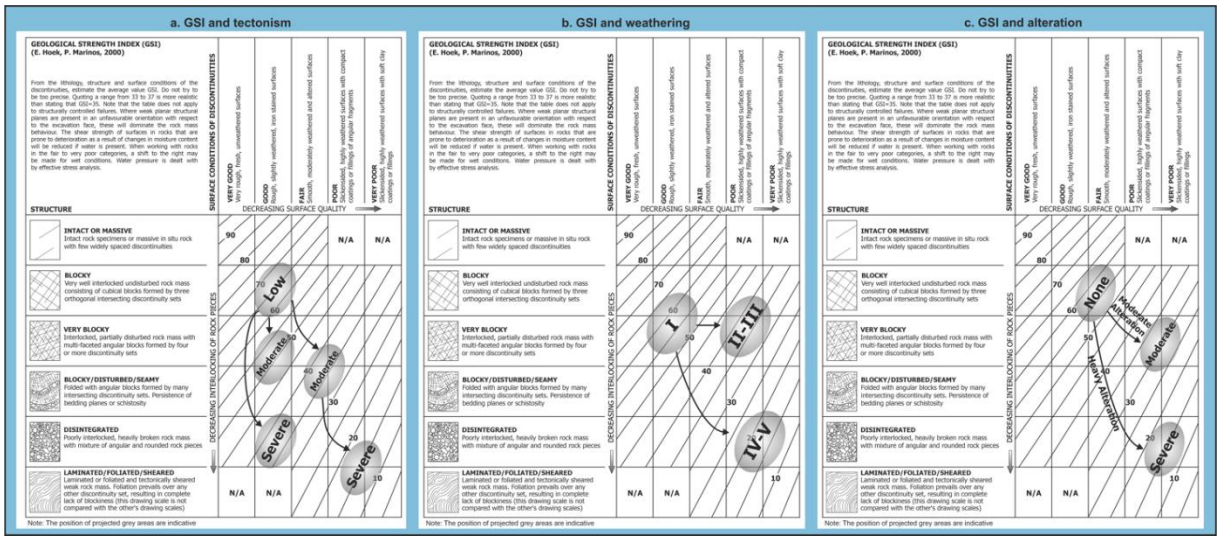

Figure 1. Indicative examples of how: (a) Tectonism, (b) Weathering and (c) Alteration affects GSI

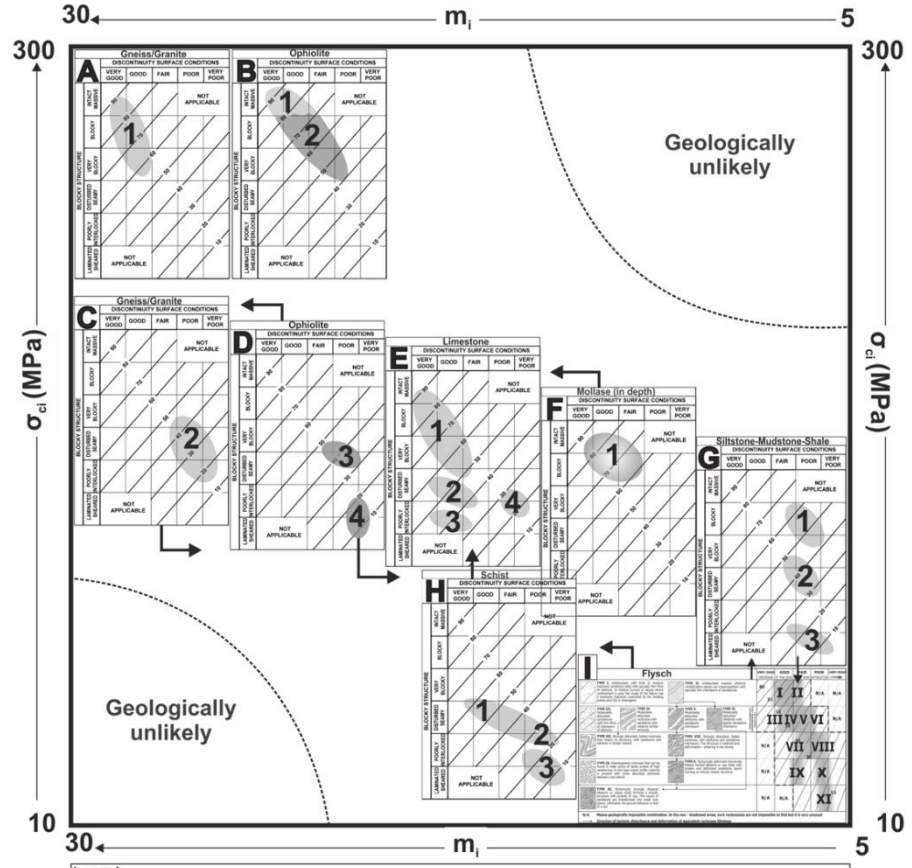

Legend

A. & C. Gneiss/Granite 1. Fresh rock masses 2. Weathered rock masses (most common range is illustrated here)	**B. & D. Ophiolite** **(Details are presented in the paper Marinos, Hoek and Marinos, 2005)** 1. Massive strong peridotite with widely spaced discontinuities. 2. Good to fair quality peridotite or compact serpentinite with discontinuities 3. Schistose serpentinite. 4. Poor to very poor quality sheared serpentinite.	**E. Limestone** 1. Massive 2. Thin bedded 3. Brecciated 4. With clay presence along the joints

F. Mollase (Details are presented in the paper Hoek, Marinos and Marinos, 2005) 1. Confined molasse at depth	**G. Siltstone-Mudstone -Shale** 1. Massive siltstones or mudstones 2. Bedded, foliated, fractured 3. Sheared, brecciated	**H. Schist** 1. Strong (e.g. micaschists) 2. Weak (e.g.chloritc schists, phyllites) 3. Sheared schist	**I. Flysch (Details are presented in the paper Marinos, 2017)** Types I to XI according to sandstone-siltstone prevalence and tectonic disturbance

Warning:
* The shaded areas are indicative only and may not be appropriate for site specific design purposes. Mean values are not suggested for indicative characterisation; the use of ranges is recommended
* The positions of the formations within the σ_{ci} - m_i chart are indicative. Exact values of σ_{ci} - m_i must be analytically defined by laboratory testing

→ The arrows show possible extension of the small scale chart

Figure 2. Most common GSI ranges for typical gneisses, granites, ophiolites, limestones, schists, siltstones/mudstones/shales, molassic and flysch formations in conjunction with a range of m_i and σ_{ci}. (Marinos & Carter, 2018).

16th International Congress of the Geological Society of Greece
17-19 October, 2022 - Patras, Greece
Bulletin of the Geological Society of Greece, Sp. Publ. 10
Ext. Abs. GSG2022-411

Limit equilibrium compared to simplified analysis for lignite mine stability during water filling reclamation practice

O. Kontopidis[1], A. Theocharis[1], I. Zevgolis[2], N. Koukouzas[1]

(1) Chemical Process & Energy Resources Institute, Centre for Research & Technology Hellas, Athens, Greece, kontopidis@certh.gr (2) School of Mining and Metallurgical Engineering, National Technical University of Athens, Greece.

Research Highlights

Slope stability is investigated for a major coal and lignite mine reclamation practice. Two approaches solving the same problem are compared and analysed presenting drastically different response.

Introduction

The vast coal mining excavations have been affected by slope failures and landslides recurrently (Zevgolis *et al*., 2019), impacting human lives and infrastructure. Sustainable reclamation of closed and abandoned coal and lignite mines is a global priority moving toward the post-coal era. One of the most common reclamation plans is the creation of pit lakes when closed excavations are flooded with water to form a lake offered to the local societies. However, during this reclamation practice, the slope stability issues might be important; thus, they are analysed by comparing limit equilibrium analysis with a recently proposed simplified approach.

Methods

A dominant factor of these phenomena is the presence of a sub-horizontal zone of low strength, which can be a thin layer or an interface between layers, named herein the weak zone. In the present work, a simplified stratigraphy was implemented, emphasising the weak zone and its effect on stability (Figure 1(a)). The height is 200m, a large but typical slope for lignite mines, and the slope angle is 10°. The weak zone was simulated with the "Weak Layer" boundary condition of Slide2 (Rocscience, 2022). The advanced "cuckoo" search method (for non-circular surfaces) was employed for the sliding surface identification, and the Mohr-Coulomb failure criterion was applied for the safety factor calculation. In parallel, Kavvadas *et al*., 2022 suggested a simplified analytical tool to calculate the evolution of the safety factor of surface lignite mining slopes after closure, considering the gradual flooding in the pit lakes. The failure of the slope was assumed to occur along a weak zone, close to the base of the slope and reaching the surface through a tension crack. The foundation of this analytical tool is a plane-type slope failure where limit equilibrium on a wedge is analysed. These two approaches both intend to provide the safety factor during water filling and are compared herein to provide further insight.

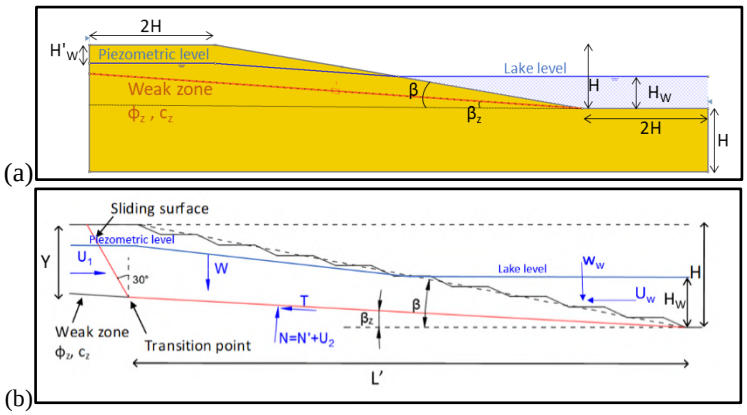

Figure 1: (a) Geometry and main parameters of the limit equilibrium computational model (b) basic elements and forces of the analytical model (after Kavvadas et al., 2022).

The groundwater regime is a crucial point of comparison. The analytical model is based on forces acting on the sliding mass (Figure 1(b)); the most crucial for the analysis are the water forces, one coming from the tension crack (named U_1) and another acting on the base of the sliding (name U_2). The basic parameter quantifying them is λ_1, which defines the fraction of the water-filled tension crack (ranging from 0 to 1, with typical values from 0.5 to 0.9). Similarly, in computational analysis, the water table's level was determined by H'_w, which is associated with the piezometric level

inside the sliding mass, as shown in Figure 1 (notice that λ_1 and H'_W are directly related, and from one the other can be calculated). The weak zone's effective friction angle and effective cohesion equal φ'_z=22° and c'_z=5 kPa, respectively. Moreover, the soil's effective friction angle and effective cohesion are φ'=28° and c' =185 kPa, and the soil unit weight γ=20 kN/m^3.

Results

Figure 2 presents the SF evolution with the water filling ratio (H_W/H). Both methods are presented for comparison; the analytical tool – with solid lines - and the limit equilibrium analysis - with dotted lines. Notice that the LEM analysis provides a sliding surface very similar to the one in Figure 1(b), underlining the effect of the weak zone defining the failure. The factor λ_1 varies from 0.5 to 0.9 and is used to characterize both approaches, being also the crucial comparison parameter.

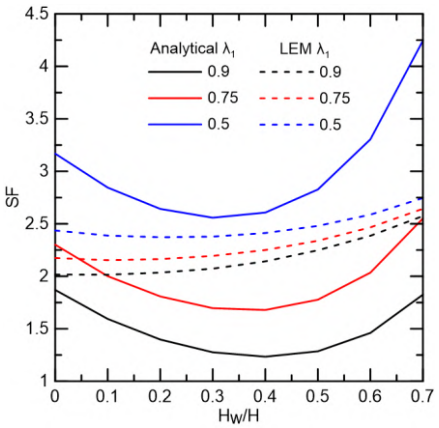

Figure 2: Safety Factor (SF) with water filling ratio (H_W/H) for various λ_1.

The difference in the results of the two methods on the SF evolution is profound and happens due to the different approaches to the groundwater regime. For the analytical method, the SF gradual decreases up to 15% while the filling ratio increases from 0 to 0.35. On the contrary, in the case of LEM, the SF practically does not decrease for the selected geometry and conditions; instead, the SF increases slowly. A further lake water elevation – especially after H_W/H>0.6-0.7 – leads to a rapid SF increase for the analytical method and a slower but significant increase for the LEM. This increase is due to the water body inside the open pit that acts as a supporting force leading to increased SF. The crucial water force U_2 is the one that, in the case of the analytical method, causes this decrease as it is dramatically larger than the pore pressures developed in the LEM approach. Finally, the factor λ_1 affects the SF tremendously regarding the analytical method; increasing λ_1 from 0.5 to 0.9 reduces the SF by approximately 43-55%. However, it affects the SF tenuously in the LEM. In particular, from 0.5 to 0.9, the SF decreases up to 15% in the initial stages of water filling, while for H_W/H greater than 0.5, the changes are negligible.

Conclusions

The present study focused on the stability analysis of lignite open pits during water filling for reclamation purposes. In that direction, two methods were compared, a simplified analytical tool recently proposed and a Limit Equilibrium analysis using commercial software. Overall, the differences between the analytical and the limit equilibrium analysis might refer to different conditions each method assumes and should be implemented in practice cautiously. The analytical method is more sensitive to changes in the piezometric and lake levels, parameters hardly precisely known in real conditions. Additionally, the impact of water evolution, especially the water forces in the tension crack and below the sliding mass, is crucial for slope stability since the SF changes rapidly as the pit-lake formation progresses. LEM analysis presents a very different situation as the pore pressures inside the slope change marginally while the lake's forces increase steadily and work for the slope's safety. In this comparison, the differences in the water forces and pore pressures between the two methods are crucial for the analysis, following the effect of the weak zone that defines the sliding mass.

Acknowledgements

This work has received funding from the European Union's Research Fund for Coal and Steel (RFCS) under the project "RAFF - Risk assessment of final pits during flooding slopes" grant agreement No 847299.

References

Kavvadas, M., Roumpos, C., Servou, A. & Paraskevis, N. 2022. Geotechnical Issues in Decommissioning Surface Lignite Mines—The Case of Amyntaion Mine in Greece. Mining 2022, 2, 278–296. https://doi.org/10.3390/mining2020015.

Zevgolis, I. E., Mikroutsikos, A., Theocharis, A. I., & Koukouzas, N. C. 2021. The effect of water filling on slope stability of open pits: A numerical investigation. In The Evolution of Geotech-25 Years of Innovation (pp. 373-379). CRC Press.

Rocscience. 2019. Slide2 Version 7.0 - 2D Limit Equilibrium Slope Stability Analysis. www.rocscience.com. Toronto, Ontario, Canada.

Rocscience. 2022. Slide2 User Guide. Documentation/Slide model/Boundaries/Weak Layer Overview. https://www.rocscience.com/help/slide2/documentation/slide-model/boundaries/weak-layer/weak-layer-overview. Accessed on 29-8-2022. Toronto, Ontario, Canada.

16th International Congress of the Geological Society of Greece
17-19 October, 2022 - Patras, Greece
Bulletin of the Geological Society of Greece, Sp. Publ. 10
Ext. Abs. GSG2022-420

Land Subsidence Phenomena in Northern Coastal Part of Korinthia Prefecture

K. Voudouris[1], Th. Chatoupis[2], M. Foumelis[1]
(1) Dept. of Geology, Aristotle University of Thessaloniki, Greece, kvoudour@geo.auth.gr (2) Geologist, Kiato, Greece

Research Highlights

The overexploitation of coastal aquifer system in combination with the susceptibility of the geological formations to compaction is the main cause of land subsidence in the north-eastern part of Korinthia Prefecture. For the mapping of land subsidence, state-of-the-art satellite-based hosted service implemented on cloud infrastructures were utilized, namely the on-demand SNAPPING service on the Geohazards Exploitation Platform.

Background

The study area, named Vocha plain, is in the northeastern part of the Korinthia prefecture, covering an area of 65 Km^2 (Fig. 1). The topographic relief slopes gently from north to south and varies from 0 to 40 m above sea level (a.s.l.). The area is characterized by xerothermic climatic conditions (the mean annual rainfall is 460 mm) and increasing water consumption, as a result of urbanization, tourist development and intense irrigated agriculture (Voudouris, 2006).

From a geological point of view, the area is formed of recent unconsolidated material consisting of sands, pebbles, breccias and fine clay to silty sand deposits. Lateral continuity of afore described deposits is disrupted by recent and older fluvio-torrential deposits originating from the streams-rivers that flow across the studied region. Within this formation sandstone, consolidated gravel, conglomerates and marly limestones of lacustrine origin exist in locally restricted intercalations. The thickness of the plain's deposits varies from 30 m to 70 m, whilst along the fluvio-torrential deposits of the river Asopos exceeds 100 m. As a result of their origin the deposits are characterized by high degree of heterogeneity and anisotropy. South of the national highway, which bounds the studied region, tyrrhenian deposits of coastal origin crop out. Usually, they consist of highly consolidated breccio-conglomerates, sand, small gravel and sporadically marl intercalations. The Pliocene deposits of the marl series occupy most of the hilly region further south of the studied region and form the bedrock of the studied aquifer system (Voudouris, 2006).

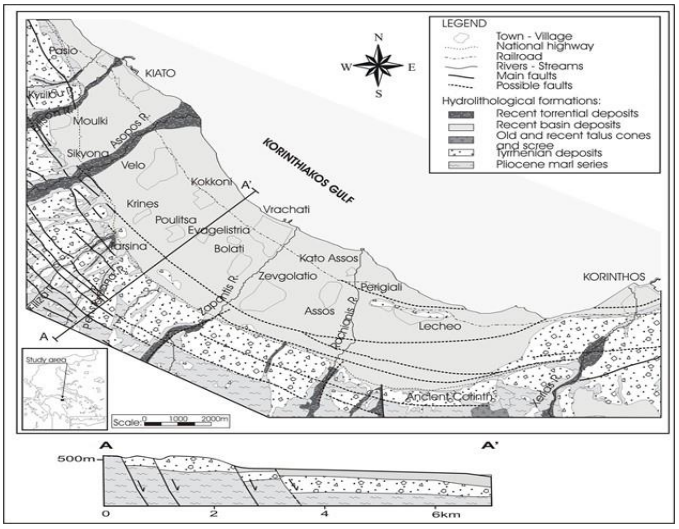

Figure 1. Geological map of the study area (Voudouris, 2006).

Within the alluvial deposits an unconfined phreatic aquifer superimposed on successive confined or semi-confined aquifers are developed. This coastal aquifer system is characterized by deficient groundwater balance. Water demands have considerably increased over the last 30 years and are mainly covered by groundwater abstracted from the alluvial aquifer via numerous boreholes, and partly by the discharge of the Asopos river. The increases in groundwater abstractions combined with prolonged dry periods, have been accompanied by declines in groundwater levels and seawater intrusion phenomena. The hydrographs show various water level fluctuations and the decline of water level during dry periods (Voudouris, 2006). Water level elevations in boreholes and wells increase steeply from the cost to island. The water table elevation is 1-3 m below ground surface (b.g.s.) in the coastal area and 15-20 m b.g.s. in the southern part of the study area (Antonakos and Lambrakis, 2021).

Methods- Results

For the monitoring of land subsidence over the study area the SNAPPING (Surface motioN mAPPING) service implemented on the Geohazards Exploitation Platform (GEP) was utilized. The Geohazards Exploitation Platform (GEP) is a cloud-based environment providing access to satellite imagery, in addition to EO processing services that allow mapping hazard prone land surfaces and monitoring terrain motion. The platform is continuously expanding by integrating a broad range of on-demand and systematic services hosted on cloud resources. Its aim is to contribute to the better understanding of geohazards and their impact through exploitation of Earth Observation (EO) services (Foumelis et al., 2019). Among the services offered to users, the on-demand Surface motioN mAPPING (SNAPPING) service consist of independent components for the PSI (Permanent Scatterer Interferometry) analysis of Copernicus Sentinel-1 mission data. The service is operational since February 2021, offering GEP users access to an automatic chain for extracting average motion rates and corresponding displacement time series (Foumelis et al., 2021). Interferometric analysis was performed initially using the SNAPPING IFG service for the generation of the interferometric stack. The IFG stack is a collection of single reference differential interferograms stored on the platform resources for consequent processing. This IFG stack was then used as input for the actual time series analysis through the SNAPPING PSI Med service at medium spatial resolution.

For the needs of the current study, the entire archive of Sentinel-1 SLC data were used, consisting of 191 dates acquired along descending track 7, well-distributed over a period of approximately 7 years (between 04/2015 and 12/2021). In practice, a total number of 374 SAR images were used, as for some consecutive data takes (same acquisition date) each covering partially the defined area of interest (AOI), concatenation was necessary. Apart from the overall stability of the area, motion rate not exceeding estimated uncertainties (mostly within -1-2 mm/yr), an interesting finding refers to a relatively large pattern spatially constraint within the broader area of Zevgolatio and Vrachati villages (Fig. 2). Along those areas motion rates reaches locally -8-10 mm/yr, whereas the spatial distribution of land subsidence does not imply a homogeneous pattern, but rather a complex one controlled by local geology. It should be underlined that the obtained measurement uncertainties were relatively low (on average ±0,38 mm/yr), underlining the robustness of the PSI motion rates. This is mainly due to the considered observation period, exceeding the generally accepted minimum time span for accurate calculating of motion based on spaceborne geodetic approaches.

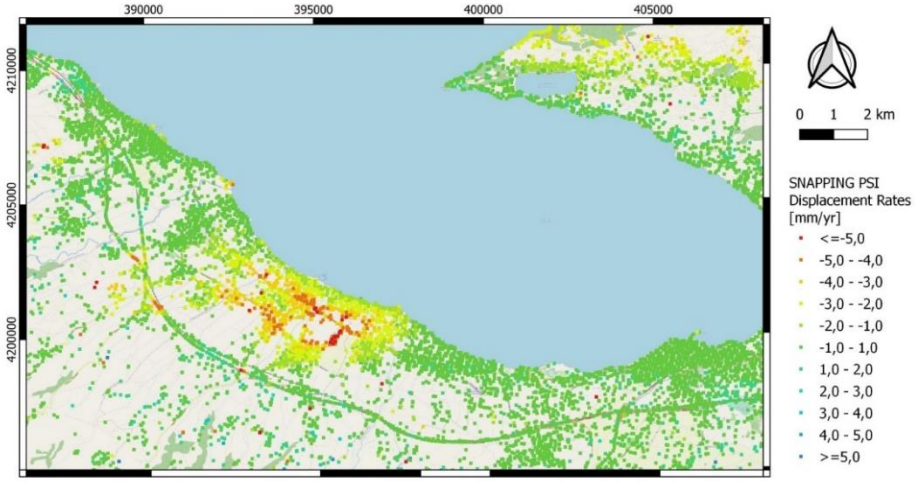

Figure 2. Land subsidence rates in the Northern coastal part of Corinth prefecture based on Sentinel-1 data acquired over the period 04/2015-12/2021, as derived using the SNAPPING service on GEP.

Conclusions

The evaluation of the results showed that the groundwater drawdown caused by overexploitation in combination with the susceptibility of the geological formations to compaction is the cause of land subsidence that occurred in the northern part of Korinthia Prefecture. The land subsidence does not imply a homogeneous pattern and the high rates are recorded in the central part of the study area.

References

Antonakos, A., Lambrakis, N., 2021. Spatial Interpolation for the Distribution of Groundwater Level in an Area of Complex Geology Using Widely Available GIS Tools. Environmental Processes 8, 993–1026.

Foumelis, M., Papadopoulou, T., Bally, Ph., Pacini, F., Provost, F., Patruno, J., 2019. Monitoring geohazards using on-demand and systematic services on ESA's geohazards exploitation platform. IEEE International Geoscience and Remote Sensing Symposium (IGARSS), Yokohama, Japan, 28 July - 2 August 2019, https://doi.org/10.1109/IGARSS.2019.8898304, 2019.

Foumelis, M., Delgado Blasco, J.M., Brito, F., Pacini, F. & Pishehvar, P., 2021. SNAPPING for Sentinel-1 mission on Geohazards Exploitation Platform: An online medium resolution surface motion mapping service. IEEE International Geoscience and Remote Sensing Symposium (IGARSS), Brussels, Belgium, 11-16 July 2021.

Voudouris, K., 2006. Groundwater balance and safe yield of the coastal aquifer system in NEastern Korinthia, Greece. Applied Geography, Vol. 26, 291-311.

16th International Congress of the Geological Society of Greece

17-19 October, 2022 - Patras, Greece

Bulletin of the Geological Society of Greece, Sp. Publ. 10

Ext. Abs. GSG2022-427

Groundwater vulnerability mapping for karst aquifers (Chelmos karst system, southern Greece)

K. Perdikaris, E.-A., Nanou, E. Zagana & M. Papailiopoulou

Laboratory of Hydrogeology, Department of geology, University of Patras, Greece

kwsthsperd7@gmail.com

1. Introduction

Groundwater from karst aquifers is considered an important resource and is extensively used for water supply (Vias *et al.* 2006). The karst landform has unique hydrogeological conditions, and it causes karst aquifers to be one of the potential water resources in many countries in the world (Yogafanny *et al.* 2021). The meaning of vulnerability assumes that the natural environment can protect groundwater to some extent. Thus, the vulnerability of groundwater is a function of both the characteristics of the aquifer system, as well as the distance from the source of pollution, the characteristics of the water and other factors that may increase the pollutant load of the specific pollutant. In Chelmos karstic system located at North Peloponnese, the COP method was applied to assess its intrinsic vulnerability. The three factors that constitute the acronym of the method are: Concentration of flow (C), Overlying layers (O) and Precipitation (P). The method is used to evaluate the physical protection of groundwater (factor O) determined by the overlying soil layers as well as to estimate how this process can be modified by infiltration (factor C) and from precipitation (factor P) (Daly, *et al*. 2002, Goldscheider, 2005). With the use of GIS tools vulnerability maps have been produced highlighting the different degrees of intrinsic vulnerability in the karst system of Chelmos.

2. Study area

The study area is located at Northern Peloponnese. The mean annual precipitation is 820 mm. The karst system consists of Cretaceous limestones, Upper Cretaceous limestones, Paleocene-Upper Eocene limestones and flysch. Planitero springs are located in the southwest foothills of the mountain Chelmos, at an altitude of 600 m and drains the Chelmos karst system. The water from the front of springs supplies the Aroanio River. The water from Planitero springs is also used for irrigation purposes.

3. Materials and methods

In this study, the COP method was applied to assess the intrinsic vulnerability of Chelmos karst system. Factor O considers the protection provided by the unsaturated zone and the properties and thickness of its layers. Daly *et al.*, (2002) proposed to subdivide the unsaturated zone into 4 layers which are: topsoil, Subsoil, karstified rocks of the unsaturated zone and non-karst rocks

Factor C (concentration of flow) is a modifier of factor O and represents the concentration of precipitation in karst systems through surface runoff with the result of point infiltration, as well as the reduction of the protective capacity offered by the overlying layers (Daly *et al.*, 2002). In this work, the following 3 parameters were considered because they describe the situation in an area where diffuse penetration occurs: The characteristics of the surface (sf), The effect of slope (s) and The effect of vegetation (v).

According to Daly *et al.*, (2002) the factor P (Precipitation) represents the amount of precipitation, the frequency and duration of those that affect infiltration. The P factor indicates the availability of water for transport and modifies the protection of the aquifer according to the amount and intensity of precipitation. Therefore, the greater the infiltration's ability to transport pollutants to the aquifer, the greater the vulnerability.

4. Results and discussion

The values of the COP index are a modification of the values of the factor O. The limits between the very high and high classes are determined by the influence of the factor C on the carbonate formations and to a lesser extent by the factor P Very Low classes represent areas where factors C and P have little influence on the protection provided by factor O. The Moderate and Low classes represent areas where the potential protection ranges from low to moderate and C and P factors have no decisive influence on vulnerability. Below is the final vulnerability map after multiplying the 3 factors (Figure 1).

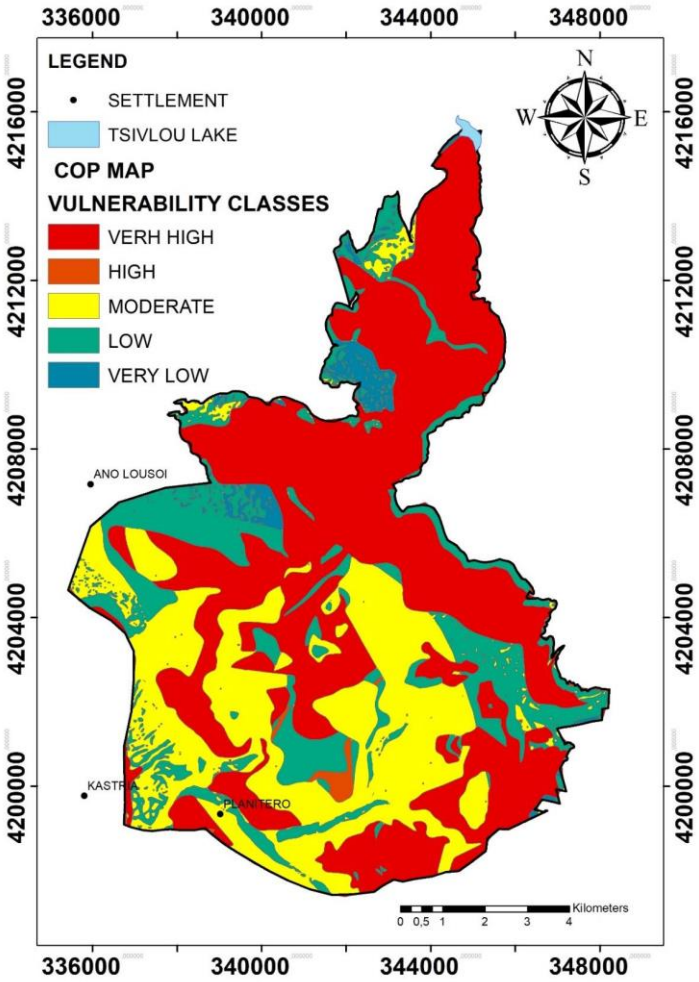

Figure 1. COP vulnerability map in the study area.

5. Conclusions

Intrinsic vulnerability in the study area ranges from very high to very low. We notice that a large part of the study area is characterized by very high vulnerability presented by the thick-platy limestones of Tripoli Zone and the platy limestones of Pindos Zone as these formations are intense karstified. As it is shown in figure 1 a large part of the map is characterized by moderate vulnerability mainly in the central and western part of the study area where Paleocene-Upper Eocene age dominate as well as Quaternary deposits such as debris cones exist.

References

Daly D., Dassargues A., Drew D., Dunne S., Goldscheider N., Neale S., Popescu C., Zwhalen F., 2002. Main concepts of the European Approach for (karst) groundwater vulnerability assessment and mapping. Hydrogeology 2, 340-345.

Goldscheider N., 2005. Karst groundwater vulnerability mapping: Application of a new method in the Swabian Alb,Germany. Hydrogeology, 13 555-564

Vias J.M., Carrasco, F., Perles M., Vadillo, I. 2006. Proposed method for groundwater vulnerability mapping in carbonate (karstic) aquifers the COP method. Hydrogeology, 14, 912-925

Yogafanny, E., Legono, D. 2021. Assessment of Groundwater Vulnerability using COP Method to Support the Groundwater Protection in Karst Area. Earth and Environmental Science, 930 012036

16th INTERNATIONAL CONGRESS of the
GEOLOGICAL SOCIETY OF GREECE

T10. Environmental Geosciences and Climate Change

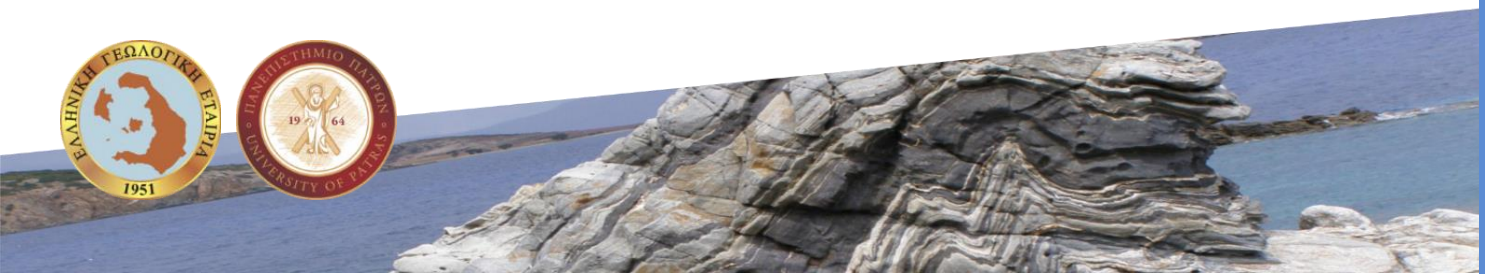

OUR EARTH, OUR HOME

16th International Congress of the Geological Society of Greece
17-19 October, 2022 - Patras, Greece
Bulletin of the Geological Society of Greece, Sp. Publ. 10
Ext. Abs. GSG2022-064

ILIDA-KIT tool: First results of near surface geophysical investigation techniques for successful management of coastal erosion

J.D. Alexopoulos[1], G.S. Mitsika[1], I.K. Giannopoulos[1], V. Gkosios[1], A. Konsolaki[1], Emm. Vassilakis[1], S.E. Poulos[1,2]

(1) Faculty of Geology and Geoenvironment, National and Kapodistrian University of Athens, jalexopoulos@geol.uoa.gr
(2) Institute of Applied and Computational Mathematics, FORTH-Hellas.

Introduction

Coastal landforms owing their formation to sediment availability and nearshore hydrodynamics, appear quite sensitive to both anthropogenic activities and effects arising from climate change. ILIDA-KIT will be an innovative and multi-parametric decision-making tool for successful management of coastal erosion and floods events, induced either by natural factors and/or human intervention (including climate change). The project ILIDA-KIT is based on multiple levels of information organized in a multi-disciplinary interactive GIS platform, which lead to the development of a set of appropriate indicators (e.g., environmental, geographical, economic). The ultimate purpose of the Tool is in the selection of the most appropriate anthropogenic intervention; the latter is based on a cost-benefit analysis that takes into account both the need for protection and the sustainable development of the coastal zone. In particular, the geophysical research aims to identify the thickness and the characteristics of the uppermost lithostarigraphic substratum of the coastal zone.

Study area

The selected location of investigation for the development of ILIDA-KIT tool is the west coast of Peloponnesus (Greece) (Fig. 1a); the coastal zone of the Helonitis Gulf and Kyparissiakos Gulf; the former is characterized by the presence of the extended Kotichi lagoon while the latter by the most extensive dune field in Greece and one of the largest along the European Mediterranean coast (Poulos *et al.* 2011).

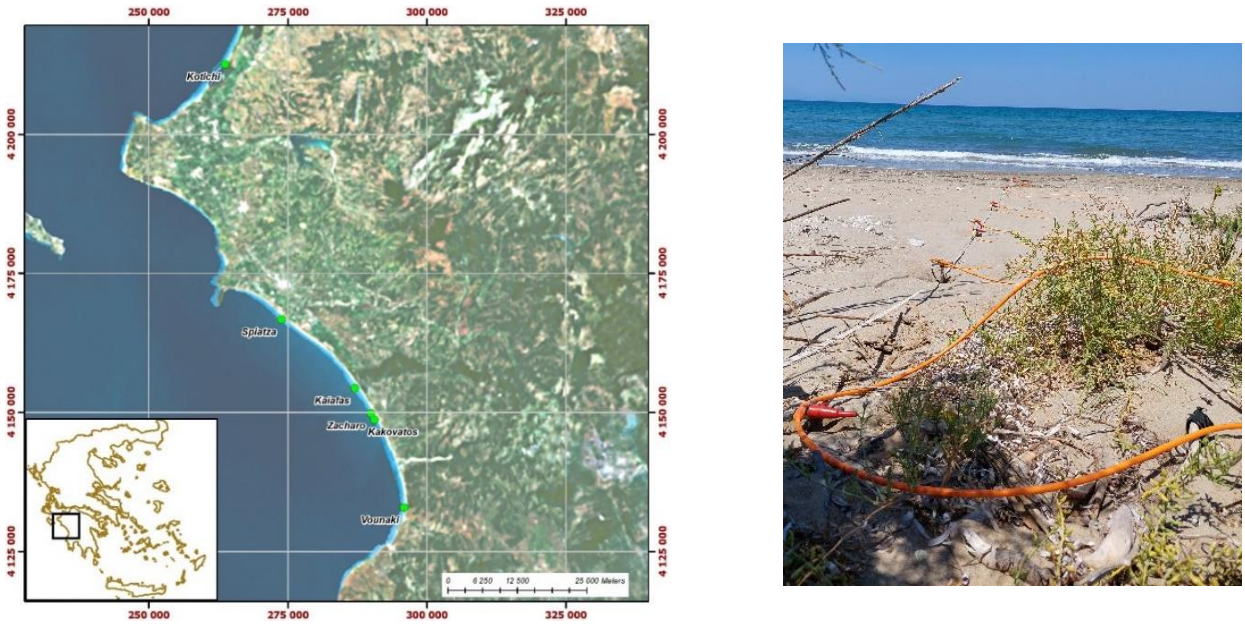

Figure 1. Index map with the sites of the geophysical campaigns (a) and data acquisition at Kotichi site (b).

Applied Methodology and Results

The geophysical techniques of electrical resistivity tomography (ERT), vertical electrical soundings (VES) and transient electromagnetic soundings (TEM) were applied. The ERT sections were carried out with a general trending normally to the shoreline whilst the VES and TEM soundings were applied at the midpoint of each ERT section. Resistivity methods have been successfully applied before in coastal environment (Alexopoulos *et al.*, 2019) and the electromagnetic method will contribute as supplementary data acquisition for detecting deeper structures and layers.

A first initiative of field data acquisition was made at Kotichi site (Fig. 1b) and the distribution of measured resistivity values, yield relatively low values near the shoreline (Fig. 2); this is in conjunction with the low relief landscape, lead to the conclusion that there is a high risk of erosion, in cases of extreme wave events and inundation.

The resistivity models of the two sounding curves (VES and TEM) appear to correlate quite well (Fig. 3). The surficial resistive layer appears in both sounding curves with resistivity values about 40 Ohm.m and the latter seems to correspond to the non-consolidated (loose) sand cover of dune. The underlying formation of relatively low resistivity (1 Ohm.m) and about 15m thickness is interpreted as a layer of saturated transgressive Holocene deposits. The deepest identified layer with resistivity values of 5-15 Ohm.m is interpreted to be Pleistocene marine deposits (Haenssler *et al.*, 2014).

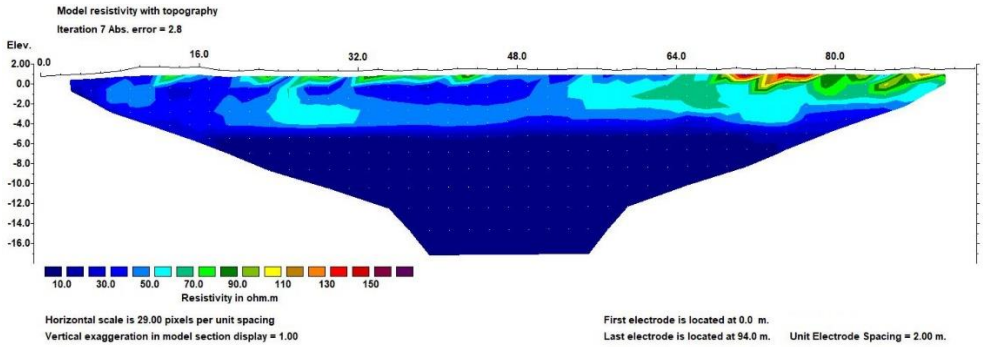

Figure 2. Electrical resistivity tomography at Kotichi site.

Table 1. Resistivity model of VES Sounding

Depth (m)	Resistivity (Ohm.m)
0-1.7	>100
1.7-7.0	45.0
7.0-20.0	1.2
	5.0

Table 2. Resistivity model of TEM Sounding

Depth (m)	Resistivity (Ohm.m)
0-8	36
8-24	1
	17

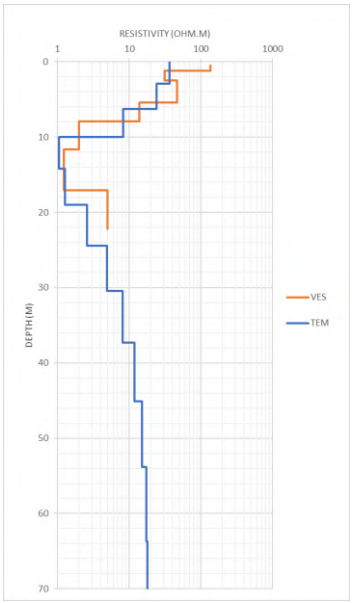

Figure 3. Resistivity models (left) of the corresponding VES and TEM sounding curves (right).

Conclusions

The combined application of the aforementioned techniques has the potential to provide valuable information regarding the thickness of the weathering layer that can be used as input data to ILIDA-KIT Tool. Additionally, the preliminary ERT results have shown that a minimum spacing of 0.5-1.0 m could provide more detailed information about the characteristics of the coastal sandy sediments and the erosion prone areas.

Acknowledgements

This research was funded by the project "Decision-making tool for the confrontation of coastal erosion and extreme wave events in the coastal zone, in the context of climate change" (MIS 5129417), financed by the Sectoral Operational Programme «Competitiveness, Entrepreneurship and Innovation» (NSRF 2014–2020) and co-financed by Greece and the European Regional Development Fund (ERDF).

References

Alexopoulos J.D., Dilalos S., Poulos S., Ghionis G., Mavroulis S. (2014). Application of geoelectrical techniques in the investigation of a coastal sand dune field. In: 20th European Meeting of Environmental and Engineering Geophysics. Vol. Tu_PA2_01. Athens, Greece; pp. 5.

Haenssler, E., Unkel, I., Dörfler, W. & Nadeau, M.-J. (2014): Driving mechanisms of Holocene lagoon development and barrier accretion in Northern Elis, Peloponnese, inferred from the sedimentary record of the Kotychi Lagoon. – E&G Quaternary Science Journal, 63 (1): 60–77.

Poulos S., Gaki-Papanastasiou K., Gialouris, P., Ghionis G. and Maroukian, H. (2011). A geomorphological investigation of the formation and evolution of the Kaiafas sand-dune field (Kyparissiakos Gulf, Ionian Sea, eastern Mediterranean) in the Late Holocene. Environmental Earth Sciences - ENVIRON EARTH SCI. 66.

16th International Congress of the Geological Society of Greece
17-19 October, 2022 - Patras, Greece
Bulletin of the Geological Society of Greece, Sp. Publ. 10
Ext. Abs. GSG2022-082

North Attica Groundwater System, Geology and Environmental Implications: The Case of Marly Limestones and Travertines

V. Giannopoulos[1], E. Andeadakis[1], E. Skourtos[1], C. Filis[1]

1 Department of Geology and Geoenvironment, National and Kapodistrian University of Athens, Athens, Greece
basilhsgiann92@gmail.com

Research Highlights

Groundwater pollution presumably takes place at Kalamos and Varnavas basins due to the groundwater flow and the significant extent of marly limestones and travertines which correlate with elevated Arsenic concentrations.

Background

The present study aims to construct an integrated hydrogeological model in the wider area covered by Kalamos and Varnavas basins at the eastern part of Oropos municipality in north Attica. The study area mainly consists of the non-metamorphic formations of the Sub-Pelagonian Unit and at a lesser extend the metamorphic rocks of Attic-Cycladic massif, that outcrops at the eastern part of the map (**figure 1**) and a large spread of Post Alpine formations mainly Neogene lacustrine sediments. The carbonate platform of the Triassic-Liassic and Upper Cretaceous limestones developed karstic forms due to its thickness and fractured mass, with the ability to contain and transfer water, hosting the karstic aquifer of NE Parnitha (Dounas et al 1980). Moreover, the Neogene lacustrine formations are capable of hosting adequate amounts of water due to their significant extent and thickness up to 300m at some cases and the development of the porous aquifer at Neogene formations (Mettos, 1992). Researchers studying the quality of groundwater in Neogene and Quaternary formations of north Attica have detected high concentrations of pollutants and specifically toxic trace elements including Arsenic, Chromium, Uranium, and Vanadium (Stamatis et al., 2011, Kampouroglou and Economou 2013, Kampouroglou and Economou 2017). Stamatis et al., (2011) referred at high Arsenic concentrations (11-247 mg/l) at the groundwater of Oropos-Markopoulo-Maurosouvala area due to lignite intercalations at marly formations and marly limestones and travertines. Moreover, they detected high Arsenic concentration at Agioi Apostoloi area at the north part of Kalamos basin up to south Evoikos gulf. Kampouroglou and Economou 2013 conclude that the elevated Arsenic concentration in the travertine limestone (61-210 ppm) and the associated soils (33-430 ppm) are considered as highly polluted soils. Furthermore, the soil contamination at the area of the Varnavas quarry by Arsenic is also attributed to natural processes, suggesting a potential environmental risk because of Arsenic contamination in soil and plants at the aforementioned basins. Kampouroglou and Economou 2017, pointed out that Arsenic contents in roots, are at most of the cases higher than normal values and also appears elevated in green vegetables as well as plants that grows in the most contaminated soils. Furthermore, the karstic system of NE Parnitha that develops in the study area also requires special protection (Cost Action 65, 1995) because of increased probability for pollution and contamination, as well as flooding phenomena.

Objectives

The use of modelling in the forthcoming study aims to assist in the following directions: i) investigation of the hydraulic connections between the geological formations of the area, ii) hydraulic connections between formations that are sources of pollutants and the water masses where they end up, iii) examination and visualization of lithology and groundwater flow in the areas of marly limestones and travertines main spread. The final objectives of this study are i) a 3D model of the lithology and tectonic structure of north Attica, ii) a 3D model of the groundwater system aquifers with determination of each aquifer geometry and interconnections, iii) Modelling of groundwater drainage pattern and groundwater routes.

Methods

To examine the groundwater flow and the routes that it follows at the wider area of north Attica and specifically through the geological formation of marly limestones and travertines that the contamination mostly takes place, the following methodology was used. i) Preprocessing and preparation of basic data such as geologic, stratigraphic, and tectonic data (cross-sections, maps) geophysical data, properties of rocks, drilling results, data from springs and wells, which are available from bibliography and case studies (Dounas et al, 1980, Mettos 1992, Lozios, 1993, Katsikatsos, 2000, 2002), ii) construction of geological cross sections along the geological map of north Attica iii) construction of virtual drillings along the cross sections to capture the bedrock structure, lithology and finally construct the aquifers with use of the virtual drillings that host water, iv) Homogenization and evaluation of every data source mention, and modification to importable data format, v) Building 3D models of lithology and the aquifers using RockWare Rockworks 2022, vi) Export of refined data answering to the main research objectives such as 3D models, cross section profiles, and fence diagrams.

Results and Conclusions

The final geological map of north Attica constructed as a following on from the IGME sheet maps Eretria, Kifissia (Katsikatsos 2000, 2002) with adjusting to later available geological, lithological and tectonic data (Mettos 1992, Lozios 1993) (**figure 1**). North Attica consist of a total of two aquifers as they were mapped and their boundaries were demarcated

(**figure 1**), the porous aquifer of Neogene Basin and the fractured NE Parnitha (Dounas et al 1980, Morphis 1995), forming the north Attica groundwater system. Neogene aquifer's drainage takes place at southern Evoikos gulf for the north part of the aquifer as the southern Varnavas-Kapandriti basin drains at the Marathon Lake (**figure 1**). The karstic aquifer of NE Parnitha develops at the carbonate platform of Sub-Pelagonian unit (Triassic-Liassic and Upper Cretaceous Limestones) and its drainage occurs at Agioi Apostopoloi springs at southern Evoikos gulf. The active karstic network of the aquifer occurs at depth of -150m (Dounas et al, 1980) at the area of the springs as the expression of the groundwater is artesian type. Based on the final 3D lithological and aquifer models as well as the groundwater drainage model for each aquifer, the present study suggests the following conclusions. i) at Kalamos basin the significant extent of marly limestones and travertines in conjunction with the extended faulting of the area increases the aforementioned formation thickness and favors the flow of the groundwater at the travertine limestones (**figure 1**, fence diagram A), ii) at Varnavas basin at the area adjacent to Marathon Lake due to the presence of Agios Georgios marbles and marly limestones and travertines there is high possibility for the development of an underground karstic network, which favors the transmission of trace elements to the groundwater and more precisely at Marathon Lake (**figure 1**, fence diagram B).

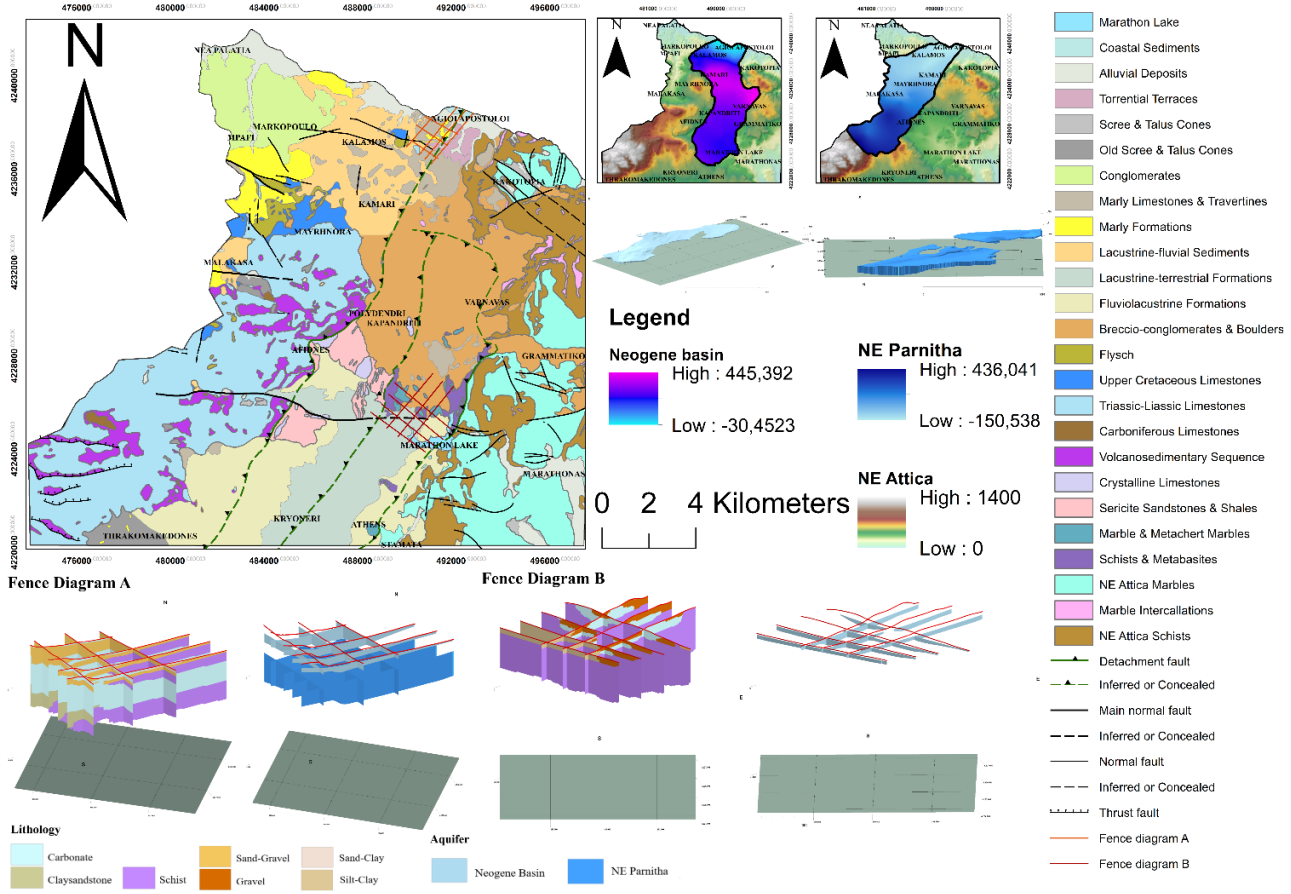

Figure 1. Geological map of north Attica together with groundwater drainage model and aquifer boundaries. Snapchat of 3D aquifer models and fence diagrams A, B of the lithology and the aquifers of the study area. The red line indicates the ground surface.

References

COST Action 65 (1995) Report of the working group: Hydrogeological Aspects of Groundwater Protection in Karstic Areas.

Dounas, A., Kallergis, G., Morphis, A., Pagounis, M. (1980). Hydrogeological study of brackish and karstic springs Agion Apostolon Kalamou. IGMR, No 31, Athens, Greece.

Kampouroglou, E., Economou-Eliopoulos, M., (2013). Natural contamination by As and heavy metals in soil, their bio-accumulation and potential sources: the case of a travertine limestone quarry, Greece. Cent. Eur. J. Geosci. 5 (1), 174–188.

Kampouroglou, E. E., & Economou-Eliopoulos, M. (2017). Assessment of arsenic and associated metals in the soil-plant-water system in Neogene basins of Attica, Greece. Catena, 150, 206–222.

Katsikatsos, G. (2000). Geological Map of Greece, Eretria Sheet 1:50.000. IGMR, Athens, Greece.

Katsikatsos, G. (2002). Geological Map of Greece, Kifissia Sheet 1:50.000. IGMR, Athens, Greece.

Lozios, S. (1993). Tectonic analysis of the metamorphic rocks in NE Attica, Ph.D. thesis, Department of Geology, University of Athens, Greece

Mettos, A.I. (1992). Geological and paleogeographical study of the continental Neogene and Quaternary deposits of NE Attica and SE Beotia, Ph.D. thesis, Department of Geology, University of Athens, Greece.

Morphis, A. (1995). Hydrogeological research karst aquifer system of NE Parnitha and the wider region of northern Attica, Ph.D. thesis, University of Patras, Greece

Stamatis, G., Alexakis, D., Gamvroula, D., Migiros, G., (2011). Groundwater quality assessment in Oropos-Kalamos basin, Attica, Greece. Environ. Earth Sci. 64 (4), 973–988.

16th International Congress of the Geological Society of Greece
17-19 October, 2022 - Patras, Greece
Bulletin of the Geological Society of Greece, Sp. Publ. 10
Ext. Abs. GSG2022-084

Greek Palygorskite and Sepiolite used for Wastewater Disinfection against E. Coli

A. Mavrikos[1], D. Vayenas[2,3], A. G. Terkelekopoulou[4], D. Venieri[5], P. Lampropoulou[1], D. Papoulis[1]

(1) Department of Geology, University of Patras, Patra, 26504, Greece, armavrikos@gmail.com (2) Department of Chemical Engineering, University of Patras, Patra, 26504, Greece (3) Institute of Chemical Engineering and High Temperature Chemical Processes (FORTH/ICE-TH), Patra, 26504, Greece (4) Department of Environmental Engineering, University of Patras, Agrinio, 30100, Greece (5) School of Environmental Engineering, Technical University of Crete, Chania, 73100, Greece

Introduction

The need for the development of effective water purification techniques is essential, due to the various inadequacies associated with the current water purification techniques. Water disinfection is achieved by removing, inactivating or killing its pathogenic microorganisms and it can occur either by chemical or natural means (Jedla *et al.*, 2022).

Clay minerals are a class of adsorbents that also act as natural antimicrobials. Their advantage over other adsorbents is their relative abundance in nature, low cost and environmental friendliness in their applications. In addition, they have large specific surface areas, high porosity, surface charge and surface functional groups that characterize them as useful adsorbents (Unuabonah *et al.*, 2017). Palygorskite and sepiolite are unique clay minerals since they are the only 2:1 clay minerals characterized by fibrous morphology and 2:1 ribbons structure. The difference between them is that sepiolite's wider b dimension can fit three Si-O group chains, instead of two in the case of palygorskite. The high specific surface of these minerals is resulting from their structure, basal spacing as well as crystal morphology and dimensions. Another outcome of these characteristics is their high adsorption capacity (Yang and Wang, 2022). Palygorskite's and sepiolite's uniqueness in combination with their characteristics as clay minerals and the minimum amount of research on this topic, makes them the perfect studying candidate clay minerals for water disinfection.

The aim of this study is to determine the optimal amount of palygorskite and sepiolite with the highest results in water disinfection at a specific waste volume and bacterial concentration, in order to be exploited for water treatment. Initial experiments took place to determine the bacteria concentration at local wastewaters and then batch kinetic experiments were carried out to determine the adsorbent's dosage.

Materials and Methods

Palygorskite from Ventzia basin (Grevena/Western Macedonia, Greece) and sepiolite from Solomos village (Corinth/ Peloponnese, Greece) were used for a series of batch experiments. The specific palygorskite deposit is exploited by Geohellas S.A. and was diagenetically formed through the smectite – silica-rich solutions interaction (Kastritis *et al.*, 2003), while the sepiolite occurrence was discovered by Papoulis *et al.*, (2018) between WNW- and ENE- trending active faults. Samples were fractionated in order to obtain powder sedimentation (< 50μm) and were characterized by XRD, FTIR and SEM that were conducted at several laboratories of the University of Patras.

The antimicrobial activity of the clay minerals was analyzed against Escherichia coli DSM498 (DSMZ-German Collection of Microorganisms and Cell Cultures Gm BH) which was obtained from the Laboratory of Environmental Microbiology, School of Chemical and Environmental Engineering, Technical University of Crete, and used as an indicator of fecal water contamination.

Batch kinetic experiments were carried out to examine the water disinfection ability of raw palygorskite and sepiolite. 250 ml conical flasks were employed and filled with 100 ml of synthetic wastewater with an initial bacterial concentration of 10^4 cfu/100ml. Different volumes (1, 2, 3, 4 and 5 g) of the clay minerals were used each time and the rpm were set at 200. Samples were taken in various time intervals (0, 10, 20, 30, 40, 50 and 60 min). The experiments took place at room temperature and the pH was set in a range from 6.5 to 7.5. The samples were filtered through 0.45 μm Whatman filters and plated onto HiCrome E.Coli agar. The plates were incubated at 38+- 2 ^oC for 24 h. After the incubation period, the colonies on each plate were counted and compared to the control sample. The removal efficiency (%) of each clay mineral was determined based on the equation (1).

$$Removal\ efficiency = \frac{C_0 - Cf}{C_0}\ \% \quad (1)$$

Where C_0 is the initial E. coli concentration and C_f is the concentration at various time intervals during the disinfection process. All antibacterial tests were performed in triplicate, and the averaged results are reported.

Results

According to the X-Ray Diffraction patterns of palygorskite and sepiolite, the purity of the sample is confirmed. Palygorskite's XRD pattern shows its basic reflections at 10.54 and 20 Å, whereas a peak at 6 Å is also shown in the pattern, due to the smectite mineral saponite which co-exist with palygorskite at Grevena's deposit. Sepiolite's XRD

pattern shows its characteristic peak at 7.2 Å, while no impurities are present. The FT-IR spectra confirmed XRD results for both clay minerals and through the SEM observations, their fibrous morphology was verified. Batch kinetic experiments indicated similar characteristics and behavior for both clay minerals used for wastewater disinfection from E. coli, with palygorskite showing slightly better results. The stirring parameter of the batch kinetic experiments has led to a re-release of the bacteria to the solution after the 50 minutes. Specifically, in case of palygorskite the decrease of adsorbent's dosage to 1,2 and 3 g, compared to 4 and 5 g, results to an increased E. coli removal at the specific parameters. The higher removal percentages are appearing at 1 and 2 g palygorskite dosages and they are close to 70% at 40 to 50 minutes, while the 3 g dosage achieved removal efficiency at about 65% and showed a more stable re-release of the bacteria to the solution due to stirring compared to the smaller dosage experiments. Sepiolite's E. coli removal efficiency reached the 55% at 40 minutes of stirring, only at the 1 g dosage. As the amount of sepiolite was increasing the removal efficiency was getting lower, respectively to that, the re-releasing time was faster than the palygorskite samples.

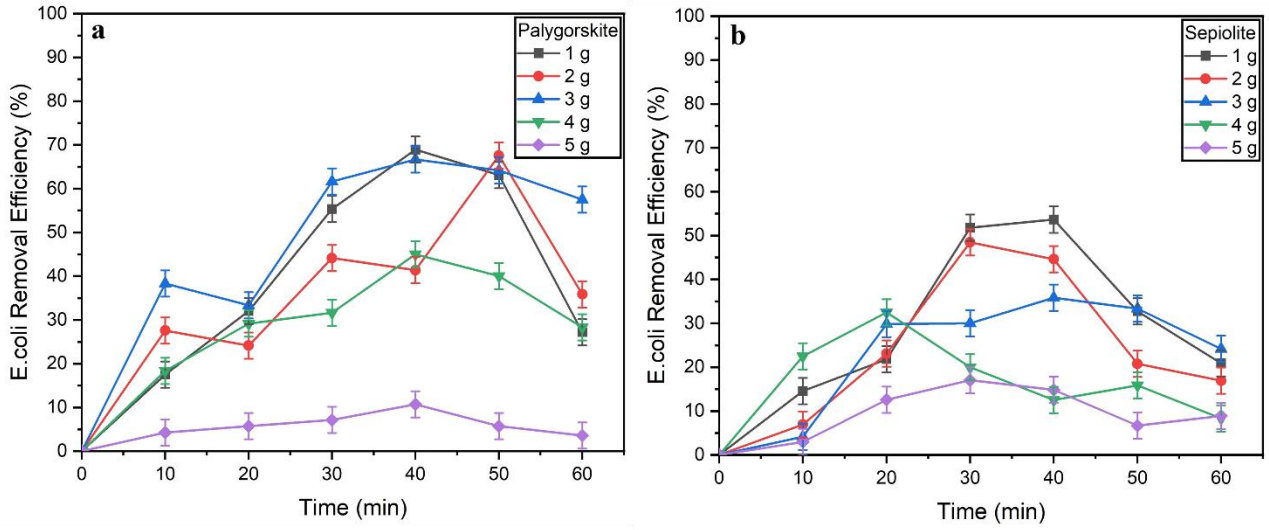

Figure 1. E. coli removal efficiency with different amounts of dosages for a) palygorskite and b) sepiolite

Conclusions

Some of the current outbreaks of diseases in the world such as diarrhea and dysentery, caused by Escherichia coli, are results of water and food infections. Thus, the development of effective and efficient water purification techniques is necessary. Greek palygorskite and sepiolite proved to be promising adsorbents of E. coli. In case of palygorskite the removal efficiency reached higher levels than sepiolite within 30-50 minutes. There is a possibility that the higher efficiency in palygorskite samples may be due to the coexistence of small percentages of smectite. In both cases the adsorbent dosage had impact, since the lower the mass, the higher the removal capacity. Also, the stirring during the process of the batch kinetic experiments appeared to have massive impact on the re-releasing of the bacteria back to the solution. Both raw palygorskite and raw sepiolite, present to be no sufficient for the main disinfection mechanism, under the effect of stirring at least. However, further research needs to be conducted, regarding the carry out of the experiment in columns where no stirring is taking place and the potential modification of the clay minerals or the combination of them with other materials.

Acknowledgements

The present work was financially supported by the «Andreas Mentzelopoulos Foundation» of the University of Patras.

References

Jedla M.R., Koneru B., Franco A., Jr., Rangappa D., Banerjee P., 2022. Recent developments in nanomaterials based adsorbents for water purification techniques**.** Biointerface Research in Applied Chemistry 12 (5), 5821-5835**.**

Kastritis I.D., Mposkos E., Kacandes G.H., 2003. The palygorskite and Mg-Fesmecite clay deposits of the Ventzia basin, western Macedonia, Greece. In Eliopoulos et al. (Eds), Millpress, Roterdam, Mineral exploration and Sustainable Development-Proceedings of the 7th SGA Meeting. 891-894.

Papoulis D., Panagiotaras D., Tsigrou P., Christoforidis K. C., Petit C., Apostolopoulou A., Koukouvelas I., 2018. Halloysite and sepiolite - TiO_2 nanocomposites: Synthesis characterization and photocatalytic activity in three aquatic wastes. Materials Science in Semiconductor Processing 85, 1-8.

Unuabonah E. I., Ugwuja C. G., Omorogie M.O., Adewuyi A., Oladoja N.A., 2018. Clays for Efficient Disinfection of Bacteria in Water. Applied Clay Science 151, 211-223.

Yang F., Wang A., 2022. Recent researches on antimicrobial nanocomposite and hybrid materials based on sepiolite and palygorskite. Applied Clay Science 219, 106454.

16th International Congress of the Geological Society of Greece
17-19 October, 2022 - Patras, Greece
Bulletin of the Geological Society of Greece, Sp. Publ. 10
Ext. Abs. GSS2022-162

Groundwater level dynamics of the Messara Basin, Crete island

I. Michalakis[1], E. Tsolaki[1], C. Loupasakis[2], K. Voudouris[3], Ch. Kontoes[4]

(1) Hellenic Survey of Geology and Mineral Exploration, Regional Branch of Crete, Rethymno, Greece, michalakis@igme.gr (2) National Technical University of Athens, Athens, Greece (3) Aristotle University of Thessaloniki, Dept. of Geology, Thessaloniki, Greece (4) National Observatory of Athens, Institute for Astronomy and Astrophysics, Space Applications and Remote Sensing, BEYOND Center for EO Research and Satellite RS, Athens, Greece.

Research Highlights

The current work presents the results acquired by the field campaigns that took place at the Messara basin during the wet and dry seasons of 2021 (Figure 1). The groundwater level has a wide range of variation between wet and dry seasons due to over-exploitation for irrigation purposes. Groundwater quality is characterized by high salinity and nitrate concentration due to seawater intrusion and intensive agriculture activities.

Figure 1. Monitoring wells and depth to water level measurements of the Messara basin. Strict quality assurance and quality control protocols were followed in the field to ensure accuracy of the measurements.

Introduction and Objectives

A proper groundwater management requires the systematic collection and accurate utilization of primary data. Although several authorities deal with the management of groundwater within a specific region, a fully developed framework at a wider scale is still missing prohibiting thus a detailed and comprehensive masterplan. Aiming to contribute into filling this gap, systematic fieldwork must be conducted, targeting on the physical borders of the groundwater systems.

During the period September 2020 to February 2022 a detailed investigation of the hydrogeological conditions of the Messara basin was carried out. Within the framework of a PhD study, field measurements took place in parallel with a wells inventory conducted by the Regional Branch of the Hellenic Survey of Geology and Mineral Exploration in Crete. The investigation took place in the administrative boundaries of five Municipalities of the island of Crete, where the Messara basin is located (Figures 1 and 2). The aim of this manuscript is to present a recent state of the groundwater head fluctuation during the wet and dry seasons of 2021.

Methods

Strict quality assurance and quality control protocols (while targeted in relation to time) were followed in the field to ensure accurate groundwater measurements (Figure 1). In addition to groundwater level measurements, parameters such as water and air temperature (ºC), E.C. (μS/cm), pH (dimensionless), D.O. (mg/l) were also measured while observations about turbidity, odor, suspended solids and color of groundwater were recorded.

The primary data that were collected, evaluated and analyzed for the compilation of groundwater prediction maps (Figure 2) come from 2,702 autopsy positions (boreholes, wells, springs) across the Messara basin, within the framework of the PhD study. Furthermore, additional data, from the archives of H.S.G.M.E., were evaluated from the wider area of interest, referring to:

- 2,824 autopsy positions (boreholes, wells, springs) across the five Municipalities of Messara basin (H.S.G.M.E./R.B.C., 2020-2022).
- 581 field measurements in 49 points of the Groundwater monitoring network of Greece (H.S.G.M.E./R.B.C., 2018-2022), in the vicinity of Messara basin (June 2018 – May 2022).

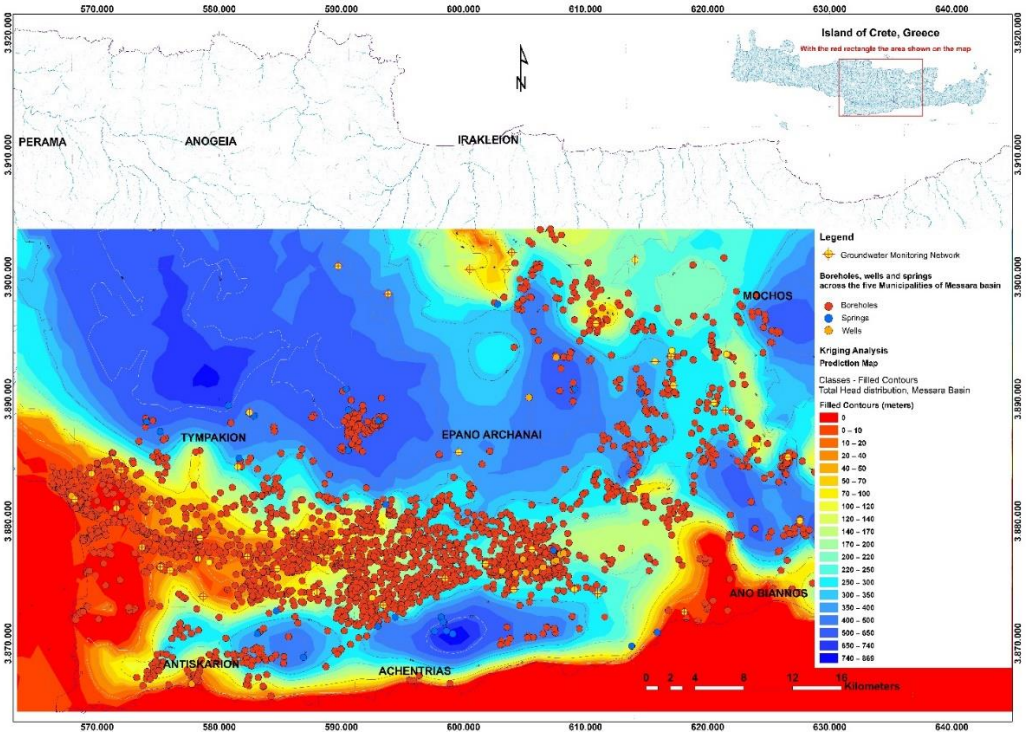

Figure 2. A Prediction map (Raster & Contours) based on geostatistical analysis of the groundwater level (Total head) distribution in the Messara basin. Groundwater head layout – Dry season 2021.

Results and Conclusions

The results of the site investigation were also integrated to enhance the knowledge of the geological and hydrogeological conditions of the island of Crete, adding more detail and confidence to future investigations in the area.

Future directions of the project will include the incorporation of all collected and available data, aiming to the publication of a hydrogeological - hydrochemical map and the investigation of the land subsidence phenomena taking place at the site as witnessed by the available DinSAR data and field survey records.

Acknowledgements

A part of the fieldwork was carried out by the executive staff of the Regional Branch of Crete in the context of the implementation of the projects: “Systematic inventory of water wells of every use throughout the country of Greece” and “Groundwater Monitoring Network of Greece”. Additional field surveys have been contacted within the framework of the PhD thesis assigned to the first author at the N.T.U.A.

References

H.S.G.M.E./R.B.C., 2020-2022. Project: “Systematic inventory of water wells of every use throughout the country of Greece” of the Municipalities: Phaistos, Gortyna, Archanon Asterousion, Minoa Pediadas, Viannos. Preliminary Technical Reports, Rethymno, Greece.

H.S.G.M.E./R.B.C., 2018-2022. Project: “Groundwater Monitoring Network of Greece”, Preliminary Reports, Rethymno, Greece.

16th International Congress of the Geological Society of Greece
17-19 October, 2022 - Patras, Greece
Bulletin of the Geological Society of Greece, Sp. Publ. 10
Ext. Abs. GSG2022-308

CCS Development Barriers and Way Forward: Road Map for CCS Deployment at National and EU levels

I. Ismail[1], T. Sketopoulos[1], E. Tartaras[1], D. Ktenas[1], A. Stefatos[1]
(1) Hellenic Hydrocarbon Resources Management, Athens, Greece, i.ismail@greekhydrocarbons.gr

Background

Despite both the urgent need for action to mitigate climate change, and the rapid uptake of renewable energy over the last two decades, emissions reductions have been slow to progress. About 80% of primary energy is still supplied by fossil fuels, as it was 50 years ago. At the heart of the climate resilience strategies is the carbon capture and storage (CCS) technology: the recent United Nations Intergovernmental Panel on Climate Change (UN IPCC) reports a critical and immediate need for technologies that capture CO_2 to offset accumulating carbon until energy storage and renewables ramp up to meet demand. CCS technologies represent a solution for capturing the CO_2 byproduct from cement and steel industries, hydrogen production from fossil fuels, and power generation, before it reaches the Earth's atmosphere. The captured CO_2 is compressed and then injected into deep underground rock formations for permanent storage. Moreover, CCS is a proven and well understood technology that reduces emissions from industrial processes that are important to the global economy (e.g., steel, cement and chemicals production). Coupled with the bioenergy used to generate electricity and produce biofuel, it is one of the few technologies that can deliver negative emissions on a scale sufficient to limit temperature rise of 1.5°-2°C.

To reach the values outlined in the policy scenarios for tackling climate change, the number of industrial-scale CCS initiatives must be increased 100-fold from the current 6 operational dedicated geological storage sites globally to over 2,000 by 2040. This is equivalent to storing 300 million tons per year by 2050.

Greece's CCS needs and main challenges

Greece emits 70 million tonnes of carbon dioxide annually, of which about 33 million tonnes are industrial emissions that require decarbonization with CCS technology. More specifically, the national energy and climate program has set a goal to reduce greenhouse gas (GHG) emissions by more than 42% compared to 1990 emissions and more than 56% compared to 2005 ones. In other words, Greece has set a goal exceeding the core EU goals for which CCS is a critical climate change mitigation technology that will enable the country to reduce its industrial emissions and meet set targets.

In Greece the regions of Volos, Mesohellenic Trough, the Axios/Thermaikos basin, the nearly depleted Prinos oil fields, as well as parts of Western Greece may have the appropriate reservoirs and/or other geologic formations (saline aquifers, salt caverns) that could serve as potential storage sites for carbon dioxide. Currently, the almost depleted oil fields in Prinos constitute the most mature candidate site for carbon storage due to the availability of extensive subsurface datasets and good knowledge of the local geology and reservoir properties. However, there is no doubt that several challenges are encountered when deploying a CCS project. The goal of this work is to identify and review the barriers to CCS development and propose ways to overcome these barriers, with a focus of four main areas, namely technical, policies and regulations, business models/funding and public perception, which have been identified as hurdles for CCS large-scale deployment.

Next, we briefly address the main challenges and we propose ways forward to overcome the main barriers.

1. Technical Challenges

To better identify the technical barriers, we review the different parts of the CCS value chain: CO_2 capture, transport and storage.

1.1. Capture Challenges

Capture technologies can remove >95% of the CO_2 from flue gases or industrial processes and waste gas streams. The CCS technology can decarbonize power generation, energy-intensive industries and large-scale hydrogen production. Importantly, for sectors such as iron and steel, cement and chemical production, the manufacturing process produce CO_2 as a by-product of chemical reactions, and CCS is one of the very few solutions to cost effectively address these "process emissions" and enable these industries to decarbonize. However, the greatest costs of a CCS project today are typically associated with the equipment and energy needed for the capture and compression phases rather than transportation and storage. The cost of CO_2 capture from industrial application ranges from 28 to 107 €/tCO2 depending on the industry. Meanwhile, the number of different capture technologies has increased steadily, which means that the general technical availability is no longer a hurdle in itself for both industrial and power applications; rather, the challenges and barriers in the capture phase of a CCS project can be identified in two main areas: 1) Economical, the high cost of capturing CO_2 at

industrial sites and power plants 2) Technical, relatively low capture rate to meet decarbonization targets. Therefore, a potential solution could be that R&I activities must receive enough funding and support to boost technological progress that will result in costs reduction as well as in increased capture rates.

1.2. Transportation Challenges

CO_2 transportation can occur through a network of pipelines, shipping or other modalities (truck etc.). Meanwhile, carbon dioxide transportation is a well understood process, that has been taking place in US and Norway for several decades both for EOR and permanent storage purposes. A central requirement for the efficient, safe design and operation of CO_2 pipeline transportation networks is the accurate transient flow modelling of fluid phase and composition of the CO_2-rich mixture along the pipeline network and at the point of injection into the storage site. Therefore, further studies are needed to assess the quality of CO_2 streams as well as CO_2 density and pressure, ensuring ongoing monitoring of CO_2 flows and pipeline safety during operations. On top of that, the development of CO_2 transport and storage infrastructure networks to connect industrial clusters with other CO_2 capture sites and finally to CO_2 storage sites and across international borders is key to progress CCS in Europe and thus need to be considered. In addition, demonstrating how crucial it is to have adequate technology for sustainable CO2 transportation by ship in order to boost CCS development and enable EU PCI projects under development to become operational.

1.3. Storage Challenges

CO_2 geological storage is a safe and mature technology ready for broad implementation, as evidenced by over twenty years of successful offshore storage in Norway, combined with more recent onshore storage in Canada, USA and Australia. Meanwhile, the uncertainty in subsurface geology understanding, storage site characterization and leakage potential of the considered sites, as well as associated legal framework obstacles, highlight the challenges and complexity of such projects. Integrated CCS projects are characterized by high uncertainty risk, thus requiring a robust risk management framework. When characterizing the storage site, we need to consider the following: the site's containment, injectivity, capacity, integrity, hydrodynamics, and monitorability in order to ensure safe and permanent storage of CO_2. This requires data availability and clarity and the close collaboration of professionals from a wide range of specialties. Furthermore, the issues of containment and liability risks for long term CO_2 storage are particularly important; a relatively challenging task is the assessment of how site operators and governments would share long-term CO_2 storage risks.

2. Policies and Regulations

A favorable policy and regulatory framework are key factors for the large-scale development of CCS technology and the kick-off of European CCS projects during the current decade. While the mitigation role of CCS technology has been adequately demonstrated and acknowledged, the legal framework for the technology is thus far limited, causing delays which is needed if we are to meet CO_2 emission reduction targets. Legal challenges that are specifically highlighted within the context of networks refer to cross-border transport of CO_2 and the coordination of CO_2 streams from different sources. Better coordination at EU and global level is needed to address existing differences in legal requirements with regards to the construction and characteristics of pipelines for cross border transport projects, as well as clear guidelines regarding specific requirements for CO_2 pipelines. At EU level, the European Commission's Directive 2009/31/EC ensures third-party access to CO_2 networks, following precise CO_2 specifications with the aim to guarantee access and compatibility in the network. The EU will still need to coordinate this network by issuing guidelines on the requirements of CO_2 streams.

3. Business Models and Funding

The biggest barrier for CCS deployment is the current market state that prevents the creation of viable business model. An internal in-depth review of different CCS projects at EU level revealed that all advanced under development projects have received governmental and/or EU support, concluding that funding mechanisms are a vital element to unlock private investments in large-scale CCS projects. In addition, the cross-value chain risks (counterparty risks) that are inherent between the different parts along any CCS value chain (capture – transport – storage) remain a high business risk. Therefore, necessary steps to support the development of 1) European CO_2 infrastructure (shared CO_2 infrastructure) 2) enabling policy framework making the CCS economically feasible for companies to invest in the whole value chain of CCS (support for both CAPEX and OPEX) 3) A functional and relevant carbon price

4. Public Acceptance/Perception

In general, there is limited public awareness of the value and benefits from CCS technology. There is a great need to clearly describe the value and also highlight how CCS technology can affect the daily life of EU citizens and consumers' choices. Bringing together policymakers at local, regional, national and EU level with companies and other societal actors, such as trade unions and environmental NGOs, will be a key driver for the development of CCS projects and raising awareness about their environmental and economic benefits.

5. Conclusions

The result of the review shows that no CCS barriers are exclusively technical, with the CCS cost/commercial aspects being the most significant hurdles in the short to medium term.

References

Budinis et al. 2018, An assessment of CCS costs, barriers and potential, Energy Strategy Reviews, 22, 61-81

Key Enablers and Hurdless Impacting CCUS Deployement with an Assessment of Current Activities to Address these Issues, Report, CCUS SET-PLAN, European Union's Horizon 2020 research and Innovation program grant agreement No 842214

16th International Congress of the Geological Society of Greece
17-19 October, 2022 - Patras, Greece
Bulletin of the Geological Society of Greece, Sp. Publ. 10
Ext. Abs. GSG2022-313

Hydrogen deployment: The EU's Pathway to Accelerate Net Zero Emission Target

E. Dimou[1], E. Kaikas[1], G.Makrodimitras[1], E. Tartaras[1], A. Stefatos[1]
(1) Hellenic Hydrocarbon Resources Management (HHRM), Athens, Greece, e.dimou@greekhydrocarbons.gr

The energy transition pathway to net zero carbon emissions by 2050 includes various climate mitigation actions and policies that support energy efficiency, renewable electricity and fuel switching to clean fuels. Hydrogen is an energy vector that can gradually replace fossil fuels and effectively decarbonize energy systems and hard-to-abate sectors. The EU strongly supports clean hydrogen deployment as one of the main pillars to achieving its zero carbon emission targets and reducing dependency on Russian fossil fuel imports. The REPowerEU has recently announced its target for clean hydrogen demand of 20 million tonnes by 2030 and this amount is projected to exceed the value of 66 million tonnes by 2050. Therefore, a hydrogen supply chain has to be accelerated and developed at affordable prices to enable the production, transportation, and storage of clean hydrogen demand in the EU. Clean hydrogen can be produced from renewable electricity using the electrolysis process (green or renewable hydrogen) and from natural gas using the methane reforming process combined with Carbon Capture and Storage (CCS) infrastructure (blue hydrogen). The produced clean hydrogen can be transported using repurposed natural gas infrastructure, new hydrogen pipelines or other distribution methods. Taking into account the large amounts of hydrogen demand and supply, as well as its large volume in atmospheric pressure conditions, Underground Hydrogen Storage (UHS) is considered a viable and promising, if not yet mature, solution for reliable, safe and cost-effective storage of large hydrogen volumes and subsequent extraction to meet seasonal demands. It is expected that the hydrogen supply chain will be developed progressively throughout time using a combination of low-cost technologies to build an affordable hydrogen economy by 2050 and satisfy the requirements for net zero emissions. This abstract aims to provide an overview of the cost-effective hydrogen supply chain options that can be applied at the European and national levels to achieve climate neutrality and energy security goals. Greece could build up a national low-cost hydrogen economy to reduce emissions and tackle climate change using its potential domestic energy resources (natural gas, offshore wind, onshore renewables) and explore opportunities for the potential use of geological formations for underground hydrogen storage.

Hydrogen Supply chain: Building a Cost-Effective Decarbonisation Pathway in the EU

Hydrogen is considered the energy fuel of the future due to its ability to replace fossil fuels and, therefore, support the emission reduction targets of hard-to-abate sectors. Hydrogen blending with natural gas can be used as a feed in natural gas-fired power generation plants and heavy industries (steel, cement) for emission reductions. Pure hydrogen can be used in fuel cells to generate electricity and heat production and power heavy truck vehicles (transport sector) producing zero emissions. Hydrogen deployment in industries and sectors requires a reliable and cost-effective hydrogen supply chain, which is expected to be gradually developed to cover the potential market demand by 2050 providing low-cost hydrogen fuel supply. The various technologies that will be employed in the hydrogen supply chain to build an affordable hydrogen economy are presented in the following sections. These technologies will enable the EU and Greece to move forward with their emissions reduction targets and to build a cost-effective hydrogen economy for the future.

Hydrogen Production: Hydrogen can be produced using two main processes; methane reforming and electrolysis process. Gray hydrogen is produced from the steam methane reforming process, where fossil fuels, mostly natural gas, react with steam and the byproduct carbon dioxide is emitted into the atmosphere. Blue hydrogen is produced when a Carbon Capture and Storage (CCS) infrastructure is added to the steam methane reforming process to capture 80-90% of the produced carbon dioxide and store it permanently in underground geological formations. Green or renewable hydrogen is produced from the electrolysis process where an electrolyzer splits water (H2O) into hydrogen (H2) and oxygen (O2) by applying an electricity input. Electricity input to the electrolyzer can be provided from either a dedicated renewable power station (offshore/onshore wind, solar) to produce renewable hydrogen or powered by a grid connection to produce green hydrogen. Blue, green, and renewable hydrogen (known as clean hydrogen) are complementary and these hydrogen sources will be combined to build a cost-effective hydrogen economy able to decarbonize faster the energy sector and heavy emission industries. Specifically, blue hydrogen is expected to provide the highest share of the hydrogen demand by 2035 due to its large-scale capacity, technology maturity, and lower levelized cost compared to green hydrogen. It is expected that renewable and green hydrogen will cover 60-80% of the worldwide hydrogen demand by 2050 since cost-effective solutions will be available to provide reduced levelized costs ranging from 1.5 USD/kg H_2 to 2 USD/kg H_2, improved efficiencies and large-scale capacities (DNV, 2022). It can be concluded that blue hydrogen is expected to act as a bridge technology from gray to green or renewable hydrogen and, in combination with green or renewable hydrogen, it can effectively support the EU's objective of gradual development of an affordable hydrogen

supply chain by 2050. Greece could develop a cost-effective hydrogen production pathway by combining promising national hydrogen sources, such as a) blue hydrogen from the utilization of the potential domestic natural gas reserves and CCS infrastructure b) renewable hydrogen from dedicated renewable electricity sources, such as the future offshore wind farms or onshore renewable projects, and c) green hydrogen from the utilization of a potential low carbon grid-connected electricity supply.

Hydrogen Transportation: Hydrogen can be transported in its gas form via pipelines, it can be liquefied, compressed, converted to ammonia or other hydrogen-based fuels for its transportation via ships or trucks. In Europe, the most cost-effective transportation option is via pipelines due to the extensive natural gas pipeline infrastructure that is currently available and its capacity to be repurposed for hydrogen transportation. Based on the European Hydrogen Backbone Study, repurposing the natural gas pipeline system for hydrogen distribution is a technically viable and cost-effective option for a major part of the EU's infrastructure, saving more than 50% of costs compared to new pipeline construction. Five European pipeline corridors have been proposed to be developed for hydrogen transportation by 2030 and one of them is the East and South-East Europe corridor, a 10,000 km large-scale hydrogen pipeline system that will use about 60% of the existing gas infrastructure to connect East European countries, such as Greece, with Central Europe (EHB, 2022). The Greek pipeline system is part of the East and South-East Europe corridor and plans have been announced by DESFA for a) repurposing the existing national gas pipeline infrastructure to receive hydrogen blending with natural gas to support the gradual expansion of the hydrogen economy b) building new natural gas pipeline systems ready to be used for pure hydrogen transportation in the future c) developing progressively new hydrogen pipeline system in parallel with the existing natural gas system to satisfy the future hydrogen demands and supply fuel specifications (Thomadakis, 2022).

Hydrogen Storage: There are various options for hydrogen storage, such as conversion to electricity and storage in batteries, above-ground tanks (in liquefied form at extremely low temperatures) and conversion to hydrogen-based fuels (e.g., ammonia). By 2050, storage options should provide an effective and low-cost solution for large-scale and long-term hydrogen storage capacity with the ability of extracting hydrogen to balance power variations and seasonal demands (energy flexibility), similar to underground natural gas storage options. Underground Hydrogen Storage (UHS) in geological formations, such as salt caverns, aquifers and depleted fields, is considered a promising option for reliable, safe and cost-effective large capacity and long-term storage of hydrogen. Research is focused on investigating the technical and economic suitability of existing underground natural gas storage sites for their potential application in hydrogen storage or developing new projects in similar geological formations. Today, UHS in salt caverns is considered a suitable and mature option for subsurface hydrogen storage since knowledge is available from four operational hydrogen storage locations in the UK and US and experience in operational performance has been obtained from 50 European underground natural gas storage projects in salt cavern formations (GIE, 2021). Hydrogen storage in aquifers or depleted fields is currently under research to investigate technical, economical and safety issues (e.g., pilot projects in Austria and Argentina). Various studies and reports have been published worldwide aiming to map out potential geological formations at the national and regional levels for hydrogen storage, mainly in salt caverns and depleted fields, due to its important role in supporting climate emission targets. In Greece, potential geological formations for hydrogen storage could be the Triassic evaporites (salt, anhydrite, gypsum, halite and dolomite) in the onshore area of Western Greece and a depleted gas field located in Northern Greece (South Kavala). Further studies must be conducted to improve knowledge of the potential geological formations for hydrogen storage and increase confidence related to the technical and economic suitability of the areas.

Conclusions

Hydrogen is an energy vector with the potential to decarbonize energy and industrial systems, contributing significantly to achieving the zero-emission target by 2050. Blue hydrogen and existing natural gas pipeline infrastructure will assist the acceleration of the hydrogen economy in combination with green or renewable hydrogen production. Greece could develop a cost-effective hydrogen production pathway by using its promising domestic energy resources, such as the potential natural gas resources and renewable electricity from the prospective offshore wind farms and onshore renewable sources. Underground hydrogen storage is considered a viable storage option providing flexibility and capacity to store large volumes by 2050, thus satisfying the energy security needs. In Greece, further studies will be initiated to identify and assess the suitability of potential storage locations in salt/evaporitic structures and depleted gas fields.

References

DNV, 2022. Hydrogen Forecast to 2050, Energy Transition Outlook 2022, retrieved from website https://www.dnv.com

European Hydrogen Backbone (EHB), 2022. Five hydrogen supply corridors for Europe in 2030. https://ehb.eu/files/downloads/EHB-Supply-corridor-presentation-Full-version.pdf

Thomadakis, M., 2022. The role of infrastructure in enabling the development the H2 value chain, Conference "Building up the Greek Hydrogen Value Chain", Athens, Greece 4th July 2022

Gas Infrastructure Europe (GIE), 2021. Regulation of Hydrogen Infrastructure, GIE Position paper. https://www.gie.eu/publications/position-papers/#2021

16th International Congress of the Geological Society of Greece
17-19 October 2022 - Patras, Greece
Bulletin of the Geological Society of Greece, Sp. Publ. 10
Ext. Abs. GSG2022-331

Estimating Morphometric Parameters and Shoreline Evolution of the Kotychi Lagoon Using Remote Sensing Techniques

Dionysios Giannikopoulos[1], Konstantinos G. Nikolakopoulos[1], Dionysios N. Apostolopoulos[1]
(1) Department of Geology, G.I.S & Remote Sensing Laboratory, University of Patras, Greece, up1060912@upnet.gr

Background: Kotychi is a lagoon situated in the northwestern part of Peloponnese, Greece and it is connected to the Ionian Sea via a small narrow tidal channel. The Kotychi Lagoon is part of the Kotychi Strofilias National Wetlands Park, and it is protected by the Ramsar Convention. It is an important ecosystem with rare species of plants and animals, natural beauty, but also a multitude of human activities, like fishing, cultivation and recreation (Ramsar Sites). So, the Kotychi Lagoon is one of the most important Greek biotopes and its diachronic water surface alterations should be monitored in order to protect the lagoon and the wetland (El Khalidi et al., 2021).

Objectives: The present study examines the spatiotemporal changes of the water surface extension of the Kotychi Lagoon. The research is based on the calculation of morphometric parameters as well as to the multitemporal movement estimation of the lagoon's shoreline, using remote sensing techniques in Geographical Information System (GIS) environment.

Methods: Several morphometric parameters and landscape metrics of the lagoon introduced by (Chubarenko et al., 2007) and used by (Ruzafa et al., 2010) and (Apostolopoulos et al., 2022), were calculated and statistically analyzed for the 1945-2016 period (table 1).

Table 1. Morphometric lagoon parameters (Chubarenko et al.,2007).

Parameter	Description
$Pr=\Sigma di/b$	Restriction ratio (Pr) is the ratio between the total width of the lagoon entrance (Σdi) and the parallel shore direction (b), $Pr \in (0, 1)$
Por=b/a	Orientation or anisotrophy parameter. The lagoon has orthogonal dimensions of the same order if $Pr \approx 1$. It is more elongated in the parallel or perpendicular to shore directions if $Pr \geq 1$ or $Pr \leq 1$, respectively (where (a) is the cross-shore length, and (b) is the along-shore length).
$Ds = l \times (4\pi A)^{-0.5}$	Shoreline development (Ds) is the ratio of the length of (l) the lagoon's perimeter and (A) is the surface area of the lagoon.
SLAG(A)	Lagoon surface (km^2)
PERI (l)	Lagoon perimeter(km)
DMAX	Maximum diameter of the lagoon (km)
DMIN	Minimum diameter of the lagoon (km)
DPER	Perpendicular distance to the open sea coastline (km)
DPAR	Parallel distance to the open sea coastline (km)
CMAR	Number of inlets or channels

In addition, the lagoon's shoreline movement onshore or offshore, was examined utilizing the Digital Shoreline Analysis System (DSAS) extension of the ArcMap Software. Different datasets such as high-resolution official orthomosaics, aerial photos, satellite, and CORONA declassified images with spatial resolution ranging from 0.25 to 5 m, were combined and processed. All of the images showed 0% cloud cover over the study area and were used to digitize the polygons of the lagoon's water surface. Satellite images and air-photos with no reference system were georeferenced to the Hellenic Geodetic Reference System of 1987 (Greek Grid) using more than 250 ground control points in Leica Photogrammetry Suite (LPS) of the ERDAS Imagine 2014 software, with root mean square (RMS) error lower than 0.5-pixel size. The official Greek orthomosaics of 1945, 2008, and 2016 were used as control datasets. The morphometric parameters that mentioned in table 1, as well as statistical parameters such as the End Point Rate (EPR) and the Linear Regression Rates (LRR) provided by the DSAS, were calculated to determinate the lagoon's water surface evolution during the 1945-2016 period.

Results: The results (table 2) showed that the water surface of the Kotychi Lagoon has been decreased over the past decades. The maximum and the minimum water surface rates (SLAG-A) of 7.55 sq. km and 4.7 sq. km, were observed in the years 1945 and 2016 respectively. Moreover, the lagoon seems to be isolated from the open sea as the restriction

rate (Pr) was very close to 0 (mean value of 0.015), while the orientation parameter (Por) was ranging from 1.42 to 2.09, with a mean value of 1.763 (>1) showing that the lagoon is more elongated in the parallel to shore direction. The shore development parameter (Ds) has a mean value of 1.644 showing that the lagoon deviates from the circular shape.

Table 2. Morphometric parameters of the Kotychi Lagoon.

Year	P_r	P_{or}	D_s	SLAG (Sq km)	PERI (km)	DMAX (km)	DMIN (km)	DPER (km)	DPAR (km)	CMAR
1945	0.015	2.095	1.856	7.55	18.07	5.14	1.67	0.06	3.53	4.00
1960	0.009	2.003	1.792	7.11	16.93	4.65	1.67	0.04	3.66	4.00
1968	0.012	2.094	1.625	6.97	15.21	4.62	1.70	0.04	4.04	4.00
1975	0.014	1.986	1.540	7.09	14.53	4.60	1.70	0.04	4.12	6.00
1987	0.020	1.599	1.555	5.96	13.45	4.09	1.69	0.05	3.59	4.00
1996	0.017	1.420	1.814	5.26	14.75	4.02	1.59	0.06	3.54	2.00
2000	0.016	1.567	1.339	4.85	10.46	3.77	1.37	0.07	3.62	2.00
2008	0.017	1.575	1.610	4.89	12.62	3.92	1.31	0.05	3.55	2.00
2016	0.018	1.526	1.670	4.70	12.85	3.88	1.25	0.04	3.64	2.00
Min	0.009	1.420	1.339	4.70	10.46	3.77	1.25	0.04	3.53	2.00
Max	0.020	2.095	1.856	7.55	18.07	5.14	1.70	0.07	3.12	6.00
Mean	0.015	1.763	1.644	6.04	14.32	4.30	1.55	0.05	3.70	3.00

Finally, for the period of 1945-2016, the LRR rates yielded that the northeastern and the southern parts of the lagoon's shoreline emerged significant accretion with rates of 17.75 m/yr and 6.46 m/yr, while the northwestern and the southern east parts experienced lower rates of accretion of 0.85 m/yr and 2.06 m/yr respectively (figure 1).

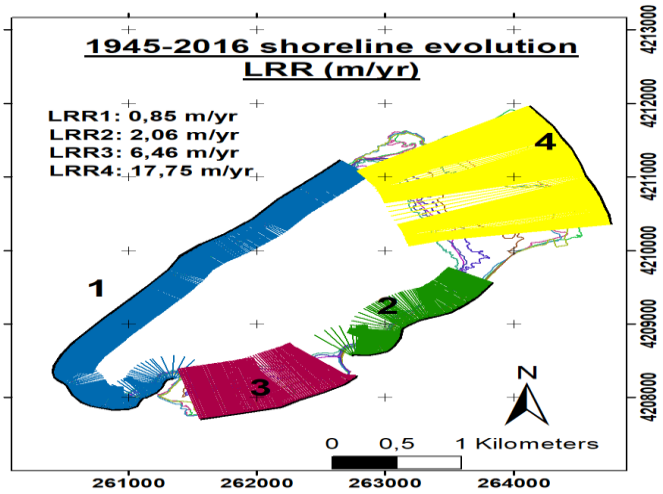

Figure 1: Four areas of different shoreline evolution during the 1945-2016 period.

Conclusions: The present study focused on the spatiotemporal changes of the water surface of the Kotychi Lagoon through several morphometric parameters' computation. The general trend is that the water area has been shrinked during the 1945-2016 period, while several fluctuations have been occurred in the intermediate years. Moreover, since 1975 the water surface area of the lagoon showed a large decrease as it seems to be covered by land and swampy areas, probably due to human activities and suspended materials discharging (Kalivas et al., 2003). In addition, the current study proved that the lagoon's ecosystem is under environmental pressure and is necessary the authorities to take action and protect its balance.

References

A.Perez-Ruzafa,C.Marcos,I.M. Perez-Ruzafa,2010.Mediterranean coastal lagoons in an ecosystem and aquatic resources management context. Physics and Chemistry of the Earth 36 (2011) 160–166.

Apostolopoulos D.,Avramidis P.,Nikolakopoulos K.,2022.Estimating Quantitative Morphometric Parameters and Spatiotemporal Evolution of the Prokopos Lagoon Using Remote Sensing Techniques.Journal of Marine Science and Engineering-July 2022.Chubarenko B.,Koutitonsky V.,Neves R.,Umgiesser G.,2007.Modeling Concepts.L1686_C06.fm page 231-306.

El Khalidi et al.,2021.Coastal land use and shoreline evolution along the Nador lagoon Coast in Morocco.Geocarto International.

Kalivas P., Kollias V., Karantounias G., 2003.A GIS for the Assessment of the Spatio-Temporal Changes of the Kotychi Lagoon, Western Peloponnese, Greece. Water Resources Management 17: 19-36, 2003.

Ramsar Sites. Available online: Ramsar Sites Information Service. rsis.ramsar.org (accessed on 2/08/2022)

16th International Congress of the Geological Society of Greece

17-19 October, 2022 - Patras, Greece

Bulletin of the Geological Society of Greece, Sp. Publ. 10

Ext. Abs. GSG2022-348

Paleoenvironmental Assessment of Bottom Waters of Amvrakikos Gulf through the Study of Foraminifera

A. Prandekou[1], M. Geraga[1], E. Dotsika[2], D. Christodoulou[1], G. Ferentinos[1], C. Koutsikopoulos[3], G. Papatheodorou[1]

(1) Laboratory of Marine Geology and Physical Oceanography, Department of Geology, University of Patras, 26500 Rio, Patras, Greece, a.prandekou@upnet.gr (2) Institute of Materials Science, National Center of Scientific Research "Demokritos", GR15310, Ag. Paraskevi Attikis, Greece (3) Department of Biology, University of Patras, 26500 Rio, Patras, Greece.

Research Highlights

- The foraminifera indicate environmental degradation of the upper sediments.
- The environmental degradation is affected by the temperature and organic fluxes.

Background

The decreasing oxygen concentration in aquatic environments is a major issue that has been observed around the world. Both anthropogenic and natural factors are responsible for its depletion, especially in enclosed or semi-enclosed water bodies (Friedrich et al., 2014). Oxygen depletion is often related to the organic matter since in order to degrade it, microbes living on the seafloor, utilize the available oxygen (Friedrich et al., 2014). Global warming and climate change affect the availability of oxygen in water since increased surface water temperatures can intensify the water column stratification, impeding the mixing and transport of oxygenated water in the deeper layers (Friedrich et al., 2014). There are various aquatic systems that are affected by oxygen depletion in Europe and especially in the Mediterranean Sea, along the coast of the Adriatic and the Ionian Seas such as Venice Lagoon, Katakolo Bay, and Amvrakikos Gulf.

Amvrakikos Gulf is a semi-enclosed gulf located on the western coast of Greece, in the Ionian Sea. It is characterized by a fjord-like oceanographic regime because of the restricted deep-water exchange with the Ionian Sea due to the shallow sill in Preveza Strait (Ferentinos et al., 2010). At the northern margin of the gulf, the two main rivers that flow into the gulf (Arachthos and Louros), create an extensive delta along with a complex lagoonal system (Kapsimalis et al., 2005) that form the largest reedbeds in Greece and a biotope to different kinds of fauna. In order to protect this unique ecosystem, the gulf is protected under many conventions (Ramsar Convention, Montreux Record, Natura 2000 network). Despite the efforts, that have been made for the protection and conservation of this unique area, the western part of the gulf is suffering from seasonal hypoxia ($DO<2\ mgL^{-1}$), whereas the eastern part is affected by seasonally anoxic conditions ($DO<0.5\ mgL^{-1}$) (Ferentinos et al., 2010) causing four major fish mortality events in fish farms since 1990. Finally, this hypoxic/anoxic environment in Amvrakikos Gulf is not a recent phenomenon, since similar oxygen depletion events were recorded in sediments from 4100 to 1600 BP (Avramidis et al., 2014).

Objectives

The main objective of this research is to investigate the palaeoenvironmental and palaeoceanographic evolution of the bottom water layer in the Amvrakikos gulf based on foraminifera analysis. Benthic foraminifera have a significant role in the assessment of palaeoenvironmental conditions (Debenay et al., 2005), and variations in benthic assemblage characteristics have been used to determine the past evolution of oxygen availability in a wide range of coastal environments (Platon et al.,2005).

Methods

For the foraminiferal analysis, 69 samples were selected from a sediment core retrieved from the western basin of the gulf. Each sample was washed over a 125μm sieve, was dried at 50 °C, and was weighed. Each specimen of foraminifera was picked and identified to the species level where possible. Foraminiferal parameters were calculated such as benthic and planktonic abundance (number of specimens per 1g of dry sediment). Furthermore, each benthic foraminifera species was categorized according to its sensitivity to organic enrichment (Dimiza et al., 2016). In addition, stable isotope analysis was conducted on benthic foraminifera at the Laboratory of Stable Isotopes and Radiocarbon, Institute of Nanoscience and Nanotechnology (NCSR Demokritos).

Results

According to an available radiocarbon dating, the sediments of the core were deposited in the last 5200 years. In total, 110 benthic foraminifera species were recognized. Though the benthic abundance is always much higher than the planktonic one their vertical distributions are in agreement (Fig. 1). More specific, both distributions indicate a decrease in abundance from 70 to 130 cm, which is accompanied by the dominance of the sensitive species. An opposite trend is recorded in the upper 70 cm, where foraminiferal abundance is increased, and the stress-tolerant taxa dominate the

foraminifera microfauna. In this interval, the depleted $\delta^{18}O$ values indicate the prevalence of high temperature (Waelbroeck et al., 2002) while the depleted $\delta^{13}C$ reflect increases in organic carbon flux (Mackensen et al., 2000).

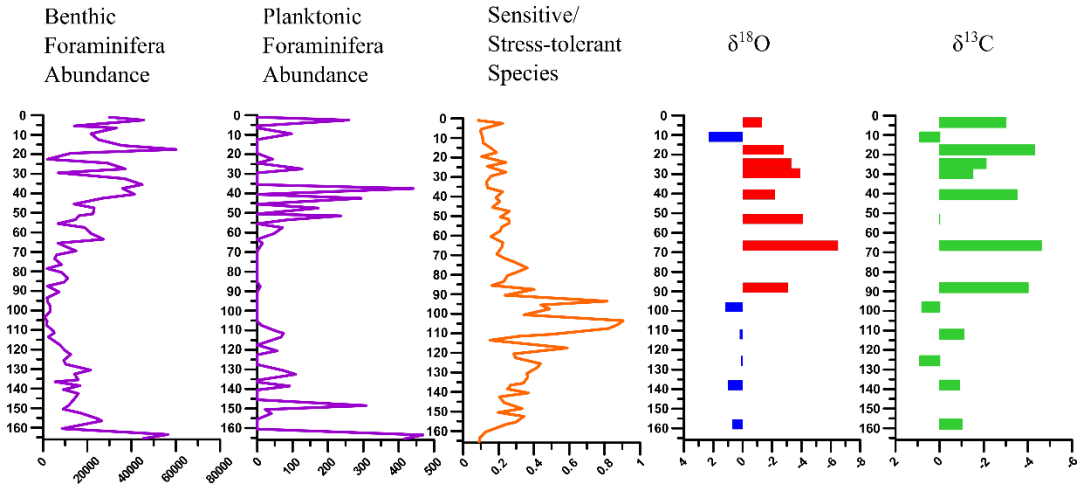

Figure 1 Vertical distributions of the proxies used. Starting from the left there are the foraminiferal abundances (in number/gr) for benthic and planktonic foraminifera respectively, followed by the depiction of the sensitive/stress-tolerant species index. In the $\delta^{18}O$ distribution, the red color indicates the negative values and thus the high temperature, while the $\delta^{13}C$ distribution is presented with green color.

Conclusions

This research shows the paleoenvironmental and paleoceanographical evolution of the Amvrakikos Gulf over the last 5000 years. The foraminifera proxies that were used present degradation of the seafloor environment over the upper Holocene, which coincides with an increase of temperature and the organic matter influx as emerged from the stable isotope analysis. The aforementioned link between foraminifera proxies and stable isotopes points out the dependent relationship between climate, organic matter, and oxygen availability.

Acknowledgements

This work was supported by the "Identification, consequences and management of the anoxic zone of Amvrakikos Gulf, NW Greece" project (European Economic Area Financial Mechanism (EEA FM) 2009–2014), HYPOX ("In situ monitoring of oxygen depletion in hypoxic ecosystems of coastal and open seas, and landlocked water bodies", FP7-EU-ENV.2008.4.1.2.1, Grand number: 226213) and the Hellenic Foundation for Research and Innovation (HFRI) under the HFRI Ph.D. Fellowship grant (Fellowship Number: 381).

References

Avramidis, P., Iliopoulos, G., Panagiotaras, D., Papoulis, D., Lambropoulou, P., Kontopoulos, N., ... & Christanis, K. 2014. Tracking Mid-to Late Holocene depositional environments by applying sedimentological, palaeontological and geochemical proxies, Amvrakikos coastal lagoon sediments, Western Greece, Mediterranean Sea. Quaternary International, 332, 19-36.

Debenay, J. P., Millet, B., & Angelidis, M. O. 2005. Relationships between foraminiferal assemblages and hydrodynamics in the Gulf of Kalloni, Greece. The Journal of Foraminiferal Research, 35(4), 327-343.

Dimiza, M. D., Triantaphyllou, M. V., Koukousioura, O., Hallock, P., Simboura, N., Karageorgis, A. P., & Papathanasiou, E. 2016. The Foram Stress Index: A new tool for environmental assessment of soft-bottom environments using benthic foraminifera. A case study from the Saronikos Gulf, Greece, Eastern Mediterranean. Ecological Indicators, 60, 611-621.

Friedrich, J., Janssen, F., Aleynik, D., Bange, H. W., Boltacheva, N., Çagatay, M. N., ... & Wenzhöfer, F. ,2014. Investigating hypoxia in aquatic environments: diverse approaches to addressing a complex phenomenon. Biogeosciences, 11(4), 1215-1259.

Ferentinos, G. Papatheodorou, G., Geraga, Iatrou, M., Fakiris, E., Christodoulou, D., Dimitriou, E., Koutsikopoulos, C. 2010.Fjord water circulation patterns and dysoxic/anoxic conditions in a Mediterranean semi-enclosed embayment in the Amvrakikos Gulf,Greece Estuarine Coastal Shelf Sci., 88 473-481.

Kapsimalis, V., Pavlakis, P., Poulos, S. E., Alexandri, S., Tziavos, C., Sioulas, A., ... & Lykousis, V. 2005. Internal structure and evolution of the Late Quaternary sequence in a shallow embayment: The Amvrakikos Gulf, NW Greece. Marine Geology, 222, 399-418.

Mackensen, A., Schumacher, S., Radke, J., & Schmidt, D. N. 2000. Microhabitat preferences and stable carbon isotopes of endobenthic foraminifera: clue to quantitative reconstruction of oceanic new production? Marine micropaleontology, 40(3), 233-258.

Platon, E., Gupta, B. K. S., Rabalais, N. N., & Turner, R. E. 2005. Effect of seasonal hypoxia on the benthic foraminiferal community of the Louisiana inner continental shelf: The 20th century record. Marine Micropaleontology, 54(3-4), 263-283.

Waelbroeck, C., Labeyrie, L., Michel, E., Duplessy, J. C., Mcmanus, J. F., Lambeck, K., ... & Labracherie, M. 2002. Sea-level and deepwater temperature changes derived from benthic foraminifera isotopic records. Quaternary science reviews, 21(1-3), 295-305

16th International Congress of the Geological Society of Greece
17-19 October, 2022 - Patras, Greece
Bulletin of the Geological Society of Greece, Sp. Publ. 10
Ext. Abs. GSG2022-389

Vegetation changes and human impact in the Argive Plain (Peloponnese, Greece) from the Bronze Age to the modern era

Cristiano Vignola[1-2] , Martina Hättestrand[3] , Anton Bonnier[4] , Martin Finné[4-5] , Adam Izdebski[1-6] , Christos Katrantsiotis[3-7] , Katerina Kouli[1-8], Georgios C. Liakopoulos[1] , Elin Norström[3-9], Maria Papadaki[1] , Nichola A. Strandberg[3-10], Erika Weiberg[4] , Alessia Masi[1-2]

(1) Palaeo-Science and History (PS&H) Independent Research Group, Max Planck Institute for the Science of Human History, Jena, Germany, vignola@shh.mpg.de. (2) Department of Environmental Biology, Sapienza University of Rome, Rome, Italy. (3) Department of Physical Geography, Stockholm University, Stockholm, Sweden. (4) Department of Archaeology and Ancient History, Uppsala University, Uppsala, Sweden. (5) Department of Social and Economic Geography, Uppsala University, Uppsala, Sweden. (6) Institute of History, Jagiellonian University in Krakow, Krakow, Poland. (7) Environmental Archaeology Laboratory, Department of Historical, Philosophical and Religious Studies, Umeå University, Umeå, Sweden. (8) Department of Geology and Geoenvironment, National and Kapodistrian University of Athens, Greece (9) Department of Geological Sciences, Stockholm University, Stockholm, Sweden (10) School of Geography and Environmental Science, University of Southampton, Southampton, United Kingdom.

Research Highlights

The pollen record from Lake Lerna provides evidence for a dynamic environmental history of the region dominated by human activities already since the mid-Holocene.

The interaction of climate with a variety of cultural, political, and socio-economic factors transformed the vegetation of the Argive Plain and caused its long-term degradation.

Introduction

This study provides new pollen data from a well dated sediment core taken in the area of ancient Lake Lerna, Peloponnese (Vignola *et al.*, 2022). By combining palaeoenvironmental and archaeological data, as well as climatic data from the same core and other regional proxies, we present a high-resolution reconstruction of the vegetation of the Argive Plain covering 5000 years. Our results show the evolution of the wetland through the study period and stress the impact of human activities on the local environments from the Early Bronze Age onwards (Figure 1).

Material and Methods

The core obtained from the ancient lake has a total length of 5 m and covers the last 5000 years. The age-depth model is based on 6 AMS radiocarbon dates of plant remains and 2 dates of organic-rich sediment. The sequence was divided into lithological units on the basis of changes in sediments and the amount of organic content (Katrantsiotis *et al.*, 2019). The analysis of pollen grains and Non-Pollen Palynomorphs (NPPs) was carried out on 84 sediment samples. The mean sampling resolution is 6 cm and the mean chronological resolution is 76 years. A known amount of dry sediment (2.8-14 g) for each sample was chemically processed with alternating treatment of HCl, HF and NaOH in order to remove mineral and organic matter from the sediments. Pollen and NPPs identification is based on literature and reference collections. The mean count of terrestrial pollen, Cyperaceae excluded, is 215 pollen grains/sample. The percentage values were calculated on different pollen sums depending on the group (Berglund and Ralska-Jasiewiczowa, 1986). Percentage, concentration and influx diagrams are plotted against depth and time scale, and pollen zonation was determined by CONISS cluster analysis and visual inspection.

Results and Discussion

Before ca. 4000 BP the coring site was a fen and mixed deciduous oak woodland prevailed on the uplands. In the plain cereals were cultivated by inhabitants of the Early Bronze Age settlements. Thereafter an increasing water level is recorded, despite the regional climatic trend shows arid conditions. In the Late Bronze Age the presence of palatial centres modified the landscape of the Argive Plain, resulting in decrease of oak woodland and increase in open land, partly used for grazing. At ca. 3310 BP the expansion of water plants marks another increase of the water depth when climatic instability is recorded. Possibly, the human management produced a permanent hydrological change at Lake Lerna, as also testified by sedimentation and lake productivity. During the following periods the alternate predominance of marsh over lake vegetation at the site is attested. From the Archaic period onwards the increasing human pressure in association with local drier conditions caused landscape instability and more sediment inflows into the lake. Roman times coincide with a forest regeneration pattern under wetter conditions and the most intensive olive cultivation. An economic landscape primarily based on pastures is established in the Byzantine period and continues until modern times, when conditions were drier, and the present-day wetland was formed at the expense of the former lake.

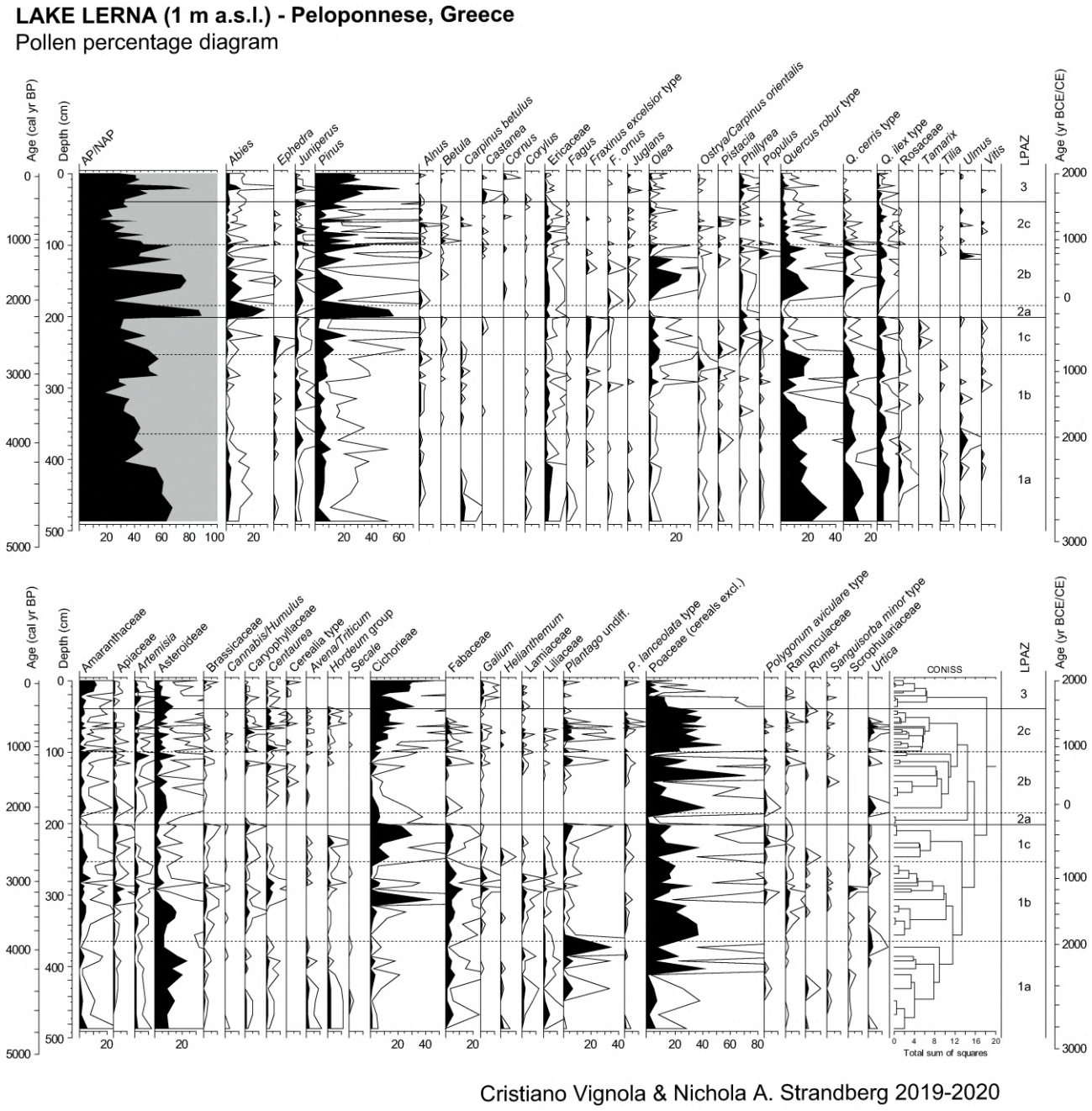

Figure 1. Pollen percentage diagram of arboreal (AP) and non-arboreal (NAP) taxa from Lake Lerna (Peloponnese).

Acknowledgments

The project is part of the Navarino Environmental Observatory (NEO) collaboration between Stockholm University, the Academy of Athens and TEMES S.S., Greece. We would like to thank the Ephorate of Antiquities of Argolida for granting the coring permit in 2016 and the Swedish Institute at Athens for help with administrative preparations.

References

Berglund, B.E., Ralska-Jasiewiczowa, M., 1986. Pollen analysis and pollen diagrams, in: Berglund B.E. (Ed.), Handbook of Holocene palaeoecology and palaeohydrology, 455-496.

Katrantsiotis, C., Norström, E., Smittenberg, R.H., Finné, M., Weiberg, E., Hättestrand, M., 2019. Climate changes in the Eastern Mediterranean over the last 5000 years and their links to the high-latitude atmospheric patterns and Asian monsoons. Glob Planet Change 175, 36-51.

Vignola, C., Hättestrand, M., Bonnier, A., Finné, M., Izdebski, A., Katrantsiotis, C., *et al.*, 2022. Mid-late Holocene vegetation history of the Argive Plain (Peloponnese, Greece) as inferred from a pollen record from ancient Lake Lerna. PLoS ONE 17(7), e0271548.

16th International Congress of the Geological Society of Greece
17-19 October, 2022 - Patras, Greece
Bulletin of the Geological Society of Greece, Sp. Publ. 10
Ext. Abs. GSG2022-408

A 9.1 ka record of paleoenvironmental variability in the South Aegean region. A case study from a semi-enclosed basin in Astypalea island.

A. Noti[1], M. Geraga[1], L. J. Lourens[2], F. Wesselingh[2,3], N. Haghipour[4], N.Georgiou[5], S. Sergiou[1], D. Christodoulou[1], X. Dimas[1], A. Vlachopoulos[6], I. Evaggelou[1], I. Foukas[1], G. Papatheodorou[1]

(1) Laboratory of Marine Geology and Physical Oceanography, Department of Geology, University of Patras, Patras, Greece, anoti@upatras.gr (2) Department of Earth Sciences, Faculty of Geosciences, Utrecht University, Utrecht, The Netherlands (3) Naturalis Biodiversity Center, 2300 RA Leiden, the Netherlands (4) Laboratory of Ion Beam Physics, Geological Institute, ETH Zürich, Zürich, Switzerland (5) Department of Environmental Sciences, Informatics and Statistics, Ca' Foscari University, Venice, Italy (6) Department of History and Archaeology, University of Ioannina, 45110 Ioannina, Greece.

Research Highlights

The Holocene paleoenvironmental evolution of a small semi-enclosed silled marine basin in the South Aegean Sea is controlled by both climatic and sea level variability.

Within the general South Aegean region, the Holocene presents a general aridification trend toward the present.

Background

Coastal restricted basins are sensitive recorders of both global and regional scale changes and thus may provide important details regarding the environmental and climatic variability over a certain region (Finné et al., 2019). Furthermore, the evolution of a silled marine basin is strongly controlled by the sea level changes and thus their deposits are encountered as valuable archives for both sea level and climate changes assessment. The south Aegean Sea acts as an interplay between the high and low latitude climatic systems (Geraga et al., 2017, 2005; Marino et al., 2007; Rohling et al., 2019), and thus contains important details regarding this climatic variability. On the other hand, the sea level changes in this region have been affected by eustatic, isostatic and tectonic factors (Lykousis et al., 2005).

Objectives

The main objective of this work is to assess the evolution of the environmental conditions developed during the Holocene in the Vathy bay located at the northeastern Astypalea island, South Aegean Sea. The bay is controlled by a 4.7 m water depth sill suggesting that the environmental evolution of the bay was depending on the sea level.

Methods

A marine sediment core (ASTC1) was retrieved from a site located at the inner part of the Vathy bay, NE Astypalea, South Aegean Sea, at 10 m water depth. The core is 320 cm long and contains sedimentary deposits of about 9.100 yrs old. The sediments of the core were analysed for the grain size distribution, the variations of nitrogen and organic carbon content using a Fisons NA1500 CN elemental analyzer and microfauna (benthic foraminifera and mollusks) composition using the standards methodologies. Stable oxygen isotopes of Ammonia spp. were measured with a Gas Bench system.

Results and Conclusions

All the acquired data sets exhibit large and almost simultaneous variations allowing the distinction of five sedimentary intervals (SI I-V, Table 1). The base of the ASTC1 core is characterized by the absence of marine specimen providing clear evidence for a terrestrial origin of the sediments of the SI-V and isolation of the bay due to the low sea levels. In the upper interval SI-IV, the sporadic presence of Charophyta together with brackish water indicative species suggest the development of an ephemeral pond or lake. The development of this freshwater body can be most probably related to increased precipitation within a period where the bay is still isolated. Moving upwards to the interval SI-III, the microfauna associations, present low abundances and are dominated by marine species which tolerate high salinity variations. This observation together with the laminated character of the sediments of this interval suggest the prevalence of a hypersaline marsh at the core site. This interval marks the first connection of the bay to the open sea, which seems to be extremely restricted at this point. In the following interval SI-II, the microfauna is dominated by species that are usually found in lagoonal environments, thus suggesting that the connection of the bay to the open sea has been established. Finally, the transition to the uppermost interval SI-I is marked by the gradual replacement of the lagoonal fauna by species thriving in shallow marine seafloors which finally dominate the faunal associations suggesting the establishment of the current conditions in the bay. The measured stable oxygen isotopic signal showed a general enrichment towards the present which is followed by the depleted Corg/N values, thus pointing out an aridification trend.

Conclusions

Our 9.1 ka BP record showed that the study area experienced different environmental conditions through time. It was found that the basin was once isolated serving as a terrestrial environment between 320 and 390 cm and then progressively

transformed into a water-logged environment, first as a lake (290-250 cm) and later as a hypersaline marsh (250-160 cm), lagoon (160-80 cm), and to finally a shallow marine basin (80-0 cm). Conditions in the bay and thus in the general South Aegean region, present an aridification trend towards the present, which can be related to the termination of the African Humid Period.

Table 1. Table which summarizes the main sedimentary intervals of the ASTC1 core, their corresponding depth, the sedimentary features, the occurring microfauna, the oxygen isotopic signal of Ammonia spp., the measured Corg/N ratio, and the environmental interpretation.

Intervals	Depth (cm)	Sedimentological features	Faunal composition	$\delta^{18}O_{Ammonia\ spp.}$ (‰)	Corg/N	Environment
V	320-290	Fine grained homogenous brownish sediments	No fauna	-	>10	Land
IV	290-250	Fine grained homogenous greyish sediments	Brackish water indicative fauna (Charophyta, Ostracods)	-	5-10	Ephemeral Pond/Lake
III	250-160	Laminated sediments	Low in abundance marine fauna (Ammonia spp., Miliolids, Peneroplis spp.	(-0.12) - 1.31	1-10	Hypersaline marsh
II	160-80	Fine grained greenish gray homogenous sediments	Lagoonal fauna (Cerastoderma glaucum s.l., Abra / Ammonia spp., Quinqueloculina spp.)	(-0.33) – 1.12	4-9	Lagoon
I	80-0	Coarser greyish homogenous sediments	Higher in abundance and in diversity Shallow marine fauna Varicorbula gibba, Bittium reticulatum / Adelosina spp., Ammonia spp., Discorbis spp., Miliolinella spp., Melonis spp., Peneroplis spp., Rosalina globularis, Quinqueloculina spp., Triloculina spp., Spiroloculina spp.)	0.19 - 1.17	2-5	Shallow marine

Acknowledgements

Part of this survey was funded by the State Scholarships Foundation (IKY). We also thank the two divers Kostas and Tasos Kouvas who carried out the sediment core acquisition.

References

Finné, M., Woodbridge, J., Labuhn, I., Roberts, C.N., 2019. Holocene hydro-climatic variability in the Mediterranean: A synthetic multi-proxy reconstruction: https://doi.org/10.1177/0959683619826634 29, 847–863. https://doi.org/10.1177/0959683619826634

Geraga, M., Papatheodorou, G., Agouridis, C., Kaberi, H., Iatrou, M., Christodoulou, D., Fakiris, E., Prevenios, M., Kordella, S., Ferentinos, G., 2017. Palaeoenvironmental implications of a marine geoarchaeological survey conducted in the SW Argosaronic gulf, Greece. J. Archaeol. Sci. Reports 12, 805–818. https://doi.org/https://doi.org/10.1016/j.jasrep.2016.08.004

Geraga, M., Tsaila-monopolis, S., Ioakim, C., Papatheodorou, G., Ferentinos, G., 2005. Short-term climate changes in the southern Aegean Sea over the last 48 , 000 years 220, 311–332. https://doi.org/10.1016/j.palaeo.2005.01.010

Lykousis, V., Karageorgis, A.P., Chronis, G.T., 2005. Delta progradation and sediment fluxes since the last glacial in the Thermaikos Gulf and the Sporades Basin, NW Aegean Sea, Greece. Mar. Geol. 222–223, 381–397. https://doi.org/https://doi.org/10.1016/j.margeo.2005.06.026

Marino, G., Rohling, E.J., Rijpstra, W.I.C., Sangiorgi, F., Schouten, S., Damsté, J.S.S., 2007. Aegean Sea as driver of hydrographic and ecological changes in the eastern Mediterranean. Geology 35, 675–678. https://doi.org/10.1130/G23831A.1

Rohling, E.J., Marino, G., Grant, K.M., Mayewski, P.A., Weninger, B., 2019. A model for archaeologically relevant Holocene climate impacts in the Aegean-Levantine region (easternmost Mediterranean). Quat. Sci. Rev. 208, 38–53. https://doi.org/10.1016/j.quascirev.2019.02.009

16th INTERNATIONAL CONGRESS of the
GEOLOGICAL SOCIETY OF GREECE

T11. Geosciences for Society, Education and Geoheritage

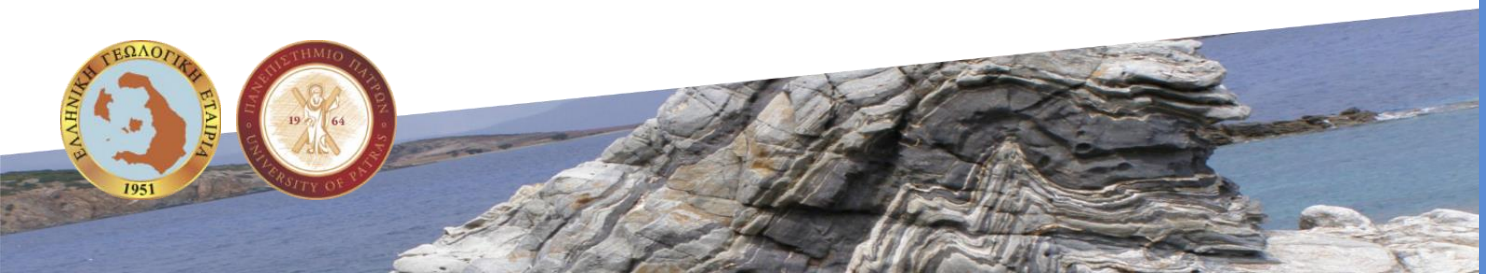

OUR EARTH, OUR HOME

16th International Congress of the Geological Society of Greece

17-19 October, 2022 - Patras, Greece

Bulletin of the Geological Society of Greece, Sp. Publ. 10

Ext. Abs. GSG2022-020

From Clay To Pottery: A Petrographic Study Of The Ceramics From The Neolithic Site Of Wutaishan In Northeast China.

P. A. Duval[1]

(1) Ecole Pratique des Hautes Etudes (EPHE), Paris, France, pauline.a.duval@gmail.com

Socio-cultural interactions highlighted by the potteries and the raw materials.

In recent years, studies on the population of Northeast China have profoundly transformed our perception of the Neolithic in this region. Traditionally, research focused on the identification of archaeological cultures: the definition of their characteristics and geochronological delimitations. The term "culture" is used here to refer to a material culture, based on ceramic typology. In other words, the potteries found on archaeological sites were classified according to morpho-stylistic criteria to highlight chronological or local variations. However, new fields of research have been developed recently, shifting the focus to humans, their behavior, and the environment and the analytical tools have diversified.

In this paper, we present a petrographic analysis of ceramics from the Neolithic site of Wutaishan, in Northeast China, dated around 5000 – 3500 BC. Quantitative analysis of the sherds based on morpho-stylistic criteria reveals three main groups in which group 1 predominates largely, which suggests a local origin. However, what does the presence of the other two minor groups mean? Are the differences limited to an aesthetic aspect or is it the influence of various phenomena? The reasons for their coexistence on the site could be: functional, chronological, socio-cultural, or geographical. Each of these hypotheses is examined.

In order to shed light in such hypotheses 20 jar sherds were selected and processed into a thin section for qualitative petrographic analysis (Quinn 2013). Their study under the polarizing microscope has permitted to distinguish four petrographic fabric groups according to their textural and compositional characteristics: fine mono-crystalline quartz fabric group, poly-crystalline quartz fabric group, potassium feldspar (microcline) fabric group and shell fragments fabric group. The compositional variability emerged through the various petrographic fabric groups established herein is indicative of exploitation of different geological sources. Thus, the petrographic approach offers possible evidence of exchange between different cultural groups.

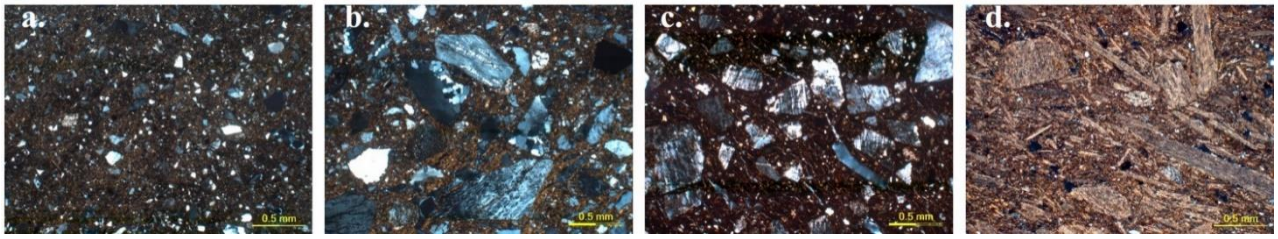

Figure 1. Thin section photomicrographs of selected Neolithic ceramics analysed in this study: fine monocrystalline quartz fabric (a.) ; polycristallin quartz fabric (b.) ; feldspar microcline fabric (c.) ; shell fragments fabric (d.)

Acknowledgements

I would like to thank Dr. Wang Yixue, Director of Changchun Museum and director of the excavation of Wutaishan site for allowing me to study this material. I would also like to thank my supervisor during this study, Professor Ioannis Iliopoulos (Patras University), always willing to discuss my work on petrographic analysis and provided me useful advices and guidance.

References

Duval, P. A., Sebillaud P., Wang Y, in progress. Étude des Tessons Néolithiques du Site de Wutaishan en Chine du Nord-Est.

Jilin Daxue Kaogu Jiaoyanshi, 1989. Nong'an Zuojiashan xinshiqi shidai yizhi. Kaogu xuebao 2, 187-212.

Eramo G., 2020. Ceramic Technology: How to Recognize Clay Processing. Archaeological and Anthropological Science 12:164, 1-24.

Quinn P. S., 2013. Ceramic petrography: the interpretation of archaeological pottery & related artefacts in thin section, Archaeopress.

16th International Congress of the Geological Society of Greece
17-19 October, 2022 - Patras, Greece
Bulletin of the Geological Society of Greece, Sp. Publ. 10
Ext. Abs. GSG2022-074

3D Geovisualization of petrified tree trunks: The case of Lesvos Geopark

K. Chaidas[1], P. Kalaitzis[1], N. Soulakellis[1], N. Zouros[1]
(1) University of the Aegean, Mytilene, Greece
Corresponding author: k.chaidas@aegean.gr

The aim of this paper is to propose a methodology for the 3D geovisualization of petrified tree trunks. The petrified tree trunks of the Natural History Museum of the Lesvos Petrified Forest were selected as a case study. This research is conducted, due to the importance of the utilization and highlighting of the geosites of Lesvos Geopark. Consequently, a methodology was developed for the purpose of recording and the 3D geovisualization of the sites and the individual fossils that appear in them. The acquisition of high-resolution aerial and terrestrial images and the collection of accurate Ground Control Points (GCPs) are the main work of the method that is being used to produce high-quality 3D models of fossilized trees. Specifically, the applied methodology consists of the following steps: (a) the GNSS RTK method is used to collect GCPs around the fossils and terrestrial and unmanned aircraft systems (UAS) images are acquired, (b) the images are photogrammetrically processed to produce DSM, orthophoto-maps, and 3D models of the petrified trees, (c) 3D geovisualization of the 3D models. In this study, the images are collected mostly based on terrestrial close-range photogrammetry, and in some cases, UAS manual flights are used to collect images of larger standing tree trunks. In total 18 petrified tree trunks of the Natural History Museum were modeled and geovisualized. The contribution of this methodology is the production of high-quality 3D models and their accurate geovisualization, which aims to environmental, touristic, educational, and cultural promotion of Geoparks.

Introduction

The Petrified Forest of Lesvos is one of the most significant natural heritage sites in the world and is situated on the island of Lesvos, Greece, covering an area of 15,000 ha. The UNESCO Global Geopark of Lesvos Island has been a founding member of the Geoparks Network since 2004 (Zafeiropoulos *et al.*, 2021). Geological sites should be preserved for cultural, scientific, historical and educational reasons. (UNESCO. Executive Board, 1999). Aerial photogrammetry methods (UAS) are mostly used for visualizing small cartographic scale geosites (Papadopoulou *et al.*, 2021), where for larger scale visualizationσ, terrestrial laser scanning (TLS), aerial and terrestrial photogrammetry are used (Bauwens *et al.*, 2017; Chatzi *et al.*, 2019; Papadopoulou *et al.*, 2020). Image-based modelling techniques are widely used for geometric surfaces. This method uses 2D images to reconstruct 3D geometrical objects (Remondino and El-Hakim, 2006). Based on the above mentioned, we propose a methodology using GNSS RTK points, terrestrial and aerial photogrammetry in order to achieve accurate and efficient 3D visualization of the tree fossils inside the Natural History Museum of the Lesvos Petrified Forest.

Methodology

The methodology proposed (**Figure *1***) consists of three steps: (a) data acquisition, (b) data processing, (c) 3D geovisualization. In the first step GNSS RTK technique is used to collect the GCPs around the fossils, that is required to georeference the high-resolution images. Afterwards, terrestrial cameras and UAS were used to obtain high-resolution images from every petrified tree trunk. In the second, GCPs were postprocessed and the images collected, were processed using computer vision algorithms to create 3D point clouds, 3D models, DSMs, and orthophoto-maps. Finally, the 3D models of the fossils were used in a 3D environment for the 3D geovisualization.

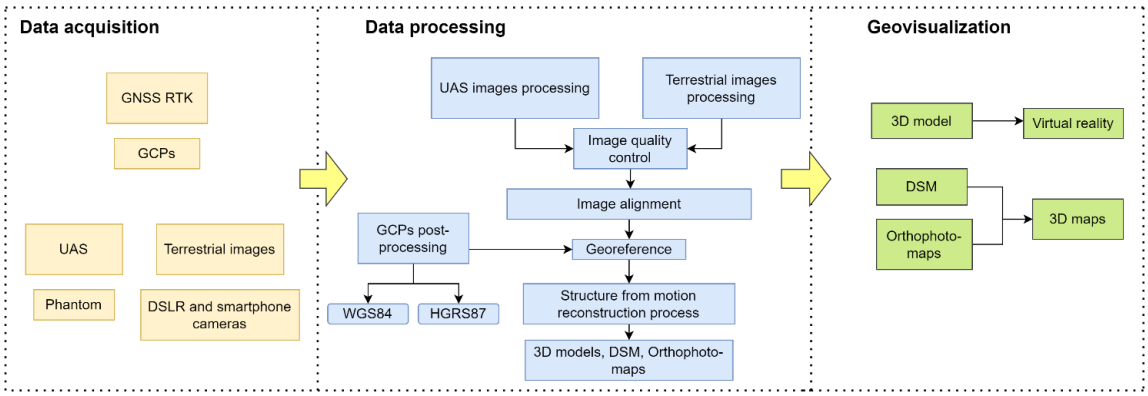

Figure 1: methodology workflow

More analytically, the collection of GCPs is mandatory for the georeferencing of the high-quality images of the fossils. This process is achieved by using the Topcon Hiper SR GNSS. The marking of GCPs, is done at the fossil sites using numbered targets which must be visible in the images. For the accurate georeferencing, 4-5 control points are distributed around the petrified tree and on it. Data collection for accurate mapping of individual fossils for a very large cartographic scale of 1:1 – 1:50, is made by a DSLR and a smartphone camera. For the reconstruction of 3D models by means of terrestrial photography the following criteria were applied:

- Capable of overlapping between photos
- Fixed focal length
- Each point of the fossil appears in at least three photographs

The high-resolution images of the individual fossils were collected with the Nikon D3400 camera and the Redmi Note 9 Pro smartphone camera. Finally, manual low flights of 5 meters are carried out to collect images of the petrified trees that were standing and tall. On these flights, the Phantom 4 Pro was used, and nadir photos of the trunks are collected for overlay needs. Approximately, 40-50 images for every site have been captured. Afterwards, the processing of both aerial and terrestrial images is carried out using the Structure from Motion (SFM) method, for producing three-dimensional representations, from sequences of overlapping two-dimensional photographs and through appropriate software. Analytically, Image quality index (IQI) was used for the quality control of the images. Image alignment was the second step, using the structure from-motion algorithm, creating a sparse point cloud. Next step is the georeference of the images, using the GCPs. Then the dense point cloud was created by applying the multi-view stereo algorithm. Reconstruction of the surface with triangulation to create 3D mesh. Finally, 3D models, DSMs and orthophoto-maps of every petrified tree trunk were generated.

Results

The results obtained from this work, were 18 3D models, DSMs and orthophoto-maps of the petrified tree trunks of the Natural History Museum Petrified Forest. The 3D point cloud of every fossilized tree was approximately 3 million points. The 3D models were processed in high quality, where the average spatial resolution of the orthophoto-maps was less than 1cm. For the geovisualization of the petrified tree trunks, their textured 3D models were used in the Sketchfab software, that is a web-based viewing, creating, and publishing tool for 3D models. Additionally, for creating 3D maps, the DSMs and the orthophoto-maps were used.

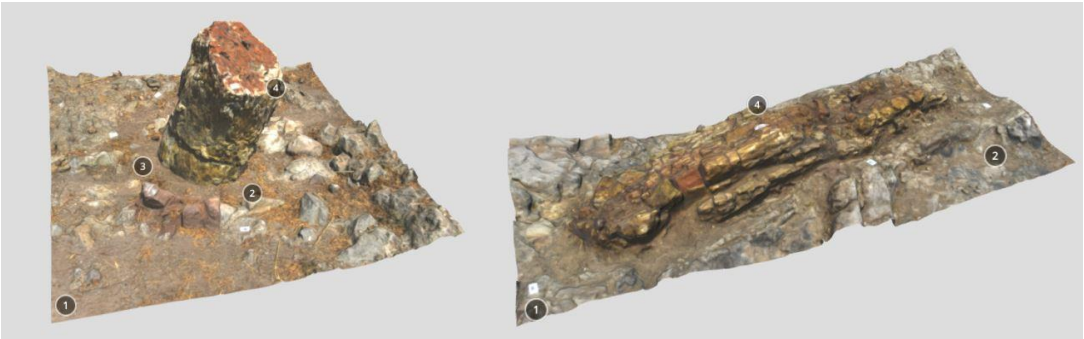

Figure 2: 3D models of petrified tree trunks

Acknowledgements

This research was funded by the Research e-Infrastructure "Interregional Digital Transformation for Culture and Tourism in Aegean Archipelagos" {Code Number MIS 5047046} which is implemented within the framework of the "Regional Excellence" Action of the Operational Program "Competitiveness, Entrepreneurship and Innovation". The action was co-funded by the European Regional Development Fund (ERDF) and the Greek State [Partnership Agreement 2014–2020].

References

Bauwens, S. *et al.* (2017) 'Terrestrial photogrammetry: a non-destructive method for modelling irregularly shaped tropical tree trunks', *Methods in Ecology and Evolution*, 8(4), pp. 460–471. doi: 10.1111/2041-210X.12670.

Chatzi, E. *et al.* (2019) '3D modelling of petrified trees: Laser scanning vs photogrammetry', *IMEKO International Conference on Metrology for Archaeology and Cultural Heritage, MetroArchaeo 2017*, (May 2018), pp. 81–86.

Papadopoulou, E. E. *et al.* (2020) 'Geovisualization of the excavation process in the Lesvos petrified forest, Greece using augmented reality', *ISPRS International Journal of Geo-Information*, 9(6). doi: 10.3390/ijgi9060374.

Papadopoulou, E. E. *et al.* (2021) 'DEM-based UAV flight planning for 3D mapping of geosites: The case of olympus tectonic window, Lesvos, Greece', *ISPRS International Journal of Geo-Information*, 10(8). doi: 10.3390/ijgi10080535.

Remondino, F. and El-Hakim, S. (2006) 'Image-based 3D Modelling: A Review', *The Photogrammetric Record*, 21(115), pp. 269–291. doi: 10.1111/j.1477-9730.2006.00383.x.

UNESCO. Executive Board (1999) 'UNESCO. UNESCO Geoparks Programme—A New Initiative to Promote a Global Network ofGeoparks Safeguarding and Developing Selected Areas Having Significant Geological Features', in. Paris, France, p. 4.

Zafeiropoulos, G. *et al.* (2021) 'From Geoheritage to Geoeducation, Geoethics and Geotourism: A Critical Evaluation of the Greek Region', *Geosciences*, 11(9), p. 381. doi: 10.3390/geosciences11090381.

16th International Congress of the Geological Society of Greece
17-19 October, 2022 - Patras, Greece
Bulletin of the Geological Society of Greece, Sp. Publ. 10
Ext. Abs. GSG2022-134

Geodidactics and CLIL: Synthesizing a syllabus for the ELT classroom through games, stories and technology

Anastasia Bozatzi[1], Argyrios Periferakis[2,3,4]

(1) Hellenic Open University, 10677 Athens, Greece, email: abozatzi@gmail.com (2) Department of Physiology, The "Carol Davila" University of Medicine and Pharmacy, 050474 Bucharest, Romania (3) Akadimia of Ancient Greek and Traditional Chinese Medicine, 16675 Athens, Greece (4) Elkyda, Research & Education Centre of Charismatheia, 17675 Athens, Greece.

Introduction

Nowadays, alternative and more creative paths, such as games, are used in the field of cultural heritage, so as to acquaint the general public and students alike, with cultural and historical concepts, in a more experiential and interactive way (Malegiannaki *et al.*, 2021). Taking into account the recent increase of public interest in places of geological and geocultural value (Drinia *et al.*, 2022) and the fact that geoeducation can not only contribute both to the understanding of the need to preserve places of geoheritage, but also enrich the curricular and extracurricular activity programs in schools and private tutoring institutions (Zafeiropoulos *et al.*, 2021), we propose a new approach, based on the latest advances in educational sciences integrating the implementation of Content and Language Integrated Learning (CLIL), through game-based, story-based and technology-based lessons, meticulously created for English language learners of different ages and English proficiency levels, according to the CEFR (Common European Framework of Reference, 2001). More specifically, this approach can be interwoven with the teaching curriculum for both primary and secondary schools in state and private sector, adhering to different subject areas, such as Environmental Education, Geography, Biology, History and Ancient Greek Language and Literature. Importantly, if implemented appropriately, this approach will provide an educational opportunity through CLIL (Cenoz, 2013), where the content of the subject and language are prioritized (Perez-Vidal, 2007), in a flexible manner (Piacentini, 2021). Here, we will focus on some of the most prominent sites of the geological heritage of Greece, briefly explain their significance as places of geoheritage, and present how they can be approached via a novel educational strategy.

The UNESCO Geoparks of Greece

The UNESCO Geoparks of Greece comprise that of Sigri in Lesvos island, Psiloritis and Sitia in Crete, Chelmos-Vouraikos, Vikos-Aoos and Grevena-Kozani. Most of these parks comprise numerous geosites, whose management is important from a standpoint of promoting the Greek geoheritage and for the effective sustainable tourism-related, economic development of the local communities (Golfinopoulos *et al.*, 2022). The influence of UNESCO Geoparks for the local communities has also been presented by Fassoulas & Zouros (2010). The ecosystems existing in the UNESCO geoparks are also important for biodiversity and ecosystem development purposes (Tsakiri *et al.*, 2022).

Mines as Centers of Geoheritage

Amongst the most important mining centers of Greece are those of Lavrion, Serifos and Naxos. Lavrion has been a well-known mining center since the times of Ancient Greece and it has an immense geocultural value (Voudouris *et al.*, 2021); their existence has shaped the history of Greece, and potentially of Europe, both during the 5th and 4th century BC and during the 19th century (Periferakis *et al.*, 2019).

The island of Naxos can be thought of as a Cordilleran metamorphic core complex and the transformation of its bauxites to emeries occurred mostly through medium to high grade metamorphism (Periferakis, 2021; and references therein). The emery deposits, also mined in ancient times, came to the foreground in the 19th century, and were pivotal in shaping the local island economy up until the 1970s when emery consumption, and therefore mining, declined. The export of emery was also quite important for the GNP of Greece, especially prior to the 1940s. The consequences of emery mining are still quite visible in the area, both from a financial and a cultural standpoint (Periferakis, 2021).

The island of Serifos represents a multiple-mineralized district (Vlachopoulos & Voudouris, 2022; and references therein) and apart from being an area rich in collection-grade minerals, is also well-known for its iron and copper mines, dating back to the time of Ancient Greece (Georgakopoulou *et al.*, 2011); an in-depth presentation of the places of geological and geocultural interest has been made by Vlachopoulos & Voudouris (2022).

Integrating games, stories and technology

Game-based, story-based and technology based-learning is proposed as the most appropriate path to promote geodidactics for all educational levels. More specifically, through games, the students are actively engaged (Smith & Mann, 2002) in a learning process where mastering the game is linked to further knowledge and skills (Prakash & Spoorthi, 2022). Simultaneously, stories not only can expand learners' knowledge of the world through imagination (Cameron, 2001) but also are a great means to cultivate cultural awareness (Davies, 2007). Moreover, technology, which can be implemented through web 2.0 tools, applications and devices in class, provides a fruitful ground for innovation, language competence

and motivation, while if integrated with CLIL practices, more successful outcomes are produced (Scott & Beadle, 2014). The use of the geosites and geoparks mentioned herein is deemed optimal, to serve as an impetus and as a thematic locus for the formulation of a game-based strategy; this approach has already been explored by Kritikou & Malegiannaki (2010).

Conclusion

Taking into consideration the needs and expectations of contemporary society, this is an attempt to arm both students and teachers with new skills, expanding their horizons; the application of this novel educational strategy is based specifically on places of geoheritage. In this vein, CLIL can be a great opportunity not only to bring motivation and cooperation but also to raise awareness about the multifaceted value and significance of various geological sites, cultivating, at the same time, the ecological and cultural competence in the English language classroom, while promoting the concomitant promulgation of the integration of a multidisciplinary educational scheme.

References

Cameron, L., 2001. Teaching Languages to Young Learners. Cambridge University Press.

Cenoz, J., 2013. Discussion: towards an educational perspective in CLIL language policy and pedagogical practice. International Journal of Bilingual Education and Bilingualism, 16, 389-394.

Council of Europe 2001. Common European Framework of Reference for Languages: Learning, teaching, assessment. Cambridge University Press

Davies, A., 2007. Storytelling in the Classroom: Enhancing Traditional Oral skills for Teachers and Pupils. Paul Chapman Publishing.

Drinia, H., Voudouris, P., Antonarakou, A., 2022. Editorial of Special Issue — "Geoheritage and Geotourism Resources: Education, Recreation, Sustainability". Geosciences, 12, 251.

Fassoulas, C., Zouros, N., 2010. Evaluating the Influence of Greek Geoparks to the Local Communities. Bulletin of the Geological Society of Greece, 43, 896-906.

Georgakopoulou, M., Bassiakos, Y., Philaniotou, O., 2011. Seriphos surfaces: A study of copper slag heaps and copper sources in the context of Early Bronze Age Aegean metal production. Archaeometry, 53, 123-145.

Golfinopoulos, V., Papadopoulou, P., Koumoutsou, E., Zouros, N., Fassoulas, C., Zelilidis, A., Iliopoulos, G., 2022. Quantitative Assessment of the Geosites of Chelmos-Vouraikos UNESCO Global Geopark (Greece). Geosciences, 11, 63.

Kritikou, S., Malegiannaki, I., 2010. Following the Traces of Naxian Emery – an Implementation of Environmental Education in Geodidactics. Proceedings of the 12th international Congress of the Geological Society of Greece, Patras, Greece, p. 2-10.

Malegiannaki, I., Daradoumis, T., Retalis, S., 2021. Using a Story-Driven Board Game to Engage Students and Adults With Cultural Heritage. International Journal of Game-Based Learning, 11, 1-19.

Perez-Vidal, C., 2007. The Need for Focus on Form (FoF) in Content and Language Integrated Approaches: An Exploratory Study. Revista Espaňola de Linguistica Aplicada, 1 (extra), 39-54.

Periferakis, A., 2021. The Emery of Naxos: A Multidisciplinary Study of the Effects of Mining at a Local and National Context. Journal NX - A Multidisciplinary Peer Reviewed Journal, 7, 93-110.

Periferakis, A., Paresoglou, I., Paresoglou, N., 2019. The significance of the Lavrion mines in Greek and European Geoheritage. European Geologist, 48, 24-27.

Piacentini, V., 2021. CLIL and Science education. A review for a Language focus in Science teaching. Journal of Theories and Research in Education, 16, 113-131.

Prakash, J.R., Spoorthi, B., 2022. Gamified Content and Language Integrated Learning Approach (CLIL): An Innovative Approach for Effective Language Teaching and Learning, Proceedings of the International Conference on Best Innovative Teaching Strategies (ICON-BITS 2021), Rajasthan India p. 141-145.

Scott, D., Beadle, S., 2014. Improving the effectiveness of language learning: CLIL and computer assisted language learning. European Commission. ICF GHK.

Smith, L. and Mann, S. (2002) Playing the Game: A Model for Gameness in Interactive Game Based Learning. Proceedings of the 15th Annual NACCQ, Montreal, Canada, p. 397-402.

Tsakiri, M., Koumoutsou, E., Kokkoris, I.P., Trigas, P., Iliadou, E., Tzanoudakis, D., Dimopoulos, P., Iatrou, G., 2022. National Park and UNESCO Global Geopark of Chelmos-Vouraikos (Greece): Floristic Diversity, Ecosystem Services and Management Implications. Land, 11, 3.

Vlachopoulos, N., Voudouris, P., 2022. Preservation of the Geoheritage and Mining Heritage of Serifos Island, Greece: Geotourism Perspectives in a Potential New Global Unesco Geopark, Geosciences, 12, 127.

Voudouris, P., Melfos, V., Mavrogonatos, C., Photiades, A., Moraiti, E., Rieck, B., Kolitsch, U., Tarantola, A., Scheffer, C., Morin, D., Vanderhaeghe, O., Spry, P.G., Ross, J., Soukis, K., Vaxevanopoulos, M., Pekov, I.V., Chukanov, N.V., Magganas, A., Kati, M., Katerinopoulos, A., Zaimis, S., 2021. The Lavrion Mines: A Unique Site of Geological and Mineralogical Heritage. Minerals, 11, 76.

Zafeiropoulos, G., Drinia, H., Antonarakou, A., Zouros, N., 2021, From Geoheritage to Geoeducation, Geoethics and Geotourism: A Critical Evaluation of the Greek Region. Geosciences, 11, 381.

16th International Congress of the Geological Society of Greece
17-19 October, 2022 - Patras, Greece
Bulletin of the Geological Society of Greece, Sp. Publ. 10
Ext. Abs. GSG2022-180

Developing a Seismic Scenario for the Arsakeia School Area of Patras in the context of the "School Seismology" Educational Program

O. Stavroulopoulou[1], G. Anagnostopoulos [1], M. Avramidi [1], E. Zampakis [1], S. Katsampas-Papageorgakopoulos [1], A. Apostolopoulou[1], P. Galiotou[1], A. Georganta[1], M Korfiati[1], E. Kamperou[1], S. Karpi[1], M. Papanikolaou[1]

(1) Arsakeio Lykeio Patras, Patra, Greece, stavroulopoulou.o@arsakeio.gr

Information Systems, use data stored in Databases and aim to produce useful information (Giakoumakis *et al.*, 2003). This paper focuses on Geographic Information Systems (G.I.S.). In the context of the "School Seismology" Educational Program, we utilized data from the accelerometer and the seismometer that have recently been installed at the Arsakeia Schools of Patras and access to Databases from the Institute of Geodynamics - National Observatory of Athens, attempting to develop a Seismic Scenario for the area of Patras where the Arsakeia Schools are located. With the help of simple programming tools that are included in the school program, spatial and descriptive data are digitized and merged into Seismic Hazard Maps.

More specifically, at our School we attempted to develop an Earthquake Scenario, aiming to draw up a response plan against earthquakes at School, control panic and also highlight the safeness of our building, regardless of the earthquake intensity. To develop the Scenario we used computer programming and digital mapping tools.

We chose one of the strongest earthquakes that occurred in the area during the past four years – period when the School's accelerometer has been operating. This was the October 26, 2018 earthquake (Zahradnik *et al.*, 2018, Theodoulidis *et al.*, 2018) which occurred at 01:54 a.m. local time. According to the Geodynamic Institute, the magnitude of the earthquake was 6.4, the focal depth was 10 kilometers and the epicenter was located in the Ionian Sea near Strofades, about 53 kilometers southeast of Zakynthos and 150 km southwest of Arsakeia Schools.

The steps followed in our research are outlined below:

1. We retrieved the earthquake record from the Database of the Geodynamic Institute.
2. Applying the epicentre location exercise on the records from our School's accelerometer, as well as those from the other accelerometers in the Geodynamic Institute's Network, we confirmed the location of the epicentre provided by the Geodynamic Institute.
3. We estimated the seismic wave directivity, i.e., its direction of propagation and calculated the epicentre distance from the Arsakeia Schools of Patras.
4. We calculated the Maximum Acceleration developed in the area where each accelerometer is located and compared it to the maximum acceleration values proposed by the Greek Earthquake Planning and Protection Organization (OASP), in their Earthquake-Resistant Design.

The following map shows the location of the Geodynamic Institute's accelerometers in the Patras area. ARSA is the one which is located at the Arsakeio School.

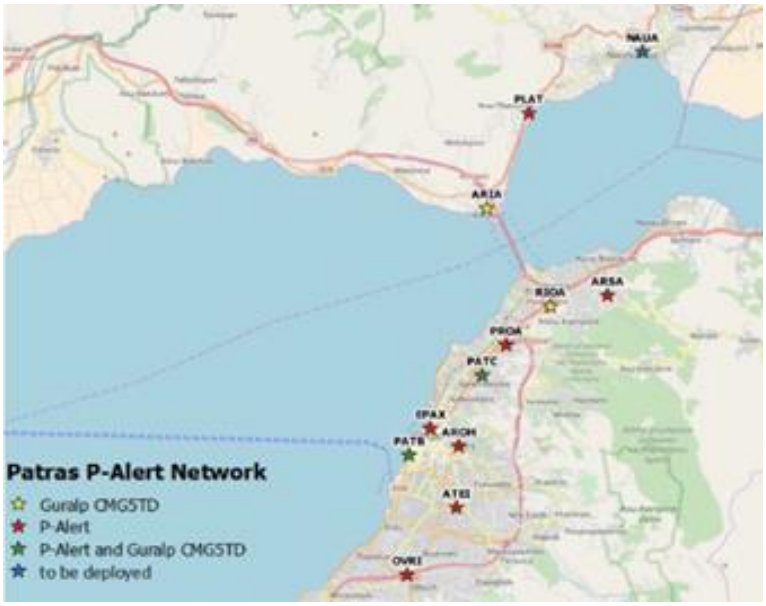

Figure 1. Accelerometer Network in Patras Area (www.gein.noa.gr)

Acknowledgements

The authors would like to thank, Dr Melis Nikolaos S., Director of Research in Institute of Geodynamics - National Observatory of Athens, for his invaluable support, guidance and criticism in completing this project, Dr Sokos Efthimios, Professor of Seismology in University of Patras, for his support and proof reading of our work and Dr Petrakis Emmanouil, Director of the Arsakeio Lykeio Patras, for his vision in developing a school open to society.

References

Zahradnik J., Sokos E., Plicka V., 2018. Zakynthos 25/10/2018, Mw 6.8 Earthquake: Superposition of Strike-Slip and Thrust. University of Patras – Greece, Report sent to EMSC on 09/11/2018.

Theodoulidis N., Karakostas X., Konstantinidou K., Lekidis B., Makra K., Margaris B., Morfidis K., Papaioannou X., Rovithis E., Salonikios T., 2018. Earthquake S. Ionian, M 6.8 in 26/10/2018, Record Analysis of Accelerometers Network of ITSAK and Damages in Natural and Built Environment. Ministry of Infrastructure & Transportation – OASP (in Greek).

Giakoumakis E., Gyrtis K., Mpelesiotis B.S., Xynos P., Stergiopoulou-Kalantzi N., 2003. IT Applications – Computers. Athens: OEDB (in Greek).

16th International Congress of the Geological Society of Greece

17-19 October, 2022 - Patras, Greece

Bulletin of the Geological Society of Greece, Sp. Publ. 10

Ext. Abs. GSG2022-268

EduSeismArtTec: Education Seismology for the School and the Society – A multidisciplinary approach through innovative theatre education methods and digital technologies.

I. Kalogeras[1], N. S. Melis[1], M. Rangoussi[2], Ch. Zoniou[3], A. Tsichli[3], A. Kastritsis[1], D. Metafas[2], A. Charitopoulos[2], P. Monachelis[2], V. Maragkou[2], E. Frentzos[1], M. Ziazia[1]

(1) National Observatory of Athens, Institute of Geodynamics, Lofos Nympon, Thissio, 11851 Athens, Greece, i.kalog@noa.gr (2) University of West Attica, Department of Electrical and Electronics Engineering, 250, Thivon Ave., 12241 Athens-Egaleo, Greece (3) University of Peloponnese, Department of Theatre Studies, 21 Vas. Constantinou St. and Terzaki St, 21100 Nafplion, Greece.

It is known that citizens who are informed - educated on natural or technological hazards behave better concerning the risk minimization before, during and after the time of crisis. This is the case with earthquakes: the scientists (seismologists) are typically expected to address the general public and transmit scientific knowledge in a popularized manner. However, the traditional ways of knowledge dissemination (brochures, posters, web pages and seminars) may fail to reach / attract the interest of specific audiences. In order to overcome this problem and reach wider population groups, synergies are required between specialized seismologists and experts of other disciplines, using innovative methods and alternative learning approaches to popularize seismology knowledge.

Less known, however, is the reverse route, i.e., the earthquake effects observations and reporting of evidence (photos etc.) from the citizens to the scientists, given that the scientists are usually not present at the meizoseismal area, while citizens are more likely to be in the vicinity of the earthquake effects. Apart from the destruction pictures taken on the spot, which are evaluated in combination with the measurements by seismic activity monitoring instruments and result to the quantification of seismological concepts (Bossu et al., 2011), the way that citizens feel the natural phenomenon (i.e. the shaking) provides socio-psychological information, useful in order to improve the education of the population (population-at-risk management).

The two-directional scheme mentioned above describes the transition from scientific seismological knowledge to Educational Seismology (or School Seismology) and further to Citizen Seismology. In Citizen Seismology, an informed and trained for earthquakes citizen becomes an observer and reports reliable information to scientists, who in turn process them and provide valuable information to the State for immediate response to the affected areas.

In the "*EduSeismArtTec*" research project, three research groups with significant experience and expertise in complementary knowledge areas, namely: the Institute of Geodynamics of the National Observatory of Athens (NOA-IG), the Department of Theatre Studies of the University of Peloponnese (UoP-DTS) and the Department of Electrical and Electronics Engineering of the University of West Attica (UWA-DEEE) collaborate to develop and disseminate a new learning culture on earthquakes. In order to maximize the learning outcomes, the project employs innovative approaches such as (i) theatre education and experiential theatre pedagogy, (ii) digital, multimedia technology for the embedding of combined physical / digital / virtual components in the educational activities. Virtual / Mixed Reality technologies as well as 3D/holographic projections are employed to this end.

As *'EduSeismArtTec'* completes two years of running, the activities and interventions carried out and the results obtained are presented and discussed in this work; future research steps are also outlined. More specifically and for indicative reasons:

In order to experimentally test and evaluate the effectiveness of the proposed approach, a *drama-in-education* intervention has been designed and implemented in an attempt to enrich the tools of Educational Seismology with those of drama-in-education methodology (see: http://eduseismarttec.gein.noa.gr/en/home-3/). The designed intervention has employed mainly the *process drama* approach (Bowell, & Heap, 2013; Schonmann, 2011; O'Toole, 1992). It has involved over 900 pupils of the primary education, over 140 pupils of the secondary education and over 60 students of the higher education, with strongly positive results.

Moreover, the "*Beat the Quake!*" theatre performance has been produced and staged, using the *devised theatre* (Oddey, 1994) and *documentary theatre* methods (Forsyth & Megson, 2009). Nine students of the Department of Theatre Studies of the University of Peloponnese, who volunteered as actors for this performance, took part in the *collaborative invention* of the play.

Another innovative aspect of *'Beat the Quake!'* is the embedding of digital components in the physical play on the stage: an explanation of the physical phenomenon has been developed for the purposes of "*EduSeismArtTec*" project. The 3D digital material was designed and developed using VR technology and specifically the Unity-3D development

platform. It involved a 'vertical' tour from the outer space into the Earth, down to lithospheric depths and then up the sea level. The simulated material (earthquake, melted mantle, volcanic eruption etc.) was projected on a holographic screen on the stage and suitably incorporated in the actors' play, complemented with real-time narration. A mixed audience of approximately 100 people attended the performance with great emotion engagement and participated in an evaluation activity after it by completing the relevant questionnaire.

Figure 1. A photograph taken from the theatre performance "*Beat the Quake!*".

The experience with schools concerning the seismology terms popularization and the understanding of precaution measures, showed the value of the educational tools. Thus, a set of improved educational tools is prepared (posters, brochures, models using mainly cheap and easy-to-find materials) and is placed in a safe water proof case, serving the aim of mobility and spread of the seismology knowledge to schools.

The development and improvement of a web platform for citizens to upload their observations for moderate / destructive earthquakes is ongoing. The platform should be able to handle observations / information in multiple forms (text, images, audio, mobile phone application products, etc.) and it should withstand heavy data traffic in cases of massive response from the public at the time of crisis. The platform via a management tool combines the operation of the strong motion network and the macroseismic bulletins (archive and present information on important past earthquake events and it will be connected to other existing databases of NOA-IG). Shake maps (Worden et al., 2020) of strong earthquakes are also included in this platform produced by the citizens observations and the instrumental recordings.

Acknowledgement

EduSeismArtTec is implemented by the National Observatory of Athens – Institude of Geodynamics (hosting coordinator Institution), the University of the Peloponnese - Department of Theatre Studies and the University of West Attika - Department of Electrical and Electronics Engineering. The research project is supported by the Hellenic Foundation for Research and Innovation (H.F.R.I.) under the "1st Call for H.F.R.I. Research Projects to support Faculty Members & Researchers and the Procurement of high-cost research equipment grant" (Project Number: 1752). The voluntary involvement of the University of the Peloponnese - Department of Theatre Studies students in the realization of the theatre performance is greatly acknowledged.

References

Bossu, R., Gilles, S., Mazet-Roux, G., and Roussel, F. (2011). "Citizen seismology: how to involve the public in earthquake response," in Comparative Emergency Management, eds D. M. Miller and J. Rivera (Boca Raton, FL), 235–257. doi: 10.1201/b10974-15

Bowell, P., & Heap, B. S. (2013). Planning Process Drama: Enriching Teaching and Learning. Routledge.

Forsyth, A., & Megson, Ch. (Eds.). (2009). Get real: documentary theatre past and present. Palgrave Macmillan.

Lee, H. (2013). 3D Holographic Technology and Its Educational Potential. TechTrends 57(4), pp 34–39.

Schonmann, S. (2011). Key Concepts in Theatre/Drama Education. Sense Publishers.

O'Toole, J. (1992). The Process of Drama: Negotiating Art and Meaning. Routledge.

Oddey, A. (1994). Devising theatre: a practical and theoretical handbook. Routledge.

Worden, CB, Thompson, EM, Hearne, M, Wald, DJ (2020) ShakeMap Manual Online: Technical Manual, User's Guide, and Software Guide. DOI: 10.5066/F7D21VPQ.

16th International Congress of the Geological Society of Greece
17-19 October, 2022 - Patras, Greece
Bulletin of the Geological Society of Greece, Sp. Publ. 10
Ext. Abs. GSG2022-304

The lignite's industrial heritage preservation as an opportunity to develop an international center of energy and environmental education in Western Macedonia, Greece

N. Karamarkos[1], A. Patra[1], I. Kapageridis[2], F. Pavloudakis[2]

(1) Western Macedonia Lignite Centre, Public Power Corporation, Ptolemaida, Greece, n.karamarkos@dei.gr (2) University of Western Macedonia, Department of Mineral Resources Engineering, Kozani, Greece.

The achievement of the objective of limiting global warming to "well below 2°C" depends to a large extent on the elimination of fossil fuels used for power generation purposes. The measures proposed by international fora (the Paris Agreement) and policies developed at an international or national level (European Green Deal) include the phase-out of coal-fired power plants and, consequently, the closure of the coal mines that were fueling them (Pavloudakis et al., 2020). This development forces many mining companies to seek solutions for the safe closure of their mines and the rehabilitation of land, well earlier than they have initially planned, while local communities are looking for new economic activities and land uses, which will mitigate the social and economic impacts at the regional level.

Regarding more specifically the new land uses that may be developed in the reclaimed mine lands, the literature presents several successful examples that promote the issue far beyond the restoration of the natural function and the improvement of the landscape aesthetics described in most environmental impact studies and required by the relevant permits. The development of several agricultural activities, including energy crops, livestock farming, recreational parks, touristic attractions as well as the siting of industrial and residential areas have in many cases been proved viable options and have contributed decisively to the strengthening of local income and the creation of new jobs (Pactwa et al., 2021; Young et al., 2021).

A critical part of recreational and tourism activities is the preservation and promotion of the industrial heritage associated with the extraction of coal and the generation of electricity (Wicke et al., 2018; Syafrini et al., 2021). The mining sites have inherent characteristics that make them impressive, such as the size and shape of the earth-moving works, the complex stratigraphy of the geological formations, the tectonic features, etc. The existence of water in the final mine pit can be exploited to improve the aesthetics of the greater area and for recreational activities. Furthermore, in a circular economy and symbiotic context, these artificial lakes can be used for irrigation and as lower reservoirs of energy storage pumping stations. Finally, the coal-fired power plants, which are usually located at a short distance from the mines, can be a second pole of attraction for visitors as they incorporate mechanical and electrical equipment and installations that are among the most complex and operationally interesting that can be demonstrated by the science and technology of 20th century (Copic et al., 2014).

The above-mentioned alternatives regarding the post-mining land uses are also valid in the case of the lignite center of Western Macedonia. It is a complex of surface mines that occupies more than 17,000 hectares, where equipment for continuous excavation, transport, and dumping of materials is installed. During the lignite's "glory" period, these mines produced more than 50 million tons of lignite and excavated more than 300 million cubic meters of rocks per year. Being a point of reference for the local economy, the lignite center traditionally receives hundreds of visitors every year, mainly politicians and officials of various national and European missions who visit the area as well as students and schools who are interested in enriching their knowledge about mining and power generation. During the period 2014-21 more than 14,000 people visited the exhibition center of Public Power Corporation, with the number of visitors during the COVID-19 pandemic period to be decreased by 70%.

For the lignite mining areas to continue to be attractive and accessible by various groups of visitors after the closure of the mines, specific interventions need to be planned and implemented towards the following main axes:

1. The preservation of the special geological, tectonic, paleontological, etc. characteristics of the lignite deposit.
2. The transport, repair, maintenance, and demonstration of the operation of certain pieces of equipment within its operating area, preferably representative of different periods of mine operation.
3. The exhibition of the findings of archaeological excavations that preceded the development of the mines.
4. The development of infrastructures capable of hosting exhibitions, conferences, accommodation, etc., with emphasis on the repurposing of existing buildings and the reduction of new constructions.
5. The establishment of a route that will unify all the visitable sites, including selected sites in restored areas that host different methods of land reclamation and land uses.
6. The optimization of planning in terms of enhancing the symbiosis of tourism, recreation, and education activities with other activities that will be located in the restored areas, such as those related to energy production: photovoltaic parks, mixed combustion units of lignite, and biomass, waste-to-energy plants, etc.
7. The incorporation into the above planning of all the necessary measures to ensure the safety of employees and visitors.

It is worth noticing that the planning and implementation of the above interventions must begin as soon as possible and, in any case, before the closure of the mines, since this will allow various works to be carried out at a lower cost while preventing arguments between various stakeholders relevant to the spatial distribution and the acreage occupied by the land uses that are considered.

Figure 1 presents schematically the spatial distribution of site visits with educational interest around the surface mines of Western Macedonia lignite center. Depending on the time that the visitor can devote, after the tour around the mining site, he can prolong his stay in the area, first, by visiting the restored waste heaps of the mines, where the largest photovoltaic park in the country has been installed, modern facilities for municipal solid waste processing and disposal are operating, and some remarkable examples of reforestation, agricultural development, and recreational sites are demonstrated. The visitor can expand further his area of interest by visiting a lignite-fired power plant and the innovative biomass combustion unit of the Amyntaio, gaining at the same time some basic knowledge about district heating systems, an idea of central heating installation that remains unknown to most Greeks. Finally, the visitor can get a full view of the main components of the country's energy system (excluding only natural gas) by visiting the hydroelectric plants of the River Aliakmonas and the Aeolian parks of Vermio Mountain, which are located within a radius of approximately 50km from the lignite mines.

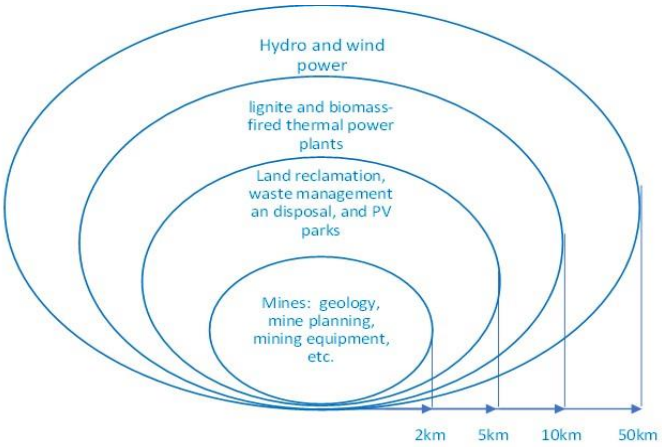

Figure 1. Spatial allocation of spaces of educational interest around the open-air lignite mines

From the above, it becomes obvious that the preservation of the industrial heritage may have a key - role in the development of domestic tourism in Western Macedonia and especially in the regional unit of Kozani, which for many decades was presented, sometimes unjustifiably, as the most polluted area of Greece. This is certainly a difficult target, considering the strong competition from other areas of Greece which exhibit particularly attractive characteristics, such as the sea, famous archaeological sites, etc. Previous efforts based on agrotourism and other categories of thematic tourism have failed.

Nevertheless, planning and acting on a symbiotic basis, the promotion of the industrial heritage, combined with some of the new uses of land that fit in the site-specific characteristics of the lignite mines and the electricity generation activities that exist in the wider mining area are composing an interesting network of site visits for entertainment but mainly for education. The presence of Western Macedonia University in the area, with many engineering, humanities, and economic departments, may contribute positively to organizing education-oriented visits, while for touristic visits there are many issues to be resolved by local authorities and the Ministries of tourism, culture, energy and environment, and education.

References

Copic, S., Djordjevic, J., Lukic, T., Stojanovic, V., Djukicin, S., Besermeji, S., Stamenkovic, I., Tumaric, A. K., Horsman, E., 2014. Transformation of industrial heritage – an example of tourism industry development in the Ruhr Area (Germany). Geographica Pannonica, 18(2), 43-50.

Pactwa, K., Konieczna-Fuławka, M., Fuławka, K., Aro, P., Jaskiewicz-Proc, I., Kozłowska-Woszczycka, A., 2021. Second Life of Post-Mining Infrastructure in Light of the Circular Economy and Sustainable Development—Recent Advances and Perspectives. Energies, 14 (7551).

Pavloudakis, F., Roumpos, C., Karlopoulos, E., Koukouzas, N., 2020. Sustainable rehabilitation of surface coal mining areas: The case of Greek lignite mines, Energies, 13 (3995).

Syafrini, D., Nurdin, M.F., Sugandi, Y.S., Miko, A., 2021. Transformation of a Coal Mining City into a Cultured Mining Heritage Tourism City in Sawahlunto, Indonesia: A Response to the Threat of Becoming a Ghost Town. Tourism Planning & Development, DOI: 10.1080/21568316.2020.1866653.

Wicke, C., Berger, S., Golombek, J. (Eds.), 2018. Industrial heritage and regional identities. Routledge Cultural Heritage and Tourism Series, Routledge.

Young, A., Barreto, M.L., Chovan, K., 2021. Towards a circular economy approach to mining operations – key concepts, drivers, and opportunities. Materials Efficiency Research Group and Enviro Integration Strategies Inc., 97p.

16th International Congress of the Geological Society of Greece
17-19 October, 2022 - Patras, Greece
Bulletin of the Geological Society of Greece, Sp. Publ. 10
Ext. Abs. GSG2022-325

The Virtual Tour of the Giannoula Aqueduct Trail (West Parnes Mountain, Attica, Greece) as an Educational Tool

I. Kampolis[1,2], Th. Georgousopoulou[3]

(1) National Technical University of Athens, Athens, Greece (2) National Center for Scientific Research "Demokritos", Agia Paraskevi, Greece, kampolisigeo@gmail.com (3) Ephorate of Antiquities of West Attica, Athens, Greece.

Research Highlights

The virtual technology applied in Giannoula Aqueduct trail can be used for the environmental awareness and education of the public.

Abstract

The geodiversity of the mountainous area of the Fyli Municipality is inseparably linked with its rich ancient history. Since the antiquity, humans took advantage of the landforms in the area and used them for their own benefit. The ancient Fortress of Fyli was constructed on a limestone horst bearing a paleo-peneplane on top of it, whereas the Cave of Pan, a well-known archaeological site located on the east bank of Gkoura Gorge, was used as a prominent cult site (Kampolis *et al.*, 2020). The Giannoula Stream, a torrential hydrographic network forming the Gkoura Gorge and known as Kelathondas River in the classical period, was exploited for its water resources from the antiquity till the historical times. The Giannoula Stream, situated in the NW area of the Fyli town, cuts through the Upper Triassic-Lower Jurassic limestones and dolomites of the Pelagonian Unit and after running on the Thriassio Plain, it discharges into the NE part of the Elefsiniakos Gulf. The large water quantities of the ancient river were exploited by ancient workers who carved water channels into the limestones close to the exit of the gorge in order to diverge the water flow and use it for drinking or irrigation purposes (Fig. 1).

Figure 1. The constructed waterway in the Limestones of the Pelagonian Unit. The carved horizontal marks can be seen on both walls of the water conduit.

Today, the trail of the Giannoula Aqueduct follows the ancient water route and the biggest part of it lies in the NATURA 2000 "OROS PARNITHA" area (GR3000001), whereas the aqueduct is protected as an archaeological site. Thus, the trail combines in a unique way the geodiversity, biodiversity and archaeological wealth of the West Parnes Mountain. The total length of the route is 1.95 km and the altitudinal difference between the starting and ending point is 2 m. Due to the smooth morphology of the trail and the richness of the concentrated features (geological, biological and archaeological), we attempted the virtual promotion of the trail in order to attract more visitors (heritage popularization, Pasquaré Mariotto and Bonali, 2021) and use the end product as a tool for geo-archaeo-educational activities. The recording of the route was accomplished by the use of the Matterport PRO2 3D camera which enables the appropriate recording of certain environments with a virtual tour as an end product. The same method has been effectively applied in other regions i.e. Lavreotiki Geopark (Kampolis *et al*., 2022). The camera captures high-resolution images (134.2 Mega Pixels) in certain station-points with 360º (horizontal) and 300º (vertical) field of view. The successive points have a constant in-between distance, allowing the successful overlap of the recorded space. The combination of all the recorded

points and captured photos results in the digital twin (3D model) of the trail (Fig. 2). Moreover, the end product is compatible with augmented reality goggles. The recording of the Giannoula Aqueduct trail was accomplished through 1425 station-points spaced every 1.5 m. The digital twin of the trail represents an unprecedented tool for geo-bio-archaeo-educational activities addressed to the public with a special target group the younger ages. The environment of the trail, although flat, poses restrictions when it comes to groups of small children. Thus, the ability of virtually visiting it, facilitates the experiential education and enhances the comprehension of the interacting nature between Geology, Biology and Archaeology. Afterall, the interaction between these disciplines is represented by the Giannoula Aqueduct trail.

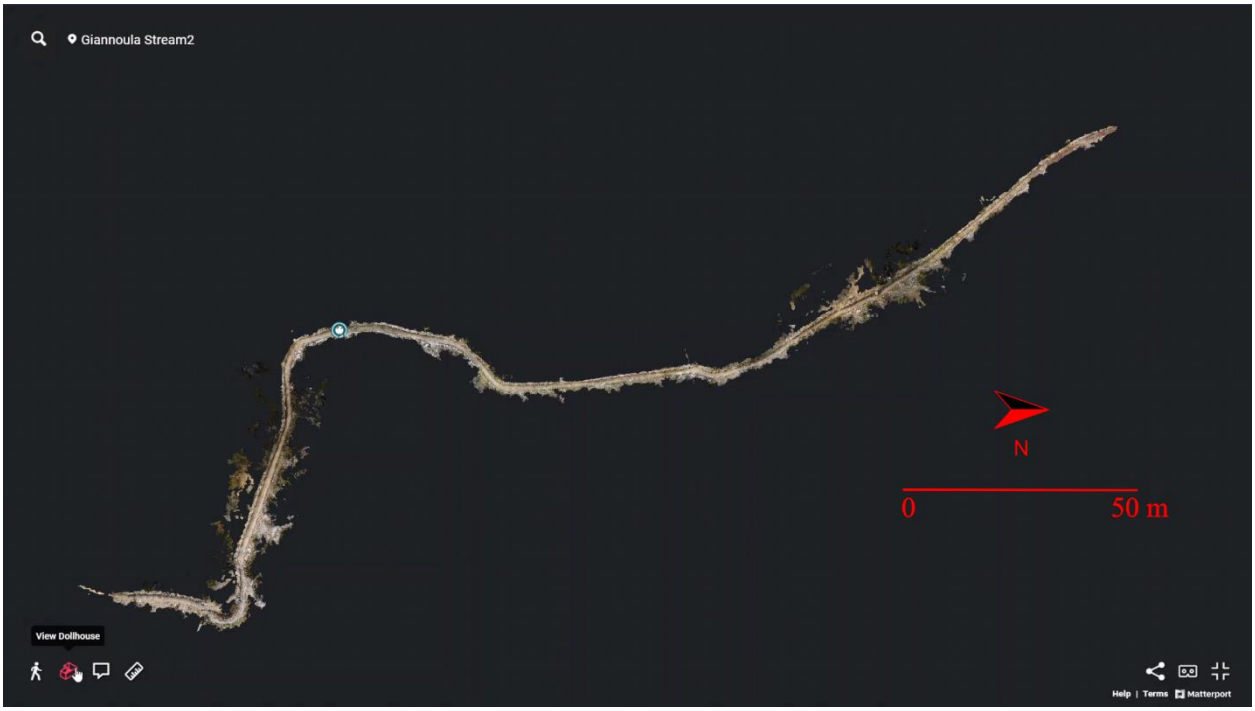

Figure 2. Top view of a section from the digital twin of Giannoula Aqueduct trail. The length of this part is 290 m.

Additionally, the Giannoula Aqueduct can stand as the best analogue in order to educate people about our dependance on water resources and in general on natural resources. The water usage for various purposes is characteristic for the progress of the human civilization. Thus, the ability of the current society to realize the stakes of water scarcity due to climate change issues and protect the natural ecosystem is vital. This environmental awareness raise can be accomplished through the Giannoula Aqueduct Trail.

Acknowledgements

We would like to express our sincere thanks to Mr. Christos Pappous, Mayor of the Fyli Municipality for the embracement and the funding of the current project. Special thanks are also, addressed to the Ephorate of Antiquities of West Attica for granting permit in order to digitally record the site.

References

Kampolis, I., Mari, A., Kampolis, A., 2020. Lychnospilia or Cave of Pan: An archaeological site with an interesting Quaternary evolution. Book of Proceedings of One-day Online Conference "The Role of Geomorphology in Modern Society" of the Hellenic Committee for Geomorphology & Environment of the Geological Society of Greece, Special Publication No 8, Bulletin of the Geological Society of Greece.

Kampolis, I., Moraiti, Ev., Barsaki, V., 2022. Virtual tour in the mining gallery 'No 80' of Lavreotiki Geopark – New technologies for the smooth transition to the post-Covid era. 3rd Conference of Greece-Cyprus UNESCO Global Geoparks «GREECE-CYPRUS UNESCO GLOBAL GEOPARKS AND SUSTAINABLE DEVELOPMENT».

Pasquaré Mariotto, F., Bonali, F.L., 2021. Virtual Geosites as Innovative Tools for Geoheritage Popularization: A Case Study from Eastern Iceland. Geosciences 2021, 11, 149.

16th International Congress of the Geological Society of Greece

17-19 October, 2022 - Patras, Greece

Bulletin of the Geological Society of Greece, Sp. Publ. 10

Ext. Abs. GSG2022-330

Contribution of Remote Sensing in geoheritage management at two scales

Z. Pantazopoulou[1], V. Tsioukas[2], A. Mouratidis[1], D. Alexakis[3]

(1) Department of Physical and Environmental Geography, Aristotle University of Thessaloniki, 54124 Thessaloniki, Greece; zpantazo@geo.auth.gr; (2) Department of Geodesy & Surveying, Aristotle University of Thessaloniki, 54124 Thessaloniki, Greece; (3) Laboratory of Geophysics - Satellite Remote Sensing & Archaeoenvironment, Institute for Mediterranean Studies, Foundation for Research and Technology Hellas (FORTH), Nikiforou Foka 130 & Melissinou, P.O. Box. 119 Rethymno 74100, Crete, Greece.

This paper examines the contribution of Remote Sensing in the management of geological heritage. The concept of geological heritage includes characteristic or even rare landforms, rocks, fossils, deposits and processes that compose the geological history of any region. The history of the Earth is linked to people and their culture. The management of the geological heritage includes a wide range of actions, starting from their identification, demarcation, mapping, monitoring and protection, and extending to its exploitation for various purposes, such as educational, research-scientific, touristic and others. Remote Sensing and especially the part related to Earth Observation, is a field of Science and Technology that has made significant progress in last few decades and has found application in many other scientific fields including Geology. The main purpose of the present paper is the study and promotion of advanced Remote Sensing methods, in the general management of geological heritage. The research is based on two case studies, which cover the range of two cartographic scales – medium (i.e. that of a local scale landform) and large (i.e. that of a fossil item) - related to geological heritage. In this context, the potential of Remote Sensing will be explored in all possible stages of geological heritage management (identification, demarcation, mapping/scanning, monitoring, protection, exploitation).

Geoheritage

The term “geoheritage” evolved from the notion of “geological heritage”. Heritage means something that has existed since the past, has been transmitted from the past, and will continue to be important in the future. Geological heritage is understood as the heritage including features of geological nature. Global, regional, and local geological elements such as igneous, metamorphic, sedimentary rocks, minerals, fossils, stratigraphic, tectonic, pedologic, palaeontologic structures, and other geosites (or geotopes) at all scales, are important sites and specimens, which offer information and insights into the formation and evolution of the Earth, the evolution of life, the climate and landscapes of the past and present, as well as the geological history of the sites where they are found. The importance of geological monuments is equally significant to the historical and archaeological monuments. Consequently, this type of information has scientific, educational, cultural, aesthetic, and tourist value. Thus, it is important to be retained for present and future generations (Zafeiropoulos, G., *et.al*, 2021, Carcavilla *et.al*, 2019, Brocx M., 2007).

Case Studies

Case study 1 Nymfopetres formation

Between the villages of Prophetis and Nymphopetra in the northern part of the basin of Mygdonia, 3.5 kilometers NW of Lake Volvi, Thessaloniki, Northern Greece, there are characteristic structures called “Nymphopetres” (Fig. 1). Nymfopetres are rock formations, which are mainly lined up in an elongated area 200 meters long and 70 meters wide. The height of the landforms reaches 8 meters, while their thickness ranges from 3 to 4 meters. They have a spongy appearance, consisting of calcium carbonate grains and are coated with a grey-black coating of calcium carbonate. They generally give a sense of a "stone forest" causing the creation of myths of the local folklore tradition. (Pavlidis S., 1997).

Figure 1 The geotope of Nymfopetres

In this particular case, the aerial remote sensing was applied. The area was scanned using Unmanned Aerial Vehicles (UAVs) and the data collected were processed via appropriate photogrammetric procedures. The objective of the scan was to test the applicability of this particular type of remote sensing at this scale of geological heritage. Through the results of the scan and the use of appropriate software, first it is possible to develop a 3D model of the area, which can be printed and given as a souvenir to visitors. Secondly, with a suitable software a remote site-visit application could be developed, which in cases of limited site-access, as it happened for safety reasons during the recent pandemic, could serve tourism. In terms of research, through scanning and the combination of measurements and the appropriate processing software, it will be possible to monitor the erosion rate of the rocks with the aim of finding appropriate protection measures to preserve them for future generations.

Case study 2 Ursus Spelaeus

The Ursus Spelaeus is a well-known endemic species that is approximately 200,000 years old. The bears fled to the caves to protect themselves from the adverse conditions of the ice age, for hibernation, and to give birth to their cubs (Koufos G. *et. al*, 2007). The sample is important, because it provides information about the paleoenvironment of the Petralona area, Halkidiki, Northern Greece in which it was found (Fig. 2). In this particular case, the terrestrial type of remote sensing was applied i.e. the sample was scanned using a laser scanner (Fig. 3). Through the results of the scan and the use of appropriate software, the possibility of 3D viewing and/or printing is given. This material can be used for research purposes as long as the fossil/object can be printed in the physical dimensions and studied simultaneously by more than one researcher. In addition, through this method, it is possible to capture and 3D-print important findings such as fossils or rocks at a large scale.

Figure 2. Fossil (cave bear skull)

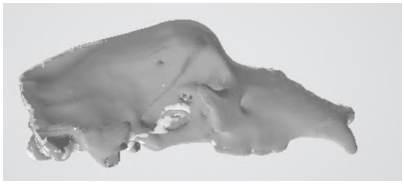

Figure 3. Result of fossil scanning with the laser scanner

Conclusions

This paper deals with the management of geological heritage with a focus on the contribution of Remote Sensing. Geological heritage includes all geosites that are an important part of the earth's history and must be preserved for future generations. The aim of the work is to highlight the methods of Remote Sensing in the management of the geological heritage. The investigation took place at two scales - large and medium. The scans produce results that can be applied to research as well as to education, tourism etc.

Acknowledgements

I would like to extend my sincere thanks to the Geology-Paleontology Museum of the School of Geology of the Aristotle University of Thessaloniki for giving me permission to use the fossil of Ursus Spelaeus and the School of Rural and Surveying Engineering for their help with scanning the fossil. The implementation of the doctoral thesis was co-financed by Greece and the EU (European Social Fund-ESF) through the Operational Programme «Human Resources Development, Education and Lifelong Learning» in the context of the Act "Enhancing Human Resources Research Potential by undertaking a Doctoral Research" Sub-action 2: IKY Scholarship Programme for PhD candidates in the Greek Universities.

References.

Vlachopoulos, N., Voudouris, P., 2022. Preservation of the Geoheritage and Mining Heritage of Serifos Island, Greece: Geotourism Perspectives in a Potential New Global Unesco Geopark. Geosciences, 12, 127. https://doi.org/ 10.3390/geosciences12030127

Zafeiropoulos, G., Drinia, H., Antonarakou, A., Zouros, N., 2021. From Geoheritage to Geoeducation, Geoethics and Geotourism: A Critical Evaluation of the Greek Region. Geosciences, 11, 381. https://doi.org/10.3390/geosciences11090381

Carcavilla, L., Díaz-Martínez, E., García-Cortés, Á., Vegas, J., 2019. Geoheritage and geodiversity, Instituto Geologico y Minero de Espana, p. 24.

UNESCO Intergovernmental Committee for the Protection of the World Cultural and Natural Heritage Operational Guidelines for the Implementation of the World Heritage Convention. 2017.

UNESCO, World Heritage Centre Operational Guidelines for the Implementation of the World Heritage Convention. Oper.Guidel. 2012.

Brocx, M., Semeniuk, V., 2007. Geoheritage and Geoconservation. History, Definition, Scope and Scale, p. 53-87, Journal of the Royal Society of Western Australia.

Koufos, G., Tsoukala, E., 2007. Petralona Cave, Aristotle University of Thessaloniki, p.70-73.

Pavlidis, S., Syrides, G., 1997. Field trip to Mygdonia basin, The 29th general assembly of the IASPEI 1997, Guide booklet.

16th International Congress of the Geological Society of Greece
17-19 October, 2022 - Patras, Greece
Bulletin of the Geological Society of Greece, Sp. Publ. 10
Ext. Abs. GSG2022-338

Developing Knowledge Management in Mine Reclamation Projects

P.-M. Spanidis[1], C. Roumpos[2], F. Pavloudakis[3], A. Servou[4], N. Paraskevis[2]

(1) ASPROFOS Engineering S.A. Athens, Greece, pspani@asprofos.gr (2) Public Power Corporation, Athens, Greece (3) University of Western Macedonia, Kozani, Greece (4) Public Power Corporation, Athens, Greece, University of Patras, Department of Geology, Patra, Greece.

Mining reclamation is a process of transforming areas excavated and disturbed due to intensive mining operations into an environmentally friendly, socially acceptable and economically usable state. Reclamation projects consist of complex, large numbers and long-duration activities aiming to restore landscape, landforms and ecosystems with beneficial returns to society and the economy. In recent decades, reclamation projects have been reformed by adopting circular economy initiatives (i.e. new supply chains for reusing and recycling disposed materials, reducing energy consumption, etc.), which take place considering the transition of post-mining sites to sustainability (Pavloudakis et al, 2022).

The knowledge of experts (mine engineers, geologists, environmentalists, economists, managers, etc.) plays an essential role in planning and executing reclamation projects. Empirical evidence shows that experts provide problem-solving ideas, consultancy on scientific and socioeconomic and administrative aspects (land use planning, landscape reshaping, soil management, water treatment, stakeholder engagement, etc.), risk management views, proposals for sustainable restoration methods (afforestation, recultivation, recreation, etc.) or methods for the extraction of valuable minerals from the remaining deposit, waste heaps or tailings and guidance on many aspects with effect to the governance and successfulness of reclamation projects (Pavloudakis et al., 2018). However, as business entities incorporate technological knowledge, mechanical infrastructures, information technologies, and specialized personnel in their production system, mining companies usually face several problems in managing effectively and efficiently the multidisciplinary experts' knowledge effectively and efficiently on an individual or collective basis. The problems of knowledge mismanagement generate criticalities and dysfunctionalities that impact the objectives of reclamation projects in terms of scope, cost, quality, timeliness and performance. In reclamation frameworks, as in most capital/knowledge-intensive projects, the most common knowledge mismanagement problems are:

1. The limited availability of experts due to changes in project organization schemes (replacement, rotation, or retirement).
2. The knowledge loss/gaps due to improper, superannuated and/or low effectiveness management of data and information collected in mining phases (exploration, development, maturity, ageing/closure and post-closure).
3. The cost and time limitations related to developing various synergies for Knowhow and Technology Transfer (KTT) established by mining companies to improve the performance of mining operations. In this context, the knowledge acquired/transferred through these synergies demonstrates a declining efficiency in the long run.

One possible way to solve the above problems is to develop a Knowledge Management (KM) system adaptable to mining companies' project management systems and operations. Literature suggests two KM approaches as applicable in businesses and projects, where knowledge represents: (a) a function/process performed within the organization's boundaries or embodied in project execution activities and (b) an entity/element of a database ("Knowledge Base"-KB), the ontological structure of which has been designed to support needs of mining management, science and technology (Project Management Institute, 2013). In this paper, the authors suggest the functional KM approach as applicable for the mining reclamation projects since it allows:

- The introduction of KM philosophy and systemic approach to the project team(s).
- The low cost and quick adaptation of KM processes to the work breakdown structure of the reclamation planning model.
- The introduction of knowledge processes in the mining company's quality management system and work procedures.
- The deployment and intra-disciplinary KB system capable of incorporating valuable information and reply to content-specific queries related to mining operations and reclamation projects execution due to the KM process system functionality and effectiveness.

The method suggested for designing KM processes is IDEF0 (Integrated DEFinition Function), a broadly applied task ontology for modelling industrial and business processes. IDEF0 enables visualization of knowledge workflow into a mining company, based on the Input-Output-Control-Mechanism (ICOM) scheme of entities, which feeds with data, information and other related materials the KM functional system. The IDEF0 design concept uses the reclamation project as a "vehicle" for knowledge transfer to the mining company (Spanidis et al., 2022). Based on literature and keeping analogies from KM systems established in project environments, the recommended KM system consists of four interacting and interlinking processes deployable in the environment of a mining company:

(a). Knowledge Acquisition (P1/KAQ): activities for data collection from legislation, international conventions,

scientific literature, best available practices of circular economy and technologies enabling transition of post-mining sites to sustainability, along with empirical evidence and lessons learned from project and risk management aspects of reclamation projects performed in the past.

(b). Knowledge Organization and Storing (P2/KOS): activities for the conceptual design, development, implementation, testing, operation and maintenance of a multidisciplinary and multi-purpose knowledge base (KB), enabling the provision of feedback and background information with practical essence, in real-time conditions, to personnel involved with long term reclamation projects of high complexity.

(c). Knowledge Transfer/Sharing (P3/KTS): activities for serving the cross-disciplinary and intra-disciplinary transactions for the delivery and distribution of knowledge on various areas related to the sustainable transformation of mines and the mitigation of all socioeconomic and environmental impacts.

(d). Knowledge Application (P4/KAP): activities related to the adaptability, maintainability and improvement of the KB content and efficiency so that the knowledge developed in the mining company becomes a company's intelligent asset and instrument of increasing the company's competitive advantages.

Figure-1 reflects an overview of the outlined IDEF0 model (the description of the KM processes tasks and ICOM entities are available upon request). IDEF0 is a low-cost, quick use and easy application tool for the functional design of industrial and business systems. As such, it provides a substantial basis for visualization and customization of a KM process model satisfying the knowledge development and performance in frameworks of mine reclamation (Jeong et al., 2009). Furthermore, the potential extension and transferability of the suggested KM model, with the necessary modifications and adaptations, is helpful for the improved(?) (re)engineering of mining operations and the purposes of academic research as well.

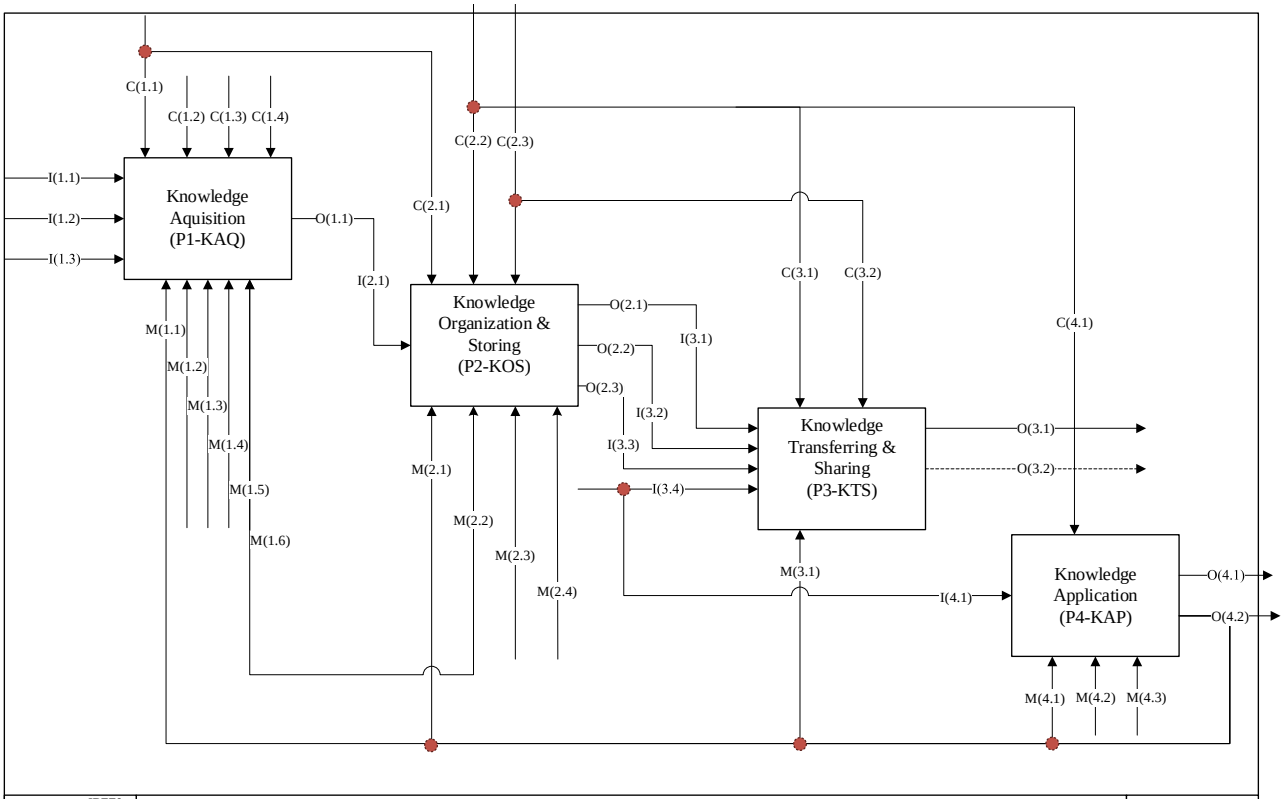

Figure 1: The IDEF0 model for Knowledge Management development in mining organizations/projects

References

Jeong, K.-Y., Wu, L., & Hong, J.-D. 2009. IDEF method-based simulation model design and development framework. Journal of Industrial Engineering and Management, *2*(2), 337–359. https://doi.org/10.3926/jiem.2009.v2n2.p337-359

Pavloudakis F., Roumpos C., Karlopoulos E., Koukouzas N. 2020. Sustainable Rehabilitation of Surface Coal Mining Areas: The Case of Greek Lignite Mines. Energies. 13(15):3995. https://doi.org/10.3390/en13153995

Project Management Institute (Ed.). (2013). *A guide to the project management body of knowledge: PMBOK® guide* (5. ed). PMI.

Spanidis, P.-M., Roumpos, C., & Pavloudakis, F. 2022. A Methodology Combining IDEF0 and Weighted Risk Factor Analysis for the Strategic Planning of Mine Reclamation. Minerals, 12(6), 713. https://doi.org/10.3390/min12060713

Pavloudakis F., Roumpos C., Spanidis P.M., 2022. Optimization of surface mining operation based on a circular economy model, Circular Economy and Sustainability, Elsevier, 395-418, https://doi.org/10.1016/B978-0-12-821664-4.00005-4

16th International Congress of the Geological Society of Greece

17-19 October, 2022 - Patras, Greece

Bulletin of the Geological Society of Greece, Sp. Publ. 10

Ext. Abs. GSG2022-340

Teaching Field Geology in the Digital Age

V. Chatzaras[1], S. Polanco[1], Y. Ibrahim[1], P.F. Rey[1]

(1) The University of Sydney, School of Geosciences, Sydney, Australia, vasileios.chatzaras@sydney.edu.au

- Students collect field data using the geological data system StraboSpot, which allows to digitally collect, store, and share field data.
- The use of digital data systems enables a transition to a more research-led teaching approach.

The traditional way of teaching geology in the field is fundamentally different from how geologists collect field data in industry and in research, nowadays. To meet the needs of an era where digital technology dominates all aspects of professional life, Earth data science is rapidly growing, information is readily available, and problem-solving and critical thinking skills are paramount, we need to reconsider our teaching strategy. The use of digital data systems seems imperative for training the next generation of field geologists.

In 2020, we restructured the field school for the third-year students in the Geology and Geophysics Major at the University of Sydney, transitioning from the traditional way of collecting field data using pencil, paper and analog tools, to a field school based entirely on digital technology. In the new format, students collect data using the geological data system StraboSpot (Walker et al., 2019) on tablets (Figure 1). StraboSpot allows users to digitally collect, store, and share field data in structural geology, sedimentology, petrology, and other field-based disciplines, integrating multiple geological fields in a single data system. The StraboSpot mobile application runs on both iOS and Android devices. The application runs in both online and offline settings. While online, students can access any base images and maps (e.g., satellite imagery, geological maps, drone imagery) they need for their projects, and download them to the device for offline use. While offline, the application can access the mobile device's GPS showing the real-time locations on the preloaded georeferenced maps and images.

The benefits of using StraboSpot data system for teaching field geology are: (1) the system includes dialog boxes and prompts, which help students organize their observations; (2) the application uses a fixed vocabulary, which reinforces learning of concepts taught in the classroom and can guide students to determine what information they need to collect in each outcrop; (3) easy access and searchability of field data (e.g., notes, orientation measurements, sketches, photographs); (4) allows easy plotting of orientation data in the Stereonet Mobile application (Allmendinger et al., 2017) for quick assessment of the structure of the study area; (5) allows easy data sharing among students, which can be useful when multiple students work together on the same project (e.g., field area). Additionally, StraboSpot has a back-end database that facilitates sharing data with the geologic community and the transition to big data science in geology (e.g., Bergen et al., 2019; Tikoff et al., 2019). Moving to an education aligned with the FAIR data principles, data collection within the StraboSpot database ensures the findability, accessibility, interoperability, and reusability of the data collected during the field school.

Having used the StraboSpot data system for teaching field geology for three years, we provide some reflections on how the use of this digital technology has improved student learning experience, based on our own observations and student feedback. The preloaded georeferenced maps and images that are provided to the students as learning resources, allowed a transition to a more research-led teaching approach; fieldwork is organised around goal-oriented assignments, designed around real-world problems. For example, by choosing field areas of ongoing scientific debate, students study relevant peer reviewed articles (along with comments and replies if available) and published geological maps, then design and implement a field data collection and analysis campaign, to test multiple hypotheses and the available geological information.

Figure 1. University of Sydney students using StraboSpot during the field school in Broken Hill, NSW, Australia.

Acknowledgements

We thank the StraboSpot team, and especially Nick Roberts, Basil Tikoff, Alexander Lusk, and Doug Walker, for their help. We thank the 2020-2022 students of GEOS3008 and GEOS3101 at the University of Sydney, who have embraced the transition to the use of digital data systems in field geology.

References

Allmendinger, R.W., Siron, C.R., and Scott, C.P., 2017. Structural data collection with mobile devices: Accuracy, redundancy, and best practices. Journal of Structural Geology, 102, 98–112.

Bergen, K.J., Johnson, P.A., de Hoop, M.V., Beroza G.C., 2019. Machine learning for data-driven discovery in solid Earth geoscience. Science, doi:10.1126/science.aau0323.

Tikoff, B., Chatzaras, V., Newman, J., Roberts, N., 2019. Big data in microstructure analysis: Building a universal orientation system for thin sections. Journal of Structural Geology, 125, 226-234.

Walker, J.D., Tikoff, B., Newman, J., Clark, R., Ash, J., Good, J., Bunse, E.G., Möller, A., Kahn, M., Williams, R.T., Michels, Z., Andrew, J.E., and Rufledt, C., 2019. StraboSpot data system for structural geology. Geosphere 15, 2, 533–547.

16th International Congress of the Geological Society of Greece
17-19October, 2022 -Patras, Greece
Bulletin of the Geological Society of Greece, Sp. Publ. 10
Ext. Abs. GSG2022-341

Space and STEM Education at school: the contribution of ESERO Greece and the opportunities for Geodidactics

A. Mouratidis[1], N. Lambrinos[2], I. Repanidou[3], Z. Pantazopoulou[4], A. Nikolaidis[5]

(1) Aristotle University of Thessaloniki, Thessaloniki, Greece, amourati@geo.auth.gr (2) Aristotle University of Thessaloniki, Thessaloniki, Greece (3) Aristotle University of Thessaloniki, Thessaloniki, Greece (4) Aristotle University of Thessaloniki, Thessaloniki, Greece (5) Aristotle University of Thessaloniki, Thessaloniki, Greece.

Young people show great excitement for space science regardless of gender or age, although interest in careers in space industry tends to follow the gender norms which exist in Sciences, in general (DeWitt and Bultitude, 2018). European Space Agency (ESA), through ESERO (European Space Education Resource Office) offices which are established all over the Europe, ensures contribution to education and endeavors to inspire students to follow career paths in space industry in the context of interdisciplinary STEM (Science, Technology, Engineering, Mathematics) Education. The dominant issue of STEM Education is to keep all the fields integrated holding their characteristics authentic and at the same time to highlight Space Education.

ESERO project aims to support Primary and Secondary Education all over Europe. Many offices have been launched in plenty of countries and more specifically in: Austria, Belgium, Czech Republic, Denmark, Estonia, France, Germany, Ireland, Italia, Luxemburg, Greece, Finland, Norway, Poland, Portugal, Romania, Spain, Sweden, UK. ESERO Greece was officially launched at 29 November 2021 and is under the leadership of Aristotle University of Thessaloniki (AUTh). The key of all ESEROs and also of ESERO Greece is their constantly growing network and national partners, who are involved in STEM and Space fields. The ESEROs use a space frame into the classroom in order to make the teaching and learning of STEM subjects more attractive and make students feel more familiar with Sciences. ESERO activities contribute to the integration of all students in STEM and Space Education, dispelling the general misconception that Science is only for geniuses. All young students are encouraged to gain new experiences, follow new challenges and find out more about Space Science in the context of STEM Education.

Unfortunately, there is a lack of space science curriculum in education which has resulted in reducing the opportunities to young people to foster space and STEM careers and thus, they are not able to discover and evolve their skills (Afful, *et al.*, 2020). Especially in Greek schools, space science content knowledge is clearly missing, contrary to the past years, where Cosmography and Astronomy subjects existed in school schedule. ESERO Greece aims to reintegrate space science in combination with STEM subjects. Greek schools need the contribution of ESERO Greece in order to strengthen the engagement of students in STEM subjects within the context of space and also to help teachers build or strengthen their teaching resources with new educational tools.

All ESERO's support five school projects suggested by ESA, which are: CanSat, Astro Pi, Mission X, Climate Detectives, Moon Camp. At this point, it is vital to describe the ESA school projects. 1) **Astro Pi** is addressed to Primary and Secondary Education (ages 7-19) and includes two levels: a) Astro Pi-Mission Zero and b) Astro Pi-Mission Space Lab. Astro Pi is a small Raspberry Pi computer where students send, in real time, a message to the astronauts of the International Space Station (ISS). At the second level, students design a project for a scientific experiment which gives information about life on Earth or life in Space. 2) **Mission X** is addressed to Primary school students (ages 8-12). Students learn about the everyday life of astronauts through experiential activities and train like real astronauts (physical exercise, nutrition etc.). 3) **Moon Camp** is referred to Primary and Secondary level of Education (ages 6-19). Students design in 3D simulation a lunar base, a space rocket, etc., with Tinkercad or Fusion 360. There are three levels of difficulty: Moon Camp discovery, Moon Camp explorers, Moon Camp pioneers. 4) **CanSat** is for Secondary Education and university students (ages 14-20). It is a simulation of a real mini-satellite in size and shape of a soda can. The challenge for students is to fit all the major subsystems which are found in a satellite, into a soda can. It is a real scientific experiment where students can fly their own satellite in a rocket. 5) **Climate Detectives** is referred to Primary and Secondary Education (ages 8-15). Students find out and investigate a climate problem by using Earth Observation data (e.g. satellite images) or by doing their own ground measurements. Then, they suggest solutions.

For many years, thousands of teachers and millions of students from all over Europe have been trained in these school projects with great success. Trainings are offered to Elementary and Secondary school teachers in cooperation with national partners, scientists, astronauts and experts in STEM and Space Education. In addition, all offices have the possibility to prepare new educational material, adapted to the national curriculum of their country in order to achieve the greatest results. Space should not be taken into account just as a subject. It can be characterized as a suitable environment for providing real synchronous models of scientific methodology, interdisciplinary collaboration and a way to inspire people for future professional engagement. The involvement of students is considered necessary in

modern society of the 21st century.

Overall, the launch of ESERO Greece in late 2021 and the high relevance of Geosciences to Space and STEM ought to be seen, among other things, as a great opportunity to promote and enhance Geodidactics all over Greece at primary and secondary school level.

References

Afful, A. M., Hamilton, M., Kootsookos, A. (2020). Towards space science education: A study of students' perceptions of the role and value of a space science program. *Acta Astronautica*, 167, 351-359, https://doi.org/10.1016/j.actaastro.2019.11.025

Astro Pi. Retrieved July 25, 2022 from www.esa.int/esearch?q=Astro+Pi

CanSat in Greece. Retrieved July 25, 2022 from https://cansat.gr/

CanSat. Retrieved July 25, 2022 from www.esa.int/esearch?q=cansat

Climate Detectives. Retrieved July 25, 2022 from www.esa.int/esearch?q=Climate+Detectives

DeWitt, J., and Bultitude, K. (2018). Space Science: the View from European School Students. *Research in Science Education*, 50, 1943–1959, doi:10.1007/s11165-018-9759-y

ESA at the forefront of space education. Retrieved July 25, 2022 from https://www.esa.int/Education/ESA_at_the_forefront_of_space_education

ESERO Greece. Retrieved July 25, 2022 from https://esero.gr/

ESERO Greece takes off to boost STEM education in school. Retrieved July 25, 2022 from https://www.esa.int/Education/Teachers_Corner/ESERO_Greece_takes_off_to_boost_STEM_education_in_school

European Space Agency. Retrieved July 25, 2022 from https://www.esa.int/

European Space Education Resource Office. Retrieved July 25, 2022 from https://www.esa.int/Education/Teachers_Corner/European_Space_Education_Resource_Office

Mission X: train like an astronaut. Retrieved July 25, 2022 from www.trainlikeanastronaut.org/greece/

Moon Camp. Retrieved July 25, 2022 from www.esa.int/esearch?q=Moon+Camp

16th International Congress of the Geological Society of Greece

17-19 October, 2022 - Patras, Greece

Bulletin of the Geological Society of Greece, Sp. Publ. 10

Ext. Abs. GSG2022-343

Towards the Establishment of a Natural History Exhibition and Paleontological Park at Isioma Karyon in Megalopolis (Peloponnese, Arcadia, Greece).

I.X. Giaourtsakis[1], P.V. Filis[1], S.D. Sklavounou[1], M.K. Georgitsis[1], D.E. Liakopoulou[1], S. Kirdis[1], E. Koumoutsea[1], N. Tsoukalas[1], S. Saltapida[2], E. Koskeridou[1], G.E. Theodorou[1]

(1) National and Kapodistrian University of Athens, Faculty of Geology and Geoenvironment, Department of Historical Geology and Palaeontology, Panepistimioupolis, GR-15784, Athens, Greece, giaourtsakis@snsb.de (2) University of the Peloponnese, School of Arts, Department of Theatre Studies, Nafplion, Greece.

The stratigraphic sequence at the intramontane basin of Megalopolis consists primarily of fluviolacustrine deposits containing lignite seams, which have been extensively mined for the production of electric energy since the 1970s. The occurrence of fossil bones in the basin was known to the ancient Greeks; they have been attributed to mythical beasts and gigantic divine beings, as testified by surviving myths and legends. During his visit in the ancient town of Megalopolis, the renowned Greek writer and geographer Pausanias reported the existence of bones of enormous proportions kept at the local sanctuary of Asclepius, which had been attributed to one of the Giants mustered by Hopladamus to fight for Rhea (*Hellados Periegesis* 8.32.5, C2nd A.D.). According to the myth, Hopladamus was one of the Kouretes Giants who gathered his brothers in defense of the goddess Rhea, when the Titan Kronos raged against her after learning that she had spirited away their infant son Zeus (*ibid*. 8.36.2-3). The extraordinary "Nichoria bone", which was discovered at the archeological excavations in the ruins of the ancient Acropolis of Nichoria, is one of the few surviving large vertebrate fossils deliberately collected and donated as an offering in the antiquity, and is believed to have originated from the nearby basin of Megalopolis (Mayor 2000).

The first scientific excavations in the basin of Megalopolis were carried out by Prof. Th. Skouphos of the National and Kapodistrian University of Athens (NKUA) (Bürchner, 1903; Skuphos, 1905). The significant palaeontological findings, now stored at the Museum of Palaeontology and Geology of the NKUA, were studied in detail much later by Prof. I. Melentis in a series of publications (e.g. Melentis, 1961, 1964), including also material from new excavations that he conducted in the area. Inevitably, precise stratigraphic information for the excavations of this early period is almost entirely missing. During the following decades, additional dedicated fieldwork and research activity revealed numerous new fossiliferous localities within the basin of Megalopolis, documenting a diverse Middle to Late Pleistocene fauna, including also decisive evidence of Paleolithic human presence and interaction (e.g. Sickenberg, 1975; Van Vugt *et al.*, 2000; Darlas, 2003; Theodorou, 2014; Panagopoulou *et al.*, 2018; Athanassiou *et al.*, 2018; Thompson *et al.*, 2018). Among the most notable encounters that have been reported at the various fossiliferous localities of the Megalopolis basin are the European straight-tusked elephant *Palaeoloxodon antiquus*, the rhinoceros *Stephanorhinus* sp., the equid *Equus* sp., the cercopithecid monkey *Macaca sylvanus*, several carnivores such as a large-sized felid *Panthera* sp., the wildcat *Felis* sp., the fox *Vulpes* sp., the wolf *Canis* sp, the weasel *Mustela* sp., and the otter *Lutra simplicidens*, numerous artiodactyls including the European hippopotamus *Hippopotamus antiquus*, the bison *Bison* sp., the wild boar *Sus scrofa*, the large-sized deer *Praemegaceros verticornis*, the red deer *Cervus elaphus*, and the fallow deer *Dama* sp., as well as several other micromammalian taxa, birds, and reptilians.

During 2009, Prof. G. Theodorou of the NKUA was invited by the local cultural association "Enosis Isiomateon Karyon" to support the idea for a local natural history exhibition and new palaeontological excavations. The mayor P. Mpouras and the council of the Megalopolis Municipality embraced the effort providing financial support for the excavations. The initial excavation by the scientific team of the NKUA was carried out during the September of 2011 at the KYT area (Kentron Yperipslis Tasis). The findings included bones from elephants and deer, as well as one disturbed lithic artifact; the latter was sent to the Ministry of Culture. The first major survey and fieldwork period was carried out during the August and September of 2012. In particular, a systematic excavation was conducted in the site "Grana tou Skouphou" at Isioma Karyon (Fig. 1), which brought to light a complete tusk and isolated molars of *P. antiquus*, as well as several deer and hippo bones. In the following year, subsequent fieldwork and survey revealed several promising excavation sites (Theodorou 2014). During the summer of 2013, the association "Enosis Isiomateon Karyon" provided a local building to facilitate the ongoing excavations and the preservation of the specimens. This building has been further utilized as an interim Information Station by the NKUA paleontological team (Fig. 1), providing regular educational presentations and cultural events ever since. In the meantime, through the combined efforts and the financial support of the Municipality of Megalopolis and the administrative Region of Peloponnese, the museum's foundations were laid on August 26, 2017. Currently, and despite some bureaucratic difficulties, the construction of the building has entered its final stage (Fig. 1). During the summer of 2022, the first post-Covid field survey has been carried out, exploring several new fossiliferous sites such as Apiditsa and Aghios Theodoros, whereas the NKUA team has also commenced with the scientific preparation of the museological and educational context for the exhibition.

Figure 1. On the left, excavating a tusk of *Palaeoloxodon antiquus* at Grana tou Skouphou (September 2012). In the middle, the new building of the natural history exhibition at Isioma Karyon (adjacent to the excavation site). On the right, detail of the current temporary exhibition at the local Information Station by the NKUA research team.

The placement of importance in the awareness and cultivation of a community's natural-history heritage as a mean of education and inspiration has been a constant plea by academia. In the case of Isioma Karyon at Megalopolis, it is the efforts and awareness of the local community, which came to acknowledge the necessity for the protection and promotion of the geological and paleontological wealth discovered in the area, which is firmly connected with its historical, cultural and socioeconomical background. Through the creation of dedicated exhibition premises, with the appropriate scientific infrastructure and educational facilities, the documentation, preservation and presentation of this exceptional geoheritage will be significantly improved and expanded. The design of the exhibition is currently under development by the multidisciplinary scientific and museological team led by the NKUA. Through the adaptation of established and contemporary museological concepts, as well as the application of modern technological tools (interactive boards and exhibits, experiential and virtual activities, 3d printing etc.), the learning experience of the visitors will be enhanced by active participation and collaborative engagement. Within this scope, the potential extension of the exhibition to a paleontological park has been further embraced and discussed by the local authorities and the cultural association, in order to connect thematically the exhibition with the adjacent fossiliferous sites, as well as other historical and cultural monuments and activities in the region. The whole effort shall add a positive contribution towards the post-lignite development and sustainability of the wider area by collectively celebrating its unique historical, cultural and geological heritage.

Acknowledgements

We kindly acknowledge the Municipality of Megalopolis, the authorities of the Region of Peloponnese (Peripheria), the cultural association Enosis Isiomateon Karyon, and the Public Power Corporation S.A. for supporting and facilitating the scientific research at the Megalopolis basin (NKUA Research Account Project Nrs. 11474 and 16996).

References

Athanassiou, A., Michailidis, D., Vlachos, E., Tourloukis, V., Thompson, N., Harvati, K., 2018. Pleistocene vertebrates from the Kyparíssia lignite mine, Megalopolis Basin, S. Greece: Testudines, Aves, Suiformes. Quaternary International 497, 178-197.

Bürchner, L., 1903. Wichtige Funde fossiler Knochen in Arkadien. Berichte des Naturwiss. Vereins zu Regensburg 9, 119–123.

Darlas, A., 2003. Palaeolithic finds from the Megalopolis Basin: their relation to the fossils of the same area. In: Vlachopoulos, A., Birtaha, K. (Eds.), Argonautis: Honorary Issue to C.G. Doumas. Kathimerini, Athens, p. 27-37.

Mayor, A., 2000. The first fossil hunters: paleontology in Greek and Roman times. Princeton University Press, Princeton.

Melentis, J.K., 1961. Die Dentition der pleistozänen Proboscidier des Beckens von Megalopolis im Peloponnes (Griechenland). Annales Géologiques des Pays Helléniques 12, 153-262.

Melentis, J.K., 1964. Die fossilen Rhinocerotiden, Hippopotamiden und andere Säugetiere aus dem Becken von Megalopolis im Peloponnes. Proceedings of the Athens Academy 39, 388–400.

Panagopoulou, E., Tourloukis, V., Thompson, N., Konidaris, G., Athanassiou, A., Giusti, D., Tsartsidou, G., Karkanas, P., Harvati, K., 2018. The Lower Palaeolithic site of Marathousa 1, Megalopolis, Greece: Overview of the evidence. Quaternary International 497, 33-46.

Sickenberg, O., 1975. Eine Säugetierfauna des Tieferen Bihariums aus dem Becken von Megalopolis (Peloponnes, Griechenland). Annales Géologiques des Pays Helléniques 27, 25-73.

Skuphos, T.G., 1905. Über die palæontologischen Ausgrabungen in Griechenland in Beziehung auf das Vorhandensein des Menschen. Comptes Rendus du Congrès International d'Archéologie, 1re session. Athènes, Grèce, p. 231–236.

Theodorou, G., 2014. Megalopolis - 112 years after the first excavation by National and Kapodistrian University of Athens (NKUA) - and the post lignite era. VIth International Conference on Mammoths and Their Relatives, Grevena-Siatista, Greece. Scientific Annals of the School of Geology, Aristotle University of Thessaloniki, Special Volume 102, p. 195-196.

Thompson, N., Tourloukis, V., Panagopoulou, E., Harvati, K., 2018. In search of Pleistocene remains at the Gates of Europe: Directed surface survey of the Megalopolis Basin (Greece). Quaternary International 497, 22-32.

Van Vugt, N., de Bruijn, H., van Kolfschoten, T., Langereis, C.G., 2000. Magneto- and cyclostratigraphy and mammal-fauna's of the Pleistocene lacustrine Megalopolis Basin, Peloponnesos, Greece. Geological Ultrajectina 189, 69-92.

16th International Congress of the Geological Society of Greece
17-19 October, 2022 - Patras, Greece
Bulletin of the Geological Society of Greece, Sp. Publ. 10
Ext. Abs. GSG2022-345

Recycling at the Upper Palaeolithic: intentionally modified bones from Melitzia Cave, Mani Peninsula, Greece (preliminary results)

M. Tzortzi[1], G. Iliopoulos[1], A. Darlas[2]

(1) Department of Geology, University of Patras, GR-26504, Rio, Patras, Greece, m.tzortzi@upatras.gr (2) Ephorate of Paleoanthropology and Speleology, Greek Ministry of Culture and Sports, Ardittou 34b, 1636 Athens, Greece.

Most ideas about recycling during the Palaeolithic are based on lithic artefacts, particularly on their surface alterations, although recycling can also be approached from the aspect of faunal remains, based on their breakage modifications. In order to maximize the nutritional value of consumed animals, hominins processed bones to extract the bone marrow, and during this process small and large sized fragments derived. Due to the fragments' morphology and the bone composition, the 'leftovers' could be considered raw material as well, an alternative to stones, and thus be appropriate materials for use as tools. In this case, the bones are selected to be used in a sustainable life cycle.

The transition from the Middle to the Upper Palaeolithic in Western Europe was characterized by the arrival of anatomically modern humans (*Homo sapiens*) and the extinction of the last Neanderthals, approximately 40,000 years ago (Burke and d'Errico, 2008). Besides the different way of lithic production, *H. sapiens* brought with him a great diversity of production demonstrated by new practices (Baumann *et al.*, 2020). Tools made of skeletal materials have been recorded from Early to Upper Palaeolithic assemblages (Julien *et al.*, 2015). Although, the Middle Palaeolithic bone industries are characterized by small typological variability, the Upper Palaeolithic ones are characterised by a great variety of shapes and manufacturing techniques. Shaped bone tools typical of the European Upper Palaeolithic have been discovered in earlier assemblages, and they are considered as a sign of "modernity" (Backwell and d'Errico, 2014), whereas unshaped tools are recorded not only in the Middle Palaeolithic assemblages but also in the Upper Palaeolithic ones.

The Mani peninsula is regarded as a key area of Greece for Palaeolithic studies due to the large number of known excavated sites containing deposits with cultural artefacts and skeletal remains from the Middle and the Upper Palaeolithic, revealing the abundance of human occupation in the wider area during the Middle-Late Pleistocene. Melitzia Cave is one of the several karstic cavities found on the western coast of Mani peninsula, used as a shelter by Late Pleistocene hominids (Darlas and Psathi 2016). The excavated layers date to the Upper Palaeolithic and more specifically to an age interval between 46,448–44,553 BP and 11,150–10,680 BP (Kolendrianou, 2021). Numerus lithic artefacts along with extremely broken, burned and modified bones testify the hominin occupation of the site.

This study presents preliminary results of a technological analysis conducted on bones from Melitzia Cave. Among the more than 3,000 bone fragments that were yielded from the excavations conducted by the Ephorate of Palaeoanthropology and Speleology from 2010 to 2016, several specimens show marks of intentional humanly-induced modifications and could be characterized as tools. Bone fragments up to 1 cm long were studied visually, without technical aids, and with the use of a Lab-20 Optika stereomicroscope as well. The technological analysis of humanly-induced fracturing relies on the presence of cortical flakes on bone remains and on percussion marks and notches from direct percussion on the bones (Tartar, 2012). The morphology of the fracture facets with a curved or V-shaped outline, an oblique angle, and a smooth surface is considered to be the evidence of fresh bone knapping (Villa and Mahieu, 1991).

Long bones are represented by diaphyseal with a circumference inferior to less than half of the original size of the bone, and the morphology of these fragments characterize human fracturing of fresh bones. The presence of notches and adhering flakes confirms this observation. Based on the certain arrangement of the damage in some of the long bone fragments, it is assumed that these were not only broken for marrow consumption but also used as tools. The key factor that distinguishes a bone used as a tool, is the morphology of the breakage at both ends, which refers to the same operating mode (Baumann *et al.*, 2020). These tools were probably used directly as a wedge, and they were the outcome of an opportunistic use of bone fragments (Baumann *et al.*, 2020). Unshaped bone tools are hardly identifiable due to the absence of standardization in their shaping, to the difficulty of being distinguished from bones that were purposefully splintered by humans to extract bone marrow or were gnawed by carnivores, and due to the mechanical and chemical modification through diagenesis (Kozlikin *et al.*, 2020).

The identification of the anatomical parts and the taxa of the referred bone tools are not always distinguishable. All of them are long bone diaphyses of medium and large mammals. Among bones, the humerus is the most prominent. The mean length of the samples is 9 cm, and their width is narrower towards one side. Most of them have one side compressed and the other shows battering marks and some removal scars on the upper surface, so most likely they were used as intermediate tools (Baumann *et al.*, 2020), meaning that the tools were hammered on one end for splitting or cutting a material with the opposite end.

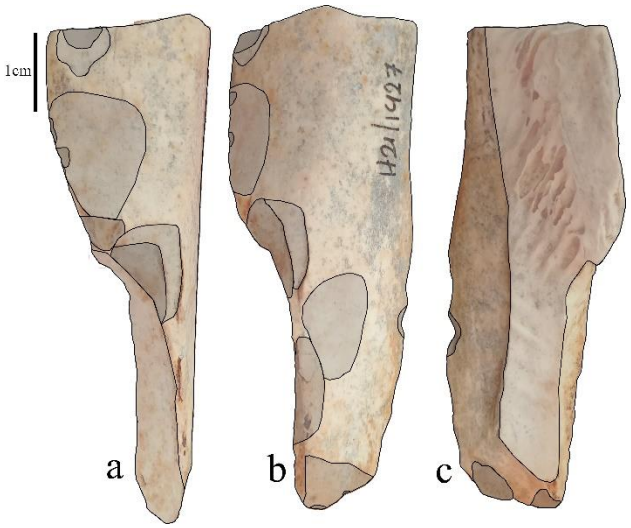

Figure 1: Humanly-induced marks on the cortical surface (a and b) and on the medullar surface (c).

Acknowledgements

We would like to thank the Ephorate of Palaeoanthropology and Speleology of the Greek Ministry of Culture and Sports and all the excavators that worked during the 2009–2016 Melitzia Cave excavations.

The implementation of the doctoral thesis was co-financed by Greece and the European Union (European Social Fund-ESF) through the Operational Programme «Human Resources Development, Education and Lifelong Learning» in the context of the Act "Enhancing Human Resources Research Potential by undertaking a Doctoral Research" Sub-action 2: IKY Scholarship Programme for PhD candidates in the Greek Universities.

References

Backwell L.R., d'Errico F. 2014 Palaeolithic bone tools, in: Smith, C. (Eds), Encyclopedia of global archaeology, Springer, 950–962

Baumann M., Plisson H., Rendu W., Maury S., Kolobova K., Krivoshapkin A., 2020. The Neandertal bone industry at Chagyrskaya cave, Altai Region, Russia. Quaternary International 559, 68-88.

Burke, A., d'Errico, F., 2008. A middle palaeolithic bone tool from Crimea (Ukraine). Antiquity 82, 843–852.

Darlas A., Psathi E., 2016. The Middle and Upper Paleolithic on the Western Coast of the Mani Peninsula (Southern Greece), in: Harvati K., Roksandic M. (Eds), Paleoanthropology of the Balkans and Anatolia: Human Evolution and Its Context, Springer, 95–118.

Julien M.A., Hardy B., Stahlschmid M.C., Uraban B., Conard N.J., 2015. Characterizing the Lower Paleolithic bone industry from Schöningen 12 II: A multi-proxy study. Journal of Human Evolution 89, 264–286.

Kolendrianou M., 2021. Palaeoenvironmental and Taphonomical study based on the microvertebrate assemblages of three Upper Pleistocene cave sites from Mani and central Greece. Ph.D. Thesis, University of Patras, Patras, Greece, 381 p.

Kozlikin, M.B., Rendu, W., Plisson, H., Baumann, M., Shunkov, M.V., 2020. Unshaped bone tools from Denisova cave, Altai.Archaeology, Ethnology & Anthropology of Eurasia 48, 16-28.

Tartar, E., 2012. The recognition of a new type of bone tools in Early Aurignacian assemblages: implications for understanding the appearance of osseous technology in Europe. Journal of Archaeological Science 39, 2348–2360.

Villa, P., Mahieu, E., 1991. Breakage patterns of human long bones. Journal of human evolution, 21(1), pp.27-48.

16th International Congress of the Geological Society of Greece
17-19 October, 2022 - Patras, Greece
Bulletin of the Geological Society of Greece, Sp. Publ. 10
Ext. Abs. GSG2022-347

Geological Heritage of Chios Island, North Aegean Sea, Greece

E. Moraiti[1], V. Barsaki[1], I. Zananiri[1], G. Chalatsis[2], G. Kakaris[3], K. Magkos[4]

(1) Hellenic Survey of Geology and Mineral Exploration (HSGME), 1 Spirou Loui str., 13677 Acharnae, Attica, Greece e-mail: moraiti@igme.gr (2) Chios Hiking, 82100, Chios (3) MSc Geographer, hiker, interested in non-urban landscape conservation, 82100, Chios (4) Honorary SPELEO member, 82100, Chios.

Geosites can be considered as the “book of the Earth”, enclosing the geological history of each region and providing information about the contemporary processes of the planet; Therefore, their recording, preservation and promotion are fundamental.

During more than 40 years of activity and participation in numerous research projects, the Hellenic Survey of Geology and Mineral Exploration [HSGME – former Institute of Geology and Mineral Exploration (IGME)] has carried out extensive work in the systematic recording of the geological heritage of Greece. As a result, a vast amount of data has been collected about geosites, geotrails and geoparks, along with several background information. In this context, more than 1400 sites have been recorded in the Greek territory, many of which have been classified as of "National Importance" and form the basis of the relevant national registry compiled by the Working Group of the Ministry of Environment and Energy. Chios island, in Northern Aegean Sea, Greece deservedly maintains two records in the Greek national catalogue of geosites (No 35: Thimiana Chiou-Paleontological findings & No 106: Chios – Ammonites; Fig. 1).

Figure 1. No 106: Chios – Ammonites (Greek national catalogue of geosites).

Chios is generally assigned to the easternmost part of the Pelagonian Zone (e.g., Jacobshagen,1986; see Meinhold et al., 2007, for discussion). Basically, it comprises two tectonostratigraphic units, an ‘autochthonous’ Lower Unit and a tectonically overlying ‘allochthonous’ Upper Unit (Herget and Roth, 1968; Besenecker et al., 1968). The Lower Unit consists of clastic sediments of Late Palaeozoic age containing blocks (of up to 100m in maximum width) of limestones, radiolarites and volcanic rocks. The Upper Unit consists of Mesozoic recrystallized limestones unconformably overlain by Cenozoic formations (Kilias, 1982). In the southeast, terrestrial, fossiliferous Neogene deposits are well exposed and small volcanic centers in the northwest and southeast, have developed during the same time interval (Besenecker and Pichler,1974).

This unique geodiversity creates a wealth of geosites (in situ or ex situ elements – collections of geological specimens) with paleontological (Fig. 1), geomorphological (Figs. 2, 3), tectonic (Fig. 4), mineralogical, petrological (Fig. 5), stratigraphical significance and of interest and is being recorded through the HSGME’s ongoing “GEOINFRA” project (funding NSRF, 2019-2023). The biodiversity of Chios further enriches its natural wealth in an admirable way (Fig. 6).

Figure 2. Geomorphological sites-karst formations in Chios island.

Figure 3. Geomorphological sites in Chios island.

Figure 4. Geosites of tectonic interest in Chios island.

Figure 5. Geosites of petrological interest in Chios island.

Figure 6. Chios biodiversity.

References

Besenecker, H., Dürr, S., Herget, G., Jacobshagen, V., Kauffmann, G., Lüdtke, G., Roth,W., Tietze, K.W., 1968. Geologie von Chios (Ägäis). Geol. et Palaeont. 2, 121–150.

Herget, G., Roth, W.,1968. Stratigraphie des Paläozoikums imNordwest-Teil der Insel Chios (Ägäis). Neues Jahrbuch für Geologie und Paläontologie, Abhandlungen 131, 46–71.

Jacobshagen, V., 1986. Geologie von Griechenland. Gebrüder Borntraeger, Berlin.

Kilias, A.A., 1982.Kleintektonische Untersuchungen im nordlich Teil der Insel Chios. Annals, Faculty of Physics and Mathematics, University of Thessaloniki 22, 3–20.

Meinhold, G., Kostopoulos, D., Reischmann, T., 2007. Geochemical constraints on the provenance and depositional setting of sedimentary rocks from the islands of Chios, Inousses and Psara, Aegean Sea, Greece: implications for the evolution of Palaeotethys. Journal of the Geological Society (London) 164, 1145–1163.

16th International Congress of the Geological Society of Greece
17-19 October, 2022 - Patras, Greece
Bulletin of the Geological Society of Greece, Sp. Publ. 10
Ext. Abs. GSG2022-371

Research Priorities and Life Cycle of the Surface Coal Mining in Greece: A Statistical and Knowledge-Based Approach

C. Roumpos[1], F. Pavloudakis[2], P.-M. Spanidis[3], A. Servou[1,4], N. Paraskevis[1]

(1) Public Power Corporation of Greece, Athens, Greece, c.roumpos@dei.gr (2) University of Western Macedonia, Kozani, Greece (3) ASPROFOS Engineering S.A. Athens, Greece (4) University of Patras, Department of Geology, Patras, Greece.

Research Highlights

The temporal evolution of scientific publications regarding mining operations follows, in general, the total ore production; however, due to the multidisciplinarity of the mining projects, some publications regard more than one life-cycle phase. The knowledge obtained from scientific works is directly connected to empirical-industrial knowledge.

Background

Lignite mining belongs to the industrial sector and, as a productive element, is characterized by the phases of a product's life cycle. Each phase spans some years or even decades, depending on the activities involved and considering that mining projects are capital-intensive and take a long time to recoup the relevant investments. However, some activities may start within a specific phase and may continue for more than one mining phase depending on the local mining conditions and lignite production evolution. For instance, considering environmental protection, land reclamation projects must start from the early mining stages and extend after the mine closure (Pavloudakis et al., 2022) to ensure sustainable mining (Pavloudakis et al., 2020). Moreover, simultaneously with the continuous technology development, the knowledge production regarding the mining projects is accelerating with tremendous speed on an interdisciplinary basis, and as a result, the number of published scientific works increases over time. The Public Power Corporation (PPC) has mainly exploited the lignite deposits in Greece since 1958, with the main works taking place in Ptolemais, Amyntaion, and Megalopolis surface mines. The industrial knowledge produced throughout these years has been combined with scientific knowledge to produce innovative strategies for each one of the mining phases.

Objectives and Research Questions

The Greek lignite mines are investigated from the perspective of the scientific works that were produced at the respective time intervals of the mining phases. In this context, the main research questions examined by the authors are:

a) Is there a correlation between the phases of the mine life cycle and the research topics?
b) Which are the main methods or tools used to investigate the relationship of the mining phases with scientific publications?
c) How was lignite production evolved compared with the theoretical models of the mine life cycle?
d) How are the mining phases temporally correlated with the market conditions and exogenous factors?

The study aims mainly to develop knowledge management, so the researchers obtain a general aspect regarding the research trends and lessons learned from the empirical procedures, skills which will encourage the evolution of scientific topics that are still underdeveloped.

Methods

Three main steps were employed in the framework of the study: a) the mining phase determination, b) the investigation of the research priorities for each mining phase, and c) the literature review regarding the research topics. Several research topics are investigated for each mining phase based on their incorporated activities. The main life-cycle mining phases that were investigated are a) the exploration, b) the development, c) the maturity, d) the ageing, and the closure/depletion phases (Roumpos and Pavloudakis, 2006, Pavloudakis et al., 2022). Figure 1 shows the real data of total lignite production distribution for all the mines and for each mine with different temporal starting points. It is observed that the maturity phase of each mine has spanned a long time, but different periods for each mine. However, it is worth noting that throughout the mining operations, the maturity phase is maintained via the opening of new mines.

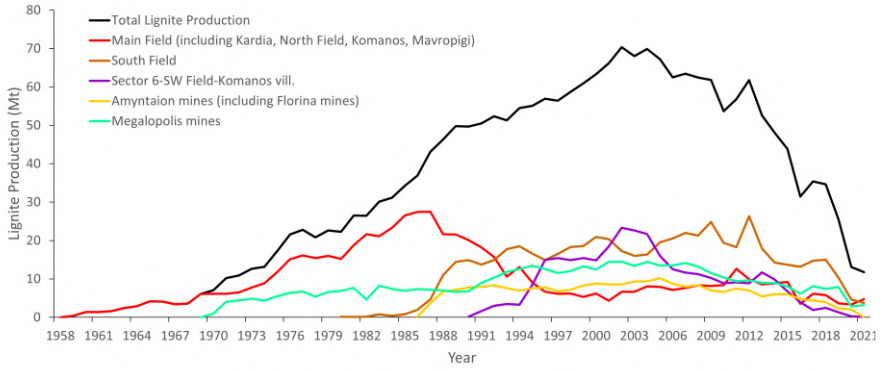

Figure 1: Lignite production evolution through time, based on the PPC's accounting data.

Due to the multidimensionality that characterizes the issue, the systematic literature review was considered the appropriate approach. Therefore, the Scopus database was used for the literature search regarding the respective research topics by choosing the most representative keywords to ensure that all the related publications have been considered and to avoid omissions if possible. Additionally, boolean operators were used to making the search more specific.

Results and Conclusions

Figure 2 presents the total lignite production from all the PPC's mines through time and the respective research scientific works published in the same time interval. Furthermore, the mining phases are distinguished through the curve fluctuation of lignite production.

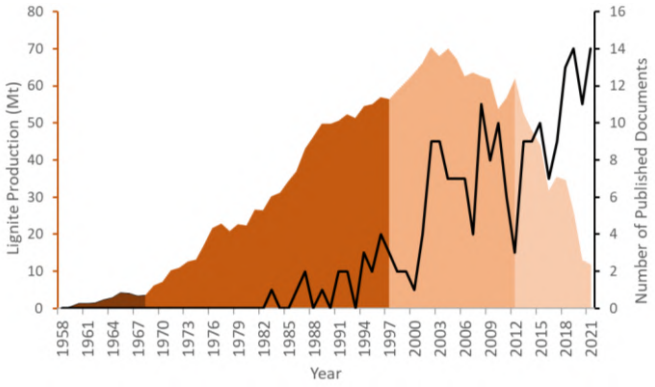

Figure 2: Surface mining life–cycle phases related to lignite production and research publications through time.

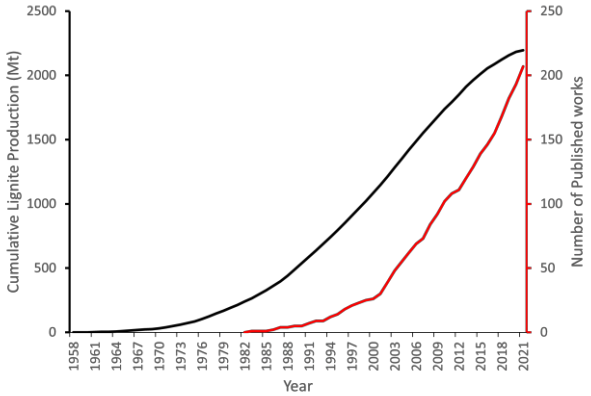

Figure 3: Cumulative distribution of published works concerning the total lignite production through time.

The literature search showed that although the mining operations began in 1958 in Greece, the first published works were observed in 1983 (Figure 3). A general increasing trend is observed until today, with a sharper increase in 2000, when the maturity mining phase was at its peak.

References

Pavloudakis, F., Roumpos, C., Karlopoulos, E., & Koukouzas, N., 2020. Sustainable Rehabilitation of Surface Coal Mining Areas: The Case of Greek Lignite Mines. Energies, 13(15), 3995.

Pavloudakis, F., Roumpos, C., & Spanidis, P. M., 2022. Optimization of surface mining operation based on a circular economy model. In Circular Economy and Sustainability, Elsevier, pp. 395–418.

Roumpos, C., Pavloudakis, F. 2006. Environmental management of surface mining projects: A comparative analysis. 8th International Symposium Continuous Surface Mining (ISCSM), Aachen, Germany, pp. 495–502.

16th International Congress of the Geological Society of Greece
17-19 October, 2022 - Patras, Greece
Bulletin of the Geological Society of Greece, Sp. Publ. 10
Ext. Abs. GSG2022-373

A Knowledge Representation Ontology for Mining Operations and Reclamation Projects

P.-M. Spanidis[1], C. Roumpos[2], F. Pavloudakis[3], N. Paraskevis[2], A. Servou[2,4]

(1) ASPROFOS Engineering S.A. Athens, Greece, pspani@asprofos.gr (2) Public Power Corporation S.A. Athens, Greece (3) University of Western Macedonia, Kozani, Greece (4) University of Patras, Department of Geology, Patra, Greece.

The mining industry is a key factor for the economy and primary energy production. The mining operations are long-term and multidisciplinary activities of high complexity aiming at producing metals, industrial minerals, and coal that modern society needs to maintain or even improve living standards. During the life cycle of a mining system, which usually lasts several decades, a vast amount of information is collected and stored in the ' 'mine's technical archives. Such information is related to the technical mine infrastructure, the geo-environmental aspects, the landform and landscape, and the administrative and managerial issues affecting the minerals production system and the local socioeconomic factors. This type and quantity of information is, by its nature, objective, recordable, formal, easily transferable and referred to in the literature as *explicit* knowledge. In parallel, a significant amount of expertise and knowledge captured during and because of the mining activity through synergies of know-how and technology transfer (KTT), problem-solving actions, and/or continuous interaction(s) with the local stakeholders (authorities, communities, NGOs, focus groups and key informants from the local municipalities) is captured, developed, and applied by the experts (managers, engineers, and operators) during the normal mining processes. This type of knowledge is (inter)personal, experience-based, subjective, hard to communicate, and referred to in the literature as *tacit* knowledge (Nonaka and Takeuchi, 1995).

A crucial problem affecting the mining operations and the post-mining reclamation projects is the dysfunctionality of using/reusing efficiently and effectively the tacit or explicit knowledge collected during a mine's life cycle. This dysfunctionality is more intensive when the mine enters a period of transition from an industrial plant of intensive extractive activity to a properly (re)engineered and sustainable land use system with environmentally friendly and socioeconomically beneficial characteristics. In the transition period, several scientific investigations, situational analyses, and engineering solutions have to be performed, and decisions on the extent, the type, and the cost-effectiveness of a reclamation project are to be ensured (Pavloudakis et al., 2022). In this transitional framework, various critical and emerging questions for the proper organization, management, and execution of the reclamation project, requiring empirical evidence and multidisciplinary knowledge, are addressed, such as:

(a). How can the knowledge created/captured/developed be effectively reused/leveraged, enabling the provision of guidance and real-time answering to queries addressed by mining experts or other users and stakeholders with authority over the reclamation project?

(b). Which tool is suitable for the conceptual representation of knowledge collected during the long-term mining operations or from lessons learned in past reclamation/repurposing projects?

(c). How effectively and efficiently can a conceptual model of a Knowledge Base (KB) appropriate for the needs of mining and post-mining projects be outlined?

One possible way to resolve the problem of dysfunctionality is for the collected knowledge to be decomposed, analyzed, classified, recomposed, and restructured through a formal ontology. This ontology aims to support database designers, information technologists, and artificial intelligence specialists in developing and operating a database system appropriate for the knowledge management and learning requirements of the mining industry and science

In this paper, the authors suggest a methodology for a knowledge-based ontology design suitable to represent the managerial, scientific, and practical content of mining knowledge. The designed ontology allows the functional representation of the knowledge domains, codification, and subdomains. Beyond, the ontology provides a substantial basis for developing a Knowledge Base (KB) that satisfies users' broader needs for knowledge searching and acquisition in mining and post-mining frameworks and initiations.

The suggested ontology is based on semantic network principles and applied in a case study adjusted to a mining reclamation project. The ontology reflects a top-bottom hierarchy and its constituent elements, which are the nodes and the hierarchical levels of the ontological structure reflected in the form of dendritic graph analysis. The ontological levels can be analyzed in more detail to constitute a multidisciplinary KB operating under the principles and requirements of relational database management systems (DBMS) (Gehani, 2006). The analysis, design, and implementation of the KB/DBMS system can be performed following the provisions of the ANSI/SPARC (1975) standard, which is usually applied in the design of database systems architecture models.

The key issues of the methodology adopted in the investigation and outlining of the conceptual model of a mining KB

ontology are the following:

1. The KB is investigated as a system analysis case study adjustable to the needs of long-term reclamation projects, where the post-mining land use model for reuse/recycle/reduction of materials and energy is repurposed and realigned according to the principles and practices of circular economy and sustainable development.
2. The nodes of the semantic ontology and the links among them are organized and classified into two levels:
   (a) An """"*Is_Kind-OF*""""" taxonomy, showing how the mining domain knowledge areas can be identified and accessed as the fundamental parts of the KB. Six (6) knowledge areas were identified: Project Management, Science & Engineering, Reclamation Technologies, Circular Economy Practices, Intra-disciplinary Database, and Inter-disciplinary Knowledge;
   (b) An """"*Is_Part-OF*""""" partonomy, showing the knowledge modules (parts) that each taxonomic level is consisted of.
3. The operational model of the KB/DBMS reflects the philosophy of the ontological structure of the main domains of knowledge, how this structure fits the DBMS processes and the feedback mechanisms for new knowledge entries, the searching for, and/or retrieving of, knowledge stored in the KB;
4. The techno-economic effects of the KB development are investigated. The KB requires time, budget, human resources, and organizational effort so that its applicability and performance are at an acceptable level of balancing costs and benefits for the mining company. For example, excess, over-demanding, costly, or high complexity database design might be helpful for specific needs as the granularity of the stored/used/reused/improved knowledge enables so. However, this might be far from being a cost-effective and quick performance solution(s) for a mining company that invests in the benefits of business knowledge management. For this reason, a substantial techno-economic evaluation of KB development alternative scenarios is required.

Figure 1 shows the scheme of the semantic ontology proposed in the paper. The ontology is suggested as an easy and low-cost technique enabling the conceptual analysis and design of a DBMS system to support: (a) the introduction of mining companies to knowledge management practices and (b) the execution of post-mining projects planned for the transition of post-mining sites to sustainability. Furthermore, the ontology is an instrument for the development of a mining KB allowing real-time access, storage, and improvement of primary knowledge, tacit and/or explicit, collected during the various mining and post-mining phases, in the way of constituting this knowledge, an asset with beneficial returns to the mining company, in the long-run.

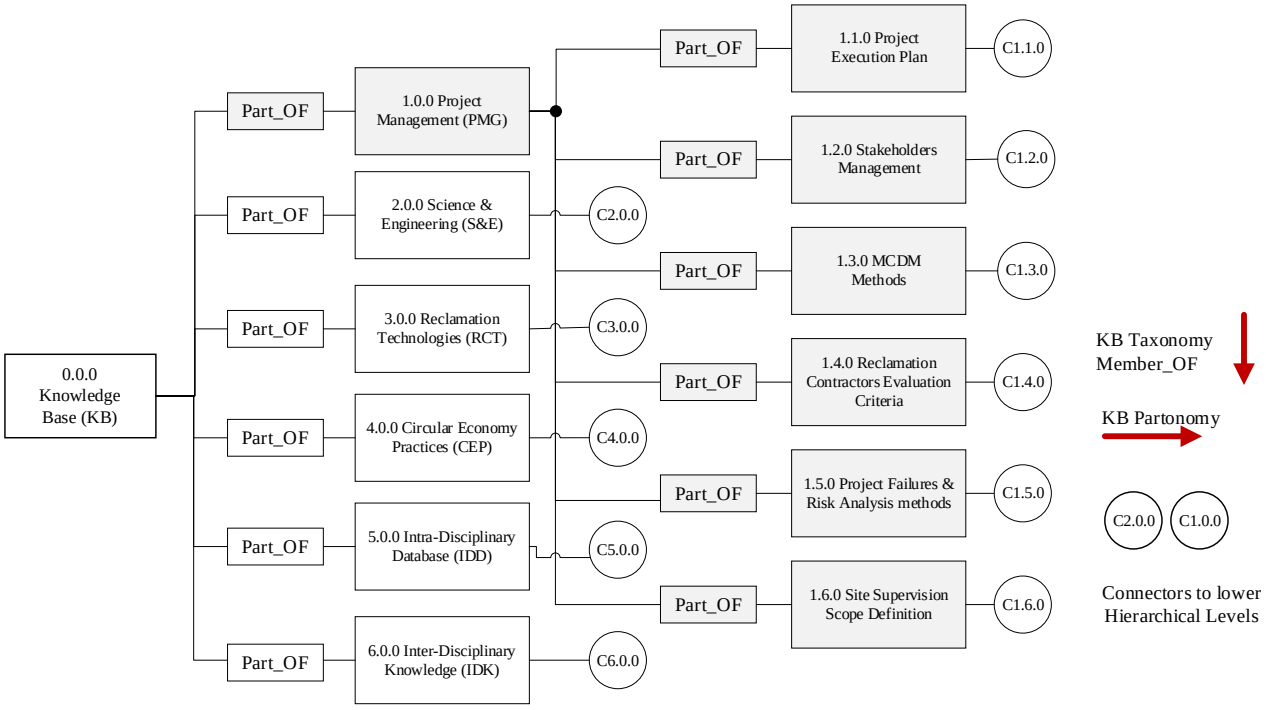

Figure-1: A Semantic Network Ontology for the development of a KB useful in Mining Reclamation Projects.

References

Nonaka, I., Takeuchi, H. 1995. The Knowledge-Creating Company: How Japanese Companies Create the Dynamics of Innovation, Oxford University Press

Pavloudakis F., Roumpos C., Karlopoulos E., Koukouzas N. 2020. Sustainable Rehabilitation of Surface Coal Mining Areas: The Case of Greek Lignite Mines. Energies. 13(15):3995. https://doi.org/10.3390/en13153995

Gehani, N. 2006. The Database Book: Principles and Practice using MySQL, 2006, 1st ed., Summit, NJ, Silicon Press

ANSI/SPARC 1975. Data Base Management System (DBMS) Model. North-Holland Pub. Co.

16th International Congress of the Geological Society of Greece

17-19 October, 2022 - Patras, Greece

Bulletin of the Geological Society of Greece, Sp. Publ. 10

Ext. Abs. GSG2022-392

Territories of multiple UNESCO designations management-Cases from China and Europe

J. Wang[1,] N, Zouros[1,2]

(1) Geography Department, University of the Aegean, Mytilene, Lesvos Island, Greece, geod18008@geo.aegean.gr (2) Natural History Museum of the Lesvos Petrified Forest, Sigri, Lesvos Island, Greece.

Earth heritage protection, conservation and management seem to attract public attention during the last decades after the establishment of Geoparks. UNESCO Global Geoparks established in 2015, is the third site designation of UNESCO after World Heritage Sites and Biosphere Reserves. Man and Biosphere Programme launched in 1971 and World Heritage Programme created in 1972, included also significant Earth heritage sites but without specific requirements regarding their conservation and management. The Man and Biosphere Programme focuses on natural resources and mainly biological diversity conservation and the World Heritage Programme concentrates on cultural sites protection and management. Consequently, the establishment of the Global Geoparks initially in 2004 and their recognition as UNESCO designation in 2015 provides the framework for the conservation and management of the abiotic nature sites.

A territory hosting geological heritage sites of international significance may also host precious biological resources, and valuable cultural relics. Thus such a territory may host multiple UNESCO designations. Due to different concepts of the Man and Biosphere Programme, World Heritage Programme and UNESCO Global Geopark, various management strategies are implemented with different tasks and focus. Sometimes the implementation of different management schemes within the same territory might cause conflicts and problems. Consequently, an integrated and effective management of areas with multiple designations in necessary.

This paper focus on multiple UNESCO designations management in UNESECO Global Geoparks in China and Europe. Huangshan UNESCO Global Geopark in China and Adamello Brenta UNESCO Global Geopark in Europe are a few cases with recognitions of World Heritage Site, Man and Biosphere Reserve as well as UNESCO Global Geopark. Hence, through presenting the co-management activities and approaches on multiple designations in these two territories, positive results of biotic and abiotic conservation as well as local development are given. The cases intend to set examples for other territories with multiple UNESCO designations to conduct co-management.

Key words: World Heritage Site; Man and Biosphere; UNESCO Global Geopark; multiple designation management

16th International Congress of the Geological Society of Greece

17-19 October, 2022 - Patras, Greece

Bulletin of the Geological Society of Greece, Sp. Publ. 10

Ext. Abs. GSG2022-397

Active Faulting In Northwest Lesvos And Earthquake Hazard Awarness Raising Activities In Lesvos Island UNESCO Global Geopark

A. Lamprakopoulos[1], N. Zouros[1]

(1) Department of Geography, University of Aegean, Greece, lamprakopoulosa@gmail.com

Background

Lesvos island, located on the Northeast Aegean region, Greece, is characterized by active tectonics associated with the evolution and deformation of the broader North East Aegean Sea. Lesvos island is recognized as a UNESCO Global Geopark and the study of active faults contributes to the development of educational activities to raise public awareness and sensitivity on seismic hazard.

The broader North East Aegean area is characterized by complex tectonics controlled by interplay of moving plates in the broader area. The area is affected by the dextral strike-slip movement of the North Anatolian fault, which ends in the Aegean basin and creates significant tectonic structures such as the North Aegean trough and the Skyros trough. The area is also affected by E-W trending normal faults

Intense volcanic activity appeared on Lesvos Island during Lower Miocene (23.5 to 16 million years ago) and the volcanic rocks are covering the 2/3 of the island's surface. The Northern part of Lesvos is covered exclusively by volcanic rocks and also there located one of the biggest volcanic centers of Lesvos, the Lepetymnos volcano.

Objectives

The study on active faults in the Northwest part of Lesvos Island gave us the opportunity to identify active tectonic structures in a broad area. The faults in the study area are variable in strike and character. Their activity level is determined based on their geological, geometrical and geomorphologic characteristics.

Results and Conclusions

In the study area found major normal and strike-slip faults. The main fault zones are linked with the presence of hydrothermal fluids and minerals in the broader area.

The results from the tectonic study are used for the educational activity "Understanding Earthquakes: natural processes and hazards on planet Earth" of the Natural History Museum of the Lesvos Petrified Forest. aiming to increase their understanding and familiarize students and citizens living on Lesvos with earthquakes, active faults and seismic hazard.

Keywords: Lesvos UNESCO Global Geopark, tectonics, fault mapping, seismic hazard, fault kinematics

References

Chatzipetros, A., Kiratzi, A., Sboras, S., Zouros, N., & Pavlides, S., 2013. Active faulting in the north-eastern Aegean Sea Islands. Tectonophysics, 597, p.106-122.

Pavlides, S., Tsapanos, T., Zouros, N., Sboras, S., Koravos, G., & Chatzipetros, A. (2009). Using active fault data for assessing seismic hazard: a case study from NE Aegean sea, Greece. In Earthquake Geotechnical Engineering Satellite Conference XVIIth International Conference on Soil Mechanics & Geotechnical Engineering 2e3 (Vol. 10, p. 2009).

Zouros, N., Pavlides, S., Soulakellis, N., Chatzipetros, A., Vasileiadou, K., Valiakos, I., & Mpentana, K. (2011). Using active fault studies for raising public awareness and sensitisation on seismic hazard: a case study from Lesvos Petrified Forest Geopark, NE Aegean Sea, Greece. Geoheritage, 3(4), p. 317-327.

16th International Congress of the Geological Society of Greece
17-19 October, 2022 - Patras, Greece
Bulletin of the Geological Society of Greece, Sp. Publ. 10
Ext. Abs. GSG2022-409

Applications of photogrammetry in geosciences: a proposed methodology for educational purposes and a virtual geological museum

V. Giamas[1], M. Giannopoulos[2], L. Kalantzi[1], P. Giannakopoulou[1], A. Rogkala[1], M. Kalpogiannaki[3], P. Petrounias[1]

(1) University of Patras (UoP), Department of Geology, Section of Earth Materials, Patras, Greece, vgiamas@upnet.gr (2) University of Gothenburg (GU), Department of Earth Sciences, Gothenburg, Sweden (3) National and Kapodistrian University of Athens, Department of Geology and Geoenvironment, Athens, Greece.

Introduction

The use of three-dimensional computer graphics and visualization techniques is becoming more and more popular because these techniques visualize more realistic object models than graphic-based object models. Thus, 3D models are nowadays used in an expanded variety of fields including archaeology, architecture, cultural heritage, engineering, manufacturing, medical industry, quality control, topographic mapping, and geology. In the last decades, the earth science community has started to construct 3D geological models typically applied to remote sensing and evaluating geoengineering properties of rock slopes and shaft tunnels of pits and mine sites as well as for mapping and deposit enclosure based upon borehole data. Although, 3D geological models across different fields of megascopic scale (Klawitter et al., 2017; Kyriou et al., 2021; Nikolakopoulos et al., 2022; Priddy et al., 2019; Schultz-Fellenz et al., 2020), there are only a few studies upon the mesoscopic scale (e.g., Yakar et al., 2011; Yilmaz et al., 2008). In this study, close-range photogrammetry is demonstrated upon a hand-sized rock sample.

Methodology

The equipment used for the photogrammetry-based 3D models includes a 24 mega-pixel digital single-lens reflex (DSLR) Nikon D5200 camera coupled with a Nikkor 35mm f/1.8G AF-S DX fixed lens. The camera was mounted on a Sony VCT-D680RM tripod in order to avoid any camera shake in hand-held photos. To further reduce micromovements and blurriness, along with the tripod, a Nikon MC-DC2 remote shutter cord was used. Camera settings for all samples considered include f/5.6 aperture stop, shutter speed of 1/125s, and 200 ISO. Photographs were acquired in a darkened room with a custom setup of three individual lights, all using identical Osram LED E27 lamp (8.5 W, 806 lm) with cool white temperature (4,000 K). Photogrammetry reconstructed 3D models require a set of photographs taken from various angles, which must cover the entire sample with significant overlap between the image sequence to digitally be reassembled into a single object. Therefore, the samples were sticked by the use of reusable adhesive on a turntable that was placed on a steady working bench. Shots were taken from three different vertical angles (approximately 0°, 20°, and 45°) at regular intervals of approximately 20°. To reconstruct the 3D models, the obtained images (~50) of each sample were imported to 3DF Zephyr Free (v. 6.006) photogrammetry software solution. The 3DF Zephyr Free software run on a 64-bit computer with Windows 10 Pro operating system, equipped with a 3.10 GHz AMD Ryzen 3 1200 Quad-core processor, 8 GB of installed RAM, and an NVIDIA GeForce GT 1030 graphics card.

After launching the 3DF Zephyr Free (v. 6.006) photogrammetry software, a new project was created and the relevant photographs were imported; ~50 photos or less for the rock sample since the free version has 50 photos limit, by drag 'n' drop the files into the window of the Project Wizard. Photographs were automatically calibrated based upon the used camera and lens setup. The specific algorithm for automatic silhouette computation of the external 3DF Masquerade tool was used for masking the initial photographs. Masks were created for both foreground elements and background elements corresponding to the rock sample and their background, respectively. After masking a few photographs, computation of foreground/background elements is automatically performed upon the remaining photographs from the sequence. It should be noted that several construction paper (i.e., white, black, red, green) were tested and used to come across with a very high contrasty background. The computed masks were automatically loaded by 3DF Zephyr Free since the relevant bim files were saved in the same directory and the Mask Images button was already checked in the project wizard. The next step for generating the 3D reconstruction can be described by the following four phases. To set up the first phase that will generate a sparse point cloud through Camera orientation settings, settings were set to advance mode selecting the highest possible settings for both matching options and reconstruction options. Similarly, settings were set to advance mode selecting the highest possible settings were used for all the other phases, including the second phase of dense point cloud, the third phase of mesh generation and the fourth phase of the texture generation of the 3D reconstruction. Following these steps, reconstruction process can start after pressing the run button in the project wizard. The computed 3D rock models can be exported through the Export Texture Mesh button in the top tool bar either as a standalone file or to other services (e.g., upload to Sketchfab).

Results

The rock model was initially exported as obj file format, and it is presented below through representative orthoslices

(Figure 1). A video of the model was also created and is freely available on Vimeo (Figure 2a), whereas the model itself is available in Sketchfab (Figure 2b). Furthermore, a short video of photomicrographs obtained using thin sections prepared from the samples, under a petrographic microscope employing both plane polarized light and crossed polar is available in Giphy (Figure 2c).

Figure 1: Orthoslices of the reconstructed 3D model.

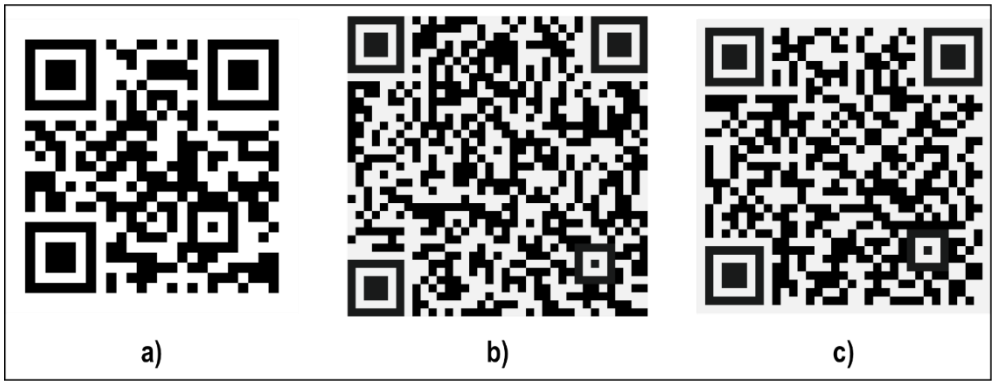

Figure 2: QR codes of a) the 3D video model, b) the 3D model, and c) photomicrographs of petrographic microscope.

Conclusions

This is an early attempt to construct rock models for precise three-dimensional macroscopic petrographic examination as well as to evaluate the applicability of close-range photogrammetry and its potential educational benefits. The sample's model was constructed by applying a scientific method in contemporary techniques that do not require expert equipment and can be achieved with low exertion since it mostly relies upon a photo acquisition custom and a photogrammetric system. This method is of low cost, whereas any tools can be transported effortlessly due to their relatively small size. It is an easily utilized and approachable way for non-experts (only basic knowledge of photography is a prerequisite) to make the most out of new technology that will guarantee the construction of a 3D model and will bridge the community with natural sciences. It could also be applied to other hand-sized specimens (e.g., fossils). Positive outcomes would be very beneficial and could possibly lead to the development of an avant-garde virtual geological museum, that every Geological and Earth Sciences Department should have nowadays, promoting geology to non-specialist and youth in a modern and more attractive way by utilizing tech-friendly applications.

References

Klawitter, M., Pistellato, D., Webster, A., & Esterle, J. (2017). Application of photogrammetry for mapping of solution collapse breccia pipes on the Colorado Plateau, USA. Photogrammetric Record, 32(160), 443–458. https://doi.org/10.1111/phor.12219

Kyriou, A., Nikolakopoulos, K., Koukouvelas, I., Lampropoulou, P. (2021). Repeated UAV Campaigns, GNSS Measurements, GIS, and Petrographic Analyses for Landslide Mapping and Monitoring. *Minerals*, *11*, 300. https://doi.org/10.3390/min11030300

Nikolakopoulos, K.G., Kyriou, A., Koukouvelas, I.K. (2022). Developing a Guideline of Unmanned Aerial Vehicle's Acquisition Geometry for Landslide Mapping and Monitoring. Appl. Sci., 12, 4598. https://doi.org/ 10.3390/app12094598

Priddy, C. L., Pringle, J. K., Clarke, S. M., & Pettigrew, R. P. (2019). Application of photogrammetry to generate quantitative geobody data in ephemeral fluvial systems. Photogrammetric Record, 34(168), 428–444. https://doi.org/10.1111/phor.12299

Schultz-Fellenz, E. S., Swanson, E. M., Sussman, A. J., Coppersmith, R. T., Kelley, R. E., Miller, E. D., Crawford, B., Lavadie-Bulnes, A., Cooley, J., Vigil, S., Townsend, M., Larotonda, J. M. (2020). High-resolution surface topographic change analyses to characterize a series of underground explosions. Remote Sensing of Environment, 246. https://doi.org/10.1016/j.rse.2020.111871

Yakar, M. (2011). Using close range photogrammetry to measure the position of inaccessible geological features. Experimental Techniques, 35(1), 54–59. https://doi.org/10.1111/j.1747-1567.2009.00583.x

Yilmaz, M. H., Yakar, M., & Yildiz, F. (2008). Digital Photogrammetry in Obtaining of 3D Model Data of Irregular Small Objects. The International Archives of the Phototgrammetry, REmote Sensing and Spatial Information Science., 37, 125–130.

16th International Congress of the Geological Society of Greece
17-19 October, 2022 - Patras, Greece
Bulletin of the Geological Society of Greece, Sp. Publ. 10
Ext. Abs. GSG2022-429

Earth Raw materials and the development of environmental awareness through the Science and Technology Museum (STM), University of Patras, Greece.

P. Theologi-Gouti[1], M. Kokkaliari[2], I. Iliopoulos[1,2]

(1) Science and Technology Museum, University of Patras, Patras, Greece, stmuseum@upatras.gr (2) Department of Geology, University of Patras, Patras, Greece.

Introduction

A Museum, according to ICOM's newly adopted Museum Definition, "*is a not-for-profit, permanent institution in the service of society that researches, collects, conserves, interprets and exhibits tangible and intangible heritage. Open to the public, accessible and inclusive, museums foster diversity and sustainability. They operate and communicate ethically, professionally and with the participation of communities, offering varied experiences for education, enjoyment, reflection and knowledge sharing*" (ICOM 2022). Tangible and intangible heritage is a complex set of natural, biological, social, cultural and political conditions that surround a human being, or an organism, and ultimately determine the form as well as the nature of its survival (UNESCO, 2002). Museums are perfectly positioned to address and enhance sustainability as they are able to work with communities to raise public awareness, support research and knowledge creation to contribute to the well-being of the planet and societies for future generations (ICOM 2022).

Realizing that Museums have an important role in addressing contemporary social issues mainly as they have been created to increase cultural awareness and education, the Science and Technology Museum responded immediately (OECD 2021). Since 2011, to years after the opening to the public, STM has organized a number of temporary exhibitions dealing with sustainability with educational programmes for group of students of all cognitive levels and special events for other members of society. The first attempt to deal with this issue in a more permanent way was made through the "Pedagogical Competence Programme" (PCP), where four-year students from the Department of Geology, at the University of Patras took part to gain pedagogical experience, through communicating various aspects of geology to students at all levels. "Geology in everyday Life" was the first educational program for high school students developed, mainly focusing on geology in human life, house construction, as well as technology and environment (Theologi-Gouti et al., 2021).

The outcome was exceptionally successful since not only school students got familiarized with the science of geology through every-day facts and examples, but also the four-year students of Geology developed personal skills and created new ways to describe informally and, even more importantly, pleasantly, various geological aspects. The programme's success encouraged the Museum to proceed with the planning of three other educational programmes for students of different cognitive levels. Thus, the museum designed and implements an educational programme for students of junior high school "Geology in our lives", an educational programme for students of 5th and 6th grade of primary school, "Littles detectives and the discovery of earth raw materials in our lives" and finally, an educational programme for students of 3rd and 4th grade of primary school "Discovering the Rawmatcity together with the Rawmat family" (Fig. 1).

Our new educational programmes are linking earth raw materials with environmental awareness. The modern way of life and the continuous growth of population, contribute to the increase of the demand for raw materials, ending in the insatiable consumption of goods and consequently their reckless use. The continuous interventions of humans in the environment to meet their needs, leads to accumulated side effects with the creation of environmental problems (increase in temperature, pollution of aquifers, presence of toxic waste, etc.).

Communicating environmental awareness through STM

Museums provide opportunities for the appreciation and understanding of natural and cultural heritage (ICOM 2017). Through the collaboration of the Department of Geology with the Science and Technology Museum (STM) of the University of Patras, educational programmes that were created aim at students of different educational levels, to get to know the science of geology, and the necessity of raw materials in our daily lives. The common denominator of all these educational programmes is the development of environmental awareness that is achieved especially through younger generations and triggering respect for the environment and its

protection.

Students participating in the Pedagogical competence programme every trimester since the academic year 2019-2020, were separated into groups, elaborating on specific thematic units related to the project, thus creating ~~an~~ educational material in the form of educational presentations, stories and fun games. The main thematic units addressed to the implementation of this program are related to the acquaintance of mineral raw materials, its usefulness in daily applications, the arise of environmental awareness, and the unpleasant environmental implications resulted from the unceasing use of minerals and earth raw materials. The supervisors evaluated the material they gathered from each group, in order to suggest improvements. The result was to create educational programmes with maximum duration of one and a half hours, including pleasant presentations, puzzles, as well as role-playing games.

After being tested, educational programmes have been implemented to school groups at the academic year 2021-2022 with great success. Their design is based on experiential, interdisciplinary and playful methods and involves school students' creativity, while developing their imagination and critical thinking. Students as museum animators through play, discovering, discussing, presentations, stories and the use of senses, help school students to enhance their critical thinking and understand the value of raw materials in our lives as well as the importance of their sustainability.

Figure 1 Screenshots of some of the interactive stories implemented during the educational programs designed.

Conclusions

Taking on its role in promoting environmental awareness and becoming a mediator between the UP Department of Geology to society, STM has developed innovative educational programmes, through including interactive games, puzzles, art activities, experiments, and entertaining short stories on the theme. Four-year students from the Department of Geology, University of Patras, contributed decisively to the completion planning and implementation of the programmes, hence developing their personal skills.

Through that strong collaboration of Geology and STM, both the society and the university gain multiplied benefits. Both the audience, and the four-year students were benefited from these programmes, by familiarizing with the science of geology and developing environmental awareness, which can be taught, and cultivated by implementing creative and entertaining educational programmes with participatory design.

The development of environmental awareness is a major issue in modern society, where human demands are constantly increasing. Younger students were educated on the necessity of both raw materials and respect for the environment, within a pleasant and creative environment.

References

UNESCO, 2002. Cultural Diversity: Common Heritage, Plural Identities. Paris: UNESCO.

ICOM 2017, ICOM Code of Ethics, Paris: ICOM

ICOM 2022 https://icom.museum/en/research/sustainability-and-local-development/, accessed 25.8.2022

OECD/ICOM 2019, Culture and Local Development: Maximising the ImpactA GUIDE FOR LOCAL GOVERNMENTS, COMMUNITIES AND MUSEUMS, Paris 2019

Theologi-Gouti, P., Iliopoulos, I., Kokkaliari, M., 2021. "Geology in Everyday Life": Designing Museum Educational Programmes (EP) with Students of Geology in the Science and Technology Museum (STM) of the University of Patras, Greece. Material Proceedings, 5, 101. https://doi.org/10.3390/materproc2021005101

16th INTERNATIONAL CONGRESS of the
GEOLOGICAL SOCIETY OF GREECE

S1. Evolving techniques in the study of sediments

OUR EARTH, OUR HOME

16th International Congress of the Geological Society of Greece
17-19 October, 2022 - Patras, Greece
Bulletin of the Geological Society of Greece, Sp. Publ. 10
Ext. Abs. GSG2022-033

Reassessing depositional conditions of the Pre-Apulian zone based on synsedimentary deformation structures during upper Paleocene to lower Miocene carbonate sedimentation, from Paxoi and Anti-Paxoi islands, northwestern end of Greece

N. Bourli[1], G. Iliopoulos[2] , A. Zelilidis[1]

(1) Laboratory of Sedimentology, Department of Geology, University of Patras, 26504 Patras, Greece, n_bourli@upnet.gr. (2) Laboratory of Paleontology and Stratigraphy, Department of Geology, University of Patras, 26504 Patras, Greece.

The studied area is situated at the northwestern Greece and corresponds to the northern end of the Pre-Apulian Zone. Pre-Apulian zone represents the margins of the Apulian Platform to the Ionian Basin and was formed during the Mesozoic to Cenozoic Eras. The proposed model is based on fieldwork, measured deformation structures and age determination. Soft sediment deformation structures (SSDS) are widespread within the upper Paleocene to lower Miocene limestones/marly limestones. These deposits are exposed in both Paxoi and Anti-Paxoi Islands, across sections of 2-3km long and up to 60m high. Soft sediment deformation structures, with a vertical thickness up to 10m, are synsedimentary or were formed just after deposition, and are cross-cut by normal faults, indicating their development during the rift stage (e.g. Fig.1).

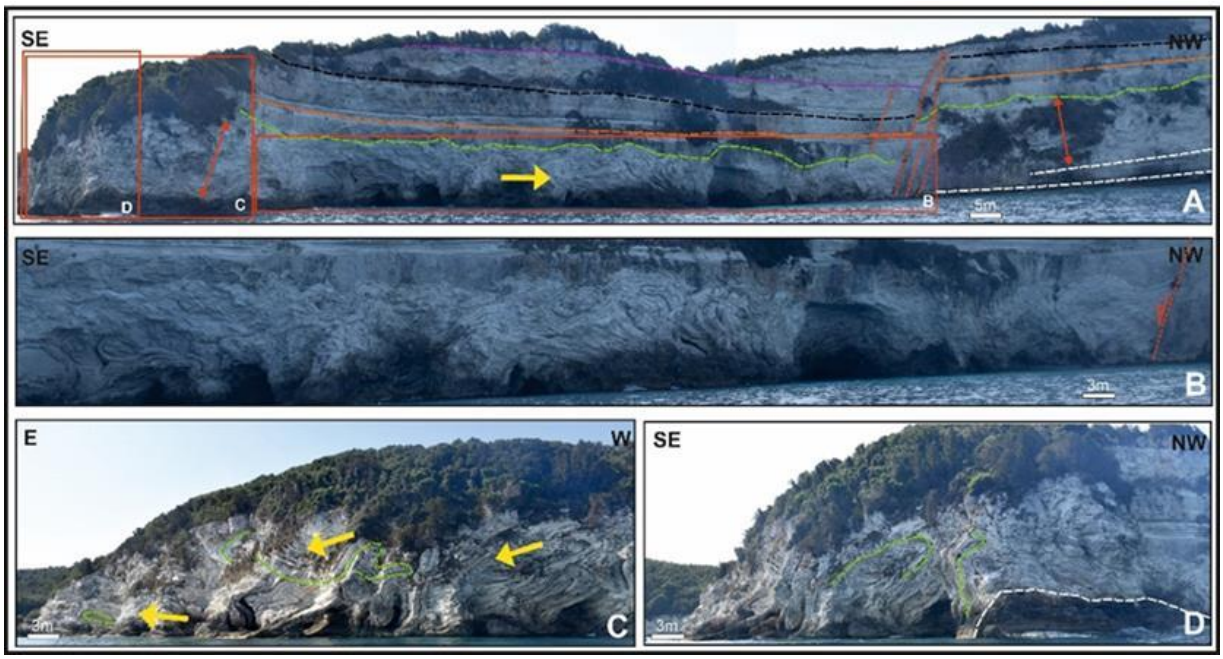

Figure 1. Strong deformation structures with an eastward progradation towards the subsiding hangingwalls, (a) shows the development of SSD structures after normal fault activity; (b) From a closer distance the SSD horizon with an up to 10m thick SSD deformation structure; (c-d) show several deformation structures within the deformed horizon.

At least five different soft sediment deformation structures horizons have been identified and exhibit an eastward or a westward progradation direction. They are classified into four different types of deformations: 1) Thick synclines and anticlines, formed because of strong synsedimentary deformation. 2) Strong and thick, soft sediment deformation structures, with erosional contacts both with the underlying and the overlying un-deformed horizons. 3) Thin slumps that display sharp contacts with the underlying undeformed horizons and erosional contacts with the overlying undeformed horizons. 4) Thin slump horizons than evolve laterally into undeformed deposits in the same horizon. Studied soft sediment deformation structures and their age of development suggest active margins between the Apulian platform and the Ionian Basin, that influenced by normal fault activity. Faults were active since the Ionian basin changed gradually to a foreland basin, after the tectonic inversion, from extension to compression, during the early to middle Eocene. The onset of compressional tectonics is post lower Miocene, and after the development of the soft sediment deformation structures (Fig. 2).

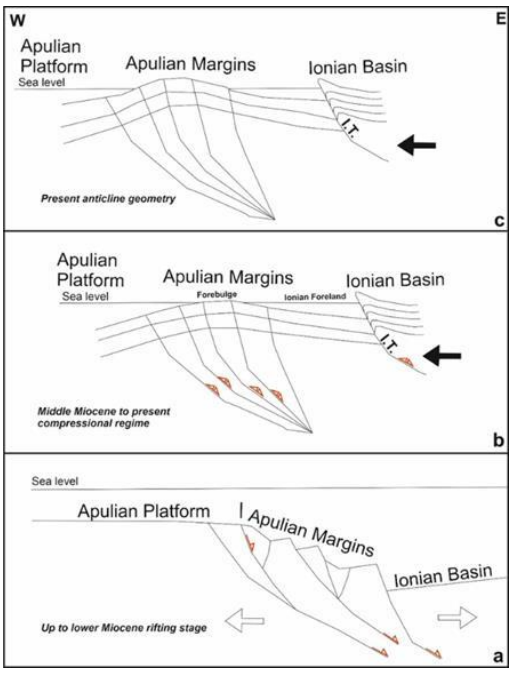

Figure 2. Evolutionary stages of development of the studied region. (a) represents the rifting stage, whereas; (b) shows the change of the extensional regime to compressional with the reactivation of normal faults as reverse faults (inverted tectonic) and the gradual change of the studied area from the Apulian Platform margins to the forebulge area of the Ionian foreland. Stage (c) represents the present morphology of the studied area where the islands Paxoi and Anti-Paxoi formed an open anticline geometry due to the Ionian Thrust movement.

The confinement of the lower Miocene deposits, both northwards and southwards (in Anti-Paxoi Island), indicates the presence of active transfer faults, with flower structure geometry, that were formed during sedimentation, producing highs and troughs (Fig. 3). The present open anticline geometry of Paxoi Island indicates that the Island represents the forebulge area of the middle Miocene Ionian Foreland due to the Ionian Thrust activity.

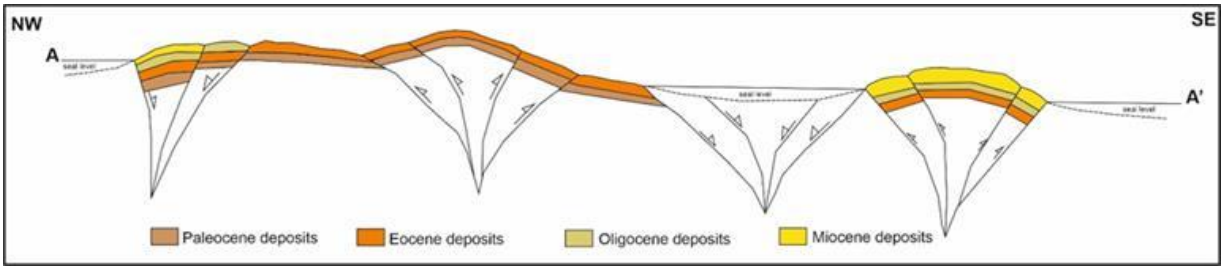

Figure 3. A cross-section along the two studied islands showing giant transfer fault zones producing negative flower structures (the reason of the separation of two islands) and a positive flower structure (the reason of the anticline-like geometry of the Paxoi Island).

Keywords: Soft-Sediment Deformation Structures, Apulian Platform Margins, Ionian Basin, Pre-Apulian Zone.

Acknowledgements

Nicolina Bourli is a Post-Doc Researcher and she was financially supported by the "Hellenic Hydrocarbon Resources Management S.A. (HHRM S.A.)". Authors would like to thank reviewers for their improvements on the manuscript.

References

Bourli, N., Iliopoulos, G., Zelilidis, A., 2022. Reassessing Depositional Conditions of the Pre-Apulian Zone Based on Synsedimentary Deformation Structures during Upper Paleocene to Lower Miocene Carbonate Sedimentation, From Paxoi and Anti-Paxoi islands, Northwestern end of Greece. Minerals 12, 201.

Bourli, N., Maravelis, A.G., Zelilidis, A., 2020. Classification of soft-sediment deformation in carbonates based on the Lower Cretaceous Vigla Formation, Kastos, Greece. International Journal of Earth Sciences 109, 2599–2614.

Zelilidis, A., Bourli, N., Zoumpouli, E., Maravelis, A., 2021. Tectonic inversion and deformation differences in the transition from Ionian basin to Apulian platform: The example from Ionian Islands, Greece. Arabian Journal of Geosciences Conference (CAJG), Sousse, Tunisia.

16th International Congress of the Geological Society of Greece
17-19 October, 2022 - Patras, Greece
Bulletin of the Geological Society of Greece, Sp. Publ. 10
Ext. Abs. GSG2022- 037

Unravelling the origin of the Messinian evaporites in Zakynthos Island, Ionian Sea: Implications for the sealing capacity in the Mediterranean Sea

A. Zelilidis[1], N. Bourli[1], K. Andriopoulos[1], E. Georgoulas[1], S. Peridis[1], D. Asimakopoulos[1], A.G. Maravelis[2]

(1) Laboratory of Sedimentology, Department of Geology, University of Patras, 26504 Patras, Greece, a.zelilidis@upatras.gr (2) Department of Geology, Aristotle University of Thessaloniki, 54124 Thessaloníki, Greece.

Zakynthos Island is located in the Pre-Apulian and Ionian zones and was influenced by the major orogenic processes that are related to the Hellenides FTB. The principal tectonic features are the Ionian and the Kalamaki Thrusts (Fig. 1). The Pre-Apulian zone lies to the east of the Apulian platform and to the west of the Ionian zone and corresponds to an edge - slope facies belt that is largely covered by the Ionian Thrust. Two sections along the south coast of Zakynthos Island (Ag. Sostis to the west and Kalamaki to the east) were selected for examining the depositional conditions of the Messinian evaporites.

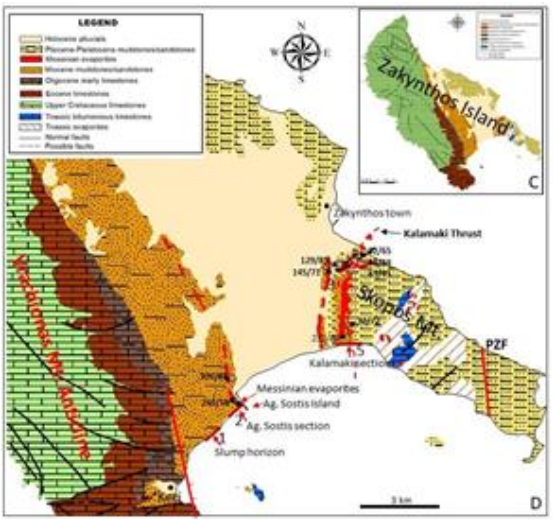

Figure 1. Geological map of western Greece with the characteristic Ionian thrust and Ionian foreland respectively.

Both sections exhibit similar sedimentological and stratigraphic features and are represented by basal lower Miocene siliciclastic shelf deposits that are overlain by Messinian evaporites. These salt deposits are then capped by lower Pliocene (Zanclean) carbonates (Trubi formation) and are interbedded with marls (Fig. 2).

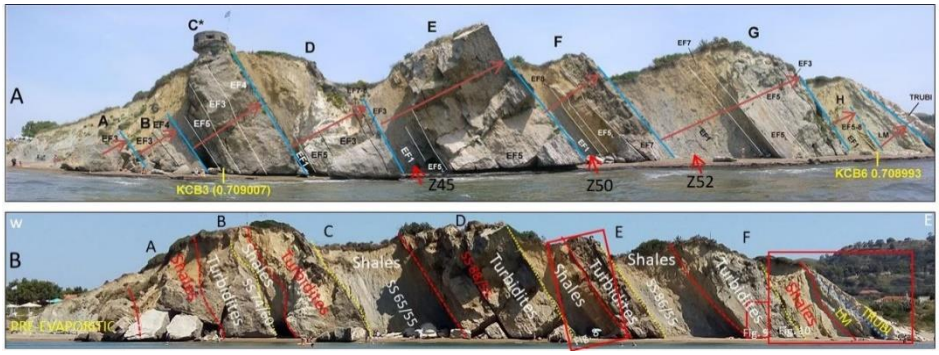

Figure 2. The Kalamaki section into two interpretations, the first (A) is according to Karakitsios et al. (2017).

The new evidence can lead to a new approach about the paleogeographic evolution of Zakynthos Island during late Miocene - Messinian to early Pliocene time: The pre-evaporitic succession (upper Miocene shelf deposits) belongs to the western end of the Pindos foreland basin and have gentle slopes (Figs. 3,4).Vrachionas anticline formed because of the Ionian Thrust activity and represent the wedge top of the Ionian thrust that took place/activated during the middle Miocene. The new Ionian Foreland is situated to the west of Zakynthos Island (in the Ionian Sea, Figs. 3,4). New results

showed that the Pre-Apulian zone represents the Apulian Platform Margins, influenced by normal faults, during the rift stage that inverted to thrust faults, during the compressional regime.

The Ionian thrust and the Kalamaki Thrust commenced just prior the Mediterranean inundation. The uplifted area between the two thrust faults exposed the pre-existing Messinian evaporites that were eroded. It is very important to understand the timing of fault activity, in regions adjacent to the Messinian evaporites, in order to understand their behaviour. The Ionian Thrust is critical in hydrocarbon exploration in the Ionian and Adriatic Seas because many exploration targets are active, and companies would like to know if there is and how it is the thickness of the in situ Messinian evaporites internally to the Ionian foreland.

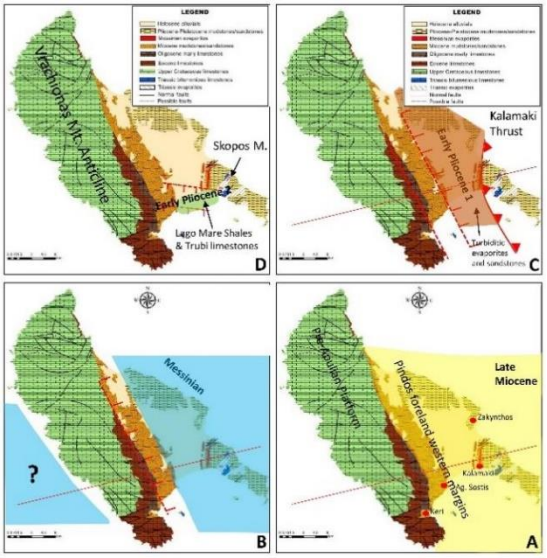

Figure 3. Paleogeographic maps showing in four stages the distribution of the sediments into the existing basins. 1. During Late Miocene, as the western part of the Pindos foreland, 2. During the Messinian, when the whole basin was desiccated, 3. During Early Pliocene, when the uplifted Messinian evaporites slide or eroded and resedimented into the Kalamaki Foreland,4. During Early Pliocene (stage 2) when the basin was restricted southwards and Lago Mare and Trubi limestones were deposited.

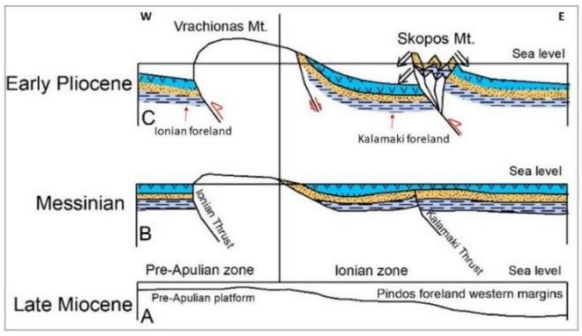

Figure 4. Cross sections showing in three stages the evolution of the area influenced from the two major thrust faults and the accompanied normal faults on their hangingwall blocks. Red line in figure 11 shows the position of cross-sections.

Keywords: Messinian evaporites, Turbiditic evaporites, Ionian Thrust, Ionian Foreland, Kalamaki Foreland.

Referens

Bourli, N., Iliopoulos, G., Zelilidis, A., 2022. Reassessing Depositional Conditions of the Pre-Apulian Zone Based on Synsedimentary Deformation Structures during Upper Paleocene to Lower Miocene Carbonate Sedimentation, From Paxoi and Anti-Paxoi islands, Northwestern end of Greece. Minerals 12, 201.

Karakitsios, V., Roveri, M., Lugli, S., Manzi V., Gennari, R., Antonarakou, A., Triantaphyllou, M., Agiadi, K., Kontakiotis, G., Kafousia, N., de Rafelis, M. 2017. A record of the Messinian salinity crisis in the eastern Ionian tectonically active domain (Greece,
eastern Mediterranean). Basin Research 29, 2, 203-233.

Zelilidis, A., Papatheodorou, G., Maravelis, A., Christodoulou, D., Tserolas, P., Fakiris, E., Dimas, X., Georgiou, N., Ferentinos, G., 2016. Interplay of thrust, back-thrust, strike-slip and salt tectonics in a Fold and Thrust Belt system: an example from Zakynthos Island, Greece. Intr.J.Earth Sciences 105, 2111-2132.

16th International Congress of the Geological Society of Greece
17-19 October, 2022 - Patras, Greece
Bulletin of the Geological Society of Greece, Sp. Publ. 10
Ext. Abs. GSG2022-047

The soft-sediment deformation structures and the siliceous concretions presence as indicators of the depositional processes

N. Dimopoulos[1], E. Zoumpouli[1], G. Iliopoulos[2], N. Bourli[1] and A. Zelilidis[1]

(1) Laboratory of Sedimentology, Department of Geology, University of Patras, 26504 Patras, Greece, nikos.dhmopoulos@gmail.com (2) Laboratory of Paleontology and Stratigraphy, Department of Geology, University of Patras, 26504 Patras, Greece.

Kefalonia Island is situated in western Greece and geologically corresponds to the Apulian Platform Margins (APM), with the Apulian platform lying to the west and the Ionian Basin to the east. The studied deposits, with a thickness up to 164.5, extend along the 650m long Agia Efimia bay, ranging from the middle Paleocene (Selandian) to the uppermost Eocene (Priabonian), during the latest part of the rift stage (Fig.1).

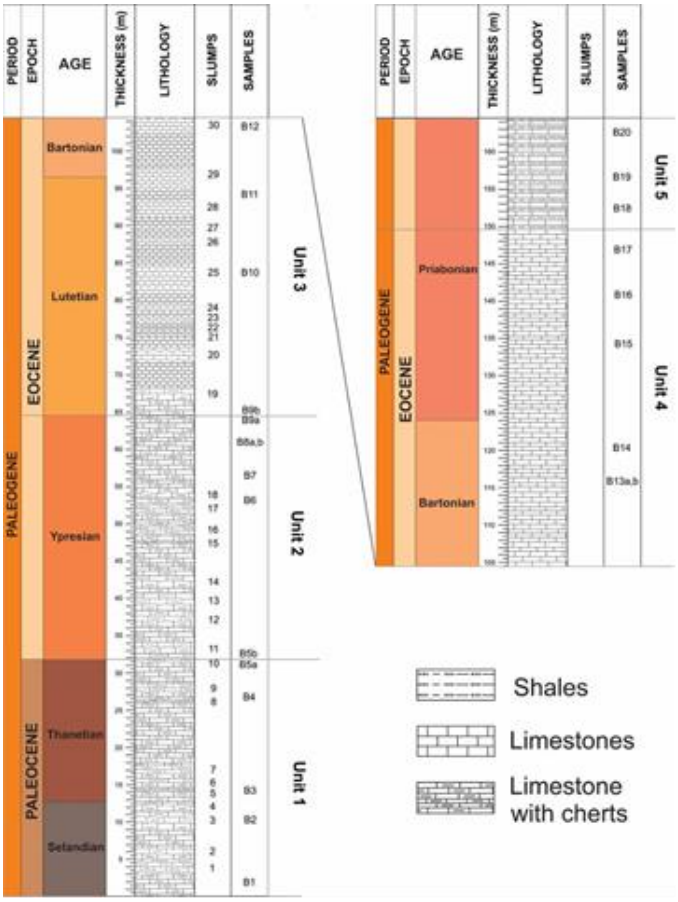

Figure 1. Detailed lithostratigraphic column of the Agia Efimia sequence with a detailed presentation of the SSDS

Fieldwork measurements of soft-sediment deformation structures (SSDS), paleocurrent directions, the size and abundance of siliceous concretions (SC) and siliceous beds (SB), and shale horizons, were correlated with the age of selected samples, and thus, the relation of the tectonic regime with the depositional conditions was presented (e.g., Fig.2).

Thirty (30) different horizons with SSDS were recognized within the lower three units of Paleocene age , whereas these are absent from the Eocene deposits, where only shale interbeds were recognized. The presence of many shale horizons in the upper unit with a late Eocene age (late Priabonian) could be related with the transportation of clastic material from the neighboring Apulian Platform.

Hosted carbonates of the SSDS showed the presence of SMF4 microfacies type that in relation with the SSDS supports the idea that extensional tectonism characterizes the APM, as far as the late Eocene (late Bartonian). Moreover, the hugesize of the SSDS structures indicates that they were produced due to an intense basin floor instability and fault activity during the extensional tectonism phase.

Figure 2. Four deformed horizons (20, 25, 26, 27) between undeformed ones. (a) Characteristic SSDS horizon (20) where the progradation of the deformation eastwards showed the transition from undeformed to deformed structures, within the same horizon, indicating the proximity with the starting point of the slumping. Red circle indicates a notebook as scale; (b) Thin to medium interbedded limestones with an SSDS horizon (25); (c) Two deformed horizons (26,27) between undeformed horizons. Red circle indicates a compass as scale.

The paleocurrent trends, measured from the SSDS, indicate a restricted basin, due to the synchronous activity of normal and transfer faults, whereas the lateral changes of the paleocurrents could be related with a shifting internally to the restricted basin.

The huge size and plenty SC in the two lower units were related with the availability of huge amounts of SiO2 transported through a dense stylolite network, during the middle to upper Paleocene (Selandian to Thanetian) and could be compared mineralogically with the neighboring SC in Sami area.

As SSDS represent an indicator of tectonic activity and instability of the basin floor, the size of the SSDS was used to identify the intensity of tectonic activity. The studied section, with a general NE-SW orientation, was subdivided into five (5) different units. The changes of these units in paleocurrent directions, the size, the abundance and the thickness of SSDS, SC and SB and the presence of shale horizons in the upper unit, characterize a gradual change of the depositional conditions in the APM, from the upper Paleocene (Selandian) to the Upper Eocene (Priabonian).

The factor that influenced the above-mentioned changes were the presence and the activity of normal faults that produced instability of the basin floor. Therefore, a reduction in tectonic activity from the Paleocene to the Eocene is suggested.

The lower three units with the SSDS that were formed during extensional faulting correspond to the syn -rift sequence, whereas the upper two units with no SSDS could be related to the post-rift sequence. The post rift sequence probably was developed after the pause of extensional faulting and sedimentation started after a period of non-deposition and/or erosion that was marked by a break-up unconformity, which removed part of the syn-rift sequence. This null area represents a long period characterized by erosion, reduced sedimentation rate, and no SSD structures.

Keywords: Soft-sediment deformation structures; siliceous concretions; Apulian Platform; Apulian Platform Margins

Acknowledgements

Nicolina Bourli is a Post-Doc Researcher, and she was financially supported by the “Hellenic Hydrocarbon Resources Management S.A. (HHRM S.A.)”. Authors would like to thank reviewers for their improvements on the manuscript.

References

Bourli, N., Iliopoulos, G., Zelilidis, A., 2022. Reassessing Depositional Conditions of the Pre-Apulian Zone Based on Synsedimentary Deformation Structures during Upper Paleocene to Lower Miocene Carbonate Sedimentation, From Paxoi and Anti-Paxoi islands, Northwestern end of Greece. Minerals 12, 201.

Bourli, N., Maravelis, A.G., Zelilidis, A., 2020. Classification of soft-sediment deformation in carbonates based on the Lower

Cretaceous Vigla Formation, Kastos, Greece. International Journal of Earth Sciences 109, 2599–2614.

Zelilidis, A., Bourli, N., Zoumpouli, E., Maravelis, A., 2021. Tectonic inversion and deformation differences in the transition from Ionian basin to Apulian platform: The example from Ionian Islands, Greece. Arabian Journal of Geosciences Conference (CAJG), Sousse, Tunisia.

16th International Congress of the Geological Society of Greece
17-19 October, 2022 - Patras, Greece
Bulletin of the Geological Society of Greece, Sp. Publ. 10
Ext. Abs. GSG2022-061

Microbial mat micro-stratification in hot springs environments and their biomineralization processes contributing to travertine deposition, at Aedipsos (Edipsos) area, Euboea (Evia) Island, Greece

Christos Kanellopoulos[1,3], Vasiliki Lamprinou[2], Artemis Politi[2], Panagiotis Voudouris[1], Ioannis Illiopoulos[3], Maria Kokkaliari[3], Leonidas Moforis[1], Athena Economou-Amilli[2]

(1) National and Kapodistrian University of Athens, Faculty of Geology and Geoenvironment, Panepistimioupolis, Ano Ilissia, 15784 Athens, Greece, ckanellopoulos@gmail.com, voudouris@geol.uoa.gr, leonidasmoforis@gmail.com (2) National and Kapodistrian University of Athens, Faculty of Biology, Department of Ecology and Systematic, Panepistimioupolis, Ano Ilissia, 15784 Athens, Greece (3) University of Patras, Department of Geology, Rio 26500, Greece.

Microbial mats are structures of microorganisms whose thickness is a few cm (Reitner & Thiel, 2011). Microbial mats are significant parts of earth ecosystems. They commonly occur in extreme environments such as hot springs, alkaline and hypersaline environments, and they are related to biomineralization processes, such as calcite, aragonite, iron-oxides. The study site is a vertical wall at Aedipsos, near the sea coast, a few meters above sea level. It is built by travertines blocks, where hot water flows through them (Fig. 1A). The water temperature was 55.8 oC, and the pH was 6.34.

Hot springs occur in Aedipsos (Euboea Island, Greece) are a combined result of active tectonics and recent volcanism of the Lichades volcanic centre. The fluids have Na-Cl geochemical type near-neutral pH, and they present chemical similarities (Kanellopoulos et al., 2017, 2020). In Aedipsos, the hot springs have been known since ancient times, and they are depositing thermogenic travertine. The travertines present several macro- and micro- facies (Kanellopoulos, 2012; 2013), with strong indications of bio-mineralization processes.

During the sampling process, sterile metal tweezers and chisels were used. Two sub-samples were collected. The first one was incubated into sterile transparent vials in the field. The second sub-sample was stored in formaldehyde solution (2.5%). Enriched cultures were obtained in flasks and Petri dishes with BG11 and BG 110 culture media. Cultures were maintained in an incubator under stable conditions and a natural diurnal cycle (north-facing window) at room temperature. The samples were studied under an optical microscope and a stereo microscope. In order to identify the species, classical and recent literature were used (Komárek and Anagnostidis, 1999, 2005; Komárek, 2014 and references within). The mineralogical study was conducted on polished sections studied under an optical microscope and powders using X-ray diffraction. Selected dehydrated samples in an alcohol series (30–100 %), critical point dried, gold-coated were studied under SEM.

Above the travertine wall, successive layers of different microorganisms, i.e. microbial mats of a few centimetres thick, occur (Fig. 1A-B). The microbial mats consist of microorganisms that belong to different taxonomic groups. In the vertical stratification of the microbial mats, cyanobacteria occupy the upper layer since they are photosynthetic organisms and need access to sunlight. The lower layer consists of other photosynthetic bacteria such as green non-sulfur bacteria, such as Chloroflexus. In the even lower layers where the necessary sunlight does not reach, non-photosynthetic bacteria live, usually sulfur-bacteria (Stal, 2000).

The collected samples present the following vertical micro-stratification (Fig. 1B): (i) Top first layer - White colour surface layer. It is abiotic and consists of calcite micritic crystals. (ii) Second layer - Blue-green colour cyanobacteria layer. It is dominated by Leptolyngbya perforans. (iii) Third layer - Oil-green colour layer, where Leptolyngbya perforans, Chloroflexus and other bacteria occur. (iv) Deeper layers, where no photosynthetic microorganisms occur.

In order to assess the cyanobacteria biodiversity, Cyanobacteria orders pie diagrams were made (Fig. 1C). The latest classification system (Hauer & Komárek, 2021) was used. Based on these, Chroococcales (37%) and Synechococcales (31%) are the dominant orders, followed by Oscillatoriales (16%) and Spirulinales (16%). Based on the microscopic study on fresh and cultured material, a total number of nineteen (19) cyanobacteria species, plus diatoms, were observed. Among them, typical thermophilic species were identified, such as Spirulina subtilissima and Chroococcus thermalis and typical limestone substrate cyanobacteria species, such as Leptolyngbya perforans.

Based mainly on SEM observations, several biomineralization processes were identified (Fig. 1D-E), mainly in the second layer, i.e. Cyanobacteria layer. Filamentous cyanobacteria trap calcite and diatoms. The extracellular polymeric substances (EPS) create crystal retention lattice contributing to the biomineralization process and also to the structure of microbial mat (Fig. 1D-E). Finally, calcified filamentous cyanobacteria sheaths were also identified, contributing to biomineralization prosses and the structure of microbial mat.

This study confirmed the importance of microbial mats for ecology, as well as for understanding biomineralization processes in extreme environments. Further research is needed, including additional sites and DNA analysis, to

comprehend the biodiversity of all the layers of the microbial mats in the area.

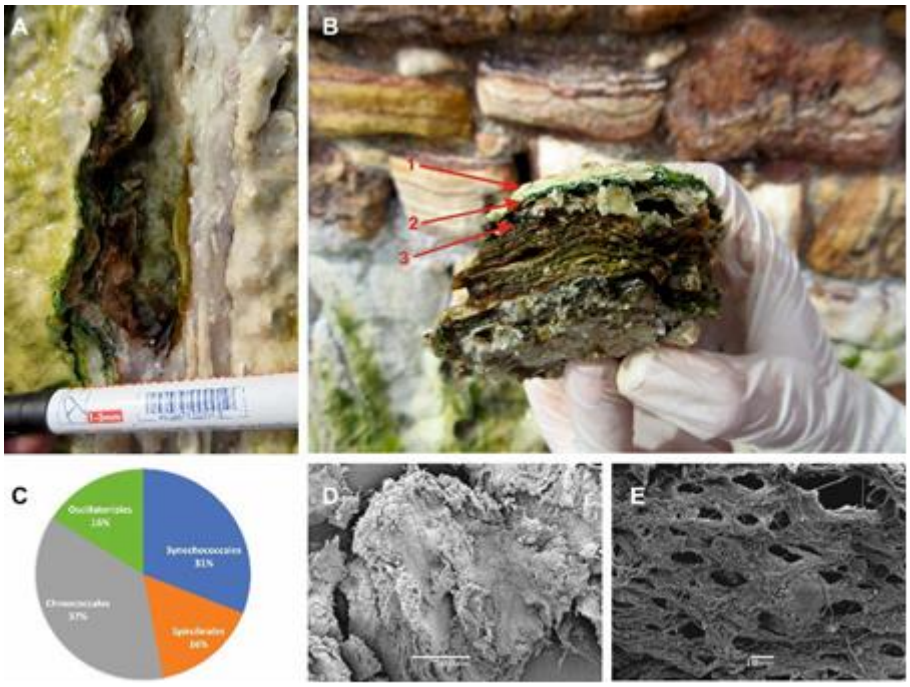

Figure 1. Field photos and sample photos (A-B), pie diagram (C) and Biomineralizing processes by cyanobacteria under SEM. (A) A vertical cut of the microbial mats, displaying the different vertical layering. (B) A full piece of microbial mats, displaying the vertical stratification: (1) top layer - the abiotic layer of travertine (white colour), (2) intense cyan-green layer of cyanobacteria and (3) olive-green layer where there is a reduction of cyanobacteria and the presence of other bacteria. (C) Pie diagrams presenting the percentage of each Cyanobacteria order. (D) Overview of dense EPS layer. (E) Closer view in other position, where the EPS creates a net along with filamentous cyanobacteria, favouring the trapping calcium carbonate crystals and diatoms.

References

Hauer, T. & Komárek, J., 2021. CyanoDB 2.0 - On-line database of cyanobacterial genera. - World-wide electronic publication, Univ. of South Bohemia & Inst. of Botany AS CR, http://www.cyanodb.cz.

Kanellopoulos, C., 2012. Distribution, lithotypes and mineralogical study of newly formed thermogenic travertines in Northern Euboea and Eastern Central Greece. Open Geosciences (former Central European Journal of Geosciences), 4(4): 545-560,.

Kanellopoulos, C., 2013. Various morphological types of thermogenic travertines in northern Euboea and Eastern Central Greece. Bull. Geol. Soc. Greece, ISSN: 0438-9557, vol. XLVII/3, p. 1929-1938.

Kanellopoulos, C., Mitropoulos, P., Valsami-Jones, E., Voudouris, P., 2017. A new terrestrial active mineralizing hydrothermal system associated with ore-bearing travertines in Greece (northern Euboea Island and Sperchios area). Journal of Geochemical Exploration 179, 9-24, https://doi.org/10.1016/j.gexplo.2017.05.003

Kanellopoulos, C., Xenakis, M., Vakalopoulos, P., Kranis, H., Christopoulou, M., Vougioukalakis, G., 2020. Seawater-dominated, tectonically controlled and volcanic related geothermal systems: the case of the geothermal area in the northwest of the Island of Euboea (Evia), Greece. International Journal of Earth Sciences, 109(6), 2081-2112, https://doi.org/10.1007/s00531-020-01889-7

Komárek, J., & Anagnostidis, K., 1989. Modern approach to the classification system of Cyanophytes 4-Nostocales. Algological Studies/Archiv für Hydrobiologie, Supplement Volumes, 247-345.

Komárek, J., & Anagnostidis, K., 1999. Cyanoprokaryota, Part 1: Chroococcales, Süsswasserflora von Mitteleuropa, Bd 19/1. Komárek, J., & Anagnostidis, K., 2005. Cyanoprokaryota, Part 2: Oscillatoriales, Süsswasserflora von Mitteleuropa, Bd 19/2. Komárek, J., Kastovsky, J., Mares, J., Johansen, J.R., 2014. Taxonomic classification of cyanoprokaryotes (cyanobacterial genera) 2014, using a polyphasic approach. Preslia, 86(4), 295-335.

Reitner, J., & Thiel, V., 2011. Encyclopedia of geobiology. Springer Science þ Business Media, ISBN: 978-1-4020-9211-4.

16th International Congress of the Geological Society of Greece
17-19 October, 2022 - Patras, Greece
Bulletin of the Geological Society of Greece, Sp. Publ. 10
Ext. Abs. GSG2022-063

Speleothems in hot spring environment and biomineralization processes by Cyanobacteria, at Aedipsos (Edipsos) area, Euboea (Evia) Island, Greece

Vasiliki Lamprinou[1], Christos Kanellopoulos[2,3], Artemis Politi[1], Panagiotis Voudouris[2], Ioannis Illiopoulos[3], Maria Kokkaliari[3], Leonidas Moforis2, Athena Economou-Amilli[1]

(1) National and Kapodistrian University of Athens, Faculty of Biology, Department of Ecology and Systematic, Panepistimioupolis, Ano Ilissia, 15784 Athens, Greece, vlampri@biol.uoa.gr (2) National and Kapodistrian University of Athens, Faculty of Geology and Geoenvironment, Panepistimioupolis, Ano Ilissia, 15784 Athens, Greece (3) University of Patras, Department of Geology, Rio 26500, Greece.

The speleothems, i.e. stalactites and stalagmites, which are secondary mineral deposits, could be created by biogenic and abiogenic processes. In the abiogenic case, the mineral precipitation is due to supersaturation of the solution due to pH changes, outgassing and evaporation. In the cases of microorganisms' contribution, biomineralization processes take place (Reitner & Thiel, 2011 and references within). The microorganisms can biologically mediate mineral formation in several ways.

Hot springs occur in three areas in Aedipsos (Euboea Island, Greece) which are a combined result of active tectonics and recent volcanism of the Lichades volcanic centre. The fluids have Na-Cl geochemical type near-neutral pH, and they present chemical similarities (Kanellopoulos et al., 2017, 2020). In Aedipsos, the hot springs have been known since ancient times, and they are depositing thermogenic travertine. The travertines present several macro- and micro- facies (Kanellopoulos, 2012; 2013), with strong indications of bio-mineralization processes.

In Aedipsos are several hot springs; some are located inside small caves. The study site is a small cave, where a hot spring occurs, in the Aedipsos area (Fig. 1A-B). At the cave roof, stalactites occur, where drops of hot water continuously fall down. The hot spring temperature, which is located just below the stalactites, is 49.2 oC, the pH is 6.05. Samples of the stalactites were collected.

During the sampling process, sterile metal tweezers and chisels were used. Two sub-samples were collected. The first one was incubated into sterile transparent vials in the field. The second sub-sample was stored in formaldehyde solution (2.5%). Enriched cultures were obtained in flasks and Petri dishes with BG11 and BG 110 culture media (Stanier et al., 1971). Cultures were maintained in an incubator under stable conditions and a natural diurnal cycle (north-facing window) at room temperature. The samples were studied under an optical microscope and a stereo microscope. In order to identify the species, classical and recent literature were used (Komárek and Anagnostidis, 1999, 2005; Komárek, 2014 and references within). The mineralogical study was conducted on polished sections studied under an optical microscope and powders using X-ray diffraction. Selected dehydrated samples in an alcohol series (30–100 %), critical point dried, gold-coated were studied under SEM.

The dominant Cyanobacteria orders (Fig. 1C), based on the latest classification system (Hauer & Komárek, 2021), are Synechococcales and Oscillatoriales with 28% and 27%, respectively and the Chroococcales and Nostocales follow with 21%, and finally, Spirulinales are also present with only 3%. By studying fresh and cultured material, the total number of twenty-nine (29) different cyanobacteria species, plus diatoms, were identified. Among them are typical thermophilic species, such as Spirulina subtilissima is among the identified species, which is a typical thermophilic cyanobacteria. As well, Chroococcus lithophilus, Leptolyngbya perforans, and Leptolyngbya ercegovicii are also present, which are typical limestone substrate cyanobacteria species.

Based mainly on SEM observations, Cyanobacteria biomineralization processes were identified in the outer layer of the samples (Fig. 1D-F). The most common was the presence of endolithic cyanobacteria, which were destroying the calcite crystals. The endolithic cyanobacteria create holes and dig channels at the crystals (Fig. 6D). These could be created by the secreted acidic substances or other factors such as EPS. In rare cases, calcified cyanobacterial sheaths were found (Fig. 1E), as well as the presence of filamentous cyanobacteria and EPS, which creates a dense net resulting in the retention of calcium carbonate crystals (Fig. 1F).

This study highlighted the importance of the geomicrobiological study of speleothems. These sites are natural labs of unique conditions. Further research ought to be conducted in the area, including additional sites and DNA analysis in order to fully comprehend the biodiversity and the biomineralization processes in these extreme environments.

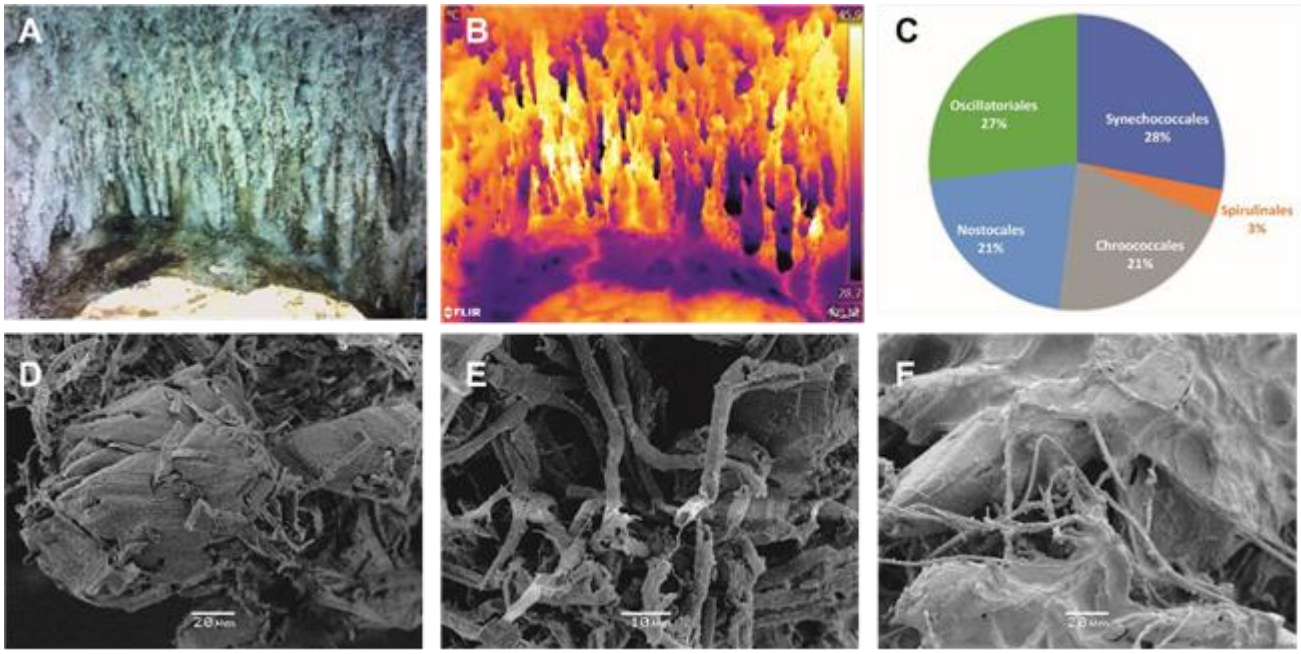

Figure 1. Paired simple and thermal images (A-B), pie diagram (C), biomineralizing processes by cyanobacteria under SEM (D-F). (A-B) Paired views of regular image and corresponding thermal image of the stalactites. (C) Pie diagrams presenting the percentage of each Cyanobacteria order. (C) Calcite crystals with distinct holes and dig channels, occupied by filamentous cyanobacteria. (E) Calcified sheaths of cyanobacteria firmaments by micritic calcium carbonate crystals. (F) EPS along with filaments.

References

Hauer, T. & Komárek, J., 2021. CyanoDB 2.0 - On-line database of cyanobacterial genera. - World-wide electronic publication, Univ. of South Bohemia & Inst. of Botany AS CR, http://www.cyanodb.cz.

Kanellopoulos, C., 2012. Distribution, lithotypes and mineralogical study of newly formed thermogenic travertines in Northern Euboea and Eastern Central Greece. Open Geosciences (former Central European Journal of Geosciences), 4(4): 545-560,.

Kanellopoulos, C., 2013. Various morphological types of thermogenic travertines in northern Euboea and Eastern Central Greece. Bull. Geol. Soc. Greece, ISSN: 0438-9557, vol. XLVII/3, p. 1929-1938.

Kanellopoulos, C., Mitropoulos, P., Valsami-Jones, E., Voudouris, P., 2017. A new terrestrial active mineralizing hydrothermal system associated with ore-bearing travertines in Greece (northern Euboea Island and Sperchios area). Journal of Geochemical Exploration 179, 9-24, https://doi.org/10.1016/j.gexplo.2017.05.003

Kanellopoulos, C., Xenakis, M., Vakalopoulos, P., Kranis, H., Christopoulou, M., Vougioukalakis, G., 2020. Seawater-dominated, tectonically controlled and volcanic related geothermal systems: the case of the geothermal area in the northwest of the Island of Euboea (Evia), Greece. International Journal of Earth Sciences, 109(6), 2081-2112, https://doi.org/10.1007/s00531-020-01889-7

Komárek, J., & Anagnostidis, K., 1989. Modern approach to the classification system of Cyanophytes 4-Nostocales. Algological Studies/Archiv für Hydrobiologie, Supplement Volumes, 247-345.

Komárek, J., & Anagnostidis, K., 1999. Cyanoprokaryota, Part 1: Chroococcales, Süsswasserflora von Mitteleuropa, Bd 19/1. Komárek, J., & Anagnostidis, K., 2005. Cyanoprokaryota, Part 2: Oscillatoriales, Süsswasserflora von Mitteleuropa, Bd 19/2. Komárek, J., Kastovsky, J., Mares, J., Johansen, J.R., 2014. Taxonomic classification of cyanoprokaryotes (cyanobacterial genera)

2014, using a polyphasic approach. Preslia, 86(4), 295-335. Reitner, J., & Thiel, V., 2011. Encyclopedia of geobiology. Springer Science þ Business Media, ISBN: 978-1-4020-9211-4.

Stanier, R.Y., Kunisawa, R., Mandel, M., Cohen-Bazire, G., 1971. Purification and properties of unicellular blue-green algae (order Chroococcales). Bacteriological reviews, 35(2), 171.

16th International Congress of the Geological Society of Greece
17-19 October, 2022 - Patras, Greece
Bulletin of the Geological Society of Greece, Sp. Publ. 10
Ext. Abs. GSG2022-076

Increased Accuracy of the Photogrammetric UAS Data Processing for the Detection of River Channel and Boulder Dimensions and Displacement after High Severity Floods

K. Gkaidatzoglou[1], A. Konsolaki[1], E. Vassilakis[1]

(1) Remote Sensing Laboratory, Department of Geology and Geoenvironment, National and Kapodistrian University of Athens, Greece.

The rapidly increasing use of Unmanned Aerial Systems (UAS) at post-flood areas, has been considered particularly useful especially in cases of necessity for accurate quantification of displacements or volumes (Tsokos et al., 2018). The number of field surveys conducted in the last decade combined with the use of UAS, especially in cases of natural disasters' mapping and management, either during the phenomenon or at the post-disaster stage has been particularly increased (Giordan et al., 2018). It's only recently, that the use of UAS combined with the Structure from Motion (SfM) photogrammetric processing technique, assisted by the positioning of precisely measured Ground Control Points (GCPs) with Global Navigation Satellite System (GNSS) equipment have been used extensively for enhancing the accuracy of field surveys and special measurements after catastrophic events.

We present a UAS-based optical granulometry method, as a new non-invasive technique of granulometric analysis based on the fusion of two individual techniques, such as the UAS photogrammetry and the optical digital granulometry, which could be considered as a significant advance in quantitative geomorphology and in the study of river and fluvial processes, in general (Graham et al., 2012; Andreadakis et al., 2020). Most of the traditional sediment analysis techniques are not suitable for clastic sedimentary material with size larger than 2 mm, while the whole process of digging, transport and sieving is time-consuming and high-cost intensive (Detert and Weitbrecht, 2013). Moreover, this technique is considered as invasive and not applicable in areas under preservation. These restrictions can be surpassed through the implementation of optical digital granulometry (Langhammer et al., 2017).

The experiment described in this work was performed by using a DJI Phantom 4 RTK, with the onboard multi-frequency GNSS receiver, which allows the adoption of NRTK (Network-based Real-Time Kinematic) approach for the data processing. The high accuracy and resolution, dense point clouds, Digital Surface Models (DSMs) and ortho-photo mosaics, which were generated after the photogrammetric processing provided us with the valuable high spatial resolution datasets as inputs for the granulometric processing.

The use of UAS systems can provide useful information for areas suffered from extended flooding events, as well as they provide the opportunity to observe and map the changes of geomorphological features, such as the region of Cephalonia, that was severely affected during the Medicane named 'Ianos', in September 2020 (Vassilakis et al., 2021). The detailed DSM model and the SfM technique products, in general, were notably useful for examining the channel geometry, and other characteristics of river flow (Fig. 1a). For the measuring of the size and the dimensions of the boulders, aerial images collected from the UAS system were used, alongside the streambed examined. We used ArcGIS software for visualizing the photogrammetry results, on which sixty-six (66) boulders that were identified, and their dimensions were measured. Alongside the riverbed examined, the size of the boulders appears to be notably reduced downstream. The a, b axis of the boulders located upstream near the northernmost GCP were measured at 0.88m and 0.55m on average, respectively, whilst the a, b axis located downstream near the furthest GCP were measured at 0.35m and 0.25m on average, respectively (Fig 1c). Consequently, the stream capacity is reduced considerably downstream in a range of 230m, which is in agreement with the flow mechanics described in the literature (see Diakakis et al., 2020 and references therein).

Since the accuracy is of high importance for the granulometry, we present a thorough analysis for the use of GCPs within the overall photogrammetric processing. The analysis yield that using GCPs demonstrates a significantly increased accuracy into the photogrammetric processing (Panagiotopoulou et al., 2021). However, despite the high accuracy, the positioning of GCPs may offer, the amount of time spent during the fieldwork (placing and measuring each GCP), as well as the time spent during the processing for locating them in the images, could be considered as unproductive and cost - effective. Therefore, the NRTK approach was adopted, since the overall accuracy is quite high and, in some cases, higher than the GCPs-only method (Fig 1b). We argue that this also allows the gaining of time, which is rather precious, especially during the post-catastrophic stage. Regarding the precision of the DSMs and the ortho-photo mosaics, the placement of six GCPs in the experiment captured area, permits the comparison between the aforementioned strategies/techniques, along with observations in high detail (in case of the boulders) larger than a few centimeters (2cm in this case). The latter can be achieved during the first few days after the disaster, as it is apparent that when time passes, the risk of losing crucial data is increased. Although the precision of the DSMs and the ortho-photo mosaics with the placement of GCPs is considerably higher, however this method provides us with more flexibility and less time is needed to complete the campaign. The well-organized field campaign for correct UAS data acquisition shortly after the post-catastrophic stage and the accurately applied SfM technique is proved to offer two considerable advantages, (i) quick

study of the affected region, especially in relatively small areas with limited access to road network, and (ii) create the basement data of the area of interest, ready to use for further examination in several ways (flood mechanics, erosion processes etc). The main objective is the assessment of a correct geospatial accuracy for the image products acquired during the aerial mapping of the affected region.

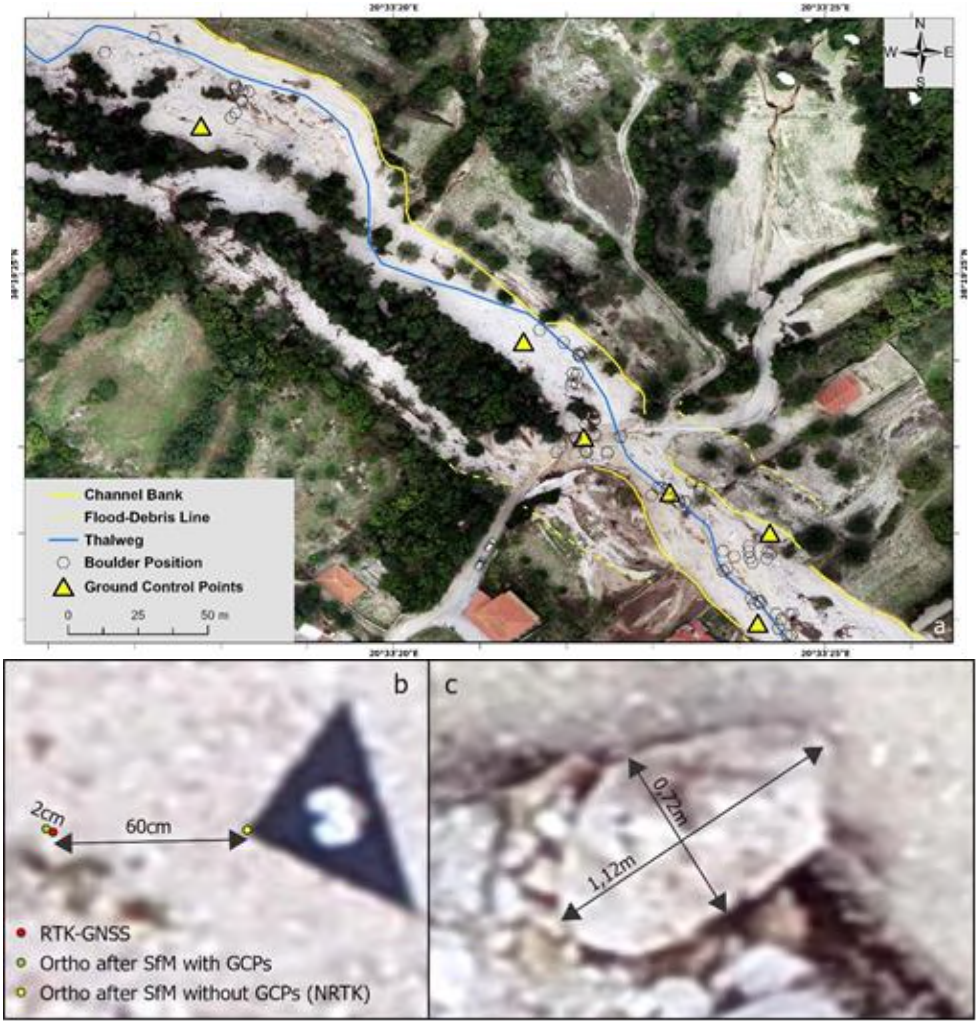

Figure 1. (a) Interpretation of the experiment river segment (see legend for symbol meanings). (b) Checking the accuracy of the final ortho-photo-mosaic with the precise coordinates of the GCP. (c) Accurately measuring the a and b axes of a boulder.

References

Andreadakis, E., Diakakis, M., Vassilakis, E., Deligiannakis, G., Antoniadis, A., Andriopoulos, P., Spyrou, N. I., & Nikolopoulos, E. I., 2020. Unmanned Aerial Systems-Aided Post-Flood Peak Discharge Estimation in Ephemeral Streams. Remote Sensing, 12(24), 4183.

Diakakis, M., Deligiannakis, G., Antoniadis, Z., Melaki, M., Katsetsiadou, N., Andreadakis, E., Spyrou, N., & Gogou, M. , 2020. Proposal of a flash flood impact severity scale for the classification and mapping of flash flood impacts. Journal of Hydrology, 590, 125452.

Detert, M., Weitbrecht, V., 2012. Automatic object detection to analyze the geometry of gravel grains--a free stand-alone tool, River flow 2012 - Proceedings of the International Conference on Fluvial Hydraulics. 1. 595-600.

Giordan, D., Hayakawa, Y. S., Nex, F., & Tarolli, P., 2018. Preface: The use of remotely piloted aircraft systems (RPAS) in monitoring applications and management of natural hazards. Natural Hazards and Earth System Sciences, 18(11), 3085–3087. Graham, D. J., Rollet, A. J., Rice, S. P., & Piégay, H. 2012. Conversions of Surface Grain-Size Samples Collected and Recorded Using Different Procedures. Journal of Hydraulic Engineering, 138(10), 839–849.

Langhammer, J., Bernsteinová, J., & Miřijovský, J., 2017. Building a High-Precision 2D Hydrodynamic Flood Model Using UAV Photogrammetry and Sensor Network Monitoring. Water, 9(11), 861.

Panagiotopoulou, S., Erkeki, A., Antonakakis, A., Grigorakakis, P., Protopapa, V., Tsiostas, G., Vlachou, K., Vassilakis, E., 2020. Evaluation of Network Real Time Kinematics contribution to the accuracy/productivity ratio for UAS-SfM Photogrammetry.

Tsokos, A., Kotsi, E., Petrakis, S., Vassilakis, E., 2018. Combining series of multi-source high spatial resolution remote sensing datasets for the detection of shoreline displacement rates and the effectiveness of coastal zone protection measures. Journal of Coastal Conservation, 22(2), 431-441.

Vassilakis, E., Konsolaki, A., Petrakis, S., Kotsi, E., Fillis, C., Lozios, S., Lekkas, E., 2021. Quantification of Mass Movements with Structure-from-Motion Techniques. The Case of Myrtos Beach in Cephalonia, After Ianos Medicane (September 2020). Bull. Of Geol. Soc. of Greece, Sp. Pub. 8, 16-20.

16th International Congress of the Geological Society of Greece
17-19 October, 2022 - Patras, Greece
Bulletin of the Geological Society of Greece, Sp. Publ. 10
Ext. Abs. GSG2022-083

Provenance and Statistical Analysis of the Lower Oligocene Gravelly Deposits in Central Pindos Foreland Basin, Western Greece: Implications for Orogenic Buildup and Unroofing

A. Kovani[1], C. Botziolis[1], A.G. Maravelis[2], G. Pantopoulos[3], G. Iliopoulos[4], A. Zelilidis[1]

(1) Laboratory of Sedimentology, Department of Geology, University of Patras, 26504, Rion, Greece, andrianakovani@gmail.com (2) Department of Geology, Aristotle University of Thessaloniki, 54124, Thessaloniki, Greece (3) Department of Earth Sciences "Ardito Desio", University of Milan, 20133, Milan, Italy (4) Laboratory of Paleontology and Stratigraphy, Department of Geology, University of Patras, 26504, Rion, Greece.

Introduction and Geological setting

This study focuses on the provenance of the Upper Eocene-Lower Oligocene submarine fan deposits in the central part of Pindos foreland basin, Greece (PFB) and integrates conglomerate clast composition and statistical analysis of conglomerate clasts, along with petrographic and cathodoluminence (CL) analysis. The conglomeratic deposits of the PFB are generally thick-bedded and occur at several stratigraphic levels, allowing for a systematic sampling and analysis at progressively higher levels, and facilitating conclusions regarding the temporal evolution of the PFB and adjacent orogen. Thus, they offer a good case study for investigating their provenance and provide information about the relative input of the different source rock types on the sedimentation. Conglomerates in other parts of the PFB have previously been investigated (Alexander *et al.*, 1990; Leigh & Hartley, 1992), but systematic provenance studies are not available. The aim of this research is to elaborate a systematic approach to define the origin of the Lower Oligocene conglomeratic deposits at the central part of the PFB and elucidate the linkage with the exhumation history of the Pindos Orogen.

Material and Methods

This study utilized several approaches including conglomerate clast composition, petrographic, CL, and statistical analyses. Facies analysis was based on sedimentological and stratigraphic criteria, as described by Botziolis *et al.*, (2021). According to this latter work, the studied outcrops correspond to inner fan deposits, and were grouped into two facies associations: the a) conglomeratic channels (FA1) and the b) internal levee deposits (FA2). The internal levees were further sub-divided in two sub-facies: the i) inner internal levees (FA2a) and the ii) outer internal levees (FA2b) (Figure 1a). The conglomerate clast composition analysis was performed on twelve outcrops, and three hundred clasts in total were described, based on the lithology, long axis, roundness, and sphericity. Additionally, twenty conglomeratic samples were collected from the same outcrops. Eighty-five carbonate and chert clasts were thin-sectioned and studied for microfacies and micropaleontological analysis. Petrographic analysis included the Gazzi-Dickinson point counting method (PC) and CL analysis on the conglomerate matrix. In each thin section 300 points were described based on the grain size, shape of the identified minerals or/and lithic fragments, and characteristics such as the undulose extinction. Statistical analysis was implemented using R software and the multivariate analysis of clast composition was carried out based on principal component analysis (PCA) and hierarchical cluster analysis.

Results

The conglomerate clast composition analysis showed that the clasts in all outcrops are mostly classified as very coarse gravel (36%), followed by coarse gravel (30%), cobble (25%), medium gravel (8%) and boulder (1%). The mean grain size exhibits a general increasing upwards trend. Regarding roundness, most of the outcrops are characterized by subangular to subrounded clasts, but both angular and rounded clasts exist. In terms of sphericity all outcrops contain non-spherical clasts. The clasts-matrix results exhibit increased clast ratios (>40%). The matrix is significant in some outcrops (57%), while in others it is generally low (14%).

The petrographic analysis applying the PC method revealed a wide range of minerals and lithic fragments composing the studied thin sections. The most common mineral grains are quartz, calcite, feldspars (K-feldspar, plagioclase) and mica (muscovite, biotite). Quartz prevails in most of thin-sections and occurs as monocrystalline, polycrystalline quartz without tectonic fabric and polycrystalline with tectonic fabric. The most common lithic fragments are extrabasinal carbonates, sandstones, cherts, and slates, while bioclasts also occur. The additional application of the QFL diagram suggests that all samples group together in the recycled orogen field, whereas in the QmFLt diagram, they plot in the field of transitional and lithic recycled orogen. The QFL diagram for the nomenclature classifies all samples as quartzolithic (Figure 1b). Based on CL analysis, the quartz grains mainly exhibit a dark brownish color, plagioclase grains preserve a greenish color and feldspars a bluish color. Calcite matrix and carbonate fragments prevail with a characteristic orange color.

According to microfacies analysis, the conglomerate clasts are dominated by carbonate and rarely by siliceous and sandstone clasts and are classified as: 1. Micritic limestones with/without structures containing planktonic foraminifera, radiolaria and/or Globotruncana spp., Globigerineloides sp., Filaments (bivalvia). 2. Micritic (mudstone) limestones with/without structures containing benthic and planktonic foraminifera, radiolaria and/or Globotruncana spp., Miliolidae,

Algae, Thaumatoporella sp., Dacycladacea, 3. Micritic limestones with peloids containing benthic foraminifera and/or Miliolidae, algae, Thaumatoporella sp. 4. Micritic limestones with ooids, fenestral cavities, structures containing algae. 5. Micritic limestones, boundstone to grainstone with fenestral cavities and structures containing benthic foraminifera, Cuneolina sp., algae, Dacycladacea, small gastropods. 6. Wackestone with planktonic foraminifera, Globotruncana spp., Hedbergella sp, 7. Microbreccia or breccia with planktonic and benthic foraminifera, algae, Discocyclina sp., Asterocyclina sp., Miscellana cf. miscella, Nummulites sp., Assilina sp., Miliolidae, 8. Chert with radiolaria.

PCA analysis revealed that the two principal components (PC 1 and 2) which control 80.75% of compositional data variation are mainly correlated with sandstone and black chert clast abundances. The bi-plot of the two main principal components recognized by PCA analysis indicated that there is a difference in clast abundance between outcrops 2, 5 and 9 (orange ellipse) in relation to the outcrops 1, 3, 4, 6 and 8 (black ellipse) and outcrops 7, 10, 11 and 12 (blue ellipse). Cluster analysis also identified three main outcrop groups based on clast lithologies same as PCA analysis (Figure 1c).

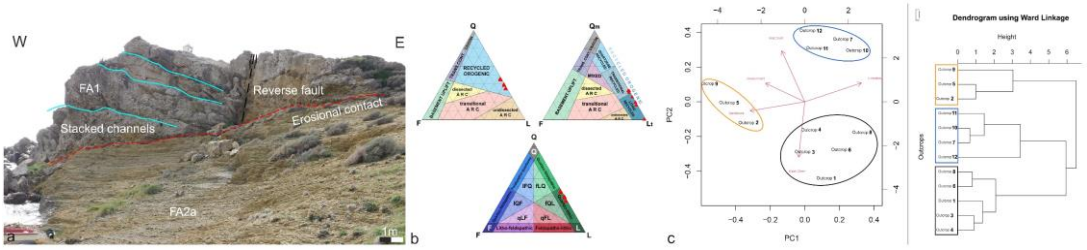

Figure 1. (a) The red line represents the erosional contact between FA1 and FA2a. (b) QFL and QmFLt tectonic setting classification diagrams of Dickinson (1985) and QFL diagram for the nomenclature (Garzanti, 2019) of the studied thin sections. (c) PCA and cluster analyses highlighting the 3 main outcrop groups.

Discussion and Conclusions

- Conglomerate clast composition analysis revealed a major carbonate source and two secondary sources, characterized by sandstone and chert lithologies.
- Petrographic analysis (PC and CL methods) seems also to agree with the previously observed sedimentary sources. According to PC results a sedimentary source is confirmed, while the appearance of undulosed quartz, polycrystalline quartz and slate fragments also indicate an additional low-grade metamorphic source. Furthermore, based on the ternary plots for compositional and tectonic setting classification, the studied samples are classified as quartzolithic deposited in a recycled orogenic setting, probably indicating recycling of the Pindos Orogen.
- Statistical analysis of clast composition (cluster and PCA analyses) highlighted 3 main outcrop groups. The limestone source was constantly active during the depositional conditions of the studied outcrops with an increasing upward trend of its contribution to the sediment bulk. The sandstone source is also active during the depositional processes and exhibits fluctuations of high and low concentrations. The chert source contributes with the red cherts concentration increasing upwards, unlike the black cherts abundance that decreases upward.
- Microfacies analysis is also in accordance with the conglomerate clast composition analysis and suggests that the detritus in the examined samples originated from a sedimentary source. This source provided mainly carbonate clasts, followed by sandstone and chert clasts: The limestone source rock is represented by the lower part of the Upper Cretaceous platy limestone ("Limestones with Globotruncanes" and the "Transitional beds") and by the Upper Jurassic to Lower Cretaceous limestones with Calpionella. The chert source rocks, rich in radiolaria and planktonic foraminifera, is most likely represented by the schist-chert formation of Late Jurassic age and the sandstone source rock by the Upper Eocene-Lower Pliocene submarine-fan deposits or the "Pindos Flysch" units.
- The low-grade metamorphic source is most likely ascribed to the Pelagonian zone that contains metamorphic rocks.
- The sedimentary succession displays a general upwards enrichment in sedimentary and metamorphic lithic fragments, along with an upwards decrease in feldspathic, and monocrystalline quartz grains. This compositional trend could be associated with the unroofing of the Pindos Orogen.

Acknowledgements

Andriana Kovani is currently a PhD student, and the presented results are part of her Master thesis. The obtained data are part of the data collected for the research project "Global climate and sea-level changes across the Latest Eocene-Early Oligocene, as reflected in the sedimentary record of Pindos foreland and Thrace basin, Greece, 80591", co-funded by the H.F.R.I.: Hellenic Foundation for Research & Innovation, Greece and G.S.R.T.: General Secretarial for Research and Technology, Greece.

References

Alexander J., Nichols G.J., Leigh S., 1990. The origins of marine conglomerates in the Pindus foreland basin, Greece. Sedimentary Geology, 13-254.

Botziolis, C., Maravelis A., Pantopoulos G., Kostopoulou S., Catuneanu O., Zelilidis A., 2021. Stratigraphic and paleogeographic development of a deep-marine foredeep: Southern Pindos foreland basin, western Greece. Marine and Petroleum Geology, 128, 105012.

Dickinson, W.R., G.G. Zuffa (Eds), 1985. Interpreting provenance relations from detrital modes of sandstones, 3–61.

Garzanti, E., 2019. Petrographic classification of sand and sandstone. Earth-Science Reviews, 192, 545–563.

Leigh S., & Hartley A. J., 1992. Mega-debris flow deposits from the Oligo-Miocene Pindos foreland basin, western mainland Greece: implications for transport mechanisms in ancient deep marine basins. Sedimentology, 39, 1003-1012.

16th International Congress of the Geological Society of Greece
17-19 October, 2022 - Patras, Greece
Bulletin of the Geological Society of Greece, Sp. Publ. 10
Ext. Abs. GSG2022-098

Depositional Environments, Diagenetic History, Economic and Strategic Importance of the Upper Cretaceous Carbonate Sediments in Ionian Zone (Epirus, Western Greece)

L. Moforis[1,2], G. Kontakiotis[1], A. Antonarakou[1], H.T. Janjuhah[3,4], A. Zambetakis-Lekkas[1], D. Galanakis[2], P. Paschos[2], C. Kanellopoulos[5,6], S. Sboras[6], E. Besiou[1], V. Karakitsios[1]

(1) National and Kapodistrian University of Athens, Faculty of Geology and Geoenvironment, Department of Historical Geology and Paleontology, Panepistimiopolis, Zografou, 15784, Athens, Greece, leonidasmoforis@gmail.com (2) [2]H.S.G.M.E., Hellenic Survey of Geology and Mineral Exploration, Athens, Greece (3) [3]Shaheed Benazir Bhutto University, Department of Geology, Sheringal 18050, KPK, Pakistan (4) Centre of Seismic Imaging, Department of Geosciences, University Technology PETRONAS, Sri Iskandar 32610, Malaysia (5) [5]National and Kapodistrian University of Athens, Faculty of Geology and Geoenvironment, Panepistimiopolis, Zografou, 15784, Athens, Greece (6) University of Patras, Department of Geology, 26504, Patras, Greece (7) National Observatory of Athens, Institute of Geodynamics, Lofos Nymphon, Thesio, Athens.

An integrated sedimentological, micropaleontological, petrophysical, and microfacies analysis of the Upper Cretaceous carbonate succession representing the Senonian limestone formation in Gardiki section of Epirus, provides new insights into the depositional and diagenetic processes of the Western Ionian Basin (External Ionian Zone) (Figure 1), as well as the synthetic paleogeographic reconstruction of the area.

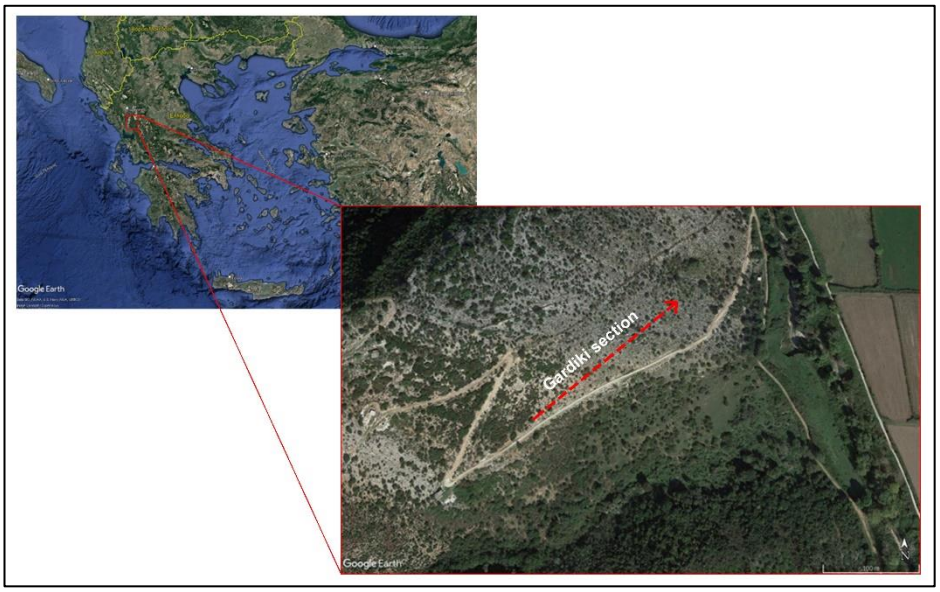

Figure 1: Google Earth map illustrating the study area. Red dashed line shows the Gardiki section (Lat: 39°20'22,09'' N, long: 20°33'5,63'' E)

The biostratigraphic analysis based on planktonic foraminifera showed that the Gardiki section covers the boundary between Upper Cretaceous (Maastrichtian) and Paleocene time span based on the coexistence of *Globotruncana* spp. and Globigerinidae. Facies analysis allowed the description of the distinguished microfacies types, including the main textural and compositional characteristics and sedimentary features related to various depositional settings or facies zones (Bourli *et al*., 2019a; Kontakiotis *et al*., 2020). Particularly, the Senonian limestone formation in this area is mainly characterized by light-grey-to-yellowish limestones with abundant planktonic foraminifera, rare radiolarians, and calcite veins. At the top of the section, siliceous intervals rarely occur as thin reddish-to-brownish chert intercalations (up to 5 cm thickness) and/or lenses within the pelagic limestone unit, with their presence of both nodular and bedded siliceous concretions to be of crucial importance on enhancing the reservoir properties (i.e., secondary porosity and permeability increase) of the hosted deposits through the fracturing and stylolites created during the nodules development and the potentiality to act as open pathways for the fluids (even for hydrocarbons). The observed siliceous nodules differ in size (up to 35 cm in diameter) and colour (red to black), and appear in a variety of shapes, mostly sub-spherical, elongated-to-flattened, or mushroom ones. They also present two or three distinct colours (development in levels probably due to differential biogenic source and mineralogic composition) from the rim to the core, such as black to the periphery, rusty red-brown to light red in the main body and again a thin blackish layer at the interior. Their existence (including the colour and shape variation observed), is consistent to the recent findings of Bourli *et al*. (2019b) for the Cretaceous nodules of the Ionian

zone deposits, about their diagenetic origin and their formation after resedimentation that follows the diagenetic events that took place into a stable basin floor, during the deposition of Senonian limestones. Overall, the main depositional facies observed into Senonian limestones in the study area is characterized by pelagic biomicrite wackestone-packstone with planktonic foraminifera and radiolarians, which is indicative of a period of basinal sedimentation with minor internal differentiation (Flügel, 2012) implying that the depositional environment during the Upper Cretaceous did not change significantly. In the study area, no coarser brecciated horizons have been observed, as usually happened within the Ionian zone in other locations of the Western Greece (Bourli *et al*., 2019b, 2021). Their absence from the Senonian limestones in Gardiki section could be attributed to the foreland basin evolution, as it is less influenced by their greater distance from the thrusts between the tectonic zones, sediment thickness and overall depositional conditions.

Furthermore, a petrographic analysis identified several distinct diagenetic features among the Senonian limestones (Figure 2), which are categorized into marine, meteoric, and burial diagenetic settings. Micrite envelop, cementation, fracture, compaction, and dissolution are the dominant diagenetic parameters identified in the study samples. This complicated diagenetic history of the carbonate rocks of Western Greece has both positive and negative effects on porosity (Janjuhah *et al*., 2019). The presence of abundant planktonic foraminifera in these deposits, in addition to the rare existence of radiolarians and filaments, denotes a relatively deep, low-energy environment.

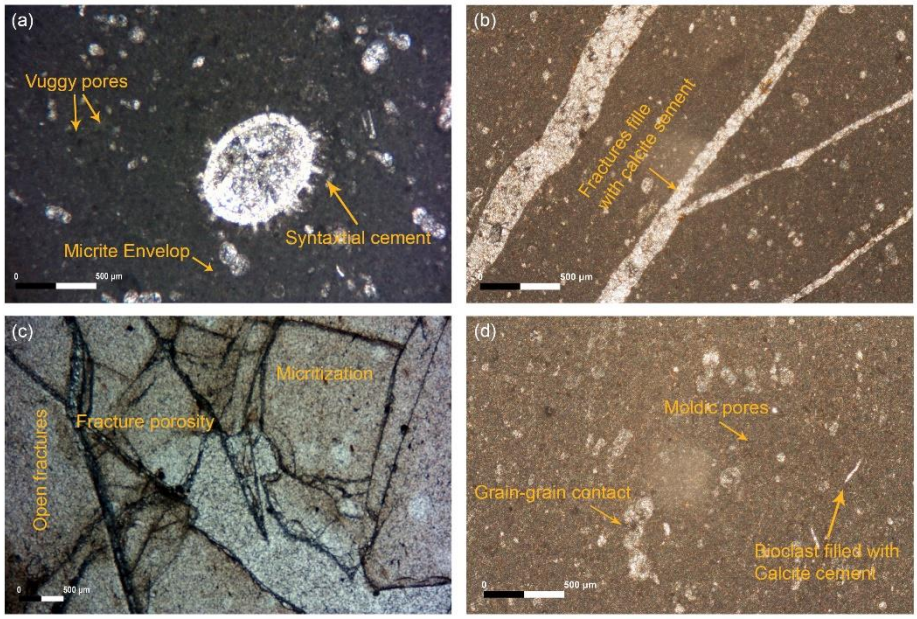

Figure 2: Petrographic analysis showing different diagenetic processes in carbonate samples collected from Ionian zone (Epirus, Western Greece), a) high micritization, vuggy pores, and syntactical overgrowth cement, b) micritization, late stage of diagenesis-fractured filled with calcite cement, c) early stage of micrite envelop, late stage of open fracture, d) moldic pores, grain-grain contact (physical compaction).

References

Bourli, N., Pantopoulos, G., Maravelis, A.G., Zoumpoulis, E., Iliopoulos, G., Pomoni-Papaioannou, F., Kostopoulou, S., Zelilidis, A. Late Cretaceous to early Eocene geological history of the eastern Ionian Basin, southwestern Greece: A sedimentological approach. Cretaceous Research 2019a, 98, 47–71.

Bourli, N., Kokkaliari, M., Iliopoulos, I., Pe-Piper, G., Piper, D.J.W., Maravelis, A.G., Zelilidis, A. Mineralogy of siliceous concretions, cretaceous of Ionian zone, western Greece: Implication for diagenesis and porosity. Marine and Petroleum Geology 2019b, 105, 45–63.

Bourli, N., Kokkaliari, M., Dimopoulos, N., Iliopoulos, I., Zoumpouli, E., Iliopoulos, G., Zelilidis, A. Comparison between Siliceous Concretions from the Ionian Basin and the Apulian Platform Margins (Pre-Apulian Zone), Western Greece: Implication of Differential Diagenesis on Nodules Evolution. Minerals 2021, 11, 890.

Flügel, E. Microfacies analysis of limestones; Springer-Verlag Berlin Heidelberg: 2012.

Janjuhah, H.T., Alansari, A., Santha, P.R. Interrelationship between facies association, diagenetic alteration and reservoir properties evolution in the Middle Miocene carbonate build up, Central Luconia, Offshore Sarawak, Malaysia. Arabian Journal for Science and Engineering 2019, 44, 341-356.

Kontakiotis, G., Moforis, L., Karakitsios, V., Antonarakou, A. Sedimentary Facies Analysis, Reservoir Characteristics and Paleogeography Significance of the Early Jurassic to Eocene Carbonates in Epirus (Ionian Zone, Western Greece). Journal of Marine Science and Engineering 2020, 8, 706.

16th International Congress of the Geological Society of Greece
17-19 October, 2022 - Patras, Greece
Bulletin of the Geological Society of Greece, Sp. Publ. 10
Ext. Abs. GSG2022-168

Sedimentary Facies Analysis and Diagenesis of the Middle-Late Eocene Carbonate Deposits of the Ceno-Tethys Ocean

A. Bilal[1], R. Yang[1,2], M.S. Mughal[3], H.T. Janjuhah[4], M. Zaheer[3], G. Kontakiotis[5]

(1) Shandong Provincial Key Laboratory of Depositional Mineralization & Sedimentary Minerals, Shandong University of Science and Technology, Qingdao 266590, China, ahmerbilal47@gmail.com (2) Laboratory for Marine Mineral Resources, Qingdao National Laboratory for Marine Science and Technology, Qingdao 266071, China (3) Institute of Geology, University of Azad Jammu and Kashmir, Muzaffarabad, 13100, Pakistan (4) Department of Geology, Shaheed Benazir Bhutto University Sheringal, Upper Dir, Khyber Pakhtunkhwa 18000, Pakistan (5) Department of Historical Geology-Paleontology, Faculty of Geology and Geoenvironment, School of Earth Sciences, National and Kapodistrian University of Athens, Panepistimiopolis, Zografou, 15784 Athens, Greece.

Research Highlights

An integrated study on the middle-late Eocene carbonate rocks has been carried out that were deposited in the Ceno-Tethys Ocean. These rocks were formed in a transgressive-regressive environment of the shallow carbonate platform. The cement generations revealed post-depositional diagenetic stages, which further enhanced the reservoir characteristics of the strata in the Indus Basin.

Background

Yadgaar Section (Figure 1) lies on the eastern margin of the Upper Indus Basin, Pakistan (Bilal *et al.*, 2022). Middle-late Eocene Margalla Hill Limestone and Chorgali Formation act as reservoir rocks in other parts of the basin (Swati *et al.*, 2013) and are also present in the Yadgaar Section. The Lack of comprehensive study in this area makes these reservoir rocks highly attractive for sedimentological evaluations and future exploration of hydrocarbons.

Objectives

Sedimentary facies analysis and diagenetic processes of the Margalla Hill Limestone and Chorgali Formation have been carried out to understand the mature development of the Ceno-Tethys Ocean in the Upper Indus Basin (UIB), Pakistan. The effect of diagenetic alterations on these reservoir rocks was also evaluated for their possible contribution to the petroleum system of the study area.

Methods

Field and sedimentological studies were used for the microfacies analysis of the Margalla Hill Limestone and Chorgali Formation, which helped us to construct the depositional environment of the strata in the area. Scanning Electron Microscopy (SEM) is used to study the cement generations for evaluating the rocks' diagenetic stages.

Results

The middle-late Eocene Margalla Hill Limestone and Chorgali Formation are divided into nine sedimentary facies: Dolomicritic mudstone-wackestone microfacies (EMI), Green algae dominating mixed foraminiferal wacke-packstone microfacies (EMII), Ostracod and green algae dominating mudstone-wackestone microfacies (EMIII), Mixed foraminiferal micritized packstone microfacies (EMIV), *Nummulites* dominating mudstone-wackestone microfacies (EMV), Algal limestone mudstone microfacies (EMVI), *Assilina* bed wackestone-packstone microfacies (EMVII), Micritized larger benthic foraminiferal wackestone microfacies (EMVIII), and Algal limestone mudstone microfacies (EMIX). The Transgressive-Regressive environment in the Ceno-Tethys Ocean leads to the deposition of the above microfacies in the restricted marine (platform interior), open marine platform, platform edge, platform margin reef, the toe of slope apron, arid-humid platform interior, platform edge, open marine platform interior and restricted marine platform interior, respectively (Flügel, 2010) (Figure 2a). Initial post-depositional diagenetic stages are identified from the base to the top of the strata by their respective cement type i.e., the base-lower middle part of the strata demonstrates eogenetic sub-stage with the appearance of drusy cement, middle section indicates mesogenetic sub-stage by the appearance of blocky cement, while the top portion again reveals eogenetic sub stage of diagenesis by the presence of a drusy and blocky type of cement. The ascending-descending hierarchy of cement generations is directly proportional to the grade of diagenesis from base to top of the carbonate strata. Variable diagenetic effects on the different parts also increase the secondary porosity range and enhance the reservoir characteristics of the formations. The presence of representative foraminiferal microfossils indicates and assigns the relative chronological age of middle-late Eocene to carbonate formations (Figure 2b).

Conclusions

The Margalla Hill Limestone and Chorgali Formation comprised nine microfacies. Benthic foraminiferal microfossils revealed that these microfacies were deposited in the middle-late Eocene time in the Ceno-Tethys Ocean. Foraminifers

and gypsum indicate shallow marine methane hydrate settings in complex lagoon conditions. Drusy and blocky types of cement indicate that the post-depositional diagenetic stages are directly proportional to each other, respectively. Moreover, as a result of these changes the reservoir rock characteristics of the Margalla Hill Limestone and Chorgali Formation are considerably enhanced.

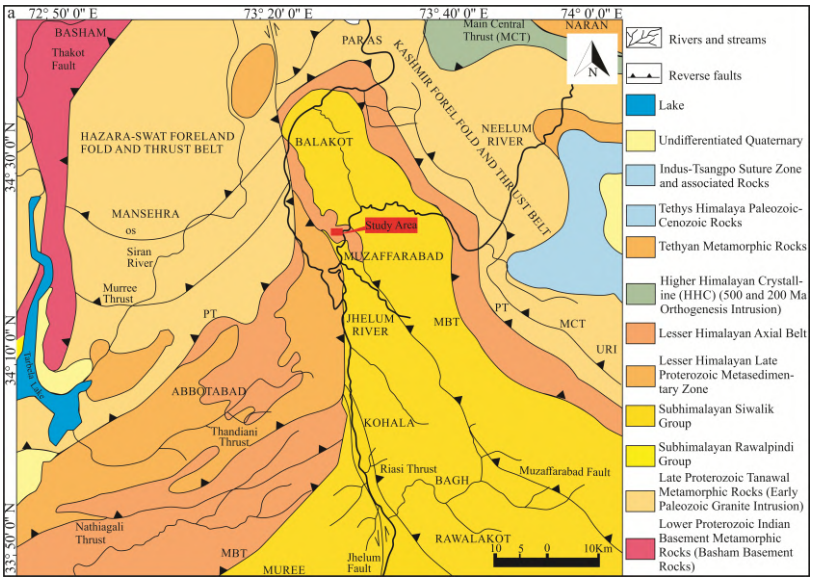

Figure 1. Showing study area of Yadgaar section in the Upper Indus Basin.

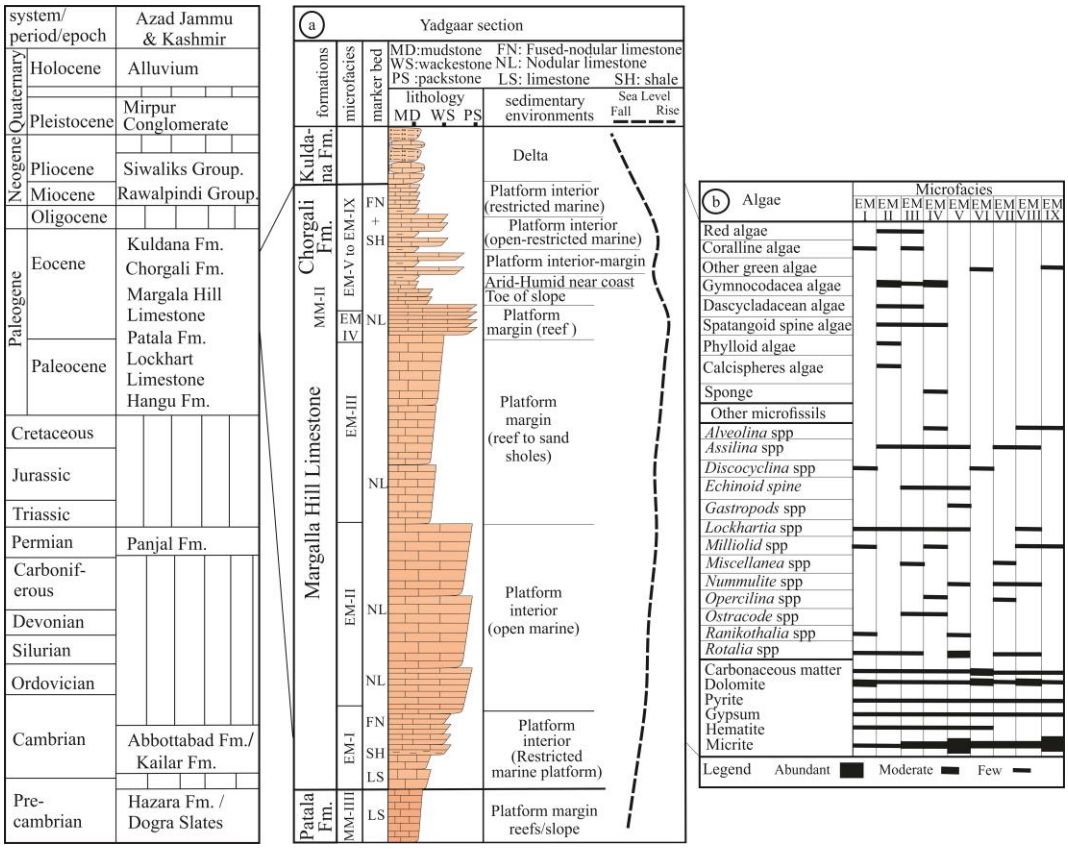

Figure 2. a) Lithology of the study Formation from Yadgaar section; b) Identified microfossils from the studied section.

References

Bilal, A., Mughal, M.S., Janjuhah, H.T., Ali, J., Niaz, A., Kontakiotis, G., Antonarakou, A., Usman, M., Hussain, S.A., Yang, R., 2022. Petrography and Provenance of the Sub-Himalayan Kuldana Formation: Implications for Tectonic Setting and Palaeoclimatic Conditions. Minerals, 12(7), 794.

Flügel, E., 2010. Microfacies of carbonate rocks: Analysis, interpretation and application, Springer-Verlag, Berlin.

Swati, M.A.F., Haneef, M., Ahmad, S., Naveed, Y., Zeb, W., Akhtar, N., Owais, 2013. Biostratigraphy and depositional environments of the Early Eocene Margalla Hill Limestone, Kohala-Bala area, Haripur, Hazara Fold-Thrust Belt, Pakistan. Journal of Himalayan Earth Sciences 46(2), 65-77.

16th International Congress of the Geological Society of Greece
17-19 October, 2022 - Patras, Greece
Bulletin of the Geological Society of Greece, Sp. Publ. 10
Ext. Abs. GSG2022-169

Sedimentation in the deep-water foredeep of the Central Pindos foreland, western Greece

C. Botziolis[1], A. G. Maravelis[2], O. Catuneanu[3] and A. Zelilidis[1]

(1) Laboratory of Sedimentology, Department of Geology, University of Patras, 26504 Rion, Greece, cbotziolis@upnet.gr (2) Department of Geology, Aristotle University of Thessaloniki, 54124 Thessaloniki, Greece (3) Department of Earth and Atmospheric Sciences, University of Alberta, Edmonton, Alberta T6G 2E3, Canada.

Introduction – Geological setting

The behavior of sediment-gravity flows is strongly influenced by the underlying seabed topography over a wide range of vertical and horizontal scales. Seabed topographic configurations control the general dispersal patterns of sediment and distribution of facies (Stevenson *et al*., 2013; Catuneanu, 2020). The origin of seabed topography may be related to active or inherited tectonic features (Li *et al.,* 2014) and depositional and erosional relief (Dakin *et al*., 2013). Submarine lobes exhibit a complicated architecture hierarchy, which generally involves lobe complex, lobe, lobe element and smaller architecture unites, although a uniform scheme remains to be established (Prélat *et al*., 2010). Gervais *et al.* (2006) noted that the composite pattern of lobe complex varied due to the variations in the confined degree of sedimentary topography, with confined lobe complex displaying lateral-migration stack while unconfined lobe complex displaying compensational stack. However, research on the differential distribution of various stacking patterns, as well as their relationships with the scale of lobe complex remain to be explored. On the Balkan Peninsula, foreland systems that were formed in response to Alpine orogenic processes are common. One of these, the Pindos foreland system (referred henceforth as PF system) in Greece, has been subjected to a few studies (e.g., Sotiropoulos *et al.*, 2008; Botziolis *et al*., 2021). The Upper Eocene - Lower Oligocene sedimentary record that is preserved in the foredeep province of the PF system (referred henceforth as PFB) offers an example of a submarine fan system with outcrops that permit the thorough analysis of facies distribution and stratigraphic architecture (Botziolis *et al*., 2021). This study provides an updated facies analysis for these deposits and links the regional stratigraphy with the evolutionary stages of the PF system.

Materials and methods

The study region is situated in the central parts of the PFB. The examined deposits are located west of the Pindos Orogen. 86 outcrops of over 1 km of cumulative length were studied and the detailed sedimentological logging, in conjunction with representative outcrop photos was employed for facies analysis. Sedimentological features, such as lithology, sedimentary structures and texture were used to define the flow types and sedimentary facies. Detailed stratigraphic cross-sections afforded the better understanding of the spatial and temporal distribution of the different depositional environments and sub-environments. The reconstruction of paleocurrent direction was achieved by 180 measurements (restored to paleohorizontal through stereonet rotation before the directions of paleoflow can be meaningfully interpreted) taken from flute and groove marks, cross-laminations, and channel-axis orientations.

Results

In the present study, the succession includes 15 depositional facies (F1 – F15). Furthermore, the different FAs are grouped together (Figure 1) and correspond to abyssal plain (FA1), outer fan (FA2 to FA5), inner fan (FA6 to FA10), and slope (FA11) settings. Basin plain deposits rise upward into outer and eventually inner fan deposits, pointing to system progradation and regional shallowing. This progradation could be due to tectonic tilting and steepening of the basin floor, increased sedimentation rates due to the Pindos thrust advance, or a combination of the two.

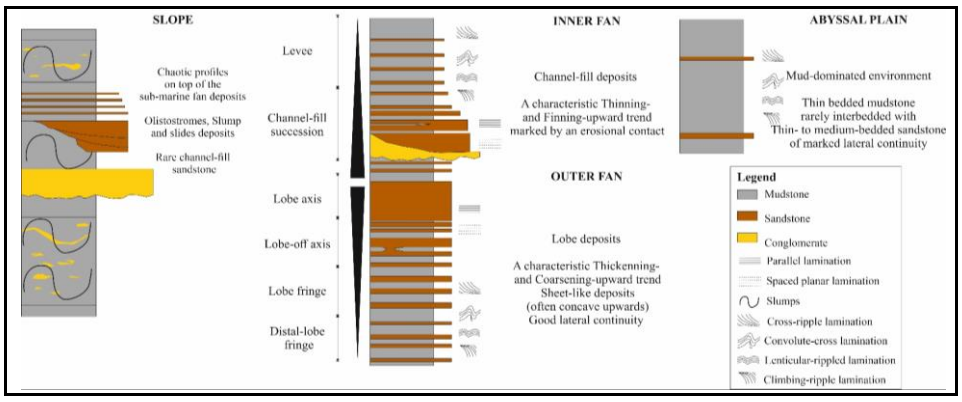

Figure 1. Facies and sequences making up the facies association characteristic of a PFB system.

Discussion - Conclusions

The sedimentary facies, sequence, and their vertical changes in facies association indicate a progressive increase in coarsening and thickening upward trends. The analysis of facies types and facies assemblages suggests an outer fan depositional environment with compensational stacking pattern. The evidence for this comes from the sand-rich lobe-axis and lobe off-axis which were built up on top of the muddy-rich lobe fringe and distal lobe fringe deposits. Such stratigraphic change entails an abrupt upward transition from mud-dominated to sand-dominated lobe deposits because there was enough room for compensation (Prelat *et al*., 2009). For this area of the PFB, an unconfined setting is postulated, as well as a relatively flat seafloor that accommodates the spatial distribution of the outer fan deposits, resulting in broad deposition. Variations in the amount of sediment available in the flows and proximity to major channels are primarily responsible for changes in the thickness and grain-size of the event beds. Each lobe can be up to 5 – 10 m thick, which is thin compared to lobe deposits found in constrained depositional conditions. The unconfined basin floor lobes exhibit markedly compensational styles of stacking to form wide and spread lobe systems (Straub and Pyles, 2012) and can be explained by the sea floor's unconfined nature, which causes system switching since sand-prone sediment cannot collect at the same location (Prelat *et al*., 2010).

However, as the deposition of the elements continued and the system progradation took place, a change in the type of stacking pattern was influenced as suggested by the internal sedimentary structures, boundary conditions, paleocurrent direction, facies, and facies association. The upwards increase in dominant sediment grain-size (from muddy abyssal plain to muddy/sandy outer and sandy/conglomeratic inner fan deposits) suggests an increase in the sediment availability because of the ongoing orogenesis. The geometry of lobes is related to the place in the basin where they were deposited. The limitation of space due to the deposition and the inherited morphology influenced the type of stacking pattern in the outer fan deposits. This setting could have caused an asymmetric basin floor in the basin, with differing degrees of confinement (Spychala *et al*., 2017). Previous unconfined settings changed to confined settings, being associated with aggradational stacking patterns (Marini *et al*., 2015). The evidence for this comes from the quick swift of paleocurrent indicators in each individual lobe-complex with absence of reflection, the sudden thickening-up of the lobe-axis (from <2 m to >4 m) deposited on top of distal-lobe/lobe fringe deposits. As a result, it is possible to conclude that at last for this area, lobe progradation had a greater impact on the PFB outer fan deposits shifting the compensation stacking (compensation) to aggradation stacking.

Acknowledgements

This research proceeded with the funding of the H.F.R.I. (Hellenic Foundation for Research & Innovation) and GSRT (General Secretarial for Research and Technology) through the research project “Global climate and sea-level changes across the latest Eocene–early Oligocene, as reflected in the sedimentary record of Pindos foreland and Thrace Basin, Greece, 80591”.

References

Botziolis, C.; Maravelis, A.; Pantopoulos, G.; Kostopoulou, S.; Catuneanu, O.; Zelilidis, A., 2021. Stratigraphic and paleogeographic development of a deep-marine foredeep: Central Pindos foreland basin, western Greece. Mar. Petrol. Geol., 128, 105012.

Catuneanu, O., 2020. Sequence stratigraphy of deep-water systems. Mar. Petrol. Geol., 114, 104238, p. 1-13.

Dakin, N., Pickering, K.T., Mohrig, D., Bayliss, N.J., 2013. Channel-like features created by erosive submarine debris flows: Field evidence from the Middle Eocene Ainsa Basin, Spanish Pyrenees, Mar. Petrol. Geol., 41, 62-71.

Gervais, A., Bruno, S., Mulder T., Gonthier E., 2006. Sandy modern turbidite lobes: A new insight from high resolution seismic data, Mar. Petrol. Geol., 23, 4, 485-502.

Li, C., Lin, J., Kulhanek, D., Williams, T., Bao, R., Briais, A., Brown, E., et al., 2014. Opening of the South China Sea and its implications for southeast Asian tectonics, climates, and deep mantle processes since the late Mesozoic. Integrated Ocean Drilling Program: Preliminary Reports (349), 1-109.

Marini, M., Milli, S., Ravnås, R., Moscatelli, M., 2015. A comparative study of confined vs. semi-confined turbidite lobes from the Lower Messinian Laga Basin (Central Apennines, Italy): implications for assessment of reservoir architecture. Mar. Petrol. Geol., 63,142-165.

Prelat, A., Hodgson, D.M., Flint, S.S., 2009. Evolution, architecture, and hierarchy of distributary deep-water deposits: a high-resolution outcrop investigation from the Permian Karoo Basin, South Africa. Sed., 56, 2132–2154.

Prélat, A., Covault, J.A., Hodgson, D.M., Fildani, A., Flint. S.S., 2010. Intrinsic controls on the range of volumes, morphologies, and dimensions of submarine lobes: Sedimentary Geol., 232, 66- 76.

Prelat, A., Hodgson, D.M., 2013. The full range of turbidite bed thickness patterns in submarine lobes: controls and implications. J. Geol. Soc., 170, 209–214.

Sotiropoulos, S., Triantaphyllou, M., Kamberis, E., Tsaila-Monopolis, S., 2008. Paleogene terrigenous (flysch) sequences in Etoloakarnania region (W. Greece), Plankton Stratigraphy and paleoenvironmental implications, Geobios, 41, 415-433.

Spychala, Y.T., Hodgson, D.M., Stevenson, C.J., Flint, S.S., 2017. Aggradational lobe fringes: The influence of subtle intrabasinal seabed topography on sediment gravity flow processes and lobe stacking patterns. Sed. 64, 582–608.

Stevenson, C.J., Talling, P.J., Wynn, R.B., Masson, D.G., Hunt, J.E., Frenz, M., Akhmetzhanhov, A., Cronin, B.T., 2013. The flows that left no trace: very large volume turbidity currents that bypassed sediment through submarine channels without eroding the sea floor: Marine and Petroleum Geology, v. 41, p. 186–205.

Straub, K.M, Pyles, D.R., 2012. Quantifying the hierarchical organization of compensation in submarine fans using surface statistics. J. Sed. Res., 82, 889–98.

16th International Congress of the Geological Society of Greece
17-19 October, 2022 - Patras, Greece
Bulletin of the Geological Society of Greece, Sp. Publ. 10
Ext. Abs. GSG2022-170

Trace fossils from Upper Eocene to Lower Oligocene deep-sea deposits of the foreland Pindos Basin, western Greece

C. Botziolis[1], A. G. Maravelis[2], A. Uchman[3] and A. Zelilidis[1]

(1) Laboratory of Sedimentology, Department of Geology, University of Patras, 26504 Rion, Greece, cbotziolis@upnet.gr (2) Department of Geology, Aristotle University of Thessaloniki, 54124 Thessaloniki, Greece (3) Jagiellonian University, Faculty of Geography and Geology, Institute of Geological Sciences, Gronostajowa 3a, 30-387 Kraków, Poland.

Introduction – geological setting

Despite advances in our understanding of deep-sea fan systems from a sedimentological point of view, there are a few studies that combine sedimentological and ichnological data. This is especially true in deep and intermediate water depth depositional systems, where only sporadic efforts have been made to distinguish the ichnological signature of various gravity-flow system types (e.g., Callow *et al.*, 2014). The study area represents a submarine fan system overlying Eocene carbonates, with a general trend from west to east, from carbonates through abyssal plain to outer (exhibiting a coarsening- and thickening-upward trend, indicative of a lobe stacking system) and inner (exhibiting a thinning- and finning-upward trend, indicative of a channel-levee stacking system) fan deposits, demonstrating system progradation (Botziolis *et al.*, 2021). Based on palaeocurrent data and facies distributions, regional palaeogeographical reconstructions show that the basin was derived from the Pindos thrust belt to the east (Alexander *et al.*, 1990; Botziolis *et al.*, 2021) and within the basin, the main flow was axial (Botziolis *et al.*, 2021).

Trace fossil assemblages

The ichnotaxa *Trichichnus* isp., *Chondrites* isp., *Planolites* isp., *Thalassinoides* isp., *Zoophycos* isp., and a variety of graphoglyptids are components the trace fossil assemblage of the examined area (Figure 1), which has a characteristic diverse upwards trend. Most of them are visible in cross section, which precludes determinations at the ichnospecies level for most of them.

Figure 1. Trace fossils of the PFB: a) *Trichichnus* isp., b) *Chondrites* isp. (note the difference in size of *Ch. intricatus* and *Ch. targionii*), c) *Planolites* isp. along with *Thalassinoides* isp., d) *Thalassinoides* isp., e) *Zoophycos* isp. with the characteristic apex, f) *Megagrapton* isp., g) *Ophiomorpha rudis*, h) *Ophiomorpha annulata*, i) *Zoophycus* isp., j) *Helminthorhaphe japonica*, k) *Scolicia strozzii*, l) *Paleodictyon* isp., m) *Helminthopsis* isp., *Helminthoidichnites* isp. and *Gordia* isp., n) *Helicolithus ramosus*.

Trace fossil abundance and distribution

The trace fossils in the lower part of the studied section (calcareous turbidities, described as transitional beds from the Eocene limestones to abyssal plain deposits) include *Trichichnus* isp., *Chondrites* isp., *Planolites* isp., *Thalassinoides* isp., and *Zoophycos* isp. Major part of the deposits consists of grey calcareous mudstone beds interbedded with calcareous sandstone beds. All ichnotaxa show a consistent record, except for *Zoophycos*, which was restricted to a few horizons. These horizons indicate an episodic increase in nutrients on the seafloor (Löwemark, 2015). The overlying section (abyssal plain deposits) consists of non-calcareous grey mudstone, which predominantly shows disrupted primary lamination indicating very shallow burrowing. *Chondrites* isp., *Planolites* isp., and *Thalassinoides* isp. are the only trace fossils which occur rarely therein. Rarely interbedded sandstone beds do not possess any evidence of bioturbation and display undisturbed ripple cross-lamination.

Up-section (outer fan deposits) the same trace fossil along with the presence of graphoglyptids rarely occur. *Chondrites* shows a less continuous record, and *Thalassinoides* isp. and *Planolites* isp. are common, while graphoglyptids occur only sporadically. Unbioturbated sandstone beds with primary lamination occur as well and record hostile episodes negatively affecting bioturbation. As the deposition of the deep-sea fan deposits progressed, a general rising trend in occurrences of

graphoglyptids was observed. Overall, ichnodiversity is high in most of the lobe-related settings investigated, with an increase in ichnodiversity from the lobe off-axis to the lobe fringe deposits. The lobe-axis deposits contain low diverse ichnoassemblages, indicating that there was limited time for substrate colonization between the emplacement of high-density turbidity currents and the environment was less stable. Furthermore, bed amalgamations imply extensive or total erosion of mudstone layers and tops of sandstone beds, reducing preservational potential pre-depositional trace fossils. Both *Ophiomorpha rudis* and *Ophiomorpha annulata* exhibit a general rise in abundance in both lobe-axis and overlaying channel-levee settings. *Scolicia* isp. is uncommon in distal lobe-fringe deposits, but it is abundant in channel-levee deposits, where it occurs in the lower and upper bedding surface. *Helminthopsis* isp., *Helminthoidichnites* isp., *Paleodictyon* isp., and *Scolicia strozzii* are the only ichnofossils found in the levee deposits.

Conclusions

The substantial changes in trace fossil assemblages within a very narrow range of depositional settings can be attributed to a number of variables. To begin with, the late Eocene basin floor environment is dominated by carbonates (micritic limestone) interbedded with calcareous turbidities, which become more common with the Eocene times. According to previous research (e.g. Uchman, 2007), mixed carbonate–siliciclastic deep-marine deposits are characterized by lower diversity of trace fossils than siliciclastic deposits. This is due in part to the monotonous pattern of sedimentation in limestone alternations, which is likely depleted of organic matter in comparison to siliciclastic sediments, which get nutrients/organic matter pulses from shallower water and the terrestrial realm. Because there are rare turbidity currents supplying well-oxygenated water, oxygenation is likely to be lower at the more distant basin floor. Oxygen levels influenced ichnodiversity, with *Trichichnus* isp. and *Chondrites* isp. being the first to appear when anoxia transits to dysoxia (e.g., Wetzel, 1991). The occurrence of *Zoophycos* isp. in the late Eocene basin floor is linked to the inflow of calcareous turbidity currents (Gianetti and McCann, 2010), and is most likely the result of opportunistic colonization of event beds (Ekdale, 1985). Graphoglyptids, which are characteristic of well oxygenated and moderately oligotrophic conditions (Rodríguez-Tovar et al., 2010), mark the commencement of siliciclastic deposition in the basin. An established oxic background, affected by episodic sediment supply in the form of gravity-flow events and the accompanying suspension clouds, is attributed to the upward increase in graphoglyptid diversity.

Previous studies (e.g. Uchman and Wetzel, 2012) suggested that proximal-to-distal relationships within typical Nereites ichnofacies yield enough differences to assign sub-ichnofacies: the Nereites (mud-rich fan fringe-basin floor environments), the Paleodictyon (sand-rich over channel and distal lobe related environments), and the Ophiomorpha rudis sub-ichnofacies (channel and proximal lobe related environments). Sub-ichnofacies like these offers a quick and easy approach to categorize underwater fan trace fossil assemblages based on their overall location within the system. However, because all these sub-ichnofacies can be found in a same stratigraphic succession, they are useless for determining precise depositional conditions. If trace fossil assemblages are to be used to reliably distinguish between sub-environments within submarine fans, detailed data on ichnodiversity and intensity trace fossil assemblages must be compiled in conjunction with sedimentological criteria-based interpretation of depositional environments.

Acknowledgements

This research proceeded with the funding of the H.F.R.I. (Hellenic Foundation for Research & Innovation) and GSRT (General Secretarial for Research and Technology) through the research project "Global climate and sea-level changes across the latest Eocene–early Oligocene, as reflected in the sedimentary record of Pindos foreland and Thrace Basin, Greece, 80591".

References

Alexander J., Nichols G.J., Leigh S., 1990. The origins of marine conglomerates in the Pindus foreland basin, Greece. Sedimentary Geol., 66, 213–254.

Botziolis C., Maravelis A., Pantopoulos G., Kostopoulou S., Catuneanu O., Zelilidis A., 2021. Stratigraphic and paleogeographic development of a deep-marine foredeep: Central Pindos foreland basin, western Greece. Mar. Petrol. Geol., 128, 105012.

Callow R.H.T., Kneller B., Dykstra M., McIlroy D., 2014. Physical, biological, geochemical and sedimentological controls on the ichnology of submarine canyon and slope channel systems, Mar. Petrol. Geol, 54, 144–166.

Ekdale A.A., 1985. Paleoecology of the marine endobenthos. Palaeogeogr. Palaeoclimat. Palaeoecol., 50: 63–81.

Giannetti A., McCann T., 2010. The Upper Paleocene of the Zumaya Section (Northern Spain): review of the ichnological content and preliminary palaeoecological interpretation. Ichnos, 17, 137–161.

Löwemark L., 2015. Evidence for targeted elasmobranch predation on thalassinidean shrimp in the Miocene Taliao sandstone formation, NE Taiwan. Lethaia, 48, 227–234.

Rodríguez-Tovar F.J., Uchman A., 2006. Ichnological analysis of the Cretaceous-Palaeogene boundary interval at the Caravaca section, SE Spain. Palaeogeogr. Palaeoclimat. Palaeoecol., 242, 313–325.

Uchman A., 2007 Deep-sea trace fossils from the mixed carbonate siliciclastic flysch of the Monte Antola Formation (Late Campanian-Maastrichtian), North Apennines, Italy. Cretaceous Res., 28, 980–1004.

Uchman A., Wetzel A., 2012. Deep-sea fans. In: Knaust D., Bromley R.G. (Eds.), Trace fossils as indicators of sedimentary environments. Developments in Sedimentology, 64, 643–672.

Wetzel A., 1991. Ecologic interpretation of deep-sea trace fossil communities. Palaeogeogr, Palaeoclimat. Palaeoecol., 85, 647–691.

16th International Congress of the Geological Society of Greece
17-19 October, 2022 - Patras, Greece
Bulletin of the Geological Society of Greece, Sp. Publ. 10
Ext. Abs. GSG2022-413

Preliminary results of coal examination through Raman Spectroscopy

A. Sougioltzis[1], V. Xanthopoulou[1,2], K. Perleros[1], S. Kalaitzidis[1], K. Christanis[1]
(1) Department of Geology, University of Patras, Patras, Greece, christan@upatras.gr (2) Laboratory of Electronic Microscopy and Microanalysis, University of Patras, Patras, Greece.

The objective of the study is the examination of coal samples of various ranks through a Raman Spectrometer in order to identify and define the Raman parameters in the obtained spectra. The aim is the affirmation of applicability of Raman Spectroscopy in coalification studies.

Polished blocks of eight samples of known coal rank (peat, lignite, subbituminous coal, bituminous coal C, bituminous coal B, bituminous coal A, anthracite and graphite) defined by vitrinite reflectance, are examined. Raman spectra were collected using Ar+ excitation source having wavelength 514 nm coupled with A Jobin-Yvon Horiba LabRam-HR micro Raman spectrometer equipped with an Olympus microscope and using a 50x objective. The laser power was about 4.3 mW and the spectra were recorded with an acquisition time of 10 accumulations per 2 seconds. The projection of the results and peak fitting is carried out through the Origin Pro 9 software. The nomenclature applied follows this proposed by Delano *et al.* (2019).

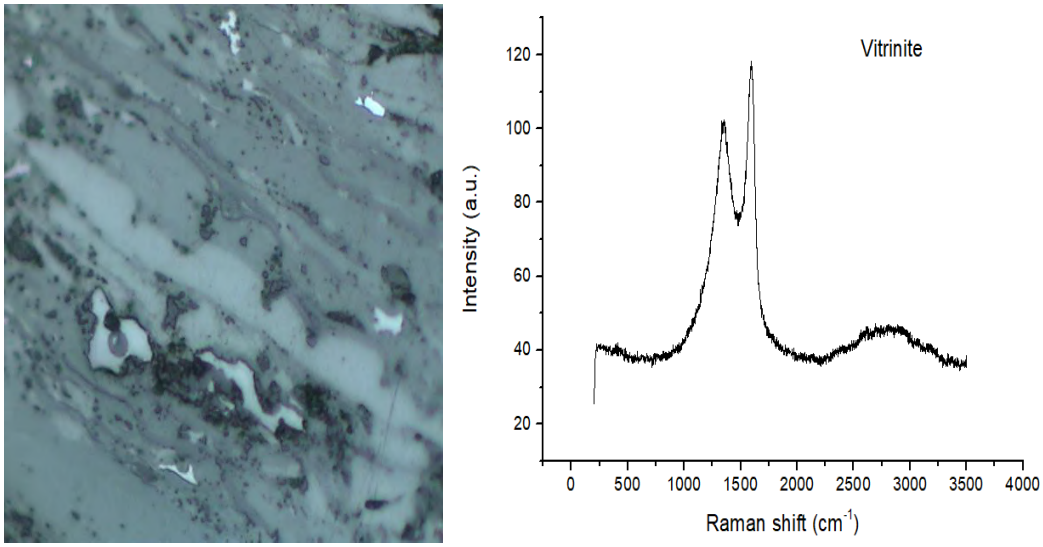

Figure 1. Raman spectrum of a vitrinite maceral in bituminous coal C (D-peak at 1352 cm^{-1} and G-peak at 1592 cm^{-1}).

Even though the parameter values in the obtained spectra slightly differ from each other, they appear to confirm a decrease in the G-FWHM, R1, D-FWHM values and an increase in the RBS values by rank increasing from bituminous B to graphite. The results correlate to those of previous studies on organic matter (Lünsdorf, 2016; Delano *et al.*, 2019) concerning the position and width of the D- (1000-1450 cm^{-1}) and G-bands (1450-1800 cm^{-1}), which are the value range of the bandwidths of interest when it comes to organic matter. Moreover, the same applies to correlation parameters such as RBS, which is the spectral distance between the positions of the D-peak (usually at 1340-1360 cm^{-1}) and the G-peak (usually at 1580 cm^{-1}). Lastly G-FWHM, the spectral width of the maximum peak of G-band at half maximum (50%) intensity of scattered phonons, along with R1, the ratio of D- to G-peak intensity, also project comparable results.

This study provides promising results concerning the applicability of Raman Spectroscopy on high rank coal, since the obtained spectra and the RBS and G-FWHM could be correlated with vitrinite reflectance. They seem to be proportional and inversely proportional, respectively, to the increase of vitrinite reflectance, hence to the rank. Low rank coal demands further study since the corresponding samples were unable to provide measurable results due to fluorescence and background noise. Smith and Dent (2005) propose the use of powdered samples concerning heterogenous fluorescent and solid organic matter, which constitutes the next step of the current research.

Acknowledgement

The authors would like to thank the Laboratory of Electron Microscopy and Microanalysis of the Faculty of Natural Sciences, University of Patras, for conducting the analysis and providing the equipment and software for the extrapolation of data.

References

Delano, G.H., Jarvis, I., Gillmore, G., Stephenson, M., 2019. Raman spectroscopy as a tool to determine the thermal maturity of organic matter: Application to sedimentary, metamorphic and structural geology. Earth-Science Reviews 198, 102936.

Lünsdorf, N.K., 2016. Raman spectroscopy of dispersed vitrinite - Methodical aspects and correlation with reflectance. International Journal of Coal Geology 153, 75-86.

Smith, E., Dent, G., 2005. Modern Raman Spectroscopy – A practical approach. Southern Gate, Chichester, John Wiley & Sons Ltd., 202 pp.

16th INTERNATIONAL CONGRESS of the
GEOLOGICAL SOCIETY OF GREECE

S2. Quaternary processes and geoenvironments in the active Corinth Rift

OUR EARTH, OUR HOME

16th International Congress of the Geological Society of Greece
17-19 October, 2022 - Patras, Greece
Bulletin of the Geological Society of Greece, Sp. Publ. 10
Ext. Abs. GSG2022-027

Did the Gulf of Corinth become a Black Sea-type basin during late Quaternary glacial periods?

F. Marret[1], E. Fatourou[2], A. Kafetzidou[2], K. Panagiotopoulos[2,3], K. Kouli[2]

(1) School of Environmental Sciences, University of Liverpool, UK, F.Marret@liverpool.ac.uk (2) National and Kapodistrian University of Athens, Natural Sciences, Geology and Geoenvironment, Greece (3) Institute of Geology and Mineralogy, University of Cologne, Germany.

The Gulf of Corinth (GoC) is a characteristically very active continental rift system, with currently two connections to the Mediterranean Sea, the shallow Rion Sill (-60m water depth) to the west and the Corinth Canal to the East (-8m water depth). Further details of its Quaternary history have been recently revealed with the findings from the IODP Exp. 381 (e.g., McNeill et al., 2019). Sedimentological, geophysical and micropalaeontological data indicated that global sea level fluctuations have played a major role in the GoC's connection to the Mediterranean Sea. Recent findings from Fatourou et al. (2022) show a detailed record of sea-surface condition indicators, highlighting periods of isolation which were characterized by brackish conditions. Interestingly, palynological indicators of brackish condition indicators were first described from the early Holocene of the Black Sea (Wall et al., 1973). The Black Sea is a unique environment, with relatively brackish conditions (salinity of ~18-19) and a narrow connection to the Mediterranean Sea through the Bosphorus Strait. It is a deep basin (~2200 m water depth) and waters are anoxic below 200m. Due to these unusual conditions, conventional palaeoceanographic proxies such as planktonic foraminifera are absent and other proxies were found to be more suitable to reconstruct the evolution of the Black Sea. Organic-walled inoflagellate cysts are produced by a major phytoplankton group, second to the diatoms and are found in many aquatic systems. They are mostly abundant in marine waters but can also thrive in freshwater conditions. Dinoflagellate cyst records from the Black Sea were able to reconstruct late Quaternary past environmental conditions, in particular the timing and the amplitude of the reconnection of the Black Sea with the Mediterranean Sea at the beginning of the Holocene (e.g., Marret al., 2009 Aksu and Hiscott, 2022).

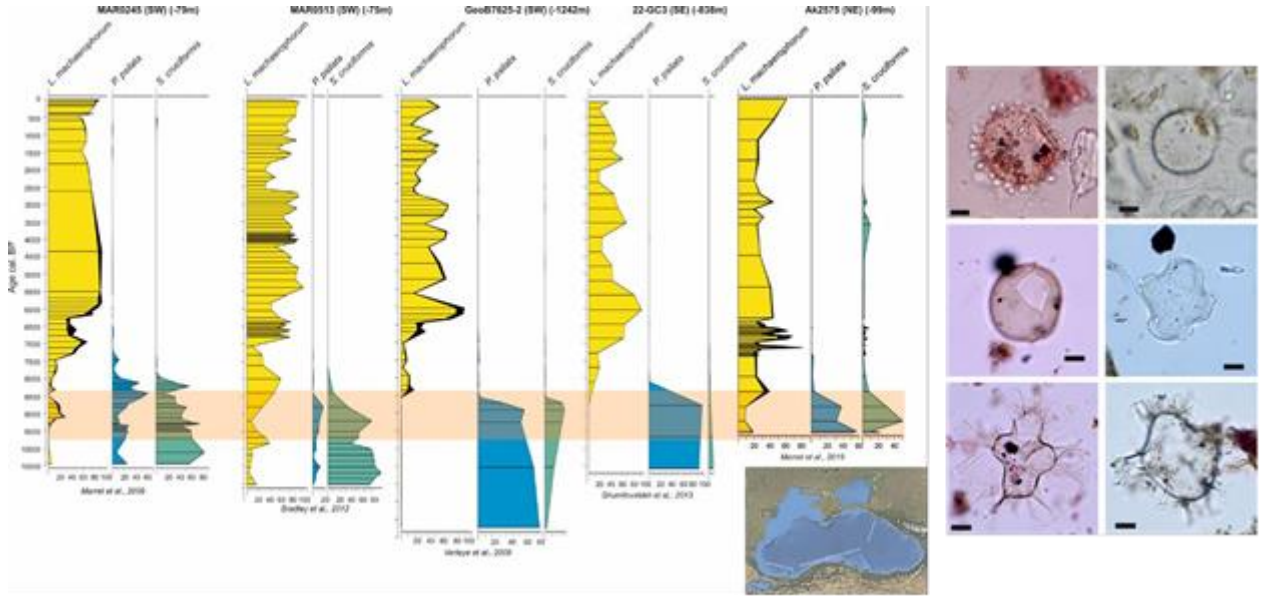

Figure 1: Compilation of dinocyst records from the Black Sea, with euryhaline species (*L. machaerophorum*) and brackish species (*P. psilata* and *S. cruciformis*). The horizontal shaded band indicates the time-interval when the reconnection between the Black Sea and the Mediterranean Sea took place. Photos of *L. machaerophorum* (top), *P. psilata* (middle) and *S. cruciformis* (bottom). Scale bar is 10 microns.

In parallel, palynological studies in the Caspian Sea enabled to better constrain the ecological affinities of certain species which were thought to be endemic to the Black Sea (Marret et al., 2004; Mudie et al., 2017). Interestingly, isolated intervals in the GoC are characterized by assemblages of dinoflagellate cysts which are typical of the early Holocene of the Black Sea, and currently occurring in the Caspian Sea. Therefore, the question ca n be asked how these brackish species of Pontian origin can regularly appear in the GoC.

Acknowledgements

The research work was supported by the Hellenic Foundation of Research and Innovation (H.F.R.I) under the "First Call for H.F.R.I. Research Projects to support Faculty members and Researchers and the procurement of high-cost research equipment grant" (Project Number: 1026, Quaternary Environmental Changes in the Corinth Rift Area: the IODP 381 palynological record: QECCoRA).

References

Aksu A. And Hiscott R.N., 2022. Persistent Holocene outflow from the Black Sea to the eastern Mediterranean Sea still contradics the Noah's Flood Hypothesis: A review of 1997-2021 evidence and a regional paleoceanographic synthesis for the latest Pleistocene-Holocene. Earth-Science Reviews 227, 103960 https://doi.org/10.1016/j.earscirev.2022.103960

Fatourou E., Kafetzidou A., Marret F., Panagiotopoulos K., Kouli K., 2022. Paleoenvironmental changes affecting dinocyst assemblages in the Corinth Gulf (NE Mediterranean Sea). Abtsract for the 16th International Congress of the Geological Society of Greece.

Marret F, Leroy S, Chalie F et al. (2004) New organic-walled dinoflagellate cysts from recent sediments of Central Asian seas. Review of Palaeobotany and Palynology 129: 1–20.

Marret F, Mudie P, Aksu A et al. (2009) A Holocene dinocyst record of a two-step transformation of the Neoeuxinian brackish water lake into the Black Sea. Quaternary International 197: 72–86.

McNeill L, Shillington DJ, Carter GDO, Everest J, Gawthorpe R, Miller C, Phillips M, Collier R, Cvetkoska A, De Gelder G, Diz Ferreiro P, Doan M.-L, Ford M, Geraga M, Gillespie J, Hemelsdael R, Herrero-Bervera E, Ismaiel M, Janikian L, Kouli K, Le Ber E, Li S, Maffione M, Mahoney C, Machlus ML, Michas G, Nixon C, Oflaz SA, Omale AP, Panagiotopoulos K, Pechlivanidou S, Sauer S, Seguin J, Sergiou S, Zhakarova N, Green S., 2019. High-resolution record reveals climate-driven environmental and sedimentary changes in an active rift. Scientific reports 9, 1-11.

Mudie, P. J., Marret, F., Mertens, K. N., Shumilovskikh, L., Leroy, S. A., 2017. Atlas of modern dinoflagellate cyst distributions in the Black Sea Corridor: from Aegean to Aral Seas, including Marmara, Black, Azov and Caspian Seas. Marine. Micropaleontology 134, 1-152. https://doi.org/10.1016/j.marmicro.2017.05.004

Wall, D., Dale, B., Harada, K., 1973. Description of new fossil dinoflagellates from the Late Quaternary of the Black Sea. Micropaleontology 19 (1), 18–31.

16th International Congress of the Geological Society of Greece
17-19 October, 2022 - Patras, Greece
Bulletin of the Geological Society of Greece, Sp. Publ. 10
Ext. Abs. GSG2022-030

Paleoenvironmental changes affecting dinocyst assemblages in the Corinth Gulf (NE Mediterranean Sea)

E. Fatourou[1], A. Kafetzidou[1], F. Marret[2], K. Panagiotopoulos[1,3], K. Kouli[1]

(1)National and Kapodistrian University of Athens, Natural Sciences, Geology and Geoenvironment, Greece, efatourou@geol.uoa.gr (2) School of Environmental Sciences, University of Liverpool, UK (3)Institute of Geology and Mineralogy, University of Cologne, Germany.

Site M0078, a 610 meters long sequence, is located at the central part of the Corinth Gulf, in central Greece, and was retrieved during the IODP Exp. 381. The area holds a long record of syn-rift sedimentation, with the earlier rifting phase being exposed onshore, while the younger phase deposits are found within the Gulf. As a result of its geomorphology, this semi-enclosed basin is sensitive to Quaternary climatic changes and sea level fluctuations. Today, the Corinth Gulf is connected at its western part with the open Mediterranean Sea through the shallow Rion sill (-60m water depth). In the past, the Gulf was repeatedly isolated from and reconnected to the Mediterranean Sea during glacial/interglacial cycles (McNeill et al., 2019a), resulting in the amplification of paleoenvironmental gradients. Alternation of marine and isolate/semi-isolated intervals and their impact on the local aquatic ecosystems were investigated through the palynological analysis of the site M0078 deposits, focusing on organic-walled dinoflagellate cysts. Dinocysts are an excellent proxy for paleoenvironmental reconstructions, as they are sensitive to environmental changes and thrive in a wide range of climatic conditions and habitats, from fresh water to the open ocean.

The M0078 site deposits were consistently sampled at a mean 2m interval, spanning several climatic cycles since the Middle Pleistocene. The chemical processing of the samples followed the protocol used during the Exp.381 (McNeill et al., 2019b). Three-hundred twenty (320) samples were analyzed and originated from both marine, isolated, and transitional intervals. An average of 200 dinoflagellate cysts were counted, while samples containing fewer than 50 cysts were not included in the analysis. The dataset was subjected to non-metric multidimensional scaling (nMDS) and to Principal Component Analysis (PCA).

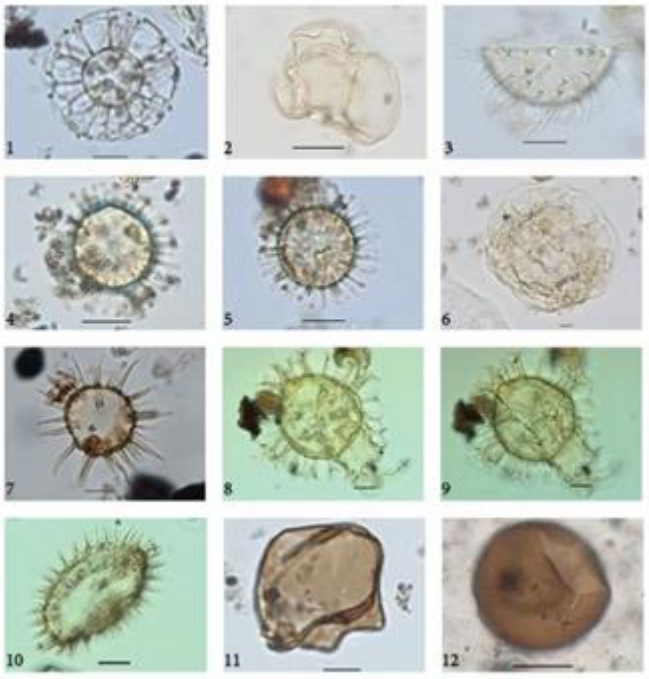

Figure 1. Marine representatives: 1. *N. labyrinthus*, 2. *A. choane*, 3. *P.zoharyi*, 4-5. *O. centrocarpum*, 6. *T. vancampoae*, 7. *L. machaerophorum* s.l., 8-9. *S. mirabilis*, 10. *S. quanta*, 11. *Q. concreta*, 12. *Brigantedinium* sp.. Scale bar: 20μm.

The microscopic analysis recorded the presence of more than 35 dinocyst species. Dinoflagellate cysts are sorted in two major ecogroups presenting alternations between marine and isolated/brackish conditions. The marine intervals are

characterized by high dinocyst diversity (30 different species), with several representatives of the *Spiniferites* group, as well as *N. labyrinthus*, *O. centrocarpum*, *L. machaerophorum* s.l., *P. zoharyi*, *T. pellitum*, *B. tepikiense* and representatives of the *Impagidinium* group.

The brackish intervals are characterized by the presence of *S. cruciformis*, *P. psilata*, *C. rugosum*, *I. caspienense* and *L. machaerophorum* with short processes (<10μm). The most characteristic species were the low-salinity indicators *S. cruciformis* and *P. psilata*. In several samples, *S. cruciformis* is dominant, characterizing the assemblage as monospecific.

The correlation between our brackish dinocyst assemblages with existing sediment core records and surface sediment samples shows many similarities with the Black-, Caspian- and Marmara- Seas (Mudie *et al*., 2017).

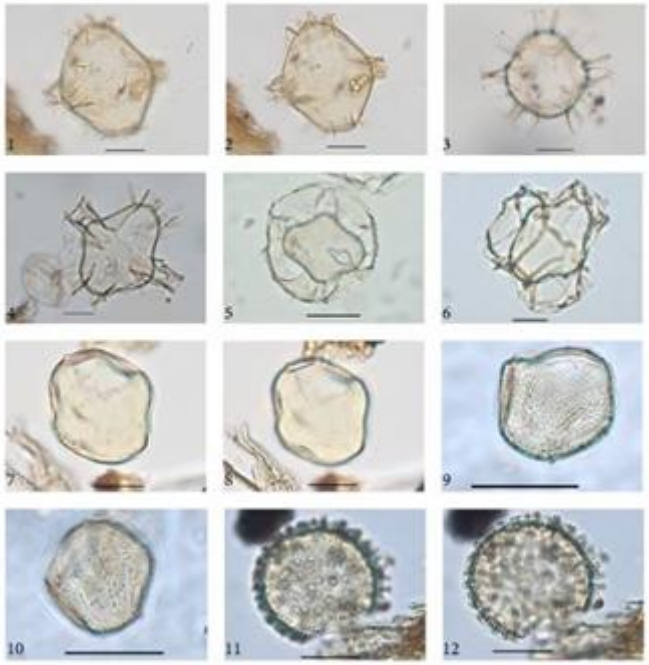

Figure 2. Low salinity indicators: 1-6. *S. cruciformis*, 7-8. *P. psilata*, 9-10. *C. rugosum*, 11-12. *L. machaerophotum* s.p.. Scale bar: 20μm.

The alternations between marine and brackish conditions recorded in the Corinth Gulf reveal changes in surface water salinity and temperature, in response to the Quaternary glacial – interglacial cycles. These seem to be in good agreement with global sea-level changes and trace orbital driven climate shifts as shown in the global Marine Isotope Record.

Acknowledgements

The research work was supported by the Hellenic Foundation of Research and Innovation (H.F.R.I) under the "First Call for H.F.R.I. Research Projects to support Faculty members and Researchers and the procurement of high-cost research equipment grant" (Project Number: 1026, Quaternary Environmental Changes in the Corinth Rift Area: the IODP 381 palynological record: QECCoRA).

References

Marret, F., Fatourou, E., Kafetzidou, A., Panagiotopoulos, K., Kouli, K., 2022. Did the Gulf of Corinth become a Black Sea-type basin during late Quaternary glacial periods?. Abtsract for the 16th International Congress of the Geological Society of Greece.

McNeill L, Shillington DJ, Carter GDO, Everest J, Gawthorpe R, Miller C, Phillips M, Collier R, Cvetkoska A, De Gelder G, Diz Ferreiro P, Doan M.-L, Ford M, Geraga M, Gillespie J, Hemelsdael R, Herrero-Bervera E, Ismaiel M, Janikian L, Kouli K, Le Ber E, Li S, Maffione M, Mahoney C, Machlus ML, Michas G, Nixon C, Oflaz SA, Omale AP, Panagiotopoulos K, Pechlivanidou S,

Sauer S, Seguin J, Sergiou S, Zhakarova N, Green S., 2019. High-resolution record reveals climate-driven environmental and sedimentary changes in an active rift. Scientific reports 9, 1-11.

McNeill, L.C., Shillington, D.J., Carter, G.D.O., Everest, J.D., Le Ber, E., Collier, R.E., Cvetkoska, A., De Gelder, G., Diz P., Doan,

M. L., Ford M., Gawthorpe, R. L., Geraga, M., Gillespie, J., Hemelsdaël, R., Herrero-Bervera, E., Ismaiel, M., Janikian, L., Kouli, K., Li, S., Machlus, M.L., Maffione, M., Mahoney, C., Michas, G., Miller, C., Nixon, C. W., Oflaz, S. A., Omale, A.P.,

Panagiotopoulos, K., Pechlivanidou, S., Phillips, M.P., Sauer S., Seguin, J., Sergiou, S., Zakharova, N.V., 2019b. Corinth active rift development. Proceedings of the International Ocean Discovery Program, 381. https://doi.org/10.14379/iodp.proc.381.104.2019

Mudie, P. J., Marret, F., Mertens, K. N., Shumilovskikh, L., Leroy, S. A., 2017. Atlas of modern dinoflagellate cyst distributions in the Black Sea Corridor: from Aegean to Aral Seas, including Marmara, Black, Azov and Caspian Seas. Marine. Micropaleontology 134, 1-152. https://doi.org/10.1016/j.marmicro.2017.05.004

16th International Congress of the Geological Society of Greece
17-19 October, 2022 - Patras, Greece
Bulletin of the Geological Society of Greece, Sp. Publ. 10
Ext. Abs. GSG2022-035

Unique shifts in the vegetation composition of a typical Mediterranean setting (Gulf of Corinth, Greece) during successive Quaternary climatic cycles

A. Kafetzidou[1], E. Fatourou [1], K. Panagiotopoulos[1,2], F. Marret[3], K. Kouli[1]

(1) Department of Geology and Geoenvironment, National and Kapodistrian University of Athens, Greece, akafetzidou@geol.uoa.gr (2) Institute of Geology and Mineralogy, University of Cologne, Germany (3) School of Environmental Sciences, University of Liverpool, UK.

The sedimentary record of site M0078, located in the Gulf of Corinth, was retrieved within the IODP Exp. 381. The Gulf of Corinth is a semi-enclosed basin, sensitive to Quaternary climatic oscillations and sea-level fluctuations and was repeatedly isolated from and reconnected to the Mediterranean Sea (McNeill et al., 2019a). The palynological analyses of the deposits are preformed within the QECCoRA project and aim to: a) study the glacial-interglacial vegetation history in the southernmost Balkan tree refugium at a millennial scale b) constrain the timing of Quaternary extinctions of Tertiary relict tree taxa, and c) distinguish global from local drivers of environmental change by studying the alternation between marine and isolated intervals and its impact on local ecosystems.

The M0078 sequence, recovered during the IODP Exp. 381 drilling campaign in late 2017, has been sampled at ~2m intervals aiming to obtain a millennial temporal resolution. The chemical processing of the samples followed the protocol used during the Exp.381 (McNeill et al., 2019b). More than 400 samples have been palynologically analyzed under a transmitted light microscope Zeiss Axiolab 5 at magnifications of ×400 and ×1000. A mean pollen sum of 250 terrestrial grains were counted, while samples containing fewer than 100 grains were not included in the analysis. Pollen, dinoflagellate cysts and all other palynomorphs were counted in the same sample allowing a direct land-sea correlation.

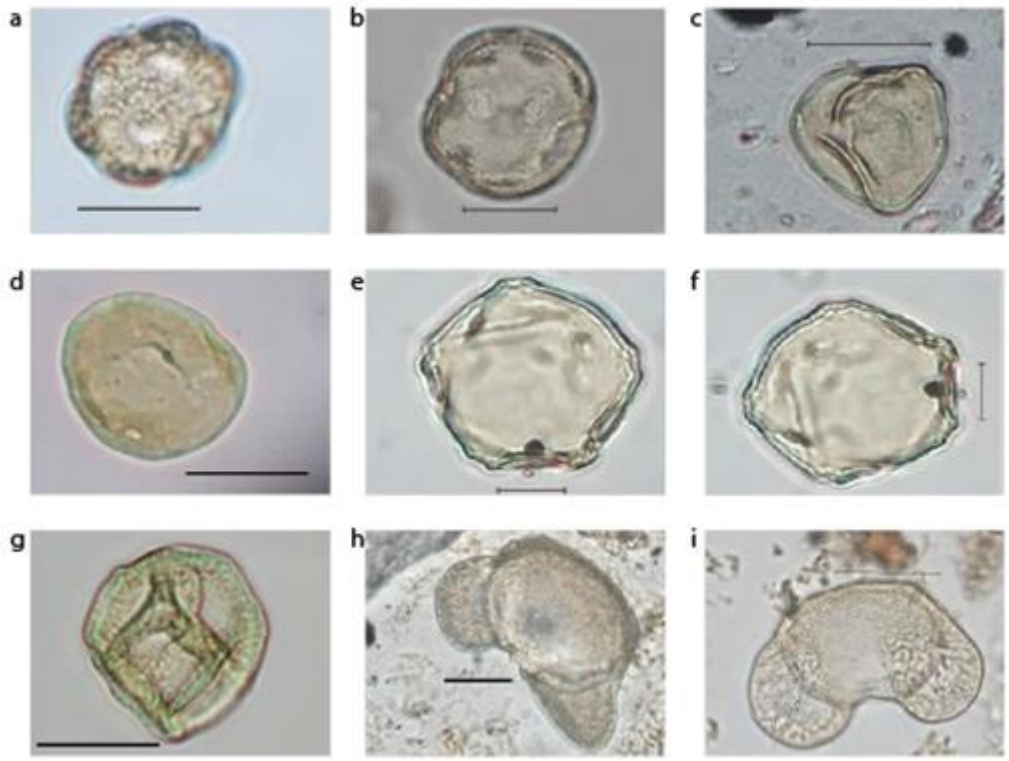

Figure 1. Light microscope photographs of selected Tertiary relict species identified in M0078A core in Corinth Gulf; a, b) *Liquidambar* sp. (21.43, 73.31 mbsf, c, d) *Carya* sp. (72.6, 73 mbsf), e, f) *Pterocarya* sp. (57.13, 60.53mbsf), g) *Tricolpoporollenites sibiricum* (514.66 mbsf), h, i) *Cedrus* sp. (54.76, 160.16 mbsf), Scale bar: 20μm.

The dinocyst assemblages record distinct alternations between marine and brackish conditions in the Gulf in response to global sea-level changes and can be correlated with global Marine Isotope Stages. At this Mediterranean setting, the vegetation response during these glacial/interglacial cycles appears to be more complex in comparison with the aquatic

ecosystem. The present study presents the unique shifts in vegetation composition and succession of Mediterranean species in the southernmost Balkan tree refugium at a millennial scale since the Middle Pleistocene. Interglacial intervals show high terrestrial pollen concentration suggesting an increase in plant biomass and vegetation cover, while during glacials, both the pollen concentration and their percentages presents a decreasing trend, which is encountered in most southern European records. However, the glacial intervals retain surprisingly high percentages of both deciduous and sclerophyllous vegetation components, that has not been previously reported. Another remarkable feature of the Corinth record is the occurrence of several Neogene relict tree taxa (Figure 1) implying their presence within the catchment until the Late Pleistocene. These findings confirm the refugial character of the Gulf of Corinth area and allow comparison with other regional reference sites such as the Lake Ohrid record (Sadori et al., 2016; Donders et al., 2021).

Acknowledgements

The research work was supported by the Hellenic Foundation of Research and Innovation (H.F.R.I) under the "First Call for H.F.R.I. Research Projects to support Faculty members and Researchers and the procurement of high-cost research equipment grant" (Project Number: 1026, Quaternary Environmental Changes in the Corinth Rift Area: the IODP 381 palynological record: QECCoRA).

References

Donders, T., Panagiotopoulos, K., Koutsodendris, A., Bertini, A., Mercuri, A. M., Masi, A., Combourieu-Nebout, N., Joannin, S., Kouli, K., Kousis, I., Peyron., O, Torri, P., Florenzano, A., Francke, Wagner, B., Sadori, L., 2021. 1.36 million years of Mediterranean forest refugium dynamics in response to glacial–interglacial cycle strength. Proceedings of the National Academy of Sciences 118, e2026111118.

McNeill L, Shillington DJ, Carter GDO, Everest J, Gawthorpe R, Miller C, Phillips M, Collier R, Cvetkoska A, De Gelder G, Diz Ferreiro P, Doan M.-L, Ford M, Geraga M, Gillespie J, Hemelsdael R, Herrero-Bervera E, Ismaiel M, Janikian L, Kouli K, Le Ber E, Li S, Maffione M, Mahoney C, Machlus ML, Michas G, Nixon C, Oflaz SA, Omale AP, Panagiotopoulos K, Pechlivanidou S, Sauer S, Seguin J, Sergiou S, Zhakarova N, Green S., 2019a. High-resolution record reveals climate-driven environmental and sedimentary changes in an active rift. Scientific reports 9, 1-11

McNeill L, Shillington DJ, Carter GDO, Everest J, Gawthorpe R, Miller C, Phillips M, Collier R, Cvetkoska A, De Gelder G, Diz Ferreiro P, Doan M.-L, Ford M, Geraga M, Gillespie J, Hemelsdael R, Herrero-Bervera E, Ismaiel M, Janikian L, Kouli K, Le Ber E, Li S, Maffione M, Mahoney C, Machlus ML, Michas G, Nixon C, Oflaz SA, Omale AP, Panagiotopoulos K, Pechlivanidou S, Sauer S, Seguin J, Sergiou S, Zhakarova N, Green S., 2019b. Corinth Active Rift Development. Proceedings of the International Ocean Discovery Program, 381: College Station, TX (International Ocean Discovery Program). https://doi.org/10.14379/iodp.proc.381.101.2019

Sadori, L., Koutsodendris, A., Panagiotopoulos, K., Masi, A., Bertini, A., Combourieu-Nebout, N., Francke, A., Kouli, K., Joannin, S., Mercuri, A.-M., Peyron, O., Torri, P., Wagner, B., Zanchetta, G., Sinopoli, G., Donders, T.H., 2016. Pollen-based paleoenvironmental and paleoclimatic change at Lake Ohrid (south-eastern Europe) during the past 500 ka. Biogeosciences 13, 1423-1437

16th International Congress of the Geological Society of Greece

17-19 October, 2022 - Patras, Greece

Bulletin of the Geological Society of Greece, Sp. Publ. 10

Ext. Abs. GSG2022-069

The middle Pleistocene evolution of Rio basin the western active margin of Corinth rift

M. Tsoni[1], I. Koukouvelas[1], P. Avramidhs[1], A. Zelilidis[1], G. Iliopoulos[1]

(1) Geology Department, University of Patras, Greece, mariatsoni@upatras.gr

Corinth rift is a region of significant stratigraphic and palaeontological interest, where several environmental changes have been recorded during the Quaternary (Ford *et al.* 2016). These changes are the result of active tectonism, related to the well-known rifting process that has been occurring in the geotectonic region of the Corinth Rift, as well as of the influence of continuous eustatic and climatic changes (Ford *et al.* 2016). Fossil assemblages from Lower to Upper Pleistocene transitional to marine and terrestrial sedimentary sequences have been analyzed herein in order to distinguish the tectonic and eustatic controls. Corinth Rift includes three basins, Corinth in the east, Rio in the center and Patras in the west. Overall, the rift system is characterised by palaeoenvironmental complexity controlled by post-Alpine structures, the present-day tectonic evolution and sea-level changes during the glacial and interglacial periods.

Rio basin is the relatively less studied area of the Corinth rift. Nevertheless, the palaeoenvironmental evolution of this basin is of great importance as it will help to address the question of the role of the Rio sill in the connection of the rift with the open sea. For this reason, a detailed stratigraphic study and micro-palaeontological analysis were carried out for the first time in the Rio basin, with micro-palaeontology as the main tool. This study revealed alternations of lakes, lagoons and shallow marine deposits.

The Rio basin was studied through the detailed stratigraphic analysis of 23 sections around the Charadros river. Micropalaeontological and the respective statistical analysis were performed on 979 samples. Four diversity indices were calculated as well as the adult/ juvenile taphonomic index for ostracods. In addition, geochemical analysis and petrographic analysis of organic-rich sediments were performed. For the age determination, two independent dating methods were used. The age of the sediments was firstly estimated, taking into account the stratigraphic ranges and stratigraphic appearances of determined species (foraminifera, ostracods and calcareous nannoplankton), and in addition, absolute dating was performed using Optically Stimulated Luminescence (OSL).

Combining data obtained from the analyses of the samples and the dating methods, a spatial and temporal palaeoenvironmental reconstruction during the late middle Pleistocene (MIS 7e-6a) was performed for the Rio basin. In addition, the elevation rate was calculated where possible, according to the relative altitude and the age of each sequence.

According to the palaeoenvironmental analysis, the studied sequences present sea level fluctuations that are mainly due to eustatism. Three main depositional environments comprise the study area :(a) lagoon/ inner lagoon environments, (b) transitional environments (between marine and lagoon), and (c) shallow marine environments). These alternations between shallow marine and lagoonal facies are well correlated to alternations of marine and isolated assemblages that McNeil *et al*. (2019) described for the Central Corinth basin (M0079 drilling site -IODP Expedition 381) (Tsoni *et al*. 2021). Furthermore, Palyvos *et al.* 2010, described a sedimentary sequence from the Aravonitsa formation (western Corinth basin) that matches well with a group of sequences in the study area. Differences in lithology or sequences' thickness could be explained either by different tectonic rates, application of the same generation process (e.g. climatic cycles and tectonics) and different provenance of the sediments, in these two different parts of the Corinth-Patras rift.

The comparison between stratigraphic and micropalaeontological results with the MIS curve shows a good correlation between stages MIS7e and 6a and allows the palaeoenvironmental reconstruction (Fig.1). This means that local climate changes are responsible for environmental changes in the main basin with corresponding changes in the aquatic environments. Accordingly, the nature and volume of accumulated sediments changes. During the interglacial stages (MIS6), laminated sediments accumulated in lacustrine environments. During the corresponding interglacial stage (MIS7), thick deposits of marine sediments were observed. Based on the above and as implied by both fauna and flora results that were observed in the respective sequences, it is concluded that the climate during MIS6d was continental, warm-temperate (Tsoni *et al.* 2021). Thus, the significant palaeoenvironmental changes demonstrated by this study are attributed to global climate variability. This is in agreement with other studies that have been done in the eastern and central part of the Corinth basin. This coherence reveals that during the Middle Pleistocene, the palaeoenvironmental evolution of the two basins was controlled by the same factors and the paleoenvironments changed proportionally. In addition, minor changes in the depositional palaeoenvironment have been observed and are attributed to the tectonic action of second-order faults. Despite the changes in the palaeoenvironment, the area remained close to sea level during the late middle Pleistocene and this is probably due to the tectonically controlled subsidence of the second-order faults that developed against the first-order faults.

This study highlights the temporal palaeoenvironmental evolution of the Rio basin during the late middle Pleistocene, which was controlled by climatic- eustatic changes, as well as by the tectonic movements of faults. Detailed stratigraphic analysis, using micropalaeontology as the main tool, revealed alternations of lakes, lagoons and shallow marine deposits.

These palaeoenvironmental changes, that characterise the study area, were caused by sea level fluctuations due to the Rio sill, which controls the connection between an isolated basin (Corinth basin) with the Patras basin and the open sea. The comparison with other studies in the eastern and central part of the Corinth basin (Palyvos *et al.* 2010, McNeil *et al.* 2019), showed that there is a coherence between the Rio and the Corinth basin. This coherence reveals that during the middle Pleistocene the palaeoenvironmental evolution of the two basins was controlled by the same factors and the palaeoenvironments were modified proportionally.

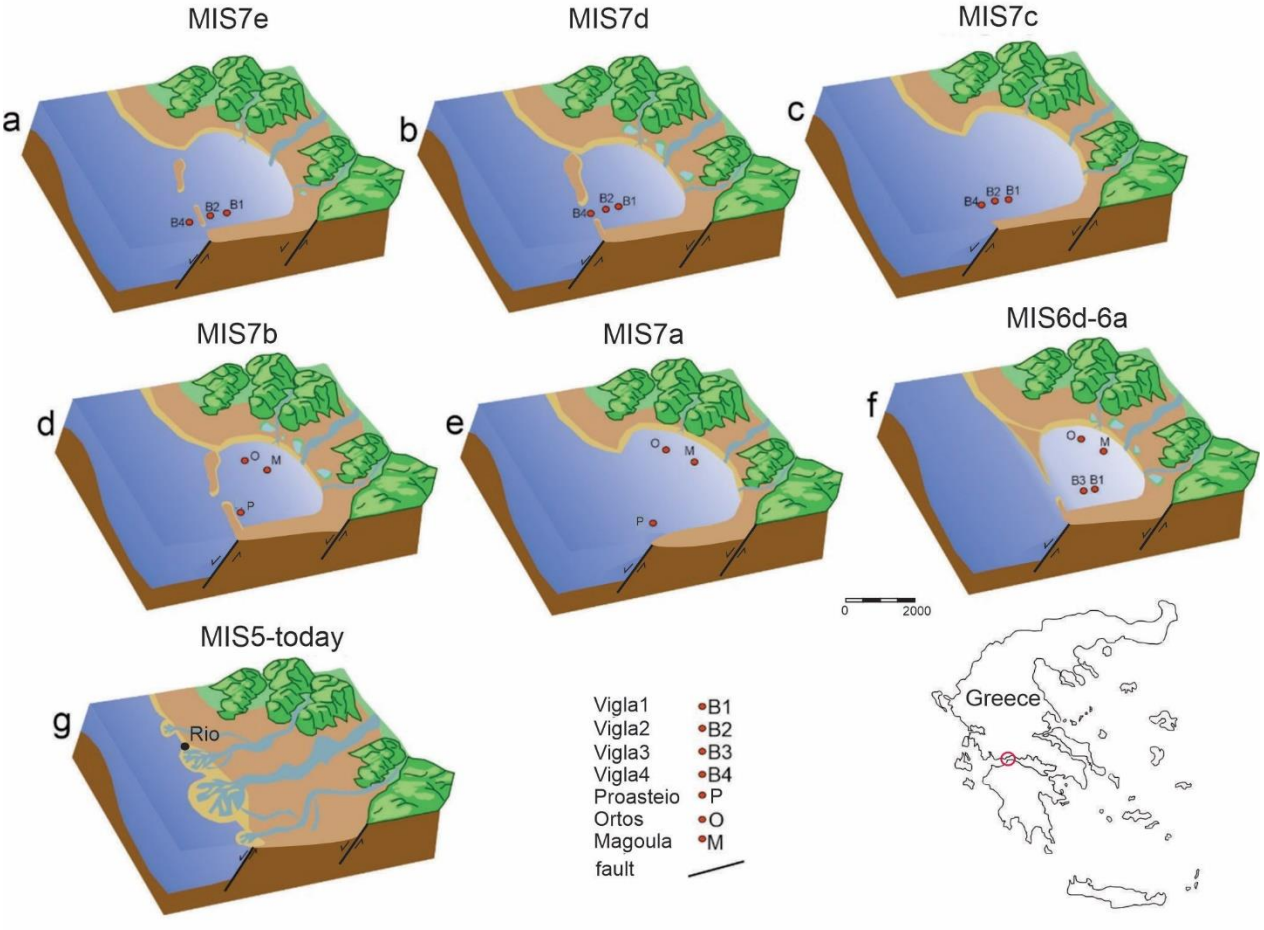

Figure 1. Palaeoenvironmental evolution of the study area between stages MIS7e to today.

References

McNeill, L.C., Shillington, D.J., Carter, G.D.O., Everest, J.D., Gawthorpe, R.L., Miller, C., Phillips, M.P., Collier, R.E.L., Cvetkoska, A., Gelder, G.D., Diz, P., Doan, M.L., Ford, M., Geraga, M., Gillespie, J., Hemelsdael, R., Herrero-Bervera, E., Ismaiel, M., Janikian, L., Kouli, K., Ber, E.L., Li, S., Maffione, M., Mahoney, C., Machlus, M., Michas, G., Nixon, C.W., Oflaz, S.A., Omale, A.P., Panagiotopoulos, K., Pechlivanidou, S., Sauer, S., Seguin, J., Sergiou, S., Zakharova, N.V. & Green, S. 2019. High-resolution record reveals climate-driven environmental and sedimentary changes in an active rift. Scientific Reports, 9, 3116. DOI: https://doi.org/10.1038/s41598-019- 40022-w

Palyvos, N., Mancini, M., Sorel, D., Lemeille, F., Pantosti, D., Julia, R., Triantaphyllou, M. & De Martini, P.M. 2010. Geomorphological, stratigraphic and geochronological evidence of fast Pleistocene coastal uplift in the westernmost part of the Corinth Rift (Greece). Geological Journal, 45: 78–104.

Ford, M., Hemelsdael, R., Mancini, M., Palyvos, N. 2016. Rift migration and lateral propagation: evolution of normal faults and sediment- routing systems of the western Corinth rift (Greece). Geological Society London Special Publications 439(1): SP439.15

Tsoni, M, Iliopoulos, G., Valavani, D., Liapi, E., Papadopoulou, P., Stamoulis, K., Koukouvelas, I., Kontopoulos, N, 2021. Palaeoenvironmental inferences on the Pleistocene deposits of the Charadros River (Rio graben, Western Corinth Gulf, Greece). Quaternary International, 589, 39-54

16th International Congress of the Geological Society of Greece
17-19 October, 2022 - Patras, Greece
Bulletin of the Geological Society of Greece, Sp. Publ. 10
Ext. Abs. GSG2022-072

Paleoceanographic conditions within the Corinth rift basin during the last interglacial (MIS 5e)

S. Sergiou[1], M. Geraga[1], S. Pechlivanidou[2], U. Ninnemann[2], R. L. Gawthorpe[2], D. Antoniou[1], D. Angelopoulou[1], A. Kastana[1]

(1) Department of Geology, University of Patras, Greece, sergiou@upatras.gr (2) Department of Earth Science, University of Bergen, Norway.

Research Highlights

The Corinth Rift basin was efficiently connected with the open sea during the MIS 5e sea level highstand. Similar sea-surface conditions were established between the Corinth basin and Ionian Sea during the sapropel S5 deposition in the eastern Mediterranean

Introduction and Objectives

In the region of the eastern Mediterranean (EM), the last interglacial period (MIS 5e; ca. 130-116 ka) was associated with enhanced humidity and increased temperature following high solar insolation (Tzedakis et al., 2003) while global sea level was about 4-6 m higher than today (Rohling et al., 2008 and references therein). These climatic conditions contributed to the deposition of the sapropel S5 in the EM (ca. 128.3-121.5 ka; Rohling et al., 2015). The deposition of S5 is well documented in the deep waters, however limited information exists regarding the formation of this layer in shallow areas of the open sea and adjacent gulfs. In this study, we examine the palaeoceanographic conditions prevailed in the Corinth Rift basin (CRb), aiming to assess the response of this semi-closed basin, at times of enhanced humidity and warm conditions as these prevailed during the S5. Hydrography within the CRb is largely influenced by a well-developed drainage system as well as water exchange patterns with the Ionian Sea. The CRb is connected to the open sea via the shallow sill (~60 m water depth) of Rio –Antirio straits. During the Quaternary, the CRb environment alternated between marine and isolated following the eustatic sea level fluctuations relative to the sill height. For the purpose of the present study, sediment samples from the drillhole M0079A, IODP Expedition 381 (McNeill et al., 2019a) are examined in terms of their microfaunal (planktic and benthic foraminifera) content and stable isotopic signal (δ18O and δ13C).

Materials and Methods

Foraminiferal analysis was performed in 28 sediment samples, collected between 175.5-180.5 mbsf from the drillhole M0079A, which according to the chronological framework of McNeill et al. (2019b) and Maffione and Herrero- Bervera, (2022), corresponds to the MIS 5e period. The analysis concerned the >125μm size fraction. Each taxon was quantified as number per gram (N/gr) and as percentage (%) of the total planktic or benthic foraminifera population respectively. For the assessment of the sea surface temperature (SST) variation we used the abundance of warm versus cool water indicator planktic species (Rohling et al., 1993; Cane et al., 2002). The warm group comprises the sum of *Gs. ruber* and SPRUDTS group (Rohling et al., 1993) while the cool group brings together *Globigerina bulloides*, Globigerinita *glutinata*, *Globorotalia inflata*, *Turborotalita quinqueloba* and *Neogloboquadrina* spp. For the assessment of the bottom water conditions we grouped the benthic foraminifera species and genera into high and low oxygen indicators (based on their response in the dissolved oxygen levels; Murray, 2006 and references therein) and into oligotrophic and eutrophic indicators (based on their preference in the organic matter content; Jorissen et al. (2018). Oxygen (δ18O) and carbon (δ13C) isotope ratios were measured on *Neogloboquadrina incompta* tests at FARLAB facilities, Department of Earth Science, University of Bergen.

Results and discussion

The investigated succession comprises fine-grained, highly bioturbated hemipelagic sediments enriched in biogenic material. In all examined samples planktic and benthic foraminifera specimens were abundant (~ 9,100 N/gr and ~ 23,500 N/gr respectively) suggesting that full marine conditions prevailed in the basin during the deposition of the examined interval. The high sea level stands (up to 4-6 m higher than modern sea level; Rohling et al., 2008) allowed the water connection between the CRb and the open sea.

The studied sediments are characterized by the dominant presence of warm indicator planktic species and light δ18O values suggesting the establishment of high SST in the basin. The detailed downcore microfaunal and isotopic variation implies two paleoenvironmental phases. The lower (phase a; 178.3-180.5 mbsf) displays high participation of *G. bulloides* and *G. glutinata* accompanying the warm ind. species thus indicating elevated surface productivity and low δ13C values indicative of increased terrigenous organic matter inflows (Schiebel and Hemleben, 2017) (Fig. 1). The benthic foraminiferal proxies suggest that the seafloor was sufficiently oxygenated and oligotrophic. The next phase (phase b; 177-178.3 mbsf) is marked by the dominance of *Gs. ruber* and SPRUDTS group in the planktic assemblages while buliminids and *Melonis* spp. prevail in the benthic microfauna thus indicating rather warm sea surface conditions and

eutrophic, low oxygen bottom waters (Fig. 1). Finally, the prevalence of *T. quinqueloba* in the planktic assemblages after the end of phase (b) together with the retreat of the warm-indicator species and the notable shift of the δ18O record to heavier values is indicative of an essential temperature lowering in the CRb (Schiebel and Hemleben, 2017).

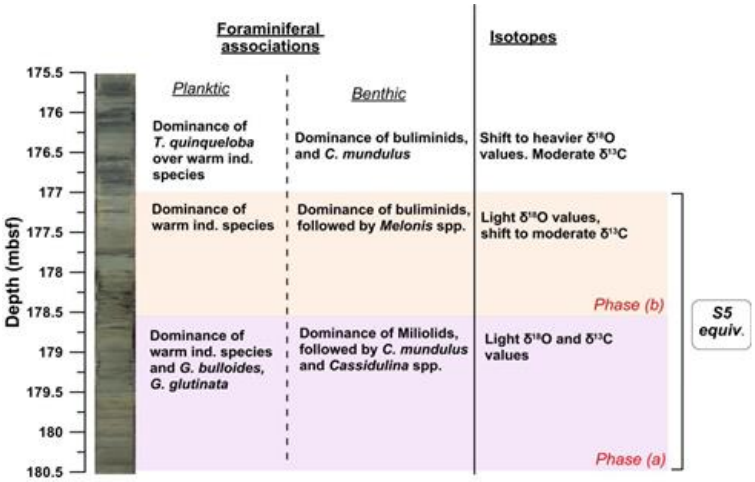

Figure 1: Discrimination of the two paleoenvironmental phases linked to sapropel S5 - equivalent conditions in the CRb.

The planktic foraminiferal associations and the isotopic composition of phases (a) and (b) are highly similar with the ones captured in records from the Ionian basin during the sapropel S5 formation (Cane et al., 2002; Capotondi et al., 2006). Hence, it is most probable that the CRb shared common surface water conditions with the open sea during that time. However, the high numbers of benthic assemblages in the examined samples suggest the deposition of sapropel-equivalent sediments rather than a pure sapropel layer in the CRb.

Phase (a) most likely signifies the onset of S5 conditions, associated with increased riverine fluxes within the basin whereas phase (b) reflects a major sea-surface warming induced by solar insolation maxima (Rohling et al., 2015). In addition, the switch from well oxygenated and oligotrophic (phase a) to oxygen-depleted and eutrophic (phase b) seafloor conditions indicates a gradual increase of water column stratification, likely associated with the combined effects of warm inflows entering the gulf from the Ionian Sea together with the high riverine runoff following elevated precipitation rates (Tzedakis et al., 2003). The sea-surface cooling after the end of phase (b) (175.5-177 mbsf) marks the termination of the S5-related conditions within the CRb.

Acknowledgements

The authors would like to thank all the scientific and technical personnel involved in the IODP Expedition 381.

References

Cane, T., Rohling, E.J., Kemp, A.E.S., Cooke, S., Pearce, R.B., 2002. High-resolution stratigraphic framework for Mediterranean sapropel S5 : defining temporal relationships between records of Eemian climate variability. Palaeogeogr. Palaeoclimatol. Palaeoecol. 183, 87–101.

Capotondi, L., Speranza, M., Morigi, C., Sangiorgi, F., Maffioli, P., Giunta, S., Negri, A., Corselli, C., 2006. Foraminiferal variations and stratigraphic implications to the deposition of sapropel S5 in the eastern Mediterranean. Palaeogeogr. Palaeoclimatol. Palaeoecol. 235, 48–65. https://doi.org/10.1016/j.palaeo.2005.09.023

Jorissen, F., Pia, M., Almogi-labin, A., Barras, C., Bergamin, L., Bicchi, E., El, A., Ferraro, L., Mcgann, M., Mor igi, C., Romano, E., Sabbatini, A., Schweizer, M., Spezzaferri, S., 2018. Developing Foram-AMBI for biomonitoring in the Mediterranean : Species assignments to ecological categories. Mar. Micropaleontol. 140, 33 –45. https://doi.org/10.1016/j.marmicro.2017.12.006

Maffione, M., Herrero-Bervera, E., 2022. A Relative Paleointensity (RPI) -Calibrated Age Model for the Corinth Syn- rift Sequence at IODP Hole M0079A (Gulf of Corinth , Greece). Front. Earth Sci. 10. https://doi.org/10.3389/feart.2022.813958

McNeill, L.C., Shillington, D.J., Carter, G.D.O. et al., 2019a. Corinth Active Rift Development. Proceedings of the International Ocean Discovery Program, 381: College Station, TX (International Ocean Discovery Program). https://doi.org/https://doi.org/10.14379/iodp.proc.381.2019

McNeill, L.C., Shillington, D.J., Carter, G.D.O. et al., 2019b. High-resolution record reveals climate-driven environmental and sedimentary changes in an active rift. Sci. Rep. 9. https://doi.org/10.1038/s41598-019-40022-w

Murray, J., 2006. Ecology and Applications of Benthic Foraminifera. Cambridge University Press.

Rohling, E.J., Grant, K., Hemleben, C., Hoogakker, B., 2008. High rates of sea-level rise during the last interglacial period. Nat. Geosci. 1. https://doi.org/10.1038/ngeo.2007.28

Rohling, E.J., Marino, G., Grant, K.M., 2015. Mediterranean climate and oceanography , and the periodic development of anoxic events (sapropels). Earth Sci. Rev. 143, 62–97. https://doi.org/10.1016/j.earscirev.2015.01.008

Schiebel, R., Hemleben, C., 2017. Planktic Foraminifers in the Modern Ocean. Springer-Verlag Berlin Heidelberg. https://doi.org/10.1007/978-3-662-50297-6

Tzedakis, C., Frogley, M., Heaton, T.H.E., 2003. Last Interglacial conditions in southern Europe: evidence from Ioannina, northwest Greece. Glob. Planet. Change 36, 157–170. https://doi.org/10.1016/S0921-8181(02)00182-0

16th International Congress of the Geological Society of Greece

17-19 October, 2022 - Patras, Greece

Bulletin of the Geological Society of Greece, Sp. Publ. 10

Ext. Abs. GSG2022-130

Controls on deep-water, syn-rift stratigraphic development of the Corinth Rift; the role of rift segment boundaries

S. Pechlivanidou[1], R.L. Gawthorpe[1], N. Fabregas[1], M. Ford[2], R.E.LI. Collier[3], G.D.O. Carter[4], L.C. McNeill[5], D.J. Shillington[6], M. Muravchik[1]

(1) University of Bergen, Bergen, Norway sofia.pechlivanidou@uib.no (2) Université de Lorraine, CNRS, CRPG, Nancy, France (3) University of Leeds, Leeds, UK (4) British Geological Survey, Edinburgh, UK (5) University of Southampton, Southampton, UK (6) Northern Arizona University, Flagstaff, Arizona, USA.

This study highlights the importance of structural highs at the ends of rift segments as a first-order control on syn-rift stratigraphic evolution (Fig. 1). Stratigraphic variability recorded within deep-water rift basins is broadly attributed to tectonic and climatic interactions that control sediment delivery at $<10^4$-10^5 yrs timescales (Cowie *et al.*, 2006, Pechlivanidou *et al.*, 2019). In semi-enclosed, marine-lacustrine rift basins, the presence of one or more structural highs at the end of rift segments has the potential to modulate the influx of marine waters from the global ocean, with implications for the syn-rift stratigraphic development. The Gulf of Corinth, is a semi-enclosed active rift basin which alternated between marine and isolated/semi-isolated (lacustrine) conditions as sea level fluctuated with respect to basin sills during Quaternary glacial/interglacial cycles. We perform a bed-scale stratigraphic analysis on two cores obtained from the IODP Expedition 381 (sites M0078 and M0079) to investigate key controls on rift stratigraphy during the Late Quaternary. Initial results from the Expedition's Science Party provided general characteristics of the drilled syn-rift succession and indicated cyclic variations in sedimentation rates and basin paleoenvironment on tens to hundreds of thousands of years timescales (McNeill *et al.*, 2019, Shillington *et al.*, 2019). Our high-resolution bed-scale analysis of the of the last ca. 800 kyr of basin-floor sedimentation reveal a range of homogeneous to laminated mud beds and sharp-based event beds. In addition, matrix-supported, intraclast-rich conglomerates and slumps form a relatively minor component of the stratigraphy. The bed-types are organized into three types of stratigraphic packages (bioturbated, bedded and laminated) that are closely linked to eustatically controlled connections to the global ocean. Bioturbated packages record interglacial marine conditions, bedded packages reflect deposition in a non-marine, lacustrine setting during glacial phases and laminated packages demonstrate seasonal variability in a dysoxic non-marine or transitional setting. The timing of stratigraphic alterations between these three packages constrained by our new age-depth model suggests changes in sill height bounding the gulf to the east and to the west controlled by eustatic variations and/or evolution of the normal fault system. The ~780 to 330 ka succession is dominated by laminated packages with thin bioturbated packages and distinct conglomerates and slumps, suggesting high sills, making ocean connections brief and transitional to lacustrine conditions prolonged. The ~330 ka to present succession shows well developed bioturbated and bedded packages, separated by thin laminated packages, suggesting brief transitions and well-developed marine conditions due to lower sills. Overall, our results show significant differences in average sedimentation rates than previously estimated considering constant sill heights, with periods of interglacial marine conditions being shorter by up to 50%.

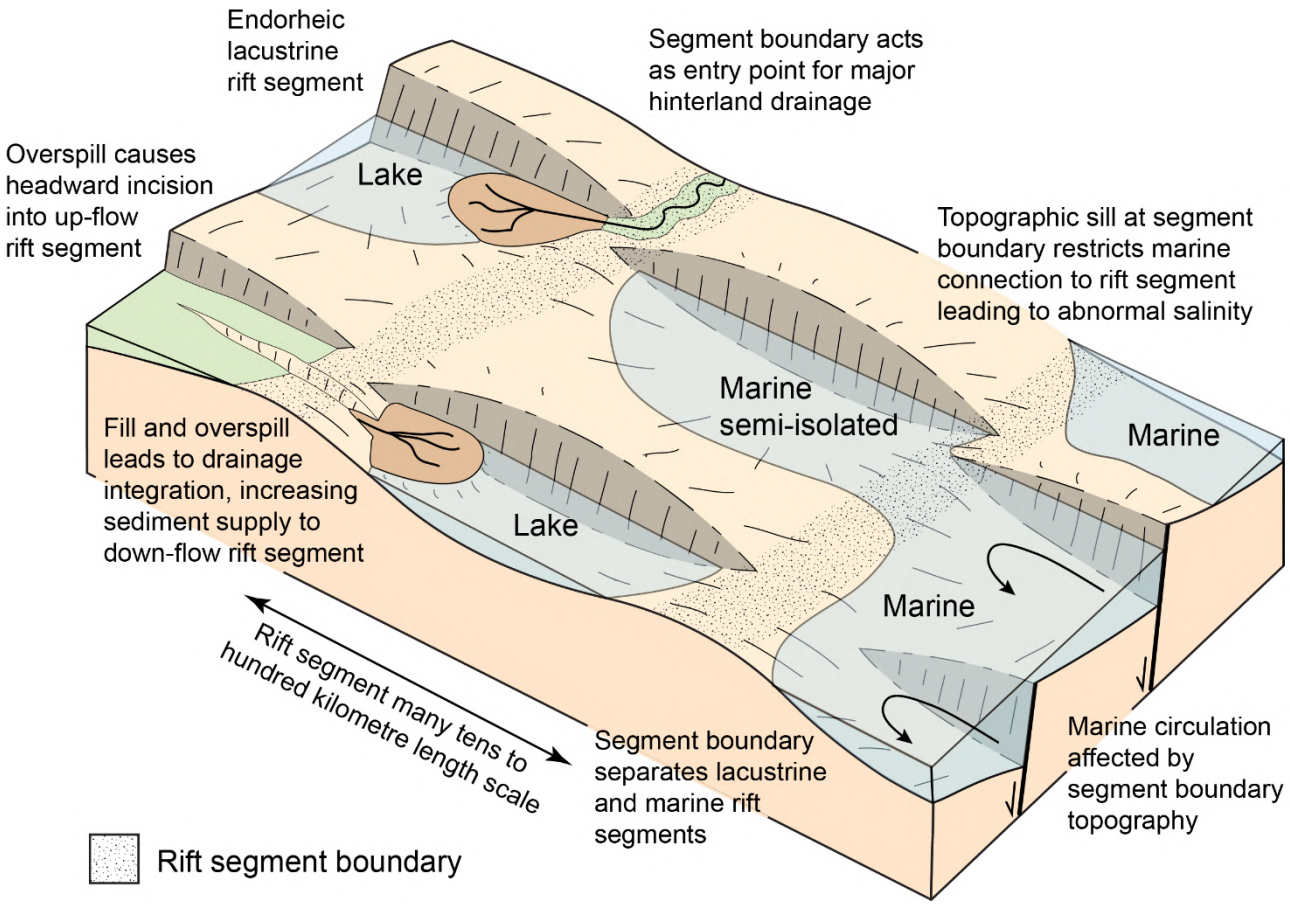

Figure 1. Schematic sketch of the varied impact of rift segment boundary structural highs on rift sedimentation in continental (left) to marine (right) settings (after Gawthorpe *et al.*, 2022)

Acknowledgements

We thank all involved with the successful completion of IODP Expedition 381, including ECORD Science Operator staff, ship and drilling crew of the D/V Fugro Synergy, and staff at MARUM, University of Bremen. The authors acknowledge support from the Research Council of Norway (DeepRift project; number 308805). RLG thanks the VISTA programme of Norwegian Academy of Science and Letters for the award of the VISTA Professorship which also provided support to SP to participate in IODP Expedition 381 and undertake post-cruise research. RELlC acknowledges NERC for grant NE/S002367/1 for supporting post-cruise research.

References

Cowie, P.A., Attal, M., Tucker, G.E., Whittaker, A.C., Naylor, M., Ganas, A., Roberts, G.P., 2006. Investigating the Surface Process Response to Fault Interaction and Linkage Using a Numerical Modelling Approach. Basin Research, 18, 231-266.

Gawthorpe, R.L., Fabregas, N., Pechlivanidou, S., Ford, M., Collier, R.E.L., Carter, G.D.O., McNeill, L.C., Shillington, D.J., 2022. Late Quaternary mud-dominated, basin-floor sedimentation of the Gulf of Corinth, Greece: Implications for deep-water depositional processes and controls on syn-rift sedimentation. Basin Research, 1-34.

McNeill, L.C., Shillington, D.J., Carter, G.D.O., Everest, J.D., Gawthorpe, R.L., Miller, C., Phillips, M.P., Collier, R.E.L., Cvetkoska, A., De Gelder, G., Diz, P., Doan, M.L., Ford, M., Geraga, M., Gillespie, J., Hemelsdael, R., Herrero-Bervera, E., Ismaiel, M., Janikian, L., Kouli, K., Le Ber, E., Li, S., Maffione, M., Mahoney, C., Machlus, M.L., Michas, G., Nixon, C.W., Oflaz, S.A., Omale, A.P., Panagiotopoulos, K., Pechlivanidou, S., Sauer, S., Seguin, J., Sergiou, S., Zakharova, N.V., Green, S., 2019. High-Resolution Record Reveals Climate-Driven Environmental and Sedimentary Changes in an Active Rift. Scientific Reports, 9, 3116.

Pechlivanidou, S., Cowie, P.A., Duclaux, G., Nixon, C.W., Gawthorpe, R.L., Salles, T., 2019. Tipping the Balance: Shifts in Sediment Production in an Active Rift Setting. Geology, 47, 259-262.

Shillington, D.J., McNeill, L.C., Carter, G.D.O., Everest, J.D., Le Ber, E., Collier, R.E.L., Cvetkoska, A., De Gelder, G., Diz, P., Doan, M.L., Ford, M., Gawthorpe, R.L., Geraga, M., Gillespie, J., Hemelsdael, R., Herrero-Bervera, E., Ismaiel, M., Janikian, L., Kouli K., Li, S., Machlus, M.L., Maffione, M., Mahoney, C., Michas, G., Miller, C., Nixon, C.W., Oflaz, S.A., Omale, A.P., Panagiotopoulos, K., Pechlivanidou, S., Phillips, M.P., Sauer, S., Seguin, J., Sergiou, S., Zakharova, N.V., 2019. Expedition 381 Preliminary Report: Corinth Active Rift Development. College Station, TX, International Ocean Discovery Program.

16th International Congress of the Geological Society of Greece
17-19 October, 2022 - Patras, Greece
Bulletin of the Geological Society of Greece, Sp. Publ. 10
Ext. Abs. GSG2022-297

Variations of Seismic Moment and Strain Rates within the Active Corinth Rift and Implications for Seismic Hazard

G. Michas[1], C. Nixon[2], L. McNeill[3], D. Shillington[4], and the IODP Expedition 381 Science party

(1) Section of Geophysics – Geothermics, Department of Geology and Geoenvironment, National and Kapodistrian University of Athens, Athens, Greece, gemichas@geol.uoa.gr (2) Department of Earth Science, University of Bergen, Bergen, Norway. (3) Ocean and Earth Science, University of Southampton, Southampton, UK. (4) School of Earth and Sustainability, Northern Arizona University, Flagstaff, Arizona, USA.

Research Highlights

- Two new seismic catalogues for historic and modern seismicity in the Corinth Rift were compiled based on the best available data sources.
- Variations of seismic moment and strain rates, compared to geological and geodetic rates, provide significant insights on the deformation patterns and seismic hazard.

Background and Objectives

The active continental Corinth Rift is a high-strain zone of extensional deformation in the back-arc region of the Hellenic subduction zone. The area presents high extension rates, some of the highest in the world, and pronounced seismicity with several large and destructive earthquakes recorded in both historic and modern times (e.g., Ambraseys and Jackson, 1997). Owing to its high deformation rates, large sedimentation fluxes and preservation of the syn-rift sediments, the Corinth Rift has recently been the site of the International Ocean Discovery Program (IODP) Expedition 381 (McNeill *et al*., 2019a; 2019b). The IODP Expedition 381 managed to drill and core the most recent ~1–2 Myr of syn-rift sediments down to a depth of 705 metres below seafloor (mbsf) during October – December 2017 (Shillington *et al*., 2019), representing the longest and highest resolution record of its kind in a young rift.

One of the primary objectives of the IODP Expedition 381 was to determine high-resolution fault slip-rates and to redefine how fault activity changed with time, reassessing the structural evolution of the Corinth Rift. Such data, integrated with the long seismic record in the area, can provide novel constraints on the regional deformation patterns and seismic hazard in one of the most seismically active areas in Europe. Herein, we focus on this objective and study the seismic moment release and seismic strain rates within the Corinth Rift for two time intervals that represent the recent and the longer-term earthquake activity in the area.

Methods

To this purpose, two new seismic catalogues were compiled based on the best available data sources. The first longer-term catalogue refers to the period between 1703 and 2019 and is considered complete in earthquakes with magnitude $M_w \geq 6$. The second catalogue refers to the modern seismicity in the rift during 1970 – 2019 and is considered complete down to magnitude $M_w = 4.1$. In both catalogues, only shallow earthquakes that contribute to the upper crustal deformation were considered.

As a first step, the regional moment-magnitude relation was determined to estimate seismic moments (M_0) from moment magnitudes (M_w) for all the events in the two catalogues. Seismic moment rates were then calculated for the two time intervals. Furthermore, to account for the seismic moment release of earthquakes below the magnitude of completeness, we considered the mathematical equation of Molnar (1979), as modified from England and Bilham (2015), which relates the seismic moment rate with the parameters of the Gutenberg-Richter relation. These parameters were adopted from the seismic zonation model of Vamvakaris *et al*. (2016) for the western, central and eastern zone of the rift, respectively.

Results

The previous methodology provides estimates regarding scalar seismic moment rates along the Corinth Rift and particularly in the western, central and eastern zones, as shown in Figure 1. Lowest moment rates appear in the central zone over the last ~50 years, while a deficit, compared to the longer-term record, also appears in the western zone. The highest moment rates over the last ~50 years appear in the eastern zone due to the 1981 Alkyonides earthquake sequence, contrasting the lower geodetic rates in this part of the rift (e.g., Briole *et al*., 2000). Looking at the longer-term moment rates, these are more consistent with the geodetic rates, showing higher rates in the western and central zones and lower rates in the eastern zone.

In addition, by using the available fault plane solutions and the Kostrov formula (Kostrov, 1974), we estimated the seismic strain rates in the three zones of the rift following the methodology described in Papazachos and Kiratzi (1992). The results of this analysis are presented in Figure 1. Seismic strain is mostly extensional in a general shallow-dipping N-S

direction, while a significant negative component in the vertical direction indicates crustal thinning. As can be seen in Figure 1, seismic strain over the last ~50 years is dominated by the 1981 Alkyonides sequence in the eastern zone, while a deficit appears in the central and western zones. The longer-term strain rates in the three zones of the rift are almost comparable in size (Figure 1).

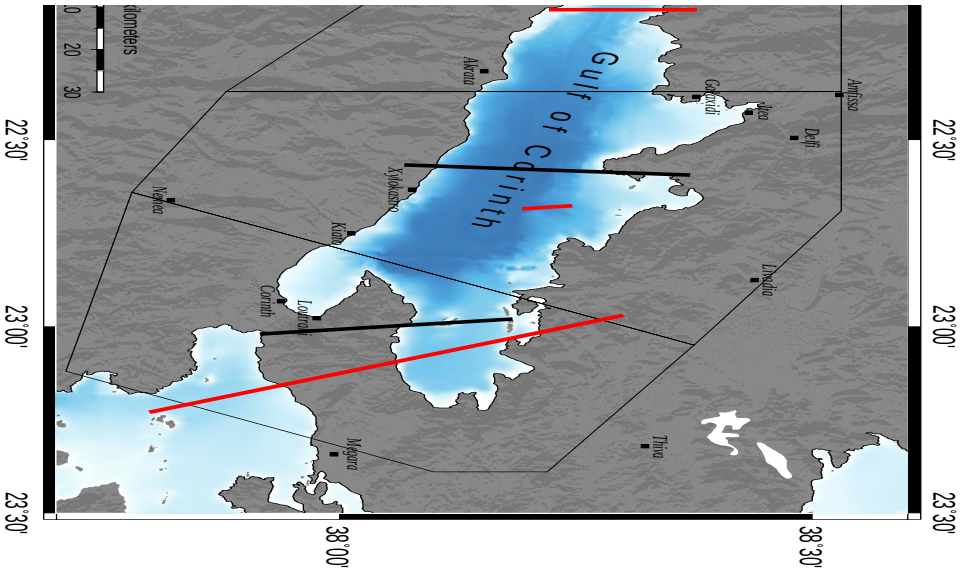

Figure 1. Map showing extensional strain rates in the Corinth Rift along the principal directions in the western, central and eastern seismic zones, calculated from the 317-yrs and the 50-yrs seismic catalogues.

Conclusions

The analysis and results provide novel insights regarding seismic moment and strain rates within the active Corinth Rift. The results further indicate a deficit in earthquake activity over the last ~50 years in the central and western zones of the rift, which could have significant implications for assessing the seismogenic hazard. Further comparing seismic strain rates with the revised fault-slip rates, as derived from the latest results of the IODP Expedition 381, can provide valuable insights on the deformation patterns and seismic hazard within the Corinth Rift.

Acknowledgements

We sincerely thank all the people involved with the successful completion of IODP Expedition 381, including ECORD Science Operator staff, ship and drilling crew of the D/V Fugro Synergy, and staff at MARUM, University of Bremen.

References

Ambraseys, N.N., Jackson, J.A., 1997. Seismicity and strain in the Gulf of Corinth (Greece) since 1694. Journal of Earthquake Engineering 1(03), 433-474.

Briole, P., Rigo, A., Lyon-Caen, H., Ruegg, J. C., Papazissi, K., Mitsakaki, C., Balodimou, A., Veis, G., Hatzfeld, D., Deschamps, A., 2000. Active deformation of the Corinth rift, Greece: results from repeated Global Positioning System surveys between 1990 and 1995. Journal of Geophysical Research: Solid Earth 105(B11), 25605-25625.

England, P., Bilham, R., 2015. The Shillong Plateau and the great 1897 Assam earthquake. Tectonics 34(9), 1792-1812.

Kostrov, V.V., 1974. Seismic moment and energy of earthquakes, and seismic flow of rock. Izv. Acad. Sci. USSR Phys. Solid Earth (Engl. Transl.) 1, 23-44.

McNeill, L.C., Shillington, D.J., Carter, G.D.O. & the Expedition 381 Participants, 2019a. Corinth Active Rift Development. Proceedings of the International Ocean Discovery Program, 381, College Station, TX, International Ocean Discovery Program.

McNeill, L.C., Shillington, D.J., Carter, G.D.O. & the Expedition 381 Participants, 2019b. High-resolution record reveals climate-driven environmental and sedimentary changes in an active rift. Scientific Reports 9, 1–11.

Molnar, P. (1979). Earthquake recurrence intervals and plate tectonics. Bulletin of the Seismological Society of America 69, 115-133.

Papazachos, C.B., Kiratzi, A.A., 1992. A formulation for reliable estimation of active crustal deformation and its application to central Greece. Geophysical Journal International 111(3), 424-432.

Shillington, D.J., McNeill, L.C., Carter, G.D.O. & the Expedition 381 Participants, 2019. Expedition 381 Preliminary Report: Corinth Active Rift Development. College Station, TX, International Ocean Discovery Program.

Vamvakaris, D.A., Papazachos, C.B., Papaioannou, C.A., Scordilis, E.M., Karakaisis, G.F., 2016. A detailed seismic zonation model for shallow earthquakes in the broader Aegean area. Natural Hazards and Earth System Sciences 16(1), 55-84.

16th International Congress of the Geological Society of Greece
17-19 October, 2022 - Patras, Greece
Bulletin of the Geological Society of Greece, Sp. Publ. 10
Ext. Abs. GSG2022-303

Understanding the Quaternary Evolution of the Corinth Rift from scientific ocean drilling, IODP Expedition 381

L.C. McNeill[1], D.J. Shillington[2], C.W. Nixon[3], R.L., Gawthorpe[3], S. Pechlivanidou[3], and IODP Expedition 381 scientists

(1) School of Ocean and Earth Science, University of Southampton, Southampton, UK, lcmn@soton.ac.uk (2) School of Earth and Sustainability, Northern Arizona University, Flagstaff, Arizona, USA, (3) Department of Earth Science, University of Bergen, Bergen, Norway.

The Corinth Rift forms an ideal laboratory for investigating Quaternary tectonic, sedimentary and environmental processes due to its young age, high levels of activity and well preserved rock record. High sedimentation rates and high fault slip rates offer the chance to establish rift development processes at very high resolution in both space and time. The form and scale of the rift also result in it being self contained in terms of sediment flux, i.e., a closed basin that is small enough that the whole rift can be evaluated.

International Ocean Discovery Program (IODP) drilling provides the only chance to sample deeper sediments within the offshore rift system. In late 2017, IODP Expedition 381 onboard the industry geotechnical vessel Fugro Synergy entered the Gulf of Corinth for operations over 2 months (Shillington et al., 2019; McNeill et al., 2019a). The primary objectives of the expedition were to a) obtain high spatial and temporal resolution records of the dynamics of the rifting process and its evolution, b) to study the interaction of climate and tectonics on sedimentary and surface processes in a rift zone, and c) to improve regional hazard assessments in one of the most seismically active regions of Europe.

The rift basin is periodically closed from marine conditions as sea level fluctuates and as the rift moves vertically due to tectonics, therefore a range of paleoenvironmental conditions are encountered, impacting microfossil assemblages and pore-water geochemistry as well as depositional processes. A dense network of interpreted marine seismic data and well-studied onshore syn-rift deposits provide the context for drilling and the potential to extend the drilling results around the entire rift system. The expedition drilled, cored and logged at 3 sites along the rift, sampling the syn-rift sedimentary deposits and collectively targeting both the temporal and spatial variation of rift processes. In total 1905 m of section were cored with 85% average recovery (1645 m recovered). At two sites a suite of logging data was collected. The first expedition results focus on how tectonic processes impact sedimentary processes, sediment flux and basin environment through time and newly resolved fault and rift development rates and timings over the Quaternary.

The new sedimentary record represents the longest and highest resolution stratigraphic record for an early phase rift. New age data from drilling have been used to obtain the timing of primary rifting events and rates of rift processes – previously timings were either very loosely constrained from onshore or from seismic stratigraphic estimates offshore. The offshore syn-rift sequence records the two most recent phases of rifting. The oldest syn-rift sedimentation in the Gulf of Corinth is now estimated to start 2-2.5 Ma, representing onset of the penultimate phase of rifting and primary creation of the Gulf. The most recent rift phase began ~0.8 Ma. A key element of the syn-rift sequence is the alternation of marine and lake conditions (controlled by sea level and tectonics). These alternations are confirmed by the drilled cores and reflected in the microfossil assemblages and sedimentary lithologies. Despite the small scale of the basin, fine-grained turbiditic and hemipelagic sediments dominate in the deep basin (Gawthorpe et al., 2022), the locations of the boreholes, while coarse sediments are largely confined to marginal systems. Finely laminated varve-like sequences are common and the marine-lake transitional sedimentary sequences are especially complex. Sediment accumulation in the basin is significantly higher during glacial periods, probably controlled by climate-driven changes in vegetation cover and increased erosion and sediment flux (McNeill et al., 2019b).

The new and confirmed ages of the rift sequence have enabled us to better resolve the fault slip rates for the Quaternary. There is the potential to resolve recent slip rates down to 10's ka timescales and potentially even less in the Holocene for some faults. We find that when the most recent rift phase started (800 ka), strain rapidly localised onto a border fault system which became linked, merging discrete depocentres and creating a more asymmetric rift (Nixon et al., 2016; submitted). The rift border fault slip rates increased up to 5-6 mm/yr at this time, with the highest rates in the centre of the rift. This central areas is a zone of relatively low seismicity today and hence a likely seismic gap.

The new results on how the earliest phase of rifting takes place and impacts the paleoenvironment in the Corinth Rift are expected to make significant advances that can be used to understand other active and ancient rifts around the world. Research continues into details of the rift tectonic development at a range of spatial scales, evidence for recent earthquakes and slope failure, resolving at high resolution the history of rifting through a range of dating techniques, extracting details of the oceanographic and environmental conditions from a wide range of microfossil and palynology assemblages as climate and the isolation of the basin changed, and exploration of the links between sedimentary processes, fault, rift and basin sill evolution, climate and sea level fluctuation over 10-100's kyr timescales.

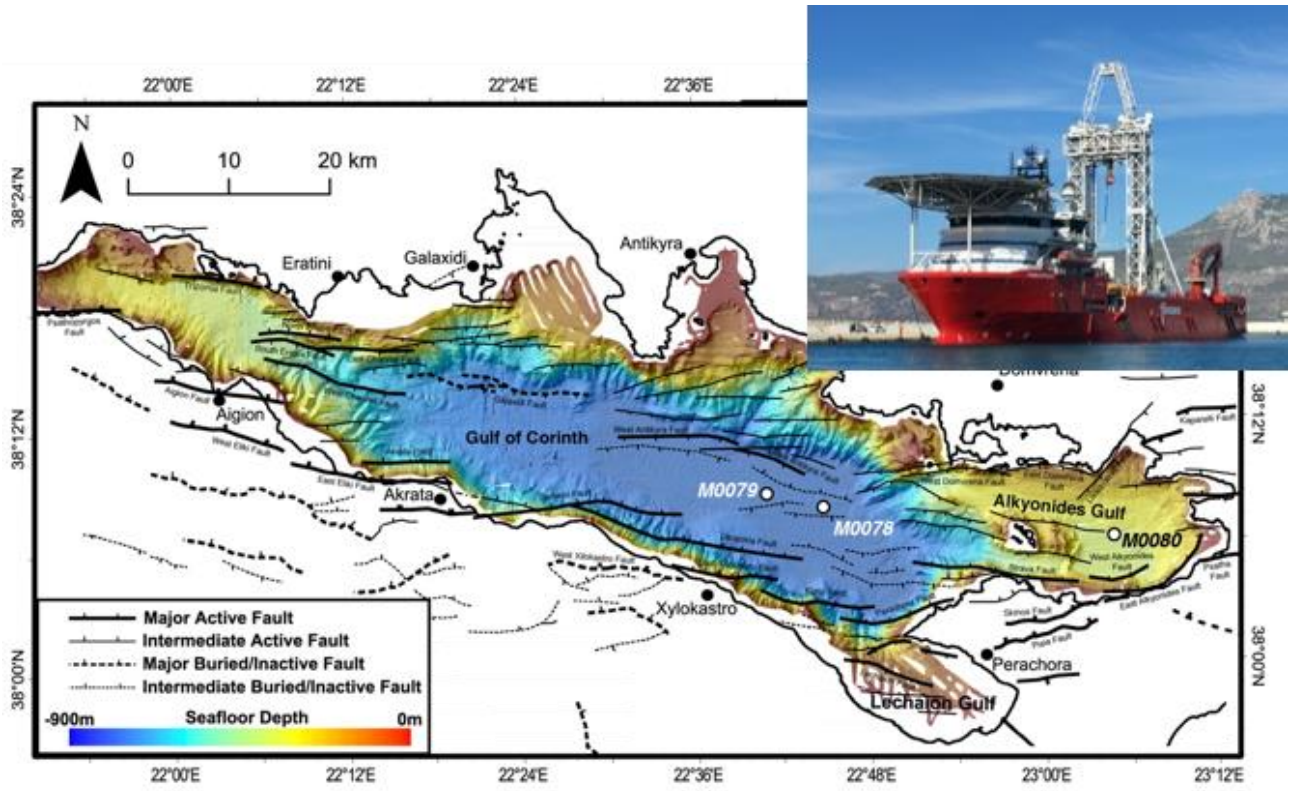

Figure 1. Fault and bathymetry map (after Nixon et al., 2016) of the Gulf of Corinth and Corinth Rift, showing the locations of the 3 IODP boreholes (M0078-M0080). Inset shows the Fugro Synergy geotechnical vessel that performed the drilling.

Acknowledgements

We thank all that contributed to IODP Expedition 381 in 2017 and 2018, including the science party both offshore and onshore, ECORD Science Operator staff, ship and drilling crew of the D/V Fugro Synergy, staff at MARUM, University of Bremen, and colleagues in Greece (in particular Dimitris Sakellariou) for providing invaluable support in terms of preparations, permissions and communications. The science party members thank their various science funding bodies for support of post-expedition research and participation in the expedition. Colleagues working on the Corinth Rift over the last few decades are thanked for contributing the scientific insights and datasets that led to this expedition.

References

Gawthorpe, R.L., Fabregas, N., Pechlivanidou, S., Ford, M., Collier, R.E.L., Carter, G.D.O., McNeill, L.C., Shillington, D.J., 2022. Late Quaternary mud-dominated, basin-floor sedimentation of the Gulf of Corinth, Greece: Implications for deep-water depositional processes and controls on syn-rift sedimentation. Basin Research, 1-34.

McNeill, L.C., Shillington, D.J., Carter, G.D.O., and the Expedition 381 Participants, 2019a. Corinth Active Rift Development. Proceedings of the International Ocean Discovery Program, 381: College Station, TX (International Ocean Discovery Program). https://doi.org/10.14379/iodp.proc.381.2019

McNeill, L.C., Shillington, D.J., Carter, G.D.O., Everest, J.D., Gawthorpe, R.L., Miller, C., Phillips, M.P., Collier, R.E.L., Cvetkoska, A., De Gelder, G., Diz, P., Doan, M.L., Ford, M., Geraga, M., Gillespie, J., Hemelsdael, R., Herrero-Bervera, E., Ismaiel, M., Janikian, L., Kouli, K., Le Ber, E., Li, S., Maffione, M., Mahoney, C., Machlus, M.L., Michas, G., Nixon, C.W., Oflaz, S.A., Omale, A.P., Panagiotopoulos, K., Pechlivanidou, S., Sauer, S., Seguin, J., Sergiou, S., Zakharova, N.V., Green, S., 2019b. High-Resolution Record Reveals Climate-Driven Environmental and Sedimentary Changes in an Active Rift. Scientific Reports, 9, 3116.

Nixon, C., McNeill, L., Bull, J.M., Bell, R.E., Gawthorpe, R.L., Henstock, T.J., Christodoulou, D., Ford, M., Taylor, B., Sakellariou, D., Ferentinos, G., Papatheodorou, G., Leeder, M.R., Collier, R.E.Ll., Goodliffe, A.M., Sachpazi, M., and Kranis, H., 2016, History of high resolution basin development within the offshore Corinth rift, central Greece. Tectonics, 35, 1225-1248, doi:10.1002/2015TC004026.

Nixon, C.W., McNeill, L.C., Gawthorpe, R.L., Shillington, D.J., Michas, G., Bell, R.E., Moyles, A., Ford, M., Zakharova, N.V., Bull, J.M., de Gelder, G., and Expedition Scientists, submitted, Increasing slip rates within the Corinth Rift: A rapidly localizing active rift fault network, Earth Planetary Science Letters.

Shillington, D.J., McNeill, L.C., Carter, G.D.O., and the Expedition 381 Participants. Expedition 381 Preliminary Report: Corinth Active Rift Development. College Station, TX, International Ocean Discovery Program. https://doi.org/10.14379/iodp.pr.381.2019

16th INTERNATIONAL CONGRESS of the
GEOLOGICAL SOCIETY OF GREECE

S3. The Hellenides: Tectonostratigraphic terranes, tectonic units and orogenic evolution

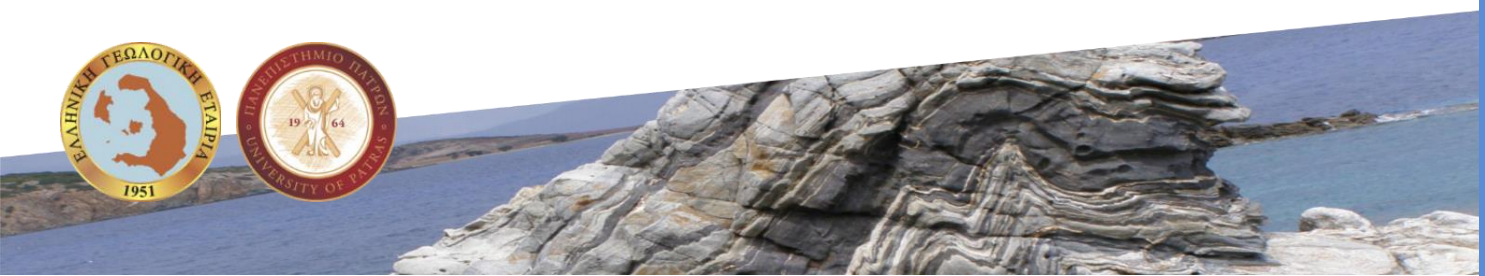

OUR EARTH, OUR HOME

16th International Congress of the Geological Society of Greece

17-19 October, 2022 - Patras, Greece

Bulletin of the Geological Society of Greece, Sp. Publ. 10

Ext. Abs. GSG2022-013

A review on thermochronometry of tectonic exhumation – the potential of solid state dosimeters for the Hellenic nappes

Constantin D. Athanassas[1]

(1)Laboratory of Geology, Department of Geological Sciences, School of Mining and Metallurgical Engineering, National Technical University of Athens (NTUA), Zografos, 15780, Athens, Greece, athanassas@mail.ntua.gr

This is a review on the current status of thermochronometry for tracking tectonic exhumation. Tectonic exhumation involves ductile thinning of the crust and, more often, tensile faulting which lifts footwall rocks towards the surface while removing overburden rock. Advection of rock towards the Earth's surface is the primary cause of crustal cooling. Historically, the principal goal of thermochronomentry (Ault et al., 2019) is to decipher the thermal maturation of sedimentary basins or orogen-scale exhumation by taking into account relationships between time, depth, and temperature. Standard (U–Th)/He or Fission-Track (FT) dating are most often used for low-temperature thermochronology, typically for understanding thermal histories associated with burial or exhumation in the upper dozen of kilometers of the Earth's crust (Ault et al., 2019; Athanassas et al., 2021).

Thermoluminescence (TL) of natural dosimeter minerals such as quartz consists of multiple spectral peaks with different closure temperatures (Fig.1). As TL of quartz arises from a discrete distribution of spectral peaks, TL can in be exploited as a thermochronometer with a number of closure temperatures. Spectral peaks arising at lower temperatures (250°C) can be exploited to estimate cooling histories over depths of exhumation less than 1 km, whereas those arising at higher temperatures can be used to reconstruct thermal histories over more than 2 km depths (Biswas et al., 2018).

As in standard systems so in TL, the combination of spectral peaks with different closure temperatures not only retains the benefits of coupled systems (e.g. (U-Th)/He of both zircon and apatite) but it may be employed to enhance the resolution of variations in exhumation rate over geologic time. The observed dose–response curves and secular dose rates may be translated into apparent closure ages and for samples down to a few km depth (e.g. Guralnik et al., 2013, Schmidt et al., 2015; King et al., 2016a,b; Ault et al., 2019).

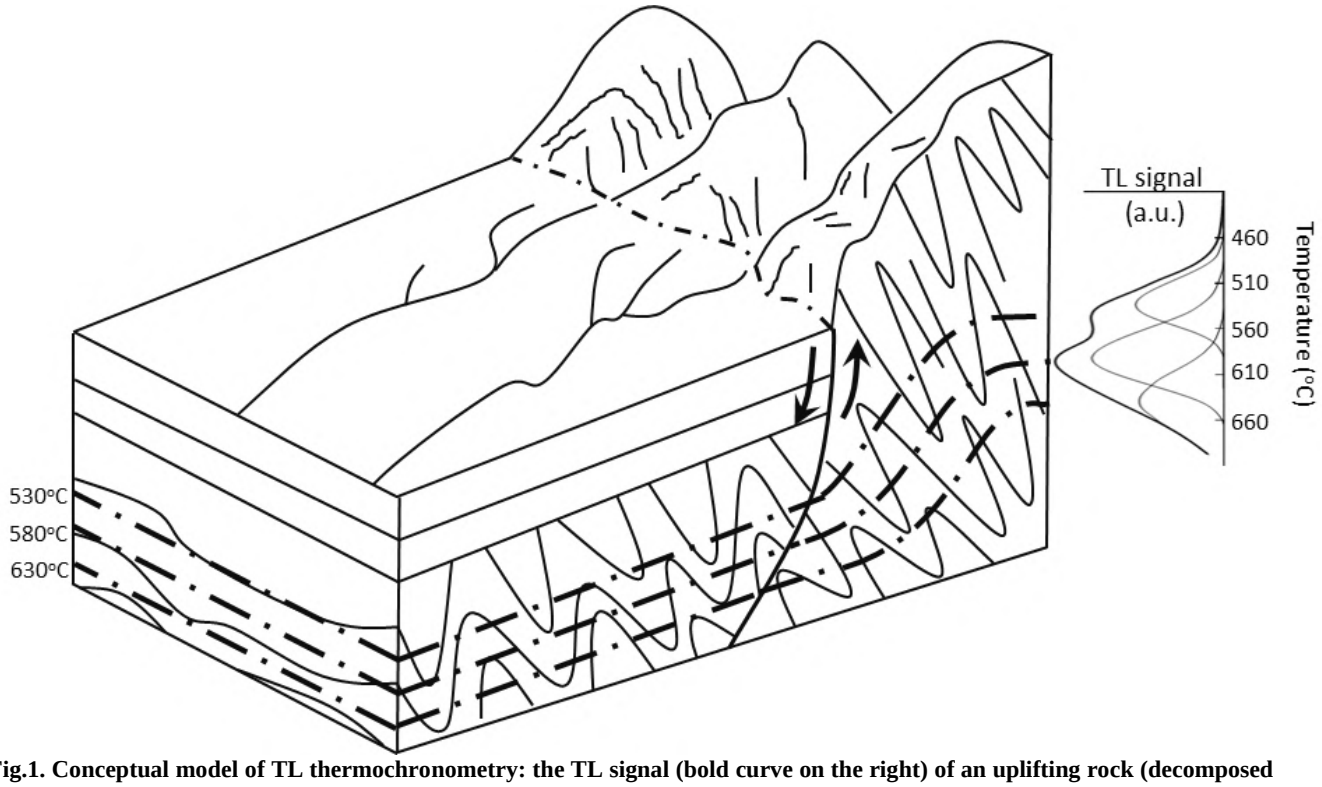

Fig.1. Conceptual model of TL thermochronometry: the TL signal (bold curve on the right) of an uplifting rock (decomposed into its spectral peaks) registers the progressively shallower isotherms that are being crossed as a series of closure temperature of progressively «shallower» spectral peaks.

Given the substantially low dose rates encountered in quartz it is possible that TL signals are not in field saturation in young and tectonically very active orogens or rapidly exhuming metamorphic nappes with quartzites. Therefore TL dating may be very useful in predicting time-dependent exhumation histories of HP metamorphic nappes (Doutsos et al., 2000; Xypolias and Doutsos, 2000). This advantage opens up the possibility for TL to be used as a competitive thermochronometer for a variety of tectonic applications, as well as for building tectonic models over the later Neogene Period (Late Miocene – Pliocene). Variation in thermochronometric TL dates over large areas of a terrain can also be used to infer the spatial patterns of exhumation. The potential of TL as a multiple, solid-state, thermochronometer of the exhumation history of metamorphic rock complexes of the southern Peloponnese is discussed.

References

Athanassas, C.D., Papanikolaou, D.I., Falkowski, S., Papanikolaou, I.D., Ntokos, D. 2021. Thermotectonic constraints on the geodynamic evolution of the Pindos fold-and-thrust-belt by low-temperature (U–Th)/He thermochronometry. *Geological Journal*, 56, 5311-5328.

Ault, A.K., Gautheron, C., King, G.E. 2019. Innovations in (U–Th)/He, Fission Track, and Trapped Charge Thermochronometry with Applications to Earthquakes, Weathering, Surface-Mantle Connections, and the Growth and Decay of Mountains. Tectonics, 38, 3705-3739.

Biswas, R.H., Herman, F., King, G.E., Braun, J. 2018. Thermoluminescence of feldspar as a multi-thermochronometer to constrain the temporal variation of rock exhumation in the recent past. Earth and Planetary Science Letters, 495, 56-68.

Doutsos, T., Koukouvelas, I., Poulimenos, G., Kokkalas, S., Xypolias, Skourlis, K. 2000. An exhumation model of the south Peloponnesus, Greece. *International Journal of Earth Sciences*, 89, 350-363.

Guralnik, B., Jain, M., Herman, F., Paris, R. B., Harrison, T. M., Murray, A. S., et al. 2013. Effective closure temperature in leaky and/or saturating thermochronometers. Earth and Planetary Science Letters, 384, 209–218.

King, G. E., Guralnik, B., Valla, P. G., & Herman, F. 2016. Trapped-charge thermochronometry and thermometry: A status review. Chemical Geology, 446, 3–17.

King, G. E., Herman, F., & Guralnik, B. 2016. Northward migration of the eastern Himalayan syntaxis revealed by OSL thermochronometry. Science, 353(6301), 800–804.

Schmidt, C., Friedrich, J., Zöller, L. 2015. Thermochronometry using red TL of quartz? Numerical simulation and observations from in-situ drill-hole samples. Radiation Measurements, 81, 98-103.

Xypolias, P. and Doutsos, T. 2000. Kinematics of rock flow in a crustal-scale shear zone: implication for the orogenic evolution of the southwestern Hellenides. *Geological Magazine*, 137, 81-96.

16th International Congress of the Geological Society of Greece

17-19 October, 2022 - Patras, Greece

Bulletin of the Geological Society of Greece, Sp. Publ. 10

Ext. Abs. GSG2022-108

Distinct periods of flysch deposition in the External Hellenides during their geodynamic evolution

Maria Triantaphyllou[1], Dimitrios Papanikolaou[1]

(1) Faculty of Geology & Geoenvironment, National and Kapodistrian University of Athens, Panepistimioupolis 15784, Zografou, Greece, mtriant@geol.uoa.gr

The Hellenides are distinguished in : 1) the External Hellenides, characterized by continuous stratigraphic columns from the early Mesozoic to the early Paleogene, and one major tectonism from early Eocene to Late Miocene and 2) the Internal Hellenides, characterized by stratigraphic unconformities mainly during the Cenomanian, that separate the pre-orogenic Triassic-Jurassic stratigraphic sequences from the post paleo-Alpine ororgenic Upper Cretaceous-Eocene transgressive sequences featured by two major phases of tectonism in Late Jurassic-Early Cretaceous and in the Eocene (Papanikolaou, 2021 and references therein). The overall evolution of the External Hellenides fold and thrust belt is marked by the onset of flysch sedimentation in its foreland, which expands as a wave from the more internal segments to the external ones, in-between late Maastrichtian to Late Miocene. This shift to younger ages towards the external segments of the belt is nevertheless not chronic but characterized by several principal breaks that correspond to major tectonic structures during the orogenic evolution, leading to subduction, metamorphism and duplication of the paleogeographic units.

The age of the transitional beds to flysch in the various geotectonic units of the Hellenides has been documented by stratigraphic and micropaleontological methods; mostly foraminiferal evidence, however calcareous nannofossil dating have been so far acquainted in several cases:

-in *Eastern Greece Unit*, the flysch onset on top of the Upper Cretaceous transgressive sediments has been constrained to Maastrichtian-Danian (Mercier & Vergely, 1984; Papanikolaou, 1986)

-the *Beotian Unit* red pelites, overlain by typical flysch deposits, have been dated in Paleocene based on the presence of globigerinids (Papanikolaou & Sideris, 1979)

-the *Parnassos Unit* red pelites, overlain by typical flysch deposits, are of Paleocene age (Aronis et al., 1964). In particular the base of red pelites (location Kokkinochoma) has been dated as late Paleocene at ~58 Ma (nannofossil biozone NP6; Richter et al., 1995); a similar age has been recorded at a flysch exposure towards to Arachova based on the contemporaneous presence of *H. kleinpellii* and *F. tympaniformis* (nannofossil biozones NP6-NP7; present study). The biozones NP7 (*H. kleinpellii, F. tympaniformis, D. mohleri, S. anarrhopus*) - NP11 (*S. conspicuus, Ch. solitus, C. crassus*) have also been recorded in the red pelites of Prosilio location; Gouliotis, 2014, present study); the recorded diachroneity is obviously associated with paleorelief differentiation due to synrifting tectonism

-the *Vardousia Unit* presents transitional beds to red pelites within Paleocene (Celet, 1979; Gouliotis, 2014)

-in *Pindos Unit* the transitional beds are of Maastrichtian-Danian age, marked by the presence of *Globotruncana* (Aubouin, 1955; Fleury, 1980). Upwards in the flysch sequence, Ananiadis et al. (2004), determined that Pindos flysch sedimentation in northern Epirus spans from Paleocene (Danian-Selandian) at ~58.5 Ma (based on the presence of *F. billii* and *P. bisulcus*; nannofossil biozones NP4-NP7, emend. this study), and in central Thessaly, transitional beds to Pindos flysch at the location of the dam of the artificial Lake of Tavropos, revealed the contemporaneous presence of *F. tympaniformis* and *H. kleinpellii* associated with the presence of NP6-NP7 biozones in Thanetian (~57 Ma, present study). In Peloponnese, Richter & Muller (1993) defined an heterochronous transition to clastic sedimentation that began in the western part of the Pindos basin in the Campanian or at the Campanian/ Maastrichtian boundary and in the eastern part not before the middle Maastrichtian or even the late Paleocene (between biozones NP1 and NP9)

-the *Arvi Unit* displays pelagic carbonates of late Maastrichtian age containing *Contusotruncana contusa, Globotruncanita stuarti, Rugoglobigerina* and Heterohelicidae that are transitional upwards to Maastrichtian-Paleocene interbedded sandstones, siltstones, shales and conglomerates (Palamakumbura et al., 2013)

-within *Ethia Unit*, the Pindos unit s.s. equivalent in Crete, flysch sedimentation begins in late Eocene/Priabonian, similarly to Gavrovo and Tripolis units (Renz, 1955; Creutzburg & Papastamatiou, 1969; Bonneau & Zambetakis, 1975)

-the *Olympus Unit* flysch sequence is overlying upper Eocene *Nummulites*-bearing limestones (Godfriaux, 1968)

-similarly the *Amorgos Unit* is featured by upper Eocene *Nummulites*-bearing limestones below the flysch deposits (Fytrolakis & Papanikolaou, 1981)

-the *Tripolis Unit* transitional beds at the base of flysch are deposited in Priabonian (Dercourt, 1964; Fleury, 1980); in Doliana Peloponnese they are dated at ~36 Ma (biozone NP19/20; Late Eocene, present study)

-within *Gavrovo Unit*, the flysch deposition started in Priabonian (IGSR & IFP, 1966; Fleury, 1980) at a mean age of ~36 Ma (nannofossil biozone NN19/20) (Triantaphyllou, 2013 and references therein)

- in the *Ionian Unit* the onset of flysch sedimentation (base of transitional beds) has been recorded in Priabonian (Renz, 1955; IGSR & IFP, 1966; Bellas, 1997) at ~36 Ma (biozone NP19/20; external/internal Ionian), and at ~41 Ma (biozone NP16; middle Ionian) (Triantaphyllou, 2013 and references therein, emend.)

-the *Mani Unit* presents early Oligocene meta-flysch with *Gl. ampliapertura* and *T. cerroazulensis* (Thiebault, 1980)

-the *Paxos Unit* on Lefkas Island exposes the classic transition to terrigenous clastics in the late Burdigalian to early Langhian (early Middle Miocene), (Bornovas, 1964; De Mulder, 1975), while Triantaphyllou (2010) documented biozones NN4-NN5 (~15 Ma; early Langhian). The basal layers of Paxos atypical flysch on Zakynthos Island have been detected in Ag. Nikolaos-Lagopodon section (Dermitzakis, 1978) and correlated with planktonic foraminiferal biozone N4 (~22 Ma).

Hence, it is evident that there exist two major breaks in the continuity of the orogenic wave (Fig. 1). The major one is observed between Paleocene (characterizing all the units from Eastern Greece to Beotia, Parnassos, Pindos and Arvi) and late Eocene (characterizing the Ethia Unit and the majority of the external carbonate platform units). The early-middle Eocene missing time interval most probably corresponds to the age of the metamorphosed flysch found at the top of subducted Cycladic units. Interestingly, this jump in the paleogeography during the orogenesis did not occur at the margins/boundaries of the tectonostratigraphic terranes but within the Pindos-Cyclades oceanic terrane H2.Thus, the synchronous onset of flysch deposition in the Pindos Unit s.s. and the Vardoussia-Parnassos units implies their paleogeographic/orogenic continuity from the inner half of the Pindos-Cyclades oceanic terrane H2 towards the Internal Carbonate Platform, H3, while Ethia Unit corresponds to the external half of the Pindos Basin towards the External Carbonate Platform H1. The second break is recorded between the late Eocene (in the Ionian Unit and the more internal segments of the platform) and Burdigalian characterizing the Paxos transitional beds. The missing period of Oligocene corresponds to the metamorphosed flysch of the subducted Mani Unit, which should be initially located between the Paxos and Ionian units. Thus, both breaks mark the lost paleogeographic areas due to subduction and metamorphism of the Metamorphic Hellenides (Papanikolaou, 1980, 1986) during Early-Middle Eocene for the Cyclades in the Medial Tectono-metamorphic Belt and during Oligocene-Early Miocene in the External Tectono-metamorphic Belt of Peloponnese-Crete.

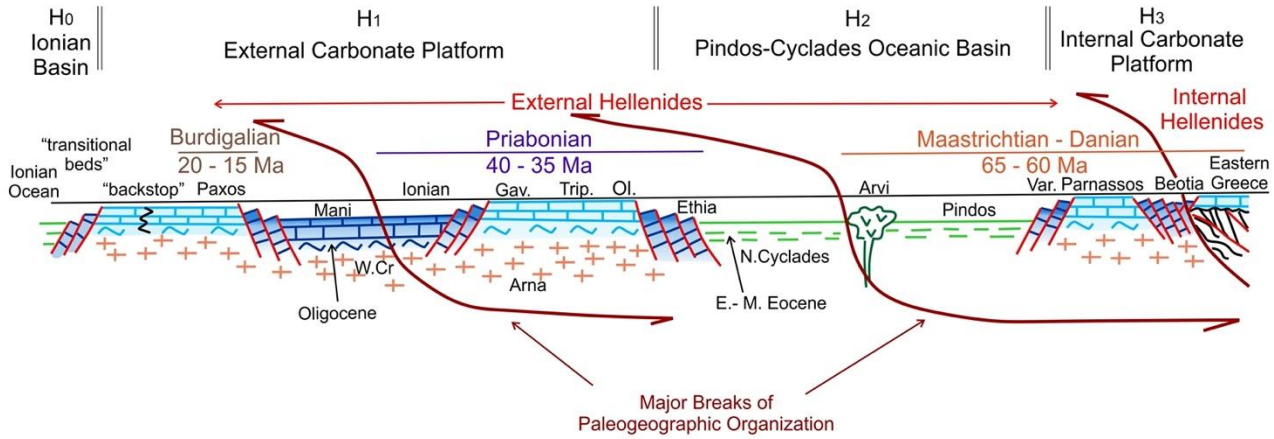

Figure 1. The orogenic evolution of the External Hellenides fold and thrust belt based on the different ages of the transitional beds to the flysch and the resulting breaks (modified from Papanikolaou, 1986; 2021; Papanikolaou & Vassilakis, 2010).

References

Ananiadis G., Vakalas I., Zelilidis A., Stoykova K., 2004. Palaeographic evolution of pindos basin during Paleogene using calcareous nannofossils. Bull. Geol. Soc. Greece vol. XXXVI, 836-845.

Bellas, S., 1997. Calcareous nannofossils of the Tertiary flysch (Post Eocene to Early Miocene) of the Ionian Zone in Epirus, NW-Greece: taxonomy and biostratigraphical correlations. Berliner Geowissenshaftliche Abhandlungen 22, 1–173.

De Mulder, E.F., 1975. Microfauna and sedimentary-tectonic history of the Oligo-Miocene of the Ionian Islands and western Epirus (Greece), Utrecht Micropaleontol. Bull., 13, 1-139.

Richter, D., Muller, C., 1993. Die Flysch-Zonen Griechenlands VI. Zur Stratigraphie des Flysches der Pindos-Zone zwischen der Querzone von Kastaniotikos und dem Südpeloponnes (Griechenland). Neues Jahrbuch fur Geologie und Palaeontologie, Monatshefte, 1993(8), 449476.

Richter, D., Muller, C., Hottinger, L., Risch, H. 1995. Die Flysch-Zonen Griechenlands X. Neue Daten zur Stratigraphie und Palaogeographie des Flysches und seiner Unterlage im Giona-Parnass-Elikon-Gebirge (Parnass-Zone, Griechenland). N.Jb.Geol.Palaont Abh., 197(3), 295- 329.

Triantaphyllou, M.V., 2010. Calcareous nannofossil biostratigraphy of Langhian deposits in Lefkas (Ionian Islands). Bull. Geol. Soc. Greece XLIII(2): 754-762.

All other references can be found in: Papanikolaou, D.I., 2021. The Geology of Greece. Springer Nature Switzerland, 389 pp.

16th International Congress of the Geological Society of Greece
17-19 October, 2022 - Patras, Greece
Bulletin of the Geological Society of Greece, Sp. Publ. 10
Ext. Abs. GSG2022-123

Structural and strain analysis of the Pelagonian nappe, Ampelakia blueschists and Olympus-Ossa unit (Eastern Thessaly, Central Greece).

I. Vrontzos[1], A. Kilias[1], E. Katrivanos[1]
(1) Department of Geology, A.U.Th., Thessaloniki, Greece, vrontzos@geo.auth.gr

Our research focuses on the study of the finite strain and structural evolution of the Pelagonian nappe, the HP/LT Ampelakia unit and the Olympus-Ossa unit in Olympus-Ossa mountainous area, in order to understand better the exhumation processes of the high-pressure rocks and the underlain Olympus-Ossa unit as a tectonic window. Shear sense kinematic indicators were used to clarify the tectonic movement.

The broader studied region constitutes a complicated tectonic nappes pile formed successively from the Jurassic to Tertiary time containing from the top to the bottom: **I.** the Jurassic Neotethyan ophiolites obducted on the Triassic-Jurassic Pelagonian platform carbonate cover, **II.** the Pelagonian nappe, composed of a Paleozoic or older poly-metamorphic crystalline basement overlain by a low grade metamorphic volcanosedimentary Permo-Triassic series and the Triassic-Jurassic carbonate cover weakly recrystallized, **III.** the metamorphosed during the Paleocene-Eocene under HP/LT conditions Ampelakia unit due to their subduction under the Pelagonian, consisted of intercalation of meta-basites and meta-sediments and **IV.** the Olympus-Ossa unit, a continuous sedimentary neritic carbonate series of Triassic to Eocene age ended up with the deposition of a Late Eocene-Early Oligocene flysch, mentioned as a part of the External Hellenides carbonate Gavrovo zone. Transgressive upper Cretaceous neritic limestones are deposited on the Ophiolites nappe and locally on the Pelagonian carbonate cover. The HP/LT Ampelakia unit together with the Pelagonian nappe and the obducted ophiolites, as well as the transgressive Cretaceous limestones were emplaced W-SW wards above the Olympus-Ossa unit during the Eocene-Oligocene (Godfriaux, 1968; Schermer, 1993; Kilias, 1995; 2021; Kilias *et al*., 2016).

For our investigation of qualitative and quantitative analysis, 52 samples were collected. For the calculation of the finite strain ellipsoid each sample was prepared in two thin sections, parallel to XZ and YZ planes and was analyzed by Rf/Φ, Fry and Panozzo methods (Fry, 1979; Ramsay & Huber, 1983; Panozzo, 1984), applying the "fabric 8" software (Wallbrecher, 1986)**.** For determining the shape of the finite strain ellipsoid and the type of deformation all these measurements are projected at the Flinn and Nadai diagrams (Fig. 1). Furthermore, for the recognition of the deformation type and sense of movement, Quartz c - axes were also measured in more than 20 thin sections using the Fedorow table and the measurements were projected in Schmidt stereograms (lower hemisphere). Finally, to define the component of the non-coaxiality, the vorticity number (Wk) was calculated, applying the mathematical formula proposed by Xypolias (2010) (Table 1).

In addition micro- and macrostructural data reveal two main stages of the Tertiary deformation related to the evolution of the nappes stacking and the exhumation processes in the studied area. The structures of the first stage consist of a main penetrative foliation Sc associated with a NE-SW trending stretching lineation Lc. It is created by the parallel development of blue amphiboles, white micas, chlorites and elongated quartz and feldspars, in the Ampelakia unit, as well as locally in deeper parts of the Pelagonian basement, indicated a HP/LT tectonometamorphic event related to compression and progressively, subduction and nappe stacking. It took place during the Paleocene-Oligocene associated with the emplacement of the Ampelakia unit and Pelagonian nappe onto the Olympus-Ossa unit (Kilias, 1995; Lips, 1998; Kilias *et al*., 2016). No clear kinematic criteria are saved of this compressional deformation stage because it is strongly replaced by the second deformation, which dominates in the studied area and is recognized with a predominant Se foliation and a same as previous NE-SW trending stretching Le lineation impressed on the Se planes. It is found with a plunge direction SW ward at the West flank of the Olympus-Ossa mountainous area and a plunge direction NE ward at the Eastern mountainous flank. Shear sense indicators shown respectively, SW sense of movement at the Western mountainous flank and opposite NE wards movement at the Eastern flank (fig. 1). If both movements took place simultaneous remains a question. Le lineation is traced by the growth of low grade metamorphism mineral parageneses, as e.g. chlorites, aktinolithe, sericites, stilpnomelane, quartz and feldspars but often due to rotation along the Se foliation planes of minerals of the previous HP/LT metamorphic event. This deformation stage developed during the Oligocene-Miocene followed the orogenic nappes stacking and has been suggested as an extensional event related to nappes tectonic denudation, uplift and exhumation of the Olympus-Ossa unit as a tectonic window. It took place under a metamorphic isothermal decompression path and is associated with the orogene collapse and crustal exhumation. The today tectonic contacts between the several nappes and the Olympus-Ossa unit are described as low angle normal detachment faults (Kilias, 1995; 2021; Kilias *et al*., 2016).

Our strain data shown that the finite strain ellipsoid is mainly of flattening type (Y>1) both at the western and eastern mountainous flanks with small deviations to near plain strain (Y=1). Furthermore, the quartz C-axes diagrams indicate significant component of a non-coaxial deformation and sense of shear analogous to the described movement direction

from the field and microscope kinematic indicators data. Finally, the calculation of the vorticity number (W_k) reveals also that the deformation is mainly characterized by a significant non-coaxial component at both mountainous flanks, W_k near 1 and it is consistent with all our other described observations.

Table 1. Strain analysis data. $W_k=\cos*\{\tan^{-1}*[(1-Rxz*\tan b^{-2})/(1+Rxz)*\tan b]\}$ (Xypolias, 2010)

SAMPLE	AVERAGE OF RF/φ - FRY AND PANOZZO METHOD			ELLIPSOID RADIUS			FLINN PARAMETRE	ANGLE	VORTICITY NUMBER
W. OSSA	RXZ	RYZ	RXY	Sx	Sy	Sz	k	b	W_k
ΚΔ 3.01	1.61	1.45	1.11	1.214	1.093	0.754	0.25	12	0.85
ΚΔ 3.02	1.57	1.45	1.08	1.193	1.102	0.760	0.18	16	0.99
ΚΔ 3.03	1.89	1.87	1.01	1.241	1.228	0.656	0.01	9	0.84
ΚΔ 2.01	1.64	1.49	1.10	1.218	1.106	0.742	0.21	9	0.88
ΚΔ 2.02	2.16	1.63	1.33	1.420	1.071	0.657	0.52	9	0.79
ΚΔ 2.03	2.19	1.83	1.20	1.379	1.152	0.630	0.24	14	0.45
ΚΔ 2.04	2.07	1.69	1.22	1.364	1.113	0.659	0.33	8	0.90
ΚΔ 1.01	2.21	1.92	1.15	1.365	1.186	0.618	0.19	10	0.76
ΚΔ 1.03	1.72	1.46	1.18	1.265	1.074	0.736	0.39	14	0.77
ΚΔ 1.04	2.11	1.87	1.13	1.335	1.183	0.633	0.15	12	0.53
ΚΔ 1.05	1.60	1.36	1.18	1.235	1.050	0.772	0.49	-	-
E. OSSA	RXZ	RYZ	RXY	Sx	Sy	Sz	k	b	W_k
ΚΑ 11	1.57	1.51	1.03	1.177	1.132	0.750	0.08	-	-
ΚΑ 12	2.08	1.51	1.37	1.420	1.031	0.683	0.74	-	-
ΚΑ 13	1.63	1.57	1.04	1.192	1.148	0.731	0.07	-	-
ΚΦ 11	1.90	1.56	1.21	1.323	1.086	0.696	0.39	8	0.88
ΚΑΑ 10	1.77	1.53	1.15	1.270	1.098	0.717	0.30	9	0.87
ΚΑΑ 11	2.79	1.86	1.49	1.612	1.074	0.578	0.58	-	-
ΚΑΑ 12	1.77	1.52	1.18	1.273	1.093	0.719	0.32	-	-

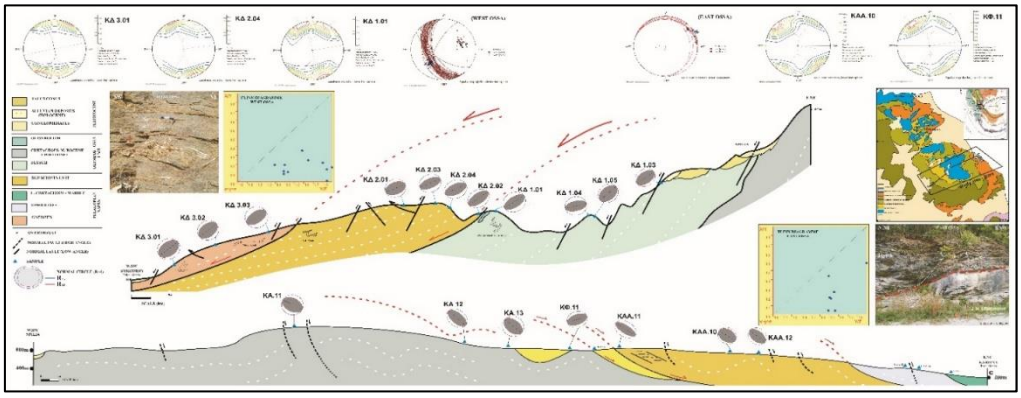

Fig 1. Cross–section through the studied area illustrating our strain and structural analysis data. Modified after geological map of Rapsani sheet (Katsikatsos et al., 1982) and geotectonic map of the Hellenides from Kilias (1995) and Kilias *et al.* (2016).

References

Fry, N., (1979): Random point distribution and strain measurement in rocks, Tectonophysics, 60, 89-105, 805-809.

Godfriaux I., (1968): Etude geologique de la region de l' Olympe (Greece), Annales Geologiques des Pays Helleniques, 19, 271 p.

Kilias, A., (1995): Tectonic Evolution of the Olympus – Ossa Mountain: Emplacement of the blueschists unit in Eastern Thessaly and exhumation of Olympus-Ossa carbonate dome as a result of Tertiary extension (central Greece), Miner Wealth, 96, 7-22.

Kilias, A.; Thomaidou, E.; Katrivanos, E.; Vamvaka, A.; Fassoulas, C.; Pipera, K.; Falalakis, G.; Avgerinas, S.; Sfeikos, A., (2016): A geological cross-section through northern Greece from Pindos to Rhodope Mountain Ranges: a field guide across the External and Internal Hellenides, journal of the Virtual Explorer, 50, paper 1, 22-35.

Kilias, A., (2021): The Hellenides: A multiphase deformed orogenic belt, its structural architecture, kinematics and geotectonic setting during the Alpine orogeny: Compression vs Extension the dynamic peer for the orogene making. A synthesis, Journal of Geology & Geoscience, 15(1), 1-56.

Katsikatsos, G.; Migiros, G.; Papazeti, E., (1982): Geological map of Rapsani sheet, scale 1:50.000, EAGME, Athens.

Lips, A.L.W. (1998): 40Ar/ 39Ar laserprobe direct dating of discrete deformational events: a continuous record of early Alpine tectonics in the Pelagonian Zone, NW Aegean area, Greece, Tectonophysics, 298, 133-153.

Panozzo, R., (1984): Two dimensional strains from orientation of lines in a plane, Journal of Structural Geology, 6, 215-221.

Ramsay, J.G.; Huber, M.I., (1983): The Techniques of Modern Structural Geology, 1, Strain analysis.

Schermer, E.R., (1993): Geometry and kinematics of continental basement deformation during the Alpine orogeny, Mt Olympus region, Greece, Journal of Structural Geology, 15 (3-5), 571-591.

Wallbrecher, E., (1986): “fabric 8” geological software, University of Graz, Austria.

Xypolias, P., (2010): Vorticity analysis in shear zones: A review of methods and applications, Journal of Structural Geology, 32, 2083.

16th International Congress of the Geological Society of Greece
17-19 October, 2022 - Patras, Greece
Bulletin of the Geological Society of Greece, Sp. Publ. 10
Ext. Abs. GSG2022-125

Formation and deformation of Triassic skarn (Uppermost Unit, Crete/Greece)

G. Zulauf[1], A. Gerdes[2], J. Krahl[3], J. Linckens[4], H. Marschall[2], L. Millonig[2], N. Neuwirth[1], R. Petschick[1], J. Pfänder[5], P. Xypolias[6]

(1) Institut für Geowissenschaften, Universität Frankfurt a.M., Germany, (g.zulauf@em.uni-frankfurt.de) (2) FIERCE, Universität Frankfurt a.M., Germany (3) Agnesstraße 45, D-80798 München, Germany (4) Tata Steel, R & D, 1970 CA Ijmuiden, The Netherlands (5) Department of Geology, TU Bergakademie Freiberg, Germany (6) Department of Geology, University of Patras, Greece.

We present new data from skarn of the blueschist-facies Preveli nappe, which is resting on top of the Pindos Unit and is overlain by Cretaceous metaflysch (Vatos nappe), Jurassic serpentinite and metagabbro (Ophiolite nappe) and a second sequence of blueschist-facies rocks (Mourne nappe) (Fig. 1).

U-Pb dating of zircons separated from felsic metavolcanics of the Preveli nappe exposed S of Lefkogia yielded Triassic emplacement ages at 237.3 ±1.8, 241.5 ±1.2 and 242.1 ±1.2 Ma. U-Pb dating of andradite-grossular of subvolcanic skarn of this area yielded the same age at 239.3 ±2.3 Ma. U-Pb garnet dating of skarn exposed SW of the Korifi and in Gerakari village (Fig. 1) yielded 232.7 ±1.5 Ma and 218.0 ±3.5 Ma, respectively, also interpreted as crystallization ages.

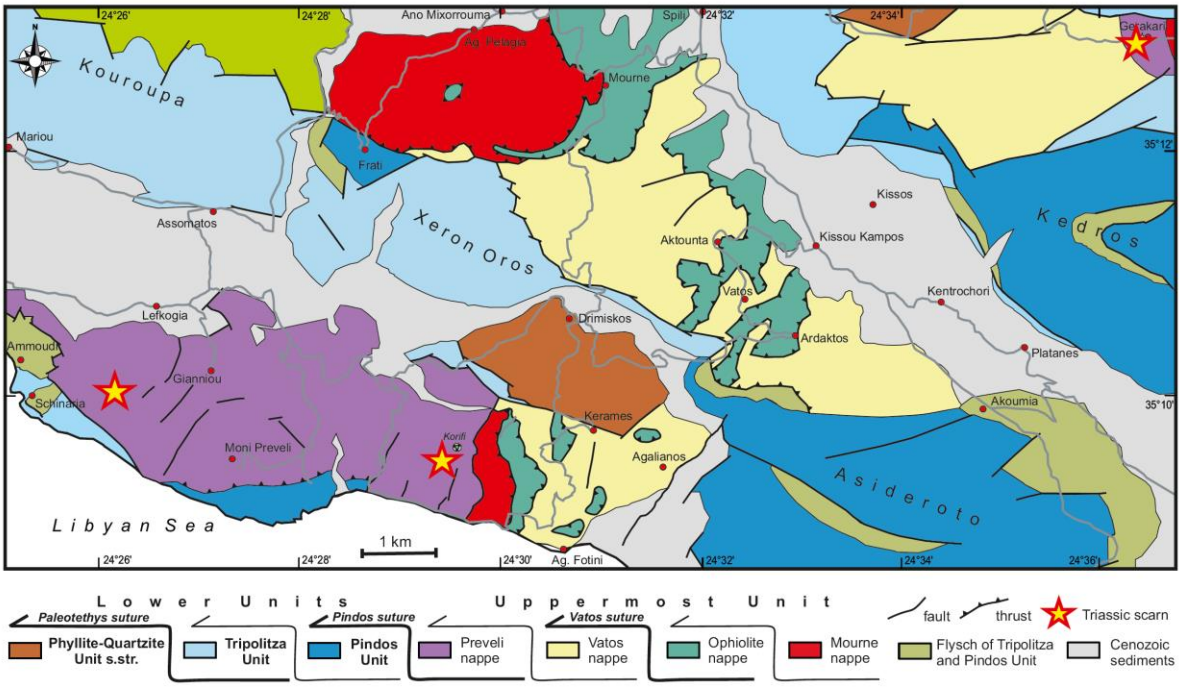

Fig. 1. Geological map of the study area in central Crete (modified after Krahl et al., 1982) with skarn localities of the Preveli nappe.

Apart from grandite, the skarn is dominated by hydrous phases (ferri-actinolite, epidote), which developed at T = 400 – 450 °C in a rift-related setting due to fluid-assisted metasomatic reactions between limestone and mafic veins. Garnet of low-strain domains is euhedral and shows a striking optical zonation in form of concentric zones differing in the degree of birefringence and following the outline of the euhedral crystal. The optical zoning of garnet is found to correlate with the chemical composition (Fig. 2) and suggests antithetic variation in Al and Fe^{3+} resulting in a change from andradite- to grossular-rich garnet, which occurred repeatedly during garnet growth. EBSD analyses of undeformed euhedral garnet revealed striking sector zoning (Fig. 2). The misorientation across the zone boundaries is < 3°.

During Eohellenic subduction, skarn and its wall rocks underwent deformation and HP-LT metamorphism. Dark blue fibers of ferri-winchite developed in tension gashes and in shear zones of skarn. Ferri-winchite in pressure shadows behind garnet grew synkinematically.

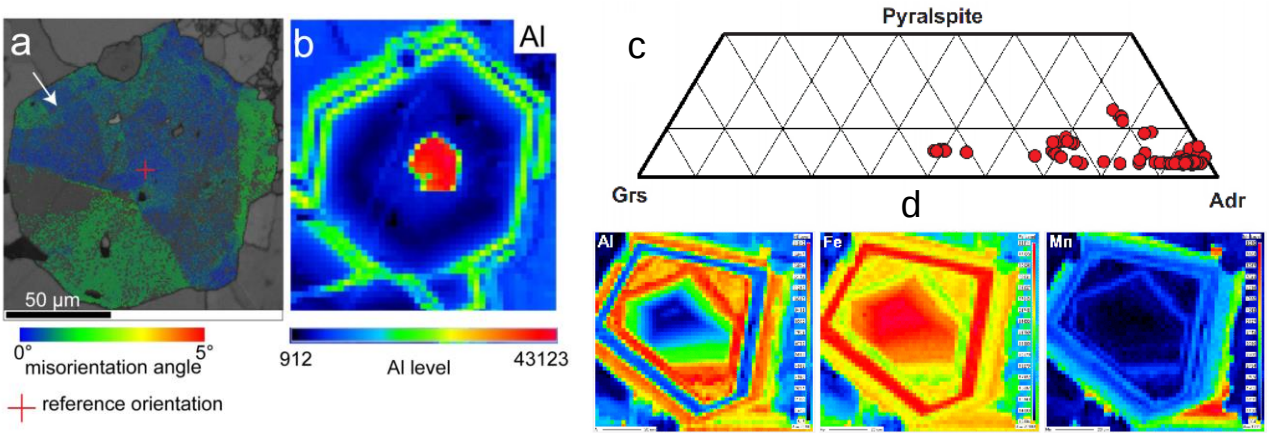

Fig. 2. Textural and chemical data of skarn garnet exposed S of Lefkogia. (a) EBSD data showing clear evidence for sector zoning, which does not correlate with the chemical zoning (Al distribution) of the garnet shown in (b). (c) Chemical composition of garnet shown in ternary diagram. (d) Element distribution maps of two-phase garnet.

^{39}Ar-^{40}Ar dating carried out on synkinematic ferri-winchite yielded a plateau age at 125 ±10 Ma. The large uncertainty is based on the low amount of potassium. Nevertheless, this value is regarded as constraining the age of Eohellenic HP-LT metamorphism related to the subduction of the Preveli rocks. An Early Cretaceous age of subduction of the Preveli rocks is in line with the Late Jurassic to Late Cretaceous flysch-type rocks of the Vatos nappe resting on top of the Preveli rocks. K-Ar dating of subcalcic hornblende (mostly barroisite) and phengite, separated from amphibolite and schist of the Mourne nappe, on the other hand, yielded Late Jurassic ages at ca. 148 Ma (Seidel et al., 1977).

The deformation microfabrics of quartz, the metamorphic index minerals, and the Si-content of white mica suggest that deformation of the Preveli rocks occurred under epidote-blueschist facies conditions at T = 360 ±40 °C and P >1.0 GPa. Despite the low deformation temperature, garnet of high-strain domains shows evidence for crystal plastic deformation in form of serrated grain boundaries and subgrains, meaning that garnet of the skarn was deformed in the brittle-ductile regime. When applying the flow law for dislocation creep of grossular under fluid-saturated conditions (Xu et al., 2013) to the HP-LT metamorphic conditions determined for the subduction stage of the Preveli rocks, the flow stress for dislocation creep is in the range of 400 – 800 MPa if a strain rate of 10^{-13} s^{-1} is assumed.

Conclusions

- Skarn of the Prevli nappe developed in Triassic times due to fluid-assisted metasomatic reactions between mafic melts of sills/and or dikes, and limestone.
- Cyclic variations in fluid composition during skarn formation are indicated by antithetic changes in garnet composition from almost pure andradite to grandite .
- Early Cretaceous (Eohellenic) subduction of the Preveli rocks led to HP-LT metamorphism and high flow stress in skarn under which grandite was deformed by both crystal plasticity and brittle fracturing. Thus, in cases of very high flow stress, dislocation creep of garnet is possible at temperatures, which are far below the threshold value (500 °C) commonly assumed for dislocation creep of garnet.
- The new ages obtained from the Preveli nappe suggest the Uppermost Unit of Crete to be derived either from the peri-Rhodope domain of the Internal Hellenides or from the Pontides of northern Turkey.

Acknowledgements

Funding by German Science Foundation, DFG (Zu 73-34) is acknowledged.

References:

Krahl, J., Herbart, H. and Katzenberger, S., 1982. Subdivision of the allochthonous ‘Ophiolites’-bearing formation upon the Pindos Group, southwestern part of Central-Crete, Greece. In: International Symposium on the Hellenic Arc and Trench (H.E.A.T.). April 8–10. 1981, Athens. Proceedings. Volume 1, p. 324–341. Αθήνα [Athens]: Εθνικό Μετσόβιο Πολυτεχνείο [Ethnikó Metsóvio Polytechneío].

Seidel, E., Schliestedt, M., Kreuzer, H., Harre, W., 1977. Metamorphic rocks of late Jurassic age as components of the ophiolitic mélange on Gavdos and Crete (Greece). Geologisches Jahrbuch 28, 3–21.

Xu, L., Mei, S., Dixon, N., Jin, Z., Suzuki, A.M., Kohlstedt, D.L., 2013. Effect of water on rheological properties of garnet at high temperatures and pressures. Earth and Planetary Science Letters, 379, 158–165

16th International Congress of the Geological Society of Greece
17-19 October, 2022 - Patras, Greece
Bulletin of the Geological Society of Greece, Sp. Publ. 10
Ext. Abs. GSG2022-155

Structural evolution of the Basal Unit (Cycladic Massif, Evia Island)

N. Gerogiannis[1], E. Aravadinou[1], V. Chatzaras[2], P. Xypolias[1]

(1) Department of Geology, University of Patras, 26500 Patras, Greece; ngerogiannis@upatras.gr (2) School of Geosciences, The University of Sydney, NSW, 2006, Sydney, Australia.

Research Highlights

Columnar calcite recognized within high-pressure marbles is used to unravel the structural evolution of the Basal Unit.

Exhumation-related deformation was localized in the western part of the Basal Unit forming three major shear zones.

Objectives

The Basal Unit is exposed on the north-western part of the Cycladic Massif (Internal Hellenides). This unit is structurally overlain by the Blueschist Unit, whereas they juxtaposed during the exhumation of the latter. Despite its critical position for understanding the tectonic evolution of the Cycladic Massif, the structure and kinematics of the Basal Unit are poorly constrained and controversial (e.g., Shaked *et al.*, 2000; Xypolias *et al.*, 2003; Chatzaras *et al.*, 2011; Spanos *et al.*, 2015). In this work, the structure and kinematics during the subduction-exhumation cycle of the Basal Unit were studied combining field-based and microstructural observations to improve our understanding of the tectonic evolution of the Hellenides orogen.

Geological framework

The Basal Unit consists of marbles of Mesozoic protolith age, which pass upwards to an early Tertiary flysch. The unit has been affected by post-middle Eocene high-pressure (HP) metamorphism followed by a greenschist facies overprint (e.g., Shaked *et al.*, 2000; Bröcker *et al.*, 2004). The Basal Thrust and the Almyropotamos Thrust represent two major structures in the Basal Unit (Xypolias *et al.*, 2003; Ring *et al.*, 2007). The Basal Thrust juxtaposes the Basal Unit with the overlying Blueschist Unit, and it was formed during the exhumation of the Blueschist Unit and the coeval underthrusting of the Basal Unit. The position of the Basal Thrust within the Cycladic Massif remains controversial (e.g., Shaked *et al.*, 2000; Xypolias *et al.*, 2003; Ring *et al.*, 2007). The Almyropotamos Thrust is inferred to be synchronous with the Basal Thrust leading to internal imbrication of the Basal Unit during subduction at Oligocene times (Xypolias *et al.*, 2003; Ring *et al.*, 2007). The kinematics of both Basal Thrust and Almyropotamos Thrust are still controversial including either W- or E-directed sense of shear (Xypolias *et al.*, 2003; Ring *et al.*, 2007).

Results

In Evia Island, the rocks of the Basal Unit were subdivided into three groups, including: a) Upper Triassic to Upper Cretaceous marbles (Lower marble sequence), b) Upper Cretaceous to Eocene marbles (Upper marble sequence), and c) undifferentiated schists interleaved within marbles. In the eastern part, marbles are characterized by a weakly developed mesoscopic foliation, whereas in the central and western part, the foliation is well-developed to mylonitic. Outcrop-scale kinematic indicators indicate a dominant top-to-the-E shearing. Map-scale shear zones developed in different structural

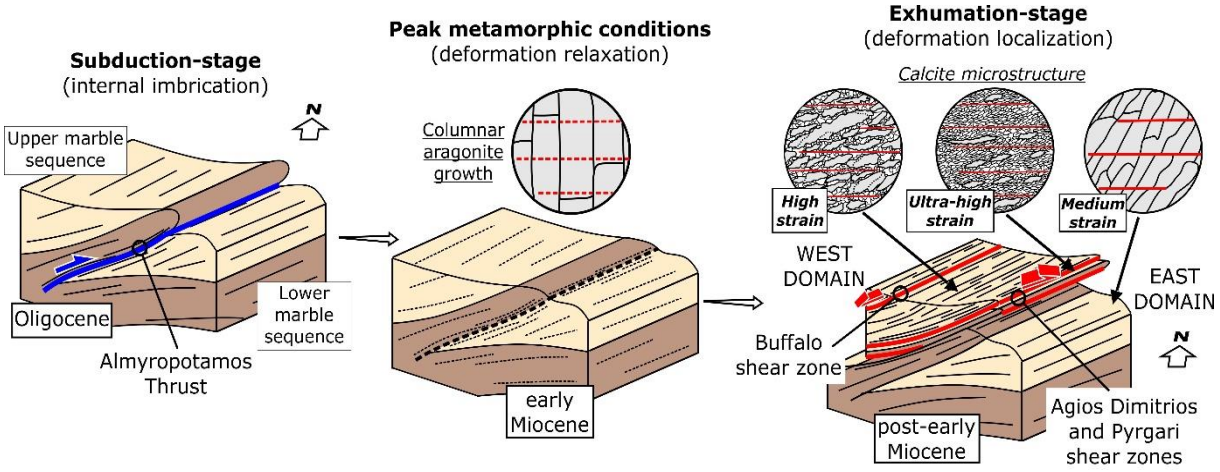

Figure 1. Tectono-metamorphic evolution of the Basal Unit in southern Evia. Block diagrams show the major structures associated with subduction, peak metamorphic conditions, and exhumation. Inset circles show aragonite and calcite microstructure.

levels of the Basal Unit. In the southern part of the study area, the Almyropotamos Thrust, brings the Lower over the Upper marble sequence. Within the thrust zone, shear sense indicators show top-to-the-SE shearing. Three shear zones were mapped in the central and western part of the study area associated with top-to-the-E (Agios Dimitrios and Pyrgari shear zones) and -WSW (Buffalo shear zone) shearing (Fig. 1).

Microstructural observations revealed that the marbles display a well-preserved columnar microstructure, defined by columnar calcite grains with their long axes oriented at high angles to the foliation (see also Brady *et al*., 2004; Gerogiannis *et al.*, 2021; Aravadinou *et al.*, 2022). This columnar microstructure possibly represents calcite pseudomorphs after aragonite. The columnar calcite was commonly sheared and affected by dynamic recrystallization. The degree of preservation of this microstructure is mainly dependent on the intensity of the subsequent ductile deformation. Based on the degree of preservation/modification of the columnar microstructure, we qualitatively classified the marble samples into four "strain" groups: low, medium, high and ultra-high strain samples. In the "low strain samples", undeformed columnar calcite characterized by a strong shape-preferred orientation (SPO) (sub-)perpendicular to the foliation is dominant (Fig. 1). Well-preserved columnar microstructure is recognized only in the eastern part of the study area, including the strongly foliated marbles of the Almyropotamos Thrust. In the "medium strain samples", columnar calcite is typically deformed displaying an inequant shape. It is characterized by a strong SPO that forms an angle of 30°–60° with the foliation (Fig. 1). Subgrain rotation (SGR) is the main recrystallization mechanism in calcite. The observed columnar calcite obliquity indicates dominant top-to-the-E shearing. In the "high/ultra-high strain samples", columnar calcite is totally recrystallized into small, sub-equant grains. These grains are oriented at small angles (<30°) to the foliation (Fig. 1). Dynamic recrystallization commenced at the SGR and continued at the bulging recrystallization field. Ultra-high strain samples are exclusively observed within the mylonites of Agios Dimitrios, Pyrgari and Buffalo shear zones (Fig. 1).

Conclusions

A columnar microstructure that represents calcite pseudomorphs after aragonite, were recorded in the marbles throughout the Basal Unit. The preservation or modification of the columnar microstructure within mylonites of map-scale shear zones, indicates that the shear zones were active during different deformation events of the subduction and exhumation history of the Basal Unit.

Well-preserved columnar calcite in the marbles of the Almyropotamos Thrust indicate that this ductile thrust was active before the growth of the columnar aragonite (Fig. 1). At peak conditions, coarsening of aragonite led to the formation of columnar crystals normal to the foliation under static conditions (Fig. 1). The Basal Unit was subdivided into two discrete exhumation-related structural domains (Fig. 1). The low to medium strain East Domain was characterized by a weakly developed mesoscopic foliation, associated with E-directed shearing. Calcite was recrystallized mainly by SGR. In contrast, the West Domain was characterized by a well-developed to mylonitic foliation, and high to ultra-high strain marbles indicating E-directed shear sense. Calcite recrystallization took place within the SGR and BLG fields. Exhumation-related deformation was localized in the West Domain leading to the formation of three major shear zones. The ductile exhumation of the Basal Unit was possibly achieved by top-to-the-E thrusting accompanied by syn-orogenic extension at upper structural levels.

Acknowledgements

This research is co-financed by Greece and the European Union (European Social Fund-ESF) through the Operational Programme « Human Resources Development, Education and Lifelong Learning» in the context of the project “Reinforcement of Postdoctoral Researchers - 2nd Cycle” (MIS-5033021), implemented by the State Scholarships Foundation (IKY) (awarded to N. Gerogiannis). Part of the field investigation was supported by Grant E045 (awarded to P. Xypolias) from the Research Committee of the University of Patras (Programme K. Karatheodori).

References

Aravadinou, E., Gerogiannis, N., Xypolias, P., 2022. Development and passive exhumation of high-pressure shear zones (Blueschist Unit, Syros): Insights from quartz and columnar calcite microstructures. Journal of Structural Geology 159, 104607.

Brady, J.B., Markley, M.J., Schumacher, J.C., Cheney, J.T., Bianciardi, G.A., 2004. Aragonite pseudomorphs in high-pressure marbles of Syros, Greece. Journal of Structural Geology 26, 3-9.

Bröcker, M., Bieling, D., Hacker, B., Gans, P., 2004. High-Si phengite records the time of greenschist facies overprinting: implications for models suggesting mega detachments in the Aegean Sea. Journal of Metamorphic Geology 22, 427-442.

Chatzaras, V., Xypolias, P., Kokkalas, S., Koukouvelas, I., 2011. Oligocene-Miocene thrusting in central Aegean: insights from the Cycladic island of Amorgos. Geological Journal 46, 619-636.

Gerogiannis, N., Aravadinou, E., Chatzaras, V., Xypolias, P., 2021. Calcite pseudomorphs after aragonite: a tool to unravel the structural history of high-pressure marbles (Evia Island, Greece). Journal of Structural Geology 148, 104373.

Ring, U., Glodny, J., Will, T., Thomson, S.N., 2007. An Oligocene extrusion wedge of blueschist-facies nappes on Evia, Aegean Sea, Greece: implications for the early exhumation of high-pressure rocks. Journal of the Geological Society 164, 637-652.

Shaked, Y., Avigad, D., Garfunkel, Z., 2000. Alpine high-pressure metamorphism at the Almyropotamos window (southern Evia, Greece). Geological Magazine 137, 367-380.

Spanos, D., Xypolias, P., Koukouvelas, I., 2015. Vorticity analysis in calcite tectonites: an example from the Attico-Cycladic massif (Attica, Greece). Journal of Structural Geology 80, 120-132

Xypolias, P., Kokkalas, S., Skourlis, K., 2003. Upward extrusion and subsequent transpression as a possible mechanism for the exhumation of HP/LT rocks in Evia Island (Aegean Sea, Greece). Journal of Geodynamics 35, 303-332.

16th International Congress of the Geological Society of Greece
17-19 October, 2022 - Patras, Greece
Bulletin of the Geological Society of Greece, Sp. Publ. 10
Ext. Abs. GSG2022-158

Structural evolution of high-pressure shear zones in the Cycladic Blueschists (Cycladic Massif, Syros Island)

E. Aravadinou[1], N. Gerogiannis[1], P. Xypolias[1]
(1) Department of Geology, University of Patras, 26500 Patras, Greece; aravantinoue@upatras.gr

Research highlights

Quartz and columnar calcite record the operation and the exhumation of the shear zones, respectively.

The shear zones were operated under increasing strain rate and slightly decreasing temperatures, whereas they were passively exhumed under weak and distributed deformation.

Introduction

In north Syros, several major high-pressure (HP) shear zones juxtaposing meta-igneous rocks with calcite marbles are exposed. Such well-preserved HP shear zones represent valuable natural laboratories for studying the deep subduction deformational processes. The HP zones have commonly been affected by very weak exhumation-related deformation that is typically difficult to be recorded. Strain sensitive, columnar calcite microstructure in HP marbles could be used as a marker for the record and quantification of this weak deformation (*e.g.*, Gerogiannis *et al.*, 2021; Aravadinou *et al.*, 2022). In this work, we study two major HP shear zones, the Kastri (KSZ) and Agios Dimitrios (ADSZ) shear zones located in north Syros Island. We combine quartz and columnar calcite microstructures to investigate the deformation conditions during the development and the exhumation of the HP shear zones providing further insights into the structural evolution of the Blueschist Unit.

Geological framework

On Syros Island, rocks of both Blueschist and Uppermost Unit of the Cycladic Massif are exposed (*e.g.*, Keiter *et al.*, 2011; Aravadinou and Xypolias, 2017). Calcite marble is the most representative rock type of Blueschist Unit, whereas meta-igneous rocks such as meta-tuffitic schists and metabasic rocks are also exposed. Peak metamorphic conditions of 1.5–1.6 GPa and 500°C for the meta-sedimentary rocks and 1.5–2.3 GPa and 500–550°C for the meta-igneous rocks have been estimated (*e.g.*, Schumacher *et al.*, 2008). Retrograde blueschist-facies metamorphism took place at temperatures 450–510°C, whereas the HP metamorphism was followed by progressive retrogression in greenschist-facies conditions (*e.g.*, Bröcker *et al.*, 2013; Cisneros *et al.*, 2021). The main deformation phase is characterized by thrusting and multiple tectonic repetitions of meta-igneous and meta-sedimentary rocks, which took place at deep subduction levels (e.g., Rosenbaum *et al.*, 2002; Keiter *et al.*, 2004) and is linked with either to top-to-(E)NE or -SSW shear sense (*e.g.*, Keiter *et al.*, 2004; Laurent *et al.*, 2016). Several works report the occurrence of columnar calcite microstructure within marbles on Syros Island (*e.g.*, Brady *et al.*, 2004; Aravadinou *et al.*, 2022). The broad preservation of this microstructure reveals that after the formation of the columnar aragonite, the rocks have not been affected by intense deformation.

Results

The hanging-wall of the ADSZ and KSZ comprises meta-tuffitic schists and metabasic rocks, whereas the footwall of both zones consists mainly of calcite marbles. The shear zones are defined by several tens of meters thick, strongly foliated rocks of both hanging-wall and footwall. The lineation in meta-igneous rocks trends generally (W)NW-(E)SE, whereas in calcite marbles trends (E)NE-(W)SW. Mesoscopic kinematic analysis focused on the hanging-wall rocks revealed a general top-to-(E)SE shear sense. Microstructural observations indicate that quartz exhibit a relatively complex dynamic recrystallization history. The dominant deformation mechanism is subgrain rotation recrystallization (SGR), but the deformation possibly commenced close to the grain boundary migration GBM/ SGR-transition field and was likely still active within the bulging recrystallization field. Static recrystallization is also sporadically present. Quartz petrofabric analysis show well- to strongly-developed preferred orientation patterns of c-axes corresponding mainly to Type-I cross-girdles pattern indicating generally plane strain conditions. A hybrid of Type-I cross-girdles or of cleft-girdles and single-girdle pattern are also obtained. All c-axis fabric diagrams are consistent with top-to-the-(E)SE sense of shear. Quartz c-axis opening-angle thermometer reveals deformation temperatures of 485°C ± 50°C. Amphibole chemistry analysis shows that acicular amphiboles defining the mylonitic foliation of meta-igneous rocks of both zones are exclusively sodic. Microstructural analysis in marbles from footwall of both zones show extensive occurrence of well-preserved columnar calcite grains oriented at high angles to the foliation. The observed obliquity between columnar calcite grains and macroscopic foliation is consistent with generally top-to-(E)NE sense of shear. Long axis orientation analysis revealed that the shear strain in both zones ranges between 0.7 and 1.0 revealing no significant spatial variation. The calcite c-axis fabric diagrams generally display a broad concentration whereas they are generally characterized by well-defined maximum rotated clockwise and at a small angle with respect to the pole of the foliation indicating top-to-(E)NE shearing.

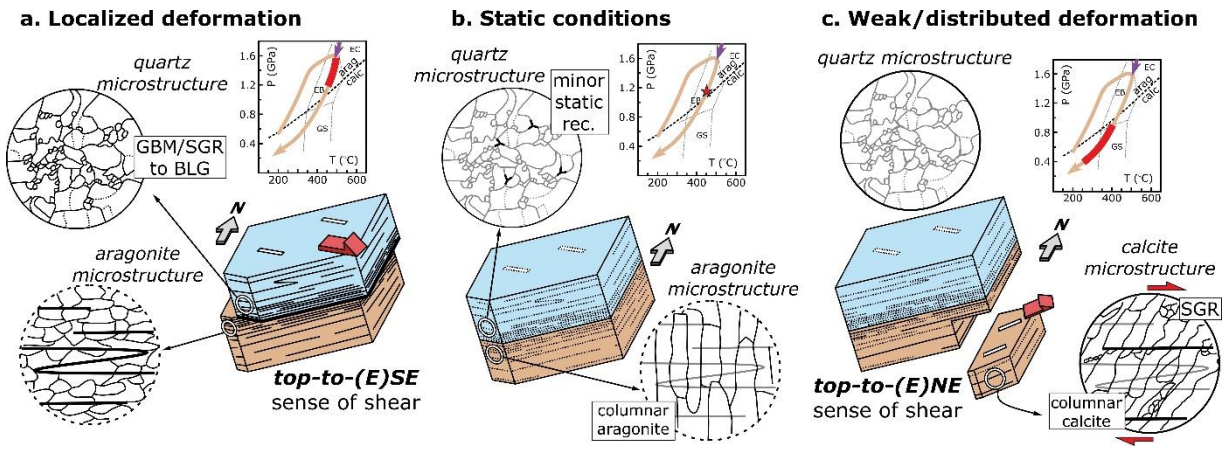

Figure 1. (a-c) 3-D block diagrams showing the evolution of Kastri and Agios Dimitrios shear zones. Circles illustrate the quartz and aragonite/calcite microstructures. Solid and dashed circles indicate observed and assumed microstructures, respectively. P–T diagrams (after Schumacher *et al.*, 2008) show the conditions of each stage.

Conclusions

Quartz microstructural/petrofabric and amphibole chemistry analysis on meta-igneous rocks revealed that the development and the operation of both ADSZ and KSZ occurred at peak and just after the peak conditions and related with top-to-the-(E)SE sense of shear under plane strain conditions (Fig. 1a). A change in both temperature and strain rate took place during the operation of the zones including a temperature decrease of ~50°C and an increase in strain rate of one order of magnitude (from 10^{-12} to 10^{-11} s^{-1}).

The formation of the columnar aragonite/calcite microstructure in the marbles of the shear zones should post-date the operation of the shear zones. This microstructure should be formed at static conditions within the stability field of aragonite (Fig. 1b). After static conditions, the shear zones should have passively been exhumed reaching at temperature below 400°C. Twinning, dynamic recrystallization within SGR field and long axis inclination of the columnar calcite reveal that the rocks were affected by weak and distributed deformation during decompression at greenschist-facies conditions (Fig. 1c). The Blueschist Unit in north Syros is characterized by a change in transport direction from (W)NW-(E)SE at the deep subduction levels to (W)SW-(E)NE during exhumation at greenschist-facies conditions. This change is linked to a change in deformation, from localized to weak and distributed revealing that the Blueschist Unit in north Syros was exhumed as a nearly rigid body.

Acknowledgements

This work was supported by Grant E045 (awarded to P. Xypolias) from the Research Committee of the University of Patras (Programme K. Karatheodori). The staff of the Laboratory of Electron Microscopy & Microanalysis (Univ. Patras) is acknowledged for their support.

References

Aravadinou, E., Gerogiannis, N., Xypolias, P., 2022. Development and passive exhumation of high-pressure shear zones (Blueschist Unit, Syros): Insights from quartz and columnar calcite microstructures. Journal of Structural Geology 159, 104607.

Aravadinou, E., Xypolias, P., 2017. Evolution of a passive crustal-scale detachment (Syros, Aegean region): insights from structural and petrofabric analyses in the hanging-wall. Journal of Structural Geology 103, 57-74.

Brady, J.B., Markley, M.J., Schumacher, J.C., Cheney, J.T., Bianciardi, G.A., 2004. Aragonite pseudomorphs in high-pressure marbles of Syros, Greece. Journal of Structural Geology 26, 3-9.

Bröcker, M., Baldwin, S., Arkudas, R., 2013. The geological significance of 40Ar/39Ar and Rb-Sr white mica ages from Syros and Sifnos, Greece: a record of continuous (re) crystallization during exhumation? Journal of Metamorphic Geology 31, 629-646.

Cisneros, M., Barnes, J.D., Behr, W.M., Kotowski, A.J., Stockli, D.F., Soukis, K., 2021. Insights from elastic thermobarometry into exhumation of high-pressure metamorphic rocks from Syros, Greece. Solid Earth 12, 1335-1355.

Gerogiannis, N., Aravadinou, E., Chatzaras, V., Xypolias, P., 2021. Calcite pseudomorphs after aragonite: a tool to unravel the structural history of high-pressure marbles (Evia Island, Greece). Journal of Structural Geology 148, 104373.

Keiter, M., Ballhaus, C., Tomaschek, F., 2011. A new geological map of the island of Syros (Aegean Sea, Greece): implications for lithostratigraphy and structural history of the Cycladic Blueschist Unit. Geological Society of America Special Paper 481, 1-43.

Keiter, M., Piepjohn, K., Ballhaus, C., Lagos, M., Bode, M., 2004. Structural development of high-pressure metamorphic rocks on Syros island (Cyclades, Greece). Journal of Structural Geology 26, 1433-1445.

Laurent, V., Jolivet, L., Roche, V., Augier, R., Scaillet, S., Cardello, G.L., 2016. Strain localization in a fossilized subduction channel: insights from the Cycladic Blueschist Unit (Syros, Greece). Tectonophysics 672-673, 150-169.

Rosenbaum, G., Avigad, D., Sánchez-Gómez, M., 2002. Coaxial flattening at deep levels of orogenic belts: evidence from blueschists and eclogites on Syros and Sifnos (Cyclades, Greece). Journal of Structural Geology 24, 1451-1462.

Schumacher, J.C., Brady, J.B., Cheney, J.T., 2008. Metamorphic style and development of the blueschist- to eclogite-facies rocks, Cyclades, Greece. IOP Conf. Series: Earth and Environmental Science 2, 012017.

16th International Congress of the Geological Society of Greece
17-19 October, 2022 - Patras, Greece
Bulletin of the Geological Society of Greece, Sp. Publ. 10
Ext. Abs. GSG2022-160

Deformation conditions and kinematics of a crustal-scale shear zone (Cycladic Massif, Ios Island): insights from quartz microstructures and petrofabrics

K.A. Tsourtis[1], N. Gerogiannis[1], E. Aravadinou[1], P. Xypolias[1]

(1) Department of Geology, University of Patras, 26500 Patras, Greece; katsourtis@gmail.com

Research Highlights

The contact between Cycladic Basement and Blueschist Unit in Ios operated at temperatures ~500-400 ºC under constrictional to plane-strain conditions.

This contact is characterized by high simple shear component of deformation associated mainly with top-to-S shearing.

Introduction/Objectives

On Ios Island, the Cycladic Massif is represented by rocks belonging to the Blueschist unit (BU) and the Cycladic Basement (CB). The contact between these two units is inferred to represent a major crustal-scale shear zone. However, the deformation conditions and the kinematics of this contact are still a matter of debate. This enigmatic contact has been interpreted both as a thrust or/and as a normal-sense detachment with controversial kinematics, whereas some researchers question the existence of a tectonic contact between the two units. In this work, quartz microstructural and c-axis fabrics analyses were carried out on rocks of the CB to evaluate the deformation conditions and kinematics of the contact between CB and BU.

Geological framework

The Cycladic Massif represents a metamorphosed nappe pile formed during the Alpine orogeny. On Ios Island, it is subdivided, from structurally higher to structurally lower, into three units/nappes: the Uppermost unit, the Blueschist unit, and the Cycladic Basement. The overlying BU consists of calcite marbles alternating with schists and ultramafic bodies (Van der Maar & Jansen, 1983, Flansburg *et al*., 2019), whereas the underlying CB consists of paragneiss, orthogneiss as well as intrusive bodies (Van der Maar & Jansen, 1983, Flansburg *et al*., 2019). Both BU and CB had experienced a blueschist to eclogite facies metamorphism during middle Eocene and were subsequently overprinted by a greenschist-facies event during Oligocene-Miocene (Henjes-Kunt & Kreuzer, 1982, Thompson *et al*., 2009). The CB has also been affected by a Hercynian amphibolite facies metamorphic event.

The contact between the BU and CB is defined by strongly deformed to mylonitic rocks from both units (Vanderberg & Lister, 1996, Huet *et al*., 2009). The nature of the contact has been interpreted as a top-to-S ductile thrust, which was active during Eocene-Oligocene and then reactivated as a top-to-N normal-sense detachment fault during Miocene (Van der Maar & Jansen, 1983, Huet *et al*., 2009). In contrast, other studies consider that the contact represents a top-to-S or a bivergent normal-sense detachment (Vanderberg & Lister, 1996, Thompson *et al*., 2009, Mizera & Behrmann, 2016). Strain and flow kinematics analyses performed in the CB reveal a pure-shear-dominated plane strain deformation (Mizera & Behrmann, 2016). In contrast, new geochronological data suggest that possibly there is no major tectonic contact between the two units (Flansburg *et al*., 2019).

Quartz microstructures

Thirty samples were collected from rocks of CB at or close to the contact with the BU. The analyzed samples represent foliation-parallel quartz veins as well as pure quartz domains, in cases phacoid, within schists and gneisses. Quartz microstructural observations indicate that large relict quartz grains with size greater than 350 μm vary in shape from slightly equant to elongated, whereas they are characterized by lobated to largely sutured/serrated boundaries (Fig. 1a). These large quartz grains are commonly characterized by intracrystalline plasticity in the form of both undulose extinction and subgrains. The subgrains display a variation in grain size (~ 40-250 μm), whereas subgrain boundaries are mainly straight, with only few cases where small-scale sutured/serrated subgrain boundaries are present (Fig. 1a). Recrystallized grains have size that range between 25 and 250 μm and is equal to that of the subgrains (Fig. 1a). In some cases, recrystallized grains decorate the large relict ones forming core-and-mantle structures. The shape of the recrystallized grains is mainly equant to slightly elongated, whereas the boundaries are mainly straight to, in few cases, small-scale sutured/serrated. Also, there are cases where the larger recrystallized grains are characterized by the presence of subgrains with size equal to that of the smaller recrystallized grains. In some cases, both large relict and recrystallized grains characterized by small-scale sutured/serrated boundaries (Fig. 1a). These microstructural features reveal that the dynamic recrystallization achieved mainly by SGR. However, quartz recrystallization possibly initiated close to grain boundary migration (GBM) / SGR transition field. Finally, the presence of small-scale sutured/serrated boundaries suggests that deformation was still active close to SGR / bulging recrystallization (BLG) field.

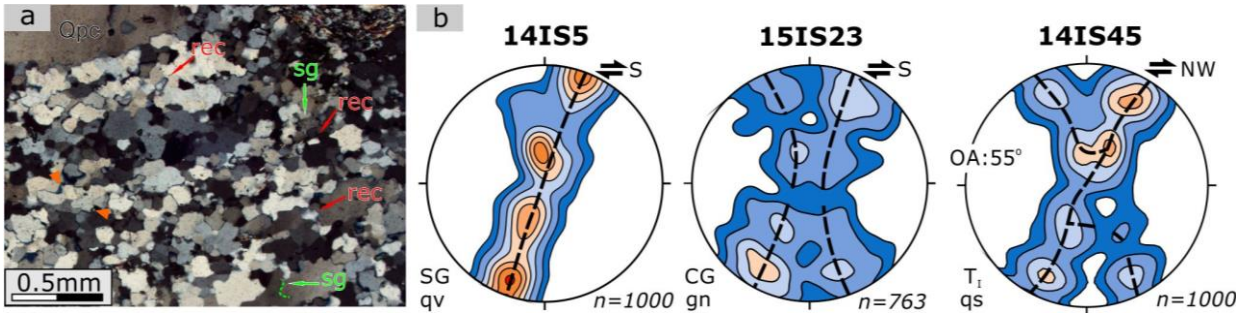

Figure 1. (a) Representative photomicrograph (cross-polarized light) showing the main quartz recrystallization features. (b) Representative quartz c-axis diagrams (contour plots, equal-area, lower hemisphere projections).

Quartz c-axis fabrics

Quartz c-axis fabrics were obtained from recrystallized grains and well-developed subgrains that occur on quartz veins and pure quartz domains within schists and gneisses. In general, 420 to 1000 quartz grains and subgrains were measured in each thin section. Generally, the analyzed samples show well- to strongly developed preferred orientation patterns. The observed c-axis fabrics can be grouped into three categories: variable-kinked single-girdle or single-girdle, cleft-girdles and Type-I cross-girdles (Fig. 1b). A systematic difference in c-axis patterns is observed between quartz veins and pure quartz domains within schists and gneisses. All six quartz vein samples display strongly developed single- to variable-kinked girdle patterns indicating top-to-S sense of shear (Fig. 1b). In contrast, pure quartz domains within quartz schists and gneisses display well-developed cleft-girdles and Type-I cross-girdles patterns (Fig. 1b). Cleft-girdles diagrams are typically slightly asymmetric in terms of density distribution and skeletal outline. Ten out of fifteen cleft-girdles patterns indicate top-to-S(SE) sense of shear, three display top-to-N(NW) asymmetry, while two diagrams are symmetric. Similarly Type-I cross-girdles diagrams are slightly asymmetric in terms of density distribution and skeletal outlines. Specifically, five Type-I cross-girdles patterns indicate a top-to-N(NW) shearing, three diagrams indicate a top-to-S(SE) sense of shear, whereas one diagram is symmetric (Fig. 1b). Quartz opening-angles were measured on well-developed Type-I cross-girdles patterns to estimate the deformation temperature. A mean opening-angle of 53° yielded a temperature of 415°C ± 50°C (Faleiros *et al*., 2016).

Conclusions

Quartz dynamic recrystallization is linked with the formation of the main foliation observed at the contact between CB and BU. Quartz was recrystallized mainly by SGR, whereas recrystallization was active from GBM/SGR to SGR/BLG transition fields. This indicates that the contact between CB and BU was likely operated under decreasing temperatures from 530-490°C to 420-390°C. Deformation temperatures of 415°C ± 50°C yielded from c-axis opening-angle thermometer is within the range of microstructural estimates, although closer to the lower temperature limit. These results correspond to an exhumation-related deformation. C-axis patterns suggest that the contact between CB and BU operated under constrictional to plane-strain conditions and is commonly associated with top-to-S sense of shear revealing a high simple shear component of deformation.

Acknowledgments

The present work was financially supported by the "Andreas Mentzelopoulos Foundation" (awarded to K.A. Tsourtis).

References

Faleiros F.M., Moraes R., Pavan M., Campanha G.A.C., A new empirical calibration of the quartz c-axis opening-angle deformation thermometer. Tectonophysics. 671, 173-182.

Flansburg, M.E., Stockli, D.F., Poulaki, E.M., & Soukis, K., 2019. Tectono-magmatic and stratigraphic evolution of the Cycladic Basement, Ios Island, Greece. Tectonics, *38*. https://doi.org/10.1029/2018TC005436

Henjes-Kunst F., Kreuzer H., 1982. Isotopic Dating of Pre-Alpine Rocks from the Island of Ios (Cyclades, Greece). Contributions to Mineralogy and Petrology, 80, 245-253.

Huet, B., L. Labrousse, and L. Jolivet (2009). Thrust or detachment? Exhumation processes in the Aegean: Insight from a field study on Ios (Cyclades, Greece), Tectonics, 28, TC3007, doi:10.1029/2008TC002397.

Mizera M., Behrmann J.H., 2016. Strain and flow in the metamorphic core complex of Ios Island (Cylades, Greece). Int. J. Earth Sci., DOI 10.1007/s00531-015-1259-y

Thomson S., Ring U., Brichau S., Glondy J., Will T.M., 2009. Timing and nature of the Ios metamorphic core complex, southern Cyclades, Greece. Geol. Society of London, Special Publications, 321, 139-167.

Van der Maar P.A., Jansen B.H., 1983. The geology of the polymetamorphric complex of Ios, Cyclades, Greece and its significance for the Cycladic Massif. Geologische Rundschau, 72, 283-299.

Vandenberg L.C., Lister G., 1996. Structural analysis of basement tectonites from the Aegean metamorphic core complex of Ios, Cyclades, Greece. J. Structural Geology. 18, 1437-1454.

16th International Congress of the Geological Society of Greece
17-19 October, 2022 - Patras, Greece
Bulletin of the Geological Society of Greece, Sp. Publ. 10
Ext. Abs. GSG2022-255

Differentiation of the structural fabric of the Skyros tectonic units from the Paleo-Alpine to the Alpine orogenic events

D. Boundi[1] and D. Papanikolaou[1]

(1) Department of Geology and Geoenvironment, National and Kapodistrian University of Athens, Panepistimioupoli Zografou, 15784_Athens_Greece_ boundi.dimitra@hotmail.com

Skyros Island is bisected by a NE-SW strike slip fault zone (Papanikolaou & Royden, 2007; Papanikolaou et al., 2022). This fault zone represents the southwest end of the southern branch of the prolongation of the North Anatolian Fault in the Aegean, passing through the Skyros Basin (Papanikolaou et al., 2019). The transverse NE-SW profiles of the northwest and the southeast blocks show the great difference of the geology of the two Skyros blocks. The southeast block is made up of only one monotonous tectonic unit, comprising a Triassic-Jurassic carbonate platform of the Sub-Pelagonian, overlain by transgressive undeformed Upper Cretaceous sediments. The northwest block comprises several Alpine tectonic units, forming a complex nappe structure with imbrications, indicated by thin interlayers of sheared ophiolite rocks. (Philippson, 1901; Ktenas, 1930; Papastamatiou, 1961; Jacobshagen et al., 1976, ; Harder et al., 1983; Jacobshagen and Wallbrecher, 1984). The northwest block is formed from base-to-top: (1) A thick Triassic-Jurassic carbonate platform, belonging to the Sub-Pelagonian unit. The platform overlies stratigraphically a Permo Triassic volcano-sedimentary sequence > 300 m thickness. (2) A thin layer of ophiolite rocks imbricated with thin tectonic wedges of the Triassic-Jurassic platform carbonates. The ophiolite outcrops belong to the Vardar/Axios oceanic basin and were tectonically emplaced on top of the carbonate platform during the Late Jurassic–Early Cretaceous (Jacobshagen et al., 1976, Papanikolaou, 2009). (3) Upper Cretaceous carbonate rocks and flysch of several hundred meters in thickness, forming tectonic wedges in between the underlying Sub-Pelagonian and ophiolite rocks and the overlying metamorphic rocks. (4) A wedge-shaped tectonic unit of metamorphic rocks, comprising meta-volcanic rocks, meta-sediments, and pelagic silicate marbles, imbricated with ophiolites. This unit was known as the "Fere-Note" formation (Ktenas, 1930; Philippson, 1901) and was renamed by Jacobshagen et al., 1976, 1983, 1984 as the "Eo-Hellenic nappe" of Skyros. In fact, it forms the lower metamorphic nappe of Skyros. Its thickness becomes more than 1 km towards the northeast, whereas towards the southwest, it thins out and there are small tectonic wedges/klippen of a few tens of meters thickness up to the western coast of Skyros. (5) On top of all previous tectonic units, there is a tectonic klippe of a metamorphic nappe, forming the highest peak of the Skyrian Olympus Mountain (403 m). This unit was known as the "Skyros tectonic unit" (Jacobshagen et al., 1983) and is now called the Upper metamorphic nappe of Skyros. It comprises pelagic silicate marbles and intercalations of gneisses-schists. Its metamorphic grade is higher than that of the underlying Lower Skyros metamorphic nappe.

Structural analysis of the four main tectonic units of Skyros comprising numerous measurements of bedding, schistosity and foliation planes, lineations and fold axes resulted in the distinction of the following main deformation phases (Figure 1).

1) The Sub-Pelagonian unit is characterized by one deformation phase with dominant NNE-NE (10º-60º) – SSW-SW (190º-240º) direction of lineations and fold axes. This deformation phase should be considered as Paleo-Alpine, during Late Jurassic – Early Cretaceous as observed also in several other outcrops of the SubPelagonian unit, beneath the undeformed unconformable Upper Cretaceous sediments, 2) The Lower Skyros unit is characterized by two deformation phases, one in the NE-SW direction (50º-60º – 230º -240º) followed by a second in the NNW-SSE direction (350º-170º). Both phases comprise lineations and fold axes but syn-metamorphic intersection lineations dominate in the first phase and post-metamorphic crenulation lineations in the second, 3) The Upper Cretaceous limestones and flysch are characterized by one deformation phase in the NW-SE direction (280º-340º – 100º-160º) expressed only by folding. The age of this deformation phase is evidently post Late Cretaceous, following the deposition of the sediments, 4) The Upper tectonic unit of Olympus is characterized by one deformation phase in the NW-SE direction (330º-150º) with dominant mineral lineations, plunging to the SE. The same direction is dominant in the striking of the bedding and foliation of the marbles and schists, which are highly inclined to sub-vertical.

Thus, the Paleo-Alpine deformation phase with structural direction in the NE-SW is present in the Sub-Pelagonian relative autochthon and in the Lower Skyros Unit as a syn-metamorphic structure. The Alpine deformation phase with structural direction in the NW-SE is present in the Cretaceous sediments only with folding, in the Upper tectonic unit of Olympus with syn-metamorphic mineral lineations and in the Lower Skyros unit with post-metamorphic crenulation lineations and folding. The newly obtained radiometric ages by the Ar/Ar method on minerals of the Upper tectonic unit of Olympus have shown Upper Cretaceous ages (Boundi, et al, 2022) confirming the Alpine nature of the NW-SE deformation phase.

The geodynamic evolution of the Skyros tectonic units comprises: 1) subduction of the Sub-Pelagonian carbonate

platform during Late Jurassic – Early Cretaceous with NE-SW syn-metamorphic structures beneath the previously subducted ophiolites and Lower Skyros Unit, resulting in the Paleo-Alpine orogenic events. 2) Deposition of Upper Cretaceous sediments with neritic limestones and flysch above the previously deformed Sub-Pelagonian unit together with the ophiolites and Lower Skyros unit. During the same period high temperature metamorphism has affected the pelagic Olympus unit in a more internal geodynamic domain, close to a magmatic/volcanic arc. 3) Alpine deformation of all units with dominant direction NW-SE. This deformation is exclusive in the Upper Cretaceous sediments (shallow level without metamorphism) and in the Olympus unit (deep level with metamorphism). In the lower units of the Sub-Pelagonian and the Lower Skyros unit this phase is secondary without metamorphism, comprising thrusting, folding and fracture cleavages with kink-folds. The tectonic vergence of the nappes indicates a direction of tectonic transport from the NE towards the SW, conformable to the other structures observed in mainland Greece.

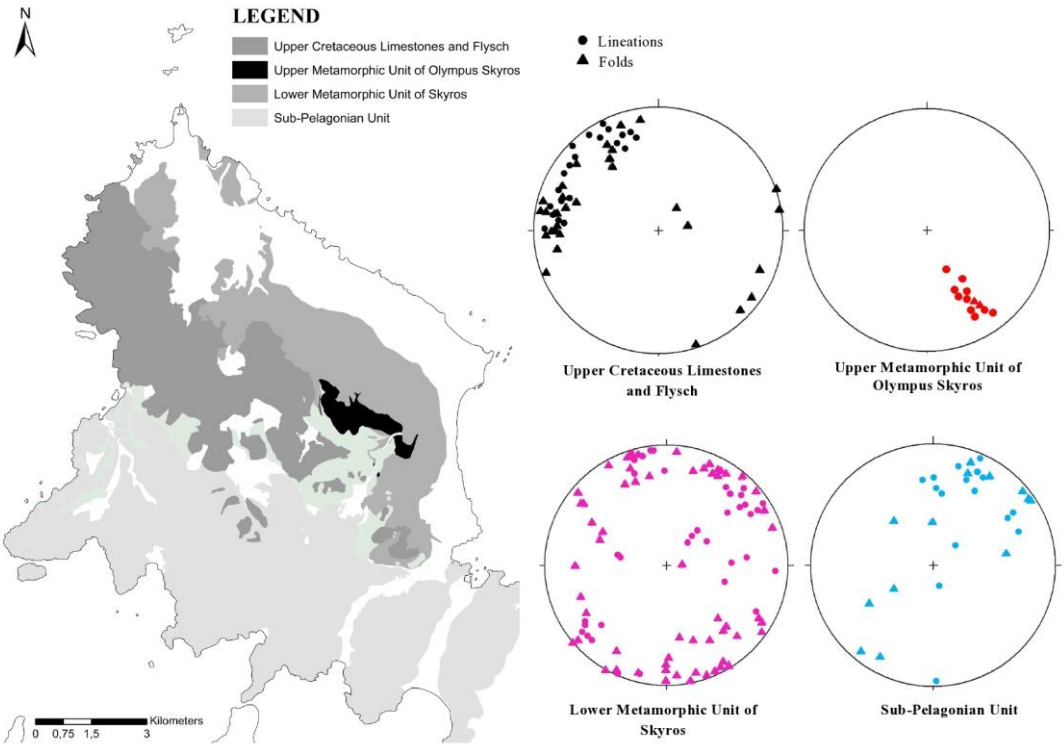

Figure 1. Representative diagrams of lineations and folds in the four tectonic units of Skyros.

References

Boundi, D., et al., 2022. Late Cretaceous Tectono-Metamorphic Events in the Skyros Upper Allochthon (Olympus Unit), Aegean Sea, Greece, International Journal of Earth Sciences [submitted]

Harder, H., et al., 1983. Geologische Entwicklung und Struktur der Insel Skyros, Nordsporaden, Griechenland. Berliner geowissenschaftliche Ab1h6andlungen 48:7-40, Berlin.

Jacobshagen, V, 1976. Die eohellenische phase. Definition und Interpretation. Zeitschrift der Deutschen Gesellschaft für Geowissenschaften 127:133-145.

Jacobshagen, V. et al.,1983. Skyros Island. Geological Map of Greece at scale 1/50,000. IGME., Athens

Jacobshagen, V., Wallbrecher, E., 1984. Pre-Neogene nappe structure and metamorphism of the North Sporades and the southern Pelion peninsula. In: Dixon JE, Robertson AHF (Eds), The Geological Evolution of the Eastern Mediterranean. Geological Society of London, Special Publication 17, pp. 591-602.

Ktenas, C., 1930. Report on the geological research effected during 1928-1929. Proceedings Academy of Athens 5:92-107.

Papanikolaou, D., Royden, L., 2007. Disruption of the Hellenic arc: Late Miocene extensional detachment faults and steep Pliocene-Quaternary normal faults - Or what happened at Corinth?. Tectonics 2007 26: TC5003

Papanikolaou, D,. 2009. Timing of tectonic emplacement of the ophiolites and terrane paleogeography in the Hellenides. Lithos 108:262-280.

Papanikolaou, D., et al., 2019. Active tectonics and seismic hazard in Skyros Basin, North Aegean Sea, Greece. Marine Geology 407:94-110.

Papanikolaou, D. et al., 2022. The onshore Skyros strike-slip system at the Southwestern tip of the North Anatolian Fault Zone: Seismotectonic and seismic hazard implications. [manuscript]

Papastamatiou, J., 1961. Quelques observations sur la géologie et la metallogénie de l'île de Skyros. Bullettin of the Geological Society of Greece IV/1:219-237.

Philippson, A., 1901. Beitrage zur Kenntnis der grienchischen Inselwelt, Peterm. Milt. Ergänzungsheft, 134:1-172.

16th International Congress of the Geological Society of Greece
17-19 October, 2022 - Patras, Greece
Bulletin of the Geological Society of Greece, Sp. Publ. 10
Ext. Abs. GSG2022-317

Eohellenic subduction and Alpine collision of Permo-Triassic rocks of the Preveli nappe (Uppermost Unit, Crete): Constraints on the age and kinematics of deformation

N. Neuwirth[1]*, G. Zulauf[1], R. Albert[2], A. Gerdes[2], D. Hezel[2], J. Krahl[3], J. Linckens[1], R. Petschick[1], J. Pfänder[4], P. Xypolias[5]

(1) Institut für Geowissenschaften, Goethe-Universität Frankfurt a.M., Altenhöferallee 1, 60438 Frankfurt a.M., Germany n.neuwirth@em.uni-frankfurt.de – corresponding author*; (2) Frankfurt Isotope & Element Research Center (FIERCE), Goethe-Universität Frankfurt a.M.,Altenhöferallee 1, 60438 Frankfurt a.M., Germany; (3) Agnesstraße 45, 80798 München, Germany; (4) Institut für Geologie, TU Bergakademie Freiberg, Bernhard-v.-Cotta-Straße 2, 09599 Freiberg, Germany; (5) Department of Geology, University of Patras, 265 04 Rio Patra, Greece.

We present new radiometric ages, which help to constrain the timing of subduction and collision of the blueschist-facies Preveli nappe in central Crete. As one of the basal nappes of the Uppermost Unit, the Preveli nappe has been thrust on top of the Pindos Unit and is overlain by Eohellenic metaflysch of the Vatos nappe, Jurassic ophiolite (Ophiolite nappe) and a second sequence of blueschist-facies rocks of the Mourne nappe (Fig. 1).

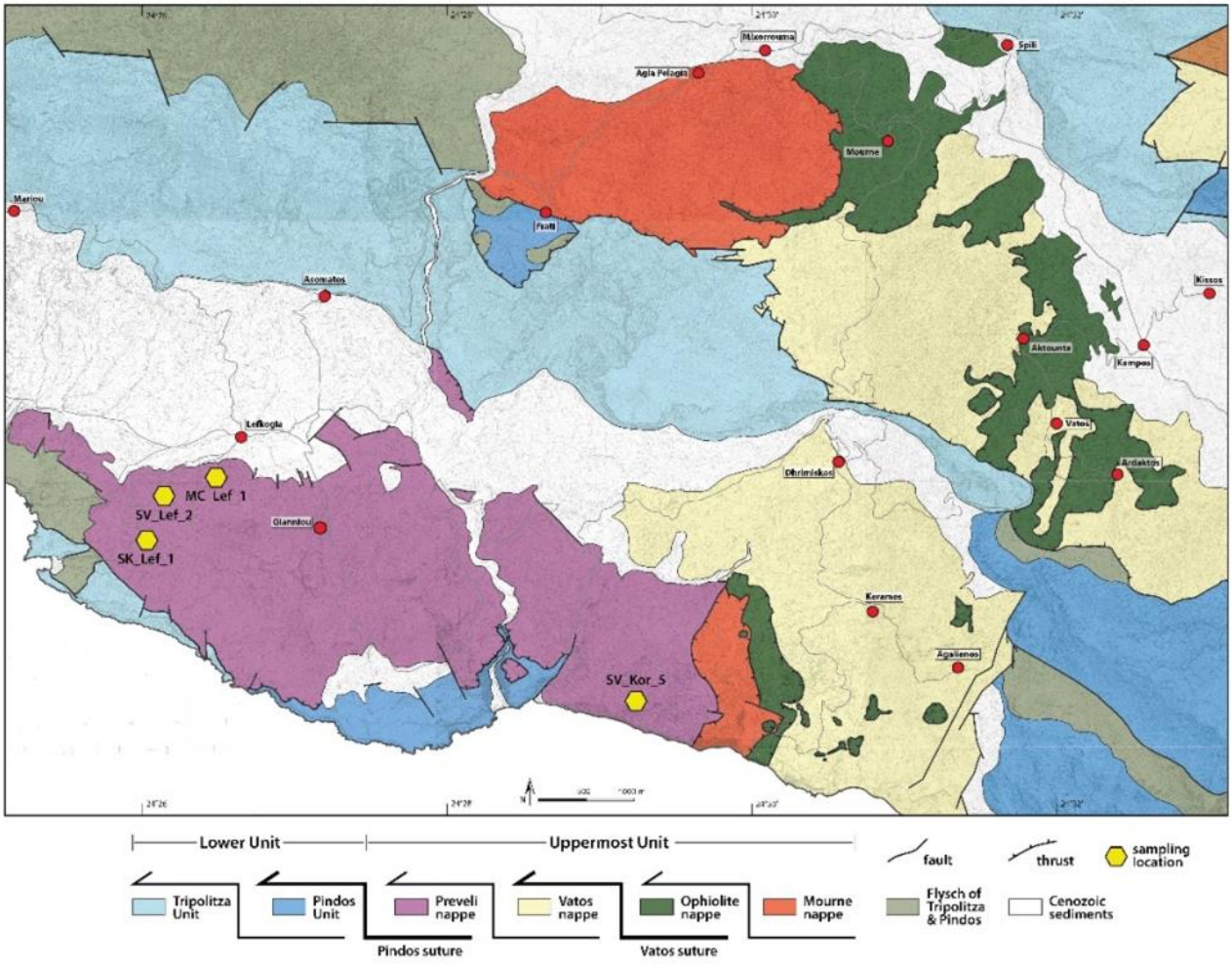

Figure 1. Geological map of the study area in central Crete (modified after Krahl et al. 1982) with sampling locations within the Preveli nappe.

U-Pb Laser ICPMS dating of rutile of mafic metavolcanics of the Preveli nappe exposed S of Lefkogia and S of Korifi summit yielded 132 ±12 and 135 ±10 Ma, respectively. ^{39}Ar-^{40}Ar dating on ferri-winchite, which grew synkinematically in pressure shadows of fractured grandite of Triassic skarn, yielded 125 ±10 Ma. Finally, U-Pb dating of calcite, which developed in a Permian limy metaconglomerate from fluid phase in pressure shadows of pebbles, exposed S of Lefkogia, yielded 31 ±9 Ma. The large uncertainty of both the U-Pb and the 39Ar-40Ar data are related to the low amount of

uranium and of potassium, respectively.

Based on quartz deformation microfabrics, metamorphic index minerals and Si-content of white mica, the meta-morphic conditions during subduction of the Preveli rocks have been constrained to the epidote-blueschist facies (T = 360 ±40°C and P >1.0 GPa). The low temperature suggests that the new radiometric ages can be regarded as crystallization ages, which reflect the time of deformation.

The U-Pb rutile und ^{39}Ar-^{40}Ar ferri-winchite ages should reflect the timing of Eohellenic HP-LT metamorphism related to the subduction of the Preveli rocks. Despite of the large uncertainty, these ages clearly indicate that subduction occurred in Early Cretaceous time (Fig. 2). An Early Cretaceous age of subduction of the Preveli rocks is compatible with both the Late Jurassic to Late Cretaceous flysch-type rocks of the Vatos nappe resting on top of the Preveli rocks and the Middle to Late Jurassic age of the Ophiolite nappe. K-Ar dating of barroisite and phengite of the Mourne nappe, on the other hand, yielded largely Late Jurassic ages (Seidel et al., 1977; Fig. 2).

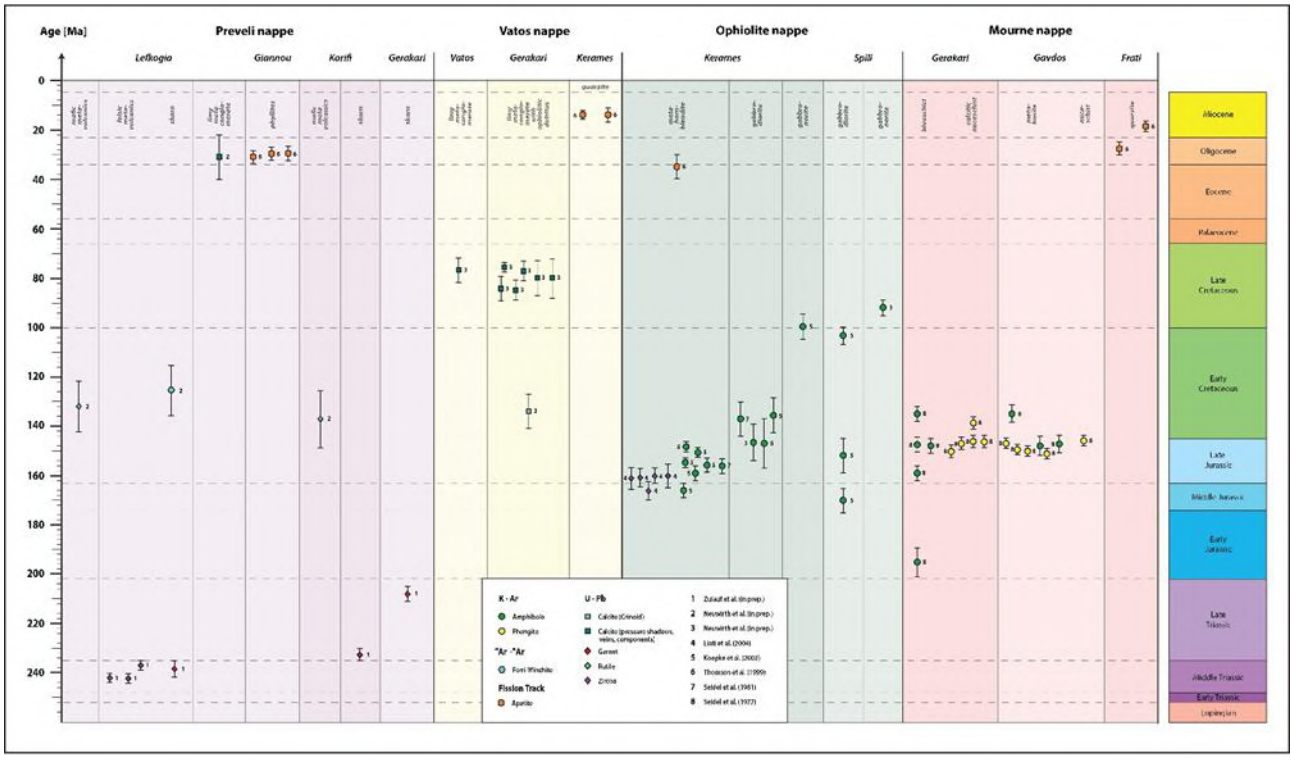

Figure 2. Radiometric ages obtained from rocks of the Preveli, Vatos, Ophiolite and Mourne nappe.

The U-Pb calcite age (31 ±9 Ma) is much younger and is attributed to top-to-the W emplacement of the Preveli nappe on top of the Pindos Unit. This late Eocene/Oligocene age of collision is consistent with the Paleocene/Eocene age of the 2nd Pindos flysch (Richter and Müller, 1992) and with apatite fission-track ages, which suggest cooling of the Preveli rocks < ca. 100° C during the early Oligocene (Thomson et al., 1999; Fig. 2).

Acknowledgements

Funding by German Science Foundation, DFG (Zu 73-34) is gratefully acknowledged

References

Krahl, J., Herbart, H. and Katzenberger, S., 1982. Subdivision of the allochthonous ‘Ophiolites’-bearing formation upon the Pindos Group, southwestern part of Central-Crete, Greece. In: International Symposium on the Hellenic Arc and Trench (H.E.A.T.). April 8–10. 1981, Athens. Proceedings. Volume 1, p. 324–341. Αθήνα [Athens]: Εθνικό Μετσόβιο Πολυτεχνείο [Ethnikó Metsóvio Polytechneío].

Richter, D., Müller, C., 1992, Die Flysch-Zonen Griechenlands, VIII. Neue Vorkommen von Böotischen Flysch im nördlichen Pindos-Gebrirge (Griechenland). Zeitschrift der Deutschen Geologischen Gesellschaft, 143, 87–94.

Seidel, E., Schliestedt, M., Kreuzer, H., Harre, W., 1977. Metamorphic rocks of late Jurassic age as components of the ophiolitic mélange on Gavdos and Crete (Greece). Geologisches Jahrbuch 28, 3–21.

Thomson, S. N., B. Stöckhert, and M. R. Brix (1999), Miocene high-pressure metamorphic rocks of Crete, Greece: rapid exhumation by buoyant escape. In: Ring, U., Brandon, M. T., Lister, G. S. & Willett, S. D. (eds) Exhumation Processes: Normal Faulting, Ductile Flow and Erosion. Geological Society, London, Special Publications, 154, 87-107.

16th International Congress of the Geological Society of Greece
17-19 October, 2022 - Patras, Greece
Bulletin of the Geological Society of Greece, Sp. Publ. 10
Ext. Abs. GSG2022-328

Deformation Processes in the Fore-Arc Mantle of the Neo-Tethyan Pindos Ocean, Greece

V. Chatzaras[1], B. Tikoff[2], M. Foley[3], M.R. Drury[4]

(1) The University of Sydney, School of Geosciences, Sydney, Australia, vasileios.chatzaras@sydney.edu.au (2) University of Wisconsin-Madison, Department of Geoscience, Madison, USA (3) The University of Sydney, Australian Centre for Microscopy and Microanalysis, Sydney, Australia (4) Utrecht University, Department of Earth Sciences, Utrecht, Netherlands.

Research Highlights

- The Mavrovouni Shear Zone (MSZ) comprises a 2 km wide, NE-SW striking and steeply dipping zone in the mantle section of the Pindos ophiolite.
- The MSZ is characterized by oblique normal sense of shear, prolate fabrics, and axial-[100] olivine CPO, consistent with transtentional deformation.

Abstract

The paleogeographic configuration of the Hellenides orogen, in Mesozoic times, was characterized by a number of microcontinents subdividing the Eastern Neo-Tethys Ocean into several small ocean basins. One of the main Mesozoic oceanic basins in Eastern Mediterranean was Pindos Ocean, which formed in the Early Jurassic and separated Apulia from Pelagonia microcontinents (e.g., Robertson et al., 1991). The Pindos Ocean closed in early Cenozoic during the Alpine orogeny. Remnants of the Pindos oceanic basin are preserved in the Pindos ophiolite, which forms part of the NW-SE trending belt of the Balkan Peninsula ophiolites extending from the Dinarides to the Hellenides. The upper mantle section of the Pindos ophiolite is interpreted to represent middle-ocean-ridge-type residue, modified by hydrous melting and metasomatism in the mantle wedge above an intra-oceanic subduction zone (e.g., Bizimis et al., 2000; Kapsiotis, 2014). The structure of the fore-arc Pindos ophiolite provides information on the early stages of the Alpine evolution of the Hellenides orogen and the deformation processes in the mantle wedge above subduction zones.

The mantle section of the Pindos ophiolite consists of deformed and variably depleted spinel peridotite, with minor plagioclase-bearing peridotite, dunite, and pyroxenite (Jones and Robertson, 1991; Ross and Zimmerman, 1996). The dominant fabric in the Pindos peridotite is a NW-SE striking foliation (e.g., Rassios and Moores, 2006). Hosted within the Pindos ophiolite are NE-SW striking shear zones (Rassios and Moores, 2006; Rassios and Dilek, 2009; Sergeev et al., 2014), although their origin and role are uncertain.

Our study focuses on the Mavrovouni Shear Zone (MSZ), which strikes NE-SW, dips steeply to the SE, and has a mineral lineation that plunges moderately to steeply to the SSW. The MSZ has a width of 2 km, which suggests that it was a major structure within the Pindos oceanic lithosphere. Harzburgite in the MSZ shows lateral transitions in the fabric and microstructure that reflect strain gradients across four structural domains: 1) Host spinel harzburgite; 2) A marginal zone with harzburgite characterized by two planar fabrics (one host rock-related and one shear zone-related); 3) A domain of strongly deformed protomylonites; and 4) A mylonitic core. Within the mylonite zone, the presence of dm-scale dunite bands – alternating with the host harzburgite – indicate channelized melt migration facilitated by deformation. Ultramylonite zones of mm-scale are present in the MSZ but their formation is not associated with the large-scale strain gradient described above.

Kinematic analysis in the protomylonites and mylonites of the MSZ indicates an oblique normal sense of shear. The three-dimensional shapes of spinel and orthopyroxene grains from the different structural domains show dominantly prolate fabric ellipsoids. Olivine crystallographic preferred orientations (CPOs) show well-developed axial-[100] and A-type patterns. Prolate fabrics and olivine axial-[100] CPO within the shear zone require some type of three-dimensional kinematics, such as occur in transtension (wrench + extension). We interpret these results to indicate transtentional deformation in the MSZ; this interpretation is constrained independently from the kinematic analysis. Deformation of fore-arc ophiolites in a transtensional setting may be associated with subduction initiation (Stewart et al., 2019). We discuss the role of the MSZ in the Mesozoic evolution of the Pindos Ocean and the implications for the structures that accommodate mantle flow in the wedge above a subducting slab.

Acknowledgements

This research was supported by a Marie Curie International Outgoing Fellowship to Vasileios Chatzaras (PIOF-GA-2012-329183). We thank Anna Rassios who originally suggested studying this zone. Melissa Meyer helped out with the fieldwork and she is gratefully acknowledged. We thank Julie Newman and Aryan Dijkstra for discussions in the field. We acknowledge the technical assistance of Sydney Microscopy & Microanalysis, the University of Sydney node of Microscopy Australia.

References

Bizimis, M., Salters, V.J.M., Bonatti, E., 2000. Trace and REE content of clinopyroxenes from supra-subduction zone peridotites: implications for melting and enrichment processes in island arcs. Chemical Geology 165, 67–85.

Kapsiotis, A., 2014. Mineralogy, geochemistry and geotectonic significance of harzburgites from the southern Dramala upper mantle suite, Pindos ophiolite complex, NW Greece. Geological Journal, doi:10.1002/gj.2626.

Rassios, A., Moores, E.M., 2006. Heterogeneous mantle complex, crustal processes, and obduction kinematics in a unified Pindos–Vourinos Ophiolitic slab (northern Greece). In: Tectonic Development of the Eastern Mediterranean Region, Robertson, A.H.F., Mountrakis, D. (eds). Geological Society of London Special Publica- tions 260, 237–266.

Rassios, A., Dilek, Y. 2009. Rotational deformation in the Jurassic Mesohellenic Ophiolites, Greece, and its tectonic significance. Lithos 108, 207–223.

Robertson, A., Clift, P., Degnan, P., Jones, G., 1991. Palaeogeographic and palaeotectonic evolution of the Eastern Mediterranean Neotethys. Palaeogeography, Palaeoclimatology, Palaeoecology 87, 289–343.

Ross, J.V., Zimmerman, J., 1996. Comparison of evolution and tectonic significance of the Pindos and Vourinos ophiolite suites, northern Greece. Tectonophysics 256, 1–15.

Sergeev, D.S., Dijkstra, A.H., Meisel, T., Brügmann, G., Sergeev A.S. 2014. Traces of ancient mafic layers in the Tethys oceanic mantle. Earth and Planetary Science Letters 389, 155–166.

Stewart, E., Newman, J., Tikoff, B., Donnelly, S., German, L., Chatzaras, V., Lamb, W., Miller, B., Kruckenberg, S., 2019. Coupled deformation and melt-migration events recording subduction initiation, Dun Mountain ophiolite, New Zealand. Memoirs, 49, 93-117.

16th International Congress of the Geological Society of Greece
17-19 October, 2022 - Patras, Greece
Bulletin of the Geological Society of Greece, Sp. Publ. 10
Ext. Abs. GSG2022-337

Morphological indicators to revisit the role of post-alpine gravity tectonics in the external Hellenides

S. Bufféral[1], M. Pubellier[2] , H. Kranis[3], E. Skourtsos[3]

(1) École Normale Supérieure, PSL University, Paris, France, simon.bufferal@ens.fr (2) CNRS-UMR8538, ENS, PSL University, Paris, France. (3) Department of Geology and Geoenvironment, National and Kapodistrian University of Athens, 15784 Zographou, Athens, Greece.

This work is part of the MOREE project, funded by the French CNRS, in collaboration with the National and Kapodistrian University of Athens and the National Observatory of Athens. This project aims at bridging the present days Peloponnese active kinematics and finite tectonics. It combines several methods: spatial and gravity geodesy; morpho-structural, microtectonic and thermochronological analyses; with elastic and viscoplastic deformation modelling. Here, we present some of the morpho-structural aspects of the project, based on the identification of active and past faults and their related stress field, in order to assess the driving forces at play.

In the Mediterranean, as along most of the South Eurasian margin, the Alpine orogenic cycle expressed itself through crustal thickening that reached its peak at the end of the Paleogene. Following the suture of the oceans responsible for the prism buildup construction, and the subsequent slowing down of convergence, most related mountain ranges ended up in a continental setting during the Neogene. As a result, the tectonics of most of these mountains worldwide has since been driven by volume forces, and they end up collapsing and eroding.

In the Peloponnese and Crete (Southern Greece), however, the configuration is different due to their location at the edge of a still active subduction zone. The region is thus dominated by the slab retreat (Sternai et al., 2014), and therefore extension, shear and vertical movements actively coexist. Yet, if the resulting extensional dynamics shaped the Neogene tectonics in the Aegean (Hatzfeld et al., 1997), the Peloponnese's response has been distinctly different. Far from being overly thinned, the region retained a crustal thickness of more than 40 km and a topography exceeding 2 km (Grigoriadis et al., 2016). This alone could explain the tilted-block collapse of its western margin towards the Matapan Trough, as in the Apennines (Vignaroli et al., 2009). There, at the edge of the trench, volume and boundary forces act here in synergy and apparently simultaneously. Nevertheless, the resulting extensional tectonics appears still at an early and brittle stage compared to that of the Aegean domain (Doutsos and Kokkalas, 2001).

Among the numerous tectonic evidences of extension and uplift occurring in the Peloponnese, we seek to identify those that result from a gravity collapse of the chain. We proceed to the systematic identification of the macro-tectonic structures, and the characterization of the associated stress orientation, in order to confront it with the theoretical direction of the sole Hellenic slab retreat. We identify or re-examine the normal faults at the rim of the Peloponnesian metamorphic cores and morphological domes. By measuring the uplift rates of these cores, we correlate their exhumation with the presence of collapsed blocks on their flanks. We finally present a series of morphological evidence to support the continuity of this tectonic style from the outcrop scale to that of the Peninsula.

In the Peloponnese, the extension expresses itself through several networks of steep to low-angle normal faults (e.g.: Ladas et al., 2004; Papanikolaou et al., 2007; Koukouvelas et al., 2010). The steepest ones are the most marked in the landscape (e.g., in Kalamata), producing offsets up to several kilometers.

Striking N150 to N180, their azimuth and active seismicity are consistent with the current kinematic field in the region (Kapetanidis and Kassaras, 2019, and references therein) and are the source of a consequent seismic hazard, including a non-negligible tsunami risk. The flattest ones, of more variable directions, participate in the thinning of the alpine nappes (Doutsos et al. 2006, Xypolias and Koukouvelas, 2001). The Gavrovo-Tripolis and Phyllite-Quartzite units, initially a few km thick, are at places reduced to a few meters each, especially around Tripoli. The Pindos nappe, the most superficial one, forms a series of short-wavelength thrusts on the NW to SW flanks of the Peloponnese. Their radial disposition around metamorphic windows suggests dynamics forced by the exhumation of central slivers such as the Mainalon Dome (Skourtsos and Kranis, 2009).

The rapid vertical velocities of these metamorphic cores suggest an isostatic response triggering the denudation of the superficial nappes, which, in turn, fastens the uplift of the deeper units. This exhumation mode may explain the turtle-back morphology of massifs such as the Mt. Parnonass, or the Taygetos Horst: the crustal block of Messenia is tilted on its western flank, on the Kalamata fault, while the one of Laconia slides to the east, on the Sparta fault. These observations suggest a potentially dominant role of the gravitational collapse of the Alpine chain in the extensional and vertical dynamics of the Peloponnese since the late Miocene. They also provide a better understanding of the current kinematic field of the region, and thus fosters the prevention of associated risk such as those from seismic and tsunami hazards.

References

Doutsos, T. and S. Kokkalas, 2001. Stress and deformation patterns in the Aegean region. Journal of Structural Geology, 23(2) :455–472.

Doutsos, T., I. K. Koukouvelas, and P. Xypolias, 2006. A new orogenic model for the External Hellenides. Geological Society of London Special Publications, 260(1) :507–520.

Grigoriadis, V. N., I. N. Tziavos, G. N. Tsokas, and A. Stampolidis, 2016. Gravity data inversion for Moho depth modeling in the Hellenic area. Pure and Applied Geophysics, 173(4) :1223–1241.

Hatzfeld, D., J. Martinod, G. Bastet, and P. Gautier, 1997. An analog experiment for the aegean to describe the contribution of gravitational potential energy. Journal of Geophysical Research, 102 :649–659.

Kapetanidis and Kassaras, 2019. Contemporary crustal stress of the Greek region deduced from earthquake focal mechanisms. Journal of Geodynamics, 123 :55–82.

Koukouvelas, I. K., S. Kokkalas, and P. Xypolias, 2010. Surface deformation during the Mw 6.4 (8 June 2008) Movri Mountain earthquake in the Peloponnese, and its implications for the seismotectonics of western Greece. International Geology Review, 52(2-3) :249–268.

Ladas, I., I. Mariolakos, and I. Fountoulis, 2004. Neotectonic deformation of eastern pylia (sw peloponnese, greece). Bulletin of the Geological Society of Greece, 36 :1652.

Papanikolaou, D., I. Fountoulis, and C. Metaxas, 2007. Active faults, deformation rates and Quaternary paleogeography at Kyparissiakos Gulf (SW Greece) deduced from onshore and offshore data. Quaternary International, 171-172 :14–30.

Skourtsos, E. and H. Kranis, 2009. Structure and evolution of the western Corinth Rift, through new field data from the Northern Peloponnesus. Geological Society of London Special Publications, 321(1) :119–138.

Sternai, P., L. Jolivet, A. Menant, and T. Gerya, 2014. Driving the upper plate surface deformation by slab rollback and mantle flow. Earth and Planetary Science Letters, 405 :110–118.

Vignaroli, G., C. Faccenna, F. Rossetti, and L. Jolivet, 2009. Insights from the Apennines metamorphic complexes and their bearing on the kinematics evolution of the orogen. Geological Society of London Special Publications, 311(1) :235–256.

Xypolias, P. and I. K. Koukouvelas, 2001. Kinematic vorticity and strain rate patterns associated with ductile extrusion in the Chelmos Shear Zone (External Hellenides, Greece). Tectonophysics, 338(1) :59–77.

16th International Congress of the Geological Society of Greece

17-19 October, 2022 - Patras, Greece

Bulletin of the Geological Society of Greece, Sp. Publ. 10

Ext. Abs. GSG2022-339

Tectono-stratigraphic Terranes and Tectono-metamorphic Belts in the Hellenides: their Geodynamic Interrelations

Dimitrios Papanikolaou[1]

(1) Faculty of Geology & Geoenvironment, National and Kapodistrian University of Athens, Panepistimioupolis 15784, Zografou, Greece, dpapan@geol.uoa.gr

The Hellenides comprise several tens of geotectonic units which are grouped from the paleogeographic point of view to 9 major tectono-stratigraphic terranes (tst) and from the tectono-metamorphic point of view to 3 tectono-metamorphic belts (tmb) (Papanikolaou, 1984; 1997; 2021). The distinction of the Metamorphic Hellenides (Papanikolaou, 1980; 1984; 1986; 2021) permitted the re-organization of the paleogeographic area of the Hellenides by introducing the metamorphosed units within the former paleogeographic schemes, which were previously based almost exclusively on the non-metamorphic Hellenides. Thus, the paleogeography included also all the omitted tectonic units that were subducted and metamorphosed during the orogenic evolution (e.g. Papanikolaou, 1986). The outcrops of the subducted and metamorphosed units of the Hellenides were grouped in three metamorphic belts (External, Medial, Internal) known previously as pre-Alpine metamorphic massifs (e.g. Brunn, 1960) incorporating pre-Alpine basement rocks together with the metamorphosed Alpine sequences. The participation of the geotectonic units and of the tst in each tmb shows that their structure and evolution is different with the most external tst occurring at the external tmb and the more internal in the medial and internal tmb. Additionally, much younger ages of tectono-metamorphism are observed towards the external part of the arc. As this will be shown in the following description the tmb do not correspond to some specific units and tst. One common feature of all three tmb is their tectonic window nature beneath non-metamorphosed units. The term metamorphic core complex can be applied in the medial and internal tmb but not in the external tmb, where there are no granitic intrusions.

The **external tmb** cropping out along **Peloponnese – Crete** comprises tectonic units exclusively of the External tst H1. The lower unit – relative autochthon- is the Mani unit, which is the metamorphosed equivalent of the Ionian unit of western Greece (Thiebault, 1977). The stratigraphy expands from the Triassic (neritic carbonates) to the Oligocene (flysch) and the tectono-metamorphism is characterized by low grade assemblages and isoclinal syn-metamorphic folding. The Arna unit forms a tectonic wedge of pre-Alpine basement rocks between the underlying Mani unit and the overlying Tripolis non-metamorphosed unit (Papanikolaou & Skarpelis, 1987). The Tyros Beds, occurring along the base of the Tripolis carbonate platform are affected by very low grade metamorphism forming the upper limit of the External tmb. The age of metamorphism is Oligocene – Early Miocene, following the subduction and internal duplication of H1. In W. Crete, there is one more duplication with the W.Crete Paleozoic metamorphic rocks and their sedimentary cover of the Trypali unit forming a nappe above the Mani unit (Papanikolaou & Vassilakis, 2010). Thus, the External carbonate platform is triplicated (Mani, Trypali, Tripolis) but the external tmb is limited beneath the Tripolis basal Triassic formations (equivalent of the Tyros Beds). In conclusion, the external tmb has been developed within the paleogeographic area of the External tst H1 with internal subduction and tectonic duplication during Oligocene – early Miocene, after the deposition of the Mani flysch.

The **medial tmb** crops out all along the Hellenides from Western Macedonia in the north to the Cyclades in the south and then to the Samos and Menderes areas in the east. Its structure is different in the Attica-Cyclades area and the Eastern Thessaly-Western Macedonia area of the former Pelagonian. The major difference is that the Internal Hellenides of the Sub-Pelagonian –Pelagonian units (H3) and the associated ophiolitic nappes (H4) are found non-metamorphosed in the **Attica-Cyclades-Samos** segments, but metamorphosed in the **Pelagonian** from Pelion to Olympus and Voras (Papanikolaou, 1986; 2013) (Fig. 1). Thus, in the south the internal carbonate platform of H3 lies above the medial tmb whereas in the north it forms the upper part of the medial tmb. The tectono-metamorphism of the medial tmb is the result of subduction of parts of the oceanic domain of H2 beneath the more internal previously deformed H3 and H4 during Eocene-Oligocene and the subsequent subduction of the internal margin of the carbonate platform of H1 during Oligocene. In the Pelagonian outcrops of Eastern Thessaly the Tertiary tectono-metamorphic events have underlain the paleo-Alpine metamorphic events of Late Jurassic-Early Cretaceous. Thus, in Attica-Cyclades-Samos the medial tmb comprises segments of H1 and H2 whereas in W. Thessaly-W. Macedonia it comprises also the H3 and H4 tst. In conclusion, the Attica-Cyclades-Samos tmb comprises the H1 and H2 tst formed during Early Cenozoic, whereas in W. Thessaly-W. Macedonia it comprises the H1 and H2 tsts at the base, overlain by the older paleo-Alpine tmb comprising segments of H3 and H4. Thus, we could separate the two areas as comprising one Early Tertiary tmb in the south but two tmb in the north formed both during the paleo-Alpine and the Alpine orogenic events. This means that there is one oceanic subduction in the south (H2) but two oceanic subductions in the north (H2 and H4). The occurrence of non-metamorphosed Upper Cretaceous transgressive sediments above the internal units of H3

and H4 is a diagnostic criterion for the different ages of metamorphism, taking into account the existence of Eocene formations at the base of the metamorphic nappe pile (e.g. Olympus, Godfriaux, 1968). It should be noted, however, that the Pelagonian outcrops in Western Macedonia do not include the H1 and H2 units, which should be found at depth, beneath the H3 and H4 units (Papanikolaou & Stojanov, 1982) (Fig. 1).

The **internal tmb** crops out in Northern Greece, extending also towards the north in southern Bulgaria and southern former Yugoslavia. Towards the west it is bounded by a tectonic zone of Tertiary thrusts with the ophiolitic rocks of the Vardar-Axios margin (Mercier, 1968) and towards the east it is terminated in the Tertiary Thrace Basin. Towards the south it occurs in Thassos and Samothraki islands with probable extensions in the North Aegean Sea up to Lesvos Island. It comprises the metamorphic rocks grouped in the so-called **Rhodope and Serbo-Macedonian** metamorphic massifs with problematic extensions in the so-called Circum-Rhodope tectonic zone surrounding the core of the tmb. Following Kockel et al, 1977; Papanikolaou and Panagopoulos, 1981; Dimitriadis, 1988, Papanikolaou, 1988 and others, the generalized structure of the internal tmb comprises four tst (H6, H7, H8, H9). The lower tectonic unit-relative autochthon of the Rhodope is the Pangeon carbonate platform (H7), overlain by the nappe of the Sidironero metamorphic basement (H9) (Papanikolaou and Panagopoulos, 1981). In the SerboMacedonian the lower unit is the Kerdylia unit (H7) and the overlying nappe of basement rocks is the Kerdylion unit (H9) (Kockel et al, 1977). In between the Volvi ophiolites (H8) separate the two basement units in Chalkidiki (Dimitriadis, 1984) and in W. Thrace the equivalent Soufli ophiolites (Maratos, 1960). On top the low grade Circum Rhodope unit (H6) with the Jurassic ophiolites covers the internal tmb from all sides. Jurassic granites and pegmatites are intruding the overall structure which should be pre-Late Jurassic (Papanikolaou, 2009).Another stratigraphic constraint is the existence of Lower Cretaceous unconformable limestones above the Circum Rhodope unit in Alexandroupolis (Maratos and Andronopoulos, 1965) and in Chalkidiki (Ivanova et al, 2015).The massive granitic intrusions during Late Cretaceous and also later in Early Tertiary mark the change of the geodynamic position/situation of the internal tmb to a volcanic arc. Thus, the tectono-metamorphic events of the internal tmb comprise the lower Mesozoic with additional tectono-magmatic events in the Late Cretaceous – Oligocene. It is likely that the internal tmb comprises also two distinct tectono-metamorphic periods/belts, one older with H7 and H8 beneath H9 and a younger with H5 beneath H6 (Fig. 1).

Some conclusions arising from the previous description of the tst in each tmb are the following:

1) Oceanic Subduction does not comprise all the oceanic areas, as major segments remain non-metamorphosed. This is observed in the Pindos unit of H2 and in the Maliac unit of H4.
2) Continental subduction of the more external carbonate platform is usually following the oceanic subduction, followed by uplift and metamorphic core complex formation. This is observed in the cases of the Pangeon unit (H7) beneath the Volvi ophiolites (H8), the Almopia unit (H3) beneath the Vardar/Axios ophiolites (H4) and the Olympus unit (H1) beneath the Northern Cyclades blueschists and ophiolites (H2).
3) The subduction is involving the external segments of the oceanic basins and the internal segments of the following carbonate platforms. Thus, the geodynamic division of the terranes results in a subducted and metamorphosed segment (Metamorphic Hellenides) and a non-metamorphosed segment with surficial tectonic transport and nappe emplacement towards the external edge of the orogenic front.

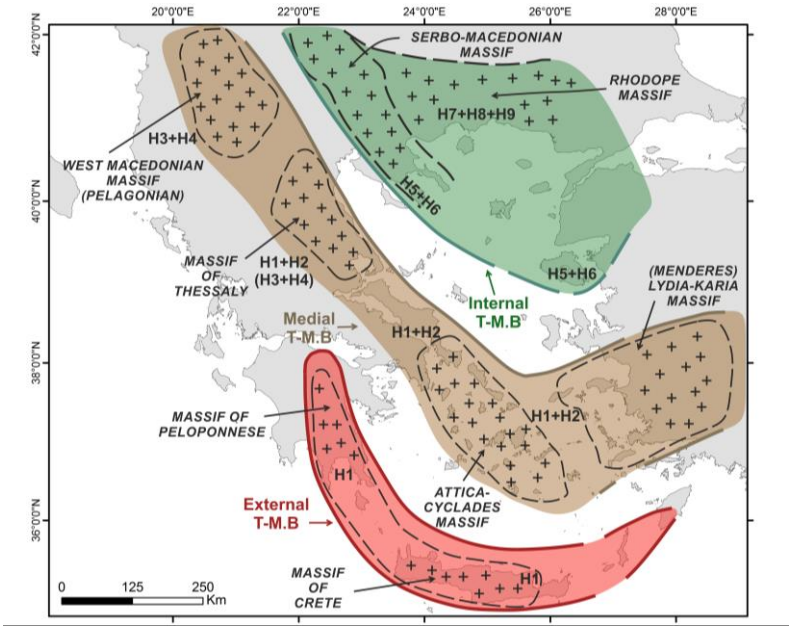

Fig. 1. The three tectono-metamorphic belts and the participating terranes (based on Papanikolaou, 1984).

References

All references can be found in:
Papanikolaou, D.I., 2021. The Geology of Greece. Springer Nature Switzerland, 389 pp.

16th International Congress of the Geological Society of Greece
17-19 October, 2022 - Patras, Greece
Bulletin of the Geological Society of Greece, Sp. Publ. 10
Ext. Abs. GSG2022-402

Tracking Extensional Structures and Exhumation in the Southeast Aegean, Greece

Konstantinos Soukis[1,2], Daniel Stockli[2], Bernhard Grasemann[3], David Schneider[4], Sofia Laskari[1], Stylianos Lozios[1], Christina Stouraiti[1], Erich Draganits[3], Vincent Roche[5], Petros Koutsovitis[6].

(1) National and Kapodistrian University of Athens, Athens, Greece (soukis@geol.uoa.gr), (2) University of Texas at Austin, Austin, USA (3) University of Vienna, Vienna, Austria (4) University of Ottawa, Ottawa, Canada, (5) Sorbonne Université, Paris, France, (6) University of Patras, Patras, Greece.

The Attic Cycladic Crystalline Complex (ACCC), situated in the back-arc area of the Hellenic subduction zone, includes mid to lower crustal rocks that were gradually exhumed through syn- to late-orogenic processes. Along the northern and southwestern side, the ACCC is flanked by crustal-scale detachments, associated with greenschist-facies ductile shear zones and brittle-ductile low-angle normal faults accompanied by ultramylonitic rocks and proto- to ultra-cataclasites. These juxtapose footwall Cycladic Blueschist Unit and Cycladic Basement Unit rocks against relics of Pelagonian-derived rocks. The detachments have been intruded by mid to late Miocene syn-extensional granitoids, and they are locally overlain by supra-detachment sediments sourced from the eroded upper plate rocks. On the other hand, the southeastern side of the ACCC is characterized mainly by ductile to brittle-ductile mylonitic shear zones and cataclastic fault zones observed at different structural levels of the hanging wall units:

- Santorini Island exposes the lowermost part of the southeast Aegean domain. On this island, the Miocene top-to SE Santorini detachment juxtaposed the Cycladic Blueschist Unit against the low-grade Pelagonian rocks (Schneider et al., 2018)
- Amorgos Island hosts top-to SE mylonitic ductile shear zones and brittle low-angle normal faults, contributing to the exhumation of the Amorgos low-grade rocks above the zircon Helium Partial Retention Zone during the early-mid Miocene (Laskari et al., 2022).
- Anafi Island includes rocks from the higher structural level of the Cycladic nappe pile, which was formed in the late Eocene - early Oligocene (Koutsovitis et al., 2022). These rocks are juxtaposed to late Miocene (supra-detachment) sediments through top-to-SSW low-angle brittle faults (Soukis and Papanikolaou 2004).
- Kalymnos Island, further east, in the northern Dodecanese, a top-to-SE brittle-ductile low angle normal fault juxtaposes the footwall late Paleozoic-Triassic Kefala (low-grade) and Marina Basement (high-grade) units from the hanging wall non-metamorphosed Marina Cover Unit of Mesozoic age (Grasemann et al., 2022).

The synthesis of local tectonostratigraphic columns produces a complete image of the eroded upper plate, at least for the southeastern part of the ACCC. Integration with structural and geochronologic data can give a glimpse of the early-mid Miocene ACCC configuration when the previously thickened south Aegean crust started to collapse.

Acknowledgements

Part of this research was funded by grants 14950, 15651, 17643, of the National and Kapodistrian University of Athens ELKE to K. Soukis and S. Lozios.

References

Grasemann, B., Schneider, D.A., Soukis, K., Roche, V. and Hubmann, B., 2022. Paleogeographic position of the central Dodecanese Islands, southeastern Greece: The push-pull of Pelagonia. Bulletin, 134(5-6), pp.1506-1528. https://doi.org/10.1130/B36095.1.

Koutsovitis, P., Soukis, K., Voudouris, P., et al., 2021. The Late Cretaceous magmatic arc of the south Aegean: geodynamic implications from petrological and geochemical studies of granitoids from Anafi Island (Cyclades – Greece). International Geology Review 63, 1-24. https://doi.org/10.1080/00206814.2021.1884906

Laskari, S., Soukis, K., Stockli, D. F., Lozios, S., & Zambetakis-Lekkas, A. 2022). Reconstructing the southern Pelagonian domain in the Aegean Sea: Insights from U-Pb detrital zircon analysis, lithostratigraphic and structural study, and zircon (U-Th)/he thermochronology on Amorgos Island (SE Cyclades, Greece). Gondwana Research, 106, 329–350. https://doi.org/10.1016/j.gr.2022.02.007

Schneider, D.A., Grasemann, B., Lion, A., Soukis, K., and Draganits, E., 2018, Geodynamic significance of the Santorini Detachment System (Cyclades, Greece): Terra Nova, v. 30, no. 6, p. 414–422, https://doi.org/10.1111/ter.12357.

Soukis, K., Papanikolaou, D., 2004. Contrasting geometry between Alpine and late to post-Alpine tectonic structures in Anafi Island (Cyclades). Bull. Geol. Soc. Greece 36 (4), 1688–1696. https://doi.org/10.12681/bgsg.16575.

16th INTERNATIONAL CONGRESS of the
GEOLOGICAL SOCIETY OF GREECE

S4. Recent Advances in InSAR and GNSS Applications for Crustal Deformation mapping and monitoring

OUR EARTH, OUR HOME

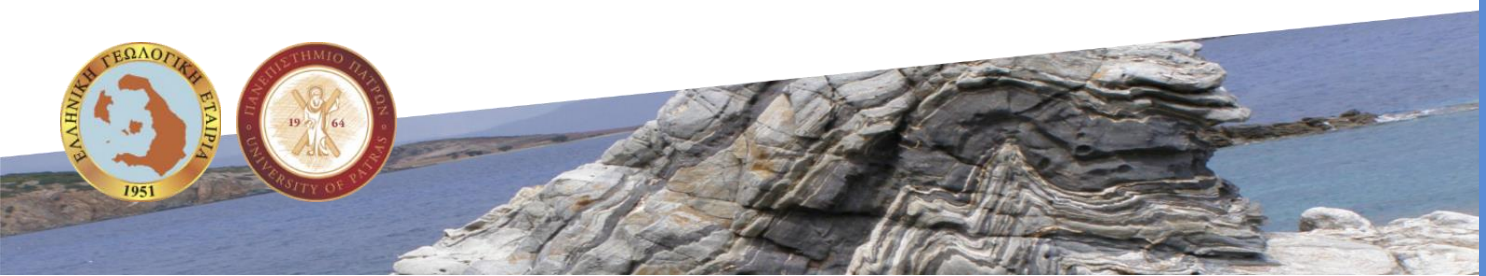

16th International Congress of the Geological Society of Greece
17-19 October, 2022 - Patras, Greece
Bulletin of the Geological Society of Greece, Sp. Publ. 10
Ext. Abs. GSG2022-029

Peculiar Vertical Ground Deformation Observed at Skyros Island (North Aegean, Greece), Consistent with Proximal Subsurface Magmatic Activity.

Ph. Kravvariti[1], V. Sakkas[1], A. Tzanis[1], S. Chailas[1]

(1) Section of Geophysics – Geothermy, Department of Geology and Geoenvironment, National and Kapodistrian Univer- sity of Athens, Greece; fedrakra@geol.uoa.gr

Research Highlights

- DGPS data at Skyros Island, North Aegean, demonstrate intermediate-term transient ground deformation with convex sinusoidal shape.
- Comparisons with analogous evidence from Santorini volcano and evidence of past subsurface magmatic activity in the vicinity of Skyros indicate the possibility of localized, low-intensity magmatic processes.

Introduction and Objectives

The analysis of GNSS data has long been utilized as a tool for evaluating the geodynamic behavior of a region. These data convey information about time-dependent changes (displacements) in the coordinates of given points on the sur- face of the Earth (geodetic stations). The shape of these changes is a strong indicator of the tectonic or volcano-tectonic characteristics of a given region; it can be used to estimate the rate of the displacement of a station. Combined with other seismological, geophysical and tectonic information, this type of data allows for the construction of robust geod y- namic models (e.g. Tzanis et al., 2020; Sakkas et al., 2020). The value of this approach is even higher in areas with little or no seismicity. Today there are several permanent, continuously recording GNSS stations in Greece, which enable almost real-time observation of the displacement rate.

Herein, we report observations of ground displacement conducted on the Island of Skyros, Greece, between May 2017 and July 2020, which are consistent with local-scale inflation/deflation with attributes similar to those observed in ac- tive volcanoes, such as Santorini (e.g. Lagios et al., 2013; Tzanis et al., 2020). These are correlated with magnetic anomalies and seismicity and thus might be interpreted in terms of low-intensity local magmatic processes.

Methods and Results

In the current study, data from 3 continuous recording permanent stations were analyzed. The raw data was obtained through METRICA S.A (https://www.metrica.gr) and concern stations SKYR on Skyros, KYMI near the city of Kyme, Euboea Island and SANT, on Santorini Island. The KYMI data were used as a control in order to assure that the obser- vations made on Skyros were local. The raw data were processed with the BERNESE v5.2 software (Darch et al., 2007) and referred to the Hellenic Geodetic Reference System 1987 (HGRS87). The acquired coordinates of the stations were used to extract the displacement that has taken place since 21 May 2017, which is used as a reference date for Skyros Island herein.

Time series of these time-dependent displacements were created for all three Cartesian components of all stations. Based on these, the trends shown in Figures 1 & 2 at the 95% confidence level were calculated with least squares. As observed in Figure 1b, ground dislocation in the vertical component of the SKYR series exhibits a convex sinusoidal trend, very similar to the one observed in the vertical component of the SANT station over the period August 2012 – May 2021, during and after the 2011-2012 unrest episode (Lagios et al., 2013; Tzanis et al., 2020). Almost nihil vertical displacement was observed at the nearest to SKYR station of KYMI, indicating that the relevant observations at SKYR were due to localized phenomena.

Discussion and Conclusions

The direct comparison and obvious similarity of vertical ground deformation at SKYR and SANT indicates that both may have been generated by analogous processes and we know that the latter was due to ground inflation and deflation in response to subsurface magmatic processes. Independent evidence of past subsurface magmatism is rather clear in the total field magnetic anomalies of the area illustrated in Figure 2: these comprise prescription signatures of intrusive magmatic bodies. The seismicity during the period of observations is also included in Figure 2; tectonic activity is plainly demonstrated but the record is grossly incomplete at the low magnitude end and does not offer much insight into the possibility of recent subsurface magmatic activity.

The GNSS and magnetic anomaly data presented herein indicate the possibility of localized, transient, low-intensity undersea/ subsurface intrusive magmatic activity proximal to station SKYR. Being located in an active and fast deform- ing domain, the area certainly has potential for subsurface magmatism. Our evidence, however, is at best substantive and by no means substatiative or conclusive. In anticipation of confirmation, it should be evaluated with due caution.

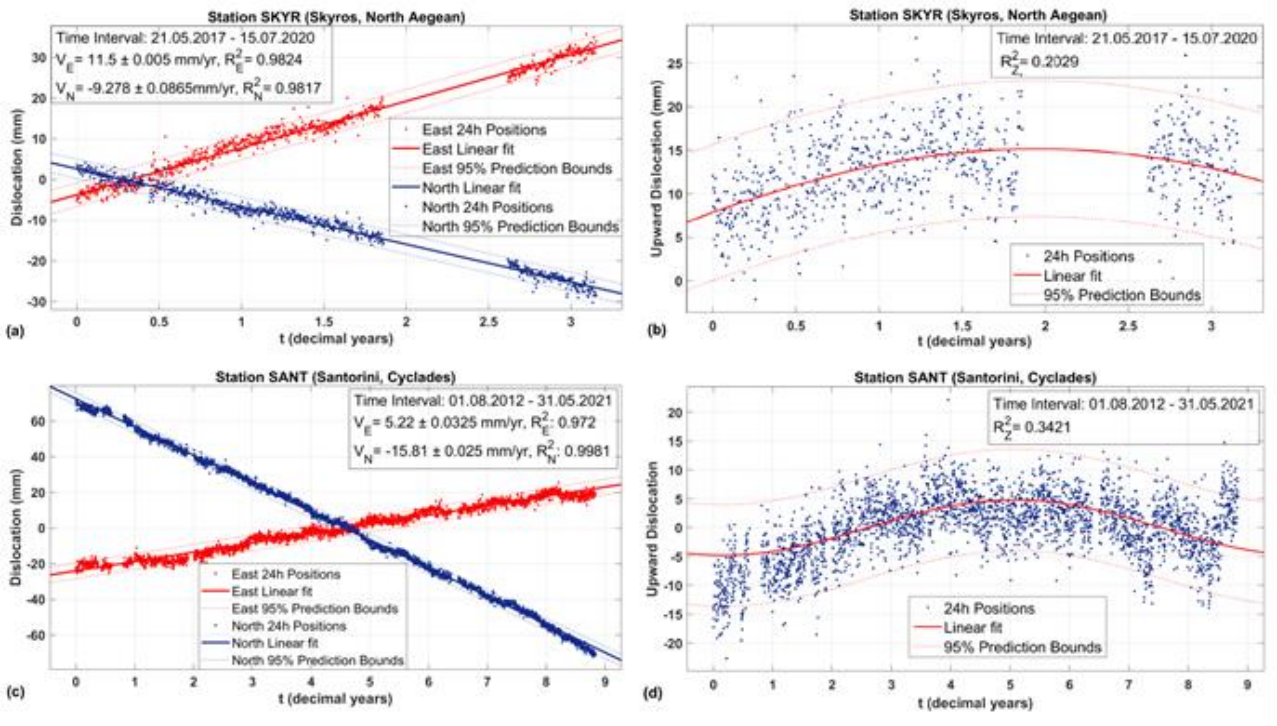

Figure 1. (a) Time series of (a) the horizontal dislocation at SKYR, (b) the vertical dislocation at SKYR, (c) the horizontal dislocation at SANT and (d) the vertical dislocation at SANT.

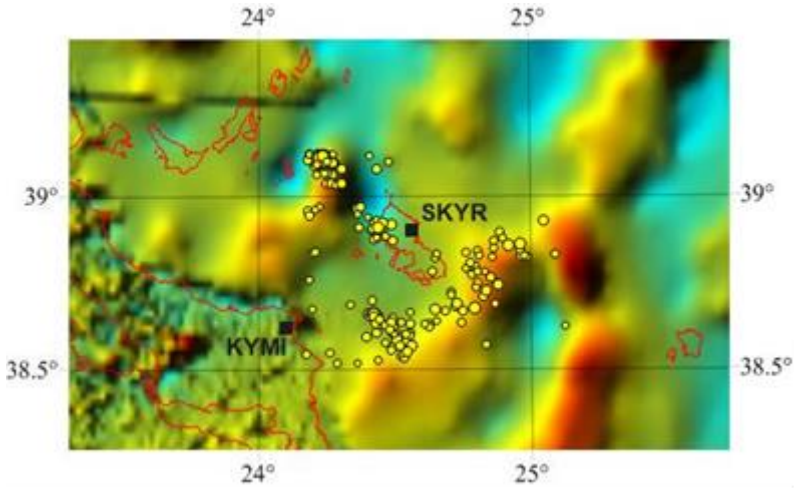

Figure 2. Reduced-to-pole magnetic anomalies (Chailas et al., 2019) and recorded during the period of GNSS observations (National Observatory of Athens, https://bbnet.gein.noa.gr/HL/databases/database); earthquakes are shown as yellow circles and have depths ≤ 30 km and magnitudes 1.0 ≤ ML ≤ 3.5. The blue square indicates the location of SKYR.

Acknowledgements

The research work was supported by the Hellenic Foundation for Research and Innovation (HFRI) under the HFRI PhD Fellowship grant (Fellowship Number: 841).

References

Chailas, S. and Tzanis A., 2019. A new improved version of the Aeromagnetic Map of Greece. Bull. Geol. Soc. Greece, Sp. Pub. 7, 289-290; https://ejournals.epublishing.ekt.gr/index.php/geosociety/issue/view/1265, accessed 22/7/2022.

Dach, R., Hugentobler, U., Fridez, P., Meindl, M., 2007. Bernese GPS Software Version 5.0. Bern: University of Bern, Astronomi cal Institute.

Lagios, E., Sakkas, V., Novali, F., Belloti, F., Ferretti, A., Vlachou, K., Dietrich, V., 2013. SqueeSARTM and GPS ground deformation monitoring f Santorini Volcano (1992–2012): tectonic implications, Tectonophysics, 594, 38–59, doi: 10.1016/j.tecto.2013.03.012

Sakkas, V., Doxa, C., Tzanis, A., and Kranis, H., 2020. Contemporary Kinematics of the South Aegean Area (Greece) Detected with Continuous GNSS Measurements, 2020 EGU General Assembly, No EGU2020-7656, doi: 10.5194/egusphere-egu2020-7656. Tzanis, A., Chailas, S., Sakkas, V., Lagios, E., 2020. Tectonic deformation in the Santorini volcanic complex (Greece) as inferred by joint analysis of gravity, magnetotelluric and DGPS observations. Geophys. J. Int., 220, 461-489, doi: 10.1093/gji/ggz461.

16th International Congress of the Geological Society of Greece
17-19 October, 2022 - Patras, Greece
Bulletin of the Geological Society of Greece, Sp. Publ. 10
Ext. Abs. GSG2022-109

Ground Deformation Study of the Ionian Islands (W. Greece) Based on Continuous GNSS Measurements

V. Sakkas[1], G. Kaviris[1], V. Kapetanidis[1], J. D. Alexopoulos[1], I. Spingos[1], I. Kassaras[1†], S. Dilalos[1], S. Mavroulis[2], M. Diakakis[2], D. Kazantzidou-Firtinidou[1], E. Vassilakis[3], E. Kotsi[2], E. Lekkas[2], N. Voulgaris[1]

(1) Section of Geophysics—Geothermics, Department of Geology and Geoenvironment, National and Kapodistrian University of Athens, 15784 Athens, Greece, vsakkas@geol.uoa.gr (2) Section of Dynamic Tectonic Applied Geology, Department of Geology and Geoenvironment, National and Kapodistrian University of Athens, 15784 Athens, Greece (3) Section of Geography & Climatology, Department of Geology and Geoenvironment, National and Kapodistrian University of Athens, 15784 Athens, Greece.

Abstract

Seismicity accompanied with intense ground deformation in the Ionian Sea (W. Greece) is mainly generated along the Cephalonia-Lefkada Transform Fault Zone (CLTFZ), in the central Ionian, and on the northwestern termination of the Hellenic subduction margin in the south. Pre- co- and post-seismic ground deformation analysis is performed at the broad Ionian area, aiming to homogeneously study the spatiotemporal evolution of the ground deformation prior to and after the occurrence of strong (M > 6) earthquakes during the last decade. The 2014 Cephalonia earthquakes (Mw6.1 and Mw5.9) were generated on a faulting system adjacent to CLTFZ, causing local ground deformation. Co-seismic displacement was recorded in the broader area after the 2015 Lefkada earthquake. The 2018 Zakynthos earthquake (Mw6.7) caused regional deformation and, alterations on the near- velocity field. In the northern Ionians, con-vergence between the Apulian platform and the Hellenic foreland occurs, exhibiting increased velocity vectors on the local GNSS sites, with respect to the southern Ionian stations.

Introduction

The area of the Ionian Islands in western Greece plays an important role in the kinematic processes of the eastern Mediterranean. This tectonically complex area is by far the most seismically active region in Greece and among the most seismogenic regions in Europe. It is characterized by the frequent occurrence of destructive large earthquakes. The area undergoes intense ground deformation. The central Ionian Islands constitute part of the Eastern Mediterranean lithosphere that is subducted beneath the Aegean lithosphere along the Hellenic Arc.

Three major tectonic features in the Ionian Islands define the regional kinematic field and control the seismic activity: the convergence of the Apulian Platform and the Hellenic foreland in the north; the long NNE–SSW Cephalonia–Lefkada Transform Fault Zone (CLTFZ) offshore and west of the respective islands in the central part; and the northwestern tip of the Hellenic Arc in the southern Ionian Sea. These major structures, together with smaller local faults, create a complex tectonic environment generating intense seismic activity and strong ground deformation. During the last decade, and mainly during the period between 2014 and 2018, increased seismicity was observed, and strong events (M > 6.0) shocked the central Ionian Islands, in 2014 in Cephalonia, in 2015 in Lefkada and in 2018 in Zakynthos Islands. The regional crustal motion along the entire Ionian Sea and western Greece, as well as the local deformation on the central Ionian Islands, have been studied and monitored with local dense Global Positioning System (GPS) networks and continuous Global Navigation Satellite System (GNSS) stations (e.g. Sakkas et al., 2022).

The present work presents an overview of the ground deformation in the broad area of Ionian Sea, extending from Corfu Island to the north to Strofades Islet in the south. The time span of the data covers the period before, during and after the occurrence of the strong 2014 to 2018 earthquakes. Pre-, co- and post-seismic deformation is quantitatively described, aiming to understand the pattern of the ground motion associated with the recorded seismicity. The geodetic data from the commercial and institutional continuous GNSS networks in the area were used on the framework of this study.

GNSS Data

Daily GNSS data from stations located in the Ionian Islands and the western mainland Greece and the Peloponnese were processed for the period from 2009 to 2022. The analysis intended to determine the crustal velocity field of the broad area, detect possible pre-seismic displacements and study co- and post-seismic deformation. The continuous GNSS stations belong to National Observatory of Athens (Ganas et al., 2008; Chousiantitis et al., 2021), to National and Kapodistrian University of Athens (Sakkas and Lagios, 2017), to PPGNET (Czech GEO/EPOS) and to commercial network of METRICA SA (HexagonSmartNet). The raw GNSS data were processed using the Bernese v5.2 software. The processing resulted in the estimation of high-precision station coordinates. Time series were formed, annual velocities were calculated (Figure 1) and co-seismic displacements were determined.

Together with the continuous GNSS stations in the Ionian Islands, stations located to in western mainland Greece and western and northwestern Peloponnese were also processed. The goal was to study the velocity field, ground deformation

and differential motions in the broad region of the Ionian Sea, focusing to on the area close to the highly activated central Ionian Islands.

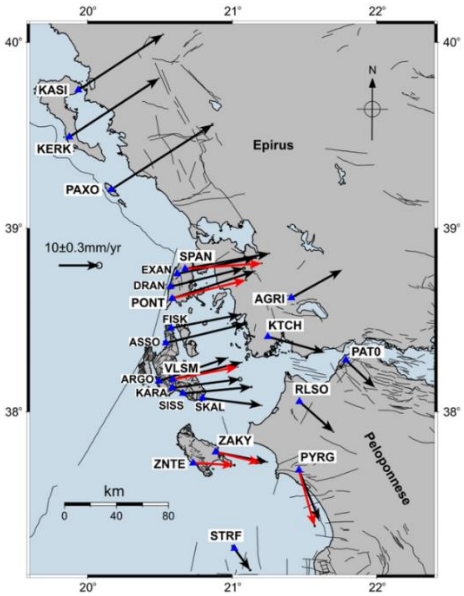

Figure 1. Horizontal velocity vectors (black arrows) for the continuous GNSS sites (blue triangles) of the broad Ionian Islands area. Red arrows indicate the horizontal velocity component estimated for the period after the strong (M>6) earthquakes in the area (ITRF 2014)..

GNSS Results

In the north Ionian Sea, where the collision between the Apulian platform and the Hellenic foreland is taking place, the velocity field of the area, deduced by GNSS stations on Corfu and Paxoi Islands, shows horizontal NW motion, transverse to the collision front. The vertical component reveals a subsiding pattern, compatible with the convergence process in the area.

The CLTFZ feature offshore of the central Ionian Islands of Cephalonia and Lefkada is the prevailing structure, generating the strong and intense seismic activity observed in the region. The 2014 Mw6.1 and Mw5.9 Cephalonia earthquakes occurred on an adjacent local faulting zone, causing strong ground displacement on the island but not in the broader area. Few months later, on 17 November 2015, another strong earthquake (Mw6.4) occurred on or parallel to the Lefkada segment of the CLTFZ. Co-seismic displacement was recorded in almost all the southern Ionian Islands, highlighting the regional character of the seismogenic source. The temporal evolution of the post-seismic ground deformation shows a long relaxation period.

The October 2018 Mw6.7 Zakynthos earthquake occurred close to the northwestern tip of the Hellenic Arc. Strong ground displacement took place on the near-field GNSS stations, as well as on Cephalonia Island and the Peloponnese. The motion field of the stations in Zakynthos and the western Peloponnese showed significant alterations with respect to the pre-seismic period, on both north and east motional components, which regained its anticipated pattern about eight months after the mainshock.

Acknowledgements

This research was funded by the project “Telemachus Innovative Seismic Risk Management Op-erational System of the Ionian Islands” (MIS 5007986) which is part of the Regional Operational Programme «Ionian Islands 2014 2020» and is co-financed by the European Regional Development Fund (ERDF) (National Strategic Reference Framework NSRF 2014 20).

References

Chousianitis, K., Papanikolaou, X., Drakatos, G., Tselentis, G.-A., 2021. NOANET: A Continuously Operating GNSS Network for Solid-Earth Sciences in Greece. Seism. Res. Lett., 92, 2050–2064. https://doi.org/10.1785/0220200340.

Czech Geo/EPOS. Available online: https://www.czechgeo.cz/en/sections-research-infrastructure-czechgeo/section-gnss-and-gravimetry/network-permanent-gnss (accessed on 13 September 2022)

Ganas, A., Drakatos, G., Rontogianni, S., Tsimi, C., Petrou, P., Papanikolaou, M., Argyrakis, P., Boukouras, K., Melis, N., Stavrakakis, G., 2008. NOANET: The new permanent GPS network for Geodynamics in Greece. Geophys. Res. Abs. 10, EGU2008-A-04380.

HexagonSmartNet METRICA S.A. Available online: https://gr.nrtk.eu/ https://hxgnsmartnet.com (accessed on 13 September 2022).

Sakkas, V., Kapetanidis, V., Kaviris, G., Spingos, I., Mavroulis, S., Diakakis, M., Alexopoulos, J.D., Kazantzidou-firtinidou, D., Kassaras, I., Dilalos, S., Vassilakis, E., Kotsi, E., Tselentis, G., Lekkas, E., Voulgaris, N., 2022. Seismological and Ground Deformation Study of the Ionian Islands (W. Greece) during 2014–2018, a Period of Intense Seismic Activity. Applied Sciences, 12 (5), art. no. 2331.

Sakkas, V., Lagios, E., 2017. Ground deformation effects from the ~M6 earthquakes (2014–2015) on Cephalonia–Ithaca Islands (Western Greece) deduced by GPS observations. Acta Geophys., 65, 207–222.

16th International Congress of the Geological Society of Greece
17-19 October, 2022 - Patras, Greece
Bulletin of the Geological Society of Greece, Sp. Publ. 10
Ext. Abs. GSG2022-122

Ground deformation and microseismicity patterns onshore Milos, Cyclades, Greece.

Athanassios Ganas[1], Andreas Karakonstantis[2], Vasilis Kapetanidis[2], Varvara Tsironi[1,3], Ioannis Karamitros[1], Eirini Efstathiou[1], Ilektra Karasante[1], and Ioannis Kassaras[2, †]

(1) Institute of Geodynamics, National Observatory of Athens, Athens, Greece aganas@noa.gr (2) Department of Geology and Geoenvironment, National and Kapodistrian University of Athens, Athens, Greece (3) Department of Geology, University of Patras, Rio, Greece.

Abstract

In this paper, we present the findings of a joint remote-sensing and seismological investigation of Milos (western Cyclades islands, Greece) using geodetic data (InSAR and GNSS) and the recordings of a local seismic network established by NOA in 2021. Our objective was to investigate the ground deformation and seismicity patterns and detect activity along fault zones of the island. We present evidence for on-going activity along a NW-SE, east-dipping fault crossing Milos.

Introduction and Objectives

Milos is a dormant stratovolcano with the most recent volcanic activity recorded about 380ka-90ka ago (Fytikas et al., 1986). As a result of the phreatic activity several overlapping craters exist on the island with diameters less than 1 km in size. Basement rocks occur in the SW, S and SE parts of the island (Fytikas et al., 1986). The seismicity around Milos is both shallow (4-15 km) and intermediate depth (70-90 km), however, no clear patterns have emerged so far due to the lack of sufficient seismic stations. Several swarms have been reported in the literature, linking seismicity and ascent of magmatic fluids but without strong evidence (Sachpazi and Hirn, 1991; Baltatzis et al., 2001).

Data and analysis

During May 2021 NOA installed a local seismic network of five (5) stations in the SE and East Milos (Fig. 1 left; blue dots). The sensors are GEOBIT C100 and were placed inside shallow (2-m) boreholes. Data telemetry is real-time (at 100 sps) using the Vodafone GSM network. During the first year of deployment, the seismic network of Milos had a fair response to the main demands such as the increase in detectability of the local microearthquakes, as well as the characterization of seismic properties of the area such as the origin of the recorded noise (natural, anthropogenic). The earthquake magnitudes range from 0.4 to 3.4 on the local magnitude (M_L) scale. The recorded activity is mainly concentrated inside the Gulf of Adamas and in Southern Milos, along the NW-SE striking fault, which might be associated with the March 1992 earthquake sequence (Delibasis and Drakopoulos, 1993; Papanikolaou et al. 1993).

In terms of geodetic data (1-D displacement time series) we used archived SAR Copernicus imagery (C-band) and we installed a local geodetic network at the SE part of the island (Fig. 1 left; red dots). For the InSAR time series analysis we applied the SBAS algorithm that is part of LiCSBAS, an open-source package (Morishita et al., 2020; Fig. 1 right). During the phase unwrapping, decorrelated areas in the interferograms are masked where the phase noise coherence is < 0.2. Wrapped and unwrapped interferograms were geocoded with a pixel spacing of 0.001 degree (~100 m) and converted to the GeoTIFF format. The accuracy of this technique is about 2-3 mm/yr (Morishita et al. 2020; Tsironi et al. 2022).

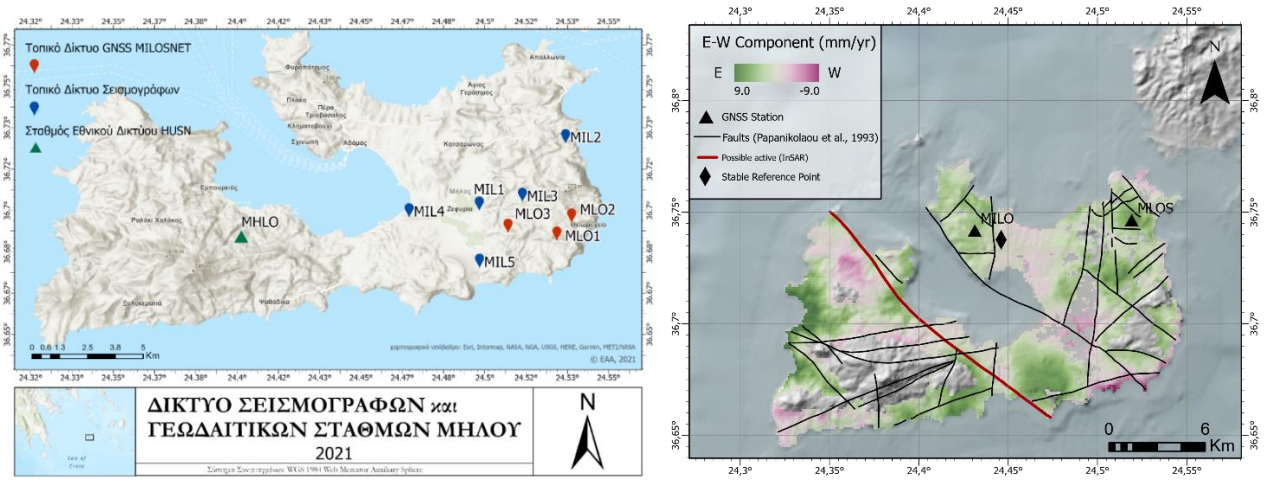

Figure 1. (left) Relief map of Milos showing seismic and GNSS networks. MHLO is a HUSN station (right) East-West velocity map based on InSAR data. Black lines indicate faults after Papanikolaou et al. (1993). Red line is active fault. Rhomb indicates the reference point used in InSAR processing. MILO & MLOS are GNSS stations on the island. Grey areas indicate no data.

Discussion and Conclusions

During 2021-2022 the local seismic network recorded tens of microearthquakes in the broader Milos area, the majority of which occurred at shallow depths (< 30 km). In order to improve the locations of hypocenters of the initial catalogue, which consists of 48 manually analyzed events and 139 additional detections through the template matching technique, we applied double-difference relocation with the HypoDD code. A set of 18 multiplets was constructed, containing a total of 147 events. Many small earthquakes are concentrated in the middle of the island (Gulf of Adamas) in tight spatial clusters, due to their strong waveform correlation. The clusters are aligned in a NW-SE orientation, following the strike of the main fault line that crosses Milos Island to the west of the epicenters. Fig. 2 (left) shows a map, where different colours represent different clusters of repeating earthquakes, as they have been recognized by means of their waveform similarity. The cross-section of Fig. 2 (right) indicates that the clustered seismicity beneath the Gulf of Adamas is located at focal depths of 5-6 km. Assuming a dip of 60° towards NE for the main fault that bounds the western shores of the Gulf, its plane would roughly cross the hypocenters. It should be noted, however, that for a more precise determination of the absolute hypocentral depths, a local velocity model is required. This could become possible with the accumulation of more data from the local network in the future.

The InSAR data processing (period 2016-2021) resulted in the production of Up-Down and E-W velocity maps (Fig. 1; right) which indicate that there is divergent ground motion (opening) across the NW-SE fault onshore Milos (see red line in Fig. 1). The velocity difference across the fault reaches 1 cm/yr, that is well above the error. In conclusion, the InSAR data provide further evidence that this fault is active and its surface trace can match an east-dipping fault plane where microseismicity is present (Fig. 2 right).

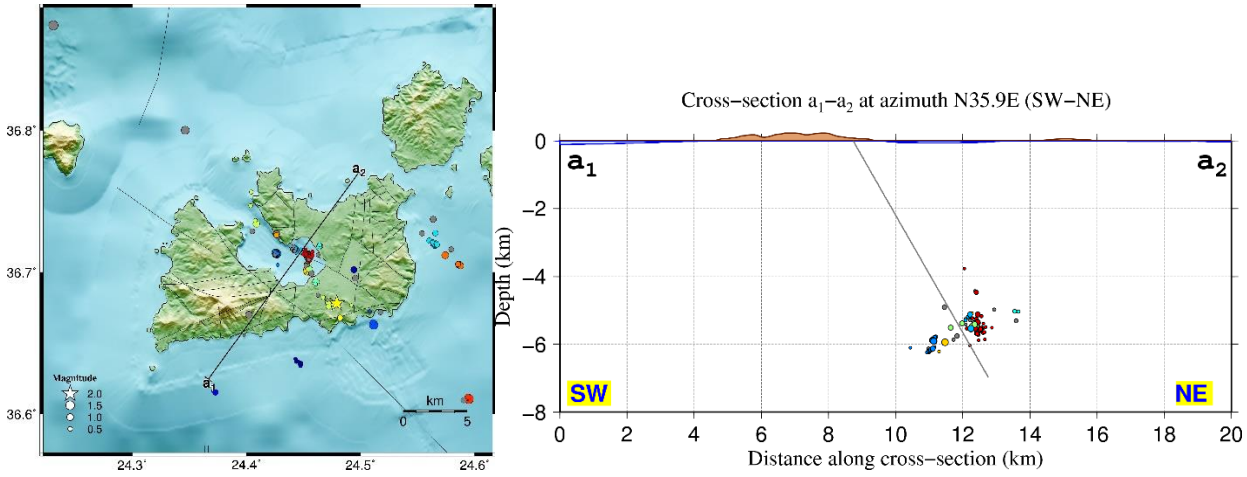

Figure 2. (left) Map of relocated seismicity (multiplets) for the period June 2021- June 2022 showing NW-SE alignment of epicentres. (right) Cross-section of hypocenters along the profile a_1-a_2, within a width of ±2km. The gray line, dipping at 60° towards NE, represents the major fault crossing Milos Island.

Acknowledgements

We thank Nikos Germenis and Fragkiskos Ninos for help with network installation. This research was partially funded by PPC Renewables SA (PPCR). This work represents the opinions of the authors and does not necessarily represent the opinions of PPCR.

References

Delibasis, N., Drakopoulos, J., 1993: The Milos island earthquake of March 20, 1992 and its tectonic significance. Pageoph, Vol. 141, No 1, p. 43-58.

Fytikas, M., Innocenti, F., Kolios, N., Manetti, P., Mazzuoli, R., Poli, G., Rita, F., Villari, L., 1986. Volcanology and petrology of volcanic products from the island of Milos and neighbouring islets. J. Volcanol. Geotherm. Res., 28: 297-317.

Morishita, Y., Lazecky, M., Wright, T. J., Weiss, J. R., Elliott, J. R., & Hooper, A. 2020. LiCSBAS: An open-source InSAR time series analysis package integrated with the LiCSAR automated Sentinel-1 InSAR processor. Remote Sensing, 12(3), 424

Papanikolaou, D., Lekkas, E., Syskakis, D., Adamopoulou, E., 1993. Correlation of neotectonic structures with the geodynamic activity in Milos during the earthquakes of March 1992. Bull. Geol. Soc. Greece, Vol. XXVIII/3, p. 413-428.

Sachpazi, M., Hirn, A., 1991. Shear-wave anisotropy across the geothermal field of Milos, Aegean Volcanic arc. Geophys. J. Int., Vol. 107, p. 763-785.

Tsironi, V., Ganas, A., Karamitros, I., Efstathiou, E., Koukouvelas, I., Sokos, E. 2022. Kinematics of Active Landslides in Achaia (Peloponnese, Greece) through InSAR Time Series Analysis and Relation to Rainfall Patterns. Remote Sens., 14(4), 844. https://doi.org/10.3390/rs14040844

Μπαλτατζής Ε., Δελήμπασης Ν., Valsami-Jones, E., Πυρλή Μ., & Baier, B. 2001. Relationship between hydrothermal fluids and microseismic activity on the south-east coast of Milos Island. Bulletin of the Geological Society of Greece, 34(4), 1441–1447. https://doi.org/10.12681/bgsg.17239 (In Greek, with English abstract).

16th International Congress of the Geological Society of Greece
17-19 October, 2022 - Patras, Greece
Bulletin of the Geological Society of Greece, Sp. Publ. 10
Ext. Abs. GSG2022-259

MT-InSAR analysis investigating the opening in the southeastern part of Thessaly Basin

Andreas Karavias[1,2], Haralambos Kranis[3], Pavlos Krassakis[1,2], Nikolaos Koukouzas[2], Issaak Parcharidis[1]

(1) Department of Geography, Harokopio University of Athens, El. Venizelou 70, Kallithea, 17671, Athens, Greece., karavias@hua.gr, (2) Centre for Research & Technology Hellas (CERTH), 15125 Athens, Greece, (3) Department of Geology and Geoenvironment, National and Kapodistrian University of Athens, Panepistimioupoli Zografou, 15784 Athens, Greece.

Introduction

This study focuses on the Eastern Thessaly basin (Central Greece) which is one of the most characteristic examples of land subsidence in the Greek region. This was mainly caused by the artificial drainage of Lake Karla in the early 1960s for the purpose of reclamation of agricultural land. The long-term pumping of water for agricultural activities and the increasing drinking water demand, in combination with the ongoing climate change trends have caused a significant reduction in groundwater reserves, resulting in substantial subsidence throughout the East Thessaly basin., Under the pressure of the local authorities, Lake Karla was recharged, a process that started in 2010, in an effort to minimize the subsidence effects. In addition, the land subsidence at the S-E part of the plain is attributed to several causes, including aquifer system compaction, and was related to the prevailing East-West (E-W) trending fault system (Caputo, 1994). The Eastern Thessaly basin is an inter-mountain basin formed during the Pliocene as a result of the post-orogenic collapse of the Hellenides (Caputo & Pavlides, 1993), and the area was affected by a NE-SW extensional regime. This caused the formation of a system of NW-SE elongated horsts and graben bounded by large normal faults. In Thessaly, this tectonic regime was active from the Pliocene, or possibly from the Latest Miocene to the Lower Pleistocene period (Caputo, 1990). From a structural point of view, this tectonic phase resulted in the formation of the NW-SE trending Larissa Basin that still dominates the morphology of this area (Caputo, 1994).

Several studies have been conducted by authors who implemented satellite remote sensing methodologies using Radar data in an attempt to investigate the overall subsidence trends with centimeter accuracy. However, most of these studies focused on the observation of subsidence patterns, before and after the recharging of Lake Karla. In a previous research (Karavias, 2021), deformation velocity was detected on the East-West (E-W) part of the basin, depicting a stretching of the Eastern Thessaly plain, but this finding requires further research and more in-depth investigation. This study aims to investigate the E-W movements and to map the impact of the recharging of Lake Karla on the subsidence pattern in the Southern part of the Eastern Thessaly plain during the period from 2015 to 2021.

Data and Methods

The input data encompass more than 300 C-band SAR scenes acquired in Interferometric Wide (IW) swath mode over Larissa plain by Sentinel-1A &1B satellites, obtained from the Copernicus Open Access Hub platform (URL:https://scihub.copernicus.eu/). In particular, 145 SAR scenes were acquired in ascending mode along track 102 and 166 SAR scenes in descending mode along track 7, respectively from March 2015 to December 2021. Moreover, rainfall data were obtained from the Meteo website (URL:https://www.meteo.gr/) of the National Observatory of Athens (NOA) to investigate the correlation of deformation patterns with the precipitation levels during the dry and wet seasons.

Multi-temporal SAR data processing was carried out following the Small BAseline Subset (SBAS) Differential InSAR (DinSAR) approach (Berardino *et al*., 2002), conducted in GAMMA software. The processing of the images included the co-registration of the entire data stack using a Shuttle Radar Topography Mission (SRTM) Digital Elevation Model (DEM), the interferogram generation, the subtraction of the topography-related based on a 30 m SRTM DEM, the phase unwrapping and filtering, as well as the geocoding of final products. The displacement decomposition was derived by combining ascending and descending cumulative displacements, in order to generate the Vertical and East-West displacement maps according to the equations of Dalla (2012).

Results

An eastward sense movement on the SE part of the Eastern Thessaly basin with a cumulative average deformation value of approximately 1.6 cm in the period of 7 years (Fig.1, a) has been detected. On the other hand, the western part is relatively stable as far as the horizontal component is concerned. Regarding the subsidence patterns, the time series analysis in both geometries shows that the recharging of Lake Karla could possibly affect the deformation rates during the dry and wet seasons. Moreover, Fig. 1(b) shows that the subsidence rates on the Stefanovikion settlement follow the changes in wet seasons by comparing the time periods 2015-2017 and 2018-2021, while in Kileler settlement, which is further from the lake, the seasonal deformation rates continue to grow. The of results the deformation times series on Sefanovikion settlement were also compared with the local GNSS station (Argyrakis *et al*., 2020) that shows similarities

on seasonal deformation patterns.

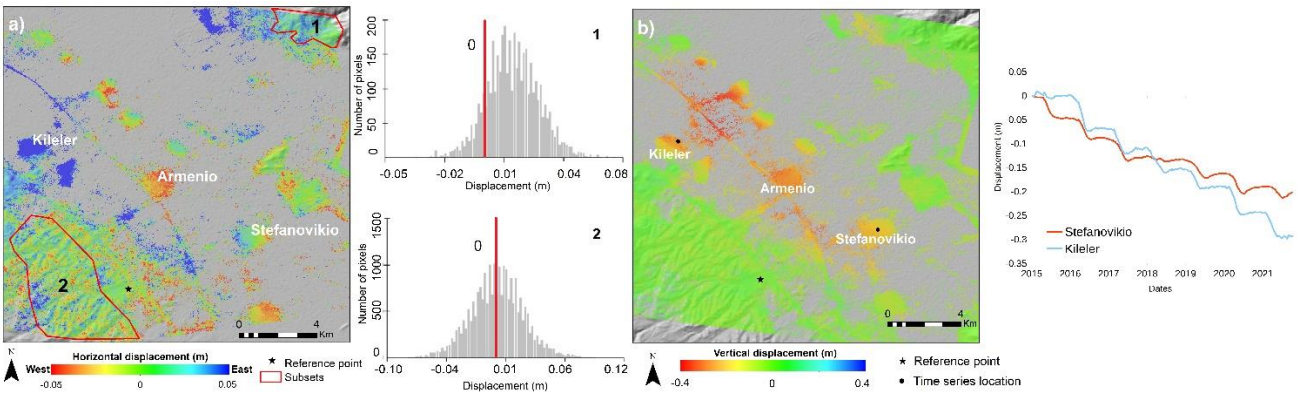

Figure 1. Displacement decomposition maps in East-West (a) and Vertical (b) components. The histograms next to the map (a) depict the distribution of displacement values in subset areas 1 and 2, while the diagram next to the map (b) presents the displacement time series analysis on Stefanovikio (red line) and Kileler (blue line) settlements based on descending geometry.

Table 1. Statistical analysis of displacement values on subset areas of Figure 1,a.

	Subset areas	
Statistics	**1**	**2**
Minimum	-0.05	-0.10
Maximum	0.08	0.12
Mean	0.01	0.00

Discussion and Conclusions

The presented methodological framework highlights the importance of multitemporal analysis of deformation trends using Earth Observation (EO) data, not only in the monitoring of land subsidence, but also in the detection of deformation patterns related to tectonic activity. The SBAS method, which is mostly applied in rural areas, is also quite useful for mountainous and urban regions thanks to the coverage extent of the generated products, thus providing a useful tool for natural hazard assessment. Therefore, a field survey could indicate the highest-risk areas for the post-incident effects. Moreover, according to the results of this study, compared to the previous findings (Karavias, 2021), the parameterization of the temporal baseline is an important factor in the accuracy of generated products. In this light, future work will focus to investigate the parameters of DinSAR analysis in order to monitor the deformation patterns of Larissa plain combined with GEOspatial INTelligence (GEOINT) approaches (Krassakis *et al*., 2022) to detect the exposure of critical infrastructures within the basin.

Acknowledgements

Maps throughout this work were created using ArcGIS® software by Esri. ArcGIS® and ArcMap™ are the intellectual property of Esri and are used herein under license. Copyright © Esri. All rights reserved. The processing of Sentinel-1 SAR SLC images was carried out on © 2021 GAMMA Remote Sensing software. The authors are grateful to the European Space Agency, who provided the Sentinel-1 datasets.

References

Caputo, R. 1990. - Geological and structural study of the recent and active brittle deformation of the Neogene-Quaternary basins of Thessaly (Central Greece). *Scientific Annals*, Aristotle University of Thessaloniki, 12, pp. 252.

Caputo, R., Pavlides, S. 1993. - Late Cainozoic geodynamic evolution of Thessaly and surroundings (central-northern Greece). *Tectonophysics*, 223, p. 339-362

Caputo, R., Bravard, J., Helly, B., 1994 The Pliocene-Quaternary tecto-sedimentary evolution of the Larissa Plain (Eastern Thessaly, Greece), *Geodinamica Acta*, 7:4, 219-231, DOI: 10.1080/09853111.1994.11105267

Berardino, P., Fornaro, G., Lanari, R., Sansosti, E., 2002. A new algorithm for surface deformation monitoring based on small baseline differential SAR interferograms. IEEE Trans. Geosci. *Remote Sens*. 40, 2375–2383. https://doi.org/10.1109/TGRS.2002.803792

Dalla Via, G.; Crosetto, M.; Crippa, B. 2012. Resolving vertical and east-west horizontal motion from differential interferometric synthetic aperture radar: The L'Aquila earthquake. J. Geophys. Res. *Solid Earth* 2012, 117, 8689.

Argyrakis, P., Ganas, A., Valkaniotis, S. et al. 2020 Anthropogenically induced subsidence in Thessaly, central Greece: new evidence from GNSS data. *Nat Hazards* 102, 179–200. https://doi.org/10.1007/s11069-020-03917-w

Karavias A. 2021 Monitoring impacts of climate change on surface subsidence using SAR Interferometry after the activation of Karla lake reservoir for water-consuming control for irrigation., *Master thesis*, Harokopio Univesity of Athens, Athens.

Krassakis P, Karavias A, Nomikou P, Karantzalos K, Koukouzas N, Kazana S, Parcharidis I. 2022 Geospatial Intelligence and Machine Learning Technique for Urban Mapping in Coastal Regions of South Aegean Volcanic Arc Islands. *Geomatics*. 2(3):297-322. https://doi.org/10.3390/geomatics2030017

16th International Congress of the Geological Society of Greece
17-19 October, 2022 - Patras, Greece
Bulletin of the Geological Society of Greece, Sp. Publ. 10
Ext. Abs. GSG2022-363

Development of a monitoring platform for permanent GNSS stations analysis in the region of the EnCeladus Hellenic Supersite, preliminary results.

D. Anastasiou[1], X. Papanikolaou[1], M. Tsakiri[1], S. Lalechos[2]

(1) National Technical University of Athens, Athens, Greece, dganastasiou@gmail.com (2) Earthquake Planning & Protection Organisation , Athens, Greece.

As part of the operation of the EnCeladus Hellenic Supersite, Dionysos Satellite Observatory (DSO) of the National Technical University of Athens (NTUA) undertook the monitoring of the Corinth Gulf area through GPS/GNSS stations and the development of a multidisciplinary platform.

Last decade, DSO has developed a platform for automatic processing of GNSS data (Papanikolaou et al., 2017) using Bernese GNSS software (Dach et al., 2015). The DSO automatic GNSS data processing platform has been significantly upgraded and strengthened in the last year. The changes made the data analysis fully compatible with the current international standards in the field of Satellite Geodesy and Navigation. The upgrades that took place mainly concern three different areas:

- adoption of new formats and information files (eg. RINEX v3).
- upgrade algorithms and methodologies (eg. Calibration files per antenna), and
- upgrade and monternize the implementation (eg. Change architecture, use Python3)

GNSS data processing results in the estimation of a number of parameters per day. The most critical is the coordinates of each station, estimated every day, in a selected reference system (IGb14). These estimates are used in a post-processing step, to create position time-series. Time series analysis follows to study the kinematics of the wider region. Time series positions are updated daily with each new solution from the automatic processing of the data. The velocity fields are calculated at regular time intervals as well as the strain field.

In this paper, data from 36 permanent GNSS stations, installed in the Gulf of Corinth, were analyzed. All available station data freely available from the providers have been used. Also, data from private organizations made available for the specific project have been used, for better coverage of the region and distribution of the stations.

The position time series were processed for all stations where the available data had a time period greater than 2.5 year for the estimation of the velocity field. The estimated velocities for each station in IGb14 and with respect to a stable Europe are presented. For the estimation of strain tensor parameters, StrainTool software (Anastasiou et al., 2019,2021) were used. A strain field estimated using the velocity field on a grid with 0.25 degrees grid step, that covers the whole region of the available stations (Figure 1). All figures and maps produced using Generic Mapping Tools software (Wessel et al.,2019)

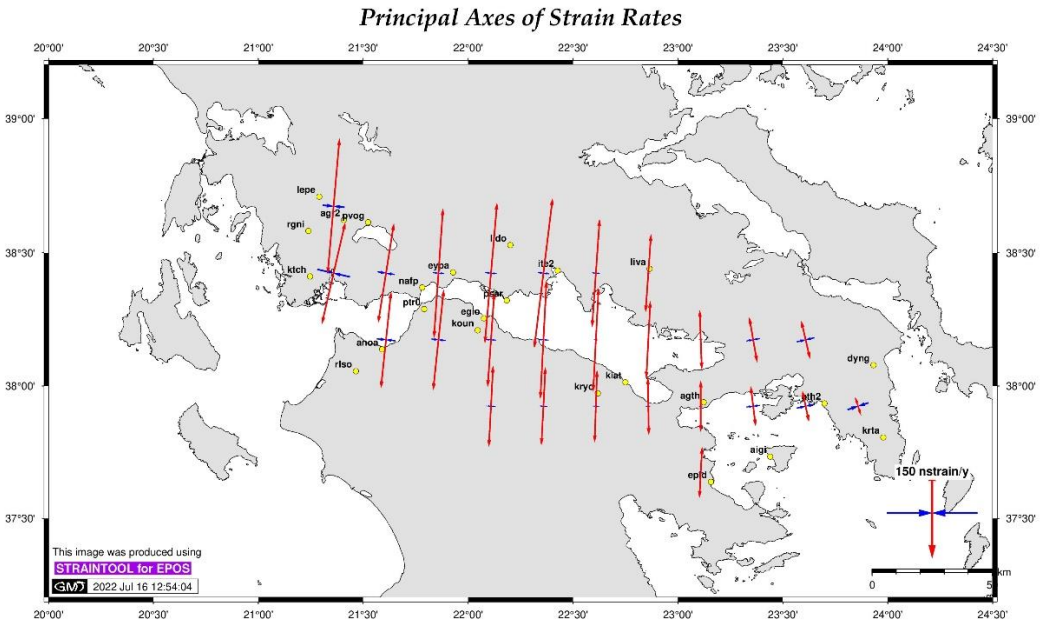

Figure 1. Strain rates field on a grid with 0.25 degrees grid step

Finally, the results are available on the web portal that has been developed as part of the DSO website. Everyone can access the results of the processing on a daily basis, while the position time series of the stations are also presented. Regularly, the velocity and strain field estimates are also updated with recent analyses.

Acknowledgements

This project was funded by Earthquake Planning & Protection Organisation (EPPO) within the framework of EnCeladus Hellenic Supersite. The authors would like to thank you National Observatory of Athens, Corinth Rift Laboratory, Geodetic Observatory Pecny for making GNSS data freely available. We would also like to thank the private companies Tree Company SA, Metrica SA, and the public organization Hellenic Cadastre for making data from specific stations free available for this project.

References

Anastasiou, D., Papanikolaou, X., Ganas, A. and Paradissis, D., 2021. StrainTool: A software package to estimate strain tensor parameters (v1.0-r1). Zenodo. DOI: 10.5281/zenodo.1297565

Anastasiou, D., Ganas, A., Legrand, J., Bruyninx, C., Papanikolaou, X., Tsironi, V., Kapetanidis, V., 2019. Tectonic strain distribution over Europe from EPN data. EGU General Assembly 2019, Geophysical Research Abstracts, Vol. 21, EGU2019-17744-1

Dach, R., Lutz, S., Walser, P., Fridez, P. (Eds.), 2015. Bernese GNSS Software Version 5.2. User manual, Astronomical Institute, University of Bern, Bern Open Publishing. DOI: 10.7892/boris.72297; ISBN: 978-3-906813-05-9.

Papanikolaou, X., Anastasiou, D., Paradissis, D., 2017. DSO contribution to EUREF densification; status and future steps. EUREF Analysis Center Workshop 2017, Royal Observatory of Belgium, Brussels, Belgium. 25-26 October.

Wessel, P., Luis, J. F., Uieda, L., Scharroo, R., Wobbe, F., Smith, W. H. F., & Tian, D., 2019. The Generic Mapping Tools version 6. Geochemistry, Geophysics, Geosystems, 20, 5556–5564. DOI:10.1029/2019GC008515

16th International Congress of the Geological Society of Greece
17-19 May 2022 - Patras, Greece
Bulletin of the Geological Society of Greece, Sp. Publ. 10
Ext. Abs. GSG2022-365

Geodetic evidence for active deformation onshore Paliki Peninsula, Cephalonia, Greece

V. Tsironi[1,2], Ath. Ganas[1], S. Valkaniotis[3], V. Kouskouna[4], I. Kassaras[4 †], Eth. Sokos[2], I. Koukouvelas[2]

(1) Institute of Geodynamics, National Observatory of Athens, Athens, Greece, vtsironi@noa.gr (2) Department of Geology, University of Patras, Rio, Greece (3) Department of Civil Engineering, Risk and Resilience Assessment Center, Democritus University of Thrace, Xanthi, Greece (4) Department of Geology and Geoenvironment, National and Kapodistrian University of Athens, Athens, Greece.

Abstract

In this paper we present new geodetic (InSAR) data (ground velocities) over the Paliki Peninsula, western Cephalonia. Greece. The data span the period 2016-2022 and were analysed with the SBAS method under the framework of the LiCSBAS open-source code. The InSAR results demonstrate that Paliki is undergoing active deformation (shear & shortening) with rates between 2-5 mm/yr in line-of-sight (LOS) direction. The town of Lixouri undergoes uplift.

Introduction and Objectives

Paliki Peninsula is located on the island of Cephalonia where it suffers from frequent earthquakes due to its proximity to the Cephalonia Transform Fault (CTF). The CTF (Louvari et al. 1999), a 140 km long dextral strike-slip fault, accommodates the relative motion between the Apulian (Africa) and Aegean (Eurasia) lithospheric plates and has a GPS slip rate of 14.3 mm/yr (Briole et al., 2021). The most recent earthquakes of Paliki include two events during early 2014 (Ganas et al. 2015); one with Mw $_{(NOA)}$=6.0 and Mw $_{(NOA)}$=5.9, which occurred on 26 January 2014 13:55 UTC and 3 February 2014 03:08 UTC, respectively. These shallow events caused widespread structural damage and environmental impacts, mainly in the western and central part of the island (Valkaniotis et al. 2014).

Any potential movements of the Earth's surface can be recorded through SAR Interferometry (InSAR). Through the analysis of time series produced by radar image processing, the rate of motion could be measured with an accuracy of 2-3 mm/yr, as well as any relative movement across an active fault could be detected (Tsironi et al., 2022). Long-term monitoring of active faults through InSAR has been successfully applied in many studies so far, not only towards identifying the respective structures, but also to monitor their spatial and temporal patterns of deformation.

Data & Analysis

The processing of InSAR time series analysis was held by the LiCSBAS, an open-source package that integrates with LiCSAR products (Morishita et al.,2020). LiCSAR produced interferograms from Sentinel-1 SLC data. Wrapped and unwrapped interferograms were geocoded with a pixel spacing of 0.001 degree (~100 m) and converted to the GeoTIFF format. We used these products for our time series analysis. We used both the ascending and the descending frames, to map ground velocities with respect to a reference point (Fig. 1). We used 2018 (ascending) and 1793 (descending track) available interferograms, respectively. In order to perform an estimate of the velocity of a surface pixel through time based upon a series of displacement data, we perform an SB (small baseline) inversion on the network of interferograms, and especially we applied the N-SBAS method. The time series analysis covers the period 2016-2022.

Discussion & Conclusions

The InSAR results show that the horizontal component of movement is dominant, which provides evidence of the existence of strike slip faulting onshore the peninsula (negative values for ascending and positive values for descending onshore Paliki peninsula; Fig. 1). The velocity pattern of the ascending track also reveal the possible post-seismic motion of the ruptured plane of the earthquake of 3 February of 2014 at the northern part of peninsula (Fig. 1 - left map; near point 15). In addition, the time series analysis reveals other possible active structures on the Paliki peninsula that need to be confirmed with geological data. The town of Lixouri is uplifting (a few mm/yr) as it observed with positive values in both satellite geometries (ascending and descending tracks). Through an East-West cross section on the LOS time-series data (Fig 2), we could determine possible velocity discontinuities (block boundaries?) which are possibly bounded by active faults. Overall, our results indicate a complex deformation pattern onshore the Paliki peninsula.

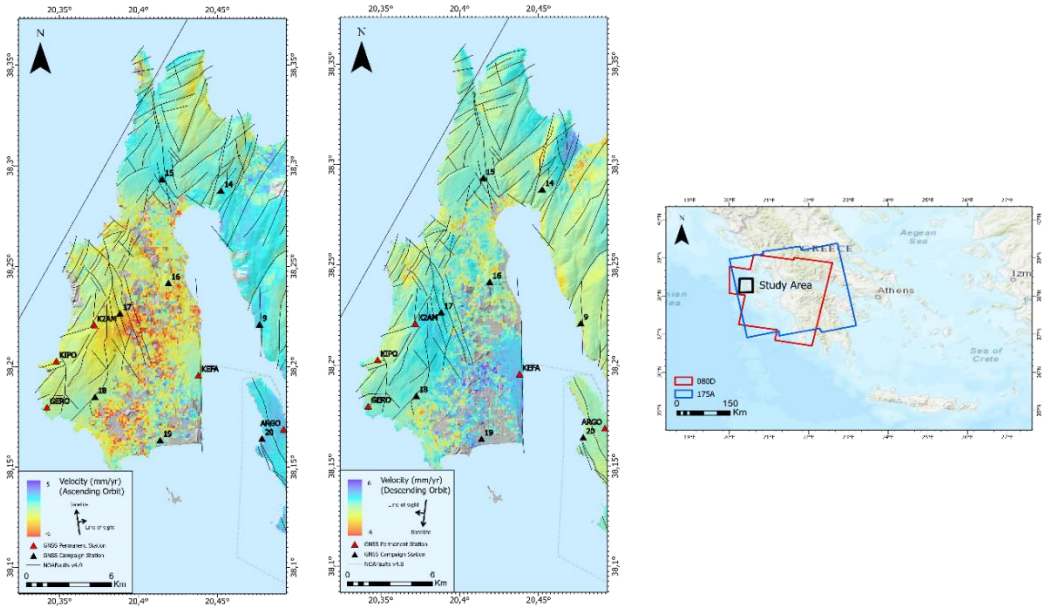

Figure 1. Left Map: Ascending ground Velocity Map of Paliki in line of sight (LOS) in mm/yr. Black lines are active faults. Centre Map: Descending ground Velocity Map in LOS in mm/yr. Triangles are the GNSS Stations in the area. Right Map: The area of interest in black box. Blue and red boxes represent the ascending and descending Sentinel-1 frames.

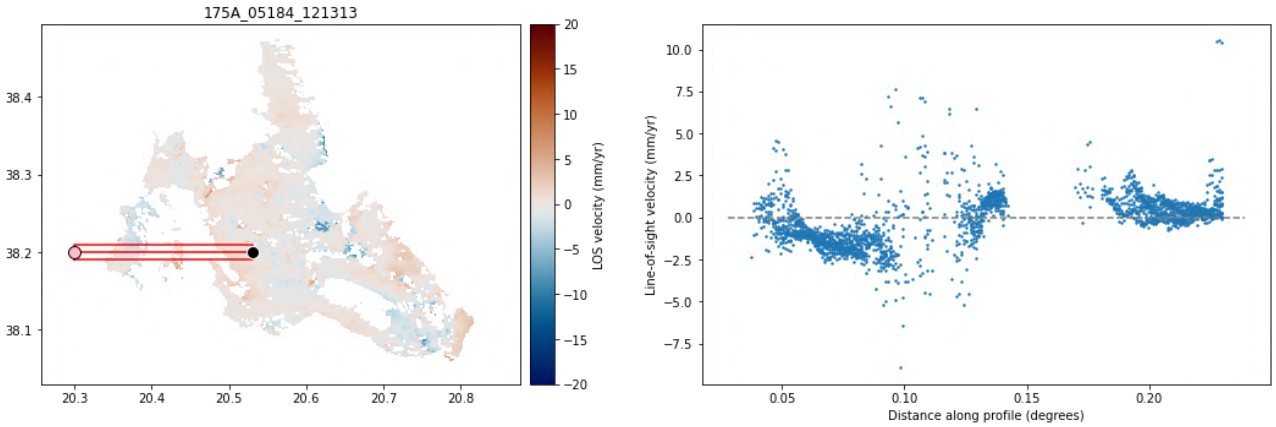

Figure 2. Left Map: Ascending ground Velocity Map of Cephalonia in line of sight (LOS) in mm/yr. Right: the velocity cross section along E-W direction. The width of data plotted on the cross section is 2 km.

Acknowledgements

We acknowledge the project '*Στρατηγικής Ολοκληρωμένης Χωρικής Επένδυσης (ΟΧΕ) στην περιοχή της Παλικής Κεφαλονιάς*' from the National Kapodistrian University of Athens for funding. This work was supported by the Hellenic Foundation for Research and Innovation (HFRI) under the 3rd Call for HFRI PhD Fellowships (Fellowship Number: 5176)

References

Briole, P., Ganas, A., Elias, P., & Dimitrov, D. 2021. The GPS velocity field of the Aegean. New observations, contribution of the earthquakes, crustal blocks model. Geophysical Journal International, 226(1), 468-492.

Ganas, A., Cannavo, F., Chousianitis, K., Kassaras, I., & Drakatos, G. 2015. Displacements recorded on continuous GPS stations following the 2014 M6 Cephalonia (Greece) earthquakes: Dynamic characteristics and kinematic implications. Acta Geodyn. Geomater, 12(1), 177, 5–27, doi:10.13168/AGG.2015.0005

Louvari, E., A.A Kiratzi, B.C Papazachos, 1999. The Cephalonia Transform Fault and its extension to western Lefkada Island (Greece), Tectonophysics, Volume 308, Issues 1–2, Pages 223-236, https://doi.org/10.1016/S0040-1951(99)00078-5

Tsironi, V., Ganas, A., Karamitros, I., Efstathiou, E., Koukouvelas, I., Sokos, E. 2022. Kinematics of Active Landslides in Achaia (Peloponnese, Greece) through InSAR Time Series Analysis and Relation to Rainfall Patterns. Remote Sens., 14(4), 844. https://doi.org/10.3390/rs14040844

Morishita, Y., Lazecky, M., Wright, T. J., Weiss, J. R., Elliott, J. R., & Hooper, A. 2020. LiCSBAS: An open-source InSAR time series analysis package integrated with the LiCSAR automated Sentinel-1 InSAR processor. Remote Sensing, 12(3), 424

Valkaniotis S., Ganas A., Papathanassiou, G., and Papanikolaou M., 2014. Field observations of geological effects triggered by the January-February 2014 Cephalonia (Ionian Sea, Greece) earthquakes, Tectonophysics, 630, 150-157, DOI:10.1016/j.tecto.2014.05.012

16th International Congress of the Geological Society of Greece

17-19 October, 2022 - Patras, Greece

Bulletin of the Geological Society of Greece, Sp. Publ. 10

Ext. Abs. GSG2022-388

A low-cost permanent GNSS network to capture transient plate tectonic motions in Greece: EU-funded deployment scheduled for 2023

J.R. Bedford[1]

(1) Ruhr University Bochum, Germany, jonathan.bedford@rub.de

Permanent GNSS stations have been successfully used to understand tectonic processes in Greece over a range of spatial and temporal timescales.

With the cost of GNSS monitoring hardware decreasing, the number of GNSS satellites increasing, and prevalence of transient motions now better recognised, it is a timely moment to densify Greece's existing continuous GNSS observations.

Various research agencies, universities, and commercial service providers operate continuous GNSS in Greece. Here I present the ongoing plans for the deployment of 72 EU-funded permanent GNSS stations in Greece. The stations will use two low-cost designs that both include multi-frequency receiver chips, and therefore it can be expected that the displacement time series, after processing, will be useful for tectonic research, as well as for other scientific applications.

In addition, I will present the preliminary analyses of the transient tectonic motion of GNSS stations in Greece using time series of existing stations recorded over the past decade and state of the art transient detection algorithms.

16th INTERNATIONAL CONGRESS of the
GEOLOGICAL SOCIETY OF GREECE

S5. Insights into the Nature of the Earth's Upper Mantle approached from the study of Ophiolites and Volcanic Rocks

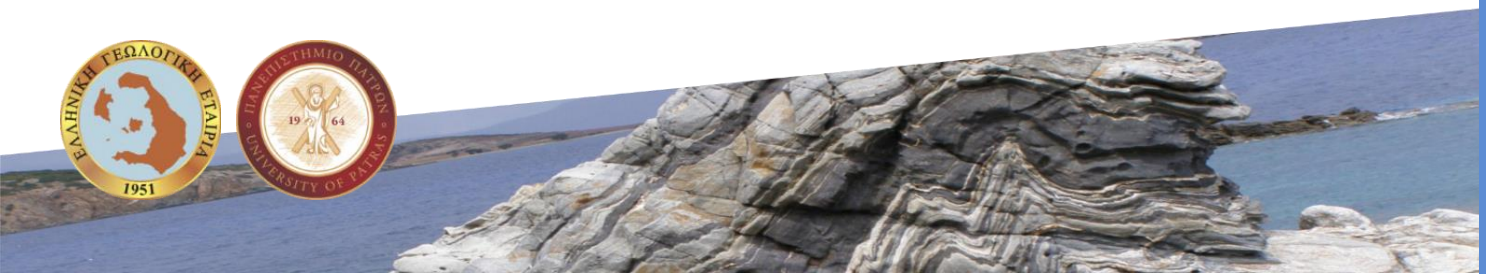

OUR EARTH, OUR HOME

16th International Congress of the Geological Society of Greece

17-19 October, 2022 - Patras, Greece

Bulletin of the Geological Society of Greece, Sp. Publ. 10

Ext. Abs. GSG2022-018

Nd-Sr-Pb Isotopes Systematics of Evros Ophiolite, Eastern Circum-Rhodope Belt, NE Greece

N. Bonev[1], Z. Dotseva[1], M. Chiaradia[2]

(1) Sofia University "St. Kliment Ohridski", Sofia, Bulgaria, niki@gea.uni-sofia.bg (2) University of Geneva, Geneva, Switzerland.

Background

The arc-related Evros ophiolite (Magganas, 1991, 2002) of Early-Middle Jurassic crystallization ages (e.g. Bonev *et al*., 2015) constitutes the essential part in the section of the eastern Circum-Rhodope Belt (eCRB), located in Thrace region of northeastern Greece (Fig.1a). In addition to the Triassic-Jurassic metasedimentary section of the eCRB (i.e. Makri unit, sedimentary part of Drimos-Melia unit), the Evros ophiolite exposes a typical upper crustal section of an ophiolite.

Objectives

Only Nd and Pb isotopes data are available from the Evros ophiolite counterpart Mandritsa unit of the eCRB in Bulgaria, which suggests a contribution of depleted MORB-type mantle in magma generation (Bonev and Stampfli, 2008). In this contribution, we present Nd-Sr-Pb isotopes systematics of the Evros ophiolite in four main outcrop areas or units (Fig. 1a), with the aim to extend our knowledge for the mantle chemical dynamics related to Jurassic intra-oceanic arc development in the Tethyan realm.

Methods

Radiogenic isotope ratios of Nd, Sr and Pb in powdered whole-rock samples were measured at the Department of Earth Sciences of the University of Geneva, Switzerland using a Thermo Neptune PLUS Multi-Collector ICP-MS. For monitoring the internal fractionation, we used $^{88}Sr/^{86}Sr = 8.375209$ for the $^{87}Sr/^{86}Sr$ ratio, $^{146}Nd/^{144}Nd = 0.7219$ for the $^{143}Nd/^{144}Nd$ ratio and $^{203}Tl/^{205}Tl = 0.418922$ for the three Pb ratios. Long-term reproducibility of the measurements was controlled by repeated measurements of the external standards SRM987 ($^{87}Sr/^{86}Sr = 0.710248$, JNdi-1 $^{143}Nd/^{144}Nd = 0.512115$), and SRM981 for Pb. Further analytical details can be found in Chiaradia *et al*., (2011). The Nd-Sr-Pb isotopic results were age corrected to the known crystallization ages of the Evros ophiolite or biostratigraphic age of associated sediments (numbers, Fig. 1a). Twelve representative samples were collected, 3 samples at the Didymotycho location (gabbro, massive basalt and basalt dyke), 2 samples from Agriani gabbro and the overlying massive basalt, respectively, 3 samples from the Drimos-Melia unit (pillow basalt, massive basalt, massive basaltic andesite), 3 samples from Petrota location and adjacent area (gabbro, anorthosite, basalt), and a single basalt sample at the village of Kornofolea (Fig. 1a).

Results

The mafic rocks show a range of Nd isotopic compositions from 0.512649 to 0.512976 with positive εNd_t values ranging from +0.2 to +6.6 and only a single exception of Kornofolea basalt εNd_t -1.3. Initial Sr isotopic compositions range from 0.703998 to 0.707584. The initial $^{206}Pb/^{204}Pb$ values fall into a range from 18.314 to 18.930 and the $^{207}Pb/^{204}Pb$ values range from 15.565 to 15.670.

Discussion

In a $^{143}Nd/^{144}Nd$ /$^{87}Sr/^{86}Sr$ diagram most of the samples parallel the mantle array and plot close to BSE, two samples plot close to BSE and one sample plot with a high $^{87}Sr/^{86}Sr$ ratio (Fig. 1b). In a $\varepsilon Nd_t/^{206}Pb/^{204}Pb$ diagram samples plot between MORB and BSE (Fig. 1c). The isotopic results indicate that the studied mafic rocks were derived from a mantle source with a relatively high time-integrated Sm/Nd ratio. The high $^{87}Sr/^{86}Sr$ ratio in some samples (Dydymotycho) and a negative εNd_t value of Kornofolea basalt suggests that crustal contamination and/or recycled sediments are involved in the magma genesis. Compared to the Mandritsa unit basalts and greenschists (Bonev and Stampfli, 2008), the Evros ophiolite samples demonstrate close isotopic compositions that are displaced toward higher $^{206}Pb/^{204}Pb$ ratios (Fig. 1c).

Conclusions

- Nd-Sr-Pb isotopic compositions demonstrate mostly a contribution of depleted MORB-type mantle source in the magma genesis of the Evros ophiolite mafic rocks.
- Crustal input is also demonstrated by more radiogenic Pb and negative εNd_t in some samples, which can be related to crustal contamination and/or recycled sediments in the arc-related, supra-subduction zone Evros ophiolite.
- Nd and Pb isotopes of the Evros ophiolite are comparable to Mandritsa unit basalts and greenschists in Bulgaria.

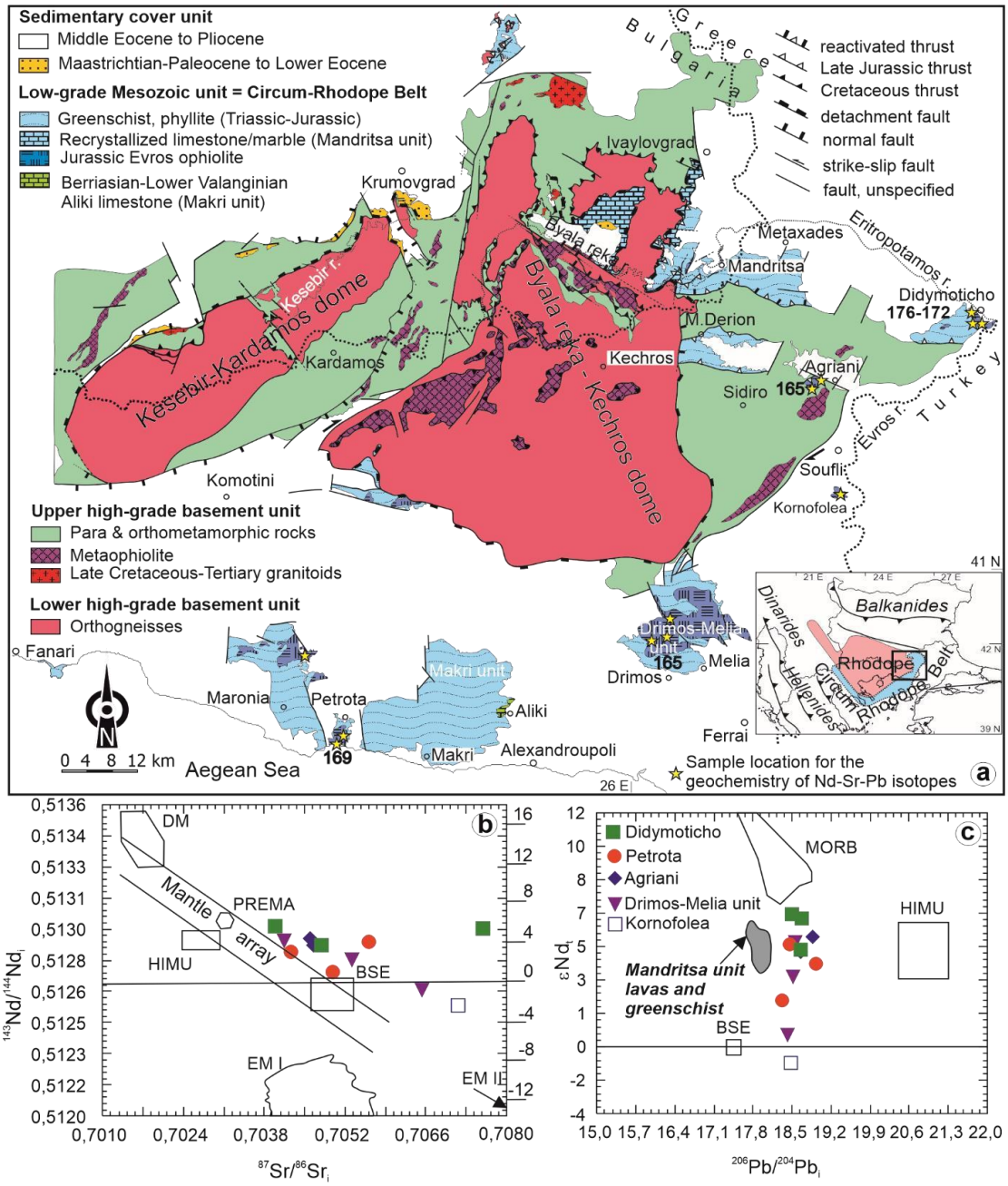

Figure 1. a) Simplified map after Bonev et al., (2015), b) $^{143}Nd/^{144}Nd$ -$^{87}Sr/^{86}Sr$ diagram, c) εNd_t-$^{206}Pb/^{204}Pb$ diagram.

Acknowledgements

The study was supported by National Science Fund (Bulgaria) contract KP-06-N54/5.

References

Bonev, N., Marchev, P., Moritz, R., Collings, D., 2015. Jurassic subduction zone tectonics of the Rhodope Massif in the Thrace region (NE Greece) as revealed by new U-Pb and $^{40}Ar/^{39}Ar$ geochronology of the Evros ophiolite and high-grade basement rocks. Gondwana Research 27, 760-775.

Bonev, N., Stampfli, G., 2008. Petrology, geochemistry and geodynamic implications of Jurassic island arc magmatism as revealed by mafic volcanic rocks in the Mesozoic low-grade sequence, eastern Rhodope, Bulgaria. Lithos 100, 210-233.

Chiaradia, M., Müntener, O., Beate, B., 2011. Enriched basaltic andesites from mid-crustal fractional crystallization, recharge, and assimilation (Pilavo volcano, Western Cordillera of Ecuador). Journal of Petrology 52, 1107-1141.

Magganas, A.C, 2002. Constraints on the petrogenesis of Evros ophiolite extrusives, NE Greece. Lithos 65, 165-182.

Magganas, A., Sideris, C., Kokinakis, A., 1991. Marginal basin-volcanic arc origin of metabasic rocks of the Circum-Rhodope Belt, Thrace, Greece. Mineralogy and Petrology 44, 235-252.

16th International Congress of the Geological Society of Greece
17-19 October, 2022 - Patras, Greece
Bulletin of the Geological Society of Greece, Sp. Publ. 10
Ext. Abs. GSG2022-044

The Ermioni back-arc depression (Argolis) versus the Arvi (Crete) seamount relative to subducting Pindos Ocean during Upper Cretaceous

S. Triantafyllidis[1], S. Kokkalas[2], S. Tombros[3]

(1) National Technical University of Athens, School of Mining and Metallurgical Engineering, Athens, Greece, striantafyllidis@metal.ntua.gr, (2) Department of Geology, University of Patras, Rio, Greece, (3) Department of Material Sciences, University of Patras, Rio, Greece

Research highlights: The major and trace element geochemistry of the footwall volcaniclastic rocks hosting the "Mafic-Pelitic" Ermioni VMS deposit (Argolis) and the pillow lavas of Arvi (Crete) point to different geotectonic position between the two units during upper Cretaceous, as the Pindos Ocean was subducting below the Pelagonian Microcontinent (Fig. 1).

Background and objectives

Earlier studies by Papanikolaou (1989) considered the Ermioni Complex in Argolis and Arvi Unit in Crete as mélanges of upper Cretaceous-to-Paleocene age. In particular, the late Cretaceous Arvi basalts were thought to be syngenetic to the late Cretaceous-to-Paleocene red shales, all found as olistoliths and olistostroms within the Arvi mélange, presenting similar geologic features to the Ermioni Complex lithologies. Later work by Palamakumbura et al. (2013) was focused on the stratigraphy and geochemistry of the lithologies comprising the Arvi Unit, resulting in a setting related to alkaline mafic volcanism of "intraplate" affinity, overlain by pelagic carbonates and terrigenous turbidites. In this study we compare the upper Cretaceous alkaline pillow basalts of Arvi (petrochemical data after Palamakumbura et al., 2013) with the intermediate volcaniclastic rocks forming the footwall of the upper Cretaceous "Mafic-Pelitic" Ermioni VMS (petrochemical data after Triantafyllidis et al., 2021) in an attempt to determine the geotectonic position of the studied areas relative to the subducting Pindos Ocean.

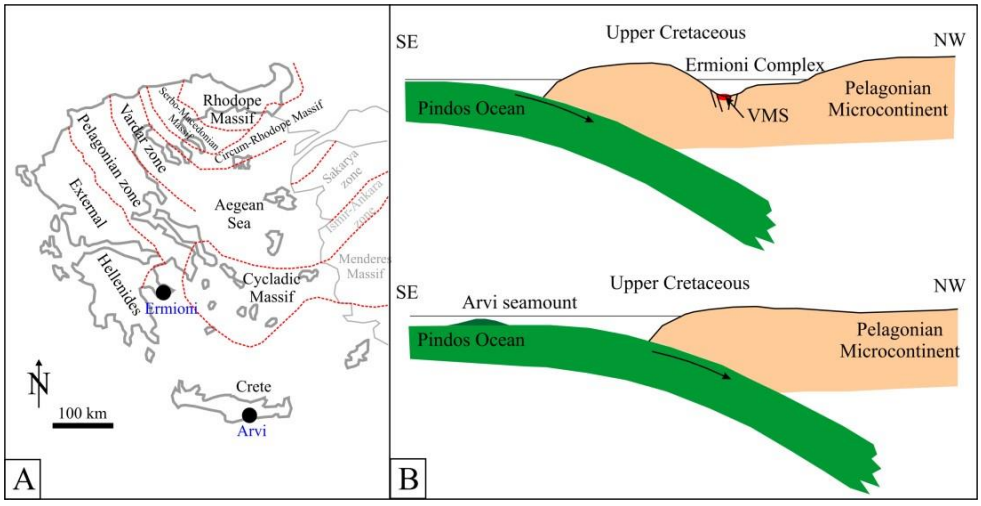

Figure 1. The Ermioni Complex and Arvi Unit (A) and their corresponding geotectonic setting during Upper Cretaceous (B) (with modifications after Triantafyllidis et al., 2021, and Palamakumbura et al., 2013).

Results and discussion

The Ermioni VMS footwall volcaniclastic rocks are arc-related andesites-to-basaltic andesites (Fig. 2A) of calc-alkaline affinity (Fig. 2A, B, C, D). Based on Palamakumbura et al. (2013), the Arvi Unit volcanic rocks are alkaline to subalkaline pillow basalts (Fig. 2A) that show relative alkaline enrichment, typical for ocean island type settings (Fig. 2B, C, D). Moreover, the degree of differentiation and/or partial melting is higher for the Ermioni volcaniclastic rocks relative to Arvi pillow basalts (higher Zr/Nb ratio, Fig. 2E), indicating formation within a back-arc basin in a suprasubduction zone setting (SSZ), while the lower Zr/Nb ratios for the Arvi lavas suggest lower degree of partial melting related to an intra-plate geotectonic setting (Fig. 2D).

Palamakumbura et al. (2013) considered the Arvi Unit as a seamount within the Pindos Ocean, with the alkaline pillow basalts forming the lowermost segment of the Unit while Pindos Ocean was subducting below the Pelagonian Microcontinent during upper Cretaceous (Fig. 1B). Interestingly, during the same period the Ermioni "Mafic-Pelitic"

VMS deposit was formed. According to Triantafyllidis et al. (2021) the VMS formation is related to hydrothermal convection along high-angle normal faults in a back-arc basin related depression (Ermioni Complex) formed due to subducted slab roll-back of the Pindos Ocean floor below the Pelagonian Microcontinent. The footwall volcaniclastic rocks have been formed prior the VMS, indicating that Pindos Ocean was already subducting during Cretaceous (Fig. 1B). The geochemistry of the pillow basalts in Arvi Unit suggests that Pindos Ocean was still active (spreading) during late Cretaceous, an indication of the different geotectonic evolution of Pindos Ocean in the west (Ermioni) and the east (Arvi) during late Cretaceous.

Despite the differences in type and age of volcanism between the two sites, there are similarities regarding the overlying sediments (turbidites and carbonates), indicating similar post-volcanism and geologic conditions of sedimentation prior emplacement on the continental margin in Paleocene-Eocene. Moreover, there are similar Fe-Mn-oxide mineralizations in both locations (Orfanoudaki and Perraki, 1997; Varnavas and Panagos, 1984), although no sulfide ores are found in Arvi. The absence of sulfides bodies in Arvi Unit is related to the low volatile content of the pillow basalts and the weak hydrothermal convection during volcanism. Such conditions have an adverse effect on massive sulfide deposition on the Pindos Ocean seafloor.

Concluding, the present study shows the effectiveness of employing ore-deposit and petrochemical data in defining the geotectonic setting of areas with diverse geological evolution, as in the case of the Ermioni Complex back-arc basin depression in respect to the Arvi seamount, where conventional and sophisticated methodologies may be proved insufficient.

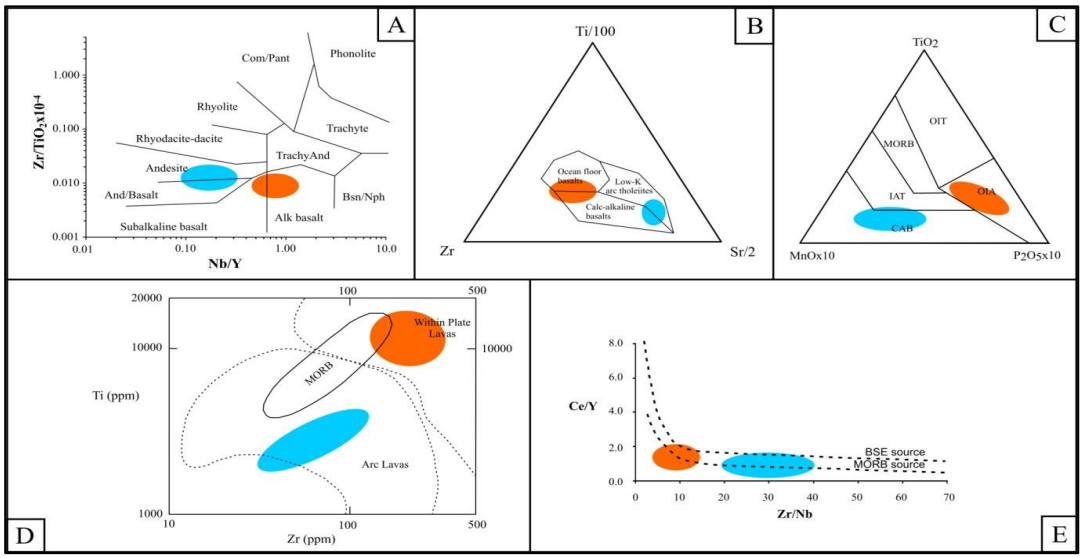

Figure 2.Geochemical diagrams of the Ermioni Complex (blue ellipses) and Arvi Unit (orange ellipses) volcanic rocks (A after Pearce, 1996; B after Pearce and Cann, 1973; C after Mullen, 1983;Dafter Pearce, 1982; E after Latin et al., 1990).

References

Latin, D.M., Dixon, J.E., Fitton, J.G., 1990. Rift-related magmatism in the North Sea Basin, in: Blundell, D.J., Gibbs, A. (Eds.), Tectonic Evolution of the North Sea Rifts. Oxford University Press, pp. 101-144.

Mullen, E.D., 1983. MnO/TiO2/P2O5: a minor element discriminant for basaltic rocks of oceanic environments and its implicatio ns for petrogenesis. Earth and Planetary Science Letters, 62, 53–62

Orfanoudaki, A., Perraki, Th., 1997. Late Cretaceous basalts of Crete and associated Manganese mineralization (in Greek with French abstract). Mineral Wealth, 102, 7-16.

Palamakumbura, R.N., Robertson, A.H.F., Dixon, J.E., 2013. Geochemical, sedimentary and micropaleontological evidence for a Late Maastrichtian oceanic seamount within Pindos ocean (Arvi Unit, S Crete, Greece). Tectonophysics, 595 -596, 250-262.

Papanikolaou, D.J., 1989. Occurrence of Arvi, Western Thessaly and Orliakas type formations in Argolis. Bulletin of the Geological Society of Greece 24, 71–84.

Pearce, J.A., 1983. Role of the sub-continental lithosphere in magma genesis at active continental margins. In: Hawkesworth, C.J., Norry, M.J. (Eds.), Continental Basalts and Mantle Xenoliths. Shiva, Nantwich, pp. 230–249.

Pearce, J.A., 1996. A user's guide to basalt discrimination diagrams, in: Wyman D.A., (Ed). Trace Element Geochemistry of Volcanic Rocks: Applications for Massive Sulphide Exploration. Sh. Cour. Not. 12, St. John's, Canada, Geo. Ass. Can., pp. 79- 113.

Pearce, J.A., Cann, J.R., 1973. Tectonic setting of basic volcanic rocks determined using trace element analyses. Earth and P lanetary Science Letters, 19, 290-300.

Varnavas, S.P., Panagos, A.G., 1984. Mesozoic metalliferous sediments from the ophiolites of Ermioni, Greece: Analogue to recent Mid-Ocean Ridge ferromanganese deposits. Chemical Geology, 42, 227-242.

Triantafyllidis, S., Tombros, S.F., Zhai, D., Kokkalas, S., 2021. The Upper Cretaceous Ermioni VMS Deposit, Argolis Peninsula, Peloponnese, Greece: type, genesis, and geotectonic setting. Ore Geology Reviews, 138, 104403.

16th International Congress of the Geological Society of Greece
17-19 October, 2022 - Patras, Greece
Bulletin of the Geological Society of Greece, Sp. Publ. 10
Ext. Abs. GSG2022-056

Variables Affecting the Tectono-Lithologic Expression of the Upper Mantle: Criteria from the Mesohellenic Ophiolites of Greece

A. Rassios[1], D. Ghikas[1], A.Batsi[1]
[1]Geopark Grevena-Kozani, Grevena, Greece, Geowonders@gmail.com

The Earth's Upper Mantle is rarely capable of inspection on an extensive scale. Dredged samples or zenoliths demonstrate a mantle petrology within single mantle regions of oceanic lithosphere: these suites contain inherent diversity in themselves; small sample collections cannot be expected to be representative of the mantle as a whole. Each "new" study of such samples seems to create a "new" model of what the oceanic mantle is like. Samples that do not fit the "new" model are reconciled as somehow aberrant.

Among ophiolites, few mantle sections display such tectonic-lithic diversity as those within the mid-Jurassic Mesohellenic Ophiolite belt, extending ~500 km from Albania and through central Greece. Age dating of magmatic rocks show similar primary ages of ~168 – 170 my; ophiolitic soles are similar in ages (again, ~168 – 170 my) and in sole temperature-pressure environments (~ 700 - 900 ^{o}C and ~5 – 10 kb). Structural and geophysical studies demonstrate that these ophiolites are contiguous and continuous in the subsurface. Thus, the upper mantle sections are co-derived from the same oceanic lithospheric slab.

Throughout the Mesohellenic slab, the upper mantle is as internally diverse as is any geologic section forming on the earth's surface. As for surficial geology, full understanding of any section requires the viewpoints from a number of geologic disciplines: mantle descriptions must include interpretation of ductile deformation, geochemistry/petrology, and geotectonics as well as the coactivity between these fields. Within the Mesohellenic ophiolite belt, we have demonstrated that the extreme diversity of the mantle rocks within a single oceanic lithospheric slab results from variations in the following formative mechanisms:

--Strato-tectonic positioning and rotations with respect to location of spreading ridge, pro-transfer, and transform environment.

--Extensional lithospheric environment with respect to development and position of a subduction zone.

--Spreading and transfer rates.

--Evolving and overlapping fluid environments: Fluid sources from subduction zones, from oceanic hydrothermal circulation, from transform concurrent circulation.

--Coactive or lack of magmatism contemporaneous to the preceding mechanisms.

The coaction of provenance, erosion rate, and depositional conditions gives rise to thousands of stratigraphic indicators within sedimentary environments. The coaction of formative mechanisms that affect the upper mantle creates a similarly complex and internally diverse setting: none of the apparently disparate members of the Mesohellenic ophiolite belt can be considered "aberrant." Rather, homogenous upper mantle sections themselves must be categorized by the same coactivity as heterogeneous sections.

16th International Congress of the Geological Society of Greece
17-19 October, 2022 - Patras, Greece
Bulletin of the Geological Society of Greece, Sp. Publ. 10
Ext. Abs. GSG2022-077

Preliminary Study of Sepiolite Occurrences of East Corinth Gulf and their Morphological Characteristics

D. Nifora[1], B. Gkoka[1], I. Koukouvelas[1], P. Lampropoulou[1], D. Panagiotaras[2], D. Papoulis[1]

(1) Department of Geology, University of Patras, Rion, Greece, geo09097@upnet.gr (2) Department of Environment, Ionian University, Zakynthos, Greece

Research Highlights

Sepiolite occurrences within fault zones provide significant information about the mineral's forming conditions.

Introduction

Sepiolite is a hydrous magnesium silicate with an ideal structural formula of $Mg_4Si_6O_{15}(OH)_2 \cdot 6H_2O$. Belonging to the same group mineral as palygorskite, sepiolite has a fibrous morphology due to its forming conditions and 2:1-unit layers. Even though it is considered to be an authigenic clay, a diagenetic transformation from smectite or illite, also sometimes from chlorite, (Murray et al., 2011) at alkaline pH (10,5-11,5) as well as the Si/Mg ratio can significantly benefit the presence of sepiolite (Ece, 1998). Deposits have been found in continental-lacustrine and marine environments, in continental soils, and in association with igneous rocks (Jones et al., 1988).

Each deposit has its own sepiolite crystal fibre morphology and textural characteristics due to the conditions of their formation (Garcia-Romero et al., 2013). Based on the structure, fibres can be categorized into laths, rods, and bundles (Singer, 1981). By the term lath, we refer to the smallest unit that can be observed under the microscope, rod is the number of laths in the crystal matrix and bundle is the formation of several rods (Singer, 1981).

In the present work, sepiolite outcrops from the broader area of Corinth, Greece were studied to assess in an initial phase its origin and morphological features. The results obtained via Electron Microscopy can provide valuable information on the mineral's physical and chemical properties, thus its forming conditions.

Geological Setting

The sepiolite occurrences in NE Peloponnese appear within Pliocene primarly malrs, with intercalations of sandstones, conglomerates, and marly limestones accumulated on top of the Sub-Pelagonian complex nappe. The Pliocene formations are affected by the presence of major faults occurring in the greater Solomos region. This sequence is deposited in brackish to lacustrine environments (Papoulis et al., 2018).

Materials and Methods

Clay samples were collected from several fault cores and fault damage zones of the area of interest as well as the wider region. The samples have been characterized through X-Ray diffraction (Bruker D8 Advance equipped with Cu-Kα radiation and Nickel filter) in order to identify the mineralogical phases and purity of each sample. Scanning Electron Microscopy (SEM) and Transmission Electron Microscopy (TEM) were conducted to assess sepiolite morphology (length, width, and curl of the fibres) and also its microtextural (arrangement of fibres) features.

Results and Conclusions

The results obtained from X-Ray diffraction showed that in the fault cores prevails the mineralogical paragenesis of sepiolite, quartz, calcite, dolomite, and chlorite, whereas in the wider region the paragenesis of smectite coexisting with sepiolite, illite, quartz, calcite, and dolomite was detected. In only a small number of samples, the presence of tremolite with smectite, serpentine, or chlorite was identified. Sepiolite and smectite are the prevailed clay minerals in the studied area, leading to the conclusion that there is a correlation between these two minerals.

SEM analysis demonstrates sepiolite fibres of different sizes, shapes, and types of aggregations. A representative SEM image is given in Fig 1. Sepiolite has formed a complex structure of rods and bundles. The length of each fibre varies, ranging from 1μm to 10nm. Furthermore, the fibre's width reaches up to 30nm. Concerning the fibre's shape, it can be completely straight or curly. The aforementioned observations can also be confirmed by TEM analysis. Additionally, all sepiolite samples have the same microtextural features, concluding that they have formed in the same paleoclimatic conditions.

In a variety of samples, sepiolite fibres are intercalated within smectite layers. Taking into account this intercalation and the absence of smectite within the fault cores, it is indicated that smectite has been replaced by sepiolite, hence smectite could be the parent mineral of sepiolite.

Based on the geological background and the results from Electron Microscopy, they could have been three possible scenarios for the presence of sepiolite within the fault zones. Either hydrothermal conditions have prevailed, or sepiolite

was formed due to the presence of Mg-rich solutions in close proximity to dolomites in the area or formed by smectite and transferred from a greater depth close to the surface very probably during seismic activity and fluid flow circulation. Nevertheless, to obtain a better understanding of the forming conditions of sepiolite, further techniques should be applied.

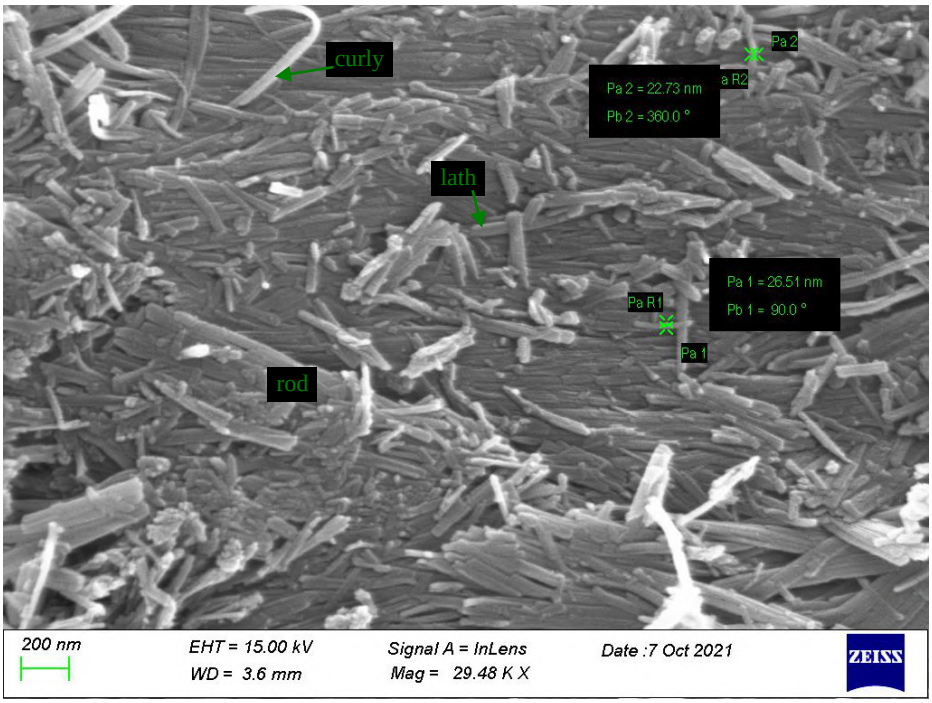

Figure 1. SEM photomicrograph of a representative sepiolite sample, depicting the fibres width, shape and type of structure.

References

Ece, O.I., 1998. Diagenetic transformation of magnesite pebbles and cobbles to sepiolite (Meerschaum) in the Miocene Eskisehir lacustrine basin, Turkey. Clays and Clay Minerals. 46, 436–445.

Garcia-Romero, E., Suarez, M., 2013. Sepiolite-palygorskite: Textural study and genetic considerations. Applied Clay Science. 86, 129-144.

Jones, B.F., Galan, E., 1988. Sepiolite and palygorskite, in: Bailey, S.W., (Eds.), Reviews in Mineralogy. Hydrous Phyllosilicates (Exclusive of Micas), 631_674.

Murray, H.H., Pozo, M., Galan, E., 2011. An introduction to palygorskite and sepiolite deposits-location, geology, and uses, in: Singer, A., Galan, E. (Eds.), Developments in Palygorskite and Sepiolite Research. A New Outlook on These Nanomaterials, 85–99.

Papoulis, D., Panagiotaras, D., Tsigrou, P., Christoforidis, K.C., C. Petit, C., Apostolopoulou, A., Stathatos, E., Komarneni, S., Koukouvelas, I., 2018: Halloysite and sepiolite -TiO_2 nanocomposites: Synthesis characterization and photocatalytic activity in three aquatic wastes, Materials Science in Semiconductor Processing, 85, 1-8.

Singer, A., 1981: The texture of palygorskite from the Rift Valley, southern Israel. Clay Minerals. 16, 415-419.

16th International Congress of the Geological Society of Greece
17-19 October, 2022 - Patras, Greece
Bulletin of the Geological Society of Greece, Sp. Publ. 10
Ext. Abs. GSG2022-113

Preliminary petrological and mineralogical results from Miocene basaltic rocks of Chios Island

L. Kalantzi[1], V. Giamas[1], P. Koutsovitis[1], P. Petrounias[1], A. Sideridis[1,] T. Ntaflos[2]

(1) University of Patras, Department of Geology, Section of Earth Materials, Patras, Greece, up1065371@upnet.gr (2) University of Vienna, Department of Lithospheric Research, Althanstr. 14, Vienna, Austria

Introduction

The island of Chios is characterized by volumetric restricted occurrences of basaltic outcrops of Miocene age (Piromallo and Morelli, 2003), that document local lithospheric thinning in Aegean microplate (Pe-Piper et al., 2007). More specifically, the back arc extension was initiated at ~13 Ma (Le Pichon et al., 1981) due to the subduction of the African plate beneath Eurasian (Jolivet and Brun, 2010). Other research results (Pe-Piper et al., 1994) has shown that these rocks are associated with alkali basaltic volcanism that also appears in the western Anatolia region. According to the same studies these rocks were affected by variable alteration processes, however some localities seem to preserve their primary mineralogical and textural features that have only been slightly affected by metasomatism.

This study is focused on the Miocene basaltic volcanic rocks of Chios Island and attempts to i) investigate the mineralogy and the textural properties of the mineral constituents, ii) preliminary petrological assessments and iii) specify the geotectonic processes related to volcanism.

Sampling and analytical methods

Rocks samples were collected from Psaronas volcano that is located at the southern part of Chios Island. The collected samples were macroscopically classified taking into account their alteration degree. The least altered samples were crushed and pulverized. Whole-rock major and trace element results were obtained by XRF and laser ablation ICP-MS at the University of Utrecht. Petrographic observations were conducted through transmitted light optical microscopy (OM) and X-ray Diffractometry (XRD) at the Research Laboratory of Rocks and Minerals of the University of Patras. Mineral chemistry analyses were conducted with a CAMECA SX-100 wavelength-dispersive (WD) electron microprobe (EPMA) at the Department of Lithospheric Research of the University of Vienna.

Results and discussion

The examined samples predominantly consist of olivine, pyroxene, plagioclase (Figure 1). Petrographically they are fairly uniform, presenting mainly pilotachytic to hyalopilitic textures that typically contain from 10 up to 20 % anhedral to subhedral phenocrysts of olivine, clinopyroxene, orthopyroxene (Figure 2a). The groundmass form mostly of microlithic plagioclase, clinopyroxene crystals, Fe-Ti oxides and glass. Although alteration is restricted, there are minor cases where the growth of uralite and sericite has formed at the expense of clinopyroxene crystals and plagioclase groundmass respectively. However, no reaction rims were observed at the crystal rims.

Mineral chemistry analyses performed upon olivine (Figure 2b) reveal that the average composition of the crystals corresponds to the forsterite-rich endmember ($Fo_{78.94}$). Following the IMA nomenclature of (Morimoto, 1988), clinopyroxene is classified as augite (avg. $En_{48.07}Fs_{9.07}Wo_{41.76}$), whereas orthopyroxene as enstatite (avg. $En_{48.07}Fs_{9.07}Wo_{41.76}$). The Mg# values (Mg# = [Mg / (Mg + Fe) x 100]) are rather high (avg. 84.58) for the

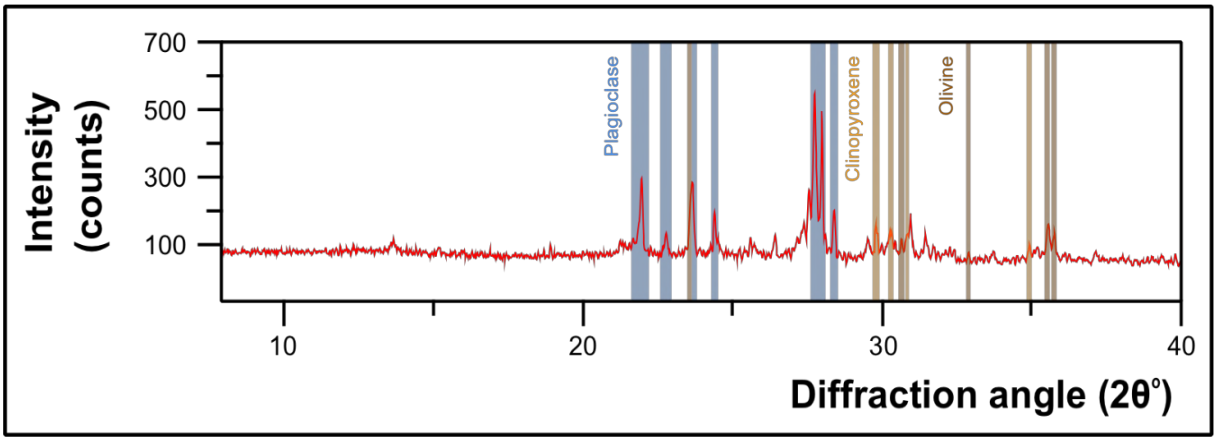

Figure 1: XRD pattern of a representative basaltic sample with major peaks of the participating mineral phases being highlighted.

clinopyroxene and moderate (avg. 74.15) for the orthopyroxene respectively. Microanalyses of feldspar matrix present intermediate composition mainly corresponding to labradorite (avg. $An_{63.52}$).

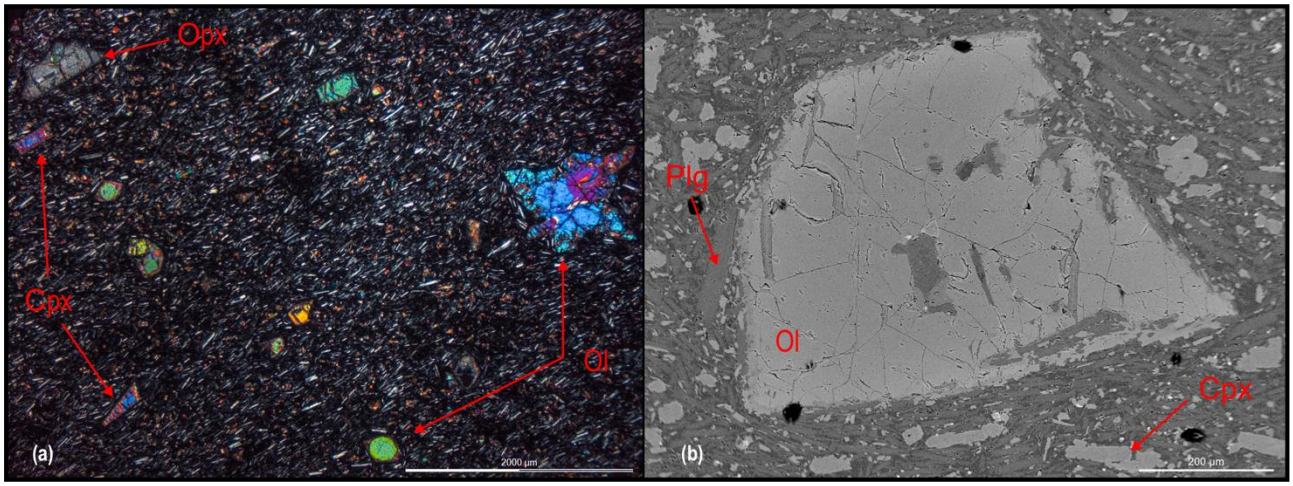

Figure 2: (a) Photomicrograph obtained through petrographic microscope under cross-polarized light. Phenocrysts of olivine (Ol) and clinopyroxene (Cpx) in an examined basaltic sample with pilotachytic groundmass. (b)Back-scattered EPMA image. Olivine phenocryst that does not display any significant zoning surrounded by matrix of plagioclase (Plg) and clinopyroxene.

Although major element geochemistry strongly suggests a classification of the examined samples regarded as andesite lithotypes, as formerly proposed by (Pe-Piper et al., 1994), there are petrographic and mineral chemistry insights suggesting that these may have a basaltic character. Moreover, microprobe results show that the phenocryst cores of olivine crystals display variability in their Fo content (Fo_{71-83}). These compositions correspond to olivine phenocrysts of magmatic origin, further confirmed by their relatively high Ca and low Ni contents. The clinopyroxene crystals are augites with Mg# ranging between 78 and 87; the range shows that the variation between core and rim compositions follows the normal fractionation trend and that some of the clinopyroxene grains may be present as xenocrysts. Orthopyroxene is enstatite with Mg# ranging between 66 and 83, values that mostly coincide with those of olivine and thus likely represent fractionation through differentiation. Also, some samples include a glassy matrix that represents a much more evolved melt than expected.

Due to the composition and variation of basaltic rocks of Chios, it seems that changes in the degrees of mantle melting likely played a significant role apart from the profound differentiation effects. Furthermore, geochemical results point to interaction with highly differentiated melts during ascending of magma to the surface. Trace element geochemistry along with geochronological data should also provide solid arguments on the volcanism and its age and further information regarding the processes and the tectonic setting of Chios.

References

Jolivet, L., Brun, J.-P., 2010. Cenozoic geodynamic evolution of the Aegean. International Journal of Earth Sciences 99, 109-138.

Le Pichon, X., Angelier, J., Osmaston, M.F., Stegena, L., Vine, F.J., Smith, A.G., 1981. The Aegean Sea. Philosophical Transactions of the Royal Society of London. Series A, Mathematical and Physical Sciences 300, 357-372.

Morimoto, N., 1988. Nomenclature of Pyroxenes. Mineralogy and Petrology 39, 55-76.

Pe-Piper, G., Piper, D.J.W., Beccaluva, L., Bianchini, G., Wilson, M., 2007. Neogene backarc volcanism of the Aegean: New insights into the relationship between magmatism and tectonics, Cenozoic Volcanism in the Mediterranean Area. Geological Society of America, p. 0.

Pe-Piper, G., Piper, D.J.W., Kotopouli, C.N., Panagos, A.G., 1994. Neogene volcanoes of Chios, Greece: the relative importance of subduction and back-arc extension. Geological Society, London, Special Publications 81, 213-231.

Piromallo, C., Morelli, A., 2003. P wave tomography of the mantle under the Alpine-Mediterranean area. Journal of Geophysical Research: Solid Earth 108.

16th International Congress of the Geological Society of Greece
17-19 October, 2022 - Patras, Greece
Bulletin of the Geological Society of Greece, Sp. Publ. 10
Ext. Abs. GSG2022-153

Preliminary analyses of lava samples from the Methana peninsula: Is there any correlation amongst volcanic eruption styles and 3D porphyric index?

V. Giamas[1], L. Kalantzi[1], P. Koutsovitis[1], P. Turberg[2], P. Petrounias[1], P. Lampropoulou[1]

(1) University of Patras (UoP), Department of Geology, Section of Earth Materials, Patras, Greece, vgiamas@upnet.gr
(2) *École Polytechnique Fédérale de Lausanne EPFL, School of Architecture, Civil and Environmental Engineering ENAC, Civil Engineering Institute IIC, Lausanne, Switzerland*

Introduction

X-ray micro–Computed Tomography (μCT) has been applied as a non-destructive technique that can reveal hidden information of the third dimension in several studies concerning various and distinctive in character geological samples (Aerden and Ruiz-Fuentes, 2020; Porfido et al., 2020; Turberg et al., 2014). Three-dimensional (3D) rock fabric analysis through μCT (Petri et al., 2020) can be efficiently performed either for the mineral phases or for the vesicles on both intrusive (Giamas et al., 2022) and extrusive igneous rocks (Voltolini et al., 2011). These parameters (i.e., size, shape, distribution, orientation) are information of significant importance in volcanology as well as in magmatic petrology since they can provide the main aspects of mineral constituents and magmatic gases. Furthermore, they provide insights regarding the established conditions of magma storage and transportation as well as the processes that led to magma crystallization. This study investigates the two major volcanic lithotypes present in the Methana peninsula aiming to correlate them with possible factors such as: i) crystallinity, ii) matrix formation, and iii) porosity volume fractions, in an attempt to specify how they can potentially affect the behavior of magma and the dynamics of gas transport.

Geological context – Analytical techniques

The subduction of the African plate beneath the Eurasian plate results in the formation of the Hellenic Volcanic Arc (HVA) along their convergent plate boundary. The present-day active HVA extends into the Aegean Sea building up from west to east by the Methana peninsula and the islands of Milos, Santorini, Kos, and Nisyros. Methana peninsula forms along with the islands of Aegina and Poros in the Saronic Gulf the western part of the HVA. The related volcanism in Methana volcanic field (MVF) is mainly characterized by calc-alkaline lavas of andesitic to dacitic composition with a general rather effusive character.

Lava samples were collected from all the domes and flows in the MVF. After macroscopic observations and categorization of all the collected samples, an andesite and a dacite were chosen to be further examined regarding their mineralogy through transmitted light optical microscopy (OM) and X-ray Diffractometry (XRD) at the Research Laboratory of Rocks and Minerals of the University of Patras (UoP). Both the two hand-sized lava samples were also analyzed at the School of Architecture, Civil and Environmental Engineering (ENAC) Platform for X-ray micro-tomography (PIXE) of the Swiss Federal Institute of Technology in Lausanne (EPFL).

Results and discussion

OM has revealed that both lava samples present hypocrystalline and inequigranular textures with plagioclase, hornblende, and biotite phenocrysts, along with micro phenocrysts of plagioclase as well as accessory oxide minerals, in a fine and glassy matrix. Minor quartz, clinopyroxene, and olivine have also been identified through XRD (Figure 1) in the andesitic sample suggesting magma mixing conditions. Although the state-of-the-art petrographic examination can reveal specific features: i) textural; such as mineral zoning, disequilibrium, reaction amongst mineral phases, and ii) mineralogical; such as the presence or absence of specific minerals, it encounters difficulties in robust quantification of the modal composition. Thin section randomness, restricted examined dimensions, non-continuous information, and variable mineral grain sizes

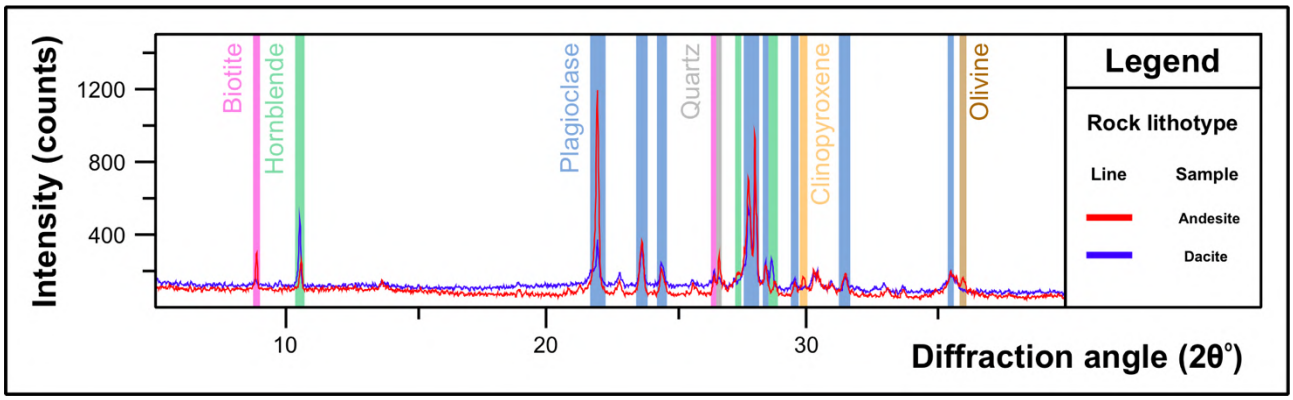

Figure 1: XRD profile patterns of the two lava samples with major peaks of the participating mineral phases being highlighted.

can be some of the major causes of inaccurate quantification calculations that all fall within a common statistic error that can be described by the known stereological bias (Giamas et al., 2022; Lätti and Adair, 2001). On the contrary, the X-ray micro-computed tomography (μCT) technique can overcome all the aforementioned limitations through the visualization in a continuous manner of the mineral constituents of a rock sample (Voltolini et al., 2011). Several recent studies have attempted to correlate the Porphyric Index and the porosity properties with a volcanic eruption (e.g., effusive, or explosive) and more importantly with eruption style (Cassidy et al., 2018; Popa et al., 2020; Wall et al., 2014). Examined sub-volumes of both lava samples demonstrate that the crystallinity of the mafic mineral group ranges between 10 to 20 vol%, whereas for the group of the high-density oxides it is typically lower than 0.5 vol%. Noteworthy is the porosity volume that may reach up to ~5 vol% which is attributed to the presence of multiple micropores and not to large vesicles. Concluding, μCT will provide a more comprehensive view regarding porphyric index and porosity in such heterogeneous lava samples and thus unravel the processes and the controls of both magma behavior and gas transport. This study will continue to evaluate the potential of the 3D porphyric index in providing data on volcanic eruption styles.

Acknowledgments

The present work was financially supported by the «Andreas Mentzelopoulos Foundation» as part of Mr. Vasileios Giamas Ph.D. research.

References

Aerden, D.G.A.M., Ruiz-Fuentes, A., 2020. X-ray computed micro-tomography of spiral garnets: A new test of how they form. Journal of Structural Geology 136, 104054.

Cassidy, M., Manga, M., Cashman, K., Bachmann, O., 2018. Controls on explosive-effusive volcanic eruption styles. Nature Communications 9, 2839.

Giamas, V., Koutsovitis, P., Sideridis, A., Turberg, P., Grammatikopoulos, T.A., Petrounias, P., Giannakopoulou, P.P., Koukouzas, N., Hatzipanagiotou, K., 2022. Effectiveness of X-ray micro-CT applications upon mafic and ultramafic ophiolitic rocks. Micron 158, 103292.

Lätti, D., Adair, B.J.I., 2001. An assessment of stereological adjustment procedures. Minerals Engineering 14, 1579-1587.

Petri, B., Almqvist, B.S.G., Pistone, M., 2020. 3D rock fabric analysis using micro-tomography: An introduction to the open-source TomoFab MATLAB code. Computers & Geosciences 138, 104444.

Popa, R.-G., Dietrich, V.J., Bachmann, O., 2020. Effusive-explosive transitions of water-undersaturated magmas. The case study of Methana Volcano, South Aegean Arc. Journal of Volcanology and Geothermal Research 399, 106884.

Porfido, C., Manzari, P., Allegretta, I., Terzano, R., De Pascale, O., Senesi, G.S., 2020. Combined micro X-ray fluorescence and micro computed tomography for the study of extraterrestrial volcanic rocks. The case of North West Africa (NWA) 8657: A shergottite martian meteorite. Talanta 217, 121114.

Turberg, P., Zeimetz, F., Grondin, Y., Elandoy, C., Buttler, A., 2014. Characterization of structural disturbances in peats by X-ray CT-based density determinations. European Journal of Soil Science 65, 613-624.

Voltolini, M., Zandomeneghi, D., Mancini, L., Polacci, M., 2011. Texture analysis of volcanic rock samples: Quantitative study of crystals and vesicles shape preferred orientation from X-ray microtomography data. Journal of Volcanology and Geothermal Research 202, 83-95.

Wall, K.T., Rowe, M.C., Ellis, B.S., Schmidt, M.E., Eccles, J.D., 2014. Determining volcanic eruption styles on Earth and Mars from crystallinity measurements. Nature Communications 5, 5090.

16th International Congress of the Geological Society of Greece

17-19 October, 2022 - Patras, Greece

Bulletin of the Geological Society of Greece, Sp. Publ. 10

Ext. Abs. GSG2022-172

The 2021 eruption in La Palma Island (Canary Islands, Spain): Volcano monitoring and crisis management conducting to a zero fatalities urban eruption.

S. Meletlidis[1], IGN Volcano Monitoring Group[2], Directorate-General of Security and Emergencies of Canary Government[3]

(1) Centro Geofísico de Canarias del IGN, Santa Cruz de Tenerife, Spain, smeletlidis@mitma.es (2) Instituto Geográfico Nacional, Madrid - Santa Cruz de Tenerife, Spain (3) Gobierno de Canarias, Las Palmas de Gran Canaria – Santa Cruz de Tenerife, Spain

The Canarian Archipelago, located along the NW margin of Africa, shows intraplate magmatism attributed to a hot spot mechanism, governed by region geodynamics. The eruptive processes were developed for more than 20 million years and in the last 500 years we had 16 eruptions, all of them being basaltic. Prior to 2021, the last two eruptions in the archipelago took place, in El Hierro Island (submarine eruption of 2011) and La Palma Island (subaerial eruption of 1971).

On 11 September 2021, the monitoring network of Instituto Geográfico Nacional (IGN) started to record an intense seismic swarm under the island and Civil Protection was alerted. In the next 5 days, the seismic energy increased and deformation patterns were detected. The day before the eruption, the habitants nearby the possible affected area were informed, and 5 hours before the onset of the eruption, an evacuation was ordered. In the first 48h of the unusual seismic activity a special Civil Protection plan concerning the volcano risk, namely PEVOLCA, was activated by the Canary Government.

On 19 September 2021, an eruption began on the island of La Palma, which lasted 85 days, until 13 December 2021. It began as a fissural one, and in less than 3 months, emitted lavas that covered a surface of >12 km2, with a bulk thickness of 12m and generated new lava deltas. The ash layer at a distance of 2 km exceeded 1m. The eruptive style was mainly effusive, with phases of moderate Strombolian explosions. Lava flows destroyed thousands of edifices, infrastructures, communication networks and extensive areas of farmlands and greenhouses, greatly affecting the local economy. Two evacuations were carried out and no casualties were reported.

The Canarian Government successfully manage the crisis through the Scientific Committee and the Steering Committee of PEVOLCA. This plan is still active (as of 31st august, 2022).

Figure 1. Researchers of IGN installing a thermal camara nearby the active cone

16th International Congress of the Geological Society of Greece
17-19 October, 2022 - Patras, Greece
Bulletin of the Geological Society of Greece, Sp. Publ. 10
Ext. Abs. GSG2022-173

Implications of Chromitites of Veria-Naousa Ophiolite (North Greece): Petrographic and Mineralogical Characteristics

A. Rogkala[1], P. Petrounias[1], P. P. Giannakopoulou[1], P. Pomonis[2], P. Koutsovitis[1], P. Lampropoulou[1], K. Hatzipanagiotou[1]

(1) University of Patras, Department of Geology, GR-26504, Rio Patras, Greece, katerinarogkala@gmail.com (2) Department of Geology and Geoenvironment, National and Kapodistrian University of Athens, Panepistimioupolis Zografou, GR-15784 Athens, Greece

Introduction

Chromitites and residual mantle peridotite in ophiolites are used as indicators of the tectonic setting in which they formed. Chromitites form in the depleted mantle sections of ophiolites in supra-subduction zone (SSZ) environments due to melt-rock interactions (Uysal *et al.*, 2012). They are commonly found in the lower part of the crustal section and within or below the 'petrologic Moho'. They hosted in the mantle section of ophiolites are known as podiform bodies, while are rarely podiform in shape, but have various morphologies (dikes, lenses, layers). The tectonic settings of podiform chromitites are related with chromitites compositions. Chromite chemistry could provide clear insights of the geochemical features of those mantle peridotites as well as chromite major elements can estimate the compositions of magmas from which they crystallised and reveal the genesis of chromitites (Zhou *et al.*, 2014). In these study, we present new petrographic data and magnesiochromite composition of Veria-Naousa chromitite in order to investigate their genesis and provide constraints for their nature and origin.

Geological setting

The Veria-Naousa ophiolitic complex is a dismembered suite, which extends between Veria and Naousa towns and belongs to the Almopias subzone of the Axios geotectonic zone. These oceanic remnants have been obducted onto Late Triassic-Jurassic platform carbonates of the Pelagonian Zone during the Upper Jurassic to Lower Cretaceous. The ophiolite consists, from base to top, of serpentinized harzburgite with subordinate lherzolite, intruded by pyroxenitic dikes, as well as gabbro, diabase and pillow basalt (Rogkala *et al.*, 2017). Moderately lherzolite is an infrequent, medium-grained rock, which is characterised by greenish black to dark green colour and conchoidal fracture. It occurs as relic, irregular bodies up to a few meters, surrounded by serpentinised harzburgite. Locally, the serpentinised harzburgite encloses lenses, pods or elongated bodies (up to few meters) of chromitite, which according to their texture and mode of occurrence, are classified as massive and disseminated podiform bodies.

Analytical methods

The mineralogical and textural characteristics of the samples were studied in polished-thin sections in optical and scanning electron microscopes (SEM). Mineral microanalyses were performed using a JEOL JSM-6300 SEM equipped with energy dispersive (EDS) and INCA software at the Laboratory of Electron Microscopy and Microanalysis, University of Patras. Operating conditions were accelerating voltage 25 kV and beam current 3.3 nA, with a 4 μm beam diameter. The total counting time was 60 s and dead-time 40%. Synthetic oxides and natural minerals were used as standards for our analyses. Detection limits are ~0.1% and accuracy better than 5% was obtained.

Petrographic features

Based on petrographic observations, two types of chromitite can be identified in the Veria-Naousa ophiolite. Massive and disseminated chromitites are primary structural types of chromitites. They are fractured and locally show cataclastic texture (Fig. 1).

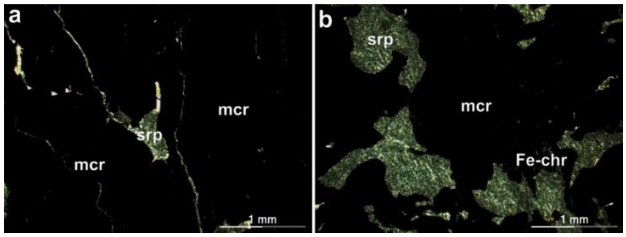

Figure 1. Photomicrographs of chromitite from Veria-Naousa ophiolite showing: a) Massive chromite (sample BE.57, + Nicols); b) Disseminated chromitite, where the interstitial areas are filled by serpentine (sample BE.158, + Nicols). Abbreviations: mcr: magnesiochromite, srp: serpentine, Fe-chr: ferritchromit.

The massive chromitites consist of magnesiochromite (~98%), serpentine and minor Cr-chlorite. Magnesiochromite crystals are anhedral to subhedral and uniform in size (2-5 mm). Disseminated chromitites are also composed of

magnesiochromite (74-85%), serpentine and Cr-chlorite (Fig. 1). Magnesiochromite crystals are subhedral to euhedral with smaller sizes (1-2 mm), unevenly distributed within the serpentine matrix. Serpentine displays mesh and less frequently interpenetrating texture. Cr-chlorite all cases surrounds the magnesiochromite or is enclosed in the magnesiochromite grains, and its mode abundance is variable. Inclusions in magnesiochromite are observed, including serpentine, Cr-chlorite and sulphides (millerite and galena). Magnesiochromite is commonly altered to ferritchromit along fractures (Fig. 1b).

Magnesiochromite and parental melt compositions

Magnesiochromites occur as primary grains in chromitites. They are characterised by relatively high Cr# [=100*Cr/(Cr+Al); avg.75.5] and Mg# [=100*Mg/(Mg+Fe^{2+}); avg. 67.3] contents, as well as lower abundances of certain trace elements (e.g. Ti, V). In Figure 2 magnesiochromites plot in the boninitic composition field.

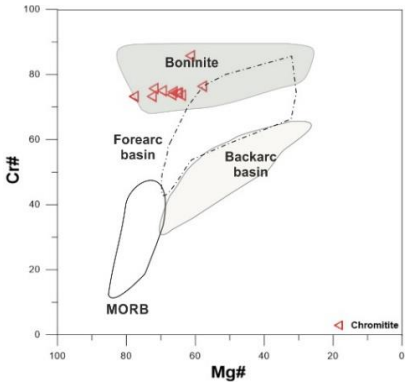

Figure 2. Compositional variations of magnesiochromite from Veria-Naousa chromitite in a Cr# vs. Mg# diagram. Compositional fields for magnesiochromite in boninite (Barnes & Roeder, 2001), forearc peridotite, backarc peridotite, and abyssal peridotite (Dick & Bullen, 1984) are shown for comparison.

Magnesiochromite can be used to compute chromitite parental melt composition applying the empirical formulae suggested by Maurel & Maurel (1982):

$$Al_2O_{3magnesiochromite}=0.035(Al_2O_3)^{2.42}_{melt} \quad (1)$$

$$\ln(FeO/MgO)_{magnesiochromite}=0.47-1.07(Al\#_{magnesiochromite})+0.64(Fe^{3+}{}_{magnesiochromite}) + \ln(FeO/MgO)_{melt} \quad (2)$$

Implications of equation (1) and equation (2) shows that the parental melt had 9.8-12.0 wt% Al_2O_3 and FeO/MgO ratios varying from 0.7 to 0.9. Our results indicate that chromitites crystallised from parental melts of high-Cr chromitites from elsewhere and comparable with those of boninites. The calculated Al_2O_3 contents and FeO/MgO ratios are consistent with boninitic compositions in parental melts, which commonly range from 10 to 14% and from 0.5 to 0.8, respectively (Dilek *et al.*, 2008). To conclude, the petrographic characteristics of chromitite and the mineralogical compositions of magnesiochromite are in favour of an arc environment for the Veria-Naousa chromitite. It is recommended that the evolution of the Veria-Naousa chromitite record the evolution of the subarc region in a broad SSZ setting from boninitic magmas in the Axios Zone of eastern Greece.

Acknowledgements

The authors kindly thank Dr. A.K. Seferlis of the Laboratory of Electron Microscopy and Microanalysis, University of Patras for his assistance with the microanalyses and SEM micrographs. We also thank M. Kalpogiannaki for her assistance with the construction of the geological map.

References

Barnes, S.J., Roeder, P.L., 2001. The range of spinel compositions in terrestrial mafic and ultramafic rocks. Journal of Petrology 42, 2279-2302.

Dick, H.J.B., Bullen, T., 1984. Chromian spinel as a petrogenetic indicator in abyssal peridotites and spatially associated lavas. Contributions to Mineralogy and Petrology 86, 54-76.

Dilek, Y., Shallo, M., Furnes, H., 2008. Geochemistry of the Jurassic Midiata Ophiolite (Abania) and the MORB to SSZ evolution of a marginal basin oceanic crust. Lithos 100, 174-209.

Maurel, C., Maurel, P., 1982. Étude experimentale de la distribution de l' aluminium entre bain silicate basique et spinelle chromifère. Implications pétrogénétiques: teneur en chrome des spinelles. Bullentin de Minéralogie 105, 197-202.

Rogkala, A., Petrounias, P., Tsikouras, V., Hatzipanagiotou, K., 2017. New occurrence of pyroxenites in the Veria-Naousa ophiolite (north Greece): Implications on their origin and petrogenetic evolution. Geosciences 7 (4), 92.

Uysal, I., Ersoy, E.Y., Karsli, O., Dilek, Y., Burthan Sadiklar, M., Ottley, C.J., Tiepolo, M., Meisel, T., 2012. Coexistence of abyssal and ultra-depleted SSZ type mantle peridotites in a neo-Tethyan ophiolite in SW Turkey: constraints from mineral composition, whole-rock geochemistry (major-rare-REE-PGE), and Re-Os isotope systematics. Lithos 132-133, 50-69.

Zhou, M.F., Robinson, P.T., Su, B.X., Gao, J.F., Li, J.W., Yang, J.S., Malpas, J., 2014. Compositions of chromite, associated minerals, and parental magmas of podiform chromite deposits: the role of slab contamination of asthenospheric melts in supra-subduction zone environments. Gondwana Research 26 (1), 262-283.

16th International Congress of the Geological Society of Greece
17-19 October, 2022 - Patras, Greece
Bulletin of the Geological Society of Greece, Sp. Publ. 10
Ext. Abs. GSG2022-203

A petrological approach on the occurrence of metasomatised alkali basaltic rocks in the region of Chronia, Evia island, Greece

M. Karalis[1], P. Koutsovitis[1], K. Lilis[1] A. Sideridis[1], C. Karkalis[2], H. Tsikos[1], I. Iliopoulos[1]
(1) University of Patras, Department of Geology, Section of Earth Materials, GR-26504 Patras, Greece, (up1056039@upnet.gr) (2) Centre for Research and Technology-Hellas (CERTH), Marousi, Attica, Greece

1. Background

Hellenic rift-related volcanism occurred mainly during two different geological eras that include the Middle-Upper Triassic and the Late Miocene (~11 Ma) to Pleistocene period. The Triassic volcanism is characterized by relatively abundant productivity, whereas the Cenozoic alkaline basaltic activity producing scattered and volumetrically limited eruptions (e.g. Volos, Patmos, Samos, Psathoura, and Chios). In both cases the volcanic rocks in their vast majority correspond to trachybasalts, exhibiting in most cases a mixed OIB geochemical imprint with an additional subduction related signature (Pe-Piper and Piper, 2002). On the other hand, Triassic alkali volcanism is the result of rift-related processes, associated with the extension of Gondwana's northeast margin, leading to the formation of the Pindos oceanic basin under fast spreading conditions (Koutsovitis et al. 2020); depending on their geochemistry they are distinguished as OIB and E-MORB lavas. They are recognized in Pindos, Koziakas, Othris, Central Greece, Argolis, Samos island and Evia. Particularly in Evia, basaltic rocks are currently exposed in the region of Chronia-Limni, occuring in the form of rather restricted outcrops, since they are partially overlain by marly sediments of the Early Pliocene. These rock types have mineralogical, textural and geochemical similarities to alkali basalts of localities in Central Evia (e.g. Danelian and Robertson, 2001).

2. Aims and Objectives

We aim to report on the occurrence of alkali basaltic rocks in the region of Chronia (Evia island, Greece), as well as to

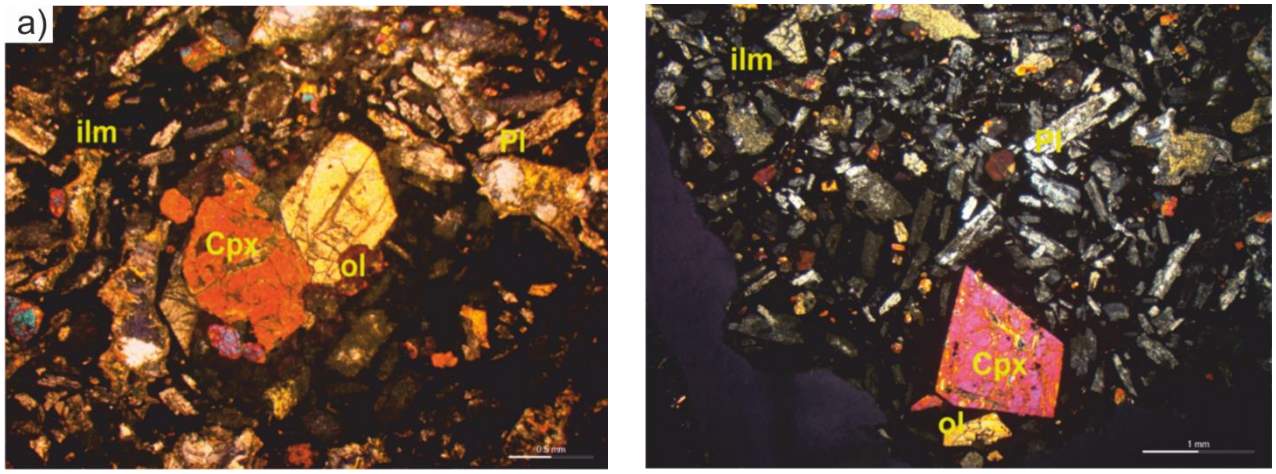

Figure 1: Representative photomicrographs (XP) of alkali basalt samples consisting of a) clinopyroxene (cpx) cumulates, olivine (ol), plagioclase (pl), ilmenite (ilm), b) euhedral clinopyroxene (cpx), olivine (ol), plagioclase (pl), ilmenite (ilm) in devitified glassy matrix

followed: a) Field work emphasized on the alkali basalts outcrop, b) Detailed petrography, c) Mineralogical analyses, d) Bulk rock chemical analyses, e) Data processing, f) Results synthesis.

3. Results and Discussion

The mineralogical primary modal composition of the alkali basalts comprises clinopyroxenes, relict plagioclases (andesine), devitrified glass, Fe-Ti oxides (ilmenite, Ti-magnetite). Secondary metasomatic phases resulted from ocean-floor alteration and include albite (partly serecitized), chlorite (mainly pycnochlorite and diabantite), epidote, pumpellyite, calcite, and serpentine (replacing olivine) (Fig1a,b). Petrographic textural features display variolitic, pilotaxic, porphyritic to glomerophyric textures between clinopyroxene and plagioclase crystals. The matrix consists of microphenocrysts of clinopyroxene and accumulates of plagioclase laths, which encompass phenocrysts of granular clinopyroxene and tabular plagioclase ; these are accompanied by interstitial alkali feldspar, partly devitrified glass and Fe-Ti oxide needles (mainly ilmenite). An interesting feature of these basalts is that they include relatively large and euhedral clinopyroxene grains (Fig. 1), that seem to resemble grains that formed after accumulation. Secondary minerals are not found exclusively within the matrix but are also present as relatively large sized crystals (calcite, chlorite, epidote/pumpellyite) filling amygdulitic vesicles. Clinopyroxene mineral chemistry is characterized by displaying high Mg# (up to ~86.0 wt.%), enriched Al and especially Ti contents; the phenocrysts are mainly classified as augite and were not subjected to significant alteration processes. Clinopyroxenes with the highest Ti and Al contents are found within the groundmass.

Based on the bulk rock geochemistry, the rocks are classified mainly as trachybasalts but also as basaltic trachyandesites (based on the TAS classification). The LOI contents are rather enhanced but dot not exceed ~3.3 wt.%; which is related to the moderate effects of metasomatism. SiO_2 values characterized as relatively low, FeO values as high, whereas the CaO and MgO values are rather moderate for alkali basalts. The same applies for Cr and Ni, with the highest values noticed in the least differentiated samples. Their silica-saturation index (S.I.; Fitton et al., 1991) values fluctuates from −12.1 to −8.9 suggesting that these lithotypes range from primitive undersaturated to moderately differentiated basalts.

The Ti/Al ratio of clinopyroxenes within basaltic lavas is regarded as a qualitative indicator to evaluate modifications in pressure conditions during crystallization (e.g. Ali and Ntaflos, 2011). The Ti/Al ratios measured in clinopyroxene grains range between 0.125 and 0.25, suggesting that initial and final crystallization conditions remained rather constant and crystallization occurred under rather enhanced pressure conditions. This estimation is further confirmed by their moderate to high Al^{VI}/Al^{IV}ratios (>0.5). To further assess the depths of magma segregation we calculated the pressure conditions during magma segregation of up to 2.3 GPa (~75 km depth), through the application of the Scarrow and Cox, (1995) pressure formula. These estimations are even higher than those determined for the generation of the vast majority of the Hellenic Triassic E-MORB lavas (Koutsovitis et al. 2020).

References

Ali, S., Ntaflos, T., 2011. Alkali basalts from Burgenland, Austria: Petrological constraints on the origin of the westernmost magmatism in the Carpathian–Pannonian Region. Lithos 121, 176–188.

Danelian, T., Robertson, A.H.F., 2001. Neotethyan evolution of eastern Greece (Pagondas Mélange, Evia island) inferred from radiolarian biostratigraphy and the geochemistry of associated extrusive rocks. Geol. Mag. 138, 345–363.

Fitton, J.G., James, D., Leeman, W.P., 1991. Basic magmatism associated with late Cenozoic extension in the Western United States compositional variations in space and time. J. Geophys. Res. 96, 13693–13711.

Koutsovitis, P., Magganas, A., Ntaflos, T., Kouzoukas, N., Rassios, A., Soukis, K., 2020. Petrogenetic constraints on the origin and formation of the Hellenic Triassic rift-related lavas. Lithos 368–369, 105604.

Pe-Piper, G., Piper, D.J.W., 2002. The Igneous Rocks of Greece. Borntraeger, Stuttgart, pp. 1–645.

16th International Congress of the Geological Society of Greece
17-19 October, 2022 - Patras, Greece
Bulletin of the Geological Society of Greece, Sp. Publ. 10
Ext. Abs. GSG2022-210

Metamorphic *versus* primary features recorded in chromitites of the East Chalkidiki meta-ultramafic bodies, Gomati and Nea Roda, Northern Greece

A. Sideridis[1], B. Tsikouras[2], P. Tsitsanis[3], P. Koutsovitis[1], F. Zaccarini[2], C. Hauzenberger[4], H. Tsikos[1]*, Konstantin Hatzipanagiotou[1]

(1) Department of Geology, Section of Earth Materials, University of Patras, 265 00 Patras, Greece, a.sideridis@upnet.gr, (2) Faculty of Science, Geosciences Programme, Universiti Brunei Darussalam, Gadong BE 1410, Brunei Darussalam, (3) Independent Researcher, Makedonias 21, 63200 Nea Moudania, Greece, (4) NAWI Graz Geocenter, University of Graz, Universitätsplatz 2, Graz 8010, Austria

Abstract

The meta-ultramafic bodies of Gomati and Nea Roda, e. Chalkidiki, are part of the Serbomacedonian Massif, which is considered an extension of the Rhodope Massif which also includes meta-ultramafic and mafic occurrences. Podiform chromitites in the East Chalkidiki have undergone metamorphism and their host rocks are pervasively serpentinized. Chromitites are widely used as petrogenetic tools to unravel the settings under which they have formed and which have subsequently affected the mantle section. Likewise, various alternating/metasomatic processes can also be studied focusing on chromitites while focusing on their mineralogy and geochemistry. Under this scope, it is important to specify primary and secondary mineralogical and chemical features in order to answer to the following questions: a) under what settings have the East Chalkidiki chromitites were generated and b) under what settings and conditions have they been modified. The answer in those questions will offer insights in the general geotectonic evolution of the Serbomacedonian Massif.

Electron microprobe (Eugen F. Stumpfl Laboratory of the Leoben University, Austria, using a Superpobe Jeol JXA 8200) and LA-ICP-MS analyses (system at the NAWI Graz Central Lab for Water, Minerals and Rocks) were conducted mainly upon spinel-group minerals. Focus was given in secondary mineral phases such as chlorite, diopside, garnet, platinum-group minerals (PGM) to further assist the interpretations. The mantle section of e. Chalkidiki hosts both Al-rich and Cr-rich chromitites. Using the normalized trace element patterns of the spinel-group minerals, the primary core was distinguished from the metamorphic rims. The main chemical differences include increase in Ti, Zn, Co, Mn during metamorphism, and those abundances point to a peak of amphibolite facies. In the pristine cores, the included PGM are primary, whereas desulphurized and zoned PGM are included in modified spinel. Garnet and chlorite were crystallized during greenschist facies, as their chemistry implies. Secondary diopside hosted in chromitite and diopsidite demonstrate subduction features (LA-ICP-MS) and this is in agreement with the serpentinite geochemistry (ICP-MS).

The platinum-group element (PGE) abundances (Instrumental Neutron Activation Analysis) of chromitites have been preserved and increase in Pd/Ir ratios in some cases are attributed to fractionation, with the main mechanism for chromitite formation being the partial melting that the mantle source has underwent. The spinel grains of the Al-rich chromitites demonstrate flat normalized trace element profiles typical of back-arc chromitites, whereas chromite from the Cr-rich chromitites demonstrate patterns related with supra subduction zone (SSZ) settings. Similar environments have been described for the chromitite occurrences of the Rhodope Massif (Colás et al., 2014; González-Jiménez et al., 2015). After their formation the ultramafic section along with the chromitites were introduced into a subduction zoned reaching amphibolite facies that were later-on overprinted by greenschist facies. These events have also been recorded upon the meta-pellitic rocks of the Serbomacedonian Massif (Kydonakis et al., 2014; Siron et al., 2018). These results point to common settings being responsible for the formation and modification of both the chromitites of Serbomacedonian and the Rhodope Massifs.

Acknowledgements

This research work was supported by the Hellenic Foundation for Research and Innovation (HFRI) under the HFRI PhD Fellowship grant (Fellowship Number: 1616). The University Centrum for Applied Geosciences (UCAG) is thanked for offering access to the Eugen F. Stumpfl electron microprobe Laboratory. Erasmus+ for traineeships is also thanked for providing the opportunity to A. Sideridis to perform analyses at the Eugen F. Stumpfl Electron Microprobe Laboratory and LA-ICP-MS facility at the NAWI Graz Central Lab for Water, Minerals and Rocks. SGS Mineral Services (Canada) and Dr. Tassos Grammatikopoulos are thanked for performing the chromitite concentrates. Prof. Dr. Luca Bindi is thanked for his contribution to the identification of the Ni grain enriched in phosphorous.

References

Colás, V., González-Jiménez, J. M., Griffin, W. L., Fanlo, I., Gervilla, F., O'Reilly, S. Y., et al. (2014). Fingerprints of metamorphism in chromite: New insights from minor and trace elements. *Chem. Geol.* 389, 137–152. doi: 10.1016/j.chemgeo.2014.10.001.

González-Jiménez, J. M., Locmelis, M., Belousova, E., Griffin, W. L., Gervilla, F., Kerestedjian, T. N., et al. (2015). Genesis and tectonic implications of podiform chromitites in the metamorphosed ultramafic massif of Dobromirtsi (Bulgaria). *Gondwana*

Res. 27, 555–574. doi: 10.1016/j.gr.2013.09.020.

Kydonakis, K., Gallagher, K., Brun, J.-P., Jolivet, M., Gueydan, F., and Kostopoulos, D. (2014). Upper Cretaceous exhumation of the western Rhodope Metamorphic Province (Chalkidiki Peninsula, northern Greece). *Tectonics* 33, 1113–1132. doi: 10.1002/2014TC003572.

Siron, C. R., Rhys, D., Thompson, J. F. H., Baker, T., Veligrakis, T., Camacho, A., et al. (2018). Structural controls on porphyry Au-Cu and Au-rich polymetallic Carbonate-hosted replacement deposits of the Kassandra mining District, Northern Greece. *Econ. Geol.* 113, 309–345. doi: 10.5382/econgeo.2018.4552.

16th International Congress of the Geological Society of Greece

17-19 October, 2022 - Patras, Greece

Bulletin of the Geological Society of Greece, Sp. Publ. 10

Ext. Abs. GSG2022-214

High-Pressure Ion-Irradiation Platform at GSI: Minerals under Multiple Extreme Conditions

I. Tzifas[1], K. Voss[1], M.E. Toimil-Molares[1], M. Lang[2], Ch. Schröck[1,3], C. Trautmann[1,4]

(1) GSI Helmholtzzentrum für Schwerionenforschung, Darmstadt, Germany (i.tzifas@gsi.de) (2) University of Tennessee, Knoxville, Tennessee, U.S.A. (3) Institute of Geosciences, Goethe University Frankfurt, Germany (4). Materialwissenschaften, Technische Universität Darmstadt, Darmstadt.

The study of materials in extreme environments is attracting more and more attention as technological and environmental demands on functional materials rapidly increase. Physical phenomena under extreme environments (pressure and temperature) also take place in the interior of the Earth and in extraterrestrial bodies. Particularly, the behavior of materials under high pressure is of interest in itself but coupling pressure with the deposition of high energy densities and defect creation opens up new possibilities. The combination of ion irradiation and pressure allows us to simulate radioactive decay events in minerals of the Earth's interior or to access thermodynamic pathways in the phase diagram such that otherwise unstable, high-pressure phases can be recovered upon pressure release (Glasmacher et al. 2006, Lang et al., 2009). To answer fundamental questions, many areas of geosciences rely on experiments where extreme conditions are created in the laboratory. During the last years, a new experimental platform has been developed at cave A at the heavy-ion synchrotron (SIS-18) of the GSI accelerator facility, where high pressure can be combined with relativistic heavy ion irradiation. Minerals are pressurized in diamond anvil cells (DAC) and then exposed to the ion beam (e.g., 60 GeV U ions). Under the simultaneous application of pressures and ion irradiation, several novel exotic effects were identified. This presentation provides an overview of existing results and reports about our new developments used to online monitor beam-induced structural changes by means of Raman spectroscopy.

References

Lang, M., Zhang, F., Zhang, J., Wang, J., Schuster, B., Trautmann, C., Neumann, R., Becker, U., Ewing, R.C. *Nanoscale manipulation of the properties of solids at high pressure with relativistic heavy ions. Nat. Mater* 2009, 8(10): p. 793-797 https://doi.org/10.1038/nmat2528

Lang, M., Zhang, F., Lian, J., Trautmann, C., Neumann, R. and Ewing, R.C. Combined high pressure and heavy-ion irradiation: a novel approach. *Journal of Synchrotron Radiation*, 2009, *16*(6), pp.773-777 https://doi.org/10.1107/S0909049509034384.

Glasmacher UA, Lang M, Keppler H, Langenhorst F, Neumann R, Schardt D, Trautmann C, Wagner GA (2006) Phase transitions in solids stimulated by simultaneous exposure to high pressure and relativistic heavy ions. Phys Rev Lett 96:195701-1–195071-4, 10.1103/PhysRevLett.96.195701

16th International Congress of the Geological Society of Greece
17-19 October, 2022 - Patras, Greece
Bulletin of the Geological Society of Greece, Sp. Publ. 10
Ext. Abs. GSG2022-217

Petrogenetic implications of a Late Cenozoic multiple injection lamproitic dike, Limnos Island, Greece

A. Magganas[1], P. Koutsovitis[2]
(1) Department of Mineralogy and Petrology, National and Kapodistrian University of Athens, Athens, Greece, amagganas@geol.uoa.gr (2) Department of Geology, University of Patras, Patras, Greece.

The volcanism in the islands of the Northern Aegean Sea was mostly realized during Miocene times and is mainly of high-K calc-alkaline to shoshonitic affinity (Gläser et al., 2022 and references therein). A multiple dike of at least Upper Oligocene age occurs in the northeastern part of Limnos Island intruding Eocene to Lower Oligocene sandstones. It has a length of about 220m and a variable thickness, which is about 1.5m initially, gradually wedging at its end (Fig. 1a). This dike has been formed by two slightly different pulses of lamproite type magma; an earlier one, which occupies its two margins, and another less voluminous in the middle. Marginal lava is flow foliated and hypocrystalline, whereas the internal lave is almost holocrystalline and more massive. Both lavas display a microporphyritic texture with mineral constituents ranging in size from fine to medium grained. The microphenocrysts consist of anhedral to subhedral clinopyroxene, former euhedral olivine pseudomorphically replaced by serpentine, and laths of Ti-phlogopite. The groundmass comprises the same minerals as the microphenocrysts and additionally Fe-Ti oxides (ilmenite, Ti-magnetite), barite, apatite, sanidine, calcite and glass usually devitrified in favor of chlorite and K-feldspar. Fine grained clinopyroxene and phlogopite either are forming trails surrounding former olivine or they are oriented subparallel to flow defining trachytic, pilotaxitic or hyalopilitic textures (Fig. 1b). Relict spinel was identified within the serpentine that replaced olivine and phlogopite. Its Cr# values are remarkably high (73.8-83.5), because the precursor olivine grains were most likely formed from accumulation of a pre-existing magma that was significantly affected by subduction-related processes.

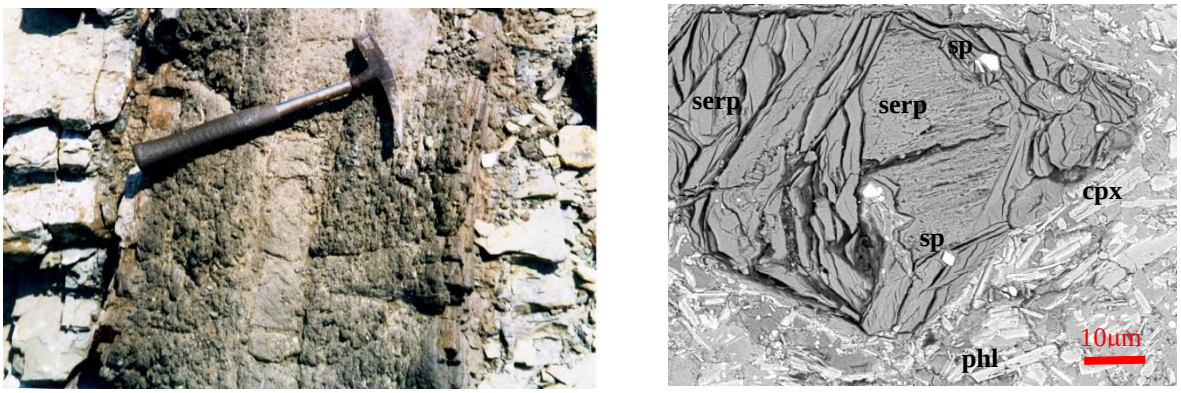

Figure 1: a) Multiple lamproitic dike crosscutting sandstone and showing light brown massive center and flow laminated greenish brown margins. b) SEM microphotograph showing euhedral spinel (sp) grains within pseudomorph serpentine (serp) after an olivine microphenocryst. Pilotaxitic and trachytic textures are defined by trails mainly of phlogopite (phl) and clinopyroxene (cpx) laths around former olivine, both oriented subparallel to flow.

Clinopyroxene grains are diopside or augite with highly variable TiO_2 and Al_2O_3 values (up to ~3.3 and up to ~8.5 wt.% respectively). The very high Ti and Al contents are assigned to clinopyroxene rims and groundmass grains (low Mg#), whereas lower values were measured from phenocryst cores, which display relatively high Mg# (up to ~89.7). Most analyses form a rather linear regression trend of Al vs Ti, pointing to clinopyroxene crystallization without significant pressure changes and are typical of clinopyroxenes present within alkali basaltic magmas. However, some clinopyroxene grains display lower Ti/Al and higher Al^{vi}/Al^{iv} ratios that indicate derivation from deeper mantle sources. The coexistence of these alkali basaltic related pyroxenes along with other phases associated with subduction-related differentiated magmas (high Cr# spinel, barite, sanidine), strongly indicate interaction of magmas from various sources, which set the basis to interpret the formation of this lamproitic volcanism. Geochemical data also show affinities typical of such rocks, such as the relatively high Mg contents along with high K, Ti and P. Trace elements also show interesting properties, such as the high Cr, Ni and Zr contents coupled with elevated LREE and also Sr, Ba and Rb, providing further support for a scarcely found rock in Eastern Mediterranean originated from an ultra K-rich mantle derived primitive magma, filling the gap of the lamproitic type volcanic belt in between North Macedonia, Lesbos and Western Anatolia (Prelević & Foley 2007; Pe-Piper et al., 2014; Casalini et al. 2021).

References

Casalini, M., Avanzinelli, R. et al. 2021. Petrogenesis of Mediterranean lamproites and associated rocks: The role of overprinted metasomatic events in the postcollisional lithospheric upper mantle. Geological Society, London, Special Publications, 513, https://doi.org/10.1144/SP513-2021-36

Gläser L., Grosche A., Voudouris P. & Haase K. 2022. The high-K calc-alkaline to shoshonitic volcanism of Limnos, Greece: implications for the geodynamic evolution of the northern Aegean. Contributions to Mineralogy and Petrology, 177:73, https://doi.org/10.1007/s00410-022-01940-7

Pe-Piper G., Zhang Y., Piper D. & Prelević D. 2014. Relationship of Mediterranean type lamproites to large shoshonite volcanoes, Miocene of Lesbos, NE Aegean Sea, Lithos, 184–187, 281–299, http://dx.doi.org/10.1016/j.lithos.2013.11.004

Prelević, D. & Foley, S.F. 2007. Accretion of arc-oceanic lithospheric mantle in the Mediterranean: evidence from extremely high-Mg olivines and Cr-rich spinel inclusions from lamproites. Earth and Planetary Science Letters,256, 120–135, https://doi.org/10.1016/j.epsl.2007.01.018

16th International Congress of the Geological Society of Greece
17-19 October, 2022 - Patras, Greece
Bulletin of the Geological Society of Greece, Sp. Publ. 10
Ext. Abs. GSG2022-228

Evidence from the CO_2 liberated from Thermal Springs in the regions of Kammena Vourla and Thermopylae

I. Georganta[1], P. Koutsovitis[2], K. Kyriakopoulos[1],

(1) National and Kapodistrian University of Athens, Department of Geology and Geoenvironment, Panepistimioupolis, Ano Ilissia, 15784, Athens, Greece (joageorg@hotmail.com) (2) University of Patras, Department of Geology, Section of Earth Materials, 26504, Rio, Greece

1. Introduction

Greece, due to its geographical location and geological structure, has a large number of hydrothermal springs. The thermal springs are differentiated according to their metallic and chemical elements, their water temperature and physical, chemical and geological properties. The present study focuses on geological findings from the hot springs in the areas of Kammena Vourla and Thermopylae, since they are characterized by comparable geological formations, in addition to their relatively proximity between them. Furthermore, some CO_2 gas measurements are analysed and conclusions are inferred concerning the activity and development of the specific hydrothermal sources.

2. Results and Discussion

The examined hydrothermal springs are connected to the recent (Quaternary) volcanic activity in the area. Some alkali basalts outcrop close to Kammena Vourla.. Their petrographic study shows crystallization of idiomorphic to hypidiomorphic olivine and clinopyroxene crystals (skeletal structures), which are surrounded by a matrix of feldspar laths and microliths (plagioclase and sanidine), clinopyroxene and glass, partly devitrified to chlorite. In addition, medium to coarse grained hypidiomorphic plagioclase phenocrysts were observed, some of which show banding (Fig. 1a,b). The accessory minerals comprise mostly of Ti-magnetite and ilmenite.

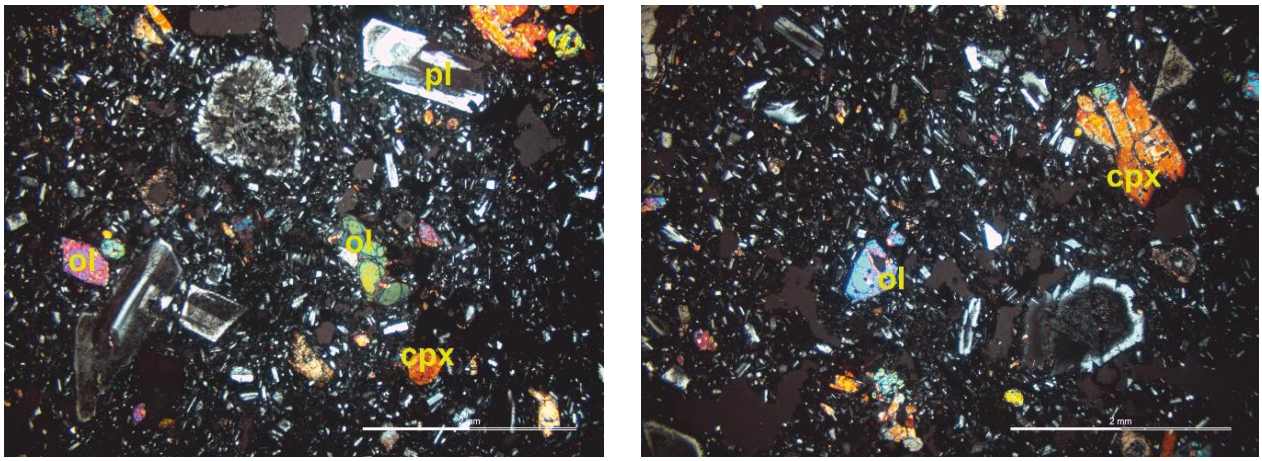

Figure 1: a) Thin section of olivine and plagioclase microphenocrysts in a devitrified matrix that comprises of feldspar microliths and Fe-Ti oxides b) The second image denotes the heterogeneous nature of the samples, since plagioclase phenocrysts are absent, whereas clinopyroxene quench shaped grains appearing with glomerophyric textures.

The gas samples were collected from the thermal springs of Kammena Vourla and Thermopylae during the period of October 2018 were four (4), corresponding to two measurements from each location (D'Alessandro et al. 2020). CO_2 and N_2 are the predominant gas phases, with the majority of the samples being dominated by CO_2 (concentrations up to ~990,000 μmol/mol). Only the gases collected at the Kammena Vourla site are rich in N_2, while helium (He) shows a wide range of values. Methane (CH_4) shows a similar behavior regarding its variability, with values reaching as high as ~16,500 μmol/mol.

The Thermopylae area stands out because the outgoing channels of the hot springs display an increased flow. In June 2018, the temperature in the outflow channels in Thermopylae decreased along its course, whereas the pH levels showed an increasing tendency. Though there is no visible stirring along the flows, the content of dissolved CO_2 decreased, implying strong CO_2 degassing by diffusion from the water surface released to the atmosphere. In addition, regarding the δ^{13} of the TDIC values along the streams, the ones measured in Thermopylae were higher compared to those present in

Kammena Vourla (D'Alessandro et al. 2020); variability of these values is consequence of the depletion of the lighter carbon isotope, which is preferentially incorporated into the CO_2 gas, which is released into the atmosphere (Caliro et al., 2005).

The total CO_2 liberation to the atmosphere in the studied localities is estimated at ~27 t/d, with the largest contribution coming from degassing along the outflow channels of the thermal springs (D'Alessandro et al., 2020). This estimate should be considered as an order of magnitude due to various uncertainties that are still present. However, the obtained value is not negligible and lies within the range of CO_2 outflows to the atmosphere of the active volcanic arc of the Southern Aegean (2.5-100 t/d). Considering the recent compilation of volcanic CO_2 emissions (Fischer et al., 2019), the studied system comes under the category of defined hydrothermal weak volcanic emissions.

3. Conclusions

In the present study, most of the gases investigated showed that CO_2 was the dominant phase, while N_2 enrichments were noticed only in Kammena Vourla. CO_2 outflow was assessed by measuring both the gas flow rates into the source reservoirs, with a floating accumulation chamber, and the non-visible to CO_2 loss ("hidden") bubbles along the outflow channels through analyses of the dissolved gas phase. The free outflow due to bubbles was always lower than the 'hidden' outflow. Overall, the total CO_2 release to the atmosphere was estimated at ~27 t/d, indicating that most of the CO_2 was degassed along the outflow channels of the thermal springs. Such an outflow is comparable to that of active volcanic systems along the South Aegean arc.

References

Caliro, S., Chiodini, G., Avino, R., Cardellini, C., Frondini, F., (2005). Volcanic degassing at Somma–Vesuvio (Italy) inferred by chemical and isotopic signatures of groundwater. Appl. Geochem. 20, 1060–1076.

D'Alessandro W., Li Vigni L., Gagliano A., Calabrese S., Kyriakopoulos K., Daskalopoulou K. (2020). CO_2 release to the atmosphere from thermal springs of Sperchios Basin and northern Euboea (Greece): The contribution of "hidden" degassing. Applied Geochemistry, Elsevier.

Fischer, T.P., Arellano, S., Carn, S., Aiuppa, A., Galle, B., Allard, P., Lopez, T., Shinohara, H., Kelly, P., Werner, C., Cardellini, C., Chiodini, G., (2019). The emissions of CO2 and other volatiles from the world's subaerial volcanoes. Sci. Rep. 9 https://doi.org/10.1038/s41598-019-54682-1, 18716.

16th International Congress of the Geological Society of Greece
17-19 October, 2022 - Patras, Greece
Bulletin of the Geological Society of Greece, Sp. Publ. 10
Ext. Abs. GSG2022-240

Assessment of petrographic and mineralogical characteristics of mafic volcanic Miocene rocks (SE Aegean) for acidic water purification applications

N. Aggelopoulou[1], E. Kosti[1], P. Petrounias[2], P. Koutsovitis[1], A. Sideridis[1]
(1) University of Patras, Department of Geology, Section of Earth Materials, 26504, Rio, Greece
(natalia.agge@gmail.com)

In the Southeastern Aegean region, the island of Patmos is located about 100 kilometers north of the Greek volcanic arc. During the Upper Miocene (~ 4.4 m.y) mafic volcanic rocks of basic to acidic composition rocks were formed (Agostini et al. 2007; Pe-Piper and Piper, 2002). The main lithological rock types comprise of basalts, andesites, trachyandesites, trachytes, rhyodacites and rhyolites. The diversity of lithotypes is mostly attributed to factors that include extent of mantle wedge partial melting, the incorporation of variable subduction-related components that are driven by the dehydration of subducted sediments, as well as fractional differentiation processes that is related with the upper crustal thickness of the hanging wall.

We focused our research efforts on compositionally intermediate and basic lithologies that seem to represent suitable lithotypes to be considered for our experimental research purposes. In particular, the intermediate lithologies consist of K-felspar, plagioclase, clinopyroxene, olivine, whereas biotite, hornblende and Fe-Ti oxides (Ti-magnetite, ilmenite) occur as rather accessory to subordinate phases. In the biotite-bearing trachyte, K-felspar and plagioclase appear as idiomorphic to subidiomorphic phenocrysts with well-defined marginal rims, that point to rather slow cooling conditions. On the contrary, the K-feldspar phenocrysts of the trachyandesites display patterns of minerals that experienced significant interaction with the differentiated melt. Plagioclase of trachyandesites and trachytes are more altered (sericitized) compared to plagioclase within biotite-bearing trachytes that mostly preserved their primary characteristics. Plagioclase of trachyandesites show compositional zoning associated with release of volatile components and with gradual cooling. Clinopyroxene phenocrysts also show indications of late-stage interaction, although in most cases they are unaltered, especially in their cores. The presence of small-sized clinopyroxene grains, along with K-feldspar and plagioclase laths within the glassy matrix, represent a differentiated melt that is texturally characterized by a microtrachytic texture, although variolitic and vitrophyric textures were also identified. Plagioclase and clinopyroxene phenocrysts in some cases display glomerophyric textures, related to the lava flow rate (Fig.1a,b).

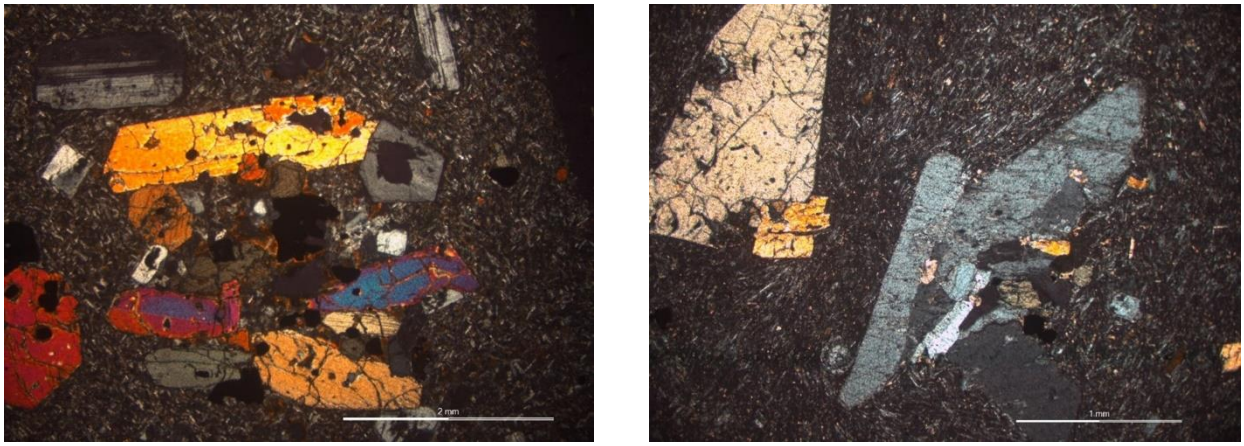

Figure 1: a) Thin section of trachyandesite ,we observed olivine and plagioclase microphenocrysts in a devitrified matrix that comprises of feldspar microliths and Fe-Ti oxides b) The second image denotes the heterogeneous nature of the samples, since plagioclase phenocrysts are absent, whereas clinopyroxene quench shaped grains appearing with glomerophyric textures, associated with cooling conditions.

In the basalts, in most cases, glass is present in higher modal amounts, indicating faster cooling conditions. The microphenocrysts comprise of olivine, plagioclase and clinopyroxene (augite). More specifically, olivine is present mostly as rather subordinate idiomorphic grains, whereas plagioclase is present as a predominant phase forming well-developed crystal twinning and zoning that suggest only minor deformation effects. The percentage it ranges around 30 – 50%, a little more from olivine's. Clinopyroxene phenocrysts may be present even as coarse grained crystals, interlocking smaller sized microphenocryst plagioclase grains. Texturally, the basalt's matrix is poikilitic to variolitic, depending on the

participation of glass component. Andesites differ by displaying higher plagioclase and K-feldspar amounts at the expense of other mafic phase; although biotite and hornblende may be present. In the basalts and andesites, the plagioclase, olivine and clinopyroxene phenocrysts show in some cases a preferable orientation. The predominant textures are porphyritic to trachytic, whereas glomerophyric textures also occur.

Amongst the examined rock types, in literature, the andesites are most often used for the development of filters (Petrounias et al. 2019, Primasari et al. 2020; Liesh 2010), although basalts have also been considered (Jiang et al. 2014). The latter however are less often used because they require specific mineralogical, textural and petrophysical properties so as to be considered for water purification application purposes. Furthermore, the mineralogical constituents of the andesites, but also of the trachyandesites, are such that increase the ability of the examined rocks to interact with water at their microsurface (adsorption). Katukiza et al. (2014) highlighted the significance of the use of crushed lava rocks to be implemented as filters so as to rastically remove pollutant loads, that may also be beneficial from the actual removement even of viruses and micropolutants. In fact the rocks used can be classified as basalts with rather enriched potassium and sodium contents. In any case, the presence of feldspars within lava samples, as well as relatively enhanced porosity properties allow the rocks to behave as natural "sponges" that withhold pollutants but that can also be beneficial for improving the pH conditions of the acidic waters. All three lithotypes can serve as proper filters for benification of water quality properties and for this purpose we intend to implement a series of experiments with the use of an electrically continuous driven flow-through experimental device, proposed by Petrounias et al. (2020), to simulate a standard continuous water recirculation system of the treated acidic runoff, in filters with a combination of specified volcanic raw materials. We expect that the trachyandesites will display the most effective rocks as filters, however we need to confirm this through the experiments with the acidic water purification experiments.

References

Katukiza, A.Y., Ronteltap, M., Niwagaba, C.B., Kansiime, F., Lens, P.N.L., 2014. A two-step crushed lava rock filter unit for grey water treatment at household level in an urban slum. Journal of Environmental Management 133, 258-267.

Liesh, A. M. 2010. Wastewater phosphorus removal by two different types of andesitic volcanic tephra. J. Nat. Resour. Life Sci. Educ., 39: 40–44.

Jiang, X., Wu, C. D., Wu, Z. R., & Zhang, B. (2014). Basic Characteristics and Application of Basalt Fiber in the Water Pollution Control. In Advanced Materials Research (Vols. 1073–1076, pp. 838–843). Trans Tech Publications, Ltd.

Petrounias, P.; Rogkala, A.; Giannakopoulou, P.P.; Tsikouras, B.; Lampropoulou, P.; Kalaitzidis, S.; Hatzipanagiotou, K.; Lambrakis, N.; Christopoulou, M.A. An Experimental Study for the Remediation of Industrial Waste Water Using a Combination of Low Cost Mineral Raw Materials. Minerals 2019, 9, 207.

Primasari B., Indah S., Afrianita R., Rahmatesa F., 2020, Biosand Filter for Removal of Organic Pollutant from Laboratory Wastewater, Journal of Physics: Conference Series 1625, 012057.

16th International Congress of the Geological Society of Greece
17-19 October, 2022 - Patras, Greece
Bulletin of the Geological Society of Greece, Sp. Publ. 10
Ext. Abs. GSG2022-272

Overview of new and rare minerals discovered in Greece: Special regards to their genesis in ophiolite complexes

F. Zaccarini[1], M. Economou-Eliopoulos[2], G. Garuti[1]

(1) Faculty of Science, Geosciences Programme, Universiti Brunei Darussalam, Gadong BE 1410, Brunei Darussalam, federicazaccarinigaruti@gmail.com, giorgio.garuti1945@gmail.com (2) Department of Geology and Geoenvironment, University of Athens, 15784 Athens, Greece, Department of Geology, econom@geol.uoa.gr

Abstract

According to the list provided by the Commission of New Minerals, Nomenclature, and Classification (CNMNC) of the International Mineralogical Association (IMA) updated to July 2022, a total of 5828 valid mineral species have been discovered so far. The list shows that 42 of the new minerals have been discovered, for the first time, in Greece. Twenty-eight of the Greek new minerals, representing about the 70%, were described in the Lavrion poly-metallic mining district, located in Attica, related with a granodioritic body and granodiorite porphyry dikes intruding metamorphic Mesozoic rocks (Voudouris et al. 2002; Skarpelis and Argyraki 2009). The new minerals of Lavrion derive from smelting activities or they occur in natural rocks such as marble representing, in most cases, the alteration products of the primary mineralization. Other Greek new minerals have been discovered in the Aghios Philippos Zn-Pb deposit, in bauxite, in metamorphic sediments and in a lava from Santorini. In 1981, the new mineral theophrastite $Ni(OH)_2$, was identified in the Vermion ophiolite and, more recently, 3 new minerals, namely tsikourasite $Mo_3Ni_2P_{(1+x)}$ ($x < 0.25$), grammatikopoulosite NiVP and eliopoulosite V_7S_8 were found in the chromitite from the Agios Stefanos deposit (Zaccarini et al. 2019, Bindi et al. 2020 a,b) and arsenotučekite $Ni_{18}Sb3AsS_{16}$ was discovered in the Eretria (Tsangli) chromium mine, located in the Othrys ophiolite complex. In this contribution we have revised and compared with literature data the mineralogical characteristics of these 5 new and rare minerals discovered in the Greek ophiolites, with the aim to better understand their genetical aspects. On the basis of their mineralogical assemblage, the formation of the new phosphides tsikourasite and grammatikopoulosite and the sulfide eliopoulosite from Agios Stefanos took place after the deposition of the host chromitite. Despite the fact that V-bearing sulfides and phosphides are common in meteorites, the probability of intercepting a fragment of a meteorite during the sampling of the studied chromitite seems very unlikely. Therefore, we can argue that they formed at lower pressure in an extremely low fO_2 and reducing environment, during the serpentinization that affected the host ophiolite. The origin of arsenotučekite in chromitites co-existing with Fe–Ni–Cu-sulfide mineralization and magnetite at Eretria (Tsangli) mine, is believed to may be related with a hydrothermal system circulation. The most salient feature of theophrastite $Ni(OH)_2$ and associated $(Ni,Co,Mn)(OH)_2$ is the development of a concentrating process. The spatial association of mixed layers of Ni-silicides with extremely tiny crystals of $Ni(OH)_2$ and (Ni,Co,Mn)-hydroxides at Vermion, may indicate that their metastability has a significant impact on the reaction process and the structural features of the reaction products. The extremely tiny crystals of these hydroxides and the spatial association of mixed layers of Ni-silicides with theophrastite may reflect the significant role of the interaction process on their reported structural features. Although the components of the revised new minerals are available in the ore forming systems of both, the Othrys and Vermion ophiolites, the strongly reducing environment and relatively higher temperature required for the formation and stability of the new minerals from the Othrys differ from those for theophrastite, forming concentrated precipitations at very low temperature and moderately oxidizing conditions. The spatial association of mixed layers of Ni-silicides with extremely tiny crystals of $Ni(OH)_2$ and (Ni,Co,Mn)-hydroxides at Vermion, may indicate that their metastability has a significant impact on the reaction process and the structural features of the reaction products. The scarcity in terrestrial samples of the new minerals revised in this paper is probably due to the required extreme physical-chemical conditions in which they can precipitate, that rarely can be achieved in a natural environment. This revision suggests that the Greek ophiolites, similarly to the Lavrion mining discrict, represent a potential source for the discovery of new minerals in the future. According to literature data, the Othrys complex, hosting 4 new minerals, ranks the second position among the Greek type localities i.e. the localities in Greece in which a new mineral species were discovered.

Acknowledgements

Many thanks are expressed to the University of Athens (grant No KE 11078) for the financial support and Evaggelos Michaelidis for his assistance with the SEM analysis.

References

Bindi, L.; Zaccarini, F., Ifandi, E., Tsikouras, B., Stanley, G., Garuti, G., Mauro, D. (2020a). Grammatikopoulosite, NiVP, a new phosphide from the chromitite of the Othrys ophiolite, Greece. *Minerals*, *10*, doi:10.3390/min10020131.

Bindi, L., Zaccarini, F., Bonazzi, P., Grammatikopoulos, T., Tsikouras, B., Stanley, C., Garuti, G. (2020b). Eliopoulosite, V_7S_8, a new sulfide from the podiform chromitite of the Othrys ophiolite, Greece. *Minerals*, *10*, doi:10.3390/min10030245.

Marcopoulos, T., Economou, M. (1981). Theophrastite, $Ni(OH)_2$, a new mineral from northern Greece. *Am. Mineral*. *66*, 1020–1021.
Skarpelis, N., Argyraki, A. (2009). Geology and origin of the supergene ore at the Lavrion Pb-Ag-Zn deposit, Attica, Greece. *Res. Geol.* 59, 1–14.
Voudouris, P, Tsolakos, A., Papanikitas, A., Solomos, Ch. (2004). New finds from Lavrion 2003. *Lapis*, 4, 13–15 (in German).
Zaccarini, F., Bindi, L., Ifandi, E., Grammatikopoulos, T., Stanley, C., Garuti, G., Mauro, D. (2019). Tsikourasite, $Mo_3Ni_2P_{1+x}$ ($x < 0.25$), a new phosphide from the chromitite of the Othrys ophiolite, Greece. *Minerals*, *9*, doi:10.3390/min9040248.
Zaccarini, F., Bindi, L., Tsikouras, B., Grammatikopoulos, T., Stanley, Ch.J., Garuti, G. (2020). Arsenotučekite, $Ni_{18}Sb_3AsS_{16}$, a new mineral from the Tsangli chromitites, Othrys ophiolite, Greece. *Mineral. Petrol*., 114, 435–442.

16th International Congress of the Geological Society of Greece
17-19 October, 2022 - Patras, Greece
Bulletin of the Geological Society of Greece, Sp. Publ. 10
Ext. Abs. GSG2022-273

Evidence for significant refertilization of depleted mantle peridotites in the Krrabi massif, Mirdita ophiolite complex, Albania

P. Koutsovitis[1], T. Ntaflos[2] K. Onuzi[3], C. Hauzenberger[4]
(1) University of Patras, Department of Geology, Rio-Patras, Greece (pkoutsovitis@upatras.gr) (2) University of Vienna, Department of Lithospheric Research, Althanstr. 14, Vienna, Austria (3) Institute of GeoSciences, Energy, Water and Environment, Tirana, Albania (4) NAWI Graz Geocenter - Petrology & Geochemistry, Austria

This study focuses on the key peridotitic massif in the northern ophiolite belt in Albania (Mirdita zone), namely Krabbi massif. Peridotites are fine to medium grained displaying secondary mosaic porphyroclastic and less often equigranular or cataclastic textures. The Krrabi peridotites comprise of olivine (Fo=~89.6 avg., NiO=0.38 avg. wt.%, CaO≤0.05 wt.%), orthopyroxene (Mg# ~89.4 avg.), clinopyroxene (Mg# ~91.5 avg.), plagioclase (bytownite), amphibole (kaersutite, pargasite) and spinel (Cr# ~0.42 avg.). Their most unique feature is the presence of microcracks, obviously alterations, existing exclusively in plagioclases that are not propagate in the neighbor minerals pointing to their relict nature. These microcracks are filled with a material composed of Fe and Mn found in no other minerals. Amphibole is frequently associated with clinopyroxene and/or surrounds spinel. The TiO_2 contents of such clinopyroxene is distinctively higher than the clinopyroxene not in contact with amphibole. In general, the TiO_2 and Cr_2O_3 contents in clinopyroxene that correlate positively, the small sized Al-rich spinel grains that are in contact with ilmenite and the presence of amphibole, indicate that these rocks have been heavily metsomatized.

Geochemically they are distinguished for displaying values that are highly comparable with fertile Primitive Mantle lherzolites. Mg# values range tightly(~90.0 avg.), whereas their CaO and Al_2O_3 contents correlate negatively with MgO abundances, being ~3.0 wt.% avg. and ~3.5 wt.% avg. respectively; bulk rock CaO/Al_2O_3 ratios values are ~0.82 avg.. The HREE are close or slightly lower than those of the Primitive Mantle [HREE = ~0.90xPM avg.]. These rocks were most likely previously depleted spinel- plagioclase peridotites that later experienced impregnation due to hydrous alkali melt interaction, leading to their significant refertilization.

16th International Congress of the Geological Society of Greece
17-19 October, 2022 - Patras, Greece
Bulletin of the Geological Society of Greece, Sp. Publ. 10
Ext. Abs. GSG2022-279

An approach to 3D rock fabric analysis of ophiolitic rocks via X-ray micro-computed tomography

V. Giamas[1], P. Koutsovitis[1], A. Sideridis[1], P. Turberg[2], T. Grammatikopoulos[3], P. Petrounias[1], P. Giannakopoulou[1], N. Koukouzas[4], K. Hatzipanagiotou[1]

(1) University of Patras (UoP), Department of Geology, Section of Earth Materials, Patras, Greece, vgiamas@upnet.gr (2) École Polytechnique Fédérale de Lausanne EPFL, School of Architecture, Civil and Environmental Engineering ENAC, Civil Engineering Institute IIC, Lausanne, Switzerland. (3) SGS Canada Inc, Lakefield, Canada. (4) Centre for Research and Technology, Hellas (CERTH), Marousi, Greece.

Abstract text

X-ray micro-computed tomography (μCT) was initially applied for medical purposes only, however during the past two decades, this technique presents an exponential character in several studies including archeology, material sciences, engineering as well as in geosciences. The reason for this is its ability to visualize in a non-destructive manner to investigate the internal features of any sample considered (i.e., the mineral constituents of a rock sample).

In this concise presentation, we will only focus on the chapter of 3D rock fabric analysis from the recently published article of Giamas et al. (2022), although their work primary investigates the effectiveness of μCT upon six geochemically different (mafic and ultramafic) ophiolitic rocks. The examined lithotypes consist of a gabbronorite and a hornblende gabbro for the mafic as well as a wehrlite, a harzburgite, a dunite and a chromitite for the ultramafic group. It should be noticed that several criteria have been taken into consideration (representative lithotypes, alteration/metasomatism, restricted number of participating minerals, primary mineral constituents with different densities and attenuation coefficient properties, variability in grain size distribution from a set of samples, textural homogeneous features within each sample). Apart from the mineral volumetric portions calculated through μCT, which were compared with other state-of-the-art- techniques (optical microscopy, mineral chemistry microanalyses-MINSQ, XRD, and QEMSCAN), fabric analysis can provide 3D information of mineral constituents regarding their textural and structural properties. Blob3D software (Ketcham, 2005) was used for mineral segmentation, separation, and mineral's volume - shape measurements that were further processed with the open-source TomoFab MATLAB code (Petri et al., 2020) for defining the individual best-fit ellipsoid that were used for the calculation of the fabric parameters (shape parameter T and anisotropy P′).

The research outcomes can be considered of major importance in terms of resolving complex petrogenetic phenomena (mantle state, magma crystallization, deformation and/or alteration processes, identification of water-bearing phases, geodynamic implications), as well as for identifying deformation fabrics that can be critical for applied research purposes (usage as aggregates or as potential storage sites for CO_2 mineralization).

References

Giamas, V., Koutsovitis, P., Sideridis, A., Turberg, P., Grammatikopoulos, T.A., Petrounias, P., Giannakopoulou, P.P., Koukouzas, N., Hatzipanagiotou, K., 2022. Effectiveness of X-ray micro-CT applications upon mafic and ultramafic ophiolitic rocks. Micron 158, 103292.

Ketcham, R.A., 2005. Computational methods for quantitative analysis of three-dimensional features in geological specimens. Geosphere 1, 32-41.

Petri, B., Almqvist, B.S.G., Pistone, M., 2020. 3D rock fabric analysis using micro-tomography: An introduction to the open-source TomoFab MATLAB code. Computers & Geosciences 138, 104444.

16th International Congress of the Geological Society of Greece
17-19 October, 2022 - Patras, Greece
Bulletin of the Geological Society of Greece, Sp. Publ. 10
Ext. Abs. GSG2022-285

Petrological and geochemical study of the successive rodingitization processes in tholeiitic, alkaline and calc-alkaline basaltic rocks from Evia Island, Greece

C. Karkalis[1], A. Magganas[2], P. Koutsovitis[3]

(1) Centre for Research & Technology Hellas, Chemical Process and Energy Resources Institute (CERTH/CPERI), 52 Egialias street, Athens GR-151 25; karkalis@certh.gr (2) Department of Geology and Geoenvironment, National & Kapodistrian University of Athens, Panepistimioupoli Zografou, Athens, GR- 15784; amagganas@geol.uoa.gr (3) Section of Earth Materials, Department of Geology, University of Patras, Patras 26504, Greece; pkoutsovitis@upatras.gr

Research Highlights

Higher vesuvianite content, as well as greater mobilization of trace and rare earth elements are noted in Mesozoic alkaline and calc-alkaline basalts than in tholeiites of Central Evia, Greece, during increasing rodingitization.

Background and Objectives

In Evia Island (Greece), rodingites crop out in the regions of Kimi and Pagondas and appear as dikes and veins that intrude variably serpentinized peridotites. Rodingites follow the foliation of the serpentinitic host-rocks trending either NNE-SSW or E-W. Their texture is coarse- to fine-grained (or even aphanitic) and massive or sheared. In Kimi region, rodingites are more metasomatized compared to those of Pagondas, as it can be seen by the formation of successive reaction zones and blackwall rims. In the Pagondas region, rodingites are mainly homogenous without reaction zones having sharp contacts with the serpentinitic country rocks. The current research aims to unravel the physicochemical and thermodynamic conditions of the successive rodingitization phenomena in Central Evia considering the behavior of significant trace elements and REE. This was accomplished via the following objectives: (a) field research and sampling, (b) mineralogical, petrographical, geochemical and isotopic analyses, (c) data processing and (d) data interpretation.

Methods

Rodingitic samples and their magmatic protoliths were selected during the field research in Central Evia. Polished thin sections were made at the ABC A HEAD Geological Research Company in Poland, and they were petrographically studied at the Department of Mineralogy and Petrology of the National and Kapodistrian University of Athens. Mineral chemistry analyses were performed at the University of Vienna, Department of Lithospheric Sciences, as well as at the Faculty of Geology and Geoenvironment of the National and Kapodistrian University of Athens. Rodingites and their magmatic protoliths were geochemically analyzed at the ACME Analytical Laboratories in Canada for major elements, trace elements and REE. Calcite was isolated from the veins of six different rodingite samples and was isotopically analyzed for $\delta^{13}C$-$\delta^{18}O$ values at the Geo-Center (North Bavaria) of the Friedrich Alexander University in Erlangen, Germany. Thermodynamic modeling of rodingitization processes was accomplished using Perple_X 6.9.0 (Connolly, 2009) and TWQ 2.32 (Berman, 2007) softwares.

Results and Conclusions

The Central Evia rodingites (Fig. 1a,b) were classified into four types based on their origin from different protoliths and their REE contents. These are Rodingites of Island-arc Tholeiitic Dolerites (RIATD) and Rodingites of Mg-rich Tholeiitic Gabbros (RMTG), which appear in the Pagondas region, as well as Rodingites of Alkaline Basalts (RAB) and Rodingites of Calc-Alkaline Basalts (RCAB), which are found in the region of Kimi. The mineralogical composition of Central Evia rodingites is closely linked with the extent of metasomatism, since rodingites were influenced by variable metasomatic degrees that in cases reached late-stage derodingitization. The qualitative mineralogical composition is relatively similar among the distinct rodingite types including garnet + clinopyroxene + vesuvianite + chlorite; though, variations on the quantitative mineralogical composition are observed between rodingites of the same or different types. Garnet is the most common mineral phase, and it is classified mainly as grossular, whereas andradite is mostly observed in RAB and RCAB. Similarly, vesuvianite was formed in RCAB and RAB but less frequently in RIATD and RTMG. Chlorite is mainly penninite and subordinately clinochlore or sheridanite. In the more metasomatized rodingites, including the derodingitized ones, chlorite tends to be FeO-richer. Clinopyroxene is distinguished into relict augite and metasomatic diopside. Accessory minerals comprise prehnite ± spinel-group minerals ± orthopyroxene ± olivine ± calcite ± amphibole ± quartz ± mica ± apatite ± allanite. Their texture is coarse-grained to aphanitic and in cases porphyroblastic or sub-ophitic.

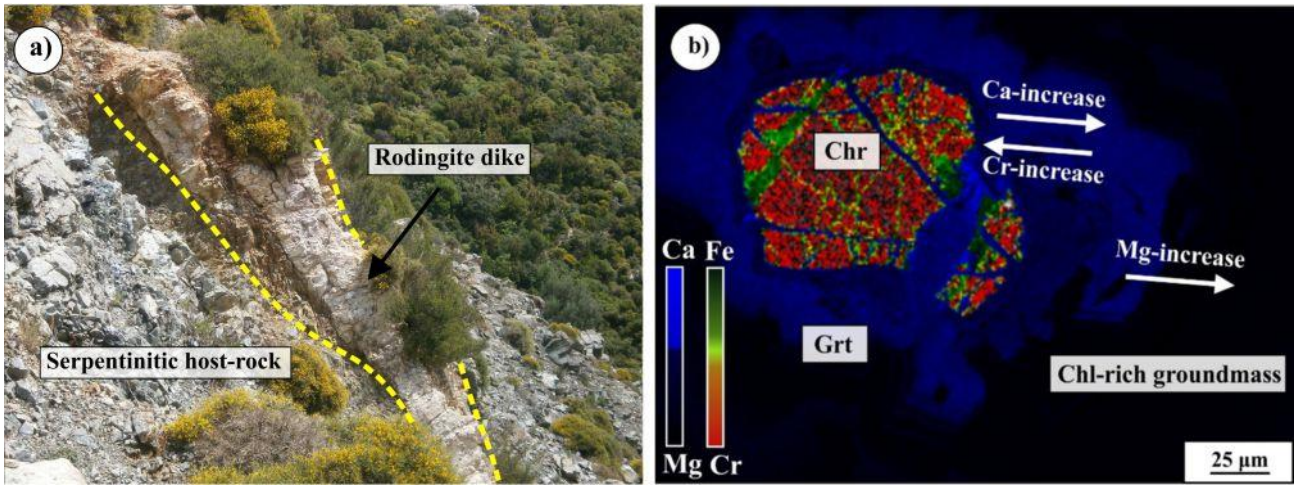

Figure 1. (a) RCAB dike of NNE-WWS direction intruding serpentinitic host-rock in the region of Kimi, (b) BSE-SEM photomicrograph of RCAB sample composed by zoning garnet (Grt) porphyroblast, chromite (Chr) and chlorite (Chl) rich groundmass.

Based on their whole rock chemistry, RIATD have variable CaO and MgO contents but relatively constant SiO_2 contents. Their chondrite normalized REE patterns are flat and they display positive Eu anomalies. In RMTG, CaO and MgO range highly, TiO_2 is low, whereas their chondrite normalized REE patterns exhibit strong positive Eu anomalies. Regarding the RAB composition, CaO and MgO vary significantly, contrary to SiO_2, which is generally constant, whereas they exhibit fractionation between their chondrite normalized LREE and HREE patterns due to LREE-enrichments. RCAB show highly ranging CaO, MgO and SiO_2 contents. Their chondrite normalized REE patterns show characteristic negative Eu-anomalies and they are sub-parallel with calc-alkaline subvolcanics from the regions of Koziakas, Pindos, Attica and East Othris (e.g. Magganas et al., 1997; Pomonis et al., 2004; Castorina et al., 2020; Koutsovitis et al., 2009). In Central Evia, rodingitization processes were linked with the serpentinization of the peridotitic country rocks and they were gradually developed in three stages during the mantle wedge exhumation at P-T conditions $\leq$ 5 kbar and $\leq$ 450 ºC. The first stage influenced all the rodingite types and it was mineralogically characterized by the crystallization of grossular, diopside, chlorite and prehnite. It also involved enrichments in Ca and volatiles, as well as Si and alkali depletions; the latter were assigned to the breakdown of magmatic clinopyroxene and amphibole. Stage-2 corresponds to the main rodingitization phenomenon that influenced mainly RAB and RCAB, and it was marked by the crystallization of vesuvianite, andradite and chlorite, as well as by REE enrichments. Metasomatic processes were completed during the third stage that involved the derodingitization of the marginal parts of some RCAB dikes, favoring the crystallization of Fe-rich chlorite + andradite and causing strong mobilization of REE and trace elements. Rodingite carbonation was part of the third metasomatic stage, in which seawater was mixed with serpentinization fluids as it is suggested by the $\delta^{13}C$-$\delta^{18}O$ values of calcite.

Acknowledgements

We would like to thank Professor Theodoros Ntaflos for his contribution in the mineral chemistry analyses and Professor Michael Joachimski for his support in the stable isotope analyses.

References

Berman, R.G., 2007. winTWQ (version 2.3): A Software Package for Performing Internally-consistent Thermobarometric Calculations. Geological Survey of Canada (Open File 5462, ed. 2.32).

Castorina, F., Magganas, A., Masi, U., Kyriakopoulos, K., 2020. Geochemical and Sr-Nd isotopic evidence for petrogenesis and geodynamic setting of Lower-Middle Triassic volcanic rocks from Central Greece: implications for the Neotethyan Pindos ocean. Mineralogy and Petrology, 114, 39-56. **[Journal Article]**

Connolly, J.A.D., 2009. The geodynamic equation of state: what and how. Geochemistry Geophysics Geosystems, 10, Q10014. **[Journal Article]**

Koutsovitis, P., Magganas, A., Katerinopoulos, A., 2009. Calc-alkaline volcanic rocks in mélange formations from the South Othris region, Greece: Petrogenetic and geotectonic implications. Geochemistry, Mineralogy and Petrology Sofia, 47, 79-95. **[Journal Article]**

Magganas, A., Kyriakopoulos, K., Lekkas, E., 1997. Early Alpine Rift volcanism in continental Greece: the case of Glykomilia Area (Koziakas Mountains). Chemie der Erde, 57, 243-255. **[Journal Article]**

Pomonis, P., Tsikouras, V., Hatzipanagiotou, K., 2004. Comparative geochemical study of the Triassic trachyandesites of Glykomilia and alkali basalts from the Koziakas ophiolite mélange (W. Thessaly): implications for their origin. Bulletin of the Geological Society of Greece 36, 587- 596. **[Journal Article]**

16th International Congress of the Geological Society of Greece
17-19 October, 2022 - Patras, Greece
Bulletin of the Geological Society of Greece, Sp. Publ. 10
Ext. Abs. GSG2022-316

Petrological and mineralogical evidence of rodingites from the region of Orliakas, Pindos ophiolite

L. Tsiarsioti[1], P. Koutsovitis [1], H. Tsikos[1], P. Pomonis[2]

(1) Section of Earth Materials, Department of Geology, University of Patras, Patras 26504, Greece; (louiztsiarsioti@gmail.com) (2) Department of Geology and Geoenvironment, National & Kapodistrian University of Athens, Panepistimioupoli Zografou, Athens, GR- 15784

1. Field evidence

In the Pindos ophiolite, exhumed thrust sheets of highly serpenitinized mantle sections outcrop at large scale in the region of Orliakas (Pelletier et al. 2008; Rassios and Moores 2006; Robertson 1990). The protoliths of these ultramafic bodies were dunites and harzburgites. These highly serpentinized rocks incorporate crosscutting dykes of highly metasomatized mafic rocks that have mostly been altered to rodingites. Even the most highly altered rocks have pseudomorphically retained the primary textural features of their precursor rocks that is evident through macroscopical observations. These rodingitized dykes are relatively thick (~0.5-2.0 m) appearing with different slope angles, which in some cases may even be either vertical or horizontal. At the rims of the dykes, we observed relatively thin black wall zones that are enriched in chlorite, which most likely represent reaction rims as the result of fluid infiltration. Another interesting feature is the fact that the dunites are in sharp contact with the crosscutting dykes, whereas in the mantle sections, harzburgites are more frequently found a few meters further away.

2. Results

The protoliths are small in size but very well preserved and are classified as olivine gabbronorites. These protoliths comprise of olivine, clinopyroxene, orthopyroxene, and plagioclase (Fig. 1a). Accessory secondary minerals include serpentinite, spinel, and sericite. Their textural features are granular to subophitic/ophitic, displaying in many cases microcrystal textural features, although porphyritic textures were also identified. The grains are mostly hypodiomorphic and even idiomorphic. The main mineralogical assemblage of the rodingites includes the following: garnet, hydrogarnet, residual clinopyroxene, actinolite, prehnite, chlorite, epidote, talc and rarely vesuvianite (Fig. 1b). Various textures were identified, with the main ones observed being porphyritic, ophitic and subophitic. Also, primary minerals were retained as confirmed by the preservation of relict clinopyroxene and even plagioclase grains, which however were subjected to albitization processes.

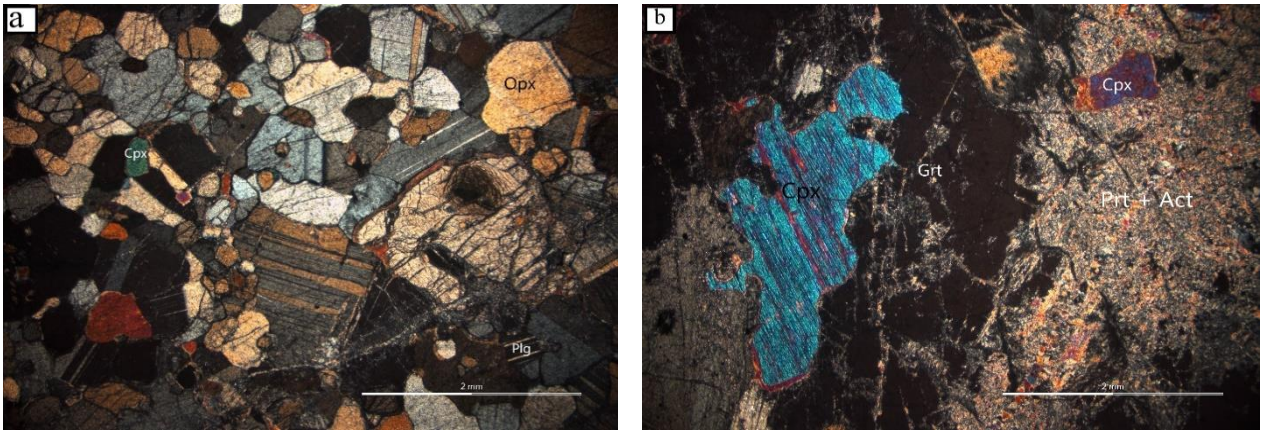

Figure 1: a) Thin section of gabbronorite protolith, mainly including Cpx, Opx, Plg, b) rodingite that encompasses a residual Cpx inherited from the gabbroic protolith, whereas other primary phases were completely replaced by secondary minerals. In addition, Grt and the Prh-Act mass are now the predominant phases. Abbreviations- Cpx: clinopyroxene, Prh: prenite, Act: actinolite, Grt: garnet.

Based upon carefully selected pairs of rodingites and their precursor protoliths that were identified in the field in proximity, we proceeded in conducting bulk-rock geochemical analyses in order to compare geochemical modifications

that took place during the percolation of metasomatism. The least altered protoliths show that they were Mg-rich rocks, whose CIPW classification reveals that they are gabbronites and olivine gabbronorites (~ 15.0 wt.% avg. MgO), with Cr and Ni contents varying from moderate to significantly high (Cr: <~1400 ppm and Ni: <~30 ppm). Their LOI contents (up to ~3.0 wt.%) reflect the fact that they were also subjected to alteration processes, although one sample (namely S1a-nb) corresponds to the lowest LOI value.

Rodingites exhibit higher LOI contents (<~8.5 wt.%), due to the higher modal composition of secondary minerals, including hydrogarnet. Regarding the major elements, we noticed Si and alkali elements decrease, whereas Ca increased slightly to significantly. Ti, Fe and Mn remained stable, whereas Al showed variability in its behavior. Amongst trace elements, Zr, Sc, Y, V, Nb and Ba remained rather stable, whereas Sr was removed from the system. Concerning the REE, The LREE were enriched, whereas the HREE were only slightly enhanced.

3. Discussion and Conclusions

The Orliakas serpentinized mantle rocks and their hosted rodingitized dykes seem to be closely associated with subduction-related processes, a feature that has also been observed in other ophiolitic outcrops in Greece (e.g. Othris: Tsikouras et al. 2009, Koutsovitis et al. 2013) This is confirmed by the occurrence of harzburgites, as well as by the interaction with high-Mg mafic intrusions that subsequently led to dunitization processes. Further diffusion of slab-derived hydrous fluids resulted in the extensive serpentinization phenomena but also seems to be related with the rodingitization processes that affected the olivine gabbronoritic dykes. Through detailed petrographic observations it is evident that rodingitization occurred at relatively low degrees, since in many cases small clusters of the protolith were found within almost all the rodingites. This is further confirmed by the relatively frequent presence prehnite and sericite along with the garnets, and in addition vesuvianite was identified in very rare cases.

Geochemical results reveal a rather significant increase in Ca and a decrease of Si, that is associated with the formation of grossular-rich garnet. Si depletion, as well as decrease in alkali contents is linked with clinopyroxene and anorthite breakdown dissolution during percolation of fluid-related metasomatism. Furthermore, the high field strength elements (HFSE) mostly remained stable due to preservation of clinopyroxene.

References

Koutsovitis, P., Magganas, A., Pomonis, P., Ntaflos, T., 2013. Subduction-related rodingites from East Othris, Greece: Mineral reactions and physicochemical conditions of formation, Lithos, 172-173, 139-157.

Pelletier L., Vils F., Kalt A., Gmeling K., 2008. Li, B and Be Contents of Harzburgites from the Dramala Complex (Pindos Ophiolite, Greece): Evidence for a MOR-type Mantle in a Supra-subduction Zone Environment.- Journal of Petrology, V. 49,(11), 2043-2080

Rassios, A.H.E., Moores, E.M., 2006. Heterogeneous mantle complex, crustal processes, and obduction kinematics in a unified Pindos-Vourinos ophiolitic slab (northern Greece). Geological Society of London, Special Publ.

Robertson, A.H.F., 1990. Late Cretaceous oceanic crust and Early Tertiary foreland basin development, Euboea, Eastern Greece. Terra Nova, 2, (4), 333-339.

Tsikouras, B., Karipi, S., Rigopoulos, I., Perraki, M., Pomonis, P., Hatzipanagiotou, K., 2009. Geochemical processes and petrogenetic evolution of rodingite dykes in the ophiolite complex of Othrys (Central Greece). Lithos, 113, 540–554.

16th International Congress of the Geological Society of Greece
17-19 October, 2022 - Patras, Greece
Bulletin of the Geological Society of Greece, Sp. Publ. 10
Ext. Abs. GSG2022-332

Deformation and Rheology of the Lithospheric Mantle Beneath the North Anatolian Fault

V. Chatzaras[1], A.D.J. Lusk[2], T. Chapman[3], E. Aldanmaz[4], J.R. Davis[5], B. Tikoff[2]

(1) The University of Sydney, School of Geosciences, Sydney, Australia, vasileios.chatzaras@sydney.edu.au (2) University of Wisconsin-Madison, Department of Geoscience, Madison, USA (3) University of New England, School of Environmental and Rural Science, Armidale, Australia (4) University of Kocaeli, Department of Geology, Izmit, Turkey (5) Carleton College, Department of Mathematics and Statistics, Northfield, USA

ABSTRACT

Research Highlights

- Mantle xenoliths from the North Anatolian Fault Zone (NAFZ) indicate transpressional deformation in the upper mantle.
- Microstructural observations, measurements of water concentration, and chemical signatures indicate a change in the deformation mechanisms with depth, where viscosity decreases at relatively constant differential stress.

Objectives

The nature of upper mantle deformation in plate boundary zones remains a major issue in geodynamics. It is increasingly recognized that transcurrent plate boundary fault systems extend into the lithospheric mantle and that they rarely are of strictly wrench deformation (Teyssier and Tikoff, 1999; Little et al., 2002; Vauchez et al., 2003). Open questions remain regarding the kinematics, strength, and rheology of the lithospheric mantle within transcurrent, plate boundary-scale faults.

Background

The North Anatolian Fault Zone (NAFZ) is a dominantly transcurrent fault system that accommodates dextral motion between the Eurasian and Anatolian plates. The NAFZ extends for more than 1200 km, from the Karlıova triple junction, widening to the west through the Sea of Marmara, and terminating in a series of splay faults into the northern Aegean Sea. The North Anatolian Fault (NAF), the most prominent strand of the NAFZ, formed at approximately 11 Ma in eastern Anatolia, propagating westward and reaching the Sea of Marmara around 200 ka. Segments of the NAF (e.g., Sea of Marmara, Ganos fault) were likely active during the late Oligocene and middle Miocene, (Zattin et al., 2005) suggesting that the entire section of the proto-NAFZ might have been active at that time. Geophysical investigations provide evidence for a lithosphere-scale fault zone extending beneath the surface expression of the NAFZ, particularly in the northern part. The fault zone appears to be localized along preexisting zones of weakness, specifically along the Intra–Pontide and Izmir–Ankara sutures (Sengör, 1979; Fichtner et al., 2013).

Methods

We analyzed xenoliths that sample the mantle portion of the NAFZ, in northwestern Turkey (Aldanmaz et al., 2005). The xenoliths were collected from two late Miocene volcanic centers (Biyikali and Çorlu) located north of the NAFZ, at distances of ~15 km north of the Ganos segment, and ~20 km north of the Sea of Marmara segment. The two volcanic centers are 35 km apart along the strike of the NAFZ. We studied the: 1) mineral element composition to determine the equilibration conditions and extraction depths of the xenoliths; 2) three-dimensional shape of spinel grains to constrain the orientation and shape of the spinel fabric ellipsoid; 3) hydroxyl content in silicate phases to constrain the hydration state; 4) record of fluid/melt-rock interaction in microstructures; 4) distribution of olivine crystallographic axes and low-angle misorientation axes, to determine the dominant slip systems and olivine CPO symmetry; and 5) olivine grain size to estimate differential stresses and strain rates in the upper mantle.

Results and Conclusions

The xenoliths consist primarily of spinel lherzolite and harzburgite. Equilibration temperatures of 757 to 1019 °C were estimated from two-pyroxene geothermometry. Pressures of 1.0 to 2.1 GPa – corresponding to depths of 38 to 75 km – were estimated using the Cr-in-clinopyroxene geobarometer and pseudosection modelling. We used X-ray computed tomography to quantify the three-dimensional shape preferred orientation of spinel grains. The spinel mean fabric ellipsoid in xenoliths from both volcanic centers exhibits oblate shape, indicative of flattening strain. Olivine crystallographic preferred orientation (CPO), determined by electron backscatter diffraction, exhibits chiefly axial-[010] and A-type patterns. The Çorlu xenoliths record orthorhombic CPOs and [100] maxima at intermediate to high angles to the spinel lineation. In contrast, the Biyikali xenoliths record axial-[010] olivine CPOs and olivine [100] maxima

subparallel to the spinel lineation . We interpret this difference to indicate that higher shear strains are recorded in Biyikali xenoliths, i.e. closer to the NAFZ. Consequently, we favor the interpretation that both the Biyikali and Çorlu xenoliths record deformation along the NAFZ, and the difference in fabrics is associated with distance to the fault. Furthermore, the axial-[010] CPO pattern is consistent with the spinel fabric that shows flattening strain, and is primarily developed in xenoliths from the volcanic center nearer to the NAFZ. Obliquity of olivine CPO to the spinel shape fabric suggests a component of simple shear. The results of spinel three-dimensional shape preferred orientation and olivine CPO combined, indicate transpressional deformation in the upper mantle (Chatzaras et al., 2021). Transpressional fabrics dominate at the change in orientation between the ~070-oriented Ganos segment and the EW-oriented Marmara segments of the NAFZ. This geometry results in a restraining bend in a right-lateral system, where transpressional deformation is expected.

We measured olivine and pyroxene water concentrations by Fourier transform infrared spectroscopy (FTIR). Calculated bulk rock water contents range between 4 and 50 wt. ppm H_2O, implying a relatively dry lithospheric mantle. Microstructural, lithologic, and chemical evidence, all indicate a multistage history of melt extraction and fluid-rock interaction, which may have affected mantle rheology. Differential stresses, calculated from olivine dynamically recrystallized grain size, range between 10-22 MPa. The lithospheric mantle beneath the NAFZ is therefore characterized by relatively constant differential stress, at least between 38 to 75 km depth and does not provide evidence for a pronounced rock strengthening with decreasing depth, as is inferred by rheological modelling at a constant strain rate. A total strain rate of 2.3×10^{-16} to 5.7×10^{-13} s^{-1} was obtained considering wet dislocation and diffusion creep. Strain rates positively correlate with temperature. Calculated viscosities range from 1.4×10^{19} to 3.5×10^{22} Pa s. Compared to a melt-free rheology, strain rates would be 5 to 20 times faster and viscosities 5 to 20 times lower at melt fractions of 5% and 10%, respectively. Our results suggest that deformation in the lithospheric mantle of the NAFZ was accommodated by different deformation mechanisms with depth. At relatively shallow depths (50 – 60 km), either phase or grain boundary sliding or wet diffusion creep in the presence of melt were the dominant modes of deformation. At depths exceeding 70 km, deformation was dominated by wet dislocation creep with or without melt. This type of vertical heterogeneity in deformation mechanisms and rheology has important consequences and should be accounted for in numerical models of post- and inter-seismic creep.

Acknowledgements

This research was supported by the U.S. National Science Foundation grant EAR-1629840 awarded to Tikoff and a research support grant from the University of Sydney awarded to Chatzaras. We thank Zach Michels and Saurabh Ghanekar for collecting the xenoliths, John Fournelle for his assistance with the electron microprobe analyses at the University of Wisconsin–Madison and Gordon Medaris for discussions on EPMA. We acknowledge the technical assistance of Sydney Microscopy & Microanalysis, the University of Sydney node of Microscopy Australia.

References

Aldanmaz, E., Gourgaud, A., Kaymakcı, N., 2005. Constraints on the composition and thermal structure of the upper mantle beneath NW Turkey: evidence from mantle xenoliths and alkali primary melts. J. Geodyn. 39, 277–316.

Chatzaras, V., Lusk, A.D.J., Chapman, T., Aldanmaz, E., Davis, J.R., Tikoff, B., 2021. Transpressional deformation in the lithospheric mantle beneath the North Anatolian Fault Zone. Tectonophysics 815, 10, 228989.

Fichtner, A., Saygin, E., Taymaz, T., Cupillard, P., Capdeville, Y., Trampert, J., 2013. The deep structure of the North Anatolian fault zone. Earth Planet. Sci. Lett. 373, 109–117.

Little, T.A., Savage, M.K., Tikoff, B., 2002. Relationship between crustal finite strain and seismic anisotropy in the mantle, Pacific–Australia plate boundary zone, South Island, New Zealand. Geophys. J. Int. 151 (1), 106–116.

Sengör, A.M.C., 1979. The North Anatolian transform fault: its age, offset and tectonic significance. J. Geol. Soc. 136 (3), 269–282.

Teyssier, C., Tikoff, B., 1998. Strike-slip partitioned transpression of the San Andreas fault system: a lithospheric-scale approach. Geol. Soc. Lond., Spec. Publ. 135 (1), 143–158.

Vauchez, A., Tommasi, A., Mainprice, D., 2012. Faults (shear zones) in the Earth's mantle. Tectonophysics 558, 1–27.

Zattin, M., Okay, A.I., Cavazza, W., 2005. Fission track evidence for late Oligocene and mid-Miocene activity along the North Anatolian fault in southwestern Thrace. Terra Nova 17, 95–101. https://doi.org/10.1111/j.1365-3121.2004.00583.x.

16th International Congress of the Geological Society of Greece
17-19 October, 2022 - Patras, Greece
Bulletin of the Geological Society of Greece, Sp. Publ. 10
Ext. Abs. GSG2022-346

Preserved High-Mg basalts within metasomatized dykes in the Pindos and Othris ophiolitic formations: A petrographic and petrogenetic approach

P. Koutsovitis[1], L. Tsiarsioti[1], M. Karalis[1], T. Makridou[1], A. Sideridis[1], K. Rogkala[1], P. Petrounias[1], P. Giannakopoulou[1], C. Karkalis[2]

(1) Section of Earth Materials, Department of Geology, University of Patras, Patras 26504, Greece; (pkoutsovitis@upatras.gr) (2) Centre for Research and Technology-Hellas (CERTH), Marousi, Attica, Greece

The Pindos and Othris ophiolitic formations in Greece are characterized by the incorporation of a wide variety of lithotypes, ranging from ultramafic to even felsic rocks (Pe-Piper et al. 2004, Magganas and Koutsovitis 2015, Koutsovitis and Magganas 2016). They were emplaced via overthrusting mechanisms upon platform carbonate rock formations due to the prolonged closure of the Pindos oceanic basin that took place after successive stages, which likely was affected by more than one subduction events (Dilek et al. 2007). Research studies have provided insights regarding the occurrence of boninitic and even picritic basaltic dykes in both the Pindos and Othris ophiolites (Pe-Piper et al. 2004, Koutsovitis and Magganas 2016). Petrogenetic constraints through the study of these rocks were challenging due to the fact that most lithologies in these ophiolitic formations were affected by rather extensive metasomatism and in some cases also by metamorphism (e.g. serpentinization). In this context, we report the occurrence of well preserved high-Mg basaltic rocks that were identified within the central parts of relatively thick metasomatized dyke formations, which in some cases were even affected by restricted rodingitization processes at their contact with serpentinized rocks. Petrographic observations showed that the rocks primarily comprise of well-preserved fine to medium grained subrounded clinopyroxene and plagioclase that additionally include olivine (in most cases unaltered), as well as slightly devitrified to chlorite glassy matrix. The clinopyroxene and plagioclase are in most cases present equigranularly, although porphyritic and even glomeroporphyritic textures were observed in microscale. Only few feldspar microlites were identified interacting with the residual glass, although in some cases plagioclase laths are in proximity with clinopyroxene forming variolithic textures. The olivine grains vary in size in their participating modal composition within each sample and only small-sized spinel grains were identified within olivine grains.

Geochemically, these rocks are classified as picrites and boninites, displaying relatively high Mg, Cr and Ni contents, features that denote the primitive nature of these rocks (associated with presence of olivine and spinel), whereas their relatively low LOI contents (<~2.5 wt.%) are amongst the lowest compared to other ophiolitic high-Mg basalts in Greece. They are classified as low-Ca boninites ($CaO/Al_2O_3 < 0.75$, Cooper et al. 2010), however, the picrites tend to display higher CaO/Al_2O_3 ratios, which is likely relate to higher participation of clinopyroxene within the mantle source at the early melting stages. CN-normalized plots reveal that the picrites have a more primitive nature, denoting that the boninites may have been formed after the effects of olivine, clinopyroxene and likely of plagioclase fractionation. Percolation of subduction process are confirmed by the LILE enrichments, whereas the higher Th and U normalized values compared to those of Nb and Ta further confirm the aforementioned effects. Application of the Petrolog3 software (Danyushevsky and Plechov 2011) with a 4 wt.% H_2O content revealed that the boninites were formed after slight to moderate (~10-20%) fractional crystallization processes.

References

Cooper, L.B., Plank, T., Arculus, R.J., Hauri, E.H., Hall, P.S., Parman, S.W. 2010. High-Ca boninites from the active Tonga Arc, J. Geophys. Res., 115, B10206

Danyushevsky, L.V., Plechov, P. 2011. Petrolog3: Integrated software for modeling crystallization processes, Geochem. Geophys. Geosyst., 12, Q07021

Dilek, Y., Furnes, H., Shallo, M., 2007. Suprasubduction zone ophiolite formation along the periphery of Mesozoic Gondwana. Gondwana Research 11, 453–475.

Koutsovitis, P., Magganas, A., 2016. Boninitic and tholeiitic basaltic lavas and dikes from dispersed Jurassic East Othris ophiolitic units, Greece: petrogenesis and geodynamic implications. Int. Geol. Rev. 58, 1983–2006.

Magganas, A., Koutsovitis, P., 2015. Composition, Melting and Evolution of the Upper Mantle beneath the Jurassic Pindos Ocean Inferred by Ophiolitic Ultramafic Rocks in East Othris, Greece. Int. J. Earth Sci. 104, 1185–1207.

Pe-Piper, G., Tsikouras, B., Hatzipanagiotou, K., 2004. Evolution of boninites and island-arc tholeiites in the Pindos Ophiolite, Greece. Geol. Mag. 141, 455–469.

16th International Congress of the Geological Society of Greece
17-19October, 2022 -Patras, Greece
Bulletin of the Geological Society of Greece, Sp. Publ. 10
Ext. Abs. GSG2022-370

Mass-balance modelling of the Thapsana Mangan Skarn, Paros, Greece.

M. Fitros[1], S. Tombros[2], A. Spiliopoulou[3], S. Triantafyllidis[3], S. Kokkalas[1], P. Voudouris[4]

(1) Department of Geology, University of Patras, Rion, 26504, Patras, Greece, geo11143@upnet.gr (2) Department of Material Sciences, University of Patras, Rio, Greece (3) School of Mining and Metallurgical Engineering, National Technical University of Athens, Iroon Polytechneiou 9, 15780, Zografou, Athens, Greece (4) Faculty of Geology and Geoenviroment, National and Kapodistrian University of Athens, Panepistimioupolis, Ano Ilisia 15784, Athens, Greece.

Research highlights: This study access the manganese mobility and its possible sources in the Thapsana mangan skarn by using mass balance modelling at constant volume over distance and the Isocon method. There is an overall increase of the MnO content in the skarns over distance which is coupled with a decrease of the MnO content in the Thapsana leucogranite and Cycladic Basement gneiss which indicates manganese contribution from both sources. The intense-to-strong loss of MnO from the leucogranite to Rdn zone (-97%) and gneiss (-55%) obtained from the Isocon method suggests the leucogranite as the main source for manganese in Thapsana mangan skarn.

Background and objectives

Mangan skarns and related manganese-oxide ore deposits are quite rare. A distinctive case of a mangan skarn in the Attico-Cycladic Massif is exposed at Thapsana mines, Paros Island. The mangan skarn occurs as lenses and NE-trending veins adjacent to the Thapsana peraluminous leucogranite hosted in the Cycladic Basement (CB) gneisses and Blueschist Unit (CBU) calcic schists, amphibolites and marbles intercalations (Fitros et al., 2018). The Thapsana mangan skarn comprises three metasomatic zones, with widths ranging up to 20 m (Fig. 1a). The Rhodonite (Rdn) zone occurs adjacent to the marbles and schists comprising rhodonite ± vesuvianite. The Rdn zone grades into the Johannsenite-Spessartine (Jhn-Sps) zone closer to the Thapsana leucogranite, comprising johannsenite and spessartine that intergrow with jacobsite, hausmannite, braunite and magnetite (stage I ore Mn-oxides). Then, the Spessartine-Cummingtonite (Sps-Cum) zone, which is closer to the Thapsana leucogranite, comprises spessartine, cummingtonite ± hornblende and phlogopite. The Sps-Cum zone is related to stage II ore Mn-oxides, comprising hollandite, cryptomelane, pyrite with gangue rhodochrosite, calcite and ankerite.

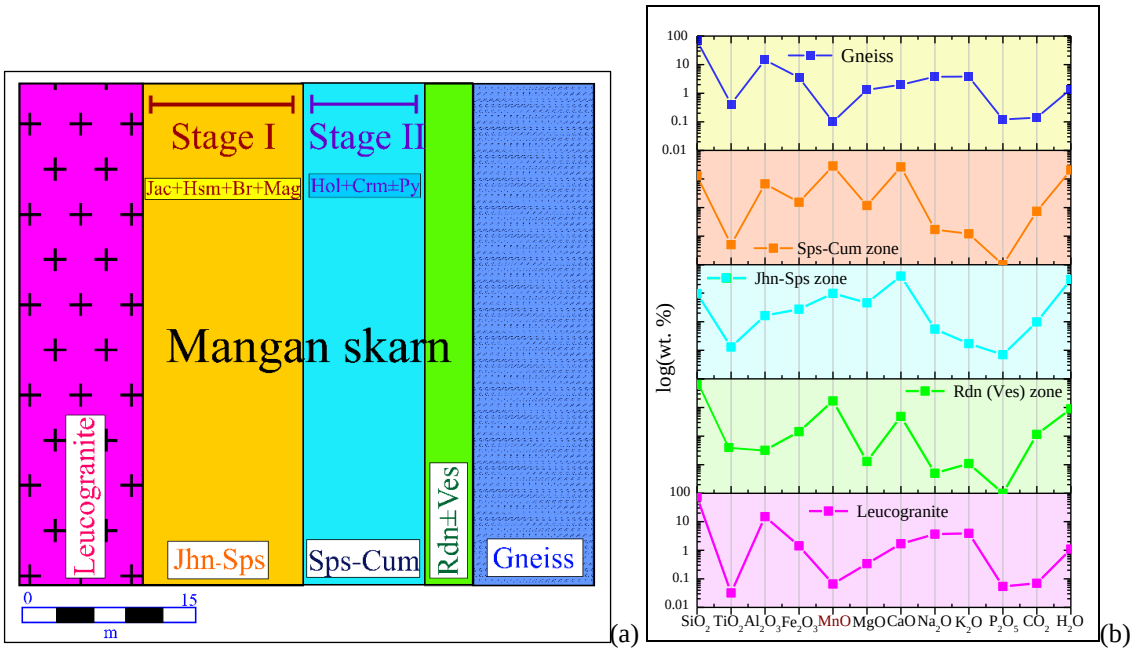

Figure 1. a) Schematic metasomatic zonation patterns at Thapsana mangan skarn from leucogranite (left) to gneiss (right) (Stage I ores: Jac = Jacobsite, Hsm = Hausmanite, Br = Braunite, Mag = Magnetite; Stage II ores: Hol = Hollandite, Crm = Cryptomelane, Py = Pyrite, Minerals abbreviations: Rdn = Rhodonite, Ves = Vesuvianite, Jhn = Johannsenite, Sps = Spessartine, Cum = Cummingtonite), b) Geochemical variations and constant volume mass balance calculations over distance (in meter-scale) from Thapsana leucogranite to host gneiss of CB.

Despite the wide acceptance of the Korzhinskii (1970) theory for metasomatic transport, there are no attempts to test his conceptual modelling in mangan skarns using petrochemical data. This study on manganese metasomatism associates with mass-balance modelling in order to quantify the mass transport and element mobility from Thapsana leucogranite and host CB gneiss, respectively towards the mangan zones.

Results and discussion

Constant volume mass balance calculations over distance (Fig. 1b) suggest a decrease of SiO_2 and TiO_2, and an increase of Fe_2O_3 and P_2O_5 from the Thapsana leucogranite towards the CB gneiss, which is interpreted as silicification of the host gneiss and precipitation of magnetite, apatite and phlogopite in the skarns and gneiss. A decrease of Al_2O_3 in the Rdn zone, coupled with an increase of the Fe_2O_3 contents in the Rdn and Jhn-Sps zones is attributed to the formation of rhodonite, johannsenite and spessartine. In the mangan zones, i.e., Rdn, Jhn-Sps and Sps-Cum zone an overall increase of their MnO contents is recognized, while there is a decrease of the MnO contents in leucogranite and gneiss which indicates manganese contribution from host lithologies in the metasomatic fluid. The MgO content decreases in the Sps-Cum zone due to the formation of cummingtonite. CaO contents increase both in leucogranite and gneiss, as well as in the three mangan skarn zones, most probably due to its competition with manganese, as calcium cannot easily enter into the manganoan minerals or Mn-oxide ores. The enrichment of calcium also suggests that diffusion was the metasomatic process prevailed during the mangan skarn formation. Finally, the CO_2 and H_2O contents increase from the Thapsana leucogranite towards the CB gneiss as the manganoan assemblages evolve from anhydrous (Rdn zone) to hydrous (Sps-Cum zone), reaction with surrounding rocks (Ca-gneiss and marble) and the coeval precipitation of rhodochrosite, calcite and ankerite (Fig. 1b).

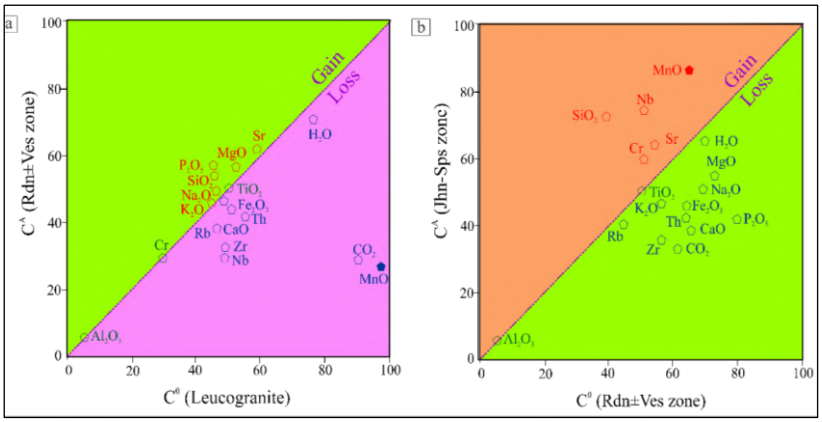

Figure 2. Representative Isocon plots after Grant (2005) displaying major and trace element gains and losses and MnO mobility from Thapsana peraluminous leucogranite towards the Rdn and Jhn-Sps skarn zones.

Additionally, we have applied the Isocon method of Grant (2005) to access the manganese mobility and its possible sources that contributed in the Thapsana mangan skarn. Manganese mobility is established by the deviation of major and trace elements from the line of constant mass denoted by the Al_2O_3 isocon, as Al_2O_3 as well as TiO_2 were immobile during mangan metasomatism (Fig. 2). The slope of isocon line defined by Al_2O_3 and TiO_2 has values of 0.44±0.01 which corresponds to ~ 40% increase of the total mass of the skarns during mangan metasomatism. Strong-to-medium gain of silica, water and alkalis in the Rdn and Jhn-Sps zones and the CB gneiss are related to the formation of anhydrous minerals (Rdn) as well as the silicification, albitization and sericitization of gneiss (see McGrath, 1999). Fe_2O_3, MgO, P_2O_5, Na_2O, Nb, Zr depletion suggest the precipitation of jacobsite, magnetite, phlogopite, apatite and cummingtonite. Loss of CO_2 from the leucogranite to the Rdn, Jhn-Sps zones and gneiss is attributed to the decarbonation reactions between the manganese-rich metasomatic fluid released from the leucogranite and the host rocks (i.e., CB gneiss and CBU marbles). Intense-to-strong loss of MnO from the leucogranite to Rdn zone (-97%) and gneiss (-55%) suggests the leucogranite as the main source for the manganese.

References

Fitros, M., Tombros, S. F., Simos, X.C., Kokkalas, S., and Hatzipanagiotou, K., 2018. Formation of Mn-skarn ores at Thapsana Mines, Paros Island, Attico-Cycladic Metallogenetic Massif, Greece, in Proceedings of the 1st International Electronic Conference on Mineral Science, p. 16-31, doi:10.3390/IECMS2018-05461.

Grant, J.A., 2005. Isocon analysis: A brief review of the method and applications: Physics and Chemistry of the Earth, 30, 997-1004.

Korzhinskii, D. S., 1970. Theory of metasomatic zoning (translated by J. Agrell), Oxford University Press, London.

McGrath, A.G., 1999. Structural and geochemical evolution of an extensional metamorphic core complex, Paros, Greece: Unpublished PhD thesis, University of Leicester, p. 196.

16th International Congress of the Geological Society of Greece
17-19 October, 2022 - Patras, Greece
Bulletin of the Geological Society of Greece, Sp. Publ. 10
Ext. Abs. GSG2022-401

Petrology and geochemistry of sandstones from the Eocene Flysch, Astypalaia Island, Dodecanese, Greece.

M. Kokkaliari[1], C. Kanellopoulos[1,2], I. Illiopoulos[1]

(1) Department of Geology, University of Patras, 26504 Patras, Greece, kokkaliari_m@upnet.gr (2) Faculty of Geology and Geoenvironment, National and Kapodistrian University of Athens, Panepistimiopolis, Zografou, 15784, Athens, Greece

Introduction

The study of sedimentary rocks yields important information about the tectonic evolution of an area, the paleoclimate conditions that occurred, and even the eventual exploitation of hydrocarbons. The purpose of this study is to thoroughly examine the petrographic features and the geochemical composition of sandstones of the Eocene Flysch, from the Astypalaia Island, Dodecanese, Aegean Sea, Greece. Petrographic and geochemical analysis are methodologies of fundamental importance, contributing in describing the mineralogical components and the texture of the lithology, the chemical composition of the material, as well as evaluating the nature of the source rocks and their depositional environment.

Geological Background

Astypalaia island is composed of sedimentary rocks, including Alpine as well as meta-Alpine lithologic formations (Christodoulou, 1966; Marnelis and Bonneau, 1977; IGME, 1986; Ring, 2001; Drouga, 2002; Chatzaras, 2010; Papoulia et al., 2013). More specifically, the geological structure of the island consists mostly of carbonate rocks (Upper Jurassic – Paleocene). The largest part of the western Astypalaia comprises Flysch (Upper Eocene – Oligocene) of pelitic composition, whereas conglomerates and sandstones also occur in higher horizons (IGME, 1986). The carbonate rocks include Upper Jurassic crystalline limestones, Senonian-Maastrichtian bituminous limestones, and Paleocene to Middle Eocene nummulitic limestones.

Materials and methods

A total number of 21 samples were collected in different sampling sites, at Vathy, Analipsi and Livadi peninsulas, in order to represent as many as possible sandstone occurrences. Each sample was used to prepare petrographic thin sections, studied by means of transmitted light microscopy. Furthermore, a small portion of it ware pulverized and homogenized in order to perform the mineralogical analysis by Powder X-Ray Diffraction Analysis to verify the mineral mode, as well as the geochemical analysis by X-Ray Fluorescence Spectroscopy to study the chemical composition.

Results and Conclusions

The petrographic study revealed similar mineralogical paragenesis among the samples (Figure 1A), usually including quartz, feldspars (mostly plagioclase), calcite, illite/muscovite, chlorite and opaque minerals. Most of the samples seem moderate to poorly sorted often characterized by cataclastic texture.

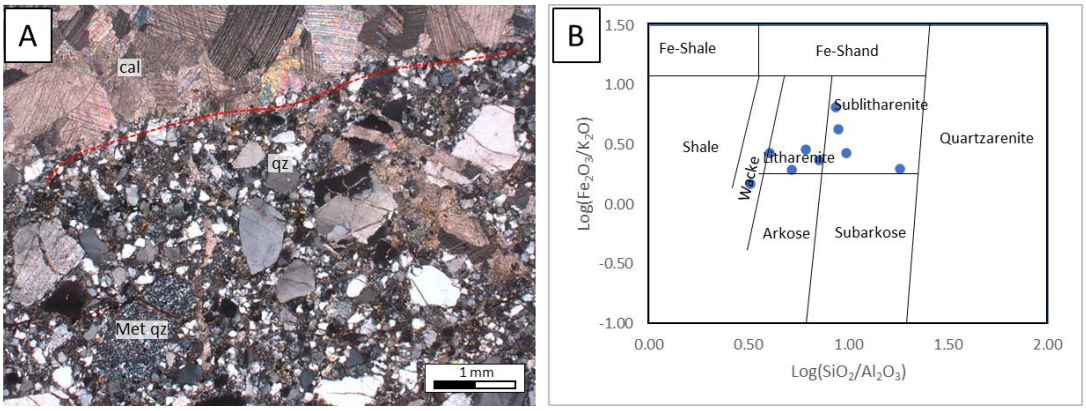

Figure 1: A. Representative microphotograph showing subangular, fragmented grains of quartz (qz) and metamorphic quartz (met qz) as well as the presence of calcite (cal) veins; B. Geochemical classification of sandstones (Herron, 1988).

The sorting of the mineralogical components probably represents a short distance of transportation and deposition of the material from the source rock. The presence of undulose extinction in quartz, micro-brecciated zones, fragmented crystal margins, as well as micro-foliations, indicate intense tectonic activity. In the $Log(Fe_2O_3/K_2O)$ *vs* $Log(SiO_2/Al_2O_3)$ discrimination diagram (Figure 1B), the samples are dispersed in many different fields representing shales, graywacke,

litharenite and sub-litharenite, and Fe-sand. In the major element Discriminant Function diagrams (DF), the studied samples are plotted mostly in the fields of quartz sedimentary, as well as felsic to intermediate igneous provenance, indicating a mixed source area. Many discrimination diagrams were used in order to enlighten the tectonic evolution of the area, where the samples are plotted mostly in the field of passive continental margins as well as in the continental island arc. The Plagioclase Index of Alteration (PIA) vs the Chemical Index of Alteration coincide with moderating towards intensive chemical weathering. The $Al_2O_3+K_2O+Na_2O$ *vs* SiO_2 imply that the sediments have deposited under humid and arid paleoclimate conditions, from cooler to hotter climate conditions. The results thatemerged from the present study are in agreement with the geotectonic evolution of the Aegean and the available literature and shed light in provenance issues of the source material.

References

Chatzaras, V. 2010. Geotraverse across the Hellenides between western Crete and the Cycladic islands, PhD dissertation, University of Patras, Greece, 206 p.

Christodoulou, G. 1966. About the geology of Astypalaia island. Scientific yearbook: issued by the Faculty of Natural and Mathematical Sciences 10, 169-180, Aristotle University of Thessaloniki, Greece.

Herron, M.M., 1988. Geochemical classification of terrigenous sands and shales from core or log data. Journal of Sedimentaty Petrology, 58, 820–829.

IGME, 1986. Geological map of Greece 1:50000, Astipalaia sheet: IGME, Athens

Marnelis, P., Bonneau, M. 1977. Stratigraphie et structure de l'île d'Astypalea (Dodécanèse, Grèce), In: G. Kallergis (ed.), VI. Colloquium on the geology of the Aegean Region 1, 323-332.

Papoulia, M., Karymbalis, E., Gaki-Papanastassiou, K., Maroukian, H. 2013. Assessment of the susceptibility of the coast of Astypalea Island (SE Aegean Sea) to sea-level rise, Bulletin of the Geological Society of Greece, vol. XLVII, No1: 305-314

Ring, U. 2001. Structure and deformation history of Astypalea island, Aegean Sea, Bulletin of Geological Society of Greece 34, 329-335.

Drouga, A. 2002. The effect of volcanic ash sedimentation and dispersion at the present and modern marine sediments of Kos, Nissyros and Astypalea islands (SE Volcanic Arc), Aegean Sea, Greece, PhD dissertation, Aristotle University of Thessaloniki, Greece, 240 p.

16th International Congress of the Geological Society of Greece
17-19 October, 2022 - Patras, Greece
Bulletin of the Geological Society of Greece, Sp. Publ. 10
Ext. Abs. GSG2022-412

Metamorphic conditions in West Rhodope massif, at Northern Drama area, Northeast Greece: preliminary results

M. Karapantzos[1], M. Kokkaliari[1], C. Kanellopoulos[2], C. Katagas[1] and I. Illiopoulos[1]

(1) Department of Geology, University of Patras, 26504 Patras, Greece, m_karapantzos@upnet.gr (2) Faculty of Geology and Geoenvironment National and Kapodistrian University of Athens, Panepistimiopolis Zografou, 15784, Athens, Greece.

Introduction

Drama area, is located in northeast Greece and comprises part of the Rhodope massif (RM), which has triggered the interest of many researchers in the field, due to the multiple metamorphic events recognized therein. More specifically, detailed petrological studies have shown that RM is influenced by three successive major metamorphic events including high pressure, medium pressure and retrograde metamorphism (Mposkos and Krohe, 2000).

Geological Background

The geological structure of the studied area is differentiated in two distinct tectonic units, i.e. the Lower and the Upper Unit, representing different metamorphic conditions (Mposkos and Kostopoulos, 2001; Mposkos and Krohe, 2000; Mposkos and Liati, 1993). The Lower Unit was subjected o lower grade of metamorphism and comprises ortho-gneisses, metabasites, marble and meta-sediments. The Upper Unit, is metamorphosed under a higher grade, and consists of basic igneous rocks and metabasites, ophiolitic rocks, ortho- and para- gneisses, as well as marbles. The aim of this work is to characterize the metamorphic events taken place in this region, by means of thorough petrological study and geochemical analyses conducted on representative samples of the various lithotypes cropping out in the study area.

Samples and Methodology

A total of 108 samples were collected from the study area during geological reconnaissance conducted by one of the co-authors (C.Katagas). Petrographic thin sections were prepared for each sample and studied by means of transmitted light microscopy under a Zeiss AxioScope A.1 polarizing microscope in order to determine the rock types and mineral modes. The mineralogy of the samples was further verified by means of X-Ray Powder Diffraction analysis (XRPD) employing a D8 Advance Bruker system in the Mineral and Rock Research Laboratory of the Department of Geology, University of Patras, Greece. The mineral chemistry was studied by means of Scanning Electron Microscopy (SEM/EDS). Furthermore, geochemical analysis helped us classify the rocks according to their protolith employing Wavelength Dispersive X-Ray Fluorescence analysis (XRF/WD), both performed at the Hellenic Survey of Geology and Mineral Exploration – HSGME, Greece.

Results and Conclusions

The petrographic examination of the studied samples offered important information about their mineralogical assemblages, indicating not only differences in the chemical composition of the protolith, but also characterizing the associated grade of metamorphism. The parageneses recognized suggest metamorphic conditions of greenschist to amphibolite facies, whereas the available geochemical data helped us to infer about the chemical composition of the protolith and determine the starting composition of the metamorphic assemblages. Low- to medium-grade metamorphic conditions of greenschist facies are characterized by the coexistence of chlorite, white mica, garnet, chloritoid and epidote (Figure 1a). The increase of the metamorphic grade to amphibolite facies is accompanied by the formation of hornblende, scapolite and pyroxene (Figure 1b). The presence of Fe-rich to Mg-rich mica (Figure 1c), and almandine which were also attested through SEM/EDS analysis, verify the petrographic observations, concluded from the mineralogical paragenesis, indicating a gradual increase in the metamorphic conditions. In rock classification diagrams the metasediments indicate sand, shale, wacke, litharenite and arkose as their potential protoliths (Figure 1d). The geochemical characteristics of meta-carbonate rocks show pure calcite and calcite-dolomite marble, as well as impure calcite marble. Finally, the geochemical features of the metabasites as well as the composition of the analyzed minerals, including chlorite, plagioclase, and amphibole among others, show a range from mafic to more acidic meta-igneous rocks. The preliminary results presented herein offer important insight to the metamorphic evolution of the area, and will help us shed further light on the P-T conditions prevailed during the metamorphism of the various lithologies.

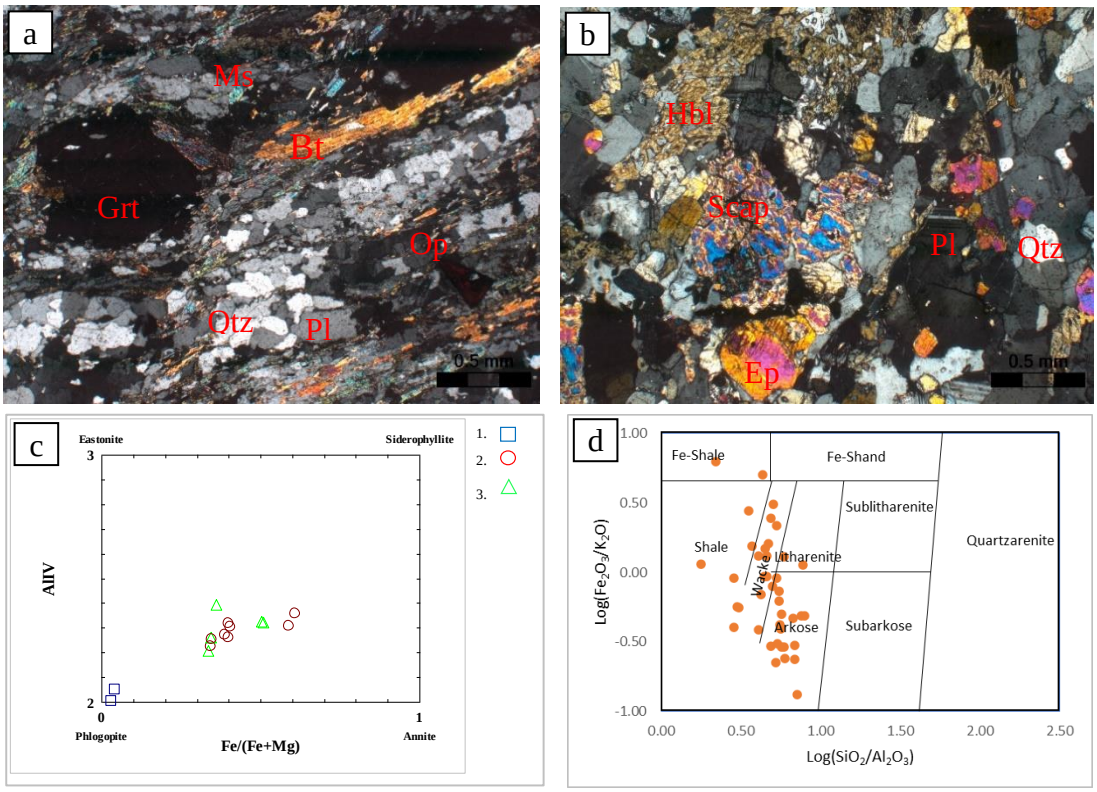

Figure 1. a) Representative microphotograph of metapelite b) Representative microphotograph of metabasite. c) Compositional range of Fe,Mg-rich mica group. D) Classification diagram of meta-sedimentary rocks modified from Herron (1988). Symbols : 1=Meta-carbonate rocks, 2=Metasedimentary rocks and 3=Metabasic rocks. Mineral abbreviations: Scap=Scapolite, Qtz=Quartz, Pl=Plagioclase, Bt=Biotite, Ms=Muscovite, Ep=Epidote, Hbl=Hornblende, Op=Opaque

References

Mposkos, E., Kostopoulos, D. 2001. Diamond, former coesite and supersilicic garnet in metasedimentary rocks from the Greek Rhodope: a new ultrahigh-pressure metamorphic province established, Earth and Planetary Science Letters 192, 497-506.

Mposkos, E., Krohe, A. 2000. Petrological and structural evolution of continental high pressure (HP) metamorphic rocks in the Alpine Rhodope Domain (N. Greece), in: Panayides, I., Xenophontos, C., Malpas, J. (Eds), Proceedings of the Third International Conference on the Geology of the Eastern Mediterranean, Geological Survey of Cyprus, Nicosia, pp. 221-232.

Mposkos E., Liati, A., (1993). Metamorphic evolution of metapelites in the high pressure terrane of the Rhodope zone Northern Greece, The Canadian. Mineralogist., 31, 401-424

Herron, M.M., 1988. Geochemical Classification of Terrigenous Sands and Shales from Core or Log Data. Journal of Sedimentary Petrology, vol. 58, no. 5, pp. 820-829.

16th INTERNATIONAL CONGRESS of the
GEOLOGICAL SOCIETY OF GREECE

S6. The Hydrocarbon prospectivity of SE Mediterranean: targets and opportunities

OUR EARTH, OUR HOME

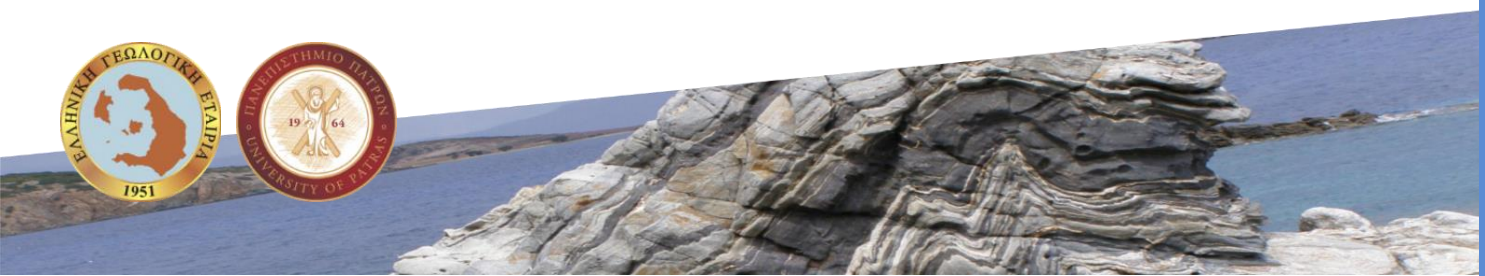

16th International Congress of the Geological Society of Greece

17-19 October, 2022 - Patras, Greece

Bulletin of the Geological Society of Greece, Sp. Publ. 10

Ext. Abs. GSG2022-034

The Lower Cretaceous "Vigla" shales potentiality to be source rocks in Ionian Basin based on TOC geochemical analysis, Greece

Nicolina Bourli[1], Nikolaos Pasadakis[2], Eleni Chamilaki[2], Maria Sianni[2], Avraam Zelilidis[1]

(1) Laboratory of Sedimentology, Department of Geology, University of Patras, 26504 Patras, Greece, n_bourli@upnet.gr
(2) Mineral Resources Engineering Department, Technical University of Crete, Chania, Greece

The Mesozoic-Paleogene Ionian basin is part of the external Hellenides orogen, bounded westwards by the Ionian Thrust and eastwards by the Gavrovo Thrust. From Triassic to upper Jurassic the basin was characterized by a pre-rift stage; whereas from upper Jurassic to early Eocene by a rift stage. During the rift-stage, the basin was sub-divided into subbasins (internal, middle, and external) due to synchronous activity of synthetic and antithetic normal faults that produced grabens and highs. The lower Cretaceous "Vigla shales" is suggested as a main source for hydrocarbon production in Ionian basin, according to previous published works. Therefore, geochemical analysis took place only in lower Cretaceous Vigla shales in both studied areas Kastos Island (external Ionian sub-basin) and NW Peloponnesus (Araxos peninsula in Gianiskari coast) (Internal Ionian sub-basin) (Fig. 1). Vigla shales ranges from 0-100m, due to the accumulation into asymmetrical subsided troughs and so on, it could be different organic carbon accumulation along and across the above asymmetrical troughs. Moreover, are composed by yellow marly or shally limestones and shales with chert intercalations, and red to green or locally black clay layers. The latter could be equivalent with the anoxic events of Selli (OAE1a) during the Aptian-Albian, Paquier Evet (OAE1b) of Early Albian age in the Ionian zone and extends to Italy and Albania.

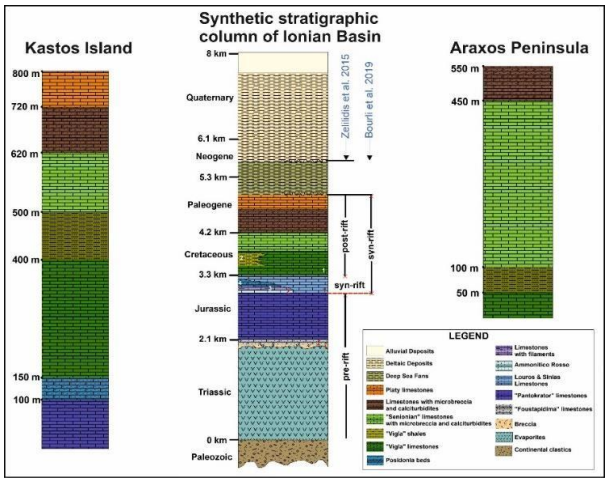

Figure 1. Detailed synthetic lithostratigraphic columns, from Kastos Island and Araxos peninsula, in relation with the synthetic stratigraphic column of Ionian zone (modified from Zelilidis et al., 2015).

Seventeen (17) samples, from Kastos Island, and thirty-one (31) samples (Figs. 2,3), from Araxos peninsula, were selected for further analysis. For the geochemical analysis ROCK-EVAL VI pyrolysis was used to show the content and quality of total organic carbon (TOC) for further analysis. The obtained data showed that TOC (0.02-3.45%) indicating good oil potential and a type II/III kerogen with the ability to produce liquid and gaseous hydrocarbons, for Kastos Island, and TOC (0.01-0.72%) with fair oil potential and type IV kerogen for Araxos peninsula (Fig. 4). The procedure was followed for further analysis was the extraction SOXHLET, and the determination of biomarkers. Four samples from Kastos Island were capable to show values, and their results based on the Odd to even predominance, OEP (27-31), OEP (2) and OEP (1), an anoxic deposition environment was indicated. The fact that there is a great difference in geochemical indices between the two studied areas during the same period, probable different depositional conditions are suggested. It seems that, the richness in Kastos Island could be related with the neighboring Apulian Platform. On the other hand, the poorness in Araxos peninsula could be related with the Gavrovo platform. An additional problem for the above differences could be the fact that these two studied areas probably are not connected to each other due to the existing intrabasinal highs that developed at the beginning of the rift stage and there are not transfer faults to connect them. Although sedimentation in Vigla shales interpreted as pelagic and basin configuration influenced by synthetic and antithetic normal faults, it seems that the presence of few samples in both areas showing terrestrial input during sedimentation could be related with the neighboring platforms.

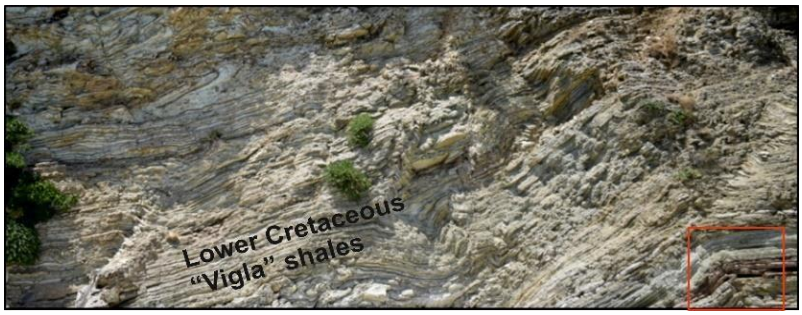

Figure 2. Representative section in Kastos Island of lower Cretaceous "Vigla shales" from where most of the samples were selected.

Figure 3. The studied outcrop along the Araxos peninsula (Gianiskari coast) with the lower Cretaceous "Vigla" shales overlying lower Cretaceous "Vigla" limestones and underlying the upper Cretaceous "Senonian" limestones (white dashed lines mark the two boundaries). Many normal faults cross-cut the sedimentary association of Vigla shales (red dashed lines) during sedimentation producing synsedimentary slumps (white circle).

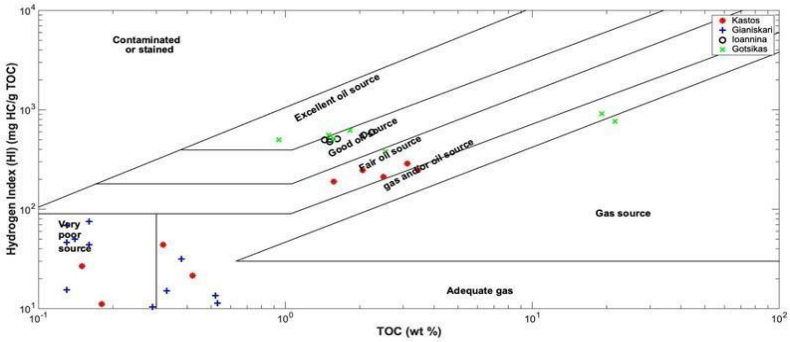

Figure 4. Diagram HI-TOC.

In other studied areas (e.g. Epirus region, according to Rigakis & Karakitsios, 1998, for middle and internal Ionian subbasins) it seems that the geochemical conditions are quite different, showing and suggesting that "Vigla" shales could be very interesting source rocks (Fig. 4). The above difference either between Epirus region (internal and middle Ionian subbasins) and between the two studied areas (internal and external Ionian sub-basins) could be related with different tectonic activity that influenced depositional conditions in these two regions, as this also highlighted by Bourli et al. (2019) studding the siliceous concretions in Kastos Island and Araxos peninsula. It seems that the great differences internal to the same sub-basin (Ioannina region VS Araxos Peninsula that belongs to the internal Ionian sub-basin) and between different sub-basins (Araxos peninsula from internal Ionian sub-basin and Kastos Island from external Ionian sub-basin) could be related with the presence-activity of transfer faults. Ionian basin cross cutted by several transfer faults, like Ag.Kyriaki, Alevrada, Amvrakikos transfer faults producing restrictions from one region to the other.

Keywords: Geochemical analysis, TOC, source rocks, Kastos Island, Araxos peninsula

References

Bourli, N., Pantopoulos, G., Maravelis, A.G., Zoumpoulis, E., Iliopoulos, G., Pomoni-Papaioannou, F., Kostopoulou, S. and Zelilidis, A., 2019. Late Cretaceous to Early Eocene geological history of the eastern Ionian Basin, southwestern Greece: An integrated sedimentological and bed thickness statistics analysis. Cretaceous Research 98, 47-71.

Rigakis, N. and Karakitsios, V., 1998. The source rock horizons of the Ionian Basin (NW Greece). Marine and Petroleum Geology 15, 593–617.

Zelilidis, A., Maravelis, A.G., Tserolas, P. and Konstantopoulos, P.A., 2015. An overview of the petroleum systems in the Ionian Zone, onshore NW Greece and Albania. Journal of Petroleum Geology 38, 331-348.

16th International Congress of the Geological Society of Greece
17-19 October, 2022 - Patras, Greece
Bulletin of the Geological Society of Greece, Sp. Publ. 10
Ext. Abs. GSG2022-048

Upper Triassic to lower Jurassic Plattenkalk series, south Peloponnesus and Crete Island, could represent source rocks

N. Bourli[1], N. Pasadakis[2], G. Iliopoulos[3], G. Makrodimitras[4], A. Nikitas[4], A. Stefatos[4], A. Zelilidis[1]

(1) Laboratory of Sedimentology, Department of Geology, University of Patras, 26504 Patras, Greece, n_bourli@upnet.gr. (2) Mineral Resources Engineering Department, Technical University of Crete, Chania, Greece (3) Laboratory of Paleontology and Stratigraphy, Department of Geology, University of Patras, 26504 Patras, Greece (4) Hellenic Hydrocarbon Resources Management S.A., Athens, Greece.

The Plattenkalk series (PS) represent the autochthonous or para-autochthonous series outcropping in Gythion-Sparta region, south Peloponnesus, and along the Crete Island, and it is considered as the equivalent to the Ionian Zone in Western Greece.

The PS is characterized as a high-pressure and low temperature metamorphic series (Fassoulas, 1978), and comprise generally a carbonate sequence up to 5km thick. The Ionian basin, and particularly the part of Upper Triassic to Lower Jurassic, consist of Triassic evaporites that pass upwards to Triassic breccia and the Foustapidima limestones and finally to Pantokrator limestones (Fig. 1). Under the Triassic evaporites, there are the Palaeozoic deposits, but they do not outcrop in western Greece. In Gythion-Sparta region, the autochthonous PS consist of dolomites, crystalline limestones, and massive marbles, up to 500m thick. PS are compared with the Pantokrator limestones of Western Greece, and they rest unconformably over Permian to Lower Triassic Phyllite basement, with up to 500m thick-outcropped deposits (Fig. 2). The characteristic point for this region is the absence of Triassic evaporites and that they unconformably overlying on the Palaeozoic (Permian) or on Upper Triassic to Lower Jurassic deposits.

Figure 1. Bedded Foustapidima formation in Igoumenitsa region. Figure 2. The deformation of Foustapidima formation due to intrusions/diapirs from the underlying.

In Crete Island, PS consist of Upper Carboniferous-Lower Permian to Eocene age deposits. Metamorphic conditions took place during Oligocene to Upper Miocene in HP-LT conditions. There are differences from west to east and from north to south in Crete Island (Figs 3,4).

In detail, PS to the east consist of dolomites and dolomitic limestones, with an outcropped thickness up to 800m. In the middle area, the PS consists of dolomites and dolomitic limestones, of Upper Triassic to Lower Jurassic age, with up to 300m thickness, which lie above banded recrystallized dolomitic stromatolites of middle Triassic age, up to 150m thick, or recrystallized limestones to marbles and dolomites, up to 100m thick. In Western Crete, the PS consists of Upper Triassic age variegated formation of schists, recrystallized limestones, and quartzite, up to 100m thick, recrystallized limestones and dolomites, up to 300m thick, and evaporites, with an outcropped thickness up to 300m (Fig. 5). The stromatolites with the interbedded black shales, the upper part of Triassic evaporites with the interbedded shales and the black Foustapidima formation, either as bedded or as deformed by diapirs – intrusions of evaporites or as interbedded with shales (Fig. 6). Depositional conditions and age determination (from selected thin sections) that are under consideration will evaluate previous mentioned indications from the field observations. Considering the above, the PS

deposits further to the west of the Crete Island could represent a potentially new source rock in the area, due to the difference in the burial history of this area.

Figure 3. Evaporites interbedded with Foustapidima carbonates. Figure 4. The Schist/shales under the Foustapidima formation and over them the grey dolomites.

Figure 5. Triassic evaporites interbedded with black schist/shales horizons. Figure 6. Interbedded black schist/shales with black carbonates and stromatolites.

PS and especially the part of Upper Triassic to Lower Jurassic deposits showed many similarities with the equivalent age deposits of Ionian basin. There are some differences concerning the Triassic evaporites, the presence of equivalent to evaporites Triassic stromatolites, the transitional deposits from evaporites to carbonates or to shales, and the Foustapidima formation just under the Pantokrator limestones. The thickness of each formation differentiates laterally, suggesting different depositional conditions.

Rock-Eval pyrolysis results showed that for the Ionian Basin, the most interesting samples are from Triassic Breccia and Foustapidima formation, in the southern studied area, close to Igoumenitsa, Parga and Vonitsa (TOC content is up to 0.90%). Additionally, the Jurassic shales north from Petousi Strike-slip fault are quite interesting (TOC is up to 5.5% and S2 up to 34 mg/g). For the southern Peloponnesus (Gythion-Sparta region), the most interesting beds are these under Pantokrator carbonates which are black shales with low metamorphosis and with an exposed thickness up to 100m, in an distance up to 7km, and with TOC content up to 0.57%. For Crete Island, the most interesting samples are from western Crete and especially from Paleozoic shales, in Bali village with TOC content up to 0.52%, and Triassic stromatolites and shales internally to Foustapidima formation, before Sisses village, in Central Crete Island, with TOC content up to 1.3%. The studied part of the PS could represent source rocks and especially three possible source rocks/formations are indicated. 1. The stromatolites with the interbedded black shales, 2. The upper part of Triassic evaporites with the interbedded shales and 3. The black Foustapidima formation, either as bedded or as deformed by diapirs intrusions of evaporites or as interbedded with shales.

Further work is needed also for the Phyllite-Quartzite series, as they showed TOC content up to 1.2%.

Keywords: Plattenkalk series, Foustapidima formation, Upper Triassic breccia, Rock-Eval analysis.

Acknowledgements

Nicolina Bourli is a Post-Doc Researcher, and she was financially supported by the “Hellenic Hydrocarbon Resources Management S.A. (HHRM S.A.)”. Authors would like to thank reviewers for their improvements on the manuscript.

References

Bourli, N., Kokkaliari, M., Dimopoulos, N., Zoumpouli, E., Iliopoulos, G. and Zelilidis, A., 2021. Comparison between siliceous concretions from the Ionian basin and the Apulian platform margins (Pre-Apulian zone), western Greece: implication of differential diagenesis on nodules evolution. Minerals 11(8), 890.

Fassoulas, C., 1998. The structural evolution of central Crete: insight into the tectonic evolution of the south Aegean (Greece). Journal of Geodynamics 27, 23-43.

16th International Congress of the Geological Society of Greece

17-19 October, 2022 - Patras, Greece

Bulletin of the Geological Society of Greece, Sp. Publ. 10

Ext. Abs. GSG2022-090

Nodular and bedded cherts as potential hydrocarbon source rocks in the Ionian Zone, Western Greece

E. Manoutsoglou[1], N. Rigakis[2], T. Thanos[2], V.I. Makri[1,3], N. Pasadakis[1,3]

(1) School of Mineral Resources Engineering, Technical University of Crete, University campus, 73100 Chania, Greece emanoutsoglou@tuc.gr, (2) Hellenic Petroleum Group of Companies, 8A Chimarras str, 15125 Maroussi, Athens, Greece, (3) Institute of GeoEnergy (FORTH/IG), Foundation for Research and Technology, M1 Building, University campus, 73100 Chania, Greece.

Source rock horizons of high hydrocarbon generation potential have been identified within multiple Alpine formations of the Ionian and Paxos zones of Greece. Yet, such horizons have not been identified in the neighboring Gavrovo zone, illustrating the importance of these two zones. The Ionian zone has a long hydrocarbon exploration history, with five main source rock horizons recognized. These are Triassic shale fragments incorporated into the Triassic breccias-evaporite formation. Lower Posidonia beds of Toarcian-Aalenian age, Upper Posidonia beds (Callovian-Tithonian) and Vigla shales (Cenomanian-Turonian). The most significant source rock of the central and western areas of the Ionian are the Lower Posidonia beds, while for the eastern areas are the Vigla shales (Rigakis & Karakitsios, 1998).

Regardless the identification of these five main source rock horizons, there is no reference on the possible microorganisms responsible for the increased TOC content in these horizons, but the main oceanic anoxic events which are responsible for the preservation of the organic matter have been studied. The well-known OAEs are the following: "Posidonienschiefer Event" of Early Toarcian age, "Selli Event" of Early Aptian, "Paquier Event" of Early Albian and the '"Bonarelli Event" of Cenomanian – Turonian age amongst others, which lead to the accumulation and preservation of organic matter. What is more, over the last decades, organic petrology and micro-spectroscopy have been used for the documentation of in situ molecular conversion and breakdown of prasinophyte (green) algae Tasmanites, as well as sponges, to petroleum during thermal maturation (Vigran, 2008).

The diagenetic evolution of nodules and siliceous beds in the early Cretaceous Vigla deposits and late Cretaceous Senonian deposits outcropping in the NW Peloponnesus (Araxos–Gianniskari area) and Kastos island, have been recently studied, highlighting that the quartz is the dominant mineral with rare to common residual calcite. The presence of moganite and opal-A minerals suggests that quartz recrystallized from original amorphous silica. A few samples from Araxos contain traces of halite and anhydrite which were associated with a different tectonic activity of these specific areas, whereas the presence of maghemite is due to the presence of iron minerals in water solutions (Bourli et al., 2019).

Following the tectonic reconstruction of Tethys during Permian/Triassic (Dornsiepen et al. 2001), major reefs were developed by the Upper Triassic and mainly during Upper Jurassic. The Upper Jurassic reefs are widespread within the shelf bordering the northern Tethyan Ocean, which today extends from Romania to Poland, southern Germany, Switzerland, France, eastern Spain to south Portugal (Keupp et al. 1990) as well as the marginal basins of the young North Atlantic Ocean. They developed in a variety of settings, ranging from the innermost platform to outer ramp settings. Compositionally they comprise the end members «coral facies», «siliceous sponge facies» and «microbial facies», yet with common transitions and successions. Important factors which determine the occurrence, and the composition of the reef facies are water depth, sedimentation rate and oxygen fluctuation. Bathymetric interpretation based on sequential analysis of shallowing upward successions shows that coral facies, mixed coral-sponge facies, and siliceous sponge facies follow each other along a deepening gradient. Additionally, according to Leinfelder (1993) the outer shelf environment was reported to be suitable for the expanse of sponge reefs.

The Plattenkalk Group (Permian-Oligocene) represents the lowermost tectonic unit under a nappe pile of metamorphic and non-metamorphic units of the External Hellenides and has undergone a prograde metamorphism ranging from anchimetamorphic to high pressure/Iow temperature facies conditions. The generally accepted belief for its depositional conditions has been derived from lithological comparisons with the succession of the Ionian zone. Extended colonies of Lithistid demosponges in the middle parts (Jurassic-Eocene) of the chert-bearing metamorphic platy limestones from the Taygetos Mountains in Peloponnese to the Ida Mountains in Crete have been identified (Manutsoglu et al., 1995; Soujon et al., 1995). The former, presenting similarities to the Campanian sponges studied in Poland (Jurkovska & Świerczewska-Gładysz, 2020) allows the deduction of the prevailing paleodepositional conditions. Different forms of bioconstructions have been recognized within these sedimentary records, leading us to conclusions about the origin of chert. As already depicted by relative studies, a big part of metamorphic chert intercalations and nodules of the Plattenkalk Group in Peloponnese and Crete is of organic origin arising from the remains of siliceous sponges. During the buildup of extensive colonies by the sponges, the latter captured essential quantities of siliceous matter which was offered for the diagenetic development of tens of meters of rocks with siliceous composition. Although after Oligocene

these rocks were subsided, metamorphism and uplift took please, while most sponges retained their outer shape and parts of their inner structure, facilitating their later recognition. The discovery of these biomes in a wide area of the Eastern Mediterranean allows a first approach and comparison of the paleogeographical area of occurrence and paleoenvironmental area of development of these organisms in the southeastern area of Tethys, with the corresponding known colonies of the northern areas of Tethys (Manutsoglu et al., 1995; Soujon et al., 1995).

Siliceous beds and nodular concretions are a prominent component of limestones in the Ionian zone of Western Greece. The color of the bedded cherts varies from white, pink to black, while the outer color of nodular cherts is white. Similar structures with biogenic characteristics (Ostia, Osculum) have also been recognized in nodular cherts of the Ionian zone. Also, the link between black cherts and high biological activity is nearly systematic from the Precambrian to recent (van Kranendonk et al., 2001).

Figure 1. Nodular cherts with prominent characteristics resembling sponge structures. Many external pores (pore/ostia) and osculum can be distinguished.

Figure 2. Gradation of black bedded cherts. Very well (left) to asymmetric chert accumulation (right).

The present study concerns TOC analyses of nodules and siliceous beds. Due to the above-mentioned, sampling of 58 chert samples was performed for the subsequent analysis of TOC. The first results from the TOC measurements of the analyzed set of samples range from 0.02 to 0.35 wt.%. Although TOC levels are low, it provides an adequate answer for the origin of cherts (nodular and bedded) of the External Ionian zone.

References

Bourli, N., Kokkaliari, M., Iliopoulos, I., Pe-Piper, G., Piper, D.J.W., Maravelis, A.G., and Zelilidis, A. 2019. A. Mineralogy of siliceous concretions, cretaceous of ionian zone, western Greece: Implication for diagenesis and porosity. Marine and Petroleum Geology, 105, 45-63.

Dornsiepen U.F., Manutsoglu E., and Mertmann D. 2001. Permian - Triassic paleogeography of the External Hellenides. Palaeogeogr., Palaeoclim. Palaeoecol. 172, 327-338.

Jurkowska, A. and Świerczewska-Gładysz, E. 2020. Evolution of Late Cretaceous Si cycling reflected in the formation of siliceous nodules (flints and cherts), Global and Planetary Change, 195, 2020, 103334, https://doi.org/10.1016/j.gloplacha.2020.103334

Keupp H., Koch R., and Leinfelder R.R. 1990. Steuerungsprozesse der Entwicklung von Oberjura-Spongiolithen Süddeutschlands: Kentnisstand, Probleme und Perspektiven. Facies, 23, 141-174.

Leinfelder R.R. 1993. Upper Jurassic reef types and controlling factors. Profil, 5, 1-45.

Manutsoglu E., Soujon A., Reitner J., and Dornsiepen U.F. 1995. Relikte lithistider Demospongiae aus der metamophen Plattenkalk-Serie der Insel Kreta (Griechenland) und ihre palaeobathymetrische Bedeutund. N. Jb. Geol. Palaeont. Mh., 1995/4, 235-247.

Rigakis N. & Karakitsios V. 1998. The source rock horizons of the Ionian Basin "NW Greece". Marine and Petroleum Geology 15, 593-617.

Soujon A., Manutsoglu, E., Reitner, J., and Jacobshagen, V. 1995. Lithistide Demospongiae aus der metamorphen Plattenkalk-Serie der Trypali Ori (Kreta/Griechenland). Berliner geowiss. Abh., E16, 559-567.

Van Kranendonk, M.J., Hickman, A.H., Williams, I.R., and Nijman, W. 2001. Archaean geology of the East Pilbara granite-greenstone terrane, West-ern Australia—A field guide: Perth, Western Australia, Geological Sur-vey of Western Australia, 134 p. (19)Micro-facies and origin of some Archaean Cherts (Pilbara, Australia).

Vigran J. O., Mørk A., Forsberg A. W., Weiss H. M., and Weitschat W. 2008. Tasmanites algae—contributors to the Middle Triassic hydrocarbon source rocks of Svalbard and the Barents Shelf. Polar Research, 27(3), 360-371.

16th International Congress of the Geological Society of Greece

17-19 October, 2022 - Patras, Greece

Bulletin of the Geological Society of Greece, Sp. Publ. 10

Ext. Abs. GSG2022-131

A geochemical analysis of the Neogene diatomites in Western Crete for their hydrocarbon potential

D. Telemenis[1], V. I. Makri[1,2], E. Manoutsoglou[1], N. Pasadakis[1,2], S. Bellas[2]

(1) School of Mineral Resources Engineering, Technical University of Crete, Chania, Greece, dimtele7@gmail.com (2) Institute of GeoEnergy (FORTH/IG), Foundation for Research and Technology - Hellas, Chania, Greece.

Diatomitic beds in Western Crete were geochemically analyzed and proven to have a good hydrocarbon potential, illustrating a prolific source rock, comparable to similar worldwide data. Diatomites are siliceous sedimentary rocks composed mainly of diatoms, silicoflagellates, sponge spicules and/or radiolaria, well-organized in cyclic light and dark color alternations (laminae), mostly connected to seasonality. Diatoms are autotrophic, silica-based, unicellular algae that form in marine and freshwater environments, and they have shown rapid evolution during Cenozoic and particularly during Oligocene - Miocene - Pliocene (Tulan, 2020). Among others, their significance relies on their high value on hydrocarbon exploration. The latter is supported by their mainly gas generation potential as suggested by several research works (Aoyagi and Omokawa 1992, 1993; Tulan, 2020), as well as their prolific hydrocarbon source rock character in many basins worldwide (Tulan, 2020).

The first reference to "laminated marls" of the lowermost part of the Khairetiana Formation resembling the Italian "tripoli" was made by Freudenthal (1969). So far, only a few research works about Miocene diatomite sections in Crete have been published and they mainly focus on stratigraphic analysis (i.e. Frydas, 1996, 2004, 2006; Frydas et al., 2008; Kontakiotis et al., 2022). These, support a pre-evaporitic Messinian age and a marine depositional environment converted to a semi-closed basin, following the transgressive and regressive cycles framework respectively.

As Western Crete diatomitic deposits have not yet been geochemically investigated, this study focuses on a combination of stratigraphic and geochemical analysis of one synthetic outcrop, located in Apokoronas Neogene Basin (south of Souda port, in Chania province). The studied outcrop is of Messinian age and is subdivided into three profiles and several subsections. These are well-laterally extended, presenting adequate thickness in relation to other reported diatomitic occurrences in Crete. Due to dense vegetation and steepness, the presently studied subsections are 12-13m high in total and have a laterally documented extend of 90-100m. Although a much greater lateral continuity was reported by Freudenthal back in 1969, nowadays is mostly covered by newly founded touristic installations. Stratigraphic analysis of the outcrop illustrates clear alternations of fine sands, siltstones/mudstones and laminated diatomaceous beds (Figure 1) from bottom to top in each subsection.

Bulk sampling of 28 samples has been carried out in this synthetic outcrop. For this set of samples, geochemical analysis has been conducted by the means of Rock-Eval 6 pyrolysis to facilitate the understanding of hydrocarbon potential. More specifically, TOC (%) values are found to reach 3.4% in the diatomites (Figure 2), while siltstone/mudstone layers encounter lower TOC (%), yet with exceptions reaching TOC levels as high as the diatomaceous facies.

Based on the above-mentioned analysis, clear outcomes have been made. Firstly, the stratigraphic analysis supports the establishment of System Tracts (ST), with transgressive ST illustrated by fining upward sequences. This is followed by a final coarsening upwards sequence suggesting a highstand ST (Telemenis et al., 2022). According to the geochemical analysis, a clear trend of very good to poor hydrocarbon generation potential is observed in the diatomites from the bottom to the top of the synthetic outcrop, in agreement with the stratigraphic interpretation. A kerogen type of II-III, leaning towards type III is documented by the analyzed set of samples. In addition to the measured TOC values, an oil-gas prone source rock of fair to very good hydrocarbon potential is pinpointed. In a nutshell, this study supports the extent of Messinian diatomites in Western Crete and their potential as source rock for hydrocarbon generation. It also demonstrates a high significance for the offshore hydrocarbon exploration in the Eastern Mediterranean, and especially in offshore Western and Southern Crete.

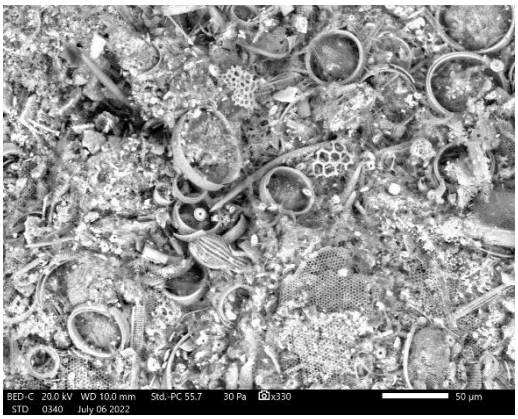

Figure 1. SEM image of marine diatomite dominated by accumulation of mostly circular diatom frustules. Sponge spicules are also present (sample 13).

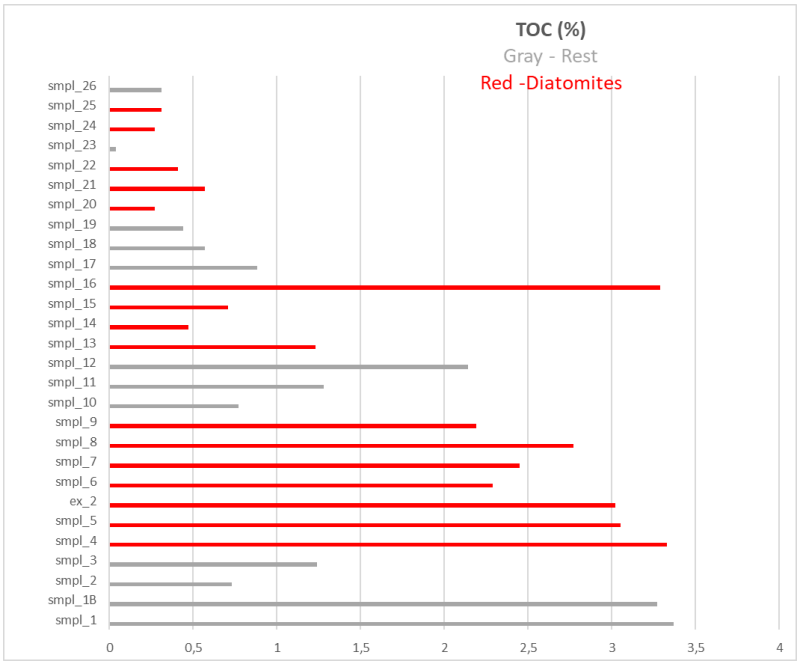

Figure 2. TOC values along the synthetic outcrop.

Acknowledgements

This study is supported by Hellenic Petroleum s.a.

References

Aoyagi, K. and Omokawa, M. 1993. Diagenesis of Neogene diatoms and their importance as a source of petroleum in Japan. The Island Arc 2, 273-279.

Aoyagi, K. and Omokawa, M. 1992. Neogene diatoms as the important source of petroleum in Japan. J. Pet. Sci. Eng. 7, 247-262.

Freudenthal, T. 1969. Stratigraphy of Neogene deposits in the Khania Province, Crete, with special reference to Foraminifera of the Family Planorbulinidae and the Genus Heterostegina. Utrecht Micropaleontological Bulletins 1, 1-208.

Frydas, D. 1996. Silicoflagellate Stratigraphy for Neogene to Quaternary marine sediments in Greece. Newsl. Stratigr. 33(2), 99-116.

Frydas, D. 2004. Calcareous and siliceous phytoplankton stratigraphy of Neogene marine sediments in central Crete (Greece). Revue de micropaléontologie 47, 87–102.

Frydas, D. 2006. Siliceous phytoplankton assemblages and biostratigraphy of the pre-evaporite Messinian diatomites on Gavdos Island, Greece. Revue de micropaléontologie 49, 86–96.

Frydas, D. et al., 2008. Stratigraphical investigations based on calcareous and siliceous phytoplankton assemblages from the Upper Cenozoic deposits of Messara Basin, Crete, Greece. Z. dt. Ges. Geowiss. 159/3, 415-437.

Kontakiotis, G. et al., 2022. Hypersalinity accompanies tectonic restriction in the eastern Mediterranean prior to the Messinian Salinity Crisis. Palaeogeography, Palaeoclimatology, Palaeoecology 592, 1-14.

Telemenis, D. et al., 2022. New evidence of Diatomitic occurrences in western Crete, Greece; A preliminary stratigraphic and geochemical approach and its implications. Special Publication BGSG (Bulletin of the Geological Society of Greece) 9, p. 85.

Tulan, E. et al., 2020. Hydrocarbon source rock potential of Miocene diatomaceous sequences in Szurdokpüspöki (Hungary) and Parisdorf/Limberg (Austria). Austrian Journal of Earth Sciences 113, 24-42.

16th International Congress of the Geological Society of Greece
17-19 October, 2022 - Patras, Greece
Bulletin of the Geological Society of Greece, Sp. Publ. 10
Ext. Abs. GSG2022-188

Distribution of Late Miocene turbidites in North Ionian: A potential reservoir level

E.K. Tripsanas[1], N. Lykakis[1]
(1) Hellenic Petroleum (HELPE) Upstream, Marousi, Greece, etripsanas@helpe.gr.

The examination of potential microbial (biogenic) gas accumulations within the Neogene siliciclastic stratigraphic section represents a newly introduced hydrocarbon play concept in North Ionian concession block. North Ionian Block is located in offshore Western Greece, west of Corfu, Paxoi, and Lefkas islands. Platform carbonates of Apulia Unit, covered by a thin (300 – 500 m) blanket of Neogene sediments, occupies the western part of the block, whereas slope to pelagic carbonates of Pre-Apulia Unit, overlaid by thick (1000 – 2000 m) Neogene sediments occur at the eastern part of the block (Figure 1A). Studies in Lefkas, Corfu, and Diapontian islands have already documented the presence of a few to several meters thick beds of sandstones and conglomerates of turbiditic origin (Clews, 1989; Makrodimitras, 2011; Tsorolas et al., 2016). Based on these studies, this work attempts to examine the presence and distribution patterns of a potential sandstone reservoir interval within the upper Miocene clastic sequence.

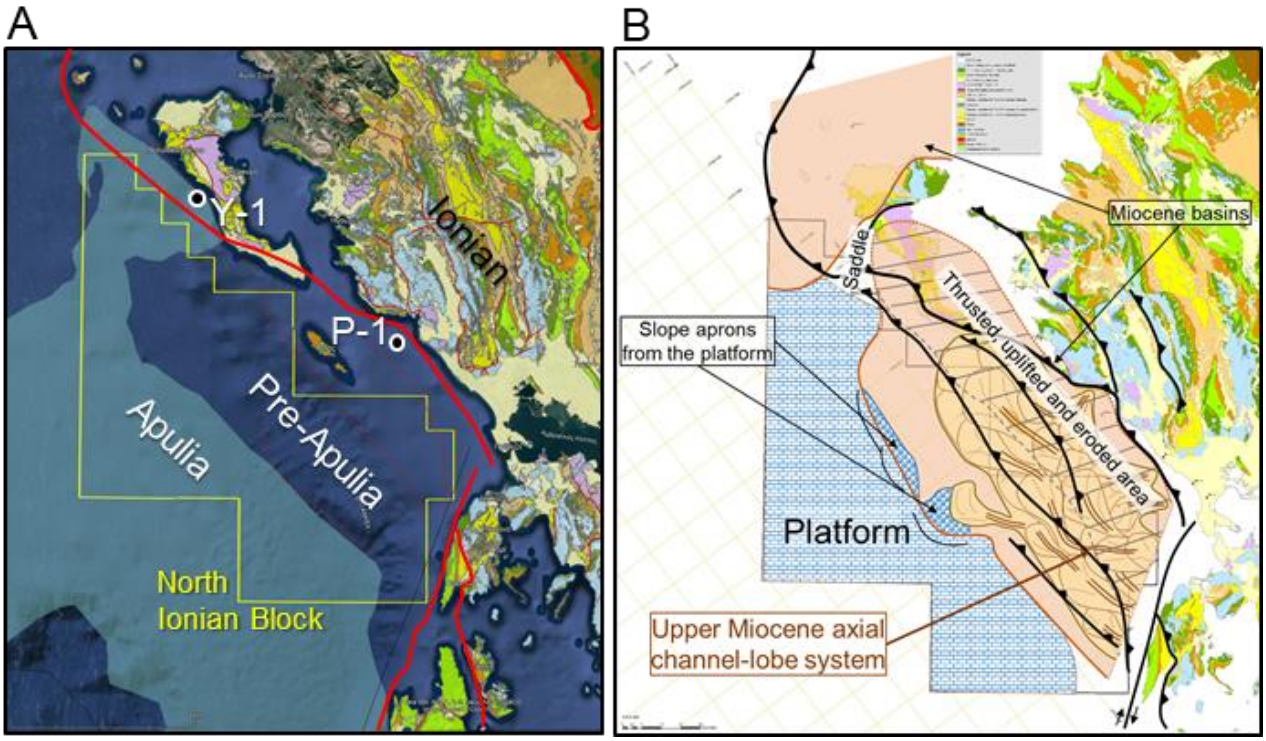

Figure 1. (A) Geological map of western Greece showing the location of the North Ionian Concession Block, and (B) map showing the distribution of the Upper Miocene fan system, as interpreted by the PGS 2D seismic profiles. Y-1: Yianades-1 well, P-1: Parga-1 well.

Gianades-1 well testifies that the Messinian Evaporitic Sequence (MES) consists of intercalations of gypsum and anhydrate beds (a few m up to 25-m-thick), and shallow marine / littoral to restricted marine packages of marly and sandy (< 5-m-thick) beds. The MES can be traced in 2013 PGS 2D seismic lines, as an interval of very high-amplitude, parallel, and continuous reflections, alternating with low to mid amplitude, discontinuous to incoherent reflections (Figure 2). Large (up to 100 ms TWTT) channel-like erosional cuts filled with low-amplitude continuous reflections are common within the MES seismic sequence. The seismic character of these erosional cuts suggest that they are mud filled. Their origin is uncertain and most likely relates to erosional fluvial processes during drying-out periods of the Messinian Salinity Crisis.

Pre-Messinian clastics are expressed in the 2D seismic profiles by three successive seismic intervals. The lower two seismic intervals consist of low to mid-amplitude, discontinuous to continuous, draping seismic facies, which especially in the lower interval might become locally incoherent (Figure 2). Such facies in the lower seismic interval are interpreted to represent argillaceous marls with possible interbedded calciturbidites and breccia in the lower seismic interval, which is consistent to outcrops descriptions from Lefkas Island (Bornovas, 1964) and the mud-log of Parga-1 well. The draping character of the seismic facies in the middle Pre-Messinian seismic interval is interpreted to represent finer-grained

argillaceous marly sediments, similar to the ones observed in Lefkas Island (Bornovas, 1964).

The Upper Pre-Messinian seismic interval consist of mid to high-amplitude convergent, base-lapping seismic facies. The base of this interval is expressed by an erosional unconformity, whereas there an increase in the dip of the seismic reflections compared to the reflections in the middle and lower Miocene seismic intervals (Figure 2). All of these elements suggest higher-energy sedimentation on a more restricted depocenter, possibly due to a late Miocene compressional event. In more detail, this upper interval consist of three seismic sections. The upper and lower sections are characterized by erosional bases and comprise discontinuous to incoherent reflections, representative of deep-sea channel-lobe complexes. On the other hand, the middle seismic section consists of continuous and parallel reflections, suggesting a lower-energy depositional setting of more distal deep-sea fans. Seismic facies distribution shows that incoherent to discontinuous reflections with common channel-cut like features are most dominant to the southeast part of the block, whereas to northwest of the block become parallel and continuous. This indicates the sediment sourcing of these Upper Miocene clastic systems was from the southeast, with the deep-sea fans to evolve axially in the foredeep basin (Figure 1B).

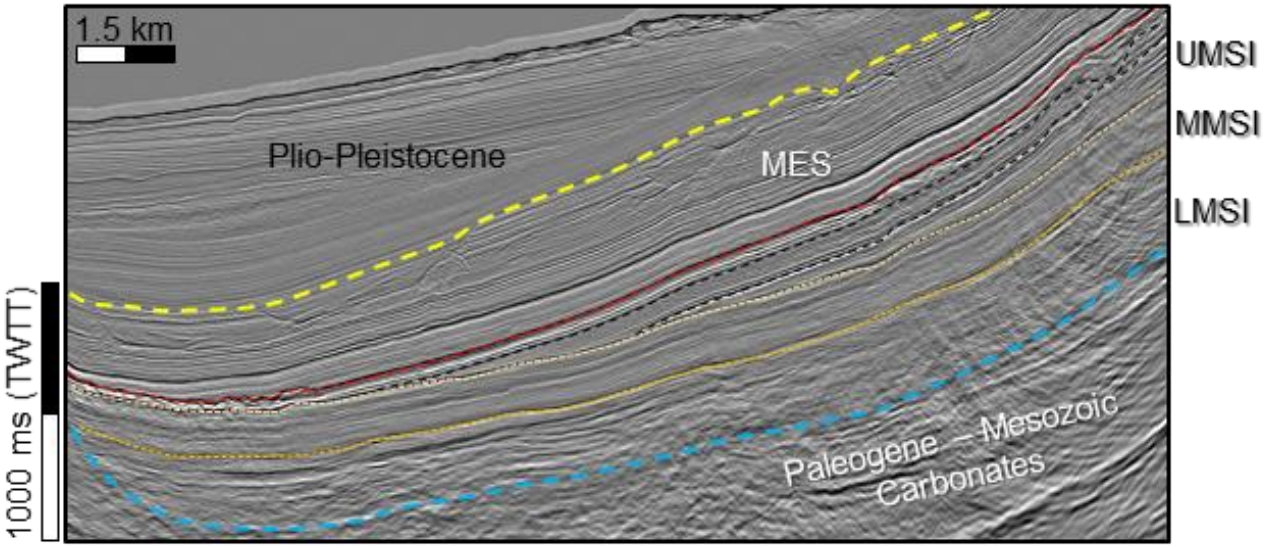

Figure 2. 2D seismic profile from the North Ionian Block, showing the Neogene seismic stratigraphy of the area. MES: Messinian Evaporitic Sequence, LMSI: lower Miocene seismic interval, MMSI: middle Miocene seismic interval, UMSI: upper Miocene seismic interval.

There are three interpretations for the development of these Late Miocene channel-lobe complexes. (1) They represent a major Late Miocene compressional event, which result in enhanced river-sourced sediment in the foredeep basin through orogenetic processes to the east. (2) The dramatic sea-level fall during the initial stages of the Messinian Salinity Crisis resulted in enhanced riverine erosion through the change of their baseline, and thus into enhanced river-sourced sediment input in the foredeep basin (similar early Messinian deep-sea clastic systems all around Mediterranean in Mousouliotis et al., 2020 and references therein). (3) A combination of the upper two interpretations could also be valid for the development of the Late Miocene channel-lobe complexes.

In conclusion, two proliferous reservoir levels are identified through this study within the Neogene clastic section in the North Ionian Block. The first consists of shallow marine to littoral sandstones within the MES, which although no distribution map is available at the moment due to the sparse seismic data, it is expected to be widespread within the area of interest. The second reservoir interval refers to widespread upper Miocene channel-lobe complexes, in which good-quality sandstone reservoirs are expected. The top seal in both reservoir levels consists of MES mudstone and gypsum / anhydrate beds.

Acknowledgements

The authors would like to acknowledge PGS and HELPE Upstream for allowing the presentation of this dataset in this publication.

References

Bornovas, J., 1964. Geological study of Levkas Island. Geological and geophysical research. Institute for Geological and Subsurface Research (now Institute for Geology and Mining Research), Report No 1 (II), Athens.

Clews, J.E., 1989. Structural controls on basin evolution: Neogene to Quaternary of the Ionina zone, Western Greece.Journal of the Geological Society, 146, 447-457.

Makrodimitras, G., 2011. Evolution of basinal sedimentation of submarine fans in Diapontia Islands, North of Corfu Island. Ph.D. Thesis, University of Patras, Patras, 301 p.

Mousouliotis, A.G., Albanakis, K., Georgakopoulos, A., Papatheodorou, G., Tripsanas, E.K., Medvedev, B., 2020. Pre-salt clastic systems in the Herodotus Basin, SE Mediterranean Sea. Marine and Petroleum Geology, 122, 19 p. (https://doi.org/10.1016/j.marpetgeo.2020.104691).

Tserolas, P., Mpotziolis, C., Maravellis, A., Zelilidis, A., 2016. Preliminary geochemical and sedimentological analysis in NW Corfu: The Miocene sediments in Agios Georgios Pagon. Bulletin of the Geological Society of Greece, 50, 402-412.

16th International Congress of the Geological Society of Greece
17-19 October, 2022 - Patras, Greece
Bulletin of the Geological Society of Greece, Sp. Publ. 10
Ext. Abs. GSG2022-191

Preliminary Results of a Biomarker Study of the Upper Triassic – Lower Jurassic Source Rocks in Ionian Zone, Epirus, NW Greece. Basin and depositional setting implications

I. Alexandridis[1], L. Schwark[2],
(1) Aristotle University of Thessaloniki, Thessaloniki, Greece, ialexandt@geo.auth.gr (2) Kiel University, Kiel, Germany

Organic-rich intervals of a Late Triassic to Early Jurassic series occur in sediments of the Epirus region, NW Greece. The well-known Toarcian shale has been studied for organic matter composition by bulk geochemical methods including TOC, Rock Eval, and $\delta^{13}C_{org}$ isotope analysis (Karakitsios and Rigakis, 1996; Kafousia et al., 2014; Alexandridis et al., 2021). Latest Triassic to Hettangian organic-rich intervals in Epirus have been identified by Alexandridis et al. (2022) and studied for bulk organic geochemical (TOC, Rock Eval 6 and Rock Eval 7S) as well as for organic petrographic parameters. Although the bulk composition of organic matter is thus well known, the molecular composition has not yet been studied in detail. Previous studies, conducted on Toarcian black shales (Farrimond et al., 1989) in Kouklesi revealed a low thermal maturity of the bitumen, allowing for biomarker-based facies reconstruction. The organic matter in Kouklesi Toarcian black shales was interpreted to have been deposited under dysaerobic conditions due to the lack of extended hopanes and originate from marine sources, predominantly from cyanobacteria as indicated by elevated hopane/sterane and nC_{17}/nC_{31} ratios. Molecular studies on sediments of Rhaetian to Pliensbachian age in NW Greece are not available.

We here report the molecular composition studied with GC-MS from three intervals in the Souli Mountains:

1. The Toarcian black shale bitumen from the Petousi site (PBS) (section A, Figure 1). This section was previously studied for bulk geochemistry by Kafousia et al. (2014).
2. The Upper Triassic-Lower Jurassic Pantokrator Shales (PSh) on Souli Mt. (SPS), (part of the section B, Figure 1).
3. The Pantokrator Shales (FPS) of Triassic/Hettangian age and black bituminous Pantokrator limestones (FPL) of Hettangian in the Frosyni section (part of the section B, Figure 1).

The bulk organic geochemical properties of the SPS, FPL and FPS are reported in Alexandridis et al. (2022).

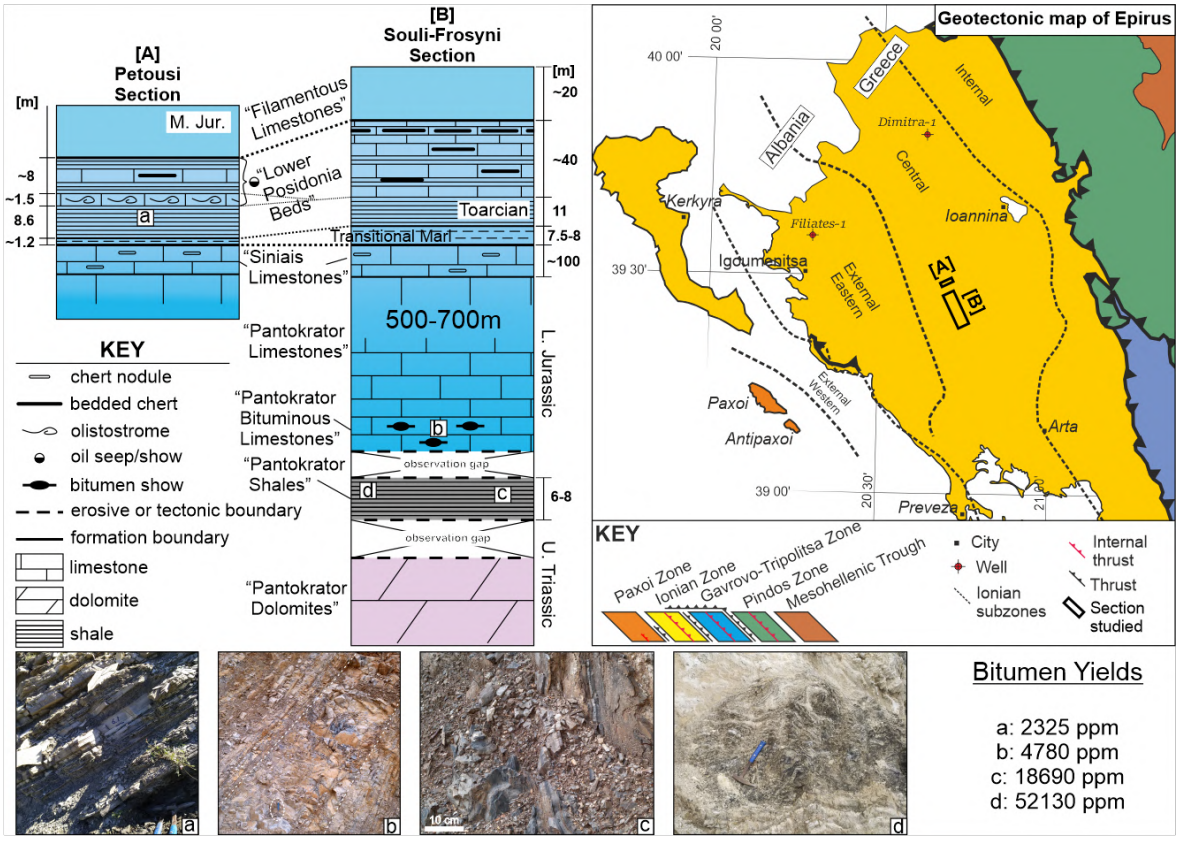

Figure 1. Geotectonic map of Epirus, stratigraphic columns of the studied sections, field photographs of the formations and their bitumen yields

Bitumen yield for the PBS reached 2,325 ppm, surpassed by the SPS with 52,130 ppm as well as the FPS with 18,690 ppm, and the FPL with 4,780 ppm, respectively. A homohopane side chain isomerization of 0.50 [C22 S/(S+SR)] and a side chain isomerization of 0.15 for C_{29}-steranes was determined for the PBS. The SPS bitumen showed homohopane isomerization of 0.58 at C22 and a side chain isomerization for C_{29}-steranes of 0.29. The Frosyni bitumen (FPL and FPS) reveals a slightly higher homohopane isomerization of 0.62 and a side chain isomerization for C_{29}-steranes of 0.40. Exceptionally low Pr/Ph ratios of 0.25 and 0.29 characterize the FPL and FPS, respectively. The SPS bitumen shows low Pr/Ph ratio of 0.42 whereas the PBS shows slightly higher Pr/Ph ratio of 0.52.

Bitumen yields indicate that the petroleum generation potential of the uppermost Rhaetian to lowermost Liassic strata in the Epirus region exceeds that of the well-known Toarcian black shales. Homohopane (C22) and C_{29}-sterane (C20) side chain isomerization indicates that the PBS are just below onset of the oil window, whereas the SPS are in the early oil window.The FPL and FPS are slightly more mature within the oil window, both having generated liquid hydrocarbons. This agrees with the organic petrographic maturity assessment by Alexandridis et al. (2022). The exceptionally low Pr/Ph ratios indicate that the depositional environment in the FPL and FPS was highly oxygen-deficient, also arguing for a highly stratified water column with potentially hypersaline bottom waters (Schwark et al., 1998). The Pr/Ph ratio of the SPS is indicative of strictly anoxic but not hypersaline conditions whereas for the PBS still denote an anoxic environment but more likely under normal saline conditions.

The biological source of the *n*-alkanes of the PBS shows a contribution of land-plant wax derived long chain analogues (C_{27} to C_{37}), whereas the SPS, FPL, and FPS lack the long chain analogues. The Pantokrator Shales sediments are assumed to have been deposited in restricted and eventually hypersaline lagoons. Terrigenic plant wax input would be expected but the exceptionally high aquatic production of short chain *n*-alkanes will mask any terrigenic influx. The carbonatic lagoon (FPL) lacked influx of terrigenic sediments rich in iron and hence reduced sulfur released by sulfate reducing bacteria interacted with lipids to form organic sulfur compounds, particularly long-chain alkylated benzothiophenes, known to occur in such restricted lagoonal settings. The carbonate-poor lagoonal sediments of the FPS yield less organic sulphur compounds but dominantly show bacterial biological sources, as evidenced by the very strong predominance of hopanes and aromatic hopanoids in the bitumen. In the FPS bitumen aromatic carotenoids including isorenieratane and its biphenylic derivative as well as aryl isoprenoids indicate the presence of *chlorobiaceae*, where the brown strain of the green sulfur bacteria execute photosynthesis under euxinic conditions. This documents an exceptionally low dynamic regime, with a strongly stratified water column supporting growth of these highly specialized microbes. Steranes derived from eukaryotic algae are scarce in the Pantokrator Shales, contribute to a slightly higher proportion in the Pantokrator limestones and are of equal abundance to hopanes in the Toarcian shales. This distribution is indicative of a dominantly microbial organic matter source in the lagoonal Pantokrator sediments and a balanced proportion of algal versus microbial producers in the Toarcian shelf settings. Apparent cyclicity in sedimentation of successive mm-thick organic-rich shale with dolomitic silt-sand alternations (Alexandridis et al., 2022), likely points to seasonably controlled productivity and clastic input (Figure 2).

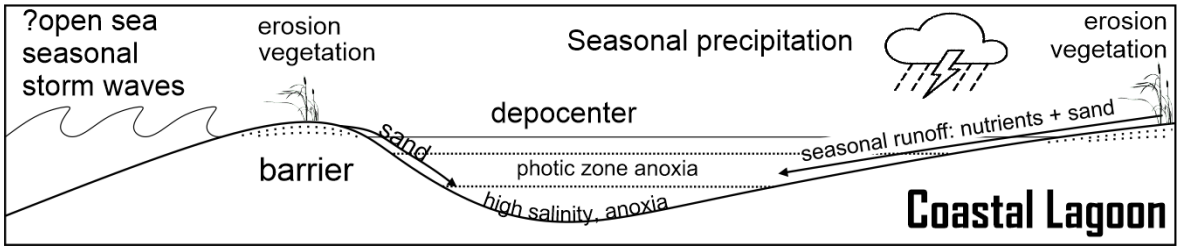

Figure 2. Pantokrator Shales depositional model sketch.

References

Alexandridis, I., Georgakopoulos, A., Carvajal-Ortiz, H., Gentzis, T., Oikonomopoulos, I., 2021. Source Rocks in Ionian Zone, western Greece. Discoveries and revisions from an outcrop study. In: Third EAGE Eastern Mediterranean Workshop. European Association of Geoscientists & Engineers, p. 1-3. DOI:10.3997/2214-4609.202137019. **[Conference Proceedings]**

Alexandridis, I., Oikonomopoulos, I., Carvajal-Ortiz, H., Gentzis, T., Kalaitzidis, S., Georgakopoulos, N. A., Christanis, K., 2022. Discovery of a new source-rock interval within the Pantokrator Formation, Ionian Zone, Epirus, western Greece: Insights from sulfur speciation and kinetics analyses. Available at SSRN: https://ssrn.com/abstract=4049379 or http://dx.doi.org/10.2139/ssrn.4049379. **[Journal Article]**

Farrimond, P., Eglinton, G., Brassell, S. C., Jenkyns, H. C., 1989. Toarcian anoxic event in Europe: An organic geochemical study. Marine and Petroleum Geology, v. 6, p. 136-147. **[Journal Article]**

Kafousia, N., Karakitsios, V., Mattioli, E., Kenjo, S., Jenkyns, H. C., 2014. The Toarcian Oceanic Anoxic Event in the Ionian Zone, Greece, Palaeogeography, Palaeoclimatology, Palaeoecology, Volume 393, P. 135-145, https://doi.org/10.1016/j.palaeo.2013.11.013. **[Journal Article]**

Karakitsios, V., and N. Rigakis, 1996, New oil source rocks cut in Greek Ionian basin: Oil & Gas Journal, v. 94, no. 7, p. 56–59. **[Journal Article]**

Schwark, L., Vliex, M., Schaeffer, P., 1998. Geochemical characterization of Malm Zeta laminated carbonates from the Franconian Alb, SW-Germany (II). Organic Geochemistry, 29, 1921–52. **[Journal Article]**

16th International Congress of the Geological Society of Greece
17-19 October, 2022 - Patras, Greece
Bulletin of the Geological Society of Greece, Sp. Publ. 10
Ext. Abs. GSG2022-196

Understanding the source rocks in Ionian and pre-Apulian units in western Greece – A review and steps ahead

I.K. Oikonomopoulos[1], S. Kalaitzidis[2], T. Gentzis[3], K. Christanis[2]

(1) Helpe Upstream, Hellenic Petroleum S.A. Maroussi, Greece, ioikonomopoulos@helpe.gr (2) Economic Geology, Section of Earth Materials, Department of Geology, University of Patras, Rio-Patras, Greece (3) Core Laboratories LP, Houston, Texas, USA.

Several organic geochemical studies, which have been performed in the past mainly by the Hellenic Petroleum S.A. and Greek universities, suggested the existence of eight source-rock intervals capable of generating both thermogenic and biogenic hydrocarbons (Alexandridis et al., 2021; Karakitsios and Rigakis, 2007; Pasadakis et al., 2016; Rigakis and Karakitsios, 1998; Rigakis et al., 2001, 2007; Tsikos et al., 2004; Zelilidis, et al., 2015). Five deep exploration wells that penetrated source rock intervals and numerous outcrops throughout the Ionian and pre-Apulian units in western Greece were studied to develop a large geochemical dataset.

Routine analyses using Rock-Eval pyrolysis instruments (e.g., RE-2 and RE-6) identified the high petroleum generating potential of the Mesozoic and post-Mesozoic source rocks, whereas maceral analysis and vitrinite/solid bitumen reflectance measurements were used to determine the kerogen/bitumen type and the level of organic matter maturity. Advanced geochemical techniques, including petroleum biomarkers and carbon/hydrogen isotopes, were also applied to correlate the surface oil exposures (oil seeps) and numerous oil/gas indications/shows in the deeper sections of the wells with the identified source-rock intervals. Organic geochemical analyses using the state-of-the-art Rock-Eval 7S instrument were performed recently by Hellenic Petroleum S.A. in collaboration with Core Laboratories L.P., in Houston, Texas, in order to understand the potential participation of sulfur in the kerogen molecular structure. These studies are on-going and will provide critical information about the kerogen kinetics that were used as input in the thermal modeling of the organic matter, which, in turn, affects the maturity threshold for liquid hydrocarbon generation (Figure 1).

The modern interpretation of the organic geochemical/petrographical datasets and the integration of such data with the geological, structural, and sedimentological context of the Ionian and the pre-Apulian units resulted in the development of thermal and maturity models in this area. The developed basin models are used to define a “most-likely” range of geological time intervals, in which the oil and/or gas generation took place - known as “timing of hydrocarbon generation” - within the various sub-basins of western Greece. However, critical issues concerning the source-rock intervals themselves and others related to the maturity of organic matter parameters remain open and need further investigation. Such issues are:

- The thickness of the eroded overburden, which is related to the maximum burial depth of the source rocks and the timing that this occurred, which affect both the maturity of the organic matter and the timing of hydrocarbon generation.
- The duration and magnitude of the Jurassic rifting in the Ionian and pre-Apulian units, which is related to the thinning of the crust and the subsequent heat flow transfer, which also affected the maturity level of the organic matter.
- The lateral extent of the identified source rocks, which is related with the capability to generate commercially viable volumes of hydrocarbons.
- The organofacies of the middle-upper Triassic/lower Jurassic source-rock intervals.

All these important questions require multidisciplinary studies, in which organic petrography along with organic geochemistry play a key role. An integration of such studies will be of great value to better define the risk of the hydrocarbon “charge” element during the evaluation of the petroleum system in western Greece.

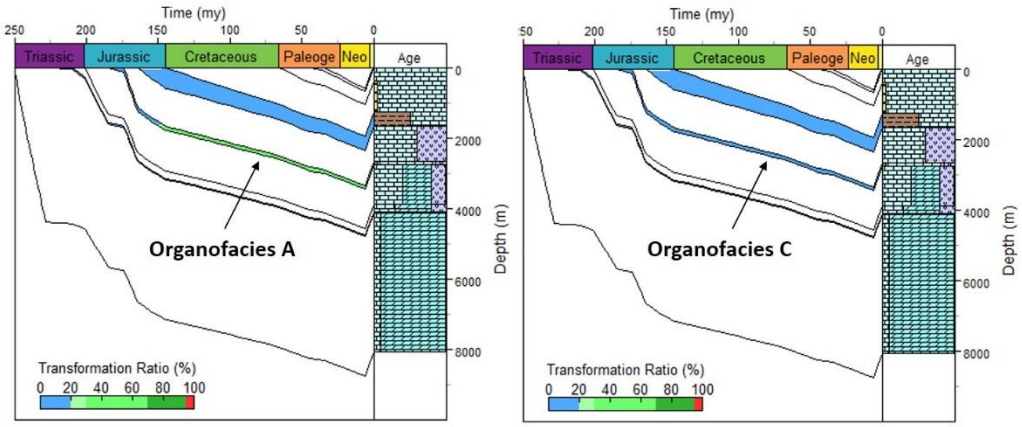

Figure 1. 1D thermal model at a hypothetical well located in offshore western Greece, illustrating the burial history with superimposed transformation ratio (colored scale) of the potential source-rock intervals. The comparison between the two diagrams highlights the critical role of organofacies type as an input to the thermal model. Organofacies A needs a lower activation energy compared to organofacies C to generate hydrocarbons because it matured at lower temperatures.

Acknowledgements

The authors would like to give many thanks to Helpe Upstream from the Hellenic Petroleum group of companies for allowing us to present the specific datasets.

References

Alexandridis, I., Georgakopoulos, A., Carvajal-Ortiz, H., Gentzis, Th., Oikonomopoulos, I. 2021. Source Rocks in Ionian Zone, western Greece. Discoveries and revisions from an outcrop study. Third EAGE Eastern Mediterranean Paper No. 19.

Karakitsios V., Rigakis N., 2007. Evolution and petroleum potential of Western Greece, Journal of Petroleum Geology, 30/3, 197-218.

Pasadakis, N., Dagounaki, V., Chamilaki, E. 2016. A comparative organic geochemical study of oils seeps in Western Greece. Energy Sources, Part A: Recovery, Utilization, and Environmental Effects. 38 (3), 362-369.

Rallakis, D., Siavalas, G., Oskay, R.G., Tsimiklis, D., Christanis, K., 2013. Maturity of dispersed organic matter in bituminous formations of the Ionian Zone (Epirus region, NW Greece). Bulletin of the Geological Society of Greece XLVII, 2013, Proceedings of the 13th International Congress, 880-889.

Rigakis, N., Karakitsios, V., 1998. The source rock horizons of the Ionian basin (NW Greece). Marine and Petroleum geology, 15, 593-617.

Rigakis, N., Nikolaou, K., Marnelis, F., Pakos, Th. 2007. The utility of oil shows in the hydrocarbon exploration of Western Greece. Bulletin of the Geological Society of Greece XXXX, 2007, Proceedings of the 11th International Congress, 959-971.

Rigakis, N., Roussos, N., Kamberis, E., Proedrou, P. 2001. Hydrocarbon gas accumulations in Greece and their origin. Bulletin of the Geological Society of Greece, 34(3), 1265-1273.

Tsikos, H., Karakitsios, V., Breugel, Y., Walswarth-Bell, B., Bombardiere, L., Petrizzo, M.R., Sinninghe Damste, J.S., Schouten, S., Erba E., Premoli Silva I., Farrimond P., Tyson R. V., Jenkyns H.C. 2004. Organic-carbon deposition in the Cretaceous of the Ionian Basin, NW Greece: the Paquier Event (OAE1b) revisited, Geological Magazine, 141/4, 401-416.

Zelilidis, A., Maravelis, A., Tserolas, P., Konstantopoulos, P. 2015. An overview of the petroleum systems in the Ionian zone, onshore NW Greece and Albania, Journal of Petroleum Geology, 38, 331-348.

16th International Congress of the Geological Society of Greece
17-19 October, 2022 - Patras, Greece
Bulletin of the Geological Society of Greece, Sp. Publ. 10
Ext. Abs. GSG2022-201

2D Marine Seismic Acquisition in Block 10 and Ionian Block

P. Gkotsis[1], A. Pagoulatos[1]
[1]Hellenic Petroleum Upstream, Marousi, Athens, pgkotsis@helpe.gr,

Hellenic Petroleum Upstream acquired 1200 km seismic reflection data within the Block 10 offshore area licensed in South Ionian Sea, as well as 1700 km in the Ionian Block licensed in North Ionian Sea during the first quarter of 2022 using 2D conventional marine seismic acquisition.

In 2D marine seismic data acquisition, the vessel tows the energy source astern (airguns) along with one seismic receiver cable line containing several hydrophones (streamer). The vessel moves along on a straight sail line and fires sequential shots, and the reflections are received by the streamer. HELPE Upstream contracted Shearwater, a reputable seismic acquisition contractor to perform this project.

In designing a 2D marine seismic survey, two main objectives must be met. The primary objective is to obtain geophysical data that provides an image of the subsurface geology, clear enough to serve the needs of seismic interpretation. The secondary objective is to acquire the maximum amount of data within a budget and time available, complying with all environmental, legal, and geographical restrictions.

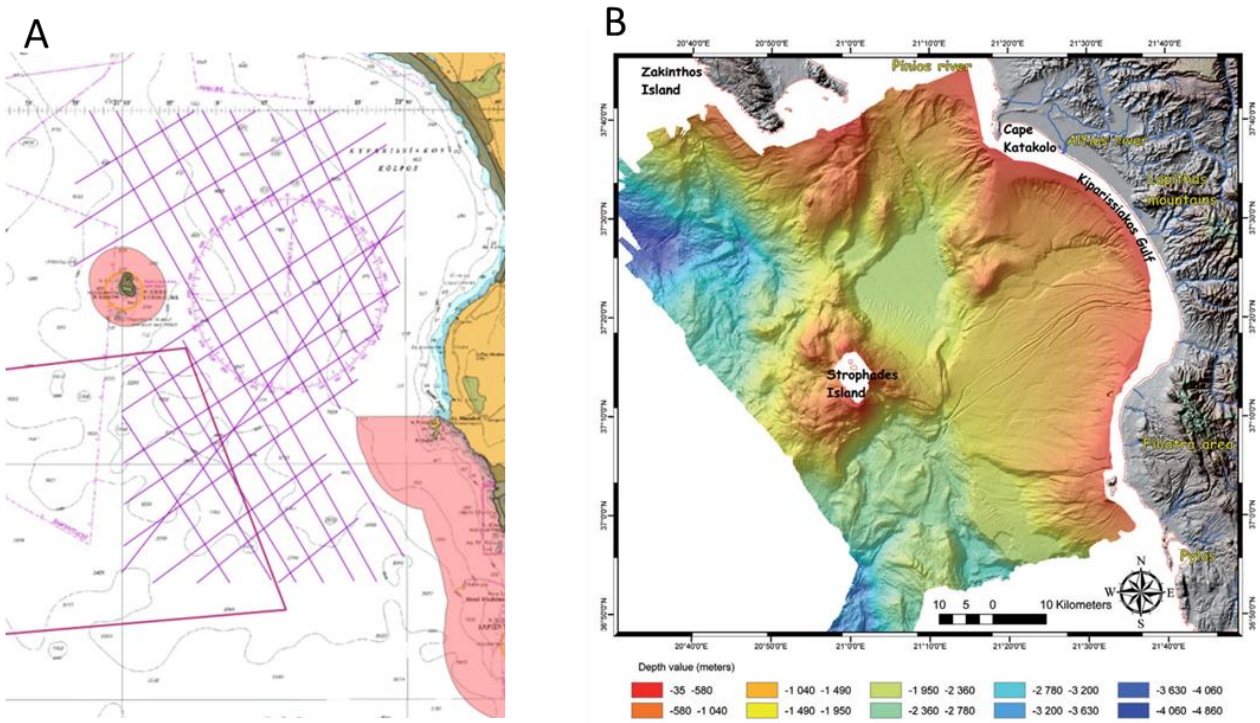

Figure 1. (A) Example of the pre-plotted lines for Block 10. The purple lines are the proposed seismic lines of 1250 km total length. The pink areas are the Natura 2000 areas plus 1km of buffer zone. Inside the natura zone, additional restrictions may apply. (B) Bathymetry map of the survey area in Block 10 (from the Island of Zakynthos to the area of Pylos), based on swath bathymetric data collected by the R/V Explora (DTM at 50 m). *ref (4)*

The methodology for marine data acquisition depends on the environment, the geology, the size of the target, and the depth of the water. It is worth mentioning that the depth of the water in the southern part of Block 10 exceeds 3000m. The smaller the structure, the tighter the line and station spacing is required. The size of the source depends on the depth of the water in the survey area as well as the target depth (Figure 1).

The target depth is determined by the geological objective. The depth range of the prospects is expected to be 2 – 3.5 km beneath the seabed. The recording length is taking into consideration the time required for the seismic wave to travel through the water column, and the targeted geological layers and then reflect the streamer's hydrophones.

Acoustic impedance contrasts (i.e., a sonic velocity or density contrast) determine if the target at a particular depth will be identified. The following three issues are closely tied to the depth and nature of the target reflectors.

1) The energy source must have adequate power at the required frequencies to create the target reflections. If the source is too strong, the dynamic range of the recording instruments may be saturated, ruining the fidelity of the data. If the source is too weak, the signal-to-noise ratio will be too low to image the target. In addition. environmental restrictions may limit the size and the type of energy sources. For the needs of the acquisition of Block 10 and the Ionian block, the source size was set to 5086 in^3.

2) There must be sufficient fold (data density) to maintain a target signal-to-noise ratio adequate for the geophysicist to make a correct interpretation. The required record length defines the shot point interval. The shot point interval needs to be long enough to maintain a clean record length at least to the depth of interest and to maintain a high signal-to-noise ratio.

3) The source/receiver geometry must have an adequately long offset to optimize velocity calculations and multiple attenuation to resolve the target properly. Often, survey parameters are optimized for the deepest target, sacrificing the quality and resolution of shallower targets.

The aforementioned parameters are produced by a simulation of ray tracing, after applying the adequate models to account for the geology in the area (Figure 2).

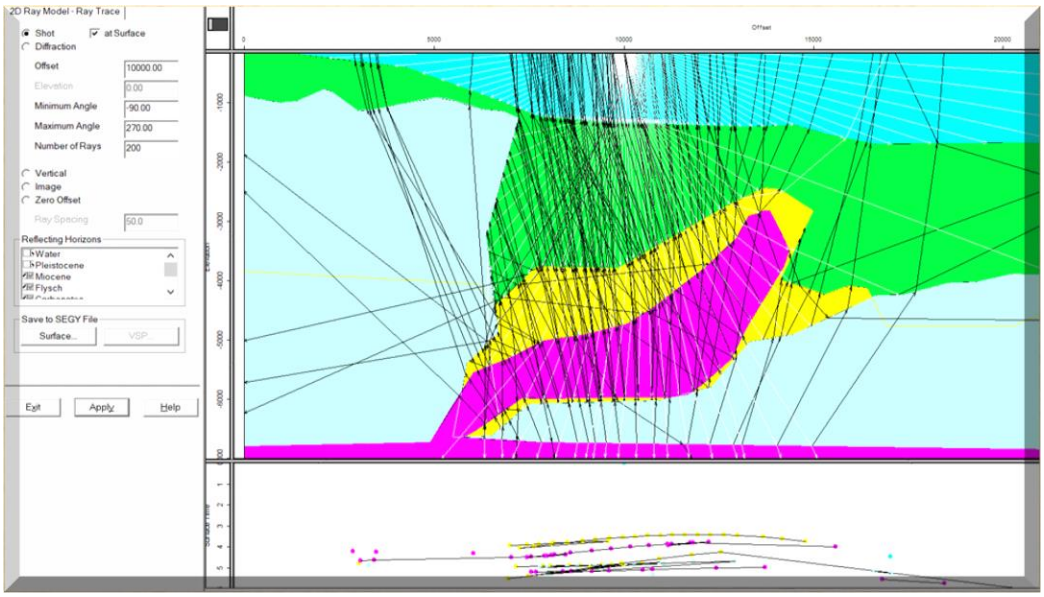

Figure 2. Simulation results of a ray tracing project for a geosection. This is an example of a salt body

The project was a success, recording high quality data that will add value in the process of H/C exploration of Greece. The processing of the acquired data is expected to be completed by the end of 2022.

References

International Association of Geophysical Contractors, Report No. 448, 2011. An Overview of marine seismic operations. Report No.448. https://offshorenorge.no/contentassets/ae812078242441fb88b75ffc46e8f849/an-overview-of-marine-seismic-operations.pdf

Brian J. Evans, No 7, 1997. A HANDBOOK FOR SEISMIC DATA ACQUISITION IN EXPLORATION, William H. Dragoset Jr, David V. Fitterman, ISBN 978-1-56080-041-5

L. Camera , J. Mascle , N. Wardell , D. Accettella, Sea Hellarc Team. June 2014. The Peloponnese continental margin from Zakynthos Island to Pylos: morphology and recent sedimentary processes. Bollettino di Geofisica Teorica ed Applicata Vol. 55, n. 2, pp. 325-342;

16th International Congress of the Geological Society of Greece
17-19 October, 2022 - Patras, Greece
Bulletin of the Geological Society of Greece, Sp. Publ. 10
Ext. Abs. GSG2022-239

Biostratigraphic and palaeoecological study of the Jurassic - Cretaceous shale formations, north of Petousi fault in Epirus

V. Golfinopoulos[1,2], A. Zelilidis[2], A. Antonarakou[3] and GIliopoulos[2]

(1) Department of Geology, Aristotle University of Thessaloniki, Thessaloniki, Greece, gkolfinopoulosv@upnet.gr (2) Department of Geology, University of Patras, Patras, Greece (3) Department of Geology and Geoenvironment, National and Kapodistrian University of Athens, Athens, Greece.

Introduction

In the last 70 years, more than 50 studies on the Ionian zone rocks have been published. These studies highlight the geological, stratigraphic, tectonic, petrographic, sedimentological and micropalaeontological aspects of these sequences. In addition, several studies on the petroleum potential of the Ionian basin have been also conducted.

The current study concerns the geological and biostratigraphic study of Jurassic formations of the middle sub-basin of the Ionian basin north of the Petousi fault, as well as the study of formations of similar age in other locations in the surrounding area. More specifically, the purpose of this study is the microfacies analysis of the shale formations. These shales differ greatly in thickness and colour, compared to equivalent and typical outcrops of these formations from other locations. In addition, the biostratigraphy of the shale formations, the palaeoecological character of these deposits, the reconstruction of the paleoenvironmental evolution of this basin will be determined and will be compared with rocks located close to this basin.

The study areas are basically two and are located in the Region of Epirus, in the regional unit of Thesprotia, approximately 5 km north of the city of Paramythia, at an altitude ranging from 650 to 1050 m, depending on the location where the sample was collected. The first study area is located southwest of Elataria village, along a tributary of Thyamis river about 1300 m long. The second study area is located along the local Elataria – Paramythia road, approximately 10 km long.

Geological Setting of Ionian Basin

The Ionian basin extends to the Ionian Islands, Epirus, Western Sterea, North-western Peloponnese, Dodecanese islands, as well as to the central – southern Peloponnese and Crete as the metamorphic Ionian equivalent (Papanikolaou, 2021) and belongs to the external Hellenides fold-and-thrust belt (Karakitsios et al., 2015). During the Mesozoic era, Epirus was part of the south-eastern passive margin of the Tethys Ocean (Karakitsios, 2013; Kontakiotis et al., 2020). This basin is restricted towards to east by the Gavrovo thrust and westwards by the Ionian thrust (Bourli et al., 2019; Kontakiotis et al., 2020).

Three stratigraphic sequences (pre-rift, syn-rift and post-rift) have been distinguished in the Ionian zone, while in recent years the syn-rift and post-rift sequences have been merged into one, the syn-rift (Bourli et al., 2019). Hence, in this study the sequences are as follow: (a) the pre-rift sequence consists of Early Triassic to Early Jurassic limestones and evaporites, (b) the syn-rift sequence is overlapping the previous one and comprises of Middle Jurassic to Late Cretaceous carbonate as well as shale formations. The second sequence was deposited throughout the rifting of the Ionian basin into small sub-basins of asymmetric half-graben geometry and its internal structural differentiation displays abrupt thickness changes within each half-graben (Bourli et al., 2019; Karakitsios, 2013, Zelilidis et al., 2015). From the Late Cretaceous to the Early Eocene, the erosion of the carbonate rocks from both Gavrovo and Apoulian platforms supplied the Ionian basin with fragments of micro-breccia. The top of this succession consists of submarine fan deposits, where during the Middle Eocene – Upper Oligocene inner fan deposits were restricted in the internal Ionian zone, while, in the middle Ionian zone fine- and medium-grained sediments were deposited (Avramidis et al., 2002; Zelilidis et al., 2015).

Materials & Methods

A total of 98 samples were collected from the two study areas. 70 samples were collected from the first one, and 28 from the second. Sampling depended on lithology and accessibility. 55 of these samples were cut and thin sections were prepared, 41 from the first area and 14 from the second. During field logging and sampling, in addition to the observations made on the lithostratigraphic properties of the rocks, rocks were continuously checked for fossils, dip and strike of beds and faults were measured, as well as the coordinates of the outcrops for the construction of a detailed geological map were recorded. Microfacies analysis of the studied thin sections allowed the determination of the changes that led to the differentiation in the thickness and lithology of the studied sub-basin.

For the classification of carbonate and shales rocks, and information on the energy levels of the depositional environments and water conditions, the classifications of Folk (1959, 1962) and Dunham (1962) were followed. The

determination and interpretation of the carbonate facies was completed using Wilson's model (Wilson, 1975), who proposed a system of 24 standard microfacies types (SMF), corresponding to 9 standard facies zones (FZ).

Results

The first study area is a small sub-basin developing along a north-south direction. This area from bottom to top, consists of limestones with microbreccia (the thickness cannot be measured), black shales and limestones occasionally with filaments, with a thickness of a few meters. These formations are overlapped by cyan shales, which in the lower part are interbedded by marls with microbreccia. The thickness of this formation is at least 200 meters.

In the second study area, almost all the formations of the Ionian zone are developed, with the thicknesses of each formation matching those of the typical outcrops of this basin. Particularly the sequence consists of Pantokrator and Siniais limestones, Lower Shales with Posidonia, Vigla Limestones and Shales, Limestones with microbreccia and Sub-lithographic Limestones. Furthermore, Upper Eocene, Oligocene and Miocene sub-marine fan deposits from Pindos Foreland basin are developed, as well as Pleistocene – Holocene alluvial deposits.

More specifically, in the Elataria study area, the following depositional environments have been recognized: deep sea and toe of slope environment. Especially, the Lower (Toarcian) to Upper Jurassic (Tithonian) Posidonia beds comprise of SMF 1 and SMF 3 (3, 3RAD and 3FIL) microfacies that were accumulated in a deep sea and toe of slope basin (FZ 1 and 3, respectively). The Lower to Upper Limestones with Filaments consist of SMF 3FIL type that are associated with deep sea environment (FZ 1). In Saloniki study area the Lower Jurassic Pantokrator Limestones consist of SMF 7 and Crystalline dolomitic microfacies, indicating a platform-margin reefs environment (FZ 5). The Upper Cretaceous Senonian Limestones comprise of SMF 5 microfacies associated with a slope environment (FZ 4). The remaining samples studied in the area of Saloniki include the following formations: Posidonia beds, Vigla Limestones and Shales, Lower Senonian Limestones, Paleocene – Eocene Limestones. These formations consist of SMF3, SMF 3-RAD and SMF 3-FOR, indicating a deep sea and/or toe of slope environment (FZ 1 and/or 3, respectively).

Conclusions

Microfacies analysis results showed that in the Elataria area, the following formations have been recognized: Lower to Upper Jurassic Limestones with filaments and Shales with Posidonia which differ greatly in thickness and colour (thicker and cyan), relative to equivalent and typical formations of this zone from other locations. In the Saloniki study area, the following formations have been recognized (almost all the formations of Ionian zone are developing, with the thicknesses of each formation matching approximately those of the typical outcrops of this basin): Lower Jurassic – Upper Triassic Pantokrator Limestones, Sinies Limestones, Jurassic Shales with Posidonia, Upper Jurassic – Lower Cretaceous Vigla Limestones and Shales, Upper Cretaceous Limestones with Microbreccia as well as Paleocene – Lower Eocene Limestones. The samples of Elataria sub-basin are characterised as SMF 3 and 1, and which were deposited in a deep sea basin and at the toe of slope (FZ 1 and 3, Limestones with filaments and Posidonia beds). The samples of Saloniki are characterised as SMF 7, 5 and 3, and which were deposited at platform-margin reefs, slope, toe of slope and/or deep sea basins (FZ 5, 4, 3 and/or 1, representing Pantokrator Limestones, Sinias Limestones, Posidonia beds, Vigla Shales and Limestones, Senonian Limestones, Limestones with microbreccia and Platy Limestones) respectively.

Acknowledgements

We would like to thank personnel in the Laboratory of thin section preparation of the Department of Geology, University of Patras.

References

Avramidis, P., Zelilidis, A., Vakalas, I., Kontopoulos, N., 2002. Interactions Between Tectonic Activity and Eustatic Sea-Level Changes in The Pindos and Mesohellenic Basins, NW Greece: Basin Evolution and Hydrocarbon Potential. Journal of Petroleum Geology 25, 53–82.

Bourli, N., Pantopoulos, G., Maravelis, A.G., Zoumpoulis, E., Iliopoulos, G., Pomoni-Papaioannou, F., Kostopoulou, S., Zelilidis, A., 2019. Late Cretaceous to early Eocene geological history of the eastern Ionian Basin, southwestern Greece: A sedimentological approach. Cretaceous Research 98.

Dunham, R.J., 1962. Classification of Carbonate Rocks According to Depositional Textures, in: Ham, W.E. (Ed.), Classification of Carbonate Rocks--A Symposium.

Folk, R.L., 1959. Practical petrographic classification of limestones. AAPG Bulletin 43.

Folk, R.L., 1962. Spectral subdivision of limestone types, in: Ham, W.E. (Ed.), Classification of Carbonate Rocks--A Symposium. American Association of Petroleum Geologists.

Karakitsios, V., 2013. Western Greece and Ionian Sea petroleum systems. AAPG Bulletin 97, 1567–1595.

Karakitsios, V., Kvaĉek, Z., Mantzouka, D., 2015. The first plant megafossil in the Early Jurassic of Greece: Brachyphyllum (Coniferales) from the Lower Posidonia Beds (Toarcian) in the Ionian zone (NW Greece) and its palaeogeographic implications. Neues Jahrbuch für Geologie und Paläontologie - Abhandlungen 278, 79–94.

Kontakiotis, G., Moforis, L., Karakitsios, V., Antonarakou, A., 2020. Sedimentary Facies Analysis, Reservoir Characteristics and Paleogeography Significance of the Early Jurassic to Eocene Carbonates in Epirus (Ionian Zone, Western Greece). Journal of Marine Science and Engineering 8.

Papanikolaou, D.I., 2021. The Geology of Greece. Springer International Publishing, Cham.

Wilson, J.L., 1975. Carbonate Facies in Geologic History. Springer New York, New York.

Zelilidis, A., Maravelis, A.G., Tserolas, P., Konstantopoulos, P.A., 2015. An overview of the petroleum systems in the Ionian zone, onshore NW Greece and Albania. Journal of Petroleum Geology 38.

16th International Congress of the Geological Society of Greece
17-19 October, 2022 - Patras, Greece
Bulletin of the Geological Society of Greece, Sp. Publ. 10
Ext. Abs. GSG2022-289

Sedimentary Evolution of Miocene Depositional Systems and Their Reservoir Potential in The Thermaikos Basin in Northern Greece

G. Makrodimitras[1], A. Nikitas[1], D. Ktenas[1], A. Maravelis[2], E. Tartaras[1], A. Stefatos[1]

(1) Hellenic Hydrocarbons Resources Management S.A., Athens, Greece, g.makrodimitras@greekhydrocarbons.gr (2) Aristotle University of Thessaloniki, Thessaloniki, Greece

Research Highlights *Miocene sandstones, with excellent reservoir properties for HC exploration or future CO_2 storage*

Background and Objectives

The Thermaikos Basin in Northern Greece corresponds to one of the Peri-Alpine basins in the Northern Aegean Sea area and was developed during the Post-Alpine period (Fig. 1C). The existence of a regional active petroleum system is confirmed by the Epanomi gas field that was discovered during the 80s at the fringes of the basin. Epanomi is a relatively small carbonate field; the production test of Epanomi-2 well yielded 19 MCF/D of gas and small quantities of light oil (Rigakis et al., 2001). The clastic deposits above this carbonate structure, further outboard to the west, in deeper parts of the basin, have gas shows within the Eocene-Oligocene and Miocene series. Additionally, the small to medium-size sandstone targets, given also their proximity to the nearby existing onshore infrastructure and the city of Thessaloniki, could present some attractive exploration opportunities, seeing that these targets could also be used potentially for future CO_2 storage. This study aims to reveal the depositional environments that constitute the clastic deposits with good reservoir properties in the Thermaikos Basin, and to examine their spatial (lateral) and temporal (stratigraphic) distribution across the onshore and offshore area.

Methods

In the first phase of the project, a correlation between offshore/onshore wells and offshore seismic data across the central part of the Thermaikos basin was performed (Fig. 1A & 1B).

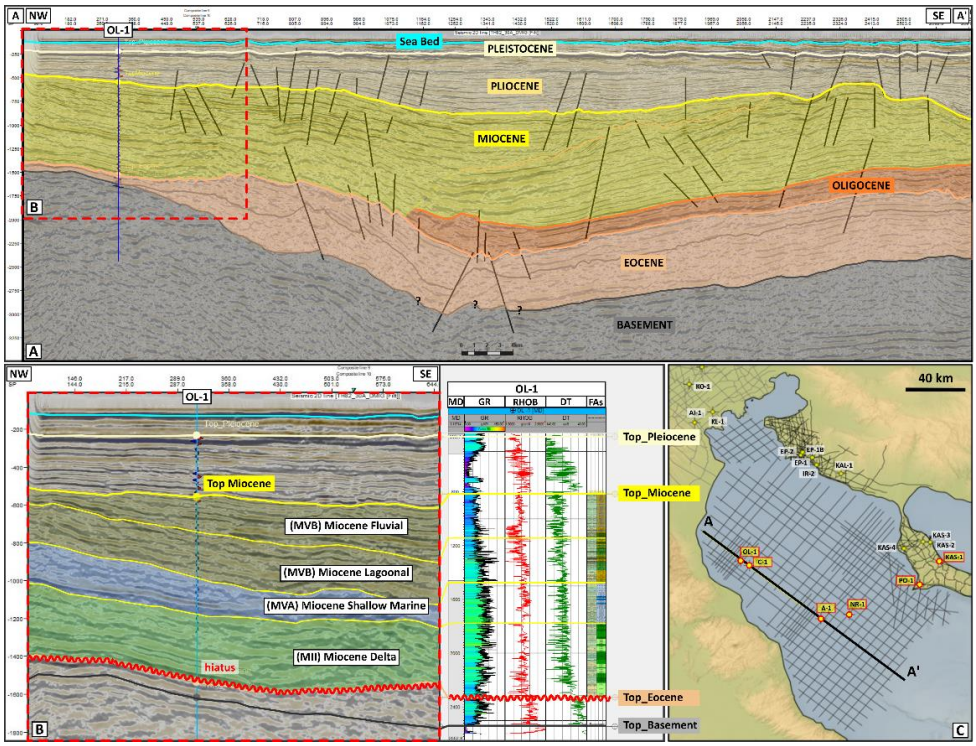

Figure 1. A. Interpreted horizons in a seismic line from the Thermaikos dataset portraying the formations above the basement. Note that the sedimentary succession is laterally continuous and forms a depocenter in the SE of the line created by the various phases of uplift in the area. B. Well to seismic tie between seismic data (TWT) and Olympia-1 well. C. Location map of Thermaikos area, and available seismic and wells dataset. The black line indicates the seismic line A.

The data set includes four (4) offshore wells: Olympia-1 (OL-1), Thermaikos C1 (C1), Thermaikos A1 (A1) and Nireas-1 (NR-1); two (2) onshore wells: Possidi-1 (PO-1) and Kassandra-1 (KAS-1); as well as 3,074.7 km of offshore and 1,047.4 km of onshore seismic data (Fig. 1C). In total, forty-seven (47) samples were evaluated for their reservoir properties. Core and cuttings data were employed to perform facies analysis. A detailed sedimentological description and interpretation of sedimentary features (e.g., color, texture and sedimentary structures) has been applied to generate the present lithotypes, depositional packages and facies associations in the available wells.

In addition to the well-log data, several seismic lines were interpreted. The interpretation revealed a laterally continuous Miocene succession with several intra-Miocene intervals (Fig. 1B) representing a differentiation in depositional systems across the basin.

Results and Conclusions

The Table 1 below summarizes the results of the sedimentological analysis in six (6) wells from the study area.

Series	Pliocene-Pleistocene	Miocene	Eocene-Oligocene
Lithology (from studied wells)	Wide range of deposits, from marls, argillaceous material, mudstone and siltstone deposits to sandstone beds and conglomerate at the base of this internal (A-1, OL-1 and NR-1) or at the fringes of the basin (POS-1). Limestone beds are also present (OL-1)	**Lower Miocene:** coarse-grained material; sandstone-mudstone interbeds with conglomerates at the base A-1) **Middle Miocene:** sandstone-mudstone interbeds with lignite beds also present (A-1) **Upper Miocene:** marl, loose sand and conglomerate deposits	Interbedded mudstone, sandstone and siltstone deposits (KAS-1, A-1, NR-1 and PO-1). Interbedded red-brownish mudstone with lignite beds, sandstone, siltstone deposits and conglomerate (C-1). Conglomerates-breccia with argillaceous and siltstone beds. Rare sandstones (OL-1).
Depositional Environment	**Lagoonal to shallow marine** depositional environment	Lower Miocene: **Fluvial-alluvial fan** depositional environment Middle Miocene: **lagoonal**, **shallow marine and deltaic** depositional environment Upper Miocene: **shallow marine** depositional environment but also **pro-delta** facies in OL-1	Sandstone beds correspond to **deep-water channel deposits** (A-1, NR-1 and PO-1). KAS-1 deposits show a relatively **deeper and "quitter" environment**. The dip of PO-1 beds at the bottom infers a tentative **shallowing depositional environment**. C-1 deposits infer **delta plain** conditions with distributary channels. OL-1 deposits and dip infer a **high energy** environment.

The Miocene sandstone series exhibit very good reservoir properties (up to 29% porosity), resulting from the absence of a matrix between the sandstone grains. However, the available 2D seismic grid limits the certainty of the lateral continuity of these sandstone lenses/beds. The Pliocene-Pleistocene deposits display very good reservoir properties (15-18% porosity). The deeper Eocene-Oligocene deposits are represented by repetitions of thin-bedded sandstone and mudstone and belong to submarine fan deposits. These sedimentary rocks exhibit low porosity (0.5-19%) and permeability (up to 1mD) values. In contrast, the KAS-1 sandstones to the East, exhibit good reservoir properties (up to 18.43% porosity). The best quality reservoir rocks are represented by the Miocene sandstones that are buried down to 1,500ms TWT. These rocks display excellent porosity values up to 29%, mainly in the central and eastern parts of the basin. These sandstone bodies exhibit good lateral continuity across the basin. The Middle to Late Miocene source rock is oil-prone, containing organic matter of type II/III kerogen and good thermal maturity levels in the deeper parts of the basin. In NR-1, deeper Eocene-Oligocene samples reveal gas-prone organic matter with good thermal maturity (PPC, 1995). The seal rocks are represented by the Pliocene-Pleistocene argillaceous/mudstone deposits that cover the stratigraphic traps (maximum thickness 2,000 m). Further, buried faults across the basin create structural traps that can be proved essential for future assessments about the hydrocarbon generation potential and the location of CO_2 storage sites. Overall, the gas shows in the Miocene series are a positive indicator for further exploration in the area. The gas potential has been confirmed by the discoveries and the gas shows of the equivalent Miocene series within the basins of the North Aegean Sea (Prinos, Orfanos and East Thassos basins).

Acknowledgements

HHRM would like to thank Angelos Tagalidis Niki-Marina Rokana and Zafiria Chatzi, for their help during their internship in 2021, and the Greek Ministry of Environment and Energy for providing the data.

References

Public Petroleum Corporation (PPC), 1995. The origin of Epanomi Hydrocarbons and the potential of Thermaikos Basin Source Rocks. Unpublished data

Rigakis, N., Roussos, N., Kamberis, E., Proedrou, P., 2001. Hydrocarbon gas accumulations in Greece and their origin. Bulletin of the Geological Society of Greece, 34(3), 1265-1273

16th International Congress of the Geological Society of Greece
17-19 October, 2022 - Patras, Greece
Bulletin of the Geological Society of Greece, Sp. Publ. 10
Ext. Abs. GSG2022-294

An integrated approach for the thermal maturity modelling re-assessment of the AY-3 well, Arta-Preveza exploration block, Western Greece

G. Moschou [1], V.I. Makri [1,2], N. Pasadakis [1,2], S. Bellas[1]

(1) Institute of GeoEnergy (FORTH/IG), Foundation for Research and Technology – Hellas, Chania, Greece, georgiamoschou@gmail.com (2) School of Mineral Resources Engineering, Technical University of Crete, Chania, Greece

Improvements to the thermal maturity model of the AY-3 well in the Internal Ionian geotectonic zone have been made, suggesting a Miocene thrusting and a Tortonian hydrocarbon expulsion. The Ionian zone belongs to the external (western) Hellenides, part of the Dinarides-Albanides-Hellenides fold-and-thrust belt and is divided into three partly thrust-bound belts (internal, middle, and external from East to West) (Aubouin, 1959). It consists of Triassic to Eocene mainly carbonate deposits and Oligo-Miocene clastics. During Late Triassic, Western Greece was dominated by carbonate platform deposits, currently overlying the Middle Triassic evaporites. Liassic rifting and subsidence formed the Ionian basin which after structural differentiation generated North-South oriented half-grabens, where the syn-rift deposition took place. An isochronous Lower Cretaceous post-rift sequence of strong thickness variations covered previous deposits prior to the Cenozoic orogenic movements (IGRS-IFP, 1966). Yet, a recent study suggested a continuous rifting from Jurassic to Early Eocene (Bourli *et al.*, 2019). So far five have been the main identified Mesozoic source rocks of Western Greece. Here, we focus on the Vigla shales, an identified source rock of Aptian-Turonian age, related to global Oceanic Anoxic Events (Karakitsios *et al.*, 2018).

For this study we utilized the available geological and geochemical data (Rigakis, 1999) to build an 1D thermal maturity model of the AY-3 well, located in the Internal Ionian zone. The goal was to re-assess the source rock maturity and hydrocarbon generation potential after Rigakis (1999) and Moschou (2021). Biomarkers and Rock-Eval data were used on top of the geothermal gradient (GG) and vitrinite reflectance (VR). Vigla shales A and B, incorporated within alternations of carbonates, cherts, and marly limestones were selected as source rock intervals, since they are considered the most prominent of the Internal Ionian zone (Karakitsios & Rigakis, 2007).

Vigla shales contain mainly kerogen type I to II, while the Rock-Eval and biomarker isomerization data suggest early to peak maturity. These biomarkers are the homohopane C32[22S/(22S+22R)] and the sterane C29aaa[20S/(20S+20R)] ratios. The former appears to exhibit values greater than 0.57 and the latter greater than 0.35, indicating that the oil window has been reached (Peters *et al.*, 2005). The generation potential is mainly good – excellent with average TOC of 2.5% and maximum of 11.35%. Also, S2 is greater than S1 illustrating the presence of residual hydrocarbon generating potential. Biostratigraphy and biomarkers (Triantaphyllou *et al.*, 2006*;* Dimopoulos *et al.*, 2019) depict a marine depositional environment with lithological intercalations, which are common in Cretaceous deposits in Southern Europe (Tiraboschi *et al.*, 2009). Vitrinite fragments are rare within the shale intervals in contrast to liptinite, supporting the prevalence of a distal basin environment. Isoprenoids (Pr, Ph) and biomarkers denote the presence of mixed organic matter, such as the distribution of C27-C29 steranes that shows slight dominance of C29aaaR steranes. The above-mentioned, underpin a submarine semi-restricted depositional environment with low water circulation and occasional terrestrial input.

For the current model, the lithologies were introduced as detailed as possible, integrating also dolomitization information. A thrust was tested to have acted during Oligocene and the concept of Early to Late Jurassic rifting was applied. Present day heat flow was set to 39mW/m^2 (Fytikas & Kolios, 1979) while GG and VR values were obtained from Rigakis (1999). In the model, a kerogen of type I (organofacies C) as mostly indicated by the geochemical data was utilized, while a kerogen of type II scenario was also tested (Pepper & Corvi, 1995). The calibration of the model was performed on the temperature (T), VR and biomarker ratio profiles. New VR models were used to assess thermal maturity and subsequent hydrocarbon generation scenarios (Schenk *et al.*, 2017).

Overall, an adequate calibration was achieved through the T, VR, and biomarker ratio trends. The Easy%RoDL and Basin%Ro VR models show significant improvements compared to the traditionally used Easy%Ro, with the former being more precise for lower VR values, as opposed to the latter (Figure 1) (Schenk e*t al.*, 2017). In that sense, the comparison of both hydrocarbon generation scenarios is crucial. The Vigla shales and more specifically Vigla shales B appear to have entered the oil window in Aquitanian using the Basin%Ro and in Langhian using the Easy%RoDL model. The generation onset appears to be during lower Oligocene (Figure 2), and the expulsion onset during Tortonian. Additionally, based on the calibration of the model, the Oligocene thrust seems to have acted during Eocene, while a total of 1950m erosion has taken place. In a nutshell, improvements to the model have been made, resulting into adequate scenarios of the thrusting age, overburden thickness, hydrocarbon generation potential and expulsion onset. We suggest that in future research, a kerogen kinetic study of this source rock would be a significant addition to the model and equally

important to the hydrocarbon exploration of the External Hellenides.

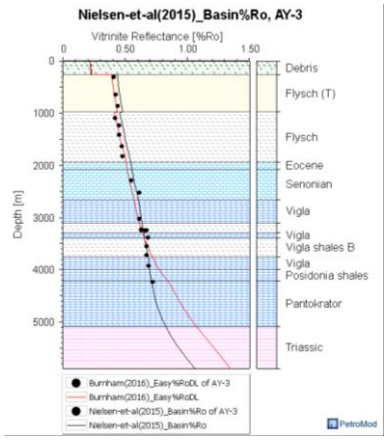

Figure 1. Vitrinite reflectance calibration with Basin%Ro and Easy%RoDL models.

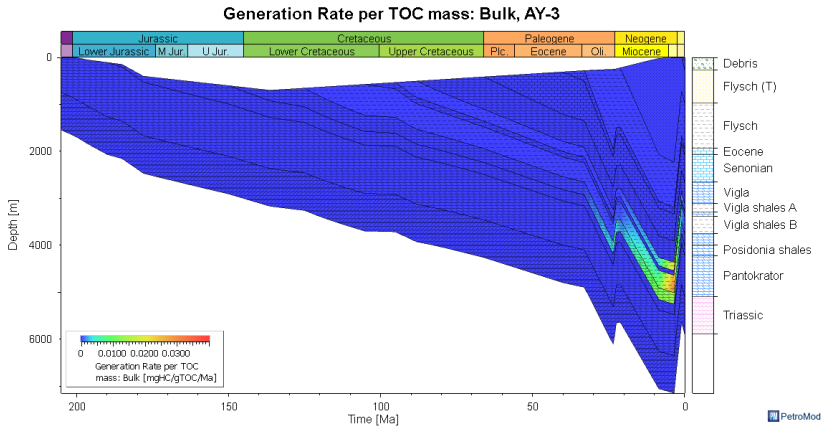

Figure 2. Generation rate per TOC mass overlay on the burial history for AY-3 well. The kinetic model used was Pepper&Corvi(1995) TI(C) .

Acknowledgements

This study is supported by Hellenic Petroleum S.A. (HELPE).

References

Aubouin, J., 1959. Contribution à l' étude géologique de la Grèce septentrionale: Le confins de l' Epire et de la Thessalie. Annales Géologiques des Pays Helléniques 10, 1-484.

Bourli, N., Pantopoulos, G., Maravelis, A.G., Zoumpoulis, E., Iliopoulos, G., Pomoni-Papaioannou, F., Kostopoulou, S., Zelilidis, A., 2019. Late Cretaceous to early Eocene geological history of the eastern Ionian Basin, southwestern Greece: A sedimentological approach. Cretaceous Research 98, 47-71.

Dimopoulos, N., Georgoulas, E., Peridis, S., Iliopoulos, G., Bourli, N., Antoniou, P., Zelilidis, A., 2019. Re-assessment of depositional conditions of Cretaceous deposits around the Amfilochia and Arta areas. Bulletin of the Geological Society of Greece 55, 241-259.

Fytikas, M.D., Kolios, N.P., 1979. Preliminary Heat Flow Map of Greece, in: Čermák, V., Rybach, L. (Eds.), Terrestrial Heat Flow in Europe, 197-205.

IGRS-IFP (Institut de Geologie et Recherches du Sous-sol-Institut Francais du Pétrole), 1966. Etude géologique de l' Epire (Grece Nord-occidentale), 306 p.

Karakitsios, V., Rigakis, N., 2007. Evolution and petroleum potential of Western Greece. Journal of Petroleum Geology 30, 197-218.

Karakitsios, V., Tsikos, H., Van Breugel, Y., Bakopoulos, I., Koletti, L., 2018. Cretaceous Oceanic Anoxic Events in Western continental Greece. Bulletin of the Geological Society of Greece 36(2), 846-855.

Moschou, G., 2021. Basin modeling study of potential source rock formation in North Ionian Sea. M.Sc thesis, Technical University of Crete, Chania, 95 p.

Pepper, A.S., Corvi, P.J., 1995. Simple kinetic models of petroleum formation. Part I: oil and gas from kerogen. Marine and Petroleum Geology 12(3), 291-319.

Peters, K., Walters, C., Moldowan, J., 2005. Source- and age-related biomarker parameters, in: Peters, K., Walters, C., Moldowan, J., (Eds.), The Biomarker Guide, 483-607.

Rigakis, N., 1999. Contribution to stratigraphic research on wells and outcrops of the Alpine formations in Western Greece, in relation to the petroleum generation efficiency of their organic matter. Ph.D Thesis, National and Kapodistrian University of Athens, Athens, 255 p.

Schenk, O., Peters, K.E., Burnham, A., 2017. Evaluation of alternatives to Easy%Ro for calibration of basin and petroleum system models, 79th EAGE Conference and Exhibition, Paris, France, 5 p.

Tiraboschi, D., Erba, E., Jenkyns, H., 2009. Origin of rhythmic Albian black shales (Piobbico core, central Italy): Calcareous nannofossil quantitative and statistical analyses and paleoceanographic reconstructions. Paleoceanography 24, 21 p.

Triantaphyllou, M.V., Karakitsios, V., Mantzouka, D., 2006. Calcareous nannofossil biostratigraphy of the basal part of Vigla shale member (Ionian zone) in Ithaki Island, preliminary results. Bulletin of the Geological Society of Greece 39(1), 126-132.

16th International Congress of the Geological Society of Greece
17-19 October, 2022 - Patras, Greece
Bulletin of the Geological Society of Greece, Sp. Publ. 10
Ext. Abs. GSG2022-307

Porosity Distribution Estimation in the Potential CO2 Storage Formations of the Mesohellenic Trough, Northern Greece, through 3D Geological Modeling

D. Ktenas[1], A. Tasianas[2], G. Makrodimitras[1], E. Tartaras[1], A. Stefatos[1]

(1) Hellenic Hydrocarbon Resources Management (HHRM), Athens, Greece, d.ktenas@greekhydrocarbons.gr (2) King Abdullah University of Science and Technology (KAUST), Thuwal, Saudi Arabia

Research Highlights *Improved spatial porosity distribution in formations for CO2 storage in the Mesohellenic Trough*

Background

Carbon Capture and Storage (CCS) has recently gained global attention as a promising technology for mitigating net CO2 emissions, as it allows removing CO2 from the atmosphere. Within this framework, the Greek government has recently announced the National Energy and Climate Plan (NEP), setting out a detailed road map regarding the attainment of specific energy and climate objectives by 2030. Consequently, the Hellenic Hydrocarbon Resources Management (HHRM) has recently become the competent authority for the licensing and monitoring of CO2 storage projects offshore and onshore Greece (HHRM, 2022). CO2 storage potential in Greece concerns saline aquifers, salt caverns and a few hydrocarbon fields (e.g., Prinos semi-depleted field). In this study we create a 3D porosity distribution model in the Mesohellenic Trough (MT) in north-western Greece, in order to help assess its CO2 storage potential. The largest share of the national stationary emissions come from NW Greece, which has been extensively mined for power generation (e.g., Ptolemaida coal-fired stations), as well as from refineries, power plants and cement industry in the nearby city of Thessaloniki. In addition, pipelines, such as the TAP and the planned IGI Poseidon are crossing the MT and, considering the rapid technology advancement, CO2, H2 and other gases could be transferred simultaneously.

The Mesohellenic Trough is a 100-130Km-long, 30-40 Km-wide intramontane sedimentary basin located in the central part of the Hellenic chain, between the Pelagonian and the Apulian geotectonic zones, in Northern Greece (Zelilidis *et al.*, 2002). Its large-scale piggyback setting (westwards) and foredeep (eastwards) structure, filled with turbiditic deposits covered by Paleogene to Neogene aged, shallow-to-deep water molassic sediments, is widely accepted by several authors (e.g., Zelilidis *et al.*, 2002). The same authors and recent studies (Arvanitis *et al.*, 2021; Makri *et al.*, 2022) have characterized the turbiditic sandstones (Pentalofos Fm and Eptachori Fm) as the most promising reservoir rocks and the overlying Tsotyli Fm as the seal rock (Fig. 1).

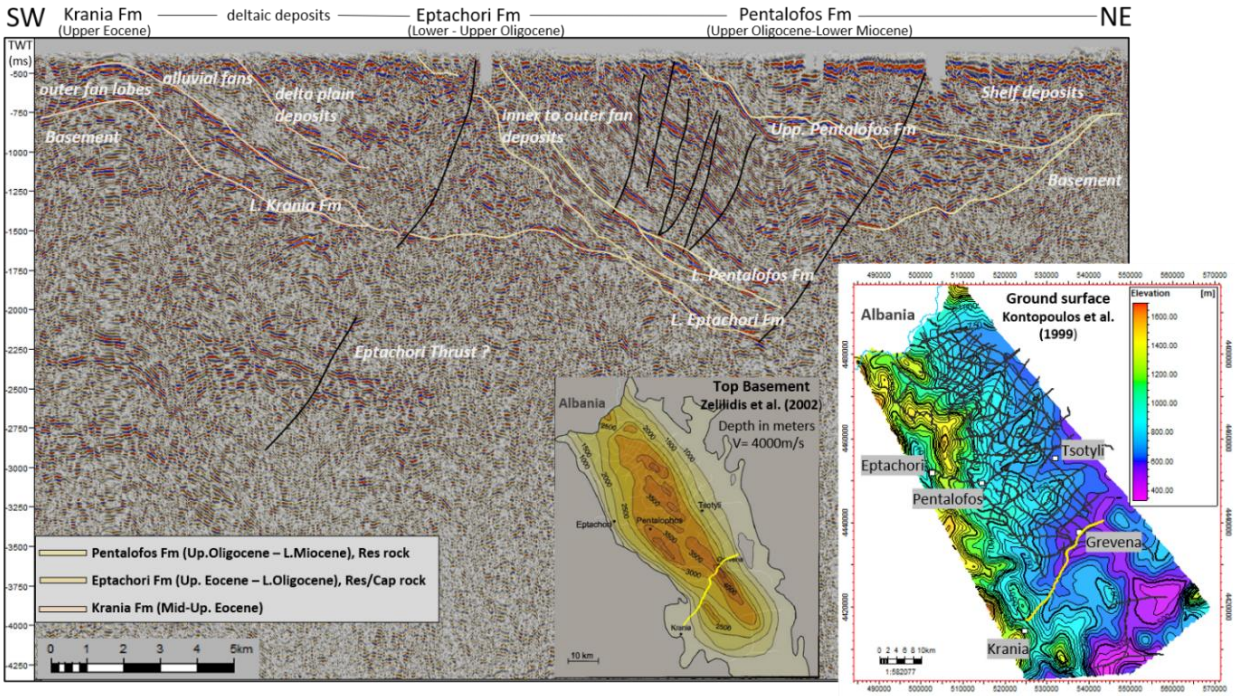

Figure 1. Seismic line GRV-734 in the southern depocenter illustrating the seismic stratigraphic architecture correlated with surface outcrops (modified after Kontopoulos *et al.*, 1999 and Zelilidis *et al.*, 2002).

Objectives

The aim of this work is to create a more advanced porosity model within the potential MT CO2 storage formations and, thus, re-evaluate the CO2 storage capacity in the Pentalofos Fm and Eptachori Fm. Furthermore, it could provide a better understanding of the interconnectivity of the various surface formations in the MT.

Methods

For creating an advanced porosity distribution model and, subsequently, estimating CO2 storage capacities, published isobath maps (Zelilidis *et al*., 2002; Tasianas and Koukouzas, 2016) were converted into surfaces and then conditioned in order to provide a more geologically realistic output. Petrophysical modeling was applied with a view to generate a layer-cake geological model. Subsequently this model was populated with characteristic reservoir properties, such as the porosities, for each stratigraphic formation (Fig. 2) (based on Koukouzas *et al*., 2021).

Results and Conclusions

Improved porosity distribution estimates have been obtained through 3D geological modeling in potential storage formations (Fig. 2). The resulting improved geological model has allowed a re-assessment of the CO2 storage capacity in the Eptachori and Pentalofos formations. The storage potential seems to be higher in the north-eastern part of the MT, whereas the reservoir (stacked sand bodies) is located at adequate depths for CO2 storage, with sufficient thickness of the Tsotyli Fm and sealed by the overlain Quaternary. These results will serve as a basis for running static and dynamic modeling to better understand potential CO2 flow and plume evolution in the Mesohellenic Trough.

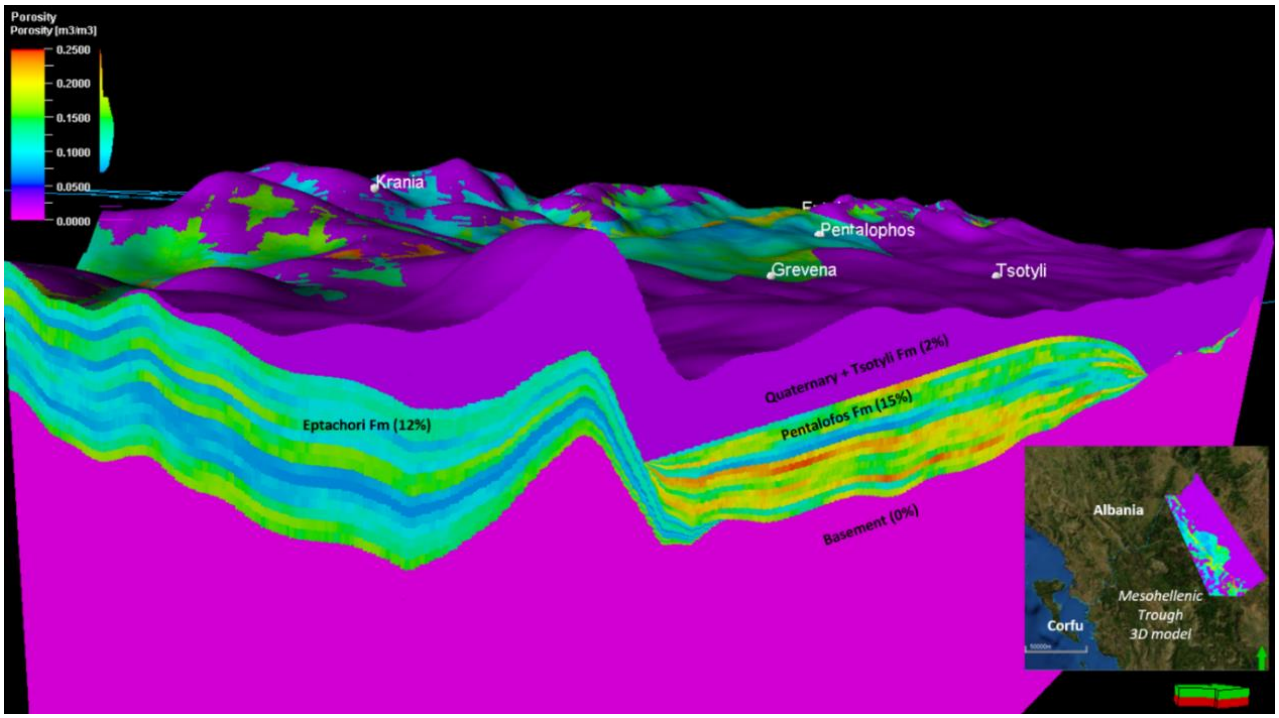

Figure 2. Porosity distribution in potential storage formations of the Mesohellenic Trough 3D model.

Acknowledgements

We thank the Ministry of the Environment and Energy for providing the data.

References

Arvanitis, A., Koutsovitis, P., Koukouzas, N., Tyrologou, P., Karapanos, D., Karkalis, C., Pomonis, P., 2020. Potential Sites for Underground Energy and CO2 Storage in Greece: A Geological and Petrological Approach. Energies, 13(11), 270.

HHRM, 2022. Expansion of scope of HHRM: Carbon Capture and Storage Projects [Press release, https://www.greekhydrocarbons.gr/news_en/PR_REL_040522_EN.html]

Kontopoulos, N., Fokianou, T., Zelilidis, A., Alexiadis, C., Rigakis, N., 1999. Hydrocarbon potential of the middle Eocene-middle Miocene Mesohellenic piggy-back basin (central Greece): A case study. Marine and Petroleum Geology, 16(8), 811-824.

Koukouzas, N., Tyrologou, P., Karapanos, D., Carneiro, J., Pereira, P., de Mesquita Lobo Veloso, F., Koutsovitis, P., Karkalis, C., Manoukian, E., Karametou, R., 2021. Carbon Capture, Utilisation and Storage as a Defense Tool against Climate Change: Current Developments in West Macedonia (Greece). Energies, 14(11), 3321.

Makri, V.I., Bellas, S., Gaganis, V., 2022. Assessing Natural Gas Versus CO2 Potential Underground Storage Sites in Greece: A Pragmatic Approach. Materials Proceedings, 5(1), 98.

Tasianas, A., Koukouzas, N., 2016. CO2 storage capacity estimate in the lithology of the Mesohellenic Trough, Greece. Energy Procedia, 86, 334-341.

Zelilidis, A., Piper, D.J.W., Kontopoulos, N., 2002. Sedimentation and basin evolution of the Oligocene-Miocene Mesohellenic basin, Greece. Aapg Bulletin, 86(1), 161-182.

16th International Congress of the Geological Society of Greece
17-19 October, 2022 - Patras, Greece
Bulletin of the Geological Society of Greece, Sp. Publ. 10
Ext. Abs. GSG2022-309

Source rock potential and spatial distribution of the pre-Evaporite sedimentary succession of the central Mediterranean Ridge: Evidence from mud volcanic deposits and seismic data

Anastasios Nikitas[1, 2], Georgios Makrodimitras[1], Maria V. Triantaphyllou[2], Nikolaos Pasadakis[3], Kimon Christanis[4], Stavros Kalaitzidis[4], Grigoris Rousakis[5], Ioannis Panagiotopoulos[2], Alexandra Gogou[5], Alexandros Papadopoulos[1], Efthimios Tartaras[1] and Aristofanis Stefatos[1]

(1) Hellenic Hydrocarbon Resources Management S.A., Athens, Greece, a.nikitas@greekhydrocarbons.gr (2) Faculty of Geology and Geoenvironment, National and Kapodistrian University of Athens, Zografou, Greece (3) Institute of Geoenergy, Foundation for Research and Technology-Hellas, University Campus, Chania, Greece (4) Department of Geology, University of Patras, Rio-Patras, Greece (5) Hellenic Centre for Marine Research, Institute of Oceanography, Anavyssos, Greece

Research Highlights: *Mud volcanoes, Mediterranean Ridge, good Miocene source rock, active petroleum system*

Background and Objectives

Due to the lack of deep wells in the greater region, the sedimentary material (mud breccia deposits) extruded from Mud Volcanoes (MVs) are considered the only source of direct information for the deeply buried sedimentary layers in the Mediterranean Ridge (MR). The study of this material in combination with the available seismic data, can lead to a better geological understanding of the study area (Fig. 1). This study is an integration of older (Panagiotopoulos et al., 2020; Nikitas et al., 2021) and new data focusing on the source rock potential evaluation of the pre-Evaporite (pre-Messinian) sedimentary succession of the central MR by examining the mud breccia deposits from 8 MVs (Gelendzhik, Heraklion, Nice, Moscow, Milano, Leipzig, Dublin and Toronto). In addition, some of the available seismic data were used, to reveal the spatial distribution of the main stratigraphic units, including the source layers of the mud breccia deposits (pre-Evaporite formations).

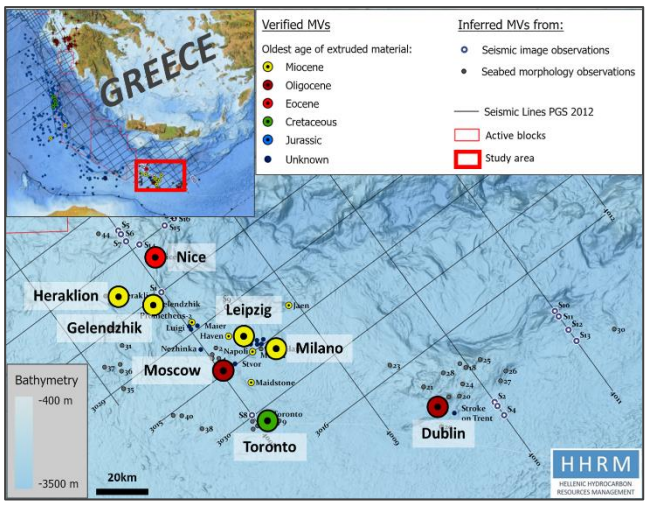

Figure 1. Sampling positions inside the study area.

Methods

For the mud breccia study, in total 97 samples (76 clasts -essentially mudstones- and 21 matrix samples) were obtained from 8 gravity cores (1 from each MV) and were macroscopically described. Calcareous nannoplankton analysis was performed to define each sample's stratigraphic origin. Subsequently, Rock-Eval pyrolysis and organic petrography examination were conducted to determine the source rock potential for each sample (TOC, kerogen type & composition, thermal maturity).

Results and Conclusions

Results show that sedimentary material of Miocene, Oligocene and Eocene age is extruded from Gelendzhik, Heraklion, Nice, Moscow, Milano, Leipzig and Dublin MVs, whereas sediments of Paleocene and Cretaceous age are extruded from Toronto MV. Concerning the geochemical analyses, there were 37 organic rich (TOC>0.5%) and 57 organic poor samples (TOC<0.5%); kerogen included is essentially of Type III and IV (but also a mixed Type II-III and minor I and II Types are present) and is considered immature for oil/gas generation (Fig. 2a, 2b). However, according to the organic petrography results, 7 samples of Miocene, mixed Oligo-Miocene, Cretaceous and unknown age have reached the early-mid oil window (V_r=0.62-0.84%). Regarding the source rock potential of the area, it can be concluded that: a) 1 mudstone clast of Miocene age (Late Serravallian) reflects the presence of an immature oil & gas prone source rock of good potential

in the subsurface, b) 20 clasts of Miocene, Eocene and undetermined age, indicate the presence of immature and early mature, gas prone source rocks of poor potential, c) a clast fragment discovered in D-10m sample originates from an oil prone source rock of excellent quality, still to be assessed and d) discovered solid hydrocarbons and oil droplets are pointing to an active petroleum system in the area.

Finally, the interpretation of available seismic reflection profiles revealed the spatial distribution of the major lithostratigraphic units (i.e., post-Evaporite, Evaporite and pre-Evaporite formations) (Fig. 2c). The burial depth of the pre-Evaporite formation (source layers of MV deposits) can greatly vary across the study area (~20 to 4970m).

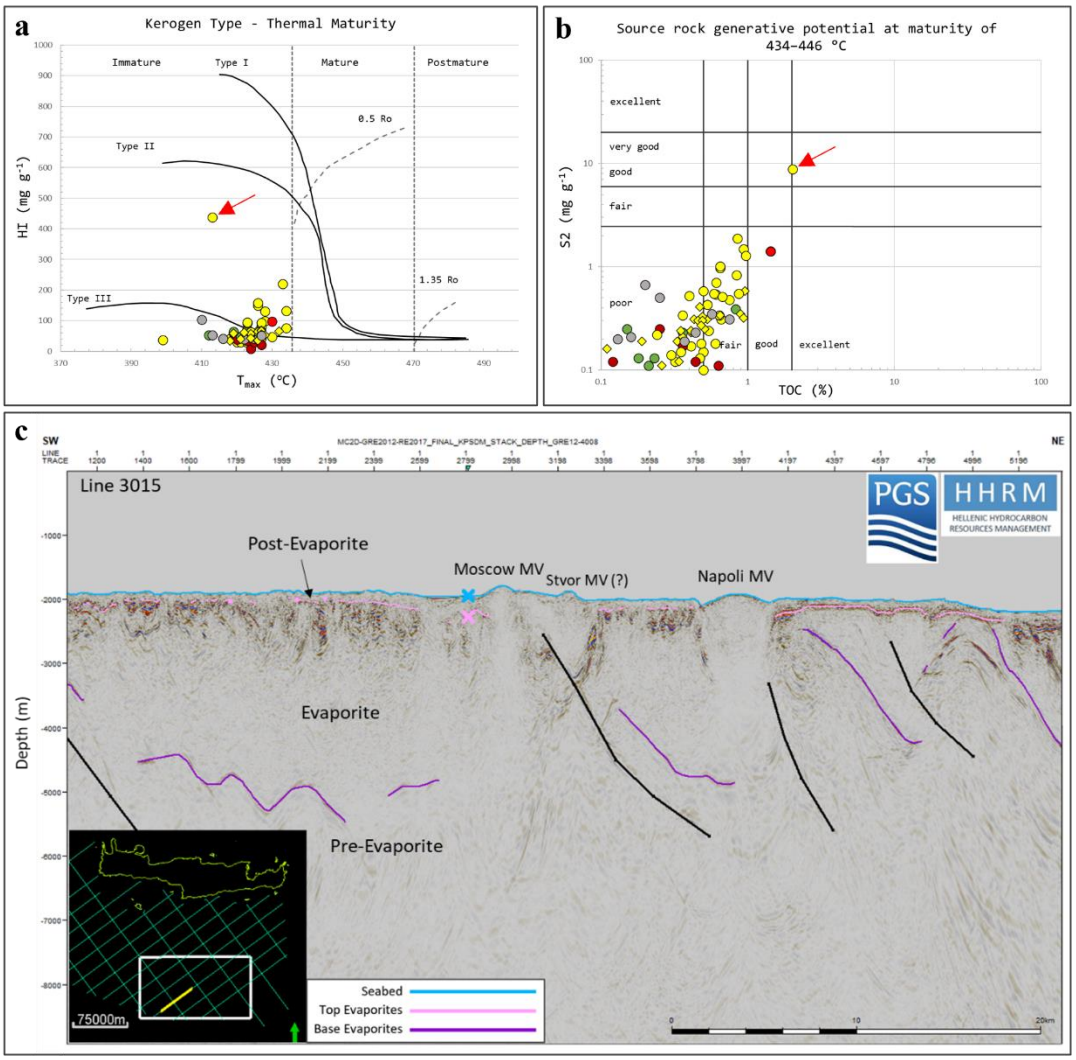

Figure 2. a, b. Source rock generative potential and kerogen type/thermal maturity diagrams of the studied samples. Yellow: Miocene; Red: Oligocene; Dark red: Oligocene; Green: Cretaceous; Grey: Undetermined. Circles: Clasts; Rhombuses: Muddy matrix; Red arrow: late Serravallian SR. c. Seismic line 3015. The mud breccia deposits originate from the pre-Evaporite layers (below the purple horizon).

Acknowledgements

This research was funded by the Hellenic Hydrocarbons Resources Management (HHRM). We are grateful to the Hellenic Center for Marine Research (HCMR) for providing the core samples for Gelendzhik, Heraklion, Nice, Moscow, Milano and Leipzig Mud Volcanic structures. We are also grateful to the British Ocean Sediment Core Research Facility (BOSCORF) for providing the core samples for Toronto and Dublin mud structures.

References

Panagiotopoulos, I.P., Paraschos, F., Rousakis, G., Hatzianestis, I., Parinos, C., Morfis, I. and Gogou, A., 2020. Assessment of the eruptive activity and identification of the mud breccia's source in the Olimpi mud volcano field, Eastern Mediterranean. Deep Sea Research Part II: Topical Studies in Oceanography, 171, p.104701.

Nikitas, A., Triantaphyllou, M.V., Rousakis, G., Panagiotopoulos, I., Pasadakis, N., Hatzianestis, I. and Gogou, A., 2021. Pre-Messinian Deposits of the Mediterranean Ridge: Biostratigraphic and Geochemical Evidence from the Olimpi Mud Volcano Field. Water, 13(10), p.1367.

16th International Congress of the Geological Society of Greece
17-19 October, 2022 - Patras, Greece
Bulletin of the Geological Society of Greece, Sp. Publ. 10
Ext. Abs. GSG2022-386

Organic geochemical signatures of the Upper Miocene (Tortonian - Messinian) sedimentary succession onshore Crete Island, Greece

A.G. Maravelis[1], G. Kontakiotis[2], S. Bellas[3], A. Antonarakou[2], C. Botziolis[4], H.T. Janjuhah[5], P. Makri[2], P. Moissette[2,6], J.-J. Cornée[7], N. Pasadakis[3], E. Manoutsoglou[8], A. Zelilidis[4], V. Karakitsios[2]

(1) Department of Geology, Aristotle University of Thessaloniki, Thessaloniki, 54124, Greece; angmar@geo.auth.gr (2) Department of Historical Geology-Paleontology, Faculty of Geology and Geoenvironment, School of Earth Sciences, National and Kapodistrian University of Athens, Panepistimiopolis, Zografou, 15784 Athens, Greece (3) Institute of Geoenergy - Foundation for Research and Technology - Hellas (FORTH/IG), Building M1, University Campus, Akrotiri, 73100 Chania, Greece (4) Laboratory of Sedimentology, Department of Geology, University of Patras, Rion, 26504, Greece (5) Department of Geology, Shaheed Benazir Bhutto University, Sheringal, KPK, 18050, Pakistan (6) Muséum National d'Histoire Naturelle, Département Origines et Evolution, UMR7207 CR2P, 8 rue Buffon, 75005 Paris, France (7) Géosciences Montpellier, Université des Antilles-Université de Montpellier-CNRS, Pointe à Pitre (FWI), Montpellier, France (8) Laboratory of Geology, School of Mineral Resources Engineering, Technical University of Crete, 73100 Chania, Greece.

Research Highlights

The definition of pre-Messinian source rocks in the Eastern Mediterranean is of paramount importance for the hydrocarbon exploration because of the ability of salt to be a high-quality seal rock. This research evaluates the organic geochemical features of the Upper Miocene (Tortonian – Messinian) sedimentary succession onshore Crete Island, Greece.

Background

The potential of onshore Crete and nearby regions to contain Tortonian to Messinian (sub-salt) source and reservoir rocks has been suggested for Gavdos Island south of Crete (Pyliotis et al., 2013), Messara and Heraklion Basins in central Crete (Pasadakis et al., 2012; Maravelis et al., 2016; Kontakiotis et al., 2020; Panagopoulos et al., 2022), and Levantine Basin in southeast Mediterranean (Grohman et al., 2019; Gardosh et al., 2006). The study employs original and published results that come from organic geochemical analyses of mudstone samples.

Objectives

This research elaborates available data from the Tortonian deposits that belong to Viannos Formation, Skinias Formation, and Faneromeni section and from the Messinian Ploutis section and additionally, presents new numerical constraints to the organic geochemical signatures of the Messinian Agios Myron Formation, providing information about the type, quantity, quality, and maturation level of the organic material. This integration of data will offer a comprehensive outlook about the existence of Tortonian - Messinian source rocks onshore Crete Island.

Methods

One hundred and one samples were examined, by using standard organic geochemistry methodology to define the origin, type, and degree of organic matter maturity. The analysis was performed using a Rock-Eval II and VI (Delsi Inc.) analyzers under standard conditions, by utilizing ~100 mg of pulverized rock. The samples were then heated in a helium atmosphere, using a suitable oven. Principal parameters, including total organic carbon content (TOC, wt%), free (S1, mg HC/g rock) and pyrolysable (S2, mg HC/g rock) hydrocarbons, total hydrocarbon generative potential (SP, S1+S2, mg HC/g rock), hydrogen index (HI, mg HC/g Corg), oxygen index (OI, mg CO2/g Corg), Tmax (◦C), and production index (PI, S1/S1+S2) were documented.

Results

The organic geochemical analysis illustrates the presence of source rocks that exhibit poor to good potential to generate hydrocarbons. Several samples yielded TOC values above 0.5 wt%, suggesting some hydrocarbon generating potential. The studied succession includes samples that could likely be interesting (TOC between 0.5 and 1.0%), and samples that are very promising (TOC above 1.0%). Most of the samples contain organic matter that is of type III and IV kerogen, suggesting gas-prone source rocks. Maturity parameters (Tmax and/or PI) suggest that the analyzed samples have not reached the oil window (Figure 1). Comparison between the studied sections exhibits a similar degree of thermal maturity, but different quantity and quality of organic material. This could be partly related to the nature of the depositional environments and sub-environments that encompass the different sections, and partly to the shoreline trajectories that are associated with their accumulation. For instance, the continental in origin Skinias Formation is less favorable for accumulation and preservation of organic material. Furthermore, even though shallow marine settings contain sufficient sources that can deliver organic material, their high oxygenation levels can prevent the formation of suitable source rocks

and can explain the unpromising geochemical signatures of the marine Skinias and Agios Myron Formations.

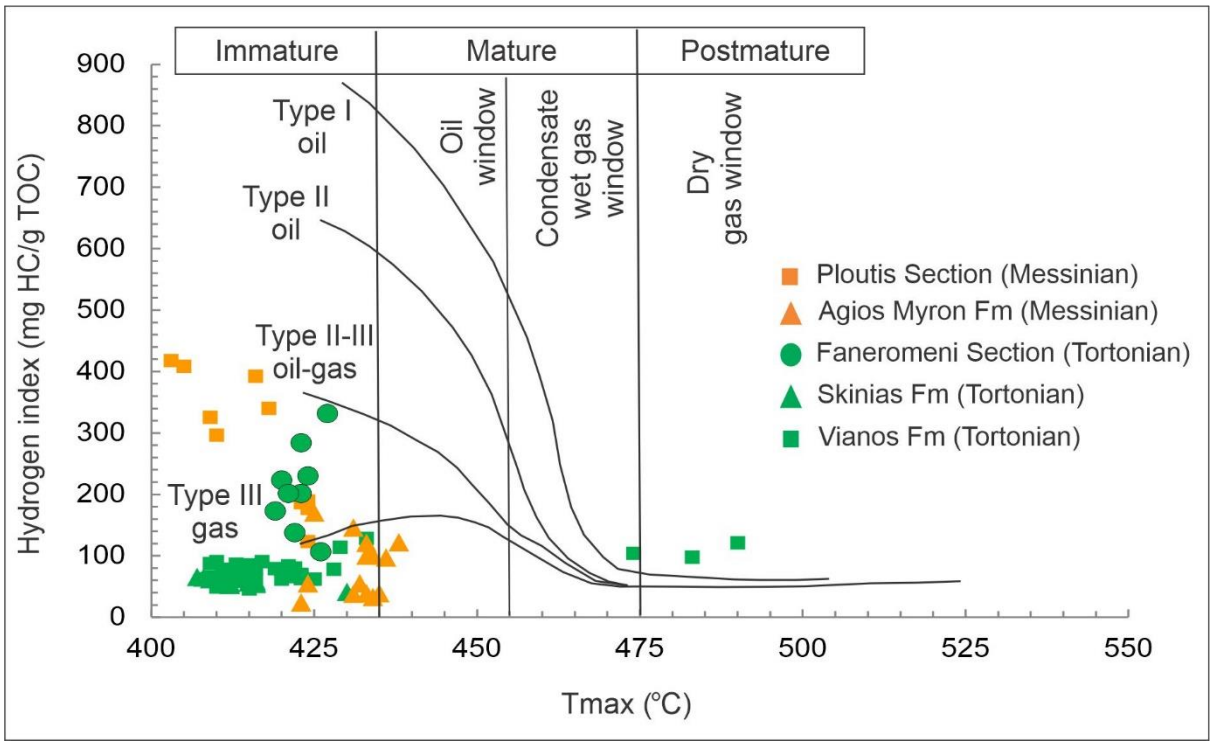

Figure 1. Assessment of maturation status of the examined samples, based on Hydrogen index vs. Tmax cross-plot. The samples derived from all formations are thermally immature. Green color refers to samples that are Tortonian in age, whereas, orange color refers to samples that are Messinian in age.

Conclusions

The data indicate that the studied samples have poor to fair, gas-prone source rock potential. These possible source rock units have not experienced great temperatures during burial and thus, their organic matter is thermally immature. The sub-salt (Tortonian – Messinian) source rock units are likely of higher thermal maturity in the western and eastern south Cretan trenches, because of tectonic subsidence and thicker sedimentary overburden. Several traps can grow in these regions, associated with normal faults, rotated blocks and unconformities (both below and above the un-conformities). This research provides the opportunity to further evaluate the hydrocarbon potential in Crete Island. It is an area that shares geological similarities with the surrounding regions that contain proven reserves and is of crucial economic and strategic importance.

References

Gardosh, M.A., Druckman, Y., 2006. Seismic stratigraphy, structure and tectonic evolution of the Levantine Basin, offshore Israel. Geological Society London Special Publications 260, 201–227. **[Journal Article]**

Grohmann, S., Romero-Sarmiento, M.-F., Nader, F.H., Baudin, F., Littke, R., 2019. Geochemical and petrographic investigation of Triassic and Late Miocene organic-rich intervals from onshore Cyprus, Eastern Mediterranean. International Journal of Coal Geology 209, 94–116. **[Journal Article]**

Kontakiotis, G., Karakitsios, V., Cornée, J.-J., Moissette, P., Zarkogiannis, S.D., Pasadakis, N., Koskeridou, E., Manoutsoglou, E., Drinia, H., Antonarakou, A., 2020. Preliminary results based on geochemical sedimentary constraints on the hydrocarbon potential and depositional environment of a Messinian sub-salt mixed siliciclastic-carbonate succession onshore Crete (Plouti section, eastern Mediterranean). Mediterranean Geoscience Reviews 2, 247–265. **[Journal Article]**

Maravelis, A.G., Panagopoulos, G., Piliotis, J., Pasadakis, N., Manoutsoglou, E., Zelilidis, A., 2016. Pre-Messinian (sub-salt) source-rock potential on back-stop basins of the Hellenic Trench System (Messara Basin, Central Crete, Greece). Oil & Gas Science and Technology - Rev. IFP Energies nouvelles 71, 1–19. **[Journal Article]**

Panagopoulos, G., Vafidis, A., Soupios, P., Manoutsoglou, E., 2022. A study on the Gas-bearing Miocene Sediments of MESSARA Basin in Crete (Greece) by Using Seismic Reflection, Geochemical and Petrophysical Data. Arabian Journal for Science and Engineering 47, 7449–7465. **[Journal Article]**

Pasadakis, N., Dagounaki, V., Chamilaki, E., Vafidis, A., Zelilidis, A., Piliotis, I., Panagopoulos, G., Manoutsoglou, E., 2012. Organic geochemical evaluation of Neogene formations in Messara (Heraklion, Crete) basin as source rocks of biogenetic methane. Mineral Wealth 166, 8–26. **[Journal Article]**

Pyliotis, I., Zelilidis, A., Pasadakis, N., Panagopoulos, G., Manoutsoglou, E., 2013. Source rock potential of the late Miocene Metochia formation of Gavdos island, Greece. Bulletin of the Geological Society of Greece 43, 871–879. **[Conference Proceedings]**

16th International Congress of the Geological Society of Greece
17-19 October, 2022 - Patras, Greece
Bulletin of the Geological Society of Greece, Sp. Publ. 10
Ext. Abs. GSG2022-400

In-situ assessment of the baseline ambient noise levels in the Ionian Sea. Reanalysis of acoustic monitoring data acquired during the HELPE's 2D/3D Marine Seismic Surveys, 2016-2022.

E. Fakiris[1]*, G. Papatheodorou[1], G. Mikoniatis[2], Y. Vavassis[2], D. Christodoulou[1], N. Georgiou[1], X. Dimas[1]
(1) Laboratory of Marine Geology and Physical Oceanography, Geology Dpt., University of Patras, Greece, fakiris@upatras.gr (2) HELPE Exploration & Production of Hydrocarbons, Athens, Greece.

Research highlights

This work describes a regional scale assessment of ambient noise in the Ionian Sea through a network of stations with a 300km longitudinal span. Sound data analysis offers the first ever baseline underwater noise levels in the area.

Background and work overview

Impacts of man-made acoustic noise on the marine environment are associated to the frequency and timing of any activity as well as the distribution and abundance of marine life. Offshore commercial operations, shipping activities, energy exploration and pile driving add noise to the already established ambient noise levels. Attention has been raised by the years to the topic of underwater noise and its effects on marine life, but the effects of underwater noise are not yet fully understood. As the adoption of the European Marine Directive (MSFD 2008/56/EC - Descriptor 11) has given great impulse to the research in this field, governments, companies and institutes are working to specify the background ambient noise levels in the European seas (OSPAR, 2009; Merchant et.al, 2015, Nienke et.al., 2022). Those studies have formed the guidelines and have set the protocols for acoustic noise monitoring and performing safer offshore operations, which are adopted by the major energy companies. Hellenic Petroleum S.A. has undertaken three Marine Seismic Surveys in the Greek territory waters of the Ionian Sea between 2016 and 2022. Those were coupled with intensive sound noise monitoring programs, including a total of 13 monitoring stations with a longitudinal span of about 300km, from Messinia regional unit to Corfu Island. Stations were mostly placed around Marine Protected Areas in coastal waters, collecting a total of more than 250 hours of sound data. The estimated Sound Pressure Levels (SPLs) gave insights into the footprints of the anthropogenic and biogenic factors on the soundscape of the Ionian Sea, including among others continuous ship traffic noises, impulsive noise and fauna sounds, offering, as far as we know, the first ever regional scale assessment of ambient noises in the Greek seas.

Methods

Realization of spot measurements has been decided to be the most efficient approach for the acoustic monitoring survey, offering flexibility and improved sound data quality (see Lillis et.al., 2018). Instead of mooring several hydrophones at the monitoring stations for the full survey period, the research vessel changed locations between the specified locations in a daily schedule, performing spot acoustic noise measurements in coastal 25-50m water depth. For each station the research vessel turned off the engines to avoid any mechanical noise and deployed the underwater recording unit at 20m water depth to uninterruptedly acquire sound data for 3 to 6 hours (Figure 1a). In each deployment the vessel was left drifting in the winds and the sea currents, hardly stabilized by using a floating anchor. More than 250 hours of raw data have been acquired from in the 13 stations (Figure 1b).

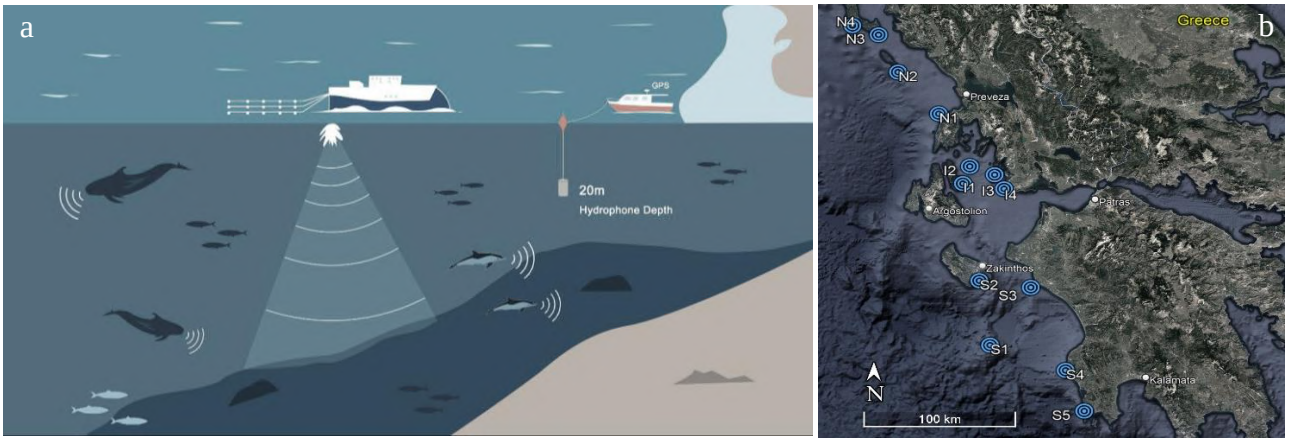

Figure 1. (a) The acoustic monitoring set-up and (b) the monitoring stations (blue circles).

Two pre-calibrated EA-SDA14 (RTsys) compact embedded recorders were used attached to two hydrophones each, a high sensitivity (170 dB dynamic range with 215 dB sensitivity) and a low sensitivity one (215 dB dynamic range with 170 dB sensitivity). Their broadband analog inputs allowed over 500 kHz bandwidth with a dynamic range greater than 100 dB, guaranteeing efficient signal to noise ratios. Both channels were recorded at 24 bits, with a sampling frequency of 78,125 Hz. The research vessel was equipped with a Hemisphere VS101 GPS, to acquire accurate positioning data in real time aligned to the recording unit for data georeferencing.

Noise sound pressure levels (SPLs) have been estimated regarding the zero to peak (SPLpeak), peak to peak (SPLp-p) and root mean square (SPLrms) definitions, as well as the sound exposure level (SEL), all integrated for 1s durations. All above SPL metrics have also been examined as a function of sound frequency components via third-octave bands (from 16 to 20,000 Hz centre bands) while 30s integrated power spectrum densities (PSD) have also been estimated. To meet the above estimations along with the necessary georeferencing of the data derivatives in an automated fashion, a suite of MATLAB codes has been implemented to perform analysis and reporting of the acquired acoustic data.

Results and Conclusions

In general, all stations exhibited high ambient sound levels concentrated close to the top limit of the bibliographic prevailing ambient noise. This is partially due to the sampling procedure, which involved shallow and close to the shore deployment, capturing high benthos noises and coastal industrial soundscape components. The average SPLrms in all the stations was 110±6 dB re 1μPa (Figures 2a) with little differences between them but for biophony and anthropophony occurrences. It was realized that the anthropophony of the area is dominated by fishing but mostly liner passenger vessels (Figures 2b,c), as well as sea-farm coastal noises, while some occurrences of military exercises from the wider Ionian – Adriatic area, involving explosives, have been detected. Biophony was a strong component of the soundscape in the area. Crustaceans produced characteristic click sounds (snapping shrimps), and dolphin whistles and clicks were recorded in a dozen of instances. Eco-acoustic indices can offer the means for assessing the rate of biophony versus anthropophony in the marine soundscape and thus assessing its ecological status. A popular index, the Normalized Difference Soundscape Index (NDSI) (Kasten et.al.,2012) was applied, which seeks to "estimate the level of anthropogenic disturbance on the soundscape by computing the ratio of human-generated (anthrophony) to biological (biophony) acoustic components". A preliminary application of NDSI index at two instances of liner ship and seismic noise showed that they yielded comparable degradation of the ecological status for the full duration of their existence, with seismic noise (impulses) producing regular “jumps” from good to bad environmental status and ship traffic noise producing a gradual degradation of the ecological status but being a persistent activity in the marine environment. Conclusively, the diversity of anthropophony and biophony in the Ionian Sea spanning from dolphin whistles and snapping shrimps, to “deafening” liner ships and sea farm noise was captured and a first assessment of anthropophony dominance in the marine soundscape of the Ionian Sea.

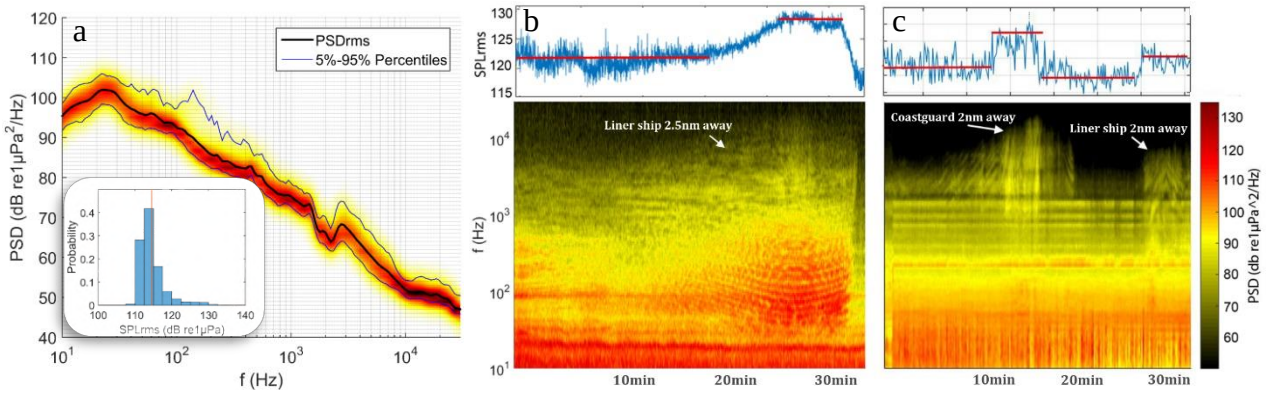

Figure 2. (a) A characteristic power spectrum density plot of the ambient noise acoustic recordings in the Ionian Sea along with the corresponding SPLrms histogram. (b, c) Spectrograms and SPLrms plots showing 3 instances of ship noise in the acoustic recordings. The ship traffic-oriented SPL increase was in the order of 5-10 dB re 1μPa.

References

OSPAR, “Assessment of the environmental impact of underwater noise 2009,” Comm. Rep., vol. Biodiversi, pp. 1–44, (2009)

N. D. Merchant, K. M. Fristrup, M. P. Johnson, P. L. Tyack, M. J. Witt, P. Blondel, and S. E. Parks, “Measuring acoustic habitats,” Methods Ecol. Evol., 6, no. 3, pp. 257–265, (2015).

van Geel NCF, Risch D, Benjamins S, Brook T, Culloch RM, Edwards EWJ, Stevens C and Wilson B (2022), Monitoring cetacean occurrence and variability in ambient sound in Scottish offshore waters. Front. Remote Sens. 3:934681.

A. Lillis, F. Caruso, T. A. Mooney, J. Llopiz, D. Bohnenstiehl, and D. B. Eggleston, “Drifting hydrophones as an ecologically meaningful approach to underwater soundscape measurement in coastal benthic habitats,” J. Ecoacoustics, vol. 2, p. (2018).

Kasten, E.P., Gage, S.H., Fox, J. & Joo, W. “The remote environmental assessment laboratory's acoustic library: an archive for studying soundscape ecology. Ecological Informatics, 12, 50-67. (2012)

16th International Congress of the Geological Society of Greece
17-19 October, 2022 - Patras, Greece
Bulletin of the Geological Society of Greece, Sp. Publ. 10
Ext. Abs. GSG2022-419

Palaeoenvironmental settings and hydrocarbon generation potential of Upper Cretaceous organic-rich layers in Parnassos-Ghiona Unit

Maria-Elli Damoulianou[1], Stavros Kalaitzidis[1] and Nikolaos Pasadakis[2]

[1] Department of Geology, University of Patras, Patras, Greece skalait@upatras.gr [2] Institute of Petroleum Research, FORTH, Chania, Greece

Research Highlights: *Coal lenses with gas generation potential in Parnassos-Ghiona Unit, Central Greece*

Background and Objectives

Evaluation of the hydrocarbon generation potential of oil- and gas-prone formations in the Greek territory has been so far focused on the Ionian geotectonic Unit (e.g. Karakitsios et al., 2018; Tserolas et al., 2019). On the contrary, the Parnassos-Ghiona Unit (PGU) is being studied mostly for the industrial interest related to the three bauxite horizons hosted (e.g. Mondillo et al., 2022). However, the discovery of a Turonian-Senonian coal layer in the area of Pera-Lakkos (PL) (Kalaitzidis et al., 2010), along with the widespread "referred" as bituminous limestone in the PGU prompted the further investigation of these strata.

In the present study, two more coal lenses, those hosted in Vagoneto (VG) and Gouves (GO) underground mines, in addition to the Pera-Lakkos one, have been studied in relation to (i) their organic petrological and geochemical features, in order to evaluate the hydrocarbon generation potential within PGU, and (ii) their mineralogical features aiming to the palaeoenvironmental reconstruction.

Methods

X-ray diffraction has been applied using a Bruker D8 X-ray Diffractometer, at the facilities of the Department of Geology, University of Patras. Rock Eval analysis has been conducted at the facilities of the Institute of Petroleum Research, FORTH, Chania. The analysis was performed using a Rock-Eval 6 Turbo (RE6) unit, in order to assess the hydrocarbons potential and to determine the kerogen types (Peters and Cassa, 1994) according to the basic methodology. Furthermore, GC-MS analysis has been conducted, as well, at the facilities of the Institute of Petroleum Research, FORTH, Chania, after Soxhlet bitumen extraction, using an open-column chromatography and gas chromatography-mass spectrometry.

Coal petrography has been conducted using a Leica DMRX coal-petrography microscope, under white incident light and blue light excitation at the facilities of the Department of Geology, University of Patras. The classification and nomenclature of macerals followed the ICCP System 1994, whereas for the solid bitumens the TSOP-ICCP nomenclature was applied (Stasiuk et al., 2002). The random reflectance measurement followed the ASTM D7708 (2014).

Results and Conclusion

The study of the coal/coaly formations of interest revealed the establishment of two different modes of organic matter depositional settings, including paralic mires on the top of the lateritic mud deposition, as well as paralic mires developed upon the Lower-Cretaceous limestone bedrock. The low/very low grade humic coal lenses at the Vagoneto and Gouves sites formed by accumulation of mostly herbaceous plants, being characterized by elevated amounts of detrovitrinite and inertinite (Figs 1a, c), and variable amounts of liptinite, mainly in the form of sporinite and alginite (Figs 1b, d).

The Rock-Eval data indicates the co-occurrence of all kerogen types, with the types III and IV generally prevailing. The *n*-alkane compound distribution, as determined by the biomarker analysis, essentially expressed by a series of OEP and CPI parameters, suggests prevalence of terrestrial organic matter. The terpane/hopane and sterane fingerprints are minor in all the studied samples; however, the relative abundance of the regular steranes clearly indicates the establishment of terrestrial conditions. Both the plots based on the DBT/P *vs.* Pr/Ph and $C_{31}R/C_{30}$ *vs.* Pr/Ph ratios indicate the establishment of hypersaline lacustrine to fluviodeltaic mire settings. Finally, the classic plot of Pr/*n*-C_{17} *vs.* Ph/*n*-C_{18} suggests mixed kerogen type II-III for all the studied coal and coaly samples.

The overall coal-petrographic data indicates an intense oxidation in the palaeomire surface, possibly related to the dry warm Turonian climate and/or the influence of brackish water. Additionally, the thermal maturity determined from vitrinite reflectance and geochemical parameters including T_{max} and biomarkers point to Medium Rank Bituminous coal or, in terms of hydrocarbon generation, to the early oil-window stage. The data suggests a good-to-excellent gas potential for Parnassos-Ghiona Unit, whereas the oil-potential seems being limited.

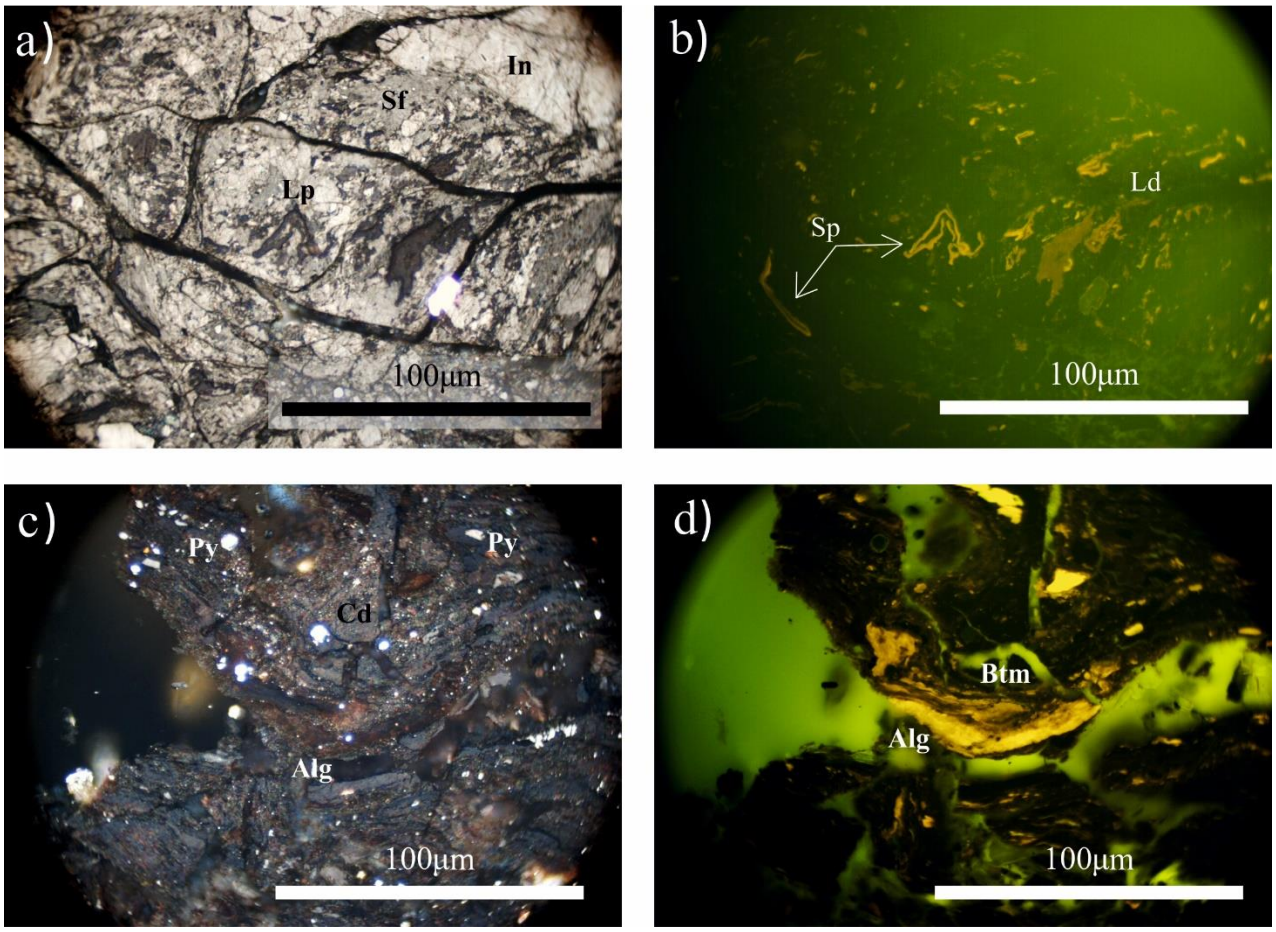

Figure 1. Photomicrographs (a-d) of the major coal-petrographic features of the studied coal and coaly samples (Alg: alginite, Btm: bituminite; Cd: collodetrinite, In: inertinite, Ld: liptodetrinite Py: pyrite, Sf: semifusinite, Sp: sporinite.

Acknowledgements

The authors would like to thank Dr. Paraskevi Lampropoulou, Section of Earth Materials, Department of Geology, University of Patras, for running the XRD analyses.

References

American Society for Testing and Materials (ASTM) D7708, 2014. Standard Test Method for Microscopical Determination of the Reflectance of Vitrinite Dispersed in Sedimentary Rocks. Annual Book of ASTM Standards: Petroleum Products, Lubricants, and Fossil Fuels; Gaseous Fuels; Coal and Coke, p. 10.

International Standard Organisation (ISO) 7404-5, 2014. Methods for the petrographic analysis of bituminous coal and anthracite—Part 5: Method of determining microscopically the reflectance of vitrinite. International Organization for Standardization, Geneva, Switzerland. 12 pp.

Kalaitzidis, S., Siavalas, G., Skarpelis, N., Araujo, C.V., Christanis, K., 2010. Late Cretaceous coal overlying karstic bauxite deposits in the Parnassus-Ghiona Unit, Central Greece: Coal characteristics and depositional environment. Int. J. Coal. Geol. 81, 211-226.

Karakitsios, V., Tzortzaki, E., Giraud, F., Pasadakis, N., 2018. First evidence for the early Aptian Oceanic Anoxic Event (OAE1a) from the Western margin of the Pindos Ocean (NW Greece). Geobios. 51, 187-210.

Mondillo, N., Di Nuzzo, M., Kalaitzidis, S., Boni, M., Santoro, L., Balassone, G., 2022. Petrographic and geochemical features of the B3 bauxite horizon (Cenomanian-Turonian) in the Parnassos-Ghiona area: a contribution towards the genesis of the Greek karst bauxites. Ore Geol. Rev., 143, 104759.

Peters, K.E. and Cassa, M.R., 1994. Applied Source-Rock Geochemistry. In: Magoon, L.B. and Dow, W.G., Eds., The Petroleum System. From Source to Trap, American Association of Petroleum Geologists, Tulsa, 93-120.

Stasiuk, L., Burgess, J., Thompson-Rizer, C., Hutton, A., Cardott B., 2002. Status report on the TSOP-ICCP dispersed organic matter classification working group. Soc. Organic Petrol. Newslett., 19 (3), p. 14.

Tserolas, P., Maravelis, A.G., Tsochandaris, N., Pasadakis, N., Zelilidis, A., 2019. Organic geochemistry of the Upper Miocene-Lower Pliocene sedimentary rocks in the Hellenic Fold and Thrust Belt, NW Corfu island, Ionian Sea, NW Greece. Mar. Pet. Geol., 106, 17–29.

16th INTERNATIONAL CONGRESS of the
GEOLOGICAL SOCIETY OF GREECE

S7. Remote Sensing Techniques in Geohazards

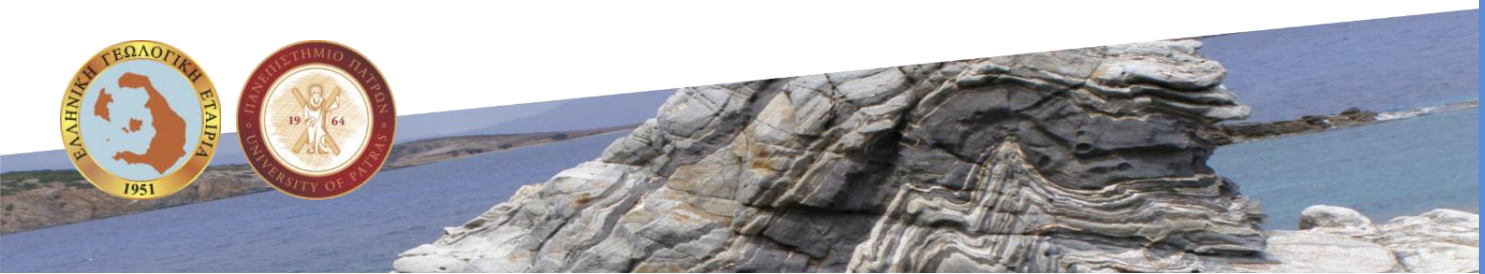

OUR EARTH, OUR HOME

16th International Congress of the Geological Society of Greece
17-19 October, 2022 - Patras, Greece
Bulletin of the Geological Society of Greece, Sp. Publ. 10
Ext. Abs. GSG2022-019

Object-based landslide mapping using ML and UAS photogrammetric products

E. Karantanellis[1], V. Marinos[2], E. Vassilakis[3], G. Papathanasiou[4]

(1) Department of Earth Science and Environmental Sciences, University of Michigan, Ann Arbor, USA, stratis@umich.edu (2) Department of Civil Engineering, National Technical University of Athens, Athens, Greece (3) Department of Geology and Geoenvironment, National and Kapodistrian University of Athens, Athens, Greece (4) Department of Geology, Aristotle University of Thessaloniki, Thessaloniki, Greece

Modeling natural hazards in 3D space constitute a significant step for managing and planning our living environment. The creation of precise maps is needed to document the impact of natural hazards such as landslides (Picarelli, 2009). Loss of life, natural resources or property transform landslide phenomenon to a natural disaster. In landslide analysis different factors can be incorporated and studied such as landslides occurrence and occurrence, their distribution, mechanisms, pattern of failures. The development of detailed and reliable maps is also crucial for determining landslide susceptibility and risk (Guzzeti, 2012). Only recently, the emerging geospatial technologies are capable to produce and combine different types of 2D and 3D data. Unmanned Aerial Vehicle (UAV) or Unmanned Aerial Systems (UAS), support the acquisition of ultra-high detailed resolution geospatial data in the 3D environment (Giordan et al. 2020). Those systems are flexible in data acquisition, with a high temporal frequency, while it is limited for site specific mapping purposes. The exploitation of 3D point-clouds has been proven remarkably efficient for analyzing data in the field of geoscience. Point cloud advantages of documenting in 3D space, data of hazardous sites at low cost and effective performance identifies them as leading primitives for site-specific 3D landslide modelling. Given the gaps between the computer vision capabilities and their applications in landslide assessment in site-specific scale, the proposed work aims at developing a general framework of predefined workflows in an object-based (Object-Based Image Analysis- OBIA) programming environment for detection (Fig.1) and characterization of landslide phenomena from ultra-high-resolution UAV-derived data.

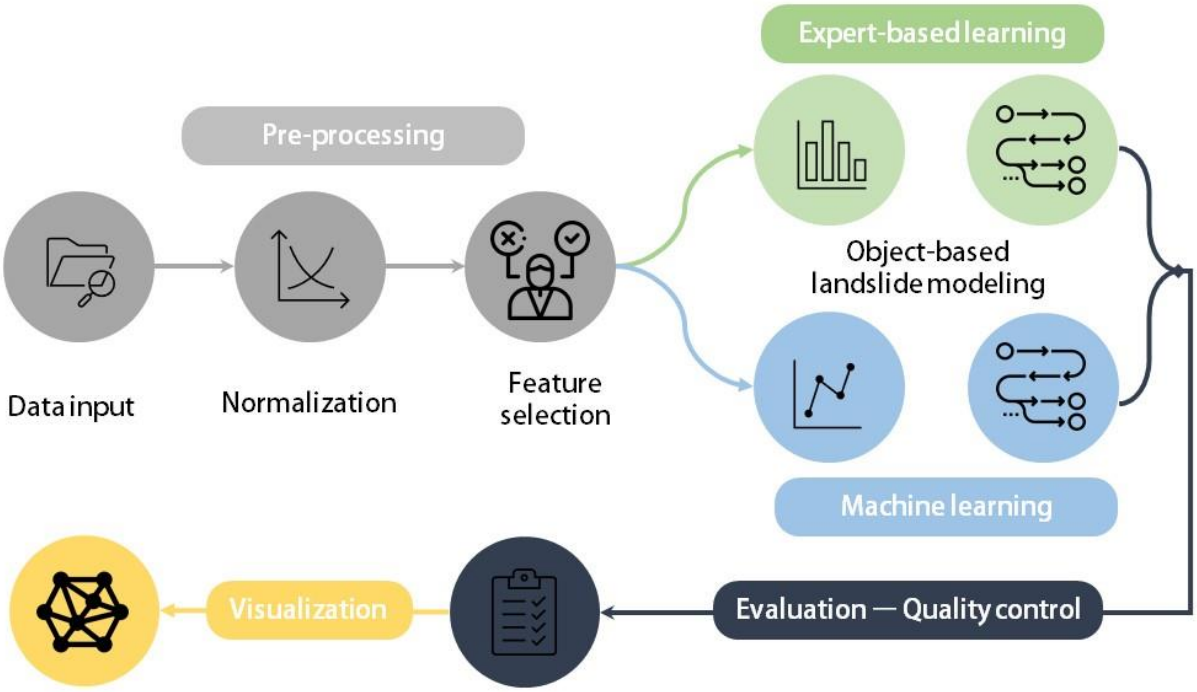

Figure 1. Developed object-based classification scheme for landslide object characterization.

The framework is built up in four distinct research phases: (a) on-site data collection, (b) data preprocessing, (c) OBIA (segmentation and classification), and (d) evaluation. These phases result in various novel component-wise solutions, which particular focus on the optimization phase of OBIA for landslide assessment. Different flight acquisition configurations were tested by varying the number of images, image overlap, flight height and focal length for selecting the optimal workflow for imagery collection always considering the site specifications (topography, landslide mechanism). Structure-from-Motion (SfM) photogrammetry has been used to provide dense 3D point clouds describing

surface morphology of landslide environments. The proposed methodology has been developed based on OBIA and fusion of multivariate data resulted from photogrammetric processing in order to take full advantage of its productivity. Several quantifiable comparative studies have been conducted to analyze the influence of topographic information, scale segmentation and evaluate the object-based classification of landslide ontologies with three state-of-the-art Machine Learning classifiers, KNN (Cover and Hart, 1967), DT (Breiman et al. 1984) and RF (Breiman, 2001) with the inclusion of spectral, spatial, and contextual characteristics. Results highlight higher performances for landslide mapping with RF when DSM information was integrated (Fig.2). Transferability constitutes a critical issue in image classification. Thus, RF presented higher predictive performance when the model was fitted and applied to a different study area. For the ML classification of landslide zones, 60% of the reference segments have been used for training and 40% for validation of the models. From all configurations tested, 54 classifications were exceed in an agreement of higher than 75% with the highest performance being with the RF classifier.

Figure 2. a) Orthophoto overlaid by the reference data, b) segmentation result and c) the final classification after refinement of the rule-based method (green: non-affected, light brown: depletion, dark brown: scarp).

Since the ultimate goal is to provide a ready-to-use landslide mapping tool, a transferability study of the final classification workflow needs to be conducted. The same object features and processes for segmentation and classification needs to follow for keeping a uniform implementation approach. Based on the F1 metrics, the RF model showcased great superiority compared with other classifiers. The proposed work illustrates the effectiveness of UAS platforms to acquire accurate photogrammetric datasets from complex surface topographies and provide an efficient and transferable objectbased framework to characterize the failure site based on semantic classification of the landslide elements on site specific scales. The outcome can be useful for prioritizing efforts to moderate the adverse consequences of landslides and provide future mitigation strategies following landslide ontologies. Complementary to the developed workflow the accomplished real-world application, this work has shown the great potential of coupling UAS photogrammetry with object-based methods for assessing the landslide features in different hierarchical scales and provide a detailed automatic classification. Desirable data for further landslide analysis and OBIA include cohesion, friction angle, plasticity values, and groundwater data. In view of the long-term and permanent nature of the landslide hazard, and the resulted risk, the only practical method of landslide mitigation is to assist local authorities and inhabitants to understand the problem and how to avoid or prepare for an event.

Acknowledgements

The authors would like to thank State Scholarships Foundation (IKY) and eCognition Trimble for their assistance and support.

References

Breiman, L. E. O. 2001. “Random Forests.” 5–32.

Breiman, Leo, Jerome H. Friedman, Richard A. Olshen, and Charles J. Stone. 1984. *Classification and Regression Trees*. Routledge

Cover, T., and P. Hart. 1967. “Nearest Neighbor Pattern Classification.” *IEEE Transactions on Information Theory* 13(1):21–27. doi: 10.1109/TIT.1967.1053964.

Giordan, Daniele, Marc S. Adams, Irene Aicardi, Maria Alicandro, Paolo Allasia, Marco Baldo, Pierluigi De Berardinis, Donatella Dominici, Danilo Godone, Peter Hobbs, Veronika Lechner, Tomasz Niedzielski, Marco Piras, Marianna Rotilio, Riccardo Salvini, Valerio Segor, Bernadette Sotier, and Fabrizio Troilo. 2020. “The Use of Unmanned Aerial Vehicles (UAVs) for Engineering

Geology Applications.” Bulletin of Engineering Geology and the Environment 79(7):3437–81. doi: 10.1007/s10064-020-01766-2.

Guzzetti, Fausto, Alessandro Cesare Mondini, Mauro Cardinali, Federica Fiorucci, Michele Santangelo, and Kang Tsung Chang. 2012. “Landslide Inventory Maps: New Tools for an Old Problem.” Earth-Science Reviews 112(1–2):42–66. doi: 10.1016/j.earscirev.2012.02.001.

Picarelli, Luciano. 2009. “Understanding to Predict.” Pp. 63–88 in *Landslides – Disaster Risk Reduction*. Berlin, Heidelberg: Springer Berlin Heidelberg

16th International Congress of the Geological Society of Greece
17-19 October, 2022 - Patras, Greece
Bulletin of the Geological Society of Greece, Sp. Publ. 10
Ext. Abs. GSG2022-050

Monitoring of the erosional phenomena next to the active fault of Psatha (Attica, Greece) with diachronic Terrestrial LiDAR data acquisition

C. Katsora[1], A. Konsolaki[1], Emm. Vassilakis[1], J.D. Alexopoulos[1]
(1) Dpt of Geology & Geoenvironment, N.K. University of Athens, Zographou, Greece, ckatsora@gmail.com

The topic of coastal erosion and the derived risk have been subjects of growing interest for public authorities and researchers. The combination of erosion along with alterations, caused by active faults in coastal areas, represents an even bigger challenge because of the apparently continuous evolving geomorphology (Abellán et al., 2006). Traditional methods for mapping such areas are generally time- as well as cost-consuming and potential to result in questionable accuracy issues (Oppikofer et al., 2009). In contrast, Light Detection And Range (LiDAR) – airborne and terrestrial – have been used in numerous case studies (Abellán et al., 2013), varying from acute natural hazard mapping (volcanoes) to fast developing landslides and rockfalls, producing remarkably precise 3D Digital Elevation Models (DEMs) (Konsolaki et al., 2020). These models are based on measuring highly accurate X, Y and Z as well as RGB values on each point of a produced cloud.

Psatha Bay represents an exemplary case for perusing the advantageous utilization of terrestrial LiDAR, as it reveals a steep coastline and anaglyph along with the visible throw of 185m, caused by the tectonic activity during the post-alpine period (Zygouri, 2008). This area became noticeable due, on the one hand, to the disastrous earthquakes of 1981, in the wide area of Eastern Gulf of Corinth and on the other hand to the frequent civil protection warnings and briefs about the rockfall threats of driving through the nearby coastal road. In terms of geology, a mix of limestone, calcite and related debris can be observed. Concerning the fault, Triassic-Jurassic limestones form the foot wall while thick Pleistocene debris covers the spectacular fault surface (Sakelariou et al., 1998). Erosion, rock falls and slope failures are present in certain parts, causing a continuous natural alteration, influenced by human intervention, namely the lately roadworks, without implementing any preventive/protective infrastructure. Since this area is outlined as highly touristic during the summer season, the construction of a risk map for estimating likely unstable areas (Ferrero et al., 2011) can be of great importance. The latter could be based on the production of a very high-resolution Digital Elevation Model (DEM) for deriving some primary topographic attributes (Agliardi & Crosta, 2003). The initial topographic information and result can be used as a reference point for future similar studies, in the frame of detecting changes on the slope, including failure widenings and rock piece detachments, quantifying them and finally introducing and/or improving risk maps (Mavroulis et al., 2022).

A multiple-phase study within a period of 11 years was conducted in the area. In the first phase, in June 2011, high resolution close range remote sensing campaign was conducted, by using a terrestrial LiDAR (a Leica ScanStation C10) for acquiring a dense point cloud, representing the micro-topography of the open to the air fault surface of the Psatha active fault (Figure 1a). It was coupled with near surface applied geophysics data, which were also conducted on the hanging wall to investigate the subsurface structure of the debris (Alexopoulos et al., 2013). A series of scanning campaigns followed during the next decade and the high-risk areas on the steep slope were located, in high detail. The research is mainly focused on the easternmost segment of the fault surface. We used a Leica P50 terrestrial LiDAR during the most recent campaign, that took place in July 2022. The data acquisition was concentrated on the contact between the debris and the carbonate fault surface, where we observed significant rockfalls and slope failures, compared to the previous campaigns (Figure 1b). Hence, this selected segment was investigated with a strategy ideal for producing a higher density point cloud generation, based on detailed scanning from different angles, which caused setting up five bases from which three were newly established.

After the necessary pre-processing of the point cloud data, which included cloud geo-rectifying, merging, cleaning and quality checking, a dataset (point cloud) with almost 150 million points has been created. The geo-rectification included high accuracy measurements with the use of Real Time Kinematics - Global Navigation Satellite System (RTK - GNSS) equipment, for ensuring the precise registration of all the datasets that have been acquired diachronically to be comparable, with the minimum error possible (Figure 1c). Several quantification techniques were applied, and specific volumes of rock particles were found displaced on top of the hanging wall due to rock falling, which in turn are mainly attributed to severe weather phenomena but also to small earthquake events, that continue to happen at the very active Gulf of Corinth.

In conclusion, we argue that the described methodology, which is a technique based on the advances of innovative surveying equipment, could be applicable to any coastal area characterized by similar features, such as steep slopes, frequent rockfalls, proximity to coastline with wide coastal front. This methodology is ideal to use in estimating any involving risks and laying out plan and protection actions/measures.

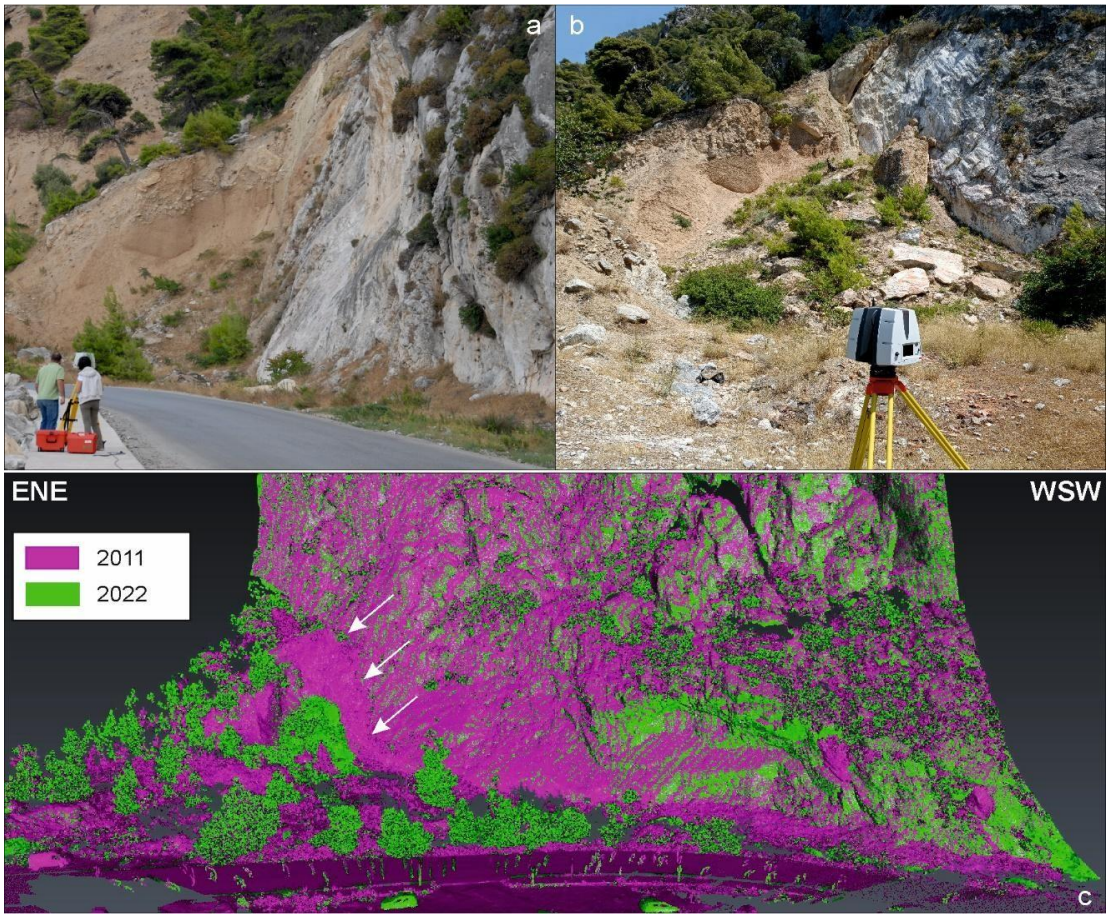

Figure 1. Aspect of the fault surface and the contact between the debris and the carbonates, during the 2011 campaign (a). Recent rock falls on the hanging wall, observed during the 2022 campaign (b). Comparative representation of the two period point clouds showing the changes during the last decade. White arrows show the debris area where most of the changes have been recorded (c).

Acknowledgements

The authors would like to thank Metrica SA (Greece) for their contribution in the field campaigns regarding the data acquisition by providing a Leica ScanStation C10 (2011, 2012) and their overall support during data processing.

References

Abellán, A., Oppikofer, T., Jaboyedoff, M., Rosser, N. J., Lim, M., Lato, M. J., 2013. Terrestrial laser scanning of rock slope instabilities. Earth Surface Processes and Landforms, John Wiley and Sons Ltd., Wiley Online Library.

Abellán, A., Vilaplana, J.M., Martinez, J., 2006. Application of a Long-range Terrestrial Laser Scanner to a Detailed Rockfall Study at Vall de Nuria (Eastern Pyrenees), Spain. Engineering Geology 8, 136-148.

Agliardi, F., Crosta, G. B., 2003. High Resolution Three-dimensional Numerical Modelling of Rockfalls. International Journal of Rock Mechanics and Mining Sciences 40, 455-471.

Alexopoulos, J.D., Vassilakis, Emm. Dilalos, S., Zaloumi, E., 2013. Quantification of Human Impact on Natural Evolution Processes at a Coastal Zone, Adjacent to an Active Fault´. 13th international Conference of Environmental Science and Technology, Athens, Greece.

Fandin, N., Feng, Q., Stephansson, O., 2003. Application of a New in Situ 3D Laser Scanner to Study the Scale Effect on the Rock Joint Surface. International Journal of Rock Mechanics and Mining Sciences 41, 329-335.

Ferrero, A. M., Migliazza, M., Roncella, R., Segalini, A., 2011. Rock Cliffs Hazard Analysis Based on Remote Geostructural Surveys: The Campione del Garda Case Study (Lake Garda, Northern Italy). Geomorphology 125, 457-471.

Konsolaki, A., Vassilakis, E., Gouliotis, L., Kontostavlos, G., Giannopoulos, V., 2020. High Resolution Digital 3D Modelling of Subsurface Morphological Structures of Koutouki Cave, Greece. Acta Carsologica 49, 163-177.

Mavroulis, S., Vassilakis, E., Diakakis, M., Konsolaki, A., Kaviris, G., Kotsi, E., Kapetanidis, V., Sakkas, V., Alexopoulos, J.D., Lekkas, E., Voulgaris, N., 2022. The Use of Innovative Techniques for Management of High-Risk Coastal Areas, Mitigation of Earthquake-Triggered Landslide Risk and Responsible Coastal Development. Applied Sciences, 12(4), 2193.

Oppikofer, T. Jaboyedoff, M., Blikra, L., Derron, M.-H., Metzger, R., 2009. Characterization and Monitoring of the Aknes Rockslide using Terrestrial Laser Scanning. Natural Hazards Earth Syst. Science 9, 1003 -1019.

Sakellariou, D., Lykousis, V., Papanikolaou, D., 1998, Neotectonic Structure and Evolution of the Gulf of Alkyonides, central Greece. Bull. Geological Society Greece, XXXII/1, 241-250.

Zygouri, V., Verroios, S., Kokkalas, S., Xypolias, P., Koukouvelas, I. and Papadopoulos, G., 2008. Growth of faults within the Gulf of Corinth. Bulletin of the Geological Society of Greece, 41, 25-33.

16th International Congress of the Geological Society of Greece

17-19 October, 2022 - Patras, Greece

Bulletin of the Geological Society of Greece, Sp. Publ. 10

Ext. Abs. GSG2022-057

Combination of close-range remote sensing data (TLS and UAS) and techniques for structural measurements across the deformation zone of the Ionian thrust in Zakynthos Isl.

Emm. Vassilakis[1], A. Konsolaki[1], S. Petrakis[1,2], E. Kotsi[1], Ch. Fillis[1], M. Triantaphyllou[1], A. Antonarakou[1], E. Lekkas[1]

(1) Dpt of Geology & Geoenvironment, N.K. University of Athens, Zographou, Greece, evasilak@geol.uoa.gr (2) Institute of Oceanography, Hellenic Centre for Marine Research (HCMR), Anavissos, Greece.

Impressive geomorphological structures are quite often interconnected with active tectonics. Most of these cases concern risky steep slopes where the necessity for careful and detailed examination is more than imperative, especially when they are located at areas of high tourist presence and therefore significant economic value. Within this work, a holistic methodology is described, including point-cloud data acquisition from a Terrestrial Laser Scanning (TLS), combined with point-cloud generation from photogrammetric processing of Unmanned Aerial Systems (UAS) imagery. The main scope is to create a reliable methodology for remote measurement of the orientation of structural features (mainly of those hard to be reached) and proceed to their tectonic analysis, as an additional tool for quantifying the surface deformation and improve our knowledge concerning the structural integrity of high-risk slopes that form geologically significant regions.

The area of interest is located at the easternmost part of Laganas beach, at Zakynthos Island, where the Ionian thrust is crosscutting the coastal area normally to the shoreline. It is near the Kalamaki locality, where the Ionian geotectonic unit is found overthrusting the Paxos unit (Papanikolaou, 1997; Papanikolaou *et al.*, 2010), causing deformation at the postalpine sediment succession that lies unconformably on top of the thrust fault. Right next to the beach, a very interesting section is formed consisting of several stratigraphic layers (Fig. 1a), corresponding to eight cycles of depositional gypsum types, which are unconformably capped by the Pliocene Trubi formation (Karakitsios *et al.*, 2017; Kontakiotis *et al.*, 2016). The entire succession consisting of intercalations of shale, limestone and several evaporite facies is tilted towards east with high angles, yielding the degree of tectonic deformation.

The slope deformation due to thrust tectonics in conjunction to the seismic activity of the wider region and the frequent human presence beneath the steep prone, constitute an ultra-high-risk coastal area. We used a combination of close-range remote sensing techniques aiming to construct a detailed 3D model of the geomorphic structure. The orientation of the area of interest was quite challenging as due to the narrow beachfront, there was not enough space on the beach for placing the equipment consisting of the tripod/TLS and establishing the several bases for scanning the steep slopes facing the sea. The shallow waters allowed for a thorough examination of the sea bottom, and we managed to locate hard ground for establishing the tripod for mounting the TLS. Geologically wise the most suitable areas for installing the tripod were at the projection of the harder strata towards offshore. We established 6 bases offshore (Fig 1a), on top of these strata, acquiring the same number of point clouds, which were linked to each other by using 4 targets that were placed along the beach (Fig 1b). Additional targets, alternating at every scan, were also placed offshore, on either side of each TLS base, for keeping the quality of the geometry of the point clouds at the highest possible level. As a result, the bundle error did not exceed 32mm for the unified TLS point cloud of the steep slopes, consisting of 84.5 million points.

The high angle of the steep slopes as well as the antithetic, almost flat, morphology of the hilltop did not allow any data acquisition from the latter. Therefore, a necessity for a different kind of surveying was raised and we used a UAS, with a built-in camera, for acquiring high-resolution, overlapping images, which were used for photogrammetric processing within the structure-from-motion approach (Westoby *et al.*, 2012). An ortho-photo mosaic and a Digital Terrain Model were produced during this procedure, which in turn were used for the extraction of a 50.2-million-point cloud, for the entire hill and not only for the steep slope facing the sea. By using the NRTK solution during the flight we ensured that the accuracy of the dataset was extremely high (27cm) and above all co-registered with the TLS one, since both were projected at the same system.

The overall result of the combination of the described datasets, that were produced based on close-range remote sensing techniques, was a merged point cloud for the entire hilly structure (Fig 1c), which allowed the creation of a 3D model, ideal for visualization and navigation in a user's personal computer. Measuring tectonic features such as strata or lineament dip and dip direction is feasible and practical within the framework of manipulating the 3D model, while using open-source software (e.g. CloudCompare, Girardeau-Montaut, 2011). We used this model for measuring, remotely, the structural orientation of the tilted blocks (e.g. lower unit bedding 55/081 and 'trubi' bedding 40/055) but also tectonic lineaments (hinge, fold axial plane intersections), which have been formed due to the compression caused by the thrust, especially at locations that cannot be reached by humans due to safety reasons, not to mention the statistical analysis of the abovementioned features through stereograms.

In conclusion, there are quite a few ways to use close-range remote sensing data and techniques for extracting geological information, but it is very crucial to take under consideration the maximum accuracy that should be succeed during the

fieldwork, especially when combing data from different sources and equipment.

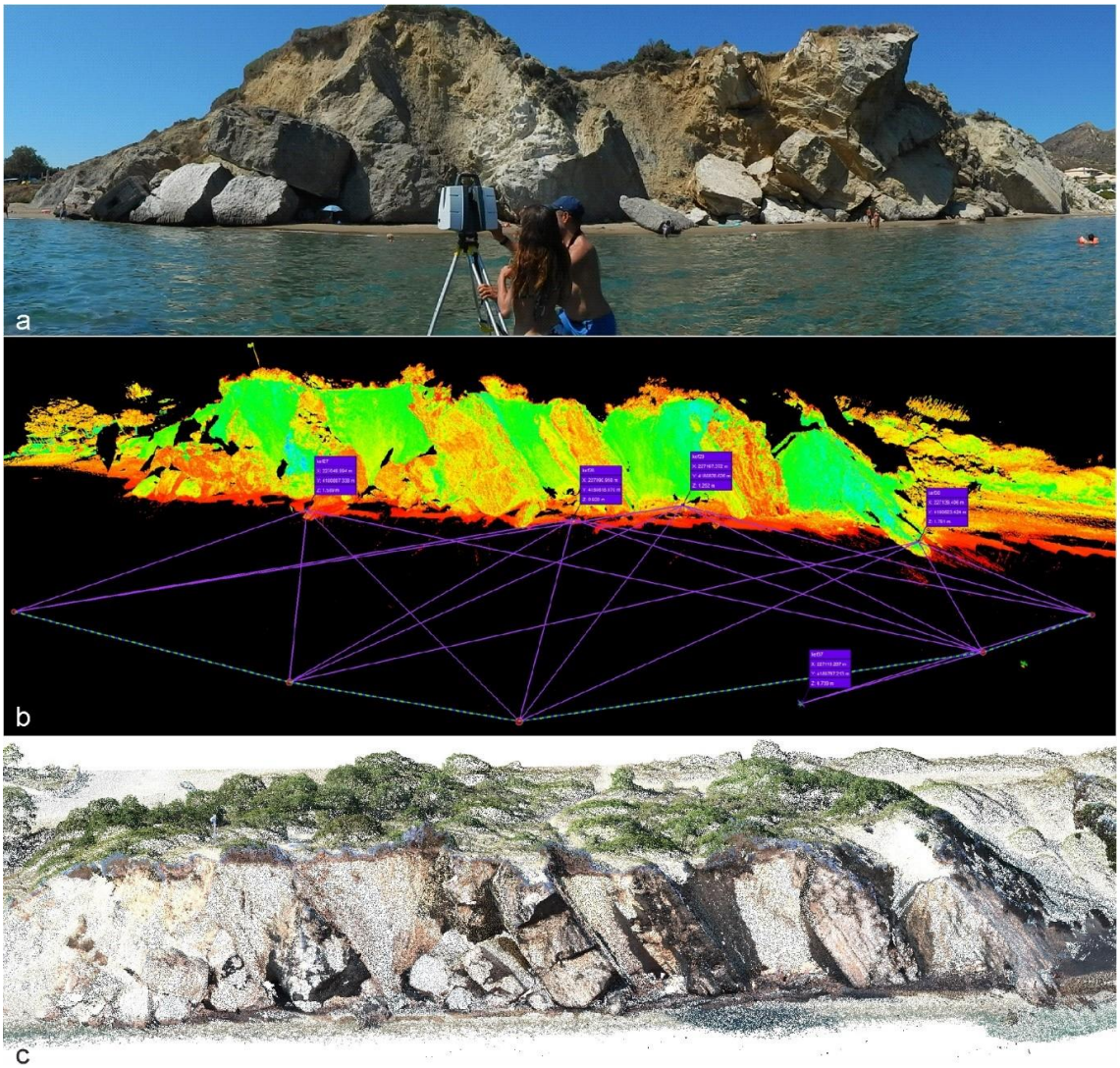

Figure 1. Using the TLS for the point-cloud data acquisition of the steep slope (a). Construction of the 3D model after the alignment of the six datasets and registration with the ground control targets (b). Combination of the two datasets of pointclouds (from TLS and UAS).

Acknowledgements

This research was funded by the "Laertis –Innovative Risk Management System in the Region of Ionian Islands" project (MIS 5010951), included in the Priority Axis "Environmental Protection and Sustainable Development" of the Regional Operational Programme "Ionian Islands 2014–2020", which is funded by the European Regional Development Fund (ERDF) and National Resources under the National Strategic Reference Framework NSRF 2014-2020.

References

Girardeau-Montaut, D., 2011. Cloud Compare v.2.12, OpenSource Project, Grenoble, France.

Karakitsios, V., Roveri, M., Lugli, S., Manzi, V., Gennari, R., Antonarakou, A., Triantaphyllou, M., Agiadi, K., Kontakiotis, G., Kafousia, N., de Rafelis, M., 2017. A record of the Messinian salinity crisis in the eastern Ionian tectonically active domain (Greece, eastern Mediterranean). Basin Research, 29(2), 203-233.

Papanikolaou, D., 1997. The tectonostratigraphic terranes of the Hellenides. Ann. Geol. Pays Hell., 37, 495-514.

Papanikolaou, M., Papanikolaou, D., Triantaphyllou, M.V., 2010. Post-alpine Late Pliocene-Middle Pleistocene uplifted marine sequences in Zakynthos Island. Proceedings of the 12th International Congress, Patras, May, 2010, Bulletin of the Geological Society of Greece XLIII(2): 475-485.

Kontakiotis, G., Karakitsios, V., Mortyn, P.G., Antonarakou, A., Drinia, H., Anastasakis, G., Agiadi, K., Kafousia, N., De Rafelis, M., 2016. New insights into the early Pliocene hydrographic dynamics and their relationship to the climatic evolution of the Mediterranean Sea. Paleogeography Paleoclimatology Paleoecology, 459, 348-364.

Westoby, M.J., Brasington, J., Glasser, N.F., Hambrey, M.J., Reynolds, J.M., 2012. 'Structure-from-Motion' photogrammetry: A lowcost, effective tool for geoscience applications. Geomorphology, 179, 300-314.

16th International Congress of the Geological Society of Greece
17-19 October, 2022 - Patras, Greece
Bulletin of the Geological Society of Greece, Sp. Publ. 10
Ext. Abs. GSG2022-059

Mapping the spatial distribution of detached boulders with the use of ultra-high resolution remote sensing data and simulation of rockfall events. The case of Kalymnos Island.

E. Vassilakis[1], A. Konsolaki[1], S. Laskari[1], I. Lialiaris[2], K. Soukis[1], E. Kotsi[1], E. Lekkas[1]

(1) Department of Geology and Geoenvironment, University of Athens, Greece, evasilak@geol.uoa.gr (2) Geodesign P.C., Athens, Greece.

We present a state-of-the-art multidisciplinary study of the Kalymnos rockfall risk, based on (i) classical geological mapping, (ii) interpretation of high-resolution satellite data, (iii) spatial distribution of rockfalls in GIS, (iv) close range remote sensing campaigns with Unmanned Aerial Systems (UAS), and (v) integrated simulation of rockfall events.

Kalymnos Island is located in SE Aegean (Greece) and is part of the northern Dodecanese. The geology of the island consists of the following groups from bottom to top (Franz *et al.*, 2005): i) the lowermost Kefala Unit comprising late Paleozoic interlayered phyllites, metapelites, and fossiliferous low-grade marble, overlain by a wild flysch with marble and ultramafic blocks, ii) the tectonically overlying Marina Basement Unit with Variscan higher grade rocks such as amphibolites, garnet mica schists, and quartzite, iii) the Marina Cover Unit, which includes Verrucano-type late Triassic, yellow to violet shales and a non-metamorphic Mesozoic sequence, with alternating neritic and pelagic facies of carbonate rocks. The contact between the Marina Basement Unit and the non-metamorphic Marina Cover Unit is a post-orogenic low-angle detachment fault, exposed at the western and central part of the island, marked by thick cataclasites with top to SSW sense of shear (Grasemann *et al.*, 2022). Due to differential weathering between the footwall and hanging wall units, this contact is spatially associated with an extended network of vertical to sub-vertical cliffs.

Detached boulders are observed throughout the entire island, making it one of the ideal places for studying rockfall events worldwide. The absence of vegetation, the existence of large vertical cliffs, and the relatively uniform geological basement, consisting of limestones (Fig. 1a-c), are the main reasons for this. The use of contemporary techniques and tools such as UAS image photogrammetric processing and high spectral and spatial resolution satellite data within GIS platform, allows the implementation of a detailed terrain model and the detection of the spatial distribution of boulders scattered on the downslope areas of steep carbonate cliffs (Gallo *et al.*, 2021).

The interpretation of WorldView-3 satellite images (8-band, 0.3m) allowed the identification of the high rockfall risk areas, related to the potential harm to human life, infrastructure, and property. Due to the very high spatial resolution, rock blocks with diameter greater than 3 meters were clearly identified. The footprint information was integrated into a geodatabase and more calculations and spatial analyses were created and stored in additional fields. More than 7,700 boulders were detected (Fig. 1d) and for each one of these entities an "identity" tab, was created with the incorporation of useful data. The next step of the methodology included new layers generation in the context of taking advantage of the rockfalls' spatial 'density' (Fig. 1e), leading to additional processing for defining high-risk rock-concentration groups, either per altitude zone or per distance from several types of infrastructures. The latter led to the definition of high importance areas at which UAS campaigns were carried out, for aerial image acquisition that were used within structurefrom-motion data processing for 3D models (Fig. 1f) construction (high resolution DSMs, Ortho-photo-mosaics, point clouds) (Vassilakis *et al.*, 2021).

A DJI Phantom 4 pro RTK drone, equipped with an FC6310R camera and a focal length of 8.8mm was used, capturing 13 areas all around Kalymnos, which according to the processing and spatial analysis within the GIS, were characterized as the most critical ones. In total, 5,700 aerial photographs were acquired, covering a total of 6,02km^2. The photogrammetric procedure was accomplished within a Network-based RTK (NRTK) module, which allows the reconstruction of highly detailed photogrammetric products without using Ground Control Points.

The processing results represent the contemporary geomorphological regime that has emerged through geological times as a result of thousands of rockfalls from specific areas. As such, the simulation of the rockfalls based on this methodology provides an inherent and significant advantage over methods based on the results of intentionally induced rockfalls along specific areas of a smaller geographical extent (e.g. quarries or isolated slopes).

The rockfalls simulation was achieved using specialized software packages providing the investigation of several different scenarios which resulted in the reliable assessment of the input parameters (Rn & Rt coefficients, friction angle, slope roughness etc.). The validation of the observed data through back-analysis approach provided the opportunity to draw valuable conclusions regarding differentiations that may arise due to either subtle changes in lithology or topographical peculiarities, which should be considered by earth scientists. The proposed design parameter ranges could enrich the "software library" and can be used in the future at geologically similar areas, leading to reliable conclusions regarding the safe design of protection measures such as rockfall barriers.

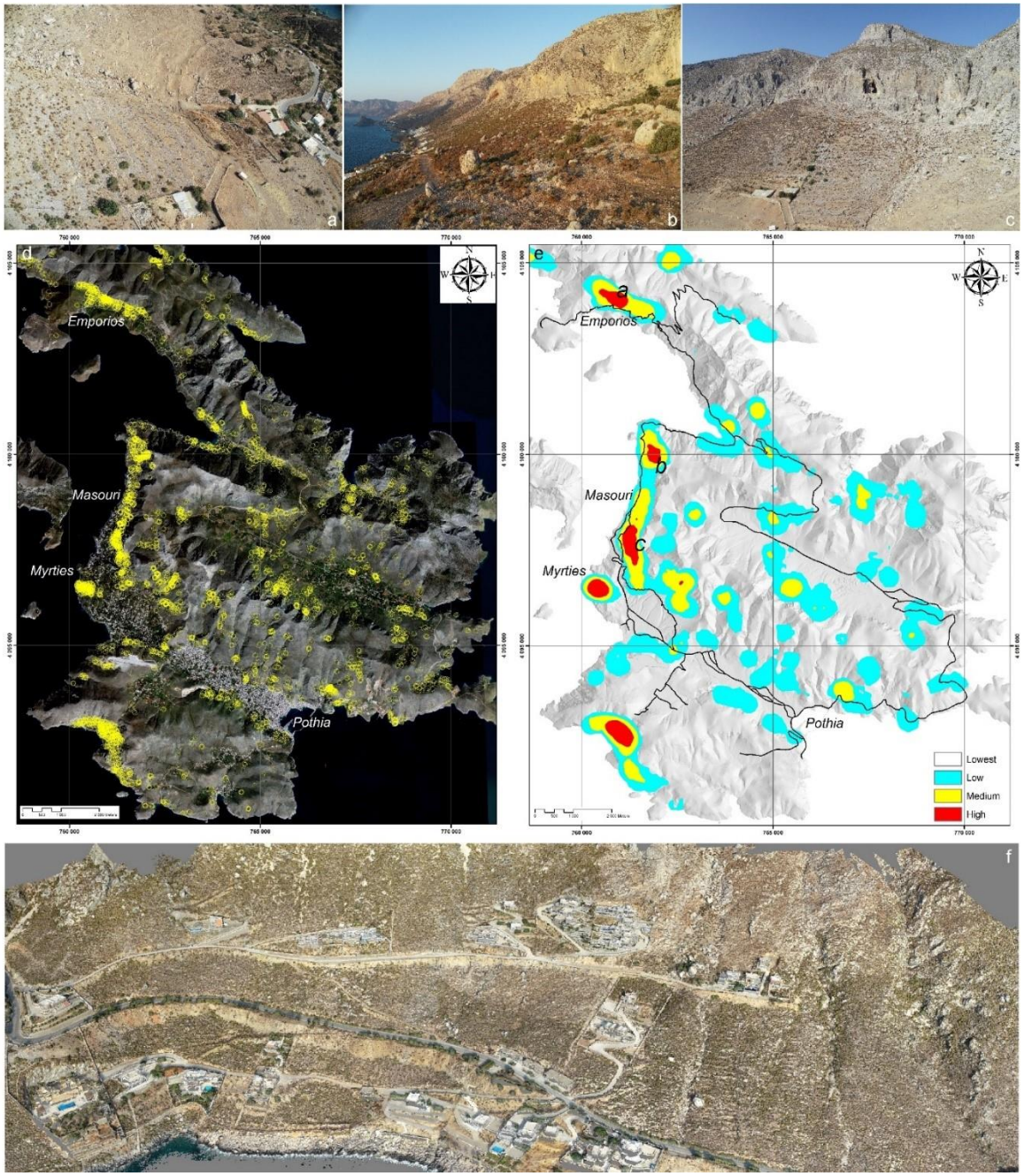

Figure 1. High risk areas due to big boulders downhill rolling towards the island infrastructure (a-c). A WorldView-3 satellite natural color image (acq. 4.3.2021) was used as a basemap for boulder detection (d). Boulder density map (e). Example of a point cloud extracted from photogrammetry processing (f).

Acknowledgements

This research was funded by the municipality of Kalymnos through the research grant "Reduction of landslide risk in areas of special geodynamic and seismotectonic regime. The island of Kalymnos".

References

Franz, L., Okrusch, M., Seidel, E., and Kreuzer, H., 2005, Polymetamorphic evolution of pre-Alpidic basement relics in the external Hellenides, Greece: Neues Jahrbuch für Mineralogie. Abhandlungen, v. 181, no. 2, p. 147–172, https://doi .org/10.1127/0077-7757/2005/0013.

Gallo, I. G., Martínez-Corbella, M., Sarro, R., Iovine, G., López-Vinielles, J., Hérnandez, M., Robustelli, G., Mateos, R. M., and García-Davalillo, J. C., 2021, An Integration of UAV-Based Photogrammetry and 3D Modelling for Rockfall Hazard Assessment: The Cárcavos Case in 2018 (Spain): Remote Sensing, v. 13, no. 17, p. 3450.

Grasemann, B., Schneider, D.A., Soukis, K., Roche, V. and Hubmann, B., 2022. Paleogeographic position of the central Dodecanese Islands, southeastern Greece: The push-pull of Pelagonia. Bulletin, 134(5-6), pp.1506-1528.

Vassilakis, E., Foumelis, M., Erkeki, A., Kotsi, E., and Lekkas, E., 2021, Post-event surface deformation of Amyntaio slide (Greece) by complementary analysis of Remotely Piloted Airborne System imagery and SAR interferometry: Applied Geomatics, v. 13, no. 1, p. 65-75.

16th International Congress of the Geological Society of Greece

17-19 October, 2022 - Patras, Greece

Bulletin of the Geological Society of Greece, Sp. Publ. 10

Ext. Abs. GSG2022-078

Using SAR data and interferometric techniques to calculate the terrain deformation after the Cumbre Vieja volcanic eruption on La Palma Island.

G. Barberis[1], A. Kyriou[1], K. Nikolakopoulos[1]

(1) University of Patras, Department of Geology, 26504 Patras, Greece, barberisgeorge@gmail.com

Research Highlights

Measuring the volcanic eruption's impact on the terrain and the provoked deformation, using remote sensing techniques.

Background-Objectives

Volcanoes are one of the most violent natural phenomena in the world. They can be very destructive and they cause a plethora of problems, like human and animal losses, destruction of properties and affections to the local or even global environment.

Remote sensing data and methods are increasingly being embedded into assessments of volcanic processes and risk. This happens thanks to their capability to provide a variety of observation and measurement opportunities to accurately sense the dynamics, magnitude, frequency, and impacts of volcanic activity. This paper describes the use of satellite remote sensing to estimate ground deformation and investigate the evolution of lava flows after the volcanic eruption on the island of La Palma. Satellite data before and after the eruption were collected for mapping and monitoring purposes. Surface displacement monitoring of La Palma was performed through Differential SAR Interferometry (DInSAR), during the various phases of the volcanic activity i.e. from the first moments of the eruption, to the lava spilling into the ocean and till the moment the lava stopped coming out from the volcano.

Methodology

The research results presented in this paper are achieved thanks to the Copernicus free satellite data (Sentinel-1 radar data and Sentinel-2 multispectral data). Interferometric techniques help us obtaining information about Earth's surface through measurements of the phase of the backscattered radar's signal. On the other hand, the offset tracking technique contributes to the measurement of the movement between two SAR images in both azimuth and slant-range direction using patch cross-correlation optimization. These systems are selected due to the fact that they provide accurate and free accessible data with the pretty good spatial resolution for earth observation (Kyriou and Nikolakopoulos, 2018). At first, radar data covering the area of the volcano some days before the explosion i.e. 19th September 2021 and when the lava flow had stopped at 13th of December 2021, had been obtained. The processing of the satellite SAR data was carried out with the SNAP (Sentinel Application Platform) software. A standard interferometric process includes the following basic steps which are: baseline estimation, SAR coregistration, interferogram formation, removal of the flat earth condition, interferogram filtering, wrapping of the phase and geocoding. Subsequently, interferograms have been created using Sentinel-1 data for each month during the eruption. Interferograms were produced from ascending and descending acquisition geometries (Table 1).

Furthermore, Sentinel -2 multispectral data (spectral bands 8, 11, 12) was used to automate the process of lava mapping using PCA(Principal Component Analysis) methods. Lastly, a comparison of results was held with the digital boundaries of lava from Sentinel-2 imagery.

Table 1. Sentinel-1 data

Ascending (60)	14/09/2021	14/10/2021	07/11/2021	01/12/2021	24/01/2022
Descending (169)	16/09/2021	1010/2021	09/11/2021	03/12/2021	20/01/2022

Results

In the generated interferograms, interferometric fringes were presented on the island of La Palma after the volcanic eruption. Figure 1 displays the areas of deformation, as resulted from the processing of Sentinel-1 and Sentinel-2 data. The results have shown that the creation of interferometric fringes in lava deformation areas is an evidence that interferometric techniques are able to measure deformation of the earth's surface with particular precision. The value of this study lies on the demonstration of the benefits that these remote sensing technologies have brought to volcano studying. With these systems more precise data can be obtained in lesser time than ever before, helping understanding the volcanic eruptions better and reducing the damage to human lives and infrastructure as much as possible.

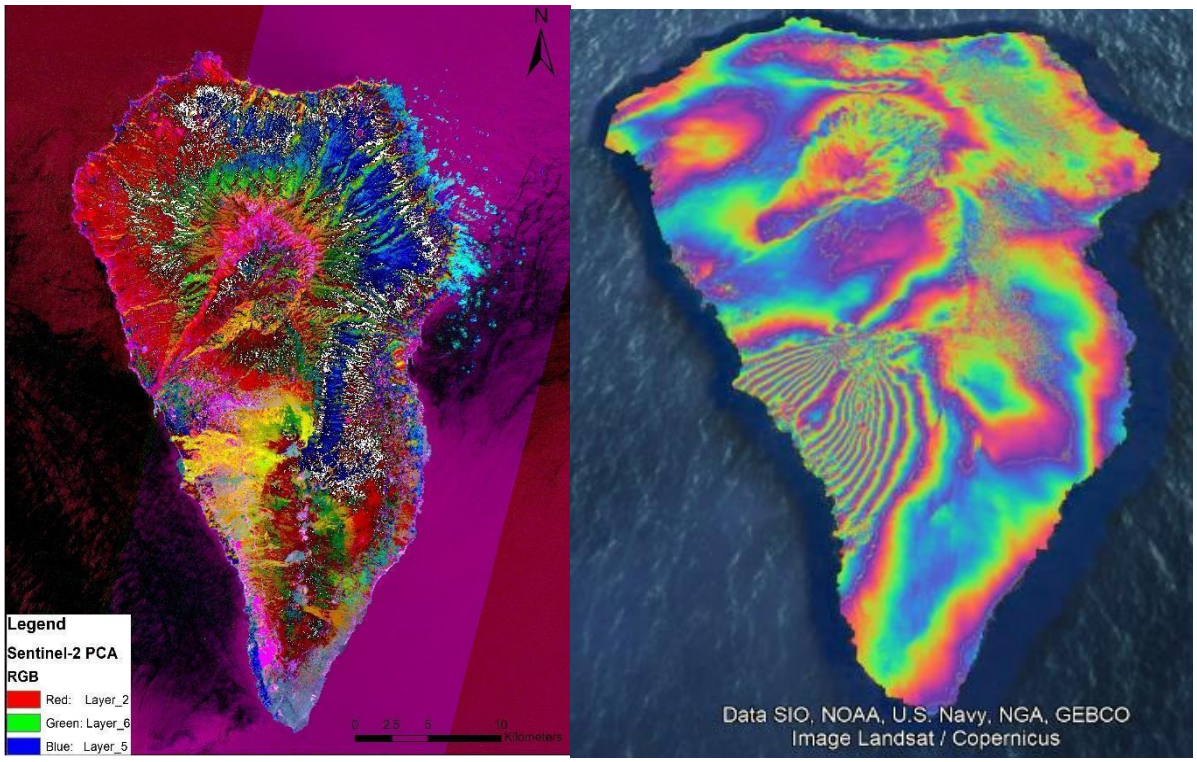

Figure 1. (Right image)A PCA image showing La Palma island from Sentinel-2 band combination. The yellow color shows the lava flow after the volcanic eruption. (Left image) Interferogram of La Palma island from the ascending orbit of Sentinel-1 data at 20th September 2021, showing the area with surface deformation.

Acknowledgements

The authors would like to thank the European Space Agency (ESA) for the provision of Sentinel-1 data through the Copernicus Open Access Hub (https://scihub.copernicus.eu/).

References

Kyriou, A., Nikolakopoulos, K., 2018. Assessing the suitability of Sentinel-1 data for landslide mapping, European Journal of Remote Sensing, 51:1, 402-411

Lekkas, E., Meletlidis, S.,Kyriakopoulos, K., Manousaki, M., Mavroulis, S., Kostaki, E., Michailidis, A., Gogou, M., Mavrouli, M., Castro-Melgar, I., Gatsios, T.,Parcharidis, I., 2021. The 2021 Cumbre Vieja volcano eruption in La Palma (Canary Islands). Newsletter of Environmental, Disaster and Crises Management Strategies, 26, ISSN 2653-9454

16th International Congress of the Geological Society of Greece
17-19 October, 2022 - Patras, Greece
Bulletin of the Geological Society of Greece, Sp. Publ. 10
Ext. Abs. GSG2022-080

Engineering geological investigation, using UAV, of extensive landslide phenomena in Tymphristos – Evritania along the road network of Lamia – Karpenisi.

T. Chatzitheodosiou[1], V. Marinos[2], E. Karantanellis[3], G. Papathanassiou[1]

(1) Laboratory of Engineering Geology & Hydrogeology, Aristotle University of Thessaloniki, 54124 Thessaloniki, Greece, themisto123@gmail.com (2) Geotechnical Division, School of Civil Engineering, National Technical University of Athens, 15780 Athens, Greece (3) Department of Earth and Environmental Science, University of Michigan, Ann Arbor, 48104 USA

Landslides are natural phenomena that affect and reshape the natural environment while causing significant environmental and socioeconomic impact worldwide. Due to the ongoing climate crisis, landslide occurrence is showing an increasing trend (Gariano and Guzzetti, 2016).

This research emphasizes on the comprehensive engineering geological assessment of a complex and large landslide, in flysch formation, at the basis of the mountain range Tymfristos in the Prefecture of Evritania, in central Greece. The study area is located a few kilometers west of the village Tymfristos, along the main road network of Lamia – Karpenisi.

The mountainous area of Evritania is considered one of the most hazardous zones, in the country, in providing landslides (Marinos *et al*., 2015). From geological perspective, landslides in the area are favored by the geological structure formed mainly in highly tectonized flysch formations involving sandstones, siltstones, and shales in alternations. In addition to frequent lithological alterations, the flysch bedrock also shows frequent variations in its tectonic structure. Extensive tectonic deformation, combined with surface weathering, forms a highly disturbed rockmass consisting of strongly weathered siltstones and shales, often with sandstone blocks, which even in its deepest parts does not provide sufficient strength.

In the past, landslide surveys in the area have been conducted using conventional survey methods, such as topographic map inspections, ground investigations and geo-research drilling programs, which were limited into a specific area along the road network. However, this landslide is much larger, has multiple and complex mechanisms and affects a wider area. The existence of a road network, in three levels of the main body of the landslide, as well as the frequent traffic on these roads, is a risk factor and landslide assessment should be considered. To formulate decision-making criteria regarding potential future intervention and remediation, innovative digital flight technologies and extensive ground surveys were integrated into this research framework to identify and monitor the evolution of the phenomenon.

In last decade, the use of Unmanned Aerial Vehicles systems (UAVs) has progressively increased and nowadays is considered as indispensable research tool for the acquisition of high-resolution imagery and topographic data over a predefined area (Giordan *et al*., 2020). High Resolution Digital Surface Models (HRDSMs), as derivatives by UAV photogrammetry, combined with computer-aided methods, offer a large set of metric and quality information that can be used to detect ground movement signatures, as well as to detect landslide morphology, with high detail (Pawluszek, 2018).

In this research, four (4) HRDSMs of the study area were constructed through Structure from Motion (SfM) photogrammetry (Westoby *et al*., 2012), to identify landslide characteristics, referring to a period between 2018 and 2020. In an effort to enhance the morphological information captured by each model, ten (10) HRDSM derivatives (slope, aspect, curvature, roughness, etc.) were transformed through the application of Principal Component Analysis (PCA), into a new set of image data consisting by a synthesis of the ten derivatives. PCA allowed the reduction of the geo-analytical redundant information of each model and the extraction of additional augmented geomorphological information. Visual interpretation of the produced dataset combined with field observations, prior and post the application of the method, led to the final recording of the boundaries for main landslide body as well as other individual sub-landslides within its area.

In terms of activity, a comparative analysis (change detection) was carried out to determine whether there is a consistent pattern of failures. This analysis concerns the automated export of quantitative results, in relation to elevation differences between the HRDSM of 2019 and an older Digital Elevation Model (DEM) created with photogrammetric techniques, from stereoscopic pairs of aerial photographs of the area, as recorded in 2007. Through the application of computational operations, between the two models, the morphological changes were captured in a 2D model, the so-called DEM of Difference (DoD). The DoD model consists of pixels with values that correspond to the difference of each pair of corresponding pixels separately between the two imported models (Williams, 2012). The results indicate that there is no clear failure pattern in the area, as many parts are not immediately visible in terms of their possible activation, and ground failure does not occur on a regular basis. However, in the western part of the complex landslide there is an active landslide characterized by intense forms of instability, which seems to be responsible for the reactivation of the total phenomenon.

In conclusion, the wider area of the landslide is under the constant influence of dynamic destabilizing factors. Processes

such as erosion and disintegration acting on the slope surface, due to numerous factors, as well as superficial and deeper slides within the landslide materials and the underlying flysch bedrock, disturb the natural balance of the slope. The landslide has not even regained a degraded long-term stability. On the contrary, especially during long term intensive rainfall periods, further instabilities appear mainly caused by slope saturation and high groundwater pore pressures development, since the materials have very low permeability. At the same time, minor local failures within the complex landslide area, such as small-scale rotational slides, soil-debris flows and rockfalls in its most stable parts, further activate the phenomenon by reshaping the geometry of the slope, burdening the landslide with additional material.

All in all, landslides in the region raise a big concern for their future development, being essentially an ever-changing system of instability that evolves over time. Therefore, investigations in the area should be constantly supplemented and revised. Finally, the methodology applied in this research (**Figure 1**) successfully demonstrates the efficiency of UAV platforms, to acquire ultra-high resolution photogrammetric datasets from environments with high relief and complex surface topography, as well as their potential for engineering geological applications.

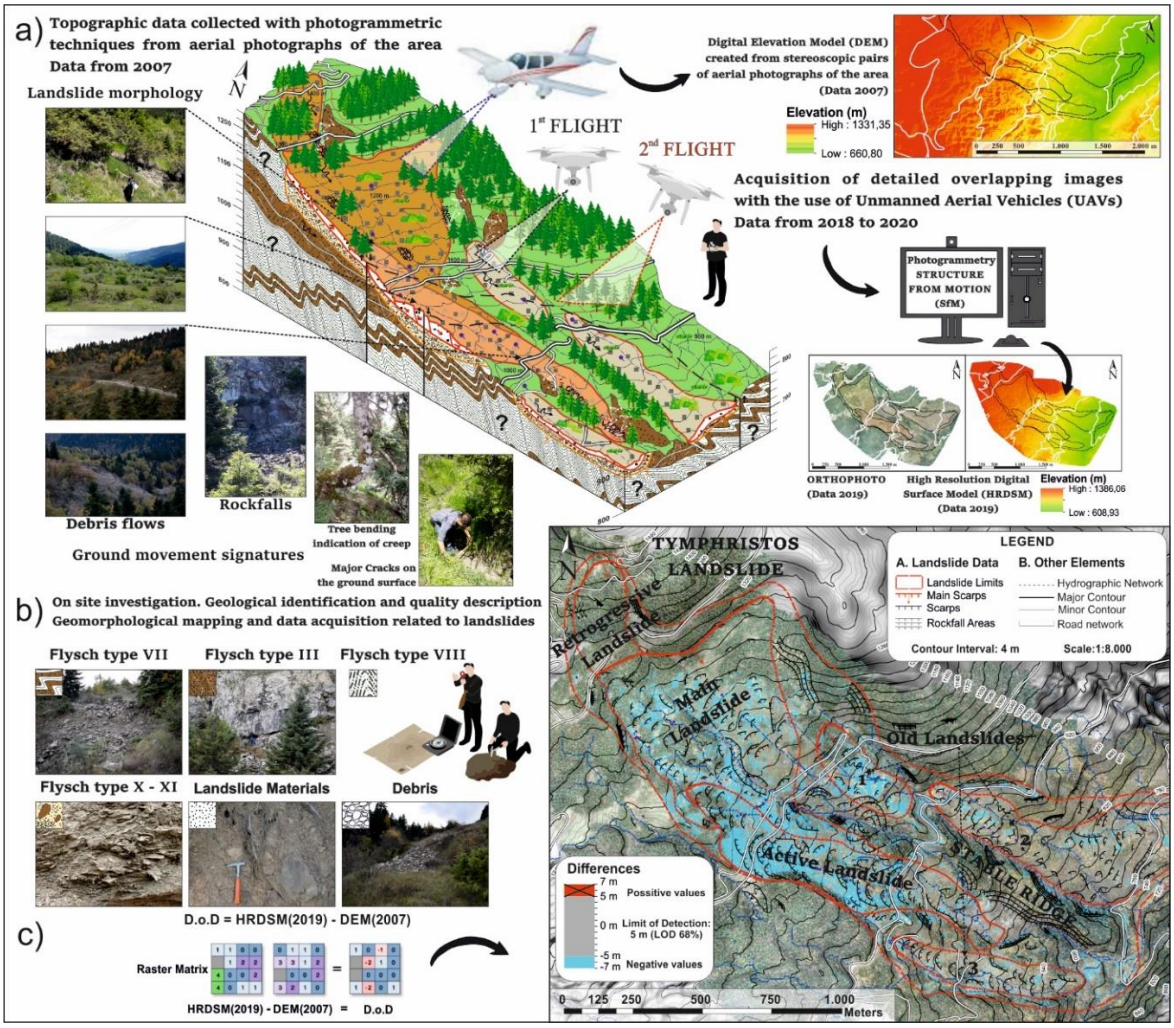

Figure 1. Schematic representation of operations followed in this research. a) Data acquisition, Geological Model and Digital Surface Models construction. b) Ground investigations. c) Change Detection analysis (DoD construction).

References

Gariano, S. L., Guzzetti, F., 2016. Landslides in a changing climate. Earth-Science Reviews, vol. 162, pp. 227 – 252.

Giordan, D., Adams, M.S., Aicardi, I. et al., 2020. The use of unmanned aerial vehicles (UAVs) for engineering geology applications. Bulletin of Engineering Geology and the Environment 79, pp. 3437 – 3481.

Marinos, V., Papathanassiou, G., Vougiouka, E., Karantanellis, E., 2015. Towards the Evaluation of Landslide Hazard in the Mountainous Area of Evritania, Central Greece. In: , et al. Engineering Geology for Society and Territory - Volume 2. Springer.

Pawluszek, K., 2018. Landslide features identification and morphology investigation using high resolution DEM derivatives. Journal of the International Society for the Prevention and Mitigation of Natural Hazards, Springer; vol. 96 (1), pp. 311 – 330.

Westoby, M. J., Brasington, J., Glasser, N. F., Hambrey, M. J., Reynolds, M. J., 2012. Structure-from-motion photogrammetry: a low-cost, effective tool for geoscience applications. Geomorphology 179, pp. 300 – 314.

Williams R. D., 2012. DEMs of Difference. In geomorphological techniques. British society of Geomorphology. Tech. 2, pp. 1 – 17.

16th International Congress of the Geological Society of Greece
17-19 October, 2022 - Patras, Greece
Bulletin of the Geological Society of Greece, Sp. Publ. 10
Ext. Abs. GSG2022-222

Landslide and rockfall investigation and mitigation design in complex natural slopes based on modern 3D reality capture technologies

V. Marinos[1], I. Farmakis[2], T. Chatzitheodosiou[1], D. Papouli[3], G. Stoumpos[4], E. Karantanellis[5], G. Prountzopoulos[6]

(1) Geotechnical Division, School of Civil Engineering, National Technical University of Athens, Greece, marinosv@civil.ntua.gr (2) Department of Geological Sciences and Geological Engineering, Queen's University, Canada (3) Engineering Geologist MSc, Geotechnical Division, School of Civil Engineering, National Technical University of Athens, 15780 Athens, Greece (4) Engineering Geologist MSc, Geotechnical Division, School of Civil Engineering, National Technical University of Athens, 15780 Athens, Greece (5) Department of Earth and Environmental Science, University of Michigan, Ann Arbor, USA (6) Independent Geotechnical Engineering Consultant

Landslides and rockfalls are among the most dominant geological hazards in both mountainous and coastal terrain with the potential to turn catastrophic when they occur in an anthropogenic environment. Various failure mechanisms can lead to the development of critical instabilities of different magnitude depending on the local geological and geomorphological conditions. Typically, landslides and rockfalls are associated with difficult terrain that poses significant accessibility challenges which may limit the effectiveness of the required engineering geological investigation. In the presented cases of the Evritania region and the islands of Kos, and Nisyros, digital solutions using primarily LiDAR and also UAV photogrammetry surveys were caried out to enhance the preliminary site investigation phase with a new set of digital applications. These applications have proven to support the required engineering geological data acquisition both in efficiency and detail, as well as the communication of the produced results and conclusions.

The cases presented in this study refer to various rock slope instabilities. They are characterized by a composite geological setting formed mainly within complex and weak rock masses. Rockfalls on coastal volcanic slopes, in highly heterogeneous pyroclastic rocks and lavas, structurally controlled failures in both mountainous and coastal areas in highly fragmented limestones and sandstone layers of flysch formations, are the main geological environments associated with this research. In addition, large-scale landslides in highly disturbed flysch rock masses, as well as smaller local rotational slides along mountainous road networks, were investigated in detail to identify and monitor their behaviour.

LiDAR and UAV photogrammetry surveys applied to a case-by-case basis depending on the study needs of the concerned area to collect valuable engineering geological information for the conceptual and/or detailed design of mitigation measures. UAV flights with a DJI Phantom 4 Pro RTK platform were performed in all cases for the compilation of dense point clouds and high-resolution Digital Surface Models (DSM). These digital models were used to enhance the engineering-geological mapping by identifying overhanging blocks that were scattered all along the slopes as well as to classify different engineering geological units (Figure 1). DSMs where also used for the construction of topographic maps for each area with an elevation interval of 1 m, while cross-sections for stability analyses were extracted from the 3D point clouds, overcoming the limitations of the classical 2.5D contour-based cross section extraction, especially at slopes with occasional inward inclinations. In sites with structurally controlled failures, such as planar slides, wedges and block toppling, a TLS LiDAR scanning was used to obtain orientation measurements and other geometric characteristics (spacing, persistence) of the discontinuity surfaces for kinematic analyses. For the calculation of these parameters, joint surfaces were extracted by locally applying Principal Component Analysis (PCA) on the XYZ space of the 3D points and subsequently forming individual clusters through density-based spatial clustering (Farmakis et al. 2020). Furthermore, potential failure areas related to overhanging blocks were indicated by the construction of depth maps (Figure 1).

In the case of Evritania a hybrid monitoring program is currently underway. This program apart from installed inclinometers, is accompanied by large-scale digital techniques for the aerial detection of ground movements and rockfall events. Specifically, the detection of surficial geometric changes between time-sequential point clouds was performed based on the M3C2 (Multiscale Model to Model Cloud Comparison) algorithm (Lague et al, 2013) with a typical example presented in Figure 2. The objective of this hybrid monitoring program, which is implemented by the research team, aims at both the point detection of subsurface movements and potential weak zones as well as the detection and quantification of surface processes such as movements, rockfalls, erosion, flows, etc.

In conclusion, with the use of these modern 3D mapping technologies, it has been possible to formulate, approach and quantitatively control and design integrated technical proposals that will successfully reduce the risk against rockfalls and landslides. All in all, through these modern digital 3D representations of the surveyed areas, excellent communication and understanding of the survey results has been achieved, contributing to a sound geotechnical design.

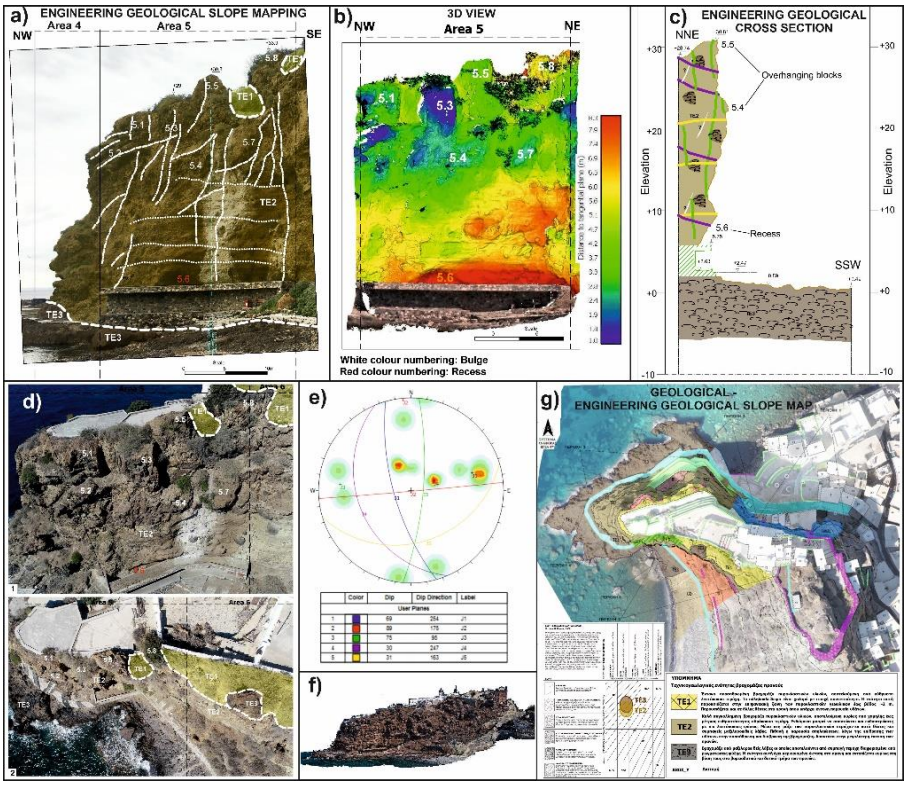

Figure 1. Overview of the digital engineering geological rock slope characterization and mapping methodology, including: a) engineering geological slope mapping view, b)3d face view, c) engineering geological cross sections, d) aerial inspection of critical structures, e) structural mapping, f) 3D point cloud view, and g) map and classification.

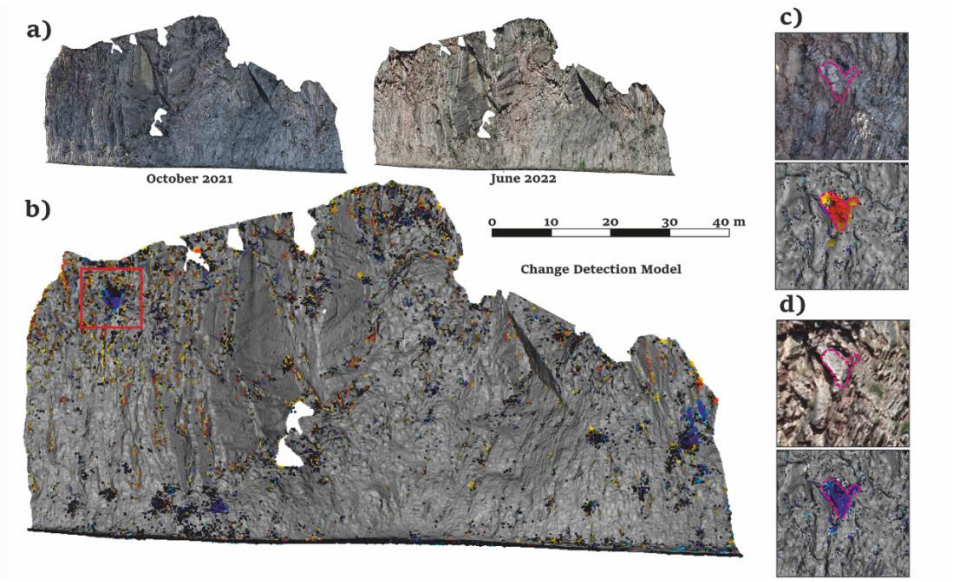

Figure 2. Change detection analysis in Evritania region, in a rockfall site towards Proussos village. The figure depicts a) the raw point clouds of the October 2021 and June 2022 UAV surveys, b) the change detection output with negative (loss) and positive (gain) changes represented by cooler and warmer colors, respectively, and c-d) a closer view of the rockfall enclosed in red square in (b), providing pre- (c) and post- (d) failure photographic (top) and point cloud (bottom) local representations.

Acknowledgements

The authors would like to thank the Prefecture of Central Greece and the Municipalities of Nisyros and Kos for funding part of this research.

References

Farmakis, I., Marinos, V., Papathanassiou, G. et al. Automated 3D Jointed Rock Mass Structural Analysis and Characterization Using LiDAR Terrestrial Laser Scanner for Rockfall Susceptibility Assessment: Perissa Area Case (Santorini). Geotech Geol Eng 38, 3007–3024 (2020).

Lague, D.; Brodu, N.; Leroux, J. Accurate 3D comparison of complex topography with terrestrial laser scanner: Application to the Rangitikei canyon (N-Z). ISPRS J. Photogramm. Remote Sens. 2013, 82, 10–26.

16th International Congress of the Geological Society of Greece
17-19 October, 2022 - Patras, Greece
Bulletin of the Geological Society of Greece, Sp. Publ. 10
Ext. Abs. GSG2022-296

Remote Sensing, GIS and Hydrologic Analysis System for Potential Dam Breach Evaluation and Landslide Mapping in Crete

E. Psomiadis[1], L. Tomanis[1], A. Papazachariou[1], A. Kavvadias[1], K.X. Soulis[1], N. Charizopoulos[1], S. Alexiou[1], I. Papanikolaou[1]

(1) Agricultural University of Athens, Iera Odos 75, 11855, Athens, Greece, mpsomiadis@aua.gr.

Introduction

A potential dam breach could have disastrous consequences for the economy and human lives. At the same time, landslides are regarded among the most hazardous and recurrently appearing natural disasters globally.

The purpose of this study is (i) to investigate the impact of a possible failure of the Bramianos dam in Lassithi Prefecture (Figure 1), comprising dam-break simulations in both overtopping and piping states; the behaviour of the flood wave, applying HEC-RAS 2D on two different elevation profiles (a Digital Elevation Model-DEM and a UAS-derived Digital Surface Model-DSM); the calculation of flood wave depth, velocity and time arrival at a given location; the risk assessment according to the downstream LULC affected, and (ii) to identify the impact of the various physical (mainly rainfall-triggered events) and anthropogenic factors (mainly road constructions and their characteristics) on landslide phenomena in Chania Prefecture (Figure 1). Moreover, through this research, we intend (i) to examine the suitability of the Earth Observation and extremely detailed DEM data in landslide detection and the assessment of potential landslide susceptibility of similar regions, and (ii) to evaluate the HEC-RAS and GIS analysis, using remote sensing data (UAS and EO) and American Society of Civil Engineers (ASCE) methodology for flood wave characteristics examination after a potential dam breach (Psomiadis *et al*., 2020; Psomiadis *et al*., 2021).

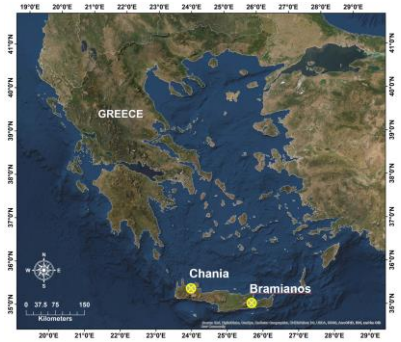

Figure 1. The study areas in the northern part of Chania prefecture and Bramianos dam in Lassithi Prefecture

Materials and Methods

The first case is dealing with the impact examination of a possible failure–collapse on a potentially affected area downstream of the existing Bramianos dam on the southwest part of Crete Island. HEC-RAS hydraulic analysis software was used to study the dam breach, and the flood wave propagation, and to estimate the extent of floods. The analysis was performed using two different relief datasets of the same area: a DEM taken from very high-resolution orthophoto images (OPH) and a detailed DSM extracted from aerial images taken by an unmanned aerial vehicle (UAV). Remote sensing data of the Sentinel-2 satellite and OPH were utilized to make a thorough land use/cover classification for the potentially flooded area (Figure 2i), which was used to assess the impact of the flood wave. Different dam breaches (overtopping and piping) and flood scenarios were also examined. The study area is dominated mainly by three geological formations with different hydrogeological characteristics (Makrylia, Ammoudares and Kalamavka formations) that dictated the positioning and structure of the dam and determine the processes that shape the geomorphology and surface roughness of the floodplain, affecting flow conditions.

The second case is related to the intense rainfalls that took place from September 2018 to February 2019 period provoked extensive landslide events in the northern part of Chania prefecture, along motorway A90. Geospatial analysis methods and earth observation data were utilized to investigate the impact of the various physical and anthropogenic factors on landslides and to evaluate landslide susceptibility. A very high-resolution DEM was produced from a dense point cloud. Sentinel-2 data were used for the detection of recent landslide events and offered suitable information for two of them.

Results and Conclusions

The results show that the impact of a potential dam break at Bramianos dam is serious, and appropriate management measures should be taken to reduce the risk. The water flow downstream of the collapsed dam depends on the water

volume stored in the reservoir. Moreover, the comparison of DSM and DEM cases shows that the detailed DSM may indicate more accurately the surface relief and existing natural obstacles such as vegetation, buildings, and greenhouses, enabling more realistic hydraulic simulation results (Figure 2ii).

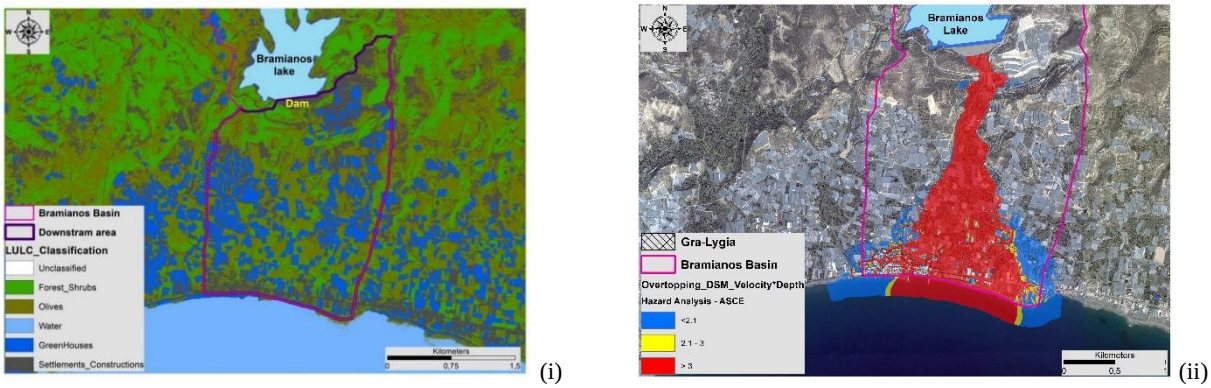

Figure 2. (i) Land use/cover classification (LULC) classification image of the Bramianos dam broader area, (ii) Map of flood arrival time, utilizing DSM in the piping scenario.

The results of the landslide events analysis proved that the triggering parameters are associated with continuous and intense rainfalls, and anthropogenic activity and, more specifically, the steep slopes along the constructed road network (this slope angle and distance to road parameters). For this reason, most of the landslide movement types are related to the debris avalanche type (Figure 3i). Moreover, the EO data revealed small landslide scars in the Stalos and Galatas regions (Figure 3ii). Landslide scars were distinctly different from the surrounding ground features and appear in dark colours since the surrounding area appears in red (vegetation cover).

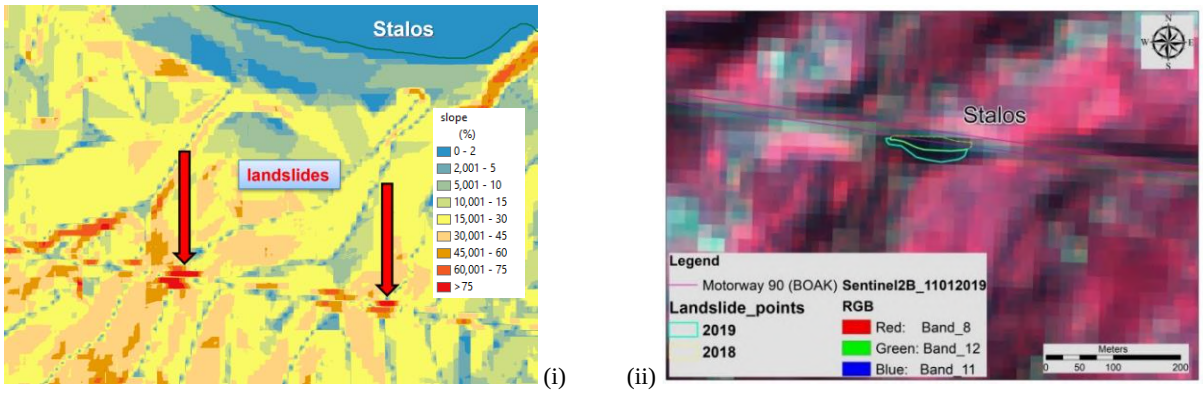

Figure 3. (i) Detailed slope map that reveals the extremely steep slopes of the landslide area, (ii) False colour composites of Sentinel-2 post-landslide event in Stalos area of motorway A90, where cyan polygon delineates the landslide scar

Conclusions

Dam breach flood simulations and innovative remote sensing data can provide valuable outcomes for engineers and stakeholders for decision-making and planning to confront the consequences of similar incidents worldwide. The results indicate the substantial effect of different break types on the hydraulic characteristics of a dam-break flood wave in the downstream areas, with the overtopping scenario being the more adverse event. Moreover, the comparison of DSM and DEM cases shows that the DSM represents the surface relief and the existing natural obstacles more accurately, providing a more precise depiction of the existing barriers, such as vegetation, buildings, and greenhouses, and, hence, more realistic hydraulic simulation results.

The landslide events analysis depicts that the preparatory and triggering mechanisms were related to extreme rainfall conditions and anthropogenic activities. Particularly in the case of the motorway A90 landslides in Chania, further studies should be performed at the local level to clarify the accurate extent site of the slope vulnerability and landslide hazard. In general, it is confirmed that the synergistic use of earth observation and geospatial analysis systems can ideally assist research regarding landslide susceptible areas. Also, despite the coarse spatial analysis of Sentinel-2 images in comparison with other very high-resolution satellites, it provides a powerful tool for landslide detection and monitoring because of its high temporal resolution (five days revisit time) and free availability.

References

Psomiadis E., Tomanis L., Kavvadias A., Soulis K.X., Charizopoulos N., Michas S., 2021. Potential Dam Breach Analysis and Flood Wave Risk Assessment Using HEC-RAS and Remote Sensing Data. A Multi-Criteria Approach. WATER, 13(3), 364. https://doi.org/10.3390/w13030364.

Psomiadis E., Papazachariou A., Soulis K.X., D.-S. Alexiou, Charalampopoulos I., 2020. Landslide mapping and risk assessment using geospatial analysis and Earth Observation data. LAND, 9(5), 133. https://doi.org/10.3390/land9050133.

16th International Congress of the Geological Society of Greece
17-19 October, 2022 - Patras, Greece
Bulletin of the Geological Society of Greece, Sp. Publ. 10
Ext. Abs. GSG2022-327

Detection and Monitoring of Total Suspended Matter (TSM) in South Evoikos Gulf, Greece after the flood event on the 9th of August 2020

D. Bafi[1], S. Tounta[1], M. Karantzia[1,2], I. Parcharidis[1]
(1) Harokopio University, Athens, Greece, gp219313@hua.gr (2) National Technical University, Athens, Greece

Research Highlights

This study's findings, present an increase in Total Suspended Matter (TSM) concentration in Evoikos Gulf as the aftermath of the flood event in the area, which is evident days after the event. Also, data for 2020-2021 are compared.

Background

Evia is the second largest island of Greece; it is located in central Greece in the Aegean Sea. The study area has two alluvial fans located in the area of Politika, and the alluvial/coastal plain of the Lilas and Messapios rivers. The Messapios river springs from Dirfys Mountain, flowing in a general direction from East to West. Messapios flows into the North Evoikos Gulf near the town of Psachna. The town is built at the confluence of the Mantania stream with the Messapios river, where a wide alluvial fan is present (Karkani *et al*., 2021). The flash flood that occurred in August 2020 mostly affected central Evia and specifically the basins of Messapios river, and Mantania, Poros, and Politika streams. Generally, the occurrence of extreme events such as floods and particularly flash floods are increasing on a global scale (Van Vliet *et al.*, 2013; IPCC, 2012). Flash floods are events occurring on a small spatial scale within a short time, under conditions of rapid production of surface runoff. (Jonkman, 2005). Such events have a major impact on human populations and infrastructure, as well as on the coastal ecosystems. During periods of floods, rivers deliver a large amount of dissolved and particulate organic and inorganic constituents to the coastal zone. Total Suspended Matter (TSM), which reaches the coastal zones via rivers and streams, is one of the main water quality indicators. It is comprised of constituents, like phytoplankton, Colored Dissolved Organic Matter (CDOM), and sediment particles. While TSM is vital for the preservation of the river deltas and provides habitat for microorganisms, it can also accumulate and transport pollutants from the upper reaches of the rivers to their estuaries, with negative effects on the physical and human environment (Vidmar *et al., 2016*).

Objectives

The objective of the present study is to utilize Copernicus satellite data to monitor the Total Suspended Matter (TSM) concentration in the South Evoikos Gulf after the flooding of Lilas river in Central Evia Island on the 9th of August. The major synoptic feature during the storm "Thalia", named by the National Observatory of Athens, between the 5th and the 9th of August 2020, was an almost stationary mid/upper-tropospheric cut-off low-pressure system in the general area of the South Adriatic Sea and the Ionian Sea (Lekkas *et al*., 2020). The extended area of impacts and fatalities is attributed mainly to the geography of hydrological basins in the area. The mountainous area of Evia has two major basins which flow into two different areas, the North and the South Evoikos Gulf. Thus, the high amounts of rainfall that fell in the central mountainous areas caused damage in two distant coastal areas in Psachna and Politika on the north and Lefkanti, Vasiliko, and Bourtzi on the south. Basins' morphology was also important, since they present high inclination at their upstream parts, leading to high flow velocities, increased erosion, and mass movement phenomena. This event caused large amounts of sediments and debris to be carried by the Lilas river to the South Evoikos Gulf and reach the shores of northeast Attica.

Methods

From satellite observations in the optical part of the spectrum, we can retrieve the concentrations of different constituents, like suspended sediments. For the detection and monitoring of TSM, 6 Sentinel-2 MSI Level-1C high-resolution satellite images were retrieved from the Copernicus Open Access Hub platform (Table 1), based on the date on which the flash flood event took place. After the Sentinel-2 images were acquired, their preprocessing was carried out, which included resampling the images to 10 m/pixel resolution and subsetting them using the open-source ESA SNAP software. The main processing of the Sentinel-2 data was carried out using the Case-2 Regional CoastColour (C2RCC) processor available in SNAP. The C2RCC, originally developed by Doerffer and Schiller (2007), uses Neural Networks (NNs) as basic technology and an extensive database of radiative transfer simulations of water-leaving radiances and top-of-atmosphere radiances, as well as different models, such as a 5-component bio-optical model. It relies on the Inherent Optical Properties (IOPs) of water, to calculate the TSM concentration. Regional parameters, such as sea surface temperature, salinity, and atmospheric pressure, were set for the study area in the processors' user interface. After performing atmospheric correction, the C2RCC uses the water leaving reflectances to determine the IOPs and finally

calculates the TSM concentration (g/m^3), using arithmetic conversion factors (Brockmann *et al*. 2016). The result is a new product that contains the TSM concentration. After, the mapping of TSM concentration was performed.

Results and Conclusions

A significant relationship was observed between TSM concentration in the Evoikos Gulf and the flash flood event. The values in the small gulf between Chalkida and Nea Lampsakos are consistent throughout the study period, ranging from 1 to 5 g/m^3. The maximum TSM concentration was observed on the 13th of August 2020, reaching up to 20 g/m^3. This is evident especially in the southern Evoikos Gulf in the aquatic areas near Lefkadi, Avlida Beach, Dilesi, and Skala Oropou, where TSM dispersed at a distance of 17,70 km from the estuary of Lilas River to the shores of north-east Attika. It is worth mentioning that higher values are observed in the North Evoikos Gulf on the 13th of August 2020 in comparison with the image acquired on the 8th of August 2020 before the event. On 07/09/2020 TSM concentration begins to decrease, but remains higher than before the event. In the 18/08/2021 image, which is acquired a year after the event, TSM concentration presents the same distribution and values in the overall area as in the image acquired before the event (Figure 1). Our study highlights the contribution of Copernicus open-access satellite data and open-source algorithms provided by the European Space Agency (ESA), to detect and monitor the ramifications of a flash flood event. In the future, the study will include Copernicus Sentinel-1 Level-2 OCN satellite data, as well as wind direction and speed data from the meteorological stations of NOA to qualitatively determine the relationship between wind direction and speed and the observed TSM direction. It is also recommended, to validate the satellite data, by using in situ data.

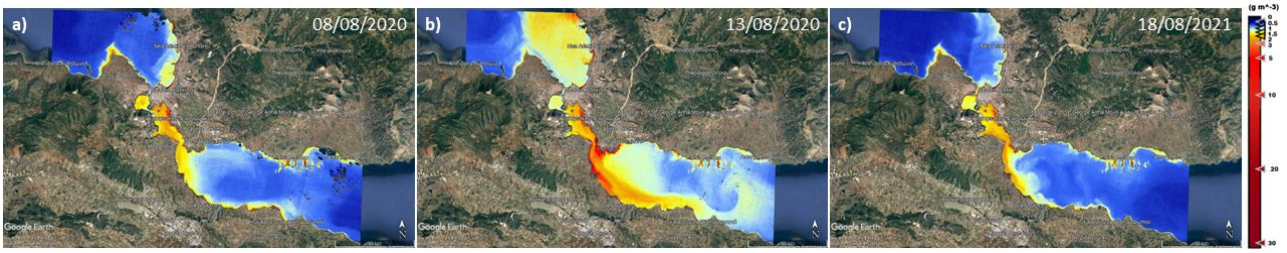

Figure 1. Total Suspended Matter (TSM) Concentration in the Central Evia region a) before the event (08/08/2020), b) after the event (13/08/2020) and c) one year after the event (18/08/2021).

Table 1. Acquisition dates of Sentinel-2 MSI Level-1C data.

Acquisition Period	Dates
Before the event	08/08/2020
Immediately after the event	13/08/2020
Monitoring of the event	18/08/2020
	28/08/2020
	07/09/2020
One year after the event	18/08/2021

Acknowledgements

We would like to thank the ESA Open Access Hub for providing free satellite images from the Sentinel Missions of the Copernicus Program.

References

Karkani A., Evelpidou N., Tzouxanioti M., Petropoulos A., Santangelo N., Maroukian H., Spyrou E., Lakidi L., 2021, Flash. Flood Susceptibility Evaluation in Human-Affected Areas Using Geomorphological Methods—The Case of 9 August 2020, Euboea, Greece. A GIS-Based Approach. Geohazards 366-382. **[Journal Article]**

Brockmann, C., Doerffer, R., Peters, M., Kerstin, S., Embacher, S., Ruescas, A. 2016. Evolution of the C2RCC neural network for Sentinel 2 and 3 for the retrieval of ocean colour products in normal and extreme optically complex waters. Proceedings of the Living Planet Symposium. http://step.esa.int/docs/extra/Evolution%20of%20the%20C2RCC_LPS16.pdf **[Conference Paper]**

Jonkman, S.N., 2005, Global perspectives on loss of human life caused by floods. Nat. Hazards Dordr., 34, 151–175. **[Journal Article]**

Lekkas, E., Spyrou N-I., Kotsi E., Filis, Ch., Diakakis, M., Lagouvardos K., Cartalis C., Kotroni V., Dafis S., Vassilakis, E., Mavrakou Th., Parcharidis I., Sartabakos P., Gogou M-E., Katsetsiadou A-N., Karagiannidis A., Barsaki V. Karavias A., Bafi D., Gougoustamos I. (2020). The August 9, 2020, Evia (Central Greece) Flood. Newsletter of Environmental, Disaster and Crises Management Strategies, 19, ISSN 2653-9454**. [Newsletter]**

Van Vliet, M. T. H., Franssen W. H. P., Yearsley J. R., Ludwig F., Haddeland I., Lettenmaier D. P., and Kabat P., 2013, Global River discharge and water temperature under climate change, Global Environ. Change, 23, 450– 464. **[Journal Article]**

Vidmar, J., Zuliani, T., Novak, P., Drincic, A., Scancar, J., Milacic, R., 2016, Elements in water, suspended particulate matter and sediments of the Sava River. Journal of Soils and Sediments, 17, 1917-1927. **[Journal Article]**

16th International Congress of the Geological Society of Greece
17-19 October, 2022 - Patras, Greece
Bulletin of the Geological Society of Greece, Sp. Publ. 10
Ext. Abs. GSG2022-329

Detection and Monitoring of Post-fire Landslides and Soil Movement Using UAS and t-LiDAR

G. Deligiannakis[1,2], I. Papanikolaou[1], S. Alexiou[1], A. Pallikarakis[1], A. Mertzanis[3], E. Psomiadis[1], K. Reicherter[4]

(1) Mineralogy-Geology Laboratory, Agricultural University of Athens, Athens, Greece, gdeligian@aua.gr (2) Hellenic Survey of Geology and Mineral Exploration, Athens, Greece (3) Department of Agribusiness & Supply Chain Management, Agricultural University of Athens, Greece (4) Institute of Neotectonics and Natural Hazards, RWTH Aachen University, Aachen, Germany.

Introduction

Wildfires impact vegetation and can increase the probability of occurrence of secondary post-fire effects such as landslides, soil erosion, and sediment transport (e.g. Shakesby *et al.*, 2006; Diakakis *et al.*, 2017). New tools such as Light Detection and Ranging (LiDAR) and Unmanned Aerial Systems (UAS) are lately being deployed, not only for detection but for monitoring purposes as well (e.g. Valkaniotis *et al.*, 2018; Koukouvelas *et al.*, 2020; Eker *et al.*, 2021; Cheng *et al.*, 2021). This paper aims to detect early surface ruptures and cracks connected to shallow landslides and debris flow after severe wildfires using UAS-based photogrammetry and t-LiDAR scanning.

Methodology

We conducted UAS and t-Lidar scans in five different locations in Central Greece (Evia, Kehries 1&2, Magoula & Drosopigi). We used a different number of Ground Control Points (GCPs) for each case, depending on the sites' extent and physical characteristics (see also Andreadakis *et al.*, 2020). In all cases, the GCPs were surveyed using a Spectra SP60 Real-Time Kinematic Global Navigation Satellite System (RTK GNSS).

A DJI Phantom 4 was used with a 1/2.3" 12.4 MP camera sensor. A minimum forward image overlapping was set at approximately 80% at the highest part of the slopes, and side overlap reached 95% in specific areas of high interest. All extracted images were photogrammetrically processed using the Agisoft PhotoScan Metashape Professional (v. 1.5.5), and point clouds were also analyzed using the Cloud Compare freeware. For the t-Lidar data acquisition, we used the Optech Ilris 3D LiDAR, following the methodology described by Alexiou *et al.*, 2021.

Results

At the Evia site, the correlation of the UAS and TLS-derived point clouds revealed two minor offsets, approximately 4–5 ±3 cm high and 1.5 m long, which could be interpreted as the initiation of a small slide. Moreover, the formation of small rills at the northern part of the slope suggests the development of a new erosional landscape after the recent wildfire.

Regarding Kehries 1, the comparison between the 08/2020 and 10/2020 scans showed an apparent movement along a major pre-existing scarp (Figure 1a). In addition, a minor crack was identified in the central part of the slope, while another crack was also revealed in the western part of the slope. The comparison between the 10/2020 and the 03/2021 scans revealed a movement in the major scarp at the eastern part of the slope. More importantly, new cracks were identified, either in the northern extension of the previously defined central scarp or in new locations that were stable during the first three months (Figure 1b). The total vertical displacement along the cracks and scarps varies from as low as 10 ± 4 cm in the smaller cracks and reaches as high as 19 ± 4 cm in the major scarp at the eastern part of the slope. Likewise, the lateral expansion of the crack in the slope's central part reaches approximately 27.5 m (Figures 1c,d&e).

Regarding the pre-existing landslide in Magoula, we identified an expansion of the slide towards the base of the slope towards the west, and two additional minor scarps at the north and south parts, respectively. The total landslide area in 10/2019 was 68 m^2, and in 06/2020 it was 74 m^2. This could be translated to an expansion rate of 0.75 m^2/month, despite the mitigation measures and assuming that the landslide is expanding at a stable pace over time.

The maximum height and length of the landslide scarp in Drosopigi location was unchanged in both orthomosaics before the 2021 Varibopi wildfire. The vegetation removal after the 2021 wildfire revealed the full extension of the pre-existing scarp towards SW (Figure 2) and allows for further research, because of the unique characteristics of this location (burned twice in 10 years, available data before and after the 2021 wildfire).

Discussion and Conclusions

UAS-derived DSM and point clouds, along with t-LiDAR point clouds, were used to detect newly formed soil cracks and monitor pre-existing landslide scarps in 5 sites with different physical characteristics. The best results were obtained from the DSMs derived from the UAS-based SfM photogrammetry in Kechries1&2 and Evia. These sites were severely burned, with insignificant vegetation regrowth for the first 7 months after the wildfire. Drosopigi and Magoula, which had experienced wildfires 7 and 10 years before our research, respectively, were not ideal for UAS or t-LiDAR scanning due

to the dense and low vegetation. However, since the 2021 Varibopi wildfire, we expect a reactivation of the Drosopigi landslide and further scan data will be elaborated.

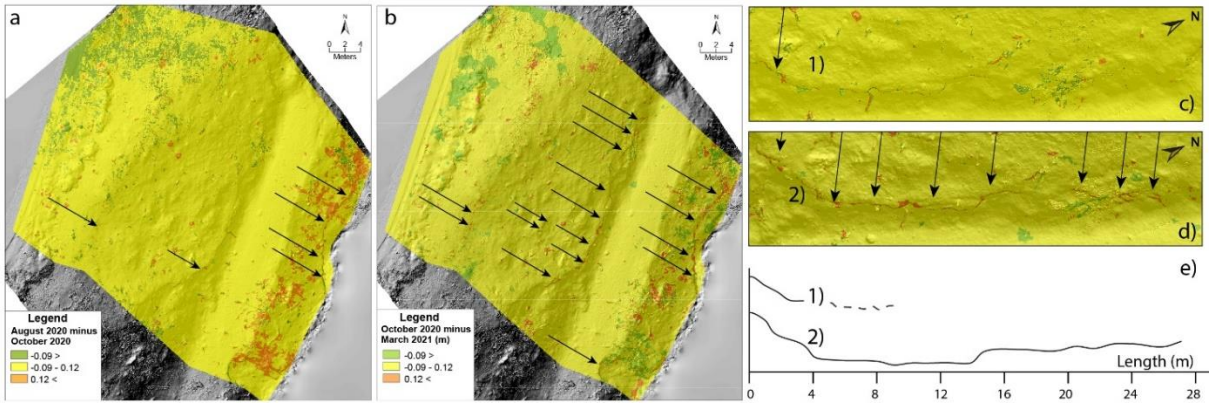

Figure 1. Kehries 1 a) DSM comparison between 08/2020 and 10/2020 scans.b) DSM comparison between 10/2020 and 03/2021 scans, c,d) gradual expansion of the major crack from approximately 4m (1) up to more than 25 m (2). d) schematic illustration of the lateral expansion of the major crack.

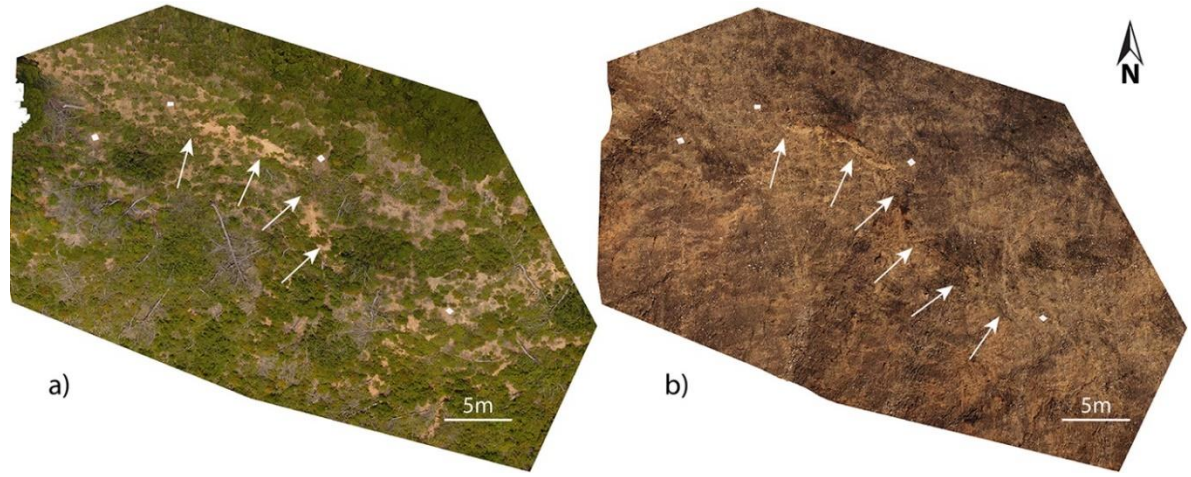

Figure 2. Orthomosaics from Drosopigi landslide, before (a) and after (b) the 2021 Varybopi wildfire. The main scarp was partly covered by vegetation but it is fully exposed after the 2021 wild fire, and its full extent is now visible.

Acknowledgements

This research was co-financed by a) GlaxoSmithKline SA through the VARIBOPI RESET initiative b) Greece and the European Union (European Social Fund) through the O.P. "Human Resources Development, Education and Lifelong Learning 2014–2020" and the Program encoded EDBM103, titled "Support for researchers with an emphasis on young researchers-cycle B", in the context of the project "Detect and describe small landslides through t-LIDAR and UAV scanning techniques" (MIS 5048452).

References

Andreadakis, E., Diakakis, M., Vassilakis, E., Deligiannakis, G., Antoniadis, A., Andriopoulos, P., Spyrou, N., Nikolopoulos, E., 2020. Unmanned Aerial Systems-Aided Post-Flood Peak Discharge Estimation in Ephemeral Streams. Remote Sens. 12, 4183.

Alexiou, S., Deligiannakis, G., Pallikarakis, A., Papanikolaou, I., Psomiadis, E., Reicherter, K., 2021. Comparing High Accuracy t-LiDAR and UAV-SfM Derived Point Clouds for Geomorphological Change Detection. ISPRS Int. J. Geo-Inf. 10, 367.

Cheng, Z., Gong,W., Tang, H., Juang, C.H., Deng, Q., Chen, J., Ye, X. 2021. UAV photogrammetry-based remote sensing and preliminary assessment of the behavior of a landslide in Guizhou, China. Eng. Geol. 289, 106172.

Diakakis, M., Nikolopoulos, E.I., Mavroulis, S., Vassilakis, E., Korakaki, E., 2017. Observational evidence on the effects of mega-fires on the frequency of hydro-geomorphic hazards. The case of the Peloponnese fires of 2007 in Greece. Sci. Total Environ. 592, 262–276.

Eker, R., Aydın, A., 2021. Long-term retrospective investigation of a large, deep-seated, and slow-moving landslide using InSAR time series, historical aerial photographs, and UAV data: The case of Devrek landslide (NW Turkey). Catena 196, 104895

Koukouvelas, I.K., Nikolakopoulos, K.G., Zygouri, V., Kyriou, A., 2020. Post-seismic monitoring of cliff mass wasting using an unmanned aerial vehicle and field data at Egremni, Lefkada Island, Greece. Geomorphology 367, 107306.

Valkaniotis, S., Papathanassiou, G., Ganas, A., 2018. Mapping an earthquake-induced landslide based on UAV imagery; case study of the 2015 Okeanos landslide, Lefkada, Greece. Eng. Geol. 245, 141–152.

Shakesby, R., 2011. Post-wildfire soil erosion in the Mediterranean: Review and future research directions. Earth-Sci. Rev. 105, 71-100.

16th International Congress of the Geological Society of Greece
17-19 October, 2022 - Patras, Greece
Bulletin of the Geological Society of Greece, Sp. Publ. 10
Ext. Abs. GSG2022-394

Towards the compilation of a landslide inventory in East Macedonia and Thrace region, Greece

S.Valkaniotis[1], G.Papathanassiou[2] , M.Taftsoglou[1], N.Klimis[1], I.Dokas[1]

(1) Democritus University of Thrace, Xanthi, Greece, svalkani@civil.duth.gr (2) Aristotle University of Thessaloniki, Thessaloniki, Greece

Background

Landslide occurrence is widespread and common over the continental and island parts of Greece, with the largest frequency and density encountered in western and southern Greece (Koukis *et al.*, 1996; Koukis *et al.*, 2005; Sabatakakis *et al.*, 2013). Most regional studies of landslides and landslide hazard rely on reports of historical and recent landslide locations and locally focused inventories (Pyrgiotis 1997; Koukis *et al.*, 2005; Chalkias *et al.*, 2014). There is also a limited number of landslide inventories from recent strong earthquakes (e.g. Papathanassiou *et al.*, 2021). Northeastern Greece, and more specifically East Macedonia and Thrace region, has a lower frequency of reported landslides, but nevertheless still significant hazard risk and risk for the local communities and infrastructure (Tsagaratos 2012). The lack of a detailed landslide dataset (rainfall- and earthquake-induced landslides) over the region, led us to the creation of a landslide inventory for the Prefecture of East Macedonia and Thrace (including the two largest islands of Thasos and Samothraki), with an approximate scale of 1:25,000-1:50,000. A concise landslide inventory should include landslide polygons and linear features traced in as much detail as possible, for both active/recent landslides and inactive/prehistoric landslides.

Methodology

The creation of the landslide inventory for East Macedonia and Thrace region was based on a geomorphological approach, using detailed digital elevation models, supplemented by remote sensing data (Keaton & Degraff, 1996; Soeters & van Westen, 1996; Burns & Madin, 2009; Burns & Mickelson, 2016; Miyagi 2021; Yagi *et al.*, 2021). Landslide mapping was performed manually, using as baseline a detailed digital surface model (DSM) with 5m resolution, provided by the Hellenic Cadastre. Landslide polygons and scarp features were traced over the DSM by using key morphological features identified in relief and slope maps. Mapped landslide features were then checked using multi-temporal aerial and satellite very high resolution imagery, in order to check validity and age of activity. Supporting data such as reported landslide occurences and satellite-derivered displacement time-series were also used to identify activity of the mapped landslide polygons. Landslide inventory coverage is limited in areas of dense forest vegetation and major built-up areas, and in parts where the DSM is missing data or appears to have artifacts. We have mapped more than 10,000 landslide polygons in the area covering the region of East Macedonia and Thrace (Figure 1). Mapped landslides are mostly deep-seated landslides, rockslides and earthflows with a significant size (from ~30m up to 1-2 km). The inventory does not include individual rockfalls and debris flows.

Results and Conclusions

- A detailed inventory of more than 10,000 active and inactive landslides for the East Macedonia and Thrace region can provide the basis for creating inventory-based susceptibility and hazard maps for rainfall- and earthquake-induced landslides in the region (Burns & Madin, 2009; Burns & Mickelson, 2016). We plan to expand the current landslide inventory by acquiring more detailed digital surface models in local and regional scale. Landslide polygons can also guide the future creation of detailed landslide maps in local scale.
- Using the new detailed inventory, we plan examine the exposure and vulnerability of critical infrastructure (built-up areas, critical facilities, major road networks etc) in East Macedonia and Thrace in order to assess the risk from landslides.

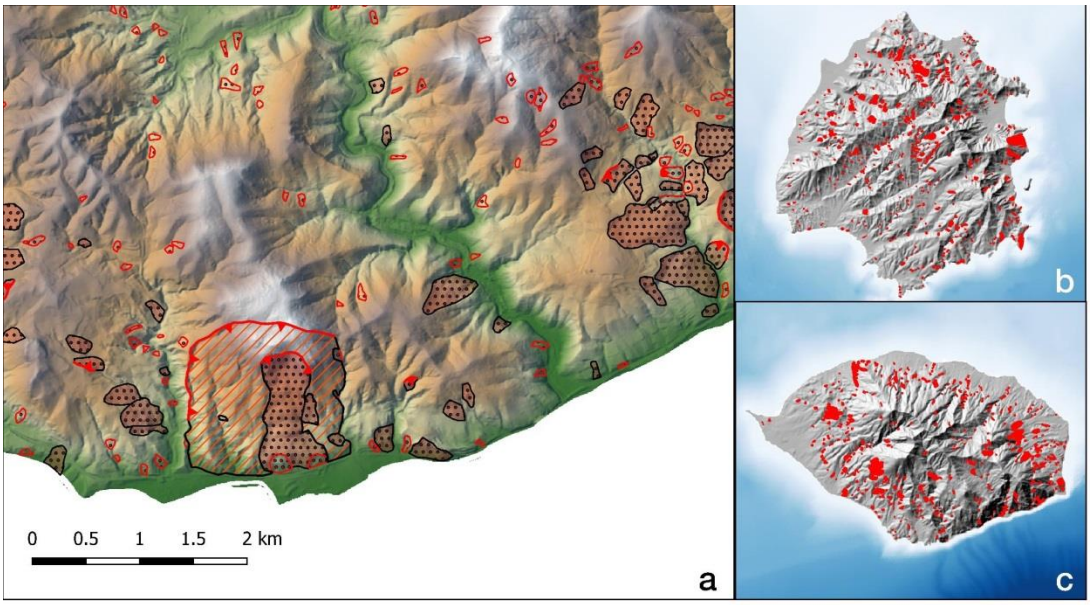

Figure 1. Examples of landslide inventory mapping in East Macedonia & Thrace Region: (a) Close-up of landslide polygons mapped in detail in the area of Loutra Eleftheron, Kavala; (b) Landslides (red polygons) mapped in Thasos Island; (c) Landslides (red polygons) mapped in Samothraki Island.

Acknowledgements

We acknowledge support of this work by the project "Risk and Resilience Assessment Center –Prefecture of East Macedonia and Thrace -Greece." (MIS 5047293) which is implemented under the Action "Reinforcement of the Research and Innovation Infrastructure", funded by the Operational Programme "Competitiveness, Entrepreneurship and Innovation" (NSRF 2014-2020) and co-financed by Greece and the European Union (European Regional Development Fund).

References

Burns, W. J., Madin, I. P., 2009. Landslide protocol for inventory mapping of landslide deposits from light detection and ranging (lidar) imagery. Oregon Department of Geology and Mineral Industries, Special Paper 42, 30 p.

Burns, W. J., Mickelson, K. A., 2016. Protocol for deep landslide susceptibility mapping. Oregon Department of Geology and Mineral Industries, Special Paper 48, 69 p.

Chalkias, C., Ferentinou, M., Polykretis, C., 2014. GIS-Based Landslide Susceptibility Mapping on the Peloponnese Peninsula, Greece. Geosciences, 4, pp. 176-190.

Keaton, J.R., Degraff, J.V., 1996. Surface observation and geologic mapping, in Turner, A.K., Schuster, R.L., (Eds.), Landslides: investigation and mitigation, Washington, D.C., National Academy Press, Transportation Research Board, National Research Council Special Report 247, pp. 178–230.

Koukis, G., Tsiambaos, G., Sabatakakis N., 1996. Landslides in Greece: Research evolution and quantitative analysis. Proceedings of the 7th International Symposium on Landslides, Trondheim. Balkema, Rotterdam, pp 1935–1940.

Koukis, G., Sabatakakis, N., Nikolau, N., Loupasakis, C., 2005. Landslide Hazard Zonation in Greece, in: Sassa, K., Fukuoka, H., Wang, F., Wang, G. (Eds), Landslides, Chapter 37, Springer, Berlin, Heidelberg.

Miyagi, T., 2021. Landslide Recognition and Mapping for Slope Disaster Risk Reduction and Management, in: Guzzetti, F., Mihalić Arbanas, S., Reichenbach, P., Sassa, K., Bobrowsky, P.T., Takara, K. (Eds.), Understanding and Reducing Landslide Disaster Risk. WLF 2020. ICL Contribution to Landslide Disaster Risk Reduction. Springer, Cham, pp. 9-31.

Papathanassiou, G., Valkaniotis, S., Ganas, A. 2021. Spatial patterns, controlling factors, and characteristics of landslides triggered by strike-slip faulting earthquakes: case study of Lefkada island, Greece. Bull. Eng. Geol. Environ., 80, pp. 3747–3765.

Pyrgiotis, L., 1997. Engineering geological conditions in Karditsa County. Landslide phenomena in flysch formations. Ph D Thesis, University of Patras, Patra Greece, 334p (in Greek, with extensive summary in English).

Sabatakakis, N., Koukis, G., Vassiliades, E., Lainas, S., 2013. Landslide susceptibility zonation in Greece. Nat. Hazards., 65, pp. 523–543.

Soeters, R., van Westen, C.J., 1996. Slope instability recognition, analysis, and zonation, in: Turner, A.K., Schuster, R.L. (Eds.), Landslides - Investigation and mitigation, Transportation Research Board Special Report 247, National Research Council, Washington, D.C., pp. 129–177.

Tsangaratos, P., 2012. Research on the engineering geological behaviour of the geological formations by the use of Information Systems. Phd Thesis, National Technical University of Athens, Athens, Greece, 363 p. (In Greek).

Yagi, H., Hayashi, K., Sato, G., 2021. Landslide Susceptibility Mapping by Interpretation of Aerial Photographs, AHP and Precise DEM, in: Guzzetti, F., Mihalić Arbanas, S., Reichenbach, P., Sassa, K., Bobrowsky, P.T., Takara, K. (Eds.), Understanding and Reducing Landslide Disaster Risk. WLF 2020. ICL Contribution to Landslide Disaster Risk Reduction. Springer, Cham, pp. 33-56.

16th INTERNATIONAL CONGRESS of the
GEOLOGICAL SOCIETY OF GREECE

S8. New perspectives for the monitoring and early detection of Geohazards

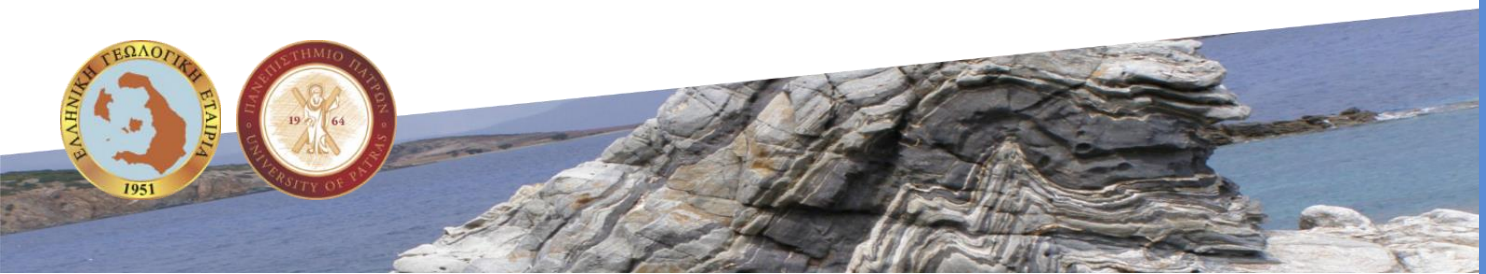

OUR EARTH, OUR HOME

16th International Congress of the Geological Society of Greece
17-19 October, 2022 - Patras, Greece
Bulletin of the Geological Society of Greece, Sp. Publ. 10
Ext. Abs. GSG2022-054

Ground Subsidence Phenomena Caused by the Overexploitation of the Aquifers in Arid Climate Regions. The Case of the Remah Area, Al Ain Region, UAE

M. El Kamali[1], I. Papoutsis[2], C. Loupasakis[3], A. Abuelgasima[1], Ch. Kontoes[2]

(1) United Arab Emirates University, Al Ain, UAE, 201890072@uaeu.ac.ae (2) National Observatory of Athens, BEYOND Center for EO Research and Satellite RS, Athens, Greece (3) National Technical University of Athens, Athens, Greece.

Research Highlights

The current study aims at investigating the deformations occurring at the Remah area, Al Ain region, UAE. Sentinel-1 data, provided by the European Space Agency (ESA), as well as Water level data, provided by the Environment Agency of Abu Dhabi (EAD), were used to guide the ground truth surveys, and determine zones affected by groundwater overexploitation.

Introduction

Applications of the InSAR technique for surface deformations in the UAE are limited due to the wide coverage of the sand dunes (more than 70% of the country) where the SAR signal experiences temporal decorrelation and there is a significant drop in interferometric coherence (Muhagir et al, 2020). The current study aims at investigating the deformations occurring at the wider Al Ain region due to the overexploitation of the aquifers by combining SAR satellite data, with ground water level measurements and ground truth surveys for the verification of the deformations. Despite the difficulties, the current study succeeded to identify a significant subsidence in the Remah and Al Wagan areas, of the wider Ai Ain region (Muhagir et al, 2021).

Al Ain region is located at the eastern part of Abu Dhabi Emirate, UAE at the border with Sultanate Oman. It is characterised by arid climate with scarce rainfall in winter and high annual evapotranspiration. The region is geomorphologically consists of Jabal Hafit and Oman mountains, a gravel plain at the western side of Oman Mountains known as Al Jaww Plain, and large Sand Dunes. Groundwater aquifers in the UAE can be classified into limestone aquifers, ophiolite aquifers, gravel aquifers, and sand dune aquifers (Elmahdy & Mohamed, 2015). Groundwater system of the Al Ain region is composed of the last two aquifers with dominant of the sand dune aquifers. This region occupies 50% of the Abu Dhabi Emirate agricultural activities consumes huge amount of groundwater with annual discharge more than 200 million m^3.

Methods

Sentinel-1 data, provided by the European Space Agency (ESA), were used to process the SAR interferometry over the study area. The dataset used consists of 37 Sentinel-1A Single Look Complex (SLC) images acquired along the ascending orbit from path 130 and frames 73 and 75, for a time span between February 2015 and May 2019. The image acquired on 22 October 2017 was selected as a primary, or master, image to increase the expected coherence due to it is minimum spatial and temporal baselines. The InSAR analysis identified an extensive land surface subsidence with a rate of 40 mm/year in the period between 2015 and 2019 (Figure 1).

Water level data were provided by the Environment Agency of Abu Dhabi (EAD), and they were used to determine zones affected by groundwater overexploitation. The water level dataset indicated an extensive cone of depression covering the area under investigation from 2013 to 2019 (Figure 1). The extended network of irrigation wells has systematically affected the unconfined sand dune aquifers unit and resulted in lowering the groundwater level with a maximum drawdown at its centre of approximately 40 to 50 m. As expected, at the perimeter of the cone, the ground water lowering gradually decreases in relation to the distance from the centre of the cone. The great discharge from the aquifer, more than 240 million m^3, along with a very low hydraulic conductivity of the aquifer and the low precipitation rates resulted in a low annual groundwater recharge.

Land surfaced subsidence evidence were identified in the field, confirming the deformations identified by the SAR interferometry product. The deformations evidence can be summarized as follow; leaning of some fracture walls caused by the differential settlements of their foundations, well casings experienced protrusion due to the land surface subsidence, and dislocated electrical pillars with the wires tensioned due to the differential surface movements (Figure 2).

Results and Conclusions

The ground water table depression cone for the water level drawdown in the study area was found in spatial correlation with the detected land surface subsidence bowl (Figure 1). So, it can be concluded that the land surface subsidence was triggered by the groundwater over extraction.

It was proved that the repeat-pass satellite SAR interferometry can provided substantial information about the actual extent of the land subsidence phenomenon. Space-based technologies are cost effective, providing high spatial coverage. So, they can fill the data and knowledge gaps and reduce the uncertainties by providing high spatial and temporal valuable information about the extend and the progress of the subsidence.

Finally, it should be noted that the detection of the phenomenon at an initial stage is extremely important, as further expansion of the affected area and damages on settlements and infrastructure can be prevented. The information provided by these studies can give rise to focused geotechnical and hydrogeological studies aiming to mitigate phenomenon.

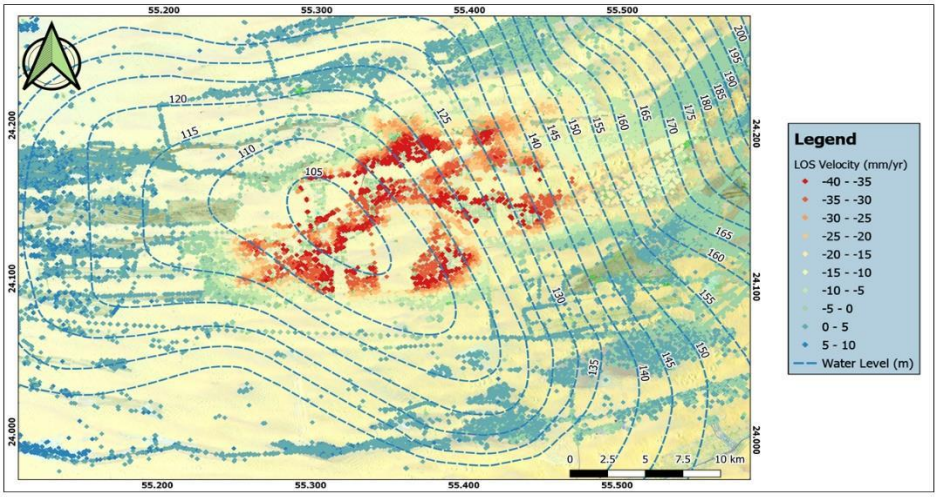

Figure 1: The ground water table contour lines of 2019 overlapped to the distribution of the deformations along the LOS.

Figure 2: Deformations and the failures, proofs of the land subsidence. Dislocated Electrical pillars with their wires tensioned, deferential settlements affecting buildings and protruding well casings, identified during the field observation

Acknowledgements

This work was supported by a grant from the United Arab Emirates University (UAEU) National Center for Water and Energy under grant number 31R155-Research Center-NWC-3-2017.

References

Elmahdy, S.I., Mohamed, M.M., 2015. Groundwater of Abu Dhabi Emirate: a regional assessment by means of remote sensing and geographic information system. Arabian Journal of Geosciences. 8, 11279-11292. https://doi.org/10.1007/s12517-015-1932-2.

Muhagir, K., Abuelgasim, A., Papoutsis, I., Loupasakis, C., Kontoes, Ch., 2020, A reasoned bibliography on SAR interferometry applications and outlook on big interferometric data processing. Remote Sensing Applications: Society and Environment 19, 100358, https://doi.org/10.1016/j.rsase.2020.100358.

Muhagir, K., Papoutsis, I., Loupasakis, C., Abuelgasim, A., Omari, K., Kontoes, Ch., 2021, Monitoring of land surface subsidence using persistent scatterer interferometry techniques and ground truth data in arid and semi-arid regions, the case of Remah, UAE. Science of The Total Environment 776, 145946, https://doi.org/10.1016/j.scitotenv.2021.145946

16th International Congress of the Geological Society of Greece
17-19 October, 2022 - Patras, Greece
Bulletin of the Geological Society of Greece, Sp. Publ. 10
Ext. Abs. GSG2022-060

Persistent Scatterer Interferometry (PSI) analysis for Landslide Detection and Mapping. The case of Chania Prefecture, Crete Island, Greece.

C. Nefros[1], S. Alatza[1,2], C. Loupasakis[1], Ch. Kontoes[2]

(1) School of Mining and Metallurgical Engineering, National Technical University of Athens, Athens, Greece, kostasnefros@central.ntua.gr (2) Institute for Astronomy, Astrophysics, Space Applications and Remote Sensing, Center for Earth Observation Research and Satellite Remote Sensing BEYOND, National Observatory of Athens, Athens, Greece

Highlights

This study aims to present the potentiality of the Persistent Scatterer Interferometry (PSI) technique, to identify and map landslides, which can be subsequently used to form a complete landslides inventory.

Introduction

Landslides consist nowadays one of the most critical geological hazards around the world (Kirschbaum et al. 2015). The landslides susceptibility assessment of an area, which is used by scientists to identify the relative causes and to reduce their impact, usually requires the existence of a complete landslides inventory database of that area. The formation of such an inventory in Greece can be a rather difficult process, since an official national inventory does not exist, and many regional inventories are mostly based on in situ observations and technical reports, which are not always publicly available (Nefros and Loupasakis 2022). Moreover, some of these regional inventories may be spatially biased, as they mostly contain landslides occurred in a short distance from populated areas or critical infrastructures, such as roads, railways, and bridges (Stanley and Kirschbaum 2017) and contain a small number or no landslides from regions, which are difficult to reach. This can result to distortions on the relevant susceptibility assessment of the whole area. Persistent Scatterer Interferometry (PSI) is a remote sensing technique, which can be used, to identify and effectively map landslides, occurred over a long time period and in difficult to reach areas (Casagli et al. 2016, Aslan et al. 2020). During this study, a timeseries analysis of Sentinel-1 images, from 2016 to 2020, has been used along with a pre-existing landslides inventory, to identify and map more than 30 new landslides in Chania Prefecture, Greece. Subsequently, the new landslides were integrated into the inventory and the updated inventory has been used for the evaluation of the landslide susceptibility assessment of that area.

Methods – Data

The last decade, several satellite-based Interferometric Synthetic Aperture Radar (InSAR) techniques served as a valuable tool in the field of landslides' detection and mapping (Casagli et al. 2016, Kontoes et al. 2021). Persistent Scatterer Interferometry (PSI) is a remote sensing technique that exploits the ability of ground targets (so called Permanent Scatterers-PS) to strongly reflect the radar signal, providing through phase history, useful information about surface deformation over time. PS can be manmade structures (e.g., buildings, roads) or natural reflectors (e.g., outcropping rocks) (Kaitantzian and Loupasakis 2016). During this research, the PSI technique was applied in Chania prefecture, Crete Island, Greece, an area with an extend of more than 2.000 km^2, as a case study, to highlight the potentiality of this method to reveal even slow-moving landslides, in difficult to reach areas and therefore to help forming a complete landslides inventory. Chania prefecture has a complicated landscape, including Lefka Ori mountain (2.400m), creating a network of rather dense plateaus and gorges, which in many cases are difficult accessed. The geology of the region mainly consists of Quaternary deposits (north), Neogene sediments (north-east), Tripolis Carbonates (north-east peninsula), Phylites-Quartzites (west, south-west), Trypalion Carbonates (central and peninsulas), Plattenkalk Limestones (south), Pindos Carbonates (west) and Flysch formations (east and south-east). The increased fragmentation of the geological formations, the intense relative relief, the dense drainage network in combination with the intense human activity (e.g., dense road network) render the study area rather vulnerable to landslides.

In this direction a multitemporal time-series analysis was performed using the parallelized PSI (P-PSI) processing chain (Papoutsis et al. 2020), developed in the Center for EO Research and Satellite Remote Sensing BEYOND of National Observatory of Athens (NOA). Sentinel-1 Single Look Complex (SLC) satellite images, were processed, covering a time span of 4 years from 2016 to 2020. Table 1 contains the basic information of the data used for that purpose.

A region in the suburbs of Chania city was selected as the reference area for all stacks. This selection was made because it is an urban area that is not characterized by intense relief and therefore is relatively stable. The reference images for the PS analysis of both ascending and descending satellite passes, presented in Table 1, were selected with the objective to achieve the minimum temporal and perpendicular baselines in the interferometric stack. As part of the P-PSI processing chain, ISCE (InSAR Scientific Computing Environment) is employed for the creation of the stack and the Stanford Method for Persistent Scatterers (StaMPS) (Hooper et al 2007) for multi-temporal SAR interferometry. Finally, TRAIN (Toolbox for Reducing Atmospheric InSAR Noise) (Bekaert et al 2015), was used to reduce the impact of the atmosphere.

Table 1: Summary of the Sentinel-1 products used in the InSAR analysis.

Path	Frame	Orbit	Time Period	SlC Stack reference	Availiable Interferograms	No. PS scatterers
102	113	Ascending	19/09/2016-27/12/2020	21/10/2018	98	291.234
109	473	Descending	08/10/2016-22/12/2020	13/04/2018	90	382.017

Results

The followed process leaded to the identification of more than 290.000 PS for both ascending and descending satellite passes and the estimation of the line of sight (LOS) velocities (Figure 1). SAR data combined with optical, geological, topographical and land use data, were used to identify and spot landslide activity. Thus, more than 30 new landslides were identified in the area of interest. This technique was rather efficient for the identification of slow-moving landslides, but it failed to recognize landslides over agricultural regions due to the resolution of Sentinel-1 data and the incoherent ability of this PSI technique to identify enough PS to these regions.

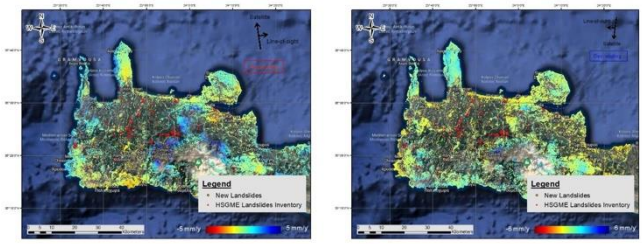

Figure 1: LOS displacements for the ascending (left) and descending (right) satellite pass. The landslides from the HSGME inventory are also presented.

Conclusions

Concluding, the Persistent Scatterer Interferometry (PSI) technique provides a significant advantage in identifying and mapping new landslides, especially over difficult to reach areas, where conventional methods usually fail or are not cost-effective. A complete landslide inventory of an area can subsequently help the researchers to better understand the local hydrological and geological conditions that can activate the landslide mechanism, to effectively evaluate the relative landslide susceptibility and to recommend the necessary precaution measures to the civil protection authorities.

Acknowledgements

Sentinel-1 images were processed with the P-PSI processing chain in the Center for EO Research and Satellite Remote Sensing BEYOND of NOA. Pre-existing landslide inventory was provided by the Hellenic Survey of Geology and Mineral Exploration (HSGME).

References

Aslan G, Foumelis M, Raucoules D, De Michele M, Bernardie S, Cakir Z. 2020. Landslide Mapping and Monitoring Using Persistent Scatterer Interferometry (PSI) Technique in the French Alps. Remote Sensing. 12(8):1305. https://doi.org/10.3390/rs12081305.

Bekaert, D.P.S., Walters, R.J., Wright, T.J., Hooper, A.J., Parker, D.J. 2015. Statistical comparison of InSAR tropospheric correction techniques. Remote Sens. Environ. 2015, 170, 40–47, https://doi.org/10.1016/j.rse.2015.08.035.

Casagli, N., Cigna, F., Bianchini, S., Hölbling, D., Füreder, P., Righini, G., Del Conte, S., Friedl, B., Schneiderbauer, S., Iasio, C., Vlcko, J., Greif, V., Proske, H., Granica, K., Falco, S., Lozzi, S., Mora, O., Arnaud, A., Novali, F., Bianchi, M. 2016. Landslide mapping and monitoring by using radar and optical remote sensing: Examples from the EC-FP7 project SAFER, Remote Sensing Applications: Society and Environment,Vol. 4, 2016, pp 92-108, ISSN 2352-9385, https://doi.org/10.1016/j.rsase.2016.07.001.

Hooper, A., Segall, P., Zebker, H. 2007. Persistent Scatterer InSAR for Crustal Deformation Analysis, with Application to Volcán Alcedo, Galápagos. J. Geophys. Res. 2007, 112, B07407, https://doi.org/10.1029/2006JB004763.

Kaitantzian, A., and Loupasakis, C. 2016. Preliminary Investigation of the Land Subsidence Phenomena Occurring at the Industrial-Commercial Area of Eleonas, Athens, Greece.Bulletin of the Geological Society of Greece,50(3), 1703–1710. https://doi.org/10.12681/bgsg.14311.

Kirschbaum, D., Stanley, T., and Zhou, Y. 2015. Spatial and temporal analysis of a global landslide catalog. Geomorphology, 249, p.4-15. https://doi.org/10.1016/j.geomorph.2015.03.016.

Kontoes C, Loupasakis C, Papoutsis I, Alatza S, Poyiadji E, Ganas A, Psychogyiou C, Kaskara M, Antoniadi S, Spanou N. 2021. Landslide Susceptibility Mapping of Central and Western Greece, Combining NGI and WoE Methods, with Remote Sensing and Ground Truth Data. Land. 10(4):402. https://doi.org/10.3390/land10040402.

Nefros, C., and Loupasakis, C. 2022. Introducing a geospatial database and GIS techniques as a decision-making tool for multicriteria decision analysis methods in landslides susceptibility assessment. Bulletin of the Geological Society of Greece, 59(1), 68–103. https://doi.org/10.12681/bgsg.29038.

Papoutsis, I.; Kontoes, C.; Alatza, S.; Apostolakis, A.; Loupasakis, C. 2020. InSAR Greece with Parallelized Persistent Scatterer Interferometry: A National Ground Motion Service for Big Copernicus Sentinel-1 Data. Remote Sens., 12, 3207. https://doi.org/10.3390/rs12193207.

Stanley, T., & Kirschbaum, D.B. 2017. Effects of Inventory Bias on Landslide Susceptibility Calculations. In Proceedings of the 3rd North American Symposium on Landslides, Roanoke, VA, USA, 4–8 June 2017.

16th International Congress of the Geological Society of Greece

17-19 October, 2022 - Patras, Greece

Bulletin of the Geological Society of Greece, Sp. Publ. 10

Ext. Abs. GSG2022-104

Temperature and Conductivity as Indicators of the Activity of a Submarine Volcano: The case of Santorini, Greece

A. Dura[1], T.J. Mertzimekis[2], P. Nomikou[1], M.D. Hannington[3], S. Petersen[3]

(1) Department of Geology and Geoenvironment, National Kapodistrian University of Athens, Zografou Campus, 15784, Athens, Greece, andura@geol.uoa.gr (2) Department of Physics, National Kapodistrian University of Athens, Zografou Campus, 15784, Athens, Greece (3) GEOMAR - Helmholtz Center for Ocean Research Kiel, 24148 Kiel, Germany

In 2017, GEOMAR, in collaboration with the National and Kapodistrian University of Athens, used an Autonomous Underwater Vehicle (AUV) to investigate the evolution of the NE–trending Santorini–Kolumbo line, where it also collected CTD data (Conductivity, Temperature, Depth). The POS510 mission lasted 25 days, 19 of which were onboard operations.

A low-temperature hydrothermal vent field (18−20°C) exists in the NE part of the northern basin, which extends over 200-300 m^2, with several hundred bacterial mounds up to 2 m high and several meters in diameter. Slightly north of this location, unusual CO_2-rich fluid pools have been discovered at the base of the caldera wall and shallower depths of 200−250 m, with temperatures ~5°C above that of the bottom waters (Camilli et al., 2015).

Previously, the Generalized Moments Method (GMM) (Lovejoy et al., 1995; Barunik et al., 2010) has been applied in two cases to study the underlying mechanisms driving CTD time series: (a) over a very active submarine hydrothermal vent field (Kolumbo, Santorini) (Bakalis et al., 2017), and (b) over a less active area (Nisyros caldera) (Bakalis et al., 2018; Dura et al., 2021). Details of the method are presented in those references, where the reported results have also established the validity of the novel approach. In this work, our focus is on the high-frequency recorded CTD data in the water column over the hydrothermal vents in the Santorini caldera and around the island.

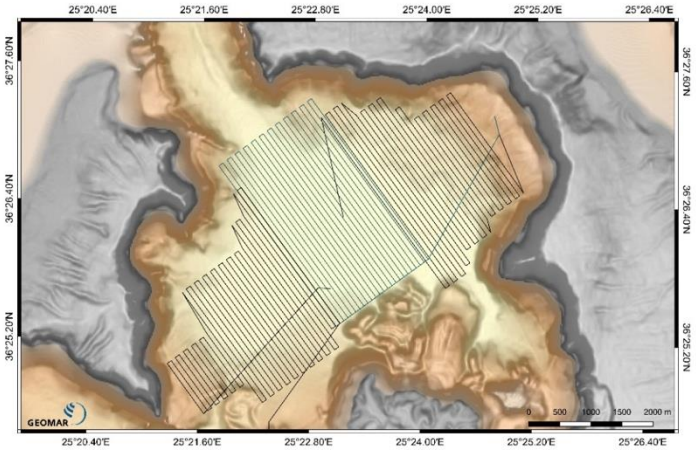

Figure 1. The North Basin of the Santorini caldera surveyed using an AUV during the POS510 mission (Nomikou et al., 2014; Hannington, M., et al., 2017).

Times series were constructed for both conductivity and temperature in the case of Santorini. Here we present the results from a half-hour sample from the survey conducted on March 11, 2017, in the NE part of the caldera after the GMM was applied. The similarity in behavior across parameters is evident with spikes appearing at the same points in time and space, in the time series and the depth profiles, respectively. Moments for temperature and conductivity are illustrated in Figure 2. For both conductivity and temperature, all the moments showed the existence of two distinct regimes with a turning point at $\Delta = 6$ s. For lag times greater than $\Delta = 6$ s, all moments are almost parallel to the time axis. This indicates that the parameters of the hydrothermal fluid equilibrate with the parameters of the surrounding water. The moments of conductivity and temperature were fitted according to the GMM for $\Delta > 6$ s and the obtained exponents were used to find the form of the structure-function, z(q), as illustrated in Figure 3. The changes in the mean-field appear to be best described by the Cauchy-Lorentz distribution.

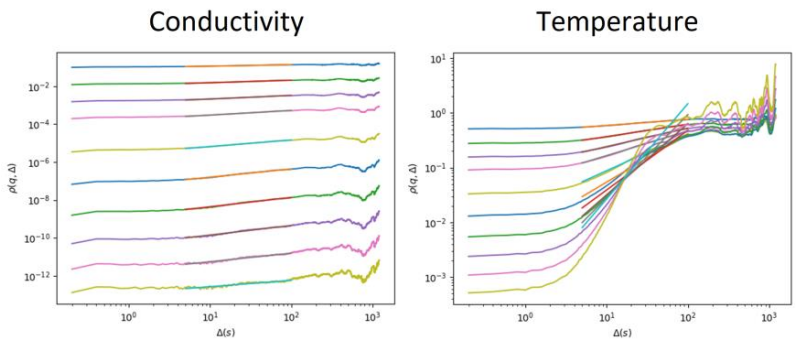

Figure 2. Conductivity and temperature moments scaling according to the 11-3-2017 survey in the North Basin of Santorini.

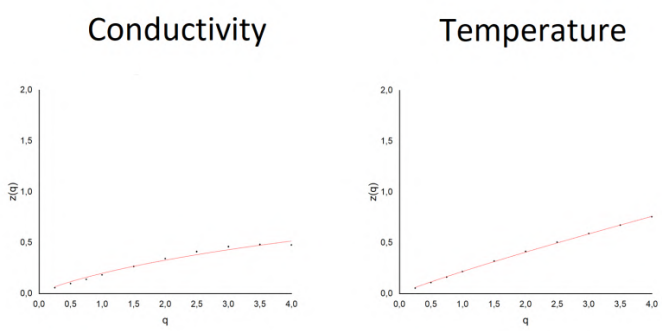

Figure 3. Conductivity and temperature structure function vs the q-moment on the 11-3-2017 survey in the North Basin of Santorini.

As the present results are the first ones produced from this expedition, they provide strong motivation for further investigation. These steps are crucial towards developing a supervised machine–learning algorithm able to provide a reliable description of the dynamic conditions over the hydrothermal vent field in near real-time fashion and potentially provide the means to predict explosive conditions. The impact of developing appropriate mechanisms and policies to avoid the associated natural hazard is expected to be significant.

Acknowledgements

The implementation of the doctoral thesis was co-financed by Greece and the European Union (European Social Fund-ESF) through the Operational Programme «Human Resources Development, Education and Lifelong Learning» in the context of the Act "Enhancing Human Resources Research Potential by undertaking a Doctoral Research" Sub-action 2: IKY Scholarship Programme for PhD candidates in the Greek Universities.

References

Bakalis, E., Mertzimekis, T.J., Nomikou, P., and Zerbetto, F., 2017. Breathing modes of Kolumbo submarine volcano (Santorini, Greece), Sci. Rep. 7, 46516.

Bakalis, E., Mertzimekis, T.J., Nomikou, P., and Zerbetto, F., 2018. Temperature and Conductivity as Indicators of the Morphology and Activity of a Submarine Volcano: Avyssos (Nisyros) in the South Aegean Sea, Greece, Geosciences 8, 193.

Barunik, J., Kristoufek, L., 2010. On Hurst exponent estimation under heavy-tailed distributions. Physica A, 389, 3844–3855

Camilli R, Nomikou P, Escartín J, Ridao P, Mallios A, Kilias SP, Argyraki A and the Caldera Science Team (2015) The KallistiLimnes, Carbon Dioxide-Accumulating Subsea Pools. Scientific Reports 3:2421.

Dura, A., Mertzimekis, T.J., Nomikou, P., Gondikas, A., Gomez Miguez M.M., Bakalis, E., Zerbetto, F., 2021. The hydrothermal vent field at the eastern edge of the Hellenic Volcanic Arc: the Avyssos caldera (Nisyros). Geosciences 2021, 11, 290. https://doi.org/10.3390/geosciences11070290

Hannington, M., 2017. Rifting and Hydrothermal Activity in the Cyclades Back-arc Basin: Cruise Report of RV Poseidon, POS510, Catania-Heraklion 06.03.17-29.03.17, 361 p.

Lovejoy, S., Schertzer, D., 1995. Multifractals and rain. In New Uncertainty Concepts in Hydrology and Water Resources. Cambridge University Press, p. 61–103.

Nomikou, P., Parks, M.M., Papanikolaou, D., Pyle, D.M., Mather, T.A. , Carey, S., Watts, A.B., Paulatto, M. , Kalnins, M.L. Livanos, I., Bejelou, K., Simou, E., Perros, I., 2014. The emergence and growth of a submarine volcano: The Kameni islands, Santorini (Greece). GeoResJ 1–2:8–18.

16th International Congress of the Geological Society of Greece
17-19 October, 2022 - Patras, Greece
Bulletin of the Geological Society of Greece, Sp. Publ. 10
Ext. Abs. GSG2022-115

Innovative tools to support hazard, exposure and risk-assessment against geohazards

E. Poyiadji[1], L. Solari[2], R.M. Mateos[3], O. Monserat[2], A. Barra[2]

(1) Hellenic Survey of Geology and Mineral Exploration (HSGME), Athens, Greece, first_author_kynpo@igme.gr (2) Centre Tecnològic de Telecomunicacions de Catalunya (CTTC/CERCA), Geomatics Division, Castelldefels, Spain, (lsolari, omonserrat)@cttc.cat (3) National Centre- Geological an Mining Institute from the National Research Council (IGME). Department of Natural Hazards and Climate Change. Granada (Spain), rm.mateos@igme.es .

Abstract

This paper focuses on the tools that have been developed and still are being improved, through a series of European projects, aiming to support hazard, exposure and risk-assessment against geohazards. This is done by mapping and monitoring the deformation activity using Sentinel-1 (S-1) data and the DInSAR (Differential Interferometric Synthetic Aperture Radar) technique and recently, after the release of the European Ground Motion Service EGMS, adapting them to the volume, format and specifications of the service.

Introduction

The use of satellite interferometry (InSAR) for the detection and monitoring of geohazards is growing exponentially. It is a methodology that allows the processing of large areas and the extraction of a high number of differential movements at short time intervals. This leads to a huge volume of data and derived products that are not easily understood by people dealing with the management of geohazards. A set of tools and methodologies developed and still being improved through a series of European projects comes to fill this gap; These are, (i) the ADA tool (Active Deformation Areas) used to semi-automatic extraction of areas with active displacements, (ii) the ADAClassifier tool, a semi-automatic tool, which aims to classify the type of phenomena behind the detected movements, and (iii) ADA-Impact tools that utilizes the outputs of the other two TOOLS to evaluate the potential impact of the detected ground instabilities.

ADA tool

ADA tool and the methodology behind it have been developed in the framework of projects that were carried out in the framework of DGECHO (Safety and U-Geohaz) and will be further exploited by the ongoing project RASTOOL. The procedure to extract the ADA areas can be summarized in three main steps (Figure 1): (i) filtering of the RDM; (ii) automatic extraction of the more reliable and relevant active areas (ADA); and (iii) Quality Index (QI) attribution to each ADA (Barra et al. 2017).

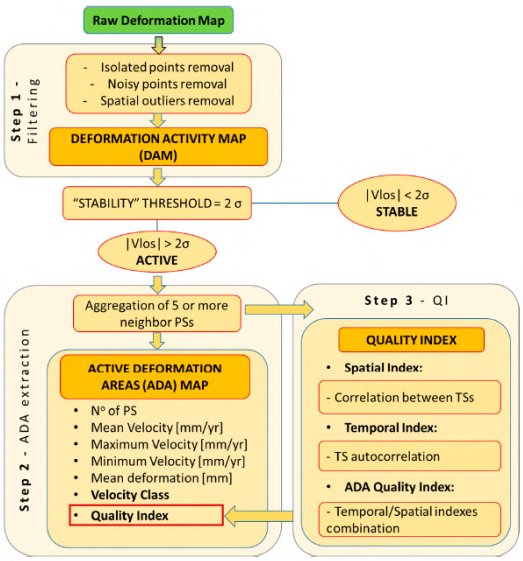

Figure 1. Flowchart of the Deformation Activity Map (DAM) and the Active Deformation Areas (ADA) maps generation (Barra et al. 2017).

The outputs of the methodology are the Deformation Activity Map (DAM), in terms of velocity map and deformation time series, and the Active Deformation Areas (ADA) map. The last one is the main product that can be exploited any not radar-expert final user, for example the Civil Protection Authorities in the risk management.

ADAClassifier tool

ADAClassifier aims to identify the kind of geological or anthropogenic process motivating the presence of ADA. Up to four different kinds of deformation phenomena are detected (Navarro et al. 2020); landslides, sinkholes, land subsidence, and constructive settlements. In the following a brief description of the ADAClassifier methodology (Navarro et al. 2019):

- **Inputs**: (1) the ADAs output by ADAfinder in ESRI shapefile format and (2) a set of thresholds controlling the classification process; optionally (3) a Digital Terrain Model (DTM), (4) landslides, sinkholes, land subsidences, infrastructures and geologic inventories (ESRI polygons) and (5) a map measuring the horizontal displacements of the PSs. When one or more optional files are absent not all the classification processes will be executed.
- **Procedure**: there are four different procedures, each one targeted at classifying the ADAs as one of the four different phenomena being tracked.
- **Output:** An ESRI file, which is a copy of the input one including four extra flags stating whether the ADA may correspond or not to any of the four deformation processes investigated.

The results from the testing of this tool to a pilot in Southeastern Italy (Navarro et al. 2020) revealed that the ADA of the area are classified as: (1) landslides (42.7%) and potential landslides (15.2%); (2) potential land subsidence (24.6%); and (3) consolidation settlement (8.8%). No potential sinkholes were identified (Figure 2).

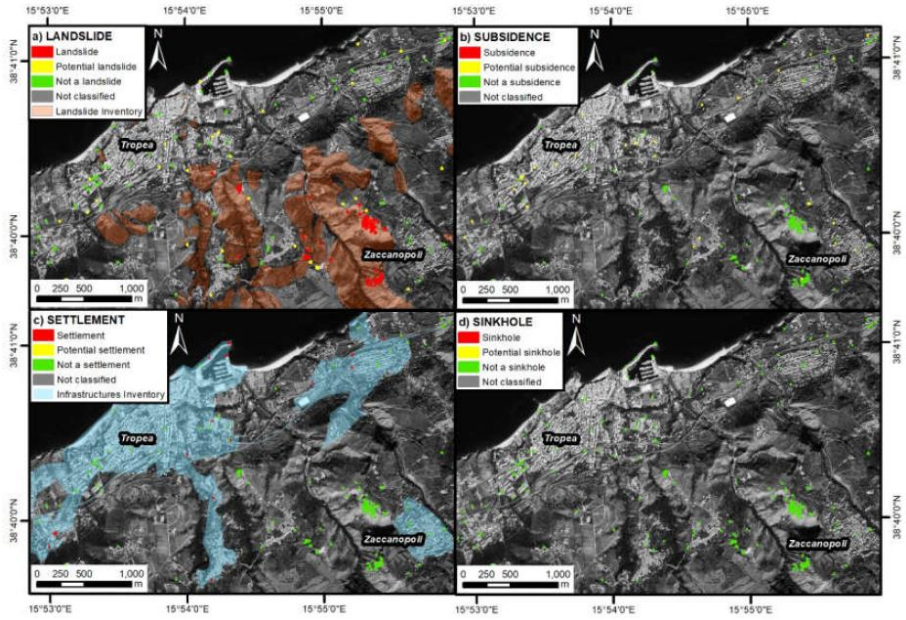

Figure 2. Classification of active deformation areas (ADA) in the study area of Tropea-Zaccanopoli, Southeastern Italy, as: a) landslides; b) subsidence; c) consolidation settlements; and d) sinkholes. (Navarro et al. 2020).

ADA-Impact tools

ADA Impact Tools are being developed in the framework of RASTOOL project (EGMS RASTOOL) with three specific objectives: (i) to identify and classify the exposed elements including critical infrastructures, (ii) to assess vulnerability of the exposed elements (for people and assets) and (iii) to provide a tool to analyse risk by crossing active hazards and vulnerability of exposed elements.

Acknowledgements

This work has been co-funded by the European Union Civil Protection through the H2020 project RASTOOL (UCPM-2021-PP - 101048474).

References

Barra, A., Solari, L., Béjar-Pizarro, M., Monserrat, O., Bianchini, S., Herrera, G., Crosetto, M., Sarro, R., González-Alonso, E., Mateos, R.M., Ligüerzana, S., López, C., Moretti, S. A Methodology to Detect and Update Active Deformation Areas Based on Sentinel-1 SAR Images. Remote Sens. 2017, 9, 1002. https://doi.org/10.3390/rs9101002 **[Journal Article]**

Navarro, J.A.; Cuevas, M.; Tomás, R.; Barra, A.; Crosetto, M. Automating the Detection and Classification of Active Deformation Areas—A Sentinel-Based Toolset. Proceedings 2019, 19, 15. https://doi.org/10.3390/proceedings2019019015 **(proceedings)**

Navarro, J.A.; Tomás, R.; Barra, A.; Pagán, J.I.; Reyes-Carmona, C.; Solari, L.; Vinielles, J.L.; Falco, S.; Crosetto, M. ADAtools: Automatic Detection and Classification of Active Deformation Areas from PSI Displacement Maps. ISPRS Int. J. Geo-Inf. 2020, 9, 584. https://doi.org/10.3390/ijgi9100584 **[Journal Article]**

EGMS RASTOOL: European ground motion risk assessment tool – RASTOOL, Project number: 101048474, UCPM Project Grants, European Commission-EU

16th International Congress of the Geological Society of Greece
17-19 October, 2022 - Patras, Greece
Bulletin of the Geological Society of Greece, Sp. Publ. 10
Ext. Abs. GSG2022-156

UAV-Based Rockfall Hazard Assessment in the Cultural Heritage Area of Kipinas Monastery, Greece.

I. Konstantinidis[1], V. Marinos[2], G. Papathanassiou[1]

(1) Laboratory of Engineering Geology & Hydrogeology, School of Geology, Aristotle University of Thessaloniki, Thessaloniki, Greece, makiskonstantinidis97@gmail.com (2) Geotechnical Division, School of Civil Engineering, National Technical University of Athens, Athens, Greece.

A semi-quantitative rockfall hazard and risk assessment was performed through the proposition and the implementation of a new Rockfall Hazard and Risk Rating System.

Background

Rockfall events consist one of the most hazardous geological phenomena in mountainous landscapes, with the potential to turn catastrophic if they occur near an anthropogenic environment. Rockfall hazard and risk analyses are inherently some of the most elaborate and challenging assessments among the geo–engineering society (Manconi *et al.,* 2016). The difficulties and the complexity of them derived from the lack of accurate data (spatial– and temporal–based), site–specific rockfall's properties, limited capabilities in the quantification and the visual interpretation of rockfall's spatial distribution and the heterogeneity of vulnerability of various elements at risk (Michoud *et al.,* 2012).

Most of the above deterring factors, during the last decade have been eased and, in many cases, surpassed by the introduction of innovative remote sensing technologies, such as Unmanned Aerial Vehicles (UAVs), as a common practice in hazard and risk assessments. The compound of them with traditional engineering geological field surveys can lead to an accurate, precise and time–effective local scale modelling of the rockfall events.

This study focuses on the cultural heritage area of Kipinas Monastery in Epirus, Greece. The site is situated into high and very steep slopes of limestone. From an engineering geological point of view, the limestone rock mass is moderately jointed, intersected by numerous major vertical fractures, which ultimately form the local face of the cliff. The limestone is karstified and voids of large dimensions are formed, undermining the rock slope. In the past years, various rockfall events occurred on the wider site area, with fallen blocks identified near the road that leads to the monastery. The impact of rockfall events generally on cultural heritage areas in the Greek territory is significant since most of the landscapes are mountainous and the sites are usually found near or on top of steep rock slopes. Adding up the significant tourist activity in such locations, the risk can be significantly increased.

Objectives

This study primarily aims to take advantage of the UAV's capabilities and perform an in–depth qualitative rockfall hazard analysis and a preliminary approach of risk analysis, based on a UAV derived dataset of the area. To achieve this goal, a new semi-quantitative rockfall hazard and risk rating system was constructed, via the modification of some preexisting systems, based on morphological and structural information of the rock mass derived from the analysis of the 3D point cloud. The factors of vulnerability and commercial impact were also considered for the risk estimation.

Methods

Initially, traditional field survey methods have been applied at the lower accessible part of the rock face, aiming to define the geometrical characteristics of the joints. According to the findings of the engineering geological field survey, two (2) main orientations were detected for the slope's face, due to its constant dip direction alternations, alongside the investigated area. Additionally, mainly three (3) major discontinuity sets and the bedding were identified. The three major discontinuity sets are characterized as very steep in general (dip angle≥80°) and two of them are transversal to the slope plane; thus, they form the rock slope face in most places. The bedding is presented as very mild up to horizontal in some (dip angle≤15°) sub-regions of the slope. Studying the engineering geological conditions that control the investigated slope, the face of the slope is generally characterized by relaxation of the rock mass, due to its high inclination. In conjunction with the spacing and the distance of discontinuities, moderate-to-large prone blocks are formatted. The main reason that these instabilities are not widespread across the slope is the superior engineering properties of the rock material, which restrain the prone-to-failure blocks, causing a temporal stability on the slope.

Simultaneously, a photogrammetry survey via a manually flown UAV was performed. The utilization of Structure from Motion (SfM) methodology enabled the production of ultra-high-resolution orthomosaic by intersecting the matched features between the overlapping offset images and interpreting them as detailed 3D point clouds. This 3D point cloud model, which consists of about 104 million points was georeferenced using the UAV sensor GPS data and a set of five artificial GCPs, and then segmented into four (4) sub-regions. The structural analysis was performed in each sub-region, in a supervised, automated manner, with the open-source DSE software (Riquelme *et al*., 2015). The result of this analysis was the extraction of the principal discontinuity sets and their main characteristics (dip, dip direction, persistence,

spacing). With all the needed information determined, a kinematic analysis was performed in order to estimate the optimal failure model for each sub-region. Then, a semi-automated procedure was performed in the 3D point cloud in order to monitor and quantify the magnitude (volume, mass) of both the already detached and fallen rock blocks and the prone ones for each sub-region. The final step was the conduction of a rockfall analysis based on trajectometry simulations. This probabilistic analysis was performed via RocFall software v.8 (RocScience Inc.) for four (4) different slope profiles, one for each sub-region, to determine the total kinetic energy of a potential rockfall event at the moment of impact, the velocity of the rock blocks and their "bounce height".

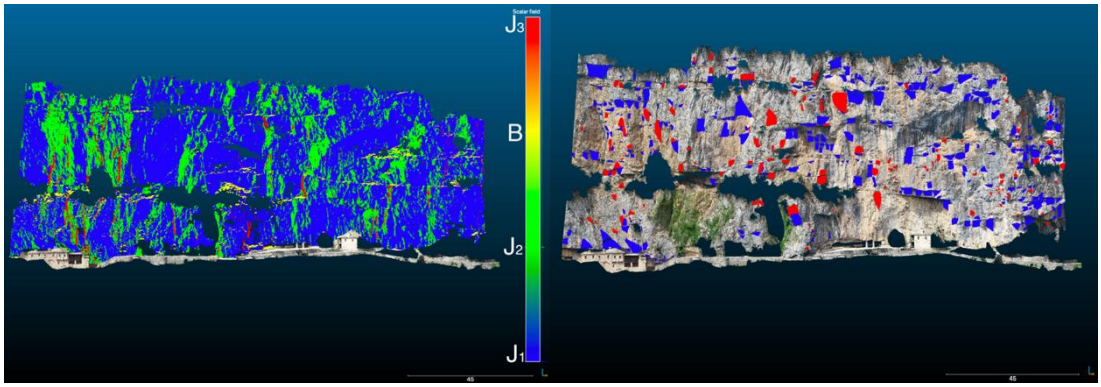

Figure 1. (Left): Allocation of each main discontinuity set on the slope. (Right): Overview of both the identified already failed (blue) and the estimated potentially unstable (red) rock blocks across the slope.

Results

With the implementation of this methodology, all the essential data were obtained in order to provide values to all of the factors of the proposed rockfall hazard and risk rating system. In general, the proposed rating system defines four (4) major parameters categories which consist of a variety of different ranking values, to estimate the total risk level for each sub-region. Three (3) of these categories are related to the hazard level (geometry factors, geoengineering factors and triggering factors) and one (1) to the impact of a potential rockfall event. Every rating factor has a different weight, which is based on the significance of each individual contribution to either the hazard and/or risk level for every sub-region. Each examined factor can be evaluated between 10 and 100, as the conditions evolve from favorable to adverse, and then should multiplied by its respective predetermined weight. The total hazard score is calculated by summing the individual score of each factor, from the first three (A, B and C) major categories. At last, the total risk score is calculated by adding the fourth category (D) to the hazard score.

After extensive application of this rating system to the investigated site, the total scores were categorized, accordingly for hazard and risk estimation, respectively. The final result of the application was a hazard and risk zonation of the cliff against rockfall occurrence.

Conclusions

It was shown that the suggested methodology, with the combination of innovative remote sensing technologies with traditional engineering geological field surveys, can lead to the extraction of all the necessary quantitative data input for the proposed rating system for any natural slope. It is important to highlight that this proposed rating system reflects the result of an initial attempt, and further development and validation by back-analyses is encouraged for the optimum adjustment of the weight for various contained factors. Specifically, its potential application in different areas and rock slopes, where most of the parameters may have a greater range, could help to evaluate the sensitivity of each factor in the final estimation of the hazard and risk level.

In a subsequent step, in order to estimate the outcome of this rockfall hazard and risk assessment and also gain important feedback for the proposed rating system, research should continue to be performed in the cultural heritage area of Kipinas Monastery. Regular monitoring of the slope, ideally per six months or annually, with a UAV is suggested in order to compare the obtained data. Through this multi-temporal change detection procedure between the different datasets, topographical changes between different epochs could be monitored and characterized for robust modelling of rockfall dynamics. Via these outcomes, an immediate evaluation and calibration, if needed, could be performed of the proposed rating system in order be as precise and accurate as possible. This constant evaluation is necessary because the main target of this proposed rockfall hazard and risk rating system is to be considered as the transitional step between qualitative and quantitative assessments.

References

Manconi, A., Giordan, D., 2016. Landslide failure forecast in near–real–time. Nat. Hazards Risk 7, 639-648.

Michoud, C., Derron, M.H., Horton, P., Jaboyedoff, M., Baillifard, F.J., Loye, A., Nicolet, P., Pedrazzini, A., Queyrel, A., 2012. Rockfall hazard and risk assessments along roads at a regional scale: Example in Swiss Alps. Nat. Hazards Earth Syst. Sci. 12, 615-629.

Riquelme, A.J., Abellán, A., Tomàs, R., 2015. Discontinuity spacing analysis in rock masses using 3D point clouds. Eng. Geol. 195, 185-195.

16th International Congress of the Geological Society of Greece
17-19 October, 2022 - Patras, Greece
Bulletin of the Geological Society of Greece, Sp. Publ. 10
Ext. Abs. GSG2022-226

Low-cost monitoring of coastal instabilities via UAV photogrammetry: Lessons learnt from the Red Beach in Santorini island, Greece

V. Marinos[1], E. Karantanellis[2], I. Farmakis[3]

(1) Department of Civil Engineering, National Technical University of Athens, Athens, Greece, marinosv@civil.ntua.gr (2) Department of Earth Science and Environmental Sciences, University of Michigan, Ann Arbor, USA (3) Queen's Geomechanics and Natural Hazards Group, Dept. of Geological Sciences & Engineering, Queen's University, Kingston, ON, Canada

In recent years, the advancements in the geoscience domain have enabled the application of efficient remote sensing tools such as Unmanned Aerial Vehicles (UAVs) to address emergency response in potentially disastrous situations. Consequently, surficial changes monitoring over large areas can be accomplished costly and timely. Structure from Motion (SfM) photogrammetry using UAV-derived images has become an indispensable such tool for the investigation of natural processes due to its flexibility of producing high-resolution three-dimensional digital replicas of steep and inaccessible cliffs (Giordan et al., 2018). This method becomes even more valuable in steep coastal settings like the outstanding Red Beach on the island complex of Santorini, Greece, where it is not possible to provide the required space for the installation of terrestrial instrumentation.

Santorini island complex, as a characteristic volcanic environment in the Aegean Sea, constitutes one of the most unique geological structures worldwide. The island is formed completely from volcanic material of dacitic and andesitic composition formed during the Pre-Minoan eruption era (Druitt T & Francaviglia, 1992). As a result, many regions in the west part of the island set to be prone in landslide and rockfall events. The Red Beach, composed of volcanic scoria cones, exhibits extended instabilities along its cliffs, placing its highly frequented touristic zones at high risk (Marinos et al, 2017).

The landscape of the Red Beach area is very steep, with volcanic slopes generally dipping up to 80º and heights reaching up to 60 m. However, sections exhibit considerably less steep slopes since the rocks have failed and slid in the past, forming an angle of 35o in the lower part of the slopes and angles of 70º – 80º in the upper sections. Negative dips are formed at the toe of a number of slopes due to wave erosion, which undermines the steep sections. The lavas consist of successive flows that can be assimilated into stratification planes. The dips of these ''beds'' are oriented toward the same direction as the inclination of the main slope of the beach where slides and rock falls develop. The main joints that are measured within the volcanic masses of the area are oriented N–S to NE–SW. These measurements are identical with the primary tectonic lineaments of the Santorini volcanic center.

Significant rock falls and slides have occurred in all sections of the beach. The combination of steep slopes, wave action erosion, and low tensile strength of scoria lead to rock mass deconfinement and tension crack formation. Rock toppling due to vertical tension and other joints represents the main failure mechanism along red beach cliffs. Rock toppling is also the principal mechanism along the old volcanic vent, where strong rock blocks, which are separated by joints resulting from the cooling of lava and vertical stress relief joints, are overhanging. Planar sliding represents a secondary failure mode along the top of the red cliff. Relief joints perpendicular to the lava flow favor planar failures, since smaller blocks are consequently formed, while water pressure and erosion are enhanced.

To deeper understand the phenomena occurring at the area, detection, and visualization of the sliding and/or falling masses in 3D space is considered essential support asset to decision-making regarding risk management. To produce such digital data, the current study proposes a low-cost monitoring solution of the active rockfall, and landslide zones based on periodically acquired UAV-derived datasets (2017 to 2022). Indeed, the movement and fall of volcanic rocks along several sections of the Red Beach cliffs were identified through this comparison and considerations of the macroscopic observations. Results in Figure 1, indicate that continuous mass movements are occurring during the year. From the comparison of the point clouds of these different periods (e.g. 2018-2020), we can observe zones that have just failed, delivering a rock fall (blue color in the upper parts of the cliffs) and their accumulation along the beach (red color next to the sea). After some period, this rock fall material next to the sea starts to wash out from wave erosion, and the same zones are depicted now (2020-2021) with blue color (volume loss).

To even more challenge this already challenging application, and investigate the potential of a low-cost application, the authors limited the survey setup down to the simplest possible. In particular, the methodology implemented for the current investigation is based only on the commercial DJI Phantom 4 Pro drone with no ground control points (GCPs) being used. Data acquisition timing variations among the survey campaigns are also present within the dataset. This practice led to the detection of sliding and/or falling masses greater that around 35cm along the displacement vector and maintained the data acquisition and processing time in very low rates. The produced failure reconstructions reveal the exact failure position, moving direction, material behavior in relation to surface changes but also the rate and quantification of the

mass movement in the area of interest. The outcome of the current research aims to highlight the implications of UAV photogrammetry as a means of efficient geotechnical field monitoring in case where accessibility and timing restriction may be implied. Furthermore, this detailed and spatially accurate visualization of the natural processes occurring along the Red Beach can support the communication of the imposed hazard and enhance public awareness.

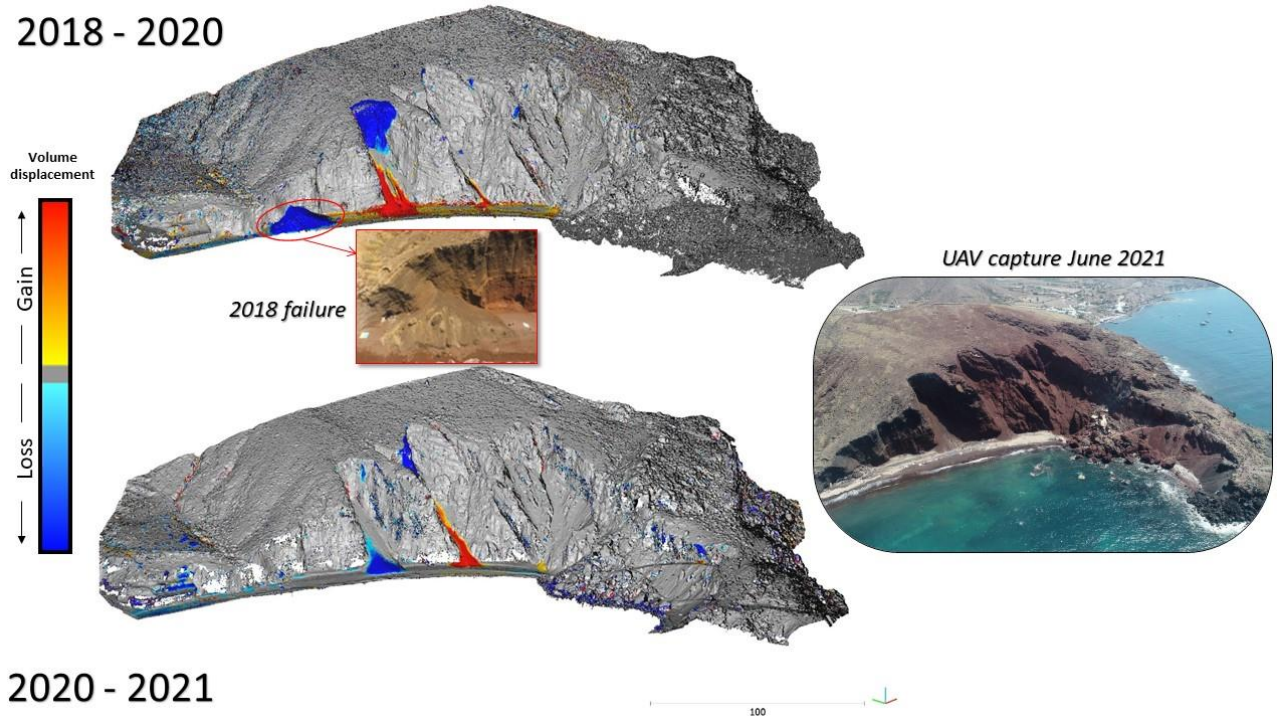

Figure 1. Change detection results between 2018 – 2020 (top) and 2020 – 2021 (bottom) showing volume loss and accumulation in cool and warm colors, respectively.

References

Druitt T, Francaviglia V.1992. Caldera formation on Santorini and the physiography of the islands in the late Bronze Age. Bull Volcanol 54:484–493

Giordan, D.; Hayakawa, Y.; Nex, F.; Remondino, F.; Tarolli, P. 2018. Review article: the use of remotely piloted aircraft systems (RPASs) for natural hazards monitoring and management. *Nat. Hazards Earth Syst. Sci.* 2018, *18*, 1079–1096, doi:10.5194/nhess-18-1079-.

Marinos, V.; Prountzopoulos, G.; Asteriou, P.; Papathanassiou, G.; Kaklis, T.; Pantazis, G.; Lambrou, E.; Grendas, N.; Karantanellis, E.; Pavlides, S. 2017. Beyond the boundaries of feasible engineering geological solutions: stability considerations of the spectacular Red Beach cliffs on Santorini Island, Greece. Environ. Earth Sci., 76, 513, doi:10.1007/s12665-017-6823-2.

16th International Congress of the Geological Society of Greece
23-25 May, 2022 - Patras, Greece
Bulletin of the Geological Society of Greece, Sp. Publ. 10
Ext. Abs. GSG2022-227

Liquefaction susceptibility map of specific areas in Thrace, Greece developed based on geomorphological-related studies

M.Taftsoglou[1], S. Valkaniotis[1], G.Papathanassiou[2] , N.Klimis[1], I.Dokas[1], S. Argyroudis[3]

(1) Democritus University of Thrace, Xanthi, Greece, mtaftsog@civil.duth.gr (2) Aristotle University of Thessaloniki, Thessaloniki, Greece (3) Brunel University London, London, United Kingdom

Background

Liquefaction is a phenomenon in which the ground material from a solid state transforms to a liquid one, due to the increase of the pore pressure and the reduction of the effective strength of the soil (Youd, 1973). Taking into consideration the age and the environment of the deposits, the liquefaction susceptibility can be assessed. Then, the liquefaction potential of the area can be evaluated based on data provided by borings with in-situ tests. The most applied methodologies concerning the regional scale assessment of liquefaction susceptibility have been proposed by Youd & Perkins (1978), the California Department of Conservation, Division of Mines (CDMG, 1999) and recently by Witter et al. (2006).

Furthermore, studies carried out in New Zealand, Italy and Greece (Wotherspoon *et al.*, 2012; Di Manna *et al.*, 2012; Bastin *et al.*, 2018; Papathanassiou *et al.*, 2015; Civico *et al.*, 2015; Villamor *et al*. 2016) concluded that active floodplains behave heterogeneously in terms of liquefaction. Recent research by Papathanassiou et al. (2022) referring to the liquefaction phenomena triggered by the March 2021, Thessaly Greece earthquake, stated that the geomorphological evolution of Pinios river floodplain impacts on the distribution of the liquefaction clusters in the area. The fact that locations with paleoenvironmental features such as oxbow lakes, former river channels and associated meanders are classified as high to very high susceptibility zones, highlights the significance of a detailed geomorphological information of the floodplain. Thus, the reliability and the accuracy of a liquefaction susceptibility map could be enhanced with a further discrimination of the geological units based on their age and their depositional environment.

This study is aiming to assess the liquefaction susceptibility of sediments in the floodplains of Nestos and Evros rivers. Study areas are located in Thrace, the north-eastern regional unit of Greece. Regarding the seismicity of Thrace, is affected not only by mapped onshore active faults (e.g Xanthi-Komotini fault, Maronia-Makri fault), but also by tectonic structures in the broader area such as western extension of North Anatolian fault (Saros fault zone). Geologically, the deposits in the region of Thrace are classified as Holocene age, mainly concentrated in the estuaries of Nestos and Evros rivers. The fact that critical infrastructures have been developed (airports and ports) on these sediments vitalizes the assessment of liquefaction susceptibility on these zones.

Methodology

In order to assess the liquefaction susceptibility of Nestos and Evros river delta, we used data provided by geologic maps published by EAGME, of 1:50000 scale, as a base layer. However, the lack of detail in these maps, concerning the classification of Holocene and Pleistocene sediments, increased the necessity for the use of supplementary data such as satellite images, aerial imagery and topographic maps. Aiming to reconstruct the geomorphological evolution in the floodplain, older imagery data were used. These data, before 1960's, depicts the area of Nestos delta without extended modifications, land reclamation and irrigation crops, making the detection of the geomorphological features more distinctive. Thus, orthophoto maps of 1945, with a ground resolution of 2 meters, were provided by Hellenic Cadastral organization and used as a basic imagery layer. Furthermore, we used declassified satellite imagery from USGS/NARA, dated before 1970. In particular, we selected KH-4 Corona frames acquired in 1960, 1967 and 1968, which were downloaded from USGS and orthorectified with the application of ERDAS IMAGINE software. The ground resolution of Corona orthoimagery is 3-4 meters.

Using orthophoto maps of 1945 and Corona satellite images in conjunction with a digital surface model of 5 meters resolution (Hellenic Cadastre), geomorphological features like floodplain deposits, estuaries, abandoned stream/meanders and oxbow lakes were mapped extensively. More recent land reclamation and surficial changes were added using Sentinel-2 and Google Earth images. Finally, information provided by bibliography and field surveys were used for the validation of the outcome concerning the spatial distribution of deposits.

Results and Conclusions

As a result of this approach, it was shown that geomorphological maps provide detailed and reliable data regarding the distribution of the deposits and thus it is suggested to be used for assessing liquefaction potential of a floodplain. Geological units of Nestos and Evros Rivers were classified into three categories, deposits younger than 500 years (fluvial and coastal deposits), Holocene (marshy and lagoonal deposits) and Pleistocene sediments. Thus, sediments,

which were formed the last 500 years are classified as high to very high susceptible to liquefaction, Holocene as moderate to low and Pleistocene as non-liquefiable.

Consequently, a liquefaction map was compiled according to the detailed distribution of <500 years, Holocene and Pleistocene deposits and their depositional environment. In the final map are delineated 4 classes, Low, Moderate, High and Very High, and also the class of the Non-liquefiable Pleistocene deposits. In the end, we calculate the total area of each susceptibility class in Nestos and Evros floodplains, with the "Very High" susceptibility areas covering 85,56 km^2 and 68,61 km^2 respectively.

Acknowledgments

We acknowledge support of this work by the project "Risk and Resilience Assessment Center –Prefecture of East Macedonia and Thrace -Greece." (MIS 5047293) which is implemented under the Action "Reinforcement of the Research and Innovation Infrastructure", funded by the Operational Programme "Competitiveness, Entrepreneurship and Innovation" (NSRF 2014-2020) and co-financed by Greece and the European Union (European Regional Development Fund).

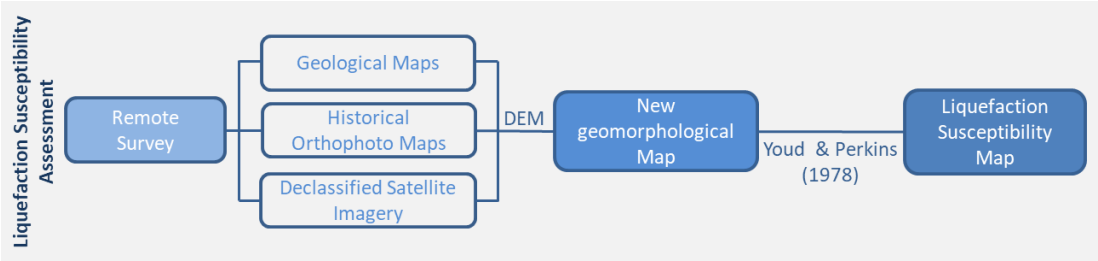

Figure 1. Flowchart of the methodological approach proposed by this study.

References

Bastin, S., Stringer, M., Green, R., Wotherspoon, L., van Ballegooy, S., Cox, B., Osuchowski, A., 2018. Geomorphological Controls on the Distribution of Liquefaction in Blenheim, New Zealand, during the 2016 Mw7.8 Kaikoura Earthquake. Geot. Earthq. Engin. Soil Dyn., V GSP 290.

CDMG.,1999. Guidelines for analyzing and mitigating liquefaction hazards in California. California Department of Conservation, Division of Mines and Geology, Special Publication 117, p. 63

Civico, R., Brunori, C.A., De Martini, P.M., Pucci, S., Cinti, F.R, Pantosti, D., 2015. Liquefaction susceptibility assessment in fluvial plains using airborne lidar: The case of the 2012 Emilia earthquake sequence area (Italy). Nat. Haz. Earth Syst. Sc., 15, pp. 2473-2483.

Di Manna, P., Guerrieri, L., Piccardi, L., Vittori, E., Castaldini, D., Berlusconi, A., Bonadeo, L., Comerci, V., Ferrario, F., Gambillara, R., Livio, F., Lucarini, M., Michetti, A.M., 2012. Ground effects induced by the 2012 seismic sequence in Emilia: implications for seismic hazard assessment in the Po Plain. Ann. Geophys., 55(4), pp. 697–703.

Mavroulis, S., Lekkas, E., Carydis, P., 2021. Liquefaction Phenomena Induced by the 26 November 2019, Mw = 6.4 Durrës (Albania) Earthquake and Liquefaction Susceptibility Assessment in the Affected Area. Geosciences. 11(5), 215, https://doi.org/10.3390/geosciences11050215

Papathanassiou, G., Mantovani A., Tarabusi, G., Rapti, D., Caputo, R., 2015. Assessment of liquefaction potential for two liquefaction prone areas considering the May 20, 2012 Emilia (Italy) earthquake, Eng. Geol., 189, pp. 1-16, https://doi.org/10.1016/j.enggeo.2015.02.002

Papathanassiou G., Valkaniotis S., Ganas Ath., Stampolidis A., Rapri D., Caputo R., 2022. Floodplain evolution and its influence on liquefaction clustering: the case study of March 2021 Thessaly, Greece, seismic sequence, Engineering Geology, in review

Villamor, P., Almond, P., Tuttle, M., Giona-Bucci, M., Langridge, R.M., Clark, K., Ries, W., Bastin, S.H., Eger, A., Vandergoes, M., 2016. Liquefaction features produced by the 2010–2011 Canterbury earthquake sequence in southwest Christchurch, New Zealand and preliminary assessment of paleoliquefaction features. Bull. Seism. Soc. Am., 106(4).

Wakamatsu, K., 1992. Evaluation of liquefaction susceptibility based on detailed geomorphological classification. In: Proceedings of the Annual Meeting of Architectural Institute of Japan, pp. 1443–1444

Witter, C.R., Knudsen, L.K., Sowers, M.J., Wentworth, M.C., Koehler, D.R., Randolph, C.E., 2006. Maps of Quaternary Deposits and liquefaction susceptibility in the Central San Francisco Bay Region, California, Open file report 2006-1037, USGS, 43

Wotherspoon, L., Pender, M., Orense, R.P., 2012. Relationship between observed liquefaction at Kaiapoi following the 2010 Darfield earthquake and former channels of the Waimakariri River. Eng. Geol., 125, pp. 45-55. https://doi.org/10.1016/j.enggeo.2011.11.001, 2012.

Youd T L., 1998. Screening guide for rapid assessment of liquefaction hazard at highway bridge site. Technical report, MCEER-98-005, pp. 58

Youd, T.L., Perkins, D.M..,1978. Mapping of Liquefaction induced Ground Failure Potential. J. Geotech. Eng. Div., 104, pp.433-446

16th International Congress of the Geological Society of Greece
17-19 October, 2022 - Patras, Greece
Bulletin of the Geological Society of Greece, Sp. Publ. 10
Ext. Abs. GSG2022-300

Combining mapping methods with advanced equipment to explore discontinuities in rock slopes and underground cavities

E. Chatzianagelis[1], N. Depountis[1]

(1) Laboratory of Engineering Geology, Department of Geology, University of Patras, 26504 Patras, Greece, up1089644@upatras.gr

Research Highlights

Exploring a mapping method with advanced equipment to investigate discontinuities in rock slopes and underground cavities

Introduction

A key task in conducting appropriate engineering geological studies in rock sites is the accurate mechanical description of the discontinuities intersecting rock masses. Either in slopes or underground cavities, the utilization of all information resulting from the study of rock discontinuities is particularly important because in combination with other geological parameters (resistance to uniaxial or triaxial compression, angle of friction, cohesion, modulus of elasticity, etc.) rock mass can be classified with RMR, GSI, and Q systems and decisions related to effective support measures can be made.

The purpose of this work is to investigate whether new technologies and their combination can easily and quickly provide the user with the required information to draw conclusions about the discontinuity parameters (orientation, spacing, persistence, aperture, roughness, etc.) and use them efficiently in rock mass classification. To investigate their effectiveness and their contribution to the overall information required, the following devices and programs were used: a) a handheld LiDAR scanner, "geoslam horizon, b) a "Phantom 3" standard drone with camera, c) a "FOIF RTS100", geodetic station, d) Cloud compare, point cloud editor and e) several design software programs.

The study aims to introduce a simple and easy-to-use mapping methodology with the use of advanced equipment to explore discontinuities in rock slopes or underground cavities that could give to the user all the necessary information, bypassing the classic procedure of the geological compass (Turanboy and Ulker, 2008; Lee et al., 2013; Assali et al., 2014). Until the completion of the objective, many difficulties and problems were identified that need further processing.

Methodology

The cave of "Koufierou" in Palaio Loutro, Municipality of Pylos - Nestoros, in the Messinia Regional Unit was the pilot area for the application of the presented methodology. The methodological procedure followed in this study included: a) aerial photographs of the cave using the "Phantom 3" standard drone with camera, b) scanning the interior of the cave with the handheld LiDAR scanner, "geoslam horizon", and c) surveying the whole site with the "FOIF RTS100" geodetic station.

During the use of these instruments, several advantages and disadvantages were observed regarding the correctness of the application of each instrument. To correctly combine the various data received from the instruments, relative measurement errors were examined as well as the compatibility and the quality of the extracted data.

Results

In the beginning an aerial survey with the "Phantom 3" standard drone – camera was done. Figure 1a shows the facade of the cave and Figure 1b the 3d display, processed with Agisoft Metashape Pro The location of the presented photos according to the data from the drone is: Latitude 37.6.30.4012, Longitude 21.46.24.5821 and Altitude 603.044 m.

Figure 1. (a) ***front view of the "Koufierou" cave, (b) 3d view with aerial photographs***

During the two flights of the drone, many photos were taken from various points, distances, and altitudes to have a complete picture of the perimeter of the cave as it is suggested by Chiabrando, et al, 2011. The height of the slopes

surrounding the cave from its lower level is approximately 55 meters. The use of the drone proved to be very important because through the shots we could have a clear picture of the condition of discontinuities in hard-to-reach places with very good image resolution. In addition, we had the opportunity to see the full path of the fault that can be seen to the right of the cave in Figure 1a. Further processing of the images gave us a general three-dimensional representation of the cave from the outside, which alone cannot give us all the necessary information.

Consequently, a survey in the surrounding area of the cave was conducted with the use of the handheld LiDAR scanner, "geoslam horizon". The lidar "geoslam horizon" survey was done before sunset to take advantage of the camera it has and is useful for coloring the cloud of points extracted by the device (Lemy et al., 2006; Gikas, 2012). Depending on the surface and the material, the coloring of the points differs. The following Figure presents the impression through the cloud of points that the device outputs with the help of the cloud compare program (CloudCompare, 2016). Through the program, it was possible to dimension the cave in any area and to export cross-sections in dwg format for further processing and data export using the autocad program.

Figure 2a shows the 3D image of the cave as captured by the "geoslam horizon" lidar. Figure 2b shows the morphology of the cave, internally and externally, with the necessary explanations. Figure 2c shows the cross-section 2-2 extracted from the program which was further processed in an autocad program, for creating drawings and making measurements.

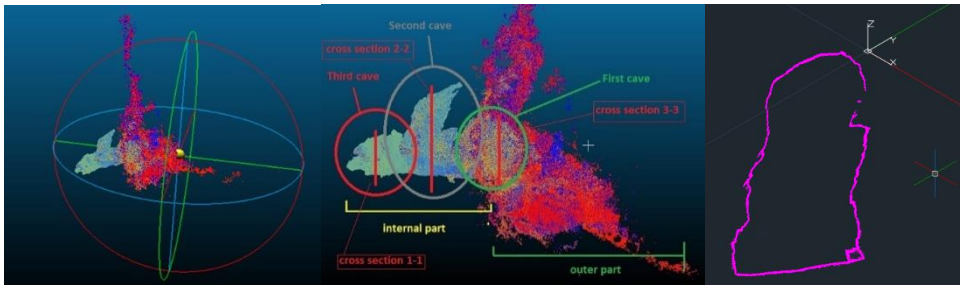

Figure 2.(a) 3d view of cave. (b) parts of cave. (c) cross section 2-2 of second cave.

Lastly, a total survey with the "FOIF RTS100", geodetic station, was performed and data was processed in the "autocad" program. To verify the correctness of the measurements from the previous two surveys, the geodetic station "FOIF RTS100" was also used as a classical survey method. The data that the geodetic station outputs are in X,Y,Z coordinates and refer to the points we have targeted. The instrument was set up in two places so that the external environment, the slope and the first cavity of the cave could be captured.

Conclusions

After the multiple mapping of the cave with different methods and instruments, the following conclusions are drawn:

a) Surveying with the drone has an advantage over others because it gives us information in places where there is no access since we have a global view of the object of study and several photos. Therefore, we are able to distinguish and process discontinuities and cracks.

b) The survey with the handheld lidar scanner gives a comprehensive and accurate survey of the space, both internally and externally, but does not give us the information regarding the discontinuities we need.

c) The mapping with the geodetic station is complementary to the above two.

It is concluded that a device that combines the advantages of the above and overcomes the referred disadvantages is a 3d camera. The creation of a detailed three-dimensional photographic model allows us to have the combination of the three dimensions, and the information needed for the later discontinuity processing.

Acknowledgments

The authors acknowledge the support of the landmark Loutridis Company which provided the geoslam horizon lidar.

References

Assali, P., Grussenmeyer, P., Villemin, T., Pollet, N., Viguier, F., 2014. Surveying and modeling of rock discontinuities by terrestrial laser scanning and photogrammetry: semiautomatic approaches for linear outcrop inspection. Journal of Structural Geology 66:102.

Chiabrando, F., Nex, F., Piatti, D., Rinaudo, F., 2011. UAV and RPV systems for photogrammetric surveys in archaelogical areas: Two tests in the Piedmont region (Italy). J. Archaeol. Sci., 38, 697–710.

CloudCompare. CloudCompare V2.8., 2016. http://www.cloudcompare.org/ [Accessed 1 Aug 2022].

Gikas, V., 2012. Three-dimensional laser scanning for geometry documentation and construction management of highway tunnels during excavation. Sensors, 12(8).

Lee, S., Suh, J., Park, H.D., 2013. Smart Compass-Clinometer: a smartphone application for easy and rapid geological site investigation. Computers & Geosciences, 61:32.

Lemy, F., Yong, S., Schulz, T., 2006. A case study of monitoring tunnel wall displacement using laser scanning technology. In: Proceedings of 10th IAEG congress 'engineering geology for tomorrow's cities'.

Turanboy A, Ulker ELIP-RM. An attempt at 3D visualization of in situ rock massstructures. Computational Geosciences 2008;12(2):181e92.

16th International Congress of the Geological Society of Greece
17-19 October, 2022 - Patras, Greece
Bulletin of the Geological Society of Greece, Sp. Publ. 10
Ext. Abs. GSG2022-399

Coastal vulnerability assessment to sea level rise for the coasts of the Ionian Islands

V. Kotinas[1], A. Karditsa[1], S.E. Poulos[1,2]

(1) National and Kapodistrian University of Athens, Athens, Greece, vkotinas@geol.uoa.gr (2) Foundation for Research and Technology, Heraklion, Crete Greece

Coastal areas around the world concentrate a large part of the population and economic activity. In Europe, more than 40% of the total population lives near the shore, while the Greek coastal zone concentrates approximately 90% of the total population. The predicted acceleration of global sea level rise could potentially pose a major threat to the coasts via erosion processes enhanced by storm events (in terms of frequency and intensity). **The scope** of this work is to identify the most vulnerable coastal areas to sea level rise, in the Ionian islands where coastal erosion is intense.

We investigate the relative vulnerability of the coasts of the main Ionian Islands, by applying the widely accepted coastal vulnerability index (CVI; Gornitz et al., 1990). We **firstly create a geodatabase** consisting of all the necessary variables for the calculation of the CVI which incorporates various geo-environmental factors i.e. coastal geomorpholology, slope, relative sea level change, shoreline displacement, tidal range and offshore significant wave height (see Table 1). Using **G.I.S. procedures we rank** the observed values, of these variables, in a scale from 1 to 5 according to the classification scheme that was proposed by Hammar Klose & Thieler (2001) and finally the coastal vulnerability index is calculated, using the square root of the geometric average of the six variables for the total coastline of the Ionian islands.

By taking into account the projected sea level rise (SLR) for the year 2100 (IPCC 2021) associated with 2 different climate change scenarios i.e. SSP 1b–2.6 (SLR: +0.47m) and SSP 4-8.5 (SLR: +0,82m) we calculated the CVI following the methodology that was presented before. **Our results** show that for the **low emissions scenario**, about 5% of the Ionian islands' coastline is characterized by high to very high vulnerability and 38% by moderate vulnerability (see Fig.1). For **the extreme (high emissions) scenario** more than 18% of the total coastline is categorized by high and/or very high vulnerability and 34% by moderate vulnerability. Corfu and Lefkas islands **demonstrate the highest vulnerability in both scenarios,** while Ithaka island the lowest one. Moreover, the coastal strips with high to very high vulnerability coincide with places of significant touristic importance. By using satellite/aerial images of the area covering an extended period of time and through extensive fieldwork we validated that the CVI works successfully in the study area (it demonstrated very good results in identifying areas that are already eroding).

Through this work, the most vulnerable areas to coastal erosion of the Ionian islands were identified, but more precise research on these areas should follow. The decision-makers and local authorities need to create an adaptation plan for sea level rise impacts and enhance their capacity against erosion and coastal flooding in the identified areas.

Table 1. The CVI variables and their ranking scheme according to Hammar Klose & Thieler (2001)

CVI	Very low (1)	Low (2)	Moderate (3)	High (4)
Geomorphology	Rocky - cliffed coasts, Artificial Constructions	Medium Cliffs, indented coasts	Low cliffs, alluvial plains, beachrocks, dunes	Cobble beaches, Estuary, Lagoon
Coastal slope (%)	>20	7-20	4-7	2.5-4
Relative sea level change (mm/yr)	<1,8	1.8 – 2.5	2.5 – 3.0	3.0 – 3.2
Shoreline erosion/ accretion(m/yr)	>2.0	1.0-2.0	-1.0-+1.0	-1.1- -2.0
Mean Tide range(m)	>6.0	4.1 – 6.0	2.0 – 4.0	1.0 – 1.9
Mean Wave	<0.55	0.55 – 0.85	0.85 – 1.05	1.05 – 1.25

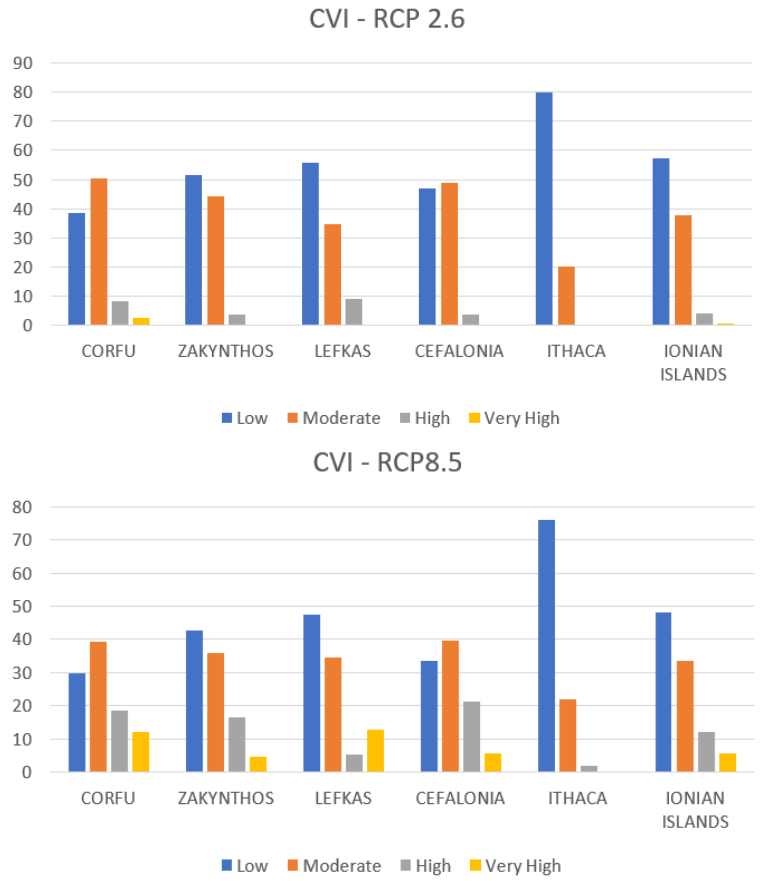

Figure 1. Coastal vulnerability index for the main islands of the Ionian Islands for 2 different emission scenarios.

Acknowledgements

V. Kotinas, A. Karditsa and S.E. Poulos acknowledge the ILIDA-KIT project (MIS 5129417) funded by the Operational Program Competitiveness, Entrepreneurship & Innovation 2014-2020 (EPAnEK).

References

Gornitz, V., White T., Cushman R., 1990. Vulnerability of the East Coast, U.S.A. to future sea level rise. Journal of Coastal Research, Special Issue No. 9, pp. 201-237.

Hammar-Klose, E., & Thieler, R. E., 2001. Coastal Vulnerability to Sea Level Rise: A Preliminary Database for the U.S. Atlantic, Pacifiv and Gulf of Mexico Coasts. In U.S.G.S. U.S.A.

IPCC, 2021: Climate Change 2021: The Physical Science Basis. Contribution of Working Group I to the Sixth Assessment Report of the Intergovernmental Panel on Climate Change [Masson-Delmotte, V., P. Zhai, A. Pirani, S.L. Connors, C. Péan, S. Berger, N. Caud, Y. Chen, L. Goldfarb, M.I. Gomis, M. Huang, K. Leitzell, E. Lonnoy, J.B.R. Matthews, T.K. Maycock, T. Waterfield, O. Yelekçi, R. Yu, and B. Zhou (eds.)]. Cambridge University Press, Cambridge, United Kingdom and New York, NY, USA, In press, doi:10.1017/9781009157896

16th INTERNATIONAL CONGRESS of the
GEOLOGICAL SOCIETY OF GREECE

S9. Geological heritage for education and sustainable development

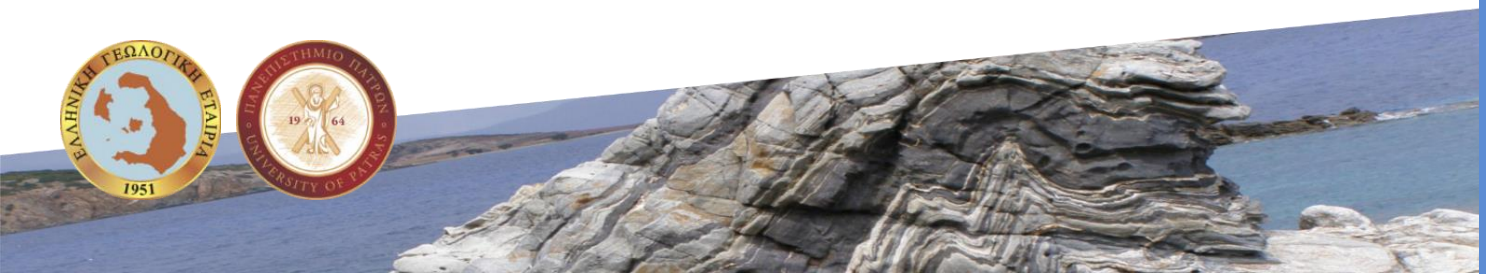

OUR EARTH, OUR HOME

16th International Congress of the Geological Society of Greece
17-19 October, 2022 - Patras, Greece
Bulletin of the Geological Society of Greece, Sp. Publ. 10
Ext. Abs. GSG2022-021

The Geoheritage of Malta from Prehistory to the Present Day

Argyrios Periferakis[1,2,3], Konstantinos Periferakis[2,4,5], Aristodemos-Theodoros Periferakis[1,3]

(1) Department of Physiology, The "Carol Davila" University of Medicine and Pharmacy, 050474 Bucharest, Romania, argyrios.periferakis0920@stud.umfcd.ro (2) Akadimia of Ancient Greek and Traditional Chinese Medicine, 16675 Athens, Greece (3) Elkyda, Research & Education Centre of Charismatheia, 17675 Athens, Greece (4) Pan-Hellenic Organization of Educational Programs (P.O.E.P), 17236 Athens, Greece (5) Orasis Acupuncture Institute, 11526 Athens, Greece

Introduction

The islands of the Archipelago of Malta represent an area of high archaeological, historical, and cultural value. Most of the sites and structures of historical and cultural significance are also associated with the geological features of the islands, given that the local limestones were widely used to construct everything, from temples to massive forts. Many of the structures and buildings of Malta are iconic and this reflects upon the materials of their construction. Indeed, the availability of geological materials made possible the construction of the impressive structures which define the cultural character of the islands.

Geology of Malta and Gozo

The Malta and Gozo islands are mostly of Tertiary age, with the Upper Coralline limestone at the top of the stratigraphic table, followed by greensand, blue clay, the Globigerina limestone, and the Lower Coralline limestone. A horst-graben structure is characteristic of Northern Malta, in an ENE axis (Pedley *et al.*, 1976). Both of the Coralline limestones form bare plateaus while the Globigerina limestone allows for the existence of a meager and modestly fertile soil. All the carbonates of the islands bear evidence of shallow water deposition. The fossil record of Malta is also rather significant (Pedley et al., 1976).

Geoheritage of the Megalithic Temples of Malta

The rich geoheritage of Malta is evident in its megalithic temples, which were built by Neolithic settlers, ca. 3600-2500 BC (Theuma & Grima, 2006). The most notable structures comprise the Ta' Hagrat, Skorba, Mnajdra, Ħagar Qim, and Tarxien temples on the island of Malta itself, and the Ggantija temple on the island of Gozo. These sites are included in the UNESCO World Heritage List (Cassar *et al.*, 2018). Based on the research of Zammit Maempel (1989), the first dwelling for the newly arrived Neolithic people was the Għar Dalam cave, a natural cave in the Lower Coralline limestone. Apart from this naturally sheltered dwelling, people of this age also carved out underground complexes of various sizes; a characteristic example is the Ħal Saflieni hypogeum (Pace, 2000).

The walls of the temples are constructed either of Globigerina limestone or Coralline limestone, but most of the elaborate structures are carved out of Globigerina limestone. This is a trend replicated in most Maltese buildings, i.e, the softer Globigerina limestone being used for ornamental purposes and the tougher Coralline limestone being used for building (Cassar, 2010). It is noteworthy that most of the stone used for the construction of these temples was available locally and only a small amount was transported from other locations on the islands (Grima, 2004). Based on the research of Evans (1971), crushed limestone was used to make the floor of some of the temples. The discovery of a number of artifacts made from stones not originating in Malta and Gozo (e.g., Stoddart *et al.*, 1993; Brown *et al.*, 1995), also indicates the existence of potential trade routes with other regions and allows for tracking human contacts in these prehistoric times.

Geoheritage of the Medieval Forts and Subsequent Structures

Following the Neolithic building phase, no further structures of note appeared on the islands, although the dwellings of the Roman period, again made out of the building materials found on the island, are noteworthy (Bonanno, 2005). During the Arab period, the Maltese buildings were frequent wholly constructed from limestone, even their roofs being made of rock rather than wood or other materials (Hughes, 1993).

Most of the villages and small towns of the island appear wherever there was an adequate supply of limestone, it being the principal building material for the inhabitants across the ages. It is striking that the existence of a vast amount of limestone enabled the construction of large churches; these were built from the limestone excavated from the crypts found underneath them (Cassar, 2010).

Arguably, the most prolific building period started with the arrival of the Order of the Knights of St. John in 1530. The majority of the building stones for the fortifications of this period were excavated on site (Spiteri, 2008). Different qualities of limestone were gradually used to cover those parts of the forts exposed to the sea and those on the landward and inward faces. The most well-known Hospitaller fortresses of Malta are Fort St. Angelo and Fort St. Elmo, while other contemporary fortifications are prominent on the island.

After a very brief French occupation, which ended the sovereignty of the Hospitaller Knights, Malta and the surrounding

islands became part of the British Empire in 1813. The British built Fort Delimara as well as Fort Benghisa, and several other fortifications, using limestone as the primary building material. Today, all the forts of the British colonial age, as well as the earlier fortifications remain pretty much intact; they are a testament to the ingenuity and skill of their builders and attest to the sturdiness of their building materials.

Discussion and Conclusions

From the aforementioned, it is evident that the geological materials of the island enabled the construction of characteristic structures which are part of the local cultural heritage. Therefore, the geoheritage of the Maltese islands is inextricably linked to the very landmarks that define the islands' historical tradition. Such is the imprint of geology in the culture of the island, that there is the Limestone Heritage Park and Gardens, which focuses on Maltese history through the scope of limestone quarrying and its use, across the centuries. It must also be mentioned that there is a rich geopharmaceutical tradition in Malta, with numerous materials associated with real or alleged medicinal properties (Duffin, 2019). There are numerous places of geoheritage in the Mediterranean islands (e.g., Periferakis, 2019, 2021; Vlachopoulos & Voudouris, 2022) and in the Mediterranean littoral areas in general (e.g., Voudouris *et al.*, 2021, Drinia et al., 2022). Malta and its surrounding islands hence form part of a rich chain of potential places where traditional tourism, i.e., that of historical/recreational interest, can be integrated with geotourism. The notion of combining different types of tourism has already been proposed by numerous authors – for the specific case of geotourism, it has more recently been proposed by Anastasiei *et al.* (2022).

Geotourism, as defined by Hose (1995), represents one of the more modern trends and concepts in tourism studies today. While arguably there exist places where geotourism can be centered just on geological features – such is the case of many geosites and geoparks – the aforementioned Maltese sites constitute places of geoheritage, where the geological materials were instrumental in creating structures of cultural and historical significance. With this in mind, Malta could well be incorporated into geotourism programs, encompassing European or Mediterranean geoheritage.

References

Anastasiei, A.-M., Niacşu, L., Enea, A., 2022. The Geoheritage value of the iconic buildings of Iaşi City, Romania. EGU General Assembly, Vienna, Austria, EGU22-8826.

Bonanno, A., 2005. Malta Phoenician, Punic, and Roman. Midsea Books.

Brown, C., Dixon, J.E., Leighton, R., 1995. Stone axes and stone axe pendants, in: Malone, C., Stoddart, S., Bonanno, A., Gouder, T., Trump, D. (Eds.), Mortuary Ritual of 4th Millennium BC Malta: The Zebbug Period Chambered Tomb from the Brochtorff Circle at Xaghra (Gozo), 303-345.

Cassar, J., 2010. The use of limestone in a historic context – the experience of Malta, in: Smith, B.J., Gomez-Heras, M., Viles, H.A., Cassar, J. (Eds.), Limestone in the Built Environment: Present-Day Challenges for the Preservation of the Past, 13-25.

Cassar, J., Cefai, S., Grima, R., Stroud, K., 2018. Sheltering archaeological sites in Malta: lessons learnt. Heritage Science, 6, 36.

Drinia, H., Voudouris, P., Antonarakou, A., 2022. Editorial of Special Issue — "Geoheritage and Geotourism Resources: Education, Recreation, Sustainability". Geosciences, 12, 251.

Duffin, C., 2019. Snakes' tongues, Serpents' eyes and sealed earths: Geology and Medicine in Malta. An Occasional Paper of the St John Historical Society.

Evans, J.D., 1971. The Prehistoric Antiquities of the Maltese Islands. Athlone Press.

Grima, R., 2004. The landscape context of megalithic architecture, in: Cilia, D. (Ed.), Malta Before History, 327-345.

Hose, T., 1995. Selling the Story of Britain's Stone. Environmental Interpretation, 10, 16–17.

Hughes, Q., 1993. The architectural development of Hospitaller Malta, in: Mallia-Milanes, V. (Ed.), Hospitaller Malta 1530-1798, 483-507.

Pace, A., 2000. The Prehistoric Hypogeum at Ħal Saflieni. PEG Ltd.

Pedley, H.M., House, M.R., Waugh, B., 1976. The Geology of Malta and Gozo. Proceedings of the Geologists' Association, 87, 325-341.

Periferakis, A., 2019. The Importance of Emery in the Cultural, Social and Economic Development of Naxos Island, Cyclades, Greece. 15th International Conference of the Geological Society of Greece, Athens, Greece, p. 708-709.

Periferakis, A., 2021. The Emery of Naxos: A Multidisciplinary Study of the Effects of Mining at a Local and National Context. Journal NX - A Multidisciplinary Peer Reviewed Journal, 7, 93-110.

Spiteri, S.C., 2008. The Art of Fortress Building in Hospitaller Malta. BDL Publishing.

Stoddart, S., Bonanno, A., Gouder, T., Malone, C. Trump, D., 1993. Cult in an island society: prehistoric Malta in the Tarxien Period. Cambridge Archaeological Journal, 3, 3-19.

Theuma, N., Grima, R., 2006. The Megalithic Temples of Malta: towards a re-evaluation of heritage, in: Leask A., Fyall, A. (Eds.), Managing World Heritage Sites, 263-272.

Vlachopoulos, N., Voudouris, P., 2022. Preservation of the Geoheritage and Mining Heritage of Serifos Island, Greece: Geotourism Perspectives in a Potential New Global Unesco Geopark, Geosciences, 12, 127.

Voudouris, P., Melfos, V., Mavrogonatos, C., Photiades, A., Moraiti, E., Rieck, B., Kolitsch, U., Tarantola, A., Scheffer, C., Morin, D., Vanderhaeghe, O., Spry, P.G., Ross, J., Soukis, K., Vaxevanopoulos, M., Pekov, I.V., Chukanov, N.V., Magganas, A., Kati, M., Katerinopoulos, A., Zaimis, S., 2021. The Lavrion Mines: A Unique Site of Geological and Mineralogical Heritage. Minerals, 11, 76.

Zammit Maempel, G., 1989. Għar Dalam Cave and Deposits. PEG Ltd.

16th International Congress of the Geological Society of Greece

17-19 October, 2022 - Patras, Greece

Bulletin of the Geological Society of Greece, Sp. Publ. 10

Ext. Abs. GSG2022-051

Introducing Interdisciplinary Innovative Techniques for Mapping Karstic Caves

A. Konsolaki[1], E. Vassilakis[1], E. Kotsi[1], G. Kontostavlos[2], E. Lekkas[1], M. Stavropoulou[1], I. Giannopoulos[1]

(1) Department of Geology and Geoenvironment, University of Athens, Greece, alikikons@geol.uoa.gr (2) Hellenic Speleological Society, Athens, Greece.

The purpose of this research is to describe a methodology for the generation of a complete 3D model of a karstic cave. We applied this methodology at two different karstic geo-environments in Cephalonia Island (Melissani and Drogarati show caves) and despite this fact, this particular methodology was successfully applied for both missions. We incorporated close-range remote sensing techniques and equipment including a Terrestrial Laser Scanner (TLS), a Handheld Laser Scanner (HLS), and an Unmanned Aerial System (UAS), maximizing the quality and precision of the 3D results. The high precision of the combined methodology is based on the use of multi-allocated control points which are established either on the surface or beneath it, throughout the area of each cave. All the coordinate measurements were calculated by using RTK-GNSS (for the surface points) and total station equipment (for the subsurface points) which allowed us to create a multi-source, high accurate, geo-rectified, dense, and above all the aforementioned, unified point cloud for each geomorphological cavity. The evolution of technology and the development of 3D space, such as computer vision, modelling, printing etc. in three-dimension, covered the needs of constructing 3D geological models for mapping, analysing and studying the earth's surface in a modern way. Nowadays, 3D modelling is applicable in every geological field such as in palaeontology, petrology, tectonics (Barreau *et al.*, 2022; Apopei *et al.*, 2021; Mavroulis *et al.*, 2022 and references within) among others. Moreover, the 3D representation of morphological structures, such as steep cliffs, gorges, karstic landforms, and caves, gives us nowadays the opportunity to study geomorphology in depth, in terms of monitoring geomorphic changes over time, erosion detection and quantification, risk management, and geo-heritage prominence and conservation (Spyrou *et al.*, 2022). Specifically in caves, a karst environment with exquisite beauty and an attraction for naturalists and tourists, 3D mapping, analysis, quality, and quantity are now essential components for their systematic study (Konsolaki *et al.*, 2020). The use of state-of-the-art equipment provide the means to map and visualize the walls, roof, and floor of a cave, including cave deposits, by constructing high quality topography inside the cave and above it as well. Cave systems are very complex environments and variant from each other, dependent on the bioclimatic conditions, formation processes, and hydro-chemical reactions taking place in a region. Therefore, the methodology to be applied, regarding the mapping and generation of the 3D model, varies and should be adapted according to the morphology of the cave. Regarding our research, there are two main parts concerning (i) the underground cavity and (ii) the open surface above, where several point clouds were constructed with two different methods. The first one is based on millions of direct measurements (TLS, HLS) whilst the second one is indirectly induced by photogrammetric processing (UAS images).

Melissani Cave is an underground lake that is situated in the northwestern part of the coastal settlement of Karavomilos (Cephalonia). The natural entrance, which is located at a collapsed doline above the cave, was created according to historical sources after a strong earthquake. A large opening (about 30m long and 20m wide) was formed at the ceiling of the underlying cavity and a spectacular subsurface lake was revealed. Continuous rockfalls resulted the concentration of large amounts of debris at several parts in the cave, forming shallow areas and emerged piles within the lake. The latter were used for placing the steady surveying equipment, whilst a boat was used for the mobile one. Specifically, the methodology included (i) terrestrial laser scanning from 6 predetermined bases on the debris pile, the artificial pier, and on a platform at the edge of the doline, constructing several point clouds for most of the floor, roof, and walls of the cave with a spatial resolution of 5mm, and (ii) handheld laser scanning by boating around the walls, where additional data acquisition was necessary either for increasing the resolution or for surveying hidden passages and hard-to-reach areas. A total of 20 control points were placed on the cavity walls where their true coordinates were measured with the total station along with 5 control points that were established on flat surfaces around the cave. The dataset was completed with a point cloud which was extracted after the photogrammetric processing of a series of georectified images (401 photos) of the open surface. They were acquired by a DJI Phantom 4 RTK, which carries an onboard multi-frequency multi-constellation GNSS receiver, allowing the adoption of the NRTK approach (Panagiotopoulou *et al.*, 2020) for the data acquisition and processing to ensure the highest accuracy of the results. The acquired point clouds were then pre-processed, cleaned, and merged, leading to the final product, a high spatial resolution cloud layer consisting of 629 million points which can be further processed and visualized in three dimensions (Fig. 1).

In contrast to Melissani, **Drogarati Cave** is a horizontal cavern, situated 1km east of the settlement of Haliotata (Cephalonia) and it consists of two main parts; (i) a collapsed doline which represents the natural entrance, and (ii) a very large chamber with dimensions of 63m*47m, divided into two sections, with 7m elevation difference, due to boulders that were detached from its roof, creating a barrier. The methodology followed, varied from the one previously described regarding handheld laser scanning, since lots of hidden passages behind columns characterize the geomorphology of this

cave, making the mobile data acquisition technique more efficient than TLS which in this case portrayed as supplementary. The latter was accomplished by establishing 5 successive bases in clear line of sight with a traverse approach.

Figure 1: The complete 3D model of Melissani Cave with the surface above it.

In total, 23 control points were established and measured throughout the cave, of which 15 were placed on the cavity walls and 8 spread across the floor. A high density 841-million-point cloud of Drogarati Cave led to the production of a 3D model, after merging the individual point clouds with the one that was extracted after surveying the open surface above the cave with the UAS and the photogrammetric processing that followed (Fig. 2).

Figure 2: The complete 3D model of Drogarati Cave with the surface above it.

In conclusion, the implementation of the described methodology at the study of the caves provides an additional tool for identifying the high-risk areas, aiming to increase the safety of the visitors. At both cases, digital measurements of the rock thickness between the roof of the underground karstic structures and the open-surface topography, as well as mapping the rock discontinuities in high detail, can be presented with very high accuracy.

Acknowledgements

This research was funded by the "Laertis –Innovative Risk Management System in the Region of Ionian Islands" project (MIS 5010951), included in the Priority Axis "Environmental Protection and Sustainable Development" of the Regional Operational Programme “Ionian Islands 2014–2020", which is funded by the European Regional Development Fund (ERDF) and National Resources under the National Strategic Reference Framework NSRF 2014-2020. Special thanks to the municipality of Sami.

References

Apopei, A., Buzgar, N., Buzatu, A., Maftei, A., and Apostoae, L., 2021, Digital 3D models of Minerals and Rocks in a nutshell: Enhancing scientific, learning, and cultural heritage environments in Geosciences by using cross-polarized light photogrammetry: Carpathian Journal of Earth and Environmental Sciences, v. 16, p. 237-249.

Barreau, J.-B., Gagnier, A., Gaugne, R., Marchand, G., Gómez, J. C., Gouranton, V., and Colleter, R., 2022, Use of Different Digitization Methods for the Analysis of Cut Marks on the Oldest Bone Found in Brittany (France): Applied Sciences, v. 12, no. 3, p. 1381.

Konsolaki, A., Vassilakis, Emm., Gouliotis L, Kontostavlos G, Giannopoulos V. High resolution digital 3D modelling of subsurface morphological structures of Koutouki Cave, Greece. Acta Carsologica [Internet]. 2020;49(2-3):163-177

Mavroulis, S., Vassilakis, E., Diakakis, M., Konsolaki, A., Kaviris, G., Kotsi, E., Kapetanidis, V., Sakkas, V., Alexopoulos, J. D., Lekkas, E., and Voulgaris, N., 2022, The Use of Innovative Techniques for Management of High-Risk Coastal Areas, Mitigation of Earthquake-Triggered Landslide Risk and Responsible Coastal Development: Applied Sciences, v. 12, no. 4, p. 2193.

Spyrou, E., Triantaphyllou, M.V., Tsourou, T., Vassilakis, E., Asimakopoulos, C., Konsolaki, A., Markakis, D., Marketou-Galari, D., Skentos, A., 2022. Assessment of Geological Heritage Sites and Their Significance for Geotouristic Exploitation: The Case of Lefkas, Meganisi, Kefalonia and Ithaki Islands, Ionian Sea, Greece. Geosciences, 12(2), 55.

Panagiotopoulou, S., Erkeki, A., Antonakakis, A., Grigorakakis, P., Protopapa, V., Tsiostas, G., Vlachou, K., Vassilakis, E., 2020. Evaluation of Network Real Time Kinematics contribution to the accuracy/productivity ratio for UAS-SfM Photogrammetry, 2020 European Navigation Conference (ENC), Dresden, Germany, pp. 1-11.

16th International Congress of the Geological Society of Greece
17-19 October, 2022 - Patras, Greece
Bulletin of the Geological Society of Greece, Sp. Publ. 10
Ext. Abs. GSG2022-070

Intangible Geoheritage: Preservation of Legends and Traditions that Interact with the Geo-environment in the region of Geopark Grevena-Kozani, Greece

A. Rassios[1], D. Ghikas[2], A.Batsi[2]

(1) Scientific Director Geopark Grevena-Kozani, Greece, rassannie@gmail.com (2) Geopark Grevena-Kozani, Grevena, Greece, Geowonders@gmail.com

Geoheritage is far more than a compendium of documentation of geosites as an "academic" database. Geoheritage is the union of the study of the geology with the recognition and importance of geology to human society. In our present study, we document legendary events in the area of the Geopark Grevena-Kozani that have their source in the unique geology, geomorphology, and geo-environments of the region. Our source material includes folk songs of the area and "living history" verbally passed on from shepherds and the memories of pioneering geologist, Jan Brunn. In addition to an "academic" presentation, this material has been presented in a "fictive" format to aid popularization, interest, and conservation of this "intangible" geoheritage.

Intangible geoheritage is a complex overlapping association of subjects rooted in a geologic base feature. An example (among many) in our Geopark is that of the subject of "dragons." The local population has called glacial tarn lakes of the Pindos "Dragon Lakes" for centuries. There are legends of the dragons inhabiting these lakes – how they arrived, how they lived, how they created these lakes as nesting sites, and then filled the lakes with their tears as they loss their mates. There are explanations for the boulders that don't match their host terrane scattered in the Pindos that are remnants of warring between dragons. Most of the dragons were subdued by Hercules in some legends, St George in others, and there are songs of the "Dragonslayers" that seem to describe seismic activity (figure 1).

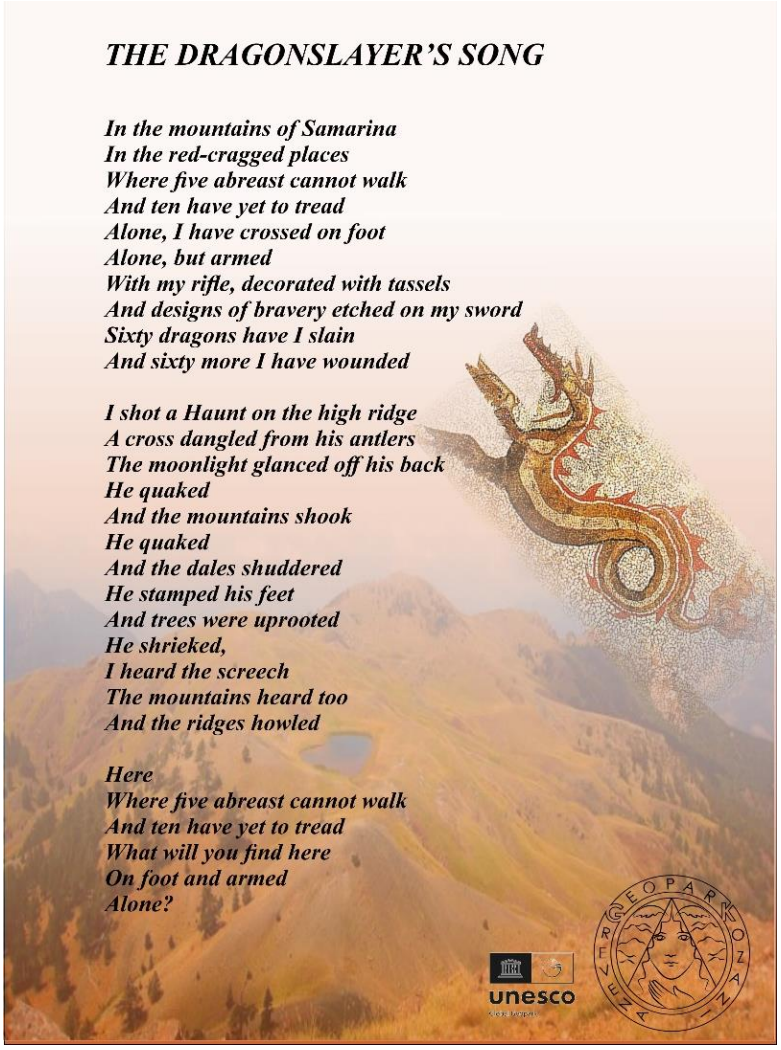

Figure 1. The Dragonslayer's Song (translated from original folk text by A. Rassios)

In addition to the Dragon Lakes, other geomorphological features add to the legends of the dragons. Fractured sandstone layers are call “dragon teeth” by inhabitants. The embayed rock of Mikrolivado is now referred to as the “Dragon’s Eye,” and the elongate peaked ridge crests as “Dragons’ Backs.” There are newts living within the Dragon Lakes that do, indeed, resemble small dragons. There are some residents even today who claim that the eagles of the Pindos may have been dragons.

Thus, this simple and elegant legend of the Pindos synthesizes biological, cultural, geomorphological, and seismic elements to an elegant mythic paradigm based in geology. We utilize this as a way to connect the geologic provenance of our Tethyan-provenance Geopark with that of the titan Tethys herself, and especially her “pet” dragon Cetus. Cetus now has an on-line game in which locating his position within the Geopark is essential and fun. With the addition of historic sources including the memories of shepherds and of Jan Brunn (1956), geological pioneer, the “living” world of intangible geoheritage has been preserved in the novel, by Rassios (2022), The Orliakada.

Acknowledgements

Thanks to the late Dimitri Ringo for introduction to the Dragonslayer’s Song. The Orliakada was published by Geowonders of Greece (Grevena) as their initial book publication.

References

Brunn, J., 1956. Contribution a L’Étude Géologique du Pinde Septentrional et D’une Partie de la Macédoine occidentale, Ann. Geol. Pays. Hellen., v. 7, pp. 1-358.

Rassios, A., 2022. The Orliakada. Geowonders of Greece. 288 pp.

16th International Congress of the Geological Society of Greece

17-19 October, 2022 - Patras, Greece

Bulletin of the Geological Society of Greece, Sp. Publ. 10

Ext. Abs. GSG2022-079

The Museums of Geology and Paleontology as Geoeducational Learning Environments for Climate Change Awareness: A Case Study.

C. Kondyli[1], M. Psychogiou[2] and H. Drinia[2]

(1) Department of History and Archaeology, National and Kapodistrian University of Athens, Athens, Greece, xristinakondyli@gmail.com (2) Department of Geology and Geoenvironment, National and Kapodistrian University of Athens, Athens, Greece, mpsychogiou@geol.uoa.gr; cntrinia@geol.uoa.gr

In the last decade, the academic community has focused its research on geoconservation and geological heritage issues (Brilha and Reynard, 2018). The term "geological heritage" is systematically linked to the broader concept of natural heritage (Zafeiropoulos et al., 2021). Palaeontological heritage is classified as a subcategory of geological heritage (Souza and Miranda, 2007). Geological heritage, or geoheritage, is divided into two categories: in situ and ex situ elements. Geosites are an example of in situ elements that contribute to geodiversity and have high scientific value. Ex situ elements are also part of geodiversity, albeit not in situ; they retain their high scientific value, as demonstrated by university collections (Brilha, 2015).

Geology and Palaeontology museums are repositories of knowledge on natural heritage, providing important information about the evolution of life on earth through their collections. Geological collections are notoriously recognized for their scientific, pedagogical, cultural and recreational values. It is true that any science museum has a greater potential to communicate scientific knowledge to a broader audience (Bud, 1997). According to Wolniewicz (2021), the educational potential of geological and paleontological exhibits could be used in informal education activities. Consequently, they could play an important role in public awareness about the protection of the environment (Jakubowski, 2004). The sensorial and affective experiences provided by the museums could provoke cocreated narratives around climate and targeted actions by the audiences (Cameron et al., 2013).

Taking the above into consideration, this paper attempts to underline the role of museums in raising awareness and inspiring action about climate change. Due to the fact that museums are social learning spaces and spaces of transformation, they are called to respond to contemporary challenges and contribute to the formation of more democratic and progressive societies (Mouliou, 2014) by creating educational experiences (Filippoupoliti, 2015). More specifically, the study focuses on both the creation and evaluation of an educational programme for the Palaeontology & Geology Museum of the University of Athens. The programme is for students in the final years of primary school and endeavours to point out the correlation between climate change and mass extinctions throughout the long history of Earth (Greshko et. al., 2019; Begum, 2021). In addition, it seeks to understand the root of the problem called climate change nowadays and simultaneously make younger generations rethink their attitude and perception about the harmonious coexistence between man and nature.

The specific educational programme was effectively developed overcoming the difficulties arising from the limited number of exhibits and interpretative material while taking the objectives, the opportunities and limitations of the museum into account. The development of the programme is based on the use of several interactive methods and tools such as AR applications as well as targeted educational material. Immersive technologies contribute to the creation of a communication bridge between visitors and the museum that facilitates the process of imparting knowledge (Khawan, 2021). The whole process created the basis for a unique museum experience, expanding the possibilities of learning and entertainment.

Furthermore, a pilot implementation and a formative evaluation by postgraduate students of the master's programme "Museum Studies" contributed significantly to the final format of the educational programme. The conclusions drawn confirmed the intended objectives and choices and contributed to the modification of certain aspects of the programme. Lastly, upon taking its final form, the programme can be presented to and evaluated by primary school students, as it was initially intended prior the covid-19 restrictions.

To conclude, this study contributes to the broader discussion of the museums around the world about the urgent need to build future citizens' environmental awareness and highlights the role of non-formal learning and museum education.

References

Begum, T. (2021, May 19). What is mass extinction and are we facing a sixth one? Retrieved from: https://www.nhm.ac.uk/discover/what-is-mass-extinction-and-are-we-facing-a-sixth-one.html [Accessed 20 July 2022].

Brilha, J.B.R. & Reynard, E. (2018). Geoheritage and geoconservation: the challenges. *Geoheritage*. https://.doi.org/10.1016/B978-0-12-809531-7.00025-3

Brilha, J.B.R. (2015). Inventory and quantitative assessment of geosites and geodiversity sites: a review. *Geoheritage 8*, 119–134. https://doi.org/10.1007/s12371-014-0139-3

Bud, R. (1997). History of science and the Science Museum. *British Journal of the History of Science 30*, 47–50.

Cameron, F., Hodge, B., & Salazarchange, J. F. (2013). Representing climate change in museum space and places. *WIREs Clim Change 4*, 9–21. Doi: 10.1002/wcc.200

Carcavilla L., López-Martínez, J., & Valsero, J.D. (2007) *Patrimonio geológico y geodiversidad: investigación, conservación y relación con los espacios naturales protegidos.* Instituto Geológico y Minero de España, Madrid

Filippoupoliti, A. (2015). Educational theories and Museum learning. In: N. Nikonanou (Ed.), *Museum Learning and experience in the 21st century*, 27-49.

Greshko, M. & National Geographic Staff (2019, September 26). What are mass extinctions, and what causes them? Retrieved from: https://www.nationalgeographic.com/science/article/mass-extinction [Accessed 20 July 2022].

Jakubowski, J.K. (2004). Geological heritage and museums. *Polish Geological Institute Special Papers, 13*. *Proceedings of the Conference "Geological heritage concept, conservation and protection policy in Central Europe", Cracow, Poland*, 21–28. Retrieved from: https://www.pgi.gov.pl/docman-tree/publikacje-2/special-papers/13/2427-13-polish-geological-institute-special-papers-13-3-jakubowski-geological-heritage-and-museums/file.html [Accessed 20 July 2022].

Khawan, S. S. (2021). Using the technology in museum environments. *SSRN Electronic Journal.* DOI: 10.2139/ssrn.3782237

Mansur, K.L. (2018). Patrimônio geológico, geoturismo e geoconservação: Uma abordagem da geodiversidade pela vertente geológica. In: Guerra AJT, Jorge MCO (eds) *Geoturismo, geodiversidade, geoconservação: abordagens geográficas e geológicas, 1-50.* Oficina de Textos, São Paulo.

Mouliou, M. (2014). Museums in the 21st century: challenges, values, roles, and practices. In: G. Bikos & A. Kaniari (Eds.), *Museology. Cultural Management and Education*, 77-111.

Souza, A.R. & Miranda, M.L.C. (2007). A produção científica acerca do patrimônio geológico: análise das referências bibliográficas brasileiras e portuguesas. *VIII ENANCIB – Encontro Nacional de Pesquisa em Ciência da Informação.* http://enancib.ibict.br/index.php/enancib/viiienancib/paper/viewFile/2978/2104

Wolniewicz, P. (2021). Beyond geodiversity sites: Exploring the educational potential of widespread geological features (rocks, minerals, and fossils). *Geoheritage 13*, 34.

Zafeiropoulos, G., Drinia, H., Antonarakou, A. & Zouros, N. (2021). From geoheritage to geoeducation, geoethics and geotourism: a critical evaluation of the Greek region. *Geosciences 11* (9), 381. https://doi.org/10.3390/geosciences11090381

16th International Congress of the Geological Society of Greece

17-19 October, 2022 - Patras, Greece

Bulletin of the Geological Society of Greece, Sp. Publ. 10

Ext. Abs. GSG2022-088

Educational Proposal For Geology Through Walk Trails In The Urban Environment Of Palaio Faliron In Athens, Greece

G. Kontokostas[1], A. Antonarakou[1], H. Drinia[1], Ch. Vasilatos[1], S. Lozios[1],

(1) National and Kapodistrian University of Athens, Department of Geology and Geoenvironment, Panepistimiopolis, Zografos, Greece, geokon@geol.uoa.gr

Background and Objectives

Educational Geological walk trails in the urban environment are proposed as a successful interdisciplinary teaching approach to Geosciences in secondary education. Geological walk trail through Palaio Faliro, using techniques entailed in the scientific/educational methodology by inquiry, contributes in forming citizens who are active, responsible and aware of contemporary environmental issues, such as natural disaster management and natural resource exploitation (Kontokostas et al. 2020).

The designed geological walk trail is a practical endorsement in which the students will use fieldwork skills to identify a variety of rocks and geological materials in the built environment, as well as learn about geological features in the area.

The research area is located between Palaio Faliron and Alimos-Kalamaki, nearby Pikrodafni stream, along the coastline from Athens to Vouliagmeni. In this area the pre-Miocene basement of the HP metamorphic units of the lower plate and the un- or weakly metamorphosed units of the upper plate are covered by Neogene marine formations and Quaternary deposits (Papanikaloaou et al. 1999, & Papanikaolaou et al. 2004).

Research Methodology

This work follows the research steps outlined by inquiry–based learning: a) trigger of interest, b) reminding of basic knowledge/formulation of hypotheses, c) experimentation/trials, d) formulation of conclusions, e) applications/generalization according to learning (Bakopoulou et al. 2016). The designed walk trail includes: Faliron War Cemetery - Estuary of Pikrodafni stream - Riverbed of Pikrodafni (figure 1). We conducted our educational research with an experimental group of students of secondary school of Attica located near geolocially interesting areas.

Results and Conclusions

The findings of our study are compared to a control group of students from the same secondary school in Attica as the experimental group. There is a remarkable improvement in students' comprehension, creativity, cooperation and critical thinking. They learned about the Pikrodafni, they recognized white marble of Pendeli, green Tinos' marble, grey marble from Thasos, granite, Botticino limestone and fossiliferous limestone. The most intriguing aspect of the study was when the students realized that the complexity of the natural world is the result of the combinations of few simple procedures.

Keywords:

Urban Environment, Educational Geological Walk Trails, field lessons, Educational Research.

Figure 1. The walk trail: (1) Faliron War Cemetery (2) Estuary of Pikrodafni stream (3) Riverbed of Pikrodafni.

References

Bakopoulou A, Antonarakou A, Loizos S, Zambetakis –Lekkas (2016). Development and precodification of a lithosphere questionnaire as a tool in education research (Geoscienses). Bulletin of the Geological Society of Greece, 50(1), 201-208.

Kontokostas, G., Antonarakou, A., Fountopoulou, M., Drinia, H., & Lozios, S. (2020). Urban geology: educational proposal for Geoscience. a case study from the inner city of Athens, Greece. Bulletin of the Geological Society of Greece, Volume 56(1), 133-146.

Papanikolaou, D., Lekkas, E., Sideris, Ch., Fountoulis, J., Danamos, G., Kranis, Ch., Lozios, S. and at the contr. of Antoniou, I., Vassilakis, E., Vasilopoulou, S., Nomikou, P., Papanikolaou, I., Skourtsos, E. & Soukis, K. (1999): Geology and tectonics of W. Attica in relation to the 7-9-99 earthquake. Newsletter of E.C.P.F.E., Council of Europe, No 3, 30-34, Athens 1999.

Papanikoalou, D., Bassi, E.-K., Kranis, Ch. and Danamos, G. (2004). Paleogeographic evolution of the Athens Basin from Upper Miocene to present. Bulletin of the Geological Society of Greece vol. XXXVI, 2004, Proceedings of the 10th International Congress, Thessaloniki, April 2004.

16th International Congress of the Geological Society of Greece
17-19 October, 2022 - Patras, Greece
Bulletin of the Geological Society of Greece, Sp. Publ. 10

Ext. Abs. GSG2022-091

"Exploring the wondrous world of a limestone island": a geoeducational program for the promotion of the geological heritage of Kalymnos island

G. Zafeiropoulos[1], H. Drinia[1], A. Antonarakou[1], N. Zouros[2]

(1) Faculty of Geology & Geoenvironment, National and Kapodistrian University of Athens, Panepistimioupolis 15784, Zographou, Greece, georzafeir@geol.uoa.gr (2) Department of Geography, University of Aegean, 81100 Mytilini, Greece

Introduction

The island complex of the Dodecanese is an area rich in geodiversity, due to the intense geotectonic regime resulting from the position of the islands in the southeastern branch of the Greek arc, at the convergence of the two lithospheric plates, the European and the African (Zafeiropoulos & Drinia 2022).

In particular, the small island of Kalymnos is characterised by a unique geological and geomorphological diversity, which includes a rich and important geoheritage as well as an impressive landscape (Zafeiropoulos & Drinia 2021). The presence of caves, deep gorges and mountains is intense throughout the island.

Kalymnos could be called the 'island of limestone', as most of the island consists of this sedimentary rock. Kalymnos is a popular climbing destination, with around 3,000 climbing routes embedded in the limestone rock of the island. Apart from the climbing routes, the island is one of the richest in limestone caves. There are about 50 caves, many of which are still unexplored due to the roughness of the terrain, which are inaccessible (some are accessible even from the sea). Depending on their morphology, these caves are classified as 'horizontal' (i.e. the most accessible), 'cave cliffs' (which are not so easily accessible) and 'underwater' caves.

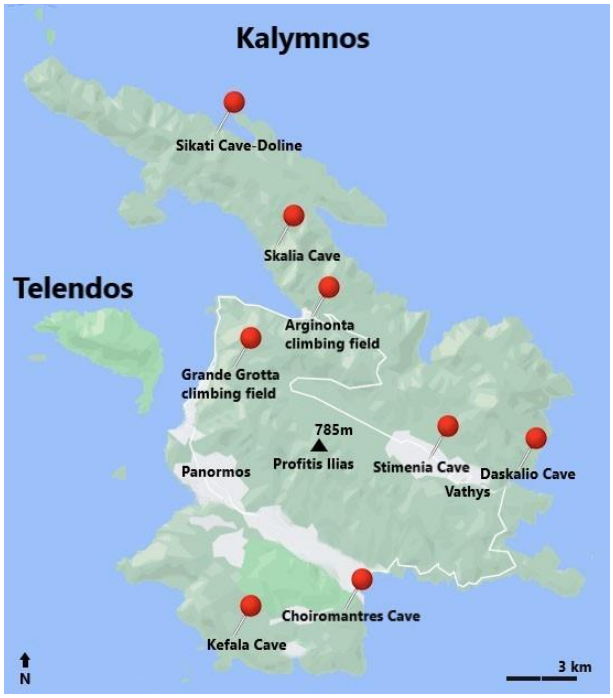

Figure 1. . Satellite map of Kalymnos island indicating the caves and climbing fields of the study area.

Despite these unique features and the strong potential in alternative forms of tourism, and in particular geotourism, that the island may have, tourism on Kalymnos has been steadily declining over the last 10-15 years, from 1,500 arrivals per week (1992-1994) to 300 arrivals per week.

In order to empower students in the knowledge, skills, values and attitudes of geocultural heritage, via the dissemination of these values, we propose an educational environmental program regarding the geocultural heritage of the rocky landforms of Kalymnos Island, entitled "Exploring the wondrous world of a limestone island".

By the implementation of the proposed geoeducational activities, we aim at understanding various geological concepts and processes in order to promote environmental awareness and respect for the value of geo-heritage. The ultimate

objective is to increase the living standards of the local population due to the influx of tourists who will discover the geological sites. This will lead to sustainable development in this area, from which future citizens of the island will also benefit. The project will mainly target secondary school students, as this is the age at which every person starts to form a culture and opinion.

Methodology

In the first stage, qualitative research was conducted among the island's locals and on secondary school students, in the form of in-depth interviews and discussions using the snowball sampling method (geological and environmental phenomena) (Simkus 2022).

At the second stage, an educational geoenvironmental program on the geocultural heritage of the limestone karstic geomorphs of Kalymnos was created, with the title "exploring the wondrous world of the limestone island". The aim of the program is to empower students' knowledge, skills, values, and attitudes [UNESCO] about the values of geocultural heritage. The objectives of Knowledge, Awareness, Attitudes and Values and Participation were identified (Ragkou 2014). According to them, students seek to mention the basic physical characteristics of caves, describe how they are created, identify them as geological heritage sites (Fermeli & Markopoulou-Diakantoni 2004) and as ecosystems, understand and realize the values of geodiversity and geoheritage, in order to develop an ethical code of conduct and a sense of responsibility for the protection and conservation of the geoenvironment.

Regarding the way to control the achievement of the goal in terms of empowering students in the values of geoheritage, the qualitative research technique of the thematic analysis of Georgousis et al. (2021) is suggested, with the main research question being whether the implementation of the environmental program "exploring the island of limestone", succeeded in empowering students in the values of geocultural heritage, Geological, Aesthetic, Cultural, Ecological and Sustainable development.

Results

The qualitative research showed a complete lack of environmental awareness as well as geo-ethical values (Zafeiropoulos et al. in prep). The relevant research on secondary school students showed that students' education on geodiversity and geoheritage is significantly underdeveloped, so that the integration of geoeducation into environmental education (geoenvironmental education) as well as the enhancement of geological heritage with holistic approaches and interdisciplinary connections are deemed necessary (Georgousis et al. 2021; Georgousis et al. 2022).

The qualitative analysis showed that the implementation of the environmental program may succeed in empowering the students in geocultural values. In addition, it appeared that students were strengthened in themes and values of geocultural heritage and sustainability as well as developed feelings of environmental sensitivity.

References

Georgousis, E.; Savelides, S.; Mosios, S.; Holokolos, M.-V.; Drinia, H., 2021. The Need for Geoethical Awareness: The Importance of Geoenvironmental Education in Geoheritage Understanding in the Case of Meteora Geomorphes, Greece. Sustainability 2021, 13, 6626, doi:10.3390/su13126626

Georgousis, E.; Savelidi, M.; Savelides, S.; Mosios, S.; Holokolos, M.-V.; Drinia, H., 2022. How Greek Students Perceive Concepts Related to Geoenvironment: A Semiotics Content Analysis. Geosciences 12, 172. https://doi.org/10.3390/geosciences12040172

Fermeli, G.; Markopoulou-Diakantoni, A., 2004. Selecting Pedagogical Geotopes in Urban Environment. Bull. Geol. Soc. Greece 36, 649–658, doi:10.12681/bgsg.16770

Ragkou, P. 2014. Didactic of Environmental Education. Aristotle University of Thessaloniki, Thessaloniki, Greece, 2014; Available online: http://eclass.auth.gr/courses/OCRS439/ [In Greek]

Simkus, J. 2022. Snowball Sampling: Definition, Method and Examples. Simply Psychology www.simplypsychology.org/snowball-sampling.html

Zafeiropoulos, G.; Drinia, H., 2021 Kalymnos Island, SE Aegean Sea: From Fishing Sponges and Rock Climbing to Geotourism Perspective. Heritage 4, 3126-3146. https://doi.org/10.3390/heritage4040175

Zafeiropoulos, G.; Drinia, H., 2022. Comparative Analysis of Two Assessment Methods for the Geoeducational Values of Geosites: A Case Study from the Volcanic Island of Nisyros, SE Aegean Sea, Greece. Geosciences 12, 82. https://doi.org/10.3390/geosciences12020082

16th International Congress of the Geological Society of Greece
17-19 October, 2022 - Patras, Greece
Bulletin of the Geological Society of Greece, Sp. Publ. 10
Ext. Abs. GSG2022-095

Geoconservation management in geoparks: The case of Vikos-Aoos (Greece) and Arouca (Portugal) UNESCO Global Geoparks

A.Koliou[1], H.Drinia[1], N.Zouros[2], J.Brilha[3]

(1) Department of Geology and Geoenvironment, National and Kapodistrian University of Athens, Panepistimiopolis, 15784 Athens, Greece, alkoliou@gmail.com (2) Department of Geography, University of Aegean, 81100 Mytilini, Greece (3) Institute of Earth Sciences, Pole of the University of Minho, Campus de Gualtar, 4710-057 Braga, Portugal

In the last two decades, a new and developing subdiscipline of applied geology has arisen: geoconservation, dealing with the preservation of non-living parts of the natural environment (Burek & Prosser, 2022), and informing us about Earth's history (Du & Girault, 2018). Geoconservation is focused on the management of geological heritage represented by geosites with scientific, educational, cultural, and touristic value (Zafeiropoulos et al. 2021).

In the context of a holistic approach to foster protection and promotion of global significant geoheritage, geoparks are an important tool. The idea of geoparks started by the end of the twentieth century. The establishment of the European Geoparks Network in 2000 that led to the establishment of the Global Geoparks Network under the auspices of UNESCO in 2004 (McKeever et al. 2010) and the approval in 2015 of the UNESCO Global Geoparks Programme placed geoconservation at the international scale.

Nowadays, UNESCO Global Geoparks (UGGp) around the world constitute one of the main conservation strategies, combining the sustainable use of geosites with benefits for the local community. Geoparks, with geosites inventory and management plans, administrative and economic measures, and education and promotion actions ensure the most efficient strategy for the protection of valuable areas (Henriques & Brilha, 2017).

With these in mind, our research will seek how different management methods shape the degree of geoheritage conservation and its effectiveness in UGGp. The aim of our research is to assess which organizational and management model offers the best geoheritage protection to Greek geoparks and to propose innovative management practices to enhance geoconservation in UGGp.

It will be presented an indicative comparison of the management structures of two UGGp, Vikos-Aoos in Greece and Arouca in Portugal, with the ultimate goal of analyzing their effectiveness in terms of geoconservation and degree of geoheritage protection. These geoparks were chosen due to their similar geomorphology, characterized by mountains and rivers, as well as similar geotouristic activities and traditional villages. Both territories have also many years of experience operating as geoparks.

Firstly, the management structure of each geopark will be described, as well as their main characteristics, protection status and action plans. It will be given particular attention to geoconservation actions, namely how effective measures are implemented and monitored.

The expected results will be included in the general framework of our research that will examine, analyze, and compare geoconservation methods and their effectiveness of all Greek geoparks and three foreign geoparks.

In order to have comparable results, we will use qualitative and quantitative models to evaluate geoconservation. If necessary, we will try to create new comparison tools in order to get a more accurate overall picture.

Acknowledgements

Special thanks to anonymous reviewers who evaluated this abstract.

References

Burek C.V., Prosser C.D., 2022.) 'The history of geoconservation: an introduction', Geological Society, 300, pp 1-5.

Du Y., Girault Y., 2018. 'A Genealogy of UNESCO Global Geopark: Emergence and Evolution', International Journal of Geoheritage and Parks, Darswin Publishing House, 6 (2), pp.1-17.

Henriques M.H., Brilha J., 2017. 'Unesc Global Geopark: a Strategy towards Global Understanding and Sustainability', Episodes, 40, pp. 349-355.

McKeever P.J., Zouros N.C., Patzak M., 2010. 'The UNESCO Global Network of National Geoparks', The George Wright Forum,27,1.

Zafeiropoulos, G.; Drinia, H.; Antonarakou, A.; Zouros, N., 2021. From Geoheritage to Geoeducation, Geoethics and Geotourism: A Critical Evaluation of the Greek Region. Geosciences 11, 381. https://doi.org/10.3390/geosciences11090381

16th International Congress of the Geological Society of Greece
17-19 October, 2022 - Patras, Greece
Bulletin of the Geological Society of Greece, Sp. Publ. 10
Ext. Abs. GSG2022-119

Quantitative Assessment of the Geosites of Chelmos-Vouraikos UNESCO Global Geopark (Greece)

V. Golfinopoulos[1], P. Papadopoulou[1], E. Koumoutsou[2,3], N. Zouros[4], C. Fassoulas[5], A. Zelilidis[1], G. Iliopoulos[1]

(1) Department of Geology, University of Patras, Patras, Greece, gkolfinopoulosv@upnet.gr (2) Chelmos-Vouraikos UNESCO Global Geopark, Kalavryta, Greece (3) Department of Biology, University of Patras, Patras, Greece (4) Department of Geography, University of the Aegean, Mytilene, Greece (5) Natural History Museum of Crete, University of Crete, Heraklion, Greece.

Introduction

Chelmos-Vouraikos geopark is one of the seven designated UNESCO Global Geoparks (UGGps) of Greece and one of 177 worldwide. UGGps have the following goals: (a) protection and conservation of their territorial geoheritage, (b) cultural and environmentally sustainable development of their territories and (c) geoscience education by promoting awareness about the history of the earth as well as sustainable development (UNESCO, Catana *et al.* 2020). Over the past three decades, several methodologies for the evaluation of geoheritage have been developed, aiming to serve geoconservation and geotourism needs (Golfinopoulos *et al.* 2022). These assessment methodologies became a useful tool for geopark managers highlighting and quantifying the priorities needed for the proper management and protection of a geopark, the priorities for geotourism and educational tourism, as well as for the geoconservation of geosites.

The main objective of this study is the evaluation of the 40 geosites of the Geopark to highlight their touristic and educational value, the need for their protection, and the evaluation of the selected methodology, through which its advantages and respective weaknesses that might need improvement, will be highlighted (Golfinopoulos *et al.* 2022).

Geopark Outline

Chelmos-Vouraikos UGGp is located in North Peloponnese, Greece. It occupies an area of 647 km^2 with a total population of approximately 27,000. The area exhibits unique geoheritage, wonderfully combined with rich biodiversity and exceptional cultural and historical elements. To date, 40 geosites have been designated in the geopark. They include unique geological formations (folds, faults, rocks and lithological formations, etc.), karstic geomorphs (caves, poljes, karstic springs), rich geomorphosites (gorges, high peaks, alpine lakes etc) and fossil sites (Golfinopoulos *et al.* 2022).

At least 485 million years (lower Palaeozoic) of geological history are "unfolded" in the geopark. The alpine basement consists of three geotectonic zones, namely Tripolis Zone, Pindos Zone and the metamorphic Phyllites–Quartzites Suite which is the oldest. Post-alpine formations, whose deposition is related to the Corinth rift and glaciers that developed during the Middle to Late Pleistocene on Chelmos Mountain, overlay the alpine basement (Golfinopoulos *et al.* 2022).

Also, the area of the geopark is valued and protected for its biodiversity and has been classified as a "National Park" as well. The local population are mainly farmers and stockbreeders, who produce among others dairy products, honey, and legumes. Additionally, tourism is important for the local economy. "Odontotos" rack railway, Kalavryta ski center, the Cave of the Lakes are classical examples which shape the local geotouristic character of this geopark. The area of geopark presents historical (e.g., Holocaust Monument at Kapi hill, Holocaust Museum etc.), archaeological (e.g., archaeological sites of ancient Lousoi and ancient Kleitoria) as well as religious interest (e.g., historic monasteries of Mega Spilaio and Agia Lavra). One more aspect of the geopark's multidimensional value is its intangible heritage, which is wonderfully expressed through popular art, especially music and poetry and mostly through the extensive mythological heritage (Golfinopoulos *et al.* 2022).

Materials & Methods

From the assessment methodologies of geopark's geosites that have been developed to date, the method proposed by Fassoulas et al. (2012) was chosen as the most suitable for the present study. Fassoulas et al. (2012) methodology is based not only on geological criteria, but also on a wider range of scientific, ecological, cultural, aesthetic, and economic criteria concerning the value of each geosite, compared to other locations at regional or/and national level. Each criterion was scored on a scale from 1 to 10, and three indexes and one factor were calculated, representing the educational (V_{edu}), touristic (V_{tour}), and need for protection (V_{prot}) indexes, and the ecological risk factor (F_{ecol}) of each geosite.

Results

The average score of the scientific criteria for the 40 assessed geosites of Chelmos-Vouraikos UGGp ranges from 2.1 to 9.5, the highest values are presented by Geosite 1 (Niamata) (9.5) and Geosite 23 (Lousoi polje) (8.5). The ecological criteria cover the full scores' range (1 to 10). Geosites 2 (Portes–Triklia), 5 (Kerpini conglomerates), 11 (the Cave of

the Lakes) and 24 (Mavrolimni) present the highest score (10). Geosites 20 and 34 (Water of Styx and Psili Korfi) are classified as slightly lower (8.8). The rating of the cultural criteria ranges from low to medium (1 to 5.9). Geosite 11 (Mega Spilaio) presents the highest score (5.9). The aesthetic criteria score shows a wide range as well (1 to 10). Geosites 11 and 17, Cave of the Lakes and Doxa Lake, present the highest value, (10). The score of the economic criteria varies from 1 to 10. Geosite 7 (Tectonic Graben of Kalavryta) has been scored with 10. The score of the criteria for potential use ranges from 3.9 to 9.5. Geosite 13 (Lousoi sinkholes) bear the highest score for this criterion (9.5).

As suitable geosites for educational activities are considered those geosites with values of V_{edu} exceeding 6. These are (in descending order) the geosites Portes-Triklia (C 02, V_{edu} = 7.3), the Cave of the Lakes (C 11, V_{edu} = 7.2), Mega Spilaio (C 28, V_{edu} = 6.8), Ntourntouvana (C 35, V_{edu} = 6.5), Niamata (C 01, V_{edu} = 6.4), Doxa lake (C 17, V_{edu} = 6.4) and Mavrolimni (C 24, V_{edu} = 6.1). Regarding the geotouristic value of the geosites index V_{tour} is considered. The highest values are presented by the Tectonic Graben of Kalavryta (C 07, V_{tour} = 7.8), Mega Spilaio (C 28, V_{tour} = 7.7), Doxa lake (C 17, V_{tour} = 7.7), the Cave of the Lakes (C 11, V_{tour} = 6.7), Portes–Triklia (C 02, V_{tour} = 6.7) and Lousoi polje (C 23, V_{tour} = 6). Geosites that, according to the V_{prot} index, show the greatest need for protection are the Tectonic Graben of Kalavryta (C 07, V_{prot} = 6.7) and the Eroded conglomerates (C 38, V_{prot} = 5.9). As far as the ecological risk factor is concerned, the highest value is held by the Eroded conglomerates geosite (C 38, F_{ecol} = 10). The F_{ecol} is also particularly high in the Tectonic Graben of Kalavryta (C 07, F_{ecol} = 5) (figure 1).

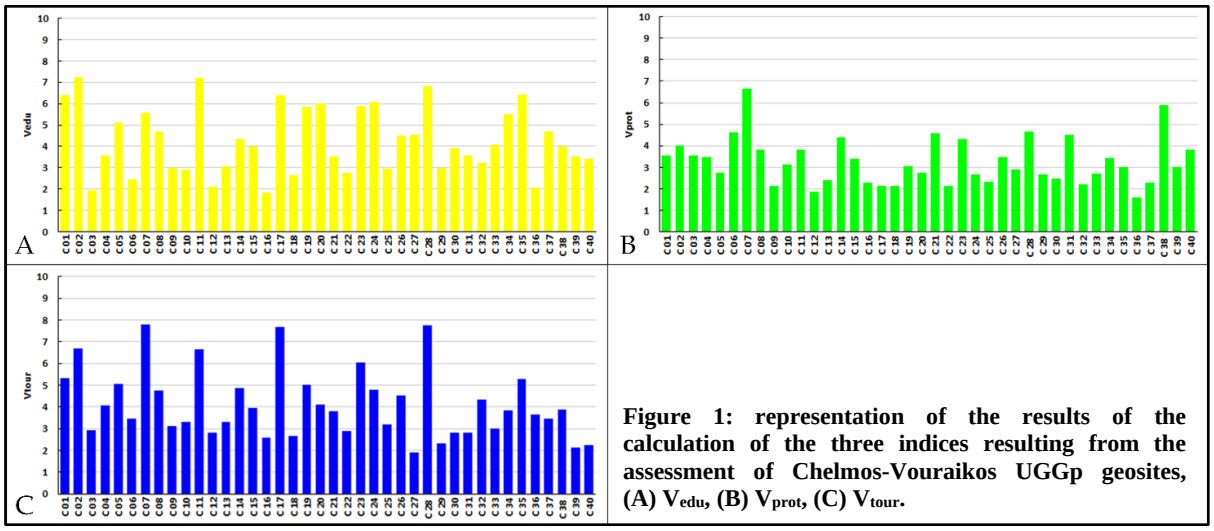

Figure 1: representation of the results of the calculation of the three indices resulting from the assessment of Chelmos-Vouraikos UGGp geosites, (A) V_{edu}, (B) V_{prot}, (C) V_{tour}.

Conclusions

Most geosites with calculated high educational value are already used for corresponding activities from the managing authorities of the geopark. Those with a very high V_{edu} index have a great improvement potential for Chelmos-Vouraikos UGGp. Geosites with high touristic value, which so far are not fully exploited, have highlighted the necessity to enhance their touristic development with various actions. Based on the assessment results, the geopark management has already planned actions to develop accessibility and promote the geosites of Chelmos Mt, and particularly the Water of Styx and Psili Korfi that were highly rated. Similarly, geosites with high protection index values, are considered as places with a great need for protection. Sometimes protection measures such as removing/reducing livestock activities and facilities around geosites are easy to be taken, whereas in other cases protection measures are difficult because of the very high human activity.

Applying the methodology of Fassoulas *et al.* (2012) in the area of Chelmos-Vouraikos made possible the identification of some malfunctions and elaboration problems related to caves, intangible heritage and the number of visitors used in the evaluation criteria. We think that these problems can be solved with further refinement and specifications in the criteria description related with the above cases.

Acknowledgements

This study is part of Golfinopoulos' Master's Thesis funded by "Andreas Mentzelopoulos Scholarships for postgraduate studies at the University of Patras", to which we are grateful. We would like to thank the personnel of Chelmos-Vouraikos UNESCO Global Geopark for all the help they provided during fieldwork and the collection of data.

References

Catana, M.M., Brilha, J.B, 2020. The Role of UNESCO Global Geoparks in Promoting Geosciences Education for Sustainability. Geoheritage, 12, 1.

Fassoulas, C., Mouriki, D., Dimitriou-Nikolakis, P., Iliopoulos, G., 2012. Quantitative Assessment of Geotopes as an Effective Tool for Geoheritage Management. Geoheritage, 4, 177–193.

Golfinopoulos, V., Papadopoulou, P., Koumoutsou, E., Zouros, N., Fassoulas, C., Zelilidis, A., Iliopoulos, G., 2022. Quantitative Assessment of the Geosites of Chelmos-Vouraikos UNESCO Global Geopark (Greece). Geosciences, 12, 63.

UNESCO. Statutes of the International Geoscience and Geoparks Programme (IGGP). Available online: https://unesdoc.unesco.org/ark:/48223/pf0000234539.locale=en (accessed on 28 December 2021).

16th International Congress of the Geological Society of Greece

17-19 October, 2022 - Patras, Greece

Bulletin of the Geological Society of Greece, Sp. Publ. 10

Ext. Abs. GSG2022-140

National Geological Park Of Nea Kameni Volcano, Santorini, Greece: A profound update of the touristic services provided to the visitors of the world-famous volcano

P. Nomikou[1], S. Kazana[1], V. Antoniou[1], G. Pehlivanides[2], P. Krassakis[3], K. Drymoni[4] D. Panousis[1], E. Nikoli[1], M. Agiomavritis[5], A. Batis[5].

(1) National and Kapodistrian University of Athens, Athens, Greece, evinom@geol.uoa.gr (2) Hands-on studio, Research & Art Direction, Branding, UX/UI Design, Project Management, Thessaloniki, Greece (3) Department of Geography, Harokopio University of Athens, El. Venizelou 70, 17671 Athens, Greece (4) Department of Earth and Environmental Sciences, University of Milan-Bicocca, 20126, Milan, Italy (5) Econtent Systems P.C, Software, Website and Mobile application development, Athens, Greece.

In the Eastern Mediterranean Sea and more specifically in the South Aegean region, the most prominent geodynamic event is the subduction of the African Lithospheric Plate beneath the Eurasian one. The latter formed the Hellenic Volcanic Arc, a nearly 600-kilometer-long chain of active volcanoes. The volcanic field of Santorini - Christianna - Kolumbo is among the most well-known of these volcanoes, and its reputation extends beyond Greece. Santorini, an island archipelago consisting of the main, crescent shape island of Thera along with the smaller islands of Therasia, Aspronisi, Palea and Nea Kameni, is famous for its caldera-forming Late Bronze Age eruption (1613-1620 BC), also known as the 'Minoan' eruption. The island of Santorini features astonishing volcanic geomorphology, with the prominent flooded caldera encompassing the central Kameni lava shield, which hosts lava domes, flows and multiple fractures as well as volcanic products that date as far back as 650.000 years. Extensive multidisciplinary studies on Santorini have only started revealing the mechanisms that drive the eruptive cycles of the volcanic center, which generally consist of a violent, Plinian eruptive phase (similar to the LBA eruption). This type was followed by a less eruptive Intra – Plinian phase with acidic lava emissions and dome building, and a final repose phase without significant activity leading up to the next Plinian eruption. Nowadays, the post-Minoan caldera activity consists of nine eruptive phases and forms the Kameni volcanic edifice, which gradually distributes in the central part of the caldera. The parts of the edifice that are above sea level form the islands of Palea and Nea Kameni.

The formation of Nea Kameni has been well documented in the historical record and diachronically shaped, affected and became part of the daily life of the residents of Santorini, who eventually learnt to live with the volcano's pulse. With the last eruption having occurred only in 1950, the islet is a treasure trove for geoscientists worldwide, and the millions of tourists that visit Santorini over the past decades. It offers its visitors the opportunity to experience the true nature of Santorini. While walking on the volcanic surface, they can observe the black, fractured dacitic lavas, identify lava flows of different ages and admire the volcanic craters with the fumarolic activity and minerals. Eventually, they can stand in awe before the panoramic view of the entire Santorini caldera, engulfing the horizon from the island's top.

A visit to Nea Kameni is a memorable experience. The island can be accessed by boat from one of the ports of Santorini. The Nea Kameni volcanic path leads to five points of interest that showcase the geological history of the volcanic eruptions. To improve the services offered by Nea Kameni Geological Park, cooperation among GEOTHIRA, the Thera Municipality and the scientific team and partners of the National and Kapodistrian University of Athens the design, construction and launch of a mobile application occurred. The "Santorini Volcano App", is a modern informative leaflet of the Nea Kameni region which accompanies a new, informative website (www.santorinivolcano.gr) with scientific accuracy and thoroughness referring to the volcanic evolution of Santorini.

The production of the first mobile virtual guide, an offline and easy-to-navigate application that can be used both in the field upon visit and remotely, is focused on providing information about the Santorini volcanic complex. It emphasizes the Minoan eruption and the subsequent creation of the Kameni islands, which are Santorini's geological and geo-touristic highlights, located inside the volcano's caldera. The app's user-friendly interface provides information about the Hellenic Volcanic Arc and the Minoan eruption, as well as general information about Santorini. It also presents a comprehensive area map featuring the volcanic path, the five points of interest on Nea Kameni, the user's position on the map, an elevation profile of the path and additional information on the points of interest. Finally, the app includes high-definition photos, videos, astonishing 360 panoramas of the region, safety tips for a safe and fulfilling visit and a prototype Geo-Dictionary which simplifies geological terms mentioned throughout the app.

Additionally, a modern informative leaflet about Nea Kameni was designed that complements the services provided by the mobile application. Its unique design revolutionizes the format of informative leaflets and excludes the traditional page-shifting template, featuring all the information within a foldable A2-sized poster. On the one side, it presents a complete 2D volcanological map of Nea Kameni depicting the volcanic path, the five points of interest, an informative legend and a QR code linked to the new Santorini Volcano website. On the other side, each fold-level features information regarding the South Aegean Volcanic Arc, the Minoan Eruption and the volcanic evolution of the Kameni islands, the

five points of interest with high-definition photos, a 3D map of the area with the elevation profile of the path and the safety tips.

The final product developed for improving the services of the National Geological Park of Nea Kameni Volcano is an informative website featuring detailed, scientifically accurate information regarding volcanism at Santorini. The website accompanies and promotes the informative leaflet and the mobile application. On the website, users can learn more about the evolution of volcanism generally along the South Aegean Volcanic Arc and Santorini volcanic complex (Minoan eruption and Kameni islands), view an interactive map with the five points of interest on Nea Kameni, download the Santorini Volcano app on their mobile devices and even admire rare and exclusive photographic material with historical eruptions at Nea Kameni.

Figure 1: Poster highlighting the different ages of lava in Palea and Nea Kameni islands and the five points of interest on the volcanic path. Snapshots from the mobile application, the website and the foldable leaflet are also visible.

Acknowledgements

The production of the mobile application, the informative poster and the Santorini Volcano website would not have been possible without the critical procedural and financial contribution and support of Thira Municipality and GEOTHIRA. Special thanks to Prof. Tim Druitt (Univ. of Clermont) for his help on the scientific text.

References

Druitt, T.H., Mellors, R.A., Pyle, D.M., and Sparks, R.S.J., (1989). Explosive volcanism on Santorini, Greece: Geological Magazine, v. 126, p. 95–126.

Druitt, T. H, Edwards L., Mellors R.M., Pyle D.M, Sparks R.S.J., Lanphere M., Davies M., & Barreirio, B. (1999). Santorini volcano, Geological Society Memoir. J. Geol. Soc.Lond. 19, 165.

Fouqué, F. (1999). Santorini and its eruptions, Translated and annotated by McBirney A.R., The Johns Hopkins Press, Baltimore.

Georgalas, G.C., (1953). L'éruption du volcan de Santorin en 1950: Bulletin Volcanologique, ser. II, v. 13, p. 39–55.

Georgalas, G., and Liatsikas, N., (1925). Sur la nouvelle éruption du volcan de Santorin (1925): Comptes Rendus Hebdomadaires des Seances de l'Academie des Sciences, v. 181, p. 1147–1149.

Georgalas, G., and Liatsikas, N., (1936). Die historische Entwickelung des Dafni-Ausbruches 1925–1926, in Reck, H., ed., Santorin: v. 2: Berlin, Dietrich Reimer, p. 1–96 (in German).

Georgalas, G.C., and Papastamatiou, J., (1953). L'éruption du volcan de Santorin en 1939–1941. L'éruption du dome Fouqué: Bulletin Volcanologique, v. 13, p. 1–38.

Kténas, C.A., (1925a). L'éruption du volcan de Santorin: Comptes Rendus Hebdomadaires des Seances de l'Academie des Sciences, v. 181, p. 376–377.

Kténas, C.A., (1925b). L'éruption du volcan de Santorin. Caractères morphologiques: Comptes Rendus Hebdomadaires des Seances de l'Academie des Sciences, v. 181, p. 518–520.

Kténas, C.A., (1926). L'éruption du volcan des Kaménis (Santorin) en 1925. Part I: Bulletin Volcanologique, v. 7–8, p. 3–64.

Kténas, C.A., (1927). L'éruption du volcan des Kaménis (Santorin) en 1925. Part II: Bulletin Volcanologique, v. 11–12, p. 7–49.

Manning, S.W., Ramsey, C.B., Kutschera, W., Higham, T., Kromer, B., Steier, P., Wild, E.M. (2006). Chronology for the Aegean Late Bronze Age 1700–1400 B.C., Science 312, 565–569.

Nomikou, P., Parks, M.M., Papanikolaou, D., Pyle, D.M., Mather, T.A., Carey, S., Watts, A.B., Paulatto, M., Kalnins, M.L., Livanos, I., Bejelou, K., Simou, E., Perros, I. (2014). The emergence and growth of a submarine volcano: the Kameni islands, Santorini (Greece), Geo. Res. J. 1–2, 8–18.

Nomikou, P., Druitt, T. H., Hübscher, C., Mather, T.A, Paulatto, M., Kalnins, L.M., Kelfoun, K., Papanikolaou, D., Bejelou, K., Lampridou, D., Pyle, D.M., Carey, S., Watts A.B, Weiß, B. & Parks, M.M. (2016). Post-eruptive flooding of Santorini caldera and implications for tsunami generation. Nat Commun 7, 13332.

Parks, M.M., Biggs, J., England, P., Mather, T.A., Nomikou, P., Palamartchouk, K., Papanikolaou, X., Paradissis, D., Parsons, B., Pyle, D.M., Raptakis, C., Zacharis, V. (2012). Evolution of Santorini Volcano dominated by episodic and rapid fluxes of melt from depth, Nat.Geosci., 5(10), 749–54.

Pyle D.M. & Elliott J.R. (2006). Quantitative morphology, recent evolution, and future activity of the Kameni Islands volcano, Santorini, Greece, Geosphere, 2, 5, 253–268.

Reck, H., ed., (1936a). Santorin. Das Werdegang eines Inselvulkans und sein Ausbruch, 1925–1928. Ergebnisse einer Deutsch-Grieschischen Arbeitgemeinschaft: Berlin, Dietrich Reimer, 3 vol. (in German).

Reck, H., (1936b). Dynamik und morphogenese des Dafni Ausbruches als beispiel einer Staukuppenbildung mit Stromerguss, in Reck, H., ed., Santorin, v. II: Berlin, Dietrich Reimer, p. 114–207 (in German).

Virlet d'Aoust, T., (1866). Histoire des Kaïmênis ou des iles volcaniques nouvelles du golfe de Santorin, dans l'archipel de la Grèce: Paris, Loignon et Cie, 21 p. (in French).

Von Fritsch, K., Reiss, W., and Stübel, A., (1867). Santorin. The Kameni islands: London, Trübner and Co., 7 p.

Watts A.B., Nomikou P., Moore J.D.P., Parks M.M., Alexandri M. (2015). Historical bathymetric charts and the evolution of Santorini subma0rine volcano, Greece. Geochemistry, Geophysics, Geosystems 16 (3), pp.847.

16th International Congress of the Geological Society of Greece

17-19 October, 2022 - Patras, Greece

Bulletin of the Geological Society of Greece, Sp. Publ. 10

Ext. Abs. GSG2022-141

Nisyros Aspiring UNESCO Global Geopark: Crucial Steps For Promoting The Volcanic Landscape's Unique Geodiversity.

P. Nomikou[1], D. Panousis[1], E. Nikoli[1], D. Emmanouloudis[2,3], P. Nastos[1], V. Antoniou[1], G. Pehlivanides[4], M. Agiomavritis[5], A. Batis[5].

(1) National and Kapodistrian University of Athens, Athens, Greece, evinom@geol.uoa.gr (2) International Hellenic University, Kavala, Greece (3) UNESCO Chair on Conservation and Ecotourism of Riparian and Deltaic Ecosystems, Kavala, Greece (4) hands-on.studio, Research & Art Direction, Branding, UX/UI Design, Project Management, Thessaloniki, Greece (5) Econtent Systems P.C, Software, Website and Mobile application development, Athens, Greece.

Nisyros Geopark, an island geopark in the Southeastern Aegean Sea, Greece, is here presented as an official candidate for the UNESCO Global Geoparks designation, featuring outstanding geological, natural and cultural characteristics. The geopark covers a total area of 481 km^2 and includes Nisyros, an active volcano and the geopark's main island, as well as the surrounding volcanic islets of Pachia, Strongyli and Pergousa, the non-volcanic islet of Kandeliousa and the marine region around them. As part of the South Aegean Volcanic Arc (also known as the Hellenic Volcanic Arc), it bears a dramatic landscape shaped after the five eruptive cycles of its geological history (Dietrich & Lagios, 2018) during the past 160,000 years, that left their scars both on the onshore and the offshore areas of the geopark (Nomikou & Papanikolaou 2011). It features a number of exceptional geosites and geomorphological features, including the central caldera, lava domes, flows, vents, fractures and even hydrothermal eruptive craters like Stefanos, one of the largest of its kind in the world (Parcharidis et al., 2018). The offshore area is the continuation of the volcanic landscape below the sea, featuring a number of basins, underwater volcanic structures like craters, lava domes and fractures as well as a pre-historic caldera, Avyssos, NE of Strongyli islet (Tibaldi et al., 2008; Nomikou et al., 2021).

Apart from geology, the Geopark features rich biodiversity protected by the two internationally designated Natura 2000 areas including its entire surface, as well as three wildlife refuge areas recognized at a national level. A great number of species of flora, avifauna and reptiles thrive within the geopark's area (Antoniou et al., 2019).

Its cultural heritage has remained immutable through time, while it exposes the splendor of art and civilization, expressed through prehistoric and historic locations and monuments. It hosts exceptional archaeological and cultural sites including fortresses, remnants of ancient habituations, numerous churches and monasteries, several thermal springs directly connected to the long tradition of its thermal baths, which all together have ultimately encapsulated the region's history and given rise to the traditions, tangible and intangible heritage of locals today.

Through a network of well-established walking trails (Antoniou et al., 2021), visitors can admire the unique geodiversity and biodiversity of the area, discover its cultural and archaeological features that are bound to its eruptive past and even listen to the rumble of the Earth itself, by walking on the bottom of Stefanos crater. Nisyros Geopark is the only area in the broader region of the Eastern Mediterranean that hosts all these features at such a restricted area, making it an ideal UNESCO Global Geopark candidate.

In the initial efforts of the management body of Nisyros Geopark and its scientific team to promote its unique geodiversity, the complete design, construction and launch of a mobile application "NISYROS VOLCANO App" and a modern informative leaflet regarding the region of Lakki, at Nisyros island, were included. A coordinated effort between the scientific team and colleagues specializing in mobile application design, graphics and websites resulted in the production of the geopark's first virtual guide, a free, offline and easy to use mobile app that focuses on providing information about the active hydrothermal region of Lakki, which is the geological and touristic highlight of the geopark, located inside the volcano's caldera. Within the app, a user-friendly interface guides visitors to information about the Hellenic Volcanic Arc and the volcanic evolution of Nisyros as well as general information about the island and the Lakki Hydrothermal Field. It also provides them with a comprehensive area map featuring the trails, the three points of interest within Lakki, along with the position of the user on the map, an elevation scale of the trails as well as additional information on the points of interest. Finally, the app includes high-definition photos, videos, astonishing 360 panoramas of the region, safety tips for a safe and fulfilling visit as well as a prototype Geo-Dictionary which simplifies geological terms mentioned throughout the app's text.

The same team also resulted in the production of a modern informative poster about Lakki, that complements the services provided by the mobile application. Its unique design revolutionizes the format of informative geopark leaflets and excludes the traditional page-shifting template, featuring all the information within a foldable A2 sized poster. On the one side, it presents a complete 2D map of the Lakki area with the proposed trails, the three points of interest, an informative legend as well as a QR code linked to the official Nisyros Geopark website. On the other side, each fold-level features information regarding the South Aegean Volcanic Arc, the volcanic evolution of Nisyros, the three points of interest with high-definition photos, a 3D map of the area with an elevation scale and the safety tips.

Figure 1: Poster highlighting the geo-biodiversity of Nisyros Geopark as well as snapshots from the mobile application, the website and the foldable leaflet.

As Nisyros Geopark (www.nisyrosgeopark.gr) continues its efforts for a sustainable touristic development and promotion of its geodiversity, biodiversity, cultural, tangible and intangible heritage, all members associated will keep brainstorming new ideas, educational activities and innovative applications to successfully lead the geopark to its eventual recognition as an official UNESCO Global Geopark.

Acknowledgements

The candidature of Nisyros Geopark as well as the production of the mobile application and the informative poster would not have been possible without the critical procedural and financial contribution and support of the Municipality of Nisyros and the Municipality of Nisyros Corporation of Public Benefit (DIKEN). Also, a special thanks must be attributed to the partners responsible for the website development, carried out by monoscopic studio, as well as for the icon set design, implemented by anifactum studio.

References

Antoniou, V., Nomikou, P., Panousis, D. and Zafeirakopoulou, E., 2021. Nisyros Volcanic Island: A Geosite through a Tailored GIS Story. Geosciences, 11(3), p.132.

Antoniou, V., Nomikou, P., Zafeirakopoulou E., Bardouli P., Ioannou T., 2019. Geo-biodiversity and cultural environment of Nisyros volcano, 15th International Congress of the Geological Society of Greece, Athens, 22-24 May, 2019 | Harokopio University of Athens, Greece. Bulletin of the Geological Society of Greece, Sp. Pub. 7 Ext. Abs. GSG2019-195.

Dietrich, V. and Lagios, E., 2018. Nisyros Volcano, The Kos - Yali - Nisyros Volcanic Field. 1st ed. Springer, Cham.

Nomikou P., Papanikolaou D. (2011). Extension of active fault zones on Nisyros volcano across the Yali-Nisyros Channel based on onshore and offshore data. Marine Geophysical Research 32 (1), pp.181. DOI 10.1007/s11001-011-9119-z.

Nomikou, P., Krassakis, P., Kazana, S., Papanikolaou, D. and Koukouzas, N., 2021. The Volcanic Relief within the Kos-Nisyros-Tilos Tectonic Graben at the Eastern Edge of the Aegean Volcanic Arc, Greece and Geohazard Implications. Geosciences, 11(6), p.231.

Parcharidis, I., Lagios, E. and Sakkas, V., 2018. Differential interferometry as a tool of an early warning system in reducing the volcano risk: the case of Nisyros volcano. Bulletin of the Geological Society of Greece, 36(2), p.913.

Tibaldi A., Pasquarè F.A., Papanikolaou D., Nomikou P. (2008). Tectonics of Nisyros Island, Greece, by field and offshore data, and analogue modeling. Journal of Structural Geology 30 (12), pp.1489.

16th International Congress of the Geological Society of Greece
17-19 October, 2022 - Patras, Greece
Bulletin of the Geological Society of Greece, Sp. Publ. 10
Ext. Abs. GSG2022-163

From Kallimarmaron Stadium... to the Odeon of Herodes Atticus–Herodeion - A geotouristic trail in the city of Athens

F. Tripolitsiotou[1], H. Drinia[1],

(1) Department of Geology and Geoenvironment, National and Kapodistrian University of Athens, Panepistimiopolis, 15784 Athens, Greece

Key words

urban geotourism, geotrail, Athens

The Attica basin was formed during the Alpine orogeny. It consists of the alpine formations (the mountains that enclose the basin), but also the hilly area in its center (Philopappou, Acropolis, Lycabettus, Turkovunia, Ardittos, Ardas, the hill of Strefi), and of the postalpine formations, that is, the sediments deposited in the Athens basin after the uplift of the mountain masses. These sediments come mainly from the erosion of the alpine formations. (Papanikolaou et al. 2004).

Athens is a city of high cultural and geological interest. The existence of the famous Sacred Rock of the Acropolis as well as the historical monuments that exist on it (Parthenon, Dionysus Theater, the Stoa of Eumenes, etc.), in addition to their cultural heritage, also has a special geological value, which is important not only for geologists but also for all visitors who arrive in this unique part of the world (Drinia et al. in press).

From this perspective, a new form of tourism has been created: urban geotourism, which according to Del Lama (2018) is defined as tourism in locations anywhere within the boundaries of a city that is related to geological concepts and features. These sites may be purely geological formations or geocultural heritage sites where there is anthropogenic intervention.

Sites of geological or geomorphological interest within a city are defined as "urban geosites' (Reynard et al. 2017). These sites may be natural or the result of geological processes, or may be derived from man-made structures that have characteristic rock types (Palacio 2014; Petrović et al. 2017). These geosites usually occupy small territorial areas within a city and may be located in the center of cities or even in their suburbs. (Zafeiropoulos-Drinia, 2021)

A route that connects geosites is called a geotrail. This paper aims to present a geotrail which has a length of 2 km. It focuses on familiarizing the visitors of the city with the geological wealth of this particular area. The geotrail begins at the Kallimarmaron Stadium, with a second stop at Agia Fotini in the Ilissus River and the adjacent Cave of God Pan. Then we encounter the Olympian Zeus columns and arrive at the Dionysus Theatre, the Thrasyllus monument, the Eumenes stoa, and the Odeon of Herodes Atticus. The geotrail is simple and the level of difficulty is low.

The Kallimarmaron stadium was built between two hills in Attica called Ardas and Ardittos. It is the only stadium in the world made entirely of Pendeli Mount's white marble. The river Ilissos used to flow in front of these hills, but the riverbed is now covered. The geological heritage is linked to the place's ancient and modern history, thanks to its unique topography in the urban environment. The following stops on the route are also linked by this landscape, which contains unique geological elements: the temple of Agia Fotini, the cave of God Pan, and the Columns of Olympian Zeus.

The following geosites on the route are primarily related to the geology of the Acropolis rock. The lithological structure of the Acropolis area is relatively simple. We mostly see Athenian schists and limestones.

The upper part of the Acropolis hill, in particular, is made of limestone with a thickness of no more than 40 m. There are erosion cavities and caves on the hill's slopes (Paraskevaides et al. 1979)

The geology of the Acropolis Hill may have influenced human history, because despite the great earthquakes that struck Attica during the historical period, this monument remained unaffected. Apart from the Parthenon, the hill has preserved earlier and later buildings and structures, some of which are over 2,500 years old.

Each monument has its own geological feature, and together they form the magnificent geoculture of Athens, particularly the sacred rock of the Acropolis.

References

Papanikolaou, D.; Lozios, S.G.; Soukis, K.I.; Skourtos, E.N. The geological structure of the allochthonous “Athens schists”. Bull. Geol. Soc. Greece Thessalon. 2004, 36, 1550–1559.

Drinia, H.; Tripolitsiotou, F.; Cheila, T.; Zafeiropoulos, G. The Geosites of the Sacred Rock of Acropolis (UNESCO World Heritage, Athens, Greece): Cultural and Geological Heritage Integrated. Geosciences 2022, 12, x.(in press)

Del Lama, E.A. Urban geotourism with an emphasis on the city of São Paulo, Brazil. In Handbook of Geotourism; Dowling, R.K., Newsome, D., Eds.; Edward Elgar Publishing: Cheltenham, UK, 2018; pp. 210–223.

Reynard, E., & Brilha, J. (Eds.). (2017). Geoheritage: assessment, protection, and management. Elsevier.

Zafeiropoulos, G.; Drinia, H.; Antonarakou, A.; Zouros, N. From Geoheritage to Geoeducation, Geoethics and Geotourism: A Critical Evaluation of the Greek Region. Geosciences 2021, 11, 381. https://doi.org/10.3390/geosciences11090381.

Paraskevaidis, H.; Chorianopoulos, P. An intersection through Mount Aegaleo. The schist of Athens. The hills of Athens. Bull. Geol. Soc. Greece 1979, 13, 116–141.

16th International Congress of the Geological Society of Greece
17-19 October, 2022 - Patras, Greece
Bulletin of the Geological Society of Greece, Sp. Publ. 10
Ext. Abs. GSG2022-189

3D Geovisualization of Bali Alonia Park in Lesvos Geopark

S. Proestakis[1], E.E. Papadopoulou[1], N. Zouros[1], N. Soulakellis[1]
[1]Department of Geography, University of the Aegean, 81100 Mytilene, Greece

The Petrified Forest in Lesvos is one of the most important geoheritage monument in the world, located in the northern part of the Aegean Sea in Greece. The aim of this study is to present the methodology followed for 3D modeling of petrified trees, by using very high-resolution images acquired by Unarmed Aerial Vehicle (UAV) and Digital Single-Lens Reflex (DSLR) camera. The derived 3D models are suitable for geovisualization, highlighting the geological heritage of the Bali Alonia Park, in the Petrified Forest of the Lesvos Geopark. More specifically, the methodology followed consists of three stages: a) data acquisition, b) data processing and c) 3D geovisualization. The data acquisition consists of the Global Navigation Satellite System (GNSS) Real Time Kinematics (RTK) method to collect Ground Control Points around the park and the fossils, flight planning for the UAV and the DSLR camera images collected for terrestrial close-range photogrammetry. Following, in the data processing, the high-resolution images was used to photogrammetrically produce Digital Surface Models (DSMs), orthophoto maps and 3D models of the park and the petrified trees. Finally, the study proposes online web cartography for highlighting fossils through 3D geovisualization, where specific petrified tree trunks of the park were selected. This research is being conducted as exploiting and highlighting the important findings of the Lesvos Geopark. Consequently, a methodology was developed for the recording and the 3D geovisualization of the park and the fossils included in it.

Introduction

The Petrified Forest of Lesvos is one geological monument and is part of UNESCO Geopark of Lesvos Island since 2004. The Petrified Forest of Lesvos Geopark consists of individual parks, located in the west part of Lesvos in the North-East Aegean in Greece [1]. The largest Park of the Lesvos Petrified Forest is the Bali Alonia Park where standing and fallen petrified tree trunks of 20,000,000 million years old [2]. These petrified tree trunks are an important element of the world's geological heritage and this makes their high-resolution recording and 3D mapping necessary [3,4]. Nowadays, the 3D mapping of areas of high geological importance begun with the use of new technological means such as UAV, DSLR cameras, terrestrial laser scanners and aerial lidars. The above means provide spatial resolution data and in combination with GNSS measurements obtain high topographic accuracy [5]. The processing of these data with specific algorithms, like the algorithm structure from motion (SfM) [6] and the methodology of image-based 3D modeling [7], can provide very accurate and precise orthophotomaps, digital surface models (DSMs), 3D dense point clouds and 3D models [8,9]. The cartographic derivatives of image based 3d modeling processing can be utilized by Geographic Information Systems (GIS) and Web Cartography[10,11] or other digital tools for their most contemporary and interactive geovisualization.

Methodology

The methodology consists of three stages:

- Creation of 3D models of fossilized trunks from images captured terrestrially and with UAVs
- Creation of online maps of the Bali Alonia Park and
- The development of online cartographic applications

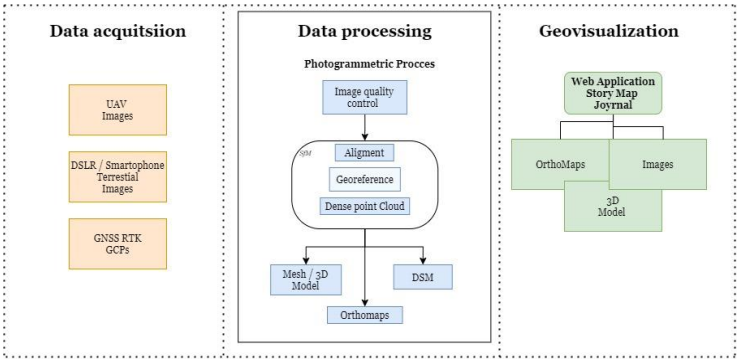

Diagram 1. Workflow of methodology.

In more detail, high-resolution images and GCPs were collected. Aerial images were captured via the DJI Matrice 300 UAV, equipped with the Zenmuse P1 camera [Sensor size (Still): 35.9×24 mm (Full frame)] on May 15, 2022, at an altitude of 40m. Images at ground level were captured with a mobile phone device (Mi 11 Lite) with camera specifications [64 MP, f/1.8, 26mm (wide), 1/1.97", 0.7μm]. The GCPs measured via GNSS and the RTK method. To generate the 3D models and the orthomosaics, the high-resolution images were processed with photogrammetric methods. More specifically, computer vision and computer graphics algorithms were utilized, namely SfM and Multi View Stereo (MVS). The processing steps followed were:

- Image alignment - SfM
- Georeference
- Dense point cloud generation
- Creation of 3D model / Mesh
- Creation of a digital surface model
- Creation of orthophoto maps and digitization of thematic levels

To share the results and create online maps, the 2D and 3D data were uploaded online. ArcGIS Pro/Online was utilized for the 2D and 3D photogrammetric results, as it provides the possibility to create interactive “Web Maps”. The online map is the basis for the development of online cartographic applications such as storytelling, or as an answer to various questions [12,13]. Additionally, the digital Mesh 3D objects were shared online, on the “SketchFab” site. Sketchfab is a 3D modeling platform website for publishing, sharing, discovering, buying, and selling 3D, VR and AR content. For the online sharing and Web Mapping process the following were used:

- Images
- Orthophoto maps
- 3D digital models (Mesh)

The online sharing of data aids in the creation of the "Web Application". In particular, a “Story Map Journal” type application was developed with information on the fossils, combined with images, Web Maps and 3D digital models. This application aims at highlighting the fossils of Bali Alonia Park.

Results

This application presents the wider area of the park and the fossils (7, 17, 18, 26, 36, 37). In more detail, the first two slides focus on information about the history of the park, and further on its boundaries, fossil sites and its walking trails as depicted in the present time. The fossilized trunks studied in this work are then presented on separate slides. On each slide, the application automatically displays the geographical location of each fossil on the main screen, while the side panel contains relevant information as presented in the Museum guide, as well as a link to the 3D projection of the tree trunk as a 3D digital object through SketchFab. At the same time, the users can navigate the map autonomously or set the scale, through the interactive and user-friendly environment. The maps, the results of photogrammetric processing along with narrative text, and very high-resolution images were utilized in the development of the “Story Map Journal”.

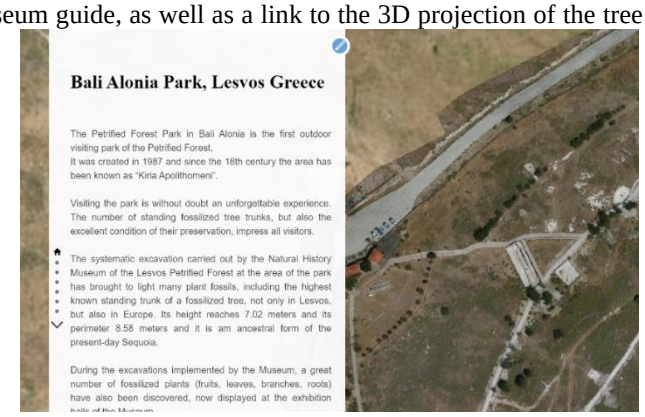

Figure 2. Image of the Web Application "A story about Park of Bali Alonia"

This type of application, as a emphasizing method, combines narrative text with maps and multimedia with embedded content to focus on the park's fossils. It contains sections displayed to users via scrolling, and each section consists of a main scene combined with an accompanying panel. Maps or other data are inserted into the main scene and the accompanying content in the side panel, to highlight the park’s wider region, fossil sites, petrified trunks and walking trails.

This study presents a web-based application for the efficient geovisualization of standing and fallen petrified trunks. Online mapping combined with online applications aims to draw special attention to the Bali Alonia Park in the Geopark of Lesvos.

Acknowledgements

This research was funded by the Research e-Infrastructure “Interregional Digital Transformation for Culture and Tourism in Aegean Archipelagos” {Code Number MIS 5047046} which is implemented within the framework of the “Regional Excellence” Action of the Operational Program “Competitiveness, Entrepreneurship and Innovation”. The action was co-funded by the European Regional Development Fund (ERDF) and the Greek State [Partnership Agreement 2014–2020].

References

[1] United Nations Educational, Scientific and Cultural Organization (UNESCO, 2006) UNESCO (2006)
[2] Zouros, Nikolas & Velitzelos, E. & Valiakos, Ilias & Labaki, O. (2007). The Plaka Petrified Forest Park in Western Lesvos - Greece. Bulletin of the Geological Society of Greece. 40. 1880-1891. 10.12681/bgsg.17182.
[3] Niedzielski, T. Applications of Unmanned Aerial Vehicles in Geosciences: Introduction. Pure Appl. Geophys. 2018, 175, 3141–3144. [Google Scholar] [CrossRef]
[4] Cayla, N.; Hobléa, F.; Reynard, E. New Digital Technologies Applied to the Management of Geoheritage. Geoheritage 2014, 6, 89–90. [Google Scholar] [CrossRef][Green Version]
[5] Chatzi, E. et al. (2019) ‘3D modelling of petrified trees: Laser scanning vs photogrammetry’, IMEKO International Conference on Metrology for Archaeology and Cultural Heritage, MetroArchaeo 2017, (May 2018).
[6] Westoby, M. J., Brasington, J., Glasser, N. F., Hambrey, M. J., & Reynolds, J. M. (2012). “Structure-from-Motion” photogrammetry: A low-cost, effective tool for geoscience applications. Geomorphology, 179, 300–314. https://doi.org/10.1016/j.geomorph.2012.08.021
[7] Hatch, M. Environmental Geophysics. Preview 2017, 2017, 32–33. [Google Scholar] [CrossRef]
[8] Papadopoulou, E. E. et al. (2021) ‘DEM-based UAV flight planning for 3D mapping of geosites: The case of olympus tectonic window, Lesvos, Greece’, ISPRS International Journal of Geo-Information, 10(8). doi: 10.3390/ijgi10080535.
[9] Antoniou, V., Nomikou, P., Panousis, D., & Zafeirakopoulou, E. (2021). Nisyros volcanic island: A geosite through a tailored gis story. Geosciences (Switzerland), 11(3). https://doi.org/10.3390/geosciences11030132
[10] OFICIAL WEB SITE OF ARCGIS ENTERPRISE retrieved through https://enterprise.arcgis.com
[11] De Reu, J. Image-Based 3D Modeling. In The Encyclopedia of Archaeological Sciences; John Wiley & Sons, Inc.: Hoboken, NJ, USA, 2018; pp. 1–4. [Google Scholar]
[12] DORMAN, M. (2020) Introduction to web mapping. https://search.ebscohost.com/login.aspx?direct=true&scope=site&db=nlebk&db=nlabk&AN=2274355.
[13]Kerski, J. Communicating with Story Maps. Available online.

16th International Congress of the Geological Society of Greece

17-19 October, 2022 - Patras, Greece

Bulletin of the Geological Society of Greece, Sp. Publ. 10

Ext. Abs. GSG2022-194

The Aliakmon Legacy Project: A Defeat for Conservation, or a Victory for Research and Education?

D. Ghikas[1], A.E. Rassios[2]

(1) Grevena-Kozani UGGp, Grevena, Greece. notconstandina@hotmail.com (2) *em.* Hellenic Survey (EAGME), Lefkovrysi, Greece.

The Aliakmon River valley in northern Greece contains exposures of the Tethyan Vourinos Ophiolite complex and suture zone with the Pelagonian landmass. It is an important geoheritage site, as the earliest geologists to visit the area were spurred by their observations to develop key concepts of what would eventually be plate tectonic theory (Brunn 1959, Moores 1969, Zimmerman 1969). Nevertheless, the area after the 1960s remained understudied, in comparison with other areas of Greece, in the context of the emerging paradigms of structural geology and kinematic indicators.

In 2004, the Public Power Corporation of Greece (PPC) began construction of a hydroelectric dam near the southwestern end of an extant hydroelectric reservoir, Lake Polyfyto. To balance the impending obliteration of this geoheritage site by a new hydroelectric reservoir, the PPC funded a multiyear, 'last-chance' initiative to document the geologic phenomena and processes of this area. From 2005-2008, over 60 undergraduate students, graduate students and professors participated in the Aliakmon Legacy Project, producing nearly 50 Bachelor's and Master's theses, and dramatically expanded the existing knowledge of regional geologic history and sparked new insights into the processes of ophiolite obduction. The student participants are now established at prestigious research institutions around the world. Publication of findings in scholarly journals continues to draw researchers to explore this area further. Recent discoveries from the area include the oldest rocks in Greece, from zircon crystals dated to ~980 mya, with geochemical signature of the Amazonian craton (Zlatkin 2014).

The findings and significance of this area are not reserved for professional geoscientists; as a long-standing practice and etiquette, the locally-based researchers who participated in the Aliakmon Legacy project regularly interact with the local population via formal and informal discussions on geoheritage and recent findings, field trips and other public events, and books aimed at non-geologists. In 2014 and 2017, researchers who had participated in the project proposed the creation of a regional geopark, to be considered for official induction into the UNESCO Global Geoparks Network. Throughout the process of proposal, evaluation and acceptance into the network, local residents and community leaders from the vicinity of the Aliakmon Legacy Project were the most vocal and proactive in supporting the aspiring geopark. They cited the recent advancements in geologic understanding in their area, the desire to preserve and promote their geoheritage, and their interest in exploring geotourism as a means to revive the depressed local economy.

The Aliakmon Legacy Project, touched off by the unavoidable loss of treasured geoheritage sites, recast a classic geologic site as a cutting-edge research destination and opened new avenues for scientific advancement as well as opportunities for regional development, via the induction of the area into the UNESCO Global Geoparks Network.

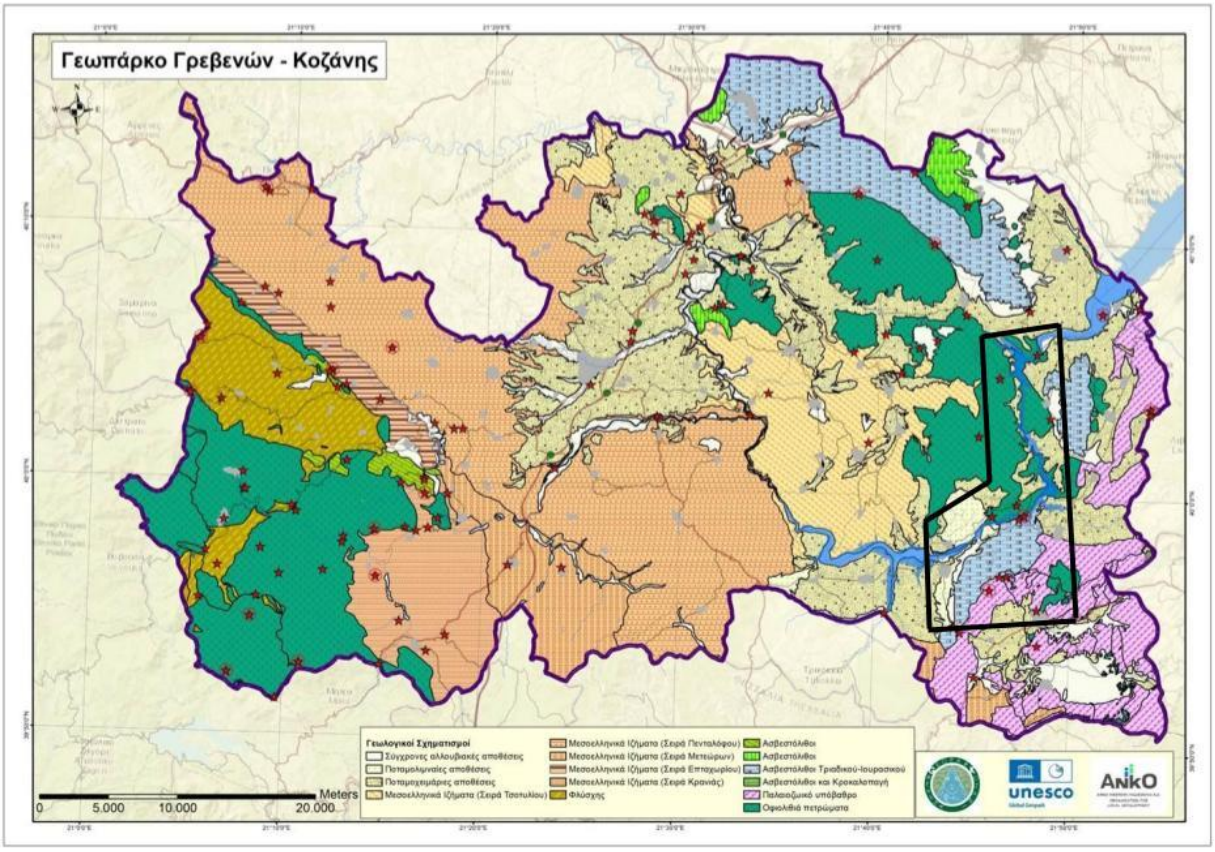

Figure 1: Geologic map of Geopark Grevena-Kozani. Black box: study area of the Aliakmon Legacy Project. Red stars: geosites of the geopark, including geoheritage localities

Acknowledgements

Many thanks to the Public Power Corporation of Greece, Regional and Sub-regional Authorities of West Macedonia, Drs. Annie Rassios, Yildirim Dilek and Giovanni Grieco, the family of Dr. Eldridge Moores, and to all the participants and supporters of the Aliakmon Legacy project.

References

Brunn, J.H., 1959. La dorsale médio-atlantique et les épanchments ophiolitiques: Compte rendues sommaire des sciences de la Société géologique de France, 234-237.

Moores, E.M., 1969. Petrology and Structure of the Vourinos Ophiolitic Complex of Northern Greece: Geological Society of America Special Paper, 118, 74 pp.

Rassios, A., Grieco, G., Batsi, A., Myhill, R. and Ghikas, D. 2016. Preserving the Non-Preservable Geoheritage of the Aliakmon River: a Case Study in Geoeducation Leading to Cutting-Edge Science. Bulletin of the Geological Society of Greece, 1, 255-264.

Zimmerman. J., 1969. The Vourinos Complex–an Allochthonous Alpine Ophiolite in Northern Greece, Abstr. Geol. Soc. Am. Ann. Mtg., 245.

16th International Congress of the Geological Society of Greece
17-19 October, 2022 - Patras, Greece
Bulletin of the Geological Society of Greece, Sp. Publ. 10
Ext. Abs. GSG2022-220

The Kefalonia-Ithaca Geopark as a Tool for Public Education, Recreation and sustainable development

E. Zoumpouli[1,2], M. Xanthakis[1], G. Drakatos[1], P. Minetos[1]

(1) Kefalonia-Ithaca Unesco Global Geopark, Management Unit of Zakynthos and Aenos National Parks and Protected Areas of the Ionian islands, Branch Office of Argostoli, Greece, zoumpouel@gmail.com (2) University of Patras Department of Geology, Patras, Greece

Kefalonia and Ithaca Geopark, this small area on planet earth represents a geopark of particular importance, which was established in 2016, and in 2022 it was designated as Kefalonia-Ithaca UNESCO Global Geopark. Kefalonia-Ithaca Geopark, has until now 50 designated geosites (Figure 1), 50 areas of outstanding natural beauty of various categories, explain the geological history of the geopark. It is a history of continental and lithospheric plate movements combined with climatic influences reflected in the geosites, creating an excellent depiction of these earth processes.

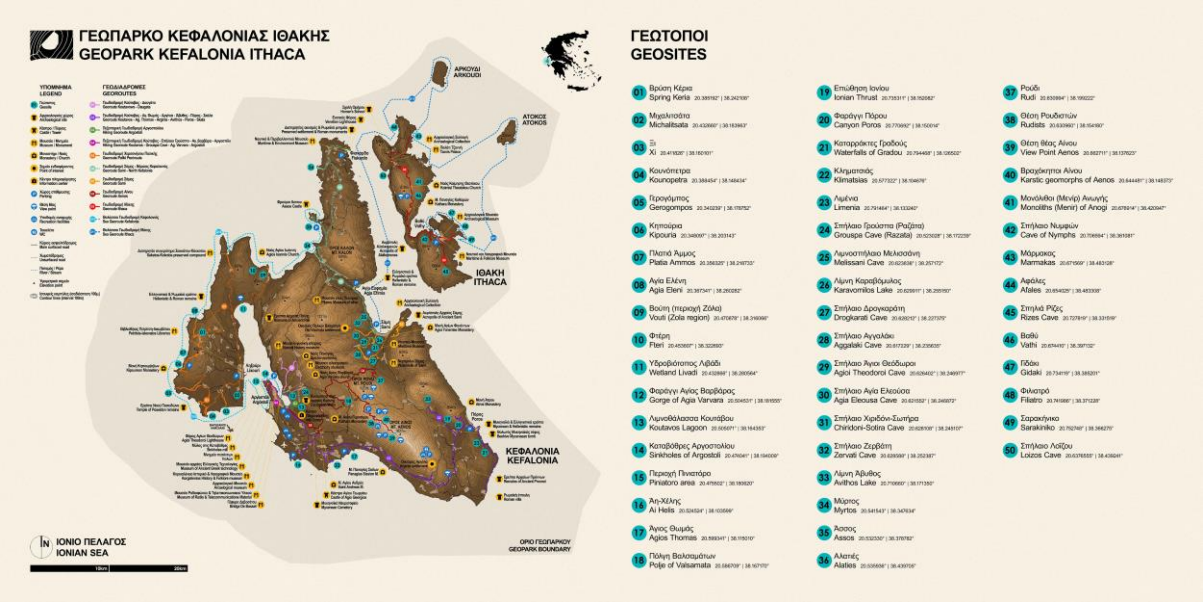

Figure 1. Map of Kefalonia-Ithaca Geopark

One of the main characteristics of Kefalonia-Ithaca Geopark, due to its geotectonic position, is the intense seismic activity. It is located in one of the most tectonically active areas of Europe. Additionally dominant role in the geopark has the intense Karstification, resulting from the dissolving action of water on limestone. The two islands are characterized by the fact that most of their surface is covered by limestone. This fact, combined with the intense tectonic activity and climatic conditions, resulted in the appearance of numerous underground and surface karstic features (Figure 2) such as caves, sinkholes, dolines, poljes, etc.

Figure 2. A) Melissani Cave B) Sinkholes of Argostoli

In addition Kefalonia and Ithaca constitute a place of great historical interest, including numerous monuments and sites of human civilization from prehistoric times to modern history, as well as precious ecosystems. The richness of its natural and cultural heritage, make the two islands a unique territory, having as its main objective a structured approach to education and geotourism strengthening knowledge, as well as heritage and cultural potential.

Consequently Kefalonia-Ithaca Geopark recognizes the importance of its contribution to the sustainable development, and for this reason it gives emphasis to public education and to geotourism (Figure 3). First of all Kefalonia-Ithaca Geopark assures its visibility through appropriate infrastructure with interpretation panels for the geosites. Also it features two Information centers which host information panels, a small exhibition of rocks and local products, useful information material, like bilingual leaflets and posters, maps with photos and information about the geopark as well as other promotional material. These environmental centers are open to the public and especially for schools for a series of educational activities concerning geodiversity and biodiversity.

Figure 3 Photos from some of the activities of Kefalonia-Ithaca Geopark promoting sustainable development

Furthermore Kefalonia-Ithaca Geopark places particular emphasis to experiential education and tours, as well as awareness-raising activities not only for students of any age but also for visitors and local community. For this reason organizes regularly educational activities, both in the classroom and in the field, and voluntary actions of cleaning Geosites in order to awaken ecological awareness, aiming for a better environment for all. On the other hand it forces also geotourism, through experiential tours we have the opportunity to experience the environment in its true dimension. The Geopark proposes ways to better disseminate and protect of the local heritage, both geological and cultural, as well as to promote unique gastronomic traditions, while providing support for local businesses and residents.

Concluding the role of Kefalonia-Ithaca Geopark is to bring people closer to the place they visit through knowledge. By visiting the geopark the images are no longer just images, we go to a deeper level, creating feelings and memories. We no longer see just a landscape; it is no longer just a nice photo. The landscape now has value; it speaks to us about its formation.

Acknowledgements

The authors are grateful to the Laboratory of Palaeontology & Stratigraphy and to Laboratory of Sedimentology, Department of Geology, University of Patras, for the helpful collaboration in the implementation of this research.

16th International Congress of the Geological Society of Greece
17-19 October, 2022 - Patras, Greece
Bulletin of the Geological Society of Greece, Sp. Publ. 10
Ext. Abs. GSG2022-232

Geodiversity and Geoheritage: The geoethical dimensions of a Geoeducation Program in the context of an experimental Lower Secondary Education school club

S. Mosios[1], E. Georgousis[1], S. Savelides[2], M. –V. Holokolos[3], H. Drinia[1]

(1) Department of Geology and Geoenvironment, National and Kapodistrian University of Athens, 15784 Athens, Greece, spymosi@geol.uoa.gr (2) Hellenic Ministry of Education and Religious Affairs, Directorate of Secondary Education of Magnesia, 38333 Volos, Greece (3) Department of Culture, Creative Media and Industries, University of Thessaly, 38221 Volos, Greece

Abstract

Due to population expansion and economic growth, human activities have become intensive and affect the geoenvironment. Widespread human activities bring significant convenience to human lives, but the geoenvironment would be damaged if not preserved, leading to a series of geohazards (e.g., surface subsidence, water and soil loss, water degradation, and land desertification). Following our previous research, which clearly showed that the latent state of students' perceptions regarding the thematic fields of the concepts of the geoenvironment can be considered particularly confused, we designed a geoeducation program aiming to empower students' understanding of geoenvironmental concepts. The geoeducational program was operated in the context of an experimental Lower Secondary Education school club (Creativity and Innovation Group) with the participation of students aged between 12 and 15 years old. Teachers throughout the school year developed and used "targeted" educational techniques and concepts highlighted by the previous research in order to help students clear up or even scientifically accept perceptions of the concepts of geodiversity, geoheritage, geoethics and geotourism in the field of the geoenvironment. It was considered necessary to measure the degree of success of the program. On account of this, students were asked to briefly answer a questionnaire, wherein each question examined their perceptions regarding the four concepts of geoenvironment: geodiversity, geoheritage, geoethics and geotourism, to assess the current state of students' perceptions regarding the thematic areas of the concepts. The qualitative research strategy approach was selected, specifically the thematic analysis. The results of the research show that the participation of students in the program led to their empowerment in the values associated with the geoenvironment.

Keywords

Geodiversity; geoheritage; geotourism; geoethics; geoeducation

16th International Congress of the Geological Society of Greece

17-19 October, 2022 - Patras, Greece

Bulletin of the Geological Society of Greece, Sp. Publ. 10

Ext. Abs. GSG2022-235

The First Geoheritage Inventory and Assessment in the Lefka Ori Mts, Crete, Greece

C. Fassoulas[1], A. Pavlaki[2], V. Perleros[3]

(1) University of Crete, Heraklion Greece, fassoulas@nhmc.uoc.gr (2) Pavlaki A. Geological Studies, Chania, Greece, (3) Perleros V. Geological Studies, Athens, Greece.

The Lefka Ori Mts (2454m.) is the largest mountain chain in Crete with more than 20 peaks over the 2000m. al. It is well known for the very deep gorges that develop mainly at its southern flanks, with Samaria being the most famous, as well as the peculiar landscape that is formed at the Alpine zone, that is commonly referred as "mountainous desert" (Rackham & Moody, 1997). The mountains are the result of the convergence between the African and the Eurasian plate and the subsequent subduction of the Mediterranean oceanic crust underneath the south Aegean. The geological evolution of the mountains is well described and studied, although geological mapping in most areas is dated back to the 70's. With the support of the Management Body of the Lefka Ori Mts and Samaria National Park we conducted a broad geological survey of the central and southern Lefka Ori mts in order, for the first time, to identify, map, record, and assess in detail, the main features of the geological heritage in the area (Pavlaki, *et al.*. 2016).

The area is mainly constituted by the lower nappes of Crete, namely the Plattenkalk (or Kriti-Mani), the Phyllites-Quartzites s.l., and Tripolitsa, hosting as well the only outcrops of the Trypali nappe of Crete (Creutzburg *et al.*, 1977; Fytrolakis, 1980). The main geological processes related with the subduction of the lower nappes of Crete (Plattenkalk, Trypali and Phyllites-Quartzites) during the late Oligocene and the subsequent exhumation in the early to middle Miocene, is very clearly observed through thrust and detachment faults, intense folded and in places overturned rocks, and neotectonic faults (Fassoulas & Nikolakakis, 2005). The present active tectonic regime is depicted at the raised beaches and notches of the southern coast, most of which are related with the 365 AD, major earthquake that devastated the whole eastern Mediterranean. Recent studies have identified that this western part of Crete is one of the most rapidly uplifted areas with rates of about 1.2 mm/a, that have resulted in a bulk crustal uplift of 2kms in the last 2 ma (Roberts et al. 2013). The vast majority of carbonate rocks that crop out in the area together with the intense erosional rates have resulted in the numerous gorges, but also in the development of the very big caves that occur at the northern slopes of the Mts (Gourgouthakas -1208m, and Leon -1100m.) that are attributed among the four deepest in Europe (Adamopoulos, 2010). Karstic landscape is dominating the Mts, and which turns into a glacial landscape with moraine relicts and U-shaped and polished valleys on the high-altitude, alpine zone (over 2000 m.).

In order to conduct this study, we collected information regarding the geodiversity of the area from all potential sources, i.e. scientific publications, popular publications, webpages related to the area, communications with cultural associations and the mountaineering club of western Crete. As the area is mainly mountainous with restricted access by vehicles in most of its parts, we additionally, collected in situ information along mountain trails, dirt roads, transects, gorges and coasts. We studied all existing geological maps in various scales and we performed rock identification and comparisons during field work in order to compile a more representative and modern geological map of the area (Mountrakis *et al.*, 2012; Pavlaki, *et al.*, 2016). Geological mapping permitted the separation in more detail of the Trypali nappe from the underlying Plattenkalk series and revealed that the lower stratigraphic horizons of the Plattenkalk series (mainly the Sisses and the stromatolitic beds) exist at the highest altitudes forming the highest peaks, whereas the typical platy marble is cropping out at the southern lower topographic areas, as for example the lower (southern) part of Samaria gorge.

For the geosite inventory and assessment we used the most modern methodologies (Fassoulas *et al.*, 2012; Zouros, 2007) compiling data from the desktop analyses and field inspection. These processes resulted in the identification of 109 geosites all over the protected area of National Park and the buffer zone, which were attributed in seven categories: Stratigraphic and petrological; Tectonic; Geomorphological; Karstic; Paleontological; Hydrogeological; and Geo-cultural. The *stratigraphic and petrological* geosites include areas where characteristic rock types of Crete exist, like the Gigilos and Trypali Formation rocks, Triassic gypsum bodies and moraine relicts, as well as some important stratigraphic sections, like the thick bedded white marbles resting with angular unconformity on top of the Stromatolitic dolomite in the area of Roussies and the very impressive alluvial fun exposed in the exit of Klados gorge. The *tectonic* category includes both fold and fault structures with the most impressive being the foldings in the gorges of Samaria and Klados, the active normal fault in the area of Agia Roumeli and the tectonic contacts between the Trypali rocks and the underlying phyllite-Quartzite and Plattenkalk series. Raised beaches as well as coastal notches existing in the areas of Sougia, Agia Roumeli, Marmara are also attributed in this category. In the *Geomorphological* category, we have allocated the numerous small and large gorges like the Samaria, Imbros, Agia Irini, Aradena, Klados etc., the alpine valleys in the areas of Ammoutsera (Fig. 1), Psari and Antropolithoi, rock landforms that form towers, pinnacles or individual shapes and coastal geomorphosites. The *Karstic* category was created to comprise all the karstic weathering

and erosion structures of the mountains. These include the large and small plateaus (like Omalos, Askifou, Tavris etc.), the deep and swallow caves like the Gourgouthakas (-1208m.), Leon (-1100m.), Mavro Skiadi (-342m.), and karstic geomorphosites like the dolines in Anopolis, in Roussies, in Amoutsera, in Modaki, in Kako Kasteli etc. The *paleontological* sites were fewer, related mainly with the sponge remnants in the platy marbles. The *hydrogeological* sites are related with wells and springs that can be found in several locations and in the gorges, with the vast majority concentrated in the Samaria area. Finally, the *geocultural* sites are related with the local stone architecture (like the old Loutro ruins), castles, and stone terraces and fences.

The qualitative assessment revealed that five geosites are of *International* importance. These are the coastal notch of Sougia, the Portes in Samaria gorge, the Ammoutsera glacial valley, the Amoutsera doline field and the Gourgouthakas Cave. Of *National* importance eight geosites can be considered: the Gigilos beds, the Samaria folds, the coastal notch at Marmara, the Agia Irini gorge, the Leon cave, the Omalos plateau, the doline fields in Modaki and the karstic landscape at Mavros Lakkos. All the rest are considered of regional or local importance. We also performed a quantitative analysis for the 62 more important of these geosites based on the methodology proposed by Fassoulas et al. (2012). This analysis revealed that the highest *touristic* value was estimated for the Portes in Samaria, the Omalos plateau, the Aradaina and Imbros gorges, and the Karstic landscape of Amoutsera. The higher *educational* value was observed for the Portes in Samaria, the Aradaina gorge, the folds in Samaria, the Imbros gorge and the Askyfou plateau. Finally, the most *vulnerable* geosites due to human and environmental pressures appear to be the scree deposits in Linoseli, the anticline in Poria, the Omalos plateau, the Linoseli spring and the scree deposits of Eligia.

In general, the geodiversity of the study area appears to be very rich with abundant and diversified geological features. As the carbonate rocks prevail, structures related with karstic weathering and erosion, like gorges, caves and karstic geomorphosites prevail. In addition, very important tectonic geosites demonstrating the geological development of Crete and the active tectonic regime are present as well. Many of these geosites have high touristic and educational values, able to support geotouristic activities of the Management Body of the National Park and of the local authorities as well, whereas on the other hand the vulnerability of the most important geosites, appears to be very low.

Figure 1. The Ammoutsera glacial valley and doline field.

Acknowledgements

The present study was financially supported by the Samaria and Lefka Ori mts National Park. We thank the staff of the park, the Chania Mountaineering Club and many locals for providing crucial information and support

References

Adamopoulos, K., 2010. 1000 and 1 caves in “Lefka Ori” massif, on Crete, GREECE. http://www.selas.org/index.php/e-mainmenu-75/doc_download/179-1100-caves-on-lefka-ori-crete.html

Creutzburg, N., et. al., 1977. Geological map of Crete (1:200.000). IGME. Athens.

Fassoulas, C., Nikolakakis, E., 2005. Landscape response to the tectonic uplift of Crete, Greece. Bull. Geol. Soc. Greece, vol. XXXVII, 201-217.

Fassoulas, C., Mouriki, D., Dimitriou-Nikolakis, P., Iliopoulos, G., 2012. Quantitative Assessment of geotopes as an effective tool for geoheritage management. Geoheritage, DOI 10.1007/s12371-011-0046-9.

Fytrolakis, N., 1980. The geological structure of Crete. Problems, observations and conclusions. Habil. thesis, Nat. Techn. Univ. Athens, 143 p.

Mountrakis, D., Kilias, A., Pavlaki,, A., Fassoulas, C., Thomaidou, E., Papazachos, C., Papaioannou, C., Roumelioti, Z., Benetatos, C., Vamvakaris, D., 2012. Neotectonic study of the Western Crete. Seismic risk evaluation of the active faults. In: (Ed.) Emmanuel Skourtsos, and Gordon S. Lister, The Geology of Greece, Journal of the Virtual Explorer, Electronic Edition, ISSN 1441-8142, vol. 42, paper 4. (DOI 10.3809/jvirtex)

Pavlaki, A., et al., 2016. Geological study & revelation of the Lefka Ori West Crete Mts. Geoenvironmental dynamism. In: 3d International Geo-Cultural Symposium, May 2016, Chania, Crete.

Rackham, O., Moody, J., 1997. The making of Cretan Landscape. Manchester University Press, Manchester, 200 p.

Roberts, G., White, N., Shaw, G., 2013. An uplift history of Crete, Greece, from inverse modeling of longitudinal river profiles. Geomorphology, 198, 177-188.

Zouros, N., 2007. Geomorphosite assessment and management in protected areas of Greece. Case study of the Lesvos Island-coastal geomorphosites. Geographica Helvetica 62(3), 69–180.

16th International Congress of the Geological Society of Greece
17-19 October, 2022 - Patras, Greece
Bulletin of the Geological Society of Greece, Sp. Publ. 10
Ext. Abs. GSG2022-252

The PalaeoScope project: augmented and virtual reality recreations of the geological and archaeological past of Athens.

A. Antonarakou[1], G. Lyras[1], G. Kontakiotis[1], G. Kotzamani[1], E. Besiou[1], M. Voulgari[1], V. Alexoudi[1], A. Grambas[1], E. Lekkas[1], E. Galanopoulos[2], N. Karydas[2], A. Iakovidis[2], K. Paraskevopoulos[2], K. Gelegenis[2]

(1) Faculty of Geology and Geoenvironment, National and Kapodistrian University of Athens, Zografos, Greece aantonar@geol.uoa.gr; (2) InDigital, Dirfis 31, Vrilissia

Research Highlights

PalaeoScope intends to present complex scientific data to the visitors of the Acropolis of Athens through artistic 3D recreations of the past. The recreations will be delivered to the visitors through technologies of virtual and augmented reality.

Background

Athens today is a modern, human-made environment. Despite the profound changes made in its recent history, the impact of geology and antiquity is still visible in the urban landscape. The most comprehensive way to transmit such kind of knowledge is with visual recreations made by the synergistic interaction between the visual arts and the sciences (Amorós *et al.*, 2021). Indeed, artistic recreations of the past are highly influential, both to the public and professionals (Witton *et al*., 2014; Davies *et al*., 2022).

Objectives

The aim of our project is to help the visitors of the Acropolis of Athens to understand some core concepts of Geology, Archaeology and History, such as landscape evolution, climate change, faunal succession, and urban development. It also aims to correct common misconceptions held by the public, such as the notion that during the Pleistocene ('Ice Age') all land was covered by ice.

Figure 1. Examples of animal reconstructions created under the PalaeoScope project.

Figure 2. Examples of palaeoenvironment reconstructions made under the PalaeoScope project. The reconstructions present views of Mount Hymettus during the Early Pleistocene and Early Holocene.

We are working on the recreation of four geologic and two historic periods of the Athens basin: Late Cretaceous, Late Miocene (Turolian), Early Pleistocene (Villafranchian), Early Holocene (Greenlandian), fifth-century BCE Athens and late 19th century. Those periods are well-documented in the palaeontological and archaeological record. The Acropolis itself is built on Late Cretaceous limestone, the Turolian is known from Pikermi, the Early Pleistocene is represented in the fossil sites of Tourkovounia and the Early Holocene is known from Vraona. Figure 1 presents some of our reconstructions which are partly based on the sites of Tourkovounia and Vraona. We selected two iconic years to demonstrate the urban development of Athens: 425 BCE (the year of completion of the temple of Athena Nike) as a representative year of the fifth-century city-state of Athens and 1873 (one year before the demolition of the Frankish tower of Acropolis) as a representative year of the 19th century modern Athens.

Methods

We are developing interactive platforms for exploring the natural (augmented reality) and virtual (virtual reality) environment of Athens. The augmented reality application will be for inexpensive, commonly-available hardware such as smartphones. It will work at specific locations on the top of Acropolis and Areopagus hills. The devices will use their video-see-through systems to overlay visuals onto the live environment and use sensors, such as digital compasses and GPS, to determine their location. The virtual reality platform will be for specialized, high performance, head mounted displays.

Results and Conclusions

Our integrated artistic reconstructions are the result of a multi-disciplinarity approach. The recreation of reconstructions has required our scientific team to push beyond typical questions and data. For example, the team had to make decisions about the spatial distribution of fauna and flora during the Miocene and Pleistocene. Such data do not exist for the Athens basin, thus our team had to rely on fossil localities elsewhere and on modern paradigms. In this way we created reconstructions, which although hypothetical, they are most certainly plausible. Figure 2 presents examples of such reconstructions for Mount Hymettus. Our recreations aim to help the public to engage with the past, and thus constitute as a cornerstone for scientific outreach.

Acknowledgements

This research was co-financed by the European Regional Development Fund of the European Union and Greek national funds through the Operational Program Competitiveness, Entrepreneurship and Innovation, under the call RESEARCH-CREATE-INNOVATE (Research project: PalaeoScope; Project code: T2EΔK-03781).

References

Amorós, G., Carrión, J.S., Ochando, J., 2021. Paleoecology and paleoart: Landscapes of the Middle Pleistocene Neanderthals in Bolomor Cave, eastern Iberia. Quaternary Science Reviews, 256, 2021, 106826.

Davis, M., Nye, B.D., Sinatra, G.M., Swartout, W., Sjöberg, M., Porter, M., Nelson, D. Kennedy, A.A.U., Herrick, I., DeNeve Weeks, D., Lindsey, E., 2022. Designing scientifically-grounded paleoart for augmented reality at La Brea Tar Pits. Palaeontologia Electronica, 25(1):a9.

Witton, M.P., Naish, D., and Conway, J., 2014. State of the Palaeoart. Palaeontologia Electronica, 17:5E.

16th International Congress of the Geological Society of Greece
17-19 October, 2022 - Patras, Greece
Bulletin of the Geological Society of Greece, Sp. Publ. 10
Ext. Abs. GSG2022-253

The presence of a Natural History Museum in a school as a geology and geological heritage educational tool

F. Tripolitsiotou[1], H. Drinia[2], A. Antonarakou[3]

(1) Natural History Museum of Arsakeia Schools P.Psychico 15452 Athens,tripolitsiotou.f@e-arsakeio.gr Greece, tripolitsiotou.f@e-arsakeio.gr (2) Department of Geology and Geoenvironment, National and Kapodistrian University of Athens, Panepistimiopolis , 15784 Athens, Greece (3) Department of Geology and Geoenvironment, National and Kapodistrian University of Athens, Panepistimiopolis , 15784 Athens

Modern museums invest in their educational role by offering integrated educational programs to students who visit them in addition to guided tours in their various departments (Plakitsi 2011). Over the last two decades, educational programs have been actively integrated into the activities of Greek museums, utilizing both their permanent and temporary collections.

The entire museum space is recognized as a different learning environment in which reality can be approached both through the exhibits and their organization in a system aimed at communication and education by museum pedagogy (Nikonanou at al. 2016).

The school space is the most appropriate location for museum experiences, the construction of new knowledge based on the interests gained during the museum visit, and finally the transformation of popularized knowledge into structured and functional knowledge. This approach to science museums has received less attention than the others (Koliopoulos at al. 2004)

Museum pedagogy has only recently been introduced into Greek school curricula. Museum curricula have an unsteady relationship with the curricula of the respective school classes (Nikonanou et al. 2016)

According to some researchers, such as Black et al. (2009), the connection between museum education programs and the school curriculum is a functionality required to fulfill teachers' requirements to enhance the school curriculum, and what matters is that students have an enjoyable and memorable experience in the museum.

Seifert et al. (2012) agree that the primary goal of museum-school collaboration is for each institution to maintain its uniqueness, i.e. museums should not be transformed into schools, but they cannot ignore basic principles of school learning and school reality.

What happens, however, when a museum is housed within a school and students have direct access to it, both as individual visitors and as participants in educational programs that are part of the school curriculum?

This paper attempts to highlight one such museum case. The Museum of Natural History of the Philekpaedeyktiki Society is located in the area of the Arsakeia Schools of Psychiko. It is one of the museums that collaborate with schools (scolarization du musée), with the goal of connecting non-formal and formal education. This link is made possible through the didactic transformation of knowledge, which serves as the foundation for the design and implementation of our museum's educational programs (Tripolitsiotou et al, 2020)

Through the use of the teaching model of Allard & Boucher et al. (1998) and Paquin et al. (1998), these programs are directly linked to the curriculum of each class, both within the framework of Natural Sciences lessons and within the framework of cross thematic programs (1995). The majority of the programs are concerned with geology and geological heritage (Tripolitsiotou et al. 2018).

Six hundred and fifty students from the first and third grades of high school participated in the survey presented in this paper by answering a 15-question questionnaire. These inquiries concern both the museum itself and the educational programs they have participated in. The results are encouraging for the continuation of the work of such a museum, which designs non-formal education programs within the school premises, giving pupils from both native and external schools who visit it the opportunity to acquire both museum and environmental awareness.

Key words

museum, educational programs, geology, geological heritage

References

Allard, M., & Boucher, S. (1998). Éduquer au musée: un modèle théorique de pédagogie muséale. Hurtubise HMH,.

Black, G. 2009. The attractive. Museums and Visitors, tr. Kotidou, S., Piraeus Group Cultural Foundation Publications:Athens

Koliopoulos, D. (2004). Didactic approach of the Museum of Natural Sciences (Greek)

Plakitsi, K., (2011). The didactic approach of the museum of natural sciences as a bridge between science and art in primary education.

Paquin, M. (1995). Didactic model of the use of cultural institutions for educational purposes in Quebec. Loisir et Société, 18(2), 309-324.

Nikonanou, N., Bounia, A., Filippoupoliti, A., Chourmouziadi, A., Giannoutsou, N. (2016). Museum learning and experience in the

21st century.
Tripolitsiotou, F., Drinia, H., Antonarakou, A., (2018): I' m cherching for the lost paleontological treasure Proceedings of the 5th conference of New Pedagogus 778-785
Tripolitsiotou, F, Drinia, H, Antonarakou, A., (2020): I know my home: Parnitha-Pendeli. An educational program of the Museum of Natural History of the Society for the promotion of Education and learning 8th Congress PEEKPE "Environmental Education with the aim of sustainability in the age of climate change" Proccedings of Conference .524-530
Tripolitsiotou,F. (2020): In the Museum… I want to see the treasures Lands & Sea An educational program of the Museum of Natural History of the Society for the promotion of Education and learning with the use of 3d sand. 11th Panhellenic Conference, The Natural Sciences in Preschool Education: Mapping the new twenty years of research and teaching practice - Proceedings (e-book) 1232-1242
Seifert, R. 2012. "Das Curriculum – Hindernis oder Chance?", στο Staupe, G. (επιμ.), Das Museum als Lernund Erfahrungsraum. Grundlagen und Praxisbeispiele, Schriften des Deutschen Hygiene-Museums Dresden, Böhlau Verlag: Köln, 102-105.

16th International Congress of the Geological Society of Greece
17-19 October, 2022 - Patras, Greece
Bulletin of the Geological Society of Greece, Sp. Publ. 10
Ext. Abs. GSG2022-254

Designing a Mammoth Herd for Augment Reality at the Acropolis of Athens

G. Lyras[1], G. Kontakiotis[1], E. Galanopoulos[2], N. Karydas[2], A. Iakovidis[2], K. Paraskevopoulos[2], K. Gelegenis[2], G. Kotzamani[1], E. Besiou[1], A. Antonarakou[1]

(1) Faculty of Geology and Geoenvironment, National and Kapodistrian University of Athens, Zografos, Greece glyras@geol.uoa.gr (2) InDigital, Dirfis 31, Vrilissia

Research Highlights

In this contribution we document the practical considerations related to the digital recreation of a *Mammuthus meridionalis* herd developed for an augmented reality app.

Background

The mammoth herd was created under our ongoing project 'PalaeoScope'. The project intends to present complex scientific data to the visitors of the Acropolis of Athens through artistic 3D recreations of the past. One of the periods under reconstruction is the Early Pleistocene. Since mammoths are the most emblematic megafaunal species of the Pleistocene, we decided that *Mammuthus meridionalis*, the Early Pleistocene mammoth of Southern Europe, should play a key role in our reconstructions.

Objectives

Mammoths are some of the first extinct creatures to be reconstructed (Witton, 2018; Manucci & Romano, 2022). Nevertheless, *M. meridionalis*, has received little attention by paleoartists. Our team designed a mammoth herd consisting of several three-dimensional, animated models of *M. meridionalis*. Through a custom augmented reality app the visitors of Acropolis will be able to see these animals roaming though the palaeoenvironment of Attica Basin. The app will be for handheld hardware such as smartphones. The devices will use their video-see-through systems to overlay visuals onto the live environment and use sensors, such as digital compasses and GPS, to determine their location.

Figure 1. Examples of some of the individuals of the mammoth herd.

Methods

The Early Pleistocene is well represented in Athens Basin. The fossil localities of Tourkovounia and Psychiko have yield fossil mammals ranging from MN16 till MNQ19. That is well within the stratigraphic range of *M. meridionalis.* Nevertheless, thus far, no fossil remains of that mammoth have been found in Athens (Athanassiou, 2022). Despite the absence of direct fossil evidence, we decided to include *M. meridionalis* in our reconstruction. The species was widespread within Greece, and thus its presence in Attika during the Early Pleistocene is plausible.

For the creation of the mammoth herd, we followed the population structure of modern elephant groups. Osteological (Haynes *et al.,* 2018) and molecular (Pečnerová *et al.,* 2017) data indicate that the social groups of wooly mammoths (*M. primigenius*) have been like that of modern elephants. Modern elephants live in social groups led by an older cow, the matriarch. Males that are sexually potent leave the herd. The only males present in the groups are juveniles. Moreover, modern healthy elephant herds have a large percentage of immature elephants (Jachmann, 1979). Thus, we reconstructed a mammoth herd comprising of several adult cows, subadult females and males. The herd is led by one older cow. We also designed a few large solitary bulls, scattered within Athens Basin.

There are some non-composite mounted skeletons of *M. meridionalis* in museums across Europe. Those mounts allow a rather accurate reconstruction of adult mammoths (e.g. Larramendi, 2016). However, the available material from juveniles is rather limited. Furthermore, a complete skull from a newborn *M. meridionalis* is unknown. We therefore modeled the mammoth calves following the skull proportions of modern species. Modern *Loxodonta* and *Elephas* calves and juveniles have small tusk sheaths and relatively long foreheads. On the contrary large adult specimens have relatively large tusk sheaths and short foreheads (van der Geer *et al.,* 2018).

Results and Conclusions

Our digital recreation of the mammoth herd (Figure 1) aims to help the public engage with the palaeontological past. Similar works have demonstrated that augmented reality apps received strong positive reviews from visitors and led to learning gains (Davies *et al.,* 2022). The mammoth herd is expected to be an appealing element of the PalaeoScope app.

Acknowledgements

This research was co-financed by the European Regional Development Fund of the European Union and Greek national funds through the Operational Program Competitiveness, Entrepreneurship and Innovation, under the call RESEARCH-CREATE-INNOVATE (Research project: PalaeoScope; Project code: T2EΔK-03781).

References

Athanassiou, A., 2022. The fossil record of continental elephants and mammoths (Mammalia: Proboscidea: Elephantidae) in Greece. in: Vlachos, E. (ed) Fossil Vertebrates of Greece Vol. 1. Springer, 345–391.

Davis, M., Nye, B.D., Sinatra, G.M., Swartout, W., Sjöberg, M., Porter, M., Nelson, D. Kennedy, A.A.U., Herrick, I., DeNeve Weeks, D., Lindsey, E., 2022. Designing scientifically-grounded paleoart for augmented reality at La Brea Tar Pits. Palaeontologia Electronica, 25(1):a9.

Haynes, G., Klimowicz, J., Wojtal, P., 2018. A comparative study of woolly mammoths from the Gravettian site Kraków Spadzista (Poland), based on estimated shoulder heights, demography, and life conditions. Quaternary Research, 90(3), 483–502.

Jachmann, H., 1979. Population dynamics of the elephants in the Kasungu National Park, Malawi. Netherlands Journal of Zoology 30(4), 622–635.

Larramendi, A., 2016. Shoulder height, body mass and shape of proboscideans. Acta Palaeontologica Polonica 61(3), 537–574.

Manucci F., Romano M., 2022. Reviewing the iconography and the central role of ‘paleoart’: four centuries of geo-palaeontological art. Historical Biology, doi:10.1080/08912963.2021.2017919

Pečnerová, P., Díez-del-Molino,D., Dussex, N., Feuerborn, T., von Seth, J., van der Plicht, J., Nikolskiy, P., Tikhonov, A., Vartanyan, S., Dalén, L., 2017. Genome-based sexing provides clues about behavior and social structure in the woolly mammoth. Current Biology, 27(22), 3505–3510.

Van der Geer, A.A.E., Lyras, G.A., Mitteroecker, P., MacPhee, R.D.E., 2018. From Jumbo to Dumbo: Cranial shape changes in elephants and hippos during phyletic dwarfing. Evolutionary Biology 45, 303–317.

Witton, M.P., 2018. The Palaeoartist's Handbook: Recreating prehistoric animals in art. U.K., Ramsbury: The Crowood Press Ltd.

16th International Congress of the Geological Society of Greece
17-19 October, 2022 - Patras, Greece
Bulletin of the Geological Society of Greece, Sp. Publ. 10
Ext. Abs. GSG2022-264

A study of students' perceptions of the Covid-19 pandemic

O. Koumoutsakou[1], A. Antonarakou[1], V. Lianou[1]
(1) National Kapodistrian University, Athens, Greece, okoumout@geol.uoa.gr.

The COVID-19 pandemic and its impact on the higher education industry is an issue being discussed worldwide (Fischer, 2020) till nowadays (Gómez-García et al. 2022). During the Covid-19 pandemic, online teaching and learning have been triggered reshaping the educational systems worldwide and changing students' lives. The guidance for the universities included moving courses for teachers and students online with the typical methods used by combining existing asynchronous teaching platforms with synchronous distance learning (i.e. pre-recorded lectures, live teaching via online platforms, and some forms of hybrid learning) (CEDEFOP, 2020). But what do students think about their studies during the Covid-19 pandemic? Online teaching and learning as experienced by the students had a positive or negative impact on them?

Methods

This study is a small-scale case study presenting the preliminary results of an analysis of students' perceptions of emergency remote teaching (ERT) (Hodges et al. (2020) during the Covid-19 pandemic. The aims of the study are: to record the students' perceptions of emergency remote teaching and learning, to record the advantages and disadvantages of the procedures, and to record students' perceptions of a hybrid education during no emergency periods. The study was conducted at the Geology and Geoenvironmental Department of National and Kapodistrian University of Athens in the years 2021 and 2022 with a descriptive method in order to measure students' beliefs by using a questionnaire survey. The questionnaire was issued via Google Form to 180 undergraduate students (4th year) and eventually, 169 students freely commented on the survey. In order for us to learn about their perceptions and experiences with online learning, a combination of wide-open questions and questions with more closed formats was preferred, and overall students displayed a wide range of responses. All quantitative and qualitative data were decoded and typed into various Word and Excel files in order to be registered in the SPSS system.

Results

The students from the Department of Geology and Geoenvironment expressed their opinions concerning the advantages and disadvantages of emergency remote teaching (ERT) during the Covid-19 pandemic. A large part of the student population (24%) considers that the greatest advantage of the ERT was the time gained while studying at home without having to travel to the University Campus. Many students indicated they got surprised at the support they had from their professors ranking this as the 2nd biggest advantage (18%). Moreover, 9 % of the students agreed that during ERT their professors used innovative teaching methods with the use of experiential exercises, concept maps, and videos, and the students had access to online materials, etc. 11% of the students responded that the use of new software was another advantage for the ERT as during the face to face education it was not so easy to understand the course material without the use of personal computers. For 6% of the students, home confinement turns out to be a home safety and an advantage during ERT though for 10% of the student population there were poor learning conditions at home. In addition, other responses were concluded as advantages of the surprisingly quick transition to distance learning as the new ways of examinations and teamwork, a smaller budget for studying, etc.

The most frequently mentioned disadvantage (13%) of the ERT was the lack of practical courses, laboratory classes, and fieldwork. Students believe that the lack of these made the course material incomprehensible and difficult to understand where it is applicable. The 2nd disadvantage mentioned was the workload with many exercise assignments in limited delivery time and an additional 8% mentioned the excessive time in front of the computer screen. The reduced or lack of professor-student interaction (10%) and the lack of interaction with friends and fellow students (5%) made the students feel unable to perform normal work or studies at the University. Although, as mentioned before, 18% of the students expressed that while there were interactions it was amazingly supportive. 8% of the students mentioned disadvantageous technical problems (internet connectivity, platforms, etc.), and an additional 6% mentioned the difficulties they had with the software due to old technology on personal computers. Research at the University of Patra students showed that the negative emotional status of their students during the pandemic turned into a positive one at the beginning of electronic classes (Karalis & Raikou, 2020). Only 4 % of the students of the Geology Department responded they held some level of depression, anxiety, increased psychological and economic stress and lack of interest and motivation for their studies during the covid-19 pandemic. Other disadvantages mentioned are related to the lack of differentiated teaching, the professors' contagiousness, difficulties during exams, courses not taken, etc.

Conclusions

Though technology can facilitate our everyday lives (Dimensional Research, 2018), according to the UN one-third of students around the globe "*do not have the appropriate connectivity, device and digital skills required to find and use educational content dependent on technology'* (UNESCO, 2021). In the Department of Geology and Geoenvironment of the University of Athens, 8% of the students could hardly access remote learning though they are people that have grown up with digital technologies. Despite the problems and the difficulties, professors made great efforts to support students and their course remote teaching and this was greatly appreciated by the students. The additional time that students had indoors from the ERT along with the use of new software and applications used, presented as major advantages for the students, should be a prompt to curriculum revision and reorganization. A previous study showed that students find insufficient, culturally and cognitively, the use of distance education in laboratory courses (Sivrikaya, 2019). In case of new recurring pandemics and crises, further research on innovative practices and the use of hybrid models for laboratory courses (eg. ISTES Organization) should be our new concern.

Acknowledgements

We have to thank all the students from the Geology and Geoenvironmental Department of National and Kapodistrian University for spending their time in filling the questionnaires.

References

Hodges, C., Moore, S., Lockee, B., Trust, T. and Bond, A., 2020. The difference between emergency remote teaching and online learning, Educause Review. (2020). Retrieved August 10, 2022, from https://medicine.hofstra.edu/pdf/faculty/facdev/facdev-article.pdf

CEDEFOP, 2020. Greece: responses to the Covid-19 outbreak. Retrieved August 19, 2022, from https://www.cedefop.europa.eu/en/news/greece-responses-covid-19-outbreak

Dimensional Research (2018). The future has arrived, are you ready for gen z? Round Rock: Dell. https://www.dellemc.com/en-us/collaterals/unauth/salesdocuments/solutions/gen-z-the- future-has-arrived-executive-summary.pdf

Fischer, K. 2020. Confronting the seismic impact of COVID-19: The need for research. Journal of International Students, 10(2), i-ii.

Gómez-García G., Ramos-Navas-Parejo M., De la Cruz-Campos J.C., Rodríguez-Jiménez, C., (2022). Impact of COVID-19 on University Students: An Analysis of Its Influence on Psychological and Academic Factors. Int. J. Environ. Res. Public Health 2022, 19, 10433.

Karalis, T., & Raikou, N. (2020). Teaching at the times of COVID-19: Inferences and implications for higher education pedagogy. International Journal of Academic Research in Business and Social Sciences, 10(5), 479-493.

Sivrikaya, O. S. (2019). Chemistry students' opinions about taking chemistry education as distance education. European Journal of Open Education and E-learning Studies, 4(2), 35-45.

Unesco, 2021. One year into COVID-19 education disruption: Where do we stand?Retrieved August 26, 2022, from: https://en.unesco.org/news/one-year-covid-19-education-disruption-where-do-we-stand

16th International Congress of the Geological Society of Greece
23-25 May, 2022 - Patras, Greece
Bulletin of the Geological Society of Greece, Sp. Publ. 10
Ext. Abs. GSG2022-265

Promoting advanced geoheritage education: the 1st Summer School of the Vikos-Aoos UNESCO Global Geopark

A. Chatzipetros[1], H. Papaioannou[2], C.L. Stergiou[1]

(1) Department of Geology, Aristotle University, Thessaloniki, Greece, ac@geo.auth.gr (2) Vikos-Aoos UGGp/ Epirus S.A., Ioannina, Greece

Geoheritage is an intangible concept that consists of the sum of geological features in a specific area, in conjunction with its interaction with the natural environment (biodiversity) and human presence and activities. The concept of geoheritage management has been introduced rather recently and was adapted by UNESCO as a significant component of an integrated approach to conservation and sustainable development. One of the main organized manifestations of geoheritage management is the concept of Geopark. UNESCO Global Geoparks are single, unified geographical areas where sites and landscapes of international geological significance are managed with a holistic concept of protection, education and sustainable development. A Geopark is a unit that consists of a number of geosites (i.e. sites with significant geological interest) in a specified area, and has set in place specific rules and administrative procedures in order to protect, highlight and promote them. To this end, the contribution of research and education is critical and a UNESCO Global Geopark, must proactively develop and promote them.

The Vikos-Aoos Geopark was established in 2010 and designated as UNESCO Global Geopark in 2015. It is managed by Epirus S.A., a development organization of local authorities, which operates within the Region of Epirus central administrative body. Some of the Geopark's main features are the deep incision Vikos and Aoos gorges, the Voidomatis river valley, the Tymphi mountain range, significant normal and oblique-slip active faults, the unique steam geothermal field of Amarantos, etc. In total, 51 well documented and accessible geosites form an integral part of the Geopark, while on-site information panels and relevant publications help disseminate the scientific knowledge to the public.

Since, as mentioned, education is one of the operational pillars of a geopark, Vikos-Aoos Geopark proposed to the Department of Geology of the Aristotle University of Thessaloniki the organization of a Summer School. Following extensive discussions with the stakeholders and the local authorities, it was decided that the School should be addressed to advanced level participants of various natural science disciplines.

The education programme of the School was designed in such a way, that it would address a broad range of relevant interests, not confined in just geological ones. The main objectives were to:

- Address advanced research and management issues.
- Introduce the participants to the geological structure of the Geopark.
- Complement lectures with hands-on experience through specially designed field trips.
- Have the participants work in teams: research, compile, develop and publicly present a specific topic of interest.
- Provide added value to the local community by introducing advanced-level participants to a relatively little-known area.

An open call was released in May 2022 and was forwarded to all relevant university departments in Greece, as well as disseminated through social media. Due to the advanced character of the programme, the call was addressed primarily to PhD and MSc students, however it was also open to senior undergraduate students as well. In total, 85 applications were received from students coming from 15 institutions in Greece and abroad. Applicants included 11 PhD and 31 MSc students, as well as 38 senior undergraduate students. Five more applications were received from graduate students.

The plan was to accept up to 25 participants; however, due to the increased interest, 39 students were finally accepted. They included 6 PhD and 15 MSc students, as well as 18 senior undergraduate students.

The programme consisted of various topics, divided into two discrete, yet complementary modes, i.e., classroom and field teaching:

- Classroom: three talks on the geological and hydrogeological features of the Geopark, three talks on research and management of geoparks and protected areas, two talks on geoarchaeology and building stones, one talk on physical dating methods and eight talks by the participants on various advanced topics.
- Field trips: Vikos gorge, Voidomatis gorge and springs and Konitsa active fault zone (Figure 1).

All lodging and subsistence expenses were sponsored by the Municipality of Konitsa, the field trip transportation by the Epirus S.A., while there were no participation fees for the attendees.

To assess the impact of the Summer School, an online structured questionnaire was sent to the participants. The questionnaire consisted of predefined weighted questions, as well as free-text fields. In total, 29 out of 39 participants returned the questionnaire (response rate: ~74%). The main outcomes are summarized as follow:

Figure 1. The group of attendees during one of the field trips, in front of a fault surface along the active Konitsa fault zone.

- 100% of the participants thought that the field trips were necessary to complement the School objectives. Almost all (96.5%) thought that their content was absolutely or very relevant to the overall programme, while most of them thought that the field trips were intensive and physically demanding.
- 100% of the participants were very content with the lecturers, while most of them (93.1%) also thought that the content of the lectures was very interesting and relevant. On the contrary, the majority of the attendees felt that the presentation programme was more intensive than they would have preferred.
- By analysing the free-text fields (comments and suggestions), the following points were drawn:
    - The level of satisfaction for both the scientific, as well as the logistical aspects of the School was very high.
    - The participants felt that the programme of the School (lecture and field trips) was intensive, and suggested a longer duration with more free time.
    - The teamwork between participants of various disciplines and levels, in order to prepare the topical presentations, was intensive, but very fruitful and with added value for potential future cooperation.
    - The participants strongly suggested the continuation of this Summer School series and most of them would wholeheartedly apply again.

It is generally accepted that a management body of a *sensu lato* natural park should not be just a strictly bureaucratic instrument, but instead it should proactively seek the advancement of scientific knowledge and the successful interaction with local communities. Educational programmes of various levels can be effective tools to help seamlessly bridge those two distinct targets. To this end, the 1st Summer School of the Vikos-Aoos UNESCO Global Geopark was a successful pilot event that brought together high-level young scientists of various disciplines and set the benchmark for subsequent events. The next steps are to establish the Summer School as a regular event with somewhat differentiated focus each year, to adjust and enhance the field trips and to expand its target audience internationally, possibly awarding ECTS points to participants.

Acknowledgements

The authors would like to sincerely thank the Municipality of Konitsa for the logistical sponsoring (lodging and subsistence) of the Summer School, as well as all the lecturers (Kati V., Kitsaki G., Melfos V., Nikolaou E., Paschos P., Stamoulis C., Telbizs T.) for participating and sharing their experience pro bono.

16th International Congress of the Geological Society of Greece
17-19 October, 2022 - Patras, Greece
Bulletin of the Geological Society of Greece, Sp. Publ. 10
Ext. Abs. GSG2022-269

Preliminary results from implementation of education through art to Geoscience Students

M. Damigou [1], O. Koumoutsakou[1], A. Antonarakou[1]
(1) National and Kapodistrian University, Athens, Greece, marousadamigou@gmail.com

This study aims to describe the students' response to the teaching method called 'education through art' in matters related to social problems. Students from the Department of Geology and Geoenvironment of Athens dealt with issues that included gender discrimination, racism, homophobia, etc. with the use of imagery art as a didactic/pedagogical tool in order to be led to unusual discoveries that may contribute to the advance and dissemination of knowledge in society. Education through art is considered the most appropriate tool in order to achieve this goal as it is an experiential process that creates a trigger for discussions (Taylor, 2015), cultivates observation and connection between various objects of knowledge (Shreeve et al. 2010), can help learners understand ethics (Williams, 2016) and has the potential to act as a means for re-examining dysfunctional assumptions.

Methods

The study is a small case study examining how an instructional method that deviates from the traditional ones can make students respond to its pedagogical endeavors. The study population consisted of Greek undergraduate students of the Department of Geology and Geoenvironment of National and Kapodistrian University of Athens. The majority of participants are currently in the phase of emerging adulthood, a phase characterized by increased socializing and self-explanatory tendencies (Arnett, 2014). Qualitative content analysis was utilized.

The main purpose of the research is to discover the degree of students' social awareness. We aimed to use the education through the art method as described by Kokkos' (2011) book so as to engage the exchange of ideas with discussion while putting the students at the center of the learning experience (Trigwell et al. 2004).

This study was contracted in two phases. During phase 1, the students were requested to fill in a questionnaire issued via Google Form. The questionnaire included topics dealing with marginalized populations (i.e. people excluded due to special needs, mental health issues, infertility, gender identity, sexual orientation, ethnicity, etc.) and was sent to 89 individuals with a total of 62 responses. Thereupon, phase 2 included the application of the teaching method of Education through Art. The students were shown a surrealistic painting that depicts the same social problems as the questionnaire mentioned above, after naming specific stereotypical phrases and assumptions. They then were asked to explicate it based on their own point of view.

Results

The participation of students in the discussion about social inequalities was quite high. The issues that were mentioned included gender roles and gender-based stereotypes, prejudices around mental health, sexual orientation, gender identity, religious discrimination, and racial/ethnic bias. The undergraduate students displayed heightened awareness of social groups that are usually discriminated against due to the race/ethnicity, sexual orientation, or gender identity of their members in both phases of the study. The way the painting was interpreted was significantly influenced by the discussion that preceded its observation, while students associated its symbols with gender equality, the refugee crisis, physical disabilities, mental health issues, climate change, the effects of colonialism, cultural diversity and the economical inequalities of our times. It is worth noting that the participants showed particular interest in the duration of the observation of the painting and the discussion that preceded it.

Conclusions

In order to foster critical thinking, a means necessary for evaluating the seriousness of synchronous social issues, it is necessary to apply the appropriate educational techniques such as education through art that unlock the mechanism of observation, questioning, and re-evaluation in student classes.

Acknowledgements

We have to thank all the students from the Department of Geology and Geoenvironment of National and Kapodistrian University that participated in this study.

References

Arnett, J.J. (2014). Emerging Adulthood: The Winding Road from the Late Teens Through the Twenties, 2nd Ed. Oxford University Press.

Shreeve, A., Sims, A.R.E, Trowler, P., 2010. A kind of exchange: Learning from art and design teaching. Higher Education Research and Development, 29(2):125-138.

Taylor, R. (2015). Using Art in the ESl. Classroom. Introduction to Teaching Overseas. Retrieved on August 16th 2022 from:

https://www.cambridge.org/elt/blog/2020/10/13/oracy-6-supporting-early-oracy- development-in-preschool-elt-students/ on June 6th, 2021.
Κόκκος, Α. και Συνεργάτες (2011). Εκπαίδευση μέσα από τις τέχνες. Αθήνα: Μεταίχμιο.

16th International Congress of the Geological Society of Greece
17-19 October, 2022 - Patras, Greece
Bulletin of the Geological Society of Greece, Sp. Publ. 10
Ext. Abs. GSG2022-283

Disaster and crisis management awareness level of local authorities in the District of Attica Municipalities before and after training courses

A. Bakopoulou[1], N.- A. Katsetsiadou[1], E. Kyriazis[1], V. Alexoudi[1], A. Grambas[1], E. Kotsi[1], E. Stamati[1], A. Antonarakou[1], E. Lekkas[1]

(1) Department of Geology and Geoenvironment, National and Kapodistrian University of Athens, Athens, Greece, abakopoulou@geol.uoa.gr.

This research is part of the adult educational program *"Training of local authorities on Disaster and Crisis Management*" under the auspices of the National and Kapodistrian University of Athens and the District of Attica Municipalities. The research aims to explore the awareness of local authorities in relation to the management of serious environmental problems, disastrous events and extended crises. To this purpose, a questionnaire tool was implemented before and after the training courses on all of the trainees, in order to compare their responses and evaluate their awareness.

Sixty-one responses out of 100 participants were reported equally before and after the courses. In this paper we present preliminary data of the pilot questionnaire implementation before and after the courses. As far as demographics are concerned, only 37% of the respondents are women and all of the rest are men. The majority of the respondents are older than 44 years while over 40% hold an M.Sc. degree, a fact that shows the high educational level of the employees. Their work experience ranges widely between 1 and 40 years with maximum frequency at about 20 years.

As far as the awareness level is concerned, it is encouraging that only 8% are unaware of the existence or not of local operational planning for disaster and crisis management, but this is not promising, as one quarter of the respondents insists on the absence of such planning in the municipality they work for. The correct answers on hazard classification reach high percentages, about 75% before to 90% after the training courses. It is an alarming precursor that more than 60% of respondents have never participated in practice drills or have never been trained on how to manage disasters and crises by the local authority they are employed in. Before the training, about 65% declare that they know how to respond in case of emergency, disaster or crisis events. Contrary to their declaration, medium scores (40%-62%) are recorded on the perception of concepts such as disaster, crisis, hazard, risk, capacity, vulnerability, risk assessment etc. Respondents' certainty on how to react in emergency cases rises to 84% (fig. 1a) after the training courses, which seem to have empowered employees' assuredness. There is a remarkable rise up to 85% in the conception of basic terminology, too, after the courses, as for example is depicted in figure 1b. Also, in figure 1b, it is noteworthy that the answer "Don't know" is dramatically decreased from 14% before the training to 0% after it. This phenomenon is thoroughly present in the responses. The answer "Don't know" records higher scores before the training program and lower to zero scores after it, which proves the increase of employees' awareness and confidence level.

Lower to medium scores of awareness from 47% to 57% appear before training, when it comes to the disaster and crisis management stages, such as prevention, readiness, response, restoration. They reach medium (47%) to higher percentages (78%) after training. Besides, lower to medium awareness level (45% to 64%) is documented as far as Emergency Plans of the Civil Protection Organization are concerned before training, while this level increases to 89% after training (i.e. Fig. 1c). Finally, the awareness level on the function, responsibilities and coordination of the National Strategy Mechanism varies from 54% to 91% before training and mounts up to 67%-100% after training courses.

In conclusion, the general awareness level of employees and executives of Municipality Organizations and Local Authorities is medium with deficient knowledge level before the training courses. Sometimes awareness level reaches higher scores, which in relation to the employees' high educational level, depicts their willingness and capacity to be trained. After the training program, the general awareness level has been improved significantly especially in the fields of terminology conception, hazard classification, emergency planning of Civil Protection and National Strategy Mechanism. On the contrary, lower improvement is recorded in the disaster and crisis management stages. This might be due to either flaws of the training courses or more demanding and specialized concepts to conceive and procedures to follow. It is obvious that the implemented adult educational program increased the disaster and crisis management awareness and confidence level of the participants. Taking into consideration a) the results of the questionnaire, b) the employee educational level, and c) the increasing frequency of disastrous and crisis events within the ongoing climate crisis, the immediate need to augment local authorities awareness through proper training and practice drills cannot be ignored. This should be a high priority action, both in the Operational Plan of each Local Authority and the National Strategy Mechanism, so that maximum risk disaster reduction and effective management of disaster and crisis is achieved.

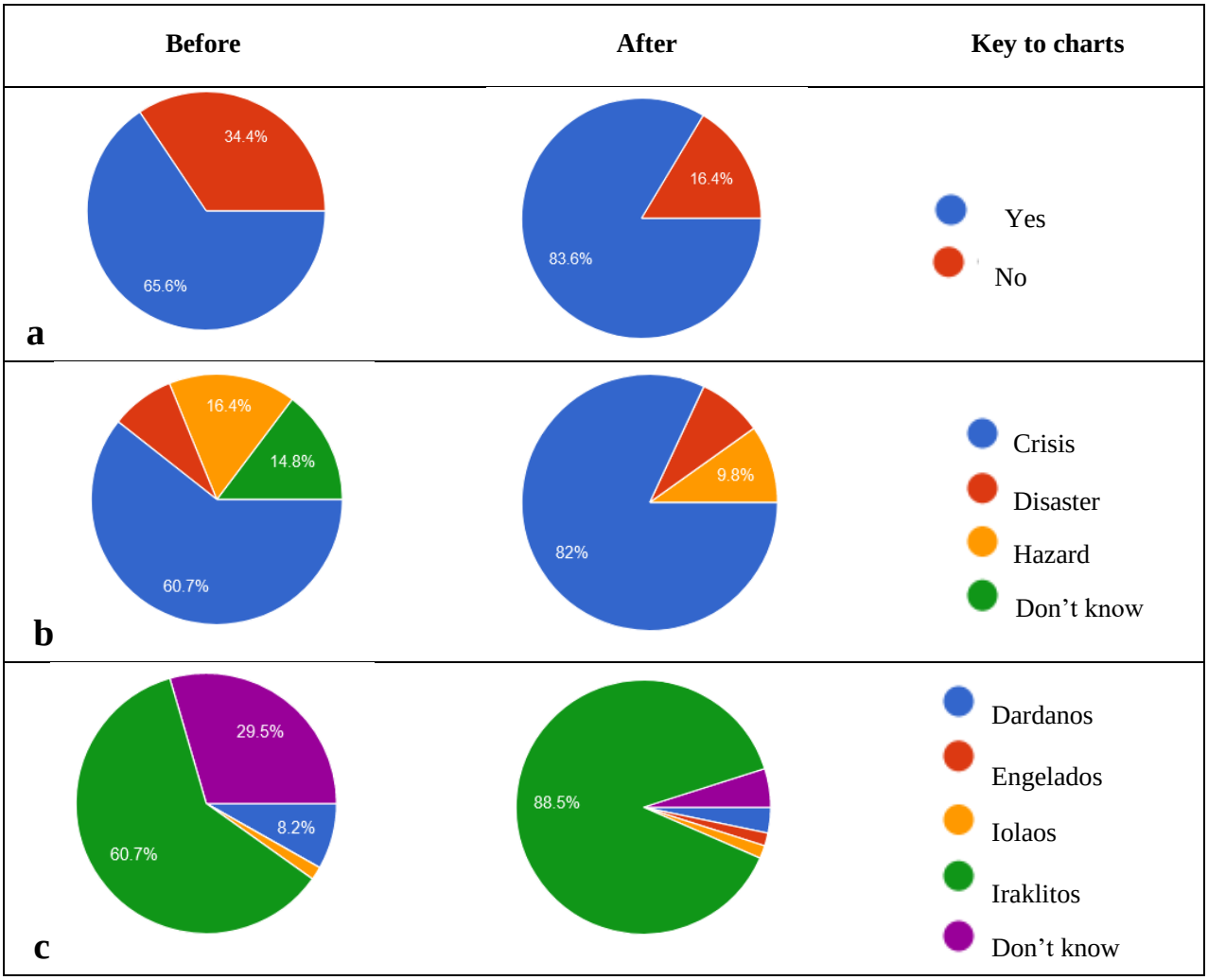

Figure 1: Changes in the responses to the questions (a) "Do you believe that you know how to respond in case of emergency?", (b) "The severe disruption of societal functions, when there is a chance of recovery and improvement, is called…"; (c) "The Emergency Plan of Greek Civil Protection for the management of Extended Technological Accidents is named…" before and after the training courses.

16th International Congress of the Geological Society of Greece
17-19 October, 2022 - Patras, Greece
Bulletin of the Geological Society of Greece, Sp. Publ. 10
Ext. Abs. GSG2022-342

The New Curriculum on Environment and Education for Sustainable Development and its Potential for Shaping Attitudes and Behaviors towards the Geoenvironment and Cultivating Geoethical Values

E. Georgousis[1], S. Mosios[1], S. Savelides[2], M. –V. Holokolos[3], H. Drinia[1]

(1) Department of Geology and Geoenvironment, National and Kapodistrian University of Athens, 15784 Athens, Greece, egeorgousis@geol.uoa.gr (2) Hellenic Ministry of Education and Religious Affairs, Directorate of Secondary Education of Magnesia, 38333 Volos, Greece (3) Department of Culture, Creative Media and Industries, University of Thessaly, 38221 Volos, Greece

Abstract

The inclusion of geodiversity, geoheritage and geoethics in the curricula contributes to the sensitization of students and their reflection on personal and social values and responsibilities, in order to redefine their needs at an individual and collective level, to lead them to a reconsideration of the value system that individuals and societies have adopted to date, and, therefore, to develop into environmentally and socially aware citizens (Georgousis et al., 2022a). Recently, the new curriculum entitled "Environment and Education for Sustainable Development" (Official Gazette of the Hellenic Republic, 2022) was prepared and published, reflecting the directions of educational policy in Greece concerning the principles and values of education for sustainable development for the coming years. It ensures the interconnection-coherence of knowledge from the first school age up to lower secondary school, creating the background for a constructive and analytical-inquiry-based learning and providing teachers with opportunities to utilize innovative elements in the context of their dissemination when teaching their subjects, in the context of "Skills workshops" and "Educational Programs of School Activities". The question was raised on whether it incorporates values of the natural world related to geology, geodiversity, geoheritage and geoethical thought, that is, whether indirectly or directly, it contributes to the awareness and empowerment of students to the values of geoethics and consequently to the development of appropriate behavior regarding the interaction of human activities with the Earth system (Georgousis et al., 2021a,b; Peppoloni & Di Capua, 2015; 2020). For the purpose of answering this question, research questions were raised concerning the presence of conceptual patterns, which refer to obvious or latent means (Thyme et al., 2013) of promoting geoethical values. In order to investigate the thematic units and the expected learning outcomes of the new compulsory education syllabus in the Greek educational system, the methodology of semiotics content analysis was followed (Bryman, 2012; Tang & Zhan, 2021; Georgousis et al., 2022b). For the content analysis, i.e., the quantification of the semantic patterns, the computer-assisted qualitative data analysis software (CAQDAS) was used (Friese, 2021). The investigation outcomes provided us with a satisfactory number of obvious semantic patterns (codes) related to geodiversity and a satisfactory number of latent meanings related to geoheritage and geoethical values. It remains for educators to understand the necessity of the new elements offered by the new curriculum in order to adopt and implement them.

Keywords

Geoethics, geodiversity, geoheritage, geoeducation, environment, sustainable development

References

Bryman, A., 2012. *Social Research Methods*. Oxford University Press, Oxford, UK.

Friese, S., 2021. *ATLAS.ti 9 User Manual*; ATLAS.ti Scientific Software Development GmbH. Berlin, Germany.

Georgousis, E., Savelides, S., Mosios, S., Holokolos, M.-V., Drinia, H., 2021a. The Need for Geoethical Awareness: The Importance of Geoenvironmental Education in Geoheritage Understanding in the Case of Meteora Geomorphes, Greece. *Sustainability*, *13*, 6626. doi:10.3390/su13126626

Georgousis, E., Savelidi, M., Savelides, S., Holokolos, M.-V., Drinia, H., 2021b. Teaching Geoheritage Values: Implementation and Thematic Analysis Evaluation of a Synchronous Online Educational Approach. *Heritage*, *4*, 3523–3542. doi:10.3390/heritage4040195

Georgousis, E., Savelidi, M., Savelides, S., Mosios, S., Holokolos, M.-V., Drinia, H., 2022a. The inclusion of Geoethical Values in the Design of Educational Policy for the Next Decade: The Case of the Greek Educational System, EGU General Assembly 2022, Vienna, Austria, 23–27 May 2022, EGU22-5915. doi:10.5194/egusphere-egu22-5915

Georgousis, E., Savelidi, M., Savelides, S., Mosios, S., Holokolos, M.-V., Drinia, H., 2022b. How Greek Students Perceive Concepts Related to Geoenvironment: A Semiotics Content Analysis. *Geosciences*, *12*, 172. doi:10.3390/geosciences12040172

Official Gazette of the Hellenic Republic, 2022. B 2820/06.06.2022. Available online: https://www.esos.gr/sites/default/files/articles-legacy/fek-2022-tefxos_b-02820-downloaded_-08_06_2022.pdf (accessed on 9 August 2022).

Peppoloni, S., Di Capua, G., 2015. The Meaning of Geoethics, in Wyss, M., Peppoloni, S. (Eds.), *Geoethics*, Elsevier, Amsterdam, The Netherlands, Volume 419, 3–14. ISBN 9780127999357.

Peppoloni, S., Di Capua, G., 2020. Geoethics as global ethics to face grand challenges for humanity. *Geol. Soc. Lond.*, *508*, 13–29.

Tang, F., Zhan, P., 2021. Does Diagnostic Feedback Promote Learning? Evidence from a Longitudinal Cognitive Diagnostic

Assessment. *AERA Open*, *7*, 1–15. doi:10.1177/23328584211060804
Thyme, K.E., Wiberg, B., Lundman, B., Graneheim, U.H., 2013. Qualitative content analysis in art psychotherapy research: Concepts, procedures, and measures to reveal the latent meaning in pictures and the words attached to the pictures. *Arts in Psychotherapy*, *40*, 101–107. doi:10.1016/j.aip.2012.11.007

16th International Congress of the Geological Society of Greece

17-19 October, 2022 - Patras, Greece

Bulletin of the Geological Society of Greece, Sp. Publ. 10

Ext. Abs. GSG2022-362

Citizen Science and Geoheritage: a Sampling Campaign for Cosmogenic ^{36}Cl Surface Exposure Dating of Glacial Deposits in Mt Parnassus National Park, Central Greece

A.D. Leontaritis[1], K. Pavlopoulos[2], M. Giorgaras[3], K. Tsalkoutis[3], N. Koukis[3]

(1) National Technical University of Athens, Greece / The Greek Mountain Project, Ioannina, Greece. aris.leontaritis@gmail.com (2) Sorbonne University Abu Dhabi, UAE. (3) Nomads Path Adevntures- Outdoor Activities Cooperative, Athens, Greece.

Research Highlights

A sampling campaign for ^{36}Cl dating of Quaternary moraines was conducted in June 2021 with an open call on social media for participation of citizens regardless of their background. The organization was jointly realized by geoscientists and mountain hiking professional guides. A multi-beneficial collaboration both for science and geoheritage was achieved which resulted in a very efficient sampling campaign. At the same time participants and professional guides were actively involved in scientific research thus gaining a deeper understanding of the geoheritage of Mt Parnassus National Park.

Paleoclimatic and geomorphological background

Evidence of former glacier occupation is present across Greece where many mountain regions exceed 2000 m asl (Leontaritis, 2021 and references therein). The most extensive glacial phase in the mountains of Greece took place during MIS 12, as established by radiometric data from Mt Tymphi (Woodward et al., 2004). These studies overturned the initial assumption that, similarly to the Alps, the most extensive glacial phase in the Balkans occurred during the global last glacial maximum (LGM) (27-23 ka). In the contrary, evidence suggests a much more restricted glacier development during the Late Pleistocene, and particularly around the LGM and during the Lateglacial Allard, et al. 2020; Leontaritis et al., 2022. The study of Pope et al. (2017) on Mt Chelmos showed that LGM glaciers were limited to the highest elevations and already in recession at 23-21ka. This is consistent with evidence from Mt Tymphi, where the presence of small glaciers at high altitudes dated to the LGM, correlated stratigraphically with many rock glaciers, has been interpreted as the result of arid climate conditions around the global LGM (Allard et al., 2020).

The Lateglacial (17.5-11.6 ka) in Europe was characterized by at least two cold periods that favored glacial advances: the Oldest (OD) and the Younger Dryas (YD) at 17.5-14.7 ka and 12.85-11.6 ka respectively. In Greece, glacial deposits from the Lateglacial are rare and have so far been dated only on Mt Olympus (OD; 15.7-14.5 ka; Styllas et al., 2018) and Mt Chelmos (YD; 12.6-10.2 ka; Pope et al., 2017). The paucity of OD or YD moraines possibly indicates that relatively unfavorable climatic conditions for glaciers formation continued throughout most of the Lateglacial.

Overall, while several glacial deposits have been identified only some have been successfully dated to the LGM, and Lateglacial. Thus glaciers response to these cold events in Greece remains largely understudied. Traces of former glaciers on the mountains of central Greece (Mt Parnassos, Mt Vardousia, Mt Gkiona) had already been identified by the first pioneer researchers like Mistardis (1937) and Pechoux (1970). The undated (likely) LGM to Lateglacial moraines in the mountains of central Greece could provide the key for testing the precipitation hypotheses of a more arid climate during the Lateglacial in northern Greece compared to the south proposed by Pope et al. (2018) and Leontaritis (2021) based on the observation of decreasing Equilibrium Line Altitudes of paleoglaciers across Greece (North to South).

Study Area, approach, and sampling campaign objectives

Mt Parnassus is (2457 m asl) is composed of a 1.5-2 km thick Upper Triassic to Palaeocene neretic carbonate sequence, terminating with a typical Palaeocene clastic sequence (flysch) (Kranis and Papanikolaou, 2001). The massif is characterised by U-shaped valleys, headed by well-developed glacial cirques, indicating extensive glacier occupancy(ies) in the past, likely linked to the Middle Pleistocene (MIS 12) (Leontaritis, 2021). Through a dedicated geomorphological field study, Leontaritis (2021) identified a few clear and well preserved, moraines within at least five high altitude (>2000m), north-facing cirques (Figure 1a). The lack of soil and vegetation, limited lichen colonisation and evidence of relatively limited weathering on the surface of these moraines indicate a likely recent (LGM to Lateglacial) age.

The scientific aim of this wider project is to constrain the age of Late Pleistocene glacial deposits on Mt Parnassus, focusing on the LGM and the Lateglacial using the cosmogenic ^{36}Cl surface exposure dating of glacial boulders - a well-proven method for limestone lithologies. Sampling focused on limestone boulders within moraines in the Liakoura, and Tsarkos NE and NW cirques (Figure 1a). Sites in Yerontovrahos and Arnovrisi cirques (panel c and d in Figure 1a) were ultimately not considered for sampling because of a lack of large boulders and the proximity to the ski runs and lifts.

Implementation of sampling campaign in the framework of Citizen Science and geoheritage

On the 26th and 27th of June 2021 a joint group of 13 persons collected 18 high quality samples from glacial boulders in

the selected moraines after hard and well-coordinated work (Figure 1b). These samples are currently under analysis in the SUERC AMS facilities in Scotland. The number of participants was significantly affected by a strong heat wave during that period with temperatures reaching 40°C in the lowlands. Several people cancelled their participation due to the prevailing conditions. The group consisted of two geoscientists coordinating and supervising the scientific work, three professional hiking guides taking responsibility of the group safety, the organization of the camp and of advising the 8 participants on tackling the challenges in this hard and remote mountain terrain.

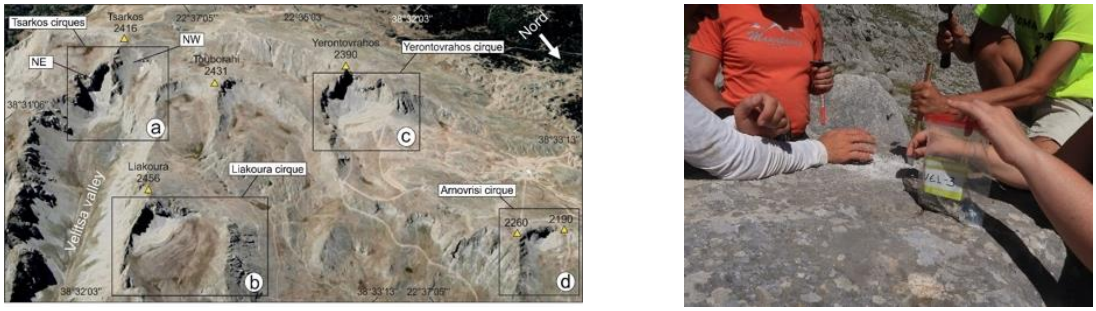

Figure 1. a) (Left) Satellite image of key sites on Mt Parnassus, b) (Right) Collaborative samples collection

The workshop started with a short review of the glacial history of Greece and the basic principles of geomorphology and geochronology and the interpretation of landforms with special focus on cryogenic processes. Special attention was given to the sampling principles for cosmogenic nuclides surface exposure dating described in Gosse and Phillips (2001). The training aimed at the understanding of the reasons why samples had to be collected in a certain way, strictly avoiding a series of inexplicable instructions. The participants and the professional guides showed great interest in expanding their knowledge through this geomorphological field study but also posed many questions on other aspects of geoscience such as the orogeny of the Greek mountains, fossils, petrology, tectonics, and geoconservation issues. These matters were openly discussed with the scientific advisors and a participating geologist with specialization in paleontology. In other words, geoheritage as discussed in Papadopoulou et al. (2022) was the focal point of arising discussions.

In summary, this pilot event of citizen geoscience (a process that involves the public in doing geoscience) raised the awareness and perception of the geoheritage of Mt Parnassus and the mountains of Greece for most participants, as it was underlined during the closing discussion of the workshop. Indeed, citizen science has been recognized to increase the participants' understanding of scientific processes and the environment, making them feel recognized and appreciated for their contribution, and potentially making participants more sensitive to and aware of certain socio-environmental issues (Haklay et al., 2021 and references therein). Thus, such actions contribute significantly towards shaping a wider perception of geoheritage and geoethics through the active participation and contribution of citizens in the development of scientific knowledge. Another important aspect is the motivation of outdoor activities professionals towards this direction as they can play a significant role in spreading this geoculture to participants in their commercial activities. The promotion of geoheritage as a natural resource of science, education, and tourism should anyway be among the main responsibilities of geoscientists and outdoor professionals supporting sustainable tourism in protected natural environments.

Acknowledgements

We would like to heartfully thank N. Batistatos, G. Bakalis, L. Giorgaras, D. Karavana, M. Kesanli, N. Manatos, A. Nizamidou, for their participation and their contribution in the sampling campaign of June 2021. Special thanks to geologist D. Mantziou-Tragaki for her valuable contribution during fieldwork.

References

Allard, L.J., Hughes, P.D., Woodward, J.C., Fink, D., Simon, K., Wilcken, K.M., 2020. Late Pleistocene glaciers in Greece: a new ^{36}Cl chronology. Quat. Sci. Rev. 245, 1–27.

Gosse, J.C., Phillips, F.M., 2001. Terrestrial in situ cosmogenic nuclides: theory and application. Quat. Sci. Rev. 20, 1475-1560.

Haklay, M., Dorler, D., Heigl, F., Manzoni, M., Hecker, S., Vohland, K., 2021a. What is citizen science? The challenges of definition. In: The Science of Citizen Science. Springer International Publishing, Cham, pp. 13–33.

Kranis, H., Papanikolaou, D., 2001. Evidence for detachment faulting on the NE Mt Parnassos (Central Greece). Bul. Geol. Soc. of Greece 34, 281-287.

Leontaritis A.D., 2021. The Late Quaternary Glacial History of Greece. PhD thesis, Harokopio University of Athens.

Leontaritis A.D., Pavlopoulos, K., Ribolini, A., Marrero, S., Spagnolo, M., Hughes, P.D., 2022. Glaciations on ophiolite terrain in the North Pindus Mountains, Greece: New geomorphological insights and preliminary ^{36}Cl exposure dating. Geomorphology 413.

Mistardis, G., 1937. Sur la morphologie des hautes montagnes de la Grece. Bul. 1st Panhel. Mount. Conf. Athens, pp. 35-41.

Pechoux, P., 1970. Traces d'activité glaciaire dans les montagnes de Grèce central. Rev. Geogr. Alp. 58, 211-224.

Papadopoulou, E.E., Papakonstantinou, A., Vasilakos , C., Zouros, N., Tataris, G., Proestakis, S., Soulakellis, N., 2022. Scale issues for geoheritage 3D mapping: The case of Lesvos Geopark, Greece. International Journal of Geoheritage and Parks 10, 435–446.

Pope, R., Hughes, P., Skourtsos, E., 2017. Glacial history of Mt Chelmos, Peloponnesus, Greece, J. Geol. Soc. Lond. 433, 211-236.

Styllas M.N., Schimmelpfennig, I., Benedetti, L., Ghilardi, M., Aumaître, G., Bourlès, D., Keddadouche, K., 2018. Late-glacial and Holocene history of the NE Mediterranean mountain glaciers - New insights from ^{36}Cl exposure dating of paleoglacier deposits on Mt Olympus, Greece. Quat. Sci. Rev. 193, 244-265.

Woodward, J.C., Macklin, M.G., Smith, G.R., 2004. Pleistocene glaciation in the mountains of Greece, IN: Quaternary glaciations - extent and chronology. Part I: Europe, Amsterdam: Elsevier, pp 155-73.

16th International Congress of the Geological Society of Greece

17-19 October, 2022 -Patras, Greece

Bulletin of the Geological Society of Greece, Sp. Publ. 10

Ext. Abs. GSG2022-372

New generation digital materials of National Geological Museum of Greece (H.S.G.M.E.)

K. Laskaridis[1], M. Fitros[1,2], V. Skliros[1,3], N. Evelpidou[4], A. Tsokos[5], D. Gkoutis[1]

(1) Hellenic Survey of Geology and Mineral Exploration, Acharnai 13672, Athens, Greece (2) Department of Geology, University of Patras, Rio 265 04, Greece, (3) School of Mining and Metallurgical Engineering, National Technical University of Athens, Iroon Polytechneiou 9, Zografou 157 80, Athens, Greece, (4) Faculty of Geology and Geoenviroment, National and Kapodistrian University of Athens, Panepistimioupolis, Ano Ilisia 15784, Athens, Greece. (5) Former General Director of Hellenic Survey of Geology and Mineral Exploration, Acharnai 13672, Athens, Greece

Research highlights:

This work discusses the current progress in the development of the new National Museum of Greece as a new ‘‘alive’’ digital museum and identify the factors that drove its development. Herein, the new digital materials of the National Geological Museum of Greece where the use of new generation tools such as Virtual Reality glasses, digital interactive applications and interpretation videos for the exhibitions which focus to provide to the user a new perspective on his experience inside the museum. The use of digital technology has improved the production process of traditional museums and galleries, greatly facilitating the interaction between visitors and collections. Although the concept of a digital museum has attracted a lot of attention over the past decade, many challenges remain.

Background and objectives

The digital transformation of museums calls for the creation of a new generation of museums with a focus on new digital technologies, thus enabling the public to interact and immerse themselves in the not so well-known science field of geology. In general, museum visitors spend less than one minute on each collection on-site. The problem focuses on how to captivate visitors’ interest in the museum exhibition. That said, digitalization of the museum has become a new research field for curation. This gives the opportunity for the physical museum’s exhibition to coexist with digital material throughout the galleries. According to Li et al. (2012) visitors’ experience can be boosted by an interactive and immersive environment in the museum. Furthermore, exhibits’ descriptions can be enhanced with digital equipment to give visitors a new perspective of experience. Based on this suggestion, the blending between the physical museum’s exhibition and digital material have been applied to the new National Geological Museum of Greece. User’s experience is enchanted with new visual material and interaction applications which promote a deeper knowledge in the field of geology. This new digital material offers visitors a valuable experience and helps improving communication between viewers, curators, and museums.

Results and discussion

Following the needs of the modern public and the evolution of technology, the new National Geological Museum has developed a wide range of educational interactive applications and digital educational material. Special digital equipment has been placed in different areas in the museum and digital activities take place through new interactive applications to familiarize the public with the field of geology, with new interactive ways, such as applications which describe the mining and processing of mineral wealth, and everyday words/phrases related to geology (Fig.1.).

Earth’s creation through animation video

There is a specially designed screening area for short animation films which describes *the Formation of the Earth*, *the Geological Evolution of Greece*, *the Cycle of the Rocks*, and *the Main Rock Units of the Country* (Fig.1). Those animations introduce visitors to the National Geological Museum of Greece. The new animation material has been created using ‘‘Unreal Engine’’ which gave the opportunity to add special effects which catches the interest of visitors of all ages.

Virtual Reality immersive experience

Throughout of the museum area VR (Virtual Reality) glasses have been installed to provide visitors with new immersive experience. In general, the problem that such a museum with geological perspective faces is that the visitors can’t experience the important geosites of Greece from a geological point of view. To solve this problem, in the Museum galleries, visitors can discover the technology of virtual reality with the use of VR glasses and can travel to important geosites of geological heritage such as Meteora, Cave-Lake Melissani, Pentelikon Mountain etc. and "dive" into the depths of the mines of Chalkidiki, Lavrion and Naxos (Fig. 2). VR technology gives the opportunity to show the visitors a new perspective of the important geological areas in Greece and this is one of the most "interactive" experiences (360º και 3D), allowing remote access and familiarization with the geology and the geological monuments of the country.

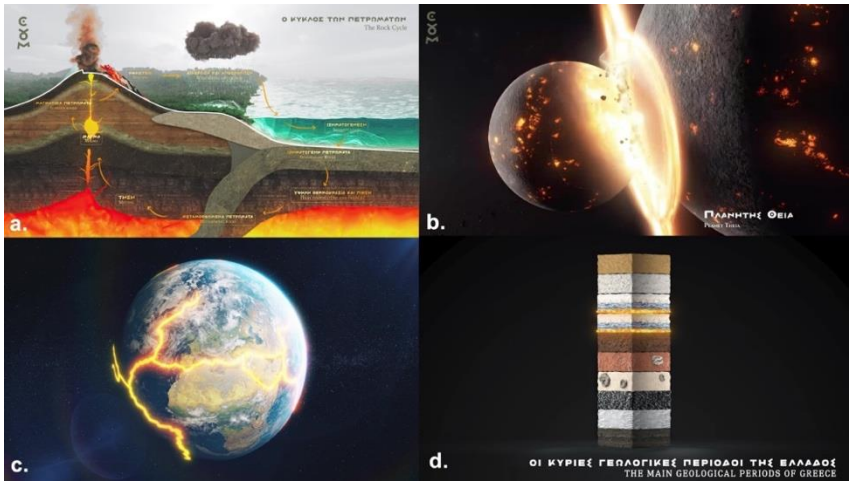

Figure 1. Example photos from the animations produced using the software ‘’Unreal Engine’’ a) the Cycle of the Rocks b) Formation of the Earth c) Evolution of Earth’s crust and d) the Rock Units of Greece

Oral and Visual Testimonial material

Visitors can’t understand the story behind the exhibits most of the times. For this reason, there is a special design of audio-visual material to bring people behind the exhibits and shed light on unknown aspects of the country's mining and metallurgical history, an area that has not been highlighted in museums of this type. Through oral testimonies exhibits can be "brought to life" and visitors can gain a more "experiential" relationship with them, taking advantage of the full use of 3D technology.

Interactive Map / The mineral wealth of Greece

An installed interactive map offers the opportunity to discover the mineral wealth of each region of Greece (Fig. 2) as well as individual information through an innovative, digital, interactive wall-map of the country. And all these, just with a touch.

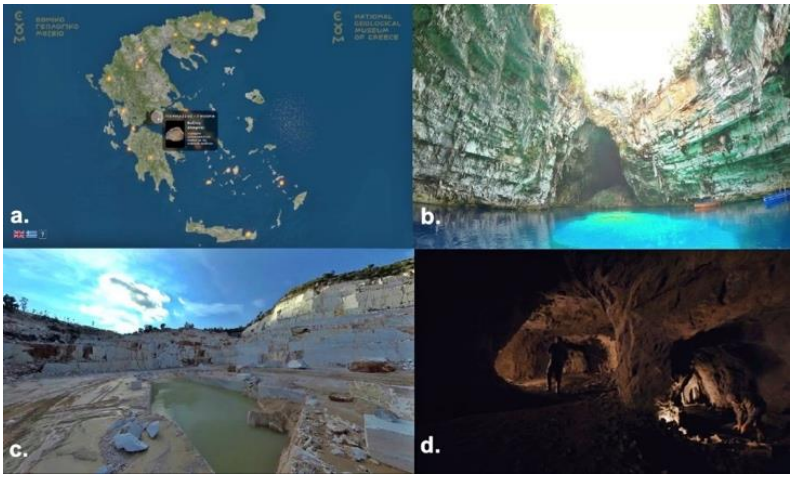

Figure 2. a) Interactive Map: The mineral wealth of Greece b) VR content from Melissani Cave-Lake c) VR content from Pentelikon Mountain and d) VR content from Lavrion mine

Augmented Experience Room (AR)

A new special area of Augmented Experience application named "Discovering the Underground Mine" has been constructed in the museum with new technology where a combination of projections, audiovisual information with special architectural design that provides the maximum interactive experience of immersion in the reality of touring in an underground mine. Finally, it will be possible for schools in the country to remotely access the educational digital material through the developed educational platform.

Conclusion

Successfully understanding the difficulties to provide visitors with a deeper knowledge of the geology, the extensive use of the technology helped to develop the new National Geological Museum of Greece with the creation of a new ‘‘living’’ digital museum, which enhances the social value of geological heritage. This work provides the methods which have been used for the development of the new museum by offering visitors a new user experience.

References

Li, Y.-C., Liew, A. W.-C., & Su, W.-P. (2012a). The digital museum: Challenges and solution. 2012 8th International Conference on Information Science and Digital Content Technology (ICIDT2012), 3, 646–649.

16th International Congress of the Geological Society of Greece
17-19 October, 2022 - Patras, Greece
Bulletin of the Geological Society of Greece, Sp. Publ. 10
Ext. Abs. GSG2022-380

The Lesvos Petrified Forest Park: "Kyria Apolithomeni", Lesvos Island UNESCO Global Geopark, Greece-Protecting And Enhancing A Historical Geological Heritage Site

I. Valiakos[1,2], N. Zouros[1,2], K. Bentana[1,2], E. Zgournios[1], E. Antonakis[1,2], A. Lamprakopoulos[1,2]

(1) Natural History Museum of the Lesvos Petrified Forest, Lesvos Island, Greece, lesvospf@otenet.gr (2) Department of Geography, University of the Aegean, Mytilini, Greece.

The Lesvos Petrified Forest Park at "Kyria Apolithomeni" site, covers an area of 40 hectares and is managed by the Lesvos Forestry Department in collaboration with the Natural History Museum of the Lesvos Petrified Forest.

The Park is located at the southern slope of a hill belonging to the mountain complex of Ordymnos. It occupies a small watershed of one of the branches of the river Tsichliodas, which forms one of the most extensive hydrographic networks of Western Lesvos.

The geological formations in the area are consisting of pyroclastic rocks of the Lower Miocene, and include:

- volcanic ash layers rich in angular pumice fragments of various dimensions
- mudstone layers containing handle fragments
- layers of volcanic cobblestones containing large-sized cobbles of volcanic origin.

Successive layers of pyroclastic materials are clearly visible in the area of the park along the walking paths and at the excavation sites. An overall view of the succession of overlapping pyroclastic formations can be seen from the area of the entrance gate, looking at the slope of the hill located south of the park. These formations were deposited in the area 20 million years ago due to successive volcanic eruptions by the main volcanic centers of Lesvos.

The Park constitutes the flagship of the Lesvos Petrified Forest, a protected Natural Monument, the most significant geological heritage area of Lesvos Island UNESCO Global Geopark. The Park is the historical site and most visited open air park of the Lesvos Petrified Forest, hosting the most emblematic petrified trees. The area in which the Park was established in 1987 has been referred to as "Kyria Apolithomeni" (Main Fossil site) since the 18th century.

This site is the first open air park of the Petrified Forest. Integrated interventions for the protection and preservation of the fossils have been conducted over the years. Since 1997 systematic excavations were carried out by the Natural History Museum of the Lesvos Petrified Forest. Walking routes were laid out and constructed in the Park, as well as various facilities for the convenience of visitors.

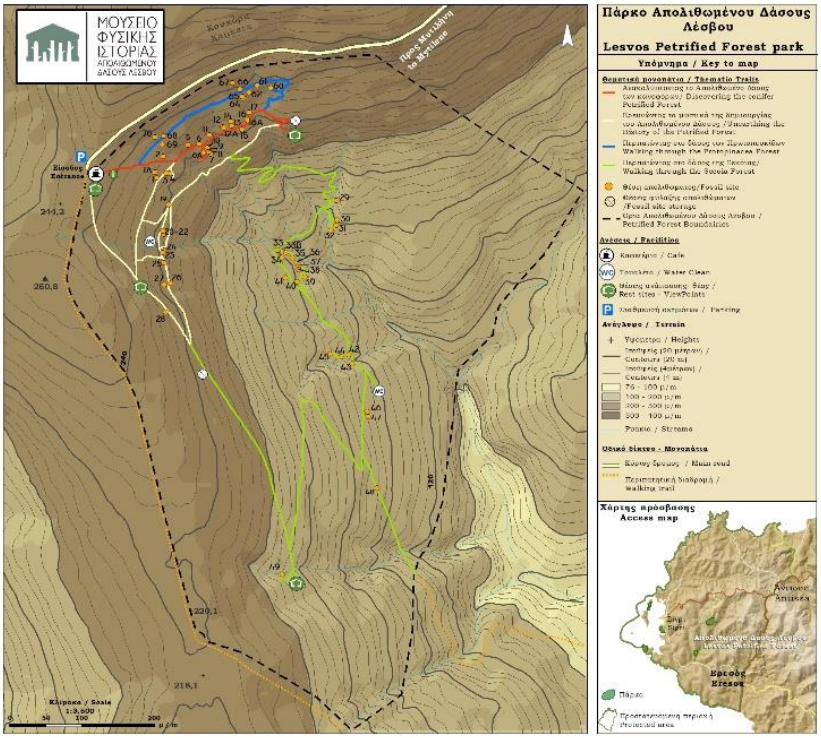

Figure 1. The area of the Lesvos Petrified Forest Park at "Kyria Apolithomeni" site

Although at first glance fossils appear hard and durable, they are in fact very fragile, and are at risk from a number of factors (called environmental parameters) that cause significant mechanical and chemical damage.

Environmental parameters are responsible for the deterioration seen in fossils. Excessive moisture causes swelling in fossils with the highest porosity and lowest hardness. Excessive dryness causes cracking and pulverization (turning surfaces into dust). Extreme heat and extreme cold respectively cause the fossils to expand and contract, leading to cracks. Rainwater enters the cracks and expands to form ice crystals due to winter frost, thus causing additional mechanical damage.

Over time, and under the influence of various corrosive factors, among which are water and air, erosion of fossils occurs, leading to the gradual disintegration and loss of fossil material. In some fossils, due to humidity, oxides are formed, and pulverization of the surfaces is observed. The soluble salts present in the soil, through moisture, move inside the fossils. These salts tend to move to drier surfaces and form hard crusts, so strong that they can cause cracks to form or pieces to break off. Fossils found in open spaces are – additionally – confronted with a multitude of biological factors. Plants often grow on the fossils themselves, causing mechanical damage such as cracks and breaks with their roots. Unfortunately, the human factor is often a danger to the fossils. Unwitting visitors have in the past caused significant damage to the fossils through vandalism, breaking and stealing pieces.

All the above led to the decision to conduct systematic conservation works to at least fifty (50) fossilized trunks in the area of the Park. All fossils conserved needed immediate protection as they have never been conserved before.

Figure 2. Conservation of the two most impressive petrified tree trunks in the area of the Lesvos Petrified Forest Park at "Kyria Apolithomeni"

Besides the conservation works there was also the need for improvement of the infrastructure and for the creation of new, aiming to the protection restoration and enhancement of the area which was necessary in order to meet the demands of the visitors. The project of the Petrified Forest Park was realized in close collaboration with the Lesvos Forestry Department.

The project included the enhancement of the Park's infrastructure, renovation of the protective fences of the Park, new pathways improving the accessibility of the fossil sites the restoration of walking routes throughout the Park as well as various works for the convenience of visitors.

Concluding, the conservation and restoration works at the petrified logs in the park that were carried out by the Natural History Museum of the Lesvos Petrified Forest as well as the actions for the enhancement of the Park's infrastructure accompanied by various activities to increase its visibility and promotion protect the fossil sites for the generations to come, improve the visitors' experience when visiting the site and benefit the geotourism potential of the Lesvos Petrified Forest Park at "Kyria Apolithomeni" site.

Acknowledgements

The conservation, protection and aesthetic enhancement of the fossilized trunks of the Petrified Forest Park in the location Kyria Apolithomeni (Bali Alonia) and the protection, restoration, enhancement and signage of the Park have been funded by the Regional Operational Program "North Aegean 2014-2020".

References

Zouros, N, Valiakos, I. 2010. Geoparks management and assessment. Bulletin of the Geological Society of Greece, 2010, Proceedings of the 12th International Congress, Patras, May, 2010,Vol. XLIII – No 2, p. 965-975

16th International Congress of the Geological Society of Greece
17-19 October, 2022 - Patras, Greece
Bulletin of the Geological Society of Greece, Sp. Publ. 10
Ext. Abs. GSG2022-383

A NEW METHODOLOGY ON GEOSITE ENCHANCEMENT USING 3D MAPPING LESVOS ISLAND UNESCO GLOBAL GEOPARK AS A CASE STUDY

E. Antonakis[1], A. Lamprakopoulos[1], N. Zouros[1], N. Soulakellis[1]
(1) University of Aegean, Mytilene, Greece, manolis.antonakis@rocketmail.com

UNESCO Global Geoparks are single, unified geographical areas where sites and landscapes of international geological significance are managed with a holistic concept of protection, education, and sustainable development. Their bottom-up approach of combining conservation with sustainable development while involving local communities is becoming increasingly popular.

Geosites/geological heritage sites are areas of special geological and geomorphological value, representative of the geological processes that form the lithosphere or of the stages of the evolution of life on earth. Thus, can be characterized as sites of the Earth's memory.

This paper aims to present a new methodology on geosite enhancement using 3D mapping. Each geosite has different dimensions and relief. Thus, we need to evaluate the needs of different geosites in order to be presented to the general public. The use of 3D mapping is necessary for educational, promotional and geoconservational purposes. A 3D model offers better observation and understanding of the large scale geosites.

The plethora of geosites within a Geopark or a protected area emphasizes the need of using digital tools and 3D mapping for a comprehensive management and interpretation of large scale geosites.

The proposed methodology aims to prioritize the needs for geosite 3D mapping based on a set of criteria and the geosite typology. We used a scale from 0-5 in order to investigate the needs for their three-dimensional mapping.

The criteria used to prioritize the needs of the different geosites are the following.

First criterion is the geosite dimension and topography. The topography of a geosite plays an important role for the selection of the geosites which will be presented through 3D mapping. This specific criterion refers to which extent a specific viewpoint (2D perspective) allows a comprehensive understanding of the geosite morphology.

Second criterion is supervision. The criterion of the supervision of a geosite, concerns to what extent the observer can have or not a comprehensive perception and understanding of the morphology of the geosite from the best viewpoint.

And the third criterion is accessibility. The criterion concerns its degree of geosite accessibility. This criterion examines the priority of approaching a geosite, i.e., whether it is easy or difficult to access for the average visitors.

Lesvos Island UNESCO Global Geopark presents a variety of geosites. The Petrified Forest protected area includes a variety of palaeobotanical and paleontological assemblages. There are also various volcanic, tectonic, karstic, stratigraphic, coastal, erosional, and human-made geosites. The above-mentioned geosite categories present different needs in order to be presented and become understandable and accessible by the general public.

Using the above-mentioned criteria, we prioritized the needs for 3D mapping of the Lesvos Geopark geosites. Geosite 3D mapping resulted to the creation of geosites 3D models which have been used in order to present them through digital applications (website, mobile app, virtual reality devices etc.) and make them accessible for the general public.

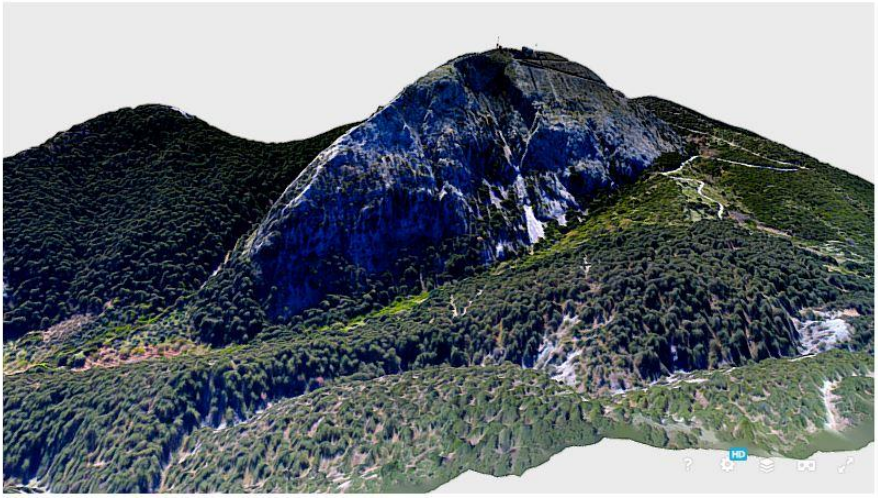

Figure 1: 3D Model Olympus, Tectonic Window, Lesvos, Greece

16th International Congress of the Geological Society of Greece
17-19 October, 2022 - Patras, Greece
Bulletin of the Geological Society of Greece, Sp. Publ. 10
Ext. Abs. GSG2022-384

Enhancement And Promotion Of The New Fossiliferous Sites Along The New Kalloni Sigri Road – An Example Of Good Practice Of Geoconservation In Lesvos Island UNESCO Global Geopark Greece.

N. Zouros[1,2], N. Soulakellis[1,2], I. Valiakos[1,2], K. Bentana[1,2], E. Theodorou[1], E. Zgournios[1], E. Antonakis[1,2], A. Lamprakopoulos[1,2]

(1) Natural History Museum of the Lesvos Petrified Forest, Lesvos Island, Greece, lesvospf@otenet.gr (2) Department of Geography, University of the Aegean, Mytilini, Greece.

In Western Lesvos Island, Greece a new road is under construction connecting Kalloni, the central town of the Island, with Sigri which is the westernmost village of the Island, where the Natural History Museum of the Lesvos Petrified Forest, the management body of Lesvos Island UNESCO Global Geopark is located. This road is of vital importance as it will improve the accessibility to Western Lesvos.

During the construction of this new road, part of which leads through the wider area of the Petrified Forest of Lesvos, a large number of astonishing sites with impressive fossilized tree trunks have been unearthed, which lay on the verge of the road.

The Natural History Museum of the Lesvos Petrified Forest aims to enhance the new fossil sites, to protect them and to create new visiting areas along the Kalloni-Sigri road. A series of interventions is underway for the protection of the improvement of the accessibility to the fossiliferous sites, interpretation and information, signage and infrastructure for visitor services. In addition to various awareness raising activities, a new campaign entitled “Walk the Forest” introduces the new fossil sites to the public.

The protection and enhancement activities include conservation of fossils, construction of stone walls, construction of wooden structures, installation of shelters, activities to enhance the fossil sites and scientific documentation - identification of the fossils. The conservation, protection and enhancement of the fossils include seven hundred (700) fossilized trunks in 15 fossil-bearing sites. Approximately two thousand (2000) fossils have been unearthed so far which include parts of fossilized trunks, roots, branches and pieces of pyroclastic material that contain leaves and twigs.

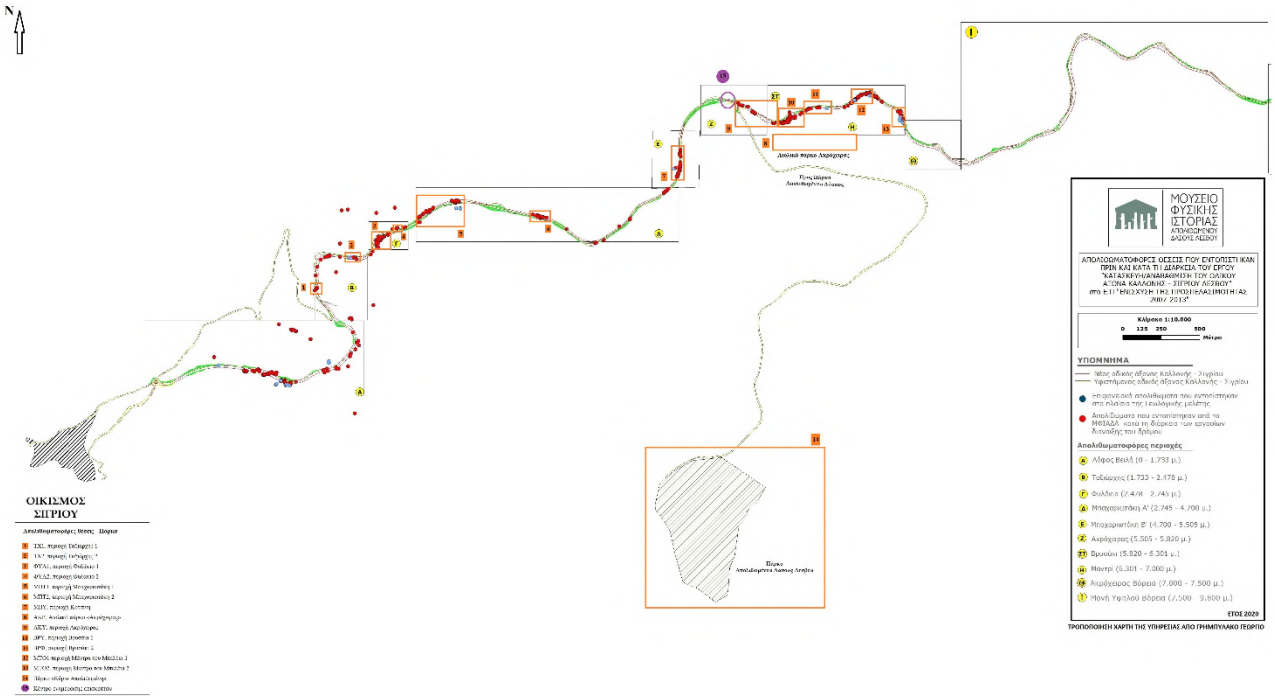

Figure 1. Map showing the fifteen (15) fossiliferous sites in the area of the Lesvos Petrified Forest in Western Lesvos

In parallel activities for the promotion of the results of the scientific work aim to make these new sites known to the wide public. An increase in the number of visitors to the area of Western Lesvos is expected with a simultaneous contribution to the economic and social development, the reduction of unemployment, and consequently the improvement of the standard of living of the inhabitants in the area.

Figure 2. Impressive fossilized tree trunk found during the construction of the Kalloni-Sigri road in the area of the Lesvos Petrified Forest in Western Lesvos

At the same time, the entire Protected Area of the Petrified Forest of Lesvos will once again be shown as a globally recognized preserved natural monument, while public opinion will understand that its effective protection is an obligation of the Greek State in the context of observing national, European and international legal commitments for the preservation of natural heritage (PD. 433/1985, Law 1650/1986, Law 2260/1994, Barcelona Treaty).

Acknowledgements

The Enhancement and promotion of the new fossiliferous sites along the new Kalloni Sigri road have been funded by the Regional Operational Program “North Aegean 2014-2020”.

References

Zouros, N, Valiakos, I. 2010. Geoparks management and assessment. Bulletin of the Geological Society of Greece, 2010, Proceedings of the 12th International Congress, Patras, May, 2010,Vol. XLIII – No 2, p. 965-975

16th International Congress of the Geological Society of Greece

17-19 October, 2022 - Patras, Greece

Bulletin of the Geological Society of Greece, Sp. Publ. 10

Ext. Abs. GSG2022-403

Educational Activities For The Visually Impaired In Lesvos Island UNESCO Global Geopark – The Erasmus+ Program "Geology for the Visually Impaired"

K. Bentana[1,2], N. Zouros[1,2], I. Valiakos[1,2],

(1) Natural History Museum of the Lesvos Petrified Forest, Lesvos Island, Greece, lesvospf@otenet.gr (2) Department of Geography, University of the Aegean, Mytilini, Greece.

The accessibility of people with visual impairments to the geological monuments, the sites of the Petrified Forest and the geosites of Lesvos Island UNESCO Global Geopark is a key priority of the Natural History Museum of the Lesvos Petrified Forest. In this direction, the Museum implements two main actions.

The first is focused on the development of educational programs for the visually impaired. The aim of the educational programs is to bring visually impaired visitors in contact with the Lesvos Petrified Forest and the geological heritage of Lesvos Island UNESCO Global Geopark. In the frames of the program, the participants have the opportunity through the senses such as touch, hearing, smell to collect information related to the characteristics of each fossil and create a complete picture of the ecosystem of the area that was fossilized during the Miocene.

At the same time, the Museum participates in the ERASMUS+ project "Geology for visually impaired people" (G4ViD). This is a project that involves the creation of educational mobile applications aiming to introduce our geological heritage and the geosites found in UNESCO Global Geopark areas to visually impaired people. Through the project, visually impaired people will have the opportunity to enjoy the experience of UNESCO Global Geoparks and the Earth Sciences will be introduced to them.

The aim of the application is that people with visual impairments and with the use of sound can perceive the geosites during a field visit. The first geosite used as a model for the app's operation was the giant fossilized sequoia tree trunk from the Lesvos Petrified Forest.

The Department of Electrical Engineering and Computer Science of the University of Patras, the Natural History Museum of the Lesvos Petrified Forest, the Liepājas Neredzīgo Biedrība (Liepāja society of the Blind) Latvia, the Red Cross special school of Cyprus, the CEIP LA JARA school from Spain and OPENCOM I.S.S.C. an ICT company in Northern Italy participate in the ERASMUS+ Program "Geology for the visually impaired".

The coordination of the actions for the selection of the appropriate geosites which will become accessible to people with visual impairments through the program was undertaken by the Natural History Museum of the Lesvos Petrified Forest. The Museum organized the collection of the necessary data for the creation of a database which contains all necessary data and content that is needed in order to get visually impaired people close to UNESCO Global Geoparks and make them familiar to geology. Apart from this, the database aims to provide all the necessary information for the development of the applications for visually impaired people related to geology. The first application is aiming to transform images and geological evidences such as fossils, rocks or petrified trees into sound files. When this happens a visually impaired person can touch a touchscreen and "feel" according to the sound changes the shape of the fossil or geological evidence. The second application refers to a mapping application. With this mapping application a visitor in a Geopark can track his path and provide a detailed route recorded into his mobile phone. This route can then be available to another visitor either if they visit the Geopark, or if they wish to virtually visit the place. The first step of the creation of the database consisted of the selection of geoparks and area of interest for the partners without a Geopark in their country:

The second step consisted of the selection of the geosites on specific criteria. The criteria for the seclection of the geosites for the database based on international criteria adjusted to the specific needs of the target group of this project. 20 geosites were selected from each project partner and in total 80 geosites were selected.

The aim is the results of the project to make our geological heritage accessible to the visually impaired giving them the opportunity to enjoy the experience of Geoparks and introduce them to the Earth Sciences.

Figure 1. A visually impaired person is testing the application by trying to understand how a petrified tree trunk looks like

Concluding we have to emphasize that a UNESCO Global Geopark is operating always with an including mentality and tries not to exclude any group of people wishing to enjoy its unique geological heritage

Acknowledgements

The programme has been funded by the Erasmus+ Program "Geology for the Visually Impaired"

References

Zouros, N, Valiakos, I. Bentana, K. 2017. Lesvos island UNESCO Global Geopark: Raising visibility and promotion, 14th EGN Conference, Abstracts Volume, Ponta Delgada, Azores, p. 42.

16th International Congress of the Geological Society of Greece
17-19 October, 2022 - Patras, Greece
Bulletin of the Geological Society of Greece, Sp. Publ. 10
Ext. Abs. GSG2022-414

Interdisciplinary studies on ancient quarries: The case of Ras serpentinite quarry, Tinos, Cyclades, Greece

A. Sideridis[1], V. Anevlavi[2], T. Jakobitsch[2], C. Hauzenberger[3], P. Koutsovitis[1] and A. Aggelopoulou[4]

(1) Department of Geology, Section of Earth Materials, University of Patras, 265 00 Patras, Greece, a.sideridis@upnet.gr (2) Austrian Archaeological Institute, Austrian Academy of Sciences, Franz-Klein-Gasse 1, 1190 Wien (3) NAWI Graz Geocenter, University of Graz, Universitätsplatz 2, Graz 8010, Austria (4) Greek Ministry of Culture and Sports, Ephorate of Antiquities of Cyclades, Epameinonda 10, 10555 Athens, Greece.

Introduction

The term marble is used in geology to describe metamorphic rocks containing carbonate minerals, in other words, the well-known white marble has been widely used from antiquity until today in the peri-Hellenic region. Colorful 'marbles' are rather rare, with small-scale quarrying activities being implemented as seen by the well-known cases of Green Thessalian stone (ophicalcite) (MELFOS, 2008) and Lapis Lacedaemonius (altered andesite) (Koutsovitis et al., 2017). These two occurrences along with the previously unexplored Ras serpentinite quarry are not classified as marbles, *stricto sensu*, but they instead represent different rock categories. The rather small quantities, relative to the white marble production in Greece, of Thessalian stone and Lapis Lacedaemonius have significant and specialized uses as decorative stones and columns for instance in the Hagia Sophia, the Santa Prassede, the St. Peter's Square etc. These prestigious usages of similar materials make the study of the ancient Ras quarry intriguing and promising.

The Ras serpentinite quarry

The serpentinite occurrence of Ras is just over 7 acres in size, whereas ancient quarrying activities are limited to a 0.9 acres area, taking into account the debris piles adjacent to the two quarries (Fig. 1a). The pits were opened using terraces forming façades with characteristic tool marks (Fig. 1b, c), only surviving in the north pit. The grooves for separating the stones from the parent rock and the holes for inserting wedges have been noticed and point to ancient activities. No modern activity was identified. The rock texture is unique, with pale-green-colored serpentine net cross-cutting the massive dark-green-colored serpentinite (Fig. 1d). dark-green serpentine is described by mesh texture under the microscope (Fig. 1e) and distinctive minerals, such as minnesotaite, have been identified during microprobe analysis (Fig. 1f), crystallized along with metal phases. Serpentinite, in places, is sheared (Fig. 1c) displaying schistosity and characteristic slippery feeling.

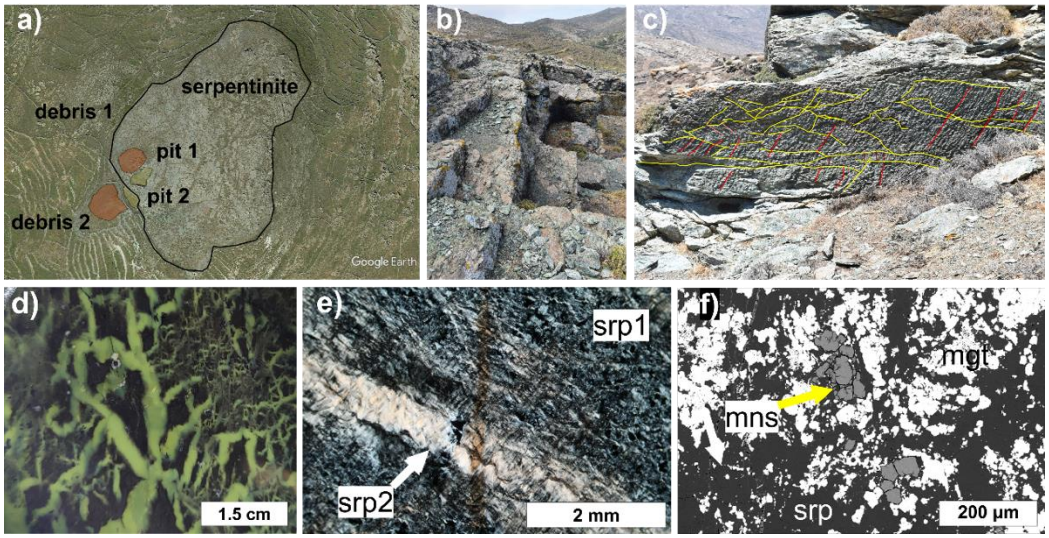

Figure 1. a) Satellite image of the Ras serpentinite occurrence, confined by the black line, open pits 1 and 2 are depicted with the yellow area whereas debris piles 1 and 2 with the orange areas; b) terraces found in the pit 1; c) serpentinite façade with tool marks (red lines) and geological discontinuities (yellow lines); d) texture of Ras serpentinite; e) photomicrograph of Ras serpentinite; f) back-scattered electron image of Ras serpentinite. Abbreviations: srp1= dark-green colored serpentine, var. antigorite; srp2= pale-green colored serpentine, var. lizardite; mgt= magnetite; mns: minnesotaite. Figures b and c © Ephorate of Antiquities of Cyclades.

Methodology and results-discussion

The serpentinite of the Ras ancient quarry has not been previously studied; hence, the geochemical imprint of the rock has been identified *via* **LA-ICP-MS** (upon serpentine-group minerals) and **EPMA** (upon serpentine-group minerals and other phases) analyses. In the serpentinite's Primitive Mantle (PM) normalized diagrams the LREE are highly depleted and the HREE concentrations are lower than the PM level. This indicates high degrees of partial melting of the mantle source, pointing to a harzburgitic source that was modified in a forearc region above a supra subduction zone (SSZ) (Deschamps et al., 2013). The elevated amounts of B, Pb and P have been incorporated during serpentinization of the harzburgitic protolith. The two different serpentine varieties, antigorite and lizardite, represent two different metamorphic stages. Antigorite formed at high grade metamorphic conditions, whereas lizardite represent lower grades, representing the healing of fractures during or after the exhumation of the Ras serpentinite. These results can be used for future provenance studies. The tool marks have been photographed and correlated with geological discontinuities (Figure 1c). The timing of the quarrying activities cannot be easily deduced from the literature, therefore the method of lichenometry is performed. By establishing a growth curve using measurements of lichen on substrates of known age (bridges, gravestones, abandoned farms, etc.), the growth rate of a species can be calculated and used to estimate the age of a lichen on a surface of unknown age, aiming to give first dating indication for the Ras quarry.

Conclusions

- The serpentinite of Ras records ancient quarrying activity, no modern practices have been deduced
- Ancient toolmarks have been preserved in the north quarry, with terraces as a method of rock extraction
- Two distinct serpentine polymorphs create the serpentinite's unique texture; minnesotaite can be used as mineral for provenance study
- Based on the geochemistry, the serpentinite had a forearc harzburgitic protolith, that was serpentinized in a subduction zone
- Fractures during the exhumation were healed with pale-green colored lizardite forming a network within the antigoritic mass

Acknowledgements

We would like to thank Prof. C. Hauzenberger for providing access on analytical equipment at the T.U. Graz and Dr. Anastasia Aggelopoulou along with the Greek Ministry of Culture and Sports, Ephorate of Antiquities of Cyclades for offering the study and publishing permissions.

References

Deschamps, F., Godard, M., Guillot, S., & Hattori, K. (2013). Geochemistry of subduction zone serpentinites: A review. Lithos, 178, 96-127. doi:https://doi.org/10.1016/j.lithos.2013.05.019

Koutsovitis, P., Kanellopoulos, C., Passa, S., Foni, K., Tsapara, E., Oikonomou, G., et al. (2017). Mineralogical, petrological and geochemical features of the unique lapis lacedaemonius (krokeatis lithos) from laconia, greece: approach on petrogenetic processes within the triassic volcanic context. Bull. Geol. Soc. Greece 50, 1903. doi: 10.12681/bgsg.14235.

Melfos, v. (2008). Green thessalian stone: the byzantine quarries and the use of a unique architectural material from the Larisa area, greece. Petrographic and geochemical characterization. Oxford J. Archaeol. 27, 387–405. doi: 10.1111/j.1468-0092.2008.00313.x.

16th International Congress of the Geological Society of Greece
17-19 October, 2022 - Patras, Greece
Bulletin of the Geological Society of Greece, Sp. Publ. 10
Ext. Abs. GSG2022-418

Links between geodiversity, floristic diversity and ecosystem services at the Chelmos-Vouraikos UNESCO Global Geopark

E. Koumoutsou[1,2,3], G. Iliopoulos[2,4], I.P. Kokkoris[3], M. Tsakiri[3], P. Papadopoulou[4,5], M. Panitsa[3], P. Dimopoulos[3]

(1) Management Unit of Chelmos – Vouraikos National Park And Protected Areas of The Northern Peloponnese (N.E.C.C.A.), Kalavryta, Greece (mdpp.northernpeloponnese@necca.gov.gr) (2) Chelmos-Vouraikos UNESCO Global Geopark (3) Laboratory of Botany, Department of Biology, University of Patras, Greece (4) Paleontology and Stratigraphy Laboratory, Department of Geology, University of Patras, 26504 Rio, Patras, Greece, (5) Natural History Museum of the Lesvos Petrified Forest, Sigri 81103, Lesvos, Greece

Background

Chelmos-Vouraikos UNESCO Global Geopark is a member of the Global Geopark Network since 2009. Except for the unique geodiversity, Chelmos – Vouraikos has a unique biodiversity as well, thus, it has been declared as a National Park since 2009. The study area (CVNP) is located in northern Peloponnese and is designated as the Protected Area of "Chelmos-Vouraikos National Park" and "UNESCO Global Geopark" covering an area of about 655 km2 (Figure 1). In this work, the diversity of the geological substrates of the 40 designated geosites of Chelmos-Vouraikos UNESCO Global Geopark (Golfinopoulos et al. 2022) is linked and correlated with the particularly valuable and often unique flora of the area.

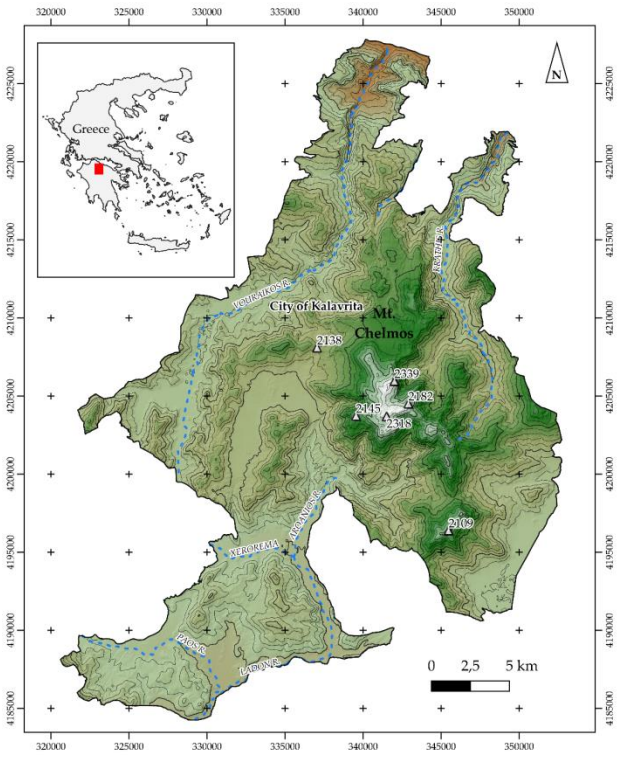

Figure 1. Map of the study, depicting, the largest city of the area (Kalavrita), major rivers and mountain peaks above 2000 m. Contours correspond to 100m intervals; contours with thicker line type correspond to 500 m intervals.

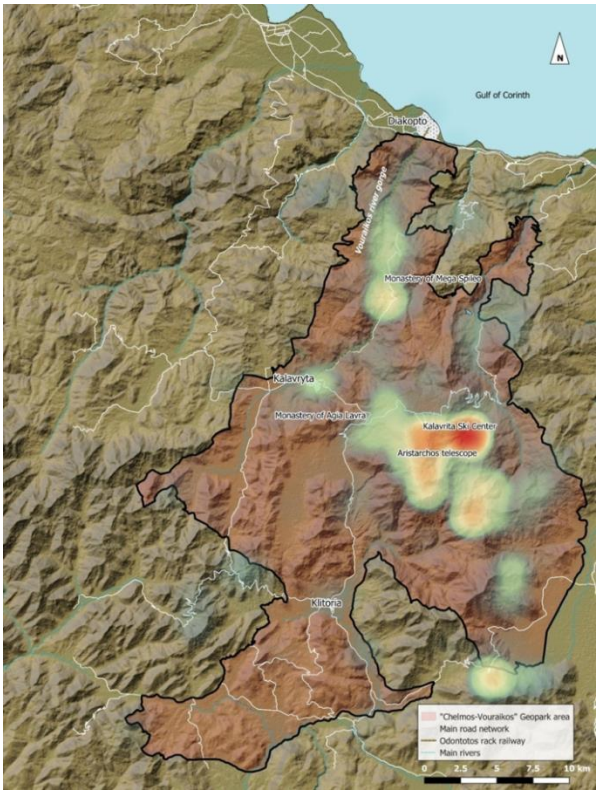

Figure 2. Hotspot area of geodiversity interaction with and endemic flora species (Mega Spilaio geosite conglomerates) at Chelmos-Vouraikos Geopark.

Objectives and Methods

The recording, assessment and understanding of natural capital and relevant ecosystem services, is a key objective for taking policy decisions and implementing management measures and actions to protect and promote natural wealth and human well-being (Tsakiri et al. 2022). Ecosystem types were delineated and mapped at the MAES (Mapping and Assessment of Ecosystem and their Services) level 3 for Greece, following Kokkoris et al. (2020) and Verde et al. (2020). Identification and assessment of ecosystem services (supply and demand) provided by the national park's ecosystem types follow Kokkoris et al. (2018) and are classified using the Common International Classification of Ecosystem Services (CICES) (Haines-Young et al. 2018). The ecosystem types throughout the Geopark have been

identified at MAES level 3 and are correlated with the elements of the flora as well as with geological diversity. Ecosystem services were identified and assessed through the recording and analysis of the main anthropogenic activities in the area of the Geopark, as well as through the determination of the impact of geosites on the conservation of specific plant species.

Results

As a case study to be considered, is the association of the local endemic species, Silene conglomeratica Melzh, with the thick conglomerate layers outcropping in the area of the Mega Spilaio Monastery geosite (Figure 3), where the very small population (known from only two locations in Mega Spilaio (locus classicus) and a neighboring area in Vouraikos gorge) of this species has a particularly limited distribution. The results are presented in heat-maps (figure 2) for the areas of geosites occurrence and the important areas of ecosystem services are identified. The areas of the Geopark with significant elements of geodiversity and the simultaneous presence of endemic flora species are recognized. These areas are highlighted as important for the provision of ecosystem services, e.g., geodiversity conservation (regulatory, conservation), biodiversity conservation (regulatory, conservation), recreation (cultural), grazing (supply, cultural).

Figure 3. Vertical conglomerate rocks, habitat of *Silene conglomeratica.*

Conclusions

In conclusion, the value of the special geodiversity and biodiversity of the Chelmos-Vouraikos UNESCO Global Geopark is highlighted in terms of ecosystem services importance that can be a competitive advantage for the integrated management of the National Park and Geopark.

References

Golfinopoulos, V., Papadopoulou, P., Koumoutsou, E., Zouros, N., Fassoulas, C., Zelilidis, A., Iliopoulos, G., 2022. Quantitative assessment of the geosites of Chelmos – Vouraikos UNESCO Global Geopark. Geosciences 11, 63.

Kokkoris, I.P., Mallinis, G., Bekri, E.S., Vlami, V., Zogaris, S., Chrysafis, I., Mitsopoulos, I., Dimopoulos, P., 2020. National set of MAES indicators in Greece: Ecosystem services and management implications. Forests 11(5), 595.

Haines-Young, R., Potschin-Young, M.B., 2018.Revision of the common international classification for ecosystem services (CICES V5.1): A policy brief. One Ecosyst 3, 1–6.

Kokkoris, I.P., Drakou, E.G., Maes, J., Dimopoulos, P., 2018. Ecosystem services supply in protected mountains of Greece: setting the baseline for conservation management. Int. J. Biodivers. Sci. Ecosyst. Serv. Manag. 14, 45-59.

Tsakiri, M., Koumoutsou, E., Kokkoris, I., Trigas, P., Iliadou, E., Tzanoudakis, D., Dimopoulos, P., Iatrou, G., 2022. National Park and UNESCO Global Geopark of Chelmos-Vouraikos (Greece): Floristic Diversity, Ecosystem Services and Management Implications. Land 11(1), 33.

Verde, N., Kokkoris, I.P., Georgiadis, C., Kaimaris, D., Dimopoulos, P., Mitsopoulos, I., Mallinis, G., 2020. National scale land cover classification for ecosystem services mapping and assessment, using multitemporal copernicus EO data and google earth engine. Remote Sensing 12(20), 3303.

Support Team

16th INTERNATIONAL CONGRESS of the GEOLOGICAL SOCIETY OF GREECE

Post Graduate Students

GEORGAKI Maria
GIAMAS Vasileios
ILIOPOULOU Georgia
KARALI Marina
KAROUTSOS Panagiotis
NANOU Eleni-Anna
NIKOLAOU Panagiota
NTOURIS Efthimios
PANETAS-FELOURIS Iasonas
PAPAILIOPOULOU Maria
PERLEROS Konstantinos
SIDERIDIS Alkiviadis
STAVROPOULOU Vasiliki
TSIARSIOTI Louiza
TSOURTIS Konstantinos
TZORTZI Marianthi
XENOU Chara

Post Doc

ARAVANTINOU Eirini
GEROGIANNIS Nikolaos
RALLAKIS Dimitrios

Under Graduate Students

ANGELOPOULOU Angeliki-Natalia
ATHANASIOU Adriana
ALEXIOU Iliana
ANASTASOPOULOU Stavroula
ANDRIKOPOULOU Angeliki-Maria
ANTONAKOPOULOS Panagiotis
ARVANITIS Angelos
ARVANITOPOULOS Marios - Ioannis
GOUKOS Konstantinos
DALGITSI Panagiota
DOUGIOS Tryphon
ZELILIDIS Panagiotis
ZIKOS Michael
ZOTOU Lydia
THEODORAKOPOULOU Dimitra
KALATZI Lemonia
KARAPANTSOS Matthew
KRATSA Zacharias
KOSTIS Efrosini
LAMPRIANIDIS Alexandros
LATTA Nikoleta
MALAMA Christina
MAVRIDIS Markos
MILIOS Nikolaos
MIHOS Panagiotis
NIKA Varvara
NIKOLAKOPOULOU Vasiliki
NICOLAOU Chrysoula-Danae
DALAKURA Ioanna
OKOUTSIDOU Konstantina
PAPAVASILOPOULOU Sofia
RAFTOPOULOS George
SAVVATIS Prokopios
SIGALA Maria-Athena
SKINTZI Pavlina
STEKA Paraskevi
TOLIAS Lukas
TSIKOURAS Pavlos
FLORAKI Spyridoula

OUR EARTH, OUR HOME

Authors Index

Dennis	Anestoudis	144									
Vasiliki	Anevlavi	414									
Dimitra	Angelopoulou	72									
Alexandra	Anifadi	181									
Marios	Anthymidis	281	298								
Emmanouil	Antonakis	380	383	384							
Asimina	Antonarakou	57	71	88	91	98	239	252	253	253	264
		269	283	357	358	386					
N	Antoniadis	223									
Dimitra	Antoniou	72									
Varvara	Antoniou	140	141								
Eleftheria	Antoniou	274									
Irini	Antoniou	351									
Christina	Antonopoulou	43									
Eleni-Apostolia	Anyfadi	230									
Emmanuel	Apostolidis	407									
Dionysios	Apostolopoulos	331									
Angeliki	Arapakou	11									
Eirini	Aravadinou	154	155	158	160						
Ariadne	Argyraki	10	126	234	236	288					
Sotirios	Argyroudis	227									
Apostolos	Arvanitis	333									
Aggelos	Arvanitis	359									
Dimitris	Asimakopoulos	37									
Paul	Asimow	221									
Argyro	Asvesta	110	112								
Anastasios	Athanasiou	350									
Constantin D.	Athanassas	13	73								
Constadinos	Athanassoulis	106									
Sophia-Ekaterini	Avgerinou	230	231								
Pavlos	Avramidis	69	114	175	185	187	190	244	354	428	
Marilou	Avramidou	292									
Despoina	Bafi	327									
Athanasia	Bakopoulou	283									
Melina	Bantouvaki	301									
Ioannis	Barbaresos	31									
Giorgos	Barberis	78									
Aggeliki	Barberopoulou	368									
Anna	Barra	115									
Vassiliki	Barsaki	322	347								
Ioannis	Bassiakos	319	321								
George	Bathrellos	142	351	357	358	387					
Aristides	Batis	140	141								
Anna	Batsi	56									

Dimitrios-Vasileios	Batzakis	146	225	318		
Ioannis	Baziotis	221	243	247		
Jonathan	Bedford	388				
Vlasoula	Bekiari	244				
Spyridon	Bellas	131	294	386		
Evangelia	Benetou	206				
Konstantina	Bentana	380	384	403		
Jasper	Berndt	100	101	243	247	
Evangelia	Besiou	71	98	252	254	
Lealem	Beza Zerihun	39				
Ahmer	Bilal	168				
Kamran	Bin Zafar	105				
Giulio	Bini	286				
Adonis	Bogris	202				
Madelaine	Böhme	238				
Pavlos	Bonatis	184				
Nikolay	Bonev	18				
Anton	Bonnier	389				
Fotios	Botsolis	178	179			
Chrysanthos	Botziolis	83	169	170	386	
Vasileios	Boumpoulis	256	350			
Dimitra	Boundi	247	255			
Nicolina	Bourli	33	34	37	47	48
Anna	Bourliva	422				
Daniel	Bowden	202				
Anastasia	Bozatzi	134				
Lindsay	Bramwell	234				
Jose	Brilha	95				
Filippo	Brugnone	183				
Lorenzo	Brusca	182				
Simon	Bufféral	337				
M.	Bulnes	28				
Gianluigi	Busico	200				
Sergio	Calabrese	116	183			
Stefano	Caliro	116				
Riccardo	Caputo	93	218	251	360	
Carlo	Cardellini	116	183			
Gareth	Carter	130				
Maria	Catania	149				
Michel	Cathelineau	89				
Octavian	Catuneanu	169				
Konstantinos	Chaidas	74				
Stylianos	Chailas	29	245	404	405	
George	Chalatsis	347				

Fotini	Chalkiopoulou	32				
Areti	Chalkioti	175				
Eleni	Chamilaki	34				
Timothy	Chapman	332				
Marianna	Charalambous	46				
Ioannis	Charalampopoulos	302				
Angelos	Charitopoulos	268				
Nikos	Charizopoulos	290	296			
Andreas	Chasiotis	148				
Vasileios	Chatzaras	154	155	328	332	340
Emmanouil	Chatziangelis	300				
Adamantia	Chatziapostolou	99				
Elissavet	Chatzicharalampous	157				
Stella	Chatzidima	248				
Panagiotis	Chatzidimitriou	281				
Athanasios	Chatziioannou	12				
Alexandros	Chatzipetros	12	229	265	335	379
Nikos	Chatzis	281	298			
Themistoklis	Chatzitheodosiou	80	222			
Georgios	Chatzopoulos	174	277			
Massimo	Chiaradia	18				
Giovanni	Chiodini	116	286			
Florina	Chitea	378				
Krystalia	Chitoglou	138				
Vassileia	Chondraki	6				
Kimon	Christanis	196	258	309	353	413
Georgios	Christidis	233	406			
Christos	Christidis	248	249			
Rozalia	Christodoulopoulou	81				
Dimitris	Christodoulou	348	364	400	408	417
Irini	Christoforou	234				
Marina	Christopoulou	148				
Anna	Chronaki	274				
Aikaterini Alexandra	Chrysafi	68				
Chrysoula	Chrysakopoulou	171				
Efthymios	Chrysanthopoulos	85	295			
Francesca R.	Cinti	97				
Riccardo	Civico	97				
Richard	Collier	130				
Jean Jacques	Cornee	386				
Eleni	Dafnioti	277				
Pavlos	Dafnis	320				
Walter	D'Alessandro	116	182	183		
Antonino	D'Alessandro	149	150	410		

Marousa	Damigou	269									
Maria-Elli	Damoulianou	419									
Ryad	Darawcheh	3									
Andreas	Darlas	345									
Kyriaki	Daskalopoulou	116	183								
Joshua R.	Davis	332									
Patrice	de Caritat	236									
Federico	Dela Peña	7									
Georgios	Deligiannakis	260	290	320	329						
Alecos	Demetriades	236									
Nikolaos	Depountis	177	199	204	256	287	299	300	350		
Michalis	Diakakis	109	215								
Paraskevas	Diakoparaskevas	137									
Nectaria	Diamanti	431									
Markos	Digenis	305									
Spyridon	Dilalos	26	31	62	109	215					
Xenophon	Dimas	364	400	408	417						
Georgios	Dimitrakakis	425									
Sarantis	Dimitriadis	110									
Eirini	Dimitriou	92									
Margarita	Dimiza	39	103								
Nikolaos	Dimopoulos	47									
Panayotis	Dimopoulos	418									
Grigoria Vasiliki	Dimou	103	175								
Effie	Dimou	313									
Ioannis	Dokas	227	394								
Despina	Dora	151	224								
Zornitsa	Dotseva	18									
Elisavet	Dotsika	55	348								
Trifon	Dougios	359									
Erich	Draganits	402									
George	Drakatos	220									
Paraskevi	Drakopoulou	38									
Chara	Drakopoulou	139									
Alexandros	Drakoulis	171									
Antonia	Dretaki	208	229	257							
Hara	Drinia	39	79	88	91	95	114	163	232	253	342
Georgios	Droukas	244									
Martyn R.	Drury	328									
Kyriaki	Drymoni	140									
Llambro	Duni	312									
Ana	Dura	104									
Edmond	Dushi	312									
Pauline A.	Duval	20									

Clara	Duverger	118		
Athena	Economou-Amilli	61	63	
Maria	Economou-Eliopoulos	272		
Eirini	Efstathiou	122		
Nikos	Efstratiou	175		
Nikolaos	Efthimiou	290		
Muhsan	Ehsan	105		
Vasiliki	Eletheriou	81		
Alexandros	Emmanouilidis	185	244	354
Dimitris	Emmanouloudis	141		
Ismail	Empliouk	86	87	
Jane	Entwistle	234		
Giuseppe	Etiope	364		
Christos	Evangelidis	246		
Dimitrios	Evangelinos	206		
	Evangelou	408		
Niki	Evelpidou	336	372	
Andriani	Exintaridi	197	407	
Natacha	Fabregas	130		
Elias	Fakiris	364	400	417
Ioannis	Farmakis	222	226	
Konstantinos	Farmakis	306		
Charalampos	Fassoulas	119	235	305
Eugenia	Fatourou	27	30	35
Sarah	Faulwetter	244		
George	Ferentinos	348		
Maria	Ferentinou	318	350	
Ludovic	Ferrière	221		
Andreas	Fichtner	202		
Anna	Figlioli	149	150	410
Ilias	Fikos	378		
Eleni	Filippaki	319	321	
Anestis	Filippidis	369		
Panagiotis	Filis	343		
Christos	Fillis	57	62	82
Martin	Finné	389		
Michalis	Fitros	370	372	
Matthew	Foley	328		
Mary	Ford	130		
	Foukas	408		
Michalis	Foumelis	420		
Ioannis	Fountoulakis	246		
Christina	Fourkalidi	274		
Emmanouil	Fragkioudakis	138		

Georgia	Giannaraki	364					
Dionysios	Giannikopoulos	331					
Ioannis Konstantinos	Giannopoulos	26	31	51	58	62	64
Vasileios	Giannopoulos	82					
Michail	Giannopoulos	409					
Ioannis	Giaourtsakis	343					
Philip	Giles	318					
Sebastian	Gilment	144					
Michalis	Giorgaras	362					
Marietta	Gkagka	106					
Konstantinos	Gkaidatzoglou	76					
Melina Dorothea	Gkari	224					
Charikleia	Gkarlaouni	207					
Anastasia	Gkeme	138					
Faidra	Gkika	246					
Ioannis	Gkiougkis	86	87				
Basiliki	Gkoka	77					
Vasileios	Gkosios	26	31	62	64		
Panagiotis	Gkotsis	201					
Myrsini	Gkouma	175					
Dionysios	Gkoutis	372					
Alexandra	Gogou	309					
Vasilis	Golfinopoulos	119	239				
Andreas	Gondikas	293					
Konstantinos	Goukos	359					
Leonidas	Gouliotis	144					
Theodoros	Gournelos	376					
Nikolaos Artemios	Gournelos	376					
Alexia	Grambas	252	283				
Tassos	Grammatikopoulos	279					
Bernhard	Grasemann	402					
Ioannis	Grendas	312	396				
E.	Grigorakou	223					
Diamantina	Griva	146	225				
Georgia	Grypaiou-Iskenderidou	406					
Yunbin	Guan	221					
Negar	Haghipour	408					
Ardit	Hajrullai	312					
Gergo	Hamar	73					
Mark	Hannington	104					
Thomas	Hasiotis	206	209				
Martina	Hättestrand	389					
Panagiotis	Hatzidimitriou	396					
Kiki	Hatzilazaridou	32					

Konstantin	Hatzipanagiotou	173	210	279							
Marie	Haut-Labourdette	185									
Christoph	Hauzenberger	210	273	414							
James	Hengesh	320									
Dominik	Hezel	317									
George	Hloupis	277									
Fabrice	Hollender	396									
Maximos-Vasileios	Holokolos	232	342								
Evangelos	Hristoforou	73									
Jinping	Hu	221									
Alexandros	Iakovidis	252	254								
Margarita	Iatrou	38									
Youseph	Ibrahim	340									
Vasileios	Ieronymakis	407									
Ioanna	Ilia	266									
George	Iliopoulos	33	47	48	69	83	119	239	291	344	345
		359	395	398	416	418					
James	Iliopoulos	355									
Ioannis	Illiopoulos	61	63	101	203	401	412	429			
Muhammad	Ishfaq	24									
Ismail	Ismail	111	308	310							
Yiannis	Issaris	14									
Adam	Izdebski	354	389								
Thorsten	Jakobitsch	414									
Hammad Tariq	Janjuhah	168	386								
Christopher	Johnson	236									
Richard	Jones	144									
Akaterina	Kafetzidou	27	30	35							
Evangelos	Kaikas	306	310	313							
George	Kakaris	347									
Triantafyllos	Kaklis	226									
Christina	Kalaitzi	138									
Stavros	Kalaitzidis	196	258	309	353	413	419	421			
Panagiotis	Kalaitzis	74									
Lemonia	Kalantzi	113	153	409							
Nikolaos	Kalligeris	207									
Vassilis	Kallimogianis	143									
Andreas	Kallioras	85	165	295							
Ioannis	Kalogeras	268									
Nikolaos	Kalogiannis	261									
G.	Kalousi	223									
Maria	Kalpogiannaki	274	374	409							
Konstantinos	Kamadanis	224									
M	Kamali	54									

Evangelos	Kamperis	334									
Isidoros	Kampolis	322	325	334	361						
Panagiotis	Kampouridis	238	311								
Stamatina	Kanakaki	246									
E	Kanaki	223									
Christos	Kanellopoulos	61	63	98	101	280	282	286	401	412	
Nikolaos	Kantiranis	66	67	171	192	195	270	366	367	369	381
		422									
Ioannis	Kapageridis	112	304								
Vasilis	Kapetanidis	36	109	122	159	161	184	215	278	284	
Konstantinos	Kappis	416									
Vassilios	Kapsimalis	6	14	225							
Maria	Karagkiozi	224									
Vasileios	Karakitsios	98	386								
Andreas	Karakonstantis	122	278	284							
Foivos	Karakostas	301									
Panagiotis	Karakoulakis	224									
Petros	Karalis	55									
Marina	Karalis	203	346								
Nestor	Karamarkos	304									
Mina	Karamesouti	290									
Ioannis	Karamitros	122									
Alexandros	Karampelas	151	224								
Efstratios	Karantanellis	19	80	222	226						
Marianthi	Karantzia	327									
Matthaios	Karapantzos	412									
Ilektra	Karasante	122									
Dimitrios	Karasogiannidis	86	87								
Vassilios	Karastathis	127	430								
Georgios	Karatzas	137									
Andreas	Karavias	216	259								
Aikaterini	Karditsa	399									
Nikolaos	Kargopoulos	238									
Christos	Karkalis	107	203	285	346						
Panagiotis	Karoutsos	164									
Maria	Karpouza	357									
Nikolaos	Karydas	252	254								
Efthimios	Karymbalis	142	146	216	225	318					
Theodora	Karympali	198									
George	Kasfikis	107									
Ioannis	Kassaras	36	109	122	215	278	284	365			
Aikaterini	Kastana	72									
Apostolos	Kastritsis	268									
Christos	Katagas	412									

Marianna	Kati	143									
Christos	Katrantsiotis	389									
Emmanouil	Katrivanos	123	335								
Olga	Katsani	244									
Katerina-Navsika	Katsetsiadou	283									
Nikolaos	Katsiavrias	45									
Chrysoula	Katsora	50									
George	Kaviris	36	62	109	159	161	184	215	278	284	357
Katerina	Kavoura	197	407								
Antonis	Kavvadias	296									
Nerantzis	Kazakis	152	200								
Stavroula	Kazana	140									
Maria	Kazantzaki	319	321								
Danai	Kazantzidou-Firtinidou	109	215								
Nikolaos	Kazilis	22									
Manuel	Keith	102									
Efstratios	Kelepertzis	43	49								
Alexandros	Kepas	407									
Athanasia	Kerkenou	356									
Hareem	Khan	305									
Stephanos P.	Kilias	102	293								
Adamantios	Kilias	123	335								
Michael	Kipp	221									
Anastasia	Kiratzi	423									
Stamatis	Kirdis	343									
Anastasia-Maria	Kiritsi	359									
Charalampos	Kkallas	267									
Reiner	Klemd	381									
Stephan	Klemme	100	101	243	247						
Nikolaos	Klimis	227	294								
Kate	Knights	236									
Rexhep	Koci	312									
Marios	Koilanitis	428									
Aliki	Kokkala	121									
Sotirios	Kokkalas	44	129	144	145	164	364	370	416		
Maria	Kokkaliari	61	63	401	412	429					
Anastasia	Kokkari	270									
Ioannis P.	Kokkoris	418									
Andrianos	Kokkoromytis	58									
Maria	Kokovaki	224									
Alexandra	Koliou	95									
Evgenia	Koltsida	295									
Christina	Kondyli	79									
George	Konidaris	138									

Aliki	Konsolaki	50	51	57	58	59	64	76		
Fotios	Konstantinakis	224								
Ioakeim	Konstantinidis	156								
Panagiotis	Konstantopoulos	144								
Garyfalia	Konstantopoulou	197	407							
George	Kontakiotis	41	42	71	98	168	252	254	315	386
Kyriakos	Kontakos	246								
Charalampos	Kontoes	54	60							
Haris	Kontoes	162								
Villy	Kontogianni	250								
George	Kontokostas	88								
Artemis	Kontomichalou	126								
Orestis	Kontopidis	411								
Ioannis	Kontos	432								
Georgios	Kontostavlos	51								
Antonis	Koroneos	186	205	208						
Maria	Koroni	202								
Efterpi	Koskeridou	343								
Efi	Kosti	240								
Dimitris S	Kostopoulos	138	139							
Vassiliki	Kostopoulou	16								
Vasileios	Kotinas	376	387	399						
Evelina	Kotsi	36	109	215						
Evangelia	Kotsi	51	57	58	59	283				
Georgia	Kotzamani	252	254							
Ilias	Koufogiannis	280								
Nikos	Koukis	362								
Olga	Koukousioura	103	175	187	190					
Ioannis	Koukouvelas	69	77	93	94	365				
Nikolaos	Koukouzas	107	147	259	274	279	375	390	411	
Prodromos	Koulelis	151								
Maria	Kouli	17								
Katerina	Kouli	27	30	35	175	185	354	389		
Nikolaos	Kouloussis	270								
Ioannis	Koumantakis	377								
Olga	Koumoutsakou	264	269							
Eirini	Koumoutsea	343								
Eleni	Koumoutsou	119	418							
Ioannis	Kourliaftis	14								
Georgia	Kourtaki	233								
Vasiliki	Kouskouna	365	368							
Argirios	Kouskouras	248								
Anna	Koutroulli	41	42							
Konstantinos	Koutroumbas	181								

Constantin	Koutsikopoulos	348									
Petros	Koutsovitis	113	153	173	203	210	217	228	240	273	279
		285	316	346	347	374	375	390	402	414	
Soultana Kyriaki	Kovaiou	270									
Andriana	Kovani	83									
Jochen	Krahl	125	317								
Haralambos	Kranis	259	314	315	337	404	405				
Pavlos	Krassakis	107	140	259							
Phaedra	Kravvariti	29									
Dimitrios	Ktenas	289	307	308							
Olga-Joan	Ktenidou	424									
Stephen C.	Kuehn	41	42								
Neki	Kuka	312									
Zacharenia	Kypritidou	96									
Chara	Kyriakidou	38									
Konstantinos	Kyriakopoulos	228									
Christina	Kyriakouli	238									
Eva	Kyriazis	283									
Aggeliki	Kyriou	78	92								
Anastasis	Ladas	138									
Anna	Ladenberger	236									
Spyros	Lalechos	363									
Nikolaos	Lambrakis	344									
Nikos	Lambrinos	341									
Sophia	Lamera	17									
Aggelos	Lamprakopoulos	380	383	384	397						
Vasiliki	Lamprinou	61	63								
Paraskevi	Lampropoulou	77	84	147	148	153	173	274	374	390	
Maik	Lang	214									
Sofia	Laskari	59	402								
Konstantinos	Laskaridis	11	32	372							
Georgios	Lazaridis	139	151	224							
Maria	Lazaridou	248									
Georgia	Lazarou	132	133								
Ilias	Lazos	127	136								
Valentine	Lefils	118									
Efthymis	Lekkas	36	51	57	58	59	109	215	252	283	
Konstantinos	Lentas	202	207								
Aris	Leontaritis	305	362								
György	Less	103									
Lorenza	Li Vigni	116	182	183							
Alexandros	Liakopoulos	126									
Spyros	Liakopoulos	246									
Georgios	Liakopoulos	354	389								

Dionysia	Liakopoulou	276	343				
Ioannis	Lialiaris	59					
Vasiliki	Lianou	264					
Eleni	Liapi	395	398				
Georgios	Liapis	390					
Konstantinos	Lilis	203					
Nikolaos	Linardos	22					
Jolien	Linckens	125	317				
Spyridon	Liogris	147					
Nikolaos	Liosis	6					
Aspasia	Litoseliti	94	374				
Isidoros	Livanos	38					
Fotis	Livanos	351					
Konstantinos	Lolos	148					
Anna Maria	Lombardi	97					
Maritza Roneen	Lopez	7					
Valia	Loukaidi	38					
Dimitrios	Loukidis	124	132	133			
George	Louloudis	107					
Constantinos	Loupasakis	54	60	81	157	162	223
Lucas	Lourens	408					
Stylianos	Lozios	88	375	402			
Federico	Lucchi	286					
Rebecca	Lunn	277					
Alexander D.J.	Lusk	332					
Nikolaos	Lykakis	188					
Evriviades	Lymperis	320					
George	Lyras	252	254	358			
Epameinondas	Lyros	323					
Chi	Ma	221					
Marta	Magán	28					
Andreas	Magganas	217	285				
Massimiliano	Maggini	360					
Konstantinos	Magkos	347					
Ifigeneia	Magremi	101					
Vagia-Ioanna	Makri	90	131	294			
Panayota	Makri	386					
Pagona	Makri	406					
Tatiana	Makridou	346					
Georgios	Makrodimitras	48	289	307	309	313	
George	Makrygiannis	178	179				
George	Malaperdas	368					
Emmanouil	Manoutsoglou	90	131	136	137	193	386
Kyriaki	Manta	38					

Vanessa	Maragkou	268									
Angelos G.	Maravelis	37	83	169	170	289	386				
Basil	Margaris	356									
Vassilios	Marinos	19	80	120	121	156	219	222	226	241	385
Konstantinos	Markantonis	295									
Fabienne	Marret	27	30	35							
Horst	Marschall	125									
Silvia	Massaro	286									
Alessia	Massi	354	389								
Micol	Mastrocicco	200									
Vasileios	Mastrokostas	390									
Rosa Maria	Mateos	115									
Sofia	Matsagou	114									
Maria	Mavraki	178	179								
Anastasios	Mavrakis	178	179								
Aristodimos	Mavrikos	84									
Constantinos	Mavrogonatos	53	100	101							
Dionysia	Mavromati	81									
Spyridon	Mavroulis	36	109	215							
Lisa	McNeill	130	297	303							
Petros	Mecaj	292									
Stavros	Meletlidis	172									
Vasilios	Melfos	66	67	100	366	381					
Margarita	Melfou	381									
Nikolaos	Melis	202	207	268							
Eleni	Mertiri	107									
Aristeidis	Mertzanis	329									
Theo J.	Mertzimekis	104	293								
Dimitrios	Metafas	268									
Ioannis	Michalakis	162									
Dionysia	Michalopoulou	81									
Maria	Michalopoulou	299									
Georgios	Michas	159	161	230	231	297					
Raymond	Michels	89									
George	Mikoniatis	400									
Leo	Millonig	125									
Giorgi	Mindiashvili	1									
Panagiotis	Minetos	220									
Muhammad Armaghan Faisal	Miraj	24	25								
Stefanos	Missias	209									
Georgia S.	Mitsika	26	31	62	64						
Leonidas	Moforis	61	63	98	315						
Pierre	Moissette	386									

Panagiotis	Monachelis	268						
Oriol	Monseratt	115						
Daniel	Moraetis	305						
Evgenia	Moraiti	322	347					
Ioannis	Morfis	38						
Georgia	Moschou	294						
Spyridon	Mosios	232	342					
Antonios	Mouratidis	330	341					
Vasiliki	Mouslopoulou	275						
Haris	Moustakas	428						
Evangelos	Mouzakiotis	127	430					
Muhammad Saleem	Mughal	168						
Andreas	Mulch	71						
Muhammad Jawad	Munawar	25						
Martin	Muravchik	130						
Christos	Mylonas	333						
Christos	Myriounis	295						
Christina	Mytiglaki	192	195	367	369			
Maria Anna	Nakasi	55						
Eleni-Anna	Nanou	427						
Panagiotis	Nastos	141						
Valentini	Navrozidou	187	190					
Constantinos	Nefros	60						
Petros	Neofotistos	167	212					
Nicolas	Neuwirth	125	317					
Maja	Nielsen	368						
Despoina	Nifora	77						
Thomas	Nikas	202						
Anastasios	Nikitas	48	289	309				
Nikolaos	Nikolaidis	305						
Anastasios	Nikolaidis	341						
Iphigeneia	Nikolaidou	224						
Konstantinos	Nikolakopoulos	78	92	93	94	244	323	331
Pantelis	Nikolakopoulos	425	426					
Nikolaos	Nikolaou	250						
Chrisoula	Nikolaou	359						
Elisavet	Nikoli	140	141					
Ioanna	Nikolopoulou	275						
Maria	Nikopoulou	66	67					
Ulysses	Ninnemann	72						
Casey	Nixon	297	303					
Brayden	Noh	8						
Paraskevi	Nomikou	102	104	140	141	293		
Elin	Norström	389						

Alexandra	Noti	408					
Vassilis	Noulis	211					
Tatyana	Novikova	430					
Theodoros	Ntaflos	113	273	375			
Sofia	Ntasioti	224					
Georgios	Ntelis	377					
Maria	Ntinou	175					
Maria Margarita	Ntona	200					
Panagiotis	Ntontos	117					
Athanasia-Violeta	Ntzoumani	244					
Gábor	Nyitrai	73					
Matthias	Ohrnberger	281					
Ioannis	Oikonomopoulos	196					
Konstantinos	Oikonomopoulos	306					
Andrés	Olivar-Castaño	281					
Kujtim	Onuzi	273					
Aristotelis	Pagoulatos	201					
Aris	Paleokrassas	209					
Aggelos	Pallikarakis	290	329				
Dionisios	Panagiotaras	77	244				
Ioannis	Panagiotopoulos	6	14	144	309		
Konstantinos	Panagiotopoulos	27	30	35			
Georgios	Panagopoulos	137	144				
Anestis	Panagopoulos	320					
Iasonas	Panetas-Felouris	416					
Maria	Panitsa	418					
Aikaterini	Panora	186	224				
Areti	Panou	312					
Dimitris	Panousis	140	141				
Sofia	Pantali	224					
Zoe	Pantazopoulou	330	341				
George	Pantopoulos	83					
Daniela	Pantosti	97					
Panagiota	Pantou	286					
Maria	Papadaki	389					
Dimitrios	Papadimitriou	192	195	367			
Panayotis	Papadimitriou	278	284				
Ioannis	Papadopoulos	216					
Christoforos	Papadopoulos	248					
Alexandros	Papadopoulos	309					
Lambrini	Papadopoulou	66		67	335	366	422
Penelope	Papadopoulou	119	353	359	418		
Ermioni Eirini	Papadopoulou	189					
Evdokia	Papadopoulou	257	379				

Maria	Papailiopoulou	427							
Haritakis	Papaioannou	265							
Christos	Papaioannou	356							
Maria	Papakonstantinou	364							
Theodosios	Papaliangas	120							
Dimitrios	Papanastassiou	142	318						
Dimitrios	Papanikolaou	108	255	339					
Ioannis	Papanikolaou	290	292	296	320	329			
Xanthos	Papanikolaou	363							
Georgia	Papapavlou	421							
George	Papathanasiou	19	80	156	227	241	251	394	
George	Papatheodorou	348	364	400	408	417			
Konstantinos	Papavasileiou	15							
Christina	Papavasileiou	179							
Joan	Papavasiliou	128	129						
Andreas	Papazachariou	296							
Constantinos	Papazachos	267	281	298	356				
Panagiotis	Papazotos	349							
Dimitra	Papouli	222							
Dimitrios	Papoulis	77	84						
Angeliki	Papoutsa	23	52						
I	Papoutsis	54							
Irena	Pappa	291							
Nikolaos	Paraskevis	338	371	373					
Konstantinos	Paraskevopoulos	252	254						
Paraskevas	Paraskevopoulos	428							
Issak	Parcharidis	81	216	223	225	259	327		
Francesco	Parello	116	183						
Nikolaos	Pasadakis	34	48	90	131	294	309	386	419
Panagiotis	Paschos	98	197	407					
Agni	Patra	112	304						
Lucian	Pavel	378							
Aikaterini	Pavlaki	235							
Spyridon	Pavlides	127	379						
Kosmas	Pavlopoulos	305	362						
Francis	Pavloudakis	304	338	371	373				
Sofia	Pechlivanidou	72	130	303					
George	Pehlivanides	140	141						
Christos	Pennos	305							
Georgia	Pe-Piper	41	42						
Martha	Perdikaki	295							
Kostantinos	Perdikaris	427							
Spyros	Perdikis	350							
Savvas	Peridis	37							

Argyrios	Periferakis	21	134	243							
Konstantinos	Periferakis	21									
Aristodemos-Theodoros	Periferakis	21									
Eftychia	Peristeridou	366									
Vasilios	Perleros	235									
Konstantis	Perleros	353	413								
Maria	Perraki	349									
Sven	Petersen	104									
Stelios	Petrakis	57	58								
Chara	Petrakou	6									
Alexandros	Petropoulos	336									
Petros	Petrounias	113	147	148	153	173	240	274	279	346	374
		390	409								
Rainer	Petschick	125	317								
Jörg	Pfänder	125	317								
Adonis	Photiades	260	261	263							
Erion-Vasilis	Pikoulis	424									
David J.W.	Piper	41	42								
Avgerinos	Pitsillis	234									
Vasilios	Pletsas	102	293								
Christina-Chrysavgi	Pliaka	86	87								
Fotios-Konstantinos	Pliakas	86	87								
Anastasios	Plougarlis	167	212								
J.	Poblet	28									
Sara	Polanco	340									
Artemis	Politi	61	63								
Paraskevi	Polymenakou	102	293								
Fotini	Pomoni-Papaioannou	16									
Panagiotis	Pomonis	173	316								
Maurizio	Poscolieri	225									
Christos	Pouliaris	295									
Serafim	Poulos	64	399								
Anastasios	Poulos	209									
Eleftheria	Poyiadji	115									
Manuel	Pozo	10									
Amalia	Prandekou	348									
Ioannis	Prevedouros	185	187	244	354						
Gloria	Prieto Rincón	236									
Stavros	Proestakis	189									
Georgios	Prountzopoulos	222									
Nikolaos	Proutsos	302									
Yiannis	Psaltakis	361									
Despoina	Psarraki	349									

Stavros	Psomadakis	229							
Emmanouil	Psomiadis	290	292	296	302	329			
Maria	Psychogiou	79							
Manuel	Pubellier	337							
Konstantina	Pyrgaki	107							
Stella	Pytharouli	277							
Dimitrios	Rallakis	89							
Alexios	Ramfos	244							
Maria	Rangoussi	268							
Dimitra	Rapti	213	218						
Anne Ewing	Rassios	56	70	194					
Michail	Ravnalis	267							
Saif-Ur	Rehman	24							
Klaus	Reicherter	290	329						
Anastasia	Rekouti	359							
Ioanna	Repanidou	341							
Patrice F.	Rey	340							
Nickos	Rigakis	90							
Alexis	Rigo	118							
Vincent	Roche	402							
Aikaterini	Rogkala	147	148	173	274	346	374	390	409
Mon Carlo	Ronquillo	7							
Zafeiria	Roumelioti	275	323	364	423	428			
Christos	Roumpos	107	338	371	373				
Grigoris	Rousakis	38	309						
Socrates	Roussiakis	238	276	311					
Davide	Russo	360							
Nikolaos	Sabatakakis	177	199	204					
Panagiotis	Sabatakakis	248							
Maria	Sagredou	245							
Dimitris	Sakellariou	38							
Vassilis	Sakkas	29	62	109	215				
Rana Faizan	Saleem	25							
Maria	Salomidi	14							
Spyridoula	Saltapida	343							
Charalampos	Sarafidis	422							
Charalambos	Saroglou	143							
Socrates	Savelides	232	342						
Maria	Savvidou	212							
Sotirios	Sboras	98	127						
Andreas	Scharf	305							
David	Schneider	402							
Christopher	Schroeck	214							
Lorenz	Schwark	191							

Salvatore	Scudero	150	410							
Foteini	Sdraka	224								
Spyridon	Sergiou	72	408	417						
Aikaterini	Servou	204	338	371	373					
Donna	Shillington	130	297	303						
Maria	Sianni	34								
Alkiviadis	Sideridis	113	210	240	279	346	414			
Evangelia	Sigala	49								
Christos	Simos	202								
Iraklis	Simos	202								
Gloria	Simubali	236								
Ioannis	Sinatkas	112								
Theodoros	Sketopoulos	308								
Hariklia	Skilodimou	142	351	357	358					
Stamatina	Sklavounou	343								
Vasilios	Skliros	372								
Emmanuel	Skourtsos	82	315	337						
Hara	Skylodimou	387								
David	Smith	236								
Krystyna	Smolinski	202								
Emilia	Sofianska	106								
Nikolaos	Sofis	421								
Efthimios	Sokos	118	246	275	323	364	365	425	426	428
Lorenzo	Solari	115								
Pinelopi	Sotiriou	241								
Apostolos	Sougioltzis	413								
Konstantinos	Soukis	52	59	100	375	402				
Nikolaos	Soulakellis	74	189	383	384					
Georgios	Soulamidis	53								
Konstantinos	Soulis	292	296							
Panteleimon	Soupios	137	223							
Philip Mark	Spanidis	338	371	373						
Natalia	Spanou	250	407							
Aikaterini	Spiliopoulou	129	370							
Ioannis	Spingos	36	109	159	161	215				
Paul G.	Spry	100								
Karen	St.Seymour	17								
Michael	Stamatakis	10	26	40						
Eleftheria	Stamati	283								
Elizabeth	Stathopoulou	55	211	314	355					
Maria	Stavropoulou	51	58							
Vasiliki	Stavropoulou	344								
Olga	Stavroulopoulou	180								
Aristofanis	Stefatos	48	111	289	306	307	308	309	310	313

Emmanouil	Steiakakis	136							
Christos	Stergiou	265							
Daniel	Stockli	402							
Georgios	Stoumpos	222							
Christina	Stouraiti	23	52	53	100	101	236	375	402
Nichola A.	Strandberg	389							
Thrasivoulos	Stylianou	132	132						
Roberto	Sulpizio	286							
Gergely	Surányi	73							
Georgia	Svorligkou	238	311						
Olga	Sykioti	96	181						
Stella	Symeonidou	369							
Georgios	Syrides	103	175	187	190				
V	Sythiakaki	223							
Maria	Taftsoglou	227	251	394					
Eleni-Maria	Takoumaki	390							
Dimitris	Tarenidis	106							
Hammad	Tariq Janjuhah	98							
Efthimios	Tartaras	111	289	307	308	309	310	313	
Alexandros	Tasianas	307							
Maria	Tassi	55							
Franco	Tassi	286							
Athanasia	Tekerlekopoulou	84							
Dimosthenis	Telemenis	131							
Maria	Teskou	266							
Tassos	Thanos	90							
Nikolaos	Theocharidis	175							
Alexandros	Theocharis	411							
Dimitra	Theodorakopoulou	359							
Christos	Theodoropoulos	287							
Marieta	Theodoropoulou	248							
Georgios	Theodorou	55	211	343					
Eleni	Theodorou	384							
Nikolaos	Theodoulidis	281	312	396					
Penelope	Theologi-Gouti	429							
Anastasios	Thermos	246							
Basil	Tikoff	328	332						
Francois	Tissot	221							
Maria Eugenia	Toimil Molares	214							
Lefteris	Tomanis	296							
Stylianos	Tombros	44	128	129	370	416			
Stamatina	Tounta	327							
Claudio	Tranne	286							
Markos	Tranos	166	167	212					

Maria	Tzima	248									
Georgios	Tzorbatzakis	315									
Ioannis	Tzorbatzakis	315									
Marianthi	Tzortzi	345									
Alfred	Uchman	170									
Antonis	Vadidis	136									
Antonis	Vafidis	137									
Nikolaos	Vagenas	177									
Ioannis	Vakalas	250	324	334	382						
Ilias	Valiakos	384	403								
Sotirios	Valkaniotis	227	251	365	394						
Kanella	Valkanou	142	146	318							
Filippos	Vallianatos	159	161	230	231	237	242	277	301		
Dimitrios	Vandarakis	6	14								
Dezso	Varga	73									
George	Vargemezis	249	378								
Antriani	Varnava	335									
Effrosyni	Varotsou	40									
Emmanouil	Varouchakis	137									
Orlando	Vaselli	286									
Charalampos	Vasilatos	23	88	96	181						
Grammatiki	Vasileiadi	354									
Eleni	Vasileiou	349	377								
Iuliana	Vasiliev	71									
Emmanuel	Vassilakis	19	50	51	57	58	59	62	64	76	109
		181	215								
Yannis	Vavassis	400									
Nikolaos	Vavlas	423									
Markos	Vaxevanopoulos	305									
Dimitris	Vayenas	84									
Paraskevi	Velli	288									
Danae	Venieri	84									
Chrisa	Ventouzi	281	298								
Dimitra	Veropoulou	292									
Sotiris	Verroios	93									
Vassilios	Vescoukis	393									
Cristiano	Vingola	354	389								
Giovanni	Vitale	149	410								
Andreas	Vlachopoulos	408									
Evangelos	Vlachos	291									
Georgios	Vogdopoulos	205									
Dimitrios	Vogiatzis	171	192	195							
Kay-Obbe	Voss	214									
Panagiotis	Voudouris	53	61	63	100	101	366	370	375	381	

Konstantinos	Voudouris	162	249								
George	Vougioukalakis	280	282	286							
Nikolaos	Voulagris	62									
Myrsini	Voulgari	252									
Nikolaos	Voulgaris	26	31	36	109	184	215	278	284		
Konstantinos	Vouvalidis	175	224								
Ioannis	Vrontzos	123									
Konstantinos	Vythoulkas	10									
Junbo	Wang	392									
Erika	Weiberg	389									
Frank	Wesselingh	408									
Małgorzata	Wojtaszek-Kalaitzidi	258									
Michalis	Xanthakis	220									
Vayia	Xanthopoulou	101	413								
Markos	Xenakis	99	333								
Stamatios	Xydous	221	243								
Paris	Xypolias	125	154	155	158	160	317				
Renchao	Yang	168									
Federica	Zaccarini	100	210	272							
George	Zafeiropoulos	91									
Eleni	Zagana	344	427								
Muhammad	Zaheer	168									
Khalid	Zahran	391									
Alexandra	Zambetakis-Lekkas	98	314								
Miltiadis	Zampos	145									
Irene	Zananiri	206	250	322	324	336	347	382			
Ioannis	Zanesis	237									
Nikolaos	Zegkinoglou	102	293								
Avraam	Zelilidis	33	34	37	47	48	69	83	119	169	170
		239	386								
Alexandra	Zervakou	263	336								
Stavroula	Zervopoulou	111									
Emmanouela	Zevgoli	292									
Ioannis	Zevgolis	411									
Efstratios	Zgournios	380	384								
Degao	Zhai	129									
Maria	Ziazia	268									
Giannis	Zidianakis	395	398								
Eleni	Zimi	6									
Andreas	Zissimos	234									
Christina	Zoniou	268									
Triantafyllia	Zorba	66									
Serafeim	Zormpas	73									
Vassilios	Zotiadis	288									

Elena	Zoumpouli	47	220								
Nikolaos	Zouros	74	91	95	119	189	353	383	384	392	395
		397	398	403							
Dimitris	Zouzias	17									
Gernold	Zulauf	125	317								
Vasiliki	Zygouri	93	102								
Angelos	Zymvragakis	36	184								

SPONSORS

PLATINUM

HEREMA
HELLENIC HYDROCARBONS AND ENERGY RESOURCES MANAGEMENT COMPANY

ΔΕΔΔΗΕ

TERNA
GEK TERNA GROUP

GOLD

Hellas GOLD

GEObit

HELPE UPSTREAM

SILVER

Δελφοι - Διστομον
μονοπρόσωπη ανώνυμος μεταλλευτική εταιρία

IMERYS

LARCO

EYDAP

ΟΛΥΜΠΙΑ ΟΔΟΣ

intrakat

geotest

JGC
mark your place
Authorised Partner of GSSI

1987
ΓΑΛΑΞΙΔΙ
ΘΑΛΑΣΣΙΕΣ ΚΑΛΛΙΕΡΓΕΙΕΣ

AIGISTOS
ΤΕΧΝΙΚΗ ΕΤΑΙΡΕΙΑ

EUROPE DIRECT
Περιφέρεια Δυτικής Ελλάδας
Region of Western Greece

BRONZE

TOPALIDIS S.A.
MARBLE & GRANITE

ΕΔΑΦΟΣ ΣΥΜΒΟΥΛΟΙ ΜΗΧΑΝΙΚΟΙ Α.Ε.
Υπερείδου 9, 105 58 Αθήνα, Τηλ: 2103222050 Fax: 2103241607 e-mail: admin@edafos.gr

ΣΥΝΔΕΣΜΟΣ ΜΕΤΑΛΛΕΥΤΙΚΩΝ ΕΠΙΧΕΙΡΗΣΕΩΝ

Marathon Data Systems

SUPPORTED BY

UNIVERSITY OF PATRAS
ΠΑΝΕΠΙΣΤΗΜΙΟ ΠΑΤΡΩΝ
MODY-ELKE
Research Funds Special Account

ΠΕΡΙΦΕΡΕΙΑ ΔΥΤΙΚΗΣ ΕΛΛΑΔΑΣ
χέρατη αντιδέσεις!

ΓΕΩΤΕΧΝΙΚΟ ΕΠΙΜΕΛΗΤΗΡΙΟ ΕΛΛΑΔΑΣ

E.P.P.O.
Earthquake Planning & Protection Organization